

THIRD EDITION

---

**TRANSFORMS**

AND

**APPLICATIONS**

---

HANDBOOK

*Editor-in-Chief*

**ALEXANDER D. POULARIKAS**

---

 CRC Press  
Taylor & Francis Group

THIRD EDITION

---

**TRANSFORMS**

AND

**APPLICATIONS**

---

HANDBOOK

# The Electrical Engineering Handbook Series

*Series Editor*

**Richard C. Dorf**

University of California, Davis

## Titles Included in the Series

*The Avionics Handbook, Second Edition*, Cary R. Spitzer  
*The Biomedical Engineering Handbook*, Third Edition, Joseph D. Bronzino  
*The Circuits and Filters Handbook*, Third Edition, Wai-Kai Chen  
*The Communications Handbook*, Second Edition, Jerry Gibson  
*The Computer Engineering Handbook*, Vojin G. Oklobdzija  
*The Control Handbook*, William S. Levine  
*CRC Handbook of Engineering Tables*, Richard C. Dorf  
*Digital Avionics Handbook*, Second Edition, Cary R. Spitzer  
*The Digital Signal Processing Handbook*, Vijay K. Madisetti and Douglas Williams  
*The Electrical Engineering Handbook*, Third Edition, Richard C. Dorf  
*The Electric Power Engineering Handbook*, Second Edition, Leonard L. Grigsby  
*The Electronics Handbook*, Second Edition, Jerry C. Whitaker  
*The Engineering Handbook*, Third Edition, Richard C. Dorf  
*The Handbook of Ad Hoc Wireless Networks*, Mohammad Ilyas  
*The Handbook of Formulas and Tables for Signal Processing*, Alexander D. Poularikas  
*Handbook of Nanoscience, Engineering, and Technology*, Second Edition,  
William A. Goddard, III, Donald W. Brenner, Sergey E. Lyshevski, and Gerald J. Iafrate  
*The Handbook of Optical Communication Networks*, Mohammad Ilyas and  
Hussein T. Mouftah  
*The Industrial Electronics Handbook*, J. David Irwin  
*The Measurement, Instrumentation, and Sensors Handbook*, John G. Webster  
*The Mechanical Systems Design Handbook*, Osita D.I. Nwokah and Yidirim Hurmuzlu  
*The Mechatronics Handbook*, Second Edition, Robert H. Bishop  
*The Mobile Communications Handbook*, Second Edition, Jerry D. Gibson  
*The Ocean Engineering Handbook*, Ferial El-Hawary  
*The RF and Microwave Handbook*, Second Edition, Mike Golio  
*The Technology Management Handbook*, Richard C. Dorf  
*Transforms and Applications Handbook*, Third Edition, Alexander D. Poularikas  
*The VLSI Handbook*, Second Edition, Wai-Kai Chen

THIRD EDITION

---

**TRANSFORMS**

AND

**APPLICATIONS**

---

HANDBOOK

*Editor-in-Chief*

ALEXANDER D. POULARIKAS



CRC Press  
Taylor & Francis Group  
Boca Raton London New York

---

CRC Press is an imprint of the  
Taylor & Francis Group, an **informa** business



MATLAB® is a trademark of The MathWorks, Inc. and is used with permission. The MathWorks does not warrant the accuracy of the text or exercises in this book. This book's use or discussion of MATLAB® software or related products does not constitute endorsement or sponsorship by The MathWorks of a particular pedagogical approach or particular use of the MATLAB® software.

CRC Press  
Taylor & Francis Group  
6000 Broken Sound Parkway NW, Suite 300  
Boca Raton, FL 33487-2742

© 2010 by Taylor and Francis Group, LLC  
CRC Press is an imprint of Taylor & Francis Group, an Informa business

No claim to original U.S. Government works

Printed in the United States of America on acid-free paper  
10 9 8 7 6 5 4 3 2 1

International Standard Book Number: 978-1-4200-6652-4 (Hardback)

This book contains information obtained from authentic and highly regarded sources. Reasonable efforts have been made to publish reliable data and information, but the author and publisher cannot assume responsibility for the validity of all materials or the consequences of their use. The authors and publishers have attempted to trace the copyright holders of all material reproduced in this publication and apologize to copyright holders if permission to publish in this form has not been obtained. If any copyright material has not been acknowledged please write and let us know so we may rectify in any future reprint.

Except as permitted under U.S. Copyright Law, no part of this book may be reprinted, reproduced, transmitted, or utilized in any form by any electronic, mechanical, or other means, now known or hereafter invented, including photocopying, microfilming, and recording, or in any information storage or retrieval system, without written permission from the publishers.

For permission to photocopy or use material electronically from this work, please access [www.copyright.com](http://www.copyright.com) (<http://www.copyright.com/>) or contact the Copyright Clearance Center, Inc. (CCC), 222 Rosewood Drive, Danvers, MA 01923, 978-750-8400. CCC is a not-for-profit organization that provides licenses and registration for a variety of users. For organizations that have been granted a photocopy license by the CCC, a separate system of payment has been arranged.

**Trademark Notice:** Product or corporate names may be trademarks or registered trademarks, and are used only for identification and explanation without intent to infringe.

---

**Library of Congress Cataloging-in-Publication Data**

---

Transforms and applications handbook / editor, Alexander D. Poularikas. -- 3rd ed.

p. cm. -- (Electrical engineering handbook ; 43)

Includes bibliographical references and index.

ISBN-13: 978-1-4200-6652-4

ISBN-10: 1-4200-6652-8

1. Transformations (Mathematics)--Handbooks, manuals, etc. I. Poularikas, Alexander D., 1933- II. Title. III. Series.

QA601.T73 2011  
515'.723--dc22

2009018410

---

Visit the Taylor & Francis Web site at  
<http://www.taylorandfrancis.com>

and the CRC Press Web site at  
<http://www.crcpress.com>

# Contents

---

Preface to the Third Edition .....	vii
Editor .....	ix
Contributors .....	xi
1 Signals and Systems .....	1-1
<i>Alexander D. Poularikas</i>	
2 Fourier Transforms .....	2-1
<i>Kenneth B. Howell</i>	
3 Sine and Cosine Transforms .....	3-1
<i>Pat Yip</i>	
4 Hartley Transform .....	4-1
<i>Kraig J. Olejniczak</i>	
5 Laplace Transforms .....	5-1
<i>Alexander D. Poularikas and Samuel Seely</i>	
6 Z-Transform .....	6-1
<i>Alexander D. Poularikas</i>	
7 Hilbert Transforms .....	7-1
<i>Stefan L. Hahn</i>	
8 Radon and Abel Transforms .....	8-1
<i>Stanley R. Deans</i>	
9 Hankel Transform .....	9-1
<i>Robert Piessens</i>	
10 Wavelet Transform .....	10-1
<i>Yulong Sheng</i>	
11 Finite Hankel Transforms, Legendre Transforms, Jacobi and Gegenbauer Transforms, and Laguerre and Hermite Transforms .....	11-1
<i>Lokenath Debnath</i>	
12 Mellin Transform .....	12-1
<i>Jacqueline Bertrand, Pierre Bertrand, and Jean-Philippe Ovarlez</i>	
13 Mixed Time–Frequency Signal Transformations .....	13-1
<i>G. Fay Boudreaux-Bartels</i>	
14 Fractional Fourier Transform .....	14-1
<i>Haldun M. Ozaktas, M. Alper Kutay, and Çağatay Candan</i>	

15	Lapped Transforms .....	15-1
	<i>Ricardo L. de Queiroz</i>	
16	Zak Transform .....	16-1
	<i>Mark E. Oxley and Bruce W. Suter</i>	
17	Discrete Time and Discrete Fourier Transforms .....	17-1
	<i>Alexander D. Poularikas</i>	
18	Discrete Chirp-Fourier Transform .....	18-1
	<i>Xiang-Gen Xia</i>	
19	Multidimensional Discrete Unitary Transforms .....	19-1
	<i>Artyom M. Grigoryan</i>	
20	Empirical Mode Decomposition and the Hilbert–Huang Transform .....	20-1
	<i>Albert Ayenu-Prah, Nii Attoh-Okine, and Norden E. Huang</i>	
	<b>Appendix A: Functions of a Complex Variable</b> .....	<b>A-1</b>
	<b>Appendix B: Series and Summations</b> .....	<b>B-1</b>
	<b>Appendix C: Definite Integrals</b> .....	<b>C-1</b>
	<b>Appendix D: Matrices and Determinants</b> .....	<b>D-1</b>
	<b>Appendix E: Vector Analysis</b> .....	<b>E-1</b>
	<b>Appendix F: Algebra Formulas and Coordinate Systems</b> .....	<b>F-1</b>
	<b>Index</b> .....	<b>IN-1</b>

# Preface to the Third Edition

---

The third edition of *Transforms and Applications Handbook* follows a similar approach to that of the second edition. The new edition builds upon the previous one by presenting additional important transforms valuable to engineers and scientists. Numerous examples and different types of applications are included in each chapter so that readers from different backgrounds will have the opportunity to become familiar with a wide spectrum of applications of these transforms. In this edition, we have added the following important transforms:

1. Finite Hankel transforms, Legendre transforms, Jacobi and Gegenbauer transforms, and Laguerre and Hermite transforms
2. Fraction Fourier transforms
3. Zak transforms
4. Continuous and discrete Chirp–Fourier transforms
5. Multidimensional discrete unitary transforms
6. Hilbert–Huang transforms

I would like to thank Richard Dorf, the series editor, for his help. Special thanks also go to Nora Konopka, the acquisitions editor for engineering books, for her relentless drive to finish the project.

**Alexander D. Poularikas**

MATLAB<sup>®</sup> is a registered trademark of The MathWorks, Inc. For product information, please contact:

The MathWorks, Inc.  
3 Apple Hill Drive  
Natick, MA 01760-2098 USA  
Tel: 508 647 7000  
Fax: 508-647-7001  
E-mail: [info@mathworks.com](mailto:info@mathworks.com)  
Web: [www.mathworks.com](http://www.mathworks.com)



# Editor

---

**Alexander D. Poularikas** received his PhD from the University of Arkansas, Fayetteville, Arkansas, and became a professor at the University of Rhode Island, Kingston, Rhode Island. He became the chairman of the engineering department at the University of Denver, Denver, Colorado, and then became the chairman of the electrical and computer engineering department at the University of Alabama in Huntsville, Huntsville, Alabama.

Dr. Poularikas has published seven books and has edited two. He has served as the editor in chief of the *Signal Processing* series (1993–1997) with Artech House and is now the editor in chief of the *Electrical Engineering and Applied Signal Processing* series as well as the *Engineering and Science Primer* series (1998 to present) with Taylor & Francis. He is a Fulbright scholar, a lifelong senior member of the IEEE, and a member of Tau Beta Pi, Sigma Nu, and Sigma Pi. In 1990 and in 1996, he received the Outstanding Educators Award of the IEEE, Huntsville Section. He is now a professor emeritus at the University of Alabama in Huntsville.

Dr. Poularikas has authored, coauthored, and edited the following books:

*Electromagnetics*, Marcel Dekker, New York, 1979.

*Electrical Engineering: Introduction and Concepts*, Matrix Publishers, Beaverton, OR, 1982.

*Workbook*, Matrix Publishers, Beaverton, OR, 1982.

*Signals and Systems*, Brooks/Cole, Boston, MA, 1985.

*Elements of Signals and Systems*, PWS-Kent, Boston, MA, 1988.

*Signals and Systems*, 2nd edn., PWS-Kent, Boston, MA, 1992.

*The Transforms and Applications Handbook*, CRC Press, Boca Raton, FL, 1995.

*The Handbook for Formulas and Tables for Signal Processing*, CRC Press, Boca Raton, FL, 1998, 2nd edn. (2000), 3rd edn. (2009).

*Adaptive Filtering Primer with MATLAB*, Taylor & Francis, Boca Raton, FL, 2006.

*Signals and Systems Primer with MATLAB*, Taylor & Francis, Boca Raton, FL, 2007.

*Discrete Random Signal Processing and Filtering Primer with MATLAB*, Taylor & Francis, Boca Raton, FL, 2009.



# Contributors

---

**Nii Attoh-Okine**

Civil Engineering Department  
University of Delaware  
Newark, Delaware

**Albert Ayenu-Prah**

Civil Engineering Department  
University of Delaware  
Newark, Delaware

**Jacqueline Bertrand**

National Center for Scientific Research  
University of Paris  
Paris, France

**Pierre Bertrand**

Department of Electromagnetism and  
Radar  
French National Aerospace Research  
Establishment (ONERA)  
Palaiseau, France

**G. Fay Boudreaux-Bartels**

University of Rhode Island  
Kingston, Rhode Island

**Çağatay Candan**

Department of Electrical and Electronics  
Engineering  
Middle East Technical University  
Ankara, Turkey

**Stanley R. Deans**

University of South Florida  
Tampa, Florida

**Lokenath Debnath**

Department of Mathematics  
University of Texas-Pan American  
Edinburg, Texas

**Artyom M. Grigoryan**

Department of Electrical and Computer  
Engineering  
The University of Texas  
San Antonio, Texas

**Stefan L. Hahn**

Warsaw University of Technology  
Warsaw, Poland

**Kenneth B. Howell**

University of Alabama in Huntsville  
Huntsville, Alabama

**Norden E. Huang**

Research Center for Adaptive Data  
Analysis  
National Central University  
Chungli, Taiwan

**M. Alper Kutay**

The Scientific and Technological Research  
Council of Turkey  
National Research Institute of Electronics  
and Cryptology  
Ankara, Turkey

**Kraig J. Olejniczak**

University of Arkansas  
Fayetteville, Arkansas

**Jean-Philippe Ovarlez**

Department of Electromagnetism and  
Radar  
French National Aerospace Research  
Establishment (ONERA)  
Palaiseau, France

**Mark E. Oxley**

Department of Mathematics and Statistics  
Graduate School of Engineering and  
Management  
Air Force Institute of Technology  
Wright-Patterson Air Force Base, Ohio

**Haldun M. Ozaktas**

Department of Electrical Engineering  
Bilkent University  
Ankara, Turkey

**Robert Piessens**

Catholic University of Leuven  
Leuven, Belgium

**Alexander D. Poularikas**

University of Alabama in Huntsville  
Huntsville, Alabama

**Ricardo L. de Queiroz**

Xerox Corporation  
Webster, New York

**Samuel Seely (deceased)**

Westbrook, Connecticut

**Yulong Sheng**

Department of Physics, Physical  
Engineering and Optics  
Laval University  
Quebec, Canada

**Bruce W. Suter**

Air Force Research Laboratory  
Information Directorate  
Rome, New York



**Xiang-Gen Xia**

Department of Electrical and Computer  
Engineering  
University of Delaware  
Newark, Delaware

**Pat Yip**

McMaster University  
Hamilton, Ontario, Canada

# Signals and Systems

1.1	Introduction to Signals .....	1-1
	Functions (Signals), Variables, and Point Sets • Limits and Continuous Functions • Energy and Power Signals	
1.2	Distributions, Delta Function .....	1-4
	Introduction • Testing Functions • Definition of Distributions • The Delta Function • The Gamma and Beta Functions	
1.3	Convolution and Correlation .....	1-13
	Convolution • Convolution Properties	
1.4	Correlation .....	1-19
1.5	Orthogonality of Signals .....	1-19
	Introduction • Legendre Polynomials • Hermite Polynomials • Laguerre Polynomials • Chebyshev Polynomials • Bessel Functions • Zernike Polynomials	
1.6	Sampling of Signals.....	1-47
	The Sampling Theorem • Extensions of the Sampling Theorem	
1.7	Asymptotic Series.....	1-52
	Asymptotic Sequence • Poincaré Sense Asymptotic Sequence • Asymptotic Approximation • Asymptotic Power Series • Operation of Asymptotic Power Series	
	References .....	1-55

Alexander D. Poularikas  
University of Alabama in Huntsville

## 1.1 Introduction to Signals

A knowledge of a broad range of signals is of practical importance in describing human experience. In engineering systems, signals may carry information or energy. The signals with which we are concerned may be the cause of an event or the consequence of an action.

The characteristics of a signal may be of a broad range of shapes, amplitudes, time duration, and perhaps other physical properties. In many cases, the signal will be expressed in analytic form; in other cases, the signal may be given only in graphical form.

It is the purpose of this chapter to introduce the mathematical representation of signals, their properties, and some of their applications. These representations are in different formats depending on whether the signals are periodic or truncated, or whether they are deduced from graphical representations.

Signals may be classified as follows:

1. Phenomenological classification is based on the evolution type of signal, that is, a perfectly predictable evolution defines a deterministic signal and a signal with unpredictable behavior is called a *random signal*.
2. Energy classification separates signals into *energy signals*, those having finite energy, and *power signals*, those with a finite average power and infinite energy.
3. Morphological classification is based on whether signals are continuous, quantitized, sampled, or digital signals.

4. Dimensional classification is based on the number of independent variables.
5. Spectral classification is based on the shape of the frequency distribution of the signal spectrum.

### 1.1.1 Functions (Signals), Variables, and Point Sets

The *rule of correspondence* from a set  $S_x$  of real or complex number  $x$  to a real or complex number

$$y = f(x) \quad (1.1)$$

is called a function of the argument  $x$ . Equation 1.1 specifies a value (or values)  $y$  of the variable  $y$  (set of values in  $Y$ ) corresponding to each suitable value of  $x$  in  $X$ . In Equation 1.1  $x$  is the *independent* variable and  $y$  is the *dependent* variable.

A function of  $n$  variables  $x_1, x_2, \dots, x_n$  associates values

$$y = f(x_1, x_2, \dots, x_n) \quad (1.2)$$

of a dependent variable  $y$  with ordered sets of values of the independent variables  $x_1, x_2, \dots, x_n$ .

The set  $S_x$  of the values of  $x$  (or sets of values of  $x_1, x_2, \dots, x_n$ ) for which the relationships (1.1) and (1.2) are defined constitutes the *domain* of the function. The corresponding set of  $S_y$  of values of  $y$  is the  $S_x$  *range* of the function.

A *single-valued* function produces a single value of the dependent variable for each value of the argument. A *multiple-valued* function attains two or more values for each value of the argument.

The function  $y=f(x)$  has an *inverse* function  $x(y)$  if  $y=f(x)$  implies  $x=x(y)$ .

A function  $y=f(x)$  is *algebraic* of  $x$  if and only if  $x$  and  $y$  satisfy a relation of the form  $F(x, y)=0$ , where  $F(x, y)$  is a polynomial in  $x$  and  $y$ . The function  $y=f(x)$  is *rational* if  $f(x)$  is a polynomial or is a quotient of two polynomials.

A real or complex function  $y=f(x)$  is bounded on a set  $S_x$  if and only if the corresponding set  $S_y$  of values  $y$  is bounded. Furthermore, a real function  $y=f(x)$  has an *upper bound*, *least upper bound* (l.u.b.), *lower bound*, *greatest lower bound* (g.l.b.), *maximum*, or *minimum* on  $S_x$  if this is also true for the corresponding set  $S_y$ .

**1.1.1.1 Neighborhood**

Given any finite real number  $a$ , an open neighborhood of the point  $a$  is the set of all points  $\{x\}$  such that  $|x - a| < \delta$  for any positive real number  $\delta$ .

An open neighborhood of the point  $(a_1, a_2, \dots, a_n)$ , where all  $a_i$  are finite, is the set of all points  $(x_1, x_2, \dots, x_n)$  such that  $|x_1 - a_1| < \delta, |x_2 - a_2| < \delta, \dots$ , and  $|x_n - a_n| < \delta$  for some positive real number  $\delta$ .

**1.1.1.2 Open and Closed Sets**

A point  $P$  is a *limit* point (accumulation point) of the point set  $S$  if and only if every neighborhood of  $P$  has a neighborhood contained entirely in  $S$ , other than  $P$  itself.

A limit point  $P$  is an interior point of  $S$  if and only if  $P$  has a neighborhood contained entirely in  $S$ . Otherwise  $P$  is a *boundary* point.

A point  $P$  is an isolated point of  $S$  if and only if  $P$  has a neighborhood in which  $P$  is the only point belonging to  $S$ .

A point set is *open* if and only if it contains only interior points.

A point set is *closed* if and only if it contains all its limit points; a finite set is closed.

**1.1.2 Limits and Continuous Functions**

1. A single-value function  $f(x)$  has a *limit*

$$\lim_{x \rightarrow a} f(x) = L, \quad L = \text{finite}$$

as  $x \rightarrow a\{f(x) \rightarrow L \text{ as } x \rightarrow a\}$  if and only if for each positive real number  $\epsilon$  there exists a real number  $\delta$  such that  $0 < |x - a| < \delta$  implies that  $f(x)$  is defined and  $|f(x) - L| < \epsilon$ .

2. A single-valued function  $f(x)$  has a limit

$$\lim_{x \rightarrow \infty} f(x) = L, \quad L = \text{finite}$$

as  $x \rightarrow \infty$  if and only if for each positive real number  $\epsilon$  there exists a real number  $N$  such that  $x > N$  implies that  $f(x)$  is defined and  $|f(x) - L| < \epsilon$ .

**TABLE 1.1** Operations with Limits

$\lim_{x \rightarrow a} [f(x) + g(x)] = \lim_{x \rightarrow a} f(x) + \lim_{x \rightarrow a} g(x)$
$\lim_{x \rightarrow a} [bf(x)] = b \lim_{x \rightarrow a} f(x)$
$\lim_{x \rightarrow a} [f(x)g(x)] = \lim_{x \rightarrow a} f(x) \lim_{x \rightarrow a} g(x)$
$\lim_{x \rightarrow a} \frac{f(x)}{g(x)} = \frac{\lim_{x \rightarrow a} f(x)}{\lim_{x \rightarrow a} g(x)} \quad (\lim_{x \rightarrow a} g(x) \neq 0)$

$a$  may be finite or infinite.

**1.1.2.1 Operations with Limits**

If limits exist, Table 1.1 gives the limit operations.

**1.1.2.2 Asymptotic Relations between Two Functions**

Given two real or complex functions  $f(x), g(x)$  of a real or complex variable  $x$ , we write

1.  $f(x) = O[g(x)]$ ;  $f(x)$  is *of the order*  $g(x)$  as  $x \rightarrow a$  if and only if there is a neighborhood of  $x = a$  such that  $|f(x)/g(x)|$  is bounded.
2.  $f(x) \sim g(x)$ ;  $f(x)$  is *asymptotically proportional* to  $g(x)$  as  $x \rightarrow a$  if and only if  $\lim_{x \rightarrow a} [f(x)/g(x)]$  exists and it is not zero.
3.  $f(x) \cong g(x)$ ;  $f(x)$  is *asymptotically equal* to  $g(x)$  as  $x \rightarrow a$  if and only if

$$\lim_{x \rightarrow a} [f(x)/g(x)] = 1.$$

4.  $f(x) = o[g(x)]$ ;  $f(x)$  becomes negligible compared with  $g(x)$  if and only if

$$\lim_{x \rightarrow a} [f(x)/g(x)] = 0.$$

5.  $f(x) = \varphi(x) + O[g(x)]$  if  $f(x) - \varphi(x) = O[g(x)]$   
 $f(x) = \varphi(x) + o[g(x)]$  if  $f(x) - \varphi(x) = o[g(x)]$

**1.1.2.3 Uniform Convergence**

1. A single-valued function  $f(x_1, x_2)$  *converges uniformly* on a set  $S$  of values of  $x_2$ ,  $\lim_{x_1 \rightarrow a} f(x_1, x_2) = L(x_2)$  if and only if for each positive real number  $\epsilon$  there exists a real number  $\delta$  such that  $0 < |x_1 - a| < \delta$  implies that  $f(x_1, x_2)$  is defined and  $|f(x_1, x_2) - L(x_2)| < \epsilon$  for all  $x_2$  in  $S$  ( $\delta$  is independent of  $x_2$ ).
2. A single-valued function  $f(x_1, x_2)$  *converges uniformly* on a set  $S$  of values of  $x_2$ ,  $\lim_{x_1 \rightarrow \infty} f(x_1, x_2) = L(x_2)$  if and only if for each positive real number  $\epsilon$  there exists a real number  $N$  such that for  $x_1 > N$  implies that  $f(x_1, x_2)$  is defined and  $|f(x_1, x_2) - L(x_2)| < \epsilon$  for all  $x_2$  in  $S$ .
3. A *sequence* of functions  $f_1(x), f_2(x), \dots$  *converges uniformly* on a set  $S$  of values of  $x$  to a finite and unique function

$$\lim_{x \rightarrow \infty} f_n(x) = f(x)$$

if and only if for each positive real number  $\epsilon$  there exists a real integer  $N$  such that for  $n > N$  implies that  $|f_n(x) - f(x)| < \epsilon$  for all  $n$  in  $S$ .

**1.1.2.4 Continuous Functions**

1. A single-valued function  $f(x)$  defined in the neighborhood of  $x = a$  is *continuous* at  $x = a$  if and only if for every positive real number  $\epsilon$  there exists a real number  $\delta$  such that  $|x - a| < \delta$  implies  $|f(x) - f(a)| < \epsilon$ .
2. A function is *continuous on a series of points* (interval or region) if and only if it is continuous at each point of the set.
3. A real function continuous on a bounded closed interval  $[a, b]$  is bounded on  $[a, b]$  and assumes every value between and including its g.l.b. and its l.u.b. at least once on  $[a, b]$ .
4. A function  $f(x)$  is *uniformly continuous* on a set  $S$  and only if for each positive real number  $\epsilon$  there exists a real number  $\delta$  such that  $|x - X| < \delta$  implies  $|f(x) - f(X)| < \epsilon$  for all  $X$  in  $S$ .

If a function is continuous in a bounded closed interval  $[a, b]$ , it is uniformly continuous on  $[a, b]$ . If  $f(x)$  and  $g(x)$  are continuous at a point, so are the functions  $f(x) + g(x)$  and  $f(x)f(x)$ .

**1.1.2.5 Limits**

1. A function  $f(x)$  of a real variable  $x$  has the *right-hand limit*  $\lim_{x \rightarrow a^+} f(x) = f(a+) = L_+$  at  $x = a$  if and only if for each positive real number  $\epsilon$  there exists a real number  $\delta$  such that  $0 < x - a < \delta$  implies that  $f(x)$  is defined and  $|f(x) - L_+| < \epsilon$ .
2. A function  $f(x)$  of a real variable  $x$  has the *left-hand limit*  $\lim_{x \rightarrow a^-} f(x) = f(a-) = L_-$  at  $x = a$  if and only if for each positive real number  $\epsilon$  there exists a real number  $\delta$  such that  $0 < a - x < \delta$  implies that  $f(x)$  is defined and  $|f(x) - L_-| < \epsilon$ .
3. If  $\lim_{x \rightarrow a} f(x)$  exists, then  $\lim_{x \rightarrow a^+} f(x) = \lim_{x \rightarrow a^-} f(x) = \lim_{x \rightarrow a} f(x)$ . Consequently,  $\lim_{x \rightarrow a^-} f(x) = \lim_{x \rightarrow a^+} f(x)$  implies the existence of  $\lim_{x \rightarrow a} f(x)$ .
4. The function  $f(x)$  is *right continuous* at  $x = a$  if  $f(a+) = f(a)$ .
5. The function  $f(x)$  is *left continuous* at  $x = a$  if  $f(a-) = f(a)$ .
6. A real function  $f(x)$  has a *discontinuity of the first kind* at point  $x = a$  if  $f(a+)$  and  $f(a-)$  exist. The greatest difference between two of these number  $f(a), f(a+), f(a-)$  is the *saltus* of  $f(x)$  at the discontinuity. The discontinuities of the first kind of  $f(x)$  constitute a discrete and countable set.
7. A real function  $f(x)$  is *piecewise continuous* in an interval  $I$  if and only if  $f(x)$  is continuous throughout  $I$  except for a finite number of discontinuities of the first kind.

**1.1.2.6 Monotonicity**

1. A real function  $f(x)$  of a real variable  $x$  is a *strongly monotonic* in the open interval  $(a, b)$  if  $f(x)$  increases as  $x$  increases in  $(a, b)$  or if  $f(x)$  decreases as  $x$  decreases in  $(a, b)$ .
2. A function  $f(x)$  is *weakly monotonic* in  $(a, b)$  if  $f(x)$  does not decrease, or if  $f(x)$  does not increase in  $(a, b)$ . Analogous definitions apply to monotonic sequences.
3. A real function of a real variable  $x$  is of *bounded variation* in the interval  $(a, b)$  if and only if there exists a real number of  $M$  such that

$$\sum_{i=1}^m |f(x_i) - f(x_{i-1})| < M \text{ for all partitions}$$

$$a = x_0 < x_1 < x_2 < \dots < x_m = b$$

of the interval  $(a, b)$ . If  $f(x)$  and  $g(x)$  are of bounded variation in  $(a, b)$ , then  $f(x) + g(x)$  and  $f(x)g(x)$  are of bounded variation also. The function  $f(x)$  is of bounded variation in every finite open interval where  $f(x)$  is bounded and has a finite number of relative maxima and minima and discontinuities (Dirichlet conditions).

A function of bounded variation in  $(a, b)$  is bounded in  $(a, b)$  and its discontinuities are only of the first kind.

Table 1.2 presents some useful mathematical functions.

**TABLE 1.2** Some Useful Mathematical Functions

1. Signum function	$\text{sgn}(t) = \begin{cases} 1 & t > 0 \\ 0 & t = 0 \\ -1 & t < 0 \end{cases}$
2. Step function	$u(t) = \frac{1}{2} + \frac{1}{2} \text{sgn}(t) = \begin{cases} 1 & t > 0 \\ 0 & t < 0 \end{cases}$
3. Ramp function	$r(t) = \int_{-\infty}^t u(\tau) d\tau = tu(t)$
4. Pulse function	$p_a(t) = u(t + a) - u(t - a) = \begin{cases} 1 &  t  < a \\ 0 &  t  > a \end{cases}$
5. Triangular pulse	$\Lambda_a(t) = \begin{cases} 1 - \frac{ t }{a} &  t  < a \\ 0 &  t  > a \end{cases}$
6. Sine function	$\sin c_a(t) = \frac{\sin at}{t}, \quad -\infty < t < \infty$
7. Gaussian function	$g_a(t) = e^{-at^2}, \quad -\infty < t < \infty$
8. Error function	$\text{erf}(t) = \frac{2}{\sqrt{\pi}} \int_0^t e^{-\tau^2} d\tau = \frac{2}{\sqrt{\pi}} \sum_{n=0}^{\infty} \frac{(-1)^n t^{2n+1}}{n!(2n+1)}$
<i>Properties:</i>	$\begin{aligned} \text{erf}(\infty) &= 1, \text{erf}(0) = 0, \text{erf}(-t) = -\text{erf}(t) \\ \text{erfc}(t) &= \text{complementary error function} \\ &= 1 - \text{erf}(t) = \frac{2}{\sqrt{\pi}} \int_t^{\infty} e^{-\tau^2} d\tau \end{aligned}$
9. Exponential function	$f(t) = e^{-at}u(t), \quad t \geq 0$
10. Double exponential	$f(t) = e^{-a t }, \quad -\infty < t < \infty$
11. Lognormal function	$f(t) = \frac{1}{t} e^{-\ln^2 t/2}, \quad 0 < t < \infty$
12. Rayleigh function	$f(t) = te^{-t^2/2}, \quad 0 < t < \infty$

### 1.1.3 Energy and Power Signals

#### 1.1.3.1 Energy Signals

If we consider any signal  $f(t)$  as denoting a voltage that exists across a  $1 \Omega$  resistor, then

$$\frac{f^2(t)}{1} = f(t) \frac{f(t)}{1} = f(t)i(t) = \text{power VA}$$

Therefore, the integral

$$E = \int_a^b f^2(t) dt \text{ joule} \quad (1.3)$$

representing the energy dissipated in the resistor during the time interval  $(a, b)$ . A signal is called *energy signal* if

$$\int_{-\infty}^{\infty} f^2(t) dt < \infty \quad (1.4)$$

#### 1.1.3.2 Power Signals

Power signals are defined by the relation

$$0 \leq \lim_{T \rightarrow \infty} \frac{1}{2T} \int_{-T}^T f^2(t) dt < \infty \quad (1.5)$$

For complex-valued signals, we must introduce  $|f(t)|^2$  instead of  $f^2(t)$ .

We may represent the energy in a finite interval in terms of the coefficients of the basis function  $\varphi_n$ ; that is, we write the energy integral in the form

$$\begin{aligned} E &= \int_a^b f^2(t) dt = \int_a^b f(t) \sum_{n=0}^{\infty} c_n \varphi_n(t) dt \\ &= \sum_{n=0}^{\infty} c_n \int_a^b f(t) \varphi_n(t) dt = \sum_{n=0}^{\infty} c_n^2 \|\varphi_n(t)\|^2 \end{aligned} \quad (1.6)$$

where

$$\int_a^b f(t) \varphi_n(t) dt = c_n \int_a^b \varphi_n^2(t) dt = c_n \|\varphi_n(t)\|^2$$

Because the square of the norm  $\|\varphi_n(t)\|^2$  is the energy associated with the  $n$ th orthogonal function, Equation 1.6 shows that the energy of the signal is the sum of the energies of its individual orthogonal components weighted by  $c_n$ . Note that this is the Parseval theorem. This equation shows that the set  $\{\varphi_n(t)\}$  forms an orthogonal (complete) set, and the signal energy can be calculated from this representation.

#### Example

$$(a) \int_0^{\infty} u^2(t) dt = \int_0^{\infty} dt = \infty; \lim_{T \rightarrow \infty} \frac{1}{2T} \int_{-T}^T u^2(t) dt = \lim_{T \rightarrow \infty} \frac{1}{2T} \int_0^T dt = \lim_{T \rightarrow \infty} \frac{1}{2T} (t|_0^T) = \frac{1}{2} < \infty.$$

This implies that  $u(t)$  is a power signal.

$$(b) \text{ The signal } e^{-at} u(t), a > 0 \text{ is an energy signal.}$$

## 1.2 Distributions, Delta Function

### 1.2.1 Introduction

The *delta function*  $\delta(t)$  often called the *impulse* or *Dirac delta function*, occupies a central place in signal analysis. Many physical phenomena such as point sources, point charges, concentrated loads on structures, and voltage or current sources, acting for very short times, can be modeled as delta functions.

Strictly speaking, delta functions are not functions in the accepted mathematical sense, and they cannot be treated with rigor within the framework of classical analysis. However, if distributions are introduced, then the concept of a delta function and operations on delta functions can be given a precise meaning.

### 1.2.2 Testing Functions

A *distribution* is a generalization of a function. Within the framework of distributions, any function encountered in applications, such as unit-step functions and pulses, may be differentiated as many times as we desire, and any convergent series of functions may be differentiated term by term.

A *testing function*  $\varphi(t)$  is a real-valued function of the real variable that can be differentiated an arbitrary number of times, and which is identical to zero outside a finite interval.

#### Example

Testing function

$$\varphi(t, a) = \begin{cases} e^{-\frac{a^2}{2t^2-t^2}} & |t| < a \\ 0 & |t| \geq a \end{cases} \quad (1.7)$$

### 1.2.2.1 Properties

1. If  $f(t)$  can be differentiated arbitrarily often

$$\Psi(t) = f(t) \varphi(t) = \text{testing function}$$

2. If  $f(t)$  is zero outside a finite interval

$$\begin{aligned} \Psi(t) &= \int_{-\infty}^{\infty} f(\tau) \varphi(t - \tau) d\tau, \quad -\infty < t < \infty \\ &= \text{testing function} \end{aligned}$$

3. A sequence of testing functions,  $\{\varphi_n\}$   $1 \leq n < \infty$ , converges to zero if all  $\varphi_n$  are identically zero outside some interval independent of  $n$  and each  $\varphi_n$ , as well as all of its derivatives, tends uniformly to zero.

**Example**

$$\varphi_n(t) = \varphi\left(t + \frac{1}{n}\right) - \varphi(t)$$

4. Testing functions belong to a set  $D$ , where  $D$  is a linear vector space, and if  $\varphi_1 \in D$  and  $\varphi_2 \in D$ , then  $\varphi_1 + \varphi_2 \in D$  and  $a\varphi_1 \in D$  for any number  $a$ .

**1.2.3 Definition of Distributions**

A *distribution* (or *generalized function*)  $g(t)$  is a process of assigning to an arbitrary test function  $\varphi(t)$  a number  $N_g[\varphi(t)]$ . A distribution is also a functional.

**Example**

An ordinary function  $f(t)$  is a distribution if

$$\int_{-\infty}^{\infty} f(t)\varphi(t)dt = N_f[\varphi(t)] \quad (1.8)$$

exists for every test function  $\varphi(t)$  in the set. For example, if  $f(t) = u(t)$  then

$$\int_{-\infty}^{\infty} u(t)\varphi(t)dt = \int_0^{\infty} \varphi(t)dt \quad (1.9)$$

The function  $u(t)$  is s distribution that assigns to  $\varphi(t)$  a number equal to its area from zero to infinity.

**1.2.3.1 Properties of Distributions**

1. Linearity-homogeneity

$$\int_{-\infty}^{\infty} g(t)[a_1\varphi_1(t) + a_2\varphi_2(t)]dt = a_1 \int_{-\infty}^{\infty} g(t)\varphi_1(t)dt + a_2 \int_{-\infty}^{\infty} g(t)\varphi_2(t)dt \quad (1.10)$$

for all test functions and all numbers  $a_i$ .

2. Summation

$$\int_{-\infty}^{\infty} [g_1(t) + g_2(t)]\varphi(t)dt = \int_{-\infty}^{\infty} g_1(t)\varphi(t)dt + \int_{-\infty}^{\infty} g_2(t)\varphi(t)dt \quad (1.11)$$

3. Shifting

$$\int_{-\infty}^{\infty} g(t - t_0)\varphi(t)dt = \int_{-\infty}^{\infty} g(t)\varphi(t + t_0)dt \quad (1.12)$$

4. Scaling

$$\int_{-\infty}^{\infty} g(at)\varphi(t)dt = \frac{1}{|a|} \int_{-\infty}^{\infty} g(t)\varphi\left(\frac{t}{a}\right)dt \quad (1.13)$$

5. Even distribution

$$\int_{-\infty}^{\infty} g(t)\varphi(t)dt = 0, \quad \varphi(t) = \text{odd} \quad (1.14)$$

6. Odd distribution

$$\int_{-\infty}^{\infty} g(t)\varphi(t)dt = 0, \quad \varphi(t) = \text{even} \quad (1.15)$$

7. Derivative

$$\begin{aligned} \int_{-\infty}^{\infty} \frac{dg(t)}{dt}\varphi(t)dt &= g(t)\varphi(t)|_{-\infty}^{\infty} - \int_{-\infty}^{\infty} g(t)\frac{d\varphi(t)}{dt}dt \\ &= - \int_{-\infty}^{\infty} g(t)\frac{d\varphi(t)}{dt}dt \end{aligned} \quad (1.16)$$

where the integrated term is equal to zero in view of the properties of testing functions.

8. The  $n$ th derivative

$$\int_{-\infty}^{\infty} \frac{d^n g(t)}{dt^n}\varphi(t)dt = (-1)^n \int_{-\infty}^{\infty} g(t)\frac{d^n \varphi(t)}{dt^n}dt \quad (1.17)$$

9. Product with ordinary function

$$\int_{-\infty}^{\infty} [g(t)f(t)]\varphi(t)dt = \int_{-\infty}^{\infty} g(t)[f(t)\varphi(t)]dt \quad (1.18)$$

provided that  $f(t)\varphi(t)$  belongs to the set of test functions.

10. Convolution

$$\begin{aligned} \int_{-\infty}^{\infty} \left[ \int_{-\infty}^{\infty} g_1(\tau)g_2(t - \tau)d\tau \right] \varphi(t)dt \\ = \int_{-\infty}^{\infty} g_1(\tau) \left[ \int_{-\infty}^{\infty} g_2(t - \tau)\varphi(t)dt \right] d\tau \end{aligned} \quad (1.19)$$

by formal change of the order of integration.

### 1.2.3.2 Definition

A sequence of distributions  $\{g_n(t)\}_1^\infty$  is said to converge to the distribution  $g(t)$  if

$$\lim_{n \rightarrow \infty} \int_{-\infty}^{\infty} g_n(t) \varphi(t) dt = \int_{-\infty}^{\infty} g(t) \varphi(t) dt \quad (1.20)$$

for all  $\varphi$  belonging to the set of test functions.

11. Every distribution is the limit, in the sense of distributions, of sequence of infinitely differentiable functions.
12. If  $g_n(t) \rightarrow g(t)$  and  $r_n(t) \rightarrow r(t)$  ( $r$  is a distribution), and the numbers  $a_n \rightarrow a$ , then

$$\begin{aligned} \frac{d}{dt} g_n(t) &\rightarrow \frac{dg(t)}{dt}, & g_n(t) + r_n(t) &\rightarrow g(t) + r(t), \\ a_n g_n(t) &\rightarrow a g(t) \end{aligned} \quad (1.21)$$

13. Any distribution  $g(t)$  may be differentiated as many times as desired. That is, the derivative of any distribution always exists and it is a distribution.

## 1.2.4 The Delta Function

### 1.2.4.1 Properties

Based on the distribution properties, the properties of the delta function are given below.

1. The delta function is a distribution assigning to the function  $\varphi(t)$  the number  $\varphi(0)$ ; thus

$$\int_{-\infty}^{\infty} \delta(t) \varphi(t) dt = \varphi(0) \quad (1.22)$$

2. Shifted

$$\int_{-\infty}^{\infty} \delta(t - t_0) \varphi(t) dt = \varphi(t_0) \quad (1.23)$$

3. Scaled

$$\int_{-\infty}^{\infty} \delta(at) \varphi(t) dt = \frac{1}{|a|} \int_{-\infty}^{\infty} \delta(t) \varphi\left(\frac{t}{a}\right) dt = \frac{1}{|a|} \varphi(0)$$

From Equation 1.22 we have the identity

$$\delta(at) = \frac{1}{|a|} \delta(t)$$

and hence ( $a = -1$ )

$$\delta(-t) = \delta(t) = \text{even} \quad (1.24)$$

4. Multiplication by continuous function

$$\int_{-\infty}^{\infty} [\delta(t)f(t)] \varphi(t) dt = \int_{-\infty}^{\infty} \delta(t)[f(t)\varphi(t)] dt = f(0)\varphi(0)$$

If  $f(t)$  is continuous at 0, then

$$f(t)\delta(t) = f(0)\delta(t) \quad (1.25)$$

and

$$t\delta(t) = 0 \quad (1.26)$$

5. Derivatives

$$\int_{-\infty}^{\infty} \frac{d\delta(t)}{dt} \varphi(t) dt = -\frac{d\varphi(0)}{dt}$$

$$\int_{-\infty}^{\infty} \frac{d\delta(t - t_0)}{dt} \varphi(t) dt = -\frac{d\varphi(t_0)}{dt} \quad (1.27)$$

$$\int_{-\infty}^{\infty} \frac{d^n \delta(t)}{dt^n} \varphi(t) dt = (-1)^n \frac{d^n \varphi(0)}{dt^n} \quad (1.28)$$

$$\begin{aligned} \int_{-\infty}^{\infty} \frac{d\delta(t)}{dt} f(t) \varphi(t) dt &= - \int_{-\infty}^{\infty} \delta(t) \frac{d[f(t)\varphi(t)]}{dt} dt \\ &= -f(0) \frac{d\varphi(0)}{dt} - \frac{df(0)}{dt} \varphi(0) \end{aligned} \quad (1.29)$$

$$f(t) \frac{d\delta(t)}{dt} = -\frac{df(0)}{dt} \delta(t) + f(0) \frac{d\delta(t)}{dt} \quad (1.30)$$

$$t \frac{d\delta(t)}{dt} = -\delta(t) \quad (1.31)$$

Set  $f(t) = \varphi(t) = 1$  in Equation 1.29 to find the relation

$$\int_{-\infty}^{\infty} \frac{d\delta(t)}{dt} dt = 0 \quad \left[ \frac{d\delta(t)}{dt} \text{ is an odd function} \right] \quad (1.32)$$

$$f(t) \frac{d^n \delta(t)}{dt^n} = \sum_{k=0}^n (-1)^k \frac{n!}{k!(n-k)!} \frac{d^k f(0)}{dt^k} \frac{d^{n-k} \delta(t)}{dt^{n-k}} \quad (1.33)$$

From

$$\begin{aligned} \int_{-\infty}^{\infty} \frac{du(t)}{dt} \varphi(t) dt &= u(t)\varphi(t) \Big|_{-\infty}^{\infty} - \int_{-\infty}^{\infty} u(t) \frac{d\varphi(t)}{dt} dt \\ &= - \int_0^{\infty} \frac{d\varphi(t)}{dt} dt = -\varphi(t) \Big|_0^{\infty} = \varphi(0) \end{aligned}$$

and comparing with Equation 1.22 we find that

$$\delta(t) = \frac{du(t)}{dt} \tag{1.34}$$

Therefore, the generalized derivatives of discontinuous function contain impulses.  $A_n$  is the jump at the discontinuity point  $t = t_n$  of the expression  $A_n \varphi(t - t_n)$ . Also

$$\frac{d\delta(t)}{dt} = \frac{d^2u(t)}{dt^2} \quad \text{or} \quad u(t) + u(-t) = 1$$

Hence

$$\frac{du(-t)}{dt} = -\delta(t) \tag{1.35}$$

$$\delta(t - t_0) = \frac{du(t - t_0)}{dt} \tag{1.36}$$

If  $r(t)$  has a finite or countably infinite number of zeros at  $t_n$  on the entire  $t$  axis and these points  $r(t)$  have a continuous derivative  $dr(t_n)/dt \neq 0$ , then

$$\delta[r(t)] = \sum_n \frac{\delta(t - t_n)}{\left| \frac{dr(t_n)}{dt} \right|} \tag{1.37}$$

Hence, we obtain

$$\delta(t^2 - 1) = \frac{1}{2}\delta(t - 1) + \frac{1}{2}\delta(t + 1) \tag{1.38}$$

$$\delta(\sin t) = \sum_{n=-\infty}^{\infty} \delta(t - n\pi) \tag{1.39}$$

In addition, the following relation is also true:

$$\frac{d\delta[r(t)]}{dt} = \sum_n \frac{\frac{d\delta(t-t_n)}{dt}}{\frac{dr(t)}{dt} \left| \frac{dr(t_n)}{dt} \right|} \tag{1.40}$$

### 6. Integrals

$$\int_{-\infty}^{\infty} A\delta(t - t_0)dt = A \tag{1.41}$$

for all  $t_0$

$$\begin{aligned} &\delta(t - t_1) * \delta(t - t_2) = \text{convolution} \\ &= \int_{-\infty}^{\infty} \delta(\tau - t_1)\delta(t - \tau - t_2)d\tau = \delta[t - (t_1 + t_2)] \end{aligned} \tag{1.42}$$

$$f(t) * \delta(t) = \int_{-\infty}^{\infty} f(t - \tau)\delta(\tau)d\tau = f(t - 0) = f(t) \tag{1.43}$$

### 1.2.4.2 Distributions as Generalized Limits

We can define a distribution as a generalized limit of a sequence  $f_n(t)$  of ordinary function. If there exists a sequence  $f_n(t)$  such that the limit

$$\lim_{n \rightarrow \infty} \int_{-\infty}^{\infty} f_n(t)\varphi(t)dt \tag{1.44}$$

exists for every test function in the set, then the result is a number depending on  $\varphi(t)$ . Hence, we may define a distribution  $g(t)$  as

$$g(t) = \lim f_n(t) \tag{1.45}$$

and, therefore, equivalently

$$\delta(t) = \lim f_n(t) \tag{1.46}$$

Consider the two sequences shown in Figure 1.1a and b. The rectangular pulse sequence is given by

$$p_\epsilon(t) = \frac{u(t) - u(t - \epsilon)}{\epsilon}$$

and has area unity whatever the value of  $\epsilon$ . Because  $\varphi(t)$  is continuous, it follows that

$$\lim_{\epsilon \rightarrow 0} \int_{-\infty}^{\infty} p_\epsilon(t)\varphi(t)dt = \lim_{\epsilon \rightarrow 0} \frac{1}{\epsilon} \int_0^\epsilon \varphi(t)dt = \lim_{\epsilon \rightarrow 0} \varphi(0) \frac{1}{\epsilon} \int_0^\epsilon dt = \varphi(0)$$

and therefore

$$\delta(t) = \lim_{\epsilon \rightarrow 0} p_\epsilon(t) \tag{1.47}$$

Similarly, from

$$\lim_{\epsilon \rightarrow 0} \frac{1}{\sqrt{\epsilon\pi}} \int_{-\infty}^{\infty} e^{-t^2/\epsilon} \varphi(t)dt \cong \frac{\varphi(0)}{\sqrt{\epsilon\pi}} \int_{-\infty}^{\infty} e^{-t^2/\epsilon} dt = \varphi(0)$$

it follows that

$$\delta(t) = \lim_{\epsilon \rightarrow 0} \frac{e^{-t^2/\epsilon}}{\sqrt{\epsilon\pi}} \tag{1.48}$$

If we use the sequence

$$\delta(t) = \lim_{\omega \rightarrow \infty} \frac{\sin \omega t}{\pi t}$$



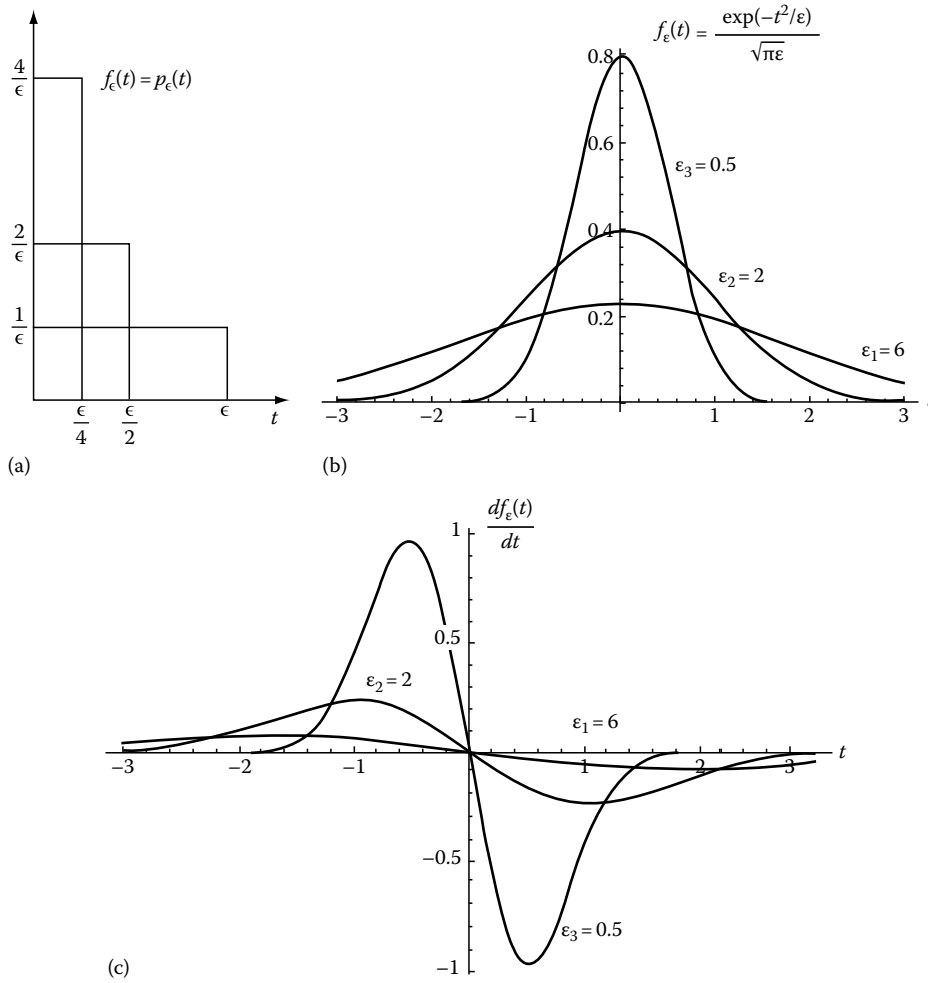


FIGURE 1.1

we find that

$$\delta(t) = \lim_{a \rightarrow \infty} \frac{1}{2\pi} \int_{-a}^a e^{+j\omega t} d\omega = \lim_{a \rightarrow \infty} \frac{\sin at}{\pi t} = \frac{1}{2\pi} \int_{-\infty}^{\infty} e^{+j\omega t} d\omega \tag{1.49}$$

Also

$$\delta(t - t_0) = \frac{1}{2\pi} \int_{-\infty}^{\infty} e^{-j\omega(t-t_0)} d\omega \tag{1.50}$$

Further

$$\begin{aligned} \int_{-\infty}^{\infty} \cos \omega t d\omega &= \lim_{\Omega \rightarrow \infty} \int_{-\Omega}^{\Omega} \cos \omega t d\omega = \lim_{\Omega \rightarrow \infty} \frac{2 \sin \Omega t}{t} \\ &= \lim_{\Omega \rightarrow \infty} 2\pi \frac{\sin \Omega t}{\pi t} = 2\pi \delta(t) \end{aligned} \tag{1.51}$$

Figure 1.1c shows the derivatives of the sequence Equation 1.48. The following examples will elucidate some of the delta properties and the use of the delta function in Table 1.3.

**Example**

Equivalence of expressions involving the delta functions:

- (a)  $(\cos t + \sin t)\delta(t) = \delta(t)$
- (b)  $\cos 2t + \sin t\delta(t) = \cos 2t$
- (c)  $1 + 2e^{-t}\delta(t-1) = 1 + 2e^{-1}\delta(t-1)$

**Example**

The values of the following integrals are

$$\begin{aligned} \int_{-\infty}^{\infty} (t^2 + 4t + 5)\delta(t)dt &= 0^2 + 4 \cdot 0 + 5 = 5, & \int_{-\infty}^{\infty} \frac{(1 + \cos t)\delta(t)}{1 + 2e^t} dt &= \frac{2}{1 + 2} \\ \int_{-\infty}^{\infty} t^2 \sum_{k=1}^n \delta(t-k)dt &= \sum_{k=1}^n k^2 = \frac{1}{6}[n(n+1)(2n+1)] \end{aligned}$$

TABLE 1.3 Delta Functional Properties

---

1.  $\delta(at) = \frac{1}{|a|} \delta(t)$
2.  $\delta\left(\frac{t-t_0}{a}\right) = |a| \delta(t-t_0)$
3.  $\delta(at-t_0) = \frac{1}{|a|} \delta\left(t-\frac{t_0}{a}\right)$
4.  $\delta(-t+t_0) = \delta(t-t_0)$
5.  $\delta(-t) = \delta(t)$ ;  $\delta(t) =$  even function
6.  $\int_{-\infty}^{\infty} \delta(t)f(t)dt = f(0)$
7.  $\int_{-\infty}^{\infty} \delta(t-t_0)f(t) = f(t_0)$
8.  $f(t)\delta(t) = f(0)\delta(t)$
9.  $f(t)\delta(t-t_0) = f(t_0)\delta(t-t_0)$
10.  $t\delta(t) = 0$
11.  $\int_{-\infty}^{\infty} A\delta(t)dt = \int_{-\infty}^{\infty} A\delta(t-t_0)dt = A$
12.  $f(t)*\delta(t) =$  convolution  $= \int_{-\infty}^{\infty} f(t-\tau)\delta(\tau)d\tau = f(t)$
13.  $\delta(t-t_1)*\delta(t-t_2) = \int_{-\infty}^{\infty} \delta(\tau-t_1)\delta(t-\tau-t_2)d\tau = \delta[t-(t_1+t_2)]$
14.  $\sum_{n=-N}^N \delta(t-nT)*\sum_{n=-N}^N \delta(t-nT) = \sum_{n=-2N}^{2N} (2N+1-|n|)\delta(t-nT)$
15.  $\int_{-\infty}^{\infty} \frac{d\delta(t)}{dt}f(t)dt = -\frac{df(0)}{dt}$
16.  $\int_{-\infty}^{\infty} \frac{d\delta(t-t_0)}{dt}f(t)dt = -\frac{df(t_0)}{dt}$
17.  $\int_{-\infty}^{\infty} \frac{d^n \delta(t)}{dt^n}f(t)dt = (-1)^n \frac{d^n f(0)}{dt^n}$
18.  $f(t)\frac{d\delta(t)}{dt} = -\frac{df(0)}{dt}\delta(t) + f(0)\frac{d\delta(t)}{dt}$
19.  $t\frac{d\delta(t)}{dt} = -\delta(t)$
20.  $t^n \frac{d^m \delta(t)}{dt^m} = \begin{cases} (-1)^n \frac{n! \delta(t)}{m!} & m = n \\ (-1)^n \frac{m!}{m-n!} \frac{d^{m-n} \delta(t)}{dt^{m-n}}, & m > n \\ 0, & m < n \end{cases}$
21.  $\int_{-\infty}^{\infty} \frac{d\delta(t)}{dt} = 0$ ,  $\frac{d\delta(t)}{dt} =$  odd function
22.  $f(t)*\frac{d\delta(t)}{dt} = \frac{df(t)}{dt}$
23.  $f(t)\frac{d^n \delta(t)}{dt^n} = \sum_{k=0}^n (-1)^k \frac{n!}{k!(n-k)!} \frac{dk f(0)}{dt^k} \frac{d^{n-k} \delta(t)}{dt^{n-k}}$
24.  $\frac{\partial \delta(yt)}{\partial y} = -\frac{1}{y^2} \delta(t)$
25.  $\delta(t) = \frac{du(t)}{dt}$
26.  $\frac{d^n \delta(-t)}{dt^n} = (-1)^n \frac{d^n \delta(t)}{dt^n}$ ,  
 $\left\{ \frac{d^n \delta(t)}{dt^n} \text{ is even if } n \text{ is even, and odd if } n \text{ is odd.} \right\}$
27.  $(\sin at)\frac{d\delta(t)}{dt} = -a\delta(t)$
28.  $\frac{d\delta(t)}{dt} = \frac{d^2 u(t)}{dt^2}$

---

TABLE 1.3 (continued) Delta Functional Properties

---

29.  $-\delta(t) = \frac{du(-t)}{dt}$
30.  $\delta(t-t_0) = \frac{du(t-t_0)}{dt}$
31.  $\frac{d\text{sgn}(t)}{dt} = 2\delta(t)$
32.  $\delta[r(t)] = \sum_n \frac{\delta(t-t_n)}{\left|\frac{dr(t_n)}{dt}\right|}$ ,  $t_n =$  zeros of  $r(t)$ ,  $\frac{dr(t_n)}{dt} \neq 0$
33.  $\frac{d\delta[r(t)]}{dt} = \sum_n \frac{\frac{d\delta(t-t_n)}{dt}}{\left|\frac{dr(t)}{dt}\right| \frac{dr(t_n)}{dt}}$ ,  $t_n =$  zeros of  $r(t)$ ,  $\frac{dr(t_n)}{dt} \neq 0$ ,  $\frac{dr(t)}{dt} \neq 0$
34.  $\delta(\sin t) = \sum_{n=-\infty}^{\infty} \delta(t-n\pi)$
35.  $\delta(t^2-1) = \frac{1}{2}\delta(t-1) + \frac{1}{2}\delta(t+1)$
36.  $\delta(r^2-a^2) = \frac{1}{2a} [\delta(t+a) + \delta(t-a)]$
37.  $\delta(t) = \lim_{\epsilon \rightarrow 0} \frac{e^{-t^2/\epsilon}}{\sqrt{\epsilon\pi}}$
38.  $\delta(t) = \lim_{\omega \rightarrow \infty} \frac{\sin \omega t}{\pi t}$
39.  $\delta(t) = \lim_{\epsilon \rightarrow 0} \frac{\epsilon}{\pi t^2 + \epsilon^2}$
40.  $\delta(t) = \frac{1}{2\pi} \int_{-\infty}^{\infty} \cos \omega t d\omega$
41.  $\frac{df(t)}{dt} = \frac{d}{dt} [tu(t) - (t-1)u(t-1) - u(t-1)]$   
 $= t\delta(t) + u(t) - (t-1)\delta(t-1) - u(t-1)\delta(t-1)$
42.  $\text{comb}_T(t) = \sum_{n=-\infty}^{\infty} \delta(t-nT)$ ,  $f(t)\text{comb}_T(t) = \sum_{n=-\infty}^{\infty} f(nT)\delta(t-nT)$   
 $\text{comb}_{\omega_0}(\omega) = \mathcal{F}\{\text{comb}_T(t)\} = \omega_0 \sum_{n=-\infty}^{\infty} \delta(\omega - n\omega_0)$ ,  $\omega_0 = \frac{2\pi}{T}$

---

**Example**

The first derivative of the functions is

$$\begin{aligned} \frac{d}{dt}(2u(t+1) + u(1-t)) &= \frac{d}{dt}(2u(t+1) + u[-(t-1)]) \\ &= 2\delta(t+1) - \delta(t-1) \end{aligned}$$

$$\begin{aligned} \frac{d}{dt}([2-u(t)] \cos t) &= \frac{d}{dt}(2 \cos t - u(t) \cos t) \\ &= -2 \sin t - \delta(t) \cos t + u(t) \sin t \\ &= (u(t)-2) \sin t - \delta(t) \end{aligned}$$

$$\begin{aligned} \frac{d}{dt} \left( \left[ u\left(t - \frac{\pi}{2}\right) - u(t - \pi) \right] \sin t \right) \\ &= \left[ \delta\left(t - \frac{\pi}{2}\right) - \delta(t - \pi) \right] \sin t + \left[ u\left(t - \frac{\pi}{2}\right) - u(t - \pi) \right] \cos t \\ &= \delta\left(t - \frac{\pi}{2}\right) + \left[ u\left(t - \frac{\pi}{2}\right) - u(t - \pi) \right] \cos t \end{aligned}$$

**Example**

The values of the following integrals are

$$\int_{-\infty}^{\infty} e^{2t} \sin 4t \frac{d^2 \delta(t)}{dt^2} dt = (-1)^2 \frac{d^2}{dt^2} [e^{2t} \sin 4t] |_{t=0} = 2 \times 2 \times 4 = 16$$

$$\begin{aligned} & \int_{-\infty}^{\infty} (t^3 + 2t + 3) \left( \frac{d\delta(t-1)}{dt} + 2 \frac{d^2\delta(t-2)}{dt^2} \right) dt \\ &= \int_{-\infty}^{\infty} (t^3 + 2t + 3) \frac{d\delta(t-1)}{dt} dt + 2 \int_{-\infty}^{\infty} (t^3 + 2t + 3) \frac{d^2\delta(t-2)}{dt^2} dt \\ &= (-1)(3t^2 + 2) |_{t=1} + (-1)^2 2(6t) |_{t=2} \\ &= -5 + 24 = 19 \end{aligned}$$

**Example**

The values of the following integrals are

$$\begin{aligned} \int_0^4 e^{4t} \delta(2t - 3) dt &= \int_0^4 e^{4t} \delta \left[ 2 \left( t - \frac{3}{2} \right) \right] dt = \frac{1}{2} \int_0^4 e^{4t} \delta \left( t - \frac{3}{2} \right) dt \\ &= \frac{1}{2} e^{4 \cdot \frac{3}{2}} = \frac{1}{2} e^6 \end{aligned}$$

$$\int_0^4 e^{4t} \delta(3 - 2t) dt = \int_0^4 e^{4t} \delta[-(2t - 3)] dt = \int_0^4 e^{4t} \delta(2t - 3) dt = \frac{1}{2} e^6$$

$$\begin{aligned} \int_{-\infty}^{\infty} e^{at} \delta(\sin t) dt &= \int_{-\infty}^{\infty} e^{at} \sum_{n=-\infty}^{\infty} \frac{\delta(t - n\pi)}{(-1)^n} dt \\ &= \sum_{n=-\infty}^{\infty} \frac{1}{(-1)^n} \int_{-\infty}^{\infty} e^{at} \delta(t - n\pi) dt \\ &= \sum_{n=-\infty}^{\infty} \frac{1}{(-1)^n} e^{an\pi} \end{aligned}$$

**Example**

The values of the following integrals are

$$\begin{aligned} \int_{-2\pi}^{2\pi} e^{at} \delta(t^2 - \pi^2) dt &= \int_{-2\pi}^{2\pi} e^{at} \frac{1}{2\pi} [\delta(t - \pi) + \delta(t + \pi)] dt \\ &= \frac{1}{2\pi} [e^{a\pi} + e^{-a\pi}] \\ &= \frac{\cosh a\pi}{\pi} \end{aligned}$$

$$\begin{aligned} \int_{-\pi}^{\pi} \cosh \theta \delta(\cos \theta) d\theta &= \int_{-\pi}^{\pi} \cosh \theta \left[ \frac{\delta(\theta + \frac{\pi}{2})}{|\sin(-\frac{\pi}{2})|} + \frac{\delta(\theta - \frac{\pi}{2})}{|\sin \frac{\pi}{2}|} \right] d\theta \\ &= \cosh \left( -\frac{\pi}{2} \right) + \cosh \frac{\pi}{2} \\ &= 2 \cosh \frac{\pi}{2} \end{aligned}$$

**1.2.5 The Gamma and Beta Functions**

The gamma function is defined by the formula

$$\Gamma(z) = \int_0^{\infty} e^{-t} t^{z-1} dt, \quad \text{Re}\{z\} > 0 \quad (1.52)$$

We shall mainly concentrate on the positive values of  $z$  and we shall take the following relationship as the basic definition of the *gamma function*:

$$\Gamma(x) = \int_0^{\infty} e^{-t} t^{x-1} dt, \quad x > 0 \quad (1.53)$$

The gamma function converges for all positive values of  $x$  are shown in Figure 1.2.

The *incomplete gamma function* is given by

$$\gamma(x, \tau) = \int_0^{\tau} t^{x-1} e^{-t} dt, \quad x > 0, \tau > 0 \quad (1.54)$$

The *beta function* is a function of two arguments and is given by

$$B(x, y) = \int_0^1 t^{x-1} (1-t)^{y-1} dt, \quad x > 0, y > 0 \quad (1.55)$$

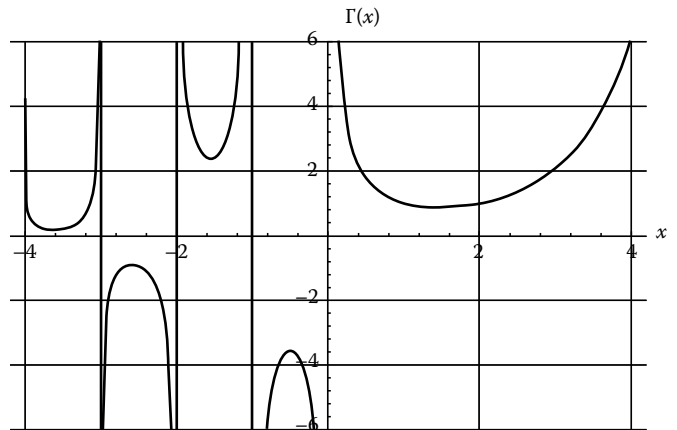


FIGURE 1.2

The beta function is related to the gamma function as follows:

$$B(x, y) = \frac{\Gamma(x)\Gamma(y)}{\Gamma(x+y)} \quad (1.56)$$

### 1.2.5.1 Integral Expressions of $\Gamma(x)$

If we set  $u = e^{-t}$  in Equation 1.54, then  $1/u = e^t$ ,  $\log_e(1/u) = t$ ,  $-(1/u)du = dt$ , and  $[\log_e(1/u)]^{x-1} = t^{x-1}$ , for the limits  $t=0$   $u=1$ , and  $t=\infty$   $u=0$ . Hence

$$\begin{aligned} \Gamma(x) &= \int_0^\infty t^{x-1} e^{-t} dt = - \int_1^0 \left[ \log_e \left( \frac{1}{u} \right) \right]^{x-1} u \frac{1}{u} du \\ &= \int_0^1 \left[ \log_e \left( \frac{1}{u} \right) \right]^{x-1} du \end{aligned} \quad (1.57)$$

Starting from the definitions and setting  $t = m^2$  ( $dt = 2m dm$ ) we obtain (limits are the same)

$$\begin{aligned} \Gamma(x) &= \int_0^\infty t^{x-1} e^{-t} dt = \int_0^\infty m^{2(x-1)} e^{-m^2} 2m dm \\ &= 2 \int_0^\infty m^{2x-1} e^{-m^2} dm \end{aligned} \quad (1.58)$$

### 1.2.5.2 Properties and Specific Evaluations of $\Gamma(x)$

Setting  $x + 1$  in place of  $x$  we obtain

$$\begin{aligned} \Gamma(x+1) &= \int_0^\infty t^{x+1-1} e^{-t} dt = \int_0^\infty t^x e^{-t} dt \\ &= - \int_0^\infty t^x d(e^{-t}) = -t^x e^{-t} \Big|_0^\infty + \int_0^\infty x t^{x-1} e^{-t} dt \\ &= x \Gamma(x) \end{aligned} \quad (1.59)$$

From the above relation we also obtain

$$\Gamma(x) = \frac{\Gamma(x+1)}{x} \quad (1.60)$$

$$\Gamma(x) = (x-1)\Gamma(x-1) \quad (1.61)$$

$$\Gamma(-x) = \frac{\Gamma(x-1)}{-x}, \quad x \neq 0, 1, 2, \dots \quad (1.62)$$

From Equation 1.53 with  $x=1$ , we find that  $\Gamma(1)=1$ . Using Equation 1.59 we obtain

$$\Gamma(2) = \Gamma(1+1) = 1\Gamma(1) = 1 \cdot 1 = 1,$$

$$\Gamma(3) = \Gamma(2+1) = 2\Gamma(2) = 2 \cdot 1,$$

$$\Gamma(4) = \Gamma(3+1) = 3\Gamma(3) = 3 \cdot 2 \cdot 1.$$

Hence we obtain

$$\Gamma(n+1) = n\Gamma(n) = n(n-1)! = n!, \quad n = 0, 1, 2, \dots \quad (1.63)$$

$$\Gamma(n) = (n-1)!, \quad n = 1, 2, \dots \quad (1.64)$$

To find  $\Gamma\left(\frac{1}{2}\right)$  we first set  $t = u^2$

$$\Gamma\left(\frac{1}{2}\right) = \int_0^\infty t^{-1/2} e^{-t} dt = \int_0^\infty 2e^{-u^2} du, \quad (t = u^2)$$

Hence its square value is

$$\begin{aligned} \Gamma^2\left(\frac{1}{2}\right) &= \left[ \int_0^\infty 2e^{-x^2} dx \right] \left[ \int_0^\infty 2e^{-y^2} dy \right] \\ &= 4 \int_0^\infty \left[ \int_0^\infty e^{-y^2} dy \right] e^{-x^2} dx = 4 \int_0^{\pi/2} \left[ \int_0^\infty e^{-r^2} r dr \right] d\theta \\ &= 4 \frac{\pi}{2} \cdot \frac{1}{2} = \pi \end{aligned}$$

and thus

$$\Gamma\left(\frac{1}{2}\right) = \sqrt{\pi} \quad (1.65)$$

Next let us find the expression for  $\Gamma\left(n + \frac{1}{2}\right)$  for integer positive value of  $n$ . From Equation 1.61 we obtain

$$\begin{aligned} \Gamma\left(n + \frac{1}{2}\right) &= \Gamma\left(\frac{2n+1}{2}\right) = \left(\frac{2n+1}{2} - 1\right) \Gamma\left(\frac{2n+1}{2} - 1\right) \\ &= \frac{2n-1}{2} \Gamma\left(\frac{2n-1}{2}\right) \\ &= \left(\frac{2n-1}{2}\right) \left(\frac{2n-3}{2}\right) \Gamma\left(\frac{2n-3}{2}\right) \end{aligned}$$

If we proceed to apply Equation 1.61, we finally obtain

$$\Gamma\left(n + \frac{1}{2}\right) = \frac{(2n-1)(2n-3)(2n-5)\dots(3)(1)\sqrt{\pi}}{2^n} \quad (1.66)$$

Similarly we obtain

$$\Gamma\left(n + \frac{3}{2}\right) = \frac{(2n+1)(2n-1)(2n-3)\dots(3)(1)\sqrt{\pi}}{2^{n+1}} \quad (1.67)$$

$$\Gamma\left(n\frac{1}{2}\right) = \frac{(2n-3)(2n-5)\dots(3)(1)\sqrt{\pi}}{2^{n-1}} \quad (1.68)$$

**Example**

To find the ratio  $\Gamma(x+n)/\Gamma(x-n)$  where  $n$  is a positive integer and  $x-n \neq 0, -1, -2, \dots$ , we proceed as follows [see Equation 1.61]:

$$\begin{aligned} \frac{\Gamma(x+n)}{\Gamma(x-n)} &= \frac{(x+n-1)\Gamma(x+n-1)}{\Gamma(x-n)} \\ &= \frac{(x+n-1)(x+n-2)\Gamma(x+n-2)}{\Gamma(x-n)} = \dots \\ &= \frac{(x+n-1)(x+n-2)(x+n-3)\dots(x+n-2n)\Gamma(x+n-2n)}{\Gamma(x-n)} \\ &= (x+n-1)(x+n-2)\dots(x-n) \end{aligned} \quad (1.69)$$

**Example**

Applying Equation 1.61 we find

$$\begin{aligned} 2^n \Gamma(n+1) &= 2^n n \Gamma(n) = 2^n n(n-1)\Gamma(n-1) \\ &= \dots = 2^n n(n-1)(n-2)\dots 2 \cdot 1 \\ &= 2^n n! = (2 \cdot 1)(2 \cdot 2)(2 \cdot 3)\dots(2 \cdot n) = 2 \cdot 4 \cdot 6 \dots 2n \end{aligned} \quad (1.70)$$

If  $n-1$  is substituted in place of  $n$ , we obtain

$$2 \cdot 4 \cdot 6 \dots (2n-2) = 2^{n-1} \Gamma(n) \quad (1.71)$$

**Example**

Based on the Legendre duplication formula

$$\frac{\Gamma(2n)}{\Gamma(n)} = \frac{\Gamma(n+\frac{1}{2})}{\sqrt{\pi} 2^{1-2n}} \quad (1.72)$$

we can find the ratio  $\Gamma(n+\frac{1}{2})/(\sqrt{\pi}\Gamma(n+1))$  as follows:

$$\begin{aligned} \frac{\Gamma(n+\frac{1}{2})}{\sqrt{\pi}\Gamma(n+1)} &= \frac{\Gamma(2n)2^{1-2n}}{\Gamma(n)\Gamma(n+1)} = \frac{\Gamma(2n)2^{1-2n}2^n}{\Gamma(n)2^n\Gamma(n+1)} \\ &= \frac{\Gamma(2n)2^{1-n}}{\Gamma(n)2 \cdot 4 \cdot 6 \dots 2n} \end{aligned}$$

(see previous example). But

$$\begin{aligned} 1 \cdot 3 \cdot 5 \dots (2n-1) &= \frac{1 \cdot 2 \cdot 3 \cdot 4 \cdot 5 \dots (2n-2)(2n-1)}{2 \cdot 4 \dots (2n-2)} \\ &= \frac{\Gamma(2n)}{2^{n-1}\Gamma(n)} \end{aligned} \quad (1.73)$$

and hence

$$\frac{\Gamma(n+\frac{1}{2})}{\sqrt{\pi}\Gamma(n+1)} = \frac{1 \cdot 3 \cdot 5 \dots (2n-1)}{2 \cdot 4 \cdot 6 \dots 2n} \quad (1.74)$$

**1.2.5.3 Remarks on Gamma Function**

1. The gamma function is continuous at every  $x$  except 0 and the negative integers.
2. The second derivative is positive for every  $x > 0$ , and this indicates that the curve  $y = \Gamma(x)$  is concave upward for all  $x > 0$ .
3.  $\Gamma(x) \rightarrow +\infty$  as  $x \rightarrow 0+$  through positive values and as  $x \rightarrow +\infty$ .
4.  $\Gamma(x)$  becomes, alternatively, negatively infinite and positively infinite at negative integers.
5.  $\Gamma(x)$  attains a single minimum for  $0 < x < \infty$  and is located between  $x = 1$  and  $x = 2$ .

The beta function is defined by

$$B(x, y) = \int_0^1 t^{x-1}(1-t)^{y-1} dt, \quad x > 0, \quad y > 0 \quad (1.75)$$

From the above definition we write

$$\begin{aligned} B(y, x) &= \int_0^1 t^{y-1}(1-t)^{x-1} dt = - \int_1^0 (1-s)^{y-1}s^{x-1} ds \\ &= \int_0^1 s^{x-1}(1-s)^{y-1} ds = B(x, y) \end{aligned} \quad (1.76)$$

where we set  $1-t=s$ .

If we set  $t = \sin^2 \theta$ ,  $dt = 2 \sin \theta \cos \theta d\theta$  and the limits of  $\theta$  are 0 and  $\pi/2$ , then

$$B(x, y) = \int_0^{\pi/2} 2 \sin^{2x-1} \theta \cos^{2y-1} \theta d\theta \quad (1.77)$$

The integral representation of the beta function is given by

$$B(x, y) = \int_0^{\infty} \frac{u^{x-1} du}{(u+1)^{x+y}}, \quad x > 0, \quad y > 0 \quad (1.78)$$

Set  $t = pt$  in Equation 1.52 and find the relation

$$\int_0^{\infty} e^{-pt} t^{z-1} dt = \frac{\Gamma(z)}{p^z}, \quad \text{Re}\{p\} > 0 \quad (1.79)$$

Next set  $p = 1+u$  and  $z = x+y$  in the above equation to find that

$$\frac{1}{(1+u)^{x+y}} = \frac{1}{\Gamma(x+y)} \int_0^{\infty} e^{-(1+u)t} t^{x+y-1} dt \quad (1.80)$$

Substituting Equation 1.80 in Equation 1.78, we obtain

$$\begin{aligned}
 B(x, y) &= \frac{1}{\Gamma(x+y)} \int_0^\infty e^{-t} t^{x+y-1} dt \int_0^\infty e^{-ut} u^{x-1} du \\
 &= \frac{\Gamma(x)}{\Gamma(x+y)} \int_0^\infty e^{-t} t^{y-1} dt = \frac{\Gamma(x)\Gamma(y)}{\Gamma(x+y)} \quad (1.81)
 \end{aligned}$$

It can be shown that

$$B(p, 1-p) = \frac{\pi}{\sin p\pi}, \quad 0 < p < 1 \quad (1.82)$$

From the identities  $\Gamma(x+1) = x\Gamma(x)$ ,  $\Gamma(-x) = \Gamma(1-x)/(-x)$ ,  $B(x, y) = \Gamma(x)\Gamma(y)/\Gamma(x+y)$  together with Equation 1.82, we obtain

$$\Gamma(p)\Gamma(1-p) = \frac{\pi}{\sin p\pi}, \quad p \text{ is nonintegral} \quad (1.83)$$

**Example**

To show that

$$\int_0^\infty t^{n-1} e^{-(a+1)t} dt = \frac{\Gamma(n)}{(a+1)^n}, \quad n > 0, a > -1$$

we set  $t = (a+1)^{-1} y$ . Hence

$$\begin{aligned}
 \int_0^\infty t^{n-1} e^{-(a+1)t} dt &= \int_0^\infty \left(\frac{y}{a+1}\right)^{n-1} e^{-y} \frac{dy}{a+1} \\
 &= (a+1)^{-n} \int_0^\infty y^{n-1} e^{-y} dy = \frac{\Gamma(n)}{(a+1)^n}
 \end{aligned}$$

**Example**

To evaluate the integral  $\int_0^\infty e^{-x^2} dx$ , we write it in the form

$$\int_0^\infty x^0 e^{-x^2} dx$$

which, if compared with the integral in Table 1.4, we have the correspondence  $a=0, b=1, c=2$ . Hence we obtain

$$\int_0^\infty e^{-x^2} dx = \frac{\Gamma\left(\frac{a+1}{c}\right)}{cb^{(a+1)/c}} = \frac{\Gamma\left(\frac{0+1}{2}\right)}{2 \cdot 1^{1/2}} = \frac{\sqrt{\pi}}{2}$$

**TABLE 1.4** Gamma and Beta Function Relations

$\Gamma(x) = \int_0^\infty e^{-t} t^{x-1} dt$	$x > 0$
$\Gamma(x) = \int_0^\infty 2u^{2x-1} e^{-u^2} du$	$x > 0$
$\Gamma(x) = \int_0^1 \left[\log\left(\frac{1}{r}\right)\right]^{x-1} dr$	$x > 0$
$\Gamma(x) = \frac{\Gamma(x+1)}{x}$	$x \neq 0, -1, -2, \dots$
$\Gamma(x) = (x-1)\Gamma(x-1)$	$x \neq 0, -1, -2, \dots$
$\Gamma(-x) = \frac{\Gamma(1-x)}{-x}$	$x \neq 0, 1, 2, \dots$
$\Gamma(n) = (n-1)!$	$n = 1, 2, 3, \dots, 0! = 1$
$\Gamma\left(\frac{1}{2}\right) = \sqrt{\pi}$	
$\Gamma\left(n + \frac{1}{2}\right) = \frac{1 \cdot 3 \cdot 5 \cdots (2n-1)\sqrt{\pi}}{2^n}$	$n = 1, 2, \dots$
$\Gamma\left(n + \frac{3}{2}\right) = \frac{(2n+1)(2n-1)(2n-3) \cdots (3)(1)\sqrt{\pi}}{2^{n+1}}$	$n = 1, 2, \dots$
$\Gamma\left(n - \frac{1}{2}\right) = \frac{(2n-3)(2n-5) \cdots (3)(1)\sqrt{\pi}}{2^{n-1}}$	$n = 1, 2, \dots$
$\Gamma(n+1) = \frac{2 \cdot 4 \cdot 6 \cdots 2n}{2^n}$	$n = 1, 2, \dots$
$\Gamma(2n) = 1 \cdot 3 \cdot 5 \cdots (2n-1)\Gamma(n)2^{1-n}$	$n = 1, 2, \dots$
$\frac{\Gamma(2n)}{\Gamma(n)} = \frac{\Gamma\left(n + \frac{1}{2}\right)}{\sqrt{\pi}2^{1-2n}}$	$n = 1, 2, \dots$
$\Gamma(x)\Gamma(1-x) = \frac{\pi}{\sin x\pi}$	$x \neq 0, \pm 1, \pm 2, \dots$
$n! = \left(\frac{n}{e}\right)^n \sqrt{2\pi n} + h$	$n = 1, 2, \dots, 0$ $< \frac{h}{n!} < \frac{1}{12n}$
$\int_0^\infty t^a e^{-bt^c} dt = \frac{\Gamma\left(\frac{a+1}{c}\right)}{cb^{(a+1)/c}}$	$a > -1, b > 0, c > 0$
$B(x, y) = \int_0^1 t^{x-1} (1-t)^{y-1} dt$	$x > 0, y > 0$
$B(x, y) = \int_0^{\pi/2} 2 \sin^{2x-1} \theta \cos^{2y-1} \theta d\theta$	$x > 0, y > 0$
$B(x, y) = \int_0^\infty \frac{u^{x-1}}{(u+1)^{x+y}} du$	$x > 0, y > 0$
$B(x, y) = \frac{\Gamma(x)\Gamma(y)}{\Gamma(x+y)}$	
$B(x, y) = B(y, x)$	
$B(x, 1-x) = \frac{\pi}{\sin x\pi}$	$0 < x < 1$
$B(x, y) = B(x+1, y) + B(x, y+1)$	$x > 0, y > 0$
$B(x, n+1) = \frac{1 \cdot 2 \cdots n}{x(x+1) \cdots (x+n)}$	$x > 0$

## 1.3 Convolution and Correlation

### 1.3.1 Convolution

Convolution of functions, although a mathematical relation, is extremely important to engineers. If the impulse response of a system is known, that is, the response of the system to a delta function input, the output of the system is the convolution of the

TABLE 1.5  $\Gamma(x)$ ,  $1 \leq x \leq 1.99$

$x$	0	1	2	3	4	5	6	7	8	9
1.0	1.0000	.9943	.9888	.9835	.9784	.9735	.9687	.9642	.9597	.9555
.1	.9514	.9474	.9436	.9399	.9364	.9330	.9298	.9267	.9237	.9209
.2	.9182	.9156	.9131	.9108	.9085	.9064	.9044	.9025	.9007	.8990
.3	.8975	.8960	.8946	.8934	.8922	.8912	.8902	.8893	.8885	.8879
.4	.8873	.8868	.8864	.8860	.8858	.8857	.8856	.8856	.8857	.8859
.5	.8862	.8866	.8870	.8876	.8882	.8889	.8896	.8905	.8914	.8924
.6	.8935	.8947	.8959	.8972	.8986	.9001	.9017	.9033	.9050	.9068
.7	.9086	.9106	.9126	.9147	.9168	.9191	.9214	.9238	.9262	.9288
.8	.9314	.9341	.9368	.9397	.9426	.9456	.9487	.9518	.9551	.9584
.9	.9618	.9652	.9688	.9724	.9761	.9799	.9837	.9877	.9917	.9958

input and its impulse response. The convolution of two functions is given by

$$g(t) \doteq f(t) * h(t) = \int_{-\infty}^{\infty} f(\tau)h(t - \tau)d\tau \quad (1.84)$$

*Proof*

Let  $f(t)$  be written as a sum of elementary  $f_i(t)$ . The output  $g(t)$  is also given by the sum of the outputs  $g_i(t)$  due to each elementary function  $f_i(t)$ . (Table 1.5) Hence

$$f(t) = \sum_i f_i(t), g(t) = \sum_i g_i(t) \quad (1.85)$$

If  $\Delta\tau$  is sufficiently small, the area of  $f_i(t)$  equals  $f(\tau_i) \Delta\tau$  (see Figure 1.3). Hence, the output is approximately  $f(\tau_i) \Delta\tau h(t - \tau_i)$  because  $f_i(t)$  is concentrated near the point  $\tau_i$ . As  $\Delta\tau \rightarrow 0$ , we thus conclude that

$$\sum_i g_i(t) \cong \sum_i f(\tau_i)h(t - \tau_i)\Delta\tau \rightarrow \int_{-\infty}^{\infty} f(\tau)h(t - \tau)d\tau$$

For casual systems, the impulse response is

$$h(t) = 0, \quad t < 0 \quad (1.86)$$

and, therefore, the output of the system becomes

$$g(t) = \int_{-\infty}^t f(\tau)h(t - \tau)d\tau = \int_0^t f(t - \tau)h(\tau)d\tau \quad (1.87)$$

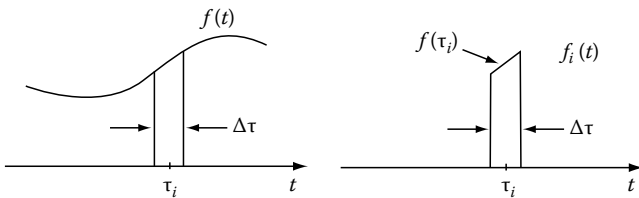


FIGURE 1.3

If, also,  $f(t) = 0$  for  $t < 0$ , then  $g(t) = 0$  for  $t < 0$ ; for  $t > 0$  we obtain

$$g(t) = \int_0^t f(\tau)h(t - \tau)d\tau = \int_0^t f(t - \tau)h(\tau)d\tau \quad (1.88)$$

The convolution does not exist for all functions. The sufficient conditions are

1. Both  $f(t)$  and  $h(t)$  must be absolutely integrable in the interval  $(-\infty, 0]$ .
2. Both  $f(t)$  and  $h(t)$  must be absolutely integrable in the interval  $[0, \infty)$ .
3. Either  $f(t)$  or  $h(t)$  (or both) must be absolutely integrable in the interval  $(-\infty, \infty)$ .

For example, the convolution  $\cos \omega_0 t * \cos \omega_0 t$  does not exist.

**Example**

If the functions to be convoluted are

$$f(t) = 1, 0 < t < 1, \quad h(t) = e^{-t}u(t)$$

then the output is given by

$$g(t) = \int_{-\infty}^{\infty} f(\tau)h(t - \tau)d\tau$$

The ranges are

1.  $-\infty < t < 0$ . No overlap of  $f(t)$  and  $h(t)$  takes place. Hence,  $g(t) = 0$ .
2.  $0 < t < 1$ . Overlap occurs from 0 to  $t$ . Hence

$$g(t) = \int_0^t 1 \cdot e^{-(t-\tau)}d\tau = e^{-t} \int_0^t e^{\tau}d\tau = 1 - e^{-t}$$

3.  $1 < t < \infty$ , Overlap occurs from 0 to 1. Hence

$$g(t) = \int_0^1 e^{-(t-\tau)} d\tau = e^{-t}(e - 1)$$

**1.3.1.1 Definition: Convolution Systems**

The convolution of any continuous and discrete system is given respectively by

$$y(t) = \int_{-\infty}^{\infty} h(t, \tau)x(\tau)d\tau \tag{1.89}$$

$$y(n) = \sum_{m=-\infty}^{\infty} h(n, m)x(m) \tag{1.90}$$

If the systems are time invariant, the kernels  $h(\cdot)$  are functions of the difference of their argument. Hence

$$h(n, m) = h(n - m), \quad h(t, \tau) = h(t - \tau)$$

and therefore

$$y(t) = \int_{-\infty}^{\infty} x(\tau)h(t - \tau)d\tau \tag{1.91}$$

$$y(n) = \sum_{m=-\infty}^{\infty} x(m)h(n - m) \tag{1.92}$$

**1.3.1.2 Definition: Impulse Response**

The impulse response  $h(t)$  of a system is the result of a delta function input to the system. Its value at  $t$  is the response to a delta function at  $t = 0$ .

**Example**

The voltage  $v_c(t)$  across the capacitor of an  $RC$  circuit in series with an input voltage source  $v(t)$  is given by

$$\frac{dv_c(t)}{dt} + \frac{1}{RC}v_c(t) = \frac{1}{RC}v(t)$$

For a given initial condition  $v_c(t_0)$  at time  $t = t_0$  the solution is

$$v_c(t) = e^{-(t-t_0)/RC}v_c(t_0) + \frac{1}{RC} \int_{t_0}^t e^{-(t-\tau)/RC}v(\tau)d\tau, \quad t \geq t_0$$

For a finite initial condition and  $t_0 \rightarrow -\infty$ , the above equation is written in the form

$$v_c(t) = \frac{1}{RC} \int_{-\infty}^{\infty} e^{-(t-\tau)/RC}u(t - \tau)v(\tau)d\tau = \left(\frac{1}{RC}e^{-t/RC}\right)*v(t)$$

Therefore, the impulse response of this system is

$$h(t) = \frac{1}{RC}e^{-t/RC}u(t)$$

**Example**

A discrete system that smooths the input signal  $x(n)$  is described by the difference equation

$$y(n) = ay(n - 1) + (1 - a)x(n), \quad n = 0, 1, 2, \dots$$

By repeated substitution and assuming zero initial condition  $y(-1) = 0$ , the output of the system is given by

$$y(n) = (1 - a) \sum_{m=0}^n a^{n-m}x(m), \quad n = 0, 1, 2, \dots \tag{1.93}$$

If we define the impulse response of the system by

$$h(n) = (1 - a)a^n, \quad n = 0, 1, 2, \dots$$

the system has an input-output relation

$$y(n) = \sum_{m=-\infty}^{\infty} h(n - m)x(m)$$

which indicates that the system is a convolution one.

**Example**

A pure delay system is defined by

$$y(t) = \int_{-\infty}^{\infty} \delta(t - t_0 - \tau)x(\tau)d\tau = x(t - t_0) \tag{1.94}$$

which shows that its impulse response is  $h(t) = \delta(t - t_0)$ .

**1.3.1.3 Definition: Nonanticipative Convolution System**

A system, discrete or continuous, is nonanticipative if and only if its impulse response is

$$h(t) = 0, \quad t < 0$$

with  $t$  ranging over the range in which the system is defined.

If the delay  $t_0$  of a pure delay system is positive, then the system is nonanticipative; and if it is negative, the system is anticipative.



### 1.3.2 Convolution Properties

*Commutative*

$$y(t) = \int_{-\infty}^{\infty} f(\tau)h(t-\tau)d\tau = \int_{-\infty}^{\infty} f(t-\tau)h(\tau)d\tau$$

Set  $t-\tau=\tau'$  in the first integral, and then rename the dummy variable  $\tau'$  to  $\tau$ .

*Distributive*

$$g(t) = f(t)*[h_1(t) + h_2(t)] = f(t)*h_1(t) + f(t)*h_2(t)$$

This property follows directly as a result of the linear property of integration.

*Associative*

$$[[f(t)*h_1(t)]*h_2(t)] = f(t)*[h_1(t)*h_2(t)]$$

*Shift invariance*

If  $g(t) = f(t) * h(t)$ , then

$$g(t-t_0) = f(t-t_0)*h(t) = \int_{-\infty}^{\infty} f(\tau-t_0)h(t-\tau)d\tau$$

Write  $g(t)$  in its integral form, substitute  $t-t_0$  for  $t$ , set  $\tau+t_0=\tau'$ , and then rename the dummy variable.

*Area property*

$$A_f = \int_{-\infty}^{\infty} f(t)dt = \text{area}$$

$$m_f = \int_{-\infty}^{\infty} tf(t)dt = \text{first moment}$$

$$K_f = \frac{m_f}{A_f} = \text{center of gravity}$$

The convolution  $g(t) = f(t) * h(t)$  leads to

$$\begin{aligned} A_g &= A_f A_h \\ K_g &= K_f + K_h \end{aligned}$$

*Proof*

$$\begin{aligned} m_g &= \int_{-\infty}^{\infty} tg(t)dt = \int_{-\infty}^{\infty} t \left[ \int_{-\infty}^{\infty} f(\tau)h(t-\tau)d\tau \right] d\tau \\ &= \int_{-\infty}^{\infty} f(\tau) \left[ \int_{-\infty}^{\infty} th(t-\tau)d\tau \right] d\tau \\ &= \int_{-\infty}^{\infty} f(\tau) \left[ \int_{-\infty}^{\infty} (\lambda+\tau)h(\lambda)d\lambda \right] d\tau, \quad t-\tau=\lambda \\ &= \int_{-\infty}^{\infty} f(\tau)d\tau \int_{-\infty}^{\infty} \lambda h(\lambda)d\lambda + \int_{-\infty}^{\infty} \tau f(\tau)d\tau \int_{-\infty}^{\infty} h(\lambda)d\lambda \\ &= A_f m_h + m_f A_h \end{aligned}$$

$$\frac{m_g}{A_f A_h} = \frac{m_g}{A_g} \doteq K_g = \frac{A_f m_h + m_f A_h}{A_f A_h} = K_h + K_f$$

*Scaline property*

If  $g(t) = f(t) * h(t)$ , then  $f\left(\frac{t}{a}\right) * h\left(\frac{t}{a}\right) = |a|g\left(\frac{t}{a}\right)$ .

*Proof*

$$\begin{aligned} \int_{-\infty}^{\infty} f\left(\frac{\tau}{a}\right)h\left(\frac{t-\tau}{a}\right)d\tau &= \int_{-\infty}^{\infty} f\left(\frac{\tau}{a}\right)h\left(\frac{t}{a}-\frac{\tau}{a}\right)d\tau \\ &= |a| \int_{-\infty}^{\infty} f(r)h\left(\frac{t}{a}-r\right)dr = |a|g\left(\frac{t}{a}\right) \end{aligned}$$

*Complex-valued functions*

$$\begin{aligned} g(t) &= f(t)*h(t) = [f_r(t) + jf_i(t)]*[h_r(t) + jfh_i(t)] \\ &= [f_r(t)*h_r(t) - f_i(t)*h_i(t)] + j[f_r(t)*h_i(t) + f_i(t)*h_r(t)] \end{aligned}$$

*Derivative of delta function*

$$\begin{aligned} g(t) &= f(t)*\frac{d\delta(t)}{dt} = \int_{-\infty}^{\infty} f(\tau)\frac{d}{dt}\delta(t-\tau)d\tau \\ &= \frac{d}{dt} \int_{-\infty}^{\infty} f(\tau)\delta(t-\tau)d\tau = \frac{df(t)}{dt} \end{aligned}$$

*Moment expansion*

Expand  $f(t-\tau)$  in Taylor series about the point  $t=0$

$$f(t-\tau) = f(t) - \tau f^{(1)}(t) + \frac{\tau^2}{2!} f^{(2)}(t) + \dots + \frac{(-\tau)^{n-1}}{(n-1)!} f^{(n-1)}(t) + e_n$$

Insert into convolution integral

$$\begin{aligned}
 g(t) &= f(t) \int_{-\infty}^{\infty} h(\tau) d\tau - f^{(1)} \int_{-\infty}^{\infty} \tau h(\tau) d\tau + \frac{f^{(2)}(t)}{2!} \int_{-\infty}^{\infty} \tau^2 h(\tau) d\tau \\
 &+ \dots + \frac{f^{(n-1)}(t)}{(n-1)!} (-1)^{n-1} \int_{-\infty}^{\infty} \tau^{n-1} h(\tau) d\tau + E_n \\
 &= m_{h0} f(t) - m_{h1} f^{(1)}(t) + \frac{m_{h2}}{2!} f^{(2)}(t) \\
 &+ \dots + \frac{(-1)^{n-1}}{(n-1)!} m_{h(n-1)} f^{(n-1)}(t) + E_n
 \end{aligned}$$

where bracketed numbers in exponents indicate order of differentiation.

*Truncation Error*

Because

$$\begin{aligned}
 e_n &= \frac{(-\tau)^n}{n!} f^{(n)}(t - \tau_1), \quad 0 \leq \tau_1 \leq \tau \\
 E_n &= \frac{1}{n!} \int_{-\infty}^{\infty} (-\tau)^n f^{(n)}(t - \tau_1) h(\tau) d\tau
 \end{aligned}$$

Because  $\tau_1$  depends on  $\tau$ , the function  $f^{(n)}(t - \tau_1)$  cannot be taken outside the integral. However, if  $f^{(n)}(t)$  is continuous and  $t^n h(t) \geq 0$ , then

$$E_n = \frac{1}{n!} f^{(n)}(t - \tau_0) \int_{-\infty}^{\infty} (-\tau)^n h(\tau) d\tau = \frac{(-1)^n m_{hn}}{n!} f^{(n)}(t - \tau_0)$$

where  $\tau_0$  is some constant in the interval of integration.

*Fourier transform*

$$\mathcal{F}\{f(t)*h(t)\} = F(\omega)H(\omega)$$

*Proof*

$$\begin{aligned}
 \int_{-\infty}^{\infty} \left[ \int_{-\infty}^{\infty} f(\tau) h(t - \tau) d\tau \right] e^{-j\omega t} dt &= \int_{-\infty}^{\infty} f(\tau) \int_{-\infty}^{\infty} h(t - \tau) e^{-j\omega t} dt d\tau \\
 &= \int_{-\infty}^{\infty} f(\tau) e^{-j\omega\tau} d\tau \int_{-\infty}^{\infty} h(r) e^{-j\omega r} dr, \quad t - \tau = r
 \end{aligned}$$

*Inverse Fourier transform*

$$\frac{1}{2\pi} \int_{-\infty}^{\infty} F(\omega)H(\omega) e^{-j\omega t} d\omega = \int_{-\infty}^{\infty} f(\tau) h(t - \tau) d\tau$$

*Band-limited function*

If  $f(t)$  is  $\sigma$ -band limited, then the output of a system is

$$g(t) = \int_{-\infty}^{\infty} f(\tau) h(t - \tau) d\tau = \sum_{n=-\infty}^{\infty} T f(nT) h_{\sigma}(t - nT)$$

where

$$h_{\sigma}(t) = \frac{1}{2\pi} \int_{-\sigma}^{\sigma} H(\omega) e^{j\omega t} d\omega$$

*Proof*

$$H_{\sigma}(\omega) = p_{\sigma}(\omega)H(\omega),$$

hence

$$\begin{aligned}
 G(\omega) &= F(\omega)H(\omega) \\
 &= \bar{F}(\omega)p_{\sigma}(\omega)H(\omega) \\
 &= \bar{F}(\omega)H_{\sigma}(\omega), \quad \bar{F}(\omega) = F(\omega) \quad \text{for } -\sigma < \omega < \sigma
 \end{aligned}$$

$$\begin{aligned}
 g(t) &= \bar{f}(t)*h_{\sigma}(t) = \left[ \sum_{n=-\infty}^{\infty} T f(nT) \delta(t - nT) \right] * h_{\sigma}(t) \\
 &= \sum_{n=-\infty}^{\infty} T f(nT) h_{\sigma}(t - nT)
 \end{aligned}$$

The convolution properties are given in Table 1.6.

### 1.3.2.1 Stability of Convolution Systems

#### 1.3.2.1.1 Definition: Bounded Input Bounded Output (BIBO) Stability

A discrete or continuous convolution system with impulse response  $h$  is BIBO stable if and only if the impulse satisfies the inequality,  $\sum_n |h| < \infty$  or  $\int_R |h(t)| dt < \infty$ . If the system is BIBO stable, then

$$\begin{aligned}
 \sup |y(n)| &\leq \sum_n |h(n)| \sup |x(n)|, \quad \sup |y(t)| \\
 &\leq \int_R |h(t)| dt \sup |x(t)|, \quad t \in R
 \end{aligned}$$

for every finite amplitude input  $x(t)$  ( $y$  is the input of the system).

#### Example

If the impulse response of a discrete system is  $h(n) = ab^n$ ,  $n = 0, 1, 2, \dots$ , then

$$\sum_{n=0}^{\infty} |h(n)| = \sum_{n=0}^{\infty} |a||b|^n = \begin{cases} |a| \frac{1}{1-|b|} & |b| < 1 \\ \infty & |b| \geq 1 \end{cases}$$

**TABLE 1.6** Convolution Properties

1. Commutative	$g(t) = \int_{-\infty}^{\infty} f(\tau)h(t - \tau)d\tau = \int_{-\infty}^{\infty} f(t - \tau)h(\tau)d\tau$
2. Distributive	$g(t) = f(t)*[h_1(t) + h_2(t)] = f(t)*h_1(t) + f(t)*h_2(t)$
3. Associative	$[[f(t)*h_1(t)]*h_2(t)] = f(t)*[h_1(t)*h_2(t)]$
4. Shift invariance	$g(t) = f(t)*h(t)$ $g(t - t_0) = f(t - t_0)*h(t) = \int_{-\infty}^{\infty} f(\tau - t_0)h(t - \tau)d\tau$
5. Area property	$A_f = \text{area of } f(t),$ $m_f = \int_{-\infty}^{\infty} tf(t)dt = \text{first moment}$ $K_f = \frac{m_f}{A_f} = \text{center of gravity}$ $A_g = A_f A_h, K_g = K_f + K_h$
6. Scaling	$g(t) = f(t) * h(t)$ $f\left(\frac{t}{a}\right) * h\left(\frac{t}{a}\right) =  a g\left(\frac{t}{a}\right)$
7. Complex-valued functions	$g(t) = f(t)*h(t) = [f_r(t)*h_r(t) - f_i(t)*h_i(t)] + j[f_r(t)*h_i(t) + f_i(t)*h_r(t)]$
8. Derivative	$g(t) = f(t)*\frac{d\delta(t)}{dt} = \frac{df(t)}{dt}$
9. Moment expansion	$g(t) = m_{h0}f(t) - m_{h1}f^{(1)}(t) + \frac{m_{h2}}{2!}f^{(1)}(t) + \dots + \frac{(-1)^{n-1}}{n-1!}m_{h(n-1)}f^{(n-1)}(t) + E_n$ $m_{hk} = \int_{-\infty}^{\infty} \tau^k h(\tau)d\tau$ $E_n = \frac{(-1)^n m_{hn}}{n!}f^{(n)}(t - \tau_0), \tau_0 = \text{constant in the interval of integration}$
10. Fourier transform	$\mathcal{F}\{f(t)*h(t)\} = F(\omega)H(\omega)$
11. Inverse Fourier transform	$\frac{1}{2\pi} \int_{-\infty}^{\infty} F(\omega)H(\omega)e^{j\omega t} d\omega = \int_{-\infty}^{\infty} f(\tau)h(t - \tau)d\tau$
12. Band-limited function	$g(t) = \int_{-\infty}^{\infty} f(\tau)h(t - \tau)d\tau = \sum_{n=-\infty}^{\infty} Tf(nT)h_{\sigma}(t - nT)$ $h_{\sigma}(t) = \frac{1}{2\pi} \int_{-\sigma}^{\sigma} H(\omega)e^{j\omega t} d\omega, f(t) = \sigma\text{-band limited} = 0,  t  > \sigma$
13. Cyclical convolution	$x(n) \otimes y(n) = \sum_{m=0}^{N-1} x((n - m) \bmod N)y(m)$
14. Discrete-time	$x(n)*y(n) = \sum_{m=-\infty}^{\infty} x(n - m)y(m)$
15. Sampled	$x(nT)*y(nT) = T \sum_{m=-\infty}^{\infty} x(nT - mT)y(mT)$

The above indicates that for  $|b| < 1$  the system is BIBO and for  $|b| \geq 1$  the system is unstable.

**Example**

If  $h(t) = u(t)$  then  $|h(t)| = \int_0^{\infty} |u(t)|dt = \infty$ , which indicates the system is not BIBO stable.

**1.3.2.1.2 Harmonic Inputs**

If the input function is of complex exponential order  $e^{j\omega t}$ , then its output is

$$y(t) = \int_{-\infty}^{\infty} h(\tau)e^{j\omega(t-\tau)} d\tau = e^{j\omega t} \int_{-\infty}^{\infty} h(\tau)e^{-j\omega\tau} d\tau = H(\omega)e^{j\omega t}$$

The above equation indicates that the output is the same as the input  $e^{j\omega t}$  with its amplitude modified by  $|H(\omega)|$  and its phase by  $\tan^{-1} (H_i(\omega)/H_r(\omega))$  where  $H_r(\omega) = \text{Re}\{H(\omega)\}$  and  $H_i(\omega) = \text{Im}\{H(\omega)\}$ .

For the discrete case we have the relation

$$y(n) = e^{j\omega n}H(e^{j\omega})$$

where

$$H(e^{j\omega}) = \sum_{n=-\infty}^{\infty} h(n)e^{-j\omega n}$$

## 1.4 Correlation

The *cross-correlation* of two different functions is defined by the relation

$$R_{fh}(t) \doteq f(t) \diamond h(t) = \int_{-\infty}^{\infty} f(\tau)h(\tau - t)d\tau = \int_{-\infty}^{\infty} f(\tau + t)h(\tau)d\tau \quad (1.95)$$

When  $f(t) = h(t)$  the correlation operation is called *autocorrelation*.

$$R_{ff}(t) \doteq f(t) \diamond f(t) = \int_{-\infty}^{\infty} f(\tau)f(\tau - t)d\tau = \int_{-\infty}^{\infty} f(\tau + t)f(\tau)d\tau \quad (1.96)$$

For complex functions the correlation operations are given by

$$R_{fh}(t) \doteq f(t) \diamond h^*(t) = \int_{-\infty}^{\infty} f(\tau)h^*(\tau - t)d\tau \quad (1.97)$$

$$R_{ff}(t) \doteq f(t) \diamond f^*(t) = \int_{-\infty}^{\infty} f(\tau)f^*(\tau - t)d\tau \quad (1.98)$$

The two basic properties of correlation are

$$f(t) \diamond h(t) \neq h(t) \diamond f(t) \quad (1.99)$$

$$\begin{aligned} |R_{ff}(t)| &\doteq |f(t) \diamond f^*(t)| = \left| \int_{-\infty}^{\infty} f(\tau)f^*(\tau - t)d\tau \right| \\ &\leq \left[ \int_{-\infty}^{\infty} |f(\tau)|^2 d\tau \right]^{1/2} \left[ \int_{-\infty}^{\infty} |f(\tau - t)|^2 d\tau \right]^{1/2} \\ &= \int_{-\infty}^{\infty} |f(\tau)|^2 d\tau \leq R_{ff}(0) \end{aligned} \quad (1.100)$$

### Example

The cross-correlation of the following two functions,  $f(t) = p(t)$  and  $h(t) = e^{-(t-3)} u(t-3)$ , is given by

$$R_{fh}(t) = \int_{-\infty}^{\infty} p(\tau)e^{-(\tau-t-3)}u(\tau-t-3)d\tau$$

The ranges of  $t$  are

1.  $t > -2$ :  $R_{fh}(t) = 0$  (no overlap of function)
2.  $-4 < t < -2$ :  $R_{fh}(t) = \int_{3+t}^1 e^{-(\tau-t-3)}d\tau = 1 - e^2 e^t$
3.  $-\infty < t < -4$ :  $R_{fh}(t) = \int_{-1}^1 e^{-(\tau-t-3)}d\tau = e^t e^2 (e^2 - 1)$

The discrete form of correlation is given by

$$x(n) \diamond y(n) = \sum_{m=-\infty}^{\infty} x(m-n)y^*(m) \equiv \text{crosscorrelation} \quad (1.101)$$

$$x(n) \diamond x(n) = \sum_{m=-\infty}^{\infty} x(m-n)x^*(m) \equiv \text{autocorrelation} \quad (1.102)$$

$$\begin{aligned} x(nT) \diamond y(nT) &= T \sum_{m=-\infty}^{\infty} x(mT-nT)y^*(mT) \\ &\equiv \text{sampled cross-correlation} \end{aligned} \quad (1.103)$$

## 1.5 Orthogonality of Signals

### 1.5.1 Introduction

Modern analysis regards some classes of functions as multidimensional vectors introducing the definition of inner products and expansion in term of orthogonal functions (base functions). In this section, functions  $\Phi(t), f(t), F(x), \dots$  symbolize either functions of one independent variable  $t$ , or, for brevity, a function of a set  $n$  independent variables  $t^1, t^2, \dots, t^n$ . Hence,  $dt = dt^1 \dots dt^n$ .

A real or complex function  $f(t)$  defined on the measurable set  $E$  of elements  $\{t\}$  is *quadratically integrable* on  $E$  if and only if

$$\int_E |f(\tau)|^2 d\tau$$

exists in the sense of Lebesque. The class  $L_2$  of all real or complex functions is quadratically integrable on a given interval if one regards the functions  $f(t), h(t), \dots$  as vectors and defines

Vector sum of  $f(t)$  and  $h(t)$  as  $f(t) + h(t)$

Product of  $f(t)$  by a scalar  $\alpha$  as  $\alpha f(t)$

The *inner product* of  $f(t)$  and  $h(t)$  is defined as

$$\langle f, h \rangle \doteq \int_I \gamma(\tau)f^*(\tau)h(\tau)d\tau \quad (1.104)$$

where  $\gamma(\tau)$  is a real nonnative function (*weighting function*) quadratically integrable on  $I$ .

*Norm*

The norm in  $L_2$  is the quantity

$$\|f\| = [\langle f, f \rangle]^{1/2} \doteq \left[ \int_I \gamma(\tau) |f(\tau)|^2 d\tau \right]^{1/2} \quad (1.105)$$

If  $\|f\|$  exists and is different from zero, the function is normalizable.

*Normalization*

$$\frac{f(t)}{\|f\|} = \text{unit norm}$$

*Inequalities*

If  $f(t)$ ,  $h(t)$ , and the nonnegative weighting function  $\gamma(t)$  are quadratically integrable on  $I$ , then

*Cauchy-Schwarz inequality*

$$|\langle f(t), h(t) \rangle| \doteq \left| \int_I \gamma(\tau) f^*(\tau) h(\tau) d\tau \right| \leq \left[ \int_I \gamma |f|^2 d\tau \right]^{1/2} \left[ \int_I \gamma |h|^2 d\tau \right]^{1/2} \doteq \langle f, f \rangle \langle h, h \rangle \quad (1.106)$$

*Minkowski inequality*

$$\begin{aligned} \|f + h\| &\doteq \left( \int_I \gamma |f + h|^2 d\tau \right)^{1/2} \\ &\leq \left( \int_I \gamma |f|^2 d\tau \right)^{1/2} + \left( \int_I \gamma |h|^2 d\tau \right)^{1/2} \\ &= \|f\| + \|h\| \end{aligned} \quad (1.107)$$

*Convergence in mean*

The space  $L_2$  admits the *distance function* (metric)

$$d(f, h) \doteq \|f - h\| \doteq \left[ \int_I \gamma(\tau) |f(\tau) - h(\tau)|^2 d\tau \right]^{1/2} \quad (1.108)$$

The root-mean-square difference of the above equation between the two functions  $f(t)$  and  $h(t)$  is equal to zero if and only if  $f(t) = h(t)$  for almost all  $t$  in  $I$ .

Every sequence in  $I$  of functions  $r_0(t)$ ,  $r_1(t)$ ,  $r_2(t)$ , ... converges in the mean to the limit  $r(t)$  if and only if

$$d^2(r_n, r) \doteq \|r_n - r\|^2 \doteq \int_I \gamma(\tau) |r_n(\tau) - r(\tau)|^2 d\tau \rightarrow 0 \quad \text{as } n \rightarrow \infty \quad (1.109)$$

Therefore we define limit in the mean

$$\lim_{n \rightarrow \infty} r_n(t) = r(t) \quad (1.110)$$

Convergence in the mean does not necessarily imply convergence of the sequence at every point, nor does convergence of all points on  $I$  imply convergence in the mean.

*Riess-Fischer Theorem*

The  $L_2$  space with a given interval  $I$  is *complete*; every sequence of quadratically integrable functions  $r_0(t)$ ,  $r_1(t)$ ,  $r_2(t)$ , ... such that  $\lim_{m \rightarrow \infty, n \rightarrow \infty} |r_m - r_n| = 0$  (*Cauchy sequence*), converges in the mean to a quadratically integrable function  $r(t)$  and defines  $r(t)$  uniquely for almost all  $t$  in  $I$ .

*Orthogonality*

Two quadratically integrable functions  $f(t)$ ,  $h(t)$  are *orthogonal* on  $I$  if and only if

$$\langle f, h \rangle = \int_I \gamma(\tau) f^*(\tau) h(\tau) d\tau = 0 \quad (1.111)$$

*Orthonormal*

A set of function  $r_i(t)$ ,  $i = 1, 2, \dots$  is an *orthonormal* set if and only if

$$\langle r_i, r_j \rangle \doteq \int_I \gamma(\tau) r_i^*(\tau) r_j(\tau) d\tau = \delta_{ij} = \begin{cases} 0 & \text{if } i \neq j \\ 1 & \text{if } i = j \end{cases} \quad (i, j = 1, 2, \dots) \quad (1.112)$$

Every set of normalizable mutually orthogonal functions is linearly independent.

*Bessel's inequalities*

Given a finite or infinite orthonormal set  $\varphi_1(t)$ ,  $\varphi_2(t)$ ,  $\varphi_3(t)$ , ... and any function  $f(t)$  quadratically integrable over  $I$

$$\sum_i |\langle \varphi_i, f \rangle|^2 \leq \langle f, f \rangle \quad (1.113)$$

The equal sign applies if and only if  $f(t)$  belongs to the space spanned by all  $\varphi_i(t)$ .

*Complete orthonormal set of functions (orthonormal bases)*

A set of functions  $\{\varphi_i(t)\}$ ,  $i = 1, 2, \dots$ , in  $L_2$  is a complete orthonormal set if and only if the set satisfies the following conditions:

1. Every quadratically integrable function  $f(t)$  can be expanded in the form

$$f(t) = \langle f, \varphi_1 \rangle \varphi_1 + \langle f, \varphi_2 \rangle \varphi_2 + \dots + \langle f, \varphi_i \rangle \varphi_i + \dots, \quad i = 1, 2, \dots$$

2. If (1) above is true, then

$$\langle f, f \rangle = |\langle f, \varphi_1 \rangle|^2 + |\langle f, \varphi_2 \rangle|^2 + \dots$$

which is the completeness relation (Parseval's identity).

3. For any pair of functions  $f(t)$  and  $h(t)$  in  $L_2$ , the relation holds

$$\langle f, h \rangle = \langle f, \varphi_1 \rangle \langle h, \varphi_1 \rangle + \langle f, \varphi_2 \rangle \langle h, \varphi_2 \rangle + \dots$$

4. The orthonormal set  $\varphi_1(t), \varphi_2(t), \varphi_3(t), \dots$  is not contained in any other orthonormal set in  $L_2$ .

The above conditions imply the following: given a complete orthonormal set  $\{\varphi_i(t)\}$ ,  $i = 1, 2, \dots$  in  $L_2$  and a set of complex numbers  $\langle f, \varphi_1 \rangle, \langle f, \varphi_2 \rangle + \dots$  such that  $\sum_{i=1}^{\infty} |\langle f, \varphi_i \rangle|^2 < \infty$ , there exists a quadratically integrable function  $f(t)$  such that  $\langle f, \varphi_1 \rangle \varphi_1 + \langle f, \varphi_2 \rangle \varphi_2 + \dots$  converges in the mean of  $f(t)$ .

*Gram-Schmidt orthonormalization process*

Given any countable (finite or infinite) set of linear independent functions  $r_1(t), r_2(t), \dots$  normalizable in  $I$ , there exists an orthogonal set  $\varphi_1(t), \varphi_2(t), \dots$  spanning the same space of functions. Hence

$$\begin{aligned} \varphi_1 &= r_1, \varphi_2 = r_2 - \frac{\int_I \varphi_1 r_2 dt}{\int_I \varphi_1^2 dt}, \varphi_3 \\ &= r_3 - \frac{\int_I \varphi_1 r_3 dt}{\int_I \varphi_1^2 dt} \varphi_1 - \frac{\int_I \varphi_2 r_3 dt}{\int_I \varphi_2^2 dt} \varphi_2, \text{ etc.} \end{aligned} \quad (1.114)$$

For creating an orthonormal set, we proceed as follows:

$$\varphi_i(t) = \frac{\mathbf{v}_i(t)}{\|\mathbf{v}_i(t)\|} = \frac{\mathbf{v}_i(t)}{+\sqrt{\langle \mathbf{v}_i, \mathbf{v}_i \rangle}}$$

$$\mathbf{v}_1(t) = r_1(t), \mathbf{v}_{i+1}(t) = r_{i+1}(t) - \sum_{k=1}^i \langle \varphi_k, r_{i+1} \rangle \varphi_k(t), \quad i = 1, 2, \dots \quad (1.115)$$

*Series approximation*

If  $f(t)$  is a quadratically integrable function, then

$$\int_I |f_n(t) - f(t)|^2 dt$$

yields the *least mean square error*. The set  $\{\varphi_i(t)\}$ ,  $i = 1, 2, \dots$  is orthonormal and the approximation to  $f(t)$  is

$$f_n(t) = a_1 \varphi_1(t) + a_2 \varphi_2(t) + \dots + a_n \varphi_n(t), \quad n = 1, 2, \dots \quad (1.116)$$

**1.5.2 Legendre Polynomials**

**1.5.2.1 Relations of Legendre Polynomials**

Legendre polynomials are closely associated with physical phenomena for which spherical geometry is important. The polynomials  $P_n(t)$  are called Legendre polynomials in honor of their discoverer, and they are given by

$$P_n(t) = \sum_{k=0}^{[n/2]} \frac{(-1)^k (2n-2k)! t^{n-2k}}{2^n k! (n-k)! (n-2k)!} \quad (1.117)$$

$$[n/2] = \begin{cases} n/2 & n \text{ even} \\ (n-1)/2 & n \text{ odd} \end{cases}$$

$$\frac{1}{\sqrt{1-2st+s^2}} = \begin{cases} \sum_{n=0}^{\infty} P_n(t) s^n & |s| < 1 \\ \sum_{n=0}^{\infty} P_n(t) s^{-n-1} & |s| > 1 \end{cases} \text{ generating function} \quad (1.117a)$$

Table 1.7 gives the first eight Legendre polynomials. Figure 1.4 shows the first six Legendre polynomials.

**TABLE 1.7** Legendre Polynomials

$P_0 = 1$
$P_1 = t$
$P_2 = \frac{3}{2}t^2 - \frac{1}{2}$
$P_3 = \frac{5}{2}t^3 - \frac{3}{2}t$
$P_4 = \frac{35}{8}t^4 - \frac{30}{8}t^2 + \frac{3}{8}$
$P_5 = \frac{63}{8}t^5 - \frac{70}{8}t^3 + \frac{15}{8}t$
$P_6 = \frac{231}{16}t^6 - \frac{315}{16}t^4 + \frac{105}{16}t^2 - \frac{5}{16}$
$P_7 = \frac{429}{16}t^7 - \frac{693}{16}t^5 + \frac{315}{16}t^3 - \frac{35}{16}t$

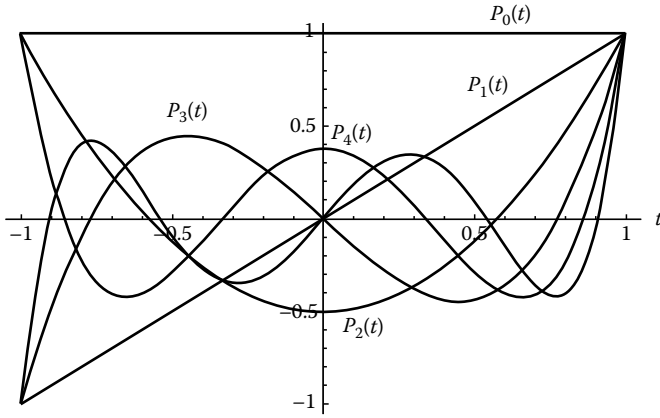


FIGURE 1.4

Rodrigues formula

$$P_n(t) = \frac{1}{2^n n!} \frac{d^n}{dt^n} (t^2 - 1)^n, \quad n = 0, 1, 2, \dots \quad (1.118)$$

Recursive formulas

$$(n + 1)P_{n+1}(t) - (2n + 1)tP_n(t) + nP_{n-1}(t) = 0, \quad n = 1, 2, \dots \quad (1.119)$$

$$P'_{n+1}(t) - tP'_n(t) = (n + 1)P_n(t), \quad (P'(t) \doteq \text{derivative of } P(t)) \quad n = 0, 1, 2, \dots \quad (1.120)$$

$$tP'_n(t) - P'_{n-1}(t) = nP_n(t) \quad n = 1, 2, \dots \quad (1.121)$$

$$P'_{n+1}(t) - P'_{n-1}(t) = (2n + 1)P_n(t) \quad n = 1, 2, \dots \quad (1.122)$$

$$(t^2 - 1)P'_n(t) = ntP_n(t) - nP_{n-1}(t) \quad (1.123)$$

$$P_0(t) = 1, P_1(t) = t \quad (1.124)$$

Example

From Equation 1.117, when  $n$  is even, implies,  $P_n(-t) = P_n(t)$  and when  $n$  is odd,  $P_n(-t) = -P_n(t)$ . Therefore

$$P_n(-t) = (-1)^n P_n(t) \quad (1.125)$$

Example

From Equation 1.123  $t = 1$  implies  $0 = nP_{n-1}(1) - nP_{n-1}(1)$  or  $P_n(1) = P_{n-1}(1)$ . For  $n = 1$  it implies  $P_1(1) = P_0(1) = 1$ . For  $n = 2$   $P_2(1) = P_1(1) = 1$ , and so forth. Hence,  $P_n(1) = 1$ . From Equation 1.125  $P_n(-1) = (-1)^n$ . Hence

$$P_n(1) = 1, P_n(-1) = (-1)^n \quad (1.126)$$

$$P_n(t) < 1 \quad \text{for } -1 < t < 1 \quad (1.127)$$

Example

From Equation 1.123 we get

$$\frac{d}{dt} [(1 - t^2)P'_n(t)] = nP'_{n-1}(t) - nP_n(t) - ntP'_n(t)$$

Use Equation 1.121 to find

$$\frac{d}{dt} [(1 - t^2)P'_n(t)] + n(n + 1)P_n(t) = 0$$

or

$$(1 - t^2)P''_n(t) - 2tP'_n(t) + n(n + 1)P_n(t) = 0 \quad (1.128)$$

We have deduced the Legendre polynomials  $y = P_n(t)$  ( $n = 0, 1, 2, \dots$ ) as the solution of the linear second-order ordinary differential equation

$$(1 - t^2)y''(t) - 2ty'(t) + n(n + 1)y(t) = 0 \quad (1.128a)$$

called the Legendre differential equation.

If we let  $x = \cos \varphi$  then the above equation transforms to the trigonometric form

$$y'' + (\cot \varphi)y' + n(n + 1)y = 0 \quad (1.128b)$$

It can be shown that Equation 1.128a has solutions of a first kind

$$y = C_0 \left[ 1 - \frac{n(n+1)}{2!}t^2 + \frac{n(n+1)(n-2)(n+3)}{4!}t^4 - \dots \right] + C_1 \left[ 1 - \frac{(n-1)(n+2)}{3!}t^3 + \frac{(n-1)(n+2)(n-3)(n+4)}{5!}t^5 - \dots \right] \quad (1.128c)$$

valid for  $|t| < 1$ ,  $C_0$  and  $C_1$  being arbitrary constants.

Schl\"afli's integral formula

$$P_n(t) = \frac{1}{2\pi j} \int_C \frac{(z^2 - 1)^n}{2^n (z - t)^{n+1}} dz \quad (1.129)$$

where  $C$  is any regular, simple, closed curve surrounding  $t$ .

1.5.2.2 Complete Orthonormal System,

$$\left\{ \left[ \frac{1}{2} (2n + 1) \right]^{1/2} P_n(t) \right\}$$

The Legendre polynomials are orthogonal in  $[-1, 1]$

$$\int_{-1}^1 P_n(t)P_m(t)dt = 0 \quad (1.130)$$

$$\int_{-1}^1 [P_n(t)]^2 dt = \frac{2}{2n + 1} \quad n = 0, 1, 2, \dots \quad (1.131)$$

and therefore the set

$$\varphi_n(t) = \sqrt{\frac{2n+1}{2}} P_n(t) \quad n = 0, 1, 2, \dots \quad (1.132)$$

is orthonormal.

### 1.5.2.2.1 Series Expansion

If  $f(t)$  is integrable in  $[-1, 1]$ , then

$$f(t) = \sum_{n=0}^{\infty} a_n P_n(t) \quad -1 < t < 1 \quad (1.132a)$$

$$a_n = \frac{2n+1}{2} \int_{-1}^1 f(t) P_n(t) dt \quad n = 0, 1, 2, \dots \quad (1.132b)$$

For even  $f(t)$ , the series will contain term  $P_n(t)$  of even index; if  $f(t)$  is odd, the term of odd index only.

If the real function  $f(t)$  is piecewise smooth in  $(-1, 1)$  and if it is square integrable in  $(-1, 1)$ , then the series Equation 1.132a converges of  $f(t)$  at every continuity point of  $f(t)$ .

### 1.5.2.2.2 Change of Range

If a function  $f(t)$  is defined in  $[a, b]$ , it is sometimes necessary in the application to expand the function in a series of orthogonal polynomials in this interval. Clearly the substitution

$$t = \frac{2}{b-a} \left[ x - \frac{b+a}{2} \right], \quad a < b, \quad \left[ x = \frac{b-a}{2} t + \frac{b+a}{2} \right] \quad (1.133)$$

transform the interval  $[a, b]$  of the  $x$ -axis into the interval  $[-1, 1]$  of the  $t$ -axis. It is, therefore, sufficient to consider the expansion in series of Legendre polynomials of

$$f \left[ \frac{b-a}{2} t + \frac{b+a}{2} \right] = \sum_{n=0}^{\infty} a_n P_n(t) \quad (1.134a)$$

$$a_n = \frac{2n+1}{2} \int_{-1}^1 f \left[ \frac{b-a}{2} t + \frac{b+a}{2} \right] P_n(t) dt \quad (1.134b)$$

The above equation can also be accomplished as follows:

$$f(t) = \sum_{n=0}^{\infty} a_n X_n(t) \quad (1.135a)$$

$$X_n(t) = \frac{1}{n!(b-a)^n} \frac{d^n(t-a)^n(t-b)^n}{dt^n} \quad (1.135b)$$

$$a_n = \frac{2n+1}{b-a} \int_a^b f(t) X_n(t) dt \quad (1.135c)$$

### Example

Suppose  $f(t)$  is given by

$$f(t) = \begin{cases} 0 & -1 \leq t < a \\ 1 & a < t \leq 1 \end{cases}$$

Then from Equation 1.132b

$$a_n = \frac{2n+1}{2} \int_a^1 P_n(t) dt$$

Using Equation 1.122, and noting that  $P_n(1) = 1$ , we obtain

$$a_n = -\frac{1}{2} [P_{n+1}(a) - P_{n-1}(a)], \quad a_0 = \frac{1}{2} (1 - a)$$

which leads to the expansion

$$f(t) \cong \frac{1}{2} (1 - a) - \frac{1}{2} \sum_{n=1}^{\infty} [P_{n+1}(a) - P_{n-1}(a)] P_n(t), \quad -1 < t < 1$$

### Example

Suppose  $f(t)$  is given by

$$f(t) = \begin{cases} -1 & -1 \leq t < 0 \\ 1 & 0 < t \leq 1 \end{cases}$$

The function is an odd function and, therefore,  $f(t)P_n(t)$  is an odd function of  $P_n(t)$  with even index. Hence,  $a_n$  are zero for  $n = 0, 2, 4, \dots$  For odd index  $n$ , the product  $f(t)P_n(t)$  is even and hence

$$a_n = \left( n + \frac{1}{2} \right) \int_{-1}^1 f(t) P_n(t) dt = 2 \left( n + \frac{1}{2} \right) \int_0^1 P_n(t) dt, \quad n = 1, 3, 5, \dots$$

Using Equation 1.122 and setting  $n = 2k + 1, k = 0, 1, 2, \dots$  we obtain

$$\begin{aligned} a_{2k+1} &= (4k+3) \int_0^1 P_{2k+1}(t) dt = \int_0^1 [P'_{2k+2}(t) - P'_{2k}(t)] dt \\ &= [P_{2k+2}(t) - P_{2k}(t)]_0^1 = P_{2k}(0) - P_{2k+2}(0) \end{aligned}$$

where we have used the property  $P_n(1) = 1$  for all  $n$ . But

$$P_{2n}(0) = \left( \frac{-1}{n} \right) = \frac{(-1)^n (2n)!}{2^{2n} (n!)^2} \quad (1.136)$$



and, thus, we have

$$\begin{aligned} a_{2k+1} &= \frac{(-1)^k(2k)!}{2^{2k}(k!)^2} - \frac{(-1)^{k+1}(2k+2)!}{2^{2k+2}[(k+1)!]^2} \\ &= \frac{(-1)^k(2k)!}{2^{2k}(k!)^2} \left[ 1 + \frac{2k+1}{2k+2} \right] = \frac{(-1)^k(2k)!(4k+3)}{2^{2k+1}k!(k+1)!} \end{aligned}$$

The expansion is

$$f(t) = \sum_{k=0}^{\infty} \frac{(-1)^k(2k)!(4k+3)}{2^{2k+1}k!(k+1)!} P_{2k+1}(t), \quad -1 \leq t \leq 1 \quad (1.137)$$

### 1.5.2.3 Associated Legendre Polynomials

If  $m$  is a positive integer and  $-1 \leq t \leq 1$ , then

$$P_n^m(t) = (1-t^2)^{m/2} \frac{d^m P_n(t)}{dt^m}, \quad m = 1, 2, \dots, n \quad (1.138)$$

where  $P_n^m(t)$  is known as the *associated Legendre function* or *Ferrer's functions*.

*Rodrigues formula*

$$P_n^m(t) = \frac{(1-t^2)^{m/2}}{2^n n!} \frac{d^{n+m}}{dt^{n+m}} (t^2-1)^n, \quad m = 1, 2, \dots, n; \quad n+m \geq 0 \quad (1.139)$$

*Properties*

$$P_n^{-m}(t) = (-1)^m \frac{(n-m)!}{(n+m)!} P_n^m(t) \quad (1.140)$$

$$P_n^0(t) = P_n(t) \quad (1.141)$$

$$(n-m+1)P_{n+1}^m(t) - (2n+1)tP_n^m(t) + (n+m)P_{n-1}^m(t) = 0 \quad (1.142)$$

$$(1-t^2)^{1/2} P_n^m(t) = \frac{1}{2n+1} [P_{n+1}^{m+1}(t) - P_{n-1}^{m+1}(t)] \quad (1.143)$$

$$(1-t^2)^{1/2} P_n^m(t) = \frac{1}{2n+1} [(n+m)(n+m-1)P_{n-1}^{m-1}(t) - (n-m+1)(n-m+2)P_{n+1}^{m-1}(t)] \quad (1.144)$$

$$P_n^{m+1}(t) = 2mt(1-t^2)^{-1/2} P_n^m(t) - [n(n+1) - m(m-1)] P_{n-1}^{m-1}(t) \quad (1.145)$$

$$\int_{-1}^1 P_n^m(t) P_k^m(t) dt = 0, \quad k \neq n \quad (1.146)$$

$$\int_{-1}^1 [P_n^m(t)]^2 dt = \frac{2}{(2n+1)} \frac{(n+m)!}{(n-m)!} \quad (1.147)$$

### Example

To evaluate the integral  $\int_{-1}^1 t^m P_n(t) dt$ , we use the Rodrigues formula and proceed as follows:

$$\begin{aligned} \int_{-1}^1 t^m P_n(t) dt &= \frac{1}{2^n n!} \int_{-1}^1 t^m D^n [(t^2-1)^n] dt, \quad \left( D^n = \frac{d^n}{dt^n} \right) \\ &= \frac{1}{2^n n!} \left[ t^m D^{n-1} (t^2-1)^n \Big|_{t=-1}^{t=1} - m \int_{-1}^1 t^{m-1} D^{n-1} [(t^2-1)^n] dt \right] \end{aligned}$$

where integration by parts was used. The left expression is zero because of the presence of the expression  $(t^2-1)^n$ .

(a) For  $m < n$  and after  $m$  integrations by parts we obtain

$$\begin{aligned} \int_{-1}^1 t^m P_n(t) dt &= \frac{(-1)^m m!}{2^n n!} \int_{-1}^1 D^{n-m} [(t^2-1)^n] dt \\ &= \frac{(-1)^m m!}{2^n n!} [D^{n-m-1} (t^2-1)^n]_{t=-1}^{t=1} = 0, \\ & \quad m < n \end{aligned}$$

(b)  $m \geq n$ . Integrate  $n$  times by parts to find the following expression:

$$\int_{-1}^1 t^m P_n(t) dt = C_{mn} \int_{-1}^1 t^{m-n} (2^2-1)^n dt$$

where

$$C_{mn} = \frac{(-1)^m m(m-1)(m-2) \cdots (m-[n-1])}{2^n n!}$$

Multiplying numerator and denominator by  $(m-n)!$  and incorporating the  $(-1)^n$  in the integrand, we obtain

$$\int_{-1}^1 t^m P_n(t) dt = \frac{m!}{2^n n! (m-n)!} \int_{-1}^1 t^{m-n} (1-t^2)^n dt, \quad m \geq n$$

If  $m-n$  is odd the integrand is an odd function and hence is equal to zero. If  $m-n$  is even then the integrand is even and hence

$$\begin{aligned} \int_{-1}^1 t^m P_n(t) dt &= \frac{m! 2}{2^n n! (m-n)!} \int_0^1 t^{m-n} (1-t^2)^n dt \\ &= \frac{m! \Gamma\left(\frac{m-n+1}{2}\right)}{2^{n-1} (m-n)! (m+n+1) \Gamma\left(\frac{m+n+1}{2}\right)}, \\ & \quad m \geq n, m-n \text{ is even} \end{aligned}$$

If  $m = n$

$$\begin{aligned} \int_{-1}^1 t^m P_n(t) dt &= \frac{n! \Gamma(\frac{1}{2})}{2^{n-1} (2n+1) \binom{2n-1}{2} \binom{2n-3}{2} \cdots \binom{3}{2} \binom{1}{2} \Gamma(\frac{1}{2})} \\ &= \frac{n! 2^n}{2^{n-1} (2n+1) (2n-1) (2n-3) \cdots (3) (1)} \\ &= \frac{n! 2^n 2^n n!}{2^{n-1} (2n+1) (2n) (2n-1) (2n-2) (2n-3) \cdots (3) (2) (1)} \\ &= \frac{2^{n+1} (n!)^2}{(2n+1)!} \end{aligned}$$

Hence,

$$\int_{-1}^1 t^m P_n(t) dt = \begin{cases} 0 & m < n \\ 0 & m \geq n, m-n \text{ is odd} \\ \frac{m! \Gamma(\frac{m-n+1}{2})}{2^{n-1} (m-n)! (m+n+1)! \Gamma(\frac{m+n+1}{2})} & m > n, m-n \text{ is even} \\ \frac{2^{n+1} (n!)^2}{(2n+1)!} & m = n \end{cases}$$

**Example**

To find  $P_{2n}(0)$  we use the summation

$$P_{2n}(t) = \frac{(-1)^n}{2^{2n-1}} \sum_{k=0}^n \frac{(-1)^k (2n+2k-1)!}{(2k)! (n+k-1)! (n-k)!} t^{2k}$$

with  $k=0$ . Hence

$$P_{2n}(0) = \frac{(-1)^n (2n-1)!}{2^{2n-1} (n-1)! n!} = \frac{(-1)^n 2n [(2n-1)!]}{2^{2n} n [(n-1)!] n!} = \frac{(-1)^n (2n)!}{2^{2n} (n!)^2}$$

**Example**

To evaluate  $\int_0^1 P_m(t) dt$  for  $m \neq 0$ , we must consider the two cases:  $m$  being odd and  $m$  being even.

(a)  $m$  is even and  $m \neq 0$

$$\begin{aligned} \int_0^1 P_m(t) dt &= \frac{1}{2} \int_{-1}^1 P_m(t) dt = \frac{1}{2} \int_{-1}^1 P_m(t) \cdot 1 dt \\ &= \frac{1}{2} \int_{-1}^1 P_m(t) P_0(t) dt = 0 \end{aligned}$$

The result is due to the orthogonality principle.

(b)  $m$  is odd and  $m \neq 0$ . From the relation (see Table 1.8)

$$\int_t^1 P_m(t) dt = \frac{1}{2m+1} [P_{m-1}(t) - P_{m+1}(t)]$$

with  $t=0$  we obtain

$$\int_0^1 P_m(t) dt = \frac{1}{2m+1} [P_{m-1}(0) - P_{m+1}(0)]$$

Using the results of the previous example, we obtain

$$\begin{aligned} \int_0^1 P_m(t) dt &= \frac{1}{2m+1} \left[ \frac{(-1)^{\frac{m-1}{2}} (m-1)!}{2^{m-1} \left[ \left( \frac{m-1}{2} \right)! \right]^2} - \frac{(-1)^{\frac{m+1}{2}} (m+1)!}{2^{m+1} \left[ \left( \frac{m+1}{2} \right)! \right]^2} \right] \\ &= \frac{(-1)^{\frac{m-1}{2}} (m-1)! (2m+1) (m+1)}{(2m+1) 2^{m+1} \left( \frac{m+1}{2} \right)! \left( \frac{m-1}{2} \right)!} = \frac{(-1)^{\frac{m-1}{2}} (m-1)!}{2^m \left( \frac{m+1}{2} \right)! \left( \frac{m-1}{2} \right)!} \end{aligned}$$

$m$  is odd.

**Example**

One hemisphere of a homogeneous spherical solid is maintained at 300°C while the other half is kept at 75°C. To find the temperature distribution we must use the equation for heat conduction

$$\frac{\partial T}{\partial t} = \frac{k}{\rho c} \left( \nabla^2 T + \frac{\partial Q}{\partial t} \right)$$

where

- $T$  is the temperature
- $t$  is the time
- $k$  is the thermal conductivity
- $\rho$  is the density
- $c$  is the specific heat
- $\partial Q/\partial t$  is the rate of heat generation

Because of the steady-state condition of the problem,  $\partial T/\partial t = \partial Q/\partial t = 0$ . Hence, the equation becomes

$$\begin{aligned} \nabla^2 T &= \frac{\partial^2 T}{\partial x^2} + \frac{\partial^2 T}{\partial y^2} + \frac{\partial^2 T}{\partial z^2} \\ &= \frac{\partial}{\partial r} \left( r^2 \frac{\partial T}{\partial r} \right) + \frac{1}{\sin \varphi} \frac{\partial}{\partial \varphi} \left( \sin \varphi \frac{\partial T}{\partial \varphi} \right) = 0 \end{aligned}$$

where  $T$  is independent of  $\theta$ .

Assuming a solution of the form

$$T = FG = f(r)g(\varphi)$$

we obtain

$$\frac{\partial T}{\partial r} = G \frac{dF}{dr}, \quad \frac{\partial^2 T}{\partial r^2} = G \frac{d^2 F}{dr^2}$$

Similarly, we obtain

$$\frac{\partial T}{\partial \varphi} = F \frac{dG}{d\varphi}, \quad \frac{\partial^2 T}{\partial \varphi^2} = F \frac{d^2 G}{d\varphi^2}$$

TABLE 1.8 Properties of Legendre and Associate Legendre Functions

1.	$\frac{1}{\sqrt{1-2tx+x^2}} = \sum_{n=0}^{\infty} P_n(t)x^n,$	$ t  \leq 1,  x  < 1$
2.	$P_n(t) = \sum_{k=0}^{[n/2]} \frac{(-1)^k (2n-2k)! t^{n-2k}}{2^n k! (n-k)! (n-2k)!},$	$[n/2] = \frac{n}{2}, \quad n \text{ is even};$ $[n/2] = (n-1)/2, \quad n \text{ is odd}$
3.	$P_0(t) = 1$	
4.	$P_{2n}(0) = \binom{-\frac{1}{2}}{n} = \frac{(-1)^n (2n)!}{2^{2n} (n!)^2},$	$n = 1, 2, \dots$
5.	$P_{2n+1}(0) = 0,$	$n = 0, 1, 2, \dots$
6.	$P_{2n}(-t) = P_{2n}(t), P_{2n+1}(-t) = -P_{2n+1}(t),$	$n = 0, 1, 2, \dots$
7.	$P_n(-t) = (-1)^n P_n(t),$	$n = 0, 1, 2, \dots$
8.	$P_n(1) = 1,$ $P_n(-1) = (-1)^n,$	$n = 0, 1, 2, \dots;$ $n = 0, 1, 2, \dots$
9.	$P_n(t) = \frac{1}{2^n n!} \frac{d^n}{dt^n} (t^2 - 1)^n = \text{Rodrigues formula},$	$n = 0, 1, 2, \dots$
10.	$(n+1)P_{n+1}(t) - (2n+1)tP_n(t) + nP_{n-1}(t) = 0,$	$n = 1, 2, \dots$
11.	$P'_{n+1}(t) - 2tP'_n(t) + P'_{n-1}(t) - P_n(t) = 0,$	$n = 1, 2, \dots$
12.	$P'_{n-1}(t) = P_n(t) + 2tP'_n(t) - P'_{n+1}(t)$	$n = 1, 2, \dots$
13.	$P'_{n+1}(t) = P_n(t) + 2tP'_n(t) - P'_{n-1}(t)$	$n = 1, 2, \dots$
14.	$P'_{n+1}(t) - tP'_n(t) = (n+1)P_n(t)$	$n = 0, 1, 2, \dots$
15.	$tP'_n(t) - P'_{n-1}(t) = nP_n(t)$	$n = 1, 2, \dots$
16.	$P'_{n+1}(t) - P'_{n-1}(t) = (2n+1)P_n(t)$	$n = 1, 2, \dots$
17.	$(1-t^2)P'_n(t) = nP_{n-1}(t) - ntP_n(t)$	$n = 1, 2, \dots$
18.	$ P_n(t)  < 1,$	$-1 < t < 1$
19.	$P_{2n}(t) = \frac{(-1)^n}{2^{2n-1}} \sum_{k=0}^n \frac{(-1)^k (2n+2k-1)!}{(2k)!(n+k-1)!(n-k)!} t^{2k},$	$n = 0, 1, 2, \dots$
20.	$(1-t^2)P'_n(t) = (n+1)[tP_n(t) - P_{n+1}(t)],$	$n = 0, 1, 2, \dots$
21.	$\int_{-1}^1 P_n(t) dt = 0,$	$n = 1, 2, \dots$
22.	$ P_n(t)  \leq 1,$	$ t  \leq 1$
23.	$\int_{-1}^1 P_n(t)P_m(t) dt = 0,$	$n \neq m$
24.	$\int_{-1}^1 [P_n(t)]^2 dt = \frac{2}{2n+1},$	$n = 0, 1, 2, \dots$
25.	$\frac{1}{2} \int_{-1}^1 t^m P_s(t) dt = \frac{m(m-2)\cdots(m-s+2)}{(m+s+1)(m+s-1)\cdots(m+1)},$	$m, s \text{ are even}$
26.	$\frac{1}{2} \int_{-1}^1 t^m P_s(t) dt = \frac{(m-1)(m-3)\cdots(m-s+2)}{(m+s+1)(m+s-1)\cdots(m+2)},$	$m, s \text{ are odd}$
27.	$\int_{-1}^1 tP_n(t)P_{n-1}(t) dt = \frac{2n}{4n^2-1},$	$n = 1, 2, \dots$
28.	$\int_{-1}^1 P_n(t)P'_{n+1}(t) dt = 2,$	$n = 0, 1, 2, \dots$
29.	$\int_{-1}^1 tP'_n(t)P_n(t) dt = \frac{2n}{2n+1},$	$n = 0, 1, 2, \dots$
30.	$\int_{-1}^1 (1-t^2)P'_n(t)P'_k(t) dt = 0,$	$k \neq n$
31.	$\int_{-1}^1 (1-t)^{-1/2} P_n(t) dt = \frac{2\sqrt{2}}{2n+1},$	$n = 0, 1, 2, \dots$
32.	$\int_{-1}^1 t^2 P_{n+1}(t)P_{n-1}(t) dt = \frac{2n(n+1)}{(4n^2-1)(2n+3)},$	$n = 1, 2, \dots$
33.	$\int_{-1}^1 (t^2-1)P_{n+1}(t)P'_n(t) dt = \frac{2n(n+1)}{(2n+1)(2n+3)},$	$n = 1, 2, \dots$
34.	$\int_{-1}^1 t^n P_n(t) dt = \frac{2^{n+1}(n!)^2}{(2n+1)!},$	$n = 0, 1, 2, \dots$
35.	$\int_{-1}^1 t^2 [P_n(t)]^2 dt = \frac{2}{(2n+1)^2} \left[ \frac{(n+1)^2}{2n+3} + \frac{n^2}{2n-1} \right]$	$n = 0, 1, 2, \dots$

**TABLE 1.8 (continued)** Properties of Legendre and Associate Legendre Functions

36.	$P_n^m(t) = (1 - t^2)^{m/2} \frac{d^m}{dt^m} P_n(t),$	$m > 0$
37.	$P_n^m(t) = \frac{1}{2^n n!} (1 - t^2)^{m/2} \frac{d^{n+m}}{dt^{n+m}} [(t^2 - 1)^n],$	$m + n \geq 0$
38.	$P_n^{-m}(t) = (-1)^m \frac{(n - m)!}{(n + m)!} P_n^m(t)$	
39.	$P_n^0(t) = P_n(t)$	
40.	$(n - m + 1)P_{n+1}^m(t) - (2n + 1)tP_n^m(t) + (n + m)P_{n-1}^m(t) = 0$	
41.	$(1 - t^2)^{1/2} P_n^m(t) = \frac{1}{2n + 1} [P_{n+1}^{m+1}(t) - P_{n-1}^{m+1}(t)]$	
42.	$(1 - t^2)^{1/2} P_n^m(t) = \frac{1}{2n + 1} [(n + m)(n + m - 1)P_{n-1}^{m-1}(t) - (n - m + 1)(n - m + 2)P_{n+1}^{m-1}(t)]$	
43.	$P_n^{m+1}(t) = 2mt(1 - t^2)^{-1/2} P_n^m(t) - [n(n + 1) - m(m - 1)]P_n^{m-1}(t)$	
44.	$\int_{-1}^1 P_n^m(t)P_k^m(t)dt = 0,$	$k \neq n$
45.	$\int_{-1}^1 [P_n^m(t)]^2 dt = \frac{2}{2n + 1} \frac{(n + m)!}{(n - m)!}$	
46.	$P_n^m(-t) = (-1)^{n+m} P_n^m(t)$	
47.	$P_n^m(\pm 1) = 0,$	$m > 0$
48.	$P_{2n}^1(0) = 0, \quad P_{2n+1}^1(0) = \frac{(-1)^n (2n + 1)!}{2^{2n} (n!)^2}$	
49.	$P_n^m(0) = 0,$	$n + m$ is odd
	$P_n^m(0) = (-1)^{(n-m)/2} \frac{(n + m)!}{2^n [(n - m)/2]! [(n + m)/2]!},$	$n + m$ is even
50.	$\int_{-1}^1 P_n^m(t)P_k^m(t)(1 - t^2)^{-1} dt = 0,$	$k \neq m$
51.	$\int_{-1}^1 (1 - t^2)^{-1/2} P_{2m}(t) dt = \left[ \frac{\Gamma(\frac{1}{2} + m)}{m!} \right]^2$	
52.	$\int_{-1}^1 t(1 - t^2)^{-1/2} P_{2m+1}(t) dt = \frac{\Gamma(\frac{1}{2} + m)\Gamma(\frac{3}{2} + m)}{m!(m + 1)!}$	
53.	$\int_t^1 P_n(t) dt = \frac{1}{2n + 1} [P_{n-1}(t) - P_{n+1}(t)]$	
54.	$\int_0^1 t^q P_n(t) dt = \Gamma(q + 1) \sum_{k=0}^n \frac{(-1)^k \Gamma(n + k + 1)}{2^k k! \Gamma(n - k + 1) \Gamma(q + k + 2)},$	$q > -1$
55.	$\int_0^1 t^{-1/2} P_n(t) dt = \begin{cases} \frac{2(-1)^{n/2}}{2n + 1} & n \text{ is even} \\ \frac{2(-1)^{(n-1)/2}}{2n + 1} & n \text{ is odd} \end{cases}$	
56.	$\int_0^1 t^{1/2} P_n(t) dt = \begin{cases} \frac{2(-1)^{(n+2)/2}}{(2n - 1)(2n + 3)} & n \text{ is even} \\ \frac{2(-1)^{(n+3)/2}}{(2n - 1)(2n + 3)} & n \text{ is odd} \end{cases}$	

Introducing these relations in the Laplacian, we obtain

$$2rG \frac{dF}{dr} + r^2 G \frac{d^2 F}{dr^2} + F \frac{dG}{d\varphi} \cot \varphi + F \frac{d^2 G}{d\varphi^2} = 0$$

or

$$\frac{2r \frac{dF}{dr} + r^2 \frac{d^2 F}{dr^2}}{F} = - \frac{\frac{dG}{d\varphi} \cot \varphi + \frac{d^2 G}{d\varphi^2}}{G}$$

Setting the above ratios equal to positive constant  $k^2$ ,  $k \neq 0$ , we obtain

$$r^2 \frac{d^2 F}{dr^2} + 2r \frac{dF}{dr} - k^2 F = 0$$

$$\frac{d^2 G}{d\varphi^2} + (\cot \varphi) \frac{dG}{d\varphi} + k^2 G = 0$$

For  $k^2 = n(n + 1)$ , we recognize that the above equation is the Legendre equation with  $G$  playing the role of  $y$ . Thus, a particular solution is

$$G = C_n P_n(\cos \varphi)$$

where  $C_n$  is an arbitrary constant. With  $k^2 = n(n + 1)$  the general solution for  $F$  is given by

$$F = S_n r^n + \frac{B_n}{r^{n+1}}$$

where  $S_n$  and  $B_n$  are arbitrary constants. Because for  $r=0$  the second term becomes infinity, we set  $B_n = 0$ . Hence, the product solution is

$$T = FG = S_n C_n r^n P_n(\cos \varphi) = D_n r^n P_n(\cos \varphi)$$

Because Legendre polynomials are continuous we must create a procedure to alleviate this problem. We denote the excess of the temperature  $T$  on the upper half of the surface over that of  $T$  on the lower half. On the bounding great circle between these halves, we arbitrarily set it equal to  $(300 - 75)/2$ . We then have

$$T_E(\varphi) = \begin{cases} 225 & 0 \leq \varphi < \pi/2 \\ 0 & \pi/2 < \varphi \leq \pi \\ 225/2 & \varphi = \pi/2 \end{cases}$$

If we let  $x = \cos \varphi$ , then  $T_E(\varphi)$  becomes  $f(x)$

$$f(x) = \begin{cases} 225 & 0 < x \leq 1 \\ 0 & -1 \leq x < 0 \\ 225/2 & x = 0 \end{cases}$$

Next we expand  $f(x)$  in the form

$$\begin{aligned} f(x) &= \sum_{n=0}^{\infty} a_n P_n(x), \quad a_n = \frac{2n+1}{2} \int_0^1 f(x) P_n(x) dx \\ &= 225 \left[ \frac{1}{2} + \frac{3}{4} P_1(x) - \frac{7}{16} P_3(x) + \frac{11}{32} P_5(x) - \dots \right] \end{aligned}$$

Setting  $D_n = a_n/R^n$ , where  $a_n$  is the coefficient of  $P_n(x)$  and  $R$  is the radius of the solid, the solution is given by

$$\begin{aligned} T(r, \varphi) &= 75 + \sum_{n=0}^{\infty} a_n \left(\frac{r}{R}\right)^n P_n(\cos \varphi) \\ &= 75 + 225 \left[ \frac{1}{2} + \frac{3}{4} \left(\frac{r}{R}\right) P_1(\cos \varphi) - \frac{7}{16} \left(\frac{r}{R}\right)^2 P_3(\cos \varphi) \right. \\ &\quad \left. + \frac{11}{32} \left(\frac{r}{R}\right)^5 P_5(\cos \varphi) - \dots \right] \end{aligned}$$

Table 1.8 gives relationships of Legendre and associated Legendre functions.

### 1.5.3 Hermite Polynomials

#### 1.5.3.1 Generating Function

If we define the Hermite polynomial by the Rodrigues formula

$$H_n(t) = (-1)^n e^{t^2} \frac{d^n e^{-t^2}}{dt^n}, \quad n = 0, 1, 2, \dots, -\infty < t < \infty \tag{1.148}$$

The first few Hermite polynomials are

$$\begin{aligned} H_0(t) &= 1, \\ H_1(t) &= 2t, \\ H_2(t) &= 4t^2 - 2, \\ H_3(t) &= 8t^3 - 12t, \\ H_4(t) &= 16t^4 - 48t^2 + 12, \\ H_5(t) &= 32t^5 - 160t^3 + 120t \end{aligned}$$

and therefore

$$H_n(t) = \sum_{k=0}^{[n/2]} \frac{(-1)^k n!}{k!(n-2k)!} (2t)^{n-2k} \tag{1.149}$$

$$[n/2] \equiv \text{largest integer} \leq n/2$$

The Hermite polynomials are orthogonal with weight  $\gamma(t) = e^{-t^2}$  on the interval  $(-\infty, \infty)$ .

The relation between Hermite polynomial and the generating function is

$$w(t, x) = e^{2tx - x^2} = \sum_{n=0}^{\infty} \frac{H_n(t)}{n!} x^n, \quad |x| < \infty \tag{1.150}$$

Because  $w(t, x)$  is the entire function in  $x$  it can be expanded in Taylor's series at  $x=0$  with  $|x| < \infty$ .

Hence the derivatives of the expansion are

$$\left( \frac{\partial^n w}{\partial x^n} \right) \Big|_{x=0} = e^{t^2} \left[ \frac{\partial^n}{\partial x^n} e^{-(t-x)^2} \right]_{x=0} = (-1)^n e^{t^2} \left[ \frac{d^n e^{-u^2}}{du^n} \right]_{u=t} \doteq H_n(t)$$

Figure 1.5 shows several Hermite polynomials.

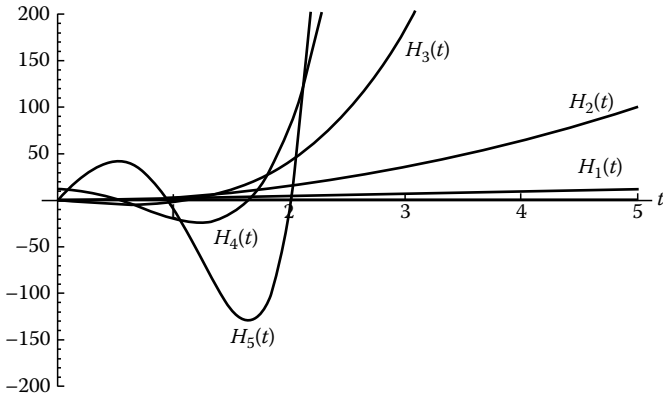


FIGURE 1.5

**Example**

Let  $t=0$  in Equation 1.150 and expand  $e^{-x^2}$  in power series. Comparing equal powers of both sides we find that

$$H_{2n}(0) = (-1)^n \frac{(2n)!}{n!}$$

Hermite polynomials are even for even  $n$  and odd for  $n$  odd. Hence,

$$H_n(-t) = (-1)^n H_n(t) \tag{1.151}$$

**1.5.3.2 Recurrence Relation**

If we substitute  $w(t, x)$  of Equation 1.150 into identity

$$\frac{\partial w}{\partial x} - 2(t - x)w = 0$$

we obtain

$$\sum_{n=0}^{\infty} \frac{H_{n+1}(t)}{n!} x^n - 2t \sum_{n=0}^{\infty} \frac{H_n(t)}{n!} x^n + 2 \sum_{n=0}^{\infty} \frac{H_n(t)}{n!} x^{n+1} = 0$$

or

$$\sum_{n=1}^{\infty} [H_{n+1}(t) - 2tH_n(t) + 2nH_{n-1}(t)] \frac{x^n}{n!} + H_1(t) - 2tH_0(t) = 0$$

But  $H_1(t) - 2tH_0(t) = 0$  and hence

$$H_{n+1}(t) - 2tH_n(t) + 2nH_{n-1}(t) = 0, \quad n = 1, 2, \dots \tag{1.152}$$

If we use

$$\frac{\partial w}{\partial x} - 2xw = 0$$

we obtain

$$H'_n(t) = 2nH_{n-1}(t), \quad n = 1, 2, \dots \tag{1.153}$$

Eliminating  $H_{n-1}(t)$  from Equations 1.153 and 1.152, we obtain

$$H_{n+1}(t) - 2tH_n(t) + H'_n(t) = 0, \quad n = 0, 1, 2, \dots \tag{1.154}$$

Differentiate Equation 1.153, combine with Equation 1.152, and use the relation  $H'_{n+1} = 2(n+1)H_{(n+1)-1}$ , we obtain

$$H''_n - 2tH'_n(t) + 2nH_n(t) = 0, \quad n = 0, 1, 2, \dots \tag{1.155}$$

From the above equation, with  $y=H_n(t)$  ( $n=0, 1, 2, \dots$ ), we observe that the Hermite polynomials are the solution to the second-order ordinary differential equation known as the *Hermite equation*

$$y'' - 2ty' + 2ny = 0 \tag{1.156}$$

**1.5.3.3 Integral Representation and Integral Equation**

The integral representation of Hermite polynomials is given by

$$H_n(t) = \frac{(-j)^n 2^n e^{t^2}}{\sqrt{\pi}} \int_{-\infty}^{\infty} e^{-x^2 + j2tx} x^n dx, \quad n = 0, 1, 2, \dots \tag{1.157}$$

The integral equation satisfied by the Hermite polynomials is

$$e^{-t^2/2} H_n(t) = \frac{1}{j^n \sqrt{2\pi}} \int_{-\infty}^{\infty} e^{jty} e^{-y^2/2} H_n(y) dy, \quad n = 0, 1, 2, \dots \tag{1.157a}$$

Also, because  $H_{2m}(t)$  is an even function and  $H_{2m+1}(t)$  is an odd function, then the above equation implies the following two integrals:

$$e^{-t^2/2} H_{2m}(t) = (-1)^m \sqrt{\frac{2}{\pi}} \int_0^{\infty} e^{-y^2/2} H_{2m}(y) \cos ty \, dy$$

$$e^{-t^2/2} H_{2m+1}(t) = (-1)^m \sqrt{\frac{2}{\pi}} \int_0^{\infty} e^{-y^2/2} H_{2m+1}(y) \sin ty \, dy,$$

$$m = 0, 1, 2, \dots \tag{1.158}$$

**1.5.3.4 Orthogonality Relation: Hermite Series**

The *orthogonality property* of the Hermite polynomials is given by

$$\int_{-\infty}^{\infty} e^{-t^2} H_m(t) H_n(t) dt = 0 \quad \text{if } m \neq n \tag{1.159}$$

and

$$\int_{-\infty}^{\infty} e^{-t^2} H_n^2(t) dt = 2^n n! \sqrt{\pi}, \quad n = 0, 1, 2, \dots \tag{1.160}$$

Therefore, the *orthonormal* Hermite polynomials are

$$\varphi_n(t) = (2^n n! \sqrt{\pi})^{-1/2} e^{-t^2/2} H_n(t), \quad n = 0, 1, 2, \dots, \\ -\infty < t < \infty \quad (1.161)$$

### THEOREM 1.1

If  $f(t)$  is piecewise smooth in every finite interval  $[-a, a]$  and

$$\int_{-\infty}^{\infty} e^{-t^2} f^2(t) dt < \infty$$

then the Hermite series

$$f(t) = \sum_{n=0}^{\infty} C_n H_n(t), \quad -\infty < t < \infty \quad (1.162)$$

$$C_n = \frac{1}{2^n n! \sqrt{\pi}} \int_{-\infty}^{\infty} e^{-t^2} f(t) H_n(t) dt \quad n = 0, 1, 2, \dots \quad (1.163)$$

converges pointwise to  $f(t)$  at every continuity point and converges at  $[f(t+) - f(t-)]/2$  at points of discontinuity.

### Example

The function  $f(t) = t^{2p}$ ,  $p = 1, 2, \dots$  satisfies Theorem 1.1 and it is even. Hence,

$$t^{2p} = \sum_{n=0}^p C_{2n} H_{2n}(t)$$

where

$$\begin{aligned} C_{2n} &= \frac{1}{2^{2n} (2n)! \sqrt{\pi}} \int_{-\infty}^{\infty} e^{-t^2} t^{2p} H_{2n}(t) dt \\ &= \frac{1}{2^{2n} (2n)! \sqrt{\pi}} \int_{-\infty}^{\infty} t^{2p} \frac{d^{2n}}{dt^{2n}} (e^{-t^2}) dt \\ &= \frac{1}{2^{2n} (2n)! \sqrt{\pi}} \frac{(2p)!}{(2p-2n)!} \int_{-\infty}^{\infty} e^{-t^2} t^{2p-2n} dt \\ &= \frac{1}{2^{2n} (2n)! \sqrt{\pi}} \frac{(2p)!}{(2p-2n)!} \Gamma\left(p-n+\frac{1}{2}\right) \end{aligned}$$

to find  $C_{2n}$ , integration by parts was performed  $n$  times.

### Example

The function  $e^{at}$ , where  $a$  is an arbitrary number, satisfies Theorem 1.1. Hence

$$e^{at} = \sum_{n=0}^{\infty} C_n H_n(t)$$

where

$$\begin{aligned} C_n &= \frac{1}{2^n n! \sqrt{\pi}} \int_{-\infty}^{\infty} e^{at} e^{-t^2} H_n(t) dt = \frac{(-1)^n}{2^n n! \sqrt{\pi}} \int_{-\infty}^{\infty} e^{at} \frac{d^n}{dt^n} (e^{-t^2}) dt \\ &= \frac{a^n}{2^n n! \sqrt{\pi}} \int_{-\infty}^{\infty} e^{at-t^2} dt = \frac{a^n}{2^n n!} e^{-a^2/4} \end{aligned}$$

### Example

The  $\text{sgn}(t)$  function is odd and hence its expansion takes the form

$$\text{sgn}(t) = \sum_{n=0}^{\infty} C_{2n+1} H_{2n+1}(t)$$

where

$$\begin{aligned} C_{2n+1} &= \frac{1}{2^{2n+1} (2n+1)! \sqrt{\pi}} \int_{-\infty}^{\infty} e^{-t^2} H_{2n+1}(t) \text{sgn}(t) dt \\ &= \frac{1}{2^{2n} (2n+1)! \sqrt{\pi}} \int_0^{\infty} e^{-t^2} H_{2n+1}(t) dt \end{aligned}$$

Use the identity

$$e^{-t^2} H_n(t) = -\frac{d}{dt} [e^{-t^2} H_{n-1}(t)]$$

which results from Equations 1.152 and 1.153, to find that

$$C_{2n+1} = \frac{H_{2n}(0)}{2^{2n} (2n+1)! \sqrt{\pi}} = \frac{(-1)^n}{2^{2n} (2n+1)! n! \sqrt{\pi}}$$

Table 1.9 gives the Hermite relationships.

## 1.5.4 Laguerre Polynomials

### 1.5.4.1 Generating Function and Rodrigues Formula

The generating function for the Laguerre polynomials is given by

$$w(t, x) = (1-x)^{-1} \exp\left[-\frac{tx}{1-x}\right] = \sum_{n=0}^{\infty} L_n(t) x^n,$$

$$|x| < 1, \quad \leq t < \infty \quad (1.164)$$

**TABLE 1.9** Properties of the Hermite Polynomials

---

1.  $H_n(t) = (-1)^n e^{t^2} \frac{d^n e^{-t^2}}{dt^n}$
2.  $H_n(t) = \sum_{k=0}^{[n/2]} \frac{(-1)^k n!}{k!(n-2k)!} (2t)^{n-2k}$   
 $[n/2] = \text{largest integer} \leq n/2$
3.  $e^{2tx-x^2} = \sum_{n=0}^{\infty} H_n(t) \frac{x^n}{n!}$
4.  $H_{2n}(0) = (-1)^n \frac{(2n)!}{n!}$
5.  $H_{2n+1}(0) = 0, H'_{2n}(0) = 0, H'_{2n+1}(0) = (-1)^n \frac{(2n+2)!}{(n+1)!}$
6.  $H_n(-t) = (-1)^n H_n(t)$
7.  $H_{2n}(t)$  are even functions,  $H_{2n+1}(t)$  are odd functions
8.  $H_{n+1}(t) - 2tH_n(t) + 2nH_{n-1}(t) = 0, n = 1, 2, \dots$
9.  $H'_n(t) = 2nH_{n-1}(t), n = 1, 2, \dots$
10.  $H_{n+1}(t) - 2tH_n(t) + H'_n(t) = 0, n = 0, 1, 2, \dots$
11.  $H''_n(t) - 2tH'_n(t) + 2nH_n(t) = 0, n = 0, 1, 2, \dots$
12.  $H_n(t) = \frac{(-j)^n 2^n e^{t^2}}{\sqrt{\pi}} \int_{-\infty}^{\infty} e^{-x^2+2tx} x^n dx, n = 0, 1, 2, \dots$
13.  $e^{-t^2/2} H_n(t) = \frac{1}{j^n \sqrt{2\pi}} \int_{-\infty}^{\infty} e^{jty} e^{-y^2/2} H_n(y) dy$   
 = integral equation
14.  $e^{-t^2/2} H_{2m}(t) = (-1)^m \sqrt{\frac{2}{\pi}} \int_0^{\infty} e^{-y^2/2} H_{2m}(y) \cos ty dy$
15.  $e^{-t^2/2} H_{2m+1}(t) = (-1)^m \sqrt{\frac{2}{\pi}} \int_0^{\infty} e^{-y^2/2} H_{2m+1}(y) \sin ty dy$
16.  $\int_{-\infty}^{\infty} e^{-t^2} H_m(t) H_n(t) dt = 0, \text{ if } m \neq n$
17.  $\int_{-\infty}^{\infty} e^{-t^2} H_n^2(t) dt = 2^n n! \sqrt{\pi}, n = 0, 1, 2, \dots$
18.  $f(t) = \sum_{n=0}^{\infty} C_n H_n(t), -\infty < t < \infty$   
 $C_n = \frac{1}{2^n n! \sqrt{\pi}} \int_{-\infty}^{\infty} e^{-t^2} f(t) H_n(t) dt$
19.  $\int_{-\infty}^{\infty} t^k e^{-t^2} H_n(t) dt = 0, k = 0, 1, 2, \dots, n-1$
20.  $\int_{-\infty}^{\infty} t^2 e^{-t^2} H_n^2(t) dt = \sqrt{\pi} 2^n n! \left( n + \frac{1}{2} \right)$
21.  $\int_{-\infty}^{\infty} x^n e^{-x^2} H_n(tx) dx = \frac{\sqrt{\pi} n!}{2} P_n(t)$
22.  $\int_{-\infty}^{\infty} e^{-2t^2} H_n^2(t) dt = 2^{n-\frac{1}{2}} \Gamma\left( n + \frac{1}{2} \right)$
23.  $\frac{d^m H_n(t)}{dt^m} = \frac{2^m n!}{(n-m)!} H_{n-m}(t), m < n$
24.  $\int_{-\infty}^{\infty} e^{-a^2 t^2} H_{2n}(t) dt = \frac{(2n)!}{n!} \frac{\sqrt{\pi}}{a} \left( \frac{1-a^2}{a^2} \right)^n, a > 0$

---

By expressing the exponential function in a series, realizing that

$$\binom{-k-1}{m} = (-1)^m \binom{k+m}{m}$$

and finally making the change of index  $m = n - k$ , Equation 1.164 leads to

$$L_n(t) = \sum_{k=0}^n \frac{(-1)^k n! t^k}{(k!)^2 (n-k)!} \quad n = 0, 1, 2, \dots, \quad 0 \leq t < \infty \tag{1.165}$$

The Rodrigues formula for creating Laguerre polynomials is given by

$$L_n(t) = \frac{e^t}{n!} \frac{d^n}{dt^n} (t^n e^{-t}), \quad n = 0, 1, 2, \dots \tag{1.166}$$

which can be verified by application of the Leibniz formula

$$\frac{d^n}{dt^n} (fg) = \sum_{k=0}^n \binom{n}{k} \frac{d^{n-k}}{dt^{n-k}} f \frac{d^k}{dt^k} g, \quad n = 1, 2, \dots \tag{1.167}$$

For a real  $a > -1$  the general Laguerre polynomials are defined by the formula

$$L_n^a(t) = e^t \frac{t^{-a}}{n!} \frac{d^n}{dt^n} (e^{-t} t^{n+a}), \quad n = 0, 1, 2, \dots \tag{1.168a}$$

Using Leibniz's formula

$$L_n^a(t) = \sum_{k=0}^n \frac{\Gamma(n+a+1)}{\Gamma(k+a+1)} \frac{(-t)^k}{k!(n-k)!} \tag{1.168b}$$

Table 1.10 gives a few Laguerre polynomials. Figure 1.6 shows several Laguerre polynomials.

### 1.5.4.2 Recurrence Relations

The generating function  $w(t, x)$ , Equation 1.164 satisfies the identity

$$(1-x^2) \frac{\partial w}{\partial x} + (t-1)w = 0 \tag{1.169}$$

Substituting Equation 1.164 in Equation 1.169 and equating the coefficients of  $x^n$  to zero, we obtain

$$(n+1)L_{n+1}(t) + (t-1-2n)L_n(t) + nL_{n-1}(t) = 0, \quad n = 1, 2, \dots \tag{1.170}$$

**TABLE 1.10** Laguerre Polynomials

---

$L_0(t) = 1$
$L_1(t) = -t + 1$
$L_2(t) = \frac{1}{2!}(t^2 - 4t + 2)$
$L_3(t) = \frac{1}{3!}(-t^3 + 9t^2 - 18t + 6)$
$L_4(t) = \frac{1}{4!}(t^4 - 16t^3 + 72t^2 - 96t + 24)$

---



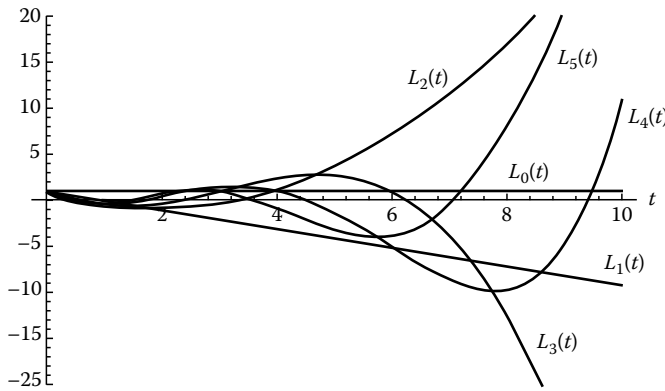


FIGURE 1.6

Similarly substituting Equation 1.164 into

$$(1-x)\frac{\partial w}{\partial t} + xw = 0 \tag{1.171}$$

we obtain the relation

$$L'_n(t) - L'_{n-1}(t) + L_{n-1}(t) = 0, \quad n = 1, 2, \dots \tag{1.172}$$

From this we obtain

$$L'_{n+1}(t) = L'_n(t) - L_n(t) \tag{1.173}$$

$$L'_{n-1}(t) = L'_n(t) + L_{n-1}(t) \tag{1.174}$$

From Equation 1.170 by differentiation we find

$$(n+1)L'_{n+1}(t) + (t-1-2n)L'_n(t) + L_n(t) + nL'_{n-1}(t) = 0 \tag{1.175}$$

Eliminating  $L'_{n+1}(t)$  and  $L'_{n-1}(t)$  by using Equations 1.173 through 1.175, we obtain

$$tL'_n(t) = nL_n(t) - nL_{n-1}(t) \tag{1.176}$$

By differentiating Equation 1.176 and using Equation 1.172, we obtain

$$tL''_n(t) + L'_n(t) = -nL_{n-1}(t)$$

Next, eliminating  $L_{n-1}(t)$  using Equation 1.176 we obtain

$$tL''_n(t) + (1-t)L'_n(t) + nL_n(t) = 0 \tag{1.177}$$

Setting  $y = L_n(t)$  ( $n = 0, 1, 2, \dots$ ), we conclude that all  $L_n(t)$  are the solution to the Laguerre equation

$$ty'' + (1-t)y' + ny = 0 \tag{1.178}$$

### 1.5.4.3 Orthogonality, Laguerre Series

The orthogonality relations for Laguerre polynomials are

$$\int_0^\infty e^{-t} L_n(t) L_m(t) dt = 0, \quad n \neq m \tag{1.179}$$

$$\int_0^\infty e^{-t} [L_n(t)]^2 dt = \frac{\Gamma(n+1)}{n!} = 1, \quad n = 0, 1, 2, \dots \tag{1.180}$$

For the generalized Laguerre polynomials, the orthogonality relations

$$\int_0^\infty e^{-t} t^a L_m^a(t) L_n^a(t) dt = 0, \quad n \neq m, \quad a > -1$$

$$\int_0^\infty e^{-t} t^a [L_n^a(t)]^2 dt = \frac{\Gamma(n+a+1)}{n!}, \quad a > -1, \quad n = 0, 1, 2, \dots \tag{1.181}$$

The orthogonal system for the generalized polynomials on the interval  $0 \leq t < \infty$  is

$$\varphi_n^a(t) = \left[ \frac{n!}{\Gamma(n+a+1)} \right]^{1/2} e^{-t/2} t^{a/2} L_n^a(t), \quad n = 0, 1, 2, \dots \tag{1.182}$$

The Laguerre series is given by

$$f(t) = \sum_{n=0}^\infty C_n L_n(t), \quad 0 \leq t < \infty \tag{1.183}$$

where

$$C_n = \int_0^\infty e^{-t} f(t) L_n(t) dt, \quad n = 0, 1, 2, \dots \tag{1.184}$$

---

#### THEOREM 1.2

If  $f(t)$  is piecewise smooth in every finite interval  $t_1 \leq t \leq t_2$ ,  $0 < t_1 < t_2 < \infty$  and

$$\int_0^\infty e^{-t} f^2(t) dt < \infty$$

then the Laguerre series converges pointwise to  $f(t)$  at every continuity point of  $f(t)$ , and at the points of discontinuity the series converges to  $[f(t+) - f(t-)]/2$ .

If we set  $a = m = \text{integer}$  ( $m = 0, 1, 2, \dots$ ), then Equation 1.168b becomes

$$L_n^m(t) = \sum_{k=0}^n \frac{(-1)^k (n+m)! t^k}{(n-k)! (m+k)! k!}, \quad m = 0, 1, 2, \dots \quad (1.185)$$

The Rodrigues formula is

$$L_n^m(t) = \frac{1}{n!} e^t t^{-m} \frac{d^n}{dt^n} (e^{-t} t^{n+m}) \quad (1.186)$$

**Example**

The function  $t^b$  can be expanded in series

$$t^b = \sum_{n=0}^{\infty} C_n L_n^a(t), \quad b > -\frac{1}{2}(a+1)$$

$$C_n = \frac{n!}{\Gamma(n+a+1)} \int_0^{\infty} t^{b+a} e^{-t} L_n(t) dt$$

$$= \frac{n!}{\Gamma(n+a+1)} \int_0^{\infty} e^{-t} t^{b+a} \frac{e^t t^{-a}}{n!} \frac{d^n}{dt^n} (t^{n+a} e^{-t}) dt$$

$$= \frac{1}{\Gamma(n+a+1)} \int_0^{\infty} t^b \frac{d^n}{dt^n} (t^{n+a} e^{-t}) dt$$

$$= \frac{(-1)^n b(b-1) \dots (b-n+1)}{\Gamma(n+a+1)} \int_0^{\infty} e^{-t} t^{b+a} dt$$

$$= (-1)^n \frac{\Gamma(b+1)}{\Gamma(n+b+1)\Gamma(b-n+1)} \int_0^{\infty} e^{-t} t^{(b+a+1)-1} dt$$

$$= (-1)^n \frac{\Gamma(b+1)\Gamma(b+a+1)}{\Gamma(n+b+1)\Gamma(b-n+1)}$$

The steps to find  $C_n$  were: (a) substitution of Equation 1.168a,b, (b) integration by parts  $n$  times, and (c) multiplication of numerator and denominator by  $\Gamma(b-n+1)$ . In particular if  $b = m = \text{positive integer}$

$$t^m = \Gamma(m+a+1)m! \sum_{n=0}^m \frac{(-1)^n L_n^a(t)}{\Gamma(n+a+1)(m-n)!}$$

$0 < t < \infty, \quad a > -1, \quad \text{and} \quad m = 0, 1, 2, \dots$

If  $a = 0$ , we obtain the expansion

$$t^m = \Gamma(m+1)m! \sum_{n=0}^m \frac{(-1)^n L_n(t)}{n!(m-n)!}$$

**Example**

The function  $f(t) = e^{-bt}$ , with  $b > -1/2$  and  $t > 0$ , is expanded as follows

$$C_n = \frac{n!}{\Gamma(n+a+1)} \int_0^{\infty} e^{-(b+1)t} t^a L_n^a(t) dt$$

$$= \frac{1}{\Gamma(n+a+1)} \int_0^{\infty} e^{-bt} \frac{d^n}{dt^n} (e^{-t} t^{n+a}) dt$$

$$= \frac{b^n}{\Gamma(n+a+1)} \int_0^{\infty} e^{-(b+1)t} t^{n+a} dt$$

$$= \frac{b^n}{(b+1)^{n+a+1}}, \quad n = 0, 1, 2, \dots$$

and thus

$$e^{-bt} = (b+1)^{-a-1} \sum_{n=0}^{\infty} \left(\frac{b}{b+1}\right)^n L_n^a(t), \quad 0 \leq t < \infty$$

For  $a = 0$

$$e^{-bt} = (b+1)^{-1} \sum_{n=0}^{\infty} \left(\frac{b}{b+1}\right)^n L_n(t), \quad 0 \leq t < \infty$$

Table 1.11 gives relationships of Laguerre polynomials.

**TABLE 1.11** Properties of the Laguerre Polynomials

1.	$L_n(t) = \sum_{k=0}^n \frac{(-1)^k n! t^k}{(k!)^2 (n-k)!}$	$0 \leq t < \infty, n = 0, 1, 2, \dots$
	$= \sum_{k=0}^n (-1)^k \frac{1}{k!} \binom{n}{k} t^k$	
2.	$L_n(t) = \frac{e^t}{n!} \frac{d^n}{dt^n} (t^n e^{-t})$	$n = 0, 1, 2, \dots$
3.	$(n+1)L_{n+1}(t) + (t-1-2n)L_n(t) + nL_{n-1}(t) = 0$	$n = 1, 2, 3, \dots$
4.	$L'_n(t) - L'_{n-1}(t) + L_{n-1}(t) = 0,$	$n = 1, 2, 3, \dots$
5.	$(n+1)L'_{n+1}(t) + (t-1-2n)L'_n(t) + L_n(t) + nL'_{n-1}(t) = 0,$	$n = 1, 2, 3, \dots$
6.	$L'_{n+1}(t) = L'_n(t) - L_n(t)$	
7.	$tL'_n(t) = nL_n(t) - nL_{n-1}(t),$	$n = 1, 2, 3, \dots$
8.	$tL''_n(t) + (1-t)L'_n(t) + nL_n(t) = 0,$ Laguerre differential equation	
9.	$w(t, x) = (1-x)^{-1} \exp\left[-\frac{tx}{1-x}\right]$ $= \sum_{n=0}^{\infty} L_n(t) x^n,$ generating function	
10.	$\int_0^{\infty} e^{-t} L_n(t) L_k(t) dt = 0,$	$k \neq n$
11.	$\int_0^{\infty} e^{-t} [L_n(t)]^2 dt = 1$	

(continued)

TABLE 1.11 (continued) Properties of the Laguerre Polynomials

12.	$f(t) = \sum_{n=0}^{\infty} C_n L_n(t),$ $C_n = \int_0^{\infty} e^{-t} f(t) L_n(t) dt$	$0 \leq t < \infty$
13.	$L_n(0) = 1, \quad L'_n(0) = -n,$ $L''_n(0) = \frac{1}{2}n(n-1)$	
14.	$L_n^{(m)}(t) = (-1)^m \frac{d^m}{dt^m} [L_{n+m}(t)],$	$m = 0, 1, 2, \dots$
15.	$L_n^{(m)}(t) = \sum_{k=0}^n \frac{(-1)^k (n+m)! t^k}{(n-k)! (m+k)! k!},$	$m = 0, 1, 2, \dots$
16.	$(n+1)L_{n+1}^{(m)}(t) + (t-1-2n-m)L_n^{(m)}(t)$ $+ (n+m)L_{n-1}^{(m)}(t) = 0$	
17.	$tL_n^{(m)'}(t) - nL_n^{(m)}(t) + (n+m)L_{n-1}^{(m)}(t) = 0$	
18.	$L_n^{(m)}(t) = \frac{1}{n!} e^t t^{-m} \frac{d^n}{dt^n} (e^{-t} t^{n+m})$ = Rodrigues formula	
19.	$L_{n-1}^{(m)}(t) + L_n^{(m-1)}(t) - L_n^{(m)}(t) = 0$	
20.	$L_n^{(m)'}(t) = -L_{n-1}^{(m+1)}(t)$	
21.	$L_n^{(m)}(0) = \frac{(n+m)!}{n!m!}$	
22.	$\int_0^{\infty} e^{-t} t^k L_n(t) dt = \begin{cases} 0 & k < n \\ (-1)^n n! & k = n \end{cases}$	
23.	$\int_0^t L_k(x) L_n(t-x) dx = \int_0^t L_{n+k}(x) dx$ $= L_{n+k}(t) - L_{n+k+1}(t)$	
24.	$\int_t^{\infty} e^{-x} L_n^m(x) dx = e^{-t} [L_n^m(t) - L_{n-1}^m(t)],$	$m = 0, 1, 2, \dots$
25.	$\int_0^t (t-x)^m L_n(x) dx = \frac{m!n!}{(m+n+1)!}$ $t^{m+1} L_{n+1}^{m+1}(t),$	$m = 0, 1, 2, \dots$
26.	$\int_0^1 x^a (1-x)^{b-1} L_n^a(x) dx$ $= \frac{\Gamma(b)\Gamma(n+a+1)}{\Gamma(n+a+b+1)} L_n^{a+b}(t),$	$a > -1, b > 0$
27.	$\int_0^{\infty} e^{-t} t^a L_n^a(t) L_k^a(t) dt = 0,$	$k \neq n, a > -1$
28.	$\int_0^{\infty} e^{-t} t^a [L_n^a(t)]^2 dt = \frac{\Gamma(n+a+1)}{n!},$	$a > -1$
29.	$\int_0^{\infty} e^{-t} t^{a+1} [L_n^a(t)]^2 dt = \frac{\Gamma(n+a+1)}{n!} (2n+a+1),$	$a > -1$
30.	$L_n^{-1/2}(t) = \frac{(-1)^n}{2^{2n} n!} H_{2n}(\sqrt{t})$	
31.	$L_n^{1/2}(t) = \frac{(-1)^n}{2^{2n+1} n!} \frac{H_{2n+1}(\sqrt{t})}{\sqrt{t}}$	
32.	$f(t) = \sum_{n=0}^{\infty} C_n L_n^m(t)$ $C_n = \frac{n!}{\Gamma(n+m+1)} \int_0^{\infty} e^{-t} t^m f(t) L_n^m(t) dt$	
33.	$t^p = p! \sum_{n=0}^p \binom{p}{n} (-1)^n L_n(t)$	
34.	$e^{-at} = (a+1)^{-1} \sum_{n=0}^{\infty} \left(\frac{a}{a+1}\right)^n L_n(t),$	$a > -\frac{1}{2}$
35.	$\int_0^{\infty} \frac{e^{-tx}}{x+1} dx = \sum_{n=0}^{\infty} \frac{L_n(t)}{n+1}$	

### 1.5.5 Chebyshev Polynomials

The Chebyshev polynomials can be derived from the Gegenbauer polynomials, and are given

$$T_n(t) = \frac{n}{2} \sum_{k=0}^{[n/2]} \frac{(-1)^k (n-k-1)!}{k!(n-2k)!} (2t)^{n-2k}, \quad -1 < t < 1 \tag{1.187}$$

The Chebyshev polynomials of the second kind are simply

$$U_n(t) = C_n^1(t), \quad n = 0, 1, 2, \dots \tag{1.188a}$$

where  $C_n^1(t)$  is the Gegenbauer polynomial with  $\lambda = 1$

$$C_n^\lambda(t) = (-1)^n \sum_{k=0}^{[n/2]} \binom{-\lambda}{n-k} \binom{n-k}{k} (2t)^{n-2k} \tag{1.188b}$$

Hence, the second kind Chebyshev polynomials are

$$U_n(t) = \sum_{k=0}^{[n/2]} \binom{n-k}{k} (-1)^k (2t)^{n-2k} \tag{1.189}$$

The recurrence are

$$T_{n+1}(t) - 2tT_n(t) + T_{n-1}(t) = 0 \tag{1.190}$$

$$U_{n+1}(t) - 2tU_n(t) + U_{n-1}(t) = 0 \tag{1.191}$$

The orthogonality properties are

$$\int_{-1}^1 (1-t^2)^{-1/2} T_n(t) T_k(t) dt = 0, \quad k \neq n \tag{1.192}$$

$$\int_{-1}^1 (1-t^2)^{1/2} U_n(t) U_k(t) dt = 0, \quad k \neq n \tag{1.193}$$

The governing differential equations for  $T_n(t)$  and  $U_n(t)$  are, respectively,

$$(1-t^2)y'' - ty' + n^2y = 0 \tag{1.194}$$

$$(1-t^2)y'' - 3ty' + n(n+2)y = 0 \tag{1.195}$$

The following are relationships between the two Chebyshev types:

$$T_n(t) = U_n(t) - tU_{n-1}(t) \tag{1.196}$$

$$(1-t^2)U_n(t) = tT_n(t) - T_{n+1}(t) \tag{1.197}$$

**TABLE 1.12** Properties of the Chebyshev Polynomials

1.  $(1 - t^2) \frac{d^2y}{dt^2} - t \frac{dy}{dt} + n^2y = 0; \quad y(t) = T_n(t)$
2.  $T_n(t) = \frac{n}{2} \sum_{k=0}^{[n/2]} \frac{(-1)^k (n-k-1)!}{k!(n-2k)!} (2t)^{n-2k},$   
 $n = 1, 2, \dots, [n/2] = \text{largest integer} \leq n/2$
3.  $T_n(t) = \frac{(-2)^n n!}{(2n)!} \sqrt{1-t^2} \frac{d^n}{dt^n} (1-t^2)^{n-\frac{1}{2}},$   
 Rodrigues formula
4.  $T_n(t) = \cos(n \cos^{-1} t)$
5.  $\frac{1-st}{1-2st+s^2} = \sum_{n=0}^{\infty} T_n(t) s^n,$  generating function
6.  $T_{n+1}(t) = 2tT_n(t) - T_{n-1}(t)$
7.  $\int_{-1}^1 \frac{T_n(t)T_m(t)}{\sqrt{1-t^2}} dt = \begin{cases} 0 & n \neq m \\ \pi/2 & n = m \neq 0 \\ \pi & n = m = 0 \end{cases}$
8.  $T_n(1) = 1, T_n(-1) = (-1)^n, T_{2n}(0) = (-1)^n, T_{2n+1}(0) = 0$

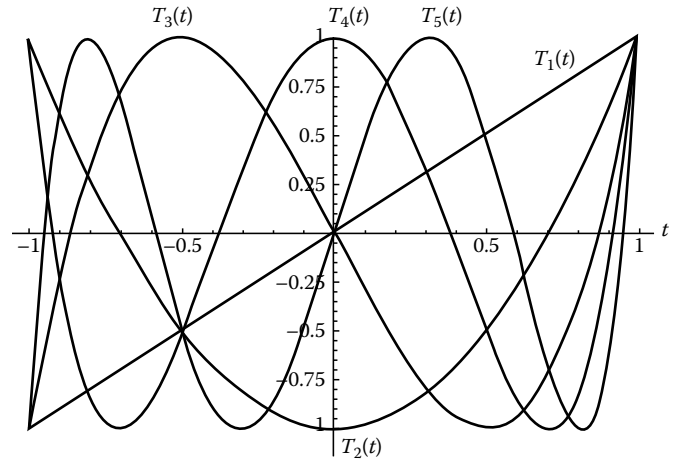


**FIGURE 1.7**

Table 1.12 gives relationships for the Chebyshev polynomials.

If we set  $t = \cos \theta$  in Equation 1.194, we find that it reduce to

$$\frac{d^2y}{d\theta^2} + n^2y = 0$$

with solution  $\cos n\theta$  and  $\sin n\theta$ . Therefore, if we set  $T_n(\cos \theta) = C_n \cos n\theta$ , we find that  $C_n = 1$  for all  $n$  because  $T_n(1) = 1$  for all  $n$ . Hence

$$T_n(t) = \cos n\theta = \cos(n \cos^{-1} t) \quad (1.198)$$

Similarly

$$U_n(t) = \frac{\sin [(n+1) \cos^{-1} t]}{\sqrt{1-t^2}} \quad (1.199)$$

The generating function for the Chebyshev polynomial is

$$\frac{1-st}{1-2st+s^2} = \sum_{n=0}^{\infty} T_n(t) s^n \quad (1.200)$$

The generalized Rodrigues formula is

$$T_n(t) = \frac{(-2)^n n!}{(2n)!} \sqrt{1-t^2} \frac{d^n}{dt^n} (1-t^2)^{n-\frac{1}{2}} \quad (1.201)$$

Figure 1.7 shows several Chebyshev polynomials.

## 1.5.6 Bessel Functions

### 1.5.6.1 Bessel Functions of the First Kind

General relations: The solution of Bessel's equation

$$y'' + \frac{1}{t}y' + \left(1 - \frac{n^2}{t^2}\right)y = 0, \quad n = 0, 1, 2, \dots \quad (1.202)$$

is the function  $y = J_n(t)$ , known as the *Bessel function of the first kind and order n*. The Bessel function is defined by the series

$$J_n(t) = \sum_{k=0}^{\infty} \frac{(-1)^k (t/2)^{n+2k}}{k!(n+k)!}, \quad -\infty < t < \infty \quad (1.203)$$

We can find Equation 1.203 by expanding the function  $w(t, x)$  in series of the two exponentials  $\exp(tx/2)$  and  $\exp(-t/2x)$  in the form

$$w(t, x) \doteq e^{\frac{1}{2}t(x-\frac{1}{x})} = \sum_{n=-\infty}^{\infty} J_n(t)x^n, \quad x \neq 0 \quad (1.204)$$

By setting  $n = -n$  in Equation 1.203 we obtain

$$J_{-n}(t) = \sum_{k=0}^{\infty} \frac{(-1)^k (t/2)^{2k-n}}{k!(k-n)!} = \sum_{k=n}^{\infty} \frac{(-1)^k (t/2)^{2k-n}}{k!(k-n)!}$$

because  $1/[(k-n)!] = 0$  for  $k = 0, 1, 2, \dots, n-1$  ( $\Gamma(n) = \infty$  for negative  $n$ ). Setting  $k = m+n$ , we obtain

$$J_{-n}(t) = \sum_{m=0}^{\infty} \frac{(-1)^{m+n} (t/2)^{2m+n}}{m!(m+n)!} \quad (1.205)$$

from which it follows that

$$J_{-n}(t) = (-1)^n J_n(t), \quad n = 0, 1, 2, \dots \quad (1.206)$$

Equating like terms in the expanded form of Equation 1.204, we obtain

$$J_0(0) = 1, \quad J_n(0) = 0, \quad n \neq 0 \quad (1.207)$$

Figure 1.8 shows several Bessel functions of the first kind and zero order.

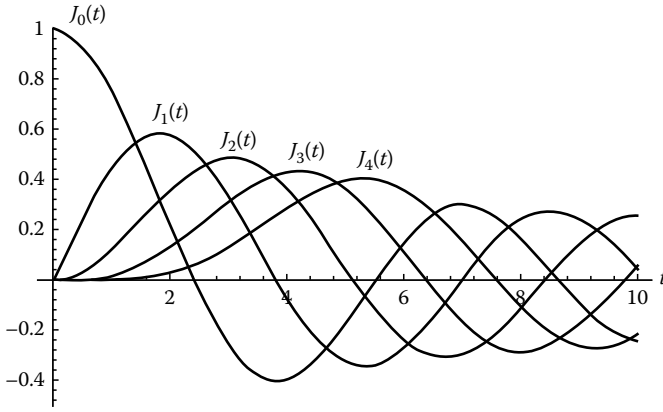


FIGURE 1.8

**1.5.6.2 Bessel Functions of Noninteger Order**

The Bessel functions of a noninteger number are give by ( $\nu$  = noninteger number)

$$J_\nu(t) = \sum_{k=0}^{\infty} \frac{(-1)^k (t/2)^{2k+\nu}}{k! \Gamma(k + \nu + 1)}, \quad \nu \geq 0 \tag{1.208a}$$

$$J_{-\nu}(t) = \sum_{k=0}^{\infty} \frac{(-1)^k (t/2)^{2k-\nu}}{k! \Gamma(k - \nu + 1)}, \quad \nu \geq 0 \tag{1.208b}$$

The two functions  $J_{-\nu}(t)$  and  $J_\nu(t)$  are linear independent for noninteger values of  $\nu$  and they do not satisfy any generating-function relation. The functions  $J_{-\nu}(0) = \infty$  and  $J_\nu(0)$  remain finite. Both share most of the properties of  $J_n(t)$  and  $J_{-n}(t)$ .

**1.5.6.3 Recurrence Relation**

$$\begin{aligned} \frac{d}{dt} [t^\nu J_\nu(t)] &= \frac{d}{dt} \sum_{k=0}^{\infty} \frac{(-1)^k (t/2)^{2k+2\nu}}{2^{2k+\nu} k! \Gamma(k + \nu + 1)} \\ &= t^\nu \sum_{k=0}^{\infty} \frac{(-1)^k (t/2)^{2k+(\nu-1)}}{k! \Gamma(k + \nu)} = t^\nu J_{\nu-1}(t) \end{aligned} \tag{1.209}$$

Similarly

$$\frac{d}{dt} [t^{-\nu} J_\nu(t)] = -t^{-\nu} J_{\nu+1}(t) \tag{1.210}$$

Differentiate Equations 1.209 and 1.210 and dividing by  $t^\nu$  and  $t^{-\nu}$ , respectively, we find

$$J'_\nu(t) + \frac{\nu}{t} J_\nu(t) = J_{\nu-1}(t) \tag{1.211}$$

$$J'_\nu(t) - \frac{\nu}{t} J_\nu(t) = -J_{\nu+1}(t) \tag{1.212}$$

Set  $\nu = 0$  in Equation 1.212 to obtain

$$J'_0(t) = -J_1(t) \tag{1.213}$$

Add and subtract Equations 1.211 and 1.212 to find, respectively, the relations

$$2J'_\nu(t) = J_{\nu-1}(t) - J_{\nu+1}(t) \tag{1.214}$$

$$\frac{2\nu}{t} J_\nu(t) = J_{\nu-1}(t) + J_{\nu+1}(t) \tag{1.215}$$

The last relation is known as the *three-term recurrence formula*. Repeated operations result in

$$\left(\frac{d}{t dt}\right)^m [t^\nu J_\nu(t)] = t^{\nu-m} J_{\nu-m}(t) \tag{1.216}$$

$$\left(\frac{d}{t dt}\right)^m [t^{-\nu} J_\nu(t)] = (-1)^m t^{-\nu-m} J_{\nu+m}(t) \quad m = 1, 2, \dots \tag{1.217}$$

**Example**

We proceed to find the following derivative

$$\begin{aligned} \frac{d}{dt} [t^\nu J_\nu(at)] &= \frac{d}{dt} \left[ \left(\frac{u}{a}\right)^\nu J_\nu(u) \right] = \frac{d}{du} \left[ \frac{u^\nu}{a^\nu} J_\nu(u) \right] \frac{du}{dt} \\ &= a^{-\nu} \frac{d}{du} [u^\nu J_\nu(u)] a = a^{1-\nu} [u^\nu J_{\nu-1}(u)] \\ &= a^{1-\nu} [(at)^\nu J_{\nu-1}(at)] = at^\nu J_{\nu-1}(at) \end{aligned}$$

where Equation 1.209 was used.

**Example**

Differentiate Equation 1.214 to find

$$\frac{d^2 J_\nu(t)}{dt^2} = \frac{1}{2} \left( \frac{dJ_{\nu-1}(t)}{dt} - \frac{dJ_{\nu+1}(t)}{dt} \right)$$

Then apply the same equation to each derivative on the right side to find

$$\begin{aligned} \frac{d^2 J_\nu(t)}{dt^2} &= \frac{1}{2} \left[ \frac{1}{2} [J_{\nu-2}(t) - J_\nu(t)] - \frac{1}{2} [J_\nu(t) - J_{\nu+2}(t)] \right] \\ &= \frac{1}{2^2} [J_{\nu-2}(t) - 2J_\nu(t) + J_{\nu+2}(t)] \end{aligned}$$

Similarly we find

$$\frac{d^3 J_\nu(t)}{dt^3} = \frac{1}{2^3} [J_{\nu-3}(t) - 3J_{\nu-1}(t) + 3J_{\nu+1}(t) - J_{\nu+3}(t)]$$

### 1.5.6.4 Integral Representation

Set  $x = \exp(-j\varphi)$  in Equation 1.204, multiply both sides by  $\exp(jn\varphi)$ , and integrate the results from 0 to  $\pi$ . Hence

$$\int_0^\pi e^{j(n\varphi - t \sin \varphi)} d\varphi = \sum_{k=-\infty}^\infty J_k(t) \int_0^\pi e^{j(n-k)\varphi} d\varphi \quad (1.218)$$

Expand on both sides the exponentials in Euler's formula; equate the real and imaginary parts and use the relation

$$\int_0^\pi \cos(n-k)\varphi d\varphi = \begin{cases} 0 & k \neq n \\ \pi & k = n \end{cases}$$

to find that all terms of the infinite sum vanish except for  $k = n$ . Hence, we obtain

$$J_n(t) = \frac{1}{\pi} \int_0^\pi \cos(n\varphi - t \sin \varphi) d\varphi, \quad n = 0, 1, 2, \dots \quad (1.219)$$

When  $n = 0$ , we find

$$J_0(t) = \frac{1}{\pi} \int_0^\pi \cos(t \sin \varphi) d\varphi \quad (1.220)$$

For a Bessel function with nonintegral order, the Poisson formula is

$$J_\nu(t) = \frac{(t/2)^\nu}{\sqrt{\pi}\Gamma\left(\nu + \frac{1}{2}\right)} \int_{-1}^1 (1-x^2)^{\nu-\frac{1}{2}} e^{jtx} dx, \quad \nu > -\frac{1}{2}, t > 0 \quad (1.221)$$

Set  $x = \cos \theta$  to obtain

$$J_\nu(t) = \frac{(t/2)^\nu}{\sqrt{\pi}\Gamma\left(\nu + \frac{1}{2}\right)} \int_0^\pi \cos(t \cos \theta) \sin^{2\nu} \theta d\theta, \quad \nu > -\frac{1}{2}, t > 0 \quad (1.222)$$

### 1.5.6.5 Integrals Involving Bessel Functions

Start with the identities

$$\frac{d}{dt} [t^\nu J_\nu(t)] = t^\nu J_{\nu-1}(t) \quad (1.223)$$

$$\frac{d}{dt} [t^{-\nu} J_\nu(t)] = -t^{-\nu} J_{\nu+1}(t) \quad (1.224)$$

and directly integrate to find

$$\int t^\nu J_{\nu-1}(t) dt = t^\nu J_\nu(t) + C \quad (1.225)$$

$$\int t^{-\nu} J_{\nu+1}(t) dt = -t^{-\nu} J_\nu(t) + C \quad (1.226)$$

where  $C$  is the constant of integration.

### Example

We apply the integration procedure to find

$$\begin{aligned} \int t^2 J_2(t) dt &= \int t^3 [t^{-1} J_2(t)] dt = - \int t^3 \frac{d}{dt} [t^{-1} J_1(t)] dt \\ &= -t^2 J_1(t) + 3 \int t J_1(t) dt = -t^2 J_1(t) - 3 \int t [-J_1(t)] dt \\ &= -t^2 J_1(t) - 3 \int t \left[ \frac{d}{dt} J_0(t) \right] dt \\ &= -t^2 J_1(t) - 3t J_0(t) + 3 \int J_0(t) dt \end{aligned}$$

The last integral has no closed solution.

### Example

If  $a > 0$  and  $b > 0$ , then [see Equation 1.220]

$$\begin{aligned} \int_0^\infty e^{-at} J_0(bt) dt &= \int_0^\infty e^{-at} dt \frac{2}{\pi} \int_0^{\pi/2} \cos(bt \sin \varphi) d\varphi \\ &= \frac{2}{\pi} \int_0^{\pi/2} d\varphi \int_0^\infty e^{-at} \cos(bt \sin \varphi) dt \\ &= \frac{2}{\pi} \int_0^{\pi/2} \frac{ad\varphi}{a^2 + b^2 \sin^2 \varphi} = \frac{1}{\sqrt{a^2 + b^2}} \end{aligned}$$

### Example

For  $a > 0$ ,  $b > 0$ , and  $\nu > -1$  ( $\nu$  is real), then

$$\begin{aligned} \int_0^\infty e^{-a^2 t^2} J_\nu(bt) t^{\nu+1} dt &= \int_0^\infty e^{-a^2 t^2} t^{\nu+1} dt \sum_{k=0}^\infty \frac{(-1)^k (bt/2)^{\nu+2k}}{k! \Gamma(k + \nu + 1)} \\ &= \sum_{k=0}^\infty \frac{(-1)^k}{k! \Gamma(k + \nu + 1)} \left(\frac{b}{2}\right)^{\nu+2k} \\ &\quad \times \int_0^\infty e^{-a^2 t^2} t^{2\nu+2k+1} dt \\ &= \sum_{k=0}^\infty \frac{(-1)^k}{k! \Gamma(k + \nu + 1)} \left(\frac{b}{2}\right)^{\nu+2k} \frac{1}{2a^{2\nu+2k+2}} \\ &\quad \times \int_0^\infty e^{-r} r^{\nu+k} dr \\ &= \frac{b^\nu}{(2a^2)^{\nu+1}} \sum_{k=0}^\infty \frac{\left(-\frac{b^2}{4a^2}\right)^k}{k!} = \frac{b^\nu}{(2a^2)^{\nu+1}} e^{-b^2/4a^2} \end{aligned} \quad (1.227)$$

where the last integral is the gamma function and the summation is the exponential expression.

The usual method of find definite integrals involving Bessel functions is to replace the Bessel function by its series representation. To illustrate the technique, let us find the value of the integral

$$\begin{aligned} I &= \int_0^{\infty} e^{-at} t^p J_p(bt) dt, \quad p > -\frac{1}{2}, \quad a > 0, \quad b > 0 \\ &= \sum_{k=0}^{\infty} \frac{(-1)^k (b/2)^{2k+p}}{k! \Gamma(k+p+1)} \int_0^{\infty} e^{-at} t^{2k+2p} dt \\ &= b^p \sum_{k=0}^{\infty} \frac{(-1)^k \Gamma(2k+2p+1)}{2^{2k+p} k! \Gamma(k+p+1)} (a^2)^{-(p+\frac{1}{2})-k} (b^2)^k \quad (1.228) \end{aligned}$$

where the last integral is in the form of a gamma function. But we know that

$$\begin{aligned} \binom{-r}{k} &= (-1)^k \binom{r+k-1}{k}, \quad \binom{n}{k} = \binom{n}{n-k} \\ \binom{n+1}{k+1} &= \binom{n}{k+1} + \binom{n}{k}, \quad 0 \leq k \leq n-1 \end{aligned}$$

and thus we obtain

$$\begin{aligned} \frac{(-1)^k \Gamma(2k+2p+1)}{2^{2k+p} k! \Gamma(k+p+1)} &= \frac{(-1)^k 2^p \Gamma\left(p+k+\frac{1}{2}\right)}{\sqrt{\pi} k!} \\ &= \frac{(-1)^k}{\sqrt{\pi}} 2^p \Gamma\left(p+\frac{1}{2}\right) \binom{p+k-\frac{1}{2}}{k} \\ &= \frac{2^p \Gamma\left(p+\frac{1}{2}\right)}{\sqrt{\pi}} \binom{-\left(p+\frac{1}{2}\right)}{k} \quad (1.229) \end{aligned}$$

Therefore, Equation 1.228 becomes

$$\begin{aligned} I &= \int_0^{\infty} e^{-at} t^p J_p(bt) dt \\ &= \frac{(2b)^p \Gamma\left(p+\frac{1}{2}\right)}{\sqrt{\pi}} \sum_{k=0}^{\infty} \binom{-\left(p+\frac{1}{2}\right)}{k} (a^2)^{-(p+(1/2)-k)} (b^2)^k \\ &= \frac{(2b)^p \Gamma\left(p+\frac{1}{2}\right)}{\sqrt{\pi} (a^2 + b^2)^{p+\frac{1}{2}}}, \quad p > -\frac{1}{2}, \quad a > 0, \quad b > 0 \quad (1.230) \end{aligned}$$

Setting  $p=0$  in this equation we find

$$\int_0^{\infty} e^{-at} J_0(bt) dt = \frac{1}{[a^2 + b^2]^{1/2}}, \quad a > 0, \quad b > 0 \quad (1.231)$$

Set  $a=0+$  in this equation to obtain

$$\int_0^{\infty} J_0(bt) dt = \frac{1}{b}, \quad b > 0 \quad (1.232)$$

By assuming the real approaches zero and writing  $a$  as pure imaginary, Equation 1.231 becomes

$$\int_0^{\infty} e^{-jat} J_0(bt) dt = \begin{cases} \frac{1}{(b^2 - a^2)^{1/2}} & b > a \\ \frac{-j}{(a^2 - b^2)^{1/2}} & b < a \end{cases} \quad (1.233)$$

The above integral, by equating real and imaginary parts, becomes

$$\int_0^{\infty} \cos(at) J_0(bt) dt = \frac{1}{(b^2 - a^2)^{1/2}}, \quad b > a \quad (1.234)$$

$$\int_0^{\infty} \sin(at) J_0(bt) dt = \frac{1}{(a^2 - b^2)^{1/2}}, \quad b < a \quad (1.235)$$

### Example

To evaluate the integral  $\int_0^b t J_0(at) dt$ , we proceed as follows:

$$\begin{aligned} \int_0^{\infty} t J_0(at) dt &= \int_0^{\infty} \frac{1}{a} \frac{d}{dt} [t J_1(at)] dt \\ &= \frac{1}{a} [t J_1(at)]_{t=0}^b = \frac{b}{a} J_1(ab), \quad a \neq 0 \quad (1.236) \end{aligned}$$

where Equation 1.209 with  $\nu=1$  was used.

### Example

To evaluate the integral  $I = \int_0^b t^2 J_0(at) dt$ , where  $a$  is a constant and nonequal to zero, we proceed as follows (set  $at=r$ ):

$$\begin{aligned} I &= \frac{1}{a^3} \int_0^{ab} r^2 J_0(r) dr = \frac{1}{a^3} \int_0^{ab} r r J_0(r) dr \\ &= \frac{1}{a^3} \int_0^{ab} r \frac{d}{dr} [r J_1(r)] dr = \frac{1}{a^3} \left[ a^2 b^2 J_1(ab) - \int_0^{ab} r J_1(r) dr \right] \end{aligned}$$

But [see Equation 1.224]

$$\int_0^{ab} rJ_1(r)dr = -\int_0^{ab} r \frac{d}{dr} [J_0(r)]dr = -rJ_0(r) \Big|_{r=0}^{ab} + \int_0^{ab} J_0(r)dr = -abJ_0(ab) + \int_0^{ab} J_0(r)dr$$

and therefore

$$I = \frac{1}{a^3} \left[ a^2 b^2 J_1(ab) + abJ_0(ab) - \int_0^{ab} J_0(r)dr \right] \quad (1.237)$$

The integral can be approximately evaluated with any desired accuracy by termwise integration of the series of  $J_0(t)$ . Hence, we write

$$\int_0^{ab} J_0(t)dt = ab - \frac{a^3 b^3}{3 \cdot 2^2} + \frac{a^5 b^5}{5 \cdot 2^4 \cdot (2!)^2} - \frac{a^7 b^7}{7 \cdot 2^6 \cdot (3!)^2} + \dots$$

### 1.5.6.6 Fourier Bessel Series

A Bessel series is a member of the class of generalized Fourier series. It is defined by

$$f(t) = \sum_{n=1}^{\infty} c_n J_\nu(t_n t), \quad 0 < t < a, \quad \nu > -\frac{1}{2} \quad (1.238)$$

where  $c$ 's are the expansion coefficient constants and  $t_n$ 's ( $n = 1, 2, 3, \dots$ ) are the zeros (positive roots) of the function

$$J_\nu(t_n t), \quad n = 1, 2, 3, \dots \quad (1.239)$$

The orthogonality property is defined as follows ( $\nu > -1$ ):

$$\int_0^a t J_\nu(t_m t) J_\nu(t_n t) dt = 0, \quad m \neq n \quad (1.240)$$

with weight  $t$ . It can also be shown that

$$\int_0^a t [J_\nu(t_n t)]^2 dt = \frac{a^2}{2} [J_{\nu+1}(t_n a)]^2 \quad (1.241)$$

---

### THEOREM 1.3

If a real function  $f(t)$  is piecewise continuous on  $(0, a)$  and is of bounded variation in every subinterval  $[t_1, t_2]$  where  $0 < t_1 < t_2 < a$ , then if the integral

$$\int_0^a \sqrt{t} |f(t)| dt$$

is finite, the Fourier–Bessel series converges to  $f(t)$  at every continuity point of  $f(t)$  and to  $[f(t+) - f(t-)]/2$  at every discontinuity point.

To begin, multiply Equation 1.238 by  $tJ_\nu(t_m t)$  and integrate from 0 to  $a$ . Assuming that termwise integration is permitted, we obtain

$$\int_0^a t f(t) J_\nu(t_m t) dt = \sum_{n=1}^{\infty} c_n \int_0^a t J_\nu(t_m t) J_\nu(t_n t) dt = c_m \int_0^a [J_\nu(t_m t)]^2 dt \quad (1.242)$$

because the integral is zero if  $n \neq m$  (see Equation 1.240). Hence, from this equation we obtain

$$c_n = \frac{2}{a^2 [J_{\nu+1}(t_n a)]^2} \int_0^a t f(t) J_\nu(t_n t) dt, \quad n = 1, 2, 3, \dots \quad (1.243)$$

### Example

Find the Fourier–Bessel series for the function

$$f(t) = \begin{cases} t & 0 < t < 1 \\ 0 & 1 < t < 2 \end{cases}$$

corresponding to the set of functions  $\{J_1(t_n t)\}$  where  $t_n$  satisfies  $J_1(2t_n) = 0$  ( $n = 1, 2, 3, \dots$ ),

Solution: We write the solution

$$f(t) = \sum_{n=1}^{\infty} c_n J_1(t_n t), \quad 0 < t < 2$$

where

$$\begin{aligned} c_n &= \frac{1}{2[J_2(2t_n)]^2} \int_0^2 t f(t) J_1(t_n t) dt \\ &= (\cdot) \int_0^1 t^2 J_1(t_n t) dt \quad (\text{let } r = t_n t) \\ &= (\cdot) \frac{1}{t_n^3} \int_0^{t_n} r^2 J_1(r) dr \quad [\text{apply Equation 1.223}] \\ &= (\cdot) \frac{1}{t_n^3} \int_0^{t_n} \frac{d}{dt} [r^2 J_2(r)] dr \\ &= \frac{1}{2[J_2(2t_n)]^2 t_n^3} t_n^2 J_2(t_n) = \frac{J_2(t_n)}{2t_n [J_2(2t_n)]^2}, \quad n = 1, 2, 3, \dots \end{aligned}$$



**Example**

To express the function  $f(t) = 1$  on the open interval  $0 < t < a$  as an infinite series of Bessel functions of zero order, we proceed as follows [see Equation 1.243]:

$$\begin{aligned} c_n &= \frac{2}{a^2 [J_1(t_n a)]^2} \int_0^a t \cdot 1 \cdot J_0(t_n t) dt \\ &= \frac{2}{a^2 [J_1(t_n a)]^2} \int_0^a \frac{1}{t_n} \frac{d}{dt} [t J_1(t_n t)] dt \quad [\text{see Equation 1.223}] \\ &= \frac{2}{a^2 t_n [J_1(t_n a)]^2} [t J_1(t_n t)]_{t=0}^a = \frac{2}{a t_n J_1(t_n a)} \end{aligned}$$

Hence the expression is

$$1 = 2 \sum_{n=1}^{\infty} \frac{J_n(t_n t)}{t_n J_1(t_n a)}, \quad 0 < t < a$$

**Example**

Let us expand the function  $f(t) = t^2, 0 \leq t \leq 1$ , in a series of the form

$$c_1 J_0(t_1 t) + c_2 J_0(t_2 t) + c_3 J_0(t_3 t) + \dots$$

where  $t_n$  denotes the  $n$ th positive zero of  $J_0(t)$ . From Equation 1.243 we obtain ( $a = 1$ )

$$\begin{aligned} c_n &= \frac{2}{[J_1(t_n)]^2} \int_0^1 t^3 J_0(t_n t) dt \\ &= \frac{2}{[J_1(t_n)]^2} \int_0^{t_n} \frac{r^3}{t_n^3} J_0(r) \frac{dr}{t_n} = \frac{2}{t_n^4 [J_1(t_n)]^2} \int_0^{t_n} r^2 \frac{d}{dr} [r J_1(r)] \\ &= \frac{2}{t_n^4 [J_1(t_n)]^2} \left[ r^3 J_1(r) \Big|_{r=0}^{t_n} - 2 \int_0^{t_n} r^2 J_1(r) dr \right] \\ &= \frac{2}{t_n^4 [J_1(t_n)]^2} \left[ t_n^3 J_1(t_n) - 2 \int_0^{t_n} \frac{d}{dr} [r^2 J_2(r)] dr \right] \\ &= \frac{2}{t_n^4 [J_1(t_n)]^2} [t_n^3 J_1(t_n) - 2 t_n^2 J_2(t_n)] \end{aligned}$$

Table 1.13 gives Bessel function relationships. Tables 1.14 and 1.15 give numerical values for Bessel functions and Table 1.16 gives the zeros of several Bessel functions.

**1.5.7 Zernike Polynomials**

Zernike polynomials are a set of complex exponentials that form a complete orthogonal set over the interior of the unit circle. Polynomial representation of optical wave fronts is essential in the analysis of interferometric test data, for example, to assess optical system performance. One such set, which is attractive for

its simple rotational properties, is the *circle polynomials* or *Zernike polynomials*. The set of these polynomials is denoted by

$$V_{nl}(x, y) = V_{nl}(r \cos \theta, r \sin \theta) = V_{nl}(r, \theta) = R_{nl}(r) e^{j l \theta} \tag{1.244}$$

where

$n$  is a nonnegative integer,  $n \geq 0$

$l$  is an integer subject to constraints:  $n - |l|$  is even and  $|l| \leq n$

$r$  is the length of vector from origin to  $(x, y)$  point

$\theta$  is the angle between  $r$ - and  $x$ -axis in the counterclockwise direction

The orthogonality property is expressed by the formula

$$\int \int_{x^2+y^2 \leq 1} V_{nl}^*(r, \theta) V_{mk}(r, \theta) r dr d\theta = \frac{\pi}{n+1} \delta_{mn} \delta_{kl} \tag{1.245}$$

where  $\delta_{ij}$  is the Kronecker symbol. The real-valued radial polynomials satisfy the orthogonality relation

$$\int_0^1 R_{nl}(r) R_{ml}(r) r dr = \frac{1}{2(n+1)} \delta_{mn} \tag{1.246}$$

The radial polynomials are given by

$$\begin{aligned} R_{n \pm |l|}(r) &= \frac{1}{\left(\frac{n-|l|}{2}\right)! r^m} \left[ \frac{d}{d(r^2)} \right]^{\frac{n-|l|}{2}} \left[ (r^2)^{\frac{n+|l|}{2}} (r^2 - 1)^{\frac{n+|l|}{2}} \right] \\ &= \sum_{s=0}^{\frac{n-|l|}{2}} (-1)^s \frac{(n-s)!}{s! \left(\frac{n+|l|}{2} - s\right)! \left(\frac{n-|l|}{2} - s\right)!} r^{n-2s} \end{aligned} \tag{1.247}$$

For all permissible values of  $n$  and  $|l|$

$$R_{n \pm |l|}(1) = 1, \quad R_{n|l|}(r) = R_{n(-|l|)}(r) \tag{1.248}$$

Table 1.17 gives the explicit form of the function  $R_{n|l|}(r)$ .

A relation between radial Zernike polynomials and Bessel functions of the first kind is given by

$$\int_0^1 R_{n|l|}(r) J_n(ur) r dr = (-1)^{\frac{n-|l|}{2}} \frac{J_{n+1}(u)}{u} \tag{1.249}$$

From Equation 1.244 we obtain the following real Zernike polynomials:

$$\begin{aligned} U_{nl} &= \frac{1}{2} [V_{nl} + V_{n(-l)}] = R_{nl}(r) \cos l\theta, \quad l \neq 0 \\ U_{n(-l)} &= \frac{1}{2j} [V_{nl} - V_{n(-l)}] = R_{nl}(r) \sin l\theta, \quad l \neq 0 \\ V_{n0} &= R_{n0}(r) \end{aligned} \tag{1.250}$$

Figure 1.9 shows the function  $U_{nl}$  for a few radial modes.

**TABLE 1.13** Properties of Bessel Functions of the First Kind

1.	$J_n(t) = \sum_{k=0}^{\infty} \frac{(-1)^k (t/2)^{n+2k}}{k!(n+k)!},$	$-\infty < t < \infty, n = 0, 1, 2, 3, \dots$
2.	$J_{-n}(t) = \sum_{m=0}^{\infty} \frac{(-1)^{m+n} (t/2)^{2m+n}}{m!(m+n)!},$	$-\infty < t < \infty, n = 0, 1, 2, 3, \dots$
3.	$J_{-n}(t) = (-1)^n J_n(t),$	$n = 0, 1, 2, 3, \dots$
4.	$J_0(0) = 1, J_n(0) = 0,$	$n \neq 0$
5.	$J_\nu(t) = \sum_{k=0}^{\infty} \frac{(-1)^k (t/2)^{2k+\nu}}{k! \Gamma(k+\nu+1)},$	$\nu \geq 0, \nu$ is noninteger
6.	$J_{-\nu}(t) = \sum_{k=0}^{\infty} \frac{(-1)^k (t/2)^{2k-\nu}}{k! \Gamma(k-\nu+1)},$	$\nu \geq 0, \nu$ is noninteger
7.	$\frac{d}{dt} [t^\nu J_\nu(t)] = t^\nu J_{\nu-1}(t)$	
8.	$\frac{d}{dt} [t^\nu J_\nu(at)] = at^\nu J_{\nu-1}(at)$	
9.	$\frac{d}{dt} [t^{-\nu} J_\nu(t)] = -t^{-\nu} J_{\nu+1}(t)$	
10.	$\frac{d^2 J_\nu(t)}{dt^2} = \frac{1}{2^2} [J_{\nu-2}(t) - 2J_\nu(t) + J_{\nu+2}(t)]$	
11.	$\frac{d^3 J_\nu(t)}{dt^3} = \frac{1}{2^3} [J_{\nu-3}(t) - 3J_{\nu-1}(t) + 3J_{\nu+1}(t) - J_{\nu+3}(t)]$	
12.	$J'_\nu(t) + \frac{\nu}{t} J_\nu(t) = J_{\nu-1}(t)$	
13.	$J'_\nu(t) - \frac{\nu}{t} J_\nu(t) = -J_{\nu+1}(t)$	
14.	$J'_0(t) = -J_1(t)$	
15.	$2J'_\nu(t) = J_{\nu-1}(t) - J_{\nu+1}(t)$	
16.	$\frac{2\nu}{t} J_\nu(t) = J_{\nu-1}(t) + J_{\nu+1}(t)$	
17.	$\left(\frac{d}{tdt}\right)^m [t^\nu J_\nu(t)] = t^{\nu-m} J_{\nu-m}(t)$	$m = 1, 2, 3, \dots$
18.	$\left(\frac{d}{tdt}\right)^m [t^{-\nu} J_\nu(t)] = (-1)^m t^{-\nu-m} J_{\nu+m}(t)$	$m = 1, 2, 3, \dots$
19.	$J'_1(0) = \frac{1}{2}, J'_n(0) = 0$	$n > 1$
20.	$J_n(t+r) = \sum_{k=-\infty}^{\infty} J_k(t) J_{n-k}(r)$	
21.	$J_0(2t) = [J_0(t)]^2 + 2 \sum_{k=1}^{\infty} (-1)^k [J_k(t)]^2$	
22.	$ J_0(t)  \leq 1,  J_n(t)  \leq \frac{1}{\sqrt{2}},$	$n = 1, 2, 3, \dots$
23.	$e^{jt \sin \theta} = \sum_{n=-\infty}^{\infty} J_n(t) e^{jn\theta}$	
24.	$\cos(t \sin \theta) = J_0(t) + 2 \sum_{n=1}^{\infty} J_{2n}(t) \cos(2n\theta)$	
25.	$\cos(t \cos \theta) = J_0(t) + 2 \sum_{n=1}^{\infty} (-1)^n J_{2n}(t) \cos(2n\theta)$	
26.	$\sin(t \sin \theta) = 2 \sum_{n=1}^{\infty} J_{2n-1}(t) \sin[(2n-1)\theta]$	
27.	$\sin(t \cos \theta) = 2 \sum_{n=0}^{\infty} (-1)^n J_{2n+1}(t) \cos[(2n+1)\theta]$	
28.	$\cos t = J_0(t) + 2 \sum_{n=1}^{\infty} (-1)^n J_{2n}(t)$	
29.	$\sin t = 2 \sum_{n=1}^{\infty} (-1)^n J_{2n-1}(t)$	
30.	$J_\nu(t) J_{1-\nu}(t) + J_{-\nu}(t) J_{\nu-1}(t) = \frac{2 \sin \nu\pi}{\pi t}$	Lommel's formula

(continued)

TABLE 1.13 (continued) Properties of Bessel Functions of the First Kind

---

31. $\frac{d}{dt} [tJ_\nu(t)J_{\nu+1}(t)] = t[[J_\nu(t)]^2 - [J_{\nu+1}(t)]^2]$	
32. $\frac{d}{dt} [t^2 J_{\nu-1}(t)J_{\nu+1}(t)] = 2t^2 J_\nu(t)J'_\nu(t)$	
33. $J_{1/2}(t) = \sqrt{\frac{2}{\pi t}} \sin t, \quad J_{-1/2}(t) = \sqrt{\frac{2}{\pi t}} \cos t$	
34. $J_{1/2}(t)J_{-1/2}(t) = \frac{\sin 2t}{\pi t}, \quad [J_{1/2}(t)]^2 + [J_{-1/2}(t)]^2 = \frac{2}{\pi t}$	
35. $[J_0(t)]^2 = \sum_{n=0}^{\infty} \frac{(-1)^n (2n)!}{(n!)^4} \left(\frac{t}{2}\right)^{2n}$	
36. $J_n(t) = \frac{1}{\pi} \int_0^\pi \cos(n\varphi - t \sin \varphi) d\varphi$	
37. $J_0(t) = \frac{1}{\pi} \int_0^\pi \cos(t \sin \varphi) d\varphi$	
38. $J_\nu(t) = \frac{(t/2)^\nu}{\sqrt{\pi} \Gamma(\nu + \frac{1}{2})} \int_{-1}^1 (1-x^2)^{\nu-\frac{1}{2}} e^{itx} dx,$	$\nu > -\frac{1}{2}, \quad t > 0$
39. $J_\nu(t) = \frac{(t/2)^\nu}{\sqrt{\pi} \Gamma(\nu + \frac{1}{2})} \int_0^\pi \cos(t \cos \theta) \sin^{2\nu} \theta d\theta,$	$\nu > -\frac{1}{2}, \quad t > 0$
40. $\int t^\nu J_{\nu-1}(t) dt = t^\nu J_\nu(t) + C,$	$C = \text{constant}$
41. $\int t^{-\nu} J_{\nu+1}(t) dt = -t^{-\nu} J_\nu(t) + C,$	$C = \text{constant}$
42. $[1 + (-1)^n] J_n(t) = \frac{2}{\pi} \int_0^\pi \cos n\varphi \cos(t \sin \varphi) d\varphi,$	$n = 0, 1, 2, \dots$
43. $J_{2k}(t) = \frac{1}{\pi} \int_0^\pi \cos 2k\varphi \cos(t \sin \varphi) d\varphi,$	$k = 0, 1, 2, \dots$
44. $J_{2k+1}(t) = \frac{1}{\pi} \int_0^\pi \sin [(2k+1)\varphi] \sin(t \sin \varphi) d\varphi,$	$k = 0, 1, 2, \dots$
45. $\int_0^\pi \cos [(2k+1)\varphi] \cos(t \sin \varphi) d\varphi = 0,$	$k = 0, 1, 2, \dots$
46. $\int_0^\pi \sin 2k\varphi \sin(t \sin \varphi) d\varphi = 0,$	$k = 0, 1, 2, \dots$
47. $J_0(t) = \frac{2}{\pi} \int_0^1 \frac{\cos tx}{\sqrt{1-x^2}} dx$	
48. $\frac{2 \sin t}{t} = \sqrt{\frac{2\pi}{t}} J_{1/2}(t)$	
49. $\int t J_0(t) dt = t J_1(t) + C$	
50. $\int t^2 J_0(t) dt = t^2 J_1(t) + t J_0(t) - \int J_0(t) dt + C$	
51. $\int t^3 J_0(t) dt = (t^3 - 4t) J_1(t) + 2t^2 J_0(t) + C$	
52. $\int J_1(t) dt = -J_0(t) + C$	
53. $\int t J_1(t) dt = -t J_0(t) + \int J_0(t) dt + C$	
54. $\int t^2 J_1(t) dt = 2t J_1(t) - t^2 J_0(t) + C$	
55. $\int t^3 J_1(t) dt = 3t^2 J_1(t) - (t^3 - 3t) J_0(t) - 3 \int J_0(t) dt + C$	
56. $\int J_3(t) dt = -J_2(t) - 2t^{-1} J_1(t) + C$	
57. $\int t^{-1} J_1(t) dt = -J_1(t) + \int J_0(t) dt + C$	
58. $\int t^{-2} J_2(t) dt = -\frac{2}{3t^2} J_1(t) - \frac{1}{3} J_1(t) + \frac{1}{3t} J_0(t) + \frac{1}{3} \int J_0(t) dt + C$	
59. $\int J_0(t) \cos t dt = t J_0(t) \cos t + t J_1(t) \sin t + C$	
60. $\int J_0(t) \sin t dt = t J_0(t) \sin t - t J_1(t) \cos t + C$	
61. $\int_0^\infty e^{-at} t^p J_p(bt) dt = \frac{(2b)^p \Gamma(p + \frac{1}{2})}{\sqrt{\pi} (a^2 + b^2)^{p+\frac{1}{2}}},$	$p > -\frac{1}{2}, \quad a > 0, \quad b > 0$
62. $\int_0^\infty e^{-at} J_0(bt) dt = \frac{1}{(a^2 + b^2)^{1/2}},$	$a > 0, \quad b > 0$
63. $\int_0^\infty J_0(bt) dt = \frac{1}{b},$	$b > 0$
64. $\int_0^\infty J_{n+1}(t) dt = \int_0^\infty J_{n-1}(t) dt,$	$n = 1, 2, \dots$
65. $\int_0^\infty J_n(at) dt = \frac{1}{a}$	$a > 0$
66. $\int_0^\infty t^{-1} J_n(t) dt = \frac{1}{n},$	$n = 1, 2, \dots$

---

**TABLE 1.13 (continued)** Properties of Bessel Functions of the First Kind

67.	$\int_0^\infty e^{-at} t^{p+1} J_p(bt) dt = \frac{2^{p+1} \Gamma(p + \frac{3}{2})}{\sqrt{\pi}} \frac{ab^p}{(a^2 + b^2)^{p+\frac{3}{2}}},$	$p > -1, a > 0, b > 0$
68.	$\int_0^\infty t^2 e^{-at} J_0(bt) dt = \frac{2a^2 - b^2}{(a^2 + b^2)^{5/2}},$	$a > 0, b > 0$
69.	$\int_0^\infty e^{-at^2} t^{p+1} J_p(bt) dt = \frac{b^p e^{-b^2/4a}}{(2a)^{p+1}},$	$p > -1, a > 0, b > 0$
70.	$\int_0^\infty e^{-at^2} t^{p+3} J_p(bt) dt = \frac{b^p}{2^{p+1} a^{p+2}} \left( p + 1 - \frac{b^2}{4a} \right) e^{-b^2/4a},$	$p > -1, a > 0, b > 0$
71.	$\int_0^\infty t^{-1} \sin t J_0(bt) dt = \arcsin\left(\frac{1}{b}\right),$	$b > 1$
72.	$\int_0^{\pi/2} J_0(t \cos \varphi) \cos \varphi d\varphi = \frac{\sin t}{t}$	
73.	$\int_0^{\pi/2} J_1(t \cos \varphi) d\varphi = \frac{1 - \cos t}{t}$	
74.	$\int_0^\infty e^{-t \cos \varphi} J_0(t \sin \varphi) t^n dt = n! P_n(\cos \varphi),$ $P_n(t) = n$ th Legendre polynomial	$0 \leq \varphi < \pi$
75.	$\int_0^\infty t(t^2 + a^2)^{-1/2} J_0(bt) dt = \frac{e^{-ab}}{b},$	$a \geq 0, b > 0$
76.	$\int_0^\infty \frac{J_p(t)}{t^m} dt = \frac{\Gamma((p+1-m)/2)}{2^m \Gamma((p+1+m)/2)},$	$m > \frac{1}{2}, p - m > -1$
77.	$\frac{1}{8}(1 - t^2) = \sum_{n=1}^\infty \frac{J_0(k_n t)}{k_n^3 J_1(k_n)},$	$0 \leq t \leq 1, J^0(k^n) = 0,$ $n = 1, 2, \dots$
78.	$t^p = 2 \sum_{n=1}^\infty \frac{J_p(k_n t)}{k_n J_{p+1}(k_n)},$	$0 < t < 1, J^p(k^n) = 0,$ $n = 1, 2, \dots$
79.	$t^{p+1} = 2^2(p+1) \sum_{n=1}^\infty \frac{J_{p+1}(k_n t)}{k_n^2 J_{p+1}(k_n)},$	$0 < t < 1, p > -1/2,$

**TABLE 1.14**

$x$	$J_0(x)$									
	0	.1	.2	.3	.4	.5	.6	.7	.8	.9
0	1.0000	.9975	.9900	.9776	.9604	.9385	.9120	.8812	.8463	.8075
1	.7652	.7196	.6711	.6201	.5669	.5118	.4554	.3980	.3400	.2818
2	.2239	.1666	.1104	.0555	.0025	-.0484	-.0968	-.1424	-.1850	-.2243
3	-.2601	-.2921	-.3202	-.3443	-.3643	-.3801	-.3918	-.3992	-.4026	-.4018
4	-.3971	-.3887	-.3766	-.3610	-.3423	-.3205	-.2961	-.2693	-.2404	-.2097
5	-.1776	-.1443	-.1103	-.0758	-.0412	-.0068	.0270	.0599	.0917	.1220
6	.1506	.1773	.2017	.2238	.2433	.2601	.2740	.2851	.2931	.2981
7	.3001	.2991	.2951	.2882	.2786	.2663	.2516	.2346	.2154	.1944
8	.1717	.1475	.1222	.0960	.0692	.0419	.0146	-.0125	-.0392	-.0653
9	-.0903	-.1142	-.1367	-.1577	-.1768	-.1939	-.2090	-.2218	-.2323	-.2403
10	-.2459	-.2490	-.2496	-.2477	-.2434	-.2366	-.2276	-.2164	-.2032	-.1881
11	-.1712	-.1528	-.1330	-.1121	-.0902	-.0677	-.0446	-.0213	.0020	.0250
12	.0477	.0697	.0908	.1108	.1296	.1469	.1626	.1766	.1887	.1988
13	.2069	.2129	.2167	.2183	.2177	.2150	.2101	.2032	.1943	.1836
14	.1711	.1570	.1414	.1245	.1065	.0875	.0679	.0476	.0271	.0064
15	-.0142	-.0346	-.0544	-.0736	-.0919	-.1092	-.1253	-.1401	-.1533	-.1650

When  $x > 15.9,$

$$J_0(x) \doteq \sqrt{\left(\frac{2}{\pi x}\right)} \left\{ \sin\left(x + \frac{1}{4}\pi\right) + \frac{1}{8x} \sin\left(x - \frac{1}{4}\pi\right) \right\}$$

$$\doteq \frac{.7979}{\sqrt{x}} \left\{ \sin(57.296x + 45^\circ) + \frac{1}{8x} \sin(57.296x - 45^\circ) \right\}$$

(continued)

TABLE 1.14 (continued)

x	$J_1(x)$									
	0	.1	.2	.3	.4	.5	.6	.7	.8	.9
0	.0000	.0499	.0995	.1483	.1960	.2423	.2867	.3290	.3688	.4059
1	.4401	.4709	.4983	.5220	.5419	.5579	.5699	.5778	.5815	.5812
2	.5767	.5683	.5560	.5399	.5202	.4971	.4708	.4416	.4097	.3754
3	.3391	.3009	.2613	.2207	.1792	.1374	.0955	.0538	.0128	-.0272
4	-.0660	-.1033	-.1386	-.1719	-.2028	-.2311	-.2566	-.2791	-.2985	-.3147
5	-.3276	-.3371	-.3432	-.3460	-.3453	-.3414	-.3343	-.3241	-.3110	-.2951
6	-.2767	-.2559	-.2329	-.2081	-.1816	-.1538	-.1250	-.0953	-.0652	-.0349
7	-.0047	.0252	.0543	.0826	.1096	.1352	.1592	.1813	.2014	.2192
8	.2346	.2476	.2580	.2657	.2708	.2731	.2728	.2697	.2641	.2559
9	.2453	.2324	.2174	.2004	.1816	.1613	.1395	.1166	.0928	.0684
10	.0435	.0184	-.0066	-.0313	-.0555	-.0789	-.1012	-.1224	-.1422	-.1603
11	-.1768	-.1913	-.2039	-.2143	-.2225	-.2284	-.2320	-.2333	-.2323	-.2290
12	-.2234	-.2157	-.2060	-.1943	-.1807	-.1655	-.1487	-.1307	-.1114	-.0912
13	-.0703	-.0489	-.0271	-.0052	.0166	.0380	.0590	.0791	.0984	.1165
14	.1334	.1488	.1626	.1747	.1850	.1934	.1999	.2043	.2066	.2069
15	.2051	.2013	.1955	.1879	.1784	.1672	.1544	.1402	.1247	.1080

When  $x > 15.9$ ,

$$\begin{aligned}
 J_1(x) &\doteq \sqrt{\left(\frac{2}{\pi x}\right)} \left\{ \sin\left(x - \frac{1}{4}\pi\right) + \frac{3}{8x} \sin\left(x + \frac{1}{4}\pi\right) \right\} \\
 &\doteq \frac{.7979}{\sqrt{x}} \left\{ \sin(57.296x - 45^\circ) + \frac{3}{8x} \sin(57.296x + 45^\circ) \right\}
 \end{aligned}$$

TABLE 1.15

x	$J_2(x)$									
	0	.1	.2	.3	.4	.5	.6	.7	.8	.9
0	.0000	.0012	.0050	.0112	.0197	.0306	.0437	.0588	.0758	.0946
1	.1149	.1366	.1593	.1830	.2074	.2321	.2570	.2817	.3061	.3299
2	.3528	.3746	.3951	.4139	.4310	.4461	.4590	.4696	.4777	.4832
3	.4861	.4862	.4835	.4780	.4697	.4586	.4448	.4283	.4093	.3879
4	.3641	.3383	.3105	.2811	.2501	.2178	.1846	.1506	.1161	.0813

When  $0 \leq x < 1, J_2(x) \doteq \frac{x^2}{8} \left(1 - \frac{x^2}{12}\right)$ .

x	$J_3(x)$									
	0	.1	.2	.3	.4	.5	.6	.7	.8	.9
0	.0000	.0000	.0002	.0006	.0013	.0026	.0044	.0069	.0102	.0144
1	.0196	.0257	.0329	.0411	.0505	.0610	.0725	.0851	.0988	.1134
2	.1289	.1453	.1623	.1800	.1981	.2166	.2353	.2540	.2727	.2911
3	.3091	.3264	.3431	.3588	.3734	.3868	.3988	.4092	.4180	.4250
4	.4302	.4333	.4344	.4333	.4301	.4247	.4171	.4072	.3952	.3811

When  $0 \leq x < 1, J_3(x) \doteq \frac{x^3}{48} \left(1 - \frac{x^2}{16}\right)$ .

x	$J_4(x)$									
	0	.1	.2	.3	.4	.5	.6	.7	.8	.9
0	.0000	.0000	.0000	.0000	.0001	.0002	.0003	.0006	.0010	.0016
1	.0025	.0036	.0050	.0068	.0091	.0118	.0150	.0188	.0232	.0283
2	.0340	.0405	.0476	.0556	.0643	.0738	.0840	.0950	.1067	.1190
3	.1320	.1456	.1597	.1743	.1891	.2044	.2198	.2353	.2507	.2661
4	.2811	.2958	.3100	.3236	.3365	.3484	.3594	.3693	.3780	.3853

When  $0 \leq x < 1, J_4(x) \doteq \frac{x^4}{384} \left(1 - \frac{x^2}{20}\right)$ .

**TABLE 1.16** Zeros of  $J_0(x), J_1(x), J_2(x), J_3(x), J_4(x), J_5(x)$

$m$	$j_{0,m}$	$j_{1,m}$	$j_{2,m}$	$j_{3,m}$	$j_{4,m}$	$j_{5,m}$
1	2.4048	3.8317	5.1356	6.3802	7.5883	8.7715
2	5.5201	7.0156	8.4172	9.7610	11.0647	12.3386
3	8.6537	10.1735	11.6198	13.0152	14.3725	15.7002
4	11.7915	13.3237	14.7960	16.2235	17.6160	18.9801
5	14.9309	16.4706	17.9598	19.4094	20.8269	22.2178
6	18.0711	19.6159	21.1170	22.5827	24.0190	25.4303
7	21.2116	22.7601	24.2701	25.7482	27.1991	28.6266
8	24.3525	25.9037	27.4206	28.9084	30.3710	31.8117
9	27.4935	29.0468	30.5692	32.0649	33.5371	34.9888
10	30.6346	32.1897	33.7165	35.2187	36.6990	38.1599

**TABLE 1.17** The Radial Polynomials  $R_{n|l|}(r)$  for  $|l| \leq 8, n \leq 8$

$\frac{n}{ l }$	0	1	2	3	4	5	6	7	8
0	1		$2r^2 - 1$		$6r^4 - 6r^2 + 1$		$20r^6 - 30r^4 + 12r^2 - 1$		$70r^8 - 140r^6 + 90r^4 - 20r^2 + 1$
1		$r$		$3r^3 - 2r$		$10r^5 - 12r^3 + 3r$		$35r^7 - 60r^5 + 30r^3 - 4r$	
2			$r^2$		$4r^4 - 3r^2$		$15r^6 - 20r^4 + 6r^2$		$56r^8 - 105r^6 + 60r^4 - 10r^2$
3				$r^3$		$5r^5 - 4r^3$		$21r^7 - 30r^5 + 10r^3$	
4					$r^4$		$6r^6 - 5r^4$		$28r^8 - 42r^6 + 15r^4$
5						$r^5$		$7r^7 - 6r^5$	
6							$r^6$		$8r^8 - 7r^6$
7								$r^7$	
8									$r^8$

**1.5.7.1 Expansion in Zernike Polynomials**

If  $f(x, y)$  is a piecewise continuous function, we can expand this function in Zernike polynomials in the form

$$f(x, y) = \sum_{n=0}^{\infty} \sum_{l=-\infty}^{\infty} A_{nl} V_{nl}(x, y), \quad n - |l| \text{ is even, } |l| \leq n \quad (1.251)$$

Multiplying by  $V_{nl}^*(x, y)$ , integrating over the unit circle, and taking into consideration the orthogonality property we obtain

$$A_{nl} = \frac{n+1}{\pi} \int_0^{2\pi} \int_0^1 V_{nl}^*(r, \theta) f(r \cos \theta, r \sin \theta) r \, dr \, d\theta$$

$$= \frac{n+1}{\pi} \int \int_{x^2+y^2 \leq 1} V_{nl}^*(x, y) f(x, y) \, dx \, dy = A_{n(-l)}^* \quad (1.252)$$

with restrictions of the values of  $n$  and  $l$  as shown above.  $A_{nl}$ 's are also known as Zernike moments.

**Example**

Expand the function  $f(x, y) = x$  in Zernike polynomials.

**SOLUTION**

We write  $f(r \cos \theta, r \sin \theta) = r \cos \theta$  and observe that  $r$  has exponent (degree) one. Therefore, the values of  $n$  will be 0, 1

and because  $n - |l|$  must be even,  $l$  will take 0, 1 and  $-1$  values. We then write

$$f(x, y) = \sum_{n=0}^{\infty} \sum_{l=-\infty}^{\infty} A_{nl} R_{nl}(r) e^{j\theta}$$

$$= \sum_{n=0}^1 (A_{n(-1)} R_{n(-1)}(r) e^{-j\theta} + A_{n0} R_{n0}(r) + A_{n1} R_{n1}(r) e^{j\theta})$$

$$= A_{00} R_{00}(r) + A_{1(-1)} R_{1(-1)}(r) e^{-j\theta} + A_{11} R_{11}(r) e^{j\theta} \quad (1.253)$$

Where three terms were dropped because they did not obey the condition that  $n - |l|$  is even. From Equation 1.248  $R_{1(-1)}(r) = R_{11}(r)$  and hence we obtain

$$A_{00} = \frac{1}{\pi} \int_0^{2\pi} \int_0^1 R_{00}(r) r \cos \theta \, r \, dr \, d\theta = 0$$

$$A_{1(-1)} = \frac{2}{\pi} \int_0^{2\pi} \int_0^1 R_{11}(r) r \cos \theta e^{-j\theta} \, r \, dr \, d\theta = \frac{1}{2}$$

$$A_{11} = \frac{2}{\pi} \int_0^{2\pi} \int_0^1 R_{11}(r) r \cos \theta e^{j\theta} \, r \, dr \, d\theta = \frac{1}{2}$$

Therefore, the expansion becomes

$$f(x, y) = \frac{1}{2} r e^{j\theta} + \frac{1}{2} r e^{-j\theta} = r \cos \theta = R_{11}(r) \cos \theta = x$$

as was expected.

The radial polynomials  $R_n(r)$  are real valued and if  $f(x, y)$  is real, that is, image intensity, it is often convenient to expand in real-values series. The real expansion corresponding to Equation 1.251

$$f(x, y) = \sum_{n=0}^{\infty} \sum_{l=0}^n (C_{nl} \cos l\theta + S_{nl} \sin l\theta) R_n(r) \quad (1.254)$$

where  $n - l$  is even and  $l < n$ . Observe that  $l$  takes only positive value. The unknown constants are found from

$$\begin{bmatrix} C_{nl} \\ S_{nl} \end{bmatrix} = \frac{2n+2}{\pi} \int_0^1 \int_0^{2\pi} r dr d\theta f (r \cos \theta, r \sin \theta) R_n(r) \begin{bmatrix} \cos l\theta \\ \sin l\theta \end{bmatrix}, \quad l \neq 0 \quad (1.255)$$

$$C_{n0} = A_{n0} = \frac{1}{\pi} \int_0^1 \int_0^{2\pi} r dr d\theta f (r \cos \theta, r \sin \theta) R_n(r), \quad l \neq 0 \quad (1.256a)$$

$$S_{n0} = 0, \quad l = 0 \quad (1.256b)$$

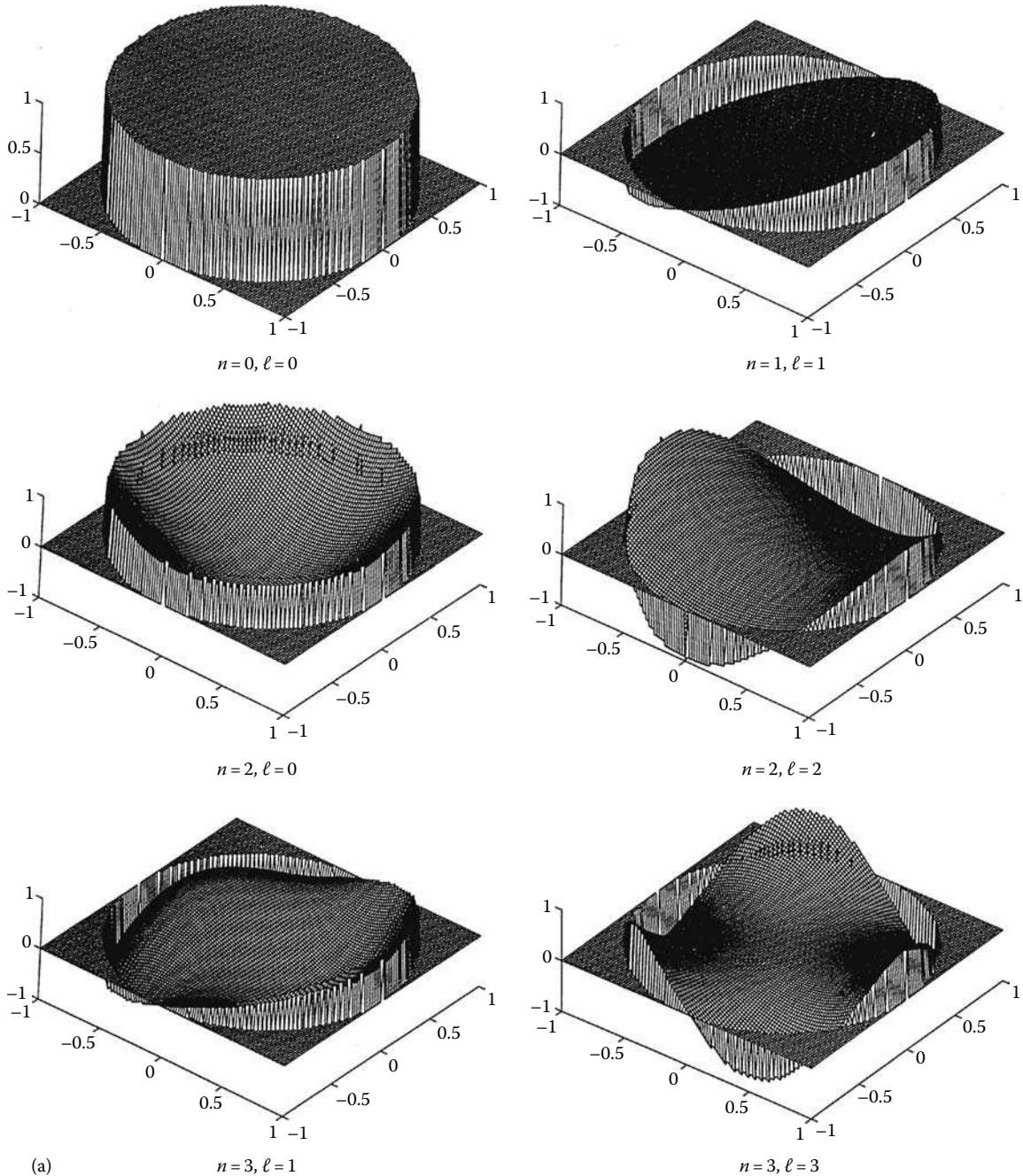


FIGURE 1.9

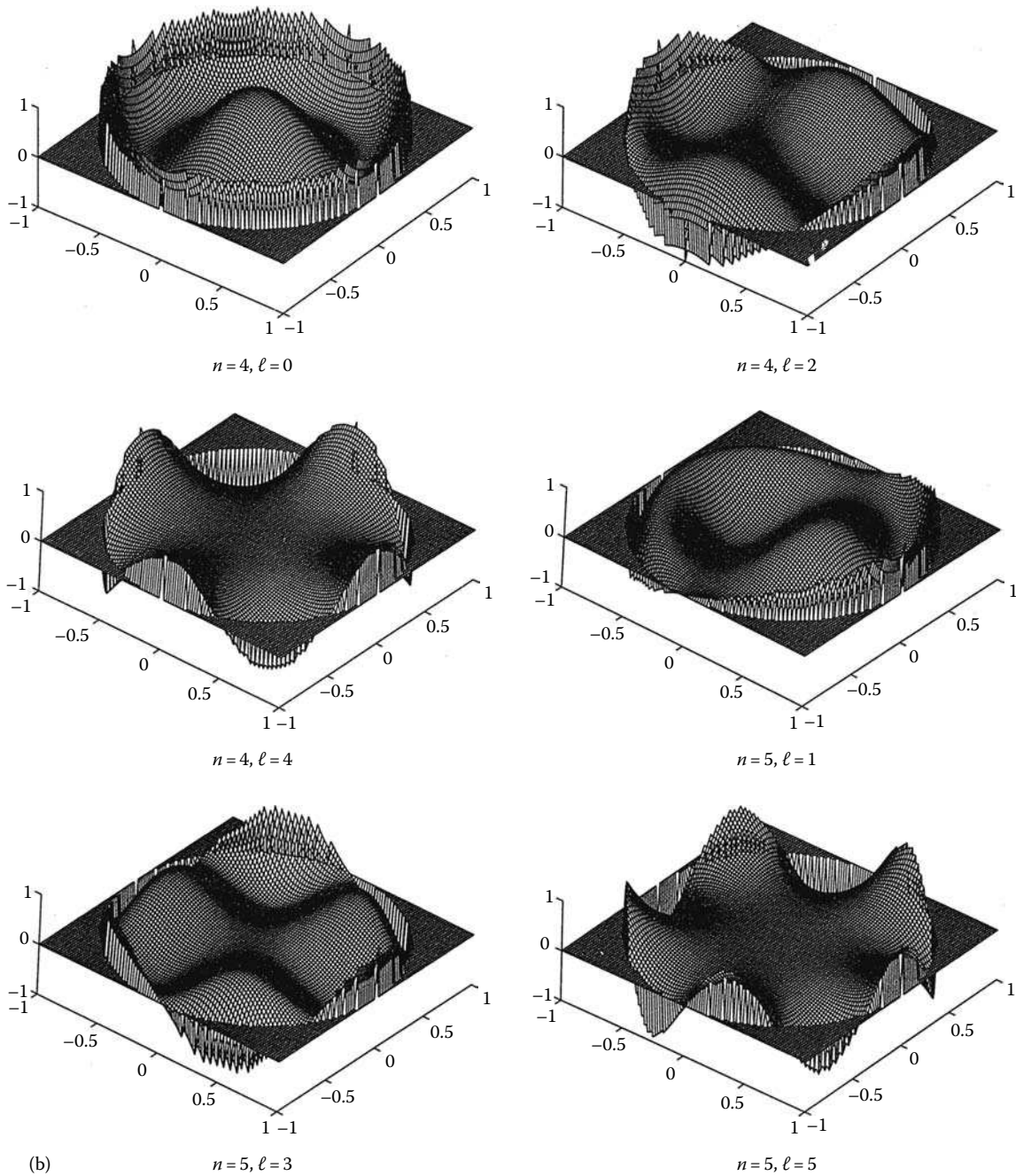


FIGURE 1.9 (continued)

If the function is axially symmetric only the cosine terms are needed. The connection between real and complex Zernike coefficients are

$$C_{nl} = 2\text{Re}\{A_{nl}\} \tag{1.257a}$$

$$S_{nl} = -2\text{Im}\{A_{nl}\} \tag{1.257b}$$

$$A_{nl} = (C_{nl} - jS_{nl})/2 = (A_{n(-l)})^* \tag{1.257c}$$

Figure 1.10 shows the reconstruction of the letter Z using different orders of Zernike moments.

## 1.6 Sampling of Signals

Two critical questions in signal sampling are: First, do the sampled values of a function adequately represent the system? Second, what must the sampling interval be in order that an



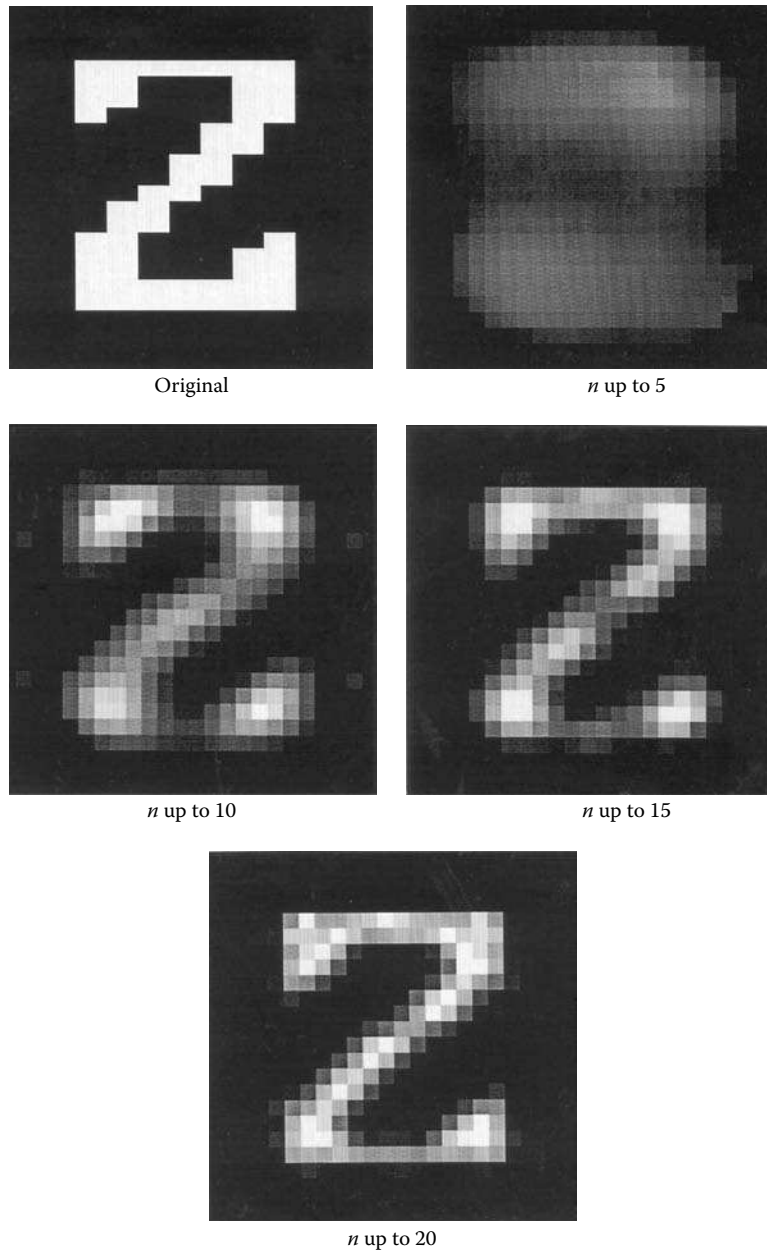


FIGURE 1.10

optimum recovery of the signal can be accomplished from the sampled values?

The value of the function at the sampling points is the *sampled value*, the time that separates the sampling points is the *sampling interval*, and the reciprocal of the sampling interval is the *sampling frequency* or *sampling rate*.

If the sampling interval  $T_s$  is chosen to be constant, and  $n = 0 \pm 1, \pm 2, \dots$ , the sampled signal is

$$f_s(t) = f(t) \sum_{n=-\infty}^{\infty} \delta(t - nT_s) = \sum_{n=-\infty}^{\infty} f(nT_s) \delta(t - nT_s) \quad (1.258)$$

Its Fourier transform is

$$\begin{aligned} F_s(\omega) &\doteq \mathcal{F}\{f_s(t)\} = \sum_{n=-\infty}^{\infty} f(nT_s) \mathcal{F}\{\delta(t - nT_s)\} \\ &= \sum_{n=-\infty}^{\infty} f(nT_s) e^{-jn\omega T_s} \end{aligned} \quad (1.259)$$

We can also represent the Fourier transform of a sampled function as follows:

$$\begin{aligned}
 F_s(\omega) &\doteq \mathcal{F}\left\{f(t) \sum_{n=-\infty}^{\infty} \delta(t - nT_s)\right\} = \frac{1}{2\pi} \mathcal{F}\{f(t)\} * \mathcal{F}\left\{\sum_{n=-\infty}^{\infty} \delta(t - nT_s)\right\} \\
 &= \frac{1}{2\pi} F(\omega) * \left[\frac{2\pi}{T_s} \sum_{n=-\infty}^{\infty} \delta(\omega - n\omega_s)\right] \\
 &= \frac{1}{T_s} \sum_{n=-\infty}^{\infty} \int_{-\infty}^{\infty} F(x) \delta(\omega - n\omega_s - x) dx = \frac{1}{T_s} \sum_{n=-\infty}^{\infty} F(\omega - n\omega_s) \\
 &= \frac{1}{T_s} \sum_{n=-\infty}^{\infty} F(\omega + n\omega_s), \quad \omega_s = \frac{2\pi}{T_s} \tag{1.260}
 \end{aligned}$$

$F_s(\omega)$  is periodic with period  $\omega_s$  in the frequency domain.

**Example**

$$\mathcal{F}\left\{e^{-|t|} \sum_{n=-\infty}^{\infty} \delta(t - nT_s)\right\} \doteq \mathcal{F}_s(\omega) = \frac{1}{T_s} \sum_{n=-\infty}^{\infty} \frac{2}{1 + (\omega - n\omega_s)^2}$$

**1.6.1 The Sampling Theorem**

It can be shown that is possible for a *band-limited* signal  $f(t)$  to be exactly specified by its sampled values provided that the time distance between sample values does not exceed a critical sampling interval.

**THEOREM 1.4**

A finite energy function  $f(t)$  having a band-limited Fourier transform,  $F(\omega)$  for  $|\omega| \geq \omega_N$ , can be completely reconstructed from its sampled values  $f(nT_s)$  (see Figure 1.11), with

$$f(t) = \sum_{n=-\infty}^{\infty} T_s f(nT_s) \left\{ \frac{\sin\left[\frac{\omega_s(t - nT_s)}{2}\right]}{\pi(t - nT_s)} \right\}, \quad \omega_s = \frac{2\pi}{T_s} \tag{1.261}$$

provided that

$$\frac{2\pi}{\omega_s} = T_s \leq \frac{\pi}{\omega_N} = \frac{1}{2f_N} = \frac{T_N}{2}$$

The function within the braces, which is the sinc function, is often called the interpolation function to indicate that it allows an interpolation between the sampled values of find  $f(t)$  for all  $t$ .

*Proof* Employ Equation 1.260 and Figure 1.11c to write

$$F(\omega) = p_{\omega_s/2}(\omega) T_s F_s(\omega) \tag{1.262}$$

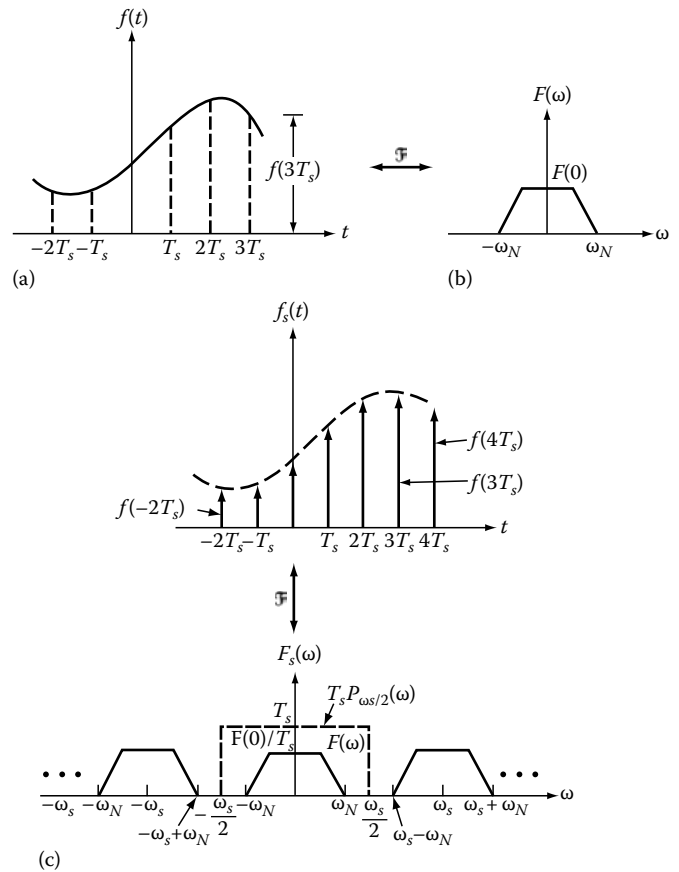


FIGURE 1.11

By Equation 1.262, the above equation becomes

$$\begin{aligned}
 f(t) &= \mathcal{F}^{-1}\{F(\omega)\} = \mathcal{F}^{-1}\left\{p_{\omega_s/2}(\omega) T_s \sum_{n=-\infty}^{\infty} f(nT_s) e^{-jn\omega T_s}\right\} \\
 &= T_s \sum_{n=-\infty}^{\infty} f(nT_s) \mathcal{F}^{-1}\{p_{\omega_s/2}(\omega) e^{-jn\omega T_s}\}
 \end{aligned}$$

By application of the frequency-shift property of the Fourier transform, this equation proves the theorem.

The sampling time

$$T_s = \frac{T_N}{2} = \frac{1}{2f_N} \tag{1.263}$$

is related to the *Nyquist interval*. It is the largest time interval that can be used for sampling of a band-limited signal and still allows recovering of the signal without distortion. If, however, the sampling time is larger than the Nyquist interval, overlap of spectra takes place, known as *aliasing*, and no perfect reconstruction of the band-limited signal is possible. Figure 1.12 shows the

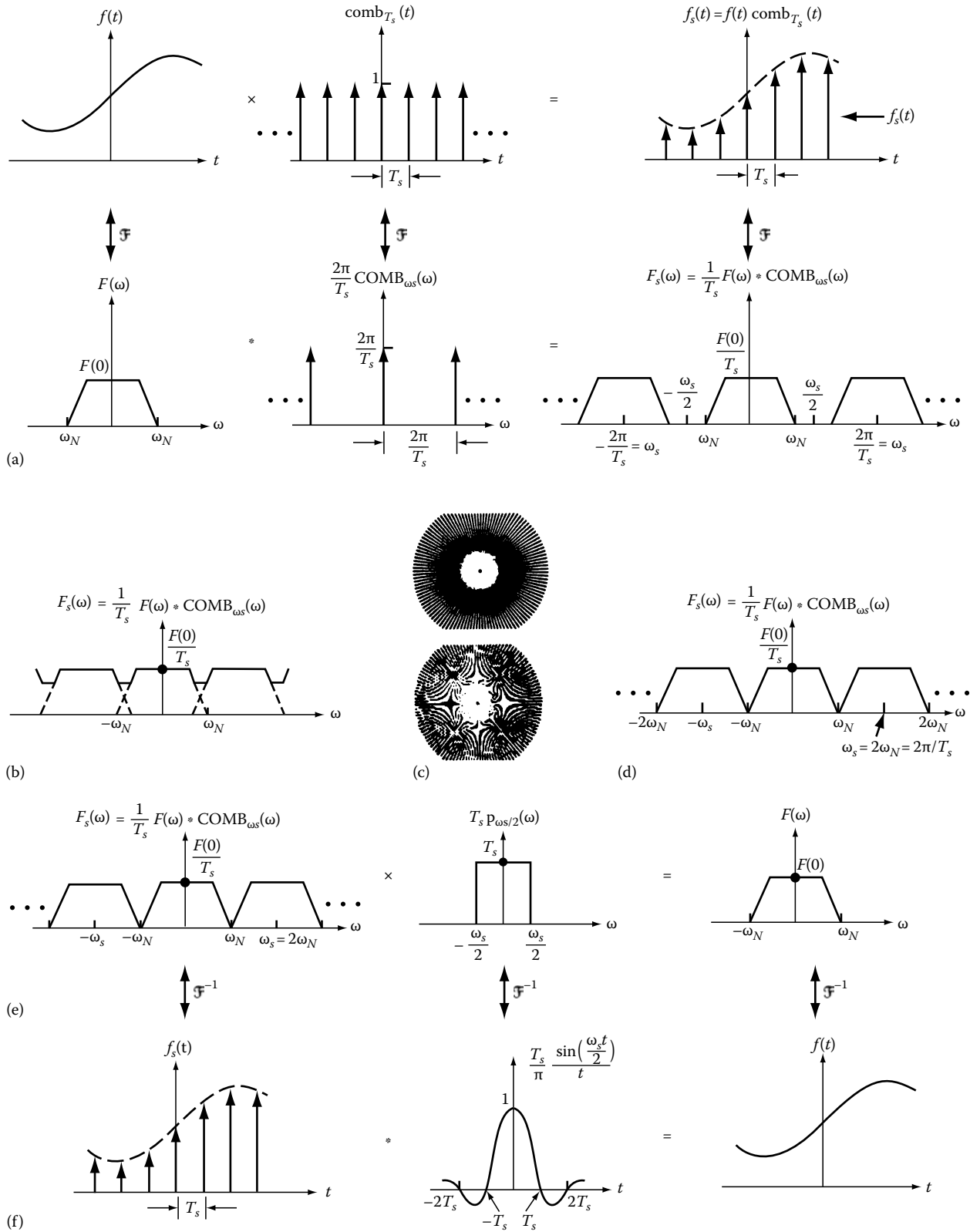


FIGURE 1.12

delta sampling representation and recovery of a band-limited signal. The following definitions have been used in the figure:

$$\text{comb}_{T_s}(t) = \sum_{n=-\infty}^{\infty} \delta(t - nT_s) \quad (1.264)$$

$$\text{COMB}_{\omega_s}(\omega) = \sum_{n=-\infty}^{\infty} \delta(\omega - n\omega_s) \quad (1.265)$$

### 1.6.1.1 Frequency Sampling

Analogous to the time-sampling theorem, a frequency-sampling equivalent also exists.

#### THEOREM 1.5

A time function  $f(t)$  that is time limited so that

$$f(t) = 0, |t| > T_N \quad (1.266)$$

possesses a Fourier transform that can be uniquely determined from its samples at distances  $n\pi/T_N$ , and is given by

$$F(\omega) = \sum_{n=-\infty}^{\infty} F\left(n\frac{\pi}{T_N}\right) \frac{\sin(\omega T_N - n\pi)}{\omega T_N - n\pi} \quad (1.267)$$

where the sampling is at the Nyquist rate.

### 1.6.1.2 Sampling with a Train of Rectangular Pulses

The Fourier transform of a band-limited function sampled with periodic pulses is given by (see Figure 1.13)

$$\begin{aligned} F_s(\omega) &= \mathcal{F}\{f(t)f_p(t)\} = \frac{1}{2\pi} F(\omega) * F_p(\omega) \\ &= \frac{1}{2\pi} F(\omega) * \left\{ \sum_{n=-\infty}^{\infty} 2\pi \frac{\sin\left(\frac{n\omega_s\tau}{2}\right)}{\frac{n\omega_s\tau}{2}} \delta(\omega - n\omega_s) \right\} \\ &= \sum_{n=-\infty}^{\infty} \frac{\sin\left(\frac{n\omega_s\tau}{2}\right)}{\frac{n\omega_s\tau}{2}} \int_{-\infty}^{\infty} \delta(x - n\omega_s) F(\omega - x) dx \\ &= \sum_{n=-\infty}^{\infty} \frac{\sin\left(\frac{n\omega_s\tau}{2}\right)}{\frac{n\omega_s\tau}{2}} F(\omega - n\omega_s) \end{aligned} \quad (1.268)$$

where  $\tau$  is the width of the pulse. The above expression indicates that as long as  $\omega_s > 2\omega_N$ , the spectrum of the sampled signal contains no overlapping spectra of  $f(t)$  and can be recovered using a low-pass filter.

### 1.6.2 Extensions of the Sampling Theorem

The sampling theorem of a band-limited function of  $n$  variables is given by the following theorem:

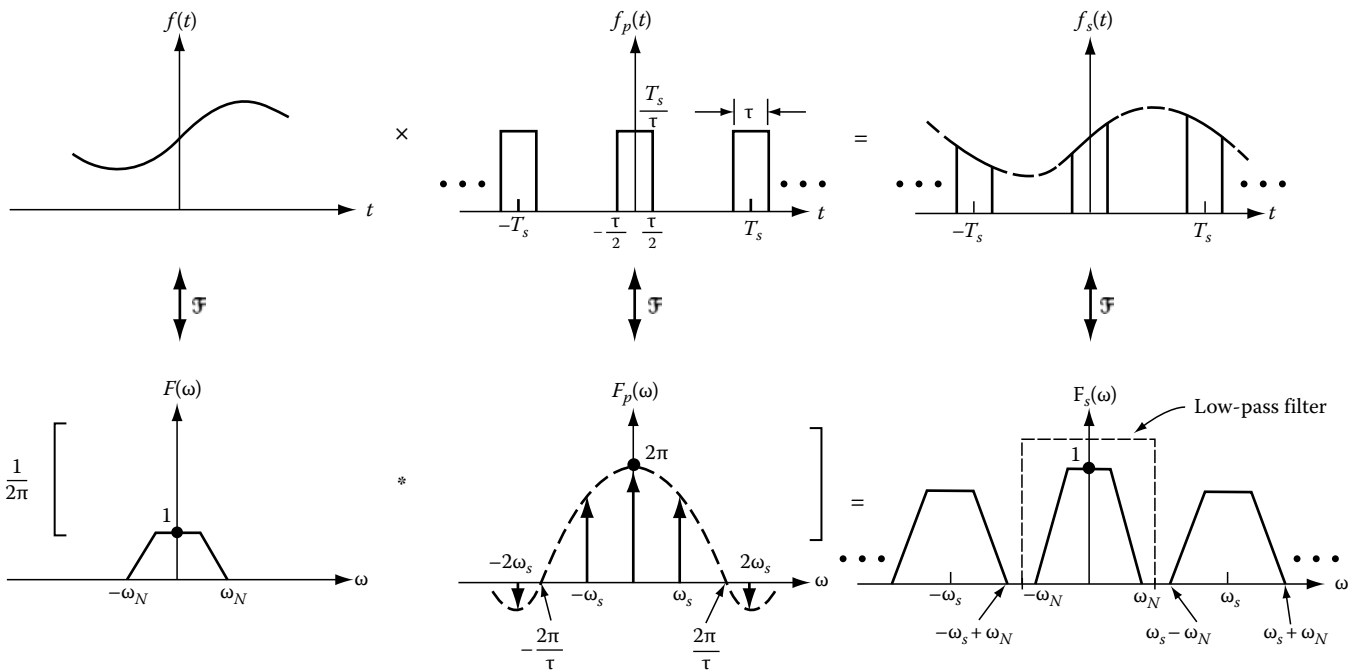


FIGURE 1.13

**THEOREM 1.6**

Let  $f(t_1, t_2, \dots, t_n)$  be a function of  $n$  real variables, whose  $n$ -dimensional Fourier integral exists and is identically zero outside an  $n$ -dimensional rectangle and is symmetrical about the origin, that is,

$$g(y_1, y_2, \dots, y_n)0, |y_k| > |\omega_k|, \quad k = 1, 2, \dots, n \quad (1.269)$$

Then

$$f(t_1, t_2, \dots, t_n) = \sum_{m_1=-\infty}^{\infty} \dots \sum_{m_n=-\infty}^{\infty} f\left(\frac{\pi m_1}{\omega_1}, \dots, \frac{\pi m_n}{\omega_n}\right) \times \frac{\sin(\omega_1 t_1 - m_1 \pi)}{\omega_1 t_1 - m_1 \pi} \dots \frac{\sin(\omega_n t_n - m_n \pi)}{\omega_n t_n - m_n \pi} \quad (1.270)$$

An additional theorem on the sampling of band-limited signals follows.

**THEOREM 1.7**

Let  $f(t)$  be a continuous function with finite Fourier transform  $F(\omega)[F(\omega) = 0 \text{ for } |\omega| > 2\pi f_N]$ . Then

$$f(t) = \sum_{k=-\infty}^{\infty} \left[ \xi(kh) + (t - kh)\xi^{(1)}(kh) + \dots + \frac{(t - kh)^R}{R!} \xi^{(R)}(kh) \right] \times \left[ \frac{\sin \frac{\pi}{h}(t - kh)}{\frac{\pi}{h}(t - kh)} \right]^{R+1} \quad (1.271)$$

where

$R$  is the highest derivative order

$$h = (R + 1)/(2f_N)$$

$\xi^{(R)}(kh)$  is the  $R$ th derivative of the function  $\xi(\cdot)$

$$\xi^{(j)}(kh) = \sum_{i=0}^j \binom{j}{i} \left(\frac{\pi}{h}\right)^{j-1} \Gamma_{R+1}^{(j-1)} f^{(i)}(kh)$$

$$\Gamma_a^{(\beta)} = \frac{d^\beta}{dt^\beta} \left[ \left(\frac{t}{\sin t}\right)^\alpha \right]_{t=0}$$

$$\Gamma_\alpha^{(0)} = 1, \Gamma_\alpha^{(2)} = \frac{\alpha}{3}, \Gamma_\alpha^{(4)} = \frac{\alpha(5\alpha + 2)}{15},$$

$$\Gamma_\alpha^{(6)} = \frac{\alpha(35\alpha^2 + 42\alpha + 16)}{63}, \dots, \Gamma_\alpha^{(\beta)} = 0 \text{ for odd } \beta$$

**1.6.2.1 Papoulis Extensions**

The band-limited signal

$$f(t) = \frac{1}{2\pi} \int_{-w_1}^{w_1} F(\omega)e^{j\omega t} d\omega \quad (1.272)$$

can be represented by

$$f(t) = \sum_{n=-\infty}^{\infty} f(nT) \frac{\sin w_0(t - nT)}{w_2(t - nT)} \quad (1.273)$$

where

$$w_2 = \frac{\pi}{T} \geq w_1, \quad w_1 \leq w_0 \leq 2w_2 - w_1$$

**THEOREM 1.8**

Given an arbitrary sequence of numbers  $\{a_n\}$ , if we form the sum

$$x(t) = \sum_{n=-\infty}^{\infty} a_n \frac{\sin w_0(t - nT)}{w_2(t - nT)} \quad (1.274)$$

then  $x(t)$  is band limited by  $w_0$ .

The sampling expansion of  $f^2(t)$  is given by

$$f^2(t) = \sum_{n=-\infty}^{\infty} f^2(nT) \frac{\sin w_0(t - nT)}{w_2(t - nT)} \quad (1.275)$$

where

$$w_2 = \frac{\pi}{T}, w_2 \geq 2w_1, 2w_1 \leq w_0 \leq 2w_2 - 2w_1, T \leq \frac{\pi}{2w_1}$$

The band-limited signal given in Equation 1.272 can be expressed in terms of the sample values  $g(nT)$  of the output

$$g(t) = \frac{1}{2\pi} \int_{-w_1}^{w_1} F(\omega)H(\omega)e^{j\omega t} d\omega \quad (1.276)$$

of a system with transfer function  $H(\omega)$  driven by  $f(t)$ . The sampling expansion of  $f(t)$  is

$$f(t) = \sum_{n=-\infty}^{\infty} g(nT)y(t - nT) \quad (1.277)$$

where

$$y(t) = \frac{1}{2w_1} \int_{-w_1}^{w_1} \frac{e^{j\omega t}}{H(\omega)} d\omega \quad (1.278)$$

**1.7 Asymptotic Series**

Functions such as  $f(z)$  and  $\varphi(z)$  are defined on a set  $R$  in the complex plane. By a neighborhood of  $z_0$  we mean an open disc

$|z - z_0| < \delta$  if  $z_0$  is at a finite distance, and a region  $|z| > \delta$  if  $z_0$  is the point at infinity.

**$f = O(\varphi)$  and  $f = o(\varphi)$  Notation**

We write  $f = O(\varphi)$  if there exists a constant  $A$  such that  $|f| \leq A|\varphi|$  for all  $z$  in  $R$ .

We also write  $f = O(\varphi)$  as  $z \rightarrow z_0$  if there exists a constant  $A$  and a neighborhood  $U$  of  $z_0$  such that  $|f| \leq A|\varphi|$  for all points in the intersection of  $U$  and  $R$ .

We write  $f = o(\varphi)$  as  $z \rightarrow z_0$  if, for any positive number  $\varepsilon$ , there exists a neighborhood  $U$  of  $z_0$  such that  $|f| \leq \varepsilon|\varphi|$  for all points  $z$  of the intersection of  $U$  and  $R$ .

More simply, if  $\varphi$  does not vanish on  $R$ ,  $f = O(\varphi)$  means that  $f/\varphi$  is bounded,  $f = o(\varphi)$  means that  $f/\varphi$  tends to zero as  $z \rightarrow z_0$ .

**1.7.1 Asymptotic Sequence**

A sequence of functions  $\{\varphi_n(z)\}$  is called an *asymptotic sequence* as  $z \rightarrow z_0$  if there is a neighborhood of  $z_0$  in which none of the functions vanish (except the point  $z_0$ ) and if for all  $n$

$$\varphi_{n+1} = o(\varphi_n) \quad \text{as } z \rightarrow z_0$$

For example, if  $z_0$  is finite  $\{(z - z_0)^n\}$  is an asymptotic sequence as  $z \rightarrow z_0$ , and  $\{z^{-n}\}$  is as  $z \rightarrow \infty$ .

**1.7.2 Poincaré Sense Asymptotic Sequence**

The formal series

$$f(z) \cong \sum_{n=0}^{\infty} a_n \varphi_n(z) \tag{1.279}$$

which is not necessarily convergent, is an asymptotic expansion of  $f(z)$  in the Poincaré sense with respect to the asymptotic sequence  $\{\varphi_n(z)\}$ , if for every value of  $m$ ,

$$f(z) - \sum_{n=0}^m a_n \varphi_n(z) = o(\varphi_m(z)) \tag{1.280}$$

as  $z \rightarrow z_0$ .

Because

$$f(z) - \sum_{n=0}^{m-1} a_n \varphi_n(z) = a_m \varphi_m(z) + o(\varphi_m(z)) \tag{1.281}$$

in partial sum

$$\sum_{n=0}^{m-1} a_n \varphi_n(z) \tag{1.282}$$

is an approximation to  $f(z)$  with an error  $O(\varphi_m)$  as  $z \rightarrow z_0$ ; this error is of the same order of magnitude as the first term omitted. If such an asymptotic expansion exists, it is unique, and the coefficients are given successively by

$$a_m = \frac{\lim_{z \rightarrow z_0} \{f(z) - \sum_{n=0}^{m-1} a_n \varphi_n(z)\}}{\varphi_m(z)} \tag{1.283}$$

Hence, for a function  $f(z)$  we write

$$f(z) \cong \sum_{n=0}^{\infty} a_n \varphi_n(z) \tag{1.284}$$

**1.7.3 Asymptotic Approximation**

A partial sum of Equation 1.284 is called an *asymptotic approximation* to  $f(z)$ . The first term is called the *dominant term*.

The above definition applies equally well for a real variable  $z$ .

**1.7.4 Asymptotic Power Series**

We shall assume that the transformation  $z' = 1/(z - z_0)$  has been done for limit points  $z_0$  located at a finite distance. Hence we can always consider expansions as  $z$  approaches infinity in a sector  $\alpha < \arg z < \beta$ ; or, for real value  $x$ , as  $x$  approaches infinity or as  $x$  approaches negative infinity.

The divergence series

$$f(z) = \sum_{n=0}^{\infty} \frac{a_n}{z^n} = a_0 + \frac{a_1}{z} + \frac{a_2}{z^2} + \dots + \frac{a_n}{z^n} + \dots$$

in which the sum of the first  $(n + 1)$  terms is  $S_n(z)$ , is said to be an *asymptotic expansion* of a function  $f(z)$  for a given range of values of  $\arg z$ , if the expansion  $R_n(z) = z^n\{f(z) - S_n(z)\}$  satisfies the condition

$$\lim_{|z| \rightarrow \infty} R_n(z) = 0 \quad (n \text{ is fixed}) \tag{1.285}$$

even though

$$\lim_{n \rightarrow \infty} |R_n(z)| = \infty \quad (z \text{ is fixed})$$

When this is true, we can make

$$|z^n\{f(z) - S_n(z)\}| < \varepsilon \tag{1.286}$$

where  $\varepsilon$  is arbitrarily small, by making  $|z|$  sufficiently large. This definition is due to Poincaré.

**Example**

For real  $x$ , integration on the real axis and repeated integration by parts, we obtain

$$f(x) = \int_x^\infty t^{-1} e^{x-t} dt = \frac{1}{x} - \frac{1}{x^2} + \frac{2!}{x^3} - \dots + \frac{(-1)^{n-1}(n-1)!}{x^n} + (-1)^n n! \int_x^\infty \frac{e^{x-t}}{t^{n+1}} dt$$

If we consider the expansion

$$u_{n-1} = \frac{(-1)^{n-1}(n-1)!}{x^n}$$

we can write

$$\sum_{m=0}^n u_m = \frac{1}{x} - \frac{1}{x^2} + \frac{2!}{x^3} - \dots + \frac{(-1)n!}{x^{n+1}} = S_n(x)$$

But  $|u_m/u_{m-1}| = mx^{-1} \rightarrow \infty$  as  $m \rightarrow \infty$ . The series  $\sum u_m$  is divergent for all values of  $x$ . However, the series can be used to calculate  $f(x)$ .

For a fixed  $n$ , we can calculate  $S_n$  from the relation

$$f(x) - S_n(x) = (-1)^{n+1}(n+1)! \int_x^\infty \frac{e^{x-t}}{t^{n+2}} dt$$

Because  $\exp(x-t) \leq 1$ ,

$$|f(x) - S_n(x)| = (n+1)! \int_x^\infty \frac{e^{x-t}}{t^{n+2}} dt < (n+1)! \int_x^\infty \frac{dt}{t^{n+2}} = \frac{n!}{x^{n+1}}$$

For large values of  $x$  the right-hand member of the above relation is very small. This shows that the value of  $f(x)$  can be calculated with great accuracy for large values of  $x$ , by taking the sum of a suitable number of terms of the series  $\sum u_m$ . From the last relation we obtain

$$|x^n \{f(x) - S_n(x)\}| < n!x^{-1} \rightarrow 0 \text{ as } x \rightarrow \infty$$

which satisfies the asymptotic expansion condition.

**1.7.5 Operation of Asymptotic Power Series**

Let the following two functions possess asymptotic expansions:

$$f(x) \approx \sum_{n=0}^\infty \frac{a_n}{x^n}, \quad g(x) \approx \sum_{n=0}^\infty \frac{b_n}{x^n} \text{ as } x \rightarrow \infty$$

on the real axis.

1. If  $A$  is constant

$$Af(x) \approx \sum_{n=0}^\infty \frac{Aa_n}{x^n} \tag{1.287}$$

2.

$$f(x) + g(x) \approx \sum_{n=0}^\infty \frac{a_n + b_n}{x^n} \tag{1.288}$$

3.

$$f(x)g(x) \approx \sum_{n=0}^\infty \frac{c_n}{x^n} \tag{1.289}$$

$$c_n = a_0b_n + a_1b_{n-1} + \dots + a_{n-1}b_1 + a_nb_0$$

4. If  $a_0 \neq 0$ , then

$$\frac{1}{f(x)} \approx \frac{1}{a_0} + \sum_{n=1}^\infty \frac{d_n}{x^n}, \quad x \rightarrow \infty \tag{1.290}$$

The function  $1/f(x)$  tends to a finite limit  $1/a_0$  as  $x$  approaches infinity. Hence,

$$\left(\frac{1}{f(x)} - \frac{1}{a_0}\right) / (1/x) = x \left(\frac{1}{a_0 + (a_1/x) + O(1/x^2)} - \frac{1}{a_0}\right) = \frac{-a_1 + O(\frac{1}{x})}{a_0[a_0 + (a_1/x) + O(1/x^2)]} \rightarrow -\frac{a_1}{a_0^2} = d_1$$

Similarly we obtain

$$\left(\frac{1}{f(x)} - \frac{1}{a_0} + \frac{a_1}{a_0^2x}\right) / \left(\frac{1}{x^2}\right) \rightarrow \frac{a_1^2 - a_0a_2}{a_0^3} = d_2$$

and so on.

In general, any rational function of  $f(x)$  has an asymptotic power series expansion provided that the denominator does not tend to zero as  $x$  approaches infinity.

5. If  $f(x)$  is continuous for  $x > a > 0$  and if  $x > a$ , then

$$F(x) = \int_x^\infty \left(f(t) - a_0 - \frac{a_1}{t}\right) dt \approx \frac{a_2}{x} + \frac{a_3}{2x^2} + \dots + \frac{a_{n+1}}{nx^n} + \dots \tag{1.291}$$

6. If  $f(x)$  has a continuous derivative  $f'(x)$ , and if  $f'(x)$  possess an analytic power series expansion as  $x$  approaches infinity, the expression is

$$f'(x) \approx - \sum_{n=2}^\infty \frac{(n-1)a_{n-1}}{x^n} \tag{1.292}$$

7. It is permissible to integrate an asymptotic expansion term-by-term. The resulting series is the expansion of the integral of the function represented by the original series.

Let

$$f(x) \approx \sum_{m=2}^{\infty} a_m x^{-m} \quad \text{and} \quad S_n = \sum_{m=2}^n a_m x^{-m}$$

Then, give any positive number  $\epsilon$ , we can find  $x_0$  such that

$$|f(x) - S_n(x)| < \epsilon |x|^{-n} \quad \text{for } x > x_0$$

Hence

$$\begin{aligned} & \left| \int_x^{\infty} f(x) dx - \int_x^{\infty} S_n(x) dx \right| \\ & \leq \int_x^{\infty} |f(x) - S_n(x)| dx < \frac{\epsilon}{(n-1)x^{n-1}} \end{aligned}$$

However,

$$\int_x^{\infty} S_n(x) dx = \frac{a_2}{x} + \frac{a_3}{2x^2} + \dots + \frac{a_n}{(n-1)x^{n-1}}$$

and therefore

$$\int_x^{\infty} f(x) dx \approx \sum_{m=2}^{\infty} \frac{a_m}{(m-1)x^{m-1}}$$

**Example**

The Fresnel integrals

$$\int_u^{\infty} \cos(\theta^2) d\theta, \quad \int_u^{\infty} \sin(\theta^2) d\theta \quad (1.293)$$

can be written in the form

$$\int_{u^2}^{\infty} \frac{\cos t}{\sqrt{t}} dt, \quad \int_{u^2}^{\infty} \frac{\sin t}{\sqrt{t}} dt$$

These are particular cases of the real and imaginary parts of the integral

$$f(x, a) = \int_x^{\infty} \frac{e^{jt}}{t^a} dt \quad (1.294)$$

Integrating by parts we obtain

$$\begin{aligned} f(x, a) &= \frac{je^{jx}}{x^a} - jaf(x, a + 1) = \frac{je^{jx}}{x^a} \sum_{r=0}^n \frac{\Gamma(a+r)}{\Gamma(a)(jx)^r} \\ &+ \frac{1}{j^{n+1}} \frac{\Gamma(a+n+1)}{\Gamma(a)} f(x, a+n+1) \end{aligned} \quad (1.295)$$

Hence

$$f(x, a) \approx \frac{je^{jx}}{x^a} \sum_{r=0}^{\infty} \frac{\Gamma(a+r)}{\Gamma(a)(jx)^r} \quad (1.296)$$

as  $x$  approaches infinity. The absolute value of the remainder after  $n+1$  terms is

$$\frac{\Gamma(a+n+1)}{\Gamma(a)} \left| \int_x^{\infty} \frac{e^{it}}{t^{a+n+1}} dt \right| \leq \frac{\Gamma(a+n+1)}{\Gamma(a)} \int_x^{\infty} \frac{dt}{t^{a+n+1}} = \frac{\Gamma(a+n)}{\Gamma(a)x^{a+n}}$$

Hence, the remainder after  $n$  terms does not exceed in absolute value the absolute value of the  $(n+1)$ th term, which proves the result.

**References**

Abdul, J. J. 1977. The Shannon sampling theorem—Its various extensions and applications: A tutorial review. *Proc. IEEE*, 65:1565–1596.

Andrews, L. C. 1985. *Special Functions for Engineers and Applied Mathematicians*. New York: Macmillan.

Copson, E. T. 1965. *Asymptotic Expansions*. New York: Cambridge University Press.

Erdélyi, A. 1956. *Asymptotic Expansions*. New York: Dover Publications.

Gel’fand, I. M. and Shilov, G.E. 1964. *Generalized Functions*. New York: Academic Press.

Hoskins, R. F. 1979. *Generalized Functions*. Chichester, U.K.: Ellis Horwood Limited.

Lebedev, N. N. 1972. *Special Functions and Their Applications*. New York: Dover Publications.

Lighthill, M. J. 1964. *Introduction to Fourier Analysis and Generalized Functions*. London, U.K.: Cambridge University Press.

Papoulis, A. 1968. *Systems and Transforms with Applications in Optics*. New York: McGraw-Hill.

Papoulis, A. 1977. *Signal Analysis*. New York: McGraw-Hill.

Sansone, G. 1959. *Orthogonal Functions*. New York: Interscience Publishers.





# 2

## Fourier Transforms

---

2.1	Introduction and Basic Definitions.....	2-1
	Basic Definition, Notation, and Terminology • Alternate Definitions • The Generalized Transforms • Further Generalization of the Generalized Transforms • Use of the Residue Theorem • Cauchy Principal Values	
2.2	General Identities and Relations.....	2-8
	Invertibility • Near-Equivalence (Symmetry of the Transforms) • Conjugation of Transforms • Linearity • Scaling • Translation and Multiplication by Exponentials • Complex Translation and Multiplication by Real Exponentials • Modulation • Products and Convolution • Correlation • Differentiation and Multiplication by Polynomials • Moments • Integration • Parseval's Equality • Bessel's Equality • The Bandwidth Theorem	
2.3	Transforms of Specific Classes of Functions.....	2-15
	Real/Imaginary Valued Even/Odd Functions • Absolutely Integrable Functions • The Bandwidth Theorem for Absolutely Integrable Functions • Square Integrable ("Finite Energy") Functions • The Bandwidth Theorem for Finite Energy Functions • Functions with Finite Duration • Band-Limited Functions • Finite Power Functions • Periodic Functions • Regular Arrays of Delta Functions • Periodic Arrays of Delta Functions • Powers of Variables and Derivatives of Delta Functions • Negative Powers and Step Functions • Rational Functions • Causal Functions • Functions on the Half-Line • Functions on Finite Intervals • Bessel Functions	
2.4	Extensions of the Fourier Transform and Other Closely Related Transforms.....	2-35
	Multidimensional Fourier Transforms • Multidimensional Transforms of Separable Functions • Transforms of Circularly Symmetric Functions and the Hankel Transform • Half-Line Sine and Cosine Transforms • The Discrete Fourier Transform • Relations between the Laplace Transform and the Fourier Transform	
2.5	Reconstruction of Sampled Signals.....	2-43
	Sampling Theorem for Band-Limited Functions • Truncated Sampling Reconstruction of Band-Limited Functions • Reconstruction of Sampled Nearly Band-Limited Functions • Sampling Theorem for Finite Duration Functions • Fundamental Sampling Formulas and Poisson's Formula	
2.6	Linear Systems.....	2-48
	Linear Shift Invariant Systems • Reality and Stability • System Response to Complex Exponentials and Periodic Functions • Casual Systems • Systems Given by Differential Equations • RLC Circuits • Modulation and Demodulation	
2.7	Random Variables.....	2-55
	Basic Probability and Statistics • Multiple Random Processes and Independence • Sums of Random Processes • Random Signals and Stationary Random Signals • Correlation of Stationary Random Signals and Independence • Systems and Random Signals	
2.8	Partial Differential Equations.....	2-62
	The One-Dimensional Heat Equation • The Initial Value Problem for Heat Flow on an Infinite Rod • An Infinite Rod with Heat Sources and Sinks • A Boundary Value Problem for Heat Flow on a Half-Infinite Rod	
2.9	Tables.....	2-65
	References.....	2-75

Kenneth B. Howell  
*University of Alabama in Huntsville*

### 2.1 Introduction and Basic Definitions

---

The Fourier transform is certainly one of the best known of the integral transforms and vies with the Laplace transform as being the most generally useful. Since its introduction by Fourier in the early 1800s, it has found use in innumerable applications and has, itself,

led to the development of other transforms. Today the Fourier transform is a fundamental tool in engineering science. Its importance has been enhanced by the development in the twentieth century of generalizations extending the set of functions that can be Fourier transformed and by the development of efficient algorithms for computing the discrete version of the Fourier transform.

There are two parts to this article on the Fourier transform. The first (Sections 2.1 through 2.4) contains the fundamental theory necessary for the intelligent use of the Fourier transform in practical problems arising in engineering. The second part (Sections 2.5 through 2.8) is devoted to applications in which the Fourier transform plays a significant role. This part contains both fairly detailed descriptions of specific applications and fairly broad overviews of classes of applications.

This particular section deals with the basic definition of the Fourier transform and some of the integrals used to compute Fourier transforms. Two definitions for the transform are given. First, the classical definition is given in Section 2.1.1. This is the integral formula for directly computing transforms generally found in elementary texts. From this formula many of the basic formulas and identities involving the Fourier transform can be derived. Inherent in the classical definition, however, are integrability conditions that cannot be satisfied by many functions routinely arising in applications. For this reason, more general definitions of the Fourier transform are briefly discussed in Sections 2.1.3 and 2.1.4. These general definitions will also help clarify the role of generalized functions in Fourier analysis.

The computation of Fourier transforms often involves the evaluation of integrals, many of which cannot be evaluated by the elementary methods of calculus. For this reason, this section also contains a brief discussion illustrating the use of the residue theorem in computing certain integrals as well as a brief discussion of how to deal with certain integrals containing singularities in the integrand.

### 2.1.1 Basic Definition, Notation, and Terminology

If  $\phi(s)$  is an absolutely integrable function on  $(-\infty, \infty)$  (i.e.,  $\int_{-\infty}^{\infty} |\phi(s)| ds < \infty$ ), then the (direct) Fourier transform of  $\phi(s)$ ,  $\mathcal{F}[\phi]$ , and the Fourier inverse transform of  $\phi(s)$ ,  $\mathcal{F}^{-1}[\phi]$ , are the functions given by

$$\mathcal{F}[\phi]|_x = \int_{-\infty}^{\infty} \phi(s)e^{-jxs} ds \tag{2.1}$$

and

$$\mathcal{F}^{-1}[\phi]|_x = \frac{1}{2\pi} \int_{-\infty}^{\infty} \phi(s)e^{jxs} ds. \tag{2.2}$$

#### Example 2.1

If  $\phi(s) = e^{-s} u(s)$ , then

$$\mathcal{F}[\phi]|_x = \int_{-\infty}^{\infty} e^{-s} u(s)e^{-jxs} ds = \int_0^{\infty} e^{-(1+jx)s} ds = \frac{1}{1+jx}$$

and

$$\begin{aligned} \mathcal{F}^{-1}[\phi]|_x &= \frac{1}{2\pi} \int_{-\infty}^{\infty} e^{-s} u(s)e^{jxs} ds = \frac{1}{2\pi} \int_0^{\infty} e^{-(1-jx)s} ds \\ &= \frac{1}{2\pi - j2\pi x}. \end{aligned}$$

#### Example 2.2

For  $\alpha > 0$ , the transform of the corresponding pulse function,

$$\rho_{\alpha}(s) = \begin{cases} 1, & \text{if } |s| < \alpha \\ 0, & \text{if } \alpha < |s| \end{cases}$$

is

$$\mathcal{F}[\rho_{\alpha}]|_x = \int_{-\alpha}^{\alpha} e^{-jxs} ds = \frac{e^{j\alpha x} - e^{-j\alpha x}}{jx} = \frac{2}{x} \sin(\alpha x).$$

A function,  $\psi$ , is said to be “classically transformable” if either

1.  $\psi$  is absolutely integrable on the real line
2.  $\psi$  is the Fourier transform (or Fourier inverse transform) of an absolutely integrable function
3.  $\psi$  is a linear combination of an absolutely integrable function and a Fourier transform (or Fourier inverse transform) of an absolutely integrable function

If  $\phi$  is classically transformable but not absolutely integrable, then it can be shown that formulas 2.1 and 2.2 can still be used to define  $\mathcal{F}[\phi]$  and  $\mathcal{F}^{-1}[\phi]$  provided the limits are taken symmetrically; that is:

$$\mathcal{F}[\phi]|_x = \lim_{a \rightarrow \infty} \int_{-a}^a \phi(s)e^{-jxs} ds$$

and

$$\mathcal{F}^{-1}[\phi]|_x = \frac{1}{2\pi} \lim_{a \rightarrow \infty} \int_{-a}^a \phi(s)e^{jxs} ds.$$

In most applications involving Fourier transforms, the functions of time,  $t$ , or position,  $x$ , are denoted using lower case letters—for example:  $f$  and  $g$ . The Fourier transforms of these functions are denoted using the corresponding upper case letters—for example:  $F = \mathcal{F}[f]$  and  $G = \mathcal{F}[g]$ . The transformed functions can be viewed as functions of angular frequency,  $\omega$ . Along these same lines it is standard practice to view a signal as a pair of functions,  $f(t)$  and  $F(\omega)$ , with  $f(t)$  being the “time domain representation of the signal” and  $F(\omega)$  being the “frequency domain representation of the signal.”

### 2.1.2 Alternate Definitions

Pairs of formulas other than formulas 2.1 and 2.2 are often used to define  $\mathcal{F}[\phi]$  and  $\mathcal{F}^{-1}[\phi]$ . Some of the other formula pairs commonly used are:

$$\begin{aligned} \mathcal{F}[\phi]|_x &= \int_{-\infty}^{\infty} \phi(s)e^{-j2\pi xs} ds, \\ \mathcal{F}^{-1}[\phi]|_x &= \int_{-\infty}^{\infty} \phi(s)e^{j2\pi xs} ds \end{aligned} \tag{2.3}$$

and

$$\begin{aligned} \mathcal{F}[\phi]|_x &= \frac{1}{\sqrt{2\pi}} \int_{-\infty}^{\infty} \phi(s)e^{-jxs} ds, \\ \mathcal{F}^{-1}[\phi]|_x &= \frac{1}{\sqrt{2\pi}} \int_{-\infty}^{\infty} \phi(s)e^{jxs} ds. \end{aligned} \tag{2.4}$$

Equivalent analysis can be performed using the theory arising from any of these pairs; however, the resulting formulas and equations will depend on which pair is used. For this reason care must be taken to ensure that, in any particular application, all the Fourier analysis formulas and equations used are derived from the same defining pair of formulas.

#### Example 2.3

Let  $\phi(t) = e^{-t} u(t)$  and let  $\psi_1$ ,  $\psi_2$ , and  $\psi_3$  be the Fourier transforms of  $\phi$  as defined, respectively, by formulas 2.1, 2.3, and 2.4. Then,

$$\begin{aligned} \psi_1(\omega) &= \int_{-\infty}^{\infty} e^{-t} u(t) e^{-j\omega t} dt = \frac{1}{1 + j\omega}, \\ \psi_2(\omega) &= \int_{-\infty}^{\infty} e^{-t} u(t) e^{-j2\pi\omega t} dt = \frac{1}{1 + j2\pi\omega}, \end{aligned}$$

and

$$\psi_3(\omega) = \frac{1}{\sqrt{2\pi}} \int_{-\infty}^{\infty} e^{-t} u(t) e^{-j\omega t} dt = \frac{1}{\sqrt{2\pi}} \cdot \frac{1}{1 + j\omega}.$$

### 2.1.3 The Generalized Transforms

Many functions and generalized functions\* arising in applications are not sufficiently integrable to apply the definitions given in Section 2.1.1 directly. For such functions it is necessary to

\* For a detailed discussion of generalized functions, see Chapter 1.

employ a generalized definition of the Fourier transform constructed using the set of “rapidly decreasing test functions” and a version of Parseval’s equation (see Section 2.2.14).

A function,  $\phi$ , is a “rapidly decreasing test function” if

1. Every derivative of  $\phi$  exists and is a continuous function on  $(-\infty, \infty)$  and
2. For every pair of nonnegative integers,  $n$  and  $p$ ,

$$|\phi^{(n)}(s)| = O(|s|^{-p}) \quad \text{as } |s| \rightarrow \infty.$$

The set of all rapidly decreasing test functions is denoted by  $\mathcal{S}$  and includes the Gaussian functions as well as all test functions that vanish outside of some finite interval (such as those discussed in Chapter 1. If  $\phi$  is a rapidly decreasing test function then it is easily verified that  $\phi$  is classically transformable and that both  $\mathcal{F}[\phi]$  and  $\mathcal{F}^{-1}[\phi]$  are also rapidly decreasing test functions. It can also be shown that  $\mathcal{F}^{-1}[\mathcal{F}[\phi]] = \phi$ . Moreover, if  $f$  and  $G$  are classically transformable, then

$$\int_{-\infty}^{\infty} \mathcal{F}[f]|_x \phi(x) dx = \int_{-\infty}^{\infty} f(y) \mathcal{F}[\phi]|_y dy \tag{2.5}$$

and

$$\int_{-\infty}^{\infty} \mathcal{F}^{-1}[G]|_x \phi(x) dx = \int_{-\infty}^{\infty} G(y) \mathcal{F}^{-1}(\phi)|_y dy. \tag{2.6}$$

If  $f$  is a function or a generalized function for which the right-hand side of Equation 2.5 is well defined for every rapidly decreasing test function,  $\phi$ , then the generalized Fourier transform of  $f$ ,  $\mathcal{F}[f]$ , is that generalized function satisfying Equation 2.5 for every  $\phi$  in  $\mathcal{S}$ . Likewise, if  $G$  is a function or generalized function for which the right-hand side of Equation 2.6 is well defined for every rapidly decreasing test function,  $\phi$ , then the generalized inverse Fourier transform of  $G$ ,  $\mathcal{F}^{-1}[G]$ , is that generalized function satisfying Equation 2.6 for every  $\phi$  in  $\mathcal{S}$ .

#### Example 2.4

Let  $\alpha$  be any real number. Then, for every rapidly decreasing test function  $\phi$ ,

$$\begin{aligned} \int_{-\infty}^{\infty} \mathcal{F}[e^{j\alpha y}]|_x \phi(x) dx &= \int_{-\infty}^{\infty} e^{j\alpha y} \mathcal{F}[\phi]|_y dy \\ &= 2\pi \left[ \frac{1}{2\pi} \int_{-\infty}^{\infty} \mathcal{F}[\phi]|_y e^{j\alpha y} dy \right] \\ &= 2\pi \mathcal{F}^{-1} [\mathcal{F}[\phi]]|_{\alpha} \\ &= 2\pi \phi(\alpha) \\ &= \int_{-\infty}^{\infty} 2\pi \delta(x - \alpha) \phi(x) dx \end{aligned}$$

where  $\delta(x)$  is the delta function. This shows that, for every  $\phi$  in  $\mathcal{S}$ ,

$$\int_{-\infty}^{\infty} 2\pi\delta(x - \alpha)\phi(x)dx = \int_{-\infty}^{\infty} e^{j\alpha y}\mathcal{F}[\phi]_y dy$$

and thus,

$$\mathcal{F}[e^{j\alpha y}]_x = 2\pi\delta(x - \alpha).$$

Any (generalized) function whose Fourier transform can be computed via the above generalized definition is called “transformable.” The set of all such functions is sometimes called the set of “tempered generalized functions” or the set of “tempered distributions.” This set includes any piecewise continuous function,  $f$ , which is also polynomially bounded, that is, which satisfies

$$|f(s)| = O(|s|^p) \quad \text{as } |s| \rightarrow \infty$$

for some  $p < \infty$ . Finally, it should also be noted that if  $f$  is classically transformable, then it is transformable, and the generalized definition of  $\mathcal{F}[f]$  yields exactly the same function as the classical definition.

### 2.1.4 Further Generalization of the Generalized Transforms

Unfortunately, even with the theory discussed in Section 2.1.3, it is not possible to define or discuss the Fourier transform of the real exponential,  $e^t$ . It may be of interest to note, however, that a further generalization that does permit all exponentially bounded functions to be considered “Fourier transformable” is currently being developed using a recently discovered alternate set of test functions. This alternate set, denoted by  $\mathcal{G}$ , is the subset of a rapidly decreasing test functions that satisfy the following two additional properties:

1. Each test function is an analytic test function on the entire complex plane.
2. Each test function,  $\phi(x + jy)$ , satisfies

$$\phi(x + jy) = O(e^{-\alpha|x|}) \quad \text{as } x \rightarrow \pm\infty$$

for every real value of  $y$  and  $\alpha$ .

The second additional property of these test functions ensures that all exponentially bounded functions are covered by this theory. The very same computations given in Example 2.4 can be used to show that, for any complex value,  $\alpha + j\beta$ ,

$$\mathcal{F}[e^{j(\alpha+j\beta)t}]|_{\omega} = 2\pi\delta_{\alpha+j\beta}(\omega),$$

where  $\delta_{\alpha+j\beta}(t)$  is “the delta function at  $\alpha + j\beta$ .” This delta function,  $\delta_{\alpha+j\beta}(t)$ , is the generalized function satisfying

$$\int_{-\infty}^{\infty} \delta_{\alpha+j\beta}(t)\phi(t)dt = \phi(\alpha + j\beta)$$

for every test function  $\phi(t)$ , in  $\mathcal{G}$ . In particular, letting  $\alpha + j\beta = -j$ ,

$$\mathcal{F}[e^t]|_{\omega} = 2\pi\delta_{-j}(\omega)$$

and

$$\mathcal{F}[\delta_j(t)]|_{\omega} = e^{\omega}.$$

In addition to allowing delta functions to be defined at complex points, the analyticity of the test functions allows a generalization of translation. Let  $\alpha + j\beta$  be any complex number and  $f(t)$  any (exponentially bounded) (generalized) function. The “generalized translation of  $f(t)$  by  $\alpha + j\beta$ ,” denoted by  $T_{\alpha+j\beta}f(t)$ , is that generalized function satisfying

$$\int_{-\infty}^{\infty} T_{\alpha+j\beta}f(t)\phi(t)dt = \int_{-\infty}^{\infty} f(t)\phi(t + (\alpha + j\beta))dt \quad (2.7)$$

for every test function,  $\phi(t)$ , in  $\mathcal{G}$ . So long as  $\beta = 0$  or  $f(t)$  is, itself, an analytic function on the entire complex plane, then the generalized translation is exactly the same as the classical translation.

$$T_{\alpha+j\beta}f(t) = f(t - (\alpha + j\beta)).$$

It may be observed, however, that Equation 2.7 defines the generalized function  $T_{\alpha+j\beta}f$  even when  $f(z)$  is not defined for nonreal values of  $z$ .

### 2.1.5 Use of the Residue Theorem

Often a Fourier transform or inverse transform can be described as an integral of a function that either is analytic on the entire complex plane, or else has a few isolated poles in the complex plane. Such integrals can often be evaluated through intelligent use of the residue theorem from complex analysis (see Appendix A). Two examples illustrating such use of the residue theorem will be given in this section. The first example illustrates its use when the function is analytic throughout the complex plane, while the second example illustrates its use when the function has poles off the real axis. The use of the residue theorem to compute transforms when the function has poles on the real axis will be discussed in Section 2.1.6.

#### Example 2.5 Transform of an Analytic Function

Consider computing the Fourier transform of  $g(t) = e^{-t^2}$ ,

$$G(\omega) = \mathcal{F}[g(t)]|_{\omega} = \int_{-\infty}^{\infty} e^{-t^2} e^{-j\omega t} dt.$$

Because

$$t^2 + j\omega t = \left(t + j\frac{\omega}{2}\right)^2 + \frac{\omega^2}{4},$$

it follows that

$$\begin{aligned}
 G(\omega) &= e^{-\frac{1}{4}\omega^2} \int_{-\infty}^{\infty} \exp\left[-\left(t + j\frac{\omega}{2}\right)^2\right] dt \\
 &= e^{-\frac{1}{4}\omega^2} \int_{-\infty + j\frac{\omega}{2}}^{\infty + j\frac{\omega}{2}} e^{-z^2} dz. \quad (2.8)
 \end{aligned}$$

Consider, now, the integral of  $e^{2z^2}$  over the contour  $C_\gamma$  where, for each  $\gamma > 0$ ,  $C_\gamma = C_{1,\gamma} + C_{2,\gamma} + C_{3,\gamma} + C_{4,\gamma}$  is the contour in Figure 2.1. Because  $e^{2z^2}$  is analytic everywhere on the complex plane, the residue theorem states that

$$\begin{aligned}
 0 &= \int_{C_\gamma} e^{-z^2} dz \\
 &= \int_{C_{1,\gamma}} e^{-z^2} dz + \int_{C_{2,\gamma}} e^{-z^2} dz + \int_{C_{3,\gamma}} e^{-z^2} dz + \int_{C_{4,\gamma}} e^{-z^2} dz.
 \end{aligned}$$

Thus,

$$- \int_{C_{3,\gamma}} e^{-z^2} dz = \int_{C_{1,\gamma}} e^{-z^2} dz + \int_{C_{2,\gamma}} e^{-z^2} dz + \int_{C_{4,\gamma}} e^{-z^2} dz. \quad (2.9)$$

Now,

$$\begin{aligned}
 \lim_{\gamma \rightarrow \infty} \int_{C_{2,\gamma}} e^{-z^2} dz &= \lim_{\gamma \rightarrow \infty} \int_{y=0}^{\omega/2} e^{-(\gamma + jy)^2} dy \\
 &= \lim_{\gamma \rightarrow \infty} e^{-\gamma^2} \int_{y=0}^{\omega/2} e^{y^2 - j2\gamma y} dy \\
 &= 0.
 \end{aligned}$$

Likewise,

$$\lim_{\gamma \rightarrow \infty} \int_{C_{4,\gamma}} e^{-z^2} dz = 0,$$

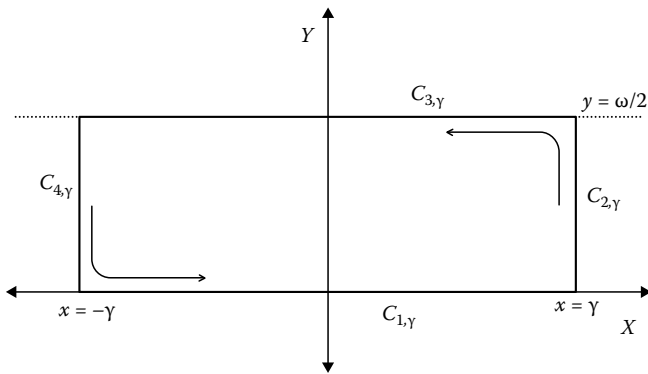


FIGURE 2.1 Contour for computing  $\mathcal{F}[e^{-t^2}]$ .

while

$$\lim_{\gamma \rightarrow \infty} \int_{C_{3,\gamma}} e^{-z^2} dz = \lim_{\gamma \rightarrow \infty} \int_{\gamma + j\frac{\omega}{2}}^{-\gamma + j\frac{\omega}{2}} e^{-z^2} dz = - \int_{-\infty + j\frac{\omega}{2}}^{\infty + j\frac{\omega}{2}} e^{-z^2} dz$$

and

$$\lim_{\gamma \rightarrow \infty} \int_{C_{1,\gamma}} e^{-z^2} dz = \lim_{\gamma \rightarrow \infty} \int_{x=-\gamma}^{\gamma} e^{-x^2} dx = \int_{-\infty}^{\infty} e^{-x^2} dx.$$

That last integral is well known and equals  $\sqrt{\pi}$ . Combining Equations 2.8 and 2.9 with the above limits yields

$$\begin{aligned}
 G(\omega) &= e^{-\frac{1}{4}\omega^2} \int_{-\infty + j\frac{\omega}{2}}^{\infty + j\frac{\omega}{2}} e^{-z^2} dz \\
 &= e^{-\frac{1}{4}\omega^2} \lim_{\gamma \rightarrow \infty} \left[ - \int_{C_{3,\gamma}} e^{-z^2} dz \right] \\
 &= e^{-\frac{1}{4}\omega^2} \lim_{\gamma \rightarrow \infty} \left[ \int_{C_{1,\gamma}} e^{-z^2} dz + \int_{C_{2,\gamma}} e^{-z^2} dz + \int_{C_{4,\gamma}} e^{-z^2} dz \right] \\
 &= e^{-\frac{1}{4}\omega^2} \sqrt{\pi}.
 \end{aligned}$$

So,

$$\mathcal{F}[e^{-t^2}]|_{\omega} = G(\omega) = \sqrt{\pi} e^{-\frac{1}{4}\omega^2}.$$

### Example 2.6 Transform of a Function with a Pole Off the Real Axis

Consider computing the Fourier inverse transform of  $F(\omega) = (1 + \omega^2)^{-1}$ ,

$$f(t) = \mathcal{F}^{-1}[F(\omega)]|_t = \frac{1}{2\pi} \int_{-\infty}^{\infty} \frac{e^{j\omega t}}{1 + \omega^2} d\omega. \quad (2.10)$$

For  $t = 0$ ,

$$f(0) = \frac{1}{2\pi} \int_{-\infty}^{\infty} \frac{1}{1 + \omega^2} d\omega = \frac{1}{2\pi} \arctan \omega|_{-\infty}^{\infty} = \frac{1}{2}. \quad (2.11)$$

To evaluate  $f(t)$  when  $t \neq 0$ , first observe that the integrand in formula 2.10, viewed as a function of the complex variable,

$$\Phi(z) = \frac{e^{jtz}}{1 + z^2},$$

has simple poles at  $z = \pm j$ . The residue at  $z = j$  is

$$\text{Res}_j[\Phi] = \lim_{z \rightarrow j} (z - j)\Phi(z) = \lim_{z \rightarrow j} (z - j) \left[ \frac{e^{jtz}}{(z - j)(z + j)} \right] = \frac{1}{2j} e^{-t},$$

while the residue at  $z = -j$  is

$$\text{Res}_{-j}[\Phi] = \lim_{z \rightarrow -j} (z + j)\Phi(z) = -\frac{1}{2j} e^t.$$

For each  $\gamma > 1$ , let  $C_\gamma$ ,  $C_{+\gamma}$ , and  $C_{-\gamma}$  be the curves sketched in Figure 2.2. By the residue theorem:

$$\int_{C_\gamma} \frac{e^{jtz}}{1 + z^2} dz + \int_{C_{+\gamma}} \frac{e^{jtz}}{1 + z^2} dz = 2\pi j \text{Res}_j[\Phi] = \pi e^{-t}$$

and

$$-\int_{C_\gamma} \frac{e^{jtz}}{1 + z^2} dz + \int_{C_{-\gamma}} \frac{e^{jtz}}{1 + z^2} dz = 2\pi j \text{Res}_{-j}[\Phi] = \pi e^t.$$

Combining these calculations with Equation 2.10 yields

$$\begin{aligned} f(t) &= \frac{1}{2\pi} \int_{-\infty}^{\infty} \frac{e^{j\omega t}}{1 + \omega^2} d\omega \\ &= \frac{1}{2\pi} \lim_{\gamma \rightarrow \infty} \int_{C_\gamma} \frac{e^{jtz}}{1 + z^2} dz \\ &= \frac{1}{2\pi} \left[ \pi e^{-t} - \lim_{\gamma \rightarrow \infty} \int_{C_{+\gamma}} \frac{e^{jtz}}{1 + z^2} dz \right] \end{aligned} \quad (2.12)$$

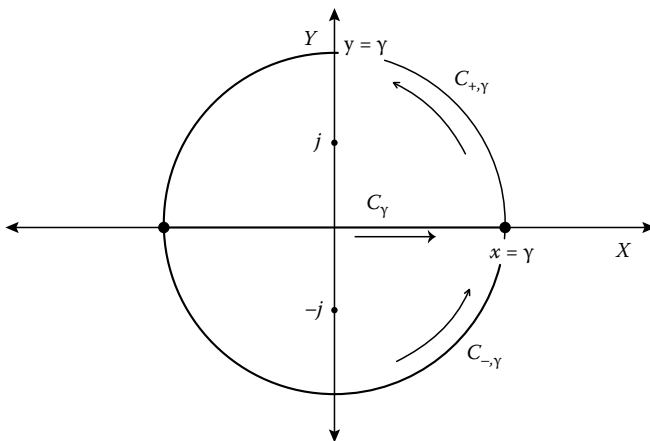


FIGURE 2.2 Contours for computing  $\mathcal{F}^{-1}[(1 + \omega^2)^{-1}]$ .

and

$$\begin{aligned} f(t) &= \frac{1}{2\pi} \int_{-\infty}^{\infty} \frac{e^{j\omega t}}{1 + \omega^2} d\omega \\ &= \frac{1}{2\pi} \lim_{\gamma \rightarrow \infty} \int_{C_\gamma} \frac{e^{jtz}}{1 + z^2} dz \\ &= \frac{1}{2\pi} \left[ \pi e^t + \lim_{\gamma \rightarrow \infty} \int_{C_{-\gamma}} \frac{e^{jtz}}{1 + z^2} dz \right]. \end{aligned} \quad (2.13)$$

Now,

$$\begin{aligned} \left| \int_{C_{+\gamma}} \frac{e^{jtz}}{1 + z^2} dz \right| &= \left| \int_0^\pi \frac{e^{j\gamma(\cos \theta + j \sin \theta)}}{1 + \gamma^2 e^{j2\theta}} \gamma e^{j\theta} d\theta \right| \\ &< \int_0^\pi \left| \frac{e^{j\gamma(\cos \theta + j \sin \theta)}}{1 + \gamma^2 e^{j2\theta}} \gamma e^{j\theta} \right| d\theta \\ &< \int_0^\pi \frac{e^{-t\gamma \sin \theta}}{\gamma^2 - 1} \gamma d\theta. \end{aligned}$$

So long as  $t > 0$  and  $0 \leq \theta \leq \pi$ ,

$$0 \leq e^{-t\gamma \sin \theta} \leq 1.$$

Thus, for  $t > 0$ ,

$$\begin{aligned} \lim_{\gamma \rightarrow \infty} \left| \int_{C_{+\gamma}} \frac{e^{jtz}}{1 + z^2} dz \right| &\leq \lim_{\gamma \rightarrow \infty} \int_0^\pi \frac{e^{-t\gamma \sin \theta}}{\gamma^2 - 1} \gamma d\theta \\ &\leq \lim_{\gamma \rightarrow \infty} \int_0^\pi \frac{\gamma}{\gamma^2 - 1} d\theta \\ &\leq \lim_{\gamma \rightarrow \infty} \frac{\pi\gamma}{\gamma^2 - 1} \\ &= 0. \end{aligned}$$

Combining this last result with Equation 2.12 gives

$$f(t) = \frac{1}{2\pi} \left[ \pi e^{-t} - \lim_{\gamma \rightarrow \infty} \int_{C_{+\gamma}} \frac{e^{jtz}}{1 + z^2} dz \right] = \frac{1}{2} e^{-t} \quad (2.14)$$

whenever  $t > 0$ .

In a similar fashion, it is easy to show that if  $t < 0$ ,

$$\begin{aligned} \lim_{\gamma \rightarrow \infty} \left| \int_{C_{-\gamma}} \frac{e^{jtz}}{1+z^2} dz \right| &\leq \lim_{\gamma \rightarrow \infty} \int_{\pi}^{2\pi} \frac{e^{-t\gamma \sin \theta}}{\gamma^2 - 1} \gamma d\theta \\ &\leq \lim_{\gamma \rightarrow \infty} \int_{\pi}^{2\pi} \frac{\gamma}{\gamma^2 - 1} d\theta \\ &= 0, \end{aligned}$$

which, combined with Equation 2.13, yields

$$f(t) = \frac{1}{2\pi} \left[ \pi e^t + \lim_{\gamma \rightarrow \infty} \int_{C_{-\gamma}} \frac{e^{jtz}}{1+z^2} dz \right] = \frac{1}{2} e^t \quad (2.15)$$

whenever  $t < 0$ .

Finally, it should be noted that formulas 2.11, 2.14, and 2.15 can be written more concisely as

$$f(t) = \frac{1}{2} e^{-|t|}.$$

### 2.1.6 Cauchy Principal Values

The Cauchy principal value (CPV) at  $x = x_0$  of an integral,  $\int_{-\infty}^{\infty} \phi(x) dx$ , is

$$\text{CPV} \int_{-\infty}^{\infty} \phi(x) dx = \lim_{\epsilon \rightarrow 0^+} \left[ \int_{-\infty}^{x_0 - \epsilon} \phi(x) dx + \int_{x_0 + \epsilon}^{\infty} \phi(x) dx \right]$$

provided the limit exists. So long as  $\phi$  is an integrable function, it should be clear that

$$\text{CPV} \int_{-\infty}^{\infty} \phi(x) dx = \int_{-\infty}^{\infty} \phi(x) dx.$$

It is when  $\phi$  is not an integrable function that the CPV is useful. In particular, the Fourier transform and Fourier inverse transform of any function with a singularity of the form  $(x - x_0)^{-1}$  can be evaluated as the CPVs at  $x = x_0$  of the integrals in formulas 2.1 and 2.2.

#### Example 2.7

Consider evaluating the inverse transform of  $F(\omega) = \omega^{-1}$ . Because of the  $\omega^{-1}$  singularity,  $f = \mathcal{F}^{-1}[F]$  is given by

$$f(t) = \frac{1}{2\pi} \text{CPV} \int_{-\infty}^{\infty} \frac{1}{\omega} e^{j\omega t} d\omega$$

or, equivalently, by

$$f(t) = \frac{1}{2\pi} \lim_{\substack{\epsilon \rightarrow 0^+ \\ R \rightarrow \infty}} \left[ \int_{-R}^{-\epsilon} \frac{1}{z} e^{jtz} dz + \int_{\epsilon}^R \frac{1}{z} e^{jtz} dz \right]. \quad (2.16)$$

Because  $\omega^{-1}$  is an odd function,  $f(0)$  is easily evaluated,

$$f(0) = \frac{1}{2\pi} \lim_{\substack{\epsilon \rightarrow 0^+ \\ R \rightarrow \infty}} \left[ \int_{-R}^{-\epsilon} \frac{1}{\omega} d\omega + \int_{\epsilon}^R \frac{1}{\omega} d\omega \right] = 0. \quad (2.17)$$

To evaluate  $f(t)$  when  $t > 0$ , first observe that the only pole of the integrand in formula 2.16,

$$\Phi(z) = \frac{1}{z} e^{jtz},$$

is at  $z = 0$ . For each  $0 < \epsilon < R$ , let  $C_{\epsilon}$  and  $C_R$  be the semicircles indicated in Figure 2.3. By the residue theorem,

$$\int_{-R}^{-\epsilon} \frac{1}{z} e^{jtz} dz + \int_{\epsilon}^R \frac{1}{z} e^{jtz} dz + \int_{C_{\epsilon}} \frac{1}{z} e^{jtz} dz + \int_{C_R} \frac{1}{z} e^{jtz} dz = 0.$$

This, combined with Equation 2.16, yields

$$f(t) = -\frac{1}{2\pi} \left[ \lim_{\epsilon \rightarrow 0^+} \int_{C_{\epsilon}} \frac{1}{z} e^{jtz} dz + \lim_{R \rightarrow \infty} \int_{C_R} \frac{1}{z} e^{jtz} dz \right], \quad (2.18)$$

provided the limits exist. Now,

$$\begin{aligned} \lim_{\epsilon \rightarrow 0^+} \int_{C_{\epsilon}} \frac{1}{z} e^{jtz} dz &= \lim_{\epsilon \rightarrow 0^+} \int_{\pi}^0 \frac{1}{\epsilon e^{j\theta}} e^{j\epsilon t (\cos \theta + j \sin \theta)} j \epsilon e^{j\theta} d\theta \\ &= j \lim_{\epsilon \rightarrow 0^+} \int_{\pi}^0 e^{-\epsilon t (\sin \theta + j \cos \theta)} d\theta \\ &= j \int_{\pi}^0 e^0 d\theta \\ &= -j\pi. \end{aligned} \quad (2.19)$$

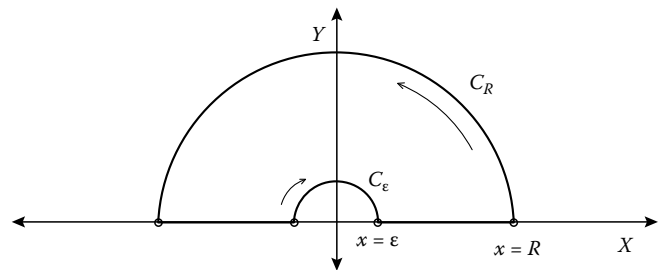


FIGURE 2.3 Contour for computing  $\mathcal{F}^{-1}[\omega^{-1}]$ .



Similarly,

$$\int_{C_R} \frac{1}{z} e^{jtz} dz = j \int_0^\pi e^{-Rt(\sin \theta + j \cos \theta)} d\theta.$$

Here, because  $t > 0$ , the integrand is uniformly bounded and vanishes as  $R \rightarrow \infty$ . Thus,

$$\lim_{R \rightarrow \infty} \int_{C_R} \frac{1}{z} e^{jtz} dz = 0. \quad (2.20)$$

With Equations 2.19 and 2.20, Equation 2.18 becomes

$$f(t) = -\frac{1}{2\pi} \left[ \lim_{\epsilon \rightarrow 0^+} \int_{C_\epsilon} \frac{1}{z} e^{jtz} dz + \lim_{R \rightarrow \infty} \int_{C_R} \frac{1}{z} e^{jtz} dz \right] = \frac{j}{2}. \quad (2.21)$$

By replacing  $C_\epsilon$  and  $C_R$  with corresponding semicircles in the lower half-plane, the approach used to evaluate  $f(t)$  when  $0 < t$ , can be used to evaluate  $f(t)$  when  $t < 0$ . The computations are virtually identical, except for a reversal of the orientation of the contour of integration, and yield

$$f(t) = -\frac{j}{2}, \quad (2.22)$$

when  $t < 0$ .

Finally, it should be noted that formulas 2.17, 2.21, and 2.22 can be written more concisely as

$$\mathcal{F}^{-1} \left[ \frac{1}{\omega} \right] \Big|_t = f(t) = \frac{j}{2} \operatorname{sgn}(t).$$

## 2.2 General Identities and Relations

Some of the more general identities commonly used in computing and manipulating Fourier transforms and inverse transforms are described here. Brief (nonrigorous) derivations of some are presented, usually employing the classical transforms (formulas 2.1 and 2.2). Unless otherwise stated, however, each identity may be assumed to hold for the generalized transforms as well.

### 2.2.1 Invertibility

The Fourier transform and the Fourier inverse transform,  $\mathcal{F}$  and  $\mathcal{F}^{-1}$ , are operational inverses, that is,

$$\psi = \mathcal{F}[\phi] \Leftrightarrow \mathcal{F}^{-1}[\psi] = \phi.$$

Equivalently,

$$\mathcal{F}^{-1}[\mathcal{F}[f]] = f \quad \text{and} \quad \mathcal{F}[\mathcal{F}^{-1}[F]] = F.$$

### Example 2.8

Because  $\mathcal{F}[e^{-t} u(t)]|_\omega = (1 + j\omega)^{-1}$  (see Example 2.1),

$$\mathcal{F}^{-1} \left[ \frac{1}{1 + j\omega} \right] \Big|_t = e^{-t} u(t).$$

### 2.2.2 Near-Equivalence (Symmetry of the Transforms)

Computationally, the classical formulas for  $\mathcal{F}[\phi(s)]|_x$  and  $\mathcal{F}^{-1}[\phi(s)]|_x$  (formulas 2.1 and 2.2) are virtually the same, differing only by the sign in the exponential and the factor of  $(2\pi)^{-1}$  in Equation 2.2. Observing that

$$\begin{aligned} \int_{-\infty}^{\infty} \phi(s) e^{-jxs} ds &= 2\pi \left[ \frac{1}{2\pi} \int_{-\infty}^{\infty} \phi(s) e^{j(-x)s} ds \right] \\ &= 2\pi \left[ \frac{1}{2\pi} \int_{-\infty}^{\infty} \phi(s) e^{jx(-s)} ds \right] \end{aligned}$$

leads to the “near equivalence” identity,

$$\mathcal{F}[\phi(s)]|_x = 2\pi \mathcal{F}^{-1}[\phi(s)]|_{-x} = 2\pi \mathcal{F}^{-1}[\phi(-s)]|_x. \quad (2.23)$$

Likewise,

$$\mathcal{F}^{-1}[\phi(s)]|_x = \frac{1}{2\pi} \mathcal{F}[\phi(s)]|_{-x} = \frac{1}{2\pi} \mathcal{F}[\phi(-s)]|_x. \quad (2.24)$$

### Example 2.9

Using near-equivalence and results of Example 2.1,

$$\mathcal{F}[e^s u(-s)]|_x = 2\pi \mathcal{F}^{-1}[e^{-s} u(s)]|_x = 2\pi \left[ \frac{1}{2\pi - j 2\pi x} \right] = \frac{1}{1 - jx}.$$

### 2.2.3 Conjugation of Transforms

Using  $z^*$  to denote the complex conjugate of any complex quantity,  $z$ , it can be observed that

$$\left( \int_{-\infty}^{\infty} f(t) e^{-j\omega t} dt \right)^* = \int_{-\infty}^{\infty} f^*(t) e^{j\omega t} dt.$$

Thus,

$$\mathcal{F}[f]^* = 2\pi \mathcal{F}^{-1}[f^*]. \quad (2.25)$$

Likewise,

$$\mathcal{F}^{-1}[f]^* = \frac{1}{2\pi} \mathcal{F}[f^*]. \quad (2.26)$$

### 2.2.4 Linearity

If  $\alpha$  and  $\beta$  are any two scalar constants, then it follows from the linearity of the integral that

$$\mathcal{F}[\alpha f + \beta g] = \alpha \mathcal{F}[f] + \beta \mathcal{F}[g]$$

and

$$\mathcal{F}^{-1}[\alpha F + \beta G] = \alpha \mathcal{F}^{-1}[F] + \beta \mathcal{F}^{-1}[G].$$

#### Example 2.10

Using linearity and the transforms computed in Examples 2.1 and 2.9,

$$\begin{aligned} \mathcal{F}[e^{-|t|}]|_{\omega} &= \mathcal{F}[e^{-t}u(t) + e^t u(-t)]|_{\omega} = \frac{1}{1+j\omega} + \frac{1}{1-j\omega} \\ &= \frac{2}{1+\omega^2} \end{aligned}$$

and

$$\begin{aligned} \mathcal{F}[\operatorname{sgn}(t)e^{-|t|}]|_{\omega} &= \mathcal{F}[e^{-t}u(t) - e^t u(-t)]|_{\omega} = \frac{1}{1+j\omega} - \frac{1}{1-j\omega} \\ &= \frac{-2j\omega}{1+\omega^2}. \end{aligned}$$

### 2.2.5 Scaling

If  $\alpha$  is any nonzero real number, then, using the substitution  $\tau = \alpha t$ ,

$$\int_{-\infty}^{\infty} f(\alpha t)e^{-j\omega t} dt = \frac{1}{|\alpha|} \int_{-\infty}^{\infty} f(\tau)e^{-j\frac{\omega}{\alpha}\tau} d\tau.$$

Letting  $F(\omega) = \mathcal{F}[f(t)]|_{\omega}$ , this can be rewritten as

$$\mathcal{F}[f(\alpha t)]|_{\omega} = \frac{1}{|\alpha|} F\left(\frac{\omega}{\alpha}\right). \quad (2.27)$$

Likewise,

$$\mathcal{F}^{-1}[F(\alpha\omega)]|_t = \frac{1}{|\alpha|} f\left(\frac{t}{\alpha}\right). \quad (2.28)$$

#### Example 2.11

Using identity 2.27 and the results from Example 2.10:

$$\mathcal{F}[e^{-|\alpha t|}]|_{\omega} = \frac{1}{|\alpha|} \cdot \frac{2}{1 + \left(\frac{\omega}{\alpha}\right)^2} = \frac{2|\alpha|}{\alpha^2 + \omega^2}.$$

## 2.2.6 Translation and Multiplication by Exponentials

If  $F(\omega) = \mathcal{F}[f(t)]|_{\omega}$  and  $\alpha$  is any real number, then

$$\mathcal{F}[f(t - \alpha)]|_{\omega} = e^{-j\alpha\omega} F(\omega), \quad (2.29)$$

$$\mathcal{F}[e^{j\alpha t} f(t)]|_{\omega} = F(\omega - \alpha), \quad (2.30)$$

$$\mathcal{F}^{-1}[F(\omega - \alpha)]|_t = e^{j\alpha t} f(t), \quad (2.31)$$

and

$$\mathcal{F}^{-1}[e^{j\alpha\omega} F(\omega)]|_t = f(t - \alpha). \quad (2.32)$$

These formulas are easily derived from the classical definitions. Identity 2.30 for example, comes directly from the observation that

$$\int_{-\infty}^{\infty} e^{j\alpha t} f(t) e^{-j\omega t} dt = \int_{-\infty}^{\infty} f(t) e^{-j(\omega - \alpha)t} dt.$$

In general, identities 2.29 through 2.32 are not valid when  $\alpha$  is not a real number. An exception to this occurs when  $f$  is an analytic function on the entire complex plane. Then identities 2.29 and 2.32 do hold for all complex values of  $\alpha$ . Likewise, identities 2.30 and 2.31 may be used whenever  $\alpha$  is complex provided  $F$  is an analytic function on the entire complex plane.

#### Example 2.12

Let  $g(t) = e^{-t^2}$ . It can be shown that  $g(t)$  is analytic on the entire complex plane and that its Fourier transform is

$$G(\omega) = \sqrt{\pi} \exp\left[-\frac{1}{4}\omega^2\right]$$

(see Example 2.5 or Example 2.18). If  $\beta$  is any real value, then

$$\begin{aligned} \mathcal{F}[e^{-t^2+2\beta t}]|_{\omega} &= \mathcal{F}[e^{j(-j2\beta)t} e^{-t^2}]|_{\omega} \\ &= \sqrt{\pi} \exp\left[-\frac{1}{4}(\omega - (-j2\beta))^2\right] \\ &= \sqrt{\pi} e^{\beta^2} \exp\left[-\frac{1}{4}\omega^2 + j\beta\omega\right]. \end{aligned}$$

## 2.2.7 Complex Translation and Multiplication by Real Exponentials

Using the “generalized” notion of translation discussed in Section 2.1.4, it can be shown that for any complex value,  $\alpha + j\beta$ ,

$$\mathcal{F}[T_{\alpha+j\beta} f(t)]|_{\omega} = e^{-j(\alpha+j\beta)\omega} F(\omega),$$

$$\mathcal{F}[e^{j(\alpha+j\beta)t} f(t)]|_{\omega} = T_{\alpha+j\beta} F(\omega),$$

$$\mathcal{F}^{-1}[T_{\alpha+j\beta} F(\omega)]|_t = e^{j(\alpha+j\beta)t} f(t),$$

and

$$\mathcal{F}^{-1}[e^{j(\alpha+j\beta)\omega}F(\omega)]_t = T_{-(\alpha+j\beta)}f(t).$$

Letting  $\alpha = 0$  and  $\beta = -\gamma$ , these identities become

$$\mathcal{F}[T_{-j\gamma}f(t)]_\omega = e^{-\gamma\omega}F(\omega),$$

$$\mathcal{F}[e^{\gamma t}f(t)]_\omega = T_{-j\gamma}F(\omega),$$

$$\mathcal{F}^{-1}[T_{-j\gamma}F(\omega)]_t = e^{\gamma t}f(t),$$

and

$$\mathcal{F}^{-1}[e^{\gamma\omega}F(\omega)]_t = T_{j\gamma}f(t).$$

Caution must be exercised in the use of these formulas. It is true that  $T_{\alpha+j\beta}f(t) = f(t - (\alpha + j\beta))$  whenever  $\beta = 0$  or  $f(z)$  is analytic on the entire complex plane. However, if  $f(z)$  is not analytic and  $\beta \neq 0$ , then it is quite possible that  $T_{\alpha+j\beta}f(t) \neq f(t - (\alpha + j\beta))$ , even if  $f(t - (\alpha + j\beta))$  is well defined. In these cases  $T_{\alpha+j\beta}f(t)$  should be treated formally.

### Example 2.13

By the above

$$\mathcal{F}[e^t u(t)]_\omega = \mathcal{F}[e^{2t} e^{-t} u(t)]_\omega = T_{-2j} \left[ \frac{1}{1 + j\omega} \right].$$

Note, however, that

$$\mathcal{F}[-e^t u(-t)]_\omega = \frac{-1}{1 - j\omega} = \frac{1}{1 + j(\omega - (-2j))}.$$

Because  $e^t u(t)$  and  $-e^t u(-t)$  certainly are not equal, it follows that their transforms are not equal,

$$T_{-2j} \left[ \frac{1}{1 + j\omega} \right] \neq \frac{1}{1 + j(\omega - (-2j))}.$$

## 2.2.8 Modulation

The “modulation formulas,”

$$\mathcal{F}[\cos(\omega_0 t)f(t)]_\omega = \frac{1}{2}[F(\omega - \omega_0) + F(\omega + \omega_0)] \quad (2.33)$$

and

$$\mathcal{F}[\sin(\omega_0 t)f(t)]_\omega = \frac{1}{2j}[F(\omega - \omega_0) - F(\omega + \omega_0)] \quad (2.34)$$

are easily derived from identity 2.30 using the well-known formulas

$$\cos(\omega_0 t) = \frac{1}{2}[e^{j\omega_0 t} + e^{-j\omega_0 t}]$$

and

$$\sin(\omega_0 t) = \frac{1}{2j}[e^{j\omega_0 t} - e^{-j\omega_0 t}].$$

### Example 2.14

For  $\alpha > 0$ , the function

$$f(t) = \begin{cases} \cos\left(\frac{\pi}{2\alpha}t\right), & \text{if } -\alpha \leq t \leq \alpha \\ 0, & \text{otherwise} \end{cases}$$

can be written as

$$f(t) = \cos\left(\frac{\pi}{2\alpha}t\right)\rho_\alpha(t).$$

Thus, using identity 2.33 and the results of Example 2.2,

$$\begin{aligned} F(\omega) &= \mathcal{F}\left[\cos\left(\frac{\pi}{2\alpha}t\right)\rho_\alpha(t)\right]_\omega \\ &= \frac{1}{2}\left[\frac{2}{\omega - \frac{\pi}{2\alpha}}\sin\left(\alpha\left[\omega - \frac{\pi}{2\alpha}\right]\right) + \frac{2}{\omega + \frac{\pi}{2\alpha}}\sin\left(\alpha\left[\omega + \frac{\pi}{2\alpha}\right]\right)\right] \\ &= \frac{4\alpha\pi}{\pi^2 - 4\alpha^2\omega^2}\cos(\alpha\omega). \end{aligned}$$

## 2.2.9 Products and Convolution

If  $F = \mathcal{F}[f]$  and  $G = \mathcal{F}[g]$ , then the corresponding transforms of the products,  $fg$  and  $FG$ , can be computed using the identities

$$\mathcal{F}[fg] = \frac{1}{2\pi}F * G \quad (2.35)$$

and

$$\mathcal{F}^{-1}[FG] = f * g, \quad (2.36)$$

provided the convolutions,  $F * G$  and  $f * g$ , exist. Conversely, as long as the convolutions exist,

$$\mathcal{F}[f * g] = FG \quad (2.37)$$

and

$$\mathcal{F}^{-1}[F * G] = 2\pi fg. \quad (2.38)$$

Identity 2.35 can be derived as follows:

$$\begin{aligned} \int_{-\infty}^{\infty} f(t)g(t)e^{-j\omega t} dt &= \int_{-\infty}^{\infty} \left( \frac{1}{2\pi} \int_{-\infty}^{\infty} F(s)e^{jst} ds \right) g(t)e^{-j\omega t} dt \\ &= \frac{1}{2\pi} \int_{-\infty}^{\infty} F(s) \int_{-\infty}^{\infty} g(t)e^{-j(\omega-s)t} dt ds \\ &= \frac{1}{2\pi} \int_{-\infty}^{\infty} F(s)G(\omega - s) ds. \end{aligned}$$

The other identities can be derived in a similar fashion.

**Example 2.15**

From direct computation, if  $\beta > 0$ , then

$$\mathcal{F}^{-1}[e^{-\beta\omega}U(\omega)]|_t = \frac{1}{2\pi} \int_0^\infty e^{(jt-\beta)\omega} d\omega = \frac{1}{2\pi} \cdot \frac{1}{\beta - jt}.$$

And so,

$$\mathcal{F}\left[\frac{1}{\beta - jt}\right]|_\omega = 2\pi e^{-\beta\omega}U(\omega).$$

Applying identity 2.35,

$$\begin{aligned} \mathcal{F}\left[\frac{1}{10 - 7jt - t^2}\right]|_\omega &= \mathcal{F}\left[\frac{1}{2 - jt} \cdot \frac{1}{5 - jt}\right]|_\omega \\ &= \frac{1}{2\pi} [2\pi e^{-2\omega}U(\omega)] * [2\pi e^{-5\omega}U(\omega)] \\ &= 2\pi \int_{-\infty}^\infty e^{-2s}U(s)e^{-5(\omega-s)}U(\omega-s)ds \\ &= \begin{cases} 0, & \text{if } \omega < 0 \\ \frac{2\pi}{3} [e^{-2\omega} - e^{-5\omega}], & \text{if } 0 < \omega. \end{cases} \end{aligned}$$

**Example 2.16**

By straightforward computations it is easily verified that for  $\alpha > 0$ ,

$$\mathcal{F}[p_{\alpha/2}(t)]|_\omega = \frac{2}{\omega} \sin\left(\frac{\alpha}{2}\omega\right)$$

and

$$p_{\alpha/2}(t) * p_{\alpha/2}(t) = \alpha\Lambda_\alpha(t),$$

where  $p_{\alpha/2}(t)$  is the pulse function,

$$p_{\alpha/2}(t) = \begin{cases} 1, & \text{if } |t| < \frac{\alpha}{2} \\ 0, & \text{if } \frac{\alpha}{2} < |t| \end{cases},$$

and  $\Lambda_\alpha(t)$  is the triangle function,

$$\Lambda_\alpha(t) = \begin{cases} 1 - \frac{|t|}{\alpha}, & \text{if } |t| < \alpha \\ 0, & \text{if } \alpha < |t| \end{cases}$$

Using identity 2.37

$$\begin{aligned} \mathcal{F}[\Lambda_\alpha(t)]|_\omega &= \frac{1}{\alpha} \mathcal{F}[p_{\alpha/2}(t) * p_{\alpha/2}(t)]|_\omega \\ &= \frac{1}{\alpha} \left(\frac{2}{\omega} \sin\left(\frac{\alpha}{2}\omega\right)\right) \left(\frac{2}{\omega} \sin\left(\frac{\alpha}{2}\omega\right)\right) \\ &= \frac{4}{\alpha\omega^2} \sin^2\left(\frac{\alpha}{2}\omega\right). \end{aligned}$$

**2.2.10 Correlation**

The cross-correlation of two functions,  $f(t)$  and  $g(t)$ , is another function, denoted by  $f(t) \star g(t)$ , given by

$$f(t) \star g(t) = \int_{-\infty}^\infty f^*(s)g(t+s)ds, \tag{2.39}$$

where  $f^*(s)$  denotes the complex conjugate of  $f(s)$ . The notation  $\rho_{fg}(t)$  is often used instead of  $f(t) \star g(t)$ . The Wiener-Khinchine theorem states that, provided the correlations exist,

$$\mathcal{F}[f(t) \star g(t)]|_\omega = F^*(\omega)G(\omega) \tag{2.40}$$

and

$$\mathcal{F}[f^*(t)g(t)]|_\omega = \frac{1}{2\pi} F(\omega) \star G(\omega), \tag{2.41}$$

where  $F = \mathcal{F}[f]$  and  $G = \mathcal{F}[g]$ . Derivations of these formulas are similar to the analogous identities involving convolution.

For a given function,  $f(t)$ , the corresponding autocorrelation function is simply the cross-correlation of  $f(t)$  with itself,

$$f(t) \star f(t) = \int_{-\infty}^\infty f^*(s)f(t+s)ds. \tag{2.42}$$

Often autocorrelation is denoted by  $\rho_f(t)$  instead of  $f(t) \star f(t)$ . For autocorrelation, formulas 2.40 and 2.41 simplify to

$$\mathcal{F}[f(t) \star f(t)]|_\omega = |F(\omega)|^2 \tag{2.43}$$

and

$$\mathcal{F}[|f(t)|^2]|_\omega = \frac{1}{2\pi} F(\omega) \star F(\omega). \tag{2.44}$$

**2.2.11 Differentiation and Multiplication by Polynomials**

If  $f(t)$  is differentiable for all  $t$  and vanishes as  $t \rightarrow \pm\infty$ , then the Fourier transform of the derivative of the function can be related

to the transform of the undifferentiated function through the use of integration by parts,

$$\begin{aligned} \int_{-\infty}^{\infty} f'(t)e^{-j\omega t} dt &= f(t)e^{-j\omega t} \Big|_{-\infty}^{\infty} + j\omega \int_{-\infty}^{\infty} f(t)e^{-j\omega t} dt \\ &= j\omega \int_{-\infty}^{\infty} f(t)e^{-j\omega t} dt. \end{aligned}$$

In more concise form this can be written

$$\mathcal{F}[f'(t)]|_{\omega} = j\omega F(\omega), \quad (2.45)$$

where  $F = \mathcal{F}[f]$ . By near equivalence, if  $G(\omega)$  is differentiable for all  $\omega$  and vanishes as  $\omega \rightarrow \pm\infty$ , then

$$\mathcal{F}^{-1}[G'(\omega)]|_t = -jtg'(t), \quad (2.46)$$

where  $g = \mathcal{F}^{-1}[G]$ . Similar derivations yield

$$\mathcal{F}[tf(t)]|_{\omega} = jF'(\omega) \quad (2.47)$$

and

$$\mathcal{F}^{-1}[\omega G(\omega)]|_t = -jg'(t), \quad (2.48)$$

provided  $tf(t)$  and  $\omega G(\omega)$  are suitably integrable.

### Example 2.17

Using identity 2.45,

$$\begin{aligned} \mathcal{F}\left[\frac{j}{(1-jt)^2}\right]|_{\omega} &= \mathcal{F}\left[\frac{d}{dt}\left(\frac{1}{1-jt}\right)\right]|_{\omega} \\ &= j\omega \mathcal{F}\left[\frac{1}{1-jt}\right]|_{\omega} \\ &= j\omega 2\pi e^{-\omega} u(\omega). \end{aligned}$$

### Example 2.18

Let  $\alpha > 0$  and  $g(t) = e^{-\alpha t^2}$ . It is easily verified that

$$\frac{dg}{dt} = -2\alpha tg(t). \quad (2.49)$$

Taking the Fourier transform of each side and using identities 2.45 and 2.47 yields

$$j\omega G(\omega) = -2aj \frac{dG}{d\omega}$$

The solution to this first-order differential equation is easily computed. It is

$$G(\omega) = A \exp\left[-\frac{1}{4\alpha}\omega^2\right].$$

The value of the constant of integration,  $A$ , can be determined\* by noting that

$$A = G(0) = \int_{-\infty}^{\infty} e^{-\alpha t^2} dt.$$

The value of this last integral is well known to be  $\sqrt{\pi/\alpha}$ . Thus,

$$G(\omega) = \sqrt{\frac{\pi}{\alpha}} \exp\left[-\frac{1}{4\alpha}\omega^2\right].$$

It should be noted that if  $f'$  and  $F'$  are assumed to be the classical derivatives of  $f$  and  $F$ , that is

$$f'(t) = \lim_{\Delta t \rightarrow 0} \frac{f(t + \Delta t) - f(t)}{\Delta t}$$

and

$$F'(\omega) = \lim_{\Delta\omega \rightarrow 0} \frac{F(\omega + \Delta\omega) - F(\omega)}{\Delta\omega},$$

then application of the above identities is limited by requirements that the functions involved be suitably smooth and that they vanish at infinity. These limitations can be eliminated, however, by interpreting  $f'$  and  $F'$  in a more generalized sense. In this more generalized interpretation,  $f'$  and  $F'$  are defined to be the (generalized) functions satisfying the "generalized" integration by parts formulas,

$$\int_{-\infty}^{\infty} f'(t)\phi(t)dt = - \int_{-\infty}^{\infty} f(t)\phi'(t)dt$$

and

$$\int_{-\infty}^{\infty} F'(\omega)\phi(\omega)d\omega = - \int_{-\infty}^{\infty} F(\omega)\phi'(\omega)d\omega,$$

for every test function,  $\phi$  (with  $\phi'$  denoting the classical derivative of  $\phi$ ). As long as the function being differentiated is piecewise smooth and continuous, then there is no difference between the classical and the generalized derivative. If however, the function,  $f(x)$ , has jump discontinuities at  $x = x_1, x_2, \dots, x_N$ , then

$$f'_{\text{generalized}} = f'_{\text{classical}} + \sum_k J_k \delta_{x_k},$$

\* A method for determining  $A$  using Bessel's equality is described in Section 2.2.15.

where  $J_k$  denotes the “jump” in  $f$  at  $x = x_k$ ,

$$J_k = \lim_{\Delta x \rightarrow 0^+} f(x_k + \Delta x) - f(x_k - \Delta x).$$

It is not difficult to show that the product rule,  $(fg)' = f'g + fg'$ , holds for the generalized derivative as well as the classical derivative.

**Example 2.19**

Consider the step function,  $u(t)$ . The classical derivative of  $u$  is clearly 0, because the graph of  $u$  consists of two horizontal half-lines (with slope zero). Using the generalized integration by parts formula, however,

$$\begin{aligned} \int_{-\infty}^{\infty} u'(t)\phi(t)dt &= - \int_{-\infty}^{\infty} u(t)\phi'(t)dt \\ &= - \int_0^{\infty} \phi'(t)dt \\ &= \phi(0) \\ &= \int_{-\infty}^{\infty} \delta(t)\phi(t)dt, \end{aligned}$$

showing that  $\delta(t)$  is the generalized derivative of  $u(t)$ .

**Example 2.20**

Using the generalized derivative and identity 2.47,

$$\begin{aligned} \mathcal{F}\left[\frac{t}{1-jt}\right]_{\omega} &= j \frac{d}{d\omega} \left( \mathcal{F}\left[\frac{1}{1-jt}\right]_{\omega} \right) \\ &= j \frac{d}{d\omega} (2\pi e^{-\omega} u(\omega)) \\ &= 2\pi j \left[ \frac{de^{-\omega}}{d\omega} u(\omega) + e^{-\omega} u'(\omega) \right] \\ &= 2\pi j [ -e^{-\omega} u(\omega) + \delta(\omega) ]. \end{aligned}$$

The extension of formulas 2.45 through 2.48 to the corresponding identities involving higher-order derivatives is straightforward. If  $n$  is any positive integer, then

$$\mathcal{F}[f^{(n)}(t)]_{\omega} = (j\omega)^n F(\omega), \tag{2.50}$$

$$\mathcal{F}^{-1}[F^{(n)}(\omega)]_t = (-jt)^n f(t), \tag{2.51}$$

$$\mathcal{F}[t^n f(t)]_{\omega} = j^n F^{(n)}(\omega), \tag{2.52}$$

and

$$\mathcal{F}^{-1}[\omega^n F(\omega)]_t = (-j)^n f^{(n)}(t). \tag{2.53}$$

Again, these identities hold for all transformable functions as long as the derivatives are interpreted in the generalized sense.

**2.2.12 Moments**

For any suitably integrable function,  $f(t)$ , and nonnegative integer,  $n$ , the “ $n$ th moment of  $f$ ” is the quantity

$$m_n(f) = \int_{-\infty}^{\infty} t^n f(t) dt.$$

Because

$$\int_{-\infty}^{\infty} t^n f(t) dt = \mathcal{F}[t^n f(t)]_{\omega},$$

it is clear from identity 2.52 that

$$m_n(f) = j^n F^{(n)}(0).$$

**2.2.13 Integration**

If  $F(\omega)$  and  $G(\omega)$  are the Fourier transforms of  $f(t)$  and  $g(t)$ , and  $g(t) = t^{-1} f(t)$ , then  $tg(t) = f(t)$  and, by identity 2.47,  $jG'(\omega) = F(\omega)$ . Integrating this gives

$$G(\omega) - G(\alpha) = -j \int_{\alpha}^{\omega} F(s) ds,$$

where  $\alpha$  can be any real number. This can be written

$$\mathcal{F}\left[\frac{f(t)}{t}\right]_{\omega} = -j \int_{\alpha}^{\omega} F(s) ds + c_{\alpha} \tag{2.54}$$

where  $c_{\alpha} = G(\alpha)$ . For certain general types of functions and choices of  $\alpha$ , the value of  $c_{\alpha}$  is easily determined. For examine, if  $f(t)$  is also absolutely integrable, then

$$\mathcal{F}\left[\frac{f(t)}{t}\right]_{\omega} = -j \int_{-\infty}^{\omega} F(s) ds, \tag{2.55}$$

while if  $f(t)$  is an even function

$$\mathcal{F}\left[\frac{f(t)}{t}\right]_{\omega} = -j \int_0^{\omega} F(s) ds, \tag{2.56}$$

provided the integrals are well defined.

It can also be shown that as long as the limit of  $\omega^{-1} F(\omega)$  exists as  $\omega \rightarrow 0$ , then for each real value of  $\alpha$  there is a constant,  $c_{\alpha}$ , such that

$$\mathcal{F}\left[\int_{\alpha}^t f(s) ds\right]_{\omega} = -j \frac{F(\omega)}{\omega} + c_{\alpha} \delta(\omega). \tag{2.57}$$

If  $f(t)$  is an even function, then

$$\mathcal{F} \left[ \int_0^t f(s) ds \right] \Big|_{\omega} = -j \frac{F(\omega)}{\omega}, \quad (2.58)$$

while if  $f(t)$  and  $\int_{-\alpha}^t f(s) ds$  are absolutely integrable, then

$$\mathcal{F} \left[ \int_{-\infty}^t f(s) ds \right] \Big|_{\omega} = -j \frac{F(\omega)}{\omega}. \quad (2.59)$$

### Example 2.21

Let  $\alpha$  and  $\beta$  be positive,

$$f(t) = e^{-\alpha|t|} - e^{-\beta|t|},$$

and

$$g(t) = \frac{f(t)}{t} = \frac{e^{-\alpha|t|} - e^{-\beta|t|}}{t}.$$

Both functions are easily verified to be transformable with

$$F(\omega) = \mathcal{F} [e^{-\alpha|t|} - e^{-\beta|t|}] \Big|_{\omega} = \frac{2\alpha}{\alpha^2 + \omega^2} - \frac{2\beta}{\beta^2 + \omega^2}.$$

Because  $f(t)$  is even, formula 2.56 applies, and

$$\begin{aligned} G(\omega) &= \mathcal{F} \left[ \frac{e^{-\alpha|t|} - e^{-\beta|t|}}{t} \right] \Big|_{\omega} = -j \int_0^{\omega} F(s) ds \\ &= -j \int_0^{\omega} \left( \frac{2\alpha}{\alpha^2 + s^2} - \frac{2\beta}{\beta^2 + s^2} \right) ds \\ &= -2j \left( \arctan \left( \frac{\omega}{\alpha} \right) - \arctan \left( \frac{\omega}{\beta} \right) \right). \end{aligned} \quad (2.60)$$

### Example 2.22

Applying the same analysis done in the previous example but using

$$f(t) = 1 - e^{-\beta|t|}$$

leads, formally, to

$$\begin{aligned} \mathcal{F} \left[ \frac{1 - e^{-\beta|t|}}{t} \right] \Big|_{\omega} &= -j \int_0^{\omega} \left( 2\pi \delta(s) - \frac{2\beta}{\beta^2 + s^2} \right) ds \\ &= -2\pi j \int_0^{\omega} \delta(s) ds + 2j \arctan \left( \frac{\omega}{\beta} \right). \end{aligned}$$

Unfortunately, this is of little value because

$$\int_{\alpha}^{\omega} \delta(s) ds$$

is not well defined if  $\alpha = 0$ . However, because

$$\lim_{\alpha \rightarrow 0^+} e^{-\alpha|t|} = 1,$$

and

$$\begin{aligned} \lim_{\alpha \rightarrow 0^+} \arctan \left( \frac{\omega}{\alpha} \right) &= \begin{cases} \frac{\pi}{2}, & \text{if } 0 < \omega \\ -\frac{\pi}{2}, & \text{if } \omega < 0 \end{cases} \\ &= \frac{\pi}{2} \operatorname{sgn}(\omega), \end{aligned}$$

it can be argued, using Equation 2.60, that

$$\begin{aligned} \mathcal{F} \left[ \frac{1 - e^{-\beta|t|}}{t} \right] \Big|_{\omega} &= \lim_{\alpha \rightarrow 0^+} \mathcal{F} \left[ \frac{e^{-\alpha|t|} - e^{-\beta|t|}}{t} \right] \Big|_{\omega} \\ &= \lim_{\alpha \rightarrow 0^+} -2j \left( \arctan \left( \frac{\omega}{\alpha} \right) - \arctan \left( \frac{\omega}{\beta} \right) \right) \\ &= -j\pi \operatorname{sgn}(\omega) + 2j \arctan \left( \frac{\omega}{\beta} \right). \end{aligned} \quad (2.61)$$

## 2.2.14 Parseval's Equality

Parseval's equality is

$$\int_{-\infty}^{\infty} f(t) g^*(t) dt = \frac{1}{2\pi} \int_{-\infty}^{\infty} F(\omega) G^*(\omega) d\omega \quad (2.62)$$

and is valid whenever the integrals make sense. Closely related to Parseval's equality and the two "fundamental identities,"

$$\int_{-\infty}^{\infty} f(x) \mathcal{F}[h] \Big|_x dx = \int_{-\infty}^{\infty} \mathcal{F}[f] \Big|_y h(y) dy \quad (2.63)$$

and

$$\int_{-\infty}^{\infty} f(y) \mathcal{F}^{-1}[H] \Big|_y dy = \int_{-\infty}^{\infty} \mathcal{F}^{-1}[F] \Big|_x H(x) dx. \quad (2.64)$$

Derivations of these identities are straightforward. Identity 2.63, for example, follows immediately from

$$\begin{aligned} \int_{-\infty}^{\infty} f(x) \left( \int_{-\infty}^{\infty} h(y) e^{-jxy} dy \right) dx &= \int_{-\infty}^{\infty} \int_{-\infty}^{\infty} f(x) h(y) e^{-jxy} dy dx \\ &= \int_{-\infty}^{\infty} \left( \int_{-\infty}^{\infty} f(x) e^{-jxy} dx \right) h(y) dy. \end{aligned}$$

Parseval's equality can then, in turn, be derived from identity 2.63 and the observation that

$$g^*(t) = \left( \mathcal{F}^{-1}[G] \Big|_t \right)^* = \frac{1}{2\pi} \int_{-\infty}^{\infty} G^*(\omega) e^{-j\omega t} d\omega = \frac{1}{2\pi} \mathcal{F}[G^*] \Big|_t.$$

### 2.2.15 Bessel's Equality

Bessel's equality,

$$\int_{-\infty}^{\infty} |f(t)|^2 dt = \frac{1}{2\pi} \int_{-\infty}^{\infty} |F(\omega)|^2 d\omega, \tag{2.65}$$

is obtained directly from Parseval's equality by letting  $g = f$ .

#### Example 2.23

Let  $\alpha > 0$  and  $f(t) = p_\alpha(t)$ , where  $p_\alpha(t)$  is the pulse function. It is easily verified that

$$F(\omega) = \mathcal{F}[p_\alpha(t)] \Big|_\omega = \int_{-\alpha}^{\alpha} e^{-j\omega t} dt = \frac{2}{\omega} \sin(\alpha\omega).$$

So, using Bessel's equality,

$$\begin{aligned} \int_{-\infty}^{\infty} \left| \frac{\sin(\alpha\omega)}{\alpha\omega} \right|^2 d\omega &= 2\pi \int_{-\infty}^{\infty} \left| \frac{1}{2\alpha} p_\alpha(t) \right|^2 dt \\ &= \frac{2\pi}{4\alpha^2} \int_{-\alpha}^{\alpha} dt \\ &= \frac{\pi}{\alpha}. \end{aligned}$$

#### Example 2.24

Let  $\alpha > 0$ . In Example 2.18 it was shown that the Fourier transform of  $g(t) = e^{-\alpha t^2}$  is  $G(\omega) = A \exp\left[-\frac{1}{4\alpha}\omega^2\right]$ . The positive constant  $A$  can be determined by noting that, by Bessel's equality,

$$\int_{-\infty}^{\infty} |e^{-\alpha t^2}|^2 dt = \frac{1}{2\pi} \int_{-\infty}^{\infty} \left| A \exp\left[-\frac{1}{4\alpha}\omega^2\right] \right|^2 d\omega.$$

Letting  $\omega = 2\alpha\tau$  this becomes, after a little simplification,

$$\int_{-\infty}^{\infty} e^{-2\alpha t^2} dt = \frac{\alpha}{\pi} A^2 \int_{-\infty}^{\infty} e^{-2\alpha\tau^2} d\tau.$$

Dividing out the integrals and solving for  $A$  yields

$$A = \sqrt{\frac{\pi}{\alpha}},$$

where the positive square root is taken because

$$A = G(0) = \int_{-\infty}^{\infty} e^{-\alpha t^2} dt > 0.$$

### 2.2.16 The Bandwidth Theorem

If  $f(t)$  is a function whose value may be considered as “negligible” outside of some interval,  $(t_1, t_2)$ , then the length of that interval,  $\Delta t = t_2 - t_1$ , is the effective duration of  $f(t)$ . Likewise, if  $F(\omega)$  is the Fourier transform of  $f(t)$ , and  $F(\omega)$  can be considered as “negligible” outside of some interval,  $(\omega_1, \omega_2)$ , then  $\Delta\omega = \omega_2 - \omega_1$  is the effective bandwidth of  $f(t)$ .

The essence of the bandwidth theorem is that there is a universal positive constant,  $\gamma$ , such that the effective duration,  $\Delta t$ , and effective bandwidth,  $\Delta\omega$ , of any function (with finite  $\Delta t$  or finite  $\Delta\omega$ ) satisfies

$$\Delta t \Delta\omega \geq \gamma.$$

Thus, it is not possible to find a function whose effective bandwidth and effective duration are both arbitrarily small.

There are, in fact, several versions of the bandwidth theorem, each applicable to a particular class of functions. The two most important versions involve absolutely integrable functions and finite energy functions. They are described in greater detail in Sections 2.3.3 and 2.3.5, respectively. Also in these sections are appropriate precise definitions of effective duration and effective bandwidth.

Because it is the basis of the Heisenberg uncertainty principle of quantum mechanics, the bandwidth theorem is often, itself, referred to as the uncertainty principle of Fourier analysis.

## 2.3 Transforms of Specific Classes of Functions

In many applications one encounters specific classes of functions in which either the functions or their transforms satisfy certain particular properties. Several such classes of functions are discussed below.



### 2.3.1 Real/Imaginary Valued Even/Odd Functions

Let  $F(\omega)$  be the Fourier transform of  $f(t)$ . Then, assuming  $f(t)$  is integrable,

$$\begin{aligned} F(\omega) &= \int_{-\infty}^{\infty} f(t)e^{-j\omega t} dt \\ &= \int_{-\infty}^{\infty} f(t)[\cos(\omega t) - j\sin(\omega t)] dt \\ &= \int_{-\infty}^{\infty} f(t)\cos(\omega t) dt - j \int_{-\infty}^{\infty} f(t)\sin(\omega t) dt. \end{aligned} \tag{2.66}$$

If  $f(t)$  is an even function, then

$$\int_{-\infty}^{\infty} f(t)\sin(\omega t) dt = 0$$

and Equation 2.66 becomes

$$F(\omega) = \int_{-\infty}^{\infty} f(t)\cos(\omega t) dt = 2 \int_0^{\infty} f(t)\cos(\omega t) dt,$$

which is clearly an even function of  $\omega$  and is real valued whenever  $f$  is real valued. Likewise, if  $f(t)$  is an odd function, then

$$\int_{-\infty}^{\infty} f(t)\cos(\omega t) dt = 0,$$

and Equation 2.66 reduces to

$$F(\omega) = -j \int_{-\infty}^{\infty} f(t)\sin(\omega t) dt = -2j \int_0^{\infty} f(t)\sin(\omega t) dt,$$

which is clearly an odd function of  $\omega$  and is imaginary valued as long as  $f$  is real valued.

These and related relations are summarized in Table 2.1.

**TABLE 2.1**  $F = \mathcal{F}[f]$

$f(t)$ is even	$\Leftrightarrow$	$F(\omega)$ is even
$f(t)$ is real and even	$\Leftrightarrow$	$F(\omega)$ is real and even
$f(t)$ is imaginary and even	$\Leftrightarrow$	$F(\omega)$ is imaginary and even
$f(t)$ is odd	$\Leftrightarrow$	$F(\omega)$ is odd
$f(t)$ is real and odd	$\Leftrightarrow$	$F(\omega)$ is imaginary and odd
$f(t)$ is imaginary and odd	$\Leftrightarrow$	$F(\omega)$ is real and odd

On occasion it is convenient to decompose a function,  $f(t)$ , into its even and odd components,  $f_e(t)$  and  $f_o(t)$ ,

$$f(t) = f_e(t) + f_o(t),$$

where

$$f_e(t) = \frac{1}{2}[f(t) + f(-t)] \quad \text{and} \quad f_o(t) = \frac{1}{2}[f(t) - f(-t)].$$

If  $f(t)$  is a real-valued function with Fourier transform

$$F(\omega) = R(\omega) + jI(\omega),$$

where  $R(\omega)$  and  $I(\omega)$  denote, respectively, the real and imaginary parts of  $F(\omega)$ , then, by the above discussion it follows that

$$F_e(\omega) = R(\omega) = \mathcal{F}[f_e(t)]|_{\omega}, \tag{2.67}$$

$$F_o(\omega) = jI(\omega) = \mathcal{F}[f_o(t)]|_{\omega}, \tag{2.68}$$

$$f_e(t) = \mathcal{F}^{-1}[F_e(\omega)]|_t = \frac{1}{\pi} \int_0^{\infty} R(\omega)\cos(\omega t) d\omega, \tag{2.69}$$

and

$$f_o(t) = \mathcal{F}^{-1}[F_o(\omega)]|_t = -\frac{1}{\pi} \int_0^{\infty} I(\omega)\sin(\omega t) d\omega. \tag{2.70}$$

Rewriting  $F(\omega)$  in terms of its amplitude,  $A(\omega) = |F(\omega)|$ , and phase,  $\phi(\omega)$ ,

$$F(\omega) = A(\omega)e^{j\phi(\omega)},$$

it is easily seen that

$$\begin{aligned} R(\omega)\cos(\omega t) - I(\omega)\sin(\omega t) &= A(\omega)[\cos\phi(\omega)\cos(\omega t) \\ &\quad - \sin\phi(\omega)\sin(\omega t)] \\ &= A(\omega)\cos(\omega t + \phi(\omega)). \end{aligned}$$

Thus, by Equations 2.69 and 2.70, if  $f(t)$  is real then,

$$f(t) = f_e(t) + f_o(t) = \frac{1}{\pi} \int_0^{\infty} A(\omega)\cos(\omega t + \phi(\omega)) d\omega. \tag{2.71}$$

### 2.3.2 Absolutely Integrable Functions

If  $f(t)$  is absolutely integrable (i.e.,  $\int_{-\infty}^{\infty} |f(t)| dt < \infty$ ) then the integral defining  $F(\omega)$ ,

$$F(\omega) = \mathcal{F}[f(t)]|_{\omega} = \int_{-\infty}^{\infty} f(t)e^{-j\omega t} dt$$

is well defined and well behaved. As a consequence,  $F(\omega)$  is well defined for every  $\omega$  and is a reasonably well behaved function on  $(-\infty, \infty)$ . One immediate observation is that for such functions,

$$F(0) = \int_{-\infty}^{\infty} f(t) dt.$$

It is also worth noting that for any  $\omega$ ,

$$|F(\omega)| = \left| \int_{-\infty}^{\infty} f(t)e^{-j\omega t} dt \right| \leq \int_{-\infty}^{\infty} |f(t)e^{-j\omega t}| dt = \int_{-\infty}^{\infty} |f(t)| dt.$$

The following can also be shown:

1.  $F(\omega)$  is a continuous function of  $\omega$  and for each  $-\infty < \omega_0 < \infty$ ,

$$\lim_{\omega \rightarrow \omega_0} F(\omega) = \int_{-\infty}^{\infty} f(t)e^{-j\omega_0 t} dt$$

2. (The Riemann–Lebesgue lemma)

$$\lim_{\omega \rightarrow \pm\infty} F(\omega) = 0.$$

As shown in the next example, care must be exercised not to assume these facts when  $f(t)$  is not absolutely integrable.

**Example 2.25**

Consider the transform,  $F(\omega)$  of  $f(t) = \text{sinc}(t) = t^{-1} \sin(t)$ . The function  $f(t)$  is not absolutely integrable. Because

$$\mathcal{F}^{-1}[\pi p_1(t)]|_{\omega} = \frac{1}{2\pi} \int_{-\infty}^{\infty} \pi p_1(t)e^{j\omega t} dt = \text{sinc}(\omega)$$

it follows that

$$F(\omega) = \mathcal{F}[\text{sinc}(t)]|_{\omega} = \pi p_1(\omega).$$

Clearly

$$\lim_{\omega \rightarrow 1^+} F(\omega) = 0 \quad \text{and} \quad \lim_{\omega \rightarrow 1^-} F(\omega) = \pi,$$

while, using the residue theorem, it is easily shown that

$$F(1) = \mathcal{F}[\text{sinc}(t)]|_{\omega=1} = \int_{-\infty}^{\infty} \text{sinc}(t)e^{jt} dt = \frac{\pi}{2}.$$

Thus,  $F(\omega)$  is not continuous.

Analogous results hold when taking inverse transforms of absolutely integrable functions. If  $F(\omega)$  is absolutely integrable and  $f = \mathcal{F}^{-1}[F]$ , then

$$f(0) = \frac{1}{2\pi} \int_{-\infty}^{\infty} F(\omega) d\omega,$$

and, for all real  $t$ ,

$$|f(t)| \leq \frac{1}{2\pi} \int_{-\infty}^{\infty} |F(\omega)| d\omega.$$

Furthermore,

1.  $f(t)$  is a continuous function of  $t$  and for each  $-\infty < t_0 < \infty$ ,

$$\lim_{t \rightarrow t_0} f(t) = \frac{1}{2\pi} \int_{-\infty}^{\infty} F(\omega)e^{j\omega t_0} d\omega.$$

2. (The Riemann–Lebesgue lemma)

$$\lim_{t \rightarrow \pm\infty} f(t) = 0.$$

**2.3.3 The Bandwidth Theorem for Absolutely Integrable Functions**

Assume that both  $f(t)$  and its Fourier transform,  $F(\omega)$ , are absolutely integrable. Let  $\bar{t}$  and  $\bar{\omega}$  be any two fixed values for  $t$  and  $\omega$  such that  $f(\bar{t}) \neq 0$  and  $F(\bar{\omega}) \neq 0$ . The corresponding effective duration,  $\Delta t$ , and the corresponding effective bandwidth,  $\Delta \omega$ , are the satisfying

$$\int_{-\infty}^{\infty} |f(t)| dt = |f(\bar{t})| \Delta t$$

and

$$\int_{-\infty}^{\infty} |F(\omega)| d\omega = |F(\bar{\omega})| \Delta \omega.$$

The bandwidth theorem for absolutely integrable functions states that

$$\Delta t \Delta \omega \geq 2\pi.$$

Moreover, using  $\bar{t} = \bar{\omega} = 0$ ,

$$\Delta t \Delta \omega = 2\pi$$

whenever  $f(t)$  and  $F(\omega)$  are both real nonnegative functions (or real nonpositive functions) and neither  $f(0)$  nor  $F(0)$  vanishes.

The choice of the values for  $\bar{t}$  and  $\bar{\omega}$  depends on the use to be made of the bandwidth theorem. One standard choice for  $\bar{t}$  and  $\bar{\omega}$  is as the centroids of  $|f(t)|$  and  $|F(\omega)|$ ,

$$\bar{t} = \frac{\int_{-\infty}^{\infty} t|f(t)|dt}{\int_{-\infty}^{\infty} |f(t)|dt} \quad \text{and} \quad \bar{\omega} = \frac{\int_{-\infty}^{\infty} \omega|F(\omega)|d\omega}{\int_{-\infty}^{\infty} |F(\omega)|d\omega}.$$

Alternatively, to minimize the values used for the effective duration and effective bandwidth,  $\bar{t}$  and  $\bar{\omega}$  can be chosen to maximize the values of  $|f(\bar{t})|$  and  $|F(\bar{\omega})|$ . Clearly, choosing  $\bar{t} = 0$  and  $\bar{\omega} = 0$  is especially appropriate if both  $f(t)$  and  $F(\omega)$  are real valued, even functions with maximums at the origin.

The above version of the bandwidth theorem is very easily derived. Because  $f(t)$  and  $F(\omega)$  are both absolutely integrable,

$$|F(\bar{\omega})| \leq \int_{-\infty}^{\infty} |f(t)|dt = |f(\bar{t})|\Delta t$$

and

$$|f(\bar{t})| \leq \frac{1}{2\pi} \int_{-\infty}^{\infty} |F(\omega)|d\omega = \frac{1}{2\pi} |F(\bar{\omega})|\Delta\omega.$$

Thus,

$$\Delta t \Delta \omega \geq \frac{|F(\bar{\omega})|}{|f(\bar{t})|} \times \frac{2\pi|f(\bar{t})|}{|F(\bar{\omega})|} = 2\pi.$$

Clearly, if both  $f(t)$  and  $F(\omega)$  are real and nonnegative and neither  $f(0)$  or  $F(0)$  vanish, then the above inequalities can be replaced with

$$F(0) = \int_{-\infty}^{\infty} f(t)dt = f(0)\Delta t,$$

$$f(0) = \frac{1}{2\pi} \int_{-\infty}^{\infty} F(\omega)d\omega = F(0)\Delta\omega,$$

and

$$\Delta t \Delta \omega = \frac{F(0)}{f(0)} \times \frac{2\pi f(0)}{F(0)} = 2\pi.$$

### Example 2.26

Let  $\alpha > 0$  and  $f(t) = e^{-\alpha|t|}$ . The transform of  $f(t)$  is

$$F(\omega) = \frac{2\alpha}{\alpha^2 + \omega^2}.$$

Observe that both  $f(t)$  and  $F(\omega)$  are even functions with maximums at the origin. It is therefore appropriate to use  $\bar{t} = 0$  and  $\bar{\omega} = 0$  to compute the effective duration and effective bandwidth,

$$\Delta t = \frac{1}{|f(0)|} \int_{-\infty}^{\infty} |f(t)|dt = \int_{-\infty}^{\infty} e^{-\alpha|t|}dt = 2 \int_0^{\infty} e^{-\alpha t}dt = \frac{2}{\alpha}$$

and

$$\Delta \omega = \frac{1}{|F(0)|} \int_{-\infty}^{\infty} |F(\omega)|d\omega = \frac{\alpha}{2} \int_{-\infty}^{\infty} \frac{2\alpha}{\alpha^2 + \omega^2}d\omega = \alpha\pi.$$

The products of these measures of effective bandwidth the duration are

$$\Delta t \Delta \omega = \left(\frac{2}{\alpha}\right)(\alpha\pi) = 2\pi.$$

as predicted by the bandwidth theorem.

## 2.3.4 Square Integrable (“Finite Energy”) Functions

A function,  $f(t)$ , is square integrable if

$$\int_{-\infty}^{\infty} |f(t)|^2 dt < \infty.$$

For many applications, it is natural to define the energy,  $E$ , in a function (or signal),  $f(t)$ , by

$$E = E[f] = \int_{-\infty}^{\infty} |f(t)|^2 dt.$$

For this reason, square integrable functions are also called finite energy functions. By Bessel’s equality,

$$E[f] = \int_{-\infty}^{\infty} |f(t)|^2 dt = \frac{1}{2\pi} \int_{-\infty}^{\infty} |F(\omega)|^2 d\omega, \quad (2.72)$$

where  $F(\omega)$  is the Fourier transform of  $f(t)$ . This shows that a function is square integrable if and only if its transform is also square integrable. It also indicates why  $|F(\omega)|^2$  is often referred to as either the “energy spectrum” or the “energy spectral density” of  $f(t)$ .

## 2.3.5 The Bandwidth Theorem for Finite Energy Functions

Assume that  $f(t)$  and its Fourier transform,  $F(\omega)$ , are finite energy functions, and let the effective duration,  $\Delta t$ , and the effective bandwidth,  $\Delta \omega$ , be given by the “standard deviations,”

$$(\Delta t)^2 = \frac{\int_{-\infty}^{\infty} (t - \bar{t})^2 |f(t)|^2 dt}{\int_{-\infty}^{\infty} |f(t)|^2 dt}$$

and

$$(\Delta \omega)^2 = \frac{\int_{-\infty}^{\infty} (\omega - \bar{\omega})^2 |F(\omega)|^2 d\omega}{\int_{-\infty}^{\infty} |F(\omega)|^2 d\omega},$$

where  $\bar{t}$  and  $\bar{\omega}$  are the mean values of  $t$  and  $\omega$ ,

$$\bar{t} = \frac{\int_{-\infty}^{\infty} t |f(t)|^2 dt}{\int_{-\infty}^{\infty} |f(t)|^2 dt} \quad \text{and} \quad \bar{\omega} = \frac{\int_{-\infty}^{\infty} \omega |F(\omega)|^2 d\omega}{\int_{-\infty}^{\infty} |F(\omega)|^2 d\omega}.$$

Using the energy of  $f(t)$ ,

$$E = \int_{-\infty}^{\infty} |f(t)|^2 dt = \frac{1}{2\pi} \int_{-\infty}^{\infty} |F(\omega)|^2 d\omega,$$

the effective duration and effective bandwidth can be written more concisely as

$$\Delta t = \sqrt{\frac{1}{E} \int_{-\infty}^{\infty} (t - \bar{t})^2 |f(t)|^2 dt}$$

and

$$\Delta \omega = \sqrt{\frac{1}{2\pi E} \int_{-\infty}^{\infty} (\omega - \bar{\omega})^2 |F(\omega)|^2 d\omega}.$$

The bandwidth theorem for finite energy functions states that, if the above quantities are well defined (and finite) and

$$\lim_{t \rightarrow \pm\infty} t |f(t)|^2 = 0,$$

then

$$\Delta t \Delta \omega \geq \frac{1}{2}.$$

Moreover, when  $\bar{t} = 0$  and  $\bar{\omega} = 0$ , then

$$\Delta t \Delta \omega = \frac{1}{2}$$

if and only if  $f(t)$  is a Gaussian,

$$f(t) = Ae^{-\alpha t^2},$$

for some  $\alpha > 0$ .

The reader should be aware that the effective duration and effective bandwidth defined in this section are not the same as the effective duration and effective bandwidth previously defined in Section 2.3.3. Nor do these definitions necessarily agree with the definitions given for the analogous quantities defined later in the sections on reconstructing sampled functions.

### Example 2.27

Let  $\alpha > 0$  and  $f(t) = e^{-\alpha|t|}$ . The transform of  $f(t)$  is

$$F(\omega) = \frac{2\alpha}{\alpha^2 + \omega^2}.$$

Because  $tf(t)$  and  $\omega F(\omega)$  are both odd functions, it is clear that  $\bar{t} = 0$  and  $\bar{\omega} = 0$ . The energy is

$$E = \int_{-\infty}^{\infty} |e^{-\alpha|t|}|^2 dt = 2 \int_0^{\infty} e^{-2\alpha t} dt = \frac{1}{\alpha}.$$

Using integration by parts, the corresponding effective duration and effective bandwidth are easily computed,

$$\begin{aligned} \Delta t &= \sqrt{\frac{1}{E} \int_{-\infty}^{\infty} (t - \bar{t})^2 |f(t)|^2 dt} \\ &= \sqrt{2\alpha \int_0^{\infty} t^2 e^{-2\alpha t} dt} \\ &= \frac{\sqrt{2}}{2\alpha} \end{aligned}$$

and

$$\begin{aligned} \Delta \omega &= \sqrt{\frac{1}{2\pi E} \int_{-\infty}^{\infty} (\omega - \bar{\omega})^2 |F(\omega)|^2 d\omega} \\ &= \sqrt{\frac{\alpha}{2\pi} \int_{-\infty}^{\infty} \omega^2 \left( \frac{2\alpha}{\alpha^2 + \omega^2} \right)^2 d\omega} \\ &= \sqrt{\frac{\alpha^3}{\pi} \int_{-\infty}^{\infty} \omega \frac{2\omega}{(\alpha^2 + \omega^2)^2} d\omega} \\ &= \alpha. \end{aligned}$$

(By comparison, treating  $f(t)$  and  $F(\omega)$  as absolutely integrable functions [Example 2.26] led to an effective duration of  $2\alpha^{-1}$  and an effective bandwidth of  $\alpha\pi$ .)

The products of these measures of bandwidth and duration computed here are

$$\Delta t \Delta \omega = \frac{\sqrt{2}}{2\alpha} \alpha = \frac{\sqrt{2}}{2} > \frac{1}{2},$$

as predicted by the bandwidth theorem for finite energy functions.

### 2.3.6 Functions with Finite Duration

A function,  $f(t)$ , has finite duration (with duration  $2T$ ) if there is a  $0 < T < \infty$  such that

$$f(t) = 0 \quad \text{whenever } T < |t|.$$

The transform,  $F(\omega)$ , of such a function is given by a proper integral over a finite interval,

$$F(\omega) = \int_{-T}^T f(t) e^{-j\omega t} dt. \quad (2.73)$$

Any piecewise continuous function with finite duration is automatically absolutely integrable and automatically has finite energy, and, so, the discussions in Sections 2.3.2 through 2.3.5 apply to such functions. In addition, if  $f(t)$  is a piecewise continuous function of finite duration (with duration  $2T$ ), then, for every nonnegative integer,  $n$ ,  $t^n f(t)$  is also a piecewise continuous finite duration function with duration  $2T$ , and using identity 2.52,

$$F^{(n)}(\omega) = \mathcal{F} [(-jt)^n f(t)]|_{\omega} = \int_{-T}^T (-jt)^n f(t) e^{-j\omega t} dt.$$

From the discussion in Section 2.3.2, it is apparent that the transform of a piecewise continuous function with finite duration must be classically differentiable up to any order, and that every derivative is continuous.

It should be noted that the integral defining  $F(\omega)$  in formula 2.73 is, in fact, well defined for every complex  $\omega = x + jy$ . It is not difficult to show that the real and imaginary parts of  $F(x + jy)$  satisfy the Cauchy–Riemann equations of complex analysis (see Appendix A). Thus,  $F(\omega)$  is an analytic function on both the real line and the complex plane. As a consequence, it follows that the transform of a finite duration function cannot vanish (or be any constant value) over any nontrivial subinterval of the real line. In particular, no function of finite duration can also be band limited (see Section 2.3.7).

Another important feature of finite duration functions is that their transforms can be reconstructed using a discrete sampling of the transforms. This is discussed more fully in Section 2.5.

### 2.3.7 Band-Limited Functions

Let  $f(t)$  be a function with Fourier transform  $F(\omega)$ . The function,  $f(t)$ , is said to be band limited if there is a  $0 < \Omega < \infty$ , such that

$$F(\omega) = 0 \quad \text{whenever } \Omega < |\omega|.$$

The quantity  $2\Omega$  is called the bandwidth of  $f(t)$ .

By the near equivalence of the Fourier and inverse Fourier transforms, it should be clear that  $f(t)$  satisfies properties analogous to those satisfied by the transforms of finite duration functions. In particular

$$f(t) = \frac{1}{2\pi} \int_{-\Omega}^{\Omega} F(\omega) e^{j\omega t} d\omega, \quad (2.74)$$

and, for any nonnegative integer,  $n$ ,  $f^{(n)}(t)$  is a well-defined continuous function given by

$$f^{(n)}(t) = \frac{1}{2\pi} \int_{-\Omega}^{\Omega} (j\omega)^n F(\omega) e^{j\omega t} d\omega.$$

Letting  $t = x + jy$  in Equation 2.74, it is easily verified that  $f(x + jy)$  is a well-defined analytic function on both the real line and on the entire complex plane. From this it follows that if  $f(t)$  is band limited, then  $f(t)$  cannot vanish (or be any constant value) over any nontrivial subinterval of the real line. Thus, no band-limited function can also be of finite duration. This fact must be considered in many practical applications where it would be desirable (but, as just noted, impossible) to assume that the functions of interest are both band-limited and of finite duration.

Another most important feature of band-limited functions is that they can be reconstructed using a discrete sampling of their values. This is discussed more thoroughly in Section 2.5.

### 2.3.8 Finite Power Functions

For a given function,  $f(t)$ , the average autocorrelation function,  $\bar{\rho}_f(t)$ , is defined by

$$\bar{\rho}_f(t) = \lim_{T \rightarrow \infty} \frac{1}{2T} \int_{-T}^T f^*(s) f(t+s) ds, \quad (2.75)$$

or, equivalently, by

$$\bar{\rho}_f(t) = \lim_{T \rightarrow \infty} \frac{1}{2T} f_T(t) \star f_T(t) \quad (2.76)$$

where the  $\star$  denotes correlation (see Section 2.2.10), and  $f_T(t)$  is the truncation of  $f(t)$  at  $t = \pm T$ ,

$$f_T(t) = f(t)p_T(t) = \begin{cases} f(t), & \text{if } -T \leq t \leq T \\ 0, & \text{otherwise} \end{cases}. \quad (2.77)$$

If  $\bar{p}_f(t)$  is a well-defined function (or generalized function), then  $f(t)$  is called a finite power function.

The power spectrum or power spectral density,  $P(\omega)$ , of a finite power function,  $f(t)$  is defined to be the Fourier transform of its average autocorrelation,

$$P(\omega) = \mathcal{F}[\bar{p}_f(t)] \Big|_{\omega} = \int_{-\infty}^{\infty} \bar{p}_f(t)e^{-j\omega t} dt. \quad (2.78)$$

Using formula 2.76 for  $\bar{p}_f(t)$  and recalling the Wiener-Khintchine theorem (Section 2.2.10).

$$\mathcal{F}[\bar{p}_f(t)] \Big|_{\omega} = \lim_{T \rightarrow \infty} \frac{1}{2T} \mathcal{F}[f_T(t) \star f_T(t)] \Big|_{\omega} = \lim_{T \rightarrow \infty} \frac{1}{2T} |F_T(\omega)|^2$$

where  $F_T(\omega)$  is the Fourier transform of  $f_T(t)$ ,

$$F_T(\omega) = \int_{-\infty}^{\infty} f(t)p_T(t)e^{-j\omega t} dt = \int_{-T}^T f(t)e^{-j\omega t} dt.$$

Thus, an alternate formula for the power spectrum is

$$P(\omega) = \lim_{T \rightarrow \infty} \frac{1}{2T} \left| \int_{-T}^T f(t)e^{-j\omega t} dt \right|^2. \quad (2.79)$$

The average power in  $f(t)$  is defined to be

$$\bar{p}_f(0) = \lim_{T \rightarrow \infty} \frac{1}{2T} \int_{-T}^T |f(s)|^2 ds. \quad (2.80)$$

Because  $P(\omega) = \mathcal{F}[\bar{p}_f(t)] \Big|_{\omega}$ , this is equivalent to

$$\bar{p}_f(0) = \mathcal{F}^{-1}[P(\omega)] \Big|_0 = \frac{1}{2\pi} \int_{-\infty}^{\infty} P(\omega) d\omega.$$

A number of properties of the average autocorrelation should be noted. They are

1.  $\bar{p}_f(t)$  is invariant under a shift in  $f(t)$ , that is, if  $g(t) = f(t - t_0)$ , then  $\bar{p}_g(t) = \bar{p}_f(t)$ .
2.  $\bar{p}_f(t)$  and  $|\bar{p}_f(t)|$  each has a maximum value at  $t = 0$ .
3.  $(\bar{p}_f(t))^* = \bar{p}_f(-t)$ . Thus, as is often the case, if  $f(t)$  is a real-valued function, then  $\bar{p}_f(t)$  is an even real-valued function.

As a consequence of the second property above, any function,  $f(t)$ , satisfying

$$\lim_{T \rightarrow \infty} \frac{1}{2T} \int_{-T}^T |f(s)|^2 ds < \infty$$

is a finite power function.

The three properties listed above are easily derived. For the first,

$$\begin{aligned} \bar{p}_g(t) &= \lim_{T \rightarrow \infty} \frac{1}{2T} \int_{-T}^T f^*(s - t_0)f(s - t_0 + t) ds \\ &= \lim_{T \rightarrow \infty} \frac{1}{2T} \int_{-T-t_0}^{T-t_0} f^*(\sigma)f(\sigma + t) ds \\ &= \lim_{T \rightarrow \infty} \frac{1}{2T} \int_{-T}^T f^*(\sigma)f(\sigma + t) d\sigma \\ &\quad + \lim_{T \rightarrow \infty} \frac{1}{2T} \int_T^{T-t_0} f^*(\sigma)f(\sigma + t) d\sigma \\ &\quad + \lim_{T \rightarrow \infty} \frac{1}{2T} \int_{-T-t_0}^{-T} f^*(\sigma)f(\sigma + t) d\sigma. \end{aligned}$$

The first limit in the last line above equals  $\bar{p}_f(t)$  while the other limits, involving integrals over intervals of fixed bounded length, must vanish.

From an application of the Schwarz inequality,

$$\left| \int_{-T}^T f^*(s)f(s+t) ds \right|^2 \leq \int_{-T}^T |f^*(s)|^2 ds \int_{-T}^T |f(s+t)|^2 ds,$$

it follows, after taking the limit, that

$$|\bar{p}_f(t)|^2 \leq |\bar{p}_f(0)|^2.$$

Hence, at  $t = 0$ ,  $|\bar{p}_f(t)|$  has a maximum (as does  $\bar{p}_f(t)$ , because  $\bar{p}_f(0) = |\bar{p}_f(0)|$ ).

Finally, using the substitution  $\sigma = s + t$ ,

$$\begin{aligned} (\bar{p}_f(t)) &= \left( \lim_{T \rightarrow \infty} \frac{1}{2T} \int_{-T}^T f^*(s)f(t+s) ds \right) \\ &= \lim_{T \rightarrow \infty} \frac{1}{2T} \int_{-T}^T f(s)f^*(t+s) ds \\ &= \lim_{T \rightarrow \infty} \frac{1}{2T} \int_{-T}^T f(\sigma - t)f^*(\sigma) d\sigma \\ &= \bar{p}_f(-t). \end{aligned}$$

If  $f(t)$  is a finite energy function, then, trivially, it is also a finite power function (with zero average power). Nontrivial examples of finite power functions include periodic functions, nearly periodic

functions, constants, and step functions. Finite energy functions also play a significant role in signal-processing problems dealing with noise.

### Example 2.28

Consider the step function,

$$u(t) = \begin{cases} 0, & \text{if } t < 0 \\ 1, & \text{if } 0 < t \end{cases}$$

For  $0 \leq t$ ,

$$\begin{aligned} \bar{\rho}_u(t) &= \lim_{T \rightarrow \infty} \frac{1}{2T} \int_{-T}^T u(s)u(s+t)ds \\ &= \lim_{T \rightarrow \infty} \frac{1}{2T} \int_0^T ds \\ &= \frac{1}{2}. \end{aligned}$$

Because the step function is a real function, its average auto-correlation function must be an even function. Thus, for all  $t$ ,

$$\bar{\rho}_u(t) = \frac{1}{2},$$

showing that the step function is a finite power function. Its average power,  $\bar{\rho}_u(0)$ , is equal to  $1/2$ , and its power spectrum is

$$P(\omega) = \mathcal{F} \left[ \frac{1}{2} \right] \Big|_{\omega} = \pi \delta(\omega).$$

### Example 2.29

Consider now the function

$$f(t) = \begin{cases} 0, & \text{if } t \leq 0 \\ \sin t, & \text{if } 0 < t \end{cases}$$

For  $0 \leq t$ ,

$$\begin{aligned} \bar{\rho}_f(t) &= \lim_{T \rightarrow \infty} \frac{1}{2T} \int_{-T}^T f(s)f(s+t)ds \\ &= \lim_{T \rightarrow \infty} \frac{1}{2T} \int_0^T \sin(s) \sin(s+t)ds \\ &= \lim_{T \rightarrow \infty} \frac{1}{2T} \int_0^T \sin(s)[\sin(s)\cos(t) + \cos(s)\sin(t)]ds \\ &= \lim_{T \rightarrow \infty} \frac{1}{2T} \int_0^T \cos(t) \int_0^T \sin^2(s)ds + \sin(t) \int_0^T \sin(s)\cos(s)ds \\ &= \lim_{T \rightarrow \infty} \frac{1}{2T} \left[ \cos(t) \left( \frac{T}{2} - \frac{\sin(2T)}{4} \right) - \sin(t) \frac{\sin^2(T)}{2} \right] \\ &= \frac{1}{4} \cos(t). \end{aligned}$$

Because  $\bar{\rho}_f(t)$  is even,

$$\bar{\rho}_f(t) = \frac{1}{4} \cos(t)$$

for all  $t$ . The average power is

$$\bar{\rho}_f(0) = \frac{1}{4},$$

and the power spectrum is

$$P(\omega) = \mathcal{F} \left[ \frac{1}{4} \cos(t) \right] \Big|_{\omega} = \frac{\pi}{4} [\delta(\omega - 1) + \delta(\omega + 1)].$$

### 2.3.9 Periodic Functions

Let  $0 < p < \infty$ . A function,  $f(t)$ , is periodic (with period  $p$ ) if

$$f(t + p) = f(t)$$

for every real value of  $t$ . The Fourier series,  $\text{FS}[f]$ , for such a function is given by

$$\text{FS}[f] \Big|_t = \sum_{n=-\infty}^{\infty} c_n e^{jn\Delta\omega t}, \quad (2.81)$$

where

$$\Delta\omega = \frac{2\pi}{p}$$

and, for each  $n$ ,

$$c_n = \frac{1}{p} \int_{\text{period}} f(t) e^{-jn\Delta\omega t} dt. \quad (2.82)$$

(Because of the periodicity of the integrand, the integral in formula 2.82 can be evaluated over any interval of length  $p$ .)

As long as  $f(t)$  is at least piecewise smooth, its Fourier series will converge, and at every value of  $t$  at which  $f(t)$  is continuous,

$$f(t) = \sum_{n=-\infty}^{\infty} c_n e^{jn\Delta\omega t}.$$

At points where  $f(t)$  has a “jump” discontinuity, the Fourier series converges to the midpoint of the jump. In any immediate neighborhood of a jump discontinuity any finite partial sum of the Fourier series,

$$\sum_{n=-N}^N c_n e^{jn\Delta\omega t},$$

will oscillate wildly and will, at points, significantly over- and undershoot the actual value of  $f(t)$  ("Ringing" or Gibbs phenomena).

Because periodic functions are not at all integrable over the entire real line, the standard integral formula, formula 2.1, cannot be used to find the Fourier transform of  $f(t)$ . Using the generalized theory, however, it can be shown that as generalized functions.

$$f(t) = \sum_{n=-\infty}^{\infty} c_n e^{jn\Delta\omega t} \quad (2.83)$$

and that the Fourier transform of  $f(t)$  is given by

$$\begin{aligned} F(\omega) &= \mathcal{F} \left[ \sum_{n=-\infty}^{\infty} c_n e^{jn\Delta\omega t} \right] \Big|_{\omega} \\ &= \sum_{n=-\infty}^{\infty} c_n \mathcal{F} [e^{jn\Delta\omega t}] \Big|_{\omega} \\ &= \sum_{n=-\infty}^{\infty} c_n 2\pi \delta(\omega - n\Delta\omega). \end{aligned}$$

It should be noted that  $F(\omega)$  is a regular array of delta functions with spacing inversely proportional to the period of  $f(t)$  (see Section 2.3.10).

If  $f(t)$  is periodic (with period  $p$ ), then  $f(t)$  is a finite power function (but is not, unless  $f(t)$  is the zero function, a finite energy function). The average autocorrelation,  $\bar{\rho}_f(t)$ , will also be periodic and have period  $p$ . Formula 2.75 reduces to

$$\bar{\rho}_f(t) = \frac{1}{p} \int_{\text{period}} f^*(s) f(s+t) ds. \quad (2.84)$$

Because  $\bar{\rho}_f(t)$  is periodic, it can also be expanded as a Fourier series,

$$\bar{\rho}_f(t) = \sum_{n=-\infty}^{\infty} a_n e^{jn\Delta\omega t}, \quad (2.85)$$

and the power spectrum is the regular array of delta functions,

$$P(\omega) = \sum_{n=-\infty}^{\infty} a_n 2\pi \delta(\omega - n\Delta\omega).$$

A useful relation between the Fourier coefficients of  $\bar{\rho}_f(t)$ ,

$$a_n = \frac{1}{p} \int_{\text{period}} \bar{\rho}_f(t) e^{-jn\Delta\omega t} dt, \quad (2.86)$$

and the Fourier coefficients of  $f(t)$ ,

$$c_n = \frac{1}{p} \int_{\text{period}} f(t) e^{-jn\Delta\omega t} dt, \quad (2.87)$$

is easily derived. Inserting formula 2.84 for  $\bar{\rho}_f(t)$  into formula 2.86, rearranging, and using the substitution  $\tau = s + t$ ,

$$\begin{aligned} a_n &= \frac{1}{p} \int_{\text{period}} \left[ \frac{1}{p} \int_{\text{period}} f^*(s) f(s+t) ds \right] e^{-jn\Delta\omega t} dt \\ &= \frac{1}{p} \int_{\text{period}} \frac{1}{p} f^*(s) \left[ \int_{\text{period}} f(s+t) e^{-jn\Delta\omega t} dt \right] ds \\ &= \frac{1}{p} \int_{\text{period}} \frac{1}{p} f^*(s) \left[ \int_{\text{period}} f(\tau) e^{-jn\Delta\omega(\tau-s)} d\tau \right] ds \\ &= \left[ \frac{1}{p} \int_{\text{period}} f^*(s) e^{jn\Delta\omega s} ds \right] \left[ \frac{1}{p} \int_{\text{period}} f(\tau) e^{-jn\Delta\omega \tau} d\tau \right] \\ &= c_n^* c_n. \end{aligned}$$

Thus,  $a_n = |c_n|^2$ .

In summary, if  $f(t)$  is periodic with period  $p$ , then so is its average autocorrelation function,  $\bar{\rho}_f(t)$ . Moreover (as generalized functions)

$$f(t) = \sum_{n=-\infty}^{\infty} c_n e^{jn\Delta\omega t}, \quad (2.88)$$

$$F(\omega) = 2\pi \sum_{n=-\infty}^{\infty} c_n \delta(\omega - n\Delta\omega), \quad (2.89)$$

$$\bar{\rho}_f(t) = \sum_{n=-\infty}^{\infty} |c_n|^2 e^{jn\Delta\omega t}, \quad (2.90)$$

and

$$P(\omega) = 2\pi \sum_{n=-\infty}^{\infty} |c_n|^2 \delta(\omega - n\Delta\omega), \quad (2.91)$$

where  $F(\omega)$  is the Fourier transform of  $f(t)$ ,  $P(\omega)$  is the power spectrum of  $f(t)$ ,

$$\Delta\omega = \frac{2\pi}{p}, \quad (2.92)$$

and, for each  $n$ ,

$$c_n = \frac{1}{p} \int_{\text{period}} f(t) e^{-jn\Delta\omega t} dt. \quad (2.93)$$

Analogous formulas are valid if  $G(\omega)$  is a periodic function with period  $P$ . In particular, its inverse transform is

$$g(t) = \sum_{k=-\infty}^{\infty} C_k \delta(t - k\Delta t), \quad (2.94)$$



where

$$\Delta t = \frac{2\pi}{p}$$

and, for each  $k$ ,

$$C_k = \frac{1}{p} \int_{\text{period}} G(\omega) e^{jk\Delta t \omega} d\omega.$$

Again, because of periodicity, the integral can be evaluated over any interval of length  $P$ .

**Example 2.30 Fourier Series and Transform of a Periodic Function**

Consider the “saw” function,

$$\text{saw}(t) = \begin{cases} t, & \text{if } -1 \leq t < 1 \\ \text{saw}(t + 2), & \text{for all } t \end{cases}$$

The graph of this saw function is sketched in Figure 2.4. Here, because the period is  $p = 2$ , formula 2.92 becomes

$$\Delta\omega = \frac{2\pi}{p} = \pi,$$

and formula 2.93 becomes

$$c_n = \frac{1}{2} \int_{-1}^1 t e^{-jn\pi t} dt = \begin{cases} 0, & \text{if } n = 0 \\ (-1)^n \frac{j}{n\pi}, & \text{if } n = \pm 1, \pm 2, \pm 3, \dots \end{cases}$$

Using Equations 2.88 and 2.90,

$$\text{saw}(t) = \sum_{\substack{n=-\infty \\ n \neq 0}}^{\infty} (-1)^n \frac{j}{n\pi} e^{jn\pi t}$$

and

$$\mathcal{F}[\text{saw}(t)]|_{\omega} = j \sum_{\substack{n=-\infty \\ n \neq 0}}^{\infty} (-1)^n \frac{2}{n} \delta(\omega - n\pi).$$

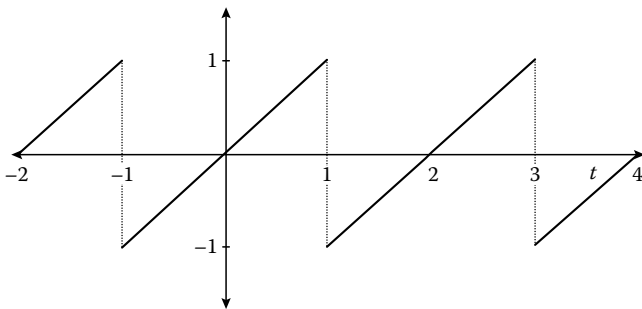


FIGURE 2.4 The saw function.

The graph of the  $N$ th partial sum approximation to  $\text{saw}(t)$ ,

$$\sum_{\substack{n=-\infty \\ n \neq 0}}^{\infty} (-1)^n \frac{j}{n\pi} e^{jn\pi t},$$

is sketched in Figure 2.5 (with  $N = 20$ ), and the graph of the imaginary part of  $\mathcal{F}[\text{saw}(t)]|_{\omega}$  is sketched in Figure 2.6. The Gibbs phenomenon is evident in Figure 2.5. Formulas 2.90 and 2.91 for the autocorrelation function,  $\bar{p}_{\text{saw}}(t)$ , and the power spectrum,  $P(\omega)$ , yield

$$\bar{p}_{\text{saw}}(t) = \frac{1}{\pi^2} \sum_{\substack{n=-\infty \\ n \neq 0}}^{\infty} \frac{1}{n^2} e^{jn\pi t}$$

and

$$P(\omega) = \frac{2}{\pi} \sum_{\substack{n=-\infty \\ n \neq 0}}^{\infty} \frac{1}{n^2} \delta(\omega - n\pi).$$

**2.3.10 Regular Arrays of Delta Functions**

Let  $\Delta x > 0$ . A function  $\phi(x)$  is called a regular array of delta functions (with spacing  $\Delta x$ ) if

$$\phi(x) = \sum_{n=-\infty}^{\infty} \phi_n \delta(x - n\Delta x),$$

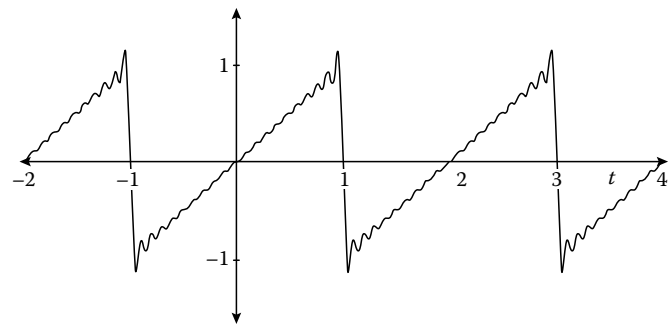


FIGURE 2.5 Partial sum of the saw function’s Fourier series.

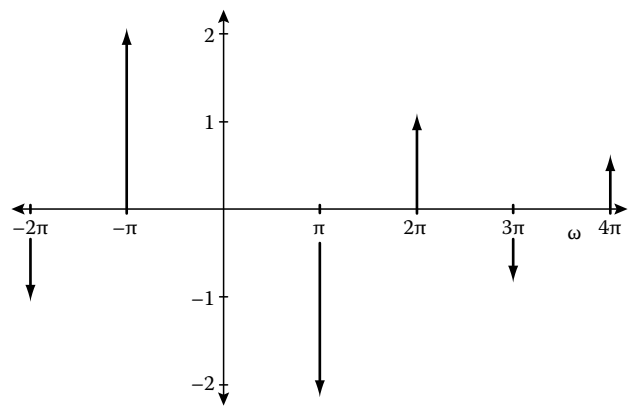


FIGURE 2.6 Fourier transform of the saw function (imaginary part).

where the  $\phi_n$ 's denote fixed values. Such arrays arise in sampling and as transforms of periodic functions. They are also useful in describing discrete probability distributions (see Examples 2.32 and 2.33 below).

**Example 2.31**

The transform of the saw function from Example 2.30,

$$\mathcal{F}[\text{saw}(t)]|_{\omega} = j \sum_{\substack{n=-\infty \\ n \neq 0}}^{\infty} (-1)^n \frac{2}{n} \delta(\omega - n\pi),$$

is a regular array of delta functions with spacing  $\Delta\omega = \pi$ .

Let  $f(t)$  be a function with Fourier transform  $F(\omega)$ . A straightforward extension and restatement of the results in Section 2.3.9 is that  $f(t)$  is periodic if and only if  $F(\omega)$  is a regular array of delta functions. The period,  $p$ , of  $f(t)$ , and the spacing,  $\Delta\omega$ , of  $F(\omega)$  are related by

$$p\Delta\omega = 2\pi.$$

Moreover,

$$f(t) = \frac{1}{2\pi} \sum_{n=-\infty}^{\infty} F_n e^{jn\Delta\omega t}$$

and

$$F(\omega) = \sum_{n=-\infty}^{\infty} F_n \delta(\omega - n\Delta\omega),$$

where, for each  $n$ ,

$$F_n = \frac{2\pi}{p} \int_{\text{period}} f(t) e^{-jn\Delta\omega t} dt. \quad (2.95)$$

Conversely, if  $g(t)$  is a function with Fourier transform  $G(\omega)$  then  $g(t)$  is a regular array of delta functions if and only if  $G(\omega)$  is periodic. The spacing of  $g(t)$ ,  $\Delta t$ , and the period of  $G(\omega)$ ,  $P$ , are related by

$$p\Delta t = 2\pi.$$

Moreover,

$$g(t) = \sum_{k=-\infty}^{\infty} g_k \delta(t - k\Delta t)$$

and

$$G(\omega) = \sum_{k=-\infty}^{\infty} g_{-k} e^{jk\Delta t \omega},$$

where, for each  $k$ ,

$$g_k = \frac{1}{p} \int_{\text{period}} G(\omega) e^{jk\Delta t \omega} d\omega.$$

**Example 2.32**

For any  $\lambda > 0$ , the corresponding Poisson probability distribution is given by

$$\phi_{\lambda}(t) = e^{-\lambda} \sum_{n=0}^{\infty} \frac{\lambda^n}{n!} \delta(t - n).$$

Its Fourier transform,  $\psi_{\lambda}(\omega)$ , is given by

$$\psi_{\lambda}(\omega) = e^{-\lambda} \sum_{n=0}^{\infty} \frac{\lambda^n}{n!} e^{-jn\omega}.$$

Recalling the Taylor series for the exponential,

$$\begin{aligned} \psi_{\lambda}(\omega) &= e^{-\lambda} \sum_{n=0}^{\infty} \frac{1}{n!} (\lambda e^{-j\omega})^n \\ &= e^{-\lambda} e^{\lambda e^{-j\omega}} \\ &= e^{-\lambda(1 - \cos \omega + j \sin \omega)}, \end{aligned}$$

which is clearly a periodic function with period  $P = 2\pi$ . It can also be seen that the amplitude,  $A(\omega)$ , and the phase,  $\Theta(\omega)$ , of  $\psi_{\lambda}(\omega)$  are given by

$$A(\omega) = e^{-\lambda(1 - \cos \omega)} \quad \text{and} \quad \Theta(\omega) = -\lambda \sin \omega.$$

**Example 2.33**

For any nonnegative integer,  $n$ , and  $0 \leq p \leq 1$ , the corresponding binomial probability distribution is given by

$$b_{n,p}(t) = \sum_{k=0}^n \binom{n}{k} p^k q^{n-k} \delta(t - k)$$

where  $q = 1 - p$ . The Fourier transform of  $b_{n,p}$  is given by

$$B_{n,p}(\omega) = \sum_{n=0}^{\infty} \binom{n}{k} p^k q^{n-k} e^{-jk\omega} = \sum_{k=0}^{\infty} \binom{n}{k} (pe^{-j\omega})^k q^{n-k}.$$

By the binomial theorem, this can be rewritten as

$$B_{n,p}(\omega) = (pe^{-j\omega} + q)^n,$$

which is clearly periodic with period  $P = 2\pi$ .

A regular array of delta functions,

$$g(t) = \sum_{k=-\infty}^{\infty} g_k \delta(t - k\Delta t),$$

cannot be a finite energy function (unless all the  $g_k$ 's vanish), but, if the  $g_k$ 's are bounded, can be treated as a finite power function with average autocorrelation function,  $\bar{\rho}_g(t)$ , and power spectrum,  $P(\omega)$ , given by

$$\bar{\rho}_g(t) = \sum_{k=-\infty}^{\infty} A_k \delta(t - k\Delta t)$$

and

$$P(\omega) = \sum_{k=-\infty}^{\infty} A_k e^{-jk\Delta t\omega},$$

where

$$A_k = \lim_{M \rightarrow \infty} \frac{1}{2M\Delta t} \sum_{m=-M}^M g_m^* g_{m+k}.$$

It should be noted, however, that if

$$\sum_{m=-\infty}^{\infty} |g_m|^2 < \infty,$$

then the  $A_k$ 's will all be zero.

### 2.3.11 Periodic Arrays of Delta Functions

Regular periodic arrays of delta functions are of considerable importance because the formulas for the discrete Fourier transforms can be based directly on formulas derived in computing transforms of regular arrays that are also periodic. For an array with spacing  $\Delta x$ ,

$$\phi(x) = \sum_{k=-\infty}^{\infty} \phi_k \delta(x - k\Delta x),$$

to also be periodic with period  $p$ ,

$$\phi(x + p) = \phi(x),$$

it is necessary that there be a positive integer,  $N$ , called the index period, such that

$$\phi_{k+N} = \phi_k \quad \text{for all } k.$$

The index period, spacing, and period of  $\phi(x)$  are related by

$$\text{period of } \phi(x) = (\text{index period of } \phi(x)) \times (\text{spacing of } \phi(x)).$$

### Example 2.34

The regular periodic array,

$$f(t) = \sum_{k=-\infty}^{\infty} f_k \delta(t - k\Delta t),$$

with spacing  $\Delta t = 1/2$ , index period  $N = 4$ , and  $(f_0, f_1, f_2, f_3) = (1, 2, 3, 3)$ , is sketched in Figure 2.7. Note that  $f_4 = f_0, f_5 = f_1, \dots$ , and that the period of  $f(t)$  is  $4\Delta t = 2$ .

Let

$$f(t) = \sum_{k=-\infty}^{\infty} f_k \delta(t - k\Delta t)$$

be a regular periodic array with spacing  $\Delta t$ , index period  $N$ , and period  $p = N\Delta t$ . From the discussion in Section 2.3.10 on regular arrays, it is evident that the Fourier transform of  $f(t)$  is also a regular periodic array of delta functions.

$$F(\omega) = \sum_{n=-\infty}^{\infty} F_n \delta(\omega - n\Delta\omega). \tag{2.96}$$

Also,  $f(t)$  can be expressed as a corresponding Fourier series,

$$f(t) = \frac{1}{2\pi} \sum_{n=-\infty}^{\infty} F_n e^{jn\Delta\omega t}. \tag{2.97}$$

The spacing,  $\Delta\omega$ , and period,  $P$ , of  $F(\omega)$  are related to the spacing,  $\Delta t$ , and period,  $p$ , of  $f(t)$  by

$$\Delta\omega = \frac{2\pi}{p} \quad \text{and} \quad P = \frac{2\pi}{\Delta t}.$$

The index period,  $M$ , of  $F(\omega)$  is given by

$$M = \frac{P}{\Delta\omega} = \frac{(2\pi/\Delta t)}{(2\pi/p)} = \frac{p}{\Delta t} = N.$$

Using Equation 2.95,

$$F_n = \frac{2\pi}{\pi} \int_{t=-\frac{\Delta t}{2}}^{p-\frac{\Delta t}{2}} \left( \sum_{k=-\infty}^{\infty} f_k \delta(\tau - k\Delta t) \right) e^{-jn\Delta\omega t} dt. \tag{2.98}$$

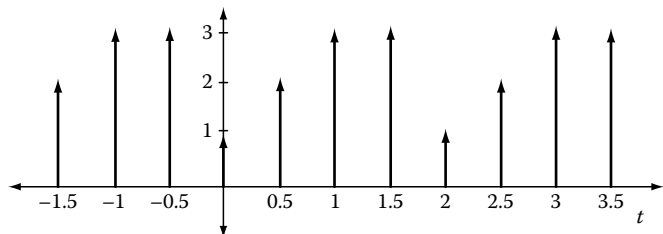


FIGURE 2.7 A regular periodic array of delta functions.

But, as is easily verified,

$$\int_{t=-\frac{\Delta t}{2}}^{t=\frac{\Delta t}{2}} \delta(t - k\Delta t) e^{-jn\Delta\omega t} dt = \begin{cases} e^{-jn\Delta\omega t}, & \text{if } 0 \leq k \leq N-1, \\ 0, & \text{otherwise} \end{cases},$$

and

$$\Delta\omega\Delta t = \frac{2\pi\Delta t}{\rho} = \frac{2\pi}{N}.$$

Thus, Equation 2.98 reduces to

$$F_n = \frac{2\pi}{N\Delta t} \sum_{k=0}^{N-1} f_k e^{-j\frac{2\pi}{N}nk}. \quad (2.99)$$

A similar set of calculations yields the inverse relation,

$$f_k = \frac{1}{N\Delta\omega} \sum_{n=0}^{N-1} F_n e^{j\frac{2\pi}{N}kn}. \quad (2.100)$$

Formulas for the autocorrelation function,  $\bar{\rho}_f(t)$ , and the power spectrum,  $P(\omega)$ , follow immediately from the above and the discussion in Sections 2.3.9 and 2.3.10. They are

$$\bar{\rho}_f(t) = \sum_{k=-\infty}^{\infty} A_k \delta(t - k\Delta t), \quad (2.101)$$

where

$$A_k = \frac{1}{N\Delta t} \sum_{m=0}^{N-1} f_m^* f_{m+k}, \quad (2.102)$$

and

$$P(\omega) = \frac{1}{2\pi} \sum_{n=-\infty}^{\infty} |F_n|^2 \delta(\omega - n\Delta\omega). \quad (2.103)$$

### Example 2.35 The Comb Function

For each  $\Delta x > 0$ , the corresponding comb function is

$$\text{comb}_{\Delta x}(x) = \sum_{k=-\infty}^{\infty} \delta(x - k\Delta x).$$

With index period  $N=1$  and with the spacing equal to the period, the comb function is the simplest possible nonzero regular period array. By the above discussion,

$$F(\omega) = \mathcal{F}[\text{comb}_{\Delta t}(t)]|_{\omega}$$

must also be a regular periodic array,

$$F(\omega) = \sum_{n=-\infty}^{\infty} F_n \delta(\omega - n\Delta\omega),$$

where

$$\Delta\omega = \frac{2\pi}{\Delta t}.$$

Because the index period of  $F(\omega)$  must also be  $N=1$ ,

$$F_n = F_0 = \frac{2\pi}{\Delta t} \sum_{k=0}^0 f_k e^{-j\frac{2\pi}{N}0 \cdot k} = \Delta\omega,$$

for all  $n$ . Combining the last few equations gives

$$\mathcal{F}[\text{comb}_{\Delta t}(t)]|_{\omega} = \sum_{n=-\infty}^{\infty} \Delta\omega \delta(\omega - n\Delta\omega) = \Delta\omega \text{comb}_{\Delta\omega}(\omega),$$

where

$$\Delta\omega = \frac{2\pi}{\Delta t}.$$

From formulas 2.101 through 2.103, the average correlation function and the power spectrum for  $\text{comb}_{\Delta t}(t)$  are given by

$$\bar{\rho}(t) = \frac{1}{\Delta t} \sum_{k=-\infty}^{\infty} \delta(t - k\Delta t) = \frac{1}{\Delta t} \text{comb}_{\Delta t}(t)$$

and

$$P(\omega) = \frac{\Delta\omega}{\Delta t} \sum_{n=-\infty}^{\infty} \delta(\omega - n\Delta\omega) = \frac{\Delta\omega}{\Delta t} \text{comb}_{\Delta\omega}(\omega).$$

In addition, using Equation 2.97, the comb function can be expressed as a Fourier series,

$$\text{comb}_{\Delta t}(t) = \frac{\Delta\omega}{2\pi} \sum_{n=-\infty}^{\infty} e^{jn\Delta\omega t} = \frac{1}{\Delta t} \sum_{n=-\infty}^{\infty} e^{jn\Delta\omega t}.$$

### 2.3.12 Powers of Variables and Derivatives of Delta Functions

In Example 2.4 it was shown that, for any real value of  $\alpha$ ,

$$\mathcal{F}[e^{j\alpha t}]|_{\omega} = 2\pi\delta(\omega - \alpha).$$

Letting  $\alpha = 0$ , this gives

$$\mathcal{F}[1]|_{\omega} = 2\pi\delta(\omega),$$

and, by symmetry or near equivalence,

$$\mathcal{F}[\delta(t)]|_{\omega} = 1.$$

Now, let  $n$  be any nonnegative integer. Because, trivially,  $x^n = x^n \cdot 1$ , it immediately follows from an application of identities 2.50 through 2.53 that

$$\mathcal{F}[t^n]|_{\omega} = j^n 2\pi \delta^{(n)}(\omega) \tag{2.104}$$

$$\mathcal{F}^{-1}[\omega^n]|_t = (-j)^n \delta^{(n)}(t), \tag{2.105}$$

$$\mathcal{F}[\delta^{(n)}(t)]|_{\omega} = (j\omega)^n, \tag{2.106}$$

and

$$\mathcal{F}^{-1}[\delta^{(n)}(\omega)]|_t = \frac{(-jt)^n}{2\pi}, \tag{2.107}$$

where  $\delta^{(n)}(x)$  is the  $n$ th (generalized) derivative of the delta function.

### 2.3.13 Negative Powers and Step Functions

The basic relation between step functions and negative powers is

$$\mathcal{F}[\text{sgn}(t)]|_{\omega} = -j \frac{2}{\omega}, \tag{2.108}$$

where  $\text{sgn}(t)$  is the signum function,

$$\text{sgn}(t) = \begin{cases} -1, & \text{if } t < 0 \\ +1 & \text{if } 0 < t \end{cases}.$$

Because the step function,

$$u(t) = \begin{cases} 0, & \text{if } t < 0 \\ 1, & \text{if } 0 < t \end{cases},$$

can be written in terms of the signum function,

$$u(t) = \frac{1}{2} [\text{sgn}(t) + 1],$$

formula 2.108 is equivalent to

$$\mathcal{F}[u(t)]|_{\omega} = \pi \delta(\omega) - j \frac{1}{\omega}. \tag{2.109}$$

A number of useful formulas can be easily derived from Equations 2.108 and 2.109 with the aid of various identities from the identities in Section 2.2. Some of these formulas are

$$\mathcal{F}\left[\frac{1}{t}\right]|_{\omega} = -j\pi \text{sgn}(\omega), \tag{2.110}$$

$$\mathcal{F}[t^{-n}]|_{\omega} = -j\pi \frac{(-j\omega)^{n-1}}{(n-1)!} \text{sgn}(\omega), \tag{2.111}$$

$$\mathcal{F}[|t|]|_{\omega} = -\frac{2}{\omega^2}, \tag{2.112}$$

$$\mathcal{F}[t^{-n} \text{sgn}(t)]|_{\omega} = (-j)^{n+1} \frac{2n}{\omega^{n+1}}, \tag{2.113}$$

$$\mathcal{F}[\text{ramp}(t)]|_{\omega} = j\pi \delta'(\omega) - \frac{1}{\omega^2}, \tag{2.114}$$

and

$$\mathcal{F}[t^n u(t)]|_{\omega} = j^n \pi \delta^{(n)}(\omega) + n! \left(\frac{-j}{\omega}\right)^{n+1}. \tag{2.115}$$

In these formulas  $n$  denotes an arbitrary positive integer.

Derivations of formulas 2.108 and 2.109 are easily obtained. One derivation starts with the observation that, for any  $\alpha < 0$ ,

$$u(t) = \int_{\alpha}^t \delta(s) ds.$$

By identity 2.57, with  $f(t) = \delta(t)$  and  $F(\omega) = \mathcal{F}[\delta(t)]|_{\omega} = 1$ ,

$$\begin{aligned} \mathcal{F}[u(t)]|_{\omega} &= \mathcal{F}\left[\int_{\alpha}^t f(s) ds\right]|_{\omega} \\ &= -j \frac{F(\omega)}{\omega} + c\delta(\omega) \\ &= -j \frac{1}{\omega} + c\delta(\omega), \end{aligned} \tag{2.116}$$

where  $c$  is some constant. From this

$$\begin{aligned} \mathcal{F}[\text{sgn}(t)]|_{\omega} &= \mathcal{F}[2u(t) - 1]|_{\omega} \\ &= 2 \left[-j \frac{1}{\omega} + c\delta(\omega)\right] - 2\pi \delta(\omega) \\ &= -j \frac{2}{\omega} + 2(c - \pi)\delta(\omega). \end{aligned} \tag{2.117}$$

Because  $\text{sgn}(t)$  is an odd function, so is  $\mathcal{F}[\text{sgn}(t)]|_{\omega}$  and, hence, so is the right-hand side of Equation 2.117. But, because the delta function is even, this is possible only if  $c = \pi$ . Plugging this only possible choice for  $c$  into Equations 2.116 and 2.117 gives formulas 2.108 and 2.109.

#### Example 2.36 Derivation of Formulas 2.112 and 2.113

Using identity 2.52,

$$\begin{aligned} \mathcal{F}[t^n \text{sgn}(t)]|_{\omega} &= j^n \frac{d^n}{d\omega^n} \mathcal{F}[\text{sgn}(t)]|_{\omega} \\ &= j^n \frac{d^n}{d\omega^n} \left(-j \frac{2}{\omega}\right) \\ &= (-j)^{n+1} \frac{2n!}{\omega^{n+1}}. \end{aligned}$$

Using this and the observation that

$$|t| = t \operatorname{sgn}(t),$$

it immediately follows that

$$\mathcal{F}[|t|]_{\omega} = \mathcal{F}[t \operatorname{sgn}(t)]_{\omega} = (-j)^{1+1} \frac{2(1!)}{\omega^{1+1}} = -\frac{2}{\omega^2}.$$

One technical flaw in the above discussion should be noted. If  $\phi(x)$  is any function continuous at  $x=0$ , and  $n \geq 1$ , then, from a strict mathematical point of view, the function  $x^{-n}\phi(x)$  is not integrable over any interval containing  $x=0$ . Because of this, it is not possible to define  $\mathcal{F}[t^{-n}]_{\omega}$  or  $\mathcal{F}^{-1}[\omega^{-n}]_t$  via the classical integral formulas. Neither is it possible for the function  $x^{-n}$  to be treated as a generalized function. However, the function  $\ln|x|$  is integrable over any finite interval and can be treated as a legitimate generalized function, as can any of its generalized derivatives (as defined in Section 2.2.11). It is possible to justify rigorously the formulas given in this section, as well as any other standard use of  $x^{-n}$ , by agreeing that  $x^{-1}$  is actually a symbol for the generalized derivative of  $\ln|x|$ , and that, more generally, for any positive integer  $n$ ,  $x^{-n}$  is a symbol for

$$\frac{(-1)^{n-1}}{(n-1)!} \frac{d^n}{dx^n} \ln|x|$$

where the derivatives are taken in the generalized sense as described in Section 2.2.11.

### 2.3.14 Rational Functions

Rational functions often turn out to be the transforms of functions of interest. The simplest nontrivial rational function is given by

$$F(\omega) = \frac{1}{(\omega - \lambda)^m},$$

where

- $m$  is a positive integer
- $\lambda$  is some complex constant

Using the elementary identities and the material from the previous section, it can be directly verified that

$$\mathcal{F}^{-1}\left[\frac{1}{(\omega - \lambda)^m}\right]_t = j \frac{(jt)^{m-1}}{(m-1)!} e^{j\lambda t} \Gamma_{\alpha}(t) \quad (2.118)$$

where  $\alpha$  is the imaginary part of  $\lambda$  and

$$\Gamma_{\alpha}(t) = \begin{cases} u(t), & \text{if } 0 < \alpha \\ \frac{1}{2} \operatorname{sgn}(t), & \text{if } \alpha = 0 \\ -u(-t), & \text{if } \alpha < 0 \end{cases}$$

More generally, if  $F(\omega)$  is any rational function, then  $F(\omega)$  can be written

$$F(\omega) = P(\omega) + R(\omega),$$

Where  $P(\omega)$  is a polynomial,

$$P(\omega) = \sum_{n=0}^N c_n \omega^n,$$

and  $R(\omega)$  is the quotient of two polynomials.

$$R(\omega) = \frac{N(\omega)}{D(\omega)},$$

in which the degree of the numerator is strictly less than the degree of the denominator. According to formula 2.104, the inverse transform of  $P(\omega)$  is simply a linear combination of derivatives of delta functions.

$$\mathcal{F}^{-1}[P(\omega)]_t = \sum_{n=0}^N (-j)^n c_n \delta^{(n)}(t).$$

Letting  $\lambda_1, \lambda_2, \dots, \lambda_K$  be the distinct roots of  $D(\omega)$  and  $M_1, M_2, \dots, M_K$  the corresponding multiplicities of the roots,  $R(\omega)$ , can be written in the partial fraction expansion,

$$R(\omega) = \sum_{k=1}^K \sum_{m=1}^{M_k} \frac{a_{k,m}}{(\omega - \lambda_k)^m}.$$

Thus, applying formula 2.118,

$$\mathcal{F}^{-1}[R(\omega)]_t = j \sum_{k=1}^K e^{j\lambda_k t} \Gamma_{\alpha_k}(t) \sum_{m=1}^{M_k} a_{k,m} \frac{(jt)^{m-1}}{(m-1)!}, \quad (2.119)$$

where, for each  $k$ ,  $\alpha_k$  is the imaginary part of  $\lambda_k$ .

Fourier transforms of rational functions can be computed using the same approach as just described for inverse transforms of rational functions.

#### Example 2.37

Let

$$F(\omega) = \frac{N(\omega)}{D(\omega)} = \frac{5\omega + 9 - 10j}{\omega^2 - 4j\omega - 13}.$$

Using the quadratic formula, the roots of  $D(\omega)$  are found to be

$$\lambda = \frac{4j \pm \sqrt{(4j)^2 + 4(13)}}{2} = \pm 3 + 2j.$$

$F(\omega)$  can then be expanded

$$F(\omega) = \frac{5\omega + 9 - 10j}{\omega^2 - 4j\omega - 13} = \frac{A}{\omega - (3 + 2j)} + \frac{B}{\omega - (-3 + 2j)}$$

Solving for  $A$  and  $B$  gives

$$F(\omega) = \frac{4}{\omega - (3 + 2j)} + \frac{1}{\omega - (-3 + 2j)}$$

whose inverse transform can be computed directly from formula 2.119,

$$\begin{aligned} f(t) &= j[4e^{j(3+2j)t}\Gamma_2(t) + e^{j(-3+2j)t}\Gamma_2(t)] \\ &= 4je^{(-2+3j)t}U(t) + je^{(-2-3j)t}U(t) \\ &= j[4e^{j3t} + e^{-j3t}]e^{-2t}U(t). \end{aligned}$$

### 2.3.15 Causal Functions

A function,  $f(t)$ , is said to be “causal” if

$$f(t) = 0 \quad \text{whenever } t < 0.$$

Such functions arise in the study of causal systems and are of obvious importance in describing phenomena that have well-defined “starting points.”

Let  $f(t)$  be a real causal function with Fourier transform  $F(\omega)$ , and let  $R(\omega)$  and  $I(\omega)$  be the real and imaginary parts of  $F(\omega)$ ,

$$F(\omega) = R(\omega) + jI(\omega).$$

Then  $R(\omega)$  is even,  $I(\omega)$  is odd, and, provided the integrals are suitably well defined,

$$f(t) = \frac{2}{\pi} \int_0^{\infty} R(\omega) \cos(\omega t) d\omega \quad \text{for } 0 < t, \quad (2.120)$$

$$f(t) = -\frac{2}{\pi} \int_0^{\infty} I(\omega) \sin(\omega t) d\omega \quad \text{for } 0 < t, \quad (2.121)$$

$$\int_0^{\infty} |f(t)|^2 dt = \frac{1}{\pi} \int_{-\infty}^{\infty} |R(\omega)|^2 d\omega, \quad (2.122)$$

and

$$\int_0^{\infty} |f(t)|^2 dt = \frac{1}{\pi} \int_{-\infty}^{\infty} |I(\omega)|^2 d\omega, \quad (2.123)$$

In addition, if  $f(t)$  is bounded at the origin, then provided the integrals exist,

$$R(\omega) = \frac{1}{\pi} \int_{-\infty}^{\infty} \frac{I(s)}{\omega - s} ds \quad (2.124)$$

and

$$I(\omega) = -\frac{1}{\pi} \int_{-\infty}^{\infty} \frac{R(s)}{\omega - s} ds. \quad (2.125)$$

The last two integrals are Hilbert transforms and may be defined using CPVs (see Section 2.1.6).

Conversely, it can be shown that  $R(\omega)$  and  $I(\omega)$  are real-valued functions (with  $R(\omega)$  even and  $I(\omega)$  odd) satisfying either Equation 2.120 or Equation 2.125, then

$$f(t) = \mathcal{F}^{-1}[R(\omega) + jI(\omega)]|_t$$

must be a causal function.

Derivations of Equations 2.120 through 2.125 are quite straightforward. First, observe that because  $f(t)$  vanishes for negative values of  $t$ , then

$$f(t) = 2f_e(t) = 2f_o(t) \quad \text{for } 0 < t,$$

where  $f_e(t)$  and  $f_o(t)$  are the even and odd components of  $f(t)$ . Equations 2.120 and 2.121 then follow immediately from Equations 2.69 and 2.70, while Equations 2.122 and 2.123 are simply Bessel's equality combined with equations from Section 2.3.1 and the subsequent observation that

$$\int_0^{\infty} |f(t)|^2 dt = 4 \int_0^{\infty} |f_e(t)|^2 dt = 2 \int_{-\infty}^{\infty} |f_e(t)|^2 dt = 2 \int_{-\infty}^{\infty} |f_o(t)|^2 dt.$$

Finally, for Equation 2.124 observe that

$$f_e(t) = f_o(t)\text{sgn}(t) \quad \text{and} \quad f_o = f_e(t)\text{sgn}(t).$$

Thus, using results from Sections 2.3.1, 2.2.9, and 2.3.13,

$$\begin{aligned} R(\omega) &= \mathcal{F}[f_e(t)]|_{\omega} \\ &= \mathcal{F}[f_o(t)\text{sgn}(t)]|_{\omega} \\ &= \frac{1}{2\pi} \mathcal{F}[f_o(t)]|_{\omega} * \mathcal{F}[\text{sgn}(t)]|_{\omega} \\ &= \frac{1}{2\pi} jI(\omega) * \left(-j\frac{2}{\omega}\right) \\ &= \frac{1}{\pi} \int_{-\infty}^{\infty} \frac{I(s)}{\omega - s} ds, \end{aligned}$$

which is Equation 2.124. Similar computations yield Equation 2.125.

**Example 2.38**

Assume  $f(t)$  is a causal function whose transform,  $F(\omega)$ , has real part

$$R(\omega) = \delta(\omega - \alpha) + \delta(\omega + \alpha),$$

for some  $\alpha > 0$ . Then, according to formula 2.120, for  $t > 0$

$$f(t) = \frac{2}{\pi} \int_0^{\infty} [\delta(\omega - \alpha) + \delta(\omega + \alpha)] \cos(\omega t) d\omega = \frac{2}{\pi} \cos(\alpha t),$$

and by formula 2.125,

$$\begin{aligned} I(\omega) &= -\frac{1}{\pi} \int_{-\infty}^{\infty} \frac{[\delta(s - \alpha) + \delta(s + \alpha)]}{\omega - s} ds \\ &= -\left[ \frac{1}{\pi(\omega - \alpha)} + \frac{1}{\pi(\omega + \alpha)} \right] \\ &= \frac{2\omega}{\pi(\alpha^2 - \omega^2)}. \end{aligned}$$

Thus,

$$f(t) = \frac{2}{\pi} \cos(\alpha t)u(t)$$

and

$$F(\omega) = \delta(\omega - \alpha) + \delta(\omega + \alpha) + j \frac{2\omega}{\pi(\alpha^2 - \omega^2)}.$$

**2.3.16 Functions on the Half-Line**

Strictly speaking, functions defined only on the half-line,  $0 < t < \infty$ , do not have Fourier transforms. Fourier analysis in problems involving such functions can be done by first extending the functions (i.e., systematically defining the values of the functions at negative values of  $t$ ), and then taking the Fourier transforms of the extensions. The choice of extension will depend on the problem at hand and the preferences of the individual. Three of the most commonly used extensions are the null extension, the even extension, and the odd extension. Given a function,  $f(t)$ , defined only for  $0 < t$ , the null extension is

$$f_{\text{null}}(t) = \begin{cases} f(t), & \text{if } 0 < t \\ 0, & \text{if } t < 0 \end{cases},$$

The even extension is

$$f_{\text{even}}(t) = \begin{cases} f(t), & \text{if } 0 < t \\ f(-t), & \text{if } t < 0 \end{cases},$$

and the odd extension is

$$f_{\text{odd}}(t) = \begin{cases} f(t), & \text{if } 0 < t \\ -f(-t), & \text{if } t < 0 \end{cases}.$$

If  $f(t)$  is reasonably well behaved (say, continuous and differentiable) on  $0 < t$ , then any of the above extensions will be similarly well behaved on both  $0 < t$  and  $t < 0$ . At  $t = 0$ , however, the extended functions is likely to have singularities that must be taken into account, especially if transforms of the derivatives are to be taken. It is recommended that the generalized derivative be explicitly used. Assume, for example, that  $f(t)$  and its first two derivatives are continuous on  $0 < t$ , and that the limits

$$f(0) = \lim_{t \rightarrow 0^+} f(t) \quad \text{and} \quad f'(0) = \lim_{t \rightarrow 0^+} f'(t)$$

exist. Let  $\hat{f}(t)$  be any of the above extensions of  $f(t)$ , and, for convenience, let  $d\hat{f}/dt$  and  $D\hat{f}$  denote, respectively, the classical and generalized derivatives of  $\hat{f}(t)$ . Recalling the relation between the classical and generalized derivatives (see Section 2.2.11),

$$D\hat{f} = \frac{d\hat{f}}{dt} + J_0\delta(t)$$

and

$$D^2\hat{f} = \frac{d^2\hat{f}}{dt^2} + J_0\delta'(t) + J_1\delta(t),$$

where  $J_0$  and  $J_1$  are the ‘‘jumps’’ in  $\hat{f}(t)$  and  $\hat{f}'(t)$  at  $t = 0$ ,

$$J_0 = \lim_{t \rightarrow 0^+} [f(t) - \hat{f}(-t)]$$

and

$$J_1 = \lim_{t \rightarrow 0^+} [f'(t) - \hat{f}'(-t)].$$

Computing these jumps for the extensions yield the following:

$$Df_{\text{null}} = \frac{df_{\text{null}}}{dt} + f(0)\delta(t), \tag{2.126}$$

$$D^2f_{\text{null}} = \frac{d^2f_{\text{null}}}{dt^2} + f(0)\delta'(t) + f'(0)\delta(t), \tag{2.127}$$

$$Df_{\text{even}} = \frac{df_{\text{even}}}{dt}, \tag{2.128}$$

$$D^2f_{\text{even}} = \frac{d^2f_{\text{even}}}{dt^2} + 2f'(0)\delta(t), \tag{2.129}$$

$$Df_{\text{odd}} = \frac{df_{\text{odd}}}{dt} + 2f(0)\delta(t), \tag{2.130}$$



and

$$D^2 f_{\text{odd}} = \frac{d^2 f_{\text{odd}}}{dt^2} + 2f(0)\delta'(t). \quad (2.131)$$

An example of the use of Fourier transforms in problems on the half-line is given in Section 2.8.4. This example also illustrates how the data in the problem determine the appropriate extension for the problem.

### 2.3.17 Functions on Finite Intervals

If a function,  $f(t)$ , is defined only on a finite interval,  $0 < t < L$ , then it can be expanded into any of a number of “Fourier series” over the interval. These series equal  $f(t)$  over the interval but are defined on the entire real line. Thus, each series corresponds to a particular extension of  $f(t)$  to a function defined for all real values of  $t$ , and, with care, Fourier analysis can be done using the series in place of the original functions. Among the best known “Fourier series” for such functions are the sine series and the cosine series.

The sine series for  $f(t)$  over  $0 < t < L$  is

$$S[f]|_t = \sum_{k=1}^{\infty} b_k \sin\left(\frac{k\pi t}{L}\right),$$

where

$$b_k = \frac{2}{L} \int_0^L f(t) \sin\left(\frac{k\pi t}{L}\right) dt.$$

This series can be viewed as an odd periodic extension of  $f(t)$ . The Fourier transform of the sine series is

$$\begin{aligned} \mathcal{F}[S[f]|_t]|_{\omega} &= j\pi \sum_{k=1}^{\infty} b_k \left[ \delta\left(\omega + \frac{k\pi}{L}\right) - \delta\left(\omega - \frac{k\pi}{L}\right) \right] \\ &= \sum_{k=-\infty}^{\infty} B_k \delta\left(\omega - \frac{k\pi}{L}\right), \end{aligned}$$

where

$$B_k = \begin{cases} -j\pi b_k, & \text{if } 0 < k \\ 0, & \text{if } k = 0 \\ j\pi b_{-k}, & \text{if } k < 0 \end{cases}.$$

The cosine series for  $f(t)$  over  $0 < t < L$  is

$$C[f]|_t = a_0 + \sum_{k=1}^{\infty} a_k \cos\left(\frac{k\pi t}{L}\right),$$

where

$$a_0 = \frac{1}{L} \int_0^L f(t) dt$$

and, for  $k \neq 0$ ,

$$a_k = \frac{2}{L} \int_0^L f(t) \cos\left(\frac{k\pi t}{L}\right) dt.$$

This series can be viewed as an even periodic extension of  $f(t)$ . The Fourier transform of the cosine series is

$$\begin{aligned} \mathcal{F}[C[f]|_t]|_{\omega} &= 2\pi a_0 \delta(\omega) + \pi \sum_{k=1}^{\infty} a_k \left[ \delta\left(\omega - \frac{k\pi}{L}\right) + \delta\left(\omega + \frac{k\pi}{L}\right) \right] \\ &= \sum_{k=-\infty}^{\infty} A_k \delta\left(\omega - \frac{k\pi}{L}\right), \end{aligned}$$

where

$$A_k = \begin{cases} \pi a_k, & \text{if } 0 < k \\ 2\pi a_0, & \text{if } k = 0 \\ \pi a_{-k}, & \text{if } k < 0 \end{cases}$$

The choice of which series to use depends strongly on the actual problem at hand. For example, because the sine functions in the sine series expansion vanish at  $t = 0$  and  $t = L$ , sine series expansions tend to be most useful when the functions of interest are to vanish at both of the end points of the interval. For problems in which the first derivatives are expected to vanish at both end points, the cosine series tends to be a better choice. Other boundary conditions suggest other choices for the appropriate Fourier series. In addition, the equations to be satisfied must be considered in choosing the series to be used. Unfortunately, the development of a reasonably complete criteria for choosing the appropriate “Fourier series” in general goes beyond the scope of this chapter. It is recommended that texts covering eigenfunction expansions and Sturm–Liouville problems be consulted.\*

### 2.3.18 Bessel Functions

#### 2.3.18.1 Solutions to Bessel’s Equations

For  $\nu \geq 0$ , the  $\nu$ th-order Bessel equation can be written as

$$t^2 y'' + ty' + (t^2 - \nu^2)y = 0. \quad (2.132)$$

\* See, for example, Boyce and DiPrima (1977), Holland (1990), or Pinsky (1991).

“Power series” solutions to this equation can be found using the method of Frobenius. From these solutions, it can be shown that the general real-valued solution to this equation on  $t > 0$  is

$$y(t) = c_1 J_\nu(t) + c_2 y_2(t)$$

where  $c_1$  and  $c_2$  are arbitrary real constants,  $J_\nu$  is the  $\nu$ th-order Bessel function of the first kind (which is a bounded function),\* and  $y_2$  is any particular real-valued solution to the Bessel equation on  $t > 0$  that is unbounded near  $t = 0$ .

Typically, one is most interested in the bounded function part of the solution to Bessel’s equation,  $c_1 J_\nu$ .

### 2.3.18.2 Zero-Order Bessel Functions

For now let  $\nu = 0$ . Equation 2.132 then simplifies to

$$ty'' + y' + ty = 0 \tag{2.133}$$

Its solution on  $t > 0$  is

$$y(t) = c_1 J_0(t) + c_2 y_2(t)$$

It is easily verified that the power series formula for  $J_0(t)$  actually defines  $J_0(t)$  as an even, analytic function on the entire real line, and that  $J_0(t)$  satisfies Equation 2.133 everywhere. It is also easily verified from the series formula for  $y_2(t)$  on  $t > 0$  that  $y_2(|t|)$  is an even function satisfying Equation 2.133 for all nonzero values of  $t$  and which behaves like  $\ln |t|$  near  $t = 0$ . Consequently, we can seek the Fourier transform of

$$y(t) = c_1 J_0(t) + c_2 y_2(|t|) \tag{2.134}$$

for any pair  $c_1$  and  $c_2$  by treating  $J_0(t)$  and  $y_2(|t|)$  as even, real-valued solutions to the Bessel equation of order zero on the real line.

Taking the Fourier transform of Equation 2.133 and using the differential identities of Section 2.2.11 results in the first-order linear equation

$$(1 - \omega^2)Y'(\omega) - \omega Y(\omega) = 0 \tag{2.135}$$

where  $Y = \mathcal{F}[y]$ . The general classical solution to this equation is easily obtained via standard methods for linear, first-order differential equations. Taking into account the possible discontinuities at  $\omega = \pm 1$ , this general solution is given by

$$Y(\omega) = \begin{cases} A(\omega^2 - 1)^{-\frac{1}{2}} & \text{if } \omega < -1 \\ B(1 - \omega^2)^{-\frac{1}{2}} & \text{if } -1 < \omega < 1 \\ C(\omega^2 - 1)^{-\frac{1}{2}} & \text{if } 1 < \omega \end{cases} \tag{2.136}$$

\* An overview of Bessel functions of the first kind is given in Chapter 1.

where  $A$ ,  $B$ , and  $C$  are “arbitrary” constants. However, here  $Y(\omega)$  must be even and real valued since it is the Fourier transform of an even, real-valued function. This forces  $A$ ,  $B$ , and  $C$  to be real constants with  $A = C$ . Thus,

$$Y(\omega) = \begin{cases} B(1 - \omega^2)^{-\frac{1}{2}} & \text{if } |\omega| < 1 \\ C(\omega^2 - 1)^{-\frac{1}{2}} & \text{if } 1 < |\omega| \end{cases},$$

or, equivalently,

$$Y(\omega) = BY_1(\omega) + CY_2(\omega)$$

where

$$Y_1(\omega) = \frac{1}{\sqrt{1 - \omega^2}} p_1(\omega)$$

and

$$Y_2(\omega) = \frac{1}{\sqrt{\omega^2 - 1}} [1 - p_1(\omega)].$$

The function  $Y_1(\omega)$  is absolutely integrable in addition to being real valued and even. Consequently,  $\mathcal{F}^{-1}[Y_1]$  is a bounded, real-valued, even function to Bessel’s equation of order zero. Thus,

$$\mathcal{F}^{-1}[Y_1(\omega)]|_t = c_1 J_0(t)$$

for some nonzero constant  $c_1$ . Conversely, then, there must be a value  $B_0$  such that  $J_0 = B_0 \mathcal{F}^{-1}[Y_1]$ . To find this value, first recall that  $J_0(0) = 1$  (see Chapter 1) and that, by elementary calculus,

$$\mathcal{F}^{-1}[Y_1(\omega)]|_0 = \frac{1}{2\pi} \int_{-1}^1 \frac{1}{\sqrt{1 - \omega^2}} d\omega = \frac{1}{2}.$$

Thus,

$$1 = J_0(0) = B_0 \mathcal{F}^{-1}[Y_1(\omega)]|_0 = \frac{B_0}{2},$$

which, in turn, means that  $B_0 = 2$ ,

$$J_0(t) = \mathcal{F}^{-1}[2Y_1(\omega)]|_t = \mathcal{F}^{-1}\left[\frac{2}{\sqrt{1 - \omega^2}} p_1(\omega)\right]|_t, \tag{2.137}$$

and

$$\mathcal{F}[J_0(t)]|_\omega = 2Y_1(\omega) \frac{2}{\sqrt{1 - \omega^2}} p_1(\omega). \tag{2.138}$$

The function  $Y_2(\omega)$  is not absolutely integrable, but it is the sum of a function that is absolutely integrable,

$$\frac{1}{\sqrt{\omega^2 - 1}} [1 - p_1(\omega)] p_2(\omega),$$

with a function that is square integrable,

$$\frac{1}{\sqrt{\omega^2 - 1}} [1 - p_1(\omega)] [1 - p_2(\omega)].$$

From this it follows that  $Y_2$  is Fourier transformable in the more general sense described in Section 2.1.3 and that its inverse transform is a function in the classical sense. The inverse transform of this function can be used for  $y_2$ , the unbounded part of Equation 2.134. A more standard choice, however, is to use  $y_2 = Y_0$  where

$$Y_0(t) = \mathcal{F}^{-1}[-2Y_2(\omega)]|_t = \mathcal{F}^{-1} \left[ \frac{-2}{\sqrt{\omega^2 - 1}} [1 - p_1(\omega)] \right] \Big|_t$$

for  $t > 0$ .

This,  $Y_0$ , is the zeroth-order Bessel function of the second kind.

### 2.3.18.3 Integral Order Bessel Functions

As with  $J_0$ , the series formula for each integral order Bessel function of the first kind  $J_n$  actually defines  $J_n$  as a bounded analytic function on the entire real line whenever  $n$  is any positive integer. Consequently, Fourier transforms for these Bessel functions exist and are well defined using, at least, the more general definitions of Section 2.1.3. The formulas for these transforms can be obtained using the above formula for  $\mathcal{F}[J_0]$ , the differentiation identities, and well-known recursion formulas for the Bessel functions (again, see Chapter 1).

In particular, since

$$J_1(t) = -J'_0(t),$$

we have

$$\mathcal{F}[J_1(t)]|_\omega = -\mathcal{F}[J'_0(t)]|_\omega = -j\omega \mathcal{F}[J_0(t)]|_\omega.$$

Combined with Equation 2.138, this gives

$$\mathcal{F}[J_1(t)]|_\omega = \frac{-2j\omega}{\sqrt{1 - \omega^2}} p_1(\omega). \quad (2.139)$$

The Fourier transforms of  $J_2(t), J_3(t), \dots$  can be obtained in a similar fashion using formulas 2.138 and 2.139, a differentiation identity, and the recursion formulas

$$J_{v+1}(t) = J_{v-1}(t) - 2J'_v(t).$$

The results of these computations can be succinctly described by the formulas

$$\mathcal{F}[J_m(t)]|_\omega = \frac{2 \cos [m \arcsin(\omega)]}{\sqrt{1 - \omega^2}} p_1(\omega) \quad \text{for } m = 0, 2, 4, \dots$$

and

$$\mathcal{F}[J_m(t)]|_\omega = \frac{-2j \sin [m \arcsin(\omega)]}{\sqrt{1 - \omega^2}} p_1(\omega) \quad \text{for } m = 1, 3, 5, \dots$$

They can be described even more succinctly by

$$\mathcal{F}[J_n(t)]|_\omega = \frac{2(-j)^n T_n(\omega)}{\sqrt{1 - \omega^2}} p_1(\omega) \quad \text{for } n = 0, 1, 2, 3, \dots$$

where  $T_n$  is the  $n$ th Chebyshev polynomial of the first kind.

The derivation of another useful set of identities starts with the observation that

$$\frac{-2j\omega}{\sqrt{1 - \omega^2}} p_1(\omega) = 2j \frac{d}{d\omega} \left[ \sqrt{1 - \omega^2} p_1(\omega) \right].$$

Combining this with Equation 2.139

$$\begin{aligned} J_1(t) &= \mathcal{F}^{-1} \left[ \frac{-2j\omega}{\sqrt{1 - \omega^2}} p_1(\omega) \right] \Big|_t \\ &= 2j \mathcal{F}^{-1} \left[ \frac{d}{d\omega} \left[ \sqrt{1 - \omega^2} p_1(\omega) \right] \right] \Big|_t \\ &= 2j \left( -jt \mathcal{F}^{-1} \left[ \sqrt{1 - \omega^2} p_1(\omega) \right] \right) \Big|_t \\ &= 2t \mathcal{F}^{-1} \left[ \sqrt{1 - \omega^2} p_1(\omega) \right] \Big|_t \end{aligned}$$

Dividing by  $t$  (which is valid since  $J_1(t) \approx \frac{t}{2}$  when  $t \approx 0$ ) then yields

$$t^{-1} J_1(t) = \mathcal{F}^{-1} \left[ 2\sqrt{1 - \omega^2} p_1(\omega) \right] \Big|_t.$$

Equivalently,

$$\mathcal{F}[t^{-1} J_1(t)]|_\omega = 2\sqrt{1 - \omega^2} p_1(\omega).$$

Continuing these computations eventually leads to the equivalent identities

$$t^{-n} J_n(t) = \mathcal{F}^{-1} \left[ \frac{2(1 - \omega^2)^{n-\frac{1}{2}}}{1 \cdot 3 \cdot 5 \cdots (2n-1)} p_1(\omega) \right] \Big|_t \quad (2.140)$$

and

$$\mathcal{F}[t^{-n} J_n(t)]|_\omega = \frac{2(1 - \omega^2)^{n-\frac{1}{2}}}{1 \cdot 3 \cdot 5 \cdots (2n-1)} p_1(\omega). \quad (2.141)$$

These identities are valid for nonnegative, integral values of  $n$  (and reduce to Equations 2.137 and 2.138 when  $n=0$ ).

### 2.3.18.4 Nonintegral Order Bessel Functions

Solving Equation 2.140 for  $J_n(t)$  and using the fact that, in terms of the gamma function,

$$1 \cdot 3 \cdot 5 \cdots (2n - 1) = \frac{2^n}{\sqrt{\pi}} \Gamma\left(n + \frac{1}{2}\right)$$

results in the following formulas:

$$J_n(t) = A_n t^n \mathcal{F}^{-1} \left[ (1 - \omega^2)^{n-\frac{1}{2}} p_1(\omega) \right] \Big|_t \quad (2.142)$$

where

$$A_n = \frac{2^{1-n} \sqrt{\pi}}{\Gamma\left(n + \frac{1}{2}\right)}.$$

This formula for  $J_n$  was obtained assuming  $n$  is any nonnegative integer. However, for  $t > 0$ , the right-hand side of Equation 2.142 remains well defined when  $n$  is any real value greater than  $-1/2$ . Moreover, through straightforward but somewhat tedious computations, it can be verified that the formula on the right-hand side of Equation 2.142 satisfies Bessel's equation of order  $|n|$  on  $t > 0$ , and is asymptotically identical to  $J_n(t)$  when  $t \rightarrow 0^+$ . It thus follows that, for any  $\mu > -1/2$ ,

$$J_\mu(t) = A_\mu t^\mu \mathcal{F}^{-1} \left[ (1 - \omega^2)^{\mu-\frac{1}{2}} p_1(\omega) \right] \Big|_t$$

where

$$A_\mu = \frac{2^{1-\mu} \sqrt{\pi}}{\Gamma\left(\mu + \frac{1}{2}\right)}.$$

Consequently, since  $\omega^2$  and  $p_1(\omega)$  are even functions,

$$\mathcal{F}^{-1} \left[ (1 - \omega^2)^{\mu-\frac{1}{2}} p_1(\omega) \right] \Big|_t = \frac{\Gamma\left(\mu + \frac{1}{2}\right)}{2\sqrt{\pi}} \left(\frac{2}{|t|}\right)^\mu J_\mu(|t|),$$

and, by near-equivalence,

$$\mathcal{F} \left[ (1 - t^2)^{\mu-\frac{1}{2}} p_1(t) \right] \Big|_\omega = \Gamma\left(\mu + \frac{1}{2}\right) \sqrt{\pi} \left(\frac{2}{|\omega|}\right)^\mu J_\mu(|\omega|),$$

whenever  $\mu > -1/2$ .

## 2.4 Extensions of the Fourier Transform and Other Closely Related Transforms

A number of applications call for transforms that are closely related to the Fourier transform. This section presents a brief survey and development of some of the transforms having a

particularly close relation to the Fourier transform. Many of them, in fact, can be viewed as natural modifications or direct extensions of the transforms defined and developed in the previous sections, or else are special cases of these modifications and extensions.

### 2.4.1 Multidimensional Fourier Transforms

The extension of Fourier analysis to handle functions of more than one variable is quite straightforward. Assuming the functions are suitably integrable, the Fourier transform of  $f(x, y)$  is

$$F(\omega, \nu) = \int_{-\infty}^{\infty} \int_{-\infty}^{\infty} f(x, y) e^{-j(\omega x + \nu y)} dx dy$$

and the Fourier transform of  $f(x, y, z)$  is

$$F(\omega, \nu, \mu) = \int_{-\infty}^{\infty} \int_{-\infty}^{\infty} \int_{-\infty}^{\infty} f(x, y, z) e^{-j(\omega x + \nu y + \mu z)} dx dy dz.$$

More generally, using vector notation with  $\mathbf{t} = (t_1, t_2, \dots, t_n)$  and  $\boldsymbol{\omega} = (\omega_1, \omega_2, \dots, \omega_n)$ , the “ $n$ -dimensional Fourier transform” is defined by

$$\mathcal{F}[f(\mathbf{t})] \Big|_\omega = \int_{-\infty}^{\infty} \int_{-\infty}^{\infty} \cdots \int_{-\infty}^{\infty} f(\mathbf{t}) e^{-j\boldsymbol{\omega} \cdot \mathbf{t}} dt_1 dt_2 \dots dt_n, \quad (2.143)$$

assuming  $f(\mathbf{t})$  is sufficiently integrable. The inverse  $n$ -dimensional Fourier inverse transform given by

$$\begin{aligned} \mathcal{F}^{-1}[F(\boldsymbol{\omega})] \Big|_{\mathbf{t}} &= (2\pi)^{-n} \int_{-\infty}^{\infty} \\ &\times \int_{-\infty}^{\infty} \cdots \int_{-\infty}^{\infty} F(\boldsymbol{\omega}) e^{-j\boldsymbol{\omega} \cdot \mathbf{t}} d\omega_1 d\omega_2 \dots d\omega_n, \end{aligned} \quad (2.144)$$

provided  $F(\boldsymbol{\omega})$  is suitably integrable.

For many functions of  $\mathbf{t}$  and  $\boldsymbol{\omega}$  that are not suitably integrable, the generalized  $n$ -dimensional Fourier and inverse Fourier transforms can be defined using the  $n$ -dimensional analogs of the rapidly decreasing test functions described in Sections 2.1.3 and 2.1.4.

Analogous to the identities discussed in Section 2.2. can be easily derived for the  $n$ -dimensional transforms. In particular,  $\mathcal{F}$  and  $\mathcal{F}^{-1}$  are inverses of each other, that is,

$$F(\boldsymbol{\omega}) = \mathcal{F}[f(\mathbf{t})] \Big|_\omega \Leftrightarrow \mathcal{F}^{-1}[F(\boldsymbol{\omega})] \Big|_{\mathbf{t}} = f(\mathbf{t}).$$

The near equivalence (or symmetry) relations for the  $n$ -dimensional transforms are

$$\mathcal{F}^{-1}[\phi(x)] \Big|_y = (2\pi)^{-n} \mathcal{F}[\phi(-x)] \Big|_y = (2\pi)^{-n} \mathcal{F}[\phi(x)] \Big|_{-y}$$

**TABLE 2.2** Identities for Multidimensional Transforms

$h(\mathbf{t})$	$H(\boldsymbol{\omega}) = \mathcal{F}[h(\mathbf{t})]_{\boldsymbol{\omega}}$
$f(\alpha \mathbf{t})$	$\frac{1}{ \alpha } F\left(\frac{\boldsymbol{\omega}}{\alpha}\right)$
$f(\mathbf{tA})$	$\frac{1}{ \mathbf{A} } F(\boldsymbol{\omegaA}^{-\text{T}})$
$f(\mathbf{t} - \mathbf{t}_0)$	$e^{-j\boldsymbol{\omega}_0 \cdot \mathbf{t}} F(\boldsymbol{\omega})$
$e^{j\boldsymbol{\omega}_0 \cdot \mathbf{t}} f(\mathbf{t})$	$F(\boldsymbol{\omega} - \boldsymbol{\omega}_0)$
$\frac{\partial f}{\partial t_k}$	$j\omega_k F(\boldsymbol{\omega})$
$t_k f(\mathbf{t})$	$j \frac{\partial F}{\partial \omega_k}$
$f(\mathbf{t})g(\mathbf{t})$	$(2\pi)^{-n} F(\boldsymbol{\omega}) * G(\boldsymbol{\omega})$
$f(\mathbf{t}) * g(\mathbf{t})$	$F(\boldsymbol{\omega})G(\boldsymbol{\omega})$
$f(\mathbf{t}) \star g(\mathbf{t})$	$F^*(\boldsymbol{\omega})G(\boldsymbol{\omega})$
$f * (\mathbf{t})g(\mathbf{t})$	$(2\pi)^{-n} F(\boldsymbol{\omega}) \star G(\boldsymbol{\omega})$

Note:  $\alpha$  is any nonzero real number,  $\mathbf{t}_0$  and  $\boldsymbol{\omega}_0$  are fixed  $n$ -dimensional points, and  $F(\boldsymbol{\omega}) = \mathcal{F}[f(\mathbf{t})]_{\boldsymbol{\omega}}$  and  $G(\boldsymbol{\omega}) = \mathcal{F}[g(\mathbf{t})]_{\boldsymbol{\omega}}$ .

and

$$\mathcal{F}[\phi(-\mathbf{x})]_{\mathbf{y}} = (2\pi)^n \mathcal{F}^{-1}[\phi(-\mathbf{x})]_{\mathbf{y}} = (2\pi)^n \mathcal{F}^{-1}[\phi(-\mathbf{x})]_{-\mathbf{y}}$$

An abbreviated listing of identities for the  $n$ -dimensional transforms are given in Table 2.2. In this table,  $\phi(\mathbf{x}) * \psi(\mathbf{x})$  and  $\phi(\mathbf{x}) \star \psi(\mathbf{x})$  denote the  $n$ -dimensional convolution and correlation,

$$\phi(\mathbf{x}) * \psi(\mathbf{x}) = \int_{-\infty}^{\infty} \int_{-\infty}^{\infty} \cdots \int_{-\infty}^{\infty} \phi(\mathbf{s})\psi(\mathbf{x} - \mathbf{s})ds_1 ds_2 \dots ds_n$$

and

$$\phi(\mathbf{x}) \star \psi(\mathbf{x}) = \int_{-\infty}^{\infty} \int_{-\infty}^{\infty} \cdots \int_{-\infty}^{\infty} \phi^*(\mathbf{s})\psi(\mathbf{x} + \mathbf{s})ds_1 ds_2 \dots ds_n.$$

There is one particularly useful  $n$ -dimensional identity that does not have a direct analog to the identities given in Section 2.2 (though it can be viewed as a generalization of the scaling formula). If  $\mathbf{A}$  is a real, invertible,  $n \times n$  matrix and  $F(\boldsymbol{\omega}) = \mathcal{F}[f(\mathbf{t})]_{\boldsymbol{\omega}}$ , then

$$\mathcal{F}[f(\mathbf{tA})]_{\boldsymbol{\omega}} = \frac{1}{|\mathbf{A}|} F(\boldsymbol{\omegaA}^{-\text{T}}) \quad (2.145)$$

where  $|\mathbf{A}|$  is the determinant of  $\mathbf{A}$  and  $\mathbf{A}^{-\text{T}}$  is the inverse of the transpose of  $\mathbf{A}$  (equivalently  $\mathbf{A}^{-\text{T}}$  is the transpose of the inverse of  $\mathbf{A}$ ),

$$\mathbf{A}^{-\text{T}} = (\mathbf{A}^{\text{T}})^{-1} = (\mathbf{A}^{-1})^{\text{T}}.$$

Likewise if  $f(\mathbf{t}) = \mathcal{F}^{-1}[F(\boldsymbol{\omega})]_{\mathbf{t}}$ , then

$$\mathcal{F}^{-1}[F(\boldsymbol{\omegaA})]_{\mathbf{t}} = \frac{1}{|\mathbf{A}|} f(\mathbf{tA}^{-\text{T}}). \quad (2.146)$$

The derivation of either of these identities is relatively simple. Lettings  $\mathbf{s} = \mathbf{tA}$  and recalling the change of variables formula for multiple integrals,

$$\begin{aligned} \mathcal{F}[f(\mathbf{tA})]_{\boldsymbol{\omega}} &= \int_{-\infty}^{\infty} \int_{-\infty}^{\infty} \cdots \int_{-\infty}^{\infty} f(\mathbf{tA})e^{-j\boldsymbol{\omega} \cdot \mathbf{t}} dt_1 dt_2 \dots dt_n \\ &= \int_{-\infty}^{\infty} \int_{-\infty}^{\infty} \cdots \int_{-\infty}^{\infty} f(\mathbf{s})e^{-j\boldsymbol{\omega} \cdot (\mathbf{sA}^{-1})} \\ &\quad \times \left| \frac{\partial(t_1, t_2, \dots, t_n)}{\partial(s_1, s_2, \dots, s_n)} \right| ds_1 ds_2 \dots ds_n. \end{aligned} \quad (2.147)$$

Now

$$\frac{\partial s_i}{\partial t_j} = A_{ji}$$

and, so, the Jacobian in Equation 2.147 is

$$\left| \frac{\partial(t_1, t_2, \dots, t_n)}{\partial(s_1, s_2, \dots, s_n)} \right| = \left| \frac{\partial(s_1, s_2, \dots, s_n)}{\partial(t_1, t_2, \dots, t_n)} \right|^{-1} = \frac{1}{|\mathbf{A}|}.$$

From linear algebra and the definition of the transpose

$$\boldsymbol{\omega} \cdot (\mathbf{sA}^{-1}) = (\boldsymbol{\omegaA}^{-1})^{\text{T}} \cdot \mathbf{s} = (\boldsymbol{\omegaA}^{-\text{T}}) \cdot \mathbf{s}.$$

Thus, Equation 2.147 can be written

$$\begin{aligned} \mathcal{F}[f(\mathbf{tA})]_{\boldsymbol{\omega}} &= \int_{-\infty}^{\infty} \int_{-\infty}^{\infty} \cdots \int_{-\infty}^{\infty} f(\mathbf{s})e^{-j(\boldsymbol{\omegaA}^{-\text{T}}) \cdot \mathbf{s}} \frac{1}{|\mathbf{A}|} ds_1 ds_2 \dots ds_n \\ &= \frac{1}{|\mathbf{A}|} F(\boldsymbol{\omegaA}^{-\text{T}}). \end{aligned}$$

An example of how Equation 2.145 can be used to compute transforms will be given in Section 2.4.2.

## 2.4.2 Multidimensional Transforms of Separable Functions

A function of two variables,  $f(x, y)$ , is separable if it can be written as the product of two single variable functions.

$$f(x, y) = f_1(x)f_2(y). \quad (2.148)$$

The transform of such a function is easily computed provided  $F_1(\omega) = \mathcal{F}[f_1(x)]_{\omega}$  and  $F_2(v) = \mathcal{F}[f_2(y)]_v$  are known. Then

$$\begin{aligned} F(\boldsymbol{\omega}, \mathbf{v}) &= \mathcal{F}[f(x, y)]_{(\boldsymbol{\omega}, \mathbf{v})} \\ &= \int_{-\infty}^{\infty} \int_{-\infty}^{\infty} f_1(x)f_2(y)e^{-j(\boldsymbol{\omega}x + \mathbf{v}y)} dx dy \\ &= \int_{-\infty}^{\infty} f_1(x)e^{-j\boldsymbol{\omega}x} dx \int_{-\infty}^{\infty} f_2(y)e^{-j\mathbf{v}y} dy \\ &= F_1(\boldsymbol{\omega})F_2(\mathbf{v}). \end{aligned}$$

More generally,  $f(\mathbf{t})$  is said to be separable if there are  $n$  functions of a single variable,  $f_1(t_1), f_2(t_2), \dots, f_n(t_n)$ , such that

$$f(t_1, t_2, \dots, t_n) = f_1(t_1)f_2(t_2) \cdots f_n(t_n). \quad (2.149)$$

The Fourier transform of such a function is another separable function

$$F(\omega_1, \omega_2, \dots, \omega_n) = F_1(\omega_1)F_2(\omega_2) \cdots F_n(\omega_n)$$

where, for each  $k$ ,  $F_k(\omega_k)$  is the one-dimensional Fourier transform of  $f_k(t_k)$ .

Likewise, if

$$F(\omega_1, \omega_2, \dots, \omega_n) = F_1(\omega_1)F_2(\omega_2) \cdots F_n(\omega_n),$$

then the  $n$ -dimensional inverse Fourier transform is

$$f(t_1, t_2, \dots, t_n) = f_1(t_1)f_2(t_2) \cdots f_n(t_n)$$

where, for each  $k$ ,  $f_k(t_k)$  is the one-dimensional inverse Fourier transform of  $F_k(\omega_k)$ .

### Example 2.39

The two-dimensional rectangular aperture function (with half-widths  $\alpha$  and  $\beta$ ) is

$$\eta_{\alpha,\beta}(x,y) = \begin{cases} 1, & \text{if } |x| < \alpha \text{ and } |y| < \beta \\ 0, & \text{if } \alpha < |x| \text{ or } \beta < |y| \end{cases}$$

or, equivalently,

$$\eta_{\alpha,\beta}(x,y) = p_\alpha(x)p_\beta(y).$$

Its Fourier transform is

$$\begin{aligned} N_{\alpha,\beta}(\omega, \nu) &= \int_{-\infty}^{\infty} \int_{-\infty}^{\infty} \eta_{\alpha,\beta}(x,y) e^{-j(\omega x + \nu y)} dx dy \\ &= \int_{-\infty}^{\infty} p_\alpha(x) e^{-j\omega x} dx \int_{-\infty}^{\infty} p_\beta(y) e^{-j\nu y} dy \\ &= \left( \frac{2 \sin(\alpha\omega)}{\omega} \right) \left( \frac{2 \sin(\beta\nu)}{\nu} \right) \\ &= \frac{4}{\omega\nu} \sin(\alpha\omega) \sin(\beta\nu). \end{aligned}$$

### Example 2.40

The three-dimensional delta function,  $\delta(x, y, z)$  is defined as the generalized function such that if  $\phi(x, y, z)$  is any function of three variables continuous at the origin,

$$\int_{-\infty}^{\infty} \int_{-\infty}^{\infty} \int_{-\infty}^{\infty} \delta(x, y, z) \phi(x, y, z) dx dy dz = \phi(0, 0, 0).$$

Because

$$\begin{aligned} &\int_{-\infty}^{\infty} \int_{-\infty}^{\infty} \int_{-\infty}^{\infty} \delta(x)\delta(y)\delta(z)\phi(x, y, z) dx dy dz \\ &= \int_{-\infty}^{\infty} \delta(z) \int_{-\infty}^{\infty} \delta(y) \int_{-\infty}^{\infty} \delta(x)\phi(x, y, z) dx dy dz \\ &= \int_{-\infty}^{\infty} \delta(z) \int_{-\infty}^{\infty} \delta(y)\phi(0, y, z) dy dz \\ &= \int_{-\infty}^{\infty} \delta(z)\phi(0, 0, z) dz \\ &= \phi(0, 0, 0), \end{aligned}$$

it is clear that

$$\delta(x, y, z) = \delta(x)\delta(y)\delta(z)$$

and

$$\mathcal{F}[\delta(x, y, z)]|_{(\omega, \nu, \mu)} = \mathcal{F}[\delta(x)]|_{\omega} \mathcal{F}[\delta(y)]|_{\nu} \mathcal{F}[\delta(z)]|_{\mu} = 1 \cdot 1 \cdot 1 = 1.$$

In using formulas 2.148 or 2.149 care must be taken to account for all the variables especially if the function depends explicitly on only a small subset of the variables. This can be done by including on the right-hand side of Equation 2.148 or Equation 2.149 the unit constant function,

$$1(s) = 1 \quad \text{for all } s,$$

for each variable,  $s$ , not explicitly involved in the computation of the function.

### Example 2.41

The vertical slit aperture of half width  $\alpha$  is the function of two variables given by

$$\text{vslit}_\alpha(x,y) = \begin{cases} 1, & \text{if } |x| < \alpha \\ 0, & \text{if } \alpha < |x| \end{cases}$$

or, equivalently,

$$\text{vslit}_\alpha(x,y) = p_\alpha(x) = P_\alpha(x)1(y).$$

Its Fourier transform is given by

$$\mathcal{F}[\text{vslit}_\alpha(x,y)]|_{(\omega, \nu)} = \mathcal{F}[p_\alpha(x)]|_{\omega} \mathcal{F}[1]|_{\nu} = \frac{2}{\omega} \sin(\alpha\omega) \cdot 2\pi\delta(\nu)$$

and not by

$$\mathcal{F}[\text{vslit}_\alpha(x,y)]|_{(\omega, \nu)} = \mathcal{F}[p_\alpha(x)]|_{\omega} = \frac{2}{\omega} \sin(\alpha\omega).$$

**Example 2.42**

The three-dimensional vertical line source function is

$$l(x, y, z) = \delta(z).$$

Its Fourier transform is

$$\begin{aligned} \mathcal{F}[l(x, y, z)]|_{(\omega, \nu, \mu)} &= \mathcal{F}[1(x)1(y)\delta(z)]|_{(\omega, \nu, \mu)} = 2\pi\delta(\omega)2\pi\delta(\nu) \cdot 1 \\ &= 4\pi^2\delta(\omega)\delta(\nu). \end{aligned}$$

Often, functions that are not separable in one set of coordinates are separable in another set of coordinates. In such cases one of the generalized scaling identities (2.145) and (2.146), can simplify the computations.

**Example 2.43**

Let  $\mathcal{P}$  be the parallelogram bounded by the lines  $y = \pm 1$  and  $x = y \pm 1$ , and consider the two-dimensional aperture function

$$\eta_{\mathcal{P}}(x, y) = \begin{cases} 1, & \text{if } (x, y) \text{ is in } \mathcal{P} \\ 0, & \text{otherwise} \end{cases}.$$

Note that  $\eta_{\mathcal{P}}(x, y) = 1$  if and only if

$$-1 < y < 1 \quad \text{and} \quad -1 < x - y < 1. \quad (2.150)$$

Let

$$\mathbf{A} = \begin{bmatrix} 1 & 0 \\ -1 & 1 \end{bmatrix}.$$

$\mathbf{A}^T$  and the determinant of  $\mathbf{A}$  are easily computed,

$$|\mathbf{A}| = 1 \quad \text{and} \quad \mathbf{A}^{-T} = \begin{bmatrix} 1 & -1 \\ 0 & 1 \end{bmatrix}^{-1} = \begin{bmatrix} 1 & 1 \\ 0 & 1 \end{bmatrix}.$$

For each  $\mathbf{x} = (x, y)$  and  $\boldsymbol{\omega} = (\omega, \nu)$ , let

$$\hat{\mathbf{x}} = (\hat{x}, \hat{y}) = \mathbf{x}\mathbf{A} = (x, y) \begin{bmatrix} 1 & 0 \\ -1 & 1 \end{bmatrix} = (x - y, y)$$

and

$$\hat{\boldsymbol{\omega}} = (\hat{\omega}, \hat{\nu}) = \boldsymbol{\omega}\mathbf{A}^{-T} = (\omega, \nu) \begin{bmatrix} 1 & 1 \\ 0 & 1 \end{bmatrix} = (\omega, \omega + \nu).$$

It is easily verified that conditions 2.150 are equivalent to

$$-1 < \hat{y} < 1 \quad \text{and} \quad -1 < \hat{x} < 1.$$

Thus,

$$\eta_{\mathcal{P}}(x, y) = \eta_{1,1}(\hat{x}, \hat{y}) = \eta_{1,1}(\mathbf{x}\mathbf{A})$$

where  $\eta_{1,1}(\hat{x}, \hat{y})$  is the rectangular aperture function of Example 2.39. Using these results and the generalized scaling identity 2.145,

$$\begin{aligned} \mathcal{F}[\eta_{\mathcal{P}}(x, y)]|_{(\omega, \nu)} &= \mathcal{F}[\eta_{1,1}(\mathbf{x}\mathbf{A})]_{\boldsymbol{\omega}} \\ &= \frac{1}{|\mathbf{A}|} N_{1,1}(\boldsymbol{\omega}\mathbf{A}^{-T}) \\ &= N_{1,1}(\boldsymbol{\omega}, \boldsymbol{\omega} + \boldsymbol{\nu}) \\ &= \frac{4}{\omega(\omega + \nu)} \sin(\omega) \sin(\omega + \nu). \end{aligned}$$

**2.4.3 Transforms of Circularly Symmetric Functions and the Hankel Transform**

Replacing  $(x, y)$  and  $(\omega, \nu)$  with their polar equivalents,

$$(x, y) = (r \cos \theta, r \sin \theta)$$

and

$$(\omega, \nu) = (\rho \cos \phi, \rho \sin \phi),$$

and using a well-known trigonometric identity, the formula for the two-dimensional Fourier transform,  $F(\omega, \nu) = \mathcal{F}[f(x, y)]|_{(\omega, \nu)}$ , becomes

$$\begin{aligned} F(\rho \cos \phi, \rho \sin \phi) &= \int_0^{\infty} \int_{-\pi}^{\pi} f(r \cos \theta, r \sin \theta) e^{-jr\rho(\cos \theta \cos \phi + \sin \theta \sin \phi)} r \, d\theta \, dr \\ &= \int_0^{\infty} \int_{-\pi}^{\pi} f(r \cos \theta, r \sin \theta) e^{-jr\rho \cos(\theta - \phi)} r \, d\theta \, dr. \end{aligned} \quad (2.151)$$

Likewise, in polar coordinates, the formula for the two-dimensional inverse Fourier transform,  $f(x, y) = \mathcal{F}[F(\omega, \nu)]|_{(x, y)}$ , is

$$\begin{aligned} f(r \cos \theta, r \sin \theta) &= \frac{1}{4\pi^2} \int_0^{\infty} \int_{-\pi}^{\pi} F(\rho \cos \phi, \rho \sin \phi) e^{jr\rho \cos(\theta - \phi)} \rho \, d\phi \, d\rho. \end{aligned} \quad (2.152)$$

If  $f(r \cos \theta, r \sin \theta)$  is separable with respect to  $r$  and  $\theta$ ,

$$f(r \cos \theta, r \sin \theta) = f_r(r)f_{\theta}(\theta),$$

then Equation 2.151 becomes

$$F(\rho \cos \phi, \rho \sin \phi) = \int_0^{\infty} f_r(r)rK^-(r\rho, \phi)dr, \quad (2.153)$$

where

$$K^-(z, \phi) = \int_{-\pi}^{\pi} f_{\theta}(\theta) e^{-jz \cos(\theta-\phi)} d\theta.$$

Observe that the integrand for  $K^-(r, \phi)$  must be periodic with period  $2\pi$ . Thus, letting  $\theta' = \theta - \phi$ ,

$$K^-(z, \phi) = \int_{-\pi}^{\pi} f_{\theta}(\theta' + \phi) e^{-jz \cos(\theta')} d\theta'. \quad (2.154)$$

Likewise, if  $F(\rho \cos \phi, \rho \sin \phi)$  is separable with respect to  $\rho$  and  $\phi$ ,

$$F(\rho \cos \phi, \rho \sin \phi) = F_{\rho}(\rho) F_{\phi}(\phi)$$

then formula 2.152 becomes

$$f(r \cos \theta, r \sin \theta) = \frac{1}{4\pi^2} \int_0^{\infty} F_{\rho}(\rho) \rho K^+(r\rho, \theta) d\rho, \quad (2.155)$$

where

$$K^+(z, \theta) = \int_{-\pi}^{\pi} F_{\phi}(\theta' + \theta) e^{jz \cos(\phi')} d\phi'. \quad (2.156)$$

The above formulas simplify considerably when circular symmetry can be assumed for either  $f(x, y)$  or  $F(\omega, \nu)$ . It follows immediately from Equations 2.153 through 2.156 that if either  $f(x, y)$  or  $F(\omega, \nu)$  is circularly symmetric, that is,

$$f(r \cos \theta, r \sin \theta) = f_r(r) \quad \text{or} \quad F(\rho \cos \phi, \rho \sin \phi) = F_{\rho}(\rho),$$

then, in fact, both  $f(x, y)$  and  $F(\omega, \nu)$  are circularly symmetric and can be written

$$f(r \cos \theta, r \sin \theta) = f_r(r) \quad \text{and} \quad F(\rho \cos \phi, \rho \sin \phi) = F_{\rho}(\rho).$$

In such cases it is convenient to use the Bessel function identity

$$2\pi J_0(z) = \int_{-\pi}^{\pi} \cos(z \cos w) dw,$$

where  $J_0(z)$  is the zeroth-order Bessel function of the first kind.\* It is easily verified that

$$\int_{-\pi}^{\pi} \sin(r\rho \cos w) dw = 0$$

\* See Chapter 1 for additional information on Bessel functions.

and so

$$K^{\pm}(r\rho, \psi) = \int_{-\pi}^{\pi} e^{\pm jr\rho \cos w} dw = \int_{-\pi}^{\pi} \cos(r\rho \cos w) dw = 2\pi J_0(r\rho)$$

and Equations 2.153 and 2.155 reduce to

$$F_{\rho}(\rho) = 2\pi \int_0^{\infty} f_r(r) J_0(r\rho) r dr \quad (2.157)$$

and

$$f_r(r) = \frac{1}{2\pi} \int_0^{\infty} F_{\rho}(\rho) J_0(r\rho) \rho d\rho. \quad (2.158)$$

The zeroth-order Hankel transform of  $g(r)$  is defined to be

$$\hat{g}(\rho) = \int_0^{\infty} g(r) J_0(r\rho) r dr.$$

Such transforms are the topic of Chapter 9. It should be noted that Equations 2.157 and 2.158 can be expressed in terms of zeroth-order Hankel transforms,

$$F_{\rho}(\rho) = 2\pi \hat{f}_r(\rho) \quad \text{and} \quad f_r(r) = \frac{1}{2\pi} \hat{F}_{\rho}(r). \quad (2.159)$$

From this it should be clear that zeroth-order Hankel transforms can be viewed as two-dimensional Fourier transforms of circularly symmetric functions. This allows fairly straightforward derivation of many of the properties of these Hankel transforms from corresponding properties of the Fourier transform. For example, letting  $g(r) = 2\pi f(r)$  in Equations 2.157 and 2.158 leads immediately to the inversion formula for the zeroth-order Hankel transform,

$$g(r) = \int_0^{\infty} \hat{g}(\rho) J_0(r\rho) \rho d\rho.$$

(For further discussion of the Hankel transforms, see Chapter 9.)

**Example 2.44**

Let  $a > 0$  and let  $f(x, y)$  be the corresponding circular aperture function,

$$f(x, y) = \begin{cases} 1, & \text{if } x^2 + y^2 < a^2 \\ 0, & \text{otherwise} \end{cases}.$$



This function is circularly symmetric with

$$f(x, y) = f_r(r) = \begin{cases} 1, & \text{if } 0 \leq r < a \\ 0, & \text{otherwise} \end{cases}.$$

Its Fourier transform must also be circularly symmetric and, using Equation 2.157, is given by

$$F(\omega, \nu) = F_\rho(\rho) = 2\pi \int_0^a J_0(r\rho)r dr. \quad (2.160)$$

Letting  $z = r\rho$  and using the Bessel function identity

$$\frac{d}{dz}[zJ_1(z)] = zJ_0(z),$$

where  $J_1(z)$  is the first-order Bessel function of the first kind, the computation of this transform is easily completed,

$$\begin{aligned} F_\rho(\rho) &= 2\pi\rho^{-2} \int_0^{a\rho} J_0(z)z dz \\ &= 2\pi\rho^{-2} \int_0^{a\rho} \frac{d}{dz}[zJ_1(z)] dz \\ &= 2\pi\rho^{-2}[a\rho J_1(a\rho)] \\ &= \frac{2\pi a}{\rho} J_1(a\rho). \end{aligned}$$

## 2.4.4 Half-Line Sine and Cosine Transforms

Half-line sine and cosine transforms are usually taken only of functions defined on just the half-line  $0 < t < \infty$ . For such a function,  $f(t)$ , the corresponding (half-line) sine transform is

$$F_S(\omega) = \mathcal{S}[f(t)]|_\omega = \int_0^\infty f(t) \sin(\omega t) dt \quad (2.161)$$

and the corresponding (half-line) cosine transform is

$$F_C(\omega) = \mathcal{C}[f(t)]|_\omega = \int_0^\infty f(t) \cos(\omega t) dt. \quad (2.162)$$

These formulas define  $F_S(\omega)$  and  $F_C(\omega)$  for all real values of  $\omega$ , with  $F_S(\omega)$  being an odd function of  $\omega$ , and  $F_C(\omega)$  being an even function of  $\omega$ .

The half-line sine and cosine transforms are directly related to the standard Fourier transforms of the odd and even extensions of  $f(t)$ ,

$$f_{\text{odd}}(t) = \begin{cases} f(t), & \text{if } 0 < t \\ -f(-t), & \text{if } t < 0 \end{cases}$$

and

$$f_{\text{even}}(t) = \begin{cases} f(t), & \text{if } 0 < t \\ f(-t), & \text{if } t < 0 \end{cases},$$

respectively. From the observations made in Section 2.3.1,

$$\mathcal{S}[f(t)]|_\omega = j\frac{1}{2}\mathcal{F}[f_{\text{odd}}]|_\omega \quad (2.163)$$

and

$$\mathcal{C}[f(t)]|_\omega = \frac{1}{2}\mathcal{F}[f_{\text{even}}(t)]|_\omega. \quad (2.164)$$

This shows that the (half-line) sine and cosine transforms can be treated as special cases of the standard Fourier transform. Indeed, by doing so it is possible to extend the class of functions that can be treated by sine and cosine transforms to include functions for which the integrals in Equations 2.161 and 2.162 are not defined.

### Example 2.45

Let  $f(t) = t^2$  for  $0 < t$ . Formula 2.162 cannot be used to define  $\mathcal{C}[f(t)]|_\omega$  because

$$\lim_{b \rightarrow \infty} \int_0^b t^2 \cos(\omega t) dt$$

does not converge. However,  $f_{\text{even}}(t) = t^2$  for all values of  $t$ , and, using formula 2.164,

$$\mathcal{C}[f(t)]|_\omega = \frac{1}{2}\mathcal{F}[t^2]|_\omega = \frac{1}{2}[-2\pi\delta''(\omega)] = -\pi\delta''(\omega).$$

All the useful identities for the sine and cosine transforms can be derived through relations 2.163 and 2.164 from the corresponding identities for the standard Fourier transform.

### Example 2.46 Inversion Formulas for the Sine and Cosine Transforms

Let  $f(t)$ ,  $F_S(\omega)$ , and  $f_{\text{odd}}(t)$  be as shown, and let

$$F_{\text{odd}}(\omega) = \mathcal{F}[f_{\text{odd}}(t)]|_\omega.$$

According to Equation 2.163

$$F_{\text{odd}}(\omega) = -2jF_S(\omega).$$

Thus, for  $0 < t$ ,

$$f(t) = \mathcal{F}^{-1}[F_{\text{odd}}(\omega)]|_t = -2j\mathcal{F}^{-1}[F_S(\omega)]|_t.$$

But, because  $F_S(\omega)$  is an odd function of  $\omega$ , the same arguments used in Section 2.3.1 yield

$$\mathcal{F}^{-1}[F_S(\omega)]|_t = \frac{1}{2\pi} \int_{-\infty}^{\infty} F_S(\omega)e^{j\omega t} d\omega = \frac{j}{\pi} \int_0^{\infty} F_S(\omega) \sin(\omega t) d\omega,$$

which, combined with the previous equation, gives the inversion formula for the sine transform,

$$f(t) = \frac{2}{\pi} \int_0^{\infty} F_S(\omega) \sin(\omega t) d\omega.$$

Precisely the same reasoning shows that the inversion formula for the cosine transform is

$$f(t) = \frac{2}{\pi} \int_0^{\infty} F_C(\omega) \cos(\omega t) d\omega.$$

In using Equations 2.163 and 2.164 to derive identities for the sine and cosine function, it is important to keep in mind that if

$$f(0) = \lim_{t \rightarrow 0^+} f(t)$$

exists, then the even extension will be continuous at  $t=0$  with  $f_{\text{even}}(0)=f(0)$ , but the odd extension will have a jump discontinuity at  $t=0$  with a jump of  $2f(0)$ . This is why most of the sine and cosine transform analogs to the differentiation formulas of Section 2.2.11 include boundary values. Some of these identities are

$$\mathcal{S}[f'(t)]|_{\omega} = -\omega F_C(\omega),$$

$$\mathcal{C}[f'(t)]|_{\omega} = \omega F_S(\omega) - f(0),$$

$$\mathcal{S}[f''(t)]|_{\omega} = \omega f(0) - \omega^2 F_S(\omega),$$

and

$$\mathcal{C}[f''(t)]|_{\omega} = -f'(0) - \omega^2 F_C(\omega),$$

where  $f'(t)$  and  $f''(t)$  denote the generalized first and second derivatives of  $f(t)$  for  $0 < t$ . (See also Section 2.3.16.)

### 2.4.5 The Discrete Fourier Transform

The discrete Fourier transform is a computational analog to the Fourier transform and is used when dealing with finite collections of sampled data rather than functions per se. Given an “Nth-order sequence” of values,  $\{f_0, f_1, f_2, \dots, f_{N-1}\}$ ,

the corresponding Nth-order discrete transform is the sequence  $\{F_0, F_1, F_2, \dots, F_{N-1}\}$  given by the formula

$$F_n = \sum_{k=0}^{N-1} e^{-j\frac{2\pi}{N}nk} f_k. \tag{2.165}$$

This can also be written in matrix form,  $\mathbf{F} = [\mathcal{F}_N]\mathbf{f}$ , where

$$\mathbf{F} = \begin{pmatrix} F_0 \\ F_1 \\ F_2 \\ \vdots \\ F_{N-1} \end{pmatrix}, \quad \mathbf{f} = \begin{pmatrix} f_0 \\ f_1 \\ f_2 \\ \vdots \\ f_{N-1} \end{pmatrix},$$

and

$$[\mathcal{F}_N] = \begin{bmatrix} 1 & 1 & 1 & \cdots & 1 \\ 1 & e^{-j\frac{2\pi}{N}} & e^{-j2\frac{2\pi}{N}} & \cdots & e^{-j(N-1)\frac{2\pi}{N}} \\ 1 & e^{-j2\frac{2\pi}{N}} & e^{-j2^2\frac{2\pi}{N}} & \cdots & e^{-j2(N-1)\frac{2\pi}{N}} \\ \vdots & \vdots & \vdots & \ddots & \vdots \\ 1 & e^{-j(N-1)\frac{2\pi}{N}} & e^{-j2(N-1)\frac{2\pi}{N}} & \cdots & e^{-j(N-1)^2\frac{2\pi}{N}} \end{bmatrix}.$$

On occasion, the matrix  $[\mathcal{F}_N]$  is itself referred to as the Nth-order discrete transform.

The inverse to formula 2.165 is given by

$$f_k = \frac{1}{N} \sum_{n=0}^{N-1} e^{j\frac{2\pi}{N}kn} F_n. \tag{2.166}$$

In matrix form this is  $\mathbf{f} = [\mathcal{F}_N]^{-1}\mathbf{F}$ , where  $[\mathcal{F}_N]^{-1}$  is the matrix

$$\frac{1}{N} \begin{bmatrix} 1 & 1 & 1 & \cdots & 1 \\ 1 & e^{j\frac{2\pi}{N}} & e^{j2\frac{2\pi}{N}} & \cdots & e^{j(N-1)\frac{2\pi}{N}} \\ 1 & e^{j2\frac{2\pi}{N}} & e^{j2^2\frac{2\pi}{N}} & \cdots & e^{j2(N-1)\frac{2\pi}{N}} \\ \vdots & \vdots & \vdots & \ddots & \vdots \\ 1 & e^{j(N-1)\frac{2\pi}{N}} & e^{j2(N-1)\frac{2\pi}{N}} & \cdots & e^{j(N-1)^2\frac{2\pi}{N}} \end{bmatrix}.$$

The similarity between the definitions for the discrete Fourier transforms, formulas 2.165 and 2.166, and formulas 2.99 and 2.100 should be noted. The discrete Fourier transforms can be treated as the regular Fourier transforms of corresponding regular periodic arrays generated from the sampled data.

#### Example 2.47

The matrices for the fourth-order discrete Fourier transforms are

$$[\mathcal{F}_4] = \begin{bmatrix} 1 & 1 & 1 & 1 \\ 1 & e^{-j\frac{\pi}{4}} & e^{-j2\frac{\pi}{4}} & e^{-j3\frac{\pi}{4}} \\ 1 & e^{-j2\frac{\pi}{4}} & e^{-j4\frac{\pi}{4}} & e^{-j6\frac{\pi}{4}} \\ 1 & e^{-j3\frac{\pi}{4}} & e^{-j6\frac{\pi}{4}} & e^{-j9\frac{\pi}{4}} \end{bmatrix} = \begin{bmatrix} 1 & 1 & 1 & 1 \\ 1 & -j & -1 & j \\ 1 & -1 & 1 & -1 \\ 1 & j & -1 & -j \end{bmatrix}$$

and

$$\begin{aligned} [\mathcal{F}_N]^{-1} &= \frac{1}{4} \begin{bmatrix} 1 & 1 & 1 & 1 \\ 1 & e^{j\frac{\pi}{4}} & e^{j2\frac{\pi}{4}} & e^{j3\frac{\pi}{4}} \\ 1 & e^{j2\frac{\pi}{4}} & e^{j4\frac{\pi}{4}} & e^{j6\frac{\pi}{4}} \\ 1 & e^{j3\frac{\pi}{4}} & e^{j6\frac{\pi}{4}} & e^{j9\frac{\pi}{4}} \end{bmatrix} \\ &= \frac{1}{4} \begin{bmatrix} 1 & 1 & 1 & 1 \\ 1 & j & -1 & -j \\ 1 & -1 & 1 & -1 \\ 1 & -j & -1 & j \end{bmatrix}. \end{aligned}$$

The discrete Fourier transform of  $\{f_0, f_1, f_2, f_3\} = \{1, 2, 3, 4\}$  is given by

$$\begin{pmatrix} F_0 \\ F_1 \\ F_2 \\ F_3 \end{pmatrix} = \begin{bmatrix} 1 & 1 & 1 & 1 \\ 1 & -j & -1 & j \\ 1 & -1 & 1 & -1 \\ 1 & j & -1 & -j \end{bmatrix} \begin{pmatrix} 1 \\ 2 \\ 3 \\ 4 \end{pmatrix} = \begin{pmatrix} 10 \\ -2 + 2j \\ -2 \\ -2 - 2j \end{pmatrix},$$

and the discrete inverse Fourier transform of  $\{F_0, F_1, F_2, F_3\} = \{10, -2 + 2j, -2, -2 - 2j\}$  is given by

$$\begin{pmatrix} f_0 \\ f_1 \\ f_2 \\ f_3 \end{pmatrix} = \frac{1}{4} \begin{bmatrix} 1 & 1 & 1 & 1 \\ 1 & j & -1 & -j \\ 1 & -1 & 1 & -1 \\ 1 & -j & -1 & j \end{bmatrix} \begin{pmatrix} 10 \\ -2 + 2j \\ -2 \\ -2 - 2j \end{pmatrix} = \begin{pmatrix} 1 \\ 2 \\ 3 \\ 4 \end{pmatrix}.$$

In practice the sample size,  $N$ , is often quite large and the computations of the discrete transforms directly from formulas 2.165 and 2.166 can be a time-consuming process even on fairly fast computers. For this reason it is standard practice to make heavy use of symmetries inherent in the computations of the discrete transforms for certain values of  $N$  (e.g.,  $N = 2^M$ ) to reduce the total number of calculations. Such implementations of the discrete Fourier transform are called “fast Fourier transforms” (FFTs).

### 2.4.6 Relations between the Laplace Transform and the Fourier Transform\*

Attention in this section will be restricted to functions of  $t$  (and their transforms) that satisfy all of the following three conditions:

1.  $f(t) = 0$  if  $t < 0$ .
2.  $f(t)$  is piecewise continuous on  $0 \leq t$ .
3. For some real value of  $\alpha$ ,  $f(t) = O(e^{\alpha t})$  as  $t \rightarrow \infty$ .

It follows from the third condition that there is a minimum value of  $\alpha_0$ , with  $-\infty \leq \alpha_0 < \infty$ , such that  $f(t)e^{-\alpha t}$  is an exponentially decreasing function of  $t$  whenever  $\alpha_0 < \alpha$ . This minimal value of  $\alpha_0$  is called the “exponential order” of  $f(t)$ .

The Laplace transform of  $f(t)$  is defined by

$$\mathcal{L}[f(t)]|_s = \int_{-\infty}^{\infty} f(t)e^{-st} dt. \quad (2.167)$$

The variable,  $s$ , in the transformed function may be any complex number whose real part is greater than the exponential order of  $f(t)$ .

There is a clear similarity between formula 2.167 defining the Laplace transform and the integral formula for the Fourier transform (formula 2.1). Comparing the two immediately yields the formal relations

$$\mathcal{L}[f(t)]|_s = \int_{-\infty}^{\infty} f(t)e^{-j(-js)t} dt = \mathcal{F}[f(t)]|_{-js}.$$

Another, somewhat more useful relation is found by taking the Fourier transform of  $f(t)e^{-xt}$  when  $x$  is greater than the order of  $f(t)$ :

$$\mathcal{F}[f(t)e^{-xt}]|_y = \int_{-\infty}^{\infty} f(t)e^{-(x+jy)t} dt = \mathcal{L}[f(t)]|_{x+jy}. \quad (2.168)$$

In particular,

$$\mathcal{F}[f(t)e^{-st}]|_0 = \mathcal{L}[f(t)]|_s.$$

The inversion formula for the Laplace transform can be quickly derived using relation 2.168. Let  $\beta$  be any real value greater than the exponential order of  $f(t)$  and observe that, letting

$$F_{\mathcal{L}}(s) = \mathcal{L}[f(t)]|_s,$$

then, by relation 2.168

$$F_{\mathcal{L}}(\beta + j\omega) = \mathcal{F}[f(t)e^{-\beta t}]|_{\omega},$$

and so,

$$\begin{aligned} f(t) &= e^{\beta t} f(t) e^{-\beta t} \\ &= e^{\beta t} \mathcal{F}^{-1}[\mathcal{F}[f(t)e^{-\beta t}]|_{\omega}]|_t \\ &= e^{\beta t} \frac{1}{2\pi} \int_{-\infty}^{\infty} \mathcal{F}[f(t)e^{-\beta t}]|_{\omega} e^{j\omega t} d\omega \\ &= \frac{1}{2\pi} \int_{-\infty}^{\infty} F_{\mathcal{L}}(\beta + j\omega) e^{(\beta + j\omega)t} d\omega. \end{aligned}$$

\* For a more complete discussion of the Laplace transform, see Chapter 5.

This formula can be expressed in slightly more compact form as a contour integral in the complex plane,

$$f(t) = \mathfrak{L}^{-1}[F_{\mathfrak{L}}(s)]|_t = \frac{1}{2j\pi} \int_{z=\beta-j\infty}^{\beta+j\infty} F_{\mathfrak{L}}(z)e^{zt} dz.$$

Alternatively, it can be left in terms of the Fourier inverse transform,

$$f(t) = \mathfrak{L}^{-1}[F_{\mathfrak{L}}(s)]|_t = e^{\beta t} \mathfrak{F}^{-1}[F_{\mathfrak{L}}(\beta + j\omega)]|_t.$$

## 2.5 Reconstruction of Sampled Signals

In practice a function is often known only by a sampling of its values at specific points. The following sections describe when such a function can be completely reconstructed using its samples and how, using methods based on the Fourier transform, the values of the reconstructed function can be computed at arbitrary points.

### 2.5.1 Sampling Theorem for Band-Limited Functions

Assume  $f(t)$  is a band-limited function with Fourier transform  $F(\omega)$  (see Section 2.3.7). Let  $2\Omega_0$  be the minimum bandwidth of  $f(t)$ , that is,  $\Omega_0$  is the smallest nonnegative value such that

$$F(\omega) = 0 \quad \text{whenever } \Omega_0 < |\omega|.$$

The Nyquist interval,  $\Delta T$ , and the Nyquist rate,  $\nu$ , for  $f(t)$  are defined by

$$\Delta T = \frac{\pi}{\Omega_0} \quad \text{and} \quad \nu = \frac{1}{\Delta T} = \frac{\Omega_0}{\pi}.$$

The sampling theorem for band-limited functions states that  $f(t)$  (and hence, also  $F(\omega)$  as well as the total energy in  $f(t)$ ) can be completely reconstructed from a uniform sampling taken at the Nyquist rate or greater. More precisely, if  $0 < \Delta t \leq \Delta T$ , then, letting  $\Omega = \pi/\Delta t$ ,

$$f(t) = \sum_{n=-\infty}^{\infty} f(n\Delta t) \frac{\sin(\Omega(t - n\Delta t))}{\Omega(t - n\Delta t)} \quad (2.169)$$

and, taking the transform

$$F(\omega) = \frac{\pi}{\Omega} \sum_{n=-\infty}^{\infty} f(n\Delta t) e^{-jn\Delta t\omega} p_{\Omega}(\omega), \quad (2.170)$$

where  $p_{\Omega}(\omega)$  is the pulse function,

$$p_{\Omega}(\omega) = \begin{cases} 1, & \text{if } |\omega| < \Omega \\ 0, & \text{if } \Omega < |\omega| \end{cases}.$$

The energy in  $f(t)$  is easily computed. Using Equations 2.72 and 2.170, and the fact that the exponentials in formula 2.170 are orthogonal on the interval  $-\Omega < \omega < \Omega$ ,

$$\begin{aligned} E &= \frac{1}{2\pi} \int_{-\infty}^{\infty} |F(\omega)|^2 d\omega \\ &= \frac{1}{2\pi} \sum_{n=-\infty}^{\infty} \left(\frac{\pi}{\Omega}\right)^2 \int_{-\Omega}^{\Omega} f(n\Delta t) f^*(n\Delta t) e^{-jn\Delta t\omega} e^{jn\Delta t\omega} d\omega \\ &= \frac{1}{2\pi} \sum_{n=-\infty}^{\infty} \left(\frac{\pi}{\Omega}\right)^2 |f(n\Delta t)|^2 2\Omega \\ &= \Delta t \sum_{n=-\infty}^{\infty} |f(n\Delta t)|^2. \end{aligned} \quad (2.171)$$

To see why formulas 2.169 and 2.170 are valid, let  $\hat{F}(\omega)$  be the periodic extension of  $F(\omega)$ ,

$$\hat{F}(\omega) = \begin{cases} F(\omega) & \text{if } -\Omega < \omega < \Omega \\ \hat{F}(\omega + 2\Omega), & \text{for all } \omega \end{cases}.$$

Observe that  $2\Omega$  is a bandwidth for  $f(t)$ , and so,

$$F(\omega) = \begin{cases} \hat{F}(\omega), & \text{if } |\omega| < \Omega \\ 0, & \text{if } \Omega < |\omega| \end{cases}. \quad (2.172)$$

This can be written more concisely using the pulse function as

$$F(\omega) = \hat{F}(\omega) p_{\Omega}(\omega).$$

From this it follows, using convolution, that

$$f(t) = \mathfrak{F}^{-1}[\hat{F}(\omega) p_{\Omega}(\omega)]|_t = \hat{f}(t) * \left(\frac{\sin(\Omega t)}{\pi t}\right), \quad (2.173)$$

where  $\hat{f}(t)$  denotes the inverse transform of  $\hat{F}(\omega)$ . By formula 2.94,

$$\hat{f}(t) = \sum_{n=-\infty}^{\infty} C_n \delta(t - n\Delta t), \quad (2.174)$$

where

$$\Delta\tau = \frac{2\pi}{2\Omega} = \Delta t$$

and, using the above,

$$\begin{aligned} C_n &= \frac{1}{2\Omega} \int_{-\Omega}^{\Omega} \hat{F}(\omega) e^{jn\Delta t\omega} d\omega \\ &= \frac{\pi}{\Omega} \left( \frac{1}{2\pi} \int_{-\infty}^{\infty} F(\omega) e^{jn\Delta t\omega} d\omega \right) \\ &= \Delta t f(n\Delta t). \end{aligned}$$

Combining this last with Equations 2.173 and 2.174, and using the shifting property of the delta function, yields

$$\begin{aligned} f(t) &= \hat{f}(t) * \left( \frac{\sin(\Omega t)}{\pi t} \right) \\ &= \sum_{n=-\infty}^{\infty} \Delta t f(n\Delta t) \delta(t - n\Delta t) * \left( \frac{\sin(\Omega t)}{\pi t} \right) \\ &= \sum_{n=-\infty}^{\infty} \Delta t f(n\Delta t) \frac{\sin(\Omega(t - n\Delta t))}{\pi(t - n\Delta t)}, \end{aligned}$$

which is the same as formula 2.169.

### 2.5.2 Truncated Sampling Reconstruction of Band-Limited Functions

Formula 2.169 employs an infinite number of samples of  $f(t)$ . Often this is impractical, and one must approximate  $f(t)$  with the truncated version of formula 2.169,

$$f(t) \approx \sum_{n=-N}^N f(n\Delta t) \frac{\sin(\Omega(t - n\Delta t))}{\Omega(t - n\Delta t)}, \quad (2.175)$$

where  $N$  is some positive integer. The pointwise error is

$$\varepsilon_N(t) = f(t) - \sum_{n=-N}^N f(n\Delta t) \frac{\sin(\Omega(t - n\Delta t))}{\Omega(t - n\Delta t)}.$$

If  $f(t)$  is a band-limited function, then the sampling theorem implies that

$$\varepsilon_N(t) = \sum_{N < |n|} f(n\Delta t) \frac{\sin(\Omega(t - n\Delta t))}{\Omega(t - n\Delta t)},$$

and it can be shown that

$$|\varepsilon_N(t)|^2 \leq \frac{E\Omega}{\pi} \sum_{N < |n|} \frac{\sin^2(\Omega(t - n\Delta t))}{\Omega^2(t - n\Delta t)^2}, \quad (2.176)$$

where  $E$  is the energy in  $f(t)$ . In addition, if the samples are known to vanish sufficiently rapidly, then one can use

$$|\varepsilon_N(t)| \leq \sqrt{\sum_{N < |n|} |f(n\Delta t)|^2}. \quad (2.177)$$

This last bound is a uniform bound directly related to expression (2.171) for the energy of a band-limited function. It can be derived after observing that  $\varepsilon_N(t)$  can be written as a proper integral,

$$\begin{aligned} \varepsilon_N(t) &= \sum_{N < |n|} f(n\Delta t) \frac{\sin(\Omega(t - n\Delta t))}{\Omega(t - n\Delta t)} \\ &= \sum_{N < |n|} f(n\Delta t) \frac{1}{2\Omega} \int_{-\Omega}^{\Omega} e^{-jn\Delta t\omega} e^{j\omega t} d\omega \\ &= \frac{1}{2\Omega} \int_{-\Omega}^{\Omega} \left( \sum_{N < |n|} f(n\Delta t) e^{-jn\Delta t\omega} \right) e^{j\omega t} d\omega. \end{aligned}$$

Using the Cauchy-Schwarz inequality,

$$\begin{aligned} |\varepsilon_N(t)|^2 &= \frac{1}{4\Omega^2} \left| \int_{-\Omega}^{\Omega} \left( \sum_{N < |n|} f(n\Delta t) e^{-jn\Delta t\omega} \right) e^{j\omega t} d\omega \right|^2 \\ &\leq \frac{1}{4\Omega^2} \left( \int_{-\Omega}^{\Omega} \left| \sum_{N < |n|} f(n\Delta t) e^{-jn\Delta t\omega} \right|^2 d\omega \right) \left( \int_{-\Omega}^{\Omega} |e^{j\omega t}|^2 d\omega \right) \\ &= \frac{1}{4\Omega^2} \left( \sum_{N < |n|} |f(n\Delta t)|^2 2\Omega \right) (2\Omega) \\ &= \sum_{N < |n|} |f(n\Delta t)|^2, \end{aligned}$$

as claimed by Equation 2.177.

#### Example 2.48

Suppose  $f(t)$  is a band-limited function (with bandwidth  $2\Omega$ ) to be approximated on the interval  $-L < t < L$ . Suppose, further, that an upper bound,  $E_0$ , is known for the energy of  $f(t)$ . Let  $N$  be any integer such that  $L < N\Delta t$ . Then, for  $-L < t < L$ , using inequality (2.176) with well-known bounds,

$$\begin{aligned} |\varepsilon_N(t)|^2 &\leq \frac{E\Omega}{\pi} \sum_{N < |n|} \frac{\sin^2(\Omega(t - n\Delta t))}{\Omega^2(t - n\Delta t)^2} \\ &\leq \frac{2E_0}{\pi\Omega} \sum_{n=N+1}^{\infty} \frac{1}{(L - n\Delta t)^2} \\ &\leq \frac{2E_0}{\pi\Omega} \int_{x=N}^{\infty} \frac{1}{(L - x\Delta t)^2} dx \\ &= \frac{2E_0}{\pi\Omega} \frac{1}{\Delta t(N\Delta t - L)} \\ &= \frac{2}{\pi^2(N\Delta t - L)} E_0. \end{aligned}$$

Thus, to ensure an error of less than  $0.05 \sqrt{E_0}$ , it suffices to choose  $N$  satisfying

$$\left( \frac{2}{\pi^2(N\Delta t - L)} \right)^{\frac{1}{2}} < 0.05$$

or, equivalently,

$$\frac{800}{\pi^2} + L < N\Delta t.$$

**Example 2.49**

Suppose that  $f(t)$  is a band-limited function (with bandwidth  $2\Omega$ ) whose transform,  $F(\omega)$ , is known to be piecewise smooth and continuous. Assume further that, for some  $A < \infty$ ,  $|F'(\omega)| < A$  for all values of  $\omega$ . Then, for each  $t$ ,

$$\begin{aligned} |tf(t)| &= |\mathcal{F}^{-1}[jF'(\omega)]|_t \\ &= \left| \frac{1}{2\pi} \int_{-\Omega}^{\Omega} jF'(\omega)e^{j\omega t} d\omega \right| \\ &\leq \frac{1}{2\pi} \int_{-\Omega}^{\Omega} |F'(\omega)| d\omega \\ &\leq A \frac{\Omega}{\pi}. \end{aligned}$$

So, for each  $n$ ,

$$|f(n\Delta t)|^2 \leq \left(\frac{A\Omega}{n\Delta t\pi}\right)^2 = \frac{1}{n^2} \frac{A^2}{\Delta t^4},$$

and inequality (2.177) becomes

$$\begin{aligned} |\varepsilon_N(t)|^2 &\leq \sum_{N < |n|} \frac{1}{n^2} \frac{A^2}{\Delta t^4} \\ &\leq \frac{2A^2}{\Delta t^4} \int_{x=N}^{\infty} \frac{1}{x^2} dx \\ &= \frac{2A^2}{N\Delta t^4}. \end{aligned}$$

**2.5.3 Reconstruction of Sampled Nearly Band-Limited Functions**

Often, one must deal with a function,  $f(t)$ , which might not necessarily be band-limited, but is “nearly” band-limited, that is, letting

$$F_{\Omega}(\omega) = F(\omega)p_{\Omega} \quad \text{and} \quad f_{\Omega}(t) = \mathcal{F}^{-1}[F_{\Omega}(\omega)]|_t,$$

one can always choose  $\Omega < \infty$  so that

$$\int_{-\infty}^{\infty} |F(\omega) - F_{\Omega}(\omega)| d\omega = \int_{\Omega < |\omega|} |F(\omega)| d\omega \quad (2.178)$$

is as small as desired. Because

$$\begin{aligned} |f(t) - f_{\Omega}(t)| &= |\mathcal{F}^{-1}[F(\omega) - F_{\Omega}(\omega)]|_t \\ &\leq \frac{1}{2\pi} \int_{-\infty}^{\infty} |F(\omega) - F_{\Omega}(\omega)| d\omega, \end{aligned}$$

it is clear that  $f_{\Omega}(t)$  can also be made as close to  $f(t)$  as desired by a suitable choice of  $\Omega$ . Any value of  $2\Omega$  that makes Equation 2.178 “sufficiently small” is called an effective bandwidth. For such a function it is reasonable to expect that if  $\Omega$  is an effective bandwidth and  $\Delta t = \pi/\Omega$ , then the interpolation formulas,

$$f_s(t) = \sum_{n=-\infty}^{\infty} f(n\Delta t) \frac{\sin(\Omega(t - n\Delta t))}{\Omega(t - n\Delta t)} \quad (2.179)$$

will be a good approximation to  $f(t)$ . Starting with the trivial observation that

$$f(t) = f_s(t) + f(t) - f_{\Omega}(t) + f_{\Omega}(t) - f_s(t),$$

one can derive

$$f(t) = f_s(t) + \varepsilon_0(t) - \varepsilon_{\Sigma}(t), \quad (2.180)$$

where

$$\begin{aligned} \varepsilon_0(t) &= \frac{1}{2\pi} \int_{\Omega < |\omega|} F(\omega) e^{j\omega t} d\omega, \\ \varepsilon_{\Sigma}(t) &= \sum_{n=-\infty}^{\infty} \varepsilon(n\Delta t) \frac{\sin(\Omega(t - n\Delta t))}{\Omega(t - n\Delta t)} \end{aligned}$$

and

$$\varepsilon(n\Delta t) = \mathcal{F}^{-1}[(1 - p_{\Omega}(\omega))F(\omega)]|_{n\Delta t} = \frac{1}{2\pi} \int_{\Omega < |\omega|} F(\omega) e^{j\omega n\Delta t} d\omega.$$

Error estimates can be obtained from Equation 2.180 provided it can be shown that  $\varepsilon(n\Delta t)$  vanishes sufficiently rapidly as  $n \rightarrow \infty$ . As Example 2.50 illustrates, finding such error estimates can be quite nontrivial.

**Example 2.50**

Suppose  $f(t)$  is an infinitely differentiable, finite duration function with duration  $2T$ . Since  $f(t)$  vanishes whenever  $|t| \geq T$ ,

$$f_s(t) = \sum_{n=-N}^N f(n\Delta t) \frac{\sin(\Omega(t - n\Delta t))}{\Omega(t - n\Delta t)}, \quad (2.181)$$

where  $N$  is the integer satisfying

$$N\Delta t < T < (N + 1)\Delta t.$$

To avoid triviality, it may be assumed that  $\Delta t < T$  and  $N \geq 1$ .

By continuity  $f(t)$  and each of its derivatives must vanish whenever  $|t| \geq T$ . Also, for each positive integer,  $m$ , there is a finite  $A_m$  such that

$$|f^{(m)}(t)| \leq A_m$$

for all  $t$ . Thus, for each nonnegative integer,  $m$ ,

$$\begin{aligned} |\omega^m F(\omega)| &= \left| \mathcal{F} \left[ f^{(m)}(t) \right] \right|_{\omega} \\ &= \left| \int_{-\infty}^{\infty} f^{(m)}(t) e^{-j\omega t} dt \right| \\ &\leq \int_{-T}^T A_m dt \\ &= 2A_m T. \end{aligned} \quad (2.182)$$

Likewise, if  $m \geq 2$ ,

$$\begin{aligned} |\omega^m F'(\omega)| &= \left| \mathcal{F} \left[ \frac{d^m}{dt^m} (tf(t)) \right] \right|_{\omega} \\ &= \left| \mathcal{F} [mf^{(m-1)}(t) + tf^{(m)}(t)] \right|_{\omega} \leq B_m \end{aligned} \quad (2.183)$$

where

$$B_m = 2mA_{m-1}T + A_m T^2.$$

It follows from inequality (2.182) that  $F(\omega)$  is absolutely integrable (and hence, nearly band-limited) and that, for  $m \geq 2$  and any  $t$ ,

$$\begin{aligned} \frac{1}{2\pi} \left| \int_{\Omega < |\omega|} F(\omega) e^{j\omega t} d\omega \right| &\leq \frac{1}{2\pi} \int_{\Omega < |\omega|} |F(\omega)| d\omega \\ &\leq \frac{1}{\pi} \int_{\Omega} 2A_m T \omega^{-m} d\omega \\ &= \frac{2A_m T}{(m-1)\pi} \Omega^{1-m} \\ &= C_m \Delta t^{m-1} \end{aligned} \quad (2.184)$$

where

$$C_m = \frac{2A_m T}{(m-1)\pi^m}.$$

Thus, in particular, for any positive integer,  $k$ ,

$$|\mathcal{E}_0(t)| = \frac{1}{2\pi} \left| \int_{\Omega < |\omega|} F(\omega) e^{j\omega t} d\omega \right| \leq C_{k+1} \Delta t^k. \quad (2.185)$$

Two bounds for  $\varepsilon(n\Delta t)$  can be derived. First, using inequality (2.184),

$$|\varepsilon(n\Delta t)| = \frac{1}{2\pi} \left| \int_{\Omega < |\omega|} F(\omega) e^{j\omega n\Delta t} d\omega \right| \leq C_m \Delta t^{m-1} \quad (2.186)$$

provided  $m \geq 2$ . For  $n \neq 0$ , observe that

$$\varepsilon(n\Delta t) = \varepsilon_+(n\Delta t) + \varepsilon_-(n\Delta t),$$

where

$$\varepsilon_{\pm}(n\Delta t) = \pm \frac{1}{2\pi} \int_{\pm\Omega}^{\pm\infty} F(\omega) e^{j\omega n\Delta t} d\omega.$$

Using integration by parts and inequalities (2.182) and (2.183),

$$\begin{aligned} |\varepsilon_{\pm}(n\Delta t)| &= \left| \frac{1}{2\pi} \int_{\pm\Omega}^{\pm\infty} F(\omega) e^{j\omega n\Delta t} d\omega \right| \\ &= \frac{1}{2\pi} \left| \frac{j}{n\Delta t} F(\pm\Omega) e^{\pm jn\Delta t \Omega} - \frac{1}{jn\Delta t} \int_{\pm\Omega}^{\pm\infty} F'(\omega) e^{jn\Delta t \omega} d\omega \right| \\ &\leq \frac{1}{2\pi} \left( \frac{2}{n\Delta t} A_m T \Omega^{-m} + \frac{1}{n\Delta t} \int_{\Omega}^{\infty} B_m \omega^{-m} d\omega \right) \\ &= \frac{1}{2\pi n} \left( \frac{2}{\Delta t} A_m T \Omega^{-m} + \frac{1}{\Delta t(m-1)} B_m \Omega^{1-m} \right) \end{aligned}$$

for any integer,  $m \geq 2$ . Because  $\Delta t \Omega = \pi$  and  $\Delta t \leq T$ , this reduces to

$$|\varepsilon_{\pm}(n\Delta t)| \leq \frac{1}{2n} D_m \Delta t^{m-2},$$

where

$$D_m = \pi^{-m} \left( \frac{2}{\pi} A_m T^2 + \frac{1}{m-1} B_m \right).$$

Thus, for all  $n \neq 0$  and  $m \geq 2$ ,

$$|\varepsilon(n\Delta t)| \leq \frac{1}{n} D_m \Delta t^{m-2}. \quad (2.187)$$

Next, observe that

$$\mathcal{E}_{\Sigma}(t) = S_1(t) + S_2(t)$$

where

$$S_1(t) = \sum_{n=-2N-1}^{2N+1} \varepsilon(n\Delta t) \frac{\sin(\Omega(t - n\Delta t))}{\Omega(t - n\Delta t)}$$

and

$$S_2(t) = \sum_{2N+1 < |n|} \varepsilon(n\Delta t) \frac{\sin(\Omega(t - n\Delta t))}{\Omega(t - n\Delta t)}.$$

Using inequality (2.186),

$$\begin{aligned} |S_1(t)| &\leq \sum_{n=-2N-1}^{2N+1} |\varepsilon(n\Delta t)| \left| \frac{\sin(\Omega(t - n\Delta t))}{\Omega(t - n\Delta t)} \right| \\ &< |\varepsilon(0)| + |\varepsilon((2N+1)\Delta t)| + |\varepsilon(-(2N+1)\Delta t)| \\ &\quad + \sum_{n=1}^{2N} (|\varepsilon(n\Delta t)| + |\varepsilon(-n\Delta t)|) \\ &\leq 3C_{k+2}\Delta t^{k+1} + 2 \sum_{n=1}^{2N} C_{k+2}\Delta t^{k+1} \\ &= C_{k+2}(3\Delta t + 4N\Delta t)\Delta t^k \\ &\leq 7TC_{k+2}\Delta t^k \end{aligned}$$

for any positive integer,  $k$ . Next, because of inequality (2.187) and the fact that  $T < (N+1)\Delta t$ , it follows that, for  $|t| \leq T$  and  $k \geq 1$ ,

$$\begin{aligned} |S_2(t)| &\leq \sum_{2N+1 < |n|} |\varepsilon(n\Delta t)| \left| \frac{\sin(\Omega(t - n\Delta t))}{\Omega(t - n\Delta t)} \right| \\ &\leq 2 \sum_{n=2N+2}^{\infty} \frac{1}{n} D_{k+1} \Delta t^{k-1} \frac{1}{\Omega(n\Delta t - |t|)} \\ &\leq 2 \sum_{n=2N+2}^{\infty} \frac{1}{n} D_{k+1} \Delta t^{k-1} \frac{1}{\Omega\Delta t(n - (N+1))} \\ &= \frac{2}{\pi} D_{k+1} \Delta t^{k-1} \sum_{n=2N+2}^{\infty} \frac{1}{n(n - N - 1)}. \end{aligned}$$

But,

$$\begin{aligned} \sum_{n=2N+2}^{\infty} \frac{1}{n(n - N - 1)} &< \int_{2N+1}^{\infty} \frac{1}{x(x - N - 1)} dx \\ &= \frac{1}{N+1} \ln \left| 2 + \frac{1}{N} \right| \\ &< \frac{2}{N+1}. \end{aligned}$$

So,

$$|S_2(t)| < \frac{2}{\pi} D_{k+1} \Delta t^k \frac{1}{\Delta t} \frac{2}{N+1} < \frac{4}{\pi T} D_{k+1} \Delta t^k.$$

Combining the bounds for  $|S_1(t)|$  and  $|S_2(t)|$  gives

$$|\mathcal{E}_{\Sigma}(t)| \leq |S_1(t)| + |S_2(t)| < E_k \Delta t^k \quad (2.188)$$

for  $|t| \leq T$  and  $k \geq 1$ , where

$$E_k = 7TC_{k+2} + \frac{4}{\pi T} D_{k+1}.$$

Combining Equations 2.180, 2.185, and 2.188 gives an error estimate for using  $f_s(t)$  as an approximation for  $f(t)$  when  $|t| \leq T$ ,

$$|f(t) - f_s(t)| \leq |\mathcal{E}_0(t)| + |\mathcal{E}_{\Sigma}(t)| < [C_{k+1} + E_k] \Delta t^k,$$

where  $k$  is any positive integer. In terms of the effective bandwidth,  $\Omega = \pi/\Delta t$ , this becomes

$$|f(t) - f_s(t)| = O(\Omega^{-k}),$$

confirming that  $f_s(t)$  can be made to approximate  $f(t)$  on  $-T < t < T$  as accurately as desired by taking the effective bandwidth,  $\Omega$ , sufficiently large.

### 2.5.4 Sampling Theorem for Finite Duration Functions

Assume  $f(t)$  is of finite duration with Fourier transform  $F(\omega)$  (see Section 2.3.6). Let  $2T_0$  be the minimum duration of  $f(t)$ , that is,  $T_0$  is the smallest nonnegative value such that

$$f(t) = 0 \quad \text{whenever } T_0 < |t|.$$

The sampling theorem for functions of finite duration states that  $F(\omega)$  and hence, also  $f(t)$  can be reconstructed from a suitable uniform sampling in the frequency domain. More precisely, if  $0 < \Delta\omega < \Delta\Omega$ , where  $\Delta\Omega$  denotes the “frequency Nyquist interval,”

$$\Delta\Omega = \frac{\pi}{T_0},$$

then, letting  $T = \pi/\Delta\omega$ ,

$$F(\omega) = \sum_{n=-\infty}^{\infty} F(n\Delta\omega) \frac{\sin(T(\omega - n\Delta\omega))}{T(\omega - n\Delta\omega)},$$

and, taking the inverse transform,

$$f(t) = \sum_{n=-\infty}^{\infty} F(n\Delta\omega) \frac{\Delta\omega}{2\pi} e^{jn\Delta\omega t} p_T(t).$$

The energy in  $f(t)$  is

$$E = \frac{\Delta\omega}{2\pi} \sum_{n=-\infty}^{\infty} |F(n\Delta\omega)|^2.$$

### 2.5.5 Fundamental Sampling Formulas and Poisson’s Formula

As long as either  $f(t)$  or its Fourier transform,  $F(\omega)$ , is absolutely integrable and has a bounded derivative, then

$$\Delta t \sum_{n=-\infty}^{\infty} f(t - n\Delta t) = \sum_{n=-\infty}^{\infty} F(n\Delta\omega) e^{jn\Delta\omega t} \quad (2.189)$$



and

$$\frac{\Delta\omega}{2\pi} \sum_{n=-\infty}^{\infty} F(\omega - n\Delta\omega) = \sum_{n=-\infty}^{\infty} f(n\Delta t)e^{-jn\Delta t\omega} \quad (2.190)$$

where  $\Delta t$  and  $\Delta\omega$  are positive constants with  $\Delta t\Delta\omega = 2\pi$ . Using these formulas it is possible to derive the sampling theorems for band-limited functions and for finite duration functions. While these formulas are not valid for periodic functions, they can be used to derive the classical Fourier series expansion for periodic functions and hence, can also be viewed as generalizations of the Fourier series expansion for periodic functions. Letting  $t = 0$  formula 2.189 yields Poisson's formula,

$$\Delta t \sum_{n=-\infty}^{\infty} f(n\Delta t) = \sum_{n=-\infty}^{\infty} F(n\Delta\omega). \quad (2.191)$$

These sampling formulas can be derived by a fairly straightforward use of properties of the delta and the comb functions along with the use of the convolution formulas of Section 2.2.9. Let

$$\phi(t) = f * \text{comb}_{\Delta t}(t).$$

Because of the properties of the delta functions making up the comb function,

$$\phi(t) = \sum_{n=-\infty}^{\infty} f * \delta(t - n\Delta t) = \sum_{n=-\infty}^{\infty} f(t - n\Delta t).$$

The Fourier transform of  $\phi(t)$  is

$$\begin{aligned} \psi(\omega) &= \mathcal{F}[f * \text{comb}_{\Delta t}(t)]|_{\omega} \\ &= F(\omega)\Delta\omega \text{comb}_{\Delta\omega}(\omega) \\ &= \Delta\omega \sum_{n=-\infty}^{\infty} F(\omega)\delta(\omega - n\Delta\omega) \\ &= \Delta\omega \sum_{n=-\infty}^{\infty} F(n\Delta\omega)\delta(\omega - n\Delta\omega). \end{aligned}$$

Thus,

$$\begin{aligned} \Delta t \sum_{n=-\infty}^{\infty} f(t - n\Delta t) &= \Delta t\phi(t) \\ &= \mathcal{F}^{-1}[\Delta t\psi(\omega)]|_t \\ &= \mathcal{F}^{-1}\left[\Delta t\Delta\omega \sum_{n=-\infty}^{\infty} F(n\Delta\omega)\delta(\omega - n\Delta\omega)\right]|_t \\ &= 2\pi \sum_{n=-\infty}^{\infty} F(n\Delta\omega)\mathcal{F}^{-1}[\delta(\omega - n\Delta\omega)]|_t \\ &= \sum_{n=-\infty}^{\infty} F(n\Delta\omega)e^{jn\Delta\omega t}, \end{aligned}$$

which is formula 2.189

Similar computations yield formula 2.190.

### Example 2.51 Evaluation of an Infinite Series

To evaluate

$$\sum_{n=-\infty}^{\infty} \frac{1}{1+n^2},$$

observe that

$$\sum_{n=-\infty}^{\infty} \frac{1}{1+n^2} = \sum_{n=-\infty}^{\infty} F(n\Delta\omega),$$

where

$$F(\omega) = \frac{1}{1+\omega^2} \quad \text{and} \quad \Delta\omega = 1.$$

The Fourier inverse transform of  $F(\omega)$  is  $f(t) = e^{-|t|}/2$ , and so, by Poisson's formula,

$$\begin{aligned} \sum_{n=-\infty}^{\infty} \frac{1}{1+n^2} &= \sum_{n=-\infty}^{\infty} F(n\Delta\omega) \\ &= 2\pi \sum_{n=-\infty}^{\infty} f(n2\pi) \\ &= 2\pi \sum_{n=-\infty}^{\infty} \frac{1}{2} e^{-|n2\pi|} \\ &= 2\pi \left[ \frac{1}{2} + \sum_{n=1}^{\infty} (e^{-2\pi})^n \right]. \end{aligned}$$

The last summation is simply a geometric series. Using the well-known formula for summing geometric series,

$$\sum_{n=-\infty}^{\infty} \frac{1}{1+n^2} = 2\pi \left[ \frac{1}{2} + \frac{e^{-2\pi}}{1-e^{-2\pi}} \right] = \pi \frac{1+e^{-2\pi}}{1-e^{-2\pi}}.$$

## 2.6 Linear Systems

Much of signal processing can be described in terms of systems that can be readily analyzed using the Fourier transform. This section gives a brief introduction to such systems and how Fourier analysis is employed to study their behavior.

Mathematically, a system,  $S$ , is an operator that takes, as input, any function,  $f_1(t)$ , from the set of functions pertinent to the problem at hand (say, finite energy functions) and modifies the inputted function according to some fixed scheme to produce a corresponding function,  $f_0(t)$ , as output. This is denoted by either

$$S: f_1(t) \rightarrow f_0(t)$$

or

$$f_0(t) = S[f_1(t)].$$

As indicated, the input function and corresponding output function will, throughout this section, be denoted via the “I” and “O” subscripts. The output,  $f_O(t)$ , is also called the system’s response to  $f_I(t)$ .

### 2.6.1 Linear Shift Invariant Systems

A system,  $S$ , is said to be linear if every linear combination of inputs leads to the corresponding linear combination of outputs. More precisely,  $S$  is linear if, given any pair of inputs,  $f_1(t)$  and  $g_1(t)$ , and any pair of constants,  $\alpha$  and  $\beta$ , then

$$S[\alpha f_1(t) + \beta g_1(t)] = \alpha f_O(t) + \beta g_O(t).$$

A system  $S$ , is said to be shift invariant if any shift in an input function leads to an identical shift in the output, that is, if

$$S[f_1(t - t_0)] = f_O(t - t_0)$$

for every real value of  $t_0$  and every allowed input,  $f_1(t)$ . Other terms commonly used instead of “shift invariant” include “translation invariant,” “time invariant,” “stationary,” and “fixed.”

An LSI system is both linear and shift invariant. If  $S$  is an LSI system, then, using both linearity and shift invariance, the following string of equalities can be verified:

$$\begin{aligned} S[f_1 * g_1(t)] &= S\left[\int_{-\infty}^{\infty} f_1(s)g_1(t-s)ds\right] \\ &= \int_{-\infty}^{\infty} f_1(s)S[g_1(t-s)]ds \\ &= \int_{-\infty}^{\infty} f_1(s)g_O(t-s)ds \\ &= f_1 * g_O(t). \end{aligned} \quad (2.192)$$

Given an LSI system,  $S$ , the system’s impulse response function, usually denoted by  $h(t)$ , is the output corresponding to an inputted delta function,

$$h(t) = S[\delta(t)].$$

The transfer function of the system is the Fourier transform of the impulse response function,

$$H(\omega) = \mathcal{F}[h(t)]|_{\omega}.$$

Combining Equation 2.192 with the fact that  $f_1 * \delta(t) = f_1(t)$  leads directly to the following important formula for computing the output of a system from any input:

$$f_O(t) = S[f_I(t)] = f_I * h(t). \quad (2.193)$$

Taking the Fourier transform gives the equally important formula

$$F_O(\omega) = F_I(\omega)H(\omega), \quad (2.194)$$

where  $F_O(\omega)$  and  $F_I(\omega)$  are the transforms

$$F_O(\omega) = \mathcal{F}[f_O(t)]|_{\omega} \quad \text{and} \quad F_I(\omega) = \mathcal{F}[f_I(t)]|_{\omega}.$$

Formulas 2.193 and 2.194 show that the effect of an LSI system on a signal is completely determined by either the system’s impulse response function or the system’s transfer function. One advantage of knowing the transfer function is that, in many cases, the transfer function provides better intuition on the effect the system has on inputted signals. Also, in many cases, the actual computations are easier using the transfer function instead of the impulse response function. Both advantages are illustrated in Example 2.52.

#### Example 2.52 Ideal Low-Pass Filter

An ideal low-pass filter with cutoff frequency  $\Omega$  (and zero delay) is an LSI system characterized by the transfer function

$$H(\omega) = \rho_{\Omega}(\omega) = \begin{cases} 1, & \text{if } |\omega| < \Omega \\ 0, & \text{if } \Omega < |\omega| \end{cases}.$$

The impulse response function is

$$h(t) = \mathcal{F}^{-1}[\rho_{\Omega}(\omega)]|_t = \frac{\sin(\Omega t)}{\pi t}.$$

Given an input signal,  $f_1(t)$ , with Fourier transform  $F_1(\omega)$ , the corresponding output,  $f_O(t)$ , is the inverse transform of

$$F_1(\omega)H(\omega) = \begin{cases} F_1(\omega), & \text{if } |\omega| < \Omega \\ 0, & \text{if } \Omega < |\omega| \end{cases}.$$

Clearly, this system passes, unaltered, the frequency components of  $f_1(t)$  corresponding to frequencies below the cutoff while completely suppressing the frequency components of  $f_1(t)$  corresponding to frequencies above the cutoff. For example, if

$$f_1(t) = \sin(\omega_0 t),$$

then

$$F_1(\omega) = \mathcal{F}[\sin(\omega_0 t)]|_{\omega} = -j\pi[\delta(\omega - \omega_0) - \delta(\omega + \omega_0)].$$

Thus,

$$\begin{aligned} F_O(\omega) &= -j\pi[\delta(\omega - \omega_0) - \delta(\omega + \omega_0)]\rho_{\Omega}(\omega) \\ &= -j\pi[\rho_{\Omega}(\omega_0)\delta(\omega - \omega_0) - \rho_{\Omega}(-\omega_0)\delta(\omega + \omega_0)] \\ &= \begin{cases} -j\pi[\delta(\omega - \omega_0) - \delta(\omega + \omega_0)] & \text{if } |\omega_0| < \Omega \\ 0, & \text{if } \Omega < |\omega_0| \end{cases} \end{aligned}$$

and

$$f_0(t) = \mathcal{F}^{-1}[F_0(\omega)]|_t = \begin{cases} \sin(\omega_0 t), & \text{if } |\omega_0| < \Omega \\ 0, & \text{if } \Omega < |\omega_0| \end{cases}.$$

Alternatively,  $f_0(t)$  could have been computed using the impulse response function,

$$\begin{aligned} f_0(t) &= \sin(\omega_0 t) * \frac{\sin(\Omega t)}{\pi t} \\ &= \int_{-\infty}^{\infty} \frac{1}{\pi(t-s)} \sin(\omega_0 s) \sin(\Omega(t-s)) ds. \end{aligned}$$

In many applications it is convenient to write the transfer function in the form

$$H(\omega) = A(\omega)e^{-j\theta(\omega)}$$

where  $A(\omega)$  and  $\theta(\omega)$  are real-valued functions (called, respectively, the amplitude and phase of  $H(\omega)$ ) with  $A(\omega)$  often assumed to be nonnegative.

### Example 2.53

In the simplest case,  $A(\omega)$  is constant and  $\phi(\omega)$  is linear,

$$A(\omega) = A_0 \quad \text{and} \quad \phi(\omega) = \tau_0 \omega.$$

In this case,

$$f_0(t) = \mathcal{F}^{-1}[F_1(\omega)A_0e^{-j\tau_0\omega}]_t = A_0 f_1(t - \tau_0)$$

Thus, a system with transfer function

$$H(\omega) = A_0 e^{-j\tau_0 \omega}$$

amplifies each inputted signal by  $A_0$  and delays it by  $\tau_0$ .

## 2.6.2 Reality and Stability

An LSI system is a “real” system if the output is a real-valued function whenever the input is a real-valued function. In practice, most physically defined systems can be assumed to be real. An equivalent condition for a system to be real is that the impulse response function,  $h(t)$ , of the system be real valued. By the discussion in Section 2.3.1, if the system is real and the transfer function is given by

$$H(\omega) = A(\omega)e^{-j\theta(\omega)},$$

where  $A(\omega)$  and  $\theta(\omega)$  are the amplitude and phase of  $H(\omega)$ , then

$$h(t) = \frac{1}{\pi} \int_0^{\infty} A(\omega) \cos(\omega t - \theta(\omega)) d\omega.$$

An LSI system is stable if there is a finite constant,  $B$ , such that

$$|f_0(t)| \leq BM \quad \text{for all } t$$

whenever

$$|f_1(t)| \leq M \quad \text{for all } t.$$

It can be shown that a system is stable if and only if its impulse response function,  $h(t)$ , is absolutely integrable and that, in this case,

$$B = \int_{-\infty}^{\infty} |h(t)| dt.$$

It follows from the discussion in Section 2.3.2 that if the transfer function,  $H(\omega)$ , is not bounded and continuous, then the system cannot be stable.

### Example 2.54

Let  $S$  be the ideal low-pass filter of Example 2.52. Because the impulse response function,

$$h(t) = \frac{1}{\pi t} \sin(\Omega t),$$

is real, so is the system. This is obvious because, if a given input,  $f_1(t)$ , is real valued, so must be

$$f_0(t) = f_1 * h(t) = \int_{-\infty}^{\infty} f_1(s) \frac{1}{\pi(t-s)} \sin(\Omega(t-s)) ds.$$

Because the transfer function,

$$H(\omega) = p_{\Omega}(\omega) \begin{cases} 1, & \text{if } |\omega| < \Omega \\ 0, & \text{if } \Omega < |\omega| \end{cases}$$

is not continuous, the system cannot be stable. This is easily verified using the input function

$$f_1(t) = \begin{cases} +1, & \text{if } 0 \leq \frac{1}{t} \sin(\Omega t) \\ -1, & \text{if } \frac{1}{t} \sin(\Omega t) < 0 \end{cases}.$$

Clearly,

$$|f_1(t)| \leq 1 \quad \text{for all } t,$$

but

$$f_1(s)h(-s) = \left| \frac{1}{s} \sin(\Omega s) \right| \quad \text{for all } s.$$

Thus,

$$\begin{aligned} f_0(t) &= f_1 * h(t) \\ &= \int_{-\infty}^{\infty} f_1(s)h(t-s)ds \\ &= \int_{-\infty}^{\infty} \left| \frac{1}{s} \sin(\Omega s) \right| ds \\ &= \infty. \end{aligned}$$

### 2.6.3 System Response to Complex Exponentials and Periodic Functions

Let  $S$  be an LSI system with impulse response function  $h(t)$  and transfer function  $H(\omega)$ . Because  $\mathcal{F}[e^{j\omega_0 t}]|_{\omega} = 2\pi\delta(\omega - \omega_0)$ ,

$$\begin{aligned} S[e^{j\omega_0 t}] &= \mathcal{F}^{-1}[2\pi\delta(\omega - \omega_0)H(\omega)]|_t \\ &= \mathcal{F}^{-1}[2\pi\delta(\omega - \omega_0)H(\omega_0)]|_t \\ &= H(\omega_0)e^{j\omega_0 t}. \end{aligned} \tag{2.195}$$

By this it is seen that the complex exponentials are eigenfunctions for  $S$  and that the transfer function gives the corresponding eigenvalues.

If  $f_1(t)$  is a periodic function with period  $p$  and with Fourier series

$$\sum_{n=-\infty}^{\infty} c_n e^{jn\Delta\omega t},$$

where  $\Delta\omega = 2\pi/p$ , then, from Equation 2.195 and the linearity of the system,

$$S[f_1(t)] = \sum_{n=-\infty}^{\infty} c_n H(n\Delta\omega) e^{jn\Delta\omega t}. \tag{2.196}$$

In particular, for  $\alpha > 0$ ,

$$S[\cos(\alpha t)] = \frac{1}{2} [H(\alpha)e^{j\alpha t} + H(-\alpha)e^{-j\alpha t}] \tag{2.197}$$

and

$$S[\sin(\alpha t)] = \frac{1}{2j} [H(\alpha)e^{j\alpha t} - H(-\alpha)e^{-j\alpha t}]. \tag{2.198}$$

If  $S$  is a real LSI system, then the imaginary parts of Equations 2.197 and 2.198 must vanish. Using this fact, it can be shown that

$$S[\cos(\alpha t)] = A(\alpha) \cos(\alpha t - \theta(\alpha))$$

and

$$S[\sin(\alpha t)] = A(\alpha) \sin(\alpha t - \theta(\alpha)),$$

where  $A(\omega)$  and  $\theta(\omega)$  are the amplitude and phase of the transfer function,

$$H(\omega) = A(\omega)e^{-j\theta(\omega)}.$$

#### Example 2.55

Let  $S$  be the ideal low-pass filter from Example 2.52 with transfer function

$$H(\omega) = \rho_{\Omega}(\omega) = \begin{cases} 1, & \text{if } |\omega| < \Omega \\ 0, & \text{if } \Omega < |\omega|. \end{cases}$$

For this example assume  $\Omega = 20.5\pi$  and let  $f_1(t)$  be the sawtooth function from Example 2.30. As seen in that example,  $\Delta\omega = \pi$  and

$$f_1(t) = \sum_{\substack{n=-\infty \\ n \neq 0}}^{\infty} (-1)^n \frac{j}{n\pi} e^{jn\pi t}.$$

From this and Equation 2.196 it follows that

$$f_0(t) = \sum_{\substack{n=-20 \\ n \neq 0}}^{20} (-1)^n \frac{j}{n\pi} e^{jn\pi t}.$$

The graphs of  $f_1(t)$  and  $f_0(t)$  are sketched in Figures 2.8 and 2.9, respectively.

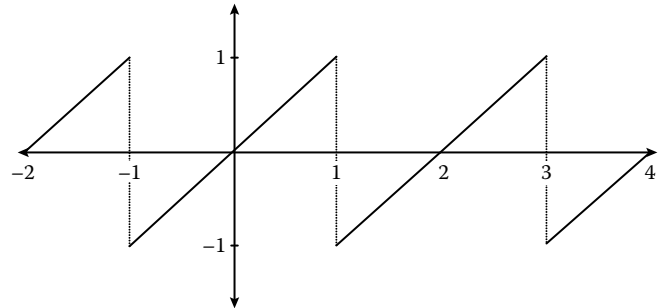


FIGURE 2.8 The saw function.

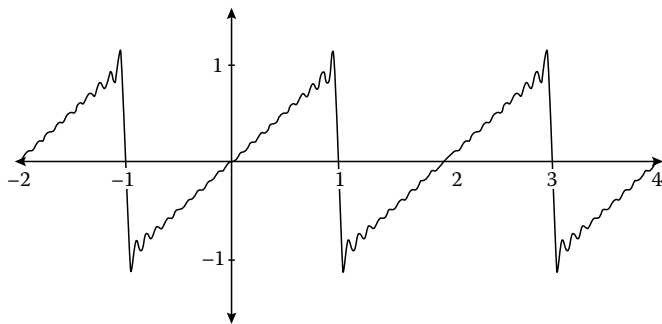


FIGURE 2.9 Low-pass filter output from a saw function input.

### 2.6.4 Casual Systems

A function,  $f(t)$ , is said to be “casual” if

$$f(t) = 0, \quad \text{whenever } t < 0.$$

An LSI system,  $S$ , is said to be “casual” if the response of the system to every causal input is a causal output. By shift invariance, this is equivalent to defining  $S$  to be casual if

$$f_1(t) = 0, \quad \text{whenever } t < t_0$$

implies that

$$f_0(t) = S[f_1(t)] = 0, \quad \text{whenever } t < t_0$$

for any real value of  $t_0$ .

If  $S$  is a casual system, then its impulse response function,  $h(t)$ , must also be casual and formula 2.193 for computing the response of a system to an input  $f_1(t)$  becomes

$$f_0(t) = \int_{-\infty}^t f_1(s)h(t-s)ds$$

or equivalently,

$$f_0(t) = \int_0^{\infty} f_1(t-s)h(s)ds.$$

If the input is also casual, then these further reduce to

$$f_0(t) = \int_0^t f_1(s)h(t-s)ds$$

and

$$f_0(t) = \int_0^t f_1(t-s)h(s)ds.$$

### 2.6.5 Systems Given by Differential Equations

Often the output,  $f_0(t)$ , of a system,  $S$ , is a solution to a non-homogeneous ordinary differential equation with the input being the nonhomogeneous part of the equation,

$$\sum_{n=0}^N A_n \frac{d^n}{dt^n} [f_0(t)] = f_1(t).$$

As long as the  $A_n$ 's are constants, it is easily verified that  $S$  is an LSI system. The impulse response function,  $h(t)$ , must satisfy

$$\sum_{n=0}^N A_n \frac{d^n h}{dt^n} = \delta(t). \quad (2.199)$$

The general solution to Equation 2.199 can be written

$$h_g(t) = h_p(t) + y_c(t),$$

where  $y_c(t)$  is the general solution to the corresponding homogeneous equation,

$$\sum_{n=0}^N A_n \frac{d^n y}{dt^n} = 0, \quad (2.200)$$

and  $h_p(t)$  is any particular solution to Equation 2.199. After a particular solution is found the undetermined constants in  $y_c(t)$  must be determined so that the resulting

$$h(t) = h_p(t) + y_c(t),$$

satisfies any additional constraints on the output (causality, finite energy, etc.).

The particular solution,  $h_p(t)$ , can be found by taking the Fourier transform of both sides of Equation 2.199. Using identity 2.50 gives an equation for  $H_p(\omega) = \mathcal{F}[h_p(t)]|_{\omega}$ ,

$$\sum_{n=0}^N A_n (j\omega)^n H_p(\omega) = 1. \quad (2.201)$$

Dividing through by

$$D(\omega) = \sum_{n=0}^N A_n (j\omega)^n$$

gives

$$H_p(\omega) = \frac{1}{D(\omega)}, \quad (2.202)$$

which is a rational function of  $\omega$ . Taking the inverse transform of  $H_p(\omega)$  (using, say, the approach described in Section 2.3.14) then yields  $h_p(t)$ .

Example 2.56 illustrates a common situation in which the obtained  $h_p(t)$  already satisfies the additional conditions and, thus, can be used directly as the impulse response function. In Example 2.57,  $h_p(t)$  is not a valid output and, so, a nontrivial solution to the corresponding homogeneous equation must be added to obtain the impulse response function.

#### Example 2.56

Let the output  $f_0(t)$ , corresponding to an input,  $f_1(t)$ , be given by the finite energy solution to

$$\frac{d^2 y}{dt^2} - y = f(t).$$

The solution to the corresponding homogeneous equation,

$$\frac{d^2y}{dt^2} - y = 0,$$

is

$$y_c(t) = c_1 e^t + c_2 e^{-t},$$

while the impulse response function must satisfy

$$\frac{d^2h}{dt^2} - h = \delta(t). \quad (2.203)$$

Letting  $h_p(t)$  denote a particular solution and taking the Fourier transform of both sides yields

$$-\omega^2 H_p(\omega) - H_p(\omega) = 1,$$

which, after some elementary algebra, reduces to

$$H_p(\omega) = \frac{-1}{1 + \omega^2}.$$

The inverse transform of this can be computed directly from tables:

$$h_p(t) = -\frac{1}{2} \mathcal{F}^{-1} \left[ \frac{2}{1 + \omega^2} \right] \Big|_t = -\frac{1}{2} e^{-|t|}.$$

The general solution to Equation 2.203 is the sum of  $h_p(t)$  and  $y_c(t)$ ,

$$h_g(t) = -\frac{1}{2} e^{-|t|} + c_1 e^t + c_2 e^{-t},$$

but, clearly, the only way  $h_g(t)$  can be a finite energy function is for  $c_1 = c_2 = 0$ . Thus, the impulse response function and the transfer function for this system are

$$h(t) = -\frac{1}{2} e^{-|t|}$$

and

$$H(\omega) = \frac{-1}{1 + \omega^2}.$$

**Example 2.57**

Assume  $S: f_i(t) \rightarrow f_o(t)$  is a causal system for which the output satisfies

$$\frac{d^2 f_o}{dt^2} + f_o = f_i(t).$$

The solution to the corresponding homogeneous equation,

$$\frac{d^2y}{dt^2} + y = 0,$$

is

$$y_c(t) = c_1 \cos(t) + c_2 \sin(t),$$

while the impulse response function must satisfy

$$\frac{d^2h}{dt^2} + h = \delta(t). \quad (2.204)$$

Letting  $h_p(t)$  denote a particular solution and taking the Fourier transform of both sides yields

$$-\omega^2 H_p(\omega) + H_p(\omega) = 1$$

which, after some elementary algebra, reduces to

$$H_p(\omega) = \frac{1}{1 - \omega^2} = \frac{1}{2} \left[ \frac{1}{\omega + 1} - \frac{1}{\omega - 1} \right].$$

Using either the tables or formula 2.118,

$$h_p(t) = \frac{1}{2} \left[ \frac{j}{2} e^{-jt} \text{sgn}(t) - \frac{j}{2} e^{jt} \text{sgn}(t) \right] = \frac{1}{2} \sin(t) \text{sgn}(t).$$

The general solution to Equation 2.204 is then

$$h_g(t) = h_p(t) + y_c(t) = \frac{1}{2} \sin(t) \text{sgn}(t) + c_1 \cos(t) + c_2 \sin(t).$$

Because  $S$  is a causal system and  $\delta(t) = 0$  for  $t < 0$ , the impulse response function must vanish for negative values of  $t$ . Thus,  $c_1$  and  $c_2$  must be chosen so that for  $t < 0$ ,

$$\begin{aligned} h_g(t) &= \frac{1}{2} \sin(t) \text{sgn}(t) + c_1 \cos(t) + c_2 \sin(t) \\ &= \left( c_2 - \frac{1}{2} \right) \sin(t) + c_1 \cos(t) \\ &= 0. \end{aligned}$$

Clearly,  $c_1 = 0$ ,  $c_2 = 1/2$ , and the impulse response function is

$$h(t) = \frac{1}{2} \sin(t) \text{sgn}(t) + \frac{1}{2} \sin(t) = \sin(t) u(t).$$

The transfer function is

$$\begin{aligned} H(\omega) &= \mathcal{F}[\sin(t) u(t)] \Big|_\omega \\ &= \frac{1}{2j} \left[ \left( \pi \delta(\omega - 1) - j \frac{1}{\omega - 1} \right) - \left( \pi \delta(\omega + 1) - j \frac{1}{\omega + 1} \right) \right] \\ &= \frac{1}{1 - \omega^2} + j \frac{\pi}{2} [\delta(\omega + 1) - \delta(\omega - 1)]. \end{aligned}$$

### 2.6.6 RLC Circuits

Consider the electric circuit sketched in Figure 2.10. This circuit consists of

- A resistor with a fixed resistance of  $R$  ohms,
- An inductor with a fixed inductance of  $L$  henries,
- A capacitor with a fixed capacitance of  $C$  farads, and
- A time varying voltage supply providing a voltage of  $E(t)$  volts.

The charge on the capacitor at time  $t$  will be denoted by  $q(t)$  and the corresponding current in the circuit by  $i(t)$ . The charge and current are related by

$$i(t) = \frac{dq}{dt}.$$

By Kirchhoff's laws

$$L \frac{d^2q}{dt^2} + R \frac{dq}{dt} + \frac{1}{C}q = E(t). \tag{2.205}$$

For a physical circuit  $R$  must be positive and  $L$  and  $C$  cannot be negative. Also, it is reasonable to assume that no charge accumulates on the capacitor if no voltage has previously been provided. Thus,  $q(t)$  can be viewed as the output corresponding to an input of  $E(t)$  to a causal LSI system. The impulse response function,  $h(t)$ , to this system satisfies

$$L \frac{d^2h}{dt^2} + R \frac{dh}{dt} + \frac{1}{C}h = \delta(t). \tag{2.206}$$

If the inductance and capacitance are nonzero, then straightforward computations, similar to those done in the examples of Sections 2.6.5 and 2.3.14 lead to

$$h(t) = \frac{1}{2L\beta} [e^{\beta t} - e^{-\beta t}]e^{-\alpha t}u(t)$$

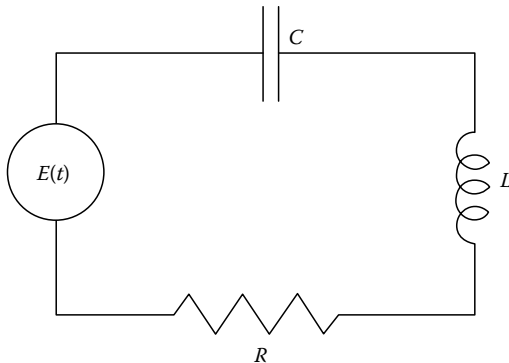


FIGURE 2.10 A simple RLC circuit.

and

$$H(\omega) = \frac{j}{2L\beta} \left[ \frac{1}{\omega - j(\alpha + \beta)} - \frac{1}{\omega - j(\alpha - \beta)} \right] = \frac{-C}{LC\omega^2 - jRC\omega - 1},$$

where

$$\alpha = \frac{R}{2L} \quad \text{and} \quad \beta = \sqrt{\left(\frac{R}{2L}\right)^2 - \frac{1}{LC}}.$$

It should be noted that, because the real part of  $\alpha \pm \beta$  is positive,  $h(t)$  is bounded by a decreasing exponential on  $0 < t$ . Hence,  $h(t)$  is absolutely integrable and the system is stable.

In practice, the current,  $i(t)$ , is often of greater interest than the charge on the capacitor. Because

$$i(t) = \frac{dq}{dt} = \frac{d}{dt}(E * h(t)) = E * h'(t),$$

it follows that the current is given by a system with impulse response function

$$h_i(t) = h'(t) = \frac{1}{2L\beta} [(\beta - \alpha)e^{\beta t} + (\beta + \alpha)e^{-\beta t}]e^{-\alpha t}u(t)$$

and transfer function

$$H_i(\omega) = j\omega H(\omega) = \frac{-jC\omega}{LC\omega^2 - jRC\omega - 1}.$$

In either case the response of the system to the impulse function will depend on whether  $\beta$  has an imaginary component. If  $\beta$  does have a nonzero imaginary component, the unit impulse response will be a sinusoidal function with an exponentially decreasing envelope. If the imaginary part of  $\beta$  is zero, then the response is simply a linear combination of decreasing exponentials.

### 2.6.7 Modulation and Demodulation

Let  $f(t)$  be any band-limited function with bandwidth  $2\Omega$ , and let  $\omega_c$  and  $t_0$  be real constants with  $\Omega < \omega_c$ . The product

$$g(t) = f(t) \cos(\omega_c t - t_0)$$

is the “modulation of the carrier signal,  $\cos(\omega t - t_0)$ , by  $f(t)$ .” The extraction of the modulating signal,  $f(t)$ , from the modulated signal provides an especially nice example of the application of Fourier analysis in signal processing.

To extract  $f(t)$ , first multiply  $g(t)$  by the carrier signal. This gives

$$\begin{aligned} g(t) \cos(\omega_c t - t_0) &= f(t) \cos^2(\omega_c t - t_0) \\ &= f(t) \left[ \frac{1}{2} + \frac{1}{2} \cos(2\omega_c t - 2t_0) \right] \\ &= \frac{1}{2}f(t) + \frac{1}{2}f(t) \cos(2\omega_c t - 2t_0). \end{aligned}$$

Using the basic identities, the Fourier transform of this is found to

$$\begin{aligned} & \frac{1}{2}F(\omega) + \frac{1}{2}F(\omega) * [\pi e^{-j4t_0\omega_c}\delta(\omega - 2\omega_c) + \pi e^{j4t_0\omega_c}\delta(\omega + 2\omega_c)] \\ &= \frac{1}{2}F(\omega) + \frac{\pi}{2}[e^{-j4t_0\omega_c}F(\omega - 2\omega_c) + e^{j4t_0\omega_c}F(\omega + 2\omega_c)]. \end{aligned}$$

Sketches of  $F(\omega)$ ,  $F(\omega - 2\omega_c)$ , and  $F(\omega + 2\omega_c)$  are given in Figure 2.11. Observe that because  $f(t)$  is a band-limited function with bandwidth  $2\Omega$  and  $\Omega < \omega_c$ , if  $H(\omega)$  is any band-limited function with bandwidth  $2\Omega_H$  satisfying  $\Omega_H < 2\omega_c - \Omega$ , then

$$\begin{aligned} & \left(\frac{1}{2}F(\omega) + \frac{\pi}{2}[e^{-j4t_0\omega_c}F(\omega - 2\omega_c) + e^{j4t_0\omega_c}F(\omega + 2\omega_c)]\right)H(\omega) \\ &= \frac{1}{2}F(\omega)H(\omega). \end{aligned}$$

In particular if  $H(\omega)$  is the perfect low-pass filter of Examples 2.52 and 2.55,

$$H(\omega) = \begin{cases} 1, & \text{if } |\omega| < \Omega_H \\ 0, & \text{if } |\omega| > \Omega_H, \end{cases}$$

with

$$\Omega < \Omega_H < 2\omega_c - \Omega,$$

then

$$\begin{aligned} & \left(\frac{1}{2}F(\omega) + \frac{\pi}{2}[e^{-j4t_0\omega_c}F(\omega - 2\omega_c) + e^{j4t_0\omega_c}F(\omega + 2\omega_c)]\right)H(\omega) \\ &= \frac{1}{2}F(\omega). \end{aligned}$$

Thus, the signal

$$g(t) = f(t) \cos(\omega_c t - t_0)$$

can be perfectly demodulated (i.e.,  $f(t)$  can be completely extracted) by first multiplying the modulated signal by the carrier and then passing the result through an appropriate ideal low-pass filter.

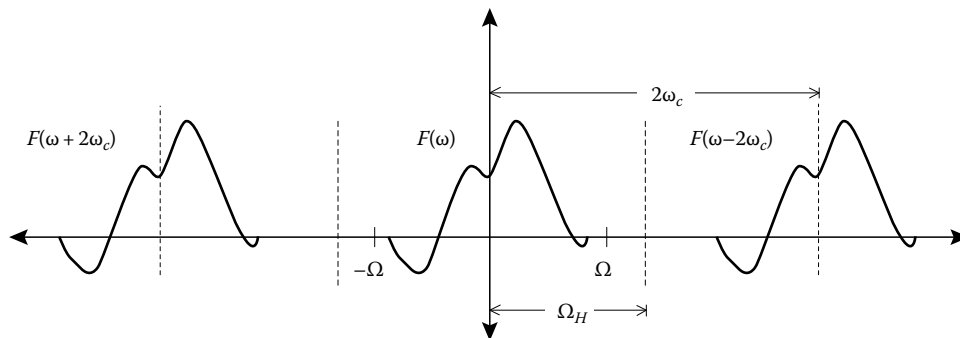


FIGURE 2.11 Translations of the transform of a band-limited function.

## 2.7 Random Variables

Because noise is an intrinsic factor in real-world systems, random variables play an important role in the mathematics of practical engineering problems. As illustrated in this section, the Fourier transform is a useful tool in analyzing signals containing a significant random component and in extracting usable information from these signals.

### 2.7.1 Basic Probability and Statistics

A nonnegative function,  $p(x)$ , is a probability density function if it satisfies

$$\int_{-\infty}^{\infty} p(x)dx = 1.$$

Such a function is absolutely integrable and so its Fourier transform,  $P(y) = \mathcal{F}[p(x)]|_y$ , must be continuous and must satisfy  $P(0) = 1$  (see Section 2.3.2).

If  $x$  denotes the outcome of a random process governed by the probability density function  $p(x)$  and if  $-\infty \leq a \leq b \leq \infty$ , then

$$\int_a^b p(x)dx$$

is the probability that  $x$  is between  $a$  and  $b$ . The “mean” or “expected value” of  $x$ , is denoted by either  $\mu$  or  $E[x]$ , and is given by the first moment of  $p(x)$ ,

$$\mu = E[x] = \int_{-\infty}^{\infty} xp(x)dx.$$

The variance of  $x$ , denoted by either  $\sigma^2$  or  $\text{Var}[x]$ , is the second moment of  $p(x)$  about its mean,

$$\sigma^2 = \text{Var}[x] = \int_{-\infty}^{\infty} (x - \mu)^2 p(x)dx,$$



and the standard deviation,  $\sigma$ , is the square root of the variance. More generally, if  $f(x)$  is any function of  $x$  then  $f(x)$  is a random variable with expected value

$$\mu = E[f(x)] = \int_{-\infty}^{\infty} f(x)p(x)dx$$

and variance

$$\text{Var}[f(x)] = \int_{-\infty}^{\infty} |f(x) - \mu|^2 p(x)dx.$$

In particular,  $\text{Var}[x] = E[|x - \mu|^2]$ . It is easy to show that the variance of  $x$ ,  $\sigma^2$ , is directly related to the first and second moments of  $p(x)$ ,

$$\sigma^2 = E[x^2] - \mu^2 = \int_{-\infty}^{\infty} x^2 p(x)dx - \left( \int_{-\infty}^{\infty} xp(x)dx \right)^2.$$

It follows from the discussion in Sections 2.2.11 and 2.2.12 that if  $p(x)$  is a probability density function, then the corresponding mean, expected value of  $x^2$ , and variance can be computed from the density function's transform,  $P(y) = \mathcal{F}[p(x)]|_y$ , by

$$\mu = jP'(0), \tag{2.207}$$

$$E[x^2] = -P''(0), \tag{2.208}$$

and

$$\sigma^2 = [P'(0)]^2 - P''(0). \tag{2.209}$$

**Example 2.58 The Normal Distribution**

A normal (or Gaussian) probability distribution is given by the density function

$$p(x) = \sqrt{\frac{\alpha}{\pi}} e^{-\alpha(x-x_0)^2},$$

where  $\alpha > 0$ . Using the tables it is easily verified that

$$P(y) = \mathcal{F}[p(x)]|_y = \exp\left[-\frac{1}{4\alpha}y^2 - jx_0y\right].$$

Furthermore,

$$P(0) = 1,$$

$$P'(y) = -\left(\frac{1}{2\alpha}y + jx_0\right)P(y),$$

and

$$P''(y) = \frac{1}{4\alpha^2}[(y + j2\alpha x_0)^2 - 2\alpha]P(y).$$

Using formulas 2.207 through 2.209 to compute the mean and variance,

$$\mu = jP'(0) = -j(0 + jx_0)P(0) = x_0,$$

$$E[x^2] = -P''(0) = -\frac{1}{4\alpha^2}[(0 + j2\alpha x_0)^2 - 2\alpha]P(0) = x_0^2 + \frac{1}{2\alpha},$$

and

$$\sigma^2 = [P'(0)]^2 - P''(0) = \frac{1}{2\alpha}.$$

Replacing  $x_0$  and  $\alpha$  in the above formulas for  $p(x)$  and  $P(y)$  it follows that the normal probability distribution with mean  $\mu$  and standard deviation  $\sigma$  is given by the density function

$$p(x) = \frac{1}{\sigma\sqrt{2\pi}} \exp\left[-\frac{1}{2}\left(\frac{x - \mu}{\sigma}\right)^2\right],$$

and that its Fourier transform is given by

$$P(y) = \exp\left[-\frac{1}{2}(\sigma y)^2 - j\mu y\right].$$

**Example 2.59 The Binomial Distribution**

Consider a process consisting of  $n$  repetitions of an experiment with exactly two outcomes, "success" and "failure." Let  $p_0$  be the probability of "success" and  $q_0$  the probability of "failure" in one experiment (hence,  $p_0 + q_0 = 1$ ). Such a process is governed by the binomial probability density function

$$p(x) = \sum_{k=0}^n \binom{n}{k} p_0^k q_0^{n-k} \delta(x - k)$$

with

$$\int_a^b p(x) dx = \sum_{a < k < b} \binom{n}{k} p_0^k q_0^{n-k}$$

being the probability that the number of "successes,"  $x$ , satisfies  $a < x < b$ .

In Example 2.33 the Fourier transform of this function was found to be

$$P(y) = (p_0 e^{-jy} + q_0)^n.$$

Assuming that  $n > 1$ ,

$$P'(y) = -jn p_0 e^{-jy} (p_0 e^{-jy} + q_0)^{n-1}.$$

and

$$P''(y) = -np_0 e^{-iy} (np_0 e^{-iy} + q_0)(p_0 e^{-iy} + q_0)^{n-2}.$$

Thus,

$$P'(0) = -jnp_0 \quad \text{and} \quad P''(0) = -np_0(np_0 + q_0).$$

So, using formulas 2.207 through 2.209 to compute the mean and variance,

$$\mu = jP'(0) = np_0,$$

$$E[x^2] = -P''(0) = np_0(np_0 + q_0),$$

and

$$\sigma^2 = [P'(0)]^2 - P''(0) = np_0q_0.$$

### 2.7.2 Multiple Random Processes and Independence

Let  $x_1$  and  $x_2$  denote the outcomes of two random processes governed, respectively, by probability density functions  $p_1(x_1)$  and  $p_2(x_2)$ , and with corresponding means  $\mu_1$  and  $\mu_2$ , and corresponding standard deviations  $\sigma_1$  and  $\sigma_2$ . Taken as a single pair,  $(x_1, x_2)$  can be viewed as the outcome of a single two-dimensional random process. This process will be governed by a probability density function of two variables,  $q(x_1, x_2)$ . Given any  $-\infty \leq a_1 \leq b_1 \leq \infty$  and  $-\infty \leq a_2 \leq b_2 \leq \infty$ , the probability that both

$$a_1 < x_1 < b_1 \quad \text{and} \quad a_2 < x_2 < b_2$$

is

$$\int_{a_1}^{b_1} \int_{a_2}^{b_2} q(x_1, x_2) dx_1 dx_2.$$

In general, the relationship between the joint density function  $q(x_1, x_2)$ , and the individual density functions,  $p_1(x_1)$  and  $p_2(x_2)$ , depends strongly on the relationship that exists between the two random processes. If  $x_1$  and  $x_2$  are, in fact, the same, then

$$q(x_1, x_2) = p_1(x_1)\delta(x_2 - x_1). \quad (2.210)$$

If the two random processes are completely independent of each other, then, for all values of  $x_1$  and  $x_2$ ,

$$q(x_1, x_2) = p_1(x_1)p_2(x_2). \quad (2.211)$$

#### Example 2.60

Let  $x$  denote the number of heads resulting from a single toss of a fair coin, and let  $x_1$  and  $x_2$  be the number of heads reported by two perfectly accurate observers, each observing

the single toss of a fair coin. The probability density function for  $x$ ,  $p(x)$ , is well known to be

$$p(x) = \frac{1}{2}\delta(x) + \frac{1}{2}\delta(x - 1).$$

If both observers are observing the same coin toss, then  $x_1 = x_2$  and, according to formula 2.210, the joint probability density function is

$$q_{\text{same}}(x_1, x_2) = \left[ \frac{1}{2}\delta(x_1) + \frac{1}{2}\delta(x_1 - 1) \right] \delta(x_2 - x_1). \quad (2.212)$$

Note that if  $\alpha$  is any real number and  $\phi(x_1, x_2)$  is any two-dimensional test function, then

$$\begin{aligned} \int_{-\infty}^{\infty} \int_{-\infty}^{\infty} \delta(x_1 - \alpha)\delta(x_1 - x_2)\phi(x_1, x_2)dx_1 dx_2 &= \phi(\alpha, \alpha) \\ &= \int_{-\infty}^{\infty} \int_{-\infty}^{\infty} \delta(x_1 - \alpha, x_2 - \alpha)\phi(x_1, x_2)dx_1 dx_2. \end{aligned}$$

This shows that, in general,

$$\delta(x_1 - \alpha)\delta(x_1 - x_2) = \delta(x_1 - \alpha, x_2 - \alpha),$$

which, in turn, verifies that formula 2.212 is completely equivalent to the formula

$$q_{\text{same}}(x_1, x_2) = \frac{1}{2}\delta(x_1, x_2) + \frac{1}{2}\delta(x_1 - 1, x_2 - 1),$$

obtained by elementary probability theory.

On the other hand, if the two observers are observing two different tosses of the coin, then the value of  $x_1$  and  $x_2$  are independent of each other and the joint density function is

$$\begin{aligned} q_{\text{indep}}(x_1, x_2) &= \left[ \frac{1}{2}\delta(x_1) + \frac{1}{2}\delta(x_1 - 1) \right] \left[ \frac{1}{2}\delta(x_2) + \frac{1}{2}\delta(x_2 - 1) \right] \\ &= \frac{1}{4}\delta(x_1)\delta(x_2) + \frac{1}{4}\delta(x_1)\delta(x_2 - 1) \\ &\quad + \frac{1}{4}\delta(x_1 - 1)\delta(x_2) + \frac{1}{4}\delta(x_1 - 1)\delta(x_2 - 1), \end{aligned}$$

which agrees with the formula

$$\begin{aligned} q_{\text{indep}}(x_1, x_2) &= \frac{1}{4}[\delta(x_1, x_2) + \delta(x_1, x_2 - 1) + \delta(x_1 - 1, x_2) \\ &\quad + \delta(x_1 - 1, x_2 - 1)] \end{aligned}$$

obtained by elementary probability theory.

Formula 2.211 gives the mathematical definition for  $x_1$  and  $x_2$  being independent random variables. Assuming  $x_1$  and  $x_2$  are independent, the mean of the product is

$$\begin{aligned}
 E[x_1x_2] &= \int_{-\infty}^{\infty} \int_{-\infty}^{\infty} x_1x_2p_1(x_1)p_2(x_2)dx_1dx_2 \\
 &= \int_{-\infty}^{\infty} x_1p_1(x_1)dx_1 \int_{-\infty}^{\infty} x_2p_2(x_2)dx_2 \\
 &= \mu_1\mu_2.
 \end{aligned}
 \tag{2.213}$$

Similar computations show that

$$\text{Var}[x_1x_2] = \sigma_1^2\sigma_2^2.$$

It should also be noted that the two-dimensional transform of the joint probability density is

$$\begin{aligned}
 Q(y_1y_2) &= \int_{-\infty}^{\infty} \int_{-\infty}^{\infty} p_1(x_1)p_2(x_2)e^{-j(x_1y_1+x_2y_2)}dx_1dx_2 \\
 &= \int_{-\infty}^{\infty} p_1(x_1)e^{-jx_1y_1}dx_1 \int_{-\infty}^{\infty} p_2(x_2)e^{-jx_2y_2}dx_2 \\
 &= P_1(y_1)P_2(y_2)
 \end{aligned}$$

where  $P_1(y_1)$  and  $P_2(y_2)$  are the Fourier transforms of  $p_1(x_1)$  and  $p_2(x_2)$ , respectively.

More generally, any number of random variables— $x_1, x_2, \dots, x_n$ —are considered to be independent if the probability density function for the vector  $(x_1, x_2, \dots, x_n)$  is the product of the density functions of the individual variables,

$$q(x_1, x_2, \dots, x_n) = p_1(x_1)p_2(x_2) \cdots p_n(x_n).$$

If  $x_1, x_2, \dots, x_n$  are independent, then the  $n$ -dimensional Fourier transform of the joint density function is simply the product of the one-dimensional Fourier transforms of the individual density functions,

$$Q(x_1, x_2, \dots, x_n) = P_1(x_1)P_2(x_2) \cdots P_n(x_n),$$

and the mean of the product of the variables and the corresponding variance are merely the products of the means and variances of the individual variables

$$E[x_1x_2 \cdots x_n] = \mu_1\mu_2 \cdots \mu_n$$

and

$$\text{Var}[x_1x_2 \cdots x_n] = \sigma_1^2\sigma_2^2 \cdots \sigma_n^2.$$

### 2.7.3 Sums of Random Processes

Let  $x_1$  and  $x_2$  denote the outcomes of two independent random processes governed, respectively, by probability density functions  $p_1(x)$  and  $p_2(x)$ , and with corresponding means  $\mu_1$  and  $\mu_2$ , and

corresponding standard deviations  $\sigma_1$  and  $\sigma_2$ . The sum of these two outcomes,

$$x_S = x_1 + x_2,$$

can be viewed as the outcomes of another random process, which is governed by the probability density function

$$p_S(x) = \int_{-\infty}^{\infty} p_1(x - \xi)p_2(\xi)d\xi = p_1 * p_2(x).$$

If  $P_1(y)$ ,  $P_2(y)$ , and  $P_S(y)$  are the Fourier transforms of  $p_1(x)$ ,  $p_2(x)$ , and  $p_S(x)$ , then, by identity 2.37,

$$P_S(y) = P_1(y)P_2(y).$$

Thus,

$$P_S(0) = P_1(0)P_2(0) = 1$$

and

$$P'_S(0) = P'_1(0)P_2(0) + P_1(0)P'_2(0) = P'_1(0) + P'_2(0).$$

From this last equation and Equation 2.207, it immediately follows that the mean of  $x_S$  is the sum of the means of  $x_1$  and  $x_2$ ,

$$\mu_S = \mu_1 + \mu_2.$$

Likewise, computing  $P''_S(0)$  and using Equations 2.208 and 2.209 leads to

$$E[x_S^2] = E[x_1^2] + E[x_2^2] + 2\mu_1\mu_2$$

and

$$\sigma_S^2 = \sigma_1^2 + \sigma_2^2.$$

More generally, if

$$x_S = x_1 + x_2 + \cdots + x_N,$$

where each  $x_n$  denotes the outcome of an independent random process governed by a probability density function,  $p_n(x)$ , and with corresponding mean and standard deviation,  $\mu_n$  and  $\sigma_n$ , then  $x_S$  is governed by the probability density function

$$p_S(x) = p_1 * p_2 * \cdots * p_N(x)$$

and has mean and variance

$$\mu_S = \mu_1 + \mu_2 + \cdots + \mu_N,$$

and

$$\sigma_S^2 = \sigma_1^2 + \sigma_2^2 + \cdots + \sigma_N^2.$$

If  $N$  is fairly large, the central limit theorem of probability theory states that under very general conditions,

$$p_S(x) \approx \frac{1}{\sigma_s \sqrt{2\pi}} \exp \left[ -\frac{1}{2} \left( \frac{x - \mu_s}{\sigma_s} \right)^2 \right]$$

or, equivalently, that

$$P_S(y) = \mathcal{F}[p_S(x)]|_y \approx \exp \left[ -\frac{1}{2} (\sigma_S y)^2 - j\mu_S y \right].$$

In practice, the “noise” in a system is often the result of a large number of random processes each of which contributes a term to the total noise. According to the above discussion, it is not necessary to describe each source of noise accurately. Instead, the aggregate can be treated as a random process governed by a normal distribution.

### 2.7.4 Random Signals and Stationary Random Signals

A signal,  $x(t)$ , is “deterministic” if it can be treated, mathematically, as a well-defined function of  $t$ , that is, if for each value of  $t$  there is a single fixed value for  $x(t)$ . The signal is “random” if, instead, for each value of  $t$ ,  $x(t)$  must be treated as the outcome of a nontrivial random process.

Assume  $x(t)$  is a random signal. For each value of  $t$  there is a corresponding probability density function,  $p(x, t)$ , with

$$\int_a^b p(x, t) dx$$

being the probability of  $a < x(t) < b$ . The corresponding mean and variance,

$$E[x(t)] = \mu(t) = \int_{-\infty}^{\infty} xp(x, t) dx$$

and

$$\text{Var}[x(t)] = \sigma^2(t) = \int_{-\infty}^{\infty} (x - \mu(t))^2 p(x, t) dx,$$

are deterministic functions of  $t$ . The Fourier transform of the density function is

$$P(y, t) = \int_{-\infty}^{\infty} p(x, t) e^{-jxy} dx.$$

If the statistical properties of the process generating  $x(t)$  do not vary with  $t$ , then the process is said to be a “stationary” random process. The corresponding signal will also be called “stationary” though its

value will certainly depend—in a random manner—on  $t$ . For a stationary random signal,  $x(t)$ , it is reasonable to expect that the long-term time average of  $x(t)$  will equal its mean,  $E[x] = \mu$ ,

$$\mu = \lim_{T \rightarrow \infty} \frac{1}{2T} \int_{-T}^T x(t) dt. \tag{2.214}$$

Mathematically, it can be shown that, under fairly broad conditions, the probability that Equation 2.214 is not correct for a given stationary random signal is vanishingly small. Likewise,

$$E[x^2(t)] = \lim_{T \rightarrow \infty} \frac{1}{2T} \int_{-T}^T |x(t)|^2 dt$$

and

$$\sigma^2 = \lim_{T \rightarrow \infty} \frac{1}{2T} \int_{-T}^T |x(t) - \mu|^2 dt.$$

Thus, stationary random signals (with finite mean and variances) can be treated as finite power functions (see Section 2.3.8). Given a stationary random signal,  $x(t)$ , the corresponding average autocorrelation function is

$$\bar{\rho}_x(t) = \lim_{T \rightarrow \infty} \frac{1}{2T} \int_{-T}^T x^*(s)x(t+s) ds.$$

The average power is

$$\bar{\rho}_x(0) = \lim_{T \rightarrow \infty} \frac{1}{2T} \int_{-T}^T |x(s)|^2 ds$$

and the power spectrum is

$$P_x(\omega) = \mathcal{F}[\bar{\rho}_x(t)]|_{\omega} = \int_{-\infty}^{\infty} \bar{\rho}_x(t) e^{-j\omega t} dt$$

or, equivalently,

$$P_x(\omega) = \lim_{T \rightarrow \infty} \frac{1}{2T} \left| \int_{-T}^T x(t) e^{-j\omega t} dt \right|^2.$$

It should be recalled that one property of the average autocorrelation function is that

$$(\bar{\rho}_x(t))^* = \bar{\rho}_x(-t). \tag{2.215}$$

Thus, if  $x(t)$  is a real random signal, then the average autocorrelation will be an even real-valued function. So, also, will the power spectrum.

### 2.7.5 Correlation of Stationary Random Signals and Independence

The average cross-correlation of two stationary random signals,  $x(t)$  and  $y(t)$ , is

$$\bar{\rho}_{xy}(t) = \lim_{T \rightarrow \infty} \frac{1}{2T} \int_{-T}^T x^*(s)y(t+s)ds,$$

or, equivalently,

$$\bar{\rho}_{xy}(t) = E[x^* \Theta_{-t} y]$$

where, for any  $\alpha$ ,  $\Theta_\alpha y$  denotes the translation of  $y$  by  $\alpha$ ,

$$\Theta_\alpha y(s) = y(s - \alpha).$$

The corresponding cross-power spectrum is

$$P_{xy}(\omega) = \mathcal{F}[\bar{\rho}_{xy}(t)] \Big|_{\omega} = \int_{-\infty}^{\infty} \bar{\rho}_{xy}(t) e^{-j\omega t} dt.$$

It should be noted that

$$\begin{aligned} [\bar{\rho}_{xy}(t)]^* &= \lim_{T \rightarrow \infty} \frac{1}{2T} \left[ \int_{-T}^T x^*(s)y(s+t)ds \right]^* \\ &= \lim_{T \rightarrow \infty} \frac{1}{2T} \int_{-T}^T x(s)y^*(s+t)ds \\ &= \lim_{T \rightarrow \infty} \frac{1}{2T} \int_{-T}^T x(\sigma-t)y^*(\sigma)d\sigma \\ &= \bar{\rho}_{yx}(-t). \end{aligned} \quad (2.216)$$

From Schwarz's inequality, it follows that

$$\left| \bar{\rho}_{xy}(t) \right|^2 \leq \bar{\rho}_x(0)\bar{\rho}_y(0).$$

A somewhat more general statement, namely, that for any  $-\infty \leq a < b \leq \infty$ ,

$$\left| \int_a^b P_{xy}(\omega) e^{j\omega t} d\omega \right|^2 \leq \int_a^b P_x(\omega) d\omega \int_a^b P_y(\omega) d\omega$$

can also be proven. This shows that if the power spectrum of a signal vanishes on an interval, then so does cross-power spectrum of that signal with any other signal.

The average cross-correlation indicates the extent to which the two processes are independent of each other. If, for example,  $x(t)$

and  $y(t)$  are generated by two completely independent stationary processes, then, following the discussion in Section 2.7.2,

$$\bar{\rho}_{xy}(t) = \mu_x^* \mu_y \quad \text{for all } t$$

and

$$P_{xy}(\omega) = 2\pi \mu_x^* \mu_y \delta(\omega).$$

In particular, if one of the two independent processes has mean zero, then

$$\bar{\rho}_{xy}(t) = 0 \quad \text{for all } t$$

and

$$P_{xy}(\omega) = 0.$$

On the other hand, if  $y(t) = \gamma x(t - \tau)$  for some pair,  $\gamma$  and  $\tau$ , of real values, then

$$\bar{\rho}_{xy}(t) = \lim_{T \rightarrow \infty} \frac{1}{2T} \int_{-T}^T x^*(s) \gamma x(s - \tau + t) ds.$$

Thus, even if the expected value of  $x(t)$  is zero,

$$\bar{\rho}_{xy}(\tau) = \gamma \lim_{T \rightarrow \infty} \frac{1}{2T} \int_{-T}^T |x(s)|^2 ds = \gamma \bar{\rho}_x(0)$$

and the cross-power spectrum,  $P_{xy}(\omega)$ , will not vanish.

Of particular interest is the average cross-correlation of a random signal,  $x(t)$ , with itself. This is the same as the average autocorrelation of  $x(t)$  and indicates the extent to which the value of  $x(t + \alpha)$  can be predicted from the value of  $x(\alpha)$ . If the expected value of  $x(t)$  is zero and, for every  $\alpha$  and nonzero value of  $t$ ,  $x(t)$  and  $x(t + \alpha)$  are outcomes of completely independent random processes, then  $x(t)$  is called "white noise." For such a signal there is a constant,  $P_0$ , such that

$$\bar{\rho}_x(t) = P_0 \delta(t)$$

and

$$P_x(\omega) = P_0.$$

### 2.7.6 Systems and Random Signals

Let  $S$  be a linear shift invariant system with impulse response function  $h(t)$  and transfer function  $H(\omega)$ . Assume the input,  $x(t)$ , is a stationary random signal with mean  $\mu_x$ , and let  $y(t)$  be the corresponding output,

$$y(t) = S[x(t)].$$

The output is also a stationary random signal. It is related to the input by

$$y(t) = h * x(t)$$

or, equivalently, by

$$Y(\omega) = H(\omega)X(\omega),$$

where  $X(\omega)$  and  $Y(\omega)$  are, respectively, the Fourier transforms of  $x(t)$  and  $y(t)$ . It should be easy to see that the expected value of the output is directly related to the expected value of the input,

$$\mu_y = S[\mu_x] = h * \mu_x = \mu_x \int_{-\infty}^{\infty} h(s) ds.$$

The auto- and cross-correlations of the input and output signals are related by

$$\bar{\rho}_y(t) = h * \bar{\rho}_{yx}(t), \quad (2.217)$$

$$\bar{\rho}_{xy}(t) = h * \bar{\rho}_x(t), \quad (2.218)$$

and

$$\bar{\rho}_y(t) = h * (h * \bar{\rho}_x)(t). \quad (2.219)$$

Taking the Fourier transforms of these relations gives the corresponding relations for the power spectra,

$$P_y(\omega) = H(\omega)P_{yx}(\omega), \quad (2.220)$$

$$P_{xy}(\omega) = H(\omega)P_x(\omega), \quad (2.221)$$

and

$$P_y(\omega) = |H(\omega)|^2 P_x(\omega). \quad (2.222)$$

Derivations of identities 2.217 through 2.219 are relatively straightforward. For identity 2.217,

$$\begin{aligned} \bar{\rho}_y(t) &= \lim_{T \rightarrow \infty} \frac{1}{2T} \int_{-T}^T y^*(s)y(s+t) ds \\ &= \lim_{T \rightarrow \infty} \frac{1}{2T} \int_{-T}^T y^*(s)[h * x(s+t)] ds \\ &= \lim_{T \rightarrow \infty} \frac{1}{2T} \int_{-T}^T y^*(s) \int_{-\infty}^{\infty} h(\lambda)x(s+t-\lambda) d\lambda ds \\ &= \int_{-\infty}^{\infty} h(\lambda) \left( \lim_{T \rightarrow \infty} \frac{1}{2T} \int_{-T}^T y^*(s)x(s+t-\lambda) ds \right) d\lambda \\ &= \int_{-\infty}^{\infty} h(\lambda) \bar{\rho}_{yx}(t-\lambda) d\lambda \\ &= h * \bar{\rho}_{yx}(t). \end{aligned}$$

Derivations of Equations 2.218 and 2.219 are similar with the derivation of Equation 2.219 aided by identities 2.215 and 2.216.

### Example 2.61

Let  $S$  be an LSI system with transfer function

$$H(\omega) = \frac{1}{j + \omega}.$$

Assume the input,  $x(t)$ , is white noise, that is, the power spectrum of  $x(t)$  is a constant,

$$P_x(\omega) = P_0.$$

The corresponding output of the system,  $y(t)$ , will have power spectrum

$$P_y(\omega) = |H(\omega)|^2 P_x(\omega) = \frac{P_0}{1 + \omega^2}$$

and autocorrelation

$$\bar{\rho}_y(t) = \mathcal{F}^{-1}[P_y(\omega)] \Big|_t = \frac{1}{2} P_0 e^{-|t|}.$$

The mean squared output is then

$$\lim_{T \rightarrow \infty} \frac{1}{2T} \int_{-T}^T |y(t)|^2 dt = \bar{\rho}_y(0) = \frac{1}{2} P_0.$$

### Example 2.62

Let  $S$  be the ideal low-pass filter from Example 2.52 with cutoff frequency  $\Omega$ . The transfer function is

$$H(\omega) = \rho_{\Omega}(\omega) = \begin{cases} 1, & \text{if } |\omega| < \Omega \\ 0, & \text{if } \Omega < |\omega| \end{cases}.$$

The power spectrum of the output,  $y(t)$ , resulting from a white noise input,  $x(t)$ , with power spectrum  $P_x(\omega) = P_0$  is

$$P_y(\omega) = |H(\omega)|^2 P_x(\omega) = P_0 \rho_{\Omega}(\omega)$$

and the autocorrelation of the output is

$$\bar{\rho}_y(t) = \mathcal{F}^{-1}[P_y(\omega)] \Big|_t = P_0 \frac{1}{\pi t} \sin(\Omega t).$$

The mean squared output of the white noise is then

$$\lim_{T \rightarrow \infty} \frac{1}{2T} \int_{-T}^T |y(t)|^2 dt = \bar{\rho}_y(0) = P_0 \lim_{t \rightarrow 0} \frac{\sin(\Omega t)}{\pi t} = \frac{\Omega}{\pi} P_0.$$

Consider, now, an input of  $f(t) + x(t)$  where  $x(t)$  is the above white noise and  $f(t)$  is a deterministic band-limited signal with bandwidth less than  $2\Omega$ . The output of this low-pass filter is then  $f(t) + y(t)$ .

The expected "intensity" of the output is

$$\begin{aligned} E[|f(t) + y(t)|^2] &= E[|f(t)|^2 + f^*(t)y(t) + f(t)y^*(t) + |y(t)|^2] \\ &= |f(t)|^2 + f^*(t)E[y(t)] + f(t)E[y^*(t)] + E[|y(t)|^2] \end{aligned}$$

Because  $x(t)$  comes from white noise,

$$E[y(t)] = E[S[x(t)]] = S[E[x(t)]] = S[0] = 0,$$

and, by the above,

$$E[|y(t)|^2] = \lim_{T \rightarrow \infty} \frac{1}{2T} \int_{-T}^T |y(t)|^2 dt = \frac{\Omega}{\pi} P_0.$$

Thus, the expected intensity of the output is

$$|f(t)|^2 + \frac{\Omega}{\pi} P_0,$$

and the ratio of the intensity of the deterministic signal to the intensity of the outputted noise (signal-to-noise ratio) is

$$\frac{\pi |f(t)|^2}{\Omega P_0}.$$

## 2.8 Partial Differential Equations

The Fourier transform is an especially useful tool for solving problems involving partial differential equations. To illustrate how the Fourier transform can be used in a variety of such problems, three different problems involving the partial differential equation describing heat flow are examined below.

### 2.8.1 The One-Dimensional Heat Equation

The next few sections concern a uniform rod of some heat conducting material positioned on the  $X$ -axis between  $x = \alpha$  and  $x = \beta$ . It is assumed that the sides of the rod are thermally insulated from the surroundings. The relevant material constants are

- $c$  = specific heat of the material
- $\rho$  = linear density of the material
- and
- $k$  = thermal diffusivity

Any heat sources (and sinks) are described by a density function,  $f(x, t)$ , where, for any  $0 \leq t_1 < t_2$  and  $\alpha \leq x_1 < x_2 \leq \beta$ ,

$$\int_{x_1}^{x_2} \int_{t_1}^{t_2} c \rho f(x, t) dt dx$$

is the total heat (in calories) generated in the rod between  $x = x_1$  and  $x = x_2$  during the period of time between  $t = t_1$  and  $t = t_2$ .

The temperature distribution throughout the rod is described by

$v(x, t)$  = the temperature at time  $t$  and position  $x$  in the rod.

Using basic thermodynamics it can be shown that  $v(x, t)$  must satisfy the "one-dimensional heat equation,"

$$\frac{\partial v}{\partial t} - k \frac{\partial^2 v}{\partial x^2} = f(x, t) \quad (2.223)$$

for  $\alpha < x < \beta$ .

In Sections 2.8.2 through 2.8.4, the above equation is solved under various conditions. In each case the Fourier transform is taken with respect to the spatial variable,  $x$ , with (assuming an infinite rod,  $\alpha = -\infty$  and  $\beta = \infty$ )

$$V = V(\xi, t) = \mathcal{F}_x[v(x, t)]|_{\xi} = \int_{-\infty}^{\infty} v(x, t) e^{-j\xi x} dx$$

and

$$F = F(\xi, t) = \mathcal{F}_x[f(x, t)]|_{\xi} = \int_{-\infty}^{\infty} f(x, t) e^{-j\xi x} dx.$$

Observe that

$$\mathcal{F}_x \left[ \frac{\partial v}{\partial t} \right] |_{\xi} = \int_{-\infty}^{\infty} \frac{\partial v}{\partial t} \Big|_{(x,t)} e^{-j\xi x} dx = \frac{\partial}{\partial t} \int_{-\infty}^{\infty} v(x, t) e^{-j\xi x} dx = \frac{\partial V}{\partial t}.$$

On the other hand, it is appropriate to use identity 2.50 to compute the transform (with respect to  $x$ ) of any partial derivatives with respect to  $x$ . In particular,

$$\mathcal{F}_x \left[ \frac{\partial^2 v}{\partial x^2} \right] |_{\xi} = (j\xi)^2 V(\xi, t) = -\xi^2 V(\xi, t).$$

Thus, taking the Fourier transform of Equation 2.223 with respect to  $x$  yields

$$\frac{\partial V}{\partial t} + k\xi^2 V = F, \quad (2.224)$$

which can be treated as an ordinary first-order linear differential equation. From the elementary theory of ordinary differential equations, the general solution to Equation 2.224 is

$$V(\xi, t) = e^{-k\xi^2 t} \int_a^t e^{k\xi^2 \tau} F(\xi, \tau) d\tau + G(\xi) e^{-k\xi^2 t} \quad (2.225)$$

where

- $a$  is any convenient value
- $G(\xi)$  is an "arbitrary" function of  $\xi$

The temperature distribution  $v(x, t)$ , is then found by taking the inverse Fourier transform with respect to the "spatial frequency" variable  $\xi$ .

### 2.8.2 The Initial Value Problem for Heat Flow on an Infinite Rod

If the rod is infinite, there are no heat sources or sinks in the rod, and the initial temperature distribution is known to be given by  $v_0(x)$ , then  $v(x, t)$  is the solution to the following system of equations:

$$\begin{aligned} \frac{\partial v}{\partial t} - k \frac{\partial^2 v}{\partial x^2} &= 0 \\ v(x, 0) &= v_0(x). \end{aligned}$$

Because  $v_0(x)$  is the initial temperature distribution, it suffices to find  $v(x, t)$  for  $0 < t$ .

Taking the Fourier transform with respect to  $x$  of each of the above equations yields the system of two equations,

$$\begin{aligned} \frac{\partial V}{\partial t} + k\xi^2 V &= 0 \\ V(\xi, 0) &= V_0(\xi), \end{aligned}$$

where

$$V_0(\xi) = \mathcal{F}[v_0(x)]|_{\xi}.$$

From formula 2.225 the general solution to the differential equation is

$$V(\xi, t) = G(\xi)e^{-k\xi^2 t}.$$

Plugging in the initial values,

$$G(\xi) = V(\xi, 0) = V_0(\xi),$$

shows that

$$V(\xi, t) = V_0(\xi)e^{-k\xi^2 t}.$$

The temperature distribution for all time is then found by taking the inverse transform (with respect to the spatial variable),

$$\begin{aligned} v(x, t) &= \mathcal{F}_{\xi}^{-1} \left[ V_0(\xi)e^{-k\xi^2 t} \right]_x \\ &= \mathcal{F}_{\xi}^{-1} [V_0(\xi)]|_x * \mathcal{F}_{\xi}^{-1} [e^{-k\xi^2 t}]|_x \\ &= v_0(x) * \left( \frac{1}{\sqrt{4\pi kt}} \exp \left[ -\frac{1}{4kt} x^2 \right] \right) \\ &= \frac{1}{\sqrt{4\pi kt}} \int_{-\infty}^{\infty} v_0(s) \exp \left[ -\frac{1}{4kt} (x-s)^2 \right] ds. \end{aligned}$$

### 2.8.3 An Infinite Rod with Heat Sources and Sinks

For this problem it is assumed that the rod is infinite, and that the initial temperature distribution is

$v(x, 0) = 0$ . The source term,  $f(x, t)$ , is assumed to be nonzero for  $0 < t$ . Because the initial temperature distribution is a constant zero and it is only necessary to find  $v(x, t)$  for  $t > 0$ , the following two assumptions may be made:

1. For  $t \leq 0$ ,  $v(x, t) = 0$ .
2. For  $t < 0$ ,  $f(x, t) = 0$ .

The heat flow problem is then one of solving the heat equation,

$$\frac{\partial v}{\partial t} - k \frac{\partial^2 v}{\partial x^2} = f(x, t) \tag{2.226}$$

for all real values of  $x$  and  $t$ , subject to conditions (1) and (2).

This problem is similar to that of finding the output to a casual LSI system. This suggests that it is convenient to find first the solution to

$$\frac{\partial h}{\partial t} - k \frac{\partial^2 h}{\partial x^2} = \delta(x)\delta(t) \tag{2.227}$$

where  $h(x, t)$  is assumed to vanish if  $t < 0$ . It is then relatively easy to verify that the solution to Equation 2.227 is given by the two-dimensional convolution of  $h(x, t)$  with  $f(x, t)$ . Because  $f(s, \tau)$  vanishes for  $\tau < 0$ , this can be written

$$\begin{aligned} v(x, t) &= f * h(x, t) \\ &= \int_{s=-\infty}^{\infty} \int_{\tau=0}^{\infty} f(s, \tau) h(x-s, t-\tau) d\tau ds. \end{aligned} \tag{2.228}$$

Taking the Fourier transform of Equation 2.227 (with respect to the spatial variable) yields

$$\frac{\partial H}{\partial t} + k\xi^2 H = \delta(t) \tag{2.229}$$

where, by the assumptions on  $h(x, t)$ ,

$$H(\xi, t) = \mathcal{F}_{\xi}[h(x, t)]|_x$$

must vanish when  $t < 0$ . From Equation 2.225 it follows that the solution to Equation 2.229 is given by

$$H(\xi, t) = e^{-k\xi^2 t} \int_a^t e^{k\xi^2 \tau} \delta(\tau) d\tau + G(\xi)e^{-k\xi^2 t}.$$

It is convenient to take  $a = -1$ . Observe, then, that

$$\int_a^t e^{k\xi^2 \tau} \delta(\tau) d\tau = \begin{cases} 1, & \text{if } 0 < t \\ 0, & \text{if } t < 0 \end{cases} = u(t).$$



Combining this with the fact that  $H(\xi, t)$  vanishes for negative values of  $t$  gives

$$0 = H(\xi, -1) = e^{-k\xi^2(-1)}u(-1) + G(\xi)e^{-k\xi^2(-1)} = G(\xi)e^{k\xi^2},$$

implying that  $G(\xi)$  vanishes and

$$H(\xi, t) = e^{-kt\xi^2}u(t).$$

Taking the inverse transform

$$h(x, t) = \mathcal{F}_\xi^{-1}[e^{-kt\xi^2}u(t)]|_x = \frac{1}{\sqrt{4\pi kt}} \exp\left[\frac{-x^2}{4kt}\right]u(t).$$

Formula 2.228 for the solution to the heat equation then becomes

$$\begin{aligned} v(x, t) &= \int_{s=-\infty}^{\infty} \int_{\tau=0}^{\infty} f(s, \tau) \frac{1}{\sqrt{4\pi k(t-\tau)}} \exp\left[\frac{-(x-s)^2}{4k(t-\tau)}\right] u(t-\tau) d\tau ds \\ &= \int_{s=-\infty}^{\infty} \int_{\tau=0}^t f(s, \tau) \frac{1}{\sqrt{4\pi k(t-\tau)}} \exp\left[\frac{-(x-s)^2}{4k(t-\tau)}\right] d\tau ds. \end{aligned}$$

### 2.8.4 A Boundary Value Problem for Heat Flow on a Half-Infinite Rod

For this problem it is assumed that the rod occupies the positive  $X$ -axis,  $0 < x$ , that there are no sources or sinks of heat in the rod, and that the initial temperature throughout the rod is zero. At  $x = 0$  the temperature is known to be given by some function,  $\Theta(t)$ , for  $0 < t$ . The temperature distribution function,  $v(x, t)$ , then must satisfy the following system of equations:

$$\begin{aligned} \frac{\partial v}{\partial t} - k \frac{\partial^2 v}{\partial x^2} &= 0, \quad 0 < x \quad \text{and} \quad 0 < t \\ v(x, 0) &= 0, \quad 0 < x \\ v(0, t) &= \Theta(t), \quad 0 < t. \end{aligned}$$

To apply the Fourier transform with respect to the spatial variable,  $v(x, t)$  must be extended to a function on all of  $x$ . A review of relations 2.126 through 2.131 along with the observation that  $v(0, t)$  is known, suggests that the odd extension,

$$\hat{v}(x, t) = \begin{cases} v(x, t), & \text{if } 0 < t \\ -v(-x, t), & \text{if } t < 0 \end{cases}$$

is appropriate. It is easily verified that  $\hat{v}(x, t)$  satisfies

$$\frac{\partial \hat{v}}{\partial t} - k \frac{\partial^2 \hat{v}}{\partial x^2} = 0$$

for all  $0 < t$  and  $x \neq 0$ . Combining this with relation 2.131,

$$D_{xx}\hat{v} = \frac{\partial^2 \hat{v}}{\partial x^2} + 2v(0, t)\delta'(x) = \frac{1}{k} \frac{\partial \hat{v}}{\partial t} + 2\Theta(t)\delta'(x),$$

gives the equation

$$\frac{\partial \hat{v}}{\partial t} - kD_{xx}\hat{v} = -2k\Theta(t)\delta'(x), \tag{2.230}$$

where  $D_{xx}\hat{v}$  explicitly denotes the second generalized derivative of  $\hat{v}(x, t)$  with respect to  $x$ . Equation 2.230 is valid for all  $x$  and is the same as Equation 2.226 with

$$f(x, t) = -2k\Theta(t)\delta'(x).$$

Because  $\hat{v}(x, t)$  also satisfies the same initial condition as assumed in Section 2.8.3, the solution derived in that section applies here,

$$\begin{aligned} \hat{v}(x, t) &= \int_{s=-\infty}^{\infty} \int_{\tau=0}^t [-2k\Theta(\tau)\delta'(s)] \frac{1}{\sqrt{4\pi k(t-\tau)}} \\ &\quad \times \exp\left[\frac{-(x-s)^2}{4k(t-\tau)}\right] d\tau ds. \end{aligned}$$

Now,

$$\begin{aligned} \int_{-\infty}^{\infty} \delta'(s)e^{-\gamma(x-s)^2} ds &= - \int_{-\infty}^{\infty} \delta(s) \frac{d}{ds} [e^{-\gamma(x-s)^2}] ds \\ &= - \int_{-\infty}^{\infty} \delta(s) 2\gamma(x-s)e^{-\gamma(x-s)^2} ds \\ &= -2\gamma xe^{-\gamma x^2}. \end{aligned}$$

Thus, for  $0 < x$  and  $0 < t$ ,

$$\begin{aligned} v(x, t) &= \hat{v}(x, t) \\ &= \int_{\tau=0}^t -2k\Theta(\tau) \frac{1}{\sqrt{4\pi k(t-\tau)}} \left( \int_{s=-\infty}^{\infty} \delta'(s) \exp\left[-\frac{(x-s)^2}{4k(t-\tau)}\right] ds \right) d\tau \\ &= \int_{\tau=0}^t -2k\Theta(\tau) \frac{1}{\sqrt{4\pi k(t-\tau)}} \left( \frac{-2}{4k(t-\tau)} x \exp\left[\frac{-x^2}{4k(t-\tau)}\right] \right) d\tau \\ &= \frac{x}{2\sqrt{\pi k}} \int_{\tau=0}^t \Theta(\tau)(t-\tau)^{-3/2} \exp\left[\frac{-x^2}{4k(t-\tau)}\right] d\tau. \end{aligned}$$

Letting  $\sigma = \frac{x}{2\sqrt{\pi k}}(t-\tau)^{-1/2}$ , this simplifies somewhat to

$$v(x, t) = 2 \int_{\sigma_0}^{\infty} \Theta\left(t - \frac{x^2}{4\pi k\sigma^2}\right) e^{-\pi\sigma^2} d\sigma,$$

where

$$\sigma_0 = \frac{x}{2\sqrt{\pi kt}}.$$

In particular, if the boundary temperature is constant,  $\Theta(t) = \Theta_0$ , then

$$v(x, t) = 2\Theta_0 \int_{\sigma_0}^{\infty} e^{-\pi\sigma^2} d\sigma = \Theta_0 \operatorname{erfc}\left(\frac{x}{2\sqrt{kt}}\right).$$

## 2.9 Tables

**TABLE 2.3** Fundamental Fourier Identities

If  $f(t)$  and  $G(\omega)$  are suitably integrable:

Integral definitions:

$$F(\omega) = \mathcal{F}[f(t)]|_{\omega} = \int_{-\infty}^{\infty} f(t)e^{-j\omega t} dt$$

$$g(t) = \mathcal{F}^{-1}[G(\omega)]|_t = \frac{1}{2\pi} \int_{-\infty}^{\infty} G(\omega)e^{j\omega t} d\omega$$

Parseval's equality:

$$\int_{-\infty}^{\infty} f(t)g^*(t)dt = \frac{1}{2\pi} \int_{-\infty}^{\infty} F(\omega)G^*(\omega)d\omega$$

Bessel's equality:

$$\int_{-\infty}^{\infty} |f(t)|^2 dt = \frac{1}{2\pi} \int_{-\infty}^{\infty} |F(\omega)|^2 d\omega$$

For all transformable functions:

Linearity:

$$\mathcal{F}[\alpha f(t) + \beta g(t)]|_{\omega} = \alpha \mathcal{F}[f(t)]|_{\omega} + \beta \mathcal{F}[g(t)]|_{\omega}$$

$$\mathcal{F}^{-1}[\alpha F(\omega) + \beta G(\omega)]|_t = \alpha \mathcal{F}^{-1}[F(\omega)]|_t + \beta \mathcal{F}^{-1}[G(\omega)]|_t$$

Near equivalence (symmetry of transforms):

$$\mathcal{F}^{-1}[\phi(x)]|_y = \frac{1}{2\pi} \mathcal{F}[\phi(-x)]|_y = \frac{1}{2\pi} \mathcal{F}[\phi(x)]|_{-y}$$

$$\mathcal{F}[\phi(x)]|_y = 2\pi \mathcal{F}^{-1}[\phi(-x)]|_y = 2\pi \mathcal{F}^{-1}[\phi(x)]|_{-y}$$

**TABLE 2.4** Commonly Used Fourier Identities

$h(t)$	$H(\omega) = \mathcal{F}[h(t)] _{\omega}$
$f(\alpha t)$	$\frac{1}{ \alpha } F\left(\frac{\omega}{\alpha}\right)$
$f(t - \alpha)$	$e^{-j\alpha\omega} F(\omega)$
$e^{j\alpha t} f(t)$	$F(\omega - \alpha)$
$\cos(\alpha t) f(t)$	$\frac{1}{2} [F(\omega - \alpha) + F(\omega + \alpha)]$
$\sin(\alpha t) f(t)$	$\frac{1}{2j} [F(\omega - \alpha) - F(\omega + \alpha)]$
$\frac{df}{dt}$	$j\omega F(\omega)$
$\frac{d^n f}{dt^n}$	$(j\omega)^n F(\omega)$
$tf(t)$	$j \frac{dF}{d\omega}$
$t^n f(t)$	$j^n \frac{d^n F}{d\omega^n}$
$\frac{f(t)}{t}$	$-j \int_{\alpha}^{\omega} F(s) ds + c_{\alpha}$
$\int_{\alpha}^t f(s) ds$	$-j \frac{F(\omega)}{\omega} + c_{\alpha} \delta(\omega)$
$f(t)g(t)$	$\frac{1}{2\pi} F(\omega) * G(\omega)$
$f(t) * g(t)$	$F(\omega)G(\omega)$
$f(t) \star g(t)$	$F^*(\omega)G(\omega)$
$f^*(t) g(t)$	$\frac{1}{2\pi} F(\omega) \star G(\omega)$

Note:  $\alpha$  is any nonzero real numbers,  $F(\omega) = \mathcal{F}[f(t)]|_{\omega}$  and  $G(\omega) = \mathcal{F}[g(t)]|_{\omega}$ .

**TABLE 2.5** Fourier Transforms of Some Common Functions

$f(t)$	$F(\omega) = \mathcal{F}[f(t)] _{\omega}$
$p_{\alpha}(t)$	$\frac{2}{\omega} \sin(\alpha\omega)$
$(\alpha -  t )p_{\alpha}(t)$	$\left(\frac{2 \sin(\frac{\alpha}{2}\omega)}{\omega}\right)^2$
$\sqrt{1-t^2}p_1(t)$	$\frac{\pi}{\omega} J_1(\omega)$
$(1-t^2)^{\alpha-1}p_1(t)$	$\Gamma(\alpha)\sqrt{\pi} \left(\frac{2}{ \omega }\right)^{\alpha-\frac{1}{2}} J_{\alpha-\frac{1}{2}}( \omega )$
$\text{sgn}(t)p_{\alpha}(t)$	$-2j \frac{1 - \cos(\alpha\omega)}{\omega}$
$\cos\left(\frac{\pi}{2\alpha}t\right)p_{\alpha}(t)$	$\frac{4\pi\alpha}{\pi^2 - 4\alpha^2\omega^2} \cos(\alpha\omega)$
$\text{Rect}_{(\beta, \gamma)}(t)$	$\frac{j}{\omega} [e^{-j\gamma\omega} - e^{-\beta\omega}]$
$e^{-(\alpha+j\beta)t}u(t)$	$\frac{1}{\alpha + j\beta + j\omega}$
$t^{\nu-1}e^{-(\alpha+j\beta)t}u(t)$	$\frac{\Gamma(\nu)}{(\alpha + j\beta + j\omega)^{\nu}}$
$e^{(\alpha+j\beta)t}u(-t)$	$\frac{1}{(\alpha + j\beta - j\omega)}$
$(-t)^{\nu-1}e^{(\alpha+j\beta)t}u(-t)$	$\frac{\Gamma(\nu)}{(\alpha + j\beta - j\omega)^{\nu}}$
$e^{-\alpha t }$	$\frac{2\alpha}{\alpha^2 + \omega^2}$
$\text{sgn}(t) e^{-\alpha t }$	$\frac{-2j\omega}{\alpha^2 + \omega^2}$
$e^{-\alpha t^2}$	$\sqrt{\frac{\pi}{\alpha}} \exp\left[-\frac{1}{4\alpha}\omega^2\right]$
$e^{-\alpha t^2 + \beta t}$	$\sqrt{\frac{\pi}{\alpha}} \exp\left[-\frac{1}{4\alpha}\omega^2 - j\frac{\beta}{2\alpha}\omega + \frac{\beta^2}{4\alpha}\right]$
$\frac{e^{-\lambda t}}{\alpha + j\beta + e^{-t}}$	$\pi(\alpha + j\beta)^{\lambda-1+j\omega} \text{csc}(\pi\lambda + j\pi\omega)$
$\text{sech}(\alpha t)$	$\frac{\pi}{\alpha} \text{sech}\left(\frac{\pi}{2\alpha}\omega\right)$
$e^{\pm j\alpha t^2}$	$\sqrt{\frac{\pi}{\alpha}} \exp\left[\mp j\frac{1}{4\alpha}(\omega^2 - \alpha\pi)\right]$
$e^{-\theta t^2}$	$[\sqrt{ \theta  + \alpha} - j \text{sgn}(\theta)\sqrt{ \theta  - \alpha}]$
$(w/\theta = \alpha + j\beta)$	$\times \frac{1}{ \theta } \sqrt{\frac{\pi}{2}} \exp\left(-\frac{1}{4\theta}\omega^2\right)$
$\frac{1}{t} \sin(\alpha t)$	$\pi p_{\alpha}(\omega)$
$\left(\frac{1}{t} \sin(\alpha t)\right)^2$	$\frac{\pi}{2} (2\alpha -  \omega )p_{2\alpha}(\omega)$
$\frac{1}{ t } \sin(\alpha t)$	$-j \text{sgn}(\omega) \ln \left  \frac{ \omega  + \alpha}{ \omega  - \alpha} \right $
1	$2\pi\delta(\omega)$
$t^n$	$j^n 2\pi\delta^{(n)}(\omega)$
$e^{j\beta t}$	$2\pi\delta(\omega - \beta)$
$\delta(t - \beta)$	$e^{-j\beta\omega}$
$\delta^{(n)}(t)$	$(j\omega)^n$
$\sin(\alpha t)$	$-j\pi [\delta(\omega - \alpha) - \delta(\omega + \alpha)]$
$\cos(\alpha t)$	$\pi[\delta(\omega - \alpha) + \delta(\omega + \alpha)]$

(continued)

**TABLE 2.5 (continued)** Fourier Transforms of Some Common Functions

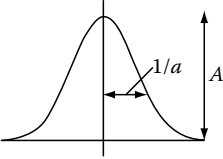
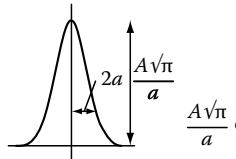
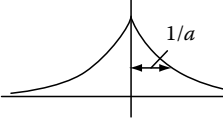
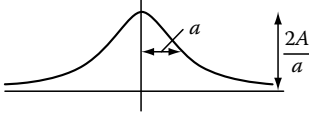
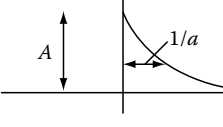
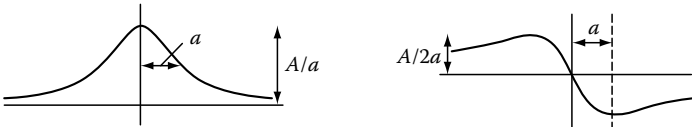
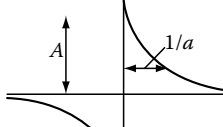
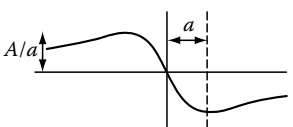
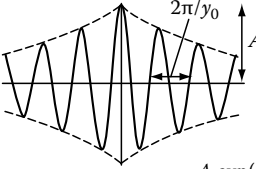
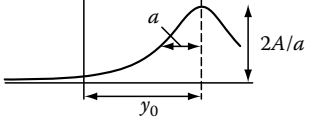
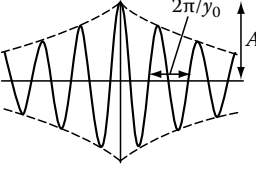
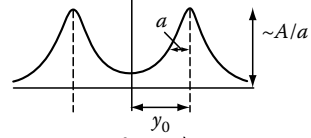
$\sin(\alpha t^2)$	$-\sqrt{\frac{\pi}{\alpha}} \sin\left[\frac{1}{4\alpha}(\omega^2 - \alpha\pi)\right]$
$\cos(\alpha t^2)$	$\sqrt{\frac{\pi}{\alpha}} \cos\left[\frac{1}{4\alpha}(\omega^2 - \alpha\pi)\right]$
$e^{-\alpha t^2} \cos(\nu t^2)$	$\frac{1}{ \theta } \sqrt{\frac{\pi}{2}} \exp\left(-\frac{\alpha}{4 \theta ^2} \omega^2\right) \times$
$(w/\theta = \alpha + j\nu)$	$\left[\sqrt{ \theta  + \alpha} \cos\left(\frac{\nu\omega^2}{4 \theta ^2}\right) + \sqrt{ \theta  - \alpha} \sin\left(\frac{\nu\omega^2}{4 \theta ^2}\right)\right]$
$e^{-\alpha t^2} \sin(\nu t^2)$	$\frac{1}{ \theta } \sqrt{\frac{\pi}{2}} \exp\left(-\frac{\alpha}{4 \theta ^2} \omega^2\right) \times$
$(w/\theta = \alpha + j\nu)$	$\left[\sqrt{ \theta  + \alpha} \cos\left(\frac{\nu\omega^2}{4 \theta ^2}\right) - \sqrt{ \theta  - \alpha} \sin\left(\frac{\nu\omega^2}{4 \theta ^2}\right)\right]$
$\text{comb}_\alpha(t)$	$\frac{2\pi}{\alpha} \text{comb}_{\frac{2\pi}{\alpha}}(\omega)$
$ \sin(\alpha t) $	$\sum_{k=-\infty}^{\infty} \frac{4}{1-4k^2} \delta(\omega - 2\alpha k)$
$ \cos(\alpha t) $	$\sum_{k=-\infty}^{\infty} (-1)^k \frac{4}{1-4k^2} \delta(\omega - 2\alpha k)$
$\text{saw}(t)$	$j \sum_{\substack{n=-\infty \\ n \neq 0}}^{\infty} (-1)^n \frac{2}{n} \delta(\omega - n\pi)$
$\sum_{m=-\infty}^{\infty} p_\alpha(t - mv)$	$\frac{4\pi\alpha}{v} \delta(\omega) + \sum_{\substack{k=-\infty \\ k \neq 0}}^{\infty} \frac{2}{k} \sin\left(\frac{2\pi k\alpha}{v}\right) \delta\left(\omega - \frac{2\pi k}{v}\right)$
$(w/2\alpha \leq v)$	
$\text{sgn}(t)$	$-j \frac{2}{\omega}$
$u(t)$	$\pi\delta(\omega) - j \frac{1}{\omega}$
$\frac{1}{t}$	$-j\pi \text{sgn}(\omega)$
$t^{-n}$	$-j\pi \frac{(-j\omega)^{n-1}}{(n-1)!} \text{sgn}(\omega)$
$ t $	$-\frac{2}{\omega^2}$
$t^n \text{sgn}(t)$	$(-j)^{n+1} \frac{2(n!)}{\omega^{n+1}}$

**TABLE 2.5 (continued)** Fourier Transforms of Some Common Functions

$\text{ramp}(t)$	$j\pi\delta'(\omega) - \frac{1}{\omega^2}$
$t^n u(t)$	$j^n \pi \delta^{(n)}(\omega) + n! \left(\frac{-j}{\omega}\right)^{n+1}$
$ t ^{-1/2}$	$\sqrt{2\pi}  \omega ^{-1/2}$
$ t ^{\lambda-1}$	$2\Gamma(\lambda) \cos\left(\frac{\lambda\pi}{2}\right)  \omega ^{-\lambda}$
$J_0(t)$	$\frac{2}{\sqrt{1-\omega^2}} p_1(\omega)$
$Y_0( t )$	$\frac{-2}{\sqrt{\omega^2-1}} [1 - p_1(\omega)]$
$J_{2n}(t)$	$\frac{2 \cos[2n \arcsin(\omega)]}{\sqrt{1-\omega^2}} p_1(\omega)$
$J_{2n+1}(t)$	$\frac{-2j \sin[(2n+1) \arcsin(\omega)]}{\sqrt{1-\omega^2}} p_1(\omega)$
$J_n(t)$	$\frac{2(-j)^n T_n(\omega)}{\sqrt{1-\omega^2}} p_1(\omega)$
$\frac{1}{t^n} J_n(t)$	$\frac{2(1-\omega^2)^{n-\frac{1}{2}}}{1 \cdot 3 \cdot 5 \cdots (2n-1)} p_1(\omega)$
$ t ^{-\alpha+\frac{1}{2}} J_{\alpha-\frac{1}{2}}( t )$	$\frac{\sqrt{2\pi}}{\Gamma(\alpha)} \left(\frac{1-\omega^2}{2}\right)^{\alpha-1} p_1(\omega)$
$\frac{1}{t} J_n(t)$	$(-j)^n \frac{2j}{n} \sqrt{1-\omega^2} U_{n-1}(\omega) p_1(\omega)$
$t^{-1/2} J_{n+\frac{1}{2}}(t)$	$(-j)^n \sqrt{2\pi} P_n(\omega) p_1(\omega)$
$\text{sgn}(t) J_0(t)$	$j \frac{2}{\sqrt{\omega^2-1}} \text{sgn}(\omega) [1 - p_1(\omega)]$
$J_0(t) u(t)$	$\frac{p_1(\omega) + j \text{sgn}(\omega) [1 - p_1(\omega)]}{\sqrt{ 1-\omega^2 }}$

Notes:  $\alpha, \beta, \gamma, \lambda, \nu,$  and  $n$  denote real numbers with  $\alpha > 0, 0 < \lambda < 1, \nu > 0,$  and  $n = 1, 2, 3, \dots$   $\Gamma(x)$ , is the Gamma function;  $P_n(x)$ , is the  $n$ th Legendre polynomial;  $J_\nu$ , is the Bessel function of the first kind of order  $\nu$ ;  $Y_\nu$ , is the Bessel function of the second kind of order  $\nu$ ;  $T_n(x)$ , is the  $n$ th Chebyshev polynomial of the first kind;  $U_n(x)$  is the  $n$ th Chebyshev polynomial of the second kind;  $\text{saw}(t)$  is the saw function of Example 2.30.

TABLE 2.6 Graphical Representations of Some Fourier Transforms

$f(x)$	$F(y)$
$\left[ f(x) = (1/2\pi) \int_{-\infty}^{+\infty} F(y)e^{+ixy} dy = FT^*\{F(y)\} \right] \qquad \left[ F(y) = \int_{-\infty}^{+\infty} f(x)e^{-ixy} dx = FT^{-}\{f(x)\} \right]$	
 <p><math>A \exp(-a^2 x^2)</math> [Gaussian]</p>	 <p><math>\frac{A\sqrt{\pi}}{a} \exp(-y^2/4a^2)</math> [Gaussian] (2.38)</p>
 <p><math>A \exp(-a x )</math></p>	 <p><math>\frac{2A}{a} \frac{a^2}{a^2 + y^2}</math> [Lorentzian] (2.39)</p>
 <p><math>A \exp(-ax) \quad [x &gt; 0]</math> <math>0 \quad [x &lt; 0]</math></p>	 <p><math>A \left\{ \frac{a - iy}{a^2 + y^2} \right\}</math> (2.40)</p>
 <p><math>A \exp(-ax) \quad [x &gt; 0]</math> <math>-A \exp(-a x ) \quad [x &lt; 0]</math></p>	 <p><math>-2iA \frac{y}{a^2 + y^2}</math> (2.41)</p>
 <p><math>A \exp(iy_0 x - a x )</math></p>	 <p><math>\frac{2A}{a} \frac{a^2}{a^2 + (y - y_0)^2}</math> (2.42)</p>
 <p><math>A \cos y_0 x \exp(-a x )</math></p>	 <p><math>\frac{A}{a} \left\{ \frac{a^2}{a^2 + (y - y_0)^2} + \frac{a^2}{a^2 + (y + y_0)^2} \right\}</math> <math>= \frac{A}{a} \left\{ \frac{2a^2 (a^2 + y_0^2 + y^2)}{(a^2 + y_0^2 - y^2)^2 + 4a^2 y^2} \right\}</math> (2.43)</p>

(continued)

TABLE 2.6 (continued) Graphical Representations of Some Fourier Transforms

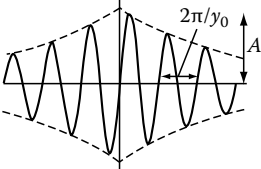
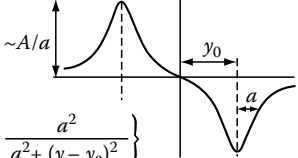
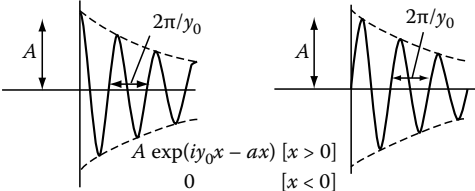
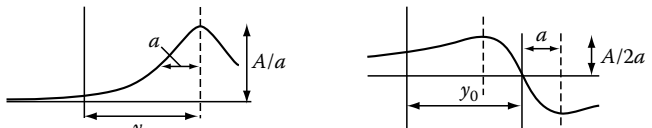
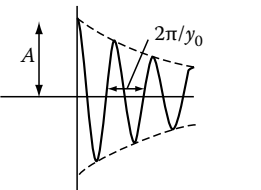
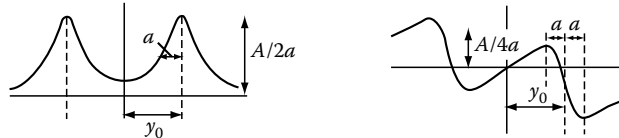
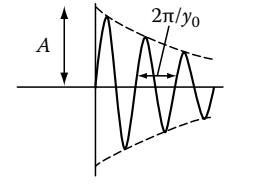
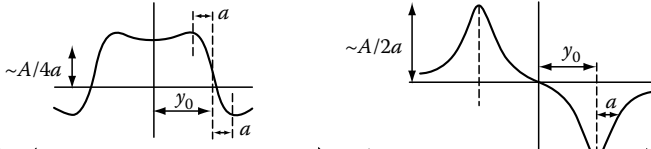
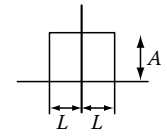
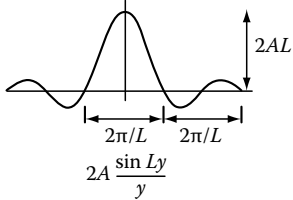
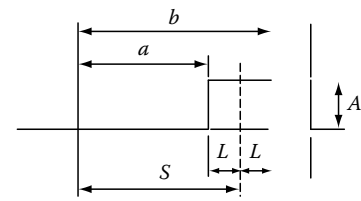
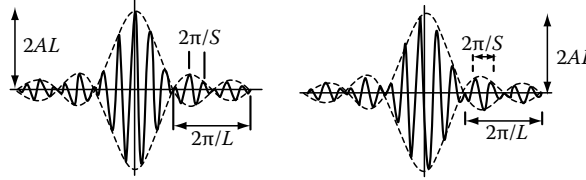
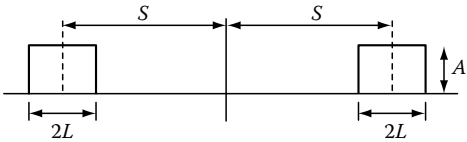
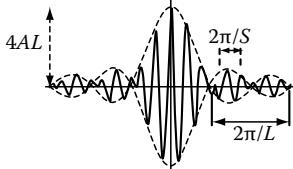
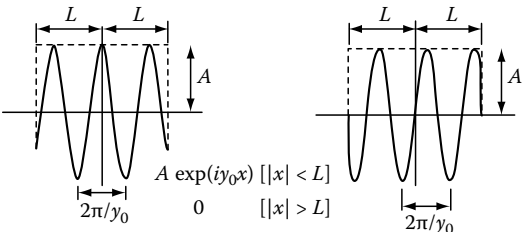
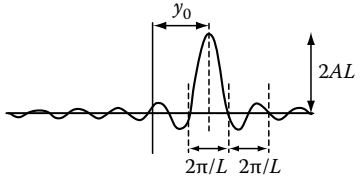
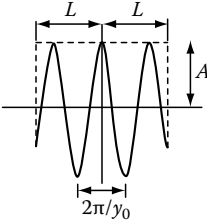
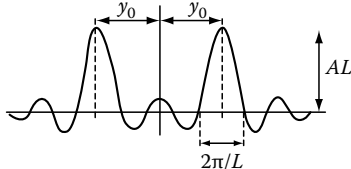
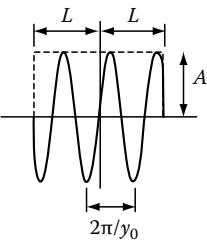
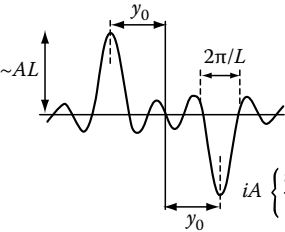
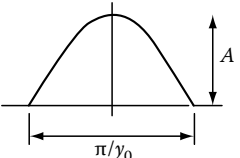
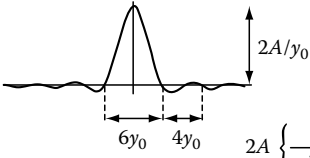
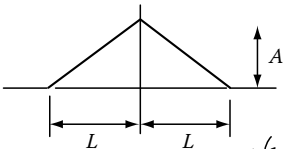
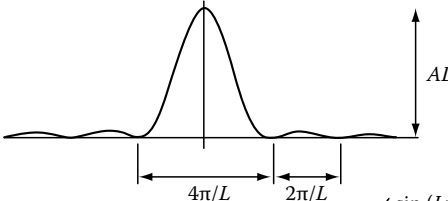
$f(x)$	$F(y)$
 <p style="text-align: center;"><math>A \sin y_0 x \exp(-a x )</math></p>	 $\frac{iA}{a} \left\{ \frac{a^2}{a^2 + (y + y_0)^2} - \frac{a^2}{a^2 + (y - y_0)^2} \right\}$ $= \frac{iA}{a} \left\{ \frac{-4a^2 y y_0}{(a^2 + y_0^2 - y^2)^2 + 4a^2 y^2} \right\} \quad (2.44)$
 <p style="text-align: center;"><math>A \exp(iy_0 x - ax) \quad [x &gt; 0]</math> <math>0 \quad [x &lt; 0]</math></p>	 $A \left\{ \frac{a + i(y_0 - y)}{a^2 + (y_0 - y)^2} \right\} = A \left\{ \frac{1}{a + i(y - y_0)} \right\} \quad (2.45)$
 <p style="text-align: center;"><math>A \cos y_0 x \exp(-ax) \quad [x &gt; 0]</math> <math>0 \quad [x &lt; 0]</math></p>	 $\frac{A}{2} \left[ \left\{ \frac{a}{a^2 + (y + y_0)^2} + \frac{a}{a^2 + (y - y_0)^2} \right\} + i \left\{ \frac{y_0 - y}{a^2 + (y_0 - y)^2} - \frac{y_0 + y}{a^2 + (y_0 + y)^2} \right\} \right]$ $A = \left\{ \frac{a(a^2 + y_0^2 - y^2) - iy(a^2 + y^2 - y_0^2)}{(a^2 + y_0^2 - y^2)^2 + 4a^2 y^2} \right\} \quad (2.46)$
 <p style="text-align: center;"><math>A \sin y_0 x \exp(-ax) \quad [x &gt; 0]</math> <math>0 \quad [x &lt; 0]</math></p>	 $\frac{A}{2} \left[ \left\{ \frac{y_0 - y}{a^2 + (y_0 - y)^2} + \frac{y_0 + y}{a^2 + (y_0 + y)^2} \right\} + i \left\{ \frac{a}{a^2 + (y_0 + y)^2} - \frac{a}{a^2 + (y_0 - y)^2} \right\} \right]$ $= Ay_0 \left\{ \frac{1}{(a^2 + y_0^2 - y^2) + i2ay} \right\} \quad (2.47)$
 <p style="text-align: center;"><math>A \quad [  x  &lt; L ]</math> <math>0 \quad [  x  &gt; L ]</math></p>	 $2A \frac{\sin Ly}{y} \quad (2.48)$
 <p style="text-align: center;"><math>A \quad [ a &lt; x &lt; b ]</math> <math>0 \quad [ x &lt; a; x &gt; b ]</math></p>	 $2A \frac{\sin Ly}{y} \exp(-iSy) = A \left[ \frac{(\sin by - \sin ay) - i(\cos ay - \cos by)}{y} \right]$ $= 2A \left[ \frac{(\sin Ly \cos Sy) - i(\sin Ly \sin Sy)}{y} \right] = \frac{iA}{y} [\exp(-iby) - \exp(-iay)] \quad (2.49)$

TABLE 2.6 (continued) Graphical Representations of Some Fourier Transforms

$f(x)$	$F(y)$
 $A \quad [(S-L) <  x  < (S+L)]$ $0 \quad [\text{otherwise}]$	 $4A \frac{\cos Sy \sin Ly}{y} \quad (2.50)$
 $A \exp(iy_0 x) \quad [ x  < L]$ $0 \quad [ x  > L]$	 $2A \frac{\sin\{L(y_0 - y)\}}{(y_0 - y)} \quad (2.51)$
 $A \cos y_0 x \quad [ x  < L]$ $0 \quad [ x  > L]$	 $A \left[ \frac{\sin L(y - y_0)}{(y - y_0)} + \frac{\sin L(y + y_0)}{(y + y_0)} \right] \quad (2.52)$
 $A \sin y_0 x \quad [ x  < L]$ $0 \quad [ x  > L]$	 $iA \left\{ \frac{\sin L(y + y_0)}{(y + y_0)} - \frac{\sin L(y - y_0)}{(y - y_0)} \right\} \quad (2.53)$
 $A \cos y_0 x \quad [ x  < (\pi/2y_0)]$ $0 \quad [ x  > (\pi/2y_0)]$	 $2A \left\{ \frac{y_0}{y_0^2 - y^2} \right\} \cos \left( \frac{\pi y}{2y_0} \right)$ <p>[See (2.52) with <math>L = \pi/2y_0</math>.] (2.54)</p>
 $A \left( 1 - \frac{ x }{L} \right) \quad [ x  < L]$ $0 \quad [ x  > L]$	 $AL \left\{ \frac{\sin(Ly/2)}{(Ly/2)} \right\}^2 \quad (2.55)$

(continued)

TABLE 2.6 (continued) Graphical Representations of Some Fourier Transforms

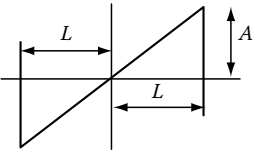
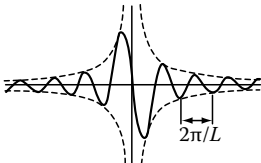
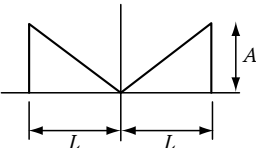
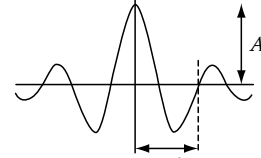
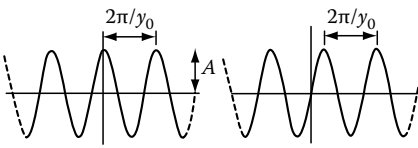
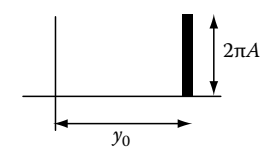
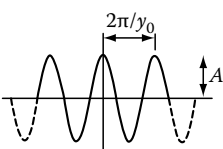
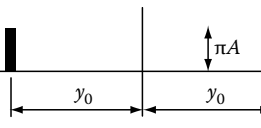
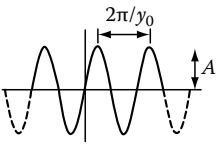
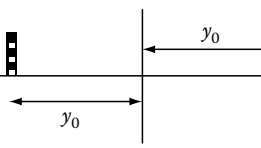
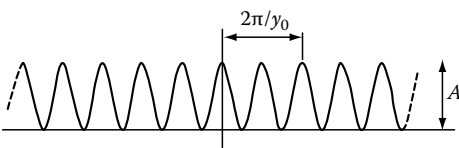
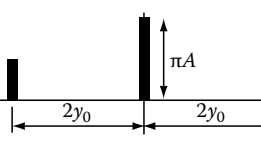
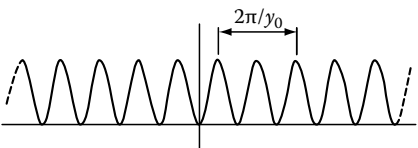
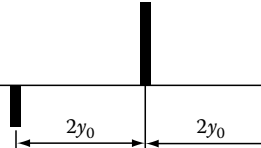
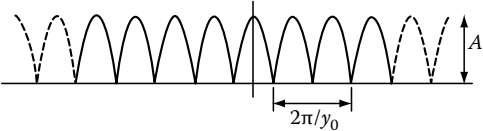
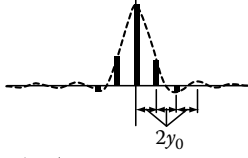
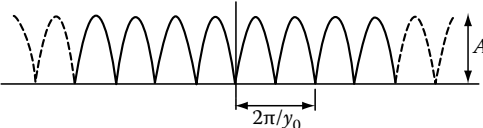
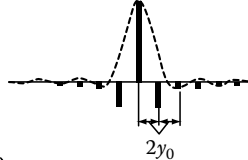
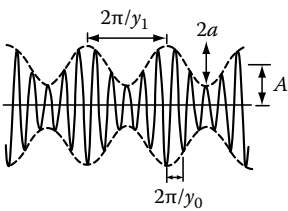
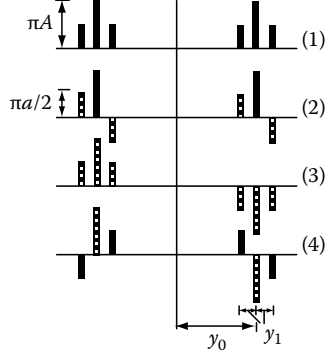
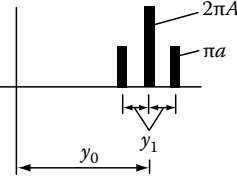
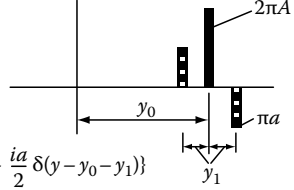
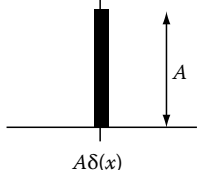
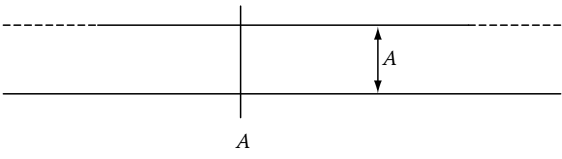
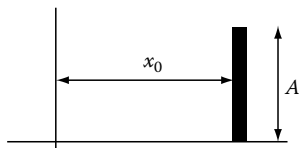
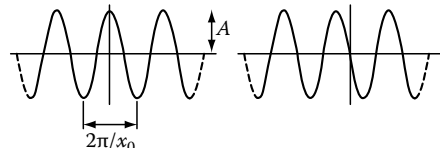
$f(x)$	$F(y)$
 $\frac{Ax}{L} \quad [  x  < L ]$ $0 \quad [  x  > L ]$	 $\frac{2iA}{y} \left\{ \cos Ly - \frac{\sin Ly}{Ly} \right\}$ <span style="float: right;">(2.56)</span>
 $\frac{A x }{L} \quad [  x  < L ]$ $0 \quad [  x  > L ]$	 $2AL \left\{ \frac{\sin Ly}{Ly} - 2 \left( \frac{\sin(Ly/2)}{Ly} \right)^2 \right\}$ <span style="float: right;">(2.57)</span>
 $A \exp(iy_0 x)$	 $2\pi A \delta(y - y_0).$ <span style="float: right;">(2.58)</span>
 $A \cos y_0 x$	 $\pi A \{ \delta(y - y_0) + \delta(y + y_0) \}$ <span style="float: right;">(2.59)</span>
 $A \sin y_0 x$	 $\pi i A \{ \delta(y + y_0) - \delta(y - y_0) \}$ <span style="float: right;">(2.60)</span>
 $A \cos^2 y_0 x$	 $\pi A \left\{ \frac{1}{2} \delta(y + 2y_0) + \delta(y) + \frac{1}{2} \delta(y - 2y_0) \right\}$ <span style="float: right;">(2.61)</span>
 $A \sin^2 y_0 x$	 $\pi A \left\{ -\frac{1}{2} \delta(y + 2y_0) + \delta(y) - \frac{1}{2} \delta(y - 2y_0) \right\}$ <span style="float: right;">(2.62)</span>

TABLE 2.6 (continued) Graphical Representations of Some Fourier Transforms

$f(x)$	$F(y)$
 <p style="text-align: center;"><math>A \cos y_0 x </math></p>	 $\sum_{n=-\infty}^{n=+\infty} 4A \left\{ \frac{y_0^2}{y_0^2 - y^2} \right\} \cos\left(\frac{\pi y}{2y_0}\right) \delta(y - 2ny_0) \quad [n = 0, \pm 1, \pm 2, \dots] \quad (2.63)$
 <p style="text-align: center;"><math>A \sin y_0 x </math></p>	 $\sum_{n=-\infty}^{n=+\infty} (-1)^n 4A \left\{ \frac{y_0^2}{y_0^2 - y^2} \right\} \cos\left(\frac{\pi y}{2y_0}\right) \delta(y - 2ny_0) \quad [n = 0, \pm 1, \pm 2, \dots] \quad (2.64)$
 <p style="text-align: center;"><math>\cos y_0 x \{A + a \cos y_1 x\} \dots (1)</math>  <math>\cos y_0 x \{A + a \sin y_1 x\} \dots (2)</math>  <math>\sin y_0 x \{A + a \cos y_1 x\} \dots (3)</math>  <math>\sin y_0 x \{A + a \sin y_1 x\} \dots (4)</math></p>	 <p style="text-align: right;"><math>F(y)</math> consists of delta functions as shown</p>
<p><math>\exp(iy_0 x) (A + a \cos y_1 x)</math></p>	$2\pi \left\{ A\delta(y - y_0) + \frac{a}{2} \delta(y - y_0 + y_1) + \frac{a}{2} \delta(y - y_0 - y_1) \right\}$  <p style="text-align: right;">(2.66)</p>
<p><math>\exp(iy_0 x) (A + a \sin y_1 x)</math></p>	$2\pi \left\{ A\delta(y - y_0) + \frac{ia}{2} \delta(y - y_0 + y_1) - \frac{ia}{2} \delta(y - y_0 - y_1) \right\}$  <p style="text-align: right;">(2.67)</p>
 <p style="text-align: center;"><math>A\delta(x)</math></p>	 <p style="text-align: right;">(2.68)</p>
 <p style="text-align: center;"><math>A\delta(x - x_0)</math></p>	 <p style="text-align: center;"><math>A \exp(-ix_0 y)</math></p> <p style="text-align: right;">(2.69)</p>

(continued)



TABLE 2.6 (continued) Graphical Representations of Some Fourier Transforms

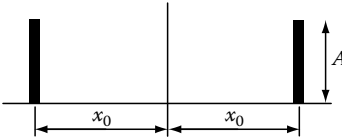
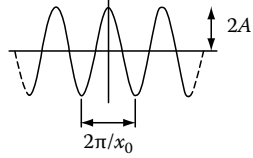
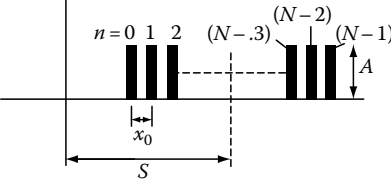
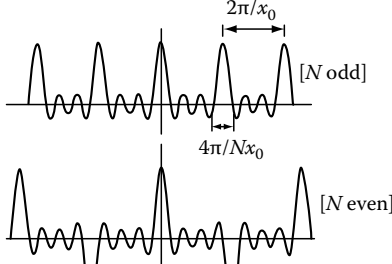
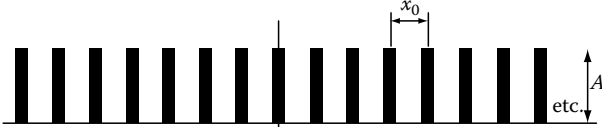
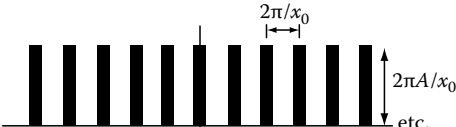
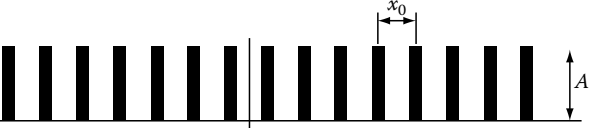
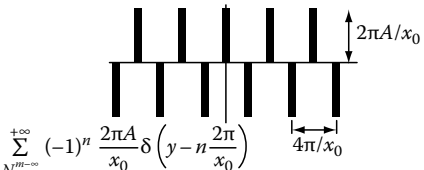
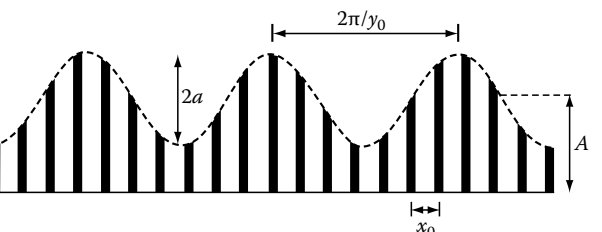
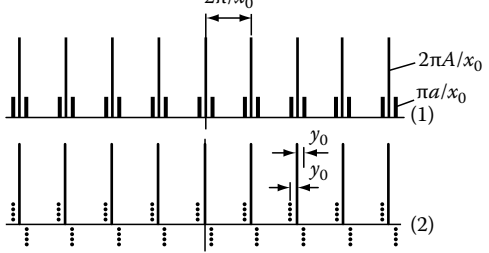
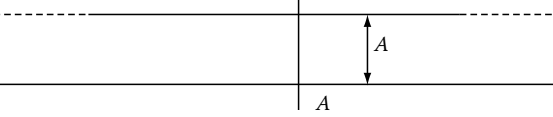
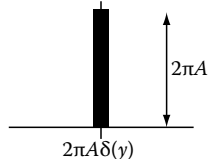
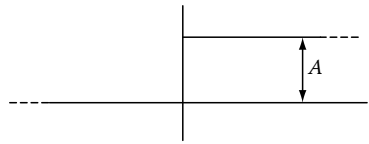
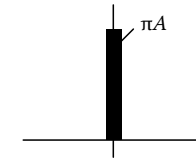
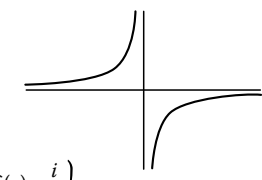
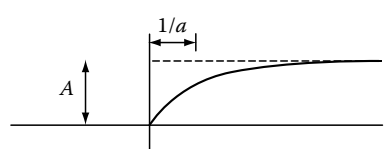
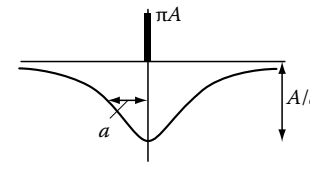
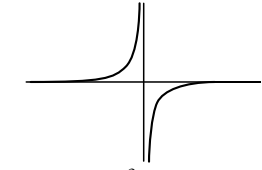
$f(x)$	$F(y)$	
 $A\{\delta(x-x_0) + \delta(x+x_0)\}$	 $2A \cos x_0 y$	(2.70)
 $\sum_{n=0}^{N-1} A \delta \left\{ x - nx_0 - S + \frac{(N-1)x_0}{2} \right\}$ <p>Set of <math>N</math> delta functions symmetrically palced about <math>x = S</math>.</p>	 $A \frac{\sin(Ny x_0/2)}{\sin(y x_0/2)} \exp(-iSy)$ <p>[Drawn for <math>S = 0</math>; <math>N = 7</math> and <math>N = 8</math>]</p>	(2.71)
 $\sum_{N^{m=-\infty}}^{+\infty} A \delta(x - nx_0)$	 $\sum_{N^{m=-\infty}}^{+\infty} \frac{2\pi A}{x_0} \delta \left( y - n \frac{2\pi}{x_0} \right)$	(2.72)
 $\sum_{N^{m=-\infty}}^{+\infty} A \delta \left( x - \frac{x_0}{2} - nx_0 \right)$	 $\sum_{N^{m=-\infty}}^{+\infty} (-1)^n \frac{2\pi A}{x_0} \delta \left( y - n \frac{2\pi}{x_0} \right)$	(2.73)
 $\sum \delta(x - nx_0) \{ A + a \cos y_0 x \}$ <p>(1)</p> $\sum \delta(x - nx_0) \{ A + a \sin y_0 x \}$ <p>(2)</p> <p>[<math>n = 0, \pm 1, \pm 2, \dots</math>]</p>	 $\sum_n \frac{2\pi}{x_0} \left\{ A \delta \left( y - n \frac{2\pi}{x_0} \right) + \frac{a}{2} \delta \left( y - n \frac{2\pi}{x_0} + y_0 \right) + \frac{a}{2} \delta \left( y - \frac{2\pi}{x_0} - y_0 \right) \right\}$ <p>(1)</p> $\sum_n \frac{2\pi}{x_0} \left\{ A \delta \left( y - n \frac{2\pi}{x_0} \right) + \frac{ia}{2} \delta \left( y - n \frac{2\pi}{x_0} + y_0 \right) - \frac{ia}{2} \delta \left( y - n \frac{2\pi}{x_0} - y_0 \right) \right\}$ <p>(2)</p> <p>[<math>n = 0, \pm 1, \pm 2, \dots</math>]</p>	(2.74)
	 $2\pi A \delta(y)$	(2.75)

TABLE 2.6 (continued) Graphical Representations of Some Fourier Transforms

$f(x)$	$F(y)$
--------	--------

	
$\begin{matrix} +A & [x > 0] \\ -A & [x < 0] \end{matrix} \quad [f(x) = A \operatorname{sgn}(x)]$	$-2iA \frac{1}{y} \quad (2.76)$

		
$\begin{matrix} A & [x > 0] \\ 0 & [x < 0] \end{matrix} \quad [f(x) = AU(x)]$	$A \left\{ \pi \delta(y) - \frac{i}{y} \right\} \quad (2.77)$	

		
$\begin{matrix} A\{1 - \exp(-ax)\} & [x > 0] \\ 0 & [x < 0] \end{matrix}$	$\pi A \delta(y) - A \left\{ \frac{a}{a^2 + y^2} + i \frac{a^2}{y(a^2 + y^2)} \right\} \quad (2.78)$	

	
$\begin{matrix} A & [ x  > L] \\ 0 & [ x  < L] \end{matrix}$	$2\pi A \delta(y) - 2A \frac{\sin Ly}{y} \quad (2.79)$

$A \exp\{i(a \cos y_0 x + bx)\}$	
$2\pi A \sum_{N=-\infty}^{+\infty} (i)^N J_N(a) \delta(y - b - ny_0) \quad (2.80)$	

$A \exp\{i(a \sin y_0 x + bx)\}$	
$2\pi A \sum_{N=-\infty}^{+\infty} J_N(a) \delta(y - b - ny_0) \quad (2.81)$	

(continued)

TABLE 2.6 (continued) Graphical Representations of Some Fourier Transforms

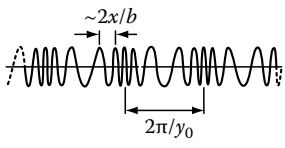
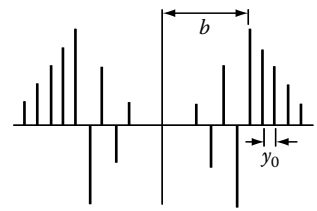
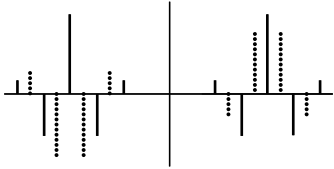
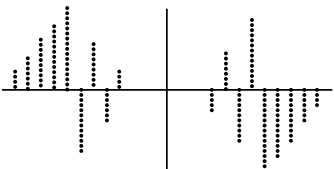
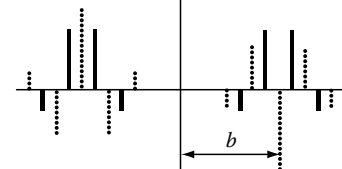
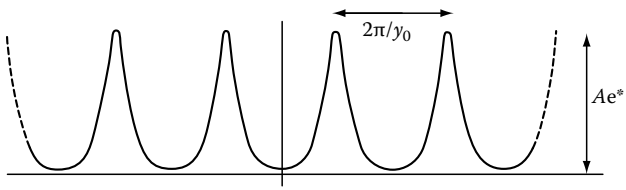
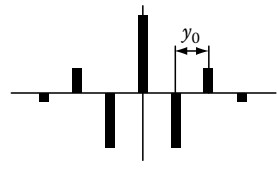
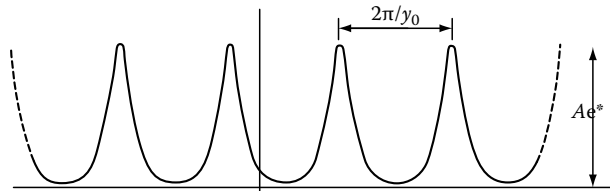
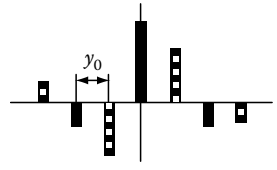
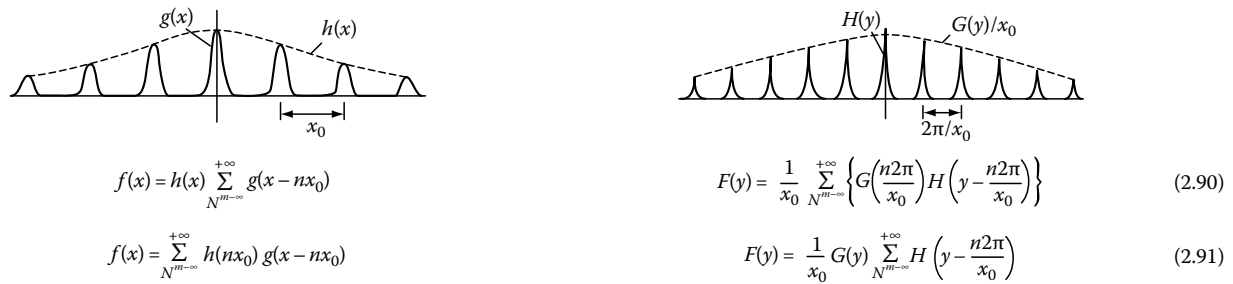
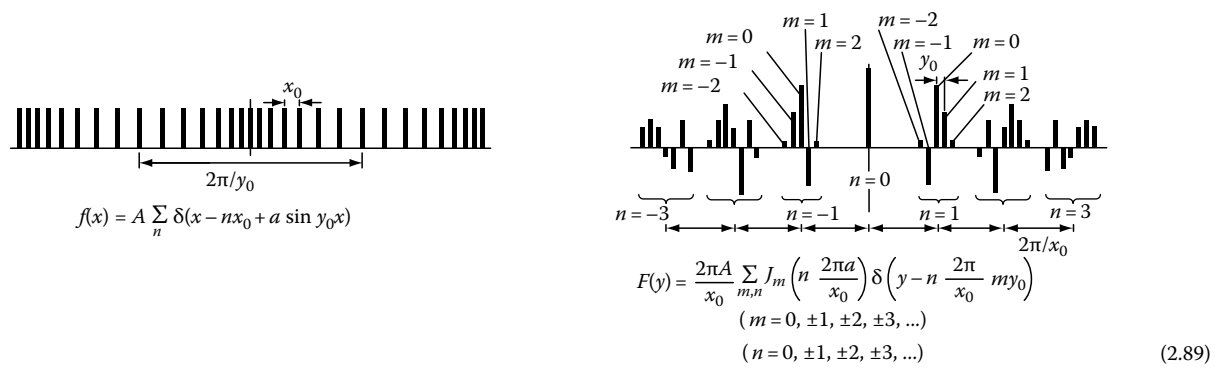
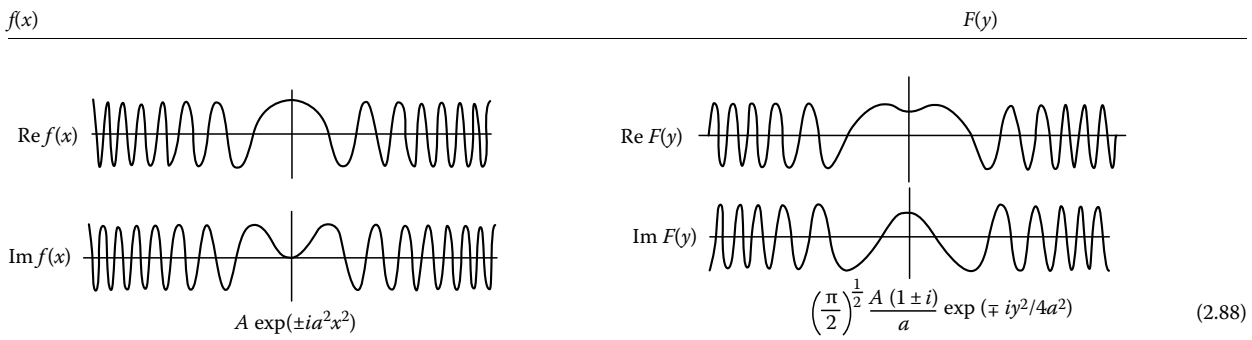
$f(x)$	$F(y)$
 <p><math>A \cos(a \sin y_0 x + bx)</math></p>	 $\pi A \sum_{N^{m=-\infty}}^{+\infty} \{J_n(a)\delta(y - b - ny_0) + J_n(a)\delta(y + b + ny_0)\}$ (2.82)
<p><math>A \cos(a \cos y_0 x + bx)</math></p>	 $\pi A \sum_{N^{m=-\infty}}^{+\infty} \{(+i)^n J_n(a)\delta(y - b - ny_0) + (-i)^n J_n(a)\delta(y + b + ny_0)\}$ (2.83)
<p><math>A \sin(a \sin y_0 x + bx)</math></p>	 $i\pi A \sum_{N^{m=-\infty}}^{+\infty} \{-J_n(a)\delta(y - b - ny_0) + J_n(a)\delta(y + b + ny_0)\}$ (2.84)
<p><math>A \sin(a \cos y_0 x + bx)</math></p>	 $i\pi A \sum_{N^{m=-\infty}}^{+\infty} \{-(-i)^n J_n(a)\delta(y - b - ny_0) + (-i)^n J_n(a)\delta(y + b + ny_0)\}$ (2.85)
 <p><math>A \exp(-a \cos y_0 x)</math></p>	 $2\pi A \sum_{N^{m=-\infty}}^{+\infty} (-1)^n J_n(a)\delta(y - ny_0)$ (2.86)
 <p><math>A \exp(-a \sin y_0 x)</math></p>	 $2\pi A \sum_{N^{m=-\infty}}^{+\infty} (i)^n J_n(a)\delta(y - ny_0)$ (2.87)

TABLE 2.6 (continued) Graphical Representations of Some Fourier Transforms



Source: Champeney, D.C., *Fourier Transforms and Their Physical Applications*, Academic Press, New York, 1973. With permission.  
 Note:  $J_n(-a) = J_{-n}(a) = (-1)^n J_n(a)$ .

## References

Abramowitz, M. and Stegun, I. 1972. *Handbook of Mathematical Functions*. New York: Dover Publications.

Arsac, J. 1966. *Fourier Transforms and the Theory of Distributions*. Englewood Cliffs, NJ: Prentice-Hall.

Boyce, W. and DiPrima, R. 1977. *Elementary Differential Equations and Boundary Value Problems*. New York: John Wiley & Sons.

Bracewell, R. 1965. *The Fourier Transform and Its Applications*. New York: McGraw-Hill.

Briggs, W. L. and Henson, V. E. 1995. *The DFT: An Owner's Manual for the Discrete Fourier Transform*. Philadelphia, PA: Society for Industrial and Applied Mathematics.

Brown, J. W. and Churchill, R. V. 2008. *Fourier Series and Boundary Value Problems* (7th edn.). New York: McGraw-Hill.

Campbell, G. A. and Poster, R. M. 1948. *Fourier Integrals for Practical Applications*. New York: D. Van Nostrand.

Champeney, D. C. 1973. *Fourier Transforms and Their Physical Applications*. New York: Academic Press.

Champeney, D. C. 1987. *A Handbook of Fourier Theorems*. Cambridge, U.K.: Cambridge University Press.

Chu, E. and George, A. 2000. *Inside the FFT Black Box: Serial and Parallel Fast Fourier Transform Algorithms*. Boca Raton, FL: CRC Press LLC.

DeVito, C. L. 2007. *Harmonic Analysis: A Gentle Introduction*. Sudbury, MA: Jones and Bartlett Publishers.

- Erdélyi, A. (Ed.) 1954. *Tables of Integral Transforms (Bateman Manuscript Project)*. New York: McGraw-Hill.
- Grafakos, L. 2004. *Classical and Modern Fourier Analysis*. Upper Saddle River, NJ: Pearson Education, Inc.
- Holland, S. 1990. *Applied Analysis by the Hilbert Space Method*. New York: Marcel Dekker.
- Howell, K. B. 2001. *Principles of Fourier Analysis*. Boca Raton, FL: Chapman & Hall/CRC.
- Körner, T. W. 1988. *Fourier Analysis*. Cambridge, U.K.: Cambridge University Press.
- Papoulis, A. 1962. *The Fourier Integrals and its Applications*. New York: McGraw-Hill.
- Papoulis, A. 1986. *Systems and Transforms with Applications in Optics*. New York: McGraw-Hill. Reprinted, Malabar, FL: Robert E. Krieger Publishing Company.
- Pinsky, M. 1991. *Partial Differential Equations and Boundary-Value Problems with Applications*. New York: McGraw-Hill.
- Strichartz, R. 1994. *A Guide to Distribution Theory and Fourier Transforms*. Boca Raton, FL: CRC Press-LLC.
- Walker, J. S. 1988. *Fourier Analysis*. New York: Oxford University Press.
- Walker, J. S. 1996. *Fast Fourier Transforms* (2nd edn.). Boca Raton, FL: CRC Press LLC.

# Sine and Cosine Transforms

3.1	Introduction.....	3-1
3.2	The Fourier Cosine Transform (FCT) .....	3-1
	Definitions and Relations to the Exponential Fourier Transforms • Basic Properties and Operational Rules • Selected Fourier Cosine Transforms • Examples on the Use of Some Operational Rules of FCT	
3.3	The Fourier Sine Transform (FST) .....	3-11
	Definitions and Relations to the Exponential Fourier Transforms • Basic Properties and Operational Rules • Selected Fourier Sine Transforms	
3.4	The Discrete Sine and Cosine Transforms (DST and DCT) .....	3-16
	Definitions of DCT and DST and Relations to FST and FCT • Basic Properties and Operational Rules • Relation to the Karhunen–Loeve Transform (KLT)	
3.5	Selected Applications.....	3-21
	Solution of Differential Equations • Cepstral Analysis in Speech Processing • Data Compression • Transform Domain Processing • Image Compression by the Discrete Local Sine Transform (DLS)	
3.6	Computational Algorithms .....	3-27
	FCT and FST Algorithms Based on FFT • Fast Algorithms for DST and DCT by Direct Matrix Factorization	
3.7	Tables of Transforms .....	3-31
	Fourier Cosine Transforms • Fourier Sine Transforms • Notations and Definitions	
	References .....	3-34

Pat Yip  
McMaster University

## 3.1 Introduction

Transforms with cosine and sine functions as the transform kernels represent an important area of analysis. It is based on the so-called half-range expansion of a function over a set of cosine or sine basis functions. Because the cosine and the sine kernels lack the nice properties of an exponential kernel, many of the transform properties are less elegant and more involved than the corresponding ones for the Fourier transform kernel. In particular, the convolution property, which is so important in many applications, will be much more complex.

Despite these basic mathematical limitations, sine and cosine transforms have their own areas of applications. In spectral analysis of real sequences, in solutions of some boundary value problems, and in transform domain processing of digital signals, both cosine and sine transforms have shown their special applicability. In particular, the discrete versions of these transforms have found favor among the digital signal-processing community. Many data compression techniques now employ, in one way or another, the discrete cosine transform (DCT), which has been found to be asymptotically equivalent to the optimal Karhunen–Loeve transform (KLT) for signal decorrelation.

In this chapter, the basic properties of cosine and sine transforms are presented, together with some selected transforms. To show the

versatility of these transforms, several applications are discussed. Computational algorithms are also presented. The chapter ends with a table of sine and cosine transforms, which is not meant to be exhaustive. The reader is referred to the References for more details and for more exhaustive listings of the cosine and sine transforms

## 3.2 The Fourier Cosine Transform (FCT)

### 3.2.1 Definitions and Relations to the Exponential Fourier Transforms

Given a real- or complex-valued function  $f(t)$ , which is defined over the positive real line  $t \geq 0$ , for  $\omega \geq 0$ , the FCT of  $f(t)$  is defined as

$$F_c(\omega) = \int_0^{\infty} f(t) \cos \omega t \, dt, \quad \omega \geq 0, \quad (3.1)$$

subject to the existence of the integral. The definition is sometimes more compactly represented as an operator  $\mathcal{F}_c$  applied to the function  $f(t)$ , so that

$$\mathcal{F}_c[f(t)] = F_c(\omega) = \int_0^{\infty} f(t) \cos \omega t \, dt. \quad (3.2)$$

The subscript  $c$  is used to denote the fact that the kernel of the transformation is a cosine function. The unit normalization constant used here provides for a definition for the inverse FCT, given by

$$\mathcal{F}_c^{-1}[F_c(\omega)] = \frac{2}{\pi} \int_0^{\infty} F_c(\omega) \cos \omega t \, d\omega, \quad t \geq 0, \quad (3.3)$$

again subject to the existence of the integral used in the definition. The functions  $f(t)$  and  $F_c(\omega)$ , if they exist, are said to form a FCT pair.

Because the cosine function is the real part of an exponential function of purely imaginary argument, that is,

$$\cos(\omega t) = \operatorname{Re}[e^{j\omega t}] = \frac{1}{2}[e^{j\omega t} + e^{-j\omega t}], \quad (3.4)$$

it is easy to understand that there exists a very close relationship between the Fourier transform and the cosine transform. To see this relation, consider an even extension of the function  $f(t)$  defined over the entire real line so that

$$f_e(t) = f(|t|), \quad t \in R. \quad (3.5)$$

Its Fourier transform is defined as

$$\mathcal{F}[f_e(t)] = \int_{-\infty}^{\infty} f_e(t) e^{-j\omega t} \, dt, \quad \omega \in R. \quad (3.6)$$

The integral in Equation 3.6 can be evaluated in two parts over  $(-\infty, 0]$  and  $[0, \infty)$ . Then using Equation 3.5 and changing the integrating variable in the  $(-\infty, 0]$  integral from  $t$  to  $-t$ , we have

$$\mathcal{F}[f_e(t)] = \left[ \int_0^{\infty} f(t) e^{-j\omega t} \, dt + \int_0^{\infty} f(t) e^{j\omega t} \, dt \right] = 2 \int_0^{\infty} f(t) \cos \omega t \, dt,$$

by Equation 3.4, and thus

$$\mathcal{F}[f_e(t)] = 2\mathcal{F}_c[f(t)], \quad \text{if } f_e(t) = f(|t|). \quad (3.7)$$

Many of the properties of the FCTs can be derived from the properties of Fourier transforms of symmetric, or even, functions. Some of the basic properties and operational rules are discussed in Section 3.2.2.

### 3.2.2 Basic Properties and Operational Rules

1. *Inverse transformation:* As stated in Equation 3.3, the inverse transformation is exactly the same as the forward transformation except for the normalization constant. This leads to the so-called Fourier cosine integral formula, which states that

$$\begin{aligned} f(t) &= \frac{2}{\pi} \int_0^{\infty} F_c(\omega) \cos \omega t \, d\omega \\ &= \frac{2}{\pi} \int_0^{\infty} \left[ \int_0^{\infty} f(\tau) \cos \omega \tau \, d\tau \right] \cos \omega t \, d\omega. \end{aligned} \quad (3.8)$$

The sufficient conditions for the inversion formula (3.3) are that  $f(t)$  be absolutely integrable in  $[0, \infty)$  and that  $f'(t)$  be piecewise continuous in each bounded subinterval of  $[0, \infty)$ . In the range where the function  $f(t)$  is continuous, Equation 3.8 represents  $f$ . At the point  $t_0$  where  $f(t)$  has a jump discontinuity, Equation 3.8 converges to the mean of  $f(t_0 + 0) + f(t_0 - 0)$ , that is,

$$\begin{aligned} &\frac{2}{\pi} \int_0^{\infty} \left[ \int_0^{\infty} f(\tau) \cos(\omega \tau) \, d\tau \right] \cos(\omega t_0) \, d\omega \\ &= \frac{1}{2} [f(t_0 + 0) + f(t_0 - 0)]. \end{aligned} \quad (3.8')$$

2. *Transforms of derivatives:* It is easy to show, because of the Fourier cosine kernel, that the transforms of even-order derivatives are reduced to multiplication by even powers of the conjugate variable  $\omega$ , much as in the case of the Laplace transforms. For the second-order derivative, using integration by parts, we can show that,

$$\begin{aligned} \mathcal{F}_c[f''(t)] &= \int_0^{\infty} f''(t) \cos(\omega t) \, dt \\ &= -f'(0) - \omega^2 \int_0^{\infty} f(t) \cos \omega t \, dt \\ &= -\omega^2 F_c(\omega) - f'(0) \end{aligned} \quad (3.9)$$

where we have assumed that  $f(t)$  and  $f'(t)$  vanish as  $t \rightarrow \infty$ . These form the sufficient conditions for Equation 3.9 to be valid. As the transform is applied to higher order derivatives, corresponding conditions for higher derivatives of  $f$  are required for the operational rule to be valid. Here, we also assume that the function  $f(t)$  and its derivative  $f'(t)$  are continuous everywhere in  $[0, \infty)$ . If  $f(t)$  and  $f'(t)$  have a jump discontinuity at  $t_0$  of magnitudes  $d$  and  $d'$ , respectively, Equation 3.9 is modified to

$$\begin{aligned} \mathcal{F}_c[f''(t)] &= -\omega^2 F_c(\omega) - f'(0) - \omega d \sin \omega t_0 \\ &\quad - d' \cos \omega t_0 \end{aligned} \quad (3.10)$$

Higher even-order derivatives of functions with jump discontinuities have similar operational rules that can be easily

generalized from Equation 3.10. For example, the FCT of the fourth-order derivative is

$$\mathcal{F}_c[f^{(iv)}(t)] = \omega^4 F_c(\omega) + \omega^2 f'(0) - f'''(0) \quad (3.11)$$

if  $f(t)$  is continuous to order three everywhere in  $[0, \infty]$ , and  $f, f',$  and  $f''$  vanish as  $t \rightarrow \infty$ . If  $f(t)$  has a jump discontinuity at  $t_0$  to order three of magnitudes  $d, d', d'',$  and  $d'''$ , then Equation 3.11 is modified to

$$\begin{aligned} \mathcal{F}_c[f^{(iv)}(t)] &= \omega^4 F_c(\omega) + \omega^2 f'(0) - f'''(0) \\ &\quad + \omega^3 d \sin \omega t_0 + \omega^2 d' \cos \omega t_0 \\ &\quad - \omega d'' \sin \omega t_0 - d''' \cos \omega t_0 \end{aligned} \quad (3.12)$$

Here, and in Equation 3.10, we have defined the magnitudes of the jump discontinuity at  $t_0$  as

$$\begin{aligned} d &= f(t_0 + 0) - f(t_0 - 0); \\ d' &= f'(t_0 + 0) - f'(t_0 - 0); \\ d'' &= f''(t_0 + 0) - f''(t_0 - 0); \\ d''' &= f'''(t_0 + 0) - f'''(t_0 - 0). \end{aligned} \quad (3.13)$$

For derivatives of odd order, the operational rules require the definition for the Fourier sine transform (FST), given in Section 3.3. For example, the FCTs of the first-order derivative is given by

$$\begin{aligned} \mathcal{F}_c[f'(t)] &= \int_0^{\infty} f'(t) \cos \omega t \, dt \\ &= -f(0) + \omega \int_0^{\infty} f(t) \sin \omega t \, dt \\ &= \omega \mathcal{F}_s[f(t)] - f(0) = \omega F_s(\omega) - f(0), \end{aligned} \quad (3.14)$$

if  $f$  vanishes as  $t \rightarrow \infty$ , and where the operator  $\mathcal{F}_s$  and the function  $F_s(\omega)$  are defined in Equation 3.78. When  $f(t)$  has a jump discontinuity of magnitude  $d$  at  $t = t_0$ , Equation 3.14 is modified to

$$\mathcal{F}_c[f'(t)] = \omega F_s(\omega) - f(0) - d \cos(\omega t_0). \quad (3.15)$$

Generalization to higher odd-order derivatives with jump discontinuities is similar to that for even-order derivatives in Equation 3.12.

3. *Scaling*: Scaling in the  $t$  domain translates directly to scaling in the  $\omega$  domain. Expansion by a factor of  $a$  in  $t$  results in the contraction by the same factor in  $\omega$ , together with a scaling down of the magnitude of the transform by the factor  $a$ . Thus, as we can show,

$$\begin{aligned} \mathcal{F}_c[f(at)] &= \int_0^{\infty} f(at) \cos \omega t \, dt \\ &= \frac{1}{a} \int_0^{\infty} f(\tau) \cos \frac{\omega \tau}{a} \, d\tau, \quad \text{by letting} \\ \tau &= at = \frac{1}{a} F_c\left(\frac{\omega}{a}\right), \quad a > 0. \end{aligned} \quad (3.16)$$

#### 4. Shifting:

- (a) Shifting in the  $t$ -domain: The shift-in- $t$  property for the cosine transform is somewhat less direct compared with the exponential Fourier transform for two reasons. First, a shift to the left will require extending the definition of the function  $f(t)$  onto the negative real line. Secondly, a shift-in- $t$  in the transform kernel does not result in a constant phase factor as in the case of the exponential kernel.

If  $f_e(t)$  is defined as the even extension of the function  $f(t)$  such that  $f_e(t) = f(|t|)$ , and if  $f(t)$  is piecewise continuous and absolutely integrable over  $[0, \infty)$ , then

$$\begin{aligned} \mathcal{F}_c[f_e(t+a) + f_e(t-a)] &= \int_0^{\infty} [f_e(t+a) + f_e(t-a)] \cos \omega t \, dt \\ &= \int_a^{\infty} f_e(\tau) \cos \omega(\tau+a) \, d\tau \\ &= \int_{-a}^{\infty} f_e(\tau) \cos \omega(\tau-a) \, d\tau. \end{aligned}$$

By expanding the compound cosine functions and using the fact that the function  $f_e(\tau)$  is even, these combine to give

$$\mathcal{F}_c[f_e(t+a) + f_e(t-a)] = 2F_c(\omega) \cos a\omega, \quad a > 0. \quad (3.17)$$

This is sometimes called the kernel-product property of the cosine transform. In terms of the function  $f(t)$ , it can be written as

$$\mathcal{F}_c[f(t+a) + f(|t-a|)] = 2F_c(\omega) \cos a\omega. \quad (3.18)$$

Similarly, the kernel-product  $2F_c(\omega) \sin(a\omega)$  is related to the FST:

$$\mathcal{F}_s[f(|t-a|) - f(t+a)] = 2F_c(\omega) \sin a\omega, \quad a > 0. \quad (3.19)$$

- (b) Shifting in the  $\omega$ -domain:

To consider the effect of shifting in  $\omega$  by the amount of  $\beta(>0)$ , we examine the following,



$$\begin{aligned}
F_c(\omega + \beta) &= \int_0^{\infty} f(t) \cos(\omega + \beta)t \, dt \\
&= \int_0^{\infty} f(t) \cos \beta t \cos \omega t \, dt - \int_0^{\infty} f(t) \sin \beta t \sin \omega t \, dt \\
&= \mathcal{F}_c[f(t) \cos \beta t] - \mathcal{F}_s[f(t) \sin \beta t]. \quad (3.20)
\end{aligned}$$

Similarly,

$$F_c(\omega - \beta) = \mathcal{F}_c[f(t) \cos \beta t] + \mathcal{F}_s[f(t) \sin \beta t]. \quad (3.20')$$

Combining Equations 3.20 and 3.20' produces a shift-in- $\omega$  operational rule involving only the FCT as

$$\mathcal{F}_c[f(t) \cos \beta t] = \frac{1}{2}[F_c(\omega + \beta) + F_c(\omega - \beta)]. \quad (3.21)$$

More generally, for  $a, \beta > 0$ , we have,

$$\mathcal{F}_c[f(at) \cos \beta t] = \frac{1}{2a} \left[ F_c\left(\frac{\omega + \beta}{a}\right) + F_c\left(\frac{\omega - \beta}{a}\right) \right]. \quad (3.22)$$

Similarly, we can easily derive

$$\mathcal{F}_c[f(at) \sin \beta t] = \frac{1}{2a} \left[ F_s\left(\frac{\omega + \beta}{a}\right) - F_s\left(\frac{\omega - \beta}{a}\right) \right]. \quad (2.22')$$

5. *Differentiation in the  $\omega$  domain:* Similar to differentiation in the  $t$  domain, the transform operation reduces a differentiation operation into multiplication by an appropriate power of the conjugate variable. In particular, even-order derivatives in the  $\omega$  domain are transformed as

$$F_c^{(2n)}(\omega) = \mathcal{F}_c[(-1)^n t^{2n} f(t)]. \quad (3.23)$$

We show here briefly, the derivation for  $n = 1$ :

$$\begin{aligned}
F_c^{(2)}(\omega) &= \frac{d^2}{d\omega^2} \int_0^{\infty} f(t) \cos \omega t \, dt \\
&= \int_0^{\infty} f(t) \frac{d^2}{d\omega^2} \cos \omega t \, dt \\
&= \int_0^{\infty} f(t) (-1)t^2 \cos \omega t \, dt \\
&= \mathcal{F}_c[(-1)t^2 f(t)].
\end{aligned}$$

For odd orders, these are related to FSTs

$$F_c^{(2n+1)}(\omega) = \mathcal{F}_s[(-1)^{n+1} t^{2n+1} f(t)]. \quad (3.24)$$

In both Equations 3.23 and 3.24, the existence of the integrals in question is assumed. This means that  $f(t)$  should be

piecewise continuous and that  $t^{2n}f(t)$  and  $t^{2n+1}f(t)$  should be absolutely integrable over  $[0, \infty)$ .

6. *Asymptotic behavior:* When the function  $f(t)$  is piecewise continuous and absolutely integrable over the region  $[0, \infty)$ , the Reimann–Lebesgue theorem for Fourier series\* can be invoked to provide the following asymptotic behavior of its cosine transform:

$$\lim_{\omega \rightarrow \infty} F_c(\omega) = 0. \quad (3.25)$$

7. *Integration:*

(a) Integration in the  $t$  domain:

Integration in the  $t$  domain is transformed to division by the conjugate variable, very similar to the cases of Laplace transforms and Fourier transforms, except the resulting transform is a FST. Thus,

$$\begin{aligned}
\mathcal{F}_c \left[ \int_t^{\infty} f(\tau) d\tau \right] &= \int_0^{\infty} \int_t^{\infty} f(\tau) d\tau \cos \omega t \, dt \\
&= \int_0^{\infty} \left[ \int_0^{\tau} \cos \omega t \, dt \right] f(\tau) d\tau
\end{aligned}$$

by reversing the order of integration. The inner integral results in a sine function and is the kernel for the FST. Therefore,

$$\mathcal{F}_c \left[ \int_t^{\infty} f(\tau) d\tau \right] = \frac{1}{\omega} \mathcal{F}_s[f(\tau)] = \frac{1}{\omega} F_s(\omega). \quad (3.26)$$

Here, again,  $f(t)$  is subject to the usual sufficient conditions of being piecewise continuous and absolutely integrable in  $[0, \infty)$ .

(b) Integration in the  $\omega$  domain:

A similar and symmetric relation exists for integration in the  $\omega$ -domain.

$$\mathcal{F}_s^{-1} \left[ \int_{\omega}^{\infty} F_c(\beta) d\beta \right] = -\frac{1}{t} f(t). \quad (3.27)$$

Note that the integration transform inversion is of the Fourier sine type instead of the cosine type. Also the asymptotic behavior of  $F_c(\omega)$  has been invoked.

8. *The convolution property:* Let  $f(t)$  and  $g(t)$  be defined over  $[0, \infty)$  and satisfy the sufficiency condition for the existence of  $F_c$  and  $G_c$ . If  $f_e(t) = f(|t|)$  and  $g_e(t) = g(|t|)$  are the

\* The Reimann–Lebesgue theorem states that if a function  $f(t)$  is piece-wise continuous over an interval  $a < t < b$ , then

$$\lim_{\gamma \rightarrow \infty} \int_a^b f(t) \cos \gamma t \, dt = \lim_{\gamma \rightarrow \infty} \int_a^b f(t) \sin \gamma t \, dt = 0.$$

even extensions of  $f$  and  $g$ , respectively, over the entire real line, then the convolution of  $f_e$  and  $g_e$  is given by

$$f_e * g_e = \int_{-\infty}^{\infty} f_e(\tau) g_e(t - \tau) d\tau \quad (3.28)$$

where  $*$  has been used to denote the convolution operation. It is easy to see that in terms of  $f$  and  $g$ , we have

$$f_e * g_e = \int_0^{\infty} f(\tau)[g(t + \tau) + g(|t - \tau|)] d\tau \quad (3.29)$$

which is an even function. Applying the exponential Fourier transform on both sides and using Equation 3.7 and convolution property of the exponential Fourier transform, we obtain the convolution property for the cosine transform:

$$\begin{aligned} 2F_c(\omega)G_c(\omega) \\ = \mathcal{F}_c \left\{ \int_0^{\infty} f(\tau)[g(t + \tau) + g(|t - \tau|)] d\tau \right\}. \end{aligned} \quad (3.30)$$

In a similar way, the cosine transform of the convolution of odd extended functions is related to the sine transforms. Thus,

$$\begin{aligned} 2F_s(\omega)G_s(\omega) \\ = \mathcal{F}_s \left\{ \int_0^{\infty} f(\tau)[g_o(t + \tau) + g_o(t - \tau)] d\tau \right\}. \end{aligned} \quad (3.31)$$

where

$$\begin{aligned} g_o(t) &= g(t) \quad \text{for } t > 0, \\ &= -g(-t) \quad \text{for } t < 0, \end{aligned} \quad (3.32)$$

is defined as the odd extension of the function  $g(t)$ .

### 3.2.3 Selected Fourier Cosine Transforms

In this section, the FCTs of some typical functions are given. Most are selected for their simplicity and application. For a more complete listing of cosine transforms, see Section 3.7 where a more extensive table is provided.

#### 3.2.3.1 FCT of Algebraic Functions

1. *The unit rectangular function:*

$$\begin{aligned} f(t) &= U(t) - U(t - a), \\ \text{where } U(t) &= 0 \quad \text{for } t < 0 = 1 \quad \text{for } t > 0 \end{aligned} \quad (3.33)$$

is the Heaviside unit step function.

$$\mathcal{F}_c[f(t)] = \int_0^a \cos \omega t dt = \frac{1}{\omega} \sin \omega a. \quad (3.34)$$

2. *The unit height tent function:*

$$\begin{aligned} f(t) &= t/a \quad 0 < t < a, \\ &= (2a - t)/a \quad a < t < 2a, \\ &= 0 \quad t > 2a. \end{aligned}$$

$$\begin{aligned} \mathcal{F}_c[f(t)] &= \int_0^a \frac{t}{a} \cos \omega t dt + \int_a^{2a} \frac{2a - t}{a} \cos \omega t dt \\ &= \frac{1}{a\omega^2} [2 \cos a\omega - \cos 2a\omega - 1]. \end{aligned} \quad (3.35)$$

3. *Delayed inverse:*

$$\begin{aligned} f(t) &= U(t - a)/t, \\ \mathcal{F}_c[f(t)] &= \int_a^{\infty} \frac{1}{t} \cos \omega t dt \\ &= \int_{a\omega}^{\infty} \frac{1}{\tau} \cos \tau d\tau = -\text{Ci}(a\omega), \end{aligned} \quad (3.36)$$

where  $\text{Ci}(\gamma) = -\int_{\gamma}^{\infty} \frac{1}{\tau} \cos \tau d\tau$  is defined as the cosine integral function.

4. *The inverse square root:*

$$\begin{aligned} f(t) &= 1/\sqrt{t}, \\ \mathcal{F}_c[f(t)] &= \int_0^{\infty} \frac{1}{\sqrt{t}} \cos \omega t dt = \sqrt{\frac{\pi}{2\omega}}. \end{aligned} \quad (3.37)$$

Equation 3.27 is obtained by letting  $t = z^2$ , and considering the integral,

$$2 \int \cos z^2 dz$$

in the complex plane (see Appendix A). Using contour integration around a pie-shape region with angle  $\pi/4$ , the result is obtained directly from the identity:

$$\int_0^{\infty} e^{jt^2} dt = \frac{1}{2} \sqrt{\frac{\pi}{2}} (1 + j).$$

## 5. Inverse linear function:

$$f(t) = (\alpha + t)^{-1} | \arg(\alpha) | < \pi.$$

$$\mathcal{F}_c[f(t)] = \int_0^{\infty} (\alpha + t)^{-1} \cos \omega t dt$$

$$= -\cos \alpha \omega \text{Ci}(\alpha \omega) - \sin \alpha \omega \text{si}(\alpha \omega). \quad (3.38)$$

Equation 3.38 is obtained by shifting the integrating variable to  $\alpha + t$ , and then expanding the compound cosine function. Here,  $\text{si}(y)$  is related to the sine integral function  $\text{Si}(y)$ , and is defined as

$$\text{si}(y) = -\int_y^{\infty} \frac{\sin x}{x} dx$$

$$= \int_0^y \frac{\sin x}{x} dx - \int_0^{\infty} \frac{\sin x}{x} dx = \text{Si}(y) - (\pi/2). \quad (3.39)$$

## 6. Inverse quadratic functions:

$$(a) f(t) = (\alpha^2 + t^2)^{-1} \quad \text{Re}(\alpha) > 0.$$

$$\mathcal{F}_c[f(t)] = \int_0^{\infty} (\alpha^2 + t^2)^{-1} \cos \omega t dt$$

$$= \frac{\pi}{2\alpha} e^{-\alpha \omega}, \quad (3.40)$$

which is obtained also by a properly chosen contour integration over the upper half-plane.

$$(b) f(t) = (\alpha^2 - t^2)^{-1} \quad a > 0,$$

$$\mathcal{F}_c[f(t)] = \text{P.V.} \int_0^{\infty} (a^2 + t^2)^{-1} \cos \omega t dt$$

$$= \frac{\pi}{2a} \sin \alpha \omega \quad (3.41)$$

where ‘‘P.V.’’ stands for ‘‘principal value’’ and the integral can be obtained by a proper contour integration in the complex plane.

$$(c) f(t) = \frac{\beta}{\beta^2 + (\alpha - t)^2} + \frac{\beta}{\beta^2 + (\alpha + t)^2} \quad \text{Im}|\alpha| < \text{Re}(\beta),$$

$$\mathcal{F}_c[f(t)] = \int_0^{\infty} \left[ \frac{\beta}{\beta^2 + (\alpha - t)^2} + \frac{\beta}{\beta^2 + (\alpha + t)^2} \right] \cos \omega t dt$$

$$= \pi \cos \alpha \omega e^{-\beta \omega} \quad (3.42)$$

where the integral can be obtained easily by considering a shift in  $t$ , applied to the result in Equation 3.40.

$$(d) f(t) = \frac{\alpha - t}{\beta^2 + (\alpha - t)^2} + \frac{\alpha + t}{\beta^2 + (\alpha + t)^2} \quad \text{Im}|\alpha| < \text{Re}(\beta),$$

$$\mathcal{F}_c[f(t)] = \int_0^{\infty} \left[ \frac{\alpha - t}{\beta^2 + (\alpha - t)^2} + \frac{\alpha + t}{\beta^2 + (\alpha + t)^2} \right] \cos \omega t dt$$

$$= \pi \sin \alpha \omega e^{-\beta \omega} \quad (3.43)$$

which can be considered as the imaginary part of the contour integral needed in Equation 3.42 when  $\alpha$  and  $\beta$  are real and positive.

## 3.2.3.2 FCT of Exponential and Logarithmic Functions

$$1. f(t) = e^{-\alpha t} \quad \text{Re}(\alpha) > 0.$$

$$\mathcal{F}_c[f(t)] = \int_0^{\infty} e^{-\alpha t} \cos \omega t dt = \frac{\alpha}{\alpha^2 + \omega^2} \quad (3.44)$$

which is identical to the Laplace transform of  $\cos \omega t$ .

$$2. f(t) = \frac{1}{t} [e^{-\beta t} - e^{-\alpha t}] \quad \text{Re}(\alpha), \text{Re}(\beta) > 0.$$

$$\mathcal{F}_c[f(t)] = \int_0^{\infty} \frac{1}{t} [e^{-\beta t} - e^{-\alpha t}] \cos \omega t dt$$

$$= \frac{1}{2} \ln \left( \frac{\alpha^2 + \omega^2}{\beta^2 + \omega^2} \right). \quad (3.45)$$

The result is easily obtained using the integration property of the Laplace transform in the phase plane.

$$3. f(t) = e^{-\alpha t^2} \quad \text{Re}(\alpha) > 0.$$

$$\mathcal{F}_c[f(t)] = \int_0^{\infty} \frac{1}{t} e^{-\alpha t^2} \cos \omega t dt$$

$$= \frac{1}{2} \sqrt{\frac{\pi}{\alpha}} e^{-\omega^2/4\alpha} \quad (3.46)$$

This is easily seen as the result of the exponential Fourier transform of a Gaussian distribution.

$$4. f(t) = \ln t [1 - U(t - 1)]$$

$$\mathcal{F}_c[f(t)] = \int_0^1 \ln t \cos \omega t dt$$

$$= -\frac{1}{\omega} \int_0^{\omega} \frac{\sin \tau}{\tau} d\tau = -\frac{1}{\omega} \text{Si}(\omega). \quad (3.47)$$

The result is obtained by integration by parts and a change of variables. The function  $\text{Si}(\omega)$  is defined as the sine integral function given by

$$\text{Si}(y) = \int_0^y \frac{\sin x}{x} dx. \quad (3.48)$$

$$5. f(t) = \frac{\ln \beta t}{(t^2 + \alpha^2)} \quad \text{Re}(\alpha) > 0$$

$$\begin{aligned} \mathcal{F}_c[f(t)] &= \int_0^{\infty} \frac{\ln \beta t}{(t^2 + \alpha^2)} \cos \omega t dt \\ &= \frac{\pi}{4\alpha} \{2e^{-\alpha\omega} \ln(\alpha\beta) + e^{\alpha\omega} \text{Ei}(-\alpha\omega) \\ &\quad - e^{-\alpha\omega} \overline{\text{Ei}}(\alpha\omega)\} \end{aligned} \quad (3.49)$$

where  $\text{Ei}(y)$  is the exponential integral function defined by,

$$\text{Ei}(y) = - \int_{-\gamma}^{\infty} \frac{e^{-t}}{t} dt, \quad |\arg(y)| < \pi,$$

and

$$\overline{\text{Ei}}(y) = (1/2)[\text{Ei}(y + j0) + \text{Ei}(y - j0)]. \quad (3.50)$$

The integral in Equation 3.49 is evaluated using contour integration.

$$6. f(t) = \ln \left| \frac{t+a}{t-a} \right|, \quad a > 0.$$

$$\begin{aligned} \mathcal{F}_c[f(t)] &= \text{P.V.} \int_0^{\infty} \ln \left| \frac{t+a}{t-a} \right| \cos \omega t dt \\ &= \frac{2}{\omega} [\text{si}(a\omega) \cos a\omega + \text{ci}(a\omega) \sin a\omega] \end{aligned} \quad (3.51)$$

where  $\text{si}(y)$  and  $\text{ci}(y) = -\text{Ci}(y)$  are defined (3.36) and (3.39), respectively. The result is obtained through integration by parts, and manifests the shift property of the cosine transform.

### 3.2.3.3 FCT of Trigonometric Functions

$$1. f(t) = \frac{\sin at}{t} \quad a > 0.$$

$$\begin{aligned} \mathcal{F}_c[f(t)] &= \int_0^{\infty} \frac{\sin at}{t} \cos \omega t dt \\ &= \pi/2 \quad \text{if } \omega < a, \\ &= \pi/4 \quad \text{if } \omega = a, \\ &= 0 \quad \text{if } \omega > a. \end{aligned} \quad (3.52)$$

The result is obtained easily after some algebraic manipulations. It is, however, better understood as the result of the inverse Fourier transform of a sinc function, which is simply a rectangular window function, as is evident in Equation 3.52.

$$2. f(t) = e^{-\beta t} \sin at, \quad a, \text{Re}(\beta) > 0.$$

$$\begin{aligned} \mathcal{F}_c[f(t)] &= \int_0^{\infty} e^{-\beta t} \sin at \cos \omega t dt \\ &= \frac{1}{2} \left[ \frac{a + \omega}{\beta^2 + (a + \omega)^2} + \frac{a - \omega}{\beta^2 + (a - \omega)^2} \right] \end{aligned} \quad (3.53)$$

The result can be easily understood as Laplace transform of the function:

$$\frac{1}{2} [\sin(a + \omega)t + \sin(a - \omega)t].$$

$$3. f(t) = e^{-\beta t} \cos \alpha t, \quad \text{Re}(\beta) > |\text{Im}(\alpha)|.$$

$$\begin{aligned} \mathcal{F}_c[f(t)] &= \int_0^{\infty} e^{-\beta t} \cos \alpha t \cos \omega t dt \\ &= \frac{\beta}{2} \left[ \frac{1}{\beta^2 + (\alpha - \omega)^2} + \frac{1}{\beta^2 + (\alpha + \omega)^2} \right], \end{aligned} \quad (3.54)$$

which is the Laplace transform of the function  $\frac{1}{2} [\cos(\alpha + \omega)t + \cos(\alpha - \omega)t]$ .

$$4. f(t) = \frac{t \sin at}{(t^2 + \beta^2)} \quad a, \text{Re}(\beta) > 0.$$

$$\begin{aligned} \mathcal{F}_c[f(t)] &= \int_0^{\infty} \frac{t \sin at}{(t^2 + \beta^2)} \cos \omega t dt \\ &= \frac{\pi}{2} e^{-a\beta} \cosh \beta \omega \quad \text{if } \omega < a \\ &= -\frac{\pi}{2} e^{-\beta \omega} \sinh a\beta \quad \text{if } \omega > a. \end{aligned} \quad (3.55)$$

The result is obtained by contour integration, as is the next cosine transform.

$$5. f(t) = \frac{\cos at}{(t^2 + \beta^2)} \quad a, \text{Re}(\beta) > 0.$$

$$\begin{aligned} \mathcal{F}_c[f(t)] &= \int_0^{\infty} \frac{\cos at}{(t^2 + \beta^2)} \cos \omega t dt \\ &= \frac{\pi}{2\beta} e^{-a\beta} \cosh \beta \omega \quad \text{if } \omega < a, \\ &= \frac{\pi}{2\beta} e^{-\beta \omega} \cosh a\beta \quad \text{if } \omega > a. \end{aligned} \quad (3.56)$$

$$6. f(t) = e^{-\beta t^2} \cos at, \quad \text{Re}(\beta) > 0.$$

$$\begin{aligned} \mathcal{F}_c[f(t)] &= \int_0^{\infty} e^{-\beta t^2} \cos at \cos \omega t dt \\ &= \frac{1}{2} \sqrt{\frac{\pi}{\beta}} e^{-(a^2 + \omega^2)/4\beta} \cosh \frac{a\omega}{2\beta}. \end{aligned} \quad (3.57)$$

### 3.2.3.4 FCT of Orthogonal Polynomials

#### 1. Legendre polynomials:

$$f(t) = P_n(1 - 2t^2) \quad 0 < t < 1, \\ = 0 \quad t > 1,$$

where the Legendre polynomial  $P_n(x)$  is defined as

$$P_n(x) = \frac{1}{2^n n!} \frac{d^n}{dx^n} (x^2 - 1)^n, \quad \text{for } |x| < 1 \\ \text{and } n = 0, 1, 2, \dots$$

$$\mathcal{F}_c[f(t)] = \int_0^1 P_n(1 - 2t^2) \cos \omega t \, dt \\ = \frac{(-1)^n \pi}{2} J_{n+\frac{1}{2}}(\omega/2) J_{-n-\frac{1}{2}}(\omega/2), \quad (3.58)$$

where  $J_\nu(z)$  is the Bessel function of the first kind, and order  $\nu$ , defined by

$$J_\nu(z) = \sum_{m=0}^{\infty} \frac{(-1)^m (z/2)^{\nu+2m}}{\Gamma(m+1)\Gamma(\nu+m+1)}, \\ |z| < \infty, |\arg z| < \pi. \quad (3.58')$$

#### 2. Chebyshev polynomials:

$$f(t) = (a^2 - t^2)^{-1/2} T_{2n}(t/a) \quad 0 < t < a, \\ = 0, \quad t > a, \\ n = 0, 1, 2, \dots$$

where the Chebyshev polynomial is defined by,

$$T_n(x) = \cos(n \cos^{-1} x), \quad n = 0, 1, 2, \dots \\ \mathcal{F}_c[f(t)] = \int_0^a (a^2 - t^2)^{-1/2} T_{2n}(t/a) \cos \omega t \, dt \\ = (-1)^n (\pi/2) J_{2n}(a\omega), \quad (3.59)$$

where  $J_{2n}(x)$  is the Bessel function defined in Equation 3.58' with  $\nu = 2n$ .

#### 3. Laguerre polynomial:

$$f(t) = e^{-t^2/2} L_n(t^2)$$

where  $L_n(x)$  is the Laguerre polynomial defined by,

$$L_n(x) = \frac{e^x}{n!} \frac{d^n}{dx^n} (x^n e^{-x}), \quad n = 0, 1, 2, \dots \\ \mathcal{F}_c[f(t)] = \int_0^{\infty} e^{-t^2/2} L_n(t^2) \cos \omega t \, dt \\ = \sqrt{\frac{\pi}{2}} \frac{1}{n!} e^{-\omega^2/2} \{\text{He}_n(\omega)\}^2, \quad (3.60)$$

where  $\text{He}_n(x)$  is the Hermite polynomial given by,

$$\text{He}_n(x) = (-1)^n e^{x^2/2} \frac{d^n}{dx^n} (e^{-x^2/2}), \quad n = 0, 1, 2, \dots$$

#### 4. Hermite polynomials:

$$(a) f(t) = e^{-t^2/2} \text{He}_{2n}(t) \quad n = 0, 1, 2, \dots$$

$$\mathcal{F}_c[f(t)] = \int_0^{\infty} e^{-t^2/2} \text{He}_{2n}(t) \cos \omega t \, dt \\ = (-1)^n \sqrt{\frac{\pi}{2}} e^{-\omega^2/2} \omega^{2n} \quad (3.61)$$

which is obtained using the Rodriques formula for the Hermite polynomial given in (3) above.

$$(b) f(t) = e^{-t^2/2} \{\text{He}_n(t)\}^2,$$

$$\mathcal{F}_c[f(t)] = \int_0^{\infty} e^{-t^2/2} \{\text{He}_n(t)\}^2 \cos \omega t \, dt \\ = n! \sqrt{\frac{\pi}{2}} e^{-\omega^2/2} L_n(\omega^2), \quad (3.62)$$

which shows a rare symmetry with Equation 3.60.

### 3.2.3.5 FCT of Some Special Functions

#### 1. The complementary error function:

$$f(t) = t \text{Erfc}(at) \quad a > 0.$$

Here the complementary error function is defined as

$$\text{Erfc}(x) = 1 - \text{Erf}(x) = \frac{2}{\sqrt{\pi}} \int_x^{\infty} e^{-t^2} \, dt. \\ \mathcal{F}_c[f(t)] = \int_0^{\infty} t \text{Erfc}(at) \cos \omega t \, dt \\ = \left[ \frac{1}{2a^2} + \frac{1}{\omega^2} \right] e^{-\omega^2/4a^2} - \frac{1}{\omega^2}. \quad (3.63)$$

#### 2. The sine integral function:

$$f(t) = \text{si}(at) \quad a > 0,$$

where  $\text{si}(x)$  is defined in Equation 3.39.

$$\mathcal{F}_c[f(t)] = \int_0^{\infty} \text{si}(at) \cos \omega t \, dt \\ = -(1/2\omega) \ln \left| \frac{\omega + a}{\omega - a} \right|, \quad \omega \neq a. \quad (3.64)$$

Note certain amount of symmetry with Equation 3.51.

3. The cosine integral function:

$$f(t) = \text{Ci}(at) = -\text{ci}(at) \quad a > 0,$$

where  $\text{ci}(x)$  is defined in Equation 3.36.

$$\begin{aligned} \mathcal{F}_c[f(t)] &= \int_0^{\infty} \text{Ci}(at) \cos \omega t \, dt \\ &= 0 \quad \text{for } 0 < \omega < a, \\ &= -\pi/2\omega \quad \text{for } \omega > a. \end{aligned} \quad (3.65)$$

4. The exponential integral function:

$$f(t) = \text{Ei}(-at) \quad a > 0,$$

where  $\text{Ei}(-x)$  is defined by

$$\begin{aligned} \text{Ei}(-x) &= -\int_x^{\infty} e^{-t}/t \, dt, \quad |\arg(x)| < \pi. \\ \mathcal{F}_c[f(t)] &= \int_0^{\infty} \text{Ei}(-at) \cos \omega t \, dt \\ &= -\frac{1}{\omega} \tan^{-1}(\omega/a). \end{aligned} \quad (3.66)$$

5. Bessel functions: We list only a few here since a more comprehensive table is available in Chapter 9:

(a)  $f(t) = J_0(at) \quad a > 0$ ,  
where  $J_n(x)$  is the Bessel function of the first kind defined in Equation 3.58'.

$$\begin{aligned} \mathcal{F}_c[f(t)] &= \int_0^{\infty} J_0(at) \cos \omega t \, dt \\ &= (a^2 - \omega^2)^{-1/2} \quad \text{for } 0 < \omega < a, \\ &= \infty, \quad \text{for } \omega = a, \\ &= 0, \quad \text{for } \omega > a. \end{aligned} \quad (3.67)$$

(b)  $f(t) = J_{2n}(at) \quad a > 0$ .

$$\begin{aligned} \mathcal{F}_c[f(t)] &= \int_0^{\infty} J_{2n}(at) \cos \omega t \, dt \\ &= (-1)^n (a^2 - \omega^2)^{-1/2} T_{2n}(\omega/a) \\ &\quad \text{for } 0 < \omega < a, \\ &= \infty, \quad \text{for } \omega = a, \\ &= 0, \quad \text{for } \omega > a. \end{aligned} \quad (3.68)$$

Here,  $T_{2n}(x)$  is the Chebyshev polynomial defined in Equation 3.59. Note the symmetry between this and Equation 3.29.

(c)  $f(t) = t^{-n} J_n(at) \quad a > 0, \quad \text{and } n = 1, 2, \dots$

$$\begin{aligned} \mathcal{F}_c[f(t)] &= \int_0^{\infty} t^{-n} J_n(at) \cos \omega t \, dt \\ &= \frac{\sqrt{\pi}}{\Gamma(n+1/2)} (2a)^{-n} (a^2 - \omega^2)^{n-1/2}, \\ &\quad 0 < \omega < a, \\ &= 0, \quad \omega > a. \end{aligned} \quad (3.69)$$

Here,  $\Gamma(x)$  is the gamma function defined by

$$\Gamma(x) = \int_0^{\infty} e^{-t} t^{x-1} \, dt. \quad (3.69')$$

(d)  $f(t) = Y_0(at) \quad a > 0$ ,  
where  $Y_\nu(x)$  is the Bessel function of the second kind defined by

$$Y_\nu(x) = \text{cosec}(\nu\pi)[J_\nu(x) \cos(\nu\pi) - J_{-\nu}(x)] \quad (3.70)$$

$$\begin{aligned} \mathcal{F}_c[f(t)] &= \int_0^{\infty} Y_0(at) \cos \omega t \, dt \\ &= 0, \quad \text{for } 0 < \omega < a, \\ &= -(\omega^2 - a^2)^{-1/2} \quad \text{for } \omega > a. \end{aligned} \quad (3.70')$$

(e)  $f(t) = t^\nu Y_\nu(at) \quad |\text{Re}(\nu)| < 1/2, a > 0$ ,

$$\begin{aligned} \mathcal{F}_c[f(t)] &= \int_0^{\infty} t^\nu Y_\nu(at) \cos \omega t \, dt \\ &= -\sqrt{\pi} (2a)^\nu [\Gamma(1/2 - \nu)]^{-1} \\ &\quad (\omega^2 - a^2)^{-\nu-1/2}, \quad \omega > a, \\ &= 0, \quad \text{for } 0 < \omega < a. \end{aligned} \quad (3.71)$$

### 3.2.4 Examples on the Use of Some Operational Rules of FCT

In this section, some simple examples on the use of operational rules of the FCT are presented. The examples are based on very simple functions and are intended to illustrate the procedure and the features in the FCT operational rules that have been discussed in Section 3.2.2.

#### 3.2.4.1 Differentiation-in- $t$

Let  $f(t)$  be defined as  $f(t) = e^{-\alpha t}$ , where  $\text{Re}(\alpha) > 0$ . Then according to Equation 3.44, its FCT is given by

$$F_c(\omega) = \frac{\alpha}{\alpha^2 + \omega^2}.$$

To obtain the FCT for  $f''(t)$ , we have, according to the differentiation-in- $t$  property, Equation 3.9

$$\begin{aligned}\mathcal{F}_c[f''(t)] &= -\omega^2 F_c(\omega) - f'(0) = -\omega^2 \frac{\alpha}{\alpha^2 + \omega^2} + \alpha \\ &= \frac{\alpha^3}{\alpha^2 + \omega^2}\end{aligned}\quad (3.72)$$

This result is verified by noting that  $f''(t) = \alpha^2 e^{-\alpha t}$ , and that its FCT is given directly also by Equation 3.72.

### 3.2.4.2 Differentiation-in- $t$ of Functions with Jump Discontinuities

Consider the function  $f(t) = tU(1-t)$ , which is sometimes called a ramp function. It has a jump discontinuity of  $d = -1$  at  $t = 1$ . Its derivative is given by  $f'(t) = U(1-t)$ , which also has a jump discontinuity at  $t = 1$ . Using the definition for FCT, we obtain

$$\mathcal{F}_c[f'(t)] = \mathcal{F}_c[U(1-t)] = \frac{\sin \omega}{\omega}. \quad (3.73)$$

The FCT rule of differentiation with jump discontinuity (3.14) can also be applied to get

$$\begin{aligned}\mathcal{F}_c[f'(t)] &= \omega F_s(\omega) - f(0) - d \cos(\omega t_0) \\ &= \omega \left[ -\frac{\cos \omega}{\omega} + \frac{\sin \omega}{\omega^2} \right] - (-1) \cos \omega, \\ &\quad (\text{because } d = -1, \text{ and } f(0) = 0.) \\ &= \frac{\sin \omega}{\omega}, \quad \text{as in Equation 3.73.}\end{aligned}$$

### 3.2.4.3 Shift-in- $t$ , Shift-in- $\omega$ , and the Kernel Product Property

Let  $f(t) = e^{-\alpha t}$ , where  $\text{Re}(\alpha) > 0$ . The FCT of a positive shift in the  $t$ -domain is easy to obtain,

$$\mathcal{F}_c[f(t+a)] = e^{-\alpha a} \frac{\alpha}{\alpha^2 + \omega^2} \quad a > 0. \quad (3.74)$$

To obtain the FCT of the function  $f(|t-a|)$ , one can apply the kernel product property in Equation 3.18 to get

$$\mathcal{F}_c[f(|t-a|)] = 2F_c(\omega) \cos a\omega - \mathcal{F}_c[f(t+a)].$$

Therefore,

$$\begin{aligned}\mathcal{F}_c[e^{-\alpha|t-a|}] &= 2 \frac{\alpha}{\alpha^2 + \omega^2} \cos a\omega - e^{-\alpha a} \frac{\alpha}{\alpha^2 + \omega^2} \\ &= \frac{\alpha}{\alpha^2 + \omega^2} [2 \cos a\omega - e^{-\alpha a}]\end{aligned}\quad (3.75)$$

which is much easier than direct evaluation.

Equation 3.21 typifies the shift-in- $\omega$  property and, when it is applied to the same function  $f(t)$  above, we obtain,

$$\mathcal{F}_c(e^{-\alpha t} \cos \beta t) = \frac{1}{2} \left[ \frac{\alpha}{\alpha^2 + (\omega + \beta)^2} + \frac{\alpha}{\alpha^2 + (\omega - \beta)^2} \right] \quad (3.76)$$

### 3.2.4.4 Differentiation-in- $\omega$ Property

This property, Equation 3.23, can often be used to generate FCTs for functions that are not listed in the tables. As an example, consider again the function  $f(t) = e^{-\alpha t}$ , where  $\text{Re}(\alpha) > 0$ . To obtain the FCT for the function  $g(t) = t^2 e^{-\alpha t}$ , we can use Equation 3.23 on  $F_c(\omega)$  for  $f(t) = e^{-\alpha t}$ . Thus,

$$F_c''(\omega) = -2\alpha \frac{\alpha^2 - 3\omega^2}{(\alpha^2 + \omega^2)^3}, \quad \text{because } \mathcal{F}_c[e^{-\alpha t}] = \frac{\alpha}{\alpha^2 + \omega^2},$$

and

$$\mathcal{F}_c[t^2 e^{-\alpha t}] = 2\alpha \frac{\alpha^2 - 3\omega^2}{(\alpha^2 + \omega^2)^3} \quad \text{using Equation 3.23 with } n = 1.$$

### 3.2.4.5 The Convolution Property

The convolution property for FCT is closely related to its kernel product property as illustrated by the following example.

Let  $f(t) = e^{-\alpha t}$ ,  $\text{Re}(\alpha) > 0$ , and  $g(t) = U(t) - U(t-a)$ ,  $a > 0$ . The FCTs of these functions are given respectively by,

$$F_c(\omega) = \frac{\alpha}{\alpha^2 + \omega^2}, \quad \text{and} \quad G_c(\omega) = \frac{\sin a\omega}{\omega}.$$

Thus,  $2F_c(\omega)G_c(\omega) = 2 \left[ \frac{\alpha}{\alpha^2 + \omega^2} \right] \left[ \frac{\sin a\omega}{\omega} \right]$ . According to the convolution property 3.20, this is the FCT of the convolution defined as

$$\int_0^{\infty} [U(\tau) - U(\tau-a)] [e^{-\alpha(t+\tau)} + e^{-\alpha|t-\tau|}] d\tau. \quad (3.77)$$

Applying the operator  $\mathcal{F}_c$  to Equation 3.77 and integrating over  $t$  first, the kernel product property in the shift-in- $t$  operation in Equation 3.18 can be invoked to give,

$$\begin{aligned}\mathcal{F}_c \left\{ \int_0^{\infty} [U(\tau) - U(\tau-a)] [e^{-\alpha(t+\tau)} + e^{-\alpha|t-\tau|}] d\tau \right\} \\ = 2 \int_0^{\infty} [U(\tau) - U(\tau-a)] \frac{\alpha}{\alpha^2 + \omega^2} \cos \omega\tau d\tau \\ = 2 \left[ \frac{\alpha}{\alpha^2 + \omega^2} \right] \left[ \frac{\sin a\omega}{\omega} \right],\end{aligned}$$

as required.

### 3.3 The Fourier Sine Transform (FST)

#### 3.3.1 Definitions and Relations to the Exponential Fourier Transforms

Similar to the FCT, the FST of a function  $f(t)$ , which is piecewise continuous and absolutely integrable over  $[0, \infty)$ , is defined by application of the operator  $\mathcal{F}_s$  as

$$F_s(\omega) = \mathcal{F}_s[f(t)] = \int_0^{\infty} f(t) \sin \omega t \, dt, \quad \omega > 0. \quad (3.78)$$

The inverse operator  $\mathcal{F}_s^{-1}$  is similarly defined

$$f(t) = \mathcal{F}_s^{-1}[F_s(\omega)] = \frac{2}{\pi} \int_0^{\infty} F_s(\omega) \sin \omega t \, d\omega, \quad t \geq 0, \quad (3.79)$$

subject to the existence of the integral. Functions  $f(t)$  and  $F_s(\omega)$  defined by Equations 3.79 and 3.78, respectively, are said to form a FST pair. It is noted in Equations 3.3 and 3.79 for the inverse FCT and inverse FST that both transform operators have symmetric kernels and that they are involutory or unitary up to a factor of  $\sqrt{(2/\pi)}$ .

FSTs are also very closely related to the exponential Fourier transform defined in Equation 3.6. Using the property that

$$\sin \omega t = \text{Im}[e^{j\omega t}] = \frac{1}{2j} [e^{j\omega t} - e^{-j\omega t}], \quad (3.80)$$

one can consider the odd extension of the function  $f(t)$  defined over  $[0, \infty)$  as

$$\begin{aligned} f_o(t) &= f(t) & t \geq 0, \\ &= -f(-t) & t < 0. \end{aligned}$$

Then the Fourier transform of  $f_o(t)$  is

$$\begin{aligned} \mathcal{F}[f_o(t)] &= \int_{-\infty}^{\infty} f_o(t) e^{-j\omega t} \, dt = - \int_0^{\infty} f(t) e^{j\omega t} \, dt + \int_0^{\infty} f(t) e^{-j\omega t} \, dt \\ &= -2j \int_0^{\infty} f(t) \sin \omega t \, dt = -2j \mathcal{F}_s[f(t)], \end{aligned}$$

and therefore,

$$\mathcal{F}_s[f(t)] = -\frac{1}{2j} \mathcal{F}[f_o(t)]. \quad (3.81)$$

Equation 3.81 provides the relation between the FST and the exponential Fourier transform. As in the case for cosine transforms, many properties of the sine transform can be related to those for the Fourier transform through this equation. We shall present some properties and operational rules for FST in the next section.

#### 3.3.2 Basic Properties and Operational Rules

1. *Inverse transformation:* The inverse transformation is exactly the same as the forward transformation except for the normalization constant. Combining the forward and inverse transformations leads to the Fourier sine integral formula, which states that,

$$\begin{aligned} f(t) &= \frac{2}{\pi} \int_0^{\infty} F_s(\omega) \sin \omega t \, d\omega \\ &= \frac{2}{\pi} \int_0^{\infty} \left[ \int_0^{\infty} f(\tau) \sin \omega \tau \, d\tau \right] \sin \omega t \, d\omega. \end{aligned} \quad (3.82)$$

The sufficient conditions for the inversion formula 3.79 are the same as for the cosine transform. Where  $f(t)$  has a jump discontinuity at  $t = t_0$ , Equation 3.82 converges to the mean of  $f(t_0 + 0)$  and  $f(t_0 - 0)$ .

2. *Transforms of derivatives:* Derivatives transform in a fashion similar to FCT, even orders involving sine transforms only and odd orders involving cosine transforms only. Thus, for example,

$$\mathcal{F}_s[f''(t)] = -\omega^2 F_s(\omega) + \omega f(0) \quad (3.83)$$

and

$$\mathcal{F}_s[f'(t)] = -\omega F_c(\omega), \quad (3.84)$$

where  $f(t)$  is assumed continuous to the first order.

For the fourth-order derivative, we apply Equation 3.83 twice to obtain,

$$\mathcal{F}_s[f^{(iv)}(t)] = \omega^4 F_s(\omega) - \omega^3 f(0) + \omega f''(0), \quad (3.85)$$

if  $f(t)$  is continuous at least to order three. When the function  $f(t)$  and its derivatives have jump discontinuities at  $t = t_0$ , Equation 3.85 is modified to become,

$$\begin{aligned} \mathcal{F}_s[f^{(iv)}(t)] &= \omega^4 F_s(\omega) + \omega^3 f(0) + \omega f''(0) - \omega^3 d \cos \omega t_0 \\ &\quad + \omega^2 d' \sin \omega t_0 + \omega d'' \cos \omega t_0 - d''' \sin \omega t_0 \end{aligned} \quad (3.86)$$

where the jump discontinuities  $d$ ,  $d'$ , and  $d'''$  are as defined in Equation 3.13. Similarly, for odd-order derivatives, when the function  $f(t)$  has jump discontinuities, the operational rule must be modified.

For example, Equation 3.84 will become

$$\mathcal{F}_s[f'(t)] = -\omega F_c(\omega) + d \sin \omega t_0. \quad (3.84')$$

Generalization to other orders and to more than one location for the jump discontinuities is straightforward.



3. *Scaling*: Scaling in the  $t$ -domain for the FST has exactly the same effect as in the case of FCT, giving,

$$\mathcal{F}_s[f(at)] = \frac{1}{a} F_s(\omega/a) \quad a > 0. \quad (3.87)$$

4. *Shifting*:

- (a) Shift in the  $t$ -domain:

As in the case of the FCT, we first define the even and odd extensions of the function  $f(t)$  as,

$$f_e(t) = f(|t|), \quad \text{and} \quad f_o(t) = \frac{t}{|t|} f(|t|). \quad (3.88)$$

Then it can be shown that:

$$\mathcal{F}_s[f_o(t+a) + f_o(t-a)] = 2F_s(\omega) \cos a\omega \quad (3.89)$$

and

$$\mathcal{F}_c[f_o(t+a) + f_o(t-a)] = 2F_s(\omega) \sin a\omega; \quad a > 0. \quad (3.90)$$

These, together with Equations 3.18 and 3.19, form a complete set of kernel-product relations for the cosine and the sine transforms.

- (b) Shift in the  $\omega$ -domain:

For a positive  $\beta$  shift in the  $\omega$ -domain, it is easily shown that

$$\mathcal{F}_s[\omega + \beta] = F_s[f(t) \cos \beta t] + F_c[f(t) \sin \beta t] \quad (3.91)$$

and combining with the result for a negative shift, we get

$$\mathcal{F}_s[f(t) \cos \beta t] = (1/2)[F_s(\omega + \beta) + F_s(\omega - \beta)]. \quad (3.92)$$

More generally, for  $a, \beta > 0$ , we have,

$$\begin{aligned} & \mathcal{F}_s[f(at) \cos \beta t] \\ &= (1/2a) \left[ F_s\left(\frac{\omega + \beta}{a}\right) + F_s\left(\frac{\omega - \beta}{a}\right) \right]. \end{aligned} \quad (3.93)$$

Similarly, we can easily show that

$$\begin{aligned} & \mathcal{F}_s[f(at) \sin \beta t] \\ &= -(1/2a) \left[ F_c\left(\frac{\omega + \beta}{a}\right) - F_c\left(\frac{\omega - \beta}{a}\right) \right]. \end{aligned} \quad (3.94)$$

The shift-in- $\omega$  properties are useful in deriving some FCTs and FSTs. As well, because the quantities being transformed are modulated sinusoids, these are useful in applications to communication problems.

5. *Differentiation in the  $\omega$ -domain*: The sine transform behaves in a fashion similar to the cosine transform when it comes to differentiation in the  $\omega$ -domain. Even-order

derivatives involve only sine transforms and odd-order derivatives involve only cosine transforms. Thus,

$$F_s^{(2n)}(\omega) = \mathcal{F}_s[(-1)^n t^{2n} f(t)],$$

and

$$F_s^{(2n+1)}(\omega) = \mathcal{F}_c[(-1)^n t^{2n+1} f(t)]. \quad (3.95)$$

It is again assumed that the integrals in Equation 3.95 exist.

6. *Asymptotic behavior*: The Reimann–Lebesgue theorem guarantees that any FST converges to zero as  $\omega$  tends to infinity, that is,

$$\lim_{\omega \rightarrow \infty} F_s(\omega) = 0. \quad (3.96)$$

7. *Integration*:

- (a) Integration in the  $t$ -domain. In analogy to Equation 3.26, we have

$$\mathcal{F}_s \left[ \int_0^t f(\tau) d\tau \right] = (1/\omega) F_c(\omega) \quad (3.97)$$

provided  $f(t)$  is piecewise smooth and absolutely integrable over  $[0, \infty)$ .

- (b) Integration in the  $\omega$ -domain. As in the FCT, integration in the  $\omega$ -domain results in division by  $t$  in the  $t$ -domain, giving,

$$\mathcal{F}_c^{-1} \left[ \int_{\omega}^{\infty} F_s(\beta) d\beta \right] = (1/t) f(t) \quad (3.98)$$

in parallel with Equation 3.27.

8. *The convolution property*: If functions  $f(t)$  and  $g(t)$  are piecewise continuous and absolutely integrable over  $[0, \infty)$ , a convolution property involving  $F_s(\omega)$  and  $G_c(\omega)$  is

$$2F_s(\omega)G_c(\omega) = \mathcal{F}_s \left\{ \int_0^{\infty} f(\tau)[g(|t-\tau|) - g(t+\tau)] d\tau \right\}. \quad (3.99)$$

Equivalently,

$$2F_s(\omega)G_c(\omega) = \mathcal{F}_s \left\{ \int_0^{\infty} g(\tau)[f(t+\tau) + f_o(t-\tau)] d\tau \right\} \quad (3.100)$$

where  $f_o(x)$  is the odd extension of the function  $f(x)$  defined as in Equation 3.88.

One can establish a convolution theorem involving only sine transforms. This is obtained by imposing an additional condition on one of the functions, say,  $g(t)$ . We define the function  $h(t)$  by,

$$h(t) = \int_t^{\infty} g(\tau) d\tau. \quad (3.101)$$

The  $g(t)$  must satisfy the condition that its integral  $h(t)$  is absolutely integrable over  $[0, \infty)$ , so that the FCT of  $h(t)$  exists. We note from Equation 3.26 that

$$H_c(\omega) = (1/\omega)G_s(\omega) \quad (3.102)$$

Applying Equation 3.99 to  $f(t)$  and  $h(t)$  yields immediately,

$$(2/\omega)F_s(\omega)G_s(\omega) = \mathcal{F}_s \left[ \int_0^{\infty} f(\tau) \int_{|t-\tau|}^{t+\tau} g(\eta) d\eta d\tau \right] \quad (3.103)$$

noting that  $g(t) = -h'(t)$ .

Because the FSTs have properties and operation rules very similar to those for the FCTs, we refer the reader to Section 3.2.4 for simple examples on the use of these rules for FCTs.

### 3.3.3 Selected Fourier Sine Transforms

In this section, selected FSTs are presented. These mostly correspond to those selected for the FCTs. It should be noted that because the sine and cosine transforms kernels are related through differentiation, many of the FSTs can be derived without direct computation by using differentiation properties listed in Sections 3.2.2 and 3.3.2. As before, we present first the FST of algebraic functions.

#### 3.3.3.1 FST of Algebraic Functions

##### 1. The unit rectangular function:

$$f(t) = U(t) - U(t - a),$$

where  $U(t)$  is the Heaviside unit step function.

$$\mathcal{F}_s[f(t)] = \int_0^a \sin \omega t dt = (1 - \cos \omega a)/\omega. \quad (3.104)$$

##### 2. The unit height tent function:

$$\begin{aligned} f(t) &= t/a, & 0 < t < a, \\ &= (2a - t)/a & a < t < 2a, \\ &= 0 & \text{otherwise.} \end{aligned}$$

$$\begin{aligned} \mathcal{F}_s[f(t)] &= \int_0^a (t/a) \sin \omega t + \int_a^{2a} [(2a - t)/a] \sin \omega t dt \\ &= \frac{1}{a\omega^2} [2 \sin a\omega - \sin 2a\omega]. \end{aligned} \quad (3.105)$$

##### 3. Delayed inverse:

$$f(t) = (1/t)U(t - a).$$

$$\begin{aligned} \mathcal{F}_s[f(t)] &= \int_a^{\infty} (1/t) \sin \omega t dt = \int_{a\omega}^{\infty} (1/\tau) \sin \tau d\tau \\ &= -\text{si}(a\omega) \end{aligned} \quad (3.106)$$

where  $\text{si}(x)$  is the sine integral function defined in Equation 3.39.

##### 4. The inverse square root:

$$f(t) = 1/\sqrt{t}.$$

$$\mathcal{F}_s[f(t)] = \int_0^{\infty} \frac{1}{\sqrt{t}} \sin \omega t dt = \sqrt{\frac{\pi}{2\omega}}. \quad (3.107)$$

##### 5. The inverse linear function:

$$f(t) = (\alpha + t)^{-1}, \quad |\arg \alpha| < \pi.$$

$$\begin{aligned} \mathcal{F}_s[f(t)] &= \int_0^{\infty} \frac{1}{\alpha + t} \sin \omega t dt \\ &= \sin \omega \alpha \text{Ci}(\omega \alpha) - \cos \omega \alpha \text{si}(\omega \alpha). \end{aligned} \quad (3.108)$$

Here  $\text{Ci}(x)$  is the cosine integral function defined in Equation 3.36.

##### 6. Inverse quadratic functions:

$$(a) f(t) = (t^2 + a^2)^{-1} \quad a > 0.$$

$$\begin{aligned} \mathcal{F}_s[f(t)] &= \int_0^{\infty} \frac{1}{a^2 + t^2} \sin \omega t dt \\ &= (1/2a)[e^{-a\omega} \overline{\text{Ei}}(a\omega) - e^{a\omega} \text{Ei}(-a\omega)] \end{aligned} \quad (3.109)$$

where  $\text{Ei}(x)$  and  $\overline{\text{Ei}}(x)$  are the exponential integral functions defined in Equation 3.50.

Here, we note that Equation 3.109 is related to the FCT of the function,

$$f(t) = -t(t^2 + a^2)^{-1}$$

by considering the derivative of Equation 3.109 with respect to  $\omega$ . Thus,

$$\mathcal{F}_c[-t(t^2 + a^2)^{-1}] = (1/2)[e^{-a\omega} \overline{\text{Ei}}(a\omega) + e^{a\omega} \text{Ei}(-a\omega)] \quad (3.110)$$

$$(b) f(t) = (a^2 - t^2)^{-1} \quad a > 0.$$

$$\begin{aligned} \mathcal{F}_s[f(t)] &= \text{P.V.} \int_0^{\infty} \frac{1}{a^2 - t^2} \sin \omega t dt \\ &= [\sin a\omega \text{Ci}(a\omega) - \cos a\omega \text{Si}(a\omega)]/a, \end{aligned} \quad (3.111)$$

where  $\text{Ci}(x)$  and  $\text{Si}(x)$  are the cosine and sine integral functions defined in Equations 3.36 and 3.39 and "P.V." denotes the principal value of the integral. Again, we

note that Equation 3.111 is related to the FCT of the function,

$$f(t) = -t(a^2 - t^2)^{-1}.$$

Thus,

$$\mathcal{F}_c[-t(a^2 - t^2)^{-1}] = \cos a\omega \operatorname{Ci}(a\omega) + \sin a\omega \operatorname{Si}(a\omega). \quad (3.112)$$

$$(c) f(t) = \frac{\beta}{\beta^2 + (a-t)^2} - \frac{\beta}{\beta^2 + (a+t)^2} \quad \operatorname{Re}(\beta) > 0.$$

$$\begin{aligned} \mathcal{F}_s[f(t)] &= \int_0^\infty \left[ \frac{\beta}{\beta^2 + (a-t)^2} - \frac{\beta}{\beta^2 + (a+t)^2} \right] \sin \omega t \, dt \\ &= \pi \sin a\omega e^{-\beta\omega}. \end{aligned} \quad (3.113)$$

$$(d) f(t) = \frac{a+t}{\beta^2 + (a+t)^2} - \frac{a-t}{\beta^2 + (a-t)^2} \quad \operatorname{Re}(\beta) > 0$$

$$\begin{aligned} \mathcal{F}_s[f(t)] &= \int_0^\infty \left[ \frac{a+t}{\beta^2 + (a+t)^2} - \frac{a-t}{\beta^2 + (a-t)^2} \right] \sin \omega t \, dt \\ &= \pi \sin a\omega e^{-\beta\omega}. \end{aligned} \quad (3.114)$$

We note here the symmetry among the transforms in Equations 3.113 and 3.114, and those in Equations 3.43 and 3.42.

### 3.3.3.2 FST of Exponential and Logarithmic Functions

$$1. f(t) = e^{-\alpha t} \quad \operatorname{Re}(\alpha) > 0.$$

$$\mathcal{F}_s[f(t)] = \int_0^\infty e^{-\alpha t} \sin \omega t \, dt = \frac{\omega}{\alpha^2 + \omega^2} \quad (3.115)$$

which is also seen to be the Laplace transform of  $\sin \omega t$ .

$$2. f(t) = \frac{e^{-\beta t} - e^{-\alpha t}}{t^2} \quad \operatorname{Re}(\beta), \operatorname{Re}(\alpha) > 0.$$

$$\begin{aligned} \mathcal{F}_s[f(t)] &= \int_0^\infty \frac{e^{-\beta t} - e^{-\alpha t}}{t^2} \sin \omega t \, dt \\ &= \frac{\omega}{2} \ln \left( \frac{\alpha^2 + \omega^2}{\beta^2 + \omega^2} \right) + \alpha \tan^{-1} \left( \frac{\omega}{\alpha} \right) - \beta \tan^{-1} \left( \frac{\omega}{\beta} \right). \end{aligned} \quad (3.116)$$

Equation 3.116 is seen to be related to the result (3.45) through the differentiation-in- $\omega$  property of the sine transform as defined in Equation 3.95.

$$3. f(t) = te^{-\alpha t^2} \quad |\arg(\alpha)| < \pi/2.$$

$$\begin{aligned} \mathcal{F}_s[f(t)] &= \int_0^\infty te^{-\alpha t^2} \sin \omega t \, dt \\ &= \frac{1}{4} \sqrt{\frac{\pi}{\alpha^3}} \omega e^{-\omega^2/4\alpha}, \end{aligned} \quad (3.117)$$

which can also be related to the cosine transform in Equation 3.46 using again the differentiation-in- $\omega$  property 3.95 of the sine transform.

$$4. f(t) = \ln t[1 - U(t-1)]$$

$$\begin{aligned} \mathcal{F}_s[f(t)] &= \int_0^\infty \ln t[1 - U(t-1)] \sin \omega t \, dt \\ &= -\frac{1}{\omega} [C + \ln \omega - \operatorname{Ci}(\omega)], \end{aligned} \quad (3.118)$$

which is obtained easily through integration in parts. Here  $C = 0.5772156649\dots$  is the Euler constant and  $\operatorname{Ci}(x)$  is the cosine integral function.

$$5. f(t) = \frac{t \ln bt}{(t^2 + a^2)} \quad a, b > 0.$$

$$\begin{aligned} \mathcal{F}_s[f(t)] &= \int_0^\infty \frac{t \ln bt}{(t^2 + a^2)} \sin \omega t \, dt \\ &= \frac{\pi}{4} [2e^{-a\omega} \ln ab - e^{a\omega} \operatorname{Ei}(-a\omega) - e^{-a\omega} \overline{\operatorname{Ei}}(a\omega)] \end{aligned} \quad (3.119)$$

Note that Equation 3.119 is related to Equation 3.49 through the differentiation-in- $\omega$  property of the FCT as defined in Equation 3.24.

$$6. f(t) = \ln \left| \frac{t+a}{t-a} \right| \quad a > 0,$$

$$\begin{aligned} \mathcal{F}_s[f(t)] &= \int_0^\infty \ln \left| \frac{t+a}{t-a} \right| \sin \omega t \, dt \\ &= \frac{\pi}{\omega} \sin a\omega. \end{aligned} \quad (3.120)$$

The result is obtained using integration by parts and the shift-in- $t$  properties 3.88 through 3.90 of the sine transform.

### 3.3.3.3 FST of Trigonometric Functions

$$1. f(t) = \frac{\sin at}{t} \quad a > 0,$$

$$\begin{aligned} \mathcal{F}_s[f(t)] &= \int_0^\infty \frac{\sin at}{t} \sin \omega t \, dt \\ &= (1/2) \ln \left| \frac{\omega + a}{\omega - a} \right|. \end{aligned} \quad (3.121)$$

This result is immediately understood when compared to Equation 3.120, taking into account the normalization used in Equations 3.78 and 3.79 for the definition of the FST.

$$2. f(t) = \frac{e^{-\beta t}}{t} \sin \alpha t \quad \text{Re}(\beta) > |\text{Im}(\alpha)|$$

$$\begin{aligned} \mathcal{F}_s[f(t)] &= \int_0^{\infty} \frac{e^{-\beta t}}{t} \sin \alpha t \sin \omega t dt \\ &= (1/4) \ln \left( \frac{\beta^2 + (\omega + \alpha)^2}{\beta^2 + (\omega - \alpha)^2} \right). \end{aligned} \quad (3.122)$$

This result follows easily from the integration-in- $\omega$  property 3.27 as applied to the cosine transform in Equation 3.53.

$$3. f(t) = e^{-\beta t} \cos \alpha t \quad \text{Re}(\beta) > |\text{Im}(\alpha)|$$

$$\begin{aligned} \mathcal{F}_s[f(t)] &= \int_0^{\infty} e^{-\beta t} \cos \alpha t \sin \omega t dt \\ &= (1/2) \left[ \frac{\omega - \alpha}{\beta^2 + (\omega - \alpha)^2} + \frac{\omega + \alpha}{\beta^2 + (\omega + \alpha)^2} \right], \end{aligned} \quad (3.123)$$

which is also recognized as the Laplace transform of the function  $\cos \alpha t \sin \omega t$ .

$$4. f(t) = \frac{t \cos at}{(t^2 + \beta^2)} \quad a, \text{Re}(\beta) > 0,$$

$$\begin{aligned} \mathcal{F}_s[f(t)] &= \int_0^{\infty} \frac{t \cos at}{(t^2 + \beta^2)} \sin \omega t dt \\ &= -\frac{\pi}{2} e^{-a\beta} \sinh \beta \omega \quad \omega < a, \\ &= \frac{\pi}{2} e^{-\beta\omega} \cosh a\beta \quad \omega > a. \end{aligned} \quad (3.124)$$

Note the symmetry of Equation 3.124 with Equation 3.55.

$$5. f(t) = \frac{\sin at}{(t^2 + \beta^2)} \quad a, \text{Re}(\beta) > 0,$$

$$\begin{aligned} \mathcal{F}_s[f(t)] &= \int_0^{\infty} \frac{\sin at}{(t^2 + \beta^2)} \sin \omega t dt \\ &= \frac{\pi}{2\beta} e^{-a\beta} \sinh \beta \omega \quad \omega < a. \\ &= \frac{\pi}{2\beta} e^{-\beta\omega} \sinh a\beta \quad \omega > a. \end{aligned} \quad (3.125)$$

The symmetry of Equation 3.125 with Equation 3.56 is apparent.

$$6. f(t) = e^{-\beta t^2} \sin at \quad \text{Re}(\beta) > 0.$$

$$\begin{aligned} \mathcal{F}_s[f(t)] &= \int_0^{\infty} e^{-\beta t^2} \sin at \sin \omega t dt \\ &= \frac{1}{2} \sqrt{\frac{\pi}{\beta}} e^{-(\omega^2 + a^2)/4\beta} \sinh \frac{a\omega}{2\beta} \end{aligned} \quad (3.126)$$

similar to Equation 3.57 for the cosine transform.

### 3.3.3.4 FST of Orthogonal Polynomials

1. *Legendre polynomial* (defined in Equation 3.58):

$$f(t) = P_n(1 - 2t^2)[1 - U(t - 1)] \quad n = 0, 1, 2, \dots$$

$$\begin{aligned} \mathcal{F}_s[f(t)] &= \int_0^1 P_n(1 - 2t^2) \sin \omega t dt \\ &= \frac{\pi}{2} \left[ J_{n+1/2} \left( \frac{\omega}{2} \right) \right]^2 \end{aligned} \quad (3.127)$$

where  $J_n(x)$  is the Bessel function of the first kind defined in Equation 3.58'.

2. *Chebyshev polynomial* (defined in Equation 3.59):

$$\begin{aligned} f(t) &= (a^2 - t^2)^{-1/2} T_{2n+1}(t/a)[1 - U(t - a)], \\ n &= 0, 1, 2, \dots \end{aligned}$$

$$\begin{aligned} \mathcal{F}_s[f(t)] &= \int_0^a (a^2 - t^2)^{-1/2} T_{2n+1}(t/a) \sin \omega t dt \\ &= (-1)^n \frac{\pi}{2} J_{2n+1}(a\omega). \end{aligned} \quad (3.128)$$

3. *Laguerre polynomials*.

$$f(t) = t^{2m} e^{-t^2/2} L_n^{2m+1}(t^2), \quad m, n = 0, 1, 2, \dots$$

$$\begin{aligned} \mathcal{F}_s[f(t)] &= \int_0^{\infty} t^{2m} e^{-t^2/2} L_n^{2m+1}(t^2) \sin \omega t dt \\ &= \sqrt{\frac{\pi}{2}} (n!)^{-1} (-1)^m e^{-\omega^2/2} \text{He}_n(\omega) \text{He}_{n+2m+1}(\omega) \end{aligned} \quad (3.129)$$

where  $L_n^a(x) = \frac{e^x x^{-a}}{n!} \frac{d^n}{dx^n} (e^{-x} x^{n+a})$ , is a Laguerre polynomial  $L_n^0(x) = L_n(x)$  as defined in Equation 3.60. Here,  $\text{He}_n(x)$  is the Hermite polynomial defined in Equation 3.61.

4. *Hermite polynomials* (defined in Equation 3.62):

$$\begin{aligned} f(t) &= e^{-t^2/2} \text{He}_{2n+1}(\sqrt{2}t) \\ \mathcal{F}_s[f(t)] &= \int_0^{\infty} e^{-t^2/2} \text{He}_{2n+1}(\sqrt{2}t) \sin \omega t dt \\ &= (-1)^n \sqrt{\frac{\pi}{2}} e^{-\omega^2/2} \text{He}_{2n+1}(\sqrt{2}\omega). \end{aligned} \quad (3.130)$$

### 3.3.3.5 FST of Some Special Functions

1. *The complementary error function* (defined in Equation 3.63):

$$f(t) = \text{Erfc}(at) \quad a > 0,$$

$$\begin{aligned}\mathcal{F}_s[f(t)] &= \int_0^{\infty} \operatorname{Erfc}(at) \sin \omega t \, dt \\ &= \frac{1}{\omega} [1 - e^{-\omega^2/4a^2}].\end{aligned}\quad (3.131)$$

2. The sine integral function (defined in Equation 3.116):

$$\begin{aligned}f(t) &= \operatorname{si}(at) \quad a > 0, \\ \mathcal{F}_s[f(t)] &= \int_0^{\infty} \operatorname{si}(at) \sin \omega t \, dt = 0 \quad 0 \leq \omega < a \\ &= -\frac{\pi}{2\omega} \quad \omega > a.\end{aligned}\quad (3.132)$$

Note the symmetry of Equation 3.132 with Equation 3.65.

3. The cosine integral function (defined in Equation 3.36):

$$\begin{aligned}f(t) &= \operatorname{Ci}(at) = -\operatorname{ci}(at) \quad a > 0 \\ \mathcal{F}_s[f(t)] &= \int_0^{\infty} \operatorname{Ci}(at) \sin \omega t \, dt \\ &= \frac{1}{2\omega} \ln \left| \frac{\omega^2}{a^2} - 1 \right|.\end{aligned}\quad (3.133)$$

4. The exponential integral function (defined in Equation 3.66):

$$\begin{aligned}f(t) &= \operatorname{Ei}(-at) \quad a > 0 \\ \mathcal{F}_s[f(t)] &= \int_0^{\infty} \operatorname{Ei}(-at) \sin \omega t \, dt \\ &= -\frac{1}{2\omega} \ln \left( \frac{\omega^2}{a^2} + 1 \right).\end{aligned}\quad (3.134)$$

5. Bessel functions (defined in Equation 3.58):

(a)  $f(t) = J_0(at) \quad a > 0$

$$\begin{aligned}\mathcal{F}_s[f(t)] &= \int_0^{\infty} J_0(at) \sin \omega t \, dt = 0, \quad 0 < \omega < a, \\ &= (\omega^2 - a^2)^{-1/2} \quad \omega > a.\end{aligned}\quad (3.135)$$

(b)  $f(t) = J_{2n+1}(at) \quad a > 0$

$$\begin{aligned}\mathcal{F}_s[f(t)] &= \int_0^{\infty} J_{2n+1}(at) \sin \omega t \, dt \\ &= (-1)^n (a^2 - \omega^2)^{-1/2} T_{2n+1}(\omega/a) \\ & \quad 0 < \omega < a, \\ &= 0 \quad \omega > a,\end{aligned}\quad (3.136)$$

where  $T_n(x)$  is the Chebyshev polynomial defined in Equation 3.59.

(c)  $f(t) = t^{-n} J_{n+1}(at), a > 0$  and  $n = 0, 1, 2, \dots$

$$\begin{aligned}\mathcal{F}_s[f(t)] &= \int_0^{\infty} t^{-n} J_{n+1}(at) \sin \omega t \, dt \\ &= \frac{\sqrt{\pi}}{\Gamma(n+1/2)} \frac{1}{2^n a^{n+1}} \omega (a^2 - \omega^2)^{n-1/2}, \\ & \quad 0 < \omega < a \\ &= 0 \quad \omega > a,\end{aligned}\quad (3.137)$$

where  $\Gamma(x)$  is the gamma function defined in Equation 3.69'.

(d)  $f(t) = Y_0(at) \quad a > 0$ .

where  $Y_\nu(x)$  is the Bessel function of the second kind (see Equation 3.70).

$$\begin{aligned}\mathcal{F}_s[f(t)] &= \int_0^{\infty} Y_0(at) \sin \omega t \, dt \\ &= \frac{2}{\pi} (a^2 - \omega^2)^{-1/2} \sin^{-1} \left( \frac{\omega}{a} \right), \\ & \quad 0 < \omega < a \\ &= \frac{2}{\pi} (\omega^2 - a^2)^{-1/2} \ln \left| \frac{\omega}{a} - \left( \frac{\omega^2}{a^2} - 1 \right)^{1/2} \right|, \\ & \quad \omega > a.\end{aligned}\quad (3.138)$$

(e)  $f(t) = t^\nu Y_{\nu-1}(at) \quad a > 0, |\operatorname{Re}(\nu)| < 1/2$

$$\begin{aligned}\mathcal{F}_s[f(t)] &= \int_0^{\infty} t^\nu Y_{\nu-1}(at) \sin \omega t \, dt \\ &= \frac{2^\nu a^{\nu-1} \sqrt{\pi}}{\Gamma(1/2 - \nu)} \omega (\omega^2 - a^2)^{-\nu-1/2} \quad \omega > a, \\ &= 0 \quad 0 < \omega < a.\end{aligned}\quad (3.139)$$

As with the cosine transforms, more detailed results are found in the sections covering Henkel transforms.

### 3.4 The Discrete Sine and Cosine Transforms (DST and DCT)

In practical applications, the computations of the Fourier sine and cosine transforms are done with sampled data of finite duration. Because of the finite duration and the discrete nature of the data, much can be gained in theory and in ease of computation by formulating the corresponding discrete sine and cosine transforms (DST and DCT) directly. In what follows, we discuss the definitions and properties of the discrete sine and cosine transforms. It is possible to define four different types of each of the DCT and the DST (for details, see Rao and Yip, 1990). We shall concentrate on Type I, which can be defined by simply discretizing the FST and FCT, within a finite rectangular window of unit height.

### 3.4.1 Definitions of DCT and DST and Relations to FST and FCT

Consider the transform kernel of the FCT given by

$$K_c(\omega, t) = \cos \omega t. \quad (3.140)$$

Let  $\omega_m = 2\pi m \Delta f$  and  $t_n = n \Delta t$  be the sampled angular frequency and time, respectively. Here,  $\Delta f$  and  $\Delta t$  are the sample intervals for frequency and time, respectively.  $m$  and  $n$  are positive integers. The kernel in Equation 3.140 can now be discretized as

$$K_c(m, n) = K_c(\omega_m, t_n) = \cos(2\pi mn \Delta f \Delta t). \quad (3.141)$$

If we further let  $\Delta f \Delta t = 1/(2N)$ , where  $N$  is a positive integer, we obtain the DCT kernel:

$$K_c(m, n) = \cos(\pi mn/N) \quad (3.142)$$

where  $m, n = 0, 1, \dots, N$ . The transform kernel in Equation 3.142 is the DCT kernel of Type I. It represents the  $mn$ th element in an  $(N+1) \times (N+1)$  transformation matrix, which, with the proper normalization, provides the definition for the DCT transformation matrix  $[C]$ . These elements are

$$[C]_{mn} = \sqrt{\frac{2}{N}} \left\{ k_m k_n \cos\left(\frac{mn\pi}{N}\right) \right\}, \quad m, n = 0, 1, \dots, N$$

where

$$\begin{aligned} k_i &= 1 \quad \text{for } i \neq 0 \text{ or } N \\ &= 1/\sqrt{2} \quad \text{for } i = 0 \text{ or } N \end{aligned} \quad (3.143)$$

The discretization can be viewed as taking a finite time duration and dividing it into  $N$  intervals of  $\Delta t$  each. Including the boundary points, there are  $N+1$  sample points to be considered. If the discrete  $N+1$  sample points are represented by a vector  $\mathbf{x}$ , the DCT of this vector is a vector  $\mathbf{X}_c$  given by,

$$\mathbf{X}_c = [C]\mathbf{x} \quad (3.144)$$

which, in an element-by-element form, means

$$\mathbf{X}_c(m) = \sqrt{\frac{2}{N}} \sum_{n=0}^N k_m k_n \cos\left(\frac{mn\pi}{N}\right) \mathbf{x}(n). \quad (3.145)$$

It can be shown that  $[C]$  is a unitary matrix. Thus, the inverse transformation is given by

$$\mathbf{x}(n) = \sqrt{\frac{2}{N}} \sum_{m=0}^N k_m k_n \cos\left(\frac{mn\pi}{N}\right) \mathbf{X}_c(m). \quad (3.146)$$

Vectors  $\mathbf{X}_c$  and  $\mathbf{x}$  are said to be a DCT pair.

Similar consideration in discretizing the FST kernel

$$K_s(\omega, t) = \sin \omega t \quad (3.147)$$

will lead to the definition of the  $(N-1) \times (N-1)$  DST transform matrix, whose elements are given by

$$[S]_{mn} = \sqrt{\frac{2}{N}} \sin\left(\frac{mn\pi}{N}\right) \quad m, n = 1, 2, \dots, N-1. \quad (3.148)$$

This matrix is also unitary and when it is applied to a data vector  $\mathbf{x}$  of length  $N-1$ , it produces a vector  $\mathbf{X}_s$ , whose elements are given by,

$$\mathbf{X}_s(m) = \sqrt{\frac{2}{N}} \sum_{n=1}^{N-1} \sin\left(\frac{mn\pi}{N}\right) \mathbf{x}(n). \quad (3.149)$$

The vectors  $\mathbf{x}$  and  $\mathbf{X}_s$  are said to form a DST pair. The inverse DST is given by

$$\mathbf{x}(n) = \sqrt{\frac{2}{N}} \sum_{m=1}^{N-1} \sin\left(\frac{mn\pi}{N}\right) \mathbf{X}_s(m). \quad (3.150)$$

It is evident in Equations 3.146 and 3.150 that both DCT and DST are symmetric transforms. Both are obtained by discretizing a finite time duration into  $N$  equal intervals of  $\Delta t$  each, resulting in an  $(N+1) \times (N+1)$  matrix for  $[C]$  because the boundary elements are not zero, and resulting in an  $(N-1) \times (N-1)$  matrix for  $[S]$  because the boundary elements are zero.

## 3.4.2 Basic Properties and Operational Rules

### 3.4.2.1 The Unitarity Property

Let  $\mathbf{c}_m$  denote the  $m$ th column vector in the matrix  $[C]$ . Consider the inner product of two such vectors:

$$\langle \mathbf{c}_m, \mathbf{c}_n \rangle = \sum_{p=0}^N k_m k_p \cos\left(\frac{mp\pi}{N}\right) k_p k_n \cos\left(\frac{pn\pi}{N}\right). \quad (3.151)$$

The summation can be carried out by defining the  $2N$ th primitive root of unity as

$$W_{2N} = e^{-j\pi/N} = \cos\left(\frac{\pi}{N}\right) - j \sin\left(\frac{\pi}{N}\right), \quad (3.152)$$

and applying it to the summation in Equation 3.151. This gives

$$\langle \mathbf{c}_m, \mathbf{c}_n \rangle = \left(\frac{k_m k_n}{N}\right) \operatorname{Re} \left[ \sum_{p=0}^{N-1} (W_{2N})^{-p(n-m)} + \sum_{p=1}^N (W_{2N})^{-p(n+m)} \right] \quad (3.153)$$

where  $\operatorname{Re}[\cdot]$  denotes the real part of  $[\cdot]$ .

Considering the first summation in Equation 3.153, and letting  $\kappa = (n - m)$ , the power series can be written as,

$$\begin{aligned} \sum_{p=0}^{N-1} (W_{2N}^{-\kappa})^p &= \frac{(1 - W_{2N}^{-N\kappa})}{(1 - W_{2N}^{-\kappa})} \\ &= \{2[1 - \cos(\kappa\pi/N)]\}^{-1} \\ &\times \left\{1 - W_{2N}^{N\kappa} - W_{2N}^{\kappa} + W_{2N}^{-(N-1)\kappa}\right\}. \end{aligned} \quad (3.154)$$

Similarly, the second series in Equation 3.153 can be summed by letting  $\lambda = (n + m)$ ,

$$\begin{aligned} \sum_{p=1}^N (W_{2N}^{-\lambda})^p &= \{2[1 - \cos(\lambda\pi/N)]\}^{-1} \\ &\times \left\{W_{2N}^{-\lambda} - W_{2N}^{-(N+1)\lambda} - 1 + W_{2N}^{-N\lambda}\right\}. \end{aligned} \quad (3.155)$$

Hence, for  $m \neq n$ , (i.e.,  $\kappa \neq 0$ ), the real part of Equation 3.154 is

$$\begin{aligned} \operatorname{Re} \left[ \sum_{p=0}^{N-1} (W_{2N}^{-\kappa})^p \right] &= \frac{[1 - (-1)^\kappa][1 - \cos(\kappa\pi/N)]}{\{2[1 - \cos(\kappa\pi/N)]\}} \\ &= [1 - (-1)^\kappa]/2, \end{aligned}$$

and the real part of Equation 3.155 is

$$\begin{aligned} \operatorname{Re} \left[ \sum_{p=1}^N (W_{2N}^{-\lambda})^p \right] &= -\frac{[1 - (-1)^\lambda][1 - \cos(\lambda\pi/N)]}{\{2[1 - \cos(\lambda\pi/N)]\}} \\ &= -[1 - (-1)^\lambda]/2. \end{aligned}$$

Combining these, and noting that  $\kappa$  and  $\lambda$  differ by  $2m$ , we obtain the orthogonality property for the inner product,

$$\langle c_m, c_n \rangle = 0 \quad \text{for } m \neq n. \quad (3.156)$$

For  $m = n \neq 0$  or  $N$ , the inner product is,

$$\langle c_m, c_n \rangle = (1/N) \operatorname{Re} \left[ \sum_{p=0}^{N-1} 1 + \sum_{p=1}^N (W_{2N}^{-2m})^p \right] = 1,$$

and for  $m = n = 0$  or  $N$ , the inner product is,

$$\langle c_m, c_n \rangle = (1/2N) \operatorname{Re} \left( \sum_{p=0}^{N-1} 1 + \sum_{p=1}^N 1 \right) = 1.$$

Therefore, the inner product satisfies the orthonormality condition,

$$\langle c_m, c_n \rangle = \delta_{mn} \quad (3.157)$$

where  $\delta_{mn}$  is the Kronecker delta and the DCT matrix  $[C]$  is shown to be unitary.

Similar considerations can be applied to the DST matrix  $[S]$  to show that it is also unitary.

### 3.4.2.2 Inverse Transformation

As alluded to in Section 3.4.1, the unitary matrices  $[C]$  and  $[S]$  are symmetric and, therefore, the inverse transformations are exactly the same as the forward transformations, based on the above unitarity properties. Therefore,

$$[C]^{-1} = [C] \quad \text{and} \quad [S]^{-1} = [S]. \quad (3.158)$$

### 3.4.2.3 Scaling

Recall that in the discretization of the FCT, the time and frequency intervals are related by

$$\Delta f \Delta t = 1/2N \quad \text{or} \quad \Delta f = \frac{1}{2N\Delta t}. \quad (3.159)$$

Because the DCT and DST deal with discrete sample points, a scaling in time has no effect in the transform, except in changing the unit frequency interval in the transform domain. Thus, as  $\Delta t$  changes to  $a\Delta t$ ,  $\Delta f$  changes to  $\Delta f/a$ , provided the number of divisions  $N$  remains the same. Hence, the properties 3.16 and 3.87 for the FCT and FST are retained, except for the  $1/a$  factor, which is absent in the cases for DCT and DST.

Equation 3.159 may also be interpreted as giving the frequency resolution of a set of discrete data points, sampled at a time interval of  $\Delta t$ . Using  $T = N\Delta t$  as the time duration of the sequence of data points, the frequency resolution for the transforms is

$$\Delta f = \frac{1}{2T}. \quad (3.160)$$

### 3.4.2.4 Shift-in-t

Because the data are sampled, we obtain the shift-in-time properties of DCT and DST by examining the time shifts in units of  $\Delta t$ . Thus, if  $\mathbf{x} = [x(0), x(1), \dots, x(N)]^T$ , we define the right-shifted sequence as  $\mathbf{x}^+ = [x(1), x(2), \dots, x(N+1)]^T$ . Their corresponding DCTs are given by

$$\mathbf{X}_c = [C]\mathbf{x} \quad \text{and} \quad \mathbf{X}_c^+ = [C]\mathbf{x}^+. \quad (3.161)$$

The shift-in-time property seeks to relate  $\mathbf{X}_c^+$  with  $\mathbf{X}_c$ . It turns out that it relates not only to  $\mathbf{X}_c$  but also to  $\mathbf{X}_s$ , the DST of  $\mathbf{x}$ . This is to be expected because the shift-in-time properties of FCT and FST are similarly related. It can be shown that the elements of  $\mathbf{X}_c^+$  are given by

$$\begin{aligned} X_c^+(m) &= \cos\left(\frac{m\pi}{N}\right)X_c(m) + k_m \sin\left(\frac{m\pi}{N}\right)X_s(m) \\ &+ \sqrt{\frac{1}{N}}k_m \left[ \left(-\frac{1}{\sqrt{2}}\right) \cos\left(\frac{m\pi}{N}\right)x(0) + \left(\frac{1}{\sqrt{2}} - 1\right)x(1) \right. \\ &\left. + (-1)^m \left(\frac{1}{\sqrt{2}} - 1\right) \cos\left(\frac{m\pi}{N}\right)x(N) + (-1)^m \frac{1}{\sqrt{2}}x(N+1) \right]. \end{aligned} \quad (3.162)$$

In Equation 3.162,  $X_c(m)$  and  $X_s(m)$  are respectively the  $m$ th element of the DCT of the vector  $[x(0), x(1), \dots, x(N)]^T$  and the  $m$ th element of the DST of the vector  $[x(1), x(2), \dots, x(N+1)]^T$ . While properties analogous to the so-called kernel-product properties for FCT in Section 3.2.2 may be developed, Equation 3.162 is more practical in that it provides for a way of updating a DCT of a given dimension without having to recompute all the components. The corresponding result of DST is

$$X_s^+(m) = \cos\left(\frac{m\pi}{N}\right)X_s(m) - \sin\left(\frac{m\pi}{N}\right)X_c(m) + \sqrt{\frac{2}{N}}\sin\left(\frac{m\pi}{N}\right)\left[\frac{1}{\sqrt{2}}x(0) - \left(1 - \frac{1}{\sqrt{2}}\right)(-1)^m x(N)\right]. \quad (3.163)$$

Here, it is noted that  $X_c(m)$  are the elements of the DCT the vector  $[x(0), \dots, x(N)]^T$ .

### 3.4.2.5 The Difference Property

For discrete sequences, the difference operator replaces the differential operator for continuous sequences. The FCT and the FST of a derivative, therefore, are analogous to the DCT and the DST of the difference operator. We can define a difference vector  $\mathbf{d}$  as

$$\mathbf{d} = \mathbf{x}^+ - \mathbf{x} \quad (3.164)$$

where  $\mathbf{x}^+$  is the right-shifted version of  $\mathbf{x}$ . It is clear that the DCT and the DST of  $\mathbf{d}$  are simply given by

$$\mathbf{D}_c = \mathbf{X}_c^+ - \mathbf{X}_c \quad \text{and} \quad \mathbf{D}_s = \mathbf{X}_s^+ - \mathbf{X}_s. \quad (3.165)$$

As we can see from Equation 3.165, the main operational advantage of the FCT and FST, namely that in the differentiation properties, have not carried over to the discrete cases. As well, properties with both integration-in- $t$  and integration-in- $\omega$  are also lost in the discrete cases.

We conclude this section by mentioning that no simple convolution properties exist in the cases of DCT and DST. For finite sequences, it is possible to define a circular convolution for two periodic sequences or a linear convolution of two nonperiodic sequences. With these, certain convolution properties for some of the DCTs may be developed. (For more details, the reader is referred to Rao and Yip, 1990). The results, however, are neither simple nor easy to apply.

### 3.4.3 Relation to the Karhunen–Loeve Transform (KLT)

While the DCT and the DST discussed here are derived by discretizing the FCT and the FST, based on some unit time interval of  $\Delta t$  and some unit frequency interval of  $\Delta f$ , their forms are closely related to the KLT in digital signal processing. KLT is an optimal transform for digital signals in that it diagonalizes the auto-covariance matrix of a data vector. It completely decorrelates the signal in the transform domain, minimizes the mean squared

errors (MSEs) in data compression and packs the most energy (variance) in the fewest number of transform coefficients.

Consider a Markov-1 signal with correlation coefficient  $\rho$ . The  $N \times N$  covariance matrix is a matrix  $[A]$ , which is real, symmetric, and Toeplitz. It is well known that a nonsingular symmetric Toeplitz matrix has an inverse of tri-diagonal form. In the case of the covariance matrix  $[A]$  for a Markov-1 signal, we can write

$$[A]^{-1} = (1 - \rho^2)^{-1} \times \begin{pmatrix} 1 & -\rho & 0 & 0 & \dots & \dots & \dots \\ -\rho & 1 + \rho^2 & -\rho & 0 & \dots & \dots & \dots \\ \dots & \dots & \dots & \dots & \dots & 1 + \rho^2 & -\rho \\ \dots & \dots & \dots & \dots & \dots & -\rho & 1 \end{pmatrix}. \quad (3.166)$$

This matrix can be decomposed into a sum of two simpler matrices,

$$[A]^{-1} = [B] + [R]$$

where

$$[B] = (1 - \rho^2)^{-1} \begin{pmatrix} 1 + \rho^2 & -\sqrt{2}\rho & 0 & \dots & \dots \\ -\sqrt{2}\rho & 1 + \rho^2 & -\rho & \dots & \dots \\ 0 & -\rho & 1 + \rho^2 & -\rho & \dots \\ \dots & \dots & \dots & \dots & \dots \\ \dots & \dots & \dots & -\sqrt{2}\rho & 1 + \rho^2 \end{pmatrix}$$

and

$$[R] = (1 - \rho^2)^{-1} \times \begin{pmatrix} -\rho^2 & (\sqrt{2}-1)\rho & 0 & \dots & \dots \\ (\sqrt{2}-1)\rho & 0 & 0 & \dots & \dots \\ \dots & \dots & \dots & 0 & (\sqrt{2}-1)\rho \\ \dots & \dots & \dots & (\sqrt{2}-1)\rho & -\rho^2 \end{pmatrix}. \quad (3.167)$$

We note that  $[R]$  is almost a null matrix and can be considered so when  $N$  is very large. Thus, the diagonalization of the matrix  $[B]$  is asymptotically equivalent to the diagonalization of the matrix  $[A]^{-1}$ . Furthermore, it is well known that the similarity transformation that diagonalizes  $[A]^{-1}$  will also diagonalize  $[A]$ . From these arguments, it is concluded that the transformation that diagonalizes  $[B]$  will, asymptotically, diagonalize  $[A]$ . The transformation that diagonalizes  $[B]$  depends on a three-terms recurrence relation that is exactly satisfied by the Chebyshev polynomials. With these, it can be shown that the matrix  $[V]$  that will diagonalize  $[B]$  and, in turn, also  $[A]$  asymptotically, is defined by

$$[V]_{mn} = k_n k_m \sqrt{\frac{2}{N-1}} \cos\left(\frac{mn\pi}{N-1}\right), \quad m, n = 0, 1, \dots, N-1. \quad (3.168)$$



As can be seen in Equation 3.168, these are the elements of the DCT matrix  $[C]$ , except that  $N$  has been replaced by  $N - 1$ . For large  $N$ , these are identical.

The foregoing has briefly demonstrated that for a Markov-1 signal, the diagonalization of the covariance matrix, which leads to the KLT, is provided by a transformation matrix  $[V]$  which is almost identical to the DCT matrix  $[C]$ . This explains why the DCT performs so well in signal decorrelation, although it is signal independent. Similar arguments can be applied to the DST.

In Figure 3.1, the basis functions forming the KLT for  $N = 16$  are shown. The signal is a Markov-1 signal with a correlation coefficient of  $\rho = 0.95$ . It is clear that the set of basis functions and, hence, the KLT is signal dependent, because they are the eigenvectors of the autocovariance matrix of the signal vector.

In Figures 3.2 and 3.3, the basis functions for  $N = 16$  of DCT and DST are shown. It is evident that they are very similar to the KLT basis functions. While it is true that the dimensions of the spaces spanned by the KLT and the DCT and DST are different, it can be shown that as  $N$  increases, both discrete transforms will asymptotically approach KLT.

However, it is true that the similarity of the basis functions does not guarantee the asymptotic behavior of the DCT and the DST, nor does it assure good performance. In applications, such as data compression and transform domain coding, the “variance distribution” of the transform coefficient is an important criterion of performance. The variance of a transform coefficient is basically a measure of the information content of that coefficient. Therefore, the higher the variances are in a few transform coefficients, the more room there is for data compression in that transform domain.

Let  $[A]$  be the data covariance matrix and let  $[T]$  be the transformation. Then, the covariance matrix in the transform domain,  $[A]_T$ , is given by,

$$[A]_T = [T][A][T]^{-1}. \tag{3.169}$$

The diagonal elements of  $[A]_T$  are the variances of the transform coefficients. In Table 3.1, comparisons are shown for the variance distributions of the DCT, the DST, and the discrete Fourier

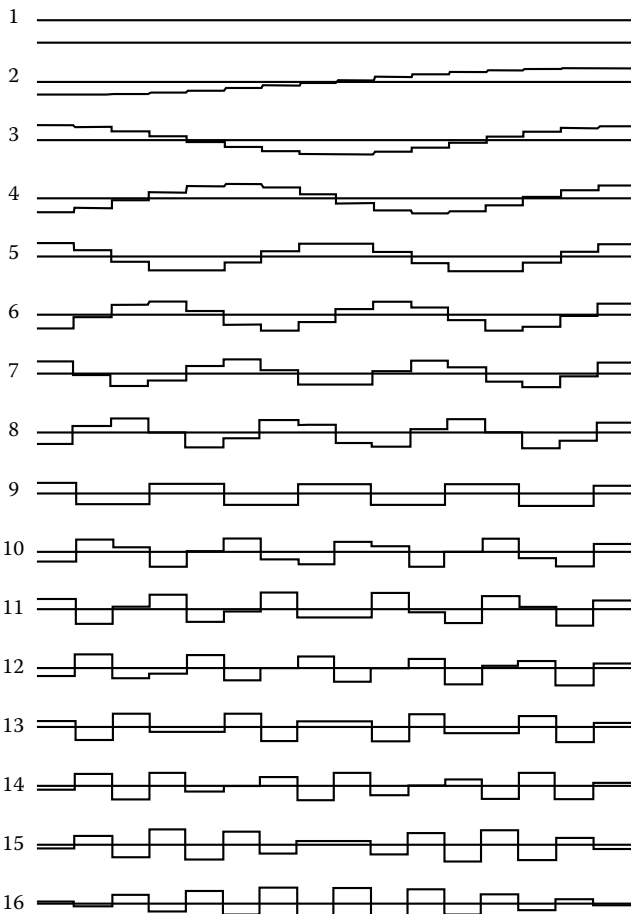


FIGURE 3.1 KLT Markov-1 signal  $\rho = 0.95, N = 16$ .

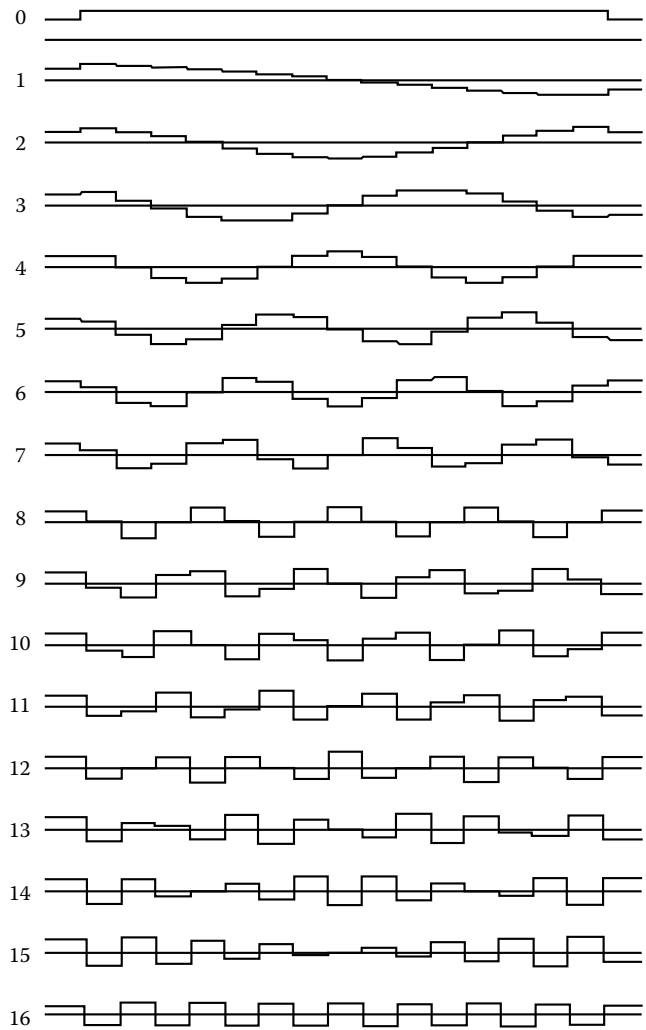
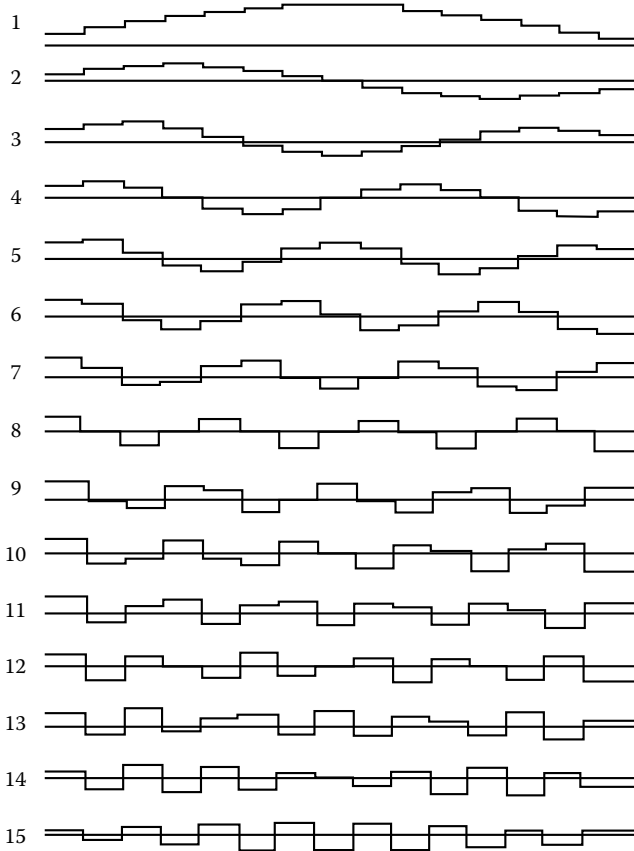


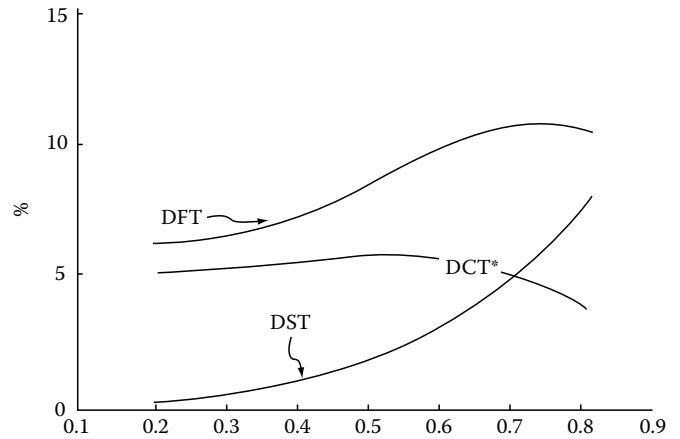
FIGURE 3.2 DCT  $N = 16$ .

FIGURE 3.3 DST  $N = 16$ .TABLE 3.1 Variance Distributions for  $N = 16$ ,  $\rho = 0.9$ 

$i$	DCT <sup>a</sup>	DST	DFT
0	9.835	9.218	9.835
1	2.933	2.640	1.834
2	1.211	1.468	1.834
3	0.581	0.709	0.519
4	0.348	0.531	0.519
5	0.231	0.314	0.250
6	0.166	0.263	0.250
7	0.129	0.174	0.155
8	0.105	0.153	0.155
9	0.088	0.110	0.113
10	0.076	0.099	0.113
11	0.068	0.078	0.091
12	0.062	0.071	0.091
13	0.057	0.061	0.081
14	0.055	0.057	0.081
15	0.053	0.054	0.078

<sup>a</sup> DCT is DCT-II here.

transform (DFT), based on a Markov-1 signal of  $\rho = 0.9$  and  $N = 16$ . It is clearly seen that both DCT and DST outperform DFT is using variance distribution as a performance criterion.

FIGURE 3.4 Percent residual correlation as a function of  $\rho$ ,  $N = 16$ .

When the transformation  $[T]$  in Equation 3.169 is not the KLT,  $[A]_T$  will not be diagonal. The nonzero off-diagonal elements in  $[A]_T$  form a measure of the “residual correlation.” The smaller the amount of residual correlation, the closer is the transform to being optimal. Figure 3.4 shows the residual correlation as a percentage of the total amount of correlation, for the transforms DCT, DST, and DFT, in a Markov-1 signal with  $N = 16$ . As can be seen, again DCT and DST outperform DFT generally.

There are other criteria of performance for a given transform, depending on what kind of signal processing is being done. However, using the KLT as a benchmark, DCT and DST are extremely good alternatives as signal independent, fast implementable transforms, because they are both asymptotic to the KLT. This asymptotic property of the discrete trigonometric transforms (particularly the DCT) has made them very important tools in digital signal processing. Although they are suboptimal, in the sense that they will not exactly diagonalize the data covariance matrix, they are signal independent and are computable using fast algorithms. KLT, though exactly optimal, is signal dependent and possesses no fast computational algorithm. Some typical applications are discussed in the next section.

## 3.5 Selected Applications

This section contains some typical applications. We begin with fairly general applications to differential equations and conclude with quite specific applications in the area of data compression. (See Churchill, 1958 and Sneddon, 1972 for more applications.)

### 3.5.1 Solution of Differential Equations

#### 3.5.1.1 One-Dimensional Boundary Value Problem

Consider the second-order differential equation,

$$y''(t) - h^2 y(t) = F(t) \quad t \geq 0 \quad (3.170)$$

with boundary conditions:  $y'(0)$  and  $0$  and  $y(\infty) = 0$ , and

$$F(t) = A \quad \text{for } 0 < t < b \\ = 0 \quad \text{otherwise.}$$

We note that  $F(t)$  can be expressed in terms of a Heaviside step function, Thus,

$$F(t) = A[1 - U(t - b)]. \quad (3.171)$$

Here, we assume  $h$ ,  $A$ , and  $b$  to be constants. Applying the operator  $\mathcal{F}_c$  to the differential equation and using the results in Equations 3.9 and 3.34, we get

$$-\omega^2 Y_c - y'(0) - h^2 Y_c = \frac{A}{\omega} \sin \omega b. \quad (3.172)$$

Applying the boundary condition and solving for  $Y_c$ , we obtain

$$Y_c = -\frac{A}{\omega(\omega^2 + h^2)} \sin \omega b \\ = -\frac{A}{h^2} \left( \frac{\sin \omega b}{\omega} - \frac{\omega \sin \omega b}{\omega^2 + h^2} \right). \quad (3.173)$$

The inversion of  $Y_c$  can be accomplished with the use of Equations 3.34, 3.55, and 3.3. Noting that the inverse FCT has a normalization factor of  $2/\pi$ , the solution for the original boundary value problem is given by

$$y(t) = -\frac{A}{h^2} [1 - U(t - b) - e^{-hb} \cosh ht] \quad t < b, \\ = -\frac{A}{h^2} [1 - U(t - b) + e^{-ht} \sinh hb] \quad \text{for } t > b.$$

These can be rewritten as

$$y(t) = \frac{A}{h^2} (e^{-hb} \cosh ht - 1) \quad \text{for } t < b, \\ = -\frac{A}{h^2} e^{-ht} \sinh hb \quad \text{for } t > b. \quad (3.174)$$

### 3.5.1.2 Two-Dimensional Boundary Value Problem

Consider a function  $v(x, y)$ , which is bounded for  $x \geq 0, y \geq 0$ . Let  $v(x, y)$  satisfy the boundary value problem:

$$\frac{\partial^2 v}{\partial x^2} + \frac{\partial^2 v}{\partial y^2} = -h(x); \quad \left. \frac{\partial v}{\partial x} \right|_{x=0} = 0, \quad v(x, 0) = f(x). \quad (3.175)$$

We further assume that  $\int_0^\infty h(x) dx = 0$ , and that the function

$$p(x) = \int_x^\infty \left[ \int_0^r h(t) dt \right] dr \quad (3.176)$$

exists and that the functions  $p(x)$  and  $f(x)$  have FCTs. We note from Equation 3.176 that

$$p''(x) = h(x) \quad \text{and} \quad p'(0) = 0,$$

leading to the following relation between their FCTs:

$$\omega^2 P_c(\omega) = H_c(\omega) \quad (3.177)$$

Applying  $\mathcal{F}_c$  for the  $x$  variable in Equation 3.175 reduces the partial differential equation to

$$-\omega^2 V_c(\omega, y) + \frac{\partial^2}{\partial y^2} V_c(\omega, y) = -\omega^2 P_c(\omega). \quad (3.178)$$

Because  $V_c(\omega, y)$  is bounded for  $y > 0$ , Equation 3.178 has the following solution,

$$V_c(\omega, y) = C e^{-\omega y} + P_c(\omega) \quad (3.179)$$

where  $C$  is an arbitrary constant, to be determined by  $v(x, 0) = f(x)$ . In the  $\omega$ -domain, this means

$$V_c(\omega, 0) = F_c(\omega). \quad (3.180)$$

Thus,

$$V_c(\omega, y) = [F_c(\omega) - P_c(\omega)] e^{-\omega y} + P_c(\omega). \quad (3.181)$$

This can be inverted and the solution in the  $(x, y)$  domain then is given by

$$v(x, y) = p(x) + \frac{1}{\pi} \int_0^\infty [f(t) - p(t)] \\ \times \left[ \frac{y}{(x+t)^2 + y^2} + \frac{y}{(x-t)^2 + y^2} \right] dt. \quad (3.182)$$

Here, we have made use of Equation 3.44 and the convolution result of Equation 3.20.

### 3.5.1.3 Time-Dependent One-Dimensional Boundary Value Problem

Consider the function  $u(x, t)$ , which is bounded for  $x, t \geq 0$ . Let this function satisfy the partial differential equation,

$$\frac{\partial u}{\partial t} + \frac{\partial^2 u}{\partial x^2} = h(x, t) \quad (3.183)$$

so that  $u(x, 0) = f(x)$  and  $u(0, t) = g(t)$  are the initial and boundary conditions.

Applying the FST for the variable  $x$  to Equation 3.183 and assuming the existence of all the integrals involved, we obtain

$$\frac{\partial U_s}{\partial t} + \omega^2 U_s = \omega g(t) + H_s(\omega, t). \quad (3.184)$$

The solution for Equation 3.184 is

$$U_s(\omega, t)e^{\omega^2 t} = \int_0^t [\omega g(\tau) + H_s(\omega, \tau)]e^{\omega^2 \tau} d\tau + C. \quad (3.185)$$

$C$  is easily found to be  $F_s(\omega)$  using the condition  $U_s(\omega, 0) = F_s(\omega)$ . With this, Equation 3.185 can be inverse transformed by applying the operator  $\mathcal{F}_s^{-1}$  to get

$$u(x, t) = \frac{2}{\pi} \int_0^{\infty} U_s(\omega, t) \sin \omega x d\omega. \quad (3.186)$$

We note that, depending on the forms of the functions  $F_s$  and  $H_s$ , the inverse FST may be obtained by table look-up.

### 3.5.2 Cepstral Analysis in Speech Processing

In cepstral analysis, a sequence is converted by a transform  $T$ , the logarithm of its absolute value is then taken and the cepstrum is then obtained by inverse transformation  $T^{-1}$ . Figure 3.5 shows the essential steps in cepstral analysis. Here,  $\{x(n)\}$  is the input speech sequence,  $\{X(k)\}$  is the transform sequence, and the output  $\{x_R(n)\}$  is called the real cepstrum.

The transform may be any invertible transform. When  $T$  is an  $N$ -point DFT, the scheme can be implemented using the DCT. In the computation to obtain the real cepstrum using the DFT, the input sequence has to be padded with trailing zeros to double its length. However, a simple relation between the DFT and the DCT for real even sequences reduces the DFT to a DCT.

Let  $x(n), n = 0, 1, 2, \dots, M$  be the input speech sequence to be analyzed. To obtain the real cepstrum  $x_R(n)$  using DFT, the sequences is padded with zeros so that  $x(n) = 0$ , for  $n = M + 1, \dots, 2M - 1$ . If we consider a symmetric sequence  $s(n)$  defined by

$$\begin{aligned} s(n) &= x(n) & 0 < n < M, \\ &= 2x(n) & n = 0, M \\ &= x(2M - n) & M < n \leq 2M - 1, \end{aligned} \quad (3.187)$$

then the DFT of  $s(n)$  can be obtained as

$$S_F(k) = 2 \left[ x(0) + (-1)^k x(M) + \sum_{n=1}^{M-1} x(n) \cos\left(\frac{nk\pi}{M}\right) \right]. \quad (3.188)$$

Equation 3.188 is clearly in the form of a DCT of the sequence  $\{x(n)\}$  up to a constant factor of normalization. Now, because

$\{s(n)\}$  is a symmetric real sequence, constructed out of  $\{x(n)\}$ , we have

$$S_F(k) = \text{Re}\{X_F(k)\}$$

where  $\{X_F(k)\}$  is the  $2M$ -point DFT of the zero-padded sequence. Combining this with Equation 3.188 we see that

$$\text{Re}\{X_F(k)\} = 2[X_c(k)] \quad (3.189)$$

where  $X_c$  is the  $(M+1)$ -point DCT of the speech sequence  $\{x(n)\}$ . Equation 3.189 is valid up to a normalization constant. Because direct sparse matrix factorization of the  $(M+1) \times (M+1)$  DCT matrix is possible, fast algorithms exist for the computation of the DCT. This means that in order to obtain the real cepstrum of  $\{x(n)\}$ , there is no need to pad the sequence with trailing zeros, and the computation for  $x_R(k)$  can be achieved through the use of DCT of the sequence  $\{x(n)\}$ .

Rather than using DCT as a means of computing the DFT, the transform  $T$  in the cepstral analysis can directly be a DCT or a DST. It has been found that the performance of speech cepstral analysis using DCT and DST is comparable to the traditional DFT cepstral analysis.

### 3.5.3 Data Compression

Data compression is an important application of transform coding when retrieval of a signal from a large database is required. Transform coefficients with large variances can be retained to represent significant features for pattern recognition, for example. Those with small variances, below a certain threshold, can be discarded. Such a scheme can be used in reducing the required bandwidth for purposes of transmission or storage.

The transforms used for these data compression purposes require maximal decorrelation of the data, with highest energy-packing efficiency possible (efficiency is defined as how much energy can be packed into the fewest number of transform coefficients). The ideal or optimal transform is the KLT, which will diagonalize the data covariance matrix and pack the most energy into the fewest transform coefficients. Unfortunately, KLT is data dependent, and has no known fast computational algorithm, and, therefore, is not practical. On the other hand, Markov models describe most of the data systems quite well, and sub-optimal but asymptotically equivalent transforms such as the DCT and the DST are data independent, and implementable using fast algorithms. Therefore, in many applications, such as storage of electrocardiogram (ECG) or vectorcardiogram (VCG) data, or video data transmission over telephone lines for video phones, suboptimal transforms such as the DCT are preferred over the optimal KLT. For such applications, depending upon the

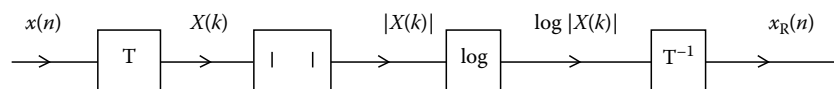


FIGURE 3.5 Block diagram for cepstral analysis for  $x(n)$ .

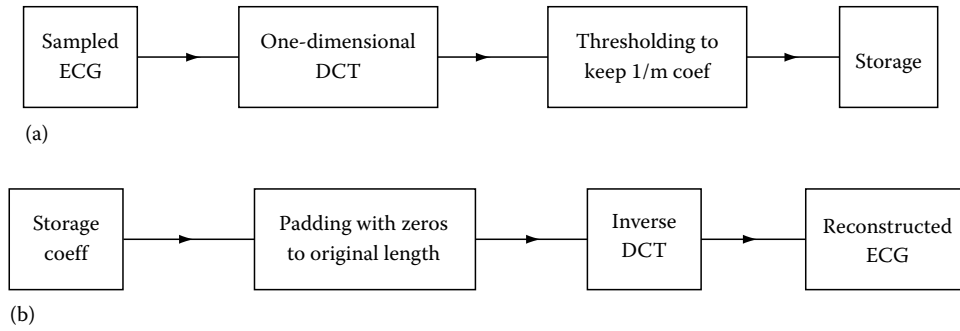


FIGURE 3.6 (a) Data compression for storage, (b) reconstruction from compressed data.

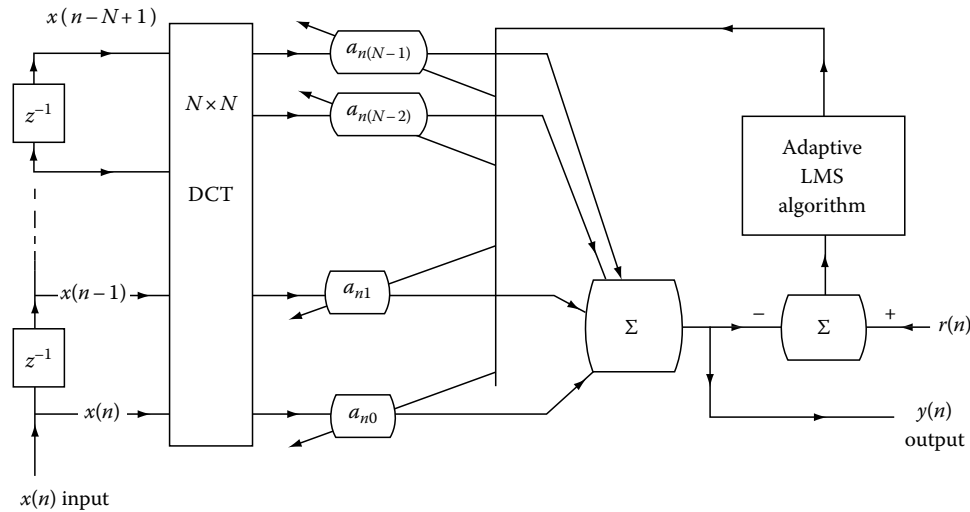


FIGURE 3.7 Adaptive transform domain LMS filtering.

required fidelity of the reconstructed data, compression ratios of up to 10:1 have been reported, and compression ratios of 3:1 to 5:1 using DCT for both ECG (one-dimensional) and VCG (two-dimensional) are commonplace.

Figure 3.6a and b show the block diagrams for processing, storage, and retrieval of a one-dimensional ECG, using  $m:1$ , compression ratio.

### 3.5.4 Transform Domain Processing

While discarding low variance coefficients in the DCT domain will provide data compression, certain details or desired features in the original data may be lost in the reconstruction. It is possible to remedy this partially by processing the transform coefficients before reconstruction. Adaptive processing can be applied based on some subjective criteria, such as in video phone applications. Coefficient quantization is another means of processing to minimize the effect of noise.

Other processing techniques such as subsampling (decimation) and up-sampling (interpolation) can also be performed in the DCT domain, effectively combining the operations of filtering and transform coding. Such processing techniques have been

successfully employed to convert high definition TV signals to the standard NTSC TV signals.

One of the most popular digital signal processing tools is the adaptive least-mean-square (LMS) filtering. This can be done either in the time domain or in the transform domain. Figure 3.7 shows the block diagram for the adaptive DCT transform domain LMS filtering. Here  $a_{n0}, a_{n1}, \dots, a_{n,N-1}$  are the adaptive weights for the transform domain filter. The desired response is  $\{r(n)\}$  and  $\{y(n)\}$  is the filtered output. It has been found that such transform domain filtering speeds up the convergence of the LMS algorithm for speech-related applications such as spectral analysis and echo cancellation.

### 3.5.5 Image Compression by the Discrete Local Sine Transform (DLS)

#### 3.5.5.1 Introduction

DCT has long been recognized as one of the best substitutes for the optimal, but data-dependent KLT, in image processing. Many standards, such as the JPEG (Joint Photographic Experts Group) and MPEG (Moving Pictures Experts Group) have adopted DCT as a standard transform technique for image compression.

While both KLT and DCT satisfy the perfect reconstruction (PR) condition when no compression (or dropping of transform coefficients) takes place in the transform domain, both suffer from the artifact of “blocking” whenever compression is done. The severity of such an artifact depends on the amount of compression. In speech and audio processing, this appears as a clicking sound in the reconstructed speech. In image compression, it appears as “tiles” overlaying the reconstituted picture.

The blocking artifact can be attributed to the fact that two-dimensional image processing by transform generally takes place with blocks of pixels, the most common sizes being  $8 \times 8$  and  $16 \times 16$ . When modification of the transform coefficients occurs in compression or other transform domain processing, the PR condition is violated. The mismatching of the edges in the reconstructed blocks produces this artifact.

Efforts to counter this compression artifact led to the development of lapped transforms (see Malvar, 1992). The transforms are based on basis functions with a wider support in the data domain than in the transform domain, leading to overlaps of the basis functions in the edge region of each block; hence, the name “lapped” transform. Many such lapped transforms can be constructed using different criteria. There are lapped orthogonal transforms (LOTs), modulated lapped transforms (MLTs), and hierarchical lapped transform (HLT). There are also lapped transforms based on the discrete sine or cosine basis functions.

In this section, one such lapped transform based on the discrete sine basis function is described. This is called DLS. The transform is applied in image compression at different compression ratios and the results are compared with other lapped transforms.

### 3.5.5.2 Elements of the Lapped Orthogonal Transform (LOT)

In general, a lapped transform will take  $N$  sample points in the data domain and transform these into  $M$  coefficients in the conjugate domain, where  $N > M$ . Very often,  $N$  can be as much as twice the size of  $M$ . In matrix vector notations, a data vector  $x_m$  of length  $N$  is transformed into a vector  $X_m$  of length  $M$ , and the transform is represented by the  $M \times N$  matrix  $\Phi^T$  in the equation

$$X_m = \Phi^T x_m \quad (3.190)$$

Here  $\Phi$  is the lapped transform matrix of dimension  $N \times M$ . One might interpret such a matrix as an  $M$ -dimensional matrix spanned by  $M$   $N$ -dimensional vectors. Specifically, if  $M = 2$  and  $N = 4$ , then the two-dimensional vector space is spanned by two linearly independent four-dimensional vectors. As can be imagined, such a scheme will provide additional flexibility in the design of the transform basis functions.

When a data sequence is to be processed by a lapped transform, the basic block transform matrix  $\Phi$  is of dimension  $N \times M$ , whereas the overall transform matrix  $\Psi$  will be in block diagonal form, given by

$$\Psi = \begin{pmatrix} \Phi & & O \\ & \Phi & \\ O & & \Phi \end{pmatrix} \quad (3.191)$$

If  $\Phi^T = \begin{bmatrix} a_{11} & a_{21} & a_{31} & a_{41} \\ a_{12} & a_{22} & a_{32} & a_{42} \end{bmatrix}$ , the matrix  $\Psi$  will appear as

$$\Psi = \begin{bmatrix} \cdot & \cdot & & & & \\ & a_{11} & a_{12} & & & \\ & a_{21} & a_{22} & & & \\ & a_{31} & a_{32} & a_{11} & a_{12} & \\ & a_{41} & a_{42} & a_{21} & a_{22} & \\ & & & a_{31} & a_{32} & \\ & & & a_{41} & a_{42} & \\ & & & & & \cdot & \cdot \end{bmatrix} \quad (3.192)$$

when the length of the overlap is 2.

For a data sequence  $x_m$  of dimension  $K$ , the lapped transformed sequence  $X_m$  is given by

$$X_m = \Psi^T x_m. \quad (3.193)$$

Evidently, in the segmented form of  $x_m$  (each segment of length  $N$ ), the data points located at the ends, in the overlapped regions, will be processed in two consecutive block transforms. One can visualize this as a sliding window of size  $N$  moving over the data sequence in shifts of size  $M$  each.

When compression or other processing is not applied, all invertible transforms should satisfy the PR condition. In terms of the transformation matrix, this PR condition is stated simply as

$$\Psi\Psi^T = I_K \quad \text{and} \quad \Psi^T\Psi = I_K \quad (3.194)$$

where  $I_K$  is a  $K \times K$  identity matrix. From Equation 3.194 conditions for the component block matrix  $\Phi$  can be stated

$$\Phi^T\Phi = I_M \quad (3.195)$$

and

$$\Phi^T W \Phi = O_M, \quad (3.196)$$

where  $W$  is an  $M \times M$  “one block shift” matrix defined by

$$W = \begin{pmatrix} O_1 & I_L \\ O_2 & O_1 \end{pmatrix}.$$

Here,  $L$  is the length of the overlap region,  $O_1$  is an  $L \times (M - L)$  null matrix,  $O_2$  is an  $(M - L) \times (M - L)$  null matrix, and  $O_M$  is an  $M \times M$  null matrix. Thus, in addition to the usual orthonormality condition 3.195, lapped transforms require the additional “lapped orthogonality” condition 3.196 to preserve the overall PR requirement.

### 3.5.5.3 The Discrete Local Sine Transform (DLS)

By properly choosing a “core” and a “lapped” region together with a specified function, a lapped transform basis set can be constructed to satisfy the PR condition. The DLS is just such a set, based on the continuous bases of Coifman and Meyer [See Coifman and Meyer, 1991.]

Let  $\Phi_s$  be the DLS transform matrix, so that

$$\Phi_s = [\Phi_0, \Phi_1, \dots, \Phi_{M-1}]. \tag{3.197}$$

Then the basis function  $\phi_r$ 's are defined by

$$\phi_r(n) = \sqrt{(2/M)} \left\{ b(n) \sin \left[ \frac{2r+1}{2} \pi \left( \frac{n}{M} - \varepsilon \right) \right] \right\}; \tag{3.198}$$

$n \in [0, M+L-1]; \quad r \in [0, M-1]$

where  $n, r$  are respectively the index for the data sample and the index of the basis function;  $\varepsilon = (L-1)/2M$ ;  $M$  is the number of basis functions in the set and  $L$  is the length of the lapped portion.  $b(n)$  is called a bell function and it controls the roll-off over the lapped portion of the basis function. It is given by

$$b(n) = \begin{cases} S_\varepsilon(n) = \sin \left[ \frac{n\pi}{2(L-1)} - \frac{1}{4} \sin \frac{2n\pi}{L-1} \right], & n = 0, \dots, L-1, \\ 1, & \text{for } n = L, \dots, M-1, \\ C_\varepsilon(n-M) = \cos \left[ \frac{(n-M)\pi}{2(L-1)} - \frac{1}{4} \sin \frac{2(n-M)\pi}{L-1} \right], & n = M, \dots, M+L-1. \end{cases}$$

Figure 3.8 shows the DLS basis functions in time and frequency domains for  $M = 8, L = 8$ . These basis functions are very similar to those of MLT developed by Malvar (1992).

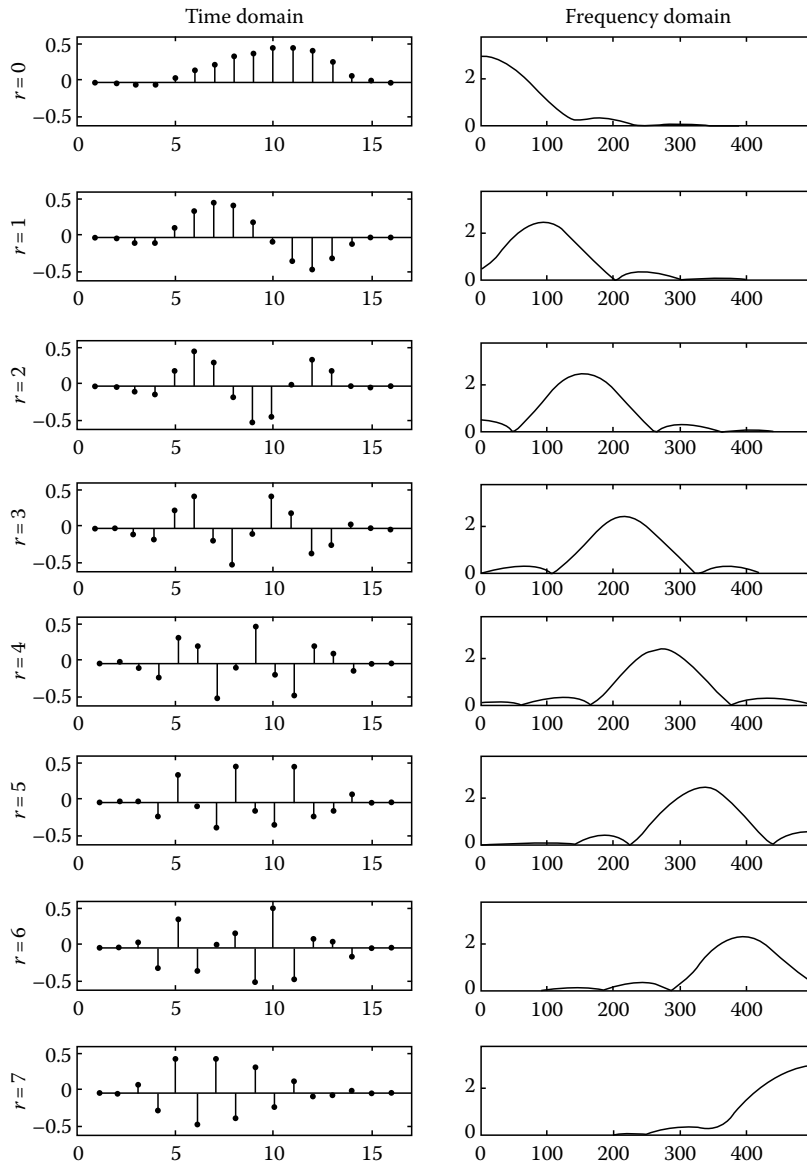


FIGURE 3.8 DLS basis functions in time and frequency domain,  $L = M = 8$ .

### 3.5.5.4 Simulation Results (For Details, See Li, 1997.)

The standard Lena image of  $256 \times 256$  pixels is used in the simulations for image compression. The original image is represented by 8 bits/pixel or 8 bpp and is shown in Figure 3.9a. Compressions based on a  $16 \times 16$  block transform ( $M=L=16$  for lapped transforms) result in reconstructed images represented by 0.4 bpp, 0.24 bpp, and 0.16 bpp. A signal-to-noise ratio is calculated for the compressed image, based on the energy (variance) of the original image and the energy of the residual image. The residual image is defined as the difference between the original image and the compressed image. For lapped transforms, zeros are padded on the actual border of the image to enable the transform.

Table 3.2 shows a comparison of the final signal-to-noise ratios for the several lapped transforms against the more conventional DCT at different compression ratios. It is obvious that the lapped transforms are superior in performance compared to the DCT.

Figures 3.9 through 3.11 depict the various reconstructed images using different lapped transforms at different compression ratios. It is seen that serious “block” artifacts are absent from the compressed images even at the very low bits per pixel rates. The performance of the DLS lies between those of the LOT and the MLT.

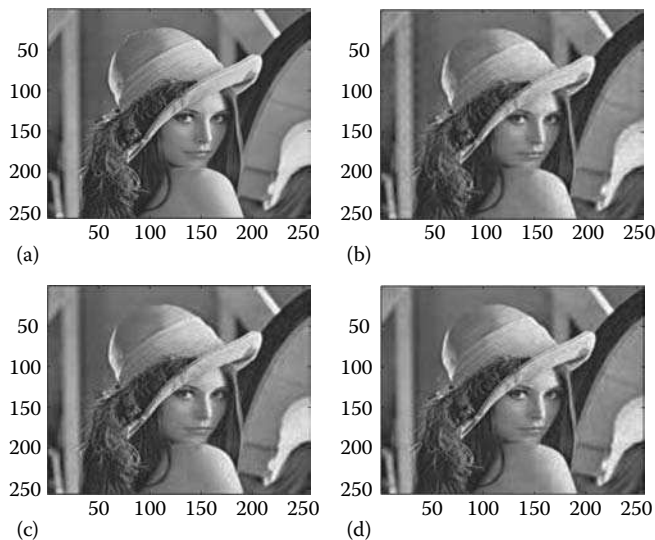


**FIGURE 3.9** Comparison of original and reconstructed image,  $M=L=16$ , at 0.4 bpp: (a) original at 8 bpp, (b) DLS, (c) LOT, (d) MLT.

**TABLE 3.2** Comparison of Signal-to-Noise Ratio (dB)

	DLS	LOT	MLT	DCT
0.4 bpp	16.3	15.8	16.5	13.9
0.24 bpp	13.8	13.6	14.3	12.2
0.16 bpp	12.2	12.2	12.7	11.2

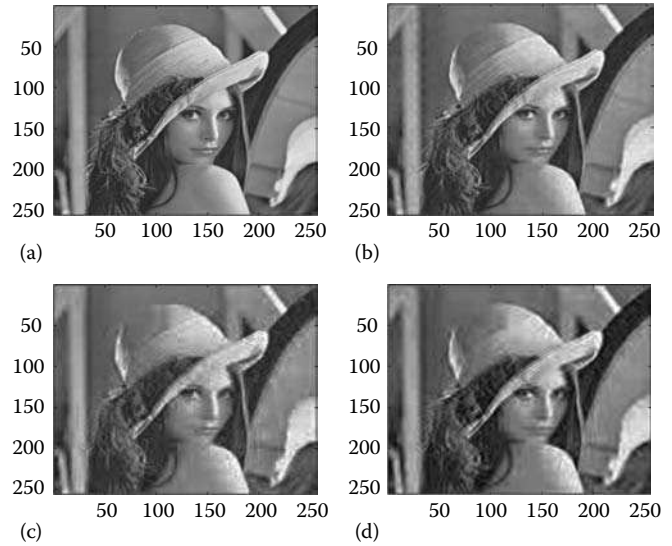


**FIGURE 3.10** Comparisons for original and reconstructed image,  $M=L=16$ , at 0.24 bpp: (a) original at 8 bpp, (b) DLS, (c) LOT, (d) MLT.

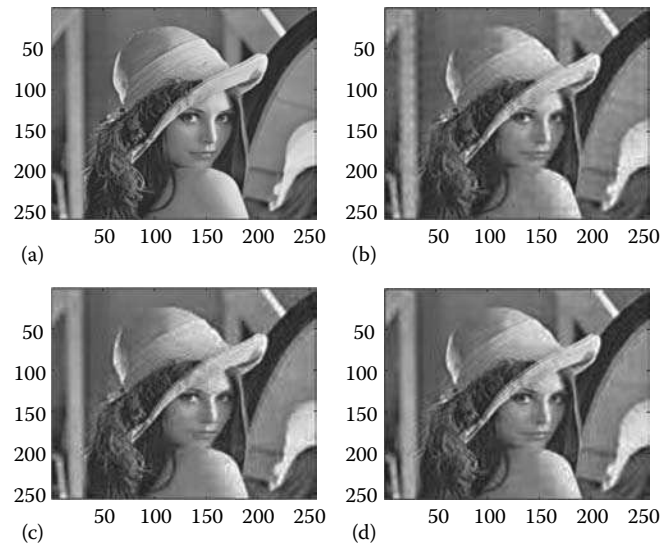


**FIGURE 3.11** Comparisons of original and reconstructed image,  $M=L=16$ , at 0.16 bpp: (a) original at 8 bpp, (b) DLS, (c) LOT, (d) MLT.

## 3.6 Computational Algorithms

In actual computations of FCT and FST, the basic integrations are performed with quadratures. Because the data are sampled and the duration is finite, most of the quadratures can be implemented via matrix computations. The fact that the FST and the FCT are closely related to the Fourier transform translates directly to the close relations between the computation of the DCT and the DST with that of the DFT. Many algorithms have been developed for the DFT. The most well known among them is the



Cooley–Tukey fast Fourier transform (FFT), which is often regarded as the single most important development in modern digital signal processing. More recently, there have been other algorithms such as the Winograd algorithm, which are based on prime-factor decomposition and polynomial factorization.

While DST and DCT can be computed using relations with DFT (thus, fast algorithms such as the Cooley–Tukey or the Winograd), the transform matrices have sufficient structure to be exploited directly, so that sparse factorizations can be applied to realize the transforms. The sparse factorization depends on the size of the transform, as well as the way permutations are applied to the data sequence. As a result, there are two distinct types of sparse factorizations, the decimation-in-time (DIT) algorithms and the decimation-in-frequency (DIF) algorithms. (DIT algorithms are of the Cooley–Tukey type while DIF algorithms are of the Sande–Tukey type).

In Section 3.6.1, the computations of FST and FCT using FFT are discussed. In Section 3.6.2, the direct fast computations of DCT and DST are presented. Both DIT and DIF algorithms are discussed. All algorithms discussed are radix-2 algorithms, where  $N$ , which is related to the sample size, is an integer power of two.

### 3.6.1 FCT and FST Algorithms Based on FFT

#### 3.6.1.1 FCT of Real Data Sequence

Let  $\{x(n), n = 0, 1, \dots, N\}$  be an  $(N + 1)$ -point sequence. Its DCT as defined in Equation 3.145 is given by

$$X_c(m) = \sqrt{\frac{2}{N}} \sum_{n=0}^N k_m k_n \cos\left(\frac{mn\pi}{N}\right) x(n),$$

where

$$\begin{aligned} k_n &= 1 && \text{for } n \neq 0 \text{ or } N \\ &= 1/\sqrt{2} && \text{for } n = 0 \text{ or } N. \end{aligned}$$

Construct an even or symmetric sequence using  $\{x(n)\}$  in the following way,

$$\begin{aligned} s(n) &= x(n) && 0 < n < N, \\ &= 2x(n) && n = 0, N, \\ &= x(2N - n) && N < n \leq 2N - 1. \end{aligned} \quad (3.199)$$

Based on the fact that the Fourier transform of a real symmetric sequence is real and is related to the cosine transform of the half-sequence, it can be shown that the DFT of  $\{s(n)\}$  is given by

$$S_F(m) = 2 \left[ x(0) + (-1)^m x(N) + \sum_{n=1}^{N-1} \cos\left(\frac{mn\pi}{N}\right) x(n) \right]. \quad (3.200)$$

Thus, the  $(N + 1)$ -point DCT of  $\{x(n)\}$  is the same as the  $2N$ -point DFT of the sequence  $\{s(n)\}$ , up to a normalization

constant as indicated by Equation 3.145. This means that the DCT of  $\{x(n)\}$  can be computed using a  $2N$ -point FFT of  $\{s(n)\}$ . We note here that

$$S_F(m) = \sum_{n=0}^{2N-1} s(n) W_{2N}^{mn}, \quad (3.201)$$

where  $W_{2N} = e^{-j2\pi/2N}$ , the principal  $2N$ th root of unity, is used for defining the DFT.

It should be pointed out that the direct  $2N$ -point DFT of a real even sequence may be considered inefficient, because inherent complex arithmetics are used to produce real coefficients in the transform. However, it is well known that a real  $2N$ -point DFT can be implemented using an  $N$ -point DFT for a complex sequence. For details, the reader is referred to Chapter 2.

#### 3.6.1.2 FST of Real Data Sequence

Let  $\{x(n), n = 1, 2, \dots, N - 1\}$  be an  $(N - 1)$ -point data sequence. Its DST as defined in Equation 3.149 is given by

$$X_s(m) = \sqrt{\frac{2}{N}} \sum_{n=1}^{N-1} \sin\left(\frac{mn\pi}{N}\right) x(n).$$

Construct a  $(2N - 1)$ -point odd or skew-symmetric sequence  $\{s(n)\}$  using  $\{x(n)\}$ ,

$$\begin{aligned} s(n) &= x(n) && 0 < n < N, \\ &= 0 && n = 0, N, \\ &= -x(2N - n) && N < n \leq 2N - 1. \end{aligned} \quad (3.202)$$

The Fourier transform of a real skew-symmetric sequence is purely imaginary and is related to the sine transform of the half-sequence. From this, it can be shown that the  $2N$ -point DFT of  $\{s(n)\}$  in Equation 3.202 is given by

$$S_F(m) = -2j \sum_{n=1}^{N-1} \sin\left(\frac{mn\pi}{N}\right) x(n). \quad (3.203)$$

Thus, the  $2N$ -point DFT of  $\{s(n)\}$  is the same as the  $(N - 1)$ -point DST of  $\{x(n)\}$ , up to a normalization constant. Again  $S_F(m)$  is as defined in Equation 3.201 and the  $2N$ -point DFT for the real sequence can be implemented using an  $N$ -point DFT for a complex sequence.

### 3.6.2 Fast Algorithms for DST and DCT by Direct Matrix Factorization

#### 3.6.2.1 Decimation-in-Time Algorithms

These are Cooley–Tukey-type algorithms, in which the time ordering of the input data sequence is permuted to allow for the sparse factorization of the transformation matrix. The essential idea is to reduce a size  $N$  transform matrix into a block

diagonal form, in which each block is related to the same transform of size  $N/2$ . Recursively applying this procedure, one finally arrives at the basic  $2 \times 2$  “butterfly.” We present here the essential equations for this reduction and also the flow diagrams for the DIT computations of DCT and DST, in block form.

1. DIT algorithm for the DCT: Let

$$X_c(m) = \sum_{n=0}^N C_N^{mn} \tilde{x}(n), \quad m = 0, 1, 2, \dots, N, \quad (3.204)$$

be the DCT of the sequence  $\{x(n)\}$  (i.e.,  $\tilde{x}(n)$  is  $x(n)$  scaled by the normalization constant and the factor  $k_n$ , while  $X_c(m)$  is scaled by  $k_m$ , as in Equation 3.145). Here we have simplified the notations using the definition

$$C_N^{mn} = \cos\left(\frac{mn\pi}{N}\right). \quad (3.205)$$

Equation 3.204 can be reduced to

$$\begin{aligned} X_c(m) &= g_c(m) + h_c(m), \\ X_c(N - m) &= g_c(m) - h_c(m), \quad \text{for } m = 0, 1, \dots, N/2, \\ \text{and } X_c(N/2) &= g_c(N/2). \end{aligned} \quad (3.206)$$

Here,  $g_c$  and  $h_c$  are related to the DCT of size  $N/2$ , defined by the following equations:

$$g_c(m) = \sum_{n=0}^{N/2} C_{N/2}^{mn} \tilde{x}(2n), \quad \text{for } m = 0, 1, \dots, N/2,$$

$$h_c(m) = \frac{1}{2C_N^m} \sum_{n=0}^{N/2} C_{N/2}^{mn} [\tilde{x}(2n + 1) + \tilde{x}(2n - 1)],$$

$$\text{for } m = 0, 1, \dots, N/2 - 1,$$

and  $h_c(N/2) = 0$  and where  $\tilde{x}(N + 1)$  is set to zero.

$$(3.207)$$

We note that both  $g_c(m)$  and  $h_c(m)$  are DCTs of half the original size. This way, the size of the transform can be reduced by a factor of two at each stage. Some combinations of inputs to the lower order DCT are required as shown by the definition for  $h_c(m)$ , as well as some scaling of the output of the DCT transform. Figure 3.12 shows a signal flow graph for an  $N = 16$  DCT. Note the reduction into two  $N = 8$  DCTs in the flow diagram.

2. DIT algorithm for DST: Let

$$X_s(m) = \sum_{n=1}^{N-1} S_N^{mn} \tilde{x}(n), \quad m = 1, 2, \dots, N - 1, \quad (3.208)$$

be the DST of the sequence  $\{x(n)\}$ , (i.e.,  $\tilde{x}(n)$  is  $x(n)$  that has been scaled with the proper normalization constant as required in Equation 3.149 and we have defined

$$S_N^{mn} = \sin\left(\frac{mn\pi}{N}\right). \quad (3.209)$$

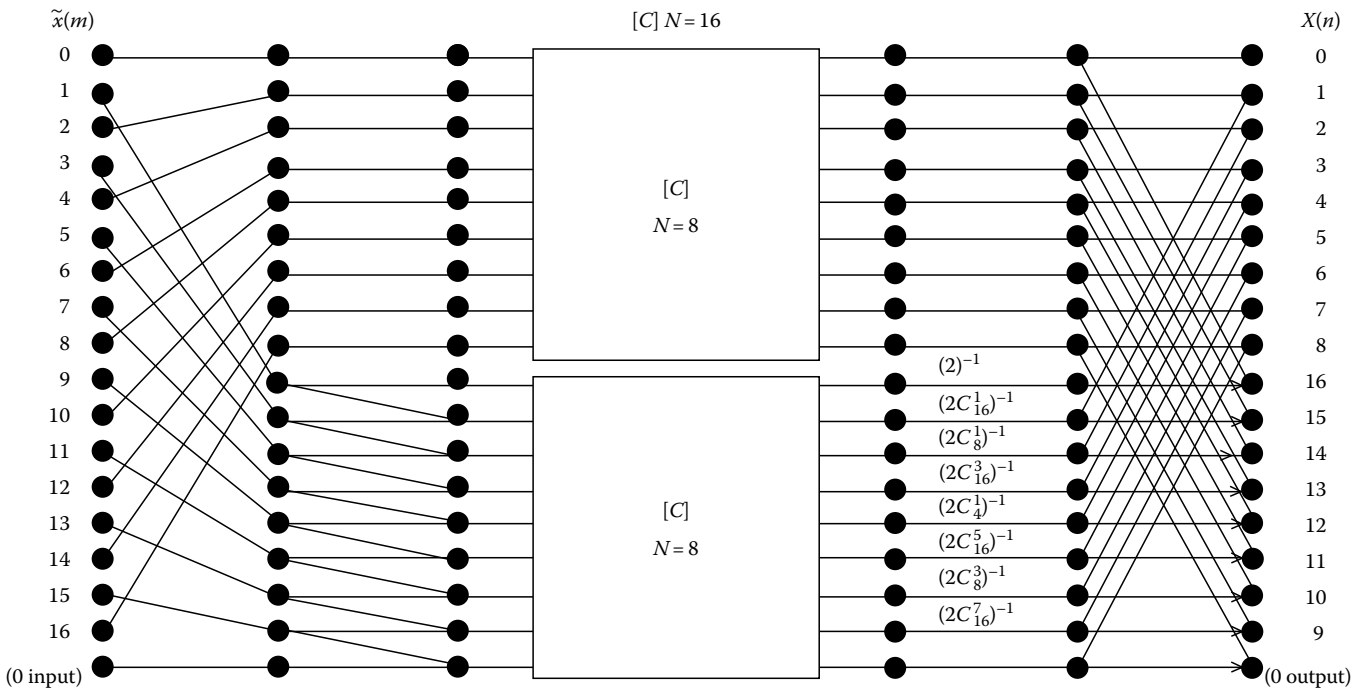


FIGURE 3.12 DIT DCT  $N = 16$  flow graph  $\rightarrow (-1)$ .

Following the same reasoning for the DIT algorithm for DCT, Equation 3.208 can be reduced to

$$\begin{aligned} X_s(m) &= g_s(m) + h_s(m), \\ X_s(N - m) &= g_c(m) - h_s(m), \quad \text{for } m = 1, 2, \dots, N/2 - 1, \text{ and} \\ X_s(N/2) &= \sum_{n=1}^{N/2-1} (-1)^n \tilde{x}(2N + 1). \end{aligned} \tag{3.210}$$

Here,  $g_s(m)$  and  $h_s(m)$  are defined as

$$\begin{aligned} g_s(m) &= \frac{1}{2C_N^m} \sum_{n=1}^{N/2-1} S_{N/2}^{mn} [\tilde{x}(2n + 1) + \tilde{x}(2n - 1)], \text{ and} \\ h_s(m) &= \sum_{n=1}^{N/2-1} S_{N/2}^{mn} \tilde{x}(2n). \end{aligned} \tag{3.211}$$

As before, it can be seen that  $g_s(m)$  and  $h_s(m)$  are the DSTs of half the original size, one involving only the odd input samples, and the other involving only the even input samples. Figure 3.13 shows a DIT signal flow graph for the  $N = 16$  DST. Note that it is reduced to two blocks of  $N = 8$  DSTs.

### 3.6.2.2 Decimation-in-Frequency Algorithms

These are Sande-Tukey-type algorithms in which the input sample sequence order is not permuted. Again, the basic principle is to reduce the size of the transform, at each stage of the computation, by a factor of two. It would be of no surprise that these algorithms are simply the conjugate versions of the DIT algorithms.

1. *The DIF algorithm for DCT:* In Equation 3.204, consider the even-ordered output points and the odd-ordered output points,

$$\begin{aligned} X_c(2m) &= G_c(m), \quad \text{for } m = 0, 1, \dots, N/2, \text{ and} \\ X_c(2m + 1) &= H_c(m) + H_c(m + 1), \\ &\text{for } m = 0, 1, \dots, N/2 - 1. \end{aligned} \tag{3.212}$$

Here,

$$\begin{aligned} G_c(m) &= \sum_{n=0}^{N/2-1} [\tilde{x}(n) + \tilde{x}(N - n)] C_{N/2}^{mn} + (-1)^m \tilde{x}(N/2), \text{ and} \\ H_c(m) &= \sum_{n=0}^{N/2-1} \frac{1}{2C_N^n} [\tilde{x}(n) - \tilde{x}(N - n)] C_{N/2}^{mn}. \end{aligned} \tag{3.213}$$

As can be seen, both  $G_c(m)$  and  $H_c(m)$  are DCTs of size  $N/2$ . Therefore, at each stage of the computation, the size of the transform is reduced by a factor of two. The overall result is a sparse factorization of the original transform matrix. Figure 3.14 shows the signal flow graph for an  $N = 16$  DIF type DCT.

2. *The GIF algorithm for DST:* Equation 3.209 can be split into even-ordered and odd-ordered output points, where

$$\begin{aligned} X_s(m) &= G_s(m), \quad \text{for } m = 1, 2, \dots, N/2 - 1, \\ X_s(2m - 1) &= H_s(m) + H_s(m - 1) + (-1)^{m+1} \tilde{x}(N/2), \\ &\text{for } m = 1, 2, \dots, N/2 - 1, \text{ and} \\ X_s(N - 1) &= H_s(N/2 - 1) + (-1)^{N/2+1} \tilde{x}(N/2). \end{aligned} \tag{3.214}$$

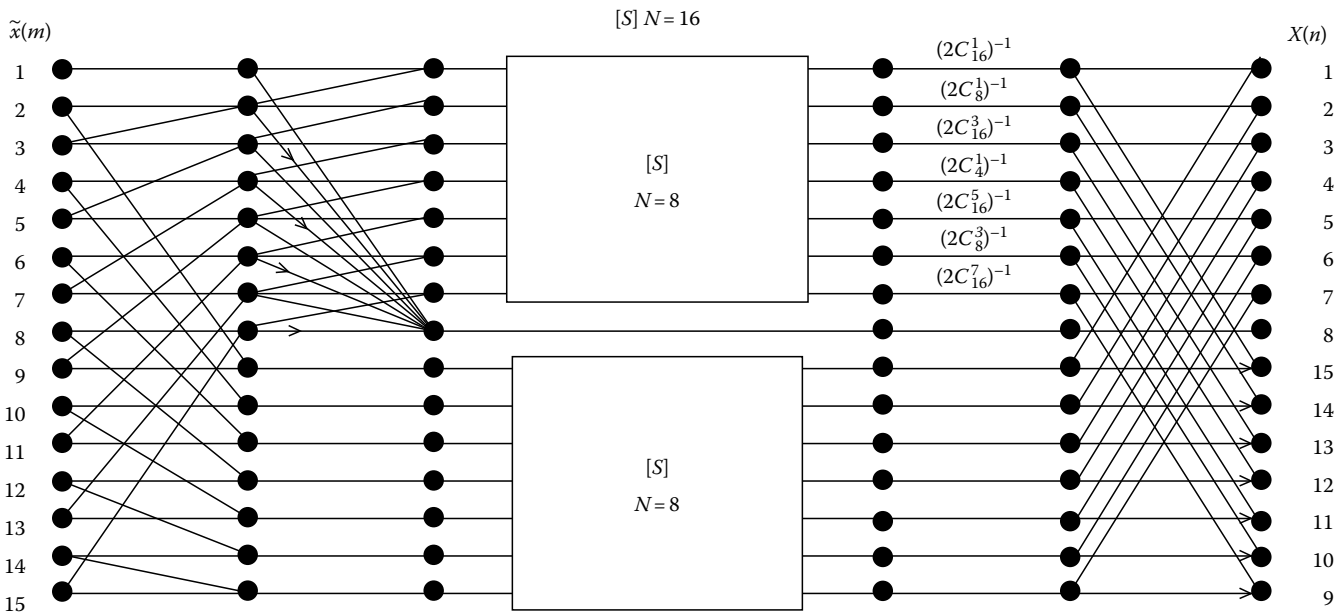


FIGURE 3.13 DIT DST  $N = 16$  flow graph  $\rightarrow (-1)$ .

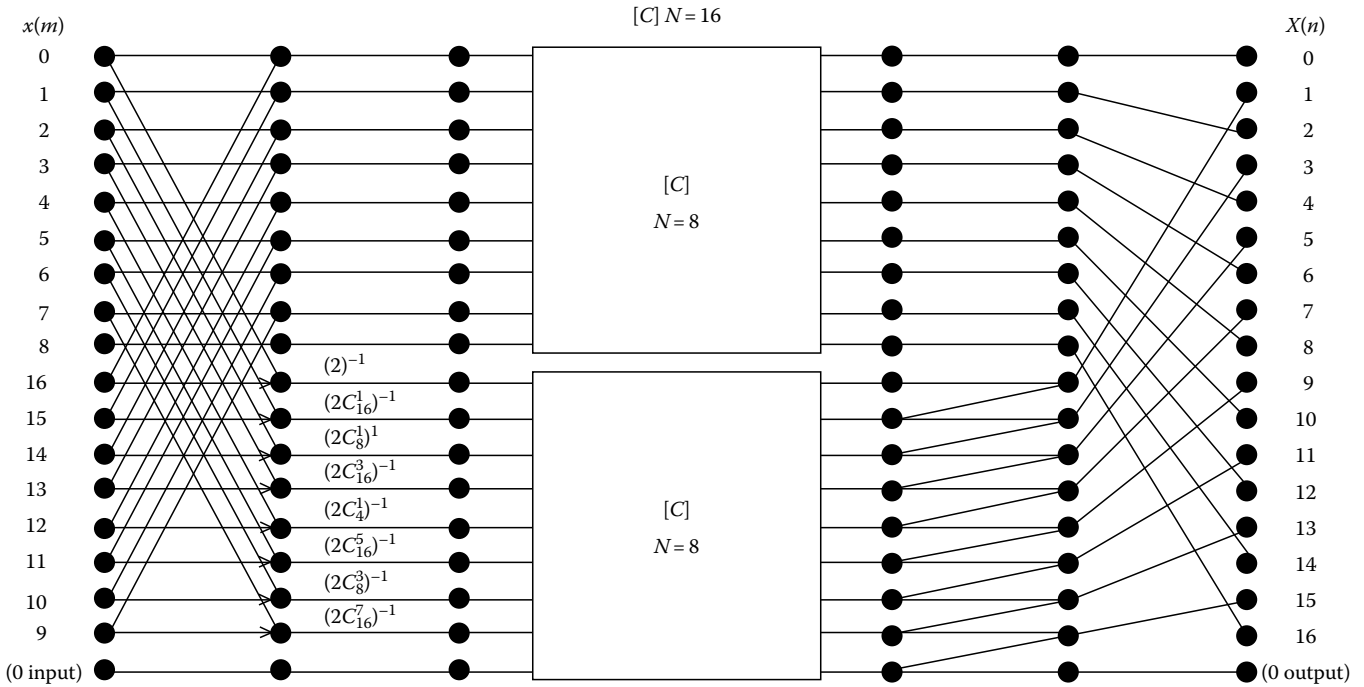


FIGURE 3.14 DIF DCT  $N = 16$  flow graph  $\rightarrow (-1)$ .

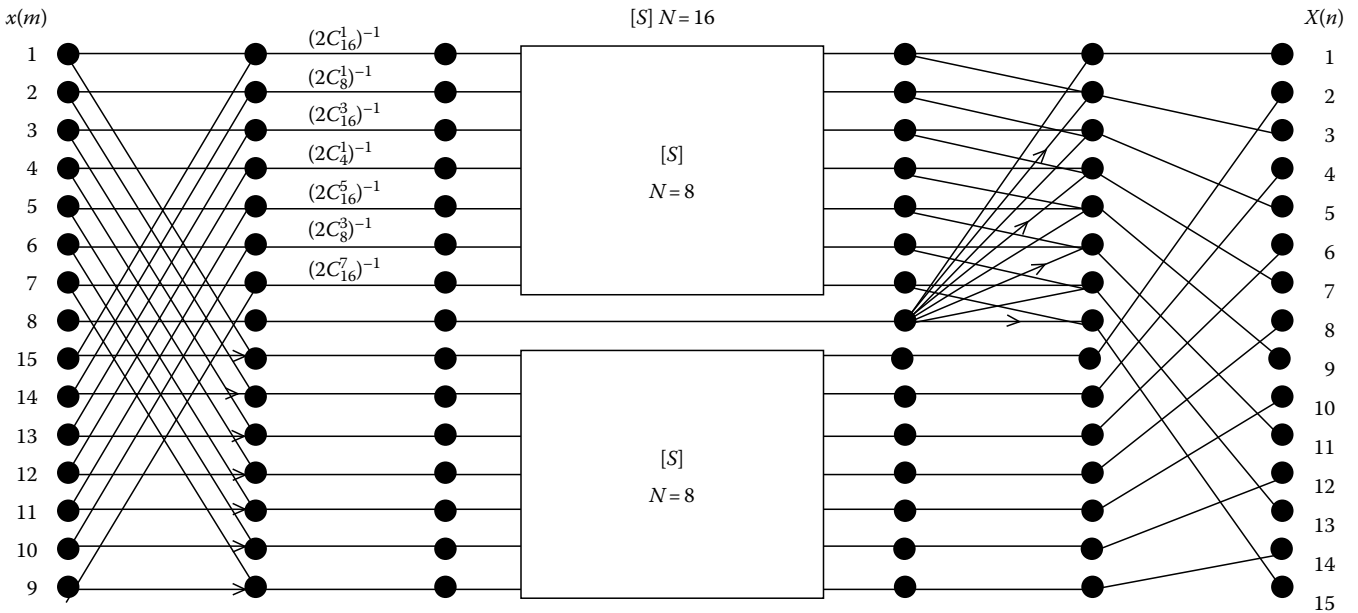


FIGURE 3.15 DIF DST  $N = 16$  flow graph  $\rightarrow (-1)$ .

Here, the outputs  $G_s(m)$  and  $H_s(m)$  are defined by DSTs of half the original size as

$$\begin{aligned}
 G_s(m) &= \sum_{n=1}^{N/2-1} [\tilde{x}(n) - \tilde{x}(N-n)] S_{N/2}^{mn}, \text{ and} \\
 H_s(m) &= \sum_{n=1}^{N/2-1} \frac{1}{2C_N^n} [\tilde{x}(n) - \tilde{x}(N-n)] S_{N/2}^{mn}.
 \end{aligned}
 \tag{3.215}$$

Figure 3.15 shows the signal graph for an  $N = 16$  DIF-type DST. Note that this flow graph is the conjugate of the flow graph shown in Figure 3.13.

### 3.7 Tables of Transforms

This section contains tables of transforms for the FCT and the FST. They are not meant to be complete. For more details and a

more complete listing of transforms, especially those of orthogonal and special functions, the reader is referred to the Bateman manuscripts (Erdelyi, 1954). Section 3.7.3 contains a list of conventions and definitions of some special functions that have been referred to in the tables.

### 3.7.1 Fourier Cosine Transforms

#### 3.7.1.1 General Properties

$f(t)$	$F_c(\omega) = \int_0^\infty f(t) \cos \omega t dt \quad \omega > 0$
1 $F_c(t)$	$(\pi/2)f(\omega)$
2 $f(at) \quad a > 0$	$(1/a)F_c(\omega/a)$
3 $f(at) \cos bt \quad a, b > 0$	$(1/2a) \left[ F_c\left(\frac{\omega+b}{a}\right) + F_c\left(\frac{\omega-b}{a}\right) \right]$
4 $f(at) \sin bt \quad a, b > 0$	$(1/2a) \left[ F_s\left(\frac{\omega+b}{a}\right) - F_s\left(\frac{\omega-b}{a}\right) \right]$
5 $t^{2n} f(t)$	$(-1)^n \frac{d^{2n}}{d\omega^{2n}} F_c(\omega)$
6 $t^{2n+1} f(t)$	$(-1)^n \frac{d^{2n+1}}{d\omega^{2n+1}} F_s(\omega)$
7 $\int_0^\infty f(r)[g(t+r) + g( t-r )]dr$	$2F_c(\omega)G_c(\omega)$
8 $\int_t^\infty f(r)dr$	$(1/\omega)F_s(\omega)$
9 $f(t+a) - f_0(t-a)$	$2F_s(\omega) \sin a\omega \quad a > 0$
10 $\int_0^\infty f(r)[g(t+r) + g_0(t-r)]dr$	$2F_s(\omega)G_s(\omega)$

#### 3.7.1.2 Algebraic Functions

$f(t)$	$F_c(\omega)$
1 $(1/\sqrt{t})$	$\sqrt{(\pi/2)}(1/\omega)^{1/2}$
2 $(1/\sqrt{t})[1 - U(t-1)]$	$(2\pi/\omega)^{1/2}C(\omega)$
3 $(1/\sqrt{t})U(t-1)$	$(2\pi/\omega)^{1/2}[1/2 - C(\omega)]$
4 $(t+a)^{-1/2} \quad  \arg a  < \pi$	$(\pi/2\omega)^{1/2} \{ \cos a\omega [1 - 2C(a\omega)] + \sin a\omega [1 - 2S(a\omega)] \}$
5 $(t-a)^{-1/2}U(t-a)$	$(\pi/2\omega)^{1/2} [\cos a\omega - \sin a\omega]$
6 $a(t^2 + a^2)^{-1} \quad a > 0$	$(\pi/2) \exp(-a\omega)$
7 $t(t^2 + a^2)^{-1} \quad a > 0$	$-1/2 [e^{-a\omega} \overline{\text{Ei}}(a\omega) + e^{a\omega} \text{Ei}(a\omega)]$
8 $(1-t^2)(1+t^2)^{-2}$	$(\pi/2)\omega \exp(-\omega)$
9 $-t(t^2 - a^2)^{-1} \quad a > 0$	$\cos a\omega \text{Ci}(a\omega) + \sin a\omega \text{Si}(a\omega)$

#### 3.7.1.3 Exponential and Logarithmic Functions

$f(t)$	$F_c(\omega)$
1 $e^{-at} \quad \text{Re } a > 0$	$a(a^2 + \omega^2)^{-1}$
2 $(1+t)e^{-t}$	$2(1 + \omega^2)^{-2}$
3 $\sqrt{t}e^{-at} \quad \text{Re } a > 0$	$\frac{\sqrt{\pi}}{2} (a^2 + \omega^2)^{-3/4} \cos [3/2 \tan^{-1}(\omega/a)]$

4 $e^{-at}/\sqrt{t} \quad \text{Re } a > 0$	$\sqrt{(\pi/2)}(a^2 + \omega^2)^{-1/2} \cdot [(a^2 + \omega^2)^{1/2} + a]^{1/2}$
5 $t^n e^{-at} \quad \text{Re } a > 0$	$n! [a/(a^2 + \omega^2)]^{n+1} \cdot \sum_{2m=0}^{n+1} (-1)^m \binom{n+1}{2m} \left(\frac{\omega}{a}\right)^{2m}$
6 $\exp(-at^2)/\sqrt{t} \quad \text{Re } a > 0$	$\pi(\omega/8a)^{1/2} \exp(-\omega^2/8a) \cdot I_{-1/4}(-\omega^2/8a)$
7 $t^{2n} \exp(-a^2 t^2) \quad  \arg a  < \pi/4$	$(-1)^n \sqrt{\pi} 2^{-n-1} a^{-2n-1} \cdot \exp[-(\omega/2a)^2] \text{He}_{2n}(2^{-1/2}\omega/a)$
8 $t^{-3/2} \exp(-a/t) \quad \text{Re } a > 0$	$(\pi/a)^{1/2} \exp[-(2a\omega)^{1/2}] \cos(2a\omega)^{1/2}$
9 $t^{-1/2} \exp(-a/\sqrt{t}) \quad \text{Re } a > 0$	$(\pi/2\omega)^{1/2} [\cos(2a\sqrt{\omega}) - \sin(2a\sqrt{\omega})]$
10 $t^{-1/2} \ln t$	$-(\pi/2\omega)^{1/2} [\ln(4\omega) + C + \pi/2]$
11 $(t^2 - a^2)^{-1} \ln t \quad a > 0$	$(\pi/2\omega) \{ \sin(a\omega) [\text{ci}(a\omega) - \ln a] - \cos(a\omega) [\text{si}(a\omega) - \pi/2] \}$
12 $t^{-1} \ln(1+t)$	$(1/2) \{ [\text{ci}(\omega)]^2 + [\text{si}(\omega)]^2 \}$
13 $\exp(-t/\sqrt{2}) \sin(\pi/4 + t/\sqrt{2})$	$(1 + \omega^4)^{-1}$
14 $\exp(-t/\sqrt{2}) \cos(\pi/4 + t/\sqrt{2})$	$\omega^2(1 + \omega^4)^{-1}$
15 $\ln \frac{a^2 + t^2}{1 + t^2} \quad a > 0$	$(\pi/\omega) [\exp(-\omega) - \exp(-a\omega)]$
16 $\ln[1 + (a/t)^2] \quad a > 0$	$(\pi/\omega) [1 - \exp(-a\omega)]$

#### 3.7.1.4 Trigonometric Functions

$f(t)$	$F_c(\omega)$
1 $t^{-1} e^{-t} \sin t$	$(1/2) \tan^{-1}(2\omega^{-2})$
2 $t^{-2} \sin^2(at) \quad a > 0$	$(\pi/2)(a - \omega/2)\omega < 2a$ $0 \quad \omega > 2a$
3 $\left(\frac{\sin t}{t}\right)^n \quad n = 2, 3, \dots$	$\frac{n\pi}{2^n} \sum_{r>0}^{r<(\omega+n)/2} \frac{(-1)^r (\omega+n-2r)^{n-1}}{r!(n-r)!}, \quad 0 < \omega < n$
4 $\exp(-\beta t^2) \cos at \quad \text{Re } \beta > 0$	$(1/2)(\pi/\beta)^{1/2} \exp\left(-\frac{a^2 + \omega^2}{4\beta}\right) \cosh\left(\frac{a\omega}{2\beta}\right)$
5 $(a^2 + t^2)^{-1}(1 - 2\beta \cos t + \beta^2)^{-1} \quad \text{Re } a > 0,  \beta  < 1$	$(1/2)(\pi/a)(1 - \beta^2)^{-1}(e^a - \beta)^{-1} \cdot (e^{a-a\omega} + \beta e^{a\omega}) \quad 0 \leq \omega < 1$
6 $\sin(at^2) \quad a > 0$	$(1/4)(2\pi/a)^{1/2} \left[ \cos\left(\frac{\omega^2}{4a}\right) - \sin\left(\frac{\omega^2}{4a}\right) \right]$
7 $\sin[a(1-t^2)] \quad a > 0$	$-(1/2)(\pi/a)^{1/2} \cos[a + \pi/4 + \omega^2/(4a)]$
8 $\cos(at^2) \quad a > 0$	$(1/4)(2\pi/a)^{1/2} \left[ \cos\left(\frac{\omega^2}{4a}\right) + \sin\left(\frac{\omega^2}{4a}\right) \right]$
9 $\cos[a(1-t^2)] \quad a > 0$	$(1/2)(\pi/a)^{1/2} \sin[a + \pi/4 + \omega^2/(4a)]$
10 $\tan^{-1}(a/t) \quad a > 0$	$(2\omega)^{-1} [e^{-a\omega} \text{Ei}(a\omega) - e^{a\omega} \text{Ei}(-a\omega)]$

### 3.7.2 Fourier Sine Transforms

#### 3.7.2.1 General Properties

$f(t)$	$F_s(\omega) = \int_0^\infty f(t) \sin \omega t dt \quad \omega > 0$
1 $F_s(t)$	$(\pi/2)f(\omega)$
2 $f(at) \quad a > 0$	$(1/a)F_s(\omega/a)$
3 $f(at) \cos bt \quad a, b > 0$	$(1/2a) \left[ F_s\left(\frac{\omega+b}{a}\right) + F_s\left(\frac{\omega-b}{a}\right) \right]$
4 $f(at) \sin bt \quad a, b > 0$	$-(1/2a) \left[ F_c\left(\frac{\omega+b}{a}\right) - F_c\left(\frac{\omega-b}{a}\right) \right]$
5 $t^{2n} f(t)$	$(-1)^n \frac{d^{2n}}{d\omega^{2n}} F_s(\omega)$
6 $t^{2n+1} f(t)$	$(-1)^{n+1} \frac{d^{2n+1}}{d\omega^{2n+1}} F_c(\omega)$
7 $\int_0^\infty f(r) \int_{ t-r }^{t+r} g(s) ds dr$	$(2/\omega) F_s(\omega) G_s(\omega)$
8 $f_o(t+a) + f_o(t-a)$	$2F_s(\omega) \cos a\omega$
9 $f_e(t-a) - f_e(t+a)$	$2F_c(\omega) \sin a\omega$
10 $\int_0^\infty f(r)[g( t-r ) - g(t+r)]dr$	$2F_s(\omega) G_c(\omega)$

#### 3.7.2.2 Algebraic Functions

$f(t)$	$F_s(\omega)$
1 $1/t$	$\pi/2$
2 $1/\sqrt{t}$	$(\pi/2\omega)^{1/2}$
3 $1/\sqrt{t}[1 - U(t-1)]$	$(2\pi/\omega)^{1/2} S(\omega)$
4 $(1/\sqrt{t})U(t-1)$	$(2\pi/\omega)^{1/2}[1/2 - S(\omega)]$
5 $(t+a)^{-1/2} \quad  \arg a  < \pi$	$(\pi/2\omega)^{1/2} \{ \cos a\omega[1 - 2S(a\omega)] - \sin a\omega [1 - 2C(a\omega)] \}$
6 $(t-a)^{-1/2} U(t-a)$	$(\pi/2\omega)^{1/2} (\sin a\omega + \cos a\omega)$
7 $t(t^2 + a^2)^{-1} \quad a > 0$	$(\pi/2) \exp(-a\omega)$
8 $t(a^2 - t^2)^{-1} \quad a > 0$	$-(\pi/2) \cos a\omega$
9 $t(a^2 + t^2)^{-2} \quad a > 0$	$(\pi\omega/4a) \exp(-a\omega)$
10 $a^2[t(a^2 + t^2)]^{-1} \quad a > 0$	$(\pi/2)[1 - \exp(-a\omega)]$
11 $t(4 + t^4)^{-1}$	$(\pi/4) \exp(-\omega) \sin \omega$

#### 3.7.2.3 Exponential and Logarithmic Functions

$f(t)$	$F_s(\omega)$
1 $e^{-at} \quad \text{Re } a > 0$	$\omega(a^2 + \omega^2)^{-1}$
2 $Te^{-at} \quad \text{Re } a > 0$	$(2a\omega)(a^2 + \omega^2)^{-2}$
3 $t(1+at)e^{-at} \quad \text{Re } a > 0$	$(8a^3\omega)(a^2 + \omega^2)^{-3}$
4 $e^{-at}\sqrt{t} \quad \text{Re } a > 0$	$\sqrt{(\pi/2)}(a^2 + \omega^2)^{-1/2} \cdot [(a^2 + \omega^2)^{1/2} - a]^{1/2}$
5 $t^{-3/2}e^{-at} \quad \text{Re } a > 0$	$(2\pi)^{1/2}[(a^2 + \omega^2)^{1/2} - a]^{1/2}$
6 $\exp(-at^2) \quad \text{Re } a > 0$	$-j(1/2)(\pi/a)^{1/2} \exp(-\omega^2/4a) \text{Erf} \left( \frac{j\omega}{2\sqrt{a}} \right)$
7 $t \exp(-t^2/4a) \quad \text{Re } a > 0$	$2a\omega\sqrt{(\pi a)} \exp(-a\omega^2)$

8 $t^{-3/2} \exp(-a/t) \quad  \arg a  < \pi/2$	$(\pi/a)^{1/2} \exp[-(2a\omega)^{1/2}] \sin(2a\omega)^{1/2}$
9 $t^{-3/4} \exp(-a/\sqrt{t}) \quad  \arg a  < \pi/2$	$-(\pi/2)(a/\omega)^{1/2} [J_{1/4}(a^2/8\omega) \cdot \cos(\pi/8 + a^2/8\omega) + Y_{1/4}(a^2/8\omega) \cdot \sin(\pi/8 + a^2/8\omega)]$
10 $t^{-1} \ln t$	$-(\pi/2)[C + \ln \omega]$
11 $t(t^2 - a^2)^{-1} \ln t \quad a > 0$	$-(\pi/2)\{ \cos a\omega[\text{Ci}(a\omega) - \ln a] + \sin a\omega[\text{Si}(a\omega) - \pi/2] \}$
12 $t^{-1} \ln(1 + a^2 t^2) \quad a > 0$	$-\pi \text{Ei}(-\omega/a)$
13 $\ln \frac{t+a}{ t-a } \quad a > 0$	$(\pi/\omega) \sin a\omega$

#### 3.7.2.4 Trigonometric Functions

$f(t)$	$F_s(\omega)$
1 $t^{-1} \sin^2(at) \quad a > 0$	$\pi/4 \quad 0 < \omega < 2a$ $\pi/8 \quad \omega = 2a \quad 0 < \omega > 2a$
2 $t^{-2} \sin^2(at) \quad a > 0$	$(1/4)(\omega + 2a) \ln  \omega + 2a  + (1/4)(\omega - 2a) \ln  \omega - 2a  - (1/2)\omega \ln \omega$
3 $t^{-2} [1 - \cos at] \quad a > 0$	$(\omega/2) \ln  (\omega^2 - a^2)/\omega^2  + (a/2) \ln  (\omega + a)/(\omega - a) $
4 $\sin(at^2) \quad a > 0$	$(\pi/2a)^{1/2} \{ \cos(\omega^2/4a) C[\omega/(2\pi a)^{1/2}] + \sin(\omega^2/4a) S[\omega/(2\pi a)^{1/2}] \}$
5 $\cos(at^2) \quad a > 0$	$(\pi/2a)^{1/2} \{ \sin(\omega^2/4a) C[\omega/(2\pi a)^{1/2}] - \cos(\omega^2/4a) S[\omega/(2\pi a)^{1/2}] \}$
6 $\tan^{-1}(a/t) \quad a > 0$	$(\pi/2\omega)[1 - \exp(-a\omega)]$

### 3.7.3 Notations and Definitions

- $f(t)$ : Piecewise smooth and absolutely integrable function on the positive real line.
- $F_c(\omega)$ : The FCT of  $f(t)$ .
- $F_s(\omega)$ : The FST of  $f(t)$ .
- $f_o(t)$ : The odd extension of the function  $f$  over the entire real line.
- $f_e(t)$ : The even extension of the function  $f$  over the entire real line.
- $C(\omega)$  is defined as the integral:

$$(2\pi)^{-1/2} \int_0^\omega t^{-1/2} \cos t dt.$$

- $S(\omega)$  is defined as the integral:

$$(2\pi)^{-1/2} \int_0^\omega t^{-1/2} \sin t dt.$$

- $\text{Ei}(x)$  is the exponential integral function defined as

$$-\int_{-x}^\infty t^{-1} e^{-t} dt, \quad |\arg(x)| < \pi.$$

9.  $\overline{\text{Ei}}(x)$  is defined as  $(1/2)[\text{Ei}(x+j0) + \text{Ei}(x-j0)]$ .

10.  $\text{Ci}(x)$  is the cosine integral function defined as

$$-\int_{-x}^{\infty} t^{-1} \cos t \, dt.$$

11.  $\text{Si}(x)$  is the sine integral function defined as

$$\int_0^x t^{-1} \sin t \, dt.$$

12.  $I_\nu(z)$  is the modified Bessel function of the first kind defined as

$$\sum_{m=0}^{\infty} \frac{(z/2)^{\nu+2m}}{m!\Gamma(\nu+m+1)}, \quad |z| < \infty, |\arg(x)| < \pi.$$

13.  $\text{He}_n(x)$  is the Hermite polynomial function defined as

$$(-1)^n \exp(x^2/2) \frac{d^n}{dx^n} [\exp(-x^2/2)].$$

14.  $C$  is the Euler constant defined as

$$\lim_{m \rightarrow \infty} \left[ \sum_{n=1}^m (1/n) - \ln m \right] = 0.5772156649 \dots$$

15.  $\text{ci}(x)$  and  $\text{si}(x)$  are related to  $\text{Ci}(x)$  and  $\text{Si}(x)$  by the equations:

$$\text{ci}(x) = -\text{Ci}(x), \quad \text{si}(x) = \text{Si}(x) - \pi/2.$$

16.  $\text{Erf}(x)$  is the error function defined by

$$(2/\sqrt{\pi}) \int_0^x \exp(-t^2) dt.$$

17.  $J_\nu(x)$  and  $Y_\nu(x)$  are the Bessel functions for the first and second kind, respectively,

$$J_\nu(x) = \sum_{m=0}^{\infty} (-1)^m \frac{(x/2)^{\nu+2m}}{m!\Gamma(\nu+m+1)}$$

and

$$Y_\nu(x) = \text{cosec}\{\nu\pi [J_\nu(x) \cos \nu\pi - J_{-\nu}(x)]\}.$$

18.  $U(t)$ : is the Heaviside step function defined as

$$U(t) = 0 \quad t < 0, \\ = 1 \quad t > 0.$$

## References

- Churchill, R.V. 1958. *Operational Mathematics*, 3rd ed. New York: McGraw-Hill.
- Coifman, R.R. and Meyer, Y. 1991. Remarques sur l'analyse de Fourier a fenetre, series I, *C.R. Acad. Sci., Paris*, 312, 259-261.
- Erdelyi, A. 1954. *Bateman Manuscript*, Vol. 1, New York: McGraw-Hill.
- Li, J. 1997. *Lapped Transforms Based on DLS and DLC Basic Function and Applications*, Ph.D. dissertation, McMaster University, Hamilton, Ontario, Canada.
- Malvar, H. 1992. *Signal Processing with Lapped Transforms*, Artech House, Boston.
- Rao, K.R. and Yip, P. 1990. *Discrete Cosine Transform: Algorithms, Advantages, Applications*. Boston: Academic Press.
- Sneddon, I.N. 1972. *The Uses of Integral Transforms*. New York: McGraw-Hill

# Hartley Transform

---

4.1	Introduction.....	4-1
4.2	Historical Background.....	4-1
4.3	Fundamentals of the Hartley Transform.....	4-2
	The Relationship between the Hartley and the Sine and Cosine Transforms •	
	The Relationship between the Hartley and Fourier Transforms • The Relationship between	
	the Hartley and Hilbert Transforms • The Relationship between the Hartley	
	and Laplace Transforms • The Relationship between the Hartley and Real Fourier	
	Transforms • The Relationship between the Hartley and the Complex	
	and Real Mellin Transforms	
4.4	Elementary Properties of the Hartley Transform.....	4-7
4.5	The Hartley Transform in Multiple Dimensions.....	4-10
4.6	Systems Analysis Using a Hartley Series Representation of a Temporal	
	or Spacial Function.....	4-10
	Transfer Function Methodology and the Hartley Series • The Hartley Series Applied	
	to Electric Power Quality Assessment	
4.7	Application of the Hartley Transform via the Fast Hartley Transform.....	4-17
	Convolution in the Time and Transform Domains • An Illustrative Example •	
	Solution Method for Transient or Aperiodic Excitations	
4.8	Table of Hartley Transforms.....	4-25
	Appendix: A Sample FHT Program.....	4-28
	Acknowledgments.....	4-31
	References.....	4-31

Kraig J. Olejniczak  
University of Arkansas

## 4.1 Introduction

The Hartley transform is an integral transformation that maps a *real-valued* temporal or special function into a *real-valued* frequency via the kernel,  $\text{cas}(vx) \equiv \cos(vx) + \sin(vx)$ . This novel symmetrical formulation of the traditional Fourier transform (FT), attributed to Ralph Vinton Lyon Hartley in 1942,<sup>1</sup> leads to a parallelism that exists between the function of the original variable and that of its transform. Furthermore, the Hartley transform permits a function to be decomposed into two *independent* sets of sinusoidal components; these sets are represented in terms of positive and negative frequency components, respectively. This is in contrast to the complex exponential,  $\exp(j\omega x)$ , used in classical Fourier analysis. For periodic power signals, various mathematical forms of the familiar Fourier series (FS) come to mind. For aperiodic energy and power signals of either finite or infinite duration, the Fourier integral can be used. In either case, signal and systems analysis and design in the frequency domain using the Hartley transform may be deserving of increased awareness due necessarily to the existence of a fast algorithm that can substantially lessen the computational burden when compared to the classical complex-valued fast Fourier transform (FFT).

Throughout the remainder of this chapter, it is assumed that the function to be transformed is real valued. In most engineering applications of practical interest, this is indeed the case. However, in the case where complex-valued functions are of interest, they may be analyzed using the novel complex Hartley transform formulation presented in Ref. [10].

## 4.2 Historical Background

Ralph V. L. Hartley was born in Spruce Mountain, approximately 50 miles south of Wells, Nevada, in 1888. After graduating with the A.B. degree from the University of Utah in 1909, he studied at Oxford for 3 years as a Rhodes Scholar where he received the B.A. and B.Sc. degrees in 1912 and 1913, respectively. Upon completing his education, Hartley returned from England and began his professional career with the Western Electric Company engineering department (New York) in September of the same year. It was here at AT&T's R&D unit that he became an expert on receiving sets and was in charge of the early development of radio receivers for the transatlantic radio telephone tests of 1915. His famous oscillating circuit, known as the Hartley oscillator, was invented during this work as well as a neutralizing circuit to offset the internal coupling of triodes that tended to cause singing.



During World War I, Hartley performed research on the problem of binaural location of a sound source. He formulated the accepted theory that direction was perceived by the phase difference of sound waves caused by the longer path to one ear then to the other. After the war, Hartley headed the research effort on repeaters and voice and carrier transmission. During this period, Hartley advanced Fourier analysis methods so that AC measurement techniques could be applied to telegraph transmission studies. In his effort to ensure some privacy for radio, he also developed the frequency-inversion system known to some as *greyqui hoy*.

In 1925, Hartley and his fellow research scientists and engineers became founding members of the Bell Telephone Laboratories when a corporate restructuring set R&D off as a separate entity. This change affected neither Hartley's position nor his work. R. V. L. Hartley was well known for his ability to clarify and arrange ideas into patterns that could be easily understood by others. In his paper entitled "Transmission of Information" presented at the International Congress of Telegraphy and Telephony in Commemoration of Volta at Lake Como, Italy, in 1927, he stated the law that was implicitly understood by many transmission engineers at that time, namely "the total amount of information which may be transmitted over such a system is proportional to the product of the frequency-range which it transmits by the time during which it is available for the transmission."<sup>2</sup> This contribution to information theory was later known by his name.

In 1929, Hartley gave up leadership of his research group due to illness. In 1939, he returned as a research consultant on transmission problems. During World War II he acted as a consultant on servomechanisms as applied to radar and fire control. Hartley, a fellow of the Institute of Radio Engineers (I.R.E.), the American Association for the Advancement of Science, the Physical and Acoustical Societies, and a member of the A.I.E.E., was awarded the I.R.E. Medal of Honor on January 24, 1946, "For his early work on oscillating circuits employing triode tubes and likewise for his early recognition and clear exposition of the fundamental relationship between the total amount of information which may be transmitted over a transmission system of limited band and the time required." Hartley was the holder of 72 patents that documented his contributions and developments. A transmission expert, he retired from Bell Laboratories in 1950 and died at the age of 81 on May 1, 1970.

### 4.3 Fundamentals of the Hartley Transform

Perhaps one of Hartley's most long-lasting contributions was a more symmetrical Fourier integral originally developed for steady-state and transient analysis of telephone transmission system problems.<sup>1</sup> Although this transform remained in a quiescent state for over 40 years, the Hartley transform was rediscovered more than a decade ago by Wang<sup>3-6</sup> and Bracewell<sup>7-9</sup> who authored definitive treatises on the subject.

The Hartley transform of a function  $f(x)$  can be expressed as either

$$H(v) = \frac{1}{\sqrt{2\pi}} \int_{-\infty}^{\infty} f(x) \text{cas}(vx) dx \quad (4.1a)$$

or

$$H(f) = \int_{-\infty}^{\infty} f(x) \text{cas}(2\pi fx) dx \quad (4.1b)$$

where the angular or radian frequency variable  $v$  is related to the frequency variable  $f$  by  $v = 2\pi f$  and

$$H(f) = \sqrt{2\pi} H(2\pi f) = \sqrt{2\pi} H(v). \quad (4.2)$$

Here the integral kernel, known as the cosine-and-sine or cas function, is defined as

$$\begin{aligned} \text{cas}(vx) &\equiv \cos(vx) + \sin(vx) \\ \text{cas}(vx) &= \sqrt{2} \sin\left(vx + \frac{\pi}{4}\right) \\ \text{cas}(vx) &= \sqrt{2} \cos\left(vx - \frac{\pi}{4}\right) \end{aligned} \quad (4.3)$$

Figure 4.1 depicts the cas function on the interval  $[0, 2\pi]$ . Additional properties of the cas function are shown in Tables 4.1 through 4.5 below.

The inverse Hartley transform may be defined as either

$$f(x) = \frac{1}{\sqrt{2\pi}} \int_{-\infty}^{\infty} H(v) \text{cas}(vx) dv \quad (4.4a)$$

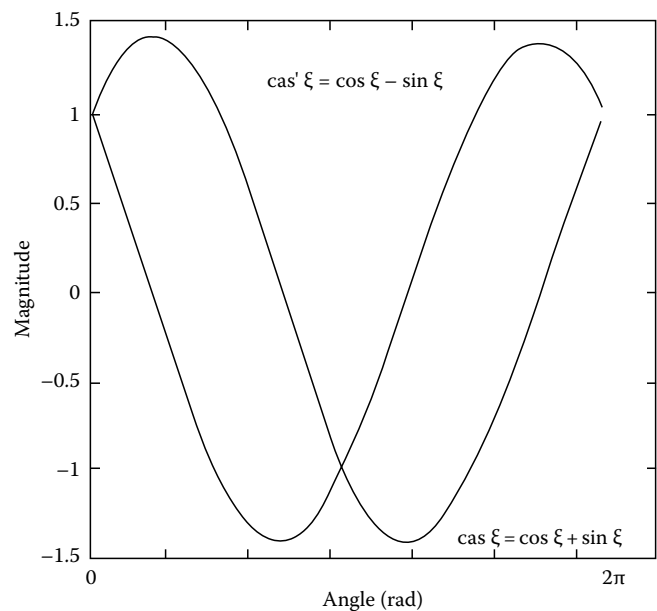


FIGURE 4.1 The cas function on the interval  $[0, 2\pi]$ .

**TABLE 4.1** Selected Trigonometric Properties of the cas Function

The cas function	$\text{cas } \xi = \cos \xi + \sin \xi$
The cas function	$\text{cas } \xi = \frac{1}{2}[(1 + j)\exp(-j\xi) + (1 - j)\exp(j\xi)]$
The complementary cas function	$\text{cas}' \xi = \text{cas}(-\xi) = \cos \xi - \sin \xi$
The complementary cas function	$\sqrt{2} \sin(\xi + \frac{3\pi}{4}) = \sqrt{2} \cos(\xi + \frac{\pi}{4})$
Relation to cos	$\cos \xi = \frac{1}{2}[\text{cas } \xi + \text{cas}(-\xi)]$
Relation to sin	$\sin \xi = \frac{1}{2}[\text{cas } \xi - \text{cas}(-\xi)]$
Reciprocal relation	$\text{cas } \xi = \frac{\csc \xi + \sec \xi}{\sec \xi + \csc \xi}$
Product relation	$\text{cas } \xi = \cot \xi \sin \xi + \tan \xi \cos \xi$
Function product relation	$\text{cas } \tau \text{ cas } \nu = \cos(\tau - \nu) + \sin(\tau + \nu)$
Quotient relation	$\text{cas } \xi = \frac{\cot \xi \sec \xi + \tan \xi \csc \xi}{\csc \xi \sec \xi}$
Double angle relation	$\text{cas } 2\xi = \text{cas}^2 \xi - \text{cas}^2(-\xi)$
Indefinite integral relation	$\int \text{cas}(\tau) d\tau = -\text{cas}(-\tau) = -\text{cas}' \tau$
Derivative relation	$\frac{d}{dt} \text{cas } \tau = \text{cas}(-\tau) = \text{cas}' \tau$
Angle-sum relation	$\text{cas}(\tau + \nu) = \cos \tau \text{ cas } \nu + \sin \tau \text{ cas}' \nu$
Angle-difference relation	$\text{cas}(\tau - \nu) = \cos \tau \text{ cas}' \nu + \sin \tau \text{ cas } \nu$
Function-sum relation	$\text{cas } \tau + \text{cas } \nu = 2 \text{cas} \frac{1}{2}(\tau + \nu) \cos \frac{1}{2}(\tau - \nu)$
Function-difference relation	$\text{cas } \tau - \text{cas } \nu = 2 \text{cas}' \frac{1}{2}(\tau + \nu) \sin \frac{1}{2}(\tau - \nu)$

**TABLE 4.2** Signs of the cas Function

Quadrant	cas
I	+
II	+ and -
III	-
IV	+ and -

**TABLE 4.3** Variations of the cas Function

Quadrant	cas
I	+1 → +1 with a maximum at $\frac{\pi}{4}$
II	+1 → -1
III	-1 → -1 with a minimum at $\frac{5\pi}{4}$
IV	-1 → +1

or

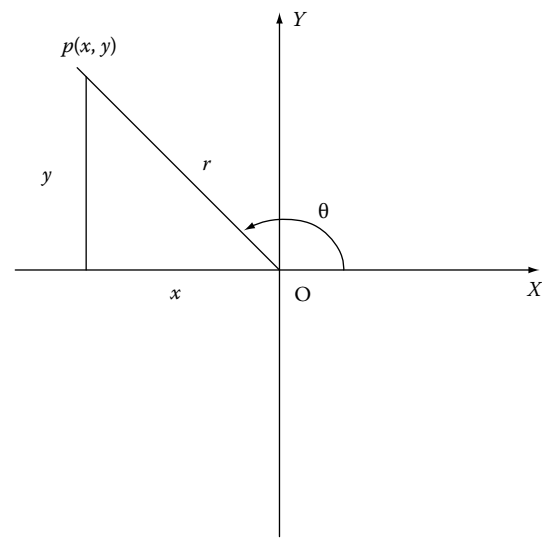
$$f(x) = \int_{-\infty}^{\infty} H(f) \text{cas}(2\pi fx) df. \quad (4.4b)$$

The angular frequency variable  $\nu$ , with units of radians per second, is equivalent to the frequency variable  $\omega$  in the Fourier domain; however, it is used here to further distinguish  $H(\nu)$ , the Hartley transform of  $f(x)$ , from the FT of  $f(x)$ ,  $F(\omega)$ . From Hartley's original formulation expressed in Equations 4.1a and 4.4a, it is clear that the inverse transformation (synthesis equation) calls for the identical integral operation as the direct transformation (analysis equation). The peculiar scaling coefficient

**TABLE 4.4** Trigonometric Functions of Some Special Angles

Angles	cas
$0^\circ = 0$	0
$30^\circ = \frac{\pi}{6}$	$\frac{1}{2}(\sqrt{3} + 1)$
$45^\circ = \frac{\pi}{4}$	$\sqrt{2}$
$60^\circ = \frac{\pi}{3}$	$\frac{1}{2}(1 + \sqrt{3})$
$90^\circ = \frac{\pi}{2}$	1
$120^\circ = \frac{2\pi}{3}$	$\frac{1}{2}(-1 + \sqrt{3})$
$150^\circ = \frac{5\pi}{6}$	$\frac{1}{2}(1 - \sqrt{3})$
$180^\circ = \pi$	-1
$270^\circ = \frac{3\pi}{2}$	-1

**TABLE 4.5** The Trigonometric Function of an Arbitrary Angle



$1/\sqrt{2\pi}$ , chosen by Hartley for the direct and inverse transformations, is used to satisfy the self-inverse condition depicted in Figure 4.2. When the independent variable is angular frequency with units of radians per second, other coefficients may be used provided that the product of the direct and inverse transform coefficients is  $1/2\pi$ .

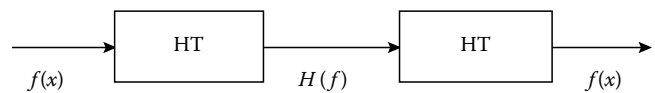


**FIGURE 4.2** The self-inverse property associated with the Hartley transform.

If one lets  $\theta$  be any angle in the  $x$ - $y$  plane and  $p(x, y)$  denotes any point on the terminal side of that angle, then denoting the positive distance from the origin to  $p$  as  $r$ ,

$$\cos \theta = \frac{x}{r} \quad \sin \theta = \frac{y}{r} \quad \text{cas } \theta = \frac{x+y}{\sqrt{x^2+y^2}}.$$

The existence of the Hartley transform of  $f(x)$  given by Equations 4.1a and b is equivalent to the existence of the FT of  $f(x)$  given by

$$f(x) = \frac{1}{2\pi} \int_{-\infty}^{\infty} \int_{-\infty}^{\infty} f(\zeta) \cos[\omega(x-\zeta)] d\zeta d\omega. \quad (4.5)$$

Equation 4.5 can also be equivalently expressed by the following three equations:

$$f(x) = \frac{1}{\sqrt{2\pi}} \int_{-\infty}^{\infty} [C(\omega) \cos(\omega x) + S(\omega) \sin(\omega x)] d\omega \quad (4.6)$$

$$\begin{aligned} C(\omega) &= \frac{1}{\sqrt{2\pi}} \int_{-\infty}^{\infty} f(x) \cos(\omega x) dx \\ &= H^e(f) = \frac{H(f) + H(-f)}{2} \end{aligned} \quad (4.7)$$

$$\begin{aligned} S(\omega) &= \frac{1}{\sqrt{2\pi}} \int_{-\infty}^{\infty} f(x) \sin(\omega x) dx \\ &= H^o(f) = \frac{H(f) - H(-f)}{2} \end{aligned} \quad (4.8)$$

where  $H^e(f)$  and  $H^o(f)$  are the even and odd part of the Hartley transform  $H(f)$ , respectively. Alternatively, Equation 4.5 can be expressed as

$$f(x) = \frac{1}{\sqrt{2\pi}} \int_{-\infty}^{\infty} F(\omega) e^{j\omega x} d\omega \quad (4.9a)$$

where

$$F(\omega) = \frac{1}{\sqrt{2\pi}} \int_{-\infty}^{\infty} f(x) e^{-j\omega x} dx. \quad (4.9b)$$

Although the transform pair defined by Equations 4.1a and 4.4a are equivalent to either Equations 4.6 through 4.8 or Equations 4.9a and b, note that the variables  $x$  and  $\nu$  are symmetrically embedded in the former but in neither of the latter.

To derive Equations 4.1a and 4.4a, let

$$H(\nu) = C(\omega) + S(\omega)|_{\omega=\nu}, \quad (4.10)$$

the linear combination of the cosine and sine transforms. Then, Equation 4.4a follows by linearity applied to Equations 4.7

and 4.8. Because  $C(\omega)$  and  $S(\omega)$  are an even and odd function of  $\omega$ , respectively, then

$$\frac{1}{\sqrt{2\pi}} \int_{-\infty}^{\infty} [C(\omega) \sin(\omega x) + S(\omega) \cos(\omega x)] d\omega = 0. \quad (4.11)$$

When Equation 4.11 is added to the right-hand side of Equations 4.1a and 4.6 results. It is interesting to note that Equations 4.5 through 4.8 are similar to Equations 4.1a and 4.4a when  $f(x)$  is real, in that  $C(\omega)$  and  $S(\omega)$  are real, as is  $H(\nu)$  via Equation 4.10. This is in stark contrast to the complex nature of Equation 4.9b when  $f(x)$  is real.

The following expressions are used to further explain the physical nature of the Hartley transform. The functions  $f(x) = f^e(x) + f^o(x)$ ,  $x > 0$ , and  $H(\nu) = H^e(\nu) + H^o(\nu)$ ,  $\nu > 0$ , can be resolved into their even and odd components as follows:<sup>1</sup>

$$f^e(x) = \frac{1}{2} [f(x) + f(-x)], \quad x > 0 \quad (4.12)$$

$$= \frac{1}{\sqrt{2\pi}} \int_{-\infty}^{\infty} H^e(\nu) \cos(\nu x) d\nu \quad (4.13)$$

$$= \frac{1}{\sqrt{2\pi}} \int_{-\infty}^{\infty} H(\nu) \cos(\nu x) d\nu$$

$$f^o(x) = \frac{1}{2} [f(x) - f(-x)], \quad x > 0 \quad (4.14)$$

$$= \frac{1}{\sqrt{2\pi}} \int_{-\infty}^{\infty} H^o(\nu) \sin(\nu x) d\nu \quad (4.15)$$

$$= \frac{1}{\sqrt{2\pi}} \int_{-\infty}^{\infty} H(\nu) \sin(\nu x) d\nu$$

$$H^e(\nu) = \frac{1}{2} [H(\nu) + H(-\nu)], \quad \nu > 0 \quad (4.16)$$

$$= \frac{1}{\sqrt{2\pi}} \int_{-\infty}^{\infty} f^e(x) \cos(\nu x) dx \quad (4.17)$$

$$= \frac{1}{\sqrt{2\pi}} \int_{-\infty}^{\infty} f(x) \cos(\nu x) dx$$

$$H^o(\nu) = \frac{1}{2} [H(\nu) - H(-\nu)], \quad \nu > 0 \quad (4.18)$$

$$= \frac{1}{\sqrt{2\pi}} \int_{-\infty}^{\infty} f^o(x) \sin(\nu x) dx \quad (4.19)$$

$$= \frac{1}{\sqrt{2\pi}} \int_{-\infty}^{\infty} f(x) \sin(\nu x) dx.$$

It is readily known that when the function to be transformed is real valued, then its FT exhibits Hermitian symmetry. That is,

$$F(-\omega) = F^*(\omega) \quad (4.20)$$

where the superscript\* denotes complex conjugation. This implies that the FT is over specified because a dependency exists between transform values for positive and negative values of  $\omega$ , respectively. This inherent redundancy is *not* present in the Hartley transform. Observe the effect of positive and negative values of  $\nu$  in Equation 4.1a. Specifically, for negative values of  $\nu$ ,

$$\text{cas}(-\nu x) = \sqrt{2} \cos\left(-\nu x - \frac{\pi}{4}\right) = \sqrt{2} \cos\left(\nu x + \frac{\pi}{4}\right). \quad (4.21)$$

For positive values of  $\nu$ ,

$$\text{cas}(\nu x) = \sqrt{2} \sin\left(\nu x + \frac{\pi}{4}\right). \quad (4.22)$$

From Equation 4.4a it is clear that the function  $f(x)$  is composed of an equal number of positive and negative frequency components. In light of the two equations above, it seems that any two components, one at  $\nu$  and the other  $-\nu$ , vary as the cosine and sine of the same angle. Thus, whereas Equations 4.7 and 4.8 represent a resolution into sine and cosine components, each of which is further decomposed into positive and negative frequencies, the Hartley transform of Equation 4.1a amalgamates these two resolutions into one. Equation 4.6 alludes to the fact that although  $C(\omega)$  and  $S(\omega)$  are each defined for positive and negative values of  $\nu$ , because of their respective symmetry properties, they are completely specified by their values over either half range alone. This is due to the Hermitian symmetry existing into the FT as shown by Equation 4.20. Note in Equation 4.1a that  $H(\nu)$  is a single function that contains no redundancy; the value of  $H(\nu)$  for  $\nu < 0$  is *independent* of that for  $\nu > 0$ . Therefore,  $H(\nu)$  must be specified over the entire range of  $\nu$ .

Although not all time functions can be represented via the Fourier integral, for those functions where such a representation exists, there is a unique relationship between the function and its FT. This is possible if and only if the integral is convergent. Sufficient conditions (although not necessary to guarantee convergence of the Fourier integral) are the well-known Dirichlet conditions, which are stated below for convenience.

1.  $\int_{-\infty}^{\infty} |f(x)| dx < \infty$ , that is,  $f(x)$  is absolutely integrable.
2.  $f(x)$  has a finite number of discontinuities over any finite interval.
3.  $f(x)$  has a finite number of local maximum and local minimum points over any finite interval.

The above sufficient conditions include most finite-energy signals of engineering interest. Unfortunately, important signals such as periodic signals and the unit step function are not absolutely integrable. If we allow the FT, and thus the Hartley

transform, to include the Dirac delta function, then even these signals can be handled using methods similar to those for finite-energy signals. This should not be surprising because the Hartley transform is simply a symmetrical representation of the FT.

### 4.3.1 The Relationship between the Hartley and the Sine and Cosine Transforms

The Hartley transform is trivially related to the cosine and sine transforms (see also Chapter 3) by the linear combination in Equation 4.10 and to each transform individually using the fifth and sixth entries of Table 4.1, respectively.

### 4.3.2 The Relationship between the Hartley and Fourier Transforms

The Hartley transform is closely related to the familiar FT. It can be easily shown via Equation 4.9b that these transforms are related in a very simple way

$$H(\nu) = [\mathcal{R}\{F(\omega)\} - \mathcal{I}\{F(\omega)\}]_{\omega=\nu} \quad (4.23)$$

where

$$\mathcal{R}\{F(\omega)\} = R(\omega) = H^e(\nu) = H^e(-\nu) \quad (4.24)$$

$$\mathcal{I}\{F(\omega)\} = I(\omega) = -H^o(\nu) = H^o(-\nu) \quad (4.25)$$

and

$$\begin{aligned} H(f) &= \frac{1+j1}{2}F(f) + \frac{1-j1}{2}F(-f) \\ H(f) &= \frac{1}{2}e^{j\pi/4}F(f) + \frac{1}{2}e^{-j\pi/4}F^*(f). \end{aligned} \quad (4.26)$$

The FT expressed in terms of the Hartley transform is

$$F(\omega) = \left[ \frac{H(\nu) + H(-\nu)}{2} - j \frac{H(\nu) - H(-\nu)}{2} \right]_{\nu=\omega} \quad (4.27)$$

$$F(\omega) = [H^e(\nu) - jH^o(\nu)]_{\nu=\omega}, \quad (4.28)$$

or alternatively as

$$F(f) = \frac{1}{2}e^{-j\pi/4}H(f) + \frac{1}{2}e^{j\pi/4}H(-f). \quad (4.29)$$

To summarize, the FT is the even part of the Hartley transform plus negative  $j$  times the odd part; similarly, the Hartley transform is the real part plus the negative imaginary part of the FT. Equation 4.23 will be used most often by the engineer when computing the Hartley transform of an arbitrary time or spacial function when the FT is known or readily available via a table lookup; when this is not the case, direct evaluation of Equation 4.1a or 4.1b is required

### 4.3.3 The Relationship between the Hartley and Hilbert Transforms

The Hilbert transform (see also Chapter 7),  $\hat{f}(x)$ , of a function  $f(x)$ , is obtained by convolving  $f(x)$  with the function  $1/\pi x$ . That is,

$$\hat{f}(x) = f(x) * \frac{1}{\pi x} = \frac{1}{\pi} \int_{-\infty}^{\infty} \frac{f(\lambda)}{x - \lambda} d\lambda$$

where the integral is assumed to be taken of its principal value. Here,  $*$  denotes linear convolution (see Property 7 in Section 4.4 and Section 1.3). The FT of  $\hat{f}(x)$  is found by convolving  $1/\pi x$  with the FT of  $f(x)$ ,  $F(f)$ . Applying Property 7 yields  $-j \operatorname{sgn} f F(f)$ . The Hartley transform of  $\hat{f}(x)$  is then found via Equation 4.23.

Thus, a Hilbert transform simply shifts all positive-frequency components by  $-90^\circ$  and all negative-frequency components by  $+90^\circ$ . The amplitude always remains constant throughout this transformation.

### 4.3.4 The Relationship between the Hartley and Laplace Transforms

Because the Hartley transform is the symmetrical form of the classical FT defined in Equations 4.9a and b, it is most convenient to review how the FT relates to the one-sided or unilateral Laplace transform (LT). Although the unilateral LT is concerned with time functions for  $t > 0$ , the FT includes both positive and negative time but falters with functions have finite average power because the concept of the Dirac delta function must be introduced.

For most functions of practical engineering significance, the conversion from the Laplace to the FT of  $f(x)$  is quite straightforward. However, more difficult situations do exist but are rarely encountered in practical engineering problems; thus, these situations will not be discussed any further.

#### 4.3.4.1 $F(s)$ with Poles in the Left-Half Plane (LHP) Only<sup>10</sup>

When the LT of a function  $f(x)$  has no poles on the  $j\omega$  axis and poles only in the LHP, the FT may be computed from the LT by simply substituting  $s = j\omega$ . These transforms include all finite-energy signals defined for positive time only. As an example, because

$$F(s) = \mathcal{L}\{e^{-\alpha t} u(t)\} = \frac{1}{s + \alpha} \mathcal{R}(s) > -\alpha$$

for all values of  $\alpha$ , then if  $\alpha$  is positive, the single pole of  $F(s)$  resides in the LHP at  $s = -\alpha$ . Thus,

$$F(\omega) = \mathcal{F}\{e^{-\alpha t} u(t)\} = F(s)|_{s=j\omega} = \frac{1}{s + \alpha} \Big|_{s=j\omega} = \frac{1}{j\omega + \alpha}.$$

Lastly, to obtain the Hartley transform of  $f(x)$ , apply Equation 4.23 to  $F(\omega)$  above, or evaluate Equation 4.4a directly. Thus,

$$H(\nu) = \mathcal{R}\left\{\frac{1}{\alpha + j\omega}\right\} - \mathcal{I}\left\{\frac{1}{\alpha + j\omega}\right\} = \frac{\alpha + \omega}{\alpha^2 + \omega^2}.$$

#### 4.3.4.2 $F(s)$ with Poles in the LHP and on the $j\omega$ Axis<sup>10</sup>

When the LT of a function  $f(x)$  has poles in the LHP and on the  $j\omega$  axis, those terms with LHP poles are treated in the same manner as described above in Section 4.3.4.1. Each simple pole on the imaginary axis will result in two terms in the Fourier domain: one is obtained by substituting  $s = j\omega$  and the other is found by the method of residues. The latter term results in a  $\delta$  function having strength of  $\pi$  times the residue at the pole. Mathematically, this is expressed as

$$F(\omega) = F(s)|_{s=j\omega} + \pi \sum_n k_n \delta(\omega - \omega_n). \quad (4.30)$$

For example, consider the LT of the function  $\cos \omega_0 t u(t)$ . Via partial fraction expansion,  $F(s)$  can be written as

$$F(s) = \frac{s}{s^2 + \omega_0^2} = \frac{\frac{1}{2}}{s + j\omega_0} + \frac{\frac{1}{2}}{s - j\omega_0}.$$

Invoking Equation 4.30 leads to the following expression in the Fourier domain

$$F(\omega) = \frac{j\omega}{\omega_0^2 - \omega^2} + \frac{\pi}{2} [\delta(\omega + \omega_0) + \delta(\omega - \omega_0)].$$

Once again, to obtain the Hartley transform of  $f(x)$ , apply Equation 4.23 to  $F(\omega)$ .

### 4.3.5 The Relationship between the Hartley and Real Fourier Transforms

The real Fourier transform (RFT) of a real signal  $f(x)$  of finite energy can be defined as

$$F(\Omega) = 2 \int_{-\infty}^{\infty} f(x) \cos [2\pi\Omega x + \Theta(\Omega)] dx \quad (4.31)$$

where

$$\Theta(\Omega) = \begin{cases} 0, & \text{if } \Omega \geq 0 \\ \frac{\pi}{2}, & \text{if } \Omega < 0 \end{cases} \quad (4.32)$$

and  $\Omega = f$  is the frequency variable with units of Hertz.

The inverse RFT is given by

$$f(x) = \int_{-\infty}^{\infty} F(\Omega) \cos [2\pi\Omega x + \Theta(\Omega)] d\Omega. \quad (4.33)$$

The transform pair (4.31) and (4.33) can also be written for  $\Omega \geq 0$  as

$$F^e(\Omega) = 2 \int_{-\infty}^{\infty} f(x) \cos(2\pi\Omega x) dx \quad (4.34)$$

$$F^o(\Omega) = 2 \int_{-\infty}^{\infty} f(x) \sin(2\pi\Omega x) dx \quad (4.35)$$

and

$$f(x) = \int_0^{\infty} [F^e(\Omega) \cos(2\pi\Omega x) + F^o(\Omega) \sin(2\pi\Omega x)] d\Omega. \quad (4.36)$$

Thus,  $F(\Omega)$  equals  $F^e(\Omega)$  for  $\Omega \geq 0$ , and  $F^o(\Omega)$  for  $\Omega < 0$ . Note the similarity between Equations 4.34 and 4.35 with Equations 4.7 and 4.8.

The Hartley transform of  $f(x)$  is related to the RFT by

$$\begin{bmatrix} H(f) \\ H(-f) \end{bmatrix} = \frac{1}{2} \begin{bmatrix} 1 & 1 \\ 1 & -1 \end{bmatrix} \begin{bmatrix} F^e(\Omega) \\ F^o(\Omega) \end{bmatrix}. \quad (4.37)$$

### 4.3.6 The Relationship between the Hartley and the Complex and Real Mellin Transforms

The Mellin transform is useful in scale-invariant image and speech recognition application.<sup>11</sup> The complex Mellin transform is given by

$$F_M(s) = \int_0^{\infty} f(x)x^{s-1} dx \quad (4.38)$$

where the complex variable  $s = \sigma + j\omega$ . If one substitutes  $\exp(-x)$  for the variable  $x$ , then Equation 4.38 becomes

$$F_M(s) = \int_{-\infty}^{\infty} f'(x)e^{-xs} dx \quad (4.39)$$

where

$$f'(x) = f(e^{-x})$$

Thus, from Equation 4.39, the complex Mellin transform is the two-sided or bilateral LT of  $f'(x)$ .

Equation 4.39 can also be written as

$$F_M(\sigma + j\omega) = \int_{-\infty}^{\infty} f''(x)e^{-j\omega x} dx \quad (4.40)$$

where

$$f''(x) = f(e^{-x})e^{-\sigma x}.$$

Thus, the complex Mellin transform is the FT of  $f''(x)$ . The Hartley transform of  $f''(x) = f(e^{-x})e^{-\sigma x}$  can then be found by direct application of Equation 4.23.

The inverse complex Mellin transform can be written as

$$f(e^{-x}) = e^{\sigma x} \int_{-\infty}^{\infty} F_M(\sigma + j\omega) e^{j\omega x} df. \quad (4.41)$$

The real Mellin transform can be written as

$$F^e(\sigma, \omega) = 2 \int_{-\infty}^{\infty} f''(x) \cos(\omega x) dx \quad (4.42)$$

and

$$F^o(\sigma, \omega) = 2 \int_{-\infty}^{\infty} f''(x) \sin(\omega x) dx. \quad (4.43)$$

By analogy to Equations 4.34 and 4.35, the Hartley transform of  $f''(x)$  is related to the real Mellin transform by

$$\begin{bmatrix} H(f) \\ H(-f) \end{bmatrix} = \frac{1}{2} \begin{bmatrix} 1 & 1 \\ 1 & -1 \end{bmatrix} \begin{bmatrix} F^e(\sigma, \omega) \\ F^o(\sigma, \omega) \end{bmatrix}. \quad (4.44)$$

The inverse real Mellin transform is given by

$$f(e^{-x}) = e^{\sigma x} \int_0^{\infty} [F^e(\sigma, \omega) \cos(\omega x) + F^o(\sigma, \omega) \sin(\omega x)] d\omega. \quad (4.45)$$

## 4.4 Elementary Properties of the Hartley Transform

In this section, several Hartley transform theorems are presented. These theorems are very useful for generating Hartley transform pairs as well as in signal and systems analysis. In most cases, proofs are presented; examples to illustrate their application are left to specific example problems contained later in this chapter.

### Property 1: Linearity

If  $f_1(x)$  and  $f_2(x)$  have the Hartley transforms  $H_1(f)$  and  $H_2(f)$ , respectively, then the sum  $\alpha f_1(x) + \beta f_2(x)$  has the Hartley transform  $\alpha H_1(f) + \beta H_2(f)$ . This property is established as follows:

$$\begin{aligned} & \int_{-\infty}^{\infty} [\alpha f_1(x) + \beta f_2(x)] \text{cas}(2\pi fx) dx \\ &= \alpha \int_{-\infty}^{\infty} f_1(x) \text{cas}(2\pi fx) dx + \beta \int_{-\infty}^{\infty} f_2(x) \text{cas}(2\pi fx) dx \\ &= \alpha H_1(f) + \beta H_2(f). \end{aligned} \quad (4.46)$$

*Property 2: Power spectrum and phase*

The power spectrum for a signal  $f(x)$  can be expressed in the Fourier domain as

$$P(f) = |F(f)|^2 = \mathcal{R}\{F(f)\}^2 + \mathcal{I}\{F(f)\}^2.$$

The power spectrum can be obtained directly from the Hartley transform using Equations 4.16 through 4.19 as follows:

$$\begin{aligned} P(f) &= |F(f)|^2 = \mathcal{R}\{F(f)\}^2 + \mathcal{I}\{F(f)\}^2 \\ &= [H^e(f)]^2 + [-H^o(f)]^2 \\ &= \frac{1}{4}[H(f) + H(-f)]^2 + \frac{1}{4}[H(f) - H(-f)]^2 \\ P(f) &= \frac{[H(f)]^2 + [H(-f)]^2}{2}. \end{aligned} \quad (4.47)$$

The phase associated with the FT of  $f(x)$  is well known; this is expressed as

$$\begin{aligned} \Phi(f) &= \tan^{-1} \left[ \frac{\mathcal{I}\{F(f)\}}{\mathcal{R}\{F(f)\}} \right] = \tan^{-1} \left[ \frac{-H^o(f)}{H^e(f)} \right] \\ \Phi(f) &= \tan^{-1} \left[ \frac{H(-f) - H(f)}{H(f) + H(-f)} \right]. \end{aligned} \quad (4.48)$$

Note that the power spectrum  $P(f)$  will always be even.

*Property 3: Scaling/Similarity*

If the Hartley transform of  $f(x)$  is  $H(f)$ , then the Hartley transform of  $f(kx)$  where  $k$  is a real constant greater than zero is determined by

$$\begin{aligned} \int_{-\infty}^{\infty} f(kx) \operatorname{cas}(2\pi fx) dx &= \int_{-\infty}^{\infty} f(x') \operatorname{cas}\left(\frac{2\pi fx'}{k}\right) \frac{dx'}{k} \\ &= \frac{1}{k} H\left(\frac{f}{k}\right). \end{aligned} \quad (4.49)$$

For  $k$  negative, the limits of integration for the new variable  $x' = kx$  are interchanged. Therefore, when  $k$  is negative, the last term in Equation 4.49 becomes  $(1/-k)H(f/k)$ . The amalgamation of these two solutions can be expressed as follows: If  $f(x)$  has the Hartley transform  $H(f)$  then  $f(k/x)$  has the Hartley transform  $(1/|k|)H(f/k)$ .

*Property 4: Function reversal*

If  $f(x)$  and  $H(f)$  are a Hartley transform pair, then the Hartley transform of  $f(-x)$  is  $H(-f)$ . This is clearly seen when  $k = -1$  is substituted into the last expression appearing in Property 3.

*Property 5: Function shift/delay*

If  $f(x)$  is shifted in time by a constant  $T$ , then by substituting  $x' = x - T$ , the Hartley transform becomes

$$H(f) = \int_{-\infty}^{\infty} f(x') \operatorname{cas}[2\pi f(x' + T)] dx'. \quad (4.50)$$

Notice that the basis function in Equation 4.50 can be expanded using the appropriate entry of Table 4.1 in the following manner:

$$\begin{aligned} \operatorname{cas}[2\pi f(x' + T)] &= \cos(2\pi fx') \cos(2\pi fT) + \cos(2\pi fx') \sin(2\pi fT) \\ &\quad + \sin(2\pi fx') \cos(2\pi fT) - \sin(2\pi fx') \sin(2\pi fT). \end{aligned}$$

Expanding Equation 4.50 into four integrals and grouping the first and third and second and fourth integrals, respectively, the final result is

$$H(f) = \cos(2\pi fT) H(f) + \sin(2\pi fT) H(-f). \quad (4.51)$$

*Property 6: Modulation*

If  $f(x)$  is modulated by the sinusoid  $\cos(2\pi f_0 x)$ , then transforming to the Hartley space via Equation 4.1b yields

$$\begin{aligned} H(f) &= \int_{-\infty}^{\infty} f(x) \cos(2\pi f_0 x) \operatorname{cas}(2\pi fx) dx \\ H(f) &= \int_{-\infty}^{\infty} f(x) \cos(2\pi f_0 x) \cos(2\pi fx) dx \\ &\quad + \int_{-\infty}^{\infty} f(x) \cos(2\pi f_0 x) \sin(2\pi fx) dx. \end{aligned} \quad (4.52)$$

Notice that if the function-product relations (i.e.,  $\cos \alpha$  and  $\cos \alpha \sin \beta$ ) are expanded and grouped accordingly, the following relation results:

$$H(f) = \frac{1}{2} H(f - f_0) + \frac{1}{2} H(f + f_0). \quad (4.53)$$

*Property 7: Convolution (\*)*

If  $f_1(x)$  has the Hartley transform  $H_1(f)$  and  $f_2(x)$  has the Hartley transform  $H_2(f)$ , then  $f_1(x) * f_2(x)$  has the Hartley transform

$$\begin{aligned} \frac{1}{2} [H_1(f)H_2(f) + H_1(-f)H_2(f) + H_1(f)H_2(-f) \\ - H_1(-f)H_2(-f)]. \end{aligned} \quad (4.54)$$

To obtain this result directly, simply substitute the convolution integral

$$f_1(x) * f_2(x) = \int_{-\infty}^{\infty} f_1(\lambda) f_2(x - \lambda) d\lambda \quad (4.55)$$

into Equation 4.1b and utilize Property 5. The result is as follows:

$$\begin{aligned}
 H(f) &= \int_{-\infty}^{\infty} [f_1(x) * f_2(x)] \text{cas}(2\pi fx) dx \\
 &= \int_{-\infty}^{\infty} \left[ \int_{-\infty}^{\infty} f_1(\lambda) f_2(x - \lambda) d\lambda \right] \text{cas}(2\pi fx) dx \\
 &= \int_{-\infty}^{\infty} f_1(\lambda) \left[ \int_{-\infty}^{\infty} f_2(x - \lambda) \text{cas}(2\pi fx) dx \right] d\lambda. \quad (4.56)
 \end{aligned}$$

Invoking the function shift/delay property (i.e., Property 5),

$$= \int_{-\infty}^{\infty} f_1(t) [\cos(2\pi f\lambda) H_2(f) + \sin(2\pi f\lambda) H_2(-f)] d\lambda.$$

Factoring the  $H_2(\cdot)$  term to the right and utilizing Equations 4.12 through 4.19, the result follows.

Note that Equation 4.54 simplifies for the following symmetries:

- If  $f_1(x)$  and/or  $f_2(x)$  is even, or if  $f_1(x)$  is even and  $f_2(x)$  is odd, or if  $f_1(x)$  is odd and  $f_2(x)$  is even, then  $f_1(x) * f_2(x) = H_1(f) H_2(f)$
- If  $f_1(x)$  is odd, then  $f_1(x) * f_2(x) = H_1(f) H_2(-f)$
- If  $f_2(x)$  is odd, then  $f_1(x) * f_2(x) = H_1(-f) H_2(f)$
- If both functions are odd, then  $f_1(x) * f_2(x) = H_1(f) H_2(f)$

In most practical situations, it is possible to shift one of the functions entering into the convolution such that it exhibits even or odd symmetry. When this is possible, Equation 4.54 simplifies to one *real* multiplication vs. the single *complex* multiplication (=four real multiplications and three real additions) in the Fourier domain.

**Property 8: Autocorrelation ( $\odot$ )**

If  $f_1(x)$  has the Hartley transform  $H_1(f)$ , then the autocorrelation of  $f_1(x)$  described by the equation below

$$f_1(x) \odot f_1(x) = f_1(x) * f_1(-x) = \int_{-\infty}^{\infty} f_1(\lambda) f_1(x + \lambda) d\lambda, \quad (4.57)$$

has the Hartley transform

$$\frac{1}{2} [H_1(f)^2 + H_1(-f)^2] = [H^e(f)]^2 + [H^o(f)]^2. \quad (4.58)$$

Comparing Equations 4.55 through 4.57, it is evident that the convolution and correlation integrals are closely related. Substituting the correlation integral of Equation 4.57 into the direct Hartley transform and utilizing Property 5, the result is as follows:

$$\begin{aligned}
 H(f) &= \int_{-\infty}^{\infty} \left[ \int_{-\infty}^{\infty} f_1(\lambda) f_1(x + \lambda) d\lambda \right] \text{cas}(2\pi fx) dx \\
 &= \int_{-\infty}^{\infty} f_1(x) \left[ \int_{-\infty}^{\infty} f_1(x + \lambda) \text{cas}(2\pi fx) dx \right] d\lambda. \quad (4.59)
 \end{aligned}$$

Invoking the function shift/delay property with  $T = -\lambda$ ,

$$= \int_{-\infty}^{\infty} f_1(x) [\cos(2\pi f\lambda) H_1(f) - \sin(2\pi f\lambda) H_1(-f)] d\lambda.$$

Factoring  $H_1(\cdot)$  to the right and utilizing Equations 4.12 through 4.19, the desired result follows.

**Property 9: Product**

If  $f_1(x)$  is multiplied by a second function  $f_2(x)$ , then the product  $f_1(x) f_2(x)$  is

$$\begin{aligned}
 &\frac{1}{2} [H_1(f) * H_2(f) + H_1(-f) * H_2(f) + H_1(f) * H_2(-f) \\
 &\quad - H_1(-f) * H_2(-f)] \\
 &= H_1^e(f) * H_2^e(f) - H_1^o(f) * H_2^o(f) + H_1^e(f) * H_2^o(f) \\
 &\quad + H_1^o(f) * H_2^e(f).
 \end{aligned}$$

**Property 10:  $n$ th derivative of a function  $f^{(n)}(x)$**

The  $n$ th derivative of a function  $f(x)$  is

$$f^{(n)}(x) = \text{cas}' \frac{n\pi}{2} (2\pi f)^n H[(-1)^n f]. \quad (4.60)$$

This property is derived by recursive application of Equation 4.23 to the FT of the function  $df(x)/dx$  and its higher-order derivatives.

A summary of the above properties appears in Table 4.6.

**TABLE 4.6** A Summary of Hartley Transform Theorems

Theorem	$f(x)$	$H(f)$
Linearity	$f_1(x) + f_2(x)$	$H_1(f) + H_2(f)$
Power spectrum	$P(f) = \frac{1}{2} \{H(f)^2 + H(-f)^2\}$	$\Phi(f) = \tan^{-1} \left[ \frac{H(-f) - H(f)}{H(f) + H(-f)} \right]$
Scaling/similarity	$f(kx)$	$\left  \frac{1}{k} \right  H\left(\frac{f}{k}\right)$
Reversal	$f(-x)$	$H(-f)$
Shift	$f(x - T)$	$H(f) = \cos(2\pi fT)H(f) + \sin(2\pi fT)H(-f)$
Modulation	$f(x) \cos(2\pi f_0 t)$	$H(f) = \frac{1}{2} H(f - f_0) + \frac{1}{2} H(f + f_0)$
Convolution	$f_1(x) * f_2(x)$	$\frac{1}{2} [H_1(f)H_2(f) + H_1(-f)H_2(f) + H_1(f)H_2(-f) - H_1(-f)H_2(-f)]$
Autocorrelation	$f_1(x) \odot f_1(x)$	$\frac{1}{2} [H_1(f)^2 + H_1(-f)^2]$
Product	$f_1(x)f_2(x)$	$\frac{1}{2} [H_1(f)*H_2(f) + H_1(-f)*H_2(f) + H_1(f)*H_2(-f) - H_1(-f)*H_2(-f)]$
$n$ th derivative	$f^{(n)}(x)$	$f^{(n)}(x) = \text{cas}' \frac{n\pi}{2} (2\pi f)^n H[(-1)^n f]$



## 4.5 The Hartley Transform in Multiple Dimensions

The Hartley transform also exists the dimensions. For a function  $f(x, y)$  the two-dimensional Hartley transform and its inverse is

$$H(u, v) = \int_{-\infty}^{\infty} \int_{-\infty}^{\infty} f(x, y) \text{cas}[2\pi(ux + vy)] dx dy \quad (4.61)$$

$$f(x, y) = \int_{-\infty}^{\infty} \int_{-\infty}^{\infty} H(u, v) \text{cas}[2\pi(ux + vy)] du dv. \quad (4.62)$$

Although a three-dimensional (3D) Hartley transform exists, it is above and beyond the scope of this treatise. That is, the user will not typically utilize the higher dimension continuous-time integral. Therefore, the reader is referred to Ref. [9] for details.

## 4.6 Systems Analysis Using a Hartley Series Representation of a Temporal or Spatial Function

The Hartley series (HS) is an infinite series expansion of a periodic signal in which the orthogonal basis functions in the series are the cosine-and-sine function,  $\text{cas}(k\nu_0 t)$ , where  $\nu_0 = 2\pi f_0 = 2\pi/T_0$  is the fundamental radian frequency. This series formulation differs from the FS in the selection of the basis functions; namely, the cas function vs. the complex exponential,  $\phi_k(t) = \exp(j2\pi kt/T_0)$ ,  $k = 0, \pm 1, \pm 2, \dots$  over the interval  $t_0 \leq t \leq t_0 + T_0$  where  $T_0$  is the fundamental period of the periodic function. The HS, so named as a result of the analogy drawn by Hartley to the FS,<sup>1</sup> is capable of representing all functions in that interval providing they satisfy certain mathematical conditions developed by Dirichlet (see Section 4.3).

If a system is linear and its impulse response is available, then the response of this system to applied inputs can be found using the principles of linearity and superposition. If the forcing function or excitation is represented as a weighted sum of individual components, called basis functions, then it is only necessary to calculate the response of the system to each of these components and add them together. This method leads to the convolution integral that was presented in Chapter 1. Before proceeding with a mathematical description of a set of basis functions  $\phi_k(t)$ , consider a desired forcing function being represented as a sum of weighted (i.e., having different strengths) impulse functions. These impulse functions produce responses that are amplitude-scaled and time-shifted versions of the response to a unit impulse. Summing all responses to each impulse results in the total response of the system to the forcing function. It seems that

the impulse function may be a type of basis function, and indeed it is.

There are a variety of basis functions that can be used for linear systems analysis. In addition to the impulse function,  $\delta(t)$ , one of the most familiar basis functions is the complex exponential  $\phi(t) = \exp(j\omega_0 t)$  corresponding to the FS. Another frequently used basis function is the complex exponential,  $\phi(t) = \exp(st)$  where  $s = \sigma + j\omega$  is a complex number. Clearly, the Fourier basis function is a specialization of  $\exp(st)$  with  $\sigma = 0$ . When applications involve linear systems analysis, sinusoidal functions are a convenient choice for basis functions. The reason for this choice is that the sum or difference of two sinusoids of the same frequency is still a sinusoid, and the derivative or integral of a sinusoid is still a sinusoid. These characteristics lend themselves well to sinusoidal steady-state analysis using the phasor concept.

Before proceeding further, it is helpful to summarize briefly properties and characteristics of basis functions. A most desirable quality of a set of basis functions is known as finality of coefficients. Referring to the equation below,

$$x(t) \approx \sum_{n=-N}^N a_n \phi_n(t), \quad (4.63)$$

a function represented by a finite number of coefficients and basis functions in the form of a linear combination can always be more accurately described by adding additional terms (i.e., increasing  $N$ ) to the linear combination without affecting any of the earlier coefficients. This desirable quality can be achieved if the basis functions are orthogonal over the time interval of interest (see also Section 1.5).

**Definition 4.1:** A set of functions  $\{\phi_n\}$ ,  $n = 0, \pm 1, \pm 2, \dots$  is an orthogonal set on the interval  $a \leq t \leq b$  if for every  $i \neq k$ ,

$$(\phi_i, \phi_k) = 0$$

where  $(\cdot, \cdot)$  denotes the inner product. Here, the inner product of two functions  $f$  and  $g$  is defined as

$$(f, g) = \int_a^b f(t)g^*(t)dt.$$

Using the integral relationship for an inner product, the condition for orthogonality of basis functions is that for all  $k$ ,

$$\int_{\tau}^{\tau+T_0} \phi_n(t)\phi_k^*(t)dt = \begin{cases} \lambda_k, & \text{if } k = n \\ 0, & \text{if } k \neq n \end{cases} \quad (4.64)$$

where  $\phi_k^*(t)$  is the complex conjugate of  $\phi_k(t)$  and the  $\lambda_k$  are real and  $\lambda_k \neq 0$ . If the basis functions are real, then  $\phi_k^*(t)$  can be

replaced by  $\phi_k(t)$ . Note that Equation 4.64 can be expressed more compactly by the following notation:

$$(\phi_n(t)\phi_k^*(t)) = \lambda_k \delta_{nk} \begin{cases} \lambda_k, & \text{if } k = n \\ 0, & \text{if } k \neq n \end{cases} \quad (4.65)$$

where  $\delta_{nk}$  is the Kronecker delta function.

In order to calculate the coefficients  $a_n$  appearing in Equation 4.63, the orthogonality property of the basis functions really demonstrates its desirable quality. If Equation 4.63 is multiplied on both sides by  $\phi_i^*(t)$ , for any  $i$ , and then integrated over the specified interval  $t$  to  $t + T$ , the following results:

$$\begin{aligned} \int_{\tau}^{\tau+T_0} \phi_i^*(t)x(t)dt &= \int_{\tau}^{\tau+T_0} \phi_i^*(t) \left[ \sum_{n=-N}^N a_n \phi_n(t) \right] dt \\ &= \sum_{n=-N}^N a_n \int_{\tau}^{\tau+T_0} \phi_i^*(t)\phi_n(t)dt. \end{aligned} \quad (4.66)$$

From Equation 4.64 above,

$$a_i = \frac{1}{\lambda_i} \int_{\tau}^{\tau+T_0} \phi_i^*(t)x(t)dt \quad (4.67)$$

when the basis functions are orthogonal. When the basis functions are complex, as in the case of the FS, a complex-valued coefficient  $a_i = \alpha_i$  will result. For real-valued signals of interest, the imaginary terms will always cancel.

Now that the coefficients to Equation 4.63 have been calculated, is it possible to find a different set of coefficients that yield a better approximation to  $x(t)$  for the same value of  $N$ ? To investigate this question, it is necessary to measure the closeness of the approximation of Equation 4.63 when  $N$  is finite and when  $N$  approaches infinity. One measure that is frequently used is the mean-squared error. This approach is generalized in detail for complex basis functions by minimizing the mean-squared error of the  $N$ -term truncation approximation to an infinite series.

The decomposition of a time function into a weighted linear combination of basis functions is an exact representation when the function is described by

$$f(t) = \sum_{k=-\infty}^{\infty} a_k \phi_k(t). \quad (4.68)$$

However, for practical numerical calculations it is computationally necessary to truncate the above sum to  $2N$  terms. In this way, an approximation to the signal  $f(t)$  may be calculated; this is guaranteed by the convergence properties of the FS via the Riemann–Lebesgue lemma. If we now denote the truncated linear combination of  $2N$  basis functions by

$$\hat{f}(t) = \sum_{k=-N}^{\infty} \hat{a}_k \phi_k(t), \quad (4.69)$$

how can the possibly complex-valued weighting factors,  $\hat{a}_k$ , be selected in order to minimize the mean-squared error between  $f(t)$  and  $\hat{f}(t)$ ? Let the mean-squared error be represented by  $\varepsilon$ , then

$$\begin{aligned} 0 \leq \varepsilon \leq \|x - \hat{x}\|^2 &= \left\| x - \sum_{k=1}^N \hat{a}_k \phi_k \right\|^2 = \left( x - \sum_k \hat{a}_k \phi_k, x - \sum_j \hat{a}_j \phi_j \right) \\ &= (x, x) - \left( x, \sum_j \hat{a}_j \phi_j \right) - \left( \sum_k \hat{a}_k \phi_k, x \right) \\ &\quad + \left( \sum_k \hat{a}_k \phi_k, \sum_j \hat{a}_j \phi_j \right) \\ &= (x, x) - \sum_j \hat{a}_j^* (x, \phi_j) - \sum_k \hat{a}_k (\phi_k, x) \\ &\quad + \sum_k \hat{a}_k \sum_j \hat{a}_j^* (\phi_k, \phi_j) \\ &= (x, x) - \sum_j \hat{a}_j^* a_j - \sum_k \hat{a}_k a_k^* + \sum_k \hat{a}_k \sum_j \hat{a}_j^* \delta_{kj}. \end{aligned} \quad (4.70)$$

Note that in the above step, the following results were used:

$$a_j = (x, \phi_j) \quad (4.71)$$

$$\hat{a}_j^* = (x, \phi_j^*) = (\phi_j, x) \quad (4.72)$$

$$(\phi_k, \phi_j) = \delta_{kj}. \quad (4.73)$$

Utilizing only one set of subscripts and adding

$$\sum_j a_j \hat{a}_j^* - \sum_j |a_j|^2$$

to the right-hand side of the previous equation,

$$\begin{aligned} &= (x, x) - \sum_j |a_j|^2 - \sum_j \hat{a}_j \hat{a}_j^* - \sum_j \hat{a}_j^* a_j + \sum_j \hat{a}_j \hat{a}_j^* + \sum_j a_j \hat{a}_j^* \\ &\in \leq (x, x) - \sum_j |a_j|^2 + \sum_j |\hat{a}_j - a_j|^2 \end{aligned} \quad (4.74)$$

where

$$\sum_j |\hat{a}_j - a_j|^2 = \sum_j (\hat{a}_j - a_j)(\hat{a}_j^* - a_j^*) = \sum_j (\hat{a}_j - a_j)(\hat{a}_j - a_j)^*$$

In Equation 4.74, the first and second terms are independent of  $\hat{a}_j$  and are strictly greater than or equal to zero. The “best choice” of  $\hat{a}_j$ ,  $j = 1, \dots, N$  is chosen such that  $\|x - \sum_{j=1}^N \hat{a}_j \phi_j\|$  is as small as possible. Therefore, choose  $\hat{a}_j = a_j$ . This results in the following:

$$0 \leq \left\| x - \sum_{j=1}^N \hat{a}_j \phi_j \right\|^2 = \|x\|^2 - \sum_j |a_j|^2.$$

From the above expression, the well-known Bessel's inequality is formed when  $N$  in the sum over  $j$  approaches  $\infty$ :

$$\sum_{j=1}^{\infty} |a_j|^2 \leq \|x\|^2.$$

When Bessel's inequality is an exact equality, the familiar Parseval's equality results. From the results presented there, it can be concluded that the  $a_j$  of Equation 4.71 are the best coefficients from the standpoint of minimizing the approximation error,  $\epsilon$ , when only a finite number of terms are used. Thus, the use of orthogonal basis functions provide two desirable qualities: they guarantee the finality of coefficients and also the same coefficients minimize the mean-squared error of the function representation.

An additional property that is vitally important in the discussion of the FS is the Riemann–Lebesgue Lemma. Briefly, this lemma states that supposing the function  $f(t)$  is absolutely integrable on the interval  $(a, b)$ , then

$$\int_a^b f(t)e^{j\omega t} dt \Rightarrow 0 \quad \text{as } |\omega| \Rightarrow \infty.$$

Because this also implies that

$$\int_a^b f(t) \cos(\omega t) dt \Rightarrow 0 \quad \text{as } |\omega| \Rightarrow \infty.$$

and

$$\int_a^b f(t) \sin(\omega t) dt \Rightarrow 0 \quad \text{as } |\omega| \Rightarrow \infty,$$

by linearity,

$$\int_a^b f(t) \text{cas}(\omega t) dt \Rightarrow 0 \quad \text{as } |\omega| \Rightarrow \infty.$$

Note that  $(a, b)$  may range from  $-\infty$  to  $\infty$ . The importance of this result foreshadows the concept of a complete set of basis functions.

A set of basis functions is termed *complete* in the sense of mean convergence if the error in the approximation of  $f(t)$  can be made arbitrarily small by making the value of  $N$  in Equation 4.63 sufficiently large.

That is,

$$\lim_{N \rightarrow \infty} \|f - S_N\| = 0$$

where  $S_N(\cdot)$ ,  $N = 1, 2, \dots$  is the partial sum of piecewise continuous functions defined on the open interval  $(a, b)$ . Also, it can be

shown that a necessary and sufficient condition for an orthonormal set  $\{\phi_n(t)\}$  to be complete is that for each function  $x$  considered, Parseval's equation

$$\sum_{n=1}^{\infty} (x, \phi_n)^2 = \|x\|^2$$

must be satisfied. Note that  $(x, \phi_n) = a_n$ .

Now, attention turns to the analog of the complex FS represented as follows:

$$x(t) = \sum_{n=-\infty}^{\infty} \alpha_n e^{jn\omega_0 t} \tag{4.75}$$

where

$$\alpha_n = \frac{1}{T_0} \int_{\tau}^{\tau+T_0} x(t) e^{-jn\omega_0 t} dt, \tag{4.76}$$

which can also be written as a single-sided series

$$x(t) = \frac{a_0}{2} + \sum_{n=1}^{\infty} [a_n \cos(n\omega_0 t) + b_n \sin(n\omega_0 t)] \tag{4.77}$$

by noting that

$$\alpha_{-n}^* = \alpha_n = \frac{1}{2}(\alpha_n - jb_n)$$

from which

$$\begin{aligned} a_n &= \alpha_n + \alpha_n^* \\ b_n &= \alpha_n - \alpha_n^* \end{aligned}$$

The properties and use of the FS are well known and well documented in the literature.

The set of basis functions used by the Hartley transform and in the HS is the set  $\{\phi_n(t)\}$ ,  $n = 0, \pm 1, \pm 2, \dots$  where  $\{\phi_n(t)\} = \text{cas}(n\nu_0 t)$ . This is an orthogonal set over the interval  $t \leq t' \leq t + T_0$  and is capable of representing any time function that the FS can in that interval. This set of time functions possesses a FS or HS if the well-known Dirichlet conditions are met as presented in Section 4.3.

Let  $\{\phi_n(t)\} = \text{cas}(n\nu_0 t)/\sqrt{2\pi}$ ,  $n = 0, \pm 1, \pm 2, \dots$  on the interval  $[-\pi, \pi]$ .

**Definition 4.2:** A set of functions  $\{\phi_n\}$ ,  $n = 0, \pm 1, \pm 2, \dots$  is an "orthonormal set" on the interval  $a \leq t \leq b$  if

$$(\phi_i, \phi_k) = \delta_{ik} = \begin{cases} 1, & \text{if } i = k \\ 0, & \text{if } i \neq k. \end{cases}$$

**Claim**

A set of functions  $\{\phi_n(t)\}$ ,  $n = 0, \pm 1, \pm 2, \dots$  where  $\{\phi_n(t)\} = \text{cas}(nv_0t)/\sqrt{2\pi}$  is an orthonormal set on the interval  $-\pi \leq t \leq \pi$ .

*Proof*

$$\begin{aligned} (\phi_i, \phi_k) &= \int_{-\pi}^{\pi} \phi_i(t) \phi_k^*(t) dt = \int_{-\pi}^{\pi} \phi_i(t) \phi_k(t) dt \\ &= \int_{-\pi}^{\pi} \frac{1}{\sqrt{2\pi}} \text{cas}(iv_0t) \cdot \frac{1}{\sqrt{2\pi}} \text{cas}(kv_0t) dt \\ &= \frac{1}{2\pi} \int_{-\pi}^{\pi} \text{cas}(iv_0t) \text{cas}(kv_0t) dt. \end{aligned}$$

If each function of the integrand in the above equation is expanded to  $\cos(\cdot) + \sin(\cdot)$  and then multiplied together, four terms result:  $\cos(\cdot) \cos(\cdot)$ ,  $\sin(\cdot) \sin(\cdot)$ , and two cross products,  $\cos(\cdot) \sin(\cdot)$  and  $\sin(\cdot) \cos(\cdot)$ . The integral of the two cross products are zero by the familiar orthogonality property for the cosine and sine functions, respectively. The other two integrands, when evaluated on the interval from  $-\pi$  to  $\pi$ , equal 0 for  $i \neq k$  and  $\pi$  when  $i = k$ . Therefore,

$$(\phi_i, \phi_k) = \begin{cases} 1, & \text{if } i = k \\ 0, & \text{if } i \neq k. \end{cases}$$

Thus, the basis functions  $\{\phi_n\}$  are an orthonormal system on the interval  $[-\pi, \pi]$ .

Let the periodic signal  $x(t)$  with period  $T_0$ ,

$$x(t + T_0) = x(t) \quad \forall t$$

be written as an orthogonal series expansion (i.e., a linear combination possessing an orthogonal set of basis functions)

$$x(t) = \sum_{i=-\infty}^{\infty} \gamma_i \phi_i(t) \quad (4.78)$$

where  $\phi_i(t)$  are orthogonal basis functions. It has been shown previously that

$$\phi_i(t) = \text{cas}(iv_0t)$$

is an orthogonal basis function over the interval  $[t, t + T_0]$

$$\int_{\tau}^{\tau+T_0} \text{cas}(iv_0t) \text{cas}(kv_0t) dt = \begin{cases} T_0, & \text{if } i = k \\ 0, & \text{if } i \neq k \end{cases}$$

where  $v_0 = 2\pi/T_0$ . Therefore the  $\gamma_i$  in Equation 4.78 are readily obtained using the orthogonality property,

$$x(t) \text{cas}(kv_0t) = \sum_{i=-\infty}^{\infty} \gamma_i \text{cas}(iv_0t) \text{cas}(kv_0t)$$

$$\frac{1}{T_0} \int_{\tau}^{\tau+T_0} x(t) \text{cas}(kv_0t) dt = 0 + 0 + 0, \dots, + \gamma_k + 0 + 0 + \dots$$

This gives what will be termed the HS,

$$\begin{aligned} x(t) &= \sum_{i=-\infty}^{\infty} \gamma_i \text{cas}(iv_0t) \\ v_0 &= \frac{2\pi}{T_0} \end{aligned}$$

$$\gamma_i = \frac{1}{T_0} \int_{\tau}^{\tau+T_0} x(t) \text{cas}(iv_0t) dt. \quad (4.79)$$

It is a simple matter to show that

$$\gamma_k = \begin{cases} \mathcal{R}\{\alpha_k\} - \mathcal{I}\{\alpha_k\} & k \neq 0 \\ \alpha_k & k = 0. \end{cases} \quad (4.80)$$

Specifically, from Equation 4.76 let

$$\begin{aligned} \mathcal{R}\{\alpha_k\} &= \frac{1}{T_0} \int_{\tau}^{\tau+T_0} x(t) \cos(k\omega_0t) dt \\ \mathcal{I}\{\alpha_k\} &= \frac{-1}{T_0} \int_{\tau}^{\tau+T_0} x(t) \sin(k\omega_0t) dt \end{aligned}$$

then

$$\mathcal{R}\{\alpha_k\} - \mathcal{I}\{\alpha_k\} = \frac{1}{T_0} \int_{\tau}^{\tau+T_0} x(t) \text{cas}(k\omega_0t) dt.$$

If  $\omega_0 = v_0$ , then the result follows. The FS coefficients are also related to the HS coefficients by

$$\alpha_i = \mathcal{E}\{\gamma_i\} - j\mathcal{O}\{\gamma_i\} \quad (4.81)$$

where  $\mathcal{E}\{\cdot\}$  and  $\mathcal{O}\{\cdot\}$  are the even and odd parts of a function,

$$\mathcal{E}\{\theta_i\} = \frac{1}{2}(\theta_i + \theta_{-i}) \quad (4.82)$$

$$\mathcal{O}\{\theta_i\} = \frac{1}{2}(\theta_i - \theta_{-i}) \quad (4.83)$$

As an example, the two-sided FS for the square wave

$$x(t) = \begin{cases} 1 & \frac{i}{2} - \frac{1}{4} < t < \frac{i}{2} + \frac{1}{4} & i \text{ even} \\ -1 & \frac{i}{2} - \frac{1}{4} < t < \frac{i}{2} + \frac{1}{4} & i \text{ odd} \end{cases}$$

is

$$x(t) = \dots + \frac{2}{5\pi} e^{-j5\omega_0 t} - \frac{2}{3\pi} e^{-j3\omega_0 t} + \frac{2}{\pi} e^{-j\omega_0 t} + 0 + \frac{2}{\pi} e^{j\omega_0 t} - \frac{2}{3\pi} e^{j3\omega_0 t} + \frac{2}{5\pi} e^{j5\omega_0 t} - \dots$$

and the HS is

$$x(t) = \dots + \frac{2}{5\pi} \text{cas}(-5\nu_0 t) - \frac{2}{3\pi} \text{cas}(-3\nu_0 t) + \frac{2}{\pi} \text{cas}(-\nu_0 t) + 0 + \frac{2}{\pi} \text{cas}(\nu_0 t) - \frac{2}{3\pi} \text{cas}(3\nu_0 t) + \frac{2}{5\pi} \text{cas}(5\nu_0 t) - \dots$$

where  $\nu_0 + \omega_0 + 2\pi$  radians per second.

From Equations 4.81 through 4.83, all of the familiar properties of the FS can be rewritten in terms of the HS. Table 4.7 summarizes some of these properties. A listing of the corresponding FS property is shown in the table for comparison. For purposes of this table, both the FS and HS of  $f(t)$  and the function  $f(t)$  itself are assumed to exist. For example, the table is read as follows: if a function  $f(t)$  possesses an HS with coefficients  $\gamma_i, -\infty < i < \infty$ , then the HS of the indefinite integral

$$\int h(t) dt$$

has coefficients  $\Gamma_i$  where

$$\Gamma_i = \frac{\gamma_{-i}}{i\nu_0},$$

The entry for convolution in Table 4.7 deserves special mention. If a periodic signal  $f(t)$  is applied to a system with impulse response  $h(t)$ , the FS of the output (i.e.,  $f(t) * h(t)$ ) has coefficient  $\alpha_i H(i\omega_0)$  where  $H(\omega)$  is the FT of  $h(t)$ ; similarly, the HS coefficients are  $\Gamma_i$ ,

$$\Gamma_i = \frac{1}{2} [\gamma_i H(i\nu_0) + \gamma_i H(-i\nu_0) + \gamma_{-i} H(i\nu_0) - \gamma_{-i} H(-i\nu_0)]. \tag{4.84}$$

Note that for the linear system response problem, the FS methodology requires one complex multiplication for each coefficient and the HS methodology requires four real multiplications and three additions. However, Equation 4.84 can also be written as

**TABLE 4.7** Selected Properties of the Hartley Series

Function	Fourier Series Coefficients	Hartley Series Coefficients
Integral $\int f(t) dt$	$\frac{-j\alpha_i}{i\omega_0}$	$\frac{\gamma_{-i}}{i\nu_0}$
Derivative $\frac{df}{dt}$	$j i \omega_0 \alpha_i$	$-i \nu_0 \gamma_{-i}$
Convolution of $f$ and $h$	$\alpha_i H(i\omega_0)$	$\frac{1}{2} [\gamma_i H(i\nu_0) + \gamma_i H(-i\nu_0) + \gamma_{-i} H(i\nu_0) - \gamma_{-i} H(-i\nu_0)]$
Time reversal $f(-t)$	$\alpha_i^*$	$\gamma_{-i}$

$$\Gamma_i = \gamma_i H^e(i\nu_0) + \gamma_{-i} H^o(i\nu_0) \tag{4.85}$$

where  $H^e(i\nu_0)$  and  $H^o(i\nu_0)$  are the even and odd parts of  $H(i\nu_0)$ , respectively. Therefore, analogous use of the HS will require only two real multiplications and one addition in general, and for certain conditions of symmetry, the number of real multiplications reduces to one.

The HS methodology may be utilized wherever the FS methodology is applicable. The HS entails no complex quantities or calculations. Under certain types of symmetry, the HS simplifies (as does the FS). Table 4.8 summarizes these symmetries. The main properties of the HS are

- HS coefficients  $\gamma_k$  are always real
- For even functions  $x(t) = x(-t)$ ,  $\gamma_{-k} = \gamma_k$
- For odd functions  $x(t) = -x(-t)$ ,  $\gamma_{-k} = -\gamma_k$
- The HS exists when the FS exists

Previously, it was mentioned that for some conditions of symmetry, the linear system response problem using the HS simplifies. The simplification refers to one real multiplication for the calculation of each HS coefficient of the output. Such is the case when the input function  $f(t)$  is an even function; in this case,  $\gamma_i = \gamma_{-i}$  in Equations 4.84 and 4.85 become

$$\Gamma_i = \gamma_i H(i\nu_0) \tag{4.86}$$

where  $H(i\nu_0)$  is the sampled Hartley transform of the system impulse response,  $H(\nu)$ , and  $\Gamma_i$  are the HS coefficients of the system output. Similarly, for odd  $f(t)$ ,

$$\Gamma_i = \gamma_i H(-i\nu_0). \tag{4.87}$$

The HS analysis technique closely parallels that of FS analysis; periodic excitation functions are resolved into a series where the system response to each term in the series is subsequently evaluated. The total response is the superposition of the individual responses. This method is applicable to a wide range of systems engineering problems, the only requirements being linearity of the system and existence of the HS (FS). Practical limitations often impose constraints in case of high bandwidth signals.

**TABLE 4.8** Simplifications in the Hartley and Fourier Series for Symmetries in  $f(t)$

Symmetry	Fourier Series Coefficients	Hartley Series Coefficients
<i>Even</i>		
$f(t) = f(-t)$	$\Im\{\alpha_i\} = 0$ $\alpha_i = \alpha_{-i}$	$\gamma_i = \gamma_{-i}$
<i>Odd</i>		
$f(t) = -f(-t)$	$\Re\{\alpha_i\} = 0$ $\alpha_i = -\alpha_{-i}$	$\gamma_i = -\gamma_{-i}$
<i>Half-wave odd</i>	$\alpha_i = 0$	$\gamma_i = 0$
$f(t) = -f(t + \frac{T}{2})$	For even $i$	For even $i$
None	$\alpha_{-i} = \alpha_i^*$	No simplification of $\gamma_i$

For such signals, the system models are often difficult to obtain accurately for frequencies far from the intended frequency band of operation. A particularly applicable area is that of industrial electric power distribution system analysis. This is the case because bandwidth limits of the power distribution system components naturally occur and thus limit the frequency range that must be accommodated in the system component models. Also, in power distribution applications, the periodicity of most currents and voltages and the behavior of these physical quantities virtually always ensure the existence of the HS (FS). In industrial distribution circuits, although switched and pulsed load currents commonly occur, these currents are nonetheless periodic; the fundamental frequency of these phenomena is the “power frequency” (i.e., 50 or 60 Hz). In three-phase power quality assessment, often times unbalanced conditions make a full phase-by-phase analysis necessary. In such cases, the faster, all-real calculations offered by the HS is particularly attractive.

#### 4.6.1 Transfer Function Methodology and the Hartley Series

The familiar transfer function methodology used with periodic signals  $x(t)$  that possess an FS is well known. If a signal  $x(t)$  is applied as an input to a linear time-invariant (LTI) system whose frequency response matrix is  $H(\omega)$ , then the output  $y(t)$ ,

$$y(t) = x(t) * h(t)$$

$$h(t) = \mathcal{F}^{-1}\{H(\omega)\}$$

may be calculated by superimposing the individual responses to the Fourier components  $\alpha_i \exp(ji\omega_0 t)$ ,

$$x(t) = \sum_i \alpha_i e^{ji\omega_0 t}$$

where  $\sum_i$  refers to the summation over  $(-\infty, \infty)$ . Thus the FS for  $y(t)$ ,

$$y(t) = \sum_i A_i e^{ji\omega_0 t}$$

is readily found, noting

$$A_i = \alpha_i H(i\omega_0). \quad (4.88)$$

This is a simple consequence of LTI systems and the impulse-shifting property that is used with the FT of  $\exp(ji\omega_0 t)$ .

An analogous result occurs when periodic  $x(t)$  is expressed as an HS. Consider  $x(t)$  applied to an LTI system. Let  $x(t)$  be written as an HS

$$x(t) = \sum_i \gamma_i \text{cas}(iv_0 t)$$

and let the system possess an impulse response  $h(t)$  whose HT is  $H(v)$ . Then, the output  $y(t)$  has an HS

$$y(t) = \sum_i \Gamma_i \text{cas}(iv_0 t)$$

where the HS coefficients are readily calculated from either Equation 4.84 or 4.85.

#### 4.6.2 The Hartley Series Applied to Electric Power Quality Assessment

Methodologies for electric power quality analysis and assessment have taken on renewed importance in recent years. This is due to two main factors: (1) the appearance of high-power switching devices and switched loads that can cause power quality problems at the distribution level and (2) the need for power quality at all power levels to avoid interference, excessive losses, and misoperation of critical loads. There are numerous fundamental issues to be resolved relating to quantifying power quality problems, instrumentation, and monitoring (especially in the environment of digital computer loads). The methodology used for the calculation of bus voltage and line current waveforms is also of salient importance.

Electric power quality assessment often involves the calculation of a bus voltage or line current. The HS methodology described above is applicable because:

1. Limited bandwidth of most electric distribution systems makes truncation of the HS practical at a reasonably low frequency (e.g.,  $v = \pm 19v_0$  or  $\pm 7163$  rad/s in a 60 Hz system,  $\pm 5969$  rad/s in a 50 Hz system)
2. Only real calculations are needed; thus microprocessor applications using elementary codes are possible
3. Waveform symmetries inherent in the operation of electric power systems makes further computational burden reduction possible

Of course, these advantages also apply to any electric circuit, but at least in (1) and (2), electric power system analysis is a particularly appropriate application.

A brief example of the HS methodology is now presented. Consider a six-pulse rectifier that is injecting an ideal current waveform  $i(t)$  into the system of Figure 4.9. This current is shown in Figure 4.3.

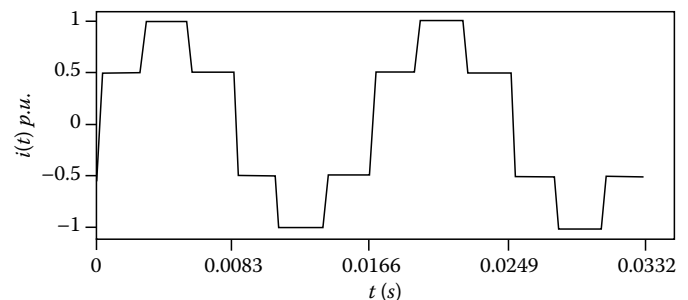


FIGURE 4.3 An ideal six-pulse rectifier load current,  $i(t)$ .

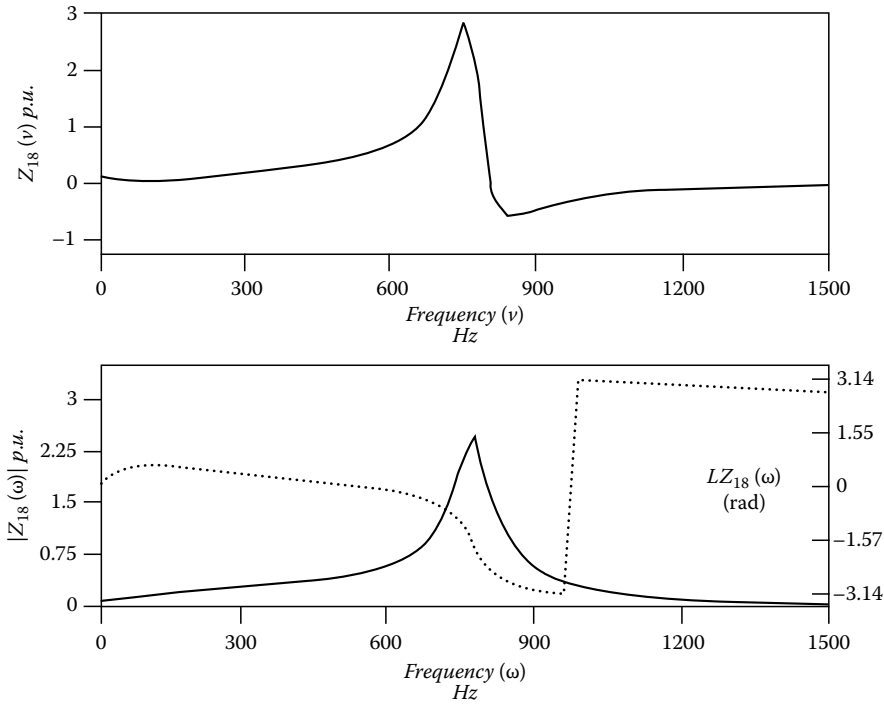


FIGURE 4.4 Transfer impedance between busses 1 and 8 in the Hartley and Fourier domains.

Working only with phase A (and using the time invariance property of the system to deduce the waveforms in the other two phases), and using  $T_0 = 1$  as a normalized period,  $v_0$  is  $2\pi$  rad/s. Let the impedance characteristic of the network be that shown in Figure 4.4.

The one-sided FS of  $i(t)$  is

$$i(t) = \sum_{\substack{k=6n\pm 1 \\ n=\text{integer}}} b_k \sin(2\pi fkt)$$

$$b_{6n\pm 1} = \frac{3}{(6n \pm 1)\pi}$$

where the sum in the equation above is carried over characteristic harmonics of order  $6n \pm 1$ ,  $n = 0, 1, 2, \dots$ , and the HS of  $i(t)$  is

$$i(t) = \dots - \frac{3}{7\pi} \text{cas}(-14\pi t) - \frac{3}{5\pi} \text{cas}(-10\pi t)$$

$$- \frac{3}{\pi} \text{cas}(-2\pi t) + \frac{3}{\pi} \text{cas}(2\pi t) + \frac{3}{5\pi} \text{cas}(10\pi t)$$

$$+ \frac{3}{7\pi} \text{cas}(14\pi t) + \dots$$

Note that  $i(t)$  is odd (actually, odd half-wave symmetric) and has HS coefficients which behave like  $\gamma_{-k} = -\gamma_k$ . An important consequence of the fact that  $i(t)$  is odd is that the convolution property in Equation 4.84 collapses to one real multiplication,

$$\Gamma_i = \gamma_i Z_{18}(-iv_0).$$

In this example, the HS of  $i(t)$  is calculated and used with samples of the transfer impedance  $Z_{18}(v)$  to find the HS of  $v_1(t)$ . Here  $Z_{18}(v)$  is the HT of  $z_{18}(t)$ , the impulse response relating the current input at bus 8 to the voltage output at bus 1. The transfer impedance,  $Z_{18}(v)$ , is displayed in Figure 4.4 along with its Fourier analog  $Z_{18}(\omega)$ . The resulting nonsinusoidal bus voltage,  $v_1(t)$ , produced by the rectifier load (i.e., only the component due to the rectifier; the 60 Hz component is excluded) is displayed in Figure 4.5. The superposition of this nonsinusoidal voltage on the 60 Hz substation bus voltage is depicted in Figure 4.6. Of course, only the phase A to neutral voltage (i.e.,  $v_{an}$ ) is calculated and the other phase voltage are deduced by shifting  $v_{an}$  by  $\pm 1/3$  s.

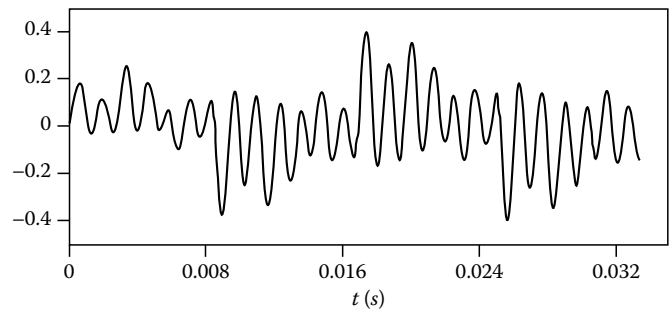


FIGURE 4.5 Substation nonsinusoidal bus voltage,  $v_1(t)$ , phase A to ground due to the current injection at bus 8.

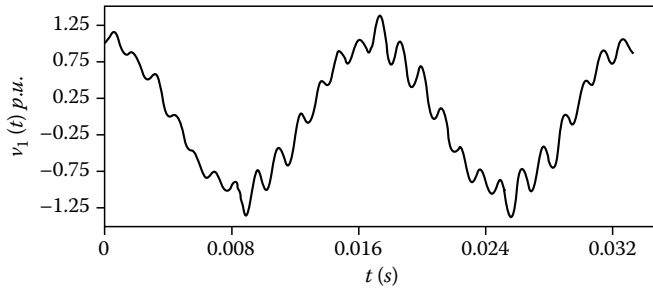


FIGURE 4.6 Superposition of the 60 Hz substation bus voltage and  $v_1(t)$ .

## 4.7 Application of the Hartley Transform via the Fast Hartley Transform

The discretized versions of the continuous Fourier and Hartley transform integrals may be put in an amenable form for digital computation. Consider the discrete Fourier transform (DFT) and inverse DFT (IDFT) of a periodic function of period  $NT$  seconds,

$$F(k\Omega_\omega) = \sum_{n=0}^{N-1} f(nT)e^{-jk\Omega_\omega nT} \quad (4.89)$$

$$f(nT) = \frac{1}{N} \sum_{k=0}^{N-1} F(k\Omega_\omega)e^{jk\Omega_\omega nT} \quad (4.90)$$

where

$T$  is the sampling time resolution of the function  $f(t)$

$N$  is the number of points in the data sequence

$\Omega_\omega$  is the frequency resolution in radians per second

$$\Omega_\omega = \frac{2\pi}{NT}.$$

Similarly, the discrete Hartley transform (DHT) is defined as

$$H(k\Omega_\nu) = \frac{1}{\sqrt{N}} \sum_{n=0}^{N-1} h(nT) \text{cas}(k\Omega_\nu nT). \quad (4.91)$$

The inverse DHT (IDHT) is

$$h(nT) = \frac{1}{\sqrt{N}} \sum_{k=0}^{N-1} H(k\Omega_\nu) \text{cas}(k\Omega_\nu nT) \quad (4.92)$$

where  $\Omega_\nu = \Omega_\omega$  is in radians per second. Note once again the ambiguity of the summation coefficients shown in these expressions. When working in radians per second, the product of the coefficients in the discrete case is  $1/N$ . The selection of  $1/\sqrt{N}$  is made in the DHT and IDHT above so that the forward and inverse transforms satisfy the self-inverse property. As expected, the real-valued DHT is related to the DFT in a very simple way

$$H(k\Omega_\nu) = \mathcal{R}\{F(k\Omega_\omega)\} - \mathcal{I}\{F(k\Omega_\omega)\}. \quad (4.93)$$

It should be noted that the continuous-time Hartley integral, although necessary for theoretical development of the DHT, is typically not utilized in solving engineering problems. In fact, it is the existence of a fast Hartley transform (FHT) algorithm that has spurred the research and use of this transform for a large number of applications. In particular, the FHT is used in single- and multiple-dimension filtering applications where the computational time is of great importance. To this end, the convolution property is of particular interest, and as such, will be discussed in some detail below.

The success of the DFT in the solution of engineering problems is largely due to the highly efficient algorithms that exist for evaluating both the DFT and IDFT. These are collectively known as the FFT algorithms. The FFT is an exact evaluation of the DFT. Numerous formulations exist when implementing the FFT; the most popular being either decimation in time or frequency and split-radix algorithms. At the crux of all FFT algorithms is the exploitation of the symmetry of  $\exp\{-j[(2\pi kn)/N]\}$  in order to render the computational burden lower. The existence of these algorithms suggests that an analog exists for rapid calculation of the DHT. This is indeed the case.

At first glance, it seems strange that the  $N$  real values of the DHT can contain the same amount of information as the  $N$  complex values of the DFT, a total of  $2N$  real numbers. Due to the Hermitian property of the DFT (i.e.,  $F(-k\Omega_\omega) = F^*(k\Omega_\omega)$ ), the DFT is redundant by a factor of two. The  $N/2$  real numbers needed to specify the cosine transform and the  $N/2$  needed for the sine transform combine to form a total of  $N$  DHT coefficients containing no degeneracy due to symmetry. This implies that the DFT, and therefore the FFT, is overspecified for performing linear filtering of real data. It should be noted that other efficient Fourier-based algorithms exist exclusively for real and real-symmetric data. Other advantages of the DHT over the DFT are

- The DHT avoids complex arithmetic
- The DHT requires only half the memory storage for real data arrays vs. complex data arrays
- For a sequence of length  $N$ , the DHT performs  $O(N \log_2 N)$  real operations vs. the DFT  $O(N \log_2 N)$  complex operations
- The DHT performs fewer operations that may lead to fewer truncation and rounding errors from computer finite word length
- The DHT is its own inverse (i.e., it has a self-inverse)

For reasons of computational advantage either occurring through waveform symmetry or simply the use of real quantities, the Hartley transform is recommended as a serious alternative to the FT for frequency-domain analysis. The salient disadvantage of the Hartley approach is that Fourier amplitude and phase information is not readily interpreted. This is not a difficulty in many applications because this information is typically used as an intermediate stage toward a final goal. Where complex numbers are needed, they can be easily constructed as a final step by Equation 4.27 or 4.28.



Due to the cited advantages above, it is clear that the Hartley transform has much to offer when engineering applications warrant digital filtering of real-valued signals. In particular, the FHT should be used when either the computation time is to be minimized; for example, in real-time signal processing. The minimization of computing time includes many other issues, such as memory allocation, real vs. complex variables, computing platforms, and so forth. However, when one is interested in computing the Hartley transform or the convolution or correlation integral, the Hartley transform is the method of choice. In general, most engineering applications based on the FFT can be reformulated in terms of the all-real FHT in order to realize a computational advantage. This is due primarily to the vast amounts of research within the past decade on FHT algorithm development as evidenced in Ref. [11]. A voluminous number of applications exist for the Hartley transform,<sup>11</sup> some of which are listed below;

- Fast convolution, correlation, interpolation, and extrapolation, finite-impulse response and multidimensional filter design
- Acoustics and speech processing, power spectrum, and cepstrum analysis
- Numerical evaluation of the LT integral and Hilbert transformation
- Multidimensional optics and imaging compression applications; image reconstruction, decorrelation, coding, restoration, identification, lensless microwave imaging, pattern/image matching, feature extraction, and rough surface classification
- Power engineering applications, which include relaying, analysis of electrical transients, harmonic propagation in electric power systems, simulation of LTI electrical systems, and electromagnetic wave propagation in multiconductor transmission systems
- Biomedical applications, which include edge enhancement of digital radiographs, pattern recognition for real-time arrhythmias, autocorrelation to improve the 3D plot of transcutaneous human electrogastrograms, functional angiographic images, electroencephalograms classification, and MRI applications
- Probability and number theory, which includes computing Wigner-Ville and pseudo-Wigner distributions, for example
  - Artificial neural network applications, which include adaptive digital filtering, tracking problems, velocity estimation, and motion analysis
  - Adaptive antenna arrays
  - Geophysical applications
  - Chemical applications
  - Astronomical applications

Because many of the above applications involve the fast, efficient evaluation of the convolution integral, additional details are provided below.

### 4.7.1 Convolution in the Time and Transform Domains

Transforms are a well-used mathematical tool in systems analysis. In engineering applications, the one-sided LT,

$$F(s) = \int_0^{\infty} f(t)e^{-st} dt, \quad (4.94)$$

$s = \alpha + j\omega$  and the two-sided FT,

$$F(\omega) = \int_{-\infty}^{\infty} f(t)e^{-j\omega t} dt, \quad (4.95)$$

are most widely used. Both the LT and FT have been widely used because of their special convolution property, which renders the convolution operation to a simple complex product in the transform domain.

Consider the two functions  $h(t)$  and  $x(t)$  and their transforms  $H(\omega)$  and  $X(\omega)$ . Let  $H(\omega)$  and  $X(\omega)$  be multiplied to form the new function  $Y(\omega)$  such that

$$Y(\omega) = H(\omega)X(\omega) \quad (4.96)$$

and consider the inverse transform,  $y(t)$ . Here,  $y(t)$  can be represented by the time-domain convolution integral

$$y(t) = \int_{-\infty}^{\infty} h(\xi)x(t - \xi)d\xi \quad (4.97)$$

or

$$y(t) = h(t) * x(t). \quad (4.98)$$

The above convolution integral can be represented in a form convenient for digital implementation as follows:

$$y(n) = T \sum_{j=0}^{N-1} h(j)x(n - j) \quad (4.99)$$

$$y(n) = T \sum_{j=0}^{N-1} x(j)h(n - j)$$

that is, as a sum of lagged products. The time required to compute  $y(n)$  from either form in Equation 4.99 is proportional to approximately  $N^2$ . If one computes the transforms of  $x$  and  $h$ , performs the complex multiplication of Equation 4.96, and then computes the inverse transform of  $Y(\omega)$ , one requires a time proportional of  $N \log_2 N$  if the FFT is utilized. The approximate ratio of computing the convolution in Equation 4.96 to that of Equation 4.99 is given by

$$\frac{N \log_2 N}{N^2} = \frac{\log_2 N}{N} = \frac{\rho}{N} \quad (4.100)$$

where  $N = 2^p$ . For example, if  $N = 2^{10}$ , the FFT requires less than 1% of the normal computing time. Timing studies have shown that for  $N$  greater than about 32, the FFT method is at least an order of magnitude faster than the lagged products approach of Equation 4.99.

The convolution property in the transform domain is of great interest. The familiar convolution property of the DFT has an analog in the Hartley space that suggests potential use of the DHT for the numerical solution of electric circuits problems. Many electric circuits problems involve the notion of convolution. A typical format of such problems is that an impedance is known, and a current associated with that impedance results in a voltage. In terms of the one-sided LT.

$$V(s) = Z(s)I(s). \quad (4.101)$$

The impedance  $Z$  may be an open-circuit driving point or a transfer impedance. Other problems are frequently encountered in electric circuit analysis, and many of these are of the same form as Equation 4.101 with  $Z(s)$  replaced by a transfer function, frequency response matrix or similar parameter. This is the case, for example, in the presence of power electronic loads and sources characterized by nonsinusoidal waveforms. "Quasiperiodic" transient inputs energizing a relaxed electric power system (i.e., zero initial conditions) at time  $0^-$ , produce responses throughout the system that may be superimposed upon the sinusoidal steady-state solution. In the time domain, the impedance  $Z(\omega)$  is, in fact, an impulse response,  $z(t)$ . In this context,  $z(t)$  is the voltage response to an input that is a unit current impulse. The responses to these quasiperiodic inputs are found analytically via the convolution integral

$$v(t) = \int_{-\infty}^{\infty} z(t - \xi)i(\xi)d\xi = z(t) * i(t) \quad (4.102)$$

and for causal systems

$$v(t) = \int_{-\infty}^t z(t - \xi)i(\xi)d\xi \quad (4.103)$$

where  $z(\cdot)$  is the impulse response satisfying  $z(t - \xi) = 0$  for  $\xi > t$ , that is,  $z(t) = 0$  for  $t < 0$ . In Equations 4.98 and 4.102,  $(*)$  denotes conventional or linear convolution. The limits of integration may be changed to  $[0, t]$  if  $i(t)$  is a causal signal, that is, if  $i(t) = 0$  for  $t < 0$ . Convolution in the time domain becomes a simple complex multiplication in the  $s$ -domain; this property makes the LT particularly attractive for systems analysis.

The familiar FT also possesses a similar convolution property

$$V(\omega) = \frac{1}{\sqrt{2\pi}} \int_{-\infty}^{\infty} v(t)e^{-j\omega t} dt \quad (4.104)$$

$$I(\omega) = \frac{1}{\sqrt{2\pi}} \int_{-\infty}^{\infty} i(t)e^{-j\omega t} dt \quad (4.105)$$

$$Z(\omega) = \frac{1}{\sqrt{2\pi}} \int_{-\infty}^{\infty} z(t)e^{-j\omega t} dt \quad (4.106)$$

$$\mathcal{F}\{v(t)\} = \mathcal{F}\{z(t)*i(t)\} = V(\omega) = Z(\omega)I(\omega). \quad (4.107)$$

Note that in Equations 4.104 through 4.107 above, the factor  $1/\sqrt{2\pi}$  is often omitted in engineering work; when this factor is included in the transform, the inverse transform is

$$v(t) = \frac{1}{\sqrt{2\pi}} \int_{-\infty}^{\infty} V(\omega)e^{j\omega t} d\omega. \quad (4.108)$$

Analogously, a salient property of the Hartley transform for this application is that convolution is rendered to a simple sum of real products under the transform,

$$\mathcal{H}\{v(t)\} = \mathcal{H}\{z(t) * i(t)\} = V(v). \quad (4.109)$$

Specifically,

$$V(v) = \frac{1}{2} [Z(v)I(v) + Z(-v)I(v) + Z(v)I(-v) - Z(-v)I(-v)] \quad (4.110)$$

$$= Z(v) \frac{[I(v) + I(-v)]}{2} + Z(-v) \frac{[I(v) - I(-v)]}{2} \quad (4.111)$$

$$= Z(v)I^e(v) + Z(-v)I^o(v) \quad (4.112)$$

$$= \frac{1}{2} [V_a(v) - V_a(-v) + V_b(v) + V_b(-v)] \quad (4.113)$$

where  $V_a(v) = Z(v)I(v)$  and  $V_b(v) = Z(v)I(-v)$ . Thus, it is possible to solve a certain class of electric circuit problems using the Hartley transform.

As with the DFT/FFT, the DHT/FHT can be readily used for performing convolution. The DHT assumes periodicity of the function being transformed; that is  $H(k\Omega_v) = H[(N+k)\Omega_v]$ . Therefore,  $H(-k\Omega_v)$  for  $-N \leq k \leq -1$ , is equivalent to  $H[(N-k)\Omega_v]$ . When convolution is represented by  $*$ , linear or time-domain convolution is implied. In the frequency domain, as a result of the characteristic modulo  $N$  operations inherent in the DFT or DHT, a different form of convolution results in the time domain. Circular or cyclic convolution, denoted by  $\oplus$ , in the time domain is the result of multiplication of two functions in the frequency domain. Let  $n$  represent the  $n$ th point of some finite-duration sequence, then cyclic convolution in the time domain is expressed as

$$f_1(n) \oplus f_2(n) = \sum_{\tau=0}^{N-1} f_1 \left( \text{mod} \left( \tau, N \right) \right) f_2 \left( \text{mod} \left( n - \tau, N \right) \right) \quad (4.114)$$

where  $\tau$  and  $n - \tau$  are depicted modulo  $N$ . The equivalent form of Equations 4.110 through 4.113 in the Hartley domain is expressed as

$$\begin{aligned}
 V(k\Omega_v) &= \frac{1}{2} [Z(k\Omega_v)I(k\Omega_v) + Z((N - k)\Omega_v)I(k\Omega_v) \\
 &\quad + Z(k\Omega_v)I((N - k)\Omega_v) \\
 &\quad - Z((N - k)\Omega_v)I((N - k)k\Omega_v)] \quad (4.115)
 \end{aligned}$$

$$= Z(k\Omega_v)I^e(k\Omega_v) + Z((N - k)\Omega_v)I^o(k\Omega_v) \quad (4.116)$$

$$\begin{aligned}
 &= \frac{1}{2} [V_a(k\Omega_v) - V_a((N - k)\Omega_v) + V_b(k\Omega_v) \\
 &\quad + V_b((N - k)\Omega_v)] \quad (4.117)
 \end{aligned}$$

where  $V_a(k\Omega_v) = Z(k\Omega_v)I(k\Omega_v)$  and  $V_b(k\Omega_v) = Z(k\Omega_v)I((N - k)\Omega_v)$ .

There are times when cyclic convolution is desired and other times when linear convolution is needed. Because both the DFT and DHT perform cyclic convolution, it would be unfortunate if methods for obtaining linear convolution by cyclic convolution were nonexistent. Fortunately, this is not the case. Linear convolution can be extracted from cyclic convolution, but at some expense. For finite-duration sequences  $f_1(n)$  and  $f_2(n)$  of length  $M$  and  $L$ , respectively, their convolution is also finite in duration. In fact, the duration is  $M + L - 1$ . Therefore, a DFT or DHT of size  $N \geq M + L - 1$  is required to represent the output sequence in the frequency domain without overlap. This implies that the  $N$ -point circular convolution of  $f_1(n)$  and  $f_2(n)$  must be equivalent to the linear convolution of  $f_1(n)$  to  $f_2(n)$ . By increasing the length of both sequences to  $N$  points (i.e., by appending zeros), and then circularly convolving the resulting sequences, the end result is as if the two sequences were linearly convolved. Clearly with zero padding, the DHT can be used to perform linear filtering. It should be clear that aliasing results in the time domain if  $N < M + L - 1$ .

When  $N$  zero values are appended to a time sequence of  $N$  data samples, the  $2N$ -point DHT reduces to that of the  $N$ -point DHT at the even index values. The odd values of the  $2N$  sequence represent the interpolated DHT values between the original  $N$ -point DHT values. The more zeros padded to the original  $N$ -point DHT, the more interpolation takes place on the sequence. In the limit,

infinite zero padding may be viewed as taking the discrete-time Hartley transform of an  $N$ -point windowed data sequence. The prevalent misconception that zero padding improves the resolution of the sequence or additional information is obtained is well known. Zero padding does not increase the resolution of the transform made from a given finite sequence, but simply provides an interpolated transform with a smoother appearance. The advantage of zero padding is that signal components with center frequencies that lie between the  $N$  frequency bins of an unpadding DHT can now be discerned. Thus, the accuracy of estimating the frequency of spectral peaks is also enhanced with zero padding.

When comparing the number of real operations performed by Equation 4.96 (with  $\omega$  replaced by  $k\Omega_\omega$ ) and Equation 4.116 or 4.117, the DHT always offers a computational advantage of two as compared to the DFT method; in many (if not most) applications, currents in electrical engineering calculations exhibit symmetry, which results in a computational advantage of four favoring the Hartley method. In the case where  $z(t)$  or  $i(t)$  in Equation 4.109 contains even symmetry, the four-term product of Equation 4.115 reduces to  $Z(k\Omega_v)I(k\Omega_v)$  or  $V_a(k\Omega_v)$ . If  $z(t)$  or  $i(t)$  is odd, then Equation 4.115 degenerates to  $Z(k\Omega_v)I((N - k)\Omega_v)$  or  $V_b(k\Omega_v)$  and  $Z((N - k)\Omega_v)I(k\Omega_v)$ , respectively. That is, only one, vs. the FFT's four real multiplications, is needed. The above symmetry conditions are more often the rule than the exception. Other symmetries exist as discussed by Bracewell for the Hartley transform.<sup>9</sup>

As a brief example of the method, consider the periodic load current shown in Figure 4.7 having the description

$$f(t) = \sum_{m=-\infty}^{\infty} f_m(t) \quad (4.118)$$

where

$$f_0(t) = f(t)[u(t) - u(t - T)] = ee^{-t}[u(t) - u(t - 1)] \quad (4.119)$$

$$f_m(t) = f_0(t - mT) \quad (4.120)$$

and  $T = 1$ . The transfer function,  $H(s)$ , for the RC network in Figure 4.7 is clearly  $1/(s + 1)$ . (Note the system is initially relaxed—zero initial conditions.) If one denotes  $y_m(t)$  as the zero-state response due to  $f_m(t)$ , then from the time shift property

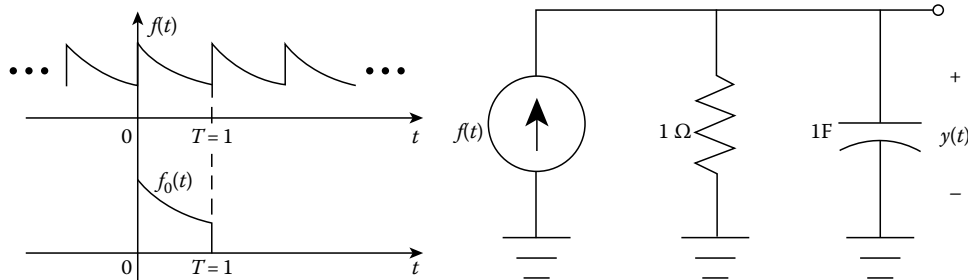


FIGURE 4.7 Injected load current into a simple RC network.

of a LTI system,  $y_m(t) = y_0(t - mT)$ . From the principle of superposition,  $y(t) = \sum y_m(t)$ . Thus, the crux of the problem is to find  $y_0(t)$ , the response for  $0 \leq t < \infty$  due to the single pulse,  $f_0(t)$ , in Figure 4.7.

The convolution of  $f_0(t)$  and the impulse response,  $h(t)$ , by the convolution integral is straightforward.

In fact, the response,  $y_0(t)$ , depicted in Figure 4.8, is readily calculated as

$$y_0(t) = \begin{cases} tee^{-t}, & \text{if } 0 \leq t \leq 1 \\ ee^{-t}, & \text{if } t > 1 \end{cases} \quad (4.121)$$

or alternatively by

$$y_0(t) = \mathcal{L}^{-1}\{Y_0(s)\} = \mathcal{L}^{-1}\left\{\frac{e - e^{-s}}{(s + 1)^2}\right\} \quad (4.122)$$

where  $Y_0(s) = F_0(s)H(s)$  and  $F_0(s) = \mathcal{L}\{f_0(t)\}$ . The calculation of the steady-state system response to the input  $f(t)$  in Figure 4.7 is more interesting. It is well known that for periodic  $y(t)$ ,

$$y(t) = \mathcal{L}^{-1}\left\{\frac{Y_0(s)}{1 - e^{-sT}}\right\} = \mathcal{L}^{-1}\{Y(s)\} \quad (4.123)$$

when  $Y_0(s)$  represents the LT of any one period of  $y(t)$  (i.e.,  $y_0(t)$ ). In general, the partial fraction expansion of  $Y(s)$  is a nontrivial computation. How then does one solve for the response  $y(t)$ ? Utilizing the assumed periodicity of the DHT (FHT), one can perform conventional convolution via circular convolution if provisions are made for aliasing (i.e., zero padding). This method of solution can be summarized by (assuming one of the convolving functions is even)

$$y(t) = f(t) \oplus h(t) = \text{DHT}\{\text{DHT}\{f(t)\} \times \text{DHT}\{h(t)\}\} \quad (4.124)$$

where  $y(t)$  is shown in Figure 4.8. An FHT software program to compute the DHT efficiently can be found in the Appendix of this section. Additional details concerning circular convolution of aperiodic inputs are discussed below.

### 4.7.2 An Illustrative Example

In this section, an illustrative example is presented from sub-transmission and distribution engineering to illustrate the calculation of nonsinusoidal waveform propagation in an electric power system. Figure 4.9 displays the distribution network model and the injected nonlinear load current into the network. The electrical load at bus 8 causes a nonsinusoidal current to

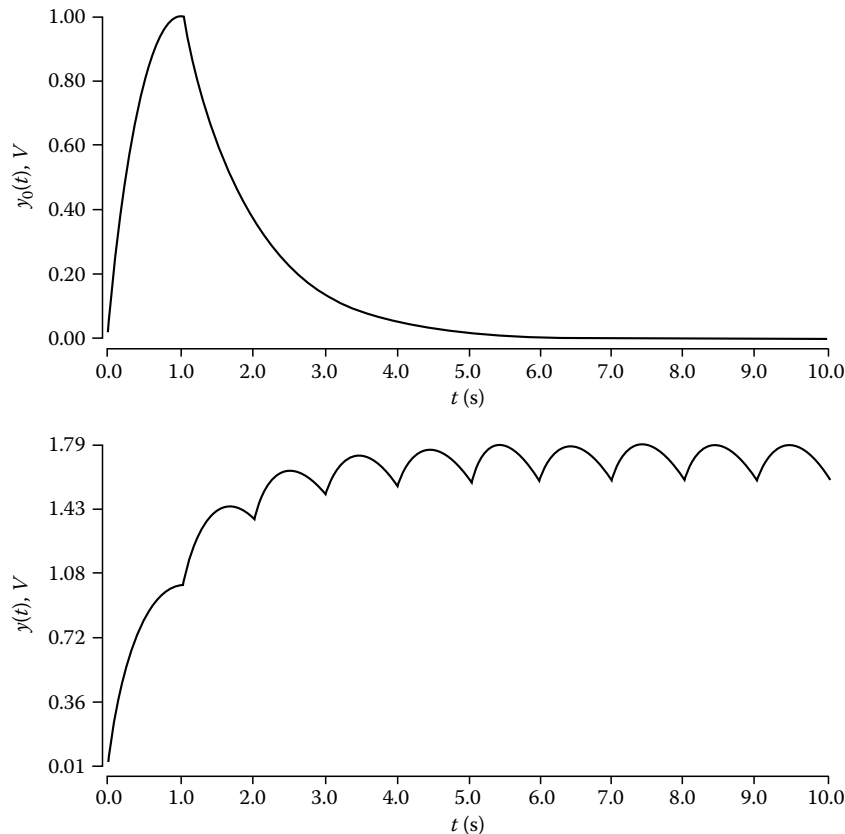


FIGURE 4.8 Output response (top)  $y_0(t)$  to the input pulse  $f_0(t)$  and (bottom)  $y(t)$  to the input  $f(t) = \sum_{m=0}^9 f_m(t) = f_0(t - m)$ .

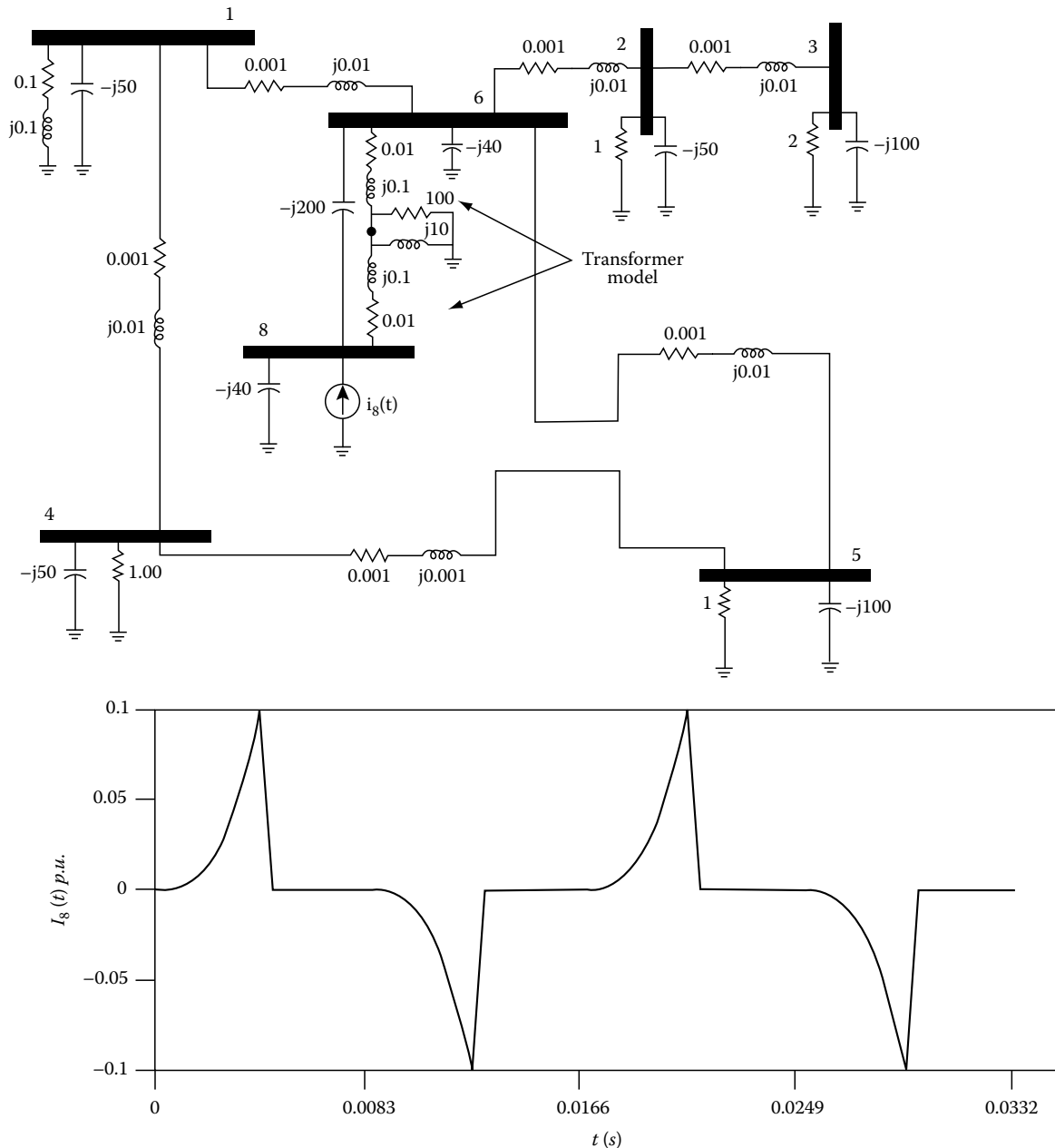


FIGURE 4.9 Load current injected at bus 8 of an example 8-bus distribution system.

propagate throughout the system and impact other loads in an unknown fashion.

The fast decay in this current results in high frequency signals in the network. An important consideration in this method is the selection of the sampling interval  $T$  and its effect on the maximum frequency component,  $\Omega_{v,max} = \pi/T$ , represented in the simulation. Because power systems are essentially band-limited due necessarily to system components designed to operate at or near the power frequency (e.g., distribution transformers), the nonlinear load current containing frequency components above  $\Omega_{v,max}$  become negligible. That is, no matter how close the current approaches an impulse (e.g., a lightning strike), the

significant energy components above  $\Omega_{v,max}$  are multiplied in the transform domain by the system impedance frequency components that are asymptotically approaching zero. This can be seen by observing the Fourier magnitude,  $|I_8(k\Omega_\omega)|$  and  $|Z_{18}(k\Omega_\omega)|$ , in Figures 4.10 and 4.11 for selected values of  $N$  (and thus  $T$ ). The Hartley transform of  $i(t)$ ,  $I_8(k\Omega_v)$ , is shown in Figure 4.12.

Load currents that decay rapidly are becoming less unusual with the advent of high-power semiconductor switches.

Referring to the system in Figure 4.9, the transformer at the load bus is modeled as a conventional  $T$  equivalent. A lumped capacitance is used to model electrostatic coupling between the primary and secondary windings, and two lumped capacitances

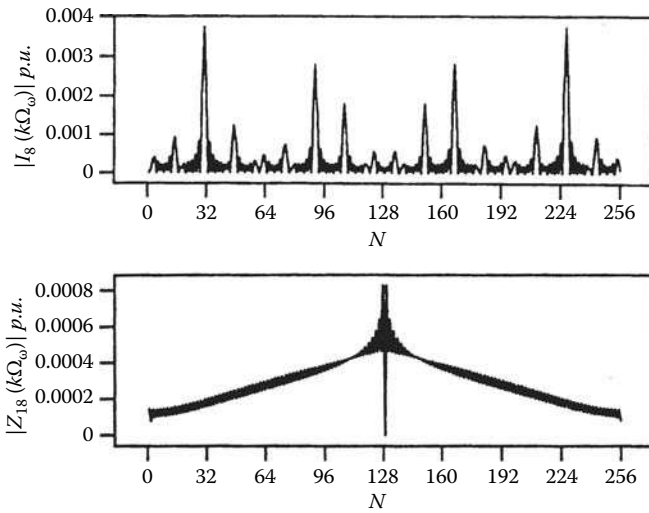


FIGURE 4.10 Fourier magnitude of the injected bus current,  $i(t)$ , and system impulse response,  $z_{18}(t)$  for  $N = 256$ .

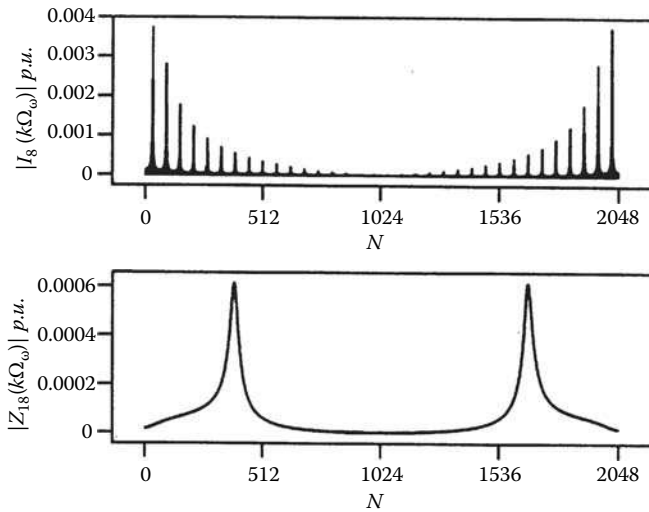


FIGURE 4.11 Fourier magnitude of the injected bus current,  $i(t)$ , and system impulse response,  $z_{18}(t)$  for  $N = 2048$ .

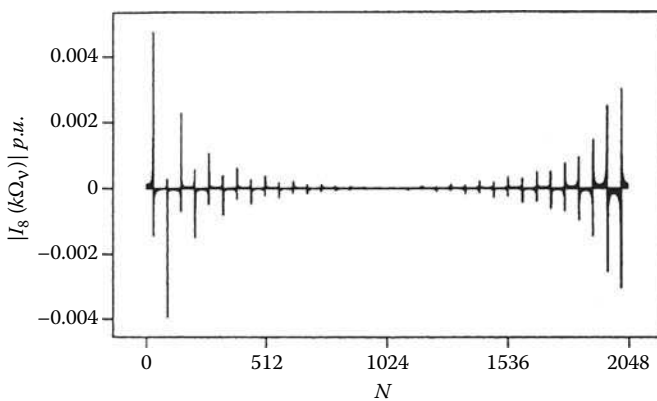


FIGURE 4.12 Hartley transform of the injected bus current,  $i(t)$ .

are used to model interwinding capacitance. Bus 1 is the substation bus and the negative-sequence impedance equivalent tie to the remainder of the network is shown as a shunt  $R$ - $L$  series branch. The circuits shown between busses are all three-phase balanced, fixed series  $R$ - $L$  branches, and frequency independent (i.e.,  $R = R(\omega)$ ). The latter assumption need not be made because frequency dependence may be included if required. The importance of frequency dependence should not be underestimated, particularly for cases in which significant energy components of the injection current spectrum lie above and beyond the 17th harmonic of 60 Hz, or approximately 1 kHz. Distributed parameter models can be readily represented as lumped parameters placed at the terminals of long lines. These refinements are quite important in actual applications, but they are omitted from this abbreviated example. If the injection current at bus 8 were “in phase” with the line to neutral voltage at that bus, the nonlinear device at bus 8 would be a source. Similarly, other phase values would result in different generation or load levels.

Each bus voltage was calculated using the Hartley transform simulation algorithm. These results were verified using an Euler predictor–trapezoidal corrector integration algorithm and time domain convolution implemented by Equation 4.99. In order to choose an adequate time step,  $T$ , for calculating the “theoretical solution” by the predictor–corrector method, it was necessary to capture all system modes. The eigenvalues calculated by the International Mathematics and Statistical Library (IMSL) subroutine EVLRG are shown in Table 4.9. Routine EVLRG computes the eigenvalues of a real matrix by first balancing the matrix; second, orthogonal similarity transformations are used to reduce this balanced matrix to a real upper Hessenberg matrix; third, the shifted QR algorithm is used to compute the eigenvalues of the Hessenberg matrix. This method is generally accepted as being most reliable.

In this example, the transfer impedance between the substation bus (bus 1) and bus 8 is of interest. Figures 4.13 and 4.14 display the DFT of  $z_{18}(t)$ ,  $Z_{18}(k\Omega_\omega)$ . Of course, two graphs are required to illustrate this transfer impedance because the DFT is

TABLE 4.9 Calculated Eigenvalues for the Example 8-Bus Power System

$\lambda_i$	$\Re\{\lambda_i\}$	$\Im\{\lambda_i\}$
$\lambda_1$	-757,718	0
$\lambda_{2,3}$	-13,548	$\pm 52,901$
$\lambda_4$	-11,988	0
$\lambda_{5,6}$	-8,976	$\pm 19,575$
$\lambda_{7,8}$	-8,690	$\pm 50,131$
$\lambda_{9,10}$	-5,033	$\pm 38,050$
$\lambda_{11,12}$	-4,245	$\pm 43,600$
$\lambda_{13}$	-1,523	0
$\lambda_{14,15}$	-214	$\pm 4,877$
$\lambda_{16}$	-40	0
$\lambda_{17}$	-3	0

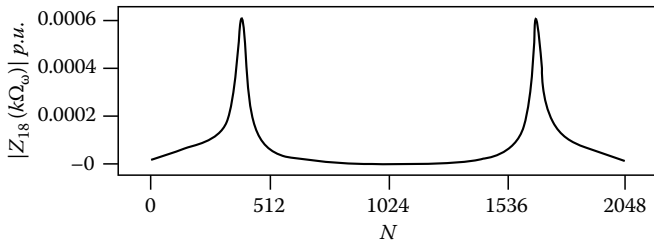


FIGURE 4.13 Fourier magnitude of the transfer impedance,  $Z_{18}(k\Omega_\omega)$ .

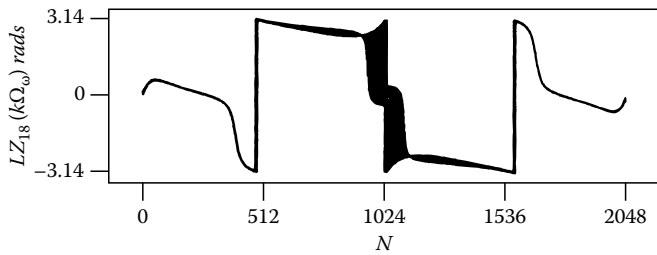


FIGURE 4.14 Fourier phase of the transfer impedance,  $Z_{18}(k\Omega_\omega)$ .

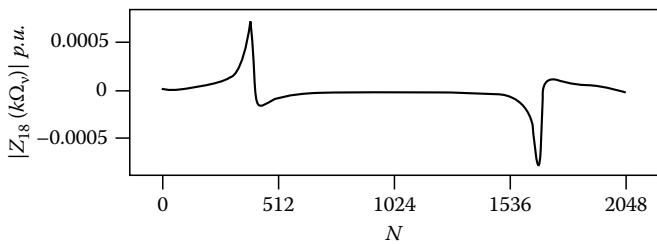


FIGURE 4.15 Hartley transform of the transfer impedance,  $Z_{18}(k\Omega_v)$ .

a complex transformation. Figure 4.15 shows the DHT of  $z_{18}(t)$ ,  $Z_{18}(k\Omega_v)$ . One figure illustrates this real transform.

The resulting bus voltages due to the current injection at bus 8 are depicted in Figures 4.16 and 4.17.

### 4.7.3 Solution Method for Transient or Aperiodic Excitations

Convolution of two finite-duration waveforms is straightforward. One simply samples the two functions every  $T$  seconds and assumes that both sampled functions are periodic with period  $N$ . If the period is chosen according to that discussed earlier, there is no overlap in the resulting convolution. As long as  $N$  is chosen correctly, discrete convolution results in a periodic function where each period approximates the continuous convolution results of Equation 4.102.

The algorithm implemented by Equation 4.124 assumed that the input is time limited and the system impulse response is band limited. That is, the periodic input is truncated to an integer multiple of its fundamental frequency and the system impulse response is of infinite duration. For stable systems, the system impulse response  $z(t)$  must decrease to zero or to negligible values for large  $|t|$ . In reality, the system impulse response cannot be both time limited and band limited; therefore, one band limits in the frequency domain such that negligible signal energy exists for  $t \geq T_0$ .

The convolution of an aperiodic excitation with the system impulse response can be regarded as a periodic convolution of functions having an equal period. Through suitable modifications to the method presented in Equation 4.124, one can use circular convolution to compute an aperiodic convolution when each function is zero everywhere outside some single time window of interest.

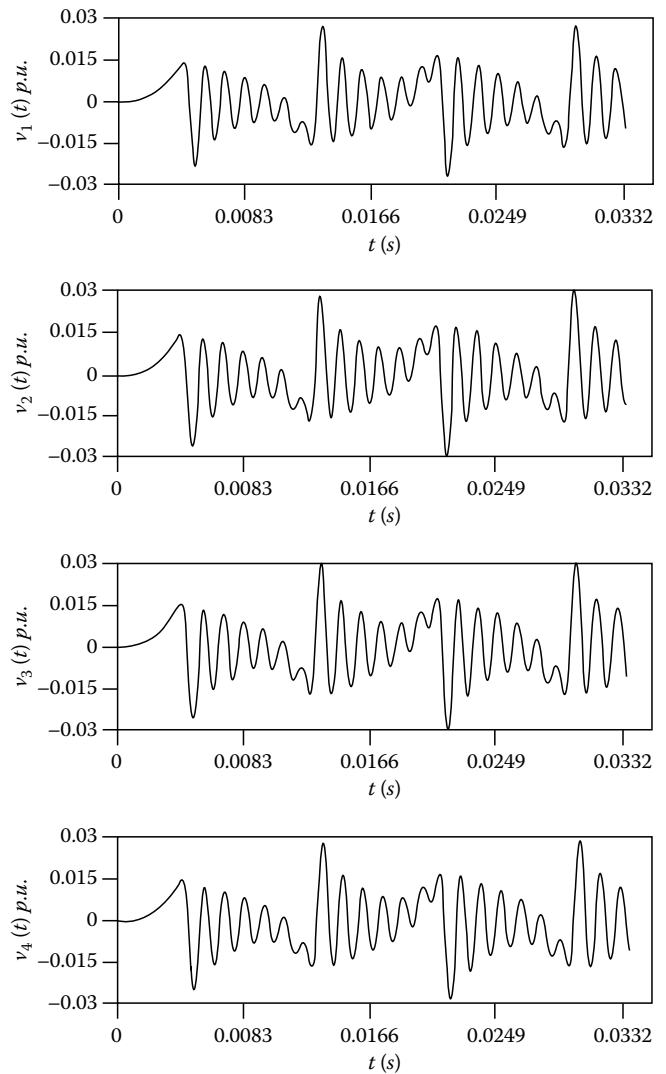


FIGURE 4.16 Resulting bus voltages due to the current injection at bus 8.

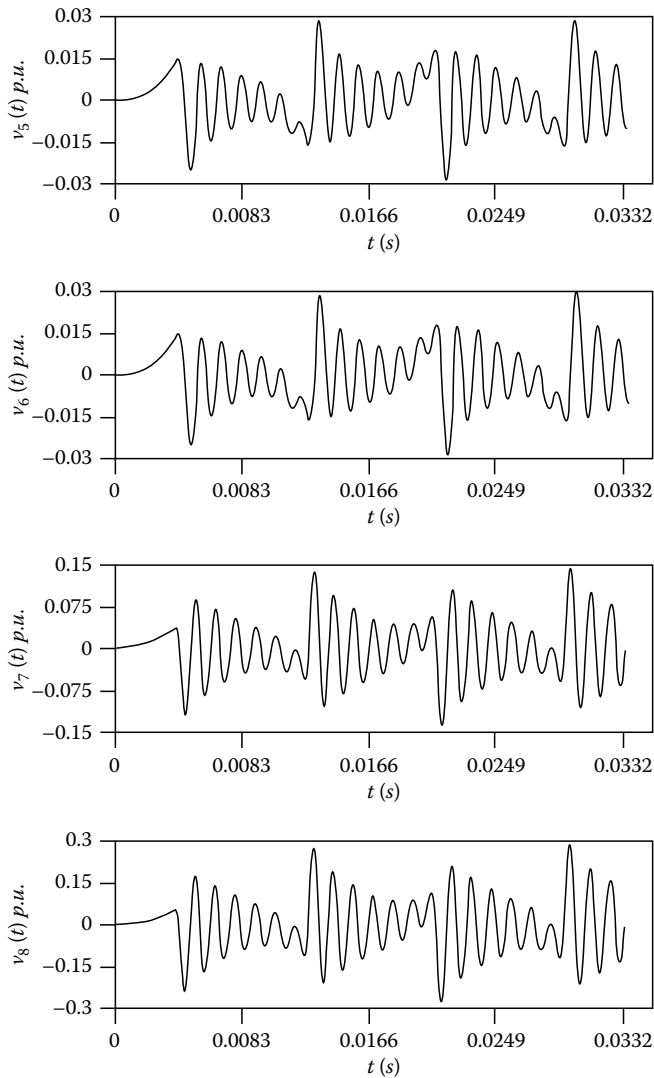


FIGURE 4.17 Resulting bus voltage due to the current injection at bus 8, continued.

Let the functions  $x(t)$  and  $h(t)$  be convolved where both functions are finite in length. Let the larger sequence,  $x(t)$ , contain  $L$  discrete points and the smaller contain  $M$  discrete points. Then the resulting convolution of these functions can be obtained by circularly or cyclically convolving suitable zero-augmented functions. That is,

$$X_{\text{pad}}(n) = \begin{cases} x(n + n_0), & \text{if } 1 \leq n \leq L \\ 0, & \text{if } L + 1 \leq n \leq N \\ x_{\text{pad}}(n + nN) & \text{otherwise} \end{cases} \quad (4.125)$$

where

$n_0$  is the first point in the function window of interest

$N$  is the smallest power of two greater than or equal to  $M + L - 1$

Similarly for  $h(t)$ , simply replace  $x$  with  $h$  and  $L$  by  $M$  in Equation 4.125. If one allows these zero-augmented functions to be periodic of period  $N$ , then the intervals of padded zeros disallow the two functions to be overlapped even though the convolution is a circular one. These periodic functions are formed by the superposition of the nonperiodic function shifted by all multiples of the fundamental period,  $T_0$  where  $T_0 = NT$ . That is,

$$f_p(t) = \sum_{k=-\infty}^{\infty} f(t + kT_0). \quad (4.126)$$

Thus, while the result is a periodic function (i.e., due to the assumed periodicity of the DHT/FHT), each period is an exact replica of the desired aperiodic convolution.

The relationship between the DHT and HT for finite-duration waveforms is different when the input  $i(t)$  is time limited. Because  $i(t)$  is time limited, its Hartley transform cannot be band limited; therefore, sampling this function leads to aliasing in the frequency domain. It is necessary to choose the sampling interval  $T$  to be sufficiently small such that aliasing is reduced to an insignificant level.

If the number of samples of the time-limited waveform is chosen as  $N$ , then it is not necessary to window in the time domain. For this set of waveforms, the only error introduced is aliasing. Errors introduced by aliasing can be reduced by choosing  $T$  sufficiently small. This allows the DHT sample values to agree reasonably well with samples of the HT.

## 4.8 Table of Hartley Transforms

Tables 4.10 through 4.12 contain the Hartley transforms of commonly encountered signals in engineering applications. When scanning the table entries, the Hartley transform entries seem to have more sophisticated expressions; this is usually the case. More exotic Hartley transforms may be generated in one of three ways. First, one can apply the elementary properties provided in Section 4.4 to the entries of Tables 4.10 and 4.11; second, one can alternatively apply Equation 4.23 to the FT entries of more comprehensive table listings such as those found in Refs. [12–14]; or third, use a DHT or FHT algorithm to evaluate numerically the Hartley transform of a discrete-time signal generated using a high-level computing language (e.g., FOTRAN, C, C++, etc.). A sample FHT algorithm, coded in the C programming language, is included in the Appendix.

Note that in the eighth entry to Table 4.11,  $\alpha_n$  is a complex number representing the FS expansion of the arbitrary periodic function. The value  $\alpha_n$  is also equal to  $1/T F_T(n/T)$  where  $F_T(f)$  is the FT of  $F(f)$  over a single period evaluated at  $n/T$ . Also, in that same entry, note that  $\gamma_n = \mathcal{R}\{\alpha_n\} - \mathcal{I}\{\alpha_n\}$ .



**TABLE 4.10** Hartley Transforms of Energy Signals

Description	$f(t)$	$F(f)$	$H(f)$
Rectangular pulse	$u(t + \frac{T}{2}) - u(t - \frac{T}{2})$	$T \frac{\sin \pi T f}{\pi T f} = T \operatorname{sinc} Tf$	Because $f(t)$ is even, $H(f) = F(f)$
Exponential	$\beta e^{-\alpha t} u(t)$	$\frac{\beta}{j\omega + \alpha}$	$\frac{\beta(\alpha + 2\pi f)}{\alpha^2 + (2\pi f)^2}$
Triangular	$1 - 2\frac{ t }{T}, \quad  t  < \frac{T}{2}$	$\frac{T}{2} \operatorname{sinc}^2\left(\frac{Tf}{2}\right) = \frac{1 - \cos \pi f T}{T \pi^2 f^2}$	Because $f(t)$ is even, $H(f) = F(f)$
Gaussian	$e^{-\alpha^2 t^2}$	$\frac{\sqrt{\pi}}{\alpha} e^{-(\pi^2 f^2 / \alpha^2)}$	Because $f(t)$ is even, $H(f) = F(f)$
Double exp	$e^{-\alpha t }$	$\frac{2\alpha}{\alpha^2 + 4\pi^2 f^2}$	Because $f(t)$ is even, $H(f) = F(f)$
Damped sine	$e^{-\alpha t} \sin(\omega_0 t) u(t)$	$\frac{\omega_0}{(\alpha + j2\pi f)^2 + \omega_0^2}$	$\frac{\omega_0(\alpha^2 + \omega_0^2 - 4\pi^2 f^2 + 4\pi f \alpha)}{(\alpha^2 + \omega_0^2 - 4\pi^2 f^2)^2 + (4\pi f \alpha)^2}$
Damped cosine	$e^{-\alpha t} \cos(\omega_0 t) u(t)$	$\frac{\alpha + j2\pi f}{(\alpha + j2\pi f)^2 + \omega_0^2}$	$\frac{(\alpha - 2\pi f)(\alpha^2 + \omega_0^2 - 4\pi^2 f^2) + (4\pi f \alpha)(\alpha + 2\pi f)}{(\alpha^2 + \omega_0^2 - 4\pi^2 f^2)^2 + (4\pi f \alpha)^2}$
One-sided exp	$\frac{1}{\beta - \alpha}(e^{-\alpha t} - e^{-\beta t})u(t)$	$\frac{1}{(\alpha + j2\pi f)(\beta + j2\pi f)}$	$\frac{\alpha\beta - 2\pi f(\alpha + \beta + 2\pi f)}{[\alpha\beta - (2\pi f)^2]^2 + [2\pi f(\alpha + \beta)]^2}$
Cosine pulse	$\cos \omega_0 t [u(t + \frac{T}{2}) - u(t - \frac{T}{2})]$	$\frac{T}{2} \left[ \frac{\sin \pi T(f-f_0)}{\pi T(f-f_0)} + \frac{\sin \pi T(f+f_0)}{\pi T(f+f_0)} \right]$	Because $f(t)$ is even, $H(f) = F(f)$

**TABLE 4.11** Hartley Transforms of Power Signals

Description	$f(t)$	$F(f)$	$H(f)$
Impulse	$K\delta(t)$	$K$	$K$
Constant	$K$	$K\delta(f)$	$K\delta(f)$
Unit step	$u(t)$	$\frac{1}{2}\delta(f) + \frac{1}{j2\pi f}$	$\frac{1}{2}\delta(f) + \frac{1}{2\pi f}$
Signum function	$\operatorname{sgnt} = \frac{t}{ t }$	$\frac{1}{j\pi f}$	$\frac{1}{\pi f}$
Cosine wave	$\cos \omega_0 t$	$\frac{1}{2}[\delta(f - f_0) + \delta(f + f_0)]$	Because $f(t)$ is even, $H(f) = F(f)$
Sine wave	$\sin \omega_0 t$	$\frac{-j}{2}[\delta(f - f_0) - \delta(f + f_0)]$	$\frac{1}{2}[\delta(f - f_0) - \delta(f + f_0)]$
Impulse train	$\sum_{-\infty}^{\infty} \delta(t - nT)$	$\frac{1}{T} \sum_{-\infty}^{\infty} \delta(f - \frac{n}{T})$	Because $f(t)$ is even, $H(f) = F(f)$
Periodic wave	$\sum_{-\infty}^{\infty} \alpha_n e^{jn2\pi f_0 t}$	$\sum_{-\infty}^{\infty} \alpha_n \delta(f - \frac{n}{T})$	$\sum_{-\infty}^{\infty} \gamma_n \delta(f - \frac{n}{T})$
Complex sinusoid	$Ae^{j\omega_0 t}$	$A\delta(f - f_0)$	$H(f) = F(f)$
Unit ramp	$tu(t)$	$\frac{j}{4\pi} \delta'(f) - \frac{1}{4\pi^2 f^2}$	$\frac{-1}{4\pi} \delta'(f) - \frac{1}{4\pi^2 f^2}$

**TABLE 4.12** Hartley Transforms of Various Engineering Signals

$f(t) = \delta(t)$	$F(v) = \pi[\delta(v - a) + \delta(v + a)]$
$F(s) = 1$	$f(t) = \sin at$
$F(v) = 1$	$F(v) = \pi[\delta(v - a) - \delta(v + a)]$
$f(t) = \delta(t - a)$	$f(t) = \cos at u(t)$
$F(s) = e^{-as}$	$F(s) = \frac{s}{s^2 + a^2}$
$F(v) = \cos av + \sin av$	$F(v) = \frac{v}{v^2 - a^2} + \frac{\pi}{2} [\delta(v - a) + \delta(v + a)]$
$f(t) = u(t)$	$f(t) = \sin at u(t)$
$F(s) = \frac{1}{s}$	$F(s) = \frac{a}{s^2 + a^2}$
$F(v) = \frac{1}{v} + \pi\delta(v)$	$F(v) = \frac{-a}{v^2 - a^2} + \frac{\pi}{2} [\delta(v - a) - \delta(v + a)]$
$f(t) = u(t - a)$	$f(t) = e^{iat}$
$F(s) = \frac{e^{-as}}{s}$	$F(v) = \pi[\delta(v - a) + \delta(v + a)] + j\pi[\delta(v - a) - \delta(v + a)]$
$F(v) = \frac{1}{v} (\cos av - \sin av) + \pi\delta(v)$	$f(t) = \sum_{n=-\infty}^{+\infty} \delta(t - nT)$
$f(t) = e^{-at} u(t), a > 0$	$F(v) = v_0 \sum_{n=-\infty}^{+\infty} \delta(v - v_0), \quad v_0 = \frac{2\pi}{T}$
$F(s) = \frac{1}{s + a}$	$f(t) = e^{-a t }, \quad a > 0$
$F(v) = \frac{a + v}{a^2 + v^2}$	$F(v) = \frac{2a}{a^2 + v^2}$
$f(t) = \cos at$	$f(t) = e^{-t^2/2\sigma^2}$
	$F(v) = \sigma\sqrt{2\pi} e^{-\sigma^2 v^2/2}$
	$f(t) = 1, \quad 0 \leq t \leq a$

**TABLE 4.12 (continued)** Hartley Transforms of Various Engineering Signals

---


$$F(s) = \frac{1-e^{-as}}{s}$$

$$F(v) = \frac{1}{v}(\sin av - \cos av + 1)$$

$$f(t) = 1, \quad -a \leq t \leq a$$

$$F(s) = \frac{\sinh as}{s}$$

$$F(v) = \frac{2 \sin av}{v}$$

$$f(t) = t, \quad 0 \leq t \leq a$$

$$F(s) = \frac{1-(1+as)e^{-as}}{s^2}$$

$$F(v) = \frac{1}{v^2}[(1-av) \cos av + (1+av) \sin av - 1]$$

$$f(t) = \begin{cases} t, & 0 \leq t \leq a \\ 2a-t, & a \leq t \leq 2a \end{cases}$$

$$F(s) = \frac{(1-e^{-as})^2}{s^2}$$

$$F(v) = \frac{1}{v^2}[2 \cos av + \sin 2av - \cos 2av - 1]$$

$$f(t) = \begin{cases} a-t, & 0 \leq t \leq a \\ a+t, & -a \leq t \leq 0 \end{cases}$$

$$F(s) = \frac{2a(\cosh as - 1)}{s^2}$$

$$F(v) = \frac{4a \sin^2(av/2)}{v^2}$$

$$f(t) = \frac{\sin at}{t}$$

$$F(v) = \pi, \quad -a \leq v \leq a$$

$$f(t) = \begin{cases} t, & 0 \leq t \leq a \\ a, & t > a \end{cases}$$

$$F(s) = \frac{1-e^{-as}}{s^2}$$

$$F(v) = \frac{1}{v^2}(\cos av - 1) + \pi a \delta(v)$$

$$f(t) = e^{-at} \cos bt u(t), \quad a > 0$$

$$F(s) = \frac{s+a}{(s+a)^2 + b^2}$$

$$F(v) = \frac{a(a^2 + b^2) + (a^2 - b^2)v + av^2 + v^3}{(a^2 + b^2 + v^2)^2 - 4b^2v^2}$$

$$f(t) = e^{-at} \sin bt u(t), \quad a > 0$$

$$F(s) = \frac{b}{(s+a)^2 + b^2}$$

$$F(v) = \frac{b(a^2 + b^2) + 2abv - bv^2}{(a^2 + b^2 + v^2)^2 - 4b^2v^2}$$

$$f(t) = \frac{e^{-\zeta\omega_n t}}{\omega_n \sqrt{1-\zeta^2}} \sin \omega_n \sqrt{1-\zeta^2} t u(t), \quad \zeta\omega_n > 0$$

$$F(s) = \frac{1}{s^2 + 2\zeta\omega_n s + \omega_n^2}$$

$$F(v) = \frac{\omega_n^2 - v^2 + 2\zeta\omega_n v}{(\omega_n^2 - v^2)^2 + (2\zeta\omega_n v)^2}$$

$$f(t) = e^{-at} \cosh bt u(t), \quad a > |b|$$

$$F(s) = \frac{s+a}{(s+a)^2 - b^2}$$

$$F(v) = \frac{a(a^2 - b^2) + (a^2 + b^2)v + av^2 + v^3}{(a^2 + b^2 + v^2)^2 - 4a^2b^2}$$

$$f(t) = e^{-at} \sinh bt u(t), \quad a > |b|$$

$$F(s) = \frac{b}{(s+a)^2 - b^2}$$

$$F(v) = \frac{b(a^2 - b^2 - 2av - v^2)}{(a^2 + b^2 + v^2)^2 - 4a^2b^2}$$

$$f(t) = \frac{a \sin bt - b \sin at}{a^2 - b^2} u(t)$$

$$F(s) = \frac{ab}{(s^2 + a^2)(s^2 + b^2)}$$

$$F(v) = \frac{ab}{(a^2 - v^2)(b^2 - v^2)} + \frac{\pi b}{2(b^2 - a^2)} [\delta(v - a) - \delta(v + a)] + \frac{\pi a}{2(a^2 - b^2)} [\delta(v - b) - \delta(v + b)]$$

$$f(t) = \frac{\cos bt - \cos at}{a^2 - b^2} u(t)$$

$$F(s) = \frac{s}{(s^2 + a^2)(s^2 + b^2)}$$

$$F(v) = \frac{1-v}{(a^2 - v^2)(b^2 - v^2)} + \frac{\pi}{2(b^2 - a^2)} [\delta(v - a) + \delta(v + a)] + \frac{\pi}{2(a^2 - b^2)} [\delta(v - b) + \delta(v + b)]$$

$$f(t) = \frac{a \sin at - b \sin bt}{a^2 - b^2} u(t)$$


---



---


$$F(s) = \frac{s^2}{(s^2 + a^2)(s^2 + b^2)}$$

$$F(v) = \frac{-v^2}{(a^2 - v^2)(b^2 - v^2)} + \frac{\pi a}{2(b^2 - a^2)} [\delta(v + a) - \delta(v - a)] + \frac{\pi b}{2(a^2 - b^2)} [\delta(v + b) - \delta(v - b)]$$

$$f(t) = \frac{a^2 \cos at - b^2 \cos bt}{a^2 - b^2} u(t)$$

$$F(s) = \frac{s^3}{(s^2 + a^2)(s^2 + b^2)}$$

$$F(v) = \frac{v^3}{(a^2 - v^2)(b^2 - v^2)} - \frac{\pi a^2}{2(b^2 - a^2)} [\delta(v + a) + \delta(v - a)] - \frac{\pi b^2}{2(a^2 - b^2)} [\delta(v + b) + \delta(v - b)]$$

$$f(t) = \frac{t^{n-1}}{(n-1)!} e^{-at} u(t), \quad a > 0, \quad n \text{ positive integer}$$

$$F(s) = \frac{1}{(s+a)^n}$$

$$F(v) = \sum_{k=0}^n \alpha_k \binom{n}{k} a^{n-k} v^k,$$

$$\alpha_k = \begin{cases} 1, & k = 4m \text{ or } k = 4m + 1 \\ -1, & k = 4m + 2 \text{ or } k = 4m + 3 \end{cases} \quad m \text{ integer}$$

$$f(t) = \frac{1}{a}(1 - e^{-at})u(t), \quad a > 0$$

$$F(s) = \frac{1}{s(s+a)}$$

$$F(v) = \frac{a-v}{v(a^2 + v^2)} + \frac{\pi}{a} \delta(v)$$

$$f(t) = \frac{1}{ab} \left(1 - \frac{b}{b-a} e^{-at} + \frac{a}{b-a} e^{-bt}\right) u(t), \quad a, b > 0$$

$$F(s) = \frac{1}{s(s+a)(s+b)}$$

$$F(v) = \frac{ab - (a+b)v - v^2}{v(a^2 + v^2)(b^2 + v^2)} + \frac{\pi}{ab} \delta(v)$$

$$f(t) = \frac{1}{ab} \left[\alpha - \frac{b(\alpha-a)}{b-a} e^{-at} + \frac{a(\alpha-b)}{b-a} e^{-bt}\right] u(t), \quad a, b > 0$$

$$F(s) = \frac{s+\alpha}{s(s+a)(s+b)}$$

$$F(v) = \frac{\alpha ab + [ab - \alpha(a+b)]v + (a+b-\alpha)v^2 - v^3}{v(a^2 + v^2)(b^2 + v^2)} + \frac{\alpha\pi}{ab} \delta(v)$$

$$f(t) = \frac{1}{b-a}(e^{-at} - e^{-bt})u(t), \quad a, b > 0$$

$$F(s) = \frac{1}{(s+a)(s+b)}$$

$$F(v) = \frac{ab + (a+b)v - v^2}{(a^2 + v^2)(b^2 + v^2)}$$

$$f(t) = \frac{1}{b-a}[(\alpha - a)e^{-at} - (\alpha - b)e^{-bt}]u(t), \quad a, b > 0$$

$$F(s) = \frac{s+\alpha}{(s+a)(s+b)}$$

$$F(v) = \frac{\alpha ab - [ab - \alpha(a+b)]v + (a+b-\alpha)v^2 + v^3}{(a^2 + v^2)(b^2 + v^2)}$$

$$f(t) = \frac{1}{b-a}(ae^{-at} - be^{-bt})u(t), \quad a, b > 0$$

$$F(s) = \frac{s}{(s+a)(s+b)}$$

$$F(v) = \frac{v^2 + (a+b)v - abv}{(a^2 + v^2)(b^2 + v^2)}$$

$$f(t) = \left[\frac{e^{-at}}{(b-a)(c-a)} + \frac{e^{-bt}}{(a-b)(c-b)} + \frac{e^{-ct}}{(a-c)(b-c)}\right] u(t), \quad a, b, c > 0$$

$$F(s) = \frac{1}{(s+a)(s+b)(s+c)}$$

$$F(v) = \frac{abc + (ab + ac + bc)v - (a+b+c)v^2 - v^3}{(a^2 + v^2)(b^2 + v^2)(c^2 + v^2)}$$

$$f(t) = \left[\frac{(\alpha-a)e^{-at}}{(b-a)(c-a)} + \frac{(\alpha-b)e^{-bt}}{(a-b)(c-b)} + \frac{(\alpha-c)e^{-ct}}{(a-c)(b-c)}\right] u(t), \quad a, b, c > 0$$

$$F(s) = \frac{s+\alpha}{(s+a)(s+b)(s+c)}$$

$$F(v) = \frac{\alpha P + (\alpha R - P)v + (R - \alpha Q)v^2 + (Q - \alpha)v^3 - v^4}{(a^2 + v^2)(b^2 + v^2)(c^2 + v^2)}$$

$$P = abc, \quad Q = a + b + c, \quad R = ab + ac + bc$$

$$f(t) = \frac{\sqrt{\alpha^2 + a^2}}{a} \sin(at + \phi)u(t), \quad \phi = \tan^{-1} \frac{a}{\alpha}$$

$$F(s) = \frac{s+\alpha}{s^2 + a^2}$$

$$F(v) = \frac{\alpha - v}{a^2 - v^2} + \frac{\pi}{2} \left[\left(1 + \frac{\alpha}{a}\right)\delta(v - a) + \left(1 - \frac{\alpha}{a}\right)\delta(v + a)\right]$$

$$f(t) = \sin(at + \theta)u(t)$$


---

(continued)

**TABLE 4.12 (continued)** Hartley Transforms of Various Engineering Signals

---


$$F(s) = \frac{s \sin \theta + a \cos \theta}{s^2 + a^2}$$

$$F(v) = \frac{a \cos \theta - v \sin \theta}{a^2 - v^2} + \frac{\pi}{2} [(\sin \theta + \cos \theta) \delta(v - a) + (\sin \theta - \cos \theta) \delta(v + a)]$$

$$f(t) = \frac{1}{a^2} (1 - \cos at) u(t)$$

$$F(s) = \frac{1}{s(s^2 + a^2)}$$

$$F(v) = \frac{1}{v(a^2 - v^2)} + \frac{\pi}{a^2} \delta(v) - \frac{\pi}{2a^2} [\delta(v - a) + \delta(v + a)]$$

$$f(t) = \left[ \frac{\alpha}{a^2} - \frac{\sqrt{\alpha^2 + a^2}}{a^2} \cos(at + \phi) \right] u(t), \quad \phi = \tan^{-1} \frac{a}{\alpha}$$

$$F(s) = \frac{s + \alpha}{s(s^2 + a^2)}$$

$$F(v) = \frac{v + \alpha}{v(a^2 - v^2)} + \frac{\alpha \pi}{a^2} \delta(v) - \frac{\pi}{2a^2} [(\alpha - a) \delta(v - a) + (\alpha + a) \delta(v + a)]$$

$$f(t) = \left[ \frac{e^{-at}}{a^2 + b^2} + \frac{1}{b\sqrt{a^2 + b^2}} \sin(bt - \phi) \right] u(t), \quad \phi = \tan^{-1} \frac{b}{a}, a > 0$$

$$F(s) = \frac{1}{(s+a)(s^2 + b^2)}$$

$$F(v) = \frac{v + \alpha}{(a^2 + v^2)(b^2 - v^2)} + \frac{\pi}{2b(b^2 - a^2)} [(a - b) \delta(v - a) - (a + b) \delta(v + a)]$$

$$f(t) = \frac{1}{b} \sqrt{(\alpha - a)^2 + b^2} e^{-at} \sin(bt + \phi) u(t), \quad \phi = \tan^{-1} \frac{b}{\alpha - a}, a > 0$$

$$F(s) = \frac{s + \alpha}{(s + a)^2 + b^2}$$

$$F(v) = \frac{\alpha(a^2 + b^2) - (a^2 + b^2 - 2\alpha a)v + (2a - \alpha)v^2 + v^3}{(a^2 + b^2 + v^2)^2 - 4b^2v^2}$$

$$f(t) = \left[ \frac{1}{a^2 + b^2} + \frac{e^{-at}}{b\sqrt{a^2 + b^2}} \sin(bt - \phi) \right] u(t), \quad \phi = \tan^{-1} \left( -\frac{b}{a} \right), a > 0$$

$$F(s) = \frac{1}{s[(s+a)^2 + b^2]}$$

$$F(v) = \frac{a^2 + b^2 - 2av - v^2}{v(a^2 + b^2 + v^2)^2 - 4b^2v^2} + \frac{\pi}{a^2 + b^2} \delta(v)$$

$$f(t) = \left[ \frac{1}{\omega_n} - \frac{e^{-\zeta \omega_n t}}{\omega_n \sqrt{1 - \zeta^2}} \sin(\omega_n \sqrt{1 - \zeta^2} t + \phi) \right] u(t), \quad \phi = \cos^{-1} \zeta, a > 0$$

$$F(s) = \frac{1}{s(s^2 + 2\zeta \omega_n s + \omega_n^2)}$$

$$F(v) = \frac{\omega_n^2 - v^2 - 2\zeta \omega_n v}{v[(\omega_n^2 - v^2)^2 + (2\zeta \omega_n v)^2]} + \frac{\pi}{\omega_n^2} \delta(v)$$

$$f(t) = \left[ \frac{e^{-ct}}{(c-a)^2 + b^2} + \frac{e^{-at}}{b\sqrt{(c-a)^2 + b^2}} \sin(bt - \phi) \right] u(t), \quad \phi = \tan^{-1} \frac{b}{c-a}, a, c > 0$$

$$F(s) = \frac{1}{(s+c)[(s+a)^2 + b^2]}$$

$$F(v) = \frac{c(a^2 + b^2) + (a^2 + b^2 + 2ac)v - (2a + c)v^2 - v^3}{[(a^2 + b^2 + v^2)^2 - 4b^2v^2](c^2 + v^2)}$$

$$f(t) = \left[ \frac{\alpha}{a^2 + b^2} + \frac{1}{b} \sqrt{\frac{(\alpha - a)^2 + b^2}{a^2 + b^2}} e^{-at} \sin(bt + \phi) \right] u(t), \quad \phi = \tan^{-1} \frac{b}{\alpha - a} - \tan^{-1} \left( -\frac{b}{a} \right), a > 0$$

$$F(s) = \frac{s + \alpha}{s[(s+a)^2 + b^2]}$$

$$F(v) = \frac{\alpha(a^2 + b^2) + (a^2 + b^2 - 2\alpha a)v + (2a - \alpha)v^2 - v^3}{v[(a^2 + b^2 + v^2)^2 - 4b^2v^2]} + \frac{\alpha \pi}{a^2 + b^2} \delta(v)$$

$$f(t) = \left[ \frac{1}{c(a^2 + b^2)} - \frac{e^{-ct}}{c[(c-a)^2 + b^2]} + \frac{e^{-at} \sin(bt - \phi)}{b\sqrt{a^2 + b^2} \sqrt{(c-a)^2 + b^2}} \right] u(t), \quad a, c > 0$$

$$\phi = \tan^{-1} \frac{b}{c-a} + \tan^{-1} \left( -\frac{b}{a} \right)$$

$$F(s) = \frac{1}{s(s+c)[(s+a)^2 + b^2]}$$

$$F(v) = \frac{c(a^2 + b^2) - (a^2 + b^2 + 2ac)v - (2a + c)v^2 + v^3}{v[(a^2 + b^2 + v^2)^2 - 4b^2v^2](c^2 + v^2)} + \frac{\pi}{c(a^2 + b^2)} \delta(v)$$

$$f(t) = \left[ \frac{\alpha}{c(a^2 + b^2)} + \frac{(c-\alpha)e^{-ct}}{c[(c-a)^2 + b^2]} + \frac{\sqrt{(\alpha - a)^2 + b^2}}{b\sqrt{a^2 + b^2} \sqrt{(c-a)^2 + b^2}} e^{-at} \sin(bt - \phi) \right] u(t), \quad a, c > 0$$


---



---


$$\phi = \tan^{-1} \frac{b}{\alpha - a} - \tan^{-1} \frac{b}{c - a} - \tan^{-1} \left( -\frac{b}{a} \right)$$

$$F(s) = \frac{s + \alpha}{s(s+c)[(s+a)^2 + b^2]}$$

$$F(v) = \frac{\alpha Bc + (cA - \alpha B)v + (A + 2ac - \alpha c)v^2 - (2a + c - \alpha)v^3 - v^4}{v[(a^2 + b^2 + v^2)^2 - 4b^2v^2](c^2 + v^2)} + \frac{\alpha \pi}{c(a^2 + b^2)} \delta(v)$$

$$A = a^2 + b^2 - 2\alpha a, B = a^2 + b^2$$

$$f(t) = \frac{1}{a^2} (1 - e^{-at} - ate^{-at}) u(t), \quad a > 0$$

$$F(s) = \frac{1}{s(s+a)^2}$$

$$F(v) = \frac{a^2 - 2av - v^2}{v(a^2 + v^2)} + \frac{\pi}{a^2} \delta(v)$$

$$f(t) = \frac{1}{a^2} [\alpha - \alpha e^{-at} + a(a - \alpha)te^{-at}] u(t), \quad a > 0$$

$$F(s) = \frac{s + \alpha}{s(s+a)^2}$$

$$F(v) = \frac{\alpha a^2 + (a^2 - 2\alpha a)v + (2a - \alpha)v^2 - v^3}{v(a^2 + v^2)^2} + \frac{\alpha \pi}{a^2} \delta(v)$$

$$f(t) = \left[ \frac{\alpha_0}{ab} + \frac{a^2 - \alpha_1 a + \alpha_0}{a(a-b)} e^{-at} - \frac{b^2 - \alpha_1 b + \alpha_0}{b(a-b)} e^{-bt} \right] u(t), \quad a, b > 0$$

$$F(s) = \frac{s^2 + \alpha_1 s + \alpha_0}{s(s+a)(s+b)}$$

$$F(v) = \frac{\alpha_0 ab + [\alpha_1 ab - \alpha_0(a+b)]v + [\alpha_1(a+b) - ab - \alpha_0]v^2 + (a+b - \alpha_1)v^3 + v^4}{v[(a^2 + b^2 + v^2)^2 - 4b^2v^2]} + \frac{\alpha_0 \pi}{ab} \delta(v)$$

$$f(t) = \left[ \frac{\alpha_0}{c^2} + \frac{1}{bc} [(a^2 - b^2 - \alpha_1 a + \alpha_0)^2 + b^2(\alpha_1 - 2a)^2]^{1/2} e^{-at} \sin(bt + \phi) \right] u(t), \quad a > 0$$

$$\phi = \tan^{-1} \frac{b(\alpha_1 - 2a)}{a^2 - b^2 - \alpha_1 a + \alpha_0} - \tan^{-1} \left( -\frac{b}{a} \right)$$

$$F(s) = \frac{s^2 + \alpha_1 s + \alpha_0}{s[(s+a)^2 + b^2]}$$

$$F(v) = \frac{\alpha_1 A + \alpha_1(A - 2a)v + (2\alpha_1 a - \alpha_1 - A)v^2 + (2a - 1)v^3 + v^4}{v[(a^2 + b^2 + v^2)^2 - 4b^2v^2]} + \frac{\alpha_0 \pi}{A} \delta(v), \quad A = a^2 + b^2$$


---

### Appendix: A Sample FHT Program

```

/ * Program
FHT . C*****
*****

/*
/* This FHT algorithm utilizes an efficient
permutation algorithm
/* developed by David M.W. Evans. Additional
details may be found
/* in: IEEE Transaction on Acoustics, Speech,
and Signal Processing,
/* vol. ASSP-35, n. 8, pp. 1120-1125, August 1987.
/*
/* This FHT algorithm, authored by Lakshmikantha
S. Prabhu, is
/* optimized for the SPARC RISC platform.
Additional details may
/* be found in his M.S.E.E. thesis referenced
below.
/*
/* L.S. Prabhu, 'A Complexity-Based Timing
Analysis of Fast
/* Real Transform Algorithms,' Master's
Thesis, University of
/* Arkansas, Fayetteville, AR, 72701-1201, 1993.
/*****
*****

```

```

/* This program assumes a maximum array length
of 2^M=N where      */
/* M=9 and N=512.    */
/* See Line 52 if the array length is increased.
*/
#include <stdio.h>
#include <math.h>
#define M 3
#define N 8
float* myFht ( );
main ( )
{
/* Read the integer values 1, . . . , N into the
vector X[N].*/
int i;
float X[N] ;
for (i=0; i<N; i++)
X[i]=i+1;
for (i=0; i<N; i++)
printf ( '\%f\n', X[i] );
myFht (X, N, M);
printf ( '\n' );
for (i=0; i<N; i++)
printf ( '\%d: \%f\n', i, X[i]/N );
/* It is assumed that the user divides by the
integer N.*/
}
float*
myFht (x, n, m)
float* x;
int n, m;
{
int i, j, k, kk, l, 10, 11, 12, 13, 14, 15, m1, n1,
n2, NN, s;
int diff=0, diff2, gamma, gamma2=2, n2.2,
n2.4, n.2, n.4, n.8, n.16;
int itemp, ntemp, phi, theta.by.2;
float ee, temp1, temp2, xtemp1, xtemp2;
float h.sec.b, x0, x1, x2, x3, x4, x5, xtemp;
double cc1, cc2, ss1, ss2;
double sine[257];
/*****
*****/
/* Digit reverse counter.      */
/*****
*****/
int powers.of.2[16], seed[256];
int firstj, log2.n, log2.seed.size;
int group.no, nn, offset;
log2.n=m >> 1;
nn=2<<(log2.n-1);
if ( (m%2) == 1 )
log2.n=log2.n+1;
seed[0]=0; seed[1]=1;
for (log2.seed.size=2; log2.seed.size <=
log2.n; log2.seed.size++)
{
for ( i=0; i < 2 << (log2.seed.size - 2);
i++)
{
seed[i]=2 * seed[i];
for (k=1; k<2; k++)
seed[ i+k * (2 << (log2.seed.size - 1))>>
1] =seed[i];
}
}
for (offset=1, offset<nn; offset++)
{
{firstj=nn * seed[offset];
i=offset; j=firstj;
xtemp=x[i];
x[i]=x[j];
x[j]=xtemp;
for ( group.no=1; group.no<seed[offset];
group.no++)
{
i=i+nn; j=firstj+seed[group.no];
xtemp=x[i];
x[i]=x[j];
x[j]=xtemp;
}
}
j=0;
n1=n-1;
n.16=n >> 4;
n.8=n >> 3;
n.4=n >> 2;
n.2=n >> 1;
/*****
*****/
/* Start the transform computation with 2-point
butterflies.*/
/*****
*****/
for (i=0; i<n; i += 2)
{
s=i+1;
xtemp=x[i];
x[i] += x[s];
x[s] =xtemp-x[s];
}
/*****
*****/
/* Now, the 4-point butterflies.*/
/*****
*****/
for ( i=0; i<N; i += 4)
{

```

```

    xtemp=x[i];
    x[i] += x[i+2];
    x[i+2]=xtemp-x[i+2];
    xtemp=x[i+1];
    x[i+1] += x[i+3];
    x[i+3]=xtemp-x[i+3];
}
/*****
*****/
/* Sine table initialization.*/
/*****
*****/
NN=n·4;
sine[0]=0;
sine[n·16]=0.382683432;
sine[n·8]=0.707106781;
sine[3·n·16]=0.923879533;
sine[n·4]=1.000000000;
h·sec·b=0.509795579;
diff=n·16;
theta·by·2=n·4 >> 3;
j=0;
while (theta·by2 >= 1)
{
    for ( i=0; i <= n·4; i += diff)
    {
        sine[j+theta·by·2]=h·sec·b * (sine[j]
+ sine[j+diff] );
        j=j+diff;
    }
    j=0;
    diff=diff >> 1;
    theta·by·2=theta·by·2 >> 1;
    h·sec·b=1 / sqrt (2+1/h·sec·b);
/*****
*****/
/* Other butterflies.*/
/*****
*****/
for ( i=3; i <= m; i++)
{
    diff=1; gamma=0;
    ntemp=0; phi=2 << (m-i) >> 1;
    ss1=sine[phi];
    cc1=sine[n·4-phi];
    n2=2 << (i-1);
    n2·2=n2 >> 1;
    n2·4=n2 >> 2;
    gamma2=n2·4;
    diff2=gamma2+gamma2-1;
    item=n2·4;
    k=0;
/*****
*****/
}
/*****
*****/
/* Initial section of stages 3, 4, . . . for which
sines & cosines are*/
/* not required.*/
/*****
*****/
for (k=0; k < (2 << (m-i) >> 1); k++)
{
    10=gamma;
    11=10+n2·2;
    13=gamma2;
    14=gamma2+n2·2;
    15=11+item;
    x0=x[10];
    x1=x[11];
    x3=x[13];
    x5=x[15];
    x10=x0+x1;
    x[11]=x0-x1;
    x[13]=x3+x5;
    x[14]=x3-x5;
    gamma=gamma+n2;
    gamma2=gamma2+n2;
}
gamma=diff;
gamma2=diff2;
/*****
*****/
/* Next sections of stages 3, 4, . . .*/
/*****
*****/
for ( j=1; j < 2 << (i-3); j++)
{
    for ( k=0; k < (2 << (m-i) >> 1); k++)
    {
        10=gamma;
        11=10+n2·2;
        13=gamma2;
        14=13+n2·2;
        x0=x[10];
        x1=x[11];
        x3=x[13];
        x4=x[14];
        x[10]=x0+x1 * cc1+x4 * ss1;
        x[11]=x0-x1 * cc1-x4 * ss1;
        x[13]=x3-x4 * cc1+x1 * ss1;
        x[14]=x3+x4 * cc1-x1 * ss1;
        gamma=gamma+n2;
        gamma2=gamma2+n2;
    }
    item=0;
    phi=phi+(2 << (m-i) >> 1);
}

```

```

ntemp = (phi < n·4) ? 0 : n·4;
ss1 = sine [phi - ntemp];
cc1 = sine [n·4 - phi + ntemp];
diff++; diff2-;
gamma = diff;
gamma2 = diff2;
}
}
}

```

## Acknowledgments

The author would like to thank Mrs. Robert William Hartley and Dr. Sheldon Hochheiser, Senior Research Associate, AT&T Archives, for their assistance in accumulating the biographical information on R.V.L. Hartley. The assistance of R.N. Bracewell, G.T. Heydt, and Z. Wang is gratefully acknowledged.

## References

1. R. V. L. Hartley, A more symmetrical Fourier analysis applied to transmission problems, *Proc. IRE*, 30, 144–150, March 1942.
2. R. V. L. Hartley, Transmission of information, *Bell Sys. Tech. J.*, 7, 535–563, July 1928.
3. Z. Wang, Harmonic analysis with a real frequency function—I. Aperiodic case, *Appl. Math. Comput.*, 9, 53–73, 1981.
4. Z. Wang, Harmonic analysis with a real frequency function—II. Periodic and bounded case, *Appl. Math. Comput.*, 9, 153–163, 1981.
5. Z. Wang, Harmonic analysis with a real frequency function—III. Data sequence, *Appl. Math. Comput.*, 9, 245–255, 1981.
6. Z. Wang, Fast algorithms for the discrete W transform and for the discrete Fourier transform, *IEEE Trans. Acoust. Speech Signal Process.*, ASSP-32, 803–816, 1984.
7. R. N. Bracewell, Discrete Hartley transform, *J. Opt. Soc. Am.*, 73, 1832–1835, December 1983.
8. R. N. Bracewell, The fast Hartley transform, *Proc. IEEE*, 72, 1010–1018, 1984.
9. R. N. Bracewell, *The Hartley Transform*, Oxford University Press, New York, 1986.
10. A. D. Poularikas and S. Seeley, *Signals and Systems*, 2nd edn., Krieger, Malabar, FL, 1994.
11. K. J. Olejniczak and G. T. Heydt, eds., Special section on the Hartley transform, *Proc. IEEE*, 82, 372–447, 1994.
12. G. A. Campbell and R. M. Foster, *Fourier Integrals for Practical Applications*, Van Nostrand, Princeton, NJ, 1948.
13. A. Erdélyi, *Tables of Integral Transforms*, Vol. 1, McGraw-Hill, New York, 1954.
14. W. Magnus and F. Oberhettinger, *Formulas and Theorems of the Special Functions of Mathematical Physics*, pp. 116–120, Chelsea, New York, 1949.



# 5

## Laplace Transforms

Alexander D. Poularikas  
University of Alabama in Huntsville

†Samuel Seely

5.1	Introduction.....	5-1
5.2	Laplace Transform of Some Typical Functions .....	5-2
5.3	Properties of the Laplace Transform .....	5-3
5.4	The Inverse Laplace Transform .....	5-10
5.5	Solution of Ordinary Linear Equations with Constant Coefficients .....	5-13
5.6	The Inversion Integral.....	5-17
5.7	Applications to Partial Differential Equations.....	5-20
5.8	The Bilateral or Two-Sided Laplace Transform.....	5-27
	References .....	5-43

### 5.1 Introduction\*

The Laplace transform has been introduced into the mathematical literature by a variety of procedures. Among these are: (a) in its relation to the Heaviside operational calculus, (b) as an extension of the Fourier integral, (c) by the selection of a particular form for the kernel in the general Integral transform, (d) by a direct definition of the Laplace transform, and (e) as a mathematical procedure that involves multiplying the function  $f(t)$  by  $e^{-st}$   $dt$  and integrating over the limits 0 to  $\infty$ . We will adopt this latter procedure.

Not all functions  $f(t)$ , where  $t$  is any variable, are Laplace transformable. For a function  $f(t)$  to be Laplace transformable, it must satisfy the Dirichlet conditions—a set of sufficient but not necessary conditions. These are

1.  $f(t)$  must be piecewise continuous; that is, it must be single valued but can have a finite number of finite isolated discontinuities for  $t > 0$ .
2.  $f(t)$  must be of exponential order; that is,  $f(t)$  must remain less than  $Me^{-a_0t}$  as  $t$  approaches  $\infty$ , where  $M$  is a positive constant and  $a_0$  is a real positive number.

For example, such functions as:  $\tan \beta t$ ,  $\cot \beta t$ ,  $e^{t^2}$  are not Laplace transformable. Given a function  $f(t)$  that satisfies the Dirichlet conditions, then

$$F(s) = \int_0^{\infty} f(t)e^{-st} dt \quad \text{written } \mathcal{L}\{f(t)\} \quad (5.1)$$

is called the Laplace transformation of  $f(t)$ . Here  $s$  can be either a real variable or a complex quantity. Observe the shorthand notation  $\mathcal{L}\{f(t)\}$  to denote the Laplace transformation of  $f(t)$ . Observe also that only ordinary integration is involved in this integral.

To amplify the meaning of condition (2), we consider piecewise continuous functions, defined for all positive values of the variable  $t$ , for which

$$\lim_{t \rightarrow \infty} f(t)e^{-ct} = 0, \quad c = \text{real constant.}$$

Functions of this type are known as functions of exponential order. Functions occurring in the solution for the time response of stable linear systems are of exponential order zero. Now we can recall that the integral  $\int_0^{\infty} f(t)e^{-st} dt$  converges if

$$\int_0^{\infty} |f(t)e^{-st}| dt < \infty, \quad s = \sigma + j\omega$$

If our function is of exponential order, we can write this integral as

$$\int_0^{\infty} |f(t)|e^{-ct} e^{-(\sigma-c)t} dt.$$

This shows that for  $\sigma$  in the range  $\sigma > 0$  ( $\sigma$  is the abscissa of convergence) the integral converges; that is

$$\int_0^{\infty} |f(t)e^{-st}| dt < \infty, \quad \text{Re}(s) > c.$$

\* All the contour integrations in the complex plane are counterclockwise.



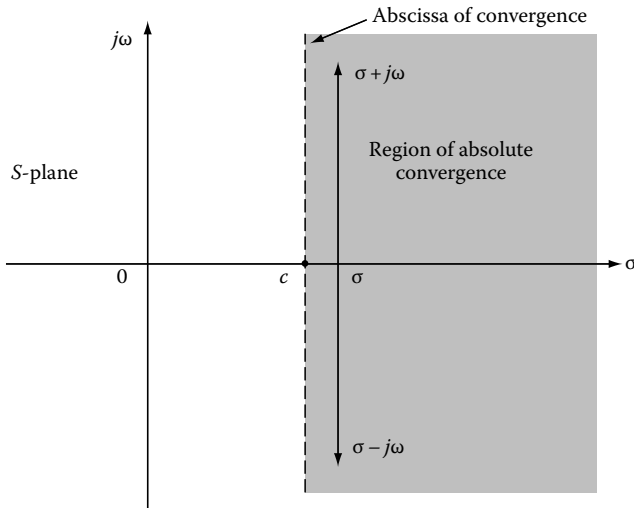


FIGURE 5.1 Path of integration for exponential order function.

The restriction in this equation, namely,  $\text{Re}(s) = c$ , indicates that we must choose the path of integration in the complex plane as shown in Figure 5.1.

## 5.2 Laplace Transform of Some Typical Functions

We illustrate the procedure in finding the Laplace transform of a given function  $f(t)$ . In all cases it is assumed that the function  $f(t)$  satisfies the conditions of Laplace transformability.

### Example 5.1

Find the Laplace transform of the unit step function  $f(t) = u(t)$ , where  $u(t) = 1, t > 0, u(t) = 0, t < 0$ .

#### SOLUTION

By Equation 5.1 we write

$$\mathcal{L}\{u(t)\} = \int_0^{\infty} u(t)e^{-st} dt = \int_0^{\infty} e^{-st} dt = \frac{e^{-st}}{s} \Big|_0^{\infty} = \frac{1}{s}. \quad (5.2)$$

The region of convergence is found from the expression  $\int_0^{\infty} |e^{-st}| dt = \int_0^{\infty} e^{-\sigma t} dt < \infty$ , which is the entire right half-plane,  $\sigma > 0$ .

### Example 5.2

Find the Laplace transform of the function  $f(t) = 2\sqrt{\frac{t}{\pi}}$

$$F(s) = \frac{2}{\sqrt{\pi}} \int_0^{\infty} t^{\frac{1}{2}} e^{-st} dt. \quad (5.3)$$

To carry out the integration, define the quantity  $x = t^{\frac{1}{2}}$ , then  $dx = \frac{1}{2} t^{-\frac{1}{2}} dt$ , from which  $dt = 2t^{\frac{1}{2}} dx = 2x dx$ . Then

$$F(s) = \frac{4}{\sqrt{\pi}} \int_0^{\infty} x^2 e^{-sx^2} dx.$$

But the integral

$$\int_0^{\infty} x^2 e^{-sx^2} dx = \frac{\sqrt{\pi}}{4s^{3/2}}.$$

Thus, finally,

$$F(s) = \frac{1}{s^{3/2}}. \quad (5.4)$$

### Example 5.3

Find the Laplace transform of  $f(t) = \text{erfc} \frac{k}{2\sqrt{t}}$ , where the error function,  $\text{erf } t$ , and the complementary error function,  $\text{erfc } t$ , are defined by

$$\text{erf } t = \frac{2}{\sqrt{\pi}} \int_0^t e^{-u^2} du, \quad \text{erfc } t = \frac{2}{\sqrt{\pi}} \int_t^{\infty} e^{-u^2} du,$$

#### SOLUTION

Consider the integral

$$I = \frac{2}{\sqrt{\pi}} \int_0^{\infty} e^{-st} \left[ \int_{\frac{\lambda}{\sqrt{t}}}^{\infty} e^{-u^2} du \right] dt \quad \text{where } \lambda = \frac{k}{2}. \quad (5.5)$$

Change the order of integration, noting that  $u = \frac{\lambda}{\sqrt{t}}, t = \frac{\lambda^2}{u^2}$

$$I = \frac{2}{\sqrt{\pi}} \int_0^{\infty} e^{-u^2} \left[ \int_{\frac{\lambda^2}{u^2}}^{\infty} e^{-st} dt \right] du = \frac{2}{s\sqrt{\pi}} \int_0^{\infty} \exp\left(-u^2 - \frac{\lambda^2 s}{u^2}\right) du$$

The value of this integral is known

$$= \frac{2}{s\sqrt{\pi}} \cdot \frac{\sqrt{\pi}}{2} e^{-2\lambda\sqrt{s}},$$

which leads to

$$\mathcal{L}\left\{\text{erfc} \frac{k}{2\sqrt{t}}\right\} = \frac{1}{s} \exp\{-k\sqrt{s}\}. \quad (5.6)$$

**Example 5.4**

Find the Laplace transform of the function  $f(t) = \sinh at$ .

**SOLUTION**

Express the function  $\sinh at$  in its exponential form

$$\sinh at = \frac{e^{at} - e^{-at}}{2}.$$

The Laplace transform becomes

$$\begin{aligned} \mathcal{L}\{\sinh at\} &= \frac{1}{2} \int_0^{\infty} [e^{-(s-a)t} - e^{-(s+a)t}] dt \\ &= \frac{a}{s^2 - a^2}. \end{aligned} \tag{5.7}$$

A moderate listing of functions  $f(t)$  and their Laplace transforms  $F(s) = \mathcal{L}\{f(t)\}$  are given in Table A.5.1.

**5.3 Properties of the Laplace Transform**

We now develop a number of useful properties of the Laplace transform; these follow directly from Equation 5.1. Important in developing certain properties is the definition of  $f(t)$  at  $t=0$ , a quantity written  $f(0+)$  to denote the limit of  $f(t)$  as  $t$  approaches zero, assumed from the positive direction. This designation is consistent with the choice of function response for  $t > 0$ . This means that  $f(0+)$  denotes the initial condition. Correspondingly,  $f^{(n)}(0+)$  denotes the value of the  $n$ th derivative at time  $t=0+$ , and  $f^{(-n)}(0+)$  denotes the  $n$ th time integral at time  $t=0+$ . This means that the direct Laplace transform can be written

$$F(s) = \lim_{\substack{R \rightarrow \infty \\ a \rightarrow 0+}} \int_a^R f(t)e^{-st} dt, \quad R > 0, a > 0. \tag{5.8}$$

We proceed with a number of theorems.

**THEOREM 5.1 Linearity**

The Laplace transform of the linear sum of two Laplace transformable functions  $f(t) + g(t)$  with respective abscissas of convergence  $\sigma_f$  and  $\sigma_g$ , with  $\sigma_g > \sigma_f$  is

$$\mathcal{L}\{f(t) + g(t)\} = F(s) + G(s). \tag{5.9}$$

*Proof* From Equation 5.8 we write

$$\mathcal{L}\{f(t) + g(t)\} = \int_0^{\infty} [f(t) + g(t)]e^{-st} dt = \int_0^{\infty} f(t)e^{-st} dt + \int_0^{\infty} g(t)e^{-st} dt,$$

$$\text{Re}(s) > \sigma_g.$$

Thus,

$$\mathcal{L}\{f(t) + g(t)\} = F(s) + G(s).$$

As a direct extension of this result, for  $K_1$  and  $K_2$  constants,

$$\mathcal{L}\{K_1f(t) + K_2g(t)\} = K_1F(s) + K_2G(s). \tag{5.10}$$

**THEOREM 5.2 Differentiation**

Let the function  $f(t)$  be piecewise continuous with sectionally continuous derivatives  $df(t)/dt$  in every interval  $0 \leq t \leq T$ . Also let  $f(t)$  be of exponential order  $e^{ct}$  as  $t \rightarrow \infty$ . Then when  $\text{Re}(s) > c$ , the transform of  $df(t)/dt$  exists and

$$\mathcal{L}\left\{\frac{df(t)}{dt}\right\} = s\mathcal{L}\{f(t)\} - f(0+) = sF(s) - f(0+). \tag{5.11}$$

*Proof* Begin with Equation 5.8 and write

$$\mathcal{L}\left\{\frac{df(t)}{dt}\right\} = \lim_{T \rightarrow \infty} \int_0^T \frac{df(t)}{dt} e^{-st} dt.$$

Write the integral as the sum of integrals in each interval in which the integrand is continuous. Thus, we write

$$\int_0^T e^{-st} f^{(1)}(t) dt = \int_0^{t_1} [ ] + \int_{t_1}^{t_2} [ ] + \dots + \int_{t_{n-1}}^T [ ].$$

Each of these integrals is integrated by parts by writing

$$\begin{aligned} u &= e^{-st} & du &= -se^{-st} dt \\ dv &= \frac{df}{dt} dt & v &= f \end{aligned}$$

with the result

$$e^{-st} f(t) \Big|_0^{t_1} + e^{-st} f(t) \Big|_{t_1}^{t_2} + \dots + e^{-st} f(t) \Big|_{t_{n-1}}^T + s \int_0^T e^{-st} f(t) dt.$$

But  $f(t)$  is continuous so that  $f(t_1 - 0) = f(t_1 + 0)$ , and so forth, hence

$$\int_0^T e^{-st} f^{(1)}(t) dt = -f(0+) + e^{-sT} f(T) + s \int_0^T e^{-st} f(t) dt.$$

However, with  $\lim_{t \rightarrow \infty} f(t)e^{-st} = 0$  (otherwise the transform would not exist), then the theorem is established.

**THEOREM 5.3 Differentiation**

Let the function  $f(t)$  be piecewise continuous, have a continuous derivative  $f^{(n-1)}(t)$  of order  $n - 1$  and a sectionally continuous derivative  $f^{(n)}(t)$  in every finite interval  $0 \leq t \leq T$ . Also, let  $f(t)$  and all its derivatives through  $f^{(n-1)}(t)$  be of exponential order  $e^{ct}$  as  $t \rightarrow \infty$ . Then the transform of  $f^{(n)}(t)$  exists when  $\text{Re}(s) > c$  and it has the following form:

$$\mathcal{L}\{f^{(n)}(t)\} = s^n F(s) - s^{n-1}f(0+) - s^{n-2}f^{(1)}(0+) - \dots - s^{n-n}f^{(n-1)}(0+). \tag{5.12}$$

*Proof* The proof follows as a direct extension of the proof of Theorem 5.2.

**Example 5.5**

Find  $\mathcal{L}\{t^m\}$  where  $m$  is any positive integer.

**SOLUTION**

The function  $f(t) = t^m$  satisfies all the conditions of Theorem 5.3 for any positive  $c$ . Thus,

$$f(0+) = f^{(1)}(0+) = \dots = f^{(m-1)}(0+) = 0$$

$$f^{(m)}(t) = m!, \quad f^{(m+1)}(t) = 0.$$

By Equation 5.12 with  $n = m + 1$  we have

$$\mathcal{L}\{f^{(m+1)}(t)\} = 0 = s^{m+1}\mathcal{L}\{t^m\} - m!.$$

It follows, therefore, that

$$\mathcal{L}\{t^m\} = \frac{m!}{s^{m+1}}.$$

**THEOREM 5.4 Integration**

If  $f(t)$  is sectionally continuous and has a Laplace transform, then the function  $\int_0^t f(\xi)d\xi$  has the Laplace transform given by

$$\mathcal{L}\left\{\int_0^t f(\xi)d\xi\right\} = \frac{F(s)}{s} + \frac{1}{s}f^{(-1)}(0+). \tag{5.13}$$

*Proof* Because  $f(t)$  is Laplace transformable, its integral is written

$$\mathcal{L}\left\{\int_{-\infty}^t f(\xi)d\xi\right\} = \int_0^\infty \left[\int_{-\infty}^t f(\xi)d\xi\right] e^{-st} dt.$$

This is integrated by parts by writing

$$u = \int_{-\infty}^t f(\xi)d\xi \quad du = f(\xi)d\xi = f(t)dt$$

$$dv = e^{-st} dt \quad v = -\frac{1}{s}e^{-st}.$$

Then

$$\mathcal{L}\left\{\int_{-\infty}^t f(\xi)d\xi\right\} = \left[-\frac{e^{-st}}{s} \int_{-\infty}^t f(\xi)d\xi\right]_0^\infty + \frac{1}{s} \int_0^\infty f(t)e^{-st} dt$$

$$= \frac{1}{s} \int_0^\infty f(t)e^{-st} dt + \frac{1}{s} \int_{-\infty}^0 f(\xi)d\xi$$

from which

$$\mathcal{L}\left\{\int_0^t f(\xi)d\xi\right\} = \frac{1}{s}F(s) + \frac{1}{s}f^{(-1)}(0+)$$

where  $[f^{(-1)}(0+)/s]$  is the initial value of the integral of  $f(t)$  at  $t = 0+$ . The negative number in the bracketed exponent indicates integration.

**Example 5.6**

Deduce the value of  $\mathcal{L}\{\sin at\}$  from  $\mathcal{L}\{\cos at\}$  by employing Theorem 5.4.

**SOLUTION**

By ordinary integration

$$\int_0^t \cos ax dx = \frac{\sin at}{a}.$$

From Theorem 5.4 we can write, knowing that  $\mathcal{L}\{\cos at\} = \frac{s}{s^2+a^2}$ .

$$\mathcal{L}\left\{\frac{\sin at}{a}\right\} = \frac{1}{s^2+a^2}.$$

so that

$$\mathcal{L}\{\sin at\} = \frac{a}{s^2+a^2}.$$

**THEOREM 5.5**

Division of the transform of a function by  $s$  corresponds to integration of the function between the limits 0 and  $t$

$$\begin{aligned} \mathcal{L}^{-1}\left\{\frac{F(s)}{s}\right\} &= \int_0^t f(\xi)d\xi \\ \mathcal{L}^{-1}\left\{\frac{F(s)}{s^2}\right\} &= \int_0^t \int_0^\xi f(\lambda)d\lambda d\xi \end{aligned} \tag{5.14}$$

and so forth, for division by  $s^n$ , provided that  $f(t)$  is Laplace transformable.

*Proof* The proof of this theorem follows from Theorem 5.4.

**THEOREM 5.6 Multiplication by  $t$**

If  $f(t)$  is piecewise continuous and of exponential order, then each of the Laplace transforms:  $\mathcal{L}\{f(t)\}$ ,  $\mathcal{L}\{tf(t)\}$ ,  $\mathcal{L}\{t^2f(t)\}$ ,... is uniformly convergent with respect to  $s$  when  $s = c$ , where  $\sigma > c$ , and

$$\mathcal{L}\{t^n f(t)\} = (-1)^n \frac{d^n F(s)}{ds^n}. \tag{5.15}$$

Further

$$\lim_{s \rightarrow \infty} \frac{d^n F(s)}{ds^n} = 0, \quad \mathcal{L}_{s \rightarrow \infty}\{t^n f(t)\} = 0, \quad n = 1, 2, 3, \dots$$

*Proof* It follows from Equation 5.8 when this integral is uniformly convergent and the integral converges, that

$$\frac{\partial F(s)}{\partial s} = \int_0^\infty e^{-st}(-t)f(t)dt = \mathcal{L}\{-tf(t)\}.$$

Further, it follows that

$$\frac{\partial^2 F(s)}{\partial s^2} = \int_0^\infty e^{-st}(-t)^2 f(t)dt = \mathcal{L}\{t^2 f(t)\}.$$

Similar procedures follow for derivatives of higher order.

**THEOREM 5.7 Differentiation of a Transform**

Differentiation of the transform of a function  $f(t)$  corresponds to the multiplication of the function by  $-t$ ; thus

$$\frac{d^n F(s)}{ds^n} = F^{(n)}(s) = \mathcal{L}\{(-t)^n f(t)\}, \quad n = 1, 2, 3, \dots \tag{5.16}$$

*Proof* This is a restatement of Theorem 5.6. This theorem is often useful for evaluating some types of integrals, and can be used to extend the table of transforms.

**Example 5.7**

Employ Theorem 5.7 to evaluate  $\partial F(s)/\partial s$  for the function  $f(t) = \sinh at$ .

**SOLUTION**

Initially we establish  $\sinh at$

$$\mathcal{L}\{\sinh at\} = \int_0^\infty e^{-st} \left[ \frac{e^{at} - e^{-at}}{2} \right] dt = \frac{a}{s^2 - a^2} = F(s).$$

By Theorem 5.7

$$\frac{\partial F(s)}{\partial s} = \int_0^\infty (-t) \sinh at e^{-st} dt = \frac{\partial}{\partial s} \left[ \frac{a}{s^2 - a^2} \right] = -\frac{2as}{(s^2 - a^2)^2}$$

from which

$$\int_0^\infty e^{-st} t \sinh at dt = \mathcal{L}\{t \sinh at\} = \frac{2as}{(s^2 - a^2)^2}.$$

We can, of course, differentiate  $F(s)$  with respect to  $a$ . In this case, Theorem 5.7 does not apply. However, the result is significant and is

$$\begin{aligned} \frac{\partial F(s)}{\partial a} &= \int_0^\infty e^{-st} (t \cosh at) dt = \mathcal{L}\{t \cosh at\} = \frac{\partial}{\partial a} \left[ \frac{a}{s^2 - a^2} \right] \\ &= \frac{s^2 + a^2}{(s^2 - a^2)^2}. \end{aligned}$$

**THEOREM 5.8 Complex Integration**

If  $f(t)$  is Laplace transformable and provided that  $\lim_{t \rightarrow 0^+} \frac{f(t)}{t}$  exists, the integral of the function  $\int_s^\infty F(s)ds$  corresponds to the Laplace transform of the division of the function  $f(t)$  by  $t$ ,

$$\mathcal{L}\left\{\frac{f(t)}{t}\right\} = \int_0^\infty F(s)ds. \tag{5.17}$$

*Proof* Let  $F(s)$  be piecewise continuous in each finite interval and of exponential order. Then

$$F(s) = \int_0^\infty e^{-st} f(t) dt$$

is uniformly convergent with respect to  $s$ . Consequently, we can write for  $\text{Re}(s) > c$  and any  $a > c$

$$\int_s^a F(s) ds = \int_s^a \int_0^\infty e^{-st} f(t) dt ds.$$

Express this in the form

$$= \int_0^\infty f(t) \int_s^a e^{-st} ds dt = \int_0^\infty \frac{f(t)}{t} (e^{-st} - e^{-at}) dt.$$

Now if  $f(t)/t$  has a limit as  $t \rightarrow 0$ , then the latter function is piecewise continuous and of exponential order. Therefore, the last integral is uniformly convergent with respect to  $a$ . Thus, as  $a$  tends to infinity

$$\int_s^\infty F(s) ds = \mathcal{L}\left\{\frac{f(t)}{t}\right\}.$$

**THEOREM 5.9 Time Delay; Real Translation**

The substitution of  $t - \lambda$  for the variable  $t$  in the transform  $\mathcal{L}\{f(t)\}$  corresponds to the multiplication of the function  $F(s)$  by  $e^{-s\lambda}$ ; that is,

$$\mathcal{L}\{f(t - \lambda)\} = e^{-s\lambda} F(s). \tag{5.18}$$

*Proof* Refer to Figure 5.2, which shows a function  $f(t)$   $u(t)$  and the same function delayed by the time  $t = \lambda$ , where  $\lambda$  is a positive constant.

We write directly

$$\mathcal{L}\{f(t - \lambda)u(t - \lambda)\} = \int_0^\infty f(t - \lambda)u(t - \lambda)e^{-st} dt.$$

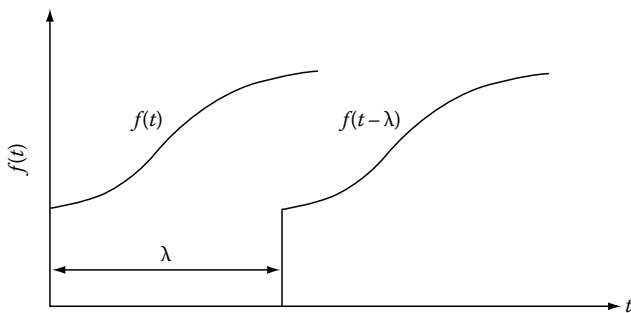


FIGURE 5.2 A function  $f(t)$  at the time  $t = 0$  and delayed time  $t = \lambda$ .

Now introduce a new variable  $\tau = t - \lambda$ . This converts this equation to the form

$$\begin{aligned} \mathcal{L}\{f(\tau)u(\tau)\} &= e^{-s\lambda} \int_{-\lambda}^\infty f(\tau)u(\tau)e^{-s\tau} d\tau = e^{-s\lambda} \int_0^\infty f(\tau)e^{-s\tau} d\tau \\ &= e^{-s\lambda} F(s) \end{aligned}$$

because  $u(\tau) = 0$  for  $-\lambda \leq t \leq 0$ .

We would similarly find that

$$\mathcal{L}\{f(t + \lambda)u(t + \lambda)\} = e^{s\lambda} F(s). \tag{5.19}$$

**Example 5.8**

Find the Laplace transform of the pulse function shown in Figure 5.3.

**SOLUTION**

Because the pulse function can be decomposed into step functions, as shown in Figure 5.3, its Laplace transform is given by

$$\mathcal{L}\{2[u(t) - u(t - 1.5)]\} = 2\left[\frac{1}{s} - \frac{1}{s}e^{-1.5s}\right] = \frac{2}{s}(1 - e^{-1.5s})$$

where the translation property has been used.

**THEOREM 5.10 Complex Translation**

The substitution of  $s + a$  for  $s$ , where  $a$  is a real or complex, in the function  $F(s + a)$ , corresponds to the Laplace transform of the product  $e^{-at}f(t)$ .

*Proof* We write

$$\int_0^\infty e^{-at}f(t)e^{-st} dt = \int_0^\infty f(t)e^{-(s+a)t} dt \quad \text{for } \text{Re}(s) > c - \text{Re}(a),$$

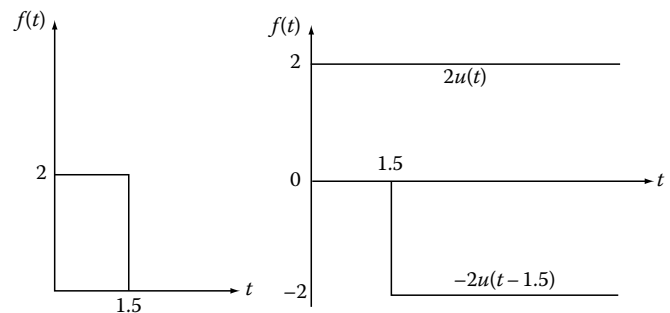


FIGURE 5.3 Pulse function and its equivalent representation.

which is

$$F(s+a) = \mathcal{L}\{e^{-at}f(t)\}. \quad (5.20)$$

In a similar way we find

$$F(s-a) = \mathcal{L}\{e^{at}f(t)\}. \quad (5.21)$$

---

### THEOREM 5.11 Convolution

The multiplication of the transforms of two sectionally continuous functions  $f_1(t)$  ( $=F_1(s)$ ) and  $f_2(t)$  ( $=F_2(s)$ ) corresponds to the Laplace transform of the convolution of  $f_1(t)$  and  $f_2(t)$ .

$$F_1(s)F_2(s) = \mathcal{L}\{f_1(t) * f_2(t)\} \quad (5.22)$$

where the asterisk  $*$  is the shorthand designation for convolution.

*Proof* By definition, the convolution of two functions  $f_1(t)$  and  $f_2(t)$  is

$$f_1(t) * f_2(t) = \int_0^\infty f_1(t-\tau)f_2(\tau)d\tau = \int_0^\infty f_1(\tau)f_2(t-\tau)d\tau. \quad (5.23)$$

Thus,

$$\begin{aligned} \mathcal{L}\{f_1(t) * f_2(t)\} &= \mathcal{L}\left\{\int_0^\infty f_1(t-\tau)f_2(\tau)d\tau\right\} \\ &= \int_0^\infty \left[\int_0^\infty f_1(t-\tau)f_2(\tau)d\tau\right] e^{-st} dt \\ &= \int_0^\infty f_2(\tau)d\tau \int_0^\infty f_1(t-\tau)e^{-st} dt. \end{aligned}$$

Now effect a change of variable, writing  $t-\tau = \xi$  and therefore  $dt = d\xi$ , then

$$= \int_0^\infty f_2(\tau)d\tau \int_{-\tau}^\infty f_1(\xi)e^{-s(\xi+\tau)}d\xi.$$

But for positive time functions  $f_1(\xi) = 0$  for  $\xi < 0$ , which permits changing the lower limit of the second integral to zero, and so

$$= \int_0^\infty f_2(\tau)e^{-s\tau}d\tau \int_0^\infty f_1(\xi)e^{-s\xi}d\xi,$$

which is

$$\mathcal{L}\{f_1(t) * f_2(t)\} = F_1(s)F_2(s).$$

### Example 5.9

Given  $f_1(t) = t$  and  $f_2(t) = e^{at}$ , deduce the Laplace transform of the convolution  $t * e^{at}$  by the use of Theorem 5.11.

#### SOLUTION

Begin with the convolution

$$\begin{aligned} t * e^{at} &= \int_0^t (t-\tau)e^{a\tau}d\tau = \frac{te^{a\tau}}{a}\Big|_0^t - \left[\frac{\tau e^{a\tau}}{a} - \frac{e^{a\tau}}{a^2}\right]_0^t \\ &= \frac{1}{a^2}(e^{at} - at - 1). \end{aligned}$$

Then

$$\mathcal{L}\{t * e^{at}\} = \frac{1}{a^2} \left( \frac{1}{s-a} - \frac{1}{s^2} - \frac{1}{s} \right) = \frac{1}{s^2} \frac{1}{(s-a)}.$$

By Theorem 5.11 we have

$$\begin{aligned} F_1(s) &= \mathcal{L}\{f_1(t)\} = \mathcal{L}\{t\} = \frac{1}{s^2}, \\ F_2(s) &= \mathcal{L}\{f_2(t)\} = \mathcal{L}\{e^{at}\} = \frac{1}{s-a}. \end{aligned}$$

and

$$\mathcal{L}\{t * e^{at}\} = \frac{1}{s^2} \frac{1}{(s-a)}.$$

---

### THEOREM 5.12

The multiplication of the transforms of three sectionally continuous functions  $f_1(t)$ ,  $f_2(t)$ , and  $f_3(t)$  corresponds to the Laplace transform of the convolution of the three functions

$$\mathcal{L}\{f_1(t) * f_2(t) * f_3(t)\} = F_1(s)F_2(s)F_3(s). \quad (5.24)$$

*Proof* This is an extension of Theorem 5.11. The result is obvious if we write

$$F_1(s)F_2(s)F_3(s) = \mathcal{L}\{f_1(t) * \mathcal{L}^{-1}\{F_2(s)F_3(s)\}\}.$$

### Example 5.10

Deduce the values of the convolution products:  $1 * f(t)$ ;  $1 * 1 * f(t)$ .

#### SOLUTION

By Equations 5.21 and 5.23 we write directly

- For  $f_1(t) = 1$ ,  $f_2(t) = f(t)$ ,  $\mathcal{L}\{1 * f(t)\} = \frac{F(s)}{s} = \mathcal{L}\left\{\int_0^t f(\xi)d\xi\right\}$  by Equation 5.14
- For  $f_1(t) = 1$ ,  $f_2(t) = 1$ ,  $f_3(t) = f(t)$ ,  $\mathcal{L}\{1 * 1 * f(t)\} = \frac{F(s)}{s^2} = \mathcal{L}\left\{\int_0^t \int_0^\xi f(\lambda)d\lambda d\xi\right\}$

**THEOREM 5.13 Frequency Convolution—*s*-Plane**

The Laplace transform of the product of two piecewise and sectionally continuous functions  $f_1(t)$  and  $f_2(t)$  corresponds to the convolution of their transforms, with

$$\mathcal{L}\{f_1(t)f_2(t)\} = \frac{1}{2\pi j} [F_1(s) * F_2(s)]. \tag{5.25}$$

*Proof* Begin by considering the following line integral in the  $z$ -plane:

$$f_2(t) = \frac{1}{2\pi j} \int_{C_2} F_2(z)e^{zt} dz, \quad \sigma_2 = \text{axis of the convergence.}$$

This means that the contour intersects the  $x$ -axis at  $x_1 > \sigma_2$  (see Figure 5.4). Then we have

$$\int_0^\infty f_1(t)f_2(t)e^{-st} dt = \frac{1}{2\pi j} \int_0^\infty f_1(t) dt \int_{C_2} F_2(z)e^{(z-s)t} dz.$$

Assume that the integral of  $F_2(z)$  is convergent over the path of integration. This equation is now written in the form

$$\begin{aligned} \int_0^\infty f_1(t)f_2(t)e^{-st} dt &= \frac{1}{2\pi j} \int_{\sigma_2-j\infty}^{\sigma_2+j\infty} F_2(z) dz \int_0^\infty f_1(t)e^{-(s-z)t} dt \\ &= \frac{1}{2\pi j} \int_{\sigma_2-j\infty}^{\sigma_2+j\infty} F_2(z)F_1(s-z) dz \triangleq \mathcal{L}\{f_1(t)f_2(t)\}. \end{aligned} \tag{5.26}$$

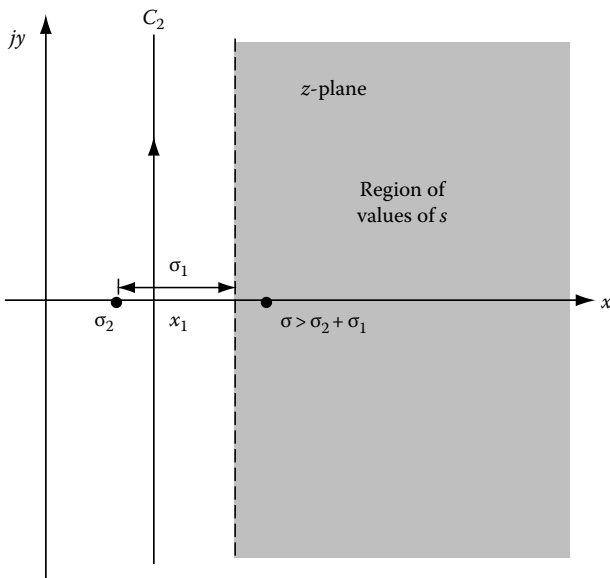


FIGURE 5.4 The contour  $C_2$  and the allowed range of  $s$ .

The Laplace transform of  $f_1(t)$ , the integral on the right, converges in the range  $\text{Re}(s - z) > \sigma_1$ , where  $\sigma_1$  is the abscissa of convergence of  $f_1(t)$ . In addition,  $\text{Re}(z) = \sigma_2$  for the  $z$ -plane integration involved in Equation 5.25. Thus, the abscissa of convergence of  $f_1(t)f_2(t)$  is specified by

$$\text{Re}(s) > \sigma_1 + \sigma_2. \tag{5.27}$$

This situation is portrayed graphically in Figure 5.4 for the case when both  $\sigma_1$  and  $\sigma_2$  are positive. As far as the integration in the complex plane is concerned, the semicircle can be closed either to the left or to the right just so long as  $F_1(s)$  and  $F_2(s)$  go to zero as  $s \rightarrow \infty$ .

Based on the foregoing, we observed the following:

- Poles of  $F_1(s - z)$  are contained in the region  $\text{Re}(s - z) < \sigma_1$
- Poles of  $F_2(z)$  are contained in the region  $\text{Re}(z) < \sigma_2$
- From (a) and Equation 5.27  $\text{Re}(z) > \text{Re}(s - \sigma_1) > \sigma_2$
- Poles of  $F_1(s - z)$  lie to the right of the path of integration
- Poles of  $F_2(z)$  are to the left of the path of integration
- Poles of  $F_1(s - z)$  are functions of  $s$  whereas poles of  $F_2(z)$  are fixed in relation to  $s$

**Example 5.11**

Find the Laplace transform of the function  $f(t) = f_1(t) f_2(t) = e^{-t} e^{-2t} u(t)$ .

**SOLUTION**

From Theorem 5.13 and the absolute convergence region for each function, we have

$$F_1(s) = \frac{1}{s + 1}, \quad \sigma_1 > -1$$

$$F_2(s) = \frac{1}{s + 2}, \quad \sigma_2 > -2.$$

Further,  $f(t) = \exp [-(2 + 1)t] u(t)$  implies that  $\sigma_f = \sigma_1 + \sigma_2 = 3$ . We now write

$$\begin{aligned} F_2(z)F_1(s - z) &= \frac{1}{z + 2} \frac{1}{s - z + 1} \\ &= \frac{1}{3 + s} \frac{1}{z - (1 + s)} - \frac{1}{3 + s} \frac{1}{z + 2}. \end{aligned}$$

To carry out the integration dictated by Equation 5.26 we use the contour shown in Figure 5.5. If we select contour  $C_1$  and use the residue theorem, we obtain

$$\begin{aligned} F(s) &= \frac{1}{2\pi j} \oint_{C_1} F_2(z)F_1(s - z) dz = 2\pi j \text{Re} s [F_2(z)F_1(s - z)]|_{z=-2} \\ &= \frac{1}{s + 3}. \end{aligned}$$

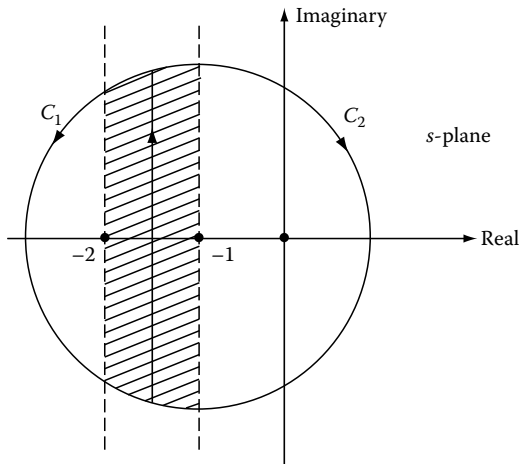


FIGURE 5.5 The contour for Example 5.11.

The inverse of this transform is  $\exp(-3t)$ . If we had selected contour  $C_2$ , the residue theorem gives

$$F(s) = \frac{1}{2\pi j} \oint_{C_2} F_2(z)F_1(s-z)dz = -2\pi j \operatorname{Re} s[F_2(z)F_1(s-z)]_{z=1+3}$$

$$= -\left[-\frac{1}{s+3}\right] = \frac{1}{s+3}.$$

The inverse transform of this is also  $\exp(-3t)$ , as to be expected.

**THEOREM 5.14 Initial Value Theorem**

Let  $f(t)$  and  $f^{(1)}(t)$  be Laplace transformable functions, then for case when  $\lim sF(s)$  as  $s \rightarrow \infty$  exists,

$$\lim_{s \rightarrow \infty} sF(s) = \lim_{t \rightarrow 0+} f(t). \tag{5.28}$$

*Proof* Begin with Equation 5.13 and consider

$$\lim_{s \rightarrow \infty} \int_0^{\infty} \frac{df}{dt} e^{-st} dt = \lim_{s \rightarrow \infty} [sF(s) - f(0+)].$$

Because  $f(0+)$  is independent of  $s$ , and because the integral vanishes for  $s \rightarrow \infty$ , then

$$\lim_{s \rightarrow \infty} [sF(s) - f(0+)] = 0.$$

Furthermore,  $f(0+) = \lim_{t \rightarrow 0+} f(t)$  so that

$$\lim_{s \rightarrow \infty} sF(s) = \lim_{t \rightarrow 0+} f(t).$$

If  $f(t)$  has a discontinuity at the origin, this expression specifies the value of the impulse  $f(0+)$ . If  $f(t)$  contains an impulse term, then the left-hand side does not exist, and the initial value property does not exist.

**THEOREM 5.15 Final Value Theorem**

Let  $f(t)$  and  $f^{(1)}(t)$  be Laplace transformable functions, then for  $t \rightarrow \infty$

$$\lim_{t \rightarrow \infty} f(t) = \lim_{s \rightarrow 0} sF(s). \tag{5.29}$$

*Proof* Begin with Equation 5.13 and Let  $s \rightarrow 0$ . Thus, the expression

$$\lim_{s \rightarrow 0} \int_0^{\infty} \frac{df}{dt} e^{-st} dt = \lim_{s \rightarrow 0} [sF(s) - f(0+)].$$

Consider the quantity on the left. Because  $s$  and  $t$  are independent and because  $e^{-st} \rightarrow 1$  as  $s \rightarrow 0$ , then the integral on the left becomes, in the limit

$$\int_0^{\infty} \frac{df}{dt} dt = \lim_{t \rightarrow \infty} f(t) - f(0+).$$

Combine the latter two equations to get

$$\lim_{t \rightarrow \infty} f(t) - f(0+) = \lim_{s \rightarrow 0} sF(s) - f(0+).$$

It follows from this that the final value of  $f(t)$  is given by

$$\lim_{t \rightarrow \infty} f(t) = \lim_{s \rightarrow 0} sF(s).$$

This result applies  $F(s)$  possesses a simple pole at the origin, but it does not apply if  $F(s)$  has imaginary axis poles, poles in the right half plane, or higher order poles at the origin.

**Example 5.12**

Apply the final value theorem to the following two functions:

$$F_1(s) = \frac{s+a}{(s+a)^2 + b^2}, \quad F_2(s) = \frac{s}{s^2 + b^2}.$$

**SOLUTION**

For the first function from  $sF_1(s)$ ,

$$\lim_{s \rightarrow 0} \frac{s(s+a)}{(s+a)^2 + b^2} = 0.$$



For the second function,

$$sF(s) = \frac{s^2}{s^2 + b^2}.$$

However, this function has singularities on the imaginary axis at  $s = \pm jb$ , and the final value theorem does not apply.

The important properties of the Laplace transform are contained in Table A.5.2.

## 5.4 The Inverse Laplace Transform

We employ the symbol  $\mathcal{L}^{-1}\{F(s)\}$ , corresponding to the direct Laplace transform defined in Equation 5.1, to denote a function  $f(t)$  whose Laplace transform is  $F(s)$ . Thus, we have the Laplace pair

$$F(s) = \mathcal{L}\{f(t)\}, \quad f(t) = \mathcal{L}^{-1}\{F(s)\}. \quad (5.30)$$

This correspondence between  $F(s)$  and  $f(t)$  is called the inverse Laplace transformation of  $f(t)$ .

Reference to Table A.5.1 shows that  $F(s)$  is a rational function in  $s$  if  $f(t)$  is a polynomial or a sum of exponentials. Further, it appears that the product of a polynomial and an exponential might also yield a rational  $F(s)$ . If the square root of  $t$  appears on  $f(t)$ , we do not get a rational function in  $s$ . Note also that a continuous function  $f(t)$  may not have a continuous inverse transform.

Observe that the  $F(s)$  functions have been uniquely determined for the given  $f(t)$  function by Equation 5.1. A logical question is whether a given time function in Table A.5.1 is the only  $t$ -function that will give the corresponding  $F(s)$ . Clearly, Table A.5.1 is more useful if there is a unique  $f(t)$  for each  $F(s)$ . This is an important consideration because the solution of practical problems usually provides a known  $F(s)$  from which  $f(t)$  must be found. This uniqueness condition can be established using the inversion integral. This means that there is a one-to-one correspondence between the direct and the inverse transform. This means that if a given problem yields a function  $F(s)$ , the corresponding  $f(t)$  from Table A.5.1 is the unique result. In the event that the available tables do not include a given  $F(s)$ , we would seek to resolve the given  $F(s)$  into forms that are listed in Table A.5.1. This resolution of  $F(s)$  is often accomplished in terms of a partial fraction expansion.

A few examples will show the use of the partial fraction form in deducing the  $f(t)$  for a given  $F(s)$ .

### Example 5.13

Find the inverse Laplace transform of the function

$$F(s) = \frac{s-3}{s^2+5s+6}. \quad (5.31)$$

### SOLUTION

Observe that the denominator can be factored into the form  $(s+2)(s+3)$ . Thus,  $F(s)$  can be written in partial fraction form as

$$F(s) = \frac{s-3}{(s+2)(s+3)} = \frac{A}{s+2} + \frac{B}{s+3}. \quad (5.32)$$

where  $A$  and  $B$  are constants that must be determined.

To evaluate  $A$ , multiply both sides of Equation 5.32 by  $(s+2)$  and then set  $s = -2$ . This gives

$$A = F(s)(s+2)|_{s=-2} = \frac{s-3}{s+3}|_{s=-2} = -5$$

and  $B(s+2)/(s+3)|_{s=-2}$  is identically zero. In the same manner, to find the value of  $B$  we multiply both sides of Equation 5.32 by  $(s+3)$  and get

$$B = F(s)(s+3)|_{s=-3} = \frac{s-3}{s+2}|_{s=-3} = 6.$$

The partial fraction form of Equation 5.32 is

$$F(s) = \frac{-5}{s+2} + \frac{6}{s+3}.$$

The inverse transform is given by

$$\begin{aligned} f(t) &= \mathcal{L}^{-1}\{F(s)\} = -5\mathcal{L}^{-1}\left\{\frac{1}{s+2}\right\} + 6\mathcal{L}^{-1}\left\{\frac{1}{s+3}\right\} \\ &= -5e^{-2t} + 6e^{-3t} \end{aligned}$$

where entry 8 in Table A.5.1, is used.

### Example 5.14

Find the inverse Laplace transform of the function

$$F(s) = \frac{s+1}{[(s+2)^2+1](s+3)}.$$

### SOLUTION

This function is written in the form

$$F(s) = \frac{A}{s+3} + \frac{Bs+C}{[(s+2)^2+1]} = \frac{s+1}{[(s+2)^2+1](s+3)}.$$

The value of  $A$  is deduced by multiplying both sides of this equation by  $(s+3)$  and then setting  $s = -3$ . This gives

$$A = (s+3)F(s)|_{s=-3} = \frac{-3+1}{(-3+2)^2+1} = -1.$$

To evaluate  $B$  and  $C$ , combine the two fractions and equate the coefficients of the powers of  $s$  in the numerators. This yields

$$\frac{-1[(s+2)^2+1] + (s+3)(Bs+C)}{[(s+2)^2+1](s+3)} = \frac{s+1}{[(s+2)^2+1](s+3)}$$

from which it follows that

$$-(s^2+4s+5) + Bs^2 + (C+3B)s + 2C = s+1.$$

Combine like-powered terms to write

$$(-1+B)s^2 + (-4+C+3B)s + (-5+3C) = s+1.$$

Therefore,

$$-1+B=0, \quad -4+C+3B=1, \quad -5+3C=1.$$

From these equations we obtain

$$B=1, \quad C=2.$$

The function  $F(s)$  is written in the equivalent form

$$F(s) = \frac{-1}{s+3} + \frac{s+2}{(s+2)^2+1}.$$

Now using Table A.5.1, the result is

$$f(t) = -e^{-3t} + e^{-2t} \cos t, \quad t > 0.$$

In many cases,  $F(s)$  is the quotient of two polynomials with real coefficients. If the numerator polynomial is of the same or higher degree than the denominator polynomial, first divide the numerator polynomial by the denominator polynomial; the division is carried forward until the numerator polynomial of the remainder is one degree less than the denominator. This results in a polynomial in  $s$  plus a proper fraction. The proper fraction can be expanded into a partial fraction expansion. The result of such an expansion is an expression of the form

$$F'(s) = B_0 + B_1(s) + \cdots + \frac{A_1}{s-s_1} + \frac{A_2}{s-s_2} + \cdots + \frac{A_{p1}}{s-s_p} + \frac{A_{p2}}{(s-s_p)^2} + \cdots + \frac{A_{pr}}{(s-s_p)^r}. \quad (5.33)$$

This expression has been written in a form to show three types of terms; polynomial, simple partial fraction including all terms with distinct roots, and partial fraction appropriate to multiple roots.

To find the constants  $A_1, A_2, \dots$  the polynomial terms are removed, leaving the proper fraction

$$F'(s) - (B_0 + B_1s + \cdots) = F(s) \quad (5.34)$$

where

$$F(s) = \frac{A_1}{s-s_1} + \frac{A_2}{s-s_2} + \cdots + \frac{A_k}{s-s_k} + \frac{A_{p1}}{s-s_p} + \frac{A_{p2}}{(s-s_p)^2} + \cdots + \frac{A_{pr}}{(s-s_p)^r}.$$

To find the constants  $A_k$  that are the residues of the function  $F(s)$  at the simple poles  $s_k$ , it is only necessary to note that as  $s \rightarrow s_k$  the term  $A_k(s-s_k)$  will become large compared with all other terms. In the limit

$$A_k = \lim_{s \rightarrow s_k} (s-s_k)F(s). \quad (5.35)$$

Upon taking the inverse transform for each simple pole, the result will be a simple exponential of the form

$$\mathcal{L}^{-1} \left\{ \frac{A_k}{s-s_k} \right\} = A_k e^{s_k t}. \quad (5.36)$$

Note also that because  $F(s)$  contains only real coefficients, if  $s_k$  is a complex pole with residue  $A_k$ , there will also be a conjugate pole  $s_k^*$  with residue  $A_k^*$ . For such complex poles

$$\mathcal{L}^{-1} \left\{ \frac{A_k}{s-s_k} + \frac{A_k^*}{s-s_k^*} \right\} = A_k e^{s_k t} + A_k^* e^{s_k^* t}.$$

These can be combined in the following way:

$$\begin{aligned} \text{response} &= (a_k + jb_k)e^{(\sigma_k + j\omega_k)t} + (a_k - jb_k)e^{(\sigma_k - j\omega_k)t} \\ &= e^{\sigma_k t} [(a_k + jb_k)(\cos \omega_k t + j \sin \omega_k t) \\ &\quad + (a_k - jb_k)(\cos \omega_k t - j \sin \omega_k t)] \\ &= 2e^{\sigma_k t} (a_k \cos \omega_k t - b_k \sin \omega_k t) \\ &= 2A_k e^{\sigma_k t} \cos(\omega_k t + \theta_k) \end{aligned} \quad (5.37)$$

where  $\theta_k = \tan^{-1}(b_k/a_k)$  and  $A_k = a_k/\cos \theta_k$ .

When the proper fraction contains a multiple pole of order  $r$ , the coefficients in the partial-fraction expansion  $A_{p1}, A_{p2}, \dots, A_{pr}$  that are involved in the terms

$$\frac{A_{p1}}{(s-s_p)} + \frac{A_{p2}}{(s-s_p)^2} + \cdots + \frac{A_{pr}}{(s-s_p)^r}$$

must be evaluated. A simple application of Equation 5.35 is not adequate. Now the procedure is to multiply both sides of Equation 5.34 by  $(s-s_p)^r$ , which gives

$$\begin{aligned} (s-s_p)^r F(s) &= (s-s_p)^r \left[ \frac{A_1}{s-s_1} + \frac{A_2}{s-s_2} + \cdots + \frac{A_k}{s-s_k} \right] \\ &\quad + A_{p1}(s-s_p)^{r-1} + \cdots \\ &\quad + A_{p(r-1)}(s-s_p) + A_{pr} \end{aligned} \quad (5.38)$$

In the limit as  $s = s_p$  all terms on the right vanish with the exception of  $A_{pr}$ . Suppose now that this equation is differentiated once with respect to  $s$ . The constant  $A_{pr}$  will vanish in the differentiation but  $A_{p(r-1)}$  will be determined by setting  $s = s_p$ . This procedure will be continued to find each of the coefficients  $A_{pk}$ . Specifically, the procedure is specified by

$$A_{pk} = \frac{1}{(r-k)!} \left\{ \frac{d^{r-k}}{ds^{r-k}} F(s)(s-s_p)^r \right\}_{s=s_p}, \quad k = 1, 2, \dots, r. \quad (5.39)$$

### Example 5.15

Find the inverse transform of the following function:

$$F(s) = \frac{s^3 + 2s^2 + 3s + 1}{s^2(s+1)}.$$

### SOLUTION

This is not a proper fraction. The numerator polynomial is divided by the denominator polynomial by simple long division. The result is

$$F(s) = 1 + \frac{s^2 + 3s + 1}{s^2(s+1)}.$$

The proper fraction is expanded into partial fraction form

$$F_p(s) = \frac{s^2 + 3s + 1}{s^2(s+1)} = \frac{A_{11}}{s} + \frac{A_{12}}{s^2} + \frac{A_2}{s+1}.$$

The value of  $A_2$  is deduced using Equation 5.35

$$A_2 = [(s+1)F_p(s)]_{s=-1} = \left. \frac{s^2 + 3s + 1}{s^2} \right|_{s=-1} = -1.$$

To find  $A_{11}$  and  $A_{12}$  we proceed as specified in Equation 5.39

$$\begin{aligned} A_{12} &= [s^2 F_p(s)]_{s=0} = \left. \frac{s^2 + 3s + 1}{s+1} \right|_{s=0} = 1 \\ A_{11} &= \frac{1}{1!} \left\{ \frac{d}{ds} s^2 F_p(s) \right\}_{s=0} = \frac{d}{ds} \left[ \frac{s^2 + 3s + 1}{s+1} \right]_{s=0} \\ &= \left. \frac{s^2 + 3s + 1}{(s+1)^2} + \frac{2s+3}{s+1} \right|_{s=0} = 4. \end{aligned}$$

Therefore,

$$F(s) = 1 + \frac{4}{s} + \frac{1}{s^2} - \frac{1}{s+1}.$$

From Table A.5.1 the inverse transform is

$$f(t) = \delta(t) + 4 + t - e^{-t}, \quad \text{for } t \geq 0.$$

If the function  $F(s)$  exists in proper fractional form as the quotient of two polynomials, we can employ the Heaviside expansion theorem in the determination of  $f(t)$  from  $F(s)$ . This theorem is an efficient method for finding the residues of  $F(s)$ . Let

$$F(s) = \frac{P(s)}{Q(s)} = \frac{A_1}{s-s_1} + \frac{A_2}{s-s_2} + \dots + \frac{A_k}{s-s_k}$$

where  $P(s)$  and  $Q(s)$  are polynomials with no common factors and with the degree of  $P(s)$  less than the degree of  $Q(s)$ .

Suppose that the factors of  $Q(s)$  are distinct constants. Then, as in Equation 5.35 we find

$$A_k = \lim_{s \rightarrow s_k} \left[ \frac{s-s_k}{Q(s)} P(s) \right].$$

Also, the limit  $P(s)$  is  $P(s_k)$ . Now, because

$$\lim_{s \rightarrow s_k} \frac{s-s_k}{Q(s)} = \lim_{s \rightarrow s_k} \frac{1}{Q^{(1)}(s)} = \frac{1}{Q^{(1)}(s_k)},$$

then

$$A_k = \frac{P(s_k)}{Q^{(1)}(s_k)}.$$

Thus,

$$F(s) = \frac{P(s)}{Q(s)} = \sum_{n=1}^k \frac{P(s_n)}{Q^{(1)}(s_n)} \cdot \frac{1}{(s-s_n)}. \quad (5.40)$$

From this, the inverse transformation becomes

$$f(t) = \mathcal{L}^{-1} \left\{ \frac{P(s)}{Q(s)} \right\} = \sum_{n=1}^k \frac{P(s_n)}{Q^{(1)}(s_n)} e^{s_n t}.$$

This is the Heaviside expansion theorem. It can be written in formal form.

---

### THEOREM 5.16: Heaviside Expansion Theorem

If  $F(s)$  is the quotient  $P(s)/Q(s)$  of two polynomials in  $s$  such that  $Q(s)$  has the higher degree and contains simple poles the factor  $s - s_k$ , which are not repeated, then the term in  $f(t)$  corresponding to this factor can be written  $\frac{P(s_k)}{Q^{(1)}(s_k)} e^{s_k t}$ .

**Example 5.16**

Repeat Example 5.13 employing the Heaviside expansion theorem.

**SOLUTION**

We write Equation 5.31 in the form

$$F(s) = \frac{P(s)}{Q(s)} = \frac{s-3}{s^2+5s+6} = \frac{s-3}{(s+2)(s+3)}.$$

The derivative of the denominator is

$$Q^{(1)}(s) = 2s + 5$$

from which, for the roots of this equation,

$$Q^{(1)}(-2) = 1, \quad Q^{(1)}(-3) = -1.$$

Hence,

$$P(-2) = -5, \quad P(-3) = -6.$$

The final value for  $f(t)$  is

$$f(t) = -5e^{-2t} + 6e^{-3t}.$$

**Example 5.17**

Find the inverse Laplace transform of the following function using the Heaviside expansion theorem:

$$\mathcal{L}^{-1} \left\{ \frac{2s+3}{s^2+4s+7} \right\}.$$

**SOLUTION**

The roots of the denominator are

$$s^2 + 4s + 7 = (s + 2 + j\sqrt{3})(s + 2 - j\sqrt{3}).$$

That is, the roots of the denominator are complex. The derivative of the denominator is

$$Q^{(1)}(s) = 2s + 4.$$

We deduce the values  $P(s)/Q^{(1)}(s)$  for each root

$$\text{For } s_1 = -2 - j\sqrt{3} \quad Q^{(1)}(s_1) = -j2\sqrt{3} \quad P(s_1) = -1 - j2\sqrt{3}$$

$$\text{For } s_2 = -2 + j\sqrt{3} \quad Q^{(1)}(s_2) = +j2\sqrt{3} \quad P(s_2) = -1 + j2\sqrt{3}.$$

Then

$$\begin{aligned} f(t) &= \frac{-1 - j2\sqrt{3}}{-j2\sqrt{3}} e^{(-2-j2\sqrt{3})t} + \frac{-1 + j2\sqrt{3}}{j2\sqrt{3}} e^{(-2+j2\sqrt{3})t} \\ &= e^{-2t} \left[ \frac{-1 - j2\sqrt{3}}{-j2\sqrt{3}} e^{-j2\sqrt{3}t} + \frac{-1 + j2\sqrt{3}}{j2\sqrt{3}} e^{j2\sqrt{3}t} \right] \\ &= e^{-2t} \left[ \frac{(e^{-j2\sqrt{3}t} - e^{j2\sqrt{3}t})}{j2\sqrt{3}} + (e^{-j2\sqrt{3}t} + e^{j2\sqrt{3}t}) \right] \\ &= e^{-2t} \left( 2 \cos 2\sqrt{3}t - \frac{1}{\sqrt{3}} \sin 2\sqrt{3}t \right) \end{aligned}$$

## 5.5 Solution of Ordinary Linear Equations with Constant Coefficients

The Laplace transform is used to solve homogeneous and non-homogeneous ordinary differential equations or systems of such equations. To understand the procedure, we consider a number of examples.

**Example 5.18**

Find the solution to the following differential equation subject to prescribed initial conditions:  $y(0+)$ ;  $(dy/dt) + ay = x(t)$ .

**SOLUTION**

Laplace transform this differential equation. This is accomplished by multiplying each term by  $e^{-st}dt$  and integrating from 0 to  $\infty$ . The result of this operation is

$$sY(s) - y(0+) + aY(s) = X(s),$$

from which

$$Y(s) = \frac{X(s)}{s+a} + \frac{y(0+)}{s+a}.$$

If the input  $x(t)$  is the unit step function  $u(t)$ , then  $X(s) = 1/s$  and the final expression for  $Y(s)$  is

$$Y(s) = \frac{1}{s(s+a)} + \frac{y(0+)}{s+a}.$$

Upon taking the inverse transform of this expression

$$y(t) = \mathcal{L}^{-1}\{Y(s)\} = \mathcal{L}^{-1} \left( \frac{1}{a} \left[ \frac{1}{s} - \frac{1}{s+a} \right] + \frac{y(0+)}{s+a} \right)$$

with the result

$$y(t) = \frac{1}{a} (1 - e^{-at}) + y(0+)e^{-at}.$$

**Example 5.19**

Find the general solution to the differential equation

$$\frac{d^2y}{dt^2} + 5\frac{dy}{dt} + 4y = 10$$

subject to zero initial conditions.

**SOLUTION**

Laplace transform this differential equation. The result is

$$s^2Y(s) + 5sY(s) + 5Y(s) = \frac{10}{s}.$$

Solving for  $Y(s)$ , we get

$$Y(s) = \frac{10}{s(s^2 + 5s + 4)} = \frac{10}{s(s + 1)(s + 4)}.$$

Expand this into partial-fraction form, thus

$$Y(s) = \frac{A}{s + 1} + \frac{B}{s + 4} + \frac{C}{s}.$$

Then

$$A = Y(s)(s + 1)|_{s=-1} = \frac{10}{s(s + 4)}|_{s=-1} = -\frac{10}{3}$$

$$B = Y(s)(s + 4)|_{s=-4} = \frac{10}{s(s + 1)}|_{s=-4} = \frac{10}{12}$$

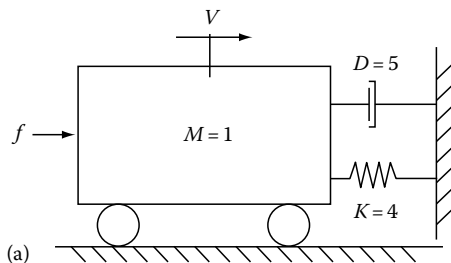
$$C = sY(s)|_{s=0} = \frac{10}{(s + 1)(s + 4)}|_{s=0} = \frac{10}{4}$$

and

$$Y(s) = 10 \left[ -\frac{1}{3(s + 1)} + \frac{1}{12(s + 4)} + \frac{1}{4s} \right].$$

The inverse transform is

$$x(t) = 10 \left[ -\frac{1}{3}e^{-t} + \frac{1}{12}e^{-4t} + \frac{1}{4} \right].$$



**Example 5.20**

Find the velocity of the system shown in Figure 5.6a when the applied force is  $f(t) = e^{-t}u(t)$ . Assume zero initial conditions. Solve the same problem using convolution techniques. The input is the force and the output is the velocity.

**SOLUTION**

The controlling equation is, from Figure 5.6b,

$$\frac{dv}{dt} + 5v + 4 \int_0^t v dt = e^{-t}u(t).$$

Laplace transform this equation and then solve for  $F(s)$ . We obtain

$$V(s) = \frac{s}{(s + 1)(s^2 + 5s + 4)} = \frac{s}{(s + 1)^2(s + 4)}.$$

Write this expression in the form

$$V(s) = \frac{A}{s + 4} + \frac{B}{s + 1} + \frac{C}{(s + 1)^2}$$

where

$$A = \frac{s}{(s + 1)^2} \Big|_{s=-4} = -\frac{4}{9}$$

$$B = \frac{1}{1!} \frac{d}{ds} \left( \frac{s}{s + 4} \right) \Big|_{s=-1} = \frac{4}{9}$$

$$C = \frac{s}{s + 4} \Big|_{s=-1} = -\frac{1}{3}.$$

The inverse transform of  $V(s)$  is given by

$$v(t) = -\frac{4}{9}e^{-4t} + \frac{4}{9}e^{-t} - \frac{1}{3}te^{-t}, \quad t \geq 0.$$

To find  $v(t)$  by the use of the convolution integral, we first find  $h(t)$ , the impulse response of the system. The quantity  $h(t)$  is specified by

$$\frac{dh}{dt} + 5h + 4 \int h dt = \delta(t)$$

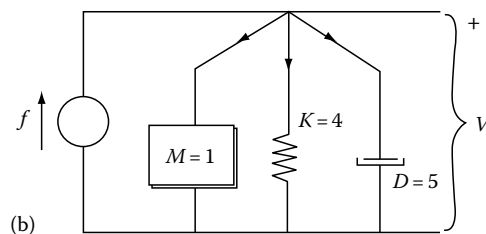


**FIGURE 5.6** The mechanical system and its network equivalent.

where the system is assumed to be initially relaxed. The Laplace transform of this equation yields

$$H(s) = \frac{s}{s^2 + 5s + 4} = \frac{s}{(s + 4)(s + 1)} = \frac{4}{3} \frac{1}{s + 4} - \frac{1}{3} \frac{1}{s + 1}.$$

The inverse transform of this expression is easily found to be

$$h(t) = \frac{4}{3}e^{-4t} - \frac{1}{3}e^{-t}, \quad t \geq 0.$$

The output of the system to the input  $e^{-t}u(t)$  is written

$$\begin{aligned} v(t) &= \int_{-\infty}^{\infty} h(\tau)f(t - \tau)d\tau = \int_0^t e^{-(t-\tau)} \left[ \frac{4}{3}e^{-4\tau} - \frac{1}{3}e^{-\tau} \right] d\tau \\ &= e^{-t} \left[ \frac{4}{3} \int_0^t e^{-3\tau} d\tau - \frac{1}{3} \int_0^t d\tau \right] = e^{-t} \left[ \frac{4}{3} \left( \frac{1}{-3} \right) e^{-3\tau} \Big|_0^t - \frac{1}{3}t \right] \\ &= -\frac{4}{9}e^{-4t} + \frac{4}{9}e^{-t} - \frac{1}{3}te^{-t}, \quad t \geq 0 \end{aligned}$$

This result is identical with that found using the Laplace transform technique.

**Example 5.21**

Find an expression for the voltage  $v_2(t)$  for  $t > 0$  in the circuit of Figure 5.7. The source  $v_1(t)$ , the current  $i_L(0^-)$  through  $L = 2$  H, and the voltage  $v_c(0^-)$  across the capacitor  $C = 1$  F at the switching instant are all assumed to be known.

**SOLUTION**

After the switch is closed, the circuit is described by the loop equations

$$\begin{aligned} \left( 3i_1 + \frac{2di_1}{dt} \right) - \left( i_2 + \frac{2di_2}{dt} \right) &= v_2(t) \\ -\left( 1i_1 + \frac{2di_1}{dt} \right) + \left( 3i_2 + \frac{2di_2}{dt} + \int i_2 dt \right) &= 0 \\ v_2(t) &= 2i_2(t). \end{aligned}$$

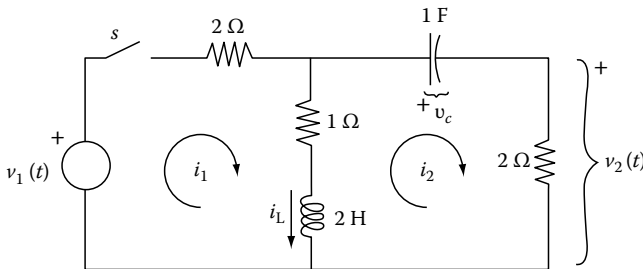


FIGURE 5.7 The circuit for Example 5.21.

All terms in these equations are Laplace transformed. The result is the set of equations

$$\begin{aligned} (3 + 2s)i_1(s) - (1 + 2s)i_2(s) &= V_1(s) + 2[i_1(0+) - i_2(0+)] \\ -(1 + 2s)i_1(s) + \left( 3 + 2s + \frac{1}{s} \right) i_2(s) &= 2[-i_1(0+) + i_2(0+)] - \frac{q_2(0+)}{s} \\ V_2(s) &= 2I_2(s). \end{aligned}$$

The current through the inductor is

$$i_L(t) = i_1(t) - i_2(t).$$

At the instant  $t = 0+$

$$i_L(0+) = i_1(0+) - i_2(0+).$$

Also, because

$$\begin{aligned} \frac{1}{C}q_2(t) &= \frac{1}{C} \int_{-\infty}^t i_2(t)dt \\ &= \frac{1}{C} \lim_{t \rightarrow 0+} \int_0^t i_2(t)dt + \frac{1}{C} \int_{-\infty}^0 i_2(t)dt = 0 + v_c(0-), \end{aligned}$$

then

$$\frac{q_2(0+)}{C} \triangleq v_c(0+) = v_c(0-) = i_L^{(-1)}(0) = \frac{q_2(0+)}{1}.$$

The equation set is solved for  $I_2(s)$ , which is written by Cramer's rule

$$\begin{aligned} I_2(s) &= \frac{\begin{vmatrix} 3 + 2s & V_1(s) + 2i_L(0+) \\ -(1 + 2s) & -2i_L(0+) - \frac{v_c(0+)}{s} \end{vmatrix}}{\begin{vmatrix} 3 + 2s & -(1 + 2s) \\ -(1 + 2s) & 3 + 2s + \frac{1}{s} \end{vmatrix}} \\ &= \frac{(3 + 2s)[-2i_L(0+) - \frac{v_c(0+)}{s}] + (1 + 2s)[V_1(s) + 2i_L(0+)]}{(3 + 2s)\left(\frac{2s^2 + 3s + 1}{s}\right) - (1 + 2s)^2} \\ &= \frac{-(2s^2 + 3s)v_c(0+) - 4si_L(0+) + (2s^2 + s)V_1(s)}{8s^2 + 10s + 3}. \end{aligned}$$

Further

$$V_2(s) = 2I_2(s).$$

Then, upon taking the inverse transform

$$v_1(t) = 2\mathcal{L}^{-1}\{I_2(s)\}.$$

If the circuit contains no stored energy at  $t = 0$ , then  $i_L(0+) = v_c(0+) = 0$  and now

$$v_2(t) = 2\mathcal{L}^{-1}\left\{ \frac{(2s^2 + s)V_1(s)}{8s^2 + 10s + 3} \right\}.$$

For the particular case when  $v_1 = u(t)$  so that  $V_1(s) = 1/s$

$$v_2(t) = 2\mathcal{L}^{-1}\left\{\frac{2s+1}{8s^2+10s+3}\right\} = 2\mathcal{L}^{-1}\left\{\frac{2s+1}{8\left(s+\frac{1}{2}\right)\left(s+\frac{3}{4}\right)}\right\}$$

$$= \frac{1}{2}\mathcal{L}^{-1}\left\{\frac{1}{s+\frac{3}{4}}\right\} = \frac{1}{2}e^{-3t/4}, \quad t \geq 0.$$

The validity of this result is readily confirmed because at the instant  $t=0+$  the inductor behaves as an open circuit and the capacitor behaves as a short circuit. Thus, at this instant, the circuit appears as two equal resistors in a simple series circuit and the voltage is shared equally.

**Example 5.22**

The input to the  $RL$  circuit shown in Figure 5.8a is the recurrent series of impulse functions shown in Figure 5.8b. Find the output current.

**SOLUTION**

The differential equation that characterizes the system is

$$\frac{di(t)}{dt} + i(t) = v(t).$$

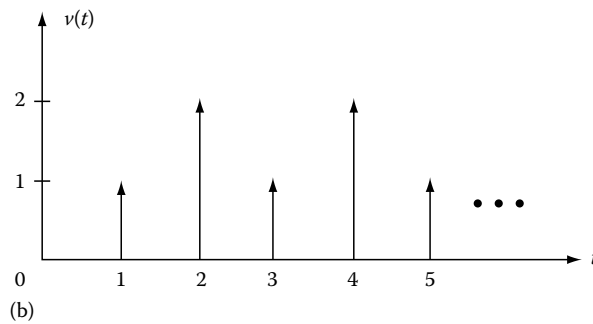
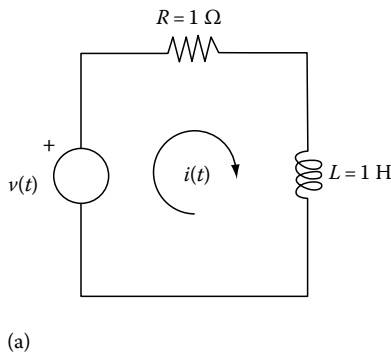


FIGURE 5.8 (a) The circuit, (b) the input pulse train.

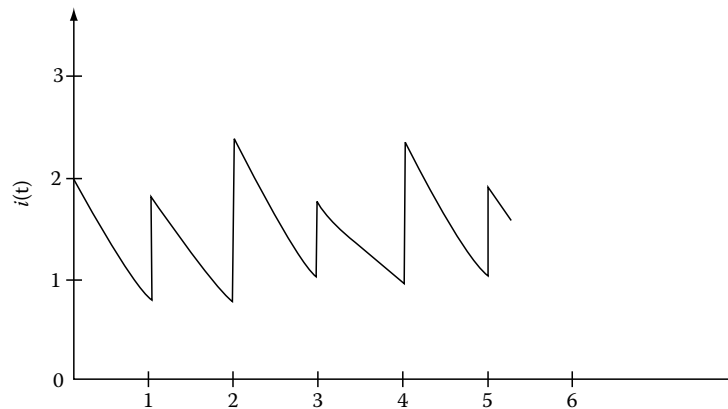


FIGURE 5.9 The response of the  $RL$  circuit to the pulse train.

For zero initial current through the inductor, the Laplace transform of the equation is

$$(s+1)I(s) = V(s).$$

Now, from the fact that  $\mathcal{L}\{\delta(t)\} = 1$  and the shifting property of Laplace transforms, we can write the explicit form for  $V(s)$ , which is

$$V(s) = 2 + e^{-s} + 2e^{-2s} + e^{-3s} + 2e^{-4s} + \dots$$

$$= (2 + e^{-s})(1 + e^{-2s} + e^{-4s} + \dots)$$

$$= \frac{2 + e^{-s}}{1 - e^{-2s}}.$$

Thus, we must evaluate  $i(t)$  from

$$I(s) = \frac{2 + e^{-s}}{1 - e^{-2s}} \frac{1}{s+1} = \frac{2}{(1 - e^{-2s})(s+1)} + \frac{e^{-s}}{(1 - e^{-2s})(s+1)}.$$

Expand these expressions into

$$I(s) = \frac{2}{s+1} (1 + e^{-2s} + e^{-4s} + e^{-6s} + \dots)$$

$$+ \frac{1}{s+1} (e^{-s} + e^{-3s} + e^{-5s} + e^{-7s} + \dots).$$

The inverse transform of these expressions yields

$$i(t) = 2e^{-t}u(t) + 2e^{-(t-2)}u(t-2) + 2e^{-(t-4)}u(t-4) + \dots \\ + e^{-(t-1)}u(t-1) + e^{-(t-3)}u(t-3) + e^{-(t-5)}u(t-5) + \dots$$

The result has been sketched in Figure 5.9.

## 5.6 The Inversion Integral

The discussion in Section 5.4 related the inverse Laplace transform to the direct Laplace transform by the expressions

$$F(s) = \mathcal{L}\{f(t)\} \tag{5.41a}$$

$$f(t) = \mathcal{L}^{-1}\{F(s)\}. \tag{5.41b}$$

The subsequent discussion indicated that the use of Equation 5.41b suggested that the  $f(t)$  so deduced was unique; that there was no other  $f(t)$  that yielded the specified  $F(s)$ . We found that although  $f(t)$  represents a real function of the positive real variable  $t$ , the transform  $F(s)$  can assume a complex variable form. What this means, of course, is that a mathematical form for the inverse Laplace transform was not essential for linear functions that satisfied the Dirichlet conditions. In some cases, Table A.5.1 is not adequate for many functions when  $s$  is a complex variable and an analytic form for the inversion process of Equation 5.41b is required.

To deduce the complex inversion integral, we begin with the Cauchy second integral theorem, which is written

$$\oint \frac{F(z)}{s-z} dz = j2\pi F(s)$$

where the contour encloses the singularity as  $s$ . The function  $F(s)$  is analytic in the half plane  $\text{Re}(s) \geq c$ . If we apply the inverse Laplace transformation to the function  $s$  on both sides of this equation, we can write

$$j2\pi \mathcal{L}^{-1}\{F(s)\} = \lim_{\omega \rightarrow \infty} \int_{\sigma-j\omega}^{\sigma+j\omega} F(z) \mathcal{L}^{-1}\left\{\frac{1}{s-z}\right\} dz.$$

But  $F(s)$  is the Laplace transform of  $f(t)$ ; also, the inverse transform of  $1/(s-z)$  is  $e^{zt}$ . Then it follows that

$$f(t) = \frac{1}{2\pi j} \lim_{\omega \rightarrow \infty} \int_{\sigma-j\omega}^{\sigma+j\omega} e^{zt} F(z) dz = \frac{1}{2\pi j} \int_{\sigma-j\infty}^{\sigma+j\infty} e^{zt} F(z) dz. \tag{5.42}$$

This equation applies equally well to both the one-sided and the two-sided transforms.

It was pointed out in Section 5.1 that the path of integration (Equation 5.42) is restricted to value of  $\sigma$  for which the direct transform formula converges. In fact, for the two-sided Laplace transform, the region of convergence must be specified in order to determine uniquely the inverse transform. That is, for the two-sided

transform, the regions of convergence for functions of time that are zero for  $t > 0$ , zero for  $t < 0$ , or in neither category, must be distinguished. For the one-sided transform, the region of convergence is given by  $\sigma$ , where  $\sigma$  is the abscissa of absolute convergence.

The path of integration in Equation 5.42 is usually taken as shown in Figure 5.10 and consists of the straight line  $ABC$  displayed to the right of the origin by  $\sigma$  and extending in the limit from  $-j\infty$  to  $+j\infty$  with connecting semicircles. The evaluation of the integral usually proceeds by using the Cauchy integral theorem, which specifies that

$$f(t) = \frac{1}{2\pi j} \lim_{R \rightarrow \infty} \oint_{\Gamma_1} F(s)e^{st} ds \\ = \sum \text{residues of } F(s)e^{st} \text{ at the singularities} \\ \text{to the left of } ABC; t > 0. \tag{5.43}$$

But the contribution to the integral around the circular path with  $R \rightarrow \infty$  is zero, leaving the desired integral along the path  $ABC$ , and

$$f(t) = \frac{1}{2\pi j} \lim_{R \rightarrow \infty} \oint_{\Gamma_2} F(s)e^{st} ds \\ = - \sum \text{residues of } F(s)e^{st} \text{ at the singularities} \\ \text{to the right of } ABC; t < 0. \tag{5.44}$$

We will present a number of examples involving these equations.

### Example 5.23

Use the inversion integral to find  $f(t)$  for the function

$$F(s) = \frac{1}{s^2 + w^2}.$$

Note that by entry 15 of Table A.5.1, this is  $\sin wt/w$ .

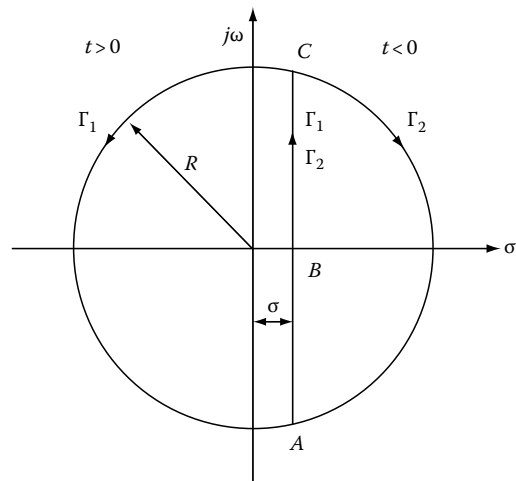


FIGURE 5.10 The path of integration in the  $s$ -plane.



**SOLUTION**

The inversion integral is written in a form that shows the poles of the integrand.

$$f(t) = \frac{1}{2\pi j} \oint \frac{e^{st}}{(s + jw)(s - jw)} ds.$$

The path chosen is  $\Gamma_1$  in Figure 5.10. Evaluate the residues

$$\begin{aligned} \text{Res} \left[ (s - jw) \frac{e^{st}}{s^2 + w^2} \right]_{s=jw} &= \frac{e^{st}}{s + jw} \Big|_{s=jw} = \frac{e^{jwt}}{2wj} \\ \text{Res} \left[ (s + jw) \frac{e^{st}}{s^2 + w^2} \right]_{s=-jw} &= \frac{e^{st}}{s - jw} \Big|_{s=-jw} = \frac{e^{-jwt}}{-2wj}. \end{aligned}$$

Therefore,

$$f(t) = \sum \text{Res} = \frac{e^{jwt} - e^{-jwt}}{2jw} = \frac{\sin wt}{w}.$$

**Example 5.24**

Evaluate  $\mathcal{L}^{-1}\{1/\sqrt{s}\}$ .

**SOLUTION**

The function  $F(s) = \sqrt{s}$  is a double-valued function because of the square root operation. That is, if  $s$  is represented in polar form by  $re^{j\theta}$ ,  $re^{j(\theta+2\pi)}$  is a second acceptable representation, and  $\sqrt{s} = \sqrt{re^{j(\theta+2\pi)}} = -\sqrt{re^{j\theta}}$ , thus showing two different values for  $\sqrt{s}$ . But a double-valued function is not analytic and requires a special procedure in its solution.

The procedure is to make the function analytic by restricting the angle of  $s$  to the range  $-\pi < \theta < \pi$  and by excluding the point  $s=0$ . This is done by constructing a branch cut along the negative real axis, as shown in Figure 5.11. The end of the branch cut, which is the origin in this case, is called a

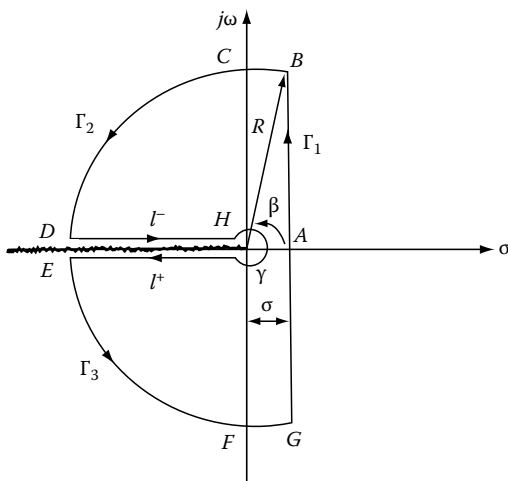


FIGURE 5.11 The integration contour for  $\mathcal{L}^{-1}\{1/\sqrt{s}\}$ .

branch point. Because a branch cut can never be crossed, this essentially ensures that  $F(s)$  is single valued. Now, however, the inversion integral (Equation 5.43) becomes for  $t > 0$

$$\begin{aligned} f(t) &= \lim_{R \rightarrow \infty} \frac{1}{2\pi j} \int_{GAB} F(s)e^{st} ds = \frac{1}{2\pi j} \int_{\sigma-j\infty}^{\sigma+j\infty} F(s)e^{st} ds \\ &= -\frac{1}{2\pi j} \left[ \int_{BC} + \int_{\Gamma_2} + \int_{\ell-} + \int_{\gamma} + \int_{\ell+} + \int_{\Gamma_3} + \int_{FG} \right], \end{aligned} \quad (5.45)$$

which does not include any singularity.

First we will show that for  $t > 0$  the integrals over the contours  $BC$  and  $CD$  vanish as  $R \rightarrow \infty$ , from which  $\int_{\Gamma_2} = \int_{\Gamma_3} = \int_{BC} = \int_{FG} = 0$ . Note from Figure 5.11 that  $\beta = \cos^{-1}(\sigma/R)$  so that the integral over the arc  $BC$  is, because  $|e^{j\theta}| = 1$ ,

$$\begin{aligned} |I| &\leq \int_{BC} \left| \frac{e^{\sigma t} e^{j\omega t}}{R^{1/2} e^{j\theta/2}} j R e^{j\theta} d\theta \right| = e^{\sigma t} \sqrt{R} \int_{\beta}^{\pi/2} d\theta \\ &= e^{\sigma t} \sqrt{R} \left( \frac{\pi}{2} - \cos^{-1} \frac{\sigma}{R} \right) = e^{\sigma t} \sqrt{R} \sin^{-1} \frac{\sigma}{R} \end{aligned}$$

But for small arguments  $\sin^{-1}(\sigma/R) = \sigma/R$ , and in the limit as  $R \rightarrow \infty$ ,  $I \rightarrow 0$ . By a similar approach, we find that the integral over  $CD$  is zero. Thus, the integrals over the contours  $\Gamma_2$  and  $\Gamma_3$  are also zero as  $R \rightarrow \infty$ .

For evaluating the integral over  $\gamma$ , let  $s = re^{j\theta} = r(\cos \theta + j \sin \theta)$  and

$$\int_{\gamma} F(s)e^{st} ds = \int_{-\pi}^{\pi} \frac{e^{r(\cos \theta + j \sin \theta)t}}{\sqrt{re^{j\theta/2}}} j r e^{j\theta} d\theta = 0 \quad \text{as } r \rightarrow 0.$$

The remaining integrals in Equation 5.45 are written

$$f(t) = -\frac{1}{2\pi j} \left[ \int_{\ell-} F(s)e^{st} ds + \int_{\ell+} F(s)e^{st} ds \right]. \quad (5.46)$$

Along path  $\ell-$ , let  $s = ue^{j\pi} = -u$ ;  $\sqrt{s} = j\sqrt{u}$ , and  $ds = -du$ , where  $u$  and  $\sqrt{u}$  are real positive quantities. Then

$$\int_{\ell-} F(s)e^{st} ds = - \int_{\infty}^0 \frac{e^{-ut}}{j\sqrt{u}} du = \frac{1}{j} \int_0^{\infty} \frac{e^{-ut}}{j\sqrt{u}} du.$$

Along path  $\ell+$ ,  $s = -ue^{j2\pi} = -u$ ,  $\sqrt{s} = -j\sqrt{u}$  (not  $+j\sqrt{u}$ ), and  $ds = -du$ . Then

$$\int_{\ell+} F(s)e^{st} ds = - \int_0^{\infty} \frac{e^{-ut}}{-j\sqrt{u}} du = \frac{1}{j} \int_0^{\infty} \frac{e^{-ut}}{j\sqrt{u}} du.$$

Combine these results to find

$$f(t) = -\frac{1}{2\pi j} \left[ \frac{2}{j} \int_0^\infty u^{-\frac{1}{2}} e^{-ut} du \right] = \frac{1}{\pi} \int_0^\infty u^{-\frac{1}{2}} e^{-ut} du,$$

which is a standard form integral with the value

$$f(t) = \frac{1}{\pi} \sqrt{\frac{\pi}{t}} = \frac{1}{\sqrt{\pi t}}, \quad t > 0.$$

**Example 5.25**

Find the inverse Laplace transform of the function

$$F(s) = \frac{1}{s(1 + e^{-s})}.$$

**SOLUTION**

The integrand in the inversion integral  $\frac{e^{st}}{s(1+e^{-s})}$  possesses simple poles at:  $s=0$  and  $s=jn\pi$ ,  $n = \pm 1, \pm 3, \pm 1 \dots$  (odd values). These are illustrated in Figure 5.12. We see that the function  $e^{st}/s(1 + e^{-s})$  is analytic in the  $s$ -plane except at the simple poles at  $s=0$  and  $s=jn\pi$ . Hence, the integral is specified in terms of the residues in the various poles. We have, specifically

$$\begin{aligned} \text{Res} \left\{ \frac{se^{st}}{s(1 + e^{-s})} \right\} \Big|_{s=0} &= \frac{1}{2} \quad \text{for } s = 0 \\ \text{Res} \left\{ \frac{(s - jn)e^{st}}{s(1 + e^{-s})} \right\} \Big|_{s=jn} &= \frac{0}{0} \quad \text{for } s = jn\pi. \end{aligned} \tag{5.47}$$

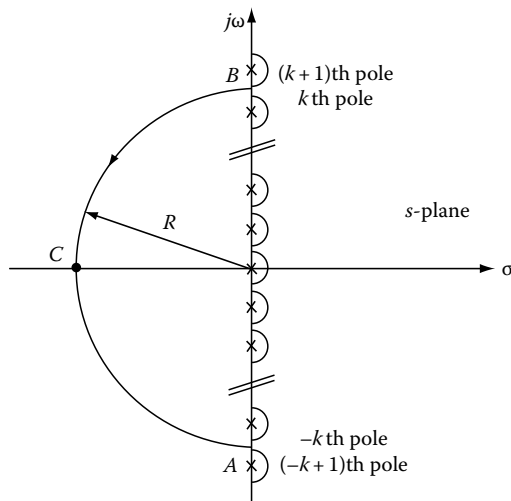


FIGURE 5.12 The pole distribution of the given function.

The problem we now face in this evaluation is that

$$\text{Res} \left\{ (s - a) \frac{n(s)}{d(s)} \right\} \Big|_{s=a} = \frac{0}{0}$$

where the roots of  $d(s)$  are such that  $s = a$  cannot be factored. However, we know from complex function theory that

$$\frac{d[d(s)]}{ds} \Big|_{s=a} = \lim_{s \rightarrow a} \frac{d(s) - d(a)}{s - a} = \lim_{s \rightarrow a} \frac{d(s)}{s - a}$$

because  $d(a) = 0$ . Combine this result with the above equation to obtain

$$\text{Res} \left\{ (s - a) \frac{n(s)}{d(s)} \right\} \Big|_{s=a} = \frac{n(s)}{\frac{d}{ds}[d(s)]} \Big|_{s=a}. \tag{5.48}$$

By combining Equation 5.48 with Equation 5.47, we obtain

$$\text{Res} \left\{ \frac{e^{st}}{s \frac{d}{ds}(1 + e^{-s})} \right\} \Big|_{s=jn\pi} = \frac{e^{jn\pi t}}{jn\pi} \quad n \text{ odd}.$$

We obtain, by adding all of residues,

$$f(t) = \frac{1}{2} + \sum_{n=-\infty}^{\infty} \frac{e^{jn\pi t}}{jn\pi}.$$

This can be rewritten as follows

$$\begin{aligned} f(t) &= \frac{1}{2} + \left[ \dots + \frac{e^{-j3\pi t}}{-j3\pi} + \frac{e^{-j\pi t}}{-j\pi} + \frac{e^{j\pi t}}{j\pi} + \frac{e^{j3\pi t}}{j3\pi} + \dots \right] \\ &= \frac{1}{2} + \sum_{\substack{n=1 \\ n \text{ odd}}}^{\infty} \frac{2j \sin n\pi t}{jn\pi}. \end{aligned}$$

This assumes the form

$$f(t) = \frac{1}{2} + \frac{2}{\pi} \sum_{k=1}^{\infty} \frac{\sin(2k - 1)\pi t}{2k - 1}. \tag{5.49}$$

As a second approach to a solution to this problem, we will show the details in carrying out the contour integration for this problem. We choose the path shown in Figure 5.12 that includes semicircular hooks around each pole, the vertical connecting line from hook to hook, and the semicircular path at  $R \rightarrow \infty$ . Thus, we examine

$$\begin{aligned} f(t) &= \frac{1}{2\pi j} \oint \frac{e^{st}}{s(1 + e^{-s})} ds \\ &= \frac{1}{2\pi j} \left[ \int_{BCA} + \int_{\text{vertical connecting lines}} + \sum \int_{\text{Hooks}} - \sum \text{Res} \right]. \end{aligned} \tag{5.50}$$

We consider the several integrals in this equation.

Integral  $I_1$ . By setting  $s = re^{j\theta}$  and taking into consideration that  $\cos \theta = -\cos \theta$  for  $\theta > \pi/2$ , the integral  $I_1 \rightarrow 0$  as  $r \rightarrow \infty$ .  
 Integral  $I_2$ . Along the  $Y$ -axis,  $s = jy$  and

$$I_2 = j \int_{-\infty}^{\infty} \frac{e^{jyt}}{jy(1 + e^{-jy})} dy.$$

Note that the integrand is an odd function, whence  $I_2 = 0$ .  
 Integral  $I_3$ . Consider a typical hook at  $s = jn\pi$ . The result is

$$\lim_{\substack{r \rightarrow 0 \\ s \rightarrow jn\pi}} \left[ \frac{(s - jn)e^{st}}{s(1 + e^{-s})} \right] = \frac{0}{0}.$$

This expression is evaluated (as for Equation 5.47) and yields  $e^{jn\pi t}/jn\pi$ . Thus, for all poles

$$\begin{aligned} I_3 &= \frac{1}{2\pi j} \int_{-\frac{\pi}{2}}^{\frac{\pi}{2}} \frac{e^{st}}{s(1 + e^{-s})} ds = \frac{j\pi}{2\pi j} \left[ \sum_{\substack{n=-\infty \\ n \text{ odd}}}^{\infty} \frac{e^{jn\pi t}}{jn\pi} + \frac{1}{2} \right] \\ &= \frac{1}{2} \left[ \frac{1}{2} + \frac{2}{\pi} \sum_{\substack{n=1 \\ n \text{ odd}}}^{\infty} \frac{\sin n\pi t}{n} \right]. \end{aligned}$$

Finally, the residues enclosed within the contour are

$$\text{Res} \frac{e^{st}}{s(1 + e^{-s})} = \frac{1}{2} + \sum_{\substack{n=-\infty \\ n \text{ odd}}}^{\infty} \frac{e^{jn\pi t}}{jn\pi} = \frac{1}{2} + \frac{2}{\pi} \sum_{\substack{n=1 \\ n \text{ odd}}}^{\infty} \frac{\sin n\pi t}{n},$$

which is seen to be twice the value around the hooks. Then when all terms are included in Equation 5.50, the final result is

$$f(t) = \frac{1}{2} + \frac{2}{\pi} \sum_{\substack{n=1 \\ n \text{ odd}}}^{\infty} \frac{\sin n\pi t}{n} = \frac{1}{2} + \frac{2}{\pi} \sum_{k=1}^{\infty} \frac{\sin(2k-1)\pi t}{2k-1}.$$

We now shall show that the direct and inverse transforms specified by Equation 5.30 and listed in Table A.5.1 constitute unique pairs. In this connection, we see that Equation 5.42 can be considered as proof of the following theorem:

---

**THEOREM 5.17**

Let  $F(s)$  be a function of a complex variable  $s$  that is analytic and of order  $O(s^{-k})$  in the half-plane  $\text{Re}(s) \geq c$ , where  $c$  and  $k$  are real constants, with  $k > 1$ . The inversion integral (Equation 5.42) written  $\mathcal{L}_t^{-1}\{F(s)\}$  along any line  $x = \sigma$ , with  $\sigma \geq c$  converges to the function  $f(t)$  that is independent of  $\sigma$ ,

$$f(t) = \mathcal{L}_t^{-1}\{F(s)\}$$

whose Laplace transform is  $F(s)$ ,

$$F(s) = \mathcal{L}\{f(t)\}, \quad \text{Re}(s) \geq c.$$

In addition, the function  $f(t)$  is continuous for  $t > 0$  and  $f(0) = 0$ , and  $f(t)$  is of the order  $O(e^{ct})$  for all  $t > 0$ .

Suppose that there are two transformable functions  $f_1(t)$  and  $f_2(t)$  that have the same transforms

$$\mathcal{L}\{f_1(t)\} = \mathcal{L}\{f_2(t)\} = F(s).$$

The difference between the two functions is written  $\phi(t)$

$$\phi(t) = f_1(t) - f_2(t)$$

where  $\phi(t)$  is a transformable function. Thus,

$$\mathcal{L}\{\phi(t)\} = F(s) - F(s) = 0.$$

Additionally,

$$\phi(t) = \mathcal{L}_t^{-1}\{0\} = 0, \quad t > 0.$$

Therefore, this requires that  $f_1(t) = f_2(t)$ . The result shows that it is not possible to find two different functions by using two different values of  $\sigma$  in the inversion integral. This conclusion can be expressed as follows:

---

**THEOREM 5.18**

Only a single function  $f(t)$  that is sectionally continuous, of exponential order, and with a mean value at each point of discontinuity, corresponds to a given transform  $F(s)$ .

---

**5.7 Applications to Partial Differential Equations**

The Laplace transformations can be very useful in the solution of partial differential equations. A basic class of partial differential equations is applicable to a wide range of problems. However, the form of the solution in a given case is critically dependent on the boundary conditions that apply in any particular case. In consequence, the steps in the solution often will call on many different mathematical techniques. Generally, in such problems the resulting inverse transforms of more complicated functions of  $s$  occur than those for most linear systems problems. Often the inversion integral is useful in the solution of such problems. The following examples will demonstrate the approach to typical problems.

**Example 5.26**

Solve the typical heat conduction equation

$$\frac{\partial^2 \varphi}{\partial x^2} = \frac{\partial \varphi}{\partial t}, \quad 0 < x < \infty, t \geq 0 \tag{5.51}$$

subject to the conditions

C-1.  $\varphi(x, 0) = f(x), \quad t = 0$

C-2.  $\frac{\partial \varphi}{\partial x} = 0, \quad \varphi(x, t) = 0 \quad x = 0.$

**SOLUTION**

Multiply both sides of Equation 5.51 by  $e^{-sx}$  and integrate from 0 to  $\infty$ .

$$\Phi(s, t) = \int_0^{\infty} e^{-sx} \varphi(x, t) dx.$$

Also

$$\int_0^{\infty} \frac{\partial^2 \varphi}{\partial x^2} e^{-sx} dx = s^2 \Phi(s, t) - s\varphi(0+) - \frac{\partial \varphi}{\partial x}(0+).$$

Equation 5.51 thus transforms, subject to C-2 and zero boundary conditions, to

$$\frac{d\Phi}{dt} - s^2 \Phi = 0.$$

The solution to this equation is

$$\Phi = Ae^{s^2 t}.$$

By an application of condition C-1, in transformed form, we have

$$\Phi = A = \int_0^{\infty} f(\lambda) e^{-s\lambda} d\lambda.$$

The solution, subject to C-1, is then

$$\Phi(s, t) = e^{+s^2 t} \int_0^{\infty} f(\lambda) e^{-s\lambda} d\lambda.$$

Now apply the inversion integral to write the function in terms of  $x$  from  $s$ ,

$$\begin{aligned} \varphi(x, t) &= \frac{1}{2\pi j} \int_{-\infty}^{\infty} e^{+s^2 t} \left[ \int_0^{\infty} f(\lambda) e^{-s\lambda} d\lambda \right] e^{sx} ds \\ &= \frac{1}{2\pi j} \int_{-\infty}^{\infty} f(\lambda) d\lambda \int_0^{\infty} e^{s^2 t - s\lambda + sx} ds. \end{aligned}$$

Note that we can write

$$s^2 t - s(x - \lambda) = \left\{ s\sqrt{t} - \frac{(x - \lambda)}{2\sqrt{t}} \right\}^2 - \frac{(x - \lambda)^2}{4t}.$$

Also write

$$s\sqrt{t} - \frac{(x - \lambda)}{2\sqrt{t}} = u.$$

Then

$$\varphi(x, t) = \frac{1}{2\pi j} \int_{-\infty}^{\infty} f(\lambda) \exp - \left[ \frac{(x - \lambda)^2}{4t} \right] d\lambda \int_0^{\infty} e^{-u^2} \frac{du}{\sqrt{t}}.$$

But the integral

$$\int_0^{\infty} e^{-u^2} du = \sqrt{\pi}.$$

Thus, the final solution is

$$\varphi(x, t) = \frac{1}{2\sqrt{\pi t}} \int_{-\infty}^{\infty} f(\lambda) e^{-\frac{(x-\lambda)^2}{4t}} d\lambda.$$

**Example 5.27**

A semi-infinite medium, initially at temperature  $\varphi = 0$  throughout the medium, has the face  $x = 0$  maintained at temperature  $\varphi_0$ . Determine the temperature at any point of the medium at any subsequent time.

**SOLUTION**

The controlling equation for this problem is

$$\frac{\partial^2 \varphi}{\partial x^2} = \frac{1}{K} \frac{\partial \varphi}{\partial t} \tag{5.52}$$

with the boundary conditions:

- a.  $\varphi = \varphi_0$  at  $x = 0, t > 0$
- b.  $\varphi = 0$  at  $t = 0, x > 0.$

To proceed, multiply both sides of Equation 5.52 by  $e^{-st}$  and integrate from 0 to  $\infty$ . The transformed form of Equation 5.52 is

$$\frac{d^2 \Phi}{dx^2} - \left( \frac{s}{K} \Phi \right) = 0, \quad K > 0.$$

The solution of this differential equation is

$$\Phi = Ae^{-x\sqrt{s/k}} + Be^{x\sqrt{s/k}}.$$

But  $\Phi$  must be finite or zero for infinite  $x$ ; therefore,  $B=0$  and

$$\Phi(s, x) = Ae^{-\sqrt{\frac{s}{K}}x}.$$

Apply boundary condition (a) in transformed form, namely

$$\Phi(0, s) = \int_0^\infty e^{-st} \varphi_0 dt = \frac{\varphi_0}{s} \quad \text{for } x = 0.$$

Therefore,

$$A = \frac{\varphi_0}{s}$$

and the solution in Laplace transformed form is

$$\Phi(s, x) = \frac{\varphi_0}{s} e^{-\sqrt{\frac{s}{K}}x}. \quad (5.53)$$

To find  $\varphi(x, t)$  requires that we find the inverse transform of this expression. This requires evaluating the inversion integral

$$\varphi(x, t) = \frac{\varphi_0}{2\pi j} \int_{\sigma-j\infty}^{\sigma+j\infty} \frac{e^{-x\sqrt{\frac{s}{K}}} e^{st}}{s} ds. \quad (5.54)$$

This integral has a branch point at the origin (see Figure 5.13). To carry out the integration, we select a path such as that shown (see also Figure 5.11). The integral in Equation 5.54 is written

$$\varphi(x, t) = \frac{\varphi_0}{2\pi j} \left[ \int_{BC} + \int_{\Gamma_2} + \int_{l^-} + \int_{\gamma} + \int_{l^+} + \int_{\Gamma_3} + \int_{FG} \right].$$

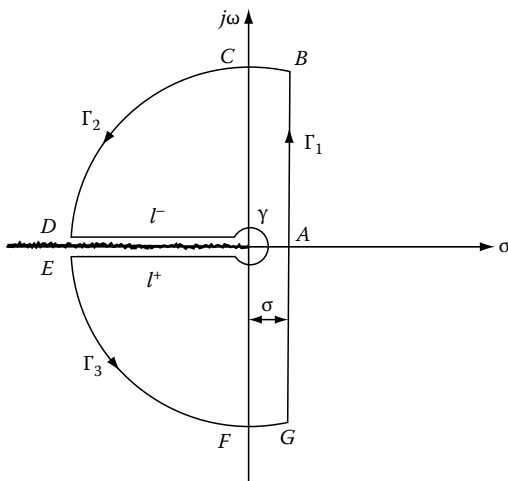


FIGURE 5.13 The path of integration.

As in Example 5.24

$$\int_{\Gamma_2} = \int_{\Gamma_3} = \int_{BC} = \int_{FG} = 0.$$

For the segments

$$\int_{l^-}, \text{ let } s = \rho e^{j\pi} \quad \text{and} \quad \int_{l^+}, \text{ let } s = \rho e^{i\pi}.$$

Then for  $l^-$  and  $l^+$ , writing this sum  $l_\ell$ ,

$$\begin{aligned} l_\ell &= \frac{1}{2\pi j} \int_0^\infty e^{-st} \left[ e^{jx\sqrt{s/K}} - e^{-jx\sqrt{s/K}} \right] \frac{ds}{s} \\ &= -\frac{1}{\pi} \int_0^\infty e^{-st} \sin x \sqrt{\frac{s}{K}} \frac{ds}{s}. \end{aligned}$$

Write

$$u = \sqrt{\frac{s}{K}}, \quad s = Ku^2, \quad ds = 2Ku \, du.$$

Then we have

$$l_\ell = -\frac{2}{\pi} \int_0^\infty e^{-Ku^2 t} \sin ux \frac{du}{u}.$$

This is a known integral that can be written

$$l_l = -\frac{2}{\sqrt{\pi}} \int_0^{\frac{x}{2\sqrt{Kt}}} e^{-u^2} du.$$

Finally, consider the integral over the hook,

$$l_\gamma = \frac{1}{2\pi j} \int_\gamma e^{st} \frac{e^{x\sqrt{s/K}}}{s} ds.$$

Let us write

$$s = re^{i\theta}, \quad ds = jre^{i\theta} d\theta, \quad \frac{ds}{s} = j\theta,$$

then

$$l_\gamma = \frac{j}{2\pi j} \int e^{tre^{i\theta}} e^{x\sqrt{r/K}} e^{i\theta/2} d\theta.$$

For  $r \rightarrow 0, l_\gamma = \frac{j2\pi}{2\pi j} = \frac{2\pi j}{2\pi j}$ , then  $l_\gamma = 1$ . Hence, the sum of the integrals in Equation 5.53 becomes

$$\varphi(t) = \varphi_0 \left[ 1 - \frac{2}{\sqrt{\pi}} \int_0^{\frac{x}{2\sqrt{kt}}} e^{-u^2} du = \varphi_0 \left[ 1 - \operatorname{erf} \frac{x}{2\sqrt{kt}} \right] \right]. \quad (5.55)$$

**Example 5.28**

A finite medium of length  $l$  is at initial temperature  $\varphi_0$ . There is no heat flow across the boundary at  $x=0$ , and the face at  $x=l$  is then kept at  $\varphi_1$  (see Figure 5.14). Determine the temperature  $\varphi(t)$ .

**SOLUTION**

Here we have to solve

$$\frac{\partial^2 \varphi}{\partial x^2} = \frac{1}{k} \frac{\partial \varphi}{\partial t}$$

subject to the boundary conditions:

- a.  $\varphi = \varphi_0 \quad t = 0 \quad 0 \leq x \leq l$
- b.  $\varphi = \varphi_1 \quad t > 0 \quad x = l$
- c.  $\frac{\partial \varphi}{\partial x} = 0 \quad t > 0 \quad x = 0$ .

Upon Laplace transforming the controlling differential equation, we obtain

$$\frac{d^2 \Phi}{dx^2} - \frac{s}{k} \Phi = 0.$$

The solution is

$$\Phi = A'e^{-x\sqrt{\frac{s}{k}}} + B'e^{x\sqrt{\frac{s}{k}}} = A \cosh x\sqrt{\frac{s}{k}} + B \sinh x\sqrt{\frac{s}{k}}.$$

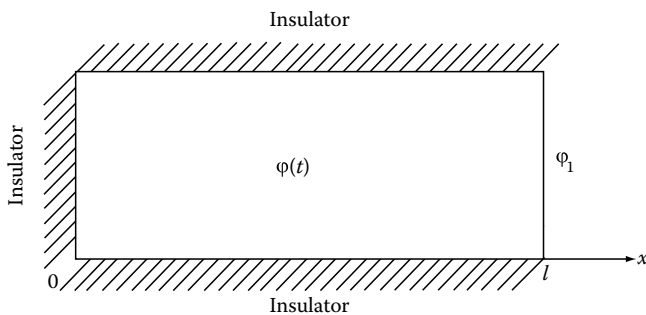


FIGURE 5.14 Details for Example 5.28.

By condition c

$$\frac{d\Phi}{dx} = 0 \quad x = 0 \quad t > 0.$$

This imposes the requirement that  $B=0$ , so that

$$\Phi = A \cosh x\sqrt{\frac{s}{k}}.$$

Now condition b is imposed. This requires that

$$\frac{\varphi_1}{s} = A \cosh \frac{l\sqrt{s}}{\sqrt{k}}.$$

Thus, by b and c

$$\Phi = \varphi_1 \frac{\cosh x\sqrt{\frac{s}{k}}}{s \cosh \frac{l\sqrt{s}}{\sqrt{k}}}.$$

Now, to satisfy c we have

$$\Phi = \frac{\varphi_0}{s} - \frac{\varphi_0}{s} \frac{\cosh x\sqrt{\frac{s}{k}}}{\cosh \frac{l\sqrt{s}}{\sqrt{k}}}.$$

Thus, the final form of the Laplace transformed equation that satisfies all conditions of the problem is

$$\Phi = \frac{\varphi_0}{s} + \frac{\varphi_1 - \varphi_0}{s} \frac{\cosh x\sqrt{\frac{s}{k}}}{\cosh \frac{l\sqrt{s}}{\sqrt{k}}}.$$

To find the expression for  $\varphi(x, t)$ , we must invert this expression. That is,

$$\varphi(x, t) = \varphi_0 + \frac{\varphi_1 - \varphi_0}{2\pi j} \int_{\sigma-j\infty}^{\sigma+j\infty} e^{st} \frac{\cosh x\sqrt{\frac{s}{k}}}{\cosh \frac{l\sqrt{s}}{\sqrt{k}}} \frac{ds}{s}. \quad (5.56)$$

The integrand is a single valued function of  $s$  with poles at  $s=0$  and  $s = -k\left(\frac{2n-1}{2}\right)^2 \frac{\pi^2}{l^2}$ ,  $n = 1, 2, \dots$

We select the path of integration that is shown in Figure 5.15. But the inversion integral over the path  $BCA(=\Gamma)=0$ . Thus, the inversion integral becomes

$$\frac{1}{2\pi j} \int_{\sigma-j\infty}^{\sigma+j\infty} e^{st} \frac{\cosh x\sqrt{\frac{s}{k}}}{\cosh \frac{l\sqrt{s}}{\sqrt{k}}} \frac{ds}{s}.$$

By an application of the Cauchy integral theorem, we require the residues of the integrand at its poles. There results

$$\operatorname{Res}|_{s=0} = 1$$

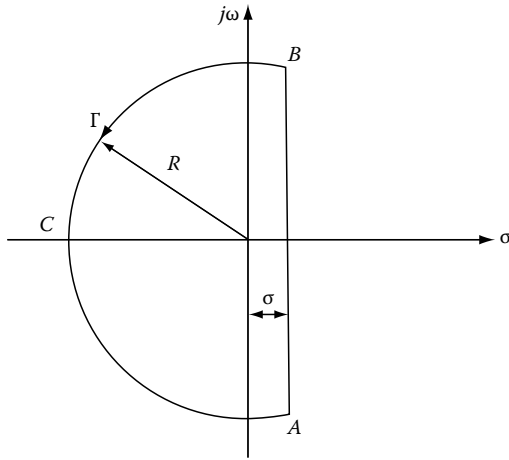


FIGURE 5.15 The path of integration for Example 5.28.

$$\text{Res}|_{s=-k(n-\frac{1}{2})^2 \frac{\pi^2}{l^2}} = \frac{e^{-k(n-\frac{1}{2})^2 \frac{\pi^2}{l^2}} \cosh j(n-\frac{1}{2}) \frac{\pi x}{l}}{\left[ s \frac{d}{ds} \{ \cosh \sqrt{\frac{s}{k}} \} \right]_{s=-k(n-\frac{1}{2})^2 \frac{\pi^2}{l^2}}}$$

Combine these with Equation 5.55 to write finally

$$\varphi(x, t) = \varphi_0 + \frac{4(\varphi_1 - \varphi_0)}{\pi} \sum_{n=1}^{\infty} \frac{(-1)^n}{2n-1} l^{-k(n-\frac{1}{2})^2 \pi^2 / l^2} \times \cos \left[ \left( n - \frac{1}{2} \right) \pi x / l \right]. \quad (5.57)$$

**Example 5.29**

A circular cylinder of radius  $a$  is initially at temperature zero. The surface is then maintained at temperature  $\varphi_0$ . Determine the temperature of the cylinder at any subsequent time  $t$ .

**SOLUTION**

The heat conduction equation in radial form is

$$\frac{\partial^2 \varphi}{\partial r^2} + \frac{1}{r} \frac{\partial \varphi}{\partial r} = \frac{1}{k} \frac{\partial \varphi}{\partial t}, \quad 0 \leq r < a, t > 0. \quad (5.58)$$

And for this problem the system is subject to the boundary conditions

- C-1.  $\varphi = 0 \quad t = 0 \quad 0 \leq r < a$
- C-2.  $\varphi = \varphi_0 \quad t > 0 \quad r = a.$

To proceed, we multiply each term in the partial differential equation by  $e^{-st}$   $dt$  and integrate. We write

$$\int_0^{\infty} \varphi e^{-st} dt = \Phi(r, s)$$

Then Equation 5.57 transforms to

$$k \left( \frac{d^2 \Phi}{dr^2} + \frac{1}{r} \frac{d\Phi}{dr} \right) - s\Phi = 0,$$

which we write in the form

$$\frac{d^2 \Phi}{dr^2} + \frac{1}{r} \frac{d\Phi}{dr} - \mu \Phi = 0, \quad \mu = \sqrt{\frac{s}{k}}.$$

This is the Bessel equation of order 0 and has the solution

$$\Phi = A I_0(\mu r) + B N_0(\mu r).$$

However, the Laplace transformed form of C-1 when  $z = 0$  imposes the condition  $B = 0$  because  $N_0(0)$  is not zero. Thus,

$$\Phi = A I_0(\mu r).$$

The boundary condition C-2 requires  $\Phi(r, a) = \frac{\varphi_0}{s}$  when  $r = a$ , hence,

$$A = \frac{\varphi_0}{s} \frac{1}{I_0(\mu a)}$$

so that

$$\Phi = \frac{\varphi_0}{s} \frac{I_0(\mu r)}{I_0(\mu a)}.$$

To find the function  $\varphi(r, t)$  requires that we invert this function. By an application of the inversion integral, we write

$$\varphi(r, t) = \frac{\varphi_0}{2\pi j} \int_{\sigma-j\infty}^{\sigma+j\infty} e^{\lambda t} \frac{I_0(\xi r)}{I_0(\xi a)} \frac{d\lambda}{\lambda}, \quad \xi = \sqrt{\frac{\lambda}{k}}. \quad (5.59)$$

Note that  $I_0(\xi r)/I_0(\xi a)$  is a single-valued function of  $\lambda$ . To evaluate this integral, we choose as the path for this integration that shown in Figure 5.16. The poles of this function are at  $\lambda = 0$  and at the roots of the Bessel function  $J_0(\xi a)$  ( $= I_0(j\xi a)$ ); these occur when  $J_0(\xi a) = 0$ , with the roots for  $J_0(\xi a) = 0$ , namely  $\lambda = -k\xi_1^2, -k\xi_2^2, \dots$ . The approximations for  $I_0(\xi r)$  and  $I_0(\xi a)$  show that when  $n \rightarrow \infty$  the integral over the path  $BCA$  tends to zero. The resultant value of the integral is written in terms of the residues at zero and when  $\lambda = k\xi_n^2$ . These are

$$\text{Res}|_{\lambda=0} = 1$$

$$\text{Res}|_{k\xi_n^2} = \frac{\lambda d I_0(\xi a)}{d\lambda} \Big|_{k\xi_n^2}.$$

Therefore,

$$\varphi(r, t) = \varphi_0 \left[ 1 + \sum_n e^{-k\xi_n^2 t} \frac{J_0(\xi_n r)}{\lambda \frac{d}{d\lambda} I_0(\xi a) |_{\lambda=k\xi_n^2}} \right].$$

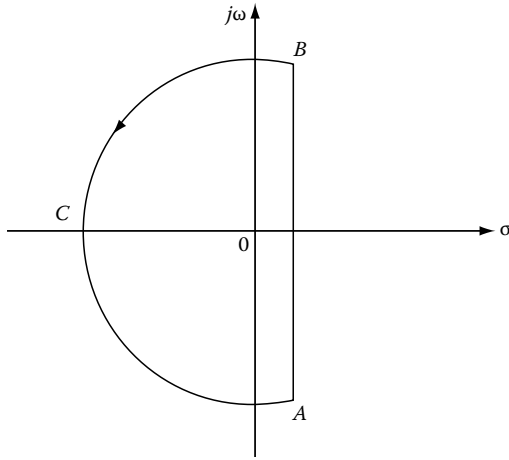


FIGURE 5.16 The path of integration for Example 5.29.

Further,  $\lambda \frac{d}{dx} I_0(\xi_n a) = \frac{1}{2} \xi_n a I_0^{(1)}(\xi_n a)$ . Hence, finally,

$$\varphi(t) = \varphi_0 \left[ 1 + \frac{2}{a} \sum_{n=1}^{\infty} e^{-k \xi_n^2 t} \frac{J_0(\xi_n t)}{\xi_n J_0^{(1)}(\xi_n a)} \right]. \quad (5.60)$$

**Example 5.30**

A semi-infinite stretched string is fixed at each end. It is given an initial transverse displacement and then released. Determine the subsequent motion of the string.

**SOLUTION**

This requires solving the wave equation

$$a^2 \frac{\partial^2 \varphi}{\partial x^2} = \frac{\partial^2 \varphi}{\partial t^2} \quad (5.61)$$

subject to the conditions

- C-1.  $\varphi(x, 0) = f(x) \quad t = 0, \quad \varphi(0, t) = 0 \quad t > 0$
- C-2.  $\lim_{x \rightarrow \infty} \varphi(x, t) = 0$ .

To proceed, multiply both sides of Equation 5.61 by  $e^{-st} dt$  and integrate. The result is the Laplace-transformed equation

$$a^2 \frac{d^2 \Phi}{dx^2} = s^2 \Phi - s\varphi(0+), \quad x > 0. \quad (5.62)$$

- C-1.  $\Phi(0, s) = 0$
- C-2.  $\lim_{x \rightarrow \infty} \Phi(x, s) = 0$ .

To solve Equation 5.62 we will carry out a second Laplace transform, but this with respect to  $x$ , that is  $\mathcal{L}\{\Phi(x, s)\} = N(z, s)$ . Thus,

$$N(z, s) = \int_0^{\infty} \Phi(x, s) e^{-zx} dx.$$

Apply this transformation to both members of Equation 5.62 subject to  $\Phi(0, s) = 0$ . The result is

$$s^2 N(z, s) - s\Phi(z) = a^2 \left[ z^2 N(z, s) - \frac{\partial \Phi}{\partial x}(0, s) \right], \quad \Phi(z) = \mathcal{L}\{\varphi_0\}.$$

We denote  $\frac{\partial \Phi}{\partial x}(0, s)$  by  $C$ . Then the solution of this equation is

$$N(z, s) = \frac{C}{z^2 - \frac{s^2}{a^2}} - \frac{s}{a^2} \Phi(z) \frac{1}{z^2 - \frac{s^2}{a^2}}.$$

The inverse transformation with respect to  $z$  is, employing convolution.

$$\Phi(x, s) = \frac{aC}{s} \sinh \frac{sx}{a} - \frac{1}{a} \int_0^x \varphi(\xi) \sinh \frac{s}{a}(x - \xi) d\xi.$$

To satisfy the condition  $\lim_{x \rightarrow \infty} \Phi(x, s) = 0$  requires that the sinh terms be replaced by their exponential forms. Thus, the factors

$$\sinh \frac{sx}{a} \rightarrow \frac{1}{2}, \quad \sinh \frac{s}{a}(x - \xi) \rightarrow \frac{e^{-s\xi/a}}{2}, \quad x \rightarrow \infty.$$

Then we have the expression

$$\Phi(x, s) = \frac{aC}{2s} - \frac{1}{2a} \int_0^x \varphi(\xi) e^{-s\xi/a} d\xi.$$

But for this function to be zero for  $x \rightarrow \infty$  requires that

$$\frac{aC}{s} = \frac{1}{a} \int_0^{\infty} \varphi(\xi) e^{-s\xi/a} d\xi, \quad x \rightarrow \infty.$$

Combine this result with  $\Phi(x, s)$  to get

$$2a\Phi(x, s) = \int_0^{\infty} \varphi(\xi) e^{-s(\xi-x)/a} d\xi - \int_0^{\infty} \varphi(\xi) e^{-s(x+\xi)/a} d\xi + \int_0^x \varphi(\xi) e^{-s(x-\xi)/a} d\xi.$$

Each integral in this expression is integrated by parts. Here we write

$$u = \varphi(\xi), \quad du = \varphi^{(1)}(\xi) d\xi; \quad dv = e^{-\frac{s(\xi-x)}{a}} d\xi, \quad v = \frac{a}{s} e^{-s(\xi-k)/a}.$$



The resulting integrations lead to

$$\Phi(x, s) = \frac{1}{s}\varphi(x) + \frac{1}{2s} \int_x^\infty \varphi^{(1)}(\xi)e^{-\frac{s(\xi-x)}{a}}d\xi - \frac{1}{2s} \int_0^\infty \varphi^{(1)}(\xi)e^{-\frac{s(x+\xi)}{a}}d\xi - \frac{1}{2s} \int_0^\infty \varphi^{(1)}(\xi)e^{-\frac{s(x-\xi)}{a}}d\xi.$$

We note by entry 61, Table A.5.1 that

$$\mathcal{L}^{-1}\left\{\frac{1}{s}e^{-\frac{s(\xi-x)}{a}}\right\} = 1 \quad \text{when } at > \xi - x \\ = 0 \quad \text{when } at < \xi - x.$$

This function of  $\xi$  vanishes except when  $\xi \leq x + at$ . Thus,

$$\mathcal{L}^{-1}\left\{\frac{1}{2} \int_x^\infty \varphi^{(1)}(\xi)e^{-s(\xi+x)/a}d\xi\right\} = \frac{1}{2} \int_x^{x+at} \varphi^{(1)}(\xi)d\xi \\ = \frac{1}{2}\varphi(x+at) - \frac{1}{2}\varphi(x).$$

Proceed in the same way for the term

$$\mathcal{L}^{-1}\left\{\frac{1}{2} \int_0^\infty \varphi^{(1)}(\xi)e^{-s(x+\xi)/a}d\xi\right\} = 1 \quad \text{when } at > x + \xi \\ = 0 \quad \text{when } at < x + \xi.$$

Thus, the second term becomes

$$\mathcal{L}^{-1}\left\{\frac{1}{2} \int_x^\infty \varphi^{(1)}(\xi)e^{-s(x+\xi)/a}d\xi\right\} = \frac{1}{2} \int_x^{x+at} \varphi^{(1)}(\xi)d\xi \\ = \frac{1}{2}\varphi(x-at).$$

The final term becomes

$$-\frac{1}{2}\varphi(x) \quad \text{when } at > x \\ -\frac{1}{2}\varphi(x) + \frac{1}{2}\varphi(x-at) \quad \text{when } at < x.$$

The final result is

$$\varphi(x, t) = \frac{1}{2}[f(at+x) - f(at-x)] \quad \text{when } t > x/a \\ = \frac{1}{2}[f(x+at) + f(x-at)] \quad \text{when } t < x/a. \quad (5.63)$$

### Example 5.31

A stretched string of length  $l$  is fixed at each end as shown in Figure 5.17. It is plucked at the midpoint and then released at  $t=0$ . The displacement is  $b$ . Find the subsequent motion.

#### SOLUTION

This problem requires the solution of

$$\frac{\partial^2 y}{\partial y^2} = c^2 \frac{\partial^2 y}{\partial t^2}, \quad 0 < y < l, t > 0 \quad (5.64)$$

subject to

$$\left. \begin{aligned} 1. \quad y &= \frac{2bx}{l} & 0 < x < l/2 \\ 2. \quad y &= \frac{2b}{l}(l-x) & l/2 < x < l \\ 3. \quad \frac{\partial y}{\partial t} &= 0 & 0 < x < l \quad t=0 \\ 4. \quad y &= 0 & x=0; \quad x=l \quad t>0. \end{aligned} \right\} t=0$$

To proceed, multiply Equation 5.63 by  $e^{-st}$  and integrate in  $t$ . This yields

$$s^2 Y - sy(0) = c^2 \frac{d^2 Y}{dx^2}$$

or

$$c^2 \frac{d^2 Y}{dx^2} - s^2 Y = sy(0) = -sf(x) \quad (5.65)$$

subject to  $Y(0, s) = Y(l, s) = 0$ . To solve this equation, we proceed as in Example 5.30; that is, we apply a transformation on  $x$ , namely  $\mathcal{L}\{Y(x, s)\} = N(z, s)$ . Thus,

$$s^2 N(z, s) - sY(0) = c^2 \left[ z^2 N(z, s) - \frac{y(0, s)}{x} \right].$$

This equation yields, writing  $sY(0)$  as  $\Phi(x, s)$ ,

$$N(z, s) = \frac{\Phi(z, s)}{z^2 - \frac{s^2}{c^2}}$$

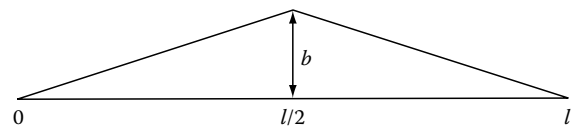


FIGURE 5.17 A stretched string plucked at its midpoint.

The inverse transform is

$$Y(x, s) = \mathcal{L}^{-1}\{N(x, s)\} = \frac{\Phi(x, s)}{c \sinh \frac{x}{c}}$$

where

$$\begin{aligned} \Phi(x, s) = & \sinh \frac{(l-x)s}{c} \int_0^x y(\xi) \sinh \frac{\xi s}{c} d\xi \\ & + \sinh \frac{xs}{c} \int_0^l y(\xi) \sinh \frac{(l-\xi)s}{c} d\xi. \end{aligned}$$

Combine these integrals with the known form of  $f(x)$  in C-1 and C-2. Upon carrying out the integrations, the resulting forms become, with  $k = \frac{s}{c}$ ,

$$\begin{aligned} \frac{lY}{2b} = & \frac{x}{s} - \frac{c}{s^2} \frac{\sinh kx}{\cosh \frac{kl}{2}}, \quad 0 \leq x \leq l/2 \\ \frac{lY}{2b} = & \frac{(l-x)}{s} - \frac{c}{s^2} \frac{\sinh k(l-x)}{\cosh \frac{kl}{2}}, \quad \frac{l}{2} \leq x \leq l. \end{aligned}$$

To find  $y(t)$ , we must invert these expressions. Note that symmetry exists and so we need consider only the first term. We use the inversion integral on the term  $\frac{1}{s^2} \frac{\sinh kx}{\cosh \frac{kl}{2}}$ . Thus, we consider the integral

$$I = \frac{1}{2\pi j} \int_{\sigma-j\infty}^{\sigma+j\infty} e^{\lambda b} \frac{\sinh \frac{\lambda x}{c}}{\cosh \frac{\lambda l}{2c}} \frac{d\lambda}{\lambda^2}.$$

We choose the path in the  $\lambda$ -plane as shown in Figure 5.18. The value of the integral over path  $\Gamma$  is zero. Thus, the value of the integral is given in terms of the residues. These occur at  $\lambda = 0$  and at the values for which  $\cosh \frac{\lambda}{2c} = 0$ , which exist where

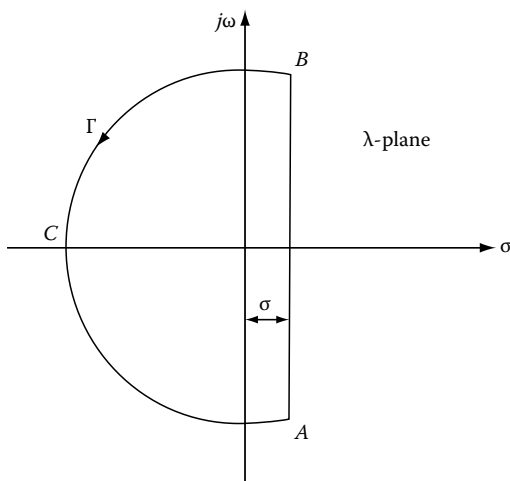


FIGURE 5.18 The path of integration for Example 5.31.

$$\frac{\lambda}{2c} = j \frac{2n-1}{l} \frac{\pi}{2} \quad \text{or} \quad \lambda = \pm j \frac{2n-1}{l} \pi c.$$

Thus, we have, by the theory of residues

$$\begin{aligned} \text{Res}|_{\lambda=0} = & \frac{x}{c} \\ \text{Res}|_{j \frac{2n-1}{l} \pi c} = & e^{j(2n-1) \frac{\pi c x}{l}} \frac{\pi c x}{l} \frac{\sinh j(2n-1) \frac{\pi x}{l}}{\frac{d}{d\lambda} [\lambda^2 \cosh \frac{\lambda l}{2c}]_{j \frac{2n-1}{l} \pi c}}. \end{aligned}$$

These poles lead to

$$= (-1)^n \frac{2l}{\pi^2 c} \frac{\sin(2n-1) \frac{\pi x}{l}}{(2n-1)^2} e^{j(2n-1) \frac{\pi c}{l} t}.$$

Thus, the poles at  $\pm j(2n-1) \frac{\pi c}{l}$  lead to

$$= (-1)^n \frac{4l}{\pi^2 c} \frac{\sin(2n-1) \frac{\pi x}{l} \cos(2n-1) \frac{\pi c}{l} t}{(2n-1)^2}.$$

Then we have

$$\begin{aligned} \frac{lY}{2b} = & x \\ & - \left\{ x + \frac{4l}{\pi^2} \sum_{n=1}^{\infty} \frac{(-1)^n}{(2n-1)^2} \sin(2n-1) \frac{\pi x}{l} \cos(2n-1) \frac{\pi c}{l} t \right\} \end{aligned}$$

so that finally

$$\begin{aligned} y = & \frac{8b}{\pi^2} \sum_{n=1}^{\infty} \frac{(-1)^{n-1}}{(2n-1)^2} \sin(2n-1) \frac{\pi x}{l} \cos(2n-1) \frac{\pi c}{l} t, \\ & 0 \leq x \leq \frac{l}{2}. \end{aligned}$$

For the string for which  $\frac{l}{2} \leq x < l$ , the corresponding expression is the same except that  $(l-x)$  replaces  $x$ .

Note that this equation can be written, with  $\eta = (2n-1) \frac{\pi}{l}$ ,

$$\sin \eta x \cos \eta c t = \frac{\sin \eta(x-ct) + \sin \eta(x+ct)}{2},$$

which shows the traveling wave nature of the solution.

## 5.8 The Bilateral or Two-Sided Laplace Transform

In Section 5.1 we discussed the fact that the region of absolute convergence of the unilateral or one-sided Laplace transform is the region to the left of the abscissa of convergence. The situation for the two-sided Laplace transform is rather different; the region

of convergence must be specified if we wish to invert a function  $F(s)$  that was obtained using the bilateral Laplace transform. This requirement is necessary because different time signals might have the same Laplace transform but different regions of absolute convergence.

To establish the region of convergence, write the bilateral Laplace transform in the form

$$F_2(s) = \int_{-\infty}^{\infty} e^{-st} f(t) dt = \int_0^{\infty} e^{-st} f(t) dt + \int_{-\infty}^0 e^{-st} f(t) dt. \quad (5.66)$$

If the function  $f(t)$  is of exponential order ( $e^{\sigma_1 t}$ ), then the region of convergence for  $t > 0$  is  $\text{Re}(s) > \sigma_1$ . If the function  $f(t)$  for  $t < 0$  is of exponential order  $\exp(\sigma_2 t)$ , then the region of convergence is  $\text{Re}(s) < \sigma_2$ . Hence, the function  $F_2(s)$  exists and is analytic in the vertical strip defined by  $\sigma_1 < \text{Re}(s) < \sigma_2$ , provided, of course, that  $\sigma_1 < \sigma_2$ . If  $\sigma_2 > \sigma_1$ , no region of convergence would exist and the inversion process could not be performed. This region of convergence is shown in Figure 5.19.

**Example 5.32**

Find the bilateral Laplace transform of the signals  $f(t) = e^{-at}u(t)$  and  $f(t) = -e^{-at}u(t)$  and specify their regions of convergence.

**SOLUTION**

Using the basic definition of the transform (Equation 5.66), we obtain

$$F_2(s) = \int_{-\infty}^{\infty} e^{-at}u(t)e^{-st} dt = \int_0^{\infty} e^{-(s+a)t} dt = \frac{1}{s+a}$$

and its region of convergence is  $\text{Re}(s) > -a$ .

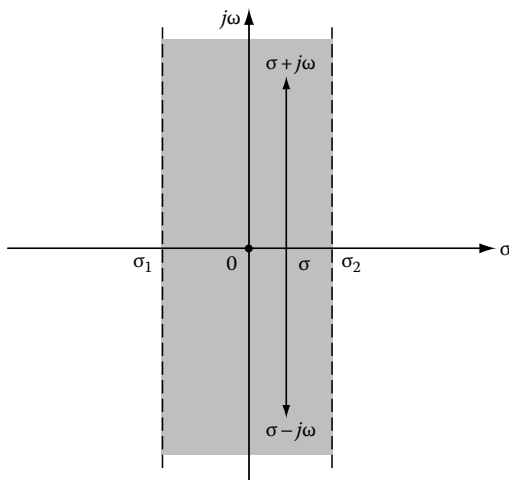


FIGURE 5.19 Region of convergence for the bilateral transform.

For the second signal,

$$F_2(s) = \int_{-\infty}^{\infty} -e^{-at}u(-t)e^{-st} dt = - \int_{-\infty}^0 e^{-(s+a)t} dt = \frac{1}{s+a}$$

and its region of convergence is  $\text{Re}(s) < -a$ .

Clearly, the knowledge of the region of convergence is necessary to find the time functions unambiguously.

**Example 5.33**

Find the function  $f(t)$ , if its Laplace transform is given by

$$F_2(s) = \frac{3}{(s-4)(s+1)(s+2)}, \quad -2 < \text{Re}(s) < -1.$$

**SOLUTION**

The region of convergence and the paths of integration are shown in Figure 5.20. For  $t > 0$  we close the contour to the left and we obtain

$$f(t) = \frac{3e^{st}}{(s-4)(s+1)} \Big|_{s=-2} = \frac{1}{2}e^{-2t}, \quad t > 0.$$

For  $t < 0$ , the contour closes to the right and now

$$f(t) = \frac{3e^{st}}{(s-4)(s+2)} \Big|_{s=-1} + \frac{3e^{st}}{(s+1)(s+2)} \Big|_{s=4} = -\frac{3}{5}e^{-t} + \frac{e^{4t}}{10}, \quad t < 0.$$

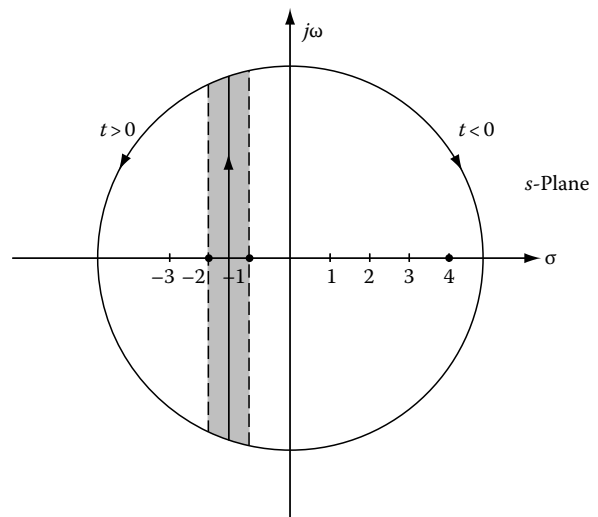


FIGURE 5.20 Illustrating Example 5.33.

## Appendix A

TABLE A.5.1 Laplace Transform Pairs

	$F(s)$	$f(t)$
1	$s^n$	$\delta^{(n)}(t)$ $n$ th derivative of the delta function
2	$s$	$\frac{d\delta(t)}{dt}$
3	1	$\delta(t)$
4	$\frac{1}{s}$	1
5	$\frac{1}{s^2}$	$t$
6	$\frac{1}{s^n} (n = 1, 2, \dots)$	$\frac{t^{n-1}}{(n-1)}$
7	$\frac{1}{\sqrt{s}}$	$\frac{1}{\sqrt{\pi t}}$
8	$s^{-3/2}$	$\sqrt{\frac{t}{\pi}}$
9	$s^{-[n+(1/2)]} (n = 1, 2, \dots)$	$\frac{2^n t^{n-(1/2)}}{1 \cdot 3 \cdot 5 \cdots (2n-1)\sqrt{\pi}}$
10	$\frac{\Gamma(k)}{s^k} (k \geq 0)$	$t^{k-1}$
11	$\frac{1}{s-a}$	$e^{at}$
12	$\frac{1}{(s-a)^2}$	$te^{at}$
13	$\frac{1}{(s-a)^n} (n = 1, 2, \dots)$	$\frac{1}{(n-1)!} t^{n-1} e^{at}$
14	$\frac{\Gamma(k)}{(s-a)^k} (k \geq 0)$	$t^{k-1} e^{at}$
15	$\frac{1}{(s-a)(s-b)}$	$\frac{1}{(a-b)} (e^{at} - e^{bt})$
16	$\frac{s}{(s-a)(s-b)}$	$\frac{1}{(a-b)} (ae^{at} - be^{bt})$
17	$\frac{1}{(s-a)(s-b)(s-c)}$	$-\frac{(b-c)e^{at} + (c-a)e^{bt} + (a-b)e^{ct}}{(a-b)(b-c)(c-a)}$
18	$\frac{1}{(s+a)}$	$e^{-at}$ valid for complex $a$
19	$\frac{1}{s(s+a)}$	$\frac{1}{a} (1 - e^{-at})$
20	$\frac{1}{s^2(s+a)}$	$\frac{1}{a^2} (e^{-at} + at - 1)$
21	$\frac{1}{s^3(s+a)}$	$\frac{1}{a^2} \left[ \frac{1}{a} - t + \frac{at^2}{2} - \frac{1}{a} e^{-at} \right]$
22	$\frac{1}{(s+a)(s+b)}$	$\frac{1}{(b-a)} (e^{-at} - e^{-bt})$
23	$\frac{1}{s(s+a)(s+b)}$	$\frac{1}{ab} \left[ 1 + \frac{1}{(a-b)} (be^{-at} - ae^{-bt}) \right]$
24	$\frac{1}{s^2(s+a)(s+b)}$	$\frac{1}{(ab)^2} \left[ \frac{1}{(a-b)} (a^2 e^{-bt} - b^2 e^{-at}) + abt - a - b \right]$
25	$\frac{1}{s^3(s+a)(s+b)}$	$\frac{1}{(ab)} \left[ \frac{a^3 - b^3}{(ab)^2(a-b)} + \frac{1}{2} t^2 - \frac{(a+b)}{ab} t + \frac{1}{(a-b)} \left( \frac{b}{a^2} e^{-at} - \frac{a}{b^2} e^{-bt} \right) \right]$
26	$\frac{1}{(s+a)(s+b)(s+c)}$	$\frac{1}{(b-a)(c-a)} e^{-at} + \frac{1}{(a-b)(c-b)} e^{-bt} - \frac{1}{(a-c)(b-c)} e^{-ct}$
27	$\frac{1}{s(s+a)(s+b)(s+c)}$	$\frac{1}{abc} - \frac{1}{a(b-a)(c-a)} e^{-at} - \frac{1}{b(a-b)(c-b)} e^{-bt} - \frac{1}{c(a-c)(b-c)} e^{-ct}$

(continued)

TABLE A.5.1 (continued) Laplace Transform Pairs

	$F(s)$	$f(t)$
28	$\frac{1}{s^2(s+a)(s+b)(s+c)}$	$\left\{ \begin{aligned} &\frac{ab(ct-1) - ac - bc}{(abc)^2} + \frac{1}{a^2(b-a)(c-a)} e^{-at} \\ &+ \frac{1}{b^2(a-b)(c-b)} e^{-bt} + \frac{1}{c^2(a-c)(b-c)} e^{-ct} \end{aligned} \right.$
29	$\frac{1}{s^3(s+a)(s+b)(s+c)}$	$\left\{ \begin{aligned} &\frac{1}{(abc)^3} [(ab+ac+bc)^2 - abc(a+b+c)] - \frac{ab+ac+bc}{(abc)^2} t + \frac{1}{2abc} t^2 \\ &- \frac{1}{a^3(b-a)(c-a)} e^{-at} - \frac{1}{b^3(a-b)(c-b)} e^{-bt} - \frac{1}{c^3(a-c)(b-c)} e^{-ct} \end{aligned} \right.$
30	$\frac{1}{s^2+a^2}$	$\frac{1}{a} \sin at$
31	$\frac{s}{s^2+a^2}$	$\cos at$
32	$\frac{1}{s^2-a^2}$	$\frac{1}{a} \sinh at$
33	$\frac{s}{s^2-a^2}$	$\cosh at$
34	$\frac{1}{s(s^2+a^2)}$	$\frac{1}{a^2} (1 - \cos at)$
35	$\frac{1}{s^2(s^2+a^2)}$	$\frac{1}{a^3} (at - \sin at)$
36	$\frac{1}{(s^2+a^2)^2}$	$\frac{1}{2a^3} (\sin at - at \cos at)$
37	$\frac{s}{(s^2+a^2)^2}$	$\frac{t}{2a} \sin at$
38	$\frac{s^2}{(s^2+a^2)^2}$	$\frac{1}{2a} (\sin at + at \cos at)$
39	$\frac{s^2-a^2}{(s^2+a^2)^2}$	$t \cos at$
40	$\frac{s}{(s^2+a^2)(s^2+b^2)} (a^2 \neq b^2)$	$\frac{\cos at - \cos bt}{b^2 - a^2}$
41	$\frac{1}{(s-a)^2 + b^2}$	$\frac{1}{b} e^{at} \sin bt$
42	$\frac{s-a}{(s-a)^2 + b^2}$	$e^{at} \cos bt$
43	$\frac{1}{[(s+a)^2 + b^2]^n}$	$\frac{e^{-at}}{4^{n-1} b^{2n}} \sum_{r=1}^n \binom{2n-r-1}{n-1} (-2t)^{r-1} \frac{d^r}{dt^r} [\cos(bt)]$
44	$\frac{s}{[(s+a)^2 + b^2]^n}$	$\left\{ \begin{aligned} &\frac{e^{-at}}{4^{n-1} b^{2n}} \left\{ \sum_{r=1}^n \binom{2n-r-1}{n-1} (-2t)^{r-1} \frac{d^r}{dt^r} [a \cos(bt) + b \sin(bt)] \right. \\ &\left. - 2b \sum_{r=1}^{n-1} r \binom{2n-r-2}{n-1} (-2t)^{r-1} \frac{d^r}{dt^r} [\sin(bt)] \right\} \end{aligned} \right.$
45	$\frac{3a^2}{s^3+a^3}$	$e^{-at} - e^{(at)/2} \left( \cos \frac{at\sqrt{3}}{2} - \sqrt{3} \sin \frac{at\sqrt{3}}{2} \right)$
46	$\frac{4a^3}{s^4+4a^4}$	$\sin at \cosh at - \cos at \sinh at$
47	$\frac{s}{s^4+4a^4}$	$\frac{1}{2a^2} (\sin at \sinh at)$
48	$\frac{1}{s^4-a^4}$	$\frac{1}{2a^3} (\sinh at - \sin at)$
49	$\frac{s}{s^4-a^4}$	$\frac{1}{2a^2} (\cosh at - \cos at)$
50	$\frac{8a^3 s^2}{(s^2+a^2)^3}$	$(1+a^2 t^2) \sin at - \cos at$
51	$\frac{1}{s} \left( \frac{s-1}{s} \right)^n$	$L_n(t) = \frac{e^t}{n!} \frac{d^n}{dt^n} (t^n e^{-t})$

TABLE A.5.1 (continued) Laplace Transform Pairs

	$F(s)$	$f(t)$
		$[L_n(t)$ is the Laguerre polynomial of degree $n$ ]
52	$\frac{1}{(s+a)^n}$	$\frac{t^{(n-1)}e^{-at}}{(n-1)!}$ where $n$ is a positive integer
53	$\frac{1}{s(s+a)^2}$	$\frac{1}{a^2}[1 - e^{-at} - ate^{-at}]$
54	$\frac{1}{s^2(s+a)^2}$	$\frac{1}{a^3}[at - 2 + ate^{-at} + 2e^{-at}]$
55	$\frac{1}{s(s+a)^3}$	$\frac{1}{a^3}\left[1 - \left(\frac{1}{2}a^2t^2 + at + 1\right)e^{-at}\right]$
56	$\frac{1}{(s+a)(s+b)^2}$	$\frac{1}{(a-b)^2}\{e^{-at} + [(a-b)t - 1]e^{-bt}\}$
57	$\frac{1}{s(s+a)(s+b)^2}$	$\frac{1}{ab^2} - \frac{1}{a(a-b)^2}e^{-at} - \left[\frac{1}{b(a-b)}t + \frac{a-2b}{b^2(a-b)^2}\right]e^{-bt}$
58	$\frac{1}{s^2(s+a)(s+b)^2}$	$\frac{1}{a^2(a-b)^2}e^{-at} + \frac{1}{ab^2}\left(t - \frac{1}{a} - \frac{2}{b}\right) + \left[\frac{1}{b^2(a-b)}t + \frac{2(a-b)-b}{b^3(a-b)^2}\right]e^{-bt}$
59	$\frac{1}{(s+a)(s+b)(s+c)^2}$	$\begin{cases} \left[\frac{1}{(c-b)(c-a)}t + \frac{2c-a-b}{(c-a)^2(c-b)^2}\right]e^{-ct} \\ + \frac{1}{(b-a)(c-a)^2}e^{-at} + \frac{1}{(a-b)(c-b)^2}e^{-bt}. \end{cases}$
60	$\frac{1}{(s+a)(s^2+\omega^2)}$	$\frac{1}{a^2 + \omega^2}e^{-at} + \frac{1}{\omega\sqrt{a^2 + \omega^2}}\sin(\omega t - \phi); \quad \phi = \tan^{-1}\left(\frac{\omega}{a}\right)$
61	$\frac{1}{s(s+a)(s^2+\omega^2)}$	$\frac{1}{a\omega^2} - \frac{1}{a^2 + \omega^2}\left(\frac{1}{\omega}\sin\omega t + \frac{a}{\omega^2}\cos\omega t + \frac{1}{a}e^{-at}\right)$
62	$\frac{1}{s^2(s+a)(s^2+\omega^2)}$	$\begin{cases} \frac{1}{a\omega^2}t - \frac{1}{a^2\omega^2} + \frac{1}{a^2(a^2 + \omega^2)}e^{-at} \\ + \frac{1}{\omega^3\sqrt{a^2 + \omega^2}}\cos(\omega t + \phi); \quad \phi = \tan^{-1}\left(\frac{a}{\omega}\right) \end{cases}$
63	$\frac{1}{[(s+a)^2 + \omega^2]^2}$	$\frac{1}{2\omega^3}e^{-at}[\sin\omega t - \omega t \cos\omega t]$
64	$\frac{1}{s^2 - a^2}$	$\frac{1}{a}\sinh at$
65	$\frac{1}{s^2(s^2 - a^2)}$	$\frac{1}{a^3}\sinh at - \frac{1}{a^2}t$
66	$\frac{1}{s^3(s^2 - a^2)}$	$\frac{1}{a^4}(\cosh at - 1) - \frac{1}{2a^2}t^2$
67	$\frac{1}{s^3 + a^3}$	$\frac{1}{3a^2}\left[e^{-at} - e^{\frac{2}{3}at}\left(\cos\frac{\sqrt{3}}{2}at - \sqrt{3}\sin\frac{\sqrt{3}}{2}at\right)\right]$
68	$\frac{1}{s^4 + 4a^4}$	$\frac{1}{4a^3}(\sin at \cosh at - \cos at \sinh at)$
69	$\frac{1}{s^4 - a^4}$	$\frac{1}{2a^3}(\sinh at - \sin at)$
70	$\frac{1}{[(s+a)^2 - \omega^2]}$	$\frac{1}{\omega}e^{-at}\sinh\omega t$
71	$\frac{s+a}{s[(s+a)^2 + \omega^2]}$	$\begin{cases} \frac{a}{b^2 + \omega^2} - \frac{1}{\omega} + \sqrt{\frac{(a-b)^2 + \omega^2}{b^2 + \omega^2}}e^{-bt}\sin(\omega t + \phi); \\ \phi = \tan^{-1}\left(\frac{\omega}{b}\right) + \tan^{-1}\left(\frac{\omega}{a-b}\right) \end{cases}$
72	$\frac{s+a}{s^2[(s+b)^2 + \omega^2]}$	$\begin{cases} \frac{1}{b^2 + \omega^2}[1 + at] - \frac{2ab}{(b^2 + \omega^2)^2} + \frac{\sqrt{(a-b)^2 + \omega^2}}{\omega(b^2 + \omega^2)}e^{-bt}\sin(\omega t + \phi) \\ \phi = \tan^{-1}\left(\frac{\omega}{a-b}\right) + 2\tan^{-1}\left(\frac{\omega}{b}\right) \end{cases}$

(continued)

TABLE A.5.1 (continued) Laplace Transform Pairs

	$F(s)$	$f(t)$
73	$\frac{s+a}{(s+c)[(s+b)^2+\omega^2]}$	$\begin{cases} \frac{a-c}{(c-b)^2+\omega^2} e^{-ct} + \frac{1}{\omega} \sqrt{\frac{(a-b)^2+\omega^2}{(c-b)^2+\omega^2}} e^{-bt} \sin(\omega t + \phi) \\ \phi = \tan^{-1}\left(\frac{\omega}{a-b}\right) - \tan^{-1}\left(\frac{\omega}{c-b}\right) \end{cases}$
74	$\frac{s+a}{s(s+c)[(s+b)^2+\omega^2]}$	$\begin{cases} \frac{a}{c(b^2+\omega^2)} + \frac{(c-a)}{c[(b-c)^2+\omega^2]} e^{-ct} \\ - \frac{1}{\omega\sqrt{b^2+\omega^2}} \sqrt{\frac{(a-b)^2+\omega^2}{(b-c)^2+\omega^2}} e^{-bt} \sin(\omega t + \phi) \\ \phi = \tan^{-1}\left(\frac{\omega}{b}\right) + \tan^{-1}\left(\frac{\omega}{a-b}\right) - \tan^{-1}\left(\frac{\omega}{c-b}\right) \end{cases}$
75	$\frac{s+a}{s^2(s+b)^3}$	$\frac{a}{b^3} t + \frac{b-3a}{b^4} + \left[ \frac{3a-b}{b^4} + \frac{a-b}{2b^2} t^2 + \frac{2a-b}{b^3} t \right] e^{-bt}$
76	$\frac{s+a}{(s+c)(s+b)^3}$	$\frac{a-c}{(b-c)^3} e^{-ct} + \left[ \frac{a-b}{2(c-b)} t^2 + \frac{c-a}{(c-b)^2} t + \frac{a-c}{(c-b)^3} \right] e^{-bt}$
77	$\frac{s^2}{(s+a)(s+b)(s+c)}$	$\frac{a^2}{(b-a)(c-a)} e^{-at} + \frac{b^2}{(a-b)(c-b)} e^{-bt} + \frac{c^2}{(a-c)(b-c)} e^{-ct}$
78	$\frac{s^2}{(s+a)(s+b)^2}$	$\frac{a^2}{(b-a)^2} e^{-at} + \left[ \frac{b^2}{(a-b)} t + \frac{b^2-2ab}{(a-b)^2} \right] e^{-bt}$
79	$\frac{s^2}{(s+a)^3}$	$\left[ 2-2at + \frac{a^2}{2} t^2 \right] e^{-at}$
80	$\frac{s^2}{(s+a)(s^2+\omega^2)}$	$\frac{a^2}{(a^2+\omega^2)} e^{-at} - \frac{\omega}{\sqrt{a^2+\omega^2}} \sin(\omega t + \phi); \quad \phi = \tan^{-1}\left(\frac{\omega}{a}\right)$
81	$\frac{s^2}{(s+a)^2(s^2+\omega^2)}$	$\begin{cases} \left[ \frac{a^2}{(a^2+\omega^2)} t - \frac{2a\omega^2}{(a^2+\omega^2)^2} \right] e^{-at} - \frac{\omega}{(a^2+\omega^2)} \sin(\omega t + \phi); \\ \phi = -2 \tan^{-1}\left(\frac{\omega}{a}\right) \end{cases}$
82	$\frac{s^2}{(s+a)(s+b)(s^2+\omega^2)}$	$\begin{cases} \frac{a^2}{(b-a)(a^2+\omega^2)} e^{-at} + \frac{b^2}{(a-b)(b^2+\omega^2)} e^{-bt} \\ - \frac{\omega}{\sqrt{(a^2+\omega^2)(b^2+\omega^2)}} \sin(\omega t + \phi); \quad \phi = -\left[ \tan^{-1}\left(\frac{\omega}{a}\right) + \tan^{-1}\left(\frac{\omega}{b}\right) \right] \end{cases}$
83	$\frac{s^2}{(s^2+a^2)(s^2+\omega^2)}$	$-\frac{a}{(\omega^2-a^2)} \sin(at) - \frac{\omega}{(a^2-\omega^2)} \sin(\omega t)$
84	$\frac{s^2}{(s^2+\omega^2)^2}$	$\frac{1}{2\omega} (\sin \omega t + \omega t \cos \omega t)$
85	$\frac{s^2}{(s+a)[(s+b)^2+\omega^2]}$	$\begin{cases} \frac{a^2}{(a-b)^2+\omega^2} e^{-at} + \frac{1}{\omega} \sqrt{\frac{(b^2-\omega^2)^2+4b^2\omega^2}{(a-b)^2+\omega^2}} e^{-bt} \sin(\omega t + \phi) \\ \phi = \tan^{-1}\left(\frac{-2b\omega}{b^2-\omega^2}\right) - \tan^{-1}\left(\frac{\omega}{a-b}\right) \end{cases}$
86	$\frac{s^2}{(s+a)^2[(s+b)^2+\omega^2]}$	$\begin{cases} \frac{a^2}{(a-b)^2+\omega^2} t e^{-at} - 2 \left[ \frac{a[(b-a)^2+\omega^2]+a^2(b-a)}{[(b-a)^2+\omega^2]^2} \right] e^{-at} \\ + \sqrt{\frac{(b^2-\omega^2)^2+4b^2\omega^2}{\omega[(a-b)^2+\omega^2]}} e^{-bt} \sin(\omega t + \phi) \\ \phi = \tan^{-1}\left(\frac{-2b\omega}{b^2-\omega^2}\right) - 2 \tan^{-1}\left(\frac{\omega}{a-b}\right) \end{cases}$
87	$\frac{s^2+a}{s^2(s+b)}$	$\frac{b^2+a}{b^2} e^{-bt} + \frac{a}{b} t - \frac{a}{b^2}$
88	$\frac{s^2+a}{s^3(s+b)}$	$\frac{a}{2b} t^2 - \frac{a}{b^2} t + \frac{1}{b^3} [b^2+a - (a+b^2)e^{-bt}]$
89	$\frac{s^2+a}{s(s+b)(s+c)}$	$\frac{a}{bc} + \frac{(b^2+a)}{b(b-c)} e^{-bt} - \frac{(c^2+a)}{c(b-c)} e^{-ct}$

TABLE A.5.1 (continued) Laplace Transform Pairs

	$F(s)$	$f(t)$
90	$\frac{s^2 + a}{s^2(s+b)(s+c)}$	$\frac{b^2 + a}{b^2(c-b)} e^{-bt} + \frac{c^2 + a}{c^2(b-c)} e^{-ct} + \frac{a}{bc} t - \frac{a(b+c)}{b^2c^2}$
91	$\frac{s^2 + a}{(s+b)(s+c)(s+d)}$	$\frac{b^2 + a}{(c-b)(d-b)} e^{-bt} + \frac{c^2 + a}{(b-c)(d-c)} e^{-ct} + \frac{d^2 + a}{(b-d)(c-d)} e^{-dt}$
92	$\frac{s^2 + a}{s(s+b)(s+c)(s+d)}$	$\frac{a}{bcd} + \frac{b^2 + a}{b(b-c)(d-b)} e^{-bt} + \frac{c^2 + a}{c(b-c)(c-d)} e^{-ct} + \frac{d^2 + a}{d(b-d)(d-c)} e^{-dt}$
93	$\frac{s^2 + a}{s^2(s+b)(s+c)(s+d)}$	$\left\{ \begin{aligned} &\frac{a}{bcd} t - \frac{a}{b^2c^2d^2} (bc + cd + db) + \frac{b^2 + a}{b^2(b-c)(b-d)} e^{-bt} \\ &+ \frac{c^2 + a}{c^2(c-b)(c-d)} e^{-ct} + \frac{d^2 + a}{d^2(d-b)(d-c)} e^{-dt} \end{aligned} \right.$
94	$\frac{s^2 + a}{(s^2 + \omega^2)^2}$	$\frac{1}{2\omega^3} (a + \omega^2) \sin \omega t - \frac{1}{2\omega^2} (a - \omega^2) t \cos \omega t$
95	$\frac{s^2 - \omega^2}{(s^2 + \omega^2)^2}$	$t \cos \omega t$
96	$\frac{s^2 + a}{s(s^2 + \omega^2)^2}$	$\frac{a}{\omega^4} - \frac{(a - \omega^2)}{2\omega^3} t \sin \omega t - \frac{a}{\omega^4} \cos \omega t$
97	$\frac{s(s+a)}{(s+b)(s+c)^2}$	$\frac{b^2 - ab}{(c-b)^2} e^{-bt} + \left[ \frac{c^2 - ac}{b-c} t + \frac{c^2 - 2bc + ab}{(b-c)^2} \right] e^{-ct}$
98	$\frac{s(s+a)}{(s+b)(s+c)(s+d)^2}$	$\left\{ \begin{aligned} &\frac{b^2 - ab}{(c-b)(d-b)^2} e^{-bt} + \frac{c^2 - ac}{(b-c)(d-c)^2} e^{-ct} + \frac{d^2 - ad}{(b-d)(c-d)} te^{-dt} \\ &+ \frac{a(bc - d^2) + d(db + dc - 2bc)}{(b-d)^2(c-d)^2} e^{-dt} \end{aligned} \right.$
99	$\frac{s^2 + a_1s + a_0}{s^2(s+b)}$	$\frac{b^2 - a_1b + a_0}{b^2} e^{-bt} + \frac{a_0}{b} t + \frac{a_1b - a_0}{b^2}$
100	$\frac{s^2 + a_1s + a_0}{s^3(s+b)}$	$\frac{a_1b - b^2 - a_0}{b^3} e^{-bt} + \frac{a_0}{2b} t^2 + \frac{a_1b - a_0}{b^2} t + \frac{b^2 - a_1b + a_0}{b^3}$
101	$\frac{s^2 + a_1s + a_0}{s(s+b)(s+c)}$	$\frac{a_0}{bc} + \frac{b^2 - a_1b + a_0}{b(b-c)} e^{-bt} + \frac{c^2 - a_1c + a_0}{c(c-b)} e^{-ct}$
102	$\frac{s^2 + a_1s + a_0}{s^2(s+b)(s+c)}$	$\frac{a_0}{bc} t + \frac{a_1bc - a_0(b+c)}{b^2c^2} + \frac{b^2 - a_1b + a_0}{b^2(c-b)} e^{-bt} + \frac{c^2 - a_1c + a_0}{c^2(b-c)} e^{-ct}$
103	$\frac{s^2 + a_1s + a_0}{(s+b)(s+c)(s+d)}$	$\frac{b^2 - a_1b + a_0}{(c-b)(d-b)} e^{-bt} + \frac{c^2 - a_1c + a_0}{(b-c)(d-c)} e^{-ct} + \frac{d^2 - a_1d + a_0}{(b-d)(c-d)} e^{-dt}$
104	$\frac{s^2 + a_1s + a_0}{s(s+b)(s+c)(s+d)}$	$\frac{a_0}{bcd} - \frac{b^2 - a_1b + a_0}{b(c-b)(d-b)} e^{-bt} - \frac{c^2 - a_1c + a_0}{c(b-c)(d-c)} e^{-ct} - \frac{d^2 - a_1d + a_0}{d(b-d)(c-d)} e^{-dt}$
105	$\frac{s^2 + a_1s + a_0}{s(s+b)^2}$	$\frac{a_0}{b^2} - \frac{b^2 - a_1b + a_0}{b} t e^{-bt} + \frac{b^2 - a_0}{b^2} e^{-bt}$
106	$\frac{s^2 + a_1s + a_0}{s^2(s+b)^2}$	$\frac{a_0}{b^2} t + \frac{a_1b - 2a_0}{b^3} + \frac{b^2 - a_1b + a_0}{b^2} t e^{-bt} + \frac{2a_0 - a_1b}{b^3} e^{-bt}$
107	$\frac{s^2 + a_1s + a_0}{(s+b)(s+c)^2}$	$\frac{b^2 - a_1b + a_0}{(c-b)^2} e^{-bt} + \frac{c^2 - a_1c + a_0}{(b-c)} t e^{-ct} + \frac{c^2 - 2bc + a_1b - a_0}{(b-c)^2} e^{-ct}$
108	$\frac{s^3}{(s+b)(s+c)(s+d)^2}$	$\left\{ \begin{aligned} &\frac{b^3}{(b-c)(d-b)^2} e^{-bt} + \frac{c^3}{(c-b)(d-c)^2} e^{-ct} + \frac{d^3}{(d-b)(c-d)} te^{-dt} \\ &+ \frac{d^2[d^2 - 2d(b+c) + 3bc]}{(b-d)^2(c-d)^2} e^{-dt} \end{aligned} \right.$
109	$\frac{s^3}{(s+b)(s+c)(s+d)(s+f)^2}$	$\left\{ \begin{aligned} &\frac{b^3}{(b-c)(d-b)(f-b)^2} e^{-bt} + \frac{c^3}{(c-b)(d-c)(f-c)^2} e^{-ct} \\ &+ \frac{d^3}{(d-b)(c-d)(f-d)^2} e^{-dt} + \frac{f^3}{(f-b)(c-f)(d-f)} te^{-ft} \\ &+ \left[ \frac{3f^2}{(b-f)(c-f)(d-f)} \right. \\ &\left. + \frac{f^3[(b-f)(c-f) + (b-f)(d-f) + (c-f)(d-f)]}{(b-f)^2(c-f)^2(d-f)^2} \right] e^{-dt} \end{aligned} \right.$

(continued)



TABLE A.5.1 (continued) Laplace Transform Pairs

	$F(s)$	$f(t)$
110	$\frac{s^3}{(s+b)^2(s+c)^2}$	$-\frac{b^3}{(c-b)^2}te^{-bt} + \frac{b^2(3c-b)}{(c-b)^3}e^{-bt} - \frac{c^3}{(b-c)^2}te^{-ct} + \frac{c^2(3b-c)}{(b-c)^3}e^{-ct}$
111	$\frac{s^3}{(s+d)(s+b)^2(s+c)^2}$	$\left\{ \begin{aligned} &-\frac{d^3}{(b-d)^2(c-d)^2}e^{-dt} + \frac{b^3}{(c-b)^2(b-d)}te^{-bt} \\ &+ \left[ \frac{3b^2}{(c-b)^2(d-b)} + \frac{b^3(c+2d-3b)}{(c-b)^3(d-b)^2} \right] e^{-bt} + \frac{c^3}{(b-c)^2(c-d)}te^{-ct} \\ &+ \left[ \frac{3c^2}{(b-c)^2(d-c)} + \frac{c^3(b+2d-3c)}{(b-c)^3(d-c)^2} \right] e^{-ct} \end{aligned} \right.$
112	$\frac{s^3}{(s+b)(s+c)(s^2+\omega^2)}$	$\left\{ \begin{aligned} &\frac{b^3}{(b-c)(b^2+\omega^2)}e^{-bt} + \frac{c^3}{(c-b)(c^2+\omega^2)}e^{-ct} \\ &-\frac{\omega^2}{\sqrt{(b^2+\omega^2)(c^2+\omega^2)}}\sin(\omega t + \phi) \\ &\phi = \tan^{-1}\left(\frac{c}{\omega}\right) - \tan^{-1}\left(\frac{\omega}{b}\right) \end{aligned} \right.$
113	$\frac{s^3}{(s+b)(s+c)(s+d)(s^2+\omega^2)}$	$\left\{ \begin{aligned} &\frac{b^3}{(b-c)(d-b)(b^2+\omega^2)}e^{-bt} + \frac{c^3}{(c-b)(d-c)(c^2+\omega^2)}e^{-ct} \\ &+ \frac{d^3}{(d-b)(c-d)(d^2+\omega^2)}e^{-dt} \\ &-\frac{\omega^2}{\sqrt{(b^2+\omega^2)(c^2+\omega^2)(d^2+\omega^2)}}\cos(\omega t - \phi) \\ &\phi = \tan^{-1}\left(\frac{\omega}{b}\right) + \tan^{-1}\left(\frac{\omega}{c}\right) + \tan^{-1}\left(\frac{\omega}{d}\right) \end{aligned} \right.$
114	$\frac{s^3}{(s+b)^2(s^2+\omega^2)}$	$\left\{ \begin{aligned} &-\frac{b^3}{b^2+\omega^2}te^{-bt} + \frac{b^2(b^2+3\omega^2)}{(b^2+\omega^2)^2}e^{-bt} - \frac{\omega^2}{(b^2+\omega^2)}\sin(\omega t + \phi) \\ &\phi = \tan^{-1}\left(\frac{b}{\omega}\right) - \tan^{-1}\left(\frac{\omega}{b}\right) \end{aligned} \right.$
115	$\frac{s^3}{s^4+4\omega^4}$	$\cos(\omega t) \cosh(\omega t)$
116	$\frac{s^3}{s^4-\omega^4}$	$\frac{1}{2}[\cosh(\omega t) + \cos(\omega t)]$
117	$\frac{s^3+a_2s^2+a_1s+a_0}{s^2(s+b)(s+c)}$	$\left\{ \begin{aligned} &\frac{a_0}{bc}t - \frac{a_0(b+c)-a_1bc}{b^2c^2} + \frac{-b^3+a_2b^2-a_1b+a_0}{b^2(c-b)}e^{-bt} \\ &+ \frac{-c^3+a_2c^2-a_1c+a_0}{c^2(b-c)}e^{-ct} \end{aligned} \right.$
118	$\frac{s^3+a_2s^2+a_1s+a_0}{s(s+b)(s+c)(s+d)}$	$\left\{ \begin{aligned} &\frac{a_0}{bcd} - \frac{-b^3+a_2b^2-a_1b+a_0}{b(c-b)(d-b)}e^{-bt} - \frac{-c^3+a_2c^2-a_1c+a_0}{c(b-c)(d-c)}e^{-ct} \\ &-\frac{-d^3+a_2d^2-a_1d+a_0}{d(b-d)(c-d)}e^{-dt} \end{aligned} \right.$
119	$\frac{s^3+a_2s^2+a_1s+a_0}{s^2(s+b)(s+c)(s+d)}$	$\left\{ \begin{aligned} &\frac{a_0}{bcd}t + \left[ \frac{a_1}{bcd} - \frac{a_0(bc+bd+cd)}{b^2c^2d^2} \right] + \frac{-b^3+a_2b^2-a_1b+a_0}{b^2(c-b)(d-b)}e^{-bt} \\ &+ \frac{-c^3+a_2c^2-a_1c+a_0}{c^2(b-c)(d-c)}e^{-ct} + \frac{-d^3+a_2d^2-a_1d+a_0}{d^2(b-d)(c-d)}e^{-dt} \end{aligned} \right.$
120	$\frac{s^3+a_2s^2+a_1s+a_0}{(s+b)(s+c)(s+d)(s+f)}$	$\left\{ \begin{aligned} &\frac{-b^3+a_2b^2-a_1b+a_0}{(c-b)(d-b)(f-b)}e^{-bt} + \frac{-c^3+a_2c^2-a_1c+a_0}{(b-c)(d-c)(f-c)}e^{-ct} \\ &+ \frac{-d^3+a_2d^2-a_1d+a_0}{(b-d)(c-d)(f-d)}e^{-dt} + \frac{-f^3+a_2f^2-a_1f+a_0}{(b-f)(c-f)(d-f)}e^{-ft} \end{aligned} \right.$
121	$\frac{s^3+a_2s^2+a_1s+a_0}{s(s+b)(s+c)(s+d)(s+f)}$	$\left\{ \begin{aligned} &\frac{a_0}{bcdf} - \frac{-b^3+a_2b^2-a_1b+a_0}{b(c-b)(d-b)(f-b)}e^{-bt} - \frac{-c^3+a_2c^2-a_1c+a_0}{c(b-c)(d-c)(f-c)}e^{-ct} \\ &-\frac{-d^3+a_2d^2-a_1d+a_0}{d(b-d)(c-d)(f-d)}e^{-dt} - \frac{-f^3+a_2f^2-a_1f+a_0}{f(b-f)(c-f)(d-f)}e^{-ft} \end{aligned} \right.$

TABLE A.5.1 (continued) Laplace Transform Pairs

	$F(s)$	$f(t)$
122	$\frac{s^3 + a_2s^2 + a_1s + a_0}{(s+b)(s+c)(s+d)(s+f)(s+g)}$	$\left\{ \begin{aligned} &\frac{-b^3 + a_2b^2 - a_1b + a_0}{(c-b)(d-b)(f-b)(g-b)} e^{-bt} + \frac{-c^3 + a_2c^2 - a_1c + a_0}{(b-c)(d-c)(f-c)(g-c)} e^{-ct} \\ &+ \frac{-d^3 + a_2d^2 - a_1d + a_0}{(b-d)(c-d)(f-d)(g-d)} e^{-dt} + \frac{-f^3 + a_2f^2 - a_1f + a_0}{(b-f)(c-f)(d-f)(g-f)} e^{-ft} \\ &+ \frac{-g^3 + a_2g^2 - a_1g + a_0}{(b-g)(c-g)(d-g)(f-g)} e^{-gt} \end{aligned} \right.$
123	$\frac{s^3 + a_2s^2 + a_1s + a_0}{(s+b)(s+c)(s+d)^2}$	$\left\{ \begin{aligned} &\frac{-b^3 + a_2b^2 - a_1b + a_0}{(c-b)(d-b)^2} e^{-bt} + \frac{-c^3 + a_2c^2 - a_1c + a_0}{(b-c)(d-c)^2} e^{-ct} \\ &+ \frac{-d^3 + a_2d^2 - a_1d + a_0}{(b-d)(c-d)} te^{-dt} \\ &+ \frac{a_0(2d-b-c) + a_1(bc-d^2)}{(b-d)^2(c-d)^2} e^{-dt} \end{aligned} \right.$
124	$\frac{s^3 + a_2s^2 + a_1s + a_0}{s(s+b)(s+c)(s+d)^2}$	$\left\{ \begin{aligned} &\frac{a_0}{bcd^2} - \frac{-b^3 + a_2b^2 - a_1b + a_0}{b(c-b)(d-b)^2} e^{-bt} - \frac{-c^3 + a_2c^2 - a_1c + a_0}{c(b-c)(d-c)^2} e^{-ct} \\ &- \frac{-d^3 + a_2d^2 - a_1d + a_0}{d(b-d)(c-d)} te^{-dt} - \frac{3d^2 - 2a_2d + a_1}{d(b-d)(c-d)} e^{-dt} \\ &- \frac{(-d^3 + a_2d^2 - a_1d + a_0)[(b-d)(c-d) - d(b-d) - d(c-d)]}{d^2(b-d)^2(c-d)^2} e^{-dt} \end{aligned} \right.$
125	$\frac{s^3 + a_2s^2 + a_1s + a_0}{(s+b)(s+c)(s+d)(s+f)^2}$	$\left\{ \begin{aligned} &\frac{-b^3 + a_2b^2 - a_1b + a_0}{(c-b)(d-b)(f-b)^2} e^{-bt} + \frac{-c^3 + a_2c^2 - a_1c + a_0}{(b-c)(d-c)(f-c)^2} e^{-ct} \\ &+ \frac{-d^3 + a_2d^2 - a_1d + a_0}{(b-d)(c-d)(f-d)^2} e^{-dt} + \frac{-f^3 + a_2f^2 - a_1f + a_0}{(b-f)(c-f)(d-f)} te^{-ft} \\ &+ \frac{(-f^3 + a_2f^2 - a_1f + a_0)[(b-f)(c-f)]}{(b-f)^2(c-f)(d-f)} e^{-ft} \\ &+ \frac{3f^2 - 2a_2f + a_1}{(b-f)(c-f)(d-f)} e^{-ft} - \frac{+(b-f)(d-f) + (c-f)(d-f)}{(b-f)^2(c-f)^2(d-f)^2} e^{-ft} \end{aligned} \right.$
126	$\frac{s}{(s-a)^{3/2}}$	$\frac{1}{\sqrt{\pi t}} e^{at} (1 + 2at)$
127	$\sqrt{s-a} - \sqrt{s-b}$	$\frac{1}{2\sqrt{\pi t^3}} (e^{bt} - e^{at})$
128	$\frac{1}{\sqrt{s+a}}$	$\frac{1}{\sqrt{\pi t}} - ae^{a^2t} \operatorname{erfc}(a\sqrt{t})$
129	$\frac{\sqrt{s}}{s-a^2}$	$\frac{1}{\sqrt{\pi t}} + ae^{a^2t} \operatorname{erf}(a\sqrt{t})$
130	$\frac{\sqrt{s}}{s+a^2}$	$\frac{1}{\sqrt{\pi t}} - \frac{2a}{\sqrt{\pi}} e^{-a^2t} \int_0^{a\sqrt{t}} e^{\lambda^2} d\lambda$
131	$\frac{1}{\sqrt{s(s-a^2)}}$	$\frac{1}{a} e^{a^2t} \operatorname{erf}(a\sqrt{t})$
132	$\frac{1}{\sqrt{s(s+a^2)}}$	$\frac{2}{a\sqrt{\pi}} e^{-a^2t} \int_0^{a\sqrt{t}} e^{\lambda^2} d\lambda$
133	$\frac{b^2 - a^2}{(s-a^2)(b+\sqrt{s})}$	$e^{a^2t} [b - a \operatorname{erf}(a\sqrt{t})] - be^{b^2t} \operatorname{erfc}(b\sqrt{t})$
134	$\frac{1}{\sqrt{s}(\sqrt{s+a})}$	$e^{a^2t} \operatorname{erfc}(a\sqrt{t})$
135	$\frac{1}{(s+a)\sqrt{s+b}}$	$\frac{1}{\sqrt{b-a}} e^{-at} \operatorname{erf}(\sqrt{b-a}\sqrt{t})$
136	$\frac{b^2 - a^2}{\sqrt{s(s-a^2)}(\sqrt{s+b})}$	$e^{a^2t} \left[ \frac{b}{a} \operatorname{erf}(a\sqrt{t}) - 1 \right] + e^{b^2t} \operatorname{erfc}(b\sqrt{t})$
137	$\frac{(1-s)^n}{s^{n+(1/2)}}$	$\left\{ \begin{aligned} &\frac{n!}{(2n)! \sqrt{\pi t}} H_{2n}(\sqrt{t}) \\ &\left[ H_n(t) = \text{Hermite polynomial} = e^{x^2} \frac{d^n}{dx^n} (e^{-x^2}) \right] \end{aligned} \right.$

(continued)

TABLE A.5.1 (continued) Laplace Transform Pairs

	$F(s)$	$f(t)$
138	$\frac{(1-s)^n}{s^{n+(3/2)}}$	$-\frac{n!}{\sqrt{\pi}(2n+1)!}H_{2n+1}(\sqrt{t})$
139	$\frac{\sqrt{s+2a}}{\sqrt{s}} - 1$	$\begin{cases} ae^{-at}[I_1(at) + I_0(at)] \\ [I_n(t) = j^{-n}J_n(jt) \text{ where } J_n \text{ is Bessel's function of the first kind}] \end{cases}$
140	$\frac{1}{\sqrt{s+a}\sqrt{s+b}}$	$e^{-(1/2)(a+b)t}I_0\left(\frac{a-b}{2}t\right)$
141	$\frac{\Gamma(k)}{(s+a)^k(s+b)^k} (k \geq 0)$	$\sqrt{\pi}\left(\frac{t}{a-b}\right)^{k-(1/2)}e^{-(1/2)(a+b)t}I_{k-(1/2)}\left(\frac{a-b}{2}t\right)$
142	$\frac{1}{(s+a)^{1/2}(s+b)^{3/2}}$	$te^{-(1/2)(a+b)t}\left[I_0\left(\frac{a-b}{2}t\right) + I_1\left(\frac{a-b}{2}t\right)\right]$
143	$\frac{\sqrt{s+2a}-\sqrt{s}}{\sqrt{s+2a}+\sqrt{s}}$	$\frac{1}{t}e^{-at}I_1(at)$
144	$\frac{(a-b)^k}{(\sqrt{s+a}+\sqrt{s+b})^{2k}} (k > 0)$	$\frac{k}{t}e^{-(1/2)(a+b)t}I_k\left(\frac{a-b}{2}t\right)$
145	$\frac{(\sqrt{s+a}+\sqrt{s})^{-2\nu}}{\sqrt{s}\sqrt{s+a}}$	$\frac{1}{a^\nu}e^{-(1/2)(at)}I_\nu\left(\frac{1}{2}at\right)$
146	$\frac{1}{\sqrt{s^2+a^2}}$	$J_0(at)$
147	$\frac{(\sqrt{s^2+a^2}-s)^\nu}{\sqrt{s^2+a^2}} (\nu > -1)$	$a^\nu J_\nu(at)$
148	$\frac{1}{(s^2+a^2)^k} (k > 0)$	$\frac{\sqrt{\pi}}{\Gamma(k)}\left(\frac{t}{2a}\right)^{k-(1/2)}J_{k-(1/2)}(at)$
149	$(\sqrt{s^2+a^2}-s)^k (k > 0)$	$\frac{ka^k}{t}J_k(at)$
150	$\frac{(s-\sqrt{s^2-a^2})^\nu}{\sqrt{s^2-a^2}} (\nu > -1)$	$a^\nu I_\nu(at)$
151	$\frac{1}{(s^2-a^2)^k} (k > 0)$	$\frac{\sqrt{\pi}}{\Gamma(k)}\left(\frac{t}{2a}\right)^{k-(1/2)}I_{k-(1/2)}(at)$
152	$\frac{1}{s\sqrt{s+1}}$	$\operatorname{erf}(\sqrt{t}); \operatorname{erf}(y) \triangleq \text{the error function} = \frac{2}{\sqrt{\pi}} \int_0^y e^{-u^2} du$
153	$\frac{1}{\sqrt{s^2+a^2}}$	$J_0(at); \text{Bessel function of 1st kind, zero order}$
154	$\frac{1}{\sqrt{s^2+a^2}+s}$	$\frac{J_1(at)}{at}; J_1 \text{ is the Bessel function of 1st kind, 1st order}$
155	$\frac{1}{[\sqrt{s^2+a^2}+s]^N}$	$\frac{N}{a^N} \frac{J_N(at)}{t}; N = 1, 2, 3, \dots, J_N \text{ is the Bessel function of 1st kind, } N\text{th order}$
156	$\frac{1}{s[\sqrt{s^2+a^2}+s]^N}$	$\frac{N}{a^N} \int_0^t \frac{J_N(au)}{u} du; N = 1, 2, 3, \dots, J_N \text{ is the Bessel function of 1st kind, } N\text{th order}$
157	$\frac{1}{\sqrt{s^2+a^2}(\sqrt{s^2+a^2}+s)}$	$\frac{1}{a}J_1(at); J_1 \text{ is the Bessel function of 1st kind, 1st order}$
158	$\frac{1}{\sqrt{s^2+a^2}[\sqrt{s^2+a^2}+s]^N}$	$\frac{1}{a^N}J_N(at); N = 1, 2, 3, \dots, J_N \text{ is the Bessel function of 1st kind, } N\text{th order}$
159	$\frac{1}{\sqrt{s^2-a^2}}$	$I_0(at); I_0 \text{ is the modified Bessel function of 1st kind, zero order}$
160	$\frac{e^{-ks}}{s}$	$S_k(t) = \begin{cases} 0 & \text{when } 0 < t < k \\ 1 & \text{when } t > k \end{cases}$
161	$\frac{e^{-ks}}{s^2}$	$\begin{cases} 0 & \text{when } 0 < t < k \\ t-k & \text{when } t > k \end{cases}$
162	$\frac{e^{-ks}}{s^\mu} (\mu > 0)$	$\begin{cases} 0 & \text{when } 0 < t < k \\ \frac{(t-k)^{\mu-1}}{\Gamma(\mu)} & \text{when } t > k \end{cases}$

TABLE A.5.1 (continued) Laplace Transform Pairs

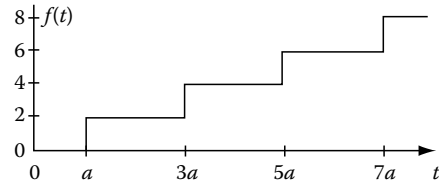
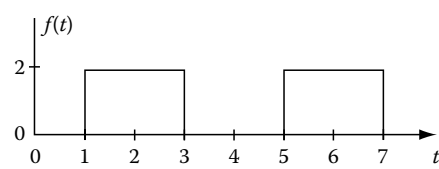
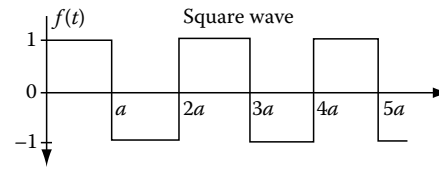
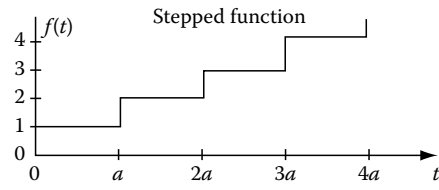
	$F(s)$	$f(t)$
163	$\frac{1 - e^{-ks}}{s}$	$\begin{cases} 1 & \text{when } 0 < t < k \\ 0 & \text{when } t > k \end{cases}$
164	$\frac{1}{s(1 - e^{-ks})} = \frac{1 + \coth \frac{1}{2} ks}{2s}$	$S(k, t) = \{n \text{ when } (n - 1)k < t < nk \text{ } (n = 1, 2, \dots)\}$
165	$\frac{1}{s(e^{+ks} - a)}$	$S_k(t) = \begin{cases} 0 & \text{when } 0 < t < k \\ 1 + a + a^2 + \dots + a^{n-1} & \text{when } nk < t < (n + 1)k \text{ } (n = 1, 2, \dots) \end{cases}$
166	$\frac{1}{s} \tanh ks$	$\begin{cases} M(2k, t) = (-1)^{n-1} & \\ & \text{when } 2k(n - 1) < t < 2nk \\ & (n = 1, 2, \dots) \end{cases}$
167	$\frac{1}{s(1 + e^{-ks})}$	$\begin{cases} \frac{1}{2}M(k, t) + \frac{1}{2} = \frac{1 - (-1)^n}{2} & \text{when } (n - 1)k < t < nk \end{cases}$
168	$\frac{1}{s^2} \tanh ks$	$\begin{cases} H(2k, t) & [H(2k, t) = k + (r - k)(-1)^n \text{ where } t = 2kn + r; \\ 0 \leq r \leq 2k; & n = 0, 1, 2, \dots] \end{cases}$
169	$\frac{1}{s \sinh ks}$	$\{2S(2k, t + k) - 2 = 2(n - 1) \text{ when } (2n - 3)k < t < (2n - 1)k \text{ } (t > 0)\}$
170	$\frac{1}{s \cosh ks}$	$\{M(2k, t + 3k) + 1 = 1 + (-1)^n \text{ when } (2n - 3)k < t < (2n - 1)k \text{ } (t > 0)\}$
171	$\frac{1}{s} \coth ks$	$\{2S(2k, t) - 1 = 2n - 1 \text{ when } 2k(n - 1) < t < 2kn\}$
172	$\frac{k}{s^2 + k^2} \coth \frac{\pi s}{2k}$	$ \sin kt $
173	$\frac{1}{(s^2 + 1)(1 - e^{-\pi s})}$	$\begin{cases} \sin t & \text{when } (2n - 2)\pi < t < (2n - 1)\pi \\ 0 & \text{when } (2n - 1)\pi < t < 2n\pi \end{cases}$
174	$\frac{1}{s} e^{-k/s}$	$J_0(2\sqrt{kt})$
175	$\frac{1}{\sqrt{s}} e^{-k/s}$	$\frac{1}{\sqrt{\pi t}} \cos 2\sqrt{kt}$
176	$\frac{1}{\sqrt{s}} e^{k/s}$	$\frac{1}{\sqrt{\pi t}} \cosh 2\sqrt{kt}$
177	$\frac{1}{s^{3/2}} e^{-k/s}$	$\frac{1}{\sqrt{\pi k}} \sin 2\sqrt{kt}$
178	$\frac{1}{s^{3/2}} e^{k/s}$	$\frac{1}{\sqrt{\pi k}} \sinh 2\sqrt{kt}$
179	$\frac{1}{s^\mu} e^{-k/s} \text{ } (\mu > 0)$	$\left(\frac{t}{k}\right)^{(\mu-1)/2} J_{\mu-1}(2\sqrt{kt})$
180	$\frac{1}{s^\mu} e^{k/s} \text{ } (\mu > 0)$	$\left(\frac{t}{k}\right)^{(\mu-1)/2} I_{\mu-1}(2\sqrt{kt})$
181	$e^{-k\sqrt{s}} \text{ } (k > 0)$	$\frac{k}{2\sqrt{\pi t^3}} \exp\left(-\frac{k^2}{4t}\right)$
182	$\frac{1}{s} e^{-k\sqrt{s}} \text{ } (k \geq 0)$	$\operatorname{erfc}\left(\frac{k}{2\sqrt{t}}\right)$
183	$\frac{1}{\sqrt{s}} e^{-k\sqrt{s}} \text{ } (k \geq 0)$	$\frac{1}{\sqrt{\pi t}} \exp\left(-\frac{k^2}{4t}\right)$
184	$s^{-3/2} e^{-k\sqrt{s}} \text{ } (k \geq 0)$	$2\sqrt{\frac{t}{\pi}} \exp\left(-\frac{k^2}{4t}\right) - k \operatorname{erfc}\left(\frac{k}{2\sqrt{t}}\right)$
185	$\frac{ae^{-k\sqrt{s}}}{s(a + \sqrt{s})} \text{ } (k \geq 0)$	$-e^{ak} e^{a^2 t} \operatorname{erfc}\left(a\sqrt{t} + \frac{k}{2\sqrt{t}}\right) + \operatorname{erfc}\left(\frac{k}{2\sqrt{t}}\right)$
186	$\frac{e^{-k\sqrt{s}}}{\sqrt{s}(a + \sqrt{s})} \text{ } (k \geq 0)$	$e^{ak} e^{a^2 t} \operatorname{erfc}\left(a\sqrt{t} + \frac{k}{2\sqrt{t}}\right)$
187	$\frac{e^{-k\sqrt{s(s+a)}}}{\sqrt{s(s+a)}}$	$\begin{cases} 0 & \text{when } 0 < t < k \\ e^{-(1/2)at} I_0\left(\frac{1}{2}a\sqrt{t^2 - k^2}\right) & \text{when } t > k \end{cases}$

(continued)

TABLE A.5.1 (continued) Laplace Transform Pairs

	$F(s)$	$f(t)$
188	$\frac{e^{-k\sqrt{s^2+a^2}}}{\sqrt{(s^2+a^2)}}$	$\begin{cases} 0 & \text{when } 0 < t < k \\ J_0(a\sqrt{t^2-k^2}) & \text{when } t > k \end{cases}$
189	$\frac{e^{-k\sqrt{s^2-a^2}}}{\sqrt{(s^2-a^2)}}$	$\begin{cases} 0 & \text{when } 0 < t < k \\ I_0(a\sqrt{t^2-k^2}) & \text{when } t > k \end{cases}$
190	$\frac{e^{-k(\sqrt{s^2+a^2}-s)}}{\sqrt{(s^2+a^2)}} \quad (k \geq 0)$	$J_0(a\sqrt{t^2+2kt})$
191	$e^{-ks} - e^{-k\sqrt{s^2+a^2}}$	$\begin{cases} 0 & \text{when } 0 < t < k \\ \frac{ak}{\sqrt{t^2-k^2}} J_1(a\sqrt{t^2-k^2}) & \text{when } t > k \end{cases}$
192	$e^{-k\sqrt{s^2+a^2}} - e^{-ks}$	$\begin{cases} 0 & \text{when } 0 < t < k \\ \frac{ak}{\sqrt{t^2-k^2}} I_1(a\sqrt{t^2-k^2}) & \text{when } t > k \end{cases}$
193	$\frac{a^v e^{-k\sqrt{s^2+a^2}}}{\sqrt{(s^2+a^2)}(\sqrt{s^2+a^2}+s)^v} \quad (v > -1)$	$\begin{cases} 0 & \text{when } 0 < t < k \\ \left(\frac{t-k}{t+k}\right)^{(1/2)v} J_v(a\sqrt{t^2-k^2}) & \text{when } t > k \end{cases}$
194	$\frac{1}{s} \log s$	$\Gamma'(1) - \log t \quad [\Gamma'(1) = -0.5772]$
195	$\frac{1}{s^k} \log s \quad (k > 0)$	$t^{k-1} \left\{ \frac{\Gamma'(k) \log t}{[\Gamma(k)]^2 \Gamma(k)} \right\}$
196	$\frac{\log s}{s-a} \quad (a > 0)$	$e^{at} [\log a - \text{Ei}(-at)]$
197	$\frac{\log s}{s^2+1}$	$\cos t \text{Si}(t) - \sin t \text{Ci}(t)$
198	$\frac{s \log s}{s^2+1}$	$-\sin t \text{Si}(t) - \cos t \text{Ci}(t)$
199	$\frac{1}{s} \log(1+ks) \quad (k > 0)$	$-\text{Ei}\left(-\frac{t}{k}\right)$
200	$\log \frac{s-a}{s-b}$	$\frac{1}{t} (e^{bt} - e^{at})$
201	$\frac{1}{s} \log(1+k^2s^2)$	$-2\text{Ci}\left(\frac{t}{k}\right)$
202	$\frac{1}{s} \log(s^2+a^2) \quad (a > 0)$	$2 \log a - 2\text{Ci}(at)$
203	$\frac{1}{s^2} \log(s^2+a^2) \quad (a > 0)$	$\frac{2}{a} [at \log a + \sin at - at \text{Ci}(at)]$
204	$\log \frac{s^2+a^2}{s^2}$	$\frac{2}{t} (1 - \cos at)$
205	$\log \frac{s^2-a^2}{s^2}$	$\frac{2}{t} (1 - \cosh at)$
206	$\arctan \frac{k}{s}$	$\frac{1}{t} \sin kt$
207	$\frac{1}{s} \arctan \frac{k}{s}$	$\text{Si}(kt)$
208	$e^{k^2s^2} \text{erfc}(ks) \quad (k > 0)$	$\frac{1}{k\sqrt{\pi}} \exp\left(-\frac{t^2}{4k^2}\right)$
209	$\frac{1}{s} e^{k^2s^2} \text{erfc}(ks) \quad (k > 0)$	$\text{erf}\left(\frac{t}{2k}\right)$
210	$e^{ks} \text{erfc}(\sqrt{ks}) \quad (k > 0)$	$\frac{\sqrt{k}}{\pi\sqrt{t(t+k)}}$
211	$\frac{1}{\sqrt{s}} \text{erfc}(\sqrt{ks})$	$\begin{cases} 0 & \text{when } 0 < t < k \\ (\pi t)^{-1/2} & \text{when } t > k \end{cases}$
212	$\frac{1}{\sqrt{s}} e^{ks} \text{erfc}(\sqrt{ks}) \quad (k > 0)$	$\frac{1}{\sqrt{\pi(t+k)}}$
213	$\text{erf}\left(\frac{k}{\sqrt{s}}\right)$	$\frac{1}{\pi t} \sin(2k\sqrt{t})$

TABLE A.5.1 (continued) Laplace Transform Pairs

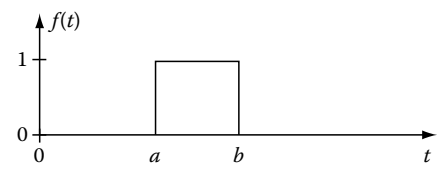
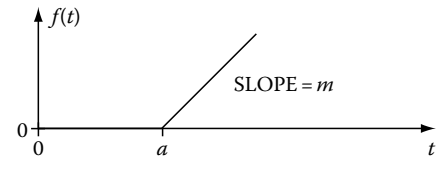
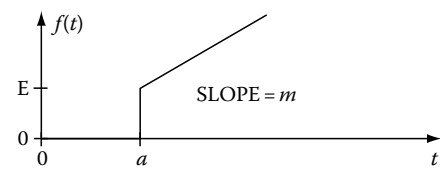
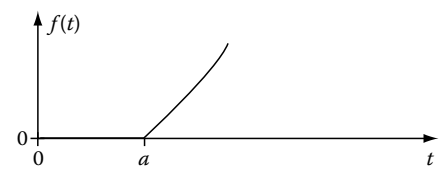
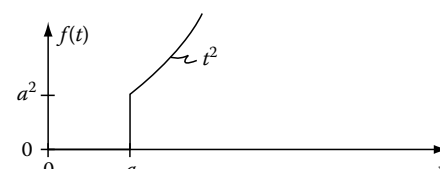
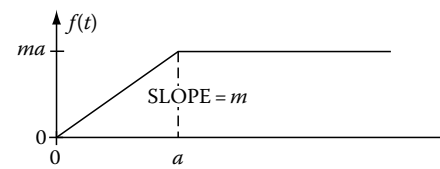
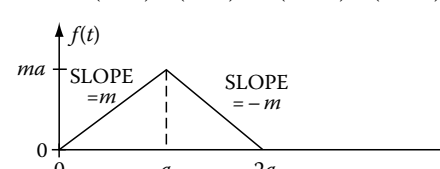
	$F(s)$	$f(t)$
214	$\frac{1}{\sqrt{s}} e^{k^2/s} \operatorname{erfc}\left(\frac{k}{\sqrt{s}}\right)$	$\frac{1}{\sqrt{\pi t}} e^{-2k\sqrt{t}}$
215	$-e^{as} \operatorname{Ei}(-as)$	$\frac{1}{t+a}; (a > 0)$
216	$\frac{1}{a} + se^{as} \operatorname{Ei}(-as)$	$\frac{1}{(t+a)^2}; (a > 0)$
217	$\left[\frac{\pi}{2} - \operatorname{Si}(s)\right] \cos s + \operatorname{Ci}(s) \sin s$	$\frac{1}{t^2 + 1}$
218	$K_0(ks)$	$\begin{cases} 0 & \text{when } 0 < t < k \\ (t^2 - k^2)^{-1/2} & \text{when } t > k \end{cases}$ [ $K_n(t)$ is Bessel function of the second kind of imaginary argument]
219	$K_0(k\sqrt{s})$	$\frac{1}{2t} \exp\left(-\frac{k^2}{4t}\right)$
220	$\frac{1}{s} e^{ks} K_1(ks)$	$\frac{1}{k} \sqrt{t(t+2k)}$
221	$\frac{1}{\sqrt{s}} K_1(k\sqrt{s})$	$\frac{1}{k} \exp\left(-\frac{k^2}{4t}\right)$
222	$\frac{1}{\sqrt{s}} e^{k/s} K_0\left(\frac{k}{s}\right)$	$\frac{2}{\sqrt{\pi t}} K_0(2\sqrt{2kt})$
223	$\pi e^{-ks} I_0(ks)$	$\begin{cases} [t(2k-t)]^{-1/2} & \text{when } 0 < t < 2k \\ 0 & \text{when } t > 2k \end{cases}$
224	$e^{-ks} I_1(ks)$	$\begin{cases} \frac{k-t}{\pi k \sqrt{t(2k-t)}} & \text{when } 0 < t < 2k \\ 0 & \text{when } t > 2k \end{cases}$
225	$\frac{1}{s \sinh(as)}$	$2 \sum_{k=0}^{\infty} u[t - (2k+1)a]$
		
226	$\frac{1}{s \cosh s}$	$2 \sum_{k=0}^{\infty} (-1)^k u(t - 2k - 1)$
		
227	$\frac{1}{s} \tanh\left(\frac{as}{2}\right)$	$u(t) + 2 \sum_{k=1}^{\infty} (-1)^k u(t - ak)$
		
228	$\frac{1}{2s} \left(1 + \coth \frac{as}{2}\right)$	$\sum_{k=0}^{\infty} u(t - ak)$
		

(continued)

TABLE A.5.1 (continued) Laplace Transform Pairs

	$F(s)$	$f(t)$
229	$\frac{m}{s^2} - \frac{ma}{2s} \left( \coth \frac{as}{2} - 1 \right)$	$mt - ma \sum_{k=1}^{\infty} u(t - ka)$ Sawtooth function 
230	$\frac{1}{s^2} \tanh \left( \frac{as}{2} \right)$	$\frac{1}{a} \left[ t + 2 \sum_{k=1}^{\infty} (-1)^k (t - ka) \cdot u(t - ka) \right]$ Triangular wave 
231	$\frac{1}{s(1 + e^{-s})}$	$\sum_{k=0}^{\infty} (-1)^k u(t - k)$ 
232	$\frac{a}{(s^2 + a^2)(1 - e^{-\frac{\pi s}{a}})}$	$\sum_{k=0}^{\infty} \left[ \sin a \left( t - k \frac{\pi}{a} \right) \right] \cdot u \left( t - k \frac{\pi}{a} \right)$ Half-wave rectification of sine wave 
233	$\left[ \frac{a}{(s^2 + a^2)} \right] \coth \left( \frac{\pi s}{2a} \right)$	$[\sin(at)] \cdot u(t) + 2 \sum_{k=1}^{\infty} \left[ \sin a \left( t - k \frac{\pi}{a} \right) \right] \cdot u \left( t - k \frac{\pi}{a} \right)$ Full-wave rectification of sine wave 
234	$\frac{1}{s} e^{-as}$	$u(t - a)$ 

TABLE A.5.1 (continued) Laplace Transform Pairs

	$F(s)$	$f(t)$
235	$\frac{1}{s}(e^{-as} - e^{-bs})$	$u(t-a) - u(t-b)$ 
236	$\frac{m}{s^2}e^{-as}$	$m \cdot (t-a) \cdot u(t-a)$ 
237	$\left[\frac{ma}{s} + \frac{m}{s^2}\right]e^{-as}$	$mt \cdot u(t-a)$ Or $[ma + m(t-a)] \cdot u(t-a)$ 
238	$\frac{2}{s^3}e^{-as}$	$(t-a)^2 \cdot u(t-a)$ 
239	$\left[\frac{2}{s^3} + \frac{2a}{s^2} + \frac{a^2}{s}\right]e^{-as}$	$t^2 \cdot u(t-a)$ 
240	$\frac{m}{s^2} - \frac{m}{s^2}e^{-as}$	$mt \cdot u(t) - m(t-a) \cdot u(t-a)$ 
241	$\frac{m}{s^2} - \frac{2m}{s^2}e^{-as} + \frac{m}{s^2}e^{-2as}$	$mt - 2m(t-a) \cdot u(t-a) + m(t-2a) \cdot u(t-2a)$ 

(continued)



TABLE A.5.1 (continued) Laplace Transform Pairs

	$F(s)$	$f(t)$
242	$\frac{m}{s^2} - \left(\frac{ma}{s} + \frac{m}{s^2}\right)e^{-as}$	$mt - [ma + m(t-a)] \cdot u(t-a)$
243	$\frac{(1 - e^{-s})^2}{s^3}$	$0.5t^2$ for $0 \leq t < 1$ $1 - 0.5(t-2)^2$ for $0 \leq t < 2$ $1$ for $2 \leq t$
244	$\left[\frac{(1 - e^{-s})^3}{s}\right]$	$0.5t^2$ for $0 \leq t < 1$ $0.75 - (t-1.5)^2$ for $1 \leq t < 2$ $0.5(t-3)^2$ for $2 \leq t < 3$ $0$ for $3 < t$
	$\frac{b}{s(s-b)} + (e^{ba} - 1)$	$(e^{bt} - 1) \cdot u(t) - (e^{bt} - 1) \cdot u(t-a) + Ke^{-b(t-a)} \cdot u(t-a)$
245	$\left[\frac{1}{s+b} - \frac{s + \frac{b}{e^{ba}-1}}{s(s-b)}\right] e^{-as}$	where $K = (e^{ba} - 1)$

TABLE A.5.2 Properties of Laplace Transforms

	$F(s)$	$f(t)$
1	$\int_0^\infty e^{-st} f(t) dt$	$f(t)$
2	$AF(s) + BG(s)$	$Af(t) + Bg(t)$
3	$sF(s) - f(+0)$	$f'(t)$
4	$s^n F(s) - s^{n-1}f(+0) - s^{n-2}f^{(1)}(+0) - \dots - f^{(n-1)}(+0)$	$f^{(n)}(t)$
5	$\frac{1}{s} F(s)$	$\int_0^t f(\tau) d\tau$
6	$\frac{1}{s^2} F(s)$	$\int_0^t \int_0^\tau f(\lambda) d\lambda d\tau$

TABLE A.5.2 Properties of Laplace Transforms

	$F(s)$	$f(t)$
7	$F_1(s)F_2(s)$	$\int_0^t f_1(t-\tau)f_2(\tau)d\tau = f_1 * f_2$
8	$-F'(s)$	$tf(t)$
9	$(-1)^n F^{(n)}(s)$	$t^n f(t)$
10	$\int_s^\infty F(x)dx$	$\frac{1}{t}f(t)$
11	$F(s-a)$	$e^{at}f(t)$
12	$e^{-bs}F(s)$	$f(t-b)$ , where $f(t) = 0; t < 0$
13	$F(cs)$	$\frac{1}{c}f\left(\frac{t}{c}\right)$
14	$F(cs-b)$	$\frac{1}{c}e^{(bt)/c}f\left(\frac{t}{c}\right)$
15	$\frac{\int_0^a e^{-st}f(t)dt}{1-e^{-as}}$	$f(t+a) = f(t)$ periodic signal
16	$\frac{\int_0^a e^{-st}f(t)dt}{1+e^{-as}}$	$f(t+a) = -f(t)$
17	$\frac{F(s)}{1-e^{-as}}$	$f_1(t)$ , the half-wave rectification of $f(t)$ in No. 16.
18	$F(s) \coth \frac{as}{2}$	$f_2(t)$ , the full-wave rectification of $f(t)$ in No. 16.
19	$\frac{p(s)}{q(s)}, q(s) = (s-a_1)(s-a_2)\cdots(s-a_m)$	$\sum_1^m \frac{p(a_n)}{q'(a_n)} e^{a_n t}$
20	$\frac{p(s)}{q(s)} = \frac{\phi(s)}{(s-a)^r}$	$e^{at} \sum_{n=1}^r \frac{\phi^{(r-n)}(a)}{(r-n)} \frac{t^{n-1}}{(n-1)} + \dots$

Sources: Campbell, G.A. and Foster, R.M., *Fourier Integrals for Practical Applications*, Van Nostrand, Princeton, NY, 1948; McLachlan, N.W. and Humbert, P., *Formulaire pour le calcul symbolique*, Gauthier-Villars, Paris, TX, 1947; A. Erdélyi and W. Magnus, Eds., *Tables of Integral Transforms*, Bateman Manuscript Project, California Institute of Technology, McGraw-Hill, New York, 1954; based on notes left by Harry Bateman.

Note: In these tables, only those entries containing the condition  $0 < g$  or  $k < g$ , where  $g$  is our  $t$ , are Laplace transforms. Several additional transforms, especially those involving other Bessel functions, can be found in sources.

## References

1. R.V. Churchill, *Modern Operational Mathematics in Engineering*, McGraw-Hill, New York, 1944.
2. J. Irving and N. Mullineux, *Mathematics in Physics and Engineering*, Academic Press, New York, 1959.
3. H.S. Carslaw and J.C. Jaeger, *Operational Methods in Applied Mathematics*, Dover Publications, Dover, NH, 1963.
4. W.R. LePage, *Complex Variables and the Laplace Transform for Engineers*, McGraw-Hill, New York, 1961.
5. R.E. Bolz and G.L. Turve, Eds., *CRC Handbook of Tables for Applied Engineering Science*, 2nd edn., CRC Press, Boca Raton, FL, 1973.
6. A.D. Poularikas and S. Seeley, *Signals and Systems*, corrected 2nd edn., Krieger Publishing Co., Melbourne, FL, 1994.
7. G.A. Campbell and R.M. Foster, *Fourier Integrals for Practical Applications*, Van Nostrand, Princeton, NJ, 1948.
8. N.W. McLachlan and P. Humbert, *Formulaire pour le calcul symbolique*, Gauthier-Villars, Paris, 1947.
9. A. Erdélyi and W. Magnus, Eds., *Tables of Integral Transforms*, Bateman Manuscript Project, California Institute of Technology, McGraw-Hill, New York, 1954; based on notes left by Harry Bateman.



# 6

## Z-Transform

Alexander D. Poularikas  
University of Alabama in Huntsville

6.1 Introduction.....	6-1
One-Sided Z-Transform • Two-Sided Z-Transform • Applications	
Appendix: Tables .....	6-36
Bibliography .....	6-44

### 6.1 Introduction

The Z-transform is a powerful method for solving difference equations and, in general, to represent discrete systems. Although applications of Z-transforms are relatively new, the essential features of this mathematical technique date back to the early 1730s when DeMoivre introduced the concept of a generating function that is identical with that for the Z-transform. Recently, the development and extensive applications of the Z-transform are much enhanced as a result of the use of the digital computers.

#### 6.1.1 One-Sided Z-Transform

##### 6.1.1.1 The Z-Transform and Discrete Functions

Let  $f(t)$  be defined for  $t \geq 0$ . The Z-transform of the sequence  $\{f(nT)\}$  is given by

$$\mathcal{Z}\{f(nT)\} \doteq F(z) = \sum_{n=0}^{\infty} f(nT)z^{-n} \quad (6.1)$$

where  $T$ , the sampling time, is a positive number.\*

To find the values of  $z$  for which the series converges, we use the ratio test or the root test. The ratio test states that a series of complex numbers

$$\sum_{n=0}^{\infty} a_n$$

with limit

$$\lim_{n \rightarrow \infty} \left| \frac{a_{n+1}}{a_n} \right| = A \quad (6.2)$$

converges absolutely if  $A < 1$  and diverges if  $A > 1$  the series may or may not converge.

The root test states that if

$$\lim_{n \rightarrow \infty} \sqrt[n]{|a_n|} = A \quad (6.3)$$

then the series converges absolutely if  $A < 1$ , and diverges if  $A > 1$ , and may converge or diverge if  $A = 1$ .

More generally, the series converges absolutely if

$$\overline{\lim}_{n \rightarrow \infty} \sqrt[n]{|a_n|} < 1 \quad (6.4)$$

where  $\overline{\lim}$  denotes the *greatest* limit points of  $\overline{\lim}_{n \rightarrow \infty} |f(nT)|^{1/n}$ , and diverges if

$$\overline{\lim}_{n \rightarrow \infty} \sqrt[n]{|a_n|} > 1 \quad (6.5)$$

If we apply the root test in Equation 6.1 we obtain the convergence condition

$$\overline{\lim}_{n \rightarrow \infty} \sqrt[n]{|f(nT)z^{-n}|} = \overline{\lim}_{n \rightarrow \infty} \sqrt[n]{|f(nT)||z^{-1}|^n} < 1$$

or

$$|z| > \overline{\lim}_{n \rightarrow \infty} \sqrt[n]{|f(nT)|} = R \quad (6.6)$$

where  $R$  is known as the *radius of convergence* for the series. Therefore, the series will converge absolutely for all points in the  $z$ -plane that lie *outside* the circle of radius  $R$ , and is centered at the origin (with the possible exception of the point at infinity). This region is called the *region of convergence* (ROC).

#### Example

The radius of convergence of  $f(nT) = e^{-anT}u(nT)$ , a positive number, is

$$|z^{-1}e^{-aT}| < 1 \quad \text{or} \quad |z| > e^{-aT}$$

\* The symbol  $\doteq$  means equal by definition.

The Z-transform of  $f(nT) = e^{-anT}u(nT)$  is

$$F(z) = \sum_{n=0}^{\infty} f(nT)z^{-n} = \sum_{n=0}^{\infty} (e^{-aT}z^{-1})^n = \frac{1}{1 - e^{-aT}z^{-1}}$$

If  $a=0$

$$F(z) = \sum_{n=0}^{\infty} u(nT)z^{-n} = \frac{1}{1 - z^{-1}} = \frac{z}{z - 1}$$

### Example

The function  $f(nT) = a^{nT} \cos nT\omega u(nT)$  has the Z-transform

$$\begin{aligned} F(z) &= \sum_{n=0}^{\infty} a^{nT} \frac{e^{jnT\omega} + e^{-jnT\omega}}{2} z^{-n} \\ &= \frac{1}{2} \sum_{n=0}^{\infty} (a^T e^{jT\omega} z^{-1})^n + \frac{1}{2} \sum_{n=0}^{\infty} (a^T e^{-jT\omega} z^{-1})^n \\ &= \frac{1}{2} \frac{1}{1 - a^T e^{jT\omega} z^{-1}} + \frac{1}{2} \frac{1}{1 - a^T e^{-jT\omega} z^{-1}} \\ &= \frac{1 - a^T z^{-1} \cos T\omega}{1 - 2a^T z^{-1} \cos T\omega + a^{2T} z^{-2}} \end{aligned}$$

The ROC is given by the relations

$$\begin{aligned} |a^T e^{jT\omega} z^{-1}| < 1 \quad \text{or} \quad |z| > |a^T| \\ |a^T e^{-jT\omega} z^{-1}| < 1 \quad \text{or} \quad |z| > |a^T| \end{aligned}$$

Therefore, the ROC is  $|z| > |a^T|$ .

## 6.1.1.2 Properties of the Z-Transform

### 6.1.1.2.1 Linearity

If there exists transforms of sequences  $\mathcal{Z}\{c_i f_i(nT)\} = c_i F_i(z)$ ,  $c_i$  are complex constants, with radii of convergence  $R_i > 0$  for  $i = 0, 1, 2, \dots, \ell$  ( $\ell$  finite), then

$$\mathcal{Z}\left\{\sum_{i=0}^{\ell} c_i f_i(nT)\right\} = \sum_{i=0}^{\ell} c_i F_i(z) \quad |z| > \max R_i \quad (6.7)$$

### 6.1.1.2.2 Shifting Property

$$\mathcal{Z}\{f(nT - kT)\} = z^{-k} F(z), \quad f(-nT) = 0 \quad n = 1, 2, \dots \quad (6.8)$$

$$\mathcal{Z}\{f(nT - kT)\} = z^{-k} F(z) + \sum_{n=1}^k f(-nT) z^{-(k-n)} \quad (6.9)$$

$$\mathcal{Z}\{f(nT + kT)\} = z^k F(z) - \sum_{n=0}^{k-1} f(nT) z^{k-n} \quad (6.10)$$

$$\mathcal{Z}\{f(nT + T)\} = z[F(z) - f(0)] \quad (6.10a)$$

### Example

To find the Z-transform of  $y(nT)$  we proceed as follows:

$$\begin{aligned} \frac{d^2 y(t)}{dt^2} &= x(t), \quad \frac{y(nT) - 2y(nT - T) + y(nT - 2T)}{T^2} = x(nT), \\ Y(z) - 2[z^{-1}Y(z) + y(-T)z^{-0}] &+ z^{-2}Y(z) + y(-T)z^{-1} \\ &+ y(-2T)z^{-0} = X(z)T^2 \end{aligned}$$

or

$$Y(z) = \frac{2y(-T) - y(-T)z^{-1} - y(-2T) + X(z)T^2}{1 - 2z^{-1} + z^{-2}}$$

### 6.1.1.2.3 Time Scaling

$$\mathcal{Z}\{a^{nT} f(nT)\} = F(a^{-T}z) = \sum_{n=0}^{\infty} f(nT)(a^{-T}z)^{-n} \quad (6.11)$$

### Example

$$\begin{aligned} \mathcal{Z}\{\sin \omega nT u(nT)\} &= \frac{z \sin \omega T}{z^2 - 2z \cos \omega T + 1} \quad |z| > 1, \\ \mathcal{Z}\{e^{-n} \sin \omega nT u(nT)\} &= \frac{e^{+1} z \sin \omega T}{e^{+2} z^2 - 2e^{+1} z \cos \omega T + 1} \quad |z| > e^{-1} \end{aligned}$$

### 6.1.1.2.4 Periodic Sequence

$$\mathcal{Z}\{f(nT)\} = \frac{z^N}{z^N - 1} \mathcal{Z}\{f_1(nT)\} = \frac{z^N}{z^N - 1} F_1(z), \quad (6.12)$$

$f_1(nT)$  = first period

where

$N$  is the number of the time units in a period,  $|z| > R$   
 $R$  is the radius of convergence of  $F_1(z)$

*Proof*

$$\begin{aligned} \mathcal{Z}\{f(nT)\} &= \mathcal{Z}\{f_1(nT)\} + \mathcal{Z}\{f_1(nT - NT)\} \\ &+ \mathcal{Z}\{f_1(nT - 2NT)\} + \dots \\ &= F_1(z) + z^{-N} F_1(z) + z^{-2N} F_1(z) + \dots \\ &= F_1(z) \frac{1}{1 - z^{-N}} = \frac{z^N}{z^N - 1} F_1(z) \end{aligned}$$

For finite sequence of  $K$  terms

$$F(z) = F_1(z) \frac{1 - z^{-N(K+1)}}{1 - z^{-N}} \quad (6.12a)$$

### 6.1.1.2.5 Multiplication by $n$ and $nT$

$R$  is the radius of convergence of  $F(z)$

$$\begin{aligned}\mathcal{Z}\{nf(nT)\} &= -z \frac{dF(z)}{dz} \\ \mathcal{Z}\{nTf(nT)\} &= -Tz \frac{dF(z)}{dz} \quad |z| > R\end{aligned}\quad (6.13)$$

*Proof*

$$\begin{aligned}\sum_{n=0}^{\infty} nTf(nT)z^{-n} &= Tz \sum_{n=0}^{\infty} f(nT) \left[ -\frac{d}{dz} z^{-n} \right] \\ &= -Tz \frac{d}{dz} \left[ \sum_{n=0}^{\infty} f(nT)z^{-n} \right] \\ &= -Tz \frac{dF(z)}{dz}\end{aligned}$$

### Example

$$\begin{aligned}\mathcal{Z}\{u(n)\} &= \frac{z}{z-1}, \quad \mathcal{Z}\{nu(n)\} = -z \frac{d}{dz} \left( \frac{z}{z-1} \right) = \frac{z}{(z-1)^2}, \\ \mathcal{Z}\{n^2u(n)\} &= -z \frac{d}{dz} \left( \frac{z}{(z-1)^2} \right) = \frac{z(z^2-1)}{(z-1)^4}\end{aligned}$$

### 6.1.1.2.6 Convolution

If  $\mathcal{Z}\{f(nT)\} = F(z)|z| > R_1$  and  $\mathcal{Z}\{h(nT)\} = H(z)|z| > R_2$ , then

$$\begin{aligned}\mathcal{Z}\{f(nT) * h(nT)\} &= \mathcal{Z}\left\{ \sum_{m=0}^{\infty} f(mT)h(nT-mT) \right\} \\ &= F(z)H(z) \quad |z| > \max(R_1, R_2)\end{aligned}\quad (6.14)$$

*Proof*

$$\begin{aligned}\mathcal{Z}\{f(nT) * h(nT)\} &= \sum_{n=0}^{\infty} \left[ \sum_{m=0}^{\infty} f(mT)h(nT-mT) \right] z^{-n} \\ &= \sum_{m=0}^{\infty} f(mT) \sum_{n=0}^{\infty} h(nT-mT)z^{-n} \\ &= \sum_{m=0}^{\infty} f(mT) \sum_{r=-m}^{\infty} h(rT)z^{-r}z^{-m} \\ &= \sum_{m=0}^{\infty} f(mT)z^{-m} \sum_{r=0}^{\infty} h(rT)z^{-r} = F(z)H(z).\end{aligned}$$

The value of  $h(nT)$  for  $n < 0$  is zero.

Additional relations of convolution are

$$\mathcal{Z}\{f(nT) * h(nT)\} = F(z)H(z) = \mathcal{Z}\{h(nT) * f(nT)\} = F(z)H(z) \quad (6.14a)$$

$$\begin{aligned}\mathcal{Z}\{(f(nT) + h(nT)) * g(nT)\} &= \mathcal{Z}\{f(nT) * g(nT)\} \\ &\quad + \mathcal{Z}\{h(nT) * g(nT)\} \\ &= F(z)G(z) + H(z)G(z)\end{aligned}\quad (6.14b)$$

$$\begin{aligned}\mathcal{Z}\{f(nT) * h(nT) * g(nT)\} &= \mathcal{Z}\{f(nT) * \{h(nT) * g(nT)\}\} \\ &= F(z)H(z)G(z)\end{aligned}\quad (6.14c)$$

### Example

The Z-transform of the output of the discrete system  $y(n) = 1/2y(n-1) + 1/2x(n)$ , when the input is the unit step function  $u(n)$  given by  $Y(z) = H(z)U(z)$ . The Z-transform of the difference equation with a delta function input  $\delta(n)$  is

$$H(z) - \frac{1}{2}z^{-1}H(z) = \frac{1}{2} \quad \text{or} \quad H(z) = \frac{1}{2} \frac{1}{1 - \frac{1}{2}z^{-1}} = \frac{1}{2} \frac{z}{z - \frac{1}{2}}$$

Therefore, the output is given by

$$Y(z) = \frac{1}{2} \frac{z}{z - \frac{1}{2}} \frac{z}{z - 1}$$

### Example

Find the  $f(n)$  if

$$F(z) = \frac{z^2}{(z - e^{-a})(z - e^{-b})} \quad a, b \text{ are constants.}$$

From this equation we obtain

$$f_1(n) = \mathcal{Z}^{-1}\left\{ \frac{z}{z - e^{-a}} \right\} = e^{-an}, \quad f_2(n) = \mathcal{Z}^{-1}\left\{ \frac{z}{z - e^{-b}} \right\} = e^{-bn}$$

Therefore,

$$\begin{aligned}f(n) &= f_1(n) * f_2(n) = \sum_{m=0}^n e^{-am} e^{-b(n-m)} = e^{-bn} \sum_{m=0}^n e^{-(a-b)m} \\ &= e^{-bn} \frac{1 - e^{-(a-b)(n+1)}}{1 - e^{-(a-b)}}\end{aligned}$$

### 6.1.1.2.7 Initial Value

$$f(0) = \lim_{z \rightarrow \infty} F(z) \quad (6.15)$$

The above value is obtained from the definition of the Z-transform. If  $f(0) = 0$ , we obtain  $f(1)$  as the limit

$$\lim_{z \rightarrow \infty} zF(z) \quad (6.15a)$$

### 6.1.1.2.8 Final Value

$$\lim_{n \rightarrow \infty} f(n) = \lim_{z \rightarrow 1} (z-1)F(z) \quad \text{if } f(\infty) \text{ exists} \quad (6.16)$$

*Proof*

$$\begin{aligned} \mathcal{Z}\{f(k+1) - f(k)\} &= \lim_{n \rightarrow \infty} \sum_{k=0}^n [f[(k+1)] - f(k)]z^{-k} \\ zF(z) - zf(0) - F(z) &= (z-1)F(z) - zf(0) \\ &= \lim_{n \rightarrow \infty} \sum_{k=0}^n [f[(k+1)] - f(k)]z^{-k} \end{aligned}$$

By taking the limit as  $z \rightarrow 1$ , the above equation becomes

$$\begin{aligned} \lim_{z \rightarrow 1} (z-1)F(z) - f(0) &= \lim_{n \rightarrow \infty} \sum_{k=0}^n [f[(k+1)] - f(k)] \\ &= \lim_{n \rightarrow \infty} \{f(1) - f(0) + f(2) - f(1) + \dots \\ &\quad + f(n) - f(n-1) + f(n+1) - f(n)\} \\ &= \lim_{n \rightarrow \infty} \{-f(0) + f(n+1)\} \\ &= -f(0) + f(\infty) \end{aligned}$$

which is the required result.

### Example

If  $F(z) = 1/[(1-z^{-1})(1-e^{-1}z^{-1})]$  with  $|z| > 1$  then

$$\begin{aligned} f(0) &= \lim_{z \rightarrow \infty} F(z) = \frac{1}{\left(1 - \frac{1}{\infty}\right)\left(1 - e^{-1} \frac{1}{\infty}\right)} = 1 \\ \lim_{n \rightarrow \infty} f(n) &= \lim_{z \rightarrow 1} (z-1) \frac{1}{(1-z^{-1})(1-e^{-1}z^{-1})} = \lim_{z \rightarrow 1} \frac{z^2}{(z-e^{-1})} \\ &= \frac{1}{(1-e^{-1})} \end{aligned}$$

### 6.1.1.2.9 Multiplication by $(nT)^k$

$$\mathcal{Z}\{n^k T^k f(nT)\} = -Tz \frac{d}{dz} \mathcal{Z}\{(nT)^{k-1} f(nT)\} \quad (6.17)$$

$k > 0$  and is an integer

As a corollary to this theorem, we can deduce

$$\begin{aligned} \mathcal{Z}\{n^{(k)} f(n)\} &= z^{-k} \frac{d^k F(z)}{d(z^{-1})^k}, \\ n^{(k)} &= n(n-1)(n-2) \cdots (n-k+1) \end{aligned} \quad (6.17a)$$

The following relations are also true:

$$\mathcal{Z}\{(-1)^k n^{(k)} f(n-k+1)\} = z \frac{d^k F(z)}{dz^k} \quad (6.17b)$$

$$\begin{aligned} \mathcal{Z}\{n(n+1)(n+2) \cdots (n+k-1)f(n)\} \\ = (-1)^k z^k \frac{d^k F(z)}{dz^k} \end{aligned} \quad (6.17c)$$

### Example

$$\begin{aligned} \mathcal{Z}\{n\} &= -z \frac{d}{dz} \left( \frac{z}{z-1} \right) = \frac{z}{(z-1)^2}, \\ \mathcal{Z}\{n^2\} &= -z \frac{d}{dz} \mathcal{Z}\{n\} = -z \frac{d}{dz} \frac{z}{(z-1)^2} = \frac{z(z+1)}{(z-1)^3}, \\ \mathcal{Z}\{n^3\} &= -z \frac{d}{dz} \frac{z(z+1)}{(z-1)^3} = \frac{z(z^2+4z+1)}{(z-1)^4} \end{aligned}$$

### 6.1.1.2.10 Initial Value of $f(nT)$

$$\begin{aligned} \mathcal{Z}\{f(nT)\} &= f(0T) + f(T)z^{-1} + f(2T)z^{-2} + \dots = F(z) \\ f(0T) &= \lim_{z \rightarrow \infty} F(z) \quad |z| > R \end{aligned} \quad (6.18)$$

### 6.1.1.2.11 Final Value for $f(nT)$

$$\lim_{n \rightarrow \infty} f(nT) = \lim_{z \rightarrow 1} (z-1)F(z) \quad f(\infty T) \text{ exists} \quad (6.19)$$

### Example

For the function

$$F(z) = \frac{1}{(1-z^{-1})(1-e^{-T}z^{-1})} \quad |z| > 1$$

we obtain

$$\begin{aligned} f(0T) &= \lim_{z \rightarrow \infty} F(z) = \frac{1}{\left(1 - \frac{1}{\infty}\right)\left(1 - \frac{e^{-T}}{\infty}\right)} = 1 \\ \lim_{n \rightarrow \infty} f(nT) &= \lim_{z \rightarrow 1} (z-1) \frac{z}{z-1} \frac{z}{1-e^{-T}} = \frac{1}{1-e^{-T}} \end{aligned}$$

### 6.1.1.2.12 Complex Conjugate Signal

$$F(z) = \sum_{n=0}^{\infty} f(nT)z^{-n} \quad |z| > R \quad \text{or} \quad F(z^*) = \sum_{n=0}^{\infty} f(nT)(z^*)^{-n}$$

or

$$F^*(z^*) = \sum_{n=0}^{\infty} f^*(nT)z^{-n} = \mathcal{Z}\{f^*(nT)\}$$

Hence,

$$\mathcal{Z}\{f^*(nT)\} = F^*(z^*) \quad |z| > R \quad (6.20)$$

6.1.1.2.13 Transform of Product

If

$$\begin{aligned} \mathcal{Z}\{f(nT)\} &= F(z) \quad |z| > R_f \\ \mathcal{Z}\{h(nT)\} &= H(z) \quad |z| > R_h \end{aligned}$$

then

$$\begin{aligned} \mathcal{Z}\{g(nT)\} &\doteq \mathcal{Z}\{f(nT)h(nT)\} \\ &= \sum_{n=0}^{\infty} f(nT)h(nT)z^{-n} \\ &= \frac{1}{2\pi j} \oint_C F(\tau)H\left(\frac{z}{\tau}\right) \frac{d\tau}{\tau} \quad |z| > R_f R_h \end{aligned} \quad (6.21)$$

where  $C$  is a simple contour encircling counterclockwise the origin with (see Figure 6.1)

$$R_f < |\tau| < \frac{|z|}{R_h} \quad (6.21a)$$

*Proof* The integration is performed in the positive sense along the circle, inside which lie all the singular points of the function  $F(\tau)$  and outside which lie all the singular points of the function  $H(z/\tau)$ . From Equation 6.21, we write

$$G(z) = \frac{1}{2\pi j} \oint_C F(\tau) \sum_{n=0}^{\infty} h(nT) \left(\frac{z}{\tau}\right)^{-n} \frac{d\tau}{\tau} \quad (6.22)$$

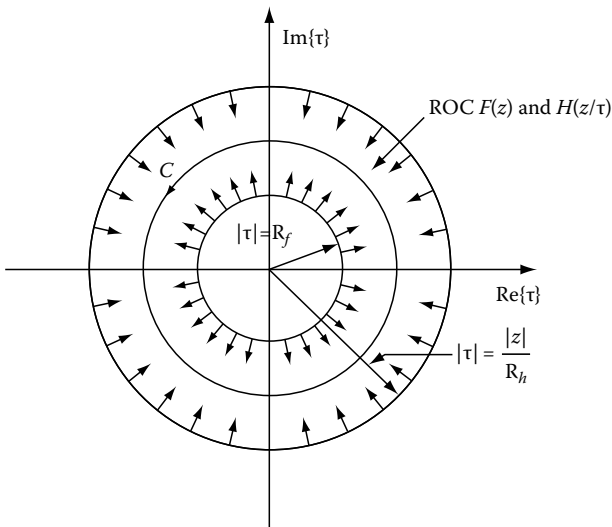


FIGURE 6.1

which converges uniformly for some choice of contour  $C$  and values of  $z$ . From Equation 6.22, we must have

$$\left| R_h \left(\frac{z}{\tau}\right)^{-1} \right| < 1 \quad \text{or} \quad \left| \frac{z}{\tau} \right| > R_h \quad \text{or} \quad |\tau| < \frac{|z|}{R_h} \quad (6.23)$$

so that the sum in Equation 6.22 converges. Because  $|z| > R_f$  and  $\tau$  takes the place of  $z$ , then Equation 6.22 implies that

$$|\tau| > R_f \quad (6.24)$$

$$R_f < |\tau| < \frac{|z|}{R_h} \quad (6.25)$$

and also

$$R_f R_h < |z|.$$

Figure 6.1 shows the ROC.

The integral is solved with the aid of the residue theorem, which yields in this case

$$G(z) = \sum_{i=1}^K \text{res}_{\tau=\tau_i} \left\{ \frac{F(\tau)H(z/\tau)}{\tau} \right\} \quad (6.26)$$

where  $K$  is the number of different poles  $\tau_i (i=1, 2, \dots, K)$  of the function  $F(\tau)/\tau$ . For the residue at the pole  $\tau_i$  of multiplicity  $m$  of the function  $F(\tau)/\tau$ , we have

$$\begin{aligned} \text{res}_{\tau=\tau_i} \left\{ \frac{F(\tau)H(z/\tau)}{\tau} \right\} &= \frac{1}{(m-1)!} \lim_{\tau \rightarrow \tau_i} \frac{d^{m-1}}{d\tau^{m-1}} \\ &\quad \times \left[ (\tau - \tau_i)^m \frac{F(\tau)H(z/\tau)}{\tau} \right] \end{aligned} \quad (6.27)$$

Hence, for a simple pole,  $m=1$ , we obtain

$$\text{res}_{\tau=\tau_i} \left\{ \frac{F(\tau)H(z/\tau)}{\tau} \right\} = \lim_{\tau \rightarrow \tau_i} (\tau - \tau_i) \left\{ \frac{F(\tau)H(z/\tau)}{\tau} \right\} \quad (6.28)$$

**Example**

See Figure 6.2 for graphical representation of the complex integration.

$$\mathcal{Z}\{nT\} \doteq H(z) = \frac{z}{(z-1)^2} T \quad |z| > 1, \quad \mathcal{Z}\{e^{-nT}\} \doteq F(z) = \frac{z}{z-e^{-T}} \quad |z| > e^{-T}$$

Hence,

$$\mathcal{Z}\{nTe^{-nT}\} = \frac{1}{2\pi j} \oint_C T \frac{z}{\tau(\tau - e^{-T})(\frac{z}{\tau} - 1)^2} d\tau.$$



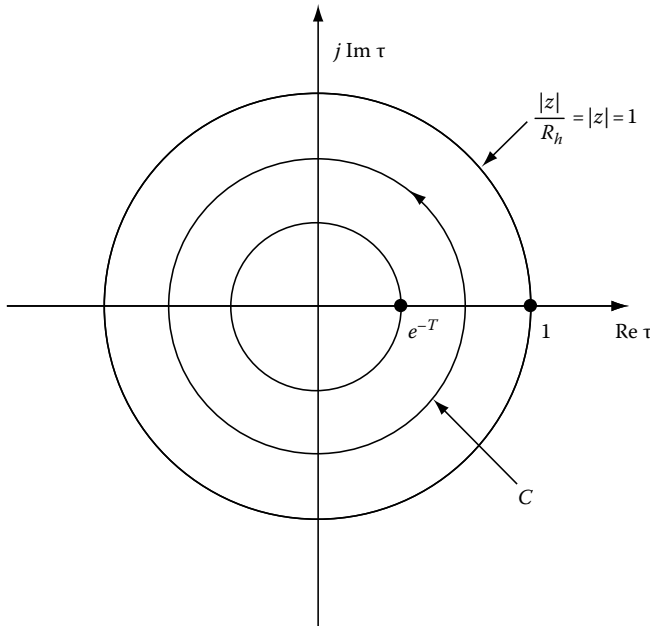


FIGURE 6.2

The contour must have a radius  $|\tau|$  of the value  $e^{-T} < |\tau| < |z| = 1$  and we have from Equation 6.28

$$\begin{aligned} \mathcal{Z}\{nTe^{-nT}\} &= \text{res}_{\tau=e^{-T}} \left\{ (\tau - e^{-T})T \frac{z\tau}{(\tau - e^{-T})(z - \tau)^2} \right\} \\ &= T \frac{ze^{-T}}{(z - e^{-T})^2} \end{aligned}$$

From Equation 6.17

$$\mathcal{Z}\{nTe^{-nT}\} = -Tz \frac{d}{dz} \left( \frac{1}{1 - e^{-T}z^{-1}} \right) = T \frac{ze^{-T}}{(z - e^{-T})^2}$$

and verifies the complex integration approach.

**6.1.1.2.14 Parseval's Theorem**

If  $\mathcal{Z}\{f(nT)\} = F(z)$ ,  $|z| > R_f$  and  $\mathcal{Z}\{h(nT)\} = H(z)$ ,  $|z| > R_h$  with  $|z| = 1 > R_f R_h$ , then

$$\sum_{n=0}^{\infty} f(nT)h(nT) = \frac{1}{2\pi j} \oint_C F(z)H(z^{-1}) \frac{dz}{z} \quad (6.29)$$

where the contour is taken counterclockwise.

*Proof* From Equation 6.21 set  $z=1$  and change the dummy variable  $\tau$  to  $z$ .

**Example**

$f(nT) = e^{-nT} u(nT)$  has the following Z-transform:

$$F(z) = \frac{1}{1 - e^{-T}z^{-1}} \quad |z| > e^{-T}$$

From Equation 6.29 and with  $C$  a unit Circle ( $R_f = e^{-T} < 1$ )

$$\begin{aligned} \sum_{n=0}^{\infty} f(nT)f(nT) &= \frac{1}{2\pi j} \oint_C \frac{1}{1 - e^{-T}z^{-1}} \frac{1}{1 - e^{-T}z} \frac{dz}{z} \\ &= \frac{1}{2\pi j} \oint_C \frac{1}{z - e^{-T}} \frac{e^T}{e^T - z} dz \\ &= \frac{2\pi j}{2\pi j} \sum_i \text{residues} = \frac{e^T}{e^T - e^{-T}} = \frac{1}{1 - e^{-2T}} \end{aligned}$$

**6.1.1.2.15 Correlation**

Let the Z-transform of the two consequences  $\mathcal{Z}\{f(nT)\} = F(z)$  and  $\mathcal{Z}\{h(nT)\} = H(z)$  exist for  $|z| = 1$ . Then the *cross correlation* is given by

$$\begin{aligned} g(nT) &\doteq f(nT) \otimes h(nT) = \sum_{m=0}^{\infty} f(mT)h(mT - nT) \\ &= \lim_{z \rightarrow 1+} \sum_{m=0}^{\infty} f(mT)h(mT - nT)z^{-m} \\ &= \lim_{z \rightarrow 1+} \mathcal{Z}\{f(mT)h(mT - nT)\} \end{aligned}$$

But  $\mathcal{Z}\{h(mT - nT)\} = z^{-n}H(z)$  and, therefore, (see Equation 6.21)

$$\begin{aligned} g(nT) &= \lim_{z \rightarrow 1+} \frac{1}{2\pi j} \oint_C F(\tau) \left(\frac{z}{\tau}\right)^{-n} H\left(\frac{z}{\tau}\right) \frac{d\tau}{\tau} \\ &= \frac{1}{2\pi j} \oint_C F(\tau)H\left(\frac{1}{\tau}\right) \tau^{n-1} d\tau \quad n \geq 1 \quad (6.30) \end{aligned}$$

This relation is the inverse Z-transform of  $g(nT)$  and, hence,

$$\begin{aligned} \mathcal{Z}\{g(nT)\} &\doteq \mathcal{Z}\{f(nT) \otimes h(nT)\} \\ &= F(z)H\left(\frac{1}{z}\right) \quad \text{for } |z| = 1 \quad (6.31) \end{aligned}$$

If  $f(nT) = h(nT)$  for  $n \geq 0$  the *autocorrelation sequence* is

$$\begin{aligned} g(nT) &\doteq f(nT) \otimes h(nT) \\ &= \sum_{m=0}^{\infty} f(mT)f(mT - nT) \\ &= \frac{1}{2\pi j} \oint_C F(\tau)F\left(\frac{1}{\tau}\right) \tau^{n-1} d\tau \quad (6.32) \end{aligned}$$

and, hence,

$$G(z) = \mathcal{Z}\{g(nT)\} = \mathcal{Z}\{f(nT) \otimes h(nT)\} = F(z)F\left(\frac{1}{z}\right) \quad (6.33)$$

If we set  $n=0$ , we obtain the Parseval's theorem in the same form it was developed above.

**Example**

The sequence  $f(t) = e^{-nT}$ ,  $n \geq 0$ , has the Z-transform

$$\mathcal{Z}\{e^{-nT}\} = \frac{z}{z - e^{-T}} \quad |z| > e^{-T}$$

The autocorrelation is given by Equation 6.32 in the form

$$\begin{aligned} G(z) \doteq \mathcal{Z}\{f(nT) \otimes f(nT)\} &= \frac{z}{z - e^{-T}} \frac{1}{z - e^{-T}} \\ &= -\frac{z}{z - e^{-T}} \frac{e^T}{z - e^T} \end{aligned}$$

The function is regular in the region  $e^{-T} < |z| < e^T$ . Using the residue theorem from Equation 6.30, we obtain

$$g(nT) = \sum_{i=1}^K \text{res}_{\tau=\tau_i} \left\{ F(\tau) H\left(\frac{1}{\tau}\right) \right\} \tau^{n-1} \quad (6.34)$$

where  $\tau_i$  are all poles of the integrand inside the circle  $|\tau| = 1$ . Similarly from Equation 6.33

$$g(nT) = \sum_{i=1}^K \text{res}_{\tau=\tau_i} \left\{ F(\tau) F\left(\frac{1}{\tau}\right) \tau^{n-1} \right\} \quad (6.35)$$

where  $\tau_i$  are the poles included inside the unit circle.

**Example**

From the previous example we obtain (only the root inside the unit circle)

$$\begin{aligned} -\frac{1}{2\pi j} \oint_C \frac{z}{z - e^{-T}} \frac{e^T}{z - e^T} z^{n-1} dz &= -\text{res}_{z=e^{-T}} \left\{ \frac{ze^T}{z - e^T} z^{n-1} \right\} \\ &= \frac{e^{2T}}{e^{2T} - 1} e^{-Tn} \end{aligned}$$

which is equal to the autocorrelation of  $f(nT) = e^{-nT}$   $u(nT)$ . Using the summation definitions, we obtain

$$\begin{aligned} &\sum_{m=0}^{\infty} e^{-mT} u(mT) e^{-T(m-n)} u(mT - nT) \\ &= e^{Tn} \sum_{m=n}^{\infty} e^{-2mT} \\ &= e^{Tn} (e^{-2nT} + e^{-2nT} e^{-2T} + e^{-2nT} e^{-4T} + \dots) \\ &= e^{-nT} (1 + e^{-2T} + (e^{-2T})^2 + \dots) \\ &= e^{-nT} \frac{1}{1 - e^{-2T}} = e^{-nT} \frac{e^{2T}}{e^{2T} - 1} \end{aligned}$$

**6.1.1.2.16 Z-Transforms with Parameters**

$$\mathcal{Z} \left\{ \frac{\partial}{\partial a} f(nT, a) \right\} = \frac{\partial}{\partial a} F(z, a) \quad (6.36)$$

$$\mathcal{Z} \left\{ \lim_{a \rightarrow a_0} f(nT, a) \right\} = \lim_{a \rightarrow a_0} F(z, a) \quad (6.37)$$

$$\mathcal{Z} \left\{ \int_{a_0}^{a_1} f(nT, a) da \right\} = \int_{a_0}^{a_1} F(z, a) da \quad \text{finite integral} \quad (6.38)$$

Table A.6.1 contains the Z-transform properties for positive-time sequences.

**6.1.1.3 Inverse Z-Transform**

The inverse Z-transform provides the object function from its given transform. We use the symbolic solution

$$f(nT) = \mathcal{Z}^{-1}\{F(z)\} \quad (6.39)$$

To find the inverse transform, we may proceed as follows:

1. Use tables
2. Decompose the expression into simpler partial forms, which are included in the tables
3. If the transform is decomposed into a product of partial sums, the resulting object function is obtained as the convolution of the partial object function
4. Use the inversion integral

**6.1.1.3.1 Power Series Method**

When  $F(z)$  is analytic for  $|z| > R$  (and at  $z = \infty$ ), the value  $f(nT)$  is obtained as the coefficient of  $z^{-n}$  in the power series expansion (Taylor's series of  $F(z)$  as a function of  $z^{-1}$ ). For example, if  $F(z)$  is the ratio of two polynomials in  $z^{-1}$ , the coefficients  $f(0T), \dots, f(nT)$  are obtained as follows:

$$\begin{aligned} F(z) &= \frac{p_0 + p_1 z^{-1} + p_2 z^{-2} + \dots + p_n z^{-n}}{q_0 + q_1 z^{-1} + q_2 z^{-2} + \dots + q_n z^{-n}} \\ &= f(0T) + f(T)z^{-1} + f(2T)z^{-2} + \dots \end{aligned} \quad (6.40)$$

where

$$\begin{aligned} p_0 &= f(0T)q_0 \\ p_1 &= f(1T)q_0 + f(0T)q_1 \\ &\vdots \\ p_n &= f(nT)q_0 + f[(n-1)T]q_1 + f[(n-2)T]q_2 + \dots + f(0T)q_n \end{aligned} \quad (6.41)$$

The same can be accomplished by synthetic division.

**Example**

$$\begin{aligned} F(z) &= \frac{1 + z^{-1}}{1 + 2z^{-1} + 3z^{-2}} = \frac{z^2 + z}{z^2 + 2z + 3} \\ &= 1 - z^{-1} - z^{-2} + 5z^{-3} + \dots \quad |z| > \sqrt{6} \end{aligned}$$

From Equation 6.41:  $1 = f(0T) \cdot 1$  or  $f(0T) = 1$ ,  $1 = f(1T) \cdot 1 + 1 \cdot 2$  or  $f(1T) = -1$ ,  $0 = f(2T) \cdot 1 + f(1T) \cdot 2 + f(0T) \cdot 3$  or  $f(2T) = +2 - 3 = -1$ ,  $0 = f(3T) \cdot 1 + f(2T) \cdot 2 + f(1T) \cdot 3 + f(0T) \cdot 0$  or  $f(3T) = 2 + 3 = 5$ , and so forth.

**6.1.1.3.2 Partial Fraction Expansion**

If  $F(z)$  is a rational function of  $z$  and analytic at infinity, it can be expressed as follows:

$$F(z) = F_1(z) + F_2(z) + F_3(z) + \dots \quad (6.42)$$

and therefore,

$$f(nT) = \mathcal{Z}^{-1}\{F_1(z)\} + \mathcal{Z}^{-1}\{F_2(z)\} + \mathcal{Z}^{-1}\{F_3(z)\} + \dots \quad (6.43)$$

For an expansion of the form

$$F(z) = \frac{F_1(z)}{(z-p)^n} = \frac{A_1}{z-p} + \frac{A_2}{(z-p)^2} + \dots + \frac{A_n}{(z-p)^n} \quad (6.44)$$

the constants  $A_i$  are given by

$$\begin{aligned} A_n &= (z-p)^n F(z)|_{z=p} \\ A_{n-1} &= \frac{d}{dz} [(z-p)^n F(z)]|_{z=p} \\ &\vdots \\ A_{n-k} &= \frac{1}{k!} \frac{d^k}{dz^k} [(z-p)^n F(z)]|_{z=p} \\ &\vdots \\ A_1 &= \frac{1}{(n-1)!} \frac{d^{n-1}}{dz^{n-1}} [(z-p)^n F(z)]|_{z=p} \end{aligned} \quad (6.45)$$

**Example**

Let

$$\begin{aligned} F(z) &= \frac{1 + 2z^{-1} + z^{-2}}{1 - \frac{3}{2}z^{-1} + \frac{1}{2}z^{-2}} = \frac{z^2 + 2z + 1}{z^2 - \frac{3}{2}z + \frac{1}{2}} \\ &= 1 + \frac{7}{2}z^{-1} + \frac{23}{4}z^{-2} + \dots \quad |z| > 1 \end{aligned}$$

Also,

$$F(z) = 1 + \frac{\frac{7}{2}z + \frac{1}{2}}{(z-1)(z-\frac{1}{2})} = 1 + \frac{A}{z-1} + \frac{B}{z-\frac{1}{2}}$$

from which we find that

$$A = \frac{(z-1)(\frac{7}{2}z + \frac{1}{2})}{(z-1)(z-\frac{1}{2})} \Big|_{z=1} = 8$$

and

$$B = \frac{(z-\frac{1}{2})(\frac{7}{2}z + \frac{1}{2})}{(z-1)(z-\frac{1}{2})} \Big|_{z=1/2} = -\frac{9}{2}$$

Hence,

$$\begin{aligned} F(z) &= 1 + \frac{8}{z-1} - \frac{9}{2} \frac{1}{z-\frac{1}{2}} \\ &= 1 + z^{-1} \frac{8z}{z-1} - \frac{9}{2} z^{-1} \frac{z}{z-\frac{1}{2}} \end{aligned}$$

and, therefore, its inverse transform is  $f(nT) = \delta(nT) + 8u(nT - T) - \frac{9}{2}(\frac{1}{2})^{n-1} u(nT - T)$  with ROC  $|z| > 1$ .

**Example**

(a) If

$$F(z) = \frac{z^2 + 1}{(z-1)(z-2)} = A + \frac{Bz}{z-1} + \frac{Cz}{z-2} \quad |z| > 2$$

then we obtain

$$\begin{aligned} A &= \frac{0 + 1}{(0-1)(0-2)} = \frac{1}{2}, \\ B &= \frac{1}{z} \frac{z^2 + 1}{(z-2)} \Big|_{z=1} = -2, \end{aligned}$$

and

$$C = \frac{1}{z} \frac{z^2 + 1}{(z-1)} \Big|_{z=2} = \frac{5}{2}$$

Hence,

$$F(z) = \frac{1}{2} - 2 \frac{z}{z-1} + \frac{5}{2} \frac{z}{z-2}$$

and its inverse is  $f(nT) = \frac{1}{2}\delta(nT) - 2u(nT) + \frac{5}{2}(2)^n u(nT)$ .

(b) If

$$F(z) = \frac{z+1}{(z-1)(z-2)} = \frac{A}{z-1} + \frac{B}{z-2}$$

then we obtain

$$A = \frac{z+1}{(z-2)} \Big|_{z=1} = -2$$

and

$$B = \frac{z+1}{(z-1)} \Big|_{z=2} = 3$$

Hence,

$$F(z) = -2 \frac{1}{(z-1)} + 3 \frac{1}{(z-2)}$$

and

$$f(nT) = -2u(nT - T) + 3(2)^{n-1}u(nT - T)$$

with ROC  $|z| > 2$ .

**Example**

If  $F(z) = \frac{z^2+1}{(z+1)(z-1)^2} = \frac{A}{z+1} + \frac{B}{z-1} + \frac{C}{(z-1)^2}$  with  $|z| > 1$ , then we find

$$A = \frac{z^2+1}{(z-1)^2} \Big|_{z=-1} = \frac{1}{2},$$

$$C = \frac{z^2+1}{z+1} \Big|_{z=1} = 1.$$

To find  $B$  we set any value of  $z$  (small for convenience) in the equality. Hence, with say  $z=2$ , we obtain

$$\frac{z^2+1}{(z+1)(z-1)^2} \Big|_{z=2} = \frac{1}{2} \frac{1}{z+1} \Big|_{z=2} + B \frac{1}{z-1} \Big|_{z=2} + \frac{1}{(z-1)^2} \Big|_{z=2}$$

or  $B = 1/2$ . Therefore,  $F(z) = \frac{1}{2} \frac{1}{z+1} + \frac{1}{2} \frac{1}{z-1} + \frac{1}{(z-1)^2}$  and its inverse transform is  $f(nT) = \frac{1}{2}(-1)^{n-1}u(nT - T) + \frac{1}{2}u(nT - T) + (nT - T)u(nT - T)$  with ROC  $|z| > 1$ .

**Example**

The function  $F(z) = z^3/(z-1)^2$  with  $|z| > 1$  can be expanded as follows:  $F(z) = z + 2 + \frac{3z-2}{(z-1)^2}$  or  $F(z) = z + 2 + \frac{3z-2}{(z-1)^2} = z + 2 + \frac{A}{z-1} + \frac{B}{(z-1)^2}$ . Therefore, we obtain  $B = \frac{(3z-2)(z-1)^2}{(z-1)^2} \Big|_{z=1} = 1$ . Set any value of  $z$  (e.g.,  $z=2$ ) in the above equality we obtain

$$2 + 2 + \frac{3 \cdot 2 - 2}{(2-1)^2} = 2 + 2 + A \frac{1}{2-1} + \frac{1}{(2-1)^2} \quad \text{or} \quad A = 3$$

Hence,

$$F(z) = z + 2 + \frac{3}{z-1} + \frac{1}{(z-1)^2}$$

and its inverse transform is

$$f(nT) = \delta(nT + T) + 2\delta(nT) + 3u(nT - T) + (nT - T)u(nT - T)$$

with ROC  $|z| > 1$ .

Tables A.6.3 and A.6.4 are useful for finding the inverse transforms.

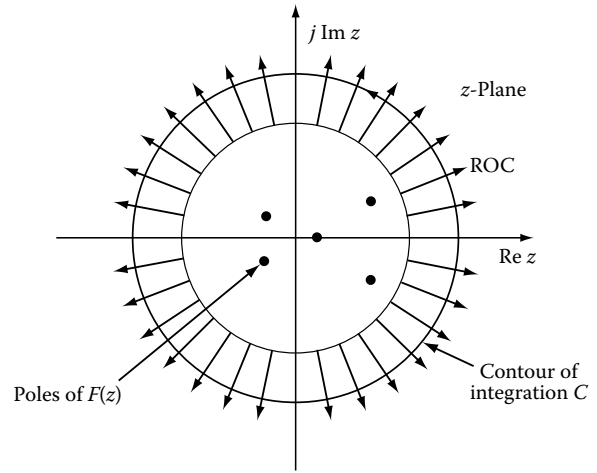


FIGURE 6.3

**6.1.1.3 Inverse Transform by Integration**

If  $F(z)$  is a regular function in the region  $|z| > R$ , then there exists a single sequence  $\{f(nT)\}$  for which  $Z\{f(nT)\} = F(z)$ , namely

$$f(nT) = \frac{1}{2\pi j} \oint_C F(z)z^{n-1} dz = \sum_{i=1}^k \text{res}_{z=z_i} \{F(z)z^{n-1}\} \quad (6.46)$$

$n = 0, 1, 2, \dots$

The contour  $C$  encloses all the singularities of  $F(z)$  as shown in Figure 6.3 and it is taken in a counterclockwise direction.

**6.1.1.3.4 Simple Poles**

If  $F(z) = H(z)/G(z)$ , then the residue at the singularity  $z = a$  is given by

$$\lim_{z \rightarrow a} (z - a)F(z)z^{n-1} = \lim_{z \rightarrow a} \left[ (z - a) \frac{H(z)}{G(z)} z^{n-1} \right] \quad (6.47)$$

**6.1.1.3.5 Multiple Poles**

The residue at the pole  $z_i$  with multiplicity  $m$  of the function  $F(z)z^{n-1}$  is given by

$$\text{res}_{z=z_i} \{F(z)z^{n-1}\} = \frac{1}{(m-1)!} \lim_{z \rightarrow z_i} \frac{d^{m-1}}{dz^{m-1}} \times [(z - z_i)^m F(z)z^{n-1}] \quad (6.48)$$

**6.1.1.3.6 Simple Poles Not Factorable**

The residue at the singularity  $a_m$  is

$$F(z)z^{n-1} \Big|_{z=a_m} = \frac{H(z)}{\frac{dG(z)}{dz}} z^{n-1} \Big|_{z=a_m} \quad (6.49)$$

6.1.1.3.7  $F(z)$  Is Irrational Function of  $z$

Let  $F(z) = [(z + 1)/z]^\alpha$ , where  $\alpha$  is a real noninteger. By Equation 6.46 we write.

$$f(nT) = \frac{1}{2\pi j} \oint_C \left(\frac{z+1}{z}\right)^\alpha z^{n-1} dz$$

where the closed contour  $C$  is that shown in Figure 6.4.

It can easily be shown that at the limit as  $z \rightarrow 0$  the integral around the small circle  $BCD$  is zero (set  $z = re^{j\theta}$  and take the limit  $r \rightarrow 0$ ). Also, the integral along  $EA$  is also zero. Because along  $AB$   $z = xe^{-j\pi}$  and along  $DE$   $z = xe^{j\pi}$ , which implies that  $x$  is positive, we obtain

$$\begin{aligned} f(nT) &= \frac{1}{2\pi j} \left[ \int_1^0 \left(\frac{xe^{-j\pi} + 1}{xe^{-j\pi}}\right)^\alpha x^{n-1} e^{-j\pi n} dx \right. \\ &\quad \left. + \int_0^1 \left(\frac{xe^{j\pi} + 1}{xe^{j\pi}}\right)^\alpha x^{n-1} e^{j\pi n} dx \right] \\ &= \frac{1}{2\pi j} \left[ - \int_0^1 (1-x)^\alpha x^{n-1-\alpha} e^{-j\pi(n-\alpha)} dx \right. \\ &\quad \left. + \int_0^1 (1-x)^\alpha x^{n-1-\alpha} e^{j\pi(n-\alpha)} dx \right] \\ &= \frac{\sin[(n-\alpha)\pi]}{\pi} \int_0^1 x^{n-1-\alpha} (1-x)^\alpha dx \end{aligned} \tag{6.50}$$

But the beta function is given by

$$B(m, k) = \frac{\Gamma(m)\Gamma(k)}{\Gamma(m+k)} = \int_0^1 x^{m-1} (1-x)^{k-1} dx \tag{6.51}$$

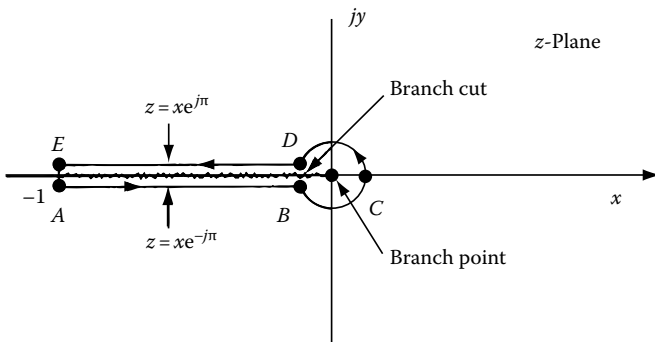


FIGURE 6.4

and, hence,

$$f(nT) = \frac{\sin[(n-\alpha)\pi]}{\pi} \frac{\Gamma(n-\alpha)\Gamma(\alpha+1)}{\Gamma(n+1)} \tag{6.52}$$

But,

$$\Gamma(m)\Gamma(1-m) = \frac{\pi}{\sin \pi m} \tag{6.53}$$

and, therefore,

$$\begin{aligned} f(nT) &= \frac{\Gamma(n-\alpha)\Gamma(\alpha+1)}{\Gamma(n+1)} \frac{1}{\Gamma(n-\alpha)\Gamma(\alpha-n+1)} \\ &= \frac{\Gamma(\alpha+1)}{\Gamma(n+1)\Gamma(\alpha-n+1)} \end{aligned} \tag{6.54}$$

The Taylor's expansion of  $F(z)$  is given as follows:

$$\begin{aligned} F(z) &= \left(\frac{z+1}{z}\right)^\alpha = (1+z^{-1})^\alpha = \sum_{n=0}^{\infty} \frac{1}{n!} \frac{d^n(1+z^{-1})^\alpha}{(dz^{-1})^n} \Big|_{z^{-1}=0} z^{-n} \\ &= \sum_{n=0}^{\infty} \frac{1}{n!} \alpha(\alpha-1)(\alpha-2) \cdots (\alpha-n+1) z^{-n} \end{aligned} \tag{6.55}$$

But,

$$\begin{aligned} \Gamma(\alpha+1) &= \alpha(\alpha-1)(\alpha-2) \cdots (\alpha-n+1)\Gamma(\alpha-n+1), \\ \Gamma(n+1) &= n! \end{aligned} \tag{6.56}$$

and, therefore, Equation 6.55 becomes

$$F(z) = \sum_{n=0}^{\infty} \frac{\Gamma(\alpha+1)}{\Gamma(n+1)\Gamma(\alpha-n+1)} z^{-n} \tag{6.57}$$

The above equation is a Z-transform expansion and, hence, the function  $F(nT)$  is that given in Equation 6.54.

**Example**

To find the inverse of the transform

$$F(z) = \frac{(z-1)}{(z+2)(z-\frac{1}{2})} \quad |z| > 2$$

we proceed with the following approaches:

1. By fraction expansion

$$\begin{aligned} \frac{(z-1)}{(z+2)(z-\frac{1}{2})} &= \frac{A}{(z+2)} + \frac{B}{z-\frac{1}{2}}, \\ A &= \frac{(z-1)}{(z-\frac{1}{2})} \Big|_{z=-2} = \frac{6}{5}, \quad B = \frac{(z-1)}{(z+2)} \Big|_{z=\frac{1}{2}} = -\frac{1}{5} \end{aligned}$$

$$f(nT) = Z^{-1} \left\{ \frac{6}{5} \frac{1}{z+2} - \frac{1}{5} \frac{1}{z-\frac{1}{2}} \right\} = \frac{6}{5} (-2)^{n-1} - \frac{1}{5} \left( \frac{1}{2} \right)^{n-1}$$

$$n \geq 1$$

2. By integration

$$f(nT) = \text{res}_{z=-2} \left\{ (z+2) \frac{z-1}{(z+2)(z-\frac{1}{2})} z^{n-1} \right\}$$

$$+ \text{res}_{z=\frac{1}{2}} \left\{ \left( z - \frac{1}{2} \right) \frac{z-1}{(z+2)(z-\frac{1}{2})} z^{n-1} \right\}$$

$$= \frac{6}{5} (-2)^{n-1} - \frac{1}{5} \left( \frac{1}{2} \right)^{n-1} \quad n \geq 1$$

3. By power expansion

$$\frac{z-1}{z^2 + \frac{3}{2}z - 1} = z^{-1} - \frac{5}{2}z^{-2} + \frac{19}{4}z^{-3} + \dots$$

$$= z^{-1} \left( 1 - \frac{5}{2}z^{-1} + \frac{19}{4}z^{-2} + \dots \right)$$

The multiplier  $z^{-1}$  indicates one time-unit shift and, hence,  $\{f(nT)\} = \left\{ 1, -\frac{5}{2}, \frac{19}{4}, \dots \right\} \quad n = 1, 2, \dots$

**Example**

1. By expansion

By  $F(z)$  has the ROC  $|z| > 5$ , then

$$F(z) = \frac{5z}{(z-5)^2} = \frac{5z}{z^2 - 10z + 25} = 5z^{-1} + 50z^{-2}$$

$$+ 375z^{-3} + \dots$$

$$= 0 \cdot 5^0 z^{-0} + 1 \cdot 5z^{-1} + 2 \cdot 5^2 z^{-2} + 3 \cdot 5^3 z^{-3} + \dots$$

Hence,  $f(nT) = n5^n \quad n = 0, 1, 2, \dots$ , which sometimes is difficult to recognize using the expansion method.

2. By fraction expansion

$$F(z) = \frac{5z}{(z-5)^2} = \frac{Az}{z-5} + \frac{Bz^2}{(z-5)^2}$$

$$B = \left. \frac{5z}{z} \right|_{z=5} = 1,$$

$$\frac{5 \times 6}{(6-1)^2} = \frac{A \times 6}{6-5} + \frac{6^2}{(6-5)^2} \quad \text{or} \quad A = -1.$$

Hence,

$$F(z) = -\frac{z}{z-5} + \frac{z^2}{(z-5)^2}$$

and  $f(nT) = -(5)^n + (n+1)5^n = n5^n, \quad n \geq 0.$

3. By integration

$$\frac{1}{(2-1)!} \frac{d^{2-1}}{dz^{2-1}} \left[ (z-5)^2 \frac{5z}{(z-5)^2} z^{n-1} \right] \Big|_{z=5} = 5nz^{n-1} \Big|_{z=5}$$

$$= n5^n, \quad n \geq 0.$$

Figure 6.5 shows the relation between pole location and type of poles and the behavior of causal signals;  $m$  stands for pole multiplicity. Table A.6.5 gives the Z-transform of a number of sequences.

**6.1.2 Two-Sided Z-Transform**

**6.1.2.1 The Z-Transform**

If a function  $f(z)$  is defined by  $-\infty < t < \infty$ , then the Z-transform of its discrete representation  $f(nT)$  is given by

$$\mathcal{Z}_{II}\{f(nT)\} \doteq F(z) = \sum_{n=-\infty}^{\infty} f(nT)z^{-n} \quad R_+ > |z| < R_- \quad (6.58)$$

where

$R_+$  is the radius of convergence for the positive time of the sequence

$R_-$  is the radius of convergence for the negative time of the sequence

**Example**

$$F(z) = \mathcal{Z}_{II}\{e^{-|nT|}\} = \sum_{n=-\infty}^{-1} e^{nT} z^{-n} + \sum_{n=0}^{\infty} e^{-nT} z^{-n}$$

$$= \sum_{n=-\infty}^0 e^{nT} z^{-n} - 1 + \sum_{n=0}^{\infty} e^{-nT} z^{-n}$$

$$= \sum_{n=0}^{\infty} e^{-nT} z^n - 1 + \sum_{n=0}^{\infty} e^{-nT} z^{-n}$$

$$= \frac{1}{1 - e^{-T}z} - 1 + \frac{1}{1 - e^{-T}z^{-1}}$$

The first sum (negative time) converges if  $|e^{-T}z| < 1$  or  $|z| < e^T$ . The second sum (positive time) converges if  $|e^{-T}z^{-1}| < 1$  or  $e^{-T} < |z|$ . Hence, the ROC is  $R_+ = e^{-T} < |z| < R_- = e^T$ . The two poles of  $F(z)$  are  $z = e^T$  and  $z = e^{-T}$ .

**Example**

The Z-transform of the functions of  $u(nT)$  and  $-u(-nT - T)$  are

$$\mathcal{Z}_{II}\{u(nT)\} = \sum_{n=0}^{\infty} u(nT)z^{-n} = \frac{1}{1 - z^{-1}} = \frac{z}{z-1} \quad |z| > 1$$

Single real poles—Causal signals

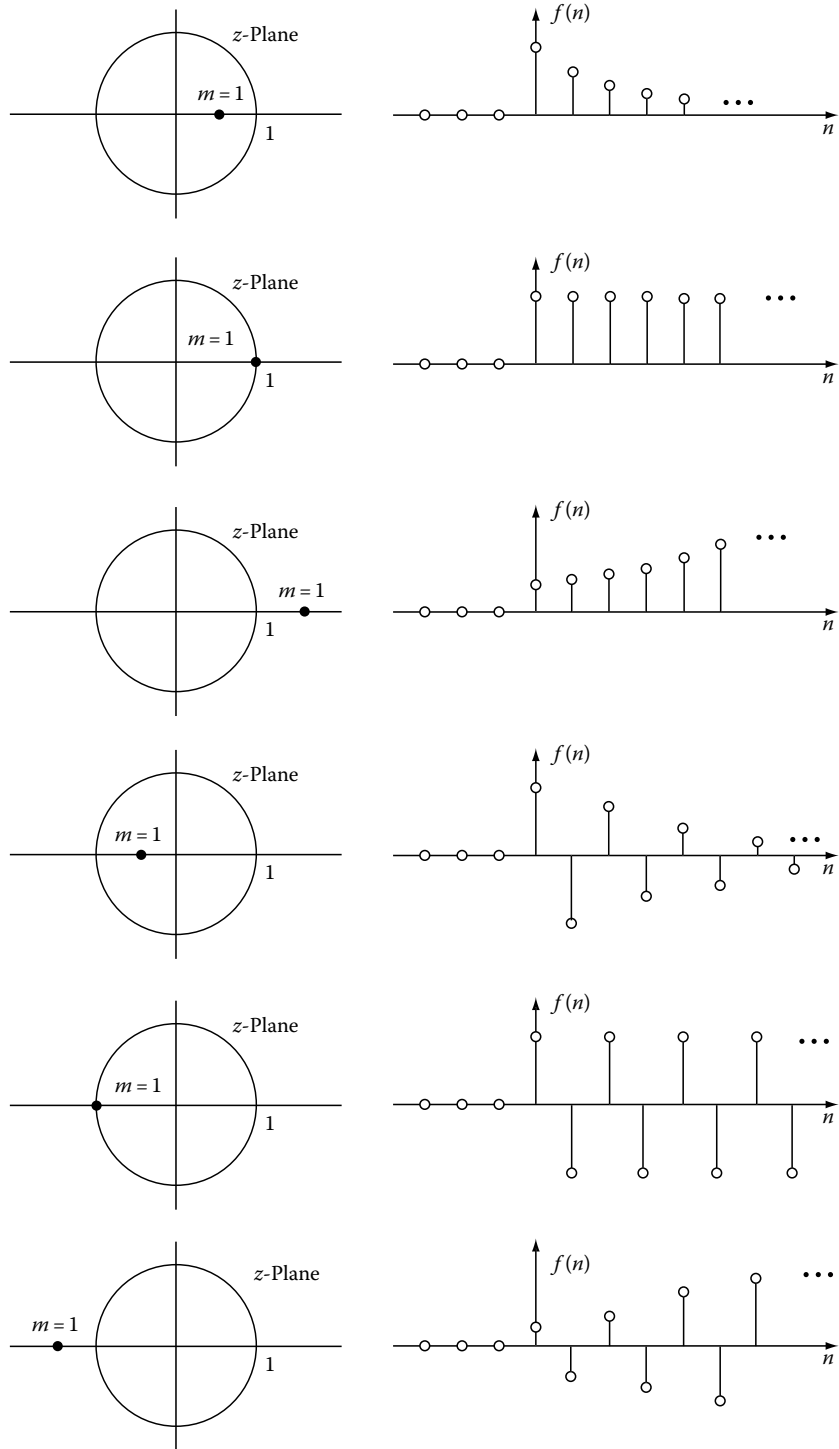


FIGURE 6.5

Double real poles—Causal signals

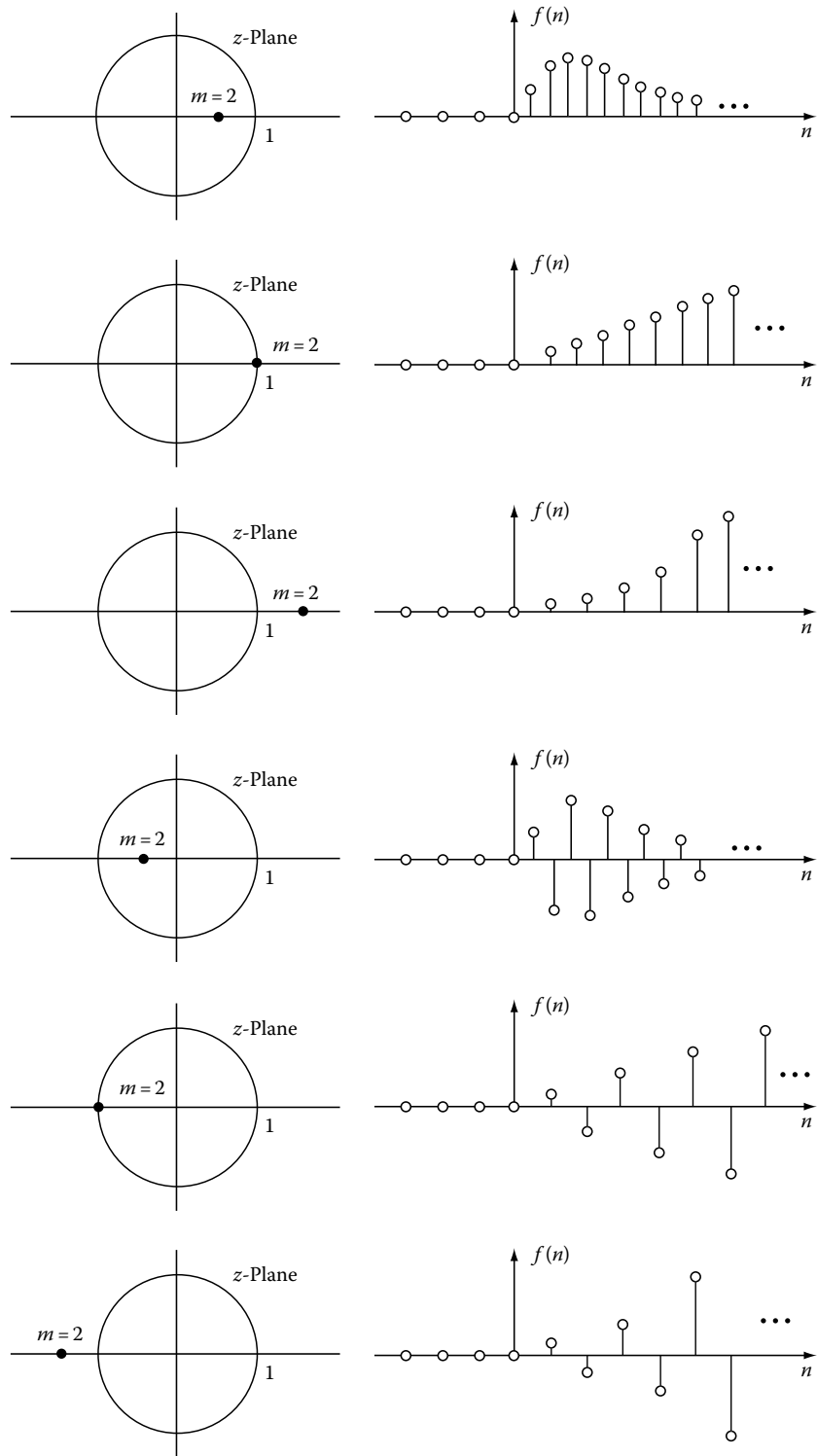


FIGURE 6.5 (continued)

(continued)



Complex-conjugate poles—Causal signals

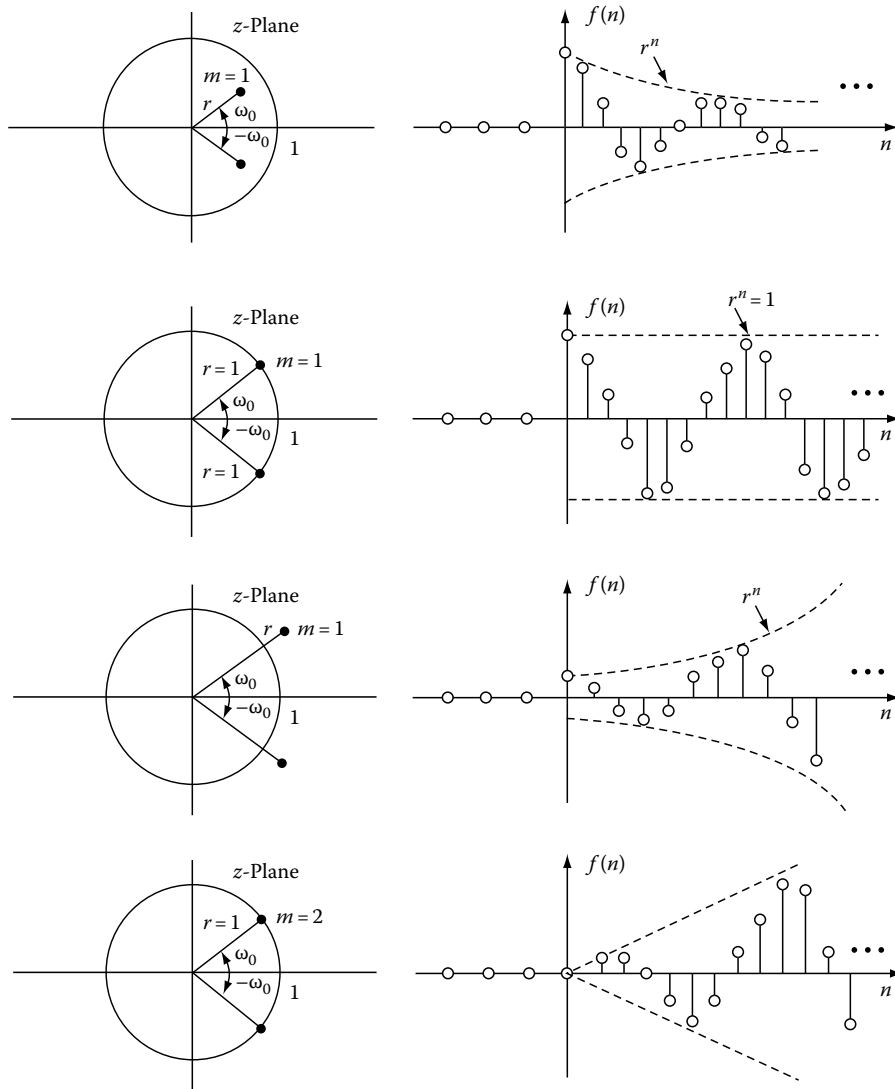


FIGURE 6.5 (continued)

$$\begin{aligned} \mathcal{Z}\{-u(-nT - T)\} &= - \sum_{n=-\infty}^{-1} u(-nT - T)z^{-n} \\ &= - \left[ \sum_{n=-\infty}^0 z^{-n} - 1 \right] \\ &= 1 - \sum_{n=0}^{\infty} z^n = 1 - \frac{1}{1-z} = \frac{z}{z-1} \quad |z| < 1 \end{aligned}$$

Although their Z-transform is identical their ROC is different. Therefore, to find the inverse Z-transform the ROC must also be given.

Figure 6.6 shows signal characteristics and their corresponding ROC.

Assuming that the algebraic expression for the Z-transform  $F(z)$  is a rational function and that  $f(nT)$  has finite amplitude, except possibly at infinities, the properties of the ROC are

1. The ROC is a ring or disc in the z-plane and centered at the origin, and  $0 \leq R_+ < |z| < R_- \leq \infty$ .
2. The Fourier transform converges also absolutely if and only if the ROC of the Z-transform of  $f(nT)$  includes the unit circle.
3. No poles exist in the ROC.
4. The ROC of a finite sequence  $\{f(nT)\}$  is the entire z-plane except possibly for  $z=0$  or  $z=\infty$ .
5. If  $f(nT)$  is left handed,  $0 \leq n < \infty$ , the ROC extends inward from the innermost pole of  $F(z)$  to infinity.
6. If  $f(nT)$  is left handed,  $-\infty < n < 0$ , the ROC extends inward from the innermost pole of  $F(z)$  to zero.

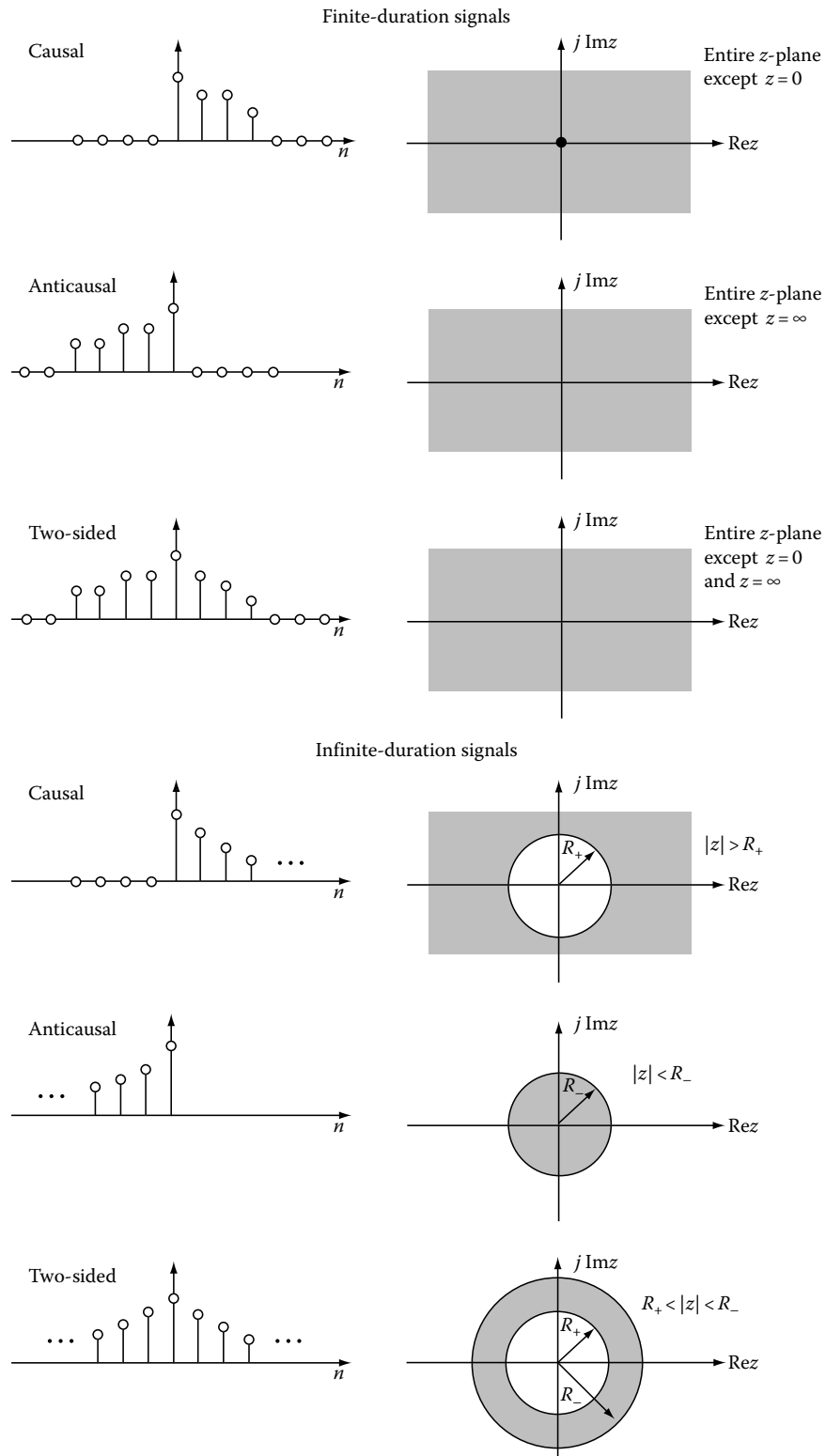


FIGURE 6.6

7. An infinite-duration two-sided sequence  $\{f(nT)\}$  has a ring as its ROC, bounded on the interior and exterior by a pole. The ring contains no poles.
8. The ROC must be a connected region.

### 6.1.2.2 Properties

#### 6.1.2.2.1 Linearity

The proof is similar to the one-sided Z-transform.

#### 6.1.2.2.2 Shifting

$$\mathcal{Z}_{II}\{f(nT \pm kT)\} = z^{\pm k}F(z) \quad (6.59) \quad \text{then}$$

*Proof*

$$\begin{aligned} \mathcal{Z}_{II}\{f(nT - kT)\} &= \sum_{n=-\infty}^{\infty} f(nT - kT)z^{-n} \\ &= z^{-k} \sum_{m=-\infty}^{\infty} f(mT)z^{-m} \end{aligned}$$

The last step results from setting  $m = n - k$ . Proceed similarly for the positive sign. The ROC of the shifted functions is the same as that of the unfinished function except at  $z=0$  for  $k > 0$  and  $z = \infty$  for  $k < 0$ .

#### Example

To find the transfer function of the system  $y(nT) - y(nT - T) + 2y(nT - 2T) = x(nT) + 4x(nT - T)$ , we take the Z-transform of both sides of the equation. Hence, we find

$$Y(z) - z^{-1}Y(z) + 2z^{-2}Y(z) = X(z) + 4z^{-1}X(z)$$

or

$$H(z) = \frac{Y(z)}{X(z)} = \frac{1 + 4z^{-1}}{1 - z^{-1} + 2z^{-2}}$$

#### Example

Consider the Z-transform

$$F(z) = \frac{1}{z - \frac{1}{2}} \quad |z| > \frac{1}{2}$$

Because the pole is inside the ROC, it implies that the function is causal. We next write the function in the form

$$F(z) = z^{-1} \frac{z}{z - \frac{1}{2}} = z^{-1} \frac{1}{1 - \frac{1}{2}z^{-1}} \quad |z| > \frac{1}{2}$$

which indicates that it is a shifted function (because of the multiplier  $z^{-1}$ ). Hence, the inverse transform is  $f(n) = \left(\frac{1}{2}\right)^{n-1} u(n-1)$  because the inverse transform of  $1/(1 - \frac{1}{2}z^{-1})$  is equal to  $\left(\frac{1}{2}\right)^n$ .

#### 6.1.2.2.3 Scaling

If

$$\mathcal{Z}_{II}\{f(nT)\} = F(z) \quad R_+ < |z| < R_-$$

then

$$\mathcal{Z}_{II}\{a^{nT}f(nT)\} = F(a^{-T}z) \quad |a^T|R_+ < |z| < |a^T|R_- \quad (6.60)$$

*Proof*

$$\begin{aligned} \mathcal{Z}_{II}\{a^{nT}f(nT)\} &= \sum_{n=-\infty}^{\infty} a^{nT}f(nT)z^{-n} = \sum_{n=-\infty}^{\infty} f(nT)(a^{-T}z)^{-n} \\ &= F(a^{-T}z) \end{aligned}$$

Because the ROC of  $F(z)$  is  $R_+ < |z| < R_-$ , the ROC of  $F(a^{-T}z)$  is

$$R_+ < |a^{-T}z| < R_- \quad \text{or} \quad R_+|a^T| < |z| < |a^T|R_-$$

#### Example

If the Z-transform of  $f(nT) = \exp(-|nT|)$  is

$$F(z) = \frac{1}{1 - e^{-nT}z} + \frac{1}{1 - e^{-nT}z^{-1}} - 1 \quad e^{-T} < |z| < e^T$$

then the Z-transform of  $g(nT) = a^{nT}f(nT)$  is

$$G(z) = \frac{1}{1 - e^{-nT}a^{-T}z} + \frac{1}{1 - e^{-nT}a^Tz^{-1}} - 1 \quad a^T e^{-T} < |z| < e^T a^T$$

#### 6.1.2.2.4 Time Reversal

If

$$\mathcal{Z}_{II}\{f(nT)\} = F(z) \quad R_+ < |z| < R_-$$

then

$$\mathcal{Z}_{II}\{f(-nT)\} = F(z^{-1}) \quad \frac{1}{R_-} < |z| < \frac{1}{R_+} \quad (6.61)$$

*Proof*

$$\mathcal{Z}_{II}\{f(-nT)\} = \sum_{n=-\infty}^{\infty} f(nT)z^{-n} = \sum_{n=-\infty}^{\infty} f(nT)(z^{-1})^{-n} = F(z^{-1})$$

and

$$\frac{1}{(n-1)!}(k+1)(k+2)\cdots(k+n-1)a^k, \quad k \leq -1 \quad \text{and} \quad |z| < \frac{1}{R_+}$$

The above means that if  $z_0$  belongs to the ROC of  $F(z)$  then  $1/z_0$  is in the ROC of  $F(z^{-1})$ . The reflection in the time domain corresponds to inversion in the  $z$ -domain.

**Example**

The Z-transform of  $f(n) = u(n)$  is  $z/(z-1)$  for  $|z| > 1$ . Therefore, the Z-transform of  $f(-n) = u(-n)$  is

$$\frac{\frac{1}{z}}{\frac{1}{z}-1} = \frac{1}{1-z}$$

Also, from the definition of the Z-transform, we write

$$\mathcal{Z}\{u(-n)\} = \sum_{n=-\infty}^0 z^{-n} = \sum_{n=0}^{\infty} z^n = \frac{1}{1-z}$$

**6.1.2.2.5 Multiplication by  $nT$**

If

$$\mathcal{Z}_{II}\{f(nT)\} = F(z) \quad R_+ < |z| < R_-$$

then

$$\mathcal{Z}_{II}\{nTf(nT)\} = -zT \frac{dF(z)}{dz} \quad R_+ < |z| < R_- \quad (6.62)$$

*Proof* A Laurent series can be differentiated term-by-term in its ROC and the resulting series has the same ROC. Therefore, we have

$$\frac{dF(z)}{dz} = \frac{d}{dz} \sum_{n=-\infty}^{\infty} f(nT)z^{-n} = \sum_{n=-\infty}^{\infty} -nf(nT)z^{-n-1}$$

for  $R_+ < |z| < R_-$

Multiply both sides by  $-zT$

$$-zT \frac{dF(z)}{dz} = \sum_{n=-\infty}^{\infty} nTf(nT)z^{-n} = \mathcal{Z}\{nTf(nT)\} \quad \text{for } R_+ < |z| < R_-$$

**Example**

If  $F(z) = \log(1 + az^{-1})$   $|z| > |a|$ , then

$$\frac{dF(z)}{dz} = \frac{-az^{-2}}{1+az^{-1}} \quad \text{or} \quad -z \frac{dF(z)}{dz} = az^{-1} \frac{1}{1-(-a)z^{-1}} \quad |z| > |a|$$

The  $z^{-1}$  implies a time shift, and the inverse transform of the fraction is  $(-a)^n$ . Hence, the inverse transform is

$a(-a)^{n-1} u(n-1)$ . From the differentiation property (with  $T = 1$ ), we obtain

$$nf(n) = a(-a)^{n-1} u(n-1) \quad \text{or} \quad f(n) = (-1)^{n-1} \frac{a^n}{n} u(n-1)$$

**Example**

If  $f(nT) = au(nT)$  then its Z-transform is  $F(z) = a/(1-z^{-1})$  for  $|z| > 1$ . Therefore,

$$\mathcal{Z}\{nTf(nT)\} = -zTa \frac{dF(z)}{dz} = aT \frac{z}{(z-1)^2} \quad |z| > 1$$

**6.1.2.2.6 Convolution**

If

$$\mathcal{Z}_{II}\{f_1(nT)\} = F_1(z) \quad \text{and} \quad \mathcal{Z}_{II}\{f_2(nT)\} = F_2(z)$$

then

$$F(z) = \mathcal{Z}_{II}\{f_1(nT) * f_2(nT)\} = F_1(z)F_2(z) \quad (6.63)$$

The ROC of  $F(z)$  is, at least, the intersection of that for  $F_1(z)$  and  $F_2(z)$ .

*Proof*

$$\begin{aligned} F(z) &= \sum_{n=-\infty}^{\infty} f(nT)z^{-n} = \sum_{n=-\infty}^{\infty} \left[ \sum_{m=-\infty}^{\infty} f_1(mT)f_2(nT-mT) \right] z^{-n} \\ &= \sum_{m=-\infty}^{\infty} f_1(mT) \left[ \sum_{n=-\infty}^{\infty} f_2(nT-mT)z^{-n} \right] \\ &= \sum_{m=-\infty}^{\infty} f_1(mT)z^{-m}F_2(z) = F_1(z)F_2(z) \end{aligned}$$

where the shifting property was invoked.

**Example**

The Z-transform of the convolution of  $e^{-n}u(n)$  and  $u(n)$  is

$$\begin{aligned} \mathcal{Z}_{II}\{(e^{-n}u(n)) * u(n)\} &= \mathcal{Z} \left\{ \sum_{m=0}^n e^{-m}u(n-m) \right\} \\ &= \mathcal{Z}\{e^{-n}\}\mathcal{Z}\{u(n)\} = \frac{z}{z-e^{-1}} \frac{z}{z-1} \end{aligned}$$

Also, from the convolution, definition we find

$$\begin{aligned} \mathcal{Z} \left\{ \sum_{m=0}^n e^{-m}u(n-m) \right\} &= \mathcal{Z} \left\{ \frac{1-e^{-n-1}}{1-e^{-1}} \right\} \\ &= \mathcal{Z} \left\{ \frac{1}{1-e^{-1}} - \frac{e^{-1}}{1-e^{-1}} e^{-n} \right\} \\ &= \frac{1}{1-e^{-1}} \left( \frac{z}{z-1} - e^{-1} \frac{z}{z-e^{-1}} \right) \\ &= \frac{z^2}{(z-1)(z-e^{-1})} \end{aligned}$$

which verifies the convolution property. The ROC for  $e^{-n}u(n)$  is  $|z| > e^{-1}$  and the ROC of  $u(n)$  is  $|z| > 1$ . The ROC of  $e^{-n}u(n) * u(n)$  is the intersection of these two ROCs and, hence, the ROC is  $|z| > 1$ .

### Example

The convolution of  $f_1(n) = \{2, 1, -3\}$  for  $n = 0, 1$ , and  $2$ , and  $f_2(n) = \{1, 1, 1, 1\}$  for  $n = 0, 1, 2$ , and  $3$  is

$$\begin{aligned} G(z) &= F_1(z)F_2(z) = (2 + z^{-1} - 3z^{-2})(1 + z^{-1} + z^{-2} + z^{-3}) \\ &= 2 + 3z^{-1} - 2z^{-4} - 3z^{-5} \end{aligned}$$

which indicates that the output is  $g(n) = \{2, 3, 0, 0, -2, -3\}$  which can easily be found by simply convoluting  $f_1(n)$  and  $f_2(n)$ .

#### 6.1.2.2.7 Correlation

If

$$\mathcal{Z}_{II}\{f_1(nT)\} = F_1(z) \quad \text{and} \quad \mathcal{Z}_{II}\{f_2(nT)\} = F_2(z)$$

then

$$\begin{aligned} \mathcal{Z}_{II}\{r_{f_1f_2}(\ell T)\} &\doteq \mathcal{Z}_{II}\{f_1(nT) \otimes f_2(nT)\} \\ &= \mathcal{Z}_{II}\left\{\sum_{n=-\infty}^{\infty} f_1(nT)f_2(nT - \ell T)\right\} \\ &= R_{f_1f_2}(z) = F_1(z)F_2(z^{-1}) \end{aligned} \quad (6.64)$$

The ROC of  $R_{f_1f_2}(z)$  is at least the intersection of that for  $F_1(z)$  and  $F_1(z^{-1})$ .

*Proof* But  $r_{f_1f_2}(\ell T) = f_1(\ell T) * f_2(-T\ell)$  and, hence, from the convolution property and the time-reversal property  $R_{f_1f_2}(z) = F_1(z)F_2(z^{-1})$ .

### Example

The transform of the autocorrelation sequencing  $f(nT) = a^{nT}u(n)$ ,  $-1 < a < 1$  is

$$R_{ff}(z) \doteq \mathcal{Z}_{II}\{r_{ff}(\ell T)\} = F(z)F(z^{-1})$$

But,

$$F(z) = \frac{1}{1 - a^T z^{-1}} \quad |z| > |a|^T \text{ causal signal}$$

and

$$F(z^{-1}) = \frac{1}{1 - a^T z} \quad |z| < \frac{1}{|a|^T} \text{ anticausal signal}$$

Hence,

$$R_{ff}(z) = \frac{1}{1 - a^T(z + z^{-1}) + a^{2T}} \quad \text{ROC} |a|^T < |z| < \frac{1}{|a|^T}$$

Because the ROC of  $R_{ff}(z)$  is a ring, it implies that  $r_{ff}(\ell T)$  is a two-sided signal.

We proceed to find the autocorrelation first

$$\begin{aligned} r_{ff}(nT) &= \sum_{m=n}^{\infty} a^{mT} a^{(m-n)T} = a^{-nT} \sum_{m=0}^{\infty} a^{2Tm} - a^{-nT} \sum_{m=0}^{n-1} a^{2Tm} \\ &= a^{-nT} \frac{1}{1 - a^{2T}} - a^{-nT} \frac{1 - a^{2Tn}}{1 - a^{2T}} = \frac{a^{nT}}{1 - a^{2T}} \quad n \geq 0 \\ r_{ff}(nT) &= \sum_{m=0}^{\infty} a^{mT} a^{(m-n)T} = a^{-nT} \frac{1}{1 - a^{2T}} \quad n \leq 0 \end{aligned}$$

and then compare by inverting the function  $F(z) F(z^{-1})$ .

#### 6.1.2.2.8 Multiplication by $e^{-anT}$

If

$$\mathcal{Z}_{II}\{f(nT)\} = F(z) \quad R_+ < |z| < R_-$$

then

$$\mathcal{Z}_{II}\{e^{-anT}f(nT)\} = F(e^{-aT}z)|e^{-aT}|R_+ < |z| < |e^{-aT}|R_-$$

*Proof*

$$\mathcal{Z}_{II}\{e^{-anT}f(nT)\} = \sum_{n=-\infty}^{\infty} f(nT)(e^{aT}z)^{-n} = F(e^{aT}z) \quad R_+ < |e^{aT}z| < R_-$$

#### 6.1.2.2.9 Frequency Translation

If the ROC of  $F(z)$  includes the unit circle and  $g(nT) = e^{j\omega_0 nT}f(nT)$ , then

$$G(\omega) = F(\omega - \omega_0) \quad (6.65)$$

*Proof* From (6.6.7)  $G(z) = F(e^{-j\omega_0 T}z)$  and has the same ROC as  $F(z)$  because  $|\exp(j\omega_0 T)| = 1$ . Therefore,

$$G(\omega) = G(z)|_{z=e^{j\omega T}} = F(e^{j(\omega - \omega_0)T}) = F(\omega - \omega_0)$$

#### 6.1.2.2.10 Product

If

$$\mathcal{Z}_{II}\{f(nT)\} = F(z) \quad R_{+f} < |z| < R_{-f} \quad (6.66)$$

$$\mathcal{Z}_{II}\{h(nT)\} = H(z) \quad R_{+h} < |z| < R_{-h} \quad (6.67)$$

$$g(nT) = f(nT)h(nT)$$

then

$$\begin{aligned} \mathcal{Z}_{II}\{f(nT)h(nT)\} &\doteq G(z) = \sum_{n=-\infty}^{\infty} f(nT)h(nT)z^{-n} \\ &= \frac{1}{2\pi j} \oint_C F(\tau)H\left(\frac{z}{\tau}\right) \frac{d\tau}{\tau} \\ &\quad R_{+f}R_{+h} < |z| < R_{-f}R_{-h} \end{aligned} \quad (6.68)$$

where  $C$  is any simple closed curve encircling the origin counter-clockwise with

$$\max\left(R_{+f}, \frac{|z|}{R_{-h}}\right) < |\tau| < \min\left(R_{-f}, \frac{|z|}{R_{+h}}\right) \quad (6.69)$$

*Proof* The series in Equation 6.68 will converge to an analytic function  $G(z)$  for  $R_{+g} < |z| < R_{-g}$ . Using the root test (see Section 6.2), we obtain

$$\begin{aligned} R_{+g} &= \overline{\lim}_{n \rightarrow \infty} (|f(nT)h(nT)|)^{1/n} \\ &\leq \overline{\lim}_{n \rightarrow \infty} (|f(nT)|)^{1/n} \overline{\lim}_{n \rightarrow \infty} (|h(nT)|)^{1/n} \\ &= R_{+f}R_{+h} \end{aligned} \quad (6.70)$$

for positive  $n$ . However,

$$F(z) = \sum_{n=-\infty}^0 f(nT)z^{-n} = \sum_{n=0}^{\infty} f(-nT)z^n \quad (6.71)$$

and this series converges if

$$|z| < \frac{1}{\overline{\lim}_{n \rightarrow \infty} (|f(-nT)|)^{1/n}} = R_{-f} \quad (6.72)$$

Hence,

$$\begin{aligned} R_{-g} &= \frac{1}{\overline{\lim}_{n \rightarrow \infty} (|f(-nT)h(-nT)|)^{1/n}} \\ &\geq \frac{1}{\overline{\lim}_{n \rightarrow \infty} (|f(-nT)|)^{1/n} \overline{\lim}_{n \rightarrow \infty} (|h(-nT)|)^{1/n}} \\ &\geq R_{-f}R_{-h} \end{aligned} \quad (6.73)$$

Replacing  $f(nT)$  in the summation of Equation 6.68 by its inversion formula 6.46, we find

$$\begin{aligned} G(z) &= \sum_{n=-\infty}^{\infty} \frac{1}{2\pi j} \oint_C F(\tau)\tau^n \frac{d\tau}{\tau} h(nT)z^{-n} \\ &= \frac{1}{2\pi j} \oint_C F(\tau) \sum_{n=-\infty}^{\infty} h(nT)\left(\frac{z}{\tau}\right)^{-n} \frac{d\tau}{\tau} \end{aligned} \quad (6.74)$$

The interchange of the sum and integral is justified if the integrand converges uniformly for some choice of  $C$  and  $z$ . The contour must be chosen so that

$$R_{+f} < |\tau| < R_{-f} \quad (6.75)$$

If

$$R_{+h} < \frac{|z|}{\tau} < R_{-h} \quad \text{or} \quad \frac{|z|}{R_{-h}} < |\tau| < \frac{|z|}{R_{+h}} \quad (6.76)$$

the series in the integrand of Equation 6.74 will converge uniformly to  $H(z/\tau)$ , and otherwise will diverge. Figure 6.7 shows the ROC for  $F(\tau)$  and  $H(z/\tau)$ . From Equations 6.75 and 6.76 we obtain

$$\begin{aligned} \frac{|z|}{R_{-h}} < R_{-f} \quad \text{or} \quad |z| < R_{-f}R_{-h} \\ \frac{|z|}{R_{+h}} > R_{+f} \quad \text{or} \quad |z| > R_{+f}R_{+h} \end{aligned}$$

or equivalently

$$R_{+f}R_{+h} < |z| < R_{-f}R_{-h} \quad (6.77)$$

When  $z$  satisfies the above equation, the intersection of the domain identified by Equations 6.75 and 6.76 is

$$\begin{aligned} (R_{+f} < |\tau| < R_{-f}) \cap \left(\frac{|z|}{R_{-h}} < |\tau| < \frac{|z|}{R_{+h}}\right) \\ = \max\left(R_{+f}, \frac{|z|}{R_{-h}}\right) < |\tau| < \min\left(R_{-f}, \frac{|z|}{R_{+h}}\right) \end{aligned} \quad (6.78)$$

The contour must be located inside the intersection.

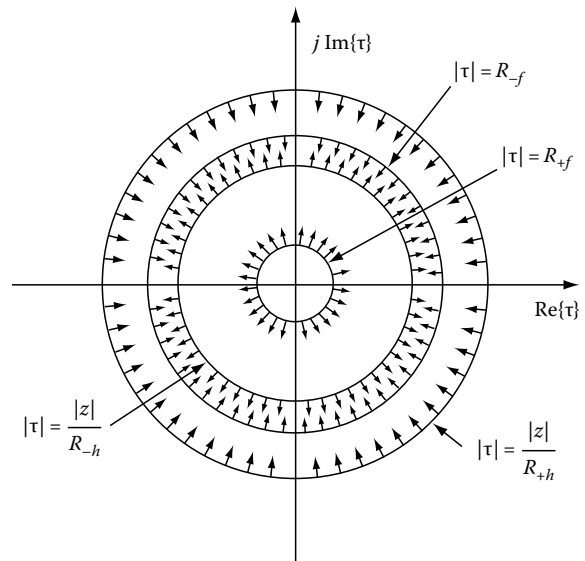


FIGURE 6.7

When signals are causal,  $R_{-f} = R_{-h} = \infty$  and the conditions 6.77 and 6.78 reduce to

$$R_{+f}R_{+h} < |z| \tag{6.79}$$

$$R_{+f} < |\tau| < \frac{|z|}{R_{+h}} \tag{6.80}$$

Hence, all of the poles of  $F(\tau)$  lie inside the contour and all the poles of  $H(z/\tau)$  lie outside the contour.

**Example**

The Z-transform of  $u(nT)$  is

$$F(z) = \frac{1}{1-z^{-1}} \quad |z| > 1 = R_{+f}, R_{-f} = \infty$$

and the Z-transform of  $h(nT) = \exp(-|nT|)$  is

$$H(z) = \frac{1 - e^{-2T}}{(1 - e^{-T}z^{-1})(1 - e^{-T}z)} \quad R_{+h} = e^{-T} < |z| < e^T = R_{-h}$$

But  $R_{-f} = \infty$  and, hence, from Equation 6.68  $1 \cdot \exp(-T) < |z| < \infty$ . The contour must lie in the region  $\max(1, |z|e^{-T}) < |\tau| < \min(-\infty, |z|e^{-T})$  as given by Equation 6.78. The pole-zero configuration and the contour are shown in Figure 6.8.

If we choose  $|z| > e^T$ , then the contour is that shown in the figure. Therefore, Equation 6.68 becomes

$$\begin{aligned} \mathcal{Z}_{II}\{u(nT)h(nT)\} &\doteq G(z) = \frac{1}{2\pi j} \oint_C \frac{1}{1-\tau^{-1}} \\ &\times \frac{1 - e^{-2T}}{(1 - e^{-T}\frac{z}{\tau})(1 - e^{-T}\frac{z}{\tau})} \frac{d\tau}{\tau} \end{aligned}$$

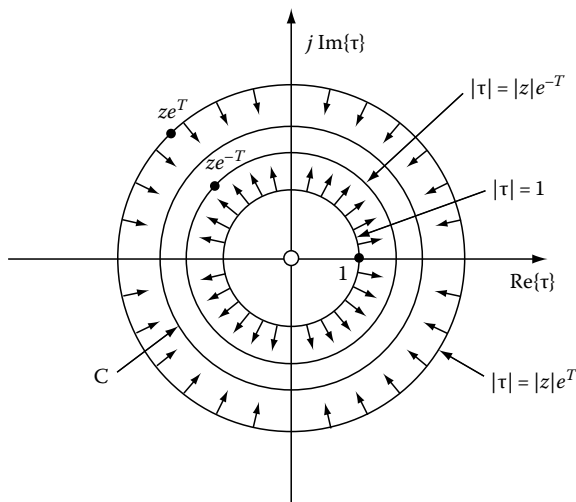


FIGURE 6.8

The poles of  $H(z/\tau)$  are at  $\tau = z \exp(-T)$  and  $\tau = z \exp(T)$ . Hence, the contour encloses the poles  $\tau = 1$  and  $\tau = z \exp(-T)$ . Applying the residue theorem next we obtain

$$G(z) = \frac{1}{(1 - e^{-T}z^{-1})} \quad |z| > e^{-T}$$

which has the inverse function  $g(nT) = e^{-nT}u(nT)$ , as expected.

**6.1.2.2.11 Parseval's Theorem**

If

$$\begin{aligned} \mathcal{Z}_{II}\{f(nT)\} &= F(z) \quad R_{+f} < |z| < R_{-f} \\ \mathcal{Z}_{II}\{h(nT)\} &= H(z) \quad R_{+h} < |z| < R_{-h} \end{aligned} \tag{6.81}$$

with

$$R_{+f}R_{+h} < |z| = 1 < R_{-f}R_{-h} \tag{6.82}$$

then we have

$$\sum_{n=-\infty}^{\infty} f(nT)h(nT) = \frac{1}{2\pi j} \oint_C F(z)H(z^{-1}) \frac{dz}{z} \tag{6.83}$$

where the contour encircles the origin with

$$\max\left(R_{+f}, \frac{1}{R_{-h}}\right) < |z| < \min\left(R_{-f}, \frac{1}{R_{+h}}\right) \tag{6.84}$$

*Proof* In Equations 6.68 and 6.69 set  $z = 1$  and replace the dummy variable  $\tau$  and  $z$  to obtain Equations 6.83 and 6.84.

For complex signals Parseval's relation 6.83 is modified as follows:

$$\sum_{n=-\infty}^{\infty} f(nT)h^*(nT) = \frac{1}{2\pi j} \oint_C F(z)H^*\left(\frac{1}{z^*}\right) \frac{dz}{z} \tag{6.85}$$

If  $f(nT)$  and  $h(nT)$  converge on the unit circle, we can use the unit circle as the contour. We then obtain

$$\begin{aligned} \sum_{n=-\infty}^{\infty} f(nT)h^*(nT) &= \frac{1}{\omega_s} \int_{-\omega_s/2}^{\omega_s/2} F(e^{j\omega T})H^*(e^{j\omega T})d\omega \\ \omega_s &= \frac{2\pi}{T} \end{aligned} \tag{6.86}$$

where we set  $z = e^{j\omega T}$ . If  $f(nT) = h(nT)$  then

$$\sum_{n=-\infty}^{\infty} |f(nT)|^2 = \frac{1}{\omega_s} \int_{-\omega_s/2}^{\omega_s/2} |F(e^{j\omega T})|^2 d\omega \tag{6.87}$$

**Example**

The Z-transform of  $f(nT) = \exp(-nT)u(nT)$  is  $F(z) = 1/(1 - e^{-T}z^{-1})$  for  $|z| > e^{-T}$ . From Equation 6.83 we obtain

$$\sum_{n=-\infty}^{\infty} f^2(nT) = \sum_{n=0}^{\infty} f^2(nT) = \frac{1}{2\pi j} \oint_C \frac{1}{1 - e^{-T}z^{-1}} \frac{1}{1 - e^{-T}z} \frac{dz}{z}$$

From Equation 6.84 we see that  $\max(e^{-T}, 0) < |z| < \min(\infty, e^T)$ . The contour encircles the pole at  $z = e^{-T}$  so that

$$\sum_{n=0}^{\infty} f^2(nT) = \text{res} \left\{ \left[ \frac{z - e^{-T}}{(z - e^{-T})(1 - e^{-T}z)} \right] \right\}_{z=e^{-T}} = \frac{1}{1 - e^{-2T}}$$

Also we find directly

$$\begin{aligned} \sum_{n=0}^{\infty} e^{-nT} e^{-nT} &= \sum_{n=0}^{\infty} e^{-2nT} = (1 + e^{-2T} + (e^{-2T})^2 + \dots) \\ &= \frac{1}{1 - e^{-2T}} \end{aligned}$$

**6.1.2.2.12 Complex Conjugate Signal**

If

$$\mathcal{Z}_{II}\{f(nT)\} = F(z) \quad R_{+f} < |z| < R_{-f}$$

then

$$\mathcal{Z}_{II}\{f \star (nT)\} = F \star (z^*) \quad R_{+f} < |z| < R_{-f} \quad (6.88)$$

*Proof* By definition we have

$$F(z) = \sum_{n=-\infty}^{\infty} f(nT)z^{-n}$$

Replacing  $z$  with  $z^*$  and taking the conjugate of both sides of the above equation, we obtain Equation 6.88.

**6.1.2.3 Inverse Z-Transform**

**6.1.2.3.1 Power Series Expansion**

The inverse Z-transform in operational form is given by

$$f(nT) = \mathcal{Z}_{II}^{-1}\{F(z)\}$$

If  $F(z)$  corresponds to a causal signal, then the signal can be found by dividing the denominator into the numerator to generate a power series in  $z^{-1}$  and recognizing that  $f(nT)$  is the coefficient of  $z^{-n}$ . Similarly, if it is known that  $f(nT)$  is zero for positive time ( $n$  positive), the value of  $f(nT)$  can be found by dividing the denominator into the numerator to generate a power series in  $z$ .

**Example**

If  $F(z) = [z(z+1)]/(z^2 - 2z + 1) = (1 + z^{-1})/(1 - 2z^{-1} + z^{-2})$  and the ROC is  $|z| > 1$ , then

$$\begin{aligned} 1 - 2z^{-1} + z^{-2} &= \sqrt{\frac{1+3z^{-1}+5z^{-2}+7z^{-3}+\dots}{1+z^{-1}}} \\ &= \frac{1 - 2z^{-1} + z^{-2}}{3z^{-1} - z^{-2}} \\ &= \frac{3z^{-1} - 6z^{-2} + 3z^{-3}}{5z^{-2} - 3z^{-3}} \\ &\dots \end{aligned}$$

and by continuing the division we recognize that

$$f(nT) = \begin{cases} 0 & n < 0 \\ (2n + 1) & n \geq 0 \end{cases}$$

If  $f(nT)$  is known to be zero for positive  $n$ , that the ROC is  $|z| < 1$ , then

$$\begin{aligned} z^{-2} - 2z^{-1} + 1 &= \sqrt{\frac{z+3z^2+5z^3+\dots}{z^{-1}+1}} \\ &= \frac{z^{-1} - 2 + z}{3 - z} \\ &= \frac{3 - 6z + 3z^2}{5z - 3z^2} \\ &\dots \end{aligned}$$

This series is recognized as

$$f(nT) = \begin{cases} -(2n + 1) & n < 0 \\ 0 & n \geq 0 \end{cases}$$

**Example**

If  $F(z) = \log(1 + 2z^{-1})$ ,  $|z| > 2$ , then using power series expansion for  $\log(1 + x)$ , with  $|x| < 1$ , we obtain

$$F(z) = \sum_{n=1}^{\infty} \frac{(-1)^{n+1} 2^n z^{-n}}{n}$$

which indicates that

$$f(nT) = \begin{cases} (-1)^{n+1} \frac{2^n}{n} & n \geq 0 \\ 0 & n \leq 0 \end{cases}$$

In general, any *improper* rational function ( $M \geq N$ ) can be expressed as

$$\begin{aligned} F(z) &= \frac{N(z)}{D(z)} = \frac{b_0 + b_1z^{-1} + \dots + b_Mz^{-M}}{1 + a_1z^{-1} + \dots + a_Nz^{-N}} \\ &= c_0 + c_1z^{-1} + \dots + c_{M-N}z^{-(M-N)} + \frac{N_1(z)}{D(z)} \end{aligned} \quad (6.89)$$



where the inverse Z-transform of the polynomial can easily be found by inspection.

A proper function ( $M < N$ ) is of the form

$$F(z) = \frac{N(z)}{D(z)} = \frac{b_0 + b_1z^{-1} + \dots + b_Mz^{-M}}{1 + a_1z^{-1} + \dots + a_Nz^{-N}} \quad a_N \neq 0, M < N$$

or

$$F(z) = \frac{N(z)}{D(z)} = \frac{b_0z^N + b_1z^{N-1} + \dots + b_Mz^{N-M}}{z^N + a_1z^{N-1} + \dots + a_N} \quad (6.90)$$

Because  $N > M$ , the function

$$\frac{F(z)}{z} = \frac{b_0z^{N-1} + b_1z^{N-2} + \dots + b_Mz^{N-M-1}}{z^N + a_1z^{N-1} + \dots + a_N} \quad (6.91)$$

is always a proper function.

### 6.1.2.3.2 Partial Fraction Expansion

*Distinct poles*

If the poles  $p_1, p_2, \dots, p_N$  on a proper function  $F(z)$  are all different, then we expand it in the form

$$\frac{F(z)}{z} = \frac{A_1}{z - p_1} + \frac{A_2}{z - p_2} + \dots + \frac{A_N}{z - p_N} \quad (6.92)$$

where all  $A_i$  are unknown constants to be determined.

The inverse Z-transform of the  $k$ th term of Equation 6.92 is given by

$$\begin{aligned} & \mathcal{Z}^{-1} \left\{ \frac{1}{1 - p_k z^{-1}} \right\} \\ &= \begin{cases} (p_k)^n u(nT) & \text{if ROC: } |z| > |p_k| \text{ (causal signal)} \\ -(p_k)^n u(-nT - T) & \text{if ROC: } |z| < |p_k| \text{ (anticausal signal)} \end{cases} \end{aligned} \quad (6.93)$$

If the signal is causal, the ROC is  $|z| > p_{\max}$ , where  $p_{\max} = \max\{|p_1|, |p_2|, \dots, |p_N|\}$ . In this case, all terms in Equation 6.92 result in causal signal components.

#### Example

(a) If  $F(z) = z(z + 3)/(z^2 - 3z + 2)$  with  $|z| > 2$  then

$$\begin{aligned} \frac{F(z)}{z} &= \frac{(z + 3)}{(z - 2)(z - 1)} = \frac{A_1}{z - 2} + \frac{A_2}{z - 1} \\ A_1 &= \left. \frac{(z + 3)(z - 2)}{(z - 2)(z - 1)} \right|_{z=2} = 5, \quad A_2 = \left. \frac{(z + 3)(z - 1)}{(z - 2)(z - 1)} \right|_{z=1} = -4 \end{aligned}$$

Therefore,

$$F(z) = 5 \frac{z}{z - 2} - 4 \frac{z}{z - 1} \quad \text{or} \quad f(nT) = 5(2)^n - 4(1)^n \quad n \geq 0$$

(b) If  $F(z) = z(z + 3)/(z^2 - 3z + 2)$  with  $1 < |z| > 2$ , then following exactly the same procedure

$$F(z) = 5 \frac{z}{z - 2} - 4 \frac{z}{z - 1}$$

However, the pole at  $z = 2$  belongs to the negative-time sequence and the pole at  $z = 1$  belongs to the positive-time sequence. Hence,

$$f(nT) = \begin{cases} -4(1)^n & n \geq 0 \\ -5(2)^n & n \leq -1 \end{cases}$$

#### Example

To determine the inverse Z-transform of  $F(z) = 1/(1 - 1.5z^{-1} + 0.5z^{-2})$  if (a) ROC:  $|z| > 1$ , (b) ROC:  $|z| < 0.5$ , and (c) ROC:  $0.5 < |z| < 1$ , we proceed as follows:

$$F(z) = \frac{z^2}{z^2 - 1.5z + 0.5} = \frac{z^2}{(z - 1)(z - \frac{1}{2})} = A + \frac{Bz}{z - 1} + \frac{Cz}{z - \frac{1}{2}}$$

or

$$F(z) = 2 \frac{z}{z - 1} - \frac{z}{z - \frac{1}{2}}$$

- (a)  $f(nT) = 2(1)^n - (1/2)^n, n \geq 0$  because both poles are outside the ROC  $|z| > 1$  (inside the unit circle).
- (b)  $f(nT) = -2(1)^n u(-nT - T) + (1/2)^n u(-nT - T), n \leq -1$  because both poles are outside the ROC (outside the circle  $|z| = 0.5$ ).
- (c) Pole at  $1/2$  provides the causal part and the pole at  $1$  provides the anticausal. Hence,

$$f(nT) = -2(1)^n u(-nT - T) - \left(\frac{1}{2}\right)^n u(nT) \quad -\infty < n < \infty$$

*Multiple poles*

If  $F(z)$  has repeated poles, we must modify the form of the expansion. Suppose  $F(z)$  has a pole of multiplicity  $m$  at  $z = p_i$ . Then one form of expansion is of the form

$$A_1 \frac{z}{z - p_i} + A_2 \frac{z^2}{(z - p_i)^2} + \dots + A_m \frac{z^m}{(z - p_i)^m} \quad (6.94)$$

The following example shows how to find  $A_i$ 's.

**Example**

Let the transfer function of each of two cascade systems be  $1/(1 - (1/2)z^{-1})$ . If the input to this system is the unit step function  $1/(1 - z^{-1})$ , then its output is

$$F(z) = \frac{1}{1 - z^{-1}} \frac{1}{(1 - \frac{1}{2}z^{-1})^2} = \frac{z^3}{(z - 1)(z - \frac{1}{2})^2}$$

$$= A_0 + \frac{A_1z}{z - 1} + \frac{A_2z}{z - \frac{1}{2}} + \frac{A_3z^2}{(z - \frac{1}{2})^2} \quad |z| > 1$$

If we set  $z=0$  in both sides, we find that  $A_0=0$ . Next we find  $A_3$  by multiplying both sides by  $(z - 1/2)^2$  and setting  $z = 1/2$ . Hence,

$$A_3 = \frac{z^3(z - \frac{1}{2})^2}{z^2(z - 1)(z - \frac{1}{2})^2} \Big|_{z=\frac{1}{2}} = \frac{\frac{1}{2}}{\frac{1}{2} - 1} = -1$$

and then we write

$$\frac{z^3}{(z - 1)(z - \frac{1}{2})^2} = \frac{A_1z}{z - 1} + \frac{A_2z}{z - \frac{1}{2}} + \frac{z^2}{(z - \frac{1}{2})^2}$$

$$= \frac{A_1z(z - \frac{1}{2})^2 + A_2z(z - 1)(z - \frac{1}{2}) - z^2(z - 1)}{(z - 1)(z - \frac{1}{2})^2}$$

$$= \frac{(A_1 + A_2 - 1)z^3 + (1 - \frac{3}{2}A_2 - A_1)z^2 + (\frac{1}{4}A_1 + \frac{1}{2}A_2)z}{(z - 1)(z - \frac{1}{2})^2}$$

Equating coefficients of equal powers, we obtain the system

$$A_1 + A_2 - 1 = 1, \quad 1 - A_1 - \frac{3}{2}A_2 = 0, \quad A_1 = 4 \quad \text{and} \quad A_2 = -2$$

Hence,

$$\frac{z^3}{(z - 1)(z - \frac{1}{2})^2} = 4 \frac{z}{z - 1} - 2 \frac{z}{z - \frac{1}{2}} - \frac{z^2}{(z - \frac{1}{2})^2}$$

and the output is

$$f(nT) = 4(1)^n - 2\left(\frac{1}{2}\right)^n - (n + 1)\left(\frac{1}{2}\right)^n \quad n \geq 0$$

Another form of expansion of a proper function (the degree of the denominator is one less than the numerator) is of the form

$$\frac{A_1}{z - p_i} + \frac{A_2z}{(z - p_i)^2} + \frac{A_3z(z + p_i)}{(z - p_i)^3} \quad (6.95)$$

and the following example explains its use (see Table A.6.4).

**Example**

Using the previous example for  $F(z)$  with  $|z| > 1$ , we obtain

$$F(z) = \frac{z^3}{(z - 1)(z - \frac{1}{2})^2} = 1 + \frac{2z^2 - \frac{5}{4}z + \frac{1}{4}}{(z - 1)(z - \frac{1}{2})^2}$$

$$= 1 + \frac{A_1}{z - 1} + \frac{A_2}{(z - \frac{1}{2})} + \frac{A_3z}{(z - \frac{1}{2})^2}$$

Hence,

$$A_1 = \frac{(2z^2 - \frac{5}{4}z + \frac{1}{4})(z - 1)}{(z - 1)(z - \frac{1}{2})^2} \Big|_{z=1} = 4,$$

$$A_3 = \frac{1}{z} \frac{(2z^2 - \frac{5}{4}z + \frac{1}{4})(z - \frac{1}{2})^2}{(z - 1)(z - \frac{1}{2})^2} \Big|_{z=\frac{1}{2}} = -\frac{1}{2},$$

$$A_2 = -\frac{3}{2}$$

where  $A_2$  was found by setting an arbitrary value of  $z$ , that is,  $z = -1$ , in both sides of the equation. Therefore, the inverse Z-transform is given by

$$f(nT) = \begin{cases} \delta(n) & n = 0 \\ 4(1)^{n-1} - \frac{3}{2}\left(\frac{1}{2}\right)^{n-1} - \frac{1}{2}n\left(\frac{1}{2}\right)^{n-1} & n \geq 1 \end{cases}$$

**Example**

Now let us assume the same example but with  $|z| < 1/2$ . This indicates that the output signal is anticausal. Hence, from

$$F(z) = 4 \frac{z}{z - 1} - 2 \frac{z}{z - \frac{1}{2}} - \frac{z^2}{(z - \frac{1}{2})^2}$$

and Table A.6.3, we obtain

$$f(nT) = -4(1)^n + 2\left(\frac{1}{2}\right)^n + (n + 1)\left(\frac{1}{2}\right)^n \quad n \leq -1$$

Similarly from

$$F(z) = 1 + 4 \frac{1}{z - 1} - \frac{3}{2} \frac{1}{z - \frac{1}{2}} - \frac{1}{2} \frac{z}{(z - \frac{1}{2})^2}$$

and Table A.6.4, we obtain

$$f(nT) = \begin{cases} \delta(n) & n = 0 \\ -4(1)^{n-1} + \frac{3}{2}\left(\frac{1}{2}\right)^{n-1} + \frac{1}{2}n\left(\frac{1}{2}\right)^{n-1} & n \leq -1 \end{cases}$$

### 6.1.2.3.3 Integral Inversion Formula

#### THEOREM 6.1

If

$$F(z) = \sum_{m=-\infty}^{\infty} f(mT)z^{-m} \quad (6.96)$$

converges to an analytic function in the annular domain  $R_+ < |z| < R_-$ , then

$$f(nT) = \frac{1}{2\pi j} \oint_C F(z)z^n \frac{dz}{z} \quad (6.97)$$

where  $C$  is any simple closed curve separating  $|z|=R_+$  from  $|z|=R_-$  and it is traced in the counterclockwise direction.

*Proof* Multiply Equation 6.96 by  $z^{n-1}$  and integrate around  $C$ . Then

$$\frac{1}{2\pi j} \oint_C F(z)z^n \frac{dz}{z} = \sum_{m=-\infty}^{\infty} f(mT) \frac{1}{2\pi j} \oint_C z^{n-m} \frac{dz}{z} \quad (6.98)$$

Set  $z = Re^{j\theta}$  with  $R_+ < R < R_-$  to obtain

$$\begin{aligned} \frac{1}{2\pi j} \oint_C z^{n-m} \frac{dz}{z} &= \frac{1}{2\pi j} \int_0^{2\pi} R^{n-m-1} e^{j\theta(n-m-1)} R j e^{j\theta} d\theta \\ &= \frac{1}{2\pi} R^k \int_0^{2\pi} e^{j\theta k} d\theta \\ &= \begin{cases} 1 & k = 0 \\ 0 & \text{elsewhere} \end{cases} \end{aligned} \quad (6.99)$$

Hence, the summation on the right-hand side of Equation 6.98 reduces to  $f(nT)$ .

Let  $\{a_k\}$  be the set of poles of  $F(z)z^{n-1}$  inside the contour  $C$  and  $\{b_k\}$  be the set of poles of  $F(z)z^{n-1}$  outside  $C$  in a finite region of the  $z$ -plane. By Cauchy's residue theorem

$$f(nT) = \sum_k \text{Res}\{F(z)z^{n-1}, a_k\} \quad n \geq 0 \quad (6.100)$$

$$f(nT) = -\sum_k \text{Res}\{F(z)z^{n-1}, b_k\} \quad n < 0 \quad (6.101)$$

#### Example

Let

$$F(z) = \frac{1}{(1-z^{-1})(1-a^T z^{-1})} \quad a < 1, |z| > 1$$

The function  $F(z)z^{n-1} = z^{n+1}/(z-1)(z-a^T)$  has two poles enclosed by  $C$  for  $n \geq 0$ . Hence,

$$\begin{aligned} f(nT) &= \text{Res}\{F(z)z^{n-1}, 1\} + \text{Res}\{F(z)z^{n-1}, a\} \\ &= \frac{1}{1-a^T} + \frac{a^{(n+1)T}}{a^T-1} \quad n \geq 0 \end{aligned}$$

#### Example

Let

$$F(z) = \frac{1-0.8^2}{(1-0.8z)(1-0.8z^{-1})} \quad 0.8 < |z| < 0.8^{-1}$$

For  $n \geq 0$  the contour  $C$  encloses only the pole  $z=0.8$  of the function  $F(z)z^{n-1}$ . Therefore,

$$\begin{aligned} f(nT) &= \text{Res}\{F(z)z^{n-1}\}_{z=0.8} = \left. \frac{(1-0.8^2)z^n(z-0.8)}{(1-0.8z)(z-0.8)} \right|_{z=0.8} \\ &= 0.8^n \quad n \geq 0 \end{aligned}$$

For  $n < 0$  only the pole  $z=1/0.8$  is outside  $C$ . Hence,

$$\begin{aligned} f(nT) &= -\text{Res}\{F(z)z^{n-1}\}_{z=1/0.8} \\ &= -\left. \frac{(1-0.8^2)0.8^{-1}z^n(z-0.8^{-1})}{-(1-0.8^{-1})(z-0.8)} \right|_{z=0.8^{-1}} = 0.8^{-n} \quad n \leq -1 \end{aligned}$$

The residue for a multiple pole of order  $k$  at  $z_0$  is given by

$$\begin{aligned} \text{Res}\{F(z)z^{n-1}\}_{z=z_0} &= \lim_{z \rightarrow z_0} \frac{1}{(k-1)!} \frac{d^{k-1}}{dz^{k-1}} \\ &\quad \times [(z-z_0)^k F(z)z^{n-1}] \end{aligned} \quad (6.102)$$

## 6.1.3 Applications

### 6.1.3.1 Solutions of Difference Equations with Constant Coefficients

Based on the relation

$$\mathcal{Z}\{f(n-m)\} = \sum_{\ell=-m}^{-1} f(\ell)z^{-(\ell+m)} = z^{-m}F(z) \quad (6.103)$$

where  $\mathcal{Z}\{f(n)\} = F(z)$ , we can solve a difference equation of the form

$$\sum_{k=0}^N a_k y(n-k) = \sum_{k=0}^L b_k f(n-k) \quad (6.104)$$

using the  $Z$ -transform approach.

**Example**

To find the solution to  $y(n) = y(n-1) + 2y(n-2)$  with initial conditions  $y(0) = 1$  and  $y(1) = 2$ , we proceed as follows:

From the difference equation

$$\begin{aligned} y(0) &= y(-1) + 2y(-2) = 1 \\ y(1) &= y(0) + 2y(-1) = 2 \end{aligned}$$

Hence,  $y(-1) = \frac{1}{2}$  and  $y(-2) = \frac{1}{4}$ . The Z-transform of the difference equation is given by

$$\begin{aligned} Y(z) &= \sum_{\ell=-1}^{-1} y(\ell)z^{-(\ell+1)} + z^{-1}Y(z) + 2\left(\sum_{\ell=-2}^{-1} y(\ell)z^{-(\ell+2)} + z^{-2}Y(z)\right) \\ &= y(-1) + z^{-1}Y(z) + 2(y(-2) + y(-1)z^{-1} + z^{-2}Y(z)) \\ &= \frac{1}{2} + z^{-1}Y(z) + \frac{1}{2} + z^{-1} + 2z^{-2}Y(z) \\ &= 1 + z^{-1} + z^{-1}Y(z) + 2z^{-2}Y(z) \end{aligned}$$

Hence,

$$\begin{aligned} Y(z) &= \frac{1}{1 - z^{-1} - 2z^{-2}} + \frac{z^{-1}}{1 - z^{-1} - 2z^{-2}} \\ &= \frac{z^2}{z^2 - z - 2} + \frac{z}{z^2 - z - 2} \end{aligned}$$

and

$$\mathcal{Z}^{-1}\{Y(z)\} \doteq y(n) = \mathcal{Z}^{-1}\left\{\frac{z^2}{z^2 - z - 2}\right\} + \mathcal{Z}^{-1}\left\{\frac{z}{z^2 - z - 2}\right\}$$

**Example**

The solution of the difference equation  $y(n) - ay(n-1) = u(n)$  with initial condition  $y(-1) = 2$  and  $|a| < 1$  proceeds as follows:

$$\begin{aligned} Y(z) - ay(-1) - az^{-1}Y(z) &= \frac{z}{z-1} \\ Y(z) &= \frac{2a}{1-az^{-1}} + \frac{z}{z-1} \frac{1}{1-az^{-1}} = \frac{2a}{1-az^{-1}} + \frac{z^2}{(z-1)(z-a)} \\ &= \frac{2a}{1-az^{-1}} + \frac{1}{1-a} \frac{1}{1-z^{-1}} + \frac{a}{a-1} \frac{1}{1-az^{-1}} \end{aligned}$$

Hence, the inverse Z-transform gives

$$\begin{aligned} y(n) &= \underbrace{2a \cdot a^n}_{\text{zero input}} + \underbrace{\frac{1}{1-a} u(n) + \frac{a}{a-1} a^n}_{\text{zero state}} \\ &= \underbrace{\frac{1}{1-a} u(n)}_{\text{steady state}} + \underbrace{\frac{2a-1}{a-1} a^{n+1}}_{\text{transient}} \quad n \geq 0 \end{aligned}$$

**6.1.3.2 Analysis of Linear Discrete Systems**

**6.1.3.2.1 Transfer Function**

From Equation 6.104 we obtain the *transfer function* by ignoring initial conditions. The result is

$$H(z) = \frac{Y(z)}{F(z)} = \frac{\sum_{k=0}^L b_k z^{-k}}{\sum_{k=0}^N a_k z^{-k}} = \text{transfer function} \quad (6.105)$$

where  $H(z)$  is the *transform of the impulse response of a discrete system*.

**6.1.3.2.2 Stability**

Using the convolution relation between input and output of a discrete systems, we obtain

$$|y(n)| = \left| \sum_{k=0}^n h(k)f(n-k) \right| \leq M \sum_{k=0}^{\infty} |h(k)| < \infty \quad (6.106)$$

where  $M$  is the maximum value of  $f(n)$ . The above inequality specifies that a discrete system is stable if to a finite input the absolute sum of its impulse response is finite. From the properties of the Z-transform, the ROC of the impulse response satisfying Equation 6.106 is  $|z| > 1$ . Hence, all the poles of  $H(z)$  of a stable system lie inside the unit circle.

The modified Schur-Cohn criterion establishes if the zeros of the denominator of the rational transfer function  $H(z) = N(z)/D(z)$  are inside or outside the unit circle.

The first step is to form the polynomial

$$D_{rp}(z) = z^N D(z^{-1}) = d_0 z^N + \dots + d_{N-1} z + d_N$$

where  $D(z^{-1}) = d_0 + \dots + d_{N-1} z^{N-1} + d_N z^N$ . This  $D_{rp}(z)$  is called the *reciprocal polynomial* associated with  $D(z)$ . The roots of  $D_{rp}(z)$  are the reciprocals of the roots of  $D(z)$  and  $|D_{rp}(z)| = |D(z)|$  on the unit circle. Next, we must divide  $D_{rp}(z)$  by  $D(z)$  starting at the high power and obtain the quotient  $\alpha_0 = d_0/d_N$  and the remainder  $D_{1rp}(z)$  of degree  $N-1$  or less, so that

$$\frac{D_{rp}(z)}{D(z)} = \alpha_0 + \frac{D_{1rp}(z)}{D(z)}$$

The division is repeated with  $D_{1rp}(z)$  and its reciprocal polynomial  $D_1(z)$  and the sequence  $\alpha_0, \alpha_1, \dots, \alpha_{N-2}$  is generated according to the rule

$$\frac{D_{k rp}(z)}{D_k(z)} = \alpha_k + \frac{D_{(k+1) rp}(z)}{D_k(z)} \quad \text{for } k = 0, 1, 2, \dots, N-2$$

The zeros of  $D(z)$  are all inside the unit circle (stable system) if and only if the following three conditions are satisfied:

1.  $D(1) > 0$
2.  $D(-1) \begin{cases} < 0 & N \text{ odd} \\ > 0 & N \text{ even} \end{cases}$
3.  $|\alpha_k| < 1$  for  $k=0, 1, \dots, N-2$

Check conditions (1) and (2) before proceeding to (3). If they are not satisfied, the system is unstable.

### Example

$$D(z) = z^3 - 0.2z^2 + z - 0.2, \quad D_{rp}(z) = -0.2z^3 + z^2 - 0.2z + 1$$

$$\alpha_0 = \frac{-0.2z^3 + z^2 - 0.2z + 1}{z^3 - 0.2z^2 + z - 0.2} = -0.2 + \frac{0.8z^2 + 0.96}{D(z)},$$

$$\alpha_1 = \frac{0.96z^2 + 0.96}{0.96z^2 + 0.96} = 1$$

Because  $|\alpha_1| = 1$ , condition (3) is not satisfied and the system is unstable.

The transfer function of a feedback system with forward (open-loop) gain  $D(z)G(z)$  and unit feedback gain is given by

$$H(z) = \frac{D(z)G(z)}{1 + D(z)G(z)}$$

Assuming that all the individual systems are causal and have rational transfer function, the open-loop gain  $D(z)G(z)$  can be written as

$$D(z)G(z) = \frac{A(z)}{B(z)}$$

where

$$A(z) = a_L z^L + \dots + a_0, \quad B(z) = z^M + b_{M-1} z^{M-1} + \dots + b_0, \quad L \leq M$$

Hence, the total transfer function becomes

$$H(z) = \frac{A(z)}{B(z) + A(z)}$$

which indicates that the system will be stable if  $B(z) + A(z)$  or  $1 + D(z)G(z)$  has zeros inside the unit circle.

#### 6.1.3.2.3 Causality

A system is causal if  $h(n) = 0$  for  $n < 0$ . From the properties of the  $Z$ -transform,  $H(z)$  is regular in the ROC and at the infinity point. For rational functions the numerator polynomial has to be at most of the same degree as the polynomial in the denominator.

The Paley-Wiener theorem provides the necessary and sufficient conditions that a frequency response characteristic  $H(\omega)$  must satisfy in order for the resulting filter to be causal.

#### 6.1.3.2.4 Paley-Wiener Theorem

If  $h(n)$  has finite energy and  $h(n) = 0$  for  $n < 0$ , then

$$\int_{-\pi}^{\pi} |\ell n |H(\omega)| d\omega < \infty$$

Conversely, if  $|H(\omega)|$  is square integrable and if the above integral is finite, then we can associate with  $|H(\omega)|$  a phase response with  $\varphi(\omega)$  so that the resulting filter with frequency response

$$H(\omega) = |H(\omega)|e^{j\varphi(\omega)}$$

is causal.

The relationship between the real and imaginary parts of an absolutely summable, causal, and real sequence is given by the relation

$$H_i(\omega) = -\frac{1}{2\pi} \int_{-\pi}^{\pi} H_r(\lambda) \cot \frac{\omega - \lambda}{2} d\lambda$$

which is known as the *discrete Hilbert transform*.

Summary of causality

1.  $H(\omega)$  cannot be zero except at a finite set of points.
2.  $|H(\omega)|$  cannot be constant in any finite range of frequencies.
3. The transition from pass band to stop band cannot be infinitely sharp.
4. The real and imaginary parts of  $H(\omega)$  are independent and are related by the discrete Hilbert transform.
5.  $|H(\omega)|$  and  $\varphi(\omega)$  cannot be chosen arbitrarily.

#### 6.1.3.2.5 Frequency Characteristics

With input  $f(n) = e^{j\omega n}$ , the output is

$$\begin{aligned} y(n) &= \sum_{k=0}^{\infty} h(k) e^{j\omega(n-k)} = e^{j\omega n} \sum_{k=0}^{\infty} h(k) e^{-j\omega k} \\ &= e^{j\omega n} H(e^{j\omega}) \end{aligned} \quad (6.107)$$

where

$$\begin{aligned} H(e^{j\omega}) &= H(z)|_{z=e^{j\omega}} = H_r(e^{j\omega}) + jH_i(e^{j\omega}) \\ &= A(\omega)e^{j\varphi(\omega)} \end{aligned} \quad (6.108)$$

$$A(\omega) = [H_r^2(e^{j\omega}) + H_i^2(e^{j\omega})]^{1/2} = \text{amplitude response} \quad (6.109)$$

$$\varphi(\omega) = \tan^{-1} [H_i(e^{j\omega})/H_r(e^{j\omega})] = \text{phase response} \quad (6.110)$$

$$\begin{aligned} \tau(\omega) &= -\frac{d\varphi(\omega)}{d\omega} = -\text{Re} \left\{ z \frac{d}{dz} \ell n H(z) \right\} \Big|_{z=e^{j\omega}} \\ &= \text{group delay characteristic} \end{aligned} \quad (6.111)$$

Because  $H(e^{j\omega}) = H(e^{j(\omega + 2\pi k)})$  it implies that the *frequency characteristics of discrete systems are periodic with period  $2\pi$* .

#### 6.1.3.2.6 Z-Transform and Discrete Fourier Transform (DFT)

If  $x(n)$  has a finite duration of length  $N$  or less, the sequence can be recovered from its  $N$ -point DFT. Hence, its  $Z$ -transform is uniquely determined by its  $N$ -point DFT. Hence, we find

$$\begin{aligned}
 X(z) &= \sum_{n=0}^{N-1} x(n)z^{-n} = \sum_{n=0}^{N-1} \left[ \frac{1}{N} \sum_{k=0}^{N-1} X(k)e^{j2\pi kn/N} \right] z^{-n} \\
 &= \frac{1}{N} \sum_{k=0}^{N-1} X(k) \sum_{n=0}^{N-1} (e^{j2\pi k/N} z^{-1})^n \\
 &= \frac{1 - z^{-N}}{N} \sum_{k=0}^{N-1} \frac{X(k)}{1 - e^{j2\pi k/N} z^{-1}} \tag{6.112}
 \end{aligned}$$

Set  $z = e^{j\omega}$  (evaluated on the unit circle) to find

$$X(e^{j\omega}) \doteq X(\omega) = \frac{1 - e^{-j\omega N}}{N} \sum_{k=0}^{N-1} \frac{X(k)}{1 - e^{-j(\omega - 2\pi k/N)}} \tag{6.113}$$

$X(\omega)$  is the Fourier transform of the finite-duration sequence in terms of its DFT.

### 6.1.3.3 Digital Filters

#### 6.1.3.3.1 Infinite Impulse Response (IIR) Filters

A discrete, linear, and time invariant system can be described by a higher-order difference equation of the form

$$y(n) - \sum_{k=1}^N a_k y(n-k) = \sum_{k=0}^M b_k x(n-k) \tag{6.114}$$

Taking the Z-transform of the above equation and solving for the ratio  $Y(z)/X(z)$ , we obtain

$$H(z) = \frac{Y(z)}{X(z)} = \frac{\sum_{k=0}^M b_k z^{-k}}{1 - \sum_{k=1}^N a_k z^{-k}} \tag{6.115}$$

The block diagram representation of Equation 6.114, in the form of the following pair of equations:

$$v(n) = \sum_{k=0}^M b_k x(n-k) \tag{6.116}$$

$$y(n) = \sum_{k=1}^N a_k y(n-k) + v(n) \tag{6.117}$$

is shown in Figure 6.9. Each appropriate rearrangement of the block diagram represents a *different* computational algorithm for implementing the *same* system.

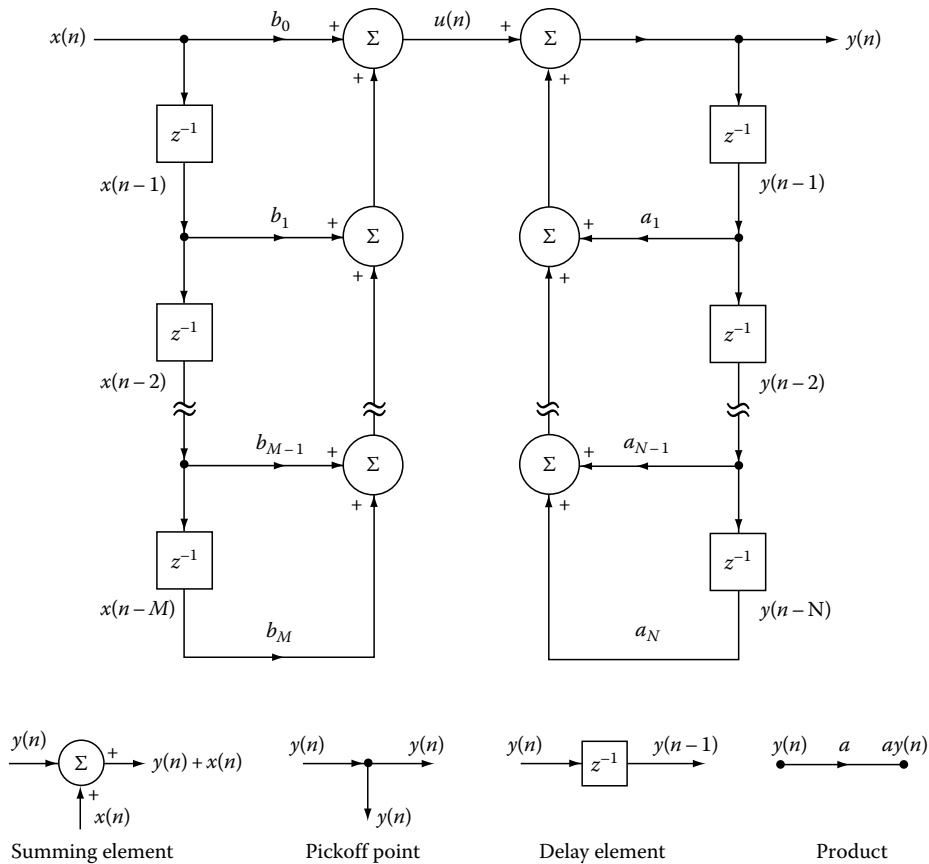


FIGURE 6.9

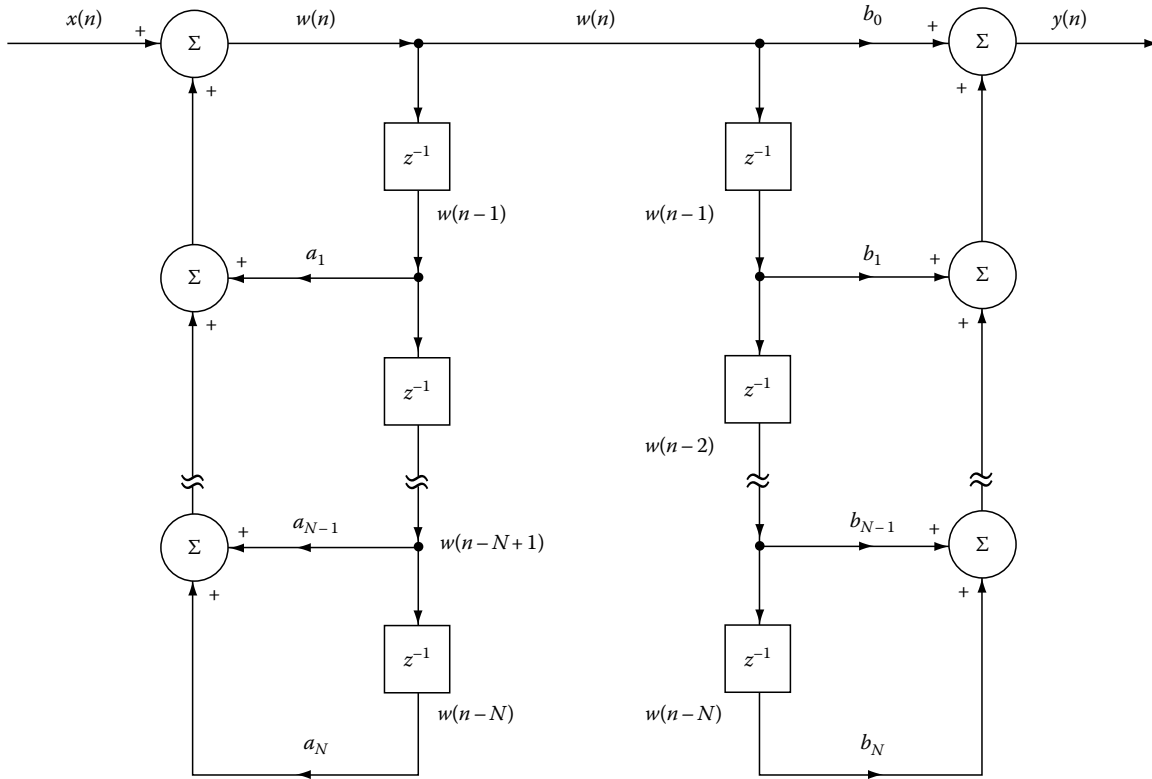


FIGURE 6.10

Figure 6.9 can be viewed as an implementation of  $H(z)$  through the decomposition

$$H(z) = H_2(z)H_1(z) = \left( \frac{1}{1 - \sum_{k=1}^N a_k z^{-k}} \right) \left( \sum_{k=0}^M b_k z^{-k} \right) \quad (6.118)$$

or through the pair of equations

$$V(z) = H_1(z)X(z) = \left( \sum_{k=0}^M b_k z^{-k} \right) X(z) \quad (6.119)$$

$$Y(z) = H_2(z)V(z) = \left( \frac{1}{1 - \sum_{k=1}^N a_k z^{-k}} \right) V(z) \quad (6.120)$$

If we arrange Equation 6.118, we can create the following two equations:

$$W(z) = H_2(z)X(z) = \left( \frac{1}{1 - \sum_{k=1}^N a_k z^{-k}} \right) X(z) \quad (6.121)$$

$$Y(z) = H_1(z)W(z) = \left( \sum_{k=0}^M b_k z^{-k} \right) W(z) \quad (6.122)$$

The last two equations are presented graphically in Figure 6.10 ( $M = N$ ).

The time domain the Figure 6.10 is the pair of equations

$$w(n) = \sum_{k=1}^N a_k w(n-k) + x(n) \quad (6.123)$$

$$y(n) = \sum_{k=0}^M b_k w(n-k) \quad (6.124)$$

Because the two internal branches of Figure 6.10 are identical, they can be combined in one branch so that Figure 6.11. Figure 6.9 represents the *direct form I* of the general  $N$ th-order system and Figure 6.11 is often referred to as the *direct form II* or *canonical direct form* implementation.

### 6.1.3.3.2 Finite Impulse Response (FIR) Filters

For causal FIR systems, the difference equation describing such a system is given by

$$y(n) = \sum_{k=0}^M b_k x(n-k) \quad (6.125)$$

which is recognized as the discrete convolution of  $x(n)$  with the impulse response

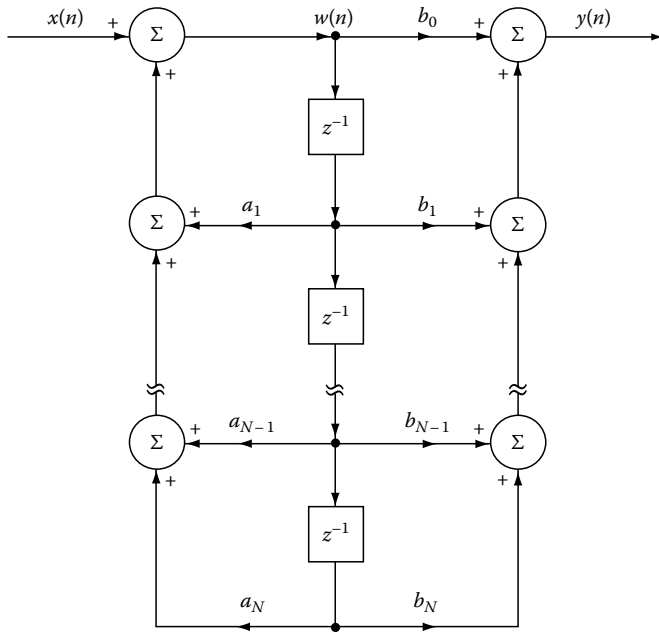


FIGURE 6.11

$$h(n) = \begin{cases} b_n & n = 0, 1, \dots, M \\ 0 & \text{otherwise} \end{cases} \quad (6.126)$$

The direct form I and direct form II structures are shown in Figures 6.12 and 6.13. Because of the chain of delay elements across the top of the diagram, this structure is also referred to as a *tapped delay line* structure or a *transversal filter* structure.

### 6.1.3.4 Linear, Time-Invariant, Discrete-Time, Dynamical Systems

The mathematical models describing dynamical systems are almost always of finite-order difference equations. If we know

the initial conditions at  $t = t_0$ , their behavior can be uniquely determined for  $t \geq t_0$ . To see how to develop a dynamic, let us consider the example below.

#### Example

Let a discrete system with input  $v(n)$  and output  $y(n)$  be described by the difference equation

$$y(n) + 2y(n - 1) + y(n - 2) = v(n) \quad (6.127)$$

If  $y(n_0 - 1)$  and  $y(n_0 - 2)$  are the initial conditions for  $n > n_0$ , then  $y(n)$  can be found recursively from Equation 6.127. Let us take the pair  $y(n - 1)$  and  $y(n - 2)$  as the state of the system at time  $n$ . Let us call the vector

$$\underline{x}(n) = \begin{bmatrix} x_1(n) \\ x_2(n) \end{bmatrix} = \begin{bmatrix} y(n - 2) \\ y(n - 1) \end{bmatrix} \quad (6.128)$$

the *state vector* for the system. From the definition above, we obtain

$$x_1(n + 1) = y(n + 1 - 2) = y(n - 1) \quad (6.129)$$

and

$$x_2(n + 1) = y(n) = v(n) - y(n - 2) - 2y(n - 1) \quad (6.130)$$

or

$$x_2(n + 1) = v(n) - x_1(n) - 2x_2(n) \quad (6.131)$$

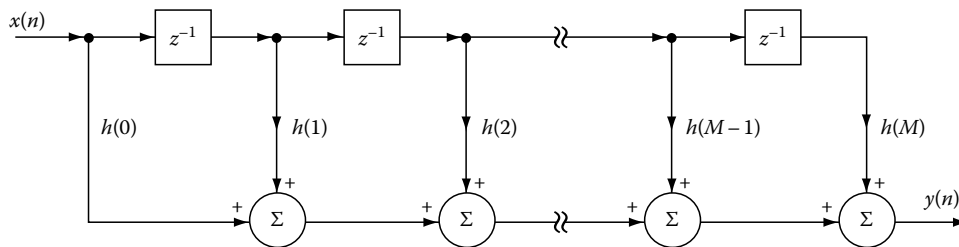


FIGURE 6.12

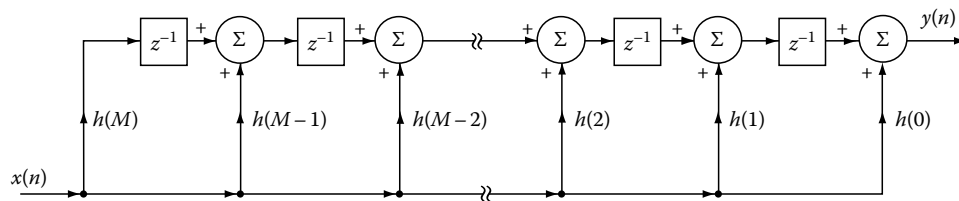


FIGURE 6.13



Equations 6.129 and 6.131 can be written in the form

$$\begin{bmatrix} x_1(n+1) \\ x_2(n+1) \end{bmatrix} = \begin{bmatrix} 0 & 1 \\ -1 & -2 \end{bmatrix} \begin{bmatrix} x_1(n) \\ x_2(n) \end{bmatrix} + \begin{bmatrix} 0 \\ 1 \end{bmatrix} \mathbf{v}(n) \quad (6.132)$$

or

$$\underline{x}(n+1) = \underline{A}\underline{x}(n) + \underline{B}\mathbf{v}(n) \quad (6.133)$$

But Equation 6.130 can be written in the form

$$y(n) = \mathbf{v}(n) - x_1(n) - 2x_2(n) = [-1 \ -2] \begin{bmatrix} x_1(n) \\ x_2(n) \end{bmatrix} + \mathbf{v}(n)$$

or

$$y(n) = \underline{C}\underline{x} + \mathbf{v}(n) \quad (6.134)$$

Hence, the system can be described by vector-matrix difference equations (6.133) and an output equation (6.134) rather than by the second-order difference equation (6.127).

A time-invariant, linear, and discrete dynamic system is described by the state equation

$$\underline{x}(nT + T) = \underline{A}\underline{x}(nT) + \underline{B}\mathbf{v}(nT) \quad (6.135)$$

and the output equation is of the form

$$y(nT) = \underline{C}\underline{x}(nT) + \underline{D}\mathbf{v}(nT) \quad (6.136)$$

where

$$\begin{aligned} \underline{x}(nT) &= N\text{-dimensional column vector} \\ \underline{v}(nT) &= M\text{-dimensional column vector} \\ y(nT) &= R\text{-dimensional column vector} \\ \underline{A} &= N \times N \text{ nonsingular matrix} \\ \underline{B} &= N \times M \text{ matrix} \\ \underline{C} &= R \times N \text{ matrix} \\ \underline{D} &= R \times M \text{ matrix} \end{aligned}$$

When the input is identically zero, Equation 6.135 reduces to

$$\underline{x}(nT + T) = \underline{A}\underline{x}(nT) \quad (6.137)$$

so that

$$\underline{x}(nT + 2T) = \underline{A}\underline{x}(nT + T) = \underline{A}\underline{A}\underline{x}(nT) = \underline{A}^2\underline{x}(nT)$$

and so on. In general we have

$$\underline{x}(nT + kT) = \underline{A}^k\underline{x}(nT) \quad (6.138)$$

The *state transition matrix* from  $n_1T$  to  $n_2T$  ( $n_2 > n_1$ ) is given by

$$\underline{\Phi}(n_2T, n_1T) = \underline{A}^{n_2-n_1} \quad (6.139)$$

This is a function only of the time difference  $n_2T - n_1T$ . Therefore, it is customary to name the matrix

$$\underline{\Phi}(nT) = \underline{A}^n \quad (6.140)$$

the state transition matrix with the understanding that  $n = n_2 - n_1$ . It follows that the system states at two times,  $n_2T$  and  $n_1T$ , are related by the relation

$$\underline{x}(n_2T) = \underline{\Phi}(n_2T, n_1T)\underline{x}(n_1T) \quad (6.141)$$

when the input is zero. From Equation 6.139 we obtain the following relationships:

$$(a) \underline{\Phi}(nT, nT) = \underline{I} = \text{identity matrix} \quad (6.142)$$

$$(b) \underline{\Phi}(n_2T, n_1T) = \underline{\Phi}^{-1}(n_1T, n_2T) \quad (6.143)$$

$$(c) \underline{\Phi}(n_3T, n_2T)\underline{\Phi}(n_2T, n_1T) = \underline{\Phi}(n_3T, n_1T) \quad (6.144)$$

If the input is not identically zero and  $\underline{x}(nT)$  is known, then the progress (later states) of the system can be found recursively from Equation 6.135. Proceeding with the recursion, we obtain

$$\begin{aligned} \underline{x}(nT + 2T) &= \underline{A}\underline{x}(nT + T) + \underline{B}\mathbf{v}(nT + T) \\ &= \underline{A}\underline{A}\underline{x}(nT) + \underline{A}\underline{B}\mathbf{v}(nT) + \underline{B}\mathbf{v}(nT + T) \\ &= \underline{\Phi}(nT + 2T, nT)\underline{x}(nT) + \underline{\Phi}(nT + 2T, nT + T)\underline{B}\mathbf{v}(nT) \\ &\quad + \underline{B}\mathbf{v}(nT + T) \end{aligned}$$

In general, for  $k > 0$  we have the solution

$$\begin{aligned} \underline{x}(nT + kT) &= \underline{\Phi}(nT + kT, nT)\underline{x}(nT) \\ &\quad + \sum_{i=n}^{n+k-1} \underline{\Phi}(nT + kT, iT + T)\underline{B}\mathbf{v}(iT) \end{aligned} \quad (6.145)$$

From Equation 6.141, when the input is zero, we obtain the relation

$$\underline{x}(n_2T) = \underline{\Phi}(n_2T - n_1T)\underline{x}(n_1T) = \underline{A}^{n_2-n_1}\underline{x}(n_1T) \quad (6.146)$$

According to Equation 6.145, the solution to the dynamic system when the input is not zero is given by

$$\begin{aligned} \underline{x}(nT + kT) &= \underline{\Phi}(nT + kT - nT)\underline{x}(nT) \\ &\quad + \sum_{i=n}^{n+k-1} \underline{\Phi}[(n+k-i-1)T]\underline{B}\mathbf{v}(iT) \end{aligned} \quad (6.147)$$

or

$$\begin{aligned} \underline{x}(nT + kT) &= \underline{\Phi}(kT)\underline{x}(nT) + \sum_{i=n}^{n+k-1} \underline{\Phi}[(n+k-i-1)T] \\ &\quad \underline{B}\mathbf{v}(iT) \quad k > 0 \end{aligned} \quad (6.148)$$

To find the solution using the Z-transform method, we define the one-sided Z-transform of an  $R \times S$  matrix function  $\underline{f}(nT)$  as the  $R \times S$  matrix

$$\underline{F}(z) = \sum_{n=0}^{\infty} \underline{f}(nT)z^{-n} \quad (6.149)$$

The elements of  $\underline{F}(z)$  are the transforms of the corresponding elements of  $\underline{f}(nT)$ . Taking the Z-transform of both sides of the state equation (6.135), we find

$$z\underline{X}(z) - z\underline{x}(0) = \underline{A}\underline{X}(z) + \underline{B}\underline{V}(z)$$

or

$$\underline{X}(z) = (z\underline{I} - \underline{A})^{-1}z\underline{x}(0) + (z\underline{I} - \underline{A})^{-1}\underline{B}\underline{V}(z) \quad (6.150)$$

From the output Equation 6.136, we see that

$$\underline{Y}(z) = \underline{C}\underline{X}(z) + \underline{D}\underline{V}(z) \quad (6.151)$$

The state of the system  $\underline{x}(nT)$  and its output  $\underline{y}(nT)$  can be found for  $n \geq 0$  by taking the inverse Z-transform of Equations 6.150 and 6.151

For a zero input, Equation 6.150 becomes

$$\underline{X}(z) = (z\underline{I} - \underline{A})^{-1}z\underline{x}(0) \quad (6.152)$$

so that

$$\underline{x}(nT) = \mathcal{Z}^{-1}\{(z\underline{I} - \underline{A})^{-1}z\}\underline{x}(0) \quad (6.153)$$

If we let  $n_1 = 0$  and  $n_2 = n$ , then Equation 6.146 becomes

$$\underline{x}(nT) = \underline{\Phi}(nT)\underline{x}(0) = \underline{A}^n\underline{x}(0) \quad (6.154)$$

Comparing Equations 6.153 and 6.154 we observe that

$$\underline{\Phi}(nT) = \underline{A}^n = \mathcal{Z}^{-1}\{(z\underline{I} - \underline{A})^{-1}z\} \quad n \geq 0 \quad (6.155)$$

or equivalently,

$$\underline{\Phi}(z) = \mathcal{Z}\{\underline{A}^n\} = (z\underline{I} - \underline{A})^{-1}z \quad (6.156)$$

The Z-transform provides straightforward method for calculating the state transition matrix.

Next combine Equations 6.150 and 6.156 to find

$$\underline{X}(z) = \underline{\Phi}(z)\underline{x}(0) + \underline{\Phi}(z)z^{-1}\underline{B}\underline{V}(z) \quad (6.157)$$

By applying the convolution theorem and the fact that

$$\mathcal{Z}^{-1}\{\underline{\Phi}(z)z^{-1}\} = \underline{\Phi}(nT - T)u(nT - T) \quad (6.158)$$

the inverse Z-transform of Equation 6.157 is given by

$$\underline{x}(kT) = \underline{\Phi}(kT)\underline{x}(0) + \sum_{i=0}^{k-1} \underline{\Phi}[(k-i)T]\underline{B}\underline{v}(iT) \quad (6.159)$$

The above equation is identical to Equation 6.148 with  $n = 0$ .

The behavior of the system with zero input depends on the location of the poles of

$$\underline{\Phi}(z) = (z\underline{I} - \underline{A})^{-1}z \quad (6.160)$$

Because

$$(z\underline{I} - \underline{A})^{-1} = \frac{\text{adj}(z\underline{I} - \underline{A})}{\det(z\underline{I} - \underline{A})} \quad (6.161)$$

where  $\text{adj}(\cdot)$  denotes the regular adjoint in matrix theory, these poles can only occur at the roots of the polynomial

$$D(z) = \det(z\underline{I} - \underline{A}) \quad (6.162)$$

$D(z)$  is known as the *characteristic polynomial* for  $\underline{A}$  (for the system) and its roots are known as the *characteristic values* or *eigenvalues* of  $\underline{A}$ . If all roots are inside the unit circle, the system is stable. If even one root is outside the unit circle, the system is unstable.

### Example

Consider the system

$$\begin{aligned} \begin{bmatrix} x_1(nT + T) \\ x_2(nT + T) \end{bmatrix} &= \begin{bmatrix} 0 & 2 \\ 0.22 & 2 \end{bmatrix} \begin{bmatrix} x_1(nT) \\ x_2(nT) \end{bmatrix} + \begin{bmatrix} 0 \\ 1 \end{bmatrix} \mathbf{v}(nT) \\ y(nT) &= [0.22 \ 2] \begin{bmatrix} x_1(nT) \\ x_2(nT) \end{bmatrix} + \mathbf{v}(nT) \end{aligned}$$

For this system we have

$$\underline{A} = \begin{bmatrix} 0 & 2 \\ 0.22 & 2 \end{bmatrix}, \quad \underline{B} = \begin{bmatrix} 0 \\ 1 \end{bmatrix}, \quad \underline{C} = [0.22 \ 2], \quad \underline{D} = [1]$$

The characteristic polynomial is

$$\begin{aligned} D(z) &= \det(z\underline{I} - \underline{A}) = \det \left[ \begin{bmatrix} z & 0 \\ 0 & z \end{bmatrix} - \begin{bmatrix} 0 & 2 \\ 0.22 & 2 \end{bmatrix} \right] \\ &= \det \begin{bmatrix} z & -2 \\ -0.22 & z-2 \end{bmatrix} \\ &= z(z-2) - 0.44 = z^2 - 2z - 0.44 = (z-2.2)(z+0.2) \end{aligned}$$

Hence, we obtain (see Equation 6.160)

$$\begin{aligned} \underline{\Phi}(z) &= \frac{z}{(z-2.2)(z+0.2)} \begin{bmatrix} z-2 & 2 \\ 0.22 & z \end{bmatrix} \\ &= \begin{bmatrix} \frac{z(z-2)}{(z-2.2)(z+0.2)} & \frac{2z}{(z-2.2)(z+0.2)} \\ \frac{0.22z}{(z-2.2)(z+0.2)} & \frac{z^2}{(z-2.2)(z+0.2)} \end{bmatrix} \end{aligned}$$

Because  $D(z)$  has a root outside the unit circle at 2.2, the system is unstable. Taking the inverse transform we find that

$$\underline{\varphi}(nT) = \begin{cases} \left[ \begin{array}{cc} \frac{1}{12}(2.2)^n + \frac{11}{12}(-0.2)^n & \frac{5}{6}(2.2)^n - \frac{5}{6}(-0.2)^n \\ \frac{11}{120}(2.2)^n - \frac{11}{120}(-0.2)^n & \frac{11}{12}(2.2)^n + \frac{1}{12}(-0.2)^n \end{array} \right] \\ n \geq 0 \end{cases}$$

To check, set  $n=0$  to find  $\underline{\varphi}(0)=\underline{1}$  and  $\underline{\varphi}(T)=\underline{A}$ .

Let  $\underline{x}(0)=0$  and the input be the unit impulse  $\underline{v}(nT)=\delta(nT)$  so that  $\underline{V}(z)=1$ . Hence, according to Equation 6.157

$$\underline{X}(z) = \underline{\Phi}(z)z^{-1}\underline{B}\underline{V}(z) = \frac{1}{(z-2.2)(z+0.2)} \begin{bmatrix} z-2 & 2 \\ 0.22 & z \end{bmatrix} \begin{bmatrix} 0 \\ 1 \end{bmatrix} \\ = \frac{1}{(z-2.2)(z+0.2)} \begin{bmatrix} 2 \\ z \end{bmatrix}$$

The inverse Z-transform gives

$$\underline{x}(nT) = \frac{5}{6} \begin{bmatrix} (2.2)^{n-1} & -(-0.2)^{n-1} \\ \frac{1}{2}(2.2)^n & -\frac{1}{2}(-0.2)^n \end{bmatrix} \quad n > 0$$

and the output is given by

$$y(nT) = \underline{C}\underline{x}(nT) + \underline{D}\underline{v}(nT) \\ = \begin{cases} 1 & n = 0 \\ \frac{5}{12}(2.2)^{n+1} - \frac{5}{12}(-0.2)^{n+1} & n > 0 \end{cases}$$

### 6.1.3.5 Z-Transform and Random Processes

#### 6.1.3.5.1 Power Spectral Densities

The Z-transform of the autocorrelation function  $R_{xx}(\tau) = E\{x(t+\tau)x(t)\}$  sampled uniformly at  $nT$  times is given by

$$S_{xx}(z) = \sum_{n=-\infty}^{\infty} R_{xx}(nT)z^{-n} \quad (6.163)$$

where the Fourier transform of  $R_{xx}(\tau)$  is designated by  $S_{xx}(\omega)$ . The *sampled power spectral density* for  $x(nT)$  is defined to be

$$S_{xx}(e^{j\omega T}) = S_{xx}(z)|_{z=e^{j\omega T}} = \sum_{n=-\infty}^{\infty} R_{xx}(nT)e^{-j\omega nT} \quad (6.164)$$

However, from the sampling theorem we have

$$S_{xx}(e^{j\omega T}) = \frac{1}{T} \sum_{n=-\infty}^{\infty} S_{xx}(\omega - n\omega_s), \quad \omega_s = 2\pi/T \quad (6.165)$$

Because  $S_{xx}(\omega)$  is real, nonnegative, and even, it follows from Equation 6.165 that  $S_{xx}(e^{j\omega T})$  is also real, nonnegative, and even. If the envelope of  $R_{xx}(\tau)$  decays exponentially for  $|\tau| > 0$ , then the ROC for  $S_{xx}(z)$  includes the unit circle. If  $R_{xx}(\tau)$  has undamped periodic components the series in Equation 6.164 converges in the distribution sense that contains impulse function.

The average power in  $x(nT)$  is

$$E\{x^2(nT)\} = R_{xx}(0) = \frac{1}{2\pi j} \oint_C S_{xx}(z) \frac{dz}{z} \quad (6.166)$$

where  $C$  is a simple, closed contour lying in the ROC and the integration is taken in counterclockwise sense. If  $C$  is the unit circle, then

$$R_{xx}(0) = \frac{1}{\omega_s} \int_{-\omega_s/2}^{\omega_s/2} S_{xx}(e^{j\omega T}) d\omega \quad \omega_s = \frac{2\pi}{T} \quad (6.167)$$

$$S_{xx}(e^{j\omega T}) \frac{d\omega}{\omega_s} = \text{average power in } d\omega \quad (6.168)$$

$S_{xy}(z)$  is called the *cross power spectral density* for two jointly wide-sense stationary processes  $x(t)$  and  $y(t)$ . It is defined by the relation

$$S_{xy}(z) = \sum_{n=-\infty}^{\infty} R_{xy}(nT)z^{-n} \quad (6.169)$$

Because  $R_{xy}(nT) = R_{yx}(-nT)$  it follows that

$$S_{xy}(z) = S_{yx}(z^{-1}), \quad S_{xx}(z) = S_{xx}(z^{-1}) \quad (6.170)$$

Equivalently, we have

$$S_{xx}(e^{j\omega T}) = S_{xx}(e^{-j\omega T}) \quad (6.171)$$

If  $S_{xx}(z)$  is a rational polynomial, it can be factored in the form

$$S_{xx}(z) = \frac{N(z)}{D(z)} = \gamma^2 G(z)G(z^{-1}) \quad (6.172)$$

where

$$G(z) = \frac{\prod_{k=1}^L (1 - \alpha_k z^{-1})}{\prod_{k=1}^M (1 - \beta_k z^{-1})} = \frac{\sum_{k=0}^L a_k z^{-k}}{\sum_{k=0}^M b_k z^{-k}}$$

$\gamma^2 > 0$ ,  $|\alpha_k| < 1$ ,  $|\beta_k| < 1$ ,  $a_k$  and  $b_k$  are real

#### 6.1.3.5.2 Linear Discrete-Time Filters

Let  $R_{xx}(nT)$ ,  $R_{yy}(nT)$ , and  $R_{xy}(nT)$  be known. Let two systems have transfer functions  $H_1(z)$  and  $H_2(z)$ , respectively. The output

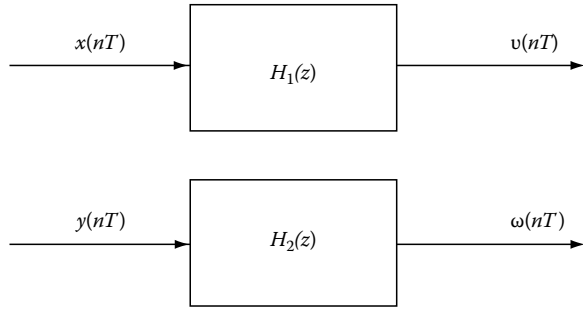


FIGURE 6.14

of these filters, when the inputs are  $x(nT)$  and  $y(nT)$  (see Figure 6.14), are

$$v(nT) = \sum_{k=-\infty}^{\infty} h_1(kT)x(nT - kT) \quad (6.173)$$

$$w(nT) = \sum_{k=-\infty}^{\infty} h_2(kT)y(nT - kT) \quad (6.174)$$

Let  $n = n + m$  in Equation 6.173, multiply by  $y(nT)$ , and take the ensemble average to find

$$\begin{aligned} R_{vy}(mT) &= \sum_{k=-\infty}^{\infty} h_1(kT)E\{x(mT + nT - kT)y(nT)\} \\ &= \sum_{k=-\infty}^{\infty} h_1(kT)R_{xy}(mT - kT) \end{aligned} \quad (6.175)$$

Hence, by taking the Z-transform we obtain

$$S_{vy}(z) = H_1(z)S_{xy}(z) \quad (6.176)$$

Similarly from Equation 6.174 we obtain

$$R_{vw}(mT) = \sum_{k=-\infty}^{\infty} h_2(kT)R_{vy}(mT + kT) \quad (6.177)$$

and

$$S_{vw}(z) = H_2(z^{-1})S_{vy}(z) \quad (6.178)$$

From Equations 6.176 and 6.178, we obtain

$$S_{vw}(z) = H_1(z)H_2(z^{-1})S_{xy}(z) \quad (6.179)$$

Also, for  $x(nT) = y(nT)$  and  $h_1(nT) = h_2(nT) = h(nT)$ , Equation 6.179 becomes

$$S_{vw}(z) = H(z)H(z^{-1})S_{xx}(z) \quad (6.180)$$

and

$$\begin{aligned} S_{vw}(e^{j\omega T}) &= H(e^{j\omega T})H(e^{-j\omega T})S_{xx}(e^{j\omega T}) \\ &= |H(e^{j\omega T})|^2 S_{xx}(e^{j\omega T}) \end{aligned} \quad (6.181)$$

### 6.1.3.5.3 Optimum Linear Filtering

Let  $y(nT)$  be an observed wide-sense stationary process and  $x(nT)$  be a desired wide-sense stationary process. The process  $y(nT)$  could be the result of the desired signal  $x(nT)$  and a noise signal  $v(nT)$ . It is desired to find a system with transfer function  $H(z)$  such that the error  $e(nT) = x(nT) - \hat{x}(nT) = x(nT) - \mathcal{Z}^{-1}\{Y(z)H(z)\}$  is minimized. Referring to Figure 6.15 and to Equation 6.180, we can write

$$S_{aa}(z) = \frac{1}{H_1(z)H_1(z^{-1})} S_{yy}(z) = \gamma^2 \quad (6.182)$$

where  $a(nT)$  is taken as white noise (uncorrelated process). We, therefore, can write

$$R_{aa}(mT) = \gamma^2 \delta(mT) \quad (6.183)$$

The signal  $a(nT)$  is known as the *innovation* process associated with  $y(nT)$ . From Figure 6.15, we obtain

$$\hat{x}(nT) = \sum_{k=-\infty}^{\infty} g(kT)a(nT - kT) \quad (6.184)$$

The mean square error is given by

$$\begin{aligned} E\{e^2(nT)\} &= E\left\{\left[x(nT) - \sum_{k=-\infty}^{\infty} g(kT)a(nT - kT)\right]^2\right\} \\ &= E\{x^2(nT)\} - 2E\left\{\sum_{k=-\infty}^{\infty} g(kT)x(nT)a(nT - kT)\right\} \\ &\quad + E\left\{\left[\sum_{k=-\infty}^{\infty} g(kT)a(nT - kT)\right]^2\right\} \\ &= R_{xx}(0) - 2 \sum_{k=-\infty}^{\infty} g(kT)R_{xa}(kT) + \gamma^2 \sum_{k=-\infty}^{\infty} g^2(kT) \\ &= R_{xx}(0) + \sum_{k=-\infty}^{\infty} \left[\gamma g(kT) - \frac{R_{xa}(kT)}{\gamma}\right]^2 - \frac{1}{\gamma^2} \sum_{k=-\infty}^{\infty} R_{xa}^2(kT) \end{aligned}$$

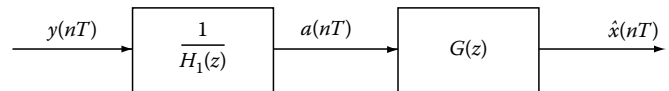


FIGURE 6.15

To minimize the error we must set the quantity in the brackets equal to zero. Hence,

$$g(nT) = \frac{1}{\gamma^2} R_{xa}(nT) \quad -\infty < n < \infty$$

and its  $Z$ -transform is

$$G(z) = \frac{1}{\gamma^2} S_{xa}(z)$$

but from Equation 6.179 (because  $v(nT) = x(nT)$  implies that  $H_1(z) = 1$ ) we have

$$S_{xy}(z) = H_1(z^{-1})S_{xa}(z) \quad \text{or} \quad S_{xa}(z) = \frac{S_{xy}(z)}{H_1(z^{-1})} \quad (6.185)$$

$$G(z) = \frac{1}{\gamma^2} \frac{S_{xy}(z)}{H_1(z^{-1})} \quad (6.186)$$

From Figure 6.15, the optimum filter is given by (see also Equation 6.182)

$$H(z) = \frac{1}{H_1(z)} G(z) = \frac{S_{xy}(z)}{\gamma^2 H_1(z) H_1(z^{-1})} = \frac{S_{xy}(z)}{S_{yy}(z)} \quad (6.187)$$

The mean square error for an optimum filter is

$$E\{e^2(nT)\} = R_{xx}(0) - \frac{1}{\gamma^2} \sum_{k=-\infty}^{\infty} R_{xa}^2(kT) \quad (6.188)$$

Applying Parseval's theorem in the above equation, we obtain

$$\begin{aligned} E\{e^2(nT)\} &= \frac{1}{2\pi j} \oint_C \left[ S_{xx}(z) - \frac{1}{\gamma^2} S_{xa}(z) S_{xa}(z^{-1}) \right] \frac{dz}{z} \\ &= \frac{1}{2\pi j} \oint_C \left[ S_{xx}(z) - \frac{S_{xy}(z) S_{xy}(z^{-1})}{S_{yy}(z)} \right] \frac{dz}{z} \\ &= \frac{1}{2\pi j} \oint_C [S_{xx}(z) - H(z) S_{xy}(z^{-1})] \frac{dz}{z} \end{aligned} \quad (6.189)$$

where  $C$  can be the unit circle.

### 6.1.3.6 Relationship between the Laplace and $Z$ -Transform

The one-sided Laplace transform and its inverse are given by the following two equations:

$$F(s) \doteq \mathcal{L}\{f(t)\} = \int_0^{\infty} f(t) e^{-st} dt \quad \text{Re}\{s\} > \sigma_c \quad (6.190)$$

$$f(t) = \mathcal{L}^{-1}\{F(s)\} = \frac{1}{2\pi j} \int_{c-j\infty}^{c+j\infty} F(s) e^{st} ds \quad c > \sigma_c \quad (6.191)$$

where  $\sigma_c$  is the abscissa of convergence.

The Laplace transform of a sampled function

$$\begin{aligned} f_s(t) &= f(t) \sum_{k=-\infty}^{\infty} \delta(t - nT) \doteq f(t) \text{comb}_T(t) \\ &= \sum_{k=-\infty}^{\infty} f(nT) \delta(t - nT) \end{aligned} \quad (6.192)$$

is given by

$$F_s(s) \doteq \mathcal{L}\{f_s(t)\} = \sum_{k=-\infty}^{\infty} f(nT) e^{-nTs} \quad (6.193)$$

because

$$\mathcal{L}\{\delta(t - nT)\} = \int_{-\infty}^{\infty} \delta(t - nT) e^{-st} dt = e^{-snT} \quad (6.194)$$

From Equation 6.193 we obtain

$$F(z) = F_s(s)|_{s=T^{-1} \ln z} \quad (6.195)$$

and, hence,

$$F(z)|_{z=e^{Ts}} = F_s(s) \doteq \mathcal{L}\{f_s(t)\} = \mathcal{L}\{f(t) \text{comb}_T(t)\} \quad (6.196)$$

If the ROC for  $F(z)$  includes the unit circle,  $|z| = 1$ , then

$$F_s(\omega) = F(z)|_{z=e^{j\omega T}} = \sum_{n=-\infty}^{\infty} f(nT) e^{-j\omega nT} \quad (6.197)$$

$$F_s(s + j\omega_s) = F_s(s) = \text{periodic} \quad \omega_s = \frac{2\pi}{T} \quad (6.198)$$

The knowledge of  $F_s(s)$  in the strip  $-\omega_s/2 < \omega \leq \omega_s/2$  determines  $F_s(s)$  for all  $s$ . The transformation  $z = e^{sT}$  maps this strip uniquely onto the complex  $z$ -plane. Therefore,  $F(z)$  contains all the information in  $F_s(s)$  without redundancy. Letting  $\sigma = s + j\omega$ , then

$$z = e^{\sigma T} e^{j\omega T} \quad (6.199)$$

Because  $|z| = e^{\sigma T}$ , we obtain

$$|z| = \begin{cases} < 1 & \sigma < 0 \\ = 1 & \sigma = 0 \\ > 1 & \sigma > 0 \end{cases} \quad (6.200)$$

Therefore, we have the following correspondence between the  $s$ - and  $z$ -planes:

1. Points in the left half of the  $s$ -plane are mapped inside the unit circle in the  $z$ -plane
2. Points on the  $j\omega$ -axis are mapped onto the unit circle
3. Points in the right half of the  $s$ -plane are mapped outside the unit circle
4. Lines parallel to the  $j\omega$ -axis are mapped into circles with radius  $|z| = e^{\sigma T}$
5. Lines parallel to the  $\sigma$ -axis are mapped into rays of the form  $\arg z = \omega T$  radians from  $z = 0$
6. The origin of the  $s$ -plane corresponds to  $z = 1$
7. The  $\sigma$ -axis corresponds to the positive  $u = \text{Re } z$ -axis
8. As  $\omega$  varies between  $-\omega_s/2$  and  $\omega_s/2$ ,  $\arg z = \omega T$  varies between  $-\pi$  and  $\pi$  radians

Let  $f(t)$  and  $g(t)$  be causal functions with Laplace transforms  $F(s)$  and  $G(s)$  that converge absolutely for  $\text{Re } s > \sigma_f$  and  $\text{Re } s > \sigma_g$  respectively; then

$$\mathcal{L}\{f(t)g(t)\} = \frac{1}{2\pi j} \int_{c-j\infty}^{c+j\infty} F(p)G(s-p)dp \quad (6.201)$$

The contour is parallel to the imaginary axis in the complex  $p$ -plane with

$$\sigma = \text{Re } s > \sigma_f + \sigma_g \quad \text{and} \quad \sigma_f < c < \sigma - \sigma_g \quad (6.202)$$

With this choice the poles  $G(s-p)$  lie to the right of the integration path. For causal  $f(t)$ , its sampling form is given by

$$\begin{aligned} f_s(t) &= f(t) \sum_{n=0}^{\infty} \delta(t-nT) \doteq f(t) \text{comb}_T(t) \\ &= \sum_{n=0}^{\infty} f(nT) \delta(t-nT) \end{aligned} \quad (6.203)$$

If

$$g(t) = \text{comb}_T(t) \doteq \sum_{n=0}^{\infty} \delta(t-nT) \quad (6.204)$$

then its Laplace transform is

$$G(s) = \mathcal{L}\{g(t)\} = \sum_{n=0}^{\infty} e^{-nTs} = \frac{1}{1-e^{-Ts}} \quad \text{Re } s > 0 \quad (6.205)$$

Because  $\sigma_g = 0$ , then Equation 6.201 becomes

$$F_s(s) = \frac{1}{2\pi j} \int_{c-j\infty}^{c+j\infty} \frac{F(p)}{1-e^{-(s-p)T}} dp \quad \sigma > \sigma_f, \sigma_f < c < \sigma \quad (6.206)$$

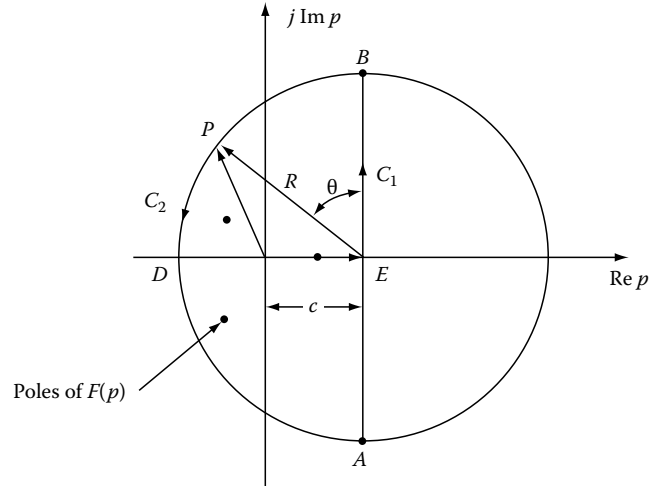


FIGURE 6.16

The distance  $p$  in Figure 6.16 is given by

$$p = c + Re^{j\theta} \quad \pi/2 \leq \theta \leq 3\pi/2 \quad (6.207)$$

If the function  $F(p)$  is analytic for some  $|p|$  greater than a finite number  $R_0$  and has a zero at infinity, then in the limit as  $R \rightarrow \infty$  the integral along the path  $BDA$  is identically zero and the integral along the path  $AEB$  averages to  $F_s(s)$ . The contour  $C_1 + C_2$  encloses all the poles of  $F(p)$ . Because of these assumptions,  $F(p)$  must have a Laurent series expansion of the form

$$F(p) = \frac{a_{-1}}{p} + \frac{a_{-2}}{p^2} + \dots = \frac{a_{-1}}{p} + \frac{Q(p)}{p^2} \quad |p| > R_0 \quad (6.208)$$

$Q(p)$  is analytic in this domain and

$$|Q(p)| < M < \infty \quad |p| > R_0 \quad (6.209)$$

Therefore, from Equation 6.208

$$a_{-1} = \lim_{p \rightarrow \infty} pF(p) \quad (6.210)$$

From the initial value theorem

$$a_{-1} = f(0+) \quad (6.211)$$

Applying Cauchy's residue theorem to Equation 6.206, we obtain

$$F_s(s) = \sum_k \text{Res} \left\{ \frac{F(p)}{1 - e^{pT} e^{-sT}} \right\} \Big|_{p=p_k} - \lim_{R \rightarrow \infty} \frac{1}{2\pi j} \int_{C_2} \frac{F(p)}{1 - e^{pT} e^{-sT}} dp \quad (6.212)$$

where  $\{p_k\}$  are the poles of  $F(p)$  and  $\sigma = \text{Re}\{s\} > \sigma_f$ .

Introducing Equations 6.208 and 6.211 into the above equation, it can be shown (see Jury, 1973)

$$F_s(s) = \sum_k \text{Res} \left\{ \frac{F(p)}{1 - e^{pT} e^{-sT}} \right\} \Big|_{p=p_k} - \frac{f(0+)}{2} \quad (6.213)$$

By letting  $z = e^{sT}$ , the above equation becomes

$$F(z) = F_s(s)_{s=\frac{1}{T} \ln z} = \sum_k \operatorname{Res} \left\{ \frac{F(p)}{1 - e^{pT} z^{-1}} \right\} \Big|_{p=p_k} - \frac{f(0+)}{2} \quad |z| > e^{\sigma_f T} \quad (6.214)$$

**Example**

The Laplace transform of  $f(t) = tu(t)$  is  $1/s^2$ . The integrand  $|te^{-\sigma t} e^{-j\omega t}| < \infty$  for  $\sigma > 0$  implies that the ROC is  $\operatorname{Re}\{s\} > 0$ . Because  $f(t)$  has a double pole at  $s = 0$ , Equation 6.214 becomes

$$F(z) = \operatorname{Res} \left\{ \frac{1}{p^2(1 - e^{pT} z^{-1})} \right\} \Big|_{p=0} - \frac{0}{2} = \frac{d}{dp} \frac{p^2}{p^2(1 - e^{pT} z^{-1})} \Big|_{p=0} = \frac{Tz^{-1}}{(1 - z^{-1})^2}$$

**Example**

The Laplace transform of  $f(t) = e^{-at} u(t)$  is  $1/(s + a)$ . The ROC is  $\operatorname{Re}\{s\} > -a$  and from Equation 6.214 we obtain

$$F(z) = \operatorname{Res} \left\{ \frac{1}{(p + a)(1 - e^{pT} z^{-1})} \right\} \Big|_{p=-a} - \frac{1}{2} = \frac{1}{1 - e^{-aT} z^{-1}} - \frac{1}{2}$$

The inverse transform is

$$f(nT) = -\frac{1}{2} \delta(n) + e^{-anT} u(nT)$$

If we had proceeded to find the Z-transform from  $f(nT) = \exp(-anT)u(nT)$ , we would have found  $F(z) = 1/(1 - e^{-aT} z^{-1})$ . Hence, to make a causal signal  $f(t)$  consistent with  $F(s)$  and the inversion formula,  $f(0)$  should be assigned the value  $f(0+)/2$ .

It is conventional in calculating with the Z-transform of causal signals to assign the value of  $f(0+)$  to  $f(0)$ . With this convention the formula for calculating  $F(z)$  from  $F(s)$  reduces to

$$F(z) = \sum_k \operatorname{Res} \left\{ \frac{F(p)}{1 - e^{pT} z^{-1}} \right\} \Big|_{p=p_k}, \quad |z| > e^{\sigma_f T} \quad (6.215)$$

**6.1.3.7 Relationship to the Fourier Transform**

The sampled signal can be represented by

$$f_s(t) = \sum_{n=-\infty}^{\infty} f(nT) \delta(t - nT) \quad (6.216)$$

with corresponding Laplace and Fourier transforms

$$F_s(s) = \sum_{n=-\infty}^{\infty} f(nT) e^{-snT} \quad (6.217)$$

$$F_s(\omega) = \sum_{n=-\infty}^{\infty} f(nT) e^{-j\omega nT} \quad (6.218)$$

If we set  $z = e^{sT}$  in the definition of the Z-transform, we see that

$$F_s(s) = F(z) \Big|_{z=e^{sT}} \quad (6.219)$$

If the ROC for  $F(z)$  includes the unit circle,  $|z| = 1$ , then

$$F_s(\omega) = F(z) \Big|_{z=e^{j\omega T}} \quad (6.220)$$

Because  $F_s(s)$  is periodic with period  $\omega_s = 2\pi/T$ , we need only consider the strip  $-\omega_s/2 < \omega \leq \omega_s/2$ , which uniquely determines  $F_s(s)$  for all  $s$ . The transformation  $z = \exp(sT)$  maps this strip uniquely onto the complex  $z$ -plane so that  $F(z)$  contains all the information in  $F_s(s)$  without the redundancy.

**Appendix: Tables**

**TABLE A.6.1** Z-Transform Properties for Positive-Time Sequences

1. Linearity	
$\mathcal{Z}\{c_i f_i(nT)\} = c_i F_i(z)$	$ z  > R_i, c_i$ are constants
$\mathcal{Z}\left\{\sum_{i=0}^{\ell} c_i f_i(nT)\right\} = \sum_{i=0}^{\ell} c_i F_i(z)$	$ z  > \max R_i$
2. Shifting property	
$\mathcal{Z}\{f(nT - kT)\} = z^{-k} F(z), f(-nT) = 0$	for $n = 1, 2, \dots$
$\mathcal{Z}\{f(nT - kT)\} = z^{-k} F(z) + \sum_{n=1}^k f(-nT) z^{-(k-n)}$	
$\mathcal{Z}\{f(nT + kT)\} = z^k F(z) - \sum_{n=0}^{k-1} f(nT) z^{k-n}$	
$\mathcal{Z}\{f(nT + T)\} = z[f(z) - f(0)]$	

TABLE A.6.1 (continued) Z-Transform Properties for Positive-Time Sequences

---

3. Time scaling	$\mathcal{Z}\{a^n f(nT)\} = F(a^{-T}z) = \sum_{n=0}^{\infty} f(nT)(a^{-T}z)^{-n} \quad  z  > a^T$
4. Periodic sequence	$\mathcal{Z}\{f(nT)\} = \frac{z^N}{z^N - 1} F_{(1)}(z) \quad  z  > R$ <p><math>N</math> = number of time units in a period  <math>R</math> = radius of convergence of <math>F_{(1)}(z)</math>  <math>F_{(1)}(z)</math> = Z-transform of the first period</p>
5. Multiplication by $n$ and $nT$	$\mathcal{Z}\{nf(nT)\} = -z \frac{dF(z)}{dz} \quad  z  > R$ $\mathcal{Z}\{nTf(nT)\} = -zT \frac{dF(z)}{dz} \quad  z  > R$ <p><math>R</math> = radius of convergence of <math>F(z)</math></p>
6. Convolution	$\mathcal{Z}\{f(nT) * h(nT)\} = F(z)H(z) \quad  z  > \max(R_1, R_2)$
7. Initial value	$f(0T) = \lim_{z \rightarrow \infty} F(z) \quad  z  > R \quad \text{if } F(\infty) \text{ exists}$
8. Final value	$\lim_{n \rightarrow \infty} f(nT) = \lim_{z \rightarrow 1} (z-1)F(z) \quad \text{if } f(\infty T) \text{ exists}$
9. Multiplication by $(nT)^k$	$\mathcal{Z}\{n^k T^k f(nT)\} = -Tz \frac{d}{dz} \mathcal{Z}\{(nT)^{k-1} f(nT)\} \quad k > 0 \text{ and is an integer}$
10. Complex conjugate signals	$\mathcal{Z}\{f(nT)\} = F(z) \quad  z  > R$ $\mathcal{Z}\{f^*(nT)\} = F^*(z^*) \quad  z  > R$
11. Transform of product	$\mathcal{Z}\{f(nT)h(nT)\} = \frac{1}{2\pi j} \oint_C F(\tau)H\left(\frac{z}{\tau}\right) \frac{d\tau}{\tau}$ <p style="text-align: center; margin-left: 100px;"><small>counterclockwise direction</small></p> <p><math> z  &gt; R_f R_h, \quad R_f &lt;  \tau  &lt; \frac{ z }{R_h}</math></p>
12. Parseval's theorem	$\sum_{n=0}^{\infty} f(nT)h(nT) = \frac{1}{2\pi j} \oint_C F(z)H(z^{-1}) \frac{dz}{z}$ <p style="text-align: center; margin-left: 100px;"><small>counterclockwise integration</small></p>
13. Correlation	$f(nT) \otimes h(nT) = \sum_{m=0}^{\infty} f(mT)h(mT-nT) = \frac{1}{2\pi j} \oint_C F(\tau)H\left(\frac{1}{\tau}\right) \tau^{n-1} d\tau \quad n \geq 1$ <p>Both <math>f(nT)</math> and <math>h(nT)</math> must exist for <math> z  &gt; 1</math>. The integration is taken in counterclockwise direction.</p>
14. Transform with parameters	$\mathcal{Z}\left\{\frac{\partial}{\partial a} f(nT, a)\right\} = \frac{\partial}{\partial a} F(z, a)$ $\mathcal{Z}\left\{\lim_{a \rightarrow a_0} f(nT, a)\right\} = \lim_{a \rightarrow a_0} F(z, a)$ $\mathcal{Z}\left\{\int_{a_0}^{a_1} f(nT, a) da\right\} = \int_{a_0}^{a_1} F(z, a) da \text{ finite interval}$

---



**TABLE A.6.2** Z-Transform Properties for Positive- and Negative-Time Sequences

## 1. Linearity

$$\mathcal{Z}_{II} \left\{ \sum_{i=0}^{\ell} c_i f_i(nT) \right\} = \sum_{i=0}^{\ell} c_i F_i(z) \quad \max R_{i+} < |z| < \min R_{i-}$$

## 2. Shifting property

$$\mathcal{Z}_{II} \{ f(nT \pm kT) \} = z^{\pm k} F(z) \quad R_+ < |z| < R_-$$

## 3. Scaling

$$\mathcal{Z}_{II} \{ f(nT) \} = F(z) \quad R_+ < |z| < R_-$$

$$\mathcal{Z}_{II} \{ a^{nT} f(nT) \} = F(a^{-T} z) \quad |a^T| R_+ < |z| < |a^T| R_-$$

## 4. Time reversal

$$\mathcal{Z}_{II} \{ f(nT) \} = F(z) \quad R_+ < |z| < R_-$$

$$\mathcal{Z}_{II} \{ f(-nT) \} = F(z^{-1}) \quad \frac{1}{R_-} < |z| < \frac{1}{R_+}$$

5. Multiplication by  $nT$ 

$$\mathcal{Z}_{II} \{ f(nT) \} = F(z) \quad R_+ < |z| < R_-$$

$$\mathcal{Z}_{II} \{ nT f(nT) \} = -zT \frac{dF(z)}{dz} \quad R_+ > |z| < R_-$$

## 6. Convolution

$$\mathcal{Z}_{II} \{ f_1(nT) * f_2(nT) \} = F_1(z) F_2(z)$$

$$\text{ROC } F_1(z) \cup \text{ROC } F_2(z^{-1}) \quad \max(R_{+f_1}, R_{+f_2}) < |z| < \min(R_{-f_1}, R_{-f_2})$$

## 7. Correlation

$$R_{f_1 f_2}(z) = \mathcal{Z}_{II} \{ f_1(nT) \otimes f_2(nT) \} = F_1(z) F_2(z^{-1})$$

$$\text{ROC } F_1(z) \cup \text{ROC } F_2(z^{-1}) \quad \max(R_{+f_1}, R_{+f_2}) < |z| < \min(R_{-f_1}, R_{-f_2})$$

8. Multiplication by  $e^{-anT}$ 

$$\mathcal{Z}_{II} \{ f(nT) \} = F(z) \quad R_+ < |z| < R_-$$

$$\mathcal{Z}_{II} \{ e^{-anT} f(nT) \} = F(e^{aT} z) \quad |e^{-aT}| R_+ < |z| < |e^{-aT}| R_-$$

## 9. Frequency translation

$$G(\omega) = \mathcal{Z}_{II} \{ e^{j\omega_0 nT} f(nT) \} = G(z)|_{z=e^{j\omega T}} = F(e^{j(\omega-\omega_0)T}) = F(\omega - \omega_0)$$

ROC of  $F(z)$  must include the unit circle

## 10. Product

$$\mathcal{Z}_{II} \{ f(nT) \} = F(z) \quad R_{+f} < |z| < R_{-f}$$

$$\mathcal{Z}_{II} \{ h(nT) \} = H(z) \quad R_{+h} < |z| < R_{-h}$$

$$\mathcal{Z}_{II} \{ f(nT) h(nT) \} = G(z) = \frac{1}{2\pi j} \oint_C F(\tau) H\left(\frac{z}{\tau}\right) \frac{d\tau}{\tau}, \quad R_{+f} R_{+h} < |z| < R_{-f} R_{-h}$$

$$\underbrace{\max\left(R_{+f}, \frac{|z|}{R_{-h}}\right) < |\tau| < \min\left(R_{-f}, \frac{|z|}{R_{+h}}\right)}_{\text{counterclockwise integration}}$$

## 11. Parseval's theorem

$$\mathcal{Z}_{II} \{ f(nT) \} = F(z) \quad R_{+f} < |z| < R_{-f}$$

$$\mathcal{Z}_{II} \{ h(nT) \} = H(z) \quad R_{+h} < |z| < R_{-h}$$

$$\sum_{n=-\infty}^{\infty} f(nT) h(nT) = \frac{1}{2\pi j} \oint_C F(z) H(z^{-1}) \frac{dz}{z} \quad R_{+f} R_{+h} < |z| = 1 < R_{-f} R_{-h}$$

$$\underbrace{\max\left(R_{+f}, \frac{1}{R_{-h}}\right) < |z| < \min\left(R_{-f}, \frac{1}{R_{+h}}\right)}_{\text{counterclockwise integration}}$$

## 12. Complex conjugate signals

$$\mathcal{Z}_{II} \{ f(nT) \} = F(z) \quad R_{+f} < |z| < R_{-f}$$

$$\mathcal{Z}_{II} \{ f^*(nT) \} = F^*(z^*) \quad R_{+f} < |z| < R_{-f}$$

**TABLE A.6.3** Inverse Transforms of the Partial Fractions of  $F(z)$

Partial Fraction Term	Inverse Transform Term in $F(z)$ Converges Absolutely for Some $ z  >  a $
$\frac{z}{z-a}$	$a^k, k \geq 0$
$\frac{z^2}{(z-a)^2}$	$(k+1)a^k, k \geq 0$
$\frac{z^3}{(z-a)^3}$	$\frac{1}{2}(k+1)(k+2)a^k, k \geq 0$
$\vdots$	$\vdots$
$\frac{z^n}{(z-a)^n}$	$\frac{1}{(n-1)!}(k+1)(k+2)\cdots(k+n-1)a^k, k \geq 0$
Partial fraction term	Inverse transform term in $F(z)$ converges absolutely for some $ z  <  a $
$\frac{z}{z-a}$	$-a^k, k \leq -1$
$\frac{z^2}{(z-a)^2}$	$-(k+1)a^k, k \leq -1$
$\frac{z^3}{(z-a)^3}$	$-\frac{1}{2}(k+1)(k+2)a^k, k \leq -1$
$\vdots$	$\vdots$
$\frac{z^n}{(z-a)^n}$	$\frac{1}{(n-1)!}(k+1)(k+2)\cdots(k+n-1)a^k, k \leq -1$

**TABLE A.6.4** Inverse Transforms of the Partial Fractions of  $F_i(z)^a$

Elementary Transform Term $F_i(z)$	Corresponding Time Sequence	
	(I) $F_i(z)$ Converges for $ z  > R_c$	(II) $F_i(z)$ Converges for $ z  < R_c$
1. $\frac{1}{z-a}$	$a^{k-1} _{k \geq 1}$	$-a^{k-1} _{k \leq 0}$
2. $\frac{z}{(z-a)^2}$	$ka^{k-1} _{k \geq 1}$	$-ka^{k-1} _{k \leq 0}$
3. $\frac{z(z+a)}{(z-a)^3}$	$k^2 a^{k-1} _{k \geq 1}$	$-k^2 a^{k-1} _{k \leq 0}$
4. $\frac{z(z^2+4az+a^2)}{(z-a)^4}$	$k^3 a^{k-1} _{k \geq 1}$	$-k^3 a^{k-1} _{k \leq 0}$

<sup>a</sup> The function must be a proper function.

**TABLE A.6.5** Z-Transform Pairs

Number	Discrete Time-Function $f(n), n \geq 0$	Z-Transform $\mathcal{F}(z) = \mathcal{Z}[f(n)] = \sum_{n=0}^{\infty} f(n)z^{-n}  z  > R$
1	$u(n) = \begin{cases} 1, & \text{for } n \geq 0 \\ 0, & \text{otherwise} \end{cases}$	$\frac{z}{z-1}$
2	$e^{-\alpha n}$	$\frac{z}{z-e^{-\alpha}}$
3	$n$	$\frac{z}{(z-1)^2}$
4	$n^2$	$\frac{z(z+1)}{(z-1)^3}$
5	$n^3$	$\frac{z(z^2+4z+1)}{(z-1)^4}$
6	$n^4$	$\frac{z(z^3+11z^2+11z+1)}{(z-1)^5}$
7	$n^5$	$\frac{z(z^4+26z^3+66z^2+26z+1)}{(z-1)^6}$

(continued)

TABLE A.6.5 (continued) Z-Transform Pairs

Number	Discrete Time-Function $f(n), n \geq 0$	Z-Transform $\mathcal{F}(z) = \mathcal{Z}[f(n)] = \sum_{n=0}^{\infty} f(n)z^{-n}  z  > R$
8	$n^k$	$(-1)^k D^k \left( \frac{z}{z-1} \right); \quad D = z \frac{d}{dz}$
9	$u(n-k)$	$\frac{z^{-k+1}}{z-1}$
10	$e^{-\alpha n} f(n)$	$\mathcal{F}(e^{\alpha} z)$
11	$n^{(2)} = n(n-1)$	$2 \frac{z}{(z-1)^3}$
12	$n^{(3)} = n(n-1)(n-2)$	$3! \frac{z}{(z-1)^4}$
13	$n^{(k)} = n(n-1)(n-2)\dots(n-k+1)$	$k! \frac{z}{(z-1)^{k+1}}$
14	$n^{[k]} f(n), n^{[k]} = n(n+1)(n+2)\dots(n+k-1)$	$(-1)^k z^k \frac{d^k}{dz^k} [\mathcal{F}(z)]$
15	$(-1)^k n(n-1)(n-2)\dots(n-k+1) f_{n-k+1}^a$	$z \mathcal{F}^{(k)}(z), \mathcal{F}^{(k)}(z) = \frac{d^k}{dz^k} \mathcal{F}(z)$
16	$-(n-1) f_{n-1}$	$\mathcal{F}^{(1)}(z)$
17	$(-1)^k (n-1)(n-2)\dots(n-k) f_{n-k}$	$\mathcal{F}^{(k)}(z)$
18	$n f(n)$	$-z \mathcal{F}^{(1)}(z)$
19	$n^2 f(n)$	$z^2 \mathcal{F}^{(2)}(z) + z \mathcal{F}^{(1)}(z)$
20	$n^3 f(n)$	$-z^3 \mathcal{F}^{(3)}(z) - 3z^2 \mathcal{F}^{(2)}(z) - z \mathcal{F}^{(1)}(z)$
21	$\frac{c^n}{n!}$	$e^{c/z}$
22	$\frac{(\ln c)^n}{n!}$	$c^{1/z}$
23	$\binom{k}{n} c^n a^{k-n}, \quad \binom{k}{n} = \frac{k!}{(k-n)!n!}, \quad n \leq k$	$\frac{(az+c)^k}{z^k}$
24	$\binom{n+k}{k} c^n$	$\frac{z^{k+1}}{(z-c)^{k+1}}$
25	$\frac{c^n}{n!}, \quad (n = 1, 3, 5, 7, \dots)$	$\sinh \left( \frac{c}{z} \right)$
26	$\frac{c^n}{n!}, \quad (n = 0, 2, 4, 6, \dots)$	$\cosh \left( \frac{c}{z} \right)$
27	$\sin(\alpha n)$	$\frac{z \sin \alpha}{z^2 - 2z \cos \alpha + 1}$
28	$\cos(\alpha n)$	$\frac{z(z - \cos \alpha)}{z^2 - 2z \cos \alpha + 1}$
29	$\sin(\alpha n + \psi)$	$\frac{z^2 \sin \psi + z \sin(\alpha - \psi)}{z^2 - 2z \cos \alpha + 1}$
30	$\cosh(\alpha n)$	$\frac{z(z - \cosh \alpha)}{z^2 - 2z \cosh \alpha + 1}$
31	$\sinh(\alpha n)$	$\frac{z \sinh \alpha}{z^2 - 2z \cosh \alpha + 1}$
32	$\frac{1}{n}, \quad n > 0$	$\ln \frac{z}{z-1}$
33	$\frac{1 - e^{-\alpha n}}{n}$	$\alpha + \ln \frac{z - e^{-\alpha}}{z-1}, \quad \alpha > 0$
34	$\frac{\sin \alpha n}{n}$	$\alpha + \tan^{-1} \frac{\sin \alpha}{z - \cos \alpha}, \quad \alpha > 0$
35	$\frac{\cos \alpha n}{n}, \quad n > 0$	$\ln \frac{z}{\sqrt{z^2 - 2z \cos \alpha + 1}}$
36	$\frac{(n+1)(n+2)\dots(n+k-1)}{(k-1)!}$	$\left(1 - \frac{1}{z}\right)^{-k}, \quad k = 2, 3, \dots$
37	$\sum_{m=1}^n \frac{1}{m}$	$\frac{z}{z-1} \ln \frac{z}{z-1}$

TABLE A.6.5 (continued) Z-Transform Pairs

Number	Discrete Time-Function $f(n), n \geq 0$	Z-Transform $\mathcal{F}(z) = \mathcal{Z}[f(n)] = \sum_{n=0}^{\infty} f(n)z^{-n}  z  > R$
38	$\sum_{m=0}^{n-1} \frac{1}{m!}$	$\frac{e^{1/z}}{z-1}$
39	$\frac{(-1)^{(n-p)/2}}{2^n \binom{n-p}{2}! \binom{n+p}{2}!}$ , for $n \geq p$ and $n-p = \text{even}$ $= 0$ , for $n < p$ or $n-p = \text{odd}$	$J_p(z^{-1})$
40	$\left\{ \begin{array}{ll} \binom{\alpha}{n/k} b^{n/k}, & n = mk, \quad (m = 0, 1, 2, \dots) \\ = 0 & n \neq mk \end{array} \right\}$	$\left( \frac{z^k + b}{z^k} \right)^\alpha$
41	$a^n P_n(x) = \frac{a^n}{2^n n!} \left( \frac{d}{dx} \right)^n (x^2 - 1)^n$	$\frac{z}{\sqrt{z^2 - 2xaz + a^2}}$
42	$a^n T_n(x) = a^n \cos(n \cos^{-1} x)$	$\frac{z(z-ax)}{z^2 - 2xaz + a^2}$
43	$\frac{L_n(x)}{n!} = \sum_{r=0}^{\infty} \binom{n}{r} \frac{(-x)^r}{r!}$	$\frac{z}{z-1} e^{-x/(z-1)}$
44	$\frac{H_n(x)}{n!} = \sum_{k=0}^{\lfloor n/2 \rfloor} \frac{(-1)^{n-k} x^{n-2k}}{k(n-2k)! 2^k}$	$e^{-x/z-1/2z^2}$
45	$a^n P_n^m(x) = a^n (1-x^2)^{m/2} \left( \frac{d}{dx} \right)^m P_n(x), \quad m = \text{integer}$	$\frac{(2m)!}{2^m m!} \frac{z^{m+1} (1-x^2)^{m/2} a^m}{(z^2 - 2xaz + a^2)^{m+1/2}}$
46	$\frac{L_n^m(x)}{n!} = \left( \frac{d}{dx} \right)^m \frac{L_n(x)}{n!}, \quad m = \text{integer}$	$\frac{(-1)^m z}{(z-1)^{m+1}} e^{-x/(z-1)}$
47	$-\frac{1}{n} \mathcal{Z}^{-1} \left[ z \frac{\mathcal{F}'(z)}{\mathcal{F}(z)} - \frac{\mathcal{G}'(z)}{\mathcal{G}(z)} \right]$ , where $\mathcal{F}(z)$ and $\mathcal{G}(z)$ are rational polynomials in $z$ of the same order	$\ln \frac{\mathcal{F}(z)}{\mathcal{G}(z)}$
48	$\frac{1}{m(m+1)(m+2) \dots (m+n)}$	$(m-1)! z^m \left[ e^{1/z} - \sum_{k=0}^{m-1} \frac{1}{k! z^k} \right]$
49	$\frac{\sin(\alpha n)}{n!}$	$e^{\cos \alpha/z} \cdot \sin \left( \frac{\sin \alpha}{z} \right)$
50	$\frac{\cos(\alpha n)}{n!}$	$e^{\cos \alpha/z} \cdot \cos \left( \frac{\sin \alpha}{z} \right)$
51	$\sum_{k=0}^n f_k g_{n-k}$	$\mathcal{F}(z)\mathcal{G}(z)$
52	$\sum_{k=0}^n k f_k g_{n-k}$	$\mathcal{F}^{(1)}(z)\mathcal{G}(z), \mathcal{F}^{(1)}(z) = \frac{d\mathcal{F}(z)}{dz}$
53	$\sum_{k=0}^n k^2 f_k g_{n-k}$	$\mathcal{F}^{(2)}(z)\mathcal{G}(z)$
54	$\frac{\alpha^n + (-\alpha)^n}{2\alpha^2}$	$\frac{1}{\alpha^2} \frac{z^2}{z^2 - \alpha^2}$
55	$\frac{\alpha^n - \beta^n}{\alpha - \beta}$	$\frac{z}{(z-\alpha)(z-\beta)}$
56	$(n+k)^{(k)}$	$k! z^k \frac{z}{(z-1)^{k+1}}$
57	$(n-k)^{(k)}$	$k! z^{-k} \frac{z}{(z-1)^{k+1}}$
58	$\frac{(n \mp k)^{(m)}}{m!} e^{\alpha(n-k)}$	$\frac{z^{1 \mp k} e^{m\alpha}}{(z - e^\alpha)^{m+1}}$
59	$\frac{1}{n} \sin \frac{\pi}{2} n$	$\frac{\pi}{2} + \tan^{-1} \frac{1}{z}$
60	$\frac{\cos \alpha(2n-1)}{2n-1}, \quad n > 0$	$\frac{1}{4\sqrt{z}} \ln \frac{z + 2\sqrt{z} \cos \alpha + 1}{z - 2\sqrt{z} \cos \alpha + 1}$
61	$\frac{\gamma^n}{(\gamma-1)^2} + \frac{n}{1-\gamma} - \frac{1}{(1-\gamma)^2}$	$\frac{z}{(z-\gamma)(z-1)^2}$

(continued)

TABLE A.6.5 (continued) Z-Transform Pairs

Number	Discrete Time-Function $f(n), n \geq 0$	Z-Transform $\mathcal{F}(z) = \mathcal{Z}[f(n)] = \sum_{n=0}^{\infty} f(n)z^{-n}  z  > R$
62	$\frac{\gamma + a_0}{(\gamma - 1)^2} \gamma^n + \frac{1 + a_0}{1 - \gamma} n + \left( \frac{1}{1 - \gamma} - \frac{a_0 + 1}{(1 - \gamma)^2} \right)$	$\frac{z(z + a_0)}{(z - \gamma)(z - 1)^2}$
63	$a^n \cos \pi n$	$\frac{z}{z + a}$
64	$e^{-\alpha n} \cos an$	$\frac{z(z - e^{-\alpha} \cos a)}{z^2 - 2ze^{-\alpha} \cos a + e^{-2\alpha}}$
65	$e^{-\alpha n} \sinh(an + \psi)$	$\frac{z^2 \sinh \psi + ze^{-\alpha} \sinh(a - \psi)}{z^2 - 2ze^{-\alpha} \cosh a + e^{-2\alpha}}$
66	$\frac{\gamma^n}{(\gamma - \alpha)^2 + \beta^2} + \frac{(\alpha^2 + \beta^2)^{n/2} \sin(n\theta + \psi)}{\beta[(\alpha - \gamma)^2 + \beta^2]^{1/2}}$ $\theta = \tan^{-1} \frac{\beta}{\alpha}$ $\psi = \tan^{-1} \frac{\alpha \beta}{\alpha - \gamma}$	$\frac{z}{(z - \gamma)[(z - \alpha)^2 + \beta^2]}$
67	$\frac{n\gamma^{n-1}}{(\gamma - 1)^3} - \frac{3\gamma^n}{(\gamma - 1)^4} + \frac{1}{2} \left[ \frac{n(n-1)}{(1-\gamma)^2} - \frac{4n}{(1-\gamma)^3} + \frac{6}{(1-\gamma)^4} \right]$	$\frac{z}{(z - \gamma)^2(z - 1)^3}$
68	$\sum_{v=0}^k (-1)^v \binom{k}{v} \frac{(n+k-v)^{(k)} e^{\alpha(n-v)}}{k!}$	$\frac{z(z-1)^k}{(z - e^{\alpha})^{k+1}}$
69	$\frac{f(n)}{n}$	$\int_z^{\infty} p^{-1} \mathcal{F}(p) dp + \lim_{n \rightarrow 0} \frac{f(n)}{n}$
70	$\frac{f_{n+2}}{n+1}, f_0 = 0, f_1 = 0$	$z \int_z^{\infty} \mathcal{F}(p) dp$
71	$\frac{1 + a_0}{(1 - \gamma)[(1 - \alpha)^2 + \beta^2]} + \frac{(\gamma + a_0)\gamma^n}{(\gamma - 1)[(\gamma - \alpha)^2 + \beta^2]} + \frac{[\alpha^2 + \beta^2]^{n/2} [(a_0 + \alpha)^2 + \beta^2]^{1/2}}{\beta[(\alpha - 1)^2 + \beta^2]^{1/2} [(\alpha - \gamma)^2 + \beta^2]^{1/2}} \times \sin(n\theta + \psi + \lambda)$ $\psi = \psi_1 + \psi_2, \psi_1 = -\tan^{-1} \frac{\beta}{\alpha - 1}, \theta = \tan^{-1} \frac{\beta}{\alpha}$ $\lambda = \tan^{-1} \frac{\beta}{a_0 + \alpha}, \psi_2 = -\tan^{-1} \frac{\beta}{\alpha - \gamma}$	$\frac{z(z + a_0)}{(z - 1)(z - \gamma)[(z - \alpha)^2 + \beta^2]}$
72	$(n + 1)e^{\alpha n} - 2ne^{\alpha(n+1)} + e^{\alpha(n-2)}(n - 1)$	$\left( \frac{z - 1}{z - e^{\alpha}} \right)^2$
73	$(-1)^n \frac{\cos \alpha n}{n}, n > 0$	$\ln \frac{z}{\sqrt{z^2 + 2z \cos \alpha} + 1}$
74	$\frac{(n+k)!}{n!} f_{n+k}, f_n = 0, \text{ for } 0 \leq n < k$	$(-1)^k z^{2k} \frac{dk}{dz^k} [\mathcal{F}(z)]$
75	$\frac{f(n)}{n+h}, h > 0$	$z^h \int_z^{\infty} p^{-(1+h)} \mathcal{F}(p) dp$
76	$-na^n \cos \frac{\pi}{2} n$	$\frac{2a^2 z^2}{(z^2 + a^2)^2}$
77	$na^n \frac{1 + \cos \pi n}{2}$	$\frac{2a^2 z^2}{(z^2 - a^2)^2}$
78	$a^n \sin \frac{\pi}{4} n \cdot \frac{1 + \cos \pi n}{2}$	$\frac{a^2 z^2}{z^4 + a^4}$
79	$a^n \left( \frac{1 + \cos \pi n}{2} - \cos \frac{\pi}{2} n \right)$	$\frac{2a^2 z^2}{z^4 - a^4}$
80	$\frac{P_n(x)}{n!}$	$e^{xz^{-1}} J_0(\sqrt{1 - x^2} z^{-1})$
81	$\frac{P_n^{(m)}(x)}{(n+m)!}, m > 0, P_n^m = 0, \text{ for } n < m$	$(-1)^m e^{xz^{-1}} J_m(\sqrt{1 - x^2} z^{-1})$

TABLE A.6.5 (continued) Z-Transform Pairs

Number	Discrete Time-Function $f(n), n \geq 0$	Z-Transform $\mathcal{F}(z) = \mathcal{Z}[f(n)] = \sum_{n=0}^{\infty} f(n)z^{-n}  z  > R$
82	$\frac{1}{(n + \alpha)^\beta}, \alpha > 0, \operatorname{Re} \beta > 0$	$\Phi(z^{-1}, \alpha, \beta),$ where $\Phi(1, \beta, \alpha) = \zeta(\beta, \alpha) =$ generalized Riemann-Zeta function
83	$a^n \left( \frac{1 + \cos \pi n}{2} + \cos \frac{\pi}{2} n \right)$	$\frac{2z^4}{z^4 - a^4}$
84	$\frac{c^n}{n}, (n = 1, 2, 3, 4, \dots)$	$\ln z - \ln(z - c)$
85	$\frac{c^n}{n}, n = 2, 4, 6, 8, \dots$	$\ln z - \frac{1}{2} \ln(z^2 - c^2)$
86	$n^2 c^n$	$\frac{cz(z + c)}{(z - c)^3}$
87	$n^3 c^n$	$\frac{cz(z^2 + 4cz + c^2)}{(z - c)^4}$
88	$n^k c^n$	$-\frac{d\mathcal{F}(z/c)}{dz}, \mathcal{F}(z) = \mathcal{Z}[n^{k-1}]$
89	$-\cos \frac{\pi}{2} n \sum_{i=0}^{(n-2)/4} \binom{n/2}{2i+1} a^{n-2-4i} (a^4 - b^4)^i$	$\frac{z^2}{z^4 + 2a^2z^2 + b^4}$
90	$n^k f(n), k > 0$ and integer	$-z \frac{d}{dz} \mathcal{F}_1(z), \mathcal{F}_1(z) = \mathcal{Z}[n^{k-1}f(n)]$
91	$\frac{(n-1)(n-2)(n-3)\dots(n-k+1)}{(k-1)!} a^{n-k}$	$\frac{1}{(z-a)^k}$
92	$\frac{k(k-1)(k-2)\dots(k-n+1)}{n!}$	$\left(1 + \frac{1}{z}\right)^k$
93	$na^n \cos bn$	$\frac{[(z/a)^3 + z/a] \cos b - 2(z/a)^2}{[(z/a)^2 - 2(z/a) \cos b + 1]^2}$
94	$na^n \sin bn$	$\frac{(z/a)^3 \sin b - (z/a) \sin b}{[(z/a)^2 - 2(z/a) \cos b + 1]^2}$
95	$\frac{na^n}{(n+1)(n+2)}$	$\frac{z(a-2z)}{a^2} \ln\left(1 - \frac{a}{z}\right) - \frac{2}{a}z$
96	$\frac{(-a)^n}{(n+1)(2n+1)}$	$2\sqrt{z/a} \tan^{-1} \sqrt{a/z} - \frac{z}{a} \ln\left(1 + \frac{a}{z}\right)$
97	$\frac{a^n \sin \alpha n}{n+1}$	$\frac{z \cos \alpha}{a} \tan^{-1} \frac{a \sin \alpha}{z - a \cos \alpha}$ $+ \frac{z \sin \alpha}{2a} \ln \frac{z^2 - 2az \cos \alpha + a^2}{z^2}$
98	$\frac{a^n \cos(\pi/2)n \sin \alpha(n+1)}{n+1}$	$\frac{z}{4a} \ln \frac{z^2 + 2az \sin \alpha + a^2}{z^2 - 2az \sin \alpha + a^2}$
99	$\frac{1}{(2n)!}$	$\cos h(z^{-1/2})$
100	$\binom{-1/2}{n} (-a)^n$	$\sqrt{z/(z-a)}$
101	$\binom{-1/2}{n/2} a^n \cos \frac{\pi}{2} n$	$\frac{z}{\sqrt{z^2 - a^2}}$
102	$\frac{B_n(x)}{n!}$ $B_n(x)$ are Bernoulli polynomials	$\frac{e^{x/z}}{z(e^{1/z} - 1)}$
103	$W_n(x) \doteq$ Chebyshev polynomials of the second kind	$\frac{z^2}{z^2 - 2xz + 1}$
104	$\left  \sin \frac{n\pi}{m} \right , m = 1, 2, \dots$	$\frac{z \sin \pi/m}{z^2 - 2z \cos \pi/m + 1} \frac{1 + z^{-m}}{1 - z^{-m}}$
105	$Q_n(x) = \sin(n \cos^{-1} x)$	$\frac{z}{z^2 - 2xz + 1}$

Source: Jury, E.I. *Theory and Application of the Z-Transform Method*, John Wiley & Sons, Inc., New York, 1964. With permission.

<sup>a</sup> It may be noted that  $f_n$  is the same as  $f(n)$ .

## Bibliography

---

- H. Freeman, *Discrete-Time Systems*, John Wiley & Sons, New York, 1965.
- R. A. Gabel and R. A. Roberts, *Signals and Linear Systems*, John Wiley & Sons, New York, 1980.
- E. I. Jury, *Theory and Application of the Z-Transform Method*, Krieger Publishing Co., Melbourne, FL, 1973.
- A. D. Poularikas and S. Seeley, *Signals and Systems*, reprinted 2nd edn., Krieger Publishing Co., Melbourne, FL, 1994.
- S. A. Tretter, *Introduction to Discrete-Time Signal Processing*, John Wiley & Sons, New York, 1976.
- R. Vich, *Z-Transform Theory and Applications*, D. Reidel Publishing Co., Boston, MA, 1987.

# 7

## Hilbert Transforms

---

7.1	Introduction.....	7-2
7.2	Basic Definitions.....	7-2
7.3	Analytic Functions Aspect of Hilbert Transformations.....	7-3
7.4	Spectral Description of the Hilbert Transformation: One-Sided Spectrum of the Analytic Signal.....	7-5
	Derivation of Hilbert Transforms Using Hartley Transforms	
7.5	Examples of Derivation of Hilbert Transforms.....	7-7
7.6	Definition of the Hilbert Transformation by Using a Distribution.....	7-9
7.7	Hilbert Transforms of Periodic Signals.....	7-10
	First Method • Second Method • Third Method: Cotangent Hilbert Transformations	
7.8	Tables Listing Selected Hilbert Pairs and Properties of Hilbert Transformations.....	7-14
7.9	Linearity, Iteration, Autoconvolution, and Energy Equality.....	7-14
	Iteration • Autoconvolution and Energy Equality	
7.10	Differentiation of Hilbert Pairs.....	7-20
7.11	Differentiation and Multiplication by $t$ : Hilbert Transforms of Hermite Polynomials and Functions.....	7-21
7.12	Integration of Analytic Signals.....	7-23
7.13	Multiplication of Signals with Nonoverlapping Spectra.....	7-27
7.14	Multiplication of Analytic Signals.....	7-28
7.15	Hilbert Transforms of Bessel Functions of the First Kind.....	7-28
7.16	Instantaneous Amplitude, Complex Phase, and Complex Frequency of Analytic Signals.....	7-32
	Instantaneous Complex Phase and Complex Frequency	
7.17	Hilbert Transforms in Modulation Theory.....	7-35
	Concept of the Modulation Function of a Harmonic Carrier • Generalized Single Side-Band Modulations • CSSB: Compatible Single Side-Band Modulation • Spectrum of the CSSB Signal • CSSB Modulation for Angle Detectors	
7.18	Hilbert Transforms in the Theory of Linear Systems: Kramers–Kronig Relations.....	7-41
	Causality • Physical Realizability of Transfer Functions • Minimum Phase Property • Amplitude-Phase Relations in DLTI Systems • Minimum Phase Property in DLTI Systems • Kramers–Kronig Relations in Linear Macroscopic Continuous Media • Concept of Signal Delay in Hilbertian Sense	
7.19	Hilbert Transforms in the Theory of Sampling.....	7-46
	Band-Pass Filtering of the Low-Pass Sampled Signal • Sampling of Band-Pass Signals	
7.20	Definition of Electrical Power in Terms of Hilbert Transforms and Analytic Signals.....	7-49
	Harmonic Waveforms of Voltage and Current • Notion of Complex Power • Generalization of the Notion of Power • Generalization of the Notion of Power for Signals with Finite Average Power	
7.21	Discrete Hilbert Transformation.....	7-54
	Properties of the DFT and DHT Illustrated with Examples • Complex Analytic Discrete Sequence • Bilinear Transformation and the Cotangent Form of Hilbert Transformations	
7.22	Hilbert Transformers (Filters).....	7-61
	Phase-Splitter Hilbert Transformers • Analog All-Pass Filters • A Simple Method of Design of Hilbert Phase Splitters • Delay, Phase Distortions, and Equalization • Hilbert Transformers with Tapped Delay-Line Filters • Band-Pass Hilbert Transformers • Generation of Hilbert Transforms Using SSB Filtering • Digital Hilbert Transformers • Methods of Design • FIR Hilbert Transformers • Digital Phase Splitters • IIR Hilbert Transformers • Differentiating Hilbert Transformers	



7.23 Multidimensional Hilbert Transformations..... 7-79  
 Evenness and Oddness of  $N$ -Dimensional Signals •  $n$ -D Hilbert Transformations •  
 2-D Hilbert Transformations • Partial Hilbert Transformations • Spectral Description  
 of  $n$ -D Hilbert Transformations •  $n$ -D Hilbert Transforms of Separable Functions •  
 Properties of 2-D Hilbert Transformations • Stark’s Extension of Bedrosian’s Theorem •  
 Appendix (Section 7.23) • Two-Dimensional Hilbert Transformers

7.24 Multidimensional Complex Signals ..... 7-88  
 Short Historical Review • Definition of the Multidimensional Complex Signal •  
 Conjugate 2-D Complex Signals • Local (or “Instantaneous”) Amplitudes, Phases,  
 and Complex Frequencies • Relations between Real and Complex Notation •  
 2-D Modulation Theory • Appendix: A Method of Labeling Orthants

7.25 Quaternionic 2-D Signals ..... 7-94  
 Quaternion Numbers and Quaternion-Valued Functions • Quaternionic Spectral Analysis •  
 Hermitian Symmetry of the 2-D Fourier Spectrum

7.26 The Monogenic 2-D Signal ..... 7-96  
 Spherical Coordinates Representation of the MS

7.27 Wigner Distributions of 2-D Analytic, Quaternionic,  
 and Monogenic Signals ..... 7-98

7.28 The Clifford Analytic Signal ..... 7-98

7.29 Hilbert Transforms and Analytic Signals in Wavelets ..... 7-99

References ..... 7-99

Stefan L. Hahn  
 Warsaw University of Technology

### 7.1 Introduction

The Hilbert transformations are of widespread interest because they are applied in the theoretical description of many devices and systems and directly implemented in the form of Hilbert analog or digital filters (transformers). Let us quote some important applications of Hilbert transformations:

1. The complex notation of harmonic signals in the form of Euler’s equation  $\exp(j\omega t) = \cos(\omega t) + j \sin(\omega t)$  has been used in electrical engineering since the 1890s and nowadays is commonly applied in the theoretical description of various, not only electrical systems. This complex notation had been introduced before Hilbert derived his transformations. However,  $\sin(\omega t)$  is the Hilbert transform of  $\cos(\omega t)$ , and the complex signal  $\exp(j\omega t)$  is a precursor of a wide class of complex signals called analytic signals.
2. The concept of the analytic signal<sup>11</sup> of the form  $\psi(t) = u(t) + jv(t)$ , where  $v(t)$  is the Hilbert transform of  $u(t)$ , extends the complex notation to a wide class of signals for which the Fourier transform exists. The notion of the analytic signal is widely used in the theory of signals, circuits, and systems. A device called the Hilbert transformer (or filter), which produces at the output the Hilbert transform of the input signal, finds many applications, especially in modern digital signal processing.
3. The real and imaginary parts of the transmittance of a linear and causal two-port system form a pair of Hilbert transforms. This property finds many applications.
4. Recently two-dimensional (2-D) and multidimensional Hilbert transformations have been applied to define 2-D and multidimensional complex signals, opening the door for applications in multidimensional signal processing.<sup>13</sup>

### 7.2 Basic Definitions

The Hilbert transformation of a 1-D real signal (function)  $u(t)$  is defined by the integral

$$v(t) = \frac{-1}{\pi} P \int_{-\infty}^{\infty} \frac{u(\eta)}{\eta - t} d\eta = \frac{1}{\pi} P \int_{-\infty}^{\infty} \frac{u(\eta)}{t - \eta} d\eta \quad (7.1)$$

and the inverse Hilbert transformation is

$$u(t) = \frac{1}{\pi} P \int_{-\infty}^{\infty} \frac{v(\eta)}{\eta - t} d\eta = \frac{-1}{\pi} P \int_{-\infty}^{\infty} \frac{v(\eta)}{t - \eta} d\eta \quad (7.2)$$

where  $P$  stands for principal value of the integral. For convenience, two conventions of the sequence of variables in the denominator are given; both have been used in studies. The left-hand side formulae is used in this chapter. The following terminology is applied: the algorithm, that is, the right-hand side of Equations 7.1 or 7.2, is called “transformation,” and the specific result for a given function, that is, the left-hand side of Equations 7.1 or 7.2, is called the “transform.” The above definitions of Hilbert transformations are conveniently written in the convolution notations

$$v(t) = u(t) * \frac{1}{\pi t} \quad (7.3)$$

$$u(t) = v(t) * \frac{1}{\pi t} \quad (7.4)$$

The integrals in definition (7.1) are improper because the integrand goes to infinity for  $\eta = t$ . Therefore, the integral is defined as the Cauchy principal value (sign  $P$ ) of the form

$$v(t) = \lim_{\substack{\varepsilon \Rightarrow 0 \\ A \Rightarrow \infty}} \frac{-1}{\pi} \left( \int_{-A}^{-\varepsilon} + \int_{\varepsilon}^A \frac{u(\eta)}{\eta - t} d\eta \right) \quad (7.5)$$

Using numerical integration in the sense of the Cauchy principal value with uniform sampling of the integrand, the origin  $\eta = 0$  should be positioned exactly at the center of the sampling interval. The limit  $\varepsilon \Rightarrow 0$  is substituted by a given value of the sampling interval and the limit  $A \Rightarrow \infty$  by a given value of  $A$ . The accuracy of the numerical integration increases with smaller sampling intervals and larger values of  $A$ .

The Hilbert transformation was originally derived by Hilbert in the frame of the theory of analytic functions. The theory of Hilbert transformations is closely related to Fourier transformation of signals of the form

$$U(\omega) = \int_{-\infty}^{\infty} u(t)e^{-j\omega t} dt; \quad \omega = 2\pi f \quad (7.6)$$

The complex function  $U(\omega)$  is called the Fourier spectrum or Fourier image of the signal  $u(t)$  and the variable  $f = \omega/2\pi$ , the Fourier frequency. The inverse Fourier transformation is

$$u(t) = \int_{-\infty}^{\infty} U(\omega)e^{j\omega t} df \quad (7.7)$$

The pair of transforms (Equations 7.6 and 7.7) may be denoted

$$u(t) \stackrel{F}{\iff} U(\omega) \quad (7.8)$$

called a Fourier pair. Similarly the Hilbert transformations (Equations 7.1 and 7.2) may be denoted

$$u(t) \stackrel{H}{\iff} v(t) \quad (7.9)$$

forming a Hilbert pair of functions. Contrary to other transformations, the Hilbert transformation does not change the domain. For example, the function of a time variable  $t$  (or of any other variable  $x$ ) is transformed to a function of the same variable, while the Fourier transformation changes a function of time into a function of frequency.

The Fourier transform (see also Chapter 2) of the kernel of the Hilbert transformation, that is,  $\Theta(t) = 1/(\pi t)$  (see Equations 7.3 and 7.4) is

$$\Theta(t) = \frac{1}{\pi t} \stackrel{F}{\iff} -j \operatorname{sgn}(\omega) \quad (7.10)$$

with the signum function (distribution) defined as follows:

$$\operatorname{sgn}(\omega) = \begin{cases} +1 & \omega > 0 \\ 0 & \omega = 0 \\ -1 & \omega < 0 \end{cases} \quad (7.11)$$

The multiplication to convolution theorem of the Fourier analysis yields the following spectrum of the Hilbert transform:

$$v(t) \stackrel{F}{\iff} V(\omega) = -j \operatorname{sgn}(\omega)U(\omega) \quad (7.12)$$

that is, the spectrum of the signal  $u(t)$  should be multiplied by the operator  $-j \operatorname{sgn}(\omega)$ . This relation enables the calculation of the Hilbert transform using the inverse Fourier transform of the spectrum defined by Equation 7.12, that is, using the following algorithm:

$$u(t) \stackrel{F}{\Rightarrow} U(\omega) \Rightarrow V(\omega) = -j \operatorname{sgn}(\omega)U \stackrel{F^{-1}}{\Rightarrow} v(t) \quad (7.13)$$

where the symbols  $F$  and  $F^{-1}$  denote the Fourier and inverse Fourier transformations, respectively. In practice, the algorithms of DFT (Discrete Fourier Transform) or FFT (Fast Fourier Transform) can be applied (Section 7.21).

### 7.3 Analytic Functions Aspect of Hilbert Transformations

The complex signal whose imaginary part is the Hilbert transform of its real part is called the *analytic signal*. The simplest example is the harmonic complex signal given by Euler's formula  $\psi(t) = \exp(j\omega t) = \cos(\omega t) + j \sin(\omega t)$ . A more general form of the analytic signal was defined in 1946 by Gabor.<sup>11</sup> The term "analytic" is used in the meaning of a complex function  $\Psi(z)$  of a complex variable  $z = t + j\tau$ , which is defined as follows:<sup>39</sup>

Consider a plane with rectangular coordinates  $(t, \tau)$  (called  $\mathbf{C}$  plane or  $\mathbf{C}$  "space") and take a domain  $\mathbf{D}$  in this plane. If we define a rule connecting to each point in  $\mathbf{D}$  a complex number  $\psi$ , we defined a complex function  $\psi(z)$ ,  $z \in \mathbf{D}$ . This function may be regarded as a complex function of two real variables:

$$\psi(z) = \psi(t, \tau) = u(t, \tau) + jv(t, \tau) \quad (7.14)$$

in the domain  $\mathbf{D} \in \mathbf{R}^2$  ( $\mathbf{R}^2$  is Euclidean plane or "space"). The complete derivative of the function  $\psi(z)$  has the form

$$d\psi = \frac{\partial \psi}{\partial z} dz + \frac{\partial \psi}{\partial z^*} dz^* \quad (7.15)$$

where  $z^* = t - j\tau$  is the complex conjugate and the partial derivatives are

$$\frac{\partial \psi}{\partial z} = \frac{1}{2} \left( \frac{\partial \psi}{\partial t} - j \frac{\partial \psi}{\partial \tau} \right); \quad \frac{\partial \psi}{\partial z^*} = \frac{1}{2} \left( \frac{\partial \psi}{\partial t} + j \frac{\partial \psi}{\partial \tau} \right) \quad (7.16)$$

The function  $\psi(z) = u(t, \tau) + jv(t, \tau)$  is called the *analytic function* in the domain  $\mathbf{D}$  if and only if  $u(t, \tau)$  and  $v(t, \tau)$  are *continuously differentiable*. It can be shown that this requirement is satisfied, if  $\partial \psi / \partial z^* = 0$ . This complex equation may be substituted by two real equations

$$\frac{\partial u}{\partial t} = \frac{\partial v}{\partial \tau}; \quad \frac{\partial u}{\partial \tau} = -\frac{\partial v}{\partial t} \quad (7.17)$$

called the *Cauchy–Riemann equations*. These equations should be satisfied if the function  $\psi(z)$  is analytic in the domain  $z \in \mathbf{D}$ . For example, the complex function

$$\psi(z) = \frac{1}{\alpha - jz} = u(t, \tau) + jv(t, \tau) \quad (7.18)$$

is analytic because

$$u(t, \tau) = \frac{(\alpha + \tau)}{(\alpha + \tau)^2 + t^2}; \quad v(t, \tau) = \frac{t}{(\alpha + \tau)^2 + t^2} \quad (7.19)$$

and the differentiation

$$\frac{\partial u(t, \tau)}{\partial t} = \frac{\partial v(t, \tau)}{\partial \tau} = \frac{-2t(\alpha + \tau)}{[(\alpha + \tau)^2 + t^2]^2} \quad (7.20)$$

verifies the Cauchy–Riemann equations.

It was shown by Cauchy that if  $z_0$  is a point inside a closed contour  $C \in \mathbf{D}$  such that  $\psi(z_0)$  is analytic inside and on  $C$ , then (see also Appendix A)

$$\psi(z_0) = \frac{1}{2\pi j} \int_C \frac{\psi(z)}{z - z_0} dz \quad (7.21)$$

$$\psi(z_0) = \frac{1}{2\pi j} \int_C \frac{\psi(y + z_0)}{y} dy \quad (7.22)$$

This is a contour integral in the  $(t, j\tau)$  plane. Let us take the contour  $C$  in the form shown in Figure 7.1. It is a sum of  $C_t + C_e + C_R$ , where  $C_t$  is a line parallel to the  $t$  axis shifted by  $\epsilon$ ,  $C_e$  is a half-circle of radius  $\epsilon$  and  $C_R$  a half-circle of radius  $R$ . The analytic signal is defined as a complex function of the real variable  $t$  given by the formula

$$\psi(t) = u(t, 0_+) + jv(t, 0_+) \quad (7.23)$$

obtained by inserting in the Equation 7.14  $\tau = 0_+$ , where the subscript  $+$  indicates that the path  $C_t$  approaches the  $t$  axis from the upside. The Equation 7.23 is the result of contour integration along the path of Figure 7.1 using the limit  $\epsilon \rightarrow 0, R \rightarrow \infty$ . We have

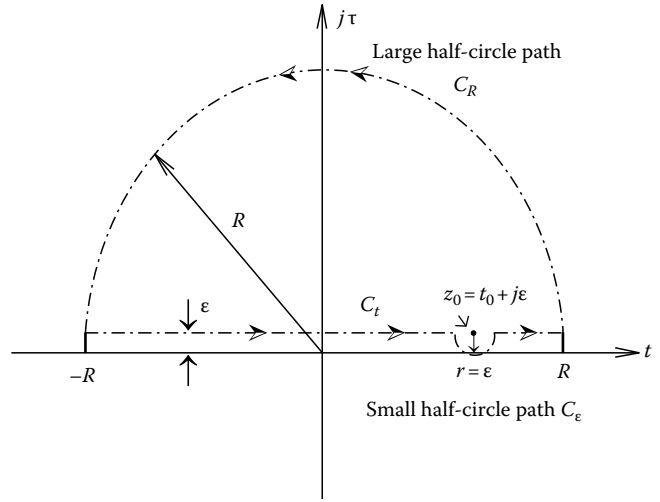


FIGURE 7.1 The integration path defining the analytic signal (Equation 7.23).

$$\begin{aligned} \psi(t_0, 0_+) &= \lim_{\epsilon \rightarrow 0, R \rightarrow \infty} \frac{1}{2\pi j} \\ &\times \left\{ P \int_{-R}^R \frac{\psi(z)}{z - z_0} dz + \int_{C_R} \frac{\psi(z)}{z - z_0} dz + \int_{C_e} \frac{\psi(z)}{z - z_0} dz \right\} \end{aligned} \quad (7.24)$$

The symbol  $P$  denotes the Cauchy principal value, that is,

$$P \int_{-R}^R = \int_{-R}^{t_0 - \epsilon} + \int_{t_0 + \epsilon}^R \quad (7.25)$$

For analytic functions the integral along  $C_R$  vanishes for  $R \rightarrow \infty$  and in the limit  $\epsilon \rightarrow 0$  the integral along the small half-circle  $C_e$  equals  $0.5 \psi(t_0, 0_+)$  since within the very small circle around  $t_0$  the function  $\psi(z) = \psi(t_0, 0_+)$  is a constant and the integral  $\int_{C_e} \frac{dz}{z - z_0} = \pi j$ . In consequence, the real and imaginary parts of the analytic signal are given by the integrals (a Hilbert pair)

$$v(t) = \frac{-1}{\pi} P \int_{-\infty}^{\infty} \frac{u(\eta, 0)}{\eta - t} d\eta \quad (7.26)$$

$$u(t) = \frac{-1}{\pi} P \int_{-\infty}^{\infty} \frac{v(\eta, 0)}{\eta - t} d\eta \quad (7.27)$$

where the subscripts  $t_0$  and  $0_+$  are deleted. The only difference between the above integrals and those defined by Equations 7.1 and 7.2 consists in notation (deleting zeros in parentheses). Therefore, the real and imaginary parts of the analytic signal

$$\psi(t) = u(t) + jv(t) \quad (7.28)$$

form a Hilbert pair of functions. For example, inserting  $\tau = 0$  in Equation 7.19 yields the Hilbert pair

$$u(t) = \frac{\alpha}{\alpha^2 + t^2} \stackrel{H}{\Leftrightarrow} v(t) = \frac{t}{\alpha^2 + t^2} \quad (7.29)$$

The signal  $u(t)$  is called the Cauchy signal and  $v(t)$  is its Hilbert transform.

A real signal  $u(t)$  may be written in terms of analytic signals

$$u(t) = \frac{\psi(t) + \psi^*(t)}{2} \quad (7.30)$$

and its Hilbert transform is

$$v(t) = \frac{\psi(t) - \psi^*(t)}{2j} \quad (7.31)$$

where  $\psi^*(t) = u(t) - jv(t)$  is the conjugate analytic signal. For this signal the Equation 7.24 takes the form  $\psi(t) = u(t, 0_-) - jv(t, 0_-)$  and the path C is in the lower half of the  $z$  plane. Notice, that the above formulae present a generalization of Euler's formulae

$$\cos(\omega t) = \frac{e^{j\omega t} + e^{-j\omega t}}{2} \quad (7.32)$$

$$\sin(\omega t) = \frac{e^{j\omega t} - e^{-j\omega t}}{2j} \quad (7.33)$$

## 7.4 Spectral Description of the Hilbert Transformation: One-Sided Spectrum of the Analytic Signal

Any real signal  $u(t)$  may be decomposed into a sum

$$u(t) = u_e(t) + u_o(t) \quad (7.34)$$

where the *even term* is defined as

$$u_e(t) = \frac{u(t) + u(-t)}{2} \quad (7.35)$$

and the *odd term*

$$u_o(t) = \frac{u(t) - u(-t)}{2} \quad (7.36)$$

The decomposition is *relative*, i.e., changes with the shift of the origin of the coordinate  $t' = t - t_0$ . In general, the Fourier image of  $u(t)$  defined by Equation 7.6 is a complex function

$$U(\omega) = U_{\text{Re}}(\omega) + jU_{\text{Im}}(\omega) \quad (7.37)$$

where the real part is given by the cosine transform

$$U_{\text{Re}}(\omega) = \int_{-\infty}^{\infty} u_e(t) \cos(\omega t) dt \quad (7.38)$$

and the imaginary part of the sine transform

$$U_{\text{Im}}(\omega) = - \int_{-\infty}^{\infty} u_o(t) \sin(\omega t) dt \quad (7.39)$$

The multiplication of the Fourier image by the operator  $-j \text{sgn}(\omega)$  changes the real part of the spectrum to the imaginary one and vice versa (see Equation 7.12). The spectrum of the Hilbert transform is

$$V(\omega) = V_{\text{Re}}(\omega) + jV_{\text{Im}}(\omega) \quad (7.40)$$

where

$$V_{\text{Re}}(\omega) = -j \text{sgn}(\omega)[jU_{\text{Im}}(\omega)] = \text{sgn}(\omega)U_{\text{Im}}(\omega) \quad (7.41)$$

and

$$V_{\text{Im}}(\omega) = -\text{sgn}(\omega)U_{\text{Re}}(\omega) \quad (7.42)$$

Therefore, the Hilbert transformation changes any even term to an odd term and any odd term to an even term. The Hilbert transforms of harmonic functions are

$$H[\cos(\omega t)] = \sin(\omega t) \quad (7.43)$$

$$H[\sin(\omega t)] = -\cos(\omega t) \quad (7.44)$$

$$H[e^{j\omega t}] = -j \text{sgn}(\omega)e^{j\omega t} = \text{sgn}(\omega)e^{j(\omega t - 0.5\pi)} \quad (7.45)$$

Therefore, the Hilbert transformation changes any cosine term to a sine term and any sine term to a reversed signed cosine term. Because  $\sin(\omega t) = \cos(\omega t - 0.5\pi)$  and  $-\cos(\omega t) = \sin(\omega t - 0.5\pi)$ , the Hilbert transformation in the time domain corresponds to a phase lag by  $-0.5\pi$  (or  $-90^\circ$ ) of all harmonic terms of the Fourier image (spectrum). Using the complex notation of the Fourier transform, the multiplication of the spectral function  $U(\omega)$  by the operator  $-j \text{sgn}(\omega)$  provides a  $90^\circ$  phase lag at all positive frequencies and a  $90^\circ$  phase lead at all negative frequencies. A linear two-port network with a transfer function  $H(\omega) = -j \text{sgn}(\omega)$  is called an ideal *Hilbert transformer* or filter. Such a filter cannot be exactly realized because of constraints imposed by causality (details in Section 7.22).

The Fourier image of the analytic signal

$$\psi(t) = u(t) + jv(t) \quad (7.46)$$

is one-sided. We have

$$u(t) \stackrel{H}{\Leftrightarrow} v(t) \quad u(t) \stackrel{F}{\Leftrightarrow} U(\omega); \quad v(t) \stackrel{F}{\Leftrightarrow} j \text{sgn}(\omega)U(\omega). \quad (7.47)$$

Therefore,

$$\psi(t) \stackrel{F}{\Leftrightarrow} U(\omega) + j[-j \text{sgn}(\omega)U(\omega)] = [1 + \text{sgn}(\omega)]U(\omega) \quad (7.48)$$

where

$$1 + \text{sgn}(\omega) = \begin{cases} 2 & \text{for } \omega > 0 \\ 1 & \text{for } \omega = 0 \\ 0 & \text{for } \omega < 0 \end{cases} \quad (7.49)$$

The Fourier image of the analytic signal is doubled at positive frequencies and canceled at negative frequencies with respect to

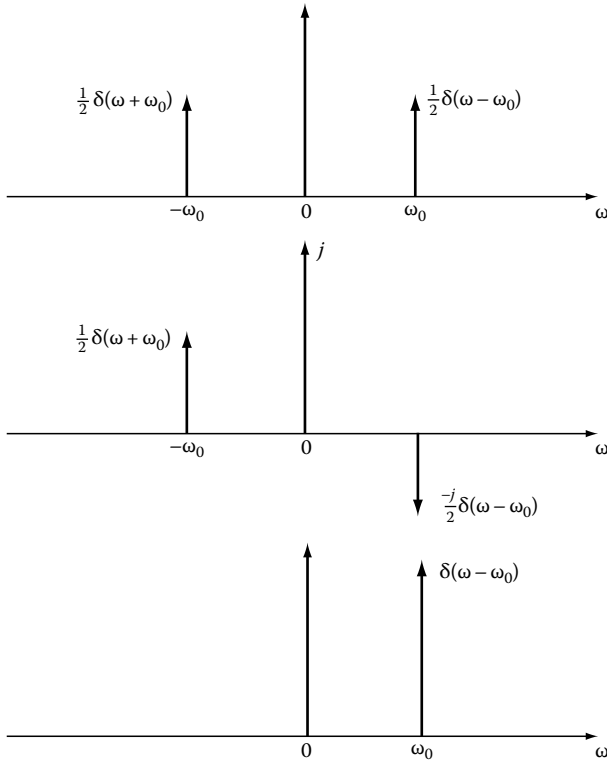


FIGURE 7.2 The spectra of  $\cos(\omega_0 t)$ ,  $\sin(\omega_0 t)$ , and of the analytic signal  $e^{j\omega_0 t}$ .

$U(\omega)$ . For the conjugate signal  $\psi^*(t) = u(t) - jv(t)$  the Fourier image is doubled at negative frequencies and canceled at positive frequencies.

**Examples**

1. Consider the analytic signal  $e^{j\omega_0 t} = \cos(\omega_0 t) + j \sin(\omega_0 t)$ . We have

$$\begin{aligned} \cos(\omega_0 t) &\stackrel{H}{\iff} \sin(\omega_0 t); \omega_0 = 2\pi f_0 \\ \cos(\omega_0 t) &\stackrel{F}{\iff} 0.5[\delta(f + f_0) + \delta(f - f_0)] \\ \cos(\omega_0 t) &\stackrel{F}{\iff} 0.5[\delta(f + f_0) + \delta(f - f_0)] \\ e^{j\omega_0 t} &\stackrel{F}{\iff} \delta(f - f_0) \end{aligned}$$

The spectra are shown in Figure 7.2.

2. Consider the analytic signal  $\psi(t) = \frac{1}{1+t^2} + j \frac{t}{1+t^2}$ . We have

$$\begin{aligned} \frac{t}{1+t^2} &\stackrel{H}{\iff} \frac{t}{1+t^2} \\ \frac{1}{1+t^2} &\stackrel{F}{\iff} \pi e^{-|\omega|}; \quad \frac{t}{1+t^2} \stackrel{F}{\iff} -j \text{sgn}(\omega) \pi e^{-|\omega|} \\ \psi(t) &\stackrel{F}{\iff} [1 + \text{sgn}(\omega)] \pi e^{-|\omega|} \end{aligned}$$

The signals and spectra are shown in Figure 7.3.

**7.4.1 Derivation of Hilbert Transforms Using Hartley Transforms**

Alternatively, the Hilbert transform may be derived using a special Fourier transformation known as Hartley transformation (See also Chapter 4); it is given by the integral

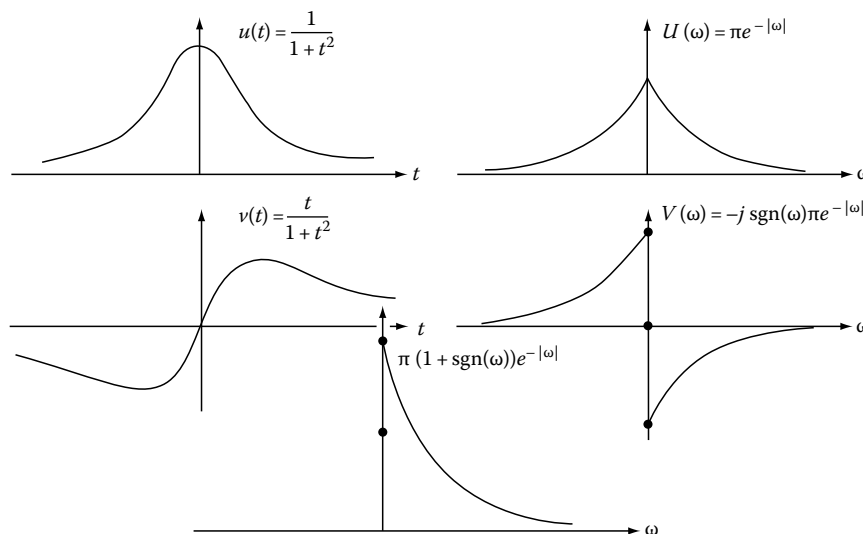


FIGURE 7.3 The Cauchy pulse, its Hilbert transform, and the corresponding spectra and the spectrum of the analytic signal  $\psi(t) = 1/(1 - jt)$ .

$$U_{\text{Ha}}(\omega) = \int_{-\infty}^{\infty} u(t) \text{cas}(\omega t) dt; \quad \omega = 2\pi f \quad (7.50)$$

and the inverse Hartley transformation is

$$u(t) = \int_{-\infty}^{\infty} U_{\text{Ha}}(\omega) \text{cas}(\omega t) df \quad (7.51)$$

where  $\text{cas}(\omega t) = \cos(\omega t) + \sin(\omega t)$ . The Hartley spectral function was denoted by the index Ha because in this chapter the index H denotes the Hilbert transform. Consider the Hartley pair

$$u(t) \stackrel{\text{Ha}}{\longleftrightarrow} U_{\text{Ha}}(\omega) \quad (7.52)$$

The Hartley spectral function of the Hilbert transform is

$$V_{\text{Ha}}(\omega) = \text{sgn}(\omega) U_{\text{Ha}}(-\omega) \quad (7.53)$$

Therefore, the Hilbert transform is given by the inverse Hartley transformation

$$v(t) = \int_{-\infty}^{\infty} \text{sgn}(\omega) U_{\text{Ha}}(-\omega) \text{cas}(\omega t) df \quad (7.54)$$

**Example**

Consider the one-sided square pulse  $\Pi_a(t - a)$  (see Figure 7.4). The Hartley transform of this pulse is

$$U_{\text{Ha}}(\omega) = \int_0^{2a} [\cos(\omega t) + \sin(\omega t)] dt = 2a \left[ \frac{\sin(2\omega a)}{2\omega a} + \frac{\sin^2(\omega a)}{\omega a} \right]$$

The spectrum of the Hilbert transform given by Equation 7.53 is

$$V_{\text{Ha}}(\omega) = 2a \text{sgn}(\omega) \left[ \frac{\sin(2\omega a)}{2\omega a} - \frac{\sin^2 \omega a}{\omega a} \right]$$

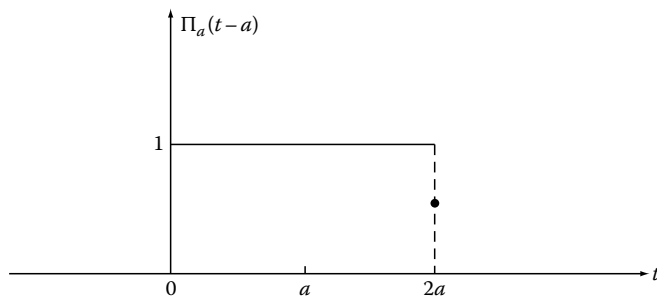


FIGURE 7.4 One-sided square pulse.

The inverse Hartley transformation of this spectrum is

$$\int_{-\infty}^{\infty} 2a \text{sgn}(\omega) \left[ \frac{\sin(2\omega a)}{2\omega a} + \frac{\sin^2(\omega a)}{\omega a} \right] [\cos(\omega t) + \sin(\omega t)] df$$

Notice that the integrals of products of opposite symmetry equal zero and the integration yields

$$v(t) = \frac{1}{\pi} \ln \left| \frac{t}{t - 2a} \right|$$

(see Equation 7.61).

## 7.5 Examples of Derivation of Hilbert Transforms

1. The harmonic signal  $u(t) = \cos(\omega t)$ ;  $\omega = 2\pi f$ , where  $f$  is a constant. The Hilbert transform of the periodic cosine signal using the defining integral (Equation 7.1) is

$$H[\cos(\omega t)] = v(t) = \frac{-1}{\pi} P \int_{-\infty}^{\infty} \frac{\cos(\omega \eta)}{\eta - t} d\eta \quad (7.55)$$

The change of variable  $y = \eta - t$ ,  $dy = d\eta$  yields

$$\begin{aligned} v(t) &= \frac{-1}{\pi} P \int_{-\infty}^{\infty} \frac{\cos[\omega(y + t)]}{y} dy \\ &= \frac{-1}{\pi} \left\{ \cos(\omega t) P \int_{-\infty}^{\infty} \frac{\cos(\omega y)}{y} dy \right. \\ &\quad \left. - \sin(\omega t) P \int_{-\infty}^{\infty} \frac{\sin(\omega y)}{y} dy \right\} \quad (7.56) \end{aligned}$$

The integrals inside the brackets are

$$P \int_{-\infty}^{\infty} \frac{\cos(\omega y)}{y} dy = 0; \quad P \int_{-\infty}^{\infty} \frac{\sin(\omega y)}{y} dy = \pi \quad (7.57)$$

Therefore,  $v(t) = \sin(\omega t)$ . The same derivation for the function  $u(t) = \sin(\omega t)$  yields  $v(t) = -\cos(\omega t)$ .

2. The two-sided symmetric unipolar square pulse

$$u(t) = \Pi_a(t) = \begin{cases} 1 & \text{for } |t| < a \\ 0.5 & \text{for } |t| = a \\ 0 & \text{for } |t| > a \end{cases} \quad (7.58)$$

The Hilbert transform of this pulse is

$$\begin{aligned}
 v(t) &= H[\Pi_a(t)] = \frac{-1}{\pi} P \int_{-\infty}^{\infty} \frac{\Pi_a(\eta)}{\eta - t} d\eta \\
 &= \lim_{\varepsilon \rightarrow 0} \left\{ \frac{-1}{\pi} \int_{-a}^{t-\varepsilon} \frac{d\eta}{\eta - t} - \frac{1}{\pi} \int_{t+\varepsilon}^a \frac{d\eta}{\eta - t} \right\} \\
 &= \lim_{\varepsilon \rightarrow 0} \left\{ -\frac{1}{\pi} \ln(\eta - t) \Big|_{-a}^{t-\varepsilon} - \frac{1}{\pi} \ln(\eta - t) \Big|_{t+\varepsilon}^a \right\} \quad (7.59)
 \end{aligned}$$

The insertion of the limits of integration yields

$$v(t) = \frac{1}{\pi} \ln \left| \frac{t+a}{t-a} \right| \quad (7.60)$$

The square pulse and its Hilbert transform are shown in Figure 7.5. Notice that the support of the square pulse is limited within the interval  $|t| \leq a$ , while the support of the Hilbert transform is infinite. This statement applies to all Hilbert transforms of functions of limited support. Of course, the inverse Hilbert transformation of the logarithmic function (Equation 7.60) restores the square pulse of limited support. The change of variable  $t' = t - a$  (time shift of the pulse) yields the Hilbert transform of a one-sided square pulse.

$$H[\Pi_a(t - a)] = \frac{1}{\pi} \ln \left| \frac{t}{t - 2a} \right| \quad (7.61)$$

3. The Hilbert transform of a constant function  $u(t) = u_0$  equals zero. This is easily seen from Equation 7.60 at the limit  $a \Rightarrow \infty$ . The mean value of a function is given by the integral

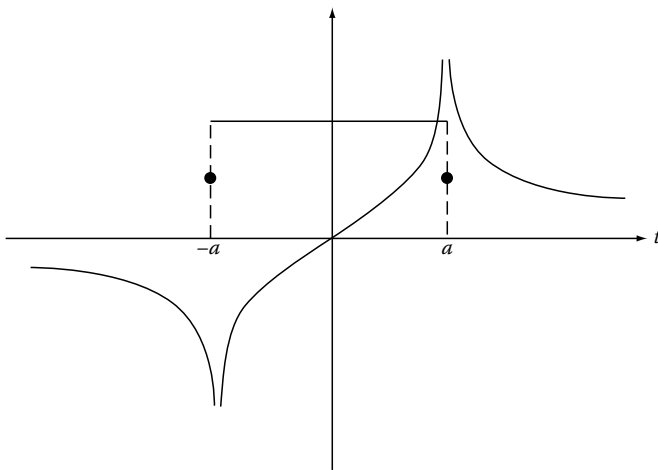


FIGURE 7.5 The square pulse  $\Pi_a(t)$  and its Hilbert transform.

$$u_0 = \lim_{T \rightarrow \infty} \frac{1}{T} \int_{-T/2}^{T/2} u(t) dt \quad (7.62)$$

Therefore, the Hilbert transform of a function  $u(t) = u_0 + u_1(t)$  is

$$H[u_0 + u_1(t)] = H[u_1(t)] \quad (7.63)$$

that is, in electrical terminology the Hilbert transformation cancels the DC term  $u_0$ .

4. Consider the Gaussian pulse and its Fourier image

$$e^{-\pi t^2} \stackrel{F}{\iff} e^{-\pi f^2}; \quad \omega = 2\pi f \quad (7.64)$$

Because for this signal the Hilbert transform defined by the integral (Equation 7.1) has no closed form, it is convenient to derive the Hilbert transform using the inverse Fourier transformation of the Fourier image (Equation 7.64). This inverse transform has the form

$$v(t) = \int_{-\infty}^{\infty} -j \operatorname{sgn}(\omega) e^{-\pi f^2} e^{j\omega t} df \quad (7.65)$$

Because the integrand is an odd function, this integral has the simplified form

$$v(t) = \int_0^{\infty} e^{-\pi f^2} \sin(\omega t) df \quad (7.66)$$

This integral has no closed solution and may be represented by a power series defining a function called  $Ei(t)$ .

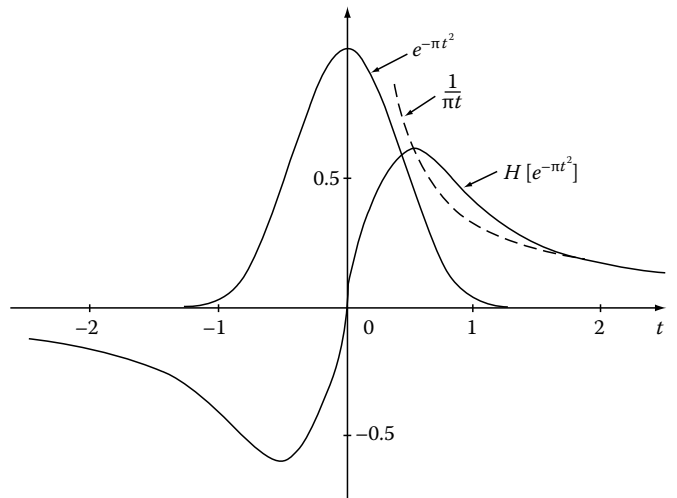


FIGURE 7.6 The Gaussian pulse and its Hilbert transform.

However, in the days of proliferation of computers it is much simpler to find a numerical solution of this integral. The Gaussian pulse and its Hilbert transform computed using Equation 7.66 are shown in Figure 7.6.

## 7.6 Definition of the Hilbert Transformation by Using a Distribution

It is well known that the concept of the delta function, the unit step, and similar functions extend the class of functions for which the Fourier transform exists. The formal Fourier integral theory restricts the functions to those satisfying Dirichlet's conditions, including the requirement of finite energy (finite value of the integral of the square). The mathematicians eliminated this restriction by introducing the concept of a distribution, giving a rigorous foundation to the notions of the delta pulse, the signum function, and so forth. The notion of a distribution is not unique, because there exist several definitions. The most accepted theory of a distributions was formulated by Schwartz,<sup>35</sup> who used the concept of a functional. Another useful approach was formulated by Mikusinski<sup>23</sup> who used sequences of approximating functions.

Equation 7.48 shows that the Fourier image of analytic signals is one-sided. A good example is the one-sided spectrum given by the doubled unit step  $2 \mathbf{1}(f)$  defined as a distribution in the Fourier frequency domain. This distribution may be decomposed into the even and odd parts:

$$2 \mathbf{1}(f) = \mathbf{1} + \text{sgn}(f) \tag{7.67}$$

where

$\mathbf{1}$  is a constant distribution  
 $\text{sgn}(f)$  is a signum distribution

The inverse Fourier transformation of this unit step is given by the integral

$$\psi_{\delta}(t) = \int_{-\infty}^{\infty} 2 \mathbf{1}(f) e^{j\omega t} df; \quad \omega = 2\pi f \tag{7.68}$$

or by the integral

$$\psi_{\delta}(t) = 2 \int_0^{\infty} e^{j\omega t} df \tag{7.69}$$

which defines the complex delta distribution of the form

$$\psi_{\delta}(t) = \delta(t) + jP \frac{1}{\pi t} = F^{-1}[2 \mathbf{1}(f)] \tag{7.70}$$

with  $P$  the Cauchy principal value. We observe, that the delta distribution and the kernel of the Hilbert transformation are forming a Hilbert pair

$$\delta(t) \stackrel{H}{\longleftrightarrow} P \frac{1}{\pi t} \tag{7.71}$$

where the Fourier images are

$$\delta(f) \stackrel{F}{\longleftrightarrow} \mathbf{1}; \quad \Theta(t) = P \frac{1}{\pi t} \stackrel{F}{\longleftrightarrow} -j \text{sgn}(\omega) \tag{7.72}$$

Therefore, the kernel of the Hilbert transformations (Equations 7.3 and 7.4) denoted by  $\Theta(t)$  has been redefined as a distribution in the form of the Hilbert transform of the delta pulse (distribution).

The *analytic signal* (Equation 7.28) may be defined in the form of a convolution of a given function (or distribution)  $u(t)$  with the *complex delta distribution*; that is,

$$\psi(t) = \psi_{\delta}(t) * u(t) = \left[ \delta(t) + jP \frac{1}{\pi t} \right] * u(t) \tag{7.73}$$

Indeed, the well-known alternative definition of the delta distribution is

$$u(t) = u(t) * \delta(t) \tag{7.74}$$

This is a convolution equation. The application of the theorem about the Hilbert transform of a convolution (see Table 7.1) yields the following two alternative forms of  $H[u(t)]$ :

$$v(t) = u(t) * \frac{1}{\pi t}; \quad v(t) = v(t) * \delta(t) \tag{7.75}$$

The complex delta distribution may be defined alternatively using approximating functions. A convenient choice is the Cauchy signal (see Equation 7.29):

$$\psi_{\delta}(t) = \lim_{\alpha \rightarrow 0} \left[ \frac{\alpha}{\pi(\alpha^2 + t^2)} + j \frac{t}{\pi(\alpha^2 + t^2)} \right] \tag{7.76}$$

(see Figure 7.7). The division by  $\pi$  is needed to get the integral of the real part equal to 1. In terms of this representation, the distribution  $\Theta(t) = 1/\pi t$  equals zero for  $t=0$ . The real and imaginary parts of the complex delta distribution, as for any analytic signal, are orthogonal; that is, the integral of their product equals zero

$$P \int_{-\infty}^{\infty} \frac{\delta(t)}{\pi t} dt = 0 \tag{7.77}$$



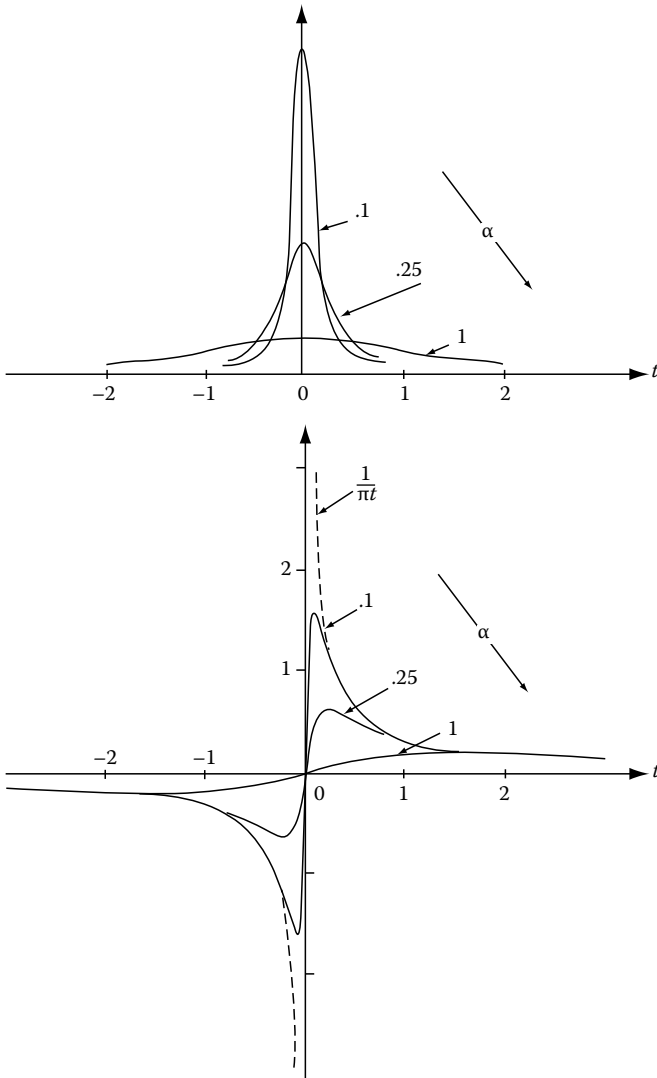


FIGURE 7.7 The approximation of the delta pulse  $\delta(t)$  and its Hilbert transform  $\Theta(t) = 1/(\pi t)$  by Cauchy pulses and its Hilbert transforms (see Figure 7.3).

## 7.7 Hilbert Transforms of Periodic Signals

A real function (signal)  $u_p(t)$  is periodic if there is some interval  $T$  (the period) for which

$$u_p(t) = u_p(t + kT) \tag{7.78}$$

for all  $t$  in  $(-\infty, \infty)$ , where  $k$  is an integer  $(-\infty, \infty)$ . The fundamental frequency is  $f=1/T$  and the fundamental angular frequency is  $\omega = 2\pi f = 2\pi/T$ . The periodic function may be alternatively defined using a periodic repetition of a so-called *generating function*  $u_T(t)$ . This repetition is represented by the infinite series

$$u_p(t) = \sum_{k=-\infty}^{\infty} u_T(t - kT) \tag{7.79}$$

where the generating function is

$$u_T(t) = \begin{cases} u_p(t) & \text{in the interval } t_0, t_0 + T \\ 0 & \text{otherwise} \end{cases} \tag{7.80}$$

Using the well-known shifting property of the convolution of a given function with the delta pulse, the periodic function (Equation 7.79) may be written in the form

$$u_p(t) = u_T(t) * \sum_{k=-\infty}^{\infty} \delta(t - kT) \tag{7.81}$$

that is, the generating function is convolved with the periodic sequence of delta pulses well known from the sampling theory.

Three different methods of derivation of the Hilbert transform of periodic functions are presented here:

1. A method using Fourier series.
2. Direct derivation in the form of infinite products.
3. The convolution with a cotangent periodic function.

### 7.7.1 First Method

The periodic function may be expanded into a Fourier series:

$$u_p(t) = U_0 + \sum_{n=1}^{\infty} U_n \cos(n\omega_0 t + \Phi_n); \quad \omega_0 = \frac{2\pi}{T} \tag{7.82}$$

The number of terms of this series may be finite or infinite. Because  $H[\cos(n\omega t + \Phi)] = \sin(n\omega t + \Phi)$ , the Hilbert transform of the periodic function  $u_p(t)$  is given by the Fourier series

$$v_p(t) = \sum_{n=1}^{\infty} U_n \sin(n\omega_0 t + \Phi_n) \tag{7.83}$$

Notice the cancellation of the constant term  $U_0$  (in electrical terminology the DC term). If the Fourier series is given using the complex notation

$$u_p(t) = \sum_{n=-\infty}^{\infty} C_n e^{jn\omega_0 t} \tag{7.84}$$

where the complex coefficient  $C_n$  is given by the integral

$$C_n = \frac{1}{T} \int_{-T/2}^{T/2} u_p(t) e^{-jn\omega_0 t} dt \tag{7.85}$$

then the Hilbert transform has the form (see Equation 7.45)

$$v_p(t) = \sum_{n=-\infty}^{\infty} -j \operatorname{sgn}(n) C_n e^{jn\omega_0 t}; \quad \omega_0 > 0 \quad (7.86)$$

Again, the constant term is eliminated ( $\operatorname{sgn}(0) = 0$ ).

**Example**

Consider the Fourier series of the periodic square wave given by the formula  $u_p(t) = \operatorname{sgn}[\cos(\omega t)]$  ( $\omega = 2\pi f - \text{a constant}$ ):

$$u_p(t) = \frac{4}{\pi} \left[ \cos(\omega t) - \frac{1}{3} \cos(3\omega t) + \frac{1}{5} \cos(5\omega t) - \frac{1}{7} \cos(7\omega t) + \dots \right] \quad (7.87)$$

The Hilbert transform has the form

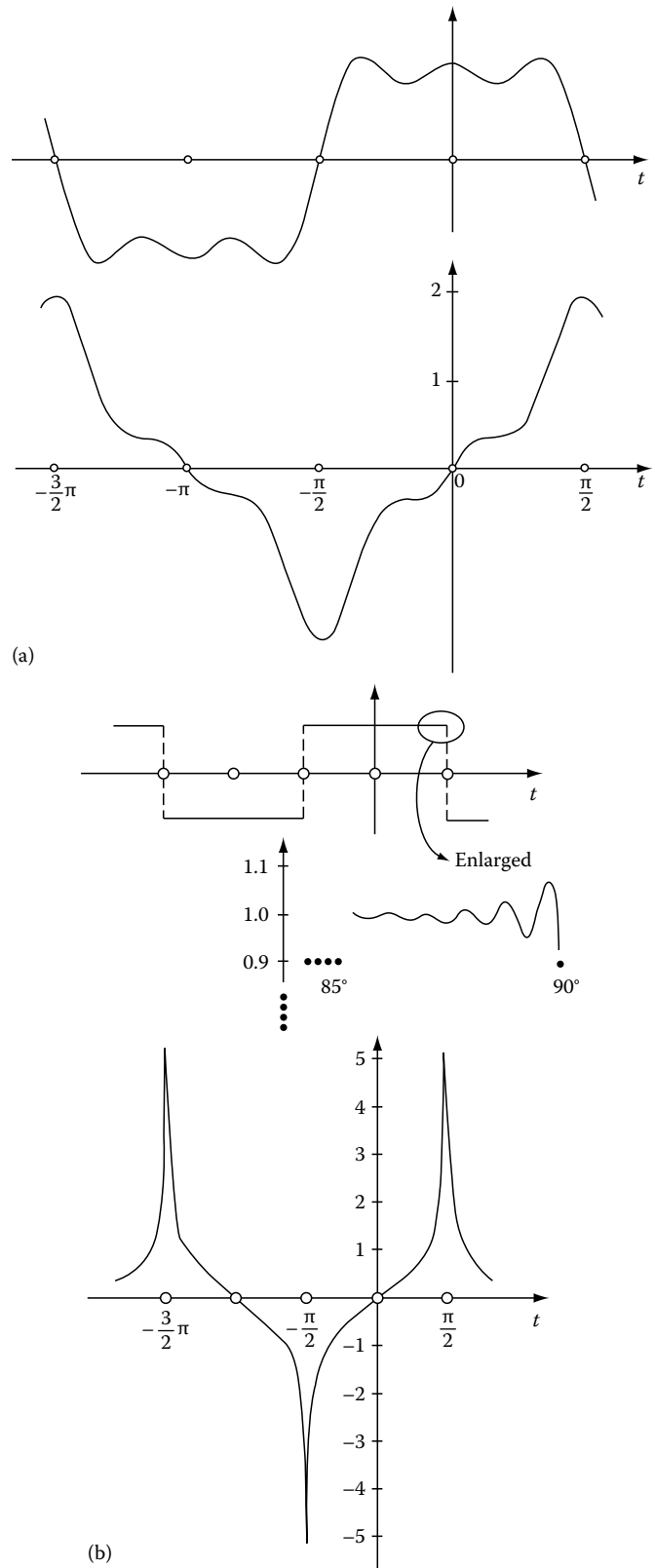
$$v_p(t) = \frac{4}{\pi} \left[ \sin(\omega t) - \frac{1}{3} \sin(3\omega t) + \frac{1}{5} \sin(5\omega t) - \frac{1}{7} \sin(7\omega t) + \dots \right] \quad (7.88)$$

Figure 7.8a and b shows the signals represented by the Fourier series (Equations 7.87 and 7.88) truncated at the fifth harmonic and at a much higher harmonic term. We observe the Gibbs peaks for the cosine series. Because in the limit, the energy of the Gibbs peaks equals zero (a zero function), the Gibbs peaks disappear for the sine series.

**7.7.2 Second Method**

The derivation of the Hilbert transform of a periodic signal directly in the time domain (or any other domain) using the basis integral definition of the Hilbert transformation given by Equation 7.1 has the form of the infinite sum of integrals over successive periods. Only one of these integrals includes the pole of the kernel  $1/(\pi t)$ . For example, the Hilbert transform of the periodic square wave (see Figure 7.9a) has the form

$$v_p(t) = -\frac{1}{\pi} \left\{ \dots \int_{-5b}^{-3b} \frac{d\eta}{\eta - t} - \int_{-3b}^{-b} \frac{d\eta}{\eta - t} + \lim_{\epsilon \Rightarrow 0} \left[ \int_{-b}^{t-\epsilon} \frac{d\eta}{\eta - t} + \int_{t+\epsilon}^b \frac{d\eta}{\eta - t} \right] - \int_b^{3b} \frac{d\eta}{\eta - t} + \int_{3b}^{5b} \frac{d\eta}{\eta - t} - \dots \right\} \quad (7.89)$$



**FIGURE 7.8** (a) The waveforms given by the truncation of the Fourier series of a square wave at the 5th harmonic number and of the corresponding Hilbert transform. (b) Analogous waveforms by the truncation at a high harmonic number.

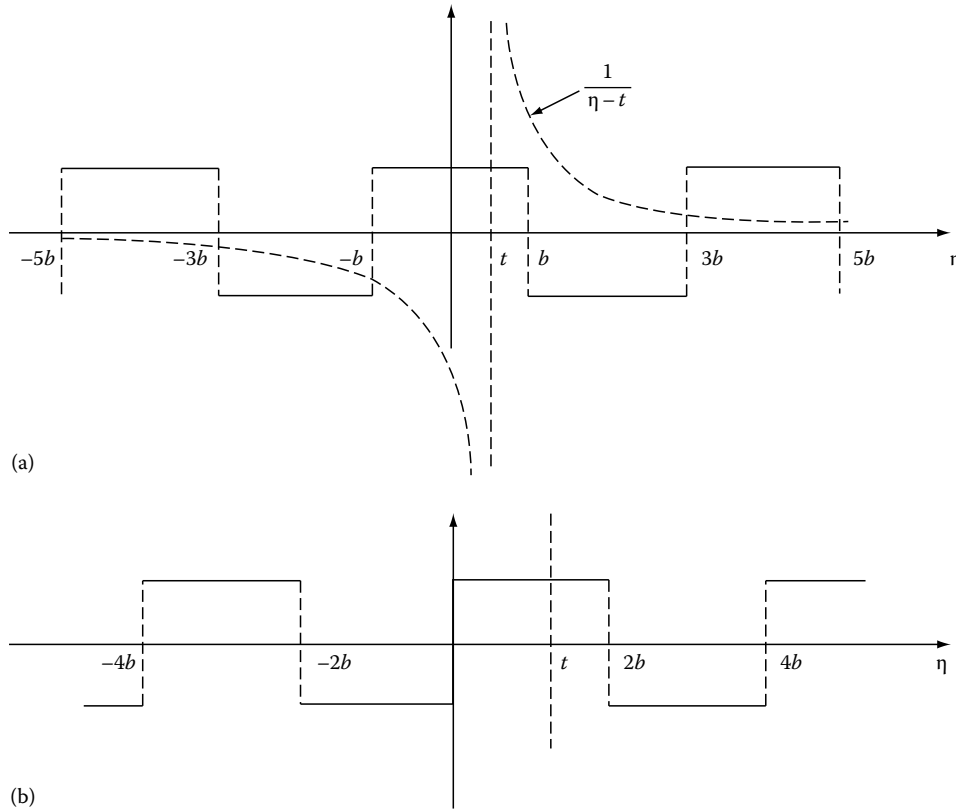


FIGURE 7.9 Illustration to the derivation of the Hilbert transform of a square wave.

where  $b = T/4$ . The result of this integration has the form

$$v_p(t) = \frac{2}{\pi} \left\{ \ln \left| \frac{\prod_{m=1}^{\infty} [2m - 1 - (1)^m x]}{\prod_{m=1}^{\infty} [2m - 1 + (1)^m x]} \right| \right\} \quad (7.90)$$

where  $x = 4t/T$  and  $m = 1, 2, 3, \dots$ . The first terms of the infinite products are

$$v_p(t) = \frac{2}{\pi} \ln \left| \frac{(1+x)(3-x)(5+x)(7-x) \dots}{(1-x)(3+x)(5-x)(7+x) \dots} \right| \quad (7.91)$$

The infinite products in the above formulas are convergent. Using the numerical evaluation of Equation 7.91 we have to truncate the products having the same number of terms in the nominator and denominator. For the odd square wave  $u_p(t) = \text{sgn}[\sin(\omega t)]$  (see Figure 7.9b), Equation 7.91 changes to

$$v_p(t) = \frac{2}{\pi} \ln \left| \frac{y(4-y^2)(16-y^2)(36-y^2) \dots}{(1-y^2)(9-y^2)(15-y^2)(7-y) \dots} \right|; \quad (7.92)$$

$y = 2x = 2t/T$

Notice that the denominator has been truncated so that a half-term of  $(49 - y^2) = (7 - y)(7 + y)$  is deleted. This is needed to

obtain a symmetrical truncation. Using a computer, the quotients in Equations 7.91 or 7.92 should be calculated using one term of the nominator divided by one term of the denominator. Otherwise there is a danger of entering in the overflow range of the computer (number too big). Let us recall that the harmonic functions have a representation in the form of infinite series.

$$\sin(z) = z \prod_{k=1}^{\infty} \left( 1 - \frac{z^2}{k^2 \pi^2} \right) \quad (7.93)$$

$$\cos(z) = \prod_{k=1}^{\infty} \left( 1 - \frac{4z^2}{(2k-1)^2 \pi^2} \right) \quad (7.94)$$

### 7.7.3 Third Method: Cotangent Hilbert Transformations

The cotangent form of the Hilbert transformation of periodic functions may be conveniently derived starting with the convolution equation (Equation 7.81). The Hilbert transform of a convolution of two functions equals the convolution of the Hilbert transform of one function (arbitrary choice) with the original of the other function (see Table 7.3). The Hilbert transform of the delta sampling sequence is

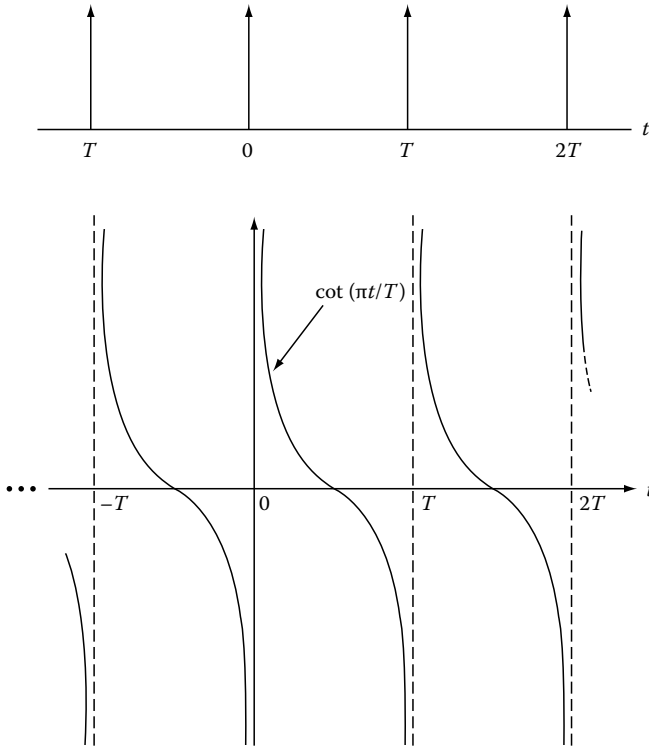


FIGURE 7.10 The periodic sequence of delta pulses and its Hilbert transform.

$$\begin{aligned} \delta_p(t) &= \sum_{k=-\infty}^{\infty} \delta(t - kT) \stackrel{H}{\iff} \Theta_p(t) \\ &= \frac{1}{T} \sum_{k=-\infty}^{\infty} \cot\left[\frac{\pi}{T}(t - kT)\right] \end{aligned} \quad (7.95)$$

This Hilbert pair is shown in Figure 7.10. The derivation is given at the end of this section. The insertion of this Hilbert transform in the convolution equation (Equation 7.75) yields the following form of the Hilbert transform of periodic functions:

$$v_p(t) = u_T(t) * \frac{1}{T} \sum_{k=-\infty}^{\infty} \cot\left[\frac{\pi}{T}(t - kT)\right] \quad (7.96)$$

where  $u_T(t)$  is the generating function defined by Equation 7.80. Contrary to Fourier series, Equation 7.96 has a closed integral form and for many generating functions a closed analytic solution. If the analytic solution does not exist, a numerical evaluation of the convolution yields the desired Hilbert transform.

**Example**

Consider again the square wave of  $\text{sgn}[\cos(\omega t)]$ . The generating function is

$$u_T(t) = \begin{cases} \text{sgn}[\cos(\omega t)] & \text{for } |t| \leq 0.5T; \quad \omega = \frac{2\pi}{T} \\ 0 & \text{otherwise} \end{cases} \quad (7.97)$$

This generating function equals  $-1$  in the intervals  $-T/2$  to  $-T/4$  and  $T/4$  to  $T/2$  and equals  $1$  in the interval  $-T/4$  to  $T/4$ . The insertion of the integration intervals (Cauchy principal value)

$$- \left| \begin{matrix} -T/4 \\ -T/2 \end{matrix} \right| + \left| \begin{matrix} t - \epsilon \\ -T/4 \end{matrix} \right| + \left| \begin{matrix} T/4 \\ t + \epsilon \end{matrix} \right| - \left| \begin{matrix} T/2 \\ T/4 \end{matrix} \right| \quad (7.98)$$

into the integral

$$\frac{1}{T} \int \cot\left[\frac{\pi}{T}(\tau - t)\right] d\tau = \frac{1}{\pi} \ln \left| \sin\left[\frac{\pi}{T}(\tau - t)\right] \right| \quad (7.99)$$

yields the following form of the Hilbert transform of the square wave

$$v_p(t) = \frac{2}{\pi} \ln \left| \frac{\sin\left[\frac{\pi}{T}\left(\frac{T}{4} - t\right)\right]}{\sin\left[\frac{\pi}{T}\left(\frac{T}{4} + t\right)\right]} \right| \quad (7.100)$$

Using trigonometric relations, we get the Hilbert pair

$$\text{sgn}[\cos(\omega t)] \stackrel{H}{\iff} \frac{2}{\pi} \ln |\tan(\omega t/2 + \pi/4)| \quad (7.101)$$

Similarly, it may be shown that

$$\text{sgn}[\sin(\omega t)] \stackrel{H}{\iff} \frac{2}{\pi} \ln |\tan(\omega t/2)| \quad (7.102)$$

The Hilbert transform of the periodic delta sequence given by Equation 7.95 may be derived as follows: We start with the Hilbert pair

$$\delta(t) \stackrel{H}{\iff} \frac{1}{\pi t} \quad (7.103)$$

The support of the Hilbert transform  $1/(\pi t)$  is infinite. Therefore, in the interval of one period, for example, the interval from 0 to  $T$ , there is a summation of successive tails of functions  $\Theta_n(t) = 1/[\pi(t - nT)]$ , i.e., the generating function of the Hilbert transform of the delta sampling sequence is

$$\Theta_T(t) = \sum_{n=-\infty}^{\infty} \frac{1}{\pi(t - nT)} = \frac{1}{T} \cot(\pi t/T) \quad (7.104)$$

that is, the infinite sum converges to the cotangent function. The repetition of this generating function yields the periodic Hilbert transform of the delta sampling sequence of the form

$$\Theta_p(t) = \sum_{k=-\infty}^{\infty} \Theta_T(t - kT) = \frac{1}{T} \sum_{k=-\infty}^{\infty} \cot\left[\frac{\pi}{T}(t - kT)\right] \quad (7.105)$$

This sequence also may be written in the convolution form

$$\Theta_p(t) = \frac{1}{T} \cot(\pi t/T) * \sum_{k=-\infty}^{\infty} \delta(t - kT) \quad (7.106)$$

The generating function  $\Theta_T(t)$  (Equation 7.104) may be alternatively derived using Fourier transforms. The well-known Fourier pair is

$$\sum_{k=-\infty}^{\infty} \delta(t - kT) \xleftrightarrow{F} \frac{1}{T} \sum_{k=-\infty}^{\infty} \delta(f - k/T) \quad (7.107)$$

The multiplication of this Fourier image by the operator  $-j \operatorname{sgn}(f)$  yields the Fourier image of the generating function  $\Theta_T(t)$ :

$$\Theta_T(t) \xleftrightarrow{F} \frac{1}{T} \sum_{n=-\infty}^{\infty} -j \operatorname{sgn}(f) \delta(f - n/T) \quad (7.108)$$

The inverse Fourier transform of this spectrum yields

$$\begin{aligned} \Theta_T(t) &= \frac{j}{T} \sum_{n=-\infty}^{\infty} e^{-j2\pi nt/T} - \frac{j}{T} \sum_{n=1}^{\infty} e^{j2\pi n/T} \\ &= \frac{2}{T} \sum_{n=1}^{\infty} \sin(2\pi nt/T) \end{aligned} \quad (7.109)$$

The insertion of the relation (in the distribution sense)

$$\sum_{n=1}^{\infty} \sin(nx) = \frac{1}{2} \cot(x/2) \quad (7.110)$$

yields  $\Theta(t)$  given by the formula 7.104. Notice that the derivation of the periodic Hilbert transform  $\Theta_p(t)$  involves two summations. The first yields the generating function  $\Theta_T(t)$  and the second gives the periodic repetition of this function (Figure 7.11).

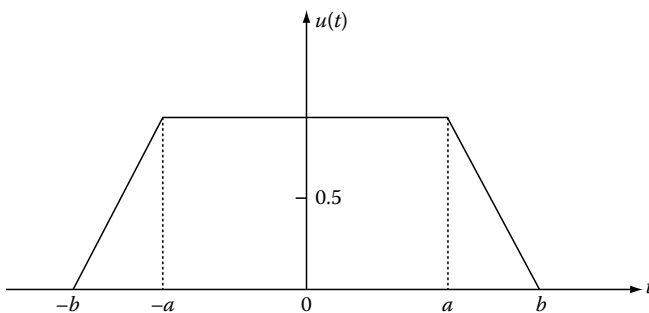


FIGURE 7.11 A trapezoidal pulse (see Table 7.1, #9.)

## 7.8 Tables Listing Selected Hilbert Pairs and Properties of Hilbert Transformations

Table 7.1 presents the Hilbert transforms of some selected a periodic signals and the two basic periodic harmonic signals  $\cos(\omega t)$  and  $\sin(\omega t)$ . The Hilbert transforms of selected other periodic signals are listed in Table 7.2. The knowledge of the Hilbert transforms listed in these tables and the application of various properties of the Hilbert transformation listed in Table 7.3 enables an easy derivation of a large variety of Hilbert transforms. Applications of the properties listed in these tables are given in Sections 7.9 through 7.15, which also include selected derivations and applications of the properties of Hilbert transformations.

## 7.9 Linearity, Iteration, Autoconvolution, and Energy Equality

The Hilbert transformation is linear and, if a complicated waveform can be decomposed into a sum of simpler waveforms, then the summation of the Hilbert transforms of each term yields the desired transform. For example, the waveform of Figure 7.12a may be decomposed into a sum of two rectangular pulses. Therefore, the Hilbert transform of this waveform is (see Table 7.1)

$$\begin{aligned} v(t) &= H[\Pi_a(t) + \Pi_b(t)] = \hat{\Pi}_a(t) + \hat{\Pi}_b(t) \\ &= \frac{1}{\pi} \left\{ \ln \left| \frac{t+a}{t-a} \right| + \ln \left| \frac{t+b}{t-b} \right| \right\} \\ &= \frac{1}{\pi} \ln \left| \frac{(t+b)(t+a)}{(t-b)(t-a)} \right| \end{aligned} \quad (7.111)$$

Let us derive in a similar way the Hilbert transform of the “ramp” pulse shown in Figure 7.12b. We decompose this pulse into a sum of one-sided square pulse and one-sided inverse triangle. The summation of Equation 7.61 and No. 8 of Table 7.1 yields

$$\begin{aligned} H[\text{ramp}] &= H[\Pi_{b/2}(t - b/2)] - H[1(t)\text{tri}(t)] \\ &= \frac{1}{\pi} \left\{ \ln \left| \frac{t}{t-b} \right| - (1 - t/a) \ln \left| \frac{t}{t+a} \right| - 1 \right\} \end{aligned} \quad (7.112)$$

### 7.9.1 Iteration

Iteration of the Hilbert transformation two times yields the original signal with the reverse sign, and the iteration four times restores the original signal  $u(t)$ . In the Fourier frequency domain the  $n$ -time iteration is translated to the  $n$ -time multiplication by the operator  $-j \operatorname{sgn}(\omega)$ . We have  $(-j \operatorname{sgn}(\omega))^2 = -1$ ,  $(-j \operatorname{sgn}(\omega))^3 = j \operatorname{sgn}(\omega)$ , and  $(-j \operatorname{sgn}(\omega))^4 = 1$ . In analog or digital signal processing, the Hilbert transform is produced approximately and with a delay. The  $n$ -time iteration is implemented using a series connection of Hilbert filters (see Section 7.22) and the time delay increases  $n$ -times.

TABLE 7.1 Selected Useful Hilbert Pairs

Number	Name	$u(t)$	$v(t)$
1	sine	$\sin(\omega t)$	$-\cos(\omega t)$
2	cosine	$\cos(\omega t)$	$\sin(\omega t)$
3	Exponential harmonic	$e^{j\omega t}$	$-j \operatorname{sgn}(\omega)e^{j\omega t}$
4	Square pulse	$\Pi_a(t)^a$	$\frac{1}{\pi} \ln \left  \frac{t+a}{t-a} \right $
5	Bipolar pulse	$\Pi_a(t) \operatorname{sgn}(t)$	$\frac{1}{\pi} \ln  1 - (a/t)^2 $
6	Double triangle	$t\Pi_a(t) \operatorname{sgn}(t)$	$\frac{1}{\pi} \ln  1 - (a/t)^2 $
7	Triangle tri(t)	$1 -  t/a ;  t  \leq a$ $0;  t  > a$	$\frac{-1}{\pi} \left\{ \ln \left  \frac{t-a}{t+a} \right  + \frac{t}{a} \ln \left  \frac{t^2}{t^2 - a^2} \right  \right\}$
8	One-sided triangle	$\mathbf{1}(t) \operatorname{tri}(t)$	$\frac{1}{\pi} \left\{ (1 - t/a) \ln \left  \frac{t}{t+a} \right  + 1 \right\}$
9	Trapezoid pulse	Waveform <sup>b</sup>	$\frac{-1}{\pi} \left\{ \frac{b}{b-a} \ln \left  \frac{(a+t)(b-t)}{(b+t)(a-t)} \right  + \frac{t}{b-a} \ln \left  \frac{a^2 - t^2}{b^2 - t^2} \right  + \ln \left  \frac{a-t}{a+t} \right  \right\}$
10	Cauchy pulse	$\frac{\alpha}{\alpha^2 + t^2}; \alpha > 0$	$\frac{t}{\alpha^2 + t^2}$
11	Gaussian pulse	$e^{-\pi t^2}$	$2 \int_0^\infty e^{-\pi f^2} \sin(\omega t) df$ $\omega = 2\pi f$
12	Parabolic pulse	$1 -  t/a ^2;  t  \leq a$ $0;  t  > a$	$\frac{-1}{\pi} \left\{ [1 - (t/a)^2] \ln \left  \frac{t-a}{t+a} \right  - \frac{2t}{a} \right\}$
13	Symmetric exponential	$e^{-a t }$	$2 \int_0^\infty \frac{2a}{a^2 + \omega^2} \sin(\omega t) df$ or $\frac{-1}{\pi} \{ \exp(-a t )E(-a t ) - \exp(a t )E(-a t ) \}$ where $E(x) = \int_x^\infty \frac{\exp(-\tau)}{\tau} d\tau$
14	Antisymmetric exponential	$\operatorname{sgn}(t)e^{-a t }$	$-2 \int_0^\infty \frac{2\omega}{a^2 + \omega^2} \cos(\omega t) df$
15	One-sided exponential	$\mathbf{1}(t)e^{-a t }$	$2 \int_0^\infty \frac{a \sin(\omega t) - \omega \cos(\omega t)}{a^2 + \omega^2} df$
16	sinc pulse	$\frac{\sin(at)}{at}$	$\frac{\sin^2(at/2)}{(at/2)} = \frac{1 - \cos(at)}{at}$
17	Video test pulse	$\cos^2(\pi t/2a);  t  \leq a$ $0;  t  > a$	$2 \int_0^\infty \frac{2a^2}{4a^2 - \omega^2} \frac{\sin(\pi\omega/2a)}{\omega} \sin(\omega t) df$
18	Constant	$a$	zero

Hyperbolic functions: Approximation by summation of Cauchy signals (see Hilbert pairs 10 and 43)<sup>c</sup>

Number	$u(t)$	$v(t)$
19	$\tanh(t) = 2 \sum_{\eta=0}^\infty \frac{t}{(\eta + 0.5)^2 \pi^2 + t^2}$	$-2\pi \sum_{\eta=0}^\infty \frac{(\eta + 0.5)}{(\eta + 0.5)^2 \pi^2 + t^2}$
<i>The part of finite energy of tanh(t) is</i>		
20	$\operatorname{sgn}(t) - \tanh(t);$	$\pi\delta(t) + 2\pi \sum_{\eta=0}^\infty \frac{(\eta + 0.5)}{(\eta + 0.5)^2 \pi^2 + t^2}$
21	$\operatorname{coth}(t) = \frac{1}{t} + 2 \sum_{\eta=1}^\infty \frac{t}{(\eta\pi)^2 + t^2};$	$-\pi\delta(t) + 2\pi \sum_{\eta=1}^\infty \frac{\eta}{(\eta\pi)^2 + t^2}$
22	$\operatorname{sech}(t) = -2\pi \sum_{\eta=0}^\infty (-1)^{(\eta-1)} \frac{(\eta + 0.5)}{(\eta + 0.5)^2 \pi^2 + t^2};$	$-2 \sum_{\eta=0}^\infty (-1)^{(\eta-1)} \frac{t}{(\eta + 0.5)^2 \pi^2 + t^2}$
23	$\operatorname{cosech}(t) = \frac{1}{t} - 2 \sum_{\eta=1}^\infty (-1)^{(\eta-1)} \frac{t}{(\eta\pi)^2 + t^2};$	$-\pi\delta(t) + 2\pi \sum_{\eta=1}^\infty (-1)^{(\eta-1)} \frac{\eta}{(\eta\pi)^2 + t^2}$

(continued)

**TABLE 7.1 (continued)** Selected Useful Hilbert Pairs

Number	$u(t)$	$v(t)$
<i>Hyperbolic functions by inverse Fourier transformation (<math>\omega = 2\pi f</math>)</i>		
24	$\text{sgn}(t) - \tanh(at/2); \text{Re } a > 0;$	$2 \int_0^\infty \left[ \frac{2\pi}{a \sinh(\pi\omega/a)} - \frac{2}{\omega} \right] \cos(\omega t) d\omega$
25	$\text{coth}(at/2) - \text{sgn}(t);$	$2 \int_0^\infty \left[ \frac{2\pi}{a} \coth(\pi\omega/a) - \frac{2}{\omega} \right] \cos(\omega t) d\omega$
26	$\text{sech}(at/2);$	$2 \int_0^\infty \frac{2\pi}{a \cosh(\pi\omega/2a)} \sin(\omega t) d\omega$
27	$\text{cosech}(at/2);$	$-2 \int_0^\infty \frac{2\pi}{a} \tanh(\pi\omega/2a) \cos(\omega t) d\omega$
28	$\text{sech}^2(at/2);$	$2 \int_0^\infty \frac{2\pi\omega}{a \sinh(\pi\omega/2a)} \sin(\omega t) d\omega$
<i>Delta distribution, <math>1/\pi t</math> distribution, and its derivatives</i>		
29	$\delta(t)$	$1/\pi t$
30	$1/\pi t$	$-\delta(t)$
31	$\delta^{(1)}(t)$	$-1/\pi t^2$
32	$1/\pi t^2$	$\delta^{(1)}(t)$
33	$\delta^{(2)}(t)$	$2/\pi t^3$
34	$1/\pi t^3$	$-0.5\delta^{(2)}(t)$
35	$\delta^{(3)}(t)$	$-6/\pi t^4$
36	$1/\pi t^4$	$(1/6)\delta^{(3)}(t)$
37	$u(t)\delta(t)$	$u(t) = (1/\pi t)u(0)$
<i>Equality of convolutions</i>		
38	$\delta(t) = \delta(t) * \delta(t)$	$\delta(t) = -(1/\pi t) * (1/\pi t)$
39	$\delta^{(1)}(t) = \delta^{(1)}(t) * \delta(t)$	$\delta^{(1)}(t) = (1/\pi t^2) * (1/\pi t)$
40	$\delta^{(2)}(t) = \delta^{(1)}(t) * \delta^{(1)}(t)$	$\delta^{(2)}(t) = -(1/\pi t^2) * (1/\pi t^2)$
41	$\delta^{(3)}(t) = \delta^{(3)}(t) * \delta(t) = \delta^{(2)}(t) * \delta^{(1)}(t)$	$\delta^{(3)}(t) = (6/\pi t^3) * (1/\pi t)$ $= (2/\pi t^3) * (1/\pi t^2)$
<i>Approximating functions to the above distributions</i>		
42	$\int \delta(a, t) dt = \frac{1}{\pi} \tan^{-1}(t/a);$	$\int \Theta(a, t) dt = \frac{\ln(a^2 + t^2)}{2\pi}$
43	$\delta(a, t) = \frac{1}{\pi} \frac{a}{a^2 + t^2};$	$\Theta(a, t) = \frac{1}{\pi} \frac{t}{a^2 + t^2}$
44	$\delta^{(1)}(a, t) = \frac{1}{\pi} \frac{-2at}{(a^2 + t^2)^2};$	$\Theta^{(1)}(a, t) = \frac{1}{\pi} \frac{a^2 - t^2}{(a^2 + t^2)^2}$
45	$\delta^{(2)}(a, t) = \frac{1}{\pi} \frac{6at^2 - 2a^2}{(a^2 + t^2)^3};$	$\Theta^{(2)}(a, t) = \frac{1}{\pi} \frac{2t^3 - 6at^2}{(a^2 + t^2)^3}$
46	$\delta^{(3)}(a, t) = \frac{1}{\pi} \frac{24a^3t - 24at^2}{(a^2 + t^2)^4};$	$\Theta^{(3)}(a, t) = \frac{1}{\pi} \frac{-6t^2 + 36a^2t^2 - 6a^4}{(a^2 + t^2)^4}$
<i>Trigonometric functions</i>		
47	$\frac{\sin(at)}{t}$	$\frac{1 - \cos(at)}{t}$
48	$\frac{\cos(at)}{t}$	$-\pi\delta(t) + \frac{\sin(at)}{t}$
49	$\frac{\sin(at)}{t^2}$	$-\pi a\delta(t) + \frac{1 - \cos(at)}{t^2}$
50	$\frac{\cos(at)}{t^2}$	$\pi\delta^{(1)}(t) - \frac{a}{t} + \frac{\sin(at)}{t^2}$
51	$\frac{\sin(at)}{t^3}$	$\pi a\delta^{(1)}(t) - \frac{a^2}{2t} + \frac{1 - \cos(at)}{t^3}$
52	$\frac{\cos(at)}{t^3}$	$-\frac{\pi}{2}\delta^{(2)}(t) + \frac{a^2\pi}{2}\delta(t) - \frac{a}{t^2} + \frac{\sin(at)}{t^3}$

<sup>a</sup> See Figure 7.5.

<sup>b</sup> See Figure 7.11.

<sup>c</sup> Notice the infinite energy of the functions  $\tanh(t)$ ,  $\text{coth}(t)$ , and  $\text{cosech}(t)$ .

**TABLE 7.2** Selected Useful Hilbert Pairs of Periodic Signals

Number	Name	$u_p(t)$	$v_p(t)$
1	Sampling sequence	$\sum_{k=-\infty}^{\infty} \delta(t - kT)$	$\frac{1}{T} \sum_{k=-\infty}^{\infty} \cot[(\pi/T)(t - kT)]$
2	Even square wave	$\text{sgn}[\cos(\omega t)]$ $\omega = 2\pi/T$	$(2/\pi) \ln  \tan(\omega t/2 + \pi/4) $
3	Odd square wave	$\text{sgn}[\sin(\omega t)]$ $\omega = 2\pi/T$	$(2/\pi) \ln  \tan(\omega t/2) $
4	Squared cosine	$\cos^2(\omega t)$	$0.5 \sin(2\omega t)$
5	Squared sine	$\sin^2(\omega t)$	$-0.5 \sin(2\omega t)$
6	Cube cosine	$\cos^3(\omega t)$	$\frac{3}{4} \sin(\omega t) + \frac{1}{4} \sin(3\omega t)$
7	Cube sine	$\sin^3(\omega t)$	$-\frac{3}{4} \cos(\omega t) + \frac{1}{4} \cos(3\omega t)$
8		$\cos^4(\omega t)$	$\frac{1}{2} \sin(2\omega t) + \frac{1}{8} \sin(4\omega t)$
9		$\sin^4(\omega t)$	$\frac{-1}{2} \sin(2\omega t) + \frac{1}{8} \sin(4\omega t)$
10		$e^{\pm j\omega t}$	$\mp j \text{sgn}(\omega) e^{\pm j\omega t}$
11	Product	$\cos(at + \varphi) \cos(bt + \psi)$ $0 < a < b$ ; $\varphi, \psi$ are constants	$\cos(at + \varphi) \sin(bt + \psi)$
12	Fourier series	$U_0 + \sum_{k=1}^n U_k \cos(k\omega t + \phi_k)$	$\sum_{k=1}^n U_k \sin(k\omega t + \phi_k)$
13	Any periodic function	$u_T(t) * \sum_{k=-\infty}^{\infty} \delta(t - kT) i^a$	$u_T(t) * \frac{1}{T} \sum_{k=-\infty}^{\infty} \cot[(\pi/T)(t - kT)]$

<sup>a</sup>  $u_T(t)$  is the generating function (see Equation 7.96).

**TABLE 7.3** Properties of the Hilbert Transformation

Number	Name	Original or Inverse Hilbert Transform	Hilbert Transform
1	Notations	$u(t)$ or $H^{-1}[v]$	$v(t)$ or $\hat{u}(t)$ or $H[u]$
2	Time domain definitions	$\begin{cases} u(t) = \frac{1}{\pi} \int_{-\infty}^{\infty} \frac{v(\eta)}{\eta - t} d\eta \\ u(t) = \frac{-1}{\pi t} * v(t) \end{cases}$ or	$\begin{cases} v(t) = \frac{-1}{\pi} \int_{-\infty}^{\infty} \frac{u(\eta)}{\eta - t} d\eta \\ v(t) = \frac{1}{\pi t} * u(t) \end{cases}$
3	Change of symmetry	$u(t) = u_{1e}(t) + u_{2o}(t)$ ;	$v(t) = v_{1o}(t) + v_{2e}(t)$
4	Fourier spectra	$u(t) \xrightarrow{F} U(\omega) = U_e(\omega) + jU_o(\omega)$ ; $U(\omega) = j \text{sgn}(\omega)V(\omega)$ ;	$v(t) \xrightarrow{F} V(\omega) = V_e(\omega) + jV_o(\omega)$ ; $V(\omega) = -j \text{sgn}(\omega)U(\omega)$
	For even functions the Hilbert transform is odd:	$U_e(\omega) = 2 \int_0^{\infty} u_{1e}(t) \cos(\omega t) dt$	$v_o(t) = 2 \int_0^{\infty} U_e(\omega) \sin(\omega t) df$
	For odd functions the Hilbert transform is even:	$U_o(\omega) = -2 \int_0^{\infty} u_{2o}(t) \sin(\omega t) dt$	$v_e(t) = 2 \int_0^{\infty} U_o(\omega) \cos(\omega t) df$
5	Linearity	$au_1(t) + bu_2(t)$	$av_1(t) + bv_2(t)$
6	Scaling and time reversal	$u(at); a > 0$ $u(-at)$	$v(at)$ $-v(-at)$
7	Time shift	$u(t - a)$	$v(t - a)$
8	Scaling and time shift	$u(bt - a)$	$v(bt - a)$
9	Iteration	$H[u(t)] = v(t)$ $H[H[u]] = -u(t)$ $H[H[H[u]]] = -v(t)$ $H[H[H[H[u]]]] = u(t)$	Fourier image $-j \text{sgn}(\omega)U(\omega)$ $[-j \text{sgn}(\omega)]^2 U(\omega)$ $[-j \text{sgn}(\omega)]^3 U(\omega)$ $[-j \text{sgn}(\omega)]^4 U(\omega)$
10	Time derivatives	$\dot{u}(t) = \frac{-1}{\pi t} * \dot{v}(t)$  $\dot{u}(t) = \left[ \frac{d}{dt} (-1/\pi t) \right] * v(t)$	First option $\dot{v}(t) = \frac{1}{\pi t} * \dot{u}(t)$ Second option $\dot{v}(t) = \left[ \frac{d}{dt} (1/\pi t) \right] * u(t)$

(continued)



TABLE 7.3 (continued) Properties of the Hilbert Transformation

Number	Name	Original or Inverse Hilbert Transform	Hilbert Transform
11	Convolution	$u_1(t) * u_2(t) = -v_1(t) * v_2(t)$	$u_1(t) * v_2(t) = v_1(t) * u_2(t)$
12	Autoconvolution equality	$\int u(\tau)u(t - \tau)d\tau = -\int v(\tau)v(t - \tau)d\tau$ for $\tau = 0$ energy equality	
13	Multiplication by $t$	$tu(t)$	$tv(t) - \int_{-\infty}^{\infty} u(\tau)d\tau$
14	Multiplication of signals with nonoverlapping spectra	$u_1(t)$ (low pass signal) $u_1(t)u_2(t)$	$u_2(t)$ (high pass signals) $u_1(t)v_2(t)$
15	Analytic signal	$\psi(t) = u(t) + jH[u(t)]$	$H[\psi(t)] = -j\psi(t)$
16	Product of analytic signals	$\psi(t) = \psi_1(t)\psi_2(t)$	$H[\psi(t)] = \psi_1(t)H[\psi_2(t)] = H[\psi_1(t)]\psi_2(t)$
17	Nonlinear transformations	$u(x)$	$v(x)$
17a	$x = \frac{c}{bt+a}$	$u_1(t) = u\left[\frac{c}{bt+a}\right]$	$v_1(t) = v\left[\frac{c}{bt+a}\right] - \frac{1}{\pi}P \int_{-\infty}^{\infty} \frac{u(t)}{t} dt$
17b	$x = a + \frac{b}{t}$	$u_1(t) = u\left[a + \frac{b}{t}\right]$	$v_1(t) = \frac{b}{a} \left\{ v\left[a + \frac{b}{t}\right] - v(a) \right\}$
	Notice that the nonlinear transformation may change the signal $u(t)$ of finite energy to a signal $u_1(t)$ of infinite energy. $P$ is the Cauchy principal value.		
18	Asymptotic value as $t \Rightarrow \infty$ for even functions of finite support: $u_e(t) = u_e(-t)$		$\lim_{t \Rightarrow \infty}  v_o(t)  = \frac{1}{\pi t} \int_S u_e(t) dt^a$

Note: e, even; o, odd.  
<sup>a</sup> S is support of  $u_e(t)$ .

### 7.9.2 Autoconvolution and Energy Equality

The energy of a real signal  $u(t) \xleftrightarrow{F} U(\omega)$  is given by the integrals

$$E_u = \int_{-\infty}^{\infty} u^2(t)dt = \int_{-\infty}^{\infty} |U(\omega)|^2 df; \quad \omega = 2\pi f \quad (7.113)$$

The above equality of the energy defined in the time domain and Fourier frequency domain is called *Parseval's theorem*. The squared magnitude of the Fourier image of the Hilbert transform  $v(t) = H[u(t)] \xleftrightarrow{F} V(\omega) = -j \operatorname{sgn}(\omega)U(\omega)$  is

$$|V(\omega)|^2 = |-j \operatorname{sgn}(\omega)U(\omega)|^2 = |U(\omega)|^2 \quad (7.114)$$

that is, the energy of the Hilbert transform is given by the integrals

$$E_v = \int_{-\infty}^{\infty} v^2(t)dt = \int_{-\infty}^{\infty} |U(\omega)|^2 df \quad (7.115)$$

Therefore, the energies  $E_u$  and  $E_v$  are equal. This property of a pair of Hilbert transforms may be used to check the algorithms of numerical evaluation of Hilbert transforms. A large discrepancy  $\Delta E = E_v - E_u$  indicates a fault in the program. A small discrepancy may be used as a measure of the accuracy. Notice that the Hilbert transformation cancels the mean value of the signal. Therefore, the energy (or the power) of this term is rejected.

The signals forming a Hilbert pair are *orthogonal*; that is, the mutual energy defined by the integral

$$\int_{-\infty}^{\infty} u(t)v(t)dt = 0 \quad (7.116)$$

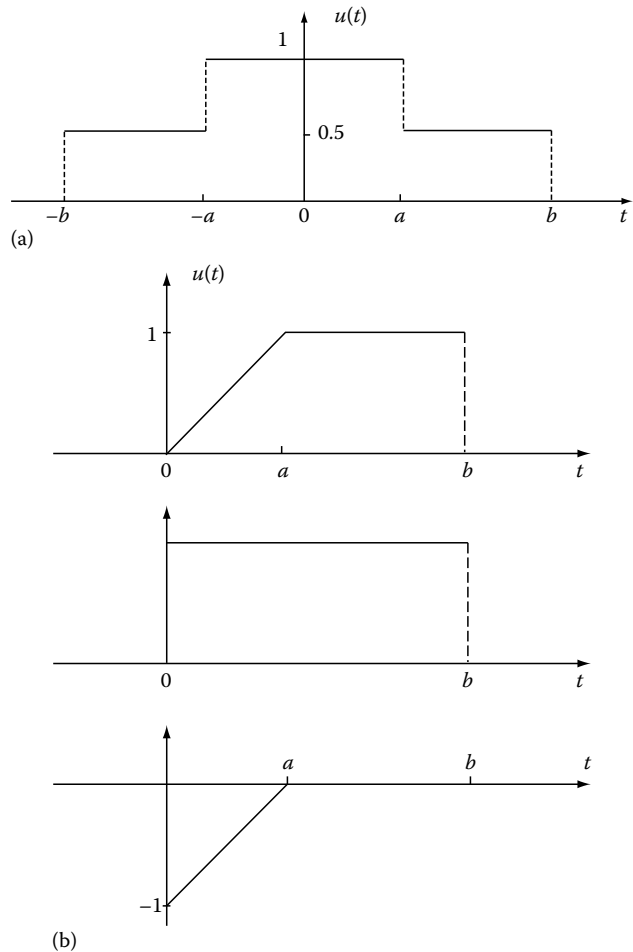


FIGURE 7.12 (a) A pulse given by the summation of two square pulses  $\Pi_a(t) + \Pi_b(t)$  and (b) The "ramp" pulse and its decomposition in two pulses.

equals zero. The *autoconvolution* of the signal  $u(t)$  is defined by the integral

$$\rho_{u-u}(t) = u(t) * u(t) = \int_{-\infty}^{\infty} u(t)u(t - \tau)d\tau \quad (7.117)$$

The autoconvolution equality theorem for a Hilbert pair of signals has the form

$$\rho_{u-u}(t) = -\rho_{v-v}(t) \quad (7.118)$$

that is, the autoconvolutions of  $u(t)$  and  $v(t)$  have the same waveform and differ only by sign.

*Proof* Let us apply the convolution to multiplication theorem of Fourier analysis to both sides of the equality (Equation 7.118). We get the Fourier pairs

$$\rho_{u-u}(t) = u(t) * u(t) \stackrel{F}{\iff} U^2(\omega) \quad (7.119)$$

$$\begin{aligned} \rho_{v-v}(t) &= v(t) * v(t) \stackrel{F}{\iff} [-j \operatorname{sgn}(\omega)U(\omega)]^2 \\ &= -U^2(\omega) \end{aligned} \quad (7.120)$$

We have shown that the functions  $\rho_{u-u}(t)$  and  $-\rho_{v-v}(t)$  have the same waveforms because they have equal Fourier transforms.

**Examples**

1. It is really amazing to observe the result of calculation of the autoconvolutions of some Hilbert pairs. Consider the Hilbert pair  $\delta(t) \stackrel{H}{\iff} \frac{1}{\pi t}$ . Because the autoconvolution of the delta pulse is  $\delta(t) = \delta(t) * \delta(t)$  (see Section 7.6), the autoconvolution equality yields the surprising result

$$\delta(t) = -\frac{1}{\pi t} * \frac{1}{\pi t} \quad (7.121)$$

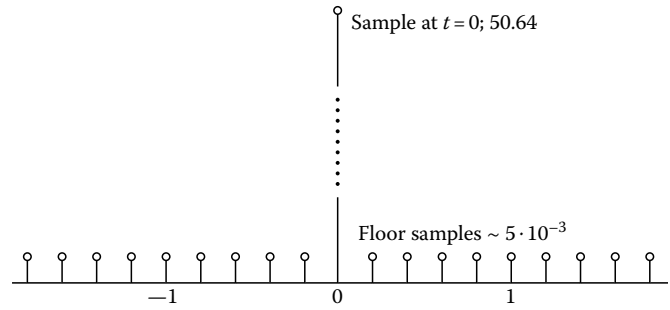


FIGURE 7.13 The discrete delta pulse obtained by numerical computing of the autoconvolution  $-1/(\pi t) * 1/(\pi t)$ .

that is, the autoconvolution of the function (distribution)  $\frac{1}{\pi t}$  of infinite support yields the delta pulse of a point support. Figure 7.13 shows the result of a numerical approximate calculation of the autoconvolution (Equation 7.121).

2. Consider the square pulse and its Hilbert transform

$$\Pi_a(t) \stackrel{H}{\iff} \frac{1}{\pi} \ln \left| \frac{t+a}{t-a} \right| \quad (7.122)$$

The waveforms are shown in Figure 7.5. The autoconvolution of the square pulse is a tri(t) (triangle) pulse of doubled support (Figure 7.14a). Again, the autoconvolution of the logarithmic function of infinite support defined by Equation 7.122, which has infinite peaks at points  $|t|=a$ , yields the triangle pulse of finite support. Indeed, we have

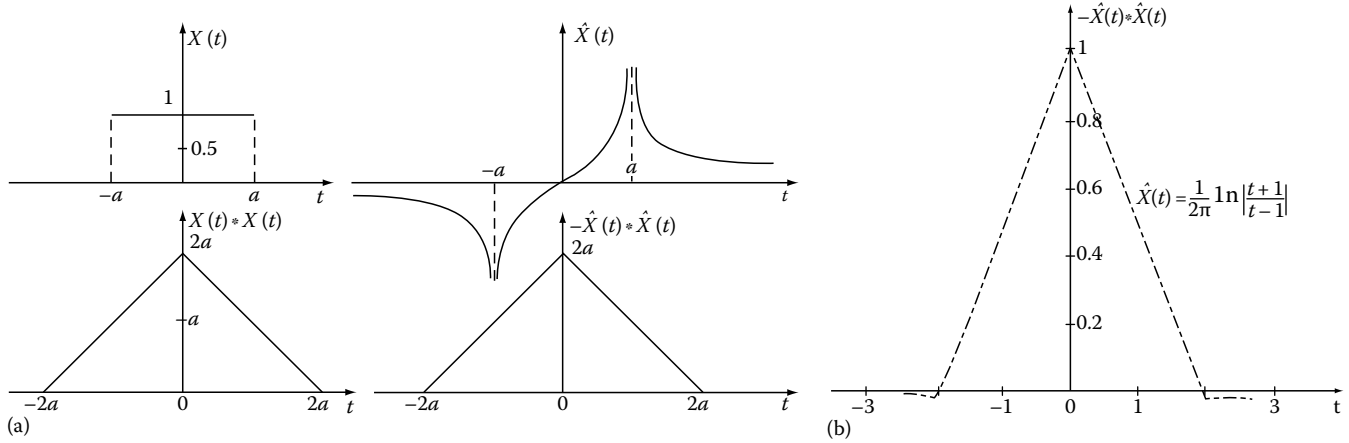


FIGURE 7.14 (a) An example of the autoconvolution equality: (left) the square pulse and its autoconvolution; (right) the Hilbert transform of the square pulse and its autoconvolution. (b) The result of numerical computing of the autoconvolution of the Hilbert transform.

$$tri(t) = -\frac{1}{\pi^2} \left\{ \ln \left| \frac{t+a}{t-a} \right| * \ln \left| \frac{t+a}{t-a} \right| \right\} \quad (7.123)$$

Figure 7.14b shows the result of a numerical evaluation of the above autoconvolution.

### 7.10 Differentiation of Hilbert Pairs

Consider a Hilbert pair  $u(t) \stackrel{H}{\Leftrightarrow} v(t)$ . Differentiation of both sides gives a new Hilbert pair:

$$\dot{u}(t) \stackrel{H}{\Leftrightarrow} \dot{v}(t) \quad (7.124)$$

Therefore, differentiation is a useful tool for creating new Hilbert pairs. Obviously, the operation can be repeated to get the next Hilbert pairs:

$$\frac{d^n u}{dt^n} \stackrel{H}{\Leftrightarrow} \frac{d^n v}{dt^n} \quad (7.125)$$

Because the signal  $\psi(t) = u(t) + jv(t)$  is an analytic function, in principle all of its derivatives exist.<sup>39</sup>

Consider the convolution notation of the Hilbert transformations:

$$u(t) = \frac{-1}{\pi t} * v(t) \stackrel{H}{\Leftrightarrow} v(t) = \frac{1}{\pi t} * u(t) \quad (7.126)$$

The derivative of a convolution has *two options*: the convolution of the derivative of the first term with the second term, or the convolution of the first term with the derivative of the second term; i.e., the *first option* has the form

$$\begin{aligned} \dot{u}(t) &= \frac{d}{dt}(t/\pi t) * v(t) \stackrel{H}{\Leftrightarrow} \dot{v}(t) = \frac{d}{dt}(t/\pi t) * u(t) \\ &= [1/(\pi t^2)] * v(t) = [-1/(\pi t^2)] * u(t) \end{aligned} \quad (7.127)$$

and the *second option* is

$$\dot{u}(t) = -\frac{1}{\pi t} * \dot{v}(t) \stackrel{H}{\Leftrightarrow} \dot{v}(t) = \frac{1}{\pi t} * \dot{u}(t) \quad (7.128)$$

*Proof* The Hilbert integrals (Equations 7.1 and 7.2) are

$$v(t) = \frac{-1}{\pi} P \int_{-\infty}^{\infty} \frac{u(\eta)}{\eta - t} d\eta; \quad u(t) = \frac{1}{\pi} P \int_{-\infty}^{\infty} \frac{v(\eta)}{\eta - t} d\eta \quad (7.129)$$

The differentiation of these integrals with respect to  $t$  yields

$$\begin{aligned} \dot{v}(t) &= \frac{1}{\pi} P \int_{-\infty}^{\infty} \frac{u(\eta)}{(\eta - t)^2} d\eta; \\ \dot{u}(t) &= \frac{-1}{\pi} P \int_{-\infty}^{\infty} \frac{v(\eta)}{(\eta - t)^2} d\eta \end{aligned} \quad (7.130)$$

These integrals have in the convolution notation the form (Equation 7.127). The change of variable  $y = \eta - t$  yields the following form of the Hilbert integrals:

$$v(t) = \frac{-1}{\pi} P \int_{-\infty}^{\infty} \frac{u(y+t)}{y} dy; \quad (7.131)$$

$$u(t) = \frac{1}{\pi} P \int_{-\infty}^{\infty} \frac{v(y+t)}{y} dy$$

and the differentiation yields

$$\dot{v}(t) = \frac{-1}{\pi} P \int_{-\infty}^{\infty} \frac{\dot{u}(y+t)}{y} dy; \quad (7.132)$$

$$\dot{u}(t) = \frac{1}{\pi} P \int_{-\infty}^{\infty} \frac{\dot{v}(y+t)}{y} dy$$

These integrals have in the convolution notation the form (Equation 7.128).

Very illustrative is the same proof in terms of the frequency domain representation:

$$v(t) = \frac{1}{\pi t} * u(t) \stackrel{F}{\Leftrightarrow} -j \operatorname{sgn}(\omega) U(\omega) \quad (7.133)$$

Time domain differentiation corresponds to the multiplication of the Fourier image by the differentiation operator  $j\omega$ . Therefore,

$$\dot{v}(t) \stackrel{F}{\Leftrightarrow} -j\omega [-j \operatorname{sgn}(\omega) U(\omega)] \quad (7.134)$$

However, the operator  $j\omega$  may be arbitrarily assigned to the first or second factor of the product in parentheses. In the time domain, this arbitrary choice corresponds to the two options of the convolution.

#### Example 1

Consider the Hilbert pair

$$\delta(t) \stackrel{H}{\Leftrightarrow} \frac{1}{\pi t} \quad (7.135)$$

The derivatives are

$$\dot{\delta}(t) \stackrel{H}{\Leftrightarrow} \frac{d}{dt}(1/\pi t) = -\frac{1}{\pi t^2} \quad (7.136)$$

The derivative  $\dot{\delta}(t)$  and, hence, the function  $d/dt(1/\pi t)$  are defined in the distribution sense (notation FP  $1/(\pi t^2)$ , where FP denotes "finite part of").<sup>35</sup> The energy of these signals is infinite.

**Example 2**

Consider the Hilbert pair

$$u(t) = \frac{1}{1+t^2} \stackrel{H}{\longleftrightarrow} \frac{t}{1+t^2} = v(t) \quad (7.137)$$

Let us differentiate  $n$ -times both sides of this equation. In this way we find an infinite series of Hilbert transform pairs as shown in Table 7.4. The derivations are simpler by using the differentiation of the analytic signal

$$\psi(t) = u(t) + jv(t) = \frac{1}{1-jt} \quad (7.138)$$

and determining the real and imaginary parts of the derivatives in the form of Hilbert pairs.

The waveforms of the first four terms of the Hilbert pairs of Table 7.4 are shown in Figure 7.15a and b. The energy was normalized to unity by division of the amplitudes by the SQR of energy. The Cauchy pulse may serve as the function approximating the delta pulse (see Equation 7.76). Therefore, the derivatives of the Cauchy-Hilbert pair may serve as the

approximating functions defining the derivatives of the complex delta distribution. For example,

$$\begin{aligned} \hat{\delta}(t) &= \lim_{\alpha \rightarrow 0} \left[ \frac{1}{\pi} \frac{-2\alpha t}{(\alpha^2 + t^2)^2} \right] \stackrel{H}{\longleftrightarrow} \hat{\delta}(t) \\ &= \lim_{\alpha \rightarrow 0} \left[ \frac{1}{\pi} \frac{\alpha^2 - t^2}{(\alpha^2 - t^2)^2} \right] \end{aligned} \quad (7.139)$$

(see Table 7.1, 42–46).

**7.11 Differentiation and Multiplication by  $t$ : Hilbert Transforms of Hermite Polynomials and Functions**

Consider the Gaussian Fourier pair:

$$e^{-t^2} \stackrel{F}{\longleftrightarrow} \pi^{0.5} e^{-\pi^2 f^2} \quad (7.140)$$

The successive differentiation of the Gaussian pulse  $\exp(-t^2)$  generates the  $n$ th order *Hermite polynomial* (see Table 7.5).

**TABLE 7.4** Hilbert Transforms of the Derivatives of the Cauchy Signal  $u(t) = 1/(1+t^2)$

$n$	Signal $u^{(n)}$	Hilbert Transform $v^{(n)}$	Analytic Signal $\psi^{(n)}$	Energy
0	$\frac{1}{1+t^2}$	$\frac{t}{1+t^2}$	$\frac{1}{1-jt}$	$\frac{\pi}{2}$
1	$\frac{-2t}{(1+t^2)^2}$	$\frac{1-t^2}{(1+t^2)^2}$	$\frac{j}{(1-jt)^2}$	$\frac{\pi}{4}$
2	$2 \frac{3t^2-1}{(1+t^2)^3}$	$2 \frac{t^3-3t}{(1+t^2)^3}$	$\frac{-2}{(1-jt)^3}$	$\frac{3\pi}{4}$
3	$-6 \frac{4t^3-4t}{(1+t^2)^4}$	$-6 \frac{t^4-6t^2+1}{(1+t^2)^4}$	$\frac{-6j}{(1-jt)^4}$	$\frac{45}{8} \pi$
4	$24 \frac{5t^4-10t^2+1}{(1+t^2)^5}$	$24 \frac{t^5-10t^3+5t}{(1+t^2)^5}$	$\frac{24}{(1-jt)^5}$	$\frac{315}{4} \pi$
$n$		$\frac{(-j)^n n!}{(1-jt)^{n+1}}$	$a$	

$$^a \text{Energy} = \int_0^\infty \frac{n! dt}{(1+t^2)^{n+1}} = \frac{(n!)^2 1.35 \dots (2n-1)}{2.46 \dots 2n} \frac{\pi}{2}$$

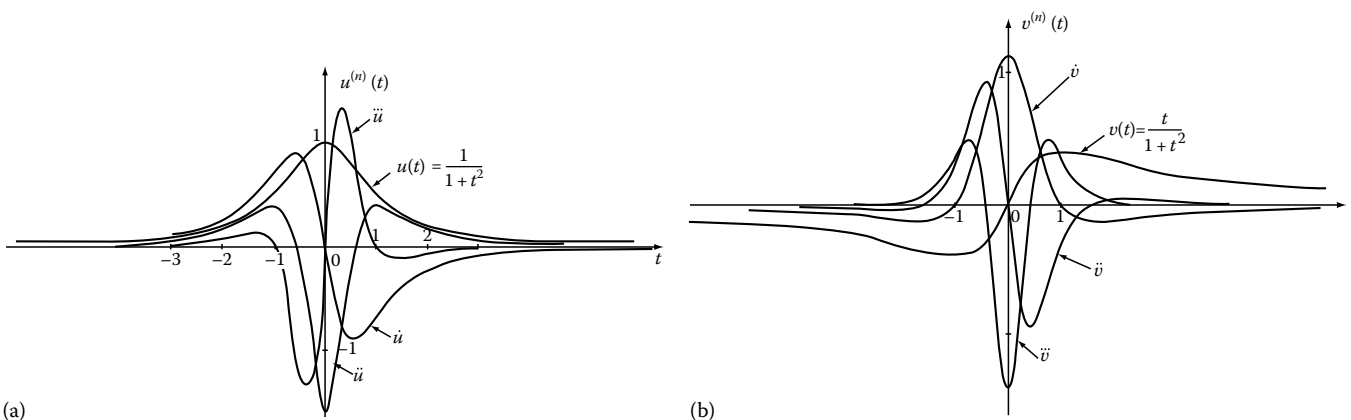


**FIGURE 7.15** (a) The waveforms of the Cauchy pulse and of its derivatives. (b) The waveforms of the corresponding Hilbert transforms.

**TABLE 7.5** Weighted Hermite Polynomials and Their Hilbert Transforms

Hermite Polynomial	Hilbert Transform	Energy
$n \quad H_n u$	$H(H_n u)$	$E$
0 $(1)u$	$2\sqrt{\pi} \int_0^\infty \exp(-\pi^2 f^2) \sin(\omega t) df$	$\sqrt{\pi/2}$
1 $(2t)u$	$-2\sqrt{\pi} \int_0^\infty \omega \exp(-\pi^2 f^2) \cos(\omega t) df$	$\sqrt{\pi/2}$
2 $(4t^2 - 2)u$	$-2\sqrt{\pi} \int_0^\infty \omega^2 \exp(-\pi^2 f^2) \sin(\omega t) df$	$3\sqrt{\pi/2}$
3 $(8t^3 - 12t)u$	$2\sqrt{\pi} \int_0^\infty \omega^3 \exp(-\pi^2 f^2) \cos(\omega t) df$	$15\sqrt{\pi/2}$
4 $(16t^4 - 48t^2 + 12)u$	$2\sqrt{\pi} \int_0^\infty \omega^4 \exp(-\pi^2 f^2) \sin(\omega t) df$	$105\sqrt{\pi/2}$
5 $(32t^5 - 160t^3 + 120t)u$	$-2\sqrt{\pi} \int_0^\infty \omega^5 \exp(-\pi^2 f^2) \cos(\omega t) df$	$945\sqrt{\pi/2}$
$n \quad H_n u = (-1)^n [2tH_{n-1}(t) - 2(n-1)H_{n-2}(t)]$	$(-1)^n 2\sqrt{\pi} \int_0^\infty \omega^n \exp(-\pi^2 f^2) \sin(\omega t + n\pi/2) df$	

Notes: Notation:  $u = \exp(-t^2)$ .

Energy =  $\int_{-\infty}^\infty u^2 H_n^2 dt = \int_{-\infty}^\infty [H(uH_n)]^2 dt = 1 \times 3 \times 5 \times \dots \times |2n - 1| \times \sqrt{\pi/2}$ .

The Hermite polynomials are defined by the formula (see also Chapter 1)

$$H_n(t) = (-1)^n e^{t^2} \frac{d^n}{dt^n} e^{-t^2} \quad (7.141a)$$

$n = 0, 1, 2, \dots; \quad t \in \pm\infty$

(Roman H is used to denote the Hermite polynomial in distinction from the italic  $H$  for the Hilbert transform). The Hermite polynomials are also defined by the recursion formula

$$H_n(t) = 2tH_{n-1}(t) - 2(n-1)H_{n-2}(t); \quad n = 1, 2, \dots \quad (7.141b)$$

The first terms of the Hermite polynomials weighted by the generating function  $\exp(-t^2)$  and their Hilbert transforms are listed in Table 7.5. The Hilbert transform of the first term was calculated using the frequency domain method represented by

the Hilbert pair (see Table 7.1, the Hilbert transform of the Gaussian pulse).

$$e^{-t^2} \xleftrightarrow{H} 2\pi^{0.5} \int_0^\infty e^{-\pi^2 f^2} \sin(\omega t) df; \quad \omega = 2\pi f \quad (7.142)$$

The next terms are obtained by calculating the successive time derivatives of both sides of this Hilbert pair. For example, the second term is

$$2te^{-t^2} \xleftrightarrow{H} -2\pi^{0.5} \int_0^\infty \omega e^{-\pi^2 f^2} \cos(\omega t) df \quad (7.143)$$

The value of the energy of successive terms is listed in the last column of Table 7.5. The waveforms are shown in Figure 7.16. Each Hilbert pair in Table 7.5 is a pair of orthogonal functions.

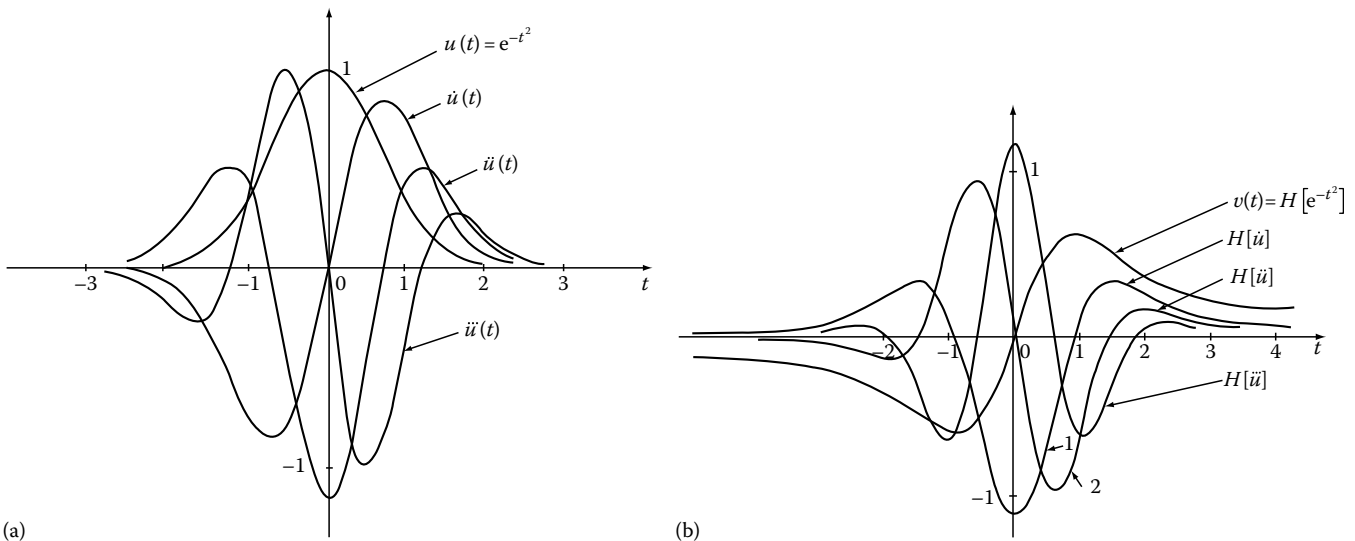


**FIGURE 7.16** (a) The waveforms of Hermite polynomials. (b) The waveforms of the corresponding Hilbert transforms.

However, the weighted Hermite polynomials do not form a set of orthogonal functions; that is, the integral of the product

$$\int_{-\infty}^{\infty} e^{-2t^2} H_n(t)H_m(t)dt \neq 0 \quad \text{for } n \neq m \quad (7.144)$$

differs from zero for  $n \neq m$ . The Hermite polynomials can be orthogonalized by replacing the weighting function  $\exp(-t^2)$  by  $\exp(-2t^2)$  because

$$\int_{-\infty}^{\infty} e^{-t^2} H_n(t)H_m(t) = \begin{cases} 0 & \text{for } n \neq m \\ 2^n n! \pi^{0.5} & \text{for } n = m \end{cases} \quad (7.145)$$

Therefore, the functions denoted by small italic  $h(t)$

$$h_n(t) = (2^n n!)^{-0.5} \pi^{-0.25} e^{-t^2/2} H_n(t); \quad n = 0, 1 \dots \quad (7.146)$$

are forming an orthonormal (energy is equal unity) set of functions called *Hermite functions*. Let us derive the Hilbert transforms of the Hermite functions. Combining the Equations 7.141 and 7.145 we get the following recurrency:

$$h_n(t) = \left\{ \frac{2(n-1)!}{n} \right\}^{0.5} t h_{n-1}(t) - (n-1) \left\{ \frac{(n-2)!}{n!} \right\}^{0.5} h_{n-2}(t) \quad (7.147)$$

The Hilbert transforms  $H[h_n(t)]$  may be derived using the multiplication by  $t$  theorem (see Table 7.3):

$$tu(t) \stackrel{H}{\iff} tv(t) - \frac{1}{\pi} \int_{-\infty}^{\infty} u(\tau) d\tau \quad (7.148)$$

*Proof* The formula 7.1 yields

$$H[tu(t)] = -\frac{1}{\pi} \int_{-\infty}^{\infty} \frac{\eta u(\eta)}{\eta - t} d\eta \quad (7.149)$$

The insertion of the new variable  $y = \eta - t$  gives

$$\begin{aligned} H[tu(t)] &= -\frac{1}{\pi} \int_{-\infty}^{\infty} \frac{(y+t)u(y+t)}{y} dy \\ &= -\frac{1}{\pi} \int_{-\infty}^{\infty} \frac{tu(y+t)}{y} dy - \frac{1}{\pi} \int_{-\infty}^{\infty} u(y+t) dy \\ &= tH[u(t)] - \frac{1}{\pi} \int_{-\infty}^{\infty} u(\tau) d\tau \end{aligned} \quad (7.150)$$

This is exactly the relation (Equation 7.148). The second term in this equation equals zero for odd functions  $u(t)$ . The first term in the recurrent formula 7.147 has the form of the product  $th(t)$  enabling the application of Equation 7.148. Therefore, the Hilbert transforms of the Hermite functions  $h_n(t)$  have the form

$$H[h_n(t)] = v_n(t) = \left[ \frac{2(n-1)!}{n!} \right]^{0.5} \left[ tv_{n-1}(t) - \frac{1}{\pi} \int_{-\infty}^{\infty} u_{n-1}(\tau) d\tau \right] - (n-1) \left[ \frac{(n-2)!}{n!} \right]^{0.5} v_{n-2}(t) \quad (7.151)$$

To derive the Hilbert transforms of Hermite functions, we have to derive by any method the first term  $v_0(t)$  and then apply the above recurrency. Let us use the frequency domain method. The function  $h_0(t)$  and its Fourier image are

$$h_0(t) = \pi^{-0.25} \exp(-t^2/2) \stackrel{F}{\iff} (4\pi)^{0.25} \exp[-2(\pi f)^2] \quad (7.152)$$

By using Equation 7.66 we obtain

$$H[h_0(t)] = v_0(t) = 2(4\pi)^{0.25} \int_0^{\infty} e^{-2\pi^2 f^2} \sin(\omega t) df \quad (7.153)$$

Introducing the abbreviated notation ( $\omega = 2\pi f$ )

$$b = \pi^{0.25}, g(t) = \int_0^{\infty} e^{-2\pi^2 f^2} \sin(\omega t) df \quad (7.154)$$

we get the form of Equation 7.152 used in Table 7.6. The next terms  $v_1, v_2, \dots$  in this table are derived by using Equation 7.150. They are listed using two notations: the recurrent and non-recurrent. The waveforms of the first four terms of the Hermite functions  $h_n(t)$  and their Hilbert transforms are shown in Figure 7.17a and b.

## 7.12 Integration of Analytic Signals

Consider the analytic signal defined by Equation 7.28 as a complex function of a real variable  $t$  in the form

$$\psi(t) = u(t) + jv(t) \quad (7.155)$$

This function is integrable in the Riemann sense in the interval  $[\alpha, \beta]$  if and only if the functions  $u(t)$  and  $v(t)$  are integrable; that is,

$$\Phi(t) = \int_{\alpha}^t \psi(t) dt = \int_{\alpha}^t u(t) dt + j \int_{\alpha}^t v(t) dt \quad (7.156)$$

**TABLE 7.6** Hilbert Transforms of Orthonormal Hermite Functions (Energy = 1)

Hermite Functions $h_n(t)$	Hilbert Transforms $v_n(t)$
<i>Recurrent notation</i>	
$h_0 = a$	$v_0 = 2\sqrt{2}bg(t)$
$h_1 = \sqrt{2}th_0$	$v_1 = \sqrt{2} \left[ tv_0 - \frac{\sqrt{2}b}{\pi} \right]$
$h_2 = th_1 - \sqrt{1/2}h_0$	$v_2 = tv_1 - \sqrt{1/2}v_0$
$h_3 = \sqrt{2/3} [th_2 - h_1]$	$v_3 = \sqrt{2/3} \left[ tv_2 - \frac{b}{\pi} - v_1 \right]$
$h_4 = \sqrt{1/2}th_3 - \sqrt{3/4}h_2$	$v_4 = \sqrt{1/2}tv_3 - \sqrt{3/4}v_2$
$h_5 = \sqrt{2/5}th_4 - \sqrt{4/5}h_3$	$v_5 = \sqrt{2/5} \left[ tv_4 - \frac{\sqrt{3}b}{2\pi} \right] - \sqrt{4/5}v_3$
$h_n = \sqrt{\frac{2(n-1)!}{n!}}th_{n-1} + (n-1)\sqrt{\frac{(n-2)!}{n!}}h_{n-2}$	$v_n = \sqrt{\frac{2(n-1)!}{n!}} \left[ tv_{n-1} + -\frac{1}{\pi} \int h_{n-1}(\tau)d\tau \right] - (n-1)\sqrt{\frac{(n-2)!}{n!}}v_{n-2}$
<i>Nonrecurrent notation</i>	
$h_0 = a1$	$2\sqrt{2}bg(t)$
$h_1 = \sqrt{2}at$	$2b[2tg(t) - \pi^{-1}]$
$h_2 = \frac{a}{\sqrt{8}}(4t^2 - 2)$	$2b[(2t^2 - 1)g(t) - t\pi^{-1}]$
$h_3 = \frac{a}{\sqrt{48}}(8t^3 - 12t)$	$\sqrt{8/3}b \left[ (2t^3 - 3t)g(t) - \frac{t^2}{\pi} + \frac{1}{2\pi} \right]$
$h_4 = \frac{a}{\sqrt{384}}(16t^4 - 48t^2 + 12)$	$\sqrt{4/3}b \left[ (2t^4 - 6t^2 + 1.5)g(t) - \frac{t^3}{\pi} + \frac{2t}{\pi} \right]$
$h_5 = \frac{a}{\sqrt{3840}}(32t^5 - 160t^3 + 120t)$	$\sqrt{8/15}b \left[ (2t^5 - 10t^3 + 7.5t)g(t) + -\frac{(t^4 - 4t^2) + 1.75}{\pi} \right]$
$h_n(t) = \frac{a}{\sqrt{2^n n!}} H_n(t)$	$H_n(t) = 2tH_{n-1}(t) - 2(n-1)H_{n-2}(t)$
$n$	0      1      2      3      4      5      ...
$\int_{-\infty}^{\infty} h_n(\tau)d\tau$	$\sqrt{2}b$ 0 $b$ 0 $\sqrt{3/4}b$ 0      ...

Note: Notations:  $h_0(t), h_1(t), \dots \Rightarrow h_0, h_1, \dots; v_0(t), v_1(t), \dots \Rightarrow v_0, v, \dots$   
 $g(t) = \int_0^{\infty} e^{-2\pi^2 f^2} \sin(2\pi f t) df; a = \pi^{-0.25} e^{-t^2/2}; b = \pi^{0.25}$

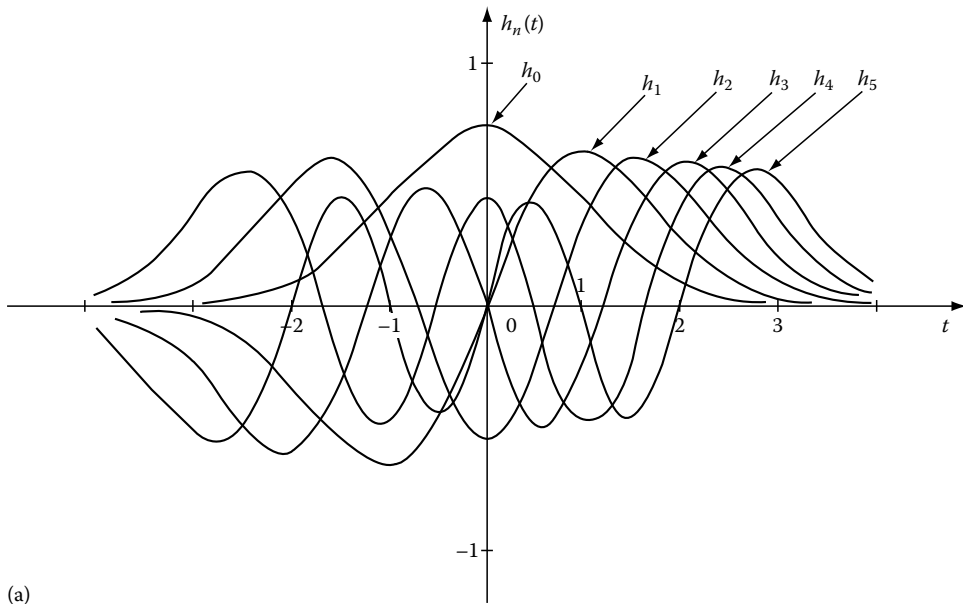


**FIGURE 7.17** (a) Waveforms of Hermite functions.

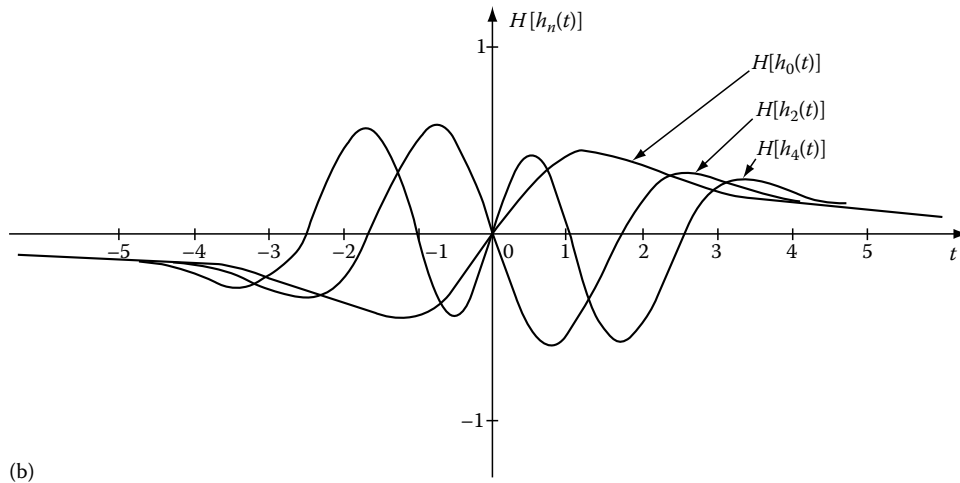


FIGURE 7.17 (continued) (b) Waveforms of the corresponding Hermite transforms.

Let us define

$$\Phi(t) = U(t) + jV(t) \tag{7.157}$$

The functions  $U(t)$  and  $V(t)$  are forming a Hilbert pair only if  $\Phi(z)$  is an analytic function of a complex variable  $z = t + j\tau$ . Therefore, let us give without a proof the following theorem:

If the function  $\psi(z) = u(t, \tau) + jv(t, \tau)$  is analytic in a simply connected domain  $D$ , then the function

$$\Phi(z) = \int_{z_0}^z \psi(z) dz \tag{7.158}$$

is also analytic, and the derivative  $\Phi'(z) = \psi(z)$ . The integral (Equation 7.158) is defined as a path integral in the plane  $(t, \tau)$ , and in the domain  $D$  the integral depends on  $z$  and  $z_0$  but not on the particular path  $\Gamma$  connecting them (Figure 7.18).<sup>39</sup>

If function 7.155 is continuous in the interval  $[\alpha, \beta]$ , then the function defined by the integral

$$\Phi(t) = \int_{\alpha}^t \psi(t) dt; \quad \alpha \leq t \leq \beta \tag{7.159}$$

is called the primary function, or antiderivative of  $\psi(t)$ , and has in the interval  $[\alpha, \beta]$  a continuous derivative  $\Phi'(t) = \psi(t)$ , the relation holds

$$\int_{\alpha}^{\beta} \psi(t) dt = \Phi(t)|_{\alpha}^{\beta} = \Phi(\beta) - \Phi(\alpha) \tag{7.160}$$

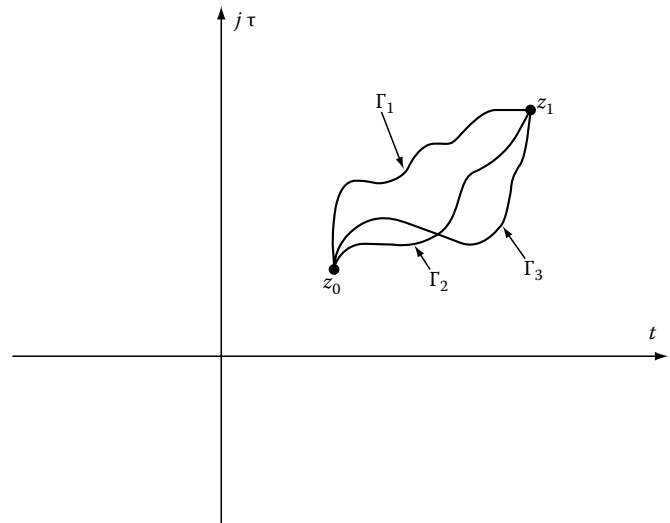


FIGURE 7.18 Passes of integration in the complex plane  $(t, j\tau)$ .

**Example**

The function  $e^{jt}$  has in the interval  $(-\infty, \infty)$  the primary function  $e^{jt}/j + c$ , where  $c$  is any complex constant. We have

$$\int_0^{\pi/2} e^{jt} dt = \frac{e^{jt}}{j} \Big|_0^{\pi/2} = \frac{e^{j\pi/2} - 1}{j} = 1 + j$$

If the analytic function has a representation in the form of a power series

$$\psi(z) = \sum_{n=0}^{\infty} d_n(z - z_0)^n \tag{7.161}$$



its integral must have a power series in the form

$$\Phi(z) = a + \sum_{n=0}^{\infty} \frac{d_n}{n+1} (z - z_0)^{n+1} \quad (7.162)$$

This means that the power series representation can be integrated term by term.

Integration in the time domain can be converted by using the Fourier transforms into integration in the frequency domain. For instance, the function  $u(t)$  can be integrated using the Fourier pairs

$$u(t) \stackrel{F}{\iff} U(\omega) \quad (7.163)$$

$$\int_{-\infty}^t u(t) dt \stackrel{F}{\iff} U(\omega) \left[ \frac{\delta(f)}{2} + \frac{1}{j\omega} \right] \quad (7.164)$$

$$\omega = 2\pi f$$

The term  $[\delta(f)/2] U(\omega)$  is equal to  $(1/2) U(0)$  and the term  $1/j\omega$  is the well-known integration operator. The same algorithm may be used to integrate the Hilbert transform  $v(t)$ .

**Example**

Consider the analytic function of the complex variable  $z = t + j\tau$

$$\psi(z) = \frac{1}{\pi} \frac{1}{\alpha - jz} = \frac{1}{\pi} \frac{1}{\alpha + \tau - jt} \quad (7.165)$$

where  $\alpha$  is a real constant ( $\alpha > 0$ ). We get

$$\psi(z) = \psi(t, \tau) = u(t, \tau) + jv(t, \tau) \quad (7.166)$$

where

$$u(t, \tau) = \frac{1}{\pi} \frac{\alpha + \tau}{(\alpha + \tau)^2 + t^2} \quad (7.167)$$

and

$$v(t, \tau) = \frac{1}{\pi} \frac{t}{(\alpha + \tau)^2 + t^2} \quad (7.168)$$

Let us integrate the function (Equation 7.165) in the interval  $[-a, t]$  where  $\alpha > 0$  is a real constant. Hence, we find

$$\begin{aligned} \Phi(z) &= \int_{-a}^t \frac{1}{\pi} \frac{dz}{\alpha - jz} = \frac{j}{\pi} \text{Ln}(\alpha - jz) \Big|_{-a}^t \\ &= \frac{j}{\pi} \text{Ln}(\alpha + \tau - jt) \Big|_{-a}^t \end{aligned} \quad (7.169)$$

The insertion of the limits of integration and change of coordinates from rectangular to polar yields

$$\begin{aligned} \Phi(t, \tau) &= \frac{1}{\pi} \left[ \tan^{-1} \left( \frac{t}{\alpha + \tau} \right) + \tan^{-1} \left( \frac{a}{\alpha + \tau} \right) \right] \\ &\quad + \frac{j}{2\pi} \text{Ln} \left[ \frac{(\alpha + \tau)^2 + t^2}{(\alpha + \tau)^2 + a^2} \right] \end{aligned} \quad (7.170)$$

Because  $\arg(\alpha - jz)$  is only determined to within a constant multiple of  $2\pi$ , the function  $(1/\pi) \text{Ln}(\alpha - jz)$  is not single valued (Notation Ln instead of ln). They prevent any winding of the integration path around  $z = -j\alpha$ , let us make a cut extending from the point  $z = -j\alpha$  to infinity. Then  $\Phi(z)$  is analytic in the remaining part of the  $z$ -plane and satisfies the Cauchy-Riemann equation (see also Appendix A).

**Example**

Consider a signal represented by the product:

$$u(t) = \text{sgn}(t)\Pi_a(t) \quad (7.171)$$

where

$\Pi_a(t)$  is defined by Equation 7.58

$\text{sgn}(t)$  is defined by Equation 7.11

We have the Fourier pair

$$0.5 \text{sgn}(t)\Pi_a(t) \stackrel{F}{\iff} \frac{1 - \cos(\omega a)}{j\omega} \quad (7.172)$$

The above Fourier spectrum is easy to derive by decomposing  $u(t)$  into right-sided and reverse sign left-sided square pulses and adding the spectra of these pulses. In a similar way we can derive the Hilbert transform by adding the two Hilbert transforms defined by Equation 7.61. The resulting Hilbert pair is

$$0.5 \text{sgn}(t)\Pi_a(t) \stackrel{H}{\iff} \frac{1}{2\pi} \ln \left| \frac{t^2}{t^2 - a^2} \right| \quad (7.173)$$

Let us integrate the signal  $u(t)$  by frequency domain integration. We get the spectrum of the primary function using the operator  $1/j\omega$ :

$$U_p(\omega) = \frac{1}{j\omega} \frac{1 - \cos(\omega a)}{j\omega} = \frac{-1 + \cos(\omega a)}{\omega^2} \quad (7.174)$$

The primary function of  $u(t)$  is the inverse Fourier transform of Equation 7.174 and has the form of a reverse-signed triangle pulse.

$$-\frac{\alpha}{2} \text{tri}(t) \stackrel{F}{\iff} \frac{-1 + \cos(\omega a)}{\omega^2} \quad (7.175)$$

The signal  $\text{tri}(t)$  is defined in Table 7.1 and its Hilbert transform is

$$-\frac{\alpha}{2} \text{tri}(t) \stackrel{H}{\iff} \frac{1}{2\pi} \left\{ a \ln \left| \frac{t-a}{t+a} \right| + \ln \left| \frac{t^2}{t^2-a^2} \right| \right\} \quad (7.176)$$

### 7.13 Multiplication of Signals with Nonoverlapping Spectra

Consider a signal of the form of the product

$$u(t) = f(t) g(t) \quad (7.177)$$

where

- $f(t)$  is a low-pass signal
- $g(t)$  a high-pass signal

The Fourier spectra of these signals do not overlap; that is, if

$$f(t) \stackrel{F}{\iff} F(\omega) \quad (7.178)$$

$$g(t) \stackrel{F}{\iff} G(\omega) \quad (7.179)$$

then ( $\omega = 2\pi f$ )

$$|F(f)| = 0 \quad \text{for } |f| > W \quad (7.180)$$

$$|G(f)| = 0 \quad \text{for } |f| < W \quad (7.181)$$

as shown in Figure 7.19. In terms of Fourier methods, the Hilbert transform of the product  $u(t) = f(t)g(t)$  may be derived using the *multiplication-convolution theorem* of the form (see also Chapter 2)

$$f(t)g(t) \stackrel{F}{\iff} \int_{-\infty}^{\infty} F(f-u)G(u)du \quad (7.182)$$

The multiplication of the spectrum by  $-j \text{sgn}(f)$  (see Equation 7.12) yields the spectrum of the Hilbert transform

$$H[f(t)g(t)] \stackrel{F}{\iff} j \text{sgn}(f) \int_{-\infty}^{\infty} F(f-u)G(u)du \quad (7.183)$$

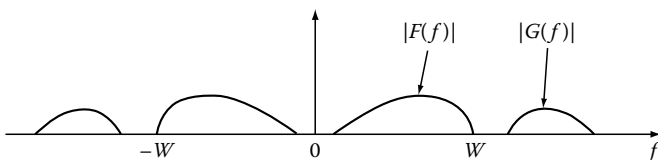


FIGURE 7.19 Nonoverlapping Fourier spectra of two signals.

However, the product  $f(t)H[g(t)]$  and its Fourier transform are

$$f(t)H[g(t)] \stackrel{F}{\iff} \int_{-\infty}^{\infty} F(f-u)[j \text{sgn}(u)G(u)]du \quad (7.184)$$

One can show<sup>4</sup> that the right-hand sides of Equations 7.183 and 7.184 are identical. Therefore, the left-hand sides are identical too, and

$$H[f(t)g(t)] = f(t)H[g(t)] \quad (7.185)$$

This equation presents Bedrosian's theorem: Only the high-pass signal in the product of low-pass and high-pass signals gets Hilbert transformed.<sup>4</sup>

#### Example

Consider a signal in the form of the amplitude-modulated harmonic function:

$$u(t) = A(t) \cos(\Omega t + \Phi); \quad \Omega = 2\pi F \quad (7.186)$$

$$A(t) \stackrel{F}{\iff} C_A(f) \quad (7.187)$$

and the magnitude  $C_A(f)$  is low-pass limited:

$$|C_A(f)| = 0 \quad \text{for } f \geq F \quad (7.188)$$

By using Bedrosian's theorem, we get

$$v(t) = H[u(t)] = A(t) \sin(\Omega t + \Phi) \quad (7.189)$$

Therefore, the amplitude-modulated signal (Equation 7.186) is a real part of the analytic signal:

$$\psi(t) = A(t) e^{j(\Omega t + \Phi)} \quad (7.190)$$

and has a geometrical representation in the form of a phasor of instantaneous amplitude  $A(t)$  and rotating with a constant regular velocity  $\Omega$ . Bedrosian's theorem was extended by Nuttall and Bedrosian<sup>25</sup> to include "frequency-translated" analytic signals. The condition, which applies to vanishing spectra at negative frequencies, can be applied more generally to signals whose Fourier spectra satisfy the condition

$$\begin{aligned} F(\omega) = F[\psi_1(t)] &= 0, & \omega < -a \\ G(\omega) = F[\psi_2(t)] &= 0, & \omega > a \end{aligned} \quad (7.191)$$

where  $a$  is an arbitrary positive constant. The extension of Bedrosian's theorem for multidimensional signals is given in Section 7.23.

## 7.14 Multiplication of Analytic Signals

The Hilbert transform of the analytic signal is given by the formula

$$H[\psi(t)] = H[u(t) + jH[u(t)]] = H[u(t)] - ju(t) = -j\psi(t) \quad (7.192)$$

where the formula  $H[H[u(t)]] = -u(t)$  (iteration) (see Table 7.3) has been applied. The Hilbert transform of the product of two analytic signals is given by the formula

$$H[\psi_1(t) \psi_2(t)] = \psi_1(t)H[\psi_2(t)] = \psi_2(t)H[\psi_1(t)] \quad (7.193)$$

that is, the Hilbert transformation should be applied to *one term of the product only* (to the first or the second).

*Proof* The product of two analytic functions is an analytic function.<sup>39</sup> Therefore, if

$$\psi(t) = \psi_1(t) \psi_2(t) \quad (7.194)$$

where  $\psi_1(t)$  and  $\psi_2(t)$  are analytic signals, then using Equation 7.192, we get

$$H[\psi(t)] = -j\psi(t) = -j\psi_1(t) \psi_2(t) \quad (7.195)$$

However, the operator  $-j$  may be assigned either to  $\psi_1(t)$  or  $\psi_2(t)$ . The application of Equation 7.193 yields two options:

$$H[\psi(t)] = H[\psi_1(t)]\psi_2(t); \quad H[\psi] = \psi_1(t)H[\psi_2(t)] \quad (7.196)$$

Let us apply Equations 7.186 and 7.190 to find the Hilbert transforms of the  $n$ th power of the analytic signal. We get

$$H[\psi^2(t)] = \psi(t)H[\psi(t)] = -j\psi^2(t) \quad (7.197)$$

$$H[\psi^n(t)] = \psi^{n-1}(t)H[\psi(t)] = -j\psi^n(t) \quad (7.198)$$

### Example

Let us find the Hilbert transform of

$$\psi^2(t) = (1 - jt)^{-2} \quad (7.199)$$

The application of Equation 7.192 gives

$$H[\psi(t)] = -j(1 - jt)^{-1} \quad (7.200)$$

and Equation 7.197 yields

$$H[\psi^2(t)] = (1 - jt)^{-1} [-j(1 - jt)^{-1}] = -j(1 - jt)^{-2}$$

Equation 7.192 has a generalized form given by the formula

$$H[\psi(at)] = -j\text{sgn}(a)\psi(at) \quad (7.201)$$

where  $a$  is a real positive or negative constant. The negative sign of  $a$  may be interpreted as time reversal. For example, the Hilbert transform of  $\exp(j\omega t)$  is

$$H(e^{j\omega t}) = -j \text{sgn}(\omega) e^{j\omega t}$$

where  $\omega$  may be positive or negative.

## 7.15 Hilbert Transforms of Bessel Functions of the First Kind

The Bessel functions (see also Chapter 1) are the solution of the second order Bessel differential equation:

$$z^2\psi''(z) + z\psi'(z) + (z^2 - \lambda^2)\psi(z) = 0 \quad (7.202)$$

where  $\psi(z)$  is a complex function of a complex variable  $z = t + j\tau$  and  $\lambda$  is a complex constant. If  $\lambda = n$ , where  $n$  is an integer ( $0, 1, 2, \dots$ ), and  $z = t$ , we get the solution in the form of Bessel functions of the first kind of the order  $n$  denoted  $J_n(t)$ . They find numerous applications in signal and system theory. For example, they are used to calculate the Fourier spectra of frequency modulated signals.

The substitution in Equation 7.202 of a solution in the form of a series  $J_n(t) = \sum_{m=0}^{\infty} a_m x^m$  gives the power series representation

$$J_n(t) = \sum_{k=0}^{\infty} \frac{(-1)^k}{k!(n-k)!} (t/2)^{n+2k}; \quad -\infty < t < \infty \quad (7.203)$$

The computation of the Bessel functions by means of this power series is inconvenient. Due to the truncation of the series at some value of  $k$ , we get divergence for large values of  $t$ . It is possible to apply Equation 7.203 up to  $t < t_1$  and calculate the values for  $t > t_1$  using the asymptotic formula

$$J_n(t) = \frac{2}{\pi t} \sin\left(t - \frac{\pi n}{2} + \frac{\pi}{4}\right) + \frac{r(t)}{t\sqrt{t}} \quad (7.204)$$

The term  $r(t)$  is a limited function for  $t \rightarrow \infty$ . However, it is much *easier* to compute the Bessel functions and its Hilbert transforms using *integral forms*, as described below.

Let us start with the periodic complex function  $\exp(jt \sin(\varphi))$  and its Hilbert transform. We have a Hilbert pair

$$e^{jt \sin(\varphi)} \stackrel{H}{\longleftrightarrow} H[e^{jt \sin(\varphi)}] = -j \text{sgn}[\sin(\varphi)] e^{jt \sin(\varphi)} \quad (7.205)$$

The Fourier series expansion of the left-hand side is

$$e^{jt \sin(\varphi)} = \sum_{n=-\infty}^{\infty} J_n(t) e^{jn\varphi} \quad (7.206)$$

The Bessel functions, i.e., the coefficients of this series, are given by the integral

$$J_n(t) = \frac{1}{2\pi} \int_{-\pi}^{\pi} e^{j(t \sin(\varphi) - n\varphi)} d\varphi \quad (7.207)$$

The odd-ordered Bessel functions are odd functions of the argument  $t$ , while the even-ordered are even functions and

$$J_{-n}(t) = (-1)^n J_n(t) \quad (7.208)$$

In fact, the integral of the imaginary part of Equation 7.207 equals zero, and due to the evenness of the real part of the integrand, we have

$$J_n(t) = \frac{1}{\pi} \int_0^{\pi} \cos [t \sin(\varphi) - n\varphi] d\varphi \quad (7.209)$$

This formula enables very efficient calculation of Bessel functions  $J_n(t)$  using numerical integration. The number of integration steps may be halved using two separate integrals:

$$J_{2n}(t) = \frac{2}{\pi} \int_0^{\pi/2} \cos [t \sin(\varphi)] \cos(2n\varphi) d\varphi \quad (7.210)$$

$$J_{2n+1}(t) = \frac{2}{\pi} \int_0^{\pi/2} \sin [t \sin(\varphi)] \sin[(2n+1)\varphi] d\varphi \quad (7.211)$$

The real part of the Fourier series (Equation 7.206) is

$$\cos [t \sin(\varphi)] = J_0(t) + 2 \sum_{n=1}^{\infty} J_{2n}(t) \cos(2n\varphi) \quad (7.212)$$

and the imaginary part is

$$\sin [t \sin(\varphi)] = 2 \sum_{n=1}^{\infty} J_{2n-1}(t) \sin[(2n-1)\varphi] \quad (7.213)$$

Inserting  $\varphi = \pi/2$  gives the well-known formulae

$$\cos(t) = J_0(t) - 2J_2(t) + 2J_4(t) - \dots \quad (7.214)$$

$$\sin(t) = 2J_1(t) - 2J_3(t) + \dots \quad (7.215)$$

The following recursion formula is very useful

$$(2n/t)J_n(t) = J_{n-1}(t) + J_{n+1}(t) \quad (7.216)$$

The derivative of a Bessel function is also given by the recursion formula

$$2j_n(t) = J_{n-1}(t) - J_{n+1}(t) \quad (7.217)$$

For example

$$j_0(t) = 0.5[J_{-1}(t) - J_1(t)] = -J_1(t) \quad (7.218)$$

(we used Equation 7.218).

The left-hand side of Equation 7.205 was expanded in the Fourier series (Equation 7.206). Similarly, due to the linearity of the Hilbert transformation, the right-hand side may be expanded in the Fourier series

$$H[e^{jt \sin \varphi}] = -j \operatorname{sgn}(\varphi) e^{jt \sin \varphi} = \sum_{n=-\infty}^{\infty} \hat{J}_n(t) e^{jn\varphi} \quad (7.219)$$

where  $\hat{J}_n(t) = H[J_n(t)]$  are the Hilbert transforms of the Bessel functions. For these functions we have the relation

$$\hat{J}_{-n}(t) = (-1)^{n+1} \hat{J}_n(t) \quad (7.220)$$

because the Hilbert transforms of odd functions are even, and vice versa (compared with Equation 7.208). The functions  $\hat{J}_n(t)$ , i.e., the coefficients of the Fourier series (Equation 7.219), are given by the integral

$$\hat{J}_n(t) = \frac{1}{2\pi} \int_{-\pi}^{\pi} H[e^{j(t \sin \varphi - n\varphi)}] d\varphi \quad (7.221)$$

As in Equation 7.207, the integral of the imaginary part equals zero and due to the evenness of the real part, we have

$$\hat{J}_n(t) = \frac{1}{\pi} \int_0^{\pi} \sin [t \sin \varphi - n\varphi] d\varphi \quad (7.222)$$

Notice that the integrand is even because it is multiplied by  $\operatorname{sgn}(\varphi)$  (see Equation 7.219). As before, using numerical integration, the Hilbert transforms of the Bessel functions can be easily computed. The first five Bessel functions and their Hilbert transforms computed using Equations 7.219 and 7.222 are shown in Figure 7.20a and b.

Let us derive the Hilbert transforms of the Bessel functions  $J_n(t)$  using Fourier transforms. The Fourier transform of the function  $J_0(t)$  is

$$J_0(t) \stackrel{F}{\iff} C_0(f) = \begin{cases} \frac{2}{(1-\omega^2)^{0.5}} & \text{for } |\omega| < 1 \\ 0 & \text{for } |\omega| > 1 \end{cases} \quad (7.223)$$

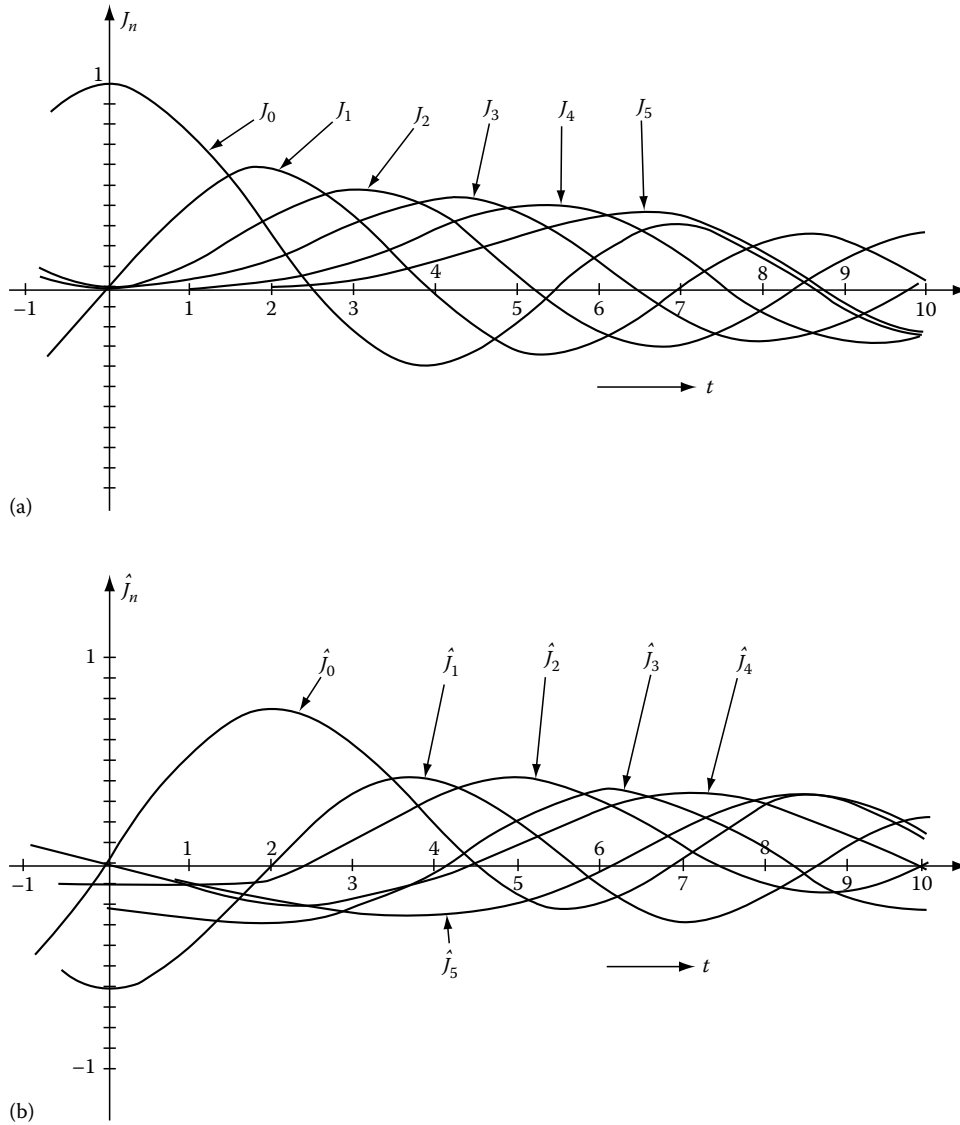


FIGURE 7.20 (a) Waveforms of the first five Bessel functions  $J_n(t)$ . (b) Waveforms of the corresponding Hilbert transforms.

*Proof* Let us find the inverse transform of this spectrum:

$$\begin{aligned}
 J_0(t) &= \frac{1}{2\pi} \int_{-1}^1 \frac{2}{(1-\omega^2)^{0.5}} \cos(\omega t) d\omega = \left\{ \begin{array}{l} \omega = \sin(\varphi) \\ d\omega = \cos(\varphi) d\varphi \end{array} \right\} \\
 &= \frac{1}{\pi} \int_0^\pi \cos[t \sin \varphi] d\varphi \tag{7.224}
 \end{aligned}$$

(See Equation 7.209) The Fourier transforms of higher-order Bessel functions can be calculated using the recursion formula (Equation 7.217) and frequency domain differentiation. We have

$$J_{n+1}(t) = J_{n-1}(t) - 2\dot{J}_n(t) \tag{7.225}$$

obtaining the following Fourier parts

$$J_0(t) \stackrel{F}{\iff} C_0(f) = \frac{2}{(1-\omega^2)^{0.5}} \tag{7.226}$$

$$J_1(t) = -\dot{J}_0(t) \stackrel{F}{\iff} -j\omega C_0(f) \tag{7.227}$$

$$J_2(t) = -J_0(t) - 2\dot{J}_1(t) \stackrel{F}{\iff} C_0(f) - 2j\omega C_1(f) \tag{7.228}$$

Successive application of the recurrency gives the Fourier spectra of the Bessel functions  $J_n(t)$  tabulated in Table 7.7. We find that

$$\dot{J}_n(t) \stackrel{F}{\iff} C_n(f) = (-j)^n 2^{n-1} T_n(t) C_0(f) \tag{7.229}$$

where  $C_0(f)$  is defined by Equation 7.226 and  $T_n(t)$  is a Chebyshev polynomial defined by the formula

**TABLE 7.7** Fourier and Hilbert Transforms of Bessel Functions of the First Kind

Bessel Function	Fourier Transform	Hilbert Transform
$J_n(t)$	$C_n(f)$	$\hat{J}_n(t) = H[J_n(t)]$
$J_0(t)$	$C_0 = \frac{2}{(1 - \omega^2)^{0.5}}; \quad  \omega  < 1$ $= 0; \quad  \omega  > 0$	$\frac{1}{\pi} \int_0^1 C_0(f) \sin(\omega t) d\omega$
$J_1(t)$	$C_1 = -j\omega C_0$	$-\frac{1}{\pi} \int_0^1  C_1(f)  \cos(\omega t) d\omega$
$J_2(t)$	$C_2 = -(2\omega^2 - 1)C_0$	$-\frac{1}{\pi} \int_0^1  C_2(f)  \sin(\omega t) d\omega$
$J_3(t)$	$C_3 = j(4\omega^3 - 3\omega)C_0$	$\frac{1}{\pi} \int_0^1  C_3(f)  \cos(\omega t) d\omega$
$J_4(t)$	$C_4 = (8\omega^4 - 8\omega^2 + 1)C_0$	$\frac{1}{\pi} \int_0^1  C_4(f)  \sin(\omega t) d\omega$
$J_5(t)$	$C_5 = -j(16\omega^5 - 20\omega^3 + 5\omega)C_0$	$-\frac{1}{\pi} \int_0^1  C_5(f)  \cos(\omega t) d\omega$
$J_6(t)$	$C_6 = -(32\omega^6 - 48\omega^4 + 18\omega^2 - 1)C_0$	$-\frac{1}{\pi} \int_0^1  C_6(f)  \sin(\omega t) d\omega$
$J_n(t)$	$C_n = (-j)^n 2^{n-1} T_n(\omega) C_0$	$\frac{(-1)^{n/2}}{\pi} \int_0^1  C_n(f)  \sin(\omega t) d\omega$ for $n = 0, 2, 4, \dots$ $\frac{(-1)^{(n+1/2)}}{\pi} \int_0^1  C_n(f)  \cos(\omega t) d\omega$ for $n = 1, 3, 5, \dots$

Note:  $T_n(\omega) = \cos[n \cos^{-1}(\omega)]$  is the Chebyshev polynomial.

$$T_n(t) = \cos [n \cos^{-1} (t)]; \quad n = 0, 1, 2, \dots \quad (7.230)$$

A recursion formula can be applied

$$T_{n+1}(t) - 2t T_n(t) + T_{n-1}(t) = 0; \quad n = 1, 2, \dots \quad (7.231)$$

Because we derived the analytical expressions for the Fourier images of the Bessel functions, the use of inverse Fourier transformations enables the evaluation of either the Bessel function  $J_n(t)$  or its Hilbert transform  $\hat{J}_n(t)$ . For example

$$J_0(t) = \frac{1}{\pi} \int_0^1 \frac{2}{(1 - \omega^2)^{0.5}} \cos(\omega t) d\omega \quad (7.232)$$

and the Hilbert transform is

$$\hat{J}_0(t) = H[J_0(t)] = \frac{1}{\pi} \int_0^1 \frac{2}{(1 - \omega^2)^{0.5}} \sin(\omega t) d\omega \quad (7.233)$$

Hence, we have an analytic signal

$$\psi_0(t) = J_0(t) + j\hat{J}_0(t) \quad (7.234)$$

Equations 7.232 and 7.233 may be regarded as alternative definitions of the Bessel functions  $J_0(t)$  and  $\hat{J}_0(t)$ . However, the computation by means of the integrals (7.209 and 7.210) ( $n = 0$ ) gives much better accuracy with a given number of integration steps.

The expressions for the Fourier images of Bessel functions and their Hilbert transforms derived using these images are listed in Table 7.7. If needed, the Fourier spectra enable the derivation of the coefficients of the power series representation of  $J_n(t)$  and  $\hat{J}_n(t)$ . Starting with the power series for  $J_n(t)$  given by Equation 7.203, let us derive the power series for  $\hat{J}_n(t)$ . We start with the expression defining the Taylor series

$$\hat{J}_n(t) = \sum_{n=0}^{\infty} \frac{\hat{J}_n^{(n)}(t=0)}{n!} \quad (7.235)$$

The derivatives  $\hat{J}_n^{(n)}(t) (t = 0)$  can be obtained by differentiation of the integrand of the integrals listed in Table 7.7. By inserting  $t = 0$ , we obtain

$$\begin{aligned} \hat{J}_0(0) &= \frac{1}{\pi} \int_0^1 \frac{2d\omega}{(1 - \omega^2)^{0.5}} \sin(0) = 0 \\ \hat{J}_0^{(1)}(0) &= \frac{1}{\pi} \int_0^1 \frac{2\omega d\omega}{(1 - \omega^2)^{0.5}} \cos(0) = \frac{2}{\pi} \\ \hat{J}_0^{(2)}(0) &= -\frac{1}{\pi} \int_0^1 \frac{2\omega^2 d\omega}{(1 - \omega^2)^{0.5}} \sin(0) = 0 \\ \hat{J}_0^{(3)}(0) &= -\frac{1}{\pi} \int_0^1 \frac{2\omega^3 d\omega}{(1 - \omega^2)^{0.5}} \cos(0) = \frac{-4}{3\pi} \end{aligned} \quad (7.236)$$

where (1), (2), ... denote the order of the derivative. Continuing the differentiation using Equation 7.235, we get the following power series:

$$\hat{j}_0(t) = \frac{2}{\pi} \left[ t - \frac{1}{9}t^3 + \frac{1}{225}t^5 - \frac{2}{33075}t^7 + \dots + \frac{(-1)^{(3+n)/2}2^{n-2}}{n!(1.3.5..n)}t^n + \dots \right] \quad (7.237)$$

In the same way one can derive the power series of higher order Hilbert transforms of the Bessel functions.

### 7.16 Instantaneous Amplitude, Complex Phase, and Complex Frequency of Analytic Signals

Signal theory needs precise definitions of various quantities such as the *instantaneous amplitude*, *instantaneous phase*, and *instantaneous frequency* if a given signal and many other quantities. Let us recall that *neither definition is true or false*. If we define something, we simply propose to make an *agreement* to use a specific name in the sense of the definition. When using this name, for instance, "instantaneous frequency," we should never forget what we have defined. The history of signal theory contains examples of misunderstanding when various authors applied the same name, instantaneous frequency, to different definitions and then tried to discuss which is true or false. Such a discussion is *meaningless*. Of course, one may discuss which definition has advantages or disadvantages from a specific point of view or whether it is compatible with other definitions or existing knowledge. The notions of the instantaneous amplitude, instantaneous phase, and instantaneous frequency of the analytic signal  $\psi(t) = u(t) + jv(t)$  may be uniquely and conveniently defined introducing the notion of a phasor rotating in the Cartesian  $(u, v)$  plane, as shown in Figure 7.21. The change of coordinates from rectangular  $(u, v)$  to polar  $(A, \varphi)$  gives

$$u(t) = A(t) \cos[\varphi(t)] \quad (7.238)$$

$$v(t) = A(t) \sin[\varphi(t)] \quad (7.239)$$

$$\psi(t) = A(t)e^{j\varphi(t)} \quad (7.240)$$

We define the instantaneous amplitude of the analytic signal equal to the length of the phasor (radius vector)  $A$ :

$$A(t) = \sqrt{u^2(t) + v^2(t)} \quad (7.241)$$

and define the instantaneous phase of the analytic signal equal to the instantaneous angle

$$\varphi(t) = \text{Tan}^{-1} \frac{v(t)}{u(t)} \quad (7.242)$$

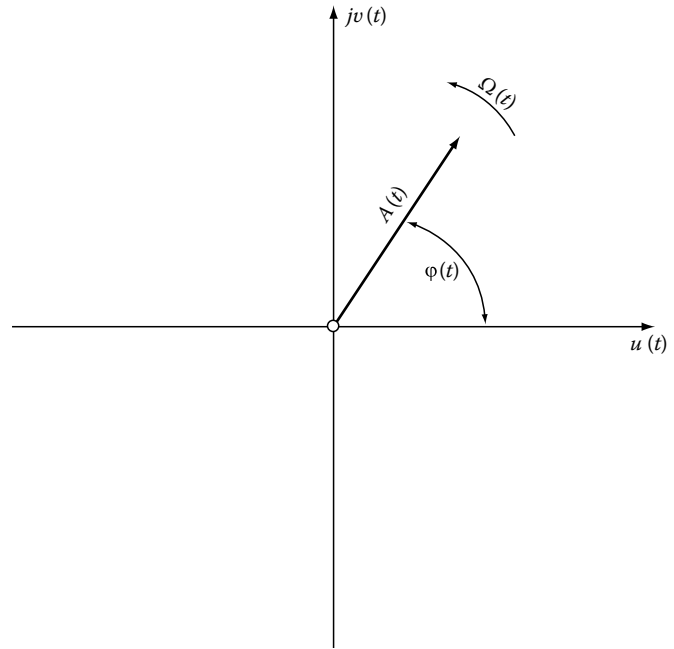


FIGURE 7.21 A phasor in the Cartesian  $(u, v)$  plane representing the analytic signal  $\psi(t) = u(t) + jv(t) = A(t)e^{j\varphi(t)}$ .

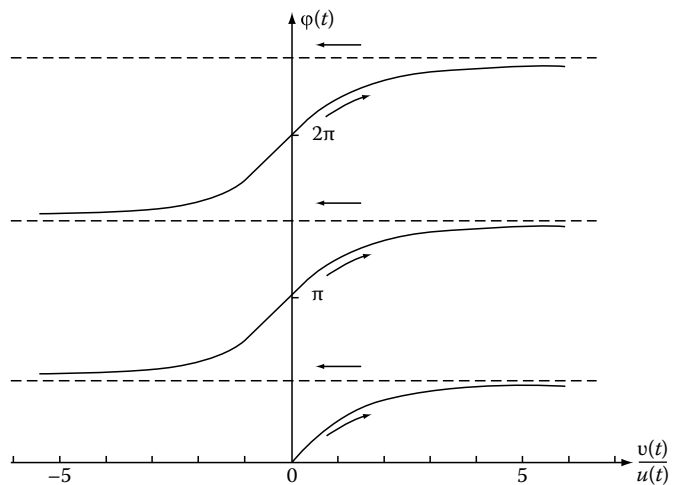


FIGURE 7.22 The multibranch function  $\varphi(t) = \tan^{-1}[v(t)/u(t)]$ . As time elapses (arrows) they are jumps from one branch to a next branch.

The notation with capital  $T$  indicates the multibranch character of the  $\text{Tan}^{-1}$  function, as shown in Figure 7.22. As times elapses, the phasor rotates in the  $(u, v)$  plane and its instantaneous angular speed defines the *instantaneous angular frequency* of the analytic signal given by the time derivative

$$\dot{\varphi}(t) = \Omega(t) = 2\pi F(t) \quad (7.243)$$

or

$$\Omega(t) = \frac{d}{dt} \tan^{-1} \frac{v(t)}{u(t)} = \frac{u(t)v'(t) - v(t)u'(t)}{u^2(t) + v^2(t)} \quad (7.244)$$

Notice the anticlock direction of rotation for positive angular frequencies. The instantaneous frequency is defined by the formula

$$F(t) = \frac{\Omega(t)}{2\pi} = \frac{1}{2\pi} \dot{\phi}(t) \quad (7.245)$$

Summarizing, using the notion of the analytic signal, we defined the instantaneous amplitude, phase, and frequency. A number of different definitions of the notion of instantaneous amplitude, phase, and frequency have developed over the years. There are many pairs of functions  $A(t)$  and  $\phi(t)$ , which inserted into Equation 7.238 reconstruct a given signal  $u(t)$ , for example, functions defining a phasor in the phase plane  $[u(t), \dot{u}(t)]$ . But only the analytic signal has the unique feature of having a one-sided Fourier spectrum. Let us recall that a real signal and its Hilbert transform are given in terms of analytic signals by Equations 7.30 and 7.31 (see Section 7.3). Figure 7.23 shows the geometrical representation of these formulae in the form of two phasors of a length  $0.5 A(t)$  and opposite direction of rotation, positive for  $\psi(t)$  and negative for  $\psi^*(t)$ . Equation 7.242 defines the instantaneous frequency of a signal regardless of the bandwidth. It is sometimes believed that the notion of instantaneous frequency has a physical meaning only for narrow-band signals (high-frequency [HF]-modulated signals). However, using adders, multipliers, dividers, Hilbert filters, and differentiators, it is possible to implement a frequency demodulator used for wide-band signals, for example, speech signals, the algorithm defined by Equation 7.244. Modern VLSI enables efficient implementation of such frequency demodulators at reasonable cost.

### 7.16.1 Instantaneous Complex Phase and Complex Frequency

Signal and systems theory widely uses the Laplace transformation of a real signal  $u(t)$  of the form

$$U(s) = \int_0^{\infty} u(t)e^{-st} dt \quad (7.246)$$

where

$$s = \alpha + j\omega; \quad \omega = 2\pi f$$

is a time-independent complex frequency ( $\alpha$  and  $\omega$  are real). The exponential kernel  $e^{-st}$  has the form of a harmonic wave with an exponentially decaying amplitude; that is, its instantaneous amplitude is

$$A(t) = e^{-\alpha t} \quad (7.247)$$

The notion of the complex frequency has been generalized by this author in 1964 defining a complex instantaneous variable frequency using the notion of the analytic signal.<sup>12</sup> It is convenient to define the *instantaneous complex frequency* as the time derivative of a complex phase. The instantaneous complex phase of the analytic signal  $\psi(t)$  is defined by the formula

$$\Phi_c(t) = \text{Ln}[\psi(t)] \quad (7.248)$$

Capital L denotes the multibranch character of the logarithmic function of the complex function  $\psi(t)$ . The insertion of the polar form of the analytic signal (see Equation 7.240) yields

$$\Phi_c(t) = \text{Ln}[A(t)] + j\phi(t) \quad (7.249)$$

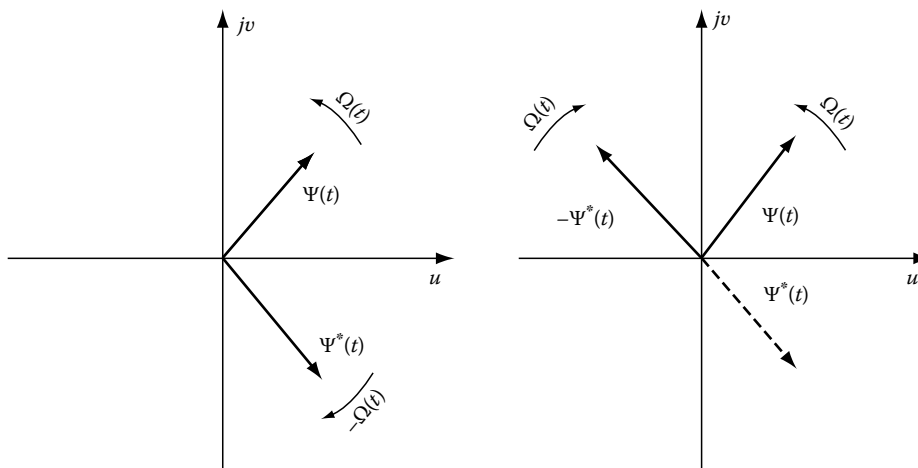


FIGURE 7.23 A pair of conjugate phasors representing the Equations 7.2.17 and 7.2.18.



The instantaneous complex frequency is defined by the derivative

$$s(t) = \dot{\Phi}_c(t) = \frac{\dot{A}(t)}{A(t)} + j\omega(t) \quad (7.250)$$

or

$$s(t) = \alpha(t) + j\omega(t) \quad (7.251)$$

where

$$\alpha(t) = \frac{\dot{A}(t)}{A(t)} \quad (7.252)$$

is the instantaneous radial frequency (a measure of the radial velocity representing the speed of changes of the radius or amplitude of the phasor), and

$$\omega(t) = \dot{\varphi}(t) \quad (7.253)$$

is the instantaneous angular frequency. Equation 7.252 has the form of a first-order differential equation. The solution of this equation yields the following form of the instantaneous amplitude

$$A(t) = A_0 e^{\int_0^t \alpha(t) dt} \quad (7.254)$$

$A_0$  is the value of the amplitude at the moment  $t=0$ . Let us introduce the notation

$$\beta(t) = \int_0^t \alpha(t) dt \quad (7.255)$$

Using this notation the complex phase can be written as

$$\Phi_c(t) = \ln A_0 + \beta(t) + j\varphi(t) \quad (7.256)$$

or

$$\Phi_c(t) = \ln A_0 + \int_0^t s(t) dt + j\Phi_0 \quad (7.257)$$

$\Phi_0$  is the integration constant or the angular position of the phasor at  $t=0$ . The introduction of the concept of a complex constant  $\psi_0 = A_0 e^{j\Phi_0}$  gives the following form of the analytic signal

$$\Psi(t) = \psi_0 e^{\int_0^t s(t) dt} \quad (7.258)$$

## Examples

1. Consider the analytic signal given by Equation 7.76:

$$\psi_\delta(t) = \frac{\alpha}{\pi(\alpha^2 + t^2)} + j \frac{t}{\pi(\alpha^2 + t^2)} \quad (7.259)$$

$\underbrace{\hspace{1.5cm}}_{u(t)} \quad \underbrace{\hspace{1.5cm}}_{v(t)}$

The polar form of this signal is

$$\psi_\delta(t) = \frac{1}{\pi \sqrt{\alpha^2 + t^2}} \exp \left[ j \underbrace{\tan^{-1}(t/\alpha)}_{\varphi(t)} \right] \quad (7.260)$$

Therefore, the instantaneous complex phase is

$$\Phi_c(t) = \ln \left\{ \frac{1}{\pi \sqrt{\alpha^2 + t^2}} \right\} + j \underbrace{\tan^{-1}(t/\alpha)}_{\varphi(t)} \quad (7.261)$$

$\underbrace{\hspace{1.5cm}}_{\beta(t)}$

and the instantaneous complex frequency is

$$s(t) = \dot{\Phi}_c(t) = \frac{-t}{\alpha^2 + t^2} + j \frac{\alpha}{\alpha^2 + t^2} \quad (7.262)$$

$\underbrace{\hspace{1.5cm}}_{\alpha(t)} \quad \underbrace{\hspace{1.5cm}}_{\omega(t)}$

Because in the limit  $\alpha \Rightarrow 0$  the signal (Equation 7.253) approximates the complex delta distribution (see Equation 7.64), the instantaneous complex phase of this distribution is

$$\Phi_{c\delta}(t) = \ln \frac{1}{\pi |t|} + j \underbrace{0.5\pi \operatorname{sgn}(t)}_{\varphi(t)} \quad (7.263)$$

$\underbrace{\hspace{1.5cm}}_{A(t)}$

and the complex frequency is

$$s_\delta(t) = \frac{-1}{t} + j \underbrace{\pi \delta(t)}_{\omega(t)} \quad (7.264)$$

$\underbrace{\hspace{1.5cm}}_{\alpha(t)}$

2. Consider the analytic signal

$$\psi(t) = \frac{\sin(at)}{at} + j \frac{\sin^2(0.5at)}{0.5at} \quad (7.265)$$

$\underbrace{\hspace{1.5cm}}_{u(t)} \quad \underbrace{\hspace{1.5cm}}_{v(t)}$

where  $u(t)$  is the well-known interpolating function of the sampling theory. Equations 7.241 and 7.242 yield, using trigonometric relations, the polar form of this signal:

$$\psi(t) = \frac{\sin(0.5at)}{0.5at} \exp \left( j \underbrace{at/2}_{\varphi(t)} \right) \quad (7.266)$$

$\underbrace{\hspace{1.5cm}}_{A(t)}$

Therefore, the instantaneous complex phase is

$$\psi_c(t) = \text{Ln} \underbrace{\left[ \frac{\sin(0.5at)}{0.5at} \right]}_{A(t)} + jat/2 \quad (7.267)$$

and the instantaneous complex frequency

$$s(t) = \frac{a}{2} \cot(0.5at) - \frac{1}{t} + j\frac{a}{2} \quad (7.268)$$

In conclusion, the interpolating function may be regarded as a signal of a variable amplitude and a constant angular frequency  $\omega = a/2$ .

- The classic complex notation of a frequency- or phase-modulated signal (Carson and Fry, 1937) has the form<sup>41</sup>

$$\psi(t) = A_0 e^{j[\Omega_0 t + \Phi_0 + \varphi(t)]}; \quad \Omega_0 = 2\pi F_0 \quad (7.269)$$

where  $\varphi(t)$  represents the angle modulation. The whole argument of the exponential function  $\Phi(t) = \Omega_0 t + \Phi_0 + \varphi(t)$  defines the instantaneous phase and its derivative, the instantaneous frequency

$$F(t) = \frac{1}{2\pi} \frac{d\Phi}{dt} = F_0 + \frac{1}{2\pi} \frac{d\varphi}{dt} \quad (7.270)$$

The signal (Equation 7.269) is represented by a phasor in the plane  $(\cos[\Phi(t)], \sin[\Phi(t)])$ , as shown in Figure 7.24. These definitions of the instantaneous phase and frequency differ from the definition using the analytic signal that is represented by a phasor in the  $(\cos[\Phi(t)],$

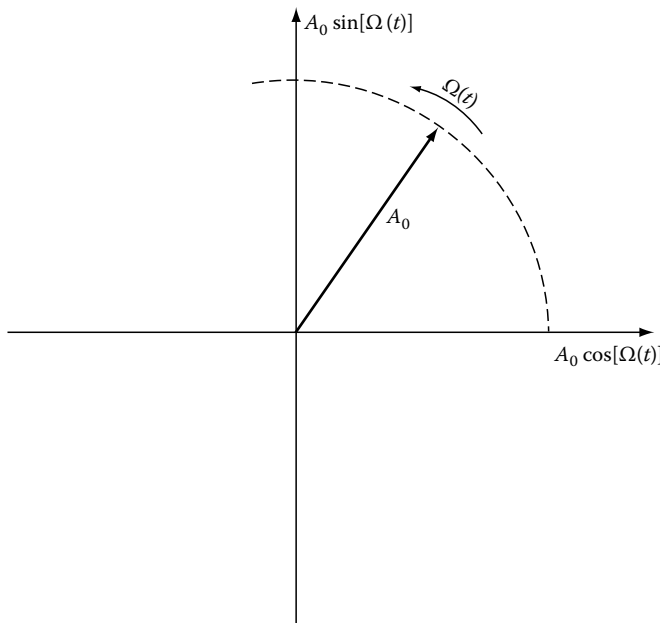


FIGURE 7.24 A phasor representing a frequency (or phase) modulated signal.

$H(\cos[\Phi(t)])$  plane, because  $\sin[\Phi(t)]$  is not the Hilbert transform of  $\cos[\Phi(t)]$  and the signal (7.269) is not an analytic function. However, it may be nearly analytic if the carrier frequency is large. If the spectra of the functions  $\cos[\varphi(t)]$  and  $\sin[\varphi(t)]$  have a limited low-pass support of a highest frequency  $|W| < |F_0|$ , then Bedrosian's theorem (see Section 7.13) may be applied and

$$\begin{aligned} H\{\cos[\Omega_0 t + \Phi_0 + \varphi(t)]\} &= \cos[\varphi(t)]H[\cos(\Omega_0 t + \Phi_0)] \\ &\quad - \sin[\varphi(t)]H[\sin(\Omega_0 t + \Phi_0)] \\ &= \sin[\Omega_0 t + \Phi_0 + \varphi(t)] \end{aligned} \quad (7.271)$$

In the case of harmonic modulation with  $\varphi(t) = \beta \sin(\omega t)$ , where  $\beta$  is the modulation index, the spectra of the function  $\cos[\varphi(t)]$  and  $\sin[\varphi(t)]$  are given by the Fourier series

$$\cos[\beta \sin(\omega t)] = J_0(\beta) + 2 \sum_{n=1}^{\infty} J_{2n}(\beta) \cos(2n\omega t) \quad (7.272)$$

$$\sin[\beta \sin(\omega t)] = 2 \sum_{n=1}^{\infty} J_{2n-1}(\beta) \sin[(2n-1)\omega t] \quad (7.273)$$

and this is not a pair of Hilbert transforms (see Section 7.7). Although the number of terms of the series is infinite, the number of significant terms is limited and for a good approximation Bedrosian's theorem may be applied for large values of  $F_0$ . Further comments are given in Reference 25.

## 7.17 Hilbert Transforms in Modulation Theory

This section is devoted to the theory of analog modulation of a harmonic carrier  $u_c(t) = A_0 \cos(2\pi F_0 t + \Phi_0)$  with emphasis on the role of Hilbert transformation, analytic signals, and complex frequencies. The theory of amplitude and angle modulation is mentioned briefly in favor of a more detailed description of the theory of single side-band (SSB) modulations. The last are conveniently defined using Hilbert transforms. Many modulators are implemented using Hilbert filters, mostly digital filters, because nowadays modulated signals can be conveniently generated digitally and converted into analog signals.

### 7.17.1 Concept of the Modulation Function of a Harmonic Carrier

The complex notation of signals is widely used in modern modulation theory. The harmonic carrier is written in the form of the analytic signal

$$\psi_c(t) = A_0 e^{j(\Omega_0 t + \Phi_0)} \quad (7.274)$$

Analog modulation is the operation of continuous change of one or more of the three parameters of the carrier: the amplitude  $A_0$ ,

the frequency  $F_0$ , or the phase  $\Phi_0$ , resulting in amplitude, frequency, or phase modulation. The complex-modulated signal has a convenient representation in the form of a product<sup>3</sup>

$$\psi(t) = \gamma(t)\psi_c(t) = A_0\gamma(t)e^{j(\Omega_0 t + \Phi_0)} \quad (7.275)$$

The function  $\gamma(t)$  is called the *modulation function*. It is a function of the modulating signal (the message)  $x(t)$ , that is,  $\gamma(t) = \gamma[x(t)]$ . Any kind of modulation, for example, amplitude, frequency, or phase modulation, is represented by a specific real or complex modulation function. We shall investigate models of modulating signals for which the Fourier transform exists and is given by the Fourier pair

$$x(t) \stackrel{F}{\iff} X(\omega); \quad \omega = 2\pi f \quad (7.276)$$

The frequency band containing the terms of the spectrum  $X(\omega)$  is called the *baseband*. In general, the modulation function is a nonlinear function of the variable  $x$ , and the spectrum of the modulation function differs from  $X(\omega)$  and is represented by the Fourier pair:

$$\gamma(t) \stackrel{F}{\iff} \Gamma(\omega) \quad (7.277)$$

The nonlinear transformations of the spectrum may have a complicated analytic representation. Usually only approximate determination of the spectrum is possible. The approximations are easier to perform if the energy of the modulating signal is nonuniformly distributed and concentrated in the low-frequency part of the baseband, for example, the energy of voice, music, or TV signals. Usually it is possible to find the terms of  $\Gamma(\omega)$  for harmonic modulating signals. In special cases, if the modulation function is proportional to the message, that is,  $\gamma(t) = mx(t)$  ( $m$  is a constant), we have

$$\Gamma(f) = mX(f) \quad (7.278)$$

The initial phase of the carrier  $\Phi_0$  is of importance only if we deal with two or more modulated carriers of the same frequency, for example, by summation or multiplication of modulated signals. It is convenient to write the modulated signal in the form

$$\psi(t) = A_0\gamma(t)e^{j\Phi_0}e^{j\Omega_0 t} \quad (7.279)$$

and define a *modified modulation function* in the form of the product

$$\gamma_1(t) = \gamma(t)e^{j\Phi_0} \quad (7.280)$$

The new Fourier spectrum is

$$\gamma_1(t) \stackrel{F}{\iff} \Gamma_1(\omega) = \Gamma(\omega)e^{j\Phi_0} \quad (7.281)$$

We observe that the spectra, in Equations 7.277 and 7.281, have the same magnitude and differ only by the phase relations.

Notice that the spectrum  $\Gamma_1(\omega)$  is defined at zero carrier frequency and the spectrum of the modulated signal is obtained by shifting this spectrum from zero to carrier frequency by the Fourier shift operator  $e^{j\Omega_0 t}$ . This approach enables us to study the spectra of modulated signals at zero carrier frequency.

Examples of modulation functions:

The modulation function for a linear full-carrier AM has the form

$$\gamma(t) = 1 + mx(t); \quad |mx(t)| < 1 \quad (7.282)$$

The number 1 represents the carrier term. Therefore, the modulation function for balanced modulation (suppressed carrier) has the simple form

$$\gamma(t) = mx(t) \quad (7.283)$$

Therefore, the spectra of the message and of the modulation function are to within the scale factor  $m$ , the same. The message may be written in the form (see Equation 7.30)

$$x(t) = \frac{\psi_x(t) + \psi_x^*(t)}{2} \quad (7.284)$$

This formula shows that the upper sideband of the AM signal is represented by the analytic signal  $\psi_x(t)$  of a one-sided spectrum at positive frequencies and the lower sideband by the conjugate analytic signal  $\psi_x^*(t)$  of a one-sided spectrum at negative frequencies. The sidebands have the geometric form of two conjugate phasors (see Figure 7.23). The instantaneous amplitude of the phasors is

$$A(t) = \frac{m}{2} |\psi_x(t)| = \frac{m}{2} \sqrt{x^2(t) + (\hat{x}(t))^2} \quad (7.285)$$

( $\hat{x}(t) = H[x(t)]$ ) and the instantaneous angular frequency is

$$\omega_x(t) = \pm \frac{d}{dt} \tan^{-1} \left[ \frac{\hat{x}(t)}{x(t)} \right] \quad (7.286)$$

Therefore, a SSB represents a signal with simultaneous amplitude and phase modulation. The multiplication of  $\psi_x(t)$  or  $\psi_x^*(t)$  with the complex carrier (Fourier shift operator)  $e^{j\Omega_0 t}$  yields the high-frequency analytic signals. The upper sideband ( $\Phi_0 = 0$ ) is (with  $mA_0 = 2$ )

$$\psi_{\text{upper}}(t) = \psi_x(t)e^{j\Omega_0 t} \quad (7.287)$$

with the modulation function  $\psi_x(t)$ , and the lower sideband is

$$\psi(t) = \psi_x^*(t)e^{j\Omega_0 t} \quad (7.288)$$

with the conjugate modulation function  $\psi_x^*(t)$ . The above signals represent the complex form of SSB AM. The real notation of these signals is

$$u_{SSB}(t) = x(t) \cos(\Omega_0 t) \mp \hat{x}(t) \sin(\Omega_0 t) \quad (7.289)$$

with the minus sign for the upper sideband and plus sign for the lower one. The products  $x(t) \cos(\Omega_0 t)$  and  $\hat{x}(t) \sin(\Omega_0 t)$  represent double side-band (DSB) compressed carrier AM signals. Therefore, an SSB modulator may be implemented, as shown in Figure 7.25.

The *angle modulation* is represented by the exponential modulation function of the form

$$\gamma(t) = e^{j\varphi[x(t)]} \quad (7.290)$$

Therefore, the complex signal representation of the angle modulation has the form

$$\Psi(t) = A_0 e^{j[\Omega_0 t + \varphi(t)]} \quad (7.291)$$

where  $\varphi$  is a function of the modulating signal  $x(t)$ . In general, this complex signal may be only approximately analytic (see Section 7.16, Example 3). In the case of a linear phase modulation, the modulation function has the form

$$\gamma(t) = e^{jmx(t)} \quad (7.292)$$

and for the linear frequency modulation

$$\gamma(t) = e^{jm \int_{-\infty}^t x(t) dt} \quad (7.293)$$

The Fourier spectrum of the modulation function is given by the integral

$$\Gamma(\omega) = \int_{-\infty}^{\infty} e^{j\varphi[x(t)]} e^{-j\omega t} dt \quad (7.294)$$

If for a specific function  $\varphi[x(t)]$  the closed form of this integral does not exist, a numerical integration may be applied. In the simplest case of linear phase modulation with a harmonic modulating signal the modulation function (Equation 7.292) has the form

$$\gamma(t) = e^{j\beta \sin(\omega_0 t)} \quad (7.295)$$

where  $\beta$  is the modulation index (in radians). The Fourier series expansion of this complex periodic function has the form:

$$\begin{aligned} \gamma(t) = & J_0(\beta) + \sum_{n=1}^{\infty} J_{2n}(\beta) \cos(2n\omega_0 t) \\ & + \sum_{n=1}^{\infty} J_{2n-1}(\beta) \sin[(2n-1)\omega_0 t] \end{aligned} \quad (7.296)$$

Using Euler's formulae (see Equations 7.32 and 7.33), this modulation function becomes

$$\begin{aligned} \gamma(t) = & J_0(\beta) + \sum_{n=1}^{\infty} J_{2n}(\beta) \left[ \frac{e^{j2n\omega_0 t} + e^{-j2n\omega_0 t}}{2} \right] \\ & + \sum_{n=1}^{\infty} J_{2n-1}(\beta) \left[ \frac{e^{j(2n-1)\omega_0 t} - e^{-j(2n-1)\omega_0 t}}{2} \right] \end{aligned} \quad (7.297)$$

Because the exponentials in the time domain are represented by delta functions in the frequency domain ( $e^{\pm jn\omega_0 t} \Leftrightarrow \delta(f \mp nf_0)$ ), the spectrum of the modulation function (zero carrier frequency) has the form shown in Figure 7.26 ( $\beta = 4$ ).

### 7.17.2 Generalized Single Side-Band Modulations

The SSB AM signal defined by Equations 7.287 and 7.288 is an example of many other possible SSB modulations. Any kind of modulation of a harmonic carrier is called SSB modulation if the modulation function is an analytic single of a one-sided spectrum at positive frequencies for the upper sideband and at negative

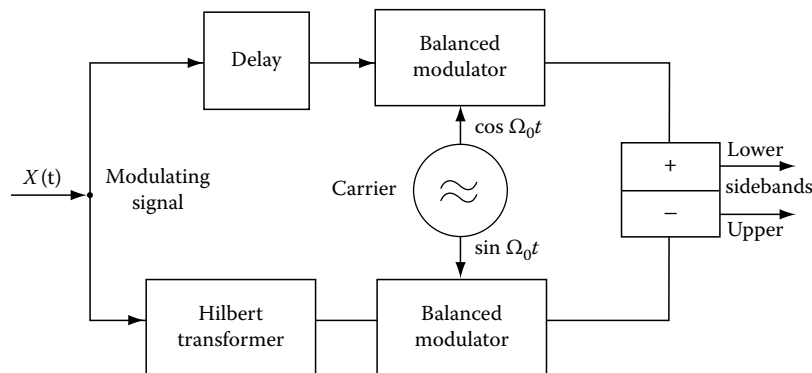


FIGURE 7.25 Block diagram of a SSB modulator (phase method) implementing Equation 7.16.16.

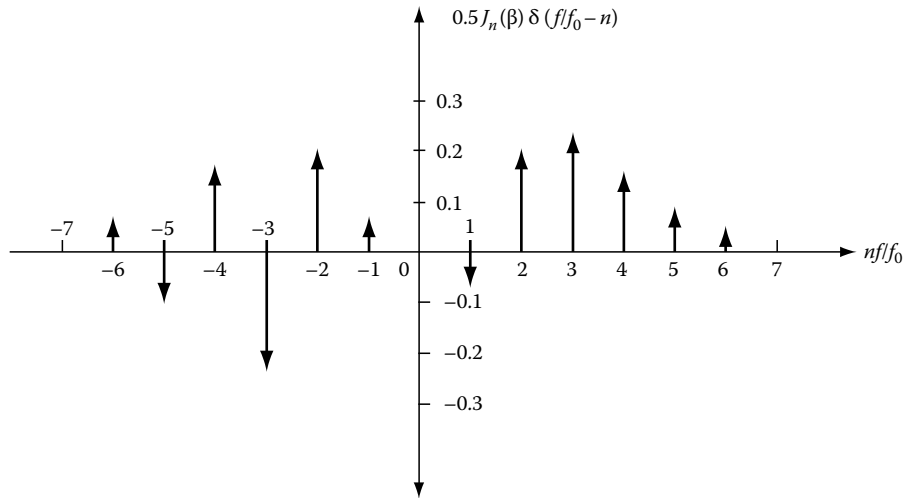


FIGURE 7.26 The spectrum of a phase modulated signal translated to zero carrier frequency, i.e., of the modulation function. Phase deviation  $\beta = 4$  radians.

frequencies for the lower sideband. Therefore, the modulation function should have the form

$$\gamma(t) = \gamma_x(t) + j\hat{\gamma}_x(t) = A(t)e^{j\phi(t)} \tag{7.298}$$

where  $\gamma_x(t) \overset{H}{\iff} \hat{\gamma}_x(t)$ . Let us use here the notion of the *instantaneous complex phase* defined by Equation 7.248 of the form

$$\phi_c(t) = \ln A(t) + j\phi(t) \tag{7.299}$$

The modulation function (Equation 7.298) can be written in the form

$$\gamma(t) = e^{\phi_c(t)} = e^{\ln[A(t)] + j\phi(t)} \tag{7.300}$$

that is, the instantaneous amplitude is written in the exponential form

$$A(t) = e^{\ln[A(t)]} \tag{7.301}$$

We now put the question: under what conditions are  $\gamma(t)$  and simultaneously  $\phi_c(t)$  analytic? That is, when is not only the relation (Equation 7.298), but also the relation

$$\ln A(t) \overset{H}{\iff} \phi(t) = \hat{\text{LN}}[A(t)] \tag{7.302}$$

satisfied? The answer comes from the dual (time domain) version of the *Paley–Wiener criterion*<sup>28</sup>

$$\int_{-\infty}^{\infty} \frac{|\text{Ln}[A(t)]|}{1+t^2} dt < \infty \tag{7.303}$$

which should be satisfied. Let us remember that  $A(t)$  is defined as a nonnegative function of time. The Paley–Wiener criterion is equivalent to a requirement that  $A(t)$  should not approach zero faster than any exponential function. This is a property of each signal with finite bandwidth that is of any practical signal.

### 7.17.3 CSSB: Compatible Single Side-Band Modulation

The CSSB signal has the same instantaneous amplitude as the conventional DSB full-carrier AM signal, that is, of the form

$$A(t) = A_0(1 + mx(t)); \quad mx(t) < 1 \tag{7.304}$$

and can be demodulated by a conventional linear diode demodulator (but not by a synchronous detector). The one-sided spectrum of the CSSB signal is achieved by a simultaneous specific phase modulation. The analytic modulation function should satisfy the requirement (Equation 7.302) and has the form

$$\gamma(t) = [1 + mx(t)]e^{j\hat{\text{LN}}[1+mx(t)]} \tag{7.305}$$

Figure 7.27 shows a block diagram of a modulator producing a high-frequency CSSB signal implemented by the use of Equation 7.305. This modulation function guarantees the exact cancellation of the undesired sideband. Using digital implementation, the level of the undesired sideband depends only on design. The bandwidth of the nonlinear logarithmic device, the Hilbert filter and phase modulator, should be several times wider than the bandwidth of the input signal. In practice it should be three to four times larger than the baseband. The instantaneous

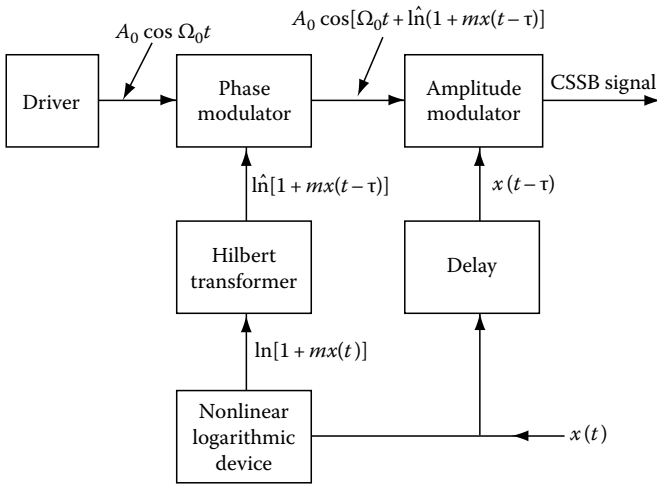


FIGURE 7.27 Diagram of the modulator producing the compatible single side-band AM signal.

amplitude  $A(t)$  should never fall to zero because the logarithm of zero equals minus infinity. Tradeoff is needed between the smallest value of  $A$  and the phase deviation.

### 7.17.4 Spectrum of the CSSB Signal

It may be a surprise that the *bandwidth* of the one-sided spectrum of the CSSB signal is *limited*. If the spectrum of the modulating signal exists in the interval  $-W < f < W$ , then the spectrum of the modulation function exists in the interval  $0 < f < 2W$ . Seemingly, the bandwidths of the CSSB and DSB AM signals are equal. However, the spectra of many messages such as speech or video signals are nonuniform, with significant terms concentrated at the lower part of the baseband. This enables us to transmit the CSSB signal in a smaller band; for example, from  $F_0$  to  $F_0 + W$  instead to  $F_0 + 2W$ , at the cost of some distortions enforced by the truncation of insignificant terms of the spectrum. Let us investigate the spectra and distortions using the model of a wide-band modulating signal given in the form of the Fourier series.

$$x(t) = \sum_{k=0}^N (-1)^k C_{2k+1} \cos[(2k+1)\omega_0 t]; \quad \omega_0 = 2\pi f_0 \quad (7.306)$$

For  $C_{2k+1} = 1/(2k+1)$  this modulating signal is a truncated Fourier series of a square wave. Its bandwidth equals  $W = (2N+1)f_0$ . The insertion of this signal in Equation 7.304 yields a periodic modulation function given by the Fourier series

$$\gamma(t) = \sum_{k=0}^{4N+2} A_k e^{jk\omega_0 t} \quad (7.307)$$

The truncation of this series at the term  $4N+2$  is not arbitrary because it will be shown that terms for  $k > 4N+2$  vanish. Therefore, the *bandwidth* of  $\gamma(t)$  equals exactly  $2W$ . To give the evidence, let us insert  $x(t)$  given by Equation 7.306 in Equation 7.305. The square of the instantaneous amplitude of so-defined modulation function is

$$A^2(t) = \left[ 1 + m \sum_{k=0}^N (-1)^k C_{2k+1} \cos[(2k+1)\omega_0 t] \right]^2 \quad (7.308)$$

The highest term of this Fourier series has the harmonic number  $4N+2$ . Analogously, the square of the instantaneous amplitude of the modulation function (Equation 7.307) is

$$A^2(t) = \left[ \sum_{k=0}^{4N+2} A_k \cos(k\omega_0 t) \right]^2 + \left[ \sum_{k=1}^{4N+2} A_k \sin(k\omega_0 t) \right]^2 \quad (7.309)$$

However, the functions 7.307 and 7.308 should be equal. Therefore, they should have the same coefficients of the Fourier series. The comparison of these coefficients yields a set of  $4N+3$  equations. The solution of these equations yields the coefficients  $A_0, A_1, A_2, \dots, A_{2N+2}$  as functions of the modulation index  $m$  and the amplitudes  $C_{2k+1}$  of the modulating signal (Equation 7.304).

### Examples

1. For the harmonic modulating signal  $x(t) = \cos(\omega_0 t)$ ,  $N=0$ ,  $C_1 = 1$ , and  $C_{2k+1} = 0$  for  $k > 0$ . The comparison of the squares of the instantaneous amplitudes yields three equations:

$$A_0^2 + A_1^2 + A_2^2 = (1 + m^2/2)C_1 \quad (7.310)$$

$$A_0 A_1 + A_1 A_2 = m C_1 \quad (7.311)$$

$$A_0 A_2 = (m C_1)^2 / 4 \quad (7.312)$$

The solution of these equations yields ( $C_1 = 1$ ): The amplitude of the zero frequency carrier

$$A_0 = 0.5 + 0.5\sqrt{1 - m^2} \quad (7.313)$$

The amplitude of the first sideband

$$A_1 = m \quad (7.314)$$

and the amplitude of the second sideband

$$A_2 = 0.5 - 0.5\sqrt{1 - m^2} \quad (7.315)$$

Figure 7.28 shows an example of the spectrum of the CSSB signal and Figure 7.29, the dependence of the amplitudes on  $m$ .

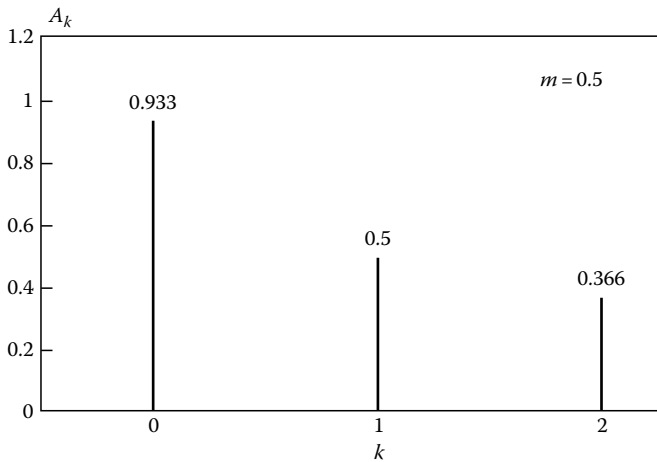


FIGURE 7.28 Example of a spectrum of the CSSB AM signal with a cosine envelope.

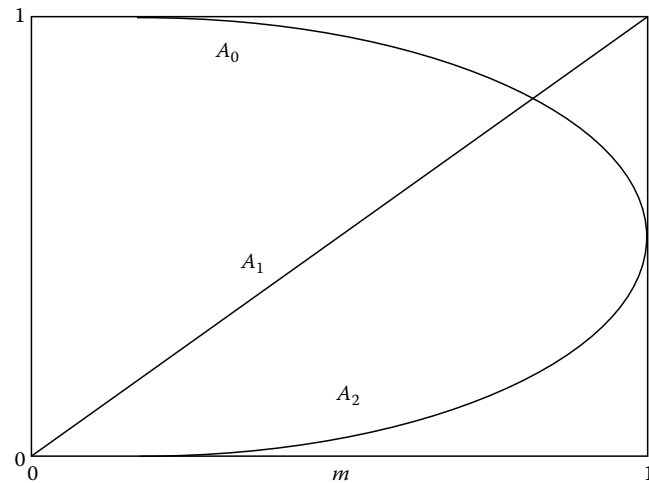


FIGURE 7.29 The dependence of the three terms of the spectrum on the modulation index  $m$ .

2. For the modulating signal  $x(t) = C_1 \cos(\omega_0 t) - C_3 \cos(3\omega_0 t)$ ,  $N=1$ , and  $C_{2k+1} = 0$  for  $k > 1$ . We get seven equations of the form

$$\sum_{k=0}^6 A_k^2 = 1 + \frac{m^2}{2}(C_1^2 + C_3^2) \quad (7.316)$$

$$\sum_{k=0}^5 A_k A_{k+1} = m C_1; \quad \sum_{k=0}^4 A_k A_{k+2} = \frac{m^2}{2}(0.5 C_1^2 - C_1 C_3) \quad (7.317)$$

$$\sum_{k=0}^3 A_k A_{k+3} = m C_3; \quad \sum_{k=0}^2 A_k A_{k+4} = \frac{-m^2}{2} C_1 C_3 \quad (7.318)$$

$$\sum_{k=0}^1 A_k A_{k+5} = 0; \quad \sum_{k=0}^0 A_k A_{k+6} = \frac{m^2}{4} C_3^2 \quad (7.319)$$

The solutions of these equations yield the seven terms of the CSSB signal. In practice it is simpler to find these terms applying any numerical method of determination of the coefficients of the Fourier series expansion of the modulation function (Equation 7.305). However, the above set of equations gives the evidence that the spectrum has a finite number of terms (example in Figure 7.30). The above equations may be used to control the accuracy of numerical calculations. Notice that Equations 7.310 and 7.316 have the form of power equality equations.

Let us quote three other modulation functions generating CSSB AM signals. The analytic modulation function of the form

$$\gamma(t) = \sqrt{1 + mx(t)} e^{j \frac{1}{2} \ln[1 + mx(t)]} \quad (7.320)$$

uses the square root of the instantaneous amplitude of an AM signal. Its spectrum is exactly one-sided. A squaring demodulator should be applied at the receiver. The phase deviation equals one-half of the phase deviation of the function (7.299). Some years ago Kahn implemented a CSSB modulator using the modulation function<sup>17</sup>

$$\gamma(t) = [1 + mx(t)] e^{j \tan^{-1} \frac{m\hat{x}(t)}{1 + mx(t)}} \quad (7.321)$$

Similarly Villard (1948) implemented a modulator using another modulation function<sup>40</sup>

$$\gamma(t) = (mx(t)) e^{jm\hat{x}(t)} \quad (7.322)$$

The last two modulation functions are not exactly analytic and their spectra are only approximately one-sided.

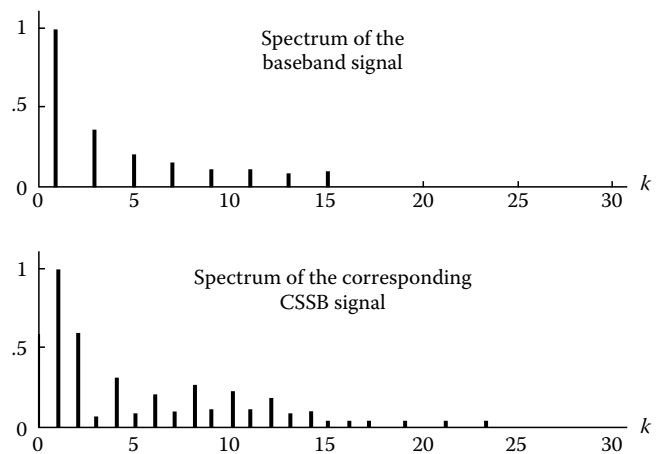


FIGURE 7.30 The spectrum of the CSSB AM signal with an envelope given by the Fourier series of a square wave truncated at the 15th harmonic number.

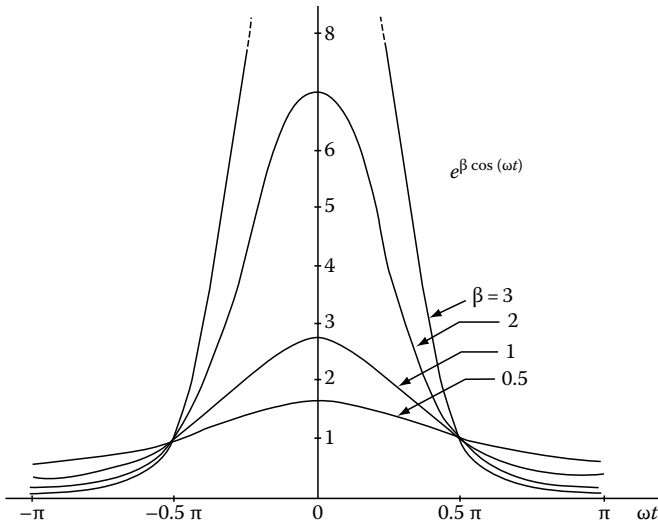


FIGURE 7.31 Envelope of the compatible with a linear FM detector single side-band FM signal.  $\beta$ -modulation index in radians.

### 7.17.5 CSSB Modulation for Angle Detectors

The modulation function of a SSB modulation compatible with a linear phase detector has the form

$$\gamma(t) = e^{-\beta \hat{x}(t) + j\beta x(t)} \quad (7.323)$$

and the modulation function of a SSB modulation compatible with a linear frequency demodulator has the form

$$\gamma(t) = e^{-m_f H \left[ \int x(t) dt \right] + jm_f \int x(t) dt} \quad (7.324)$$

where  $\beta$  and  $m_f$  are modulation indexes of phase or frequency modulation (in radians). The above modulation functions are analytic. Therefore, their spectra are exactly one-sided due to the simultaneous amplitude and angle modulation. Notice the exponential amplitude modulation function. For large modulation indexes the required dynamic range of the amplitude modulator is extremely large. An example is the modulating signal  $x(t) = \sin(\omega_0 t)$ . Here, the instantaneous amplitude has the form  $A(t) = \exp[\beta \cos(\omega_0 t)]$  and is shown in Figure 7.31. Figure 7.32 shows the amplitudes of the one-sided spectrum in dependence of  $\beta$ .

## 7.18 Hilbert Transforms in the Theory of Linear Systems: Kramers–Kronig Relations

The notions of *impedance*, *admittance*, and *transfer function* are commonly used to describe the properties of *linear, time-invariant* (LTI) systems. If the signal at the input port of the LTI system varies in time as  $\exp(j\omega t)$ , the signal at the output is a sine wave of the same frequency with a different amplitude and phase.

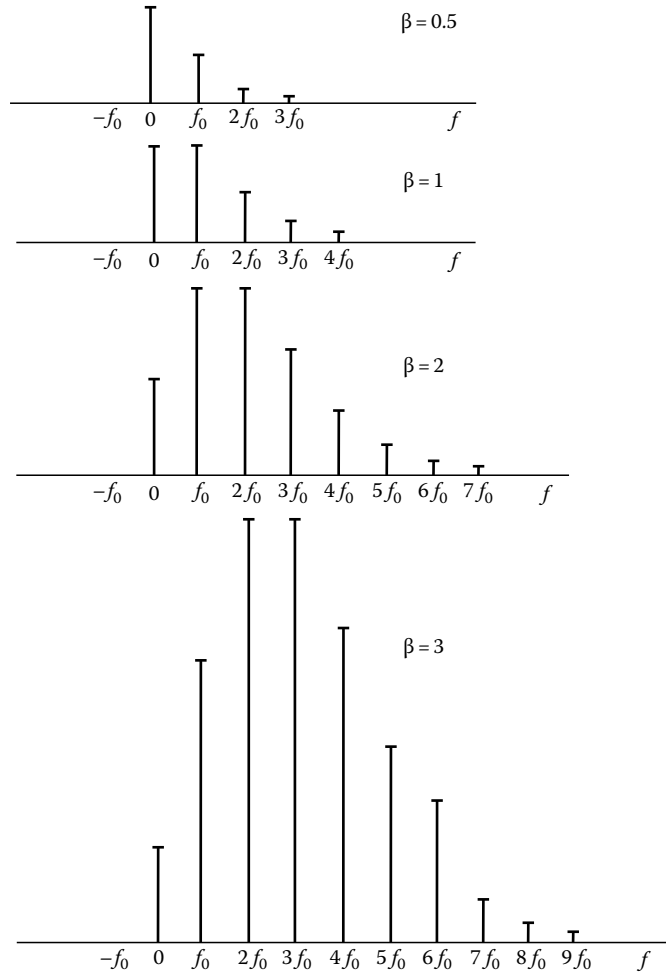


FIGURE 7.32 One-sided spectrum of the modulation function of the compatible with a linear detector FM signal.

In other words, the LTI conserves the waveform of sine signals. A pure sine waveform is a mathematical entity. However, it is easy to generate physical quantities that vary in time practically as  $\exp(j\omega t)$ . Signal generators producing nearly ideal sine waves are widely used in many applications, including precise measurements of the behavior of circuits and systems. The transfer function of the LTI system is defined as a quotient of the output and input analytic signals

$$H(j\omega) = \frac{\psi_2(t)}{\psi_1(t)} = \frac{A_2 e^{j(\omega t + \varphi_2)}}{A_1 e^{j(\omega t + \varphi_1)}} \quad (7.325)$$

This transfer function describes the steady-state, input-output relations. Theoretically, the input sine wave should be applied at the time at minus infinity. In practice, the steady state arrives if the transients die out. The transfer function is time independent because the term  $\exp(j\omega t)$  may be deleted from the nominator and denominator of Equation 7.325.

The frequency domain description by means of the transfer function can be converted into the time-domain description



using the Fourier transformation. A response of the LTI system to the delta pulse, i.e., the *impulse response*, is defined by the Fourier pair:

$$h(t) = \delta(t) * h(t) \stackrel{F}{\iff} 1H(j\omega) = H(j\omega) \quad (7.326)$$

where  $\delta(t) \stackrel{F}{\iff} 1$ .

### 7.18.2 Causality

All physical systems are causal. Causality implies that any response of a system at the time  $t$ , depends only on excitations at earlier times. For this reason, the impulse response of a causal system is one-sided; that is,  $h(t) = 0$  for  $t < 0$ . But one-sided time signals have analytic spectra (see Section 7.4). Therefore, the spectrum of the impulse response given by Equation 7.326, and thus the transfer function of a causal system is an analytic function of the complex frequency  $s = \alpha + j\omega$ . The analytic transfer function

$$H(s) = A(\alpha, \omega) + jB(\alpha, \omega) \quad (7.327)$$

satisfies the Cauchy–Riemann equations (see Equation 7.17)

$$\frac{\partial A}{\partial \alpha} = \frac{\partial B}{\partial \omega}; \quad \frac{\partial A}{\partial \omega} = -\frac{\partial B}{\partial \alpha} \quad (7.328)$$

and the real and imaginary parts ( $\alpha = 0$ ) of the transfer function form a Hilbert pair:

$$A(\omega) = \frac{-1}{\pi} P \int_{-\infty}^{\infty} \frac{B(\lambda)}{\lambda - \omega} d\lambda \quad (7.329)$$

$$B(\omega) = \frac{1}{\pi} P \int_{-\infty}^{\infty} \frac{A(\lambda)}{\lambda - \omega} d\lambda \quad (7.330)$$

A one-sided impulse response can be regarded as a sum of *noncausal* even and odd parts (see Equations 7.35 and 7.36)

$$h(t) = h_e(t) + h_o(t) \quad (7.331)$$

because  $h(t)$  is real, we have the following Fourier pairs:

$$h_e(t) = \frac{1}{2} [h(t) + h(-t)] \stackrel{F}{\iff} A(\omega) \quad (7.332)$$

$$h_o(t) = \frac{1}{2} [h(t) - h(-t)] \stackrel{F}{\iff} jB(\omega) \quad (7.333)$$

The causality of  $h(t)$  yields the relations

$$h_e(t) = \text{sgn}(t)h_o(t) \quad (7.334)$$

$$h_o(t) = \text{sgn}(t)h_e(t) \quad (7.335)$$

These products are the time-domain representation of the convolution integrals (Equations 7.329 and 7.330) (convolution to multiplication theorem).

### 7.18.3 Physical Realizability of Transfer Functions

The Hilbert relations between real and imaginary parts of transfer functions are valid for physically realizable transfer functions. The terminology “physically realizable” may be misleading because a transfer function given by a closed algebraic form is a mathematical representation of a model of a circuit built using ideal inductances, capacitances, and resistors or amplifiers. Such models are a theoretical, approximate description of physical systems. The physical realizability of a particular transfer function in the sense of circuit (or systems) theory is defined by means of causality. A general question of whether a particular amplitude characteristic can be realized by a causal system (filter) is answered by the Paley–Wiener criterion. Consider a specific magnitude of a transfer function  $|H(j\omega)|$  (an even function of  $\omega$ ). It can be realized by means of a causal filter if and only if the integral

$$\int_{-\infty}^{\infty} \frac{\ln |H(j\omega)|}{1 + \omega^2} d\omega < \infty \quad (7.336)$$

is bounded.<sup>28</sup> Then a phase function exists such that the impulse response  $h(t)$  is causal. The Paley–Wiener criterion is satisfied only if the support of  $|H(j\omega)|$  is unbounded, otherwise  $|H(j\omega)|$  would be equal to zero over finite intervals of frequency resulting in infinite values of the logarithm ( $\ln |H(j\omega)| = -\infty$ ).

### 7.18.4 Minimum Phase Property

Transfer functions satisfying the Paley–Wiener criterion have a general form:

$$H(j\omega) = H_\varphi(j\omega)H_{ap}(j\omega) \quad (7.337)$$

where  $H_\varphi(j\omega)$  is called a *minimum phase transfer function* and  $H_{ap}(j\omega)$  is an all-pass transfer function. The minimum phase transfer function

$$H_\varphi(j\omega) = |H(j\omega)|e^{j\varphi(\omega)} = A_\varphi(\omega) + jB_\varphi(\omega) \quad (7.338)$$

has a minimum phase lag  $\varphi(\omega)$  for a given magnitude characteristic. The minimum phase transfer function  $H_\varphi(s)$  has all the zeros lying in the left half-plane (i.e.,  $\alpha < 0$ ) of the  $s$ -plane. The minimum phase transfer function is analytic and its real and imaginary parts form a Hilbert pair

$$A_\varphi(\omega) \stackrel{H}{\iff} -B_\varphi(\omega) \quad (7.339)$$

An important feature of the minimum phase transfer function is that the *propagation function*

$$\gamma(s) = \ln [H(s)] = \beta(\alpha, \omega) + j\varphi(\alpha, \omega) \quad (7.340)$$

is analytic in the right half-plane. It is so because all zeros are in the left half-plane and, because we postulate stability, all poles are in the left half-plane, too. Then the real and imaginary part of the propagation function form a Hilbert pair:

$$\varphi(\omega) = \frac{-1}{\pi} P \int_{-\infty}^{\infty} \frac{\beta(\lambda)}{\lambda - \omega} d\lambda = \frac{-1}{\pi} P \int_{-\infty}^{\infty} \frac{\ln |H(j\lambda)|}{\lambda - \omega} d\lambda \quad (7.341)$$

$$\beta(\omega) = \frac{1}{\pi} P \int_{-\infty}^{\infty} \frac{\varphi(\lambda)}{\lambda - \omega} d\lambda \quad (7.342)$$

These relations can be converted to take the form of the well-known *Bode phase-integral* theorem:

$$\varphi(\omega_0) = \frac{\pi}{2} \left| \frac{d\beta}{du} \right|_0 + \frac{1}{\pi} P \int_{-\infty}^{\infty} \left[ \left| \frac{d\beta}{du} \right| - \left| \frac{d\beta}{du} \right|_0 \right] \ln [\coth |u/2|] du \quad (7.343)$$

where

$u = \ln(\omega/\omega_0)$  is the normalized logarithmic frequency scale  
 $d\beta/du$  is the slope of the  $\beta$ -curve in  $\ln$ - $\ln$  scale

The Bode formula shows that for the minimum-phase transfer functions the phase depends on the slope of the  $\beta$ -curve ( $\beta$  is the damping coefficient). The factor  $\ln[\coth |u/2|]$  is peaked at  $u = 0$  (or  $\omega = \omega_0$ ) and, hence, the phase at a given  $\omega_0$  is mostly influenced by the slope  $d\beta/du$  in the vicinity of  $\omega_0$ .

The all-pass part of the *nonminimum phase transfer function* defined by Equation 7.337 may be written in the form

$$H_{ap}(j\omega) = e^{j\psi(\omega)} \quad (7.344)$$

Therefore, the total phase function has two terms:

$$\arg [H(j\omega)] = \varphi(\omega) + \psi(\omega) \quad (7.345)$$

where

$\varphi(\omega)$  is the minimum phase  
 $\psi(\omega)$  is the nonminimum phase part of the total phase

### 7.18.5 Amplitude-Phase Relations in DLTl Systems

A discrete, linear, and time-invariant system (DLTI) is characterized by the  $Z$ -pair (see also Chapter 6)

$$h(i) \stackrel{Z}{\iff} H(z); \quad z = e^{j\psi} \quad (7.346)$$

The sequence  $h(i)$  ( $i = 0, 1, 2, \dots$ ) is the impulse response of the system to the excitation by the *Kronecker delta* and  $H(z)$  is the one-sided  $Z$  transform of the impulse response called the transfer function (or frequency characteristic) of the DLTl system, a function of the *dimensionless* normalized frequency  $\psi = 2\pi f/f_s$ , where  $f$  is the actual frequency and  $f_s$  the sampling frequency. For causal systems the impulse response is one-sided ( $h(i) = 0$  for  $i < 0$ ). The transfer function  $H(e^{j\psi})$  is periodic with the period equal to  $2\pi$ . This periodic function may be expanded into a Fourier series

$$H(e^{j\psi}) = \sum_{i=-\infty}^{\infty} h(i)e^{-j\psi i} = \sum_{i=0}^{\infty} h(i)e^{-j\psi i} \quad (7.347)$$

The Fourier coefficients  $h(i)$  are equal to the terms of the impulse response and are given by the Fourier integral:

$$h(i) = \frac{1}{2\pi} \int_{-\pi}^{\pi} H(e^{j\psi}) e^{j\psi i} d\psi \quad (7.348)$$

In general, the transfer function is a complex quantity

$$H(e^{j\psi}) = A(\psi) + jB(\psi) \quad (7.349)$$

Analogously to Equation 7.331 the causal impulse response  $h(i)$  can be regarded as a sum of two noncausal even and odd parts of the form

$$h(i) = h(0) + h_e(i) + h_o(i) \quad (7.350)$$

The even part is defined by the equation

$$h_e(i) = 0.5[h(i) + h(-i)]; \quad |i| > 0 \quad (7.351)$$

and the odd part by the equation:

$$h_o(i) = 0.5[h(i) - h(-i)] \quad (7.352)$$

Let us write the Fourier series (Equation 7.347) term by term. We get

$$H(e^{j\psi}) = h(0) + \sum_{i=1}^{\infty} h(i) \cos(\psi i) - j \sum_{i=1}^{\infty} h(i) \sin(\psi i) \quad (7.353)$$

The comparison of Equations 7.349 and 7.353 shows that

$$H(\psi) = h(0) + \sum_{i=1}^{\infty} h(i) \cos(\psi i) = h(0) + F^{-1}[h_e(i)] \quad (7.354)$$

and

$$B(\psi) = - \sum_{i=1}^{\infty} h(i) \sin(\psi i) = F^{-1}[h_o(i)] \quad (7.355)$$

and we have a Hilbert pair

$$A(\psi) \stackrel{H}{\longleftrightarrow} B(\psi) \quad (7.356)$$

We used the relations  $H[h(0)] = 0$  and  $H[\cos(\psi i)] = \sin(\psi i)$ . Because  $A(\psi)$  and  $B(\psi)$  are periodic functions of  $\psi$ , we may apply the cotangent form of the Hilbert transform (see Section 7.7).

$$B(\psi) = \frac{1}{2\pi} P \int_{-\pi}^{\pi} A(\Theta) \cot[(\Theta - \psi)/2] d\Theta \quad (7.357)$$

and

$$A(\psi) = h(0) - \frac{1}{2\pi} P \int_{-\pi}^{\pi} B(\Theta) \cot[(\Theta - \psi)/2] d\Theta \quad (7.358)$$

### 7.18.6 Minimum Phase Property in DLTI Systems

Analogous to Equations 7.337 and 7.338 the transfer function of DLTI system may be written in the form:

$$H(z) = H_{\varphi}(z)H_{\text{ap}}(z) \quad (7.359)$$

where

$H_{\varphi}(z)$  satisfies the constraints of a *minimum phase transfer function*; that is, has all the zeros inside the unit circle of the  $z$ -plane

$H_{\text{ap}}(z)$  is an *all-pass function* consisting of a cascade of factors of the form

$$H_{\text{ap}}(z) = [z^{-1} - z_i]/[1 - z_i^* z^{-1}] \quad (7.360)$$

The all-pass function has a magnitude of one, hence,  $H(z)$  and  $H_{\varphi}(z)$  have the same magnitude.  $H_{\varphi}(z)$  differs from  $H(z)$  in that the zeros of  $H(z)$ , lying outside the unit circle at points  $z = 1/z_i$ , are reflected inside the unit circle at  $z = z_i^*$ . Let us take the complex logarithm of  $H_{\varphi}(e^{j\psi})$ :

$$\ln [H_{\varphi}(e^{j\psi})] = \ln |H_{\varphi}(e^{j\psi})| + j \arg [H_{\varphi}(e^{j\psi})] \quad (7.361)$$

and analogous to Equations 7.341 and 7.342, we have a Hilbert pair

$$\ln |H_{\varphi}(e^{j\psi})| = \ln [h(0)] - \frac{1}{2\pi} P \int_{-\pi}^{\pi} \arg [H_{\varphi}(e^{j\Theta})] \cot [(\Theta - \psi)/2] d\Theta \quad (7.362)$$

$$\arg [H_{\varphi}(e^{j\psi})] = \frac{1}{2\pi} P \int_{-\pi}^{\pi} \log |H_{\varphi}(e^{j\Theta})| \cot [(\Theta - \psi)/2] d\Theta \quad (7.363)$$

It can be proved that the relations (Equations 7.362 and 7.363) are valid for transfer functions with zeros on the unit circle. In general, a stable and causal system has all its poles inside, while its zero may lie outside the unit circle. However, starting from a nonminimum-phase transfer function, a minimum-phase function can be constructed by reflecting those zeros lying outside the unit circle, inside it.

### 7.18.7 Kramers–Kronig Relations in Linear Macroscopic Continuous Media

The amplitude-phase relations of the circuit theory are known in the macroscopic theory of continuous lossy media as the Kramers–Kronig relations.<sup>18,19</sup> Almost all media display some degree of frequency dependence of some parameters, called *dispersion*. Let us take the example of a linear and isotropic electromagnetic medium. The simplest constitutive macroscopic relations describing this medium are<sup>32</sup>

$$D = \varepsilon \varepsilon_0 E = (1 + \chi_e) \varepsilon_0 E \quad (7.364)$$

$$B = \mu \mu_0 H = (1 + \chi_m) \mu_0 H \quad (7.365)$$

and

$$P = \chi_e \varepsilon_0 E \quad (7.366)$$

$$M = \chi_m H \quad (7.367)$$

where

$E$  [V/m] is the electric field vector

$H$  [A/m] is the magnetic field vector

$D$  [C/m<sup>2</sup>] is the electric displacement

$B$  [Wb/m<sup>2</sup>] is the magnetic induction

$\mu_0 = 4\pi \cdot 10^{-7}$  [Hy/m] is the permeability

$\varepsilon_0 = 1/36\pi \cdot 10^{-9}$  [F/m] is the permittivity of free space

$\varepsilon$ ,  $\mu$ ,  $\chi_m$ , and  $\chi_e$  are dimensionless constants

The vectors  $P$  and  $M$  are called polarization and magnetization of the medium. If we substitute the electrostatic field vector  $E$  with a field varying in time as  $\exp(j\omega t)$ , then the properties of the medium are described by the frequency-dependent complex susceptibility

$$\chi(j\omega) = \chi'(\omega) - j\chi''(\omega) \quad (7.368)$$

where  $\chi'$  is an even and  $\chi''$  an odd function of  $\omega$ . The imaginary term  $\chi''$  represents the conversion of electric energy into heat; that is, losses of the medium. In fact,  $\chi(j\omega)$  plays the same role as the transfer function in circuit theory and is defined by the equation

$$\chi(j\omega) = \frac{P_m e^{j(\omega t + \varphi)}}{\varepsilon_0 E_m e^{j\omega t}} = \frac{P_m}{\varepsilon_0 E_m} e^{j\varphi} \quad (7.369)$$

Let us apply Fourier spectral methods to examine Equations 7.366 and 7.369. We consider a disturbance  $E(t)$  given by the Fourier pair

$$E(t) \stackrel{F}{\iff} \mathbf{X}_E(j\omega) \quad (7.370)$$

The response  $P(t)$  is represented by the Fourier pair

$$P(t) \stackrel{F}{\iff} \mathbf{X}_P(j\omega) \quad (7.371)$$

where

$$X_p(j\omega) = \varepsilon_0 \chi(j\omega) \mathbf{X}_E(j\omega) \quad (7.372)$$

The multiplication convolution theorem yields the time-domain solution

$$P(t) = \varepsilon_0 \int_{-\infty}^{\infty} h(\tau) E(t - \tau) d\tau \quad (7.373)$$

where  $h(t)$  is given by the Fourier pair

$$h(t) \stackrel{F}{\iff} \chi(j\omega) \quad (7.374)$$

is the “impulse response” of the medium; that is, the response to the excitation  $\delta(t)$ . For any physical medium, the impulse response is causal. This is possible if  $\chi(j\omega)$  is analytic. Therefore, its real and imaginary parts form a Hilbert pair

$$\chi''(\omega) = -\frac{1}{\pi} P \int_{-\infty}^{\infty} \frac{\chi'(\eta)}{\eta - \omega} d\eta \quad (7.375)$$

$$\chi'(\omega) = \frac{1}{\pi} P \int_{-\infty}^{\infty} \frac{\chi''(\eta)}{\eta - \omega} d\eta \quad (7.376)$$

These relations are known as the Kramers–Kronig relations and are a direct consequences of causality. They apply for many media; for example, in optics, the real and imaginary parts of the complex reflection coefficient form a Hilbert pair.

### 7.18.8 Concept of Signal Delay in Hilbertian Sense

Consider a signal and its Fourier transform

$$x(t) \stackrel{F}{\iff} X(j\omega) \quad (7.377)$$

Let us assume that the Fourier spectrum  $X(j\omega)$  may be written in the form of a product defined by Equation 7.337

$$X(j\omega) = X_1(j\omega) X_2(j\omega) \quad (7.378)$$

where

$X_1(j\omega)$  fulfills the constraints of a minimum-phase function  $X_2(j\omega)$  is an “all-pass” function of the magnitude equal to one and the phase function  $\psi(\omega)$ ; that is,  $X_2(j\omega) = e^{j\psi(\omega)}$

The application of the convolution-multiplication theory yields the convolution

$$x(t) = x_1(t) * x_2(t) \quad (7.379)$$

where  $x_1(t) \stackrel{F}{\iff} X_1(j\omega)$  is defined as a minimum-phase signal satisfying relations (7.341 and 7.342); that is,

$$\arg [X_1(j\omega)] \stackrel{H}{\iff} \ln |X_1(j\omega)| \quad (7.380)$$

and the signal

$$x_2(t) \stackrel{F}{\iff} X_2(j\omega) = e^{j\psi(\omega)} \quad (7.381)$$

is defined as the nonminimum-phase part of the signal  $x(t)$ . Let us formulate the following definitions:

---

**Definition 7.1** The minimum phase signal  $x_1(t)$  has a zero delay in the Hilbert sense.

---

**Definition 7.2** The delay of the signal relative to the moment  $t=0$  is defined by a specific property of the signal  $x_2(t)$ . Krylov and Ponomariev<sup>20</sup> used the name “ambiguity function” for  $x_2(t)$  and proposed to define the delay by the position of its maximum. Another possibility is to define the delay using the position of the center of gravity of  $x_2(t)$ .

#### Examples

1. If the function  $x_2(t) = \delta(t)$ , the delay equals zero because

$$x(t) = x_1(t) * \delta(t) = x_1(t) \quad (7.382)$$

2. If the function  $x_2(t) = \delta(t - t_0)$ , the delay equals  $t_0$  because

$$x(t) = x_1(t) * \delta(t - t_0) = x_1(t - t_0) \quad (7.383)$$

3. Consider a phase-delayed harmonic signal and its Fourier image:

$$\cos(\omega_0 t - \varphi_0) \stackrel{F}{\iff} \pi \delta(\omega + \omega_0) e^{j\varphi_0} + \pi \delta(\omega - \omega_0) e^{-j\varphi_0} \quad (7.384)$$

or

$$\cos \omega_0 t * \delta \left( t - \frac{\varphi_0}{\omega_0} \right) \stackrel{F}{\iff} \pi [\delta(\omega + \omega_0) + \delta(\omega - \omega_0)] e^{-j\varphi_0 \operatorname{sgn} \omega} \quad (7.385)$$

Evidently the ambiguity function  $x_2(t)$  is

$$x_2(t) = \delta\left(t - \frac{\varphi_0}{\omega_0}\right) \stackrel{F}{\iff} e^{-j\varphi_0 \operatorname{sgn} \omega} \quad (7.386)$$

and the time delay is, of course,  $t_0 = \varphi_0/\omega_0$ , as we could expect.

4. Consider the series connection of the first-order low-pass with the transfer function

$$X_1(j\omega) = \frac{1}{1 + j\omega\tau} \quad (7.387)$$

and the first-order all-pass with the phase function of the form

$$\arg [X_2(j\omega)] = \tan^{-1} \frac{2\omega\tau}{(\omega\tau)^2 - 1} \quad (7.388)$$

The impulse response of the low-pass is

$$x_1(t) = F^{-1} \left[ \frac{1}{1 + j\omega\tau} \right] = 1(t)e^{-t/\tau} \quad (7.389)$$

and satisfies the definition of the minimum-phase signal. The impulse response of the all-pass plays here the role of the ambiguity function and has the form

$$x_2(t) = F^{-1} \left[ \exp \frac{-2\omega\tau}{\omega^2\tau^2 - 1} \right] = 1(t) \frac{2}{\tau} e^{-t/\tau} - \delta(t)$$

We observe that the maximum of  $x_2(t)$  is at  $t=0$ . However, we expect that the all-pass introduces some delay. In this case it would be advisable to define the delay using the center of gravity of the signal  $x_2(t)$ .

### 7.19 Hilbert Transforms in the Theory of Sampling

The generation of a sequence of samples of a continuous signal (sampling) and the recovery of this signal from its samples (interpolation) is a widely used procedure in modern signal processing and communications techniques. Basic and advanced theory of sampling and interpolation is presented in many textbooks. This section presents the role of Hilbert transforms in the theory of sampling and interpolation. Figure 7.33, for reference, is the usual means by which the sequence of samples is produced. In general, the sampling pulses may be nonequidistant. However, this section presents the role of Hilbert transforms in the basis WKS (Wittaker, Kotelnikow, Shannon) theory of periodic sampling and interpolation.

The periodic sequence of sampling pulses may be written in the form (see Equation 7.81)

$$p(t) = p_T(t) * \sum_{k=-\infty}^{\infty} \delta(t - kT) \quad (7.390)$$

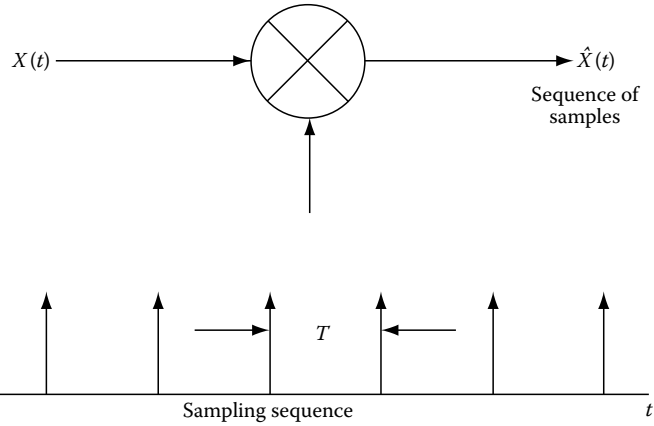


FIGURE 7.33 A method of generation of a sequence  $\hat{x}(t)$  of samples of the analog signal  $x(t)$ .

where

$p_T(t)$  defines the waveform of the sampling pulse (the generating function of the periodic sequence of pulses)  
 $f = 1/T$  is the sampling frequency

From the point of view of the presentation of the role of Hilbert transforms in sampling and interpolation, it is sufficient to use the delta sampling sequence inserting  $p_T(t) = \delta(t)$ . The *delta sampling sequence* is given by the formula (remember that  $\delta(t) * \delta(t) = \delta(t)$ )

$$p(t) = \sum_{k=-\infty}^{\infty} \delta(t - kT) \quad (7.391)$$

For convenience, let us write here the Hilbert transform of this sampling sequence (see Section 7.7, Equation 7.95)

$$\sum_{k=-\infty}^{\infty} \delta(t - nT) \stackrel{H}{\iff} \frac{1}{T} \sum_{k=-\infty}^{\infty} \cot [(\pi/T)(t - kT)] \quad (7.392)$$

The Fourier image of the delta sampling sequence is given by another periodic delta sequence

$$\sum_{k=-\infty}^{\infty} \delta(t - kT) \stackrel{F}{\iff} \frac{1}{T} \sum_{k=-\infty}^{\infty} \delta(f - k/T) \quad (7.393)$$

The sampler produces as an output a sequence of samples given by the formula

$$x_s(t) = \sum_{k=-\infty}^{\infty} x(kT)\delta(t - kT) \quad (7.394)$$

that is, a sequence of delta functions weighted by the samples of the signal  $x(t)$ . Let us recall the basic WKS sampling theorem. Consider a signal  $x(t)$  and its Fourier image  $X(f)$ ,  $\omega = 2\pi f$ .

If the Fourier image is low-pass band limited, i.e.,  $|X(jf)| = 0$  for  $|f| > W$ , then  $x(t)$  is completely determined by the sequence of its samples taken at the moments  $t_k$  spaced  $T = 1/2W$  apart. The sampling frequency  $f_s = 2W$  is called the Nyquist rate. The multiplication to convolution theorem yields the spectrum of the sequence of samples

$$X_s(jf) = X(jf) * \frac{1}{T} \sum_{k=-\infty}^{\infty} \delta(f - k/T) \quad (7.395)$$

Figure 7.34 shows an example of a low-pass band-limited spectrum of a signal  $x(t)$  and the well-known three spectra of the sequence of samples: the spectrum of oversampled signal with no aliasing with the sampling frequency  $f_s = 1/T > 2W$ , the limit case with  $f_s = 2W$ , and the spectrum of undersampled signal

with  $f_s < 2W$ . Notice that the sequence of samples given by Equation 7.394 may be regarded as a model of a signal with pulse amplitude modulation (PAM). The original signal  $x(t)$  may be recovered by filtering this PAM signal using the ideal noncausal and physically unrealizable low-pass filter defined by the transfer function

$$Y(jf) = \begin{cases} 1 & \text{for } |f| < W \\ 0.5 & \text{for } |f| = W \\ 0 & \text{for } |f| > W \end{cases} \quad (7.396)$$

The noncausal impulse response of this filter is

$$h(t) = F^{-1}[Y(jf)] = 2W \frac{\sin(2\pi Wt)}{2\pi Wt} \quad (7.397)$$

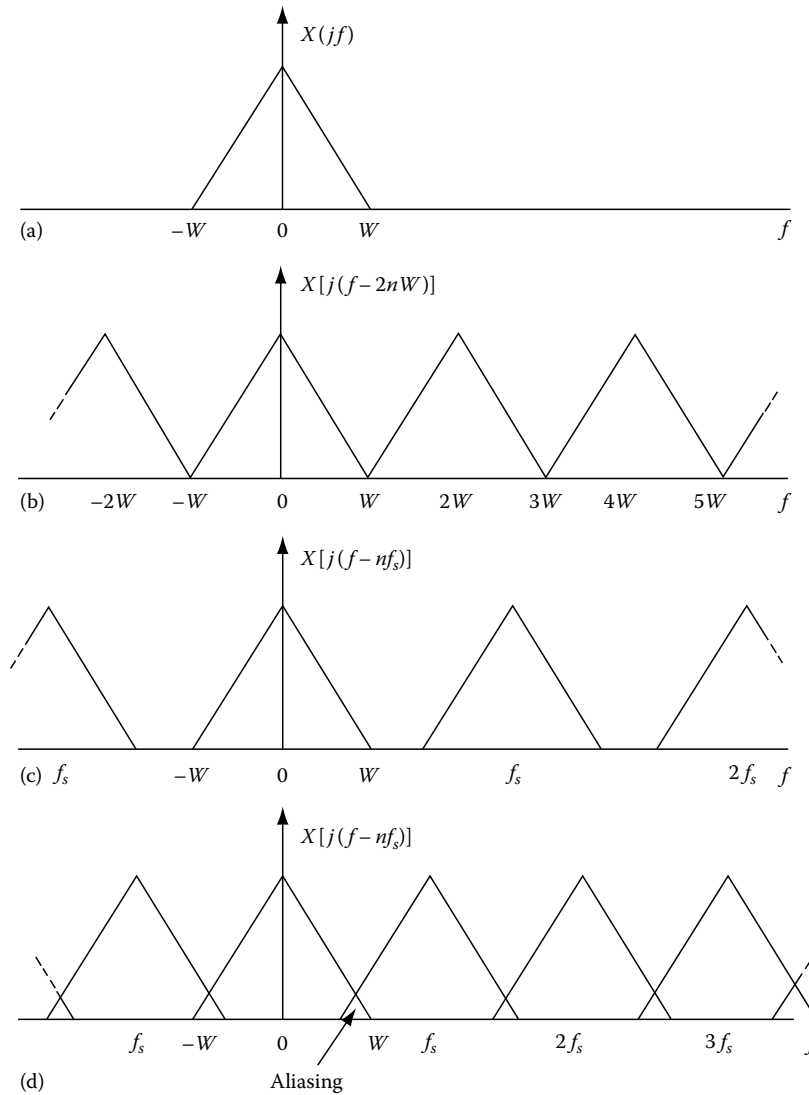


**FIGURE 7.34** (a) A band-limited low-pass spectrum of a signal, (b) the corresponding spectrum of the sequence of sampled with Nyquist rate of sampling  $f_s < 2W$ , (c) spectrum by oversampling  $f_s > 2W$ , and (d) spectrum by undersampling  $f_s < 2W$  showing the aliasing of the sidebands.

and is called the *interpolatory function*. The total response is a sum of responses to succeeding samples giving the well-known *interpolatory expansion* ( $f_s = 2W$ ):

$$x(t) = \sum_{k=-\infty}^{\infty} x\left[\frac{k}{2W}\right] \frac{\sin\left[2\pi W\left(t - \frac{k}{2W}\right)\right]}{2\pi W\left(t - \frac{k}{2W}\right)} \quad (7.398)$$

The summation exactly restores the original signal  $x(t)$ . In the following text the argument of the interpolatory function will be written using the notation

$$2\alpha(t, k) = 2\pi W\left(t - \frac{k}{2W}\right) \quad (7.399)$$

giving the following form of the interpolation expansion

$$x(t) = \sum_{k=-\infty}^{\infty} x\left(\frac{k}{2W}\right) \frac{\sin[2\alpha(t, k)]}{2\alpha(t, k)} \quad (7.400)$$

Notice that the sampling of the function  $x(t) = a$  (a constant) yields the formula

$$\sum_{k=-\infty}^{\infty} \frac{\sin[2\alpha(t, k)]}{2\alpha(t, k)} = 1 \quad (7.401)$$

This equation may be used to calculate the accuracy of the interpolation due to any truncation of the summation.

The Whittaker's interpolatory function and its Hilbert transform are forming the Hilbert pair

$$\frac{\sin[2\alpha(t, k)]}{2\alpha(t, k)} \xleftrightarrow{H} \frac{\sin^2[\alpha(t, k)]}{\alpha(t, k)} \quad (7.402)$$

Therefore, the interpolatory expansion of the Hilbert transform  $H[x(t)] = \hat{x}(t)$ , due to the linearity property, is given by the formula

$$\hat{x}(t) = \sum_{k=-\infty}^{\infty} x\left[\frac{k}{2W}\right] \frac{\sin^2[\alpha(t, k)]}{\alpha(t, k)} \quad (7.403)$$

This formula may be applied to calculate the Hilbert transforms of low-pass signals using their samples. The transfer function of the low-pass Hilbert filter (transformer) is given by the Fourier transform of the impulse response given by the right-hand side of Equation 7.402:

$$\begin{aligned} Y_H(jf) &= F\left[\frac{\sin^2(\alpha, k)}{\alpha(t, k)}\right] \\ &= -j \operatorname{sgn}(f) Y(f) \\ &= \begin{cases} j & \text{for } |f| < W \\ 0 & \text{for } f = 0; 0.5 \text{ for } |f| \\ -j & \text{for } |f| < W \end{cases} \quad (7.404) \end{aligned}$$

The sampling of the function  $x(t) = a$  yields

$$\sum_{k=-\infty}^{\infty} \frac{\sin^2[\alpha(t, k)]}{\alpha(t, k)} = 0 \quad (7.405)$$

The expansion of the analytic signal  $\psi(t) = x(t) + j\hat{x}(t)$  using interpolatory functions has the form

$$\psi(t) = \sum_{k=-\infty}^{\infty} x\left[\frac{k}{2W}\right] \left[ \frac{\sin[2\alpha(t, k)]}{2\alpha(t, k)} + j \frac{\sin^2[\alpha(t, k)]}{\alpha(t, k)} \right] \quad (7.406)$$

and using trigonometric identities we get the following form of the interpolatory expansion of the analytic signal:

$$\psi(t) = -j \sum_{k=-\infty}^{\infty} x\left[\frac{k}{2W}\right] \frac{e^{j2\alpha(t, k)} - 1}{2\alpha(t, k)} \quad (7.407)$$

### 7.19.1 Band-Pass Filtering of the Low-Pass Sampled Signal

Consider the ideal band-pass with a physically unrealizable transfer function in the form of a "spectral window" as shown in Figure 7.35. The impulse response of this filter is

$$h(t) = 2(f_2 - f_1) \frac{\sin[\pi(f_2 - f_1)t]}{\pi(f_2 - f_1)t} \cos[\pi(f_1 + f_2)t] \quad (7.408)$$

The insertion  $f_1 = W$  and  $f_2 = 3W$  yields

$$h(t) = 4W \frac{\sin(2\pi Wt)}{2\pi Wt} \cos(4\pi Wt) \quad (7.409)$$

If the sequence of samples of the signal  $x(t)$  is applied to the input of this band-pass, the output signal  $z(t)$  is given by the interpolatory expansion of the form

$$z(t) = \sum_{k=-\infty}^{\infty} \left\{ x(k/(2W)) \frac{\sin[2\alpha(t, k)]}{2\alpha(t, k)} \cos[4\alpha(t, k)] \right\} \quad (7.410)$$

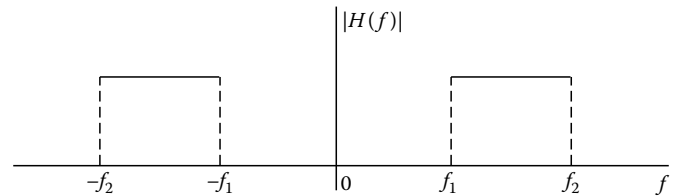


FIGURE 7.35 The magnitude of the transfer function of an ideal band-pass.

where  $\alpha(t, k)$  is given by Equation 7.399. We obtained the compressed-carrier amplitude-modulated signal of the form

$$z(t) = x(t) \cos(4\pi Wt) \quad (7.411)$$

with a carrier frequency  $2W$ . Therefore, the AM-balanced modulator may be implemented using a sampler and a band-pass. Multiplication of the carrier frequency is possible using band-pass filters with  $f_1 = 3W$  and  $f_2 = 5W$  or  $f_1 = 5W$ , and  $f_2 = 7W, \dots$ . The conclusion is that in principle one may multiply the carrier frequency of AM signals getting undistorted sidebands (envelope). The comparison of Equations 7.400 and 7.411 enables us to write the signal  $z(t)$  in the form

$$z(t) = \left\{ \sum_{k=-\infty}^{\infty} x \left[ \frac{k}{2W} \right] \frac{\sin [2\alpha(t, k)]}{2\alpha(t, k)} \right\} \cos(4\pi Wt) \quad (7.412)$$

and because  $\cos(4\pi Wt - k2\pi) = \cos(4\pi Wt)$ , in the form

$$z(t) = \sum_{k=-\infty}^{\infty} x \left[ \frac{k}{2W} \right] \frac{\sin [2\alpha(t, k)]}{2\alpha(t, k)} \cos(4\pi Wt) \quad (7.413)$$

Analogously, a SSB AM signal may be produced by band-pass filtering of the sequence of samples using a filter with  $f_1 = 2W$  and  $f_2 = 3W$  (upper sideband). The impulse response of this filter is

$$h(t) = 2W \frac{\sin(\pi Wt)}{\pi Wt} \cos(5\pi Wt) \quad (7.414)$$

and the interpolatory expansion is

$$z_{SSB}(t) = \sum_{k=-\infty}^{\infty} x \left[ \frac{k}{2W} \right] \frac{\sin [2\alpha(t, k)]}{\alpha(t, k)} \cos [5\alpha(t, k)] \quad (7.415)$$

This SSB signal may be written in the standard form given by Equation 7.289 (see Section 7.17)

$$z_{SSB}(t) = x(t) \cos(4\pi Wt) - \hat{x}(t) \sin(4\pi Wt) \quad (7.416)$$

Let us derive the above form starting with Equation 7.414. Using the trigonometric identity  $\cos(5\alpha) = \cos \alpha \cos(4\alpha) - \sin \alpha \sin(4\alpha)$ , Equation 7.415 becomes

$$z_{SSB}(t) = \sum_{k=-\infty}^{\infty} x \left[ \frac{k}{2W} \right] \left\{ \frac{\sin [2\alpha(t, k)]}{2\alpha(t, k)} \cos [4\alpha(t, k)] - \frac{\sin^2 [\alpha(t, k)]}{\alpha(t, k)} \sin [4\alpha(t, k)] \right\} \quad (7.417)$$

It may be shown in the same manner as before that Equations 7.416 and 7.417 have identical left-hand sides.

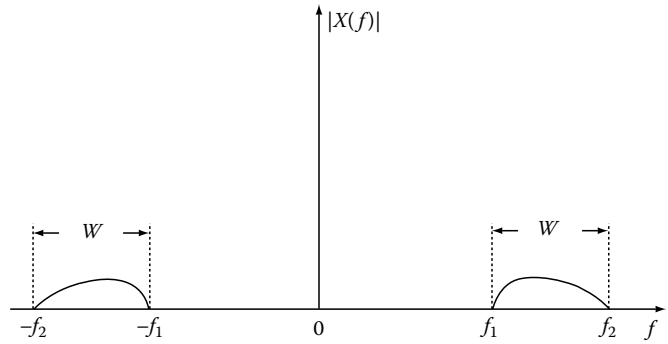


FIGURE 7.36 The magnitude of the spectrum of a band-pass signal.

### 7.19.2 Sampling of Band-Pass Signals

Consider a band-pass signal  $f(t)$  with the spectrum limited in band  $f_1 < |f| < f_2 = f_1 + W$  (see Figure 7.36). In general, a so-called second-order sampling should be applied to recover, using interpolation, the signal  $f(t)$ . However, it may be shown that alternatively, first-order sampling at the rate  $W$  may be applied with simultaneous sampling of the signal  $f(t)$  and of its Hilbert transform  $H[f(t)] = \hat{f}(t)$ . The following interpolation formula has to be applied to recover the signal using the sequences of samples  $f(k/W)$  and  $\hat{f}(k/W)$ .

$$f(t) = \sum_{k=-\infty}^{\infty} f \left( \frac{n}{W} \right) s \left( t - \frac{n}{W} \right) + \hat{f} \left( \frac{n}{W} \right) \hat{s} \left( t - \frac{n}{W} \right) \quad (7.418)$$

where the interpolating functions are given by the impulse response of the band-pass

$$s(t) = \frac{\sin(\pi Wt)}{\pi Wt} \cos \left[ 2\pi \left( f_1 + \frac{W}{2} \right) t \right] \quad (7.419)$$

and of a band-pass Hilbert filter (see Section 7.22)

$$\hat{s}(t) = \frac{\sin(\pi Wt)}{\pi Wt} \sin \left[ 2\pi \left( f_1 + \frac{W}{2} \right) t \right] \quad (7.420)$$

## 7.20 Definition of Electrical Power in Terms of Hilbert Transforms and Analytic Signals

The problem of efficient energy transmission from the source to the load is of importance in electrical systems. Usually the voltage and current waveforms may be regarded as sinusoidal. However, many loads are nonlinear and, therefore, nonsinusoidal cases should be investigated. In many applications the voltages and currents are nearly periodic, unperiodic, or even random. Therefore, some generalizations of theories developed for periodic cases are needed.



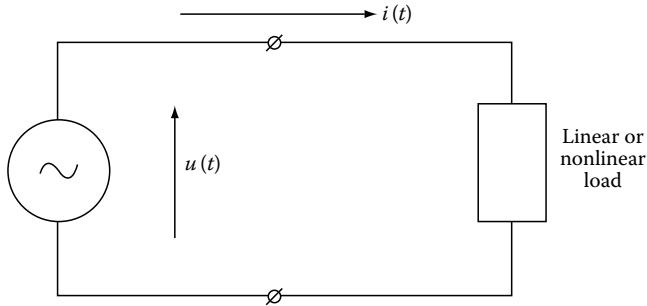


FIGURE 7.37 An electrical one-port where  $u(t)$  is the instantaneous voltage and  $i(t)$  the instantaneous current.

Consider an electrical one-port (linear or nonlinear) as shown in Figure 7.37. The *instantaneous power* is defined by the equation

$$P(t) = u(t)i(t) \quad (7.421)$$

where

$u(t)$  is the instantaneous voltage across the load  
 $i(t)$  the instantaneous current in the load

We arbitrarily assign a positive sign to  $P$  if the energy  $P(t)dt$  is delivered from the source to the load and a negative sign for the opposite direction. The above formal definition of power involves *all limitations* associated with the definition of voltage, current, and the electrical one-port.

Let us introduce the notion of *quadrature instantaneous power* defined by the equation

$$Q(t) = u(t)\hat{i}(t) = -\hat{u}(t)i(t) \quad (7.422)$$

where  $\hat{u}$  and  $\hat{i}$  are Hilbert transforms of the voltage and current waveforms.

## 7.20.2 Harmonic Waveforms of Voltage and Current

Consider the classical case of a linear load with sine waveforms of  $u(t)$  and  $i(t)$ . We have

$$u(t) = U \cos(\omega t + \varphi_u) \quad (7.423)$$

$$i(t) = J \cos(\omega t + \varphi_i) \quad (7.424)$$

The instantaneous power is

$$P(t) = UJ \cos(\omega t + \varphi_u) \cos(\omega t + \varphi_i) \quad (7.425)$$

The Fourier series expansion of  $P(t)$  is

$$P(t) = 0.5UJ \cos(\varphi_i - \varphi_u) + 0.5UJ [\cos[2(\omega t + \varphi_i)] \cos(\varphi_i - \varphi_u) - \sin[2(\omega t + \varphi_i)] \sin(\varphi_i - \varphi_u)] \quad (7.426)$$

The instantaneous quadrature power is

$$Q(t) = UJ \cos(\omega t + \varphi_u) \sin(\omega t + \varphi_i) \quad (7.427)$$

The Fourier series expansion of  $Q(t)$  is

$$Q(t) = 0.5UJ \sin(\varphi_i - \varphi_u) + 0.5UJ [\sin[2(\omega t + \varphi_i)] \cos(\varphi_i - \varphi_u) + \cos[2(\omega t + \varphi_i)] \sin(\varphi_i - \varphi_u)] \quad (7.428)$$

The mean value of  $P(t)$  defined by the equation

$$\bar{P} = \frac{1}{T} \int_0^T P(t) dt = 0.5UJ \cos(\varphi_i - \varphi_u); \quad \omega = \frac{2\pi}{T} \quad (7.429)$$

is called the *active power* and it is a measure of the unilateral energy transfer from the source to the load. The mean value of the quadrature power  $Q(t)$  defined by the equation

$$\bar{Q} = \frac{1}{T} \int_0^T Q(t) dt = 0.5UJ \sin(\varphi_i - \varphi_u) \quad (7.430)$$

is called the *reactive power*. The value of the reactive power depends on energy that is delivered periodically back and forth between the source and the load with no net transfer. The waveform of the instantaneous power given by Equation 7.426 is shown in Figure 7.38 (for convenience  $\varphi_u = 0$ ). The energy transfer from the source to the load is given by the integral

$$E_+ = \frac{1}{\omega} \int_{-\pi/2}^{\pi/2 - \varphi_i} UI \cos(\omega t) \cos(\omega t + \varphi_i) d\omega t \\ = \frac{UI}{2\omega} [(\pi - \varphi) \cos \varphi + \sin \varphi] \quad (7.431)$$

and the energy transfer from the load to the source during the remaining part of the half-period is

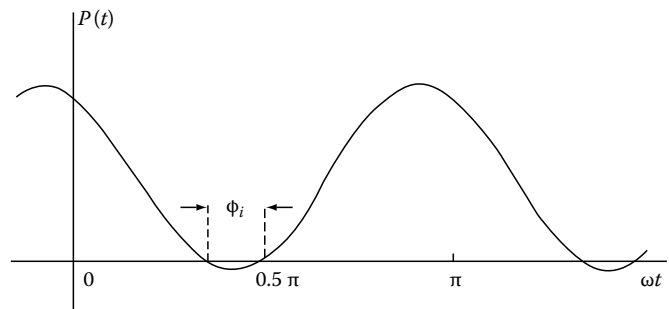


FIGURE 7.38 The waveform of the instantaneous power given by Equation 7.425.

$$E_- = \frac{1}{\omega} \int_{\pi/2-\varphi_i}^{\pi/2} UI \cos(\omega t) \cos(\omega t + \varphi_i) d\omega t$$

$$= \frac{UI}{2\omega} [\varphi \cos \varphi - \sin \varphi] \quad (7.432)$$

Therefore, the net energy transfer toward the load is

$$E = E_+ - E_- = \frac{UIT}{4} \cos(\varphi_i) \quad (7.433)$$

The division of this energy by  $0.5T$  gives the mean value of the power equal to the active power. However, the division of  $E_-$  by  $0.5T$  yields

$$\bar{P}_- = \frac{2E}{T} [\varphi \cos \varphi_i - \sin \varphi_i] \quad (7.434)$$

and this mean power differs from the reactive power defined by Equation 7.430. Therefore, the notions of active and reactive power differ considerably. The active power equals the time-independent or constant term of the instantaneous power given by the Fourier series (Equation 7.426) while the reactive power equals the amplitude of the quadrature (or sine) term of Equation 7.426. Notice that in the Fourier series (Equation 7.428) the role of both quantities is reversed. Let us recall that the quantity

$$S = 0.5UJ = U_{RMS}J_{RMS} \quad (7.435)$$

is called the *apparent power* and the quantity

$$\rho = \cos(\varphi_i - \varphi_u) = \frac{\bar{P}}{S} \quad (7.436)$$

is called the *power factor*. The power factor may be regarded as a normalized correlation coefficient of the voltage and current signals while  $\sin(\varphi_i - \varphi_u) = \text{SQR}(1 - \rho^2)$  may be called the anticorrelation coefficient. The quantities  $S$ ,  $\bar{P}$ , and  $\bar{Q}$  satisfy the relation

$$S^2 = \bar{P}^2 + \bar{Q}^2 \quad (7.437)$$

### 7.20.3 Notion of Complex Power

Consider the analytic (complex) form of the voltage and current harmonic signals defined by Equations 7.423 and 7.424. We have  $\psi_u(t) = U \exp(j\omega t + \varphi_u)$  and  $\psi_i(t) = J \exp(j\omega t + \varphi_i)$ . The complex power is defined by the equation

$$S = \frac{1}{2} \psi_u(t) \psi_i^*(t) = 0.5 U J \exp[j(\varphi_i - \varphi_u)] \quad (7.438)$$

In the following text, the symbol  $S$  will be used to denote the complex power. We have

$$S = P + jQ = |S| \exp[j(\varphi_i - \varphi_u)] \quad (7.439)$$

The real part of  $S$  equals the active power and the imaginary part equals the reactive power. The module of the complex power equals the apparent power and the argument equals the phase angle  $\varphi_i - \varphi_u$ .

### 7.20.4 Generalization of the Notion of Power

The above-described well-known notions of apparent, active, and reactive power were in the past generalized by several authors for nonsinusoidal cases and later for signals with finite average power. The nonsinusoidal periodic waveforms of  $u(t)$  and  $i(t)$  may be described in the frequency domain by the Fourier series:

$$u(t) = U_0 + \sum_{n=1}^N U_n \cos(n\omega t + \varphi_{un}) \quad (7.440)$$

$$i(t) = I_0 + \sum_{n=1}^N J_n \cos(n\omega t + \varphi_{in}) \quad (7.441)$$

where

$\omega$  is a constant equal to the fundamental angular frequency,

$$\omega = 2\pi/T$$

$T$  is the period

Some or even all harmonics of the voltage waveform may not be included in the current waveform and vice versa. The active power may be defined using the same equation (Equation 7.429) as for sinusoidal waveforms. Inserting Equations 7.440 and 7.441 into Equation 7.429 yields

$$\bar{P} = U_0J_0 + \sum 0.5 U_nJ_n \cos(\varphi_{in} - \varphi_{un}) \quad (7.442)$$

The summation involves terms included in both waveforms. Analogously, the reactive power is defined using Equation 7.430:

$$\bar{Q} = \sum 0.5 U_nJ_n \sin(\varphi_{in} - \varphi_{un}) \quad (7.443)$$

This definition of the reactive power was proposed in 1927 by Budeanu<sup>6</sup> and is nowadays commonly accepted. It has been sometimes criticized as “lacking of physical meaning.” Another definition of reactive power was introduced by Fryze<sup>10</sup> who proposed to resolve the current waveform in two components:

$$i(t) = i_p(t) + i_q(t) \quad (7.444)$$

The “in-phase” component is given by the relation

$$i_p(t) = \frac{\frac{1}{T} \int_0^T i u dt}{\frac{1}{T} \int_0^T u^2 dt} u(t) = \frac{\bar{P}}{U_{RMS}^2} u(t) \quad (7.445)$$

$U_{\text{RMS}}$  is the root mean square (RMS) value of the voltage. The “quadrature” component is

$$i_q = i - i_p \tag{7.446}$$

and satisfies the orthogonality property

$$\int_0^T i_q i_p dt = 0 \tag{7.447}$$

This orthogonality yields for the RMS values:

$$I_{\text{RMS}}^2 = I_{p,\text{RMS}}^2 + I_{q,\text{RMS}}^2 \tag{7.448}$$

The reactive power is defined by the product

$$Q = U_{\text{RMS}} I_{q,\text{RMS}} \tag{7.449}$$

The comparison of Budeanu’s and Fryze’s definitions of the reactive power shows how misleading it is to apply the same name, “reactive power,” for notions having *different* definitions. Let us illustrate this statement with an example. A source of a cosine voltage is loaded with the ideal diode with a nonlinear characteristic (see Figure 7.39)

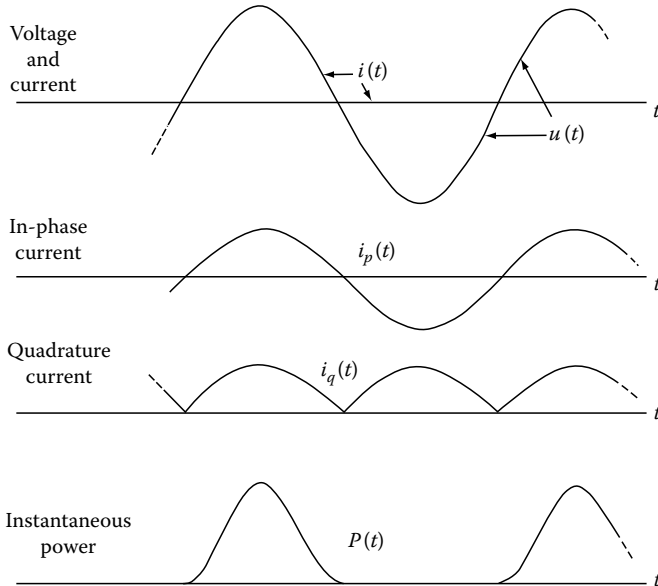
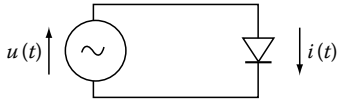


**FIGURE 7.39** (a) A source of sine voltage loaded with a diode, (b) the voltage and current waveforms, (c) the in-phase component of the current, (d) the quadrature component of the current, and (e) the waveform of the instantaneous power.

$$\begin{aligned} i &= Gu & \text{if } u > 0 \\ i &= 0 & \text{if } u < 0 \end{aligned} \tag{7.450}$$

The current has the waveform of a half-wave rectified cosine (see Figure 7.39a) and may be resolved into the in-phase and quadrature components. The Fourier series expansion of the current has the form

$$i(t) = \frac{U}{\pi} \left[ 1 - \frac{\pi}{2} \cos(\omega t) + \frac{2}{3} \cos(2\omega t) - \frac{2}{15} \cos(4\omega t) + \frac{2}{35} \cos(6\omega t) - \dots \right] \tag{7.451}$$

The in-phase component is

$$i_p(t) = \frac{U}{2} \cos(\omega t) \tag{7.452}$$

and the Fourier series of the quadrature component (full-wave rectified cosine) is

$$i_q(t) = \frac{U}{\pi} \left[ 1 + \frac{2}{3} \cos(2\omega t) - \frac{2}{15} \cos(4\omega t) + \frac{2}{35} \cos(6\omega t) - \dots \right] \tag{7.453}$$

The reactive power defined by Equation 7.443 equals zero while the reactive power is defined by Equation 7.449 equals

$$Q = \frac{U^2}{8} \tag{7.454}$$

However, the instantaneous power (Figure 7.39) is always positive, so there is no energy oscillating back and forth between the source and load. Therefore, we should expect that the reactive power equals zero. This requirement is satisfied using Budeanu’s definition but not Fryze’s definition.

### 7.20.5 Generalization of the Notion of Power for Signals with Finite Average Power

A generalized theory of electric power by use of Hilbert transforms was presented by Nowomiejski.<sup>24</sup> He considered voltages and currents with *finite average power*; that is, finite RMS defined by the equations

$$U_{\text{RMS}} = \sqrt{\lim_{T \rightarrow \infty} \frac{1}{2T} \int_{-T}^T u^2(t) dt} \tag{7.455}$$

$$I_{\text{RMS}} = \sqrt{\lim_{T \rightarrow \infty} \frac{1}{2T} \int_{-T}^T i^2(t) dt} \tag{7.456}$$

The apparent power is defined as

$$S = U_{\text{RMS}} I_{\text{RMS}} \quad (7.457)$$

and the active and reactive powers are defined by means of the relations

$$\bar{P} = \lim_{T \rightarrow \infty} \frac{1}{2T} \int_{-T}^T u(t)i(t)dt \quad (7.458)$$

and

$$\bar{Q} = \lim_{T \rightarrow \infty} \frac{1}{2T} \int_{-T}^T \hat{u}(t)i(t)dt \quad (7.459)$$

or

$$\bar{Q} = - \lim_{T \rightarrow \infty} \frac{1}{2T} \int_{-T}^T \hat{u}(t)i(t)dt \quad (7.460)$$

where  $\hat{\phantom{x}}$  indicates the Hilbert transform. Nowomieski has not explicitly defined the notion of the quadrature power (see Equation 7.422) but in fact the integrand in Equations 7.459 and 7.460 equals  $Q(t)$ . However, a new quantity called *distortion power* was defined. Generally, for each value of  $T$  the identity

$$\int_{-T}^T u^2(t)dt \int_{-T}^T i^2(t)dt = \left| \int_{-T}^T u(t)i(t)dt \right|^2 + \int_{-T}^T \int_{-T}^T \frac{1}{2} [u(t)i(\tau) - u(\tau)i(t)]^2 dt d\tau \quad (7.461)$$

holds true, and because the limit exists

$$S^2 \left\{ \lim_{T \rightarrow \infty} \frac{1}{2T} \int_{-T}^T u^2(t)dt \right\} \left\{ \lim_{T \rightarrow \infty} \frac{1}{2T} \int_{-T}^T i^2(t)dt \right\} \quad (7.462)$$

the quantity  $D$ , called distortion power, may be defined by means of the equation

$$\bar{D} = \sqrt{\lim_{T \rightarrow \infty} \left[ \frac{1}{2T} \int_{-T}^T \int_{-T}^T \frac{1}{2} [u(t)i(\tau) - u(\tau)i(t)]^2 dt d\tau \right]} \quad (7.463)$$

Based on Equation 7.461 we arrive at

$$S^2 = \bar{P}^2 + \bar{D}^2 \quad (7.464)$$

In the case

$$i(t) = \text{const } u(t) \quad (7.465)$$

the quadrature component defined by Equation 7.439 equals zero and the distortion power equals zero, too. Otherwise, the distortion power is given by

$$\bar{D} = U \sqrt{\lim_{T \rightarrow \infty} \frac{1}{2T} \int_{-T}^T i_q^2(t)dt} \quad (7.466)$$

Let us define a power factor  $\rho_D$  using the relation

$$\rho_D = \frac{\bar{P}}{\bar{P}^2 + \bar{D}^2} \quad (7.467)$$

The power factor is a measure of the efficiency of the utilization of the power supplied to the load being equal to unity only, if the distortion power  $D=0$ . The cross-correlation of the instantaneous voltage and current waveforms is defined by the integral

$$\rho_{ui}(\tau) = \lim_{T \rightarrow \infty} \frac{1}{2T} \int_{-T}^T u(t)i(t-\tau)dt \quad (7.468)$$

This function enables us to introduce the frequency domain interpretations of the above-defined powers. The *cross-power spectrum*  $\Theta(\omega)$  is defined by the Fourier pair

$$\rho_{u-i}(\tau) \stackrel{F}{\Leftrightarrow} \Theta(\omega) \quad (7.469)$$

It may be shown that the active power is given by the integral of the power spectrum

$$\bar{P} = \frac{1}{2\pi} \int_{-\infty}^{\infty} \Theta(\omega)d\omega \quad (7.470)$$

In general,  $\Theta(\omega)$  is a complex function, but the integral of the odd imaginary part equals zero. The reactive power is given by

$$\bar{Q} = \frac{1}{2\pi j} \int_{-\infty}^{\infty} \text{sgn}(\omega)\Theta(\omega)d\omega \quad (7.471)$$

Hence, the *complex power* is

$$S = \bar{P} + j\bar{Q} = \frac{1}{2\pi} \int_{-\infty}^{\infty} [1 + \text{sgn}(\omega)]\Theta(\omega)d\omega \quad (7.472)$$

Because the integrand presents a one-sided complex power spectrum, the complex power is an analytic function and  $\bar{P}$  and  $\bar{Q}$  form a pair of Hilbert transforms. If at least one of the signals  $u(t)$

or  $i(t)$  does not contain a constant component, Equation 7.472 reduces to the form

$$S = \bar{P} + j\bar{Q} = \frac{1}{\pi} \int_{-\infty}^{\infty} \Theta(\omega) d\omega \quad (7.473)$$

Notice that the Wiener-Khinchin relation (Equation 7.469) holds for stationary and ergodic processes. If the load presents a linear, time-invariant, and strictly stable system defined by the Fourier pair

$$h(t) \xleftrightarrow{F} H(j\omega) \quad (7.474)$$

(where  $h(t)$  is the impulse response and  $H(j\omega)$  is the transfer function) then the autocorrelation function of the voltage and its power spectrum are given by the Fourier pair

$$\rho_{u-u}(\tau) \xleftrightarrow{F} \Phi(\omega) \quad (7.475)$$

and the RMS values of the voltage and current have the form

$$U_{\text{RMS}}^2 = \rho_{u-u}(0); \quad I_{\text{RMS}}^2 = \frac{1}{2\pi} \int_{-\infty}^{\infty} \Phi(\omega) |H(j\omega)|^2 d\omega \quad (7.476)$$

and the complex power is given by

$$S = \bar{P} + j\bar{Q} = \frac{1}{\pi} \int_{-\infty}^{\infty} \Phi(\omega) H^*(\omega) d\omega \quad (7.477)$$

## 7.21 Discrete Hilbert Transformation

The theory and applications of the discrete Hilbert transformation (DHT) are closely tied with the principles of digital signal processing.<sup>26,30</sup> Because discrete transforms will be included in another handbook in this series, this section presents only basic concepts. The formulas for the DFT and for the Z-transformation are given to fix the notations because there are various notations (definitions) of the DFT.

For reference, let us recall the Fourier transformations given by Equations 7.6 or 7.7 and defined using the exponential kernels  $\exp(-j2\pi ft)$  and  $\exp(j2\pi ft)$ , respectively ( $\omega = 2\pi f$ ). In digital signal processing, a time signal  $u(t)$  is substituted by a sequence of samples  $u(i)$ . Therefore, in the DFT the time variable  $t$  is replaced by the discrete integer variable  $i$ ,  $0 \leq i \leq N-1$ , where  $N$  is the length of the sequence. The discrete signal has the form of a sequence of samples  $u(0), u(1), u(2), \dots, u(N-1)$ . The DFT of this sequence is defined by the formula

$$U(k) = \sum_{i=0}^{N-1} u(i) e^{-jkw}; \quad w = 2\pi ik/N \quad (7.478)$$

where  $k$  is a discrete integer frequency variable,  $0 \leq k \leq N-1$ . The discrete spectrum is periodic; that is  $U(k) = U(k+N) = U(k+2N), \dots$ . The inverse transformation denoted  $\text{DFT}^{-1}$  has the form

$$u(i) = \frac{1}{N} \sum_{k=0}^{N-1} U(k) e^{jkw} \quad (7.479)$$

The sequence generated by this inverse transformation is periodic; that is,  $u(t) = u(i+N) = u(i+2N) = \dots$ . Usually of interest is the basic period. The comparison of Fourier integrals with the DFT shows that integration is replaced by summation and the exponential kernel  $\exp(\pm j\omega t)$  is replaced by  $\exp(\pm jkw)$ . The discrete Fourier pair may be shortened to

$$u(i) \xleftrightarrow{\text{DFT}} U(k) \quad (7.480)$$

In general, for real sequences  $u(i)$  is the spectral function  $U(k)$  is complex, i.e.,

$$U(k) = U_{\text{re}}(k) + j U_{\text{im}}(k) \quad (7.481)$$

The real part is defined by the cosine DFT of the form

$$U_{\text{re}}(k) = \sum_{i=0}^{N-1} u(i) \cos(w) \quad (7.482)$$

and the imaginary part by the sine DFT of the form

$$U_{\text{im}}(k) = \sum_{i=0}^{N-1} u(i) \sin(w) \quad (7.483)$$

A given sequence may be resolved in two parts

$$u(i) = u_e(i) + u_o(i) \quad (7.484)$$

where for even values of  $N$  the even and odd parts are given by

$$u_e(i) = \frac{u(N/2+i) + u(N/2-i)}{2}; \quad (7.485)$$

$$u_o(i) = \frac{u(N/2+i) - u(N/2-i)}{2}$$

with  $N/2 \leq i \leq N-1$ . The cosine transform depends only on  $u_e(i)$  and the sine transform on  $u_o(i)$ . Using the complex form (Equation 7.481) the inverse DFT may be written in the form

$$u(i) = \frac{1}{N} \sum_{k=0}^{N-1} [U_{\text{re}}(k) \cos(w) - U_{\text{im}}(k) \sin(w)] \quad (7.486)$$

The one-sided Z-transformation of the sequence  $u(i)$  is defined by the formula (see also Chapter 6)

$$U(z) = \sum_{i=0}^{N-1} u(i) z^{-i} \quad (7.487)$$

where the complex frequency variable  $z = x + jy$  is continuous differently than the discrete frequencies used in the DFTs. We shall denote the Z-pair by

$$u(i) \stackrel{z}{\Leftrightarrow} U(z) \quad (7.488)$$

The discrete one-sided convolution is defined by the equation

$$y(i) = \sum_{m=0}^{N-1} h(i-m)u(m) \quad (7.489)$$

and if  $h(i) \stackrel{z}{\Leftrightarrow} H(z)$  and  $u(i) \stackrel{z}{\Leftrightarrow} U(z)$  then the well-known convolution to multiplication property yields the Z-pair

$$y(i) \stackrel{z}{\Leftrightarrow} H(z)U(z) \quad (7.490)$$

Because the DFT is periodic, it is a periodic function of the normalized frequency

$$\psi = 2\pi k/N \quad (7.491)$$

The basic period equals the interval  $0 \leq \psi < 2\pi$ , the next period is  $2\pi \leq \psi < 4\pi$ , and so forth. The DFT equals the Z-transform for values of  $z$  given by

$$z = e^{j\psi}; \quad \psi = 2\pi k/N \quad (7.492)$$

that is, equally spaced on the unit circle of the  $z$ -plane (see Figure 7.40). The half-period  $0 \leq \psi < \pi$  (upper half-circle) is classified as positive frequencies and the other half-period,  $\pi \leq \psi < 2\pi$ , as negative frequencies. The insertion of Equation 7.492 in Equation 7.490) yields the  $k$ -domain form of the multiplication to convolution theorem

$$y(i) = u(i)*h(i) \stackrel{\text{DFT}}{\Leftrightarrow} U(k)H(k) \quad (7.493)$$

The discrete equivalent of the delta pulse is the Kronecker delta sample

$$\delta_K(i) = \begin{cases} 1 & \text{for } i = 0 \\ 0 & \text{for } i \neq 0 \end{cases} \quad (7.494)$$

The impulse response of the DLTI system defined as the response to the  $\delta_K$  sample and the transfer function  $H(z)$  of the system are forming a Z-pair

$$h(i) \stackrel{z}{\Leftrightarrow} H(z) \quad (7.495)$$

The insertion  $z = e^{j\psi}$  ( $\psi = 2\pi k/N$ ) yields the relation

$$h(i) \stackrel{\text{DFT}}{\Leftrightarrow} H(k) \quad (7.496)$$

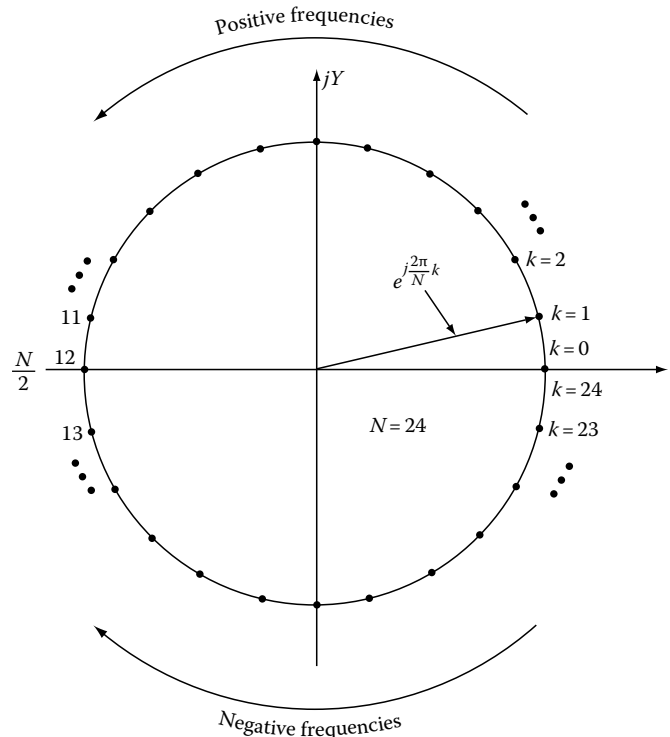


FIGURE 7.40 The unit circle in the  $z = x + jy$  plane (see Equation 7.492,  $N = 24$ ).

The transfer function of an ideal discrete Hilbert filter is defined by the equation ( $N$  even)<sup>7</sup>

$$H(k) = \begin{cases} -j & \text{for } k = 1, 2, \dots, N/2 - 1 \\ 0 & \text{for } k = 0 \text{ and } N/2 - 1 \\ j & \text{for } k = N/2 + 1, N/2 + 2, \dots, N - 1 \end{cases} \quad (7.497)$$

This transfer function may be written in the closed form

$$H(k) = -j \operatorname{sgn}(N/2 - k) \operatorname{sgn}(k) \quad (7.498)$$

where

$$\operatorname{sgn}(x) = \begin{cases} 1 & \text{for } x > 0 \\ 0 & \text{for } x = 0 \\ -1 & \text{for } x < 0 \end{cases} \quad (7.499)$$

The output sequence  $v(i)$  of the Hilbert filter by a given input sequence  $u(i)$  defines the discrete Hilbert pair

$$u(i) \stackrel{\text{DHT}}{\Leftrightarrow} v(i) \quad (7.500)$$

The impulse response of the Hilbert filter is given by the inverse DFT of  $H(k)$ :

$$h(i) = \frac{1}{N} \sum_{k=0}^{N-1} H(k)e^{jkw} = \frac{1}{N} \sum_{k=0}^{N-1} -j \operatorname{sgn}(N/2 - k) \operatorname{sgn}(k) e^{jkw}$$

$$= \frac{1}{N} \sum_{k=0}^{N-1} \sin(w) \tag{7.501}$$

( $w = 2\pi ik/N$ ). The closed form of this sum is (see Figure 7.41)

$$h(i) = \frac{2}{N} \sin^2(\pi i/2) \cot(\pi i/N) \quad i = 0, 1, \dots, N - 1 \tag{7.502}$$

Therefore, the impulse response is given by the samples of the cotangent function (compare with Equation 7.104 with the even samples ( $i = 0, 2, 4, \dots, N$ ) canceled by the term  $\sin^2(\pi i/2)$ ). The convolution to multiplication theorem (Equation 7.493) yields the DHT in the form of the convolution

$$v(i) = -u(i) \otimes h(i) = -u(i) \otimes \frac{2}{N} \sin^2(\pi i/2) \cot(\pi i/N)$$

$$i = 0, 1, \dots, N - 1 \quad (N \text{ even}) \tag{7.503}$$

where the sign  $\otimes$  denotes a so-called circular convolution. This convolution may be written in the form

$$v(i) = \sum_{r=0}^{N-1} h(i - r)u(r) \tag{7.504}$$

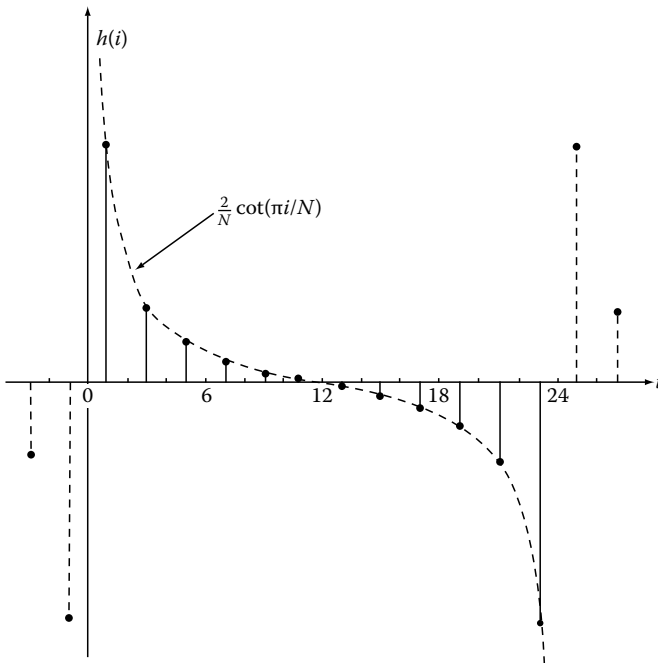


FIGURE 7.41 The noncausal impulse response of a Hilbert filter (see Equation 7.20.5),  $N = 24$ .

Concluding, the DHT of a given sequence  $u(i)$  may be calculated using the above circular convolution or alternatively via the DFT using the algorithm

$$u(i) \xrightarrow{\text{DFT}} U(k) \Rightarrow V(k) = -j \operatorname{sgn}(N/2 - k) \operatorname{sgn}(k) U(k)$$

$$\xrightarrow{\text{DFT}^{-1}} v(i) \quad i = 0, 1, \dots, N - 1 \quad (N \text{ even}) \tag{7.505}$$

Both algorithms give exactly the same result. Of course, the convolution algorithm is faster, because it involves only a single summation. However, the DFT may be replaced by the FFT.

The above formulas apply for even values of  $N$ . If  $N$  is odd, the transfer function of the Hilbert filter has the form

$$k) = \begin{cases} -j & \text{for } k = 1, 2, \dots, (N - 1)/2 \\ 0 & \text{for } k = 0 \\ j & \text{for } k = N/2 + 1, (N + 1)/2, \dots, N - 1 \end{cases} \tag{7.506}$$

and the impulse response is

$$h(i) = \frac{2}{N} \sum_{k=1}^{(n-1)/2} \sin(2\pi ik/N); \quad i = 0, 1, 2, \dots, N - 1 \tag{7.507}$$

or

$$h(i) = \frac{1}{N} \left[ 1 - \frac{\cos(\pi i)}{\cos(\pi i/N)} \cot(\pi i/N) \right] \tag{7.508}$$

### 7.21.1 Properties of the DFT and DHT Illustrated with Examples

#### 7.21.1.1 Parseval's Theorem

Consider the discrete Fourier part  $u(i) \xleftrightarrow{\text{DFT}} U(k)$ . The discrete form of the Parseval's energy (or power) equality has the form

$$E[u(i)] = \sum_{i=0}^{N-1} |u(i)|^2 = \frac{1}{N} \sum_{k=0}^{N-1} |U(k)|^2 \tag{7.509}$$

This equation may be used to check the correctness of calculations of DFTs and DHTs. However, the energies of the sequences  $u(i)$  and its DHT,  $v(i)$ , may differ, in general,

$$E[u(i)] \neq E[v(i)] \tag{7.510}$$

The explanation is given by Equation 7.505. The operator  $-j \operatorname{sgn}(N/2 - k) \operatorname{sgn}(k)$  cancels the spectral terms  $U(0)$  and  $U(N/2)$ . The term  $U(0)$  has the form

$$U(0) = \sum_{i=0}^{N-1} u(i) = N u_{\text{DC}} \tag{7.511}$$

where  $u_{DC}$  is the mean value of the signal sequence  $u(i)$ , or in electrical terminology, the DC term. The algorithm of DHT cancels this term. Therefore, the sequence  $v(i)$  is defined by the DHT pair

$$u_{AC}(i) \stackrel{\text{DFT}}{\iff} v(i) \tag{7.512}$$

where  $u_{AC}(i) = u(i) - u_{DC}$  is the alternate current component of the signal sequence (with DC term removed). The energies of the sequences  $u_{AC}(i)$  and  $v(i)$  are given by the equation

$$\sum_{i=1}^{N-1} |u_{AC}(i)|^2 = \sum_{i=1}^{N-1} |v(i)|^2 + \frac{|U(N/2)|^2}{N} \tag{7.513}$$

that is, the energies differ by the energy of the spectral term  $U(N/2)$  and only if this term equals zero are both energies equal.

**Example**

Consider the signal given by a Kronecker delta  $u(0) = \delta_k(i)$  and  $u(i) = 0$  for  $i \geq 1, N = 8$ . This sequence and its DFT are shown in Figure 7.42a and b. The circular convolution (Equation 7.503) yields in this case

$$v(i) = -\delta_k(i)^* \frac{1}{4} \sin^2(\pi i/2) \cot(\pi i/N) \tag{7.514}$$

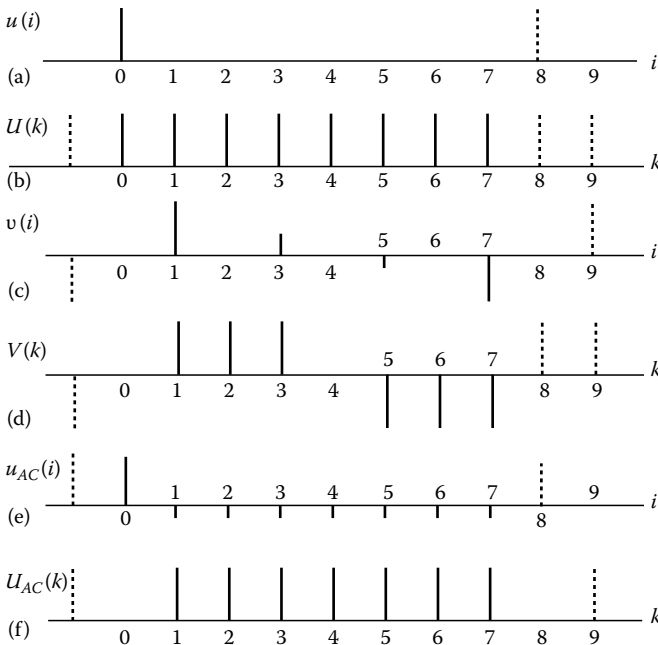


**FIGURE 7.42** (a) The sequence  $u(i)$  consisting of a single sample  $\delta_k(i)$ , (b) its spectrum  $U(k)$  given by the DFT, (c) the samples of the discrete Hilbert transform, (d) the corresponding spectrum  $V(k)$ , (e) the samples of the AC component of  $u(i)$ , and (f) the corresponding spectrum  $U_{AC}(k)$ .

that is, the following sequence

$i$	0	1	2	3	4
$v(i)$	0	$[\cot(\pi/8)]/4$	0	$[\cot(3\pi/8)]/4$	0
		5	6	7	
		$-[\cot(3\pi/8)]/4$	0	$-[\cot(\pi/8)]/4$	

where

$$[\cot(\pi/8)]/4 = (\sqrt{2} + 1)/4 = 0.6035 \dots$$

$$[\cot(3\pi/8)]/4 = (\sqrt{2} - 1)/4 = 0.1035 \dots$$

The sequence  $v(i)$  and its DFT are shown in Figure 7.42c and d. The DC term defined by Equation 7.511 is  $u_{DC} = 1/N = 0.125$ . For convenience, Figure 7.42e and f shows the sequence  $u_{AC}(i)$  and its DFT. The energies are  $E[u(i)] = 1$ ,  $E[u_{AC}(i)] = 1 - 1^2/N = 0.875$ ,  $E[v(i)] = 1 - 1^2/N - 1^2/N = 1 - 2/N = 0.75$ .

**7.21.1.2 Shifting Property**

Consider the discrete Fourier pair  $u(i) \stackrel{\text{DFT}}{\iff} U(k)$ . It can be shown that

$$u(i + m) \stackrel{\text{DFT}}{\iff} e^{j2\pi mk/N} U(k) \tag{7.515}$$

where  $m$  is an integer.

**Example**

The spectrum of Figure 7.42b is real with all samples equal to 1. The shifted-by-one interval ( $m = 1$ ) delta pulse and its spectrum are

$$\delta_k(i - m) \stackrel{\text{DFT}}{\iff} e^{-j2\pi mk/N} \tag{7.516}$$

This spectrum is complex and of the form

$k$	0	1	2	3	4	5	6	7
$U_{re}(k)$	1	$\sqrt{2}/2$	0	$-\sqrt{2}/2$	-1	$-\sqrt{2}/2$	0	$\sqrt{2}/2$
$U_{im}(k)$	0	$-\sqrt{2}/2$	-1	$-\sqrt{2}/2$	0	$\sqrt{2}/2$	1	$\sqrt{2}/2$
$ U(k) $	1	1	1	1	1	1	1	1

This example shows the general rule that shift changes in phase relations will have no effect on the magnitude of the spectrum.

**7.21.1.3 Linearity**

Consider the discrete Fourier pairs  $u_1(i) \stackrel{\text{DFT}}{\iff} U_1(k)$  and  $u_2(i) \stackrel{\text{DFT}}{\iff} U_2(k)$ . Due to the linearity property the summation of the sequences yields

$$au_1(i) + bu_2(i) \stackrel{\text{DFT}}{\iff} aU_1(k) + bU_2(k) \tag{7.517}$$



where  $a$  and  $b$  are constants. The linearity property applies also for the DHTs:

$$au_1(i) + bu_2(i) \stackrel{\text{DFT}}{\iff} av_1(i) + bv_2(i) \quad (7.518)$$

**Example**

Consider the sequence of two deltas  $u(i) = \delta_k(i) + \delta_k(i - 1)$  for  $i = 0$  and  $1$  and  $u(i) = 0$  for  $1 < i \leq N - 1$ ,  $N = 8$ . The DFT of this sequence may be obtained by adding to each term of the real part of the spectrum given by Equation 7.516 the number 1; that is, the terms of the spectrum of  $\delta_k(i)$  (see Figure 7.42b). This yields the complex spectrum

$k$	0	1	2	3	4	5	6	7
$U_{re}(k)$	2	$1 + \sqrt{2}/2$	1	$1 - \sqrt{2}/2$	0	$1 - \sqrt{2}/2$	1	$1 + \sqrt{2}/2$
$U_{im}(k)$	0	$-\sqrt{2}/2$	-1	$-\sqrt{2}/2$	0	$\sqrt{2}/2$	1	$\sqrt{2}/2$
$ U(k) $	2	1.847...	$\sqrt{2}$	0.765...	0	0.765...	$\sqrt{2}$	1.847...

Notice that the term  $U(N/2) = U(4)$  equals zero. Therefore, the energies  $E[u_{AC}(i)] = E[v(i)] = 2 - 2^2/N = 1.5$  are equal. The DC term  $u_{DC} = 2/N = 0.25$ .

**Example**

Consider the sequence

$$u(i) = e^{-0.05\pi((N-1)/2 - i)^2}; \quad N = 16 \quad (7.519)$$

representing a sample Gaussian pulse as shown in Figure 7.43 (top). Figure 7.43 (middle/bottom) shows the DFT of this pulse and the DHT calculated via the DFT. The DC term equals  $u_{DC} = 0.2795\dots$ . The energies are  $E[u(i)] = 3.1622\dots$ ,  $E[u_{AC}(i)] = E[v(i)] = 1.9122\dots$ , that is, the energy difference is negligible due to the negligible value of the term  $U(N/2)$ .

**7.21.2 Complex Analytic Discrete Sequence**

A sequence of complex samples of a signal and its discrete Hilbert transform does not represent an analytic signal in the sense of the definition of the analytic function. However, it is possible to define the analytic sequence of the form of a sequence of samples

$$\psi(i) = u(i) + jv(i) \quad (7.520)$$

where  $v(i)$  is the DHT of  $u(i)$ . Let us derive the spectrum of the sequence  $\psi(i)$ . If  $u(i) \stackrel{\text{DFT}}{\iff} U(k)$ , then the spectrum of  $v(i)$  given by Equation 7.505, and due to the linearity property, the spectrum of the complex sequence  $\psi(i)$  is

$$\psi(i) \stackrel{\text{DFT}}{\iff} U(k) + j[ -j \operatorname{sgn}(N/2 - k) \operatorname{sgn}(k)]U(k)$$

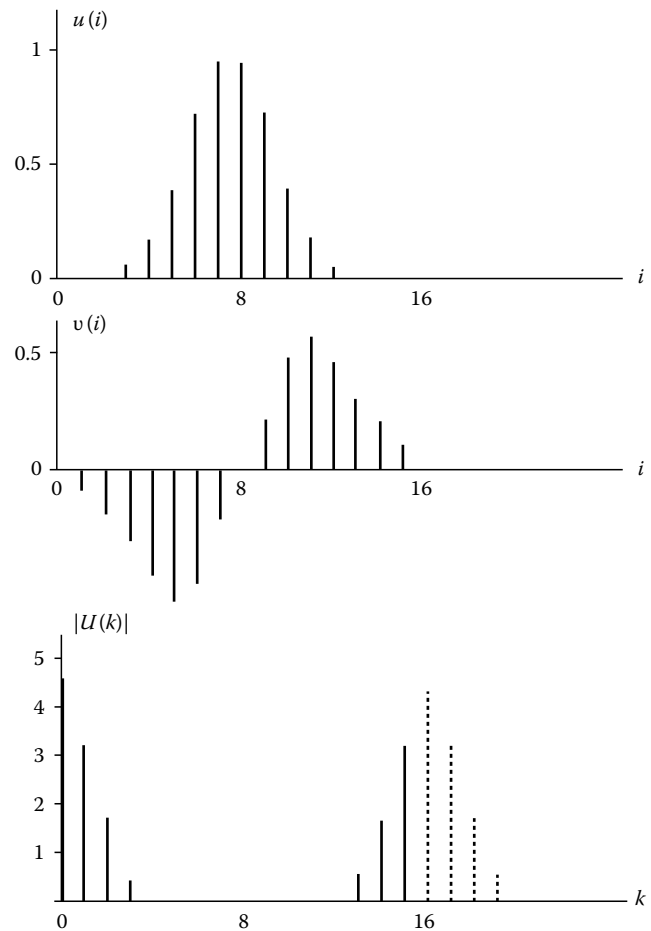


**FIGURE 7.43** (Top) A sequence of samples of a Gaussian pulse, (middle) the samples of the DHT, and (bottom) the samples of the magnitude of the DFT of the Gaussian pulse.

that is,

$$\psi(i) \stackrel{\text{DFT}}{\iff} [1 + \operatorname{sgn}(N/2 - k) \operatorname{sgn}(k)]U(k) \quad (7.521)$$

$k = 0, 1, \dots, N - 1 (N \text{ even})$

The spectrum is doubled at positive frequencies and canceled at negative frequencies.

**Example**

Consider the signals and spectra of Figure 7.42. Figure 7.44 shows the real spectra of the delta pulse and its DHT and the resulting spectrum of the complex sequence. The terms of the spectrum of  $u(i)$  are canceled at negative frequencies and doubled at positive frequencies. The DC term, i.e.,  $U(0)$ , is unaltered. The property that analytic sequences have a one-sided spectrum makes it possible to implement antialiasing schemes of sampling.

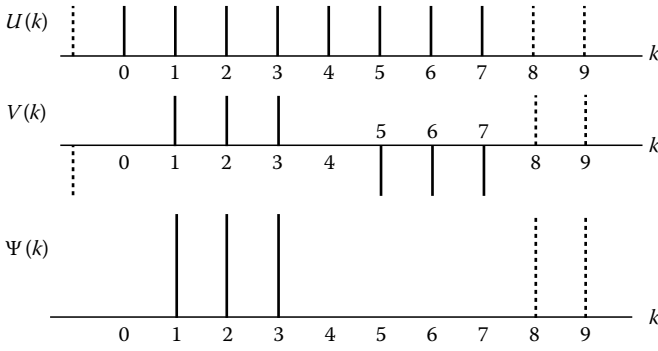


FIGURE 7.44 (Top, middle) The spectra  $U(k)$  and  $V(k)$  of Figure 7.42; (bottom) the corresponding spectrum of the analytic sequence.

### 7.21.3 Bilinear Transformation and the Cotangent Form of Hilbert Transformations

The transfer function of an analog LTI system is defined as the quotient of the output-to-input analytic signals (see Equation 7.325), and if analytical, is an analytic function of the complex frequency  $s = \alpha + j\omega$ . Similarly, the transfer function of the DLTI system defined by Equation 7.495, if analytical, is an analytic function of the complex variable  $z = x + jy$ . Let us study the problem of a *conformal mapping* of the  $s$ -plane into the  $z$ -plane by means of the *bilinear transformations* defined by the formulae

$$z = \frac{1 + s}{1 - s} \tag{7.522}$$

and

$$s = \frac{z - 1}{z + 1} \tag{7.523}$$

where  $s$  is a normalized complex frequency (normalized  $s = s/f_s = s\Delta t$ , where  $f_s$  is the sampling frequency and  $\Delta t$  the sampling period). Inserting  $s = \alpha + j\omega$  into Equation 7.522 and equating the real and imaginary parts yields

$$x = \frac{1 - \alpha^2 - \omega^2}{(1 - \alpha)^2 + \omega^2}; y = \frac{2\omega}{(1 - \alpha)^2 + \omega^2} \tag{7.524}$$

These equations are mapping a family of orthogonal lines  $a = \text{const.}$  and  $\omega = \text{const.}$  of the  $s$ -plane into a family of orthogonal of the  $z$ -plane, as shown in Figure 7.45. The magnitude of the variable is  $|z| = \text{SQR}(x^2 + y^2)$  giving

$$|z| = \sqrt{\frac{(1 + \alpha)^2 + \omega^2}{(1 - \alpha)^2 + \omega^2}} \tag{7.525}$$

and the argument

$$\psi = \arg(z) = \tan^{-1} \left[ \frac{2}{1 - \alpha^2 - \omega^2} \right] \tag{7.526}$$

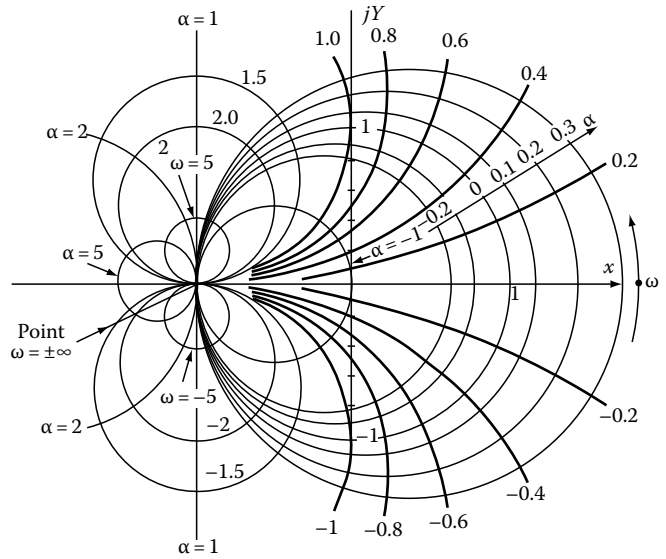


FIGURE 7.45 The mapping of the  $s$ -plane,  $s = \alpha + j\omega$ , into the  $z$ -plane,  $z = x + jy$ , defined Equation 7.524. Let us introduce the notations

This equation defines the nonlinear dependence between the angular frequency  $\omega$  and the normalized frequency  $\psi$  defined by the representation  $z = e^{j\psi}$  (see Equation 7.492). For  $s = j\omega$ ; that is,  $\alpha = 0$ , Equation 7.526 takes the form of a quadratic equation

$$\tan(\psi)\omega^2 + 2\omega - \tan(\psi) = 0 \tag{7.527}$$

The roots of this equation are

$$\omega = \tan(\psi/2) \tag{7.528}$$

and

$$\omega = -\cot(\psi/2) \tag{7.529}$$

Let us use these nonlinear relations to derive a new form of Hilbert transformations. We start with the Hilbert transformation

$$B(\omega) = -\frac{1}{\pi} P \int_{-\infty}^{\infty} \frac{A(\eta)}{\eta - \omega} d\eta \tag{7.530}$$

Let us introduce the notations

$$\eta = \tan(\phi/2); \omega = \tan(\psi/2) \tag{7.531}$$

and  $d\eta = 0.5[1 + \tan^2(\phi/2)]d\phi$ . We get

$$B(\psi) = \frac{1}{\pi} P \int_{-\pi}^{\pi} \frac{A[\tan(\phi/2)]}{\tan(\phi/2) - \tan(\psi/2)} 0.5[1 + \tan^2(\phi/2)]d\phi \tag{7.532}$$

By means of the trigonometric relation

$$\frac{1 + \tan^2(\phi/2)}{\tan(\phi/2) - \tan(\psi/2)} = \tan(\phi/2) + \cot[(\phi - \psi)/2] \quad (7.533)$$

we get

$$B(\psi) = -\frac{1}{2\pi} \int_{-\pi}^{\pi} A[\tan(\phi/2)] \tan(\phi/2) d\phi - \frac{1}{2\pi} \int_{-\pi}^{\pi} A[\tan(\phi/2)] \cot[(\phi - \psi)/2] d\phi \quad (7.534)$$

If we start with the inverse Hilbert transformation

$$A(\omega) = \frac{1}{\pi} P \int_{-\infty}^{\infty} \frac{B(\eta)}{\eta - \omega} d\eta \quad (7.535)$$

the same derivation gives

$$A(\psi) = \frac{1}{2\pi} \int_{-\pi}^{\pi} B[\tan(\phi/2)] \tan(\phi/2) d\phi + \frac{1}{2\pi} \int_{-\pi}^{\pi} B[\tan(\phi/2)] \cot[(\phi - \psi)/2] d\phi \quad (7.536)$$

The first term of Equation 7.534 is a constant depending only on the even part of  $A[\tan(\phi/2)]$ , while the first term of Equation 7.536 depends only on the odd part of  $B[\tan(\psi/2)]$ .

If we use instead of Equation 7.528 the next root defined by Equation 7.529, then Hilbert transformations (7.534) and (7.536) have the alternative form:

$$B(\psi) = \frac{-1}{2\pi} \int_0^{2\pi} A[-\cot(\phi/2)] \cot(\phi/2) d\phi - \frac{1}{2\pi} \int_0^{2\pi} A[-\cot(\phi/2)] \cot[(\phi - \psi)/2] d\phi \quad (7.537)$$

$$A(\psi) = \frac{1}{2\pi} \int_0^{2\pi} B[-\cot(\phi/2)] \cot(\phi/2) d\phi + \frac{1}{2\pi} \int_0^{2\pi} B[-\cot(\phi/2)] \cot[(\phi - \psi)/2] d\phi \quad (7.538)$$

The Hilbert transforms in the cotangent form are periodic functions of the variable  $\psi$ .

**Example**

Consider the square function

$$A(\omega) = \begin{cases} 1 & \text{for } |\omega| < a \\ 0.5 & \text{for } |\omega| = a \\ 0 & \text{for } |\omega| > a \end{cases} \quad (7.539)$$

Introducing  $\omega = \tan(\psi/2)$  gives

$$A[\tan(\psi/2)] = \begin{cases} 1 & \text{for } |\psi| < \psi_p = 2 \tan^{-1}(a) \\ 0.5 & \text{for } |\psi| = \psi_p \\ 0 & \text{for } |\psi| > \psi_p \end{cases} \quad (7.540)$$

The Hilbert transform defined by Equation 7.538 is here

$$B(\psi) = -\frac{1}{2\pi} \int_{-\psi_p}^{\psi_p} \tan\left[\frac{\phi}{2}\right] d\phi - \frac{1}{2\pi} \int_{-\psi_p}^{\psi_p} \cot\left[\frac{\phi - \psi}{2}\right] d\phi \quad (7.541)$$

The first integral equals zero and the result of the second integration (Cauchy Principal Value (CPV) value) is

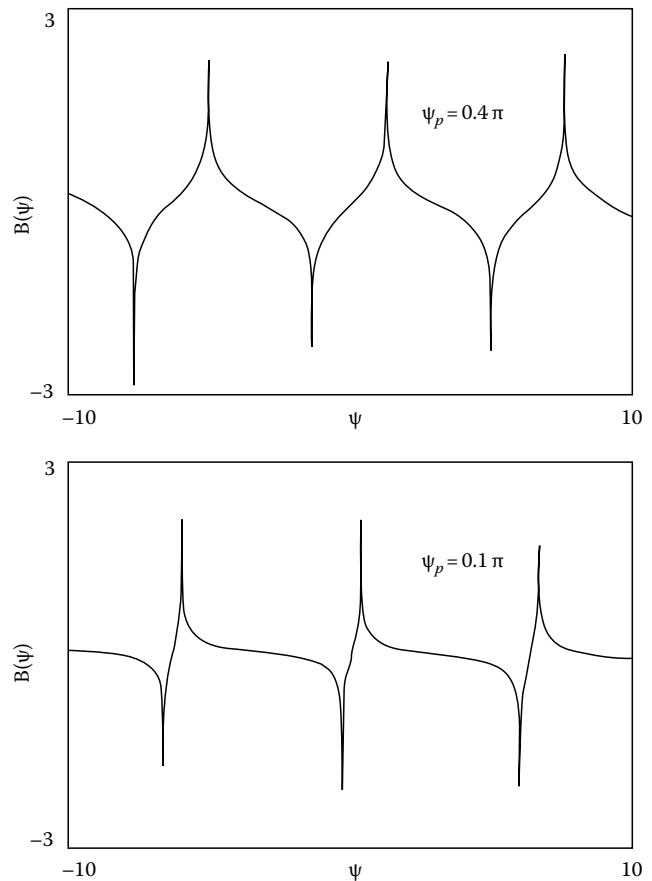


FIGURE 7.46 The function  $B(\psi)$  given by Equation 7.542.

$$B(\psi) = \frac{1}{\pi} \ln \left| \frac{\sin \frac{\psi_p + \psi}{2}}{\sin \frac{\psi_p - \psi}{2}} \right| \quad (7.542)$$

Figure 7.46 shows  $B(\psi)$  for two values of  $\psi_p$ :  $0.4\pi$  and  $0.1\pi$  corresponding to the normalized frequencies  $\omega \cong 0.726$  and  $0.155$ . The functions  $A(\psi)$  and  $B(\psi)$  are periodic with the period of  $2\pi$ .

## 7.22 Hilbert Transformers (Filters)

The *Hilbert transformer*, also called a *quadrature filter* or wide-band  $90^\circ$  phase shifter, is a device in the form of a linear two-port whose output signal is a Hilbert transform of the input signal. Hilbert transformers find numerous applications, for example, in radar systems, SSB modulators, speech processing, measurement systems, schemes of sampling band-pass signals, and many other systems. They are implemented as analog or digital filters. The transfer function of the ideal analog Hilbert filter is (see Equation 7.10)

$$H(jf) = F[1/(\pi t)] = |H(jf)|e^{j\varphi(f)} = -j \operatorname{sgn}(f) \quad (7.543)$$

Hence, the transfer function is given by

$$H(jf) = \begin{cases} -j & \text{for } f > 0 \\ 0 & \text{for } f = 0 \\ j & \text{for } f < 0 \end{cases} \quad (7.544)$$

The magnitude is  $|H(jf)| = 1$  and the phase function is

$$\varphi(f) = \arg [H(jf)] = -(\pi/2) \operatorname{sgn}(f) \quad (7.545)$$

Notice that the convention with a +sgn by  $\varphi(f)$  results in a negative slope of the phase function. The last equation explains the terminology “quadrature filter” or “wide-band  $90^\circ$  phase shifter.” The ideal Hilbert filter is noncausal and physically unrealizable. Causality implies the introduction of an infinite delay. In any practical implementation of the Hilbert filter, the output signal is a delayed and more or less distorted Hilbert transform of the input signal. The spectrum of the input signal should be band-limited between the low-frequency edge  $f_1$  and high-frequency edge  $f_2$  of the pass-band. The necessary delay depends only on  $f_1$ . Inside the pass-band  $W = f_2 - f_1$ , it is possible to get an approximate version of the transfer function defined by Equation 7.543. Good approximations require sophisticated methods of design and implementations.

Hilbert transformers can be implemented in the form of analog or digital convolvers using the time definition of the Hilbert transforms given by Equations 7.3 and 7.4 (analog convolutions) or by Equation 7.503 (discrete circular convolution). An other implementation uses so-called quadrature filters.

The performance of analog Hilbert transformers depends on design and alignment. Having in mind that ideal alignment is impossible and that even by good initial alignment it is deteriorated by aging and various physical changes; for example, temperature, humidity, pressure, vibrations, and others, the use of extremely sophisticated design methods and implementations may be unreasonable. Differently, the performance of digital Hilbert transformers may depend only on design.

Because the magnitude of the transfer function defined by Equation 7.544 equals 1, all-pass filters are frequently used in analog and digital implementations of Hilbert transformers.

### 7.22.1 Phase-Splitter Hilbert Transformers

Analog Hilbert transformers are mostly implemented in the form of a phase splitter consisting of two parallel all-pass filters with a common input port and separated output ports, as shown in Figure 7.47. The transfer functions of the all-pass filters are

$$H_1(jf) = e^{j\varphi_1(f)}; \quad H_2(jf) = e^{j\varphi_2} \quad (7.546)$$

The magnitude of both functions equals 1. The antisymmetry of the phase functions allows us to consider only the positive frequency part. The phase difference of the harmonic signals at the output ports of the phase splitter should be

$$\delta(f) = \varphi_1(f) - \varphi_2(f) = -\pi/2; \quad \text{all } f > 0 \quad (7.547)$$

The realization of this requirement is possible in a limited frequency band between the low-frequency edge  $f_1$  and the high-frequency edge  $f_2$ , as shown in Figures 7.52 through 7.55. Therefore, the spectrum of the input signal should be band limited between  $f_1$  and  $f_2$ . Due to unavoidable amplitude and phase errors, the output signals of the phase splitter approximately are forming a Hilbert pair. The phase functions of the all-pass filters defined by Equation 7.546 should be inside the band  $W = f_2 - f_1$ , approximately linear in the logarithmic frequency scale, but are nonlinear in a linear scale. This nonlinearity introduces phase distortions. Therefore, the output signals are form-

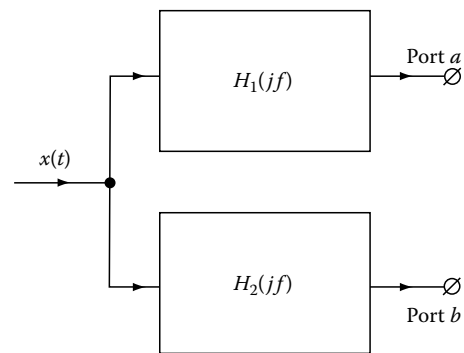


FIGURE 7.47 A phase splitter Hilbert transformer, where  $H_1(jf)$  and  $H_2(jf)$  are all-pass transfer functions.

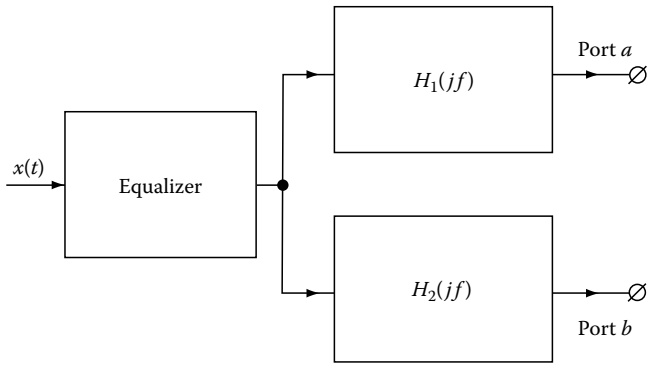


FIGURE 7.48 The series connection of a phase equalizer and the Hilbert transformer of Figure 7.47.

ing a distorted in relation to the input signal Hilbert pair. The distortions can be removed using a suitable phase equalizer connected in series to the input port, as shown in Figure 7.48. By proper phase equalization the output signals are forming an undistorted pair of Hilbert transforms.

### 7.22.2 Analog All-Pass Filters

Hilbert transformers in the form of phase splitters are implemented using all-pass filters. A convenient choice is the all-pass consisting of two complementary filters, a low-pass and a high-pass, as shown in Figure 7.49a. The impedance  $Z(j\omega) = X(j\omega)$  is a loss-less one-port (pure reactance). The transfer function of this all-pass has the form

$$H(j\omega) = \frac{R - jX(\omega)}{R + jX(\omega)}; \quad \omega = 2\pi f \quad (7.548)$$

The magnitude of this function equals one for all  $f$  and the phase function is

$$\varphi(\omega) = \arg[(R - jX(\omega))^2] = \tan^{-1} \left[ \frac{2RX(\omega)}{R^2 - X^2(\omega)} \right] \quad (7.549)$$

The insertion  $X = 1/\omega C$  (see Figure 7.49b) yields the phase function of a first-order all-pass

$$\varphi(y) = \tan^{-1} \left[ \frac{-2\gamma}{1 - \gamma^2} \right]; \quad y = \omega RC = \omega\tau \quad (7.550)$$

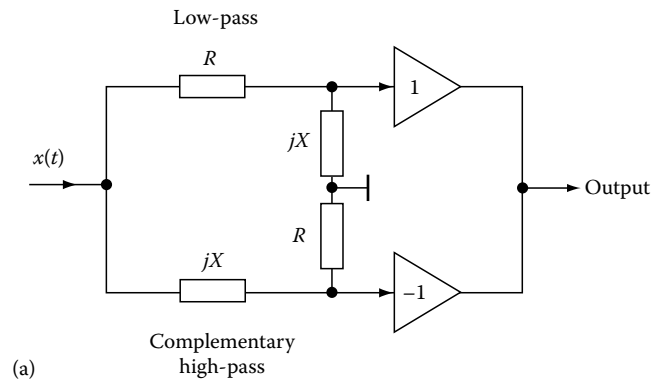
The insertion  $X = \omega L - 1/\omega C$  (see Figure 7.49c) yields a phase function of a second-order all-pass

$$\varphi(y) = \tan^{-1} \left[ \frac{2(1 - y^2)qy}{(1 - y^2)^2 - q^2y^2} \right] \quad (7.551)$$

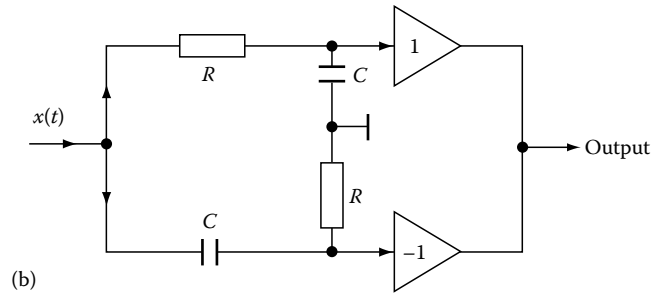
where

$$y = \omega/\omega_r, \omega_r = 1/\sqrt{LC}$$

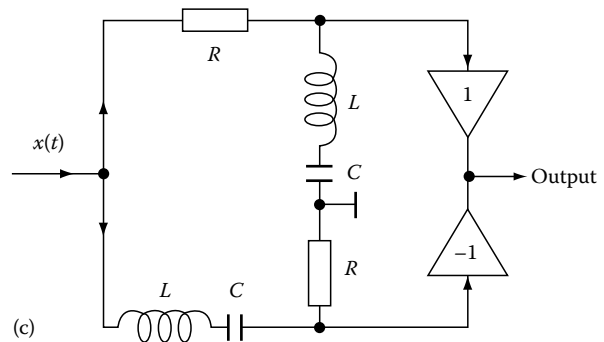
$$q = \omega_r RC = R\sqrt{C/L}$$



(a)



(b)



(c)

FIGURE 7.49 An all-pass consisting of (a) a low-pass and a complementary high-pass, (b) a first-order RC low-pass and complementary CR high-pass, and (c) a second-order RLC low-pass and complementary RLC high-pass.

The phase functions defined by Equations 7.550 and 7.551 are shown in Figure 7.50 in linear and logarithmic frequency scales. The second-order function best shows linearity in the logarithmic scale for  $q = 4$ . Notice that the phase functions are continuous if we remove the phase jumps by  $\pi$  by changing the branch of a multiple-valued  $\tan^{-1}$  function, similar to that in Figure 7.22. To get a wider frequency range of Hilbert transformers, higher order all-passes have to be applied. But more practical is the use of a series connection of first-order all-passes with appropriate staggering of the individual phase functions. For a given frequency band  $W = f_2 - f_1$ , optimum staggering yields the smallest value of the RMS phase error. The local value of the phase error is defined as a difference between  $\delta(f)$  given by Equation 7.547 and  $-\pi/2$ . Therefore, the local error is

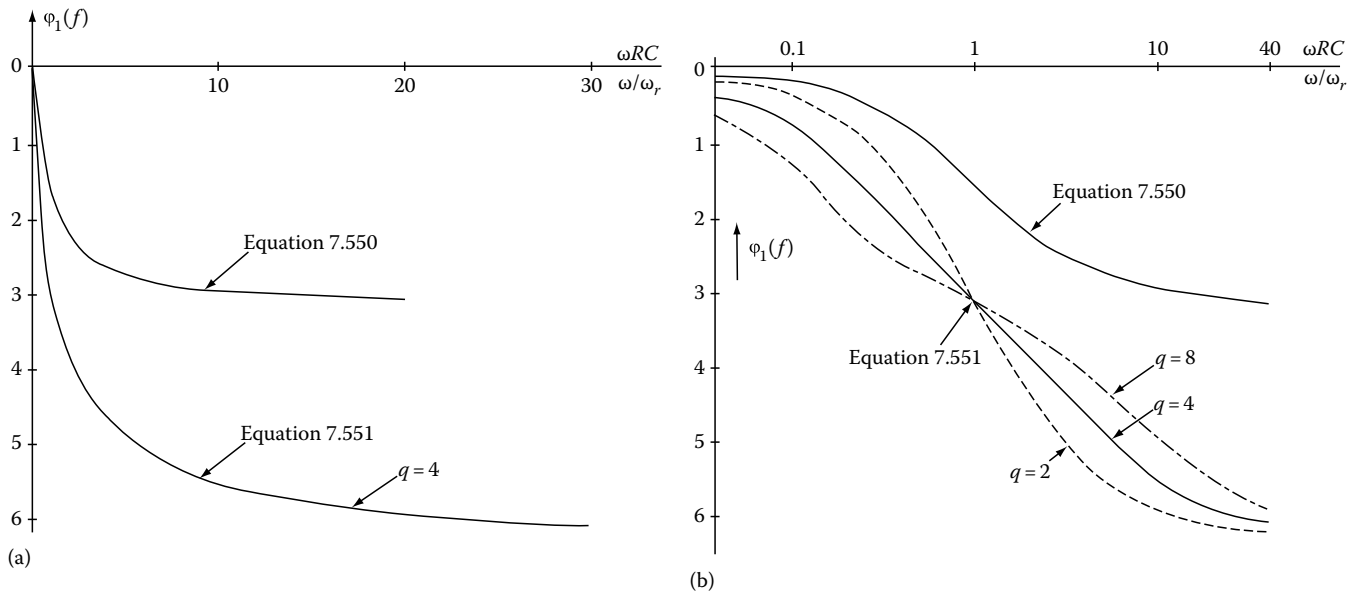


FIGURE 7.50 (a) Nonlinear phase functions of the first-order all-pass given by Equation 7.550 and the second-order all-pass given by Equation 7.551. (b) The same functions in a logarithmic frequency scale. The second-order function shows best linearity for  $q = 4$ .

$$\varepsilon(f) = \delta(f) + \pi/2 \quad (7.552)$$

The design methods of  $90^\circ$  phase splitters were described by Dome<sup>9</sup> in 1946. Later Darlington,<sup>8</sup> Orchard,<sup>27</sup> Weaver,<sup>38</sup> and Saraga<sup>33</sup> described design methods based on a Chebyshev approximation of a desired phase error. Tables and diagrams of these approximations can be found in Bedrosian.<sup>2</sup>

### 7.22.3 A Simple Method of Design of Hilbert Phase Splitters

Analog Hilbert transformers are designed using models of a given filter consisting of loss-less capacitors, low-loss inductors, ideal resistors, and ideal operational amplifiers. More accurate models that take into account spurious capacitances, inductances, and other spurious effects are sophisticated and rarely applied at the design stage. The alignment of circuits with an accuracy better than 0.5%–1% is difficult to achieve. Having in mind the above arguments, the required accuracy of design of the parameters of the phase splitter is limited. Therefore, the simple method of design using a personal computer may be effective in many applications and is presented here.

The method consists of two steps. In the first step, the phase function  $\varphi_1(f)$ , given by Equation 7.546, is linearized in the logarithmic frequency scale. In the second step, the phase function  $\varphi_2(f)$  is obtained by shifting the function  $\varphi_1(f)$  in order to get a minimum value of the RMS phase error defined by Equation 7.547. The lower and upper frequency edges  $f_1$  and  $f_2$  are chosen as abscissae at which the error function diverges. The method is illustrated by four examples of design of Hilbert transformers given by the circuit models in Figure 7.51.

### Example

First example: The Hilbert transformer of this example is implemented using two first-order all-pass filters (see Figure 7.51a). The phase function of the first filter is

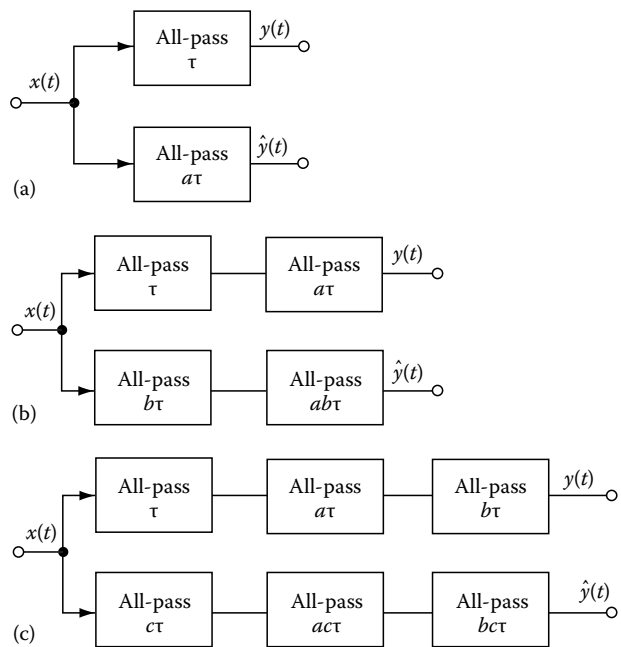


FIGURE 7.51 The phase splitter Hilbert transformer using (a) first-order all-pass filters, (b) a series connection of two first-order all-passes, (c) three first-order all-passes, and

(continued)

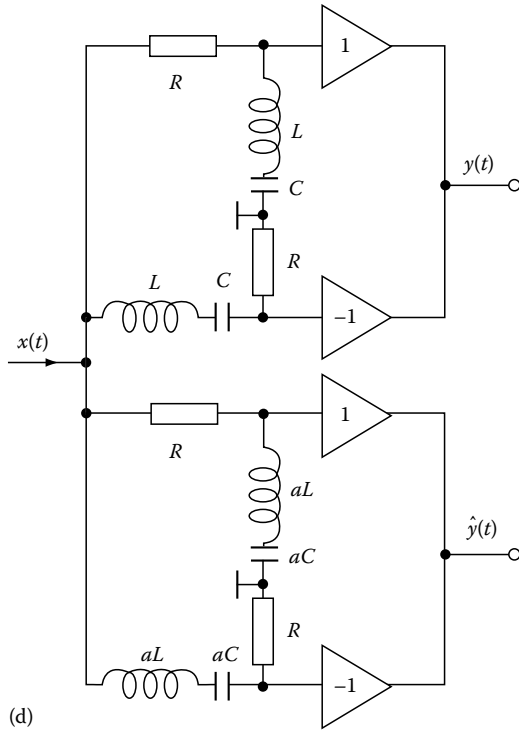


FIGURE 7.51 (continued) (d) second-order all-passes.

(see Equation 7.550  $\varphi_1(f) = \tan^{-1} \left[ \frac{-2y}{y^2 - 1} \right]$ ;  
 $y = 2\pi f RC = 2\pi f \tau$  (7.553)

The first step is abandoned because  $\varphi_1(f)$  has no degree of freedom for linearization. In the second step we have to find the shift parameter denoted  $a$  in the phase function

$$\varphi_2(f) = \tan^{-1} \left[ \frac{-2ay}{a^2y^2 - 1} \right], \quad Y = 2\pi f RC \quad (7.554)$$

giving the minimum RMS phase error. The functions  $\varphi_1(f)$ ,  $\varphi_2(f)$ , and the error function  $\epsilon(f)$  are shown in Figure 7.52. Simple computer calculations yield the value of  $a = 0.167$  giving the normalized frequency edges  $y_1 = 1.75$  and  $y_2 = 3, 5$ , and the RMS phase error  $\epsilon_{RMS} = 0.012$ . The pass-band equals one octave.

Second example: The phase splitter of this example is implemented using two first-order all-pass filters in each chain (see Figure 7.51b). The phase function of the first filter is

$$\varphi_1(f) = \tan^{-1} \left[ \frac{-2y}{y^2 - 1} \right] + \tan^{-1} \left[ \frac{-2ay}{a^2y^2 - 1} \right], \quad Y = 2\pi f RC \quad (7.555)$$

In the first step, we have to find the shift parameter  $a$  to get the best linearity of  $\varphi_1(f)$  in the logarithmic scale. Small changes of  $a$  introduce a tradeoff between the RMS phase error and the pass-band of the Hilbert transformer. In the second step we have to find the value of the shift parameter  $b$  in the phase function

$$\varphi_2(f) = \tan^{-1} \left[ \frac{-2by}{b^2y^2 - 1} \right] + \tan^{-1} \left[ \frac{-2aby}{a^2b^2y^2 - 1} \right], \quad y = 2\pi f R. \quad (7.556)$$

yielding the minimum of the RMS phase error. Figure 7.53 shows an example with  $a = 0.08$  and  $b = 0.24$  giving the normalized edge frequencies  $y_1 = 1.6$  and  $y_2 = 30$  ( $f_2/f_1 = 18.75$  or more than 4 octaves) with  $\epsilon_{RMS} = 0.016$ .

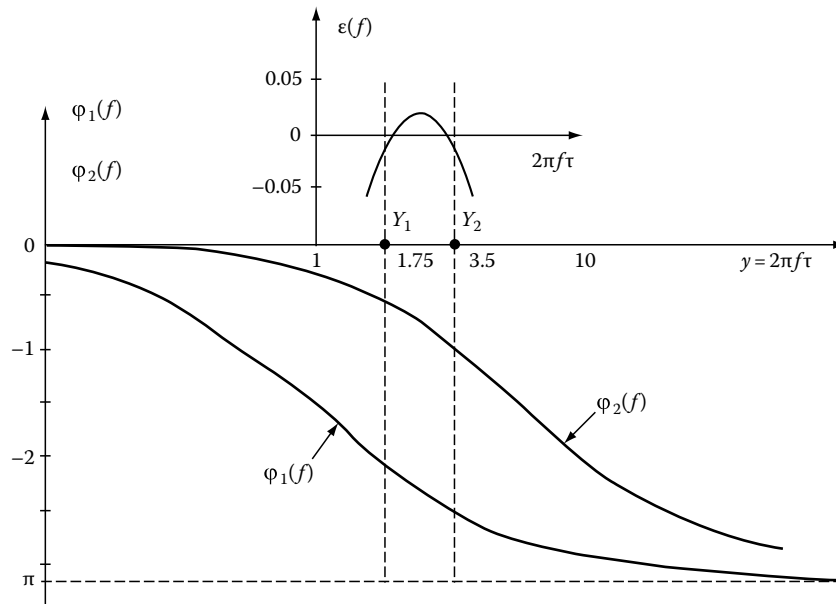


FIGURE 7.52 The phase functions and the phase error of the Hilbert transformer of Figure 7.51a.

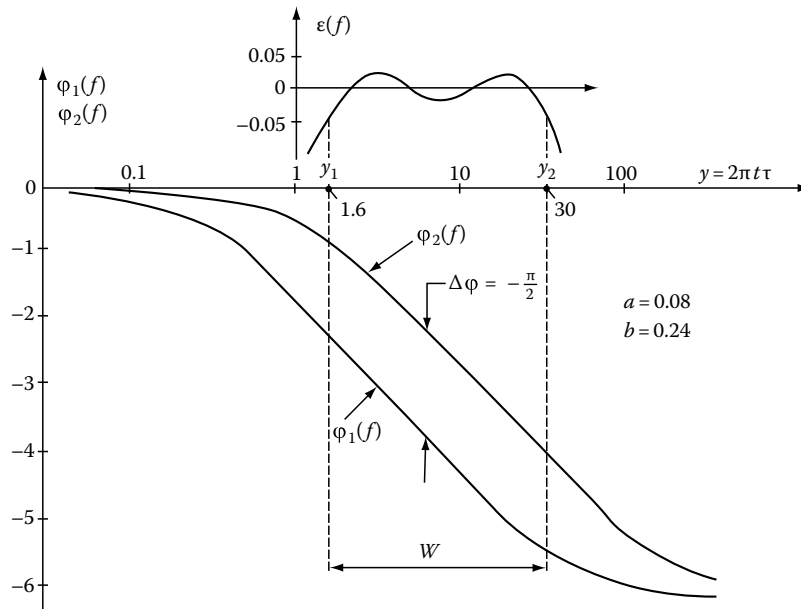


FIGURE 7.53 The phase functions and the phase error of the Hilbert transformer of Figure 7.51b.

Third example: The phase splitter consists of three first-order all-passes in each chain (see Figure 7.51c). The phase functions are

$$\begin{aligned} \varphi_1(f) = & \tan^{-1} \left[ \frac{-2y}{y^2 - 1} \right] + \tan^{-1} \left[ \frac{-2ay}{a^2y^2 - 1} \right] \\ & + \tan^{-1} \left[ \frac{-2by}{b^2y^2 - 1} \right] \end{aligned} \quad (7.557)$$

and

$$\begin{aligned} \varphi_2(f) = & \tan^{-1} \left[ \frac{-2cy}{c^2y^2 - 1} \right] + \tan^{-1} \left[ \frac{-2cay}{c^2a^2y^2 - 1} \right] \\ & + \tan^{-1} \left[ \frac{-2cby}{c^2b^2y^2 - 1} \right] \end{aligned} \quad (7.558)$$

Good linearity of the phase function  $\varphi_1(f)$  depend on the shift parameters  $a$  and  $b$ . The first step yields  $a = 0.08$  and  $b = 0.008$ . In the second step the parameter  $c = 0.24$  yields the minimum value of the RMS phase error. Figure 7.54 shows the phase functions and the error distribution  $\epsilon(f)$ . The RMS phase error is  $\epsilon_{RMS} = 0.025$ . The edge frequencies are  $y_1 = 1.8, y_2 = 300$  giving  $f_2/f_1 = 166$  (more than 7 octaves). A smaller phase error may be achieved at the cost of frequency range.

Fourth example: The phase splitter consists of one second-order all-pass in each chain (see Figure 7.51d). The phase functions are

$$\varphi_1(f) = \tan^{-1} \left[ \frac{2(1 - y^2)qy}{(1 - y^2)^2 - q^2y^2} \right], \quad Y = 2\pi f RC \quad (7.559)$$

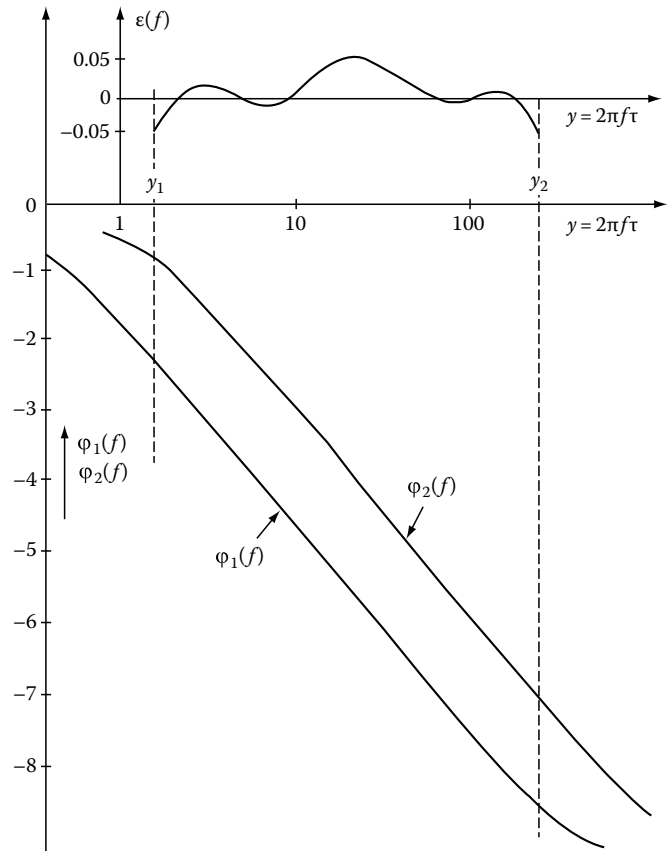


FIGURE 7.54 The phase functions and the phase error of the Hilbert transformer of Figure 7.51c.



$$\varphi_2(f) = \tan^{-1} \left[ \frac{2(1 - a^2 y^2) q a y}{(1 - a^2 y^2)^2 - q^2 a^2 y^2} \right], \quad Y = 2\pi f RC \quad (7.560)$$

Good linearity of  $\varphi_1(f)$  yields the value  $q = 4$  (see Figure 7.55). The minimum value of the RMS phase error yields the shift parameter  $a = 0.232$ . The phase functions and the error distribution are shown in Figure 7.50. The edge frequencies are  $y_1 = 0.5$  and  $y_2 = 9$  giving  $f_2/f_1 = 18$  with  $\epsilon_{RMS} = 0.0186$ . The bandwidth is about the same as in the second example with two first order all-passes in each chain.

### 7.22.4 Delay, Phase Distortions, and Equalization

The phase functions of the all-pass filters used to implement the Hilbert transformer are, disregarding the small phase errors, linear in the logarithmic frequency scale, but nonlinear in a linear frequency scale. Let us investigate the phase distortions due to that nonlinearity for the Hilbert filter of the second example. Consider a wide-band test signal given by the Fourier series of a square wave truncated at the seventh harmonic term:

$$x(t) = \frac{4}{\pi} \left[ \sin(\omega_1 t) + \frac{1}{3} \sin(3\omega_1 t) + \frac{1}{5} \sin(5\omega_1 t) + \frac{1}{7} \sin(7\omega_1 t) \right] \quad (7.561)$$

where  $\omega_1 = 2\pi f_1 = 1.75/\tau$  was chosen near the low-frequency edge of the pass-band  $W$ . The spectrum of this signal is enclosed inside  $W$ . The waveforms of this signal and its Hilbert transform are shown in Figure 7.56a. The phase-distorted Hilbert pair at the output ports of the phase splitter is shown in Figure 7.56b. The phase distortions can be removed by connecting a phase equalizer in series to the input port, predistorting the input signal (see the waveform of Figure 7.56d). The required phase functions of the equalizer may have the form

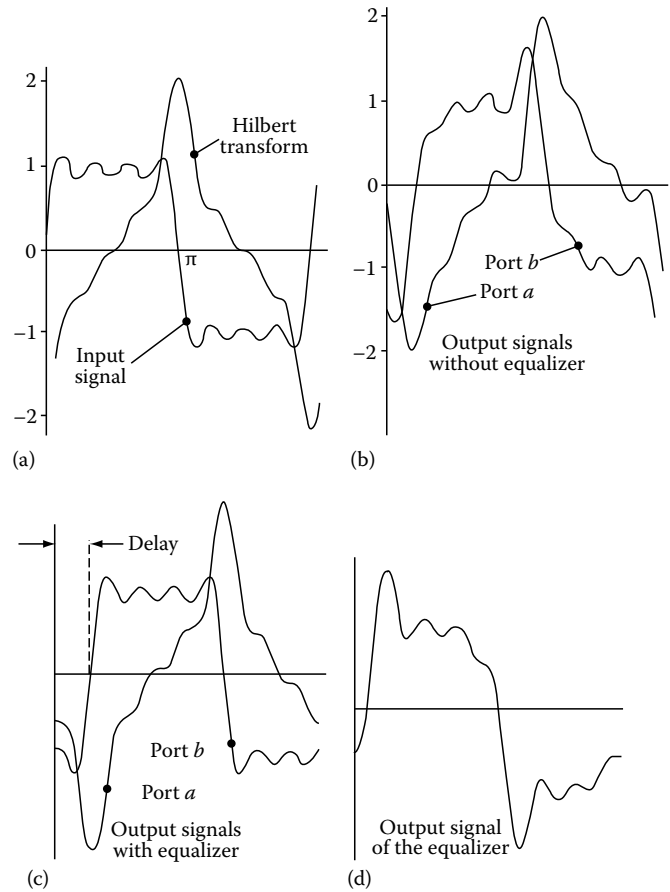


FIGURE 7.56 The waveform given by (a) the truncated Fourier series (7.557) and of its Hilbert transform, (b) the distorted Hilbert pair at the output with no equalization, (c) the equalized undistorted and delayed Hilbert pair, and (d) the input signal predistorted by the equalizer.

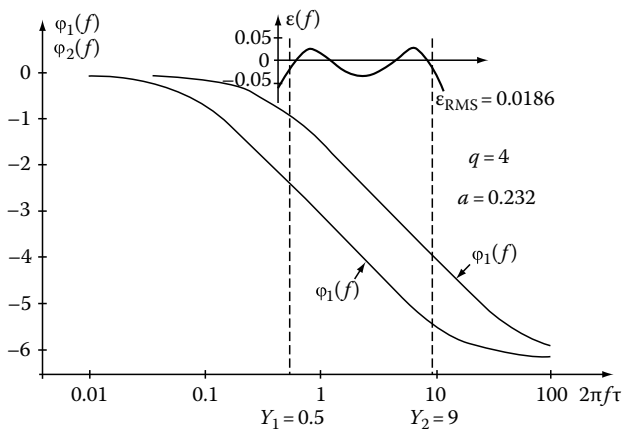


FIGURE 7.55 The phase functions and the phase error of the Hilbert transformer of Figure 7.51d.

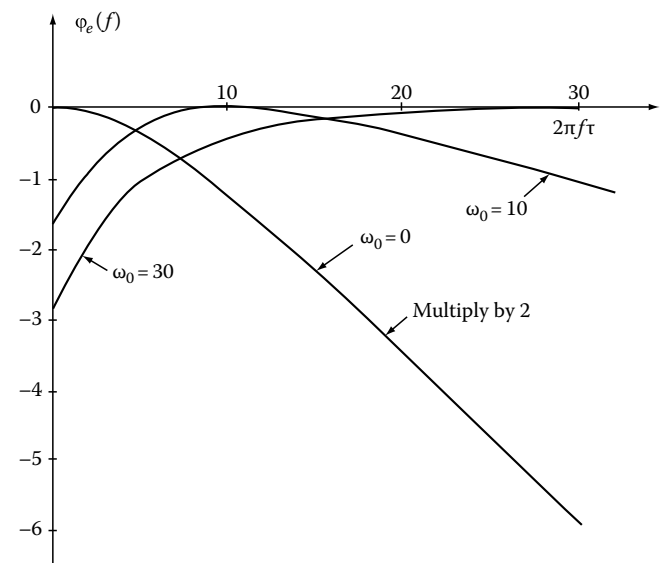


FIGURE 7.57 The phase functions of the equalizer given by Equation 7.552 for the phase function  $\varphi_2(f)$  given by Equation 7.556.

$$\varphi_{\text{equalizer}}(f) = \varphi_L(f) - \varphi_2(f) \quad (7.562)$$

where  $\varphi_2(f)$  is given by Equation 7.550 and

$$\varphi_L(f) = \varphi_2(f_0) + \left. \frac{d\varphi_2(f)}{df} \right|_{f=f_0} (f - f_0) \quad (7.563)$$

is a linear phase function tangential to  $\varphi_2(f)$  at  $f=f_0$ . Figure 7.57 shows the phase function of the equalizer for three different values of the abscissae  $f_0$ . Figure 7.56c shows the delayed and practically undistorted output waveforms of the equalized Hilbert transformer with  $f_0 = 0$ . The delay is given by the slope of the phase function

$$t_0 = \left. \frac{d\varphi_2(f)}{df} \right|_{f_0=0} = 2\tau b(1 + a) \quad (7.564)$$

giving the delay  $t_0 = 0.5065$  s ( $\tau = 1$ ). Another method of linearization of the phase function is given in Ref. 21.

### 7.22.5 Hilbert Transformers with Tapped Delay-Line Filters

Tapped delay-line filters often referred to as transversal filters may be used as phase equalizers. Such a filter enables the approximation of a given transmittance  $H(jf)$  with a desired accuracy. Therefore, a Hilbert filter may be implemented using a tapped delay line,<sup>15,34</sup> (see Figure 7.58). If the spectrum of the input signal is band-pass limited such that  $X(f) = 0$  for  $|f| > W$ , then the transfer function of the ideal Hilbert transformer given by Equation 7.544 may be truncated at  $|f| = W$ . The tapped delay-line Hilbert filter may be designed using a periodic repetition of this truncated function, as shown in Figure 7.59. The expansion of this function in a Fourier series yields, using truncation, the following approximate form of the transfer function

$$H_N(jf) = 2j \sum_{i=1}^{(N-1)/2} b(i) \sin [i2\pi f t_0]; \quad t_0 = \frac{1}{2W} \quad (7.565)$$

with

$$b(i) = -\frac{2}{\pi i} \sin^2 \left[ \frac{\pi i}{2} \right] \quad (7.566)$$

Different from the implementations of Hilbert transformers with all-pass filters, where the design amplitude equals error zero and the phase error is distributed over the pass-band, here the roles are interchanged. The amplitude error is distributed over the pass-band and there is no phase error (linear phase). The RMS amplitude ripple decreases with the increasing number of tapes of the delay line (increasing number of coefficients  $b(n)$ ). The transversal Hilbert transformer, disregarding the small distortions due to the amplitude ripple, produces at the output a delayed undistorted signal and its Hilbert transform. However, analog implementations are rarely used in favor of digital implementations in the form of FIR (Finite Impulse Response) Hilbert transformers.

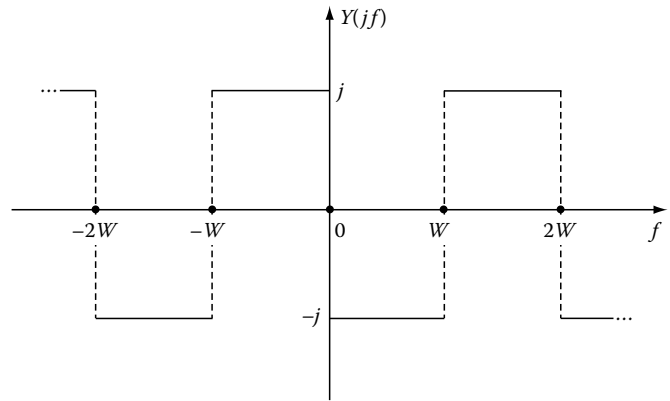


FIGURE 7.59 A truncated at  $\pm W$  and periodically repeated transfer function of an ideal Hilbert transformer (see Equation 7.544).

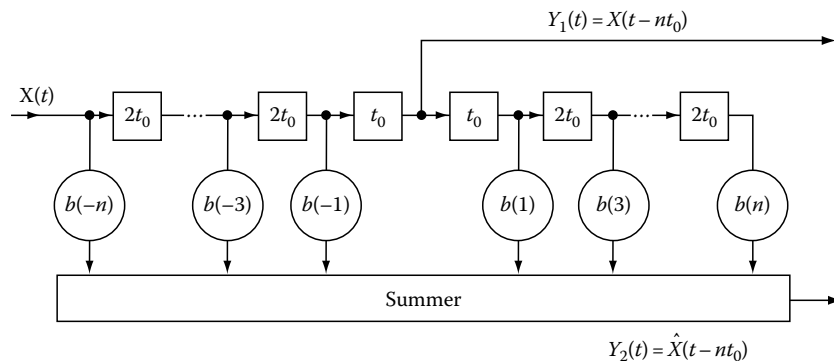


FIGURE 7.58 A tapped delay line Hilbert transformer.

### 7.22.6 Band-Pass Hilbert Transformers

The transfer function of a band-pass Hilbert transformer may be defined as the frequency-translated transfer function of a low-pass Hilbert transformer. The transfer function of an ideal low-pass with linear phase is given by the formula

$$H_{LP}(jf) = \Pi[f/(2W)]e^{-j2\pi f\tau} \quad (7.567)$$

where  $\tau$  is the time delay and  $\Pi(x)$  has the form

$$\Pi(x) = \begin{cases} 1 & \text{for } |x| < 0.5 \\ 0.5 & \text{for } |x| = 0.5 \\ 0 & \text{for } |x| > 0.5 \end{cases} \quad (7.568)$$

This is illustrated in Figure 7.60. The impulse response of this filter is

$$h_{LP}(t) = F^{-1}[H_{LP}(jf)] = 2W \frac{\sin X}{X} \quad (7.569)$$

where  $X = 2\pi W(t - \tau)$ . The response, as shown in Figure 7.61 is noncausal, but for large delays  $\tau$  is nearly causal. The transfer function of the Hilbert transformer derived from Equation 7.567 is given by

$$H_H(jf) = H_{LP}(jf) e^{-j[0.5\pi \operatorname{sgn}(f) + 2\pi f\tau]} \quad (7.570)$$

as illustrated in Figure 7.60a and c. The impulse response of such a Hilbert transformer is

$$h_H(t) = F^{-1}[H_H(jf)] = \frac{1}{\pi(t - \tau)} [1 - \cos 2\pi W(t - \tau)] \quad (7.571)$$

or

$$h_H(t) = \frac{2 \sin^2 [\pi W(t - \tau)]}{\pi(t - \tau)} \quad (7.572)$$

This is illustrated in Figure 7.61b. If  $W$  goes to infinity the mean value of  $h_H(t)$  taken over the period  $T = 1/W$  approximates the distribution  $1/(\pi(t - \tau))$ . The transfer function of an ideal band-pass filter is given by

$$H_{BP}(jf) = \left\{ \Pi \left[ \frac{f + f_0}{2W} \right] + \Pi \left[ \frac{f - f_0}{2W} \right] \right\} e^{-j2\pi f\tau} \quad (7.573)$$

This is illustrated in Figure 7.62a and b. The impulse response of this filter is

$$h_{BP}(t) = 2W \frac{\sin X}{X} \cos [2\pi f_0(t - \tau)] \quad (7.574)$$

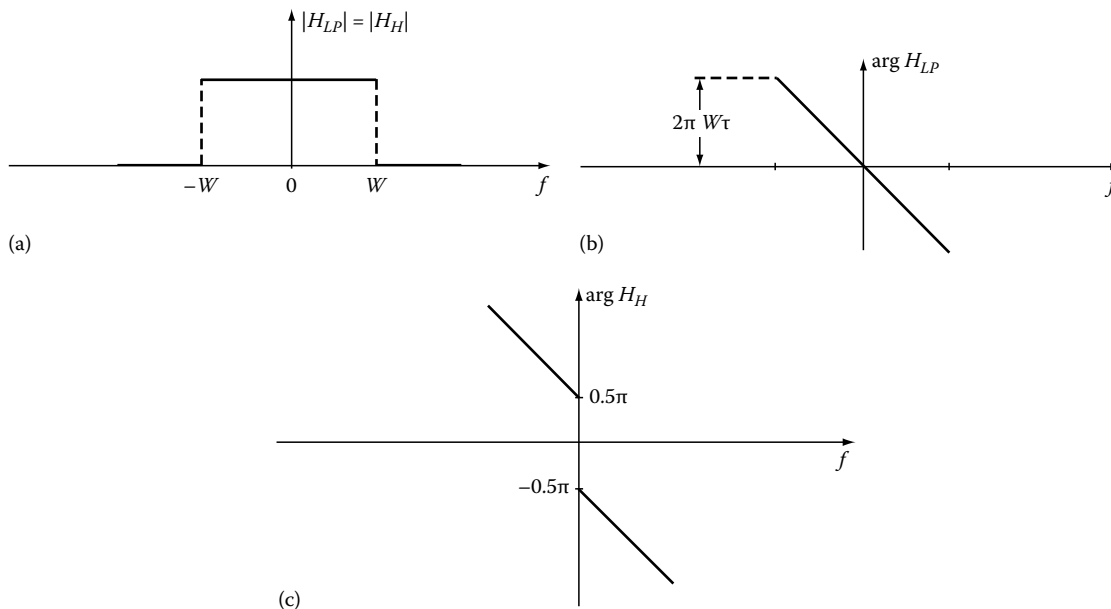


**FIGURE 7.60** The transfer function of the ideal low-pass: (a) magnitude, (b) linear phase function, and (c) phase function of a Hilbert transformer derived from the low-pass function.

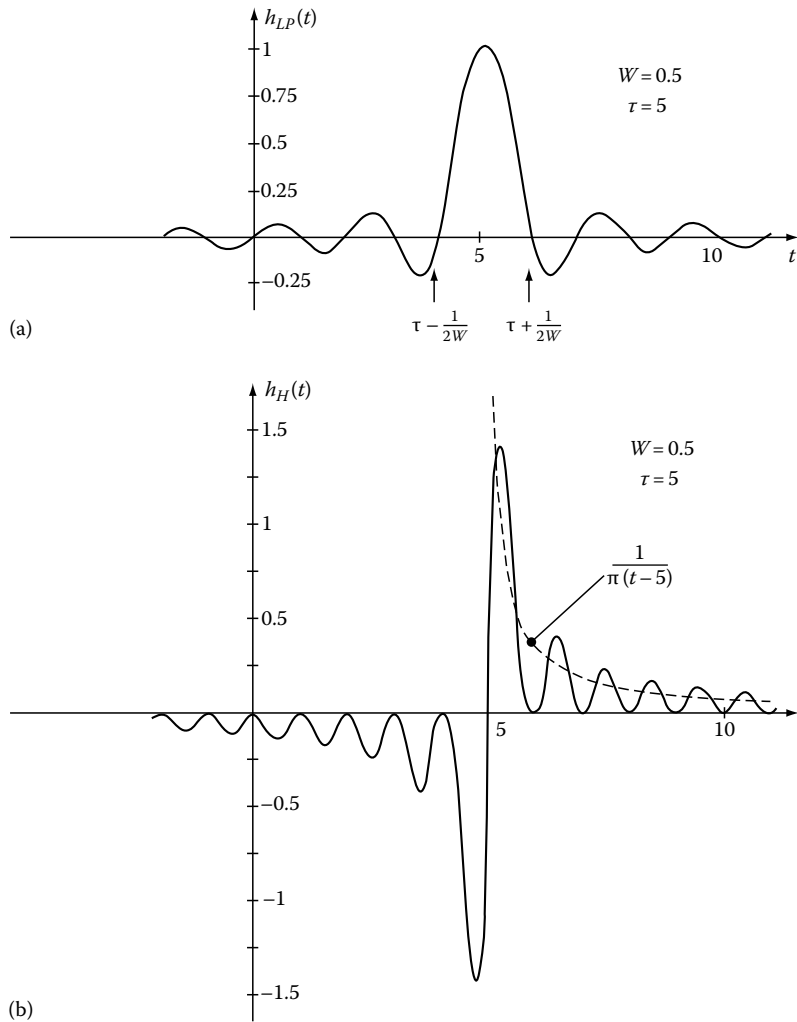


FIGURE 7.61 Impulse responses of (a) the low-pass and (b) the corresponding Hilbert transformer. Transfer functions are shown in Figure 7.60.

and is shown in Figure 7.63a. The transfer function of an ideal band-pass Hilbert transformer derived from the transfer function (Equation 7.573) is

$$H_{HBP}(jf) = H_{BP}(jf) \exp\{-j 0.5\pi[\text{sgn}(f + f_0) + \text{sgn}(f - f_0)]\} \quad (7.575)$$

This is illustrated in Figure 7.62a and c. The impulse response of this Hilbert transformer is

$$h_{HBP}(t) = \frac{2 \sin^2 [\pi W(t - \tau)]}{\pi(t - \tau)} \cos [2\pi f_0(t - \tau)] \quad (7.576)$$

and is shown in Figure 7.63b.

Consider the response of the band-pass Hilbert transformer to a band-pass signal  $u_1(t) = x(t) \cos (2\pi f_0 t)$  where  $x(t)$  has no spectral terms for  $|f| > W$  and  $f_0 > W$ . This response has the form

$$u_2(t) = \hat{x}(t - \tau) \cos [2\pi f_0(t - \tau)] \quad (7.577)$$

that is, the modulating signal  $x(t)$  is replaced by the delayed version of its Hilbert transform. Notice that due to Bedrosian's theorem the Hilbert transform of the input signal (see Section 7.13) has the form

$$u_2(t) = x(t - \tau) \sin [2\pi f_0(t - \tau)] \quad (7.578)$$

that is, only the carrier is Hilbert transformed, compared to signal (7.577), for which the envelope is transformed. The transfer function of a band-pass producing at the output the Hilbert transform in agreement with Bedrosian's theorem is given by the equation

$$H_{HBP}(jf) = -j \text{sgn}(f) H_{BP}(jf) \quad (7.579)$$

where  $H_{BP}(jf)$  is given by Equation 7.21.31 and is shown in Figure 7.64.

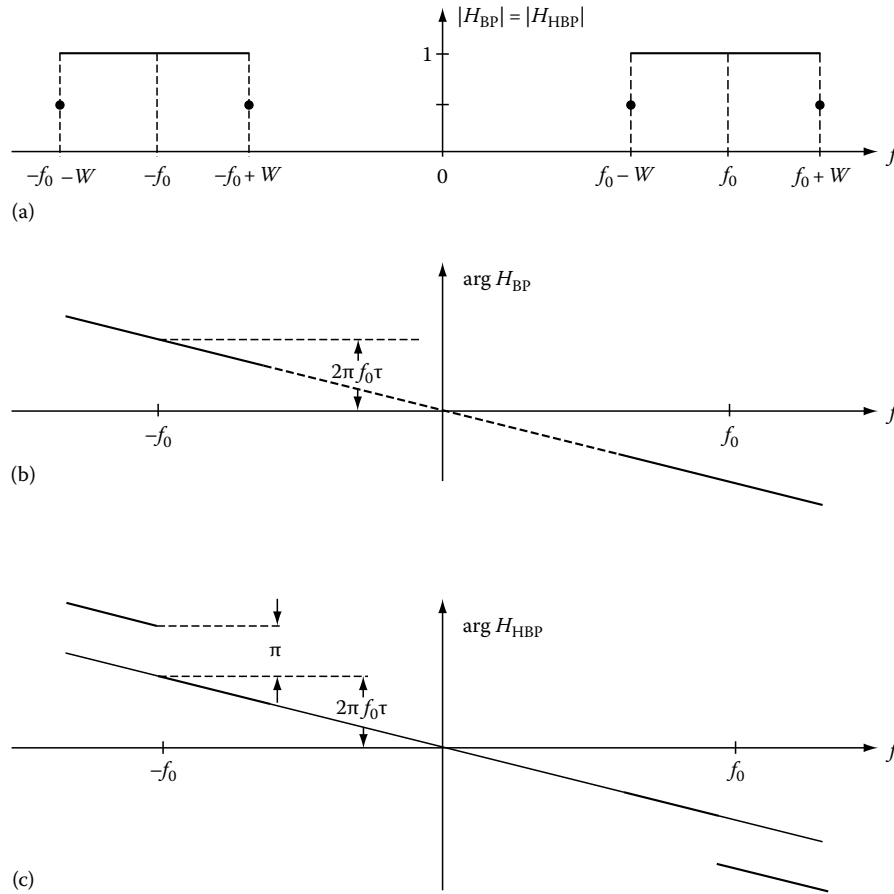


**FIGURE 7.62** The transfer functions of an ideal band-pass filter and of the corresponding Hilbert transformer: (a) the magnitude, (b) the phase function of the band-pass, and (c) the Hilbert transformer.

A possible implementation of a band-pass Hilbert transformer defined by Equation 7.573 is shown in Figure 7.65. It consists of a linear phase lower side-band band-pass, analogous upper side-band, band-pass, and a subtractor. Figure 7.66 shows the implementation of such a Hilbert transformer by use of a SAW (surface acoustic wave) filter.

### 7.22.7 Generation of Hilbert Transforms Using SSB Filtering

The Hilbert transform of a given signal may be obtained by band-pass filtering of a DSB AM signal. The SSB signal has the form (see Section 7.17)

$$u_{SSB}(t) = x(t) \cos(2\pi F_0 t) \pm \hat{x}(t) \sin(2\pi F_0 t) \quad (7.580)$$

where  $F_0$  is the carrier frequency. Such a signal can be obtained by band-pass filtering of a DSB AM signal. A synchronous demodulator using the quadrature carrier  $\sin(2\pi F_0 t)$  generates at his output the Hilbert transform  $\hat{x}(t)$ .

### 7.22.8 Digital Hilbert Transformers

The ideal discrete-time Hilbert transformer is defined as an all-pass with a pure imaginary transfer function, that is, if

$$\begin{aligned} H(e^{j\psi}) &= H_r(\psi) + jH_i(\psi), \quad \text{then} \\ H_r(\psi) &= 0 \quad \text{all } \psi \end{aligned} \quad (7.581)$$

and

$$H(e^{j\psi}) = jH_i(\psi) = \begin{cases} -j & 0 < \psi < \pi \\ 0 & \psi = 0, |\psi| = \pi \\ j & -\pi < \psi < 0 \end{cases} \quad (7.582)$$

or in another equivalent notation

$$\begin{aligned} H(e^{j\psi}) &= -j \operatorname{sgn}(\sin \psi) = -\operatorname{sgn}(\sin \psi) e^{j\pi/2} \\ &= |H(\psi)| e^{j \arg H(\psi)} \end{aligned} \quad (7.583)$$

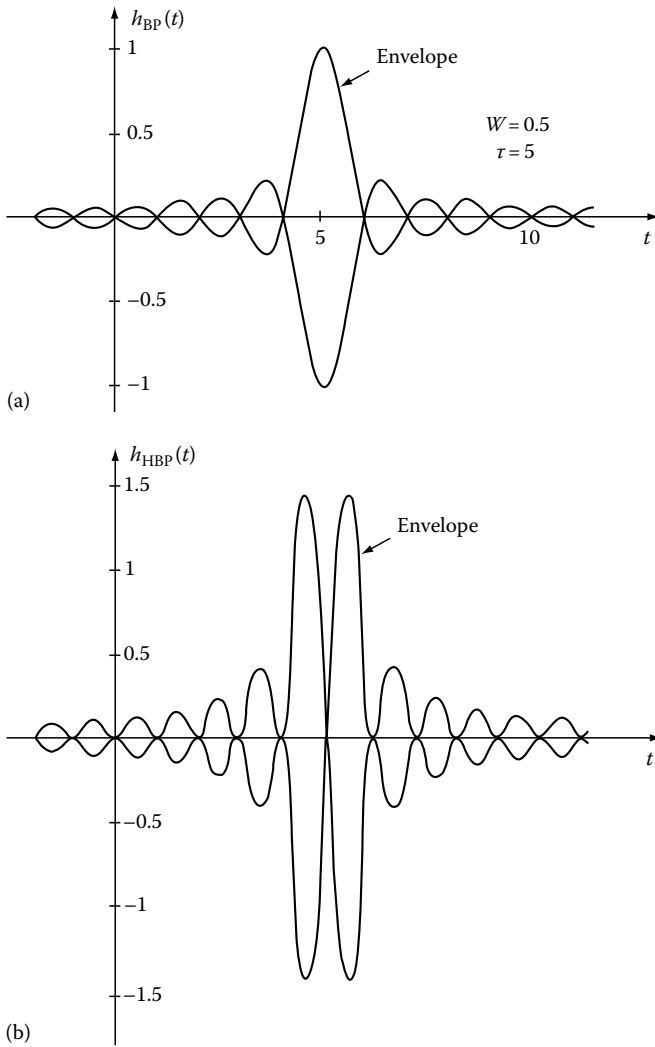


FIGURE 7.63 The envelopes of the impulse responses of (a) a band-pass and (b) the Hilbert transformer. Transfer functions are shown in Figure 7.62.

The magnitude (see Figure 7.67) has the form

$$|H(\psi)| = |\text{sgn}(\sin \psi)| = \begin{cases} 1, & 0 < |\psi| < \pi \\ 0, & \psi = 0, |\psi| = \pi \end{cases} \quad (7.584)$$

and the phase function is

$$\arg[H(\psi)] = -(\pi/2)\text{sgn}(\sin \psi) \quad (7.585)$$

Notice that  $\psi = 2\pi f_n$ , where  $f_n = f/f_s$  is a frequency normalized against the sampling frequency  $f_s$ .

The basic period has the interval from  $-\pi$  to  $\pi$  corresponding to the values of  $f_n$  from  $-0.5$  to  $0.5$ .

The noncausal infinite range impulse response of the ideal Hilbert transformer has the form of the antisymmetric sequence

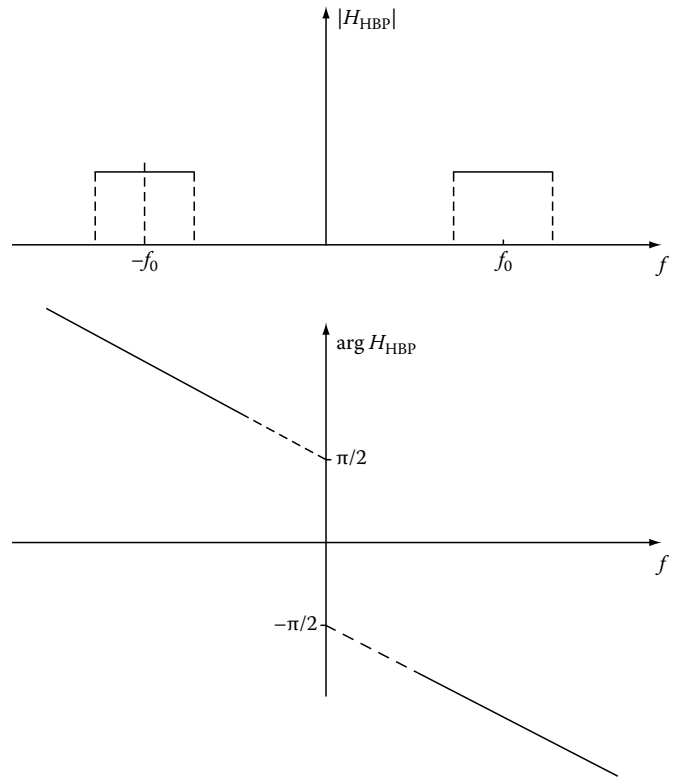


FIGURE 7.64 The transfer function of a Hilbert transformer that transforms the carrier signal with no change of the waveform of the envelope.

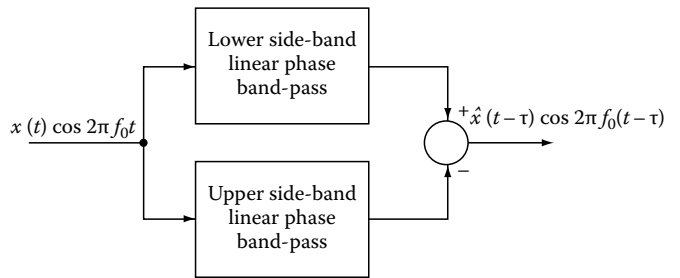


FIGURE 7.65 The implementation of the Hilbert transformer of the transfer function defined in Figure 7.62 using two band-pass filters.

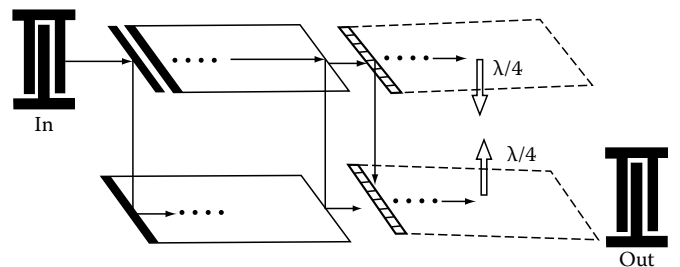


FIGURE 7.66 A SAW filter implementing the band-pass Hilbert transformer of Figure 7.21.19.

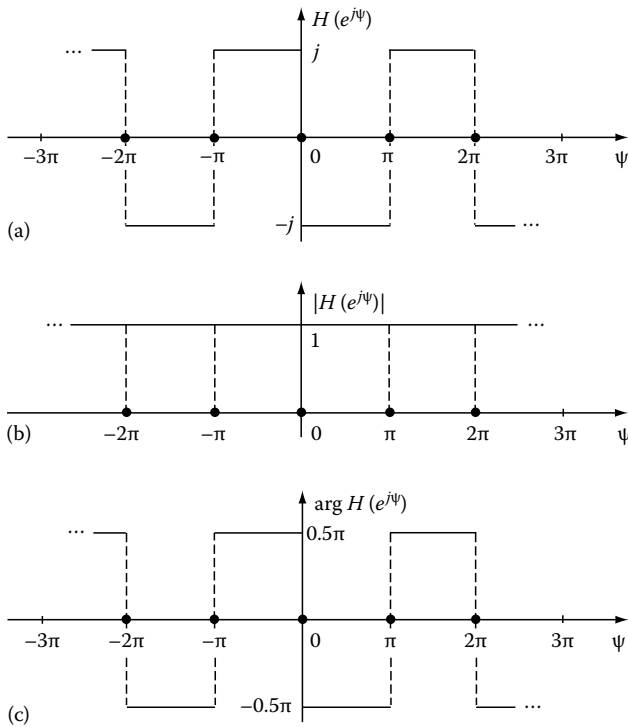


FIGURE 7.67 An ideal discrete-time Hilbert transformer's (a) transfer function, (b) magnitude, and (c) phase function.

$$h(i) = (2/\pi i)\sin^2(i\pi/2) \tag{7.586}$$

If one allows the addition of a linear phase term in the ideal frequency response introducing a frequency-independent group delay (in samples), then the transfer function (Equation 7.582) takes the form

$$H(e^{j\psi}) = \begin{cases} -je^{-j\psi\tau} & 0 < \psi < \pi \\ 0 & \psi = 0, |\psi| = \pi \\ je^{-j(\psi - 2\pi)\tau} & \pi < \psi < 2\pi \end{cases} \tag{7.587}$$

and the impulse response takes the form

$$h(i) = (2/\pi) \frac{\sin^2[(\pi/2)(i - \tau)]}{i - \tau}, \quad i = 0, \pm 1, 2, \dots \tag{7.588}$$

The important feature of the impulse response given by Equation 7.586 is that even-numbered samples are exactly zero, and that the samples are antisymmetric, that is,

$$h(i) = -h(-i); \quad i = 0, 1, \dots \tag{7.589}$$

### 7.22.9 Methods of Design

There are several methods of realizing digital Hilbert transformers. The three basic implementations are as follows:

1. The FIR Hilbert transformer
2. The IIR (Infinite Impulse Response) Hilbert transformer
3. Digital phase splitter Hilbert transformer

It is possible to realize a differentiating Hilbert transformer that produces at the output the derivative of the Hilbert transform of the input signal.

### 7.22.10 FIR Hilbert Transformers<sup>25,31</sup>

The FIR Hilbert transformer is a digital version of the taped delay line Hilbert transformer (see Section 7.22). Its structure is shown in Figure 7.68. The string of  $z^{-1}$  delays acts as a discrete taped delay line. Such a filter is inherently stable and its

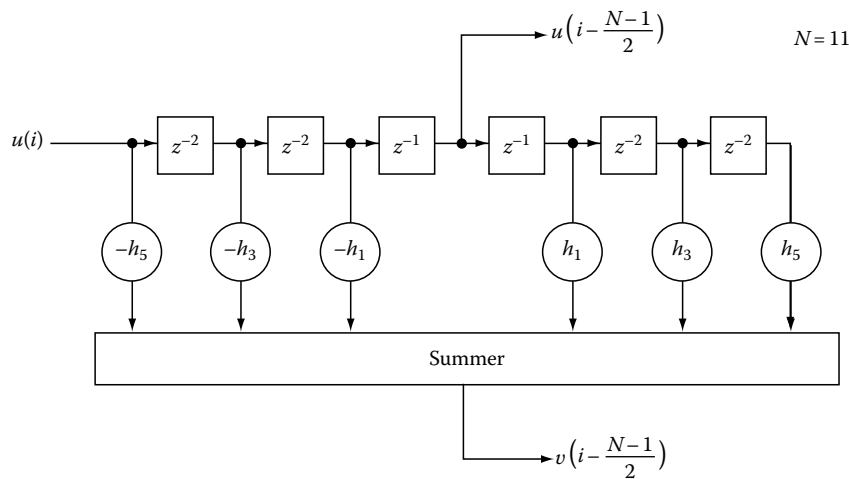


FIGURE 7.68 The structure of the FIR Hilbert transformer.

impulse response is given by the coefficients (gains)  $h(0), h(1), h(2), \dots, h(i), \dots, h(N-1)$ , that is, has the length of  $N$  samples. An example of the impulse response of the FIR Hilbert transformer is shown in Figure 7.69b, where for convenience,  $N$  is an odd number. This causal impulse response is obtained by a truncation and shifting by  $(N-1)/2$  samples of the finite impulse response of the ideal Hilbert transformer in Figure 7.69a. The transfer function of the Hilbert filter defined by the causal impulse response (see Equations 7.487 and 7.488 is given by the Z-transform

$$H_H(z) = \sum_{i_1=0}^{N-1} h_1(i_1)z^{-i_1} \quad (7.590)$$

where  $i_1$  is the discrete coordinate given in the Equation 7.591. The shifted causal impulse response  $h_1(i_1)$  and the noncausal impulse  $h(i)$  of Figure 7.69a satisfy the relation

$$h_1[i + (N-1)/2] = h(i), \quad i_1 = i + (N-1)/2, \\ i = \frac{N-1}{2}, \dots, 0, \dots, \frac{N-1}{2} \quad (7.591)$$

The insertion of  $z = e^{j\psi}$  in Equation 7.590 (see Equation 7.492) and using Equation 7.591 yields

$$H_H(e^{j\psi}) = e^{-j\psi(N-1)/2} \sum_{i=-(N-1)/2}^{(N-1)/2} h(i)e^{-j\psi i} \quad (7.592)$$

Using Euler's formula for the sine function and the relation  $h(i) = -h(-i)$ , this transfer function takes the form

$$H_H(e^{j\psi}) = e^{-j\psi(N-1)/2} \sum_{i=1}^{(N-1)/2} -j2h(i) \sin(\psi i) \quad (7.593)$$

Because every second sample of the impulse response equals zero, the summation should be written: from  $i=1$  to  $(N-1)/2$  step 2. Let us denote this by

$$G(e^{j\psi}) = - \sum_{i=1}^{(N-1)/2} 2h(i) \sin(\psi i) \quad (7.594)$$

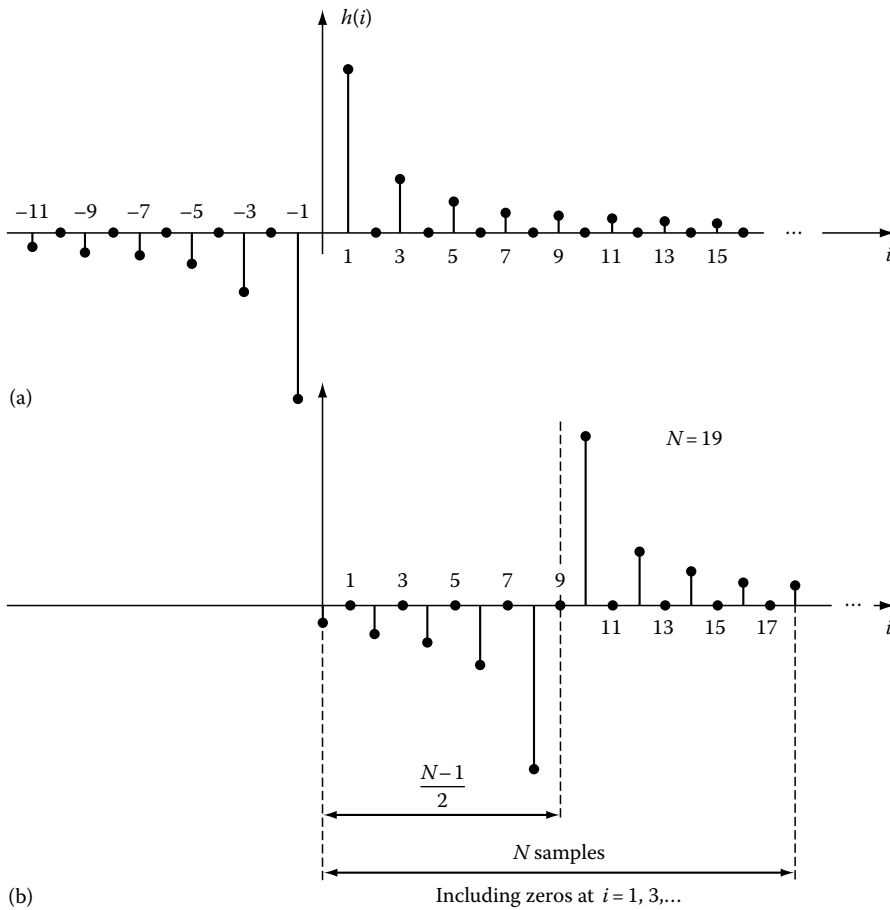


FIGURE 7.69 Impulse responses of (a) the ideal discrete time Hilbert transformer (see Equation 7.586) and (b) a FIR Hilbert transformer given by the truncation and shifting of the impulse response shown in (a).



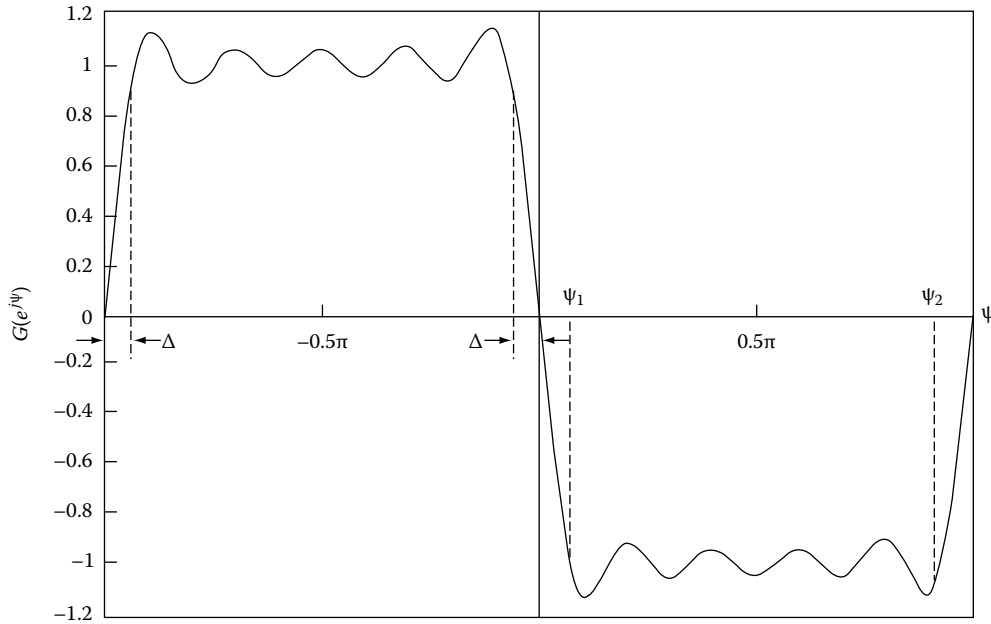


FIGURE 7.70 The  $G(e^{j\psi})$  function of a FIR Hilbert transformer defined by the Fourier series (7.597).

This function has the form of a Fourier series and defines the amplitude of the transfer function of the Hilbert transformer (this is not the magnitude  $G(e^{j\psi})$  has positive and negative values). An example is shown in Figure 7.70. The normalized dimensionless pass-band of this Hilbert transformer is given by the edge frequencies

$$W_\psi = \psi_2 - \psi_1 = \pi - 2\Delta \tag{7.595}$$

Because  $\psi = 2\pi f/f_s$ , where  $f$  is the frequency in hertz [Hz] and  $f_s$  is the sampling frequency, the pass-band in hertz is

$$W_f[\text{Hz}] = \frac{\pi - 2\Delta}{2\pi} f_s \tag{7.596}$$

The pass-band increases and the amplitude  $\delta$  of the ripple decreases with increasing length  $N$  of the impulse response; that is, at the cost of the delay, which equals  $(N - 1)/2$  samples. The amplitude ripple in the pass-band depends on the coefficients  $h(i)$  in the Fourier series (Equation 7.594). Let us consider three cases:

1. The coefficients  $h(i)$  are given by the Fourier series of an odd square periodic function of the form

$$G(e^{j\psi}) = -\frac{4}{\pi} \left[ \sin(\psi) + \frac{1}{3} \sin(3\psi) + \frac{1}{5} \sin(5\psi) \dots + \frac{1}{2i+1} \sin[\psi i(N-1)/2] \right] \tag{7.597}$$

corresponding to the truncation of the Fourier series by a rectangular window. This yields a nonequiripple amplitude distribution with “Gibbs peaks” at the edges of the pass-band, as shown in Figure 7.70.

2. The coefficients  $h(i)$  in the above Fourier series are changed using an appropriate spectral window function; for example, Blackman, Hamming, or Kaiser windows. This yields a more uniform amplitude ripple.
3. The coefficients  $h(i)$  are calculated to obtain an equiripple amplitude distribution in the pass-band in the mini-max or Chebyshev sense; for example, using the Parks–McClellan algorithm.<sup>22</sup> Figure 7.71 shows an example for  $N=19$ . The product of  $N$  and  $\Delta$  is given by the asymptotic relation derived by Kaiser<sup>29</sup>

$$N\Delta \cong 0.61 \log_{10} \delta \tag{7.598}$$

Concluding, the FIR Hilbert transformer has a linear-phase characteristic and an amplitude ripple in the pass-band depending on design. Odd values of  $N$  are preferred. Design with even  $N$  is possible but inconvenient because all the impulse response coefficients are nonzero and the frequency response cannot have the required symmetry. A symmetric FIR Hilbert transformer (odd  $N$ ) may be eventually derived from the corresponding designs of symmetric half-band FIR filters.<sup>16</sup>

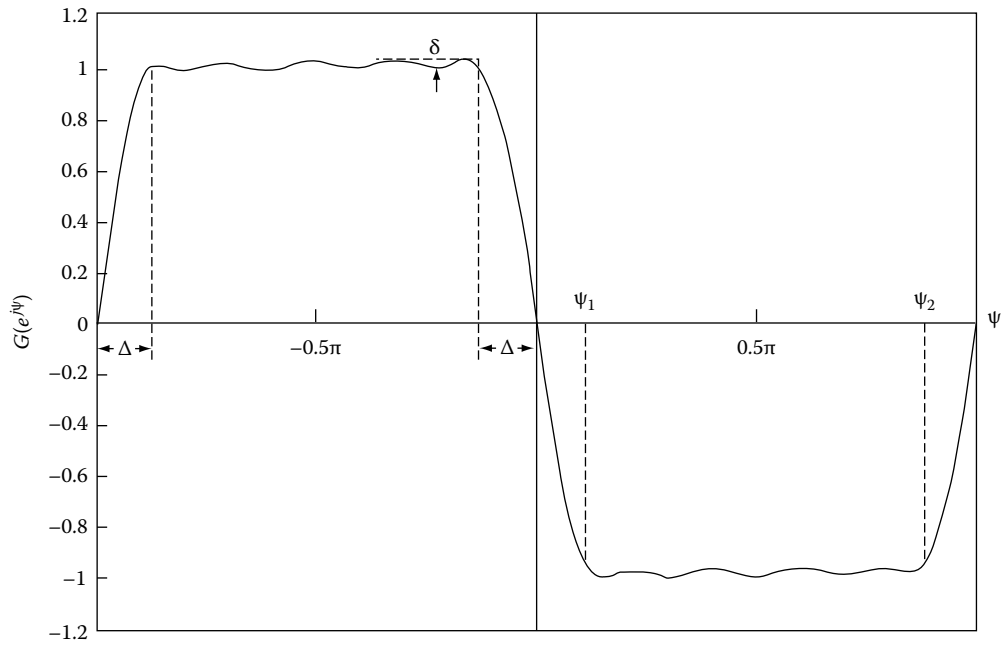


FIGURE 7.71 The equiripple  $G(e^{j\psi})$  function of a FIR Hilbert transformer designed in the mini-max or Chebyshev sense.

### 7.22.11 Digital Phase Splitters

A digital Hilbert transformer may be implemented in the form of a digital phase splitter as shown in Figure 7.72. The transfer functions of the all-pass filters may be derived directly from the analog transfer functions by use of the bilinear frequency transformation (see Section 7.21). Details of the procedure can be found in any textbook on digital filters. All basic properties of the analog implementation are conserved. Without a phase equalizer the output Hilbert pair is distorted in reference to the

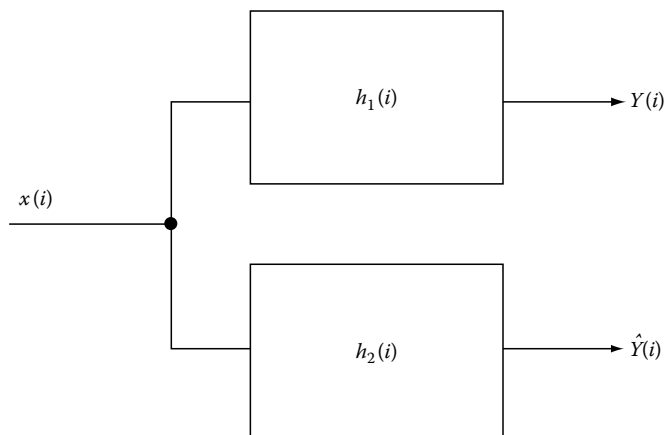


FIGURE 7.72 The discrete-time (or digital) version of the phase splitter Hilbert transformer of Figure 7.21.1

input signal. Nonlinearity of the bilinear transformation introduces some tradeoffs not present in the analog case.

### 7.22.12 IIR Hilbert Transformers

IIR Hilbert transformers may be derived using noncausal generalized half-band filters. Generalized half-band filters are derived by modifying the conventional elliptic filter design so that all poles of the half-band filter lie on the imaginary axis. The IIR ideal half-band transfer function proposed by Ansari<sup>1</sup> has the form

$$H_{HB}(z) = 1 + z^{-1}G(z^2) \tag{7.599}$$

where  $G(z^2)$  is an all-pass filter with unit magnitude. The ideal example of this transfer function is shown in Figure 7.73a. Let us show that the transfer function of an ideal IIR Hilbert transformer is given by

$$H_H(z) = z^{-1}G(-z^2) \tag{7.600}$$

This is illustrated step by step in Figure 7.73. The term

$$F(z) = z^{-1}G(-z^2) \tag{7.601}$$

is an all-pass with  $F(e^{j\psi})$  shown in Figure 7.73b. It has a unit magnitude and a phase function equal to zero in the pass-band and  $\pm\pi$  in the stop-band as shown in Figure 7.73d. This phase function can be written in the form

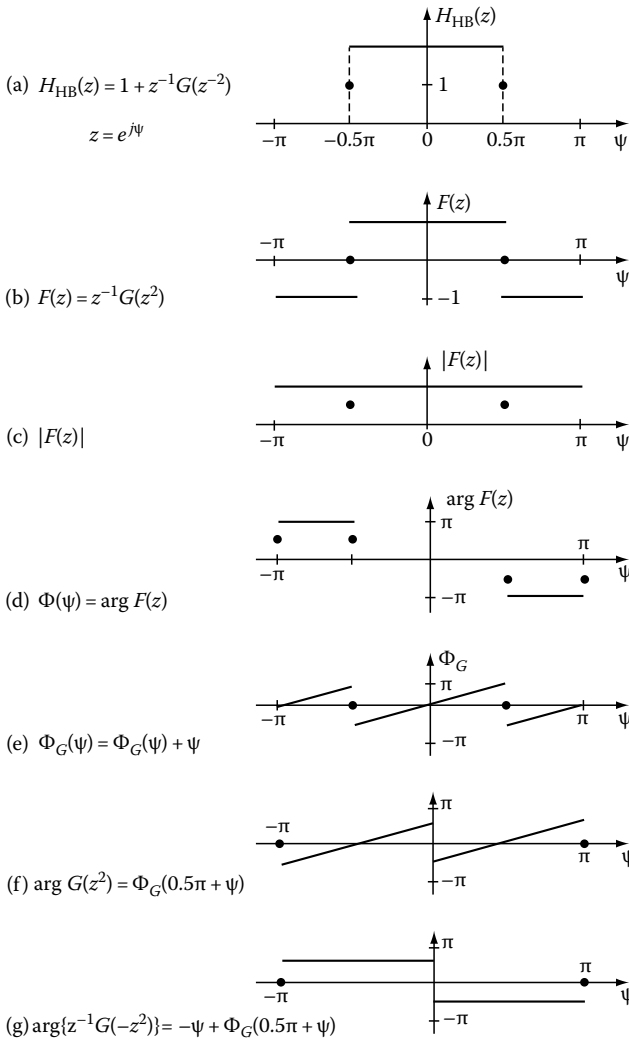


FIGURE 7.73 Step-by-step derivation of the IIR transfer function of a Hilbert transformer defined by Equation 7.600, starting from the transfer function of the ideal half-band filter given by Equation 7.599.

$$\Phi(\psi) = 0.5\pi[\text{sgn}(\sin(2\psi)) - \text{sgn}(\psi)] \quad (7.602)$$

The term  $F(z)$  can be written in the form ( $z = e^{j\psi}$ )

$$F(e^{j\psi}) = e^{-j\psi} e^{j\Phi_G(\psi)} = e^{j\Phi(\psi)} \quad (7.603)$$

where

$$\Phi_G(\psi) = \Phi(\psi) + \psi \quad (7.604)$$

This phase function is shown in Figure 7.73e. Because  $z^2 = e^{j2\psi}$  and  $-z^2 = e^{j2(0.5\pi + \psi)}$ , we have

$$H_H(e^{j\psi}) = e^{-j\psi} e^{j\Phi_G(0.5\pi + \psi)} \quad (7.605)$$

The phase function  $\Phi_G(0.5\pi + \psi)$  is shown in Figure 7.73f and is the same as the phase function of the ideal Hilbert transformer (see Equation 7.579) and finally the phase function of  $H_H(z)$  is shown in Figure 7.73g.

Differently than FIR transformers, the above IIR Hilbert transformer is designed with an equiripple phase function and exact amplitude. The explicit form of the noncausal transfer function may have the form

$$H(z) = z^{-1} \sum_{i=1}^N \frac{1 - a_i z^2}{z^2 - a_i} \quad (7.606)$$

where  $N$  is an integer. Let us present an example. Consider the IIR Hilbert transformer with the low-frequency edge  $\psi_1 = 0.02\pi$ , the high-frequency edge  $\psi_2 = 0.98\pi$  ( $\Delta = 0.02\pi$ ), and with the required amplitude of the phase ripple  $|\Delta\Phi| \leq 0.01\pi$ . The following relation between the phase ripple and the stop-band amplitude ripple of the half-band filter was derived<sup>1</sup>

$$\delta = \sin(0.5\Delta\Phi) \quad (7.607)$$

Inserting  $\Delta\Phi = 0.01\pi$  gives  $\delta = 0.0157$ . The design procedure described in Reference 1a was applied to find the filter coefficients  $a(i)$  giving  $a(1) = 5.36078$ ,  $a(2) = 1.2655$ ,  $a(3) = 0.94167$ , and  $a(4) = 0.53239$ . The insertion of the coefficients in Equation 7.606 enabled the calculation of the phase function shown in Figure 7.74. The phase error has a symmetric distribution around  $\Psi = 0.5\pi$ , i.e., half of the sampling frequency. The pass-band of this Hilbert transformer covers about 4.5 octaves. The phase ripple in the pass-band may be eliminated using half-band Butterworth IIR filters. For this kind of filter the coefficients  $a(i)$  in Equation 7.606 are given by a simple formula

$$a_i = \tan^2[\pi i / 2N + 1]; \quad i = 1, 2, \dots, N \quad (7.608)$$

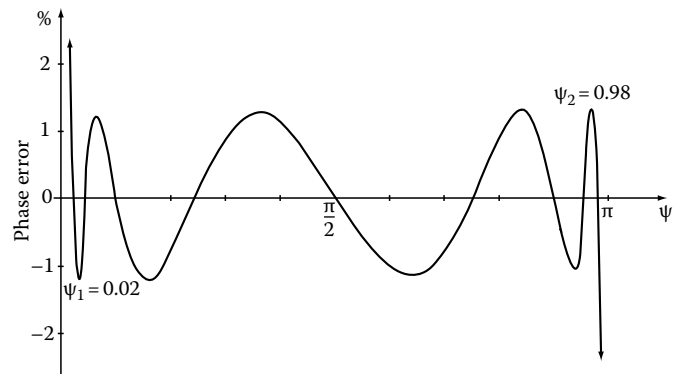


FIGURE 7.74 An example of the equiripple phase function of the IIR Hilbert transformer.

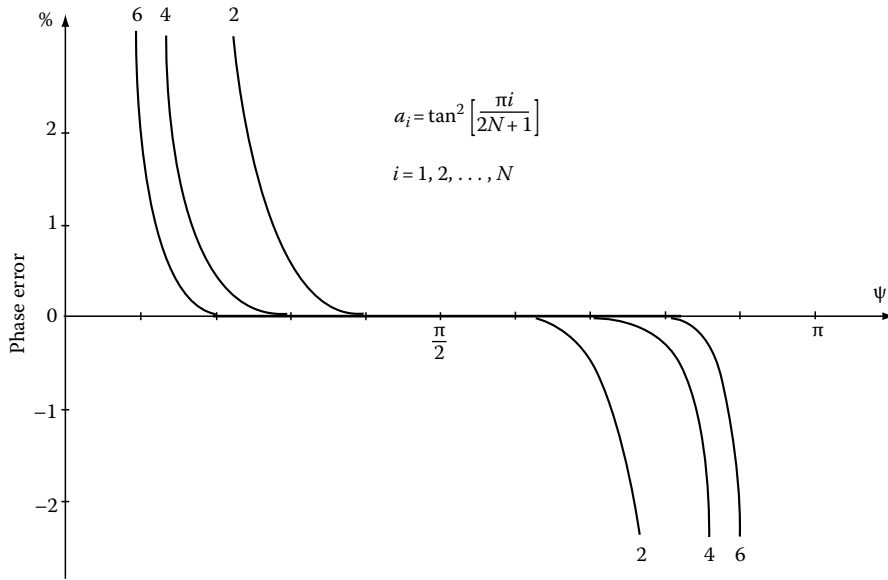


FIGURE 7.75 Phase errors of Butterworth IIR Hilbert transformers.

Figure 7.75 shows a family of maximum flat phase functions for  $N=2, 4,$  and  $6$ . The pass-band depends considerably on the permissible phase error at the edges. The edge frequencies for edge errors 0.1% and 1% are given in the table:

$N$	2		4		6	
	$\psi_1$	$\psi_2$	$\psi_1$	$\psi_2$	$\psi_1$	$\psi_2$
0.1%	0.36	0.64	0.24	0.76	0.165	0.835
1%	0.265	0.735	0.165	0.835	0.115	0.885

The widest pass-band for  $N=6$  and 1% error covers about 3 octaves and the smallest for  $N=2$  and 0.1% only 1 octave. The frequency around which the phase function is maximally flat equals  $\psi = 0.5\pi$ . It can be shifted by use of a suitable digital-to-digital frequency transformation. The disadvantage of the Butterworth filter is that the ratio of the first to the last coefficient is very large and increases with  $N$ .

### 7.22.13 Differentiating Hilbert Transformers

The differentiating Hilbert transformer is defined as a linear system the output of which is the derivative of the Hilbert transform of the input signal. In principle, a differentiating Hilbert transformer may be implemented as a cascade connection of a differentiator and a Hilbert transformer as shown in Figure 7.76. However, it may be designed as a specialized FIR filter. Due to the cascade connection, the transfer function of the differentiating discrete Hilbert transformer is given by the product of the transfer function of the discrete Hilbert transformer given by Equation 7.587 and the transfer function of the ideal discrete differentiator of the form<sup>29</sup>

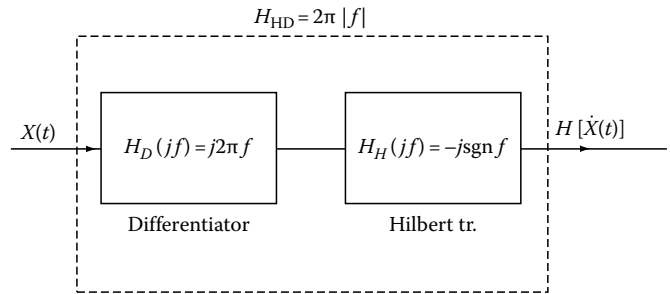


FIGURE 7.76 A cascade connection of a Hilbert transformer and a differentiating filter.

$$H_D(e^{j\psi}) = \begin{cases} j\psi e^{-j\psi\tau} & 0 < \psi < \pi \\ 1 & |\psi| = k\pi; \quad k = 0, 1, 2 \\ j(\psi - 2\pi)e^{-j(\psi-2\pi)\tau} & \pi < \psi < 2\pi \end{cases} \quad (7.609)$$

or using the equivalent notation

$$H_D(e^{j\psi}) = [\psi + \text{sgn}(\sin(\psi)) - 1] e^{j[0.5\pi - \psi\tau - \pi\tau(\text{sgn}(\sin(\psi)) - 1)]} \quad 0 < \psi < 2\pi \quad (7.610)$$

The product of both transfer functions may be written in the form

$$H_{HD}(e^{j\psi}) = [\psi + \pi(\text{sgn}(\sin(\psi)) - 1)] \text{sgn}(\sin(\psi)) e^{-j[2\psi\tau - \pi\tau(\text{sgn}(\sin(\psi)) - 1)]} \quad (7.611)$$

The magnitude and the phase function of this transfer function of the differentiating Hilbert transformer are shown in

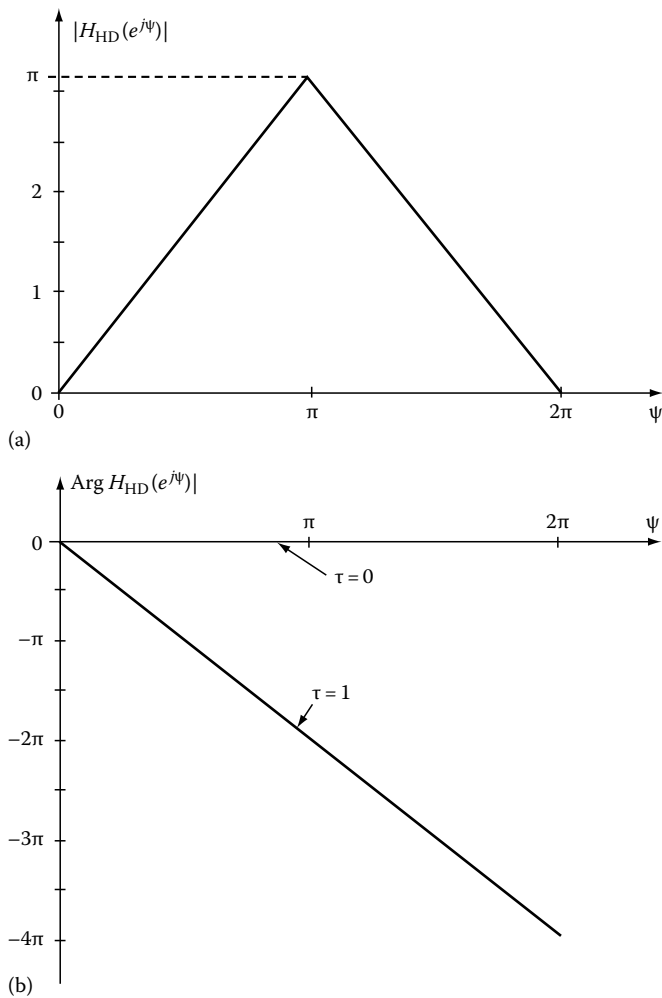


FIGURE 7.77 The transfer function of a differentiating Hilbert transformer: (a) magnitude and (b) phase function.

Figure 7.77. The inverse Fourier transform with  $(\tau = 0)$  yields the noncausal, even, and of infinite duration impulse response:

$$h_{HD}(i) = \begin{cases} a(i) = -[2 \sin^2(0.5\pi i)]/(\pi i^2); & i \neq 0 \\ 0.5\pi & i = 0 \end{cases} \quad (7.612)$$

This is illustrated in Figure 7.78a. The design method is the same as for the discrete Hilbert filter. The impulse response should be truncated to include  $N$  samples and shifted by  $\tau = (N - 1)/2$  samples as shown in Figure 7.77b. The  $G(e^{j\psi})$  function defined by Equation 7.21.52 here takes the form

$$G_{HD}(e^{j\psi}) = [\psi + \pi(\text{sgn}(\sin(\psi)) - 1)] \text{sgn}(\sin(\psi)); \quad 0 < \psi < 2\pi \quad (7.613)$$

and in this case is equal to the magnitude of the transfer function (see Figure 7.77). The truncated Fourier series is

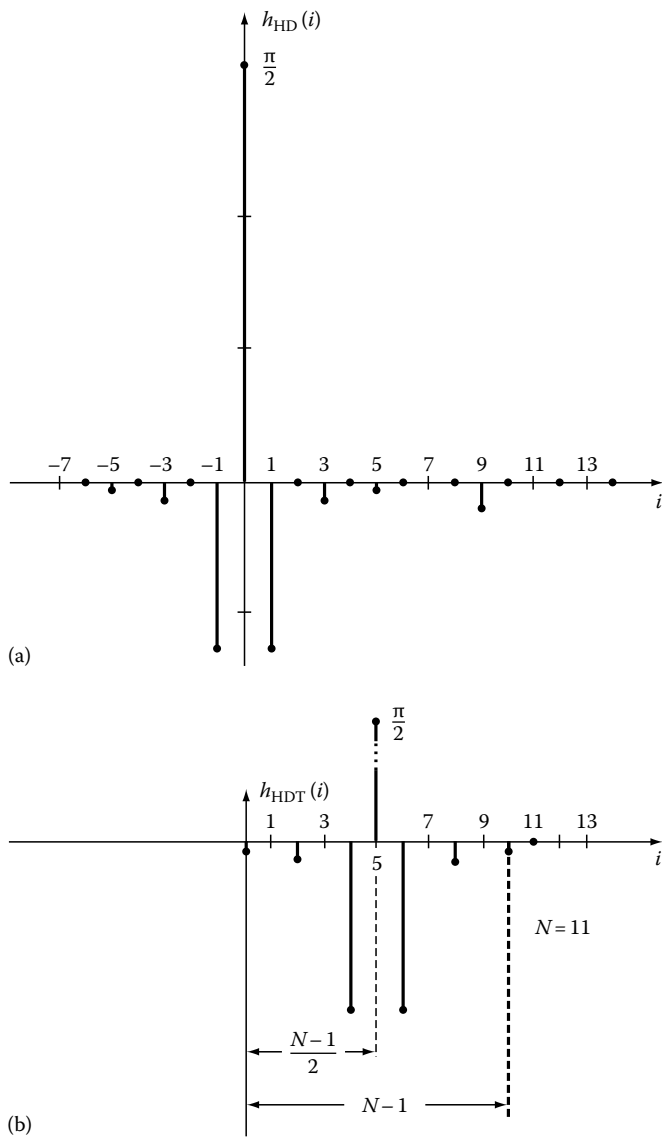


FIGURE 7.78 The impulse responses of the differentiating Hilbert transformer: (a) noncausal ideal and (b) truncated and causal.

$$G_{HDT}(e^{j\psi}) = 0.5\pi - \sum_{i=1}^{(N-1)/2} 2a(i) \cos(\psi i) \quad (7.614)$$

Compare this function with the analogous function of the FIR Hilbert transformer (see Equation 7.573). The design methods to get the desired amplitude ripple are the same as described in the three points following Equation 7.594. However, the Fourier series given by Equation 7.595 takes for the differentiating Hilbert transformer the form

$$G_{HDT}(e^{j\psi}) = \frac{\pi}{2} - \left(\frac{4}{\pi}\right) \left[ \cos \psi + \left(\frac{1}{9}\right) \cos 3\psi + \left(\frac{1}{25}\right) \cos 5\psi + \dots \right] \quad (7.615)$$

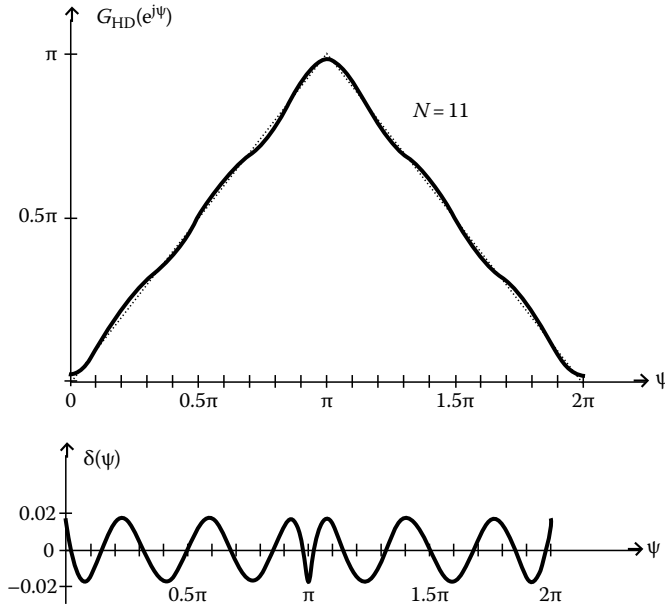


FIGURE 7.79 The  $G(e^{j\psi})$  function of a FIR differentiating Hilbert transformer.

TABLE 7.8 Coefficients of FIR Differentiating Hilbert Transformer

	Pass-Band Edges				
	$\psi_1 = 0$ $N = 7$	$\psi_2 = \pi$ $N = 11$	$N = 19$	$\psi_1 = 0.2\pi$ $N = 11$	$\psi_2 = 0.8\pi^a$ $N = 19$
$a(1)$	0.6426919	0.6388893	0.6373537	0.6068935	0.6184231
$a(3)$	0.0997952	0.07348499	0.0715001	0.0450341	0.05423771
$a(5)$		0.0459263	0.0263422	0.00615878	0.0118350 <sup>a</sup>
$a(7)$			0.0140561		0.00260689
$a(9)$			0.0020769		0.0003889

Source: Cizek, V.V., Differentiating FIR Hilbert transformer, in *Proc. 1989 URSI Internat Symp. Signals, Syst., Electron.*, Erlangen, Germany, September 1989.

<sup>a</sup> Corrected by Cizek.

This Fourier series differs by three important features from the series given by Equation 7.595. First, it converges faster (coefficients  $1/i^2$  instead  $1/i$ ) and, second, there are no Gibbs peaks at the edges of the pass-band. Third, the function is unipolar with the mean value equal to  $\pi/2$ . An example of the magnitude designed in the minimax sense is shown in Figure 7.79. The coefficients are given in Table 7.8.

## 7.23 Multidimensional Hilbert Transformations

Multidimensional transformations are applied in modern multidimensional digital signal processing. The theory of complex notation of multidimensional signals uses multidimensional

Hilbert transforms. These are the reasons basic definitions and properties of multidimensional Hilbert transformations are presented here. As in the one-dimensional case, the theory of Hilbert transformations is closely tied with multidimensional Fourier transformations.

Let us define the  $n$ -dimensional signal  $u(\mathbf{x})$  as a function of the  $n$ -dimensional variable  $\mathbf{x} = \{x_1, x_2, \dots, x_n\}$ , an  $n$ -D real column vector. For example, a single frame of a video black-and-white signal may be described by the 2-D signal  $u(x_1, x_2)$ .

### 7.23.1 Evenness and Oddness of $N$ -Dimensional Signals

Let us remember that the 1-D signal may be resolved in a sum of the even and odd parts (see Equations 7.35 and 7.36). Therefore, it has two degrees of freedom concerning evenness or oddness. In general, the  $n$ -dimensional real signal  $u(\mathbf{x})$  has  $2^n$  degrees of freedom in this respect. For example, a 2-D function may be resolved into a sum of four terms:

$$u(x_2, x_1) = u_{ee}(x_2, x_1) + u_{eo}(x_2, x_1) + u_{oe}(x_2, x_1) + u_{oo}(x_2, x_1) \tag{7.616}$$

where the indices “e” and “o” indicate evenness or oddness in respect to the variables  $x_1$  and  $x_2$ . Notice that the indices “ee,” “eo,” “oe” and “oo” are written in the natural order of binary numbers using “e” = 0 (zero) and “o” = 1, i.e., 00, 01, 10, 11. The even-even part is given by

$$u_{ee}(x_2, x_1) = \frac{u(x_2, x_1) + u(x_2, -x_1) + u(-x_2, x_1) + u(-x_2, -x_1)}{4} \tag{7.617}$$

the even-odd part by

$$u_{eo}(x_2, x_1) = \frac{u(x_2, x_1) - u(x_2, -x_1) + u(-x_2, x_1) - u(-x_2, -x_1)}{4} \tag{7.618}$$

the odd-even part by

$$u_{oe}(x_2, x_1) = \frac{u(x_2, x_1) + u(x_2, -x_1) - u(-x_2, x_1) + u(-x_2, -x_1)}{4} \tag{7.619}$$

and the odd-odd part by

$$u_{oo}(x_2, x_1) = \frac{u(x_2, x_1) - u(x_2, -x_1) - u(-x_2, x_1) + u(-x_2, -x_1)}{4} \tag{7.620}$$

We used a reversed order of the indices, that is,  $(x_2, x_1)$  instead of  $(x_1, x_2)$  and as before used the order 00, 01, 10, 11. The sign of a given term in nominators of Equations 7.617 through 7.620 is

equal to the product of the signs of odd indexed variables. If only one variable is odd, as in Equations 7.618 or 7.613, its sign decides. For example, in Equation 7.619 we have  $-u(-x_2, x_1)$  and  $-u(-x_2, -x_1)$  because only the variable  $x_2$  is odd indexed.

A 3-D function may be resolved into a sum of eight terms:

$$u(x_3, x_2, x_1) = u_{eee} + u_{e eo} + u_{e oe} + u_{e oo} + u_{oe e} + u_{oe o} + u_{oo e} + u_{ooo} \tag{7.621}$$

Using the same rules as above, we get

$$u_{eee}(x_3, x_2, x_1) = \frac{u(x_3, x_2, x_1) + u(x_3, x_2, -x_1) + u(x_3, -x_2, x_1) + u(x_3, -x_2, -x_1)}{16} + \frac{u(-x_3, x_2, x_1) + u(-x_3, x_2, -x_1) + u(-x_3, -x_2, x_1) + u(-x_3, -x_2, -x_1)}{16} \tag{7.622}$$

$$u_{e eo}(x_3, x_2, x_1) = \frac{u(x_3, x_2, x_1) - u(x_3, x_2, -x_1) + u(x_3, -x_2, x_1) - u(x_3, -x_2, -x_1)}{16} + \frac{u(-x_3, x_2, x_1) - u(-x_3, x_2, -x_1) + u(-x_3, -x_2, x_1) - u(-x_3, -x_2, -x_1)}{16} \tag{7.623}$$

$$u_{e oe}(x_3, x_2, x_1) = \frac{u(x_3, x_2, x_1) + u(x_3, x_2, -x_1) - u(x_3, -x_2, x_1) - u(x_3, -x_2, -x_1)}{16} + \frac{-u(-x_3, x_2, x_1) - u(-x_3, x_2, -x_1) + u(-x_3, -x_2, x_1) + u(-x_3, -x_2, -x_1)}{16} \tag{7.624}$$

$$u_{e oo}(x_3, x_2, x_1) = \frac{u(x_3, x_2, x_1) - u(x_3, x_2, -x_1) - u(x_3, -x_2, x_1) + u(x_3, -x_2, -x_1)}{16} + \frac{-u(-x_3, x_2, x_1) + u(-x_3, x_2, -x_1) + u(-x_3, -x_2, x_1) - u(-x_3, -x_2, -x_1)}{16} \tag{7.625}$$

It is possible to introduce a geometric interpretation of the decomposition of a function into even and odd terms, as shown in Figure 7.80, and to define the “distance” between the terms. The distance  $D$  is

$$1 > D > n \tag{7.626}$$

For example, the distance between  $f_e$  and  $f_o$  or between  $f_{eo}$  and  $f_{oo}$  equals 1, between  $f_{ee}$  and  $f_{oo}$  equals 2.

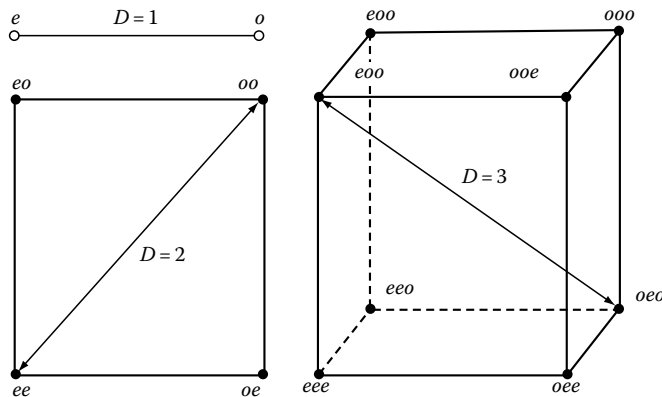


FIGURE 7.80 The geometrical interpretation of the “distance” concerning the evenness and oddness of 1-D, 2-D, and 3-D functions.

### 7.23.2 n-D Hilbert Transformations

The  $n$ -dimensional ( $n$ -D) Hilbert transformation of the  $n$ -D function  $u(\mathbf{x})$  is defined by the  $n$ -fold integral<sup>37</sup>

$$v(\mathbf{x}) = H_n[u(\mathbf{x})] = \frac{1}{\pi^n} P \int_{-\infty}^{\infty} \dots \int_{-\infty}^{\infty} \frac{u(H)}{\prod_{k=1}^n (x_k - \eta_k)} dH; \tag{7.627}$$

$$H = \{\eta_1, \eta_2, \dots, \eta_n\}$$

$$dH = d\eta_1, d\eta_2, \dots, d\eta_n$$

where

$P$  denotes the CPV

$H_n$  is the operator of the  $n$ -D Hilbert transformation

The inverse transformation is

$$u(\mathbf{x}) = H_n^{-1}[v(\mathbf{x})] = \frac{(-1)^n}{\pi^n} P \int_{-\infty}^{\infty} \dots \int_{-\infty}^{\infty} \frac{v(H)}{\prod_{k=1}^n (x_k - \eta_k)} dH \tag{7.628}$$

The  $n$ -D Hilbert pair will be denoted by

$$u(\mathbf{x}) \overset{n-H}{\iff} v(\mathbf{x}) \tag{7.629}$$

Analogous to the 1-D case, the  $n$ -D Hilbert transformation changes the indices of the terms in equations, such as Equations 7.616 or 7.621, from even to odd and from odd to even. Similar to the 1-D case, the  $n$ -D Hilbert transformation may be derived from the  $n$ -D Cauchy integral

$$f(z) = \frac{1}{(2\pi i)^n} \int_{\Gamma} \frac{f(\zeta) d\zeta}{(\zeta - z)} \quad z = \{z_1, \dots, z_n\} \quad \zeta = \{\zeta_1, \dots, \zeta_n\} \tag{7.630}$$

where  $\Gamma = \partial D_1 \times \dots \times \partial D_n$  is an  $n$ -D surface, being the bound of  $\partial D$ , where the region  $D$  has the form of the Cartesian product  $D = D_1 \times \dots \times \partial D_n$ .

### 7.23.3 2-D Hilbert Transformations

The 2-D Hilbert transformation is given by Equation 7.627 with  $n = 2$  and has the form<sup>36</sup>

$$\begin{aligned} v(\mathbf{x}) &= H[u(\mathbf{x})] \\ &= \frac{1}{\pi^2} P \int_{-\infty}^{\infty} \int_{-\infty}^{\infty} \frac{u(\eta_1, \eta_2)}{(x_1 - \eta_1)(x_2 - \eta_2)} d\eta_1 d\eta_2 \end{aligned} \quad (7.631)$$

and because  $n$  is even, the inverse Hilbert transformation has the same form

$$\begin{aligned} u(\mathbf{x}) &= H[v(\mathbf{x})] \\ &= \frac{1}{\pi^2} P \int_{-\infty}^{\infty} \int_{-\infty}^{\infty} \frac{v(\eta_1, \eta_2)}{(x_1 - \eta_1)(x_2 - \eta_2)} d\eta_1 d\eta_2 \end{aligned} \quad (7.632)$$

The 2-D Hilbert transformation may be written using the convolution notation

$$v(x_1, x_2) = u(x_1, x_2) ** \frac{1}{\pi^2 x_1 x_2} \quad (7.633)$$

$$u(x_1, x_2) = v(x_1, x_2) ** \frac{1}{\pi^2 x_1 x_2} \quad (7.634)$$

### 7.23.4 Partial Hilbert Transformations

The partial Hilbert transformation of the  $n$ -D function  $u(\mathbf{x})$ ,  $\mathbf{x} = \{x_1, x_2, \dots, x_n\}$  is defined as the Hilbert transformation in respect to a part of the variables. For example, the partial transformation of a 2-D function in respect to  $x_1$  has the form

$$v_1(x_1, x_2) = \frac{1}{\pi} P \int_{-\infty}^{\infty} \frac{u(\eta_1, x_2)}{(x_1 - \eta_1)} d\eta_1 \quad (7.635)$$

and in respect to the variable  $x_2$

$$v_2(x_1, x_2) = \frac{1}{\pi} P \int_{-\infty}^{\infty} \frac{u(x_1, \eta_2)}{(x_2 - \eta_2)} d\eta_2 \quad (7.636)$$

For 3-D functions it is possible to derive three first-order partial Hilbert transforms denoted  $v_1, v_2, v_3$  and three second-order Hilbert transforms denoted  $v_{12}, v_{13}, v_{23}$ . For example,

$$v_1(x_1, x_2, x_3) = \frac{1}{\pi} P \int_{-\infty}^{\infty} \frac{u(\eta_1, x_2, x_3)}{(x_1 - \eta_1)} d\eta_1 \quad (7.637)$$

and

$$v_{12}(x_1, x_2, x_3) = \frac{1}{\pi^2} P \int_{-\infty}^{\infty} \int_{-\infty}^{\infty} \frac{u(\eta_1, \eta_2, x_3)}{(x_1 - \eta_1)(x_2 - \eta_2)} d\eta_1 d\eta_2 \quad (7.638)$$

### 7.23.5 Spectral Description of $n$ -D Hilbert Transformations

The  $n$ -D Fourier transformation of  $u(\mathbf{x})$  is defined by the  $n$ -fold integral

$$U(\Omega) = F_n[u(\mathbf{x})] = \int_{-\infty}^{\infty} \dots \int_{-\infty}^{\infty} u(\mathbf{x}) \exp(-j\Omega^T \mathbf{x}) d\mathbf{x} \quad (7.639)$$

where  $\Omega = \{\omega_1, \omega_2, \dots, \omega_n\}$  is the  $n$ -D column vector of Fourier frequencies. The index "T" denotes transpose. Therefore, the exponential kernel of the  $n$ -D Fourier transformation has the form

$$\exp(-j\Omega^T \mathbf{x}) = e^{-j(\omega_1 x_1 + \omega_2 x_2 + \dots + \omega_n x_n)} \quad (7.640)$$

The inverse Fourier transformation is defined by the  $n$ -fold integral

$$\begin{aligned} u(\mathbf{x}) &= F_n^{-1}[U(\Omega)] \\ &= \int_{-\infty}^{\infty} \dots \int_{-\infty}^{\infty} U(\Omega) \exp(j\Omega^T \mathbf{x}) df_1 df_2 \dots df_n \end{aligned} \quad (7.641)$$

where  $df_i = d\omega_i/2\pi$  ( $i = 1, 2, \dots, n$ ). The  $n$ -D Fourier pair may be denoted

$$u(\mathbf{x}) \stackrel{n-F}{\longleftrightarrow} U(\Omega) \quad (7.642)$$

The  $n$ -D Fourier image of the Hilbert transform is given by the formula

$$V(\Omega) = F_n\{H_n[u(\mathbf{x})]\} = (-j)^n \left[ \prod_{k=1}^n \text{sgn}(\omega_k) \right] U(\Omega) \quad (7.643)$$

*Proof* By the definition given by Equation 7.639

$$\begin{aligned} F_n\{H_n[u(\mathbf{x})]\} &= \frac{1}{\pi^n} \int_{-\infty}^{\infty} \left\{ \int_{-\infty}^{\infty} \frac{U(H)}{\prod_{k=1}^n (x_k - \eta_k)} dH \right\} \\ &\quad \times \exp(-j\Omega^T \mathbf{x}) d\mathbf{x} \end{aligned} \quad (7.644)$$



where  $\mathbf{H} = \{\eta_1, \eta_2, \dots, \eta_n\}$ ,  $d\mathbf{H} = d\eta_1, d\eta_2, \dots, d\eta_n$  and for convenience the  $n$ -fold integrals are denoted by a single integral sign. Formally

$$\begin{aligned}
 F_n\{H_n[u(\mathbf{x})]\} &= \frac{1}{\pi^n} \int_{-\infty}^{\infty} u(\mathbf{H}) d\mathbf{H} \int_{-\infty}^{\infty} \frac{\exp(-j\Omega^T \mathbf{x})}{\prod_{k=1}^n (x_k - \eta_k)} d\mathbf{x} \\
 &= \int_{-\infty}^{\infty} u(\mathbf{H}) d\mathbf{H} \prod_{k=1}^n \left( \frac{1}{\pi} \int_{-\infty}^{\infty} \frac{\exp(-j\omega_k x_k)}{x_k - \eta_k} dx_k \right)
 \end{aligned} \tag{7.645}$$

In the 1-D case, we have

$$H[\exp(-j\omega x)] = j \operatorname{sgn}(\omega) \exp(-j\omega x) \tag{7.646}$$

Hence,

$$\begin{aligned}
 F_n\{H_n[u(\mathbf{x})]\} &= (-j)^n \left[ \prod_{k=1}^n \operatorname{sgn}(\omega_k) \right] \\
 &\quad \times \int_{-\infty}^{\infty} u(\mathbf{x}) \exp(-j\Omega^T \mathbf{x}) d\mathbf{x}
 \end{aligned} \tag{7.647}$$

and this is equal to Equation 7.643.

This equation enables the calculation of the  $n$ -D Hilbert transform using the inverse Fourier transform of the spectrum given by the above equation, i.e., using the algorithm

$$\begin{aligned}
 u(\mathbf{x}) \stackrel{n-F}{\Rightarrow} U(\Omega) &\Rightarrow V(\Omega) \\
 &= (-j)^n \left[ \prod_{k=1}^n \operatorname{sgn}(\omega_k) \right] U(\Omega) \stackrel{2-F^{-1}}{\Rightarrow} v(\mathbf{x})
 \end{aligned} \tag{7.648}$$

For example, in the 2-D case the Hilbert transform is given by

$$\begin{aligned}
 v(x_1, x_2) &= \int_{-\infty}^{\infty} \int_{-\infty}^{\infty} \\
 &\quad - \operatorname{sgn}(\omega_1) \operatorname{sgn}(\omega_2) U(\omega_1, \omega_2) e^{j(\omega_1 x_1 + \omega_2 x_2)} df_1 df_2
 \end{aligned} \tag{7.649}$$

( $\omega_1 = 2\pi f_1$ ,  $\omega_2 = 2\pi f_2$ ). This general formula may be simplified, if the signal given by Equation 7.610 has only a part of the four terms.

**Example<sup>14</sup>**

Consider the 2-D Gaussian signal and its Fourier image given by the Fourier pair

$$u(x_1, x_2) = e^{-\pi(x_1^2 + x_2^2)} \stackrel{2-F}{\Leftrightarrow} U(\omega_1, \omega_2) = e^{-\pi(f_1^2 + f_2^2)} \tag{7.650}$$

where

$$\begin{aligned}
 \omega_1 &= 2\pi f_1 \\
 \omega_2 &= 2\pi f_2
 \end{aligned}$$

The Fourier image of the Hilbert transform is

$$V(\omega_1, \omega_2) = -\operatorname{sgn}(\omega_1) \operatorname{sgn}(\omega_2) e^{-\pi(f_1^2 + f_2^2)} \tag{7.651}$$

Because this spectral function is real and odd-odd, the 2-D inverse Fourier transformation takes the simplified form

$$v(x_1, x_2) = 4 \int_0^{\infty} \int_0^{\infty} e^{-\pi(f_1^2 + f_2^2)} \sin(\omega_1 x_1) \sin(\omega_2 x_2) df_1 df_2 \tag{7.652}$$

**7.23.6  $n$ -D Hilbert Transforms of Separable Functions**

The  $n$ -D function  $u(\mathbf{x})$  is said to be *separable* in the coordinates  $\mathbf{x} = \{x_1, x_2, \dots, x_n\}$  if it is given by the product of 1-D functions

$$u(\mathbf{x}) = f_1(x_1) f_2(x_2) \dots f_n(x_n) \tag{7.653}$$

Let us denote by  $g_1(x_1), g_2(x_2), \dots, g_n(x_n)$  the Hilbert transforms of the terms of this product. Because the Fourier image of a separable function is a separable function of the Fourier coordinates  $\Omega = \{\omega_1, \omega_2, \dots, \omega_n\}$  the inverse Fourier transform is a product of 1-D integrals. Therefore, the Hilbert transform of a separable function has the form

$$v(\mathbf{x}) = g_1(x_1) g_2(x_2) \dots g_n(x_n) \tag{7.654}$$

Analogously, the partial Hilbert transforms of  $u(\mathbf{x})$  are separable functions; for example, a first-order partial transform is

$$v(\mathbf{x}) = g_1(x_1) f_2(x_2) \dots f_n(x_n) \tag{7.655}$$

and a second-order partial transform is

$$v_{12}(\mathbf{x}) = g_1(x_1) g_2(x_2) f_3(x_3) \dots f_n(x_n) \tag{7.656}$$

**Examples**

1. The 2-D delta pulse is a separable distribution of the form

$$\delta(x_1, x_2) = \delta(x_1) \delta(x_2) \tag{7.657}$$

Because  $\delta(x_1) \stackrel{H}{\iff} 1/(\pi x_1)$  and  $\delta(x_2) \stackrel{H}{\iff} 1/(\pi x_2)$ , the Hilbert transform of the 2-D delta pulse has the form

$$\delta(x_1, x_2) \stackrel{2-H}{\iff} 1/(\pi^2 x_1 x_2) \quad (7.658)$$

and the partial transforms are

$$\begin{aligned} v(x_1, x_2) &= \delta(x_2)/(\pi x_1); \\ v_1(x_1, x_2) &= \delta(x_1)/(\pi x_2); \end{aligned} \quad (7.659)$$

2. The 2-D signal has the form

$$u(x_1, x_2) = \Pi_a(x_1)\Pi_b(x_2) \quad (7.660)$$

The Hilbert transform takes the form (see Table 7.1, 4)

$$v(x_1, x_2) = \frac{1}{\pi^2} \ln \left| \frac{x_1 + a}{x_1 - a} \right| \ln \left| \frac{x_2 + b}{x_2 - b} \right| \quad (7.661)$$

and the partial transforms are

$$\begin{aligned} v(x_1, x_2) &= \frac{1}{\pi} \ln \left| \frac{x_1 + a}{x_1 - a} \right| \Pi_b(x_2); \\ v_2(x_1, x_2) &= \frac{1}{\pi} \Pi_a(x_1) \ln \left| \frac{x_2 + b}{x_2 - b} \right| \end{aligned} \quad (7.662)$$

3. Derivation of the Hilbert Transform of a nonseparable function defined by the equation

$$\begin{aligned} u(x_1, x_2) &= \frac{h}{a}(a - |x_1| - |x_2|); & (x_1, x_2) \in S \\ u(x_1, x_2) &= 0; & (x_1, x_2) \notin S \end{aligned} \quad (7.663)$$

The support  $S$  is shown in Figure 7.81b. This function has the geometric form of a pyramid (Figure 7.81a). The Hilbert transform of this function is

$$\begin{aligned} v(x_1, x_2) &= \frac{h}{\pi^2 a} \left\{ P \int_0^a \int_0^{a-x_2} \frac{a - \eta - \gamma}{(x_1 - \eta)(x_2 - \gamma)} d\gamma d\eta \right. \\ &+ P \int_0^{-a} \int_{-a+x_2}^0 \frac{a - \eta - \gamma}{(x_1 - \eta)(x_2 - \gamma)} d\gamma d\eta \\ &+ P \int_{-a}^0 \int_0^{-a+x_2} \frac{a - \eta - \gamma}{(x_1 - \eta)(x_2 - \gamma)} d\gamma d\eta \\ &\left. + P \int_{-a}^0 \int_{-a-x_2}^0 \frac{a - \eta - \gamma}{(x_1 - \eta)(x_2 - \gamma)} d\gamma d\eta \right\} \quad (7.664) \end{aligned}$$

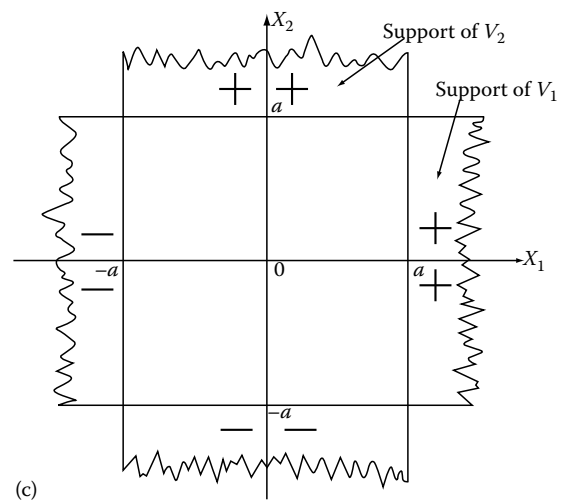
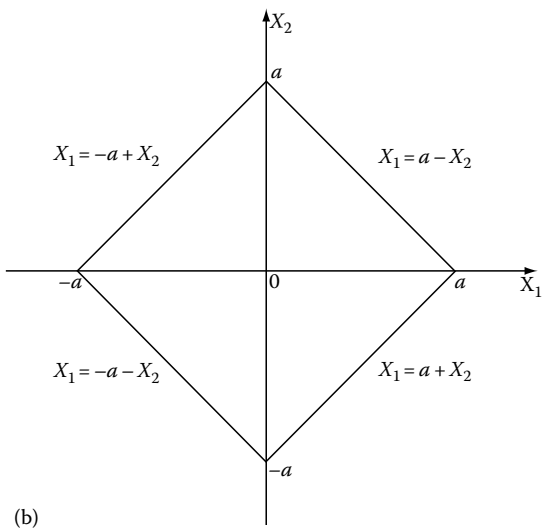
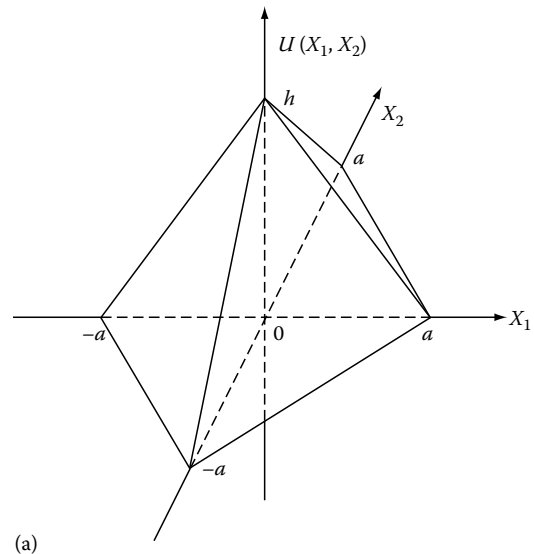


FIGURE 7.81 (a) The pyramid pulse. (b) The support of the pyramid pulse. (c) The supports of the partial Hilbert transforms of this pulse.

The integration yields

$$v(x_1, x_2) = \frac{h}{\pi^2 a} \left\{ 2x_1 \ln|x_1| \ln \left| \frac{x_2 - a}{x_2 + a} \right| + P \int_0^a \frac{(x_1 + \gamma - a) \ln|x_1 + \gamma - a| + (x_1 + a - \gamma) \ln|x_1 + a - \gamma|}{x_2 - \gamma} d\gamma + P \int_{-a}^0 \frac{(x_1 - a - \gamma) \ln|x_1 - a - \gamma| + (a + x_1 + \gamma) \ln|a + x_1 + \gamma|}{x_2 - \gamma} d\gamma \right\} \quad (7.665)$$

The 1-D integrals do not have a closed solution and a numerical integration should be applied. Notice that the support of the Hilbert transform (Equation 7.665) is infinite, which is different than the finite support of  $u(x_1, x_2)$ . The partial Hilbert transforms, defined by Equations 7.635 and 7.636 are

$$v_1(x_1, x_2) = \frac{h}{\pi a} [-2x_1 \ln|x_1| + (x_1 + x_2 - a) \ln|x_1 + x_2 - a| + (x_1 + a - x_2) \ln|x_1 + a - x_2|] \quad (7.666)$$

$$v_2(x_1, x_2) = \frac{h}{\pi a} [-2x_2 \ln|x_2| + (x_2 + x_1 - a) \ln|x_2 + x_1 - a| + (x_2 + a - x_1) \ln|x_2 + a - x_1|] \quad (7.667)$$

The supports of these functions are shown in Figure 7.81c. They are infinite in one dimension and finite in a band  $(-a, a)$  in the second dimension.

### 7.23.7 Properties of 2-D Hilbert Transformations

Selected properties of 2-D Hilbert transformations are summarized in Table 7.9.

#### 7.23.7.1 Orthogonality

The terms of the 1-D Hilbert pair form a pair of orthogonal functions satisfying the condition

$$E = \int u(t)v(t)dt = 0 \quad (7.668)$$

that is, the *mutual energy* of both signals equals zero. In general, the terms of the 2-D Hilbert pair are not orthogonal; that is, the mutual energy

$$E = \iint u(x_1, x_2)v(x_1, x_2)dx_1 dx_2 \neq 0 \quad (7.669)$$

does not equal zero. However, this integral equals zero for 2-D separable signals and for nonseparable signals with certain symmetry; for example, the pyramid signal defined by Equation 7.657. For separable signals the above double integral takes form of a product of single integrals, each of which equals zero.

#### Example

Consider the 2-D Gaussian signal of the form<sup>14</sup>

$$u(x_1, x_2) = [2\pi\sigma_1\sigma_2\text{SQR}(1 - \rho^2)]^{-1} \times \exp\{-(1 - \rho^2)^{-1} [(x_1/\sigma_1)^2 + (x_2/\sigma_2)^2 - 2\rho x_1 x_2 / (\sigma_1 \sigma_2)]\} \quad (7.670)$$

**TABLE 7.9** Properties of 2-D Hilbert Transformations

Number	Name	Original Signal or the Inverse Transform	Hilbert Transform
1	Notations	$u(x_1, x_2) = H_2^{-1}[v(x_1, x_2)]$ ;	$v(x_1, x_2) = H_2[u(x_1, x_2)]$
2	Signal domain definitions	$u(x_1, x_2) = 1/(\pi^2 x_1 x_2) ** v(x_1, x_2)$ ; <sup>a</sup>	$v(x_1, x_2) = 1/(\pi^2 x_1 x_2) ** u(x_1, x_2)$ ; <sup>b</sup>
3	Fourier spectra	$u(x_1, x_2) \xleftrightarrow{2-F} U(\omega_1, \omega_2) = -\text{sgn}(\omega_1)\text{sgn}(\omega_2)V(\omega_1, \omega_2)$	$v(x_1, x_2) \xleftrightarrow{2-F} V(\omega_1, \omega_2) = -\text{sgn}(\omega_1)\text{sgn}(\omega_2)U(\omega_1, \omega_2)$
4	Linearity	$au_a(x_1, x_2) + bu_b(x_1, x_2)$ ;	$av_a(x_1, x_2) + bv_b(x_1, x_2)$
5	Change of symmetry	$u_{ee} + u_{oo} + u_{eo} + u_{oe}$ ;	$v_{oo} + v_{ee} - v_{oe} - v_{eo}$ <sup>c</sup>
6	Iteration	$v(x_1, x_2) \xleftrightarrow{2-H} u(x_1, x_2)$	
7	Energy quality	$\int \int u^2(x_1, x_2) dx_1 dx_2 = \int \int v^2(x_1, x_2) dx_1 dx_2$	
8	Product of low-pass and high-pass signals with strongly separated spectra	$u_{LP}(x_1, x_2)$ $u_{HP}(x_1, x_2)$	Low-pass signal High-pass signal
9	Separable functions	$H_2(u_{LP}u_{HP}) = u_{LP}[H_2(u_{HP})]$	
	Total Hilbert tr.	$f_1(x_1) \xleftrightarrow{H} g_1(x_1); f_2(x_2) \xleftrightarrow{H} g_2(x_2)$	$v(x_1, x_2) = g_1 g_2$
	Partial Hilbert tr.	$u(x_1, x_2) = f_1 f_2$ $v_1(x_1, x_2) = g_1 f_2$	$v_2(x_1, x_2) = f_1 g_2$

Note: Indices: e, even, o, odd.

<sup>a</sup> See Equation 7.632.

<sup>b</sup> See Equation 7.631.

This function is well known in probability theory. It is a separable function if the parameter  $\rho = 0$ . Otherwise, for  $0 < \rho < 1$ , it is a nonseparable function. Its Hilbert transform may be calculated using the inverse Fourier transform of the Fourier image, which has the form

$$U(\omega_1, \omega_2) = \exp\{-0.5[\sigma_1^2\omega_1^2 + \sigma_2^2\omega_2^2 + 2\rho\sigma_1\sigma_2\omega_1\omega_2]\} \quad (7.671)$$

Because  $U$  is a real function, the inverse Fourier transformation has the simplified form

$$\begin{aligned} \mathbf{v}(x_1, x_2) &= \int_{-\infty}^{\infty} \int_{-\infty}^{\infty} -\text{sgn}(\omega_1)\text{sgn}(\omega_2)U(\omega_1, \omega_2) \\ &\times \cos(\omega_1x_1 + \omega_2x_2)df_1df_2 \end{aligned} \quad (7.672)$$

and the partial Hilbert transforms are given by the integrals

$$\begin{aligned} \mathbf{v}_1(x_1, x_2) &= \int_{-\infty}^{\infty} \int_{-\infty}^{\infty} -\text{sgn}(\omega_1)U(\omega_1, \omega_2) \\ &\times \sin(\omega_1x_1 + \omega_2x_2)df_1df_2 \end{aligned} \quad (7.673)$$

$$\begin{aligned} \mathbf{v}_2(x_1, x_2) &= \int_{-\infty}^{\infty} \int_{-\infty}^{\infty} -\text{sgn}(\omega_2)U(\omega_1, \omega_2) \\ &\times \sin(\omega_1x_1 + \omega_2x_2)df_1df_2 \end{aligned} \quad (7.674)$$

Because these integrals cannot be expressed in the closed form, a numerical integration scheme must be used for their approximation. Figure 7.82 shows the equal-value contour lines of the Gaussian function  $u(x_1, x_2)$  and the total and partial Hilbert transforms ( $\rho = 0.5, \sigma_1 = 1, \sigma_2 = 2$ ). The numerical integration yields the value of the mutual energy  $E \cong 0.25$  (relative to the signal energy).  $E$  equals zero only if  $\rho = 0$ , i.e., for separable Gaussian signals.

### 7.23.8 Stark's Extension of Bedrosian's Theorem<sup>37</sup>

Bedrosian's theorem defines the Hilbert transform of a product of low-pass and high-pass signals. Stark formulated an extension of this theorem for 2-D signals. A 2-D function  $u_{LP}(x_1, x_2) \stackrel{2-F}{\iff} U_{LP}(\omega_1, \omega_2)$  is said to be low-pass with cutoff vector  $\Omega_0 = \{\omega_{10}, \omega_{20}\}$  if

$$\begin{aligned} \max |\omega_1| = \omega_{10} \quad \text{and} \quad \max |\omega_2| = \omega_{20} \\ \text{all } \omega_1 \in \text{supp } U_{LP}(\omega_1, \omega_2) \quad \text{all } \omega_2 \in U_{LP}(\omega_1, \omega_2) \end{aligned} \quad (7.675)$$

where  $\text{supp } U_{LP}$  denotes the support of the Fourier image; that is, the set of points for which  $U_{LP}(\omega_1, \omega_2)$  is not zero. Analogously, the function  $U_{HP}(x_1, x_2) \stackrel{2-F}{\iff} U_{HP}(\omega_1, \omega_2)$  is said to be high-pass with cutoff vector  $\Omega_0 = \{\omega_{10}, \omega_{20}\}$  if

$$\begin{aligned} \min |\omega_1| = \omega_{10} \quad \text{and} \quad \min |\omega_2| = \omega_{20} \\ \text{all } \omega_1 \in \text{supp } U_{HP}(\omega_1, \omega_2) \quad \text{all } \omega_2 \in U_{HP}(\omega_1, \omega_2) \end{aligned} \quad (7.676)$$

The signals  $u_{LP}$  and  $u_{HP}$  are said to be strongly spectrally separable if the conditions (Equations 7.675 and 7.676) are satisfied. We say that the functions  $U_{LP}$  and  $U_{HP}$  are spectrally disjointed if they have nonoverlapping supports. However, spectral disjointedness may not coincide with strong separability, as shown in Figure 7.83. Stark's extension of Bedrosian's theorem has the form

$$H_2[u_{LP}(x_1, x_2)u_{HP}(x_1, x_2)] = u_{LP}(x_1, x_2)H_2[u_{HP}(x_1, x_2)] \quad (7.677)$$

that is, only the high-pass term of the product is transformed.

### 7.23.9 Appendix (Section 7.23)

Consider the 2-D signal given by Equation 7.616. Its 2-D Fourier transform is (Table 7.10)

$$\begin{aligned} U(\omega_1, \omega_2) &= \int_{-\infty}^{\infty} \int_{-\infty}^{\infty} u(x_1, x_2)e^{-j(\omega_1x_1 + \omega_2x_2)}dx_1dx_2 \\ &= U_{Re} + jU_{Im} \\ &= U_{ee} - U_{oo} - j(U_{eo} + U_{oe}) \end{aligned} \quad (7.678)$$

where (Tables 7.11 and 7.12)

$$U_{ee}(\omega_1, \omega_2) = \int_{-\infty}^{\infty} \int_{-\infty}^{\infty} u_{ee}(x_1, x_2) \cos(\omega_1x_1) \cos(\omega_2x_2) dx_1dx_2 \quad (7.679)$$

$$U_{oo}(\omega_1, \omega_2) = \int_{-\infty}^{\infty} \int_{-\infty}^{\infty} u_{oo}(x_1, x_2) \sin(\omega_1x_1) \sin(\omega_2x_2) dx_1dx_2 \quad (7.680)$$

$$U_{oe}(\omega_1, \omega_2) = \int_{-\infty}^{\infty} \int_{-\infty}^{\infty} u_{oe}(x_1, x_2) \sin(\omega_1x_1) \cos(\omega_2x_2) dx_1dx_2 \quad (7.681)$$

$$U_{eo}(\omega_1, \omega_2) = \int_{-\infty}^{\infty} \int_{-\infty}^{\infty} u_{eo}(x_1, x_2) \cos(\omega_1x_1) \sin(\omega_2x_2) dx_1dx_2 \quad (7.682)$$

Using computer programs for numerical integration, the insertion in these integrals of  $u(x_1, x_2)$  instead of  $u_{ee}, u_{oo}, \dots$  does not change the result because the trigonometric kernels are selecting the right terms themselves. Because the Fourier image of the Hilbert transform is

$$V(\omega_1, \omega_2) = -\text{sgn}(\omega_1)\text{sgn}(\omega_2)[U_{ee} - U_{oo} - j(U_{oe} + U_{eo})] \quad (7.683)$$

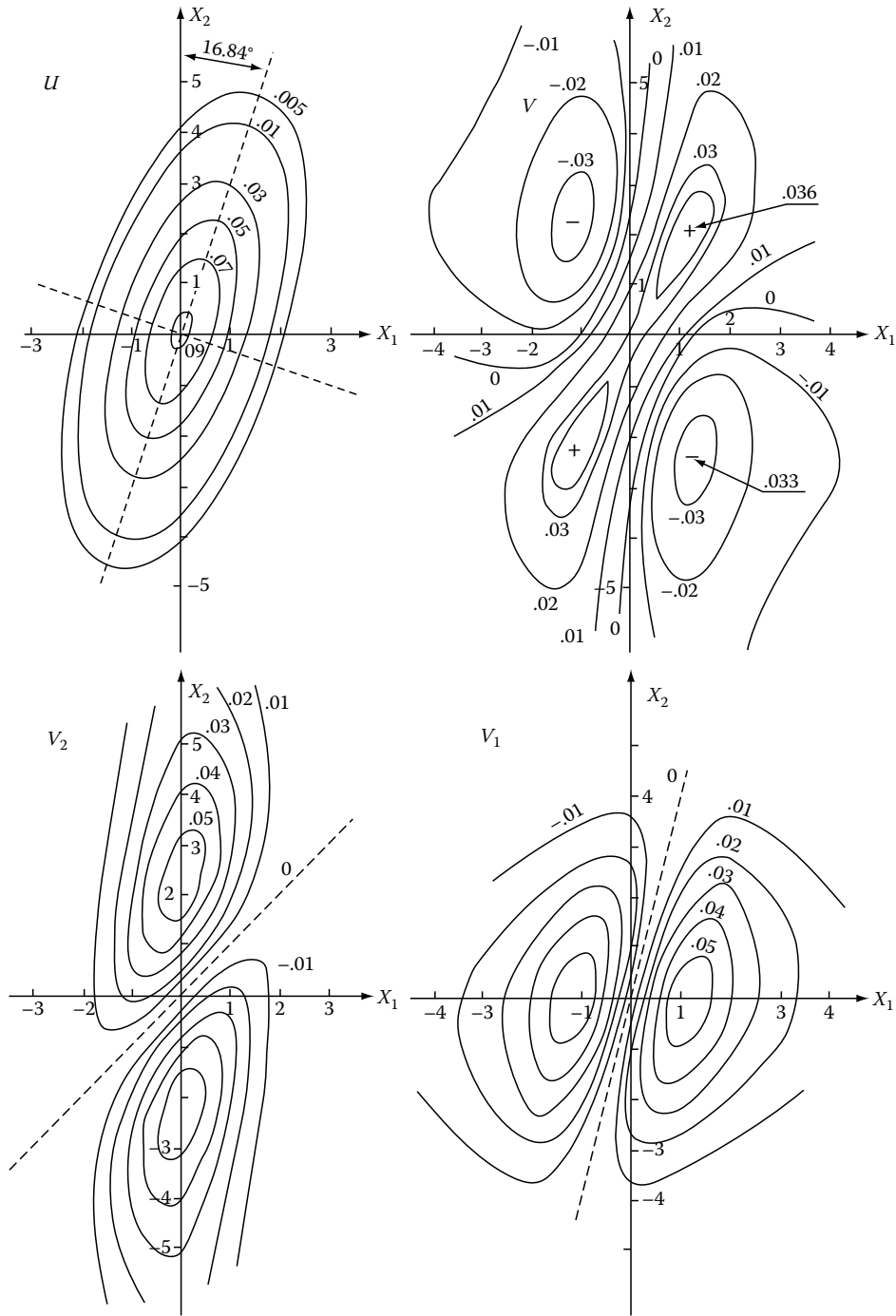


FIGURE 7.82 The elliptical equal-value contours of a nonseparable Gaussian function (see Equation 7.670) and of the Hilbert transforms  $v, v_1,$  and  $v_2$ , where  $\rho = 0.5, \sigma_1 = 1, \sigma_2 = 2$ .

the inverse Fourier transform yields the Hilbert transform

$$v(x_1, x_2) = v_{ee} + v_{oo} + v_{oe} + v_{eo} \quad (7.684)$$

$$V_{ee}(x_1, x_2) = 4 \int_0^\infty \int_0^\infty U_{ee}(\omega_1, \omega_2) \cos(\omega_1 x_1) \cos(\omega_2 x_2) df_1 df_2 \quad (7.685)$$

where due to the symmetry conditions, the terms of  $u$  may be given by one-sided integrals

$$V_{oo}(x_1, x_2) = 4 \int_0^\infty \int_0^\infty U_{oo}(\omega_1, \omega_2) \sin(\omega_1 x_1) \sin(\omega_2 x_2) df_1 df_2 \quad (7.686)$$

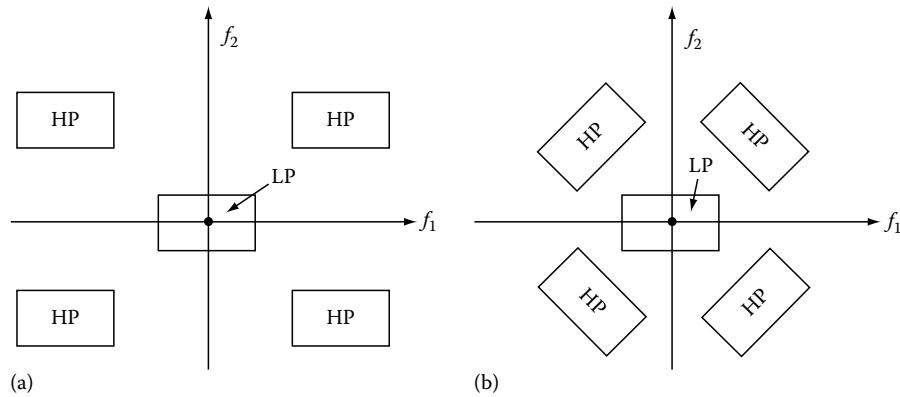


FIGURE 7.83 (a) LP is the support of the spectrum of a low-pass signal, HP is the support of the spectrum of a high-pass signal strongly separable from the low-pass. (b) Analogous spectra with spectral disjointedness.

TABLE 7.10 2-D Total and Partial Hilbert Transforms

Number	Name	Original Signal, Total, and Partial Hilbert Transforms	
1	Delta	$u = \delta(x_1, x_2)$	$v = 1/(\pi^2 x_1 x_2)$
		$v_1 = \delta(x_2)/(\pi x_1)$	$v_2 = \delta(x_1)/(\pi x_2)$
2	Gaussian pulse	$u = e^{-\pi(x_1^2 + x_2^2)}$	$\omega_1 = 2\pi f_1; \omega_2 = 2\pi f_2$
		$v = 4 \int_0^\infty \int_0^\infty e^{-\pi(f_1^2 + f_2^2)}$	$\sin(\omega_1 x_1) \sin(\omega_2 x_2) df_1 df_2$
		$v_1 = 4 \int_0^\infty \int_0^\infty e^{-\pi(f_1^2 + f_2^2)}$	$\sin(\omega_1 x_1) \cos(\omega_2 x_2) df_1 df_2$
		$v_2 = 4 \int_0^\infty \int_0^\infty e^{-\pi(f_1^2 + f_2^2)}$	$\cos(\omega_1 x_1) \sin(\omega_2 x_2) df_1 df_2$
3	Cauchy pulse	$u = \frac{ab}{(a^2 + x_1^2)(b^2 + x_2^2)}$	$v = \frac{x_1 x_2}{(a^2 + x_1^2)(b^2 + x_2^2)}$
		$v_1 = \frac{x_1 b}{(a^2 + x_1^2)(b^2 + x_2^2)}$	$v_2 = \frac{ax_2}{(a^2 + x_1^2)(b^2 + x_2^2)}$
4	Cube pulse	$u = \Pi_a(x) \Pi_b(x_2)$	$v = \frac{1}{\pi^2} \ln \left  \frac{x_1 + a}{x_1 - a} \right  \ln \left  \frac{x_2 + b}{x_2 - b} \right $
		$v_1 = \frac{1}{\pi} \ln \left  \frac{x_1 + a}{x_1 - a} \right  \Pi_b(x_2)$	$v_2 = \frac{1}{\pi} \ln \left  \frac{x_2 + b}{x_2 - b} \right  \Pi_a(x_1)$
5	Sinc pulse	$u = \frac{\sin(ax_1) \sin(bx_2)}{abx_1 x_2}$	$v = 4 \frac{\sin^2(ax_1/2) \sin^2(bx_2/2)}{abx_1 x_2}$
		$v_1 = 2 \frac{\sin^2(ax_1/2) \sin(bx_2)}{abx_1 x_2}$	$v_2 = 2 \frac{\sin(ax_1) \sin^2(bx_2/2)}{abx_1 x_2}$
6	Nonseparable Gaussian pulse	See Equations 7.670 through 7.674	
7	Pyramid pulse	See Equations 7.663 through 7.667	
8	2-D periodic signals	See Table 7.11	

Note: Notations:  $u(x_1, x_2)$ , original signal;  $v(x_1, x_2)$ , total Hilbert transform;  $v_1(x_1, x_2)$  or  $v_2(x_1, x_2)$ , partial Hilbert transforms.

$$V_{oe}(x_1, x_2) = 4 \int_0^\infty \int_0^\infty U_{oe}(\omega_1, \omega_2) \sin(\omega_1 x_1) \cos(\omega_2 x_2) df_1 df_2 \tag{7.687}$$

$$V_{eo}(x_1, x_2) = 4 \int_0^\infty \int_0^\infty U_{eo}(\omega_1, \omega_2) \cos(\omega_1 x_1) \sin(\omega_2 x_2) df_1 df_2 \tag{7.688}$$

### 7.23.9 Two-Dimensional Hilbert Transformers

The transfer function of the ideal “noncausal” 2-D Hilbert transformer is given by a product of 1-D transfer functions (see Equations 7.553 through 7.555). Therefore,

$$H_{2-H}(f_1, f_2) = [-j \operatorname{sgn}(f_1)] [-j \operatorname{sgn}(f_2)] = |H_{2-H}| e^{j\Phi(f_1, f_2)} \tag{7.689}$$

**TABLE 7.11** 2-D Total and Partial Hilbert Transforms of Periodic Functions

Number	Original Signal, Total, and Partial Hilbert Transforms	
1	$u = \cos(\omega_1 x_1) \cos(\omega_2 x_2)$ $v_1 = \sin(\omega_1 x_1) \cos(\omega_2 x_2)$	$v = \sin(\omega_1 x_1) \sin(\omega_2 x_2)$ $v_2 = \cos(\omega_1 x_1) \sin(\omega_2 x_2)$
2	$u = \sin(\omega_1 x_1) \sin(\omega_2 x_2)$ $v_1 = -\cos(\omega_1 x_1) \sin(\omega_2 x_2)$	$v = \cos(\omega_1 x_1) \cos(\omega_2 x_2)$ $v_2 = -\sin(\omega_1 x_1) \cos(\omega_2 x_2)$
3	$u = \cos(\omega_1 x_1 + \omega_2 x_2)$ $v_1 = \sin(\omega_1 x_1 + \omega_2 x_2)$	$v = -\cos(\omega_1 x_1 + \omega_2 x_2)$ $v_2 = \sin(\omega_1 x_1 + \omega_2 x_2)$
4	$u = \sin(\omega_1 x_1 + \omega_2 x_2)$ $v_1 = -\cos(\omega_1 x_1 + \omega_2 x_2)$	$v = -\sin(\omega_1 x_1 + \omega_2 x_2)$ $v_2 = \cos(\omega_1 x_1 + \omega_2 x_2)$
5	$u = e^{j(\omega_1 x_1 + \omega_2 x_2)}$ $v_1 = -j \operatorname{sgn}(\omega_1) e^{j(\omega_1 x_1 + \omega_2 x_2)}$	$v = -\operatorname{sgn}(\omega_1) \operatorname{sgn}(\omega_2) e^{j(\omega_1 x_1 + \omega_2 x_2)}$ $v_2 = -j \operatorname{sgn}(\omega_2) e^{j(\omega_1 x_1 + \omega_2 x_2)}$
6	$u = \operatorname{sgn}[\cos(\omega_1 x_1)] \operatorname{sgn}[\cos(\omega_2 x_2)]$ (2-D square wave) $v = (4/\pi^2) \ln  \tan(\omega_2 x_1/2 + \pi/4)  \ln  \tan(\omega_1 x_2/2 + \pi/4) $ $v_1 = (2/\pi) \ln  \tan(\omega_1 x_1/2 + \pi/4)  \operatorname{sgn}[\cos(\omega_2 x_2)]$ $v_2 = (2/\pi) \ln  \tan(\omega_2 x_2/2 + \pi/4)  \operatorname{sgn}[\cos(\omega_1 x_1)]$	
7	$u = \sum_{n=-\infty}^{\infty} \sum_{m=-\infty}^{\infty} \delta(x_1 - na, x_2 - mb)$ (2-D delta sampling sequence) $v = \frac{1}{ab} \sum_{n=-\infty}^{\infty} \sum_{m=-\infty}^{\infty} \cot[(\pi/a)(x_1 - na)] \cot[(\pi/b)(x_2 - mb)]$ $v_1 = \frac{1}{a} \sum_{n=-\infty}^{\infty} \sum_{m=-\infty}^{\infty} \cot[(\pi/a)(x_1 - na)] \delta(x_2 - mb)$ $v_2 = \frac{1}{b} \sum_{n=-\infty}^{\infty} \sum_{m=-\infty}^{\infty} \cot[(\pi/b)(x_2 - mb)] \delta(x_1 - na)$	

Note: Notations:  $u(x_1, x_2)$ , original signal;  $v(x_1, x_2)$ , total Hilbert transforms;  $v_1(x_1, x_2)$  or  $v_2(x_1, x_2)$ , partial Hilbert transforms.

**TABLE 7.12**  $n$ -D Hilbert Transforms of Harmonic Functions

$n$	Function	Hilbert Transform
1	$\cos(\omega t)$ $\sin(\omega t)$	$\sin(\omega t)$ $-\cos(\omega t)$
2	$\cos(\omega_1 x_1 + \omega_2 x_2)$ $\sin(\omega_1 x_1 + \omega_2 x_2)$	$-\cos(\omega_1 x_1 + \omega_2 x_2)$ $-\sin(\omega_1 x_1 + \omega_2 x_2)$
3	$\cos(\omega_1 x_1 + \omega_2 x_2 + \omega_3 x_3)$ $\sin(\omega_1 x_1 + \omega_2 x_2 + \omega_3 x_3)$	$-\sin(\omega_1 x_1 + \omega_2 x_2 + \omega_3 x_3)$ $\cos(\omega_1 x_1 + \omega_2 x_2 + \omega_3 x_3)$
4	$\cos(\omega_1 x_1 + \omega_2 x_2 + \omega_3 x_3 + \omega_4 x_4)$ $\sin(\omega_1 x_1 + \omega_2 x_2 + \omega_3 x_3 + \omega_4 x_4)$	$\cos(\omega_1 x_1 + \omega_2 x_2 + \omega_3 x_3 + \omega_4 x_4)$ $\sin(\omega_1 x_1 + \omega_2 x_2 + \omega_3 x_3 + \omega_4 x_4)$
1	$e^{j\omega t}$	$-j \operatorname{sgn}(\omega) e^{j\omega t}$
2	$e^{j(\omega_1 x_1 + \omega_2 x_2)}$	$-\operatorname{sgn}(\omega_1) \operatorname{sgn}(\omega_2) e^{j(\omega_1 x_1 + \omega_2 x_2)}$
3	$e^{j(\omega_1 x_1 + \omega_2 x_2 + \omega_3 x_3)}$	$-j \operatorname{sgn}(\omega_1) \operatorname{sgn}(\omega_2) \operatorname{sgn}(\omega_3) e^{j(\omega_1 x_1 + \omega_2 x_2 + \omega_3 x_3)}$
4	$e^{j(\omega_1 x_1 + \omega_2 x_2 + \omega_3 x_3 + \omega_4 x_4)}$	$\operatorname{sgn}(\omega_1) \operatorname{sgn}(\omega_2) \operatorname{sgn}(\omega_3) \operatorname{sgn}(\omega_4) e^{j(\omega_1 x_1 + \omega_2 x_2 + \omega_3 x_3 + \omega_4 x_4)}$

The magnitude equals 1 and the phase function is

$$\Phi(f_1, f_2) = -\frac{\pi}{2} \operatorname{sgn}(f_1) - \frac{\pi}{2} \operatorname{sgn}(f_2) \quad (7.690)$$

## 7.24 Multidimensional Complex Signals

### 7.24.1 Short Historical Review

The complex notation of harmonic signals in the form of Euler's equation  $e^{j\omega t} = \cos(\omega t) + j \sin(\omega t)$  was introduced to electrical

engineering at the end of the nineteenth century (E. Kennedy and C. Steinmetz) and soon proliferated to many science and engineering disciplines. Restating the equation in the form  $\cos(\omega t) = 0.5(e^{j\omega t} + e^{-j\omega t})$  introduces the concept of *negative frequencies*, commonly used in modern Fourier spectral analysis. In 1946, Gabor<sup>11</sup> introduced the extension of the complex notation of time signals in the form of the *analytic signal*  $\psi(t) = u(t) + jv(t)$  where  $v(t)$  is the Hilbert transform of  $u(t)$  (see Section 7.4). It has the unique feature that its Fourier transform is one-sided. In 1964 this author<sup>12</sup> used the analytic signal to define the notion of the instantaneous complex frequency. This section presents

how the complex notation of signals and the notion of the analytic signal can be *generalized for* multidimensional signals. This generalization has been recently developed by this author.<sup>13</sup>

### 7.24.2 Definition of the Multidimensional Complex Signal

Let us remember that no definition is “true” or “false.” However, it is very desirable that a definition of the  $n$ -D complex signal satisfy certain requirements. The basic requirement is the *compatibility* with the 1-D case, i.e., with the definition of the analytic signal. Many other requirements may be formulated, such as usefulness in applications. The definition of the multidimensional complex signal introduced in Ref. 13 is based on the frequency domain description of the multidimensional signals given by the Fourier pair

$$u(x) \stackrel{n-F}{\iff} U(\Omega) \quad (7.691)$$

where  $x = \{x_1, x_2, \dots, x_n\}$  and  $\Omega = \{\omega_1, \omega_2, \dots, \omega_n\}$  are  $n$ -D real column vectors (see Section 7.23). Let us remember that the *kernels* of the  $n$ -D Fourier transformations are in 1-D  $e^{\pm j\omega t}$ , in 2-D  $e^{\pm j(\omega_1 x_1 + \omega_2 x_2)}$ , in 3-D  $e^{\pm j(\omega_1 x_1 + \omega_2 x_2 + \omega_3 x_3)}$ , and in  $n$ -D  $e^{\pm j(\omega_1 x_1 + \dots + \omega_n x_n)}$ . These kernels have the form of complex signals of a constant amplitude  $A = 1$  and *linear phase* in respect to the variables  $x_1, x_2, \dots, x_n$ . Therefore, a compatible definition of a multidimensional complex signal should define  $n$ -dimensional complex harmonic signals in the form of the above kernels  $n$ -D Fourier transformation. Because the 1-D complex analytic signal has a one-sided spectrum at positive frequencies, let us define the  $n$ -D complex signal using the inverse Fourier transform of its spectrum canceled at all *orthants* of the Fourier frequencies space except in the first orthant. In 1-D this space has two *half-axes*, in 2-D four *quadrants*, in 3-D eight *octants*, and in general  $2^n$  *orthants*. Mathematicians denote the orthant with all the axis of positive sign by  $R^+$ . Therefore, the  $n$ -D complex signal is defined by the Fourier pair

$$\psi(x) \stackrel{n-F}{\iff} \Gamma(\Omega) = 2^n \mathbf{1}(\Omega) U(\Omega) \quad (7.692)$$

The cancellation of the spectrum in all but the first orthant is achieved by multiplication of the  $n$ -D Fourier image by the  $n$ -D *unit step function* (or distribution)  $\mathbf{1}(\Omega)$  defined by the formula ( $\Omega = \{\omega_1, \omega_2, \dots, \omega_n\}$ )

$$\mathbf{1}(\Omega) = \begin{cases} 1 & \text{all } \omega > 0 \\ 0.5 & \text{all } \omega = 0 \\ 0 & \text{all } \omega < 0 \end{cases} \quad (7.693)$$

The numerical factor  $2^n$  is used to normalize the energy of the complex signal. The  $n$ -D unit step may be written in the form of a product of 1-D unit steps; that is, given by the formula

$$\mathbf{1}(\Omega) = \mathbf{1}(\omega_1) \otimes \mathbf{1}(\omega_2) \otimes \dots \otimes \mathbf{1}(\omega_n) \quad (7.694)$$

where  $\otimes$  denotes a *tensor product* of distributions. In the following text we will suppress the symbol  $\otimes$  because here it has a pure formal meaning. The 1-D unit step may be written in the form  $\mathbf{1}(\omega) = 0.5[1 + \text{sgn}(\omega)]$  (see Equation 7.49). The insertion of this form in Equation 7.694 yields

$$\mathbf{1}(\Omega) = [0.5 \text{sgn}(\omega_1)] [0.5 + 0.5 \text{sgn}(\omega_2)] \dots [0.5 + 0.5 \text{sgn}(\omega_n)] \quad (7.695)$$

The application of the convolution to multiplication theorem of Fourier analysis to the spectrum  $\Gamma(\Omega)$  defined by Equation 7.692 yields the signal domain definition of the  $n$ -D complex signal in the form of the  $n$ -fold convolution

$$\psi(\mathbf{x}) = \psi_\delta(\mathbf{x}) * \dots * u(\mathbf{x}) \quad (7.696)$$

where the signal  $\psi_\delta(\mathbf{x})$  is given by the inverse Fourier transform of the unit step; that is,

$$\psi_\delta(\mathbf{x}) \stackrel{n-F}{\iff} 2^n \mathbf{1}(\Omega) \quad (7.697)$$

The  $n$ -D delta pulse (distribution)  $\delta(\mathbf{x}) = \delta(x_1) \delta(x_2) \dots \delta(x_n)$  may be defined by the inverse Fourier transform of the spectrum  $U(\Omega) = \mathbf{1}$ , i.e., by the Fourier pair

$$\delta(\mathbf{x}) \stackrel{n-F}{\iff} 1 \quad (7.698)$$

Therefore, the signal  $\psi_\delta(\mathbf{x})$  defines the  $n$ -D *complex delta distribution* (see the 1-D case, Section 7.6, Equation 7.67 and a more detailed description in the next part of this section). Notice that Equations 7.692 and 7.696 uniquely define the  $n$ -D complex signal due to the uniqueness theorem of the Fourier analysis.

To get the structure of the  $n$ -D complex signal  $\psi(\mathbf{x})$  let us insert in the spectrum  $\Gamma(\Omega)$  defined by Equation 7.692 the developed form of the multiple product given by Equation 7.695, as shown in Table 7.13. The real part of the complex signals  $\psi_1$  in Table 7.13 corresponds to the spectral terms obtained by multiplication of  $\Gamma(\Omega)$  by 1,  $\text{sgn}(\omega_1) \text{sgn}(\omega_2), \dots, \text{sgn}(\omega_1) \text{sgn}(\omega_2) \text{sgn}(\omega_3) \text{sgn}(\omega_4), \dots$ ; that is, by a product of an even number of signum functions, and the imaginary part by  $\text{sgn}(\omega_1), \dots, \text{sgn}(\omega_1) \text{sgn}(\omega_2) \text{sgn}(\omega_3), \dots$ ; that is, by a product of an odd number of signum functions.

#### Example

Consider the 2-D harmonic signal  $u = \cos(\omega_1 x_1) \cos(\omega_2 x_2)$ . The Hilbert transforms are (see Table 7.11)  $\mathbf{v} = \sin(\omega_1 x_1) \sin(\omega_2 x_2)$ ,  $\mathbf{v}_1 = \sin(\omega_1 x_1) \cos(\omega_2 x_2)$ ,  $\mathbf{v}_2 = \cos(\omega_1 x_1) \sin(\omega_2 x_2)$ . The insertion of  $u, \mathbf{v}, \mathbf{v}_1$ , and  $\mathbf{v}_2$  into Equation 7.700 yields the complex signal



**TABLE 7.13** The  $n$ -D Complex Signals and Their Fourier Spectra

$n$ -D	Complex Signal	Fourier Image	
1-D	$\psi_1 = u + jv$	$\Gamma(\omega) = [1 + \text{sgn}(\omega)]U(\omega)$	(7.699)
2-D	$\psi_1 = u - v + j(v_1 + v_2)$	$\Gamma(\omega_1, \omega_2) = U(\omega_1, \omega_2) \times [1 + \text{sgn}(\omega_1) + \text{sgn}(\omega_2) + \text{sgn}(\omega_1) \text{sgn}(\omega_2)]$	(7.700)
3-D	$\psi_1 = u - v_{12} - v_{13} - v_{23} + j(v_1 + v_2 + v_3 - v)$	$\Gamma(\omega_1, \omega_2, \omega_3) = U(\omega_1, \omega_2, \omega_3) \times [1 + \text{sgn}(\omega_1) + \text{sgn}(\omega_2) + \text{sgn}(\omega_3) + \text{sgn}(\omega_1) \text{sgn}(\omega_2) + \text{sgn}(\omega_1) \text{sgn}(\omega_3) + \text{sgn}(\omega_2) \text{sgn}(\omega_3) + \text{sgn}(\omega_1) \text{sgn}(\omega_2) \text{sgn}(\omega_3)]$	(7.701)
	$\vdots$	$\vdots$	
$n$ -D	$\psi_1 = F^{-1}[\Gamma(\Omega)]$	$[\Gamma(\Omega)] = 2^n \mathbf{1}(\Omega)U(\Omega)$	(7.702)

Note:  $u$  is the original signal,  $v$  is its total Hilbert transform,  $v_1, v_2, v_3$  are the first-order partial Hilbert transform  $v_{12}, v_{13}, v_{23}$  are the second-order partial Hilbert transforms. For notations ease, the dependence of  $u, v, v_1, \dots$  on  $x_1, x_2, x_3, \dots$  is omitted. The index 1 in  $\psi_1$  indicates a complex signal with a single orthant spectrum in the first orthant (in  $R^+$ ).

**TABLE 7.14** 2-D Complex Signals with Single-Quadrant Spectra in Successive Quadrants of the Fourier Frequency Plane ( $\omega_1, \omega_2$ )

Quadrant	Complex Signal	Fourier Image
1	$\psi_1 = u - v + j(v_1 + v_2)$	$\Gamma_1(\omega_1, \omega_2) = 4 \mathbf{1}(\omega_1, \omega_2)U(\omega_1, \omega_2) = U[1 + \text{sgn}(\omega_1) + \text{sgn}(\omega_2) + \text{sgn}(\omega_1) \text{sgn}(\omega_2)]$
2	$\psi_2 = u + v - j(v_1 - v_2)$	$\Gamma_2(\omega_1, \omega_2) = 4 \mathbf{1}(-\omega_1, \omega_2)U(\omega_1, \omega_2) = U[1 - \text{sgn}(\omega_1) + \text{sgn}(\omega_2) - \text{sgn}(\omega_1) \text{sgn}(\omega_2)]$
3	$\psi_3 = u + v + j(v_1 - v_2)$	$\Gamma_3(\omega_1, \omega_2) = 4 \mathbf{1}(\omega_1, -\omega_2)U(\omega_1, \omega_2) = U[1 + \text{sgn}(\omega_1) - \text{sgn}(\omega_2) - \text{sgn}(\omega_1) \text{sgn}(\omega_2)]$
4	$\psi_4 = u - v - j(v_1 + v_2)$	$\Gamma_4(\omega_1, \omega_2) = 4 \mathbf{1}(-\omega_1, -\omega_2)U(\omega_1, \omega_2) = U[1 - \text{sgn}(\omega_1) - \text{sgn}(\omega_2) + \text{sgn}(\omega_1) \text{sgn}(\omega_2)]$

Note: Two pairs of conjugate signals:  $\psi_1 = \psi_4^*$  and  $\psi_3 = \psi_2^*$ . Notations: See Table 7.13.

$$\begin{aligned} \psi_1(x_1, x_2) &= \cos(\omega_1, x_1) \cos(\omega_2, x_2) - \sin(\omega_1, x_1) \sin(\omega_2, x_2) \\ &+ j[\sin(\omega_1, x_1) \cos(\omega_2, x_2) \\ &+ \cos(\omega_1, x_1) \sin(\omega_2, x_2)] \end{aligned} \quad (7.703)$$

The application of standard trigonometric relations yields

$$\psi_1(x_1, x_2) = e^{j(\omega_1 x_1 + \omega_2 x_2)} \quad (7.704)$$

Notice that the real part of the signal  $u - v = \cos(\omega_1 x_1 + \omega_2 x_2)$  and is not equal to  $u$ . Then  $n$ -D generalization of the above signal is  $u(\mathbf{x}) = \cos(\omega_1 x_1) \cos(\omega_2 x_2) \dots \cos(\omega_n x_n)$ , yielding the complex signal

$$\psi(x) = e^{j(\omega_1 x_1 + \omega_2 x_2 + \dots + \omega_n x_n)} \quad (7.705)$$

This formula gives evidence that the important requirement of compatibility of the definition of a multidimensional complex signal with the 1-D case is satisfied by complex signals with single orthant spectra.

**Example**

Consider the 2-D delta pulse distribution  $\delta(x_1, x_2) = \delta(x_1) \delta(x_2)$ . The Hilbert transforms are given in Table 7.14 and Equation 7.700 yields the following form of the 2-D complex delta distribution

$$\begin{aligned} \psi_\delta(x_1, x_2) &= \delta(x_1, x_2) - 1/(\pi^2 x_1 x_2) + j[\delta(x_2)/(\pi x_1) \\ &+ \delta(x_1)/(\pi x_2)] \end{aligned} \quad (7.706)$$

The insertion in Equation 7.701 of the appropriate Hilbert transforms of the 3-D delta pulse  $\delta(x_1, x_2, x_3)$  yields the following form of the 3-D complex delta distribution

$$\begin{aligned} \psi_\delta(x_1, x_2, x_3) &= \delta(x_1, x_2, x_3) - \frac{\delta(x_3)}{\pi^2 x_1 x_2} - \frac{\delta(x_2)}{\pi^2 x_1 x_3} - \frac{\delta(x_1)}{\pi^2 x_2 x_3} \\ &+ j \left( \frac{\delta(x_2, x_3)}{\pi x_1} + \frac{\delta(x_1, x_3)}{\pi x_2} + \frac{\delta(x_1, x_2)}{\pi x_3} - \frac{1}{\pi^3 x_1 x_2 x_3} \right) \end{aligned} \quad (7.707)$$

**7.24.3 Conjugate 2-D Complex Signals**

The 2-D complex signal defined by Equation 7.700 has the single quadrant spectrum in the first quadrant. Let us define 2-D complex signals with single quadrant spectra in successive quadrants. The accepted numeration of the quadrants is shown in Figure 7.84. The so-defined complex signals and their spectra are shown in Table 7.14.

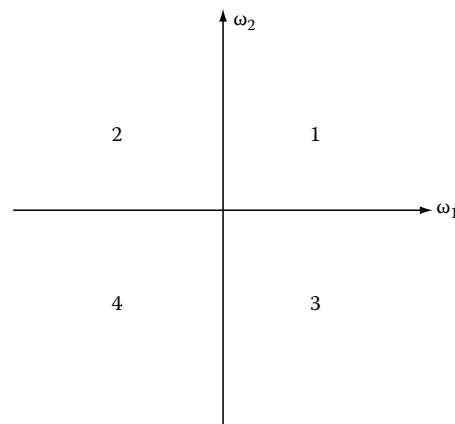


**FIGURE 7.84** The numeration of quadrants (see Appendix 7.24.7).

### 7.24.4 Local (or “Instantaneous”) Amplitudes, Phases, and Complex Frequencies

Let us write the complex signals of Table 7.14 in polar coordinates:

$$\psi_1(x_1, x_2) = \psi_4^*(x_1, x_2) = A_1(x_1, x_2)e^{j\Phi_1(x_1, x_2)} \quad (7.708)$$

$$\psi_3(x_1, x_2) = \psi_2^*(x_1, x_2) = A_2(x_1, x_2)e^{j\Phi_2(x_1, x_2)} \quad (7.709)$$

This representation defines the *local* (or “instantaneous”) *amplitudes*

$$A_1(x_1, x_2) = \text{SQR}\{[u(x_1, x_2) - v(x_1, x_2)]^2 + [v_1(x_1, x_2) + v_2(x_1, x_2)]^2\} \quad (7.710)$$

$$A_2[x_1, x_2] = \text{SQR}\{[u(x_1, x_2) + v(x_1, x_2)]^2 + [v_1(x_1, x_2) + v_2(x_1, x_2)]^2\} \quad (7.711)$$

and the *local* (or “instantaneous”) *phases*

$$\Phi_1(x_1, x_2) = \tan^{-1} \frac{v_1(x_1, x_2) + v_2(x_1, x_2)}{u(x_1, x_2) - v(x_1, x_2)} \quad (7.712)$$

$$\Phi_2(x_1, x_2) = \tan^{-1} \frac{v_1(x_1, x_2) - v_2(x_1, x_2)}{u(x_1, x_2) + v(x_1, x_2)} \quad (7.713)$$

of the real signal  $u(x_1, x_2)$ . Analogous to the 1-D case (see Section 7.16, Equation 7.249) let us define the *complex phases*

$$\Phi_{1c}(x_1, x_2) = \text{Ln } \psi_1(x_1, x_2) \quad (7.714)$$

$$\Phi_{2c}(x_1, x_2) = \text{Ln } \psi_3(x_1, x_2) \quad (7.715)$$

and the *partial* instantaneous complex frequencies

$$s_{1x_1}(x_1, x_2) = \frac{\partial \Phi_{1c}(x_1, x_2)}{\partial x_1} = \alpha_{1x_1}(x_1, x_2) + j\omega_{1x_1}(x_1, x_2) \quad (7.716)$$

$$s_{1x_2}(x_1, x_2) = \frac{\partial \Phi_{1c}(x_1, x_2)}{\partial x_2} = \alpha_{1x_2}(x_1, x_2) + j\omega_{1x_2}(x_1, x_2) \quad (7.717)$$

$$s_{2x_1}(x_1, x_2) = \frac{\partial \Phi_{2c}(x_1, x_2)}{\partial x_1} = \alpha_{2x_1}(x_1, x_2) + j\omega_{2x_1}(x_1, x_2) \quad (7.718)$$

$$s_{2x_2}(x_1, x_2) = \frac{\partial \Phi_{2c}(x_1, x_2)}{\partial x_2} = \alpha_{2x_2}(x_1, x_2) + j\omega_{2x_2}(x_1, x_2) \quad (7.719)$$

In Equations 7.716 and 7.718  $x_2$  is a parameter and the complex frequencies are defined along the lines parallel to the  $x_1$  axis. Similarly, Equations 7.717 and 7.719 define complex frequencies parallel to the  $x_2$  axis.

For separable 2-D signals (see Equation 7.653), the amplitudes  $A_1$  and  $A_2$  defined by Equations 7.710 and 7.711 are equal and given by the formula

$$A(x_1, x_2) = \text{SQR}[u^2 + v^2 + v_1^2 + v_2^2] \quad (7.720)$$

and the phases (Equations 7.712 and 7.713) are

$$\Phi_1(x_1, x_2) = \varphi_1(x_1) + \varphi_2(x_2) \quad (7.721)$$

$$\Phi_2(x_1, x_2) = \varphi_1(x_1) - \varphi_2(x_2) \quad (7.722)$$

where  $\varphi_1 = \tan^{-1}(g_1/f_1)$  (see Equation 7.653). The complex frequencies have, for separable signals, the simplified form

$$s_{1x_1} = s_{2x_1} = \alpha_1 + j\omega_1 \quad (7.723)$$

$$s_{1x_2} = s_{2x_2}^* = \alpha_2 + j\omega_2 \quad (7.724)$$

### Example

Consider the 2-D signal of the form

$$u(x_1, x_2) = \frac{\sin(ax_1) \sin(bx_2)}{abx_1x_2} \quad (7.725)$$

The insertion of this signal and its Hilbert transforms  $v$ ,  $v_1$ , and  $v_2$  (see Table 7.10) in Equation 7.720 using certain trigonometric relations yields

$$A(x_1, x_2) = \left| \frac{1 - \cos(ax_1)}{\sin(ax_1)} \right| \left| \frac{1 - \cos(bx_2)}{\sin(bx_2)} \right| \quad (7.726)$$

The phase functions (Equations 7.721 and 7.722) take the form

$$\Phi_1(x_1, x_2) = \tan^{-1} \frac{1 - \cos(ax_1)}{\sin(ax_1)} + \tan^{-1} \frac{1 - \cos(bx_2)}{\sin(bx_2)} = \frac{a}{2}x_1 + \frac{b}{2}x_2 \quad (7.727)$$

$$\Phi_2(x_1, x_2) = \tan^{-1} \frac{1 - \cos(ax_1)}{\sin(ax_1)} - \tan^{-1} \frac{1 - \cos(bx_2)}{\sin(bx_2)} = \frac{a}{2}x_1 - \frac{b}{2}x_2 \quad (7.728)$$

The local partial angular frequencies defined by the imaginary parts of (7.723) and (7.724) are  $\omega_1 = a/2$  and  $\omega_2 = b/2$ . The local amplitude (7.726) is a product of local amplitudes of the separable terms of the signal (7.725), and the phase is a sum (or difference) of phases of these terms. The phase functions in this example are linear (a constant slope if we remove the jumps of the multibranch  $\tan^{-1}$  function), giving constant values of the angular frequencies.

### 7.24.5 Relations between Real and Complex Notation

In one dimension, we have the following well-known relations:

$$u(t) = \frac{\psi(t) + \psi^*(t)}{2}; \quad v(t) = \frac{\psi(t) - \psi^*(t)}{2j} \quad (7.729)$$

In two dimensions, the corresponding relations become (see Table 7.14)

$$u(x_1, x_2) = \frac{\psi_1 + \psi_2 + \psi_3 + \psi_4}{4} \quad (7.730)$$

$$v(x_1, x_2) = \frac{\psi_1 - \psi_2 + \psi_3 - \psi_4}{4} \quad (7.731)$$

$$v_1(x_1, x_2) = \frac{\psi_1 - \psi_2 + \psi_3 - \psi_4}{4j} \quad (7.732)$$

$$v_2(x_1, x_2) = \frac{\psi_1 + \psi_2 - \psi_3 - \psi_4}{4j} \quad (7.733)$$

Using the relations  $\psi_1 = \psi_4^*$  and  $\psi_3 = \psi_2^*$ , the real part of the complex signal  $\psi_1$  takes the form

$$u - v = 0.5(\psi_1 + \psi_4) = 0.5(\psi_1 + \psi_1^*) \quad (7.734)$$

and the real part of  $\psi_3$  is

$$u + v = 0.5(\psi_2 + \psi_3) = 0.5(\psi_2 + \psi_2^*) \quad (7.735)$$

Notice that the spectra of these two signals exist in two quadrants of the Fourier frequency plane. The insertion of the polar representations (Equations 7.708 and 7.709) into Equations 7.734 and 7.735 yield

$$u - v = A_1 \cos(\Phi_1) \quad (7.736)$$

$$u + v = A_2 \cos(\Phi_2) \quad (7.737)$$

The summation (or subtraction) yields the following relations:

$$u(x_1, x_2) = \frac{A_1 \cos(\Phi_1) + A_2 \cos(\Phi_2)}{2} \quad (7.738)$$

$$v(x_1, x_2) = \frac{A_2 \cos(\Phi_2) + A_1 \cos(\Phi_1)}{2} \quad (7.739)$$

and analogous derivation yields

$$v_1(x_1, x_2) = \frac{A_1 \sin(\Phi_1) + A_2 \sin(\Phi_2)}{2} \quad (7.740)$$

$$v_2(x_1, x_2) = \frac{A_2 \sin(\Phi_2) - A_1 \sin(\Phi_1)}{2} \quad (7.741)$$

For separable signals, these relations have the simplified form

$$u(x_1, x_2) = A \cos[\varphi_1(x_1)] \cos[\varphi_2(x_2)] \quad (7.742)$$

$$v(x_1, x_2) = A \sin[\varphi_1(x_1)] \sin[\varphi_2(x_2)] \quad (7.743)$$

$$v_1(x_1, x_2) = A \sin[\varphi_1(x_1)] \cos[\varphi_2(x_2)] \quad (7.744)$$

$$v_2(x_1, x_2) = A \cos[\varphi_1(x_1)] \sin[\varphi_2(x_2)] \quad (7.745)$$

In three dimensions the number of octants equals eight and the relation between the real and complex notation becomes

(we applied the method of numeration of octants given in Appendix 7.24.7),

$$u(x_1, x_2, x_3) = \frac{\psi_1 + \psi_2 + \psi_3 + \psi_4 + \psi_5 + \psi_6 + \psi_7 + \psi_8}{8} \quad (7.746)$$

Using the relations  $\psi_1 = \psi_8^* = A_1 e^{j\Phi_1}$ ,  $\psi_2 = \psi_7^* = A_2 e^{j\Phi_2}$ ,  $\psi_3 = \psi_6^* = A_3 e^{j\Phi_3}$ , and  $\psi_4 = \psi_5^* = A_4 e^{j\Phi_4}$ , the above formula takes the form

$$(x_1, x_2, x_3) = \frac{A_1 \cos(\Phi_1) + A_2 \cos(\Phi_2) + A_3 \cos(\Phi_3) + A_4 \cos(\Phi_4)}{8} \quad (7.747)$$

For separate signals all amplitudes are equal and the phase functions are

$$\Phi_1(x_1, x_2, x_3) = \varphi_1(x_1) + \varphi_2(x_2) + \varphi_3(x_3) \quad (7.748)$$

$$\Phi_2(x_1, x_2, x_3) = -\varphi_1(x_1) + \varphi_2(x_2) + \varphi_3(x_3) \quad (7.749)$$

$$\Phi_3(x_1, x_2, x_3) = \varphi_1(x_1) - \varphi_2(x_2) + \varphi_3(x_3) \quad (7.750)$$

$$\Phi_4(x_1, x_2, x_3) = -\varphi_1(x_1) - \varphi_2(x_2) + \varphi_3(x_3) \quad (7.751)$$

The insertion of these phase functions in Equation 7.747 yields

$$u(x_1, x_2, x_3) = A \cos[\varphi_1(x_1)] \cos[\varphi_2(x_2)] \cos[\varphi_3(x_3)] \quad (7.752)$$

Similar formulae for  $u, u_1,$  and  $u_2$  may be easily derived or written directly by comparison with the 2-D case. In general, for the  $n$ -D separable signal of the form  $u(\mathbf{x}) = \prod_{k=1}^n a_k f(x_k)$  this formula takes the form  $u(\mathbf{x}) = A \prod_{k=1}^n \cos[\varphi(x_k)]$ , where  $A = \prod_{k=1}^n a_k$ . If all  $a_k$ 's are equal to  $a$ , then  $A = a^n$  or  $a = \sqrt[n]{A}$ .

### Example

Consider again the signal  $u(x_1, x_2) = \cos(\omega_{10}x_1) \cos(\omega_{20}x_2)$  of the previous example. The four complex signals of Table 7.14 and their spectra are

Quadrant	Complex Signal	Fourier Image
1	$\psi_1 = e^{j(\omega_{10}x_1 + \omega_{20}x_2)}$	$\delta(\omega_1 - \omega_{10}, \omega_2 - \omega_{20})$
2	$\psi_2 = e^{j(-\omega_{10}x_1 + \omega_{20}x_2)}$	$\delta(\omega_1 + \omega_{10}, \omega_2 - \omega_{20})$
3	$\psi_3 = e^{j(\omega_{10}x_1 - \omega_{20}x_2)}$	$\delta(\omega_1 - \omega_{10}, \omega_2 + \omega_{20})$
4	$\psi_4 = e^{j(-\omega_{10}x_1 - \omega_{20}x_2)}$	$\delta(\omega_1 + \omega_{10}, \omega_2 + \omega_{20})$

The spectrum of the signal  $u$  is shown in Figure 7.85. The insertion of these functions in Equations 7.730 through 7.741 gives the verifications of these relations.

## 7.24.6 2-D Modulation Theory

The 1-D modulated signal has the complex representation in the form of a product of the *modulation function* and the complex

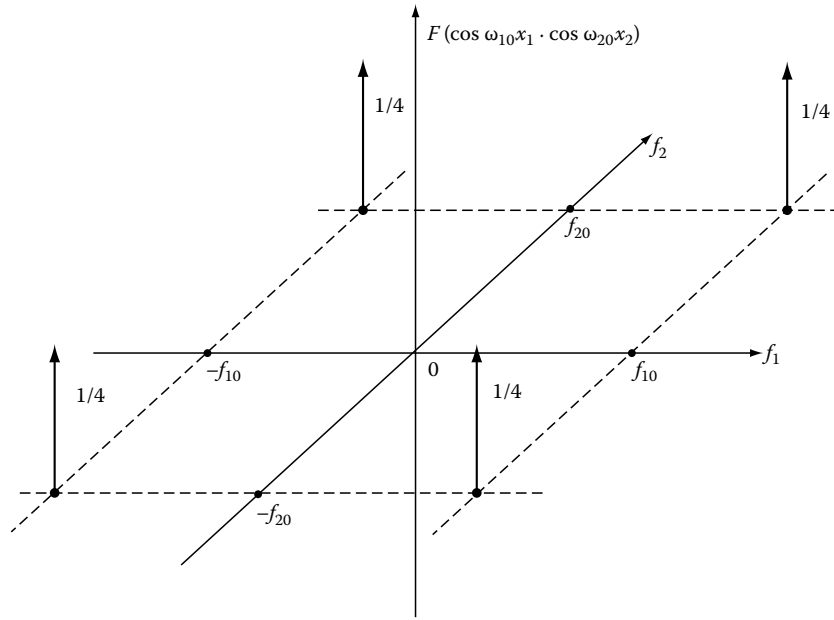


FIGURE 7.85 The Fourier spectrum of the 2-D harmonic signal  $u(x_1, x_2) = \cos(\omega_{10}x_1) \cos(\omega_{20}x_2)$ .

harmonic carrier (see Section 7.17, Equation 7.279). From the formal point of view, the concept of the modulation function can be extended to multidimensional modulating signals with multidimensional harmonic carriers. The  $n$ -D complex harmonic carrier has the form

$$\Psi_c(\mathbf{x}) = A_0 e^{j(\omega_{10}x_1 + \varphi_1 + \omega_{20}x_2 + \varphi_2 + \dots + \omega_{n0}x_n + \varphi_n)} \quad (7.753)$$

We define the  $n$ -D modulated signal in the form of a product

$$\psi(\mathbf{x}) = \gamma(\mathbf{x})\psi_c(\mathbf{x}) \quad (7.754)$$

where  $\gamma(\mathbf{x}) = f[u(\mathbf{x})]$  is called the  $n$ -D modulation function and  $f[u(\mathbf{x})]$  is a function of the  $n$ -D message  $u(\mathbf{x})$ . As in the 1-D case, the function  $f$  defines a specific type of modulation. The 2-D modulated signal has the form

$$\Psi(x_1, x_2) = \gamma(x_1, x_2)A_0 e^{j(\omega_{10}x_1 + \omega_{20}x_2)} \quad (7.755)$$

where for convenience, the phases  $\varphi_1 = \varphi_2 = 0$ .

**Example**

Consider a 2-D low-pass message and its Fourier image

$$u(x_1, x_2) \stackrel{2-F}{\iff} U(j\omega_1, j\omega_2) \quad (7.756)$$

with the base-band spectrum band limited such that  $U(j\omega_1, j\omega_2) = 0$  for  $|\omega_1| > a$  and  $|\omega_2| > b$ . The modulation function of the 2-D suppressed carrier amplitude modulation is

$$\gamma_{AM}(x_1, x_2) = mu(x_1, x_2) \quad (7.757)$$

Figure 7.86 shows the spectra of the base-band signal  $u$  and of the modulated signal.

The 2-D equivalent of the 1-D SSB modulation is the *single quadrant modulation (SQM)*. The modulation function is given by the inverse Fourier transform of the base-band single quadrant spectrum

$$\begin{aligned} \gamma_{SQM}(x_1, x_2) &= F^{-1}[4\mathbf{1}(\omega_1, \omega_2) U(\omega_1, \omega_2)] \\ &= u(x_1, x_2) - \mathbf{v}(x_1, x_2) + j[\mathbf{v}_1(x_1, x_2) + \mathbf{v}_2(x_1, x_2)] \end{aligned} \quad (7.758)$$

that is, in the form of the complex signal (7.700) in Table 7.13. The insertion of this modulation function in Equation 7.745 yields the complex SQM signal

$$\begin{aligned} \Psi_{SQM}(x_1, x_2) &= \{u(x_1, x_2) - \mathbf{v}(x_1, x_2) + j[\mathbf{v}_1(x_1, x_2) \\ &\quad + \mathbf{v}_2(x_1, x_2)]\}A_0 e^{j(\omega_{10}x_1 + \omega_{20}x_2)} \end{aligned} \quad (7.759)$$

and its real notation is

$$\begin{aligned} u_{SQM}(x_1, x_2) &= u \cos(\omega_{10}x_1) \cos(\omega_{20}x_2) + \mathbf{v} \sin(\omega_{10}x_1) \sin(\omega_{20}x_2) + \\ &\quad - \mathbf{v}_1 \sin(\omega_{10}x_1) \cos(\omega_{20}x_2) - \mathbf{v}_2 \cos(\omega_{10}x_1) \sin(\omega_{20}x_2) \end{aligned} \quad (7.760)$$

Figure 7.87 shows the supports of the spectra of  $\gamma_{SQM}$ ,  $\Psi_{SQM}$ , and  $u_{SQM}$ .

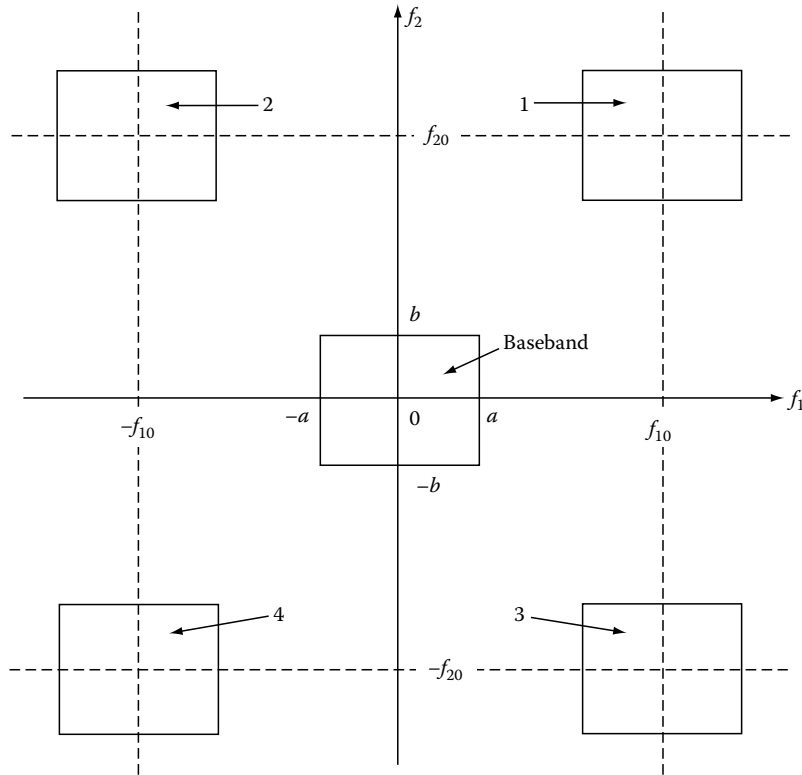


FIGURE 7.86 The supports of the spectrum of a 2-D carrier with 2-D amplitude modulation.

### 7.24.7 Appendix: A Method of Labeling Orthants

The applied numbering method of successive orthants is the following: we assign the binary number zero to a plus sign and the binary number 1 to a minus sign of the variable  $\omega$ . For example, the unit step function  $\mathbf{I}(\omega_4, -\omega_3, -\omega_2, \omega_1)$  corresponds to the binary number 0110. If the decimal-coded binary number is  $a$ , we assign to the given orthant the decimal number  $l = a + 1$ . So, we have in four dimensions:

$l = a + 1$	Binary	Sign of the $\Omega$ Axis			
		$\omega_4$	$\omega_3$	$\omega_2$	$\omega_1$
1	0000	+	+	+	+
2	0001	+	+	+	-
3	0010	+	+	-	+
4	0011	+	+	-	-
16	1111	-	-	-	-

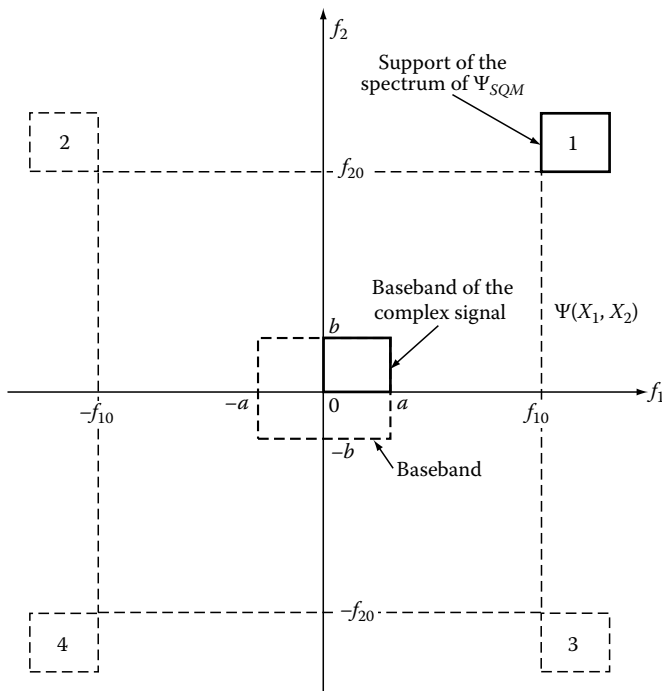


FIGURE 7.87 The supports of the spectrum of a 2-D signal with single quadrant modulation (SQM).

## 7.25 Quaternionic 2-D Signals

### 7.25.1 Quaternion Numbers and Quaternion-Valued Functions

The concept of the quaternion number was introduced by Hamilton in 1843 and defined by the formula

**TABLE 7.15** The Algebra of Imaginary Units

1	$I$	$j$	$k$
$i$	$i^2 = -1$	$ij = k$	$ik = -j$
$j$	$ji = -k$	$j^2 = -1$	$jk = i$
$k$	$ki = j$	$kj = -i$	$k^2 = -1$

$$q = 1a + ib + jc + kd \tag{7.761}$$

where  $a, b, c, d \in \mathbb{R}$  and imaginary units  $i, j, k$  obey the algebra presented in Table 7.15.

Note, that this algebra is noncommutative, i.e.,  $ij \neq ji$ . If we replace the constants  $a, b, c$ , and  $d$  with 2-D functions, we get a quaternion-valued function:

$$\psi_q(x_1, x_2) = a(x_1, x_2) + ib(x_1, x_2) + jc(x_1, x_2) + kd(x_1, x_2) \tag{7.762}$$

### 7.25.2 Quaternionic Spectral Analysis

The 2-D Fourier transformation of a real signal  $u(x_1, x_2)$  is defined by the Equation 7.639 for  $n = 2$ :

$$U(f_1, f_2) = \int_{-\infty}^{\infty} \int_{-\infty}^{\infty} e^{-j\omega_1 x_1} u(x_1, x_2) e^{-j\omega_2 x_2} dx_1 dx_2 \tag{7.763}$$

where we intentionally have written the kernel  $e^{-j(\omega_1 x_1 + \omega_2 x_2)}$  in a separate form to get a comparison with the corresponding quaternionic Fourier transformation (QFT)

$$U_q(f_1, f_2) = \int_{-\infty}^{\infty} \int_{-\infty}^{\infty} e^{-i\omega_1 x_1} u(x_1, x_2) e^{-j\omega_2 x_2} dx_1 dx_2 \tag{7.764}$$

Here the order of the terms of the integrand cannot be changed. It can be shown [46] that

$$U_q(f_1, f_2) = \frac{1-k}{2} U(f_1, f_2) + \frac{1+k}{2} U(-f_1, f_2) \tag{7.765}$$

The signal  $u(x_1, x_2)$  can be decomposed in a union of four terms given by the Equation 7.616. This yields the following form of the 2-D FT:

$$U(f_1, f_2) = U_{ee} - U_{oo} - j(U_{oe} + U_{eo}) \tag{7.766}$$

The corresponding quaternionic spectrum is

$$U_q(f_1, f_2) = U_{ee} - iU_{oe} - jU_{eo} + kU_{oo} \tag{7.767}$$

where

$\alpha_1 = 2\pi f_1 x_1$  and  $\alpha_2 = 2\pi f_2 x_2$ . Note, that the 2-D FT and the QFT are defined by the same four terms indexed ee, oo, ee, and eo (see Equations 7.616 through 7.619). For even-even signals both transforms are real and equal, i.e., 2-D FT = QFT.

### 7.25.3 Hermitian Symmetry of the 2-D Fourier Spectrum

An important feature of the 2-D FT is the Hermitian symmetry defined by the equations

$$\begin{aligned} U(f_1, f_2) &= U^*(-f_1, -f_2) \\ U(-f_1, f_2) &= U^*(f_1, -f_2) \end{aligned} \tag{7.768}$$

where “\*” denotes the complex conjugate. Due to this symmetry, the signal can be recovered from its *half-plane spectrum*, for example, the half-plane  $f_1 > 0$  (Remark: A half-plane may be defined w.r.t. any line crossing the origin. However, the choice of a coordinate axis yields simpler relations). The spectrum in the complementary half-plane is *redundant*. We say that all spectral information about the real signal  $u(x)$  is given by a half-plane spectrum. A half-plane is a union of two quadrants. In general, the single-quadrant spectra of a half-plane differ. However, for separable signals of the form of a product of 1-D signals  $u(x_1, x_2) = f_1(x_1)f_2(x_2)$ , the spectral information in both quadrants is the same. More specifically, the two single-quadrant spectra are forming a mirror image w.r.t. the axis separating these quadrants.

#### 7.25.3.1 Quaternionic Hermitian Symmetry of the QFT<sup>44</sup>

The quaternionic spectrum defined by the QFT obeys the rules of the quaternionic Hermitian symmetry defined by the relations

$$\begin{aligned} U_q(-f_1, f_2) &= \alpha_j [U_q(f_1, f_2)], \\ U_q(-f_1, -f_2) &= \alpha_k [U_q(f_1, f_2)], \\ U_q(f_1, -f_2) &= \alpha_i [U_q(f_1, f_2)] \end{aligned} \tag{7.769}$$

where the functions  $\alpha_i$ ,  $\alpha_j$ , and  $\alpha_k$  are called involutions of  $U_q$  and are defined as follows:

$$\begin{aligned} \alpha_i(f_1, f_2) &= -iU_q i = U_{ee} - iU_{oe} + jU_{eo} - kU_{oo}, \\ \alpha_j(f_1, f_2) &= -jU_q j = U_{ee} + iU_{oe} - jU_{eo} - kU_{oo}, \\ \alpha_k(f_1, f_2) &= -kU_q k = U_{ee} + iU_{oe} + jU_{eo} + kU_{oo} \end{aligned} \tag{7.770}$$

Due to the quaternionic Hermitian symmetry all spectral information is contained in a single-quadrant spectrum. The information in the other three quadrants is *redundant*.

### 7.25.3.2 The Quaternionic Signal with Single-Quadrant Spectrum

The quaternionic signal QS with a single-quadrant spectrum is defined by the inverse QFT of the form

$$\begin{aligned} \psi_q(x_1, x_2) = & \int_{-\infty}^{\infty} \int_{-\infty}^{\infty} e^{j2\pi f_1 x_1} [1 + \operatorname{sgn}(f_1) + \operatorname{sgn}(f_2) \\ & + \operatorname{sgn}(f_1) \operatorname{sgn}(f_2)] U_q(f_1, f_2) e^{j2\pi f_2 x_2} df_1 df_2 \end{aligned} \quad (7.771)$$

The integration yields the following QS:

$$\psi_q(x_1, x_2) = u + iv_1 + jv_2 + kv, \quad (7.772)$$

where  $v_1$ ,  $v_2$ , and  $v$  are the same Hilbert transforms as used in Table 7.14 for 2-D analytic signals with single-quadrant spectra. The polar notation of this signal is

$$\psi_q(x_1, x_2) = A_q e^{i\phi_1} e^{k\phi_k} e^{j\phi_j} \quad (7.773)$$

where the amplitude is given by the formula

$$A_q(x_1, x_2) = \sqrt{u^2 + v_1^2 + v_2^2 + v^2} \quad (7.774)$$

and the phase functions are

$$\phi_i(x_1, x_2) = 0.5 \operatorname{Tan}^{-1} \left[ \frac{2(uv_1 + vv_2)}{u^2 - v_1^2 + v_2^2 - v^2} \right] \quad (7.775)$$

$$\phi_j(x_1, x_2) = 0.5 \operatorname{Tan}^{-1} \left[ \frac{2(uv_2 + vv_1)}{u^2 + v_1^2 - v_2^2 - v^2} \right] \quad (7.776)$$

$$\phi_k(x_1, x_2) = 0.5 \sin^{-1} \left[ \frac{D^2}{A_q^2} \right] \quad (7.777)$$

where  $D^2 = 2(uv - v_1v_2)$ .

### 7.25.3.3 Comparison of the Polar Notation of 2-D Analytic Signals and Quaternionic Signals

Let us write the local amplitudes of the 2-D analytic signal given by the Equations 7.711 and 7.712 in the form

$$A_1(x_1, x_2) = \sqrt{A_q^2 + D^2} = A_q \sqrt{1 + \sin(2\phi_k)} \quad (7.778)$$

$$A_2(x_1, x_2) = \sqrt{A_q^2 - D^2} = A_q \sqrt{1 - \sin(2\phi_k)} \quad (7.779)$$

Therefore,

$$A_q = \sqrt{\frac{A_1^2 + A_2^2}{2}} \quad (7.780)$$

and

$$\sin(2\phi_k) = \frac{A_1^2 - A_2^2}{A_1^2 + A_2^2}. \quad (7.781)$$

We see that the angle  $\phi_k \in (-\pi/4, \pi/4)$  and  $\phi_k = \pm\pi/4$  if  $A_1 = A_2$ . It can be shown that the quaternionic phase functions  $\phi_i$  and  $\phi_j$  are related to the analytic phase functions  $\phi_1$  and  $\phi_2$  by the equations

$$\operatorname{Tan}(2\phi_i) = \operatorname{Tan}(\phi_1 + \phi_2), \quad \text{i.e., } \phi_i = 0.5(\phi_1 + \phi_2) \quad (7.782)$$

$$\operatorname{Tan}(2\phi_j) = \operatorname{Tan}(\phi_1 - \phi_2), \quad \text{i.e., } \phi_j = 0.5(\phi_1 - \phi_2) \quad (7.783)$$

The real signal  $u(x_1, x_2)$  can be reconstructed in terms of two analytic signals with single-quadrant spectra using the Equation 7.730:

$$u(x_1, x_2) = \frac{A_1 \cos(\phi_1) + A_2 \cos(\phi_2)}{2} \quad (7.738)$$

The reconstruction formula for the quaternionic signal is

$$\begin{aligned} u(x_1, x_2) = & A_q [\cos(\phi_i) \cos(\phi_j) \cos(\phi_k) \\ & - \sin(\phi_i) \sin(\phi_j) \sin(\phi_k)] \end{aligned} \quad (7.784)$$

In both cases the reconstruction requires four functions. In the analytic case two amplitudes and two phase functions and in the quaternionic case a single amplitude and three phase functions. The methods are equivalent and the choice may depend on secondary arguments. However, for separable signals of the form  $u(x_1, x_2) = f_1(x_1)f_2(x_2)$  all the amplitudes are equal  $A = A_q = A_1 = A_2$ , the quaternionic angle  $\phi_k = 0$ . The phase functions of the analytic functions are given by the Equations 7.721 and 7.722. This yields the following form of the reconstruction formula (Equation 7.739)

$$u(x_1, x_2) = A \cos[\varphi_1(x_1)] \cos[\varphi_2(x_2)]. \quad (7.785)$$

The same formula applies for the quaternionic case replacing (7.784).

## 7.26 The Monogenic 2-D Signal

Another generalization of the notion of the 1-D AS for 2-D is the monogenic signal (MS) developed and described in detail in [45]. Let us present shortly the notion of the MS. It has the form

$$\psi_M(x_1, x_2) = u(x_1, x_2) + iv_{r1}(x_1, x_2) + jv_{r2}(x_1, x_2). \quad (7.786)$$

It is a quaternion-valued function. In comparison to the QS (Equation 7.772), the partial Hilbert transforms  $v_1$  and  $v_2$  are substituted by the Riesz transforms  $v_{r1}$  and  $v_{r2}$  and the term  $kv$  is deleted. The

Riesz transforms, called also *isotropic Hilbert transforms*,<sup>47</sup> have the form of a convolution of the signal  $u$  with Riesz kernels, i.e.,

$$v_{r1}(x_1, x_2) = u(x_1, x_2) ** r_1(x_1, x_2), \quad (7.787)$$

$$v_{r2}(x_1, x_2) = u(x_1, x_2) ** r_2(x_1, x_2), \quad (7.788)$$

where the Riesz kernels are

$$r_1(x_1, x_2) = \frac{x_1}{2\pi \left[ \sqrt{x_1^2 + x_2^2} \right]^3}, \quad (7.789)$$

$$r_2(x_1, x_2) = \frac{x_2}{2\pi \left[ \sqrt{x_1^2 + x_2^2} \right]^3}. \quad (7.790)$$

Note that the Riesz transforms are defined using the convolution of  $u$  with  $r_1$  or  $r_2$  w.r.t. both variables  $x_1$  and  $x_2$ , as in the case of the total Hilbert transform (Equation 7.631 or 7.633) and not as in the case of partial Hilbert transforms (Equations 7.635 and 7.636). It may be shown that the total energy of the monogenic signal equals twice the energy of the real signal. However, only the sum of the energies of  $v_{r1}$  and  $v_{r2}$  equals the energy of  $u$ , since the energies of  $v_{r1}$  and  $v_{r2}$  may be different.

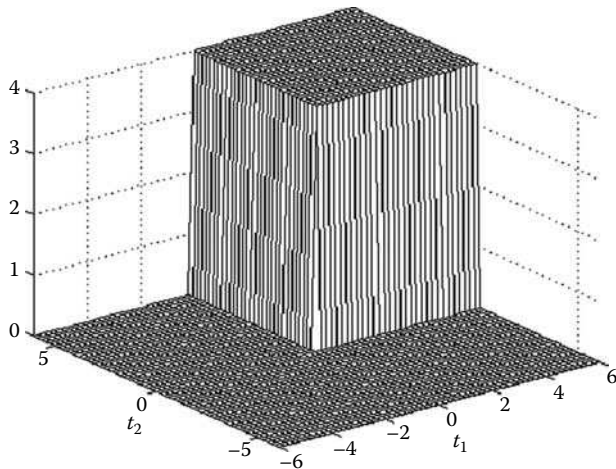
The Fourier transforms of the Riesz kernels are<sup>46</sup>

$$U_{r1}(f_1, f_2) = \frac{-jf_1}{\sqrt{f_1^2 + f_2^2}} \quad (7.791)$$

$$U_{r2}(f_1, f_2) = \frac{-jf_2}{\sqrt{f_1^2 + f_2^2}} \quad (7.792)$$

The insertion of the above 2-D FT's in (Equation 7.765) yields the corresponding QFT's

$$\text{QFT}[r_1(x_1, x_2)] = \frac{-jf_1}{\sqrt{f_1^2 + f_2^2}} \quad (7.793)$$



(a)

$$\text{QFT}[r_2(x_1, x_2)] = \frac{-jf_2}{\sqrt{f_1^2 + f_2^2}}. \quad (7.794)$$

In comparison to (7.791), for QFT[ $r_1$ ] the “ $j$ -unit” is replaced by the “ $i$ -unit”, with no change for QFT[ $r_2$ ]. The quaternionic spectrum of the MS has the form

$$\text{QFT}[\psi_M(x_1, x_2)] = \text{QFT}[u] \left[ 1 + \frac{f_1 + f_2}{\sqrt{f_1^2 + f_2^2}} \right] \quad (7.795)$$

where QFT[ $u$ ] is given by Equation 7.795). The comparison with 2-D analytic signals with single-quadrant spectra (see Table 7.14) shows that Equation 7.796 is not a spectrum with a single-quadrant support. Figure 7.88 compares the single-quadrant operator of Table 7.14 with the operator of Equation 7.795. Note the four quadrant support of the last one and the negative values in the quadrant ( $f_1 < 0, f_2 < 0$ ).

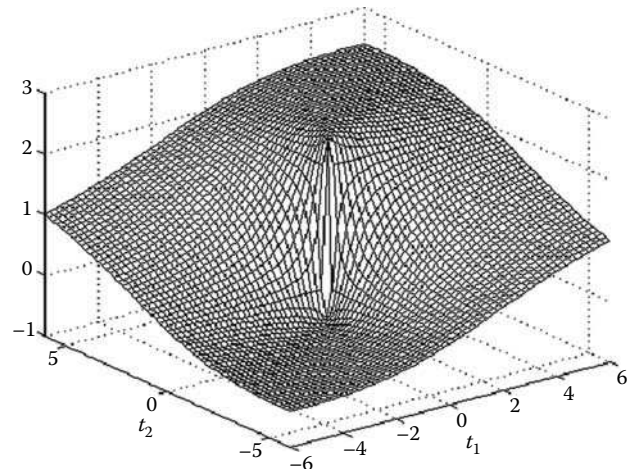
### 7.26.1 Spherical Coordinates Representation of the MS

The spherical coordinates representation of the MS (see Figure 7.89) defines its amplitude

$$A_M(x_1, x_2) = \sqrt{u^2 + v_{r1}^2 + v_{r2}^2} \quad (7.796)$$

and two angles  $\Theta$  and  $\Phi$ . The angle  $\Phi$  is called by the authors of [45] the orientation angle and  $\Theta$  is called the phase. They are given by the equations

$$\Phi(x_1, x_2) = \text{Tan}^{-1} \left( \frac{v_{r2}}{v_{r1}} \right) \quad (7.797)$$



(b)

FIGURE 7.88 (a) The single-quadrant operator  $[1 + \text{sgn}(f_1)][1 + \text{sgn}(f_2)]$ . (b) The operator  $1 + \frac{f_1 + f_2}{\sqrt{f_1^2 + f_2^2}}$  used in (7.790).



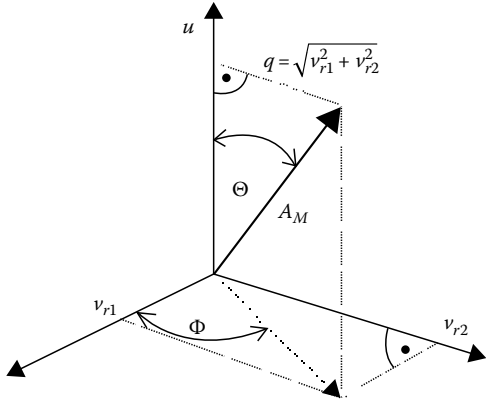


FIGURE 7.89 Spherical coordinates of the monogenic signal.

and

$$\Theta(x_1, x_2) = \cos^{-1} \left( \frac{u}{A_M} \right) = \tan^{-1} \left( \frac{\sqrt{v_{r1}^2 + v_{r2}^2}}{u} \right). \quad (7.798)$$

In terms of  $(A_M, \Phi, \Theta)$ , the MS has the form

$$\psi_M = A_M [\cos \Theta + i \sin \Theta \cos \Phi + j \sin \Theta \sin \Phi]. \quad (7.799)$$

## 7.27 Wigner Distributions of 2-D Analytic, Quaternionic, and Monogenic Signals

The time-frequency Wigner distribution of the 1-D analytic signal  $\psi(t) = u(t) + jv(t)$  is defined by the Fourier transform of the correlation product  $r(t, \tau) = \psi(t + 0.5\tau)\psi^*(t - 0.5\tau)$  w.r.t. the time shift variable  $\tau$ :

$$W(t, f) = \int_{-\infty}^{\infty} r(t, \tau) e^{-j2\pi f \tau} d\tau \quad (7.800)$$

This function is one-sided in the frequency domain (zero values in the half-plane  $f < 0$ ). The use of the analytic signal avoids the generation of the cross terms between the analytic signal  $\psi(t)$  and its conjugate  $\psi^*(t)$ . Note that the real signal has the form  $u(t) = 0.5[\psi(t) + \psi^*(t)]$ . In consequence the Wigner distribution of a real signal produces cross-terms due to the interaction of  $\psi(t)$  with  $\psi^*(t)$  (see Chapter 12). The Wigner distribution of any signal, real or complex, is a real function.

The Wigner distribution can be defined for  $n$ -D signals  $\psi(\mathbf{x}), \mathbf{x} \in (x_1, x_2, \dots, x_n)$ . The extension for 2-D signals is not unique. The Wigner distribution can be defined for analytic signals  $\psi_A(x_1, x_2)$ , quaternionic signals  $\psi_Q(x_1, x_2)$  and monogenic signals  $\psi_M(x_1, x_2)$ . It is a 4-D function given by the Fourier

transforms of the correlation products: The analytic correlation product

$$r_A(x_1, x_2, \chi_1, \chi_2) = \psi_A(x_1 + 0.5\chi_1, x_2 + 0.5\chi_2) \times \psi_A^*(x_1 - 0.5\chi_1, x_2 - 0.5\chi_2) \quad (7.801)$$

the quaternionic correlation product

$$r_Q(x_1, x_2, \chi_1, \chi_2) = \psi_Q(x_1 + 0.5\chi_1, x_2 + 0.5\chi_2) \times \psi_Q^*(x_1 - 0.5\chi_1, x_2 - 0.5\chi_2) \quad (7.802)$$

and the monogenic correlation product

$$r_M(x_1, x_2, \chi_1, \chi_2) = \psi_M(x_1 + 0.5\chi_1, x_2 + 0.5\chi_2) \times \psi_M^*(x_1 - 0.5\chi_1, x_2 - 0.5\chi_2) \quad (7.803)$$

The 4-D Wigner distribution is defined by the Fourier transform

$$W_K(x_1, x_2, f_1, f_2) = \int_{-\infty}^{\infty} \int_{-\infty}^{\infty} e^{-i2\pi f_1 \chi_1} r_K(x_1, x_2, \chi_1, \chi_2) e^{-j2\pi f_2 \chi_2} d\chi_1 d\chi_2 \quad (7.804)$$

In the analytic case  $r_K = r_A$  and we apply a normal Fourier transformation inserting the imaginary unit  $i_1 = j_1$ . In the quaternionic and monogenic case we apply the quaternionic Fourier transformation inserting  $r_K = r_Q$  or  $r_K = r_M$ .

The 4-D Wigner distribution of the 2-D analytic signal with single-quadrant Fourier support remains a real function. However, in general, a given signal is represented by two distributions of signals analytic signals, for example,  $\psi_1$  and  $\psi_3$  (see Table 7.14). Differently, the Wigner distributions of quaternionic or monogenic signals are represented by a single quaternion-valued function [46].

## 7.28 The Clifford Analytic Signal<sup>56</sup>

The  $n$ -D analytic signal with single orthant spectra are described in Section 7.24. For example, the 3-D analytic signal corresponding to the real signal  $u(\mathbf{x}), \mathbf{x} \in (x_1, x_2, x_3)$  has in the  $\mathbf{x}$  domain the form

$$\psi_A(x_1, x_2, x_3) = u(x_1, x_2, x_3) \delta(x_1) + j \frac{1}{\pi x_1} \times \left[ \delta(x_2) + j \frac{1}{\pi x_2} \right] \left[ \delta(x_3) + j \frac{1}{\pi x_3} \right] \quad (7.805)$$

The 3-D Fourier transform of this signal is

$$\Gamma(f_1, f_2, f_3) = [1 + \text{sgn}(f_1)] [1 + \text{sgn}(f_2)] [1 + \text{sgn}(f_3)] U(f_1, f_2, f_3) \quad (7.806)$$

where  $u(\mathbf{x}) \stackrel{3-F}{\Leftrightarrow} U(\mathbf{f}), \mathbf{f} \in (f_1, f_2, f_3)$ . The  $n$ -D hypercomplex analytic signal is defined using the notion  $n$ -D Clifford Fourier transform given by [56]

$$U_C(\mathbf{f}) = \int_{\mathbb{R}^n} u(\mathbf{x}) \prod_{k=1}^n \exp(-e_k f_k x_k) d^n \mathbf{x} \quad (7.807)$$

where

$$\mathbf{f} = (f_1, f_2, \dots, f_n), \mathbf{x} = (x_1, x_2, \dots, x_n)$$

$e_1, e_2, \dots, e_n$  are basis unit vectors of the Clifford algebra  $\mathbb{R}_{0,n}$

The  $n$ -D hypercomplex analytic signal is defined by the formula

$$\psi_C(\mathbf{x}) = \prod_{i=1}^n \left[ \delta(x_i) + \frac{e_i}{\pi x_i} \right] \quad (7.808)$$

and is given by the inverse Clifford Fourier transform of the form

$$\Gamma_C(\mathbf{f}) = u(\mathbf{x})^* \prod_{i=1}^n [1 + \operatorname{sgn}(f_i)] U_C(\mathbf{f}) \quad (7.809)$$

## 7.29 Hilbert Transforms and Analytic Signals in Wavelets

In this handbook properties of wavelet transforms are described in Chapter 10. This short note presents in a descriptive manner the role of Hilbert transforms and analytic signals in wavelets. In [47] the authors describe the following four problems with real wavelets: (1) Oscillations: Since wavelets are band-pass functions, the wavelet coefficients tend to oscillate around the singularities. (2) Shift invariance: A small shift of the signal greatly perturbs the wavelet oscillation pattern around singularities. (3) Aliasing: see [47]. (4) Lack of directionality in 2-D wavelets. All this shortcomings of real wavelets can be considerably deleted by using complex wavelets. In principle, analytic wavelets should be applied. For 1-D signals the Fourier transform of an analytic signal should be a one-sided function at positive frequencies. However, a complex wavelet has the form of an envelope of finite support modulated with a pair of oscillating orthogonal functions (a pair of Hilbert transforms). The modulus of the Fourier transform of such a signal has leakage into negative frequencies region. Such a signal is called quasi-analytic. In practice various kinds of complex wavelets are quasi-analytic. Examples are described in [48–51]. For 2-D signals the Fourier transform of an analytic signal should have a single-quadrant support (see [13] and Section 7.24). The notion of quasianalyticity can be extended for 2-D signals. The authors of [48] describe 2-D quasi-analytic wavelets. Analogous 2-D wavelets using quaternionic and monogenic signals are described in [53–55].

## References

1. Ansari, R. IIR discrete-time Hilbert transformers, *IEEE Trans. ASSP*, ASSP-35(8), August 1987, 1116–1119.
- 1a. Ansari, R. Elliptic filter design for generalized half-band filters. ASSP-33, October 1985, 1146–1150.
2. Bedrosian, S. D. Normalised design of 90° phase-difference networks. *Trans. Inst. Radio Eng.*, CT-7, 1960, 128–136.
3. Bedrosian, E. The analytic signal representation of modulated waveforms. *Proc. IEEE*, 50(10), October 1962, 2071–2076.
4. Bedrosian, E. A product theorem for Hilbert transforms. *Proc. IEEE (Lett.)*, 51(5), May 1963, 868–869.
5. Bedrosian, E. and Stark, H. Comments on “An extension of the Hilbert transform product theorem,” *Proc. IEEE*, 60, February 1972, 228–229.
6. Budeanu, C. Reactive and fictitious powers, *Romanian National Inst. Publ.*, No. 2, 1927, Bucharest, Romanian.
7. Čížek, V. Discrete Hilbert transform. *IEEE Trans*, AU-18 (4), December 1970, 340–343.
8. Darlington, S. Realization of a constant phase difference. *Bell Syst. Tech. J.*, 29, 1950, 94–104.
9. Dome, R. B. Wide-band phase shift networks. *Electronics*, 19, December 1946, 112–115.
10. Fryze, S., Wirk- und Blind- und Scheinleistung in Elektrischen Stromkreisen mit nichtstunusoidalen foremigen Verlauf von Strom and Spannung. *Elektrotech. Z.*, 53(25), 1932, 696–599 (Active, reactive, and apparent power in electrical circuits with nonsinusoidals currents and voltages).
11. Gabor, D. Theory of communications. *J. Inst. EE*, Pt. III, 93, November 1946, 429–457.
12. Hahn, S. L. Complex variable frequency electric circuit theory. *Proc. IEEE (Lett.)*, 52(6), June 1964, 735–736.
13. Hahn, S. L. Multidimensional complex signals with single-orthant spectra. *Proc. IEEE*, 80(8), August 1992, 1287–1300.
14. Hahn, S. L. Amplitudes, phases and complex frequencies of 2-D Gaussian signals, *Bull. Polish Acad. Sci.*, 40(3), 1992, 289–311.
15. Hermann, O. Transversalfilter zur Hilbert-Transformation. *Arch. Elektr. Übertr.*, 23, Heft 12, 1969, 581–587 (Transversal filters as Hilbert transformers).
16. Jackson, L. B. On the relationship between digital Hilbert transformers and certain low-pass filters. *IEEE Trans. ASSP*, 23(8), August 1975, 381–383.
17. Kahn, L. R. Compatible single sideband. *Proc. IRE*, 49, October 1961, 1503–1527.
18. Kramers, H. A. *Phys. Z.*, 30, 1929, 522.
19. Kronig, R. de L. On the theory of dispersion of x-rays. *J. Opts. Soc. Am.*, 12, 1926, 547–567.
20. Krylov, W. W. and Ponomariev, D. M. Definition of the signal delay in linear two-ports using the Hilbert transform (in Russian). *Radiotekhnika i Elektronika*, 5, 1980, 204–206.
21. Klyagin, L. Ye. Linearization of the phase characteristics of wide-band phase shifters (translated from Russian). *Telecommun. Radio Eng.*, Part 2 (USA) 1967, 82–87.

22. McClellan, J. H. A. computer program for designing optimum FIR linear phase digital filters. *IEEE Trans.*, AU-21(6), December 1973, 506–526.
23. Mikusinski, J. The elementary theory of distributions. *Rozprawy Matematyczne XII*, Warsaw: PWN, 1957.
24. Nowomiejski, Z. Generalized theory of electric power, *Archiv. f. Elektrotechnik*, 63, 1981, 177–182, 1972, 1361–1362.
25. Nuttall, A. and Bedrosian, E. On the quadrature approximation of the Hilbert transform of modulated signals. *Proc. IEEE (Lett.)*, 54, October 1966, 1458–1459.
26. Oppenheim, A. V. and Schaffer, R. W. *Digital Signal Processing*. Englewood Cliffs, NJ: Prentice-Hall, 1975.
27. Orchard, H. J. The synthesis of RC networks to have prescribed transfer functions. *Proc. IRE*, 39, April 1951, 428–432.
28. Paley, E. A. C. and Wiener, N. *Fourier Transforms in the Complex Domain*. Vol. 19, American Mathematical Society, New York: Colloquium Publications, 1934.
29. Rabiner, L. R. and Schaffer, R. W. On the behaviour of minimax FIR digital Hilbert transformers. *Bell Syst. Tech. J.*, 53(2), February 1974, 363–390, and On the behaviour of minimax relative error FIR differentiators, 333–362.
30. Rabiner, L. R. and Gold, B. *Theory and Applications of Digital Signal Processing*. Englewood Cliffs, NJ: Prentice-Hall, 1975.
31. Rabiner, L. R. et al. FIR digital filter design techniques using weighted Chebyshev approximation. *Proc. IEEE*, 63(4), April 1975, 585–610.
32. Robinson, F. N. H. *Macroscopic Electromagnetism*, Oxford, U.K.: Pergamon Press, 1973.
33. Saraga, W. The design of wide-band two-phase networks, *Proc. Inst. Electron. Eng.*, 38, 1950, 754–770.
34. Schneider, W. Quadraturfilter nach der methode der angezapften Laufzeitketten. *Telefunken-Ztg.*, 40, 1967 (Quadrature filter using the method of a tapped-delay line).
35. Schwartz, L. *Methodes Mathematique Pour les Science Physique*. Paris: Hermann, 1965.
36. Stark, H. and Tuteur, F. B. Modern electrical communications. *Theory and Systems*. Englewood Cliffs, NJ: Prentice-Hall, 1979.
37. Stark, H. An extension of the Hilbert transform product theorem, *Proc. IEEE*, 59(9), September 1971, 1359–1360.
38. Weaver, D. K. Design of RC wide-band 90-degree phase difference networks. *Proc. IRE*, 42, April 1954, 671–676.
39. Weinberger, H. F. *Partial Differential Equations with Complex Variables and Transform Methods*. New York: Blaisdell Publishing Co., 1965.
40. Villard, O. G., Jr. Composite amplitude and phase modulation. *Electronics*, 21, Nov. 1948, 86–89.
41. Carson, J. R. and Fry, C. F. Variable frequency electric circuit theory with application to the theory of frequency modulation, *Bell Syst. Tech. J.*, 6(4), 1954, 513–530.
42. Hahn, S. L. On the uniqueness of the definition of the amplitude and phase of the analytic signal. *Signal Process.*, 82 (2002), 1815–1820.
43. Hahn, S. L. Complex signals with single-orthant spectra as boundary distributions of multidimensional analytic functions. *Bull. Polish Acad. Sci.* 51(2), 2003, 155–161 (see also the Appendix in reference: Hahn S. L., Snopek K. M., Wigner Distributions and Ambiguity Functions of 2-D Quaternionic and Monogenic Signals, *IEEE Trans. Signal Process.*, 53(8), August 2005, 3129–3140.
44. Bülow, T. and Sommer, G. The hypercomplex signal—A novel extension of the analytic signal to the multidimensional case. *IEEE Trans. Signal Process.*, 49(11), November 2001, 2844–2852.
45. Felsberg, M. and Sommer, G. The monogenic signal. *IEEE Trans. Signal Process.*, 49(12), December 2001, 3136–3140.
46. Hahn S. L. and Snopek K. M., Wigner Distributions and Ambiguity Functions of 2-D Quaternionic and Monogenic Signals, *IEEE Trans. Signal Process.*, 53(8), August 2005, 3129–3140.
47. Larkin, K. G., Bone, D., and Oldfield, M. A. Natural demodulation of two-dimensional fringe patterns: General background of the spiral phase quadrature transform. *J. Opt. Soc. Am.* 18(8), August 2001, 1862–1870.
48. Selesnick, W. I., Baraniuk, R. G., and Kingsbury, N. G. The dual-tree complex wavelet transform, *IEEE Signal Process. Mag.*, November 2005, 123–150.
49. Selesnick, W. I., Hilbert transform pairs of wavelet bases, *IEEE Signal Process. Lett.*, 8(6), June 2001, 170–173.
50. Selesnick, W. I., The design of approximate Hilbert transform pairs of wavelet bases, *IEEE Trans. Signal Process.*, 50(5), May 2002, 1144–1152.
51. Tay, D. B. H., Kingsbury, N. G., and Palaniswami, M. Orthonormal Hilbert-pair of wavelets with (almost) maximum vanishing moments, *IEEE Signal Process. Lett.*, 13(9), September 2006, 533–536.
52. Dumitrescu, B. SDP approximation of a fractional delay and the design of a dual-tree wavelet transform, *IEEE Trans. Signal Process.*, 56(9), September 2008, 4255–4262.
53. Chan, W. L., Choi, H., and Baraniuk, B. Coherent multi-scale image processing using dual-tree quaternion wavelets, *IEEE Trans. Image Process.*, 17(7), July 2008, 1069–1082.
54. Olhede, S. C. and Metikas, G., The hyperanalytic wavelet transform, Imperial College Statistics Section Technical Report TR-06-02, February 2008, 1–49.
55. Cerejeiras, P., Ferriera, M., and Kähler, U., Monogenic wavelets over the unit ball, *Zeitschrift für Analysis und ihre Anwendungen*, 24, 841–852, 2005.
56. Sommer, G. (Ed.), *Geometric Computing with Clifford Algebras*, Berlin, Germany: Springer-Verlag, 2001.

# Radon and Abel Transforms

8.1	Introduction.....	8-1
	Organization of the Chapter • Remarks about Notation	
8.2	Definitions.....	8-3
	Two Dimensions • Three Dimensions • Higher Dimensions • Probes, Structure, and Transforms • Transforms between Spaces, Central-Slice Theorem	
8.3	Basic Properties.....	8-7
	Linearity • Similarity • Symmetry • Shifting • Differentiation • Convolution	
8.4	Linear Transformations .....	8-9
8.5	Finding Transforms .....	8-10
8.6	More on Derivatives .....	8-15
	Transform of Derivatives • Derivatives of the Transform	
8.7	Hermite Polynomials.....	8-17
8.8	Laguerre Polynomials.....	8-18
8.9	Inversion.....	8-19
	Two Dimensions • Three Dimensions	
8.10	Abel Transforms.....	8-21
	Singular Integral Equations, Abel Type • Some Abel Transform Pairs • Fractional Integrals • Some Useful Examples	
8.11	Related Transforms and Symmetry, Abel and Hankel.....	8-27
	Abel Transform • Hankel Transform • Spherical Symmetry, Three Dimensions	
8.12	Methods of Inversion .....	8-30
	Backprojection • Backprojection of the Filtered Projections • Filter of the Backprojections • Direct Fourier Method • Iterative and Algebraic Reconstruction Techniques	
8.13	Series .....	8-34
	Circular Harmonic Decomposition • Orthogonal Functions on the Unit Disk	
8.14	Parseval Relation .....	8-39
8.15	Generalizations and Wavelets .....	8-41
8.16	Discrete Periodic Radon Transform .....	8-42
	The Discrete Version of the Image • A Discrete Transform • The Inverse Transform • Good News and Bad News	
	Appendix 8.A: Functions and Formulas .....	8-43
	Appendix 8.B: Short List of Abel and Radon Transforms.....	8-45
	References .....	8-47

Stanley R. Deans  
University of South Florida

## 8.1 Introduction

The Austrian mathematician Johann Radon (1887–1956) wrote a classic paper in 1917, “Über die Bestimmung von Funktionen durch ihre Integralwerte längs gewisser Mannigfaltigkeiten” (on the determination of functions from their integrals along certain manifolds) (Radon, 1917). This work forms the foundation for what we now call the Radon transform. English translations are available in the monograph by Deans (1983, 1993) and the translation by Parks (1986). The problem of determining a function  $f(x, y)$  from knowledge of its line integrals (the two-dimensional (2D) case), or a function  $f(x, y, z)$  from integrals over planes (the three-dimensional [3D] case) arises in widely diverse fields. These include medical imaging, astronomy,

crystallography, electron microscopy, geophysics, optics, and material science. In these applications the central aim is to obtain certain information about the internal structure of an object either by passing some probe (such as x-rays) through the object or by using information from the source itself when it is self-emitting, such as an organ in the body that contains a radioactive isotope, or perhaps the interior of the Earth when motions occur. Comprehensive reviews of these and other applications are contained in Brooks and Di Chiro (1976), Scudder (1978), Barrett (1984), Chapman (1987), and Deans (1983, 1993).

The general problem of unfolding internal structure of an object by observations of projections is known as the problem of *reconstruction from projections*. Many situations arise when it is possible to determine (reconstruct) various structural

properties of an object or substance by methods that utilize projected information and leave the object in an essentially undamaged state. The Radon transform and its inversion forms the mathematical framework common to a large class of these problems. This problem of reconstructing a function from knowledge of its projections emerges naturally in fields so diverse that those working in one area seldom communicate with their counterparts in the other areas. This was especially true prior to the advent of computerized tomography in the 1970s. As a consequence, there is an interesting history of the independent development of applications of the Radon transform by individuals who were not aware of the original work by Radon in 1917, or of contemporary work in other fields. Those interested in pursuing these historical matters can consult Cormack (1973, 1982, 1984), Barrett et al. (1983), and Deans (1985, 1993).

Also, the Radon transform has varying degrees of relevance in three Nobel prizes: (Medicine 1979, Allan M. Cormack and Godfrey N. Hounsfield) (DiChiro and Brooks, 1979, 1980), (Cormack, 1980), and (Hounsfield, 1980); (Chemistry 1982, Aaron Klug) (Caspar and DeRosier, 1982); (Chemistry 1991, Richard R. Ernst) (Amato, 1991).

As short a time as a decade ago, the Radon transform was known by very few engineers and scientists. Only those working directly on reconstruction from projections in one of the major areas of application had knowledge of this transform. Today, the Radon transform is widely known by working scientists in medicine, engineering, physical science, and mathematics. It has made its way into the image processing texts (Kak, 1984, 1985), (Kak and Slaney, 1988), (Jain, 1989), (Jähne, 1993), and is widely appreciated in many diverse areas; among the best known include: medical imaging (Herman, 1980), (Macovski, 1983), (Natterer, 1986), (Swindell and Webb, 1988), (Parker, 1990), (Russ, 1992), (Cho et al., 1993); optics and holographic interferometry (Vest, 1979); geophysics (Claerbout, 1985), (Chapman, 1987), (Ruff, 1987), (Bregman et al., 1989); radio astronomy (Bracewell, 1979); and pure mathematics (Grinberg and Quinto, 1990), (Gindikin and Michor, 1994).

The purpose of this chapter is to review (and illustrate with examples) important properties of Radon and Abel transforms and indicate some of the applications, along with important sources for applications. Because the Abel transform is a special case of the Radon transform, most of the discussion is for the more general transform. This is especially important to keep in mind for applications where the Abel transform can be used. Section 8.10 is devoted to Abel integral equations and Abel transforms. The formal connection between Abel and Radon transforms is made in Section 8.11; the reader primarily interested in Abel transforms may want to look at those two sections first.

The overall goal is to provide the reader with basic material that can be used as a foundation for understanding current research that makes use of the transforms. A conscientious attempt is made to present essential mathematical material in a way that is easily understood by anyone having a basic knowledge of Fourier transforms. In keeping with this goal, the emphasis will be on the 2D and 3D cases. The extension to

higher dimensions will be mentioned at various times, especially when the extension is rather obvious. For the most part, derivations are kept as simple and intuitive as possible. Reference is made to more rigorous discussions and abstract applications. The same policy is followed for highly technical problems related to sampling and numerical implementation of inversion algorithms. These are ongoing research problems that lie a level above the basic treatment presented here. Section 8.1.1 contains a brief summary of how the chapter is organized. An attempt is made to cross reference the various sections, so the reader interested in a given topic can go directly to that topic without having to read everything that precedes. Finally, it is to be noted that liberal use is made of material contained in books by the author on the same subject (Deans, 1983, 1993).

### 8.1.1 Organization of the Chapter

Section 8.2 is devoted mainly to fundamental definitions, concepts, and spaces. The definitions are given several ways and for various dimensions to make it easier for the reader to make connection with usage in the current literature. The section on probes, structure, and transforms outlines the connection of the Radon transform to physical applications. A very important theorem known as the central-slice theorem serves to relate three spaces of special importance: feature space, Radon space, and Fourier space. A proof is provided for the 2D case and an example is given to illustrate how a function transforms among the three spaces.

Some of the most basic properties of the Radon transform are presented in Section 8.3 and compared with the corresponding properties for the Fourier transform. These properties are used many times throughout the sections that follow.

A brief, but important, discussion of the Radon transform of a linear transformation is in Section 8.4. This provides the foundation for powerful methods to calculate transforms of various functions. In Section 8.5 this idea is combined with the basic properties to illustrate, by several examples, just how the Radon transform works when applied to certain special functions. These examples are selected to bring out subtle points that emerge when actually computing a transform.

More advanced topics on derivatives and the transform are in Section 8.6. This work serves as background for transforms involving Hermite polynomials in Section 8.7 and Laguerre polynomials in Section 8.8.

The important problem of inversion is initiated in Section 8.9. Details are given for two and three dimensions, and the foundation is provided for some of the currently utilized inversion methods outlined in sections that follow.

Abel transforms and Abel-type integral equations are discussed in Section 8.10. Four different types of Abel transforms are defined along with the corresponding inverses. Interrelationships among the transforms are illustrated along with several useful examples. A rule is given to establish a method for finding Abel transforms from extensive tables of Riemann–Liouville and Weyl (fractional) integrals. The way the Radon and Fourier transforms relate to the Abel and Hankel transforms is developed

in Section 8.11. An important observation is that the Abel transform is a special case of the Radon transform. Examples are given to demonstrate the connection for specific cases.

The earlier work on inversion is supplemented in Section 8.12 by some methods that form the basis for modern algorithms for numerical inversion of discrete data using backprojection and convolution methods. Diagrams that clearly illustrate the various options are included in this section.

Series methods for inversion are discussed in Section 8.13, with emphasis on two and three dimensions. Special attention is given to functions defined on the unit disk in feature space. Several examples are provided to illustrate both techniques and the connection with earlier sections.

The Parseval relation for the Radon transform is given in Section 8.14 for the general  $n$ -dimensional case. A useful example in two dimensions serves to highlight the difference between the Fourier and Radon cases.

Extensions and emerging concepts are mentioned briefly in Section 8.15. An especially exciting area involves the use of the wavelet transform to facilitate inversion of the Radon transform.

Finally, Appendix 8.A contains a compilation of formulas and special functions used throughout the chapter, and a list of selected Radon and Abel transforms appears in Appendix 8.B.

### 8.1.2 Remarks about Notation

The Radon transform is defined on real Euclidean space for two and higher dimensions. Many results are just as easy to obtain for the  $n$ -dimensional transform as for the 2D transform. However, most illustrations (and applications) of the transform are easier in two or three dimensions. Consequently, several equivalent notations are appropriate for vectors. Various notations are given here and the policy throughout the entire discussion is to change freely from one notation to the other with absolutely no apology.

Both component and matrix notations will be used. In component notation, all of the following expressions are used,

$$\mathbf{x} = \mathbf{r}(x, y) \quad \mathbf{x} = (x_1, x_2) \quad \mathbf{y} = (y_1, y_2).$$

In matrix notation these would be:

$$\mathbf{x} = \mathbf{r} = \begin{pmatrix} x \\ y \end{pmatrix} \quad \mathbf{x} = \begin{pmatrix} x_1 \\ x_2 \end{pmatrix} \quad \mathbf{y} = \begin{pmatrix} y_1 \\ y_2 \end{pmatrix}.$$

Similar notations are used for three dimensions by appending  $z$  or  $x_3$  or  $y_3$ . For the  $n$ -dimensional case we use:

$$\mathbf{x} = (x_1, \dots, x_n) \quad \mathbf{y} = (y_1, \dots, y_n),$$

or the equivalent matrix form. When there is no confusion about which variables are being integrated, the abbreviated notation

$$\int f(\mathbf{x}) dx \equiv \int_{-\infty}^{\infty} \dots \int_{-\infty}^{\infty} f(x_1, \dots, x_n) dx_1 \dots dx_n$$

will be used for integration over all space.

## 8.2 Definitions

In a discussion of the Radon transform it is convenient to identify three spaces. These spaces are designated by *feature space*, *Radon space*, and *Fourier space*.

Feature space is just Euclidean space in two, three, or  $n$  dimensions, designated by 2D, 3D, or  $n$ D. This is where the spatial distribution  $f$  of some physical property is defined. Radon space and Fourier space designate the spaces for the corresponding transforms of this distribution. Functions in feature space that represent the distribution are designated by  $f(x, y)$ ,  $f(x, y, z)$ , and  $f(x_1, \dots, x_n)$ , depending on the dimensions of the transform. For the purposes of this presentation, these functions  $f$  are selected from some nice class of functions, such as the class of infinitely differentiable ( $C^\infty$ ) functions with compact support or rapidly decreasing  $C^\infty$  functions (Schwartz, 1966). This assumption serves well for the current discussion; however, it can be relaxed in more general treatments (Gel'fand et al., 1966; Lax and Phillips, 1970, 1979; Helgason, 1980; Grinberg and Quinto, 1990; Mikusiński and Zayed, 1993; Gindikin and Michor, 1994).

The transformation from one space to another can be represented symbolically as a mapping operation. Let  $\mathfrak{R}$  be the operator that transforms  $f$  to Radon space. If the corresponding function in Radon space is designated by  $\tilde{f}$ , the mapping operation is expressed by

$$\tilde{f} = \mathfrak{R}f. \quad (8.1)$$

In a similar way, the transformation to Fourier space is written:

$$\tilde{f} = \mathfrak{F}f. \quad (8.2)$$

These operations will be made more precise in the next sections where explicit definitions are given for various dimensions.

### 8.2.1 Two Dimensions

The Radon transform of the function  $f(x, y)$  is defined as the line integral of  $f$  for all lines  $\ell$  defined by the parameters  $\phi$  and  $p$ , illustrated in Figure 8.1. There are several ways this can be expressed. In terms of integrals along  $\ell$ ,

$$\tilde{f}(p, \phi) = \int_{-\infty}^{\infty} f(\mathbf{r}) dl, \quad (8.3)$$

where  $\mathbf{r} = (x, y)$  is a general position vector. Another way to write this is to define the unit vector  $\boldsymbol{\xi} = (\cos \phi, \sin \phi)$  and the perpendicular vector  $\boldsymbol{\xi}' = (-\sin \phi, \cos \phi)$ , then the position vector is given by  $\mathbf{r} = p \boldsymbol{\xi} + t \boldsymbol{\xi}'$  and (note that  $r^2 = p^2 + t^2$ )

$$\tilde{f}(p, \boldsymbol{\xi}) = \int_{-\infty}^{\infty} f(p\boldsymbol{\xi} + t\boldsymbol{\xi}') dt. \quad (8.4)$$

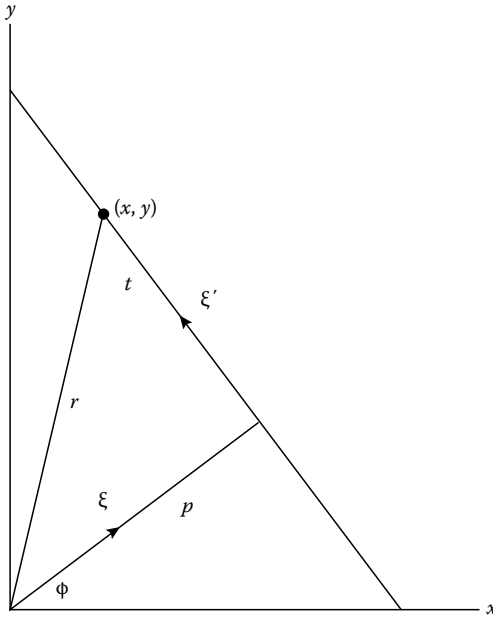


FIGURE 8.1 Coordinates in feature space used to define the Radon transform. The equation of the line is given by  $p = x \cos \phi + y \sin \phi$ .

An equivalent definition making use of the delta function (see Chapter 1) is most convenient for the current discussion,

$$\tilde{f}(p, \phi) = \int_{-\infty}^{\infty} \int_{-\infty}^{\infty} f(x, y) \delta(p - x \cos \phi - y \sin \phi) dx dy. \quad (8.5)$$

Note that due to the property of the delta function and the fact that the normal form for the equation of the line  $\ell$  is given by  $p = x \cos \phi + y \sin \phi$ , the integral over the plane reduces to a line integral in agreement with the previous definitions. A slightly different form proves especially useful for generalization to higher dimensions. In terms of the vector  $\mathbf{r}$  and  $\xi$ ,

$$\tilde{f}(p, \xi) = \int_{-\infty}^{\infty} \int_{-\infty}^{\infty} f(\mathbf{r}) \delta(p - \xi \cdot \mathbf{r}) dx dy, \quad (8.6)$$

where  $\xi \cdot \mathbf{r} = \xi_1 x + \xi_2 y = x \cos \phi + y \sin \phi$ .

It is important to understand that  $\tilde{f}$  is *not* defined on a circular polar coordinate system. The appropriate space is on the surface of a half-cylinder. Consider an infinite cylinder of radius unity. Let the parameter  $p$  measure length along the cylinder from  $-\infty$  to  $+\infty$ , and let the angle  $\phi$  measure the angle of rotation with respect to an arbitrary reference position. A point on an arbitrary cross section of the cylinder is represented by  $(p, \phi)$  as illustrated in Figure 8.2.

Observe that from the definition of the transform, if  $\tilde{f}$  is known for  $-\infty < p < \infty$ , then only values of  $\phi$  in the range  $0 \leq \phi < \pi$  are needed. To verify this, recall that the delta function

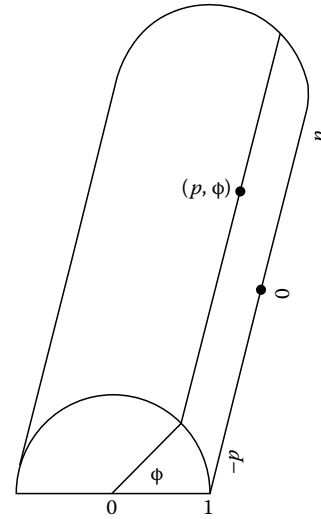


FIGURE 8.2 Coordinates in Radon space on the surface of a cylinder.

is even  $\delta(x) = \delta(-x)$ , and the change  $\phi \rightarrow \phi + \pi$  corresponds to  $\xi \rightarrow -\xi$ . Hence, the coordinates  $(-p, \phi)$  and  $(p, \phi + \pi)$  denote the same point in Radon space. Likewise, the function  $\tilde{f}$  is completely defined for  $0 \leq p < \infty$  and  $0 \leq \phi < 2\pi$ . More will be said about properties of  $\tilde{f}$  in Section 8.3.

Now, suppose we unroll the half-cylinder in Figure 8.2. The resulting surface is a plane with points represented by  $(p, \phi)$  on a rectangular grid. It is convenient to let  $p$  vary along the vertical axis and  $\phi$  along the horizontal axis, restricted to the range 0 to  $\pi$ . This construction is especially useful for illustrations because the values of  $\tilde{f}$  can be represented as a surface in the third dimension perpendicular to this plane. Also, note that for most practical applications the object of interest in feature space does not extend to infinity. Suppose  $f(\mathbf{r}) = 0$  for  $|\mathbf{r}| > R$ , where  $R$  is finite. It follows that  $\tilde{f} = 0$  for  $|p| > R$ , and  $p$  varies on a finite interval.

To help interpret Equation 8.6 let  $f(x, y)$  represent the density (in 2D) for some finite mass distributed throughout the plane. (Here, we are considering a special case of the more general result in  $nD$  discussed by Gel'fand et al. (1966). If  $\mathcal{M}(p, \xi)$  denotes the total mass in the region  $\xi \cdot \mathbf{r} < p$ , then

$$\mathcal{M}(p, \xi) = \int \int_{\xi \cdot \mathbf{r} < p} f(x, y) dx dy = \iint f(x, y) \mathcal{U}(p - \xi \cdot \mathbf{r}) dx dy,$$

where  $\mathcal{U}(\cdot)$  denotes the unit step function. Now from the relation  $\frac{\partial \mathcal{U}(p)}{\partial p} = \delta(p)$  for generalized functions, the above equation becomes

$$\frac{\partial \mathcal{M}(p, \xi)}{\partial p} = \int_{-\infty}^{\infty} \int_{-\infty}^{\infty} f(\mathbf{r}) \delta(p - \xi \cdot \mathbf{r}) dx dy = \mathfrak{R}\{f(x, y)\}. \quad (8.7)$$

This result shows that if  $f(x, y)$  denotes a density with which a finite mass is distributed throughout space, its Radon transform is

$$\tilde{f}(p, \xi) = \frac{\partial \mathcal{M}(p, \xi)}{\partial p}.$$

where  $\mathcal{M}(p, \xi)$  is the mass in the half-space  $\xi \cdot \mathbf{r} < p$ , and the derivative with respect to  $p$  is assumed to exist. It is important to observe that to have complete knowledge of the Radon transform one must know the mass distribution for all values of the variable  $p$  and  $\xi$ . If the transform is found for only selected values of these variables, we may call the result a *sample* of the Radon transform. The next example illustrates this idea.

**Example 8.1**

Find a sample of the Radon transform for the case shown in Figure 8.3, for the case where the mass is proportional to the area. For simplicity, let the proportionality constant be unity. The equation of the line specified in the figure  $x = p$  and the angle is  $\phi = 0$ . The required sample is found from

$$\tilde{f} = \frac{\partial A}{\partial p},$$

where  $A$  is the area in the neighborhood of the line  $x = p$ . This example is simple enough to yield, by simple calculus for finding areas, an explicit expression for  $A$  as a function of  $p$ ,

$$A(p) = 2 \int_0^p \sqrt{1 - x^2} dx.$$

It follows that  $\tilde{f} = 2\sqrt{1 - p^2}$ .

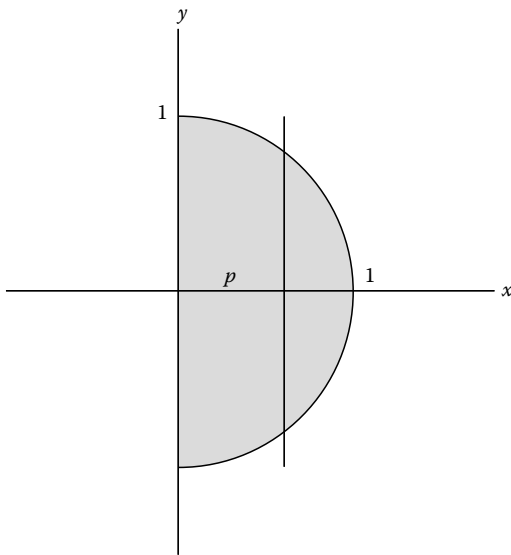


FIGURE 8.3 A semicircle of unit radius. The equation of the line is  $x = p$ .

In this example, it is worth noting that although a sample of the Radon transform is found, the result has relevance to the entire Radon transform for circular symmetry. More will be said about this in several of the sections that follow. Also, observe that  $\tilde{f}$  depends on how  $A$  changes with  $p$  where the derivative is taken, and not on how much area lies to the left or right of the line  $x = p$ .

From Equation 8.3 the Radon transform can also be defined by

$$\tilde{f}(p, \phi) = \int_{\xi \cdot \mathbf{r} = p} f(x, y) ds, \tag{8.8}$$

where the integration is taken along the line  $\mathbf{X} \cdot \mathbf{r} = p$  and  $ds$  is an infinitesimal element on the line. Observe specifically that each line can be uniquely specified by the two coordinates  $\phi$  and  $p$ .

In terms of rotated coordinates of Figure 8.4, Equations 8.5 and 8.8 can be expressed in the form (with  $x = p \cos \phi - t \sin \phi$ ,  $y = p \sin \phi + t \cos \phi$ )

$$\tilde{f}(p, \phi) = \int_{-\infty}^{\infty} f(p \cos \phi - t \sin \phi, p \sin \phi + t \cos \phi) dt. \tag{8.9}$$

This reflects a rotation of the coordinate axes by  $\phi$  such that the  $p$  axis is perpendicular to the original line  $\mathbf{X} \cdot \mathbf{r} = p$ . The above equation can also be interpreted as follows: if  $f_\phi(p, t)$  is the representation of  $f(x, y)$  with respect to the rotated coordinate system, then  $\tilde{f}_\phi(p)$  is the integral of  $f_\phi(p, t)$  with respect to  $t$  for fixed  $\phi$ . That is

$$\tilde{f}_\phi(p) = \int_{-\infty}^{\infty} f_\phi(p, t) dt, \tag{8.10}$$

where  $f_\phi(p, t) = f(p \cos \phi - t \sin \phi, p \sin \phi + t \cos \phi)$ . The interpretation given here covers those cases where the Radon

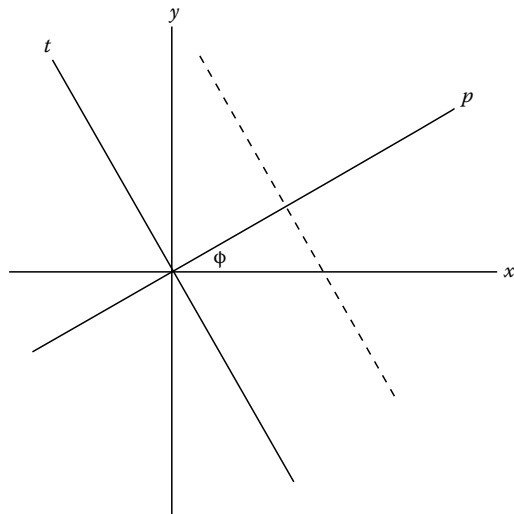


FIGURE 8.4 Rotated coordinates so the line of integration (dashed) is perpendicular to the  $p$  axis.



transform is treated as a function of a single variable  $p$  with the angle  $\phi = \Phi$  viewed as a parameter. In this case the functions of  $p$  for various of  $\Phi$  are called the *projections* of  $f(x, y)$  at angle  $\Phi$ .

### 8.2.2 Three Dimensions

The definition given by Equation 8.6 is easy to extend to three dimensions. Let the line  $\ell$  be replaced by a plane, and let the vector  $\xi$  be a unit vector from the origin such that the vector  $p\xi$  is perpendicular to the plane. That is, the perpendicular distance from the origin to the plane is  $p$  and the vector  $\xi$  defines the direction. Now, the equation of the plane is given by  $p = \xi \cdot \mathbf{r}$ , where the position vector is extended to three dimension,  $\mathbf{r} = (x, y, z)$ . The Radon transform of this function is given by

$$\tilde{f}(p, \xi) = \int_{-\infty}^{\infty} \int_{-\infty}^{\infty} \int_{-\infty}^{\infty} f(\mathbf{r}) \delta(p - \xi \cdot \mathbf{r}) dx dy dz. \quad (8.11)$$

Here, it is understood that the integral is over all planes defined by the equation  $p = \xi \cdot \mathbf{r}$ .

### 8.2.3 Higher Dimensions

The extension to higher dimensions is accomplished by defining the position vector  $\mathbf{r} = (x_1, \dots, x_n)$ , extending the unit vector  $\xi$  to  $n$  dimensions, and integrating over all hyperplanes with equation given by  $p = \xi \cdot \mathbf{r}$ ,

$$\tilde{f}(p, \xi) = \int_{-\infty}^{\infty} \dots \int_{-\infty}^{\infty} f(\mathbf{r}) \delta(p - \xi \cdot \mathbf{r}) dx_1 \dots dx_n. \quad (8.12)$$

Although we do not emphasize use of the transform in higher dimensions in this discussion, it should be noted that the  $nD$  version is just a natural extension of the 3D transform. And, as might be expected, most of the major properties and theorems are just logical extensions of the corresponding results for two and three dimensions (Ludwig, 1966; Helgason, 1980).

### 8.2.4 Probes, Structure, and Transforms

The Radon transform encompasses the appropriate mathematical formalism for solving a large class of practical problems related to reconstruction from projections. This is easy to see by the following considerations. Suppose there exists some physical probe that is capable of producing a projection (profile) that approximates a cumulative measurement of some property of the internal structure of an object. For a fixed angle  $\phi$  this corresponds to knowledge of  $\tilde{f}$  at each point along a line on the cylinder of Figure 8.2. We say that the distribution (represented by  $f$ ) of some physical property of the object is measured by the probe to produce the indicated profile. The correspondence is that:

[physical probe] acting on (Distribution)  $\rightarrow$  Profile

corresponds to

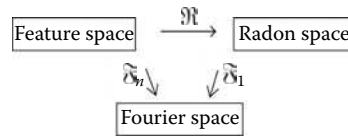
$$[\text{Radon transform}] \text{ acting on } (f) \rightarrow \tilde{f}_\phi$$

for a fixed value of the angle  $\phi = \Phi$ . Here, the notation  $\tilde{f}_\phi$  is used to emphasize that a single profiles serves only to determine a sample of the function  $f$ . A complete determination of  $\tilde{f}$  requires the measurement of the profiles for all angles  $0 \leq \phi < \pi$ .

In applications, typical probes include x-rays, gamma rays, visible light, microwaves, electrons, protons, heavy ions, sound waves, and magnetic resonance signals. These probes are used to obtain information about a wide variety of internal distributions: various types of attenuation coefficients, various densities, isotope distributions, index of refraction distributions, solar microwave distributions, radar brightness distributions, synthetic seismograms, and electron momentum in solids. References for applications and reviews of applications are given in Section 8.1.

### 8.2.5 Transforms between Spaces, Central-Slice Theorem

The general result is that the  $nD$  Fourier transform  $\mathfrak{F}_n$  of  $f(\mathbf{r})$  is equivalent to the Radon transform of  $f(\mathbf{r})$  followed by a 1D Fourier transform  $\mathfrak{F}_1$  on the variable  $p$ . This can be represented by the diagram



Or, in operator equation form

$$\mathfrak{F}_1 \mathfrak{R}f = \mathfrak{F}_1 \tilde{f} = \mathfrak{F}_n f = \tilde{f}. \quad (8.13)$$

This result is important enough to have a special name. It is known as the *central-slice theorem*, very nicely illustrated and discussed by Swindell and Barrett (1977). This designation follows from the observation that the 1D Fourier transform of a projection of  $f$  for a fixed angle is a slice of the  $nD$  Fourier transform of  $f$  for the same fixed angle. A proof is given for  $n = 2$ . The extension to higher dimensions is not difficult.

Start with the 2D Fourier transform.

$$\tilde{f}(u, v) = \int_{-\infty}^{\infty} \int_{-\infty}^{\infty} f(x, y) e^{-i2\pi(ux+vy)} dx dy. \quad (8.14)$$

By using the delta function, this can be rewritten as

$$\tilde{f}(u, v) = \int_{-\infty}^{\infty} dx \int_{-\infty}^{\infty} dy \int_{-\infty}^{\infty} ds f(x, y) e^{-i2\pi s} \delta(s - ux - vy).$$

Next, interchange the order of integration and let  $s = qp$  with  $q > 0$ . This gives

$$\tilde{f}(u, v) = q \int_{-\infty}^{\infty} dp \int_{-\infty}^{\infty} dx \int_{-\infty}^{\infty} dy f(x, y) e^{-i2\pi qp} \delta(qp - ux - vy).$$

In Fourier space, let  $u = q \cos \phi$  and  $v = q \sin \phi$ . Then the variable  $q$  can be factored from the delta function by use of the general property (see Section 1.2)  $\delta(ax) = \delta(x)/|a|$ ,

$$\tilde{f}(u, v) = \int_{-\infty}^{\infty} dp e^{-i2\pi qp} \int_{-\infty}^{\infty} dx \int_{-\infty}^{\infty} dy f(x, y) \delta(p - x \cos \phi - y \sin \phi).$$

This integral over the  $(x, y)$  plane is just the Radon transform of  $f$  from Equation 8.5, and the desired result follows easily

$$\tilde{f}(q \cos \phi, q \sin \phi) = \int_{-\infty}^{\infty} \tilde{f}(p, \phi) e^{-i2\pi qp} dp \quad (8.15)$$

It is interesting to observe the simple result obtained if the coordinates are selected such that the angle  $\phi$  is fixed and equal to zero,  $\Phi = 0$ , then

$$\tilde{f}(q, 0) = \int_{-\infty}^{\infty} \tilde{f}(p, 0) e^{-i2\pi qp} dp. \quad (8.16)$$

By thinking about what the last two equations mean it should be clear that the 1D Fourier transform of a projection of  $f$  for fixed angle  $\phi = \Phi$  is a slice of the 2D Fourier transform of  $f$ , and this slice in Fourier space is defined by the angle  $\Phi$ . One further remark is in order here. This result is sometimes referred to as the *projection-slice theorem*; however, for higher dimensions this designation may have a slightly different meaning as used by Mersereau and Oppenheim (1974). To avoid confusion, in the current presentation (Equation 8.13) is called the  $n$ D form of the central-slice theorem.

For historical purposes, it is to be noted that Bracewell (1956) derived and used this theorem without prior knowledge of the theory of the Radon transform.

**Example 8.2**

A simple example is useful to illustrate the use of transforms between spaces. Suppose the feature space function is the 2D Gaussian

$$f(x, y) = e^{-x^2 - y^2}.$$

First, compute the Fourier transform. Let  $x = r \cos \theta$  and  $y = r \sin \theta$ , then the polar form of Equation 8.14 is given by

$$\tilde{f}(u, v) = \int_0^{\infty} dr r e^{-r^2} \int_0^{2\pi} d\theta e^{[-i2\pi q r \cos(\theta - \phi)]},$$

with  $u = q \cos \phi$  and  $v = q \sin \phi$ . The integral over  $\theta$  is given by  $2\pi J_0(2\pi qr)$ , where  $J_0$  is a Bessel function of order zero (see Section 1.5.6). The remaining integral is a Hankel transform of order zero.

It follows that

$$\tilde{f} = 2\pi \int_0^{\infty} r e^{-r^2} J_0(2\pi qr) dr = \pi e^{-\pi^2 q^2}.$$

Now use Equation 8.12 in the form

$$\tilde{f} = \mathcal{R}^{-1} \tilde{f},$$

to obtain (see Appendix 8.A)

$$\tilde{f}(p, \xi) = \pi \int_{-\infty}^{\infty} e^{-\pi^2 q^2} e^{i2\pi qp} dq = \sqrt{\pi} e^{-p^2}. \quad (8.17)$$

In this example the path from feature space to Radon space was taken through Fourier space for purposes of illustration. Actually, in this case, it is easier to compute the Radon transform directly; see Example 8.3 in Section 8.5.

**8.3 Basic Properties**

Important properties of the Radon transform follow directly from the definition. These properties can be compared with the corresponding properties of the Fourier transform discussed in detail by Bracewell (1986). In this section these basic properties (theorems) are given for the 2D case, along with the corresponding results for the Fourier transform. The slight loss in generality suffered by using 2D illustrations is compensated for by being able to show details that are familiar from a knowledge of elementary calculus. It proves useful to keep the notation for the components of the unit vector  $\xi$  as simple as possible. Rather than always using  $(\cos \phi, \sin \phi)$  for these components, the notation  $(\xi_1, \xi_2)$  is often convenient, where it is understood that

$$\xi_1 = \cos \phi, \quad \xi_2 = \sin \phi, \quad \text{and} \quad \xi_1^2 + \xi_2^2 = 1. \quad (8.18)$$

This means that for the discussion in this Section 8.2.5 may be modified to read

$$\tilde{f}(p, \xi_1, \xi_2) = \int_{-\infty}^{\infty} \int_{-\infty}^{\infty} f(x, y) \delta(p - x\xi_1 - y\xi_2) dx dy. \quad (8.19)$$

The 2D Fourier transform is still given by Equation 8.14. Also, in the following discussion it is always assumed that the transforms actually exist. The reader interested in examples can look ahead

to Section 8.5 where several of these basic properties are used to illustrate ways to find transforms. The reader should also consult Chapter 2 for detail exposition of the Fourier transform properties.

### 8.3.1 Linearity

The Radon and Fourier transforms are both linear. If  $f(x, y)$  and  $g(x, y)$  are functions in feature space, then for any constants  $a$  and  $b$ ,

$$\mathfrak{R}[af + bg] = a\tilde{f} + b\tilde{g} \quad (8.20)$$

and

$$\mathfrak{F}[af + bg] = a\tilde{f} + b\tilde{g}. \quad (8.21)$$

### 8.3.2 Similarity

If  $\mathfrak{R}f(x, y) = \tilde{f}(p, \xi_1, \xi_2)$ , then for arbitrary constants  $a$  and  $b$  the Radon transform of  $f(ax, by)$  is given by

$$\mathfrak{R}f(ax, by) = \frac{1}{|ab|} \tilde{f}\left(p, \frac{\xi_1}{a}, \frac{\xi_2}{b}\right). \quad (8.22)$$

This follows immediately by making the change of variable  $x' = ax$  and  $y' = by$  in the expression

$$\int_{-\infty}^{\infty} \int_{-\infty}^{\infty} f(ax, by) \delta(p - x\xi_1 - y\xi_2) dx dy.$$

The corresponding scaling equation for Fourier transforms: If  $\mathfrak{F}f(x, y) = \tilde{f}(u, v)$  then

$$\mathfrak{F}f(ax, by) = \frac{1}{|ab|} \tilde{f}\left(\frac{u}{a}, \frac{v}{b}\right). \quad (8.23)$$

### 8.3.3 Symmetry

A similar technique can be applied to give an important *symmetry* property. Examine the expression

$$\tilde{f}(ap, a\xi) = \int_{-\infty}^{\infty} \int_{-\infty}^{\infty} f(x, y) \delta(ap - ax\xi_1 - ay\xi_2) dx dy.$$

The constant  $a$  can be factored from the delta function to yield

$$\tilde{f}(ap, a\xi) = |a|^{-1} \tilde{f}(p, \xi). \quad (8.24)$$

If  $a = -1$  this demonstrates that the Radon transform is an even homogenous function of degree  $-1$ ,

$$\tilde{f}(-p, -\xi) = \tilde{f}(p, \xi). \quad (8.25)$$

Another useful form for the symmetry property is

$$\tilde{f}(p, s\xi) = |s|^{-1} \tilde{f}\left(\frac{p}{s}, \xi\right). \quad (8.26)$$

### 8.3.4 Shifting

Given that  $\mathfrak{R}f(x, y) = \tilde{f}(p, \xi)$ , then for arbitrary constants  $a$  and  $b$  the Radon transform of  $f(x - a, y - b)$  is found by

$$\mathfrak{R}f(x - a, y - b) = \tilde{f}(p - a\xi_1 - b\xi_2, \xi). \quad (8.27)$$

As in the previous case, the proof follows immediately by introducing a change of variables. Let  $x' = x - a$  and  $y' = y - b$  in the expression

$$\int_{-\infty}^{\infty} \int_{-\infty}^{\infty} f(x - a, y - b) \delta(p - x\xi_1 - y\xi_2) dx dy.$$

The corresponding theorem for the Fourier transform is a little different, involving a phase change

$$\mathfrak{F}f(x - a, y - b) = e^{-i2\pi(au+bv)} \tilde{f}(u, v). \quad (8.28)$$

### 8.3.5 Differentiation

Details of the derivation are given for the Radon transform of  $\partial f / \partial x$ . Other results follow directly by using the same method. First note that

$$\frac{\partial f}{\partial x} = \lim_{\epsilon \rightarrow 0} \frac{f[x + (\epsilon/\xi_1), y] - f(x, y)}{\epsilon/\xi_1}$$

Now take the Radon transform of both sides and apply Equation 8.27 with  $a = -\epsilon/\xi_1$  and  $b = 0$  to get

$$\mathfrak{R} \frac{\partial f}{\partial x} = \xi_1 \lim_{\epsilon \rightarrow 0} \frac{\tilde{f}(p + \epsilon, \xi) - \tilde{f}(p, \xi)}{\epsilon}.$$

By definition of a partial derivative it follows that

$$\mathfrak{R} \frac{\partial f}{\partial x} = \xi_1 \frac{\partial \tilde{f}(p, \xi)}{\partial p} \quad (8.29a)$$

Likewise, differentiation with respect to  $y$  yields

$$\mathfrak{R} \frac{\partial f}{\partial y} = \xi_2 \frac{\partial \tilde{f}(p, \xi)}{\partial p} \quad (8.29b)$$

Using the same approach, the second derivatives are given by

$$\begin{aligned} \mathfrak{R} \frac{\partial^2 f}{\partial x^2} &= \xi_1^2 \frac{\partial^2 \tilde{f}(p, \xi)}{\partial p^2} \\ \mathfrak{R} \frac{\partial^2 f}{\partial x \partial y} &= \xi_1 \xi_2 \frac{\partial^2 \tilde{f}(p, \xi)}{\partial p^2} \\ \mathfrak{R} \frac{\partial^2 f}{\partial y^2} &= \xi_2^2 \frac{\partial^2 \tilde{f}(p, \xi)}{\partial p^2}. \end{aligned} \quad (8.30)$$

The derivative theorems for the 2D Fourier transform are

$$\mathfrak{F} \frac{\partial f}{\partial x} = 2\pi i u \tilde{f}(u, v), \quad \mathfrak{F} \frac{\partial f}{\partial y} = 2\pi i v \tilde{f}(u, v), \quad (8.31)$$

and

$$\begin{aligned} \mathfrak{F} \frac{\partial^2 f}{\partial x^2} &= -4\pi^2 u^2 \tilde{f}(u, v) \\ \mathfrak{F} \frac{\partial^2 f}{\partial x \partial y} &= -4\pi^2 uv \tilde{f}(u, v) \\ \mathfrak{F} \frac{\partial^2 f}{\partial y^2} &= -4\pi^2 v^2 \tilde{f}(u, v). \end{aligned} \quad (8.32)$$

### 8.3.6 Convolution

The convolution of two functions  $f$  and  $g$  is commonly designated by  $f * g$ , regardless of the dimension. Here, this convention is modified slightly to emphasize the distinction between convolution in one and two dimensions. We write 2D convolution as

$$f ** g = \int_{-\infty}^{\infty} \int_{-\infty}^{\infty} f(x', y') g(x - x', y - y') dx' dy'. \quad (8.33)$$

The Fourier convolution theorem is very simple, yielding a simple product in Fourier space,

$$\mathfrak{F}(f ** g) = \tilde{f}(u, v) \tilde{g}(u, v). \quad (8.34)$$

The corresponding theorem for the Radon transform is considerably more complicated. If  $f = g ** h$ , then the Radon transform of  $f$  is given by a 1D convolution in Radon space, rather than a simple product as in the Fourier case,

$$\check{f}(p, \xi) = \mathfrak{R}(g ** h) = \check{g} * \check{h} = \int_{-\infty}^{\infty} \check{g}(\tau, \xi) \check{h}(p - \tau, \xi) d\tau. \quad (8.35)$$

The proof follows by applying the definition followed by some tricky manipulations with double integrals and delta functions. The details are given by Deans (1983, 1993).

## 8.4 Linear Transformations

A practical method for finding Radon transforms involves making a change of variables. This approach can be related to the Radon transform of a function of a linear transformation of coordinates. Here, inner products are designated by

$$\xi \cdot \mathbf{x} = \xi_1 x_1 + \xi_2 x_2 + \cdots + \xi_n x_n. \quad (8.36)$$

Or, in matrix notation

$$\begin{aligned} \xi^T \mathbf{x} &= (\xi_1 \ \xi_2 \ \cdots \ \xi_n) \begin{pmatrix} x_1 \\ x_2 \\ \vdots \\ x_n \end{pmatrix} \\ &= \xi_1 x_1 + \xi_2 x_2 + \cdots + \xi_n x_n, \end{aligned} \quad (8.37)$$

where T means transpose.

Let A be a nonsingular  $n \times n$  matrix with real elements, then a change of coordinates follows by matrix multiplication

$$\mathbf{y} = \mathbf{A}\mathbf{x}. \quad (8.38)$$

An important identity, in matrix notation, is

$$\xi^T \mathbf{y} = \xi^T \mathbf{A}\mathbf{x} = (\mathbf{A}^T \xi)^T \mathbf{x} \quad (8.39)$$

and the same identity in the “dot” notation is

$$\xi \cdot \mathbf{y} = \xi \cdot \mathbf{A}\mathbf{x} = \mathbf{A}^T \xi \cdot \mathbf{x}. \quad (8.40)$$

Because A is nonsingular, the inverse exists. For convenience, let  $\mathbf{B} = \mathbf{A}^{-1}$ , then  $\mathbf{x} = \mathbf{B}\mathbf{y}$ . The Radon transform of  $f(\mathbf{A}\mathbf{x})$  follows:

$$\begin{aligned} \mathfrak{R} f(\mathbf{A}\mathbf{x}) &= \int f(\mathbf{A}\mathbf{x}) \delta(p - \xi \cdot \mathbf{x}) d\mathbf{x} \\ &= |\det \mathbf{B}| \int f(\mathbf{y}) \delta(p - \xi \cdot \mathbf{B}\mathbf{y}) d\mathbf{y} \\ &= |\det \mathbf{B}| \int f(\mathbf{y}) \delta(p - \mathbf{B}^T \xi \cdot \mathbf{y}) d\mathbf{y} \\ &= |\det \mathbf{B}| \check{f}(p, \mathbf{B}^T \xi). \end{aligned} \quad (8.41)$$

The term  $|\det \mathbf{B}|$  appears because the Jacobian of the transformation is just the magnitude of the determinant of the matrix B. Because  $\mathbf{A} = \mathbf{B}^{-1}$ , an equivalent result is

$$\mathfrak{R} f(\mathbf{B}^{-1} \mathbf{x}) = |\det \mathbf{B}| \check{f}(p, \mathbf{B}^T \xi). \quad (8.42)$$

A word of caution is in order here. It may be that  $\mathbf{B}^T \xi$  is not a unit vector. In such case, it is a good idea to define  $s$  equal to the magnitude of the vector  $\mathbf{B}^T \xi$  and observe that

$$\boldsymbol{\mu} = \frac{\mathbf{B}^T \xi}{s} \quad (8.43)$$

is a unit vector. Now from the results of Section 8.3.3 the right side of Equation 8.42 becomes

$$|\det \mathbf{B}| \check{f}(p, \mathbf{B}^T \xi) = |\det \mathbf{B}| \check{f}(p, s\boldsymbol{\mu}) = \frac{|\det \mathbf{B}|}{s} \check{f}\left(\frac{p}{s}, \boldsymbol{\mu}\right). \quad (8.44)$$

Finally, we have the useful result that

$$\mathfrak{R} f(B^{-1}\mathbf{x}) = \frac{|\det B|}{s} \check{f}\left(\frac{p}{s}, \boldsymbol{\mu}\right), \quad \text{with } s = |B^T \boldsymbol{\xi}|. \quad (8.45)$$

There are two important special cases that deserve attention. First, suppose  $B$  is orthogonal. Then  $B^{-1} = B^T = A$ , with  $|\det B| = 1$ , and

$$\mathfrak{R} f(A\mathbf{x}) = \check{f}(p, A\boldsymbol{\xi}), \quad (8.46)$$

where  $A\boldsymbol{\xi}$  is a unit vector. The other special case is for  $A$  equal to a multiple of the identity. If  $A = cI$  with  $c$  real, then  $B = A^{-1} = c^{-1}I$ , and

$$\mathfrak{R} f(c\mathbf{x}) = \frac{1}{|c|^n} \check{f}\left(p, \frac{\boldsymbol{\xi}}{c}\right) = \frac{1}{|c|^{n-1}} \check{f}(cp, \boldsymbol{\xi}). \quad (8.47)$$

### 8.5 Finding Transforms

In this section some simple examples are worked out in detail to illustrate the use of the various formulas developed in the previous sections. These examples demonstrate how to find transforms and point out pitfalls that sometimes occur during a calculation. The definite integrals that occur in the calculations are tabulated in Appendix 8.A.

#### Example 8.3

Recall from Example 8.2 in Section 8.2 that the Radon transform of

$$f(x, y) = e^{-x^2 - y^2}$$

was found by going through Fourier space to yield

$$\check{f}(p, \boldsymbol{\xi}) = \sqrt{\pi} e^{-p^2}.$$

In this example the Radon transform is calculated directly. Suppose the matrix  $A$  from Section 8.4 is given in terms of the components of the unit vector  $\boldsymbol{\xi} = (\cos \phi, \sin \phi)$ ,

$$A = \begin{pmatrix} \xi_1 & \xi_2 \\ -\xi_2 & \xi_1 \end{pmatrix}.$$

Now define the components of the transformed vector by

$$\begin{pmatrix} u \\ v \end{pmatrix} = A \begin{pmatrix} x \\ y \end{pmatrix} = \begin{pmatrix} \xi_1 x + \xi_2 y \\ -\xi_2 x + \xi_1 y \end{pmatrix}.$$

Observe that  $A$  is orthogonal and Equation 8.46 applies. Also, note that  $u^2 + v^2 = x^2 + y^2$  and  $u = \xi_1 x + \xi_2 y$ . It follows that

$$\begin{aligned} \mathfrak{R} f(A\mathbf{x}) &= \mathfrak{R} f(u, v) = \int_{-\infty}^{\infty} \int_{-\infty}^{\infty} e^{-u^2 - v^2} \delta(p - u) du dv \\ &= e^{-p^2} \int_{-\infty}^{\infty} e^{-v^2} dv = \sqrt{\pi} e^{-p^2}. \end{aligned}$$

Because this result is not dependent on  $\boldsymbol{\xi}$ , or equivalently  $\phi$ , it follows that

$$\mathfrak{R}\{e^{-x^2 - y^2}\} = \sqrt{\pi} e^{-p^2} \quad (8.48)$$

The lack of dependence on  $\phi$  is certainly expected because the Gaussian is symmetric and centered at the origin.

#### Example 8.4

Extend the result in the previous example to three dimensions. Let the orthogonal transformation matrix be selected as

$$A = \begin{pmatrix} \xi_1 & \xi_2 & \xi_3 \\ \frac{-\xi_1 \xi_2}{s} & s & \frac{-\xi_2 \xi_3}{s} \\ \frac{-\xi_3}{s} & 0 & \frac{\xi_1}{s} \end{pmatrix}$$

where  $s = (\xi_1^2 + \xi_2^2)^{1/2}$  and  $|\boldsymbol{\xi}| = 1$ . If the components of the transformed vector are given by  $(u, v, w)$  then after the substitutions are made in Equation 8.46 the transform is given by the integral

$$\int_{-\infty}^{\infty} \int_{-\infty}^{\infty} \int_{-\infty}^{\infty} e^{-u^2 - v^2 - w^2} \delta(p - u) du dv dw = \pi e^{-p^2}.$$

The final result above is obtained by use of the delta function and the evaluation of the two remaining Gaussian integrals over  $v$  and  $w$ . Once again by the invariance argument it follows that

$$\mathfrak{R}\{e^{-x^2 - y^2 - z^2}\} = \sqrt{\pi} e^{-p^2}. \quad (8.49)$$

#### Example 8.5

If the results of the previous example are extended on  $n$  dimensions, then

$$\mathfrak{R}\{\exp(-x_1^2 - \dots - x_n^2)\} = (\sqrt{\pi})^{n-1} e^{-p^2}. \quad (8.50)$$

#### Example 8.6

Start with  $f(x, y) = \exp(-x^2 - y^2)$  and apply Equation 8.47 with  $n = 2$  and  $c = 1/\sigma\sqrt{2}$ . This yields the Radon transform of the symmetric Gaussian probability density function. Note that

$$f(A\mathbf{x}) = \exp\left(-\frac{x^2}{2\sigma^2} - \frac{y^2}{2\sigma^2}\right)$$

and

$$\frac{1}{c} \tilde{f}(cp, \xi) = \sigma\sqrt{2\pi} e^{-p^2/2\sigma^2}.$$

An overall division by  $2\pi\sigma^2$  yields the standard form,

$$\begin{aligned} \Re \left\{ \frac{1}{2\pi\sigma^2} \exp\left(-\frac{x^2}{2\sigma^2} - \frac{y^2}{2\sigma^2}\right) \right\} \\ = \frac{1}{\sigma\sqrt{2\pi}} \exp\left(-\frac{p^2}{2\sigma^2}\right) \end{aligned} \quad (8.51)$$

**Example 8.7**

The problem here is to find the Radon transform of

$$\exp\left[-\left(\frac{x}{a}\right)^2 - \left(\frac{y}{b}\right)^2\right]$$

with both  $a$  and  $b$  real. Again, the starting function is selected to be

$$f(x, y) = e^{-x^2 - y^2}.$$

Now we use Equation 8.45 with

$$B = \begin{pmatrix} a & 0 \\ 0 & b \end{pmatrix}, \quad B^{-1} = \begin{pmatrix} \frac{1}{a} & 0 \\ 0 & \frac{1}{b} \end{pmatrix}, \quad |\det B| = |ab|.$$

In this example

$$B^T \xi = \begin{pmatrix} a \cos \phi \\ b \sin \phi \end{pmatrix}$$

is not a unit vector, having magnitude

$$s = (a^2 \cos^2 \phi + b^2 \sin^2 \phi)^{1/2}.$$

With these observations, Equation 8.45 yields

$$\Re \left\{ \exp\left[-\left(\frac{x}{a}\right)^2 - \left(\frac{y}{b}\right)^2\right] \right\} = \frac{|ab|\sqrt{\pi}}{s} \exp\left(-\frac{p^2}{s^2}\right). \quad (8.52)$$

Note that once the symmetry is lost in feature space the angle  $\phi$  appears in the transform.

**Example 8.8**

Use the similarity theorem to obtain Equation 8.52. Application of Equation 8.22 with

$$f(x, y) = e^{-x^2 - y^2} \quad \text{and} \quad \tilde{f}(p, \xi) = \sqrt{\pi} e^{-p^2}$$

yields

$$\Re f\left(\frac{x}{a}, \frac{y}{b}\right) = |ab| \tilde{f}\left(p, \frac{\xi_1}{a}, \frac{\xi_2}{b}\right)$$

This is not in the desired form, so we let  $\mu = (a\xi_1/s, b\xi_2/s)$  with  $s$  defined as in the previous example so  $\mu$  is a unit vector. Now the right side of the above equation becomes

$$|ab| \tilde{f}(p, s\mu) = \frac{|ab|}{s} \tilde{f}\left(\frac{p}{s}, \mu\right) = \frac{|ab|\sqrt{\pi}}{s} \exp\left(-\frac{p^2}{s^2}\right) \quad (8.53)$$

as in the previous example.

**Example 8.9**

Find the Radon transform of the characteristic function of a unit disk, sometimes called the cylinder function,  $\text{cyl}(r)$ . This function is given by

$$f(x, y) = \begin{cases} 1, & \text{for } x^2 + y^2 \leq 1 \\ 0, & \text{for } x^2 + y^2 > 1. \end{cases} \quad (8.54a)$$

By inspection, the transform is given by the length of a chord at a distance  $p$  from the center and is independent of the angle  $\phi$ ,

$$\tilde{f}(p, \phi) = \begin{cases} 2(1 - p^2)^{1/2}, & \text{for } p \leq 1 \\ 0, & \text{for } p > 1. \end{cases} \quad (8.54b)$$

**Example 8.10**

Find the Radon transform of the characteristic function of an ellipse where  $f$  is given by

$$f(x, y) = \begin{cases} 1, & \text{for } (x/a)^2 + (y/b)^2 \leq 1 \\ 0, & \text{for } (x/a)^2 + (y/b)^2 > 1. \end{cases} \quad (8.55a)$$

If the matrix  $B$  is selected as in Example 8.7 above, then from the result in Example 8.9 it follows immediately that

$$\tilde{f}(p, \phi) = \begin{cases} \frac{2|ab|}{s} \left[1 - \left(\frac{p}{s}\right)^2\right]^{1/2}, & \text{for } \frac{|p|}{s} \leq 1 \\ 0, & \text{for } \frac{|p|}{s} > 1 \end{cases} \quad (8.55b)$$

where  $s = (a^2 \cos^2 \phi + b^2 \sin^2 \phi)^{1/2}$ .

**Example 8.11**

Use the method of Example 8.3 to find a general expression for the Radon transform of a function defined on the unit disk,

and zero outside the unit disk. From the matrix in A Example 8.3, it follows that (see Figure 8.4 with  $(p, t) \rightarrow (u, v)$ )

$$x = u \cos \phi - v \sin \phi \quad \text{and} \quad y = u \sin \phi + v \cos \phi.$$

Therefore,

$$\begin{aligned} \check{f}(p, \phi) &= \int_{\text{disk}} f(x, y) \delta(p - x \cos \phi - y \sin \phi) dx dy \\ &= \int_{\text{disk}} f(u \cos \phi - v \sin \phi, u \sin \phi + v \cos \phi) \delta(p - u) du dv. \end{aligned}$$

After the integration over  $u$ ,

$$\check{f}(p, \phi) = \int_{-\sqrt{1-p^2}}^{\sqrt{1-p^2}} f(p \cos \phi - v \sin \phi, p \sin \phi + v \cos \phi) dv. \tag{8.56}$$

**Example 8.12**

Find the Radon transform over the unit square, situated as indicated in Figure 8.5. It is adequate to consider the transform for  $0 < \phi \leq \pi/4$ .

$$\check{f}(p, \phi) = \begin{cases} \frac{p}{\sin \phi \cos \phi} & \text{for region 1, } 0 < p < \sin \phi \\ \sec \phi & \text{for region 2, } \sin \phi < p < \cos \phi \\ \frac{\sin \phi + \cos \phi - p}{\sin \phi \cos \phi} & \text{for region 3, } \cos \phi < p < \sin \phi + \cos \phi. \end{cases} \tag{8.57a}$$

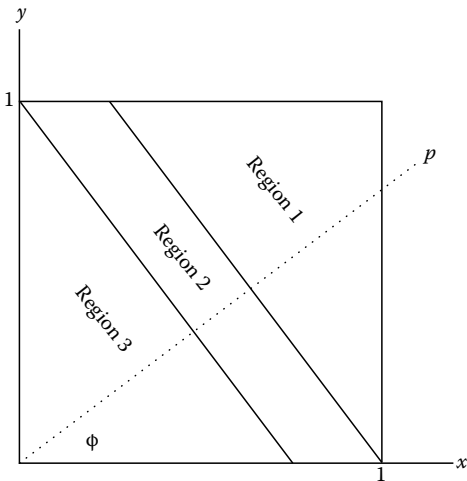


FIGURE 8.5 Coordinates for unit square with regions defined as  $p$  varies along dotted line.

By symmetry, for  $\pi/4 \leq \phi < \pi/2$ ,

$$\check{f}(p, \phi) = \begin{cases} \frac{p}{\sin \phi \cos \phi} & \text{for region 1, } 0 < p < \cos \phi \\ \csc \phi & \text{for region 2, } \cos \phi < p < \sin \phi \\ \frac{\sin \phi + \cos \phi - p}{\sin \phi \cos \phi} & \text{for region 3, } \sin \phi < p < \sin \phi + \cos \phi. \end{cases} \tag{8.57b}$$

**Example 8.13**

The shift theorem from Section 8.3.4 can be written as

$$\mathfrak{R}\{f(\mathbf{x} - \mathbf{a})\} = \check{f}(p - p_0, \xi), \quad \text{with } p_0 = \xi \cdot \mathbf{a}.$$

Apply this equation with

$$\mathbf{a} = (a, b) \quad \text{and} \quad p_0 = a \cos \phi + b \sin \phi$$

to the result of Example 8.6 above. This gives the transform of a 2D Gaussian density function

$$\begin{aligned} \mathfrak{R}\left\{ \frac{1}{2\pi\sigma^2} \exp\left(-\frac{(x-a)^2}{2\sigma^2} - \frac{(y-b)^2}{2\sigma^2}\right) \right\} \\ = \frac{1}{\sigma\sqrt{2\pi}} \exp\left(-\frac{(p-p_0)^2}{2\sigma^2}\right). \end{aligned} \tag{8.58}$$

Again, note that the loss of rotational symmetry about the origin in feature space causes the function in Radon space to have explicit dependence of the angle  $\phi$ .

**Example 8.14**

In the previous example, if the limit  $\sigma \rightarrow +0$  is taken, both sides are convergent  $\delta$  sequences.

$$\mathfrak{R}\{\delta(x-a)\delta(y-b)\} = \delta(p-p_0), \tag{8.59}$$

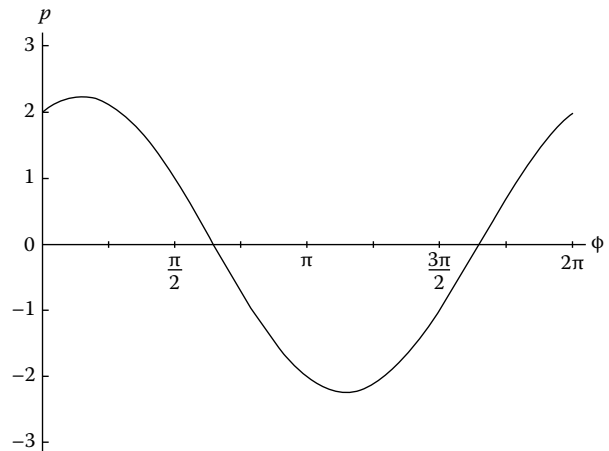


FIGURE 8.6 The impulse function maps to a sinusoidal curve.

with  $p_0 = a \cos \phi + b \sin \phi$ . This result also follows easily by substitution of

$$f(x, y) = \delta(x - a)\delta(y - b) \equiv \delta(x - a, y - b)$$

into the definition of the Radon transform, Section 8.2.5. This example has some special significance because it demonstrates how an impulse function centered at  $(a, b)$  in feature space transforms to Radon space. In Radon space  $(p, \phi)$  there is an impulse function everywhere along a sinusoidal curve with the equation of the curve given by

$$p = a \cos \phi + b \sin \phi. \tag{8.60}$$

An illustration is given in Figure 8.6 for  $p = 2 \cos \phi + \sin \phi$ .

**Example 8.15**

Another way to approach the transform of the delta function is to observe that for the delta function centered at the origin  $\delta(x, y) = \delta(p, t)$ . Then, in the rotated system (see Figure 8.4) it follows that

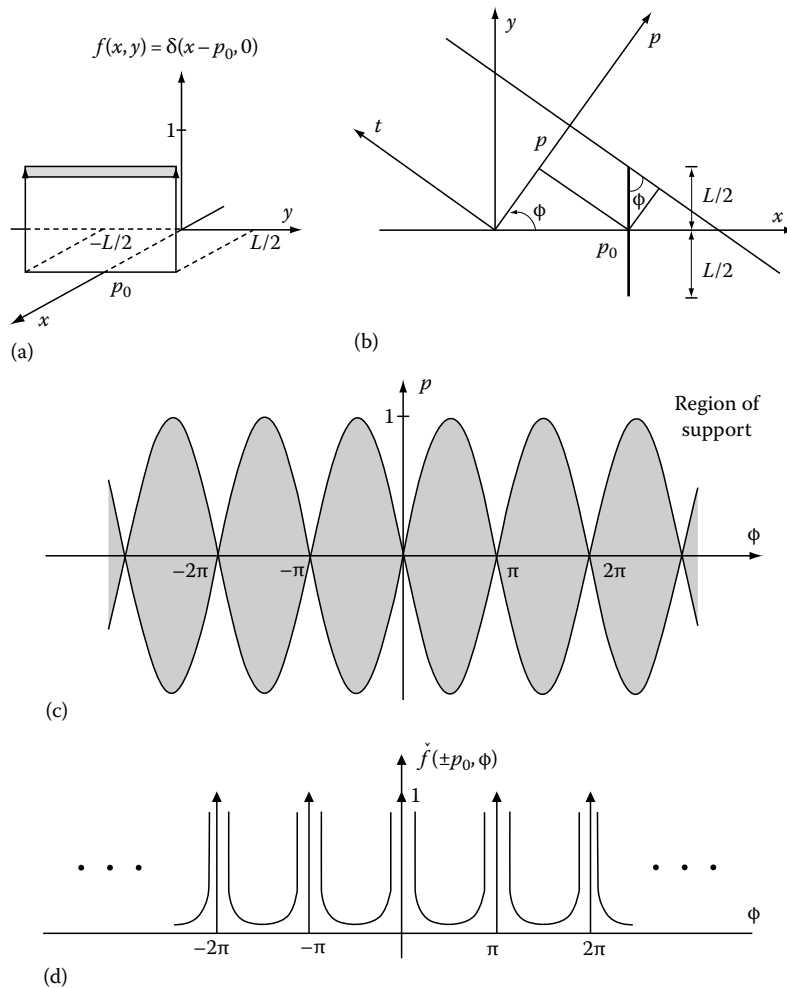


FIGURE 8.7 Radon transform of finite-extended delta function.

$$\int_{-\infty}^{\infty} \delta(p, t) dt = \delta(p).$$

This result can be used to obtain the transform of the shifted delta function. By use of Section 8.3.4 it follows that Equation 8.59 holds. If  $\phi_0 = \tan^{-1} \frac{b}{a}$  and  $r_0 = \sqrt{a^2 + b^2}$ , then  $p_0 = r_0 \cos(\phi_0 - \phi)$  and

$$\mathfrak{R}\{\delta(x - a, y - b)\} = \delta[p - r_0 \cos(\phi_0 - \phi)].$$

As with the example in Figure 8.6, the region of support for the delta function is a sinusoidal curve in Radon space.

**Example 8.16**

Find the Radon transform of a finite-extended delta function (see Figure 8.7a),

$$f(x, y) = \begin{cases} \delta(x - p_0), & \text{for } |y| < L/2 \\ 0, & \text{for } |y| \geq L/2. \end{cases}$$



We write

$$\begin{aligned} \tilde{f}(p, \phi) &= \int_{-\frac{L}{2}}^{\frac{L}{2}} \delta(p \cos \phi - t \sin \phi - p_0) dt \\ &= \begin{cases} L\delta(p - p_0), & \text{for } \phi = 2n\pi \\ L\delta(p + p_0), & \text{for } \phi = (2n + 1)\pi. \end{cases} \end{aligned}$$

However, if the angle  $\phi$  is different from a multiple of  $\pi$ , then we obtain (see Section 1.2)

$$\tilde{f}(p, \phi) = \begin{cases} |\sin \phi|^{-1}, & \text{for } |p - p_0 \cos \phi| \leq \frac{L}{2} \sin \phi \\ 0, & \text{otherwise.} \end{cases}$$

The inequality can be deduced from the geometry of Figure 8.7b. The region of support is shown in Figure 8.7c and the transform is illustrated in Figure 8.7d.

This example illustrates a useful property of the Radon transform; namely, its ability to serve as an instrument for the detection of line segments in images. A slightly more general version of this example is given by Deans (1985).

**Example 8.17**

Find the Radon transform of the cylinder function defined in Example 8.9 displaced at the point  $(x_0, y_0)$  as shown in Figure 8.8a. The solution follows immediately from the solution of Example 8.9 combined with the shifting property

in Section 8.3.4. Also, the solution can be deduced from the geometry in Figure 8.8a. When  $d = 1$ , the length  $t = 0$ ; also, for  $p$  such that the line of integration passes through the cylinder,

$$t = 2\sqrt{1 - [p - r_0 \cos(\phi_0 - \phi)]^2}.$$

Further, when  $\phi$  varies, the values  $p$  can assume follow from the geometry. The transform is

$$\tilde{f}(p, \phi) = \begin{cases} 2\sqrt{1 - [p - r_0 \cos(\phi_0 - \phi)]^2}, & -1 + r_0 \cos(\phi_0 - \phi) \leq p \leq 1 + r_0 \cos(\phi_0 - \phi) \\ 0, & \text{otherwise.} \end{cases}$$

Figure 8.8b shows the (sinusoidal) region of support of the transform.

**Example 8.18**

Suppose the points in feature space lie along a line defined by parameters  $p_0$  and  $\phi_0$  as indicated in Figure 8.9. All of these collinear points map to sinusoidal curves in Radon space; moreover, these curves all intersect at the same point  $(p_0, \phi_0)$  in Radon space. By selecting an appropriate threshold and only plotting values of  $\tilde{f}$  above the threshold it follows that a single point in Radon space serves to identify a line of collinear points in feature space. It is in this sense that the Radon transform is sometimes regarded as a line-to-point transformation. This idea has been used by various authors

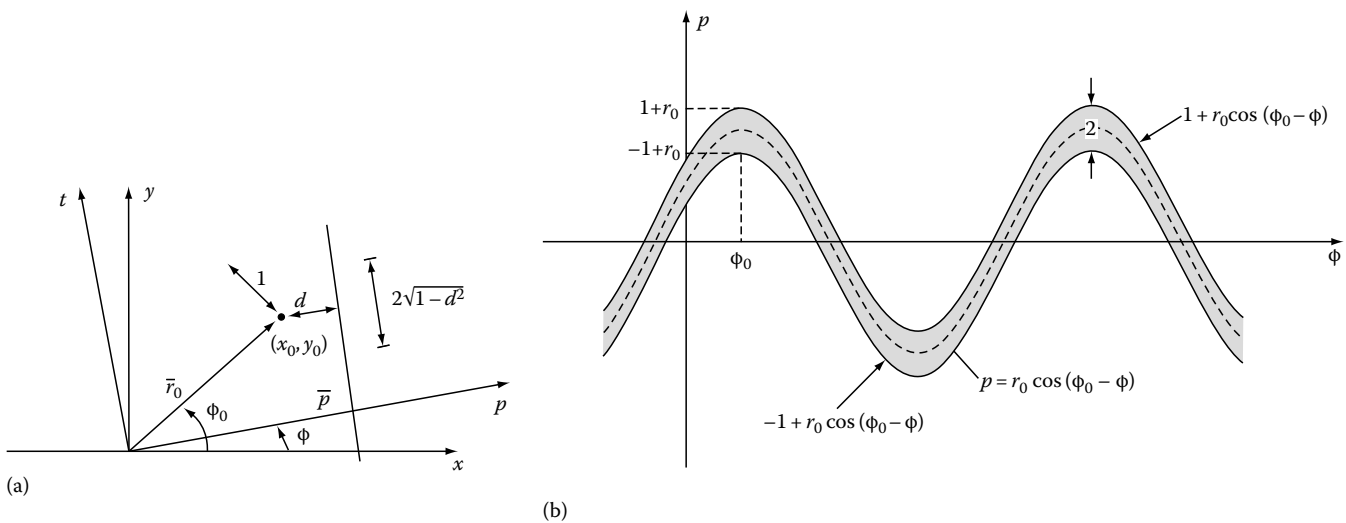
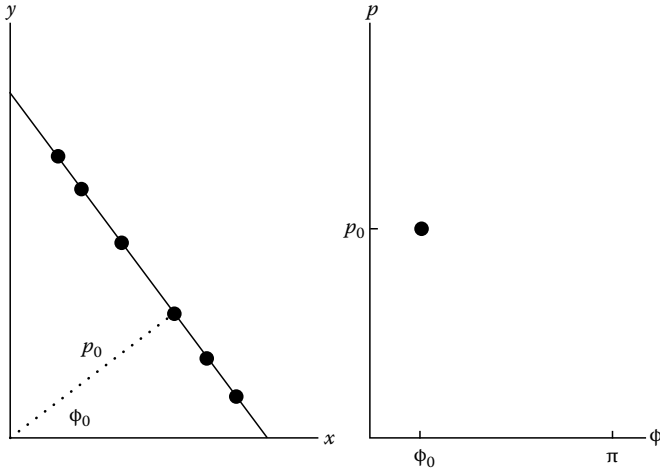


FIGURE 8.8 Displaced cylinder function and region of support of the transform.



**FIGURE 8.9** After thresholding, a single point in Radon space corresponds to a line in feature space.

interested in detecting lines in digital images: Duda and Hart (1972) and Shapiro and Iannino (1979). When the Radon transform is used in this fashion, it is often referred to as the Hough transform after the work of Hough (1962).

## 8.6 More on Derivatives

In Section 8.3.5 basic equations were given for the Radon transform of derivatives in two dimensions. Clearly, these results can be generalized and it is useful to do that, especially in connection with using the Radon transform in connection with partial differential equations and series expansions. Another use of derivatives is related to the derivatives of the Radon transform. Both of these cases are covered in this section.

### 8.6.1 Transform of Derivatives

Let  $f(\mathbf{x}) = f(x_1, \dots, x_n)$ . The generalization of Equations 8.29a and b is

$$\mathfrak{R}\left\{\frac{\partial f}{\partial x_k}\right\} = \xi_k \frac{\partial \tilde{f}(p, \xi)}{\partial p} \quad (8.61)$$

where  $\xi_k$  is the  $k$ th component of the unit vector  $\xi$ . The linearity property (Equation 8.20) can be used to find the transform of the sum

$$\sum_{k=1}^n a_k \frac{\partial f}{\partial x_k}$$

for arbitrary constants  $a_k$ . If the constants are components of the vector  $\mathbf{a}$ , then

$$\mathfrak{R}\left\{\sum_{k=1}^n a_k \frac{\partial f}{\partial x_k}\right\} = (\mathbf{a} \cdot \xi) \frac{\partial \tilde{f}(p, \xi)}{\partial p}. \quad (8.62)$$

#### Example 8.19

Let  $n = 3$ , and let  $\nabla$  be the gradient operator ( $\partial/\partial x_1, \partial/\partial x_2, \partial/\partial x_3$ ). Now Equation 8.62 is interpreted as the Radon transform of a directional derivative.

$$\mathfrak{R}\{\mathbf{a} \cdot \nabla f\} = (\mathbf{a} \cdot \xi) \frac{\partial \tilde{f}(p, \xi)}{\partial p}. \quad (8.63)$$

Another obvious generalization from Section 8.3.5 is

$$\mathfrak{R}\left\{\frac{\partial^2 f}{\partial x_l \partial x_k}\right\} = \xi_l \xi_k \frac{\partial^2 \tilde{f}(p, \xi)}{\partial p^2}. \quad (8.64)$$

Consequently, for arbitrary constant vectors  $\mathbf{a}$  and  $\mathbf{b}$ ,

$$\mathfrak{R}\left\{\sum_{l=1}^n \sum_{k=1}^n a_l b_k \frac{\partial^2 f}{\partial x_l \partial x_k}\right\} = (\mathbf{a} \cdot \xi)(\mathbf{b} \cdot \xi) \frac{\partial^2 \tilde{f}(p, \xi)}{\partial p^2} \quad (8.65)$$

#### Example 8.20

There is a very important special case of the last equation. Suppose the product  $a_l b_k$  reduces to the Kronecker delta,

$$a_l b_k = \delta_{lk} = \begin{cases} 1, & \text{for } l = k \\ 0, & \text{for } l \neq k. \end{cases}$$

Now the operator is just the Laplacian operator

$$\nabla^2 = \frac{\partial^2}{\partial x_1^2} + \dots + \frac{\partial^2}{\partial x_n^2}$$

and

$$\mathfrak{R}\{\nabla^2 f(\mathbf{x})\} = |\xi|^2 \frac{\partial^2 \tilde{f}(p, \xi)}{\partial p^2} = \frac{\partial^2 \tilde{f}(p, \xi)}{\partial p^2}. \quad (8.66)$$

Note that  $|\xi| = 1$  has been used.

Results of this type have been used by John (1955) in applications of the Radon transform to partial differential equations.

**Example 8.21**

Suppose  $f$  is a function of both time and space variables. For example, if  $n=3$ , then  $f=f(x,y,z,t)$ . The wave equation in three dimensions is given by

$$\frac{\partial^2 f}{\partial x^2} + \frac{\partial^2 f}{\partial y^2} + \frac{\partial^2 f}{\partial z^2} = \frac{\partial^2 f}{\partial t^2}. \quad (8.67)$$

Because the operator  $\mathfrak{R}$  does not involve time, it must commute with the time derivative operator  $\partial/\partial t$ . Thus, the Radon transform of the wave equation yields

$$\frac{\partial^2 \tilde{f}}{\partial p^2} = \frac{\partial^2 \tilde{f}}{\partial t^2} \quad (8.68)$$

where it is understood that  $\tilde{f}$  now depends on time,  $\tilde{f} = \tilde{f}(p, \xi; t) = \mathfrak{R}\{f(x,y,z,t)\}$ . The important significance is that the wave equation in three spatial dimensions has been reduced to a wave equation in one spatial dimension.

**8.6.2 Derivatives of the Transform**

Here we investigate what happens when  $\tilde{f}$  is differentiated with respect to one of the components of the unit vector  $\xi$ . To facilitate this, an identity related to derivatives of the delta function is needed. First, note that

$$\frac{\partial}{\partial y} \delta(x-y) = -\frac{\partial}{\partial x} \delta(x-y)$$

and if  $y$  is replaced by  $ay$ ,

$$\frac{\partial}{\partial(ay)} \delta(x-ay) = \frac{1}{a} \frac{\partial}{\partial y} \delta(x-ay) = -\frac{\partial}{\partial x} \delta(x-ay).$$

In  $n$  dimensions

$$\frac{\partial}{\partial y_j} \delta(\mathbf{x}-\mathbf{y}) = -\frac{\partial}{\partial x_j} \delta(\mathbf{x}-\mathbf{y}).$$

From these equations it is easy to see that

$$\frac{\partial}{\partial \eta_j} \delta(p - \boldsymbol{\eta} \cdot \mathbf{x}) = -x_j \frac{\partial}{\partial p} \delta(p - \boldsymbol{\eta} \cdot \mathbf{x}). \quad (8.69)$$

This identity is in terms of  $\boldsymbol{\eta} \cdot \mathbf{x}$  where  $\boldsymbol{\eta}$  must not be restricted to being a unit vector; however, the desired derivatives are in terms of components of the unit vector  $\xi$ . The way to deal with this is to

take derivatives with respect to components of  $\boldsymbol{\eta}$  and then evaluate the results at  $\boldsymbol{\eta} = \xi$ . This prescription is followed starting with

$$\begin{aligned} \tilde{f}(p, \boldsymbol{\eta}) &= \int f(\mathbf{x}) \delta(p - \boldsymbol{\eta} \cdot \mathbf{x}) d\mathbf{x}, \\ \frac{\partial \tilde{f}}{\partial \xi_k} &= \left[ \frac{\partial \tilde{f}(p, \boldsymbol{\eta})}{\partial \eta_k} \right]_{\boldsymbol{\eta}=\xi} = \left[ \int f(\mathbf{x}) \frac{\partial}{\partial \eta_k} \delta(p - \boldsymbol{\eta} \cdot \mathbf{x}) d\mathbf{x} \right]_{\boldsymbol{\eta}=\xi} \\ &= -\frac{\partial}{\partial p} \int x_k f(\mathbf{x}) \delta(p - \xi \cdot \mathbf{x}) d\mathbf{x}. \end{aligned}$$

This gives the desired formula,

$$\frac{\partial \tilde{f}}{\partial \xi_k} = \left[ \frac{\partial}{\partial \eta_k} \mathfrak{R}\{f(\mathbf{x})\} \right]_{\boldsymbol{\eta}=\xi} = -\frac{\partial}{\partial p} \mathfrak{R}\{x_k f(\mathbf{x})\}. \quad (8.70)$$

**Convention:** Whenever the transformed function  $\tilde{f}$  is differentiated with respect to a component of the unit vector  $\xi$ , it is understood that

$$\frac{\partial \tilde{f}(p, \xi)}{\partial \xi_k} \equiv \left[ \frac{\partial \tilde{f}(p, \boldsymbol{\eta})}{\partial \eta_k} \right]_{\boldsymbol{\eta}=\xi}. \quad (8.71)$$

The following example clearly illustrates the need for caution when taking derivatives of  $f$ .

**Example 8.22**

Start with

$$f(x,y) = e^{-x^2-y^2} \quad \text{and} \quad \tilde{f}(p, \xi) = \sqrt{\pi} e^{-p^2}.$$

Apply the scaling relation (Equation 8.26) with

$$\boldsymbol{\eta} = s\xi \quad \text{and} \quad s = (\eta_1^2 + \eta_2^2)^{1/2},$$

to obtain

$$\tilde{f}(p, \boldsymbol{\eta}) = \tilde{f}(p, s\xi) = \frac{\sqrt{\pi}}{s} e^{-p^2/s^2}.$$

Now use

$$\frac{\partial}{\partial \eta_k} = \frac{\partial s}{\partial \eta_k} \frac{\partial}{\partial s}, \quad (k=1,2),$$

to get

$$\begin{aligned} \frac{\partial \tilde{f}}{\partial \eta_k} &= \sqrt{\pi} \frac{\eta_k}{s} \frac{\partial}{\partial s} (s^{-1} e^{-p^2/s^2}) \\ &= \sqrt{\pi} \frac{\eta_k}{s^2} (2p^2 - s^2) e^{-p^2/s^2}. \end{aligned}$$

The desired derivative is found when this expression is evaluated at  $\boldsymbol{\eta} = \boldsymbol{\xi}$ , or equivalently for  $s = 1$ ,

$$\frac{\partial \tilde{f}}{\partial \xi_k} = \sqrt{\pi} \xi_k (2\rho^2 - 1) e^{-\rho^2}.$$

The significance of this result becomes more apparent when compared with Example 8.27 in Section 8.7.

### Example 8.23

In Example 8.43 of Section 8.13 it is shown that the Radon transform of  $x^2 + y^2$  confined to the unit disk and zero outside the disk is given by

$$\mathfrak{R}\{x^2 + y^2\} = \frac{2}{3} \sqrt{1 - \rho^2} (1 + 2\rho^2),$$

and in Example 8.45 of the same section

$$\mathfrak{R}\{x(x^2 + y^2)\} = \frac{2}{3} \rho \sqrt{1 - \rho^2} (1 + 2\rho^2) \cos \phi.$$

It is left as an exercise for the reader to demonstrate that Equation 8.70 is satisfied by this pair of transforms. That is, verify that

$$\left[ \frac{\boldsymbol{\eta}_1}{s} \frac{\partial \tilde{f}(p, \boldsymbol{\eta})}{\partial s} \right]_{\boldsymbol{\eta}=\boldsymbol{\xi}} = -\frac{\partial}{\partial p} \mathfrak{R}\{x(x^2 + y^2)\},$$

where

$$\tilde{f}(p, \boldsymbol{\eta}) = \frac{2}{3} s^{-4} \sqrt{s^2 - p^2} (s^2 + 2p^2).$$

This can be done by showing that both sides reduce to

$$\frac{2}{3} \cos \phi (1 - \rho^2)^{-1/2} (8\rho^4 - 4\rho^2 - 1).$$

There are some rather obvious generalizations for derivatives of higher order. These results follow immediately by differentiating Equation 8.70; it is understood that the convention (Equation 8.71) always applies. For second derivatives

$$\frac{\partial^2 \tilde{f}(p, \boldsymbol{\xi})}{\partial \xi_i \partial \xi_k} = \frac{\partial^2}{\partial p^2} \mathfrak{R}\{x_i x_k f(\mathbf{x})\}. \quad (8.72)$$

For higher derivatives the procedure is to differentiate this expression. For example, one of the third derivatives is given by

$$\frac{\partial^3 \tilde{f}(p, \boldsymbol{\xi})}{\partial \xi_i \partial \xi_k^2} = \frac{\partial^3}{\partial p^3} \mathfrak{R}\{x_i x_k^2 f(\mathbf{x})\}. \quad (8.73)$$

Note that there is an alternating sign, + for even derivatives and – for odd derivatives. One final example is given here. Additional examples involving derivatives are given in Section 8.7.

### Example 8.24

If  $f = f(x, y)$  is a 2D function, a generalization of Equation 8.73 to arbitrarily high derivatives provides a method for finding many additional transforms of functions in two dimensions,

$$\frac{\partial^{l+k} \tilde{f}(p, \boldsymbol{\xi})}{\partial \xi_1^l \partial \xi_2^k} = \left( -\frac{\partial}{\partial p} \right)^{l+k} \mathfrak{R}\{x^l y^k f(x, y)\}. \quad (8.74)$$

## 8.7 Hermite Polynomials

In this section the discussion is confined to two dimensions, and the components of  $\boldsymbol{\xi}$  are written as  $(\xi_1, \xi_2) = (\cos \phi, \sin \phi)$  to emphasize the dependence of the transform on  $\phi$ . The extension to higher dimensions does not involve complications except that the formulas contain more variables. The previous section on derivatives can be used to find transforms of functions of the form

$$H_l(x) H_k(y) e^{-x^2 - y^2}$$

where  $H_l$  and  $H_k$  are Hermite polynomials of order  $l$  and  $k$ , respectively. More information on these polynomials is contained in Appendix 8.A of this chapter and in Section 1.5.

We start with the Rodrigues formula for Hermite polynomials (Rainville 1960),

$$e^{-x^2} H_l(x) = (-1)^l \left( \frac{\partial}{\partial x} \right)^l e^{-x^2}. \quad (8.75)$$

A similar formula holds for the variable  $y$ . When these are combined, the joint formula is

$$H_l(x) H_k(y) e^{-x^2 - y^2} = (-1)^{l+k} \left( \frac{\partial}{\partial x} \right)^l \left( \frac{\partial}{\partial y} \right)^k e^{-x^2 - y^2}. \quad (8.76)$$

From the methods developed in Section 8.6, we deduce that

$$\mathfrak{R} \left\{ \left( \frac{\partial}{\partial x} \right)^l \left( \frac{\partial}{\partial y} \right)^k f(x, y) \right\} = (\cos \phi)^l (\sin \phi)^k \left( \frac{\partial}{\partial p} \right)^{l+k} \tilde{f}(p, \boldsymbol{\xi}).$$

By using this derivative relation, it follows that the Radon transform of the Rodrigues formula gives

$$\mathfrak{R}\{H_l(x) H_k(y) e^{-x^2 - y^2}\} = (-1)^{l+k} (\cos \phi)^l (\sin \phi)^k \left( \frac{\partial}{\partial p} \right)^{l+k} \sqrt{\pi} e^{-p^2}.$$

By application of the Rodrigues formula in one variable to the right side of this equation, the basic formula for transforms of Hermite polynomials is

$$\mathfrak{R}\{H_l(x) H_k(y) e^{-x^2 - y^2}\} = \sqrt{\pi} (\cos \phi)^l (\sin \phi)^k e^{-p^2} H_{l+k}(p). \quad (8.77)$$

The importance of the last equation becomes more apparent after observing that members of the sequence

$$1, x, y, x^2, xy, y^2, \dots, x^l y^k, \dots$$

can be expressed in terms of Hermite polynomials. Some examples are given to illustrate the way transforms of members of this sequence are found.

### Example 8.25

Find the Radon transform of  $xy^2 e^{-x^2-y^2}$ . From Appendix 8.A,

$$xy^2 = \frac{1}{8}H_1(x)H_2(y) + \frac{1}{4}H_1(x)H_0(y).$$

It follows immediately from the fundamental relation (Equation 8.77) that

$$\begin{aligned} \mathfrak{R}\{xy^2 e^{-x^2-y^2}\} &= \frac{\sqrt{\pi}}{8}[\cos \phi \sin^2 \phi H_3(p) \\ &\quad + 2 \cos \phi H_1(p)]e^{-p^2}. \end{aligned} \quad (8.78)$$

This result can be modified by using explicit expressions for the Hermite polynomials, from Appendix 8.A,

$$\begin{aligned} \mathfrak{R}\{xy^2 e^{-x^2-y^2}\} &= \frac{\sqrt{\pi}}{2}e^{-p^2}[2p^3 \cos \phi \sin^2 \phi \\ &\quad + p \cos \phi (1 - 3 \sin^2 \phi)]. \end{aligned} \quad (8.79)$$

### Example 8.26

The method used for the previous example can be applied to obtain some basic results; then other theorems can be applied to get easy extensions. The linear property is especially useful. Given that

$$\mathfrak{R}\{x e^{-x^2-y^2}\} = \sqrt{\pi} p e^{-p^2} \cos \phi. \quad (8.80)$$

By just changing  $x$  to  $y$  and  $\cos \phi$  to  $\sin \phi$  it follows that

$$\mathfrak{R}\{y e^{-x^2-y^2}\} = \sqrt{\pi} p e^{-p^2} \sin \phi. \quad (8.81)$$

Now, by linearity

$$\mathfrak{R}\{(x+y)e^{-x^2-y^2}\} = \sqrt{\pi} p e^{-p^2} (\cos \phi + \sin \phi). \quad (8.82)$$

The same technique can be applied to obtain:

$$\mathfrak{R}\{x^2 e^{-x^2-y^2}\} = \frac{\sqrt{\pi}}{2}(2p^2 \cos^2 \phi + \sin^2 \phi)e^{-p^2}; \quad (8.83)$$

$$\mathfrak{R}\{y^2 e^{-x^2-y^2}\} = \frac{\sqrt{\pi}}{2}(2p^2 \sin^2 \phi + \cos^2 \phi)e^{-p^2}; \quad (8.84)$$

$$\mathfrak{R}\{(x^2 + y^2)e^{-x^2-y^2}\} = \frac{\sqrt{\pi}}{2}(2p^2 + 1)e^{-p^2}. \quad (8.85)$$

### Example 8.27

It is instructive to relate the transforms in the last example to earlier results. We focus attention on formula (Equation 8.80),

$$\mathfrak{R}\{x e^{-x^2-y^2}\} = \sqrt{\pi} p e^{-p^2} \cos \phi.$$

From Example 8.22 of Section 8.6.2 with  $k=1$ ,

$$\frac{\partial \tilde{f}}{\partial \xi_1} = \sqrt{\pi} \cos \phi (2p^2 - 1) e^{-p^2}.$$

Now, from formula (Equation 8.70) it should be true that this is the same as

$$-\frac{\partial}{\partial p} \left\{ \sqrt{\pi} p e^{-p^2} \right\},$$

and, of course, the consistency is verified by doing the differentiation. This explicitly demonstrates that

$$\frac{\partial \tilde{f}}{\partial \xi_1} = -\frac{\partial}{\partial p} \mathfrak{R}\{x e^{-x^2-y^2}\}.$$

### Example 8.28

It is easy to find the extension of Equation 8.77 for scaled variables. By use of Equation 8.22 with  $a=b=c$ ,

$$\mathfrak{R}\left\{H_l(cx)H_k(cy)e^{-c^2(x^2+y^2)}\right\} = \frac{\sqrt{\pi}}{c}(\cos \phi)^l(\sin \phi)^k e^{-c^2 p^2} H_{l+k}(cp). \quad (8.86)$$

## 8.8 Laguerre Polynomials

Here, a very brief introduction to transforms of Laguerre polynomials is given. A much more extensive treatment is given by Deans (1983, 1993), where several examples and applications are provided. Additional applications are contained in the work by Maldonado and Olsen (1966) and Louis (1985). As in the previous section, the discussion is confined to two dimensions and the angle  $\phi$  appears explicitly in the transform. The approach is the same as with the Hermite polynomials. We start with the Rodrigues formula for the Laguerre polynomials (Szegő, 1939; Rainville, 1960),

$$e^{-t} t^l L_k^l(t) = \frac{1}{k!} \left( \frac{\partial}{\partial t} \right)^k e^{-t} t^{l+k}, \quad (8.87)$$

and derive a generalized expression that accommodates the Radon transform,

$$\begin{aligned} \left( \frac{\partial}{\partial x} \pm i \frac{\partial}{\partial y} \right)^l \left( \frac{\partial^2}{\partial x^2} + \frac{\partial^2}{\partial y^2} \right)^k e^{-x^2-y^2} \\ = (-1)^{l+k} 2^{2k+l} k! (x \pm iy)^l e^{-x^2-y^2} L_k^l(x^2 + y^2). \end{aligned} \quad (8.88)$$

From the two previous sections, the Radon transform of the left side is

$$\begin{aligned} & \mathfrak{R} \left\{ \left( \frac{\partial}{\partial x} \pm i \frac{\partial}{\partial y} \right)^l \left( \frac{\partial^2}{\partial x^2} \pm \frac{\partial^2}{\partial y^2} \right)^k e^{-x^2-y^2} \right\} \\ &= (-1)^{2k+l} \sqrt{\pi} e^{\pm il\phi} e^{-p^2} H_{l+2k}(p), \end{aligned}$$

leading to the expression

$$\begin{aligned} & \mathfrak{R} \left\{ (-1)^k 2^{2k+l} k! (x \pm iy)^l e^{-x^2-y^2} L_k^l(x^2 + y^2) \right\} \\ &= \sqrt{\pi} e^{\pm il\phi} e^{-p^2} H_{l+2k}(p). \end{aligned} \quad (8.89)$$

A more standard form is obtained by making substitutions,

$$x^2 + y^2 = r^2, \quad (x \pm iy)^l = (x^2 + y^2)^{l/2} e^{\pm il\theta} \quad \text{with } \theta = \tan^{-1} \left( \frac{y}{x} \right),$$

and defining a normalization constant by

$$N_k^l = \frac{1}{2^{2k+l}} \left[ \frac{1}{k!(l+k)!} \right]^{1/2}. \quad (8.90)$$

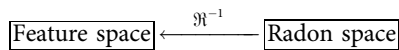
These changes lead to the standard form for the transform of expressions that involve Laguerre polynomials,

$$\begin{aligned} & \mathfrak{R} \left\{ (-1)^k \left[ \frac{k!}{(l+k)!} \right]^{1/2} r^l e^{\pm il\theta} L_k^l(r^2) \right\} \\ &= N_k^l e^{\pm il\phi} e^{-p^2} H_{l+2k}(p). \end{aligned} \quad (8.91)$$

## 8.9 Inversion

Inversion of the Radon transform is especially important because it yields information about an object in feature space when some probe has been used to produce projection data. This inversion is the solution of the problem of “reconstruction from projections” when the projections can be interpreted as the Radon transform of some function in feature space.

There are several routes that can be followed to go from Radon space to feature space. The direct route illustrated by the diagram



is probably the most difficult to derive and certainly the most difficult to implement in practical situations; however, see the alternative method used by Nievergelt (1986). The direct method is discussed in some detail by John (1955) and Deans (1983, 1993).

For those already familiar with Fourier transforms, the route through Fourier space pioneered by Bracewell (1956) may be easier. Other important early references include Helgason (1965)

and Ludwig (1966). The route from feature space to Fourier space and the route from Radon space to Fourier space is discussed in Section 8.2.5. The basic ideas presented there can be used to derive formulas for the inverse Radon transform.

It turns out that there is a fundamental difference between inversion in even dimension and inversion in odd dimension. Although this may seem a bit strange at first, it is something that is quite common in the study of partial differential equations and Green’s function for the wave equation: Morse and Feshbach (1953) and Wolf (1979). This difference is discussed in connection with the Radon transform by Shepp (1980), Barrett (1984), Berenstein and Walnut (1994), and Olson and DeStefano (1994). The important observation is that the operations required for the inverse in two dimensions are global; the transform must be known over all of Radon space. By contrast, in three dimensions, because derivatives are required, the inversion operations are local. Hence, the procedure here is to give separate derivations for two and three dimensions. It is not very much more difficult to do the derivation for general even and odd dimensions; however, it is a bit easier to follow the specific cases. And, after all, these are the most important for applications anyway. The method used is patterned after that used by Barrett (1984) and Deans (1985).

### 8.9.1 Two Dimensions

The notation is the same as used previously for vectors,  $\mathbf{x} = (x, y)$  and  $\boldsymbol{\xi} = (\cos \phi, \sin \phi)$ . The coordinates in Fourier space are designated by  $(u, v) = (q \cos \phi, q \sin \phi) = q \boldsymbol{\xi}$ . The starting point is Equation 8.15,

$$\tilde{f}(q\boldsymbol{\xi}) = \mathfrak{F}_1 \mathfrak{R} f(x, y) \quad (8.92)$$

along with the observation that  $f$  is given by the inverse 2D Fourier transform,

$$f(x, y) = \mathfrak{F}_2^{-1} \tilde{f}(u, v).$$

In polar form,

$$\begin{aligned} f(x, y) &= \int_{-\infty}^{\infty} dq |q| \int_0^{\pi} d\phi \tilde{f}(q\boldsymbol{\xi}) e^{i2\pi q \boldsymbol{\xi} \cdot \mathbf{x}} \\ &= \int_0^{\pi} d\phi \left[ \int_{-\infty}^{\infty} dq |q| \tilde{f}(q\boldsymbol{\xi}) e^{i2\pi q p} \right]_{p=\boldsymbol{\xi} \cdot \mathbf{x}}. \end{aligned} \quad (8.93)$$

Now the term in square brackets is the inverse 1D Fourier transform of the product  $|q| \tilde{f}$  and this is to be evaluated at  $p = \boldsymbol{\xi} \cdot \mathbf{x}$ . The convolution theorem for Fourier transforms can be used to obtain

$$\mathfrak{F}_2^{-1} \{ |q| \tilde{f}(q\boldsymbol{\xi}) \} = \mathfrak{F}_2^{-1} \{ |q| \} * \mathfrak{F}_2^{-1} \{ \tilde{f}(q\boldsymbol{\xi}) \}.$$

From Section 8.2.5 the last term on the right is just the Radon transform  $\check{f}(p, \xi)$ . This observation leads to

$$f(x, y) = \int_0^\pi d\phi [\check{f}(p, \xi) * \check{\delta}^{-1}\{|q|\}]_{p=\xi \cdot \mathbf{x}}. \quad (8.94)$$

The inverse Fourier transform in this equation is interpreted in terms of generalized functions to give (Lighthill, 1962; Bracewell, 1986)

$$\check{\delta}^{-1}\{|q|\} = \check{\delta}^{-1}\{2\pi i q\} * \check{\delta}^{-1}\left\{\frac{\text{sgn } q}{2\pi i}\right\}.$$

Here, we have written

$$|q| = q \text{sgn } q = 2\pi i q \frac{\text{sgn } q}{2\pi i},$$

where

$$\text{sgn } q = \begin{cases} +1, & \text{for } q > 0 \\ 0, & \text{for } q = 0 \\ -1, & \text{for } q < 0. \end{cases} \quad (8.95)$$

The methods needed to work with these inverse Fourier transforms is given by Lighthill (1962) and Bracewell (1986). By use of the derivative theorem

$$\check{\delta}^{-1}\{2\pi i q\} = \delta'(p),$$

where the prime denotes first order derivative with respect to variable  $p$ . The other transform is given in terms of a Cauchy principal value,

$$\check{\delta}^{-1}\left\{\frac{\text{sgn } q}{2\pi i}\right\} = \frac{1}{2\pi^2} \mathcal{P}\left(\frac{1}{p}\right).$$

It follows that

$$\check{\delta}^{-1}\{|q|\} = \delta'(p) * \frac{1}{2\pi^2} \mathcal{P}\left(\frac{1}{p}\right).$$

Now, Equation 8.94 becomes

$$f(x, y) = \frac{1}{2\pi^2} \int_0^\pi d\phi \left[ \check{f}(p, \xi) * \delta'(p) * \mathcal{P}\left(\frac{1}{p}\right) \right]_{p=\xi \cdot \mathbf{x}}. \quad (8.96)$$

By using the derivative theorem for convolution and the properties of the delta function,

$$\check{f}(p, \xi) * \delta'(p) = \frac{\check{f}(p, \xi)}{\partial p} * \delta(p) = \frac{\check{f}(p, \xi)}{\partial p}.$$

It is convenient to use the subscript notation for partial derivatives and write

$$\check{f}_p(p, \xi) \equiv \frac{\check{f}(p, \xi)}{\partial p}.$$

Now the term in square brackets in Equation 8.96 can be written as

$$\begin{aligned} \left[ \check{f}_p(p, \xi) * \mathcal{P}\left(\frac{1}{p}\right) \right]_{p=\xi \cdot \mathbf{x}} &= \left[ \mathcal{P} \int_{-\infty}^{\infty} \frac{\check{f}_t(t, \xi)}{p-t} \right]_{p=\xi \cdot \mathbf{x}} \\ &= -\mathcal{P} \int_{-\infty}^{\infty} \frac{\check{f}_t(t, \xi)}{t-\xi \cdot \mathbf{x}} dt. \end{aligned}$$

Note that  $t$  is a dummy variable in the last integral, and can be replaced by  $p$  to agree with earlier notation. The final formula follows by substituting this result in Equation 8.96 to get

$$f(x, y) = \frac{-1}{2\pi^2} \mathcal{P} \int_0^\pi d\phi \int_{-\infty}^{\infty} \frac{\check{f}_p(p, \xi)}{p-\xi \cdot \mathbf{x}} dp. \quad (8.97)$$

Here, the Cauchy principal value is related to the integral over  $p$ . It has been placed outside for convenience. Sometimes the  $\mathcal{P}$  is dropped altogether; in this case it is “understood” that the singular integral is interpreted in terms of the Cauchy principal value.

The inversion formula (Equation 8.97) can be expressed in terms of a Hilbert transform (see also Chapter 7). The Hilbert transform of  $f(t)$  is defined by Sneddon (1972) and Bracewell (1986),

$$\mathcal{H}_i[f(t); t \rightarrow x] = \frac{1}{\pi} \int_{-\infty}^{\infty} \frac{f(t) dt}{t-x}, \quad (8.98)$$

where the Cauchy principal value is understood. Thus, the inversion formula can be written as

$$f(x, y) = \frac{-1}{2\pi} \int_0^\pi \mathcal{H}_i[\check{f}_p(p, \xi); p \rightarrow \xi \cdot \mathbf{x}] d\phi. \quad (8.99)$$

For reasons that will become apparent in the subsequent discussion it is extremely desirable to make the following definition for the Hilbert transform of the derivative of some function, say  $g$ ,

$$\bar{g}(t) = \frac{-1}{4\pi} \mathcal{H}_i[g_p(p); p \rightarrow t] \quad \text{for } n=2. \quad (8.100)$$

If this is done, the inversion formula for  $n=2$ , is given by

$$f(x, y) = 2 \int_0^\pi d\phi \left[ \bar{f}(t, \xi) \right]_{t=\xi \cdot \mathbf{x}}. \quad (8.101)$$

### 8.9.2 Three Dimensions

The inversion formula in three dimensions is actually easier to derive because no Hilbert transforms emerge. The path through Fourier space is used again with the unit vector  $\xi$  given in terms of the polar angle  $\theta$  and azimuthal angle  $\phi$ ,

$$\xi = (\sin \theta \cos \phi, \sin \theta \sin \phi, \cos \theta).$$

The feature space function  $f(\mathbf{x}) = f(x, y, z)$  is found from the inverse 3D Fourier transform,

$$f(\mathbf{x}) = \mathfrak{F}_3^{-1} \tilde{f}(q\xi) = \int_0^\infty dq q^2 \int_{|\xi|=1} d\xi \tilde{f}(q\xi) e^{i2\pi q\xi \cdot \mathbf{x}}. \quad (8.102)$$

Here, the integral over the unit sphere is indicated by

$$\int_{|\xi|=1} d\xi = \int_0^{2\pi} d\phi \int_0^\pi \sin \theta d\theta.$$

Now recall that  $\tilde{f}$  is given by the 1D Fourier transform of  $\check{f}$ , and from the symmetry properties of  $\check{f}$  the integral over  $q$  from 0 to  $\infty$  can be replaced by one-half the integral from  $-\infty$  to  $\infty$ .

$$\begin{aligned} f(\mathbf{x}) &= \frac{1}{2} \int_{|\xi|=1} d\xi \left[ \int_{-\infty}^\infty dq q^2 \tilde{f}(q\xi) e^{i2\pi q\xi \cdot \mathbf{x}} \right]_{p=\xi \cdot \mathbf{x}} \\ &= \frac{1}{2} \int_{|\xi|=1} d\xi \mathfrak{F}^{-1} [q^2 \check{f}(q\xi)]_{p=\xi \cdot \mathbf{x}} \end{aligned}$$

Now from the inverse of the 1D derivative theorem

$$\mathfrak{F}^{-1} [q^2 \check{f}] = \frac{-1}{4\pi} \frac{\partial^2 \check{f}}{\partial p^2} = \frac{-1}{4\pi} \check{f}_{pp},$$

one form of the inversion formula is

$$f(\mathbf{x}) = \frac{-1}{8\pi^2} \int_{|\xi|=1} d\xi \left[ \check{f}_{pp}(p, \xi) \right]_{p=\xi \cdot \mathbf{x}}. \quad (8.103)$$

Another form for Equation 8.103 comes from the observation that for any function of  $\xi \cdot \mathbf{x}$

$$\nabla^2 \psi(\xi \cdot \mathbf{x}) = |\xi|^2 [\psi_{pp}(p)]_{p=\xi \cdot \mathbf{x}} = [\psi_{pp}(p)]_{p=\xi \cdot \mathbf{x}}.$$

The last equality follows because  $\xi$  is a unit vector. These observations lead to the inversion formula

$$f(\mathbf{x}) = \frac{-1}{8\pi^2} \nabla^2 \int_{|\xi|=1} \check{f}(\xi \cdot \mathbf{x}, \xi) d\xi. \quad (8.104)$$

## 8.10 Abel Transforms

In this section we focus attention on a particular class of singular integral equations and how transforms known as Abel transforms emerge. Actually, it is convenient to define four different Abel transforms. Although all of these transforms are called Abel transforms at various places in the literature, there is no agreement regarding the numbering. Consequently, an arbitrary decision is made here in that respect. There is an intimate connection with the Radon transform; however, that discussion is delayed until Section 8.11. There are some very good recent references devoted primarily to Abel integral equations, Abel transforms, and applications. The monograph by Gorenflo and Vessella (1991) is especially recommended for both theory and applications. Also, the chapter by Anderssen and de Hoog (1990) contains many applications along with an excellent list of references. A recent book by Srivastava and Bushman (1992) is valuable for convolution integral equations in general. Other general references include Kanwal (1971), Widder (1971), Churchill (1972), Doetsch (1974), and Knill (1994). Another valuable resource is the review by Lonseth (1977). His remarks on page 247 regarding Abel's contributions "back in the spring-time of analysis" are required reading for those who appreciate the history of mathematics. Other references to Abel transforms and relevant resource material are contained in Section 8.11 and in the following discussion.

### 8.10.1 Singular Integral Equations, Abel Type

An integral equation is called singular if either the range of integration is infinite or the kernel has singularities within the range of integration. Singular integral equations of Volterra type of the first kind are of the form (Tricomi, 1985)

$$g(x) = \int_0^x k(x, y) f(y) dy \quad x > 0, \quad (8.105)$$

where the kernel satisfies the condition  $k(x, y) \equiv 0$  if  $y > x$ . If  $k(x, y) = k(x - y)$ , then the equation is of convolution type. The type of kernel of interest here is

$$k(x - y) = \frac{1}{(x - y)^\alpha} \quad 0 < \alpha < 1.$$

This leads to an integral equation of Abel type,

$$g(x) = \int_0^x \frac{f(y)}{(x - y)^\alpha} dy = f(x)^* \frac{1}{x^\alpha}, \quad x > 0, \quad (8.106)$$

$$0 < \alpha < 1.$$

Integral equations of the type in Equation 8.106 were studied by the Norwegian mathematician Niels H. Abel (1802–1829) with particular attention to the connection with the tautochrone



problem. This work by Abel (1823, 1826a,b) served to introduce the subject of integral equations. The connection with the tautochrone problem emerges when  $\alpha = 1/2$  in the integral equation. This is the problem of determining a curve through the origin in a vertical plane such that the time required for a massive particle to slide without friction down the curve to the origin is independent of the starting position. It is assumed that the particle slides freely from rest under the action of its weight and the reaction of the curve (smooth wire) that constrains its movement. Details of this problem are discussed by Churchill (1972) and Widder (1971).

One way to solve Equation 8.105 when  $k(x, y) = k(x - y)$  is by use of the Laplace transform (see Chapter 5); this yields

$$G(s) = F(s)K(s). \tag{8.107}$$

The solution for  $F(s)$  can be written in two forms,

$$F(s) = \frac{G(s)}{K(s)} = [sG(s)] \left[ \frac{1}{sK(s)} \right] \tag{8.108}$$

The second form is used when the inverse Laplace transform of  $1/K(s)$  does not exist.

**Example 8.29**

Solve Equation 8.106 for  $f(x)$ . From Equation 8.107 and Laplace transform tables (Chapter 5),

$$G(s) = \mathfrak{L}\{f(x)\} \mathfrak{L}\left\{\frac{1}{x^\alpha}\right\} = F(s)s^{\alpha-1}\Gamma(1-\alpha).$$

To find  $F(s)$  we must invert the equation

$$F(s) = \frac{s}{\Gamma(\alpha)\Gamma(1-\alpha)} [\Gamma(\alpha)s^{-\alpha}G(s)].$$

The inversion yields

$$\begin{aligned} f(x) &= \mathfrak{L}^{-1}\left\{\frac{s}{\Gamma(\alpha)\Gamma(1-\alpha)} [\Gamma(\alpha)s^{-\alpha}G(s)]\right\} \\ &= \mathfrak{L}^{-1}\left\{\frac{s}{\Gamma(\alpha)\Gamma(1-\alpha)} \mathcal{L}\left\{\int_0^x (x-y)^{\alpha-1}g(y)dy\right\}\right\}. \end{aligned}$$

By invoking the property  $df(x)/dx = \mathfrak{L}^{-1}\{s\mathfrak{L}\{f(x)\}\}$  the above equation becomes

$$f(x) = \frac{\sin \alpha\pi}{\pi} \frac{d}{dx} \int_0^x (x-y)^{\alpha-1}g(y)dy. \tag{8.109}$$

Here, use is made of the gamma function identity

$$\Gamma(\alpha)\Gamma(1-\alpha) = \frac{\pi}{\sin \alpha\pi}.$$

Another form of Equation 8.108 can be found if  $g(y)$  is differentiable. One way to find this other solution is to use integration by parts,  $\int u dv = uv - \int v du$ , with  $u = g(y)$  and  $dv = (x - y)^{\alpha-1}dy$ ,

$$\int_0^x (x-y)^{\alpha-1}g(y)dy = \frac{g(+0)x^\alpha}{\alpha} + \frac{1}{\alpha} \int_0^x (x-y)^\alpha g'(y)dy.$$

When this expression is multiplied by  $\sin \alpha\pi/\pi$  and differentiated with respect to  $x$  the alternative expression for Equation 8.109 follows,

$$f(x) = \frac{\sin \alpha\pi}{\pi} \left[ \frac{g(+0)}{x^{1-\alpha}} + \int_0^x \frac{g'(y)}{(x-y)^{1-\alpha}} dy \right]. \tag{8.110}$$

**Remark**

It is tempting to take a quick look at Equation 8.106 and assume that  $g(0) = 0$ . This is wrong! The proper interpretation is to do the integral first and then take the limit as  $x \rightarrow 0$  through positive values. This is why we have written  $g(+0)$  in Equation 8.110.

The above Equation 8.110 also follows by taking into consideration the convolution properties and derivatives for the Laplace transform. We observe that Equation 8.108 can be written in two alternative forms,

$$F(s) = s[G(s)H(s)] = [sG(s)] [H(s)],$$

Where  $H(s)$  is defined by

$$H(s) = \frac{1}{sK(s)}.$$

The inversion gives

$$f(x) = \frac{d}{dx} \int_0^x g(y)h(x-y)dy, \tag{8.111a}$$

or

$$f(x) = g(0)h(x) + \int_0^x g'(y)h(x-y)dy. \tag{8.111b}$$

The previous equations can be used to solve an integral equation of the form

$$g(x) = \int_0^x f(y)k(x^2 - y^2)dy. \tag{8.112}$$

After making the substitutions,

$$x = u^{\frac{1}{2}}, \quad y = v^{\frac{1}{2}}, \quad f_1(v) = \frac{1}{2} f(v^{\frac{1}{2}}) v^{-\frac{1}{2}}, \quad g_1(u) = g(u^{\frac{1}{2}}),$$

Equation 8.112 becomes

$$g_1(u) = \int_0^u f_1(v) k(u-v) dv. \quad (8.113)$$

This equation is identical to Equation 8.105 with  $k(x, y) = k(x - y)$  and the solution is given by Equations 8.111a and b with  $k$  replaced by  $h$ ,

$$\begin{aligned} f_1(u) &= \frac{d}{du} \int_0^u g_1(v) h(u-v) dv \\ &= g_1(0)h(u) + \int_0^u g_1'(v) h(u-v) dv, \end{aligned}$$

where  $h(x) = \mathcal{L}^{-1}\{1/sK(s)\}$ . Using the substitutions in reverse gives

$$\frac{f(x)}{2x} = \frac{1}{2x} \frac{d}{dx} \int_0^x g(y)h(x^2 - y^2) 2y dy,$$

or

$$f(x) = 2 \frac{d}{dx} \int_0^x y g(y) h(x^2 - y^2) dy, \quad (8.114a)$$

and if the derivative of  $g$  exists,

$$f(x) = 2xg(0)h(x^2) + 2x \int_0^x g'(y) h(x^2 - y^2) dy. \quad (8.114b)$$

**Example 8.30**

Find the solution of Equation 8.112 if the kernel is  $k(x) = x^{-\alpha}$  and  $0 < \alpha < 1$ . With this kernel the equation to be solved is

$$g(x) = \int_0^x \frac{f(y) dy}{(x^2 - y^2)^\alpha}. \quad (8.115a)$$

We need the inverse Laplace transform of  $H(s) = 1/sK(s)$ . From

$$K(s) = \int_0^\infty e^{-sx} x^{-\alpha} dx = \Gamma(1 - \alpha)s^{\alpha-1},$$

it follows that

$$h(x) = \mathcal{L}^{-1} \left\{ \frac{1}{\Gamma(1 - \alpha) s^\alpha} \right\} = \frac{1}{\Gamma(\alpha)\Gamma(1 - \alpha)} x^{\alpha-1} = \frac{\sin \alpha\pi}{\pi} x^{\alpha-1}.$$

Now the solution follows directly from Equation 8.114a,

$$f(x) = \frac{2 \sin \alpha\pi}{\pi} \frac{d}{dx} \int_0^x \frac{y g(y) dy}{(x^2 - y^2)^{1-\alpha}}. \quad (8.115b)$$

**Example 8.31**

Apply Equation 8.114b to find an alternative expression for the inverse Equation 8.115b. Note that

$$h(x^2) = \frac{\sin \alpha\pi}{\pi} x^{2\alpha-2}$$

follows from Example 8.30. Consequently, the desired equation is

$$f(x) = \frac{2 \sin \alpha\pi}{\pi} \left[ g(0)x^{2\alpha-1} + x \int_0^x \frac{g'(y) dy}{(x^2 - y^2)^{1-\alpha}} \right]. \quad (8.115c)$$

There are other integral equations similar to the one in Example 8.30 that are of particular interest here. The relevant results are given without proof. The derivations are very similar to the procedures used above. A transform pair related to the pair of Equation 8.115a,b is

$$g(x) = \int_x^\infty \frac{f(y) dy}{(y^2 - x^2)^\alpha}, \quad 0 < \alpha < 1, f(\infty) = 0, \quad (8.116a)$$

and

$$f(x) = -\frac{2 \sin \alpha\pi}{\pi} \frac{d}{dx} \int_x^\infty \frac{y g(y) dy}{(y^2 - x^2)^{1-\alpha}}. \quad (8.116b)$$

Another pair of interest is

$$g(x) = 2 \int_x^\infty \frac{y f(y) dy}{(y^2 - x^2)^\alpha} \quad 0 < \alpha < 1, f(\infty) = 0, \quad (8.117a)$$

and

$$f(x) = -\frac{\sin \alpha \pi}{\pi} \int_x^\infty \frac{g'(y)dy}{(y^2 - x^2)^{1-\alpha}}. \quad (8.117b)$$

### 8.10.2 Some Abel Transform Pairs

If the choice  $\alpha = \frac{1}{2}$  is made in Equations 8.115 through 8.117 the resulting transforms are known as Abel transforms. In order, these are designated by  $\mathcal{A}_1\{f\}$ ,  $\mathcal{A}_2\{f\}$ , and  $\mathcal{A}_3\{f\}$ . The numerical designation is not standard, and some authors leave  $\alpha$  in the equations. With the exception of a constant factor, Sneddon (1972) uses the same notation for  $\mathcal{A}_1\{f\}$  and  $\mathcal{A}_2\{f\}$ . Bracewell (1986) introduces only  $\mathcal{A}_3\{f\}$ , and uses the notation  $\mathcal{A}\{f\}$ . This is the transform most directly related to the Radon transform. It is discussed in much more detail in Section 8.11. Also, for completeness we add a fourth transform. It is related to Riemann–Liouville (fractional) integrals of order  $1/2$ , discussed in Section 8.10.3.

Explicitly, the transforms are designated by

$$\hat{f}_1(x) \equiv \mathcal{A}_1\{f_1(r); x\} = \int_0^x \frac{f_1(r)dr}{(x^2 - r^2)^{\frac{1}{2}}}, \quad x > 0 \quad (8.118a)$$

$$\hat{f}_2(x) \equiv \mathcal{A}_2\{f_2(r); x\} = \int_x^\infty \frac{f_2(r)dr}{(r^2 - x^2)^{\frac{1}{2}}}, \quad x > 0 \quad (8.118b)$$

$$\hat{f}_3(x) \equiv \mathcal{A}_3\{f_3(r); x\} = 2 \int_x^\infty \frac{r f_3(r)dr}{(r^2 - x^2)^{\frac{1}{2}}}, \quad x > 0 \quad (8.118c)$$

$$\hat{f}_4(x) \equiv \mathcal{A}_4\{f_4(r); x\} = 2 \int_0^x \frac{r f_4(r)dr}{(x^2 - r^2)^{\frac{1}{2}}}, \quad x > 0. \quad (8.118d)$$

Note the change from  $y \rightarrow r$  to agree with the short tables of transforms given in Appendix 8.B. Also note the change  $g \rightarrow \hat{f}$ , and the use of subscripts to keep track of which transform is being applied.

The corresponding inversion expressions are

$$f_1(r) = \frac{2}{\pi} \frac{d}{dr} \int_0^r \frac{x \hat{f}_1(x)dx}{(r^2 - x^2)^{\frac{1}{2}}} \quad (8.119a)$$

$$f_2(r) = -\frac{2}{\pi} \frac{d}{dr} \int_r^\infty \frac{x \hat{f}_2(x)dx}{(x^2 - r^2)^{\frac{1}{2}}} \quad (8.119b)$$

$$f_3(r) = -\frac{1}{\pi r} \frac{d}{dr} \int_r^\infty \frac{x \hat{f}_3(x)dx}{(x^2 - r^2)^{\frac{1}{2}}} \quad (8.119c)$$

$$f_4(r) = \frac{1}{\pi r} \frac{d}{dr} \int_0^r \frac{x \hat{f}_4(x)dx}{(r^2 - x^2)^{\frac{1}{2}}}. \quad (8.119d)$$

There are alternative ways to write the above inverses. The results can be verified by integrating by parts before taking the derivative with respect to  $r$ :

$$f_1(r) = \frac{2\hat{f}_1(0)}{\pi} + \frac{2r}{\pi} \int_0^r \frac{\hat{f}_1'(x)dx}{(r^2 - x^2)^{\frac{1}{2}}} \quad (8.120a)$$

$$f_2(r) = -\frac{2r}{\pi} \int_r^\infty \frac{\hat{f}_2'(x)dx}{(x^2 - r^2)^{\frac{1}{2}}} \quad (8.120b)$$

$$f_3(r) = -\frac{1}{\pi} \int_r^\infty \frac{\hat{f}_3'(x)dx}{(x^2 - r^2)^{\frac{1}{2}}} \quad (8.120c)$$

$$f_4(r) = \frac{\hat{f}_4(0)}{\pi r} + \frac{1}{\pi} \int_0^r \frac{\hat{f}_4'(x)dx}{(r^2 - x^2)^{\frac{1}{2}}}. \quad (8.120d)$$

In these equations it is assumed that the transform vanishes at infinity,  $\hat{f}(\infty) \equiv 0$ , and the prime means derivative with respect to  $x$ .

There is yet another form that is useful for  $f_3$ . The result comes from a study of the Radon transform (Deans, 1983, 1993):

$$f_3(r) = -\frac{1}{\pi} \frac{d}{dr} \int_r^\infty \frac{r \hat{f}_3(x)dx}{x(x^2 - r^2)^{\frac{1}{2}}}. \quad (8.121)$$

To verify that this indeed reduces to Equation 8.120c, let the integration by parts be done in Equation 8.121 with

$$u = r \hat{f}_3(x), \quad du = r \hat{f}_3'(x)dx, \quad v = \frac{1}{r} \cos^{-1} \frac{r}{x},$$

$$dv = \frac{dx}{x(x^2 - r^2)^{\frac{1}{2}}}.$$

After doing the integration by parts, take the derivative with respect to  $r$  to get Equation 8.120c.

#### Some important observations

From the definitions of the transforms  $\mathcal{A}_i$ , it follows that

$$\mathcal{A}_3\{f(r)\} = 2\mathcal{A}_2\{rf(r)\} \quad (8.122a)$$

$$\mathcal{A}_4\{f(r)\} = 2\mathcal{A}_1\{rf(r)\} \quad (8.122b)$$

$$\mathcal{A}_4\{r^{-1}f_1(r)\} = 2\hat{f}_1(x) \quad (8.122c)$$

$$\mathcal{A}_3\{r^{-1}f_2(r)\} = 2\hat{f}_2(x) \quad (8.122d)$$

$$f_1(r) \equiv \mathcal{A}_1^{-1}\{\hat{f}_1(x)\} = \frac{2}{\pi} \frac{d}{dr} \mathcal{A}_1\{x \hat{f}_1(x)\} \quad (8.122e)$$

$$f_2(r) \equiv \mathcal{A}_2^{-1}\{\hat{f}_2(x)\} = -\frac{2}{\pi} \frac{d}{dr} \mathcal{A}_2\{x \hat{f}_2(x)\}. \quad (8.122f)$$

These equations (along with obvious variations) can be used to find transforms and inverse transforms. A few samples are provided in the examples of Section 8.10.4.

### 8.10.3 Fractional Integrals

The Abel transforms are related to the Riemann–Liouville and Weyl (fractional) integrals of order  $1/2$ ; these are discussed along with an extensive tabulation in Chapter 13 of Erdélyi et al. (1954). In the notation of this reference, the Riemann–Liouville integral is given by

$$g(y; \mu) = \frac{1}{\Gamma(\mu)} \int_0^y f(x)(y-x)^{\mu-1} dx, \quad (8.123)$$

and the Weyl integral is given by

$$h(y; \mu) = \frac{1}{\Gamma(\mu)} \int_y^\infty f(x)(x-y)^{\mu-1} dx. \quad (8.124)$$

Now in Equation 8.123 let  $\mu = 1/2$ , make the replacement  $y \rightarrow x^2$ , and change the variable of integration  $x = r^2$  to obtain.

$$\sqrt{\pi} g\left(x^2, \frac{1}{2}\right) = 2 \int_0^x \frac{rf(r^2)dr}{(x^2 - r^2)^{\frac{1}{2}}}.$$

Clearly, this form of the Riemann–Liouville integral can be converted to Equation 8.118d by the appropriate replacements. By a similar argument, the Weyl integral (Equation 8.124) can be converted to Equation 8.118c. This leads to the following useful rule for finding Abel transforms  $\mathcal{A}_3$  and  $\mathcal{A}_4$  from the tables in Chapter 13 of Erdélyi et al. (1954).

**Rule**

1. Replace:  $\mu \rightarrow \frac{1}{2}$
2. Replace:  $x \rightarrow r^2$  (column on left).
3. Replace:  $y \rightarrow x^2$  and multiply the transform by  $\sqrt{\pi}$  (column on right).

It is easy to verify that this rule works by its application to cases that yield results quoted in Appendix 8.B for  $\mathcal{A}_3$ . Verification of the rule for  $\mathcal{A}_4$  follows immediately from the use of standard integral tables. Although the rule works most directly for the  $\mathcal{A}_3$  and  $\mathcal{A}_4$  transforms, it can be extended to apply to finding  $\mathcal{A}_1$  and  $\mathcal{A}_2$  transforms by use of the formulas in Equations 8.122a through f. Finally, it is interesting to note that these integrals lead to an interpretation for fractional differentiation and fractional integration. A good resource for details on this concept is the monograph by Gorenflo and Vessella (1991).

### 8.10.4 Some Useful Examples

We close this section with a few useful examples. These are especially valuable for those concerned with the analytic computation of Abel transforms or inverse Abel transforms.

#### Example 8.32

Consider the Abel transform

$$\hat{f}_1(x) = \mathcal{A}_1\{a-r\} = \frac{\pi a}{2} - x.$$

This is a simple case where  $\hat{f}_1(x)$  is not zero at  $x=0$ ; here,  $\hat{f}_1(0) = \pi a/2$  and  $\hat{f}'_1(x) = -1$ . If Equation 8.120a is used to verify the transform, the calculation is

$$f_1(r) = \frac{2}{\pi} \frac{\pi a}{2} + \frac{2r}{\pi} \int_0^r \frac{-dx}{(r^2 - x^2)^{\frac{1}{2}}} = a - r.$$

Verification of this inverse for Equation 8.119a follows by using the appropriate integral formulas from Appendix 8.A, and application of the derivative with respect to  $r$ :

$$\frac{2}{\pi} \frac{d}{dr} \int_0^r \frac{\frac{1}{2}\pi ax - x^2}{(r^2 - x^2)^{\frac{1}{2}}} dx = a - r.$$

From Equation 8.122c we know the transform

$$\mathcal{A}_4\{r^{-1}(a-r)\} = \pi a - 2x.$$

Inversion formulas (Equation 8.119d) and (Equation 8.120d) apply for this case.

#### Example 8.33

It is instructive to apply inversion formulas (8.119c), (8.120c), and (8.121) to the same problem. From Appendix 8.B, we use

$$\mathcal{A}_3\{\chi(r/a)\} = 2(a^2 - x^2)^{\frac{1}{2}}\chi(x/a).$$

Application of Equation 8.119c gives

$$\begin{aligned} -\frac{1}{\pi r} \frac{d}{dr} \int_r^a \frac{2x(a^2 - x^2)^{\frac{1}{2}} dx}{(x^2 - r^2)^{\frac{1}{2}}} &= -\frac{2}{\pi r} \frac{d}{dr} \int_r^a \frac{x(a^2 - x^2) dx}{(a^2 - x^2)^{\frac{1}{2}}(x^2 - r^2)^{\frac{1}{2}}} \\ &= -\frac{2}{\pi r} \frac{d}{dr} \int_r^a \frac{a^2 x dx}{(a^2 - x^2)^{\frac{1}{2}}(x^2 - r^2)^{\frac{1}{2}}} \\ &\quad + \frac{2}{\pi r} \frac{d}{dr} \int_r^a \frac{x^3 dx}{(a^2 - x^2)^{\frac{1}{2}}(x^2 - r^2)^{\frac{1}{2}}} \\ &= -\frac{2}{\pi r} \frac{d}{dr} \left(\frac{a^2 \pi}{2}\right) + \frac{2}{\pi r} \frac{d}{dr} (a^2 + r^2) \frac{\pi}{4} \\ &= 0 + 1 = 1. \end{aligned}$$

Application of Equation 8.120c gives

$$-\frac{1}{\pi} \int_r^a \frac{-2x dx}{(a^2 - x^2)^{\frac{1}{2}}(x^2 - r^2)^{\frac{1}{2}}} = \frac{2}{\pi} \int_r^a \frac{x dx}{(a^2 - x^2)^{\frac{1}{2}}(x^2 - r^2)^{\frac{1}{2}}} = 1.$$

Application of Equation 8.121 gives

$$\begin{aligned} -\frac{1}{\pi} \frac{d}{dr} \int_r^a \frac{2r(a^2 - x^2)^{\frac{1}{2}} dx}{x(x^2 - r^2)^{\frac{1}{2}}} &= -\frac{2}{\pi} \frac{d}{dr} \int_r^a \frac{r(a^2 - x^2) dx}{x(a^2 - x^2)^{\frac{1}{2}}(x^2 - r^2)^{\frac{1}{2}}} \\ &= -\frac{2}{\pi} \frac{d}{dr} \int_r^a \frac{ra^2 dx}{x(a^2 - x^2)^{\frac{1}{2}}(x^2 - r^2)^{\frac{1}{2}}} \\ &\quad + \frac{2}{\pi} \frac{d}{dr} \int_r^a \frac{rx dx}{(a^2 - x^2)^{\frac{1}{2}}(x^2 - r^2)^{\frac{1}{2}}} \\ &= -\frac{2}{\pi} \frac{d}{dr} (a^2 r) \left( \frac{\pi}{2ar} \right) + \frac{2}{\pi} \frac{d}{dr} \left( \frac{r\pi}{2} \right) \\ &= 0 + 1 = 1. \end{aligned}$$

Evaluation of the various integrals above follows from material in Appendix 8.A.

### Example 8.34

The following Bessel function identities are used in this example.

$$\frac{\partial}{\partial x} \{x^v J_v(bx)\} = bx^v J_{v-1}(bx). \quad (8.125a)$$

$$\frac{\partial}{\partial x} \{x^{-v} J_v(bx)\} = -bx^{-v} J_{v+1}(bx). \quad (8.125b)$$

It follows from the formulas

$$\frac{\pi}{2} J_0(bx) = \int_0^x \frac{\cos br dr}{(x^2 - r^2)^{\frac{1}{2}}}, \quad \frac{\pi}{2} J_0(bx) = \int_x^\infty \frac{\sin br dr}{(r^2 - x^2)^{\frac{1}{2}}},$$

for the Bessel function  $J_0$  that

$$\mathcal{A}_1\{\cos br\} = \frac{\pi}{2} J_0(bx),$$

and

$$\mathcal{A}_2\{\sin br\} = \frac{\pi}{2} J_0(bx).$$

Differentiation of the previous two expressions with respect to the parameter  $b$  yields the formulas

$$\mathcal{A}_1\{r \sin br\} = \frac{\pi x}{2} J_1(bx)$$

and

$$\mathcal{A}_2\{r \cos br\} = -\frac{\pi x}{2} J_1(bx).$$

From formula (Equation 8.122e) with  $\hat{f}_1(x) = \sin bx$ ,

$$\frac{2}{\pi} \frac{d}{dt} \mathcal{A}_1\{x \sin bx\} = \frac{2}{\pi} \frac{d}{dt} \left\{ \frac{1}{2} \pi t J_1(bt) \right\} = bt J_0(bt).$$

This means that

$$\mathcal{A}_1^{-1}\{\sin bx\} = bt J_0(bt),$$

or equivalently

$$\mathcal{A}_1\{r J_0(br)\} = \frac{\sin bx}{b}.$$

And by the same technique, from Equation 8.122f

$$\mathcal{A}_2\{r J_0(br)\} = \frac{\cos bx}{b}.$$

From Equation 8.122f with  $\hat{f}_2(x) = x^{-1} \sin bx$ ,

$$\begin{aligned} \mathcal{A}_2^{-1}\{x^{-1} \sin bx\} &= -\frac{2}{\pi} \frac{d}{dt} \mathcal{A}_2\{\sin bx\} = -\frac{2}{\pi} \frac{d}{dt} \left\{ \frac{1}{2} \pi J_0(bt) \right\} \\ &= b J_1(bt) \end{aligned}$$

or

$$\mathcal{A}_2\{J_1(br)\} = \frac{\sin bx}{bx}.$$

From the formulas developed above for the  $\mathcal{A}_2$  transforms and Equation 8.122a,

$$\mathcal{A}_3\{\cos br\} = -\pi x J_1(bx),$$

$$\mathcal{A}_3\{r^{-1} \sin br\} = \pi J_0(bx),$$

$$\mathcal{A}_3\{J_0(br)\} = \frac{2 \cos bx}{b},$$

and

$$\mathcal{A}_3\{r^{-1} J_1(br)\} = \frac{2 \sin bx}{bx}.$$

Additional formulas similar to those in the previous example are contained in Sneddon (1972) and Gorenflo and Vessella (1991). These authors also make use of the formulas of this example to make the connection between the Abel transform and the Hankel transform. This connection is also discussed in Section 8.11 in the more general context of the Radon transform.

### Example 8.35

Use the rule in Section 8.10.3 to compute

$$\mathcal{A}_4\{r^{2v-2}\}.$$

From item (7) of Table 13.1, Riemann–Liouville fractional integrals, of Erdélyi et al. (1954)

$$\mathcal{A}_4\{r^{2\nu-2}\} = \frac{\sqrt{\pi}\Gamma(\nu)}{\Gamma(\nu + \frac{1}{2})} x^{2\nu-1}.$$

A special case is provided by  $\nu = 2$ . This leads to the expression

$$2 \int_0^x \frac{r^3 dr}{(x^2 - r^2)^{\frac{1}{2}}} = \frac{4x^3}{3}.$$

## 8.11 Related Transforms and Symmetry, Abel and Hankel

The direct connection of the Radon transform and the Fourier transform is used extensively throughout earlier sections of this chapter. Several other transforms are also related to the Radon transform. Some of these are related by circumstances that involve some type of symmetry. The Abel and Hankel transforms emerge naturally in this context. Other related transforms follow more naturally from considerations of orthogonal function series expansions. In this section some of these relations are explored and examples provided to help illustrate the connections.

### 8.11.1 Abel Transform

The Abel transform is closely connected with a generalization of the tautochrone problem. This is the problem of determining a curve through the origin in a vertical plane such that the time required for a particle to slide without friction down the curve to the origin is independent of the starting position. It was the generalization of this problem that led Abel to introduce the subject of integral equations (see Section 8.10). More recent applications of Abel transforms in the area of holography and interferometry with phase objects (of practical importance in aerodynamics, heat and mass transfer, and plasma diagnostics) are discussed by Vest (1979), Schumann et al. (1985) and Ladouceur and Adiga (1987). A very good description of the relation of the Abel and Radon transform to the problem of determining the refractive index from knowledge of a holographic interferogram is provided by Vest (1979); in particular, see Chapter 6, where many references to original work are cited. Minerbo and Levy (1969), Sneddon (1972), and Bracewell (1986) also contain useful material on the Abel transform. Many other references are contained in Section 8.10.

Suppose the feature space function  $f(x,y)$  is rotationally symmetric and depends only on  $(x^2 + y^2)^{1/2}$ . Now, knowledge of one set of projections, for any angle  $\phi$ , serves to define the Radon transform for all angles. For simplicity, let  $\phi = 0$  in the definition (Equation 8.5). Then  $\tilde{f}(p, \phi) = \tilde{f}(p, 0)$ ; because there is no dependence on angle there is no loss of generality by writing this as  $\tilde{f}(p)$ . With these modifications taken into account, the definition becomes

$$\begin{aligned} \tilde{f}(p) &= \int_{-\infty}^{\infty} \int_{-\infty}^{\infty} f(\sqrt{x^2 + y^2}) \delta(p - x) dx dy \\ &= \int_{-\infty}^{\infty} f(\sqrt{p^2 + y^2}) dy \\ &= 2 \int_0^{\infty} f(\sqrt{p^2 + y^2}) dy. \end{aligned}$$

Clearly, because  $p$  appears only as  $p^2$ , the function  $\tilde{f}(p)$  is even and it is sufficient to always choose  $p > 0$ . A change of variable  $r^2 = (p^2 + y^2)$  yields

$$\tilde{f}(p) = 2 \int_{|p|}^{\infty} \frac{rf(r)}{(r^2 - p^2)^{1/2}} dr.$$

This equation is just the defining equation for the Abel transform (Bracewell, 1986), designated by

$$f_A(p) = \mathcal{A}\{f(r)\} = 2 \int_{|p|}^{\infty} \frac{rf(r)}{(r^2 - p^2)^{1/2}} dr. \quad (8.126)$$

The absolute value can be removed if  $p$  is restricted to  $p > 0$  and  $f_A(p) = f_A(-p)$ .

**Remark about notation:** The Abel transform used here is  $\mathcal{A}_3$  of Section 8.10; that is,  $\mathcal{A} \equiv \mathcal{A}_3$ .

The Abel transform can be inverted by using the Laplace transform, Section 8.10, or by using the Fourier transform (Bracewell, 1986). For purposes of illustration, the method employed by Barrett (1984) is used here. Equation 8.13, with  $n = 2$ , coupled with the observation that the Radon transform operator  $\mathfrak{R} = \mathcal{A}$  when  $f(x,y)$  has rotational symmetry, becomes

$$\mathfrak{F}_1 \mathcal{A} f = \mathfrak{F}_2 f. \quad (8.127)$$

Moreover, for rotationally symmetric functions, the  $\mathfrak{F}_2$  operator is just the Hankel transform operator of order zero,  $\mathcal{H}_0$ . (More on the Hankel transform appears in Section 8.12 and in Chapter 9.) This means that

$$\mathfrak{F}_2 f = f_H(q) = 2\pi \int_0^{\infty} f(r) J_0(2\pi qr) r dr.$$

From the observation that  $\mathfrak{F}_2 = \mathcal{H}_0$ , and from the reciprocal property of the Hankel transform,  $\mathcal{H}_0 = \mathcal{H}_0^{-1}$ , we have

$$\mathcal{H}_0 f = \mathfrak{F}_1 f_A$$

or

$$f = \mathcal{H}_0^{-1} \mathcal{F}_1 f_A = \mathcal{H}_0 \mathcal{F}_1 f_A.$$

It follows that the inverse Abel transform operator is given by

$$\mathcal{A}^{-1} = \mathcal{H}_0 \mathcal{F}_1. \quad (8.128)$$

From Equation 8.128 the first step in finding the inverse Abel transform is to determine the Fourier transform of  $f_A$ ,

$$\mathcal{F} f_A = \int_{-\infty}^{\infty} f_A(p) e^{-i2\pi q p} dp = 2 \int_0^{\infty} f_A(p) \cos(2\pi q p) dp.$$

The last step follows because  $f_A(p)$  is an even function. Integration by parts gives

$$\mathcal{F} f_A = \frac{-1}{\pi q} \int_0^{\infty} f'_A(p) \sin(2\pi q p) dp,$$

where it is assumed that  $f_A(p) \rightarrow 0$  as  $p \rightarrow \infty$ . The prime means differentiation with respect to  $p$ . Now the inverse of Equation 8.126 is given by

$$f(r) = 2\pi \int_0^{\infty} dq q J_0(2\pi q r) \left( \frac{-1}{\pi q} \right) \int_0^{\infty} f'_A(p) \sin(2\pi q p) dp$$

or, after simplification and interchanging the order of integration,

$$f(r) = -2 \int_0^{\infty} dp f'_A(p) \int_0^{\infty} dq \sin(2\pi q p) J_0(2\pi q r).$$

The integral over  $q$  is tabulated (Gradshteyn et al., 1994); it vanishes for  $0 < p < r$  and gives

$$\frac{1}{2\pi} (p^2 - r^2)^{-1/2} \quad \text{for } 0 < r < p.$$

Hence, the inverse is found from

$$f(r) = -\frac{1}{\pi} \int_r^{\infty} f'_A(p) (p^2 - r^2)^{-1/2} dp. \quad (8.129)$$

This equation and Equation 8.126 are an Abel transform pair. Other forms for the inversion are given in Section 8.10. It may be useful to observe that, for rotationally symmetric functions, if the angle  $\phi$  in the Radon transform is chosen  $\phi = 0$ , then the  $p$  that appears in these formulas is just the same as  $x$ , the projection of the radius  $r$  on the horizontal axis. For this reason, in many discussions of the Abel transform the variable  $p$  used here is

replaced by the variable  $x$ . This notation is used in Section 8.10 and in Appendix 8.B.

Because the Abel transform is a special case of the Radon transform, all of the various basic theorems for the Radon transform apply to the Abel transform. One way to make use of this is to apply the theory of the Radon transform to obtain general results. Then observe that for all rotationally symmetric functions the same results apply to the Abel transform. Some examples of Radon transforms already worked out illustrate the idea.

### Example 8.36

Consider Example 8.3 in Section 8.5. The feature space function has the required rotational symmetry, so it follows immediately that the corresponding Abel transform is

$$\mathcal{A}\{e^{-r^2}\} = \sqrt{\pi} e^{-p^2}. \quad (8.130)$$

From Example 8.9 of that same section, if  $\chi(r)$  represents the characteristic function of a unit disk, then

$$\mathcal{A}\{\chi(r)\} = \begin{cases} 2(1 - p^2)^{1/2}, & \text{for } p < 1 \\ 0, & \text{for } p > 1. \end{cases} \quad (8.131)$$

Another rotationally symmetric case worked out for the Radon transform is from the last part of Example 8.26 in Section 8.7. The corresponding Abel transform is

$$\mathcal{A}\{r^2 e^{-r^2}\} = \frac{\sqrt{\pi}}{2} (2p^2 + 1) e^{-p^2}. \quad (8.132)$$

### Example 8.37

In some cases it is just as easy to apply the definition of the Abel directly; for example, the transform of  $(a^2 + r^2)^{-1}$  is given by

$$\mathcal{A}\{(a^2 + r^2)^{-1}\} = 2 \int_p^{\infty} \frac{r dr}{(r^2 - p^2)^{1/2} (r^2 + a^2)}.$$

The change of variables  $z^2 = r^2 + a^2$  leads to a form that is easy to evaluate; see Appendix 8.A,

$$\mathcal{A}\{(a^2 + r^2)^{-1}\} = \frac{\pi}{(p^2 + a^2)^{1/2}}. \quad (8.133)$$

### Example 8.38

Suppose the desired transform is of  $(1 - r^2)^{1/2}$  restricted to the unit disk or

$$f(r) = (1 - r^2)^{1/2} \chi(r).$$

One way to do this is to find the Radon transform of this function and identify the result with the Abel transform. From the definition of the Radon transform, taking  $\phi = 0$ , and restricting the integral to the unit disk  $D$ ,

$$\tilde{f}(r, \phi) = \int_D (1 - x^2 - y^2)^{1/2} \delta(p - x) dx dy.$$

The integral over  $x$  is easy using the delta function, and the remaining integral over  $y$  is accomplished by observing that over the unit disk  $y^2 + p^2 = 1$ , thus

$$\tilde{f} = \int_{-\sqrt{1-p^2}}^{\sqrt{1-p^2}} [(1 - p^2) - y^2]^{1/2} dy.$$

This integral can be evaluated by use of trigonometric substitution or from integral tables (Appendix 8.A). The result is the Abel transform

$$\tilde{f} = \mathcal{A}\{(1 - r^2)^{1/2} \chi(r)\} = \frac{\pi}{2} (1 - p^2) \chi(p). \quad (8.134)$$

Now suppose it is desired to scale this result to a disk of radius  $a$ . The scaling can be accomplished by application of Section 8.3.2 in the form

$$\mathfrak{R} f\left(\frac{x}{a}, \frac{y}{a}\right) = a^2 \tilde{f}(p, a\xi) = a \tilde{f}\left(\frac{p}{a}, \xi\right).$$

The scaled Abel transform follows, with  $r \rightarrow r/a$ ,

$$\mathcal{A}\left\{\left(1 - \frac{r^2}{a^2}\right)^{1/2} \chi\left(\frac{r}{a}\right)\right\} = \frac{\pi a}{2} \left(1 - \frac{p^2}{a^2}\right) \chi\left(\frac{p}{a}\right)$$

or

$$\mathcal{A}\left\{(a^2 - r^2)^{1/2} \chi\left(\frac{r}{a}\right)\right\} = \frac{\pi}{2} (a^2 - p^2) \chi\left(\frac{p}{a}\right). \quad (8.135)$$

By following the approach used in the last example, it is possible to find a whole class of Abel transforms. These are listed in Appendix 8.B. More results for Abel transforms appear in sections that follow, especially in the section on transforms restricted to the unit disk.

### 8.11.2 Hankel Transform

See Chapter 9 for details about Hankel transforms. By using an approach similar to that in Section 8.11.1 it is possible to find the connection between the Hankel transform of order  $\nu$  and the Radon transform. Note that throughout this discussion, if  $\nu = 0$  the results here correspond to results for the Abel transform. Let the feature space function be given by a rotationally symmetric function multiplied by  $e^{i\nu\theta}$ ,

$$f(x, y) = f(r) e^{i\nu\theta}.$$

The polar form of the 2D Fourier transform is given by

$$\tilde{f}(q, \phi) = \int_0^{2\pi} \int_0^\infty e^{i\nu\theta} e^{-i2\pi q r \cos(\theta - \phi)} r f(r) dr d\theta.$$

Now, after the change of variables  $\beta = \theta - \phi$ , followed by an interchange of the order of integration,

$$\tilde{f}(q, \phi) = e^{i\nu\phi} \int_0^\infty dr r f(r) \int_0^{2\pi} d\beta e^{i(\nu\beta - 2\pi q r \cos \beta)}.$$

The integral over  $\beta$  can be related to a Bessel function identity from Appendix 8.A to yield

$$\tilde{f}(q, \phi) = 2\pi e^{i\nu\phi} e^{-i\nu\pi/2} \int_0^\infty f(r) J_\nu(2\pi q r) r dr.$$

This is where the Hankel transform of order  $\nu$  comes in, by definition,

$$\mathcal{H}_\nu\{f(r)\} = 2\pi \int_0^\infty f(r) J_\nu(2\pi q r) r dr. \quad (8.136)$$

Thus,

$$\tilde{f}(q, \phi) = (-i)^\nu e^{i\nu\phi} \mathcal{H}_\nu\{f(r)\}. \quad (8.137)$$

This equation can be related to the Radon transform by first finding the Radon transform of  $f$ , and then applying the Fourier transform as indicated in Equation 8.13. In polar form,

$$\tilde{f}(p, \phi) = \int_0^{2\pi} \int_0^\infty e^{i\nu\theta} f(r) \delta[p - r \cos(\theta - \phi)] r dr d\theta.$$

Once again, the change of variables  $\beta = \theta - \phi$  is employed to obtain

$$\tilde{f}(p, \phi) = e^{i\nu\phi} \int_0^\infty dr r f(r) \int_0^{2\pi} d\beta e^{i\nu\beta} \delta(p - r \cos \beta).$$

The integration over  $\beta$  in this expression has been discussed by many authors, including Cormack (1963, 1964) and Barrett (1984), where details can be found leading to

$$\tilde{f}(p, \phi) = 2e^{i\nu\phi} \int_{|p|}^\infty f(r) T_\nu\left(\frac{p}{r}\right) \left(1 - \frac{p^2}{r^2}\right)^{-1/2} dr. \quad (8.138)$$

Some of the more useful properties of the Chebyshev polynomials of the first kind  $T_\nu$  are given in Appendix 8.A. For more details, see the summary by Arfken (1985) and the interesting discussion by Van der Pol and Weijers (1934).



It is useful to identify a Chebyshev transform by

$$\mathcal{T}_v\{f(r)\} = 2 \int_{|p|}^{\infty} f(r) T_v\left(\frac{p}{r}\right) \left(1 - \frac{p^2}{r^2}\right)^{-1/2} dr. \quad (8.139)$$

Then,

$$\check{f}(p, \phi) = e^{iv\phi} \mathcal{T}_v\{f(r)\}.$$

The Fourier transform of Equation 8.138 must be equal to Equation 8.137. It follows that the Hankel transform is given in terms of the Radon transform by

$$(-i)^v e^{iv\phi} \mathcal{H}_v\{f(r)\} = \mathcal{R}f = e^{iv\phi} \mathcal{T}_v\{f(r)\}. \quad (8.140)$$

Or, in terms of the Chebyshev transform, because the  $e^{iv\phi}$  term cancels,

$$\mathcal{H}_v\{f(r)\} = i^v \mathcal{R} \mathcal{T}_v\{f(r)\}. \quad (8.141)$$

Note that an operator identity follows immediately,

$$\mathcal{H}_v = i^v \mathcal{R} \mathcal{T}_v. \quad (8.142)$$

This relation between the Hankel transform and the Fourier transform of the Radon transform is a useful expression because it serves as the starting point for finding Hankel transforms without having to do integrals over Bessel functions. Several authors have made contributions in this area. For applications and references to the literature see Hansen (1985), Higgins and Munson (1987, 1988), and Suter (1991).

In this section we have concentrated on how the Hankel transform relates to the Radon transform. A logical extension of some of the ideas presented in this discussion appear in Section 8.13 on circular harmonic decomposition.

### 8.11.3 Spherical Symmetry, Three Dimensions

An interesting generalization of the above cases arises when the function  $f(x, y, z)$  has spherical symmetry. In this case, the Radon transform of  $f$  can be found by letting both the polar angle  $\theta$  and the azimuthal angle  $\phi$  be zero. Now the unit vector  $\xi = (0, 0, 1)$ , and formula (Equation 8.7) is given by

$$\begin{aligned} \check{f}(p) &= \int_{-\infty}^{\infty} \int_{-\infty}^{\infty} \int_{-\infty}^{\infty} f\left(\sqrt{x^2 + y^2 + z^2}\right) \delta(p - z) dx dy dz \\ &= \int_{-\infty}^{\infty} \int_{-\infty}^{\infty} f\left(\sqrt{x^2 + y^2 + p^2}\right) dx dy \\ &= \int_0^{2\pi} \int_0^{\infty} f\left(\sqrt{\rho^2 + p^2}\right) \rho d\rho d\phi \\ &= 2\pi \int_0^{\infty} f\left(\sqrt{\rho^2 + p^2}\right) \rho d\rho. \end{aligned}$$

In these equations the transformation  $x = \rho \cos \phi$ ,  $y = \rho \sin \phi$  is used. One more transformation,  $\rho^2 + p^2 = r^2$ , leads to

$$\check{f}(p) = 2\pi \int_p^{\infty} f(r) r dr, \quad p > 0. \quad (8.143)$$

Note that the lower limit follows from  $r = (p^2)^{1/2}$  when  $\rho = 0$ . The interesting point is that for this highly symmetric case, the original function  $f$  can be found by differentiation,

$$\frac{d\check{f}(p)}{dp} = -2\pi p f(p).$$

In this equation, the variable  $p$  is actually a dummy variable and it can be replaced by  $r$ ,

$$f(r) = \frac{-1}{2\pi r} \check{f}'(r). \quad (8.144)$$

This same result can be found directly from the inversion methods of Section 8.9.2. Also, Barrett (1984) does the same derivation and he makes the interesting observation that (Equation 8.144) was given in the optics literature by Vest and Steel (1978), but was actually known much earlier by Du Mond (1929) in connection with Compton scattering, and by Stewart (1957) and Mijnaerends (1967) in connection with positron annihilation.

## 8.12 Methods of Inversion

The inversion formulas given by Radon (1917) and the formulas given in Section 8.9 serve only as a beginning for an applied problem. This point is emphasized by Shepp and Kruskal (1978). The main problem is that these formulas are rigorously valid for an infinite number of projections, and in practical situations the projections are a discrete set. This discrete nature of the projections gives rise to subtle and difficult questions. Most of these are related in some way to the "Indeterminacy Theorem" by Smith et al. (1977). After a little rephrasing, the theorem establishes that: *a function  $f(x, y)$  with compact support is uniquely determined by an infinite set of projections, but not by any finite set of projections.* This clearly means that uniqueness must be sacrificed in applications. Experience with known images shows that this is not so serious if one can come close to the actual  $\check{f}$  and then apply an approximate reconstruction algorithm. Moreover, some encouragement comes from another theorem by Hamaker et al. (1980). The main thrust of this theorem is that arbitrarily good approximations to  $f$  can be found by utilization of an arbitrarily large number of projections. Perhaps the way to express all of this is to say: even though you can't win you must never give up!

There are several other considerations about inversion. The inverse Radon transform is technically an *ill-posed problem*. Small errors in knowledge of the function  $\check{f}$  can lead to very large errors in the reconstructed function  $f$ . Hence, problems of

stability, ill-posedness, accuracy, resolution, and optimal methods of sampling must be addressed when working with experimental data. These are obviously very important problems, and the subject of ongoing research. A thorough discussion would have to be highly technical and inappropriate for inclusion here. For those concerned with these matters, the papers by Lindgren and Rattey (1981), Rattey and Lindgren (1981), Louis (1984), Madych and Nelson (1986), Hawkins and Barrett (1986), Hawkins et al. (1988), Kruse (1989), Madych (1990), Faridani (1991), Faridani et al. (1992), Maass (1992), Desbat (1993), Natterer (1993), Olson and DeStefano (1994), and the books by Herman (1980) and Natterer (1986) are good starting points for methods and references to other important work. Good examples illustrating many of the difficulties encountered when dealing with real data along with defects in the reconstructed image associated with the performance of various algorithms are given in Chapter 7 of the book by Russ (1992).

There are several methods that serve as the basis for the development of algorithms that can be viewed as discrete implementations of the inversion formula. Our purpose here is to present several of these along with reference to their implementation. Those interested in more detail and other flow charts may want to see Barrett and Swindell (1977) and Deans (1983, 1993). The first topic below, the operation of *backprojection*, is an essential step in some of the reconstruction algorithms. Also, this operation is closely related to the adjoint of the Radon transform, discussed in Section 8.14. More on inversion methods is contained in Section 8.13 on series.

### 8.12.1 Backprojection

Let  $G(p, \phi)$  be an arbitrary function of a radial variable  $p$  and angle  $\phi$ . The backprojection operation is defined by replacing  $p$  by  $x \cos \phi + y \sin \phi$  and integrating over the angle  $\phi$ , to obtain a function of  $x$  and  $y$ ,

$$g(x, y) = \mathcal{B} G(p, \phi) = \int_0^\pi G(x \cos \phi + y \sin \phi, \phi) d\phi. \quad (8.145)$$

*Note:* From the definition of the backprojection operator it follows that the inversion formula (Equation 8.101) can be written as

$$f(x, y) = 2 \mathcal{B} \tilde{f}(t, \phi). \quad (8.146)$$

### 8.12.2 Backprojection of the Filtered Projections

The algorithm known as the *filtered backprojection algorithm* is presently the optimum computational method for reconstructing a function from knowledge of its projections. This algorithm can be considered as an approximate method for computer implementation of the inversion formula for the Radon transform. Unfortunately, there is some confusion associated with the name, because the filtering of the projections is done *before* the backprojection operation. Hence, a better name is the one chosen

for the title of this section. There are several ways to derive the basic formula for this algorithm. Because we want to emphasize its relation to the inversion formula, the starting point is Equation 8.146. First, rewrite that equation as

$$f = 2 \mathcal{B} \tilde{\mathcal{F}}^{-1} \tilde{\mathcal{F}} \tilde{f}. \quad (8.147)$$

Here, the identity operator for the 1D Fourier transform is used. Now, making use of various operations from Section 8.9.1, we obtain

$$\begin{aligned} f &= \frac{2\mathcal{B}}{4\pi^2} \tilde{\mathcal{F}}^{-1} \left\{ \tilde{\mathcal{F}} \frac{\partial}{\partial p} \left[ \frac{1}{p} \tilde{f}(p, \phi) \right] \right\} \\ &= \frac{\mathcal{B}}{2\pi^2} \tilde{\mathcal{F}}^{-1} \left\{ (i2\pi k) \left[ \tilde{\mathcal{F}} \left( \frac{1}{p} \right) \right] [\tilde{\mathcal{F}} \tilde{f}(p, \phi)] \right\} \\ &= \frac{\mathcal{B}}{2\pi^2} \tilde{\mathcal{F}}^{-1} \{ (i2\pi k) (i\pi \text{sngn} k) \tilde{\mathcal{F}} \tilde{f}(p, \phi) \} \\ &= \mathcal{B} \tilde{\mathcal{F}}^{-1} \{ |k| \tilde{\mathcal{F}} \tilde{f}(p, \phi) \}. \end{aligned} \quad (8.148)$$

The inverse Fourier transform operation converts a function of  $k$  to a function of some other radial variable, say  $s$ . This observation leads to a natural definition; for convenience of notation, define

$$F(s, \phi) = \tilde{\mathcal{F}}^{-1} \{ |k| \tilde{\mathcal{F}} \tilde{f}(p, \phi) \} = \tilde{\mathcal{F}}^{-1} \{ |k| \tilde{f}(k, \phi) \}. \quad (8.149)$$

Now the feature space function is recovered by backprojection of  $F$ ,

$$f(x, y) = \mathcal{B} F(s, \phi) = \int_0^\pi F(x \cos \phi + y \sin \phi, \phi) d\phi. \quad (8.150)$$

The beautiful part of this formula is that the need to use the Hilbert transform has been eliminated. From a computational viewpoint this is a real plus. For additional information on computationally efficient algorithms based on these equations, see Rowland (1979) and Lewitt (1983).

#### 8.12.2.1 Convolution Methods

Due to the presence of the  $|k|$  in Equation 8.149 the story is not over. This causes a problem with numerical implementation due to the behavior for large values of  $k$ . It would be desirable to have a well-behaved function, say  $g$ , such that  $\tilde{\mathcal{F}}g = |k|$ . Then Equation 8.149 could be modified to read

$$F(s, \phi) = \tilde{\mathcal{F}}^{-1} [(\tilde{\mathcal{F}}g)(\tilde{\mathcal{F}} \tilde{f})].$$

And, by the convolution theorem,

$$F(s, \phi) = \tilde{f} * g = \int_{-\infty}^{\infty} \tilde{f}(p, \phi) g(s - p) dp. \quad (8.151)$$

A function  $g$  such that  $\tilde{\mathcal{F}}g = |k|$  can be found, but is not well behaved. In fact, it is a singular distribution (Lighthill, 1962).

In view of these difficulties a slight compromise is in order. Rather than looking for a function whose Fourier transform equals  $|k|$ , try to find a well-behaved function with a Fourier transform that approximates  $|k|$ . The usual approach is to define a filter function in terms of a window function; that is, let

$$\mathfrak{F}g = |k|w(k). \tag{8.152}$$

Then Equation 8.151 can be used to find the function  $F$  used in the backprojection equation. One advantage of this approach is that there is no need to find the Fourier transform of the projection data  $\tilde{f}$ ; however, it is necessary to compute the convolver function

$$g(s) = \mathfrak{F}^{-1}\{|k|w(k)\} \tag{8.153}$$

before implementing Equation 8.151. This signal space convolution approach is discussed in some detail by Rowland (1979). An approach directly aimed toward computer implementation is in Rosenfeld and Kak (1982). Excellent practical discussions of windows and filters are given by Harris (1978) and by Embree and Kimble (1991).

### 8.12.2.2 Frequency Space Implementation

It should be noted that there are times when it is desirable to implement the filter in Fourier space and use Equation 8.149 in the form

$$F(s, \phi) = \mathfrak{F}^{-1}\{|k|w(k)\mathfrak{F}\tilde{f}(p, \phi)\} = \mathfrak{F}^{-1}\{|k|w(k)\tilde{f}(k, \phi)\}, \tag{8.154}$$

to approximate  $F$  before backprojecting. This has been emphasized by Budinger et al. (1979) for data where noise is an important consideration.

A diagram of the options associated with the algorithm for backprojection of the filtered projections is given in Figure 8.10.

### 8.12.3 Filter of the Backprojections

In this approach to reconstruction, the backprojection operation is applied first and the filtering or convolution comes last. When the backprojection operator is applied to the projections, the result is a blurred image that is related to the true image by a 2D convolution with  $1/r$ . Let this blurred image of the backprojected projections be designated by

$$b(x, y) = \mathcal{B}\tilde{f}(p, \phi) = \int_0^\pi \tilde{f}(x \cos \phi + y \sin \phi, \phi) d\phi. \tag{8.155}$$

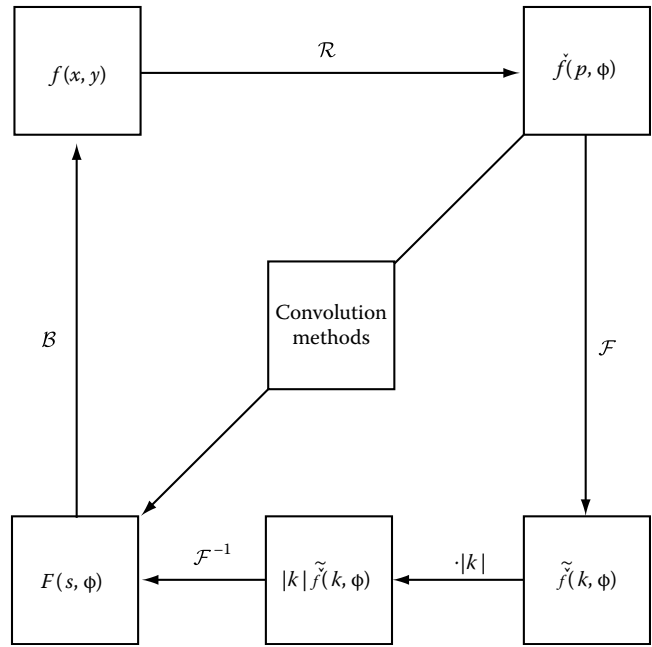


FIGURE 8.10 Filtered backprojection, convolution.

The true image is related by  $b$  by

$$b(x, y) = f(x, y) ** \frac{1}{r} = \int_{-\infty}^{\infty} \int_{-\infty}^{\infty} \frac{f(x', y') dx' dy'}{[(x - x')^2 + (y - y')^2]^{1/2}}. \tag{8.156}$$

This is not an obvious result; it can be deduced by considering Equation 8.13 in the form

$$\tilde{f} = \mathfrak{F}_1^{-1} \mathfrak{F}_2 f.$$

Apply the backprojection operator to obtain

$$b = \mathcal{B}\tilde{f} = \mathcal{B}\mathfrak{F}_1^{-1} \mathfrak{F}_2 f. \tag{8.157}$$

(In this section, subscripts on the Fourier transform operator are shown explicitly to avoid any possible confusion.) There is a subtle point lurking in this equation. Suppose the 2D Fourier transform of  $f$  produces  $\tilde{f}(u, v)$ . The inverse 1D operator  $\mathfrak{F}_1^{-1}$  is understood to operate on a radial variable in Fourier space. This means  $\tilde{f}(u, v)$  must be converted to polar form, say  $\tilde{f}(q, \phi)$  before doing the inverse 1D Fourier transform. The variable  $q$  is the radial variable in Fourier space,  $q^2 = u^2 + v^2$ . If we designate the inverse 1D Fourier transform of  $\tilde{f}(q, \phi)$  by  $f(s, \phi)$ , then

$$b(x, y) = \mathcal{B}f(s, \phi) = \mathcal{B} \int_{-\infty}^{\infty} \tilde{f}(q, \phi) e^{i2\pi sq} dq.$$

Explicitly, the backprojection operation with  $s \rightarrow x \cos \phi + y \sin \phi$  gives

$$b(x, y) = \int_0^\pi \int_{-\infty}^\infty dq \tilde{f}(q, \phi) e^{i2\pi q(x \cos \phi + y \sin \phi)}$$

$$= \int_0^{2\pi} \int_{-\infty}^\infty q^{-1} \tilde{f}(q, \phi) e^{i2\pi q r \cos(\theta - \phi)} q dq d\phi,$$

where the replacements  $x = r \cos \theta$  and  $y = r \sin \theta$  have been made, and the radical integral is over positive values of  $q$ . We observe that the expression on the right is just the inverse 2D Fourier transform,

$$b(x, y) = \tilde{\mathcal{F}}_2^{-1}\{|q|^{-1}\tilde{f}\}, \tag{8.158}$$

and from the convolution theorem

$$b(x, y) = [\tilde{\mathcal{F}}_2^{-1}\{\tilde{f}\}] ** [\tilde{\mathcal{F}}_2^{-1}\{|q|^{-1}\}]. \tag{8.159}$$

The last term on the right is just the Hankel transform of  $|q|^{-1}$  that gives  $|r|^{-1}$ , and the other term yields  $f(x, y)$ . These substitutions immediately verify Equation 8.156.

The desired algorithm follows by taking the 2D Fourier transform of Equation 8.158,

$$\tilde{\mathcal{F}}_2 b(x, y) = |q|^{-1} \tilde{f}(u, v)$$

or

$$\tilde{f}(u, v) = |q| \tilde{\mathcal{F}}_2 b.$$

Application of  $\tilde{\mathcal{F}}_2^{-1}$  to both sides of this equation, along with the replacement  $b = \mathcal{B}f$ , yields the basic reconstruction formula for filter of the backprojected projections.

$$f(x, y) = \tilde{\mathcal{F}}_2^{-1}\{|q| \tilde{\mathcal{F}}_2 \mathcal{B}f\}. \tag{8.160}$$

Just as in the previous section a window function can be introduced, but this time it must be a 2D function. Let

$$\tilde{g}(u, v) = |q| w(u, v).$$

Now Equation 8.160 becomes

$$f(x, y) = \tilde{\mathcal{F}}_2^{-1}\{\tilde{g} \tilde{\mathcal{F}}_2 \mathcal{B}f\}$$

$$= [\tilde{\mathcal{F}}_2^{-1}\{\tilde{g}\}] ** [\mathcal{B}f]$$

$$= g(x, y) ** b(x, y). \tag{8.161}$$

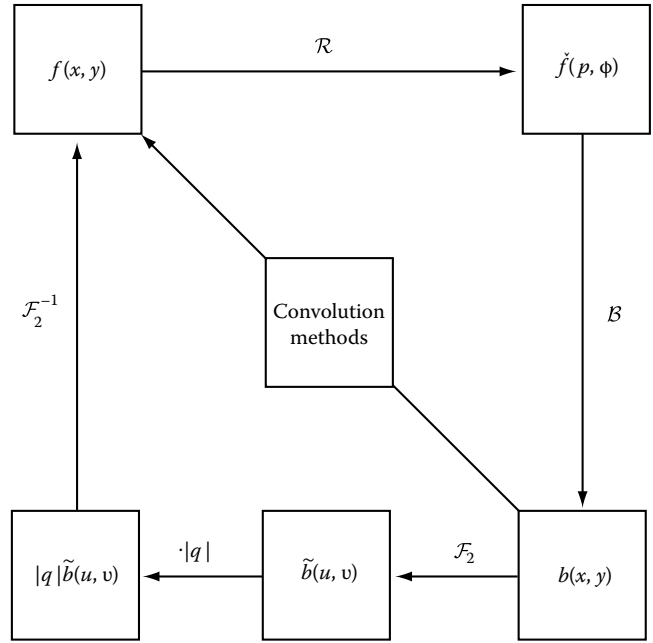


FIGURE 8.11 Filter of backprojections and convolution,  $q = \sqrt{x^2 + v^2}$ .

Once the window function is selected,  $g$  can be found in advance by calculating the inverse 2D Fourier transform, and the reconstruction is accomplished by a 2D convolution with the back-projection of the projections.

Options for implementation of these results are illustrated in Figure 8.11. Important references for applications and numerical implementation of this algorithm are Bates and Peters (1971), Smith et al. (1973), Gullberg (1979), and Budinger et al. (1979).

### 8.12.4 Direct Fourier Method

The direct Fourier method follows immediately from the central-slice theorem, Section 8.2.5, in the form

$$f = \tilde{\mathcal{F}}_2^{-1} \tilde{\mathcal{F}} f. \tag{8.162}$$

The important point is that the 1D Fourier transform of the projections produces  $\tilde{f}(q, \phi)$  defined on a polar grid in Fourier space. An interpolation is needed to get  $\tilde{f}(u, v)$  and then apply  $\tilde{\mathcal{F}}_2^{-1}$  to recover  $f(x, y)$ . The procedure is illustrated in Figure 8.12. Although this appears to be the simplest inversion algorithm, it turns out that there are computational problems associated with the interpolation and there is a need to do a 2D inverse Fourier transform. For a detailed discussion see: Mersereau (1976), Stark et al. (1981), and Sezan and Stark (1984).

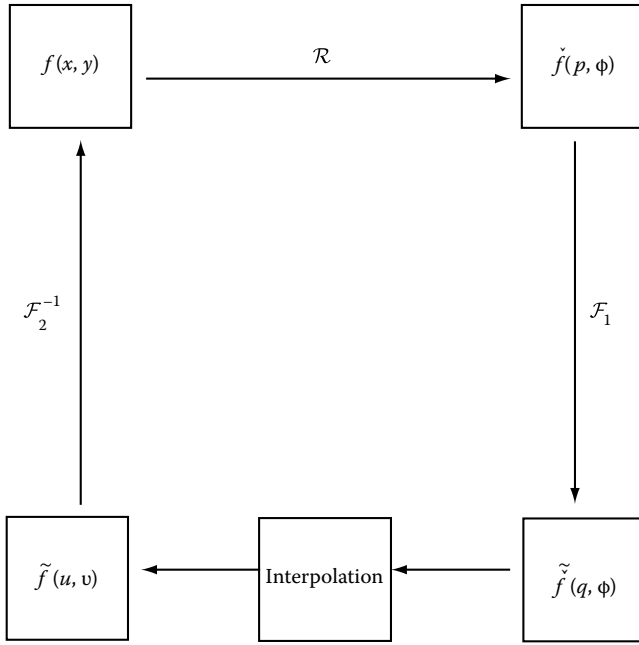


FIGURE 8.12 Direct Fourier method.

### 8.12.5 Iterative and Algebraic Reconstruction Techniques

The so-called algebraic reconstruction techniques (ART) form a large family of reconstruction algorithms. They are iterative procedures that vary depending on how the discretization is performed. There is a high computational cost associated with ART, but there are some advantages, too. Standard numerical analysis techniques can be applied to a wide range of problems and ray configurations, and a priori information can be incorporated in the solution. Details about various methods, the history, and extensive reference to original work is provided by Herman (1980), Rosenfeld and Kak (1982), and Natterer (1986). Also, the discrete Radon transform and its inversion is described by Beylkin (1987) and Kelley and Madisetti (1993), where both the forward and inverse transforms are implemented using standard methods of linear algebra.

## 8.13 Series

There are many series approaches to finding an approximation to the original feature space function  $f$  when given sufficient information about the corresponding function  $\tilde{f}$  in Radon space. The particular method selected usually depends on the physical situation and the quality of the data. The purpose of this section is to present some of the more useful approaches and observe that the basic ideas developed here carry over to other series techniques not discussed.

The approach is to give details for some of the 2D cases and quote results and references for higher dimensional cases. The first method discussed, the circular harmonic expansion, is the

method used by Cormack (1963, 1964) in his now famous work that many regard as the beginning of modern computed tomography.

### 8.13.1 Circular Harmonic Decomposition

The basic ideas developed in Section 8.11.2 can be extended to obtain the major results. First, note that in polar coordinates in feature space, functions that represent physical situations are periodic with period  $2\pi$ . This immediately leads to a consideration of expanding the function in a Fourier series. If  $f(x, y)$  is written for  $f(r, \theta)$ , then the decomposition is

$$f(r, \theta) = \sum_l h_l(r) e^{il\theta}. \tag{8.163}$$

The sum is understood to be from  $-\infty$  to  $\infty$ , and the Fourier coefficient  $h_l$  is given by

$$h_l(r) = \frac{1}{2\pi} \int_0^{2\pi} f(r, \theta) e^{-il\theta} d\theta. \tag{8.164}$$

The Radon transform of  $f$  can also be expanded in a Fourier series of the same form,

$$\tilde{f}(p, \phi) = \sum_l \tilde{h}_l(p) e^{il\phi}, \tag{8.165}$$

where

$$\tilde{h}_l(p) = \frac{1}{2\pi} \int_0^{2\pi} \tilde{f}(p, \phi) e^{-il\phi} d\phi, \quad p \geq 0, \tag{8.166a}$$

and

$$\tilde{h}_l(-p) = (-1)^l \tilde{h}_l(p). \tag{8.166b}$$

The connection between the Fourier coefficients in the two spaces can be determined by taking the Radon transform of  $f$ , as given by Equation 8.163. The polar form of the transform gives

$$\tilde{f}(p, \phi) = \sum_l \int_0^\infty \int_0^{2\pi} e^{il\theta} h_l(r) \delta[p - r \cos(\theta - \phi)] r dr d\theta.$$

Now, the change of variables  $\beta = \theta - \phi$  leads to an expression similar to one obtained in Section 8.11.2,

$$\tilde{f}(p, \phi) = \sum_l e^{il\phi} \int_0^\infty dr r h_l(r) \int_0^{2\pi} d\beta e^{il\beta} \delta(p - r \cos \beta). \tag{8.167}$$

From the linear independence of the functions  $e^{i\beta}$ , it follows by comparison of Equations 8.165 and 8.167 that

$$\check{h}_l(p) = \int_0^\infty dr r h_l(r) \int_0^{2\pi} d\beta e^{i\beta} \delta(p - r \cos \beta).$$

From Equation 8.138 this gives the connection between the Fourier coefficients in terms of a Chebyshev transform,

$$\check{h}_l(p) = 2 \int_p^\infty h_l(r) T_l\left(\frac{p}{r}\right) \left(1 - \frac{p^2}{r^2}\right)^{-1/2} dr, \quad p \geq 0. \quad (8.168a)$$

One form of the inverse is

$$h_l(r) = -\frac{1}{\pi r} \int_r^\infty \check{h}_l(p) T_l\left(\frac{p}{r}\right) \left(\frac{p^2}{r^2} - 1\right)^{-1/2} dp, \quad r > 0. \quad (8.168b)$$

Here the prime means derivative with respect to  $p$ .

The inverse (Equation 8.168b) can be found by various techniques. These include use of the Mellin transform, contour integration, and orthogonality properties of the Chebyshev polynomials of the first and second kinds. The method used by Barrett (1984) is easy to follow, and he provides extensive reference to other derivations and some of the subtleties related to the stability and uniqueness of the inverse. The problem with this expression for the inverse is that  $T_l$  increases exponentially as  $l \rightarrow \infty$  and  $\check{h}_l$  is a rapidly oscillating function. The integration of the product of these two functions leads to severe cancellations and numerical instability. For a further discussion of stability, uniqueness, and other forms for the inverse, see Hansen (1981), Hawkins and Barrett (1986), and Natterer (1986). Additional details on the circular harmonic Radon transform are given by Chapman and Cary (1986).

### 8.13.1.1 Extension to Higher Dimensions

The extension to higher dimensions is presented in detail by Ludwig (1966). Other relevant references include Deans (1978, 1979) and Barrett (1984). The  $nD$  counterpart of the transform pair is given by Equations 8.168a and b is a Gegenbauer transform pair for the radial functions,

$$\check{h}_l(p) = \frac{(4\pi)^\nu \Gamma(l+1) \Gamma(\nu)}{\Gamma(l+2\nu)} \int_p^\infty r^{2\nu} h_l(r) C_l^\nu\left(\frac{p}{r}\right) \left(1 - \frac{p^2}{r^2}\right)^{\nu-\frac{1}{2}} dr, \quad (8.169a)$$

and

$$h_l(r) = \frac{(-1)^{2\nu+1} \Gamma(l+1) \Gamma(\nu)}{2\pi^{\nu+1} \Gamma(l+2\nu) r} \int_p^\infty \check{h}_l(p) C_l^\nu\left(\frac{p}{r}\right) \left(\frac{p^2}{r^2} - 1\right)^{\nu-\frac{1}{2}} dp. \quad (8.169b)$$

In these equations,  $r \geq 0$ ,  $p \geq 0$ ,  $\check{h}_l^{-(2\nu+1)} = (d/dp)^{(2\nu+1)} \check{h}_l(p)$ ,  $\check{h}_l(-p) = (-1)^l \check{h}_l(p)$ , and  $\nu$  is related to dimension  $n$  by  $\nu = (n-2)/2$ .

The Gegenbauer polynomials  $C_l^\nu$  are orthogonal over the interval  $[-1, +1]$  (Rainville, 1960) and (Szegő, 1939). This leads to questions about the integration in Equation 8.169b. And, just as mentioned in connection with Equation 8.168b, this formula is not practical for numerical implementation. However, the integral can be understood because it is possible to define Gegenbauer functions  $G_l^\nu(z)$  analytic in the complex  $z$  plane cut from  $-1$  to  $-\infty$ . For a discussion and proofs, see Durand et al. (1976).

### 8.13.1.2 Three Dimensions

The 3D version of the expansion (Equation 8.163) is in terms of the real orthonormal spherical harmonics  $S_{lm}(\omega)$ , discussed by Hochstadt (1971),

$$f(r, \omega) = \sum_{l,m} A_{lm} h_l(r) S_{lm}(\omega). \quad (8.170)$$

The  $A_{lm}$  are real constants and  $\omega$  is a 3D unit vector,

$$\omega = (\sin \theta \cos \phi, \sin \theta \sin \phi, \cos \theta).$$

The corresponding expansion in Radon space is

$$\check{f}(p, \xi) = \sum_{l,m} A_{lm} \check{h}_l(r) S_{lm}(\xi). \quad (8.171)$$

It follows from the orthogonality of the spherical harmonics that

$$A_{lm} \check{h}_l(p) = \int_{|\xi|=1} \check{f}(p, \xi) S_{lm}(\xi) d\xi, \quad (8.172)$$

where  $d\xi$  is the surface element on a unit sphere. The Gegenbauer transform Equations 8.169a and b reduces to a Legendre transform for  $n = 3$ ,  $\nu = \frac{1}{2}$ , and the radial functions satisfy

$$\check{h}_l(p) = 2\pi \int_p^\infty r h_l(r) P_l\left(\frac{p}{r}\right) dr, \quad (8.173a)$$

$$h_l(r) = \frac{1}{2\pi r} \int_r^\infty \check{h}_l(p) P_l\left(\frac{p}{r}\right) dp. \quad (8.173b)$$

The spherical harmonics  $Y_{lm}(\theta, \phi)$ , discussed by Arfken (1985), are probably more familiar to engineers and physicists. These can be used in place of the  $S_{lm}$  suggested here. However, various properties (real, orthonormal, symmetry) of the  $S_{lm}$  make them more suitable for use in connection with problems involving the general  $nD$  Radon transform (Ludwig, 1966).

For the 3D case, one possible connection is given by

$$S_{lm} = \begin{cases} \frac{Y_{lm} + Y_{lm}^*}{\sqrt{2}}, & \text{for } m = 1, 2, \dots, l \\ Y_{l0}, & \text{for } m = 0 \\ \frac{Y_{lm} - Y_{lm}^*}{i\sqrt{2}}, & \text{for } m = -1, -2, \dots, -l, \end{cases}$$

where  $Y_{l,-m} = (-1)^m Y_{lm}^*$ . Note that under the parity operation

$$(x \rightarrow -x, y \rightarrow -y, z \rightarrow -z),$$

the well known result  $Y_{lm} \rightarrow (-1)^l Y_{lm}$  carries over to the  $S_{lm}(\omega)$ , giving

$$S_{lm}(-\omega) = (-1)^l S_{lm}(\omega).$$

### 8.13.2 Orthogonal Functions on the Unit Disk

In most practical reconstruction problems the function in feature space is confined to a finite region. This region can always be scaled to fit inside a unit disk. Hence, the development of an orthogonal function expansion on the unit disk holds promise as a useful approach for inversion using series methods. (In this connection, note that when the problem is confined to the unit disk the infinite upper limit on all integrals in the previous section can be replaced by unity.) Orthogonal polynomials that have been used for many years in optics are especially good candidates. These are the Zernike polynomials; a standard reference is Born and Wolf (1975); also see Chapter 1. A more recent reference, Kim and Shannon (1987), contains a graphic library of 37 selected Zernike expansion terms. One reason why these functions are desirable is that their transforms ( $\mathfrak{R}$  and  $\mathfrak{F}$ ) lead to orthogonal function expansions in both Radon and Fourier space. This choice for basis functions in reconstruction has been discussed by Cormack (1964), Marr (1974), Zeitler (1974), and Hawkins and Barrett (1986), and examples similar to those given here are given by Deans (1983, 1993).

The approach is to assume that  $f(x, y)$  can be approximated by a sum of monomials of the form  $x^k y^j$ . Then  $x^k y^j$  can be written as  $r^{k+j}$  multiplied by some function of  $\sin \theta$  and  $\cos \theta$ . This leads to the consideration of an expansion of the form

$$f(r, \theta) = \sum_{l=-\infty}^{\infty} h_l(r) e^{il\theta} = \sum_{s=0}^{\infty} \sum_{l=-\infty}^{\infty} A_{ls} Z_{|l|+2s}^{|l|}(r) e^{il\theta}, \quad (8.174)$$

in terms of complex constants  $A_{ls}$  and Zernike polynomials  $Z_m^l(r)$ , with  $m = |l| + 2s$ . The Radon transform of this expression can be found exactly, and it contains the same constants. These constants are evaluated in Radon space, and the feature space function is found by the expansion (Equation 8.174). There are several subtle points associated with this process, and it is useful to break the problem into separate parts. First, we discuss

relevant properties of the Zernike polynomials, and give some simple examples. This is followed with the transform to Radon space, and more examples. Next, the expression for the constants  $A_{ls}$  is found in terms of  $f$ , which is assumed known from experiment. Finally, to emphasize that this application also extends to Fourier space, the transform to Fourier space is illustrated, along with some observations regarding three different orthonormal basis sets.

#### 8.13.2.1 Zernike Polynomials

The Zernike polynomials (see Section 1.5) can be found by orthogonalizing the powers

$$r^l, r^{l+2}, r^{l+4}, \dots$$

with weight function  $r$  over the interval  $[0, 1]$ . The exponent  $l$  is a nonnegative integer. The resulting polynomial  $Z_m^l(r)$  is a degree  $m = l + 2s$  and it contains no powers of  $r$  less than  $l$ . The polynomials are even if  $l$  is even and odd if  $l$  is odd. This leads to an important symmetry relation,

$$Z_m^l(-r) = (-1)^l Z_m^l(r). \quad (8.175)$$

The orthogonality condition is given by

$$\int_0^1 Z_{l+2s}^l(r) Z_{l+2t}^l(r) r dr = \frac{1}{2(l+2s+1)} \delta_{st}. \quad (8.176)$$

It follows that the expansion coefficients are given by

$$A_{ls} = \frac{2(l+2s+1)}{2\pi} \int_0^{2\pi} \int_0^1 f(r \cos \theta, r \sin \theta) Z_{l+2s}^l(r) e^{-il\theta} r dr d\theta. \quad (8.177a)$$

In this equation  $l \geq 0$ . To find the expansion coefficient for negative values of  $l$ , use the complex conjugate,

$$A_{-l,s} = A_{ls}^*. \quad (8.177b)$$

Some simple examples are useful to gain an understanding of just how the expansion works. A short table of Zernike polynomials is given in Appendix 8.A. Methods for extending the table and many other properties are given by Born and Wolf (1975).

#### Example 8.39

Let the feature space function be given by  $f(x, y) = y$  in the unit circle and zero outside the circle. Thus, in terms of  $r$ ,

$$f(x, y) = r \sin \theta.$$

Here, the degree is 1 and  $|| + 2s \leq 1$ . The series expansion (Equation 8.174) reduces to

$$f(x, y) = A_{00}Z_0^0 + A_{10}Z_1^1e^{i\theta} + A_{-10}Z_1^1e^{-i\theta}.$$

This case is easy enough to do by inspection of the table of Zernike polynomials in Appendix 8.A. The coefficients are  $A_{00} = 0, A_{10} = \frac{1}{2}, A_{-10} = -\frac{1}{2}$ . This choice gives

$$f(x, y) = r \frac{e^{i\theta} - e^{-i\theta}}{2i} = Z_1^1(r) \sin \theta.$$

**Example 8.40**

This time let  $f(x, y) = xy$ , so  $f(r, \theta) = r^2 \cos \theta \sin \theta$ . It follows immediately from the angular part of the integral in Equation 8.177a that the only nonzero coefficients are given by  $A_{20} = \frac{1}{4}$  and  $A_{-20} = \frac{1}{4}$ . This leads to the expansion

$$f(x, y) = (A_{20}e^{2i\theta} + A_{-20}e^{-2i\theta})Z_2^2(r)$$

or

$$f(x, y) = r^2 \frac{e^{2i\theta} - e^{-2i\theta}}{4i} = r^2 \cos \theta \sin \theta.$$

**Example 8.41**

Let  $f(x, y) = x(x^2 + y^2)$ . Now, changing to  $r$  and  $\theta$  gives  $f(r, \theta) = r^3 \cos \theta$ . It is tempting to take a quick look at the table and say the expansion must contain  $A_{30}$  and  $Z_3^3$  because this polynomial is equal to  $r^3$ . This is *not* the correct thing to do! A quick inspection of the angular part of Equation 8.177a reveals that  $A_{30}$  vanishes. The nonzero constants are  $A_{11} = A_{-11} = \frac{1}{6}$ , and  $A_{10} = A_{-10} = \frac{1}{3}$ . This gives the correct expansion

$$f(x, y) = \frac{1}{3}Z_3^1(r) \cos \theta + \frac{2}{3}Z_1^1(r) \cos \theta = r^3 \cos \theta.$$

**8.13.2.2 Transform of the Zernike Polynomials**

We need to find the Radon transform of a function of the form

$$f(x, y) = Z_m^l(r)e^{il\theta}.$$

It is adequate to consider  $l \geq 0$ , because the negative case follows by complex conjugation. The angular part transforms to  $e^{il\phi}$  and the radial part must satisfy Equation 8.168a with upper limit 1,

$$\check{h}_l(p) = 2 \int_p^1 Z_m^l(r) T_l\left(\frac{p}{r}\right) \left(1 - \frac{p^2}{r^2}\right)^{-1/2} dr, \quad p \geq 0. \quad (8.178)$$

There are various ways to evaluate this integral, and the details are not shown here. The method used by Zeitler (1974) and Deans (1983, 1993) makes use of the path through Fourier space to find the transformed function in Radon space. The important result is that the orthogonal set of Zernike polynomials transforms to the orthogonal set of Chebyshev polynomials of the second kind,

$$\mathfrak{R}\{Z_m^l(r)e^{il\theta}\} = \frac{2}{m+1} \sqrt{1-p^2} U_m(p)e^{il\phi}, \quad (8.179)$$

with  $m = l + 2s$ . Basic properties of the  $U_m$  are given in Appendix 8.A, and summaries are given by Arfken (1985) and Erdélyi et al. (1953).

The Radon transform of Equation 8.174 follows immediately by use of Equation 8.179,

$$\check{f}(p, \phi) = \sum_{s=0}^{\infty} \sum_{l=-\infty}^{\infty} A_{ls} \frac{2}{|l| + 2s + 1} \times \sqrt{1-p^2} U_{|l|+2s}(p)e^{il\phi}. \quad (8.180)$$

Some more examples serve to illustrate how the method developed here relates to transforms found in earlier sections when the function is confined to the unit disk. Also, these examples are designed to point out ways certain pitfalls can be avoided.

**Example 8.42**

If  $f(x, y) = 1$  on the unit disk and zero elsewhere, the expansion in terms of Zernike polynomials is just  $f = Z_0^0$ , with  $A_{00} = 1$ . From Equation 8.180,  $f = 2\sqrt{1-p^2}$ , because  $U_0 = 1$ . Note that this is just another way of doing Example 8.9.

**Example 8.43**

If  $f(x, y) = x^2 = r^2 \cos^2 \theta = \frac{1}{2}r^2(1 + \cos 2\theta)$  on the unit disk, then

$$f(x, y) = \frac{1}{4}(Z_0^0 + Z_2^0) + \frac{1}{2}Z_2^2 \cos 2\theta.$$

This serves to identify the coefficients  $A_{ls}$  and by use of Equation 8.180

$$\check{f} = \sqrt{1-p^2} \left[ \frac{1}{4} \left( 2U_0 + \frac{2}{3}U_2 \right) + \frac{1}{3}U_2 \cos 2\phi \right].$$

After simplification,

$$\mathfrak{R}\{x^2\} = \sqrt{1-p^2} \left[ 2p^2 \cos^2 \phi + \frac{2}{3}(1-p^2) \sin^2 \phi \right].$$

Now note that if  $f(x, y) = y^2 = \frac{1}{2}r^2(1 - \cos 2\theta)$ , the change is  $(\cos \phi \leftrightarrow \sin \phi)$  in the equation for  $\mathfrak{R}\{x^2\}$ , and

$$\mathfrak{R}\{y^2\} = \sqrt{1-p^2} \left[ 2p^2 \sin^2 \phi + \frac{2}{3}(1-p^2) \cos^2 \phi \right].$$



Finally, by linearity, the transform of  $f(x, y) = x^2 + y^2$  is given by the sum of the above transforms

$$\mathfrak{R}\{x^2 + y^2\} = \frac{2}{3} \sqrt{1 - p^2} (2p^2 + 1).$$

### Example 8.44

Let  $f(x, y) = 1 - r^2$  on the unit disk. By using the methods of the earlier examples in this section

$$f = z_0^0 - \frac{1}{2}(z_0^0 + z_2^0) = \frac{1}{2}z_0^0 - \frac{1}{2}z_2^0.$$

From Equation 8.180

$$\check{f} = \frac{1}{2} 2\sqrt{1 - p^2} U_0 - \frac{1}{2} \frac{2}{3} \sqrt{1 - p^2} U_2.$$

Or, after substitution for  $U_0$  and  $U_2$  from Appendix 8.A,

$$\check{f} = \frac{4}{3} (1 - p^2) \sqrt{1 - p^2}.$$

Another way to obtain this is to use Examples 8.42 and 8.43 and linearity.

### Example 8.45

For  $f(x, y) = x(x^2 + y^2)$  as in Example 8.41, it follows from knowing that  $A_{ls}$  that

$$\begin{aligned} \check{f} &= \frac{1}{3} \sqrt{1 - p^2} \left[ \frac{1}{2} U_3 + 2U_1 \right] \cos \phi \\ &= \frac{2}{3} p (2p^2 + 1) \sqrt{1 - p^2} \cos \phi. \end{aligned}$$

### Example 8.46

It may be worthwhile to emphasize that there are certain transforms that cannot be found by a naive application of the Zernike polynomials. To illustrate, suppose  $f(x, y) = x\sqrt{x^2 + y^2}$ . Although this has the form  $f = xr = Z_2^2 \cos \theta$ , it is not a simple sum over monomials  $x^k y^j$ , and the method of this section does not apply. The transform can be found by use of the technique in Example 8.11 of Section 8.5. The solution is

$$\check{f}(p, \phi) = 2p \cos \phi \left[ \frac{1}{2} \sqrt{1 - p^2} + \frac{p^2}{2} \log \left( \frac{1 + \sqrt{1 - p^2}}{p} \right) \right].$$

Clearly, this does not follow by Zernike decomposition of  $xr$ .

### 8.13.2.3 Evaluation in Radon Space

In the previous section, Equation 8.180 was used to find Radon transforms when the constants  $A_{ls}$  can be determined by knowing the feature space function. Here the idea is to determine the same constants by knowledge of the Radon space function  $\check{f}$ . It is easy to solve for the constants directly from Equation 8.180. Multiply both sides by  $e^{-il\phi} U_{|l|+2s}$  and integrate over  $p$  and  $\phi$ . Then use the orthogonality equation for the  $U_m$  in Appendix 8.A to find the constants,

$$A_{ls} = \frac{|l| + 2s + 1}{2\pi^2} \int_0^{2\pi} \int_{-1}^1 \check{f}(p, \phi) e^{-il\phi} U_{|l|+2s} dp d\phi. \quad (8.181)$$

### Example 8.47

This simplest test of Equation 8.181 is for the inverse of the problem of Example 8.42. We assume that  $\check{f} = 2\sqrt{1 - p^2}$  with  $l = s = 0$ , then  $f = 1$  on the unit disk

$$\begin{aligned} A_{00} &= \frac{1}{2\pi^2} \int_0^{2\pi} \int_{-1}^1 2\sqrt{1 - p^2} dp d\phi \\ &= \frac{2}{\pi} \int_{-1}^1 \sqrt{1 - p^2} dp = 1. \end{aligned}$$

### 8.13.2.4 Transform to Fourier Space

The Radon transform of the basis set given in Equation 8.179 transformed one orthogonal set to another orthogonal set. It is interesting to examine the Fourier transform of the basis set. It turns out that this also leads to another orthogonal set. Details are given by Zeitler (1974) and Deans (1983, 1993). The important result is that

$$\mathfrak{F}_2 \{ Z_{l+2s}^l(r) e^{il\theta} \} = (-i)^l (-1)^s e^{il\phi} \frac{J_{l+2s+1}(2\pi q)}{q}. \quad (8.182)$$

This equation is obtained using the symmetric form of the Fourier transform (see Equation 8.14). These Bessel functions are orthogonal with respect to weight function  $q^{-1}$ , and have been studied by Wilkins (1948),

$$\int_0^\infty J_{|l|+2s+1}(q) J_{|l|+2t+1}(q) q^{-1} dq = \frac{\delta_{st}}{2(|l| + 2s + 1)}.$$

The Fourier space version of Equation 8.174 is

$$\check{f}(q, \phi) = \sum_{s=0}^\infty \sum_{l=-\infty}^\infty (-i)^l (-1)^s A_{ls} e^{il\phi} \frac{J_{|l|+2s+1}(2\pi q)}{q}. \quad (8.183)$$

**Example 8.48**

The Fourier transform of the characteristic function of the unit disk, Example 8.42, with  $A_{00}=1$  and  $l=s=0$ , is given by  $J_1(2\pi q)/q$ .

**Example 8.49**

For the function in Example 8.44, the expansion (Equation 8.183), with  $A_{00} = \frac{1}{2}$  and  $A_{01} = -\frac{1}{2}$ , yields

$$\tilde{\mathfrak{F}}_2\{1 - r^2\} = \frac{J_1(2\pi q)}{2q} + \frac{J_3(2\pi q)}{2q} = \frac{J_2(2\pi q)}{\pi q^2}.$$

The last equality follows from the Bessel function identity

$$J_{n-1}(z) + J_{n+1}(z) = \frac{2n}{z} J_n(z)$$

with  $n=2$  and  $z=2\pi q$ .

**Example 8.50**

Repeat Example 8.43 with transforms to Fourier space using Equation 8.183.

$$\begin{aligned} \tilde{\mathfrak{F}}_2\{x^2\} &= \frac{J_1(2\pi q)}{4q} - \frac{J_3(2\pi q)}{4q} - \frac{J_3(2\pi q)}{2q} \cos 2\phi \\ \tilde{\mathfrak{F}}_2\{y^2\} &= \frac{J_1(2\pi q)}{4q} - \frac{J_3(2\pi q)}{4q} + \frac{J_3(2\pi q)}{2q} \cos 2\phi \\ \tilde{\mathfrak{F}}_2\{x^2 + y^2\} &= \frac{J_1(2\pi q)}{2q} - \frac{J_3(2\pi q)}{2q} = \frac{J_1(2\pi q)}{q} - \frac{J_2(2\pi q)}{\pi q^2}. \end{aligned}$$

The last part follows from the identity in Example 8.49. Also, note that the result for  $x^2 + y^2$  follows directly from Examples 8.48 and 8.49 and linearity.

**8.13.2.5 Some Final Observations**

It is possible to find orthogonal function expansions that transform to each other in all three spaces. In feature space the Zernike polynomials, defined on the unit disk, are orthogonal with weight function  $r$  over the interval  $0 \leq r \leq 1$ . In Radon space the Chebyshev polynomials of the second kind emerge, orthogonal on the interval  $-1 \leq p \leq 1$  with weight function  $\sqrt{1-p^2}$ . These are both defined on finite intervals and consequently, as is to be expected, in Fourier space the interval is infinite,  $0 \leq q \leq \infty$ . The orthogonal functions are no longer polynomials, they are orthogonal Bessel functions with weight function  $q^{-1}$ . The orthogonality integrals over the three spaces, including the angles, are given by

$$\begin{aligned} &\int_0^{2\pi} \int_0^1 \left[ Z_{|l|+2s}^{|l|}(r) e^{il\theta} \right]^* Z_{|l'|+2s'}^{|l'|}(r) e^{il'\theta} r dr d\theta \\ &= \frac{\pi}{|l| + 2s + 1} \delta_{ll'} \delta_{ss'}, \end{aligned} \tag{8.184a}$$

$$\begin{aligned} &\int_0^{2\pi} \int_{-1}^1 \left[ U_{|l|+2s}^{|l|}(p) e^{il\phi} \right]^* U_{|l'|+2s'}^{|l'|}(p) e^{il'\phi} \sqrt{1-p^2} dp d\phi \\ &= \pi^2 \delta_{ll'} \delta_{ss'}, \end{aligned} \tag{8.184b}$$

$$\begin{aligned} &\int_0^{2\pi} \int_0^\infty \left[ J_{|l|+2s+1}^{|l|}(q) e^{il\phi} \right]^* J_{|l'|+2s'+1}^{|l'|}(q) e^{il'\phi} q^{-1} dq d\phi \\ &= \frac{\pi}{|l| + 2s + 1} \delta_{ll'} \delta_{ss'}. \end{aligned} \tag{8.184c}$$

**8.14 Parseval Relation**

In the notation of Section 8.1.2, let inner products in  $nD$  be designated by

$$\langle f, g \rangle = \int f^*(\mathbf{x})g(\mathbf{x})d\mathbf{x}.$$

If the  $nD$  Fourier transforms of  $f$  and  $g$  are designated by  $\tilde{f}$  and  $\tilde{g}$ , the Parseval relation for the Fourier transform is given by

$$\langle f, g \rangle = \langle \tilde{f}, \tilde{g} \rangle. \tag{8.185}$$

The integral on the right is over all Fourier space. If  $g=f$ , then the integrals are normalization integrals. This guarantees that if  $f$  is normalized to unity, then its Fourier transform is also normalized to unity.

The corresponding expression for the Radon transform is considerably more complicated, and we need to extend some of the previous work in order to give a general result. First, define the *adjoint* for the Radon transform. If inner products in Radon space are designated by square brackets, then  $\mathfrak{N}^\dagger$  is ense that

$$\langle f, \mathfrak{N}^\dagger g \rangle = [\mathfrak{N} f, G]. \tag{8.186}$$

Here,  $G$  is a function of the variables in Radon space,  $G = G(p, \xi)$ , and the adjoint operator  $\mathfrak{N}^\dagger$  converts  $G$  to a function of  $\mathbf{x}$ , designated by  $g(\mathbf{x}) = \mathfrak{N}^\dagger G(p, \xi)$ . For example, in 2D the adjoint is just two times the backprojection operator,  $\mathfrak{N}^\dagger = 2\mathfrak{B}$ .

**Example 8.51**

It is instructive to see how Equation 8.186 comes from the definitions,

$$\begin{aligned}
 \langle f, \mathfrak{R}^\dagger g \rangle &= \int d\mathbf{x} f(\mathbf{x}) g(\mathbf{x}) \\
 &= \int d\mathbf{x} f(\mathbf{x}) \int_{|\xi|=1} d\xi G(\xi \cdot \mathbf{x}, \xi) \\
 &= \int d\mathbf{x} f(\mathbf{x}) \int_{|\xi|=1} d\xi \int_{-\infty}^{\infty} dp G(p, \xi) \delta(p - \xi \cdot \mathbf{x}) \\
 &= \int_{|\xi|=1} d\xi \int_{-\infty}^{\infty} dp \int d\mathbf{x} f(\mathbf{x}) \delta(p - \xi \cdot \mathbf{x}) G(p, \xi) \\
 &= \int_{|\xi|=1} d\xi \int_{-\infty}^{\infty} dp \tilde{f}(p, \xi) G(p, \xi) \\
 &= [\mathfrak{R}f, G].
 \end{aligned}$$

The significance of this result is more apparent after making a generalization of Section 8.9 to include the  $nD$  inversion formula. Define the operator  $\mathbf{Y}$  to cover both the even and odd dimension cases (Ludwig, 1966), (Deans, 1983, 1993):

$$\begin{aligned}
 y\bar{g}(t) &= \mathbf{Y}g \\
 &= \begin{cases} N_n \left[ \left( \frac{\partial}{\partial p} \right)^{n-1} g(p) \right]_{p=t} & n \text{ odd} \\ \frac{N_n}{i} \left[ \mathfrak{H}_i \left\{ \left( \frac{\partial}{\partial p} \right)^{n-1} g(p) \right\} \right]_{p=t} & n \text{ even,} \end{cases} \quad (8.187)
 \end{aligned}$$

where  $N_n = \frac{1}{2}(2\pi)^{1-n}$ . This reduces to Equation 8.100 for  $n=2$  and to Equation 8.103 for  $n=3$ .

With this definition the inversion formula for the Radon transform is given by

$$f = \mathfrak{R}^\dagger \bar{f} = \mathfrak{R}^\dagger \mathbf{Y} \tilde{f} = \mathfrak{R}^\dagger \mathbf{Y} \mathfrak{R} f. \quad (8.188)$$

This leads to the operator identity *operating in feature space*,

$$I = \mathfrak{R}^\dagger \mathbf{Y} \mathfrak{R}. \quad (8.189)$$

By starting with

$$\mathfrak{R}^\dagger G = g = I g = \mathfrak{R}^\dagger \mathbf{Y} \mathfrak{R} \mathfrak{R}^\dagger G,$$

it follows that the identity *operating on functions in Radon space* is given by

$$I = \mathbf{Y} \mathfrak{R} \mathfrak{R}^\dagger. \quad (8.190)$$

When Equations 8.186 and 8.190 are combined, we obtain the desired form for the Parseval relation for the Radon transform,

$$\begin{aligned}
 \langle f, g \rangle &= \langle f, \mathfrak{R}^\dagger G \rangle \\
 &= [\mathfrak{R}f, IG] \\
 &= [\mathfrak{R}f, \mathbf{Y} \mathfrak{R} \mathfrak{R}^\dagger G] \\
 &= [\mathfrak{R}f, \mathbf{Y} \tilde{g}] \\
 &= [\tilde{f}, \mathbf{Y} \tilde{g}] \quad (8.191)
 \end{aligned}$$

An important special case is for  $g=f$ , then

$$\langle f, f \rangle = [\tilde{f}, \mathbf{Y} \tilde{f}]. \quad (8.192)$$

**Example 8.52**

Verify the Parseval relation (Equation 8.192) explicitly in all three spaces for  $f(x, y) = e^{-x^2 - y^2}$ . This looks simple, but it demonstrates the difficulty of dealing with Radon space compared with feature space and Fourier space.

*Feature space:*

$$\begin{aligned}
 \langle f, f \rangle &= \int_{-\infty}^{\infty} \int_{-\infty}^{\infty} e^{-x^2 - y^2} e^{-x^2 - y^2} dx dy \\
 &= \int_{-\infty}^{\infty} \int_{-\infty}^{\infty} e^{-2x^2 - 2y^2} dx dy \\
 &= \frac{\sqrt{\pi}}{\sqrt{2}} \frac{\sqrt{\pi}}{\sqrt{2}} = \frac{\pi}{2}.
 \end{aligned}$$

*Fourier space:* Note that  $q^2 = u^2 + v^2$ . Then

$$\begin{aligned}
 \langle \tilde{f}, \tilde{f} \rangle &= \int_{-\infty}^{\infty} \int_{-\infty}^{\infty} \pi e^{-\pi^2(u^2+v^2)} \pi e^{-\pi^2(u^2+v^2)} du dv \\
 &= \pi^2 \int_{-\infty}^{\infty} \int_{-\infty}^{\infty} e^{-2\pi^2 u^2} e^{-2\pi^2 v^2} du dv \\
 &= \pi^2 \frac{\sqrt{\pi}}{\sqrt{2\pi^2}} \frac{\sqrt{\pi}}{\sqrt{2\pi^2}} = \frac{\pi}{2}.
 \end{aligned}$$

*Radon space:* Verification in Radon space is not as easy as the other two cases due to the presence of the Hilbert transform. The entire calculation is shown in detail, because there are some tricky parts. First note that  $\partial \tilde{f} / \partial p = -2\sqrt{\pi} p e^{-p^2}$ . Then Equation 8.192 is

$$\begin{aligned}
 [\tilde{f}, \mathbf{Y} \tilde{f}] &= \left[ \sqrt{\pi} e^{-p^2}, \frac{-1}{4\pi} \mathfrak{H}_i \left( \frac{\partial \tilde{f}}{\partial p} \right) \right] \\
 &= \left[ \sqrt{\pi} e^{-p^2}, \left( \frac{-1}{4\pi} \right) (-2\sqrt{\pi}) \mathfrak{H}_i(p e^{-p^2}) \right] \\
 &= \frac{1}{2} \left[ e^{-p^2}, \mathfrak{H}_i(p e^{-p^2}) \right].
 \end{aligned}$$

Because there is no angle dependence, the integral  $\int_{|\xi|} d\xi = 2\pi$ . Hence, the last inner product becomes

$$\begin{aligned} [\tilde{f}, Y\tilde{f}] &= \frac{2\pi}{2} \int_{-\infty}^{\infty} dp e^{-p^2} \frac{1}{\pi} \int_{-\infty}^{\infty} ds \frac{se^{-s^2}}{s-p} \\ &= \int_{-\infty}^{\infty} dp e^{-p^2} \int_{-\infty}^{\infty} ds \frac{se^{-s^2}}{s-p}. \end{aligned}$$

Now the problem is to demonstrate that this double integral yields  $\pi/2$ . Change the order of integration to get

$$[\tilde{f}, Y\tilde{f}] = \int_{-\infty}^{\infty} ds se^{-s^2} \int_{-\infty}^{\infty} dp \frac{e^{-p^2}}{s-p}.$$

From page 227 of Davis and Rabinowitz (1984), this becomes

$$[\tilde{f}, Y\tilde{f}] = \int_{-\infty}^{\infty} ds se^{-s^2} \sqrt{\pi} se^{-s^2} \int_{-1}^1 dp e^{s^2 p^2}.$$

Another change in the order of integration followed by evaluation of the definite integrals (Appendix 8.A) yields the desired result,

$$\begin{aligned} [\tilde{f}, Y\tilde{f}] &= \sqrt{\pi} \int_{-1}^1 dp \int_{-\infty}^{\infty} ds s^2 e^{-(2-p^2)s^2} \\ &= \frac{\sqrt{\pi}\sqrt{\pi}}{2} \int_{-1}^1 \frac{dp}{(2-p^2)^{3/2}} \\ &= \pi \int_0^1 \frac{dp}{(2-p^2)^{3/2}} \\ &= \frac{\pi}{2}. \end{aligned}$$

## 8.15 Generalizations and Wavelets

Mathematical generalization of the Radon transform and some of the more technical applications are discussed in the recent publications edited by Grinberg and Quinto (1990) and Gindikin and Michor (1994). There are many other references and the reader interested in some of the more abstract treatments will find these two books good entry points to the literature.

A generalization that has important applicability in the area of image reconstruction in nuclear medicine is known as the *attenuated* Radon transform. One way to define this transform is to modify Equation 8.4 to read

$$\begin{aligned} \tilde{f}_{\mu}(p, \phi) &= \int_{-\infty}^{\infty} f(p\xi + t\xi') \\ &\quad \exp \left[ - \int_t^{\infty} \mu(p\xi + s\xi') ds \right] dt. \end{aligned} \quad (8.193)$$

If the attenuation term  $\mu$  is a constant, say  $\mu_0$ , that vanishes outside a finite region, then this equation reduces to what is often referred to as the *exponential* Radon transform,

$$\tilde{f}_{\mu_0}(p, \phi) = \int_{-\infty}^{\infty} e^{\mu_0 t} f(p\xi + t\xi') dt. \quad (8.194)$$

These transforms are fundamental in single photon emission computed tomography (SPECT), and to a lesser degree in positron emission tomograph (PET) where corrections can be introduced to compensate for attenuation (Budinger et al., 1979). For details see Natterer (1979, 1986), Tretiak and Metz (1980), Clough and Barrett (1983), Hawkins et al. (1988), Hazou and Solmon (1989), and Nievergelt (1991).

One of the most recent and certainly one of the most exciting new developments is the use of the wavelet transform in connection with the Radon transform. The application of wavelets to inversion of the Radon transform has been investigated by Kaiser and Streater (1992). They make use of a change of variables to connect a generalized version of the Radon transform to a continuous wavelet transform. Work along related lines was done by Holschneider (1991) where the inverse wavelet transform is used to obtain a pointwise and uniformly convergent inversion formula for the Radon transform.

Berenstein and Walnut (1994) use the theory of the continuous wavelet transform to derive inversion formulas for the Radon transform. The inversion formula they obtain is "local" in even dimensions in the following sense (stated for 2D): to recover  $f$  to a given accuracy in a circle of radius  $r$  about a point  $(x_0, y_0)$  it is sufficient to know only those projections through a circle of radius  $r + \alpha$  about  $(x_0, y_0)$  for some  $\alpha > 0$ . The accuracy increases as  $\alpha$  increases. In a related paper, Walnut (1992) demonstrates how the Gabor and wavelet transforms relate to the Radon transform. He finds inversion formulas for  $\tilde{f}$  based on Gabor and wavelet expansions by a direct method and by the filtered backprojection method.

More work on wavelet localization of the Radon transform is in the papers by Olson and DeStefano (1994), and Olson (1995). As mentioned in Section 8.9, they emphasize that one problem with the Radon transform in two dimensions (most relevant in medical imaging) is that the inversion formula is globally dependent upon the line integral of the object function  $f$ . A fundamental important aspect of their work is that they are able to develop a stable algorithm that uses properties of wavelets to "essentially localize" the Radon transform. This means collect line integrals which pass through the region of interest, plus a small number of integrals not through the region. Recent work by Rashid-Farrokhi et al. (1997) makes use of the properties of wavelets with many vanishing moments to reconstruct local regions of a cross section using almost completely local data. A comprehensive discussion of the Radon transform and local tomography is given in the book by Ramm and Katsevich (1996).

The work by Donoho (1992) on nonlinear solution of linear inverse problems by wavelet-vaguelette decomposition is relevant

to the inversion of Abel-type transforms and Radon transforms. This method serves as a substitute for the singular value decomposition of an inverse problem, and applies to a large class of ill-posed inverse problems.

Another important applied generalization is related to fan beam and cone beam tomography. Recent work in these areas can be found in papers by Natterer (1993), Kudo and Saito (1990, 1991), Rizo et al. (1991), Gullberg et al. (1991), and in the book by Natterer (1986).

In recent work by Wood and Barry (1994), the Winger distribution is combined with the Radon transform to facilitate the analysis of multicomponent linear FM signals. These authors provide several references to other applications of this combined transform, now known as the Radon-Wigner transform.

### 8.16 Discrete Periodic Radon Transform

A natural extension of the continuous Radon transform that can be used for discrete data sets has been developed by Gertner (1988). Further work by Hsung et al. (1996) demonstrates many details regarding both the forward and inverse discrete periodic Radon transform (DPRT). The application of this transform to  $N \times N$  sets of data when  $N$  is prime will be demonstrated here. This is the simplest case; however, further generalizations are possible and for these we refer the reader to Hsung et al. (1996).

Clearly, a prime factor algorithm is not greatly restrictive since there are primes just a little greater than any power of two and zeros can be added with absolutely no consequence of importance. The purpose here is to make as much contact with the continuous transform as possible, while defining a discrete transform and its inverse. The extension here is applied directly to the continuous transform defined in Section 8.2.1 for two dimensions.

#### 8.16.1 The Discrete Version of the Image

The function  $f$  defines the image in terms of coordinates  $(x, y)$ . Here we let  $x$  and  $y$  be discrete and vary from 0 to  $P - 1$ , where  $P$  is prime. Moreover, for values of  $x$  and  $y$  greater than or equal to  $P$  we define the periodic extension of  $f$  such that for positive integers  $l, n$

$$f(x + lP, y + nP) = f(x, y).$$

This means that knowledge of  $f(x, y)$  for  $x$  and  $y$  in the set  $\{0, 1, 2, \dots, P - 1\}$  serves to define  $f$  everywhere. For example, suppose  $P = 3$ , then  $f(4, 1) = f(1, 1)$  and  $f(6, 8) = f(0, 2)$ . To make this more precise, if the residue of  $a$  modulo  $P$  is designated by

$$a \bmod P \equiv [a]_P, \quad \text{Definition}$$

then

$$f(x, y) = f([x]_P, [y]_P).$$

This square bracket notation is especially useful for some of the formulas. In terms of an image, this amounts to reproducing the image over and over again in both the vertical and horizontal directions. This will be illustrated when interpreting the discrete transform.

#### 8.16.2 A Discrete Transform

The prime factor DPRT is defined by three equations:

$$\check{f}(b, \downarrow) = \sum_{y=0}^{P-1} f(b, y) \quad \text{vertical}$$

$$\check{f}(b, 0) \equiv \check{f}(b, \leftrightarrow) = \sum_{x=0}^{P-1} f(x, b) \quad \text{horizontal}$$

$$\check{f}(b, m) = \sum_{x=0}^{P-1} f(x, [b + mx]_P) \quad m = 1, 2, \dots, P - 1.$$

In all of these equations  $b = 0, 1, \dots, P - 1$ . Note that for computational and coding purposes the last two equations can be combined by letting  $m$  vary from 0 to  $P - 1$ . At this point, an example followed by a generalization will be especially valuable.

#### Example 8.53

Suppose  $P = 5$  and we wish to calculate  $\check{f}(1, 2)$ . Set  $b = 1$  and  $m = 2$ , then

$$\check{f}(1, 2) = f(0, 1) + f(1, 3) + f(2, 0) + f(3, 2) + f(4, 4).$$

The graphical interpretation is shown in Figure 8.13, where the periodic extension is shown explicitly on the right. Also, note that for this  $P = 5$  case:

$$\tan \theta = m \text{ for } m = 1, 2 \text{ and } \tan \theta = m - P \text{ for } m = 3, 4.$$

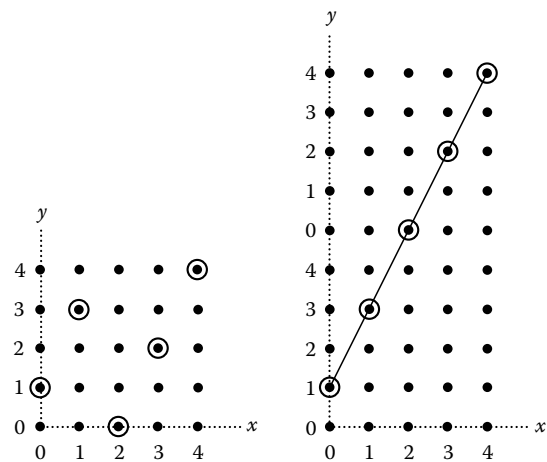


FIGURE 8.13 Use of the periodic property.

The generalization of the previous example to arbitrary values of  $P$  follows by induction. The slope variable takes on the values

$$m = 1, 2, \dots, \frac{P-1}{2}, \frac{P+1}{2}, \dots, P-1.$$

The angles  $\theta$  (slope angle) and  $\phi$  (used in continuous case) are related by

$$\begin{aligned} \tan \theta &= m, \quad 1 \leq m \leq \frac{P-1}{2}, \quad 0 < \theta < \frac{\pi}{2}, \quad \phi = -\left(\frac{\pi}{2} - \theta\right), \\ \tan \theta &= m - P, \quad \frac{P+1}{2} \leq m \leq P-1, \quad \frac{\pi}{2} < \theta < \pi, \quad \phi = \theta - \frac{\pi}{2}. \end{aligned}$$

**A Word of Caution**

The equations apply to a function  $f(x, y)$  where  $x$  is horizontal and  $y$  is vertical as indicated in Figure 8.13. If you are using a matrix of numbers  $M(i, j)$  where  $i$  designates rows and  $j$  designates columns, you will have to make some changes, since  $x$  actually labels columns and  $y$  labels rows. Also  $(x, y) = (0, 0)$  is in the lower left corner and often  $M(0, 0)$  is in the upper left corner.

**8.16.3 The Inverse Transform**

The inverse transform is given by

$$\begin{aligned} f(x, y) &= \frac{1}{P} \sum_{m=0}^{P-1} \tilde{f}([y - mx + P^2]_P, m) \\ &\quad - \frac{1}{P} \sum_{b=0}^{P-1} \tilde{f}(b, \uparrow) + \frac{1}{P} \tilde{f}(x, \uparrow). \end{aligned}$$

This can be derived by using a discrete version of the projection-slice theorem in Section 8.2.5 along with the discrete 2D Fourier transform. It is important to realize that this result is exact. See Hsung et al. (1996) for more details and extensions.

**Example 8.54**

We illustrate the transform with a  $5 \times 5$  matrix of data  $f(x, y)$

$y$							
	4	1	2	1	4	5	
	3	6	0	1	9	3	
	2	4	5	8	0	1	
	1	0	3	4	7	6	
	0	0	1	2	3	8	
		0	1	2	3	4	$x$

The transform  $\tilde{f}(b, m)$  is given by

$m$							
	4	9	12	16	23	24	
	3	9	16	18	18	23	
	↓	11	11	16	23	23	
	2	16	7	27	25	9	
	1	25	18	14	18	9	
	↔	14	20	18	19	13	
		0	1	2	3	4	$b$

**8.16.4 Good News and Bad News**

The discrete transform and inversion algorithm given here represents a natural evolution from the continuous case to the discrete case. It yields exact results, is simple and very fast (the inverse is free of multiplications). It is completely different from algorithms used in commercial machines designed for tomography. Those algorithms are usually based on filtered backprojection, convolution techniques, and utilize projections at equal angle increments, Huesman et al. (1977), Brooks and Di Chiro (1976), Rosenfeld and Kak (1982). The prime factor discrete algorithm here requires specific slopes that translate to an irregular sampling with respect to angle. This results in a tradeoff. Although this algorithm is exact and fast, it may not be easy to implement in an experimental setting. Also, if the prime factor  $P$  is large (greater than about 13) the angles are very closely spaced as the slope parameter  $m$  approaches the vertical. Moreover, the algorithm requires the use of periodicity and in experimental situations this is likely to be a problem.

**Appendix 8.A: Functions and Formulas**

Various functions and formulas are recorded here for the convenience of the reader. (Also, see Chapter 1 and Appendices.) The information here can be found in standard sources. In particular, those used here include Abramowitz and Stegun (1972), Arfken (1985), Born and Wolf (1975), Erdélyi et al. (1953), Gradshteyn et al. (1994), Lide (1993), Rainville (1960), and Szegő (1939).

**8.A.1 Chebyshev Polynomials:  
First Kind:  $T_1(x)$**

*Definitions*

$$\begin{aligned} T_l(x) &= \cos(l \arccos x), \quad 0 < x < 1 \\ T_l(x) &= \cosh(l \cosh^{-1} x), \quad 1 < x < \infty \\ T_l(x) &= \frac{1}{2} \left(x + \sqrt{x^2 - 1}\right)^l + \frac{1}{2} \left(x - \sqrt{x^2 - 1}\right)^l, \quad 0 < x < \infty \\ T_l(1) &= 1, \quad T_l(0) = \cos \frac{l\pi}{2}, \quad T_l(-x) = (-1)^l T_l(x) \end{aligned}$$

## Orthogonality

$$\int_{-1}^1 T_l(x)T_m(x)(1-x^2)^{-1/2} dx = \begin{cases} 0, & \text{for } l \neq m \\ \frac{\pi}{2}, & \text{for } l = m \neq 0 \\ \pi, & \text{for } l = m = 0 \end{cases}$$

## Recurrence and derivations

$$\begin{aligned} T_{l+1} &= 2xT_l - T_{l-1} \\ (1-x^2)T_l' &= lT_{l-1} - lxT_l \\ (1-x^2)T_l'' - xT_l' + l^2T_l &= 0 \end{aligned}$$

## First few

$$\begin{aligned} T_0 &= 1 \\ T_1 &= x \\ T_2 &= 2x^2 - 1 \\ T_3 &= 4x^3 - 3x \end{aligned}$$

## Useful integrals

$$\begin{aligned} \int_a^b \frac{T_l(x/a)T_l(x/b)dx}{x(b^2-x^2)^{1/2}(x^2-a^2)^{1/2}} &= \frac{\pi}{2ab} \\ \int_a^b \frac{dx}{x(b^2-x^2)^{1/2}(x^2-a^2)^{1/2}} &= \frac{\pi}{2ab} \\ \int_a^b \frac{x dx}{(b^2-x^2)^{1/2}(x^2-a^2)^{1/2}} &= \frac{\pi}{2} \\ \int_a^b \frac{x^3 dx}{(b^2-x^2)^{1/2}(x^2-a^2)^{1/2}} &= \frac{\pi}{4}(a^2+b^2) \end{aligned}$$

## 8.A.2 Chebyshev Polynomials: Second Kind: $U_l(x)$

## Definitions

$$\begin{aligned} U_{l-1}(x) &= \frac{\cos(l \arccos x)}{\sqrt{1-x^2}}, \quad 0 < x < 1 \\ U_{l-1}(x) &= \frac{\sinh(l \cosh^{-1} x)}{\sqrt{x^2-1}}, \quad 1 < x < \infty \\ U_{l-1}(x) &= \frac{(x+\sqrt{x^2-1})^l - (x-\sqrt{x^2-1})^l}{2\sqrt{x^2-1}}, \quad 0 < x < \infty, \quad x \neq 1 \\ U_l(-x) &= (-1)^l U_l(x), \quad U_l(1) = l+1, \quad U_l(0) = \cos \frac{l\pi}{2} \end{aligned}$$

## Orthogonality

$$\int_{-1}^1 U_l(x)U_m(x)(1-x^2)^{1/2} dx = \frac{\pi}{2} \delta_{lm}$$

## Recurrence and derivatives

$$\begin{aligned} U_{l+1} &= 2xU_l - U_{l-1} \\ (1-x^2)U_l' &= (l+1)U_{l-1} - lxU_l \\ (1-x^2)U_l'' - 3xU_l' + l(l+2)U_l &= 0 \end{aligned}$$

## First few

$$\begin{aligned} U_0 &= 1 \\ U_1 &= 2x \\ U_2 &= 4x^2 - 1 \\ U_3 &= 8x^3 - 4x \\ U_4 &= 16x^4 - 12x^2 + 1 \end{aligned}$$

## Miscellaneous connections

$$\begin{aligned} U_{l-1} &= \frac{1}{l} T_l', \quad l \geq 1 \\ T_l &= U_l - xU_{l-1}, \quad l \geq 1 \\ (1-x^2)U_l &= xT_{l+1} - T_{l+2} \\ \frac{T_l}{\sqrt{x^2-1}} - U_{l-1} &= \frac{(x-\sqrt{x^2-1})^l}{\sqrt{x^2-1}} = \frac{(x+\sqrt{x^2-1})^{-l}}{\sqrt{x^2-1}}, \quad x \neq 1 \end{aligned}$$

## 8.A.3 Hermite Polynomials: $H_l(x)$

## Generating function

$$e^{2xt-t^2} = \sum_{l=0}^{\infty} \frac{H_l(x)t^l}{l!}$$

## Orthogonality

$$\int_{-\infty}^{\infty} H_l(x)H_m(x)e^{-x^2} dx = \sqrt{\pi} 2^l l! \delta_{lm}$$

## Recurrence and derivatives

$$\begin{aligned} H_{l+1} &= 2xH_l - 2lH_{l-1} \\ H_l' &= 2lH_{l-1} \\ H_l'' - 2xH_l' + 2lH_l &= 0 \end{aligned}$$

Special values

$$H_l(x) = (-1)^l H_l(-x)$$

$$H_{2l}(0) = (-1)^l \frac{(2l)!}{l!}$$

$$H_{2l+1}(0) = 0$$

First few

$$H_0 = 1$$

$$H_1 = 2x$$

$$H_2 = 4x^2 - 2$$

$$H_3 = 8x^3 - 12x$$

$$H_4 = 16x^4 - 48x^2 + 12$$

Reverse expansions

$$x^0 = H_0$$

$$x^1 = \frac{1}{2} H_1$$

$$x^2 = \frac{1}{4} (H_2 + 2H_0)$$

$$x^3 = \frac{1}{8} (H_3 + 6H_1)$$

$$x^4 = \frac{1}{16} (H_4 + 12H_2 + 12H_0)$$

### 8.A.4 Zernike Polynomials: $Z_{lm}(r)$

Definition

The Zernike polynomials can be defined in terms of the more general Jacobi polynomials  $P_n^{(\alpha, \beta)}(z)$  by

$$Z_{l+2s}^l(r) = r^l P_s^{(0, l)}(2r^2 - 1).$$

An extensive discussion of the Zernike polynomials is given by Born and Wolf (1975). Jacobi polynomials are discussed by the other references cited at the beginning of this appendix.

First few

$$Z_0^0 = 1$$

$$Z_1^1 = r$$

$$Z_2^0 = 2r^2 - 1$$

$$Z_2^2 = r^2$$

$$Z_3^1 = 3r^3 - 2r$$

$$Z_3^3 = r^3$$

$$Z_4^0 = 6r^4 - 6r^2 + 1$$

$$Z_4^2 = 4r^4 - 3r^2$$

$$Z_4^4 = r^4$$

### 8.A.5 Selected Integral Formulas

$$\int_{-\infty}^{\infty} e^{-\alpha x^2} dx = \sqrt{\frac{\pi}{\alpha}}$$

$$\int_{-\infty}^{\infty} x^2 e^{-\alpha x^2} dx = \frac{1}{2\alpha} \sqrt{\frac{\pi}{\alpha}}$$

$$\int_{-a}^a \sqrt{a^2 - x^2} dx = \frac{a\pi}{2}$$

$$\int \frac{x dx}{\sqrt{a^2 - x^2}} = -\sqrt{a^2 - x^2}$$

$$\int \frac{dx}{\sqrt{x^2 \pm a^2}} = \log(x + \sqrt{x^2 \pm a^2})$$

$$\int \frac{dx}{x\sqrt{x^2 - a^2}} = \frac{1}{a} \cos^{-1}\left(\frac{a}{x}\right)$$

$$\int \frac{dx}{x^2\sqrt{x^2 - a^2}} = \frac{\sqrt{x^2 - a^2}}{a^2 x}$$

$$\int \frac{dx}{(a^2 - x^2)^{3/2}} = \frac{x}{a^2\sqrt{a^2 - x^2}}$$

$$\int \frac{dx}{\sqrt{a^2 - x^2}} = \sin^{-1}\left(\frac{x}{a}\right)$$

$$\int \frac{x^2 dx}{\sqrt{a^2 - x^2}} = -\frac{x}{2}\sqrt{a^2 - x^2} + \frac{a^2}{2}\sin^{-1}\left(\frac{x}{a}\right)$$

$$\int \frac{x^3 dx}{\sqrt{a^2 - x^2}} = \frac{1}{3}\sqrt{(a^2 - x^2)^3} - a^2\sqrt{a^2 - x^2}$$

$$\int \frac{dx}{x^2\sqrt{a^2 - x^2}} = -\frac{\sqrt{a^2 - x^2}}{a^2 x}$$

$$\int \frac{\sqrt{a^2 - x^2} dx}{x^2} = -\frac{\sqrt{a^2 - x^2}}{x} - \sin^{-1}\left(\frac{x}{a}\right)$$

$$\int_0^{\pi/2} \cos^n x dx = \frac{1 \cdot 3 \cdot 5 \dots (n-1)}{2 \cdot 4 \cdot 6 \cdot 8 \dots n} \frac{\pi}{2}, \quad \text{for } n \text{ even integer}$$

$$\int_0^{\pi/2} \cos^n x dx = \frac{2 \cdot 4 \cdot 6 \dots (n-1)}{1 \cdot 3 \cdot 5 \cdot 7 \dots n}, \quad \text{for } n \text{ odd integer}$$

### Appendix 8.B: Short List of Abel and Radon Transforms

The list of transforms recorded here is by no means complete. It contains some of the more common and useful transforms that can be found in closed form. Other Radon and Abel transforms



are scattered throughout this chapter. The notation for the Abel transforms is the same as in Section 8.10.2, and the notation for the 2D Radon transform is the same as in other parts of the chapter.

Also, just to remind the user of these tables, the sinc function is defined by

$$\text{sine } x = \frac{\sin \pi x}{\pi x},$$

and the characteristic function for the unit disk, designated by  $\chi(r)$  is defined by

$$\chi(r) = \begin{cases} 1, & \text{for } 0 \leq r \leq 1 \\ 0, & \text{for } r > 1. \end{cases}$$

The complete elliptic integral of the first kind is designated by  $F(\frac{1}{2}\pi, t)$  and the complete elliptic integral of the second kind is designated by  $E(\frac{1}{2}\pi, t)$ . A good source for these is the tabulation by Gradshteyn et al. (1994). The constant  $C(n)$  in the table for  $\mathcal{A}_3$  is  $C(n) = 2 \int_0^{\pi/2} \cos^n x \, dx$ , with  $n \geq 1$ ; it can be calculated from Appendix 8.A. Bessel functions of the first kind  $J_\nu$ , and second kind  $N_\nu$  (Neumann functions) conform to the standard definitions in Arfken (1985) and Gradshteyn et al. (1994). In these tables,  $a > 0$  and  $b > 0$ .

**Abel Transforms  $\mathcal{A}_1$**

$f(r)$	$\mathcal{A}_1\{f(r); x\}$
$\chi(r/a)$	$\sin^{-1}(\frac{a}{x}), \quad x > a$
$\delta(r - a)$	$(x^2 - a^2)^{-\frac{1}{2}}, \quad x > a$
$(a^2 - r^2)^{-\frac{1}{2}}$	$a^{-1}F(\frac{\pi}{2}, \frac{x}{a}), \quad x < a$
$(a^2 - r^2)^{\frac{1}{2}}$	$a E(\frac{\pi}{2}, \frac{x}{a}), \quad x < a$
$r^2(a^2 - r^2)^{-\frac{1}{2}}$	$a [F(\frac{\pi}{2}, \frac{x}{a}) - E(\frac{\pi}{2}, \frac{x}{a})], \quad x < a$
$a - r$	$\frac{1}{2}\pi a - x, \quad x < a$
$\cos br$	$\frac{1}{2}\pi J_0(bx)$
$r \sin br$	$\frac{1}{2}\pi x J_1(bx)$
$r J_0(br)$	$b^{-1} \sin bx$
$J_\nu(br)$	$\frac{1}{2}\pi \left[ J_{\frac{\nu}{2}}(\frac{bx}{2}) \right]^2$
$r^{\nu+1} J_\nu(br)$	$\pi^{\frac{1}{2}}(2b)^{-\frac{1}{2}} x^{\nu+\frac{1}{2}} J_{\nu+\frac{1}{2}}(bx)$

**Abel Transforms  $\mathcal{A}_2$**

$f(r)$	$\mathcal{A}_2\{f(r); x\}$
$\chi(r/a)$	$\log \left( \frac{a + \sqrt{a^2 - x^2}}{x} \right), \quad x < a$
$\delta(r - a)$	$(a^2 - x^2)^{-\frac{1}{2}}, \quad x < a$
$(a^2 - r^2)^{-\frac{1}{2}} \chi(r/a)$	$a^{-1} F(\frac{1}{2}\pi, t), \quad x < a$
$(a^2 - r^2)^{\frac{1}{2}} \chi(r/a)$	$a [F(\frac{1}{2}\pi, t) - E(\frac{1}{2}\pi, t)], \quad x < a$

$r^2(a^2 - r^2)^{-\frac{1}{2}} \chi(r/a)$	$a E(\frac{1}{2}\pi, t); \quad x < a$
$(a - r) \chi(r/a)$	$\log \left( \frac{a + \sqrt{a^2 - x^2}}{x} \right) - \sqrt{a^2 - x^2}, \quad x < a$
$\sin br$	$\frac{1}{2}\pi J_0(bx)$
$r \cos br$	$-\frac{1}{2}\pi x J_1(bx)$
$r J_0(br)$	$b^{-1} \cos bx$

Note:  $t = a^{-1} \sqrt{a^2 - x^2}$ .

**Abel Transforms  $\mathcal{A}_3$**

$f(r)$	$\mathcal{A}_3\{f(r); x\}$
$(a^2 - r^2)^{-\frac{1}{2}} \chi(r/a)$	$\pi \chi(x/a)$
$\chi(r/a)$	$2(a^2 - x^2)^{\frac{1}{2}} \chi(x/a)$
$(a^2 - r^2)^{\frac{1}{2}} \chi(r/a)$	$\frac{1}{2}\pi(a^2 - x^2) \chi(r/a)$
$(a^2 - r^2) \chi(r/a)$	$\frac{4}{3}(a^2 - x^2)^{\frac{3}{2}} \chi(x/a)$
$(a^2 - r^2)^{\frac{3}{2}} \chi(r/a)$	$\frac{3\pi}{8}(a^2 - x^2)^2 \chi(x/a)$
$(a^2 - r^2)^2 \chi(r/a)$	$\frac{15}{16}(a^2 - x^2)^{\frac{5}{2}} \chi(x/a)$
$(a^2 - r^2)^{\frac{n-1}{2}} \chi(r/a)$	$C(n)(a^2 - x^2)^{\frac{n}{2}} \chi(x/a)$
$(a^2 + r^2)^{-1}$	$\pi(a^2 + x^2)^{-\frac{1}{2}}$
$(a^2 + r^2)^{-\frac{3}{2}}$	$2(a^2 + x^2)^{-1}$
$e^{-r^2}$	$\sqrt{\pi} e^{-x^2}$
$r^2 e^{-r^2}$	$\frac{1}{2}\sqrt{\pi}(2x^2 + 1)e^{-x^2}$
$\text{sine } 2ar$	$\frac{1}{2a} J_0(2\pi ax)$
$\cos br$	$-\pi x J_1(bx)$
$J_0(br)$	$2b^{-1} \cos bx$
$r^{-1} J_1(br)$	$2(bx)^{-1} \sin bx$
$r^{-1} J_\nu(br)$	$-\pi J_{\frac{\nu}{2}}(\frac{bx}{2}) N_{\frac{\nu}{2}}(\frac{bx}{2})$
$r^{-1} N_\nu(br)$	$\frac{1}{2}\pi \left[ J_{\frac{\nu}{2}}(\frac{bx}{2}) \right]^2 - \frac{1}{2}\pi \left[ N_{\frac{\nu}{2}}(\frac{bx}{2}) \right]^2$

**Radon Transforms**

$f(x, y)$	$\check{f}(p, \phi)$
$e^{-x^2 - y^2}$	$\sqrt{\pi} e^{-p^2}$
$(x^2 + y^2) e^{-x^2 - y^2}$	$\frac{1}{2}\sqrt{\pi}(2p^2 + 1)e^{-p^2}$
$x e^{-x^2 - y^2}$	$\sqrt{\pi} e^{-p^2} \cos \phi$
$y e^{-x^2 - y^2}$	$\sqrt{\pi} e^{-p^2} \sin \phi$
$x^2 e^{-x^2 - y^2}$	$\frac{1}{2}\sqrt{\pi}(2p^2 \cos^2 \phi + \sin^2 \phi) e^{-p^2}$
$y^2 e^{-x^2 - y^2}$	$\frac{1}{2}\sqrt{\pi}(2p^2 \sin^2 \phi + \cos^2 \phi) e^{-p^2}$
$\exp \left[ -\left(\frac{x}{a}\right)^2 - \left(\frac{y}{a}\right)^2 \right]$	$\frac{ ab \sqrt{\pi}}{s} \exp \left[ -\left(\frac{p}{s}\right)^2 \right]$
$\delta(x - a) \delta(y - b)$	$\delta(p - p_0)$
$\chi(r)$	$2(1 - p^2)^{\frac{1}{2}} \chi(p)$

$\chi(\text{ellipse})$	(See Example 8.10)
$\chi(\text{square})$	(See Example 8.12)
$x^2\chi(r)$	$(1 - p^2)^{\frac{1}{2}}[2p^2 \cos^2 \phi + \frac{2}{3}(1 - p^2) \sin^2 \phi]$
$y^2\chi(r)$	$(1 - p^2)^{\frac{1}{2}}[2p^2 \sin^2 \phi + \frac{2}{3}(1 - p^2) \cos^2 \phi]$
$(x^2 + y^2)\chi(r)$	$\frac{2}{3}(1 - p^2)^{\frac{1}{2}}(2p^2 + 1)$

The following notation is used in the above table,

$$s = (a^2 \cos^2 \phi + b^2 \sin^2 \phi)^{\frac{1}{2}}, \quad r = \sqrt{x^2 + y^2},$$

$$p_0 = a \cos \phi + b \sin \phi.$$

Formulas for Radon transforms involving Hermite polynomials, Laguerre polynomials, and Zernike polynomials appear in Sections 8.7, 8.8, and 8.13, respectively.

## References

- Abel, N. H. Solution de quelque problèmes à l'aide d'intégrales définies. In *Oeuvres Complètes*, Vol. 1, pp. 11–27, Christiania, Oslo, Norway, 1823.
- Abel, N. H. Résolution d'un problème de mécanique. In *Oeuvres Complètes*, Vol. 1, pp. 97–101, Christiania, Oslo, Norway, 1826a.
- Abel, N. H. Auflösung einer mechanischen Aufgabe. *Journal für die reine und angewandte Mathematik*, 1, 153–157, 1826b.
- Abramowitz, M. and Stegun, A., Eds. *Handbook of Mathematical Functions with Formulas, Graphs, and Mathematical Tables*, National Bureau of Standards Applied Mathematics Series 55, 10th printing. U.S. Government Printing Office, Washington, DC, 1972.
- Amato, I. Nobel Prizes'91. *Science*, 254, 518–519, 1991.
- Anderssen, R. R. and de Hoog, F. R. Abel integral equations. In *Numerical Solution of Integral Equations*, Ed. M. A. Golberg, pp. 373–410. Plenum Press, New York and London, U.K., 1990.
- Arfken, G. *Mathematical Methods for Physicists*, 3rd edn. Academic Press, San Diego, CA, 1985.
- Barrett, H. H. The Radon transform and its applications. In *Progress in Optics*, Ed. E. Wolfe, Vol. 21, pp. 219–286. Elsevier, Amsterdam, the Netherlands, 1984.
- Barrett, H. H., Hawkins, W. G., and Joy, M. L. Historical note on computed tomography. *Radiology*, 147, 72, 1983.
- Barrett, H. H. and Swindell, W. Analog reconstruction methods for transaxial tomography. *Trans. IEEE*, 65, 89–107, 1977.
- Bates, R. H. T. and Peters, T. M. Towards improvements in tomography. *N. Z. J. Sci.*, 14, 883–896, 1971.
- Berenstein, C. and Walnut D. Local inversion of the Radon transform in even dimensions using wavelets. In *75 Years of Radon Transform*, Eds. S. Gindikin and P. Michor, pp. 45–69. International Press, Cambridge, MA, 1994.
- Beylkin, G. Discrete Radon transform. *IEEE Trans. Acoust. Speech Signal Process.*, 35(2), 162–172, 1987.
- Born, M. and Wolf, E. *Principles of Optics*, 5th edn. Pergamon Press, New York, 1975.
- Bracewell, R. N. Strip integration in radio astronomy. *Aust. J. Phys.*, 9, 198–217, 1956.
- Bracewell, R. N. Image reconstruction in radio astronomy. In *Image Reconstruction from Projections*, Ed. G. T. Herman, pp. 891–104. *Topics in Applied Physics*, Vol. 32, Springer-Verlag, New York, 1979.
- Bracewell, R. N. *The Fourier Transform and Its Applications*, 2nd edn. revised. McGraw-Hill, New York, 1986.
- Bregman, N. D., Bailey, R. C., and Chapman, C. H. Crosshole seismic tomography. *Geophysics*, 54, 200–215, 1989.
- Brooks, R. A. and Di Chiro, G. Principles of computer assisted tomography (CAT) in radiographic and radioisotopic imaging. *Phys. Med. Biol.*, 21, 689–732, 1976.
- Budinger, T. F., Gullberg, G. T., and Huesman, R. H. Emission computed tomography. In *Image Reconstruction from Projections*, Ed. G. T. Herman, pp. 147–246. *Topics in Applied Physics*, Vol. 32. Springer-Verlag, New York, 1979.
- Caspar, D. L. D. and De Rosier, D. J. The 1982 Nobel Prize in chemistry. *Science*, 218, 653–655, 1982.
- Chapman, C. H. The Radon transform and seismic tomography. In *Seismic Tomography*, Ed. G. Nolet, pp. 25–47. D. Reidel, Dordrecht, Holland, the Netherlands, 1987.
- Chapman, C. H. and Cary, P. W. The circular harmonic Radon transform. *Inverse Probl.*, 2, 23–49, 1986.
- Cho, Z. H., Jones, J. P., and Singh, M. *Foundations of Medical Imaging*. Wiley, New York, 1993.
- Churchill, R. V. *Operational Mathematics*, 3rd edn. McGraw-Hill, New York, 1972.
- Claerbout, J. F. *Imaging the Earth's Interior*. Blackwell Scientific, Palo Alto, CA, 1985.
- Clough, A. V. and Barrett, H. H. Attenuated Radon and Abel transforms. *J. Opt. Soc. Am.*, 73(11), 1590–1595, 1983.
- Cormack, A. M. Representation of a function by its line integrals, with some radiological applications. *J. Appl. Phys.*, 34, 2722–2727, 1963.
- Cormack, A. M. Representation of a function by its line integrals, with some radiological applications. II. *J. Appl. Phys.*, 35, 2908–2913, 1964.
- Cormack, A. M. Reconstruction of densities from their projections, with applications in radiological physics. *Phys. Med. Biol.*, 18, 195–207, 1973.
- Cormack, A. M. Nobel Prize address, Dec. 8, 1979. Early two-dimensional reconstruction and recent topics stemming from it. *Med. Phys.*, 7, 277–282, 1980.
- Cormack, A. M. Computed tomography: Some history and recent developments. *Proc. Symp. Appl. Math.*, 27, 35–42, 1982.
- Cormack, A. M. Radon's problem—Old and new. In *SIAM-AMS Proc., Inverse Problems*, Vol. 14, pp. 33–39. American Mathematical Society, Providence, RI, 1984.

- Davis, P. J. and Rabinowitz, P. *Methods of Numerical Integration*, 2nd edn. Academic Press, Orlando, FL, 1984.
- Deans, S. R. A Unified Radon inversion formula. *J. Math. Phys.*, 19(11), 2346–2349, 1978.
- Deans, S. R. Gegenbauer transforms via the Radon transform. *SIAM J. Math. Anal.*, 10(3), 577–585, 1979.
- Deans, S. R. *The Radon Transform and Some of Its Applications*. Wiley-Interscience, New York, 1983.
- Deans, S. R. The Radon transform. In *Mathematical Analysis of Physical Systems*, Ed. R. E. Mickens, pp. 81–133. Van Nostrand Reinhold, New York, 1985.
- Deans, S. R. *The Radon Transform and Some of Its Applications*, Revised edition. Krieger, Malbar, FL, 1993.
- Desbat, L. Efficient sampling on coarse grids in tomography. *Inverse Probl.*, 9, 251–269, 1993.
- Di Chiro, G. and Brooks, R. A. The 1979 Nobel Prize in physiology or medicine. *Science*, 205, 1060–1062, 1979.
- Di Chiro, G. and Brooks, R. A. The 1979 Nobel Prize in physiology or medicine. *J. Comput. Assisted Tomogr.*, 4, 241–245, 1980.
- Doetsch, G. *Introduction to the Theory and Application of the Laplace Transformation*. Springer-Verlag, New York, 1974.
- Donoho, D. L. Nonlinear solution of linear inverse problems by wavelet-vaguelette decomposition, Tech. Rept., Statistics, Stanford, CA, 1992.
- Duda, R. O. and Hart, P. E. Use of the Hough transform to detect lines and curves in pictures. *Commun. Assoc. Comput. Mach.*, 15, 11–15, 1972.
- DuMond, J. W. M. Compton modified line structure and its relation to the electron theory of solid bodies. *Phys. Rev.*, 33(5), 643–658, 1929.
- Durand, L., Fishbane, P. M., and Simmons, L. M., Jr. Expansion formulas and addition theorems for Gegenbauer functions. *J. Math. Phys.*, 17(11), 1933–1948, 1976.
- Embree, P. M. and Kimble, B. *C Language Algorithms for Digital Signal Processing*. Prentice-Hall, Englewood Cliffs, NJ, 1991.
- Erdélyi, A., Magnus, W., Oberhettinger, F., and Tricomi, F. G. *Higher Transcendental Functions*, Vol. II. McGraw-Hill, New York, 1953.
- Erdélyi, A., Magnus, W., Oberhettinger, F., and Tricomi, F. G. *Tables of Integral Transforms*, Vol. II. McGraw-Hill, New York, 1954.
- Faridani, A. Reconstruction from efficiently sampled data in parallel-beam computed tomography. In *Inverse Problems and Imaging*, Ed. G. F. Roach, pp. 68–102. Pitman Research Notes in Mathematics, Vol. 245. Longman Press, London, U.K., 1991.
- Faridani, A., Ritman, E. L., and Smith, K. T. Local tomography. *SIAM J. Appl. Math.*, 52(2), 459–484, and Examples of local tomography. *SIAM J. Appl. Math.*, 52(4), 1193–1198, 1992.
- Gel'fand, I. M., Graev, M. I., and Vilenkin, N. Ya. *Generalized Functions*, Vol. 5. Academic, New York, 1966.
- Gertner, I. A new efficient algorithm to compute the two-dimensional discrete Fourier transform. *IEEE Trans. Acoust. Speech Signal Process.*, 36, 1036–1050, 1988.
- Gindikin, S. and Michor, P. *75 Years of Radon Transform*, Eds. S. Gindikin and P. Michor, International Press, Cambridge, MA, 1994.
- Gorenflo, R. and Vessella, S. *Abel Integral Equations, Lecture Notes in Mathematics 1461*, Eds. A. Dold, B. Eckmann, and F. Takens. Springer-Verlag, Berlin, Germany, 1991.
- Gradshteyn, I. S., Ryzhik, I. M., and Jeffrey, A. *Table of Integrals, Series, and Products*, 5th edn. Academic Press, San Diego, CA, 1994.
- Grinberg, E. and Quinto, E. T. Preface. In *Contemporary Mathematics*, Vol. 113: *Integral Geometry and Tomography*, Eds. E. Grinberg and E.T. Quinto. American Mathematical Society, Providence, RI, 1990.
- Gullberg, G. T. The reconstruction of fan-beam data by filtering the back-projection. *Comput. Graph. Image Proc.*, 10, 30–47, 1979.
- Gullberg, G. T., Christian, P. E., Zeng, G. L., Datz, F. L., and Morgan, H. T. Cone beam tomography of the heart using single-photon emission-computed tomography. *Invest. Radiol.*, 26, 681–688, 1991.
- Hamaker C., Smith, K. T., Solmon, D. C., and Wagner, S. L. The divergent beam x-ray transform. *Rocky Mountain J. Math.*, 10, 253–283, 1980.
- Hansen, E. W. Circular harmonic image reconstruction: Experiments. *Appl Opt.*, 20, 2266–2274, 1981.
- Hansen, E. W. Fast Hankel transform algorithm. *IEEE Trans. Acoust. Speech Signal Process.*, 33, 666–671, 1985, [Erratum, 34, 623–624 (1986).]
- Harris, F. J. On the use of windows for harmonic analysis with the discrete Fourier transform. *Proc. IEEE*, 66(1), 51–83, 1978.
- Hawkins, W. G. and Barrett, H. H. A numerically stable circular harmonic reconstruction algorithm. *SIAM J. Numer. Anal.*, 23, 873–890, 1986.
- Hawkins, W. G., Leichner, P. K., and Yang, N.-C. The circular harmonic transform for SPECT reconstruction and boundary conditions on the Fourier transform of the sinogram. *IEEE Trans. Med. Imaging*, 7, 135–148, 1988.
- Hazou, I. A. and Solmon, D. C. Filtered-backprojection and the exponential Radon transform. *J. Math. Anal. Appl.*, 141, 109–119, 1989.
- Helgason, S. The Radon transform on Euclidean spaces, compact two-point homogeneous spaces and Grassmann manifolds. *Acta Math.*, 113, 153–180, 1965.
- Helgason, S. *The Radon Transform*. Birkhäuser, Boston, MA, 1980.
- Herman, G. T. *Image Reconstruction from Projections*. Academic Press, New York, 1980.
- Higgins, W. E. and Munson, D. C. Jr. An algorithm for computing general integer-order Hankel transforms. *IEEE Trans. Acoust. Speech Signal Process.*, 35, 86–97, 1987.
- Higgins, W. E. and Munson, D. C. Jr. A Hankel transform approach to tomographic image reconstruction. *IEEE Trans. Med. Imag.*, 7, 59–72, 1988.
- Hochstadt, H. *The Functions of Mathematical Physics*, Wiley, New York, 1971.

- Holschneider, M. Inverse Radon transforms through inverse wavelet transforms. *Inverse Probl.*, 7, 853–861, 1991.
- Hough, P. V. C. Method for recognizing complex patterns. U.S. Patent 3 096 654, 1962.
- Hounsfield, G. N. Nobel Prize address, Dec. 8, 1979. Computed medical imaging. *Med. Phys.*, 7, 283–290, 1980. (also in *J. Comput. Assisted Tomogr.*, 4, 665–674 and *Science*, 210, 22–28.)
- Huesman, R. H., Gullberg, G. T., Greenberg, W. L., and Budinger, T. F. RECLBL Library Users Manual—Donner algorithms for reconstruction tomography, Tech. Report PUB 214, Lawrence Berkeley Laboratory, Berkeley, CA, 1977.
- Hsung, T., Lun, D. P. K., and Siu, W. The discrete periodic Radon transform. *IEEE Trans. Signal Process.*, 44, 2651–2657, 1996.
- Jähne, B. *Digital Image Processing*, 2nd edn. Springer-Verlag, Berlin, Germany, 1993.
- Jain, A. K. *Fundamentals of Digital Image Processing*. Prentice-Hall, Englewood Cliffs, NJ, 1989.
- John, F. *Plane Waves and Spherical Means Applied to Partial Differential Equations*. Interscience, New York, 1955.
- Kaiser, G. and Streater, R. F. Windowed Radon transforms, analytic signals, and the wave function. In *Wavelets: A Tutorial in Theory and Applications*, Ed. C. K. Chui, pp. 399–441. Academic Press, San Diego, CA, 1992.
- Kak, A. C. Image reconstructions from projections. In *Digital Image Processing Techniques*, Ed. M. P. Ekstron, pp. 111–167. Academic Press, Orlando, FL, 1984.
- Kak, A. C. Tomographic imaging with diffracting and non-diffracting sources. In *Array Signal Processing*, Ed. S. Haykin, pp. 351–428. Prentice-Hall, Englewood Cliffs, NJ, 1985.
- Kak, A. C. and Slaney, M. *Principles of Computerized Tomographic Imaging*. IEEE Press, New York, 1988.
- Kanwal, R. P. *Linear Integral Equations*. Academic Press, New York, 1971.
- Kelley, B. T. and Madisetti, V. K. The fast discrete Radon transform—I: Theory. *IEEE Trans. Image Proc.*, 2(3), 382–400, 1993.
- Kim, C.-J. and Shannon, R. R. Catalog of Zernike polynomials. In *Applied Optics and Optical Engineering*, Eds. R. R. Shannon and J. C. Wyant, Vol. 10, pp. 193–221. Academic Press, San Diego, CA, 1987.
- Knill, O. Diagonalization of Abel's integral operator. *SIAM J. Appl. Math.*, 54(5), 1250–1253, 1994.
- Kruse, H. Resolution of reconstruction methods in computerized tomography. *SIAM J. Sci. Stat. Comput.*, 10, 447–474, 1989.
- Kudo, H. and Saito, T. Feasible cone beam scanning methods for exact reconstruction in three-dimensional tomography. *J. Opt. Soc. Am. A.*, 7, 2169–2183, 1990.
- Kudo, H. and Saito, T. Sinogram recovery with the method of convex projections for limited-data reconstruction in computed tomography. *J. Opt. Soc. Am. A.*, 8, 1148–1160, 1991.
- Ladouceur, H. D. and Adiga, K. C. The application of Abel inversion to combustion diagnostics. In *Some Topics on Inverse Problems*, Ed. P. C. Sabatier, pp. 369–390. World Scientific, Singapore, 1987.
- Lax, P. D. and Phillips, R. S. The Paley-Wiener theorem for the Radon transform. *Comm. Pure Appl. Math.*, 23, 409–424, 1970.
- Lax, P. D. and Phillips, R. S. Translation representation for the solution of the non-Euclidean wave equation. *Commun. Pure Appl. Math.*, 32, 617–667, 1979 [Correction. *Comm. Pure Appl. Math.*, 33, 685, 1980.]
- Lewitt, R. M. Reconstruction algorithms: Transform methods. *Proc. IEEE*, 71, 390–408, 1983.
- Lide, D. R., Ed. *Handbook of Chemistry and Physics*, 74th edn. CRC Press, Inc., Boca Raton, FL, 1993.
- Lindgren, A. G. and Rattey, P. A. The inverse discrete Radon transform with applications to tomographic imaging using projection data. In *Advances in Electronics and Electron Physics*, Ed. C. Marton, Vol. 56, pp. 359–410. Academic Press, New York, 1981.
- Lighthill, M. J. *Fourier Analysis and Generalized Functions*. Cambridge University Press, Cambridge, U.K., 1962.
- Lonseth, A.T. Sources and applications of integral equations. *SIAM Rev.*, 19, 241–278, 1977.
- Louis, A. K. Orthogonal function series expansions and the null space of the Radon transform. *SIAM J. Math. Anal.*, 15, 621–633, 1984.
- Louis, A. K. Laguerre and computerized tomography: Consistency conditions and stability of the Radon transform. In *Polynômes Orthogonaux et Applications*, Eds. C. Brezinski et al., pp. 524–531. *Lecture Notes in Mathematics 1171*. Springer-Verlag, Berlin, Germany, 1985.
- Ludwig, D. The Radon transform on Euclidean space. *Commun. Pure Appl. Math.*, 19, 49–81, 1966.
- Maass, P. The interior Radon transform. *SIAM J. Appl. Math.*, 52(3), 710–724, 1992.
- Macovski, A. *Medical Imaging Systems*. Prentice-Hall, Englewood Cliffs, NJ, 1983.
- Madych, W. R. and Nelson, S. A. Reconstruction from restricted Radon transform data: Resolution and ill-conditionedness. *SIAM J. Math. Anal.*, 17, 1447–1453, 1986.
- Madych, W. R. Summability and approximate reconstruction from Radon transform data. In *Contemporary Mathematics, Vol. 113: Integral Geometry and Tomography*, Eds. E. Grinberg and E. T. Quinto, pp. 189–219. American Mathematical Society, Providence, RI, 1990.
- Maldonado, C. D. and Olsen, H. N. New method for obtaining emission coefficients from emitted spectral intensities. Part II: Asymmetrical sources. *J. Opt. Soc. Am.*, 56, 1305–1313, 1966.
- Marr, R. R. On the reconstruction of a function on a circular domain from a sampling of its line integrals. *J. Math. Anal. Appl.*, 45, 357–374, 1974.
- Mersereau, R. M. Direct Fourier transform techniques in 3-D image reconstruction. *Comput. Biol. Med.*, 6, 247–258, 1976.
- Mersereau, R. M. and Oppenheim, A. V. Digital reconstruction of multidimensional signals from their projections. *Proc. IEEE*, 62, 1319–1338, 1974.

- Mijnarends, P. E. Determination of anisotropic momentum distribution in positron annihilation. *Phys. Rev.*, 160, 512–519, 1967.
- Mikusinski, P. and Zayed, A. An extension of the Radon transform. In *Generalized Functions and their Applications*, Ed. R. S. Pathak, pp. 141–147. Plenum Press, New York, 1993.
- Minerbo, G. N. and Levy, M. E. Inversion of Abel's integral equation by means of orthogonal polynomials. *SIAM J. Num. Anal.*, 6(4), 598–616, 1969.
- Morse, P. M. and Feshbach, H. *Methods of Theoretical Physics*. McGraw-Hill, New York, 1953.
- Natterer, F. On the inversion of the attenuated Radon transform. *Numer. Math.*, 32, 431–438, 1979.
- Natterer, F. *The Mathematics of Computerized Tomography*. John Wiley & Sons, New York, 1986.
- Natterer, F. Sampling in fan beam tomography. *SIAM J. Appl. Math.*, 53(2), 358–380, 1993.
- Nievergelt, Y. Elementary inversion of Radon's transform. *SIAM Rev.*, 28(1), 79–84, 1986.
- Nievergelt, Y. Elementary inversion of the exponential x-ray transform. *IEEE Trans. Nucl. Sci.*, 38(2), 873–876, 1991.
- Olson, T. and DeStefano, J. Wavelet localization of the Radon transform. *IEEE Trans. Signal Process.*, 42(8), 2055–2067, 1994.
- Olson, T. Optimal time-frequency projections for local tomography. *Ann. Biomed. Eng.*, 23, 622–636, 1995.
- Parker, J. A. *Image Reconstruction in Radiology*. CRC Press, Inc., Boca Raton, FL, 1990.
- Parks, P. C. On the determination of functions from their integral values along certain manifolds. (Translated by P.C. Parks) *IEEE Trans. Med. Imag.*, 5, 170–176, 1986.
- Radon, J. Über die Bestimmung von Funktionen durch ihre Integralwerte längs gewisser Mannigfaltigkeiten. *Berichte Sachsische Akademie der Wissenschaften, Leipzig, Mathematische-Physikalische Klasse*, 69, 262–267, 1917.
- Rainville, E. D. *Special Functions*. Chelsea, New York, 1960.
- Ramm, A. G. and Katsevich, A. I. *The Radon Transform and Local Tomography*. CRC Press, Boca Raton, FL, 1996.
- Rashid-Farrokh, F., Liu, K. J. R., Berenstein, C. A., and Walnut, D. Wavelet-based multiresolution local tomography. *IEEE Trans. Image Process.*, 6, 1412–1430, 1997.
- Rathey, P. A. and Lindgren, A. G. Sampling the 2D Radon transform. *IEEE Trans. Acoust. Speech Signal Process.*, 29(5), 994–1002, 1981.
- Rizo, P., Grangeat, P., Sire, P., Lemasson, P., and Melennec, P. Comparison of two three-dimensional x-ray cone-beam reconstruction algorithms with circular source trajectories. *J. Opt. Soc. Am. A*, 8, 1639–1648, 1991.
- Rosenfeld, A. and Kak, A. C. *Digital Picture Processing*, 2nd edn., Vol. I and II. Academic Press, New York, 1982.
- Rowland, S. W. Computer implementation of image reconstruction formulas. In *Image Reconstruction from Projections*, Ed. G. T. Herman, *Topics in Applied Physics* Vol. 32. Springer-Verlag, New York, 1979.
- Ruff, J. L. Tomographic imaging of seismic sources. In *Seismic Tomography*, Ed. G. Nolet, pp. 339–366. D. Reidel, Dordrecht, Holland, the Netherlands, 1987.
- Russ, J. C. *The Image Processing Handbook*, CRC Press, Inc., Boca Raton, FL, 1992.
- Schumann, W., Zürcher, J.-P., and Cuhe, D. *Holography and Deformation Analysis*, Springer-Verlag, Berlin, Germany, 1985.
- Schwartz, L. *Mathematics for the Physical Sciences*, Addison-Wesley, Reading, MA, 1966.
- Scudder, H. J. Introduction to computer aided tomography. *Proc. IEEE*, 66, 628–637, 1978.
- Sezan, M. I. and Stark, H. Tomographic image reconstruction from incomplete view data by convex projections and direct Fourier inversion. *IEEE Trans. Med. Imag.*, 3, 91–98, 1984.
- Shapiro, S. D. and Iannino, A. Geometric constructions for predicting Hough transform performance. *IEEE Trans. Pattern Anal. Mach. Intell.*, 1, 310–317, 1979.
- Shepp, L. A. Computerized tomography and nuclear magnetic resonance. *J. Comput. Assisted Tomogr.*, 4(1), 94–107, 1980.
- Shepp, L. A. and Kruskal, J. B. Computerized tomography: The new medical x-ray technology. *Am. Math. Month*, 85, 420–439, 1978.
- Smith, K. T., Solmon, D. C., and Wagner, S. L. Practical and mathematical aspects of the problem of reconstructing objects from radiographs. *Bull. Am. Math. Soc.*, 83, 1227–1270, 1977.
- Smith, P. R., Peters, T. M., and Bates, R. H. T. Image reconstruction from finite numbers of projections. *J. Phys. A: Math. Nucl. Gen.*, 6, 361–382, 1973.
- Sneddon, I. N. *The Use of Integral Transforms*. McGraw-Hill, New York, 1972.
- Srivastava, H. M. and Bushman, R. G. *Theory and Applications of Convolution Integral Equations*. Kluwer Academic Publishers, Dordrecht, the Netherlands, 1992.
- Stark, H., Woods, J. W., Paul, I., and Hingorani, R. An investigation of computerized tomography by direct Fourier inversion and optimum interpolation. *IEEE Trans. Biomed. Eng.*, 28, 496–505, 1981.
- Stewart, A. T. Momentum distribution of metallic electrons by positron annihilation. *Can. J. Phys.*, 35, 168–183, 1957.
- Suter, B. W. Fast Nth-order Hankel transform algorithm. *IEEE Trans. Signal Process.*, 39, 532–536, 1991.
- Swindell, W. and Barrett, H. H. Computerized tomography. *Phys. Today*, 30(12), 32–41, 1977.
- Swindell, W. and Webb, S. X-ray transmission computed tomography. In *The Physics of Medical Imaging*, Ed. S. Webb, pp. 98–127. Institute of Physics Publishing, Bristol and Philadelphia, PA, 1988.
- Szegö, G. *Orthogonal Polynomials*, American Mathematical Society Colloquium Publications, Vol. 23. American Mathematical Society, Providence, RI, 1939.
- Tretiak, O. J. and Metz, C. The exponential Radon transform. *SIAM J. Appl. Math.*, 39, 341–354, 1980.

- Tricomi, F. G. *Integral Equations*. Dover Publications, New York, 1985.
- Van der Pol, B. and Weijers, Th. Tchebycheff polynomials and their relation to circular functions, Bessel functions and Lissajous-figures. *Physica*, 1, 78–96, 1934.
- Vest, C. M. *Holographic Interferometry*. John Wiley & Sons, New York, 1979.
- Vest, C. M. and Steel, D. G. Reconstruction of spherically symmetric objects from slit-imaged emission: Application to spatially resolved spectroscopy. *Opt. Lett.*, 3, 54–56, 1978.
- Walnut, D. Applications of Gabor and wavelet expansions to the Radon transform. In *Probabilistic and Stochastic Methods in Analysis, with Applications*, Eds. J. S. Byrnes et al., pp. 187–205. Kluwer Academic Publishers, Dordrecht, the Netherlands, 1992.
- Widder, D. V. *An Introduction to Transform Theory*. Academic Press, New York, 1971.
- Wilkins, J. E. Jr. Neumann series of Bessel functions. *Transactions Am. Math. Soc.*, 64, 359–385, 1948.
- Wolf, K. B. *Integral Transforms in Science and Engineering*. Plenum Press, New York, 1979.
- Wood, J. C. and Barry, D. T. Tomographic time-frequency analysis and its application toward time-varying filtering and adaptive kernel design for multicomponent linear-FM signals. *IEEE Trans. Signal Process*, 42(8), 2094–2104, and Linear signal synthesis using the Radon-Wigner transform. *IEEE Trans. Signal Process*, 42(8), 2105–2111, 1994.
- Zeitler, E. The reconstruction of objects from their projections. *Optik.*, 39, 396–415, 1974.



# Hankel Transform

9.1	Introductory Definitions and Properties.....	9-1
9.2	Definition of the Hankel Transform.....	9-2
9.3	Connection with the Fourier Transform.....	9-2
9.4	Properties and Examples.....	9-3
9.5	Applications.....	9-6
	The Electrified Disc • Heat Conduction • The Laplace Equation in the Half-Space $z > 0$ , with a Circularly Symmetric Dirichlet Condition at $z = 0$ • An Electrostatic Problem	
9.6	The Finite Hankel Transform.....	9-9
9.7	Related Transforms.....	9-10
9.8	Need of Numerical Integration Methods.....	9-10
9.9	Computation of Bessel Function Integrals over a Finite Interval.....	9-11
	Integration between the Zeros of $J_\nu(x)$ • Modified Clenshaw–Curtis Quadrature	
9.10	Computation of Bessel Function Integrals over an Infinite Interval.....	9-13
	Integration between the Zeros of $J_\nu(x)$ and Convergence Acceleration • Transformation into a Double Integral • Truncation of the Infinite Interval	
9.11	Tables of Hankel Transforms.....	9-15
	References.....	9-15

Robert Piessens  
Catholic University of Leuven

Hankel transforms are integral transformations whose kernels are Bessel functions. They are sometimes referred to as Bessel transforms. When we are dealing with problems that show circular symmetry, Hankel transforms may be very useful. Laplace's partial differential equation in cylindrical coordinates can be transformed into an ordinary differential equation by using the Hankel transform. Because the Hankel transform is the two-dimensional Fourier transform of a circularly symmetric function, it plays an important role in optical data processing.

## 9.1 Introductory Definitions and Properties

Bessel functions are solutions of the differential equation

$$x^2 y'' + xy' + (x^2 - p^2)y = 0 \quad (9.1)$$

where  $p$  is a parameter.

Equation 9.1 can be solved using series expansions. The Bessel function  $J_p(x)$  of the first kind and of order  $p$  is defined by

$$J_p(x) = \left(\frac{1}{2}x\right)^p \sum_{k=0}^{\infty} \frac{\left(-\frac{1}{4}x^2\right)^k}{k!\Gamma(p+k+1)}. \quad (9.2)$$

The Bessel function  $Y_p(x)$  of the second kind and of order  $p$  is another solution that satisfies

$$W(x) = \det \begin{bmatrix} J_p(x) & Y_p(x) \\ J'_p(x) & Y'_p(x) \end{bmatrix} = \frac{2}{\pi x}.$$

Properties of Bessel function have been studied extensively (see Refs. [7,22,26]).

Elementary properties of the Bessel functions are

1. *Asymptotic forms.*

$$J_p(x) \sim \sqrt{\frac{2}{\pi x}} \cos\left(x - \frac{1}{2}p\pi - \frac{1}{4}\pi\right), \quad x \rightarrow \infty. \quad (9.3)$$

2. *Zeros.*  $J_p(x)$  and  $Y_p(x)$  have an infinite number of real zeros, all of which are simple, with the possible exception of  $x = 0$ . For nonnegative  $p$  the  $s$ th positive zero of  $J_p(x)$  is denoted by  $j_{p,s}$ . The distance between two consecutive zeros tends to  $\pi$ :  $\lim_{s \rightarrow \infty} (j_{p,s+1} - j_{p,s}) = \pi$ .

3. *Integral representations.*

$$J_p(x) = \frac{\left(\frac{1}{2}x\right)^p}{\pi^{1/2}\Gamma(p+1/2)} \int_0^\pi \cos(x \cos \theta) \sin^{2p} \theta \, d\theta. \quad (9.4)$$



If  $p$  is a positive integer or zero, then

$$\begin{aligned}
 J_p(x) &= \frac{1}{\pi} \int_0^\pi \cos(x \sin \theta - p\theta) d\theta \\
 &= \frac{j^{-n}}{\pi} \int_0^\pi e^{jx \cos \theta} \cos(p\theta) d\theta.
 \end{aligned}
 \tag{9.5}$$

4. Recurrence relations.

$$J_{p-1}(x) - \frac{2p}{x} J_p(x) + J_{p+1}(x) = 0 \tag{9.6}$$

$$J_{p-1}(x) - J_{p+1}(x) = 2J'_p(x) \tag{9.7}$$

$$J'_p(x) = J_{p-1}(x) - \frac{p}{x} J_p(x) \tag{9.8}$$

$$J'_p(x) = -J_{p+1}(x) + \frac{p}{x} J_p(x). \tag{9.9}$$

5. *Hankel's repeated integral.* Let  $f(r)$  be an arbitrary function of the real variable  $r$ , subject to the condition that

$$\int_0^\infty f(r) \sqrt{r} dr$$

is absolutely convergent. Then for  $p \geq -1/2$

$$\int_0^\infty s ds \int_0^\infty f(r) J_p(sr) J_p(su) r dr = \frac{1}{2} [f(u+) + f(u-)] \tag{9.10}$$

provided that  $f(r)$  satisfies certain Dirichlet conditions.

For a proof, see Ref. [26]. The reader should also refer to Section 1.5.6 for more information regarding Bessel functions.

## 9.2 Definition of the Hankel Transform

Let  $f(r)$  be a function defined for  $r \geq 0$ . The  $\nu$ th-order Hankel transform of  $f(r)$  is defined as

$$F_\nu(s) \equiv \mathcal{H}_\nu\{f(r)\} \equiv \int_0^\infty r f(r) J_\nu(sr) dr. \tag{9.11}$$

If  $\nu > -1/2$ , Hankel's repeated integral immediately gives the inversion formula

$$f(r) = \mathcal{H}_\nu^{-1}\{F_\nu(s)\} \equiv \int_0^\infty s F_\nu(s) J_\nu(sr) ds. \tag{9.12}$$

The most important special cases of the Hankel transform correspond to  $\nu=0$  and  $\nu=1$ . Sufficient but not necessary conditions for the validity of Equations 9.11 and 9.12 are

1.  $f(r) = O(r^{-k})$ ,  $r \rightarrow \infty$  where  $k > 3/2$
2.  $f'(r)$  is piecewise continuous over each bounded subinterval of  $[0, \infty)$
3.  $f(r)$  is defined as  $[f(r+) + f(r-)]/2$

These conditions can be relaxed.

## 9.3 Connection with the Fourier Transform

We consider the two-dimensional Fourier transform of a function  $\varphi(x, y)$ , which shows a circular symmetry. This means that  $\varphi(r \cos \theta, r \sin \theta) \equiv f(r, \theta)$  is independent of  $\theta$ .

The Fourier transform of  $\varphi$  is

$$\Phi(\zeta, \eta) = \frac{1}{2\pi} \int_{-\infty}^\infty \int_{-\infty}^\infty f(x, y) e^{-j(x\zeta + y\eta)} dx dy. \tag{9.13}$$

We introduce the polar coordinates

$$x = r \cos \theta, \quad y = r \sin \theta$$

and

$$\zeta = s \cos \varphi, \quad \eta = s \sin \varphi.$$

We have then

$$\begin{aligned}
 \phi(s \cos \varphi, s \sin \varphi) &\equiv F(s, \varphi) = \frac{1}{2\pi} \int_0^\infty r dr \int_0^{2\pi} e^{-jrs \cos(\theta-\varphi)} f(r) d\theta \\
 &= \frac{1}{2\pi} \int_0^\infty r f(r) dr \int_0^{2\pi} e^{-jrs \cos \alpha} d\alpha \\
 &= \int_0^\infty r f(r) J_0(rs) dr.
 \end{aligned}$$

This result shows that  $F(s, \varphi)$  is independent of  $\varphi$ , so that we can write  $F(s)$  instead of  $F(s, \varphi)$ . Thus, the two-dimensional Fourier transform of a circularly symmetric function is, in fact, a Hankel transform of order zero.

This result can be generalized: the  $N$ -dimensional Fourier transform of a circularly symmetric function of  $N$  variables is related to the Hankel transform of order  $N/2 - 1$ . If  $f(r, \theta)$  depends on  $\theta$ , we can expand it into a Fourier series

$$f(r, \theta) = \sum_{n=-\infty}^\infty f_n(r) e^{jn\theta} \tag{9.14}$$

and, similarly

$$F(s, \varphi) = \frac{1}{2\pi} \int_0^\infty r dr \int_0^{2\pi} e^{-jrs \cos(\theta-\varphi)} f(r, \theta) d\theta = \sum_{n=-\infty}^\infty F_n(s) e^{jn\varphi} \quad (9.15)$$

where

$$f_n(r) = \frac{1}{2\pi} \int_0^{2\pi} f(r, \theta) e^{-jn\theta} d\theta \quad (9.16)$$

and

$$F_n(s) = \frac{1}{2\pi} \int_0^{2\pi} F(s, \varphi) e^{-jn\varphi} d\varphi. \quad (9.17)$$

Substituting Equation 9.15 into Equation 9.17 and using Equation 9.14, we obtain

$$\begin{aligned} F_n(s) &= \frac{1}{(2\pi)^2} \int_0^{2\pi} e^{-jn\varphi} d\varphi \int_0^{2\pi} d\theta \int_0^\infty f(r, \theta) e^{jsr \cos(\theta-\varphi)} r dr \\ &= \frac{1}{(2\pi)^2} \int_0^{2\pi} e^{-jn\varphi} d\varphi \int_0^\infty r dr \int_0^{2\pi} e^{jsr \cos(\theta-\varphi)} d\theta \times \sum_{m=-\infty}^\infty f_m(r) e^{jm\theta} \\ &= \frac{1}{(2\pi)} \int_0^\infty r dr \int_0^{2\pi} e^{-jn\alpha} e^{jsr \cos \alpha} f_n(r) d\alpha \\ &= \int_0^\infty r f_n(r) J_n(sr) dr \\ &= \mathcal{H}_n\{f_n(r)\}. \end{aligned}$$

In a similar way, we can derive

$$f_n(r) = \mathcal{F}_n\{F_n(s)\}. \quad (9.18)$$

## 9.4 Properties and Examples

Hankel transforms do not have as many elementary properties as do the Laplace or the Fourier transforms.

For example, because there is no simple addition formula for Bessel functions, the Hankel transform does not satisfy any simple convolution relation.

1. *Derivatives.* Let

$$F_\nu(s) = \mathcal{H}_\nu\{f(x)\}.$$

Then

$$G_\nu(s) = \mathcal{H}_\nu\{f'(x)\} = s \left[ \frac{\nu+1}{2\nu} F_{\nu-1}(s) - \frac{\nu-1}{2\nu} F_{\nu+1}(s) \right]. \quad (9.19)$$

*Proof*

$$\begin{aligned} G_\nu(s) &= \int_0^\infty x f'(x) J_\nu(sx) dx \\ &= [x f(x) J_\nu(sx)]_0^\infty - \int_0^\infty f(x) \frac{d}{dx} [x J_\nu(sx)] dx. \end{aligned}$$

In general, the expression between the brackets is zero, and

$$\frac{d}{dx} [x J_\nu(sx)] = \frac{sx}{2\nu} [(\nu+1) J_{\nu-1}(sx) - (\nu-1) J_{\nu+1}(sx)].$$

Hence, we have Equation 9.19.

2. *The Hankel transform of the Bessel differential operator.*

The Bessel differential operator

$$\Delta_\nu \equiv \frac{d^2}{dr^2} + \frac{1}{r} \frac{d}{dr} - \left(\frac{\nu}{r}\right)^2 = \frac{1}{r} \frac{d}{dr} r \frac{d}{dr} - \left(\frac{\nu}{r}\right)^2$$

is derived from the Laplacian operator

$$\nabla^2 = \frac{\partial^2}{\partial r^2} + \frac{1}{r} \frac{\partial}{\partial r} + \frac{1}{r^2} \frac{\partial}{\partial \theta^2} + \frac{\partial^2}{\partial z^2}$$

after separation of variables in cylindrical coordinates  $(r, \theta, z)$ .

Let  $f(r)$  be an arbitrary function with the property that  $\lim_{r \rightarrow \infty} f(r) = 0$ . Then

$$\mathcal{H}_\nu\{\Delta_\nu f(r)\} = -s^2 \mathcal{H}_\nu\{f(r)\}. \quad (9.20)$$

This result shows that the Hankel transform may be a useful tool in solving problems with cylindrical symmetry and involving the Laplacian operator.

*Proof* Integrating by parts, we have

$$\begin{aligned} \mathcal{H}_\nu\{\Delta_\nu f(r)\} &= \int_0^\infty \left[ \frac{d}{dr} r \frac{df}{dr} - \frac{\nu^2}{r} f(r) \right] J_\nu(sr) dr \\ &= \int_0^\infty \left[ s^2 J_\nu''(sr) + \frac{s}{x} J_\nu'(sr) - \frac{\nu^2}{r^2} J_\nu(sr) \right] f(r) r dr \\ &= -s^2 \int_0^\infty r f(r) J_\nu(rs) dr \\ &= -s^2 \mathcal{H}_\nu\{f(r)\}. \end{aligned}$$

This property is the principal one for applications of the Hankel transforms to solving differential equations. See Refs. [2,3,24,25,28].

3. *Similarity.*

$$\mathcal{H}_\nu\{f(ar)\} = \frac{1}{a^2} F_\nu\left(\frac{s}{a}\right). \quad (9.21)$$

4. *Division by r.*

$$\mathcal{H}_\nu\{r^{-1}f(r)\} = \frac{s}{2\nu} [F_{\nu-1}(s) + F_{\nu+1}(s)]. \quad (9.22)$$

5.

$$\mathcal{H}_\nu\left\{r^{\nu-1} \frac{d}{dr} [r^{1-\nu} f(r)]\right\} = -s F_{\nu-1}(s). \quad (9.23)$$

6.

$$\mathcal{H}_\nu\left\{r^{-\nu-1} \frac{d}{dr} [r^{\nu+1} f(r)]\right\} = s F_{\nu+1}(s). \quad (9.24)$$

7. *Parseval's theorem.* Let

$$F_\nu(s) = \mathcal{H}_\nu\{f(r)\}$$

and

$$G_\nu(s) = \mathcal{H}_\nu\{g(r)\}.$$

Then

$$\begin{aligned} \int_0^\infty F_\nu(s) G_\nu(s) s ds &= \int_0^\infty F_\nu(s) s ds \int_0^\infty r g(r) J_\nu(sr) dr \\ &= \int_0^\infty r g(r) dr \int_0^\infty s F_\nu(s) J_\nu(sr) ds \\ &= \int_0^\infty r g(r) f(r) dr. \end{aligned} \quad (9.25)$$

**Example 9.1**

From the Fourier pair (see Chapter 2)  $\mathfrak{F}\{e^{-a(x^2+y^2)}\} = (\pi/a)e^{-(\zeta^2+\eta^2)/4a}$  and the Fourier transform relationship  $\mathfrak{F}\left\{f\left(\sqrt{x^2+y^2}\right)\right\} = 2\pi F_0\left(\sqrt{\zeta^2+\eta^2}\right) \equiv 2\pi F_0(s)$ , we obtain the Hankel transform

$$\mathcal{H}\left\{e^{-ar^2}\right\} = \frac{1}{2a} e^{-s^2/4a}, \quad a > 0.$$

**Example 9.2**

From the relationship  $\int_0^a r J_0(sr) dr = \int_0^a (1/s)(d/dr)[r J_1(sr)] = [a J_1(as)]/s$  (see Section 1.5.6), we conclude that

$$\mathcal{H}_0\{p_a(r)\} = \frac{a J_1(as)}{s}$$

where  $p_a(r) = 1$  for  $|r| < a$  and zero otherwise.

**Example 9.3**

From the identity  $\int_0^\infty J_0(sr) dr = 1/s, s > 0$  (see Section 1.5.6), we obtain

$$\mathcal{H}_0\left\{\frac{1}{r}\right\} = \frac{1}{s}.$$

**Example 9.4**

Since  $\int_0^\infty r \delta(r-a) J_0(sr) dr = a J_0(as)$  (see Section 1.2.4), we obtain

$$\mathcal{H}_0\{\delta(r-a)\} = a J_0(as), \quad a > 0$$

and because of symmetry

$$\mathcal{H}_0\{a J_0(ar)\} = \delta(s-a), \quad a > 0.$$

*Convolution Identity*

Let  $f_1(r)$  and  $f_2(r)$  have Hankel transforms  $F_1(s)$  and  $F_2(s)$ , respectively. From Section 2.4.1 above, we have

$$\begin{aligned} \mathfrak{F}\left\{\int_{-\infty}^\infty \int_{-\infty}^\infty f_1\left(\sqrt{x_1^2+y_1^2}\right) f_2\left(\sqrt{(x-x_1)^2+(y-y_1)^2}\right) dx_1 dy_1\right\} \\ = 4\pi^2 F_1(s) F_2(s). \end{aligned}$$

Hence, we have

$$\mathcal{H}_0\{f_1(r)**f_2(r)\} = \frac{1}{2\pi} \mathfrak{F}_{(2)}\{f_1(r)**f_2(r)\} = 2\pi F_1(s) F_2(s).$$

Therefore, to find the inverse Hankel transform of  $2\pi F_1(s) F_2(s)$ , we convolve  $f_1\left(\sqrt{x^2+y^2}\right)$  with  $f_2\left(\sqrt{x^2+y^2}\right)$ , and in the answer we replace  $\sqrt{x^2+y^2}$  by  $r$ . We can also write the above relationship in the form

$$\mathcal{H}_0\{2\pi f_1(r) f_2(r)\} = F_1(s) \star \star F_2(s).$$

**Example 9.5**

If  $f_1(r) = f_2(r) = [J_1(ar)]/r$  then from the convolution identity above, we obtain

$$\mathcal{H}_0 \left\{ 2\pi \frac{J_1^2(ar)}{r^2} \right\} = \frac{1}{a^2} P_a(s) \star \star P_a(s)$$

where

$$p_a(s) \star \star p_a(s) = \left( 2 \cos^{-1} \frac{s}{2a} - \frac{s}{a} \sqrt{1 - \frac{s^2}{4a^2}} \right) a^2.$$

Hence,

$$\mathcal{H}_0 \left\{ 2\pi \frac{J_1^2(ar)}{r^2} \right\} = \left( 2 \cos^{-1} \frac{s}{2a} - \frac{s}{a} \sqrt{1 - \frac{s^2}{4a^2}} \right) p_{2a}(s)$$

$$p_{2a}(s) = \begin{cases} 1 & |s| \leq 2a \\ 0 & \text{otherwise} \end{cases}$$

**Example 9.6**

From the definition, the Hankel transform of  $r^\nu h(a-r)$ ,  $a > 0$  is given by

$$\mathcal{H}_\nu \{ r^\nu h(a-r) \} = \int_0^a r^{\nu+1} J_\nu(sr) dr = \frac{1}{s^{\nu+2}} \int_0^{as} x^{\nu+1} J_\nu(x) dx$$

since  $h(a-r)$  is the unit step function with value equal to 1 for  $r \leq a$  and 0 for  $r > a$ . But  $\int t^\nu J_{\nu-1}(t) dt = t^\nu J_\nu(t) + C$  (see Table 1.13) and hence,

$$\mathcal{H}_\nu \{ r^\nu h(a-r) \} = \frac{(as)^{\nu+1}}{s^{\nu+2}} J_{\nu+1}(as) = \frac{a^{\nu+1}}{s} J_{\nu+1}(as),$$

$$a > 0, \nu > -\frac{1}{2}.$$

**Example 9.7**

The Hankel transform of  $r^{\nu-1} e^{-ar}$ ,  $a > 0$  is given by

$$\mathcal{H}_\nu \{ r^{\nu-1} e^{-ar} \} = \int_0^\infty r^\nu e^{-ar} J_\nu(sr) dr = \frac{1}{s^{\nu+1}} \int_0^\infty t^\nu J_\nu(t) e^{-\frac{a}{s}t} dt$$

$$= \frac{1}{s^{\nu+1}} \mathcal{L} \left\{ t^\nu J_\nu(t); p = \frac{a}{s} \right\}$$

where we set  $t = rs$  and  $\mathcal{L}$  is the Laplace transform operator (see also Chapter 5). But

$$t^\nu J_\nu(t) = \sum_{n=0}^\infty \frac{(-1)^n t^{2n+2\nu}}{n! \Gamma(n+\nu+1) 2^{2n+\nu}}$$

and, hence,

$$\mathcal{L} \{ t^\nu J_\nu(t); p \} = \sum_{n=0}^\infty \frac{(-1)^n}{n! \Gamma(n+\nu+1) 2^{2n+\nu}} \mathcal{L} \{ t^{2n+2\nu}; p \}$$

$$= \sum_{n=0}^\infty \frac{(-1)^n \Gamma(2n+2\nu+1)}{n! \Gamma(n+\nu+1) 2^{2n+\nu} p^{2n+2\nu+1}}.$$

From Section 1.2.5, the duplication formula of the gamma function gives the relationship

$$\frac{\Gamma(2n+2\nu+1)}{\Gamma(n+\nu+1)} = \frac{1}{\sqrt{\pi}} 2^{2n+2\nu} \Gamma\left(n+\nu+\frac{1}{2}\right)$$

and, therefore, the Laplace transform relation becomes

$$\mathcal{L} \{ t^\nu J_\nu(t); p \} = \frac{2^\nu}{\sqrt{\pi} p^{2\nu+1}} \sum_{n=0}^\infty \frac{(-1)^n \Gamma(n+\nu+\frac{1}{2})}{n!} \left(\frac{1}{p^2}\right)^n.$$

The last series can be summed by using properties of the binomial series

$$(1+x)^{-b} = \sum_{n=0}^\infty \binom{-b}{n} x^n = \sum_{n=0}^\infty \frac{(-1)^n \Gamma(n+b)}{n! \Gamma(b)} x^n, \quad |x| < 1$$

where the relation

$$\binom{-b}{n} = \frac{(-1)^n b(b+1) \cdots (b+n-1)}{n!} = \frac{(-1)^n \Gamma(n+b)}{n! \Gamma(b)}$$

was used. The Laplace transform now becomes

$$\mathcal{L} \{ t^\nu J_\nu(t); p \} = \frac{2^\nu \Gamma(\nu+\frac{1}{2})}{\sqrt{\pi} (p^2+1)^{\nu+\frac{1}{2}}} = \frac{2^\nu \Gamma(\nu+\frac{1}{2})}{\sqrt{\pi} \left[ \left(\frac{a}{s}\right)^2 + 1 \right]^{\nu+\frac{1}{2}}}, \quad \text{Re}(p) > 1$$

and, hence,

$$\mathcal{H}_\nu \{ r^{\nu-1} e^{-ar} \} = \frac{1}{s^{\nu+1}} \frac{2^\nu \Gamma(\nu+\frac{1}{2})}{\sqrt{\pi} \left[ \left(\frac{a}{s}\right)^2 + 1 \right]^{\nu+\frac{1}{2}}} = \frac{s^\nu 2^\nu \Gamma(\nu+\frac{1}{2})}{\sqrt{\pi} (a^2+s^2)^{\nu+\frac{1}{2}}},$$

$$\nu > -\frac{1}{2}.$$

If we set  $\nu=0$  and  $a=0$  in the above equation, we obtain the results of Example 9.3. If we set  $\nu=0$ , we obtain

$$\mathcal{H}_0 \{ r^{-1} e^{-ar} \} = \frac{1}{\sqrt{a^2+s^2}}, \quad a > 0.$$

**Example 9.8**

The Hankel transform  $\mathcal{H}_0\{e^{-ar}\}$  is given by

$$\begin{aligned} \mathcal{H}_0\{e^{-ar}\} &= \mathcal{L}\{r J_0(sr); r \rightarrow a\} = -\frac{d}{da} \left[ (s^2 + a^2)^{-1/2} \right] \\ &= \frac{a}{[s^2 + a^2]^{3/2}}, \quad a > 0 \end{aligned}$$

since multiplication by  $r$  corresponds to differentiation in the Laplace transform domain.

**Example 9.9**

From Section 1.5.6, we have the following identity:

$$\frac{d^2 r_n(x)}{dx^2} + \frac{1}{x} \frac{dr_n(x)}{dx} + r_n(x) = 2nr_{n+1}(x),$$

where  $r_n(x) = J_n(x)/x^n$ .

Using the Hankel transform property of the Bessel operator, we obtain the relationship

$$(1 - s^2)R_n(s) = 2nR_{n+1}(s)$$

or

$$R_{n+1}(s) = \frac{1 - s^2}{2n} R_n(s) = \dots = \frac{(1 - s^2)^n}{2^n n!} R_1(s).$$

But from Example 9.2,  $\mathcal{H}_0\left\{\frac{J_1(r)}{r}\right\} = p_1(s)$  and, hence,

$$\mathcal{H}_0\left\{\frac{J_n(r)}{r^n}\right\} = \frac{(1 - s^2)^{n-1}}{2^{n-1}(n-1)!} p_1(s)$$

where  $p_1(s)$  is a pulse of width 2 centered at  $s = 0$ .

**Example 9.10**

If the impulse response of a linear space invariant system is  $h(r)$  and the input to the system is  $f(r)$ , then its output is  $g(r) = f(r) \star \star h(r)$  and, hence,

$$G(s) = 2\pi F(s)H(s).$$

Since  $\mathcal{H}_0\{J_0(ar)\} = [\delta(s - a)]/a$  (see Example 9.4) and  $\varphi(s)\delta(s - a) = \varphi(a)\delta(s - a)$ , we conclude that if the input is  $f(r) = J_0(ar)$ , then

$$G(s) = \frac{2\pi}{a} \delta(s - a)H(s) = \frac{2\pi H(a)}{a} \delta(s - a).$$

Therefore, the output is

$$g(r) = 2\pi H(a)J_0(ar).$$

## 9.5 Applications

### 9.5.1 The Electrified Disc

Let  $v$  be the electric potential due to a flat circular electrified disc, with radius  $R = 1$ , the center of the disc being at the origin of the three-dimensional space and its axis along the  $z$ -axis.

In polar coordinates, the potential satisfies Laplace's equation

$$\nabla^2 v \equiv \frac{\partial^2 v}{\partial r^2} + \frac{1}{r} \frac{\partial v}{\partial r} + \frac{\partial^2 v}{\partial z^2} = 0. \tag{9.26}$$

The boundary conditions are

$$v(r, 0) = v_0, \quad 0 \leq r < 1 \tag{9.27}$$

$$\frac{\partial v}{\partial z}(r, 0) = 0, \quad r > 1. \tag{9.28}$$

In Equation 9.27,  $v_0$  is the potential of the disc. Condition (Equation 9.28) arises from the symmetry about the plane  $z = 0$ .

Let

$$V(s, z) = \mathcal{H}_0\{v(r, z)\}$$

so that

$$\mathcal{H}_0\{\nabla^2 v\} = -s^2 V(s, z) + \frac{\partial^2 V}{\partial z^2}(s, z) = 0.$$

The solution of this differential equation is

$$V(s, z) = A(s)e^{-sz} + B(s)e^{sz}$$

where  $A$  and  $B$  are functions that we have to determine using the boundary conditions.

Because the potential vanishes as  $z$  tends to infinity, we have  $B(s) \equiv 0$ . By inverting the Hankel transform, we have

$$v(r, z) = \int_0^\infty sA(s)e^{-sz}J_0(sr)ds. \tag{9.29}$$

The boundary conditions are now

$$v(r, 0) = \int_0^\infty sA(s)J_0(rs)ds = v_0, \quad 0 \leq r < 1 \tag{9.30}$$

$$\frac{\partial v}{\partial z}(r, 0) = \int_0^\infty s^2 A(s)J_0(rs)ds = 0, \quad r > 1. \tag{9.31}$$

Using entries (Equations 9.8 and 9.9) of Table 9.1 (see Section 9.11), we see that  $A(s) = \sin s/s^2$  so that

TABLE 9.1 Hankel Transforms of Order 0

	$f(r)$	$F_0(s) = \mathcal{H}_0\{f(r)\}$
(1)	$\frac{1}{r}$	$\frac{1}{s}$
(2)	$r^{-\mu}, \frac{1}{2} < \mu < 2$	$2^{1-\mu} \frac{\Gamma(1-\frac{\mu}{2})}{\Gamma(\frac{\mu}{2})} \frac{1}{s^{2-\mu}}$
(3)	$h(a-r)$	$\frac{a}{s} J_1(as)$
(4)	$e^{-ar}$	$\frac{a}{(s^2+a^2)^{3/2}}$
(5)	$\frac{e^{-ar}}{r}$	$\frac{1}{\sqrt{s^2+a^2}}$
(6)	$\frac{1-e^{-ar}}{r^2}$	$\log\left(\frac{a+\sqrt{a^2+s^2}}{s}\right)$
(7)	$\log\left(1+\frac{a^2}{r^2}\right)$	$\frac{2}{s} \left[ \frac{1}{s} - a K_1(as) \right]$
(8)	$\frac{\sin r}{r}$	$\frac{1}{\sqrt{1-s^2}}, \quad s < 1$ $0, \quad s > 1$
(9)	$\frac{\sin r}{r^2}$	$\frac{\pi}{2}, \quad s \leq 1$ $\arcsin \frac{1}{s}, \quad s > 1$
(10)	$\frac{\sin(ar)}{r^2+b^2}$	$\frac{\pi}{2} e^{-ab} I_0(bs), \quad 0 < s < a$
(11)	$\frac{\cos(ar)}{r^2+b^2}$	$\cosh(ab) K_0(bs), \quad a < s < \infty$
(12)	$e^{-a^2 r^2}$	$\frac{e^{-s^2/4a^2}}{2a^2}$
(13)	$\frac{1}{r(r+a)}$	$\frac{\pi}{2} [H_0(as) - Y_0(as)]$
(14)	$\frac{1}{r^2+a^2}$	$K_0(as)$
(15)	$\frac{1}{r(r^2+a^2)}$	$\frac{\pi}{2a} [I_0(as) - L_0(as)]$
(16)	$\frac{1}{1+r^4}$	$-\text{Kei}(s)$
(17)	$\frac{r^3}{1+r^4}$	$\text{Ker}(s)$
(18)	$\frac{1}{\sqrt{r^2+a^2}}$	$\frac{e^{-sa}}{s}$
(19)	$\frac{1}{\sqrt{r^4+a^4}}$	$K_0(as/\sqrt{2}) J_0(as/\sqrt{2})$
(20)	$\frac{1-J_0(ar)}{r^2}$	$\log \frac{a}{s}, \quad s \leq a$ $0, \quad s \geq a$
(21)	$\frac{a}{r} J_1(ar)$	$1, \quad \text{if } 0 < s < a$ $0, \quad \text{if } s > a$
(22)	$\frac{1}{r} J_0(2\sqrt{ar})$	$\frac{1}{s} J_0\left(\frac{a}{s}\right)$

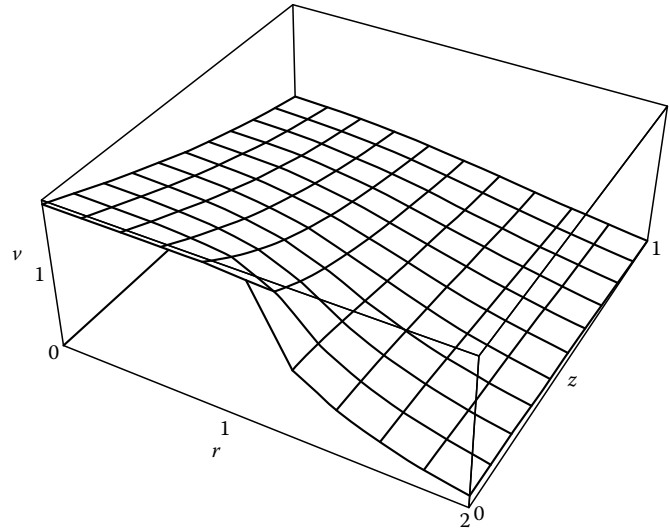


FIGURE 9.1 Electrical potential due to an electrified disc.

$$\int_0^\infty f(t) t^{2\alpha} J_\nu(xt) dt = a(x), \quad 0 \leq x < 1 \quad (9.33)$$

$$\int_0^\infty f(t) J_\nu(xt) dt = 0, \quad x > 1 \quad (9.34)$$

where  $a(x)$  is given and  $f(x)$  is to be determined.

The solution of Equation 9.29 can be expressed as a repeated integral:<sup>12</sup>

$$f(x) = \frac{2^{-\alpha} x^{1-\alpha}}{\Gamma(\alpha+1)} \int_0^1 s^{-\nu-\alpha} J_{\nu+\alpha}(xs) \frac{d}{ds} \int_0^s a(t) t^{\nu+1} (s^2-t^2)^\alpha dt ds, \quad -1 < \alpha < 0 \quad (9.35)$$

$$f(x) = \frac{(2x)^{1-\alpha}}{\Gamma(\alpha)} \int_0^1 s^{-\nu-\alpha+1} J_{\nu+\alpha}(xs) \int_0^s a(t) t^{\nu+1} (s^2-t^2)^{\alpha-1} dt ds, \quad 0 < \alpha < 1. \quad (9.36)$$

If  $a(x) = x^\beta$ , and  $\alpha < 1, 2\alpha + \beta > -3/2, \alpha + \nu > -1, \nu > -1$ , then

$$f(x) = \frac{\Gamma(1+\frac{\beta+\nu}{2}) x^{-(2\alpha+\beta+1)}}{2^\alpha \Gamma(1+\alpha+\frac{\beta+\nu}{2})} \int_0^x t^{\alpha+\beta+1} J_{\nu+\alpha}(t) dt. \quad (9.37)$$

With  $\beta = \nu$  and  $\alpha < 1, \alpha + \nu > -1, \nu > -1$  further simplification is possible:

$$f(x) = \frac{\Gamma(\nu+1)}{(2x)^\alpha \Gamma(\nu+\alpha+1)} J_{\nu+\alpha+1}(x). \quad (9.38)$$

$$v(r, z) = \frac{2v_0}{\pi} \int_0^\infty \frac{\sin s}{s} e^{-sz} J_0(sr) ds. \quad (9.32)$$

In Figure 9.1, the graphical representation of  $v(r, z)$  for  $v_0 = 1$  is depicted on the domain  $0 \leq r \leq 2, 0 \leq z \leq 1$ . The evaluation of  $v(r, z)$  requires numerical integration.

Equations 9.30 and 9.31 are special cases of the more general pair of equations

### 9.5.2 Heat Conduction

Heat is supplied at a constant rate  $Q$  per unit area and per unit time through a circular disc of radius  $a$  in the plane  $z=0$ , to the semi-infinite space  $z>0$ . The thermal conductivity of the space is  $K$ . The plane  $z=0$  outside the disc is insulated. The mathematical model of this problem is very similar to that of Section 9.5.1. The temperature is denoted by  $v(r, z)$ . We have again the Laplace Equation 9.26 in polar coordinates, but the boundary conditions are now

$$-K \frac{\partial v(r, z)}{\partial z} = Q, \quad r < a, \quad z = 0 \tag{9.39}$$

$$= 0, \quad r > a, \quad z = 0.$$

The Hankel transform of the differential equation is again

$$\frac{\partial^2 V}{\partial z^2}(s, z) - s^2 V(s, z) = 0. \tag{9.40}$$

We can now transform also the boundary condition, using formula (3) in Table 9.1:

$$-K \frac{\partial V}{\partial z}(s, 0) = QaJ_1(as)/s. \tag{9.41}$$

The solution of Equation 9.39 must remain finite as  $z$  tends to infinity. We have

$$V(s, z) = A(s)e^{-sz}.$$

Using condition (Equation 9.41) we can determine

$$A(s) = QaJ_1(as)/(Ks^2).$$

Consequently, the temperature is given by

$$v(r, z) = \frac{Qa}{K} \int_0^\infty e^{-sz} J_1(as) J_0(rs) s^{-1} ds. \tag{9.42}$$

### 9.5.3 The Laplace Equation in the Half-Space $z > 0$ , with a Circularly Symmetric Dirichlet Condition at $z = 0$

We try to find the solution  $v(r, z)$  of the boundary value problem

$$\begin{cases} \frac{\partial^2 v}{\partial r^2} + \frac{1}{r} \frac{\partial v}{\partial r} + \frac{\partial^2 v}{\partial z^2} = 0, & z > 0, \quad 0 < r < \infty \\ v(r, 0) = f(r). \end{cases} \tag{9.43}$$

Taking the Hankel transform of order 0 yields

$$\frac{\partial^2 V}{\partial z^2}(s, z) - s^2 V(s, z) = 0$$

and

$$V(s, 0) = \int_0^\infty rf(r)J_0(sr)dr.$$

The solution is

$$V(s, z) = e^{-sz} \int_0^\infty rf(r)J_0(sr)dr$$

so that

$$v(r, z) = \int_0^\infty se^{-sz} J_0(sr) ds \int_0^\infty pf(p)J_0(sp)dp. \tag{9.44}$$

For the special case

$$f(r) = h(a - r)$$

where  $h(r)$  is the unit step function, we have the solution

$$v(r, z) = a \int_0^\infty e^{-sz} J_0(sr) J_1(as) ds. \tag{9.45}$$

### 9.5.4 An Electrostatic Problem

The electrostatic potential  $Q(r, z)$  generated in the space between two grounded horizontal plates at  $z = \pm \ell$  by a point charge  $q$  at  $r = 0, z = 0$  shows a singular behavior at the origin. It is given by

$$v(r, z) = \varphi(r, z) + q(r^2 + z^2)^{-1/2}. \tag{9.46}$$

where  $\varphi(r, z)$  satisfies Laplace's Equation 9.26. The boundary conditions are

$$\varphi(r, \pm \ell) + q(r^2 + \ell^2)^{-1/2} = 0 \tag{9.47}$$

Taking the Hankel transform of order 0, we obtain

$$\frac{\partial^2 \Phi}{\partial z^2}(s, z) - s^2 \Phi(s, z) = 0 \tag{9.48}$$

$$\Phi(s, \pm \ell) = -\frac{qe^{-s\ell}}{s} \tag{9.49}$$

(see formula (18) in Table 9.1).

The solution is

$$A(s)e^{-sz} + B(s)e^{sz}$$

where  $A(s)$  and  $B(s)$  must satisfy

$$A(s)e^{+s\ell} + B(s)e^{-s\ell} = -\frac{qe^{-s\ell}}{s}$$

$$A(s)e^{-s\ell} + B(s)e^{s\ell} = -\frac{qe^{-s\ell}}{s}.$$

Hence,

$$A(s) = B(s) = -\frac{qe^{-s\ell}}{2s \cosh(s\ell)}$$

and

$$\Phi(s, z) = -\frac{qe^{-s\ell}}{s} \frac{\cosh(sz)}{\cosh(s\ell)}.$$

Hence,

$$\varphi(r, z) = \frac{q}{\sqrt{r^2 + z^2}} - q \int_0^\infty e^{-st} \frac{\cosh(sz)}{\cosh(s\ell)} J_0(sr) ds. \quad (9.50)$$

## 9.6 The Finite Hankel Transform

We consider the integral transformation

$$F_\nu(\alpha) = H_\nu\{f, \alpha\} = \int_0^1 rf(r)J_\nu(\alpha r)dr. \quad (9.51)$$

A property of this transformation is that

$$H_\nu(\Delta_\nu f, \alpha) = -\alpha^2 F_\nu(\alpha) + [J_\nu(\alpha)f'(1) - \alpha J'_\nu(\alpha)f(1)]$$

where  $\Delta_\nu$  is the Bessel differential operator.

If  $\alpha$  is equal to the  $s$ th positive zero  $j_{\nu,s}$  of  $J_\nu(x)$ , we have

$$H_\nu(\Delta_\nu f, j_{\nu,s}) = -j_{\nu,s}^2 H_\nu(f, j_{\nu,s}) + j_{\nu,s} J_{\nu+1}(j_{\nu,s})f(1).$$

If  $\alpha$  is equal to the  $s$ th positive root  $\beta_{\nu,s}$  of

$$hJ_\nu(x) + xJ'_\nu(x) = 0$$

where  $h$  is a nonnegative constant, we have

$$H_\nu(\Delta_\nu f, \beta_{\nu,s}) = -\beta_{\nu,s}^2 H_\nu(f, \beta_{\nu,s}) + J_\nu(\beta_{\nu,s})[hf(1) + f'(1)].$$

The transformation Equation 9.51 with  $\alpha = j_{\nu,s}$ ,  $s = 1, 2, \dots$  is the finite Hankel transform. It maps the function  $f(r)$  into the vector  $(F_\nu(j_{\nu,1}), F_\nu(j_{\nu,2}), F_\nu(j_{\nu,3}), \dots)$ . The inversion formula can be obtained from the well-known theory of Fourier-Bessel series

$$f(r) = 2 \sum_{s=1}^\infty \frac{F_\nu(j_{\nu,s})}{J_{\nu+1}^2(j_{\nu,s})} J_\nu(j_{\nu,s}r). \quad (9.52)$$

The transformation Equation 9.51 with  $\alpha = \beta_{\nu,s}$ ,  $s = 1, 2, \dots$  is the modified finite Hankel transform. The inversion formula is

$$f(r) = 2 \sum_{s=1}^\infty \frac{\beta_{\nu,s}^2 F_\nu(\beta_{\nu,s})}{h^2 + \beta_{\nu,s}^2 - \nu^2} \frac{J_\nu(\beta_{\nu,s}r)}{J'_\nu(\beta_{\nu,s})}. \quad (9.53)$$

If  $h = 0$ ,  $\beta_{\nu,s}$  is the  $s$ th positive zero of  $J'_\nu(x)$ , denoted by  $j'_{\nu,s}$ .

Formulas for the computation of  $j_{\nu,s}$  and  $j'_{\nu,s}$  are given by Olver.<sup>15</sup> Values of  $j_{\nu,s}$  and  $j'_{\nu,s}$  are tabulated in Ref. [1]. A Fortran program for the computation of  $j_{\nu,s}$  and  $j'_{\nu,s}$  is given in Ref. [18].

### Application

We calculate the temperature  $v(r, t)$  at time  $t$  of a long solid cylinder of unit radius. The initial temperature is unity and radiation takes place at the surface into the surrounding medium maintained at zero temperature.

The mathematical model of this problem is the diffusion equation in polar coordinates

$$\frac{\partial^2 v}{\partial r^2} + \frac{1}{r} \frac{\partial v}{\partial r} = \frac{\partial v}{\partial t}, \quad 0 \leq r < 1, t > 0 \quad (9.54)$$

The initial condition is

$$v(r, 0) = 1, \quad 0 \leq r \leq 1. \quad (9.55)$$

The radiation at the surface of the cylinder is described by the mixed boundary condition

$$\frac{\partial v}{\partial r}(1, t) = -hv(1, t) \quad (9.56)$$

where  $h$  is a positive constant.

Transformation of Equation 9.54 by the modified finite Hankel transform yields

$$\frac{dV}{dt}(\beta_{0,s}, t) = -\beta_{0,s}^2 V(\beta_{0,s}, t) \quad (9.57)$$

where

$$V(\alpha, t) = \int_0^1 rv(r, t)J_0(\alpha r)dr$$

so that

$$V(\alpha, 0) = \int_0^1 rJ_0(\alpha r)dr = \frac{J_1(\alpha)}{\alpha}. \quad (9.58)$$



The solution of Equation 9.57, with the initial condition (Equation 9.58), is

$$V(\beta_{0,s}, t) = \frac{J_1(\beta_{0,s})}{\beta_{0,s}} e^{-\beta_{0,s}^2 t}.$$

Using the inversion formula, we obtain

$$v(r, t) = 2 \sum_{j=1}^{\infty} e^{-\beta_{0,s}^2 t} \frac{\beta_{0,s} J_1(\beta_{0,s})}{h^2 + \beta_{0,s}^2} \frac{J_0(\beta_{0,s} r)}{J_0^2(\beta_{0,s})}. \quad (9.59)$$

## 9.7 Related Transforms

For some applications, Hankel transforms with a more general kernel may be useful. We give one example.

We consider the cylinder function

$$Z_\nu(s, r) = J_\nu(sr)Y_\nu(s) - Y_\nu(sr)J_\nu(s). \quad (9.60)$$

Using this function as a kernel, we can construct the following transform pair:

$$F_\nu(s) = \int_1^{\infty} r f(r) Z_\nu(s, r) dr \quad (9.61)$$

$$f(r) = \int_0^{\infty} s F_\nu(s) \frac{Z_\nu(s, r)}{J_\nu^2(s) + Y_\nu^2(s)} ds \quad (9.62)$$

The inversion formula follows immediately from Weber's integral theorem (see Watson<sup>26</sup>):

$$\int_1^{\infty} u du \int_0^{\infty} f(s) Z_\nu(r, u) Z_\nu(s, u) s ds = \frac{1}{2} [J_\nu^2(r) + Y_\nu^2(r)] [f(r+) + f(r-)]. \quad (9.63)$$

For this reason, we will refer to Equations 9.61 and 9.62 as the Weber transform. This transform has the following important property:

If

$$f(x) = g''(x) + \frac{1}{x} g'(x) - \frac{\nu^2}{x^2} g(x) \quad (9.64)$$

then

$$F_\nu(s) = -s^2 G_\nu(s) - \frac{2}{\pi} g(1). \quad (9.65)$$

We may expect that this transform is useful for solving Laplace's equation in cylindrical coordinates, with a boundary condition at  $r = 1$ .

### Example

We want to compute the steady-state temperature  $u(r, z)$  in a horizontal infinite homogeneous slab of thickness  $2\ell$ , through which there is a vertical circular hole of radius 1. The horizontal faces are held at temperature zero and the circular surface in the hole is at temperature  $T_0$ .

The mathematical model is

$$\begin{aligned} \frac{\partial^2 u}{\partial r^2} + \frac{1}{r} \frac{\partial u}{\partial r} + \frac{\partial^2 u}{\partial z^2} &= 0 \\ u(r, \ell) = u(r, -\ell) &= 0 \\ u(1, z) &= T_0. \end{aligned} \quad (9.66)$$

Taking the Weber transform of order zero, we have

$$\frac{\partial^2 U_0}{\partial z^2}(s, z) - s^2 U_0(s, z) = \frac{2}{\pi} T_0.$$

The solution of this ordinary differential equation, satisfying the boundary condition, is

$$U_0(s, z) = \frac{2T_0}{\pi s^2} \left[ \frac{\cosh sz}{\cosh s\ell} - 1 \right].$$

Consequently, we have

$$u(r, z) = \frac{2T_0}{\pi} \int_0^{\infty} \frac{1}{s} \left[ \frac{\cosh sz}{\cosh s\ell} - 1 \right] \frac{Z_0(s, r)}{J_0^2(s) + Y_0^2(s)} ds \quad (r > 1). \quad (9.67)$$

## 9.8 Need of Numerical Integration Methods

When using the Hankel transform for solving partial differential equations, the solution is found as an integral of the form

$$I(a, p, \nu) = \int_0^a J_\nu(px) f(x) dx \quad (9.68)$$

where  $a$  is a positive real number or infinite. In most cases, analytical integration of Equation 9.68 is impossible, and numerical integration is necessary. But integrals of type (Equation 9.68) are difficult to evaluate numerically if

1. The product  $ap$  is large
2.  $a$  is infinite
3.  $f(x)$  shows a singular or oscillatory behavior

In cases 1 and 2, the difficulties arise from the oscillatory behavior of  $J_\nu(x)$  and they grow when the oscillations become stronger.

We give here a survey of numerical methods that are especially suited for the evaluation of  $I(a, p, \nu)$  when  $ap$  is large or  $a$  is infinite. We restrict ourselves to cases where  $f(x)$  is smooth, or where  $f(x) = x^\alpha g(x)$  where  $g(x)$  is smooth and  $\alpha$  is a real number.

## 9.9 Computation of Bessel Function Integrals over a Finite Interval

Integral Equation 9.68 can be written as

$$I(a, p, \nu) = a^{\alpha+1} \int_0^1 x^\alpha J_\nu(apx)g(ax)dx. \quad (9.69)$$

We assume that  $\alpha + \nu > -1$ . If  $(\alpha + \nu)$  is not an integer, there is an algebraic singularity of the integrand at  $x=0$ . If  $ap$  is large, then the integrand is strongly oscillatory.

If  $(\alpha + \nu)$  is an integer and  $ap$  is small, classical numerical integration methods, such as Romberg integration, Clenshaw–Curtis integration of Gauss–Legendre integration (see Davis and Rabinowitz<sup>4</sup>) are applicable. If  $(\alpha + \nu)$  is not an integer and  $ap$  is small, the only difficulty is the algebraic singularity at  $x=0$ , and Gauss–Jacobi quadrature or Iri–Moriguti–Takesawa (IMT) integration<sup>4</sup> can be used. If  $ap$  is large, special methods should be applied that take into account the oscillatory behavior of the integrand. We describe two methods here.

### 9.9.1 Integration between the Zeros of $J_\nu(x)$

We denote the  $s$ th positive zero of  $J_\nu(x)$  by  $j_{\nu,s}$  and we set  $j_{\nu,0} = 0$ . Then

$$I(a, p, \nu) = \sum_{k=1}^N (-1)^{k+1} I_k + \int_{j_{\nu,N/p}}^a J_\nu(px)f(x)dx \quad (9.70)$$

where

$$I_k = \int_{j_{\nu,k-1/p}}^{j_{\nu,k/p}} |J_\nu(px)|f(x)dx \quad (9.71)$$

and where  $N$  is the largest natural number for which  $j_{\nu,N} \leq ap$ . This means that  $N$  is large when  $ap$  is large.

Using a transformation attributed to Longman,<sup>10</sup> the summation in Equation 9.70 can be written as

$$\begin{aligned} S = & \sum_{k=1}^N (-1)^{k+1} I_k = \frac{1}{2}I_1 - \frac{1}{4}\Delta I_1 + \frac{1}{8}\Delta^2 I_1 + \cdots + (-1)^{p-1} 2^{-p} \Delta^{p-1} I_1 \\ & + (-1)^{N-1} \left[ \frac{1}{2}I_N + \frac{1}{4}\Delta I_{N-1} + \frac{1}{8}\Delta^2 I_{N-2} + \cdots + 2^{-p} \Delta^{p-1} I_{N-p+1} \right] \\ & + 2^{-p} (-1)^p \left[ \Delta^p I_1 - \Delta^p I_2 + \Delta^p I_3 - \cdots + (-1)^{N-1-p} \Delta^p I_{N-p} \right]. \end{aligned}$$

Assuming now that  $N$  and  $p$  are large and that high-order differences are small, the last bracket may be neglected and

$$\begin{aligned} S \simeq & \frac{1}{2}I_1 - \frac{1}{4}\Delta I_1 + \frac{1}{8}\Delta^2 I_1 - \cdots + (-1)^{N-1} \\ & \times \left[ \frac{1}{2}I_N + \frac{1}{4}\Delta I_{N-1} + \frac{1}{8}\Delta^2 I_{N-2} + \cdots \right]. \end{aligned} \quad (9.72)$$

The summations in Equation 9.72 may be truncated as soon as the terms are small enough. For the evaluation of  $I_k$ ,  $k=1, 2, \dots$ , classical integration methods (e.g., Lobatto's rule) can be used, but special Gauss quadrature formulas (see Piessens<sup>16</sup>) are more efficient. If the integral  $I_1$  has an algebraic singularity at  $x=0$ , then the Gauss–Jacobi rules or the IMT rule are recommended.

### 9.9.2 Modified Clenshaw–Curtis Quadrature

The Clenshaw–Curtis quadrature method is a well-known and efficient method for the numerical evaluation of an integral  $I$  with a smooth integrand. This method is based on a truncated Chebyshev series approximation of the integrand. However, when the integrand shows a singular or strongly oscillatory behavior, the classical Clenshaw–Curtis method is not efficient or even applicable, unless it is modified in an appropriate way, taking into account the type of difficulty of the integrand. We call this method then a modified Clenshaw–Curtis method (MCC method). The principle of the MCC method is the following: the integration interval is mapped onto  $[-1, +1]$  and the integrand is written as the product of a smooth function  $g(x)$  and a weight function  $w(x)$  containing the singularities or the oscillating factors of the integrand; that is

$$I = \int_{-1}^{+1} w(x)g(x)dx. \quad (9.73)$$

The smooth function is then approximated by a truncated series of Chebyshev polynomials

$$g(x) \simeq \sum_{k=0}^N {}'c_k T_k(x), \quad -1 \leq x \leq 1. \quad (9.74)$$

Here the symbol  $\Sigma'$  indicates that the first term in the sum must be halved. For the computation of the coefficients  $c_k$  in Equation 9.74 several good algorithms, based on the fast Fourier transform, are available.

The integral in Equation 9.73 can now be approximated by

$$I \simeq \sum_{k=0}^N {}'c_k M_k \quad (9.75)$$

where

$$M_k = \int_{-1}^{+1} w(x) T_k(x) dx$$

are called modified moments.

The integration interval may also be mapped onto  $[0, 1]$  instead of  $[-1, 1]$ , but then the shifted Chebyshev polynomials  $T_k^*(x)$  are to be used.

We now consider the computation of the integral Equation 9.69,

$$I = \int_0^1 x^\alpha J_\nu(\omega x) g(x) dx. \quad (9.76)$$

If

$$g(x) \simeq \sum_{k=0}^N c_k T_k'(x) \quad (9.77)$$

then

$$I \simeq \sum_{k=0}^N c_k M_k(\omega, \nu, \alpha) \quad (9.78)$$

where

$$M_k(\omega, \nu, \alpha) = \int_0^1 x^\alpha J_\nu(\omega x) T_k^*(x) dx. \quad (9.79)$$

These modified moments satisfy the following homogeneous, linear, nine-term recurrence relation:

$$\begin{aligned} & \frac{\omega^2}{16} M_{k+4} + \left[ (k+3)(k+3+2\alpha) + \alpha^2 - \nu^2 - \frac{\omega^2}{4} \right] M_{k+2} \\ & + [4(\nu^2 - \alpha^2) - 2(k+2)(2\alpha - 1)] M_{k+1} \\ & - \left[ 2(k^2 - 4) + 6(\nu^2 - \alpha^2) - 2(2\alpha - 1) - \frac{3\omega^2}{8} \right] M_k \\ & + [4(\nu^2 - \alpha^2) + 2(k-2)(2\alpha - 1)] M_{k-1} \\ & + \left[ (k-3)(k-3-2\alpha) + \left( \alpha^2 - \nu^2 - \frac{\omega^2}{4} \right) \right] M_{k-2} + \frac{\omega^2}{16} M_{k-4} = 0. \end{aligned} \quad (9.80)$$

Because of the symmetry of the recurrence relation of the shifted Chebyshev polynomials, it is convenient to define

$$T_{-k}^*(x) = T_k^*(x), \quad k = 1, 2, 3, \dots$$

and consequently

$$M_{-k}(\omega, \nu, \alpha) = M_k(\omega, \nu, \alpha).$$

To start the recurrence relation with  $k = 0, 1, 2, 3, \dots$  we need only  $M_0, M_1, M_2$ , and  $M_3$ . Using the explicit expressions of the shifted Chebyshev polynomials, we obtain

$$\begin{aligned} M_0 &= G(\omega, \nu, \alpha) \\ M_1 &= 2G(\omega, \nu, \alpha + 1) - G(\omega, \nu, \alpha) \\ M_2 &= 8G(\omega, \nu, \alpha + 2) - 8G(\omega, \nu, \alpha + 1) + G(\omega, \nu, \alpha) \\ M_3 &= 32G(\omega, \nu, \alpha + 3) - 48G(\omega, \nu, \alpha + 2) \\ &+ 18G(\omega, \nu, \alpha + 1) - G(\omega, \nu, \alpha) \end{aligned} \quad (9.81)$$

where

$$G(\omega, \nu, \alpha) = \int_0^1 x^\alpha J_\nu(\omega x) dx. \quad (9.82)$$

Because

$$\begin{aligned} \omega^2 G(\omega, \nu, \alpha + 2) &= [\nu^2 - (\alpha + 1)^2] G(\omega, \nu, \alpha) \\ &+ (\alpha + \nu + 1) J_\nu(\omega) - \omega J_{\nu-1}(\omega) \end{aligned} \quad (9.83)$$

we need only  $G(\omega, \nu, \alpha)$  and  $G(\omega, \nu, \alpha + 1)$ .

Luke<sup>12</sup> has given the following formulas:

1. A Neumann series expansion that is suitable for small  $\omega$

$$\begin{aligned} G(\omega, \nu, \alpha) &= \frac{2}{\omega(\alpha + \nu + 1)} \\ &\times \sum_{k=0}^{\infty} \frac{(\nu + 2k + 1) \binom{\nu - \alpha + 1}{2}}{\binom{\nu + \alpha + 3}{2}_k} J_{\nu + 2k + 1}(\omega) \end{aligned} \quad (9.84)$$

2. An asymptotic expansion that is suitable for large  $\omega$

$$G(\omega, \nu, \alpha) = \frac{2^\alpha \Gamma(\frac{\nu + \alpha + 1}{2})}{\omega^{\alpha + 1} \Gamma(\frac{\nu - \alpha + 1}{2})} - \sqrt{\frac{2}{\pi \omega^3}} (g_1 \cos \theta + g_2 \sin \theta) \quad (9.85)$$

where

$$\theta = \omega - \nu\pi/2 + \pi/4$$

and

$$g_1 \sim \sum_{k=0}^{\infty} (-1)^k a_{2k} \omega^{-2k}, \quad \omega \rightarrow \infty$$

$$g_2 \sim \sum_{k=0}^{\infty} (-1)^k a_{2k+1} \omega^{-2k-1}, \quad \omega \rightarrow \infty$$

$$a_k = \frac{(1/2 - \nu)_k (1/2 + \nu)_k}{2^k k!} b_k$$

$$b_0 = 1$$

$$b_{k+1} = 1 + \frac{2(k+1)(\alpha - k - 1/2)}{(\nu - k - 1/2)(\nu + k + 1/2)} b_k.$$

If  $\alpha$  and  $\nu$  are integers, the following formulas are useful:<sup>1</sup>

$$\int_0^1 J_{2\nu}(\omega x) dx = \int_0^1 J_0(\omega x) dx - \frac{2}{\omega} \sum_{k=0}^{\nu-1} J_{2k+1}(\omega)$$

$$\int_0^1 J_{2\nu+1}(\omega x) dx = \frac{1 - J_0(\omega)}{\omega} - \frac{2}{\omega} \sum_{k=1}^{\nu} J_{2k}(\omega).$$

For the evaluation of

$$\int_0^1 J_0(\omega x) dx$$

Chebyshev series approximations are given by Luke.<sup>11</sup> We now discuss the numerical aspect of the recurrence formula (Equation 9.80). The numerical stability of forward recursion depends on the asymptotic behavior of  $M_k(\omega, \nu, \alpha)$  and of eight linearly independent solutions  $y_{i,k}$ ,  $i = 1, 2, \dots, 8$ ,  $k \rightarrow \infty$ .

Using the asymptotic theory of Fourier integrals, we find

$$\begin{aligned} |y_{1,k}| &\sim k^{-2} \\ |y_{2,k}| &\sim k^{-4} \\ |y_{3,k}| &\sim k^{-2(\alpha+1)-2\nu} \\ |y_{4,k}| &\sim k^{-2(\alpha+1)+2\nu}, \quad \text{if } \nu \neq 0 \\ &\sim k^{-2(\alpha+1)} \ell n k, \quad \text{if } \nu = 0 \\ |y_{5,k}| &\sim |y_{6,k}| \sim \left(\frac{\omega}{4k}\right)^k e^k k^\alpha \\ |y_{7,k}| &\sim |y_{8,k}| \sim \left(\frac{4k}{\omega}\right)^k e^{-k} k^\alpha \end{aligned} \tag{9.86}$$

and

$$\begin{aligned} M_k(\omega, \nu, \alpha) &\sim -\frac{1}{2} J_\nu(\omega) k^{-2} \\ &+ (-1)^k 2^{-3\nu-2\alpha-1} \frac{\omega^\nu}{\Gamma(\nu+1)} \cos[\pi(\alpha+1)] \\ &\times \Gamma(2\alpha+2) k^{-2\alpha-2\nu-2}. \end{aligned} \tag{9.87}$$

The asymptotically dominant solutions are  $y_{7,k}$  and  $y_{8,k}$ . The asymptotically minimal solutions are  $y_{5,k}$  and  $y_{6,k}$ . We may conclude that forward and backward recursion are asymptotically unstable. However, the instability of forward recursion is less pronounced if  $k \leq \omega/2$ . Indeed, practical experiments demonstrate that  $M_k(\omega, \nu, \alpha)$  can be computed accurately using forward recursion for  $k \leq \omega/2$ . For  $k > \omega/2$  the loss of significant figures increases and forward recursion is no longer applicable. In that case, Oliver's algorithm<sup>14</sup> has to be used. This means that Equation 9.80 has to be solved as a boundary value problem with six initial values and two end values. The solution of this boundary

value problem requires the solution of a linear system of equations having a band structure.

An important advantage of the MCC method is that the function evaluations of  $g$ , needed for the computation of the coefficients  $c_k$  of the Chebyshev series expansion, are independent of the value of  $\omega$ . Consequently, the same function evaluations may be used for different values of  $\omega$ , and have to be computed only once.

Numerical examples can be found in Refs. [19,20].

## 9.10 Computation of Bessel Function Integrals over an Infinite Interval

In this section we consider methods for the computation of

$$I(p, \nu) = \int_0^\infty J_\nu(px) f(x) dx. \tag{9.88}$$

### 9.10.1 Integration between the Zeros of $J_\nu(x)$ and Convergence Acceleration

We have

$$I(p, \nu) = \sum_{k=1}^\infty (-1)^{k+1} I_k \tag{9.89}$$

where

$$I_k = \int_{j_{\nu,k-1}/p}^{j_{\nu,k}/p} |J_\nu(px)| f(x) dx. \tag{9.90}$$

Using Euler's transformation,<sup>4</sup> the convergence of series Equation 9.89 can be accelerated

$$I(p, \nu) = \frac{1}{2} I_1 - \frac{1}{4} \Delta I_1 + \frac{1}{8} \Delta^2 I_1 - \frac{1}{16} \Delta^3 I_1 + \dots \tag{9.91}$$

It is not always desirable to start the convergence acceleration with  $I_1$ , but with some later term, say  $I_m$ , so that

$$\begin{aligned} I(p, \nu) &= \int_0^{j_{\nu,m-1}/p} J_\nu(px) f(x) dx + (-1)^{m-1} \\ &\times \left[ \frac{1}{2} I_m - \frac{1}{4} \Delta I_m + \frac{1}{8} \Delta^2 I_m - \dots \right]. \end{aligned}$$

Other convergence accelerating methods, for example the  $\epsilon$ -algorithm,<sup>23</sup> are also applicable (for an example, see Ref. [21]).

### 9.10.2 Transformation into a Double Integral

Substituting the integral expression

$$J_\nu(x) = 2 \frac{(x/2)^\nu}{\Gamma(\nu + 1/2)\sqrt{\pi}} \int_0^1 (1-t^2)^{\nu-1/2} \cos(xt) dt \quad (9.92)$$

into Equation 9.88 and changing the order of integration, we obtain

$$I(p, \nu) = \frac{2(p/2)^\nu}{\Gamma(\nu + 1/2)\sqrt{\pi}} \int_0^1 (1-t^2)^{\nu-1/2} F(t) dt \quad (9.93)$$

where

$$F(t) = \int_0^\infty x^\nu f(x) \cos(pxt) dx. \quad (9.94)$$

We assume that the integral in Equation 9.94 is convergent. If we want to evaluate Equation 9.93 using an  $N$ -point Gauss–Jacobi rule, then we have to compute the Fourier integral Equation 9.94 for  $N$  values of  $t$ . Because  $F(t)$  shows a peaked or even a singular behavior especially when  $f(x)$  is slowly decaying, a large enough  $N$  has to be chosen.

This method is closely related to Linz’s method,<sup>8</sup> which is based on the Abel transformation of  $I(p, \nu)$ .

TABLE 9.2 Hankel Transforms of General Order  $\nu$

	$f(r)$	$F_\nu(s) = \mathcal{H}_\nu\{f(r)\}$
(1)	$\frac{1}{r}$	$\frac{1}{s}$
(2)	$r^{-\mu}, \quad \frac{1}{2} < \mu < \nu + 2$	$\frac{2^{1-\mu} \Gamma(\frac{\nu+2-\mu}{2})}{s^{2-\mu} \Gamma(\frac{\nu+\mu}{2})}$
(3)	$x^\nu(a^2 - r^2)^\mu h(a - r), \mu > -1$	$2^\mu a^{\mu+\nu+1} s^{-\mu-1} \Gamma(\mu + 1) J_{\nu+\mu+1}(as)$
(4)	$\frac{\sin ar}{r}$	$\frac{1}{(s^2 - a^2)^{1/2}} \sin\left(\nu \arcsin\left(\frac{a}{s}\right)\right) \quad s > a$ $\cos\left(\frac{\nu\pi}{2}\right) \frac{1}{(a^2 - s^2)^{1/2}} \frac{s^\nu}{\left(a + (a^2 - s^2)^{1/2}\right)^\nu} \quad s < a$
(5)	$\frac{\sin ar}{r^2}$	$\frac{\nu^{-1} s^\nu}{(a + \sqrt{a^2 - s^2})^\nu} \sin \frac{\nu\pi}{2} \quad s \leq a$ $\nu^{-1} \sin\left(\nu \arcsin\left(\frac{a}{s}\right)\right) \quad s > a$
(6)	$\frac{e^{-ar}}{r}$	$\frac{(\sqrt{s^2 + a^2} - a)^\nu}{s^\nu \sqrt{s^2 + a^2}}$
(7)	$\frac{e^{-ar}}{r^2}$	$\frac{(\sqrt{s^2 + a^2} - a)^\nu}{\nu s^\nu}$
(8)	$r^{\nu-1} e^{-ar}$	$\frac{(2s)^\nu \Gamma(\nu + 1/2)}{(s^2 + a^2)^{\nu+1/2} \sqrt{\pi}}$
(9)	$r^\nu e^{-ar}$	$\frac{2a(2s)^\nu \Gamma(\nu + 3/2)}{(s^2 + a^2)^{\nu+3/2} \sqrt{\pi}}$
(10)	$e^{-a^2 r^2} r^\nu$	$\frac{s^\nu}{(2a^2)^{\nu+1}} \exp\left(-\frac{s^2}{4a^2}\right)$
(11)	$e^{-a^2 r^2} r^\mu$	$\frac{\Gamma((\nu + \mu + 2)/2) \left(\frac{1}{2} \frac{s}{a}\right)^\nu}{2a^{\mu+2} \Gamma(\nu + 1)} \times {}_1F_1\left(\frac{\nu + \mu + 2}{2}; \nu + 1; -\frac{s^2}{4a^2}\right)$
(12)	$\frac{r^\nu}{(r^2 + a^2)^{\mu+1}}$	$\frac{s^\mu a^{\nu-\mu}}{2^\mu \Gamma(\mu + 1)} K_{\nu-\mu}(as)$
(13)	$\frac{r^\nu}{(r^4 + 4a^4)^{\nu+\frac{1}{2}}}$	$\frac{\left(\frac{1}{2} s\right)^\nu \sqrt{\pi}}{(2a)^{2\nu} \Gamma(\nu + \frac{1}{2})} J_\nu(as) K_\nu(as)$
(14)	$\frac{r^{\nu+2}}{(r^4 + 4a^4)^{\nu+\frac{1}{2}}}$	$\frac{\left(\frac{1}{2} s\right)^\nu \sqrt{\pi}}{2(2a)^{2\nu-2} \Gamma(\nu + \frac{1}{2})} J_{\nu-1}(as) K_{\nu-1}(as)$
(15)	$r^{\mu-\nu} J_\mu(ar)$	$0 \quad 0 < s < a$ $\frac{2^{\mu-\nu+1} a^\mu (s^2 - a^2)^{\nu-\mu-1}}{s^\nu \Gamma(\nu - \mu)} \quad a < s$

### 9.10.3 Truncation of the Infinite Interval

If  $a$  is an arbitrary positive real number, we can write

$$I(p, v) = \int_0^a J_v(px) f(x) dx + R(p, a) \tag{9.95}$$

where

$$R(p, a) = \int_a^\infty J_v(px) f(x) dx. \tag{9.96}$$

The first integral in the right side of Equation 9.95 can be computed using the methods of Section 9.9

If  $a$  is sufficiently large and  $f$  is strongly decaying, then we may neglect  $R(p, a)$ . If

$$f(x) \sim \frac{c_1}{x} + \frac{c_2}{x^2} + \dots \tag{9.97}$$

is an asymptotic series approximation which is sufficiently accurate in the interval  $[a, \infty)$ , then

$$R(p, a) \simeq \sum_k c_k \int_a^\infty \frac{J_v(px)}{x^k} dx. \tag{9.98}$$

Longman<sup>9</sup> has tabulated the values of the integrals in Equation 9.98 for some values of  $v$  and  $ap$ .

Using Hankel's asymptotic expansion,<sup>1</sup> for  $x \rightarrow \infty$

$$J_v(px) \sim \sqrt{\frac{2}{\pi px}} [P_v(px) \cos \chi - Q_v(px) \sin \chi] \tag{9.99}$$

where  $\chi = px - (v/2 + 1/4)\pi$ , and where  $P_v(x)$  and  $Q_v(x)$  can be expressed as a well-known asymptotic series,  $R(p, a)$  can be written as the sum of two Fourier integrals.

Especially, if  $a = (8 + v/2 + 1/4)\pi/p$ , we have

$$R(p, a) = \int_0^\infty \sqrt{\frac{2}{\pi p(u+a)}} P_v(p(u+a)) f(u+a) \cos pu \, du - \int_0^\infty \sqrt{\frac{2}{\pi p(u+a)}} Q_v(p(u+a)) f(u+a) \sin pu \, du. \tag{9.100}$$

For the computation of the Fourier integrals in Equation 9.100, tailored methods are available.<sup>4</sup>

## 9.11 Tables of Hankel Transforms

Table 9.1 lists the Hankel transform of some particular functions for the important special case  $v=0$ . Table 9.2 lists Hankel transforms of general order  $v$ . In these tables,  $h(x)$  is the unit step function,  $I_\nu$  and  $K_\nu$  are modified Bessel functions,  $L_0$  and  $H_0$  are Struve functions, and Ker and Kei are Kelvin functions as defined in Abramowitz and Stegun.<sup>1</sup> Extensive tables are given by Erdélyi et al.,<sup>6</sup> Ditkin and Prudnikov,<sup>5</sup> Luke,<sup>11</sup> Wheelon,<sup>27</sup> Sneddon,<sup>24</sup> and Oberhettinger.<sup>13</sup>

## References

1. M. Abramowitz and I. N. Stegun, *Handbook of Mathematical Functions*, Dover Publications, New York, 1965.
2. R. N. Bracewell, *The Fourier Transform and Its Applications*, McGraw-Hill, New York, 1978.
3. B. Davies, *Integral Transforms and Their Applications*, Springer-Verlag, New York, 1978.
4. P. J. Davis and P. Rabinowitz, *Methods of Numerical Integration*, Academic Press, New York, 1975.
5. V. A. Ditkin and A. P. Prudnikov, *Integral Transforms and Operational Calculus*, Pergamon Press, Oxford, NY, 1965.
6. A. Erdélyi, W. Magnus, F. Oberhettinger, and F. G. Tricomi, *Tables of Integral Transforms*, Vol. 2, McGraw-Hill, New York, 1954.
7. A. Gray and G. B. Mathews, *A Treatise on Bessel Functions and Their Applications to Physics*, Dover Publications, New York, 1966.
8. P. Linz, A method for computing Bessel function integrals, *Math. Comp.*, 20, 504–513, 1972.
9. I. M. Longman, A short table of  $\int_x^\infty J_0(t)t^{-n} dt$  and  $\int_x^\infty J_1(t)t^{-n} dt$ , *Math. Tables Aids Comp.*, 13, 306–311, 1959.
10. I. M. Longman, A method for the numerical evaluation of finite integrals of oscillatory functions, *Math. Comp.*, 14, 53–59, 1960.
11. Y. L. Luke, *The Special Functions and Their Approximations*, Vol. 2, Academic Press, New York, 1969.
12. Y. L. Luke, *Integrals of Bessel Functions*, McGraw-Hill, New York, 1962.
13. F. Oberhettinger, *Table of Bessel Transforms*, Springer-Verlag, Berlin, Germany, 1971.
14. J. Oliver, The numerical solution of linear recurrence relations, *Numer. Math.*, 11, 349–360, 1968.
15. F. W. J. Olver, *Bessel Functions, Part III: Zeros and Associated Values*, Cambridge University Press, Cambridge, U.K., 1960.
16. R. Piessens, Gaussian quadrature formulas for integrals involving Bessel functions, Microfiche section of *Math. Comp.*, 26, 1972.
17. R. Piessens, Automatic computation of Bessel function integrals, *Comp. Phys. Commun.*, 25, 289–295, 1982.
18. R. Piessens, On the computation of zeros and turning points of Bessel functions, in E. A. Lipitakis (Ed.), *Advances*

- on *Computer Mathematics and Its Applications*, World Scientific, Singapore, pp. 53–57, 1993.
19. R. Piessens and M. Branders, Modified Clenshaw–Curtis method for the computation of Bessel function integrals, *Bit*, 23, 370–381, 1983.
  20. R. Piessens and M. Branders, A survey of numerical methods for the computation of Bessel function integrals, *Rend. Sem. Mat. Univers. Politecn. Torino*, Fascicolo speciale, pp. 250–265, 1985.
  21. R. Piessens, E. de Doncker-Kapenga, C. W. Ueberhuber, and D. K. Kahaner, *Quadpack, A Subroutine Package for Automatic Integration*, Springer-Verlag, Berlin, Germany, 1983.
  22. F. E. Relton, *Applied Bessel Functions*, Dover Publications, New York, 1965.
  23. D. Schanks, Non-linear transformations of divergent and slowly convergent sequences, *J. Math. Phys.*, 34, 1–42, 1955.
  24. I. N. Sneddon, *The Use of Integral Transforms*, McGraw-Hill, New York, 1972.
  25. C. J. Tranter, *Integral Transforms in Mathematical Physics*, Methuens & Co., London, U.K., 1951.
  26. G. N. Watson, *A Treatise on the Theory of Bessel Functions*, Cambridge University Press, Cambridge, U.K., 1966.
  27. A. D. Wheelon, *Table of Summable Series and Integrals Involving Bessel Functions*, Holden-Day, San Francisco, CA, 1968.
  28. K. B. Wolf, *Integral Transforms in Science and Engineering*, Plenum Press, New York, 1979.

# 10

## Wavelet Transform

---

10.1	Introduction.....	10-2
	Continuous Wavelet Transform • Time-Frequency Space Analysis • Short-Time Fourier Transform • Wigner Distribution and Ambiguity Functions	
10.2	Properties of the Wavelets .....	10-6
	Admissible Condition • Regularity • Multiresolution Wavelet Analysis • Linear Transform Property • Examples of the Wavelets	
10.3	Discrete Wavelet Transform.....	10-14
	Timescale Space Lattices • Wavelet Frame	
10.4	Multiresolution Signal Analysis .....	10-16
	Laplacian Pyramid • Subband Coding • Scale and Resolution	
10.5	Orthonormal Wavelet Transform .....	10-18
	Multiresolution Signal Analysis Bases • Orthonormal Bases • Orthonormal Subspaces • Wavelet Series Decomposition • Reconstruction • Biorthogonal Wavelet Bases	
10.6	Filter Bank.....	10-27
	FIR Filter Bank • Perfect Reconstruction • Orthonormal Filter Bank • Orthonormal Filters in Time Domain • Biorthogonal Filter Bank	
10.7	Wavelet Theory.....	10-33
	Orthonormality • Two Scale Relations in Frequency Domain • Orthogonal Filters in Time Domain • Wavelet and Subband Filters • Regularity	
10.8	Some Orthonormal Wavelet Bases.....	10-42
	B-Spline Bases • Lemarie and Battle Wavelet Bases • Daubechies Bases	
10.9	Fast Wavelet Transform .....	10-47
	Wavelet Matrices • Number of Operations • Time-Bandwidth Product	
10.10	Applications of the Wavelet Transform.....	10-50
	Multiresolution Analysis of Power System Signal • Signal Detection • Image Edge Detection • Image Compression	
	References .....	10-53

Yulong Sheng  
*Laval University*

The wavelet transform is a new mathematical tool developed mainly since the middle of the 1980s. It is efficient for local analysis of nonstationary and fast transient wideband signals. The wavelet transform is a mapping of a time signal to the timescale joint representation, that is used in the short-time Fourier transform, the Wigner distribution and the ambiguity function. The temporal aspect of the signals is preserved. The wavelet transform provides multiresolution analysis with dilated windows. The higher frequency analysis is done using narrower windows and the lower frequency analysis is done using wider windows. Thus, the wavelet transform is a constant-Q analysis.

The basis functions of the wavelet transform, the wavelets, are generated from a basic wavelet function by dilations and translations. They satisfy an admissible condition so that the original signal can be reconstructed by the inverse wavelet transform. The wavelets satisfy also the regularity condition so that the wavelet coefficients decrease fast with the decreasing of the scale. The wavelet transform is local not only in time but also in frequency domain.

To reduce the time-bandwidth product of the wavelet transform output, the discrete wavelet transform with discrete dilations and translations of the continuous wavelets can be used. The orthonormal wavelet transform is implemented in the multiresolution signal analysis framework, which is based on the scaling functions. The discrete translates of the scaling functions form an orthonormal basis at each resolution level. The wavelet basis is generated from the scaling function basis. The two bases are mutually orthogonal at each resolution level. The scaling function is an averaging function. The orthogonal projection of a function onto the scaling function basis is an averaged approximation. The orthogonal projection onto the wavelet basis is the difference between two approximations at two adjacent resolution levels. Both the scaling functions and the wavelets satisfy the orthonormality conditions and the regularity conditions.

The discrete orthonormal wavelet series decomposition and reconstruction are computed in the multiresolution analysis framework with recurring two discrete low-pass and high-pass filters, that are, in fact, the 2-band paraunitary perfect reconstruction



quadrature mirror filters, developed in the subband coding theory, with the additional regularity. The tree algorithm operating the discrete wavelet transform requires only  $O(L)$  operations where  $L$  is the length of the data vector. The time–bandwidth product of the wavelet transform output is only slightly increased with respect to that of the signal.

The wavelet transform is powerful for multiresolution local spectrum analysis of nonstationary signals, such as the sound, radar, sonar, seismic, electrocardiographic signals, and for image compression, image processing and pattern recognition.

In this chapter all integrations extend from  $-\infty$  to  $\infty$ , if not stated otherwise. The formulation of the wavelet transform in this chapter is one-dimensional (1-D). The wavelet transform can be easily generalized to any dimensions.

## 10.1 Introduction

### 10.1.1 Continuous Wavelet Transform

**Definition** Let  $L^2(\mathbf{R})$  denote the vector space of measurable, square-integrable functions. The continuous wavelet transform of a function  $f(t) \in L^2(\mathbf{R})$  is a decomposition of  $f(t)$  into a set of basis functions  $h_{s,\tau}(t)$  called the wavelets:

$$W_f(s, \tau) = \int f(t) h_{s,\tau}^*(t) dt \quad (10.1)$$

where  $*$  denotes the complex conjugate. However, most wavelets are real valued. The wavelets are generated from a single basic wavelet (mother wavelet)  $h(t)$  by scaling and translation:

$$h_{s,\tau}(t) = \frac{1}{\sqrt{s}} h\left(\frac{t-\tau}{s}\right) \quad (10.2)$$

where

- $s$  is the scale factor
- $\tau$  is the translation factor

We usually consider only positive scale factor  $s > 0$ . The wavelets are dilated when the scale  $s > 1$  and are contracted when  $s < 1$ . The wavelets  $h_{s,\tau}(t)$  generated from the same basic wavelet have different scales  $s$  and locations  $\tau$ , but all have the identical shape.

The constant  $s^{-1/2}$  in the expression (Equation 10.2) of the wavelets is for energy normalization. The wavelets are normalized in terms of energy as

$$\int |h_{s,\tau}(t)|^2 dt = \int |h(t)|^2 dt = 1$$

so that all the wavelets scaled by the factor  $s$  would have the same energy. The wavelets can also be normalized in terms of amplitude as

$$\int |h_{s,\tau}(t)| dt = 1$$

In this case, the normalization constant is  $s^{-1}$  instead of  $s^{-1/2}$ , and the wavelets are generated from the basic wavelet as

$$h_{s,\tau}(t) = \frac{1}{s} h\left(\frac{t-\tau}{s}\right) \quad (10.3)$$

In this chapter we consider mostly the normalization of the wavelet in terms of energy.

On substituting Equation 10.2 into Equation 10.1 we express the wavelet transform of  $f(t)$  as a correlation between the signal and the scaled wavelets  $h(t/s)$ :

$$W_f(s, \tau) = \frac{1}{\sqrt{s}} \int f(t) h^*\left(\frac{t-\tau}{s}\right) dt \quad (10.4)$$

#### 10.1.1.1 Wavelet Transform in Frequency Domain

The Fourier transform of the wavelet is

$$\begin{aligned} H_{s,\tau}(\omega) &= \int \frac{1}{\sqrt{s}} h\left(\frac{t-\tau}{s}\right) \exp(-j\omega t) dt \\ &= \sqrt{s} H(\omega) \exp(-j\omega\tau) \end{aligned} \quad (10.5)$$

where  $H(\omega)$  is the Fourier transform of the basic wavelet  $h(t)$ . In the frequency domain the Fourier transform of the wavelet is scaled by  $1/s$ , multiplied by a phase factor  $\exp(-j\omega\tau)$  and by a normalization factor  $s^{1/2}$ . The amplitude of the scaled wavelet is proportional to  $s^{-1/2}$  in the time domain and is proportional to  $s^{1/2}$  in the frequency domain. Note that when the wavelets are normalized in terms of amplitude, their Fourier transforms of different scales will have the same amplitude. This is suitable for implementation of the continuous wavelet transform using the frequency domain filtering.

Equation 10.5 shows a well known concept that a dilatation  $t/s$  ( $s > 1$ ) of a function in the time domain produces a contraction  $s\omega$  of its Fourier transform. The term  $1/s$  has a dimension of frequency and is equivalent here to the frequency. However, we prefer the term “scale” to the term “frequency” for the wavelet transform. The term “frequency” is reserved to be a parameter related to the Fourier transform.

The correlation between the signal and the wavelets in the time domain can be written as the inverse Fourier transform of the product of the Fourier transform of the wavelets and the Fourier transform of the signal:

$$W_f(s, \tau) = \frac{\sqrt{s}}{2\pi} \int F(\omega) H^*(s\omega) \exp(j\omega\tau) d\omega \quad (10.6)$$

The Fourier transforms of the wavelets  $\sqrt{s}H(s\omega)$  are referred to as the wavelet transform filters, and the impulse response of the wavelet transform filter is the scaled wavelet  $s^{-1/2}h(t/s)$ , where the explicit phase shift  $\exp(j\omega\tau)$  in the frequency and translation  $\tau$  in the time are removed. Therefore, the wavelet transform is a bank of wavelet transform filters with different scales  $s$ .

In the definition of the wavelet transform, the kernel function, wavelet, is not specified. This is a difference between the wavelet transform and other transforms such as the Fourier transform.

The theory of wavelet transform deals with general properties of the wavelet and the wavelet transform, such as the admissibility, regularity, and orthogonality. The wavelet basis is built to satisfy these basic conditions. The wavelets can be given as analytical or numerical functions. They can be orthonormal or nonorthonormal, continuous or discrete. One can choose or even build himself a proper wavelet basis for a specific application. Therefore, when talking about the wavelet transform one used to specify what wavelet is used in the transform.

The most important properties of the wavelets are the admissibility and regularity. As we shall see below, according to the admissible condition the wavelet must oscillate to have its mean value equal to zero. According to the regularity condition the wavelet have exponential decay so that its first low order moments are equal to zero. Therefore, in the time domain the wavelet is just like a small wave that oscillates and vanishes, as that described by the name wavelet. The wavelet transform is a local operator in the time domain.

The orthonormality is a property which belongs to the discrete wavelet transform. We shall discuss the discrete orthonormal and biorthonormal wavelet transforms in Sections 10.3 through 10.9.

## 10.1.2 Time–Frequency Space Analysis

The wavelets transform of a 1-D signal is a two-dimensional (2-D) function of the scale  $s$  and the time shift  $\tau$ , that represents the signal in the timescale space and is referred to as the timescale joint representation. The timescale wavelet representation is equivalent to the time–frequency joint representation, which is familiar in the analysis of nonstationary and fast transient signals.

### 10.1.2.1 Nonstationary Signals

The wavelet transform is of particular interest for analysis of nonstationary and fast transient signals. Signals are stationary if their properties do not change during the course of signals. The concept of the stationarity is well defined in the theory of stochastic processes. A stochastic process is called strict-sense stationary if its statistical properties are invariant to a shift of the origin of the time axis. A stochastic process is called wide-sense (or weak) stationary if its second-order statistics is invariant to shift in time and depends only on the time difference.

Most signals in the nature are nonstationary. Examples of nonstationary signals are speech, radar, sonar, seismic, electrocardiographic signals, and music. The nonstationary signals are in general characterized by their local features rather than by their global features. 2-D images are also nonstationary as the image features such as edges, textures, and deterministic objects are distributed in different locations and orientations.

### 10.1.2.2 Time–Frequency Joint Representation

An example of the nonstationary signal is music. The frequency spectrum of a music signal changes with the time. At a specific time, for instance, a piano key is knocked, that gives rise to a sound which has a specific frequency spectrum. At another time, another key will be knocked generating another spectrum.

The notation of music score is an example of the time–frequency joint representation. A piece of music can be described accurately by air pressure as a function of time. It can be equally accurately described by the Fourier transform of the pressure function. However, neither of the those two signal representations would be useful for a musician, who wants to perform a certain piece. Musicians prefer a 2-D plot, with time and logarithmic frequency as axes. The music scores tell them when and what notes should be played.

### 10.1.2.3 Fourier Analysis of Nonstationary Signals

The Fourier transform is widely used in signal analysis and processing. When the signal is periodic and sufficiently regular, the Fourier coefficients decay quickly with the increasing of the frequency. For nonperiodic signals, the Fourier integral gives a continuous spectrum. The fast Fourier transform (FFT) permits efficient numerical Fourier analysis.

The Fourier transform is not satisfactory for analyzing signals whose spectra vary with time, such as the music signals. The Fourier transform is a decomposition of a signal into two series of orthogonal functions  $\cos \omega t$  and  $j \sin \omega t$  with  $j = (-1)^{1/2}$ . The Fourier bases are of infinite duration along the time axis. They are perfectly local in frequency, but are global in time. A signal may be reconstructed from its Fourier components, which are the Fourier basis functions of infinite duration weighted by the corresponding Fourier coefficients of the signal. Most signals that we are interested in are, however, of finite extent. Outside this finite time duration window, its Fourier components, which are nonzero, must be canceled by their own summation. A short pulse that is local in time is not local in frequency. Its Fourier spectrum decays slowly with frequency. The reconstruction of the pulse from its Fourier components depends on the cancellation of the high frequency Fourier components heavily and, therefore, is sensitive to high frequency noise.

The Fourier spectrum analysis is global in time and is basically not suitable to analyze nonstationary and fast varying transient signals. Many temporal aspects of the signal, such as the start and end time of a finite signal and the instant of appearance of a singularity in a transient signal, are not preserved in the Fourier spectrum. The Fourier transform does not provide any information regarding the time evolution of spectral characteristics of the signal.

The short-time Fourier transform also referred to as the Gabor transform, the Wigner distribution and the ambiguity function are usually used to overcome the drawback of the Fourier analysis for nonstationary and fast transient signals. The Wigner distribution and the ambiguity function are not linear, but are bilinear transforms.

### 10.1.3 Short-Time Fourier Transform

---

**Definition** An intuitive way to analyze a nonstationary signal is to perform a time-dependent spectral analysis. A nonstationary signal is divided into a sequence of time segments in which the

signal may be considered as quasistationary. Then, the Fourier transform is applied to each of the local segments of the signal.

The short-time Fourier transform is associated with a window of fixed width. Gabor in 1946 was the first to introduce the short-time Fourier transform [1] which is known as the sliding window Fourier transform. The transform is defined as

$$S_f(\omega', \tau) = \int f(t)g^*(t - \tau) \exp(-j\omega't) dt$$

where  $g(t)$  is a square integrable short-time window, which has a fixed width and is shifted along the time axis by a factor  $\tau$ .

### 10.1.3.1 Gabor Functions

The Gabor transform may also be regarded as an inner product between the signal and a set of kernel functions, called the Gabor functions:  $g(t - \tau) \exp(j\omega't)$ . The Gabor basis is generated from a basic window function  $g(t)$  which is translated along the time axis by  $\tau$ . The phase modulation  $\exp(j\omega't)$  corresponds to translation of the Gabor function spectrum along the frequency axis by  $\omega'$ . The Fourier transform of the basic Gabor function  $g(t) \exp(j\omega't)$  is expressed as

$$\int g(t) \exp(j\omega't) \exp(-j\omega t) dt = G(\omega - \omega')$$

The Fourier transform  $G(\omega)$  of the basic window function  $g(t)$  is shifted along the frequency axis by  $\omega'$ . The short-time Fourier transform of a 1-D signal is a complex valued function of two real parameters: time  $\tau$  and frequency  $\omega'$  in the 2-D time–frequency space.

### 10.1.3.2 Inverse Short-Time Fourier Transform

When  $\tau$  and  $\omega'$  are continuous variables, the signal  $f(t)$  may be reconstructed completely by integrating the Gabor functions weighted by the short-time Fourier transform coefficients:

$$f(t) = \frac{1}{2\pi} \iint S_f(\omega', \tau) g(t - \tau) \exp(j\omega't) d\omega' d\tau$$

and this holds for any chosen window  $g(t)$ . The inverse short-time Fourier transform may be proved by the following calculation:

$$\begin{aligned} & \iint S_f(\omega', \tau) g(t - \tau) \exp(j\omega't) d\omega' d\tau \\ &= \iiint f(t') g^*(t' - \tau) \exp(-j\omega't') g(t - \tau) \exp(j\omega't) d\omega' d\tau dt' \\ &= \iint 2\pi \delta(t' - t) f(t') g^*(t' - \tau) g(t - \tau) d\tau dt' \\ &= 2\pi f(t) \int |g(t - \tau)|^2 d\tau = 2\pi f(t) \end{aligned}$$

provided that the window function is normalized as

$$\int |g(t)|^2 dt = 1 \quad (10.7)$$

### 10.1.3.3 Time and Frequency Resolution

In the short-time Fourier transform the signal is multiplied by a sliding window that localizes the signal in time domain, but is blurring the signal in the frequency domain. The narrower the window, the better we localize the signal and the poorer we localize its spectrum.

The width  $\Delta t$  of the window  $g(t)$  in time domain and the bandwidth  $\Delta\omega$  of the window  $G(\omega)$  in frequency domain are defined respectively as

$$\Delta t^2 = \frac{\int t^2 |g(t)|^2 dt}{\int |g(t)|^2 dt} \quad \Delta\omega^2 = \frac{\int \omega^2 |G(\omega)|^2 d\omega}{\int |G(\omega)|^2 d\omega} \quad (10.8)$$

where the denominator is the energy of the window in time and frequency domains, respectively.

The two sinusoids can be discriminated only if they are more than  $\Delta\omega$  apart. Thus,  $\Delta\omega$  is the resolution in the frequency domain of the short-time Fourier transform. Similarly, two pulses in time domain can be discriminated only if they are more than  $\Delta t$  apart. Note that once a window has been chosen for the short-time Fourier transform, the time and frequency resolutions given by Equation 10.8 are fixed over the entire time–frequency plane. The short-time Fourier transform is a fixed window Fourier transform.

### 10.1.3.4 Uncertainty Principle

The time–frequency joint representation has an intrinsic limitation: the product of the resolutions in time and frequency is limited by the uncertainty principle:

$$\Delta t \Delta\omega \geq 1/2 \quad (10.9)$$

This is also referred to as Heisenberg inequality, familiar in quantum mechanics and important for time–frequency joint representation. A signal cannot be represented as a point in the time–frequency space. One can only determine its position in the time–frequency space within a rectangle of  $\Delta t \Delta\omega$ .

### 10.1.3.5 Gaussian Window

The time–bandwidth product  $\Delta t \Delta\omega$  must obey the uncertainty principle. We can only trade time resolution for frequency resolution or vice versa. Gabor proposed the Gaussian function as the window function. The Gaussian function has the minimum time–bandwidth product determined by the uncertainty principle Equation 10.9. The Fourier transform of the Gaussian window is still a Gaussian as

$$g(t) = \frac{1}{\sqrt{2\pi s}} \exp\left(-\frac{t^2}{2s^2}\right) \quad \text{and} \quad G(\omega) = \exp(-s^2\omega^2/2)$$

which have a minimum spread. A simple calculation using Equation 10.8 shows that

$$\Delta t^2 = \frac{s^2}{2} \quad \text{and} \quad \Delta\omega^2 = \frac{1}{2s^2}$$

which satisfies the uncertainty principle Equation 10.9 and achieves the minimum time–bandwidth product  $\Delta t \Delta \omega = 1/2$ .

The short-time Fourier analysis depends critically on the choice of the window. Its application requires a priori information concerning the time evolution of the signal properties in order to make a priori choice of the window function. Once a window is chosen, the width of the window along both time and frequency axes are fixed in the entire time–frequency plane.

### 10.1.3.6 Discrete Short-Time Fourier Transform

When the translation factors of the Gabor functions along the time and the frequency axes,  $\tau$  and  $\omega$ , take discrete values,  $\tau = n\tau_0$  and  $\omega = m\omega_0$  with  $m$  and  $n \in \mathbf{Z}$ , the discrete Gabor functions are written as

$$g_{m,n}(t) = g(t - n\tau_0) \exp(jm\omega_0 t)$$

and their Fourier transforms are

$$G_{m,n}(\omega) = G(\omega - m\omega_0) \exp[j(\omega - m\omega_0)n\tau_0]$$

The discrete Gabor transform is

$$S_f(m,n) = \int f(t) g^*(t - n\tau_0) \exp(-jm\omega_0 t) dt$$

The signal  $f(t)$  can still be recovered from the coefficients  $S_f(m,n)$ , provided that  $\tau_0$  and  $\omega_0$  are suitably chosen. Gabor's original choice was  $\omega_0 \tau_0 = 2\pi$ .

### 10.1.3.7 Regular Lattice

If the window function is normalized as shown in Equation 10.7 and is also centered to the origin in the time–frequency space, so that:

$$\int t |g(t)|^2 dt = 0 \quad \int \omega |G(\omega)|^2 d\omega = 0$$

then the locations of the Gabor functions in the time–frequency space are determined by

$$\int t |g_{m,n}(t)|^2 dt = \int t |g(t - n\tau_0)|^2 dt = n\tau_0$$

and

$$\int \omega |G_{m,n}(\omega)|^2 d\omega = \int \omega |G(\omega - m\omega_0)|^2 d\omega = m\omega_0$$

The discrete Gabor function set will be represented by a regular lattice with the equal intervals  $\tau_0$  and  $\omega_0$  in the time–frequency space, as will be shown in Figure 10.2a.

## 10.1.4 Wigner Distribution and Ambiguity Functions

The Wigner distribution function and the ambiguity function are second-order transform or bilinear transforms, that perform mapping of the signals into the time–frequency space.

### 10.1.4.1 Wigner Distribution Function

The Wigner distribution function [2] is an alternative to the short-time Fourier transform for nonstationary and transient signal analysis. The Wigner distribution of a function  $f(t)$  is defined in the time domain as

$$W_f(\tau, \omega) = \int f\left(\tau + \frac{t}{2}\right) f^*\left(\tau - \frac{t}{2}\right) \exp(-j\omega t) dt \quad (10.10)$$

that is the Fourier transform of the product,  $f(\tau + t/2)f^*(\tau - t/2)$ , between the dilated signal  $f(t/2)$  and the dilated by 2 and inverted signal  $f^*(-t/2)$ . Furthermore, the product is shifted along the time axis by  $\tau$ . The Wigner distribution is a complex valued function in the time–frequency space and is a time–frequency joint representation of the signal. In the frequency domain the Wigner distribution function is expressed as

$$W_f(\tau, \omega) = \frac{1}{2\pi} \int F\left(\omega + \frac{\xi}{2}\right) F^*\left(\omega - \frac{\xi}{2}\right) \exp(j\tau\xi) d\xi \quad (10.11)$$

where  $F(\omega)$  is the Fourier transform of  $f(t)$ .

The inverse relations of the Wigner distribution function can be obtained from the inverse Fourier transforms of Equations 10.10 and 10.11. With the changes of variables  $t_1 = \tau + t/2$  and  $t_2 = \tau - t/2$ , the inverse Fourier transform of the Wigner distribution of Equation 10.10 gives

$$f(t_1) f^*(t_2) = \frac{1}{2\pi} \int W_f\left(\frac{t_1 + t_2}{2}, \omega\right) \exp[j(t_1 - t_2)\omega] d\omega \quad (10.12)$$

Similarly, with the changes of variables  $\omega_1 = \omega + (\xi/2)$  and  $\omega_2 = \omega - (\xi/2)$  the inverse Fourier transform of Equation 10.11 gives

$$F(\omega_1) F^*(\omega_2) = \int W_f\left(\tau, \frac{\omega_1 + \omega_2}{2}\right) \exp[-j(\omega_1 - \omega_2)\tau] d\tau$$

The signal  $f(t)$  can be recovered from the inverse Wigner distribution function. Let  $t_1 = t$  and  $t_2 = 0$ , Equation 10.12 becomes

$$f(t) f^*(0) = \frac{1}{2\pi} \int W_f\left(\frac{t}{2}, \omega\right) \exp(j\omega t) d\omega$$

where  $f^*(0)$  is a constant. Hence, the function  $f(t)$  is reconstructed from the inverse Fourier transform of the Wigner distribution function  $W_f(t/2, \omega)$ , dilated by 2 in the time domain.

As the basic properties of the Wigner distribution function we mention that the projection of  $W_f(\tau, \omega)$  along the  $\tau$ -axis in the time–frequency space gives the square modulus of  $F(\omega)$ , because according to Equation 10.11 the projection along the  $\tau$ -axis is

$$\begin{aligned} \int W_f(\tau, \omega) d\tau &= \frac{1}{2\pi} \iint F\left(\omega + \frac{\xi}{2}\right) F^*\left(\omega - \frac{\xi}{2}\right) \exp(j\tau\xi) d\tau d\xi \\ &= |F(\omega)|^2 \end{aligned}$$

The projection of  $W_f(\tau, \omega)$  along the  $\omega$ -axis gives the square modulus of  $f(t)$ , because according to Equation 10.11 the projection along the  $\omega$ -axis is

$$\int W_f(\tau, \omega) d\omega = \iint f\left(\tau + \frac{t}{2}\right) f^*\left(\tau - \frac{t}{2}\right) \exp(-j\omega t) dt d\omega = 2\pi |f(t)|^2$$

Furthermore, there is the conservation of energy of the Wigner distribution in the time–frequency joint representation:

$$\frac{1}{2\pi} \int W_f(\tau, \omega) d\tau d\omega = \frac{1}{2\pi} \int |F(\omega)|^2 d\omega = \int |f(t)|^2 dt$$

### 10.1.4.2 Ambiguity Function

The ambiguity function is a mapping of a transient time function signal  $f(t)$  into the time–frequency space. The ambiguity function is defined in the time domain as [3]

$$A_f(t, \omega) = \int f\left(\tau + \frac{t}{2}\right) f^*\left(\tau - \frac{t}{2}\right) \exp(-j\omega\tau) d\tau \quad (10.13)$$

In the frequency domain, the ambiguity function is expressed as

$$A_f(\tau, \omega) = \frac{1}{2\pi} \int F\left(\xi + \frac{\omega}{2}\right) F^*\left(\xi - \frac{\omega}{2}\right) \exp(j\tau\xi) d\xi$$

The ambiguity function can be viewed as a time–frequency autocorrelation function of the signal with the time delay  $t$  and the Doppler frequency shift  $\omega$ . The ambiguity function has found wide applications for radar signal processing.

According to the definitions (Equations 10.10 and 10.13) the double Fourier transform of the product  $f(\tau + t/2)f^*(\tau - t/2)$  with respect to both variables  $t$  and  $\tau$  gives the relation between the Wigner distribution function and the ambiguity function

$$\int A_f(t, \omega) \exp(-j\omega t) dt = \int W_f(\tau, \omega) \exp(-j\omega\tau) d\tau$$

The cross ambiguity function is defined as the Fourier transform of the product  $f(\tau)g^*(\tau)$  of two functions  $f(\tau)$  and  $g(\tau)$

$$A(t, \omega) = \int f\left(\tau + \frac{t}{2}\right) g^*\left(\tau - \frac{t}{2}\right) \exp(j\omega\tau) d\tau$$

High value of  $A(t, \omega)$  means that the two functions are ambiguous. The function  $g(\tau)$  can also be considered as a window function of fixed width that is shifted along the time axis by  $t/2$ . Hence, the cross ambiguity function is the fixed-window short-time Fourier transform. The cross Wigner distribution function is defined as

$$W(\tau, \omega) = \int f\left(\tau + \frac{t}{2}\right) g^*\left(\tau - \frac{t}{2}\right) \exp(j\omega t) dt$$

that can be seen as the Fourier transform of the signal  $f(t)$  dilated by a factor of two and multiplied with an inverted window  $g(-t)$  which is also dilated by a factor of two and shifted by  $\tau$ .

Both the ambiguity function and the Wigner distribution function are useful for active and passive transient signal analysis. Both transforms are bilinear transform. However, the mapping of a summation of signals  $f_1(t) + f_2(t)$  into the time–frequency space with the ambiguity function or with the Wigner distribution function produces cross-product interference terms that might be a nuisance in the projections in the time–frequency space and in the reconstruction of the signal.

## 10.2 Properties of the Wavelets

In this section we discuss some basic properties of the wavelets. One of them is related to the fact that we must be able to reconstruct the signal from its wavelet transform. This property involves the resolution of identity, the energy conservation in the timescale space and the wavelet admissible condition. First any square integrable function which has finite energy and satisfies the wavelets admissible condition can be a wavelet. The second basic property is related to the fact that the wavelet transform should be a local operator in both time and frequency domains. Hence, the regularity condition is usually imposed on the wavelets. The third basic property is related to the fact that the wavelet transform is a multiresolution signal analysis.

### 10.2.1 Admissible Condition

#### 10.2.1.1 Resolution of Identity

The wavelet transform of a 1-D signal is a 2-D timescale joint representation. No information should be lost during the wavelet transform. Hence, the resolution of identity must be satisfied, that is expressed as

$$\int \frac{ds}{s^2} \int d\tau \langle f_1, h_{s,\tau} \rangle \langle h_{s,\tau}, f_2 \rangle = c_h \langle f_1, f_2 \rangle \quad (10.14)$$

where  $\langle, \rangle$  denotes the inner product so that  $\langle f_1, h_{s,\tau} \rangle$  is the wavelet transform of  $f_1$  as defined in Equation 10.4 and  $c_h$  is a constant. In the left-hand side of Equation 10.14 the extra factor  $1/s^2$  in the integral is the Haar invariant measure, owing to the timescale space differential elements,  $d\tau d(1/s) = d\tau ds/s^2$ . We have assumed positive dilation  $s > 0$ . Using the expression (Equation 10.6) for the wavelet transform in the Fourier domain we have

$$\begin{aligned} & \int \frac{ds}{s^2} \int d\tau \langle f_1, h_{s,t} \rangle \langle h_{s,\tau}, f_2 \rangle \\ &= \frac{1}{4\pi^2} \int \frac{ds}{s^2} \int d\tau \iint s F_1(\omega_1) H^*(s\omega_1) F_2^*(\omega_2) H(s\omega_2) e^{j\tau(\omega_1\omega_2)} d\omega_1 d\omega_2 \\ &= \frac{1}{2} \iint F_1(\omega_1) F_2^*(\omega_1) |H(s\omega_1)|^2 \frac{ds}{s} d\omega_1 \\ &= \frac{c_h}{2\pi} \iint F_1(\omega_1) F_2^*(\omega_1) d\omega_1 \end{aligned}$$

where we used the change of variables  $\omega = s\omega_1$  and  $ds = d\omega/|\omega_1|$ , so that  $ds$  and  $d\omega$  are of the same sign. Because  $s > 0$ , we have  $ds/s = d\omega/|\omega|$ , then we defined the constant

$$c_h = \int |H(\omega)|^2 \frac{d\omega}{|\omega|}$$

According to the Parseval's equality in the Fourier transform we have

$$\frac{1}{2\pi} \int F_1(\omega_1) F_2^*(\omega_1) d\omega_1 = \int f_1(t) f_2^*(t) dt = \langle f_1, f_2 \rangle$$

Hence, the resolution of identity is satisfied on the condition that

$$c_h = \int \frac{|H(\omega)|^2}{|\omega|} d\omega < +\infty \quad (10.15)$$

### 10.2.1.2 Admissible Condition

The condition (Equation 10.15) is the admissible condition of the wavelet, which implies that the Fourier transform of the wavelet must be equal to zero at the zero frequency:

$$|H(\omega)|^2|_{\omega=0} = 0 \quad (10.16)$$

Equivalently, in the time domain the wavelet must be oscillatory, like a wave, to have a zero-integrated area, or a zero-mean value:

$$\int h(t) dt = 0 \quad (10.17)$$

### 10.2.1.3 Energy Conservation

When  $f_1 = f_2$ , the resolution of identity, Equation 10.14 becomes

$$\iint |W_f(s, \tau)|^2 d\tau \frac{ds}{s^2} = c_h \int |f(t)|^2 dt \quad (10.18)$$

This is the energy conservation relation of the wavelet transform, equivalent to the Parseval energy relation in the Fourier transform.

### 10.2.1.4 Inverse Wavelet Transform

By withdrawing  $f_2$  from the both sides of the resolution of identity (Equation 10.14) we have directly

$$f(t) = \frac{1}{c_h} \iint W_f(s, \tau) \frac{1}{\sqrt{s}} h\left(\frac{t-\tau}{s}\right) d\tau \frac{ds}{s^2} \quad (10.19)$$

This is the inverse wavelet transform. The function  $f(t)$  is recovered from the inverse wavelet transform by the integrating in the timescale space the wavelets  $h_{s,\tau}(t)$  weighted by the wavelet transform coefficients  $W_f(s, \tau)$ .

Thus, the wavelet transform is a decomposition of a function into a linear combination of the wavelets. The wavelet transform coefficients  $W_f(s, \tau)$  are the inner products between the function and the wavelets. The  $W_f(s, \tau)$  indicate how close the function  $f(t)$  is to the corresponding basis functions  $h_{s,\tau}(t)$ .

### 10.2.1.5 Reproducing Kernel

The inverse wavelet transform shows that the original signal may be synthesized by summing up all the projections of the signal onto the wavelet basis. In this sense, the continuous wavelet transform behaves like an orthogonal transform. We refer to this property of the continuous wavelet transform as the quasi-orthogonality. Obviously, a set of the wavelet basis functions  $h_{s,\tau}(t)$  with continuously varying scale and shift is not orthogonal, but is heavily redundant.

Applying the wavelet transforms in the two sides of Equation 10.19 yields

$$W_f(s_0, \tau_0) = \iint W_f(s, \tau) K(s_0, s; \tau_0, \tau) d\tau \frac{ds}{s^2}$$

where the reproducing kernel

$$K(s_0, s; \tau_0, \tau) = \frac{1}{c_h} \frac{1}{\sqrt{ss_0}} \int h^*\left(\frac{t-\tau_0}{s_0}\right) h\left(\frac{t-\tau}{s}\right) dt$$

is not zero with continuously varying factors  $s_0, s, \omega_0$  and  $\omega$ . This expression describes the intrinsic redundancy between the values of the wavelets at  $(s, \tau)$  and at  $(s_0, \tau_0)$ .

Any square integrable function satisfying the admissible condition may be a wavelet. When the wavelets satisfy the admissible condition, the signal can be recovered by the inverse wavelet transform. No signal information is lost.

## 10.2.2 Regularity

The wavelets should be local in both time and frequency domains. This is achieved by applying the regularity condition to the wavelet. The regularity is not an obligated condition, but is usually required as an important property of the wavelet.

### 10.2.2.1 Regularity of Wavelet

For the sake of simplicity, let the translation of the wavelet  $\tau = 0$  and consider the convergence to zero of the wavelet transform coefficients with increasing of  $1/s$  and decreasing of  $s$ . The signal  $f(t)$  is expanded into the Taylor series at  $t=0$  until order  $n$ . The wavelet transform coefficients become [4]

$$\begin{aligned} W_f(s, 0) &= \frac{1}{\sqrt{s}} \int f(t) h^*\left(\frac{t}{s}\right) dt \\ &= \frac{1}{\sqrt{s}} \left[ \sum_{p=0}^n f^{(p)}(0) \int \frac{t^p}{p!} h\left(\frac{t}{s}\right) dt + \int R(t) h\left(\frac{t}{s}\right) dt \right] \quad (10.20) \end{aligned}$$

where the remainder in the Taylor series is

$$R(t) = \int_0^t \frac{(t-t')^n}{n!} f^{(n+1)}(t') dt'$$

and  $f^{(p)}(0)$  denotes the  $p$ th derivative of  $f(t)$  at  $t=0$ . Denoting the moments of the wavelets by  $M_p$

$$M_p = \int t^p h(t) dt$$

it is easy to show that the last term in the right-hand side of Equation 10.20 which is the wavelet transform of the remainder, decreases as  $s^{n+2}$ . We have then a finite development as

$$W_f(s, 0) = \frac{1}{\sqrt{s}} \left[ f(0)M_0s + \frac{f'(0)}{1!}M_1s^2 + \frac{f''(0)}{2!}M_2s^3 + \dots + \frac{f^{(n)}(0)}{n!}M_ns^{n+1} + O(s^{n+2}) \right] \quad (10.21)$$

According to the admissible condition of the wavelet,  $M_0 = 0$ , the first term in the right-hand side of Equation 10.21 must be zero. The speed of convergence to zero of the wavelet transform coefficients  $W_f(s, \tau)$  with decreasing of the scale  $s$  or increasing of  $1/s$  is then determined by the first nonzero moment of the basic wavelet  $h(t)$ . It is in general required that the wavelets have the first  $n+1$  moments until order  $n$ , equal to zero:

$$M_p = \int t^p h(t) dt = 0 \quad \text{for } p = 0, 1, 2, \dots, n \quad (10.22)$$

Then, according to Equation 10.21 the wavelet transform coefficient  $W_f(s, \tau)$  decays as fast as  $s^{n+(1/2)}$  for a smooth signal  $f(t)$ . This regularity condition leads to localization of the wavelet transform in the frequency domain.

The wavelet satisfying the condition (Equation 10.22) is called the wavelet of order  $n$ . In frequency domain, this condition is equivalent to the derivatives of the Fourier transform of the wavelet  $h(t)$  up to order  $n$  to be zero at the zero frequency  $\omega = 0$ :

$$H^{(p)}(0) = 0 \quad \text{for } p = 0, 1, 2, \dots, n. \quad (10.23)$$

The Fourier transform of the wavelet has a zero of order  $n+1$ . The order  $(n+1)$  is a measure of the flatness of the wavelet in the frequency domain about  $\omega = 0$ .

### 10.2.2.2 Time-Bandwidth Product

While the wavelet transform of an 1-D function is 2-D, the wavelet transform of a 2-D function is four-dimensional. As a consequence we would have an explosion of the time-bandwidth product with the wavelet transform, which is in contradiction with the restrictions of many applications, such as data compression and

pattern classification, where the signals need to be characterized efficiently by fewer transform coefficients.

We usually impose the regularity property to the wavelets such that the wavelet transform coefficients decrease fast with decreasing of the scale  $s$  and increasing of  $1/s$ . For this purpose, the Fourier transform,  $H(\omega)$ , of the basic wavelet should have some smoothness and concentration in the frequency domains, according to the wavelet transform in the frequency domain Equation 10.6. The wavelet transform should be a local operator in frequency domain.

## 10.2.3 Multiresolution Wavelet Analysis

The wavelet transform performs the multiresolution signal analysis with the varying scale factor  $s$ . The purpose of the multiresolution signal analysis is decomposing the signal in multiple frequency bands in order to process the signal in multiple frequency bands differently and independently. Hence, we need the wavelet to be local in both time and frequency domains. Historically, looking for a kernel function which is local in both time and frequency domains has been a hard research topic and has conducted to invention of the wavelet transform.

### Example

Figure 10.1 shows a typical wavelet multiresolution analysis for an electrical power system transient signal. The signal is decomposed with different resolutions corresponding to different scale factors of the wavelets. The signal components in multiple frequency bands and the times of occurrence of those components are well presented in the figure. This figure is a timescale joint representation, with the vertical axis in each discrete scale representing the amplitude of wavelet components. More detailed discussion will be given in Section 10.10.1.

### 10.2.3.1 Localization in Time Domain

According to the admissible condition the wavelet must oscillate to have a zero mean. According to the regularity condition the wavelet of order  $n$  has first  $n+1$  vanishing moments and decays as fast as  $t^{-n}$ . Therefore, in the time domain the wavelet must be a small wave that oscillates and vanishes, as that described by the name wavelet. The wavelet is localized in the time domain.

### 10.2.3.2 Localization in Frequency Domain

According to the regularity condition the wavelet transform with a wavelet of order  $n$  decays with  $s$  as  $s^{n+(1/2)}$  for a smooth signal. According to the frequency domain wavelet transform, Equation 10.6 when the scale  $s$  decreases the wavelet  $H(s\omega)$  in the frequency domain is dilated to cover a large frequency band of the signal Fourier spectrum. Therefore, the decay with  $s$  as  $s^{n+(1/2)}$  of the wavelet transform coefficient implies that the Fourier transform of the wavelet must decay fast with the frequency  $\omega$ . The wavelet must be local in frequency domain.

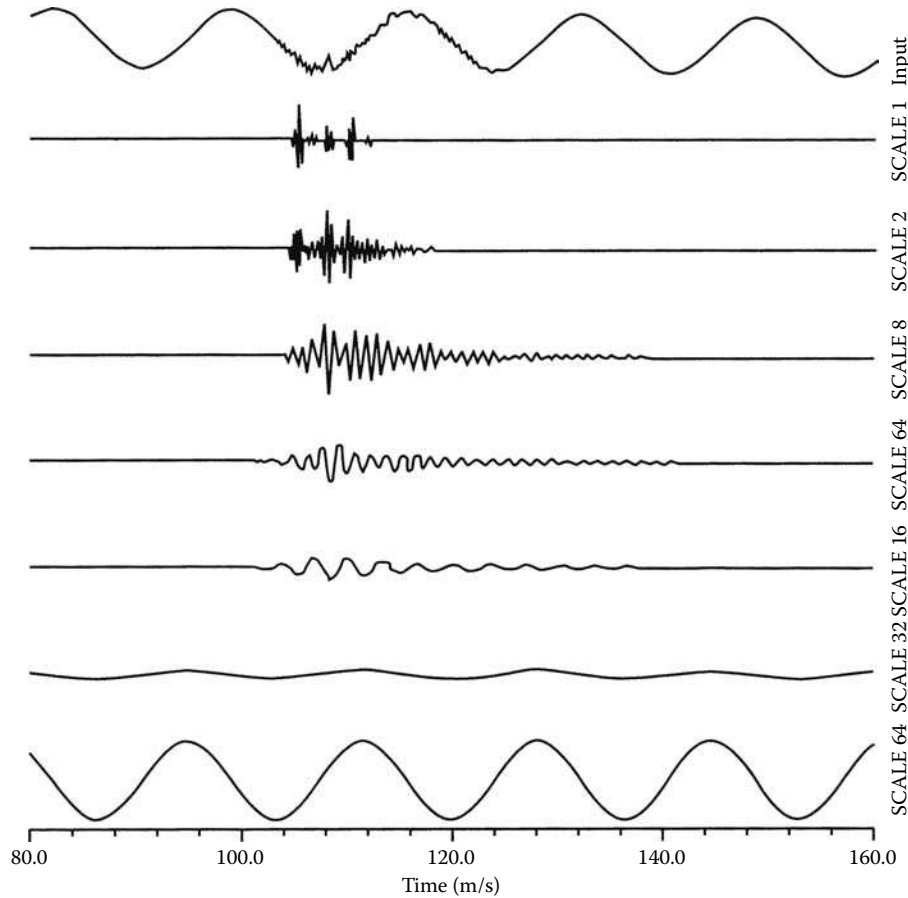


FIGURE 10.1 Multiresolution wavelet analysis of a transient signal in the electrical power system. (From Robertson, D. C. et al., *Proc. SPIE*, 2242, 474, 1994. With permission.)

### 10.2.3.3 Band-Pass Filters

In the frequency domain, the wavelet is localized according to the regularity condition, and is equal to zero at the zero frequency according to the admissible condition. Therefore, the wavelet is intrinsically a band-pass filter.

### 10.2.3.4 Bank of Multiresolution Filters

The wavelet transform is the correlation between the signal and the dilated wavelets. The Fourier transform of the wavelet is a filter in the frequency domain. For a given scale, the wavelet transform is performed with a wavelet transform filter  $\sqrt{s}H(s\omega)$  in the frequency domain, which is in the time domain the scaled wavelet  $h(t/s)$ . When the scale  $s$  varies, the wavelet transform performs a multiscale signal analysis.

In the timescale joint representation, as shown in Figure 10.1, in each horizontal stripe along the time axis the wavelet transform coefficient is computed by the correlation between the signal and the wavelets  $h(t/s)$  at a given scale. When the scale is small the wavelet is concentrated in time, the wavelet analysis gives detailed view of the signal. When the scale increases the wavelet becomes spread out in time, the wavelet analysis gives global view and takes into account the longtime behavior

of the signal. Hence, the wavelet transform is a bank of multi-resolution filters.

The wavelet transform is a bank of multiresolution band-pass filters.

### 10.2.3.5 Constant Fidelity Analysis

Scale change of the wavelet permits the wavelet analysis to zoom in on the discontinuities, singularities and edges, and to zoom out for a global view. This is a unique property of the wavelet transform, important for nonstationary and fast transient signal analysis. The fixed window short-time Fourier transform has not this ability.

With the bank of multiresolution wavelet transform filters, the signal is divided into different frequency subbands. In each subband the signal is analyzed with a resolution matched to the scales of the wavelets. When the scale changes, the bandwidth  $(\Delta\omega)_s$  of the wavelet transform filter becomes, according to the definition of the bandwidth Equation 10.8:

$$(\Delta\omega)_s^2 = \frac{\int \omega^2 |H(s\omega)|^2 d\omega}{\int |H(s\omega)|^2 d\omega} = \frac{\int (s\omega)^2 |H(s\omega)|^2 d(s\omega)}{s^2 \int |H(s\omega)|^2 d(s\omega)} = \frac{1}{s^2} (\Delta\omega)^2$$



The fidelity factor  $Q$  refers to, in general, the central frequency divided by the bandwidth of a filter and is, by this definition, the inverse of the relative bandwidth. The relative bandwidths of the wavelet transform filters are constant because

$$\frac{1}{Q} = \frac{(\Delta\omega)_s}{1/s} = (\Delta\omega) \quad (10.24)$$

which is independent of the scale  $s$ . Hence, the wavelet transform is a constant- $Q$  analysis. At low frequency, corresponding to a large scale factor,  $s$ , the wavelet transform filter has a small bandwidth, which implies a broad time window with a low time resolution. At high frequency, corresponding to a small scale factor,  $s$ , the wavelet transform filter has a wide bandwidth, which implies a narrow time window with high time resolution. The time resolution of the wavelet analysis increases with decrease of the window size. This adaptive window property is desirable for time–frequency analysis.

When the constant- $Q$  relation (Equation 10.24) is satisfied, the frequency bandwidth  $\Delta\omega$  changes with the center frequency  $1/s$  of the wavelet transform filter. The product  $\Delta\omega\Delta t$  satisfies still the uncertainty principle (Equation 10.9). In the wavelet transform the time window size,  $\Delta t$ , can be arbitrarily small at small scale and the frequency window size,  $\Delta\omega$ , can be arbitrarily small at large scale. Figure 10.2 shows the coverage of the time–scale space for the wavelet transform and, as a comparison, that for the short-time Fourier transform.

### 10.2.3.6 Scale and Resolution

The scale is related to the window size of the wavelet. The wavelet transform of a large scale performs an analysis of global view, and that of a small scale performs an analysis of detailed view. The resolution is related to the frequency of the wavelet oscillation. For a given wavelet function, reducing the scale will reduce the window size and increase the resolution in the same time. For some wavelets, such as the Gabor-wavelets the scale and frequency may be chosen separately.

#### Example

Figure 10.3a shows the cos-Gaussian wavelets in comparison with the real part of the Gabor transform basis functions.

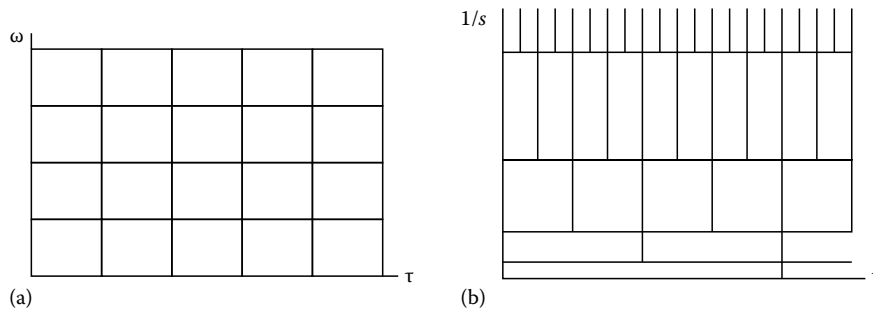


**FIGURE 10.2** Coverage of the time frequency space with (a) the short-time Fourier transform, where  $\Delta\omega$  and  $\Delta t$  are fixed in the whole plane; (b) the wavelet transform, where the frequency bandwidth  $\Delta\omega$  increases and the time resolution  $\Delta t$  improves with increase of  $\Delta(1/s)$ .

Both functions consist of a cosine function with a Gaussian window. The basic cos-Gaussian wavelet is

$$h(t) = \frac{1}{\sqrt{2\pi}} \cos(\omega_0 t) \exp\left(\frac{-t^2}{2}\right)$$

where  $\omega_0 = 5$  in Figure 10.3a. The wavelets  $h_{s,\tau}(t)$  are generated from  $h(t)$  by dilation and translation

$$h_{s,\tau} = \frac{1}{\sqrt{s}} h\left(\frac{t - \tau}{s}\right)$$

with the discrete scale factor  $s = 2^m$  and the discrete translation factor  $(\tau/s) = n$  where  $m$  and  $n$  are integers, the wavelets become discrete as  $h_{m,n}(t)$

The discrete Gabor function  $g_{m,n}(t)$  is defined as

$$g_{m,n}(t) = g(t - n\tau_0) \exp(jm\omega_0 t)$$

where  $\omega_0 = \pi$  in Figure 10.3a and  $g(t)$  is the Gaussian window with a fixed width

In Figure 10.3a we see that the wavelets are with the dilated window. All the dilated wavelets contain the same number of oscillations. The wavelet transform performs multiresolution analysis with high frequency analysis for narrow windowed signals and low frequency analysis for wide windowed signals. This constant- $Q$  analysis property makes the wavelet transform surpass the fixed-window short-time Fourier transform for analysis of local property of signals.

Figure 10.3b shows a comparison between the wavelet transform and the Gabor transform for a step function input. The wavelets are with the dilated windows. The Gabor functions are with windows of fixed width. The timescale joint representation  $\log s - t$  of the wavelet transform and the time–frequency joint representation  $\log \omega - t$  of the Gabor transform are also shown. The wavelet transform with very small scale  $s$  and very narrow window is able to “zoom in” on the discontinuity and to indicate the arrival time of the step signal, while the Gabor transform cannot do this.

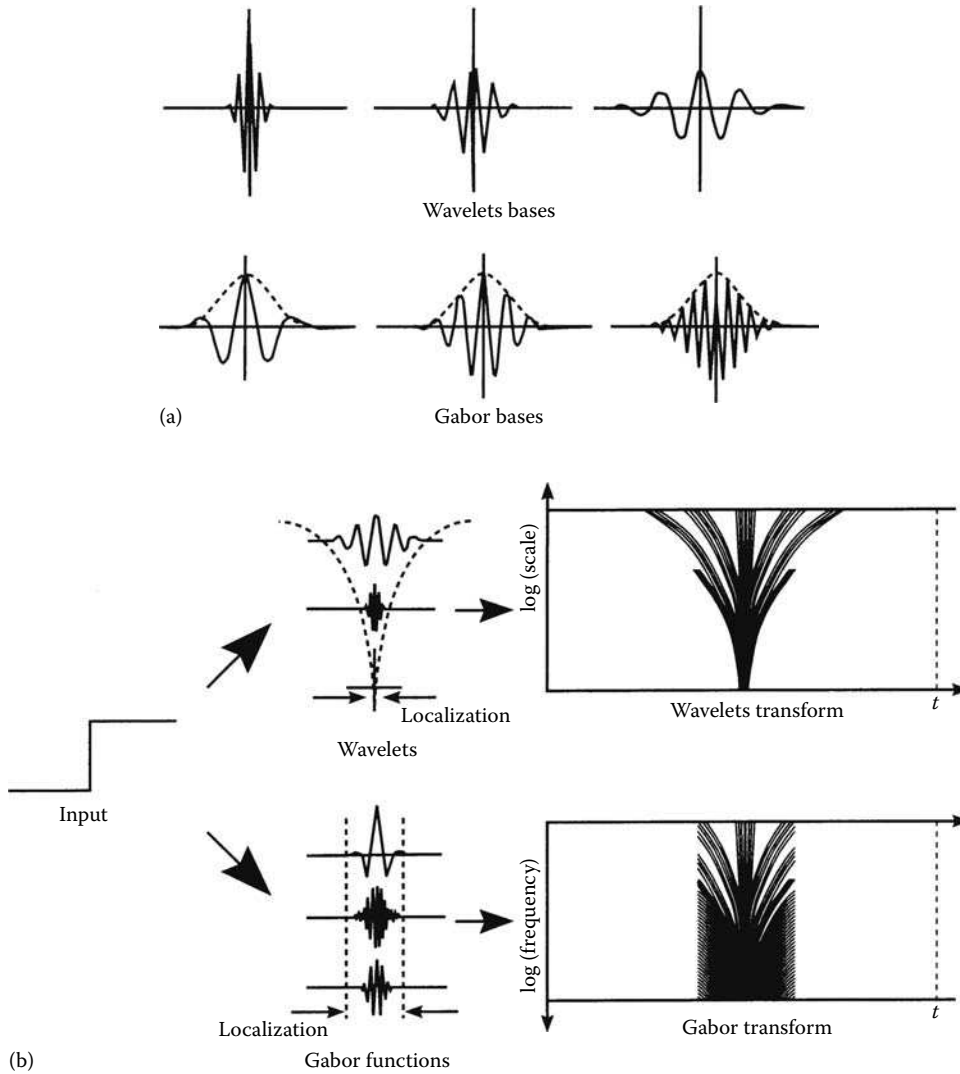


**FIGURE 10.3** (a) The cos-Gaussian wavelets  $h_{m,n}(t)$  and the real part of the Gabor functions  $g_{m,n}(t)$ , with the scale factor  $s = 2^m$  and the translation factor  $\tau = ns$  for different values of  $m$ . The wavelets have a dilated window. The Gabor functions have a window with fixed width. (b) Time-scale joint representation of the wavelet transform and time-frequency joint representation of the Gabor transform for a step function. (From Szu, H. et al. *Appl. Optics*, 31(17), 1992. Freeman, M.O. *Photonics New*, August 1995, 8–14. With permission.)

### 10.2.4 Linear Transform Property

By definition the wavelet transform is a linear operation. Given a function  $f(t)$ , its wavelet transform  $W_f(s, \tau)$  satisfies the following relations

1. Linear superposition without the cross terms

$$W_{f_1+f_2}(s, \tau) = W_{f_1}(s, \tau) + W_{f_2}(s, \tau),$$

2. Translation

$$W_{f(t-t_0)}(s, \tau) = W_{f(t)}(s, \tau - t_0)$$

3. Rescale

$$W_{\alpha^{1/2}f(\alpha t)}(s, \tau) = W_{f(t)}(\alpha s, \alpha \tau)$$

Different from the standard Fourier transform and other transforms, the wavelet transform is not ready for closed form solution apart from some very simple functions such as:

1. For  $f(t) = 1$ , from the definition (Equation 10.4) and the admissible condition of the wavelets, Equation 10.17 we have

$$W_f(s, \tau) = 0$$

The wavelet transform of a constant is equal to zero.

2. For a sinusoidal function  $f(t) = \exp(j\omega_0 t)$ , we have directly from the Fourier transform of the wavelets (Equation 10.6) that

$$W_f(s, \tau) = \sqrt{s} H^*(s\omega_0) \exp(j\omega_0 \tau)$$

The wavelet transform of a sinusoidal function is a sinusoidal function of the time shift  $\tau$ . Its modulus  $|W_f(s, \tau)|$  depends on the scale  $s$  as  $\sqrt{s}|H^*(s\omega_0)|$ .

3. For a linear function  $f(t) = t$ , we have

$$\begin{aligned} W_f(s, \tau) &= \frac{1}{\sqrt{s}} \int t h^*\left(\frac{t-\tau}{s}\right) dt \\ &= s^{3/2} \int t h^*(t-\tau') dt = \frac{s^{3/2}}{j} \left. \frac{dH^*(\omega)}{d\omega} \right|_{\omega=0} \end{aligned}$$

Hence, if the wavelet  $h(t)$  is regular and of order  $n \geq 1$  so that its moments of order  $n \geq 1$  is equal to zero and its derivatives of first-order is equal to zero at  $\omega = 0$ , then the wavelet transform of  $f(t) = t$  is equal to zero.

### 10.2.4.1 Wavelet Transform of Regular Signals

According to what discussed in the precedent the wavelet transform of a constant is zero. The wavelet transform of a linear signal is zero, when the wavelet has the first-order vanishing moment:  $M_1 = 0$ . The wavelet transform of a quadratic signal could be zero, when the wavelet has the first-and second-order vanishing moments:  $M_1 = M_2 = 0$ . The wavelet transform of a polynomial signal of degree  $m$  could be equal to zero, when the wavelet has the vanishing moments up to the order  $n \geq m$ .

Thus, the wavelet transform is efficient for detecting singularities in signal and analyzing nonstationary, transient signal.

For most functions the wavelet transforms have no closed analytical solutions and can be calculated only by numerical computer or by optical analog computer. The optical continuous wavelet transform is based on the explicit definition of the wavelet transform Equation 10.4 and implemented using a bank of optical wavelet transform filters as described in Equation 10.6 in the Fourier plane in an optical correlator [21–23].

## 10.2.5 Examples of the Wavelets

In this section we give some examples of the wavelets, mainly used for the continuous wavelet transform. Examples of the wavelets for the discrete orthonormal wavelet transform will be given in Section 10.8.

### 10.2.5.1 Haar Wavelet

The Haar wavelet was historically introduced by Haar [5] in 1910. It is a bipolar step function:

$$h(t) = \begin{cases} 1 & \text{when } 0 < t < 1/2 \\ -1 & \text{when } 1/2 < t < 1 \\ 0 & \text{otherwise} \end{cases}$$

The Haar wavelet can be written as a correlation between a dilated rectangle function  $\text{rect}(2t)$  and two delta functions

$$\begin{aligned} h(t) &= \text{rect}\left(2\left(t - \frac{1}{4}\right)\right) - \text{rect}\left(2\left(t - \frac{3}{4}\right)\right) \\ &= \text{rect}(2t)^* \left[ \delta\left(t - \frac{1}{4}\right) - \delta\left(t - \frac{3}{4}\right) \right] \end{aligned}$$

where the rectangular function is defined as

$$\text{rect}(t) = \begin{cases} 1 & \text{when } -1/2 < t < 1/2 \\ 0 & \text{otherwise} \end{cases}$$

The Haar wavelet is real-valued and antisymmetric with respect to  $t = 1/2$ , as shown in Figure 10.4. The wavelet admissible condition (Equation 10.17) is satisfied. The Fourier transform of the Haar wavelet is complex valued and is equal to the product of a sine function and a sinc function.

$$\begin{aligned} H(\omega) &= 2j \exp\left(-j\frac{\omega}{2}\right) \text{sinc}\left(\frac{\omega}{4}\right) \sin\left(\frac{\omega}{4}\right) \\ &= 4j \exp\left(-j\frac{\omega}{2}\right) \frac{1 - \cos\frac{\omega}{2}}{\omega} \end{aligned} \quad (10.25)$$

whose amplitude is even and symmetric to  $\omega = 0$ . That is a band-pass filter, as shown in Figure 10.4. The phase factor  $\exp(-j\omega/2)$  is related to the shift of  $h(t)$  to  $t = 1/2$ , which is necessary for the causal filtering of time signals.

The Haar wavelet transform involves a bank of multiresolution filters that yield the correlations between the signal and the Haar wavelets scaled by factor  $s$ . The Haar wavelet transform is a local operation in the time domain. The time resolution depends on the scale  $s$ . When the signal is constant, the Haar wavelet transform is

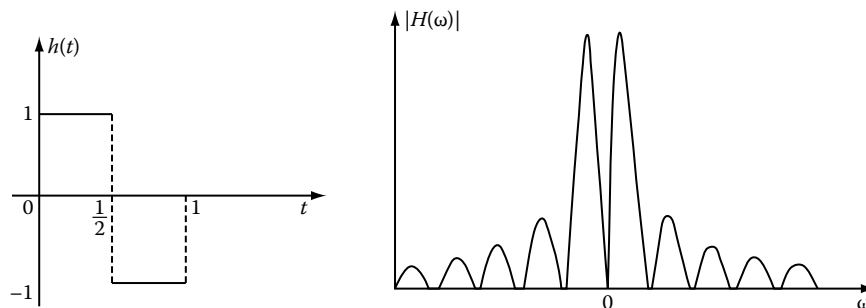


FIGURE 10.4 Haar basic wavelet  $h(t)$  and its Fourier transform  $H(\omega)$ . (From Sheng, Y. et al. *Opt. Eng.*, 31, 1840, 1992. With permission.)

equal to zero. The amplitude of the Haar wavelet transform has high peak values when there are discontinuities of the signal.

The Haar wavelet is irregular. Its first derivative is discontinuous and its first-order moment is not zero. According to Equation 10.25 the amplitude of Fourier spectrum of the Haar wavelet converges to zero slowly as  $1/\omega$ . According to Equation 10.21 the Haar wavelet transform decays with increasing of  $1/s$  at least as slowly as  $(1/s)^{-3/2}$ . The Haar wavelet transform has not found many practical applications because of its poor localization property in the frequency domain.

The set of discrete dilations and translations of the Haar wavelets constitute the simplest discrete orthonormal wavelet basis. We shall use the Haar wavelets as an example of the orthonormal wavelet basis in Sections 10.5 and 10.7.

### 10.2.5.2 Gaussian Wavelet

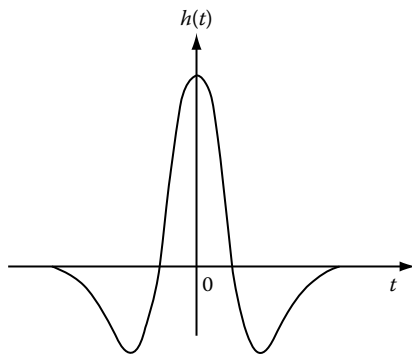
The Gaussian function is perfectly local in both time and frequency domains and is infinitely derivable. In fact, a derivative of any order  $n$  of the Gaussian function may be a wavelet. The Fourier transform of the  $n$ th-order derivative of the Gaussian function is

$$H(\omega) = (j\omega)^n \exp\left(-\frac{\omega^2}{2}\right)$$

that is the Gaussian function multiplied by  $(j\omega)^n$ , so that  $H(0) = 0$ . The wavelet admissible condition is satisfied. The derivatives up to  $n$ th-order of the Gaussian wavelets  $H^{(n-1)}(0) = 0$ . The Gaussian wavelet is a regular wavelet of order  $n$ . Both  $h(t)$  and  $H(\omega)$  are infinitely derivable. The Gaussian wavelet transform coefficients decay with increasing of  $1/s$  as fast as  $(1/s)^{n-(1/2)}$ .

### 10.2.5.3 Mexican-Hat Wavelet

The Mexican-hat like wavelet was first introduced by Gabor. It is the second-order derivative of the Gaussian function [7]:



The Mexican-hat wavelet is even and real valued. The wavelet admissible condition is satisfied. The Fourier transform of the Mexican-hat wavelet is

$$H(\omega) = -\omega^2 \exp\left(-\frac{\omega^2}{2}\right)$$

that is also even and real-valued, as shown in Figure 10.5.

The 2-D Mexican-hat wavelet is well known as the Laplacian operator, widely used, for instance, for zero-crossing image edge detection.

### 10.2.5.4 Gabor-Wavelet

The Gabor function in the short-time Fourier transform with Gaussian window is defined as

$$h(t) = \exp(j\omega_0 t) \exp\left(-\frac{(t-\tau)^2}{2}\right)$$

Its real part is a cosine-Gaussian and its imaginary part is a sine-Gaussian function. The Gaussian window in the Gabor function has a fixed width and is shifted along the time axis by  $\tau$ . The Fourier transform of the Gabor function is again a Gaussian window shifted along the frequency axis by  $\omega_0$ .

The Gabor function can also have a dilated window and is defined as

$$h(t) = \exp(j\omega_0 t) \exp\left(-\frac{t^2}{2s^2}\right)$$

where the scale factor  $s$  is also the width of the Gaussian window. The term  $\exp(j\omega_0 t)$  introduces a translation in the spectrum of

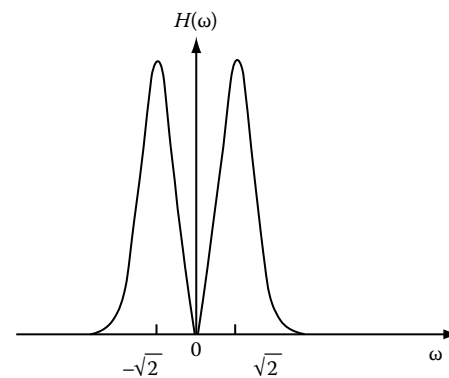


FIGURE 10.5 Mexican hat wavelet  $h(t)$  and its Fourier transform  $H(\omega)$ . (From Sheng, Y. et al. *Opt. Eng.*, 31, 1840, 1992. With permission.)

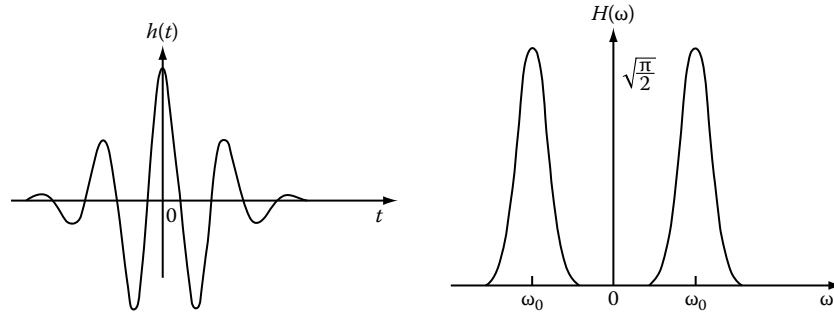


FIGURE 10.6 Cos-Gaussian wavelet  $h(t)$  and its Fourier transform  $H(\omega)$ . (From Sheng, Y. et al. *Opt. Eng.*, 31, 1840, 1992. With permission.)

the Gabor wavelet. The Gabor function with the dilation of both window and Fourier kernel is the Gabor-wavelet. This wavelet has been used by Martinet, Morlet, and Grossmann for analysis of sound patterns [6]. The Morlet's basic wavelet function is the Fourier basis multiplied with a Gaussian window. Its real part is the cosine-Gaussian wavelet, whose Fourier transform consists of two Gaussian functions shifted to  $\omega_0$  and  $-\omega_0$ , respectively:

$$H(\omega) = \sqrt{2\pi}\pi \left[ \exp\left(-\frac{(\omega - \omega_0)^2}{2}\right) + \exp\left(-\frac{(\omega + \omega_0)^2}{2}\right) \right]$$

that are real positive-valued, even and symmetric to the origin  $\omega = 0$ . The Gaussian window is perfectly local in both time and frequency domains and achieves the minimum time-bandwidth product determined by the uncertainty principle, as shown by Equation 10.9. The cos-Gaussian wavelets are band-pass filters in frequency domain. They converge to zero like the Gaussian function as the frequency increases. Figure 10.6 shows the cosine-Gaussian wavelet and its Fourier spectrum.

The Gabor wavelets do not satisfy the wavelet admissible condition, because

$$H(0) \neq 0$$

that leads to  $c_h = +\infty$ . But the value of  $H(0)$  is very close to zero provided that the  $\omega_0$  is sufficiently large. When  $\omega_0 = 5$ , for example,

$$H(0) = (2\pi)^{3/2} \exp\left(-\frac{25}{2}\right)$$

that is of the order of magnitude of  $10^{-5}$  and can be practically considered as zero in numerical computations.

### 10.3 Discrete Wavelet Transform

The continuous wavelet transform is a mapping of a 1-D time signal into a 2-D timescale joint representation. The time-bandwidth product of the continuous wavelet transform output

is the square of that of the signal. For most applications, however, the goal of signal processing is to represent the signal efficiently with fewer parameters. The use of the discrete wavelet transform can reduce the time-bandwidth product of the wavelet transform output.

By the term discrete wavelet transform we mean, in fact, the continuous wavelets with the discrete scale and translation factors. The wavelet transform is then evaluated at discrete scales and translations. The discrete scale is expressed as  $s = s_0^i$ , where  $i$  is integer and  $s_0 > 1$  is a fixed dilation step. The discrete translation factor is expressed as  $\tau = k\tau_0 s_0^i$ , where  $k$  is integer. The translation depends on the dilation  $s_0^i$ . The corresponding discrete wavelets are written as

$$\begin{aligned} h_{i,k}(t) &= s_0^{-i/2} h(s_0^{-i}(t - k\tau_0 s_0^i)) \\ &= s_0^{-i/2} h(s_0^{-i}t - k\tau_0) \end{aligned} \tag{10.26}$$

The discrete wavelet transform with the dyadic scaling factor with  $s_0 = 2$  is effective in the computer implementation.

#### 10.3.1 Timescale Space Lattices

The discrete wavelet transform evaluated at discrete times and scales performs a sampling in the timescale space. The timescale joint representation of a discrete wavelet transform is a grid along the scale and time axes. To show the sampling we consider localization points of the discrete wavelets in the timescale space.

The sampling along the time axis has the interval  $\tau_0 s_0^i$ , that is proportional to the scale  $s_0^i$ . The time sampling step is small for small scale wavelet analysis and is large for large scale wavelet analysis. With the varying scale the wavelet analysis will be able to “zoom in” on singularities of the signal using more concentrated wavelets of very small scale. For this detailed analysis the time sampling step is very small. As only the signal detail is of interest, only a few small time translation steps would be needed. Therefore, the wavelet analysis provides a more efficient way to represent transient signals.

There is an analogy between the wavelet analysis and the microscope. The scale factor  $s_0^i$  corresponds to the magnification

or the resolution of microscope. The translation factor  $\tau$  corresponds to the location where one makes observation with the microscope. If one looks at very small details, the magnification and the resolution must be large, that corresponds to a large and negative-valued  $i$ . In this case the wavelet is very concentrated. The step of translation is small, that justifies the choice  $\tau = k\tau_0 s_0^i$ . For large and positive-valued  $i$ , the wavelet is spread out, and the large translation steps  $k\tau_0 s_0^i$  are adapted to this wide width of the wavelet analysis function. This is another interpretation of the constant-Q analysis property of the wavelet transform, discussed in Section 10.2.3.

The behavior of the discrete wavelets depends on the scale and time steps  $s_0$  and  $\tau_0$ . When  $s_0$  is close to 1 and  $\tau_0$  is small, the discrete wavelets are close to the continuous wavelets. For a fixed scale step  $s_0$ , the localization points of the discrete wavelets along the scale axis are logarithmic as  $\log s = i \log s_0$ , as shown in Figure 10.7.

The frequency sampling interval has the unit as octave in the music. One octave is the interval between two frequencies having a ratio of two. One octave frequency band has the bandwidth equal to one octave.

The discrete time step is  $\tau_0 s_0^i$ . We choose usually  $\tau_0 = 1$ . Hence, the time sampling step is a function of the scale and is equal to  $2^i$  for the dyadic wavelets with  $s_0 = 2$ . Along the  $\tau$ -axis the localization points of the discrete wavelets depends on the scale. The intervals between the localization points at the same scale are equal and are proportional to the scale  $s_0^i$ . The translation steps are small for small positive-valued  $i$  with the small scale wavelets, and are large for large positive-valued  $i$  with large scale wavelets. In the localization of the discrete wavelets in the timescale space shown in Figure 10.7, where the scale axis is logarithmic,  $\log s = i \log 2$ , and the localization is uniform along the time axis  $\tau$  with the time steps proportional to the scale factor  $s = 2^i$ .

### 10.3.2 Wavelet Frame

With the discrete wavelet basis a continuous function  $f(t)$  is transformed to a sequence of wavelet coefficients

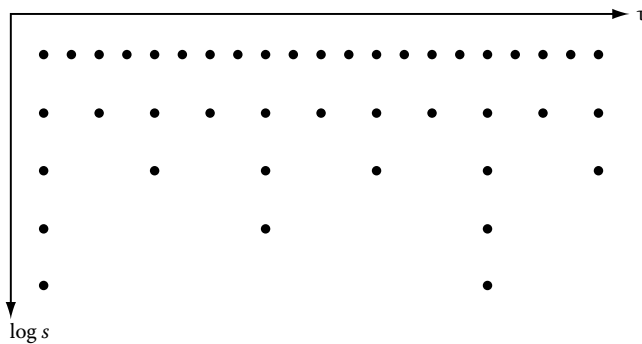


FIGURE 10.7 Localization of the discrete wavelets in the time-scale space.

$$W_f(i, k) = \int f(t) h_{i,k}^*(t) dt = \langle f, h_{i,k} \rangle \quad (10.27)$$

A raising question for the discrete wavelet transform is how well the function  $f(t)$  can be reconstructed from the discrete sequence of wavelet coefficients:

$$f(t) = A \sum_i \sum_k W_f(i, k) h_{i,k}(t) \quad (10.28)$$

where  $A$  is a constant that does not depend on  $f(t)$ . Obviously, if  $s_0$  is close enough to 1 and  $\tau_0$  is small enough, the set of wavelets approaches as continuous. The reconstruction (Equation 10.28) is then close to the inverse continuous wavelet transform. The signal reconstruction takes place without restrictive conditions other than the admissible condition on the wavelet  $h(t)$ . On the other hand, if the sampling is sparse,  $s_0 = 2$  and  $\tau_0 = 1$ , the reconstruction (Equation 10.28) can be achieved only for some special choices of the wavelet  $h(t)$ .

The theory of wavelet frames provides a general framework, that covers the above-mentioned two extreme situations. It permits one to balance between the redundancy, which is the sampling density in the scale-time space, and the restriction on the wavelet  $h(t)$  for the reconstruction scheme (Equation 10.28) to work. If the redundancy is large with high over-sampling, then only mild restrictions are put on the wavelet basis. If the redundancy is small with critical sampling, then the wavelet basis functions are very constrained.

Daubechies [8] has proven that the necessary and sufficient condition for the stable reconstruction of a function  $f(t)$  from its wavelet coefficients  $W_f(i, k)$  is that the energy, which is the sum of square moduli of  $W_f(i, k)$ , must lie between two positive bounds:

$$A \|f\|^2 \leq \sum_{j,k} |\langle f, h_{i,k} \rangle|^2 \leq B \|f\|^2 \quad (10.29)$$

where  $\|f\|^2$  is the energy of  $f(t)$ ,  $A > 0$ ,  $B < \infty$  and  $A, B$  are independent of  $f(t)$ . When  $A = B$ , the energy of the wavelet transform is proportional to the energy of the signal. This is similar to the energy conservation relation (Equation 10.18) of the continuous wavelet transform. When  $A \neq B$  there is still some proportional relation between the energies of the signal and its wavelet transform.

When Equation 10.29 is satisfied, the family of the wavelet basis functions  $\{h_{i,k}(t)\}$  with  $i, k \in \mathbf{Z}$  is referred to as a frame and  $A, B$  are termed frame bounds. Hence, when proportionality between the energy of the function and the energy of its discrete transform function is bounded between something greater than zero and less than infinity for all possible square integrable functions, then the transform is complete. No information is lost and the signal can be reconstructed from its decomposition.

Daubechies has shown that the accuracy of the reconstruction is governed by the frame bounds  $A$  and  $B$ . The frame bounds  $A$  and  $B$  can be computed from the dilation step  $s_0$ , the translation

step  $\tau_0$  and the basis function  $h(t)$ . The closer  $A$  and  $B$ , the more accurate the reconstruction. When  $A = B$ , the frame is tight and the discrete wavelets behave exactly like an orthonormal basis. When  $A = B = 1$  Equation 10.29 is simply the energy conservation equivalent to the Parseval relation of the Fourier transform. It is important to note that the same reconstruction works even when the wavelets are not orthogonal to each other.

When  $A \neq B$  the reconstruction can still work exactly for the discrete wavelet transform if for reconstruction we use the synthesis function basis, which is different from the decomposition function basis for analysis. The former constitute the dual frame of the later.

## 10.4 Multiresolution Signal Analysis

The multiresolution signal analysis is a technique that permits us to analyze signals in multiple frequency bands. Two existing approaches of multiresolution analysis are the Laplacian pyramid and the subband coding, which were developed independently on the wavelet transform in the late 1970s and early 1980s. Meyer and Mallat [9] found in 1986 that the orthonormal wavelet decomposition and reconstruction can be implemented in the multiresolution signal analysis framework.

### 10.4.1 Laplacian Pyramid

The multiresolution signal analysis was first proposed by Burt and Adelson in 1983 [10] for image decomposition, coding, and reconstruction.

#### 10.4.1.1 Gaussian Pyramid

The multiresolution signal analysis is based on a weighting function, which is also called a smoothing function. The original data, represented as a sequence of real numbers,  $c_0(n)$ ,  $n \in \mathbf{Z}$ , is averaged in neighboring pixels by the weighting function, which can be a Gaussian function and used as the impulse response of a low-pass filter. The correlation of the signal with the weighting function reduces the resolution of the signal. Hence, after the averaging process the data sequence is down-sampled by a factor of two. The resultant data sequence  $c_1(n)$  is the averaged approximation of  $c_0(n)$ .

The averaging and down-sampling process can be iterated. For instance, they are applied at the level  $i=1$  to the averaged approximation data  $c_1(n)$  with the smoothing function, which is also dilated by a scale factor of two. Then, they are applied to  $c_2(n)$  with the smoothing function, which is again dilated by two, and so on. In the iteration process the smoothing function is dilated with dyadic scales  $2^i$  with  $i \in \mathbf{Z}$  to average the signals at multiple resolutions. Hence, the original data is represented by a set of successive approximations. Each approximation corresponds to a smoothed version of the original data at a given resolution.

Assume that the original data are of size  $2^N$ . Then, the smoothed sequence  $c_1(n)$  has a reduced size  $2^{N-1}$ . By iterating

the process, the successive averaging and down-sampling result in a set of data sequences of exponentially decreasing size. If we imagine these data sequences stacked on top of one another, then they constitute an hierarchical pyramid structure with  $\log_2 N$  pyramid levels.

The original data  $c_0(n)$  are at the bottom or zero level of the pyramid. At  $i$ th pyramid level the signal sequence is obtained from the data sequence in the  $(i-1)$ th level by

$$c_i(n) = \sum_k p(k-2n)c_{i-1}(k) \quad (10.30)$$

where  $p(n)$  is the weighting function. The operation described in Equation 10.30 is a correlation between  $c_{i-1}(k)$  and  $p(k)$  followed by a down-sampling by two. Note that a shift by two in  $c_{i-1}(k)$  results in a shift by one in  $c_i(n)$ . The sampling interval in level  $i$  is double of that in the previous level  $i-1$ . The size of the sequence  $c_i(n)$  is half as long as its predecessor  $c_{i-1}(n)$ . When the weighting function is the Gaussian function, the pyramid of the smoothed sequences is referred to as the Gaussian pyramid. Figure 10.8 shows a part of the Gaussian pyramid.

#### 10.4.1.2 Laplacian Pyramid

By the low-pass filtering with the weighting function  $p(n)$ , the high frequency detail of the signal is lost. The lost information can be recovered by computing the difference between two successive Gaussian pyramid levels of different size. In this process we have to first expand the data sequence  $c_i(n)$  in two steps: (1) inserting a zero between every samples of  $c_i(n)$ , that is up-sampling  $c_i(n)$  by two; (2) interpolating the sequence with a filter whose impulse response is  $p'(n)$ . The expand process results in a sequence  $c'_{i-1}(n)$  that has the same size as the size of  $c_{i-1}(n)$ . In general  $c'_{i-1}(n) \neq c_{i-1}(n)$ . The difference can be represented by a sequence  $d_{i-1}(n)$

$$d_{i-1}(n) = c_{i-1}(n) - c'_{i-1}(n) \quad (10.31)$$

which contains the lost detail information of the signal. All the differences between each pair in the sequences of successive Gaussian pyramid levels form a set of sequences  $d_i(n)$  that constitute another pyramid, referred to as the Laplacian pyramid. The original signal can be reconstructed exactly by summing the Laplacian pyramid levels.

The Laplacian pyramid contains the compressed signal data in the sense that the pixel to pixel correlation of the signal is removed by the averaging and subtracting process. If the original data is an image that is positively valued, then the values on the Laplacian pyramid nodes are both positive and negative. Their absolute values are smaller and are shifted toward zero, so that they can be represented by fewer bits. The multiresolution analysis is useful for image coding and compression.

The Laplacian pyramid signal representation is redundant. One stage of the pyramid decomposition leads to a half size, low resolution signal and a full size, difference signal, resulting in

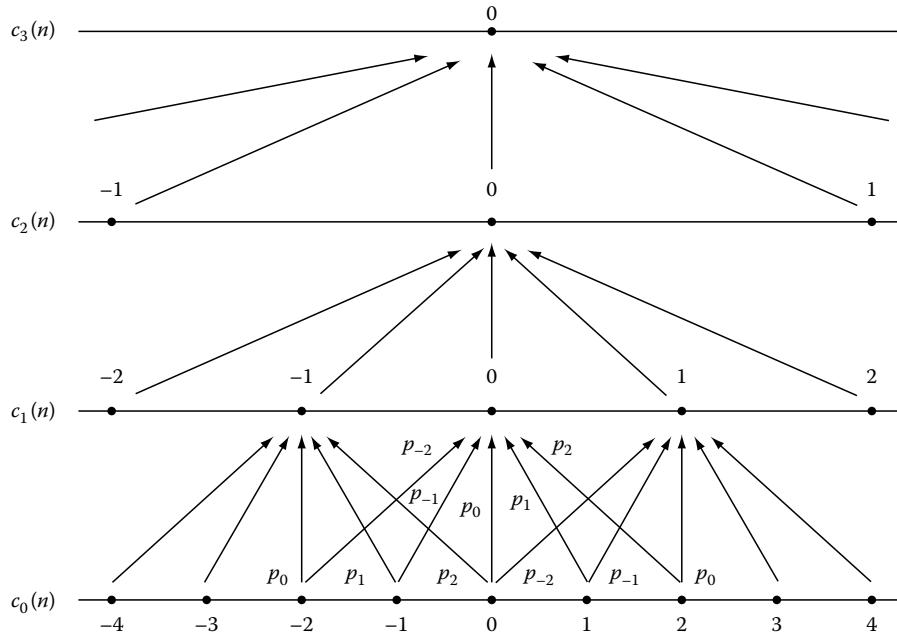


FIGURE 10.8 Multiresolution analysis Gaussian pyramid. The weighting function is  $p(n)$  with  $n = 0 \pm 1, \pm 2$ . The even and odd number nodes in  $c_0(n)$  have different connections to the nodes in  $c_1(n)$ .

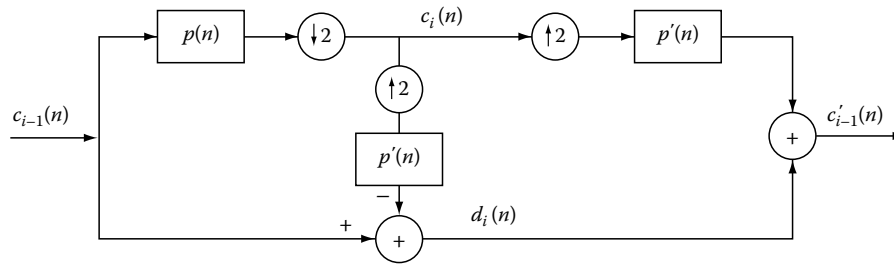


FIGURE 10.9 Schematic pyramid decomposition and reconstruction.

an increase in the number of signal samples by 50%. Figure 10.9 shows the scheme for building the Laplace pyramid.

$$c_1(n) = \sum_k p(k - 2n)c_0(k) \quad (10.32)$$

### 10.4.2 Subband Coding

Subband coding [11] is a multiresolution signal processing approach that is different from the Laplacian pyramid. The basic objective of the subband coding is to divide the signal spectrum into independent subbands in order to treat the signal in individual subbands for different purposes. Subband coding is an efficient tool for multiresolution spectral analysis and has been successful in speech signal processing.

#### 10.4.2.1 Analysis Filtering

Given an original data sequence  $c_0(n)$ ,  $n \in \mathbf{Z}$ , the lower resolution approximation of the signal is derived by low-pass filtering with a filter having its impulse response  $p(n)$ .

which is the correlation between  $c_0(k)$  and  $p(k)$  down-sampled by a factor of two. The process is exactly the same as the averaging process in the Laplacian pyramid decomposition, as described in Equation 10.30. In order to compute the detail information that is lost by the low-pass filtering with  $p(n)$ , a high-pass filter with the impulse response  $q(n)$  is applied to the data sequence  $c_0(n)$  as

$$d_1(n) = \sum_k q(k - 2n)c_0(k) \quad (10.33)$$

which is the correlation between  $c_0(k)$  and  $q(k)$  down-sampled by a factor of two. Hence, the subband decomposition leads to a half size low resolution signal and a half size detail signal.



### 10.4.2.2 Synthesis Filtering

To recover the signal  $c_0(n)$  from the down-sampled approximation  $c_1(n)$  and the down-sampled detail  $d_1(n)$ , both  $c_1(n)$  and  $d_1(n)$  are up-sampled by a factor of two. The up-sampling is performed by first inserting a zero between each node in  $c_1(n)$  and  $d_1(n)$  and then interpolating with the filters  $p'(n)$  and  $q'(n)$  respectively. Finally, adding together the two up-sampled sequences yields  $c_0(n)$ . Figure 10.10 shows the scheme of the two-channel subband system.

The reconstructed signal  $c'_0(n)$ , in general, is not identical to the original  $c_0(n)$ , unless the filters meet a specific constraint, that the analysis filters  $P(n)$ ,  $Q(n)$  and the synthesis filters  $p'(n)$ ,  $q'(n)$  satisfy the perfect reconstruction condition, which will be discussed in Section 10.6.2.

The scheme shown in Figure 10.10 is a two-channels system with a bank of two-band filters. The two-band filter bank can be extended to  $M$ -band filter bank by using a bank of  $M$  analysis filters followed by down-sampling and a bank of  $M$  up-samplers followed by  $M$  synthesis filters.

The two-band filter bank and the  $M$ -band filter bank can also be iterated: the filter bank divides the input spectrum into two equal subbands, yielding the low (L) and high (H) bands. Then, the two-band filter bank can be again applied to these (L) and (H) half bands to generate the quarter bands: (LL), (LH), (HL) and (HH). The scheme of this multiresolution analysis has a tree structure.

### 10.4.3 Scale and Resolution

In the multiresolution signal analysis each layer in the pyramid is generated by a bank of low-pass and high-pass filters at a given scale, that corresponds to the scale of that layer.

In general, scale and resolution are different concept. Scale change of a continuous signal does not alter its resolution. The resolution of a continuous signal is related to its frequency bandwidth. In a geographic map a large scale means a global view and a small scale means a detailed view. However, if the size of the map is fixed, then enlarging the map scale would require reducing the resolution.

In the multiresolution signal analysis the term of scale is that of the low-pass and high-pass filters. At each scale, the down-sampling by two, which follows the low-pass filtering, halves the resolution. When a signal is transferred from a scale level  $i$  to a

larger scale level  $i + 1$ , its resolution is reduced by two. The size of the approximation signal also is reduced by two. Therefore, each scale level corresponds to a specific resolution. The larger the scale, the lower the resolution.

## 10.5 Orthonormal Wavelet Transform

The first orthonormal wavelet basis was found by Meyer when he looked for the orthonormal wavelets that are localized in both time and frequency domains. The multiresolution Laplacian pyramid ideas of hierarchal averaging the signal and computing the difference triggered Mallat and Meyer to view the orthonormal wavelet bases as a vehicle for multiresolution analysis [9]. The multiresolution analysis is now a standard way to construct orthonormal wavelet bases and to implement the orthonormal wavelets transforms. Most orthonormal wavelet bases are now constructed from the multiresolution analysis framework.

In the multiresolution analysis framework the dyadic orthonormal wavelet decomposition and reconstruction use the tree algorithm that permits very fast computation of the orthonormal wavelet transform in the computer.

### 10.5.1 Multiresolution Signal Analysis Bases

#### 10.5.1.1 Scaling Functions

The multiresolution analysis is based on the scaling function. The scaling function is a continuous, square integrable and, in general, real-valued function. The scaling function does not satisfy the wavelet admission condition: the mean value of the scaling function  $\phi(t)$  is not equal to zero, but is usually normalized to unity.

The basic scaling function  $\phi(t)$  is dilated by dyadic scale factors. At each scale level the scaling function is shifted by discrete translation factors as

$$\phi_{i,k}(t) = 2^{-i/2} \phi(2^{-i}t - k) \quad (10.34)$$

where  $k \in \mathbf{Z}$  and the coefficient  $2^{-i/2}$  is a normalization constant. Here, the scaling function basis is normalized in the  $L^2(\mathbf{R})$  norm, similar to the normalization of the wavelet described by Equation 10.2. We shall restrict ourselves to the dyadic scaling with

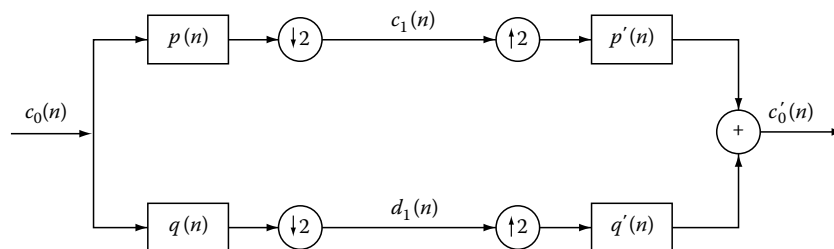


FIGURE 10.10 Schematic two-channel subband coding decomposition and reconstruction.

the scaling factor  $2^i$  for  $i \in \mathbf{Z}$ . The scaling functions of all scales  $2^i$  with  $i \in \mathbf{Z}$  generated from the same  $\phi(t)$  are all similar in shape. At each resolution level  $i$  the set of the discrete translations of the scaling functions,  $\phi_{i,k}(t)$ , forms a function basis that spans a subspace  $V_i$ .

A continuous signal function may be decomposed into the scaling function bases. At each resolution level  $i$ , the decomposition is evaluated at discretely translated points. The scaling functions play a role of the average and smoothing function in the multiresolution signal analysis.

At each resolution level, the correlation between the scaling function and the signal produces the averaged approximation of signal, which is sampled at a set of discrete points. After the averaging by the scaling functions, the signal is down-sampled by factor of two that halves the resolution. Then, the approximated signal is decomposed into the dilated scaling function basis at the next coarser resolution.

### 10.5.1.2 Wavelets

In the multiresolution analysis framework the wavelet bases are generated from the scaling function bases. In order to emphasize the dependence of the wavelets to the scaling functions in the multiresolution analysis framework, from now on we change the notation of the wavelet and use  $\psi(t)$  to denote the wavelet in the discrete wavelet transform instead of  $h(t)$  in the previous sections for the continuous wavelet transform.

Similarly to the scaling function, the wavelet is scaled with dyadic scaling factors and is translated at each resolution level as

$$\psi_{i,k}(t) = 2^{-i/2} \psi(2^{-i}t - k) \quad (10.35)$$

where  $k \in \mathbf{Z}$  and the coefficient  $2^{-i/2}$  is a normalization constant. The wavelet basis is normalized in the  $L^2(\mathbf{R})$  norm for energy normalization, as discussed in Section 10.1. At each resolution level  $i$ , the set of the discrete translations of the wavelets,  $\psi_{i,k}(t)$ , forms a function basis, that spans a subspace  $W_i$ . A signal function may be decomposed into the wavelet bases. At each resolution level, the decomposition is evaluated at discrete translated points.

In the multiresolution analysis framework the orthonormal wavelet transform is the decomposition of a signal into approximations at lower and lower resolutions with less and less detail information by the projections of the signal onto the orthonormal scaling function bases. The differences between each two successive approximations are computed with the projections of the signal onto the orthonormal wavelet bases, as shown in the next.

### 10.5.1.3 Two-Scale Relation

The two-scale relation is the basic relation in the multiresolution analysis with the dyadic scaling. The scaling functions and the wavelets form two bases at every resolution level by their discrete translates. Let  $\phi(t)$  be the basic scaling function whose translates

with integer step span the subspace  $V_0$ . At the next finer resolution the subspace  $V_{-1}$  is spanned by the set  $\{\phi(2t - k)\}$ , that is generated from the scaling function  $\phi(t)$  by a contraction with a factor of two and by translations with half integer steps. The set  $\{\phi(2t - k)\}$  can also be considered as a sum of two sets of even and odd translates,  $\{\phi(2t - 2k)\}$  and  $\{\phi[2t - (2k + 1)]\}$ , all are with integer steps  $k \in \mathbf{Z}$ . The scaling function at resolution  $i = 0$  may be decomposed as linear combination of the scaling functions at the higher resolution level  $i = -1$ , as

$$\phi(t) = \sum_k p(k) \phi(2t - k) \quad (10.36)$$

where the discrete decomposition coefficient sequence  $p(k)$  is called the interscale coefficients, that will be used in the wavelet decomposition as the discrete low-pass filter and will be discussed in Section 10.5.4. This decomposition may be considered as the projection of the basis function  $\phi(t) \in V_0$  onto the finer resolution subspace  $V_{-1}$ . The two scale relation, or called the two-scale difference equation, (Equation 10.36) is the fundamental equation in the multiresolution analysis. The basic ingredient in the multiresolution analysis is a scaling function such that the two scale relation holds for some  $p(k)$ . The sequence  $p(k)$  of the interscale coefficients in the two scale relation governs the structure of the scaling function  $\phi(t)$ .

Let  $\psi(t) \in V_0$  be the basic wavelet, which can also be expanded onto the scaling function basis  $\{\phi(2t - k)\}$  in the finer resolution subspace  $V_{-1}$  as

$$\psi(t) = \sum_k q(k) \phi(2t - k) \quad (10.37)$$

where the sequence  $q(k)$  is the interscale coefficients that will be used in the wavelet decomposition as the discrete high-pass filter and will be discussed in Section 10.5.4. Equation 10.37 is a part of the two scale relation, and is useful for generating the wavelets from the scaling functions, as shown in the next.

On the both sides of the two scale relations, (Equations 10.36 and 10.37)  $\phi(t)$  and  $\psi(t)$  are continuous scaling function and wavelet. On the right-hand side of the two scale relations, the interscale coefficients,  $p(k)$  and  $q(k)$ , are discrete with  $k \in \mathbf{Z}$ . The two scale relations express the relations between the continuous scaling function  $\phi(t)$  and wavelet  $\psi(t)$  and the discrete sequences of the interscale coefficients  $p(k)$  and  $q(k)$ .

## 10.5.2 Orthonormal Bases

We should show in this section first how the discrete translates of the scaling function and of the wavelet form the orthonormal bases at each given scale level, and then how the scaling function generates the multiresolution analysis.

### 10.5.2.1 Orthonormal Scaling Function Basis

At a given scale level the discrete translates of a basic scaling function  $\phi(t)$  can form an orthonormal basis, if  $\phi(t)$  satisfies

some orthonormality conditions. The scaling function can be made orthonormal to its own translates. When a basic scaling function  $\phi(t)$  has its discrete translates that form an orthonormal set  $\{\phi(t-k)\}$ , we have

$$\langle \phi_{i,k}, \phi_{i,k'} \rangle = 2^{-i} \int \phi_i(t-k)\phi_i(t-k')dt = \delta_{k,k'} \quad (10.38)$$

### 10.5.2.2 Orthonormal Wavelet Basis

Similarly, the discrete translates of a basic wavelet  $\psi(t)$  can form an orthonormal basis, if  $\psi(t)$  satisfies some orthonormality condition. At the same scale level, the wavelet can be made orthonormal to its own translates. When a basic wavelet  $\psi(t)$  has its discrete translates that form an orthonormal set  $\{\psi(t-k)\}$ , we have

$$\langle \psi_{i,k}, \psi_{i,k'} \rangle = 2^{-i} \int \psi_i(t-k)\psi_i(t-k')dt = \delta_{k,k'} \quad (10.39)$$

### 10.5.2.3 Cross-Orthonormality

The orthonormal wavelet basis is not only orthogonal to their own translates at the same scale level. The set of the wavelet translates is also orthogonal to the set of the scaling function translates at the same scale level

$$\langle \phi_{i,k}, \psi_{i,n} \rangle = 2^{-i} \int \phi_i(t-k)\psi_i(t-n)dt = 0 \quad (10.40)$$

for all  $k$  and  $n \in \mathbf{Z}$ .

#### Example: Orthonormal Haar's Bases

An simple example for the orthonormal wavelet basis is the historical Haar wavelet. The Haar scaling function is the simple rectangle function in the interval  $[0, 1)$ .

$$\phi(t) = \begin{cases} 1 & 0 \leq t < 1 \\ 0 & \text{otherwise} \end{cases}$$

Obviously, the translations with integer steps of this rectangular function form an orthonormal set, satisfying Equation 10.38 because the translates  $\phi(t-k)$  and  $\phi(t-k')$  with  $k, k' \in \mathbf{Z}$  and  $n \neq k$  do not overlap.

The contracted Haar scaling function  $\phi(2t)$  is a rectangular function in the interval  $[0, 1/2)$ . Its discrete translates with half integer steps form an orthonormal basis  $\{\phi(2t-k)\}$ . Automatically, within every fixed scale  $2^{-i}$ , the Haar scaling functions form an orthonormal basis with the translation step of  $2^{-i}$

As  $\phi(2t-k)$  are of half integer width, the  $\phi(t)$  in  $\mathbf{V}_0$  can be expressed as a linear combination of the even and odd translates of  $\phi(2t)$  in  $\mathbf{V}_{-1}$ :

$$\phi(t) = \frac{1}{\sqrt{2}}[\phi(2t) + \phi(2t-1)]$$

This is the two-scale relation for the Haar's basis described in Equation 10.36 with the interscale coefficients

$$\begin{aligned} p(0) &= \frac{1}{\sqrt{2}}, & p(1) &= \frac{1}{\sqrt{2}}, \\ p(k) &= 0 & \text{for } k \neq 0, 1 \end{aligned}$$

The Haar's basic wavelet has a compact support of  $[0, 1)$ :

$$\psi(t) = \begin{cases} 1 & 0 \leq t < 1/2 \\ -1 & 1/2 \leq t < 1 \\ 0 & \text{otherwise} \end{cases}$$

Obviously, The integer translates of  $\psi(t)$  constitute an orthonormal basis  $\{\psi(t-k)\}$ , because the translated wavelets  $\psi(t-k)$  and  $\psi(t-k')$  do not overlap for  $k$  and  $k' \in \mathbf{Z}$  and  $k \neq k'$ . Also, within every fixed scale level  $i$  the discrete translates of the Haar wavelets form an orthonormal basis. Furthermore, the Haar wavelets are orthogonal to the Haar scaling function because

$$\int \phi(t-k)\psi(t-n)dt = 0$$

The Haar wavelet can be expressed as a linear combination of the Haar scaling functions in a higher resolution level:

$$\psi(t) = \frac{1}{\sqrt{2}}[\phi(2t) - \phi(2t-1)]$$

This is the two scale relation for the Haar' basis described in Equation 10.37 with the interscale coefficients

$$\begin{aligned} q(0) &= \frac{1}{\sqrt{2}}, & q(1) &= -\frac{1}{\sqrt{2}} \\ q(k) &= 0 & \text{for } k \neq 0, 1 \end{aligned}$$

The Haar wavelets are orthonormal at the same scale and also orthonormal across the scales. One can verify that

$$\int \psi_{i,k}(t)\psi_{m,n}(t)dt = \delta_{i,m}\delta_{k,n}$$

## 10.5.3 Orthonormal Subspaces

Assume that the basic scaling function  $\phi(t)$  satisfies some orthogonality condition at a given scale level, so that its discrete translates  $\{\phi(t-k)\}$  with integer translations  $k \in \mathbf{Z}$  form an orthonormal set. The projection of a function  $f(t) \in L^2(\mathbf{R})$  on the orthonormal basis  $\{\phi(t-k)\}$  is a correlation between the original function  $f(t)$  and the scaling function  $\phi(t)$  sampled at integer intervals.

The scaling function plays the role of a smoothing function in the multiresolution analysis. The projection of  $f(t)$  on the scaling function basis results in a blurred approximation of  $f(t)$ . All the approximations of  $f(t) \in L^2(\mathbf{R})$  form a subspace  $V_0 \in L^2(\mathbf{R})$ . The vector space  $V_0$  can be interpreted as the set of all possible approximations of functions in  $L^2(\mathbf{R})$  generated by the orthonormal set  $\{\phi(t-k)\}$ . The space  $V_0$  is spanned by the basis  $\{\phi(t-k)\}$ .

Now we consider the dilation of the scaling function. All the scaling functions are generated from the basic scaling function  $\phi(t)$  by dyadic dilations and discrete translations. The basic scaling function  $\phi(t)$  generates the orthonormal basis  $\{\phi(t-k)\}$  of  $V_0$  with integer translation step. The dilated scaling function  $\phi(t/2)$  will generate the orthonormal basis  $\{\phi(2^{-1}t-k)\}$  of  $V_1$  with translation step of two, and the dilated scaling function  $\phi(t/4)$  will generate the orthonormal basis  $\{\phi(2^{-2}t-k)\}$  of  $V_2$  with translation step of four, and so on. There is then a set of orthogonal bases of scaling functions. Each scaling function basis is orthonormal at its own scale level.

The projections of functions in  $L^2(\mathbf{R})$  on the set of orthonormal scaling function bases form a set of subspaces  $V_i$ . Each subspace  $V_i$  is the set of all possible approximations of functions in  $L^2(\mathbf{R})$  generated by the orthonormal scaling function basis  $\{\phi(2^{-i}t-k)\}$ . The subspace  $V_i$  is spanned by the orthonormal scaling function basis at the scale level  $i$ . Hence, the scaling function  $\phi(t)$  generates the subspaces of the multiresolution analysis.

Similarly, the projection of a signal function  $f(t)$  on the orthonormal wavelet bases, at a given resolution level  $i$ , is a correlation between  $f(t)$  and  $\psi_i(t)$  sampled at discrete intervals. The projections of all functions in  $L^2(\mathbf{R})$  on the orthonormal wavelet basis  $\{\psi(2^{-i}t-k)\}$  form a subspace  $W_i$ . The subspace  $W_i$  is spanned by  $\{\psi(2^{-i}t-k)\}$ .

Because of the cross-orthonormality between the wavelet set and the scaling function set,  $\{\phi(2^{-i}t-k)\}$  is orthogonal to  $\{\psi(2^{-i}t-k)\}$ , the subspace  $W_i$  is an orthogonal complement of  $V_i$ :

$$W_i \perp V_i$$

Both  $V_i$  and  $W_i$  are the subspaces on  $V_{i-1} \in V_i$ ,  $W_i \in V_{i-1}$ . Since  $W_i$  is orthogonal to  $V_i$ , the subspace  $V_{i-1}$  is the direct sum of  $V_i$  and  $W_i$ .

$$V_{i-1} = V_i \oplus W_i$$

### 10.5.3.1 Properties of the Multiresolution Subspaces

The multiresolution analysis associated with the scaling function has some interesting properties. The approximates of a function  $f(t)$  at different resolutions must be similar, because they are all generated by the same scaling function only with different scales. The approximation spaces  $V_i$  then may be deduced from each other by simple dilation.

$$f(t) \in V_i \Leftrightarrow f(2t) \in V_{i-1}$$

All the information useful to compute the approximate function at the coarser resolution and large scale level  $i$  are contained in the approximate function at the finer resolution and smaller scale level  $(i-1)$ . The  $V_i$  is a subspace in  $V_{i-1}$ . This is a causality property. We have a fine-to-coarse sequence as

$$\cdots V_2 \subset V_1 \subset V_0 \subset V_{-1} \subset V_{-2} \cdots \subset L^2(\mathbf{R})$$

where  $i \in \mathbf{Z}$ . When the resolution increases with  $i$  tending to  $-\infty$  the approximated function should converge to the original function. Any function in  $L^2(\mathbf{R})$  can be approximated as closely as desired by its project in  $V_i$  when  $i$  tends to  $-\infty$ . This property may be described as

$$\bigcup_i V_i = L^2(\mathbf{R})$$

Conversely, when the resolution decreases to zero with  $i$  tending to  $+\infty$ , the approximations contain less and less information and converges to zero:

$$\bigcap_i V_i = \{0\}$$

In summary, the multiresolution analysis is generated by the scaling function  $\phi(t)$ . The  $\phi(t)$  is scaled with the dyadic scaling factor  $2^i$ . The discrete translates  $\phi(2^{-i}t-k)$  form an orthonormal basis and span the subspace  $V_i$  at the resolution level  $i$ . All the dilates and translates of the scaling function bases and the wavelet bases are generated from a single basic scaling function and are, therefore, not linearly independent.

## 10.5.4 Wavelet Series Decomposition

In this section we show how the wavelet series decomposition and reconstruction can be implemented by iterating the discrete filter bank. A function  $f(t) \in V_0$  can be represented as a linear superposition of the translated scaling functions  $\phi(t-k)$  in  $V_0$

$$f(t) = \sum_k c_0(k)\phi(t-k) \quad (10.41)$$

where the coefficients in the combination can be obtained using the orthonormality of the scaling function set as

$$c_0(k) = \int f(t)\phi(t-k)dt = \langle f, \phi_{0,k} \rangle \quad (10.42)$$

We now apply the entire multiresolution analysis to the function  $f(t)$ .

### 10.5.4.1 Orthonormal Projections on the Subspaces

The function to be analyzed is in  $V_0$ . At the next coarser resolution  $i=1$ , there are two mutually orthogonal subspaces

$V_1$  and  $W_1$ , spanned by the orthonormal bases,  $\{\phi_{1,k}(t)\}$  and  $\{\psi_{1,k}(t)\}$  respectively. The subspace  $W_1$  is the orthogonal complement of  $V_1$ . Because  $V_0$  is the direct sum of  $V_1$  and  $W_1$ ,  $V_0 = V_1 \oplus W_1$ , there is one and only one way to express a function  $f(t) \in V_0$  as the sum of two functions in  $V_1$  and  $W_1$ , respectively:

$$f = P_1 f + Q_1 f \quad (10.43)$$

where the two terms on the right-hand side are the orthonormal projections of  $f(t)$  on  $V_1$  and  $W_1$ , with  $P_1$  and  $Q_1$  denoting the orthonormal projection operators on the subspaces  $V_1$  and  $W_1$  respectively.

$$\begin{aligned} P_1 f &= \sum_n c_1(k) \phi_{1,k} \\ Q_1 f &= \sum_n d_1(k) \psi_{1,k} \end{aligned} \quad (10.44)$$

where the explicit time dependence in  $f$ ,  $\phi_{i,k}$  and  $\psi_{i,k}$  is not shown for ease of notation.

Because the scaling function set  $\{\phi_{1,k}\}$  is orthonormal in  $V_1$  and the wavelet set  $\{\psi_{1,k}\}$  is orthonormal in  $W_1$  and they are mutually orthogonal, multiplying the scaling function  $\phi_{1,k}$  with both sides of the expansions (Equation 10.43) and computing the inner products yields

$$\langle \phi_{1,k}, f \rangle = \langle \phi_{1,k}, P_1 f \rangle \quad (10.45)$$

Multiplying  $\phi_{1,k}$  with both sides of Equation 10.44, computing the inner products and using Equation 10.45 yields

$$c_1(k) = \langle \phi_{1,k}, P_1 f \rangle = \langle \phi_{1,k}, f \rangle \quad (10.46)$$

$$d_1(k) = \langle \psi_{1,k}, Q_1 f \rangle = \langle \psi_{1,k}, f \rangle \quad (10.47)$$

The discrete sequences,  $c_1(k)$  and  $d_1(k)$ , are the coefficients in the decomposition of a continuous function  $f(t)$  onto the bases  $\{\phi_{1,k}\}$  in  $V_1$  and  $\{\psi_{1,k}\}$  in  $W_1$ , respectively, where both scaling functions and wavelets are continuous. The sequence  $c_1$  is the averaged approximation of  $f(t)$  and referred to as the discrete approximation of  $f(t)$ . The sequence  $d_1$  represents the difference between the original  $f(t)$  and the approximation  $P_1 f$  and is referred to as the discrete wavelet transform coefficients of  $f(t)$  at the coarse resolution level  $i = 1$ .

#### 10.5.4.2 Low-Pass and High-Pass Filters

The discrete expansion coefficient sequence,  $c_1(k)$  and  $d_1(k)$ , may be calculated by

$$c_1(k) = 2^{-1/2} \sum_n p(n-2k) c_0(n) \quad (10.48)$$

$$d_1(k) = 2^{-1/2} \sum_n q(n-2k) c_0(n) \quad (10.49)$$

These are the correlations between the signal data  $c_0$  and  $p(n)$  and  $q(n)$  respectively. The correlation results are down-sampled by a factor of two, because of the double-shift of  $p(n)$  and  $q(n)$  in the correlations. The discrete interscale coefficients  $p(n)$  and  $q(n)$  are called the discrete low-pass and high-pass filters, respectively.

The Equations 10.48 and 10.49 may be proved as follows: substituting Equation 10.41 into Equations 10.46 and 10.47 yields:

$$\begin{aligned} c_1(k) &= \sum_n \langle \phi_{1,k}, \phi_{0,n} \rangle c_0(n) \\ d_1(k) &= \sum_n \langle \psi_{1,k}, \phi_{0,n} \rangle c_0(n) \end{aligned} \quad (10.50)$$

The inner product between the scaling function and the wavelet sets  $\{\phi_{1,k}\}$  and  $\{\psi_{1,k}\}$  at the scale  $i = 1$  and the scaling function set,  $\{\phi_{0,n}\}$ , at the next finer scale level  $i = 0$  can be computed as

$$\begin{aligned} \langle \phi_{1,k}, \phi_{0,n} \rangle &= 2^{-1/2} \int \phi\left(\frac{t}{2} - k\right) \phi(t - n) dt \\ &= 2^{1/2} \int \phi(t) \phi[2t - (n - 2k)] dt \end{aligned} \quad (10.51)$$

$$\langle \psi_{1,k}, \phi_{0,n} \rangle = 2^{1/2} \int \psi(t) \phi[2t - (n - 2k)] dt \quad (10.52)$$

Substituting the two scale relation:

$$\begin{aligned} \phi(t) &= \sum_n p(n) \phi(2t - n) \\ \psi(t) &= \sum_n q(n) \phi(2tn) \end{aligned}$$

into Equations 10.51 and 10.52 and using the orthonormality of the set  $\{\phi(2t)\}$  we obtain

$$\langle \phi_{1,k}, \phi_{0,n} \rangle = 2^{-1/2} p(n - 2k) \quad (10.53)$$

$$\langle \psi_{1,k}, \phi_{0,n} \rangle = 2^{1/2} q(n - 2k) \quad (10.54)$$

Substituting Equations 10.53 and 10.54 into Equation 10.50 results in Equation 10.49.

#### 10.5.4.3 Recursive Projections

The projection procedure can be iterated. The orthonormal projections at one resolution level can continue to the next coarser resolution. At the next coarser resolution the subspace  $V_2$  and  $W_2$  are orthogonal complement,  $V_1 = V_2 \oplus W_2$ , and  $V_1$  is the direct sum of  $V_2$  and  $W_2$ . We can decompose  $P_1 f \in V_1$  into two components along  $V_2$  and  $W_2$

$$P_1 f = P_2 f + Q_2 f \quad (10.55)$$

with

$$P_2 f = \sum_n c_2(n) \phi_{2,n} \quad (10.56)$$

$$Q_2 f = \sum_n d_2(n) \psi_{2,n} \quad (10.57)$$

Multiplying by  $\phi_{2,k}$  both sides of expansions (Equation 10.56) and using the orthonormality of the set  $\{\phi_{2,n}\}$ , and multiplying by  $\psi_{2,k}$  both sides of expansions (Equation 10.55) and using the mutual orthonormality between  $\phi_{2,n}$  and  $\psi_{2,k}$  we obtain the discrete approximation  $c_2(k)$  as

$$\begin{aligned} c_2(k) &= \langle \phi_{2,k}, P_2 f \rangle = \langle \phi_{2,k}, P_1 f \rangle \\ &= \sum_n \langle \phi_{2,k}, \phi_{1,n} \rangle c_1(n) \end{aligned}$$

Similarly, multiplying  $\psi_{2,k}$  with both sides of expansions (Equations 10.55 and 10.57) and using the orthonormality of  $\{\phi_{2,n}\}$  and the mutual orthogonality between  $\phi_{2,k}$  and  $\psi_{2,n}$  within the same scale we obtain the discrete wavelet coefficients  $d_2(k)$  as

$$\begin{aligned} d_2(k) &= \langle \psi_{2,k}, Q_2 f \rangle = \langle \psi_{2,k}, P_1 f \rangle \\ &= \sum_n \langle \psi_{2,k}, \phi_{1,n} \rangle c_1(n) \end{aligned}$$

The decomposition into smoothed approximations and details at larger scale can be continued as far as wanted. The procedure can be iterated as many times as wanted. The successive projections  $P_i f$  correspond to more and more blurred version of  $f(t)$ . The successive projections  $Q_i f$  correspond to the differences between the two approximations of  $f(t)$  at two successive scale levels. At every step  $i$  one has the orthonormal projection of  $P_{i-1} f$  along the subspaces  $V_i$  and  $W_i$

$$\begin{aligned} P_{i-1} f &= P_i f + Q_i f \\ &= \sum_k c_i(k) \phi_{i,k} + \sum_k d_i(k) \psi_{i,k} \end{aligned} \quad (10.58)$$

It is easy to verify that similarly to Equations 10.53 and 10.54 and independently of the scale level we have for scale level  $i$ :

$$\begin{aligned} \langle \phi_{i,k}, \phi_{i-1,n} \rangle &= 2^{1/2} p(n-2k) \\ \langle \psi_{i,k}, \phi_{i-1,n} \rangle &= 2^{1/2} q(n-2k) \end{aligned} \quad (10.59)$$

It follows that

$$\begin{aligned} c_i(k) &= 2^{-1/2} \sum_n p(n-2k) c_{i-1}(n) \\ d_i(k) &= 2^{-1/2} \sum_n q(n-2k) c_{i-1}(n) \end{aligned} \quad (10.60)$$

We define the low-pass and high-pass filtering operators  $L$  and  $H$  respectively such that the operations on a sequence  $\alpha(n)$  are

$$\begin{aligned} (L\alpha)(k) &= 2^{-1/2} \sum_n p(n-2k) \alpha(n) \\ (H\alpha)(k) &= 2^{-1/2} \sum_n q(n-2k) \alpha(n) \end{aligned}$$

Then, Equation 10.60 can be shortened to

$$\begin{aligned} C_i &= L C_{i-1} \\ d_i &= H C_{i-1} \end{aligned}$$

#### 10.5.4.4 Wavelet Series Decomposition

The approximation  $c_{i-1}(n)$  is recursively decomposed into the sequences  $c_i(n)$  and  $d_i(n)$  by iterating the low-pass and high-pass filters, according to Equation 10.60. The successive discrete approximation sequences  $c_i(n)$  are lower and lower resolution versions of the original data  $c_0(n)$ , each sampled twice as sparsely as their predecessor. The successive wavelet coefficient sequence  $d_i(n)$  represents the difference between the two approximations at resolutions levels  $i$  and  $i-1$ .

Continuing up to resolution  $M$  we can represent the original function  $f(t)$  by a series of detail functions plus one smoothed approximation

$$f(t) = P_M L + Q_M f + Q_{M-1} f + \cdots + Q_1 f$$

and

$$\begin{aligned} f(t) &= \sum_{k \in \mathbb{Z}} 2^{-M/2} c_M(k) \phi(2^{-M} t - k) \\ &+ \sum_{i=1}^M \sum_{k \in \mathbb{Z}} 2^{-i/2} d_i(k) \psi(2^{-i} t - k) \end{aligned} \quad (10.61)$$

Equation 10.61 is referred to as the wavelet series decomposition. The function  $f(t)$  is represented as an approximation at resolution  $i=M$  plus the sum of  $M$  detail components at dyadic scales. The first term in the right-hand side of Equation 10.61 is the smoothed approximation of  $f(t)$  at very low resolution  $i=M$ . When  $M$  approaches to infinity the projection of  $f(t)$  on with the scaling functions of very large scale would smooth out any signal detail and converge to a constant. The function  $f(t)$  is then represented as a series of its orthonormal projections on the wavelet bases.

The wavelet series decomposition is a practical representation of the wavelet expansion and points out the complementary role of the scaling function in the wavelet decomposition. Note that in the wavelet series decomposition the function  $f(t)$ , the scaling function bases  $\phi(t)$  and the wavelet bases  $\psi(t)$  are all continuous. The approximation coefficients  $c_M(k)$  and the wavelet coefficients  $d_i(k)$  with  $i=1, 2, \dots, M$  are discrete. In this sense, the wavelet series decomposition is similar to the Fourier series decomposition.

The discrete approximations  $c_i(n)$  and the discrete wavelet coefficients  $d_i(n)$  can be computed with an iterative algorithm, described by Equation 10.60. This is essentially a discrete algorithm implemented by recursive applications of the discrete

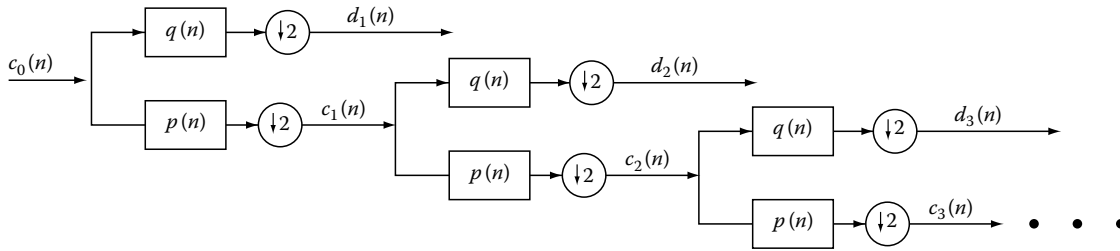


FIGURE 10.11 Schematic wavelet series decomposition in the tree algorithm.

low-pass and high-pass filter bank to the discrete approximations  $c_i(n)$ . The algorithm is called the tree algorithm. The first two stages of the tree algorithm for computing the wavelet decomposition is shown in Figure 10.11. The decomposition into coarser smoothed approximations and details can be continued as far as wanted.

**Example: Decomposition with Haar Wavelets**

A simple example for orthonormal wavelet decomposition is that with the Haar’s orthonormal bases. Let subspace  $\mathbf{V}_0$  be spanned by the Haar scaling function basis,  $\{\phi(t - k)\}$ , defined as a rectangular function of unit width  $[0, 1)$ . The projection of a function  $f(t)$  on  $\mathbf{V}_0$  is an approximation of  $f(t)$  that is piecewise constant over the integer interval. The projection of  $f(t)$  on  $\mathbf{V}_{-1}$  with the orthonormal basis  $\{\phi(2t - k)\}$  of the next finer resolution is piecewise constant over the half integer interval. Since  $\mathbf{V}_{-1} = \mathbf{V}_0 + \mathbf{W}_0$ , and

$$P_{-1}f = P_0f + Q_0f$$

with the projection  $Q_0f$  represents the difference between the approximation in  $\mathbf{V}_0$  and the approximation in  $\mathbf{V}_{-1}$ . The approximations  $P_0f$  in  $\mathbf{V}_0$  and  $P_{-1}f$  in  $\mathbf{V}_{-1}$  and the detail  $Q_0f$  are shown in Figure 10.12. In the figure the projection  $Q_0f$  is constant over half integer intervals, which can be added to the approximation  $P_0f$  to provide the next finer approximation  $P_{-1}f$ .

When the scale level  $i$  approaches minus infinity with finer and finer resolution the approximations  $P_{-i}f$  will converge to the original function  $f(t)$  as closely as desired.

The projection of  $f(t)$  onto the subspace  $\mathbf{V}_i$  spanned by the Haar scaling function basis at the resolution level  $i$  is

$$P_i f = \sum_k c_i(k) \phi_{i,k}$$

with the discrete approximation coefficients

$$c_i(k) = \langle f, \phi_{i,k} \rangle = 2^{-i/2} \int_{2^i k}^{2^i(k+1)} f(t) dt$$

As  $\phi_{i+1,k}$  is a rectangular function with width of  $2^{i+1}$  and  $\phi_{i,k}$  is with width of  $2^i$ , it is easy to verify that

$$\begin{aligned} \phi_{i+1,k} &= 2^{-1/2}(\phi_{i,2k} + \phi_{i,2k+1}) \\ \psi_{i+1,k} &= 2^{-1/2}(\phi_{i,2k} - \phi_{i,2k+1}) \end{aligned} \tag{10.62}$$

The discrete approximation  $c_{i+1}(k)$  can be obtained directly by the orthonormal projection of  $f(t)$  onto  $\mathbf{V}_{i+1}$

$$c_{i+1}(k) = \langle f, \phi_{i+1,k} \rangle = 2^{-1/2}(c_i(2k) + c_i(2k + 1)) \tag{10.63}$$

The difference between the two successive approximations is obtained using Equation 10.62 and

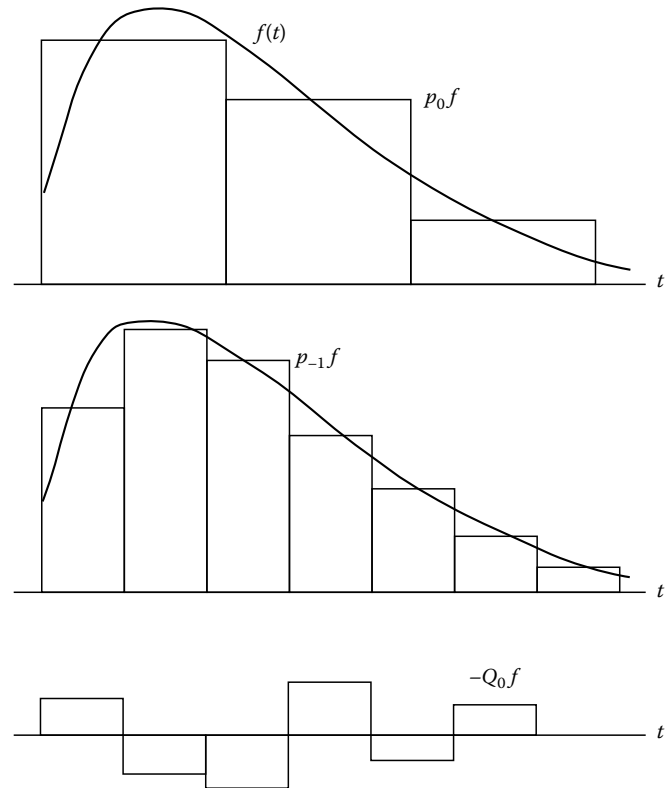


FIGURE 10.12 Orthogonal projections  $P_0f$  and  $Q_0f$  onto the Haar scaling function and wavelet bases. The projection at the next finer resolutions,  $P_{-1}f = P_0f + Q_0f$ . (From Akansu, A. N. and Haddad, R. A. *Multiresolution Signal Decomposition*, Academic Press, Boston, 1992. With permission.)

$$\begin{aligned}
P_i f - P_{i+1} f &= \sum_k [c_i(k)\phi_{i,k} - c_{i+1}(k)\phi_{i+1,k}] \\
&= \sum_k [(c_i(2k)\phi_{i,2k} + c_i(2k+1)\phi_{i,2k+1}) \\
&\quad - 2^{-1/2}(c_i(2k) + c_i(2k+1))2^{-1/2}(\phi_{i,2k} + \phi_{i,2k+1})] \\
&= \frac{1}{2} \sum_k (c_i(2k) - c_i(2k+1))(\phi_{i,2k} - \phi_{i,2k+1}) \\
&= \frac{1}{2} \sum_k (c_i(2k) - c_i(2k+1))\psi_{i+1,k}
\end{aligned}$$

Hence, the projection of  $f(t)$  onto the subspace  $W_{i+1}$  is the difference between  $P_i f$  and  $P_{i+1} f$

$$Q_{i+1,k} = \sum_k d_{i+1}(k)\psi_{i+1,k} = P_i f - P_{i+1} f$$

provided that

$$d_{i+1}(k) = 2^{-1/2}(c_i(k) - c_i(2k+1)) \quad (10.64)$$

The interscale coefficients that are the discrete low-pass and high-pass filters,  $p(n)$  and  $q(n)$ , are given for the Haar's bases have been given in Section 10.5.2. Hence, the iterated filtering by the low-pass and high-pass filters becomes

$$\begin{aligned}
c_{i+1}(k) &= \frac{1}{\sqrt{2}} \sum_n p(n-2k)c_i(n) = \frac{1}{\sqrt{2}}(c_i(2k) + c_i(2k+1)) \\
d_{i+1}(k) &= \frac{1}{\sqrt{2}} \sum_n q(n-2k)c_i(n) = \frac{1}{\sqrt{2}}(c_i(2k) - c_i(2k+1))
\end{aligned}$$

that are agree with Equations 10.63 and 10.64.

## 10.5.5 Reconstruction

### 10.5.5.1 Recursive Reconstruction

The original signal sequence  $c_0(n)$  can be reconstructed from the sequences of the approximation coefficients  $c_i(n)$  and of the wavelet coefficients  $d_i(n)$  with  $0 < i \leq M$ , where  $i = M$  is the lowest resolution in the decomposition. At each resolution level  $i$  we have the wavelet decomposition described by Equations 10.58 and 10.60. On multiplying the both sides of Equation 10.58 by  $\phi_{i-1,n}$  and integrating the both sides we obtain

$$\begin{aligned}
c_{i-1}(n) &= \langle P_{i-1} f, \phi_{i-1,n} \rangle \\
&= \sum_k c_i(k) \langle \phi_{i,k}, \phi_{i-1,n} \rangle + \sum_k d_i(k) \langle \psi_{i,k}, \phi_{i-1,n} \rangle \\
&= 2^{-1/2} \sum_k c_i(k)p(n-2k) + 2^{-1/2} \sum_k d_i(k)q(n-2k)
\end{aligned} \quad (10.65)$$

where the inner products  $\langle \phi_{i,k}, \phi_{i-1,n} \rangle$  and  $\langle \psi_{i,k}, \psi_{i-1,n} \rangle$  are obtained in Equation 10.59 as the interscale coefficients  $p(n-2k)$  and  $q(n-2k)$ . Hence, the discrete approximation  $c_{i-1}(n)$  at the next finer resolution can be obtained as the sum of two convolutions between the discrete approximation  $c_i(n)$  and the low-pass synthesis filter  $p(n)$  and between the wavelet coefficients  $d_i(n)$  and the high-pass synthesis filter  $q(n)$ .

The synthesis filters are identical to the analysis filters. But the filtering operations become the convolutions for synthesis and reconstruction instead of the correlations for analysis and decomposition. To compute the convolution with the synthesis filters in Equation 10.65 one must first put zeros between each sample of the sequences  $c_i(n)$  and  $d_i(n)$  before convolving the resulting sequences with the synthesis low-pass and high-pass filters  $p(n)$  and  $q(n)$ . The process is quite similar to the expand operation in the reconstruction algorithm of the multiresolution Laplacian pyramid and the subband coding. The reconstruction process can be repeated by iterations. We define the synthesis filtering operators  $L_0$  and  $H_0$  as

$$(L_0 \alpha)(n) = \frac{1}{\sqrt{2}} \sum_k p(n-2k)\alpha(k)$$

$$(H_0 \alpha)(n) = \frac{1}{\sqrt{2}} \sum_k q(n-2k)\alpha(k)$$

and rewrite Equation 10.65 in a shorten form

$$c_{i-1} = L_0 c_i + H_0 d_i$$

The block diagram shown in Figure 10.13 illustrates the reconstruction algorithm, where the up-sampling by two means putting zeros between the sample of the sequences.

To reconstruct the original data  $c_0(n)$  we start from the lowest resolution approximation  $c_M$ . According to Equation 10.65 we have

$$\begin{aligned}
c_{M-1} &= H_0 d_M + L_0 c_M \\
c_{M-2} &= H_0 d_{M-1} + L_0(H_0 d_M + L_0 c_M) \\
&= H_0 d_{M-1} + L_0 H_0 d_M + (L_0)^2 c_M
\end{aligned}$$

When the discrete approximation  $c_{i-1}$  is obtained from  $c_i(n)$  and  $d_i(n)$ , the next finer approximation  $c_{i-2}(n)$  can be obtained from the approximation  $c_{i-1}(n)$  and the wavelet coefficients  $d_{i-1}(n)$ .

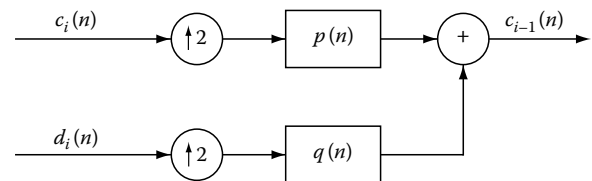


FIGURE 10.13 Schematic wavelet reconstruction.



The process can continue until the original sequence  $c_0(n)$  is reconstructed. The reconstruction formula for the original sequence is

$$c_0 = \sum_{i=1}^M (L_0)^{i-1} H_0 d_i + (L_0)^M c_M \quad (10.66)$$

In this reconstruction procedure it is the low-pass filtering operator  $L_0$  that is iteratively applied to generate the finer resolution discrete approximations.

### 10.5.5.2 Discussion

In summary, we have introduced in this section the orthonormal wavelet series decomposition and reconstruction. In the multi-resolution analysis framework, the basic function of the orthonormal wavelet transform is the scaling function  $\phi(t)$  that satisfies the two scale relation. The discrete translates of the scaling functions form the orthonormal bases within each resolution level. The discrete translates of the wavelets also form the orthonormal bases within each resolution level. The scaling and the wavelet function bases are mutually orthogonal within the same resolution level. The recursive orthonormal projections on the multiresolution subspaces yield the wavelet series decomposition.

The wavelet series decomposition and reconstruction are computed by iterating the discrete low-pass filters  $p(n)$  and the discrete high-pass filters  $q(n)$ , in the tree algorithms, in order to compute a set of discrete wavelet transform coefficients  $d_i(n)$  and a set of discrete approximation coefficients  $c_i(n)$ .

The scaling function and wavelet bases are orthonormal only with discrete translations and dilations. The decomposition of a continuous function onto the orthonormal scaling and wavelet function bases yields discrete sequences of expansion coefficients. Hence, there is an analogy of the orthonormal wavelet transform with the Fourier series decomposition.

## 10.5.6 Biorthogonal Wavelet Bases

The biorthogonal wavelet bases give more flexibility to the filter design. We define in the multiresolution framework two hierarchies of approximation subspaces:

$$\begin{aligned} \cdots V_2 \subset V_1 \subset V_0 \subset V_{-1} \subset V_{-2} \cdots \\ \cdots \bar{V}_2 \subset \bar{V}_1 \subset \bar{V}_0 \subset \bar{V}_{-1} \subset \bar{V}_{-2} \cdots \end{aligned}$$

where the subspaces  $V_i$  are spanned by the translates of the scaling function  $\phi(t)$ , and  $\bar{V}_i$  are spanned by the translates of the dual scaling function  $\bar{\phi}(t)$ . The wavelet subspace  $W_i$  is complementary to  $V_i$  in the finer resolution subspace  $V_{i-1}$ , but is not an orthogonal complement. Instead,  $W_i$  is the orthogonal complement to  $\bar{V}_i$ . Similarly, the dual wavelet subspace  $\bar{W}_i$  is the orthogonal complement to  $V_i$ . Thus,

$$\begin{aligned} W_i \perp \bar{V}_i \quad \text{and} \quad \bar{W}_i \perp V_i \\ \bar{V}_{i-1} = \bar{V}_i \oplus W_i \quad \text{and} \quad V_{i-1} = V_i \oplus \bar{W}_i \end{aligned}$$

The orthogonality between the wavelet and the dual scaling function and between the scaling function and the dual wavelet can also be expressed as

$$\begin{aligned} \langle \bar{\phi}(t-k), \psi(t-n) \rangle &= 0 \\ \langle \bar{\psi}(t-k), \phi(t-n) \rangle &= 0 \end{aligned}$$

for any  $n, k \in \mathbf{Z}$ . We expect also the orthogonality between the scaling function and its dual and between the wavelet and its dual:

$$\begin{aligned} \langle \bar{\phi}(t-k), \phi(t-n) \rangle &= \delta_{k,n} \\ \langle \bar{\psi}(t-k), \psi(t-n) \rangle &= \delta_{k,n} \end{aligned}$$

The orthogonality expressed in the four preceding equations is referred to as the biorthogonality. Indeed, the biorthogonal scaling functions and wavelets can be found with the polynomial B-splines scaling functions and wavelets. The cross scale orthogonality of the wavelet and its dual can also be obtained

$$\langle \psi_{i,k}, \bar{\psi}_{m,n} \rangle = \delta_{i,m} \delta_{k,n}$$

Any function  $f \in L^2(\mathbf{R})$  can be expanded onto the biorthogonal scaling function and the wavelet bases as

$$\begin{aligned} f(t) &= \sum_i \sum_k \langle f, \bar{\psi}_{i,k} \rangle \psi_{i,k}(t) \\ &= \sum_i \sum_k \langle f, \psi_{i,k} \rangle \bar{\psi}_{i,k}(t) \end{aligned}$$

and also

$$\begin{aligned} f(t) &= \sum_i \sum_k \langle f, \bar{\phi}_{i,k} \rangle \phi_{i,k}(t) \\ &= \sum_i \sum_k \langle f, \phi_{i,k} \rangle \bar{\phi}_{i,k}(t) \end{aligned}$$

The implementation of the wavelet transform on the biorthogonal bases is also with the discrete low-pass and high-pass filters  $p(n)$  and  $q(n)$  in the multiresolution framework. In the reconstruction from the biorthogonal wavelet transform, however, the discrete synthesis filters  $p_0(n)$  and  $q_0(n)$  are not identical to the analysis filters  $p(n)$  and  $q(n)$ . They can have no equal length. We shall discuss the low-pass and high-pass filters for the biorthogonal wavelet transform in detail in Section 10.6.4 in the framework of the subband coding theory. The discrete iterated filters are introduced with the two scale relations as

$$\begin{aligned} \phi(t) &= \sum_n p(n) \phi(2t-n) \\ \bar{\phi}(t) &= \sum_n p_0(-n) \bar{\phi}(2t-n) \end{aligned}$$

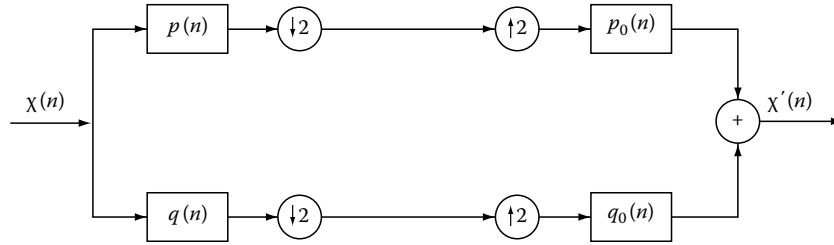


FIGURE 10.14 Schematic wavelet decomposition and reconstruction with the biorthogonal scaling function and wavelet bases.

and

$$\begin{aligned}\psi(t) &= \sum_n q(n)\phi(2t - n) \\ \bar{\psi}(t) &= \sum_n q_0(-n)\bar{\phi}(2t - n)\end{aligned}$$

One stage of the wavelet decomposition and reconstruction with the biorthogonal filter bank is shown in Figure 10.14.

### 10.5.6.1 Biorthogonal Wavelet Decomposition

Similar to the orthogonal decomposition in Equation 10.60 the decomposition with the biorthogonal wavelets is implemented with the biorthogonal analysis filters  $p(n)$  and  $q(n)$  as:

$$c_i(k) = 2^{-1/2} \sum_n p(n - 2k)c_{i-1}(n)$$

and

$$d_i(k) = 2^{-1/2} \sum_n q(n - 2k)c_{i-1}(n)$$

### 10.5.6.2 Biorthogonal Wavelet Reconstruction

Similar to the reconstruction with the orthonormal wavelet transform (Equation 10.65) the signal is reconstructed with the biorthogonal synthesis filters  $p_0(n)$  and  $q_0(n)$  as

$$c_{i-1}(n) = 2^{-1/2} \sum_k c_i(k)p_0(n - 2k) + 2^{-1/2} \sum_k d_i(k)q_0(n - 2k)$$

We shall discuss the biorthogonal analysis and synthesis filters in Section 10.6.

## 10.6 Filter Bank

The discrete and dyadic wavelet transform is computed in the multiresolution signal analysis framework with the recurring low-pass and high-pass filters, that can be designed in the multiresolution signal analysis framework with the subband coding theory. The properties of the filters may be studied equivalently in the time domain and in the frequency or the  $z$ -transform domain.

## 10.6.1 FIR Filter Bank

### 10.6.1.1 Two Channel Filter Bank

The two-channel filter bank, shown in the Figure 10.14, is a building block of the discrete wavelet transform and subband coding. An input signal  $x(k)$  is filtered in the two channels by the low-pass filter  $p(k)$  and high-pass filter  $q(k)$ , which are the analysis filters for decomposing the signal. The analysis filtering is followed by a down-sampling by two. The filters  $p_0(k)$  and  $q_0(k)$  are the synthesis filters for reconstructing the signal. There is up-sampling before the synthesis filters.

The low-pass and high-pass filters  $p(k)$  and  $q(k)$  are discrete and usually real-valued sequences with  $k \in \mathbf{Z}$ . For the sake of consistency with the wavelet decomposition described in Section 10.5, we define that the analysis filtering is a correlation operation, and the synthesis filtering is a convolution operation.

### 10.6.1.2 Finite Impulse Response (FIR) Filters

Digital filters can be classified into two groups. In the first group, the filter is a finite-extent sequence, called the finite impulse response (FIR) filter. In the second group, the filter is of infinite extent, called the infinite impulse response (IIR) filters. The FIR filters have compact supports. Only a finite number of  $p(k)$  and  $q(k)$  are not zero:  $p(k) \neq 0$  and  $q(k) \neq 0$ , for  $0 \leq k \leq N - 1$ . However, in the biorthonormal filter banks the low-pass and high-pass filters can have different lengths.

The Fourier transforms of the FIR filters  $p(k)$  and  $q(k)$  with compact support would have no fast decay. There is a trade-off between the compactness and the regularity of the FIR filter.

### 10.6.1.3 Transfer Functions

Both filters  $p(k)$  and  $q(k)$  for  $k \in \mathbf{Z}$  have limited lengths (FIR filters). The filter length is  $N$ . Their Fourier transforms exist as

$$\begin{aligned}P(\omega) &= \sum_k p(k) \exp(-jk\omega) \\ Q(\omega) &= \sum_k q(k) \exp(-jk\omega)\end{aligned}\tag{10.67}$$

where  $k = 0, 1, 2, \dots, N - 1$  and the Fourier transforms of the filters, i.e., the transfer functions,  $P(\omega)$  and  $Q(\omega)$ , are complex-valued continuous functions. Note that Equation 10.67 may be considered as the Fourier series expansions of  $P(\omega)$  and  $Q(\omega)$ , therefore, both  $P(\omega)$  and  $Q(\omega)$  are periodic functions of period  $\omega = 2\pi$ .

The Fourier series expansions (Equation 10.67) are equivalent to the  $z$ -transform of the sequences  $p(k)$  and  $q(k)$ . With the definition of  $z$  as  $z = \exp(j\omega)$ , Equation 10.67 can be rewritten as the Laurent polynomial:

$$\begin{aligned} P(z) &= \sum_k p(k)z^{-k} \\ Q(z) &= \sum_k q(k)z^{-k} \end{aligned} \quad (10.68)$$

where  $k = 0, 1, 2, \dots, N-1$  and both  $P(z)$  and  $Q(z)$  are complex-valued continuous functions of the complex variable  $z$ .

The degree of the Laurent polynomial  $P(z)$  is then equal to  $N-1$ , i.e., the length of the FIR filter  $p(k)$  minus one.

The analysis filtering is a correlation operation. In the frequency domain, the filtering of the signal  $x(k)$  by the low-pass and high-pass filters,  $p(k)$  and  $q(k)$ , is equivalent to multiplying the Fourier transform of  $x(k)$ ,  $X(z)$ , by the transfer functions  $P(z)$  and  $Q(z)$ . That yields  $X(z)P(z^{-1})$  and  $X(z)Q(z^{-1})$ , respectively, where  $P(z^{-1})$  and  $Q(z^{-1})$  are complex conjugated  $P(z)$  and  $Q(z)$ , used in the correlation operations. Note that the coefficients  $p(k)$  and  $q(k)$  are real-valued in the Laurent polynomial Equation 10.68.

#### 10.6.1.4 Time Delay and Causality

If the signal  $x(n)$  is a time sequence, then the filtering convolution operation with a filter  $g(k)$  is written as

$$\sum_k g(k)x(n-k) = g(0)x(n) + g(1)x(n-1) + \dots$$

where  $x(n)$  is the current input,  $x(n-1)$  is the input earlier by one time step etc. The output has a time delay with respect to the input. The filter  $g(k)$  is a causal filter, and  $g(-k)$  must be zero, because the output cannot be a function of the later input. For instance, if  $g(-1) \neq 0$ , then the filtering output would contain a term of  $g(-1)x(n+1)$ , where  $x(n+1)$  is the input of one time step later. According to the causality principle the filtering output at a time step  $n$  cannot be a function of  $x(n+1)$  so that  $g(-1)$  must be zero.

#### 10.6.1.5 Linear-Phase Filters

The low-pass FIR filters  $p(k)$  are usually real-valued and symmetric. In this case, the transfer function  $P(\omega)$  as the Fourier transform of  $p(k)$  is itself a real-valued and even function, with zero phase. Because  $p(k)$  is causal,  $p(-k)$  is not allowed. Therefore, the filter  $p(k)$  must be shifted in time domain, centered at  $N/2$ , that corresponds to a time delay, where  $N$  is the length of the FIR filter. Hence, the symmetric and antisymmetric filters should be

$$\begin{aligned} \text{Symmetric} \quad p(k) &= p(N-k) \\ \text{Antisymmetric} \quad p(k) &= -p(N-k) \end{aligned} \quad (10.69)$$

Their transfer function  $P(\omega)$  would have a linear phase, and becomes  $P(\omega)\exp(-jm\omega)$ , or  $P(z)z^{-m}$ . Its modulus  $|P(\omega)|$  would be even.

In some wavelet bases, such as the Daubechies bases, the low-pass filters are not symmetric. A nonsymmetric filter would introduce a nonlinear phase to the transfer function, that can distort the proper registration of different frequency components. For instance, in image processing applications of the non-symmetrical filters will introduce important image distortions.

#### 10.6.1.6 Binary Coefficient Filters

A binary coefficients or dyadic coefficient is an integer divided by a power of 2. In the computer, multiplication by a binary number can be executed entirely by shifts and adds without round-off error. Also, in some architectures, the filters need less time and less space. We are therefore highly interested in binary coefficient filters.

### 10.6.2 Perfect Reconstruction

#### 10.6.2.1 Down-Sampling

The down-sampling by factor of two is a decimation operation, that is to save the even-numbered and discard the odd-numbered components of data sequence. The down-sampling by two can be considered as being achieved in two steps. First, the signal  $x(n)$  is sampled with the double sampling interval:

$$x'(n) = \begin{cases} x(n) & \text{for } n = 0, \pm 2, \pm 4, \dots \\ 0 & \text{otherwise} \end{cases}$$

The intermediate signal  $x'(n)$  has the same time clock rate as that of  $x(n)$ . Then, the time clock rate is reduced by two to obtain the down-sampled signal  $y(n)$  as

$$y(n) = x'(2n) \quad \text{for } n = 0, \pm 1, \pm 2, \dots$$

Its spectrum  $Y(\omega)$  in the Fourier domain is two-times larger than  $X(\omega)$ , because  $Y(\omega) = X'(\omega/2)$ .

Discarding the odd-numbered components leads to a loss in information. This loss of information is definitive. In the frequency domain this is aliasing error. The down-sampling process is not invertible.

The down-sampling is not shift-invariant. By the down-sampling by two of its output, the convolution of a filter becomes a convolution with the filter that is shifted only by even numbers, i.e., a double-shift convolution. Therefore, when the input signal is shifted by an odd number, the results of the double shift convolution can change dramatically. The Laplacian pyramid, discrete and dyadic wavelet transform, subband coding and all other multiresolution analysis using the down-sampling are all highly dependent of the relative alignment of the input signal with the sub-sampling lattices and are not shift-invariant.

### 10.6.2.2 Up-Sampling

The up-sampling by factor of two is an expansion operation, that is to insert zeros as the odd-numbered components into the data sequence. The up-sampling is also implemented in two steps. First, insert zeros between nodes of the down-sampled signal  $y(n)$  and then increase the time clock rate by two and let

$$y'(n) = \begin{cases} y(n/2) & \text{for } n = 0, \pm 2, \pm 4, \dots \\ 0 & \text{otherwise} \end{cases}$$

In the Fourier domain the spectrum of the up-sampled data  $Y'(\omega)$  is compressed by two with respect to the original  $Y(\omega)$ , because  $Y'(\omega) = Y(2\omega)$ . Thus, a low-pass filter should be used for smoothing the up-sampled signal. The up-sampling processes also is not shift-invariant. When the input signal is shifted by an odd number, the results of the up-sampling can change dramatically.

### 10.6.2.3 Aliasing Cancellation

Aliasing error is introduced by the down-sampling. The signal  $x(k)$  is filtered in the two channels by the low-pass and high-pass filters. The filtered signals are described in the frequency domain as  $X(z)P(z^{-1})$  and  $X(z)Q(z^{-1})$  before the down-sampling. The combination process of the down-sampling followed by the up-sampling would put to zero all the odd-numbered components of the filtered signals. This corresponds in the  $z$ -domain to keep only the even powers of  $z$  in  $X(z)P(z^{-1})$  and  $X(z)Q(z^{-1})$ , that can be represented as [12]

$$\begin{aligned} \text{Low - pass channel output} & \quad \frac{1}{2}[X(z)P(z^{-1}) + X(-z)P(-z^{-1})] \\ \text{High - pass channel output} & \quad \frac{1}{2}[X(z)Q(z^{-1}) + X(-z)Q(-z^{-1})] \end{aligned} \quad (10.70)$$

or equivalently in the frequency domain

$$\begin{aligned} & \frac{1}{2}[X(\omega)P^*(\omega) + X(\omega + \pi)P^*(\omega + \pi)] \\ & \frac{1}{2}[X(\omega)Q^*(\omega) + X(\omega + \pi)Q^*(\omega + \pi)] \end{aligned} \quad (10.71)$$

where the terms  $X(-z)P(-z^{-1})$  and  $X(-z)Q(-z^{-1})$  are aliasing errors introduced by the down-sampling, which are not canceled by the up-sampling.

In the two channel filter bank, the alias terms  $X(-z)P(-z^{-1})$  and  $X(-z)Q(-z^{-1})$  can be canceled in the synthesis step by the synthesis filters  $P_0(z)$  and  $Q_0(z)$  with the aliasing term,  $X(-z)P(-z^{-1})$ , in the low-pass channel multiplied by  $P_0(z)$  and the aliasing term,  $X(-z)Q(-z^{-1})$ , in the high-pass channel multiplied by  $Q_0(z)$ . Hence, the aliasing terms are canceled, if the condition

$$P_0(z)P(-z^{-1}) + Q_0(z)Q(-z^{-1}) = 0 \quad (10.72)$$

is satisfied. The Equation 10.72 is the antialiasing condition.

### 10.6.2.4 Perfect Reconstruction Condition

The perfect reconstruction requires  $\hat{x}(n) = cx(n)z^{-m}$ , i.e., the output is equal to the input in the building block shown in Figure 10.14 with an extra constant  $c$ . When the input  $x(n)$  passes the two channels without divided by two, but the data from the two channels are added up in the end for the output, we have  $c = 2$ . If the analysis and synthesis filters are normalized to remove the constant  $c$ , we have  $c = 1$ . The extra phase shift  $z^{-m}$  with  $m \in \mathbf{Z}$  corresponds to a possible time delay between the output and the input data sequences. The filter bank can be causal.

Now, the signal passes both the low-pass filter and high-pass filter channels. Each is followed by down-sampling and up-sampling, respectively as expressed in Equation 10.70. We then multiply each by the synthesis filters,  $P_0(z)$  and  $Q_0(z)$ , respectively and sum them up. When the antialiasing condition (Equation 10.72) is satisfied, and the two aliasing terms  $X(-z)P(-z^{-1})$  and  $X(-z)Q(-z^{-1})$  in Equation 10.70 are canceled, the output could be identical to the input, and the building block could behave like an identity operation if:

$$P_0(z)P(z^{-1}) + Q_0(z)Q(z^{-1}) = cz^{-m} \quad (10.73)$$

The ensemble of Equation 10.73 for perfect reconstruction and Equation 10.72 for aliasing error cancellation is referred to as the perfect reconstruction condition.

### 10.6.2.5 Modulation Matrix

Two  $2 \times 2$  modulation matrices are defined as

$$\begin{aligned} M(z) &= \begin{bmatrix} P(z) & P(-z) \\ Q(z) & Q(-z) \end{bmatrix} \quad \text{and} \\ M_0(z) &= \begin{bmatrix} P_0(z) & P_0(-z) \\ Q_0(z) & Q_0(-z) \end{bmatrix} \end{aligned} \quad (10.74)$$

where  $M(z)$  is the analysis modulation matrix and  $M_0(z)$  is the synthesis modulation matrix.

The perfect reconstruction conditions (Equations 10.72 and 10.73) condition may be summarized to

$$[P_0(z) \quad Q_0(z)]M(z^{-1}) = c[1 \quad 0] \quad (10.75)$$

where the constant extra time delay  $z^{-m}$  are removed in the sake of simplicity. If we want the synthesis filters,  $P_0(-z)$  and  $Q_0(-z)$ , to play the same role as  $P_0(z)$  and  $Q_0(z)$ , then the aliasing cancellation Equation 10.72 becomes

$$P_0(-z)P(-z^{-1}) + Q_0(-z)Q(-z^{-1}) = 0$$

and the perfect reconstruction condition (Equation 10.73) becomes

$$P_0(-z)P(z^{-1}) + Q_0(-z)Q(z^{-1}) = cz^{-m}$$

then combining with Equation 10.75 we have

$$M_0(z)^t M(z^{-1}) = cI \quad (10.76)$$

where  $I$  is the identity matrix. Note that in the time domain, the filters with the transfer function  $P_0(-z)$  and  $Q_0(-z)$ , are only shifted by one with respect to that with the transfer function  $P_0(z)$  and  $Q_0(z)$ . Moreover, if we need the two modulation matrices be even reversible, then we need also the perfect reconstruction condition as

$$M(z^{-1})M_0(z)^t = cI \quad (10.77)$$

that will introduce the cross-filter relation as shown in the next sections.

### 10.6.3 Orthonormal Filter Bank

#### 10.6.3.1 Paraunitary Matrix

The orthogonal filter bank is the perfect reconstruction filter bank with the synthesis filters equal to the analysis filters,  $P_0(z) = P(z)$  and  $Q_0(z) = Q(z)$ , in the building block shown in Figure 10.14. Therefore, for the orthogonal filter bank we have from Equations 10.76 and 10.77

$$M(z)^t M(z^{-1}) = cI \quad \text{and} \quad M(z^{-1})M(z)^t = cI \quad (10.78)$$

The modulation matrix  $M(z)$  is a para-unitary matrix, if the constant factor  $c$  in the right-hand side of Equation 10.78 is not considered. Hence, the low-pass and high-pass filters for the discrete wavelet transform are the two-channel paraunitary filter bank.

#### 10.6.3.2 Orthonormality Condition

From the paraunitary filter bank condition (Equation 10.78) it follows that

$$\begin{aligned} |P(z)|^2 + |P(-z)|^2 = c \quad \text{and} \quad |P(\omega)|^2 + |P(\omega + \pi)|^2 = c \\ |Q(z)|^2 + |Q(-z)|^2 = c \quad \text{and} \quad |Q(\omega)|^2 + |Q(\omega + \pi)|^2 = c \end{aligned} \quad (10.79)$$

We call both  $|P(z)|^2$  and  $|Q(z)|^2$  the half-band filters and shall discuss their properties later in this section. The relation (Equation 10.79) can be also obtained from the orthonormality condition of the scaling function and wavelet bases in the frequency domain, as will be shown in Section 10.7.

#### 10.6.3.3 Cross-Filter Orthonormality

From the paraunitary filter bank condition (Equation 10.78) it also follows that

$$\begin{aligned} P(z^{-1})Q(z) + P(-z^{-1})Q(-z) = 0 \\ Q(z^{-1})P(z) + Q(-z^{-1})P(-z) = 0 \end{aligned} \quad (10.80)$$

The relation (Equation 10.80) can be also obtained from the cross-orthonormality condition of the scaling function and wavelet bases in the frequency domain, as will be shown in Section 10.7.

In this section we introduced the paraunitary filter bank, which leads to the orthonormality and cross-filter orthonormality conditions. The paraunitary filter bank is a solution of the aliasing error cancellation and perfect reconstruction conditions (Equation 10.75), which becomes the modulation matrix Equations 10.76 and 10.77 with the additional constraints. In Section 10.7 we shall demonstrate the orthonormality and cross-filter orthonormality conditions on the low-pass and high-pass filters, and then use the orthonormality and cross-filter orthonormality conditions to demonstrate the paraunitary filter bank condition.

#### 10.6.3.4 Alternating Flip

It is easy to verify that the solution

$$Q(z) = (-z)^{-(N-1)} P(-z^{-1}) \quad (10.81)$$

satisfies the cross-filter orthonormality condition (Equation 10.80), with an arbitrary even number  $N$ , which is the length of the filter in time domain.

The inverse  $z$ -transform of the solution (Equation 10.81) gives the relation between the low-pass filters  $p(n)$  and high-pass filters  $q(n)$  in the time domain. In multiresolution signal analysis, the wavelet bases are generated by the basic scaling functions. Similarly, the high-pass filters in the filter bank are generated from the low-pass filter by the alternating flip relation. In the orthonormal wavelet transform the high-pass filters  $q(n)$  are obtained from the low-pass filters  $p(n)$ , by the inverse  $z$ -transform of Equation 10.81:

$$q(n) = (-1)^n p(N-1-n) \quad \text{for } n = 0, 1, 2, \dots, N-1 \quad (10.82)$$

for an even  $N$ , such that the low-pass and high-pass filters  $p(n)$  and  $q(n)$  satisfy the cross-filter orthogonality, where  $N$  is the length of the FIR filters, or can be any even number. Note that an arbitrary even number can be added to  $N$ , resulting in an even number shift of  $p(N-1-n)$ .

#### 10.6.3.5 Quadrature Mirror Filters (QMF)

The alternating flip filters are a solution of the cross-filter orthonormality condition (Equation 10.80). For the alternating flip filter bank, the low-pass and high-pass filters satisfy

$$\begin{aligned} |Q(z)|^2 = |P(-z^{-1})|^2 \quad \text{or equivalently} \\ |Q(\omega)|^2 = |P(\omega + \pi)|^2 \end{aligned} \quad (10.83)$$

and are referred to as a pair of quadrature mirror filters. If the high-pass filter  $Q(\omega)$  is such that  $Q(\omega)|_{\omega=0} = 0$ , then from the quadrature mirror property (Equation 10.83) we have  $P(\omega)|_{\omega=\pi} = 0$ . If the low-pass filter  $P(\omega)$  is normalized such that  $P(\omega)|_{\omega=0} = 1$ , then from the quadrature mirror property (Equation 10.83) the high-pass filter would be such that  $Q(\omega)|_{\omega=\pi} = 1$ .

### 10.6.3.6 Mirror Filters

A pair of FIR filters  $L(\omega)$  and  $H(\omega)$  are referred to as mirror filters, if

$$L(z) = H(-z) \quad \text{or equivalently} \quad L(\omega) = H(\omega + \pi) \quad (10.84)$$

In the time domain the two FIR mirror filters with real-valued coefficients satisfy the relation

$$l(k) = (-1)^k h(k) \quad (10.85)$$

that is the inverse  $z$ -transform of Equation 10.84.

The filter pair  $L(\omega)$  and  $H(\omega)$  are mirror filters because on substituting for  $\omega$  by  $\omega - \pi/2$  in Equation 10.84 and noting that the low-pass filter  $L(n)$  is real valued, and  $|L(\omega)|$  is an even function of  $\omega$ , we obtain

$$\left| H\left(\frac{\pi}{2} + \omega\right) \right| = \left| L\left(\frac{\pi}{2} - \omega\right) \right| \quad (10.86)$$

This is the mirror image property of  $|L(\omega)|$  and  $|H(\omega)|$  about  $\omega = \pi/2$ .

### 10.6.3.7 Ideal Half-Band Filters

Intuitively, if a low-pass filter is an ideal low-pass filter:  $L(\omega) = 1$  for  $-\pi/2 \leq \omega \leq \pi/2$  and  $P(\omega) = 0$  elsewhere, then its mirror filter  $H(\omega)$  is the ideal half-band high-pass filter:  $H(\omega) = 0$  for  $-\pi/2 \leq \omega \leq \pi/2$  and equal to 1 elsewhere. They are both brick-wall filters and are rectangular functions. Hence, the input spectrum in the full band  $-\pi \leq \omega \leq \pi$  is divided into two equal subbands by the analysis mirror filters  $L(\omega)$  and  $H(\omega)$ .

### 10.6.3.8 Half-Band Filters

The idea half-band filters are orthonormal. In practice of multi-resolution signal analysis, it is not necessary to use the ideal low-pass and high-pass filters. A filter  $G(z)$  is a half-band filter if

$$G(z) + G(-z) = 2 \quad \text{or equivalently} \\ G(\omega) + G(\omega + \pi) = 2 \quad (10.87)$$

The filter  $G(\omega)$  is half-band because on substituting for  $\omega$  by  $\omega - \pi/2$  in Equation 10.87 and noting that the low-pass filter  $g(n)$  is real valued, and  $|G(\omega)|$  is an even function of  $\omega$ , we obtain

$$\left| G\left(\frac{\pi}{2} - \omega\right) \right| = \left| G\left(\frac{\pi}{2} + \omega\right) \right| \quad (10.88)$$

There is the mirror image property of  $|G(\omega)|$  about  $\omega = \pi/2$ , which is referred to as the half-band frequency.

In the Laurent polynomial (Equation 10.68) of the half-band filters  $G(z)$  all the even powers of  $z$  must be zero, and all the odd powers of  $z$  must be canceled by each others, except the zero power term  $G(0) = 1$ .

Note that the low-pass and high-pass filters in the multiresolution signal analysis are not themselves half-band, but their square modula are half-band filters, according to Equation 10.79 and are the quadrature mirror filters according to Equation 10.83.

### 10.6.3.9 Power Complementary Filters

The filter pair  $\{L(\omega), H(\omega)\}$  are referred to as the power complementary filters if

$$|L(\omega)|^2 + |H(\omega)|^2 = c \quad (10.89)$$

where the constant  $c = 1$  or  $2$ . This relation shows the energy complementary property of the low-pass and high-pass filters. From the orthonormality condition (Equation 10.79) and quadrature mirror condition (Equation 10.83) it follows that  $P(\omega)$  and  $Q(\omega)$  are complementary, because:

$$\begin{aligned} |P(z)|^2 + |Q(z)|^2 &= c \quad \text{or} \\ |P(\omega)|^2 + |Q(\omega)|^2 &= c|P(-z)|^2 + |Q(-z)|^2 = c \quad \text{or} \\ |P(\omega + \pi)|^2 + |Q(\omega + \pi)|^2 &= c \end{aligned} \quad (10.90)$$

## 10.6.4 Orthonormal Filters in Time Domain

From the orthonormal filter condition (Equation 10.79) both  $|P(z)|^2$  and  $|Q(z)|^2$  are half-band filters so that in their Laurent polynomials all the even powers of  $z$  must be zero. Note that  $P(z)$  and  $Q(z)$  are the Fourier transforms of the time domain filters  $p(k)$  and  $q(k)$  respectively. The inverse Fourier transform of the square modulus  $|P(z)|^2$  is the autocorrelation of  $p(k)$ . Let a product filter  $\text{Pr}(z) = |P(z)|^2$ . In the Laurent polynomial of  $\text{Pr}(z)$ , the coefficients  $p_r(2n) = 0$  for  $n \neq 0$  and  $p_r(0) = 1$ . Hence, the time domain low-pass filter has the double-shift orthogonality as

$$\sum_k p(k)p(k-2n) = \delta(n)$$

and similarly for the high-pass filter

$$\sum_k q(k)q(k-2n) = \delta(n)$$

From the cross-filter orthonormality (Equation 10.80) and using the similar process we can have the cross-filter orthonormality in the time domain as

$$\sum_k p(k)q(k-2n) = 0$$

All the filters are shifted in the time domain by even integers in the correlations. Therefore, at the same resolution level, the low-pass filter  $p(n)$  is orthonormal to its own translates by two or by any even numbers. The high-pass filter  $q(n)$  also is orthonormal to its own translates by two or by any even numbers. Also, the low-pass

and high-pass filters translated by two, or any even numbers, are mutual orthogonal. This is the double-shift orthonormality of the low-pass and high-pass filters in the time domain.

In the multiresolution signal analysis, the double-shift of the low-pass and high-pass filters in the time domain correspond to the filtering followed by the down-sampling by factor of two.

The double-shift orthonormality implies that the orthonormal wavelet transform filters  $p(n)$  and  $q(n)$  must have even lengths.

### 10.6.5 Biorthogonal Filter Bank

In the two-channel filter bank, shown in Figure 10.14, the synthesis filters may be different from the analysis filters, that brings more freedom in the filter design. The perfect reconstruction conditions should be still satisfied. The filter bank in this case is biorthogonal.

The choice for the synthesis filters  $P_0(z)$  and  $Q_0(z)$  as

$$\begin{aligned} P_0(z) &= Q(-z^{-1}) \\ Q_0(z) &= -P(-z^{-1}) \end{aligned} \quad (10.91)$$

satisfies the alias cancellation equation:

$$P_0(z)P(-z^{-1}) + Q_0(z)Q(-z^{-1}) = 0$$

Thus, the synthesis filters are associated to the analysis filters. The low-pass synthesis filter is equal to the high-pass analysis filter. They have the same length. The high-pass synthesis filter is equal to the low-pass analysis filter. They have the same length. The synthesis filters cancels the alias errors, caused by the analysis filters, and the down- and up-sampling.

#### 10.6.5.1 Product Filters

With the choice (Equation 10.91) for the synthesis filters the perfect reconstruction Equation 10.73

$$P_0(z)P(z^{-1}) + Q_0(z)Q(z^{-1}) = 2z^{-m}$$

becomes

$$P_0(z)P(z^{-1}) - P_0(-z)P(-z^{-1}) = 2z^{-m} \quad (10.92)$$

The left-hand side of Equation 10.92 is an odd function of  $z$ . Therefore, in the right-hand side of Equation 10.92 the power  $-m$  of  $z$  must be odd. We define the product filter  $\text{Pr}(z)$  as:

$$\text{Pr}(z) = P_0(z)P(z^{-1}) \quad (10.93)$$

and the normalized product filter as

$$\tilde{\text{Pr}}(z) = P_0(z)P(z^{-1})z^m$$

where  $m$  is an odd number. Then, the perfect reconstruction condition (Equation 10.92) becomes

$$\tilde{\text{Pr}}(z) + \tilde{\text{Pr}}(-z) = 2 \quad (10.94)$$

The normalized product filter  $\tilde{\text{Pr}}(z)$  has to be a half-band filter. Hence, all the even powers of  $z$  in  $\tilde{\text{Pr}}(z)$  must be zero, except for zero power term  $\tilde{\text{Pr}}(0) = 2$ . There are only the odd powers of  $z$  in the polynomial  $\tilde{\text{Pr}}(z)$  and all the odd powers must be canceled by each others,

#### 10.6.5.2 Degrees and Symmetries

Because the normalized product filter is half-band, and  $m$  is an odd number, the product filter  $\text{Pr}(z) = P_0(z)P(z^{-1})$  must be a polynomial in  $z$  of even degrees. Its two factors, the low-pass analysis and synthesis filters,  $P(z^{-1})$  and  $P_0(z)$ , must both have even degrees or both have odd degrees. In the time domain, the low-pass analysis and synthesis filters must be both of odd lengths or both of even length.

The symmetric or antisymmetric filters are linear-phase filters. The product filter can be symmetric, but can not be antisymmetric, because the half-band filter  $\tilde{\text{Pr}}(0) \neq 0$  also the low-pass filter can not have a zero mean:  $\sum p(k) \neq 0$ . Hence, the low-pass analysis and synthesis filters,  $P(z^{-1})$  and  $P_0(z)$ , can only be both symmetric. In this case, the low-pass analysis and synthesis filters in the time domain, are both symmetric and have either both odd lengths or both even lengths.

The synthesis filters are obtained from the analysis filters as shown in Equation 10.91:

$$\begin{aligned} P_0(z) &= Q(-z^{-1}) \\ Q_0(z) &= -P(-z^{-1}) \end{aligned}$$

by changing  $-z$  to  $z$  that alters the signs of all the coefficients of the high-pass filters in time domain,  $q(k)$  and  $q_0(k)$ . When  $P(z^{-1})$  and  $P_0(z)$  are symmetric and of odd lengths, changing  $-z$  to  $z$  does not change the symmetry of the high-pass filters. Then, the high-pass filters are also both symmetric and of odd lengths. When  $P(z^{-1})$  and  $P_0(z)$  are symmetric and of even lengths, changing  $-z$  to  $z$  and changing the signs of the  $p_0(k)$  and  $q_0(k)$  of odd  $k$  do change the symmetry to antisymmetry, so that the high-pass filters of even lengths are both antisymmetric.

#### 10.6.5.3 Design Biorthonormal Filters

The biorthonormal filter bank is design to satisfy the perfect reconstruction condition (Equation 10.92). First, one chooses the product filter  $\tilde{\text{Pr}}(z)$  satisfying the half-band condition (Equation 10.94). If the analysis and synthesis filters in the time domain have the lengths  $N$  and  $N_0$ , respectively, the degrees of the polynomials  $P(z^{-1})$  and  $P_0(z)$  would be  $N-1$  and  $N_0-1$ , respectively. Then, the degree of the polynomial  $\tilde{\text{Pr}}(z)$  will be  $N+N_0-2$ , which is usually determined at the beginning. Then,

one factorize the product filter  $\text{Pr}(z)$  into the low-pass analysis and synthesis filters  $P(z^{-1})$  and  $P_0(z)$ . The high-pass filters can be finally determined according to the alternating flip relation (Equation 10.91). Splitting  $\text{Pr}(z)$  into  $P(z^{-1})$  and  $P_0(z)$  can have some degrees of freedom which can be used for providing some useful properties, such as the linear phase filters (symmetry or antisymmetry).

In one of design methods the product filter  $\text{Pr}(z)$  takes the form as

$$\text{Pr}(z) = \left( \frac{1+z^{-1}}{2} \right)^M F(z) \quad (10.95)$$

where the first term is the Fourier spectrum of a low-pass filter whose corresponding scaling function is a spline function, as will be discussed in Section 10.8.1. Note that  $z = e^{j\omega}$  and  $|(1 + e^{-j\omega})/2| = |\cos \omega|$ . Hence, this term insures  $|\text{Pr}(\omega)|$  to have a zero of order  $M$  at  $z = -1$  and at  $\omega = \pi$ , and to have  $M$  vanishing derivatives at  $\omega = 0$ . The second term  $F(z)$  insures the  $\text{Pr}(z)$  to satisfy the perfect reconstruction condition and being a half-band filter.

The biorthonormal wavelet transform filter banks can be designed with the lifting steps and the polyphase representation. Readers interested in the polyphase, lifting and spectral factorization are referred to other reference books [24]. The lifting steps can be considered as a balancing operation between the smoothness of the analysis and synthesis filters [24], that is moving the factor  $(1 + z^{-1})/2$  from the synthesis filter  $P_0(z)$  to the analysis filter  $P(z^{-1})$  where  $P_0(z)$  and  $P(z^{-1})$  are two factors in the same product filter  $\text{Pr}(z) = P_0(z)P(z^{-1})$ . Multiplying  $(1 + z^{-1})/2$  to  $P(z^{-1})$  corresponds to in the time domain

$$p^{\text{new}}(k) = \frac{1}{2}[p^{\text{old}}(k) + p^{\text{old}}(k-1)]$$

The synthesis filter  $P_0(z)$  is divided by  $(1 + z^{-1})/2$  then

$$P_0^{\text{new}}(z) = P_0^{\text{old}}(z) \left( \frac{1+z^{-1}}{2} \right)^{-1} \quad \text{and}$$

$$P_0^{\text{new}}(z) = 2P_0^{\text{old}}(z) - z^{-1}P_0^{\text{new}}(z)$$

Hence, the synthesis filter in the time domain is changed as

$$p_0^{\text{new}}(k) = [2p_0^{\text{old}}(k) - p_0^{\text{new}}(k-1)]$$

The biorthonormality is preserved because

$$P^{\text{new}}(z^{-1})P_0^{\text{new}}(z) = P^{\text{old}}(z^{-1})P_0^{\text{old}}(z)$$

This process also maintains the binary coefficients of the filters [24].

### Example

The pair of low-pass analysis and synthesis filters

$$p_1 = [1] \quad \text{and} \quad p_0^7 = [-1 \ 0 \ 9 \ 16 \ 9 \ 0 \ -1]/16$$

are symmetric and binary coefficient filters. Balancing will produce 2/6 and 3/5 filters as

$$p_2 = [11]/2 \quad \text{and} \quad p_0^6 = [-1 \ 1 \ 8 \ 8 \ 1 \ -1]/8$$

$$p_3 = [1 \ 2 \ 1]/4 \quad \text{and} \quad p_0^5 = [-1 \ 2 \ 6 \ 2 \ -1]/4$$

These filters are biorthonormal and of binary coefficients.

## 10.7 Wavelet Theory

The dyadic discrete wavelet decomposition and reconstruction are computed by iterating the discrete low-pass and high-pass filters in the tree algorithm in the multiresolution signal analysis framework. The low-pass and high-pass filters for the orthonormal wavelet transform are the paraunitary 2-band perfect reconstruction (PR) quadrature mirror filter (QMF) bank, which can be designed using the subband coding theory.

When computing the discrete wavelet transform one is given by a bank of low-pass and high-pass filters to iterate. The wavelet and scaling function are not given by explicit expressions during the wavelet transform computation. They even have no closed forms for many wavelets.

However, in the wavelet theory an extra regularity condition is imposed on the scaling function and the wavelets. The orthonormal wavelet transform can be applied to continuous functions and therefore serves as a transform tool for analytic signals. The multiresolution Laplacian pyramid and the subband coding are discrete. The multiresolution wavelet transform algorithm is also essentially discrete. But the algorithm leads to a wavelet series expansion that decomposes a continuous function into a series of continuous wavelet functions.

The novelties in the wavelet theory with respect to that developed in the subband theory are the wavelet decomposition of continuous signal functions into the continuous scaling function and wavelet bases; the regularity of the scaling function, wavelet as well as the quadrature mirror filters; the localization of the scaling function and wavelet in both time and frequency domains; the zero-mean condition on the high-pass filter and the generation of the continuous scaling function and wavelet by iterating the low-pass and high-pass filters.

The basic properties of the orthonormal scaling functions and wavelets are the orthonormality and regularity, which are applied to the discrete low-pass and high-pass filters as well. Most analysis on the filter properties will be done in the Fourier domain. The knowledge on those properties is useful for designing and using the wavelet bases.



### 10.7.1 Orthonormality

The scaling function and the wavelets can be orthonormal to their own discrete translates at each resolution level, constructing orthonormal bases, in the condition that the scaling function and wavelet satisfy the orthonormality conditions. The orthonormality conditions can be expressed in the frequency domain.

#### 10.7.1.1 Orthonormality Conditions

Consider a generic basic scaling function  $\phi(t)$  that is, in most cases, real valued. At a given scale, its discrete translations form an orthonormal set  $\{\phi(t-k)\}$ , such that:

$$\int \phi(t-k)\phi(t-k')dt = \delta_{k,k'} \quad k, k' \in \mathbf{Z}$$

The orthonormality of the discrete translations of  $\phi(t)$  is equivalent to the fact that the autocorrelation of  $\phi(t)$  evaluated at discrete time steps  $(k-k')$  must be zero everywhere except at the origin  $k=k'$ . The Fourier transform of the autocorrelation of a function is equal to the squared modulus of the Fourier transform of that function. Hence, the orthonormality of the basic scaling function in the Fourier domain may be written as

$$\int |\Phi(\omega)|^2 \exp(-jn\omega)d\omega = 2\pi\delta_{n,0} \quad (10.96)$$

where  $n=k-k'$  with  $n \in \mathbf{Z}$ , and  $\Phi(\omega)$  is the Fourier transform of  $\phi(t)$ . Hence, the Fourier transform of the scaling function,  $|\Phi(\omega)|^2$ , evaluated at discrete frequency steps  $n$  must be equal to zero except at the origin  $n=0$ . We shall prove that the orthonormality condition (Equation 10.96) for the basic scaling function may be expressed as

$$\sum_n |\Phi(\omega + 2n\pi)|^2 = 1 \quad (10.97)$$

The sum of the series of its Fourier spectrum intensity  $|\Phi(\omega)|^2$  discretely translated by  $2n\pi$  must be equal to one.

Similarly, the orthogonality condition for a basic wavelet is that its Fourier spectrum satisfies:

$$\sum_n |\Psi(\omega + 2n\pi)|^2 = 1 \quad (10.98)$$

#### 10.7.1.2 Poisson Summation Formula

To prove the orthonormality condition (Equations 10.97 and 10.98) we need to use the Poisson summation formula

$$\sum_n f(x + 2\pi n) = \frac{1}{2\pi} \sum_n F(n) \exp(jnx) \quad (10.99)$$

If  $f(x)$  is a delta function, then Equation 10.99 is the well known Fourier transform of a comb function. If  $f(x)$  is continuous and has a compact support smaller than  $2\pi$ , then the left-hand side of Equation 10.99 is a periodic function, and the right-hand side of Equation 10.99 is the Fourier series expansion of that periodic function, where  $F(n)$  is the Fourier transform of  $f(x)$ . The Poisson summation formula then corresponds to the simple Fourier series decomposition of the periodic function  $\sum f(x + 2n\pi)$ . The Poisson summation formula is valid when  $f(x)$  satisfies some regularity conditions and has a compact support such that the series  $\sum f(x + 2n\pi)$  converges to a periodic function of period  $2\pi$ .

Assume that the Fourier spectrum  $|\Phi(\omega)|^2$  of the basic scaling function  $\phi(t)$  is regular, and has a compact support. Let  $|\Phi(\omega)|^2$  be the  $f(x)$  in the Poisson summation formula, (Equation 10.99), we obtain

$$\sum_n |\Phi(\omega + 2n\pi)|^2 = \frac{1}{2\pi} \sum_n R(n) \exp(jn\omega)$$

where  $R(n)$  is the Fourier transform of  $|\Phi(\omega)|^2$ . If  $\Phi(\omega)$  satisfy the orthonormality condition (Equation 10.96)  $R(n)$  would be equal to zero for  $n \neq 0$  and equal to  $2\pi$  for  $n=0$ , that proves the orthonormality condition (Equation 10.97), and similarly we have Equation 10.98.

#### 10.7.1.3 Discussion

To gain an insight of the orthonormality condition (Equation 10.97) we expand a function  $g(t)$  onto the orthonormal basis of the translates  $\{\phi(t-k)\}$  with  $k \in \mathbf{Z}$  that is

$$g(t) = \sum_k c(k)\phi(t-k) = \phi(t) * \sum_k c(k)\delta(t-k)$$

where  $*$  denotes the convolution and  $c(k)$  are the coefficients of expansion. In the Fourier domain this expansion becomes

$$G(\omega) = \Phi(\omega) \sum_k c(k) \exp(-jk\omega) = \Phi(\omega)M(\omega)$$

where  $M(\omega)$  is defined as

$$M(\omega) = \sum_k c(k) \exp(-jk\omega)$$

which is a periodic with period  $2\pi$ :  $M(\omega) = M(\omega + 2n\pi)$ . According to the Parseval's relation of the Fourier transform

$$\frac{1}{2\pi} \int_0^{2\pi} |M(\omega)|^2 d\omega = \sum_n |c(n)|^2$$

We can compute the energy of  $g(t)$  by

$$\begin{aligned} \int_{-\infty}^{\infty} |g(t)|^2 dt &= \frac{1}{2\pi} \int_{-\infty}^{\infty} |\Phi(\omega)|^2 |M(\omega)|^2 d\omega \\ &= \frac{1}{2\pi} \sum_{n=-\infty}^{\infty} \int_{2\pi n}^{2\pi(n+1)} |\Phi(\omega)|^2 |M(\omega)|^2 d\omega \\ &= \frac{1}{2\pi} \sum_{n=-\infty}^{\infty} \int_0^{2\pi} |\Phi(\omega + 2n\pi)|^2 |M(\omega + 2n\pi)|^2 d\omega \\ &= \frac{1}{2\pi} \int_0^{2\pi} |M(\omega)|^2 \sum_{n=-\infty}^{\infty} |\Phi(\omega + 2n\pi)|^2 d\omega \end{aligned}$$

where we used the property that  $\Phi(\omega + 2n\pi)$  is periodic of period  $2\pi$ . From the orthogonality condition (Equation 10.97) we can write

$$\int |g(t)|^2 dt = \sum_n |c(n)|^2 \quad (10.100)$$

This is the energy conservation relation for the expansion onto the orthonormal scaling function and wavelet bases, and is similar to the energy conservation relation (Equation 10.18) for the continuous wavelet transform in Section 10.2.1. According to the wavelet frame theory in Section 10.3.2, Equation 10.100 means the frame is tight, the discrete scaling function basis behaves like an orthonormal basis.

## 10.7.2 Two Scale Relations in Frequency Domain

The two scale relations in the multiresolution analysis are the basic relations between the continuous scaling function  $\phi(t)$ , wavelet  $\psi(t)$  and the discrete low-pass and high-pass filters,  $p(n)$  and  $q(n)$ :

$$\begin{aligned} \phi(t) &= \sum_k p(k)\phi(2t - k) \\ \psi(t) &= \sum_k q(k)\phi(2t - k) \end{aligned}$$

In the multiresolution wavelet decomposition the low-pass filter  $p(n)$  plays the role of the weighting function and the high-pass filter  $q(n)$  is used to compute the detail information. The Fourier transform of the two scale relations gives

$$\begin{aligned} \Phi(\omega) &= \sum_k p(k) \int \phi(2t - k) \exp(-j\omega t) dt \\ &= \frac{1}{2} \left[ \sum_k p(k) \exp(jk\omega/2) \right] \Phi\left(\frac{\omega}{2}\right) \\ &= P\left(\frac{\omega}{2}\right) \Phi\left(\frac{\omega}{2}\right) \end{aligned} \quad (10.101)$$

and similarly,

$$\Psi(\omega) = Q\left(\frac{\omega}{2}\right) \Phi\left(\frac{\omega}{2}\right) \quad (10.102)$$

where  $P(\omega)$  and  $Q(\omega)$  are the Fourier transform of the sequences of the low-pass and high-pass filters, as defined in Equations 10.67 and 10.68. Both  $P(\omega)$  and  $Q(\omega)$  are periodic functions of period  $2\pi$ .

According to Equation 10.101 the Fourier transform  $\Phi(\omega)$  of the coarser resolution scaling function  $\phi(t)$  is the product of the twice wider Fourier transforms  $\Phi(\omega/2)$  of the finer resolution scaling function  $\phi(2t)$  and that of the low-pass filter  $P(\omega/2)$ . Equation 10.101 is a recursion equation. The recursion can be repeated  $m$  times to yield  $\Phi(\omega/2)$ ,  $\Phi(\omega/4)$ ... so on, that gives

$$\Phi(\omega) = \prod_{i=1}^m P\left(\frac{\omega}{2^i}\right) \Phi\left(\frac{\omega}{2^m}\right) \quad (10.103)$$

When  $m$  approaches to infinity and  $1/2^m$  tends to zero we have the Fourier transform of the continuous scaling function expressed as

$$\Phi(\omega) = \prod_{i=1}^{\infty} P\left(\frac{\omega}{2^i}\right) \quad (10.104)$$

provided that the scaling function  $\phi(t)$  is normalized with respect to the  $L^1(\mathbf{R})$  as

$$\int \phi(t) dt = \Phi(0) = 1$$

Similarly, we can replace the second term  $\Phi(\omega/2)$  in the right-hand side of Equation 10.102 with the infinite product derived in Equation 10.104 and obtain

$$\Psi(\omega) = Q\left(\frac{\omega}{2}\right) \prod_{i=2}^{\infty} P\left(\frac{\omega}{2^i}\right) \quad (10.105)$$

It can be proved that if for some  $\varepsilon > 0$  the sequence of interscale coefficients  $p(n)$  satisfies

$$\sum_n |p(n)| |n|^\varepsilon < \infty$$

then the infinite product on the right-hand side of Equation 10.104 converges pointwise and the convergence is uniform. That is, the low-pass filter  $p(n)$  decays as fast as  $n^\varepsilon$ . This is a very mild condition, because in most practical cases the low-pass filters  $p(n)$  are the FIR filters with only a limited number of  $p(n) \neq 0$ .

The two Equations 10.104 and 10.105 express relations between the Fourier transforms of the continuous scaling function and wavelet and the infinite product of the Fourier transforms of the low-pass and high-pass filters.

### 10.7.2.1 Filters Orthonormality

Using the Fourier domain two scale relation (Equation 10.101) and the orthonormality condition (Equation 10.97) we can write

$$\begin{aligned} \sum_n |\Phi(2\omega + 4n\pi)|^2 &= |P(\omega)|^2 \sum_n |\Phi(\omega + 2n\pi)|^2 = |P(\omega)|^2 \\ \sum_n |\Phi(2\omega + 2(2n+1)\pi)|^2 &= |P(\omega + \pi)|^2 \sum_n |\Phi(\omega + (2n+1)\pi)|^2 \\ &= |P(\omega + \pi)|^2 \end{aligned}$$

which correspond to the summation of  $\Phi(\omega)$  translated by  $4n\pi$  and by  $(2n+1)2\pi$  respectively. Adding these two equations and applying again the orthonormality condition (Equation 10.97) to the two summations of  $\Phi(\omega)$  on the left-hand side of the preceding equations we have

$$|P(\omega)|^2 + |P(\omega + \pi)|^2 = 2 \quad (10.106)$$

This is the orthonormality condition for the square modulus of the low-pass filter  $P(\omega)$  in the Fourier domain. Similarly, the orthonormality condition for the high-pass filter  $\psi(\omega)$  in the Fourier domain is

$$|Q(\omega)|^2 + |Q(\omega + \pi)|^2 = 2 \quad (10.107)$$

Both Equations 10.106 and 10.107 are identical to Equation 10.79 introduced in Section 10.6.3.

### 10.7.2.2 Cross-Filter Orthogonality

The scaling functions and the wavelets must be mutually orthogonal within the same scale:

$$\int \phi(t - n')\psi(t - k)dt = 0$$

for all  $n', k \in \mathbf{Z}$ . In the Fourier domain the condition for the cross-filter orthogonality can be written as

$$\int \Phi(\omega)\Psi^*(\omega) \exp(-jn\omega)d\omega = 0 \quad (10.108)$$

where  $n = n' - k$  and  $n \in \mathbf{Z}$ . Using the Poisson summation formula (Equation 10.99):

$$\sum_n f(x + 2n\pi) = \frac{1}{2\pi} \sum_n F(n) \exp(jnx)$$

and assuming that the product  $\Phi(\omega)\Psi^*(\omega)$  is regular and of finite support and let it be the  $f(x)$  in the Poisson summation formula, and using the cross-filter orthogonality condition (Equation 10.108) we have the Fourier transform of  $\Phi(\omega)\Psi^*(\omega)$  equal to zero and

$$\sum_n \Phi(\omega + 2n\pi)\Psi^*(\omega + 2n\pi) = 0 \quad (10.109)$$

We separate the translations of  $4k\pi$  and of  $(2k+1)2\pi$  of the product  $\Phi(\omega)\Psi^*(\omega)$  an rewrite (Equation 10.109) as

$$\begin{aligned} \sum_n \Phi(2\omega + 4n\pi)\Psi^*(2\omega + 4n\pi) \\ + \sum_n \Phi(2\omega + 2(2n+1)\pi)\Psi^*(2\omega + 2(2n+1)\pi) = 0 \end{aligned}$$

On substituting the Fourier domain two scale relations (Equations 10.101 and 10.102) for  $\Phi(\omega)$  and  $\Psi^*(\omega)$  into the above expression and using the periodicity of period  $2\pi$  of  $P(\omega)$  and  $Q(\omega)$  we have

$$\begin{aligned} P(\omega)Q^*(\omega) \sum_n |\Phi(\omega + 2n\pi)|^2 + P(\omega + \pi)Q^*(\omega + \pi) \\ \times \sum_n |\Phi(\omega + (2n+1)\pi)|^2 = 0 \end{aligned}$$

Using the orthonormality condition for  $\Phi(\omega)$  described in Equation 10.97 we have

$$\begin{aligned} P(\omega)Q^*(\omega) + P(\omega + \pi)Q^*(\omega + \pi) &= 0 \\ P^*(\omega)Q(\omega) + P^*(\omega + \pi)Q(\omega + \pi) &= 0 \end{aligned}$$

This is the cross filter orthogonality condition on the low-pass and high-pass filters  $P(\omega)$  and  $Q(\omega)$  in the Fourier domain, which is identical to Equation 10.80 introduced in Section 10.6.3.

### 10.7.2.3 Paraunitary Matrix

We observe the orthonormality conditions for the low-pass and high-pass filters and the cross-filter orthogonality in terms of the  $z$ -transform as

$$\begin{aligned} P(z)P(z^{-1}) + P(-z)P(-z^{-1}) &= 2 \\ Q(z)Q(z^{-1}) + Q(-z)Q(-z^{-1}) &= 2 \\ P(z)Q(z^{-1}) + P(-z)Q(-z^{-1}) &= 0 \\ P(z^{-1})Q(z) + P(-z^{-1})Q(-z) &= 0 \end{aligned} \quad (10.110)$$

and choose the alternating flip filter bank as a solution for the cross-filter orthogonality as Equation 10.81

$$Q(z) = (-z)^{-(N-1)}P(-z^{-1}) \quad (10.111)$$

where  $N$  is an arbitrary even number. That leads to

$$|Q(z)|^2 = |P(-z)|^2 \quad \text{and} \quad |Q(\omega)|^2 = |P(\omega + \pi)|^2 \quad (10.112)$$

The conjugate quadrature filters  $|P(-z)|^2$  and  $|Q(z)|^2$  are the mirror filters, as defined in Equation 10.84.

The first two equations in 10.110 are

$$\begin{aligned} |P(z)|^2 + |P(-z)|^2 &= 2 \\ |Q(z)|^2 + |Q(-z)|^2 &= 2 \end{aligned} \quad (10.113)$$

From Equations 10.112 and 10.113 we have

$$\begin{aligned} |P(z)|^2 + |Q(z)|^2 &= 2 \quad \text{and} \quad |P(\omega)|^2 + |Q(\omega)|^2 = 2 \\ |P(-z)|^2 + |Q(-z)|^2 &= 2 \quad \text{and} \\ |P(\omega + \pi)|^2 + |Q(\omega + \pi)|^2 &= 2 \end{aligned} \quad (10.114)$$

The filter pair  $\{P(z), Q(z)\}$  are power complementary as defined in Equation 10.90. The orthogonality conditions described in Equation 10.110 and the power complementary properties described in Equation 10.114 are equivalent to the requirement that the  $2 \times 2$  modulation matrix defined in Equation 10.74 should be paraunitary:

$$\begin{vmatrix} p(z^{-1}) & P(-z^{-1}) \\ Q(z^{-1}) & Q(-z^{-1}) \end{vmatrix} \begin{vmatrix} p(z) & Q(z) \\ P(-z) & Q(-z) \end{vmatrix} = 2 \begin{vmatrix} 1 & 0 \\ 0 & 1 \end{vmatrix} \quad (10.115)$$

The paraunitary properties are useful for designing the compactly supported orthonormal scaling function and the wavelet bases. All the properties for orthonormality, cross-filter orthonormality, alternating flip filters, conjugate quadrature mirror filters, complementary filters and the paraunitary filter banks, and relations (Equations 10.106 through 10.115) have been introduced and discussed in Section 10.6. from the perfect reconstruction property of the filter bank. However, the orthonormality of  $P(\omega)$  and  $Q(\omega)$  and the cross-filter orthonormality are obtained here from the orthonormality of the scaling function and wavelet bases.

### Example: Orthonormality of the Haar's Bases

Let us consider the orthonormality condition for the Haar's bases, as an example. We know that the Haar's bases are orthonormal at every scale. The Fourier transforms of the Haar scaling functions and wavelets are

$$\begin{aligned} \Phi(\omega) &= e^{-j\omega/2} \frac{\sin(\omega/2)}{\omega/2} \\ \Psi(\omega) &= e^{-j\omega/2} \frac{\sin^2(\omega/2)}{\omega/4} \end{aligned}$$

We have for the scaling function  $\Phi(\omega)|_{\omega=0} = 1$  and for the wavelet  $\Psi(\omega)|_{\omega=0} = 0$ . It can be verified that the orthonormality condition expressed as

$$\begin{aligned} \sum_n |\Phi(\omega + 2n\pi)|^2 &= 1 \\ \sum_n |\Psi(\omega + 2n\pi)|^2 &= 1 \end{aligned}$$

are satisfied.

The two-scale relations of the Haar scaling functions and the Haar wavelets are obtained in Section 10.5.2. On substituting the interscale coefficients of the Haar's bases:  $p(n) = 1/\sqrt{2}$  for  $n = 0, 1$  and  $p(n) = 0$  otherwise,  $q(0) = 1/\sqrt{2}$ ,  $q(1) = -1/\sqrt{2}$  and  $q(n) = 0$  otherwise according to Equations 10.63 and 10.64 into the Fourier transform of  $p(n)$  and  $q(n)$ , we obtain the quadrature mirror filters of the Haar's bases as

$$\begin{aligned} P(\omega) &= 2^{-1/2} \cos \frac{\omega}{2} \exp(-j\omega/2) \\ Q(\omega) &= j2^{-1/2} \sin \frac{\omega}{2} \exp(-j\omega/2) \end{aligned}$$

It is easy to verify that the Haar's quadrature mirror filters satisfy all the orthonormality conditions because:

$$\begin{aligned} |P(\omega)|^2 + |P(\omega + \pi)|^2 &= \frac{1}{2} \left[ \cos^2 \left( \frac{\omega}{2} \right) + \cos^2 \left( \frac{\omega + \pi}{2} \right) \right] = 1 \\ |Q(\omega)|^2 + |Q(\omega + \pi)|^2 &= \frac{1}{2} \left[ \sin^2 \left( \frac{\omega}{2} \right) + \sin^2 \left( \frac{\omega + \pi}{2} \right) \right] = 1 \end{aligned}$$

and

$$\begin{aligned} P(\omega)Q^*(\omega) + P(\omega + \pi)Q^*(\omega + \pi) \\ = -j\frac{1}{2} \cos \frac{\omega}{2} \sin \frac{\omega}{2} - j\frac{1}{2} \cos \frac{\omega + \pi}{2} \sin \frac{\omega + \pi}{2} = 0 \end{aligned}$$

We have also that

$$\begin{aligned} |P(\omega)|^2 + |Q(\omega)|^2 &= 1 \\ |P(-\omega)|^2 + |Q(-\omega)|^2 &= 1 \end{aligned}$$

and that the matrix

$$\begin{vmatrix} p(\omega) & Q(\omega) \\ P(\omega + \pi) & Q(\omega + \pi) \end{vmatrix}$$

are paraunitary.

## 10.7.3 Orthogonal Filters in Time Domain

### 10.7.3.1 Double-Shift Orthonormality

When the basic scaling function and the wavelet satisfy the orthonormality condition, their discrete translates with integer translation steps form two orthonormal bases, and those two bases are mutually orthogonal

$$\begin{aligned} \langle \Phi_{0,k}, \Phi_{0,n} \rangle &= \delta_{k,n} \\ \langle \Psi_{0,k}, \Psi_{0,n} \rangle &= \delta_{k,n} \\ \langle \Psi_{0,k}, \Phi_{0,n} \rangle &= 0 \end{aligned}$$

In Section 10.5.4 we obtained (Equations 10.53 and 10.54) from the two scale relations

$$\begin{aligned}\langle \phi_{1,k}, \phi_{0,n} \rangle &= 2^{-1/2} p(n-2k) \\ \langle \psi_{1,k}, \phi_{0,n} \rangle &= 2^{-1/2} q(n-2k)\end{aligned}$$

Hence, at the resolution level  $i=1$  the inner products of two translated scaling functions and wavelets may be written in terms of  $p(n)$  and  $q(n)$  as

$$\begin{aligned}\langle \phi_{1,k}, \phi_{1,k'} \rangle &= \sum_{n,m} p(n-2k)p(m-2k') \langle \phi_{0,n}, \phi_{0,m} \rangle \\ &= \sum_n p(n-2k)p(n-2k') = \delta_{k,k'} \\ \langle \psi_{1,k}, \psi_{1,k'} \rangle &= \sum_{n,m} q(n-2k)q(m-2k') \langle \phi_{0,n}, \phi_{0,m} \rangle \\ &= \sum_n q(n-2k)q(n-2k') = \delta_{k,k'} \\ \langle \psi_{1,k}, \phi_{1,k'} \rangle &= \sum_{n,m} q(n-2k)p(m-2k') \langle \phi_{0,n}, \phi_{0,m} \rangle \\ &= \sum_n q(n-2k)p(n-2k') = 0\end{aligned}$$

The double-shift orthonormality and cross-filter orthonormality also have been obtained from the paraunitary matrix properties of the filter bank in Section 10.6.4.

### 10.7.3.2 Equal Contribution Constraint

The low-pass filter  $p(n)$  in time domain should satisfy the equal contribution constraint, stipulating that all the node in one resolution level contribute the same total amount to the next level and that the sum of all the weights for a given node  $n$  is independent of  $n$ . Hence, the weighting function should satisfy:

$$\sum_n p(2n) = \sum_n p(2n+1)$$

In an example of multiresolution signal analysis shown in Figure 10.8 the odd number nodes and the even number nodes in the data sequence  $c_{i-1}(n)$  have two different connections with the low-pass filter  $p(n)$  because of the down-sampling by 2 of  $c_i(k)$ . The even nodes in  $c_0(n)$  are connected to  $c_1(n)$  with the weighting factors  $p(-2)$ ,  $p(0)$ , and  $p(2)$ , the odd nodes are connected to  $c_1(n)$  with the weighting factors  $p(-1)$  and  $p(1)$ . When the preceding relation is satisfied the sums of the weights are equal for odd and even nodes in  $c_1(n)$ .

From the orthonormality condition (Equation 10.97)

$$\sum_k |\Phi(\omega + 2k\pi)|^2 = 1$$

we find that if the scaling function is normalized such that its mean value is unity

$$\int \phi(t) dt = 1 \quad \text{and} \quad \Phi(0) = 1$$

then at  $\omega=0$ , we have  $\Phi(2k\pi) = 0$  for  $k=1, 2, \dots$ . Therefore, we have  $\sum_k |\Phi[2(2k+1)\pi]|^2 = 0$ . Using the two scale relation

$$\Phi(2\omega) = P(\omega)\Phi(\omega)$$

at  $\omega = (2k+1)\pi$  we have

$$\sum_k |P[(2k+1)\pi]|^2 |\Phi[(2k+1)\pi]|^2 = 0$$

As  $\Phi[(2k+1)\pi] \neq 0$  we must have  $P[(2k+1)\pi] = 0$  and equivalently for the low-pass filter in the time domain we have, according to the Fourier transform (Equation 10.67)

$$P(\pi) = \sum_k (-1)^k p(k) = 0$$

but

$$P(0) = \sum_k p(k) = 1$$

Addition and subtraction of the two preceding equations yield, respectively

$$\sum_k p(2k) = 1 \quad \text{and} \quad \sum_k p(2k+1) = 1$$

This is the equal constraint condition for the multiresolution signal analysis filters.

### 10.7.4 Wavelet and Subband Filters

The discrete orthonormal wavelet transform low-pass and high-pass filters are simply the 2-band paraunitary perfect reconstruction quadrature mirror filters developed in the subband coding theory. The novelties of the wavelet transform are

#### 1. Continuous function bases

The wavelet transform is defined on the scaling function and wavelet bases, which are continuous function bases of continuous variables, so that the wavelet transform can serve as a mathematical transform tool to analogue signal functions. The subband coding technique is based on the discrete filters and applied to discrete data.

#### 2. Zero-mean high-pass filter:

Applying the wavelet admissible condition  $\Psi(\omega)|_{\omega=0} = 0$  to the Fourier domain two-scale relation (Equation 10.105), it follows that

$$Q(\omega)|_{\omega=0} = 0 \quad (10.116)$$

The high-pass filter  $q(n)$  in the time domain must have a zero mean.

### 3. Regularity of the scaling function and wavelet

On substituting the zero mean property of the high-pass filter,  $Q(\omega)|_{\omega=0} = 0$ , into the quadrature mirror filter property (Equation 10.112) we have  $P(\omega)|_{\omega=\pi} = 0$ . The low-pass filter  $P(\omega)$  must contain at least one term of  $(1 + e^{-j\omega})$  or  $(1 + z^{-1})$ , which equals to zero at  $\omega = \pi$  or  $z = -1$ . The regularity of the low-pass filter  $P(\omega)$  insures the iterations of the low-pass filter to converge, as will be discussed in Section 10.7.5.

## 10.7.5 Regularity

The regularity of the wavelet basis functions is an important property of the wavelet transform, that results in the localization of the wavelet transform in both time and frequency domains. In Section 10.2.2 we discussed the regularity condition for the continuous wavelet transform. For the wavelet transform coefficients to decay as fast as  $s^{n+1/2}$  with an increase of  $(1/s)$ , where  $s$  is the scale factor, the wavelet  $\psi(t)$  must have the first  $n+1$  moments of the order  $0, 1, \dots, n$  equal to zero, and equivalently, the Fourier transform  $\Psi(\omega)$  of the wavelets must have the first  $n$  derivatives of the order up to  $n$  equal to zero about zero frequency  $\omega = 0$ .

In this section we shall discuss the regularity condition on the orthonormal scaling functions and wavelets, and on the quadrature mirror filters  $P(\omega)$  and  $Q(\omega)$  in the multiresolution analysis framework. We shall discuss the regularity condition in a slightly different way from that in Section 10.2.2. The regularity conditions are applied for ensuring convergence of the reconstruction from the orthonormal wavelet decomposition. However, the regularity conditions obtained in both approaches are equivalent.

### 10.7.5.1 Smoothness Measure

The regularity is a measure of smoothness for scaling functions and wavelets. The regularity of the scaling function is determined by the decay of its Fourier transform  $\Phi(\omega)$  and is defined as the maximum value of  $r$  such that

$$|\Phi(\omega)| \leq \frac{c}{(1 + |\omega|)^r}$$

for  $\omega \in \mathbf{R}$ . Hence, the  $|\Phi(\omega)|$  has exponential decay as  $\omega^{-M}$ , where  $M \leq r$ . This in turn implies that  $\phi(t)$  is  $(M-1)$ -times continuously differentiable, and both  $\phi(t)$  and  $\psi(t)$  are smooth functions.

### 10.7.5.2 Convergence of Wavelet Reconstruction

The reconstruction from the wavelet series decomposition is described by Equation 10.66

$$c_0 = \sum_{i=1}^M (L_0)^{i-1} H_0 d_i + (L_0)^M c_M$$

where the synthesis filtering operators applied to a sequence  $\alpha(k)$ ,  $L_0$  and  $H_0$ , are defined as

$$(L_0\alpha)(n) = \frac{1}{\sqrt{2}} \sum_k p(n-2k)\alpha(k)$$

$$(H_0\alpha)(n) = \frac{1}{\sqrt{2}} \sum_k q(n-2k)\alpha(k)$$

Note that in the reconstruction it is the low-pass filter  $L_0$  that is iterated.

The problem of the convergence of the wavelet reconstruction may be formulated for a particular example, where the original function to be decomposed is the scaling function itself. In this case the wavelet series coefficients must be  $c_M = \delta_{0,n}$  and  $d_0 = \dots = d_M = 0$ , where the sequence  $\delta_{0,n}$  has only one non-zero entry for  $n=0$ . The reconstruction formula becomes

$$c_0(n) = (L_0)^M c_M$$

It is therefore important to study the behavior of the iterated filtering operator  $(L_0)^i c_M$  for large  $i$ . Ideally we want  $(L_0)^i c_M$  to converge to a reasonably regular function when  $i$  tends to infinity. However, when  $i$  approaches to infinity  $(L_0)^i c_M$  can converge to a continuous function, or to a function with finite discontinuities, even to a fractal function. The sequence  $(L_0)^i c_M$  may also not converge at all. The condition for the reconstruction to converge is the regularity of the scaling function.

With a graphic representation shown in Figure 10.15, we represent the sequence  $c_M(n)$  at the resolution level  $i=M$  by a rectangular function  $\eta_0(t)$ :

$$\eta_0(t) = \begin{cases} 1 & -1/2 \leq t \leq 1/2 \\ 0 & \text{otherwise} \end{cases}$$

Assume that the sequence  $c_M(n)$  has the time clock rate of 1. At the next finer resolution level  $i=M-1$  the sequence  $c_{M-1}(n)$  is

$$c_{M-1}(n) = L_0 c_M(n) = \sum_k p(n-2k)\delta_{0,k} = p(n)$$

In fact, to compute  $c_{M-1}(n)$  we first increase the time clock rate such that  $c_M(n)$  is with a time interval of length  $1/2$ . The  $c_M(n)$  is then convolved with the discrete filter  $p(n)$  that has also the time interval of  $1/2$ . The amplitude of  $c_{M-1}(n)$  is equal exactly to  $p(n)$ , as shown in Figure 10.14. We represent  $c_{M-1}(n)$  by a piecewise constant function,  $\eta_1(t)$ , that is constant over the interval of  $1/2$ . It is easy to see that the  $\eta_1(t)$  may be expressed as

$$\eta_1(t) = \sum_n p(n)\eta_0(2t-n)$$

Continuing for computing  $c_{M-2}(n) = (L_0)^2 c_M(n)$  we put a zero between each node of the sequence  $c_{M-1}(n)$  and increase the time

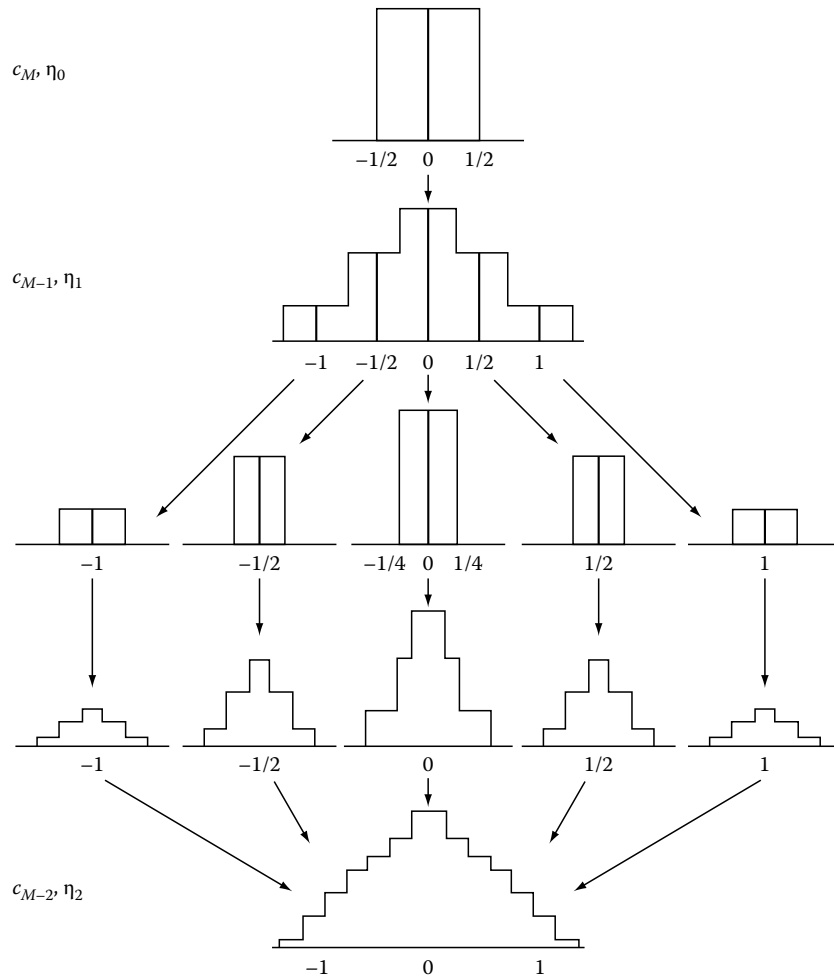


FIGURE 10.15 Reconstruction from  $c_M(n) = 1, \text{ for } n = 0$  and  $c_M(n) = 0$  for  $n \neq 0$  and the corresponding rectangle function  $\eta_0(t)$ . The time clock rate is equal to 1 for  $c_M(n)$ ,  $1/2$  for  $c_{M-1}(n)$  and  $1/4$  for  $c_{M-2}(n)$ . (From Daubechies, I., *Commun. on Pure and Appl. Math*, XLI, 909, 1988. With permission.)

clock rate. Thus, at this resolution level both the data sequences  $c(n)$  and the filter  $p(n)$  have the time interval of  $1/4$ . Their convolution yields the sequence  $c_{M-2}(n)$ . We represent  $c_{M-2}(n)$  by the piecewise constant function  $\eta_2(t)$  of a step of length  $1/4$ , as shown in Figure 10.15. It is easy to verify that

$$\eta_2(t) = \sum_n p(n)\eta_1(2t - n)$$

Similarly  $\eta_i(t) = (L_0)^i c_M(n)$  is a piecewise constant function with a step of length  $2^{-i}$  and

$$\eta_i(t) = \sum_n p(n)\eta_{i-1}(2t - n)$$

When  $i$  approaches to infinity  $(L_0)^i c_M$  can converge to  $\eta_\infty$  and

$$\lim_{i \rightarrow \infty} \eta_i(t) = \phi(t)$$

in the condition that the scaling function  $\phi(t)$  is regular, that we shall discuss next.

### 10.7.5.3 Construction of Scaling Function

The above recursion process with the low-pass filter operator  $L_0$ , associated to the low-pass filter  $p(n)$ , is a reconstruction of the scaling function  $\phi(t)$ . Starting from the rectangular function  $\eta_0$ , the recursion gives the values of  $\phi(t)$  of half-integers. Then, the recursion gives  $\phi(t)$  at the quarter-integers, and ultimately, at all dyadic point  $t = k/2^i$ . Finer and finer detail of  $\phi(t)$  is achieved by the recursion when the number of iterations  $i$  approaches to infinity. Therefore, the basic scaling function  $\phi(t)$  is constructed from the discrete low-pass filter  $p(n)$ . This process is useful to compute the continuous scaling and wavelet functions,  $\phi(t)$  and  $\psi(t)$  from the discrete low-pass and high-pass filters,  $p(n)$  and  $q(n)$ .

### 10.7.5.4 Regularity of Quadrature Mirror Filter

The regularity of the scaling function should not only ensure that the reconstructed scaling function  $\eta_\infty(t)$  converges, but also ensure that (1)  $\eta_\infty(t)$  is sufficiently regular or the Fourier transform of  $\eta_\infty(t)$  has sufficient decay, and (2)  $\eta_i(t)$  converges to  $\eta_\infty(t)$  point-wisely when  $i$  approaches to infinity. Daubechies [13]

has proven that the above two conditions can be satisfied when the Fourier transform of the low-pass filter  $p(n)$ , satisfies

$$P(\omega) = \left( \frac{1 + e^{-j\omega}}{2} \right)^M F(e^{-j\omega}) \quad (10.117)$$

or, written in terms of the  $z$ -transform, as

$$P(z^{-1}) = \left( \frac{1 + z^{-1}}{2} \right)^M F(z^{-1})$$

where  $M > 1$  and  $F(z^{-1})$  is a polynomial in  $z^{-1}$ , or in  $e^{-j\omega}$  with real coefficients and satisfies some conditions so that the infinite product

$$\left| \prod_{k=0}^{\infty} F(z^{k/2}) \right| \leq 2^{k(N-M-1)} \quad (10.118)$$

converges and is bounded. Because the low-pass filter  $p(n)$  is a FIR filter,  $p(n) \neq 0$  only for  $n = 0, 1, \dots, N-1$ , then its Fourier transform,  $P(\omega)$ , is a polynomial in  $e^{-j\omega}$  or in  $z^{-1}$ , of degree  $N-1$ . Hence,  $F(z^{-1})$  is a polynomial in  $z^{-1}$  of degree  $N-1-M$  where  $N$  is the length of  $p(n)$ .

According to Equation 10.117 the quadrature mirror filter  $P(\omega)$  must have  $M$  zeros at  $\omega = \pi$  or  $z = -1$ . We know that  $P(\omega)$  must have at least one zero at  $\omega = \pi$ , because according to the wavelet admissible condition for the high-pass filter (Equation 10.116):

$$Q(\omega)|_{\omega=0} = 0$$

and the quadrature mirror filter condition (Equation 10.112)

$$|P(\omega + \pi)|^2 = |Q(\omega)|^2$$

Hence,

$$P(\omega)|_{\omega=\pi} = 0$$

$P(\omega)$  must contain at least one term of  $(1 + e^{-j\omega})$ , the power  $M$  in Equation 10.117 must be at least equal to one. However, the regularity condition (Equation 10.117) requires  $P(\omega)$  to have more zeros with  $M > 1$  to insure convergence of the wavelet reconstruction.

### 10.7.5.5 Regularity of Scaling Function

Regularity condition (Equation 10.117) implies that

$$|P(\omega)| = \left| \cos \frac{\omega}{2} \right|^M |F(e^{-j\omega})|$$

On substituting the preceding relation into the infinite product form (Equation 10.104) of the Fourier transform  $\Phi(\omega)$  of the scaling function we obtain the regularity condition on  $\Phi(\omega)$  as

$$|\Phi(\omega)| = \prod_{i=1}^{\infty} \left| \cos \frac{\omega}{2^{i+1}} \right|^M \cdot \left| \prod_{i=1}^{\infty} F(e^{-j\omega/2^i}) \right| \quad (10.119)$$

but

$$\cos \frac{\omega}{2} = \frac{\sin \omega}{2 \sin (\omega/2)}$$

The first infinite product term in Equation 10.119 is therefore

$$\begin{aligned} \lim_{M \rightarrow \infty} \left| \prod_{i=1}^M \frac{\sin (\omega/2^i)}{2 \sin (\omega/2^{i+1})} \right|^M &= \lim_{M \rightarrow \infty} \left| \frac{\sin (\omega/2)}{2^M \sin (\omega/2^{M+1})} \right|^M \\ &= \left[ \frac{\sin (\omega/2)}{(\omega/2)} \right]^M \end{aligned}$$

and

$$|\Phi(\omega)| = \left| \frac{\sin (\omega/2)}{\omega/2} \right|^M \left| \prod_{i=1}^{\infty} F(e^{-j\omega/2^i}) \right| \quad (10.120)$$

The first term in the right-hand side of Equation 10.120 contributes to the exponential decay of  $\Phi(\omega)$  as  $\omega^{-M}$ . The second term is bounded according to the condition (Equation 10.118).

The number  $M$  of zeros of the quadrature mirror filter  $P(\omega)$  at  $\omega = \pi$ , or at  $z = -1$  is a measure of flatness of  $P(\omega)$  at  $\omega = \pi$ . From the regularity conditions (Equations 10.117 and 10.120) we see that the exponential decay of the scaling function  $\Phi(\omega)$  and the flatness of the quadrature mirror filter  $P(\omega)$  are equivalent. When the scaling function  $\Phi(\omega)$  has the exponential decay as  $\omega^{-M}$ , the quadrature mirror filter  $P(\omega)$  has number  $M$  of zero at  $\omega = \pi$ .  $M$  is a measure of the regularity of the scaling function.

### 10.7.5.6 Smoothness in Time Domain

The regularity also implies the smoothness of the low-pass filter  $p(n)$  in the time domain. We rewrite Equation 10.117 as

$$P(\omega) = \exp(-jM\omega/2) \left( \cos \frac{\omega}{2} \right)^M F(\omega)$$

Its  $r$ th derivative is

$$\frac{d^r P(\omega)}{d\omega^r} = \left( \cos \frac{\omega}{2} \right)^{M-r} g_r(\omega) \quad (10.121)$$

where  $[\cos(\omega/2)]^{M-r}$  is the minimum power of  $\cos(\omega/2)$  that the  $r$ th derivative contains and  $g_r(\omega)$  is the residual terms of the derivative. The term  $[\cos(\omega/2)]^{M-r}$  makes the  $r$ th derivative of  $P(\omega)$  equal to zero at  $\omega = \pi$  for  $r = 0, 1, \dots, M-1$ . On the other hand, because  $P(\omega)$  is the Fourier transform of  $p(n)$ , we have

$$\frac{d^r P(\omega)}{d\omega^r} = \sum_n (-jn)^r p(n) \exp(-jn\omega)$$



Then,

$$\left. \frac{d^r P(\omega)}{d\omega^r} \right|_{\omega=\pi} = (-j)^r \sum_n n^r (-1)^n p(n) = 0 \quad (10.122)$$

for  $r = 0, 1, \dots, M - 1$ . Hence, the low-pass filter  $p(n)$  is a smooth filter. Substituting the alternating flip filter expression

$$Q(z) = (-z)^{-(N-1)} P(-z^{-1})$$

where  $N$  is an even number, into the regularity condition (Equation 10.122) we have

$$Q(z) = \left( \frac{1-z}{2} \right)^M z^{-N} F(-z^{-1})$$

or in terms of the Fourier transform frequency  $\omega$  as

$$Q(\omega) = \left( \sin \frac{\omega}{2} \right)^M g_r(\omega)$$

where  $g_r(\omega)$  is the residual terms. The  $[\sin(\omega/2)]^M$  term insures that  $Q(\omega)$  has the vanishing derivatives at  $\omega = 0$

$$\left. \frac{d^r Q(\omega)}{d\omega^r} \right|_{\omega=0} = 0$$

As  $Q(\omega)$  is the Fourier transform of  $q(n)$ , the  $r$ th derivative of  $Q(\omega)$  is equal to zero at  $\omega = 0$  for  $r = 0, 1, \dots, M - 1$

$$\sum_n r^n q(n) = 0 \quad (10.123)$$

The high-pass filter  $q(n)$  has vanishing moment of order  $r$ .

Both the low-pass filter  $p(n)$  and high-pass filter  $q(n)$  are FIR filters:  $p(n) \neq 0$  only for  $n = 0, 1, \dots, N - 1$  and  $N$  is the length of  $p(n)$ . The compactness of  $p(n)$  and  $q(n)$ , described by  $(N - 1)$  is in contrast with the regularity of  $P(\omega)$  and  $Q(\omega)$  and of the scaling and wavelet functions, described by  $M$ , because according the regularity condition (Equation 10.119)  $M < N - 1$ . There is a trade-off between the compactness of the filters and the regularity of the scaling function and wavelet. We will discuss this issue in Section 10.8.3.

## 10.8 Some Orthonormal Wavelet Bases

In this section we summarize some orthonormal wavelet bases. In general, the orthonormal wavelet bases generated in the multiresolution analysis framework are associated to the orthonormal scaling function bases. Different orthonormal scaling function and wavelet bases are designed to satisfy the

orthonormality condition and the regularity condition in slightly different ways.

More filter banks and wavelet filter coefficients may be founded in MATLAB<sup>®</sup> Wavelet Toolbox and in WaveLab (<http://playfair.stanford.edu/~wavelab>), and in many other computer software.

### 10.8.1 B-Spline Bases

One of the basic methods for constructing the orthonormal wavelet families involves the B-spline functions, which are familiar in the approximation theory for interpolating a given sequence of data points. In this section we give a brief description of the multiresolution analysis with the B-spline scaling function and wavelet bases, and the related low-pass and high-pass filters.

#### 10.8.1.1 B-Spline

The B-spline of degree  $n$  is generated by repeated  $(n + 1)$ -fold convolutions [14] of the rectangular function:

$$\beta^0(t) = \begin{cases} 1 & \text{for } 0 \leq t < 1 \\ 0 & \text{otherwise} \end{cases} \quad (10.124)$$

where  $n$  is an arbitrary positive integer. The  $n$ th degree B-spline is then

$$\begin{aligned} \beta^n(t) &= (\beta^{n-1} * \beta^0)(t) \\ &= \int_{-\infty}^{\infty} \beta^{n-1}(t-x) \beta^0(x) dx = \int_0^1 \beta^{n-1}(t-x) dx \end{aligned} \quad (10.125)$$

Equation 10.125 is recursive. Because of the repeated convolutions, the  $n$ th degree B-spline has a support of size  $(0, n + 1)$  in time. This support increases with the degree  $n$ . The B-spline is a bell-shaped and symmetric function with respect to the center of its support  $t = 1/2$ . There is also the central B-spline which is defined such that it is symmetric with respect to the origin.

The B-spline of zero degree  $\beta^0(t)$  has been used as the Haar scaling function. It is not even differentiable. The B-spline of first degree is the linear spline, which is a triangle function, called the hat function. Its first derivative is not continuous. The B-spline of second degree is the quadratic spline. It has continuous first derivatives. The B-spline of degree 3 is the cubic spline. It has the first and second continuous derivatives. The higher-order B-splines with the degree  $n > 1$  are smooth bell shaped functions and have continuous derivatives of orders up to  $n - 1$ .

According to the definition, the Fourier transform of the B-spline of degree  $n$  is

$$B^n(\omega) = \left( \frac{1 - e^{-j\omega}}{j\omega} \right)^{n+1} = e^{-j(n+1)\omega/2} \left( \frac{\sin(\omega/2)}{\omega/2} \right)^{n+1} \quad (10.126)$$

Its modulus,  $|B^n(\omega)|$  has the exponential decay as  $1/\omega^{n+1}$ . When  $n$  increases, the B-spline becomes more regular but its support becomes less compact. There is then the typical trade-off between the regularity and the compactness of the B-splines.

### 10.8.1.2 Spline Interpolation

The polynomial splines are linear combinations of the translated B-splines. The polynomial splines  $f^n(t)$  can be used to interpolate a given sequence of data point  $\{s(k)\}$ :

$$f^n(t) = \sum_k c(k)\beta^n(t-k)$$

When the polynomial coefficients equal to the signal data  $c(k) = s(k)$ ,  $f^n(t)$  is a cardinal spline interpolator, that has piecewise polynomial segments of  $n$ -degree. Hence, the B-spline of degree  $n$  is the interpolation function. When  $n = 0$ , the sequence of points  $\{s(k)\}$  with equal intervals is interpolated by  $\beta^0(t)$  which is a staircase function, as that shown in the case of the Haar scaling function approximation. When  $n = 1$ , the sequence of points are connected by the straight line segment in each interval  $[k, k+1]$ . When  $n > 2$ , the data points is interpolated by a function that is, in each interval, a polynomial in degree  $n$ .

### 10.8.1.3 Spline Scaling Function

The B-spline itself can be used as the scaling function. The scaling function can be dilated and translated to form the spline scaling function bases at different resolution levels. However, the B-spline of degree  $n$  has a support of  $(0, n+1)$ . Their integer translates do not necessarily form an orthonormal basis within a resolution level.

When the B-spline of degree  $m-1$  is used as the scaling function  $\Phi(\omega) = B^{m-1}(\omega)$ , the corresponding low-pass filter  $P(\omega)$  can be derived as that follows. From the two-scale relation (Equation 10.101)

$$\Phi(2\omega) = P(\omega)\Phi(\omega)$$

and Equation 10.126 we have

$$\left(\frac{1-e^{-2j\omega}}{2j\omega}\right)^m = P(\omega)\left(\frac{1-e^{-j\omega}}{j\omega}\right)^m \quad \text{and}$$

$$P(\omega) = \left(\frac{1+e^{-j\omega}}{2}\right)^m = \left(\frac{1+z^{-1}}{2}\right)^m \quad (10.127)$$

The coefficients of the corresponding low-pass filter,  $p(k)$ , in the time domain can be obtained from Equation 10.127 by the inverse  $z$ -transform.

### Example

When the cubic spline is the scaling function in the multi-resolution analysis, the corresponding low-pass filter

$$P(z) = [(1+z^{-1})/2]^4 = (1+4z^{-1}+6z^{-2}+4z^{-3}+z^{-4})/16$$

Hence, the low-pass filter in time is  $p(k) = [1, 4, 6, 4, 1]$ .

## 10.8.2 Lemarie and Battle Wavelet Bases

The Lemarie and Battle wavelet bases are a family of orthonormal scaling functions and wavelets, that are associated to the B-spline, with an additional condition that the Lemarie and Battle polynomial scaling functions and wavelets are orthonormal within the given resolution level. The orthonormality is obtained by imposing the orthonormality constraints on the B-spline scaling functions and wavelets.

### 10.8.2.1 Nonorthonormal Spline Basis

When the spline of degree  $m-1$ ,  $\beta^{m-1}(\omega)$ , is used as the scaling function. The orthonormality condition is not satisfied, because from Equation 10.126 we have

$$\sum_k |\beta^{m-1}(\omega + 2\pi k)|^2 = \sum_k \left( \frac{\sin[(\omega/2) + \pi k]}{((\omega/2) + \pi k)} \right)^{2m}$$

$$= \sin^{2m}(\omega/2) \sum_{2m} \left( \frac{\omega}{2} \right) \quad (10.128)$$

where with  $x = \omega/2$  we define

$$\sum_{2m}(x) \equiv \sum_k \left( \frac{1}{x + \pi k} \right)^{2m}$$

From the complex analysis we have

$$\cot x = \lim_{n \rightarrow \infty} \sum_{k=-n}^n \frac{1}{x + nk}$$

We can differentiate this identity  $2m-1$  times to obtain

$$\sum_{2m}(x) = \sum_k \frac{1}{(x + \pi k)^{2m}} = -\frac{1}{(2m-1)!} \frac{d^{2m-1}}{dx^{2m-1}} \cot x \quad (10.129)$$

Substituting Equation 10.129 into Equation 10.128, we obtain

$$\sum_k |\beta^{m-1}(\omega + 2\pi k)|^2 = \frac{-\sin^{2m}(x)}{(2m-1)!} \frac{d^{2m-1}}{dx^{2m-1}} \cot x \quad (10.130)$$

where  $x = \omega/2$ . Hence, for the zero-degree spline  $m = 1$ , we have

$$\sum_k |\beta^0(\omega + 2\pi k)|^2 = 1$$

The Haar scaling function is orthonormal. However, for the spline with  $m = 2$ , we have

$$\sum_k |\beta^1(\omega + 2\pi k)|^2 = \frac{1}{3} + \frac{2}{3} \cos^2\left(\frac{\omega}{2}\right)$$

which is between  $1/3$  and  $1$ . The linear spline scaling function basis is not orthonormal. In general, the higher degree spline scaling function bases are not orthogonal.

**10.8.2.2 Lemarie–Battle Basis**

The Lemarie and Battle’s multiresolution basis [15] is built from the B-spline. Lemarie has found a scaling function that is associated to the  $(m - 1)$ th degree splines and its integer translates form an orthonormal basis within the same resolution level. The Lemarie–Battle scaling function is given by its Fourier transform as

$$\begin{aligned} \Phi(\omega) &= \frac{1}{\omega^m} \left( \sum_k \left( \frac{1}{(\omega + 2\pi k)^{2m}} \right) \right)^{-1/2} \\ &= \frac{1}{\omega^m \sqrt{\sum_{2m}(\omega)}} \end{aligned} \tag{10.131}$$

---


$$\begin{aligned} \Phi(\omega) &= \omega^{-4} \left[ \sum (\omega + 2\pi k)^{-8} \right]^{-1/2} = 8\omega^{-4} \left( \frac{1}{315} \frac{d^7}{d\omega^7} \cot \frac{\omega}{2} \right)^{-1/2} \\ &= \frac{16\sqrt{315 \sin^4(\omega/2)}}{\omega^{-4} \sqrt{315 \cos^6(\omega/2) + 515 \cos^4(\omega/2) \sin^2(\omega/2) + 231 \cos^2(\omega/2) \sin^4(\omega/2) + 17 \sin^6(\omega/2)}} \end{aligned}$$


---

It is easy to verify that the orthonormality condition

$$\sum_k |\Phi(\omega + 2\pi k)|^2 = 1$$

is satisfied. The Lemarie–Battle scaling function  $\Phi(\omega)$  defined in Equation 10.131 can be computed using Equation 10.129.

**10.8.2.3 Quadrature Mirror Filters**

The low-pass quadrature mirror filter  $P(\omega)$  can be obtained from the two scale relation in the Fourier domain, described (Equation 10.101)

$$\Phi(2\omega) = P(\omega)\Phi(\omega)$$

According to Equation 10.131 we obtain

$$P(\omega) = \sqrt{\frac{\sum_{2m}(\omega)}{2^m \sum_{2m}(2\omega)}} \tag{10.132}$$

The Fourier transform of the corresponding orthonormal wavelet can be derived also from the two scale relation

$$\Psi(\omega) = Q\left(\frac{\omega}{2}\right)\Phi\left(\frac{\omega}{2}\right)$$

where the conjugate quadrature mirror filter  $Q(\omega)$  satisfying the orthonormal condition is obtained from the alternating flip property as described in Equation 10.82

$$\begin{aligned} Q(z) &= (-z)^{-(N-1)}P(-z^{-1}) \\ Q(\omega) &= e^{-j(N-1)(\omega+\pi)}P^*(\omega + \pi) \end{aligned}$$

where  $N$  is an even number. Hence,

$$\Psi(\omega) = e^{-j(N-1)(\omega+\pi)/2}P^*\left(\frac{\omega + \pi}{2}\right)\Phi\left(\frac{\omega}{2}\right) \tag{10.133}$$

**Example**

The Lemarie and Battle scaling function basis from the cubic spline with  $m - 1 = 3$  can be obtained from Equations 10.129 and 10.131 as [25]

From the expression for  $\sum_{2m}(\omega)$ , the Fourier transforms  $\Phi(\omega)$  and  $\Psi(\omega)$  of the scaling function and wavelet and the quadrature mirror filters,  $P(\omega)$  and  $Q(\omega)$ , can be calculated. Table 10.1 gives the first 12 coefficients of the discrete low-pass filter  $p(n)$  that are the impulse response of  $P(\omega)$  useful for the wavelet series decomposition. The coefficients of the

**TABLE 10.1** Low-Pass Filter  $p(k)$  of the Lemarie–Battle Wavelet Basis Associated with the Cubic B-Spline

$k$	$p(k)$	$q(k)$	$k$	$p(k)$	$q(k)$
0	0.542	-0.189	6	0.012	0.005
1	0.307	0.099	7	-0.013	0.054
2	-0.035	0.312	8	0.006	0.027
3	-0.078	0.099	9	0.006	0.018
4	0.023	-0.189	10	-0.003	0.017
5	-0.030	-0.161	11	-0.002	0.000

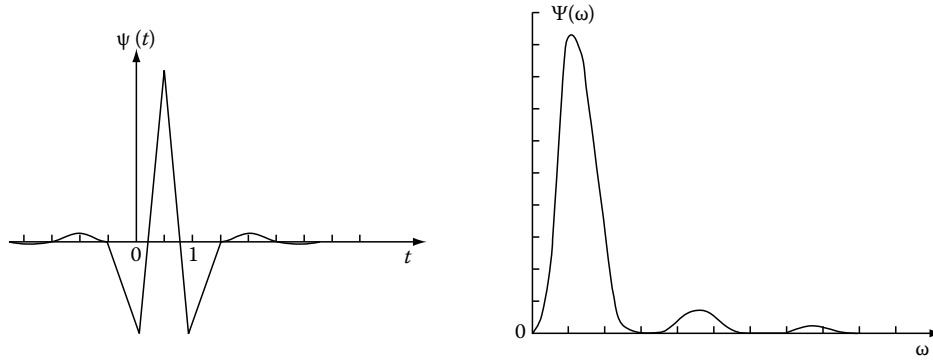


**FIGURE 10.16** Lemarie–Battle wavelet and its Fourier transform associated with the second order B-spline. (From Sheng, Y. et al. *Opt. Eng.*, 31, 1840, 1992. With permission.)

high-pass filter  $q(n)$  obtained from the low-pass filter  $p(n)$  with Equation 10.133 are also given.

Figure 10.16 shows the Lemarie–Battle wavelet  $\psi(t)$  and its Fourier transform  $\Psi(\omega)$ , which is given by Equation 10.133. The wavelet is associated to the linear spline of degree  $m = 1$ . Hence, the wavelet consists of the straight line segments between the discrete nodes. When  $m$  increases the Lemarie–Battle scaling function and wavelet associated to high order B-splines become smoother. The Lemarie–Battle wavelet is symmetrical to  $t = 1/2$  and has no compact support. The wavelet  $\psi(t)$  decays slowly with time  $t$ .

The square modulus of the low-pass filter  $|P(\omega)|^2$  is half-band. The length  $N$  of the discrete low-pass filters  $p(n)$  is to be chosen first. The discrete high-pass filters  $q(n)$  has the same length of  $N$ . The low-pass filter  $p(n)$  of a compact support of length  $N$  is the FIR filter or called the  $N$ -tap filter,  $p(n) \neq 0$  only for  $n = 0, 1, \dots, N - 1$ . Its Fourier transform  $P(\omega)$  is a polynomial in  $e^{-j\omega}$  of degree  $N - 1$ , according to the definition (Equation 10.67):

$$P(\omega) = \sum_{k=0}^{N-1} p(k) \exp(-jk\omega)$$

### 10.8.3 Daubechies Bases

The Daubechies wavelet basis [13] is a family of orthonormal, compactly supported scaling and wavelet functions, that have the maximum regularity and the maximum flatness at  $\omega = 0$  and  $\omega = \pi$  for a given length of the support of the quadrature mirror filters. The Daubechies basis is not given in closed form. The decomposition and the reconstruction are implemented by iterating the discrete low-pass and high-pass filters  $p(n)$  and  $q(n)$ .

In the regularity condition (Equation 10.117),  $M > 1$  is the regularity, and  $F(e^{-j\omega})$  is a polynomial in  $e^{-j\omega}$  with real coefficients. Since  $P(\omega)$  is a polynomial in  $e^{-j\omega}$  of degree  $N - 1$ , the polynomial  $F(e^{-j\omega})$  in  $e^{-j\omega}$  is of degree  $N - 1 - M$ . The quadrature mirror filter  $P(\omega)$  and its impulse response  $p(n)$  is determined by the choice of the polynomial  $F(e^{-j\omega})$ .

We consider the square modulus relation for  $|P(\omega)|^2$ , which is, from Equation 10.117:

$$|P(\omega)|^2 = \left(\cos^2 \frac{\omega}{2}\right)^M |F(e^{-j\omega})|^2 \tag{10.134}$$

#### 10.8.3.1 Maximum Flatness Filter

The Daubechies scaling and wavelet functions are built based on the consideration for the regularity condition, (Equation 10.117), and the orthonormality, (Equation 10.106), on the quadrature mirror filter  $P(\omega)$  in the Fourier domain, expressed as

where  $|P(\omega)|^2$  should be a polynomial in  $\cos^2(\omega/2)$  and  $\sin^2(\omega/2)$  of degree  $N - 1$ . Because the polynomial  $F(e^{-j\omega})$  has real-valued coefficients,  $F^*(e^{-j\omega}) = F(e^{j\omega})$  and  $|F(e^{-j\omega})|^2$  is a symmetric polynomial and can be rewritten as a polynomial in  $\cos \omega$  or, equivalently, as a polynomial in  $\sin^2(\omega/2)$ , rewritten as  $G[\sin^2(\omega/2)]$ :

$$P(\omega) = \left(\frac{1 + e^{-j\omega}}{2}\right)^M F(e^{-j\omega})$$

$$|F(e^{-j\omega})|^2 = G\left(\sin^2 \frac{\omega}{2}\right)$$

and

which is of degree

$$|P(\omega)|^2 + |P(\omega + \pi)|^2 = 1$$

$$L = N - 1 - M \tag{10.135}$$

Introducing a variable  $y = \cos^2(\omega/2)$ , Equation 10.134 can be written as

$$\begin{aligned} |P(\omega)|^2 &= (y)^M G(1 - y) \\ |P(\omega + \pi)|^2 &= (1 - y)^M G(y) \end{aligned} \tag{10.136}$$

Combining these regularity conditions with the orthonormality condition we obtain

$$y^M G(1 - y) + (1 - y)^M G(y) = 1$$

This equation can be solved for  $G(y)$ , which is a polynomial in  $y$  of minimum degree  $M - 1$ . Daubechies chose the minimum degree for  $G(y)$  as  $L = M - 1$ . Compared with Equation 10.135, we have

$$M = N/2$$

Hence, the term  $(\cos^2(\omega/2))^M$  has the maximum value of  $M$ . The regularity  $M$  of the Daubechies scaling function is then the maximum and increases linearly with the width of their support, i.e., with the length  $N$  of the discrete filters  $p(n)$  and  $q(n)$ , because  $M = N/2$ .

In Equation 10.136 the term  $[\cos(\omega/2)]^M$  insures  $|P(\omega)|$  to have  $M$  zeros at  $\omega = \pi$ , and to have  $M$  vanishing derivatives at  $\omega = 0$ . The term  $G(\sin^2(\omega/2))$  ensures  $|P(\omega + \pi)|$  to have  $L = (M - 1)$  zeros at  $\omega = 0$ , and to have  $M - 1$  vanishing derivatives at  $\omega = \pi$ . This corresponds to the unique maximally flat magnitude response of the frequency responses of the Daubechies low-pass and high-pass filters. Daubechies solved for  $P(\omega)$  from  $|P(\omega)|^2$  by spectral factorization.

### 10.8.3.2 Daubechies Filters in Time Domain

The values of the coefficients  $p_M(n)$  for the cases  $M = 2, 3, \dots, 10$  are listed in Table 10.2, where the filter length  $N = 2M$ . For the most compact support  $M = 2$  and  $N = 4$  the discrete low-pass filter is given as

$$\begin{aligned} p(0) &= \frac{1}{4}(1 + \sqrt{3})/\sqrt{2} = 0.483 \\ p(1) &= \frac{1}{4}(3 + \sqrt{3})/\sqrt{2} = 0.836 \\ p(2) &= \frac{1}{4}(3 - \sqrt{3})/\sqrt{2} = 0.224 \\ p(3) &= \frac{1}{4}(1 - \sqrt{3})t/\sqrt{2} = -0.13 \end{aligned} \tag{10.137}$$

The discrete high-pass filter  $q(n)$  can be obtained from  $p(n)$  by the alternating flip relation

**TABLE 10.2** The Low-Pass Filter of the Daubechies Wavelet Bases with the Support of the Filter  $N = 2M$  and  $M = 2, 3, \dots, 10$

	$n$	$P_M(n)$		$n$	$P_M(n)$
$M = 2$	0	.482962913145	$M = 8$	0	.054415842243
	1	.836516303738		1	.312871590914
	2	.224143868042		2	.675630736297
$M = 3$	3	-.129409522551	3	.585354683654	
	0	.332670552950	4	-.015829105256	
	1	.806891509311	5	-.284015542962	
	2	.459877502118	6	.000472484574	
	3	-.135011020010	7	.128747426620	
$M = 4$	4	-.085441273882	8	-.017369301002	
	5	.035226291882	9	-.044088253931	
	0	.230377813309	10	.013981027917	
	1	.714846570553	11	.008746094047	
	2	.630880767930	12	-.004870352993	
	3	-.027983769417	13	-.000391740373	
	4	-.187034811719	14	.000675449406	
$M = 5$	5	.030841381836	15	-.000117476784	
	6	.032883011667	$M = 9$	0	.038077947364
	7	-.010597401785	1	.243834674613	
	0	.160102397974	2	.604823123690	
	1	.603829269797	3	.657288078051	
	2	.724308528438	4	.133197385825	
	3	.138428145901	5	-.293273783279	
	4	-.242294887066	6	-.096840783223	
	5	-.032244869585	7	.148540749338	
$M = 6$	6	.077571493840	8	.030725681479	
	7	-.006241490213	9	-.067632829061	
	8	-.012580751999	10	.000250947115	
	9	.003335725285	11	.022361662124	
	0	.111540743350	12	-.004723204758	
	1	.494623890398	13	-.004281503682	
	2	.751133908021	14	.001847646883	
	3	.315250351709	15	.000230385764	
	4	-.226264693965	16	-.000251963189	
	5	-.129766867567	17	.000039347320	
	6	.097501605587	$M = 10$	0	.026670057901
$M = 7$	7	.027522865530	1	.188176800078	
	8	-.031582039318	2	.527201188932	
	9	.000553842201	3	.688459039454	
	10	.004777257511	4	.281172343661	
	11	-.001077301085	5	-.249846424327	
	0	.007852054085	6	-.195946274377	
	1	.396539319482	7	.127369340336	
	2	.729132090846	8	.093057364604	
	3	.469782287405	9	-.071394147166	
	4	-.143906003929	10	-.029457536822	
	5	-.224036184994	11	.033212674059	
	6	.071309219267	12	.003606553567	
	7	.080612609151	13	-.010733175483	
8	-.038029936935	14	.001395351747		
9	-.016574541631	15	.001992405295		
10	.012550998556	16	-.000685856695		
11	.000429577973	17	-.000116466855		
12	-.001801640704	18	.000093588670		
13	.000353713800	19	-.000013264203		

Source: Daubechies, I., *Commun. on Pure and Appl. Math.*, XLI, 909, 1988. With permission.

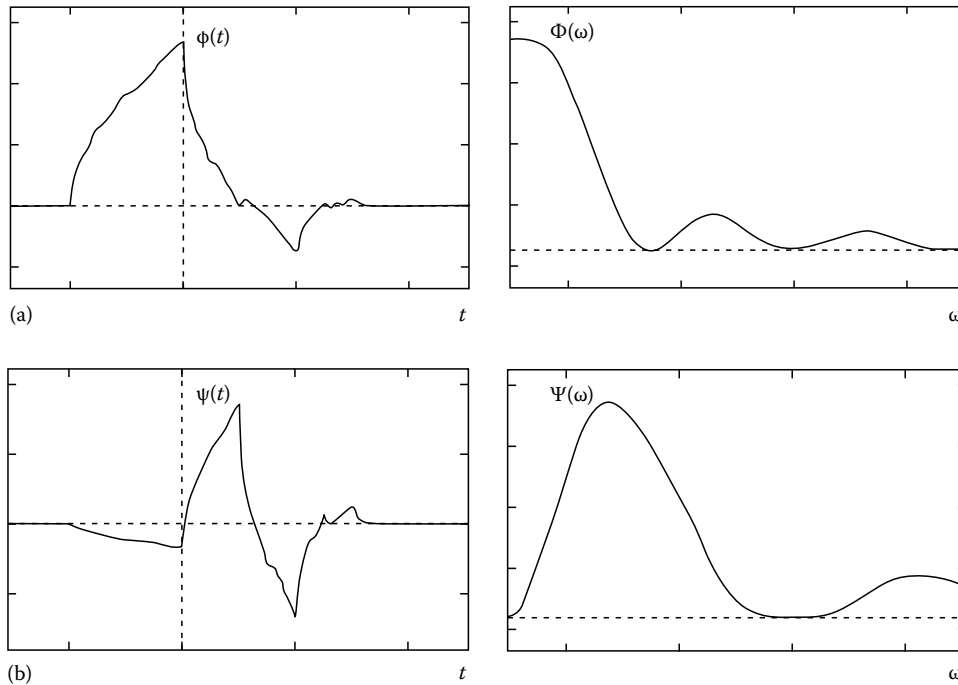


**FIGURE 10.17** Daubechies scaling function (a) and wavelet (b) and their Fourier transforms with the compact support  $N = 4$ . (From Daubechies, I., *Commun. on Pure and Appl. Math.*, XLI, 909, 1988. With permission.)

$$q(n) = (-1)^n p(N - 1 - n)$$

where  $N$  is an even number and  $n = 0, 1, 2, \dots, N$ .

It is easy to verify that the translates of  $p(n)$  and  $q(n)$  with double integer steps are orthonormal, respectively. Figure 10.17a and b show the Daubechies scaling function and wavelet with compact support  $M=2$  and  $N=4$  and their Fourier transforms. The scaling function is generated from the quadrature mirror filter  $p(n)$  given with the method of reconstruction discussed in Section 10.5.5. Those functions have the most compact support, but are neither smooth nor regular. When the length of the filters  $p(n)$  and  $q(n)$  increase the Daubechies scaling functions and wavelets become smoother and more regular, at the cost of larger number of nonzero coefficients of  $p(n)$  and  $q(n)$  that results in large support widths for the scaling functions and wavelets.

Another important feature of Figure 10.17 is the lack of any symmetry or antisymmetry axis for the Daubechies scaling function and wavelet. Daubechies has shown that it is impossible to obtain an orthonormal and compactly supported wavelet that is either symmetric or antisymmetric around any axis, except for the trivial Haar wavelets.

## 10.9 Fast Wavelet Transform

The wavelet transform is not ready for explicit calculus. Only for few simple functions the wavelet transform have analytical solutions as given in Section 10.2.4. For most functions the wavelet

transforms must be computed in the digital computer. In the multiresolution analysis framework, the orthonormal wavelet transform is implemented by iterating the quadrature mirror filters in the tree algorithm. In the computer both the function to be transformed and the iterated quadrature mirror filters are discrete. The orthonormal wavelet series decomposition and reconstruction are essentially discrete. The wavelet tree algorithm permits the fast wavelet transform. One of the main reasons for the recent success of the wavelet transform is the existence of this fast wavelet transform algorithm which only requires a number  $O(L)$  of the operations where  $L$  is the size of the initial data.

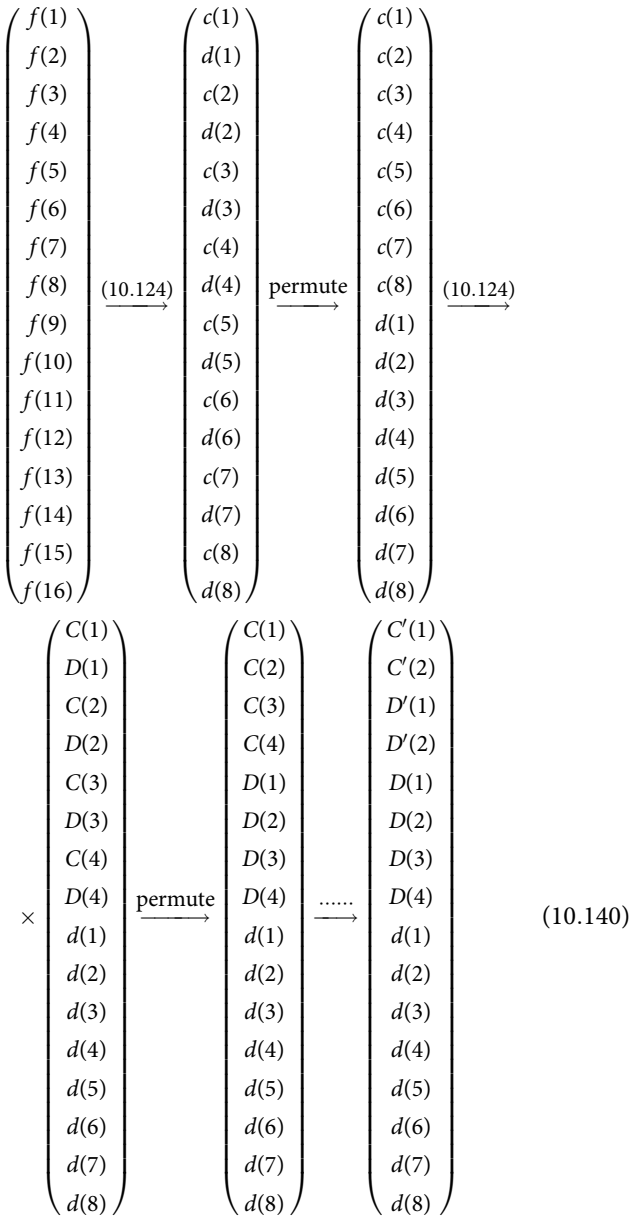
The discrete wavelet decomposition and reconstruction algorithms are discussed in Sections 10.5.4 and 10.5.5. In this section we implement the algorithm by matrix operations and introduce the discrete wavelet matrix and we discuss the number of operations, the time-bandwidth product of the wavelet transform output.

### 10.9.1 Wavelet Matrices

The discrete orthonormal wavelet transform is a linear operation. Given a vector of data that has a length of an integer power of two, the wavelet decomposition and reconstruction are numerically computed by recurring two conjugate quadrature mirror filters  $p(n)$  and  $q(n)$  that are the FIR filters compactly supported with a finite number  $N$  of nonzero coefficients. The degree of the Laurent polynomial of the transfer function of



side of Equation 10.138 as shown in the following diagram with  $N = 16$ .



If the length of the data vector  $N > 16$  there would be more stages of applying (Equation 10.140) and permuting. The final output vector will always be a vector with two approximation coefficients  $C(1)$  and  $C(2)$  at the lowest resolution and a hierarchy of the wavelet coefficients  $D(1), D(2)$  for the lowest resolution and  $D(1) - D(4)$  for higher resolution and  $d(1) - d(8)$  for still higher resolution, etc. Notice that once the wavelet coefficients  $d$ 's are generated, they simply propagate through to all subsequent stages without further computation.

The discrete wavelet reconstruction can be computed by simple reversed procedure, starting with the lowest resolution level

in the hierarchy and working from right to left with the diagram (Equation 10.140). The inverse wavelet transform matrix (Equation 10.139), is used instead of Equation 10.138.

The above wavelet transform matrix method shows a clear figure of the discrete wavelet decomposition and reconstruction. The wavelet transform can also be computed with other methods iterating the discrete filters in the tree algorithms without using the wavelet transform matrix.

### 10.9.2 Number of Operations

We consider now the number of operations required for the discrete orthonormal wavelet transform of a vector of data. Let  $L$  be the length of the data vector and  $N$  the length of the FIR filters  $p(n)$  and  $q(n)$ . As the wavelet transform is a local operation usually  $N \ll L$ . At the highest frequency band the first stage of decomposition requires  $2NL$  multiplies and adds. In the tree algorithm at the next coarser frequency band the vector length of the discrete approximation  $c(n)$  is reduced to  $N/2$ . Therefore the next stage of decomposition requires  $2(NL/2)$  multiplies and adds. The total number of operations of the orthonormal wavelet decomposition is then

$$2 \left( NL + \frac{NL}{2} + \frac{NL}{4} + \dots \right) = 2NL \left( 1 + \frac{1}{2} + \frac{1}{4} + \dots \right) \approx 4NL$$

As  $N$  is a small number, the orthonormal wavelet transform requires only an  $O(L)$  computations. This is even faster than the FFT for the Fourier transform, that requires  $O(L \log_2 L)$  multiplies and adds, due to its global nature.

### 10.9.3 Time-Bandwidth Product

The wavelet transform is a mapping of a function of time, in 1-D case, to the 2-D timescale joint representation. At first glance the time-bandwidth product of the wavelet transform output would be squared of that of the signal. In the multiresolution analysis framework, however, the size of the data vector is reduced by a factor of two in moving from one frequency band to the next coarser resolution frequency band. The time-bandwidth product also is reduced by a factor of two. If the original data vector  $c_0(n)$  has  $L$  samples, in the tree algorithm for the wavelet decomposition shown in Figure 10.11 the first stage wavelet coefficients outputs  $d_1(n)$  has  $L/2$  samples, that of the second stage has  $L/4$  samples etc. Let the length of the data vector  $L = 2^K$ , the total time-bandwidth product of the wavelet decomposition including all the wavelet coefficients  $d_i(n)$  with  $i = 1, 2, \dots, K - 1$  and the lowest resolution approximation  $c_{k-1}(n)$  is equal to the original data vector length

$$L \left( \frac{1}{2} + \frac{1}{4} + \dots \right) \approx L$$



## 10.10 Applications of the Wavelet Transform

In this section we present some popular applications of the wavelet transform for multiresolution transient signal analysis and detection, image edge detection, and compression with some simple examples.

### 10.10.1 Multiresolution Analysis of Power System Signal

In this section we show an example of multiresolution analysis for a simple transient signal. Transient signals in the power system are nonstationary time-varying voltage and current that can occur as a result of changes in the electrical configuration and in industrial and residential loads, and of a variety of disturbances on transmission lines, including capacitor switching, lightning strikes and short-circuits. The waveform data of the transient signals are captured by digital transient recorders. Analysis and classification of the power system disturbance can help to provide more stability and efficiency in power delivery by switching transmission lines to supply additional current or switching capacitor banks to balance inductive loads, and help to prevent system failures.

The power system transient signals contain a range of frequencies from a few hertz to impulse components with microsecond rise times. The normal 60 Hz sinusoidal voltage and current waveforms are interrupted or superimposed with impulses, oscillations, and reflected waves. An experienced power engineer can visually analyze the waveform data in order to determine the type of system disturbance. However, the Fourier analysis with its global operation nature is not as appropriate for the transient signals as the timescale joint representation provided by the wavelet transform.

#### 10.10.1.1 Multiresolution Wavelet Decomposition of Transient Signal

The wavelet transform provides a decomposition of power system transient signals into meaningful components in multiple frequency bands, and the digital wavelet transform is computationally efficient [18]. Figure 10.1 in Section 10.1 shows the wavelet components in the multiple frequency bands. At the top is the input voltage transient signal. There is a disturbance of a capacitor bank switching on a three-phase transmission line. Below the first line are the wavelet components as a function of the scale and time shift. The scales of the discrete wavelets increase by a factor of two successively from SCALE 1 to SCALE 64, corresponding to the dyadic frequency bands. The vertical axis in each discrete scale is the normalized magnitude of the signal component in voltage. The three impulses in high frequency band SCALE 1 correspond to the successive closing of each phase of the three-phase capacitor bank. SCALE 2 and SCALE 4 are the bands of system response frequencies. SCALE 4 contains most energy from the resonant frequency caused by the addition

of a capacitor bank to a primarily inductive circuit. The times of occurrence of all those components can be determined on the time axis. SCALE 64 contains only the basic signal of continuous 60 Hz.

The wavelet analysis decomposes the power system transient into the meaningful components, whose modulus maxima then can be used for further classification. The nonorthogonal multiresolution analysis wavelets with FIR quadratic spline wavelet filters were used in this example of application.

#### 10.10.1.2 Shift Invariance

One problem in this application and many other applications with the dyadic wavelet transform is the lack of shift invariance. The dyadic wavelet transform is not shift invariant. In the wavelet decomposition the analysis low-pass and high-pass filters are double shifted by two as described by Equation 10.60. If the input signal is shifted by one sampling interval distance, then the output of the dyadic wavelet transform is not simple shifted by the same distance, but the values of the wavelet coefficients would be changed dramatically. This aliasing error is caused by the down-sampled by factor of two in the multiresolution signal analysis and is discussed in Section 10.6.2. This is a disadvantage of the dyadic wavelet transform, because many applications such as real-time signal analysis and pattern recognition require shift invariant wavelet transform. In the above example of application, the orthonormal quadrature mirror filters has been found sensitive to translations of the input. Hence, nonorthonormal quadratic spline wavelets have been used.

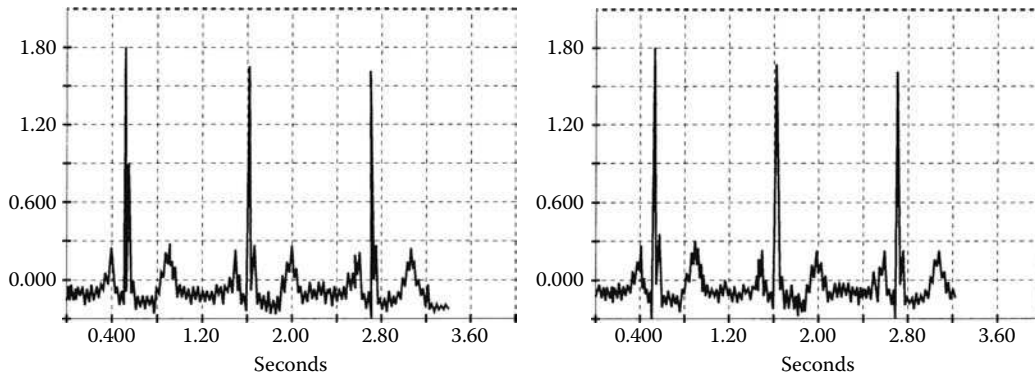
### 10.10.2 Signal Detection

The detection of weak signals embedded in a stronger stationary stochastic process, such as the detection of radar and sonar signals in zero-mean Gaussian white noise, is a well-studied problem. If the shape of the expected signal is known, the correlation and the matched filter provide optimum solution in terms of the signal-to-noise ratio in the output correlation.

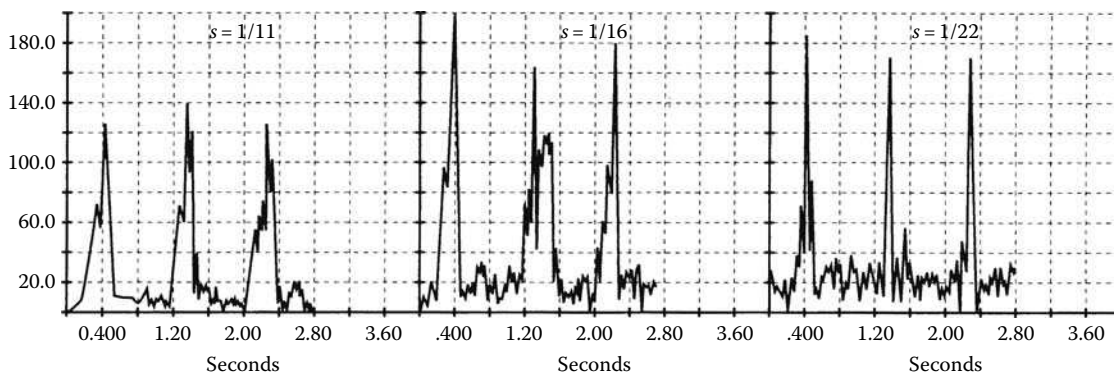
In the detection of speech or biomedical signals, the exact shape of the signal is unknown. The Fourier spectrum analysis could be effective for those applications, only when the expected signal has spectral features that are clearly distinguished from the noise. The effectiveness of the Fourier spectrum analysis is generally proportional to the ratio of the signal to noise energy. For short-time, low-energy transients, the change in the Fourier spectrum is not easily detected. Such transient signals can be detected by the wavelet transform. An example of electrocardiogram signal detection follows [19].

Figure 10.18 shows the clinical electrocardiogram with normal QRS peaks and an abnormality called ventricular late potentials (VLP) right after the second QRS peak. The amplitude of the VLP signal is about 5% of the QRS peaks. Its duration was about 0.1 s, or a little less than 10% of the pulse period. The VLP's are weak signals, swamped by noise, and they occur somewhat randomly.

Figure 10.19 shows the magnitude of continuous wavelet transform with the cos-Gaussian wavelets of scale  $s=1/11$ ,



**FIGURE 10.18** (Left) Normal electrocardiogram, (right) electrocardiogram with VLP abnormality. (From Combes, J. M. et al., *Wavelets*, 2nd ed. Springer-Verlag, Berlin, 1990. With permission.)



**FIGURE 10.19** Wavelet transform of the abnormal electrocardiogram for scale factor  $s = 11, 16, 22$ . The bulge to the right of the second QRS peak for  $s = 1/16$  indicates the presence of the VLP. (From Combes, J. M. et al., *Wavelets*, 2nd ed. Springer-Verlag, Berlin, 1990. With permission.)

1/16 and 1/22. The peak after the second QRS spike observed for  $s = 1/16$  is very noticeable and gives a clear indication of the presence of the VLP.

### 10.10.3 Image Edge Detection

Edges and boundaries, representing shapes of objects, intersections between surfaces and between textures, are among the most important features of images, useful for image segmentation and pattern recognition. An edge in image is a set of locally connected pixels, which are characterized by sharp intensity variation in their neighborhood in one direction, i.e., the maximum of the gradient of intensity, and smooth intensity variation in the direction perpendicular to the gradient. Edges are local features of an image.

The wavelet transform is a local operation. The wavelet transform of a constant is equal to zero and the wavelet transform of a polynomial function of degree  $n$  is also equal to zero if the Fourier transform of the wavelet has the zero of order  $n + 1$  about the frequency  $\omega = 0$ , as described in Section 10.2.4. Hence, the wavelet transform is useful for detecting singularities of functions and edges of images.

#### 10.10.3.1 Edge Detectors

The edge detectors smooth first an image at various scales and then detect sharp variation from the first- or second-order derivative of the smoothed images. The extrema of the first-order derivative correspond to the zero crossing of the second-order derivative and to the inflection points of the image.

An simple example of edge detector is the first- or second-order derivative of the Gaussian function  $g(x, y)$ . The Gaussian function  $g_s(x, y)$  is scaled by a factor  $s$ . The first- and second-order derivative, i.e., the gradient and the Laplacian, of  $g_s(x, y)$  are the Gaussian wavelets satisfying the wavelet admissible condition, as described in Section 10.2.5.

By the definition, the wavelet transform of an image  $f(x, y)$  is correlation between  $f(x, y)$  and the scaled wavelets. We derive that

$$W_f(s; x, y) = f^*(s\nabla g_s) = s\nabla(f^*g_s)(x, y)$$

where  $*$  denotes the correlation with the first-order derivative Gaussian wavelet and  $s$  is the scale factor, so that

$$W_f(x, y) = f^*(s^2\Delta^2 g_s) = s^2\Delta^2(f^*g_s)(x, y)$$

with the second-order derivative Gaussian wavelet, which is the Mexican-hat wavelet. The wavelet transform is then the gradient or the Laplacian of the image smoothed by the Gaussian function  $g_s(x, y)$  at the scale  $s$ .

The local maxima of the wavelet transform with the first-derivative of Gaussian wavelet can be extracted as edges. This is the Canny edge detector. The zero-crossing of the wavelet transform with the Mexican-hat wavelet corresponds to the inflection points of the smoothed image  $f^*g_s(x, y)$ , which can be extracted as edges. This is the zero-crossing Laplacian edge detector.

### 10.10.3.2 Two-Dimensional Wavelet Transform

The wavelet transform can be easily extended to 2-D case for image processing applications. The wavelet transform of a 2-D image  $f(x, y)$  is

$$W_f(s_x, s_y; u, v) = \frac{1}{\sqrt{s_x s_y}} \iint f(x, y) \psi\left(\frac{x-u}{s_x}, \frac{y-v}{s_y}\right) dx dy$$

that is a four-dimensional function. It is reduced to a set of two-dimension functions of  $(u, v)$  with different scales, when the scale factors  $s_x = s_y = s$ . When  $\psi(x, y) = \psi(r)$  with  $r = (x^2 + y^2)^{1/2}$ , the wavelets are isotropic and have no selectivity for spatial orientation. Otherwise, the wavelet can have particular orientation. The wavelet can also be a combination of the 2-D wavelets with different particular orientations, so that the 2-D wavelet transform has orientation selectivity.

At each resolution the pair of the 1-D low-pass and high-pass filters are first applied to each row of the image, that results in a horizontally approximation image and a horizontal detail image. Then the pair of the 1-D filters are applied to each column of the two horizontally filtered images. The down-sampling by two is

applied after each filtering. The two-step filtering and down-sampling result in four subband images : (LL) for the low-pass filtered both horizontally and vertically image, (HH) for the high-pass filtered both horizontally and vertically image, (LH) for low-pass filtered in horizontal direction and high-pass filtered in vertical direction image and (HL) for high-pass filtered in vertical direction and high-pass filtered in horizontal direction image, as shown in Figure 10.20 [16].

All the four images have the half size of the input image. We put the detail images (LH), (HL) and (HH) in three respective quadrants as shown in Figure 10.21. The image (LL) is the approximation image in both horizontal and vertical directions and is down-sampled in both directions. Then, we apply the whole process of two-step filtering and down-sampling again to the image (LL) in this lower resolution level. The iteration can continue many times until, for instance, the image (LL) has only a size of  $2 \times 2$ . Figure 10.21 show a disposition of the detail images (LH), (HL) and (HH) at three resolution levels (1, 2, 3) and the approximation image (LL) at the fourth low resolution level (4). If the original image has  $L^2$  pixels at the resolution  $i = 0$ , then each image (LH), (HL) and (HH) at resolution level  $i$  has  $(L/2^i)^2$  pixels ( $i > 0$ ) The total number of pixels of the orthonormal wavelet representation is therefore still equal to  $L^2$ , as shown in Figure 10.21. The dyadic wavelet transform does not increase the volume of data. This is owing to the orthonormality of the discrete wavelet decomposition.

### 10.10.3.3 Multiscale Edges

The wavelet transform of a 2-D image for edge detection is performed at a set of dyadic scales, generating a set of detail images. Similarly to the reconstruction process described in Section 10.5.5, the detail images from the wavelet decomposition can be used to reconstruct the original image.

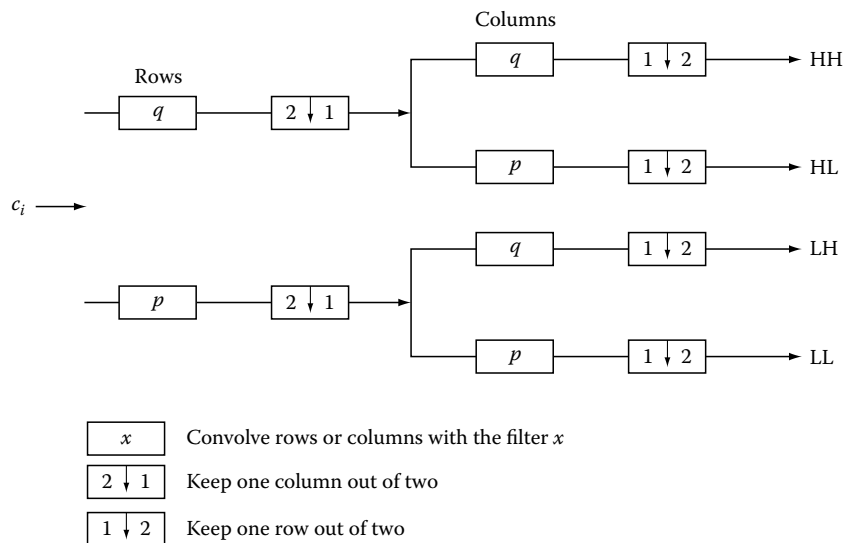


FIGURE 10.20 Schematic two-dimensional wavelet decomposition with quadrature mirror low-pass and high-pass filters  $p(n)$  and  $q(n)$ .

(LL) <sub>3</sub>	(HL) <sub>3</sub>	(HL) <sub>2</sub>	(HL) <sub>1</sub>
(LH) <sub>3</sub>	(HH) <sub>3</sub>		
(LH) <sub>2</sub>		(HH) <sub>2</sub>	
(LH) <sub>1</sub>			(HH) <sub>1</sub>

**FIGURE 10.21** Presentation of the two-dimensional wavelet decomposition. The detail images  $d_i^n$  and the approximation  $c_i$  are defined by Equations (10.9.5) and (10.9.7).

If the wavelet is the first-order derivative of the Gaussian smoothing function and we retain the modulus maxima of the wavelet components then we obtain the edge images, which correspond to the maximum variation of the smoothed image at a scale  $s$ . The multiscale edge information provided by the wavelet transform can also be used to analyze the regularity of the image function by observing the propagation of the modulus maxima from one scale to next scale. A similar approach is used to reduce the noise in the image, since the noise has different regularity than that of the image and image edges.

#### 10.10.4 Image Compression

Image compression is to use fewer bits to represent the image information for different purposes, such as image storage, image transmission, and feature extraction. The general idea behind is to remove the redundancy in an image to find more compact representation.

A popular method for image compression for removing the spatial redundancy is so-called transform coding, that represents the image in the transformation basis such that the transformation coefficients are decorrelated. We see in Section 10.5.4 that the multiresolution wavelet decomposition is projections onto subspaces spanned by scaling function basis and the wavelet basis. The projections on the scaling function basis yield approximations of the signal and the projections on the wavelet basis yield the differences between the approximations at two adjacent resolution levels. Therefore, the wavelet detail images are decorrelated and can be used for image compression. Indeed, the

detail images obtained from the wavelet transform consist of edges in the image. There is only few correlation among the values on pixels in the edge images.

One example of image compression applications is the gray-scale fingerprint image compression using the wavelet transform [20]. The fingerprint images are captured as 500 pixels per inch and 256 gray levels. The wavelet subband decomposition is accomplished by the tree algorithm described by Figure 10.20. The dominant ridge frequency in fingerprint images is in roughly  $\omega = \pi/8$  up to  $\omega = \pi/4$  bands. Because the wavelet decomposition removes the correlation among image pixels, only the wavelet coefficients with large magnitude are retained. The wavelet decomposition uses pairs of symmetric biorthogonal wavelet filters with 7 and 9 taps.

Most wavelet transform coefficients are equal or close to zero in the regions of smooth image intensity variation. After a thresholding on the wavelet coefficients the retained coefficients are subsequently coded according to a scalar quantizer and are mapped to a set of 254 symbols for Huffman encoding using the classical image coding technique. The thresholding and the Huffman coding can achieve high compression ratio.

The analysis low-pass and high-pass filters, the quantization rule and the Huffman code table are included with the compressed images, so that a decoder can reconstruct approximations of the original images by performing the inverse wavelet transform. After compression at 20:1, the reconstructed images conserve the ridge features: ridge ending or bifurcations that are definitive information useful for determination.

## References

1. D. Gabor, Theory of communication, *J. Inst. Elec. Eng.* 93, 429–457 (1946).
2. E. Wigner, On the quantum correction for thermodynamic equilibrium, *Phys. Rev.* 40, 749–759 (1932).
3. A. W. Rihaczek, *Principles of High Resolution Radar*, McGraw-Hill, New York (1969).
4. C. Gasquet and P. Witomski, *Analyse de Fourier et Applications*, Chap. XII, Masson, Paris (1990).
5. A. Harr, Zur theorie des orthogonalen funktionen systeme, *Math. Annal.* 69, 331–371 (1910).
6. R. K. Martinet, J. Morlet, and A. Grossmann, Analysis of sound patterns through wavelet transforms, *Int. J. Pattern Recogn. Artif. Intell.* 1(2), 273–302 (1987).
7. D. Marr and E. Hildreth, Theory of edge detection, *Proc. R. Soc. Lond. B* 207, 187–217 (1980).
8. I. Daubechies, The wavelet transform: Time-frequency localization and signal analysis, *IEEE Trans. Inform. Theory* 36(5), 961–1005 (1990).
9. S. G. Mallat, Multifrequency channel decompositions of images and wavelet models, *Trans. IEEE Acoust. Speech Signal Process.* ASSP-37 12, 2091–2110 (1989).
10. P. J. Burt and E. H. Adelson, The Laplacian pyramid as a compact image code, *IEEE Trans. Commun.* 31(4), 532–540 (1983).

11. A. N. Akansu and R. A. Haddad, *Multiresolution Signal Decomposition*, Academic, Boston, MA (1992).
12. G. Strang, Wavelets and dilation equations: A brief introduction, *SIAM Rev.* 31(4), 614–627 (1989).
13. I. Daubechies, Orthonormal bases of compactly supported wavelets, *Commun. Pure Appl. Math.* XLI, 909–996 (1988).
14. C. K. Chui, Ed., *Wavelets: A Tutorial Theory and Applications*, Vol. 2, Academic, Boston, MA (1992).
15. P. G. Lemarie and Y. Meyer, Ondelettes et bases Hilbertiennes, *Rev. Mat. Iberoam.* 1Y2, 2 (1986).
16. S. Mallat, A theory for multiresolution signal decomposition: The wavelet representation, *IEEE Trans. Pattern Anl. Machine Intell.* PAMI-31 11, 674–693 (1989).
17. W. H. Press et al., *Numerical Recipes*, 2nd edn., Chap 13, Cambridge, London, U.K. (1992).
18. D. C. Robertson, O. I. Camps, and J. Mayer, Wavelets and power system transients: Feature detection and classification, *Proc. SPIE* 2242, 474–487 (1994).
19. J. M. Combes, A. Grosmann, and P. Tchamitchian, Eds., *Wavelets*, 2nd edn., Springer-Verlag, Berlin, Germany (1990).
20. T. Hopper, Compression of gray-scale fingerprint images, *Proc. SPIE* 2242, 180–187 (1994).
21. Y. Sheng, D. Roberge, and H. Szu, Optical wavelet transform, *Opt. Eng.* 31, 1840–1845 (1992).
22. H. Szu, Y. Sheng, and J. Chen, The wavelet transform as a bank of matched filters, *Appl. Opt.* 31(17), 3267–3277 (1992).
23. M. O. Freeman, Wavelet signal representations with important advantages, *Opt. & Photonics News* 4(8), 8–14, August (1995).
24. G. Strang and T. Hguyen, *Wavelets and Filter Banks*, Cambridge-Wellesley, Wellesley, MA (1996).
25. R. L. Allen et al., Laplacian and orthogonal wavelet pyramid decomposition in coarse-to-fine registration, *IEEE Trans. Signal Process.* 41(12), 3536–3540 (1993).

## Finite Hankel Transforms, Legendre Transforms, Jacobi and Gegenbauer Transforms, and Laguerre and Hermite Transforms

---

11.1	Finite Hankel Transforms.....	11-1
	Introduction • Definition of the Finite Hankel Transform and Examples • Basic Operational Properties • Applications of Finite Hankel Transforms • Additional Relations	
11.2	Legendre Transforms.....	11-5
	Introduction • Definition of the Legendre Transform and Examples • Basic Operational Properties of Legendre Transforms • Applications of Legendre Transforms to Boundary Value Problems • Additional Relations	
11.3	Jacobi and Gegenbauer Transforms.....	11-11
	Introduction • Definition of the Jacobi Transform and Examples • Basic Operational Properties • Applications of Jacobi Transforms to the Generalized Heat Conduction Problem • The Gegenbauer Transform and Its Basic Operational Properties • Application of the Gegenbauer Transform	
11.4	Laguerre Transforms.....	11-16
	Introduction • Definition of the Laguerre Transform and Examples • Basic Operational Properties • Applications of Laguerre Transforms • Additional Relations	
11.5	Hermite Transforms.....	11-21
	Introduction • Definition of the Hermite Transform and Examples • Basic Operational Properties • Additional Relations	
	References.....	11-27

Lokenath Debnath  
*University of Texas-Pan American*

### 11.1 Finite Hankel Transforms

---

#### 11.1.1 Introduction

This chapter is devoted to the study of the *finite Hankel transform* and its basic operational properties. The usefulness of this transform is shown by solving several initial-boundary problems of physical interest. The method of finite Hankel transforms was first introduced by Sneddon (1946).

#### 11.1.2 Definition of the Finite Hankel Transform and Examples

Just as problems on finite intervals  $-a < x < a$  lead to Fourier series, problems on finite intervals  $0 < r < a$ , where  $r$  is the cylindrical polar coordinate, lead to the *Fourier-Bessel series* representation of a function  $f(r)$ , which can be stated in the following theorem.

---

#### THEOREM 11.1

If  $f(r)$  is defined in  $0 \leq r \leq a$  and

$$\tilde{f}_n(k_i) = \int_0^a r f(r) J_n(rk_i) dr, \quad (11.1)$$

then  $f(r)$  can be represented by the Fourier-Bessel series as

$$f(r) = \frac{2}{a^2} \sum_{i=1}^{\infty} \tilde{f}_n(k_i) \frac{J_n(rk_i)}{J_{n+1}^2(ak_i)}, \quad (11.2)$$

where  $k_i (0 < k_1 < k_2 < \dots)$  are the roots of the equation  $J_n(ak_i) = 0$ , which means

$$J'_n(ak_i) = J_{n-1}(ak_i) = -J_{n+1}(ak_i), \quad (11.3)$$

due to the standard recurrence relations among  $J'_n(x), J_{n-1}(x)$ , and  $J_{n+1}(x)$ .

*Proof* We write the Bessel series expansion of  $f(r)$  formally as

$$f(r) = \sum_{i=1}^{\infty} c_i J_n(rk_i), \quad (11.4)$$

where the summation is taken over all the positive zeros  $k_1, k_2, \dots$  of the Bessel function  $J_n(ak_i)$ . Multiplying Equation 11.4 by  $rJ'_n(rk_i)$ , integrating both sides of the result from 0 to  $a$ , and then using the orthogonal property of the Bessel functions, we obtain

$$\int_0^a rf(r)J_n(rk_i)dr = c_i \int_0^a rJ_n^2(rk_i)dr.$$

Or,

$$\tilde{f}_n(k_i) = \frac{a^2 c_i}{2} J_{n+1}^2(ak_i),$$

hence, we obtain

$$c_i = \frac{2}{a^2} \frac{\tilde{f}_n(k_i)}{J_{n+1}^2(ak_i)}. \quad (11.5)$$

Substituting the value of  $c_i$  into Equation 11.4 gives Equation 11.2.

**Definition 11.1:** The finite Hankel transform of order  $n$  of a function  $f(r)$  is denoted by  $\mathcal{H}_n\{f(r)\} = \tilde{f}_n(k_i)$  and is defined by

$$\mathcal{H}_n\{f(r)\} = \tilde{f}_n(k_i) = \int_0^a rf(r)J_n(rk_i)dr. \quad (11.6)$$

The inverse finite Hankel transform is then defined by

$$\mathcal{H}_n^{-1}\{\tilde{f}_n(k_i)\} = f(r) = \frac{2}{a^2} \sum_{i=1}^{\infty} \tilde{f}_n(k_i) \frac{J_n(rk_i)}{J_{n+1}^2(ak_i)}, \quad (11.7)$$

where the summation is taken over all positive roots of  $J_n(ak) = 0$ .

The zero-order finite Hankel transform and its inverse are defined by

$$\mathcal{H}_0\{f(r)\} = \tilde{f}_0(k_i) = \int_0^a r f(r)J_0(rk_i)dr, \quad (11.8)$$

$$\mathcal{H}_0^{-1}\{\tilde{f}_0(k_i)\} = f(r) = \frac{2}{a^2} \sum_{i=1}^{\infty} \tilde{f}_0(k_i) \frac{J_0(rk_i)}{J_1^2(ak_i)}, \quad (11.9)$$

where the summation is taken over the positive roots of  $J_0(ak) = 0$ .

Similarly, the first-order finite Hankel transform and its inverse are

$$\mathcal{H}_1\{f(r)\} = \tilde{f}_1(k_i) = \int_0^a rf(r)J_1(rk_i)dr, \quad (11.10)$$

$$\mathcal{H}_1^{-1}\{\tilde{f}_1(k_i)\} = f(r) = \frac{2}{a^2} \sum_{i=1}^{\infty} \tilde{f}_1(k_i) \frac{J_1(rk_i)}{J_2^2(ak_i)}, \quad (11.11)$$

where  $k_i$  is chosen as a positive root of  $J_1(ak) = 0$ . ■

We now give examples of *finite Hankel transforms* of some functions.

### Example 11.1

If  $f(r) = r^n$ , then

$$\mathcal{H}_n\{r^n\} = \int_0^a r^{n+1} J_n(rk_i)dr = \frac{a^{n+1}}{k_i} J_{n+1}(ak_i). \quad (11.12)$$

When  $n = 0$ ,

$$\mathcal{H}_0\{1\} = \frac{a}{k_i} J_1(ak_i). \quad (11.13)$$

■

### Example 11.2

If  $f(r) = (a^2 - r^2)$ , then

$$\mathcal{H}_0\{(a^2 - r^2)\} = \int_0^a r(a^2 - r^2)J_0(ak_i)dr = \frac{4a}{k_i^3} J_1(ak_i) - \frac{2a^2}{k_i^2} J_0(ak_i).$$

Since  $k_i$  are the roots of  $J_0(ak) = 0$ , we find

$$\mathcal{H}_0\{(a^2 - r^2)\} = \frac{4a}{k_i^3} J_1(ak_i). \quad (11.14)$$

■

## 11.1.3 Basic Operational Properties

We state the following operational properties of *finite Hankel transforms*:

$$\mathcal{H}_n\{f'(r)\} = \frac{k_i}{2n} [(n-1)\mathcal{H}_{n+1}\{f(r)\} - (n+1)\mathcal{H}_{n-1}\{f(r)\}], n \geq 1, \quad (11.15)$$

provided  $f(r)$  is finite at  $r = 0$ .

When  $n = 1$ , we obtain the finite Hankel transform of derivatives

$$\mathcal{H}_1\{f'(r)\} = -k_i \mathcal{H}_0\{f(r)\} = -k_i \tilde{f}_0(k_i). \quad (11.16)$$

$$\mathcal{H}_n \left[ \frac{1}{r} \frac{d}{dr} \{r f'(r)\} - \frac{n^2}{r^2} f(r) \right] = -k_i^2 \tilde{f}_n(k_i) - a k_i f(a) J'_n(a k_i). \quad (11.17)$$

When  $n = 0$

$$\mathcal{H}_0 \left[ f''(r) + \frac{1}{r} f'(r) \right] = -k_i^2 \tilde{f}_0(k_i) + a k_i f(a) J_1(a k_i). \quad (11.18)$$

If  $n = 1$ , Equation 11.17 becomes

$$\mathcal{H}_1 \left[ f''(r) + \frac{1}{r} f'(r) - \frac{1}{r^2} f(r) \right] = -k_i^2 \tilde{f}_1(k_i) - a k_i f(a) J'_1(a k_i). \quad (11.19)$$

Results (Equations 11.18 and 11.19) are very useful for finding solutions of differential equations in cylindrical polar coordinates.

The proofs of the above results are elementary exercises for the reader.

### 11.1.4 Applications of Finite Hankel Transforms

#### Example 11.3 (Temperature Distribution in a Long Circular Cylinder)

Find the solution of the axisymmetric heat conduction equation

$$\frac{\partial u}{\partial t} = \kappa \left( \frac{\partial^2 u}{\partial r^2} + \frac{1}{r} \frac{\partial u}{\partial r} \right), \quad 0 \leq r \leq a, t > 0 \quad (11.20)$$

with the boundary and initial conditions

$$u(r, t) = f(t) \quad \text{on} \quad r = a, t > 0 \quad (11.21)$$

$$u(r, 0) = 0, \quad \text{on} \quad 0 \leq r \leq a. \quad (11.22)$$

Application of the *finite Hankel transform* defined by

$$\tilde{u}(k_i, t) = \mathcal{H}_0\{u(r, t)\} = \int_0^a r J_0(r k_i) u(r, t) dr, \quad (11.23)$$

yields the given system with the boundary condition

$$\begin{aligned} \tilde{u}_t + \kappa k_i^2 \tilde{u} &= \kappa a k_i J_1(a k_i) f(t), \\ \tilde{u}(k_i, 0) &= 0. \end{aligned} \quad (11.24a,b)$$

The solution of the first-order system is

$$\tilde{u}(k_i, t) = \kappa a k_i J_1(a k_i) \int_0^t f(\tau) \exp\{-\kappa k_i^2(t - \tau)\} d\tau \quad (11.25)$$

The inverse transform gives the formal solution

$$u(r, t) = \left( \frac{2\kappa}{a} \right) \sum_{i=1}^{\infty} \frac{k_i J_0(r k_i)}{J_1(a k_i)} \int_0^t f(\tau) \exp\{-\kappa k_i^2(t - \tau)\} d\tau. \quad (11.26)$$

In particular, if  $f(t) = T_0 = \text{constant}$ ,

$$u(r, t) = \left( \frac{2T_0}{a} \right) \sum_{i=1}^{\infty} \frac{J_0(r k_i)}{k_i J_1(a k_i)} [1 - \exp(-\kappa k_i^2 t)]. \quad (11.27)$$

Using the inverse version of Equation 11.7 gives the final solution

$$u(r, t) = T_0 - \left( \frac{2T_0}{a} \right) \sum_{i=1}^{\infty} \frac{J_0(r k_i)}{k_i J_1(a k_i)} \exp(-\kappa k_i^2 t). \quad (11.28)$$

This solution representing the temperature distribution consists of the steady-state term, and the transient term which decays to zero as  $t \rightarrow \infty$ . Consequently, the steady temperature is attained in the limit as  $t \rightarrow \infty$ . ■

#### Example 11.4 (Unsteady Viscous Flow in a Rotating Long Circular Cylinder)

The axisymmetric unsteady motion of a viscous fluid in an infinitely long circular cylinder of radius  $a$  is governed by

$$u_t = \nu \left( u_{rr} + \frac{1}{r} u_r - \frac{u}{r^2} \right), \quad 0 \leq r \leq a, \quad t > 0, \quad (11.29)$$

where  $u = u(r, t)$  is the tangential fluid velocity and  $\nu$  is the constant kinematic viscosity of the fluid.

The cylinder is initially at rest at  $t = 0$ , and it is then allowed to rotate with constant angular velocity  $\Omega$ . Thus, the boundary and initial conditions are

$$u(r, t) = a\Omega \quad \text{on} \quad r = a, t > 0, \quad (11.30)$$

$$u(r, t) = 0 \quad \text{at} \quad t = 0 \quad \text{for} \quad 0 < r < a. \quad (11.31)$$

We solve the problem by using the joint *Laplace* and the *finite Hankel transform* of order one defined by

$$\tilde{\tilde{u}}(k_i, s) = \int_0^{\infty} e^{-st} dt \int_0^a r J_1(k_i r) u(r, t) dr, \quad (11.32)$$

where  $k_i$  are the positive roots of  $J_1(a k_i) = 0$ .

Application of the joint transform gives

$$s \tilde{\tilde{u}}(k_i, s) = -\nu k_i^2 \tilde{\tilde{u}}(k_i, s) - \frac{\nu a^2 \Omega k_i}{s} J'_1(a k_i).$$

Or,

$$\tilde{\tilde{u}}(k_i, s) = -\frac{\nu a^2 \Omega k_i J'_1(a k_i)}{s(s + \nu k_i^2)}. \quad (11.33)$$



The inverse Laplace transform gives

$$\tilde{u}(k_i, t) = -\frac{a^2 \Omega}{k_i} J_1'(ak_i) [1 - \exp(-\nu t k_i^2)]. \quad (11.34)$$

Thus, the final solution is found from Equation 11.34 by using the *inverse Hankel transform* with  $J_1'(ak_i) = -J_2(ak_i)$  in the form

$$u(r, t) = 2\Omega \sum_{i=1}^{\infty} \frac{J_1(rk_i)}{k_i J_2(ak_i)} [1 - \exp(-\nu t k_i^2)]. \quad (11.35)$$

This solution is the sum of the steady-state and the transient fluid velocities.

In view of Equation 11.12 for  $n = 1$ , we can write

$$r = \mathcal{H}_1^{-1} \left\{ \frac{a^2}{k_i} J_2(ak_i) \right\} = 2 \sum_{i=1}^{\infty} \frac{J_1(rk_i)}{k_i J_2(ak_i)}. \quad (11.36)$$

This result is used to simplify Equation 11.35 so that the final solution for  $u(r, t)$  takes the form

$$u(r, t) = r\Omega - 2\Omega \sum_{i=1}^{\infty} \frac{J_1(rk_i)}{k_i J_2(ak_i)} \exp(-\nu t k_i^2). \quad (11.37)$$

In the limit as  $t \rightarrow \infty$ , the transient velocity component decays to zero, and the ultimate steady state flow is attained in the form

$$u(r, t) = r\Omega. \quad (11.38)$$

Physically, this represents the rigid body rotation of the fluid inside the cylinder. ■

### Example 11.5 (Vibrations of a Circular Membrane)

The free symmetric vibration of a thin circular membrane of radius  $a$  is governed by the wave equation

$$u_{tt} = c^2 \left( u_{rr} + \frac{1}{r} u_r \right), \quad 0 < r < a, \quad t > 0 \quad (11.39)$$

with the initial and boundary data

$$u(r, t) = f(r), \quad \frac{\partial u}{\partial t} = g(r) \quad \text{at } t = 0 \quad \text{for } 0 < r < a, \quad (11.40a, b)$$

$$u(a, t) = 0 \quad \text{for all } t > 0. \quad (11.41)$$

Application of the zero-order *finite Hankel transform* of  $u(r, t)$  defined by Equation 11.23 in Equation 11.39 through 11.41 gives

$$\frac{d^2 \tilde{u}}{dt^2} + c^2 k_i^2 \tilde{u} = 0, \quad (11.42)$$

$$\tilde{u} = \tilde{f}(k_i) \quad \text{and} \quad \left( \frac{d\tilde{u}}{dt} \right)_{t=0} = \tilde{g}(k_i). \quad (11.43ab)$$

The solution of this system is

$$\tilde{u}(k_i, t) = \tilde{f}(k_i) \cos(ckt_i) + \frac{\tilde{g}(k_i)}{ck_i} \sin(ckt_i). \quad (11.44)$$

The inverse transform yields the formal solution

$$u(r, t) = \frac{2}{a^2} \sum_{i=1}^{\infty} f(k_i) \cos(ckt_i) \frac{J_0(rk_i)}{J_1^2(ak_i)} + \frac{2}{ca^2} \sum_{i=1}^{\infty} g(k_i) \sin(ckt_i) \frac{J_0(rk_i)}{k_i J_1^2(ak_i)}, \quad (11.45)$$

where the summation is taken over all positive roots of  $J_0(ak_i) = 0$ .

We consider a more general form of the *finite Hankel transform* associated with a more general boundary condition

$$f'(r) + h f(r) = 0 \quad \text{at } r = a, \quad (11.46)$$

where  $h$  is a constant.

We define the *finite Hankel transform* of  $f(r)$  by

$$\mathcal{H}_n \{ f(r) \} = \tilde{f}_n(k_i) = \int_0^a r J_n(rk_i) f(r) dr, \quad (11.47)$$

where  $k_i$  are the roots of the equation

$$k_i J_n'(ak_i) + h J_n(ak_i) = 0. \quad (11.48)$$

The corresponding inverse transform is given by

$$f(r) = \mathcal{H}_n^{-1} \{ \tilde{f}_n(k_i) \} = 2 \sum_{i=1}^{\infty} \frac{k_i^2 \tilde{f}_n(k_i) J_n(rk_i)}{\{ (k_i^2 + h^2) a^2 - n^2 \} J_n^2(ak_i)}. \quad (11.49)$$

This *finite Hankel transform* has the following operational property

$$\mathcal{H}_n \left[ \frac{1}{r} \frac{d}{dr} \{ r f'(r) \} - \frac{n^2}{r^2} f(r) \right] = -k_i^2 \tilde{f}_n(k_i) + a [f'(a) + h f(a)] J_n(ak_i), \quad (11.50)$$

which is, by Equation 11.48

$$= -k_i^2 \tilde{f}_n(k_i) - \frac{ak_i}{h} [f'(a) + h f(a)] J_n'(ak_i). \quad (11.51)$$

Thus, result (Equation 11.51) involves  $f'(a) + hf(a)$  as the boundary condition. ■

We apply these more general *finite Hankel transform* pairs (Equations 11.47 and 11.49) to solve the following axisymmetric initial-boundary value problem.

### Example 11.6 (Temperature Distribution of Cooling of a Circular Cylinder)

Solve the axisymmetric heat conduction problem for an infinitely long circular cylinder of radius  $r=a$  with the initial constant temperature  $T_0$ , and the cylinder cooling by radiation of heat from its boundary surface at  $r=a$  to the outside medium at zero temperature according to Newton's law of cooling, which satisfies the boundary condition

$$\frac{\partial u}{\partial r} + hu = 0 \quad \text{at } r = a, \quad t > 0, \quad (11.52)$$

where  $h$  is a constant.

The problem is governed by the axisymmetric heat conduction equation

$$u_t = \kappa \left( u_{rr} + \frac{1}{r} u_r \right), \quad 0 \leq r \leq a, \quad t > 0, \quad (11.53)$$

with the boundary condition (Equation 11.52) and the initial condition

$$u(r, 0) = T_0 \quad \text{at } t = 0, \quad \text{for } 0 < r < a. \quad (11.54)$$

Application of the zero-order *Hankel transform* (Equation 11.47) with (Equation 11.48) to the system (Equations 11.52 through 11.54) gives

$$\frac{d\tilde{u}}{dt} + \kappa k_i^2 \tilde{u} = 0, \quad t > 0 \quad (11.55)$$

$$\tilde{u}(k_i, 0) = T_0 \int_0^a r J_0(rk_i) dr = \frac{aT_0}{k_i} J_1(ak_i). \quad (11.56)$$

The solution of Equations 11.55 and 11.56 is

$$\tilde{u}(k_i, t) = \left( \frac{aT_0}{k_i} \right) J_1(ak_i) \exp(-\kappa t k_i^2). \quad (11.57)$$

The inverse transform (Equation 11.49) with  $n=0$  and  $k_i J_0'(ak_i) + h J_0(ak_i) = 0$ , that is,  $k_i J_1(ak_i) = h J_0(ak_i)$ , leads to the formal solution

$$u(r, t) = \left( \frac{2hT_0}{a} \right) \sum_{i=1}^{\infty} \frac{J_0(rk_i) \exp(-\kappa t k_i^2)}{(k_i^2 + h^2) J_0(ak_i)}, \quad (11.58)$$

where the summation is taken over all the positive roots of  $k_i J_1(ak_i) = h J_0(ak_i)$ . ■

### 11.1.5 Additional Relations

1.  $\mathcal{H}_n \left\{ \frac{J_n(\alpha r)}{J_n(\alpha a)} \right\} = \frac{ak_i}{(\alpha^2 - k_i^2)} J_n'(ak_i)$
2. If  $\mathcal{H}_n\{f(r)\}$  is the *finite Hankel transform* of  $f(r)$  defined by Equation 11.6, and if  $n > 0$ , then
  - (a)  $\mathcal{H}_n\{r^{-1}f'(r)\} = \frac{1}{2}k_i[\mathcal{H}_{n+1}\{r^{-1}f(r)\} - \mathcal{H}_{n-1}\{r^{-1}f(r)\}]$ ,
  - (b)  $\mathcal{H}_0\{r^{-1}f'(r)\} = k_i \mathcal{H}_1\{r^{-1}f(r)\} - f(a)$ .

3. If we define the *finite Hankel transform* of  $f(r)$  by

$$\mathcal{H}_n\{f(r)\} = \tilde{f}_n(k_i) = \int_a^b r f(r) A_n(rk_i) dr, \quad b > a,$$

where

$$A_n(rk_i) = J_n(rk_i)Y_n(ak_i) - Y_n(rk_i)J_n(ak_i),$$

and  $Y_n(x)$  is the Bessel function of the second kind of order  $n$ , then the inverse transform is

$$\mathcal{H}_n^{-1}\{\tilde{f}_n(k_i)\} = f(r) = \frac{\pi^2}{2} \sum_{i=1}^{\infty} \frac{k_i^2 \tilde{f}_n(k_i) A_n(rk_i) J_n^2(bk_i)}{J_n^2(ak_i) - J_n^2(bk_i)},$$

where  $k_i$  are the positive roots of  $A_n(bk_i) = 0$ .

4. For the transform defined in problem 3, then

$$\mathcal{H}_n \left[ f''(r) + \frac{1}{r} f'(r) - \frac{n^2 f(r)}{r^2} \right] = -k_i^2 \tilde{f}_n(k_i) + \frac{2}{\pi} \left[ f(b) \frac{J_n(ak_i)}{J_n(bk_i)} - f(a) \right].$$

## 11.2 Legendre Transforms

### 11.2.1 Introduction

We consider in this chapter the Legendre transform with a Legendre polynomial as kernel and discuss basic operational properties including the convolution theorem. Legendre transforms are then used to solve boundary value problems in potential theory. This chapter is based on papers by Churchill (1954) and Churchill and Dolph (1954).

### 11.2.2 Definition of the Legendre Transform and Examples

Churchill (1954) defined the *Legendre transform* of a function  $f(x)$  defined in  $-1 < x < 1$  by the integral

$$\mathcal{T}_n\{f(x)\} = \tilde{f}(n) = \int_{-1}^1 P_n(x) f(x) dx, \quad (11.59)$$

provided the integral exists and where  $P_n(x)$  is the *Legendre polynomial* of degree  $n$  ( $\geq 0$ ). Obviously  $\mathcal{T}_n$  is a linear integral transformation.

When  $x = \cos \theta$ , Equation 11.59 becomes

$$\mathcal{T}_n\{f(\cos \theta)\} = \tilde{f}(n) = \int_0^\pi P_n(\cos \theta) f(\cos \theta) \sin \theta d\theta. \quad (11.60)$$

The *inverse Legendre transform* is given by

$$f(x) = \mathcal{T}_n^{-1}\{\tilde{f}(n)\} = \sum_{n=0}^{\infty} \left(\frac{2n+1}{2}\right) \tilde{f}(n) P_n(x). \quad (11.61)$$

This follows from the expansion of any function  $f(x)$  in the form

$$f(x) = \sum_{n=0}^{\infty} a_n P_n(x), \quad (11.62)$$

where the coefficient  $a_n$  can be determined from the orthogonal property of  $P_n(x)$ . It turns out that

$$a_n = \left(\frac{2n+1}{2}\right) \int_{-1}^1 P_n(x) f(x) dx = \left(\frac{2n+1}{2}\right) \tilde{f}(n), \quad (11.63)$$

and hence, result (Equation 11.61) follows.

### Example 11.7

$$\mathcal{T}_n\{\exp(i\alpha x)\} = \left(\frac{2\pi}{\alpha}\right)^{1/2} i^n J_{n+1/2}(\alpha), \quad (11.64)$$

where  $J_\nu(x)$  is the Bessel function.

We have, by definition,

$$\mathcal{T}_n\{\exp(i\alpha x)\} = \int_{-1}^1 \exp(i\alpha x) P_n(x) dx,$$

which is, by a result in Copson (1935, p. 341),

$$= \sqrt{\frac{2\pi}{\alpha}} i^n J_{n+1/2}(\alpha).$$

Similarly,

$$\mathcal{T}_n\{\exp(\alpha x)\} = \sqrt{\frac{2\pi}{\alpha}} I_{n+1/2}(\alpha), \quad (11.65)$$

where  $I_\nu(x)$  is the modified Bessel function of the first kind.

### Example 11.8

$$\text{a. } \mathcal{T}_n\{(1-x^2)^{-1/2}\} = \pi P_n^2(0) \quad (11.66)$$

$$\text{b. } \mathcal{T}_n\left\{\frac{1}{2(t-x)}\right\} = Q_n(t), \quad |t| > 1, \quad (11.67)$$

where  $Q_n(t)$  is the Legendre function of the second kind given by

$$Q_n(t) = \frac{1}{2} \int_{-1}^1 (t-x)^{-1} P_n(x) dx.$$

These results are easy to verify with the aid of results given in Copson (1935, p. 292, 310). ■

### Example 11.9

If  $|r| \leq 1$ , then

$$\text{a. } \mathcal{T}_n\{(1-2rx+r^2)^{-1/2}\} = \frac{2r^n}{(2n+1)}, \quad (11.68)$$

$$\text{b. } \mathcal{T}_n\{1-2rx+r^2\}^{-3/2} = \frac{2r^n}{(1-r^2)}. \quad (11.69)$$

We have, from the generating function of  $P_n(x)$ ,

$$(1-2rx+r^2)^{-1/2} = \sum_{n=0}^{\infty} r^n P_n(x), \quad |r| < 1.$$

Multiplying this result by  $P_n(x)$  and using the orthogonality condition of the Legendre polynomial gives

$$\int_{-1}^1 (1-2rx+r^2)^{-1/2} P_n(x) dx = \frac{2r^n}{(2n+1)}. \quad (11.70)$$

In particular, when  $r=1$ , we obtain

$$\mathcal{T}_n\{(1-x)^{-1/2}\} = \frac{2\sqrt{2}}{(2n+1)}. \quad (11.71)$$

Differentiating Equation 11.70 with respect to  $r$  gives

$$\frac{1}{2} \int_{-1}^1 (1-2rx+r^2)^{-3/2} (2rx-2r^2) P_n(x) dx = \frac{2nr^n}{(2n+1)},$$

so that

$$-\mathcal{T}_n\{(1-2rx+r^2)^{-1/2}\} + (1-r^2) \mathcal{T}_n\{(1-2rx+r^2)^{-3/2}\} = \frac{2nr^n}{(2n+1)}.$$

Using Equation 11.68, we obtain Equation 11.69. ■

### Example 11.10

If  $|r| < 1$  and  $\alpha > 0$ , then

$$\mathcal{T}_n\left\{\int_0^r \frac{t^{\alpha-1} dt}{(1-2xt+t^2)^{1/2}}\right\} = \frac{2r^{n+\alpha}}{(2n+1)(n+\alpha)}. \quad (11.72)$$

We replace  $r$  by  $t$  in Equation 11.68 and multiply the result by  $t^{\alpha-1}$  to obtain

$$\mathcal{T}_n\{t^{\alpha-1}(1-2xt+t^2)^{-1/2}\} = \frac{2t^{n+\alpha-1}}{(2n+1)}.$$

Integrating this result on  $(0, r)$  we find Equation 11.72. ■

### Example 11.11

If  $H(x)$  is a Heaviside unit step function, then

$$\mathcal{T}_n\{H(x)\} = \begin{cases} 1, & n = 0 \\ \frac{P_{n-1}(0) - P_{n+1}(0)}{(2n+1)}, & n \geq 1 \end{cases}. \quad (11.73)$$

Obviously,

$$\mathcal{T}_n\{H(x)\} = \int_0^1 P_n(x) dx = 1 \quad \text{when } n = 0$$

However, for  $n > 1$ , we use the *recurrence relation* for  $P_n(x)$  as

$$(2n+1)P_n(x) = P'_{n+1}(x) - P'_{n-1}(x) \quad (11.74)$$

to derive

$$\begin{aligned} \mathcal{T}_n\{H(x)\} &= \frac{1}{(2n+1)} \int_0^1 [P'_{n+1}(x) - P'_{n-1}(x)] dx \\ &= \frac{1}{2n+1} [P_{n+1}(0) - P_{n-1}(0)]. \end{aligned}$$

Debnath and Harrel (1976) introduced the *associated Legendre transform* defined by

$$\mathcal{T}_{n,m}\{f(x)\} = \tilde{f}(n,m) = \int_{-1}^1 (1-x^2)^{-m/2} P_n^m(x) f(x) dx, \quad (11.75)$$

where  $P_n^m(x)$  is the *associated Legendre function* of the first kind.

The inverse transform is given by

$$f(x) = \mathcal{T}_{n,m}^{-1}\{\tilde{f}(n,m)\} = \sum_{n=0}^{\infty} \frac{(2n+1)(n-m)!}{2(n+m)!} \tilde{f}(n,m) (1-x^2)^{m/2} P_n^m(x). \quad (11.76)$$

The reader is referred to Debnath and Harrel (1976) for a detailed discussion of this transform. ■

## 11.2.3 Basic Operational Properties of Legendre Transforms

### THEOREM 11.2

If  $f'(x)$  is continuous and  $f''(x)$  is bounded and integrable in each subinterval of  $-1 \leq x \leq 1$ , and if  $\mathcal{T}_n\{f(x)\}$  exists and

$$\lim_{|x| \rightarrow 1} (1-x^2)f(x) = \lim_{|x| \rightarrow 1} (1-x^2)f'(x) = 0, \quad (11.77)$$

then

$$\mathcal{T}_n\{R[f(x)]\} = -n(n+1)\tilde{f}(n), \quad (11.78)$$

where  $R[f(x)]$  is a differential form given by

$$R[f(x)] = \frac{d}{dx} \left[ (1-x^2) \frac{d}{dx} f(x) \right], \quad n > 0. \quad (11.79)$$

*Proof* We have, by definition,

$$\mathcal{T}_n\{R[f(x)]\} = \int_{-1}^1 \frac{d}{dx} \left[ (1-x^2) \frac{d}{dx} f(x) \right] P_n(x) dx$$

which is, by integrating by parts together with Equation 11.77,

$$= - \int_{-1}^1 (1-x^2) P_n'(x) \frac{d}{dx} f(x) dx.$$

Integrating this result by parts again, we obtain

$$\begin{aligned} \mathcal{T}_n\{R[f(x)]\} &= -[(1-x^2)P_n'(x)f(x)]_{-1}^1 \\ &\quad + \int_{-1}^1 \frac{d}{dx} [(1-x^2)P_n'(x), f(x)] dx. \end{aligned}$$

Using Equation 11.77 and the differential equation for the Legendre polynomial

$$\frac{d}{dx} \left[ (1-x^2) \frac{dy}{dx} \right] + n(n+1)y = 0, \quad (11.80)$$

we obtain the desired result

$$\mathcal{T}_n\{R[f(x)]\} = -n(n+1)\tilde{f}(n).$$

We may extend this result to evaluate the Legendre transforms of the differential forms  $R^2[f(x)]$ ,  $R^3[f(x)]$ ,  $\dots$ ,  $R^k[f(x)]$ . ■

Clearly

$$\begin{aligned} \mathcal{T}_n\{R^2[f(x)]\} &= \mathcal{T}_n\{R[R[f(x)]]\} \\ &= -n(n+1)\mathcal{T}_n\{R[f(x)]\} = n^2(n+1)^2\tilde{f}(n), \end{aligned} \quad (11.81)$$

provided  $f'(x)$  and  $f''(x)$  satisfy the conditions of Theorem 11.2.

Similarly,

$$\mathcal{T}_n\{R^3[f(x)]\} = (-1)^3 n^3(n+1)^3\tilde{f}(n). \quad (11.82)$$

More generally, for a positive integer  $k$ ,

$$\mathcal{T}_n\{R^k[f(x)]\} = (-1)^k n^k(n+1)^k\tilde{f}(n). \quad (11.83)$$

---

**COROLLARY 11.1**

If  $\mathcal{T}_n\{R[f(x)]\} = -n(n+1)\tilde{f}(n)$ , then

$$\mathcal{T}_n\left\{\frac{1}{4}f(x) - R[f(x)]\right\} = \left(n + \frac{1}{2}\right)^2\tilde{f}(n). \quad (11.84)$$

*Proof* We replace  $n(n+1)$  by  $(n + \frac{1}{2})^2 - \frac{1}{4}$  in Equation 11.78 to obtain

$$\mathcal{T}_n\{R[f(x)]\} = -\left[\left(n + \frac{1}{2}\right)^2 - \frac{1}{4}\right]\tilde{f}(n). \quad (11.85)$$

Rearranging the terms in Equation 11.85 gives

$$\mathcal{T}_n\left\{\frac{1}{4}f(x) - R[f(x)]\right\} = \left(n + \frac{1}{2}\right)^2\tilde{f}(n).$$

In general, this result can be written as

$$\begin{aligned} &(-1)^k \mathcal{T}_n\{R^k[f(x)] - 4^{-k}f(x)\} \\ &= \sum_{r=0}^{k-1} (-1)^r \binom{k}{r} \left[4^{-r} \left(n + \frac{1}{2}\right)^{2k-2r}\right]\tilde{f}(n). \end{aligned} \quad (11.86)$$

The proof of Equation 11.86 follows from Equation 11.83 by replacing  $n(n+1)$  with  $(n + \frac{1}{2})^2 - \frac{1}{4}$  and using the binomial expansion. ■

**Example 11.12**

$$\mathcal{T}_n\{\log(1-x)\} = \begin{cases} 2(\log 2 - 1), & n = 0 \\ -\frac{2}{n(n+1)}, & n > 0 \end{cases}. \quad (11.87)$$

Clearly,

$$R[\log(1-x)] = \frac{d}{dx} \left[ (1-x^2) \frac{d}{dx} \log(1-x) \right] = -1.$$

Although  $\frac{d}{dx} \log(1-x)$  does not satisfy the conditions of Theorem 11.2, we integrate by parts to obtain

$$\begin{aligned} \mathcal{T}_n\{R[\log(1-x)]\} &= \int_{-1}^1 R[\log(x)]P_n(x)dx \\ &= [-(1+x)P_n(x)]_{-1}^1 + \int_{-1}^1 (1+x)P'_n(x)dx, \end{aligned}$$

which is, since  $(1+x) = -(1-x^2) \frac{d}{dx} \log(1-x)$ , and by integrating by parts,

$$= -2 + \int_{-1}^1 \log(1-x) \frac{d}{dx} [(1-x^2)P'_n(x)]dx. \quad (11.88)$$

By integrating by parts twice, result (Equation 11.88) gives

$$\mathcal{T}_n\{R[\log(1-x)]\} = -2 + \int_{-1}^1 \frac{d}{dx} \left[ (1-x^2) \frac{d}{dx} \log(1-x) \right] P_n(x)dx,$$

which is, by Equation 11.78,

$$= -2 - n(n+1)\tilde{f}(n), \quad (11.89)$$

where  $\tilde{f}(n) = \mathcal{T}_n\{\log(1-x)\}$ .

However,  $R[\log(1-x)] = -1$  so that  $\mathcal{T}_n\{R[\log(1-x)]\} = 0$  for all  $n > 0$  and hence, result (Equation 11.89) gives

$$\mathcal{T}_n[\log(1-x)] = \tilde{f}(n) = -\frac{2}{n(n+1)}.$$

On the other hand, since  $P_0(x) = 1$ , we have

$$\mathcal{T}_0\{\log(1-x)\} = \int_{-1}^1 \log(1-x)dx,$$

which is, by direct integration,

$$= -[(1-x)\{\log(1-x) - x\}]_{-1}^1 = 2(\log 2 - 1). \quad \blacksquare$$

---

**THEOREM 11.3**

If  $f(x)$  and  $f'(x)$  are piecewise continuous in  $-1 < x < 1$ ,  $R^{-1}[f(x)] = h(x)$ , and  $f(0) = \int_{-1}^1 f(x)dx = 0$ , then

$$\mathcal{T}_n^{-1} \left\{ \frac{\tilde{f}(n)}{n(n+1)} \right\} = A - \int_0^x \frac{ds}{(1-s^2)} \int_{-1}^s f(t)dt, \quad (11.90)$$

where  $A$  is an arbitrary constant of integration.

*Proof* We have

$$R[h(x)] = f(x)$$

or,

$$\frac{d}{dx} \left[ (1-x^2) \frac{d}{dx} h(x) \right] = f(x).$$

Integrating over  $(-1, x)$  gives

$$\int_{-1}^x f(t)dt = (1-x^2) \frac{d}{dx} h(x), \quad (11.91)$$

which is a continuous function of  $x$  in  $|x| < 1$  with limit zero as  $|x| \rightarrow 1$ .

Integration of Equation 11.91 gives

$$h(x) = \int_0^x \frac{ds}{(1-s^2)} \int_{-1}^s f(t)dt - A,$$

where  $A$  is an arbitrary constant. Clearly,  $h(x)$  satisfies the conditions of Theorem 11.2, and there exists a positive real constant  $m < 1$  such that

$$|h(x)| = O\{(1-x^2)^{-m}\} \text{ as } |x| \rightarrow 1.$$

Hence,  $\mathcal{T}_n\{R[h(x)]\}$  exists, and by Theorem 11.2, it follows that

$$\begin{aligned} \mathcal{T}_n\{R[h(x)]\} &= -n(n+1)\mathcal{T}_n\{h(x)\} \\ &= -n(n+1)\mathcal{T}_n\{R^{-1}\{f(x)\}\}, \end{aligned} \quad (11.92)$$

from which it turns out that

$$\mathcal{T}_n\{R^{-1}\{f(x)\}\} = -\frac{\tilde{f}(n)}{n(n+1)}. \quad (11.93)$$

Inversion leads to the results

$$\begin{aligned} \mathcal{T}_n^{-1} \left\{ \frac{f(n)}{n(n+1)} \right\} &= -R^{-1}\{f(x)\} = -h(x) \\ &= A - \int_0^x \frac{ds}{1-s^2} \int_{-1}^s f(t)dt. \end{aligned} \quad (11.94)$$

This proves the theorem. ■

---

**THEOREM 11.4**

If  $f(x)$  is continuous in each subinterval of  $(-1, 1)$  and a continuous function  $g(x)$  is defined by

$$g(x) = \int_{-1}^x f(t)dt, \quad (11.95)$$

then

$$\mathcal{T}_n\{g'(x)\} = \tilde{f}(n) = g(1) - \int_{-1}^1 g(x)P'_n(x)dx. \quad (11.96)$$

*Proof* We have, by definition,

$$\mathcal{T}_n\{g'(x)\} = \int_{-1}^1 g'(x) P_n(x)dx,$$

which is, by integrating by parts,

$$= [P_n(x)g(x)]_{-1}^1 - \int_{-1}^1 g(x)P'_n(x)dx.$$

Since  $P_n(1) = 1$  and  $g(-1) = 0$ , the preceding result becomes Equation 11.96. ■

---

**COROLLARY 11.2**

If result (Equation 11.96) is true and  $g(x)$  is given by Equation 11.95, then

$$\left. \begin{aligned} \mathcal{T}_n\{g(x)\} &= f(0) - f(1) && \text{when } n = 0 \\ &= \frac{\tilde{f}(n-1) - \tilde{f}(n+1)}{(2n+1)} && \text{when } n > 1 \end{aligned} \right\}. \quad (11.97)$$

*Proof* We write  $\tilde{f}(n-1)$  and  $\tilde{f}(n+1)$  using Equation 11.96 and then subtract so that the resulting expression gives Equation 11.97 with the help of Equation 11.74. ■

---

**COROLLARY 11.3**

If  $g'(x)$  is a sectionally continuous function and  $g(x)$  is the continuous function given by Equation 11.95, then

■

$$\left. \begin{aligned} \mathcal{T}_n\{g'(x)\} &= g(1), \quad \text{when } n = 0 \\ &= g(1) - (2n - 1)\tilde{g}(n - 1) - (2n - 5)\tilde{g}(n - 3) \\ &\quad - \cdots - g(0) \quad \text{when } n = 1, 3, 5, \dots \\ &= g(1) - 2(2n - 1)\tilde{g}(n - 1) - (2n - 5)\tilde{g}(n - 3) \\ &\quad - \cdots - 3g(1) \quad \text{when } n = 2, 4, 6, \dots \end{aligned} \right\} \quad (11.98)$$

These results can readily be verified using Equations 11.74 and 11.96. ■

**THEOREM 11.5 (Convolution)**

If  $\mathcal{T}_n\{f(x)\} = \tilde{f}(n)$  and  $\mathcal{T}_n\{g(x)\} = \tilde{g}(n)$ , then

$$\mathcal{T}_n\{f(x) * g(x)\} = \tilde{f}(n)\tilde{g}(n), \quad (11.99)$$

where the convolution  $f(x) * g(x)$  is given by

$$f(x) * g(x) = h(x) = \frac{1}{\pi} \int_0^\pi f(\cos \mu) \sin \mu \, d\mu \int_0^\pi g(\cos \lambda) d\beta, \quad (11.100)$$

with

$$x = \cos \nu \quad \text{and} \quad \cos \lambda = \cos \mu \cos \nu + \sin \mu \sin \nu \cos \beta. \quad (11.101)$$

*Proof* We have, by definition (Equation 11.60),

$$\begin{aligned} \tilde{f}(n)\tilde{g}(n) &= \int_0^\pi f(\cos \mu) P_n(\cos \mu) \sin \mu \, d\mu \int_0^\pi g(\cos \lambda) P_n(\cos \lambda) \sin \lambda \, d\lambda \\ &= \int_0^\pi f(\cos \mu) \sin \mu \left[ \int_0^\pi g(\cos \lambda) P_n(\cos \lambda) P_n(\cos \mu) \sin \lambda \, d\lambda \right] d\mu, \end{aligned} \quad (11.102)$$

where  $f(x) = f(\cos \mu)$  and  $g(x) = g(\cos \lambda)$ .

With the aid of an addition formula (see Sansone, 1959, p. 169) given as

$$P_n(\cos \lambda) P_n(\cos \mu) = \frac{1}{\pi} \int_0^\pi P_n(\cos \nu) d\alpha, \quad (11.103)$$

where  $\cos \nu = \cos \lambda \cos \mu + \sin \lambda \sin \mu \cos \alpha$ , the product can be rewritten in the form

$$\tilde{f}(n)\tilde{g}(n) = \frac{1}{\pi} \int_0^\pi f(\cos \mu) \sin \mu \left[ \int_0^\pi \int_0^\pi g(\cos \mu) P_n(\cos \mu) \sin \lambda d\alpha d\lambda \right] d\mu. \quad (11.104)$$

We next use Churchill and Dolph's (1954, pp. 94–96) geometrical arguments to replace the double integral inside the square bracket by

$$\int_0^\pi \int_0^\pi g(\cos \mu \cos \nu + \sin \mu \sin \nu \cos \beta) P_n(\cos \nu) \sin \nu \, d\nu. \quad (11.105)$$

Substituting this result in Equation 11.102 and changing the order of integration, we obtain

$$\begin{aligned} \tilde{f}(n)\tilde{g}(n) &= \frac{1}{\pi} \int_0^\pi P_n(\cos \nu) \sin \nu \left[ \int_0^\pi \int_0^\pi f(\cos \mu) \sin \mu g(\cos \lambda) d\mu d\beta \right] d\nu \\ &= \int_0^\pi h(\cos \nu) P_n(\cos \nu) \sin \nu \, d\nu, \end{aligned} \quad (11.106)$$

where

$$\cos \lambda = \cos \mu \cos \nu + \sin \mu \sin \nu \cos \beta, \quad (11.107)$$

and

$$h(\cos \nu) = \frac{1}{\pi} \int_0^\pi f(\cos \mu) \sin \mu \, d\mu \int_0^\pi g(\cos \lambda) d\beta.$$

This proves the theorem.

In particular, when  $\nu = 0$ , result Equation 11.100 becomes

$$h(1) = \int_{-1}^1 f(t)g(-t)dt, \quad (11.108)$$

and when  $\nu = \pi$ , Equation 11.100 gives

$$h(-1) = \int_{-1}^1 f(t)g(-t)dt. \quad (11.109)$$

■

**11.2.4 Applications of Legendre Transforms to Boundary Value Problems**

We solve the *Dirichlet problem* for the *potential*  $u(r, \theta)$  inside a unit sphere  $r = 1$ , which satisfies the Laplace equation

$$\frac{\partial}{\partial r} \left[ r^2 \frac{\partial u}{\partial r} \right] + \frac{\partial}{\partial x} \left[ (1 - x^2) \frac{\partial u}{\partial x} \right] = 0, \quad 0 < r < 1, \quad (11.110)$$

with the boundary condition ( $x = \cos \theta$ )

$$u(1, x) = f(x), \quad -1 < x < 1. \quad (11.111) \quad \text{which is, in terms of } w,$$

We introduce the ‘‘Legendre transform’’  $\tilde{u}(r, n) = \mathcal{T}_n\{u(r, \theta)\}$  defined by Equation 11.59. Application of this transform to Equations 11.110 and 11.111 gives

$$r^2 \frac{d^2 \tilde{u}(r, n)}{dr^2} + 2r \frac{d\tilde{u}}{dr} - n(n+1)\tilde{u}(r, n) = 0, \quad (11.112)$$

$$\tilde{u}(1, n) = \tilde{f}(n), \quad (11.113)$$

where  $\tilde{u}(r, n)$  is to be continuous function for  $r$  for  $0 \leq r < 1$ .

The bounded solution of Equations 11.112 and 11.113 is

$$\tilde{u}(r, n) = \tilde{f}(n)r^n, \quad 0 \leq r < 1, \quad \text{for } n = 0, 1, 2, 3, \dots \quad (11.114)$$

Thus, the solution for  $u(r, x)$  can be found by the inverse transform so that

$$u(r, x) = \sum_{n=0}^{\infty} \left( n + \frac{1}{2} \right) \tilde{f}(n) r^n P_n(x) \quad \text{for } 0 < r \leq 1, |x| < 1. \quad (11.115)$$

The convolution theorem allows us to give another representation of the solution. In view of Equation 11.69, we find

$$\mathcal{T}_n^{-1}\{r^n\} = \frac{1}{2}(1-r^2)(1-2rx+r^2)^{-3/2}.$$

Thus, it follows from Equation 11.114 that

$$\begin{aligned} u(r, \cos \theta) &= \mathcal{T}_n^{-1}\{\tilde{f}(n)r^n\} \\ &= \frac{1}{2\pi} \int_0^\pi f(\cos \mu) \sin \mu \, d\mu \int_0^\pi \frac{(1-r^2)d\lambda}{(1-2r \cos \nu + r^2)^{3/2}}, \end{aligned} \quad (11.116)$$

where

$$\cos \nu = \cos \mu \cos \theta + \sin \mu \sin \theta \cos \lambda. \quad (11.117)$$

Integral Equation 11.116 is called the *Poisson integral formula* for the potential inside the unit sphere for the Dirichlet problem.

On the other hand, for the Dirichlet exterior problem, the potential  $w(r, \cos \theta)$  outside the unit sphere ( $r > 1$ ) can be obtained with the boundary condition  $w(1, \cos \theta) = f(\cos \theta)$ . The solution of the Legendre transformed problem is

$$\tilde{w}(r, n) = \frac{1}{r} \tilde{f}(n) r^{-n}, \quad n = 0, 1, 2, \dots, \quad (11.118)$$

$$w(r, \cos \theta) = \frac{1}{r} w\left(\frac{1}{r}, \cos \theta\right), \quad r > 1 \quad (11.119)$$

$$= \frac{1}{2\pi} \int_0^\pi f(\cos \mu) \sin \mu \, d\mu \int_0^\pi \frac{(r^2-1)d\lambda}{(1-2r \cos \nu + r^2)^{3/2}}, \quad (11.120)$$

where  $\cos \nu$  is given by Equation 11.117.

## 11.2.5 Additional Relations

1. If  $|r| < 1$ ,

$$\text{a. } \mathcal{T}_n\{x^n\} = \frac{2^{n+1}(n!)^2}{(2n+1)!}$$

$$\text{b. } \mathcal{T}_n \left[ \log \left\{ \frac{r-x+(1-2rx+r^2)^{1/2}}{1-x} \right\} \right] = \frac{2r^{n+1}}{(n+1)(2n+1)}.$$

$$\begin{aligned} \text{c. } \mathcal{T}_n \left[ \{2r(1-rx+r^2)^{-1/2}\} \right. \\ \left. - \log \left\{ \frac{r-x+(1-2rx+r^2)^{1/2}}{1-x} \right\} \right] &= \frac{2r^{n+1}}{(n+1)}. \end{aligned}$$

$$\begin{aligned} \text{d. } \mathcal{T}_n \left[ -\log \frac{1}{2} \{1-rx+(1-2rx+r^2)^{1/2}\} \right] \\ = \begin{cases} 0, & n=0 \\ \frac{2r^n}{n(2n+1)}, & n>0 \end{cases} \end{aligned}$$

$$\begin{aligned} \text{e. } \mathcal{T}_n \left[ (1-2rx+r^2)^{-\frac{1}{2}} \right. \\ \left. - \frac{1}{2} \log \left\{ \frac{1-rx+(1-2rx+r^2)^{1/2}}{2} \right\} \right] = \frac{r^n}{n}. \end{aligned}$$

## 11.3 Jacobi and Gegenbauer Transforms

### 11.3.1 Introduction

This chapter deals with Jacobi and Gegenbauer transforms and their basic operational properties. The former is a fairly general finite integral transform in the sense that both Gegenbauer and Legendre transforms follow as special cases of the Jacobi transform. Some applications of both Jacobi and Gegenbauer transforms are discussed. This chapter is based on the papers by Debnath (1963, 1967), Scott (1953), Conte (1955), and Lakshmanarao (1954). All these special transforms have been unified by Eringen (1954) in his paper on the finite Sturm–Liouville transform.



### 11.3.2 Definition of the Jacobi Transform and Examples

Debnath (1963) introduced the *Jacobi transform* of a function  $F(x)$  defined in  $-1 < x < 1$  by the integral

$$J\{F(x)\} = f^{(\alpha,\beta)}(n) = \int_{-1}^1 (1-x)^\alpha (1+x)^\beta P_n^{(\alpha,\beta)}(x) F(x) dx, \quad (11.121)$$

where  $P_n^{(\alpha,\beta)}(x)$  is the Jacobi polynomial of degree  $n$  and orders  $\alpha (> -1)$  and  $\beta (> -1)$ .

We assume that  $F(x)$  admits the following series expansion

$$F(x) = \sum_{n=0}^{\infty} a_n P_n^{(\alpha,\beta)}(x). \quad (11.122)$$

In view of the orthogonal relation

$$\int_{-1}^1 (1-x)^\alpha (1+x)^\beta P_n^{(\alpha,\beta)}(x) P_m^{(\alpha,\beta)}(x) dx = \delta_n \delta_{mn}, \quad (11.123)$$

where  $\delta_{nm}$  is the Kronecker delta symbol,

$$\delta_n = \frac{2^{\alpha+\beta+1} \Gamma(n+\alpha+1) \Gamma(n+\beta+1)}{n! (\alpha+\beta+2n+1) \Gamma(n+\alpha+\beta+1)}, \quad (11.124)$$

and the coefficients  $a_n$  in Equation 11.122 are given by

$$a_n = \frac{1}{\delta_n} \int_{-1}^1 (1-x)^\alpha (1+x)^\beta F(x) P_n^{(\alpha,\beta)}(x) dx = \frac{f^{(\alpha,\beta)}(n)}{\delta_n}. \quad (11.125)$$

Thus, the *inverse Jacobi transform* is given by

$$J^{-1}\{f^{(\alpha,\beta)}(n)\} = F(x) = \sum_{n=0}^{\infty} (\delta_n)^{-1} f^{(\alpha,\beta)}(n) P_n^{(\alpha,\beta)}(x). \quad (11.126)$$

Note that both  $J$  and  $J^{-1}$  are linear transformations.

#### Example 11.13

If  $F(x)$  is a polynomial of degree  $m < n$ , then

$$J\{F(x)\} = 0. \quad (11.127)$$

#### Example 11.14

$$J\{P_m^{(\alpha,\beta)}(x)\} = \delta_{mn}. \quad (11.128)$$

#### Example 11.15

From the uniformly convergent expansion of the generating function for  $|z| < 1$

$$2^{\alpha+\beta} Q^{-1} (1-z+Q)^{-\alpha} (1+z+Q)^{-\beta} = \sum_{n=0}^{\infty} z^n P_n^{(\alpha,\beta)}(x), \quad (11.129)$$

where  $Q = (1 - 2xz + z^2)^{\frac{1}{2}}$ , it turns out that

$$\begin{aligned} J\{2^{\alpha+\beta} Q^{-1} (1-z+Q)^{-\alpha} (1+z+Q)^{-\beta}\} \\ = \sum_{n=0}^{\infty} z^n \int_{-1}^1 (1-x)^\alpha (1+x)^\beta P_n^{(\alpha,\beta)}(x) P_n^{(\alpha,\beta)}(x) dx \\ = \sum_{n=0}^{\infty} (\delta_n) z^n. \end{aligned} \quad (11.130)$$

#### Example 11.16

$$\begin{aligned} J\{x^n\} &= \int_{-1}^1 (1-x)^\alpha (1+x)^\beta P_n^{(\alpha,\beta)}(x) x^n dx \\ &= 2^{n+\alpha+\beta+1} \frac{\Gamma(n+\alpha+1) \Gamma(n+\beta+1)}{\Gamma(n+\alpha+\beta+1)}. \end{aligned} \quad (11.131)$$

#### Example 11.17

If  $p > \beta - 1$ , then

$$\begin{aligned} J\{(1+x)^{p-\beta}\} &= \int_{-1}^1 (1-x)^\alpha (1+x)^p P_n^{(\alpha,\beta)}(x) dx \\ &= \binom{n+\alpha}{n} 2^{\alpha+p+1} \frac{\Gamma(p+1) \Gamma(\alpha+1) \Gamma(p-\beta+1)}{\Gamma(\alpha+p+n+2) \Gamma(p-\beta+n+1)}. \end{aligned} \quad (11.132)$$

In particular, when  $\alpha = \beta = 0$ , the above results reduce to the corresponding results for the *Legendre transform* defined by Equation 11.59 so that

$$\begin{aligned} \mathcal{T}_n\{(1+x)^p\} &= \int_{-1}^1 (1+x)^p P_n(x) dx \\ &= \frac{2^{p+1} \{\Gamma(1+p)\}^2}{\Gamma(p+n+2) \Gamma(p+n+1)}, \quad (p > -1). \end{aligned} \quad (11.133)$$

**Example 11.18**

If  $\text{Re } \sigma > -1$ , then

$$\begin{aligned} J\{(1-x)^{\sigma-\alpha}\} &= \int_{-1}^1 (1-x)^{\sigma}(1+x)^{\beta} P_n^{(\alpha,\beta)}(x) dx, \quad \text{Re } \sigma > -1, \\ &= \frac{2^{\sigma+\beta+1}}{n! \Gamma(\alpha-\sigma)} \cdot \frac{\Gamma(\sigma+1)\Gamma(n+\beta+1)\Gamma(\alpha-\sigma+n)}{\Gamma(\beta+\sigma+n+2)}, \end{aligned} \quad (11.134)$$

■

**Example 11.19**

If  $\text{Re } \sigma > -1$  then

$$\begin{aligned} J\{(1+x)^{\sigma-\beta} P_m^{(\alpha,\sigma)}(x)\} &= \int_{-1}^1 (1-x)^{\alpha}(1+x)^{\sigma} P_n^{(\alpha,\beta)}(x) P_m^{(\alpha,\sigma)}(x) dx \\ &= \frac{2^{\alpha+\sigma+1} \Gamma(n+\alpha+1) \Gamma(\alpha+\beta+m+n+1) \Gamma(\sigma+m+1)}{m!(n-m)! \Gamma(\alpha+\beta+n+1) \Gamma(\alpha+\sigma+m+n+2)} \\ &\quad \times \frac{\Gamma(\sigma-\beta+1)}{\Gamma(\alpha-\beta+m+1)}. \end{aligned} \quad (11.135)$$

■

**11.3.3 Basic Operational Properties****THEOREM 11.6**

If  $J\{F(x)\} = f^{(\alpha,\beta)}(n)$ ,

$$\lim_{|x| \rightarrow 1} (1-x)^{\alpha+1} (1+x)^{\beta+1} F(x) = 0, \quad (11.136a)$$

$$\lim_{|x| \rightarrow 1} (1-x)^{\alpha+1} (1+x)^{\beta+1} F'(x) = 0, \quad (11.136b)$$

$$R[F(x)] = (1-x)^{-\alpha} (1+x)^{-\beta} \frac{d}{dx} \left[ (1-x)^{\alpha+1} (1+x)^{\beta+1} \frac{d}{dx} F(x) \right], \quad (11.137)$$

then  $J\{R[F(x)]\}$  exists and is given by

$$J\{R[F(x)]\} = -n(n+\alpha+\beta+1) f^{(\alpha,\beta)}(n), \quad (11.138)$$

where  $n=0, 1, 2, 3, \dots$

*Proof* We have, by definition,

$$J\{R[F(x)]\} = \int_{-1}^1 \frac{d}{dx} \left[ (1-x)^{\alpha+1} (1+x)^{\beta+1} \frac{dF}{dx} \right] P_n^{(\alpha,\beta)}(x) dx,$$

which is, by integrating by parts and using the orthogonal relation (Equation 11.123),

$$\begin{aligned} &= -n(n+\alpha+\beta+1) \int_{-1}^1 (1-x)^{\alpha} (1+x)^{\beta} P_n^{(\alpha,\beta)}(x) F(x) dx \\ &= -n(n+\alpha+\beta+1) f^{(\alpha,\beta)}(n). \end{aligned}$$

This completes the proof.

If  $F(x)$  and  $R[F(x)]$  satisfy the conditions of Theorem 11.6, then  $J\{[R[F(x)]]\}$  exists and is given by

$$\begin{aligned} J\{R^2[F(x)]\} &= J\{R[R[F(x)]]\} \\ &= (-1)^2 n^2 (n+\alpha+\beta+1)^2 f^{(\alpha,\beta)}(n). \end{aligned} \quad (11.139)$$

More generally, if  $F(x)$  and  $R^k[F(x)]$  satisfy the conditions of Theorem 11.6, where  $k=1, 2, \dots, m-1$ , and  $m$  is a positive integer then

$$J\{R^m[F(x)]\} = (-1)^m n^m (n+\alpha+\beta+1)^m f^{(\alpha,\beta)}(n). \quad (11.140)$$

When  $\alpha = \beta = 0$ ,  $P_n^{(0,0)}(x)$  becomes the Legendre polynomial  $P_n(x)$  and the Jacobi transform pairs (Equations 11.121 and 11.125) reduce to the Legendre transform pairs (Equations 11.59 and 11.61). All results for the Jacobi transform also reduce to those given in Chapter 14.

**11.3.4 Applications of Jacobi Transforms to the Generalized Heat Conduction Problem**

The one-dimensional generalized heat equation for temperature  $u(x, t)$  is

$$\frac{\partial}{\partial x} \left[ \kappa \frac{\partial u}{\partial x} \right] + Q(x, t) = \rho c \frac{\partial u}{\partial t}, \quad (11.141)$$

where

$\kappa$  is the thermal conductivity

$Q(x, t)$  is a continuous heat source within the medium

$\rho$  and  $c$  are density and specific heat, respectively

If the thermal conductivity is  $\kappa = a(1-x^2)$ , where  $a$  is a real constant, and the source is  $Q(x, t) = (\mu x + \nu) \frac{\partial u}{\partial x}$ , then the heat Equation 11.141 reduces to

$$\frac{\partial}{\partial x} \left[ (1-x^2) \frac{\partial u}{\partial x} \right] + \left( \frac{\mu x + \nu}{a} \right) \frac{\partial u}{\partial x} = \left( \frac{\rho c}{a} \right) \frac{\partial u}{\partial t}. \quad (11.142)$$

We consider a nonhomogeneous beam with ends at  $x = \pm 1$  whose lateral surface is insulated. Since  $\kappa = 0$  at the ends, the ends of the beam are also insulated. We assume the initial conditions as

$$u(x, 0) = G(x) \quad \text{for all } -1 < x < 1, \quad (11.143)$$

where  $G(x)$  is a suitable function so that  $J\{G(x)\}$  exists.

If we write  $\frac{\mu}{a} = -(\alpha + \beta)$  and  $\frac{\nu}{a} = \beta - \alpha$  so that  $(\alpha, \beta) = -\left(\frac{\mu + \nu}{2a}, \frac{\mu - \nu}{2a}\right)$ , the left-hand side of Equation 11.142 becomes

$$\begin{aligned} & \frac{\partial}{\partial x} \left[ (1-x^2) \frac{\partial u}{\partial x} \right] + [(\beta - \alpha) - (\beta + \alpha)x] \frac{\partial u}{\partial x} \\ &= \frac{\partial}{\partial x} \left[ (1-x^2) \frac{\partial u}{\partial x} \right] + [(1-x)\beta - (1+x)\alpha] \frac{\partial u}{\partial x} \\ &= (1-x)^{-\alpha} (1+x)^{-\beta} \left\{ (1-x)^\alpha (1+x)^\beta \frac{\partial}{\partial x} \left[ (1-x^2) \frac{\partial u}{\partial x} \right] \right. \\ & \quad \left. + [\beta(1+x)^\beta (1-x)^{\alpha+1} - \alpha(1-x)^\alpha (1+x)^{\beta+1}] \frac{\partial u}{\partial x} \right\} \\ &= (1-x)^{-\alpha} (1+x)^{-\beta} \left\{ \frac{\partial}{\partial x} \left[ (1-x)^{\alpha+1} (1+x)^{\beta+1} \frac{\partial u}{\partial x} \right] \right\} \\ &= R[u(x, t)]. \end{aligned}$$

Thus, Equation 11.142 reduces to

$$R[u(x, t)] = \left(\frac{1}{d}\right) \frac{\partial u}{\partial t}, \quad d = \left(\frac{a}{\rho c}\right). \quad (11.144)$$

Application of the *Jacobi transform* to Equations 11.143 and 11.144 gives

$$\frac{d}{dt} u^{(\alpha, \beta)}(n, t) = -dn(n + a + \beta + 1)u^{(\alpha, \beta)}(n, t), \quad (11.145)$$

$$u^{(\alpha, \beta)}(n, 0) = g^{(\alpha, \beta)}(n). \quad (11.146)$$

The solution of this system is

$$u^{(\alpha, \beta)}(n, t) = g^{(\alpha, \beta)}(n) \exp[-n(n + \alpha + \beta + 1)td]. \quad (11.147)$$

The *inverse Jacobi transform* gives the formal solution

$$u(x, t) = \sum_{n=0}^{\infty} \delta_n^{-1} g^{(\alpha, \beta)}(n) P_n^{(\alpha, \beta)}(x) \exp[-n(n + \alpha + \beta + 1)td], \quad (11.148)$$

where  $\alpha = -\frac{1}{2a}(\mu + \nu)$  and  $\beta = \frac{1}{2a}(\mu - \nu)$ .

### 11.3.5 The Gegenbauer Transform and Its Basic Operational Properties

When  $\alpha = \beta = \nu - \frac{1}{2}$ , the *Jacobi polynomial*  $P_n^{(\alpha, \beta)}(x)$  becomes the *Gegenbauer polynomial*  $C_n^\nu(x)$  which satisfies the self-adjoint differential form

$$\frac{d}{dx} \left[ (1-x^2)^{\nu+\frac{1}{2}} \frac{dy}{dx} \right] + n(n+2\nu)(1-x^2)^{\nu-1}y = 0, \quad (11.149)$$

and the orthogonal relation

$$\int_{-1}^1 (1-x^2)^{\nu-\frac{1}{2}} C_m^\nu(x) C_n^\nu(x) dx = \delta_n \delta_{mn}, \quad (11.150)$$

where

$$\delta_n = \frac{2^{1-2\nu} \pi \Gamma(n+2\nu)}{n! (n+\nu) [\Gamma(\nu)]^2}. \quad (11.151)$$

Thus, when  $\alpha = \beta = \nu - \frac{1}{2}$ , the Jacobi transform pairs (Equations 11.121 and 11.126) reduce to the *Gegenbauer transform* pairs, in the form

$$G\{F(x)\} = f^{(\nu)}(n) = \int_{-1}^1 (1-x^2)^{\nu-\frac{1}{2}} C_n^\nu(x) F(x) dx, \quad (11.152)$$

$$G^{-1}\{f^{(\nu)}(n)\} = F(x) = \sum_{n=0}^{\infty} \delta_n^{-1} C_n^\nu(x) f^{(\nu)}(n), \quad -1 < x < 1. \quad (11.153)$$

Obviously,  $G$  and  $G^{-1}$  stand for the Gegenbauer transformation and its inverse respectively. They are linear integral transformations.

When  $\alpha = \beta = \nu - \frac{1}{2}$ , the differential form (Equation 11.137) becomes

$$R[F(x)] = (1-x^2) \frac{d^2 F}{dx^2} - (2\nu+1)x \frac{dF}{dx}, \quad (11.154)$$

which can be expressed as

$$R[F(x)] = (1-x^2)^{\frac{1}{2}-\nu} \frac{d}{dx} \left[ (1-x^2)^{\nu+\frac{1}{2}} \frac{dF}{dx} \right]. \quad (11.155)$$

Under the Gegenbauer transformation  $G$ , the differential form (Equation 11.154) is reduced to the algebraic form

$$G\{R[F(x)]\} = -n(n+2\nu)f^{(\nu)}(n). \quad (11.156)$$

This follows directly from the relation (Equation 11.138).

Similarly, we obtain

$$G\{R^2[F(x)]\} = (-1)^2 n^2 (n+2\nu)^2 f^{(\nu)}(n). \quad (11.157)$$

More generally,

$$G\{R^k[F(x)]\} = (-1)^k n^k (n+2\nu)^k f^{(\nu)}(n), \quad (11.158)$$

where  $k = 1, 2, \dots$

**CONVOLUTION THEOREM 11.7**

If  $G\{F(x)\} = f^{(\nu)}(n)$  and  $G\{G(x)\} = g^{(\nu)}(n)$ , then

$$f^{(\nu)}(n)g^{(\nu)}(n) = G\{H(x)\} = h^{(\nu)}(n), \quad (11.159)$$

where

$$H(x) = G^{-1}\{h^{(\nu)}(n)\} = G^{-1}\{f^{(\nu)}(n)g^{(\nu)}(n)\} = F(x) * G(x), \quad (11.160)$$

and  $H(x)$  is given by

$$H(\cos \psi) = A(\sin \psi)^{1-2\nu} \int_0^\pi \int_0^\pi F(\cos \theta)G(\cos \phi)(\sin \theta)^{2\nu} \\ \times (\sin \phi)^{2\nu-1}(\sin \lambda)^{2\nu-1} d\theta d\alpha, \quad (11.161)$$

where  $\alpha$  is defined by Equation 11.167.

*Proof* We have, by definition,

$$f^{(\nu)}(n)g^{(\nu)}(n) = \int_{-1}^1 F(x)(1-x^2)^{\nu-\frac{1}{2}} C_n^\nu(x) dx \\ \times \int_{-1}^1 G(x)(1-x^2)^{\nu-\frac{1}{2}} C_n^\nu(x) dx \\ = \int_0^\pi F(\cos \theta)(\sin \theta)^{2\nu} C_n^\nu(\cos \theta) d\theta \\ \times \int_0^\pi G(\cos \phi)(\sin \phi)^{2\nu} C_n^\nu(\cos \phi) d\phi \\ = \int_0^\pi F(\cos \theta)(\sin \theta)^{2\nu} \left[ \int_0^\pi G(\cos \phi) C_n^\nu(\cos \phi) \right. \\ \left. \times C_n^\nu(\cos \phi)(\sin \phi)^{2\nu} d\phi \right] d\theta. \quad (11.162)$$

The addition formula for the Gegenbauer polynomial (see Erdélyi, 1953, p. 177) is

$$C_n^\nu(\cos \theta)C_n^\nu(\cos \phi) = A \int_0^\pi C_n^\nu(\cos \psi)(\sin \lambda)^{2\nu-1} d\lambda, \quad (11.163)$$

where

$$A = \{\Gamma(n+2\nu)/n!2^{2\nu-1}\Gamma^2(\nu)\}, \quad (11.164)$$

and

$$\cos \psi = \cos \theta \cos \phi + \sin \theta \sin \phi \cos \lambda. \quad (11.165)$$

In view of this formula, result (Equation 11.162) assumes the form

$$f^{(\nu)}(n)g^{(\nu)}(n) = A \int_0^\pi F(\cos \theta)(\sin \theta)^{2\nu} \left[ \int_0^\pi \int_0^\pi G(\cos \phi) C_n^\nu(\cos \psi) \right. \\ \left. \times (\sin \phi)^{2\nu}(\sin \lambda)^{2\nu-1} d\lambda d\phi \right] d\theta. \quad (11.166)$$

We next introduce a new variable  $\alpha$  defined by the relation

$$\cos \phi = \cos \theta \cos \psi + \sin \theta \sin \psi \cos \alpha. \quad (11.167)$$

Thus, under transformation of coordinates defined by Equations 11.165 and 11.167, the elementary area  $d\lambda d\phi = (\sin \psi/\sin \phi) \times d\psi d\alpha$ , where  $(\sin \psi/\sin \phi)$  is the Jacobian of the transformation. In view of this transformation, the square region of the  $\phi$ - $\lambda$  plane given by  $(0 \leq \phi \leq \pi \leq \lambda \leq \pi)$  transforms into a square region of the same dimension in the  $\psi$ - $\alpha$  plane. Consequently, the double integral inside the square bracket in Equation 11.166 reduces to

$$\int_0^\pi \int_0^\pi G(\cos \phi) C_n^\nu(\cos \psi)(\sin \phi)^{2\nu-1}(\sin \lambda)^{2\nu-1} \sin \psi d\psi d\alpha, \quad (11.168)$$

where  $\cos \psi$  is defined by Equation 11.165 and  $\cos \phi$  is defined by Equation 11.167. If the double integral (Equation 11.168) is substituted into Equation 11.166, and if the order of integration is interchanged, Equation 11.166 becomes

$$f^{(\nu)}(n)g^{(\nu)}(n) = \int_0^\pi (\sin \psi)^{2\nu} C_n^\nu(\cos \psi) H(\cos \psi) d\psi = G\{H(\cos \psi)\}, \quad (11.169)$$

where

$$H(\cos \psi) = A(\sin \psi)^{1-2\nu} \int_0^\pi \int_0^\pi F(\cos \theta)G(\cos \phi)(\sin \theta)^{2\nu} \\ \times (\sin \phi)^{2\nu-1}(\sin \lambda)^{2\nu-1} d\theta d\alpha. \quad (11.170)$$

When  $\nu = \frac{1}{2}$ ,  $C_n^{\frac{1}{2}}(x)$  becomes the Legendre polynomial, the Gegenbauer transform pairs (Equations 11.152 and 11.153) reduce to the Legendre transform pairs (Equations 11.59 and 11.61), and the convolution theorem 11.7 reduces to the corresponding convolution theorem 11.5 for the Legendre transform.

### 11.3.6 Application of the Gegenbauer Transform

The generalized one-dimensional heat equation in a nonhomogeneous solid beam for the temperature  $u(x,t)$  is

$$\frac{\partial}{\partial x} \left[ (1-x^2) \frac{\partial u}{\partial x} \right] - (2\nu + 1)x \frac{\partial u}{\partial x} = \frac{1}{d} \frac{\partial u}{\partial t}, \quad (11.171)$$

where  $\kappa = (1-x^2)$  is the thermal conductivity,  $d = \left(\frac{a}{\rho c}\right)$ , and the second term on the left-hand side represents the continuous source of heat within the solid beam. We assume that the beam is bounded by the planes at  $x = \pm 1$  and its lateral surfaces are insulated. The initial condition is

$$u(x, 0) = G(x) \quad \text{for } -1 < x < 1, \quad (11.172)$$

where  $G(x)$  is a given function so that its Gegenbauer transform exists.

Application of the Gegenbauer transform to Equations 11.171 and 11.172 and the use of Equation 11.156 gives

$$\frac{d}{dt} u^{(v)}(n, t) = -d n(n + 2\nu) u^{(v)}(n, t), \quad (11.173)$$

$$u^{(v)}(n, 0) = g^{(v)}(n). \quad (11.174)$$

This solution of this system is

$$u^{(v)}(n, t) = g^{(v)}(n) \exp[-n(n + 2\nu)td]. \quad (11.175)$$

The inverse transform gives the formal solution

$$u(x, t) = \sum_{n=0}^{\infty} \delta_n^{-1} C_n^{\nu}(x) g^{(v)}(n) \exp[-n(n + 2\nu)td], \quad (11.176)$$

where  $\delta_n$  is given by Equation 11.151.

## 11.4 Laguerre Transforms

### 11.4.1 Introduction

This chapter is devoted to the study of the Laguerre transform and its basic operational properties. It is shown that the Laguerre transform can be used effectively to solve the heat conduction problem in a semi-infinite medium with variable thermal conductivity in the presence of a heat source within the medium.

### 11.4.2 Definition of the Laguerre Transform and Examples

Debnath (1960) introduced the *Laguerre transform* of a function  $f(x)$  defined in  $0 \leq x < \infty$  by means of the integral

$$L\{f(x)\} = \tilde{f}_{\alpha}(n) = \int_0^{\infty} e^{-x} x^{\alpha} L_n^{\alpha}(x) f(x) dx, \quad (11.177)$$

where  $L_n^{\alpha}(x)$  is the *Laguerre polynomial* of degree  $n(\geq 0)$  and order  $\alpha(> -1)$ , which satisfies the ordinary differential equation expressed in the self-adjoint form

$$\frac{d}{dx} \left[ e^{-x} x^{\alpha+1} \frac{d}{dx} L_n^{\alpha}(x) \right] + n e^{-x} x^{\alpha} L_n^{\alpha}(x) = 0. \quad (11.178)$$

In view of the orthogonal property of the Laguerre polynomials

$$\int_0^{\infty} e^{-x} x^{\alpha} L_n^{\alpha}(x) L_m^{\alpha}(x) dx = \binom{n+\alpha}{n} \Gamma(\alpha+1) \delta_{nm} = \delta_n \delta_{nm}, \quad (11.179)$$

where  $\delta_{nm}$  is the Kronecker delta symbol, and  $\delta_n$  is given by

$$\delta_n = \binom{n+\alpha}{n} \Gamma(\alpha+1). \quad (11.180)$$

The *inverse Laguerre transform* is given by

$$f(x) = L^{-1}\{\tilde{f}_{\alpha}(n)\} = \sum_{n=0}^{\infty} (\delta_n)^{-1} \tilde{f}_{\alpha}(n) L_n^{\alpha}(x). \quad (11.181)$$

When  $\alpha = 0$ , the Laguerre transform pairs due to McCully (1960) follow from Equations 11.177 and 11.181 in the form

$$L\{f(x)\} = \tilde{f}_0(n) = \int_0^{\infty} e^{-x} L_n(x) f(x) dx, \quad (11.182)$$

$$L^{-1}\{\tilde{f}_0(n)\} = f(x) = \sum_{n=0}^{\infty} \tilde{f}_0(n) L_n(x), \quad (11.183)$$

where  $L_n(x)$  is the Laguerre polynomial of degree  $n$  and order zero.

Obviously,  $L$  and  $L^{-1}$  are linear integral transformations. The following examples (Debnath, 1960) illustrate the Laguerre transform of some simple functions.

#### Example 11.20

$$\text{If } f(x) = L_m^{\alpha}(x) \text{ then } L\{L_m^{\alpha}(x)\} = \delta_n \delta_{nm}. \quad (11.184)$$

This follows directly from the definitions (Equations 11.177 and 11.179). ■

#### Example 11.21

If  $f(x) = x^{s-1}$  where  $s$  is a positive real number, then

$$L\{x^{s-1}\} = \int_0^{\infty} e^{-x} x^{\alpha+s-1} L_n^{\alpha}(x) dx = \frac{\Gamma(s+\alpha)\Gamma(n-s+1)}{n!\Gamma(1-s)}, \quad (11.185)$$

in which a result due to Howell (1938) is used. ■

**Example 11.22**

If  $a > -1$ , and  $f(x) = e^{-ax}$ , then

$$L\{e^{-ax}\} = \int_0^\infty e^{-x(1+a)} x^\alpha L_n^\alpha(x) dx = \frac{\Gamma(n + \alpha + 1) a^n}{n!(a + 1)^{n+\alpha+1}}, \quad (11.186)$$

where the result in Erdélyi et al. (1954, vol. 2, p. 191) is used. ■

**Example 11.23**

If  $f(x) = e^{-ax} L_m^\alpha(x)$ , then

$$L\{e^{-ax} L_m^\alpha(x)\} = \int_0^\infty e^{-x(a+1)} x^\alpha L_n^\alpha(x) L_m^\alpha(x) dx,$$

which is, due to Howell (1938),

$$\begin{aligned} &= \frac{1}{n! m!} \frac{\Gamma(n + \alpha + 1) \Gamma(m + \alpha + 1)}{\Gamma(1 + \alpha)} \cdot \frac{(a - 1)^{n-m+\alpha+1}}{a^{n+m+2\alpha+2}} \\ &\times {}_2F_1\left(n + \alpha + 1, \frac{m + a + 1}{a + 1}, \frac{1}{a^2}\right), \end{aligned} \quad (11.187)$$

where  ${}_2F_1(x, \alpha, \beta)$  is the hypergeometric function. ■

**Example 11.24**

$$L\{f(x)x^{\beta-\alpha}\} = \int_0^\infty e^{-x} x^\beta L_n^\alpha(x) f(x) dx.$$

We use a result from Erdélyi (1953, vol. 2, p. 192)

$$L_n^\alpha(x) = \sum_{m=0}^n (m!)^{-1} (\alpha - \beta)_m L_{n-m}^\beta(x) \quad (11.188)$$

to obtain the following result:

$$L\{f(x)x^{\beta-\alpha}\} = \sum_{m=0}^n (m!)^{-1} (\alpha - \beta)_m \tilde{f}_\beta(n - m). \quad (11.189)$$

In particular, when  $\beta = \alpha - 1$ , we obtain

$$L\left\{\frac{f(x)}{x}\right\} = \sum_{m=0}^n (m!)^{-1} \tilde{f}_{\alpha-1}(n - m). \quad \blacksquare$$

**Example 11.25**

$$L\{e^x x^{-\alpha} \Gamma(\alpha, x)\} = \sum_{n=0}^\infty \frac{\delta_n}{(n + 1)}, \quad -1 < \alpha < 0. \quad (11.190)$$

We use a result from Erdélyi (1953, vol. 2, p. 215) as

$$e^x x^{-\alpha} \Gamma(\alpha, x) = \sum_{n=0}^\infty (n + 1)^{-1} L_n^\alpha(x), \quad (\alpha > -1, x > 0),$$

in the definition (Equation 11.177) to derive Equation 11.190. ■

**Example 11.26**

If  $\beta > 0$ , then

$$L\{x^\beta\} = \Gamma(\alpha + \beta + 1) \sum_{n=0}^\infty \frac{(-\beta)_n \delta_n}{\Gamma(n + \alpha + 1)}. \quad (11.191)$$

Using the result from Erdélyi (1953, vol. 2, p. 214)

$$x^\beta = \Gamma(\alpha + \beta + 1) \sum_{n=0}^\infty \frac{(-\beta)_n}{\Gamma(n + \alpha + 1)} L_n^\alpha(x),$$

where

$$-\beta < 1 + \min\left(\alpha, \frac{\alpha}{2} - \frac{1}{4}\right), \quad x > 0, \alpha > -1,$$

we can easily obtain Equation 11.191. ■

**Example 11.27**

If  $|z| < 1$  and  $\alpha \geq 0$ , then

a.  $L\left\{(1 - z)^{-(\alpha+1)} \exp\left(\frac{xz}{z-1}\right)\right\} = \sum_{n=0}^\infty \delta_n z^n, \quad (11.192)$

b.  $L\left\{(xz)^{-\frac{\alpha}{2}} e^z J_\alpha\left[2\sqrt{xz}\right]\right\} = \sum_{n=0}^\infty \frac{\delta_n z^n}{\Gamma(n + \alpha + 1)}. \quad (11.193)$

We have the following generating functions (Erdélyi, 1953, vol. 2, p. 189)

$$(1 - z)^{-(\alpha+1)} \exp\left(\frac{xz}{z-1}\right) = \sum_{n=0}^\infty L_n^\alpha(x) z^n, \quad |z| < 1,$$

$$(xz)^{-\alpha/2} e^z J_\alpha\left[2\sqrt{xz}\right] = \sum_{n=0}^\infty \frac{z^n L_n^\alpha(x)}{\Gamma(n + \alpha + 1)}, \quad |z| < 1.$$

In view of these results combined with the orthogonality relation (Equation 11.179), we obtain Equations 11.192 and 11.193. ■

**Example 11.28**

(Recurrence Relations).

a.  $\tilde{f}_{\alpha+1}(n) = (n + \alpha + 1)\tilde{f}_{\alpha}(n) - (n + 1)\tilde{f}_{\alpha}(n + 1),$  (11.194)

b.  $n! \tilde{f}_{m-n}(n) = (-1)^{n-m} m! \sum_{k=0}^m (k!)^{-1} (2n - 2m)_k \tilde{f}_{m-n}(m - k).$   
(11.195)

We have

$$\tilde{f}_{\alpha+1}(n) = \int_0^{\infty} e^{-x} x^{\alpha+1} L_n^{\alpha+1}(x) f(x) dx,$$

which is, by using the recurrence relation for the Laguerre polynomial,

$$\begin{aligned} &= \int_0^{\infty} e^{-x} x^{\alpha} [(n + \alpha + 1)L_n^{\alpha}(x) - (n + 1)L_{n+1}^{\alpha}(x)] f(x) dx \\ &= (n + \alpha + 1)\tilde{f}_{\alpha}(n) - (n + 1)\tilde{f}_{\alpha}(n + 1). \end{aligned}$$

Similarly, we find

$$n! \tilde{f}_{m-n}(n) = \int_0^{\infty} e^{-x} x^{m-n} n! L_n^{m-n}(x) f(x) dx.$$

We next use the following result due to Howell (1938)

$$n! L_n^{m-n}(x) = (-1)^{n-m} m! L_m^{n-m}(x)$$

to obtain

$$\begin{aligned} n! \tilde{f}_{m-n}(n) &= (-1)^{n-m} m! \int_0^{\infty} e^{-x} x^{m-n} L_m^{n-m}(x) f(x) dx \\ &= (-1)^{n-m} m! \sum_{k=0}^m (k!)^{-1} (2n - 2m)_k \tilde{f}_{m-n}(m - k). \end{aligned}$$

■

**11.4.3 Basic Operational Properties**

We obtain the Laguerre transform of derivatives of  $f(x)$  as

$$L\{f'(x)\} = \tilde{f}_{\alpha}(n) - \alpha \sum_{k=0}^n f_{\alpha-1}(k) + \sum_{k=0}^{n-1} f_{\alpha}(k), \quad (11.196)$$

$$\begin{aligned} L\{f''(x)\} &= \tilde{f}_{\alpha}(n) - 2\alpha \sum_{m=0}^n \tilde{f}_{\alpha-1}(n - m) + 2 \sum_{m=0}^{n-1} \tilde{f}_{\alpha}(n - m - 1) \\ &\quad - 2\alpha \sum_{m=0}^{n-1} (m + 1)\tilde{f}_{\alpha+1}(n - m - 1) + \alpha(\alpha - 1) \\ &\quad \times \sum_{m=0}^n (m + 1)f_{\alpha-2}(n - m) + \sum_{m=0}^{n-2} (m + 1)\tilde{f}_{\alpha}(n - m - 2) \end{aligned} \quad (11.197)$$

and so on for the Laguerre transforms of higher derivatives.

We have, by definition,

$$\begin{aligned} L\{f'(x)\} &= \int_0^{\infty} e^{-x} x^{\alpha} L_n^{\alpha}(x) f'(x) dx \\ &= [e^{-x} n^{\alpha} L_n^{\alpha}(x) f(x)]_0^{\infty} + \int_0^{\infty} e^{-x} x^{\alpha} L_n^{\alpha}(x) f(x) dx \\ &\quad - \alpha \int_0^{\infty} e^{-x} x^{\alpha-1} L_n^{\alpha}(x) f(x) dx - \int_0^{\infty} e^{-x} x^{\alpha} \left[ \frac{d}{dx} L_n^{\alpha}(x) \right] f(x) dx, \end{aligned}$$

which is, due to Erdélyi et al (1954, vol. 2, p. 192),

$$= \tilde{f}_{\alpha}(n) - \alpha \sum_{k=0}^n \tilde{f}_{\alpha-1}(k) + \sum_{k=0}^{n-1} f_{\alpha}(k).$$

Similarly, we can derive Equation 11.197.

---

**THEOREM 11.8**

If  $g(x) = \int_0^x f(t) dt$  so that  $g(x)$  is absolutely continuous and  $g'(x)$  exists, and if  $g'(x)$  is bounded and integrable, then

$$\tilde{f}_{\alpha}(n) - \tilde{f}_{\alpha}(n - 1) = \tilde{g}_{\alpha}(n) - \alpha \tilde{g}_{\alpha-1}(n), \quad (11.198)$$

and

$$L \left\{ \int_0^x f(t) dt \right\} = \tilde{f}_0(n) - \tilde{f}_0(n - 1), \quad (11.199)$$

where  $L$  stands for the zero-order Laguerre transform defined by Equation 11.182.

*Proof* We have

$$\tilde{f}_{\alpha}(n) = \int_0^{\infty} e^{-x} x^{\alpha} L_n^{\alpha}(x) g'(x) dx,$$

which is, by integrating by parts,

$$\begin{aligned} &= \int_0^{\infty} e^{-x} x^{\alpha} L_n^{\alpha}(x) g(x) dx - \alpha \int_0^{\infty} e^{-x} x^{\alpha-1} L_n^{\alpha}(x) g(x) dx \\ &\quad - \int_0^{\infty} e^{-x} x^{\alpha} \left[ \frac{d}{dx} L_n^{\alpha}(x) \right] g(x) dx. \end{aligned}$$

Thus,

$$\begin{aligned} \tilde{f}_{\alpha}(n) - \tilde{f}_{\alpha}(n+1) &= \int_0^{\infty} e^{-x} x^{\alpha} [L_n^{\alpha}(x) - L_{n+1}^{\alpha}(x)] g(x) dx \\ &\quad + \alpha \int_0^{\infty} e^{-x} x^{\alpha} [L_{n+1}^{\alpha}(x) - L_n^{\alpha}(x)] g(x) dx \\ &\quad - \int_0^{\infty} e^{-x} x^{\alpha} \frac{d}{dx} [L_n^{\alpha}(x) - L_{n+1}^{\alpha}(x)] g(x) dx. \end{aligned}$$

Thus,

$$\begin{aligned} \tilde{f}_{\alpha}(n) - \tilde{f}_{\alpha}(n+1) &= \int_0^{\infty} e^{-x} x^{\alpha} [L_n^{\alpha}(x) - L_{n+1}^{\alpha}(x)] g(x) dx \\ &\quad + \alpha \int_0^{\infty} e^{-x} x^{\alpha} L_{n+1}^{\alpha-1}(x) g(x) dx - \int_0^{\infty} e^{-x} x^{\alpha} L_n^{\alpha}(x) g(x) dx \\ &= -\tilde{g}_{\alpha}(n+1) + \alpha \tilde{g}_{\alpha-1}(n+1). \end{aligned}$$

This proves Equation 11.198.

Putting  $\alpha = 0$  and replacing  $n$  by  $n-1$  gives

$$\tilde{g}_0(n) = \tilde{f}_0(n) - \tilde{f}_0(n-1).$$

Or,

$$L \left\{ \int_0^x f(t) dt \right\} = \tilde{f}_0(n) - \tilde{f}_0(n-1).$$

■

### THEOREM 11.9

If  $L\{f(x)\} = \tilde{f}_{\alpha}(n)$  exists, then

$$L\{R[f(x)]\} = -n\tilde{f}_{\alpha}(n), \quad (11.200)$$

where  $R[f(x)]$  is the differential operator given by

$$R[f(x)] = e^x x^{-\alpha} \frac{d}{dx} \left[ e^{-x} x^{\alpha+1} \frac{d}{dx} f(x) \right]. \quad (11.201)$$

*Proof* We have, by definition,

$$L\{R[f(x)]\} = \int_0^{\infty} L_n^{\alpha}(x) \frac{d}{dx} \left[ e^{-x} x^{\alpha+1} \frac{df}{dx} \right] dx,$$

which is, by integrating by parts and using Equation 11.178,

$$= -n \int_0^{\infty} e^{-x} x^{\alpha} L_n^{\alpha}(x) f(x) dx = -n\tilde{f}_{\alpha}(n).$$

This completes the proof of the basic operational property. This result can easily be extended as follows:

$$L\{R^2[f(x)]\} = L\{R[R[f(x)]]\} = (-1)^2 n^2 \tilde{f}_{\alpha}(n). \quad (11.202)$$

More generally,

$$L\{R^m[f(x)]\} = (-1)^m n^m \tilde{f}_{\alpha}(n), \quad (11.203)$$

where  $m$  is a nonnegative integer. ■

The convolution theorem for the Laguerre transform can be stated as follows:

---

### THEOREM 11.10 (Convolution Theorem)

If  $L\{f(x)\} = \tilde{f}_{\alpha}(n)$  and  $L\{g(x)\} = \tilde{g}_{\alpha}(n)$ , then

$$L^{-1}\{\tilde{f}_{\alpha}(n)\tilde{g}_{\alpha}(n)\} = h(x), \quad (11.204)$$

where  $h(x)$  is given by the following repeated integral

$$\begin{aligned} h(x) &= \frac{\Gamma(n+\alpha+1)}{\sqrt{\pi}\Gamma(n+1)} \int_0^{\infty} e^{-t} t^{\alpha} f(t) dt \int_0^{\pi} \exp(-\sqrt{xt} \cos \phi) \\ &\quad \times \sin^{2\alpha} \phi g(x+t+2\sqrt{xt} \cos \phi) \frac{J_{\alpha-\frac{1}{2}}(\sqrt{xt} \sin \phi) d\phi}{\left[\frac{1}{2}(\sqrt{xt} \sin \phi)\right]^{\alpha-\frac{1}{2}}}. \end{aligned} \quad (11.205)$$

In order to avoid long proof of this convolution theorem 11.10, we will not present the proof here, but refer the reader to the article of Debnath (1969). However, when  $\alpha = 0$  and  $\phi$  is replaced by  $(\pi - \theta)$ , and the standard result

$$J_{-\frac{1}{2}}(x) = \sqrt{\frac{2}{\pi x}} \cos x \quad (11.206)$$

is used, the convolution theorem 11.10 reduces to that of McCully's (1960). We now state and prove *McCully's convolution theorem* as follows:



**THEOREM 11.11 (McCully's Theorem)**

If  $L\{f(x)\} = \tilde{f}_0(n)$  and  $L\{g(x)\} = \tilde{g}_0(n)$ , then

$$L^{-1}\{\tilde{f}_0(n)\tilde{g}_0(n)\} = h(x), \quad (11.207)$$

where  $h(x)$  is given by the formula

$$h(x) = \frac{1}{\pi} \int_0^{\infty} e^{-t} f(t) dt \int_0^{\pi} \exp(\sqrt{xt} \cos \theta) \cos(\sqrt{xt} \sin \theta) \\ \times g(x + t - 2\sqrt{xt} \cos \theta) d\theta. \quad (11.208)$$

*Proof* We have, by definition,

$$\tilde{f}_0(n)\tilde{g}_0(n) = \int_0^{\infty} e^{-x} L_n(x) f(x) dx \int_0^{\infty} e^{-y} L_n(y) g(y) dy \\ = \int_0^{\infty} e^{-x} f(x) dx \int_0^{\infty} e^{-y} L_n(x) L_n(y) g(y) dy. \quad (11.209)$$

This can be written in the form

$$\tilde{f}_0(n)\tilde{g}_0(n) = L\{h(t)\} = \int_0^{\infty} e^{-t} L_n(t) h(t) dt.$$

This shows that  $h$  is the convolution of  $f$  and  $g$  and has the representation

$$h(x) = f(x) * g(x). \quad (11.210)$$

It follows from a formula of Bateman (1944, p. 457) that

$$L_n(x)L_n(y) = \frac{1}{\pi} \int_0^{\pi} e^{\sqrt{xy} \cos \theta} \cos(\sqrt{xy} \sin \theta) L_n(x+y-2\sqrt{xy} \cos \theta) d\theta. \quad (11.211)$$

In view of this result, Equation 11.209 becomes

$$\pi \tilde{f}_0(n)\tilde{g}_0(n) = \int_0^{\infty} e^{-x} f(x) dx \left[ \int_0^{\infty} e^{-y} g(y) \int_0^{\pi} \exp(\sqrt{xy} \cos \theta) \\ \times \cos(\sqrt{xy} \sin \theta) L_n(x+y-2\sqrt{xy} \cos \theta) d\theta dy \right]. \quad (11.212)$$

Using  $\sqrt{y}$  as the variable of integration combined with polar coordinates, the integral inside the square bracket in Equation 11.212 can be reduced to the form

$$\int_0^{\infty} e^{-t} L_n(t) dt \int_0^{\pi} \exp(\sqrt{xt} \cos \phi) \cos(\sqrt{xt} \sin \phi) \\ \times g(x+t-2\sqrt{xt} \cos \phi) d\phi, \quad (11.213)$$

so that Equation 11.212 becomes

$$\tilde{f}_0(n)\tilde{g}_0(n) = L\{h(t)\} = \int_0^{\infty} e^{-t} L_n(t) h(t) dt,$$

where  $h(x)$  is given by

$$h(x) = \frac{1}{\pi} \int_0^{\infty} e^{-t} f(t) dt \int_0^{\pi} \exp(\sqrt{xt} \cos \theta) \cos(\sqrt{xt} \sin \theta) \\ \times g(x+t-2\sqrt{xt} \cos \theta) d\theta. \quad (11.214)$$

This proves the McCully's theorem for the Laguerre transform (Equation 11.182). ■

**11.4.4 Applications of Laguerre Transforms****Example 11.29 (Heat Conduction Problem)**

The diffusion equation for one-dimensional linear flow of heat in a semi-infinite medium  $0 \leq x < \infty$  with a source  $Q(x, t)$  in the medium is

$$\frac{\partial}{\partial x} \left[ \kappa \frac{\partial u}{\partial x} \right] + Q(x, t) = \rho c \frac{\partial u}{\partial t}, \quad t > 0, \quad (11.215)$$

where  $\kappa = \kappa(x) = \lambda e^{-x} x^{\beta}$  is the variable thermal conductivity;  $Q(x, t) = \mu e^{-x} x^{\beta'} \frac{\partial u}{\partial x}$ ;  $\rho = \nu e^{-x} x^{\beta'}$ ;  $\lambda, \mu, \nu$  and  $c$  are constants; and  $\beta \geq 1$  and  $\beta - \beta' = 1$ . Thus, the above equation reduces to

$$\frac{\partial}{\partial x} \left[ e^{-x} x^{\beta} \frac{\partial u}{\partial x} \right] + \frac{\mu}{\lambda} e^{-x} x^{\beta'} \frac{\partial u}{\partial x} = \frac{\nu c}{\lambda} e^{-x} x^{\beta'} \frac{\partial u}{\partial t}. \quad (11.216)$$

The initial condition is

$$u(x, 0) = g(x), \quad 0 \leq x < \infty \quad (11.217)$$

Clearly, Equation 11.216 assumes the form

$$e^x x^{-\alpha} \frac{\partial}{\partial x} \left( e^{-x} x^{\alpha+1} \frac{\partial u}{\partial x} \right) = \gamma \frac{\partial u}{\partial t}, \quad (11.218)$$

where  $\alpha = \frac{\mu}{\lambda} + \beta - 1$  and  $\gamma = \frac{\nu c}{\lambda}$ .

Application of the Laguerre transform to Equation 11.218 gives

$$\frac{d}{dt} u_\alpha(n, t) = -\frac{n}{\gamma} u_\alpha(n, t), \quad u_\alpha(n, 0) = g_\alpha(n).$$

Thus, the solution of this system is

$$u_\alpha(n, t) = g_\alpha(n) \exp\left(-\frac{nt}{\gamma}\right). \quad (11.219)$$

The inverse transform (Equation 11.181) gives the formal solution

$$u(x, t) = \sum_{n=0}^{\infty} (\delta_n)^{-1} g_\alpha(n) L_n^\alpha(x) \exp\left(-\frac{nt}{\gamma}\right), \quad (11.220)$$

where  $\delta_n$  is given by Equation 11.180. ■

**Example 11.30 (Diffusion Equation)**

Solve Equation 11.215 with

$$\kappa = xe^{-x}, \quad Q(x, t) = e^{-x}f(t), \quad \text{and} \quad \rho c = e^{-x}.$$

In this case, the diffusion Equation 11.215 becomes

$$\frac{\partial u}{\partial t} = e^x \frac{\partial}{\partial x} \left( x e^{-x} \frac{\partial u}{\partial x} \right) + f(t), \quad 0 \leq x < \infty, t > 0, \quad (11.221)$$

and has to be solved with the initial-boundary data

$$\left. \begin{aligned} u(x, 0) &= g(x), & 0 \leq x < \infty \\ \frac{\partial}{\partial t} u(x, t) &= f(x), & \text{at } t = 0, \text{ for } x > 0 \end{aligned} \right\}. \quad (11.222)$$

Application of the Laguerre transform  $L\{u(x, t)\} = \tilde{u}_0(n, t)$  to Equations 11.221 and 11.222 gives

$$\tilde{u}_0(n, t) = g_0(n)e^{-nt}, \quad n = 1, 2, 3, \dots \quad (11.223)$$

$$\tilde{u}_0(0, t) = g_0(0) + \int_0^t f(\tau) d\tau. \quad (11.224)$$

The inverse Laguerre transform (Equation 11.181) leads to the formal solution

$$\begin{aligned} u(x, t) &= g_0(0) + \int_0^t f(\tau) d\tau + \sum_{n=1}^{\infty} g_0(n) e^{-nt} L_n(x) \\ &= \int_0^t f(\tau) d\tau + \sum_{n=0}^{\infty} g_0(n) e^{-nt} L_n(x). \end{aligned} \quad (11.225)$$

In view of the convolution theorem 11.11, this result takes the form

$$\begin{aligned} u(x, t) &= \int_0^t f(\tau) d\tau + \frac{1}{\pi} \int_0^\infty e^{-\tau} (e^\tau - 1)^{-1} \exp\left(\frac{-\tau}{e^\tau - 1}\right) \\ &\quad \times \int_0^\pi \exp(\sqrt{x\tau} \cos \theta) \cos(\sqrt{x\tau} \sin \theta) g(x + \tau - 2\sqrt{x\tau} \cos \theta) d\theta d\tau. \end{aligned} \quad (11.226)$$

This result is obtained by McCully (1960).

Another application of the Laguerre transform to the problem of oscillations of a very long and heavy chain with variable tension was discussed by Debnath (1961).

We conclude this chapter by adding references of recent work on the Laguerre–Pinney transformation and the Wiener–Laguerre transformation by Glaeske (1981, 1986). For more details, the reader is referred to these papers. ■

**11.4.5 Additional Relations**

1. If  $L\{f(x)\} = f_0(n) = \int_0^\infty e^{-x} L_n(x) f(x) dx$ , and  $a > 0$ , show that
  - a.  $L\{\sin ax\} = \frac{a^n}{(1+a^2)^{\frac{n+1}{2}}} \sin\left[n \tan^{-1}\left(\frac{1}{a}\right) + \tan^{-1}(-a)\right]$ ,
  - b.  $L\{\cos ax\} = \frac{a^n}{(1+a^2)^{\frac{n+1}{2}}} \cos\left[n \tan^{-1}\left(\frac{1}{a}\right) + \tan^{-1}(-a)\right]$ .
2. If  $L\{f(x)\} = \tilde{f}_0(n) = \int_0^\infty e^{-x} L_n(x) f(x) dx$ , show that:
  - a.  $L\{xf'(x)\} = -(n+1)\tilde{f}_0(n+1) + n\tilde{f}_0(n)$ ,
  - b.  $L\left[e^x \frac{d}{dx} \{x e^{-x} f'(x)\}\right] = -n\tilde{f}_0(n)$ ,
  - c.  $L\left[e^{-x} \frac{d}{dx} \{x e^x f'(x)\}\right] = n\tilde{f}_0(n) - 2(n+1)\tilde{f}_0(n+1)$ ,
  - d.  $L\left[\frac{d}{dx} \{xf'(x)\}\right] = -(n+1)\tilde{f}_0(n+1)$ .

**11.5 Hermite Transforms**

**11.5.1 Introduction**

In this chapter we introduce the Hermite transform with a kernel involving a Hermite polynomial and discuss its basic operational properties, including the convolution theorem. Debnath (1964) first introduced this transform and proved some of its basic operational properties. This chapter is based on papers by Debnath (1964, 1968) and Dimovski and Kalla (1988).

**11.5.2 Definition of the Hermite Transform and Examples**

Debnath (1964) defined the *Hermite transform* of a function  $F(x)$  defined in  $-\infty < x < \infty$  by the integral

$$H\{F(x)\} = f_H(n) = \int_{-\infty}^{\infty} \exp(-x^2) H_n(x) F(x) dx, \quad (11.227)$$

where  $H_n(x)$  is the well-known *Hermite polynomial* of degree  $n$ .

The inverse Hermite transform is given by

$$H^{-1}\{f_H(n)\} = F(x) = \sum_{n=0}^{\infty} (\delta_n)^{-1} f_H(n) H_n(x), \quad (11.228)$$

where  $\delta_n$  is given by

$$\delta_n = \sqrt{\pi} n! 2^n. \quad (11.229)$$

This follows from the expansion of any function  $F(x)$  in the form

$$F(x) = \sum_{n=0}^{\infty} a_n H_n(x), \quad (11.230)$$

where the coefficients  $a_n$  can be determined from the orthogonal relation of the Hermite polynomial  $H_n(x)$  as

$$\int_{-\infty}^{\infty} \exp(-x^2) H_n(x) H_m(x) dx = \delta_{nm} \delta_n. \quad (11.231)$$

Multiplying Equation 11.230 by  $\exp(-x^2) H_m(x)$  and integrating over  $(-\infty, \infty)$  and using Equation 11.230, we obtain

$$a_n = \delta_n^{-1} f_H(n) \quad (11.232)$$

so that Equation 11.228 follows immediately.

**Example 11.31**

If  $F(x)$  is a polynomial of degree  $m$ , then

$$f_H(n) = 0 \quad \text{for } n > m. \quad (11.233)$$

**Example 11.32**

If  $F(x) = H_m(x)$ , then

$$H\{H_m(x)\} = \int_{-\infty}^{\infty} \exp(-x^2) H_n(x) H_m(x) dx = \delta_n \delta_{nm}. \quad (11.234)$$

**Example 11.33**

If

$$\exp(2xt - t^2) = \sum_{n=0}^{\infty} \frac{t^n}{n!} H_n(x) \quad (11.235)$$

is the generating function of  $H_n(x)$ , then

$$H\{\exp(2xt - t^2)\} = \sqrt{\pi} \sum_{n=0}^{\infty} (2t)^n, \quad |t| < \frac{1}{2}. \quad (11.236)$$

We have, by definition,

$$\begin{aligned} H\{\exp(2xt - t^2)\} &= \sum_{n=0}^{\infty} \frac{t^n}{n!} \int_{-\infty}^{\infty} \exp(-x^2) H_n^2(x) dx \\ &= \sum_{n=0}^{\infty} \delta_n \frac{t^n}{n!} = \sqrt{\pi} \sum_{n=0}^{\infty} (2t)^n, \quad |t| < \frac{1}{2}. \end{aligned}$$

**Example 11.34**

If  $F(x) = H_m(x) H_p(x)$ , then

$$H\{H_m(x) H_p(x)\} = \begin{cases} \frac{\sqrt{\pi} 2^k m! n! p!}{(k-m)!(k-n)!(k-p)!} & m+n+p=2k, \\ & k \geq m, n, p \\ 0, & \text{otherwise} \end{cases} \quad (11.237)$$

This follows from a result proved by Bailey (1939).

**Example 11.35**

If  $F(x) = H_m^2(x) H_n(x)$ , then

$$H\{H_m^2(x) H_n(x)\} = 2^m \delta_n \sum_{k=0}^n \binom{m}{k} \binom{n}{k} \binom{2k}{k}, \quad (11.238)$$

if  $m > n$ .

Using a result proved by Feldheim (1938), Equation 11.238 follows immediately.

**Example 11.36**

If  $F(x) = H_{n+p+q}(x) H_p(x) H_q(x)$ , then

$$H\{F(x)\} = \delta_{n+p+q}. \quad (11.239)$$

We have, by definition,

$$H\{F(x)\} = \int_{-\infty}^{\infty} \exp(-x^2) H_{n+p+q}(x) H_p(x) H_q(x) dx = \delta_{n+p+q},$$

where a result due to Bailey (1939) is used and  $\delta_n$  is given by Equation 11.229.

**Example 11.37**

If  $F(x) = \exp(ax)$ , then

$$H\{\exp(ax)\} = \sqrt{\pi} \sum a^n \exp\left(\frac{1}{4} a^2\right). \quad (11.240)$$

This result follows from the standard result

$$\int_{-\infty}^{\infty} \exp(-x^2 + 2bx)H_n(x)dx = \sqrt{\pi}(2b)^n \exp(b^2).$$

■

**Example 11.38**

If  $|z| < 1$ , show that

$$H\left\{\exp(z^2)\sin(\sqrt{2}xz)\right\} = \begin{cases} 0, & n \neq 2m+1 \\ \sqrt{\pi} \sum_{m=0}^{\infty} (-1)^m (2z)^{2m+1}, & n = 2m+1 \end{cases} \quad (11.241)$$

We have, by definition,

$$H\left\{\exp(z^2)\sin(\sqrt{2}xz)\right\} = \int_{-\infty}^{\infty} \exp(z^2 - x^2)H_n(x)\sin(\sqrt{2}xz)dx.$$

We use a result (see Erdélyi et al., 1954, vol. 2, p. 194)

$$\exp(z^2)\sin(\sqrt{2}xz) = \sum_{m=0}^{\infty} (-1)^m H_{2m+1}(x) \frac{z^{2m+1}}{(2m+1)!}, \quad (11.242)$$

to derive

$$\begin{aligned} H\left\{\exp(z^2)\sin(\sqrt{2}xz)\right\} &= \sum_{m=0}^{\infty} (-1)^m \frac{z^{2m+1}}{(2m+1)!} \int_{-\infty}^{\infty} \exp(-x^2)H_n(x)H_{2m+1}(x)dx \\ &= \begin{cases} \sqrt{\pi} \sum_{m=0}^{\infty} (-1)^m (2z)^{2m+1}, & n = 2m+1 \\ 0, & n \neq 2m+1 \end{cases} \end{aligned}$$

■

**Example 11.39**

$$H\left[(1-z^2)^{-\frac{1}{2}} \exp\left\{\frac{2xyz - (x^2 + y^2)z^2}{(1-z^2)}\right\}\right] = \sqrt{\pi} \sum_{m=0}^{\infty} z^m H_m(y)\delta_{mn}. \quad (11.243)$$

We use a result (see Erdélyi et al., 1954, vol. 2, p. 194)

$$(1-z^2)^{-\frac{1}{2}} \exp\left\{\frac{2xyz - (x^2 + y^2)z^2}{(1-z^2)}\right\} = \sum_{m=0}^{\infty} \left(\frac{1}{2}z\right)^m \frac{1}{m!} H_m(x)H_m(y)$$

to derive

$$\begin{aligned} &H\left[(1-z^2)^{-\frac{1}{2}} \exp\left\{\frac{2xyz - (x^2 + y^2)z^2}{(1-z^2)}\right\}\right] \\ &= \sum_{m=0}^{\infty} \left(\frac{1}{2}z\right)^m \frac{1}{m!} H_m(y) \int_{-\infty}^{\infty} \exp(-x^2)H_n(x)H_m(x)dx \\ &= \sum_{m=0}^{\infty} \left(\frac{1}{2}z\right)^m \frac{1}{m!} H_m(y)\delta_m \delta_{mn} = \sqrt{\pi} \sum_{m=0}^{\infty} z^m H_m(y)\delta_{mn}. \end{aligned}$$

**11.5.3 Basic Operational Properties**

**THEOREM 11.12**

If  $F'(x)$  is continuous and  $F''(x)$  is bounded and locally integrable in the interval  $-\infty < x < \infty$ , and if  $H\{F(x)\} = f_H(n)$ , then

$$H\{R[F(x)]\} = -2n f_H(n), \quad (11.244)$$

where  $R[F(x)]$  is the differential form given by

$$R[F(x)] = \exp(x^2) \frac{d}{dx} \left[ \exp(-x^2) \frac{dF}{dx} \right]. \quad (11.245)$$

*Proof* We have, by definition,

$$H\{R[F(x)]\} = \int_{-\infty}^{\infty} \frac{d}{dx} \left[ \exp(-x^2) \frac{dF}{dx} \right] H_n(x)dx$$

which is, by integrating by parts and using the orthogonal relation (Equation 11.234),

$$= -2n \int_{-\infty}^{\infty} \exp(-x^2) H_n(x) F(x)dx = -2n f_H(n).$$

Thus, the theorem is proved.

If  $F(x)$  and  $R[F(x)]$  satisfy the conditions of Theorem 11.12, then

$$H\{R^2[F(x)]\} = H\{R[R[F(x)]]\} = (-1)^2(2n)^2 f_H(n). \quad (11.246)$$

$$H\{R^3[F(x)]\} = (-1)^3(2n)^3 f_H(n). \quad (11.247)$$

More generally,

$$H\{R^m[F(x)]\} = (-1)^m(2n)^m f_H(n), \quad (11.248)$$

where  $m = 1, 2, \dots, m-1$

■

**THEOREM 11.13**

If  $F(x)$  is bounded and locally integrable in  $-\infty < x < \infty$ , and  $f_H(0) = 0$ , then  $H\{F(x)\} = f_H(n)$  exists and for each constant  $C$ ,

$$\begin{aligned}
 H^{-1}\left\{-\frac{f_H(n)}{2n}\right\} &= R^{-1}[F(x)] \\
 &= \int_0^x \exp(s^2) \int_{-\infty}^s \exp(-t^2) F(t) dt ds + C,
 \end{aligned}
 \tag{11.249}$$

where  $R^{-1}$  is the inverse of the differential operator  $R$  and  $n$  is a positive integer.

*Proof* We write

$$R^{-1}[F(x)] = Y(x)$$

so that  $Y(x)$  is a solution of the differential equation

$$R[Y(x)] = F(x). \tag{11.250}$$

Since  $f_H(0) = 0$ , and  $H_0(x) = 1$ , then

$$\int_{-\infty}^{\infty} \exp(-x^2) F(x) dx = 0.$$

The first integral of Equation 11.250 is

$$\exp(-x^2) Y'(x) = \int_{-\infty}^x \exp(-t^2) F(t) dt,$$

which is a continuous function of  $x$  and tends to zero as  $|x| \rightarrow \infty$ . The second integral

$$Y(x) = \int_0^x \exp(s^2) \int_{-\infty}^s \exp(-t^2) F(t) dt ds + C,$$

where  $C$  is an arbitrary constant, is also continuous. Evidently,

$$\lim_{|x| \rightarrow \infty} \exp(-x^2) Y(x) = 0$$

provided  $Y(x)$  is bounded.

Then  $H\{Y(x)\}$  exists and

$$H\{R[Y(x)]\} = -2n H\{Y(x)\}.$$

Or,

$$H\{F(x)\} = -2n H\{Y(x)\}.$$

Hence,

$$f_H(n) = -2n H\{R^{-1}[F(x)]\}.$$

Thus, for any positive integer  $n$ ,

$$H\{R^{-1}[F(x)]\} = -\frac{f_H(n)}{2n}.$$

**THEOREM 11.14**

If  $F(x)$  has bounded derivatives of order  $m$  and if  $H\{F(x)\} = f_H(n)$  exists, then

$$H\{F^{(m)}(x)\} = f_H(n + m). \tag{11.251}$$

*Proof* We have, by definition,

$$H\{F'(x)\} = \int_{-\infty}^{\infty} \exp(-x^2) H_n(x) F'(x) dx,$$

which is, by integrating by parts,

$$\begin{aligned}
 &= [\exp(-x^2) F(x) H_n(x)]_{-\infty}^{\infty} - \int_{-\infty}^{\infty} F(x) \frac{d}{dx} [e^{-x^2} H_n(x)] dx \\
 &= 2 \int_{-\infty}^{\infty} x \exp(-x^2) H_n(x) F(x) dx - \int_{-\infty}^{\infty} F(x) \exp(-x^2) H'_n(x) dx.
 \end{aligned}
 \tag{11.252}$$

We use the *recurrence relations* for the Hermite polynomial

$$\begin{aligned}
 H_{n+1}(x) - 2xH_n(x) + 2nH_{n-1}(x) &= 0 \\
 H'_n(x) &= 2xH_{n-1}(x)
 \end{aligned}$$

to rewrite Equation 11.252 in the form

$$\begin{aligned}
 H\{F'(x)\} &= \int_{-\infty}^{\infty} \exp(-x^2) [H_{n+1}(x) + 2nH_{n-1}(x)] F(x) dx \\
 &\quad - 2n \int_{-\infty}^{\infty} \exp(-x^2) H_{n-1}(x) F(x) dx \\
 &= \int_{-\infty}^{\infty} \exp(-x^2) H_{n+1}(x) F(x) dx = f_H(n + 1).
 \end{aligned}$$

Proceeding in a similar manner, we can prove

$$H\{F^{(m)}(x)\} = f_H(n + m).$$

Thus, the theorem is proved. ■

**THEOREM 11.15**

If the Hermite transforms of  $F(x)$  and  $x F^{(m-1)}(x)$  exist, then

$$H\{x F^{(m)}(x)\} = n f_H(m+n-1) + \frac{1}{2} f_H(m+n+1). \quad (11.253)$$

*Proof* We have, by definition,

$$\begin{aligned} H\{x F^{(m)}(x)\} &= \int_{-\infty}^{\infty} \exp(-x^2) H_n(x) \left\{ x \frac{d^m F(x)}{dx^m} \right\} dx \\ &= [x \exp(-x^2) H_n(x) F^{(m-1)}(x)]_{-\infty}^{\infty} \\ &\quad - \int_{-\infty}^{\infty} \frac{d}{dx} [x \exp(-x^2) H_n(x)] F^{(m-1)}(x) dx. \end{aligned}$$

Thus,

$$\begin{aligned} H\{x F^{(m)}(x)\} &= \int_{-\infty}^{\infty} 2x^2 \exp(-x^2) H_n(x) F^{(m-1)}(x) dx \\ &\quad - \int_{-\infty}^{\infty} \exp(-x^2) H_n(x) F^{(m-1)}(x) dx \\ &\quad - n \int_{-\infty}^{\infty} 2x \exp(-x^2) H_{n-1}(x) F^{(m-1)}(x) dx, \end{aligned}$$

which is, by the recurrence relations (Equations 11.253, 11.254 and 11.251),

$$\begin{aligned} &= \int_{-\infty}^{\infty} x \exp(-x^2) [H_{n+1}(x) + 2n H_{n-1}(x)] F^{(m-1)}(x) dx \\ &\quad - n \int_{-\infty}^{\infty} \exp(-x^2) [H_n(x) + 2(n-1) H_{n-2}(x)] F^{(m-1)}(x) dx \\ &\quad - f_H(n+m+1) \\ &= \frac{1}{2} \int_{-\infty}^{\infty} \exp(-x^2) [H_{n+2}(x) + 2(n+1) H_n(x)] F^{(m-1)}(x) dx \\ &\quad + n \int_{-\infty}^{\infty} \exp(-x^2) [H_n(x) + 2(n-1) H_{n-2}(x)] F^{(m-1)}(x) dx \\ &\quad - n f_H(n+m-1) - 2n(n-1) f_H(n+m-3) - f_H(n+m+1) \\ &= \frac{1}{2} f_H(n+m+1) + (n+1) f_H(n+m-1) \\ &\quad + n [f_H(n+m-1) + 2(n-1) f_H(n+m-3)] \\ &\quad - n f_H(n+m-1) - 2n(n-1) f_H(n+m-3) - f_H(n+m+1) \\ &= n f_H(n+m-1) + \frac{1}{2} f_H(n+m+1). \end{aligned}$$

In particular, when  $m=1$  and  $m=2$ , we obtain

$$H\{x F'(x)\} = n f_H(n) + \frac{1}{2} f_H(n+2), \quad (11.254)$$

$$H\{x F''(x)\} = n f_H(n+1) + \frac{1}{2} f_H(n+3). \quad (11.255)$$

The reader is referred to a paper by Debnath (1968) for other results similar to those of Equations 11.254 and 11.255.

**Definition 11.2: (Generalized Convolution)** The generalized convolution of  $F(x)$  and  $G(x)$  for the Hermite transform defined by

$$H\{F(x) * G(x)\} = \mu_n H\{F(x)\} H\{G(x)\} = \mu_n f_H(n) g_H(n), \quad (11.256)$$

where  $\mu_n$  is a nonzero quantity given by

$$\mu_n = \sqrt{\pi} (-1)^n \left\{ 2^{2n+1} \Gamma\left(n + \frac{3}{2}\right) \right\}^{-1}. \quad (11.257)$$

Debnath (1968) first proved the convolution theorem of the Hermite transform for odd functions. However, Dimovski and Kalla (1988) extended the theorem for both odd and even functions. We follow Dimovski and Kalla to state and prove the convolution theorem of the Hermite transform. Before we discuss the theorem, it is observed that, if  $F(x)$  is an odd function, then

$$H\{F(x); 2n\} = f_H(2n) = \int_{-\infty}^{\infty} \exp(-x^2) H_{2n}(x) F(x) dx = 0, \quad (11.258)$$

but

$$H\{F(x); 2n+1\} = f_H(2n+1) \neq 0. \quad (11.259)$$

On the other hand, if  $F(x)$  is an even function, then

$$H\{F(x); 2n+1\} = f_H(2n+1) = 0, \quad (11.260)$$

but

$$H\{F(x); 2n\} = f_H(2n) \neq 0. \quad (11.261)$$

**THEOREM 11.16 (Convolution of the Hermite Transform for Odd Functions)**

If  $F(x)$  and  $G(x)$  are odd functions and  $n$  is an odd positive integer, then

$$H\{F(x) \circledast G(x); 2n + 1\} = \mu_n f_H(2n + 1)g_H(2n + 1), \quad (11.262)$$

where  $\circledast$  denotes the convolution operation for odd functions and is given by

$$F(x) \circledast G(x) = \frac{x}{\pi} \int_{-\infty}^{\infty} \exp(-t^2)tF(t)dt \int_0^{\pi} \exp(-xt \cos \phi) \sin \phi \times \int_0^{\pi} \frac{G[(x^2 + t^2 + 2xt \cos \phi)]^{\frac{1}{2}}}{(x^2 + t^2 + 2xt \cos \phi)^{\frac{3}{2}}} J_0(xt \sin \phi) d\phi, \quad (11.263)$$

and  $J_0(z)$  is the Bessel function of the first kind of order zero.

*Proof* We have, by definition,

$$f_H(2n + 1) = \int_{-\infty}^{\infty} \exp(-x^2)H_{2n+1}(x)F(x)dx. \quad (11.264)$$

We replace  $H_{2n+1}(x)$  by using a result for Erdélyi (1953, vol. 2, p. 1993)

$$H_{2n+1}(x) = (-1)^n 2^{2n+1} n! x L_n^{\frac{1}{2}}(x^2), \quad (11.265)$$

where  $L_n^{\alpha}(x)$  is the Laguerre polynomial of degree  $n$  and order  $\alpha$  so that Equation 11.264 reduces to the form

$$f_H(2n + 1) = (-1)^n 2^{2n+2} n! \int_0^{\infty} x \exp(-x^2) L_n^{\frac{1}{2}}(x^2) F(x) dx. \quad (11.266)$$

Invoking the change of variable  $x^2 = t$ , we obtain

$$H\{F(x); 2n + 1\} = (-1)^n 2^{2n+1} n! \int_0^{\infty} \sqrt{t} \exp(-t) L_n^{\frac{1}{2}}(t) \frac{F(\sqrt{t})}{\sqrt{t}} dt. \quad (11.267)$$

It is convenient to introduce the transformation  $T$  by

$$(TF)(t) = \frac{F(\sqrt{t})}{\sqrt{t}}, \quad 0 \leq t < \infty \quad (11.268)$$

so that the inverse of  $T$  is given by

$$T^{-1}(\Phi)(x) = x \Phi(x^2). \quad (11.269)$$

Consequently, Equation 11.267 takes the form

$$H\{F(x); 2n + 1\} = (-1)^n 2^{2n+1} n! L\{TF(x)\}, \quad (11.270)$$

where  $L$  is the Laguerre transformation of degree  $n$  and order  $\alpha = \frac{1}{2}$  defined by (11.227).

The use of Equation 11.270 allows us to write the product of two Hermite transforms as the product of two Laguerre transforms as

$$f_H(2n + 1)g_H(2n + 1) = 2^{4n+2} (n!)^2 L\{TF(x)\}L\{TG(x)\}. \quad (11.271)$$

We now apply the convolution theorem for the Laguerre transform (when  $\alpha = 0$ ) proved by Debnath (1969) in the form

$$L\{F \tilde{\ast} G(x)\} = \frac{n! \sqrt{\pi}}{\Gamma(n + \frac{3}{2})} L\{F(x)\}L\{G(x)\}, \quad (11.272)$$

where  $F \tilde{\ast} G$  is given by

$$F \tilde{\ast} G(x) = \int_0^{\infty} \exp(-\tau) \sqrt{\tau} F(\tau) d\tau \int_0^{\pi} \exp(-\sqrt{t\tau} \cos \phi) \sin \phi \times G(t + \tau + 2\sqrt{t\tau} \cos \phi) J_0(\sqrt{t\tau} \sin \phi) d\phi. \quad (11.273)$$

Substituting Equation 11.272 into 11.271, we obtain

$$f_H(2n + 1)g_H(2n + 1) = \pi^{-\frac{1}{2}} 2^{4n+2} n! \Gamma\left(n + \frac{3}{2}\right) L\{TF \tilde{\ast} TG\},$$

which is, by Equation 11.270,

$$= \frac{2^{2n+1} \Gamma\left(n + \frac{3}{2}\right)}{(-1)^n \sqrt{\pi}} H\{T^{-1}(TF \tilde{\ast} TG)\}. \quad (11.274)$$

or, equivalently,

$$H\{F \circledast G(x); 2n + 1\} = \mu_n H\{F(x)\}H\{G(x)\}, \quad (11.275)$$

where

$$F \circledast G(x) = T^{-1}\{TF \circledast TG(x)\}. \quad (11.276)$$

This coincides with Equation 11.263. Thus, the proof is complete.

**THEOREM 11.17 (Convolution of the Hermite Transform for Even Functions)**

If  $F(x)$  and  $G(x)$  are even functions and  $n$  is an even positive integer, then

$$H\{F(x) \star G(x); 2n\} = \mu_n H\{F(x); 2n\} H\{G(x); 2n\}. \quad (11.277)$$

*Proof* We use result (Equation 11.251), that is,

$$H\{F'(x); n\} = H\{F(x); n + 1\}$$

so that

$$H\{I F(x); 2n + 1\} = H\{F(x); 2n\}, \quad (11.278)$$

where

$$I F(x) = \int_0^x F(t) dt \quad \text{and} \quad [I F(x)]' = F(x).$$

Obviously,

$$\begin{aligned} H\{F(x) \star G(x); 2n\} &= H\{[I F(x) \star I G(x)]'; 2n\} \\ &= H\{I F(x) \star I G(x); 2n + 1\} \\ &= \mu_n H\{I F(x); 2n + 1\} H\{I G(x); 2n + 1\} \\ &= \mu_n H\{F(x); 2n\} H\{G(x); 2n\}. \end{aligned}$$

This proves the theorem. ■

**THEOREM 11.18**

If  $F(x)$  and  $G(x)$  are two arbitrary functions such that their Hermite transforms exist, then

$$H\{F(x) \star G(x); n\} = \mu_{[n/2]} H\{F(x); n\} H\{G(x); n\}, \quad (11.279)$$

where

$$F(x) \star G(x) = F_0(x) \circ G_0(x) + F_e(x) \star G_e(x), \quad (11.280)$$

and

$$\begin{aligned} F_0(x) &= \frac{1}{2} [F(x) - F(-x)] \quad \text{and} \\ F_e(x) &= \frac{1}{2} [F(x) + F(-x)]. \end{aligned} \quad (11.281)$$

*Proof* We first note that arbitrary functions  $F(x)$  and  $G(x)$  can be expressed as sums of even and odd functions, that is,  $F(x) = F_0(x) + F_e(x)$  and  $G(x) = G_0(x) + G_e(x)$  so that result (Equation 11.281) follows.

Suppose  $n$  is odd. Then

$$H\{F(x); n\} = H\{F_0(x); n\}, H\{G(x); n\} = H\{G_0(x); n\},$$

and

$$H\{F(x) + G(x); n\} = H\{F_0(x) + G_0(x); n\}.$$

Clearly,

$$\begin{aligned} H\{F(x) \star G(x); 2n + 1\} &= H\{F_0(x) \star G_0(x); 2n + 1\} + H\{F_e(x) \star G_e(x); 2n + 1\} \\ &= \mu_n H\{F_0(x)\} H\{G_0(x)\} = \mu_n H\{F(x)\} H\{G(x)\}. \end{aligned}$$

Similarly, the case for even  $n$  can be handled without any difficulty.

We conclude this chapter by citing some recent work on the generalized Hermite transformation by Glaeske (1983, 1986, 1987). These papers include some interesting discussion on operational properties and convolution structure of the generalized Hermite transformations. For more details, the reader is referred to these papers.

**11.5.4 Additional Relations**

1. The relation below

$$H\{x^n\} = \sqrt{\pi} n! P_n(1),$$

Is true, where  $P_n(x)$  is the Legendre polynomial.

2. Also

$$H\{H_n^2(x)\} = \sqrt{\pi} \sum_{r=0}^n \binom{n}{r} 2^{r+n} (2r)! n!.$$

**References**

Bailey, W. N. (1939). On Hermite polynomials and associated Legendre functions, *J. Lond. Math. Soc.*, 14, 281-286.  
 Bateman, H. (1944). *Partial Differential Equations of Mathematical Physics*, Dover Publications, New York.  
 Churchill, R. V. (1954). The operational calculus of Legendre Transforms, *J. Math. and Physics*, 33, 165-178.  
 Churchill, R. V. and Dolph, C. L. (1954). Inverse transforms of products of Legendre transforms. *Proc. Am. Math Soc.*, 5, 93-100.  
 Conte, S. D. (1955). Gegenbauer transforms, *Quart. J. Math. Oxford* (2), 6, 48-52.



- Copson, E. T. (1935). *An Introduction to the Theory of Functions of a Complex Variable*, Oxford University Press, Oxford.
- Debnath, L. (1960). On Laguerre transform, *Bull. Calcutta Math. Soc.*, 55, 69–77.
- Debnath, L. (1961). Applications of Laguerre transform to the problem of oscillations of a very long and heavy chain, *Annali dell' Univ. di Ferrara, Sezione VII-Scienze Matematiche*, IX, 149–151.
- Debnath, L. (1963). On Jacobi transforms, *Bull. Calcutta Math. Soc.*, 55, 113–120.
- Debnath, L. (1964). On Hermite transforms, *Mathematicioki*, 1 (16), 285–292.
- Debnath, L. (1967). Solutions of partial differential equations by the Jacobi transform, *Bull. Calcutta Math. Soc.*, 59, 155–158.
- Debnath, L. (1968). Some operational properties of the Hermite transform, *Math. Vesnik*, 5 (20), 29–36.
- Debnath, L. (1969). An asymptotic treatment of the transient development of surface waves, *Appl. Sci. Res.*, 21, 24–36.
- Debnath, L. and Harrel, C. W. (1976). The operational calculus of associated Legendre transforms-I, *Indian J. Pure Appl. Math.*, 7, 278–291.
- Dimorski, I. H. and Kalla, S. L. (1988). Convolution for Hermite transforms, *Math. Japonica*, 33, 345–351.
- Erdélyi, A. (1953). *Higher Transcendental Functions*, Vols. 1 and 2, McGraw-Hill, New York.
- Erdélyi, A., Magnus, W., Oberhettinger, F., and Tricomi, F. (1954). *Tables of Integral Transforms*, Vols. 1 and 2, McGraw-Hill, New York.
- Eringen, A. C. (1954). The finite Sturm–Liouville transform, *Quart. J. Math. Oxford* (2), 5, 120–129.
- Feldheim, E. (1938). Quelques nouvelles relations pour les polynômes d'Itermite, *J. Lond. Math. Soc.*, 13, 22–29.
- Glaeske, H. J. (1981). Die Laguerre–Pinney transformation, *Aequationes Math.*, 22, 73–85.
- Glaeske, H. J. (1983). On a convolution structure of a generalized Hermite transformation, *Serdica Bulgaricae Math. Publ.*, 9, 223–229.
- Glaeske, H. J. (1986). On the Wiener–Laguerre transformation, *Riv. Téc. Ing. Univ. Zulia*, 9, 27–34.
- Glaeske, H. J. (1987). Operational properties of generalized Hermite transformations, *Aequationes Math.*, 32, 155–170.
- Howell, R. (1938). A definite integral for Legendre functions, *Phil. Mag.*, 25, 1113–1115.
- Lakshmanarao, S. K. (1954). Gegenbauer transforms, *Math. Student*, 22, 161–165.
- McCully, J. (1960). The Laguerre transform, *SIAM Review*, 2, 185–191.
- Sanson, G. (1959). *Orthogonal Functions*, Interscience Publishers, New York.
- Scott, E. J. (1953). Jacobi transforms, *Quart. J. Math.*, 4, 36–40.
- Sneddon, I. N. (1946). Finite Hankel transforms, *Phil. Mag.*, 37, 17–25.

# 12

## Mellin Transform

---

Jacqueline Bertrand  
*University of Paris*

Pierre Bertrand  
*French National Aerospace Research  
Establishment (ONERA)*

Jean-Philippe Ovarlez  
*French National Aerospace Research  
Establishment (ONERA)*

12.1	Introduction.....	12-1
12.2	The Classical Approach and Its Developments .....	12-2
	Generalities on the Transformation • Standard Applications	
12.3	Alternative Approach Related to the Dilation Group and Its Representations.....	12-17
	Theoretical Aspects • Discretization and Fast Computation of the Transform • Practical Use in Signal Analysis	
	Appendix 12.A: Some Special Functions Frequently Occurring as Mellin Transforms.....	12-33
	Appendix 12.B: Summary of Properties of the Mellin Transformation .....	12-35
	References .....	12-36

### 12.1 Introduction

---

In contrast to Fourier and Laplace transformations that were introduced to solve physical problems, Mellin's transformation arose in a mathematical context. In fact, the first occurrence of the transformation is found in a memoir by Riemann in which he used it to study the famous Zeta function. References concerning this work and its further extension by M. Cahen are given in Ref. [1]. However, it is the Finnish mathematician, R. H. Mellin (1854–1933), who was the first to give a systematic formulation of the transformation and its inverse. Working in the theory of special functions, he developed applications to the solution of hypergeometric differential equations and to the derivation of asymptotic expansions. The Mellin contribution gives a prominent place to the theory of analytic functions and relies essentially on Cauchy's theorem and the method of residues. A biography of R. H. Mellin including a sketch of his works can be found in Ref. [2]. Actually, the Mellin transformation can also be placed in another framework, which in some respects conforms more closely to the original ideas of Riemann.

In this approach, the transformation is seen as a Fourier transformation on the multiplicative group of positive real numbers (i.e., group of dilations) and its development parallels the group-theoretical presentation of the usual Fourier transform.<sup>3,4</sup> One of the merits of this alternative presentation is to emphasize the fact that the Mellin transformation corresponds to an isometry between Hilbert spaces of functions. Besides its use in mathematics, Mellin's transformation has been applied in many different areas of physics and engineering.

Maybe the most famous application is the computation of the solution of a potential problem in a wedge-shaped region where the unknown function (e.g., temperature or electrostatic potential) is supposed to satisfy Laplace's equation with given

boundary conditions on the edges. Another domain where Mellin's transformation has proved useful is the resolution of linear differential equations in  $x(d/dx)$  arising in electrical engineering by a procedure analogous to Laplace's. More recently, traditional applications have been enlarged and new ones have emerged. A new impulse has been given to the computation of certain types of integrals by Marichev,<sup>5</sup> who has extended the Mellin method and devised a systematic procedure to make it practical.

The alternative approach to Mellin's transformation involving the group of dilations has specific applications in signal analysis and imaging techniques. Used in place of Fourier's transform when scale invariance is more relevant than shift invariance, Mellin's transform suggests new formal treatments. Moreover, a discretized form can be set up and allows the fast numerical computation of general expressions in which dilated functions appear, such as wavelet coefficients and time-frequency transforms.

This chapter is divided into two parts that can be read independently. The first part (Section 12.2) deals with the introduction of the transformation as a holomorphic function in the complex plane, in a manner analogous to what is done with Laplace's transform. The definition of the transform is given in Section 12.2.1; its properties are described in detail and illustrated by examples. Emphasis is put in Section 12.2.1.6 on inversion procedures that are essential for a practical use of the transform. The applications considered in this first part (Section 12.2.2) are well-known for the most part: summation of series, computation of integrals depending on a parameter, solution of differential equations, and asymptotic expansion. The last example (Section 12.2.2.6), however, concerns a fairly recent application to the asymptotic analysis of harmonic sums arising in the analysis of algorithms.<sup>6</sup>

The second part (Section 12.3), which is especially oriented towards signal analysis and imaging, deals with the introduction of the Mellin transform from a systematic study of dilations. In Section 12.3.1, some notions of group theory are recalled in the special case of the group of positive numbers (dilation group) and Mellin's transformation is derived together with properties relevant to the present setting. The discretization of the transformation is performed in Section 12.3.2. A choice of practical applications is then presented in Section 12.3.3.

## 12.2 The Classical Approach and Its Developments

### 12.2.1 Generalities on the Transformation

#### 12.2.1.1 Definition and Relation to Other Transformations

**Definition 12.1:** Let  $f(t)$  be a function defined on the positive real axis  $0 < t < \infty$ . The Mellin transformation  $\mathcal{M}$  is the operation mapping the function  $f$  into the function  $F$  defined on the complex plane by the relation:

$$\mathcal{M}[f; s] \equiv F(s) = \int_0^{\infty} f(t)t^{s-1} dt \quad (12.1)$$

The function  $F(s)$  is called the Mellin transform of  $f$ . In general, the integral does exist only for complex values of  $s = a + jb$  such that  $a < a_1 < a_2$ , where  $a_1$  and  $a_2$  depend on the function  $f(t)$  to transform. This introduces what is called the *strip of definition* of the Mellin transform that will be denoted by  $S(a_1, a_2)$ . In some cases, this strip may extend to a half-plane ( $a_1 = -\infty$  or  $a_2 = +\infty$ ) or to the whole complex  $s$ -plane ( $a_1 = -\infty$  and  $a_2 = +\infty$ ).

#### Example 12.1

Consider

$$f(t) = H(t - t_0)t^z \quad (12.2)$$

where

- $H$  is Heaviside's step function
- $t_0$  is a positive number
- $z$  is complex

The Mellin transform of  $f$  is given by

$$\mathcal{M}[f; s] = \int_{t_0}^{\infty} t^{z+s-1} dt = -\frac{t_0^{z+s}}{z+s} \quad (12.3)$$

provided  $s$  is such that  $\text{Re}(s) < -\text{Re}(z)$ . In this case the function  $f(s)$  is holomorphic in a half-plane.

#### Example 12.2

The Mellin transform of the function:

$$f(t) = e^{-pt} \quad p > 0 \quad (12.4)$$

is equal, by definition, to

$$\mathcal{M}[f; s] = \int_0^{\infty} e^{-pt} t^{s-1} dt \quad (12.5)$$

Using the definition (see Appendix 12.A) of the Gamma function, we obtain

$$\mathcal{M}[f; s] = p^{-s}\Gamma(s) \quad (12.6)$$

Recalling that the Gamma function is analytic in the region  $\text{Re}(s) > 0$ , we conclude that the strip of holomorphy is a half-plane as in the first example.

#### Example 12.3

Consider the function:

$$f(t) = (1+t)^{-1} \quad (12.7)$$

Its Mellin transform can be computed directly using the calculus of residues. But another method consists in changing the variables in Equation 12.1 from  $t$  to  $x$  defined by

$$t+1 = \frac{1}{1-x}, \quad x = \frac{t}{t+1}, \quad dx = \frac{dt}{(t+1)^2} \quad (12.8)$$

The transform of Equation 12.7 is then expressed by

$$\mathcal{M}[f; s] = \int_0^1 x^{s-1}(1-x)^{-s} dx \quad (12.9)$$

with the condition  $0 < \text{Re}(s) < 1$ . This integral is known (Appendix 12.A) to define the beta function  $B(s, 1-s)$  which can also be written in terms of Gamma functions. The result is given by the expression:

$$\begin{aligned} \mathcal{M}[f; s] &= B(s, 1-s) \\ &= \Gamma(s)\Gamma(1-s) \end{aligned} \quad (12.10)$$

which is analytic in the strip of existence of Equation 12.9. An equivalent formula is obtained using a property (Appendix 12.A) of the Gamma function:

$$\mathcal{M}[f; s] = \frac{\pi}{\sin \pi s} \quad (12.11)$$

valid in the same strip.

12.2.1.1.1 Relation to Laplace and Fourier Transformations

Mellin's transformation is closely related to an extended form of Laplace's. The change of variables defined by

$$t = e^{-x}, \quad dt = -e^{-x} dx \tag{12.12}$$

transforms the integral (Equation 12.1) into

$$F(s) = \int_{-\infty}^{\infty} f(e^{-x})e^{-sx} dx \tag{12.13}$$

After the change of function:

$$g(x) \equiv f(e^{-x}) \tag{12.14}$$

one recognizes in Equation 12.13 the *two-sided* Laplace transform of  $g$  usually defined by

$$\mathcal{L}[g; s] = \int_{-\infty}^{\infty} g(x)e^{-sx} dx \tag{12.15}$$

This can be written symbolically as

$$\mathcal{M}[f(t); s] = \mathcal{L}[f(e^{-x}); s] \tag{12.16}$$

The occurrence of a strip of holomorphy for Mellin's transform can be deduced directly from this relation. The usual right-sided Laplace transform is analytic in a half-plane  $\text{Re}(s) > \sigma_1$ . In the same way, one can define a left-sided Laplace transform analytic in the region  $\text{Re}(s) < \sigma_2$ . If the two half-planes overlap, the region of holomorphy of the two-sided transform is thus the strip  $\sigma_1 < \text{Re}(s) < \sigma_2$  obtained as their intersection.

To obtain Fourier's transform, write now  $s = a + 2\pi j\beta$  in Equation 12.13:

$$F(s) = \int_{-\infty}^{\infty} f(e^{-x}) e^{-ax} e^{-j2\pi\beta x} dx \tag{12.17}$$

The result is

$$\mathcal{M}[f(t); a + j2\pi\beta] = \mathfrak{F}[f(e^{-x})e^{-ax}; \beta] \tag{12.18}$$

where  $\mathfrak{F}$  represents the Fourier transformation defined by

$$\mathfrak{F}[f; \beta] = \int_{-\infty}^{\infty} f(x)e^{-j2\pi\beta x} dx \tag{12.19}$$

Thus, for a given value of  $\text{Re}(s) = a$  belonging to the definition strip, the Mellin transform of a function can be expressed as a Fourier transform.

12.2.1.2 Inversion Formula

A direct way to invert Mellin's transformation (Equation 12.1) is to start from Fourier's inversion theorem. As is well known, if  $\tilde{f} = \mathfrak{F}[f; \beta]$  is the Fourier transform (Equation 12.19) of  $f$ , the original function is recovered by

$$f(x) = \int_{-\infty}^{\infty} \tilde{f}(\beta)e^{j2\pi\beta x} d\beta \tag{12.20}$$

Applying this formula to Equation 12.17 with  $s = a + j2\pi\beta$  yields:

$$f(e^{-x})e^{-ax} = \int_{-\infty}^{\infty} F(s) e^{j2\pi\beta x} d\beta \tag{12.21}$$

Hence, going back to variables  $t$  and  $s$ :

$$f(t) = t^{-a} \int_{-\infty}^{\infty} F(s) t^{-j2\pi\beta} d\beta \tag{12.22}$$

The inversion formula finally reads:

$$f(t) = (1/2\pi j) \int_{a-j\infty}^{a+j\infty} F(s) t^{-s} ds \tag{12.23}$$

where the integration is along a vertical line through  $\text{Re}(s) = a$ . Here a few questions arise. What value of  $a$  has to be put into the formula? What happens when  $a$  is changed? Is the inverse unique? In what case is  $f$  a function defined for all  $t$ 's?

It is clear that if  $F$  is holomorphic in the strip  $S(a_1, a_2)$  and vanishes sufficiently fast when  $\text{Im}(s) \rightarrow \pm\infty$ , then by Cauchy's theorem, the path of integration can be translated sideways inside the strip without affecting the result of the integration. More precisely, the following theorem holds:<sup>7,8</sup>

---

**THEOREM 12.1**

If, in the strip  $S(a_1, a_2)$ ,  $F(s)$  is holomorphic and satisfies the inequality:

$$|F(s)| \leq K|s|^{-2} \tag{12.24}$$

for some constant  $K$ , then the function  $f(t)$  obtained by formula (Equation 12.23) is a continuous function of the variable  $t \in (0, \infty)$  and its Mellin transform is  $F(s)$ .

Remark that this result gives only a sufficient condition for the inversion formula to yield a continuous function.

From a practical point of view, it is important to note that the inversion formula applies to a function  $F$ , holomorphic in a given strip, and that the uniqueness of the result holds only with respect to that strip. In fact, a Mellin transform consists of a pair: a function  $F(s)$  and a strip of holomorphy  $S(a_1, a_2)$ . A unique function  $F(s)$  with several disjoint strips of holomorphy will in general have several reciprocals, one for each strip. Some examples will illustrate this point.

**Example 12.4**

The Mellin transform of the function:

$$f(t) = (H(t - t_0) - H(t))t^z \tag{12.25}$$

is given by

$$\mathcal{M}[f; s] = -\frac{t_0^{z+s}}{(z+s)} \tag{12.26}$$

provided  $\text{Re}(s) > -\text{Re}(z)$ . Comparing Equations 12.3 and 12.26, we see an example of two functions  $F(s)$  having the same analytical expression but considered in two distinct regions of holomorphy: the inverse Mellin transforms, given respectively by Equations 12.2 and 12.25 are indeed different (see Figure 12.1).

**Example 12.5 Gamma function continuation**

From the result of Example 12.2 considered for  $p = 1$ , the function  $f(t) = e^{-t}$ ,  $t > 0$  is known to be the inverse Mellin transform of  $\Gamma(s)$ ,  $\text{Re}(s) > 0$ . Besides, it may be checked that  $\Gamma(s)$  satisfies the hypotheses of Theorem 12.1; this is done by

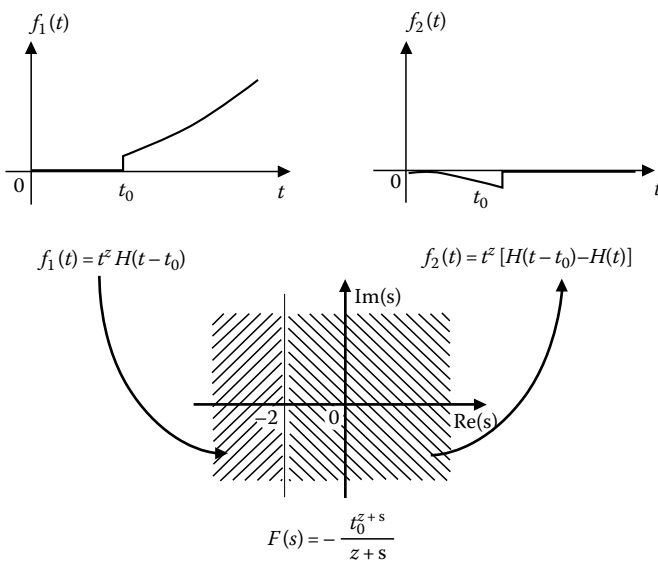


**FIGURE 12.1** Examples of results when the regions of holomorphy are changed.

using Stirling's formula which implies the following behavior of the Gamma function:<sup>5</sup>

$$|\Gamma(a + ib)| \sim \sqrt{2\pi}|b|^{a-1/2} e^{-|b|\pi/2}, \quad |b| \rightarrow \infty \tag{12.27}$$

Thus, the inversion formula (Equation 12.23) can be applied here and gives an integral representation of  $e^{-t}$  as

$$e^{-t} \equiv (1/2\pi j) \int_{a-j\infty}^{a+j\infty} \Gamma(s)t^{-s} ds, \quad a > 0 \tag{12.28}$$

It is known that the  $\Gamma$ -function can be analytically continued in the left half-plane except for an infinite number of poles at the negative or zero integers. The inverse Mellin transform of the Gamma function for different strips of holomorphy will now be obtained by transforming the identity (Equation 12.28). The contour of integration can be shifted to the left and the integral will only pick up the values of the residues at each pole (Figure 12.2). Explicitly, if  $a > 0$  and  $-N < a' < -N, N$  integer, we have

$$(1/2\pi j) \int_{a-j\infty}^{a+j\infty} \Gamma(s)t^{-s} ds = \sum_{n=0}^{N-1} \frac{(-1)^n}{n!} t^n + (1/2\pi j) \int_{a'-j\infty}^{a'+j\infty} \Gamma(s)t^{-s} ds \tag{12.29}$$

Hence, the inversion formula of the  $\Gamma$ -function in the strip  $S(-N, -N + 1)$  gives the result:

$$(1/2\pi j) \int_{a'-j\infty}^{a'+j\infty} \Gamma(s)t^{-s} ds = e^{-t} - \sum_{n=0}^{N-1} \frac{(-1)^n}{n!} t^n, \quad -N < a' < -N + 1 \tag{12.30}$$

The integral term represents the remainder in the Taylor expansion of  $e^{-t}$  and can be shown to vanish in the limit  $N \rightarrow \infty$  by applying Stirling formula.

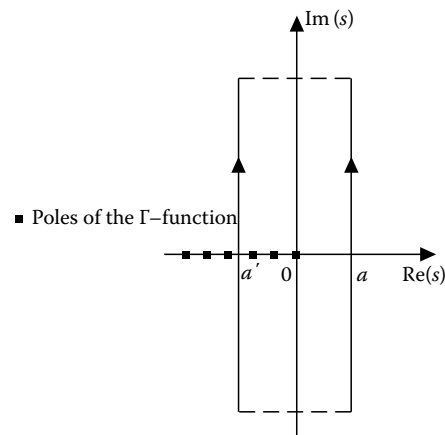


**FIGURE 12.2** Different contours of integration for the inverse Mellin transform of the Gamma function. The contributions from the horizontal parts go to zero as  $\text{Im}(s)$  goes to infinity.

As a corollary of the inversion formula, a Parseval relation can be established for suitable classes of functions.

**COROLLARY 12.1**

Let  $\mathcal{M}[f; s]$  and  $\mathcal{M}[g; s]$  be the Mellin transforms of functions  $f$  and  $g$  with strips of holomorphy  $S_f$  and  $S_g$ , respectively, and suppose that some real number  $c$  exists such that  $c \in S_f$  and  $1 - c \in S_g$ . Then Parseval's formula can be written as

$$\int_0^\infty f(t)g(t) dt = \frac{1}{2\pi j} \int_{c-j\infty}^{c+j\infty} \mathcal{M}[f; s]\mathcal{M}[g; 1-s] ds \quad (12.31)$$

This formula may be established formally by computing the right-hand side of Equation 12.31 using definition (12.1):

$$\frac{1}{2\pi j} \int_{c-j\infty}^{c+j\infty} \mathcal{M}[f; s]\mathcal{M}[g; 1-s] ds = \frac{1}{2\pi j} \int_{c-j\infty}^{c+j\infty} \mathcal{M}[g; 1-s] \int_0^\infty f(t)t^{s-1} dt ds \quad (12.32)$$

Exchanging the two integrals:

$$\frac{1}{2\pi j} \int_{c-j\infty}^{c+j\infty} \mathcal{M}[f; s]\mathcal{M}[g; 1-s] ds = \frac{1}{2\pi j} \int_0^\infty f(t) \int_{c-j\infty}^{c+j\infty} \mathcal{M}[g; 1-s]t^{s-1} dt ds \quad (12.33)$$

and using the inverse formula (Equation 12.23) for  $g$  leads to Equation 12.31.

Different sets of conditions ensuring the validity of this Parseval formula may be stated (see Ref. [9, p. 108]). The crucial point is the interchange of integrals that cannot always be justified.

**12.2.1.3 Transformation of Distributions**

The extension of the correspondence (Equation 12.1) to distributions has to be considered to introduce a larger framework in which Dirac delta and other singular functions can be treated straightforwardly. The distributional setting of Mellin's transformation has been studied mainly by Kang,<sup>10</sup> Zemanian,<sup>7</sup> and Misra and Lavoine.<sup>8</sup> We refer the interested reader to these works for a thorough treatment. As we will see, several approaches of the subject are possible as it was the case for Fourier's transformation.

It is possible to define the Mellin transform for all distributions belonging to the space  $\mathcal{D}'_+$  of distributions on the half-line  $(0, \infty)$ . The procedure<sup>10</sup> is to start from the space  $\mathcal{D}(0, \infty)$  of infinitely differentiable functions of compact support on  $(0, \infty)$  and to consider the set  $Q$  of their Mellin transforms. It can be shown that it is a space of entire functions which is isomorphic, as a linear topological space, to the space  $Z$  of Gelfand and

Shilov.<sup>11</sup> This space can be used as a space of test functions and the one-to-one correspondence thus defined between elements of spaces  $\mathcal{D}(0, \infty)$  and  $Q$  can then be carried (i.e., transposed) to the dual spaces  $\mathcal{D}'_+$  and  $Q'$ . In this operation, a Mellin transform is associated with any distribution in  $\mathcal{D}'_+$  and the result belongs to a space  $Q'$  formed of analytic functionals (see Example 12.6 for an illustration). The situation is quite analogous to that encountered with the Fourier transformation where a correspondence between distributions spaces  $\mathcal{D}'$  and  $Z'$  are established.

Actually, it may be efficient to restrict the class of distributions for which the Mellin transformation will be defined, as is usually done in Fourier analysis with the introduction of the space  $\mathcal{S}'$  of tempered distributions.<sup>11</sup> In the present case, a similar approach can be based on the possibility to single out subspaces of  $\mathcal{D}'_+$  whose elements are Mellin-transformed into functions which are analytic in a given strip. This construction will now be sketched.

The most practical way to proceed is to give a new interpretation of formula (Equation 12.1) by considering it as the application of a distribution  $f$  to a test function  $t^{s-1}$ :

$$F(s) = \langle f, t^{s-1} \rangle \quad (12.34)$$

A suitable space of test functions  $\mathcal{T}(a_1, a_2)$  containing all functions  $t^{s-1}$  for  $s$  in the region  $a_1 < \text{Re}(s) < a_2$  may be introduced as follows.<sup>8</sup> The space  $\mathcal{T}(a_1, a_2)$  is composed of functions  $\phi(t)$  defined on  $(0, \infty)$  and with continuous derivatives of all orders going to zero as  $t$  approaches either zero or infinity. More precisely, there exists two positive numbers  $\zeta_1, \zeta_2$ , such that, for all integers  $k$ , the following conditions hold:

$$t^{k+1-a_1-\zeta_1} \phi^{(k)}(t) \rightarrow 0, \quad t \rightarrow 0 \quad (12.35)$$

$$t^{k+1-a_2-\zeta_2} \phi^{(k)}(t) \rightarrow 0, \quad t \rightarrow \infty \quad (12.36)$$

A topology on  $\mathcal{T}$  is defined accordingly, it can be verified that all functions in  $\mathcal{D}(0, \infty)$  belong to  $\mathcal{T}(a_1, a_2)$ .<sup>\*</sup> The space of distributions  $\mathcal{T}'(a_1, a_2)$  is then introduced as a linear space of continuous linear functionals on  $\mathcal{T}(a_1, a_2)$ . It may be noticed that if  $\alpha_1, \alpha_2$  are two real numbers such that  $a_1 < \alpha_1 < \alpha_2 < a_2$ , then  $\mathcal{T}(\alpha_1, \alpha_2)$  is included in  $\mathcal{T}(a_1, a_2)$ . One may so define a whole collection of ascending spaces  $\mathcal{T}(a_1, a_2)$  with compatible<sup>†</sup> topologies, thus ensuring the existence of limit spaces when  $a_1 \rightarrow -\infty$  and/or  $a_2 \rightarrow \infty$ .

Hence, the dual spaces of distributions are such that  $\mathcal{T}'(a_1, a_2) \subset \mathcal{T}'(\alpha_1, \alpha_2)$  and  $\mathcal{T}'(-\infty, +\infty)$  is included in all of them. Moreover, as a consequence of the status of  $\mathcal{D}(0, \infty)$  relatively to  $\mathcal{T}(a_1, a_2)$ , the space  $\mathcal{T}'(a_1, a_2)$  is a subspace of distributions in  $\mathcal{D}'_+$ . The precise construction of these spaces is explained in Ref. [8]. A slightly different presentation is given in Ref. [7] and leads to these same spaces denoted by  $\mathcal{M}(a_1, a_2)$ .

<sup>\*</sup> More precisely, one can show that  $\mathcal{D}(0, \infty)$  is dense in  $\mathcal{T}(a_1, a_2)$

<sup>†</sup> In fact,  $\mathcal{T}(-\infty, a_2)$ ,  $\mathcal{T}(a_1, +\infty)$ , and  $\mathcal{T}(-\infty, +\infty)$  are defined as inductive limits.

With the above definitions, the Mellin transform of an element  $f \in \mathcal{T}'(a_1, a_2)$  is defined by

$$\mathcal{M}[f; s] \equiv F(s) = \langle f, t^{s-1} \rangle \quad (12.37)$$

The result is always a conventional function  $F(s)$  holomorphic in the strip  $a_1 < \text{Re}(s) < a_2$ .

In summary, every distribution in  $\mathcal{D}'_+$  has a Mellin transform which, as a rule, is an analytic functional. Besides, it is possible to define subspaces  $\mathcal{T}'(a_1, a_2)$  of  $\mathcal{D}'_+$  whose elements,  $f$ , are Mellin transformed by formula (Equation 12.37) into functions  $F(s)$  holomorphic in the strip  $S(a_1, a_2)$ . Any space,  $\mathcal{T}'$ , contains in particular Dirac distributions and arbitrary distributions of bounded support. They are stable under derivation and multiplication by a smooth function. Their complete characterization is given by the following theorems.

---

### THEOREM 12.2

(Uniqueness theorem<sup>7</sup>) Let  $\mathcal{M}[f; s] = F(s)$  and  $\mathcal{M}[h; s] = H(s)$  be Mellin transforms with strips of holomorphy  $S_f$  and  $S_h$ , respectively. If the strips overlap and if  $F(s) \equiv H(s)$  for  $s \in S_f \cap S_h$ , then  $f \equiv h$  as distributions in  $\mathcal{T}'(a_1, a_2)$  where the interval  $(a_1, a_2)$  is given by the intersection of  $S_f \cap S_h$  with the real axis.

---

### THEOREM 12.3

(Characterization of the Mellin transform of a distribution in  $\mathcal{T}'(a_1, a_2)$ .<sup>7,8</sup> A necessary and sufficient condition for a function  $F(s)$  to be the Mellin transform of a distribution  $f \in \mathcal{T}'(a_1, a_2)$  is

- $F(s)$  is analytic in the strip  $a_1 < \text{Re}(s) < a_2$ ,
- For any closed substrip  $\alpha_1 \leq \text{Re}(s) \leq \alpha_2$  with  $a_1 < \alpha_1 < \alpha_2 < a_2$  there exists a polynomial  $P$  such that  $|F(s)| \leq P(|s|)$  for  $\alpha_1 \leq \text{Re}(s) \leq \alpha_2$ .

#### Example 12.6 (Example of analytic functional)

The function  $t^z$ ,  $z$  complex, defines a distribution in  $\mathcal{D}'_+$  according to

$$\langle t^z, \phi \rangle = \int_0^{\infty} t^z \phi(t) dt, \quad \phi \in \mathcal{D}(0, \infty) \quad (12.38)$$

But it may seem that this distribution does not belong to any of the spaces  $\mathcal{T}'(a_1, a_2)$ . Its Mellin transform may nevertheless be defined by the following formula:

$$\langle \mathcal{M}[t^z], \psi \rangle_M = \langle t^z, \phi \rangle \quad (12.39)$$

where  $\langle, \rangle_M$  denotes duality in the space of Mellin transforms,  $\phi \equiv \mathcal{M}^{-1}\psi$  is an element of  $\mathcal{D}(0, \infty)$  and, consequently,  $\psi$  is an entire function.

According to Equation 12.39 and Definition 12.1, we obtain:

$$\begin{aligned} \langle \mathcal{M}[t^z], \Psi \rangle_M &= \mathcal{M}[\phi; z+1] \\ &= \psi(z+1) \end{aligned} \quad (12.40)$$

Since distribution  $\mathcal{M}[t^z]$  applied to  $\psi$  gives the value of  $\psi$  in a point of the complex plane, it can be symbolized by a delta function. To introduce the notation, we need the explicit form of duality  $\langle, \rangle_M$  which comes out of Parseval formula. According to Equation 12.31, it is given for entire functions  $\chi, \psi$  by

$$\langle \chi, \psi \rangle_M = \frac{1}{2\pi j} \int_{c-j\infty}^{c+j\infty} \chi(s)\psi(1-s) ds \quad (12.41)$$

where  $c$  is any real number. A more usual form is obtained by setting:

$$\tilde{\psi}(s) \equiv \psi(1-s) \quad (12.42)$$

and

$$\langle \chi, \tilde{\psi} \rangle \equiv \langle \chi, \psi \rangle_M \quad (12.43)$$

$$= \frac{1}{2\pi j} \int_{c-j\infty}^{c+j\infty} \chi(s)\tilde{\psi}(s) ds \quad (12.44)$$

With these definitions, Equation 12.40 can be written:

$$\langle \mathcal{M}[t^z], \tilde{\psi} \rangle = \tilde{\psi}(-z) \quad (12.45)$$

and the notation:

$$\mathcal{M}[t^z] = \delta(s+z) \quad (12.46)$$

can be proposed. Such Dirac distributions in the complex plane are defined in Ref. [11].

#### Example 12.7

The Mellin transform of the Dirac distribution  $\delta(t-t_0)$  is found by applying the general rule:

$$\langle \delta(t-t_0), \phi \rangle = \phi(t_0) \quad (12.47)$$

to the family of functions  $\phi(t) = t^{s-1}$ . One obtains:

$$\begin{aligned} \mathcal{M}[\delta(t - t_0); s] &= \langle \delta(t - t_0), t^{s-1} \rangle \\ &= t_0^{s-1} \end{aligned} \quad (12.48)$$

for any value of the positive number  $t_0$ . Moreover the result is holomorphic in the whole complex  $s$ -plane.

It is instructive to verify explicitly the inverse formula on this example. According to Equation 12.23, the inverse Mellin transform  $\mathcal{M}^{-1}[t_0^{s-1}; t]$  can be written as

$$\mathcal{M}^{-1}[t_0^{s-1}; t] = \frac{1}{2\pi j t_0} \int_{-j\infty}^{j\infty} \left(\frac{t}{t_0}\right)^{-s} ds \quad (12.49)$$

since the choice  $a = 0$  is allowed by the holomorphy property of the integrand in the whole plane. Setting  $s = j\beta$  in Equation 12.49 and performing the integration leads to the equivalent expressions:

$$\begin{aligned} \mathcal{M}^{-1}[t_0^{s-1}; t] &= \frac{1}{2\pi t_0} \int_{-\infty}^{\infty} e^{-j\beta \ln(t/t_0)} d\beta \\ &= t_0^{-1} \delta(\ln t - \ln t_0) \end{aligned} \quad (12.50)$$

The expected result:

$$\mathcal{M}^{-1}[t_0^{s-1}; t] = \delta(t - t_0) \quad (12.51)$$

comes out by using the classical formula:

$$\delta(f(t)) = |f'(t_0)|^{-1} \delta(t - t_0) \quad (12.52)$$

in which  $f(t)$  is a function having a simple zero in  $t = t_0$ .

**Example 12.8**

Consider the distribution:

$$f = \sum_{n=1}^{\infty} \delta(t - pn), \quad p > 0 \quad (12.53)$$

Its Mellin transform is given by

$$\begin{aligned} \left\langle \sum_{n=1}^{\infty} \delta(t - pn), t^{s-1} \right\rangle &= \sum_{n=1}^{\infty} (pn)^{s-1} \\ &= p^{s-1} \sum_{n=1}^{\infty} n^{s-1} \end{aligned} \quad (12.54)$$

The sum converges uniformly for  $\text{Re}(s) < 0$  and can be expressed in terms of Riemann's Zeta function<sup>13</sup> (see Appendix 12.A). Explicitly, we have

$$\mathcal{M} \left[ \sum_{n=1}^{\infty} \delta(t - pn); s \right] = p^{s-1} \zeta(1 - s), \quad \text{Re}(s) < 0 \quad (12.55)$$

**12.2.1.4 Some Properties of the Transformation**

This paragraph describes the effect on the Mellin transform  $\mathcal{M}[f; s]$  of some special operations performed on  $f$ . The resulting formulas are very useful for deducing new correspondences from a given one.

Let  $F(s) = \mathcal{M}[f; s]$  be the Mellin transform of a distribution which is supposed to belong to  $\mathcal{T}'(\sigma_1, \sigma_2)$  and denote by  $S_f = \{s: \sigma_1 < \text{Re}(s) < \sigma_2\}$  its strip of holomorphy ( $\sigma_1$  is either finite or  $-\infty$ ,  $\sigma_2$  is finite or  $\infty$ ). Then the following formulas hold with the regions of holomorphy as indicated. The notation of functions will be used but this must not obscure the fact that  $f$  is a distribution and that all operations performed on  $f$ , especially differentiation, must be understood in the generalized sense of distributions.

- *Scaling of the original variable by a positive number:*

$$\mathcal{M}[f(rt); s] = r^{-s} F(s), \quad s \in S_f, r > 0 \quad (12.56)$$

- *Raising of the original variable to a real power:*

$$\mathcal{M}[f(t^r); s] = |r|^{-1} F(r^{-1} s), \quad r^{-1} s \in S_f, r \text{ real } \neq 0 \quad (12.57)$$

- *Multiplication of the original function by  $\ln t$ :*

$$\mathcal{M}[(\ln t)^k f(t); s] = \frac{d^k}{ds^k} F(s), \quad s \in S_f, k \text{ positive integer} \quad (12.58)$$

- *Multiplication of the original function by some power of  $t$ :*

$$\mathcal{M}[(t)^z f(t); s] = F(s + z), \quad s + z \in S_f, z \text{ complex} \quad (12.59)$$

- *Derivation of the original function:*

$$\begin{aligned} \mathcal{M} \left[ \frac{d^k}{dt^k} f(t); s \right] &= (-1)^k (s - k)_k F(s - k), \\ & \quad s - k \in S_f, \quad k \text{ positive integer} \end{aligned} \quad (12.60)$$

where the symbol  $(s - k)_k$  is defined for  $k$  integer by

$$(s - k)_k \equiv (s - k)(s - k + 1) \dots (s - 1) \quad (12.61)$$

Formulas (Equation 12.59) and (Equation 12.60) can be used in various ways to find the effect of linear combinations of differential operators such that  $t^k(d/dt)^m$ ,  $k, m$  integers. The most remarkable result is

$$\mathcal{M} \left[ \left( t \frac{d}{dt} \right)^k f(t); s \right] = (-1)^k s^k F(s) \quad (12.62)$$

Other combinations can be computed. We have, for example,

$$\mathcal{M} \left[ \frac{d^k}{dt^k} t^k f(t); s \right] = (-1)^k (s - k)_k F(s) \quad (12.63)$$



$$\mathcal{M} \left[ t^k \frac{d^k}{dt^k} f(t); s \right] = (-1)^k (s)_k F(s) \quad (12.64)$$

where  $s \in S_f$ ,  $k$  is a positive integer and

$$(s)_k \equiv s(s+1) \dots (s+k-1) \quad (12.65)$$

These relations are easily verified on infinitely differentiable functions. It is important to stress that they are essentially true for distributions. That implies in particular that all derivatives occurring in the formulas are to be taken according to the distribution rules. An example dealing with a discontinuous function will make this manifest.

**Example 12.9**

Consider the function:

$$f(t) = H(t - t_0)t^z, z \text{ complex} \quad (12.66)$$

According to the results of Example 12.1, the Mellin transform of  $f$  is given by

$$\mathcal{M}[f; s] \equiv F(s) = -\frac{t_0^{z+s}}{z+s} \quad (12.67)$$

Applying formula (Equation 12.60) for  $k=1$  yields:

$$\begin{aligned} \mathcal{M} \left[ \frac{df}{dt}; s \right] &= -(s-1)F(s-1) \\ &= (s-1) \frac{t_0^{z+s-1}}{z+s-1} \end{aligned} \quad (12.68)$$

which can be rewritten as

$$\mathcal{M} \left[ \frac{df}{dt}; s \right] = -z \frac{t_0^{z+s-1}}{z+s-1} + t_0^{z+s-1} \quad (12.69)$$

or, recognizing the Mellin transforms obtained in Examples 12.1 and 12.7:

$$\mathcal{M} \left[ \frac{df}{dt}; s \right] = \mathcal{M} [zH(t - t_0)t^{z+s-1}; s] + \mathcal{M} [t_0^z \delta(t - t_0); s] \quad (12.70)$$

This result shows explicitly that, in formula (Equation 12.60),  $f$  is differentiated as a distribution. The first term in Equation 12.70 corresponds to the derivative of the function for  $t \neq t_0$  and the second term is the Dirac distribution arising from the discontinuity at  $t = t_0$ .

Additional results on the Mellin transforms of primitives can be established for particular classes of functions. Namely, if  $x > 1$ , integration by parts leads to the result:

$$\begin{aligned} \mathcal{M} \left[ \int_x^\infty f(t) dt; s \right] &= \int_0^\infty s^{-1} x^s f(x) dx \\ &= s^{-1} F(s+1) \end{aligned} \quad (12.71)$$

provided the integrated part  $s^{-1}x^s \int_x^\infty f(t) dt$  is equal to zero for  $x=0$  and  $x=\infty$ .

In the same way, but with different conditions on  $f$ , one establishes:

$$\mathcal{M} \left[ \int_0^x f(t) dt; s \right] = -s^{-1} F(s+1) \quad (12.72)$$

**12.2.1.5 Relation to Multiplicative Convolution**

The usual convolution has the property of being changed into multiplication by either a Laplace or a Fourier transformation. In the present case, a multiplicative convolution,<sup>10</sup> also called Mellin-type convolution,<sup>7,8</sup> is defined which has a similar property with respects to Mellin's transformation. In the same way as the usual convolution of two distributions in  $\mathcal{D}(\mathbb{R})$  does not necessarily exist, the multiplicative convolution of distributions in  $\mathcal{D}'_+$  can fail to define a distribution. To avoid such problems, we shall restrict our considerations to spaces  $\mathcal{T}'(a_1, a_2)$ .

**Definition 12.2:** Let  $f, g$  be two distributions belonging to some space  $\mathcal{T}'(a_1, a_2)$ . The multiplicative convolution of  $f$  and  $g$  is a functional  $(f \vee g)$  whose action on test functions  $\theta \in \mathcal{T}(a_1, a_2)$  is given by

$$\langle f \sim g, \theta \rangle = \langle f(t), \langle g(\tau), \theta(t\tau) \rangle \rangle \quad (12.73)$$

It can be shown that  $f \vee g$  is a distribution which belongs to the space  $\mathcal{T}'(a_1, a_2)$ .

If the distributions  $f$  and  $g$  are represented by locally integrable functions, definition (Equation 12.73) can be written explicitly as

$$\langle f \sim g, \theta \rangle = \int_0^\infty \int_0^\infty f(t)g(\tau)\theta(t\tau) dt d\tau \quad (12.74)$$

A change of variables then leads to the following expression for the multiplicative convolution of the functions  $f$  and  $g$ :

$$(f \sim g)(\tau) = \int_0^\infty f(t)g\left(\frac{\tau}{t}\right) \frac{dt}{t} \quad (12.75)$$

The so-called exchange formula for usual convolution has an analog for multiplicative convolution. It is expressed by the following theorem.<sup>7,8</sup>

**THEOREM 12.4 (Exchange Formula)**

The Mellin transform of the convolution product  $f \vee g$  of two distributions belonging to  $\mathcal{T}'(a_1, a_2)$  is given by the formula:

$$\mathcal{M}[f \vee g; s] = F(s)G(s), a_1 < \operatorname{Re}(s) < a_2 \quad (12.76)$$

where  $F(s)$  and  $G(s)$  are the Mellin transforms of distributions  $f$  and  $g$ , respectively.

The proof is a simple application of the definitions. According to Equation 12.37, the Mellin transform of distribution  $f \vee g \in \mathcal{T}'(a_1, a_2)$  is given by

$$\mathcal{M}[f \vee g; s] = \langle f \vee g, t^{s-1} \rangle, a_1 < \operatorname{Re}(s) < a_2 \quad (12.77)$$

or, using the definition (Equation 12.73) of convolution:

$$\mathcal{M}[f \sim g; s] = \langle f(t), \langle g(\tau), (t\tau)^{s-1} \rangle \rangle \quad (12.78)$$

which can be rewritten as

$$\mathcal{M}[f \sim g; s] = \langle f(t), t^{s-1} \rangle \langle g(\tau), \tau^{s-1} \rangle \quad (12.79)$$

Formula (Equation 12.73) allows to consider the multiplicative convolution of general distributions not belonging to space  $\mathcal{T}'(a_1, a_2)$ . However, in that case, it is not ensured that the product exists as a distribution.

**12.2.1.5.1 General Properties of the Multiplicative Convolution**

In this paragraph,  $f$  and  $g$  are distributions which belong to  $\mathcal{T}'(a_1, a_2)$  and  $k$  is a positive integer. The following properties are easy to verify. In fact, some of them are a direct consequence of the exchange formula.

1. *Commutativity*

$$f \vee g = g \vee f \quad (12.80)$$

2. *Associativity*

$$(f \vee g) \vee h = f \vee (g \vee h) \quad (12.81)$$

3. *Unit element*

$$f \vee \delta(t-1) = f \quad (12.82)$$

4. *Action of the operator  $t(d/dt)$* 

$$\begin{aligned} \left( t \frac{d}{dt} \right)^k (f \sim g) &= \left[ \left( t \frac{d}{dt} \right)^k f \right] \sim g \\ &= f \sim \left[ \left( t \frac{d}{dt} \right)^k g \right] \end{aligned} \quad (12.83)$$

i.e., it is sufficient to apply the operator to one of the factors.

5. *Multiplication by  $\ln t$ .*

$$(\ln t)(f \vee g) = [(\ln t)f] \vee g + f \vee [(\ln t)g] \quad (12.84)$$

6. *Convolution with Dirac distributions and their derivatives*

$$\delta(t-a) \sim f = a^{-1}f(a^{-1}t) \quad (12.85)$$

$$\delta(t-p) \sim \delta(t-p') = \delta(t-pp'), \quad p, p' > 0 \quad (12.86)$$

$$\delta^{(k)}(t-1) \sim f = (d/dt)^k(t^k f) \quad (12.87)$$

*Proof of relation (12.87)*

According to the definition of the  $k$ -derivative of the Dirac distribution, the multiplicative convolution of  $f$  with  $\delta^{(k)}(t-1)$  is given by

$$\begin{aligned} \langle f \sim \delta^{(k)}(t-1), \theta(t) \rangle &= \langle f(t), \langle \delta^{(k)}(\tau-1), \theta(t\tau) \rangle \rangle \\ &= \left\langle f(t), \left\langle \delta(\tau-1), (-1)^k \left( \frac{d}{d\tau} \right)^k \theta(t\tau) \right\rangle \right\rangle \end{aligned} \quad (12.88)$$

or, after performing an ordinary differentiation and applying the definition of  $\delta$ :

$$\langle f \sim \delta^{(k)}(t-1), \theta(t) \rangle = \langle f(t), (-1)^k t^k \theta^{(k)}(t) \rangle \quad (12.89)$$

The usual rules of calculus with distributions and the commutativity of convolution yield:

$$\langle \delta^{(k)}(t-1) \sim f, \theta(t) \rangle = \left\langle \left( \frac{d}{dt} \right)^k (t^k f(t)), \theta(t) \right\rangle \quad (12.90)$$

Finally, identity (Equation 12.87) follows from the fact that Equation 12.90 holds for any function  $\theta$  belonging to  $\mathcal{T}(a_1, a_2)$ .

**12.2.1.6 Hints for a Practical Inversion of the Mellin Transformation**

In many applications, it is essential to be able to perform explicitly the Mellin inversion. This is often the most difficult part of the computation and we now give some indications on different ways to proceed.

*Compute the inversion integral:* This direct approach is not always the simplest. In some cases, however, the integral Equation 12.23 can be computed by the method of residues.

*Use rules of Section 12.2.1.4 to exploit the inversion formula:* Property (Equation 12.62) in particular can be used to extend the domain of practical utility of the inversion formula (Equation 12.23). Indeed, in the case where the Mellin transform  $F(s)$ , holomorphic in the strip  $S(a_1, a_2)$  with  $(a_1, a_2)$  finite, does not satisfy condition (Equation 12.24), suppose that a positive integer  $k$  can be found such that:

$$|s^{-k}F(s)| \leq K|s|^{-2} \quad (12.91)$$

The inversion formula (Equation 12.23) can now be used on the function  $G(s)$  defined by

$$G(s) = (-1)^k s^{-k} F(s), \quad a_1 < \text{Re}(s) < a_2 \quad (12.92)$$

and yields a continuous function  $g(t)$ . Using rule (Equation 12.62) and the uniqueness of the Mellin transform, we conclude that the reciprocal of  $F(s)$  is the distribution  $f$  defined by

$$f = \left( t \frac{d}{dt} \right)^k g(t) \quad (12.93)$$

In spite of the fact that the continuous function  $g(t)$  is not necessarily differentiable everywhere, formula (Equation 12.93) remains meaningful since derivatives are taken in the sense of distributions. In fact, the above procedure corresponds to generalizing Theorem 12.1 in the following form:

---

**THEOREM 12.5<sup>7,8</sup>**

Let  $F(s)$  be a function holomorphic in the strip  $S(a_1, a_2)$  with  $a_1, a_2$  finite. If there exists an integer  $k \geq 0$  such that  $s^{2-k} F(s)$  is bounded as  $|s|$  goes to infinity, then the inverse Mellin transform of  $F(s)$  is the unique distribution  $f$  given by

$$f = \left( t \frac{d}{dt} \right)^k g(t) \quad (12.94)$$

where  $g(t)$  is a continuous function obtained by the formula:

$$g(t) = \frac{(-1)^k}{2\pi j} \int_{a-j\infty}^{a+j\infty} F(s) s^{-k} t^{-s} ds \quad (12.95)$$

with  $a \in S(a_1, a_2)$ .

Other inversion formulas may be obtained in the same way,<sup>8</sup> by using rules (Equation 12.63) and (Equation 12.64), respectively. They are

$$f = t^k \left( \frac{d}{dt} \right)^k g(t), \quad \text{where } g(t) = \frac{(-1)^k}{2\pi j} \int_{a-j\infty}^{a+j\infty} \frac{F(s)}{(s)_k} t^{-s} ds \quad (12.96)$$

$$f = \left( \frac{d}{dt} \right)^k t^k g(t), \quad \text{where } g(t) = \frac{(-1)^k}{2\pi j} \int_{a-j\infty}^{a+j\infty} \frac{F(s)}{(s-k)_k} t^{-s} ds \quad (12.97)$$

*Use the tables:* In simple cases, exploitation of tables<sup>14-16</sup> and use of the rules of calculus exhibited in Section 12.2.1.4 are sufficient to obtain the result.

In more difficult cases, it may be rewarding to use the systematic approach developed by Marichev<sup>5</sup> and applicable to a large number of functions. Suppose we are given a function  $F(s)$  holomorphic in the strip  $S(\sigma_1, \sigma_2)$  and we want to find its inverse Mellin transform. The first step is to try and cast  $F$  into the form of a fraction involving only products  $\Gamma$ -functions, the variable  $s$  appearing only with the coefficient  $\pm 1$ . This looks quite restrictive, but in fact many simple functions can be so rewritten using the properties of  $\Gamma$ -functions, recalled in Appendix 12.A. Thus,  $F(s)$  is brought to the form:

$$F(s) = C \prod_{i,j,k,l} \frac{\Gamma(a_i + s)\Gamma(b_j - s)}{\Gamma(c_k + s)\Gamma(d_l - s)} \quad (12.98)$$

where  $C, a_i, b_j, c_k, d_l$  are constants and where  $\text{Re}(s)$  is restricted to the strip  $S(\sigma_1, \sigma_2)$  now defined in terms of these.

For such functions, the explicit computation of the inversion integral Equation 12.23 can be performed by the theory of residues and yields a precise formula given in Ref. [5] as Slater's theorem. The result has the form of a function of hypergeometric type. The important point is that most special functions are included in this class. For a thorough description of the method, the reader is referred to Marichev's book<sup>5</sup> which contains simple explanations along with all the proofs and exhaustive tables.

*Special forms related to the use of polar coordinates:*<sup>17</sup> The analytical solution of some two-dimensional problems in polar coordinates  $(r, \theta)$  is obtained by using a Mellin transformation with respect to the radial variable  $r$ . In this approach, one can be faced with the task of inverting expressions of the type  $\cos(s\theta) F(s)$  or  $\sin(s\theta) F(s)$ . We will show that, for a large class of problems, the reciprocals of the products  $\cos(s\theta)F(s)$  and  $\sin(s\theta)F(s)$  can be obtained straightforwardly from the knowledge of the reciprocal of  $F(s)$ .

Let  $f(r), f$  real-valued, be the inverse Mellin transform of  $F(s)$  in strip  $S(a_1, a_2)$  and suppose that  $f$  can be analytically continued into a function  $f(z), z \equiv re^{j\theta}$ , in some sector  $|\theta| < \beta$  of the complex plane. If the rule of scaling (Equation 12.56) can be extended to the complex numbers, we have

$$\mathcal{M}[f(re^{j\theta}); s] = e^{-j\theta s} \mathcal{M}[f(r); s] \quad (12.99)$$

where the Mellin transforms are with respect to  $r$ .

In fact, this formula can be established by contour integration in a sector  $|\arg z| < \beta$  where the function  $f$  is such that:

$$z^s f(z) \rightarrow 0 \text{ as } |z| \rightarrow 0 \text{ or } \infty \quad (12.100)$$

Remark that since  $f$  has a Mellin transform with strip of definition  $S(a_1, a_2)$ , this condition already holds on the real axis when  $a_1 < \text{Re}(s) < a_2$ .

Recalling that  $f$  is real-valued, we can take the real and imaginary parts of Equation 12.99 and obtain, for real  $s$ , the formulas:

$$\mathcal{M}[\operatorname{Re}(f(re^{j\theta})); s] = \cos(s\theta)F(s) \quad (12.101)$$

$$\mathcal{M}[\operatorname{Im}(f(re^{j\theta})); s] = -\sin(s\theta)F(s) \quad (12.102)$$

These can be extended to complex  $s$  and yield the inverse Mellin transforms of  $\cos(s\theta)F(s)$  and  $\sin(s\theta)F(s)$  for  $a_1 < \operatorname{Re}(s) < a_2$  and  $|\theta| < \beta$ .

---

**EXAMPLE 12.10**<sup>17</sup>

To illustrate the use of the above rules, we shall perform explicitly the inversion of

$$F(s) = \frac{\cos s\theta}{s \cos s\alpha}, \alpha \text{ real} \quad (12.103)$$

in the strip  $0 < \operatorname{Re}(s) < \pi/(2\alpha)$ .

Using the result of Example 12.3 and rule (Equation 12.57), we obtain:

$$\mathcal{M}[(1+r^2)^{-1}; s] = \frac{\pi}{2 \sin(\pi s/2)}, \quad 0 < \operatorname{Re}(s) < 1 \quad (12.104)$$

Recalling that

$$\int_r^\infty \frac{dx}{1+s^2} = \pi/2 - \tan^{-1} r \quad (12.105)$$

and using rule (Equation 12.71) gives

$$\mathcal{M}[\pi/2 - \tan^{-1} r; s] = \frac{\pi}{2s \cos \pi s/2}, \quad 0 < \operatorname{Re}(s) < 1 \quad (12.106)$$

Using again property (Equation 12.57) but with  $\nu = \pi/2\alpha$  finally gives

$$\mathcal{M}[\pi/2 - \tan^{-1} r^\nu; s] = \frac{\pi}{2s \cos(\pi s/2\nu)}, \quad 0 < \operatorname{Re}(s) < \nu \quad (12.107)$$

To find the domain in which function  $f(z) = \pi/2 - \tan^{-1} z^\nu$ , where  $z = re^{j\theta}$ , verifies the condition (Equation 12.100), we write it under the form:

$$f(z) = (1/2j) \ln \left( \frac{z^\nu + j}{z^\nu - j} \right) \quad (12.108)$$

subject to the choice of the determination for which  $0 < \tan^{-1} r < \pi/2$ . The results is  $|\theta| \equiv |\arg(z)| < \pi/2$ . Relation (Equation 12.101) yields the result:

$$\mathcal{M}^{-1} \left[ \frac{\cos(s\theta)}{s \cos(s\alpha)}; s \right] = \operatorname{Re}(\pi/2 - \tan^{-1} z^\nu), \quad 0 < \operatorname{Re}(s) < \pi/(2\alpha), |\theta| < \pi/2 \quad (12.109)$$

The real part of  $f(re^{j\theta})$  is given explicitly by

$$\operatorname{Re}(\pi/2 - \tan^{-1} z^\nu) = \begin{cases} 1 - \pi^{-1} \tan^{-1} \frac{2r^\nu \cos \nu\theta}{1 - r^{2\nu}} & 0 \leq r < 1 \\ \pi^{-1} \tan^{-1} \frac{2r^\nu \cos \nu\theta}{r^{2\nu-1}} & r > 1 \end{cases}$$

## 12.2.2 Standard Applications

### 12.2.2.1 Summation of Series

Even if a numerical computation is intended, Mellin's transformation may be used with profit to transform slowly convergent series either into integrals that can be computed exactly or into more rapidly convergent series.

Let  $S$  represent a series of the form:

$$S = \sum_{n=1}^{\infty} f(n) \quad (12.110)$$

in which the terms are samples of a function  $f(t)$  for integer values of the variable  $t \in (0, \infty)$ . If this function has a Mellin transform  $F(s)$  with  $S(a_1, a_2)$  as strip of holomorphy, it can be written:

$$f(t) = (2\pi j)^{-1} \int_{a-j\infty}^{a+j\infty} F(s)t^{-s} ds, \quad a_1 < a < a_2 \quad (12.111)$$

Substituting this identity in Equation 12.110 yields:

$$S = (2\pi j)^{-1} \sum_{n=1}^{\infty} \int_{a-j\infty}^{a+j\infty} F(s)n^{-s} ds \quad (12.112)$$

Now, if  $F(s)$  is such that sum and integral can be exchanged, an integral expression for  $S$  is obtained:

$$S = (2\pi j)^{-1} \int_{a-j\infty}^{a+j\infty} F(s)\zeta(s) ds \quad (12.113)$$

where  $\zeta(s)$  is the Riemann zeta function defined by

$$\zeta(s) = \sum_{n=1}^{\infty} n^{-s} \quad (12.114)$$

The integral Equation 12.113 is then evaluated by the methods of Section 12.2.1.6. The calculus of residues may give the result as an infinite sum which, hopefully, will be more rapidly convergent than the original series.

Some care is necessary when going from Equations 12.112 and 12.113. Actually, if the interchange of summation and integration is not justified, the expression (Equation 12.113) can fail to represent the original series (see Ref. [17, p. 216], for an example).

**Example 12.11**

Compute the sum:

$$S(y) = \sum_{n=1}^{\infty} \frac{\cos ny}{n^2} \tag{12.115}$$

From Table 12.1 and properties (12.56) and (12.59), one finds:

**TABLE 12.1** Some Standard Mellin Transform Pairs

Original Function	Mellin Transform	
$f(t), t > 0$	$\mathcal{M}[f; s] \equiv \int_0^{\infty} f(t) t^{s-1} dt$	Strip of Holomorphy
$e^{-pt}, p > 0$	$p^{-s}\Gamma(s)$	$\text{Re}(s) > 0$
$H(t-a)t^b, a > 0$	$-\frac{a^{b+s}}{b+s}$	$\text{Re}(s) < -\text{Re}(b)$
$(H(t-a) - H(t))t^b$	$-\frac{a^{b+s}}{b+s}$	$\text{Re}(s) > -\text{Re}(b)$
$(1+t)^{-1}$	$\frac{\pi}{\sin(\pi s)}$	$0 < \text{Re}(s) < 1$
$(1+t)^{-a}$	$\frac{\Gamma(s)\Gamma(a-s)}{\Gamma(a)}$	$0 < \text{Re}(s) < \text{Re}(a)$
$(1-t)^{-1}$	$\pi \cot(\pi s)$	$0 < \text{Re}(s) < 1$
$H(1-t)(1-t)^{b-1}, \text{Re}(b) > 0$	$\frac{\Gamma(s)\Gamma(b)}{\Gamma(s+b)}$	$\text{Re}(s) > 0$
$H(t-1)(t-1)^{-b}$	$\frac{\Gamma(b-s)\Gamma(1-b)}{\Gamma(1-s)}$	$\text{Re}(s) < \text{Re}(b) < 1$
$H(t-1) \sin(a \ln t)$	$\frac{a}{s^2 + a^2}$	$\text{Re}(s) < - \text{Im}(a) $
$H(1-t) \sin(-a \ln t)$	$\frac{a}{s^2 + a^2}$	$\text{Re}(s) >  \text{Im}(a) $
$(H(t) - H(t-p)) \ln(p/t), p > 0$	$\frac{p^s}{s^2}$	$\text{Re}(s) > 0$
$\ln(1+t)$	$\frac{\pi}{s \sin(\pi s)}$	$-1 < \text{Re}(s) < 0$
$H(p-t) \ln(p-t)$	$-p^s s^{-1} [\psi(s+1) + p^{-1} \ln p]$	$\text{Re}(s) > 0$
$t^{-1} \ln(1+t)$	$\frac{\pi}{(1-s) \sin(\pi s)}$	$0 < \text{Re}(s) < 1$
$\ln \left  \frac{1+t}{1-t} \right $	$(\pi/s) \tan(\pi s)$	$-1 < \text{Re}(s) < 1$
$(e^t - 1)^{-1}$	$\Gamma(s)\zeta(s)$	$\text{Re}(s) > 1$
$t^{-1} e^{-t^{-1}}$	$\Gamma(1-s)$	$-\infty < \text{Re}(s) < 1$
$e^{-x^2}$	$(1/2)\Gamma(s/2)$	$0 < \text{Re}(s) < +\infty$
$e^{iat}$	$a^{-s}\Gamma(s)e^{i\pi(s/2)}$	$0 < \text{Re}(s) < 1$
$\tan^{-1}(t)$	$\frac{-\pi}{2s \cos(\pi s/2)}$	$-1 < \text{Re}(s) < 0$
$\cotan^{-1}(t)$	$\frac{\pi}{2s \cos(\pi s/2)}$	$0 < \text{Re}(s) < 1$
$\delta(t-p), p > 0$	$p^{s-1}$	Whole plane
$\sum_{n=1}^{\infty} \delta(t-pn), p > 0$	$p^{s-1} \zeta(1-s)$	$\text{Re}(s) < 0$
$J_\nu(t)$	$\frac{2^{s-1}\Gamma[(s+\nu)/2]}{\Gamma[(1/2)(\nu-s)+1]}$	$-\nu < \text{Re}(s) < 3/2$
$\sum_{n=-\infty}^{+\infty} p^{-nr} \delta(t-p^n)$	$\frac{1}{\ln p} \sum_{n=-\infty}^{+\infty} \delta\left(\beta - \frac{n}{\ln p}\right)$	$s = r + j\beta$
$p > 0, r \text{ real}$	$\beta = \text{Im}(s)$	
$t^b$	$\delta(b+s)$	None (analytic functional)

$$\mathcal{M}\left[\frac{\cos ty}{t^2}; s\right] = -y^{2-s}\Gamma(s-2)\cos(\pi s/2), \quad 2 < \text{Re}(s) < 3 \quad (12.116)$$

Hence, the sum can be rewritten as

$$S = -(1/2\pi j) \int_{a-j\infty}^{a+j\infty} y^{2-s}\Gamma(s-2)\cos(\pi s/2)\zeta(s) ds \quad (12.117)$$

where the interchange of summation and integration is justified by absolute convergence. The integral can be rearranged by using Riemann's functional relationship (see Ref. [17] and Appendix 12.A):

$$\pi^s \zeta(1-s) = 2^{1-s}\Gamma(s)\cos(\pi s/2)\zeta(s) \quad (12.118)$$

Then Equation 12.117 becomes:

$$S = -(1/2\pi j) \int_{a-j\infty}^{a+j\infty} y^{2-s}2^{s-1}\pi^s \frac{\zeta(1-s)}{(s-1)(s-2)} ds \quad (12.119)$$

The integral is easily computed by the method of residues, closing the contour to the left where the integrand goes to zero. The function  $\zeta(s)$  is analytic everywhere except at  $s = 1$  where it has a simple pole with residue equal to 1. The result is

$$S = \frac{y^2}{4} - \frac{\pi y}{2} + \frac{\pi^2}{6} \quad (12.120)$$

### 12.2.2.2 Computation of Integrals Depending on a Parameter

Essentially, the technique concerns integrals which can be brought to the form:

$$K(x) = \int_0^\infty K_0(t) K_1(x/t) \frac{dt}{t}, \quad x > 0 \quad (12.121)$$

One recognizes the expression of a multiplicative convolution. Such an integral can be computed by performing the following steps:

- Mellin transform functions  $K_0$  and  $K_1$  to obtain  $\mathcal{M}[K_0; s]$  and  $\mathcal{M}[K_1; s]$ .
- Multiply the transforms to obtain  $\mathcal{M}[K; s] \equiv \mathcal{M}[K_0; s] \mathcal{M}[K_1; s]$ .
- Find the inverse Mellin transform of  $\mathcal{M}[K; s]$  using the tables. The result will in general be expressed as a combination of generalized hypergeometric series.

For the last operation, the book by Marichev<sup>5</sup> can be of great help as previously mentioned in Section 12.2.1.6. The method can be extended to allow the computation of integrals of the form:

$$K(x_1, \dots, x_N) = \int_0^\infty K_0(t) \left[ \prod_{i=1}^n K_i\left(\frac{x_i}{t}\right) \right] \frac{dt}{t} \quad (12.122)$$

where  $x_1, \dots, x_N$  are positive variables.

It can be verified that the multiple Mellin transform defined by

$$[K; s_1, \dots, s_N] = \int_0^\infty \dots \int_0^\infty K(x_1, \dots, x_N) x_1^{s_1-1} \dots x_N^{s_N-1} dx_1 \dots dx_N \quad (12.123)$$

allows the expression (Equation 12.122) to be factored as

$$\mathcal{M}[K; s_1, \dots, s_N] = \mathcal{M}[K_0; s_1 + s_2 + \dots + s_N] \prod_{i=1}^N \mathcal{M}[K_i; s_i] \quad (12.124)$$

Techniques of inversion for this expression are developed in a book by Sasiella<sup>18</sup> devoted to the propagation of electromagnetic waves in turbulent media.

### 12.2.2.3 Mellin's Convolution Equations

These are not always expressed with integrals of type (Equation 12.75) but also with differential operators which are polynomials in  $(t(d/dt))$ . Such equations are of the general form:

$$Lu(t) \equiv \left( a_n \left( t \frac{d}{dt} \right)^n + a_{n-1} \left( t \frac{d}{dt} \right)^{n-1} + \dots + a_0 \right) u(t) = g(t) \quad (12.125)$$

By using the identity:

$$(t(d/dt))^k u(t) \equiv [(t(d/dt))^k \delta(t-1)] \sim u(t) \quad (12.126)$$

they can be written as a convolution:

$$\sum_{k=0}^n a_k (t(d/dt))^k \delta(t-1) \sim u(t) = g(t) \quad (12.127)$$

The more usual Euler–Cauchy differential equation, which is written as

$$(b_n t^n (d/dt)^n + b_{n-1} t^{n-1} (d/dt)^{n-1} + \dots + b_0) u(t) = g(t) \quad (12.128)$$

can be brought to the form (Equation 12.125) by using relations such that:

$$\left(t \frac{d}{dt}\right)^2 = t \frac{d}{dt} + t^2 \frac{d^2}{dt^2} \tag{12.129}$$

It can also be transformed directly into a convolution which reads:

$$\sum_{k=0}^n b_k t^k \delta^{(k)}(t-1) \sim u(t) = g(t) \tag{12.130}$$

The Mellin treatment of convolution equations will be explained in the case of Equation 12.127 since it is the most characteristic.

Suppose that the known function  $g$  has a Mellin transform  $\mathcal{M}[g; s] = G(s)$  that is holomorphic in the strip  $S(\sigma_b, \sigma_r)$ . We shall seek solution  $u$  which admit a Mellin transform  $U(s)$  holomorphic in the same strip or in some substrip. The Mellin transform of Equation 12.127 is obtained by using the convolution property and relation (Equation 12.62):

$$A(s)U(s) = G(s) \tag{12.131}$$

where

$$A(s) \equiv \sum_{k=0}^{\infty} a_k (-1)^k s^k \tag{12.132}$$

Two different situations may arise.

1. Either  $A(s)$  has no zeros in the strip  $S(\sigma_b, \sigma_r)$ . In that case,  $U(s)$  given by  $G(s)/A(s)$  can be inverted in the strip. According to Theorems 12.2 and 12.3, the unique solution is a distribution belonging to  $\mathcal{F}'(\sigma_1, \sigma_2)$ .
2. Or  $A(s)$  has  $m$  zeros in the strip. The main strip  $S(\sigma_b, \sigma_r)$  can be decomposed into adjacent substrips

$$\sigma_l < \text{Re}(s) < \sigma_1, \sigma_1 < \text{Re}(s) < \sigma_2, \dots, \sigma_m < \text{Re}(s) < \sigma_r \tag{12.133}$$

The solution in the  $k$ -substrip is given by the Mellin inverse formula:

$$u(t) = \frac{1}{2\pi j} \int_{c-j\infty}^{c+j\infty} \frac{G(s)t^{-s}}{A(s)} ds \tag{12.134}$$

where  $\sigma_k < c < \sigma_{k+1}$ . There is a different solution in each strip, two solutions differing by a solution of the homogeneous equation.

### 12.2.2.4 Solution of a Potential Problem in a Wedge<sup>7,8,17</sup>

The problem is to solve Laplace's equation in an infinite two-dimensional wedge with Dirichlet boundary conditions. Polar coordinates with origin at the apex of the wedge are used and the sides are located at  $\theta = \pm \alpha$ . The unknown function  $u(r, \theta)$  is supposed to verify:

$$\Delta u = 0, \quad 0 < r < \infty, \quad -\alpha < \theta < \alpha \tag{12.135}$$

with the following boundary conditions:

1. On the sides of the wedge, if  $R$  is a given positive number:

$$u(r, \pm\alpha) = \begin{cases} 1 & \text{if } 0 < r < R \\ 0 & \text{if } r > R \end{cases} \tag{12.136}$$

or, equivalently:

$$u(r, \pm\alpha) = H(R - r) \tag{12.137}$$

2. When  $r$  is finite,  $u(r, \theta)$  is bounded.
3. When  $r$  tends to infinity,  $u(r, \theta) \sim r^{-\beta}$ ,  $\beta > 0$ .

In polar coordinates, Equation 12.135 multiplied by  $r^2$  yields:

$$r^2 \frac{\partial^2 u}{\partial r^2} + r \frac{\partial u}{\partial r} + \frac{\partial^2 u}{\partial \theta^2} = 0 \tag{12.138}$$

The above conditions on  $u(r, \theta)$  ensure that its Mellin transform  $U(s, \theta)$  with respect to  $r$  exists as a holomorphic function in some region  $0 < \text{Re}(s) < \beta$ . The equation satisfied by  $U$  is obtained from Equation 12.138 by using property (Equation 12.59) of the Mellin transformation and reads:

$$\frac{d^2 U}{d\theta^2}(s, \theta) + s^2 U(s, \theta) = 0 \tag{12.139}$$

The general solution of this equation can be written as

$$U(s, \theta) = A(s)e^{js\theta} + B(s)e^{-js\theta} \tag{12.140}$$

Functions  $A, B$  are to be determined by the boundary condition (Equation 12.137) which leads to the following requirement on  $U$ :

$$U(s, \pm\alpha) = R^s s^{-1} \quad \text{for } \text{Re}(s) > 0 \tag{12.141}$$

Explicitly, this is written as

$$A(s)e^{js\alpha} + B(s)e^{-js\alpha} = a^s s^{-1} \tag{12.142}$$

$$A(s)e^{-js\alpha} + B(s)e^{js\alpha} = a^s s^{-1} \tag{12.143}$$

and leads to the solution:

$$A(s) = B(s) = \frac{R^s}{2s \cos(s\alpha)} \tag{12.144}$$

The solution of the form (Equation 12.140) which verifies Equation 12.141 is given by

$$U(s, \theta) = \frac{R^s \cos(s\theta)}{s \cos(s\alpha)} \tag{12.145}$$

This function  $U$  is holomorphic in the strip  $0 < \text{Re}(s) < \pi/(2\alpha)$ . Its inverse Mellin transform is a function  $u(r, \theta)$  that is obtained from the result of Example 12.10.

### 12.2.2.5 Asymptotic Expansion of Integrals

The Laplace transform  $I[f; \lambda]$  defined by

$$I[f; \lambda] = \int_0^{\infty} e^{-\lambda t} f(t) dt \quad (12.146)$$

has an asymptotic expansion as  $\lambda$  goes to infinity which is characterized by the behavior of the function  $f$  when  $t \rightarrow 0+$ .<sup>9,14,19</sup> With the help of Mellin's transformation, one can extend this type of study to other transforms of the form:

$$I[f; \lambda] = \int_0^{\infty} h(\lambda t) f(t) dt \quad (12.147)$$

where  $h$  is a general kernel.

Examples of such  $h$ -transforms<sup>9</sup> are

- Fourier transform:  $h(\lambda t) = e^{i\lambda t}$
- Cosine and Sine transforms:  $h(\lambda t) = \cos(\lambda t)$  or  $\sin(\lambda t)$
- Laplace transform:  $h(\lambda t) = e^{-\lambda t}$
- Hankel transform:  $h(\lambda t) = J_\nu(\lambda t)(\lambda t)^{1/2}$  where  $J_\nu$  is the Bessel function of the first kind
- Generalized Stieltjes transform:  $h(\lambda t) = \lambda^\nu \int_0^{\infty} f(t)/(1 + \lambda t)^\nu dt$

A short formal overview of the procedure will be given below. The theory is exposed in full generality in Ref. [9]. It includes the study of asymptotic expansions when  $\lambda \rightarrow 0+$  in relation with the behavior of  $f$  at infinity and the extension to complex values of  $\lambda$ . The case of oscillatory  $h$ -kernels is given special attention.

Suppose from now on that  $f$  and  $h$  are locally integrable functions such that the transform  $I[f; \lambda]$  exists for the large  $\lambda$ . The different steps leading to an asymptotic expansion of  $I[f; \lambda]$  in the limit  $\lambda \rightarrow +\infty$  are the following:

1. *Mellin transform the functions  $h$  and  $f$  and apply Parseval's formula.* The Mellin transforms  $\mathcal{M}[f; s]$  and  $\mathcal{M}[h; s]$  are supposed to be holomorphic in the strips  $\eta_1 < \text{Re}(s) < \eta_2$  and  $\alpha_1 < \text{Re}(s) < \alpha_2$ , respectively. Assuming that Parseval's formula may be applied and using property (Equation 12.56), one can write Equation 12.146 as

$$I[f; \lambda] = \frac{1}{2\pi j} \int_{r-j\infty}^{r+j\infty} \lambda^{-s} \mathcal{M}[h; s] \mathcal{M}[f; 1-s] ds \quad (12.148)$$

where  $r$  is any real number in the strip of analyticity of the function  $G$  defined by

$$G(s) = \mathcal{M}[h; s] \mathcal{M}[f; 1-s], \quad \max(\alpha_1, 1 - \eta_2) < \text{Re}(s) < \min(\alpha_2, 1 - \eta_1) \quad (12.149)$$

2. *Shift of the contour of integration to the right and use of Cauchy's formula.* Suppose  $G(s)$  can be analytically continued in the right half-plane  $\text{Re}(s) \geq \min(\alpha_2, 1 - \eta_1)$  as a meromorphic function. Remark that this assumption implies that  $\mathcal{M}[f; s]$  may be continued to the right half-plane  $\text{Re}(s) > \alpha_2$  and  $\mathcal{M}[h; s]$  to the left  $\text{Re}(s) < \eta_1$ . Suppose moreover that the contour of integration in Equation 12.148 can be displaced to the right as far as the line  $\text{Re}(s) = R > r$ . A sufficient condition ensuring this property is that

$$\lim_{|b| \rightarrow \infty} G(a + jb) = 0 \quad (12.150)$$

for all  $a$  in the interval  $[r, R]$ .

Under these conditions, Cauchy's formula may be applied and yields:

$$I[f; \lambda] = - \sum_{r < \text{Re}(s) < R} \text{Res}(\lambda^{-s} G(s)) + \frac{1}{2\pi j} \int_{R-j\infty}^{R+j\infty} \lambda^{-s} G(s) ds \quad (12.151)$$

where the discrete summation involves the residues (denoted  $\text{Res}$ ) of function  $\lambda^{-s} G(s)$  at the poles lying inside the region  $r < \text{Re}(s) < R$ .

3. *The asymptotic expansion.* The relation (Equation 12.151) is an asymptotic expansion provided the error bound hold. A sufficient condition to ensure that the integral term is of order  $O(\lambda^{-R})$  is that  $G$  satisfy:

$$\int_{-\infty}^{\infty} |G(R + jb)| db < \infty \quad (12.152)$$

The above operations can be justified step by step when treating a particular case. The general theory gives a precise description of the final form of the asymptotic expansion, when it exists, in terms of the asymptotic properties of  $h$  when  $t \rightarrow +\infty$  and of  $f$  when  $t \rightarrow 0+$ .

The above procedure is easily adapted to give the asymptotic expansion of  $I[f; \lambda]$  when  $\lambda \rightarrow 0+$ .

### Example 12.12

Consider the case where the kernel,  $h$ , is given by

$$h(t) = \frac{1}{1+t} \quad (12.153)$$

The integral under consideration is thus:

$$I[f; \lambda] = \int_0^{\infty} \frac{f(t)}{1 + \lambda t} dt \quad (12.154)$$



The function  $f$  must be such that the integral exists. In addition, it is supposed to have a Mellin transform holomorphic in the strip  $\sigma_1 < \text{Re}(s) < \sigma_2$  and to have an asymptotic development as  $t \rightarrow 0$  of the form:

$$f \sim \sum_{m=0}^{\infty} t^{a_m} p_m \quad (12.155)$$

where the numbers  $\text{Re}(a_m)$  increase monotonically to  $+\infty$  as  $m \rightarrow +\infty$  and the numbers  $p_m$  may be arbitrary.

To apply the method, we first compute the Mellin transform of  $h$  which is given by

$$\mathcal{M}[(1+t)^{-1}; s] = \frac{\pi}{\sin \pi s}, \quad 0 < \text{Re}(s) < 1 \quad (12.156)$$

It can be continued in the half-plane  $\text{Re}(s) > 0$  where it has simple poles at  $s = 1, 2, \dots$  and decays along imaginary lines as follows:

$$\frac{\pi}{\sin \pi(a+jb)} = O(e^{-\pi|b|}) \quad \text{for all } a \quad (12.157)$$

As for function  $f$ , its behavior given by Equation 12.155 ensures<sup>9</sup> that the Mellin transform  $\mathcal{M}[f; s]$  has an analytic continuation in the half-plane  $\text{Re}(s) \leq \sigma_1 = -\text{Re}(a_0)$  which is a meromorphic function with poles at the points  $s = -a_m$ . Moreover, one finds the following behavior at infinity for the continued Mellin transform:

$$\lim_{|b| \rightarrow \infty} \mathcal{M}[f; a+jb] = 0, \quad \text{for all } a < \sigma_2 \quad (12.158)$$

In this situation, the method will lead to an asymptotic expansion which can be written explicitly. For example, in the case where  $a_m \neq 0, 1, 2, \dots$ , the poles of  $\mathcal{M}[f; 1-s]$ , which occur at  $1-s = -a_m$  are distinct from those of  $\mathcal{M}[h; s]$  at  $s = m+1$  and the expansion of  $l$  is given by

$$\begin{aligned} l[f; \lambda] \sim & \sum_{m=0}^{\infty} \lambda^{-1-a_m} \frac{\pi}{\sin(\pi a_m)} \text{Res}_{s=1+a_m} \{\mathcal{M}[f; 1-s]\} \\ & + \sum_{m=0}^{\infty} \lambda^{-1-m} \mathcal{M}[f; -m] \text{Res}_{s=m+1} \left\{ \frac{\pi}{\sin(\pi s)} \right\} \end{aligned} \quad (12.159a)$$

Hence,

$$l[f; \lambda] \sim \sum_{m=0}^{\infty} \lambda^{-1-a_m p_m} \frac{\pi}{\sin(\pi a_m)} + \sum_{m=0}^{\infty} (-1)^m \lambda^{-1-m} \mathcal{M}[f; -m] \quad (12.159b)$$

In particular, if  $f(t) = (1/t)e^{-(1/t)}$ , all the  $p_m$  are equal to zero and the expansion is just:

$$l[f; \lambda] \sim \sum_{n=0}^{\infty} (-1)^n (\lambda)^{-n-1} \Gamma(n+1) \quad (12.160)$$

### 12.2.2.6 Asymptotic Behavior of Harmonic Sums

A more recent application of Mellin's transformation concerns the study of functions defined by series of the following type:

$$g(x) \equiv \sum_k \lambda_k f(\mu_k x), \quad k \text{ integer, } x > 0 \quad (12.161)$$

where  $\lambda_k$  and  $\mu_k$  are real parameters.<sup>20,21</sup> Such functions, which can be interpreted as a superposition of generalized harmonics associated with a base function  $f(x)$ , are referred to as harmonic sums,<sup>6</sup> the parameters  $\lambda_k, \mu_k$  being interpreted as amplitude and frequency, respectively. Those expressions arise in applications of combinatorial theory, especially in the evaluation of algorithms where the problem is to find the behavior of  $g(x)$  when  $x$  tends to 0 or infinity.<sup>22</sup> Mellin's transformation comes in as an essential tool to obtain asymptotic expansions of this type of function. In the following, a brief account of the method will be given and an example will be treated. For further details, the reader should refer to the review paper by Flajolet et al.<sup>6</sup> which contains precise theorems and numerous examples of application.

The first step in establishing an asymptotic expansion of the function  $g(x)$  defined by Equation 12.161 is to find the expression of its Mellin transform  $\mathcal{M}[g; s] \equiv G(s)$ . When the sum on  $k$  is finite, the linearity of the transformation and the property (Equation 12.56) relative to scaling allow one to write:

$$G(s) \equiv \mathcal{M}[g; s] = \Lambda(s)F(s) \quad (12.162)$$

where

$$F(s) \equiv \mathcal{M}[f; s] \quad (12.163)$$

and the function  $\Lambda(s)$  is defined by

$$\Lambda(s) \equiv \sum_k \lambda_k \mu_k^{-s} \quad (12.164)$$

Thus, the Mellin transformation performs a separation between the base function  $f(x)$  and the parameters  $\lambda_k, \mu_k$ . In the more general case of an infinite sum, the validity of the procedure, which involves interchanging sum and integral, will depend on the properties of the functions  $f(x)$  and  $\Lambda(s)$ ; the latter has the form of a generalized Dirichlet series for which convergence theorems exist. From now on, we suppose that the Mellin transform of  $g(x)$  has the form (Equation 12.162) and, in addition, is holomorphic in a strip  $S(\sigma_1, \sigma_2)$  and satisfies the conditions of Theorem 12.1. In that case, the inversion formula (Equation 12.23) allows to recover  $g(x)$  by an integration in the complex  $s$  plane along an imaginary line in the strip of holomorphy according to

$$g(x) = (1/2\pi j) \int_{a-j\infty}^{a+j\infty} \Lambda(s)F(s)x^{-s} ds \quad (12.165)$$

With  $\sigma_1 < a < \sigma_2$ .

The second step relies on the possibility to continue the function  $G(s)$  in a half plane as a meromorphic function of sufficient decrease at infinity. The asymptotic development of  $g(x)$  as  $x \rightarrow 0$  is then given by the approximate computation of Equation 12.165 using the method of residues in the left half-plane  $P_l$ :

$$g(x) \sim \sum_{P_l} \text{Res}[G(s)x^{-s}] \quad (12.166)$$

The development for  $x \rightarrow \infty$  is likewise obtained by considering the right half-plane  $P_r$ :

$$g(x) \sim - \sum_{P_r} \text{Res}[G(s)x^{-s}] \quad (12.167)$$

This formal procedure is valid under general conditions involving the separate behaviors of the functions  $\Lambda(s)$ , associated with the parameters, and  $F(s)$ , characterizing the base function. The result is a systematic correspondence between the properties of the poles of  $G(s)$  in the complex plane and the terms of the asymptotic series of  $g(x)$ .<sup>6,21</sup> A simple example will illustrate this procedure.

**Example 12.13**

Consider the sum

$$g(x) = \sum_{k=1}^{\infty} d(k)e^{-kx} \quad (12.168)$$

where  $d(k)$  represents the number of divisors of  $k$ . The Mellin transform is given by

$$\mathcal{M}[g; s] \equiv G(s) = \sum_{k=1}^{\infty} d(k)k^{-s}\Gamma(s) \quad (12.169)$$

The identity<sup>12</sup>

$$\sum_{k=1}^{\infty} d(k)k^{-s} = \zeta^2(s) \quad (12.170)$$

allows us to write

$$G(s) = \zeta^2(s)\Gamma(s) \quad (12.171)$$

The holomorphy domain of  $G(s)$  is  $\text{Re}(s) > 1$ . Recall that the Zeta function has a simple pole at  $s = 1$  and simple zeros at the pair negative integers. Hence, taking also into account the properties of the Gamma function, we find that  $G(s)$  has a double pole in  $s = 1$  and simple poles at  $s = 0$  and  $s = -2n - 1$ ,  $n$  integer. The singular terms of the Laurent expansion of  $G(s)$  are

At  $s = 1$

$$G(s) \sim \frac{1}{(s-1)^2} + \frac{\gamma}{s-1}, \quad \gamma = \text{Euler constant}$$

At  $s = 0$

$$G(s) \sim \frac{1}{4s} \quad (12.172)$$

At  $s = -2n - 1$

$$G(s) \sim - \frac{\zeta^2(-2n-1)}{(2n+1)(s+2n+1)}$$

In addition, the decreasing properties of  $G(s)$  when  $|s| \rightarrow +\infty$  allow to write:

$$G(s) \sim \sum_{\text{Re}(s) \leq 1} \text{Res}(G(s)x^{-s}) \quad (12.173)$$

Computation of the residue at  $s = 1$  gives

$$\text{Res}_{s=1}(G(s)x^{-s}) = \frac{d}{ds} [(s-1)^2 G(s)x^{-s}]_{s=1} \quad (12.174)$$

or using Equation 12.172:

$$\text{Res}_{s=1}(G(s)x^{-s}) = (\gamma - \ln x)x^{-1} \quad (12.175)$$

The other residues are at simple poles and the asymptotic expansion of  $g(x)$  for  $x \rightarrow 0$  finally reads:

$$g(x) = (\gamma - \ln x) \frac{1}{x} + \frac{1}{4} + \sum_{k=0}^{\infty} \frac{\zeta^2(-2n-1)}{(2n+1)} x^{2n+1} \quad (12.176)$$

The value of  $\zeta(-2n-1)$  can be found in tables in Ref. [16].

In this example, the use of Mellin's transformation has led easily to the  $x=0$  behavior of  $g(x)$  which was not obvious on the definition (Equation 12.168). Other types of series involving poles in the complex domain of  $s$  can be handled in an analogous way.<sup>6</sup>

## 12.3 Alternative Approach Related to the Dilation Group and Its Representations

### 12.3.1 Theoretical Aspects

#### 12.3.1.1 Construction of the Transformation

Rather than start directly by giving the explicit formula of the Mellin transformation, we will construct it explicitly as a tool especially devoted to the computation of functionals involving scalings of a variable. Such an introduction of the transform may be found, for example, in the book by Vilenkin<sup>3</sup> or, in a more applied context, in articles.<sup>23-25</sup>

If  $Z(\nu)$  is a function defined on the positive half-axis  $(0, \infty)$ , a scaling of the variable  $\nu$  by a positive number  $a$  leads to a new function  $Z'(\nu)$  which is related to  $Z(\nu)$  by the change of variable:

$$v \rightarrow av \quad (12.177)$$

The set of such transformations forms a group which is isomorphic to the multiplicative group of positive real numbers. In practice, the scaled function is often defined by the transformation:

$$Z(v) \rightarrow a^{1/2}Z(av) \quad (12.178)$$

which does not change the value of the usual scalar product:

$$(Z_1, Z_2) \equiv \int_0^{\infty} Z_1(v) Z_2^*(v) dv \quad (12.179)$$

in which the symbol \* denotes complex conjugation. However, there are serious physical reasons to consider more general transformations of the form:

$$\mathcal{D}_a \cdot Z(v) \rightarrow (\mathcal{D}_a Z)(v) \equiv a^{r+1}Z(av) \quad (12.180)$$

where  $r$  is a given real number. The general correspondence  $a \leftrightarrow \mathcal{D}_a$  is such that:

$$\begin{aligned} \mathcal{D}_a \mathcal{D}_{a'} &= \mathcal{D}_{aa'} \\ \mathcal{D}_1 \mathcal{D}_a &= \mathcal{D}_a \mathcal{D}_1 = \mathcal{D}_a \\ (\mathcal{D}_a)^{-1} &= \mathcal{D}_{a^{-1}} \end{aligned} \quad (12.181)$$

Thus, for any value of  $r$ , the set of  $\mathcal{D}_a$  operations constitutes a representation of a group. These transformations preserve the following scalar product:

$$(Z_1, Z_2) \equiv \int_0^{\infty} Z_1(v) Z_2^*(v) v^{2r+1} dv \quad (12.182)$$

that is to say, we have

$$(\mathcal{D}_a Z_1, \mathcal{D}_a Z_2) = (Z_1, Z_2) \quad (12.183)$$

The scalar product (Equation 12.182) defines a norm for the functions  $Z(v)$  on the positive axis  $\mathbb{R}^+$ . We have

$$\|Z\|^2 \equiv \int_0^{\infty} |Z(v)|^2 v^{2r+1} dv \quad (12.184)$$

The corresponding Hilbert space will be denoted by  $L^2(\mathbb{R}^+, v^{2r+1} dv)$ . It is handled in the same manner as an ordinary  $L^2$  space with the measure  $dv$  replaced by  $v^{2r+1} dv$  in all formulas. In this space, the meaning of Equation 12.183 is that the set of operations  $\mathcal{D}_a$  constitutes a unitary representation of the multiplicative group of positive numbers.

The value of  $r$  will be determined by the specific applications to be dealt with. Examples of adjustments of this parameter are given in Ref. [26] where the occurrence of dilations in radar imaging is analyzed.

When confronted with expressions involving functions modified by dilations of the form (Equation 12.180), it may be advantageous to use a Hilbert space basis in which the operators  $\mathcal{D}_a$  have a diagonal expression. This leads to a decomposition of functions  $Z$  into simpler elements on which the scaling operation breaks down to a mere multiplication by a complex number. Such a procedure is familiar when considering the operation which translates a function  $f(t)$ ,  $t \in \mathbb{R}$  according to

$$f(t) \rightarrow f(t - t_0) \quad (12.185)$$

In that case, the exponentials  $e^{\lambda t}$ ,  $\lambda$  complex, are functions that are multiplied by a number  $e^{\lambda t_0}$  in a translation. If  $\lambda = j\alpha$ ,  $\alpha$  real, these functions are unitary representations of the translation group in  $L^2(\mathbb{R})$  and provide a generalized\* orthonormal basis for functions in this space. The coefficients of the development of function  $f(t)$  on this basis are obtained by scalar product with the basis elements and make up the Fourier transform. In the present case, analogous developments will connect the Mellin transformation to the unitary representations of the dilation group in  $L^2(\mathbb{R}^+, v^{2r+1} dv)$ .

For simplicity and for future reference, the diagonalization of  $\mathcal{D}_a$  will be performed on its infinitesimal form defined by the operator  $\mathcal{B}$  whose action on function  $Z(v)$  is given by

$$(\mathcal{B}Z)(v) \equiv -\frac{1}{2\pi j} \frac{d}{da} [( \mathcal{D}_a Z)(v)]_{(a=1)} \quad (12.186)$$

The computation yields:

$$\mathcal{B} = -\frac{1}{2\pi j} \left( v \frac{d}{dv} + r + 1 \right) \quad (12.187)$$

The operator  $\mathcal{B}$  is a self-adjoint operator and the unitary representation  $\mathcal{D}_a$  is recovered from  $\mathcal{B}$  by exponentiation:†

$$\mathcal{D}_a = e^{-2\pi j a \mathcal{B}} \quad (12.188)$$

where the exponential of the operator is defined formally by the infinite series:

$$e^{-2\pi j a \mathcal{B}} = \sum_{n=0}^{\infty} (-1)^n \frac{(2\pi j a \mathcal{B})^n}{n!} \quad (12.189)$$

\* Such families of functions which do not belong to the Hilbert space under consideration but are treated like bases by physicists are called *improper bases*. Their use can be rigorously justified.

† This is known as Stone's theorem.

Here, we only need to find the eigenfunctions of  $\mathcal{B}$ , i.e., the solutions of the differential equation:

$$\mathcal{B}Z(v) = \beta Z(v) \quad (12.190)$$

with  $\beta$  real.

The solution is, up to an arbitrary factor:

$$E_\beta(v) = v^{-2\pi j\beta - r - 1} \quad (12.191)$$

As ensured by the construction, any member of this family of functions  $E_\beta$  is just multiplied by a phase when a scaling is performed:

$$\mathcal{D}_a: E_\beta(v) \rightarrow a^{-2\pi j\beta} E_\beta(v) \quad (12.192)$$

Moreover, the family  $\{E_\beta\}$  is orthonormal and complete as will now be shown. The orthonormality is obtained by setting  $v = e^{-x}$  in the expression:

$$(E_\beta, E_{\beta'}) = \int_0^\infty v^{-2\pi j(\beta - \beta') - 1} dv \quad (12.193)$$

which becomes

$$(E_\beta, E_{\beta'}) = \int_{-\infty}^\infty e^{2\pi j(\beta - \beta')x} dx \quad (12.194)$$

The result is

$$(E_\beta, E_{\beta'}) = \delta(\beta - \beta') \quad (12.195)$$

To show completeness, we compute:

$$\int_{-\infty}^\infty E_\beta(v) E_{\beta'}^*(v') d\beta \equiv \int_{-\infty}^\infty e^{-2\pi j\beta \ln(v/v')} (vv')^{-r-1} d\beta \quad (12.196)$$

$$= (vv')^{-r-1} \delta(\ln(v) - \ln(v')) \quad (12.197)$$

and, using the rule of calculus with delta functions recalled in Equation 12.52, we obtain:

$$\int_{-\infty}^\infty E_\beta(v) E_{\beta'}^*(v') d\beta = v^{-2r-1} \delta(v - v') \quad (12.198)$$

Any function  $Z$  in  $L^2(\mathbb{R}^+, v^{2r+1} dv)$  can thus be decomposed on the basis  $E_\beta$  with coefficients  $\mathcal{M}[Z](\beta)$  given by

$$\mathcal{M}[Z](\beta) = (Z, E_\beta) \quad (12.199)$$

or explicitly:

$$\mathcal{M}[Z](\beta) = \int_0^\infty Z(v) v^{2\pi j\beta + r} dv \quad (12.200)$$

The set of coefficients, considered as a function of  $\beta$ , constitutes what is called the Mellin transform of function  $Z$ . This definition coincides with the usual one (12.1) provided we set  $s = r + 1 + 2\pi j\beta$ . Thus,

$$\mathcal{M}[Z](\beta) \equiv \mathcal{M}[Z; r + 1 + 2\pi j\beta] \quad (12.201)$$

But the viewpoint here is different. The value of  $\text{Re}(s) = r + 1$  is fixed once and for all as it is forced upon us by the representation of dilations occurring in the physical problem under study. Thus, the situation is closer to the Fourier than to the Laplace case and an  $L^2$  theory is developed naturally.

The property (Equation 12.198) of completeness for the basis implies that the Mellin transformation (Equation 12.199) from  $Z(v)$  to  $\mathcal{M}[Z](\beta)$  is norm-preserving:

$$\int_{-\infty}^\infty |\mathcal{M}[Z](\beta)|^2 d\beta = (Z, Z) \quad (12.202)$$

A Parseval formula (also called unitarity property) follows immediately:

$$\int_{-\infty}^\infty \mathcal{M}[Z_1](\beta) \mathcal{M}^*[Z_2](\beta) d\beta = (Z_1, Z_2) \quad (12.203)$$

where

$$\mathcal{M}^*[Z](\beta) \equiv [\mathcal{M}[Z](\beta)]^* \quad (12.204)$$

The decomposition formula of function  $Z(v)$  on basis  $\{E_\beta(v)\} \equiv v^{-2\pi j\beta - r - 1}$  which can be obtained from Equations 12.198 and (12.200) constitutes the inversion formula for the Mellin transformation:

$$Z(v) = \int_{-\infty}^\infty \mathcal{M}[Z](\beta) v^{-2\pi j\beta - r - 1} d\beta \quad (12.205)$$

By construction, the Mellin transformation performs the diagonalization of the operators  $\mathcal{B}$  and  $\mathcal{D}_a$ . Indeed, by definition (Equation 12.199), the Mellin transform of the function  $(\mathcal{B}Z)(v)$  is given by

$$\mathcal{M}[\mathcal{B}Z](\beta) = (\mathcal{B}Z, E_\beta) \quad (12.206)$$

or, using the fact that  $\mathcal{B}$  is self-adjoint and that  $E_\beta$  is an eigenfunction of  $\mathcal{B}$ :

$$\mathcal{M}[\mathcal{B}Z](\beta) = \beta(Z, E_\beta) \quad (12.207)$$

Thus,

$$\mathcal{M}[\mathcal{B}Z](\beta) = \beta \mathcal{M}[Z](\beta) \quad (12.208)$$

In the same way, the Mellin transform of  $\mathcal{D}_a Z$  is computed using the unitarity of  $\mathcal{D}_a$ :

$$\begin{aligned} \mathcal{M}[\mathcal{D}_a Z](\beta) &= (\mathcal{D}_a Z, E_\beta) \\ &= (Z, \mathcal{D}_{a^{-1}} E_\beta) \end{aligned} \quad (12.209)$$

Thus,

$$\mathcal{M}[\mathcal{D}_a Z](\beta) = a^{-2\pi j\beta} \mathcal{M}[Z](\beta) \quad (12.210)$$

All these results can be summed up in the following proposition.

---

### THEOREM 12.6

Let  $Z(\nu)$  be a function in  $L^2(\mathbb{R}^+, \nu^{2r+1} d\nu)$ . Its Mellin transform defined by

$$\mathcal{M}[Z](\beta) = \int_0^\infty Z(\nu) \nu^{2\pi j\beta+r} d\nu \quad (12.211)$$

belongs to  $L^2(\mathbb{R})$ .

The inversion formula is given by

$$Z(\nu) = \int_{-\infty}^\infty \mathcal{M}[Z](\beta) \nu^{-2\pi j\beta-r-1} d\beta \quad (12.212)$$

An analog of Parseval's formula (unitarity) holds as

$$\int_{-\infty}^\infty \mathcal{M}[Z_1](\beta) \mathcal{M}^*[Z_2](\beta) d\beta = \int_0^\infty Z_1(\nu) Z_2^*(\nu) \nu^{2r+1} d\nu \quad (12.213)$$

For any function  $Z$ , the Mellin transform of the dilated function

$$(\mathcal{D}_a Z)(\nu) \equiv a^{r+1} Z(a\nu) \quad (12.214)$$

is given by

$$\mathcal{M}[\mathcal{D}_a Z](\beta) = a^{-2\pi j\beta} \mathcal{M}[Z](\beta) \quad (12.215)$$

### 12.3.1.2 Uncertainty Relations

As in the case of the Fourier transformation, there is a relation between the spread of a function and the spread of its Mellin transform. To find this relation, we will consider the first two moments of the density functions  $|Z(\nu)|^2$  and  $|\mathcal{M}[Z](\beta)|^2$  connected by Equation 12.213. The mean value of  $\nu$  with density  $|Z(\nu)|^2$  is defined by the formula:

$$\bar{\nu} \equiv \frac{(Z, \nu Z)}{(Z, Z)} \quad (12.216)$$

The mean value of  $\nu^2$  is defined by an analogous formula. The mean square deviation  $\sigma_\nu^2$  of variable  $\nu$  can then be computed according to

$$\sigma_\nu^2 \equiv \overline{(\nu - \bar{\nu})^2} \quad (12.217)$$

In the same way, in the space of Mellin transforms, the mean value of  $\beta$  is defined by

$$\bar{\beta} \equiv \frac{(\tilde{Z}, \beta \tilde{Z})}{(\tilde{Z}, \tilde{Z})} \quad (12.218)$$

where  $\tilde{Z}$  denotes the Mellin transform of  $Z$ . Using Parseval formula (Equation 12.213) and property (Equation 12.208), one can also rewrite this mean value in terms of the original function  $Z(\nu)$  as

$$\bar{\beta} = \frac{(Z, \mathcal{B}Z)}{(Z, Z)} \quad (12.219)$$

where the operator  $\mathcal{B}$  has been defined by formula (Equation 12.187). At this point, it is convenient to introduce the following notation for any operator  $\mathcal{O}$  acting on  $Z$ :

$$\langle \mathcal{O} \rangle \equiv \frac{(Z, \mathcal{O}Z)}{(Z, Z)} \quad (12.220)$$

and to rewrite Equation 12.219 as

$$\bar{\beta} = \langle \mathcal{B} \rangle \quad (12.221)$$

The mean square deviation  $\sigma_\beta^2$  of variable  $\beta$  can also be expressed in terms of the operator  $\mathcal{B}$  according to

$$\sigma_\beta^2 = \langle (\mathcal{B} - \bar{\beta})^2 \rangle \quad (12.222)$$

A simple way to obtain a lower bound on the product  $\sigma_\beta \sigma_\nu$  is to introduce the operator  $\mathcal{X}$  defined by

$$\mathcal{X} \equiv \mathcal{B} - \bar{\beta} + j\lambda(\nu - \bar{\nu}) \quad (12.223)$$

where  $\lambda$  is a real parameter. The obvious requirement that the norm of  $\mathfrak{X}Z(\nu)$  must be positive or zero whatever the value of  $\lambda$  is expressed by the inequality:

$$\|\mathfrak{X}Z\|^2 = \langle Z, \mathfrak{X}^* \mathfrak{X}Z \rangle \geq 0 \quad (12.224)$$

where  $\mathfrak{X}^*$  denotes the adjoint of  $\mathfrak{X}$ . This constraint implies the positivity of the expression:

$$\langle (\mathcal{B} - \bar{\beta} + j\lambda(\nu - \bar{\nu}))(\mathcal{B} - \bar{\beta} - j\lambda(\nu - \bar{\nu})) \rangle \quad (12.225)$$

Developing and using relations (Equation 12.217) and (Equation 12.222), we obtain:

$$\lambda^2 \sigma_\nu^2 + j\lambda \langle \nu \mathcal{B} - \mathcal{B} \nu \rangle + \sigma_\beta^2 \geq 0 \quad (12.226)$$

The computation of  $\nu \mathcal{B} - \mathcal{B} \nu$  yields:

$$(\nu \mathcal{B} - \mathcal{B} \nu)Z(\nu) = \frac{-1}{2\pi j} \left( \nu^2 \frac{d}{d\nu} - \nu \frac{d}{d\nu} \nu \right) Z(\nu) \quad (12.227)$$

$$= \frac{1}{2\pi j} \nu Z(\nu) \quad (12.228)$$

With this result, condition (Equation 12.226) becomes

$$\lambda^2 \sigma_\nu^2 + (\lambda/2\pi)\bar{\nu} + \sigma_\beta^2 \geq 0 \quad (12.229)$$

The left member is a quadratic expression of the parameter  $\lambda$ . Its positivity whatever the value of  $\lambda$  means that the coefficients of the expression verify:

$$\sigma_\nu \sigma_\beta \geq \bar{\nu}/4\pi \quad (12.230)$$

The functions for which this product is minimal are such that there is equality in Equation 12.224. Hence, they are solutions of the equation:

$$[\mathcal{B} - \bar{\beta} - j\lambda(\nu - \bar{\nu})]Z(\nu) = 0 \quad (12.231)$$

and are found to be

$$K(\nu) \equiv e^{-2\pi\lambda\nu} \nu^{2\pi\lambda\bar{\nu} - r - 1 - 2\pi j\bar{\beta}} \quad (12.232)$$

These functions, first introduced by Klauder,<sup>27</sup> are the analogs of Gaussians in Fourier theory.

### 12.3.1.3 Extension of the Mellin Transformation to Distributions

The definition of the transformation has to be extended to distributions to be able to treat generalized functions such as Dirac's which are currently used in electrical engineering. Section 12.2.1.3 can be read at this point for a general view of the possible approaches. Here we only give a succinct definition that will

generally be sufficient and we show on explicit examples how computations can be performed.

First, a test function  $\mathcal{T}$  is constructed so as to contain the functions  $\nu^{2\pi j\beta+r}$ ,  $\nu > 0$ ,  $\beta \in \mathbb{R}$  for a fixed value of  $r$ . Examples of such spaces are the spaces  $\mathcal{T}(a_1, a_2)$  of Section 12.2.1.3 provided  $a_1, a_2$  are chosen verifying the inequality  $a_1 < r + 1 < a_2$ .<sup>7,8</sup> Then the space of distributions  $\mathcal{T}'$  is defined as usual as a linear space  $\mathcal{T}'$  of continuous functionals on  $\mathcal{T}$ . It can be shown that the space  $\mathcal{T}'$  contains the distributions of bounded support on the positive axis and, in particular, the Dirac distributions.

The Mellin transform of a distribution  $Z$  in a space  $\mathcal{T}'$  can always be obtained as the result of the application of  $Z$  to the set of test functions  $\nu^{2\pi j\beta+r}$ ,  $\beta \in \mathbb{R}$ , i.e., as

$$\mathcal{M}[Z](\beta) \equiv \langle Z, \nu^{2\pi j\beta+r} \rangle \quad (12.233)$$

With this extended definition, it is easily verified that relations (Equation 12.208) and (Equation 12.215) still hold. One more property that will be useful, especially for discretization, is relative to the effect of translations on the Mellin variable. Computing  $\mathcal{M}[Z]$  for the value  $\beta + c$ ,  $c$  real, yields:

$$\begin{aligned} \mathcal{M}[Z](\beta + c) &= \langle Z, \nu^{2\pi j(\beta+c)+r} \rangle \\ &= \langle Z \nu^{2\pi jc}, \nu^{2\pi j\beta+r} \rangle \end{aligned} \quad (12.234)$$

and the result

$$\mathcal{M}[Z](\beta + c) = \mathcal{M}[Z \nu^{2\pi jc}](\beta) \quad (12.235)$$

#### Example 12.14

The above formula (Equation 12.233) allows to compute the Mellin transform of  $\delta(\nu - \nu_0)$  by applying the usual definition of the Dirac distribution:

$$\langle \delta(\nu - \nu_0), \phi \rangle = \phi(\nu_0) \quad (12.236)$$

to the function  $\phi(\nu) = \nu^{2\pi j\beta+r}$ , thus giving

$$\mathcal{M}[\delta(\nu - \nu_0)](\beta) \equiv \langle \delta(\nu - \nu_0), \nu^{2\pi j\beta+r} \rangle = \nu_0^{2\pi j\beta+r} \quad (12.237)$$

#### Example 12.15 The Geometric Dirac Comb

In problems involving dilations, it is natural to introduce a special form of the Dirac comb defined by

$$\begin{aligned} \Delta_A^r(\nu) &\equiv \sum_{n=-\infty}^{+\infty} A^{-nr} \delta(\nu - A^n) \\ &\equiv \sum_{n=-\infty}^{+\infty} A^{nr} \delta(\nu - A^{-n}) \end{aligned} \quad (12.238)$$

where  $A$  is a positive number. The values of  $v$  which are picked out by this distribution form a geometric progression of ratio  $A$ . Moreover, the comb  $\Delta_A^r$  is invariant in a dilation by an integer power of  $A$ . Indeed, using definition (Equation 12.214), we have

$$\mathcal{D}_A \Delta_A^r(v) \equiv A^{r+1} \Delta_A^r(Av) \tag{12.239}$$

$$= \sum_{n=-\infty}^{\infty} A^{-(n-1)r} \delta(v - A^{n-1}) \tag{12.240}$$

$$= \Delta_A^r(v) \tag{12.241}$$

The distribution  $\Delta_A^r$  will be referred to as the geometric Dirac comb and is represented in Figure 12.3.

Distribution  $\Delta_A^r$  does not belong to  $\mathcal{F}'$  and, hence, its Mellin transform cannot be obtained by formula (Equation 12.233). However, the property of linearity of the Mellin transformation and result (Equation 12.237) allow to write:

$$\mathcal{M}[\Delta_A^r](\beta) = \sum_{n=-\infty}^{+\infty} A^{2j\pi\beta n} \tag{12.242}$$

The right-hand side of Equation 12.242 is a Fourier series which can be summed by Poisson's formula:

$$\ln A \sum_{n=-\infty}^{\infty} e^{2j\pi n\beta \ln A} = \sum_{n=-\infty}^{\infty} \delta\left(\beta - \frac{n}{\ln A}\right) \tag{12.243}$$

This leads to

$$\mathcal{M}[\Delta_A^r](\beta) = \frac{1}{\ln A} \sum_{n=-\infty}^{+\infty} \delta\left(\beta - \frac{n}{\ln A}\right) \tag{12.244}$$

Thus, the Mellin transform of a geometric Dirac comb  $\Delta_A^r$  on  $\mathbb{R}^+$  is an arithmetic Dirac comb on  $\mathbb{R}$  (Figure 12.3).

### 12.3.1.4 Transformations of Products and Convolutions

The relations between product and convolution that are established by a Fourier transformation have analogs here. Classical convolution and usual product in the space of Mellin transforms correspond respectively to a special invariant product and a

multiplicative convolution in the original space. The latter operations can also be defined directly by their transformation properties under a dilation as will now be explained.

#### Invariant product

The dilation-invariant product of the functions  $Z_1$  and  $Z_2$  which will be denoted by the symbol  $\circ$  is defined as

$$(Z_1 \circ Z_2)(v) \equiv v^{r+1} Z_1(v) Z_2(v) \tag{12.245}$$

It is nothing but the usual product of the functions multiplied by the  $(r+1)$ th power of the variable. Relation (Equation 12.245) defines an internal law on the set of functions that is stable by dilation since:

$$\mathcal{D}_a[Z_1] \circ \mathcal{D}_a[Z_2] = \mathcal{D}_a[Z_1 \circ Z_2] \tag{12.246}$$

where  $\mathcal{D}_a$  is the operation (Equation 12.180).

Now, we shall compute the Mellin transform of the product  $Z_1 \circ Z_2$ . According to definition (Equation 12.211), this is given by

$$\mathcal{M}[Z_1 \circ Z_2](\beta) = \int_0^{+\infty} v^{r+1} Z_1(v) Z_2(v) v^{2j\pi\beta+r} dv \tag{12.247}$$

Replacing  $Z_1$  and  $Z_2$  by their inverse Mellin transforms given by Equation 12.212 and using the orthogonality relation (Equation 12.195) to perform the  $v$ -integration, we obtain:

$$\mathcal{M}[Z_1 \circ Z_2](\beta) = \int_{-\infty}^{\infty} d\beta_1 \int_{-\infty}^{\infty} \mathcal{M}[Z_1](\beta_1) \mathcal{M}[Z_2](\beta_2) d\beta_2 \delta(\beta - \beta_1 - \beta_2) \tag{12.248a}$$

$$= \int_{-\infty}^{\infty} \mathcal{M}[Z_1](\beta_1) \mathcal{M}[Z_2](\beta - \beta_1) d\beta_1 \tag{12.248b}$$

where we recognize the classical convolution of the Mellin transforms.

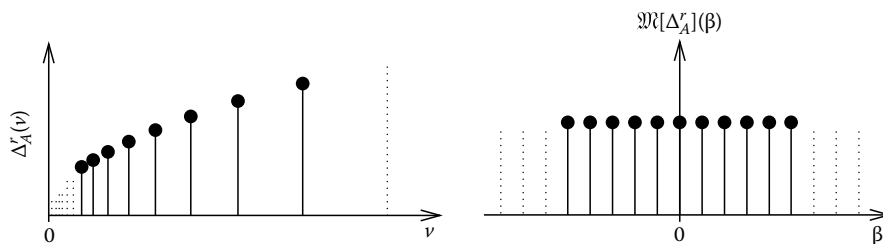


FIGURE 12.3 Geometrical dirac comb in  $\mathbb{R}^+$ -space and corresponding arithmetical Dirac comb in the Mellin space (case  $r = -1/2$ ).

**THEOREM 12.7**

The Mellin transform of the invariant product (Equation 12.245) of the two functions  $Z_1$  and  $Z_2$  is equal to the convolution of their Mellin transforms:

$$\mathcal{M}[Z_1 \circ Z_2](\beta) = (\mathcal{M}[Z_1]^* \cdot \mathcal{M}[Z_2])(\beta) \quad (12.249)$$

*Multiplicative convolution:* For a given function  $Z_1$  (resp  $Z_2$ ), the usual convolution  $Z_1 * Z_2$  can be seen as the most general linear operation commuting with translations that can be performed on  $Z_1$  (resp  $Z_2$ ). By analogy, the *multiplicative convolution* of  $Z_1$  and  $Z_2$  is defined as the most general linear operation on  $Z_1$  (resp  $Z_2$ ) that commutes with dilations. More precisely, suppose that a linear operate  $\mathcal{A}$  is defined in terms of a kernel function  $A(v, v')$  according to

$$\mathcal{A}[Z_1](v) = \int_0^{+\infty} A(v, v') Z_1(v') dv' \quad (12.250)$$

Then the requirement that transformation  $\mathcal{D}_a$  applied either on  $Z_1$  or  $\mathcal{A}[Z_1]$  yield the same results implies that:

$$a^{r+1} \mathcal{A}[Z_1](av) = a^{r+1} \int_0^{+\infty} A(v, v') Z_1(av') dv' \quad (12.251)$$

must be true for any function  $Z_1$ . Comparing Equation 12.251 to Equation 12.250, we thus obtain the following constraint on the kernel  $A(v, v')$ :

$$A(v, v') \equiv a A(av, av') \quad (12.252)$$

valid for any  $a$ . For  $a = v'^{-1}$ , we obtain the identity:

$$A(v, v') \equiv \frac{1}{v'} A\left(\frac{v}{v'}, 1\right) \quad (12.253)$$

which shows that the operator  $\mathcal{A}$  can be expressed by using a function of a single variable. Thus, any linear transformation acting on function  $Z_1$  and commuting with dilations can be written in the form:

$$\int_0^{+\infty} Z_1(v') Z_2\left(\frac{v}{v'}\right) \frac{dv'}{v'} \quad (12.254)$$

where  $Z_2(v)$  is an arbitrary function.

It can be verified, by changing variables, that the above expression is symmetrical with respect to the two functions  $Z_1$  and  $Z_2$ . It defines the multiplicative convolution of these functions which is usually denoted by  $Z_1 \sim Z_2$ :

$$Z_1 \sim Z_2 \equiv \int_0^{+\infty} Z_1(v') Z_2\left(\frac{v}{v'}\right) \frac{dv'}{v'} \quad (12.255)$$

On this definition, it can be observed that dilating one of the factors  $Z_1$  or  $Z_2$  of the multiplicative convolution is equivalent to dilating the result, i.e.,

$$\mathcal{D}_a[(Z_1 \sim Z_2)(v)] \equiv [Z_1 \sim (\mathcal{D}_a Z_2)](v) \quad (12.256)$$

$$\equiv [(\mathcal{D}_a Z_1) \sim Z_2](v) \quad (12.257)$$

where  $\mathcal{D}_a$  is defined in Equation 12.214.

For applications, an essential property of the multiplicative convolution is that it is converted into a classic product when a Mellin transformation is performed.

$$\mathcal{M}[Z_1 \sim Z_2](\beta) = \mathcal{M}[Z_1](\beta) \cdot \mathcal{M}[Z_2](\beta) \quad (12.258)$$

To prove this result, we write the definition of  $\mathcal{M}[Z_1 \sim Z_2](\beta)$  which is, according to Equations 12.211 and 12.255:

$$\mathcal{M}[Z_1 \sim Z_2](\beta) = \int_0^{\infty} v^{2\pi/\beta+r} Z_1(v') Z_2\left(\frac{v}{v'}\right) \frac{dv'}{v'} dv \quad (12.259)$$

The change of variables from  $v$  to  $x = v/v'$  yields the result.

**THEOREM 12.8**

The Mellin transform of the multiplicative convolution (Equation 12.255) of functions  $Z_1$  and  $Z_2$  is equal to the product of their Mellin transforms:

$$\mathcal{M}[Z_1 \sim Z_2](\beta) = \mathcal{M}[Z_1](\beta) \cdot \mathcal{M}[Z_2](\beta) \quad (12.260)$$

*Remark*

It can be easily verified that the above theorems remain true if  $Z_1, Z_2$  are distributions provided the composition laws involved in the formulas may be applied.

**12.3.2 Discretization and Fast Computation of the Transform**

Discretization of the Mellin transform (Equation 12.211) is performed along the same lines as discretization of the Fourier transform. It concerns signals with support practically limited, both in  $v$ -space and in  $\beta$ -space. The result is a discrete formula giving a linear relation between  $N$  geometrically spaced samples of  $Z(v)$  and  $N$  arithmetically spaced samples of  $\mathcal{M}[Z](\beta)$ .<sup>24,25,28</sup> The fast computation of this discretized transform involves the same algorithms as used in the fast Fourier transformation (FFT).



Before proceeding to the discretization itself, we introduce the special notions of sampling and periodizing that will be applied to the function  $Z(v)$ .

**12.3.2.1 Sampling in Original and in Mellin Variables**

Sampling and periodizing are operations that are well defined in the Mellin space of functions  $\tilde{Z}(\beta)$  and can be expressed in terms of Dirac combs. We shall show that the corresponding operations in the space of original functions  $Z(v)$  involve the geometrical Dirac combs introduced in Section 12.3.1.3.

**12.3.2.1.1 Arithmetic Sampling in Mellin Space**

Given a function  $M(\beta) \equiv \mathcal{M}[Z](\beta)$ , the arithmetically sampled function  $M_s(\beta)$  with sample interval  $1/\ln Q, Q$  real, is usually defined by

$$M_s(\beta) \equiv \frac{1}{\ln Q} \sum_{n=-\infty}^{+\infty} \mathcal{M}[Z](\beta) \delta\left(\beta - \frac{n}{\ln Q}\right) \quad (12.261)$$

Remark that besides sampling, this definition contains a factor  $1/\ln Q$  that is a matter of convenience.

To compute the inverse Mellin transform of this function  $M_s(\beta)$ , we remark that, due to relation (Equation 12.244), it can also be written as a product of Mellin transform in the form:

$$M_s(\beta) = \mathcal{M}[Z](\beta) \mathcal{M}[\Delta_Q^r](\beta) \quad (12.262)$$

where  $\Delta_Q^r$  is the geometric Dirac comb (Equation 12.238). Applying now theorem 12.8, we write  $M_s$  as

$$M_s(\beta) = \mathcal{M}[Z \sim \Delta_Q^r](\beta) \quad (12.263)$$

This relation implies that the inverse Mellin transform of the impulse function  $M_s(\beta)$  is the function  $Z^D(v)$  given by

$$Z^D(v) \equiv (Z \vee \Delta_Q^r)(v) \quad (12.264)$$

The definition of  $Z^D$  can be cast into a more explicit form by using the definition of the multiplicative convolution and the expression (Equation 12.238) of  $\Delta_Q^r$ :

$$(Z \sim \Delta_Q^r)(v) = \int_0^{+\infty} Z\left(\frac{v}{v'}\right) \left[ \sum_{n=-\infty}^{+\infty} Q^{nr} \delta(v' - Q^{-n}) \right] \frac{dv'}{v'} \quad (12.265)$$

The expression (Equation 12.264) finally becomes

$$Z^D(v) = \sum_{n=-\infty}^{+\infty} Q^{n(r+1)} Z(Q^n v) \quad (12.266)$$

As seen on Figure 12.4, function  $Z^D$  is constructed by juxtaposing dilated replicas of  $Z$ . This operation will be referred to as *dilatocycling* and the function  $Z^D$  itself as the *dilatocycled form* of  $Z$  with ratio  $Q$ . In the special case where the support of function  $Z$  is the interval  $[v_1, v_2]$  and the ratio  $Q$  verifies  $Q \geq [v_2/v_1]$ , the restriction of  $Z^D$  to the support  $[v_1, v_2]$  is equal to the original function  $Z$ .

*Result*

The Mellin transform  $M_s(\beta)$  of the dilatocycled form  $Z^D$  of a signal  $Z$  is equal to a regular sampled form of the Mellin transform of  $Z$ . Explicitly, we have

$$Z^D(v) = (\Delta_Q^r \vee Z)(v) \quad (12.267)$$

where

$$\Delta_Q^r(v) \equiv \sum_{n=-\infty}^{+\infty} Q^{nr} \delta(v - Q^{-n}) \quad (12.268)$$

and the result is

$$M_s(\beta) \equiv \frac{1}{\ln Q} \sum_{n=-\infty}^{+\infty} \mathcal{M}[Z](\beta) \delta\left(\beta - \frac{n}{\ln Q}\right) \quad (12.269)$$

**12.3.2.1.2 Geometric Sampling in the Original Space**

Given a function  $Z(v)$ , its geometrically sampled version is defined as the function  $Z_s$  equal to the invariant product (Equation 12.245) of  $Z$  with the geometric Dirac comb  $\Delta_q^r$ , i.e., as

$$Z_s \equiv Z \circ \Delta_q^r \quad (12.270)$$

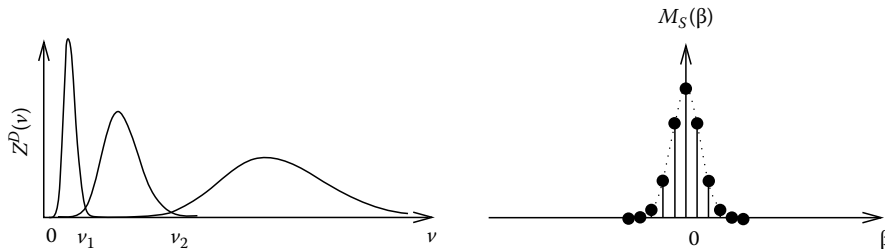


FIGURE 12.4 Correspondence between the dilatocycled form of a function and its Mellin transform.

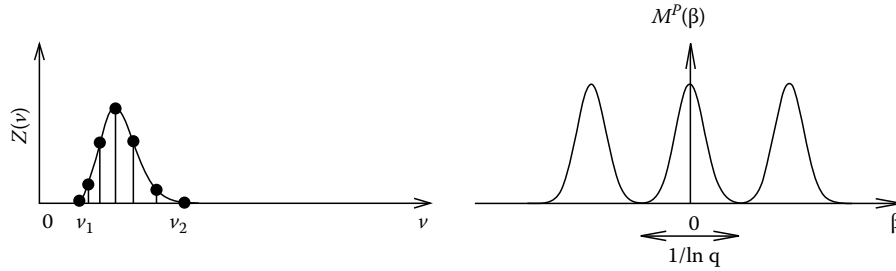


FIGURE 12.5 Correspondence between the geometrically sampled function and its Mellin transform.

or, using the expression (Equation 12.238):

$$Z_S(v) = Z(v) \sum_{n=-\infty}^{+\infty} q^{-nr} \delta(v - q^n) v^{r+1} \quad (12.271)$$

$$= \sum_{n=-\infty}^{+\infty} q^n Z(q^n) \delta(v - q^n) \quad (12.272)$$

The result is a function made of impulses located at points forming a geometric progression in  $v$ -space (Figure 12.5).

Let us compute the Mellin transform  $M^P(\beta)$  of  $Z_S(v)$ . Using definition (Equation 12.270) and property (Equation 12.249), we can write:

$$M^P(\beta) \equiv \mathcal{M}[Z_S](\beta) \quad (12.273)$$

$$= \mathcal{M}[Z \circ \Delta_q^r](\beta) \quad (12.274)$$

$$= (\mathcal{M}[Z]^* \mathcal{M}[\Delta_q^r])(\beta) \quad (12.275)$$

Thus, function  $M^P(\beta)$  is equal to the convolution between  $\mathcal{M}[Z]$  and the transform  $\mathcal{M}[\Delta_q^r]$  which has been shown in Equation 12.244 to be a classical Dirac comb. As a consequences, it is equal to the classical periodized form of  $\mathcal{M}[Z](\beta)$  which is given explicitly by

$$M^P(\beta) \equiv \frac{1}{\ln q} \sum_{n=-\infty}^{+\infty} \mathcal{M}[Z] \left( \beta - \frac{n}{\ln q} \right) \quad (12.276)$$

If the function  $M(\beta) \equiv \mathcal{M}[Z](\beta)$  is equal to zero outside the interval  $[\beta_1, \beta_2]$ , then to avoid aliasing, the period  $1/\ln q$  must be chosen such that:

$$\frac{1}{\ln q} \geq \beta_2 - \beta_1 \quad (12.277)$$

In that case, the functions  $M^P(\beta)$  and  $(1/\ln q)M(\beta)$  coincide on the interval  $[\beta_1, \beta_2]$ .

**Result**

The geometrically sampled form of  $Z(v)$  defined by

$$Z_S(v) \equiv \sum_{n=-\infty}^{+\infty} q^n Z(q^n) \delta(v - q^n) \quad (12.278)$$

is connected by Mellin's correspondence to the periodized form of  $\mathcal{M}[Z](\beta)$  given by

$$M^P(\beta) = \frac{1}{\ln q} \sum_{n=-\infty}^{+\infty} \mathcal{M}[Z] \left( \beta - \frac{n}{\ln q} \right) \quad (12.279)$$

**12.3.2.2 The Discrete Mellin Transform**

Let  $Z(v)$  be a function with Mellin transform  $M(\beta)$  and suppose that these functions can be approximated by their restriction to the intervals  $[v_1, v_2]$  and  $[\beta_1, \beta_2]$ , respectively, (see Figure 12.6a and b). For such functions, it is possible to write down a discretized form of the transform which is very similar to what is done for the Fourier transformation. One may obtain the explicit formulas by performing the following steps:

*Dilatocycle function  $Z(v)$  with ratio  $Q$ .* This operation leads to the function  $Z^D$  defined by Equation 12.267. To avoid aliasing, the real number  $Q$  must be chosen such that:

$$Q \geq \frac{v_2}{v_1} \quad (12.280)$$

The Mellin transform of  $Z^D$  is the sampled function  $M_S$  defined by Equation 12.269 in terms of  $\mathcal{M}[Z](\beta) \equiv M(\beta)$  (Figure 12.6d).

*Periodize  $M_S(\beta)$  with a period  $1/\ln q$ .* This is performed by rule (Equation 12.279) and yields a function  $M_S^P(\beta)$  given by

$$M_S^P(\beta) = \frac{1}{\ln q} \sum_{n=-\infty}^{+\infty} M_S \left( \beta - \frac{n}{\ln q} \right) \quad (12.281)$$

To avoid aliasing in  $\beta$ -space, the period must be chosen greater than the approximate support of  $\mathcal{M}[Z](\beta)$  and this leads to the condition:

$$\frac{1}{\ln q} \geq \beta_2 - \beta_1 \quad (12.282)$$

The inverse Mellin transform of  $M_S^P$  is the geometrically sampled form of  $Z^D$  (Figure 12.6e) given, according to Equation 12.278, by

$$Z_S^D(v) = \sum_{n=-\infty}^{+\infty} q^n Z^D(q^n) \delta(v - q^n) \quad (12.283)$$

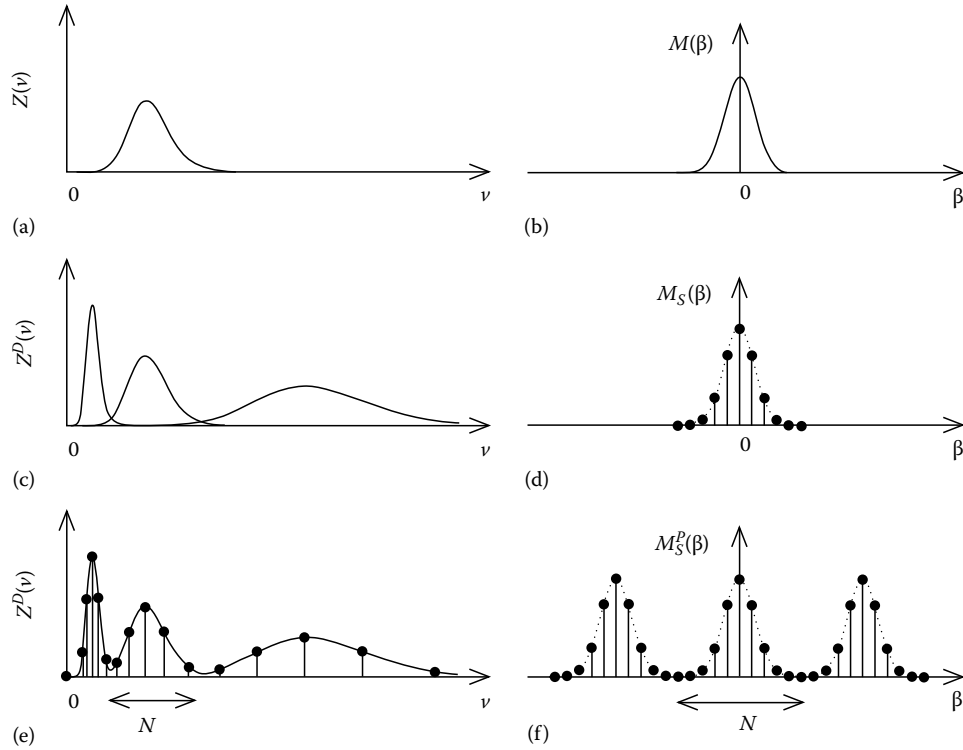


**FIGURE 12.6** Steps leading to the discrete Mellin transform. Continuous form of the function  $Z(v)$  (a) and its Mellin transform  $M(\beta)$  (b). Dilatocycled function (c) and its Mellin transform (d). Correspondence between samples of a cycle (e) in  $v$ -space and samples of a period (f) in  $\beta$ -space.

The use of Equation 12.269 allows to rewrite definition (Equation 12.281) as

$$M_S^p(\beta) = \frac{1}{\ln q \ln Q} \sum_{n,p=-\infty}^{\infty} M\left(\frac{p}{\ln Q}\right) \delta\left(\beta - \frac{n}{\ln q} - \frac{p}{\ln Q}\right) \quad (12.284)$$

We now impose that the real numbers  $q$  and  $Q$  be connected by the relation:

$$Q = q^N, N \text{ positive integer} \quad (12.285)$$

This ensures that the function  $M_S^p$  defined by Equation 12.281 is of periodic impulse type which can be written as

$$M_S^p(\beta) = \frac{1}{\ln q \ln Q} \sum_{n,p=-\infty}^{\infty} M\left(\frac{p}{N \ln q}\right) \delta\left(\beta - \frac{nN+p}{N \ln q}\right) \quad (12.286)$$

or, changing the  $p$ -index to  $k \equiv p + nN$ :

$$M_S^p(\beta) = \frac{1}{\ln q \ln Q} \sum_{n,k=-\infty}^{\infty} M\left(\frac{k}{N \ln q} - \frac{n}{\ln q}\right) \delta\left(\beta - \frac{k}{N \ln q}\right) \quad (12.287)$$

Thus, recalling definition (Equation 12.279)

$$M_S^p(\beta) = \frac{1}{\ln Q} \sum_{k=-\infty}^{\infty} M^p\left(\frac{k}{\ln Q}\right) \delta\left(\beta - \frac{k}{\ln Q}\right) \quad (12.288)$$

Connect the  $v$  and  $\beta$  samples. This is done by writing explicitly that  $M_S^p$  as given by Equation 12.288 is the Mellin transform (Equation 12.211) of  $Z_S^D$  and computing:

$$M_S^p(\beta) = \sum_{n=-\infty}^{\infty} q^{n(r+1)} Z^D(q^n) e^{2j\pi n \beta \ln q} \quad (12.289)$$

This formula shows that  $q^{n(r+1)} Z^D(q^n)$  for different values of  $n$  are the Fourier series coefficients of the periodic function  $M_S^p(\beta)$ . They are computed as

$$\begin{aligned} Z^D(q^n) &= q^{-n(r+1)} \ln q \int_0^{1/\ln q} \frac{1}{\ln Q} \sum_{k=-\infty}^{\infty} \delta\left(\beta - \frac{k}{\ln Q}\right) \\ &\quad \times M^p\left(\frac{k}{\ln Q}\right) e^{-j2\pi n \beta \ln q} d\beta \\ &= \frac{q^{-n(r+1)}}{N} \sum_{k=K}^{K+N-1} M^p\left(\frac{k}{\ln Q}\right) e^{-2j\pi kn/N} \end{aligned} \quad (12.290)$$

where the summation is on these values of  $\beta$  lying inside the interval  $[\beta_1, \beta_2]$ . The integer  $K$  is thus given by the integer part of  $\beta_1 \ln Q$ .

Inversion of Equation 12.290 is performed using the classical techniques of discrete Fourier transform (DFT). This leads to the discrete Mellin transform formula:

$$M^P\left(\frac{m}{\ln Q}\right) = \sum_{n=J}^{J+N-1} q^{n(r+1)} Z^D(q^n) e^{2j\pi nm/N} \quad (12.291)$$

where the integer  $J$  is given by the integer part of  $\ln v_1/\ln q$ . In fact, since the definition of the periodized  $M^P$  contains a factor  $N/\ln Q = 1/\ln q$ , the true samples of  $M(\beta)$  are given by  $(\ln Q/n) M^P(m/\ln Q)$ .

It is clear on formulas (Equation 12.290) and (Equation 12.291) that their implementation can be performed with a FFT algorithm.

Choose the number of samples of handle. The number of samples  $N$  is related to  $q$  and  $Q$  according to Equation 12.285 by

$$N = \frac{\ln Q}{\ln q} \quad (12.292)$$

The conditions for nonaliasing given by Equations 12.280 and (12.282) lead to the sampling condition:

$$N \geq (\beta_2 - \beta_1) \ln\left(\frac{v_2}{v_1}\right) \quad (12.293)$$

which gives the minimum number of samples to consider in terms of the spreads of  $Z(v)$  and  $\mathcal{M}[Z](\beta)$ . In practice, the spread of the Mellin transform of a function is seldom known. However, as we will see in the applications, there are methods to estimate it.

### 12.3.2.3 Interpolation Formula in $v$ -Space

In the same way as the Fourier transformation is used to reconstruct a band-limited function from its regularly spaced samples, Mellin's transformation allows to recover a function  $Z(v)$  with limited spread in the Mellin space from its samples spaced according to a geometric progression. If the Mellin transform  $\mathcal{M}[Z]$  has a bounded support  $[-\beta_0/2, \beta_0/2]$ , it will be equal on this interval to its periodized form with period  $1/\ln q = \beta_0$ . Thus,

$$\mathcal{M}[Z](\beta) = \sum_{n=-\infty}^{+\infty} \mathcal{M}[Z]\left(\beta - \frac{n}{\ln q}\right) g\left(\frac{\beta}{\beta_0}\right) \quad (12.294)$$

where the window function  $g$  is the characteristic function of the  $[-1/2, 1/2]$ -interval.

The inverse Mellin transform of this product is the multiplicative convolution of the two functions  $Z_1$  and  $Z_2$  defined as

$$Z_1(v) = \ln q \sum_{n=-\infty}^{+\infty} q^n Z(q^n) \delta(v - q^n) \quad (12.295)$$

and

$$Z_2(v) = \int_{-\infty}^{\infty} g\left(\frac{\beta}{\beta_0}\right) v^{-2j\pi\beta-r-1} d\beta \quad (12.296)$$

$$= v^{-r-1} \frac{\sin(\pi\beta_0 \ln v)}{\pi \ln v} \quad (12.297)$$

The multiplicative convolution between  $Z_1$  and  $Z_2$  takes the following form:

$$Z(v) = \int_0^{+\infty} \ln q \sum_{n=-\infty}^{+\infty} q^n Z(q^n) \delta(v' - q^n) \left(\frac{v}{v'}\right)^{-r-1} \frac{\sin(\pi\beta_0 \ln(\frac{v}{v'}))}{\pi \ln(\frac{v}{v'})} \frac{dv'}{v'} \quad (12.298)$$

which reduces to

$$Z(v) = v^{-r-1} \sum_{n=-\infty}^{+\infty} q^{n(r+1)} Z(q^n) \frac{\sin \pi \left( \left( \frac{\ln v}{\ln q} \right) - n \right)}{\pi \left( \left( \frac{\ln v}{\ln q} \right) - n \right)} \quad (12.299)$$

where the relation  $\beta_0 = 1/\ln q$  has been used.

This is the interpolation formula of a function  $Z(v)$  from its geometrically spaced samples  $Z(q^n)$ .

## 12.3.3 Practical Use in Signal Analysis

### 12.3.3.1 Preliminaries

As seen above, Mellin's transformation is essential in problems involving dilations. Thus, it is not surprising that it has come to play a dominant role in the development of analytical studies of wideband signals. In fact, expressions involving dilations arise in signal theory any time the approximation of small relative bandwidth is not appropriate. Recent examples of the use of the Mellin transform in this context can be found in time-frequency analysis where it has contributed to the introduction of several classes of distributions.<sup>29-36</sup> This fast growing field cannot be explored here but an illustration of the essential role played by Mellin's transformation in the analysis of wide-band signals will be given in Section 12.3.3.2 where Cramer-Rao bound for velocity estimation is derived.<sup>37</sup>

Numerical computation of Mellin's transform has been undertaken in various domains such as signal analysis,<sup>38,39</sup> optical image processing,<sup>40</sup> or pattern recognition.<sup>41-43</sup> In the past, however, all these applications have been restricted by the difficulty of assessing the validity of the results, due to the lack of definite sampling rules. Such a limitation does not exist any more as we will show in Section 12.3.3.3 by deriving a sampling theorem and a practical way to use it. The technique will be applied in Sections 12.3.3.4 and 12.3.3.5 to the computation of a wavelet coefficient and of an affine time-frequency distribution.<sup>47-49</sup>

### 12.3.3.2 Computation of Cramer–Rao Bounds for Velocity Estimation in Radar Theory<sup>37</sup>

In a classical radar or sonar experiment, a real signal is emitted and its echo is processed in order to find the position and velocity of the target. In simple situations, the received signal will differ from the original one only by a time shift and a Doppler compression. In fact, the signal will also undergo an attenuation and a phase shift; moreover, the received signal will be embedded in noise.

The usual procedure, which is adapted to narrow-band signals, is to represent the Doppler effect by a frequency shift.<sup>44</sup> This approximation will not be made here so that the results will be valid whatever the extent of the frequency band. Describing the relevant signals by their positive frequency parts (so-called analytic signals), we can write the expression of the received signal  $x(t)$  in terms of the emitted signal  $z(t)$  and noise  $n(t)$  as

$$x_{a'}(t) = a_1'^{-1/2} A_0 z(a_1'^{-1}t - a_2') e^{j\phi} + n(t) \quad (12.300)$$

where  $A_0$  and  $\phi$  characterize the unknown changes in amplitude and phase and the vector  $\mathbf{a}' \equiv (a_1', a_2')$  represents the unknown parameters to be estimated. The parameter  $a_2'$  is the delay and  $a_1'$  is the Doppler compression given in terms of the target velocity  $v$  by

$$a_1' = \frac{c+v}{c-v}, \quad c \text{ velocity of light} \quad (12.301)$$

The noise  $n(t)$  is supposed to be a zero mean Gaussian white noise with variance equal to  $\sigma^2$ . Relation (Equation 12.300) can be written in terms of the Fourier transforms  $Z, X, N$  of  $z, x, n$  (defined by Equation 12.19):

$$X_{a'}(f) = a_1'^{1/2} A_0 e^{-j\pi f a_2'} Z(a_1' f) e^{j\phi} + N(f) \quad (12.302)$$

The signal  $Z(f)$  is supposed normalized so that:

$$\|Z(f)\|^2 \equiv \int_0^{\infty} |Z(f)|^2 df = 1 \quad (12.303)$$

Hence, the delayed and compressed signal will also be of norm equal to one. Remark that here we work in the space  $L^2(\mathbb{R}^+, f^{2r+1} df)$  with  $r = -1/2$  (cf Section 12.3.1.1).

We will consider the maximum-likelihood estimates  $\hat{a}_i$  of the parameters  $a_i'$ . They are obtained by maximizing the likelihood function  $\Lambda(\mathbf{a}', \mathbf{a})$  which is given in the present context by

$$\Lambda(\mathbf{a}', \mathbf{a}) \equiv \frac{1}{2\sigma^2} |A(\mathbf{a}', \mathbf{a})|^2 \quad (12.304)$$

where

$$A(\mathbf{a}', \mathbf{a}) \equiv \int_0^{\infty} X_{a'}(f) Z^*(a_1 f) e^{2j\pi a_1 a_2 f} df \quad (12.305)$$

is the broad-band ambiguity function.<sup>45</sup>

The efficiency of an estimator  $\hat{a}_i$  is measured by its variance  $\sigma_{ij}^2$  defined by

$$\sigma_{ij}^2 \equiv E[(\hat{a}_i - a_i)(\hat{a}_j - a_j)] \quad (12.306)$$

where the mean value operation  $E$  includes an average on noise.

For an unbiased estimator ( $E(\hat{a}_i) = a_i$ ), this variance satisfies the Cramer–Rao inequality<sup>46</sup> given by

$$\sigma_{ij}^2 \geq (J^{-1})_{ij} \quad (12.307)$$

where the matrix  $J$ , the so-called Fisher information matrix, is defined by

$$J_{ij} = \left( -E \left[ \frac{\partial^2 \Lambda}{\partial a_i \partial a_j} \right] \right)_{ij} \quad (12.308)$$

with the partial derivatives evaluated at the true values of the parameters. The minimum value of the variance given by

$$(\sigma_{ij}^0)^2 = (J^{-1})_{ij} \quad (12.309)$$

is called the Cramer–Rao bound and is attained in the case of an efficient estimator such as the maximum-likelihood one.

The determination of the matrix (Equation 12.308) by classical methods is intricate and does not lead to an easily interpretable result. On the contrary, we shall see how the use of Mellin's transformation allows a direct computation and leads to a physical interpretation of the matrix coefficients.

The computation of  $J$  is done in the vicinity of the value  $\mathbf{a} = \mathbf{a}'$  which maximizes the likelihood function  $\Lambda$  and, without loss of generality, all partial derivatives will be evaluated at the point  $a_1 = 1, a_2 = 0$ . Using Parseval's formula (Equation 12.213), we can write the ambiguity function  $A(\mathbf{a}', \mathbf{a})$  as

$$A(\mathbf{a}', \mathbf{a}) = \int_{-\infty}^{+\infty} \mathcal{M}[X](\beta) \mathcal{M}^*[Z_{a_2}](\beta) a_1^{2j\pi\beta} d\beta \quad (12.310)$$

with

$$Z_{a_2} \equiv Z(f) e^{-2j\pi a_2 f} \quad (12.311)$$

On this form, the partial derivatives with respect to  $\mathbf{a}$  are easily computed and the result is

$$\left\{ \frac{\partial A}{\partial a_1} \right\} = 2j\pi \int_{-\infty}^{+\infty} \beta \mathcal{M}[X](\beta) \mathcal{M}^*[Z](\beta) d\beta \quad (12.312)$$

$$\left\{ \frac{\partial A}{\partial a_2} \right\} = 2j\pi \int_{-\infty}^{+\infty} \mathcal{M}[X](\beta) \mathcal{M}^*[fZ(f)](\beta) d\beta \quad (12.313)$$

$$= 2j\pi \int_0^{\infty} f X(f) Z^*(f) df \quad (12.314)$$

$$\left\{ \frac{\partial^2 A}{\partial a_1 \partial a_2} \right\} = -4\pi^2 \int_{-\infty}^{+\infty} \beta \mathcal{M}[X](\beta) \mathcal{M}^* [fZ(f)](\beta) d\beta \quad (12.315)$$

$$\left\{ \frac{\partial^2 A}{\partial a_1^2} \right\} = 2j\pi \int_{-\infty}^{+\infty} \beta (2j\pi\beta - 1) \mathcal{M}[X](\beta) \mathcal{M}^* [Z](\beta) d\beta \quad (12.316)$$

$$\left\{ \frac{\partial^2 A}{\partial a_2^2} \right\} = -4\pi^2 \int_0^{+\infty} f^2 X(f) Z^*(f) df \quad (12.317)$$

where the curly brackets mean that the functions are evaluated for the values  $a_1 = a'_1 = 1$ ,  $a_2 = a'_2 = 0$ .

The corresponding Fisher information matrix can now be computed. To obtain  $J_{11}$ , we substitute the expression (Equation 12.304) in definition (Equation 12.308) and use (Equation 12.312) and (Equation 12.316):

$$\begin{aligned} J_{11} &= -\frac{1}{\sigma^2} E \left[ \operatorname{Re} \left( A^* \left\{ \frac{\partial^2 A}{\partial a_1^2} \right\} + \left\{ \left| \frac{\partial A}{\partial a_1} \right|^2 \right\} \right) \right] \quad (12.318) \\ &= -\frac{1}{\sigma^2} \operatorname{Re} \int_{-\infty}^{+\infty} \int_{-\infty}^{+\infty} E[\mathcal{M}[X](\beta_1) \mathcal{M}^* [X](\beta_2)] \mathcal{M}^* [Z](\beta_1) \mathcal{M}[Z](\beta_2) \\ &\quad \times [2j\pi\beta_1(2j\pi\beta_1 - 1) + 4\pi^2\beta_1\beta_2] d\beta_1 d\beta_2 \quad (12.319) \end{aligned}$$

The properties of the zero mean white Gaussian noise  $n(t)$  lead to the following expression for the covariance of the Mellin transform of  $X$ :

$$E[\mathcal{M}[X](\beta_1) \mathcal{M}^* [X](\beta_2)] = A_0^2 \mathcal{M}[Z](\beta_1) \mathcal{M}^* [Z](\beta_2) + \sigma^2 \delta(\beta_1 - \beta_2) \quad (12.320)$$

Substituting this relation in Equation 12.319, we obtain the expression of the  $J_{11}$  coefficient:

$$J_{11} = \frac{4\pi^2 A_0^2}{\sigma^2} \sigma_\beta^2 \quad (12.321)$$

where the variance  $\sigma_\beta^2$  of parameter  $\beta$  defined in Equation 12.217 is given explicitly by

$$\begin{aligned} \sigma_\beta^2 &= \int_{-\infty}^{+\infty} (\beta - \bar{\beta})^2 |\mathcal{M}[Z](\beta)|^2 d\beta, \\ \bar{\beta} &= \int_{-\infty}^{+\infty} \beta |\mathcal{M}[Z](\beta)|^2 d\beta \end{aligned} \quad (12.322)$$

The computation of the  $J_{22}$  coefficient is performed in the same way and leads to

$$J_{22} = \frac{4\pi^2 A_0^2}{\sigma^2} \sigma_f^2 \quad (12.323)$$

where

$$\sigma_f^2 = \int_{-\infty}^{+\infty} (f - \bar{f})^2 |Z(f)|^2 df, \quad \bar{f} = \int_{-\infty}^{+\infty} f |Z(f)|^2 df \quad (12.324)$$

The computation of the symmetrical coefficient  $J_{12} = J_{21}$  is a little more involved. Writing the definition in the form:

$$J_{12} = -\frac{1}{\sigma^2} E \left[ \operatorname{Re} \left( A^* \left\{ \frac{\partial^2 A}{\partial a_1 \partial a_2} \right\} + \left\{ \frac{\partial A^*}{\partial a_1} \frac{\partial A}{\partial a_2} \right\} \right) \right] \quad (12.325)$$

and using relations (Equations 12.312 through 12.315), (Equation 12.320), we get

$$\begin{aligned} J_{12} &= \frac{4\pi^2 A_0^2}{\sigma^2} \operatorname{Re} \left[ \int_{-\infty}^{+\infty} \beta_1 \mathcal{M}^* [fZ(f)](\beta_1) \mathcal{M}[Z](\beta_1) d\beta_1 \right. \\ &\quad \left. - \int_{-\infty}^{+\infty} \mathcal{M}^* [fZ(f)](\beta_1) \mathcal{M}[Z](\beta_1) d\beta_1 \int_{-\infty}^{+\infty} \beta_2 |\mathcal{M}[Z](\beta_2)|^2 d\beta_2 \right] \quad (12.326) \end{aligned}$$

This expression is then transformed to the frequency domain using the Parseval formula (Equation 12.213) and the property (Equation 12.208) of the operator  $\mathcal{B}$  defined by Equation 12.187 (with  $r = -1/2$ ). The result is

$$\begin{aligned} J_{12} &= \frac{4\pi^2 A_0^2}{\sigma^2} \left[ \operatorname{Re} \int_0^{+\infty} \mathcal{B}Z(f) f Z^*(f) df - \overline{\beta f} \right] \\ &= \frac{4\pi^2 A_0^2}{\sigma^2} [M - \overline{\beta f}] \quad (12.327) \end{aligned}$$

where  $M$  is the broad-band modulation index defined by

$$M \equiv \frac{1}{2\pi} \operatorname{Im} \int_0^{+\infty} f^2 \frac{dZ^*}{df} Z(f) df \quad (12.328)$$

The inversion of the matrix  $J$  just obtained leads according to Equation 12.307 to the explicit expression of the Cramer-Rao bound for the case of delay and velocity estimation with broad-band signals:

$$\left( \sigma_{ij}^0 \right)^2 = \frac{\sigma^2}{4\pi^2 A_0^2 (\sigma_f^2 \sigma_\beta^2 - (M - \overline{\beta f}))^2} \begin{pmatrix} \sigma_f^2 & \overline{\beta f} - M \\ \overline{\beta f} - M & \sigma_\beta^2 \end{pmatrix} \quad (12.329)$$

Relation (Equation 12.301) allows to deduce from this result the minimum variance of the velocity estimator:

$$E[(v - \hat{v})^2] = \frac{c^2}{4} E[(a_1 - \hat{a}_1)^2] \quad (12.330)$$

$$= \frac{c^2}{4} (\sigma_{11}^0)^2 \quad (12.331)$$

Comparing these results to the narrow-band case, we see that the delay resolution measured by  $\sigma_{22}^0$  is still related to the spread of the signal in frequency:

$$(\sigma_{22}^0)^2 \geq \frac{\sigma^2}{4\pi^2 A_0^2} \frac{1}{\sigma_f^2} \quad (12.332)$$

while the velocity resolution now depends in an essential way on the spread in Mellin's space:

$$E[(v - \hat{v})^2] \geq \frac{c^2 \sigma^2}{16\pi^2 A_0^2 \sigma_\beta^2} \quad (12.333)$$

Thus, for wide-band signals, it is not the duration of the signal that determines the velocity resolution, but the spread in the dual Mellin variable measured by the variance  $\sigma_\beta^2$ .

As an illustrative example, consider the hyperbolic signal defined by

$$Z(f) = f^{-2j\pi\beta_0 - 1/2} \quad (12.334)$$

Its Mellin transform which is equal to  $\delta(\beta - \beta_0)$  can be considered to have zero spread in  $\beta$ . Hence, such a signal cannot be of any help if seeking a finite velocity resolution.

These remarks can be developed and applied to the construction of radar codes with given characteristics in the variables  $f$  and  $\beta$ .<sup>37</sup>

The above results can be seen as a generalization to arbitrary signals of a classical procedure since, in the limit of narrow band, the variance of the velocity estimator can be shown to tend toward its usual expression:

$$E[(v - \hat{v})^2] = \frac{c^2 \sigma^2}{16\pi^2 A_0^2 f_0^2} \frac{\sigma_f^2}{\sigma_t^2 \sigma_f^2 - (m - f_0 t_0)^2} \quad (12.335)$$

where the modulation index  $m$  is given by

$$m = \frac{1}{2\pi} \text{Im} \int_{-\infty}^{+\infty} tz^*(t) \frac{dz}{dt} dt = \frac{1}{2\pi} \text{Im} \int_{-\infty}^{+\infty} tZ(f) \frac{dZ^*}{df} df \quad (12.336)$$

and the variance  $\sigma_t^2$  by

$$\sigma_t^2 = \int_{-\infty}^{\infty} (t - \bar{t})^2 |z(t)|^2 dt, \quad \bar{t} = \int_{-\infty}^{\infty} t |z(t)|^2 dt \quad (12.337)$$

### 12.3.3.3 Interpretation of the Dual Mellin Variable in Relation to Time and Frequency

Consider a signal defined by a function of time  $z(t)$  such that its Fourier transform  $Z(f)$  has only positive frequencies (so-called analytic signal). In that case a Mellin transformation can be applied to  $Z(f)$  and yields a function  $\mathcal{M}[Z](\beta)$ . But while variables  $t$  and  $f$  have a well defined physical meaning as time and frequency, the interpretation of variable  $\beta$  and its relation to physical parameters of the signal has still to be worked out. This will be done in the present paragraph, thus allowing a formulation of the sampling condition (Equation 12.293) for the Mellin transform in terms of the time and frequency spreads of the signal.

As seen in Section 12.3.1.1, the Mellin transform  $\mathcal{M}[Z](\beta)$  gives the coefficients of the decomposition of  $Z$  on the basis  $\{E_\beta(f)\}$ :

$$Z(f) = \int_{-\infty}^{\infty} \mathcal{M}[Z](\beta) E_\beta(f) d\beta \quad (12.338)$$

The elementary parts:

$$E_\beta(f) = f^{-2\pi j\beta - r - 1} \equiv f^{-r-1} e^{j\phi(f)} \quad (12.339)$$

can be considered as filters with group delay given by

$$\begin{aligned} T(f) &\equiv -\frac{1}{2\pi} \frac{d\phi(f)}{df} \\ &= \frac{\beta}{f} \end{aligned} \quad (12.340)$$

As seen on this expression, the variable  $\beta$  has no dimension and labels hyperbolas in a time-frequency half-plane  $f > 0$ . Hyperbolas displaced in time, corresponding to a group delay  $t = \xi + \beta/f$  are obtained by time shifting the filters  $E_\beta$  to  $E_\beta^\xi(f)$  defined by

$$E_\beta^\xi(f) = e^{-2\pi j\xi f} f^{-2\pi j\beta - r - 1} \quad (12.341)$$

A more precise characterization of signals (Equation 12.339) and, hence, of variable  $\beta$  is obtained from a study of a particular affine time-frequency distribution which is to dilations what Wigner-Ville's is to frequency translations. We give only the practical results of the study, referring the interested reader to the literature.<sup>28-31</sup> The explicit form of the distribution is

$$P_0(t, f) = f^{2r+2} \int_{-\infty}^{+\infty} (\lambda(u)\lambda(-u))^{r+1} Z(f\lambda(u)) Z^*(f\lambda(-u)) e^{2j\pi ftu} du \quad (12.342)$$

where function  $\lambda$  is given by

$$\lambda(u) = \frac{ue^{u/2}}{2 \sinh u/2} \quad (12.343)$$

This distribution realizes an exact localization of hyperbolic signals defined by Equation 12.341 on hyperbolas of the time-frequency half-plane as follows:

$$Z(f) = e^{-2\pi j \xi f} f^{-r-1} f^{-2j\pi\beta} \rightarrow P_0(t, f) = f^{-1} \delta(t - \xi - \beta/f) \quad (12.344)$$

It can be shown that the affine time-frequency distribution (Equation 12.342) has the so-called tomographic property<sup>29-31</sup> which reads:

$$\int_{-\infty}^{+\infty} dt \int_0^{+\infty} P_0(t, f) \delta(t - \xi - \beta/f) f^{-1} df = |\mathcal{M}[Z](\beta)|^2 \quad (12.345)$$

Formulas (Equation 12.344) and (Equation 12.345) are basic for the interpretation of the  $\beta$  variable. It can be shown that for a signal  $z(t) \leftrightarrow Z(f)$  having a duration  $T = t_2 - t_1$  and a bandwidth  $B = f_2 - f_1$ , distribution  $P_0$  has a support approximately localized in a bounded region of the half-plane  $f > 0$  (see Figure 12.7) around the time  $\xi = (t_1 + t_2)/2$  and the mean frequency  $f_0 = (f_1 + f_2)/2$ . Writing that the hyperbolas at the limits of this region have the equation:

$$t = \xi \pm \beta_0/f \quad (12.346)$$

and pass through the points of coordinates  $\xi \pm T/2, f_0 + B/2$ , we find:

$$\beta_0 = (f_0 + B/2)(T/2) \quad (12.347)$$

The support  $[\beta_1, \beta_2]$  of the Mellin transform  $\mathcal{M}[Z](\beta)$  thus can be written in terms of  $B$  and  $T$  as

$$\beta_2 - \beta_1 = 2\beta_0 \quad (12.348)$$

The condition (Equation 12.293) to avoid aliasing when performing a discrete Mellin transform can now be written in terms of

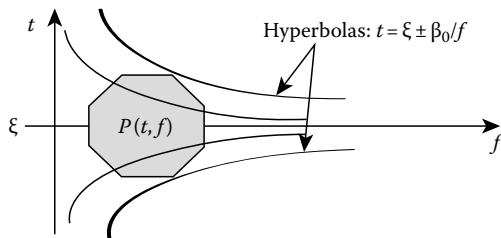


FIGURE 12.7 Time-frequency localization of a signal between hyperbolas with equations  $t = \xi + \beta_0/f$  and  $t = \xi - \beta_0/f$ .

the time-bandwidth product  $BT$  and the relative bandwidth  $R$  defined by

$$R \equiv \frac{B}{f_0} \quad (12.349)$$

The result giving the minimum number of samples to treat is

$$N \geq BT \left( \frac{1}{2} + \frac{1}{R} \right) \ln \frac{1 + R/2}{1 - R/2} \quad (12.350)$$

### 12.3.3.4 The Mellin Transform and the Wavelet Transform<sup>47,48</sup>

The Mellin transform is well suited to the computation of expressions containing dilated functions and, in particular, of scalar products such as

$$(Z_1, \mathcal{D}_a Z_2) = a^{r+1} \int_0^{+\infty} Z_1(f) Z_2^*(af) f^{2r+1} df \quad (12.351)$$

Because of the dilation parameter, a numerical computation of these functions of  $a$  by standard techniques (such as DFT) requires the use of oversampling and interpolation. By contrast, the Mellin transform allows a direct and more efficient treatment. The method will be explained on the example of the wavelet transform for one-dimensional signals. But it can also be used in more general situations such as those encountered in radar imaging.<sup>47,48</sup>

Let  $s(t)$  be a real signal with Fourier transform  $S(f)$  defined by

$$S(f) = \int_{-\infty}^{+\infty} s(t) e^{-2j\pi f t} dt \quad (12.352)$$

The reality of  $s$  implies that:

$$S(-f) = S^*(f) \quad (12.353)$$

Given a real function  $\phi(t)$  (the so-called mother wavelet), one defines the continuous wavelet transform of signal  $s(t)$  as a function  $C(a, b)$  of two variables  $a > 0, b$  real given by

$$C(a, b) = \frac{1}{\sqrt{a}} \int_{-\infty}^{+\infty} z(t) \phi^* \left( \frac{t-b}{a} \right) dt \quad (12.354)$$

Transposed to the frequency domain by a Fourier transformation and the use of property (Equation 12.353), the definition becomes:

$$C(a, b) = 2\text{Re} \left\{ \sqrt{a} \int_0^{+\infty} Z(f) \Phi^*(af) e^{2j\pi f b} df \right\} \quad (12.355)$$

where  $\Phi$  denotes the Fourier transforms of  $\phi$ .



If we define the function  $Z_b(f)$  by

$$Z_b(f) \equiv Z(f)e^{2j\pi bf} \quad (12.356)$$

the scale invariance property (Equation 12.215) of the Mellin transform with  $r = -1/2$  and the unitarity property (Equation 12.213) allow to write Equation 12.355 in Mellin's space as

$$C(a, b) = 2\text{Re} \left\{ \int_{-\infty}^{+\infty} \mathcal{M}[Z_b(\beta)] \mathcal{M}^*[\Phi](\beta) a^{2j\pi\beta} d\beta \right\} \quad (12.357)$$

In this form, there are no more dilations and the computation of the wavelet coefficient reduces to Fourier and Mellin transforms which can all be performed using an FFT algorithm. First the Mellin transform of the wavelet is computed once and for all. Then, for each value of  $b$ , one computes the Mellin transform of  $Z_b$  and the inverse Fourier transform with respect to  $\beta$  of the product  $\mathcal{M}[Z_b](\beta) \mathcal{M}^*[\Phi](\beta)$ . The complexity of this algorithm is given by  $(2M + 1)$  FFT with  $2N$  points if the wavelet coefficients are discretized in  $(N, M)$  points on the  $(a, b)$  variables. The signal and the mother wavelet are supposed geometrically sampled with the same geometric ratio  $q$ .

The same procedure can be applied to the computation of the broad band ambiguity function.<sup>45</sup> This function is used in problems of radar theory involving target detection and estimation of its characteristics (range, velocity, angle, ...). It is defined for an analytic signal  $z(t)$  with Fourier transform  $Z(f)$  by

$$X(a, b) = \frac{1}{\sqrt{a}} \int_{-\infty}^{+\infty} z(t) z^* \left( \frac{t}{a} - b \right) dt \quad (12.358)$$

$$= \sqrt{a} \int_{-\infty}^{+\infty} Z(f) Z^*(af) e^{2j\pi abf} df \quad (12.359)$$

The parameters  $a$  and  $b$  are respectively called the Doppler compression factor and the time shift.

### 12.3.3.5 Numerical Computation of Affine Time-Frequency Distributions<sup>49</sup>

In this section, the Mellin transformation is applied to the fast computation of the affine time-frequency distribution<sup>29-31</sup> given by

$$P_0(t, f) = f^{2r+2-q} \int_{-\infty}^{+\infty} (\lambda(u)\lambda(-u))^{r+1} Z(f\lambda(u)) Z^*(f\lambda(-u)) e^{2j\pi ftu} du \quad (12.360)$$

where the function  $\lambda$  is defined by

$$\lambda(u) = \frac{ue^{\frac{u}{2}}}{2 \sinh\left(\frac{u}{2}\right)} \quad (12.361)$$

and where  $r$  and  $q$  are real numbers.

Setting

$$\gamma = ft \quad \text{and} \quad \tilde{P}_0(\gamma, f) = P_0(t, f) \quad (12.362)$$

one can write Equation 12.360 as

$$f^{-r-1+q} \tilde{P}_0(\gamma, f) = \int_{-\infty}^{+\infty} (\lambda(u)\lambda(-u))^{r+1} [f^{r+1} Z(f\lambda(u)) Z^*(f\lambda(-u))] e^{2j\pi\gamma u} du \quad (12.363)$$

To perform the Mellin transformation of this expression with respect to  $f$ , we notice that the term in brackets represents the invariant product of the two functions of  $f$  defined by  $Z(f\lambda(u))$  and  $Z^*(f\lambda(-u))$ . By relation (Equation 12.249), we know that the Mellin transform of this product is equal to the convolution of the functions  $\mathcal{M}[Z(f\lambda(u))]$  and  $\mathcal{M}[Z^*(f\lambda(-u))]$ . Besides, the scaling property (Equation 12.215) allows to write:

$$\mathcal{M}[Z(f\lambda(u))](\beta) = \lambda(u)^{-2j\pi\beta-r-1} \mathcal{M}[Z](\beta) \quad (12.364)$$

and

$$\mathcal{M}[Z^*(f\lambda(-u))](\beta) = \lambda(-u)^{-2j\pi\beta-r-1} \mathcal{M}^*[Z](-\beta) \quad (12.365)$$

where

$$\mathcal{M}^*[Z](-\beta) \equiv [\mathcal{M}[Z](-\beta)]^* \quad (12.366)$$

Introducing the notation:

$$X(\beta, u) \equiv \lambda(u)^{-2j\pi\beta} \mathcal{M}[Z](\beta) \quad (12.367)$$

we can write the convolution between Equations 12.364 and 12.365 as

$$(\lambda(u)\lambda(-u))^{-r-1} \int_{-\infty}^{+\infty} X(\beta_1, u) X^*(\beta_1 - \beta, -u) d\beta_1 \quad (12.368)$$

The Mellin transform of expression (Equation 12.363) is now written as

$$\mathcal{M}[f^{-r-1+q} \tilde{P}_0(\gamma, f)](\beta) = \int_{-\infty}^{+\infty} \left[ \int_{-\infty}^{+\infty} X(\beta_1, u) X^*(\beta_1 - \beta, -u) d\beta_1 \right] e^{2j\pi\gamma u} du \quad (12.369)$$

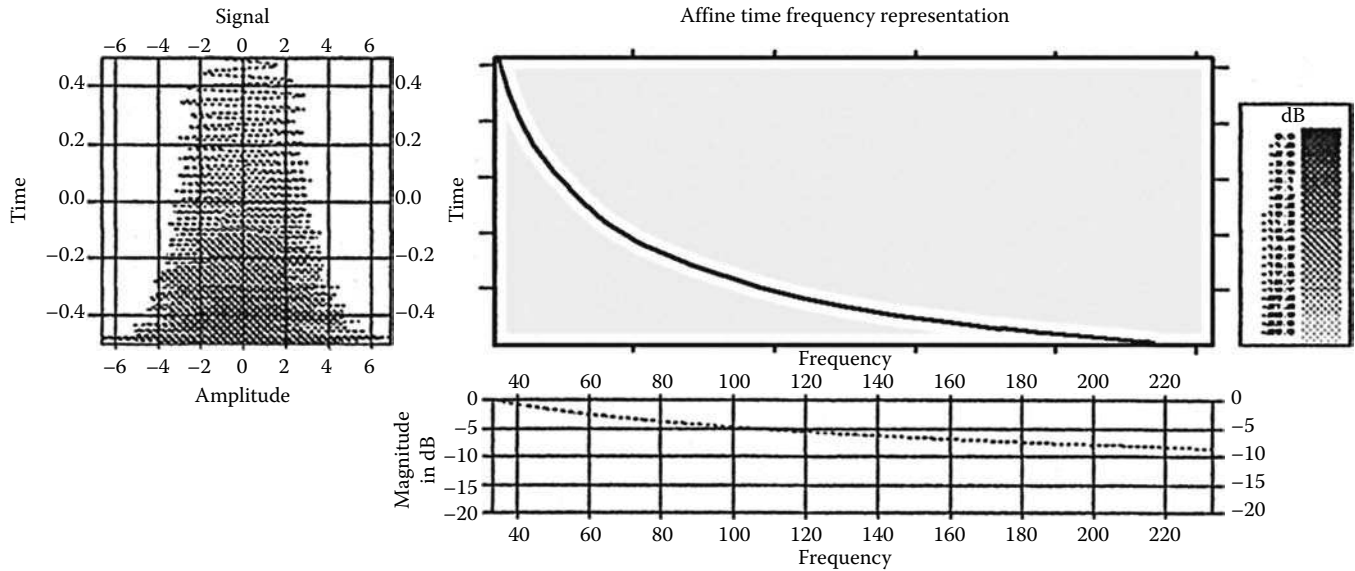


FIGURE 12.8 Affine time-frequency representation of a hyperbolic signal.

The cross-correlation inside brackets is computed in terms of the Fourier transform of  $X(\beta, u)$  defined by

$$F(\theta, u) = \int_{-\infty}^{+\infty} X(\beta, u) e^{-2j\pi\theta\beta} d\beta \quad (12.370)$$

and Equation 12.369 becomes

$$\mathcal{M}[f^{-r-1+q} \tilde{P}_0(\gamma, f)](\beta) = \int_{-\infty}^{+\infty} \int_{-\infty}^{+\infty} F(\theta, u) F^*(\theta, -u) e^{2j\pi\theta\beta} e^{2j\pi\gamma u} d\theta du \quad (12.371)$$

Finally, inverting the Mellin transform by Equation 12.212, recalling Equation 12.362 and taking into account the property of the integrand in the change  $u \rightarrow -u$ , one obtains the following form of the affine Wigner function  $P_0$ :

$$P_0(t, f) = 2\text{Re} \left\{ f^{-q} \int_0^{+\infty} F(\ln f, u) F^*(\ln f, -u) e^{2j\pi f u} du \right\} \quad (12.372)$$

where  $\text{Re}$  denotes the real part operation. In this form, the numerical computation of  $P_0$  has been reduced to a Fourier transform. The operations leading from  $Z$  to  $F$  are a Fourier and a Mellin transform, both of which are performed using the Fast Fourier Transform algorithm. The approximate complexity of the whole algorithm for computing  $P_0$  can be expressed in terms of the number of FFT performed. If the time-frequency

distribution  $P_0(t, f)$  is characterized by  $(M, N)$  points, respectively, in time and frequency, we have to deal with  $2M + \text{FFT}$  of  $2N$  points and  $N$  FFT of  $M$  points. The Figure 12.8 gives an example of affine distribution computed by this method.

## Appendix 12.A: Some Special Functions Frequently Occurring as Mellin Transforms

### 12.A.1 The Gamma Function (See Also Chapter 1)

**Definition:** The gamma function  $\Gamma(s)$  is defined on the complex half-plane  $\text{Re}(s) > 0$  by the integral:

$$\Gamma(s) = \int_0^{\infty} e^{-t} t^{s-1} dt \quad (12.A.1)$$

*Analytic continuation.* The analytically continued gamma function is holomorphic in the whole plane except at the points  $s = -n, n = 0, 1, 2, \dots$  where it has a simple pole.

*Residues at the poles*

$$\text{Re } s_{s=-n}(\Gamma(s)) = \frac{(-1)^n}{n!} \quad (12.A.2)$$

*Relation to the factorial*

$$\Gamma(n + 1) = n! \quad (12.A.3)$$

Functional relations

$$\Gamma(s + 1) = s\Gamma(s) \tag{12.A.4}$$

$$\Gamma(s)\Gamma(1 - s) = \frac{\pi}{\sin(\pi s)} \tag{12.A.5}$$

$$\Gamma\left(\frac{1}{2}\right) = \sqrt{\pi} \tag{12.A.6}$$

$$\Gamma(2s) = \pi^{-1/2} 2^{2s-1} \Gamma(s)\Gamma(s + 1/2) \tag{12.A.7}$$

(Legendre's duplication formula)

$$\Gamma(ms) = m^{ms-1/2} (2\pi)^{(1-m)/2} \prod_{k=0}^{m-1} \Gamma(s + k/m), \quad m = 2, 3, \dots \tag{12.A.8}$$

(Gauss-Legendre multiplication formula<sup>5</sup>)

Stirling asymptotic formula

$$\Gamma(s) \sim \sqrt{2\pi} s^{-1/2} \exp\left[-s\left(1 + \frac{1}{12s} + O(s^{-2})\right)\right] \quad s \rightarrow \infty, \quad |\arg(s)| < \pi \tag{12.A.9}$$

### 12.A.2 The Beta Function

**Definition:**

$$B(x, y) \equiv \int_0^1 t^{x-1} (1-t)^{y-1} dt \tag{12.A.10}$$

Relation to the gamma function

$$B(x, y) = \frac{\Gamma(x)\Gamma(y)}{\Gamma(x+y)} \tag{12.A.11}$$

### 12.A.3 The Psi Function (Logarithmic Derivative of the Gamma Function)

**Definition:**

$$\Psi(s) \equiv \frac{d}{ds} \ln \Gamma(s) \tag{12.A.12}$$

$$= -\gamma + \sum_{n=0}^{\infty} \left( \frac{1}{n+1} - \frac{1}{s+n} \right) \tag{12.A.13}$$

Euler's constant  $\gamma$ , also called C, is defined by

$$\gamma \equiv -\Gamma'(1)/\Gamma(1) \tag{12.A.14}$$

and has value  $\gamma \cong 0.577 \dots$

### 12.A.4 Riemann's Zeta Function<sup>12,13</sup>

**Definition:**

$$\zeta(z) \equiv \sum_{n=1}^{\infty} \frac{1}{n^z}, \quad \text{Re}(z) > 1 \tag{12.A.15}$$

Other forms of the definition, which are valid for all complex values of  $z$ , have been written down. They coincide with Equation 12.A.15 for  $\text{Re}(z) > 1$  and allow the continuation of  $\zeta(z)$  as a meromorphic function in the whole complex  $z$ -plane. The resulting function has only one pole, situated in  $z = 1$ ; it is simple, with residue equal to  $+1$ . In addition, the  $\zeta$ -function has simple zeros at  $z = -2n, n \neq 0$ . All other zeros are in the strip  $0 \leq \text{Re}(z) \leq 1$ .

Functional equation

$$\pi^{-z/2} \Gamma(z/2) \zeta(z) = \pi^{1/2(z-1)} \Gamma\left(\frac{1-z}{2}\right) \zeta(1-z) \tag{12.A.16}$$

Other forms of this equation can be obtained by using the properties of the Gamma function.

*Asymptotic estimates.* Let  $\sigma \equiv \text{Re}(z)$  and  $t \equiv \text{Im}(z)$ . The behavior of  $\zeta(z)$  when  $|t| \rightarrow \infty$  is such that:

$$|\zeta(z)| < C(\epsilon) |t|^{\mu(\sigma)+\epsilon}, \quad \epsilon > 0 \tag{12.A.17}$$

where  $C(\epsilon)$  is a constant and  $\mu(\sigma)$  is a function defined as follows:

$$\begin{aligned} \mu(\sigma) &= 0 & \sigma > 1 \\ \mu(\sigma) &\leq \frac{1-\sigma}{2} & 0 < \sigma < 1 \\ \mu(\sigma) &= \frac{1}{2} - \sigma & \sigma < 0 \end{aligned} \tag{12.A.18}$$

For  $\sigma = 1/2$ , more precise estimates have been proven. In particular:<sup>12</sup>

$$\zeta(1/2 + it) = O(|t|^{9/56+\epsilon}), \quad \epsilon > 0 \tag{12.A.19}$$

## Appendix 12.B: Summary of Properties of the Mellin Transformation

**Definition:** The Mellin transformation of a function  $f(t)$ ,  $0 < t < \infty$  is defined by

$$\mathcal{M}[f; s] \equiv \int_0^{\infty} f(t)t^{s-1} dt$$

and the result is a function holomorphic in the strip  $S_f$  of the complex plane  $s$ .

When the real part  $\text{Re}(s) \equiv r + 1$  of  $s$  is held fixed, the Mellin transform is defined by

$$\mathcal{M}[f](\beta) \equiv \mathcal{M}[f; r + 1 + 2\pi j\beta]$$

In that case, it is an isomorphism between the space  $L^2(\mathbb{R}^+, t^{2r+1} dt)$  of functions  $f(t)$  on  $(0, \infty)$  equipped with the scalar product:

$$(f, g) \equiv \int_0^{\infty} f(t)g^*(t)t^{2r+1} dt$$

and the space  $L^2(\mathbb{R})$  of functions  $\mathcal{M}[f](\beta)$ .

Moreover, the scaled function defined by

$$\mathcal{D}_a f(t) \equiv a^{r+1}f(at)$$

is transformed according to

$$\mathcal{M}[\mathcal{D}_a f](\beta) = a^{-j2\pi\beta} \mathcal{M}[f](\beta)$$

*Inversion formulas*

$$f(t) = (1/2\pi j) \int_{a-j\infty}^{a+j\infty} \mathcal{M}[f; s]t^{-s} ds$$

$$f(t) = \int_{-\infty}^{+\infty} \mathcal{M}[f](\beta)t^{-2j\pi\beta-r-1} d\beta$$

*Parseval formulas*

$$\int_0^{\infty} f(t)g(t)dt = \frac{1}{2\pi j} \int_{c-j\infty}^{c+j\infty} \mathcal{M}[f; s]\mathcal{M}[g; 1-s]ds$$

$$\int_0^{\infty} f(t)g^*(t)t^{2r+1} dt = \int_{-\infty}^{\infty} \mathcal{M}[f](\beta)\mathcal{M}^*[g](\beta)d\beta$$

Other basic formulas involving the Mellin transforms  $\mathcal{M}[f; s]$  and  $\mathcal{M}[f](\beta)$  are recalled in Tables 12.2 and 12.3.

**TABLE 12.2** Properties of the Mellin Transform in  $s$  Variable (Definition (12.1))

Original Function	Mellin Transform	
$f(t), t > 0$	$\mathcal{M}[f; s] \equiv \int_0^{\infty} f(t)t^{s-1} dt$	Strip of Holomorphy
$f(t)$	$F(s)$	$S_f$
$f(at), a > 0$	$a^{-s} F(s)$	$S_f$
$f(t^a), a \text{ real } \neq 0$	$ a ^{-1} F(a^{-1} s)$	$a^{-1} s \in S_f$
$(\ln t)^k f(t)$	$\frac{d^k}{ds^k} F(s)$	$s \in S_f$
$(t)^z f(t), z \text{ complex}$	$F(s+z)$	$s+z \in S_f$
$\frac{d^k}{dt^k} f(t)$	$(-1)^k (s-k)_k F(s-k)$	$s-k \in S_f$
	$(s-k)_k \equiv (s-k)(s-k+1)\dots(s-1)$	
$\left[ t \frac{d}{dt} \right]^k f(t)$	$(-1)^k s^k F(s)$	$s \in S_f$
$\frac{d^k}{dt^k} t^k f(t)$	$(-1)^k (s-k)_k F(s)$	$s \in S_f$
$t^k \frac{d^k}{dt^k} f(t)$	$(-1)^k (s)_k F(s)$	$s \in S_f$
	$(s)_k \equiv s(s+1)\dots(s+k-1)$	
$\int_t^{\infty} f(x) dx$	$s^{-1} F(s+1)$	
$\int_0^t f(x) dx$	$-s^{-1} F(s+1)$	
$\int_0^{\infty} f_1(\tau)f_2(t/\tau)(d\tau/\tau)$	$F_1(s) F_2(s)$	$s \in S_{f_1} \cap S_{f_2}$

*Note:* Here  $k$  is a positive integer.

**TABLE 12.3** Some Properties of the Mellin Transform in  $\beta$  Variable (Definition (12.200))

Original Function	Mellin Transform
$f(t), t > 0$	$\mathcal{M}[f](\beta) \equiv \int_0^\infty f(t) t^{2\pi\beta+r} dt$
$f(t)$	$M(\beta)$
$\mathcal{D}_a f(t) \equiv a^{r+1} f(at), a > 0$	$a^{-2\pi\beta} M(\beta)$
$t^{2\pi jc} f(t), c$ real	$M(\beta + c)$
$\frac{-1}{2j\pi} \left[ t \frac{d}{dt} + r + 1 \right] f(t)$	$\beta M(\beta)$

*Multiplicative convolution.* It is defined by

$$(f \sim g)(t) \equiv \int_0^\infty f(\tau) f(t/\tau) (d\tau/\tau)$$

$$f \sim \delta(t-1) = f$$

$$\left[ t \frac{d}{dt} \right]^k (f \sim g) = \left[ \left( t \frac{d}{dt} \right)^k f \right] \sim g$$

$$= f \sim \left[ \left( t \frac{d}{dt} \right)^k g \right]$$

$$(\ln t)(f \vee g) = [(\ln t)f] \vee g + f \vee [(\ln t)g]$$

$$\delta(t-a) \vee f = a^{-1} f(a^{-1}t)$$

$$\delta(t-p) \vee \delta(t-p') = \delta(t-pp'), p, p' > 0$$

$$\delta^{(k)}(t-1) \vee f = (d/dt)^k (t^k f)$$

*Invariant product.* It is defined by

$$(f \circ g)(t) \equiv t^{r+1} f(t) g(t)$$

$$\mathcal{D}_a[f] \circ \mathcal{D}_a[g] = \mathcal{D}_a[f \circ g]$$

$$\mathcal{M}[f \circ g](\beta) = (\mathcal{M}[f] * \mathcal{M}[g])(\beta)$$

*Useful formulas for discretization.* In the following, the variable  $\nu$  goes from 0 to  $\infty$  and  $Z(\nu)$  is a (possibly generalized) function.

Geometric Dirac comb:

$$\Delta_Q^r(\nu) \equiv \sum_{n=-\infty}^{+\infty} Q^{-nr} \delta(\nu - Q^n), \quad Q > 0$$

Dilatocycled form of function Z:

$$Z^D(\nu) \equiv \sum_{n=-\infty}^{+\infty} Q^{n(r+1)} Z(Q^n \nu), \quad Q > 0$$

$$Z^D(\nu) \left[ \Delta_Q^r \sim Z \right] (\nu)$$

$$\mathcal{M}[Z^D](\beta) = \frac{1}{\ln Q} \sum_{n=-\infty}^{+\infty} \mathcal{M}[Z](\beta) \delta\left(\beta - \frac{n}{\ln Q}\right)$$

Geometrically sampled form of function Z:

$$Z_s(\nu) \equiv \sum_{n=-\infty}^{+\infty} q^n Z(q^n) \delta(\nu - q^n)$$

$$Z_s(\nu) = \left( Z \circ \Delta_q^r \right) (\nu)$$

$$\mathcal{M}[Z_s](\beta) = \frac{1}{\ln q} \sum_{n=-\infty}^{+\infty} \mathcal{M}[Z] \left( \beta - \frac{n}{\ln q} \right)$$

*Discrete Mellin transform pair.*

$$M^P \left( \frac{m}{N \ln q} \right) = \sum_{n=M}^{M+N-1} q^{n(r+1)} Z^D(q^n) e^{2j\pi nm/N}$$

$$Z^D(q^n) = \frac{q^{-n(r+1)}}{N} \sum_{k=K}^{K+N-1} M^P \left( \frac{k}{N \ln q} \right) e^{2j\pi kn/N}$$

where  $N$  is the number of samples. In practice, the choice of the ratio  $q$  is facilitated by the time-frequency interpretation of the signal  $Z(\nu)$  (see Section 12.3.3.3).

## References

1. Titchmarsh, E. C., 1975. *Introduction to the Theory of Fourier Integrals*, Clarendon Press, Oxford, U.K.
2. Elfving, G., 1981. *The History of Mathematics in Finland 1828–1918*, Frencckell, Helsinki, Finland (ISBN 951-653-098-2).
3. Vilenkin, N. Ya., 1968. *Special Functions and the Theory of Group Representations*, American Mathematical Society, Providence, RI.
4. Reid, C. E. and Passin, T. B., 1992. *Signal Processing in C*, John Wiley & Sons, New York.
5. Marichev, O. I., 1982. *Handbook of Integral Transforms of Higher Transcendental Functions: Theory and Algorithmic Tables*, Ellis Horwood Ltd., Chichester, U.K.
6. Flajolet, P., Gourdon, X., and Dumas, P., 1995. Mellin transforms and asymptotics: Harmonic sums, *Theoret. Comput. Sci.*, 144, 3–58.
7. Zemanian, A. H., 1987. *Generalized Integral Transformations*, Dover Publications, New York.
8. Misra, O. P. and Lavoine, J. L., 1986. *Transform Analysis of Generalized Functions*, North-Holland Mathematics Studies, Vol. 119, Elsevier, Amsterdam, the Netherlands.
9. Bleistein, N. and Handelsman, R. A., 1986. *Asymptotic Expansions of Integrals*, Dover Publications, New York.
10. Kang, F., 1958. Generalized Mellin transforms I, *Sc. Sinica*, 7, 582–605.

11. Gelfand, I. M. and Shilov, G. E., 1964. *Generalized Functions*, Vol. 1, Academic Press, Inc., New York.
12. Patterson, S. J., 1989. *An Introduction to the Theory of the Riemann Zeta-Function*, Cambridge University Press, Cambridge, U.K.
13. Edwards, H. M., 1974. *Riemann's Zeta Function*, Academic Press, New York.
14. Ditkin, V. A. and Prudnikov, A. P., 1965. *Integral Transforms and Operational Calculus*, Pergamon Press, Oxford, New York; Prudnikov, A. P., Brychkov, Yu. A., and Marichev, O. I., 1990. *Integrals and Series*, Vol. 3: *More Special Functions*, Gordon and Breach, New York.
15. Oberhettinger, F., 1974. *Tables of Mellin Transforms*, Springer-Verlag, New York.
16. Gradshteyn, I. S. and Ryzhik, I. M., 1994. *Table of Integrals, Series and Products*, A. Jeffrey (Ed.), 5th edn., Academic Press, New York.
17. Davies, B., 1984. *Integral Transforms and their Applications*, 2nd edn., Springer-Verlag, New York.
18. Sasiela, R. J., 1994. *Electromagnetic Wave Propagation in Turbulence - Evaluation and Application of Mellin Transforms*, Springer series on Wave Phenomena, Vol. 18, Springer-Verlag, New York.
19. Doetsch, G., 1943. *Laplace Transformation*, Dover Publications, New York.
20. De Bruijn, N. G., Knuth, D. E., and Rice, S. O., 1972. The average height of planted plane trees, in *Graph Theory and Computing*, R.C. Read (Ed.), Academic Press, New York.
21. Vitter, J. S. and Flajolet, P., 1990. Average-case analysis of algorithms and data structures, in *Handbook of Theoretical Computer Science, Vol. A: Algorithms and Complexity*, J. van Leeuwen (Ed.), Chapter 9, Elsevier, Amsterdam, the Netherlands.
22. Bellman, R., 1980. *Analytic Number Theory, An Introduction*, Benjamin-Cummings, Reading, MA.
23. Moses, H. E. and Quesada, A. F., 1974. The power spectrum of the Mellin transformation with applications to scaling of physical quantities, *J. Math. Phys.*, 15(6), 748–752.
24. Bertrand, J., Bertrand, P., and Ovarlez, J.P., 1990. Discrete Mellin transform for signal analysis, *Proc. IEEE-ICASSP*, Albuquerque, NM.
25. Bertero, M., 1992. Sampling theory, resolution limits and inversion methods, in *Inverse Problems in Scattering and Imaging*, M. Bertero and E. R. Pike (Eds.), Malvern Physics Series, Adam Hilger, Bristol.
26. Bertrand, J., Bertrand, P., and Ovarlez, J. P., 1991. Dimensionalized wavelet transform with application to radar imaging, *Proc. IEEE-ICASSP*, Toronto, Ontario, Canada.
27. Klauder, J., 1980. In *Functional Integration: Theory and Applications*, J. P. Antoine and E. Tirapegui (Eds.), Plenum Press, New York.
28. Ovarlez, J. P., 1992. La Transformation de Mellin: un Outil pour l'Analyse des Signaux à Large-Bande, Doctoral thesis, University Paris 6, Paris.
29. Bertrand, J. and Bertrand, P., 1984. Représentations temps-fréquence des signaux, *C.R. Acad. Sci. Paris*, 299, 635–638.
30. Bertrand, J. and Bertrand, P., 1992. Affine time-frequency distributions, in *Time-Frequency Signal Analysis—Methods and Applications*, B. Boashash (Ed.), Chapter V, Longman-Cheshire, Australia.
31. Bertrand, J. and Bertrand, P., 1992. A class of affine Wigner functions with extended covariance properties, *J. Math. Phys.*, 33 (7), 2515–2527.
32. Altes, R.A., 1990. Wide-band, proportional-bandwidth Wigner-Ville analysis, *IEEE Trans. Acoust., Speech, Signal Process.*, 38, 1005–1012.
33. Eichmann, G. and Marinovich, N. M., 1984. Scale invariant Wigner distribution and ambiguity functions, *Proc. Int. Soc. Opt. Eng. SPIE*, 519, 18–24.
34. Marinovich, N. M., 1986. The Wigner distribution and the ambiguity function: Generalizations, enhancement, compression and some applications, PhD thesis, City University of New York, New York.
35. Cohen, L., 1993. The scale representation, *IEEE Trans. Signal Process.*, 41(12), 3275–3292.
36. Hlawatsch, F., Papandreou, A., and Boudreaux-Bartels, F. G., 1993. Hyperbolic Class, *IEEE Trans. Signal Process.*, 41(12), 3425–3444.
37. Ovarlez, J. P., 1993. Cramer-Rao bound computation for velocity estimation in the broad band case using the Mellin transform, *Proc. IEEE-ICASSP*, Minneapolis, MN.
38. Altes, R. A., 1978. The Fourier-Mellin transform and mammalian hearing, *J. Acoust. Soc. Am.*, 63, 174–183.
39. Zwicke, P. E. and Kiss, I., Jr., March 1983. A new implementation of the Mellin transform and its application to radar classification of ships, *IEEE Trans. Pattern Anal. Mach. Intell.*, 5(2), 191–199.
40. Casasent, D. and Psaltis, S., May 1978. Position, rotation and scale invariant optical correlation, *Appl. Opt.*, 17, 1559–1561; Deformation invariant, space-variant optical pattern recognition, in *Progress in Optics XVI*, E. Wolf (Ed.), pp. 291–355, North-Holland, Amsterdam, the Netherlands.
41. Sheng, Y. and Arsenault, H. H., 1986. Experiments on pattern recognition using invariant Fourier-Mellin descriptors, *J. Opt. Soc. Am.*, 3(6), 771–884.
42. Sheng, Y. and Duvernoy, J., 1986. Circular-Fourier-radial-Mellin transform descriptors for pattern recognition, *J. Opt. Soc. Am.*, 3(6), 885–887.
43. Casasent, D. and Psaltis, S., 1977. New optical transforms for pattern recognition, *Proc. IEEE*, 5, 77–84.
44. Woodward, P. M., 1953. *Probability and Information Theory with Applications to Radar*, Pergamon Press, New York.
45. Kelly, E. J. and Wishner, R. P., 1965. Matched filter theory for high velocity accelerating targets, *IEEE Trans. Military Elect.*, Mil 9, 56–69.
46. Van Trees, H. L., 1971. *Detection, Estimation and Modulation Theory, Parts I, II and III*, John Wiley & Sons, New York.

47. Bertrand, J., Bertrand, P., and Ovarlez, J. P., 1993. The wavelet approach in radar imaging and its physical interpretation, in *Progress in Wavelet Analysis and Applications*, Y. Meyer and S. Roques (Eds.), Editions Frontières, Gif-sur-yvette, France.
48. Bertrand, J., Bertrand, P., and Ovarlez, J. P., 1994. Frequency directivity scanning in laboratory radar imaging, *Int. J. Imaging Sys. Technol.*, 5, 39–51.
49. Ovarlez, J. P., Bertrand, J., and Bertrand, P., 1992. Computation of affine time-frequency distributions using the fast Mellin transform, *Proc. IEEE-ICASSP*, San Francisco, CA.

# 13

## Mixed Time–Frequency Signal Transformations

---

13.1	Introduction.....	13-1
13.2	One-Dimensional Spectral Representations.....	13-2
	Fourier Transform • Instantaneous Frequency and Group Delay	
13.3	Classical Time–Frequency Representations .....	13-4
	Short-Time Fourier Transform • Wigner Distribution and Woodward Ambiguity Function • Altes Q or “Wideband” Wigner Distribution • TFR Warping • Bertrand $P_k$ Distributions • Cross Terms of Quadratic Time–Frequency Representations	
13.4	Desirable Properties of Time–Frequency Representations .....	13-13
	Covariance Properties • Statistical Energy Density Distribution Properties • Signal Analysis Properties • Signal Localization • Preserving Inner Products	
13.5	Classes of TFRs with Common Properties.....	13-23
	Cohen’s Class of TFRs • Affine Class of TFRs • Affine-Cohen Subclass • Hyperbolic Class of TFRs • $\kappa$ th Power Class	
13.6	Summary .....	13-40
	Acknowledgments.....	13-40
	References .....	13-40

G. Fay Boudreaux-Bartels  
*University of Rhode Island*

### 13.1 Introduction

---

Mixed time–frequency representations are transformations of time-varying signals that depict how the spectral content of a signal is changing with time. They are multidimensional, time-varying extensions to conventional Fourier transform spectral analysis of signals and systems. Most time–frequency representations (TFRs) transform a one-dimensional signal,  $x(t)$ , into a two-dimensional function of time and frequency,  $T_x(t, f)$ . These transformations represent a surface above the time–frequency “plane” which gives an indication as to which spectral components of the signal are present at a given time and their relative amplitude. They are conceptually similar to a musical score with time running along one axis and frequency along the other.<sup>37,50</sup> Just as the location and the shape of the notes on a musical score represent the pitch, time of occurrence, and duration of each sound in a piece of music, so too does the location of the local maximum and the shape of the surface of the TFR give an indication as to the frequency content, onset, and duration of various dominant signal components. Such representations are useful for the analysis, modification, synthesis, and detection of a variety of nonstationary signals with time-varying spectral content.<sup>1–4,30,91</sup>

The purpose of this chapter is to give an overview of many of the linear and quadratic time–frequency representations that have been developed over the past 60 years. The chapter first

reviews various one-dimensional spectral representations, such as the Fourier transform, the instantaneous frequency, and the group delay. A brief discussion follows of a few commonly used TFRs such as the short-time Fourier transform (STFT), the Wigner distribution (WD), the Altes Q distribution, and the Bertrand unitary  $P_0$  distribution. These TFRs will be used as examples in the subsequent section, which describes many useful properties that an ideal TFR should satisfy. Unfortunately, no one TFR exists which satisfies all of these desirable properties. The relative merits of these TFRs can be understood by grouping them into “classes” of TFRs that share two or more properties. The remainder of the chapter is devoted to defining and understanding these classes. Important insights into these classes of TFRs can be gained by examining a set of five two-dimensional kernel functions that are unique to each TFR. These kernels greatly simplify the analysis and application of TFRs.

Other tutorials that discuss properties of TFRs satisfy or that give references to a variety of interesting applications can be found in Refs. [1–6,8,10,12,13,16–18,20,22–30,37–39,41–43,45, 47,49,54,56,60,61,63–69,71–75,81,84,86,87–92,97,99,100,103,104, 109–111,113–119,121]. Although this chapter deals primarily with the TFRs of continuous-time signals and systems, issues related to discrete-time implementation algorithms for TFRs are discussed in Refs. [12,18,21,24,34,38,45,47–49,60,78,85,93–95, 102–104,106,107].



## 13.2 One-Dimensional Spectral Representations

### 13.2.1 Fourier Transform

Conventional spectral analysis of a signal has been based on Fourier transform techniques. The Fourier transform of a signal  $x(t)$ ,\*

$$X(f) = \int x(t)e^{-j2\pi ft} dt, \tag{13.1}$$

is a useful tool for analyzing the spectral content of a stationary signal and for transforming the difficult operations of convolution, differentiation, and integration into relatively simple algebraic operations in the Fourier dual domain.<sup>32,33,101,105</sup> The inverse Fourier transform or synthesis equation

$$x(t) = \int X(f)e^{j2\pi ft} df, \tag{13.2}$$

represents the signal  $x(t)$  as a linear combination of infinite duration complex sinusoids,  $e^{j2\pi ft}$ . Throughout this chapter, the double arrow will be used to denote a Fourier transform pair:

$$x(t) \leftrightarrow X(f).$$

A variety of useful Fourier transform pairs and properties are summarized in Table 13.1. For example, the first entry states that  $\delta(t - t_0)$ , which is a Dirac impulse<sup>101,105</sup> centered at time  $t_0$ , has a Fourier transform that is a complex exponential whose phase is proportional to  $t_0$ . The next entry is the “dual” Fourier transform relationship for a Dirac impulse centered at the frequency  $f_0$ . In fact, by making use of the Duality property of Fourier transforms, given in entry 13 in Table 13.1, almost all of the Fourier transforms can be written in dual pairs:

(i)  $x(t) \leftrightarrow X(f)$  and (ii)  $y(t) = X(t) \leftrightarrow Y(f) = x(-f)$ .

For example, in entry 2 in Table 13.1, since the Fourier transform of a rectangular function in the time domain is a sinc function in the frequency domain, then by the duality property, the Fourier transform of a sinc function in the time domain must be a rectangular function in frequency. In this example, the frequency reversal of the duality property has no effect as the rectangular function is an even function. The dilation property in entry 12 of Table 13.1 states that if a recorded segment of speech is played back on a tape recorder at five times the original recording speed ( $a = 5$ ), then the bandwidth of the accelerated speech will be increased by a factor of 5. So compressing the signal in one domain has the inverse effect of

TABLE 13.1 Table of Fourier Transform Pairs and Properties

	Signal or Property	$y(t)$	$Y(f) = \int y(t)e^{-j2\pi ft} dt$
1	Impulse $\leftrightarrow$ exponential	$\delta(t - t_0)$ $e^{j2\pi f_0 t}$	$e^{-j2\pi f t_0}$ $\delta(f - f_0)$
2	Box $\leftrightarrow$ Sinc	$\text{rect}_a(t)$ $\frac{\sin(2\pi at)}{\pi t}$	$\frac{\sin(2\pi af)}{\pi f}$ $\text{rect}_a(f)$
3	One-sided exponential	$e^{-\alpha t} \tilde{u}(t), \alpha > 0$ $\frac{1}{\alpha + j2\pi t}$	$\frac{1}{\alpha + j2\pi f}$ $e^{\alpha} \int \tilde{u}(-f), \alpha > 0$
4	Two-sided exponential	$e^{-\alpha t }, \alpha > 0$ $\frac{2\alpha}{\alpha^2 + 4\pi^2 t^2}$	$\frac{2\alpha}{\alpha^2 + 4\pi^2 f^2}$ $e^{-\alpha f }, \alpha > 0$
5	Unit step	$\tilde{u}(t)$ $\frac{1}{2} \delta(t) - j \frac{1}{2\pi t}$	$\frac{1}{2} \delta(f) - j \frac{1}{2\pi f}$ $\tilde{u}(-f)$
6	Signum function	$\text{sgn}(t)$ $\frac{1}{j2\pi t}$	$\frac{1}{j2\pi f}$ $\text{sgn}(-f) = -\text{sgn}(f)$
7	Gaussian $\leftrightarrow$ Gaussian	$\frac{1}{\sqrt{\sigma}} e^{-\pi(t/\sigma)^2}$	$\sqrt{\sigma} e^{-\pi(f/\sigma)^2}$
8	Linear FM chirp	$e^{j\pi\alpha t^2}$	$\frac{1}{\sqrt{-j\alpha}} e^{-j\pi f^2/\alpha}$
9	Axis reversal	$x(-t)$	$X(-f)$
10	Convolution $\leftrightarrow$ multiplication	$\int x(\tau)h(t - \tau)d\tau$ $x(t)h(t)$	$X(f)H(f)$ $\int X(v)H(f - v)dv$
11	Differentiation	$\frac{d^n}{dt^n} x(t)$	$(j2\pi f)^n X(f)$
	Mult. by Fourier parameter	$(-j2\pi t)^n x(t)$	$\frac{d^n}{df^n} X(f)$
12	Dilation $\leftrightarrow$ compression	$x(at)$	$\frac{1}{ a } X\left(\frac{f}{a}\right)$
13	Duality	$X(t)$	$x(-f)$
14	Linearity	$\alpha x(t) + \beta q(t)$	$\alpha X(f) + \beta Q(f)$
15	Translation $\leftrightarrow$ phase change	$x(t - t_0)$ $x(t)e^{j2\pi f_0 t}$	$X(f)e^{-j2\pi f t_0}$ $X(f - f_0)$

Note: Here,  $\text{rect}_a = \begin{cases} 1, & |t| < |a| \\ 0, & |t| > |a| \end{cases}$ ,  $\tilde{u}(t) = \begin{cases} 1, & t > 0 \\ 0, & t < 0 \end{cases}$ , and  $\text{sgn}(t) = \begin{cases} 1, & t > 0 \\ -1, & t < 0 \end{cases}$  are the rectangular, unit step, and signum functions, respectively.  $x(t) \leftrightarrow X(f)$  and  $q(t) \leftrightarrow Q(f)$  are Fourier transform pairs.

dilating the signal in the Fourier dual domain. The effects of linear convolution, differentiation, dilation, and translation on a signal or its Fourier transform will be exploited throughout this chapter.

Traditional Fourier transform analysis techniques have several disadvantages. In the synthesis equation (Equation 13.2), the value  $X(f_0)$  of the Fourier transform at the frequency  $f_0$  can be thought of as the weighting coefficient of the complex sinusoidal basis function,  $e^{j2\pi f_0 t}$ . Since these sinusoidal basis functions are infinite duration, Fourier analysis implicitly assumes that each sinusoidal component with nonzero weighting coefficient is always present, and hence that the spectral content of the signal under analysis is unchanging, i.e., stationary. However, many

\* Unless otherwise noted, all limits of integration are assumed to be from  $-\infty$  to  $\infty$  and  $j = \sqrt{-1}$ . Also, throughout the text, lowercase letters denote a time-domain signal and uppercase letters denote its Fourier transform.

naturally occurring signals, such as speech, music, biosonar, etc., intrinsically have spectral characteristics that change with time. For example, from the Fourier transform of a piece of music, it would be relatively easy to discern the frequency or pitch of various notes that were played, but relatively difficult to extract when each note was played. Hence, Fourier transform spectral decomposition techniques are inadequate for the analysis of most real-world signals.

An example of the dichotomy that exists between time-domain analysis versus frequency-domain analysis accomplished via a Fourier transform is depicted in Figure 13.1. The time-domain signal,  $x(t)$ , which is plotted at the bottom of the figure, consists of three successive tone bursts. The exact value of the frequency of each tone is not immediately obvious. Its Fourier transform, whose squared magnitude  $|X(f)|$  is plotted vertically on the left side of Figure 13.1, clearly shows the frequencies of the three tones, but obscures the time of their onset. In such a situation, it is desirable to have the ideal TFR,  $T_x(t, f)$ , such as the one plotted in the middle of Figure 13.1, which facilitates simultaneous analysis in both the time domain and the frequency domain.

### 13.2.2 Instantaneous Frequency and Group Delay

The instantaneous frequency and the group delay of a signal are one-dimensional transformations which attempt to represent

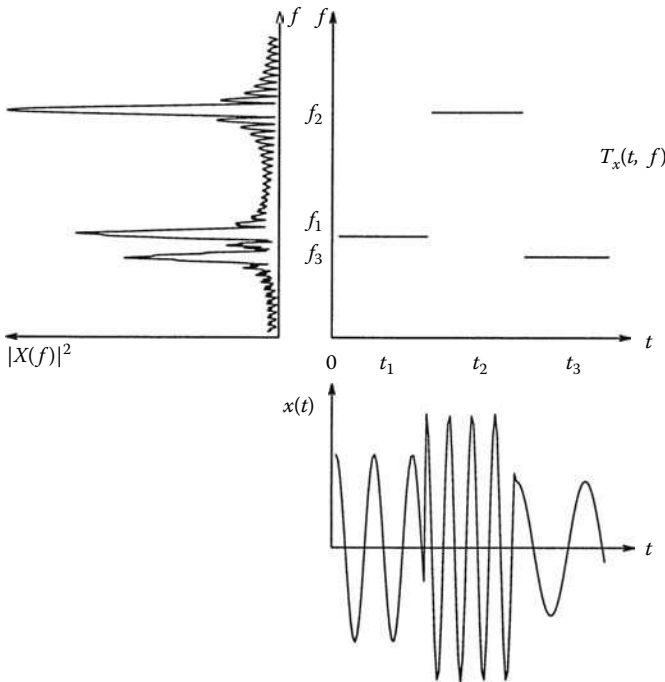


**FIGURE 13.1** Ideal time–frequency representation for a signal that consists of three consecutive, short-duration tones of frequencies,  $f_1$ ,  $f_2$ , and  $f_3$ , respectively. The corresponding time-domain signal is plotted on the bottom and its Fourier spectrum is plotted vertically along the left-hand side.

temporal and spectral signal characteristics simultaneously. They work best for phase modulated signals, i.e.,  $x(t) = e^{j2\pi\theta(t)}$  or  $X(f) = e^{j2\pi\phi(f)}$ , where  $\theta(t), \phi(f) \in \Re$ , have only one frequency component present at any given time or one temporal component present at any given frequency, respectively. However, most signals that occur in nature are a rich mixture of spectral components. Further, even if the signal is mono-component, it is often corrupted by environmental or measurement noise.

An understanding of the definition of the instantaneous frequency, which has been frequently used in communication theory,<sup>101,119</sup> can be gained by examining a complex exponential. The (constant) frequency,  $f_0$ , of the complex exponential,  $x(t) = e^{j2\pi f_0 t}$ , is proportional to the derivative of the phase of the signal, i.e.,  $f_0 \propto \frac{d}{dt}(2\pi f_0 t)$ . The instantaneous frequency of a time-varying signal is thus defined as the instantaneous change in the phase of that signal,

$$f_x(t) = \frac{1}{2\pi} \frac{d}{dt} \arg x(t). \quad (13.3)$$

For example, the signal  $x(t) = e^{j\pi\alpha t^2}$  is called a linear FM chirp since its instantaneous frequency is the line  $f_x(t) = \alpha t$ . The slope or “sweep rate”  $\alpha$  gives the change in frequency per unit time.

A dual concept, known as group delay, is useful in filter analysis. If an ideal complex exponential of frequency  $f_0$  is put into a linear time-invariant filter whose frequency response\* is  $H(f) = e^{-j2\pi f\tau}$ , then the output of the filter is equal to the input delayed by  $\tau$ .<sup>101</sup> Thus, in this simple case, temporal translation information can be obtained by looking at the derivative of the phase response of a filter, commonly known as its group delay,

$$\tau_h(f) = -\frac{1}{2\pi} \frac{d}{df} \arg H(f). \quad (13.4)$$

For linear phase systems, the group delay is nondispersive, i.e., constant for all frequencies.

These time-varying spectral representations give counterintuitive information for multicomponent signals. For example, let

$$\begin{aligned} y(t) &= e^{j2\pi f_1 t} + e^{j2\pi f_2 t}, \quad a_1, a_2 \in \Re \\ &= e^{j2\pi\theta(t)}, \quad \text{where } \theta(t) = \arctan \left[ \frac{\sin(2\pi f_1 t) + \sin(2\pi f_2 t)}{\cos(2\pi f_1 t) + \cos(2\pi f_2 t)} \right] \end{aligned} \quad (13.5)$$

be the sum of two complex exponentials of frequency  $f_1$  and  $f_2$ . The instantaneous frequency of  $y(t)$  can be derived in closed form using the property  $\frac{d}{da} \arctan b = \frac{1}{1+b^2} \frac{db}{da}$ ,

\* The frequency response of a linear, time-invariant filter is the Fourier transform of the filter’s impulse response,  $h(t)$ .<sup>101</sup>

$$\begin{aligned}
f_y(t) &= \frac{1}{2\pi} \frac{d}{dt} \arctan \left[ \frac{\sin(2\pi f_1 t) + \sin(2\pi f_2 t)}{\cos(2\pi f_1 t) + \cos(2\pi f_2 t)} \right] \\
&= \frac{1}{2\pi} \frac{1}{1 + (\sin(2\pi f_1 t) + \sin(2\pi f_2 t))^2 / (\cos(2\pi f_1 t) + \cos(2\pi f_2 t))^2} \\
&\quad \times 2\pi \left[ \frac{f_1 (\cos(2\pi f_1 t) + f_2 \cos(2\pi f_2 t))}{\cos(2\pi f_1 t) + \cos(2\pi f_2 t)} - \frac{(\sin(2\pi f_1 t) + \sin(2\pi f_2 t))(-f_1 \sin(2\pi f_1 t) - f_2 \sin(2\pi f_2 t))}{(\cos(2\pi f_1 t) + \cos(2\pi f_2 t))^2} \right] \\
&= \frac{f_1 + f_2}{2}
\end{aligned} \tag{13.6}$$

Thus, the instantaneous frequency of this signal is the numerical average of the frequency of its two sinusoidal components. This is not very useful information, in general, as there are an infinite number of pairs of frequencies, e.g.,  $f_1 + \varepsilon$  and  $f_2 - \varepsilon$ , which have the same numerical average for all  $\varepsilon$ . In addition, letting  $f_2 = -f_1$  in Equation 13.5, shows that the real signal  $2 \cos(2\pi f_1 t)$  has an instantaneous frequency equal to zero, which is clearly unintuitive.

### 13.3 Classical Time–Frequency Representations

In this section, several commonly used linear and quadratic TFRs are described. The first TFR is the STFT, which is a linear transformation of the signal. The remaining TFRs that are discussed in this section, such as the spectrogram, the WD, the Altes Q distribution, and the unitary form of the Bertrand  $P_0$  distribution, are quadratic functions of the signal.

#### 13.3.1 Short-Time Fourier Transform

The most commonly used and easy to understand TFR is the STFT,

$$\text{STFT}_x(t, f; \Gamma) = \int x(\tau) \gamma^*(\tau - t) e^{-j2\pi f \tau} d\tau \tag{13.7}$$

$$= e^{-j2\pi f t} \int X(f') \Gamma^*(f' - f) e^{j2\pi f' t} df', \tag{13.8}$$

which is a linear function of the signal  $x(t)$ .<sup>47,68,69,92,103,104,107,112</sup>

The first STFT equation in Equation 13.7 indicates that the STFT can be thought of as the Fourier transform of a windowed segment of the data,  $[x(\tau) \gamma^*(\tau - t)]$ . Typically, the analysis window,  $\gamma(t)$ , is real and even, so that the STFT is equivalent to the Fourier transform of a segment of the signal centered at the output time,  $t$ . The second STFT equation in Equation 13.8 illustrates that the STFT can also be thought of as filtered version of the signal. If the analysis window is a lowpass function, then evaluating the STFT is equivalent to sending the signal through a band-pass filter  $\Gamma^*(f' - f)$  centered at the output frequency,  $f$ . Thus, the STFT can be thought of as the frequency content of the signal near the output time  $t$  or the temporal fluctuations of the signal spectrum near the output frequency  $f$ . Analog STFT techniques known as spectrograms<sup>9,83</sup> were originally used to

analyze the local frequency content of speech signals. In the TFR literature, the squared magnitude of the STFT is sometimes referred to as the spectrogram:

$$\begin{aligned}
\text{SPEC}_x(t, f; \Gamma) &= |\text{STFT}_x(t, f; \Gamma)|^2 \\
&= \left| \int x(\tau) \gamma^*(\tau - t) e^{-j2\pi f \tau} d\tau \right|^2 \\
&= \left| \int X(f') \Gamma^*(f' - f) e^{j2\pi f' t} df' \right|^2.
\end{aligned} \tag{13.9}$$

The following two simple examples provide insight into the STFT. First, consider the case of the STFT of an impulsive signal,  $x(t) = \delta(t - t_0)$ . Using Equation 13.7, it can be shown that the STFT of a Dirac impulse simplifies to the complex conjugate of the shifted STFT analysis window,  $\gamma(t)$ , modulated by a complex exponential:

$$\begin{aligned}
\text{STFT}_x(t, f; \Gamma) &= \int \delta(\tau - t_0) \gamma^*(\tau - t) e^{-j2\pi f \tau} d\tau \\
&= \gamma^*(t_0 - t) e^{-j2\pi f t_0}.
\end{aligned} \tag{13.10}$$

Hence, if the window is real and even, then the nonzero support region of the STFT will be centered at  $t = t_0$ . The time duration of the STFT in this example is equal to the duration of the analysis window. The second example is that of a complex exponential whose Fourier transform,  $Y(f) = \delta(f - f_0)$ , is perfectly concentrated at the frequency  $f_0$ . Using Equation 13.8 reveals that the magnitude of the STFT will be equal to the magnitude of the Fourier transform of the analysis window, shifted by an amount proportional to the frequency  $f_0$  of the signal

$$\begin{aligned}
\text{STFT}_y(t, f; \Gamma) &= e^{-j2\pi f t} \int \delta(f'' - f_0) \Gamma^*(f' - f) e^{j2\pi f'' t} df' \\
&= \Gamma^*(f_0 - f) e^{-j2\pi (f - f_0) t}.
\end{aligned} \tag{13.11}$$

The STFT's region of nonzero support about  $f_0$  in this example is equal to the content bandwidth of the analysis window for all output frequencies. Thus, the STFT gives a constant bandwidth or fixed resolution time-varying analysis.

There are several advantages and drawbacks to the STFT. The STFT is a linear signal transformation, i.e.,

$$y(t) = \alpha x_1(t) + \beta x_2(t) \implies$$

$$\text{STFT}_y(t, f, \Gamma) = \alpha \text{STFT}_{x_1}(t, f, \Gamma) + \beta \text{STFT}_{x_2}(t, f, \Gamma). \tag{13.12}$$

It is easy to understand and compute and has been widely used in the analysis of quasistationary signals. In general, however, the STFT is complex-valued and its time duration and bandwidth are greater than that of the signal, producing a spreading of the support of the signal in the time–frequency plane. Second, there is a tradeoff between time resolution and frequency resolution. Consider the following multicomponent signal:  $q(t) = \delta(t - t_0) + e^{j2\pi f_0 t}$ . Using the linearity of the STFT in Equation 13.12, it can be shown that the STFT of  $q(t)$  is the sum of the two STFTs derived in Equations 13.10 and 13.11. If the analysis window is the Gaussian function in Table 13.1,

$$\gamma(t) = \frac{1}{\sqrt{\sigma}} e^{-\pi(t/\sigma)^2} \leftrightarrow \Gamma(f) = \sqrt{\sigma} e^{-\pi(\sigma f)^2}, \quad (13.13)$$

then it can be shown using Equations 13.10 through 13.12 that the STFT of  $q(t)$  is as follows:

$$\begin{aligned} \text{STFT}_q(t, f; \Gamma) &= \frac{1}{\sqrt{\sigma}} e^{-\pi(t-t_0)^2/\sigma^2} e^{-j2\pi f t_0} \\ &+ \sqrt{\sigma} e^{-\pi\sigma^2(f-f_0)^2} e^{-j2\pi(f-f_0)t}. \end{aligned} \quad (13.14)$$

This STFT corresponds to a two-dimensional Gaussian function centered at  $t_0$  and  $f_0$ . Ideally, the STFT would be highly concentrated about the time  $t = t_0$  and the frequency  $f = f_0$ , corresponding to the fact that the signal contains an impulse in time and an impulse in frequency at those locations. However, for the STFT  $q(t, f; \Gamma)$  to be highly concentrated in time, Equation 13.14 reveals that the Gaussian analysis window must be very short duration, i.e.,  $\sigma \approx 0$ . For the STFT to be highly concentrated in frequency about  $f = f_0$ , then the analysis window must be very narrowband, i.e.,  $\sigma \gg 0$ . Clearly, both conditions on  $\sigma$  cannot be met simultaneously. The STFT can achieve either good time resolution or good frequency resolution but generally not both. Hence, the STFT works best on quasistationary signals, which are signals whose spectral content is changing slowly with time.

### 13.3.2 Wigner Distribution and Woodward Ambiguity Function

The first TFR proposed was the WD in the field of quantum mechanics.<sup>37,60,88,120</sup> The WD of a signal  $x(t)$ ,

$$\text{WD}_x(t, f) = \int x\left(t + \frac{\tau}{2}\right) x^*\left(t - \frac{\tau}{2}\right) e^{-j2\pi f \tau} d\tau \quad (13.15)$$

$$= \int X\left(f + \frac{\nu}{2}\right) X^*\left(f - \frac{\nu}{2}\right) e^{j2\pi t \nu} d\nu \quad (13.16)$$

$$= \int \int \text{AF}_x(\tau, \nu) e^{j2\pi(t\nu - f\tau)} d\tau d\nu, \quad (13.17)$$

can be obtained using either the signal in Equation 13.15 or its Fourier transform in Equation 13.16. Equation 13.17 shows that

the WD is related to the Woodward narrowband ambiguity function (AF),

$$\text{AF}_x(\tau, \nu) = \int x\left(t + \frac{\tau}{2}\right) x^*\left(t - \frac{\tau}{2}\right) e^{-j2\pi \nu t} dt \quad (13.18)$$

$$\begin{aligned} &= \int X\left(f + \frac{\nu}{2}\right) X^*\left(f - \frac{\nu}{2}\right) e^{j2\pi f \tau} df \\ &= \int \int \text{WD}_x(t, f) e^{-j2\pi(\nu t - \tau f)} dt df, \end{aligned} \quad (13.19)$$

via a two-dimensional Fourier transform. The AF is a two-dimensional auto-correlation function commonly used in radar and sonar to track the distance (range) and velocity (range rate) of a moving target.<sup>39,109,114,115,121</sup>

For real, band-limited signals, replacing the signal in Equations 13.15 through 13.17 with its corresponding analytic signal,

$$z_x(t) = x(t) + j\hat{x}(t) \leftrightarrow Z_x(f) = \begin{cases} 2X(f), & f > 0 \\ X(f), & f = 0 \\ 0, & f < 0 \end{cases} \quad (13.20)$$

often simplifies the analysis. Here,

$$\hat{x}(t) = \frac{\text{PV}}{\pi} \int \frac{x(\tau)}{t - \tau} d\tau$$

is the Hilbert transform<sup>101,105</sup> of  $x(t)$  and PV indicates principal value. The spectrum of the analytic signal in Equation 13.20 is proportional to that of the original signal for positive frequencies, but is equal to zero for negative frequencies. For real signals, this zeroing out of the negative frequency signal components results in no loss of information as the Fourier transform of a real signal is conjugate symmetric, i.e.,  $X(f) = X^*(-f)$ . The TFR that results from this substitution

$$\text{WD}_{z_x}(t, f) = \int z_x\left(t + \frac{\tau}{2}\right) z_x^*\left(t - \frac{\tau}{2}\right) e^{-j2\pi f \tau} d\tau, \quad (13.21)$$

is often referred to as the Wigner–Ville distribution.<sup>24,60,61,119</sup> Using Wigner–Ville distribution instead of the WD greatly simplifies the analysis of band-limited signals, but can distort the analysis of lowpass signals.

The WD can be computed in closed form for a variety of signals, as is indicated in Table 13.2. The first entry in Table 13.2 states that a Dirac impulse at  $t = t_0$ ,  $x(t) = \delta(t - t_0)$ , has a WD that is also an impulse concentrated at the same time  $t = t_0$ .

*Proof* Let  $x(t) = \delta(t - t_0)$ .

$$\begin{aligned} \text{WD}_x(t, f) &= \int \delta(t + \tau/2 - t_0) \delta(t - \tau/2 - t_0) e^{-j2\pi f \tau} d\tau \\ &= 2\delta(2(t - t_0)) e^{-j4\pi f(t - t_0)} = \delta(t - t_0). \end{aligned}$$

TABLE 13.2 Signals with Closed-Form Equations for Their Wigner Distribution and Ambiguity Function

Signal, $x(t)$	Fourier Transform, $X(f)$	Wigner Distribution, $WD_x(t, f)$	Ambiguity Function, $AF_x(\tau, \nu)$
$\delta(t - t_i)$	$e^{-j2\pi ft_i}$	$\delta(t - t_i)$	$e^{-j2\pi \nu t_i \delta(\tau)}$
$e^{j2\pi f_i t}$	$\delta(f - f_i)$	$\delta(f - f_i)$	$e^{j2\pi f_i \tau \delta(\nu)}$
$e^{+j\pi \alpha t^2}$	$\frac{1}{\sqrt{-j\alpha}} e^{-j\pi f^2/\alpha}$	$\delta(f - \alpha t)$	$\delta(\nu - \alpha \tau)$
$\frac{1}{\sqrt{j\alpha}} e^{j\pi t^2/\alpha}$	$\frac{1}{e^{-j\pi f^2/\alpha}}$	$\delta(t - \alpha f)$	$\delta(\tau - \alpha \nu)$
$e^{j\pi(\alpha t^2 + 2ft + c)}$	$\frac{1}{\sqrt{-j\alpha}} e^{j\pi[c - (f - f_i)^2/\alpha]}$	$\delta(f - f_i - \alpha t)$	$\delta(\nu - \alpha \tau) e^{j2\pi f_i \tau}$
$\frac{1}{\sqrt{\sigma}} e^{-\pi(t/\alpha)^2}$	$\sqrt{\sigma} e^{-\pi(\sigma f)^2}$	$\sqrt{2} e^{-2\pi[(t/\sigma) + (\sigma f)^2]}$	$\frac{1}{\sqrt{2}} e^{-\pi(2)[(\tau/\sigma)^2 + (\sigma \nu)^2]}$
$\frac{1}{\sqrt{\sigma}} e^{-\pi(t/\sigma)^2} e^{j\pi \alpha t^2}$	$\frac{1}{\sqrt{\sigma[\sigma^{-2} - j\alpha]}} \exp\left[-\pi f^2 \frac{\sigma^{-2} + j\alpha}{\alpha^{-4} + \alpha^2}\right]$	$\sqrt{2} e^{-2\pi[(t/\sigma) + (\sigma f)^2 + (\sigma f - \alpha t)^2]}$	$\frac{1}{\sqrt{2}} e^{-\pi(2)[(\tau/\sigma)^2 + (\sigma \nu)^2 + (\nu - \alpha \tau)^2]}$
$\frac{1}{\sqrt{\sigma}} e^{-\pi[(t-t_i)/\sigma]^2} e^{j2\pi f_i t}$	$\sqrt{\sigma} e^{-\pi \sigma^2 (f - f_i)^2} e^{-j2\pi (f - f_i) t_i}$	$\sqrt{2} e^{-2\pi[(t-t_i)/\sigma]^2 + \sigma^2 (f - f_i)^2}$	$\frac{1}{\sqrt{2}} e^{-\pi(2)[(\tau/\sigma)^2 + (\sigma \nu)^2]} e^{j2\pi (f_i \tau - t_i \nu)}$
$\text{rect}_a(t)$	$\frac{\sin(2\pi a f)}{\pi f}$	$\frac{\sin[4\pi(a -  t )f]}{\pi f} \text{rect}_a(t)$	$\frac{\sin[\pi \nu(2a -  \tau )]}{\pi \nu} \text{rect}_{2a}(\tau)$
$\frac{\sin(2\pi a t)}{\pi t}$	$\text{rect}_a(f)$	$\frac{\sin[4\pi(a -  f )t]}{\pi t} \text{rect}_a(f)$	$\frac{\sin[\pi \tau(2a -  \nu )]}{\pi \tau} \text{rect}_{2a}(\nu)$
$e^{j\pi \alpha t^2} \text{rect}_a(t)$	$\frac{1}{\sqrt{-j\alpha}} \int e^{-\frac{j\pi}{\alpha}(f-\beta)^2} \frac{\sin 2\pi a \beta}{\pi \beta} d\beta$	$\frac{\sin[4\pi(a -  t )(f - \alpha t)]}{\pi(f - \alpha t)} \text{rect}_a(t)$	$\frac{\sin[\pi(\nu - \alpha \tau)(2a -  \tau )]}{\pi(\nu - \alpha \tau)} \text{rect}_{2a}(\tau)$
$\tilde{u}(t) = \begin{cases} 1, & t > 0 \\ 0, & t < 0 \end{cases}$	$\frac{\delta(f)}{2} - \frac{j}{2\pi f}$	$\frac{\sin(4\pi f t)}{\pi f} \tilde{u}(t)$	$\left[\frac{\delta(\nu)}{2} - \frac{j}{2\pi \nu}\right] e^{-j\pi \nu  \tau }$
$e^{-\sigma t} \tilde{u}(t)$	$\frac{1}{\sigma + j2\pi f}$	$e^{-2\sigma t} \frac{\sin 4\pi f t}{\pi f} \tilde{u}(t)$	$\frac{e^{-(\sigma + j\pi \nu) \tau } - 1}{2\sigma + j2\pi \nu}$
$u_n(t), n = 0, 1, \dots$	$(-j)^n u_n(f)$	$2e^{-2\pi(t^2 + f^2)} L_n(4\pi(t^2 + f^2))$	$e^{-\pi(\tau^2 + \nu^2)/2} L_n(\pi(\tau^2 + \nu^2))$
$\cos(2\pi f_i t)$	$[\delta(f + f_i) + \delta(f - f_i)]/2$	$[\delta(f + f_i) + \delta(f - f_i) + 2\delta(f) \cos(4\pi f_i t)]/4$	$[\delta(\nu + 2f_i) + \delta(\nu - 2f_i) + 2\delta(\nu) \cos(2\pi f_i \tau)]/4$
$\sin(2\pi f_i t)$	$j[\delta(f + f_i) - \delta(f - f_i)]/2$	$[\delta(f + f_i) + \delta(f - f_i) - 2\delta(f) \cos(4\pi f_i t)]/4$	$-[\delta(\nu + 2f_i) + \delta(\nu - 2f_i) - 2\delta(\nu) \cos(2\pi f_i \tau)]/4$
$\delta(t - t_i) + \delta(t - t_m)$	$e^{-j2\pi f t_i} + e^{-j2\pi f t_m}$	$\delta(t - t_i) + \delta(t - t_m) + 2\delta\left(t - \frac{t_i + t_m}{2}\right) \cos(2\pi(t_i - t_m)f)$	$[e^{-j2\pi \nu t_i} + e^{-j2\pi \nu t_m}] \delta(\tau) + e^{-j\pi \nu(t_i + t_m)} [\delta(\tau - (t_i - t_m)) + \delta(\tau + (t_i - t_m))]$
$e^{j2\pi f_i t} + e^{j2\pi f_m t}$	$\delta(f - f_i) + \delta(f - f_m)$	$\delta(f - f_i) + \delta(f - f_m) + 2\delta\left(f - \frac{f_i + f_m}{2}\right) \cos(2\pi(f_i - f_m)t)$	$[e^{j2\pi f_i \tau} + e^{j2\pi f_m \tau}] \delta(\nu) + e^{j\pi(f_i + f_m)\tau} [\delta(\nu - (f_i - f_m)) + \delta(\nu + (f_i - f_m))]$
$\sum_k c_k e^{j2\pi k f_0 t}$	$\sum_k c_k \delta(f - k f_0)$	$\sum_k  c_k ^2 \delta(f - k f_0) + \sum_k \sum_{m \neq k} c_k c_m^* \delta\left(f - \frac{k + m}{2} f_0\right) e^{j2\pi(k - m)f_0 t}$	$\sum_k  c_k ^2 e^{j2\pi k f_0 \tau} \delta(\tau) + \sum_k \sum_{m \neq k} c_k c_m^* e^{j\pi(k + m)f_0 \tau} \delta(\nu - (k - m)f_0)$

Note: Here,  $\sigma > 0$ ,  $a, \alpha, c \in \mathbb{R}$ ,  $\text{sgn}(a)$ , and  $\text{rect}_a(t)$  are defined in Table 13.1;  $u_n(t) = \frac{2^{1/4}}{\sqrt{n!}} e^{-\pi t^2} H_n(2\sqrt{\pi}t)$ ,  $H_n(t) = (-1)^n e^{t^2/2} \frac{d^n}{dt^n} e^{-t^2/2}$  is the  $n$ th order Hermite polynomial;  $L_n(t) = \frac{1}{n!} e^t \frac{d^n}{dt^n} (t^n e^{-t}) = \sum_{k=0}^n \frac{n!}{k!(n-k)!} (-t)^k$  is the  $n$ th-order Laguerre polynomial.

In a dual manner, the second entry in Table 13.2 indicates that the WD of a complex exponential, i.e.,  $X(f) = \delta(f - f_0)$ , is Dirac function centered at the same frequency  $f = f_0$ . The next entry in Table 13.2 is that of WD of a linear FM signal,  $x(t) = e^{j\pi \alpha t^2}$  with a sweep rate  $\alpha$ . Its WD is a Dirac function perfectly concentrated along the signal's linear instantaneous frequency,  $f_x(t) = \alpha t$ .

*Proof* Let  $x(t) = e^{j\pi \alpha t^2}$ . Using Equation 13.15, one obtains the following proof:

$$\begin{aligned} WD_x(t, f) &= \int e^{j\pi \alpha(t+\tau/2)^2} e^{-j\pi \alpha(t-\tau/2)^2} e^{-j2\pi f \tau} d\tau, \\ &= \int e^{j\pi \alpha(t^2 + t\tau + \tau^2/4 - t^2 + t\tau - \tau^2/4)} e^{-j2\pi f \tau} d\tau \\ &= \int e^{-j2\pi(f - \alpha t)\tau} d\tau = \delta(f - \alpha t). \end{aligned}$$

Another interesting example is that of the WD of a Gaussian signal. Recall from Equation 13.13, the Fourier transform of a

Gaussian signal is itself a Gaussian function, but one with inversely proportional variance. The WD of this Gaussian signal is the two-dimensional Gaussian function given in Table 13.2.

*Proof* Let  $g(t) = \frac{1}{\sqrt{\sigma}} e^{-\pi(t/\sigma)^2}$ .

$$\begin{aligned} \text{WD}_g(t, f) &= \frac{1}{\sigma} \int e^{-\pi[(t+\tau/2)/\sigma]^2} e^{-\pi[(t-\tau/2)/\sigma]^2} e^{-j2\pi f\tau} d\tau, \\ &= \frac{1}{\sigma} \int e^{-\pi(t^2+t\tau+\tau^2/4+t^2-t\tau+\tau^2/4)/\sigma^2} e^{-j2\pi f\tau} d\tau \\ &= \frac{1}{\sigma} \int e^{-2\pi(t/\sigma)^2} \int e^{-\pi\tau^2/(2\sigma^2)} e^{-j2\pi f\tau} d\tau \\ &= \sqrt{2} e^{-2\pi[(t/\sigma)^2 + (\sigma f)^2]}. \end{aligned} \quad (13.22)$$

Note that if  $\sigma$  is very small, then the Gaussian signal  $g(t)$  is very short duration, but its Fourier transform  $G(f)$  is broadband in frequency; likewise, Equation 13.22 reveals that the WD of  $g(t)$  will be concentrated in time but broadband in frequency.

The AF of a variety of signals is given in the right-hand column of Table 13.2. Equations 13.17 and 13.19 indicate that the WD and the AF are two-dimensional Fourier transform pairs. hence, we can exploit the Fourier transform properties in Table 13.1 to gain insight into the relationship between the AF and the WD of any signal. Some of these relationships are given in Table 13.3, which lists the effects of signal operations on the WD and AF. For example, the first entry in Table 13.3 shows that the WD is insensitive to the phase of proportionality constants, i.e.,

$$y(t) = e^{j\alpha} x(t) \implies \text{WD}_y(t, f) \equiv \text{WD}_x(t, f), \forall \alpha \in \mathfrak{R}. \quad (13.23)$$

The WD and the AF are not one-to-one signal transformations; rather, they are only unique to a unit amplitude proportionality factor as indicated in Equation 13.23. The next entry in Table 13.3 shows that reversing the time axis of the signal in turn reverses its frequency axis as well; this produces a corresponding reversal in both the time and frequency axes of the WD and the AF. The fifth entry in Table 13.3 states that if a signal is

**TABLE 13.3** Effects of Signal Operations on the Wigner Distribution and Ambiguity Function

Signal, $y(t)$	Fourier Transform, $Y(f)$	Wigner Distribution, $\text{WD}_y(t, f)$	Ambiguity Function, $\text{AF}_y(\tau, \nu)$
$ax(t)$	$aX(f)$	$ a ^2 \text{WD}_x(t, f)$	$ a ^2 \text{AF}_x(\tau, \nu)$
$x(-t)$	$X(-f)$	$\text{WD}_x(-t, -f)$	$\text{AF}_x(-\tau, -\nu)$
$\sqrt{ a }x(at)$	$\frac{1}{\sqrt{ a }}X(f/a)$	$\text{WD}_x(at, f/a)$	$\text{AF}_x(a\tau, \nu/a)$
$\sqrt{ a }X(at)$	$\frac{1}{\sqrt{ a }}x(-f/a)$	$\text{WD}_x(-f/a, at)$	$\text{AF}_x(-\nu/a, a\tau)$
$x(t) = \pm x(\pm t)$	$X(f) = \pm X(\pm f)$	$\pm 2\text{AF}_x(2t, 2f)$	$\pm \frac{1}{2} \text{WD}_x(\tau/2, \nu/2)$
$x^*(t)$	$X^*(-f)$	$\text{WD}_x^*(\tau, -\nu)$	$\text{AF}_x^*(\tau, -\nu)$
$x(t - t_i)e^{j2\pi f t_i}$	$X(f - f_i)e^{-j2\pi(f - f_i)t_i}$	$\text{WD}_x(t - t_i, f - f_i)$	$\text{AF}_x(\tau, \nu)e^{j2\pi(f_i\tau - t_i\nu)}$
$x(t)h(t)$	$\int X(f')H(f - f')df'$	$\int \text{WD}_x(t, f')\text{WD}_h(t, f - f')df'$	$\int \text{AF}_x(\tau, \nu')\text{AF}_h(\tau, \nu - \nu')d\nu'$
$\int x(t')h(t - t')dt'$	$X(f)H(f)$	$\int \text{WD}_x(t', f)\text{WD}_h(t - t', f)dt'$	$\int \text{AF}_x(\tau', \nu)\text{AF}_h(\tau - \tau', \nu)d\tau'$
$x(t)e^{j\pi\alpha t^2}$	$\frac{1}{\sqrt{-j\alpha}} \int X(f - f')e^{-j\pi f'^2/\alpha}df'$	$\text{WD}_x(t, f - \alpha t)$	$\text{AF}_x(\tau, \nu - \alpha\tau)$
$\int \sqrt{ \alpha }e^{j\pi\alpha u^2}x(t - u)du$	$\sqrt{j\text{sgn}(\alpha)}X(f)e^{-j\pi f^2/\alpha}$	$\text{WD}_x(t - f/\alpha, f)$	$\text{AF}_x(\tau - \nu/\alpha, \nu)$
$\sum_{i=0}^{N-1} x(t - (i - \frac{N-1}{2})T_r),$ $T_r > 0$	$X(f) \frac{\sin(\pi T_r N f)}{\sin(\pi T_r f)}$	$\sum_{i=0}^{N-1} \text{WD}_x\left[t - \left(i - \frac{N-1}{2}\right)T_r, f\right]$ $+ 2 \sum_{i=0}^{N-2} \sum_{m=i+1}^{N-1} \text{WD}_x\left(t - \frac{(i+m) - (N-1)}{2}T_r, f\right)$ $\times \cos[2\pi T_r(i - m)f]$	$\sum_{n=-N+1}^{N-1} \text{AF}_x(\tau - nT_r, \nu)$ $\frac{\sin \pi \nu T_r (N -  n )}{\sin(\pi \nu T_r)}$
$\sum_{i=1}^N x(t - t_i)e^{j2\pi f t_i}$	$\sum_{i=1}^N X(f - f_i)e^{-j2\pi(f - f_i)t_i}$	$\sum_{i=1}^N \text{WD}_x(t - t_i, f - f_i)$ $+ 2 \sum_{i=1}^{N-1} \sum_{m=i+1}^N \text{WD}_x\left(t - \frac{t_i + t_m}{2}, f - \frac{f_i + f_m}{2}\right)$ $\times \cos 2\pi$ $\left[(f_i - f_m)t - (t_i - t_m)f + \frac{f_i + f_m}{2}(t_i - t_m)\right]$	$\text{AF}_x(\tau, \nu) \sum_{i=1}^N e^{j2\pi(f_i\tau - \nu t_i)}$ $+ \sum_{i=1}^N \sum_{\substack{m=1 \\ m \neq i}}^N \text{AF}_x(\tau - (t_i - t_m), \nu - (f_i - f_m))$ $\exp\left[j2\pi\left(\frac{f_i + f_m}{2}\tau - \frac{t_i + t_m}{2}\nu\right)\right]$ $+ (f_i - f_m)\frac{t_i + t_m}{2}$

Note: Here,  $\sigma > 0$ ,  $a, \alpha, \sigma, c \in \mathfrak{R}$ , and  $\text{sgn}(a)$  is the Signum function defined in Table 13.1.

even or odd, then its WD and AF are scaled versions of one another. For example, if  $x(t) = x(-t)$  is even, then its AF  $AF_x(\tau, \nu) = \frac{1}{2} WD_x\left(\frac{\tau}{2}, \frac{\nu}{2}\right)$ .

*Proof* Let  $x(t) = x(-t)$ .

$$\begin{aligned} AF_x(\tau, \nu) &= \int x(t + \tau/2)x^*(t - \tau/2)e^{-j2\pi\nu t} dt \\ &= \int x(t + \tau/2)x^*(-(t - \tau/2))e^{-j2\pi\nu t} dt \\ &= \frac{1}{2} \int x\left(\frac{\tau}{2} + \frac{\gamma}{2}\right)x^*\left(\frac{\tau}{2} - \frac{\gamma}{2}\right)e^{-j2\pi(\nu/2)\gamma} d\gamma \\ &= \frac{1}{2} WD_x\left(\frac{\tau}{2}, \frac{\nu}{2}\right). \end{aligned}$$

Just as Table 13.1 indicates that time shifts in a signal change the phase of its Fourier transform, so too does Table 13.3 indicate that time or frequency shifts in the WD cause phase changes in its Fourier transform, the AF.

*Proof* Let  $WD_y(t, f) = WD_x(t - t_0, f - f_0)$  in (13.19).

$$\begin{aligned} AF_y(\tau, \nu) &= \int \int WD_x(t - t_0, f - f_0)e^{-j2\pi(\nu t - \tau f)} dt df \\ &= \int \int WD_x(t', f')e^{-j2\pi[\nu(t'+t_0) - \tau(f'+f_0)]} dt' df' \\ &= e^{-j2\pi(\nu t_0 - \tau f_0)} AF_x(\tau, \nu) \end{aligned}$$

### 13.3.3 Altes Q or “Wideband” Wigner Distribution

The Altes Q distribution was originally proposed as a “wideband” version of the WD.<sup>6,97</sup>

$$\begin{aligned} Q_X(t, f) &= f \int X(fe^{u/2})X^*(fe^{-u/2})e^{j2\pi t f u} du, \quad f > 0 \\ &= f \int_0^\infty X(f\sqrt{\alpha})X^*(f/\sqrt{\alpha})e^{j2\pi t f^{-1} \alpha} d\alpha \end{aligned} \quad (13.24)$$

$$= \int \int HAF_x(\zeta, \beta)e^{j2\pi(t f \beta - \zeta \ln(f/f_r))} d\zeta d\beta. \quad (13.25)$$

Here,  $f_r$  is a positive reference frequency. Marinovich proposed a dual formulation to Equation 13.24, called the scale-invariant WD,

$$MSIWD_x(t, c) = \int x(te^{\sigma/2})x^*(te^{-\sigma/2})e^{-j2\pi c \sigma} d\sigma,$$

which used the time-domain version of the signal  $x(t)$  instead of the signal spectrum used in Equation 13.24.<sup>51,57,86</sup> The Q distribution is related to the hyperbolic AF (HAF),

$$\begin{aligned} HAF_x(\zeta, \beta) &= \int_0^\infty X(fe^{\beta/2})X^*(fe^{-\beta/2})e^{j2\pi\zeta \ln(f/f_r)} df \\ &= f_r \int e^b X(f_r e^{b+\beta/2})X^*(f_r e^{b-\beta/2})e^{j2\pi\zeta b} db \end{aligned} \quad (13.26)$$

$$= \int_0^\infty \int_{-\infty}^\infty Q_X(t, f)e^{-j2\pi(t f \beta - [\ln(f/f_r)]\zeta)} dt df \quad (13.27)$$

$$= \int \int Q_X\left(\frac{c}{f_r e^b}, f_r e^b\right)e^{-j2\pi(\beta c - \zeta b)} dc db, \quad (13.28)$$

via Fourier and Mellin transformations. Like the Mellin transform,<sup>32,60,94</sup>

$$MT_x(s) = \int_0^\infty X(u)e^{-j2\pi s \ln(u)} \frac{du}{u} \quad (13.29)$$

$$= \int X(e^\beta)e^{-j2\pi s \beta} d\beta, \quad (13.30)$$

the Altes Q distribution is useful for analyzing signals that have undergone scale change, e.g., the compressions or dilations that occur in wideband Doppler analysis of a moving target. Both Equations 13.27 and 13.28 and Equations 13.29 and 13.30 demonstrate that the Mellin transform is equivalent to the Fourier transform if the argument of the function being transformed is first prewarped in an exponential fashion. This allows the Mellin transform and the Altes Q distribution to be implemented efficiently using fast Fourier transform (FFT) techniques.<sup>95,106</sup>

The Altes Q distribution and the HAF of several signals are given in Table 13.4. This table shows that the Q distribution is well matched to signals with hyperbolic group delay. For example, the second entry in Table 13.4 states that the analytic signal  $Y(f) = \frac{1}{\sqrt{f}}e^{-j2\pi c \ln f/f_r} \tilde{u}(f)$  has a Q distribution that is perfectly localized along the signal’s hyperbolic group delay,  $\tau_y(f) = c/f, f > 0$ .

*Proof* Let  $Y(f) = \frac{1}{\sqrt{f}}e^{-j2\pi c \ln f/f_r} \tilde{u}(f) = \frac{1}{\sqrt{f_r}}\left(\frac{f}{f_r}\right)^{-j2\pi c - \frac{1}{2}} \tilde{u}(f)$  where  $\tilde{u}(f)$  is the unit step function defined in Table 13.1.

$$\begin{aligned} Q_Y(t, f) &= f \int \frac{1}{\sqrt{f}e^{u/2}} e^{-j2\pi c \ln(fe^{u/2}/f_r)} \frac{1}{\sqrt{f}e^{-u/2}} e^{j2\pi c \ln(fe^{-u/2}/f_r)} \\ &\quad e^{j2\pi t f u} du, f > 0 \\ &= \int e^{-j2\pi c \ln e^u} e^{j2\pi t f u} du \\ &= \int e^{j2\pi(t f - c)u} du = \delta(t f - c) = \frac{1}{|f|} \delta(t - c/f). \end{aligned} \quad (13.31)$$

**TABLE 13.4** Signals with Closed form Expressions for Their Altes Q Distribution and Hyperbolic Ambiguity Function

Analytic Signal $Y(f), f > 0$	Altes Distr., $Q_Y(t, f), f > 0$	Hyperbolic AF, $\text{HAF}_Y(\zeta, \beta)$
$\sqrt{\frac{f_r}{f}} X(f_r \ln(f/f_r))$	$\text{WD}_X\left(\frac{tf}{f_r}, f_r \ln \frac{f}{f_r}\right)$	$\text{AF}_X\left(\frac{\zeta}{f_r}, f_r \beta\right)$
$\sqrt{\frac{f_r}{f}} e^{-j2\pi t f_r \ln(f/f_r)} = \left(\frac{f}{f_r}\right)^{-j2\pi t f_r - \frac{1}{2}}$	$\left \frac{f_r}{f}\right  \delta\left(t - \frac{t f_r}{f}\right)$	$f_r e^{-j2\pi t f_r \beta} \delta(\zeta)$
$\sqrt{e^{f_i/f_r}} \delta(f - f_r e^{f_i/f_r})$	$ e^{f_i/f_r}  \delta(f - f_r e^{f_i/f_r})$	$\frac{1}{f_r} e^{j2\pi f_i \zeta / f_r \beta}$
$\sqrt{\frac{f_r}{f}} e^{-j\pi \alpha f_r^2 (\ln(f/f_r))^2}$	$\left \frac{f_r}{f}\right  \delta\left(t - \alpha f_r^2 \frac{\ln(f/f_r)}{f}\right)$	$f_r \delta(\zeta - \alpha f_r^2 \beta)$
$\sqrt{\frac{f_r}{f}} e^{-j\pi \alpha f_r^2 (\ln(f/f_r))^2} e^{-j2\pi t f_r \ln(f/f_r)}$	$\left \frac{f_r}{f}\right  \delta\left(t - \frac{f_r t_i}{f} - \alpha f_r^2 \frac{\ln(f/f_r)}{f}\right)$	$f_r \delta(\zeta - \alpha f_r^2 \beta) e^{-j2\pi t_i \zeta / f_r}$
$\sqrt{\frac{f_r}{-j\alpha f}} e^{j\pi [c - (f_r \ln(f/f_r) - f)^2 / \alpha]}$	$\left \frac{f_r}{\alpha f}\right  \delta\left(t - \frac{f_r^2 \ln(f/f_r)}{\alpha f} + \frac{f f_r}{\alpha f}\right)$	$\frac{1}{f_r} \delta\left(\beta - \frac{\alpha}{f_r^2} \zeta\right) e^{j2\pi f_i \zeta / f_r}$
$\sqrt{e^{f_i/f_r}} \delta(f - f_r e^{f_i/f_r}) + \sqrt{e^{-f_i/f_r}} \delta(f - f_r e^{-f_i/f_r})$	$ e^{f_i/f_r}  \delta(f - f_r e^{f_i/f_r}) +  e^{-f_i/f_r}  \delta(f - f_r e^{-f_i/f_r}) + 2\delta(f - f_r) \cos(4\pi f_i t f)$	$\left[\delta\left(\beta + \frac{2f_i}{f_r}\right) + \delta\left(\beta - \frac{2f_i}{f_r}\right) + 2\delta(\beta) \cos(2\pi f_i \zeta / f_r)\right] / f_r$
$\sqrt{\frac{f_r}{f}} \frac{\sin(2\pi a f_r \ln(f/f_r))}{\pi f_r \ln(f/f_r)}$	$\frac{\sin[4\pi(a f_r -  t f ) \ln(f/f_r)]}{\pi f_r \ln(f/f_r)} \text{rect}_a\left(\frac{t f}{f_r}\right)$	$f_r \frac{\sin[\pi \beta(2a f_r -  \zeta )]}{\pi \zeta} \text{rect}_{2a}\left(\frac{\zeta}{f_r}\right)$
$\sqrt{\frac{f_r}{f}} \left[ \frac{\delta(f - f_r)}{2} - \frac{j}{2\pi f_r \ln(f/f_r)} \right]$	$\frac{\sin 4\pi t f \ln(f/f_r)}{\pi f_r \ln(f/f_r)} \tilde{u}(t f / f_r)$	
$\sqrt{\frac{\sigma f_r}{f}} e^{-\pi(\sigma f_r \ln(f/f_r))^2}$	$\sqrt{2} \exp\left(-\pi \left[ \left(\frac{t f}{\sigma f_r}\right)^2 + (\sigma f_r \ln(f/f_r))^2 \right]\right)$	$\frac{1}{\sqrt{2}} \exp\left(-\frac{\pi}{2} \left[ \left(\frac{\zeta}{f_r \sigma}\right)^2 + (\sigma f_r \beta)^2 \right]\right)$
$(-j)^n \sqrt{\frac{f_r}{f}} u_n(f_r \ln(f/f_r))$	$2 \exp(-2\pi [(t f / f_r)^2 + (f_r \ln(f/f_r))^2]) \times L_n(4\pi((t f / f_r)^2 + (f_r \ln(f/f_r))^2))$	$\exp\left(-\frac{\pi}{2} [(\zeta / f_r)^2 + (f_r \beta)^2]\right) \times L_n(\pi((\zeta / f_r)^2 + (f_r \beta)^2))$

Note that all signals in column one are assumed to be analytic, i.e.,  $Y(f) = 0, f < 0$ . Here,  $\tilde{u}(t)$  and  $\text{rect}_a(t)$  are the unit step function and the rectangular function defined in Table 13.1.  $u_n(t) = \frac{2^{1/4}}{\sqrt{n!}} e^{-\pi t^2} H_n(2\sqrt{\pi}t), H_n(t) = (-1)^n e^{t^2/2} \frac{d^n}{dt^n} e^{-t^2/2}$  is the  $n$ th-order Hermite polynomial, and  $L_n(t) = \frac{1}{n!} e^t \frac{d^n}{dt^n} (t^n e^{-t}) = \sum_{k=0}^n \frac{n!}{k!(n-k)!} (-t)^k$  is the  $n$ th-order Laguerre polynomial.

### 13.3.4 TFR Warping

The Altes Q and the WDs are warped versions of each other.<sup>6,97,100</sup>

$$Q_X(t, f) = \text{WD}_{\text{WX}}\left(\frac{t f}{f_r}, f_r \ln \frac{f}{f_r}\right) \quad (13.32)$$

$$\text{WD}_X(t, f) = Q_{W^{-1}X}(t e^{-f/f_r}, f_r e^{f/f_r}) \quad (13.33)$$

In Equations 13.32 and 13.33, the signal is first prewarped using the following unitary signal transformations,

$$(WX)(f) = \sqrt{e^{f/f_r}} X(f_r e^{f/f_r}) \quad (13.34)$$

$$(W^{-1}X)(f) = \sqrt{\frac{f_r}{f}} X\left(f_r \ln \frac{f}{f_r}\right), \quad f > 0, \quad (13.35)$$

respectively, followed by a warping of the time–frequency axis. Since  $W$  and  $W^{-1}$  in Equations 13.34 and 13.35 are inverse

operators, i.e.,  $(W^{-1}WX)(f) = X(f)$ , then Equation 13.32 can also be written as

$$Q_{W^{-1}X}(t, f) = \text{WD}_X\left(\frac{t f}{f_r}, f_r \ln \frac{f}{f_r}\right), \quad (13.36)$$

which is the first entry in Table 13.4. Likewise, it can be shown that the Woodward AF in Equation 13.18 and the HAF in Equation 13.26 are related by a simple axis scaling, once the signal has been prewarped appropriately<sup>97,100</sup>:

$$\text{HAF}_X(\zeta, \beta) = \text{AF}_{\text{WX}}(\zeta/f_r, f_r \beta) \quad (13.37)$$

$$\text{HAF}_{W^{-1}X}(\zeta, \beta) = \text{AF}_X(\zeta/f_r, f_r \beta) \quad (13.38)$$

Consequently, and table of WD and AF pairs, such as Table 13.2, can be transformed into an equivalent table of the Altes Q and HAF transform pairs by using Equation 13.35 to warp the signal spectrum and Equations 13.36 and 13.38 to warp the WD and the AF. For example, the second entry of Table 13.2 can be used to derive the third entry in Table 13.4.



*Proof* From the second entry in Table 13.2, let

$$\begin{aligned} X(f) = \delta(f - f_i) &\Rightarrow \text{WD}_x(t, f) = \delta(f - f_i) \\ &\Rightarrow \text{AF}_x(\tau, \nu) = e^{j2\pi f_i \tau} \delta(\nu). \end{aligned}$$

By prewarping  $X(f)$  to form

$$\begin{aligned} Y(f) = (W^{-1}X_i)(f) &= \sqrt{\frac{f_r}{f}} \delta\left(f_r \ln \frac{f}{f_r} - f_i\right) \\ &= \sqrt{e^{f_i/f_r}} \delta(f - f_r e^{f_i/f_r}), \end{aligned}$$

one obtains using Equations 13.36 and 13.38

$$\begin{aligned} Q_Y(t, f) &= \text{WD}_x\left(\frac{tf}{f_r}, f_r \ln \frac{f}{f_r}\right) \\ &= \delta\left(f_r \ln \frac{f}{f_r} - f_i\right) = |e^{f_i/f_r}| \delta(f - f_r e^{f_i/f_r}) \\ \text{HAF}_Y(\zeta, \beta) &= \text{AF}_x(\zeta/f_r, f_r \beta) = e^{j2\pi f_i \zeta/f_r} \delta(f_r \beta) \end{aligned}$$

which corresponds to the third entry in Table 13.4.

### 13.3.5 Bertrand $P_k$ Distributions

The  $P_k$  distributions proposed by the Bertrands,<sup>19,20,95</sup>

$$\begin{aligned} &BP_k D_X(t, f; \mu) \\ &= f \int X(f \lambda_k(u)) X^*(f \lambda_k(-u)) \mu(u) e^{j2\pi t f (\lambda_k(u) - \lambda_k(-u))} du, \\ &f > 0 \end{aligned} \quad (13.39)$$

with

$$\begin{aligned} \lambda_0(u) &= \frac{u/2 e^{u/2}}{\sinh(u/2)} = \frac{u}{1 - e^{-u}}, \\ \lambda_1(u) &= \exp\left[1 + \frac{ue^{-u}}{e^{-u}-1}\right], \\ \lambda_k(u) &= \left[k \frac{e^{-u}-1}{e^{-ku}-1}\right]^{\frac{1}{k-1}}, \quad k \neq 0, 1, \end{aligned}$$

and  $\mu(u) = \mu^*(-u)$ , are affine TFRs that are covariant to all affine time transformations on analytic signals, i.e.,

$$\begin{aligned} Y(f) &= \frac{1}{\sqrt{|a|}} X\left(\frac{f}{a}\right) e^{-j2\pi f t_0}, \quad f > 0 \\ &\Rightarrow BP_k D_Y(t, f; \mu) = BP_k D_X\left(a(t - t_0), \frac{f}{a}; \mu\right), \quad f > 0. \end{aligned}$$

This affine covariance is useful in wideband Doppler applications. By properly selecting,  $k$ , the versatile  $P_k$  distributions also have extended covariance to dispersive, i.e., nonconstant, time

shifts on the signal including those proportional to power, hyperbolic, or logarithmic functions of frequency:

$$\begin{aligned} k \neq 0, 1; Y(f) &= \frac{1}{\sqrt{|a|}} e^{-j2\pi(bf+cf^k)} X\left(\frac{f}{a}\right) \\ &\Rightarrow BP_k D_Y(t, f; \mu) \\ &= BP_k D_X\left(a(t - b - kcf^{k-1}), \frac{f}{a}; \mu\right) \end{aligned} \quad (13.40)$$

$$\begin{aligned} k = 0; Y(f) &= \frac{1}{\sqrt{|a|}} e^{-j2\pi(bf+c \ln f)} X\left(\frac{f}{a}\right) \\ &\Rightarrow BP_0 D_Y(t, f; \mu) = BP_0 D_X\left(a\left(t - b - \frac{c}{f}\right), \frac{f}{a}; \mu\right) \end{aligned} \quad (13.41)$$

$$\begin{aligned} k = 1; Y(f) &= \frac{1}{\sqrt{|a|}} e^{-j2\pi(bf+cf \ln f)} X\left(\frac{f}{a}\right) \\ &\Rightarrow BP_1 D_Y(t, f; \mu) \\ &= BP_1 D_X\left(a(t - b - c[1 + \ln f]), \frac{f}{a}; \mu\right). \end{aligned} \quad (13.42)$$

Note that the dispersive time shifts in the Bertrand  $P_k$  distributions in Equations 13.40 and 13.42 are equivalent to the change in the group delay of  $X(f)$  brought about by multiplication with the complex exponential terms used to form  $Y(f)$ . The most commonly used Bertrand distribution is the unitary form of the  $k=0$  or  $P_0$  Bertrand distribution:

$$\begin{aligned} BP_0 D_X(t, f; \mu_0) &= f \int X\left(f \frac{u/2 e^{u/2}}{\sinh u/2}\right) X^*\left(f \frac{u/2 e^{-u/2}}{\sinh u/2}\right) \\ &\frac{u/2}{\sinh u/2} e^{j2\pi t f u} du, \quad f > 0. \end{aligned} \quad (13.43)$$

This special form of the  $P_0$  distribution in Equation 13.39 with  $\mu_0(u) = \frac{u/2}{\sinh u/2}$  is called the unitary  $P_0$  as the resulting TFR preserves inner products:

$$\int_0^\infty \int_0^\infty BP_0 D_X(t, f; \mu_0) BP_0 D_Y^*(t, f; \mu_0) dt df = \left| \int_0^\infty X(f) Y^*(f) df \right|^2.$$

### 13.3.6 Cross Terms of Quadratic Time-Frequency Representations

The spectrogram, Wigner, Altes Q, and Bertrand  $P_k$  distributions, as well as several other “energetic” TFRs listed in later sections, are quadratic functions of the signal. These nonlinear functions produce “cross terms” which can make visual analysis of TFRs difficult. For example, the nonlinear operation,

$$|x(t) + y(t)|^2 = |x(t)|^2 + |y(t)|^2 + 2\text{Real}\{x(t)y^*(t)\},$$

is equal to the sum of the two “auto” terms  $|x(t)|^2$ ,  $|y(t)|^2$  plus the cross term  $2\text{Real}\{x(t)y^*(t)\}$ . The following discussion will focus on the characteristics of the cross terms of the WD.<sup>52,70,82</sup>

The WD of a multicomponent signal,

$$y(t) = \sum_{i=1}^N x_i(t) \Rightarrow$$

$$\text{WD}_y(t, f) = \sum_{i=1}^N \text{WD}_{x_i}(t, f) + 2 \sum_{i=1}^{N-1} \sum_{k=i+1}^N \text{Real}\{\text{WD}_{x_i x_k}(t, f)\},$$
(13.44)

consists of  $N$  auto-terms,  $\text{WD}_{x_i}(t, f)$ , and  $\frac{N(N-1)}{2}$  cross terms,

$$\text{WD}_{x_i x_k}(t, f) = \int x_i(t + \tau/2) x_k^*(t - \tau/2) e^{-j2\pi f \tau} d\tau$$

$$= \text{WD}_{x_k x_i}^*(t, f).$$
(13.45)

An intuitive understanding of these cross terms can be obtained by analyzing the WD and the AF of the multicomponent signal  $y(t)$  in Equation 13.44 for the special case that each signal component,  $x_i(t)$ , is a shifted version of basic envelope  $x(t)$ , i.e.,

$$x_i(t) = x(t - t_i) e^{j2\pi f_i t}. \quad (13.46)$$

The WD and the AF given below were taken from the last entry in Table 13.3:

$$\text{WD}_y(t, f) = \sum_{i=1}^N \text{WD}_x(t - t_i, f - f_i)$$

$$+ 2 \sum_{i=1}^{N-1} \sum_{m=i+1}^N \text{WD}_x\left(t - \frac{t_i + t_m}{2}, f - \frac{f_i + f_m}{2}\right)$$

$$\times \cos 2\pi \left[ (f_i - f_m)t - (t_i - t_m)f + \frac{f_i + f_m}{2}(t_i - t_m) \right]$$
(13.47)

$$\text{AF}_y(\tau, \nu) = \text{AF}_x(\tau, \nu) \sum_{i=1}^N e^{j2\pi(f_i \tau - \nu t_i)}$$

$$+ \sum_{i=1}^{N-1} \sum_{\substack{m=1 \\ m \neq i}}^N \text{AF}_x(\tau - (t_i - t_m), \nu - (f_i - f_m))$$

$$\times \exp \left[ j2\pi \left( \frac{f_i + f_m}{2} \tau - \frac{t_i + t_m}{2} \nu + (f_i - f_m) \frac{t_i + t_m}{2} \right) \right]$$
(13.48)

The  $i$ th auto WD term in the first sum in Equation 13.47 has been shifted by  $(t_i, f_i)$  in the same way that the basic signal component  $x_i(t)$  in Equation 13.46 was shifted. In the second summation, the cross WD term corresponding to the pair of auto terms  $x_i(t)$  and  $x_m(t)$  is equal to the WD of the envelope  $x(t)$ , shifted to midway in the time–frequency plane, i.e.,  $\left(\frac{t_i + t_m}{2}, \frac{f_i + f_m}{2}\right)$ , between the pair of auto signal components;

the cross term oscillates with a spatial frequency proportional to the distance  $(t_i - t_m, f_i - f_m)$  between the pair of auto terms. This is depicted in Figure 13.2. In Equation 13.48, the AF of each auto term is equal to the AF of the envelope multiplied by a complex exponential; all auto AF terms map on top of one another at the origin of the AF plane. The cross terms in the second summation correspond to the AF of the basic envelope,  $x(t)$ , shifted away from the origin of the  $(\tau, \nu)$  plane by an amount equal to the distance between each pair of signal terms, as indicated in Figure 13.3. Signal components which occur at the same time, i.e.,  $t_i = t_m$ , or at the same frequency,  $f_i = f_m$ , have cross terms which are shifted along the axes in the AF plane. The greater the separation between any two signal components, the more rapidly the corresponding cross term in Equation 13.47 oscillates in the WD plane and the farther away from the origin the cross term in Equation 13.48 maps to in the AF plane. For example, Table 13.2 indicates that the WD of a cosine,

$$x(t) = \cos(2\pi f_i t) \leftrightarrow X(f) = [\delta(f + f_i) + \delta(f - f_i)]/2 \quad (13.49)$$

$$\Rightarrow \text{WD}_x(t, f) = [\delta(f + f_i) + \delta(f - f_i) + 2\delta(f) \cos(4\pi f_i t)]/4,$$
(13.50)

consists of two auto terms, which are the impulses located at  $f = \pm f_i$ , plus the oscillatory cross term located at mid-frequency  $f = 0$ . Increasing the sinusoidal frequency  $f_i$  increases the oscillation rate of the cross term, but produces no change in its location. The AF of this cosine,

$$x(t) = \cos(2\pi f_i t) \Rightarrow \text{AF}_x(\tau, \nu)$$

$$= [\delta(\nu) \{e^{j2\pi f_i \tau} + e^{-j2\pi f_i \tau}\} + \delta(\nu + 2f_i) + \delta(\nu - 2f_i)]/4,$$

has two auto terms which always map to the origin of the AF plane and two cross terms which occur at  $\nu = \pm 2f_i$ .

The characteristics of the cross terms of the spectrogram, Altes Q, and the Bertrand,  $P_k$  are described in Refs. [12,46,62,65,76,82]. The spectrogram contains undulating cross terms that occur wherever the STFT of the auto signal components  $x_i(t)$  overlap in the time–frequency plane. Using Equation 13.11 and the cosine example from Equation 13.49, one can show that

$$x(t) = \cos(2\pi f_i t) \Rightarrow$$

$$\text{SPEC}_x(t, f; \Gamma) = \frac{1}{4} [|\Gamma(f_i - f)|^2 + |\Gamma(-f_i - f)|^2$$

$$+ 2\text{Real}\{\Gamma^*(f_i - f)\Gamma(-f_i - f)e^{j2\pi(2f_i)t}\}].$$
(13.51)

If the bandwidth of the analysis window,  $\Gamma(f)$ , is greater than the sinusoidal frequency  $f_i$ , i.e.,  $|\Gamma(\pm f_i)| \neq 0$ , then the cross term in Equation 13.51 is nonzero and is modulated by a cosine whose frequency,  $2f_i$ , equals the distance between the signal’s spectral components at  $f = \pm f_i$ . Likewise, the Bertrand  $P_k$  distributions produce an oscillatory cross term corresponding to each air of signal components; closed form expression can be obtained for some of the  $P_k$  distributions revealing that their cross terms occur

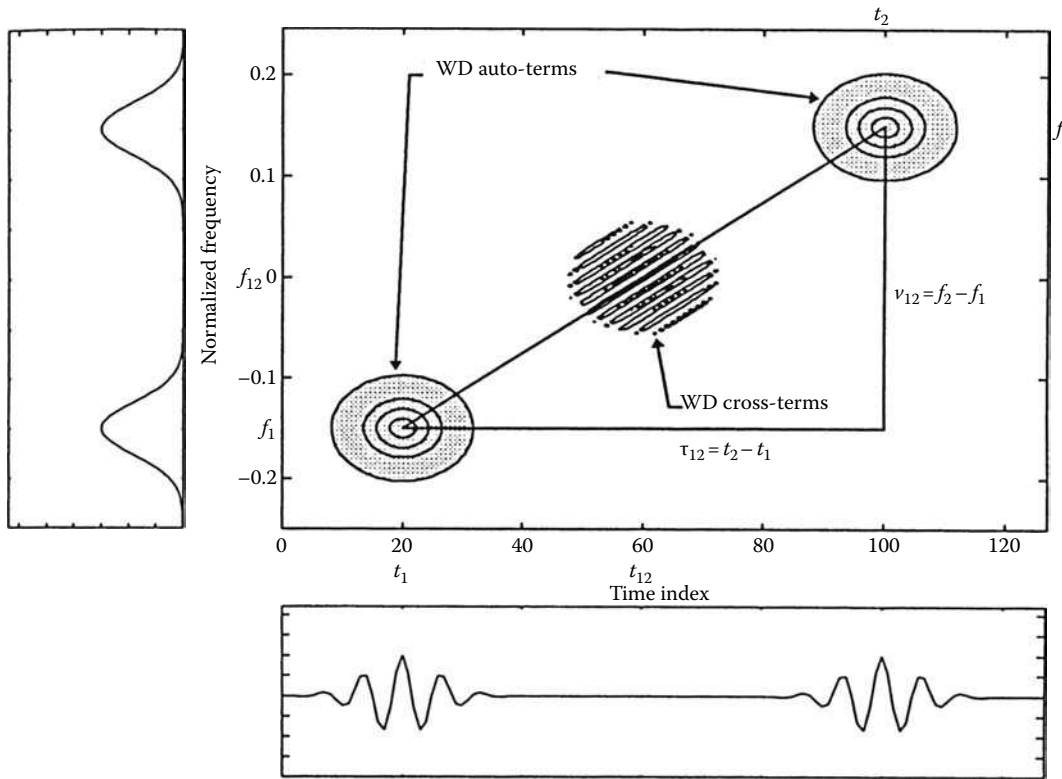


**FIGURE 13.2** Interference geometry of the Wigner distribution (WD) of a two-component signal  $y(t) = \sum_{i=1}^2 x(t - t_i)e^{j2\pi f_i t}$ . The signal is plotted at the bottom of the figure and its Fourier spectrum is plotted vertically along the left. The two auto terms are centered at  $(t_1, f_1)$  and  $(t_2, f_2)$ . The oscillatory WD cross term occurs midway between term at  $(t_{12}, f_{12}) = \left(\frac{t_1 + t_2}{2}, \frac{f_1 + f_2}{2}\right)$ . (From Costa, A.H., *Multiform, tiltable time–frequency representations and masked auto Wigner distribution synthesis*, Ph.D. thesis, University of Rhode Island, Kingston, RI, 1994. With permission.)

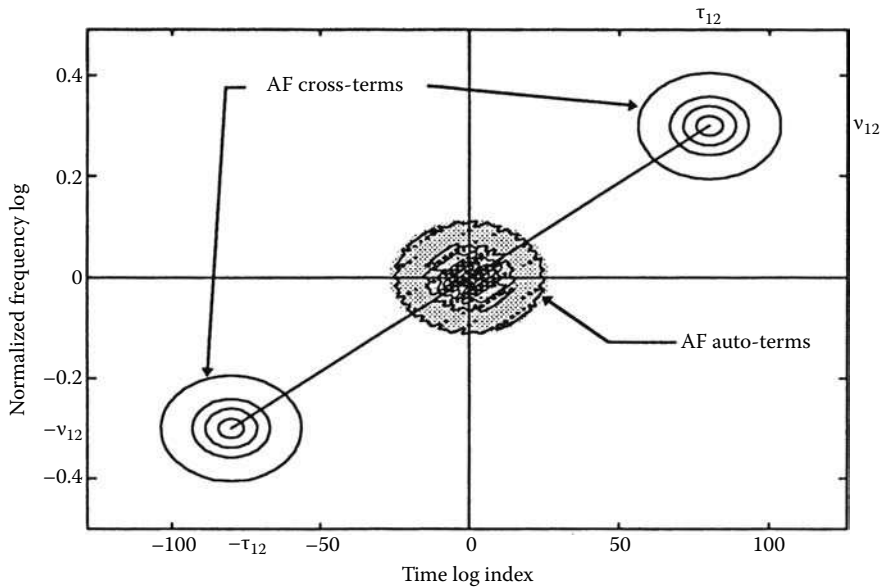


**FIGURE 13.3** Interference geometry of the ambiguity function (AF) of a two-component signal  $y(t) = \sum_{i=1}^2 x(t - t_i)e^{j2\pi f_i t}$ . The two AF auto terms map to the origin, while the cross term maps away from the origin to the locations corresponding to  $(\tau_{12}, \nu_{12})$  and  $(-\tau_{12}, -\nu_{12})$ , where  $\tau_{12} = t_2 - t_1$  is the temporal separation and  $\nu_{12} = f_2 - f_1$  is the spectral separation between the two Wigner distribution auto terms in Figure 13.2. (From Costa, A.H., *Multiform, tiltable time–frequency representations and masked auto Wigner distribution synthesis*, Ph.D. thesis, University of Rhode Island, Kingston, RI, 1994. With permission.)

**TABLE 13.5** Many TFRs are Equivalent to Smoothed or Warped Wigner Distributions

TFR Name	TFR Formulation
Cohen's class	$C_x(t, f; \Psi_C) = \iint \psi_C(t - t', f - f') \text{WD}_x(t', f') dt' df'$
Pseudo Wigner	$\text{PWD}_x(t, f; \Gamma) = \int \text{WD}_\gamma(0, f - f') \text{WD}_x(t, f') df'$
Scalogram	$\text{SCAL}_x(t, f; \Gamma) = \iint \text{WD}_\gamma\left(\frac{f}{f_r}(t' - t), \frac{f'}{f_r}\right) \text{WD}_x(t', f') dt' df'$
Smoothed pseudo Wigner Spectrogram	$\text{SPWD}_x(t, f; \Gamma, s) = \iint s(t - t') \text{WD}_\gamma(0, f - f') \text{WD}_x(t', f') dt' df'$ $\text{SPEC}_x(t, f; \Gamma) = \iint \text{WD}_\gamma(t' - t, f' - f) \text{WD}_x(t', f') dt' df'$
Altes Q	$Q_x(t, f) = \text{WD}_{\text{WX}}\left(\frac{tf}{f_r}, f_r \ln \frac{f}{f_r}\right)$
$\kappa$ th power Wigner	$\text{WD}_X^{(\kappa)}(t, f) = \text{WD}_{\text{WX}}\left(\frac{t}{\kappa f/f_r ^{\kappa-1}}, f_r \text{sgn}(f) f/f_r ^\kappa\right), \quad \kappa \neq 0$
Hyperbologram	$\text{HYP}_x(t, f; \Gamma) = \int \int_0^\infty \text{WD}_{\text{WT}}\left(t' - \frac{tf}{f_r}, f' - f_r \ln \frac{f}{f_r}\right) \text{WD}_{\text{WX}}(t', f') dt' df'$
Pseudo Altes Q	$\text{PQ}_x(t, f; \Gamma) = f_r \int_0^\infty \text{WD}_{\text{WT}}\left(0, f_r \ln \frac{f}{f_r}\right) \text{WD}_{\text{WX}}\left(\frac{tf}{f_r}, f_r \ln \frac{f}{f_r}\right) \frac{df'}{f'}$
Smoothed pseudo Altes Q	$\text{SPQ}_x(t, f; \Gamma, s) = f_r \int_{-\infty}^\infty \int_0^\infty s(tf - c) \text{WD}_{\text{WT}}\left(0, f_r \ln \frac{f}{f_r}\right) \times \text{WD}_{\text{WX}}\left(\frac{c}{f_r}, f_r \ln \frac{f}{f_r}\right) dc \frac{df'}{f'}$

Note: Alternative formulations for these TFRs can be found in Tables 13.9, 13.11, 13.13, and 13.15. Here  $f_r > 0$  is a positive reference frequency,  $(W X)(f) = \sqrt{e^{f/f_r} X(f_r e^{f/f_r})}$ ,  $(W_\kappa X)(f) = |\kappa| |f/f_r|^{(\kappa-1)/\kappa} |f|^{-1/2} X(f_r \text{sgn}(f)|f/f_r|^{1/\kappa})$ ,  $\kappa \neq 0$ , and  $\text{sgn}(f)$  is defined in Table 13.1. Also  $\psi_c(t, f) \leftrightarrow \Psi_C(\tau, \nu)$  and  $\gamma(t) \leftrightarrow \Gamma(f)$  are Fourier transform pairs.

at the location corresponding to the generalized mean of the locations of the corresponding pair of auto terms.

The presence of cross terms can make visual analysis of non-linear TFRs difficult. Two basic approaches are used to minimize the effects of these cross terms. The first approach is to use the analytic form of real, bandpass signals to zero out redundant negative frequency axis components of the signal's Fourier transform. The advantage of replacing real signals with their analytic counterpart can be demonstrated by comparing the Wigner–Ville distribution in Equation 13.21 for a band-limited cosine,

$$\begin{aligned} x(t) = \cos(2\pi f_i t) &\Rightarrow z_x(t) = x(t) + j\hat{x}(t) = e^{j2\pi f_i t} \\ &\Rightarrow \text{WD}_{z_x}(t, f) = \delta(f - f_i). \end{aligned} \quad (13.52)$$

The analytic signal corresponding to the cosine is a single tone located at  $Z_x(f) = \delta(f - f_i)$ , and as such its WD is a simple impulse at  $f = f_i$ . Comparison of Equation 13.50 with Equation 13.52 demonstrates that using the Wigner–Ville distribution for band-limited signals removes all cross WD terms that arise from signal components occurring on the negative frequency axis. The second approach to cross term removal exploits the fact that cross terms which oscillate rapidly in the time–frequency plane can be removed by smoothing or lowpass filtering the WD. Applying an ideal lowpass filter to the WD is equivalent to multiplying the signal's AF by a function that (1) approximately equal to one in the region near the origin where the auto AF

terms map to in Equation 13.48 and (2) is approximately zero in the region away from the origin of the AF plane where the AF cross terms map. Examples of TFRs that are a smoothed version of the WD are given in Table 13.5. The most commonly known smoothed WD is the spectrogram in Equation 13.9. The pseudo WD and the smoothed pseudo WD use lowpass analysis windows  $\gamma(\tau)$  and  $s(t)$  to smooth out the oscillatory cross terms. Unfortunately, the cost to be paid for smoothing away of cross terms is a loss of resolution between signal components in the time–frequency plane,<sup>55,80</sup> and, as we shall see in Section 13.4, a loss of desirable TFR properties.<sup>39</sup>

## 13.4 Desirable Properties of Time–Frequency Representations

One way of selecting which TFR to use is to examine which one has the most desirable properties for the particular application at hand. This section is a summary of several such properties, listed in Table 13.6. This table can be broken up conceptually into the following categories of ideal TFR properties: covariance, statistical or energy distribution, signal analysis, localization, and inner products.<sup>10,24,39,43,60,68,69</sup>

In the following section, each of the ideal TFR properties are discussed individually and at least one example is given demonstrating how to prove whether or not a certain TFR satisfies that property. Additional proofs can be found in Refs. [10,25,39,60,81,103,111].

TABLE 13.6 Ideal Time-Frequency Representation (TFR) Properties

Property Name	TFR Property
$P_1$ : Frequency-shift covariance	$T_y(t, f) = T_x(t, f - f_0)$ for $y(t) = x(t)e^{j2\pi f_0 t}$
$P_2$ : Time-shift covariance	$T_y(t, f) = T_x(t - t_0, f)$ for $y(t) = x(t - t_0)$
$P_3$ : Scale covariance	$T_y(t, f) = T_x(at, f/a)$ for $y(t) = \sqrt{ a }x(at)$
$P_4$ : Hyperbolic time shift	$T_y(t, f) = T_x(t - c/f, f)$ if $Y(f) = \exp\left(-j2\pi c \ln \frac{f}{f_0}\right)X(f)$
$P_5$ : Convolution covariance	$T_y(t, f) = \int T_h(t - \tau, f)T_x(\tau, f) d\tau$ for $y(t) = \int h(t - \tau)x(\tau)d\tau$
$P_6$ : Modulation covariance	$T_y(t, f) = \int T_h(t, f - f')T_x(t, f') df'$ for $y(t) = h(t)x(t)$
$P_7$ : Real-valued	$T_x^*(t, f) = T_x(t, f)$
$P_8$ : Positivity	$T_x(t, f) \geq 0$
$P_9$ : Time marginal	$\int T_x(t, f)df =  x(t) ^2$
$P_{10}$ : Frequency marginal	$\int T_x(t, f)dt =  X(f) ^2$
$P_{11}$ : Energy distribution	$\iint T_x(t, f)dt df = \int  X(f) ^2 df$
$P_{12}$ : Time moments	$\iint t^n T_x(t, f)dt df = \int t^n  x(t) ^2 dt$
$P_{13}$ : Frequency moments	$\iint f^n T_x(t, f)dt df = \int f^n  X(f) ^2 df$
$P_{14}$ : Finite time support	$T_x(t, f) = 0$ for $t \notin (t_1, t_2)$ if $x(t) = 0$ for $t \notin (t_1, t_2)$
$P_{15}$ : Finite freq. support	$T_x(t, f) = 0$ for $f \notin (f_1, f_2)$ if $X(f) = 0$ for $f \notin (f_1, f_2)$
$P_{16}$ : Instantaneous freq.	$\frac{\int f T_x(t, f) x(f) df}{\int T_x(t, f) df} = \frac{1}{2\pi} \frac{d}{dt} \arg\{x(t)\}$
$P_{17}$ : Group delay	$\frac{\int t T_x(t, f) dt}{\int T_x(t, f) dt} = -\frac{1}{2\pi} \frac{d}{df} \arg\{X(f)\}$
$P_{18}$ : Fourier transform	$T_y(t, f) = T_x(-f, t)$ for $y(t) = X(t)$
$P_{19}$ : Freq. localization	$T_x(t, f) = \delta(f - f_0)$ for $X(f) = \delta(f - f_0)$
$P_{20}$ : Time localization	$T_x(t, f) = \delta(t - t_0)$ for $x(t) = \delta(t - t_0)$
$P_{21}$ : Linear chirp localization	$T_x(t, f) = \delta(t - cf)$ for $X(f) = e^{-j\pi cf^2}$
$P_{22}$ : Hyperbolic localization	$T_x(t, f) = \frac{1}{f} \delta\left(t - \frac{c}{f}\right), f > 0$ if $X_c(f) = \frac{1}{\sqrt{f}} e^{-j2\pi c \ln \frac{f}{f_0}}, f > 0$
$P_{23}$ : Chirp convolution	$T_y(t, f) = T_x(t - f/c, f)$ for $y(t) = \int x(t - \tau) \sqrt{ c } e^{j\pi c \tau^2} d\tau$
$P_{24}$ : Chirp multiplication	$T_y(t, f) = T_x(t, f - ct)$ for $y(t) = x(t) e^{j\pi c t^2}$
$P_{25}$ : Moyal's Formula	$\iint T_x(t, f) T_y^*(t, f) dt df = \left  \int x(t) y^*(t) dt \right ^2$

### 13.4.1 Covariance Properties

The covariance properties  $P_1 - P_6$  in Table 13.6 state that certain operations on the signal, such as translation, dilation, or convolution, should be preserved in the TFR. That is, if the signal is changed in some way, then its TFR should change in exactly the same fashion.

#### $P_1$ : Frequency-shift covariance

$$y(t) = x(t)e^{j2\pi f_0 t} \Rightarrow Y(f) = X(f - f_0) \Rightarrow T_y(t, f) = T_x(t, f - f_0)$$

Property  $P_1$  states that if a signal is modulated or shifted in frequency by an amount  $f_0$ , then the TFR of that signal should also be shifted by  $f_0$ . This property is very important for analyzing a variety of signals such as speech, music, or sonar. Both the WD and the spectrogram satisfy this property; the STFT does not.

*Proof* Let  $Y(f) = X(f - f_0)$ .

$$\begin{aligned} \text{WD}_y(t, f) &= \int Y(f + \nu/2) Y^*(f - \nu/2) e^{j2\pi \nu t} d\nu \\ &= \int X([f + \nu/2] - f_0) X^*([f - \nu/2] - f_0) e^{j2\pi \nu t} d\nu \\ &= \int X([f - f_0] + \nu/2) X^*([f - f_0] - \nu/2) e^{j2\pi \nu t} d\nu \\ &= W_x(t, f - f_0) \end{aligned}$$

$$\begin{aligned} \text{STFT}_y(t, f; \Gamma) &= e^{-j2\pi t f} \int Y(f') \Gamma^*(f' - f) e^{j2\pi t f'} df' \\ &= e^{-j2\pi t f} \int X(f' - f_0) \Gamma^*(f' - f) e^{j2\pi t f'} df' \\ &= e^{-j2\pi t f} \int X(\nu) \Gamma^*(\nu + f_0 - f) e^{j2\pi t (\nu + f_0)} d\nu \\ &= e^{-j2\pi [f - f_0] t} \int X(\nu) \Gamma^*(\nu - [f - f_0]) e^{j2\pi t \nu} d\nu \\ &= e^{-j2\pi [f - f_0] t} \text{STFT}_x(t, f - f_0; \Gamma) \neq \text{STFT}_x(t, f - f_0; \Gamma) \\ \text{SPEC}_y(t, f; \Gamma) &= |\text{STFT}_y(t, f; \Gamma)|^2 = |e^{-j2\pi [f - f_0] t} \text{STFT}_x(t, f - f_0; \Gamma)|^2 \\ &= \text{SPEC}_x(t, f - f_0; \Gamma) \end{aligned}$$

**P<sub>2</sub>: Time-shift covariance**

$$y(t) = x(t - t_0) \Rightarrow T_y(t, f) = T_x(t - t_0, f)$$

Property  $P_2$  states that any time translations in the signal should be preserved in its TFR. Equivalently,  $P_2$  states that an ideal TFR should be covariant to any constant shift in the signal's group delay. The WD and the spectrogram satisfy this property, but the STFT does not.

*Proof* Let

$$y(t) = x(t - t_0) \leftrightarrow Y(f) = e^{-j2\pi f t_0} X(f) \Rightarrow \tau_y(f) = \tau_x(f) - t_0.$$

$$\begin{aligned} \text{WD}_y(t, f) &= \int y\left(t + \frac{\tau}{2}\right) y^*\left(t - \frac{\tau}{2}\right) e^{-j2\pi f \tau} d\tau \\ &= \int x\left(t + \frac{\tau}{2} - t_0\right) x^*\left(t - \frac{\tau}{2} - t_0\right) e^{-j2\pi f \tau} d\tau \\ &= \int x\left([t - t_0] + \frac{\tau}{2}\right) x^*\left([t - t_0] - \frac{\tau}{2}\right) e^{-j2\pi f \tau} d\tau \\ &= W_x(t - t_0, f) \end{aligned}$$

$$\begin{aligned} \text{STFT}_y(t, f; \Gamma) &= \int y(\tau) \gamma^*(\tau - t) e^{-j2\pi f \tau} d\tau \\ &= \int x(\tau - t_0) \gamma^*(\tau - t) e^{-j2\pi f \tau} d\tau \\ &= \int x(\beta) \gamma^*(\beta + t_0 - t) e^{-j2\pi f [\beta + t_0]} d\beta \\ &= e^{-j2\pi f t_0} \int x(\beta) \gamma^*(\beta - [t - t_0]) e^{-j2\pi f \beta} d\beta \\ &= e^{-j2\pi f t_0} \text{STFT}_x(t - t_0, f; \Gamma) \neq \text{STFT}_x(t - t_0, f; \Gamma) \end{aligned}$$

$$\begin{aligned} |\text{STFT}_y(t, f; \Gamma)|^2 &= |e^{-j2\pi f t_0} \text{STFT}_x(t - t_0, f; \Gamma)|^2 \\ &= |\text{STFT}_x(t - t_0, f; \Gamma)|^2 \end{aligned}$$

**P<sub>3</sub>: Scale covariance**

$$y(t) = \sqrt{|a|} x(at) \Rightarrow T_y(t, f) = T_x\left(at, \frac{f}{a}\right)$$

To understand property  $P_3$ , recall that the dilation property in Table 13.1 indicates that if the time axis of a signal is compressed by a scalar factor  $a$ , then its Fourier transform is expanded by a factor of  $1/a$ . That is, if  $y(t) = \sqrt{|a|} x(at)$ , then  $Y(f) = \frac{1}{\sqrt{|a|}} X\left(\frac{f}{a}\right)$ . Hence, property  $P_3$  states that if the signal's time axis is compressed by a scale factor  $a$ , then its TFR's time axis should also be compressed by  $a$  and its frequency axis expanded by the factor  $1/a$ . The WD, the Altes Q distribution, and the Bertrand  $P_k$  distributions are scale covariant, but the STFT is not for any nontrivial scale factor  $a \neq 1$ .

*Proof* Let  $y(t) = \sqrt{|a|} x(at) \leftrightarrow Y(f) = \frac{1}{\sqrt{|a|}} X\left(\frac{f}{a}\right)$ .

$$\begin{aligned} \text{WD}_y(t, f) &= \int y\left(t + \frac{\tau}{2}\right) y^*\left(t - \frac{\tau}{2}\right) e^{-j2\pi f \tau} d\tau \\ &= |a| \int x\left(\left[t + \frac{\tau}{2}\right] a\right) x^*\left(\left[t - \frac{\tau}{2}\right] a\right) e^{-j2\pi f \tau} d\tau \\ &= \int x\left(at + \frac{u}{2}\right) x^*\left(at - \frac{u}{2}\right) e^{-j2\pi f / a} du \\ &= W_x\left(at, \frac{f}{a}\right) \end{aligned}$$

$$\begin{aligned} Q_Y(t, f) &= f \int Y(fe^{u/2}) Y^*(fe^{-u/2}) e^{j2\pi f u} du, \quad f > 0 \\ &= \frac{f}{a} \int X\left(\frac{f}{a} e^{u/2}\right) X^*\left(\frac{f}{a} e^{-u/2}\right) e^{j2\pi (at)(f/a)u} du, \quad a > 0 \\ &= Q_X\left(at, \frac{f}{a}\right) \end{aligned}$$

$$\begin{aligned} \text{BP}_k D_Y(t, f; \mu) &= f \int Y(f \lambda_k(u)) Y^*(f \lambda_k(-u)) \mu(u) e^{j2\pi t f (\lambda_k(u) - \lambda_k(-u))} du, \quad f > 0 \\ &= \frac{f}{a} \int X\left(\frac{f}{a} \lambda_k(u)\right) X^*\left(\frac{f}{a} \lambda_k(-u)\right) \mu(u) e^{j2\pi (at)(f/a)(\lambda_k(u) - \lambda_k(-u))} du, \quad a > 0 \\ &= \text{BP}_k D_Y\left(at, \frac{f}{a}; u\right) \end{aligned}$$

$$\begin{aligned} \text{STFT}_Y(t, f; \Gamma) &= \int \sqrt{|a|} x(a\tau) \gamma^*(\tau - t) e^{-j2\pi f \tau} d\tau \\ &= \frac{1}{\sqrt{|a|}} \int x(t') \gamma^*\left(\frac{t'}{a} - t\right) e^{-j2\pi f t' / a} dt', \quad a > 0 \\ &= \int x(t') \tilde{\gamma}^*(t' - at) e^{-j2\pi (f/a) t'} dt', \quad \text{where } \tilde{\gamma}(t) \\ &= \frac{1}{\sqrt{|a|}} \gamma\left(\frac{t}{a}\right) \\ &= \text{STFT}_x\left(at, \frac{f}{a}; \tilde{\Gamma}\right) \\ &\neq \text{STFT}_x\left(at, \frac{f}{a}; \Gamma\right) \text{ unless } a = 1 \end{aligned}$$

**P<sub>4</sub>: Hyperbolic time-shift covariance**

$$Y(f) = \exp\left(-j2\pi c \ln \frac{f}{f_r}\right) X(f) \Rightarrow T_y(t, f) = T_x\left(t - \frac{c}{f}, f\right)$$

Property  $P_4$  states that an ideal TFR should be covariant to hyperbolic changes in this signal's group delay. If the signal's Fourier transform or spectrum undergoes a logarithmic phase change, then its group delay undergoes a hyperbolic shift, i.e.,  $\tau_y(f) = \tau_x(f) + \frac{c}{f}$ . Property  $P_4$  states that an ideal TFR of a logarithmic FM-modulated signal should correspond to the

TFR of the original signal, but with a dispersive temporal shift equal to the hyperbolic change in the group delay. The Altes Q distribution and the general form of the Bertrand  $P_0$  distribution satisfy this property.

*Proof* Let  $Y(f) = \exp\left(-j2\pi c \ln \frac{f}{f_t}\right) X(f) \Rightarrow \tau_y(f) = \tau_x(f) + \frac{c}{f}$ .

$$\begin{aligned} Q_Y(t, f) &= f \int Y(fe^{u/2}) Y^*(fe^{-u/2}) e^{j2\pi f u} du, \quad f > 0 \\ &= f \int X(fe^{u/2}) e^{-j2\pi c \ln(fe^{u/2}/f_t)} \\ &\quad X^*(fe^{-u/2}) e^{j2\pi c \ln(fe^{-u/2}/f_t)} e^{j2\pi f u} du \\ &= f \int X(fe^{u/2}) X^*(fe^{-u/2}) \\ &\quad \times e^{-j2\pi c [\ln(f/f_t) + u/2 - \ln(f/f_t) + u/2]} e^{j2\pi f u} du \\ &= f \int X(fe^{u/2}) X^*(fe^{-u/2}) e^{j2\pi [t - c/f] f u} du \\ &= Q_X(t - c/f, f) \end{aligned}$$

$$\begin{aligned} BP_0 D_Y(t, f; \mu) &= f \int X\left(f \frac{u/2 e^{u/2}}{\sinh u/2}\right) e^{-j2\pi c \ln\left(\frac{f}{f_t} \frac{u/2 e^{u/2}}{\sinh u/2}\right)} \\ &\quad X^*\left(f \frac{u/2 e^{-u/2}}{\sinh u/2}\right) e^{j2\pi c \ln\left(\frac{f}{f_t} \frac{u/2 e^{-u/2}}{\sinh u/2}\right)} \mu(u) e^{j2\pi f u} du \\ &= f \int X\left(f \frac{u/2 e^{u/2}}{\sinh u/2}\right) \\ &\quad X^*\left(f \frac{u/2 e^{-u/2}}{\sinh u/2}\right) e^{-j2\pi c \ln e^u} \mu(u) e^{j2\pi f u} du \\ &= f \int X\left(f \frac{u/2 e^{u/2}}{\sinh u/2}\right) X^*\left(f \frac{u/2 e^{-u/2}}{\sinh u/2}\right) \\ &\quad \times \mu(u) e^{j2\pi(t - c/f) f u} du \\ &= BP_0 D_X(t - c/f, f; \mu) \end{aligned}$$

### $P_5$ : Convolution covariance

$$y(t) = \int h(t - \tau) x(\tau) d\tau \Rightarrow T_y(t, f) = \int T_h(t - \tau, f) T_x(\tau, f) d\tau$$

Property  $P_5$  states that convolving two signals together in the time domain should produce the equivalent effect of convolving their corresponding TFRs together in the frequency domain. The WD is one of the few TFRs that satisfies this property.

*Proof* Let  $y(t) = \int h(t - \tau) x(\tau) d\tau$ .

$$\begin{aligned} WD_y(t, f) &= \int y(t + t'/2) y^*(t - t'/2) e^{-j2\pi f t'} dt' \\ &= \int \left[ \int h(t + t'/2 - \alpha) x(\alpha) d\alpha \right] \\ &\quad \times \left[ \int h^*(t - t'/2 - \gamma) x^*(\gamma) d\gamma \right] e^{-j2\pi f t'} dt' \end{aligned}$$

Substituting  $\alpha = \tau + p/2$ ,  $\gamma = \tau - p/2$ , and  $t' = q + p$  produces

$$\begin{aligned} WD_y(t, f) &= \iiint h\left((t - \tau) + \frac{q}{2}\right) h^*\left((t - \tau) - \frac{q}{2}\right) x\left(\tau + \frac{p}{2}\right) \\ &\quad x^*\left(\tau - \frac{p}{2}\right) e^{-j2\pi f(q+p)} dq d\tau dp \\ &= \int WD_h(t - \tau, f) WD_x(\tau, f) d\tau. \end{aligned}$$

### $P_6$ : Modulation covariance

$$\begin{aligned} y(t) &= h(t)x(t) \Rightarrow Y(f) = \int H(f - f') X(f') df' \\ \Rightarrow T_y(t, f) &= \int T_h(t, f - f') T_x(t, f') df' \end{aligned}$$

If two signals are modulated together in time, then Table 13.1 indicates that their Fourier transforms are convolved together in frequency. Similarly, property  $P_6$  states that whenever the Fourier transforms of two signals are convolved together in the frequency domain, then the TFR of the resulting signal should be equal to the convolution in frequency of the two signals' respective TFRs. It can be shown using the dual to the proof in  $P_5$  above that the WD satisfies this property.

## 13.4.2 Statistical Energy Density Distribution Properties

The second category of properties in Table 13.6 originates from the desire to generalize the concepts of the one-dimensional instantaneous signal energy,  $|x(t_0)|^2$ , and power spectral density,  $|X(f)|^2$ , into a two-dimensional instantaneous signal probability density function or an energy distribution,  $T_x(t_0, f_0)$ , which would ideally provide a measure of the local signal energy or the probability that a signal contains a sinusoidal component of the frequency  $f_0$  at the time  $t_0$ . Properties  $P_7$ – $P_{13}$  state that such an energy distribution TFR should be real, nonnegative, and have its marginal distributions equal to the signal's temporal and spectral energy densities,  $|x(t)|^2$  and  $|X(f)|^2$ , respectively. A TFR should also preserve the signal energy, mean, variance, and other higher order moments of the signal's temporal and spectral energy density. These ideal statistical or energy density TFR properties are described below.

### $P_7$ : Real

$$T_x(t, f) = T_x^*(t, f), \forall x(t)$$

For a TFR to be real, it must be equal to its own complex conjugate for all signals. The WD, the Altes Q distribution, and the spectrogram are always real valued. Equations 13.10 and 13.11 are examples of the fact that the STFT is complex, which is why its squared magnitude, the spectrogram, is usually used for visual analysis.

*Proof*

$$\begin{aligned}
\text{WD}_x^*(t, f) &= \left[ \int x\left(t + \frac{\tau}{2}\right)x^*\left(t - \frac{\tau}{2}\right)e^{-j2\pi f\tau} d\tau \right]^* \\
&= \int x^*\left(t + \frac{\tau}{2}\right)x\left(t - \frac{\tau}{2}\right)e^{j2\pi f\tau} d\tau \\
&= \int x^*\left(t - \frac{t'}{2}\right)x\left(t + \frac{t'}{2}\right)e^{-j2\pi ft'} dt' = W_x(t, f) \\
Q_X^*(t, f) &= f \int X^*(fe^{u/2})X(fe^{-u/2})e^{-j2\pi fu} du \\
&= f \int X^*(fe^{-\beta/2})X(fe^{\beta/2})e^{j2\pi f\beta} d\beta = Q_X(t, f)
\end{aligned}$$

**P<sub>8</sub>: Positivity**

$$T_x(t, f) \geq 0, \forall x(t)$$

If a TFR is to be interpreted as a two-dimensional distribution of signal energy, then it should be nonnegative. By definition, since the spectrogram is equal to the squared magnitude of the STFT, it is always nonnegative. However, Tables 13.2 and 13.4 reveal that the WD and the Q distribution, respectively, have negative values for some signals. For example, Table 13.2 states that the WD of a rectangular box function is a variable width sinc function, which is frequently negative. The last five entries in Table 13.2 correspond to the WD of multicomponent signals. Each has a WD with cross terms that oscillate about zero.

**P<sub>9</sub>: Time marginal preservation**

$$\int T_x(t, f) df = |x(t)|^2, \forall x(t)$$

If TFR is to be interpreted as a signal's two-dimensional energy distribution over the time–frequency plane, then integrating out the frequency variable should result in the signal's instantaneous energy in the time domain. The WD satisfies this property; the spectrogram does not.

*Proof*

$$\begin{aligned}
\int W_x(t, f) df &= \iint x(t + \tau/2)x^*(t - \tau/2)e^{-j2\pi f\tau} d\tau df \\
&= \int x(t + \tau/2)x^*(t - \tau/2)\delta(\tau) d\tau = |x(t)|^2 \\
\int |\text{STFT}_x(t, f; \Gamma)|^2 df &= \iint \left[ \int x(\tau)\gamma^*(\tau - t)e^{-j2\pi f\tau} d\tau \right] \\
&\quad \times \left[ \int x^*(t')\gamma(t' - t)e^{j2\pi ft'} dt' \right] df \\
&= \iint x(\tau)x^*(t')\gamma^*(\tau - t)\gamma(t' - t)\delta(\tau - t') d\tau dt' \\
&= \int |x(t')|^2 |\gamma(t' - t)|^2 dt'.
\end{aligned}$$

Hence, the marginal distribution corresponding to the two-dimensional spectrogram is equal to a weighted average of the signal's instantaneous signal energy,  $|x(t')|^2$ , in the neighborhood of the output time  $t$ . The weighting function is a shifted version of the analysis window. The spectrogram only satisfies  $P_9$  if the analysis window is a Dirac impulse in time.

**P<sub>10</sub>: Frequency marginal preservation**

$$\int T_x(t, f) dt = |X(f)|^2, \quad \forall x(t)$$

If the TFR is the signal's two-dimensional energy distribution, then integrating out the time axis should result in the signal's spectral density function,  $|X(f)|^2$ . The Wigner and Altes Q distributions satisfy this property; the spectrogram does not.

*Proof*

$$\begin{aligned}
\int \text{WD}_x(t, f) dt &= \iint X(f + \nu/2)X^*(f - \nu/2)e^{j2\pi\nu t} d\nu dt \\
&= \int X(f + \nu/2)X^*(f - \nu/2)\delta(\nu) d\nu = |X(f)|^2 \\
\int Q_X(t, f) dt &= \int f \int X(fe^{u/2})X^*(fe^{-u/2})e^{j2\pi fu} du dt \\
&= f \int X(fe^{u/2})X^*(fe^{-u/2})\delta(fu) du = |X(f)|^2 \\
\int |\text{STFT}_x(t, f; \Gamma)|^2 dt &= \iint \left[ \int e^{-j2\pi tf} X(f')\Gamma^*(f' - f)e^{j2\pi t f'} df' \right] \\
&\quad \times \left[ \int e^{j2\pi t f} X^*(\nu)\Gamma(\nu - f)e^{-j2\pi t \nu} d\nu \right] dt \\
&= \iint X(f')X^*(\nu)\Gamma^*(f' - f)\Gamma(\nu - f) \\
&\quad \times \delta(\nu - f') df' d\nu \\
&= \int |X(f')|^2 |\Gamma(f' - f)|^2 df'.
\end{aligned}$$

Hence, the spectrogram does not satisfy  $P_{10}$  unless the Fourier transform of the STFT analysis window is a Dirac function.

**P<sub>11</sub>: Energy preservation**

$$\iint T_x(t, f) dt df = \int |X(f)|^2 df = E_x$$

If the TFR is a distribution of the signal's energy over the whole time–frequency plane, then integrating the TFR should give you back the total signal energy,  $E_x$ . The Wigner and Altes Q distributions satisfy this property. The proof is simplified by making use of the fact that they were shown to preserve the frequency-domain marginals in  $P_{10}$  above.



*Proof*

$$\begin{aligned}\iint \text{WD}_x(t, f) dt df &= \int |X(f)|^2 df = E_x \\ \iint Q_x(t, f) dt df &= \int |X(f)|^2 df = E_x.\end{aligned}$$

### $P_{12}$ : Time moment preservation

$$\iint t^n T_x(t, f) dt df = \int t^n |x(t)|^2 dt$$

The  $n$ th moment of a signal  $g(t)$  is defined to be

$$m_g(n) = \int t^n g(t) dt.$$

Property  $P_{12}$  states that the value of the  $n$ th time moment of the signal's instantaneous energy,  $|x(t)|^2$ , and the  $n$ th time moment of the signal's TFR should be identical. The WD satisfies this property.

*Proof*

$$\begin{aligned}\iint t^n \text{WD}_x(t, f) dt df &= \iiint t^n x(t + \tau/2) x^*(t - \tau/2) e^{-j2\pi f \tau} \\ &\quad \times d\tau dt df \\ &= \iint t^n x(t + \tau/2) x^*(t - \tau/2) \delta(\tau) d\tau dt \\ &= \int t^n |x(t)|^2 dt.\end{aligned}\quad (13.53)$$

### $P_{13}$ : Frequency moment preservation

$$\iint f^n T_x(t, f) dt df = \int f^n |X(f)|^2 df$$

The  $n$ th moment of the power spectral density,  $|X(f)|^2$ , and the  $n$ th frequency moment of the signal's TFR should be identical. The Wigner and the Altes Q distributions satisfy this property.

*Proof*

$$\begin{aligned}\iint f^n \text{WD}_x(t, f) dt df &= \iiint f^n X(f + \nu/2) X^*(f - \nu/2) e^{j2\pi \nu t} \\ &\quad dv dt df \\ &= \iint f^n X(f + \nu/2) X^*(f - \nu/2) \delta(\nu) dv df \\ &= \int f^n |X(f)|^2 df\end{aligned}\quad (13.54)$$

$$\begin{aligned}\iint f^n Q_x(t, f) dt df &= \iint \int f^{n+1} X(fe^{u/2}) X^*(fe^{-u/2}) e^{j2\pi f u} du dt df \\ &= \iint f^{n+1} X(fe^{u/2}) X^*(fe^{-u/2}) \delta(fu) du df \\ &= \int f^n |X(f)|^2 df.\end{aligned}\quad (13.55)$$

Note that an alternative way to prove that the WD and the Altes Q distribution satisfy the energy preservation property  $P_{11}$  is to evaluate Equations 13.54 and 13.55 for the special case of  $n = 0$ .

### 13.4.3 Signal Analysis Properties

The next category of properties in Table 13.6 is  $P_{14}$  through  $P_{18}$  which arise from signal processing considerations. A TFR should have the same nonzero support, i.e., duration and bandwidth, as the signal under analysis. At any given time,  $t$ , the average or mean frequency should equal the instantaneous frequency of the signal, while the average or center of gravity of the TFR in the time direction should equal the group delay of the signal. These two properties have been used to analyze the distortion of audio systems and the complex FM sonar signals used by bats and whales for echolocation.<sup>5,7,24,53,69,75</sup> Property  $P_{18}$  is the TFR equivalent of the duality property of Fourier transforms in Table 13.1.

#### $P_{14}$ : Finite time support

$$x(t) = 0 \quad \text{for } t \notin (t_1, t_2) \Rightarrow T_x(t, f) = 0 \quad \text{for } t \notin (t_1, t_2)$$

Property  $P_{14}$  states that if a signal starts at time  $t_1$  and stops at time  $t_2$ , then an ideal TFR should also start and stop at the same time. This is a very intuitive property for the TFR to have if it is to be interpreted as a two-dimensional energy distribution; there should be no nonzero values of the TFR at any time before the signal starts up nor after the signal has stopped. However, this property is sometimes referred to as "weak" time support,<sup>43</sup> as it simply guarantees that the TFR will have the same global time support as the signal under analysis. It does not guarantee that the TFR will be equal to zero whenever the signal or its spectrum are equal to zero. The WD satisfies the finite support property, but the STFT does not for any analysis window  $\gamma(t) \neq k\delta(t)$ .

*Proof* Assume  $x(t) = 0$  for  $t \notin (t_1, t_2)$ .

A sufficient condition for the WD of  $x(t)$  in Equation 13.15 to be equal to zero is that the signal product  $[x(t + \tau/2)x^*(t - \tau/2)]$  inside the integral be zero everywhere, or equivalently, that the nonzero support region of these two shifted signals do not overlap. Since  $x(t + \tau/2) = 0$  for  $t \notin (2(t_1 - t), 2(t_2 - t))$  and  $x^*(t - \tau/2) = 0$  for  $t \notin (2(t - t_2), 2(t - t_1))$ , then the WD in Equation 13.15 will be equal to zero whenever the nonzero support region of  $x(t + \tau/2)$  lies entirely to the right or entirely to the left of that of  $x^*(t - \tau/2)$ , i.e.,  $2(t - t_1) < 2(t_1 - t)$  or  $2(t - t_2) > 2(t_2 - t)$ , respectively. Simplifying these last two inequalities, we see that the WD of a finite duration signal is identically zero for  $t < t_1$  and  $t > t_2$ .

**P<sub>15</sub>: Finite frequency support**

$$|X(f)| = 0 \text{ for } f \notin (f_1, f_2) \Rightarrow T_x(t, f) = 0 \text{ for } f \notin (f_1, f_2), f_1 < f_2$$

Property  $P_{15}$  is the dual to the finite time support property above. It states that if the Fourier transform of the signal is band limited, then its TFR should also have the same nonzero support in the frequency domain. It is easy to show using the “frequency-domain” formulations of the WD and the STFT in Equations 13.16 and 13.8, respectively, that the WD satisfies this property, but the STFT does not unless the Fourier transform of the analysis window is  $\Gamma(f) = c\delta(f)$ . Again,  $P_{15}$  is a “weak” frequency support property, as it only guarantees that the global bandwidth of the TFR matches that of the signal spectrum.

**P<sub>16</sub>: Instantaneous frequency**

$$\frac{\int f T_x(t, f) df}{\int T_x(t, f) df} = f_x(t) = \frac{1}{2\pi} \frac{d}{dt} \arg\{x(t)\} \quad (13.56)$$

Property  $P_{16}$  states that the first normalized moment in frequency of the TFR should be equal to the instantaneous frequency of the signal. Hence, this property asserts that the TFR’s average value or center of gravity in the frequency direction should correspond to the signal’s instantaneous frequency in Equation 13.3. The WD satisfies this property.

*Proof* First, write the signal in terms of its polar form,  $x(t) = A(t)e^{j2\pi\phi(t)}$ , where  $A(t) > 0$  is the real amplitude function and  $\phi(t)$  is the phase of the signal. The proof will first evaluate the numerator of the expression in Equation 13.56 and then denominator. Let the following notation be used to represent the partial time derivative of a function, followed by that derivative being evaluated at the time  $t_0$ :

$$\dot{g}(t_0) = \left. \frac{\partial}{\partial \tau} g(\tau) \right|_{\tau=t_0} \quad (13.57)$$

$$\begin{aligned} \int f \text{WD}_x(t, f) df &= \int f \int A(t + \tau/2) e^{j2\pi\phi(t + \tau/2)} \\ &\quad \times A(t - \tau/2) e^{-j2\pi\phi(t - \tau/2)} e^{-j2\pi f\tau} d\tau df \\ &= \int A(t + \tau/2) A(t - \tau/2) e^{-j2\pi[\phi(t - \tau/2) - \phi(t + \tau/2)]} \\ &\quad \times \left[ \int f e^{-j2\pi f\tau} df \right] d\tau \\ &= \int A(t + \tau/2) A(t - \tau/2) e^{-j2\pi[\phi(t - \tau/2) - \phi(t + \tau/2)]} \\ &\quad \times \frac{1}{j2\pi} \frac{\partial}{\partial \tau} \delta(\tau) d\tau = \frac{1}{j2\pi} \\ &\quad \times \left. \frac{\partial}{\partial \tau} \left[ A(t + \tau/2) A(t - \tau/2) e^{-j2\pi[\phi(t - \tau/2) - \phi(t + \tau/2)]} \right] \right|_{\tau=0} \\ &= \frac{1}{j2\pi} [\dot{A}(t)A(t)/2 - A(t)\dot{A}(t)/2 + A^2(t)j2\pi\dot{\phi}(t)] \\ &= A^2(t)\dot{\phi}(t) \quad (13.58) \end{aligned}$$

$$\int \text{WD}_x(t, f) df = |x(t)|^2 = A^2(t) \text{ from } P_9. \quad (13.59)$$

Dividing Equation 13.58 by 13.59, one obtains

$$\frac{\int f \text{WD}_x(t, f) df}{\int \text{WD}_x(t, f) df} = \frac{A^2(t)\dot{\phi}(t)}{A^2(t)} = \dot{\phi}(t) = f_x(t). \quad (13.60)$$

This property is very useful for the analysis of FM signals. For example, we see from the third entry in Table 13.2 that the WD of a linear FM chirp in the time domain is a Dirac function centered along the chirp’s linear instantaneous frequency. Since a Dirac function is symmetrical, this also shows that the average value or center of gravity of the chirp’s WD in the frequency direction is also located along the signal’s linear instantaneous frequency. Table 13.2 shows that all even signals modulated by a linear FM chirp have a WD that is symmetric with respect to the instantaneous frequency of the chirp; hence, the center of gravity of the WD in the frequency direction is equal to the signal’s instantaneous frequency.

In general, the spectrogram does not satisfy this property.<sup>39</sup> Its center of gravity,

$$\frac{\int f \text{SPEC}_x(t, f; \Gamma) df}{\int \text{SPEC}_x(t, f; \Gamma) df} = \frac{\int \dot{\phi}(\tau) |x(\tau)|^2 |\gamma(\tau - t)|^2 d\tau}{\int |x(\tau)|^2 |\gamma(\tau - t)|^2 d\tau},$$

is only equal to the instantaneous frequency if the analysis window is a Dirac function.

**P<sub>17</sub>: Group delay**

$$\frac{\int t T_x(t, f) dt}{\int T_x(t, f) dt} = -\frac{1}{2\pi} \frac{d}{df} \arg \{X(f)\}$$

Property  $P_{17}$  is the dual to property  $P_{16}$ . It states that the TFR’s normalized average value or center of gravity in the time direction should be equal to the group delay of the signal in Equation 13.4. The WD satisfies this property. The proof is similar to that of  $P_{16}$  above except that the signal’s Fourier transform is expressed in polar form and the frequency-domain formulation of the WD in Equation 13.16 is used. The spectrogram does not satisfy this property.<sup>39</sup>

**P<sub>18</sub>: Fourier transform**

$$y(t) = X(t) \Rightarrow Y(f) = x(-f) \Rightarrow T_y(t, f) = T_x(-f, t)$$

Property  $P_{18}$  is the TFR equivalent of the duality property of the Fourier transform in Table 13.1, which states what happens to the Fourier transform if the time and frequency-domain forms of a signal  $x(t)$  are switched. If  $y(t)$  is set equal to the Fourier transform of  $x(t)$ , i.e.,  $y(t) = X(t)$ , then the Fourier transform of  $y(t)$  is equal to  $x(t)$ , but with its argument replaced by  $t = -f$ , i.e.,  $Y(f) = x(-f)$ . Property  $P_{18}$  states that the TFR of the dual signal

$y(t) = X(t)$  should likewise have the role of time and frequency interchanged, but with the frequency variable negated. The WD satisfies this property.

*Proof* Let  $y(t) = X(t)$ .

$$\begin{aligned} \text{WD}_y(t, f) &= \int y(t + \tau/2) y^*(t - \tau/2) e^{-j2\pi f \tau} d\tau \\ &= \int X(t + \tau/2) X^*(t - \tau/2) e^{-j2\pi f \tau} d\tau \\ &= \int X(t + \nu/2) X^*(t - \nu/2) e^{j2\pi(-f)\nu} d\nu \\ &= \text{WD}_x(-f, t). \end{aligned}$$

This useful property can be used to simplify the derivation of many TFRs. For example, it has been shown in many articles that the WD of a rectangular function is a variable width sinc function.<sup>37,103</sup> See Table 13.2. Since the rectangular and sinc functions are Fourier transform pairs in Table 13.1, then property  $P_{18}$  shows that the WD of a sinc function is equal to the WD of a rectangle, but with the time and frequency variables interchanged. That is, if

$$\begin{aligned} x(t) = \text{rect}_a(t) &= \begin{cases} 1, & |t| < a \\ 0, & |t| > a \end{cases} \Rightarrow \text{WD}_x(t, f) \\ &= \frac{\sin[4\pi(a - |t|)f]}{\pi f} \text{rect}_a(t), \end{aligned}$$

then

$$\begin{aligned} y(t) = X(t) &= \frac{\sin 2\pi a t}{\pi t} \Rightarrow \text{WD}_y(t, f) = \text{WD}_x(-f, t) \\ &= \frac{\sin [4\pi(a - |-f|)t]}{\pi t} \text{rect}_a(-f) \\ &= \frac{\sin [4\pi(a - |f|)t]}{\pi t} \text{rect}_a(f). \end{aligned}$$

The negation of the frequency axis has no effect in this example since the magnitude and rectangular functions are even functions.

### 13.4.4 Signal Localization

The group of properties  $P_{19}$  through  $P_{24}$  in Table 13.6 are ideal TFR localization properties that are desirable for high-resolution capabilities. These properties state that if a signal is perfectly concentrated in time or frequency (i.e., the signal is an impulse or a sinusoid) then its TFR should also be perfectly concentrated at the same time or frequency, respectively. Properties  $P_{21}$  and  $P_{22}$  state that the TFRs of a linear or hyperbolic spectral FM chirp signal should be perfectly concentrated along that signal's group delay. Property  $P_{24}$  states that a signal modulated by a linear FM chirp should have a TFR whose frequency axis has been sheared by an amount equal to the linear instantaneous frequency of the chirp.  $P_{23}$  is the dual to property  $P_{24}$ ; it states that multiplication by a linear FM chirp in the frequency domain should shear the

time axis of the TFR by an amount equal to the group delay of the chirp.

#### $P_{19}$ : Frequency localization

$$X(f) = \delta(f - f_0) \Rightarrow T_x(t, f) = \delta(f - f_0)$$

This property states that if the signal is a complex sinusoid whose Fourier transform is perfectly concentrated about a certain frequency,  $f_0$ , then its TFR should also be perfectly concentrated about that same frequency. The WD and the Altes Q distribution satisfy this property. As Equation 13.11 shows, the STFT does not, unless the Fourier transform of the analysis window is proportional to a Dirac function.

*Proof* Let  $X(f) = \delta(f - f_0)$ .

$$\begin{aligned} \text{WD}_x(t, f) &= \int \delta(f + \nu/2 - f_0) \delta(f - \nu/2 - f_0) e^{j2\pi \nu t} d\nu \\ &= 2\delta\left(f + \frac{2(f - f_0)}{2} - f_0\right) e^{j4\pi(f - f_0)t} = \delta(f - f_0) \end{aligned}$$

$$\begin{aligned} Q_x(t, f) &= f \int X(fe^{u/2}) X^*(fe^{-u/2}) e^{j2\pi t f u} du \\ &= f \int \delta(fe^{u/2} - f_0) \delta(fe^{-u/2} - f_0) e^{j2\pi t f u} du \\ &= f \int \left[ \frac{\delta(u - 2 \ln(f_0/f))}{|\frac{1}{2} f e^{u/2}|} \right] \left[ \frac{\delta(u + 2 \ln(f_0/f))}{|-\frac{1}{2} f e^{-u/2}|} \right] e^{j2\pi t f u} du \\ &= \frac{4}{|f|} \delta(4 \ln(f_0/f)) e^{j4\pi t f \ln(f_0/f)} \\ &= \frac{4}{|f|} \frac{\delta(f - f_0)}{\left| 4 \frac{f}{f_0} \left[ \frac{-f_0}{f^2} \right] \right|} e^{j4\pi t f \ln(f_0/f)} = \delta(f - f_0). \end{aligned}$$

#### $P_{20}$ : Time localization

$$x(t) = \delta(t - t_0) \Rightarrow T_x(t, f) = \delta(t - t_0)$$

This property states that if the signal is an impulse perfectly localized at time  $t = t_0$ , then its TFR should also be concentrated at time  $t = t_0$ . The WD satisfies this property. The proof is the dual to that used in property  $P_{19}$  above with the time-domain WD formulation in Equation 13.15 being used in place of Equation 13.16. The STFT does not satisfy this property in general; as Equation 13.10 indicates, the STFT experiences spreading about  $t = t_0$  equal to the duration of the analysis window.

#### $P_{21}$ : Linear chirp localization

$$X(f) = e^{-j\pi c f^2} \Rightarrow T_x(t, f) = \delta(t - cf)$$

This property states that if a signal's Fourier transform is equal to a linear FM chirp, then its TFR should be perfectly concentrated along the chirp's linear group delay,  $\tau_x(f) = cf$ . The WD satisfies this property.

*Proof* Let  $X(f) = e^{-j\pi cf^2}$ .

$$\begin{aligned} \text{WD}_x(t, f) &= \int e^{-j\pi c(f+v/2)^2} e^{j\pi c(f-v/2)^2} e^{j2\pi vt} dv \\ &= \int e^{-j\pi c[f^2+fv+v^2/4-f^2+fv-v^2/4]} e^{j2\pi vt} dv \\ &= \int e^{j2\pi v(t-cf)} dv = \delta(t - cf). \end{aligned} \quad (13.61)$$

When property  $P_{18}$  is coupled with  $P_{21}$ , it can be shown that the WD also satisfies a dual property to linear chirp localization. If the signal is a linear FM time-domain chirp, then its TFR should be concentrated along its instantaneous frequency. Thus, if  $x(t) = e^{-j\pi ct^2}$ , then  $\text{WD}_x(t, f) = \delta(f + ct)$ .

*Proof* Let  $X(f) = e^{-j\pi cf^2}$  with WD,  $\text{WD}_x(t, f) = \delta(t - cf)$  derived in Equation 13.61. Coupling properties  $P_{18}$  and  $P_{21}$ , one can show that if  $y(t) = X(t) = e^{-j\pi ct^2}$ , then  $\text{WD}_y(t, f) = \text{WD}_x(-f, t) = \delta(f + ct)$ .

### $P_{22}$ : Hyperbolic chirp localization

$$X_c(f) = \frac{1}{\sqrt{f}} e^{-j2\pi c \ln \frac{f}{f_t}}, \quad f > 0 \Rightarrow T_{x_c}(t, f) = \frac{1}{f} \delta\left(t - \frac{c}{f}\right), \quad f > 0$$

This property is useful for analyzing FM signals whose group delay is hyperbolic. That is, signals with logarithmic phase spectra should have TFRs that are perfectly concentrated along its hyperbolic group delay,  $\tau_x(f) = \frac{c}{f} \tilde{u}(f)$ . Chirps with logarithmic phase are Doppler invariant; they have been used to model the biosonar signals used by bats.<sup>7,53</sup> The Atles Q distribution and the Unitary Bertrand  $P_0$  distribution are two of the few distributions that satisfy this property.

*Proof* Let  $X(f) = \frac{1}{\sqrt{f}} e^{-j2\pi c \ln(f/f_t)} \tilde{u}(f)$ .

$$\begin{aligned} Q_X(t, f) &= f \int \frac{1}{\sqrt{fu/2}} e^{-j2\pi c \ln[fe^{u/2}/f_t]} \frac{1}{\sqrt{fe^{-u/2}}} \\ &\quad \times e^{-j2\pi c \ln[fe^{-u/2}/f_t]} e^{j2\pi ftu} du, \quad f > 0 \\ &= \int e^{-j2\pi c[\ln(f/f_t)+u/2-(\ln f/f_t)+u/2]} e^{j2\pi ftu} du \\ &= \int e^{j2\pi(t-c/f)fu} du = \delta(t - c/f). \end{aligned}$$

### $P_{23}$ : Chirp convolution

$$y(t) = \int x(t - \tau) \sqrt{|c|} e^{j\pi c\tau^2} d\tau \Rightarrow T_y(t, f) = T_x\left(t - \frac{f}{c}, f\right)$$

To understand this property, recall from Table 13.1 that a Gaussian signal and its Fourier transform have inversely proportional variances. Thus, time-domain convolution of a signal  $x(t)$  with a linear FM chirp with sweep rate  $c$  is equivalent to multiplying the Fourier transform of the signal with a linear FM chirp of sweep rate  $-1/c$ :

$$\begin{aligned} y(t) &= \int x(t - \tau) \sqrt{|c|} e^{j\pi c\tau^2} d\tau \leftrightarrow Y(f) \\ &= X(f) \sqrt{|c|} e^{-j\pi f^2/c} \end{aligned} \quad (13.62)$$

$$|Y(f)| = |X(f)| \quad (13.63)$$

$$\tau_y(f) = \tau_x(f) + f/c. \quad (13.64)$$

This multiplication in Equation 13.62 of the signal spectrum with a linear FM chirp leaves the magnitude of  $X(f)$  unchanged in Equation 13.63, but changes the signal's group delay in Equation 13.64 by the group delay of the chirp. Because changes in the group delay correspond to a temporal translation of each spectral component, property  $P_{23}$  states that the TFR of the convolution output  $y(t)$  in Equation 13.62 should therefore be equal to the TFR of  $x(t)$ , but with the time axis adjusted for the frequency-dependent change in the group delay brought about by the convolution. Note that this results in a shearing of the TFR. Such shearing has been exploited in RADAR analysis.<sup>109,114</sup> By definition in Equation 13.39, the Bertrand  $k=2$  distribution in Equation 13.40 satisfies this property. The WD is one of the few other TFRs that satisfies this property.

*Proof* Let  $Y(f) = X(f) \sqrt{|c|} e^{-j\pi f^2/c}$ .

$$\begin{aligned} \text{WD}_Y(t, f) &= \int X(f + v/2) \sqrt{|c|} e^{-j\pi(f+v/2)^2/c} X^*(f - v/2) \\ &\quad \times \sqrt{-|c|} e^{j\pi(f-v/2)^2/c} e^{j2\pi vt} dv \\ &= \int X(f + v/2) X^*(f - v/2) \\ &\quad \times e^{-j\pi[f^2+fv+v^2/4-f^2+fv-v^2/4]/c} e^{j2\pi vt} dv \\ &= \int X(f + v/2) X^*(f - v/2) e^{j2\pi v(t-f/c)} dv \\ &= \text{WD}_X(t - f/c, f). \end{aligned}$$

### $P_{24}$ : Chirp multiplication

$$y(t) = x(t) e^{j\pi ct^2} \Rightarrow T_y(t, f) = T_x(t, f - ct)$$

This property is the dual to property  $P_{23}$  with multiplication by a linear FM chirp occurring in the time domain rather than in the frequency domain as before. If a signal is multiplied in the time domain by a linear FM chirp with sweep rate  $c$ , then its magnitude is unchanged, but its instantaneous frequency is changed by the linear instantaneous frequency of the linear FM chirp, i.e.,  $f_y(t) = f_x(t) - ct$ . Property  $P_{24}$  states that the TFR of  $y(t)$  should correspond to the TFR of  $x(t)$  but with the frequency axis corrected to account for the time-dependent change in the signal's instantaneous frequency. The WD is one of the few TFRs to satisfy this property. The proof is similar to that of  $P_{23}$  except that the time-domain formulation of the WD in Equation 13.15 is used. An alternative proof is to use the fact that the WD satisfies the convolution covariance property  $P_5$  coupled with the

fact that the WD of a linear FM chirp in Table 13.2 is a Dirac function centered around its instantaneous frequency:

$$y(t) = x(t)e^{j\pi ct^2} \Rightarrow \text{WD}_y(t, f) = \int \text{WD}_x(t, f') \delta((f - f') - ct) df' \\ = \text{WD}_x(t, f - ct).$$

### Example

Table 13.2 states that the rectangular signal,

$$x(t) = \text{rect}_a(t) \Rightarrow \text{WD}_x(t, f) = \frac{\sin [4\pi(a - |t|)f]}{\pi f} \text{rect}_a(t),$$

has a WD that is equal to a sinc function whose mainlobe width varies with time. Near  $t=0$ , the sinc function is a relatively narrow function of frequency centered near  $f=0$ . For time values near the edges of the rectangle, the spectral width of the sinc's main lobe is very broad. This is an intuitive result as the middle of the rectangle is very smooth, so its WD should be narrowband and lowpass; however, near the edges of the rectangle, where a sharp discontinuity exists, the WD is broadband. Property  $P_{24}$  states that the WD of a chirp modulated rectangle,

$$y(t) = \text{rect}_a(t)e^{j\pi ct^2} \Rightarrow \text{WD}_y(t, f) \\ = \text{WD}_x(t, f - ct) = \frac{\sin [4\pi(a - |t|)(f - ct)]}{\pi(f - ct)} \text{rect}_a(t),$$

is a variable width sinc function as before, but centered along the chirp's linear instantaneous frequency,  $f = ct$ , in the time-frequency plane.

*Proof* Let  $y(t) = \text{rect}_a(t)e^{j\pi ct^2}$ .

$$\text{WD}_y(t, f) = \int e^{j\pi c(t+\tau/2)^2} \text{rect}_a(t + \tau/2) e^{-j\pi c(t-\tau/2)^2} \\ \times \text{rect}_a(t - \tau/2) e^{-j2\pi f\tau} d\tau \\ = \int \text{rect}_a(t + \tau/2) \text{rect}_a(t - \tau/2) e^{-j2\pi(f-ct)\tau} d\tau \\ = 2 \int \text{rect}_a(t') \text{rect}_a(2t - t') e^{-j4\pi(f-ct)(t'-t)} dt' \\ = \begin{cases} 0, & 2t + a < -a \\ 2 \int_{-a}^{2t+a} e^{-j4\pi(f-ct)(t'-t)} dt' \\ = \frac{\sin 4\pi(f-ct)(a+t)}{\pi(f-ct)}, & -a < 2t + a < a \\ 2 \int_{2t-a}^a e^{-j4\pi(f-ct)(t'-t)} dt' \\ = \frac{\sin 4\pi(f-ct)(a-t)}{\pi(f-ct)}, & -a < 2t - a < a \\ 0, & 2t - a > a \end{cases} \\ = \frac{\sin 4\pi(f-ct)(a - |t|)}{\pi(f-ct)} \text{rect}_a(t).$$

### 13.4.5 Preserving Inner Products

The last property in Table 13.6, known as Moyal's formula<sup>39,60</sup> or the unitarity property, states that TFRs should preserve the signal projections, inner products, and norm metrics which are used frequently in signal detection, synthesis, approximation theory, and pattern recognition.<sup>24,28,56,60,69,72,77,96,108</sup> It also states that if two basis functions are orthogonal, i.e., their inner product is equal to zero, then their respective TFRs should also be orthogonal. Hence, TFRs that satisfy Moyal's formula can be used to induce a set of two-dimensional, orthogonal basis functions,  $T_{g_i}(t, f)$  from a set of one-dimensional orthogonal basis functions,  $g_i(t)$ ,  $i = 1, \dots, N$ .

#### $P_{25}$ : Moyal's formula

$$\left| \int x(t)y^*(t)dt \right|^2 = \iint T_x(t, f) T_y^*(t, f) dt df$$

This property states that an ideal TFR should preserve inner products. It is analogous to Parseval's theorem for the Fourier transform.<sup>101,105</sup>

$$\int x(t)y^*(t)dt = \int X(f)Y^*(f)df,$$

which states that the inner product of two signals in the time domain should be equal to the inner product of their respective Fourier transforms in the frequency domain. The Wigner, Altes Q, and the Unitary Bertrand  $P_0$  distributions satisfy this property.

*Proof*

$$\iint \text{WD}_x(t, f) \text{WD}_y^*(t, f) dt df \\ = \iint \left[ \int x(t + u/2) x^*(t - u/2) e^{-j2\pi fu} du \right] \\ \times \left[ \int y^*(t + t'/2) y(t - t'/2) e^{j2\pi ft'} dt' \right] dt df \\ = \iint \int x(t + u/2) y^*(t + t'/2) x^*(t - u/2) y(t - t'/2) \\ \times \delta(t' - u) du dt dt' \\ = \iint [x(t + u/2) y^*(t + u/2)] [x(t - u/2) \\ \times y^*(t - u/2)]^* du dt \\ = \left| \int x(t) y^*(t) dt \right|^2$$

$$\begin{aligned}
& \iint Q_X(t, f) Q_Y^*(t, f) dt df \\
&= \iint \left[ f \int X(fe^{u/2}) X^*(fe^{-u/2}) e^{j2\pi f u} du \right] \\
&\quad \times \left[ f \int Y^*(fe^{\beta/2}) Y(fe^{-\beta/2}) e^{-j2\pi f \beta} d\beta \right] dt df \\
&= \iint \int f^2 X(fe^{u/2}) Y^*(fe^{\beta/2}) X^*(fe^{-u/2}) Y(fe^{-\beta/2}) \\
&\quad \times \delta(f(u - \beta)) du d\beta df \\
&= \iint f X(fe^{u/2}) Y^*(fe^{u/2}) X^*(fe^{-u/2}) Y(fe^{-u/2}) du df \\
&= \left| \int X(a) Y^*(a) da \right|^2, \quad f > 0
\end{aligned}$$

## 13.5 Classes of TFRs with Common Properties

The list of ideal TFR properties given in Section 13.4 is far from exhaustive; others have been proposed in Refs. [1,4,12,43,60,84,122]. Nonetheless, the checklist summary in Table 13.7 reveals that no known TFR satisfies all such properties. To understand the relative advantages of various TFRs, and to understand their inter-relationships, this section will group TFRs into classes. Each class is defined by the two or three ideal TFR properties that all member TFRs must satisfy. A review will be given of Cohen's class of shift covariant TFRs, the affine class of affine covariant TFRs, the hyperbolic class, developed for signals with hyperbolic group delay, and the power class, which is useful for signals with power group delay.<sup>43,60,69,73,97,98,100</sup>

The grouping of TFRs into classes sharing common properties has the following advantages. It provides very helpful insight as to which types of TFRs will work best in different situations. For example, many members of Cohen's class TFRs are well suited to constant bandwidth analysis whereas several affine class TFRs are best suited for multiresolution analysis. Within a given class, each TFR is completely characterized by a unique set of TFR-dependent kernels that can be compared against the list of class-dependent kernel constraints in Table 13.8 to quickly determine which ideal properties a given TFR satisfies. The shape of these kernels can be analyzed to ascertain which is best for auto term preservation or cross term removal in a particular application.

### 13.5.1 Cohen's Class of TFRs

$$\begin{aligned}
\text{Cohen's class} &= \{T_x(t, f) | y(t) = x(t - t_0) e^{j2\pi f_0 t} \Rightarrow T_y(t, f) \\
&= T_x(t - t_0, f - f_0)\}.
\end{aligned}$$

Cohen's class consists of all quadratic TFRs that satisfy the frequency-shift and time-shift covariance properties. Several TFRs in Cohen's class are listed in Table 13.9. Since each

Cohen's-class TFR automatically satisfies properties  $P_1$ – $P_2$  in Table 13.6, then it must have a check mark in the first two property rows in Table 13.7.<sup>39–41,43,60,69</sup> Time- and frequency-shift covariance are very useful properties in the analysis of speech, narrowband Doppler systems, and multipath environments.

#### 13.5.1.1 Alternative Formulations

Any TFR in Cohen's class can be written in one of the four equivalent "Normal Forms,"<sup>39,60,69</sup>

$$\begin{aligned}
C_x(t, f; \Psi_C) &= \iint \varphi_C(t - t', \tau) x \\
&\quad \times \left(t' + \frac{\tau}{2}\right) x^* \left(t' - \frac{\tau}{2}\right) e^{-j2\pi f \tau} dt' d\tau \quad (13.65)
\end{aligned}$$

$$= \iint \Phi_C(f - f', \nu) X \left(f' + \frac{\nu}{2}\right) X^* \left(f' - \frac{\nu}{2}\right) e^{j2\pi f \nu} df' d\nu \quad (13.66)$$

$$= \iint \psi_C(t - t', f - f') \text{WD}_x(t', f') dt' df' \quad (13.67)$$

$$= \iint \Psi_C(\tau, \nu) \text{AF}_x(\tau, \nu) e^{j2\pi(\nu - f\tau)} d\tau d\nu, \quad (13.68)$$

or in the "bi-frequency" form

$$\begin{aligned}
C_x(t, f; \Psi_C) &= \iint \Gamma_C(f - f_1, f - f_2) \\
&\quad \times X(f_1) X^*(f_2) e^{j2\pi(f_1 - f_2)t} df_1 df_2. \quad (13.69)
\end{aligned}$$

Each normal form is characterized by one of the four kernel  $\varphi_C(t, \tau)$ ,  $\Phi_C(f, \nu)$ ,  $\psi_C(t, f)$ , and  $\Psi_C(\tau, \nu)$ , which are interrelated by the following Fourier transforms,

$$\begin{aligned}
\varphi_C(t, \tau) &= \iint \Phi_C(f, \nu) e^{j2\pi(f\tau + \nu t)} df d\nu \\
&= \int \Psi_C(\tau, \nu) e^{j2\pi \nu t} d\nu \\
&\leftrightarrow \Phi_C(f, \nu) \quad (13.70)
\end{aligned}$$

$$\begin{aligned}
\psi_C(t, f) &= \iint \Psi_C(\tau, \nu) e^{j2\pi(\nu t - f\tau)} d\tau d\nu \\
&= \int \Phi_C(f, \nu) e^{j2\pi \nu t} d\nu \\
&\leftrightarrow \Psi_C(\tau, \nu) \quad (13.71)
\end{aligned}$$

$$\Gamma_C(f_1, f_2) = \Phi_C\left(\frac{f_1 + f_2}{2}, f_2 - f_1\right). \quad (13.72)$$

The kernels for the TFRs in Cohen's class are given in Table 13.10. They can be combined with Equations 13.65 through 13.69 to provide alternative formulations for any of the Cohen's-class TFRs given in Table 13.9. These kernels can also be compared against the constraints in the second column of Table 13.8 to determine which properties a given Cohen's-class TFR satisfies.



14	Finite time support	✓	✓	✓	✓	✓	✓	✓	✓	✓	✓	✓	✓	✓	✓	✓	✓	✓	✓
15	Finite frequency support	✓	✓	✓	✓	✓	✓	✓	✓	✓	✓	✓	✓	✓	✓	✓	✓	✓	✓
16	Instantaneous frequency	✓	✓	✓	✓	✓	✓	✓	✓	✓	✓	✓	✓	✓	✓	✓	✓	✓	✓
17	Group delay	✓	✓	✓	✓	✓	✓	✓	✓	✓	✓	✓	✓	✓	✓	✓	✓	✓	✓
18	Fourier transform	✓	✓	✓	✓	✓	✓	✓	✓	✓	✓	✓	✓	✓	✓	✓	✓	✓	✓
19	Frequency localization	✓	✓	✓	✓	✓	✓	✓	✓	✓	✓	✓	✓	✓	✓	✓	✓	✓	✓
20	Time localization	✓	✓	✓	✓	✓	✓	✓	✓	✓	✓	✓	✓	✓	✓	✓	✓	✓	✓
21	Linear chirp localization	✓	✓	✓	✓	✓	✓	✓	✓	✓	✓	✓	✓	✓	✓	✓	✓	✓	✓
22	Hyperbolic localization	✓	✓	✓	✓	✓	✓	✓	✓	✓	✓	✓	✓	✓	✓	✓	✓	✓	✓
23	Chirp convolution	✓	✓	✓	✓	✓	✓	✓	✓	✓	✓	✓	✓	✓	✓	✓	✓	✓	✓
24	Chirp multiplication	✓	✓	✓	✓	✓	✓	✓	✓	✓	✓	✓	✓	✓	✓	✓	✓	✓	✓
25	Moyal's formula	✓	✓	✓	✓	✓	✓	✓	✓	✓	✓	✓	✓	✓	✓	✓	✓	✓	✓

In the second row, the letters c, a, h, and p indicate that the corresponding TFR is a member of the Cohen, affine, hyperbolic, and κth power class, respectively. A ✓ indicates that the tfr. can be shown to hold the given property, a number following the ✓ indicates that additional constraints are needed to satisfy the property. The Constraints are as follows: (1)  $M = N$ ; (2)  $M > 1/2$ ; (3)  $N > 1/2$ ; (4)  $g(\tau)$  even; (5)  $|\alpha| < 1/2$ ; (6)  $M = 1/2$ ; (7)  $N = 1/2$ ; (8)  $\int_0^{\infty} |\Gamma(f)|^2 df = 1$ ; (9)  $\alpha = 1$ ; (10)  $r = 0, \alpha = 1, \gamma = 1/4$ ; (11)  $\alpha \neq 1$ ; (12)  $|\rho_r(0)|^2 = \frac{1}{f_r}$ ; (13)  $|\gamma(0)| = 1$ ; (14)  $\gamma(0) = 1$ ; (15)  $s(\beta)$  even; (16)  $\int |\Gamma(b)|^2 \frac{db}{|b|}$  Real; (18)  $s(t) \in \text{Real}$ ; (19)  $S(0)|\gamma(0)|^2 = 1$ ; (20)  $\int |\gamma(t)|^2 dt = 1$ .



TABLE 13.8 Kernel Constraints Needed to Satisfy Ideal TFR Properties for the TFRs in Cohen's Affine and kth Power Classes

Property Name	Kernel Constraints for Cohen's Class	Kernel Constraints for the Affine Class	Kernel Constraints for the Hyperbolic Class	Kernel Constraints for the kth Power Class
$P_1$ : Frequency shift covariant	Always satisfied	$\Psi_A^{(A)}(\zeta, \beta) = S_A(\zeta\beta)e^{-j2\pi\zeta}$	$\Psi_H^{(H)}(\zeta, \beta) = S_{AH}(\beta)e^{-j2\pi\zeta}$ in $\mu_0(\beta)$	$\Gamma_{PC}^{(k)}(b_1, b_2) = \int \delta(b_1 - \lambda_k(u)) \times \delta(b_2 - \lambda_k(-u))\mu(u)du$
$P_2$ : Time shift covariant	Always satisfied	Always satisfied	with $\mu_0(\beta) = \frac{\sin h(\beta/2)}{\beta/2}$	Always satisfied
$P_3$ : Scale covariant	$\Psi_C(\tau, \nu) = S_C(\tau \nu)$	Always satisfied	Always satisfied	
$P_4$ : Hyperbolic time shift		$\Phi_A^{(A)}(b, \beta) = G_A^{(A)}(\beta)\delta\left(b + \frac{\beta}{2} \coth \frac{\beta}{2}\right)$	Always satisfied	
$P_5$ : Convolution covariant	$\Psi_C(\tau_1 + \tau_2, \nu) = \Psi_C(\tau_1, \nu)\Psi_C(\tau_2, \nu)$	$\Psi_A^{(A)}(\zeta_1 + \zeta_2, \beta) = \Psi_A^{(A)}(\zeta_1, \beta)\Psi_A^{(A)}(\zeta_2, \beta)$	$\Phi_H^{(H)}(b_1, \beta)\Phi_H^{(H)}(b_2, \beta) = e^{b_1}\Phi_H(b_1, \beta)\delta(b_1 - b_2)$	$\Phi_{PC}^{(A)}(b, \beta) = \Phi_{PC}^{(A)*}(b, -\beta)$
$P_6$ : Modulation covariant	$\Psi_C(\tau_1, \nu_1 + \nu_2) = \Psi_C(\tau_1, \nu_1)\Psi_C(\tau_1, \nu_2)$			
$P_7$ : Real-valued	$\Psi_C^*(-\tau, -\nu) = \Psi_C(\tau, \nu)$	$\Phi_A^{(A)}(b, \beta) = \Phi_A^{(A)*}(b, -\beta)$	$\Psi_H^{(H)*}(-\zeta, -\beta) = \Psi_H^{(H)}(\zeta, \beta)$	
$P_8$ : Positivity	$\Psi_C(\tau, \nu) = AF_\gamma(-\tau, -\nu)$		$\Psi_H^{(H)*}(\zeta, \beta) = \text{HAF}\Gamma(-\zeta, -\beta)$	
$P_9$ : Time marginal	$\Psi_C(0, \nu) = 1$	$\int \Phi_A^{(A)}(b, 2b) \frac{db}{ b } = 1$		
$P_{10}$ : Frequency marginal	$\Psi_C(\tau, 0) = 1$	$\Phi_A^{(A)}(b, 0) = \delta(b+1)$	$\Psi_H^{(H)}(\zeta, 0) = 1$	$\Phi_{PC}^{(A)}(b, 0) = \delta(b+1)$
$P_{11}$ : Energy distribution	$\Psi_C(0, 0) = 1$	$\int \Phi_A^{(A)}(b, 0) \frac{db}{ b } = 1$	$\Psi_H^{(H)}(0, 0) = 1$	$\int \Phi_{PC}^{(A)}(b, 0) \frac{db}{ b } = 1$
$P_{12}$ : Time moments	$\Psi_C(0, \nu) = 1$			
$P_{13}$ : Frequency moments	$\Psi_C(\tau, 0) = 1$			
$P_{14}$ : Finite time support	$\varphi_C(t, \tau) = 0, \left \frac{t}{\tau}\right  > \frac{1}{2}$	$\varphi_A^{(A)}(c, \zeta) = 0, \left \frac{c}{\zeta}\right  > \frac{1}{2}$	$\Phi_H^{(H)}(c, \zeta) = 0, \left \frac{c}{\zeta}\right  > \frac{1}{2}$	$\Phi_{PC}^{(A)}(b, \beta) = 0, \left \frac{b+1}{\beta}\right  > \frac{1}{2}$
$P_{15}$ : Finite freq. support	$\Phi_C(f, \nu) = 0, \left \frac{f}{\nu}\right  > \frac{1}{2}$	$\Phi_A^{(A)}(b, \beta) = 0, \left \frac{b+1}{\beta}\right  > \frac{1}{2}$		
$P_{16}$ : Instantaneous Frequency	$\Psi_C(0, \nu) = 1$ and $\frac{\partial}{\partial \tau} \Psi_C(\tau, \nu) _{\tau=0} = 0$			
$P_{17}$ : Group delay	$\Psi_C(\tau, 0) = 1$ and $\frac{\partial}{\partial \nu} \Psi_C(\tau, \nu) _{\nu=0} = 0$	$\Phi_A^{(A)}(b, 0) = \delta(b+1)$ and $\frac{\partial}{\partial \beta} \Phi_A^{(A)}(b, \beta) _{\beta=0} = 0$	$\Psi_H^{(H)}(\zeta, 0) = 1$ and $\frac{\partial}{\partial \beta} \Psi_H^{(H)}(\zeta, \beta) _{\beta=0} = 0$	$\Phi_{PC}^{(A)}(b, 0) = \delta(b+1)$ and $\frac{\partial}{\partial \beta} \Phi_{PC}^{(A)}(b, \beta) _{\beta=0} = 0$
$P_{18}$ : Fourier transform	$\Psi_C(-\nu, \tau) = \Psi_C(\tau, \nu)$			
$P_{19}$ : Freq. localization	$\Psi_C(\tau, 0) = 1$			
$P_{20}$ : Time localization	$\Psi_C(0, \nu) = 1$			
$P_{21}$ : Linear chirp localization	$\Psi_C(\tau, \nu) = 1$			
$P_{22}$ : Hyperbolic localization	$\Psi_C\left(\tau - \frac{\nu}{\zeta}, \nu\right) = \Psi_C(\tau, \nu)$			
$P_{23}$ : Chirp convolution	$\Psi_C(\tau, \nu - c\tau) = \Psi_C(\tau, \nu)$			
$P_{24}$ : Chirp multiplication	$ \Psi_C(\tau, \nu)  = 1$	$\int \Phi_A^{(A)*}(b\beta, \tilde{\eta}\beta)\Phi_A^{(A)}(\beta, \tilde{\eta}\beta)d\beta = \delta(b-1), \forall \tilde{\eta}$	$ \Psi_H^{(H)}(\zeta, \beta)  = 1$	$\int \Phi_{PC}^{(A)*}(b\beta, \alpha\beta)\Phi_{PC}^{(A)}(\beta, \alpha\beta)d\beta = \delta(b-1), \forall \alpha$

Note: Here,  $\lambda_k(u)$  is Defined in (13.39) and  $\mu(u) = \mu^*(-u)$ .

TABLE 13.9 Cohen’s Class TFRs

Cohen’s-Class Distribution	Formula
Ackroyd	$AC K_x(t, f) = \text{Re}\{x^*(t)X(f)e^{j2\pi ft}\}$
Affine-Cohen subclass	$AC_x(t, f; S_{AC}) = \iint \frac{1}{ \tau } S_{AC}\left(\frac{t-t'}{\tau}\right) x\left(t' + \frac{\tau}{2}\right) x^*\left(t' - \frac{\tau}{2}\right) e^{-j2\pi f \tau} dt' d\tau$
Born–Jordan	$BJD_x(t, f) = \iint \frac{\sin(\pi\tau\nu)}{\pi\tau\nu} AF_x(\tau, \nu) e^{j2\pi(t\nu-f\tau)} d\tau d\nu$ $= \int \frac{1}{\tau} \left[ \int_{t- \tau /2}^{t+ \tau /2} x\left(t' + \frac{\tau}{2}\right) x^*\left(t' - \frac{\tau}{2}\right) dt' \right] e^{-j2\pi f \tau} d\tau$
Butterworth	$BUD_x(t, f; M, N) = \iint \left(1 + \left(\frac{\tau}{\tau_0}\right)^{2M} \left(\frac{\nu}{\nu_0}\right)^{2N}\right)^{-1} AF_x(\tau, \nu) e^{j2\pi(t\nu-f\tau)} d\tau d\nu$
Choi–Williams (Exponential)	$CWD_x(t, f; \sigma) = \iint e^{-(2\pi\tau\nu)^{2/\sigma}} AF_x(\tau, \nu) e^{j2\pi(t\nu-f\tau)} d\tau d\nu$ $= \int \int \sqrt{\frac{\sigma}{4\pi}} \frac{1}{ \tau } \exp\left[-\frac{\sigma}{4} \left(\frac{t-t'}{\tau}\right)^2\right] x\left(t' + \frac{\tau}{2}\right) x^*\left(t' - \frac{\tau}{2}\right) e^{-j2\pi f \tau} dt' d\tau$
Cone Kernel	$CKD_x(t, f) = \iint g(\tau)  \tau  \frac{\sin(\pi\tau\nu)}{\pi\tau\nu} AF_x(\tau, \nu) e^{j2\pi(t\nu-f\tau)} d\tau d\nu$
Cummulative attack spectrum	$CAS_x(t, f) = \left  \int_{-\infty}^t x(\tau) e^{-j2\pi f \tau} d\tau \right ^2$
Cummulative decay spectrum	$CDS_x(t, f) = \left  \int_t^{\infty} x(\tau) e^{-j2\pi f \tau} d\tau \right ^2$
Generalized exponential	$GED_x(t, f) = \iint \exp\left[-\left(\frac{\tau}{\tau_0}\right)^{2M} \left(\frac{\nu}{\nu_0}\right)^{2N}\right] AF_x(\tau, \nu) e^{j2\pi(t\nu-f\tau)} d\tau d\nu$
Generalized rectangular	$GRD_x(t, f) = \int \text{rect}_1( \tau ^{M/N}  \nu /\sigma) AF_x(\tau, \nu) e^{j2\pi(t\nu-f\tau)} d\tau d\nu$
Generalized Wigner	$GWD_x(t, f; \tilde{\alpha}) = \int x\left(t + \left(\frac{1}{2} + \tilde{\alpha}\right)\tau\right) x^*\left(t - \left(\frac{1}{2} - \tilde{\alpha}\right)\tau\right) e^{-j2\pi f \tau} d\tau$
Levin	$LD_x(t, f) = -\frac{d}{dt} \left  \int_t^{\infty} x(\tau) e^{-j2\pi f \tau} d\tau \right ^2$
Margineau–Hill	$MH_x(t, f) = \text{Re}\{x(t)X^*(f) e^{-j2\pi ft}\}$
Multiform tilttable kernel	$MT_x(t, f; S) = \iint S\left(\tilde{\mu}\left(\frac{\tau}{\tau_0}, \frac{\nu}{\nu_0}; \alpha, r, \beta, \gamma\right)^{2\lambda}\right) AF_x(\tau, \nu) e^{j2\pi(t\nu-f\tau)} d\tau d\nu$ $S_{MTED}(\beta) = e^{-\pi\beta}, S_{MTBUD}(\beta) = [1 + \beta]^{-1}$
Nutall	$ND_x(t, f) = \iint \exp\left\{-\pi \left[\left(\frac{\tau}{\tau_0}\right)^2 + \left(\frac{\nu}{\nu_0}\right)^2 + 2r\left(\frac{\tau\nu}{\tau_0\nu_0}\right)\right]\right\} AF_x(\tau, \nu) e^{j2\pi(t\nu-f\tau)} d\tau d\nu$
Page	$PD_x(t, f) = 2 \text{Re}\left\{x^*(t) e^{j2\pi ft} \int_{-\infty}^t x(\tau) e^{-j2\pi f \tau} d\tau\right\}$
Pseudo Wigner	$PWD_x(t, f; \Gamma) = \int x\left(t + \frac{\tau}{2}\right) x^*\left(t - \frac{\tau}{2}\right) \gamma\left(\frac{\tau}{2}\right) \gamma^*\left(-\frac{\tau}{2}\right) e^{-j2\pi f \tau} d\tau$ $= \int WD_\gamma(0, f - f') WD_x(t, f') df'$
Reduced interference	$RID_x(t, f) = \iint \frac{1}{ \tau } s\left(\frac{t-t'}{\tau}\right) x\left(t' + \frac{\tau}{2}\right) x^*\left(t' - \frac{\tau}{2}\right) e^{-j2\pi f \tau} dt' d\tau$ with $S(\beta) \in \Re, S(0) = 1, \frac{d}{d\beta} S(\beta) _{\beta=0} = 0, \left\{S(\alpha) = 0 \text{ for }  \alpha  > \frac{1}{2}\right\}$
Rihaczek	$RD_x(t, f) = x(t)X^*(f) e^{-j2\pi ft}$
Smoothed Pseudo Wigner	$SPWD_x(t, f; \Gamma, s) = \int s(t-t') PWD_x(t', f; \Gamma) dt'$ $= \iint s(t-t') WD_\gamma(0, f - f') WD_x(t', f') dt' df'$
Spectrogram	$SPEC_x(t, f; \Gamma) = \left  \int x(\tau) \gamma^*(\tau - t) e^{-j2\pi f \tau} d\tau \right ^2 = \left  \int X(f') \Gamma^*(f' - f) e^{j2\pi t f'} df' \right ^2$
Wigner	$WD_x(t, f) = \int x\left(t + \frac{\tau}{2}\right) x^*\left(t - \frac{\tau}{2}\right) e^{-j2\pi f \tau} d\tau = \int X\left(f + \frac{\nu}{2}\right) X^*\left(f - \frac{\nu}{2}\right) e^{j2\pi t \nu} d\nu$

Note: Here,  $\text{rect}_a(t) = \begin{cases} 1, & |t| < |a| \\ 0, & |t| > |a| \end{cases}$ ,  $AF_x(\tau, \nu)$  is defined in Equation 13.18, and  $\tilde{\mu}(\tilde{\tau}, \tilde{\nu}; \alpha, r, \beta, \gamma) = \tilde{\tau}^2(\tilde{\nu}^2)^\alpha + (\tilde{\tau})^\alpha \tilde{\nu}^2 + 2r((\tilde{\tau}\tilde{\nu})^\beta)^\gamma$ . Functions with lower- and uppercase letters, e.g.,  $\gamma(t)$  and  $\Gamma(f)$ , are Fourier transform pairs.

TABLE 13.10 Kernels of Cohen's Shift Covariant Class of TFRs Defined in Table 13.9

TFR	$\Psi_C(t, f)$	$\Psi_C(\tau, \nu)$	$\varphi_C(t, \tau)$	$\Phi_C(f, \nu)$
AC	$\int \frac{1}{ \tau } s_{AC}\left(\frac{t}{\tau}\right) e^{-j2\pi f \tau} d\tau$	$S_{AC}(\tau\nu)$	$\frac{1}{ \tau } s_{AC}\left(\frac{t}{\tau}\right)$	$\frac{1}{ \nu } s_{AC}\left(-\frac{f}{\nu}\right)$
ACK	$2\cos(4\pi t f)$	$\cos(\pi\tau\nu)$	$\frac{\delta(t + \tau/2) + \delta(t - \tau/2)}{2}$	$\frac{\delta(f - \nu/2) + \delta(f + \nu/2)}{2}$
BJD		$\frac{\sin(\pi\tau\nu)}{\pi\tau\nu}$	$\begin{cases} \frac{1}{ \tau }, &  t/\tau  < 1/2 \\ 0, &  t/\tau  > 1/2 \end{cases}$	$\begin{cases} \frac{1}{ \nu }, &  f/\nu  < 1/2 \\ 0, &  f/\nu  > 1/2 \end{cases}$
BUD		$\left(1 + \left(\frac{\tau}{\tau_0}\right)^{2M} \left(\frac{\nu}{\nu_0}\right)^{2N}\right)^{-1}$		
CWD	$\sqrt{\frac{\sigma}{4\pi}} \int \frac{1}{ \beta } \exp\left[-\frac{\sigma}{4} \left(\frac{t}{\beta}\right)^2\right] e^{-j2\pi f \beta} d\beta$	$e^{-(2\pi \tau \nu)^2 / \sigma}$	$\sqrt{\frac{\sigma}{4\pi}} \frac{1}{ \tau } \exp\left[-\frac{\sigma}{4} \left(\frac{t}{\tau}\right)^2\right]$	$\sqrt{\frac{\sigma}{4\pi}} \frac{1}{ \nu } \exp\left[-\frac{\sigma}{4} \left(\frac{f}{\nu}\right)^2\right]$
CKD		$g(\tau) \tau  \frac{\sin(\pi\tau\nu)}{\pi\tau\nu}$	$\begin{cases} g(\tau), &  t/\tau  < 1/2 \\ 0, &  t/\tau  > 1/2 \end{cases}$	
CAS		$\left[\frac{1}{2}\delta(\nu) + \frac{1}{j\nu}\right] e^{-j\pi \tau \nu}$		
CDS		$\left[\frac{1}{2}\delta(-\nu) - \frac{1}{j\nu}\right] e^{j\pi \tau \nu}$		
GED		$\exp\left[-\left(\frac{\tau}{\tau_0}\right)^{2M} \left(\frac{\nu}{\nu_0}\right)^{2N}\right]$	$\frac{\nu_0}{2\sqrt{\pi}} \left \frac{\tau_0}{\tau}\right ^M \exp\left[\frac{-\nu_0^2 \tau_0^{2M} t^2}{4\tau^{2M}}\right]$ $N = 1$ only	$\frac{\tau_0}{2\sqrt{\pi}} \left \frac{\nu_0}{\nu}\right ^N \exp\left[\frac{-\tau_0^2 \nu_0^{2N} f^2}{4\nu^{2N}}\right]$ $M = 1$ only
GRD		$\begin{cases} 1, & \left \frac{ \tau ^{M/N}  \nu /\sigma}{ \tau ^{M/N}  \nu /\sigma}\right  < 1 \\ 0, & \left \frac{ \tau ^{M/N}  \nu /\sigma}{ \tau ^{M/N}  \nu /\sigma}\right  > 1 \end{cases}$	$\frac{\sin(2\pi \sigma t/ \tau ^{M/N})}{\pi t}$	
GWD	$\frac{1}{ \tilde{\alpha} } e^{j2\pi t f / \tilde{\alpha}}$	$e^{j2\pi \tilde{\alpha} \tau \nu}$	$\delta(t + \tilde{\alpha}\tau)$	$\delta(f - \tilde{\alpha}\nu)$
LD		$e^{j\pi \tau \nu}$	$\delta(t +  \tau /2)$	
MH	$2 \cos(4\pi t f)$	$\cos(\pi\tau\nu)$	$\frac{\delta(t + \tau/2) + \delta(t - \tau/2)}{2}$	$\frac{\delta(f - \nu/2) + \delta(f + \nu/2)}{2}$
MT		$S\left(\tilde{\mu}\left(\frac{\tau}{\tau_0}, \frac{\nu}{\nu_0}; \alpha, r, \beta, \gamma\right)^{2\lambda}\right)$		
ND		$\exp\left[-\pi\tilde{\mu}\left(\frac{\tau}{\tau_0}, \frac{\nu}{\nu_0}; 0, r, 1, 1\right)\right]$		
PD		$e^{-j\pi \tau \nu}$	$\delta(t -  \tau /2)$	$\left[\delta\left(f + \frac{\nu}{2}\right) + \delta\left(f - \frac{\nu}{2}\right) + j\frac{\nu}{\pi(f^2 - \nu^2/4)}\right]/2$
PWD	$\delta(t)WD_\gamma(0, f)$	$\gamma(\tau/2)\gamma^*(-\tau/2)$	$\delta(t)\gamma(\tau/2)\gamma^*(-\tau/2)$	$W D_\gamma(0, f)$
RGWD	$\frac{1}{ \tilde{\alpha} } \cos(2\pi t f / \tilde{\alpha})$	$\cos(2\pi \tilde{\alpha} \tau \nu)$	$\frac{\delta(t + \tilde{\alpha}\tau) + \delta(t - \tilde{\alpha}\tau)}{2}$	$\frac{\delta(f - \tilde{\alpha}\nu) + \delta(f + \tilde{\alpha}\nu)}{2}$
RID	$\int \frac{1}{ \beta } s\left(\frac{t}{\beta}\right) e^{-j2\pi f \beta} d\beta$	$S(\tau\nu),$ $S(\beta) \in \Re, S(0) = 1, \frac{d}{d\beta} S(\beta)\Big _{\beta=0} = 0$	$\frac{1}{ \tau } s\left(\frac{t}{\tau}\right),$ $s(\alpha) = 0,  \alpha  > \frac{1}{2}$	$\frac{1}{ \nu } s\left(-\frac{f}{\nu}\right),$ $s(\alpha) = 0,  \alpha  > \frac{1}{2}$
RD	$2e^{-j4\pi t f}$	$e^{-j\pi\tau\nu}$	$\delta(t - \tau/2)$	$\delta(f + \nu/2)$
SPWD	$s(t)WD_\gamma(0, f)$	$S(\nu)\gamma\left(\frac{\tau}{2}\right)\gamma^*\left(-\frac{\tau}{2}\right)$	$s(t)\gamma\left(\frac{\tau}{2}\right)\gamma^*\left(-\frac{\tau}{2}\right)$	$S(\nu)WD_\gamma(0, f)$
SPEC	$WD_\gamma(-t, -f)$	$AF_\gamma(-\tau, -\nu)$	$\gamma\left(-t - \frac{\tau}{2}\right)\gamma^*\left(-t + \frac{\tau}{2}\right)$	$\Gamma\left(-f - \frac{\nu}{2}\right)\Gamma^*\left(-f + \frac{\nu}{2}\right)$
WD	$\delta(t)\delta(f)$	1	$\delta(t)$	$\delta(f)$

Here,  $\tilde{\mu}(\tilde{\tau}, \tilde{\nu}; \alpha, r, \beta, \gamma) = ((\tilde{\tau})^2((\tilde{\nu})^2)^\alpha((\tilde{\tau})^\alpha(\tilde{\nu})^2 + 2r((\tilde{\tau}\tilde{\nu})^\beta)^\gamma)$ . Functions with Lowercase and Uppercase Letters, e.g.,  $\gamma(t)$  and  $\Gamma(f)$ , Indicate Fourier Transform Pairs.

A checklist summary of the properties that each Cohen’s-class TFRs satisfies is given in Table 13.7.

### 13.5.1.2 Implementation Considerations

The formulations in Equations 13.65 through 13.69 provide alternative ways of understanding and computing a given Cohen’s-class TFR. For example, inserting the Choi–Williams or exponential distribution kernels in Table 13.10 into Equations 13.65 through 13.69 yields the following five equivalent formulations for this popular TFR.<sup>35</sup>

$$\begin{aligned} \text{CWD}_x(t, f; \sigma) &= \sqrt{\frac{\sigma}{4\pi}} \iint \frac{1}{|\tau|} \exp\left(\frac{-\sigma}{4} \left[\frac{t-t'}{\tau}\right]^2\right) x\left(t' + \frac{\tau}{2}\right) \\ &\quad \times x^*\left(t' - \frac{\tau}{2}\right) e^{-j2\pi f\tau} dt' d\tau \end{aligned} \quad (13.73)$$

$$\begin{aligned} &= \sqrt{\frac{\sigma}{4\pi}} \iint \frac{1}{|v|} \exp\left(\frac{-\sigma}{4} \left[\frac{f-f'}{v}\right]^2\right) X\left(f' + \frac{v}{2}\right) \\ &\quad \times X^*\left(f' - \frac{v}{2}\right) e^{j2\pi tv} df' dv \end{aligned} \quad (13.74)$$

$$\begin{aligned} &= \sqrt{\frac{\sigma}{4\pi}} \iiint \frac{1}{|u|} \exp\left(\frac{-\sigma}{4} \left[\frac{t-t'}{u}\right]^2\right) e^{-j2\pi(f-f')u} \\ &\quad \times \text{WD}_x(t', f') du dt' df' \end{aligned} \quad (13.75)$$

$$= \iint e^{-(2\pi\tau v)^2/\sigma} \text{AF}_x(\tau, v) e^{j2\pi(tv-f\tau)} d\tau dv \quad (13.76)$$

$$\begin{aligned} &= \sqrt{\frac{\sigma}{4\pi}} \iint \frac{1}{|f_1 - f_2|} \\ &\quad \times \exp\left(\frac{-\sigma}{4} \left[\frac{f - (f_1 + f_2)/2}{f_1 - f_2}\right]^2\right) \\ &\quad \times X(f_1) X^*(f_2) e^{j2\pi t(f_1 - f_2)} df_1 df_2. \end{aligned} \quad (13.77)$$

The Choi–Williams exponential distribution (CWD) is often used as a compromise between the high-resolution but cluttered WD versus the smeared, but easy to interpret spectrogram.<sup>24,35,79</sup> The most intuitive formulation for the CWD is Equation 13.76, which states that the CWD is the two-dimensional Fourier transform of the product of the AF of the signal with a lowpass kernel. This kernel,  $\Psi_{\text{CWD}}(\tau, v) = \exp[-(2\pi\tau v)^2/\sigma]$ , is a Gaussian function when evaluated at the product of the kernel arguments  $\tau v$ . The disadvantage of Equation 13.76 is that the signal must be known for all time before the AF can be computed. Fast algorithms for calculating the CWD are frequently implemented using Equation 13.73, which can be computed directly from the signal  $x(t)$ . If  $\sigma$  is large, then the Gaussian kernel in Equation 13.73 falls off quickly to zero, which means that the integration requires knowledge of only short, local segments of the signal, making real-time implementations a possibility. If the spectrum of the signal is very narrowband, then the frequency-domain formulations in Equation 13.74 or 13.77 may prove more computationally efficient. The bi-frequency formulation

in Equation 13.77 states explicitly how signal components from different spectral bands interact and how they are weighted to produce the quadratic CWD.

Hence, the four normal forms offer various computational and analysis advantages. The first two normal forms in Equations 13.65 and 13.66 can be computed directly from the signal,  $x(t)$ , or its Fourier transform,  $X(f)$ , via a one-dimensional convolution with  $\varphi_C(t, \tau)$  or  $\Phi_C(f, v)$ , respectively. If the kernel  $\varphi_C(t, \tau)$  is fairly short duration, then it may be possible to implement a discrete-time version of Equation 13.65 on a digital computer in real time using only a small number of local signal samples. The third normal form in Equation 13.67 indicates that any TFR in Cohen’s-shift covariant class can be computed by convolving the TFR-dependent kernel  $\psi_C(t, f)$ , with the WD of the signal, defined in Equation 13.15 through 13.17. Hence, the WD is one of the key members of Cohen’s class and many TFRs correspond to smoothed WDs, as can be seen in the top of Table 13.5. Equation 13.71 and the fourth normal form in Equation 13.68 indicate that the two-dimensional convolution in Equation 13.67 transforms to multiplication of the Fourier transform of the kernel,  $\psi_C(t, f)$ , with the Fourier transform of the WD, which is the AF. This last normal form provides an intuitive interpretation that the “AF-domain” kernel,  $\Psi_C(\tau, v)$ , can be thought of as the frequency response of a two-dimensional filter. Equation 13.48 reveals that this AF plane kernel should be an ideal lowpass filter in order to retain AF auto terms which map to the origin and to reduce AF cross terms which map away from the origin in the AF plane.

### 13.5.1.3 Determination of TFR Properties by Kernel Constraints

The kernels in Equations 13.65 through 13.69 are signal-independent and provide valuable insight into the performance of each Cohen’s-class TFR, regardless of the input signal. The kernels can be used to evaluate which ideal TFR property a given TFR satisfies and the relative merits of one TFR over another. Given on the left in each row in Table 13.8 is one of the ideal TFR properties discussed earlier; provided in the second column are the corresponding constraints that a TFR’s kernel in Equation 13.65 through 13.68 must satisfy for the ideal property to hold. For example, the second column in Table 13.8 reveals that the time–frequency marginal, moment, and localization properties are automatically satisfied by any Cohen’s-class TFR whose AF plane kernel  $\Psi_C(\tau, v)$  in Table 13.10 is equal to one along its axes, i.e.,  $\Psi_C(0, v) = 1 = \Psi_C(\tau, 0)$ . The row for  $P_{25}$  in Table 13.8 indicates that Moyal’s formula is satisfied by any Cohen’s class TFR whose AF-domain kernel has unit modulus. Hence, it can be easily seen by examining the third column of Table 13.10 that the WD with unit kernel  $\Psi_{\text{WD}}(\tau, v) = 1$  trivially satisfies these properties. In fact, the checklist in Table 13.7 indicates that the WD satisfies  $P_1$ – $P_7$ ,  $P_9$ – $P_{21}$ , and  $P_{23}$ – $P_{25}$ . The product kernels,  $\Psi_C(\tau, v) = S(\tau, v)$ , used in the reduced interference distributions (RID) and the CWD<sup>35,79</sup> can easily be made to satisfy the time–frequency moment, marginal, and localization properties simply by normalizing the kernel to be

one at its origin, i.e.,  $S(0) = 1$ . In addition, if  $S(\underline{\beta})$  is an even function, then these distributions automatically satisfy the instantaneous frequency, group delay, and Fourier transform properties as well.

There is a tradeoff between Cohen's class TFRs that have good cross-term reduction versus those TFRs that satisfy Moyal's formula or the marginal, moment, or localization properties. The WD kernel,  $\Psi_{\text{WD}}(\tau, \nu) = 1$ , satisfies the constraint for Moyal's formula, but it unfortunately acts as an allpass filter in the AF-domain formulation in Equation 13.68, passing all cross terms in Equation 13.48. For good cross-term reduction and little auto-term distortion, the kernel  $\Psi_{\text{C}}(\tau, \nu)$  given in Table 13.8 should be as close as possible to an ideal lowpass filter. Kernels that are equal to one along the axes in the AF plane satisfy the time–frequency marginal, moment, and localization properties, but they cannot reduce the cross terms in Equation 13.48 that occur along the AF plane axes, i.e., those across terms which correspond to pairs of signal components that occur at the same time or at the same frequency. The Born-Jordan, Butterworth, Choi-Williams, generalized exponential, Auger generalized rectangular, reduced interference, and multiform tiltable kernel distributions<sup>11,43,45,60</sup> all use one-dimensional prototype kernels in the third column of Table 13.10 that were designed to be lowpass and to be equal to one along the axes. For example, the CWD has equal amplitude iso-contours along hyperbolas in the  $(\tau, \nu)$  plane; it is equal to one along the AF plane axes and decreases to zero away from the AF plane origin in a Gaussian fashion. It can be used to reduce those cross terms in Equation 13.48 that map away from the axes. The CWD scaling factor  $\sigma$  determines the width of the passband region in the AF plane; small values for  $\sigma$  allow the user to select a narrow passband for good cross-term reduction whereas large values of  $\sigma$  produce good auto-term preservation; unfortunately, both are not always possible with CWD. The generalized exponential, Butterworth, and the multiform tiltable distributions are extensions to the CWD and the RID that use nonlinear axis mappings with several degrees of freedom that can be exploited to satisfy both passband and stopband constraints. Although the lowpass nature of produce kernels is useful for cross-term reduction, it prevents any such TFR from satisfying Moyal's formula or the linear chirp localization property.

### 13.5.2 Affine Class of TFRs

$$\begin{aligned} \text{Affine class} &= \left\{ T_x(t, f) | y(t) = \sqrt{|a|} x(a(t - t_0)) \Rightarrow T_y(t, f) \right. \\ &= \left. T_x\left(a(t - t_0), \frac{f}{a}\right) \right\} \end{aligned}$$

TFRs that are covariant to scale changes and time translations, i.e., properties  $P_2$  to  $P_3$  in Table 13.6, are members of the affine class.<sup>19,20,60,63,111</sup> Several such TFRs are given in Table 13.11.

The scale covariance property,  $P_3$ , is useful for several applications, including wideband Doppler systems, signals with fractal structure,<sup>58</sup> octave band systems like the cochlea of the inner ear, and short duration “transients.”<sup>2,3,30,36,81,90,91</sup>

#### 13.5.2.1 Alternative Formulations

Any affine class TFR can be written in the four normal forms and bi-frequency form equations similar to those of Cohen's class<sup>60,100,111</sup>:

$$\begin{aligned} A_x(t, f; \Psi_A^{(A)}) &= |f| \iint \varphi_A^{(A)}(f(t - t'), f\tau) x(t' + \tau/2) \\ &\quad \times x^*(t' - \tau/2) dt' d\tau \end{aligned} \quad (13.78)$$

$$\begin{aligned} &= \frac{1}{|f|} \iint \Phi_A^{(A)}\left(-\frac{f'}{f}, \frac{\nu}{f}\right) X(f' + \nu/2) \\ &\quad \times X^*(f' - \nu/2) e^{j2\pi t\nu} df' d\nu \end{aligned} \quad (13.79)$$

$$\begin{aligned} &= \iint \Psi_A^{(A)}\left(f(t - t'), -\frac{f'}{f}\right) \\ &\quad \times \text{WD}_x(t', f') dt' df' \end{aligned} \quad (13.80)$$

$$= \iint \Psi_A^{(A)}\left(f\tau, \frac{\nu}{f}\right) \text{AF}_x(\tau, \nu) e^{j2\pi t\nu} d\tau d\nu \quad (13.81)$$

$$\begin{aligned} &= \frac{1}{|f|} \iint \Gamma_A^{(A)}\left(\frac{f_1}{f}, \frac{f_2}{f}\right) X(f_1) \\ &\quad \times X^*(f_2) e^{j2\pi t(f_1 - f_2)} df_1 df_2. \end{aligned} \quad (13.82)$$

The affine-class kernels are interrelated by the same Fourier transforms given in Equations 13.70 and 13.71, i.e.,

$$\varphi_A^{(A)}(c, \zeta) \leftrightarrow \Phi_A^{(A)}(b, \beta)$$

$$\Psi_A^{(A)}(c, b) \leftrightarrow \Psi_A^{(A)}(\zeta, \beta).$$

The bi-frequency kernel is related to the normal form kernels by the following equation:

$$\Gamma_A^{(A)}(b_1, b_2) = \Phi_A^{(A)}\left(-\frac{b_1 + b_2}{2}, b_1 - b_2\right).$$

Note that the third normal form of the affine class in Equation 13.80 involves an affine smoothing of the WD of the signal, i.e., the output frequency  $f$  is inversely proportional to the amount of time smoothing and proportional to the amount of frequency smoothing.<sup>63</sup> In Table 13.11, various members of the affine class, such as the Bertrand  $P_0$  distribution, the scalogram, and the Unterberger distributions, are defined.

The four normal form kernels used to formulate affine-class TFRs in Equations 13.78 through 13.81 are listed in Table 13.12.

TABLE 13.11 TFRs in the Affine Class

Affine Class Distr.	Formula
Ackroyd	$ACK_x(t, f) = \text{Re}\{x^*(t)X(f)e^{j2\pi ft}\}$
Affine-Cohen Subclass	$AC_x(t, f; S_{AC}) = \iint \frac{1}{ \tau } S_{AC}\left(\frac{t-t'}{\tau}\right) x\left(t' + \frac{\tau}{2}\right) x^*\left(t' - \frac{\tau}{2}\right) e^{-j2\pi f\tau} dt' d\tau$
Affine-Hyp. Subclass	$AH_X(t, f; S_{AH}) = f \int S_{AH}(f(t-t')) B P_0 D_X(t', f; \mu_0) dt'$ $= f \int X\left(f \frac{\beta/2 e^{\beta/2}}{\sinh \beta/2}\right) X^*\left(f \frac{\beta/2 e^{-\beta/2}}{\sinh \beta/2}\right) S_{AH}(\beta) \frac{\beta/2}{\sinh \beta/2} e^{j2\pi t f \beta} d\beta$
(Unitary) Bertrand $P_0$	$BP_0 D_X(t, f; \mu_0) = f \int X\left(f \frac{u/2 e^{u/2}}{\sinh(u/2)}\right) X^*\left(f \frac{u/2 e^{-u/2}}{\sinh(u/2)}\right) \frac{u/2}{\sinh(u/2)} e^{j2\pi t f u} du$
(General) Bertrand $P$ 0	$BP_0 D_X(t, f; \mu) =  f  \int X\left(f \frac{\beta/2}{\sinh \beta/2} e^{\beta/2}\right) X^*\left(f \frac{\beta/2}{\sinh \beta/2} e^{-\beta/2}\right) \mu(\beta) e^{j2\pi t f \beta} d\beta$ $=  f  \int X\left(f \left[\frac{u}{2} \coth \frac{u}{2} + \frac{u}{2}\right]\right) X^*\left(f \left[\frac{u}{2} \coth \frac{u}{2} - \frac{u}{2}\right]\right) \mu(u) e^{j2\pi t f u} du$
Bertrand $P_k$	$BP_k D_X(t, f; \mu) = f \int X(f\lambda_k(u)) X^*(f\lambda_k(-u)) \mu(u) e^{j2\pi t f (\lambda_k(u) - \lambda_k(-u))} du,$ $\lambda_0(u) = \frac{u/2 e^{u/2}}{\sinh(u/2)}, \lambda_1(u) = \exp\left[1 + \frac{ue^{-u}}{e^{-u}-1}\right], \lambda_k(u) = \left[k \frac{e^{-u}-1}{e^{-ku}-1}\right]^{\frac{1}{k-1}}, k \neq 0, 1 \text{ and } \mu(u) = \mu^*(-u)$
Born-Jordan	$BJD_x(t, f) = \iint \frac{\sin(\pi\tau\nu)}{\pi\tau\nu} A F_x(\tau, \nu) e^{j2\pi(t\nu-f\tau)} d\tau d\nu$
Choi–Williams Exp.	$CWD_x(t, f; \sigma) = \iint e^{-(2\pi\tau\nu)^2/\sigma} A F_x(\tau, \nu) e^{j2\pi(t\nu-f\tau)} d\tau d\nu$
Flandrin $D$	$FD_x(t, f) = f \int X\left(f\left[1 + \frac{u^2}{4}\right]\right) X^*\left(f\left[1 - \frac{u^2}{4}\right]\right) \left[1 - \left(\frac{u}{4}\right)^2\right] e^{j2\pi t f u} du$
Generalized Wigner	$GWD_x(t, f; \alpha) = \int x\left(t + \left(\frac{1}{2} + \alpha\right)\tau\right) x^*\left(t - \left(\frac{1}{2} - \alpha\right)\tau\right) e^{-j2\pi f\tau} d\tau$
Localized Affine	$LA_X(t, f; G^{(A)}, F^{(A)}) = f \int X(f(-F^{(A)}(\beta) + \beta/2)) X^*(f(-F^{(A)}(\beta) - \beta/2)) G^{(A)}(\beta) e^{j2\pi t f \beta} d\beta$
Margineau-Hill	$MH_x(t, f) = \text{Re}\{x(t)X^*(f)e^{-j2\pi ft}\}$
Reduced Interference	$RID_x(t, f) = \iint \frac{1}{ \tau } s\left(\frac{t-t'}{\tau}\right) x\left(t' + \frac{\tau}{2}\right) x^*\left(t' - \frac{\tau}{2}\right) e^{-j2\pi f\tau} dt' d\tau$ with $S(\beta) \in \Re, S(0) = 1, \frac{d}{d\beta} S(\beta) _{\beta=0} = 0, \left\{s(\alpha) = 0 \text{ for }  \alpha  > \frac{1}{2}\right\}$
Rihaczek	$RD_x(t, f) = x(t)X^*(f)e^{-j2\pi t f}$
Scalogram	$SCAL_x(t, f; \Gamma) = \left  \int x(\tau) \sqrt{\left \frac{f}{f_t}\right } \gamma^*\left(\frac{f}{f_t}(\tau-t)\right) d\tau \right ^2 = \left \frac{f_t}{f}\right  \left  \int X(\hat{f}) \Gamma^*\left(\frac{\hat{f}}{f_t}\right) e^{j2\pi t \hat{f}} d\hat{f} \right ^2$
Unterberger Active	$UAD_X(t, f) = f \int_0^\infty X(fu) X^*(f/u) [1 + u^{-2}] e^{j2\pi t f (u-1/u)} du$ $= f \int X\left(f\left(\sqrt{1 + (\beta/2)^2} + \beta/2\right)\right) X^*\left(f\left(\sqrt{1 + (\beta/2)^2} - \beta/2\right)\right) e^{j2\pi t f \beta} d\beta$
Unterberger Passive	$UPD_X(t, f) = 2f \int_0^\infty X(fu) X^*(f/u) \left[\frac{1}{u}\right] e^{j2\pi t f (u-1/u)} du$ $= f \int X\left(f\left(\sqrt{1 + \left(\frac{\beta}{2}\right)^2} + \frac{\beta}{2}\right)\right) X^*\left(f\left(\sqrt{1 + \left(\frac{\beta}{2}\right)^2} - \frac{\beta}{2}\right)\right) \frac{1}{\sqrt{1 + (\beta/2)^2}} e^{j2\pi t f \beta} d\beta$
Wigner	$WD_x(t, f) = \int x\left(t + \frac{\tau}{2}\right) x^*\left(t - \frac{\tau}{2}\right) e^{-j2\pi f\tau} d\tau = \int X\left(f + \frac{\nu}{2}\right) X^*\left(f - \frac{\nu}{2}\right) e^{j2\pi t \nu} d\nu$

The Bertrand  $P_0$ , Generalized WD, Unterberger active and passive, and the Wigner distributions are special cases of the localized affine distributions with  $g^{(a)}(\beta)$  and  $f^{(a)}(\beta)$  defined accordingly, e.g.,  $F_{UAD}^{(A)}(\beta) = -\sqrt{1 + (\beta/2)^2}$  and  $G_{UAD}^{(A)}(\beta) = 1$ .

TABLE 13.12 Kernels of Affine-Class TFRs Defined in Table 13.11

TFR	$\Psi_{\mathcal{A}}^{(A)}(c, b)$	$\Psi_{\mathcal{A}}^{(A)}(\zeta, \beta)$	$\Phi_{\mathcal{A}}^{(A)}(c, \zeta)$	$\Phi_{\mathcal{A}}^{(A)}(b, \beta)$
AC	$\int \frac{1}{ \zeta } S_{AC}\left(\frac{1}{\zeta}\right) e^{-j2\pi c(1+b)\zeta} d\zeta$	$S_{AC}(\zeta\beta) e^{-j2\pi \zeta}$	$\frac{1}{ \zeta } S_{AC}\left(\frac{c}{\zeta}\right) e^{-j2\pi \zeta}$	$\frac{1}{ \beta } S_{AC}\left(-\frac{1+b}{\beta}\right)$
AH	$\int \frac{S_{AH}(\beta) \beta/2}{\sinh \beta/2} \delta\left(b + \frac{\beta}{2} \coth \frac{\beta}{2}\right) e^{j2\pi c\beta} d\beta$	$\frac{S_{AH}(\beta)\beta/2}{\sinh \beta/2} e^{-j2\pi \zeta \left[\frac{\beta}{2} \coth \frac{\beta}{2}\right]}$	$\int \frac{S_{AH}(\beta)\beta/2}{\sinh \beta/2} e^{-j2\pi(\zeta \left[\frac{\beta}{2} \coth \frac{\beta}{2}\right] - c\beta)} d\beta$	$\frac{S_{AH}(\beta)\beta/2}{\sinh \beta/2} \delta\left(b + \frac{\beta}{2} \coth \frac{\beta}{2}\right)$
Unitary	$\int \frac{\beta/2}{\sinh \beta/2} \delta\left(b + \left[\frac{\beta}{2} \coth \frac{\beta}{2}\right]\right) e^{j2\pi c \beta} d\beta$	$\frac{\beta/2}{\sinh \beta/2} e^{-j2\pi \zeta \left[\frac{\beta}{2} \coth \frac{\beta}{2}\right]}$	$\int \frac{\beta/2}{\sinh \beta/2} e^{-j2\pi(\zeta \left[\frac{\beta}{2} \coth \frac{\beta}{2}\right] - c\beta)} d\beta$	$\frac{\beta/2}{\sinh \beta/2} \delta\left(b + \left[\frac{\beta}{2} \coth \frac{\beta}{2}\right]\right)$
$B P_0 D$				
General	$\int \mu(\beta) \delta\left(b + \frac{\beta}{2} \coth \frac{\beta}{2}\right) e^{j2\pi c\beta} d\beta$	$\mu(\beta) e^{-j2\pi \zeta \left[\frac{\beta}{2} \coth \frac{\beta}{2}\right]}$	$\int \mu(\beta) e^{-j2\pi(\zeta \left[\frac{\beta}{2} \coth \frac{\beta}{2}\right] - c\beta)} d\beta$	$\mu(\beta) \delta\left(b + \frac{\beta}{2} \coth \frac{\beta}{2}\right)$
$B P_0 D_{\mu}$				
FD	$\int \left[1 - \left(\frac{\beta}{4}\right)^2\right] \delta\left(b + \left[1 + \left(\frac{\beta}{4}\right)^2\right]\right) e^{j2\pi c\beta} d\beta$	$\left[1 - \left(\frac{\beta}{4}\right)^2\right] e^{-j2\pi \zeta [1 + (\beta/4)^2]}$	$\int \left[1 - \left(\frac{\beta}{4}\right)^2\right] e^{-j2\pi(\zeta [1 + (\beta/4)^2] - c\beta)} d\beta$	$\left[1 - \left(\frac{\beta}{4}\right)^2\right] \delta(b + [1 + (\beta/4)^2])$
GWD	$\frac{1}{ \tilde{\alpha} } e^{j2\pi c(1+b)/\tilde{\alpha}}$	$e^{-j2\pi \zeta [1 - \tilde{\alpha}\beta]}$	$e^{-j2\pi \zeta} \delta(c + \tilde{\alpha}\zeta)$	$\delta(b + 1 - \tilde{\alpha}\beta)$
LA	$\int G(\beta) \delta(b - F(\beta)) e^{j2\pi c\beta} d\beta$	$G(\beta) e^{+j2\pi \zeta F(\beta)}$	$\int G(\beta) e^{+j2\pi(\zeta F(\beta) + c\beta)} d\beta$	$G(\beta) \delta(b - F(\beta))$
SCAL	$WD_{\gamma}(-c/f_r, -f_r b)$	$AF_{\gamma}(-\zeta/f_r, -f_r \beta)$	$\frac{1}{f_r} \gamma\left(\frac{1}{f_r}(-c - \zeta/2)\right)$ $\gamma^*\left(\frac{1}{f_r}(-c + \zeta/2)\right)$ $= \frac{1}{f_r} u_{\Gamma}(-c/f_r, -\zeta/f_r)$	$f_r \Gamma\left(f_r\left(-b - \frac{\beta}{2}\right)\right)$ $\Gamma^*\left(f_r\left(-b + \frac{\beta}{2}\right)\right)$ $= f_r U_{\Gamma}(-f_r b, -f_r \beta)$
UAD	$\int \delta\left(b + \sqrt{1 + \beta^2/4}\right) e^{j2\pi c\beta} d\beta$	$e^{-j2\pi \zeta \sqrt{1 + \beta^2/4}}$	$\int e^{-j2\pi(\zeta \sqrt{1 + \beta^2/4} - c\beta)} d\beta$	$\delta\left(b + \sqrt{1 + \beta^2/4}\right)$
UPD	$\int \left[1 + \frac{\beta^2}{4}\right]^{-\frac{1}{2}} \delta\left(b + \sqrt{1 + \frac{\beta^2}{4}}\right) e^{j2\pi c\beta} d\beta$	$\left[1 + \frac{\beta^2}{4}\right]^{-\frac{1}{2}} e^{-j2\pi \zeta \sqrt{1 + \beta^2/4}}$	$\int \left[1 + \frac{\beta^2}{4}\right]^{-\frac{1}{2}} e^{-j2\pi(\zeta \sqrt{1 + \beta^2/4} - c\beta)} d\beta$	$\left[1 + \frac{\beta^2}{4}\right]^{-\frac{1}{2}} \delta\left(b + \sqrt{1 + \beta^2/4}\right)$
WD	$\delta(b + 1)\delta(c)$	$e^{-j2\pi \zeta}$	$e^{-j2\pi \zeta} \delta(c)$	$\delta(b + 1)$

Members of the affine-Cohen (AC) subclass in the first row include the Ackroyd, Margineau-Hill, Born-Jordan, Choi-Williams, generalized Wigner, reduced interference, Rihaczek, and Wigner distributions. They have the following kernels:  $S_{ACK}(b) = S_{MH}(b) = \cos \pi b$ ,  $S_{BJD}(b) = \sin \pi b / \pi b$ ,  $S_{CWD}(b) = e^{-(2\pi b)^2 / \sigma}$ ,  $S_E(b) = e^{j2\pi \tilde{\alpha} b}$ ,  $S_{RID}(b) = S_{RID}(b) * (\sin \pi b / \pi b)$ ,  $S_{RD}(b) = e^{-j\pi b}$ , where \* denotes convolution and  $s_{wd}(b) = 1$ , respectively. Here,  $u_{\Gamma}(c, \zeta) = \gamma(c + \zeta/2)\gamma^*(c - \zeta/2)$  and  $u_{\Gamma}(b, \beta) = \Gamma(b + \beta/2)\Gamma^*(b - \beta/2)$ , where  $\gamma(t) \leftrightarrow \Gamma(f)$  are Fourier transform pairs.

These kernels can be compared with the constraints listed in the third column of Table 13.8 to determine which of the ideal properties a given affine TFR satisfies. A checklist summary of the properties that the affine-class TFRs satisfy is provided in Table 13.7. Any affine-class TFR must necessarily have a check mark in the rows for  $P_2$  and  $P_3$ . Because of the scale covariance property, many TFRs in the affine class exhibit constant-Q behavior, permitting multiresolution analysis.<sup>60,112</sup>

The scalogram<sup>60,111</sup> in Table 13.11 is the squared magnitude of the recently introduced wavelet transform (WT)<sup>2,3,36,49,60,69,89,112,118</sup>:

$$WT_x(t, f; \Gamma) = \int x(\tau) \sqrt{\left|\frac{f}{f_0}\right|} \gamma^*\left(\frac{f}{f_0}(\tau - t)\right) d\tau \quad (13.83)$$

$$= \int X(f') \sqrt{\left|\frac{f_0}{f}\right|} \Gamma^*\left(\frac{f_0}{f} f'\right) e^{j2\pi t f'} df'. \quad (13.84)$$

It uses a special sliding analysis window,  $\gamma(t)$ , called the mother wavelet, to analyze local spectral information of the signal  $x(t)$ .

The mother wavelet is either compressed or dilated to give a multiresolution signal representation. Assume that  $\gamma(t)$  is a band-pass filter centered near time  $t=0$  and frequency  $f=f_0$  with (approximate) time duration  $D$  and one-sided spectral bandwidth  $B$ , i.e.,  $|\gamma(t)| \approx 0$ ,  $|t| > D$  and  $|\Gamma(f)| \approx 0$ ,  $|f - f_0| > B$ . Then the scaled mother wavelet in Equation 13.83 is centered near the

output time  $t$  and its time duration is  $\left|\frac{f_0}{f} D\right|$ .

Likewise,  $\Gamma^*\left(\frac{f_0}{f}f'\right)$  in Equation 13.84 is centered near the output frequency,  $f$ , and has spectral bandwidth  $B\left|\frac{f}{f_0}\right|$ . Hence, for  $f > f_0$ , the WT in Equation 13.83 compresses the time duration of the mother wavelet while simultaneously expanding its spectral bandwidth in Equation 13.84. In fact, the WT implements a “constant-Q” signal analysis, since the mother wavelet’s quality factor,<sup>60</sup>

$$Q = \frac{\text{Center frequency}}{\text{Bandwidth}} = \frac{f}{B|f/f_0|} = \frac{f_0}{\beta}, \quad f > 0,$$

is constant for all output frequencies.

Thus, the scalogram can be thought of as the multiresolution output of a parallel bank of octave band filters.<sup>69,111,112</sup> High-frequency regions of the WT domain have very good time resolution, whereas low-frequency regions of the WT domain have very good spectral resolution. The wavelet transform has been used to code images, to model the mid- to high-frequency operation of the cochlea, to track transients such as speech pitch and the onset of the QRS complex in ECG signals, and to analyze fractal and chaotic signals.<sup>1–4,30,36,60,91,118</sup> One drawback of the scalogram is its poor temporal resolution at low-frequency regions of the time–frequency plane and poor spectral resolution at high frequencies. The quadratic scalogram produces cross terms whenever signal components overlap.<sup>82</sup> Further, many discrete WT implementations do not preserve the important time-shift covariance property.

### 13.5.3 Affine-Cohen Subclass

$$\begin{aligned} \text{Affine-Cohen subclass} &= \left\{ T_y(t, f) | y(t) = \sqrt{|a|} x(a(t - t_0)) e^{j2\pi f_0 t} \right. \\ &\Rightarrow T_y(t, f) = T_x\left(a(t - t_0), \frac{f - f_0}{a}\right) \end{aligned}$$

Those TFRs listed in both Tables 13.9 and 13.11 are members of the intersection of Cohen’s class of time–frequency shift-covariant TFRs with the affine class of affine-covariant TFRs. This intersection is depicted graphically in Figure 13.4. All shift-scale covariant TFRs must satisfy properties  $P_1$ – $P_3$  in Table 13.6. This subclass is characterized by those Cohen’s-class TFRs whose AF-domain kernel,  $\Psi_C(\tau, \nu) = f \text{cn}(\tau \nu)$ , is a product kernel, that is, a one-dimensional function evaluated at the product  $\tau \nu$ . Inspection of the third column of Table 13.10 reveals that the affine-Cohen subclass includes the Ackroyd, Margineau-Hill, Born-Jordon, Choi–Williams, generalized Wigner, reduced interference, Rihaczek, and WDs. Further, the affine-class kernels used in Equations 13.78 through 13.81 and the Cohen’s-class kernels used in Equations 13.65 through 13.68 of each shift scale covariant TFR are related as follows:

$$\begin{aligned} \psi_{AC}^{(A)}(c, b) &= \psi_{AC}(c, 1 + b) \longleftrightarrow \Psi_{AC}^{(A)}(\zeta, \beta) = \Psi_{AC}(\zeta, \beta) e^{-j2\pi\zeta} \\ &= S_{AC}(\zeta\beta) e^{-j2\pi\zeta} \\ \varphi_{AC}^{(A)}(c, \zeta) &= \varphi_{AC}(c, \zeta) e^{-j2\pi\zeta} \longleftrightarrow \Phi_{AC}^{(A)}(b, \beta) = \Phi_{AC}(1 + b, \beta). \end{aligned}$$

### 13.5.4 Hyperbolic Class of TFRs

Hyperbolic class

$$\begin{aligned} &= \left\{ T_X(t, f) | Y(f) = \frac{1}{\sqrt{|a|}} X\left(\frac{f}{a}\right) \frac{1}{\sqrt{f}} e^{-j2\pi c \ln(f/f_0)} \Rightarrow T_Y(t, f) \right. \\ &= T_X\left(a\left(t - \frac{c}{f}\right), \frac{f}{a}\right) \end{aligned}$$

The hyperbolic class of TFRs consists of all TFRs that are covariant to scale changes and hyperbolic time shifts on analytic signals, i.e., properties  $P_3$  and  $P_4$  in Table 13.6.<sup>97,98,100</sup> They can be analyzed using the following alternative forms, valid for  $f > 0$ ,

$$\begin{aligned} H_X(t, f; \Psi_H^{(H)}) &= \iint \varphi_H^{(H)}(tf - c, \zeta) \\ &\times v_X(c, \zeta) e^{-j2\pi[\ln(f/f_0)]\zeta} d\zeta \quad (13.85) \end{aligned}$$

$$\begin{aligned} &= \iint \Phi_H^{(H)}\left(\ln\frac{f}{f_r} - b, \beta\right) f_r e^b X(f_r e^{b+\beta/2}) \\ &\times X^*(f_r e^{b-\beta/2}) e^{j2\pi t f \beta} db d\beta \quad (13.86) \end{aligned}$$

$$= \iint_0^\infty \psi_H^{(H)}\left(tf - t'f', \ln\frac{f}{f'}\right) Q_X(t', f') dt' df' \quad (13.87)$$

$$\begin{aligned} &= \iint \Psi_H^{(H)}(\zeta, \beta) \text{HAF}_X(\zeta, \beta) \\ &\times e^{j2\pi(tf\beta - [\ln(f/f_0)]\zeta)} d\zeta d\beta \quad (13.88) \end{aligned}$$

$$\begin{aligned} &= \frac{1}{f} \int_0^\infty \int_0^\infty \Gamma_H^{(H)}\left(\frac{f_1}{f}, \frac{f_2}{f}\right) X(f_1) \\ &\times X^*(f_2) e^{j2\pi t f \ln(f_1/f_2)} df_1 df_2, \quad (13.89) \end{aligned}$$

where  $Q_X(t, f)$  is the Altes Q distribution defined in Equation 13.24,  $\text{HAF}_X(\zeta, \beta)$  is the hyperbolic ambiguity function defined in Equation 13.26, and the quadratic signal product,

$$\begin{aligned} v_X(c, \zeta) &= \left( \int_0^\infty X(f) \left(\frac{f}{f_r}\right)^{j2\pi(c+\zeta/2)} \frac{df}{\sqrt{f}} \right) \\ &\times \left( \int_0^\infty X^*(\nu) \left(\frac{\nu}{f_r}\right)^{-j2\pi(c-\zeta/2)} \frac{d\nu}{\sqrt{\nu}} \right) \quad (13.90) \end{aligned}$$

$$= \frac{1}{f_r} \rho_x([c + \zeta/2]/f_r) \rho_x^*([c - \zeta/2]/f_r), \quad (13.91)$$



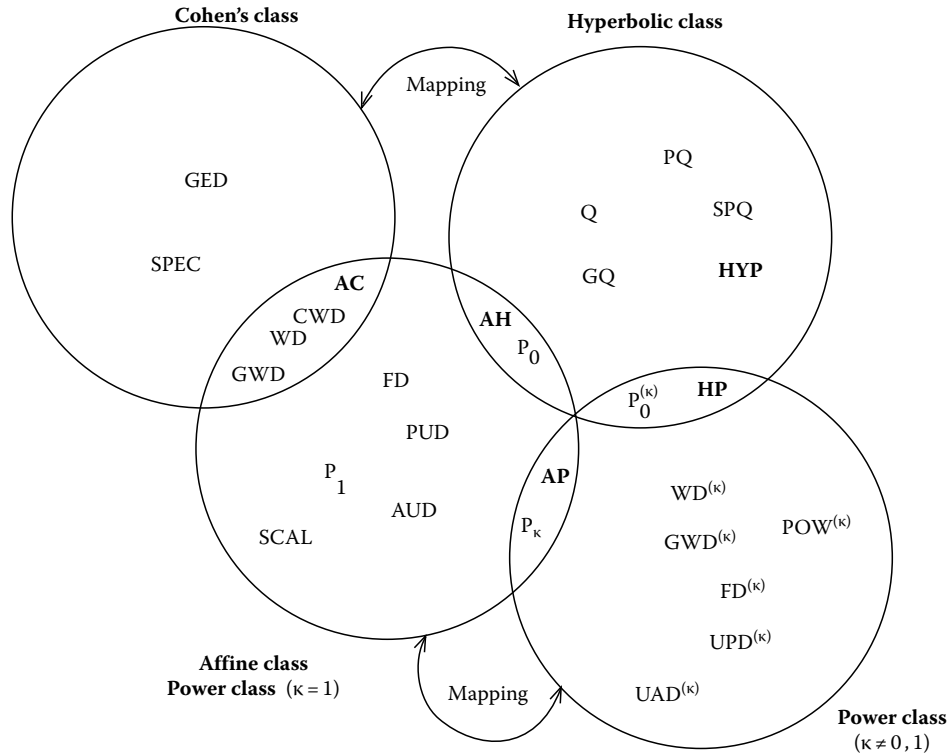


**FIGURE 13.4** A pictorial summary of the different classes of QTFRs considered in this manuscript: Cohen’s class, affine class, hyperbolic class, and  $\kappa$ th power class ( $\kappa \neq 0, 1$ ) together with their intersection subclasses and some important QTFR members. The spectrogram (SPEC), the Wigner distribution (WD), the generalized WD (GWD), the Choi–Williams exponential distribution (CWD), and the generalized exponential distribution (GED) are members of Cohen’s class. The WD, GWD, CWD, scalogram (SCAL), Flandrin  $D$  (FD), passive Unterberger (UPD), active Unterberger (UAD), Bertrand  $P_0$ -distribution, Bertrand  $P_1$ -distribution, and Bertrand  $P_\kappa$ -distributions,  $\kappa \neq 0, 1$ , are members of the affine class. The affine-Cohen’s intersection (AC) contains the WD, GWD, and CWD. The hyperbologram (HYP), the Altes-Marinovich Q-distribution (Q), the generalized Q (GQ), the pseudo Q (PQ), the smoothed pseudo Q (SPQ), the Bertrand  $P_0$ -distribution, and the  $\kappa$ th power form of the Bertrand  $P_0$ -distribution ( $P_0^{(\kappa)}$ ) are members of the hyperbolic class. The affine-hyperbolic intersection (AH) contains the Bertrand  $P_0$ -distribution. The powergram,  $POW^{(\kappa)}$ ; the power Wigner distribution  $WD^{(\kappa)}$ ; the generalized  $WD^{(\kappa)}$ ,  $GWD^{(\kappa)}$ ; the Bertrand  $P_\kappa$ -distributions; the power Bertrand  $P_0$ -distribution,  $P_0^{(\kappa)}$ ; the power FD,  $FD^{(\kappa)}$ ; the power UPD,  $UPD^{(\kappa)}$ ; and the power UAD,  $UAD^{(\kappa)}$ ; are all  $P_\kappa$ -distributions. The hyperbolic and Cohen’s classes, and the affine and power classes are related through unitary mappings.

is proportional to the product of modified Mellin transformations of the signal spectrum, where

$$\begin{aligned} \rho_x(t) &= \int \sqrt{e^{f/f_r}} X(f_r e^{f/f_r}) e^{j2\pi f t} df \leftrightarrow (WX)(f) \\ &= \sqrt{e^{f/f_r}} X(f_r e^{f/f_r}), \end{aligned} \tag{13.92}$$

$$= \sqrt{f_r} \int_0^\infty X(v) \left(\frac{v}{f_r}\right)^{j2\pi f t} \frac{dv}{\sqrt{v}} \tag{13.93}$$

corresponds to the unitary warping of the frequency axis of the signal given in Equation 13.34. The four normal form kernels in Equations 13.85 through 13.88 are interrelated via the Fourier transforms in Equations 13.70 and 13.71. The relationship of the hyperbolic bi-frequency kernel (Equation 13.89) to the normal form II kernel in Equation 13.86 is as follows:

$$\Gamma_H^{(H)}(b_1, b_2) = \frac{1}{\sqrt{|b_1 b_2|}} \Phi_H^{(H)} \left( -\ln \sqrt{|b_1 b_2|}, \ln(b_1/b_2) \right).$$

Table 13.13 reveals that the Altes Q distribution, the Bertrand  $P_0$  distribution, and the hyperbologram are members of the hyperbolic class. Their corresponding hyperbolic kernels are given in Table 13.14. Listed in the fourth column of Table 13.8 are the constraints on these hyperbolic kernels needed for the corresponding TFR to satisfy the ideal properties listed in the first column. A summary of the ideal properties that the hyperbolic class TFRs satisfy is provided in Table 13.7. Note that any member of the hyperbolic class must, by definition, have the rows for properties  $P_3$  and  $P_4$  checked off.

The hyperbolic class TFRs give highly concentrated TFR representations for signals with hyperbolic group delay. They are well suited for the analysis of self-similar random processes or of wideband Doppler-invariant signals similar to the biosonar signals used by bats and dolphins for echolocation.<sup>7,53,59,69,100</sup>

TABLE 13.13 Hyperbolic TFRs

Hyperbolic TFR	Formula, $f > 0$
Affine-Hyperbolic Subclass	$AH_X(t, f; S_{AH}) =  f  \int S_{AH}(f(t - t')) B P_0 D_X(t', f; \mu_0) dt'$ $=  f  \int X\left(f\left(\frac{\beta}{2} \coth \frac{\beta}{2} + \frac{\beta}{2}\right)\right) X^*\left(f\left(\frac{\beta}{2} \coth \frac{\beta}{2} - \frac{\beta}{2}\right)\right) S_{AH}(\beta) \frac{\beta/2}{\sinh \beta/2} e^{j2\pi t f \beta} d\beta$ $=  f  \int X\left(f \frac{\beta/2}{\sinh \beta/2} e^{\beta/2}\right) X^*\left(f \frac{\beta/2}{\sinh \beta/2} e^{-\beta/2}\right) S_{AH}(\beta) \frac{\beta/2}{\sinh \beta/2} e^{j2\pi t f \beta} d\beta$
Altes	$Q_X(t, f) = f \int X(f e^{u/2}) X^*(f e^{-u/2}) e^{j2\pi t f u} du$
Unitary Bertrand $P_0$	$BP_0 D_X(t, f; \mu_0) = f \int X\left(f \frac{u/2}{\sinh(u/2)} e^{u/2}\right) X^*\left(f \frac{u/2}{\sinh(u/2)} e^{-u/2}\right) \frac{u/2}{\sinh(u/2)} e^{j2\pi t f u} du,$
General Bertrand $P_0$	$BP_0 D_X(t, f; \mu) = f \int X\left(f \frac{\beta/2}{\sinh \beta/2} e^{\beta/2}\right) X^*\left(f \frac{\beta/2}{\sinh \beta/2} e^{-\beta/2}\right) \mu(\beta) e^{j2\pi t f \beta} d\beta,$ $= f \int X\left(f\left(\frac{\beta}{2} \coth\left(\frac{\beta}{2}\right) + \frac{\beta}{2}\right)\right) X^*\left(f\left(\frac{\beta}{2} \coth\left(\frac{\beta}{2}\right) - \frac{\beta}{2}\right)\right) \mu(\beta) e^{j2\pi t f \beta} d\beta$
Generalized Altes	$GQ_X(t, f; \tilde{\alpha}) = f \int e^{-\tilde{\alpha} u} X\left(f e^{\left(\frac{1}{2} - \tilde{\alpha}\right) u}\right) X^*\left(f e^{-\left(\frac{1}{2} + \tilde{\alpha}\right) u}\right) e^{j2\pi t f u} du$
Hyp. Choi–Williams	$HCWD_X(t, f; \sigma) = \iint e^{-(2\pi t v)^2 / \sigma} A F_{WX}(\tau, v) e^{j2\pi(t v f / f_r - \tau f_r \ln f / f_r)} d\tau dv$
$\kappa$ th Hyp. Power Subclass	$HP_X^{(\kappa)}(t, f; G^{(H)}) = f \int X\left(f\left(\frac{\kappa\beta/2}{\sinh(\kappa\beta/2)}\right)^{1/\kappa} e^{\beta/2}\right) X^*\left(f\left(\frac{\kappa\beta/2}{\sinh(\kappa\beta/2)}\right)^{1/\kappa} e^{-\beta/2}\right) \left(\frac{\kappa\beta/2}{\sinh(\kappa\beta/2)}\right)^{1/\kappa} G^{(H)}(\beta) e^{j2\pi t f \beta} d\beta$ $= \left \frac{f}{\kappa}\right  \int g^{(H)}\left(\frac{f}{\kappa}[t - t']\right) BP_0 D_X^{(\kappa)}(t', f; \mu_0) dt'$
Hyperbologram	$HYP_X(t, f; \Gamma) = \left \frac{f_r}{f}\right  \left \int_0^\infty X(\xi) \Gamma^*\left(\frac{f_r}{f} \xi\right) e^{j2\pi t f \ln(\xi/f_r)} d\xi\right ^2$ $= \int_{-\infty}^\infty \int_0^\infty Q_\Gamma\left(\frac{1}{f_r} \frac{f}{f'}(t' f' - t f), f_r \frac{f'}{f}\right) Q_X(t', f') dt' df'$
Localized Hyp. Subclass	$LH_X(t, f; G^{(H)}, F^{(H)}) = f \int X(f e^{-F^{(H)}(\beta) + \beta/2}) X^*(f e^{-F^{(H)}(\beta) - \beta/2}) e^{-F^{(H)}(\beta)} G^{(H)}(\beta) e^{j2\pi t f \beta} d\beta$
Power-Warp Hyp. Subclass	$PWH_X(t, f; s^{(H)}) = \int s^{(H)}(-\eta) GQ_X(t, f; \eta) d\eta$
Pseudo Altes	$PQ_X(t, f; \Gamma) = f_r \int_0^\infty Q_\Gamma\left(0, f_r \frac{f}{f'}\right) Q_X\left(\frac{t f}{f_r}, f'\right) \frac{df'}{f'}$
Smoothed Pseudo Altes	$SPQ_X(t, f; \Gamma, s) = \int s(t f - c) PQ_X\left(\frac{c}{f}, f; \Gamma\right) dc$ $= f_r \int \int_0^\infty s(t f - c) Q_\Gamma\left(0, f_r \frac{f}{f'}\right) Q_X\left(\frac{c}{f_r}, f'\right) dc \frac{df'}{f'}$
Warped Cohen Class	$H_X(t, f; \Psi_H^{(H)}) = C_{H_{WX}}\left(\frac{t f}{f_r}, f_r \ln \frac{f}{f_r}; \Psi_{C_H}\right)$

Members of the localized hyperbolic (lh) subclass include the affine hyperbolic (ah) and the  $\kappa$ th hyperbolic power subclasses as well as the altes, bertrand  $p_0$ , and generalized altes distributions.  $(wx)(f)$  is the unitary signal warping defined in Equation 13.34, and  $\underline{\mu}(u) = \mu^*(-u)$  is a real and even function.

Each hyperbolic-class TFR, kernel, and property corresponds to a warped version of a Cohen’s-class TFR, kernel, and property, respectively.<sup>14,15,44,97,100</sup> That is, each hyperbolic-class TFR,  $H$ , corresponds to an axis-warped version of a corresponding Cohen’s class TFR,  $C_H$ ,

$$H_X(t, f; \Psi_H^{(H)}) = C_{H_{WX}}\left(\frac{t f}{f_r}, f_r \ln \frac{f}{f_r}; \Psi_{C_H}\right) \quad (13.94)$$

$$C_{H_X}(t, f; \Psi_{C_H}) = H_{W^{-1}X}\left(t e^{-f/f_r}, f_r e^{f/f_r}; \Psi_H^{(H)}\right), \quad (13.95)$$

provided that the signal is first prewarped by  $WX$  or  $W^{-1}X$  defined in Equations 13.34 and 13.35, respectively. Examples are given in the bottom of Table 13.5. Also, in Equation 13.32, the Altes  $Q$  distribution is equal to the WD after warping both the signal and the time–frequency axes. In this case,  $H=Q$  and  $C_H=WD$  in Equation 13.94. Likewise, the hyperbologram is a warped version of the spectrogram, provided that both the signal and the analysis window are prewarped:

TABLE 13.14 Kernels of the Hyperbolic Class of TFRs Defined in Table 13.13

TFR	$\Psi_H^{(H)}(c, b)$	$\Psi_H^{(H)}(\zeta, \beta)$	$\Phi_H^{(H)}(c, \zeta)$	$\Phi_H^{(H)}(b, \beta)$
AH	$\int S_{AH}(\beta) \delta\left(b - \ln \frac{\sin \beta/2}{\beta/2}\right) \times e^{j2\pi c\beta} d\beta$	$S_{AH}(\beta)$	$\int S_{AH}(\beta)$	$S_{AH}(\beta)$
Unitary $B P_0D$	$\int \delta(b + \ln \mu_0(\beta)) e^{j2\pi c\beta} d\beta$	$e^{j2\pi\zeta \left  \ln \frac{\sinh \beta/2}{\beta/2} \right }$ $e^{-j2\pi\zeta \ln \mu_0(\beta)}$	$\times e^{j2\pi(\zeta \left  \ln \frac{\sinh \beta/2}{\beta/2} \right  + c\beta)} d\beta$ $\int e^{j2\pi(c\beta - \zeta \ln \mu_0(\beta))} d\beta$	$\times \delta\left(b - \ln \left(\frac{\sinh \beta/2}{\beta/2}\right)\right)$ $\delta(b + \ln \mu_0(\beta))$
General $B P_0D$	$\int \frac{\mu(\beta)}{\mu_0(\beta)} \delta(b + \ln \mu_0(\beta)) e^{j2\pi c\beta} d\beta$	$\frac{\mu(\beta)}{\mu_0(\beta)} e^{-j2\pi\zeta \ln \mu_0(\beta)}$	$\int \frac{\mu(\beta)}{\mu_0(\beta)} e^{j2\pi(c\beta - \zeta \ln \mu_0(\beta))} d\beta$	$\frac{\mu(\beta)}{\mu_0(\beta)} \delta(b + \ln \mu_0(\beta))$
Power $B P_0D^{(\kappa)}$	$\int \delta(b - F^{(\kappa)}(\beta)) e^{j2\pi c\beta} d\beta$	$e^{+j2\pi\zeta F^{(\kappa)}(\beta)}$	$\int e^{j2\pi(c\beta + \zeta F^{(\kappa)}(\beta))} d\beta$	$\delta(b - F^{(\kappa)}(\beta))$
GQ	$\frac{1}{ \tilde{\alpha} } e^{j2\pi c b / \tilde{\alpha}}$	$e^{j2\pi \tilde{\alpha} \zeta \beta}$	$\delta(c + \tilde{\alpha} \zeta)$	$\delta(b - \tilde{\alpha} \beta)$
$HP^{(\kappa)}$	$\int G^{(H)}(\beta) \delta(b - F^{(\kappa)}(\beta)) \times e^{j2\pi c\beta} d\beta$	$G^{(H)}(\beta) e^{j2\pi\zeta F^{(\kappa)}(\beta)}$	$\int G^{(H)}(\beta) \times e^{j2\pi[\zeta F^{(\kappa)}(\beta) + c\beta]} d\beta$	$G^{(H)}(\beta) \times \delta\left(b - \frac{1}{\kappa} \ln \left(\frac{\sinh(\kappa\beta/2)}{\kappa\beta/2}\right)\right)$
HYP	$Qr\left(\frac{-c}{f_r e^{-b}}, f_r e^{-b}\right)$ $= WD_{W\Gamma}\left(\frac{-c}{f_r}, -bf_r\right)$	$HAF_{\Gamma}(-\zeta, -\beta)$ $= AF_{W\Gamma}\left(\frac{-\zeta}{f_r}, -f_r\beta\right)$	$v_{\Gamma}(-c, -\zeta)$ $= \frac{1}{f_r} u_{W\Gamma}(-c/f_r, -\zeta/f_r)$	$V_{\Gamma}(-b, -\beta)$ $= f_r U_{W\Gamma}(-f_r b, -f_r \beta)$
LH	$\int G^{(H)}(\beta) \delta(b - F^{(H)}(\beta)) e^{j2\pi c\beta} d\beta$	$G^{(H)}(\beta) e^{j2\pi\zeta F^{(H)}(\beta)}$	$\int G^{(H)}(\beta) e^{j2\pi[\zeta F^{(H)}(\beta) + c\beta]} d\beta$	$G^{(H)}(\beta) \delta(b - F^{(H)}(\beta))$
PQ	$f_r \delta(c) Q_{\Gamma}(0, f_r e^b)$ $= \delta(c/f_r) WD_{W\Gamma}(0, f_r b)$	$f_r v_{\Gamma}(0, \zeta)$ $= u_{W\Gamma}(0, \zeta/f_r)$	$f_r \delta(c) v_{\Gamma}(0, \zeta)$ $= \frac{1}{f_r} \delta\left(\frac{c}{f_r}\right) u_{W\Gamma}(0, \zeta/f_r)$	$f_r Q_{\Gamma}(0, f_r e^b)$ $= f_r WD_{W\Gamma}(0, f_r b)$
PWH	$\int s^{(H)}(\eta) \frac{1}{ \eta } e^{-j2\pi \frac{b}{\eta}} d\eta$	$S^{(H)}(\zeta\beta)$	$\frac{1}{ \zeta } s^{(H)}\left(\frac{c}{\zeta}\right)$	$\frac{1}{ \beta } s^{(H)}\left(\frac{b}{\beta}\right)$
Q	$\delta(c)\delta(b)$	1	$\delta(c)$	$\delta(b)$
SPQ	$f_r s(c) Q_{\Gamma}(0, f_r e^b)$ $= s(c/f_r) WD_{W\Gamma}(0, f_r b)$	$f_r S(\beta) v_{\Gamma}(0, \zeta)$ $= S(f_r \beta) u_{W\Gamma}(0, \zeta/f_r)$	$f_r s(c) v_{\Gamma}(0, \zeta)$ $= \frac{1}{f_r} s(c/f_r) u_{W\Gamma}(0, \zeta/f_r)$	$f_r S(\beta) Q_{\Gamma}(0, f_r e^b)$ $= f_r S(f_r \beta) WD_{W\Gamma}(0, f_r b)$
Warped $C_H$	$\Psi_{C_H}(c/f_r, f_r b)$	$\Psi_{C_H}(\zeta/f_r, f_r \beta)$	$\frac{1}{f_r} \Phi_{C_H}(c/f_r, \zeta/f_r)$	$f_r \Phi_{C_H}(f_r b, f_r \beta)$

Note: Here, HAF is the Hyperbolic AF,  
 $AF, \mu_0(\beta) = \frac{\beta/2}{\sinh(\beta/2)}, \mu(\beta) = S_{AH}(\beta)\mu_0(\beta), V_{\Gamma}(b, \beta) = f_r e^b \Gamma(f_r e^{b+\beta/2})$   
 $\Gamma^*(f_r e^{b-\beta/2}), F^{(\kappa)}(\beta) = \frac{1}{\kappa} \ln \frac{\sinh(\kappa \beta/2)}{\kappa \beta/2}, u_{\Gamma}(c, \zeta) = \gamma(c + \zeta/2)\gamma^*(c + \zeta/2), U_{\Gamma}(b, \beta) = \Gamma(b + \beta/2)\Gamma^*(b + \beta/2)$ , and  $v_{\Gamma}(c, \zeta)$  and  $(W\Gamma)(f)$  are defined in Equations 13.90 and 13.34, respectively.

$$HYP_X(t, f; \Gamma) = SPEC_{WX}\left(\frac{tf}{f_r}, f_r \ln \frac{f}{f_r}; W\Gamma\right)$$

$$SPEC_X(t, f; \Gamma) = HYP_{W^{-1}X}(te^{-f/f_r}, f_r e^{f/f_r}; W^{-1}\Gamma). \quad (13.96)$$

The constant bandwidth analysis of many Cohen's-class TFRs, such as the spectrogram, is mapped into the multiresolution, constant Q analysis of many of the hyperbolic-class TFRs. Equation 13.96 demonstrates that the relatively new hyperbologram can be computed using standard spectrogram implementations. This one-to-one correspondence between TFRs in the Cohen and the hyperbolic classes greatly facilitates their analysis and gives alternative methods for calculating various TFRs.<sup>34,106</sup>

The hyperbolic and Cohen's-class kernels are related by a simple scaling factor, provided that any analysis windows are warped appropriately:<sup>100</sup>

$$\Psi_H^{(H)}(c, b) = \Psi_{C_H}\left(\frac{c}{f_r}, f_r b\right) \leftrightarrow \Psi_H^{(H)}(\zeta, \beta) = \Psi_{C_H}\left(\frac{\zeta}{f_r}, f_r \beta\right)$$

$$\Phi_H^{(H)}(c, \zeta) = \frac{1}{f_r} \Phi_{C_H}\left(\frac{c}{f_r}, \frac{\zeta}{f_r}\right) \leftrightarrow \Phi_H^{(H)}(b, \beta) = f_r \Phi_{C_H}(f_r b, f_r \beta)$$

$$\Gamma_H^{(H)}(b_1, b_2) = \frac{1}{\sqrt{|b_1 b_2|}} \Phi_{C_H}\left(-\ln \sqrt{b_1 b_2}, \ln(b_1/b_2)\right).$$

For example, comparing the WD kernels in Table 13.10 with the Altes Q kernels in Table 13.14 reveals that the Altes kernel

$$\psi_Q^{(H)}(c, b) = \psi_{WD}(c/f_r, f_r b) = \delta(c/f_r)\delta(f_r b) = \delta(c)\delta(b)$$

is identical to that of the WD; similarly, examining the spectrogram and hyperbologram kernels reveals that the kernels are related by an axis scaling and a warping of the spectrogram analysis window:

$$\psi_{HYP}^{(H)}(c, b) = \psi_{SPEC}(c/f_r, f_r b) = WD_{WT}(-c/f_r, -bf_r)$$

Properties of Cohen's-class TFRs also map in a one-to-one fashion to properties of the hyperbolicclass TFRs.<sup>100</sup> For example, the WD's perfect localization of linear FM chirps ( $P_{22}$ ) warps to the Altes Q distribution's perfect localization for hyperbolic FM chirps ( $P_{23}$ ).

### 13.5.4.1 Affine-Hyperbolic Subclass

Affine-hyperbolic subclass

$$\begin{aligned} &= \left\{ T_Y(t, f) | Y(f) = \frac{1}{\sqrt{|a|}} X\left(\frac{f}{a}\right) e^{-j2\pi c \ln(f/f_r)} e^{j2\pi f t_0} \right. \\ &\Rightarrow T_Y(t, f) = T_X\left(a\left(t - t_0 - \frac{c}{f}\right), \frac{f}{a}\right) \left. \right\} \end{aligned}$$

TFRs that satisfy properties  $P_2$ – $P_4$  in Table 13.6 are members of the intersection of the affine class with the hyperbolic class, as depicted graphically in Figure 13.4. The most commonly known member of the affine-hyperbolic subclass is the unitary form of the Bertrand  $P_0$  distribution. The first entry in Table 13.13 indicates that any member of the affine-hyperbolic subclass can be written as an affine smoothed version of the unitary Bertrand  $P_0$  distribution. Evaluation of the first entry in Table 13.14 reveals that the two-dimensional kernels of the TFRs in this subclass simplify to a function of a one-dimensional prototype  $S_{AH}(\beta)$ . This greatly simplifies the kernel constraints in Table 13.8.

### 13.5.5 $\kappa$ th Power Class

$\kappa$ th power class

$$\begin{aligned} &= \left\{ T_X(t, f) | Y(f) = \frac{1}{\sqrt{|a|}} X\left(\frac{f}{a}\right) \exp(-j2\pi c [\text{sgn}(f)] |f/f_r|^\kappa) \right. \\ &\Rightarrow T_Y(t, f) = T_X\left(a\left(t - \frac{\kappa}{f_r} \left|\frac{f}{f_r}\right|^{\kappa-1}\right), \frac{f}{a}\right) \left. \right\} \end{aligned}$$

The power classes of TFRs consists of many classes of TFRs, each indexed by  $-\infty < \kappa < \infty$ .<sup>73,100</sup> These TFRs are scale covariant (property  $P_3$ ) and power time-shift covariant, i.e.,

$$\begin{aligned} PC_Y^{(\kappa)}(t, f) &= PC_X^{(\kappa)}\left(t - c \frac{d}{df} \xi_\kappa(f/f_r), f\right) \quad \text{for } Y(f) \\ &= e^{-j2\pi c \xi_\kappa(f/f_r)} X(f) \\ &= PC_X^{(\kappa)}\left(t - c \frac{\kappa}{f_r} \left|\frac{f}{f_r}\right|^{\kappa-1}, f\right) \end{aligned} \quad (13.97)$$

where

$$\xi_\kappa(f) = \text{sgn}(f) |f|^\kappa \quad \text{for } \kappa \neq 0 \quad (13.98)$$

is a one-to-one phase function involving the  $\kappa$ th power of frequency,  $f$ .<sup>73,98,100</sup> Consequently, the  $\kappa$ th power class perfectly represents dispersive group delay changes in the signal that are proportional to powers of frequency. When  $\kappa=1$ , the power class is equivalent to the affine class in Equation 13.78. Any member of the power class can be written in the following four normal forms and the corresponding bi-frequency form:

$$\begin{aligned} PC_X^{(\kappa)}\left(t, f; \Psi_{PC}^{(A)}\right) &= \left| \xi_\kappa\left(\frac{f}{f_r}\right) \right| \left| \int \varphi_{PC}^{(A)}\left(\xi_\kappa\left(\frac{f}{f_r}\right) \left[\frac{t}{\tau_\kappa(f)} - c\right], \right. \right. \\ &\quad \left. \left. \times \xi_\kappa\left(\frac{f}{f_r}\right) \zeta\right) \nu_X^{(\kappa)}(c, \zeta) dc d\zeta \right. \end{aligned} \quad (13.99)$$

$$\begin{aligned} &= \frac{1}{\left| \xi_\kappa\left(\frac{f}{f_r}\right) \right|} \iint \Phi_{PC}^{(A)}\left(\frac{-b}{\xi_\kappa\left(\frac{f}{f_r}\right)}, \frac{\beta}{\xi_\kappa\left(\frac{f}{f_r}\right)}\right) \\ &\quad \times V_X^{(\kappa)}(b, \beta) e^{j2\pi \frac{t}{\tau_\kappa(f)} \beta} db d\beta \end{aligned} \quad (13.100)$$

$$\begin{aligned} &= \iint \psi_{PC}^{(A)}\left(\xi_\kappa\left(\frac{f}{f_r}\right) \left[\frac{-t'}{\tau_\kappa(f')} + \frac{t}{\tau_\kappa(f)}\right], \right. \\ &\quad \left. -\xi_\kappa\left(\frac{f'}{f_r}\right)\right) WD_X^{(\kappa)}(t', f') dt' df' \end{aligned} \quad (13.101)$$

$$\begin{aligned} &= \iint \psi_{PC}^{(A)}\left(\xi_\kappa\left(\frac{f}{f_r}\right) \zeta, \frac{\beta}{\xi_\kappa\left(\frac{f}{f_r}\right)}\right) \\ &\quad \times AF_X^{(\kappa)}(\zeta, \beta) e^{j2\pi \frac{t}{\tau_\kappa(f)} \beta} d\zeta d\beta \end{aligned} \quad (13.102)$$

$$\begin{aligned} &= \frac{1}{|f|} \iint \Gamma_{PC}^{(A)(\kappa)}\left(\frac{f_1}{f}, \frac{f_2}{f}\right) e^{j2\pi \frac{t}{\tau_\kappa(f)} [\xi_\kappa\left(\frac{f_1}{f_r}\right) - \xi_\kappa\left(\frac{f_2}{f_r}\right)]} \\ &\quad \times X(f_1) X^*(f_2) df_1 df_2. \end{aligned} \quad (13.103)$$

Below are the definitions of the  $\kappa$ th signal product,

$$\begin{aligned} \nu_X^{(\kappa)}(c, \zeta) &= \rho_X^{(\kappa)}(c + \zeta/2) \rho_X^{(\kappa)*}(c - \zeta/2), \quad \text{with} \\ \rho_X^{(\kappa)}(c) &= \int X(f) \sqrt{|\tau_\kappa(f)|} e^{j2\pi c \xi_\kappa(f/f_r)} df, \end{aligned} \quad (13.104)$$

the  $\kappa$ th power signal spectrum product,

$$\begin{aligned} V_X^{(\kappa)}(b, \beta) &= \frac{f_r}{|\kappa| |b^2 - \beta^2/4|^{\frac{\kappa-1}{2\kappa}}} X(f_r \xi_\kappa^{-1}(b + \beta/2)) \\ &\quad X^*(f_r \xi_\kappa^{-1}(b - \beta/2)) \\ &= f_r (W_\kappa X)([b + \beta/2] f_r) (W_\kappa X)^*([b - \beta/2] f_r) \end{aligned} \quad (13.105)$$

the  $\kappa$ th central member,

$$\begin{aligned} \text{WD}_X^{(\kappa)}(t, f) &= \text{WD}_{W_\kappa X} \left( \frac{t}{f_r \tau_\kappa(f)}, f_r \xi_\kappa \left( \frac{f}{f_r} \right) \right) \\ &= \frac{|f|}{|\kappa|} \int \frac{1}{\left| 1 - \frac{\beta^2}{4} \right|^{\frac{\kappa-1}{2\kappa}}} X \left( f \xi_\kappa^{-1} \left( 1 + \frac{\beta}{2} \right) \right) \\ &\quad \times X^* \left( f \xi_\kappa^{-1} \left( 1 - \frac{\beta}{2} \right) \right) e^{j2\pi \frac{t}{f} \beta} d\beta, \end{aligned} \quad (13.106)$$

the  $\kappa$ th power AF,

$$\begin{aligned} \text{AF}_X^{(\kappa)}(\zeta, \beta) &= \text{AF}_{W_\kappa X} \left( \frac{\zeta}{f_r}, f_r \beta \right) \\ &= \int \frac{f_r}{|\kappa| \left| b^2 - \frac{\beta^2}{4} \right|^{\frac{\kappa-1}{2\kappa}}} X \left( f_r \xi_\kappa^{-1} (b + \beta/2) \right) \\ &\quad \times X^* \left( f_r \xi_\kappa^{-1} \left( b - \frac{\beta}{2} \right) \right) e^{j2\pi \zeta b} db, \end{aligned} \quad (13.107)$$

the  $\kappa$ th power inverse phase function,

$$\xi_\kappa^{-1}(b) = \text{sgn}(b)|b|^{1/\kappa}, \quad f \in \Re, \quad \kappa \neq 0, \quad (13.108)$$

the  $\kappa$ th power group delay,

$$\tau_\kappa(f) = \frac{d}{df} \xi_\kappa \left( \frac{f}{f_r} \right) = \frac{\kappa}{f_r} \left| \frac{f}{f_r} \right|^{\kappa-1}, \quad f \in \Re \text{ for } \kappa \neq 0, \quad (13.109)$$

and the  $\kappa$ th power signal warping.

$$\begin{aligned} (W_\kappa X)(f) &= \frac{1}{\sqrt{|f_r| \tau_\kappa \left( f_r \xi_\kappa^{-1} \left( \frac{f}{f_r} \right) \right)}} X \left( f_r \xi_\kappa^{-1} \left( \frac{f}{f_r} \right) \right) \\ &= \frac{1}{\sqrt{|\kappa| |f/f_r|^{\frac{\kappa-1}{2\kappa}}}} X \left( f_r \text{sgn}(f) |f/f_r|^{1/\kappa} \right). \end{aligned} \quad (13.110)$$

TABLE 13.15  $\kappa$ th Power Class TFRs

$\kappa$ th PC TFR	Formula	
Affine Class	$A_x(t, f; \Psi_A^{(A)})$	$= PC_X^{(1)}(t, f; \Psi_A^{(A)})$
Hyperbolic-Power	$H P_X^{(\kappa)}(t, f; G^{(H)})$	$= \frac{ f }{ \kappa } \int g^{(H)} \left( \frac{f}{\kappa} (t - t') \right) B P_0 D_X^{(\kappa)}(t', f; \mu_0) dt', \quad f > 0$
Localized-Power	$LP_X^{(\kappa)}(t, f; G^{(A)}, F^{(A)})$	$= \frac{ f }{ \kappa } \int \frac{G^{(A)}(\beta)}{\left  -F^{(A)^2}(\beta) - \beta^2/4 \right ^{\frac{\kappa-1}{2\kappa}}} X \left( f \xi_\kappa^{-1} (-F^{(A)}(\beta) + \beta/2) \right) \\ \times X^* \left( f \xi_\kappa^{-1} (-F^{(A)}(\beta) - \beta/2) \right) e^{j2\pi t f \beta / \kappa} d\beta$
Pow. Unitary $P_0$	$BP_0 D_X^{(\kappa)}(t, f; \mu_0)$	$= f \int X \left( f \left( \frac{\kappa\beta/2}{\sinh \kappa\beta/2} \right)^{1/\kappa} e^{\beta/2} \right) X^* \left( f \left( \frac{\kappa\beta/2}{\sinh \kappa\beta/2} \right)^{1/\kappa} e^{-\beta/2} \right) \left( \frac{\kappa\beta/2}{\sinh \kappa\beta/2} \right)^{1/\kappa} e^{j2\pi t f \beta} d\beta$
Bertrand $P_\kappa$	$BP_\kappa D_X(t, f; \mu)$	$= f \int X(f\lambda_\kappa(u)) X^*(f\lambda_\kappa(-u)) \mu(u) e^{j2\pi t f (\lambda_\kappa(u) - \lambda_\kappa(-u))} du, \quad f > 0$ with $\lambda_\kappa(u) = \left[ k \frac{e^{-u} - 1}{e^{-ku} - 1} \right]^{\frac{1}{\kappa-1}}, \quad k \neq 0, 1, \lambda_1(u) = \exp \left[ 1 + \frac{ue^{-u}}{e^{-u} - 1} \right]$ , and $\mu(u) = \mu^*(-u)$
Power Flandrin	$FD_X^{(\kappa)}(t, f)$	$= \left  \xi_\kappa \left( \frac{f}{f_r} \right) \right  \int V_X^{(\kappa)} \left( \xi_\kappa \left( \frac{f}{f_r} \right) \left[ 1 + \left( \frac{\beta}{4} \right)^2 \right], \xi_\kappa \left( \frac{f}{f_r} \right) \beta \right) \left[ 1 - \left( \frac{\beta}{4} \right)^2 \right] e^{j2\pi t f \beta / \kappa} d\beta$
Powegram	$POW_X^{(\kappa)}(t, f; \Gamma)$	$= \frac{f_r}{ f } \left  \int X(f') \Gamma^*(f_r f' / f) e^{j2\pi \frac{t}{f_r} \xi_\kappa(f' / f)} df' \right ^2$
Pow. Unterberger Act.	$UAD_X^{(\kappa)}(t, f)$	$=  \xi_\kappa(f/f_r)  \int V_X^{(\kappa)}(\xi_\kappa(f/f_r) \left[ \sqrt{1 + (\beta/2)^2} \right], \xi_\kappa(f/f_r) \beta) e^{j2\pi t f \beta / \kappa} d\beta$
Pow. Unterberger Pass.	$UAD_X^{(\kappa)}(t, f)$	$=  \xi_\kappa(f/f_r)  \int V_X^{(\kappa)}(\xi_\kappa(f/f_r) \left[ \sqrt{1 + (\beta/2)^2} \right], \xi_\kappa(f/f_r) \beta) \frac{1}{\sqrt{1 + (\beta/2)^2}} e^{j2\pi t f \beta / \kappa} d\beta$
Power Generalized	$GWD_X^{(\kappa)}(t, f; \tilde{\alpha})$	$= \frac{f_r}{ \kappa } \int \frac{1}{\left  (\xi_\kappa(f/f_r) - \tilde{\alpha}\beta)^2 - \beta^2/4 \right ^{\frac{\kappa-1}{2\kappa}}} X \left( f_r \xi_\kappa^{-1} (\xi_\kappa(f/f_r) - \tilde{\alpha}\beta + \beta/2) \right) X^* \left( f_r \xi_\kappa^{-1} (\xi_\kappa(f/f_r) - \tilde{\alpha}\beta - \beta/2) \right) e^{j2\pi \frac{t}{f_r} \beta} d\beta$
Power Wigner	$WD_X^{(\kappa)}(t, f)$	$= \frac{ f }{ \kappa } \int \frac{1}{\left  1 - \beta^2/4 \right ^{\frac{\kappa-1}{\kappa}}} X \left( f \xi_\kappa^{-1} (1 + \beta/2) \right) X^* \left( f \xi_\kappa^{-1} (1 - \beta/2) \right) e^{j2\pi t f \beta / \kappa} d\beta$

Note:  $v_X^{(\kappa)}(c, \zeta)$  and  $V_X^{(\kappa)}(b, \beta)$  are power signal products defined in Equations 13.104 and 13.105, and the power functions  $\xi_\kappa(b)$  and  $\tau_\kappa(f)$  are given in Equations 13.98 and 13.109, respectively.

The bi-frequency kernel in Equation 13.103 is related to the normal form kernels as follows:

$$\Gamma_{PC}^{(A)(\kappa)}(b_1, b_2) = \begin{cases} \left| \xi'_\kappa(\sqrt{|b_1 b_2|}) \right| \\ \Phi_{PC}^{(A)}\left(-\frac{\xi_\kappa(b_1) + \xi_\kappa(b_2)}{2}, \right. \\ \left. \xi_\kappa(b_1) - \xi_\kappa(b_2) \right), & \kappa \neq 0 \\ \Gamma_{PC}^{(A)}(b_1, b_2), & \kappa = 1. \end{cases}$$

A list of power-class TFRs is given in Table 13.15. These PC TFRs are well matched to power chirps and dispersive power-time shifts, e.g.,

$$\begin{aligned} X(f) &= \sqrt{\tau_X(f)} e^{-j2\pi\xi_X(f/f_r)} \Rightarrow \text{WD}_X^{(\kappa)}(t, f) \\ &= |\tau_\kappa(f)| \delta(t - c\tau_\kappa(f)). \end{aligned}$$

The best known among them are the Bertrand  $P_\kappa$  distributions. The PC TFR kernels for us in Equations 13.99 through 13.102 are given in Table 13.16. The last column in Table 13.7 lists the kernel constrains for a given power class TFR to have ideal

properties.<sup>100</sup> All TFRs, kernels, and properties of the power class correspond to a warped version of the TFRs, kernels, and properties, respectively, of the affine class. Every TFR,  $A_{PC}$ , in the affine class that is covariant to scale changes and constant time shifts, maps to a corresponding power-class TFR

$$\text{PC}_X^{(\kappa)}\left(t, f; \Psi_{PC}^{(A)}\right) = A_{W_\kappa, X}\left(\frac{t}{f_r \tau_\kappa(f)}, f_r \xi_\kappa\left(\frac{f}{f_r}\right); \Psi_{A_{PC}}^{(A)}\right) \quad (13.111)$$

that is covariant to scale changes and the dispersive time shifts in Equation 13.97 that are proportional to powers of frequency. Just as in Cohen’s-class to hyperbolic-class mapping in Equation 13.94, the transformation in Equation 13.111 involves a unitary warping of the signal and a scaling of the time–frequency axes. Likewise, affine-class TFR kernels and their corresponding PC TFR kernels are equivalent, provided any analysis windows are prewarped appropriately. For example, the affine-class Unterberger active distribution,  $\text{UAD}_X(t, f)$ , in Table 13.11 maps to the power-class TFR,  $\text{UAD}_X^{(\kappa)}(t, f)$ , in Table 13.15. Their respective kernels in Tables 13.12 and 13.16 are identical. The scalogram in Table 13.11 maps to the powergram in Table 13.15; their respective kernels in Tables 13.12 and 13.16 differ only in the power warping in Equation 13.110 of the analysis window spectrum  $\Gamma(f)$ .

TABLE 13.16 Normal Form Kernels of the Power-Class TFRs Defined in Table 13.15

PC TFR	$\Psi_{PC}^{(A)}(\zeta, \beta)$	$\Psi_{PC}^{(A)}(\zeta, \beta)$	$\Phi_{PC}^{(A)}(c, \zeta)$	$\Phi_{PC}^{(A)}(b, \beta)$
Unitary	$\int \frac{\beta/2}{\sinh \beta/2} \delta\left(b + \frac{\beta}{2} \coth(\beta/2)\right) e^{j2\pi c\beta} d\beta$	$\frac{\beta/2}{\sinh \beta/2} e^{-j2\pi \zeta \frac{\beta}{2} \coth \frac{\beta}{2}}$	$\int \frac{\beta/2}{\sinh \beta/2} e^{j2\pi(c\beta - \zeta \frac{\beta}{2} \coth \beta/2)} d\beta$	$\frac{\beta/2}{\sinh \beta/2} \delta\left(b + \frac{\beta}{2} \coth \frac{\beta}{2}\right)$
$BP_0D^{(\kappa)}$				
$LP^{(\kappa)}$	$\int G^{(A)}(\beta) \delta(b - F^{(A)}(\beta)) e^{j2\pi c\beta} d\beta$	$G^{(A)}(\beta) e^{j2\pi \zeta F^{(A)}(\beta)}$	$\int G^{(A)}(\beta) e^{j2\pi(\zeta F^{(A)}(\beta) + c\beta)} d\beta$	$G^{(A)}(\beta) \delta(b - F^{(A)}(\beta))$
$FD^{(\kappa)}$	$\int \left(1 - \left(\frac{\beta}{4}\right)^2\right) \delta\left(b + \left(1 + \left(\frac{\beta}{4}\right)^2\right)\right) e^{j2\pi c\beta} d\beta$	$\left[1 - \left(\frac{\beta}{4}\right)^2\right] e^{-j2\pi \zeta \left(1 + \left(\frac{\beta}{4}\right)^2\right)}$	$\int \left(1 - \left(\frac{\beta}{4}\right)^2\right) e^{j2\pi(c\beta - \zeta \left(1 + \left(\frac{\beta}{4}\right)^2\right))} d\beta$	$\left[1 - \left(\frac{\beta}{4}\right)^2\right] \delta\left(b + \left(1 + \left(\frac{\beta}{4}\right)^2\right)\right)$
$GWD^{(\kappa)}$	$\frac{1}{ \tilde{\alpha} } e^{j2\pi(c(b+1)/\tilde{\alpha})}$	$e^{j2\pi \zeta(\tilde{\alpha}\beta - 1)}$	$e^{-j2\pi \zeta} \delta(c + \tilde{\alpha}\zeta)$	$\delta(b + 1 - \tilde{\alpha}\beta)$
$LP^{(\kappa)}$	$\int G^{(A)}(\beta) \delta(b - F^{(A)}(\beta)) e^{j2\pi c\beta} d\beta$	$G^{(A)}(\beta) e^{j2\pi \zeta F^{(A)}(\beta)}$	$\int G^{(A)}(\beta) e^{j2\pi(c\beta + \zeta F^{(A)}(\beta))} d\beta$	$G^{(A)}(\beta) \delta(b - F^{(A)}(\beta))$
$POW^{(\kappa)}$	$\text{WD}_\Gamma^{(\kappa)}(-\tau_\kappa(f_r \xi_\kappa^{-1}(b))c, -f_r \xi_\kappa^{-1}(b))$ $= \text{WD}_{W_\kappa \Gamma}(-c/f_r, -f_r b)$	$AF_\Gamma^{(\kappa)}(-\zeta, -\beta)$ $= AF_{W_\kappa \Gamma}(-\zeta/f_r, -f_r \beta)$	$\mathbf{v}_\Gamma^{(\kappa)}(-c, -\zeta)$	$V_\Gamma^{(\kappa)}(-b, -\beta)$ $= f_r U_{W_\kappa \Gamma}(-bf_r, -f_r \beta)$
$UAD^{(\kappa)}$	$\int \delta\left(b + \sqrt{1 + \left(\frac{\beta}{2}\right)^2}\right) e^{j2\pi c\beta} d\beta$	$e^{-j2\pi \zeta \sqrt{1 + \left(\frac{\beta}{2}\right)^2}}$	$\int e^{j2\pi(c\beta - \zeta \sqrt{1 + \left(\frac{\beta}{2}\right)^2})} d\beta$	$\delta\left(b + \sqrt{1 + \left(\frac{\beta}{2}\right)^2}\right)$
$UPD^{(\kappa)}$	$\int \left[1 + \left(\frac{\beta}{2}\right)^2\right]^{-1/2} \delta\left(b + \sqrt{1 + \left(\frac{\beta}{2}\right)^2}\right) \times e^{j2\pi c\beta} d\beta$	$\left[1 + \left(\frac{\beta}{2}\right)^2\right]^{-1/2} \times e^{-j2\pi \zeta \sqrt{1 + \left(\frac{\beta}{2}\right)^2}}$	$\int \left[1 + \left(\frac{\beta}{2}\right)^2\right]^{-1/2} \times e^{j2\pi(c\beta - \zeta \sqrt{1 + \left(\frac{\beta}{2}\right)^2})} d\beta$	$\left[1 + \left(\frac{\beta}{2}\right)^2\right]^{-1/2} \times \delta\left(b + \sqrt{1 + \left(\frac{\beta}{2}\right)^2}\right)$
$WD^{(\kappa)}$	$\delta(c) \delta(b + 1)$	$e^{-j2\pi \zeta}$	$e^{-j2\pi \zeta} \delta(c)$	$\delta(b + 1)$

Note: Here,  $AF_X^{(\kappa)}(\zeta, \beta)$ ,  $\mathbf{v}_\Gamma^{(\kappa)}(c, \zeta)$ ,  $V_\Gamma^{(\kappa)}(b, \beta)$ , and  $(W_\kappa X)(f)$  are defined in Equations 13.104, 13.105, 13.107, and 13.110, respectively, and  $U_\Gamma(b, \beta) = \Gamma(b + \beta/2) \Gamma^*(b - \beta/2)$ .

## 13.6 Summary

This chapter has focused on linear and quadratic TFRs and the different types of properties that they should satisfy. Properties of the Fourier transform, Mellin transform, and unitary operators were used to understand the relative merits of these time-varying spectral representations. No known TFR is ideal for all applications, so the search continues for new ones. There are many other TFRs in the literature that are highly nonlinear functions of the signal; they have been proposed to adapt automatically to changes in the signal, to be always nonnegative, to extend the concepts of higher order cumulants and spectra, or to solve time-varying constrained optimization problems.<sup>1,4,24,103,116</sup> Recent research has focused on the mapping of known TFRs to multidimensional representations of arbitrary variables.<sup>44</sup>

## Acknowledgments

The author would like to acknowledge the help given by Dr. A. Papandreou-Suppappola proofreading this chapter, by S. Praveenkumar and R. Murray in formatting some of the tables, and by Dr. Papandreou-Suppappola and Dr. A. Costa in generating the figures.

## References

1. *Proceedings IEEE-SP International Symposium of Time-Frequency and Time-Scale Analysis*, Victoria, Canada, October 1992.
2. Special issue on wavelet transforms and multiresolution signal analysis, in *IEEE Trans. Inform. Theory*, 38, 1992.
3. Special issue on wavelets and signal processing, in *IEEE Trans. Signal Process.*, 1993.
4. *Proceedings IEEE-SP International Symposium on Time-Frequency and Time-Scale Analysis*, Philadelphia, PA, October 1994.
5. R. A. Altes, Detection, estimation, and classification with spectrograms, *J. Acoust. Soc. Am.*, 67, 1232–1246, April 1980.
6. R. A. Altes, Wide-band, proportional-bandwidth Wigner-Ville analysis, *IEEE Trans. Acoust. Speech Signal Process.*, 38(6), 1005–1012, June 1990.
7. R. A. Altes and E. L. Titlebaum, Bat signals as optimally Doppler tolerant waveforms, *J. Acoust. Soc. Am.*, 48(4), 1014–1020, October 1970.
8. M. G. Amin, Time-frequency spectrum analysis and estimation for non-stationary random processes, in *Time-Frequency Signal Analysis*, B. Boashash (Ed.) pp. 208–232, Longman-Cheshire, Melbourne, Australia, 1992.
9. J. C. Anderson. Speech analysis/synthesis based on perception, Technical Report 707, MIT Lincoln Laboratory, Lexington, MA, November 1984.
10. F. Auger, Représentations temps-fréquence des signaux non-stationnaires: Synthèse et contribution, PhD thesis, Université de Nantes, Nantes, France, December 1991.
11. F. Auger, Some simple parameter determination rules for the generalized Choi-Williams and Butterworth distributions, *IEEE Signal Proc. Lett.*, 1994.
12. F. Auger and C. Doncarli, Quelques commentaires sur des représentations temps-fréquence proposées récemment, *Traitement du Signal*, 9(1), 3–25, 1992.
13. F. Auger and P. Flandrin, The why and how of time-frequency reassignment, *IEEE-SP International Symposium on Time-Frequency and Time-Scale Analysis*, pp. 197–200, Philadelphia, PA, October 1994.
14. R. G. Baraniuk, Warped perspectives in time-frequency analysis, *IEEE-SP International Symposium on Time-Frequency and Time-Scale Analysis*, pp. 528–531, Philadelphia, PA, October 1994.
15. R. G. Baraniuk and D. L. Jones, Unitary equivalence: A new twist on signal processing, *IEEE Trans. Signal Process.*, to appear.
16. R. G. Baraniuk and D. L. Jones, Shear madness: New orthonormal bases and frames using chirp functions, *IEEE Trans. Signal Process.*, 41, 3543–3549, December 1993.
17. R. G. Baraniuk and D. L. Jones, A signal-dependent time-frequency representation: Optimal kernel design, *IEEE Trans. Signal Process.*, 41, 1589–1602, April 1993.
18. M. Basseville, P. Flandrin, and N. Martin, Signaux non-stationnaires, analyse temps-fréquence et segmentation. fiches descriptives d'algorithmes, *Traitement du Signal*, 9 (1 supplement), 1992.
19. J. Bertrand and P. Bertrand, Affine time-frequency distributions, in *Time-Frequency Signal Analysis—Methods and Applications*, B. Boashash (Ed.), Chapter 5, pp. 118–140, Longman-Cheshire, Melbourne, Australia, 1992.
20. J. Bertrand and P. Bertrand, A class of affine Wigner functions with extended covariance properties, *J. Math. Phys.*, 33, 2515–2527, 1992.
21. J. Bertrand, P. Bertrand, and J. P. Ovarlez, Discrete Mellin transform for signal analysis, *Proceedings IEEE International Conference on Acoustics, Speech, and Signal Processing*, pp. 1603–1606, Albuquerque, NM, April 1990.
22. R. E. Blahut, W. Miller, and C. H. Wilcox, *Radar and Sonar, Part I*, Springer-Verlag, New York, 1991.
23. B. Boashash, Time-frequency signal analysis, in *Advances in Spectrum Estimation*, pp. 418–517, S. Haykin (Ed.), Prentice Hall, Inc., Englewood Cliffs, NJ, 1990.
24. B. Boashash, (Ed.), *Time-frequency Signal Analysis—Methods and Applications*. Longman-Cheshire, Melbourne, Australia, 1992.
25. G. F. Boudreaux-Bartels, Time-frequency signal processing algorithms: Analysis and synthesis using Wigner distributions, PhD thesis, Rice University, Houston, TX, December 1983.

26. G. F. Boudreaux-Bartels, Time-varying signal processing using the Wigner-distribution time-frequency signal representation, in *Advances in Geophysical Data Processing, Vol. 2. Two Dimensional Transforms*, M. Simaan (Ed.), pp. 33–79, JAI Press Inc., Greenwich, CT, 1985.
27. G. F. Boudreaux-Bartels, On the use of operators vs. warpings vs. axiomatic derivations of new time-frequency-scale (operator) representations, *Proceedings Twenty-Eighth Asilomar Conference on Signals, Systems and Computers*, Pacific Grove, CA, October/November 1994.
28. G. F. Boudreaux-Bartels, Time-varying signal processing using Wigner distribution synthesis techniques, in *The Wigner Distribution—Theory and Applications in Signal Processing*, W. Mecklenbräuker (Ed.), North Holland Elsevier Science Publishers, Amsterdam, the Netherlands, 1995.
29. G. F. Boudreaux-Bartels, Useful equations for time-frequency-scale representations, Technical Report 0895–0001, University of Rhode Island, Electrical Eng. Dept., Kingston, RI, 1995.
30. G. F. Boudreaux-Bartels and F. Hlawatsch, References for the short-time Fourier transform, Gabor expansion, wavelet transform, Wigner distribution, ambiguity function, and other time-frequency and time-scale signal representations, Technical Report 0492–0001, University of Rhode Island, Electrical Eng. Dept., Kingston, RI, April 1992.
31. G. F. Boudreaux-Bartels and R. L. Murray, Time-frequency signal representations for biomedical signals, in *Biomedical Engineering Handbook*, Chapter 57, pp. 866–855, CRC Press, Inc., Boca Raton, FL, 1995.
32. R. N. Bracewell, *The Fourier Transform and Its Applications*, 2nd edn., revised, McGraw-Hill, New York, 1986.
33. E. O. Brigham, *The Fast Fourier Transform and Its Applications*, Prentice-Hall, Englewood Cliffs, NJ, 1988.
34. K. G. Canfield and D. L. Jones, Implementing time-frequency representations for Non-Cohen Classes, *Proceedings Twenty-Seventh Asilomar Conference on Signals, Systems and Computers*, Pacific Grove, CA, November 1993.
35. H. I. Choi and W. J. Williams, Improved time-frequency representation of multicomponent signals using exponential kernels, *IEEE Trans. Acoust. Speech Signal Process.*, 37, 862–871, June 1989.
36. C. K. Chui (Ed.), *Wavelets: A Tutorial in Theory and Applications*, Academic Press, Inc., Boston, MA, 1992.
37. T. A. C. M. Claasen and W. F. G. Mecklenbräuker, The Wigner distribution—A tool for time-frequency signal analysis, Part I: Continuous-time signals, *Philips J. Res.*, 35, 217–250, 1980.
38. T. A. C. M. Claasen and W. F. G. Mecklenbräuker, The Wigner distribution—A tool for time-frequency signal analysis, Part II: Discrete-time signals, *Philips J. Res.*, 35, 276–300, 1980.
39. T. A. C. M. Claasen and W. F. G. Mecklenbräuker, The Wigner distribution—A tool for time-frequency signal analysis, Part III: Relations with other time-frequency signal transformations, *Philips J. Res.*, 35, 372–389, 1980.
40. L. Cohen, Generalized phase-space distribution functions, *J. Math. Phys.*, 7, 781–786, 1966.
41. L. Cohen, Time-frequency distribution—A review, *Proceedings IEEE*, 77, 941–981, July 1989.
42. L. Cohen, A primer on time-frequency analysis, in *Time-Frequency Signal Analysis*, B. Boashash (Ed.), pp. 3–42, John Wiley & Sons, Inc., New York, 1992.
43. L. Cohen, *Time Frequency Analysis*, Prentice-Hall, Inc., Englewood Cliffs, NJ, 1995.
44. L. Cohen and R. G. Baraniuk, Joint distributions for arbitrary variables, *IEEE-SP International Symposium on Time-Frequency and Time-Scale Analysis*, pp. 520–523, Philadelphia, PA, October 1994.
45. A. H. Costa, Multifform, tilttable time-frequency representations and masked auto Wigner distribution synthesis, PhD thesis, University of Rhode Island, Kingston, RI, May 1994.
46. G. Courbebaisse, Transformée bilinéaire temps-échelle des signaux asymptotiques d'énergie finie, in *14ème Coll. GRETSI*, Juan-les-Pins, France, 1993.
47. R. E. Crochiere and L. R. Rabiner, *Multi-Rate Digital Signal Processing*, Prentice Hall, Inc., Englewood Cliffs, NJ, 1983.
48. G. S. Cunningham and W. J. Williams, Fast implementation of generalized discrete time-frequency distributions, *IEEE Trans. Signal Process.*, 42, 1496–1508, 1994.
49. I. Daubechies, *Ten Lectures on Wavelets*, Society for Industrial and Applied Mathematics, Philadelphia, PA, 1992.
50. N. G. DeBruijn, A theory of generalized functions with applications to Wigner distribution and Weyl correspondence, *Nieuw Archief voor Wiskunde*, 21(3), 205–280, 1973.
51. G. Eichmann and N. M. Marinovich, Scale-invariant Wigner distribution and ambiguity functions, *Proceedings of SPIE*, 519, 18–24, 1985.
52. P. Flandrin, Some features of time-frequency representations of multicomponent signals, *Proceedings IEEE International Conference on Acoustics, Speech, and Signal Processing*, pp. 41B.4.1–4, San Diego, CA, March 1984.
53. P. Flandrin, Time-frequency processing of bat sonar signals, in *Animal Sonar Systems Symposium*, Hilsinger, Denmark, September 1986.
54. P. Flandrin, Représentations temps-fréquence des signaux non-stationnaires, PhD thesis, Institut National Polytechnique de Grenoble, France, 1987.
55. P. Flandrin, Maximum signal energy concentration in a time-frequency domain, *Proceedings IEEE International Conference on Acoustics, Speech, and Signal Processing*, pp. 2176–2179, 1988.
56. P. Flandrin, A time-frequency formulation of optimum detection, *IEEE Trans. Acoust. Speech Signal Process.*, 36, 1377–1384, September 1988.
57. P. Flandrin, Scale-invariant Wigner spectra and self-similarity, *Proceedings European Signal Processing Conference, EUSIPCO—90*, pp. 149–152, Barcelona, Spain, September 1990.



58. P. Flandrin, Fractional Brownian motion and wavelets, in *Wavelets, Fractals and Fourier transforms—New Developments and New Applications*, M. Farge, J. C. R. Hunt, and J. C. Vassilicos (Eds.), Oxford University Press, Oxford, U.K., 1991.
59. P. Flandrin, On the time-scale analysis of self similar processes, In *The Role of Wavelets in Signal Processing Applications*, B. W. Suter, M. E. Oxley, and G. T. Warhola (Eds.), No. AFIT/EN-TR-92-3, pp. 137–150, 1992.
60. P. Flandrin, *Temps-Fréquence*, Hermès, Paris, 1993.
61. P. Flandrin and B. Escudié, Time and frequency representation of finite energy signals: A physical property as a result of a Hilbertian condition, *Signal Process.*, 2, 93–100, 1980.
62. P. Flandrin and P. Gonçalves, Geometry of affine distributions, *IEEE-SP International Symposium on Time-Frequency and Time-Scale Analysis*, pp. 80–83, Philadelphia, PA, October 1994.
63. P. Flandrin and O. Rioul, Affine smoothing of the Wigner-Ville distribution, *Proceedings IEEE International Conference on Acoustics, Speech, and Signal Processing*, pp. 2455–2458, Albuquerque, NM, April 1990.
64. D. Gabor, Theory of communication, *J. IEEE*, 93(III), 429–457, November 1946.
65. P. Gonçalves, Représentations temps-fréquence et temps-échelle bilinéaires: synthèse et contributions, PhD thesis, Institut National Polytechnique de Grenoble, France, November 1993.
66. F. Hlawatsch, *A study of bilinear time-frequency signal representations with applications to time-frequency signal synthesis*, PhD thesis, Technische Universität Wien, Vienna, Austria, 1988.
67. F. Hlawatsch, Duality and classification of bilinear time-frequency signal representations, *IEEE Trans. Signal Process.*, 39(7), pp. 1564–1574, July 1991.
68. F. Hlawatsch, Time-frequency methods for signal processing, Technical Report 1291-0001, University of Rhode Island, Electrical Eng. Dept., Kingston, Rhode Island, December 1991.
69. F. Hlawatsch and G. F. Boudreaux-Bartels, Linear and quadratic time-frequency signal representations, *IEEE Signal Process. Mag.*, 9(2), 21–67, April 1992.
70. F. Hlawatsch and P. Flandrin, The interference structure of the Wigner distribution and related time-frequency signal representations, in *The Wigner Distribution—Theory and Applications in Signal Processing*, W. Mecklenbräuker (Ed.), North Holland Elsevier Science Publishers, Amsterdam, the Netherlands, 1995.
71. F. Hlawatsch and W. Krattenthaler, Bilinear signal synthesis, *IEEE Trans. Signal Process.*, 40(2), 352–363, February 1992.
72. F. Hlawatsch and W. Krattenthaler, Signal synthesis algorithms for bilinear time-frequency signal representations, in *The Wigner Distribution—Theory and Applications in Signal Processing*, W. Mecklenbräuker (Ed.), North Holland Elsevier Science Publishers, Amsterdam, the Netherlands, 1995.
73. F. Hlawatsch, A. Papandreou, and G. F. Boudreaux-Bartels, The power classes of quadratic time-frequency representations: A generalization of the affine and hyperbolic classes, *Proceedings Twenty-Seventh Asilomar Conference on Signals, Systems and Computers*, pp. 1265–1270, Pacific Grove, CA, November 1993.
74. F. Hlawatsch and R. L. Urbanke, Bilinear time-frequency representations of signals: The shift-scale invariant class, *IEEE Trans. Signal Process.*, 42(2), 357–366, February 1994.
75. C. P. Janse and A. J. M. Kaizer, Time-frequency distributions of loudspeakers: The application of the Wigner distribution, *J. Audio Eng. Soc.*, 31, pp. 198–223, April 1983.
76. J. Jeong and W. J. Williams, On the cross-terms in spectrograms, *Proc. IEEE Int. Symp. Ckts. Syst.*, pp. 1565–1568, 1990.
77. J. Jeong and W. J. Williams, Time-varying filtering and signal synthesis using the extended discrete-time Wigner distribution. In B. Boashash and P. Boles (Eds.), *Proc. ISSPA90, Sig. Proc., Theories, Impl. Appl.*, pp. 895–898, 1990.
78. J. Jeong and W. J. Williams, Alias-free generalized discrete-time time-frequency distributions, *IEEE Trans. Signal Process.*, 40, 2757–2765, November 1992.
79. J. Jeong and W. J. Williams, Kernel design for reduced interference distributions, *IEEE Trans. Signal Process.*, 40(2), 402–412, February 1992.
80. D. L. Jones and T. W. Parks, A resolution comparison of several time-frequency representations, *IEEE Trans. Signal Process.*, 40, 413–420, February 1992.
81. S. Kadambe, The application of time-frequency and time-scale representations in speech analysis, PhD thesis, University of Rhode Island, Kingston, RI, 1991.
82. S. Kadambe and G. F. Boudreaux-Bartels, A comparison of the existence of “cross terms” in the Wigner distribution and the squared magnitude of the wavelet transform and the short-time Fourier transform, *IEEE Trans. Signal Process.*, 40(10), 2498–2517, October 1992.
83. R. Koenig, H. K. Dunn, and L. Y. Lacy, The sound spectrograph, *J. Acoust. Soc. Amr.*, 18, pp. 19–49, 1946.
84. P. Loughlin, J. Pitton, and L. E. Atlas, Bilinear time-frequency representations: New insights and properties, *IEEE Trans. Signal Process.*, 41, 750–767, 1993.
85. N. Marinovich and U. G. Oklobdzija, VLSI chip architecture for real time ambiguity function computation, *Proceedings of the Asilomar Conference on Signals, Systems and Computers*, pp. 74–78, Pacific Grove, CA, November 1991.
86. N. M. Marinovich, The Wigner distribution and the ambiguity function: Generalizations, enhancement, compression and some applications, PhD thesis, The City University of New York, New York, 1986.

87. W. F. G. Mecklenbräuker, A tutorial on non-parametric bilinear time–frequency signal representations, in *Time and Frequency Representations of Signals and Systems*, G. Longo and B. Picinbono (Eds.), Springer-Verlag, New York, 1989, pp. 11–68.
88. W. F. G. Mecklenbräuker (Ed.), *The Wigner Distribution: Theory and Applications in Signal Processing*, North Holland Elsevier Science Publishers, Amsterdam, the Netherlands, 1995.
89. Y. Meyer, *Wavelets—Algorithms and Applications*, Society for Industrial and Applied Mathematics, Philadelphia, PA, 1993.
90. R. L. Murray, Dyadic wavelet transform based QRS detector, Master's thesis, University of Rhode Island, Electrical Eng. Dept., Kingston, RI, 1993.
91. R. L. Murray, Biomedical applications of time–frequency signal processing, Technical Report 0195–0001, University of Rhode Island, Electrical Eng. Dept., Kingston, RI, January 1995.
92. S. H. Nawab and T. F. Quatieri, Short-term Fourier transform, In *Advanced Topics in Signal Processing*, J. S. Lim and A. V. Oppenheim (Eds.), Prentice Hall, Englewood Cliffs, NJ, 1988.
93. A. H. Nuttall, Alias-free smoothed Wigner distribution function for discrete-time samples, Technical Report TR 8785, Naval Underwater Systems Center, New London, CT, October 1990.
94. J. P. Ovarlez, La Transformation de Mellin: Un Outil Pour L'Analyse des Signaux à Large Bande, PhD thesis, Thèse Univ. Paris 6, 1992.
95. J. P. Ovarlez, J. Bertrand, and P. Bertrand, Computation of affine time–frequency distributions using the fast Mellin transform, *Proceedings of IEEE International Conference on Acoustics, Speech, and Signal Processing*, vol. 5, pp. 117–120, San Francisco, CA, 1992.
96. A. Papandreou, G. F. Boudreaux-Bartels, and S. M. Kay, Detection and estimation of generalized chirps using time–frequency representations, *Proceedings Twenty-Eighth Asilomar Conference on Signals, Systems, and Computers*, Pacific Grove, CA, October/November 1994.
97. A. Papandreou, F. Hlawatsch, and G. F. Boudreaux-Bartels, The hyperbolic class of quadratic time–frequency representations, Part I: Constant-Q warping, the hyperbolic paradigm, properties, and members, *IEEE Trans. Signal Process.*, 41, 3425–3444, December 1993.
98. A. Papandreou, F. Hlawatsch, and G. F. Boudreaux-Bartels, A unified framework for the scale covariant affine, hyperbolic, and power class time–frequency representations using generalized time-shifts, *Proceedings 1995 International Conference on Acoustics, Speech and Signal Processing*, Detroit, MI, May 1995.
99. A. Papandreou, S. M. Kay, and G. F. Boudreaux-Bartels, The use of hyperbolic time–frequency representations for optimum detection and parameter estimation of hyperbolic chirps, *IEEE-SP International Symposium on Time–Frequency and Time-Scale Analysis*, pp. 369–372, Philadelphia, PA, October 1994.
100. A. Papandreou-Suppappola, New classes of quadratic time–frequency representations with scale covariance and generalized time-shift covariance: Analysis, detection and estimation, PhD thesis, University of Rhode Island, Kingston, RI, May 1995.
101. A. Papoulis, *Signal Analysis*, McGraw-Hill, New York, 1977.
102. E. Peyrin and R. Prost, A unified definition for the discrete-time, discrete-frequency, and discrete-time/frequency Wigner distributions, *IEEE Trans. Acoust., Speech, Signal Process.*, 34, 858–867, 1986.
103. B. Porat, *Digital Processing of Random Signals: Theory and Methods*, Prentice-Hall, Inc., Englewood Cliffs, NJ, 1993.
104. M. R. Portnoff, Time–frequency representations of digital signals and systems based on short-time Fourier analysis, *IEEE Trans. Acoust. Speech Signal Process.*, 28, 55–69, February 1980.
105. A. Poularikas and S. Seeley, *Signals and Systems*, 2nd edn., PWD-Kent Publ., Boston, MA, 1991.
106. V. S. Praveenkumar, Implementation of hyperbolic class of time frequency distributions and removal of cross-terms, Master's thesis, University of Rhode Island, Kingston, RI, May 1995.
107. L. R. Rabiner and R. W. Schafer, *Digital Processing of Speech Signals*, Prentice Hall, Englewood Cliffs, NJ, 1978.
108. S. Raz, Synthesis of signals from Wigner distributions: Representations in biorthogonal bases, *Signal Process.*, 20, 303–314, 1990.
109. A. W. Rihaczek, *Principles of High Resolution Radar*, McGraw Hill, New York, 1969.
110. M. D. Riley, *Speech Time–Frequency Representations*, Kluwer Academic, Boston, MA, 1989.
111. O. Rioul and P. Flandrin, Time-scale energy distributions: A general class extending wavelet transforms, *IEEE Trans. Signal Process.*, 40(7), 1746–1757, July 1992.
112. O. Rioul and M. Vetterli, Wavelets and signal processing, *IEEE Signal Process. Mag.*, 8, 14–38, October 1991.
113. R. G. Shenoy and T. W. Parks, Affine Wigner distributions, *Proceedings IEEE International Conference on Acoustics, Speech, and Signal Processing*, 5, 185–188, San Francisco, CA, March 1992.
114. M. I. Skolnik, *Introduction to Radar Systems*, McGraw Hill, New York, 1962.
115. J. M. Speiser, Wide-band ambiguity function, *IEEE Trans. Inform. Theory*, 13, 122–123, 1967.
116. L. B. Stanković, S. B. Stanković, and Z. L. Usković, *Time–Frequency Signal Analysis*, Epsilon and Montenegropublic, Podgorica, Montenegro, 1994.
117. E. F. Velez, Transient Analysis of Speech Using the Wigner-Ville Distribution, PhD thesis, University of Vermont, Burlington, VT, 1989.
118. M. Vetterli and J. Kovačević, *Wavelets and Subband Coding*, Prentice-Hall, Inc., Englewood Cliffs, NJ, 1995.

119. J. Ville, Théorie et applications de la notion de signal analytique, *Câbles et Transmission*, 2A, 61–74, 1948. Translated into English by I. Selin, RAND Corporation Report T-92, Santa Monica, CA, August 1958.
120. E.P.Wigner, On the quantum correction for thermodynamic equilibrium, *Phys. Rev.*, 40, 749–759, 1932.
121. P. M. Woodward. Information theory and the design of radar receivers, *Proc. Inst. Radio Eng.*, 39, 1521–1524, 1951.
122. Y. Zhao, L. E. Atlas, and R. J. Marks, The use of cone-shaped kernels for generalized time–frequency representations of nonstationary signals, *IEEE Trans. Acoust., Speech, Signal Process.*, 38(7), 1084–1091, July 1990.

# Fractional Fourier Transform<sup>\*</sup>

Haldun M. Ozaktas

*Bilkent University*

M. Alper Kutay

*The Scientific and Technological  
Research Council of Turkey*

Çağatay Candan

*Middle East Technical University*

14.1	Introduction.....	14-1
14.2	Definition and Essential Properties.....	14-2
14.3	Fractional Fourier Domains.....	14-4
14.4	Fractional Fourier Transforms of Some Common Functions .....	14-6
14.5	Basic and Operational Properties of the Fractional Fourier Transform .....	14-6
14.6	Dual Operators and Their Fractional Generalizations .....	14-8
14.7	Time-Order and Space-Order Representations.....	14-9
14.8	Linear Canonical Transforms.....	14-11
14.9	Basic and Operational Properties of Linear Canonical Transforms.....	14-13
14.10	Filtering in Fractional Fourier Domains.....	14-14
14.11	Fractional Fourier Domain Decompositions .....	14-17
14.12	Discrete Fractional Fourier Transforms.....	14-18
14.13	Digital Computation of the Fractional Fourier Transform.....	14-20
14.14	Applications.....	14-21
	Applications in Signal and Image Processing • Applications in Communications •	
	Applications in Optics and Wave Propagation • Other Applications	
	References.....	14-22

## 14.1 Introduction

The ordinary Fourier transform and related techniques are of great importance in many areas of science and engineering. The fractional Fourier transform (FRT) is a generalization of the ordinary Fourier transform with an order (or power) parameter  $a$ . This chapter provides an introduction to the fractional Fourier transform and discusses some of its more important properties. The FRT also has a growing list of applications in several areas. An overview of applications that have received interest so far are provided at the end of this chapter. Those interested in learning about the transform and its applications in greater depth are referred to [23,122,123,129].

Mathematically the  $a$ th order fractional Fourier transform operator is the  $a$ th power of the ordinary Fourier transform operator. (Readers not familiar with functions of operators may think of them in analogy with functions of matrices. In the discrete case, where the discrete ordinary and fractional Fourier transform operators are represented by matrices, this is actually the case.) If we denote the ordinary Fourier transform operator by  $\mathcal{F}$ , then the  $a$ th order fractional Fourier transform operator is denoted by  $\mathcal{F}^a$ . The zeroth-order fractional Fourier transform

operator  $\mathcal{F}^0$  is equal to the identity operator  $\mathcal{I}$ . The first-order fractional Fourier transform operator  $\mathcal{F}^1$  is equal to the ordinary Fourier transform operator. Integer values of  $a$  correspond to repeated application of the Fourier transform; for instance,  $\mathcal{F}^2$  corresponds to the Fourier transform of the Fourier transform.  $\mathcal{F}^{-1}$  corresponds to the inverse Fourier transform operator. The  $a$ 'th order transform of the  $a$ th order transform is equal to the  $(a' + a)$ th order transform; that is  $\mathcal{F}^{a'} \mathcal{F}^a = \mathcal{F}^{a'+a}$ , a property referred to as index additivity. For instance, the 0.5th fractional Fourier transform operator  $\mathcal{F}^{0.5}$ , when applied twice, amounts to ordinary Fourier transformation. Or, the 0.4th transform of the 0.3rd transform is the 0.7th transform. The order  $a$  may assume any real value, however the operator  $\mathcal{F}^a$  is periodic in  $a$  with period 4; that is  $\mathcal{F}^{a+4j} = \mathcal{F}^a$  where  $j$  is any integer. This is because  $\mathcal{F}^2$  equals the parity operator  $\mathcal{P}$  which maps  $f(u)$  to  $f(-u)$  and  $\mathcal{F}^4$  equals the identity operator. Therefore, the range of  $a$  is usually restricted to  $(-2, 2]$  or  $[0, 4)$ . Complex-ordered transforms have also been discussed by some authors, although there remains much to do in this area both in terms of theory and applications.

The same facts can also be thought of in terms of the functions which these operators act on. For instance, the zeroth-order fractional Fourier transform of the function  $f(u)$  is merely

\* Parts of this chapter appeared in or were adapted from Ozaktas and Kutay [121].

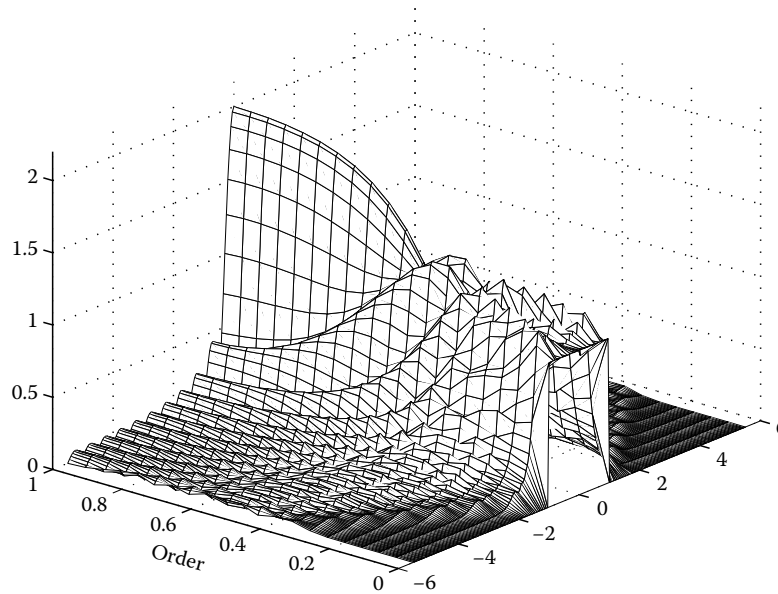


**FIGURE 14.1** Magnitude of the fractional Fourier transform of the rectangle function as a function of the transform order. (From Ozaktas, H. M. and Kutay, M. A., *Proceedings of the European Control Conference*. European Union Control Association and University of Porto, Porto, Portugal, 2001. With permission.)

the function itself, and the first-order transform is its ordinary Fourier transform  $F(\mu)$ , where  $\mu$  denotes the frequency domain variable. The  $a$ th fractional Fourier transform of  $f(u)$  is denoted by  $f_a(u)$  so that  $f_0(u) = f(u)$  and  $f_1(\mu) = F(\mu)$  (or  $f_1(u) = F(u)$  since the functional equality does not depend on the dummy variable employed).

An example is given in Figure 14.1, where we see the magnitude of the fractional Fourier transforms of the rectangle function for different values of the order  $a \in [0, 1]$ . We observe that as  $a$  varies from 0 to 1, the rectangle function evolves into a sinc function, which is the ordinary Fourier transform of the rectangle function.

The earliest known references dealing with the transform go back to the 1920s and 1930s; since then the transform has been reinvented several times. It has received the attention of a few mathematicians during the 1980s [100,106,109]. However, interest in the transform really grew with its reinvention/reintroduction by researchers in the fields of optics and signal processing, who noticed its relevance for a variety of application areas [8,88,102,117,124,125]. A detailed account of the history of the transform may be found in [129].

Fractionalization of the Fourier transform has led to interest in fractionalization of other transforms [5,91,175] such as the Hilbert transform [137] and the cosine-sine and Hartley transforms [30,134], and extensions to the study of time-frequency distributions [130,132,143]. These will not be dealt with in this chapter.

Throughout this chapter, the imaginary unit is denoted by  $i$  and the square root is defined such that the argument of the result lies in the interval  $(-\pi/2, \pi/2]$ .

The first three to five sections can be read as a tutorial on the fractional Fourier transform, and the other sections can be read or consulted as needed.

## 14.2 Definition and Essential Properties

The most straightforward way of defining the fractional Fourier transform is as a linear integral transform as follows:

$$f_a(u) = \int_{-\infty}^{\infty} K_a(u, u') f(u') du', \quad (14.1)$$

$$K_a(u, u') = \sqrt{1 - i \cot \alpha} \exp [i\pi(\cot \alpha u^2 - 2 \csc \alpha uu' + \cot \alpha u'^2)],$$

$$\alpha = \frac{a\pi}{2},$$

when  $a \neq 2j$  for integer  $j$ . When  $a = 4j$  the transform is defined as  $K_a(u, u') = \delta(u - u')$  and when  $a = 4j + 2$  the transform is defined as  $K_a(u, u') = \delta(u + u')$ . It can be shown that the above kernel for  $a \neq 2j$  indeed approaches these delta function kernels as  $a$  approaches even integers. For  $0 < |a| < 2$ , the factor  $\sqrt{1 - i \cot \alpha}$  can be written as  $\exp\{-i[\pi \operatorname{sgn}(\alpha)/4 - \alpha/2]\}/\sqrt{|\sin \alpha|}$  where  $\operatorname{sgn}(\cdot)$  is the sign function. It is easy to show that when  $a = 1$  the kernel reduces to  $\exp(-i2\pi uu')$ , corresponding to the ordinary Fourier transform, and that when  $a = -1$  the kernel reduces to  $\exp(i2\pi uu')$ , corresponding to the ordinary inverse Fourier transform.

It is not easy to see from the above definition that the transform is indeed the operator power of the ordinary Fourier transform. In order to find the operator power of the ordinary Fourier transform, we first consider its eigenvalue equation:

$$\mathcal{F}\psi_n(u) = e^{-in\pi/2}\psi_n(u). \quad (14.2)$$

Here the eigenfunctions  $\psi_n(u)$ ,  $n = 0, 1, 2, \dots$  are the Hermite-Gaussian functions defined as  $\psi_n(u) = (2^{1/4}/\sqrt{2^n n!}) H_n(\sqrt{2\pi} u) \exp(-\pi u^2)$ , where  $H_n(u)$  are the standard Hermite polynomials.  $\exp(-in\pi/2)$  is the eigenvalue associated with the  $n$ th eigenfunction  $\psi_n(u)$ . Now, following a standard procedure also used to define functions of matrices, the fractional Fourier transform may be defined such that it has the same eigenfunctions, but the eigenvalues raised to the  $a$ th power:

$$\mathcal{F}^a \psi_n(u) = (e^{-in\pi/2})^a \psi_n(u). \quad (14.3)$$

This definition is not unique for at least two reasons. First, it depends on the choice of the Hermite-Gaussian set as the set of eigenfunctions (which is not the only such possible set). Second, it depends on how we resolve the ambiguity in evaluating  $[\exp(-in\pi/2)]^a$ . The particular definition, which has so far received the greatest attention, has the most elegant properties, and which has found the most applications, follows from choosing  $[\exp(-in\pi/2)]^a = \exp(-ian\pi/2)$ . With this choice, the fractional Fourier transform of a square-integrable function  $f(u)$  can be found by first expanding it in terms of the set of Hermite-Gaussian functions  $\psi_n(u)$  as

$$f(u) = \sum_{n=0}^{\infty} C_n \psi_n(u), \quad (14.4)$$

$$C_n = \int_{-\infty}^{\infty} \psi_n(u) f(u) du, \quad (14.5)$$

and then applying  $\mathcal{F}^a$  to both sides to obtain

$$\mathcal{F}^a f(u) = \sum_{n=0}^{\infty} C_n \mathcal{F}^a \psi_n(u), \quad (14.6)$$

$$f_a(u) = \sum_{n=0}^{\infty} C_n e^{-ian\pi/2} \psi_n(u), \quad (14.7)$$

$$f_a(u) = \int_{-\infty}^{\infty} \left[ \sum_{n=0}^{\infty} e^{-ian\pi/2} \psi_n(u) \psi_n(u') \right] f(u') du' \quad (14.8)$$

The final form can be shown to be equal to that given by Equation 14.1 through a standard identity (for instance, see Table 2.8.9 in [129]).

Alternative definitions of the transform will arise if we make different choices regarding the eigenfunctions or in taking the fractional powers of the eigenvalues [31,77]. For instance, if the ambiguity in evaluating  $z^a$  is resolved by choosing the principal power of  $z$ , it turns out that the  $a$ th fractional Fourier transform of  $f(u)$  can be expressed as a linear combination of the form

$$\beta_0(a)f(u) + \beta_1(a)F(u) + \beta_2(a)f(-u) + \beta_3(a)F(-u), \quad (14.9)$$

where

$F(u)$  is the ordinary Fourier transform of  $f(u)$

$\beta_k(a)$  are the order-dependent coefficients of the linear combination (page 139 of [129])

This definition is merely a linear combination of a function and its Fourier transform (and their time-reversed versions). It is worth emphasizing that the definition of the FRT which is the subject of this chapter not only does not correspond to choosing the principal powers, it does not correspond to any unambiguous way of specifying the power function  $z^a$ . The special nature of resolving the ambiguity in evaluating  $[\exp(-in\pi/2)]^a$  by taking it equal to  $\exp(-ian\pi/2)$  is further discussed in [129].

The fractional Fourier transform  $f_a(u)$  of a function  $f(u)$  also corresponds to the solution of the following differential equation, with  $f_0(u) = f(u)$  acting as the initial condition:

$$\left[ -\frac{1}{4\pi} \frac{\partial^2}{\partial u^2} + \pi u^2 - \frac{1}{2} \right] f_a(u) = i \frac{2}{\pi} \frac{\partial f_a(u)}{\partial a}. \quad (14.10)$$

The solution to Equation 14.10 can be expressed as

$$f_a(u) = \int_{-\infty}^{\infty} K_a(u, u') f_0(u') du', \quad (14.11)$$

where  $K_a(u, u')$  is the same kernel as defined in Equation 14.1, a fact which can be shown by direct substitution. Equation 14.10 is the quantum-mechanical harmonic oscillator differential equation, which can be obtained from the classical harmonic oscillator equation through standard procedures [84]. In this interpretation, the order parameter  $a$  corresponds to time and  $f_a(u)$  gives us the time evolution of the wave function. The kernel  $K_a(u, u')$  is sometimes referred to as the harmonic oscillator Green's function: it is the response of the system to  $f_0(u) = \delta(u - u')$  [95]. (To be precise, we must note that the harmonic oscillator differential equation differs from equation 10 by the term  $-1/2$ ; see [129].) Further discussion of the relationship of the fractional Fourier transform to harmonic oscillation may be found in [13,84].

The fractional Fourier transform operator can also be expressed in hyperdifferential form:

$$\mathcal{F}^a = e^{-i(a\pi/2)\mathcal{H}}, \quad (14.12)$$

$$\mathcal{H} = \pi(\mathcal{D}^2 + \mathcal{U}^2) - \frac{1}{2},$$

where

$\mathcal{U}$  is the coordinate multiplication operator defined as

$$\mathcal{U}f(u) = uf(u)$$

$\mathcal{D}$  is the differentiation operator defined as  $\mathcal{D}f(u) =$

$$(i2\pi)^{-1} df(u)/du$$

With these definitions, Equation 14.12 corresponds to the following expression in the time domain:

$$f_a(u) = \mathcal{F}^a f(u) = \exp \left[ -i \left( \frac{a\pi}{2} \right) \left( -\frac{1}{4\pi} \frac{d^2}{du^2} + \pi u^2 - \frac{1}{2} \right) \right] f(u). \tag{14.13}$$

We can convince ourselves that this way of expressing the fractional Fourier transform is equivalent to earlier expressions by noting that the differential equation 10 can be written as  $\mathcal{H}f_a(u) = i(2/\pi)\partial f_a(u)/\partial a$ . The solution of this equation can be formally expressed as  $f_a(u) = \exp(-i(a\pi/2)\mathcal{H})f_0(u)$  where  $f_0(u)$  serves as the initial or boundary condition, which is the same as Equation 14.12. In other words, Equation 14.12 is simply the solution of the differential equation given in Equation 14.10, expressed in hyperdifferential form.

We will conclude this section with a derivation that links together several of the concepts presented above. Let us recall the eigenvalue equation (Equation 14.3):

$$\mathcal{F}^a \psi_n(u) = e^{-ian\pi/2} \psi_n(u) = e^{-i\alpha n} \psi_n(u), \tag{14.14}$$

where  $\alpha = a\pi/2$  and  $\psi_n(u)$  are the Hermite–Gaussian functions satisfying the differential equation (Table 2.8.6 of [129])

$$\left[ \frac{d^2}{du^2} + 4\pi^2 \left( \frac{2n+1}{2\pi} - u^2 \right) \right] \psi_n(u) = 0. \tag{14.15}$$

Now, starting from the last two equations, let us seek a hyperdifferential representation for  $\mathcal{F}^a$  of the form  $\exp(-i\alpha\mathcal{H})$ . Differentiating

$$\exp(-i\alpha\mathcal{H})\psi_n(u) = e^{-i\alpha n} \psi_n(u) \tag{14.16}$$

with respect to  $\alpha$  and setting  $\alpha = 0$ , we obtain

$$\mathcal{H}\psi_n(u) = n\psi_n(u), \tag{14.17}$$

which upon comparison with Equation 14.15 leads to

$$\mathcal{H}\psi_n(u) = \left( -\frac{1}{4\pi} \frac{d^2}{du^2} + \pi u^2 - \frac{1}{2} \right) \psi_n(u). \tag{14.18}$$

By expanding arbitrary  $f(u)$  in terms of the  $\psi_n(u)$ , we obtain

$$\mathcal{H}f(u) = \left( -\frac{1}{4\pi} \frac{d^2}{du^2} + \pi u^2 - \frac{1}{2} \right) f(u), \tag{14.19}$$

by virtue of the linearity of  $\mathcal{H}$ . Now, in abstract operator form, we may write

$$\mathcal{H} = \pi(\mathcal{D}^2 + \mathcal{U}^2) - \frac{1}{2}, \tag{14.20}$$

precisely corresponding to Equation 14.12.

A brief list of the fractional Fourier transforms of common functions is provided in Section 14.4. Many of the elementary and operational properties of the FRT are collected in

Section 14.5, which can be recognized as generalizations of the corresponding properties of the ordinary Fourier transform.

### 14.3 Fractional Fourier Domains

One of the most important concepts in Fourier analysis is the concept of the Fourier (or frequency) domain. This “domain” is understood to be a space where the Fourier transform representation of the signal lives, with its own interpretation and qualities. This naturally leads one to inquire into the nature of the domain where the fractional Fourier transform representation of a function lives. This is best understood by referring to Figure 14.2, which shows the phase space spanned by the axes  $u$  (usually time or space) and  $\mu$  (temporal or spatial frequency). This phase space is also referred to as the time–frequency or space–frequency plane in the signal processing literature. The horizontal axis  $u$  is simply the time or space domain, where the original function lives. The vertical axis  $\mu$  is simply the frequency (or Fourier) domain where the ordinary Fourier transform of the function lives. Oblique axes making angle  $\alpha$  constitute domains where the  $a$ th order fractional Fourier transform lives, where  $a$  and  $\alpha$  are related through  $\alpha = a\pi/2$ . Notice that this description is consistent with the fact that the second Fourier transform is equal to the parity operation (associated with the  $-u$  axis), the fact that the  $-1$ st transform corresponds to the inverse Fourier transform (associated with the  $-\mu$  axis), and the periodicity of  $f_a(u)$  in  $a$  (adding a multiple of 4 to  $a$  corresponds to adding a multiple of  $2\pi$  to  $\alpha$ ).

For those familiar with phase spaces from a mechanics—rather than a signal analysis—perspective, we note that the correspondence between spatial frequency and momentum allows one to construct a correspondence between the familiar mechanical phase space of a single degree of freedom (defined by the space axis and the momentum axis), and the phase space of signal analysis (defined by the space axis and the spatial frequency axis). What is important to understand for the present purpose is that the phase space or time– and/or space–frequency planes we are talking about is essentially the same physical construct as the classical phase space of mechanics.

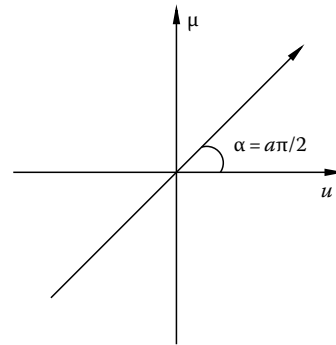


**FIGURE 14.2** Phase space and the  $a$ th order fractional Fourier domain. (From Ozaktas, H. M. and Kutay, M. A., *Proceedings of the European Control Conference*. European Union Control Association and University of Porto, Porto, Portugal, 2001. With permission.)

Referring to axes making angle  $\alpha = a\pi/2$  with the  $u$  axis as the “ $a$ th fractional Fourier domain” is supported by several of the properties of the fractional Fourier transform to be discussed further in Section 14.5. However, the most substantial justification is based on the fact that

*fractional Fourier transformation corresponds to rotation in phase space.*

This can be formulated in many ways, the most straightforward being to consider a phase-space distribution (or time/space–frequency representation) of the function  $f(u)$ , such as the Wigner distribution  $W_f(u, \mu)$ , which is defined as

$$W_f(u, \mu) = \int_{-\infty}^{\infty} f(u + u'/2) f^*(u - u'/2) e^{-i2\pi\mu u'} du'. \quad (14.21)$$

The many properties of the Wigner distribution [37,67] support its interpretation as a function giving the distribution of signal energy in phase space (the time- or space-frequency plane). That is, the Wigner distribution answers the question “How much of the signal energy is located near this time and frequency?” (Naturally, the answer to this question can only be given within limitations imposed by the uncertainty principle.) Three of the important properties of the Wigner distribution are

$$\int_{-\infty}^{\infty} W_f(u, \mu) d\mu = \mathcal{R}_0[W_f(u, \mu)] = |f(u)|^2, \quad (14.22)$$

$$\int_{-\infty}^{\infty} W_f(u, \mu) du = \mathcal{R}_{\pi/2}[W_f(u, \mu)] = |F(\mu)|^2, \quad (14.23)$$

$$\int_{-\infty}^{\infty} \int_{-\infty}^{\infty} W_f(u, \mu) du d\mu = \|f\|^2 = \text{Signal energy}. \quad (14.24)$$

Here  $\mathcal{R}_\alpha$  denotes the integral projection (or Radon transform) operator which takes an integral projection of the two-dimensional function  $W_f(u, \mu)$  onto an axis making angle  $\alpha$  with the  $u$  axis, to produce a one-dimensional function (page 56 of [129]).

Now, it is possible to show that the Wigner distribution  $W_{f_a}(u, \mu)$  of  $f_a(u)$  is a clockwise rotated version of the Wigner distribution  $W_f(u, \mu)$  of  $f(u)$ . Mathematically,

$$W_{f_a}(u, \mu) = W_f(u \cos \alpha - \mu \sin \alpha, u \sin \alpha + \mu \cos \alpha). \quad (14.25)$$

That is, the act of fractional Fourier transformation on the original function, corresponds to rotation of the Wigner distribution [88,107,117]. An immediate corollary of this result, supported by Figure 14.3, is

$$\mathcal{R}_\alpha[W_f(u, \mu)] = |f_a(u)|^2, \quad (14.26)$$

which is a generalization of Equations 14.22 and 14.23. This equation means that the projection of the Wigner distribution of  $f(u)$  onto the axis making angle  $\alpha$  gives us  $|f_a(u)|^2$ , the squared magnitude of the  $a$ th fractional Fourier transform of the function. Since projection onto the  $u$  axis (the time or space domain) gives  $|f(u)|^2$  and projection onto the  $\mu = u_1$  axis (the frequency domain) gives  $|F(\mu)|^2$ , it is natural to refer to the axis making angle  $\alpha$  as the  $a$ th order fractional Fourier domain.

Closely related to the Wigner distribution is the ambiguity function  $A_f(\bar{u}, \bar{\mu})$  of the function  $f(u)$ , defined as

$$A_f(\bar{u}, \bar{\mu}) = \int_{-\infty}^{\infty} f(u' + \bar{u}/2) f^*(u' - \bar{u}/2) e^{-i2\pi\bar{\mu}u'} du'. \quad (14.27)$$

Whereas the Wigner distribution is the prime example of an *energetic* time-frequency representation, the ambiguity function

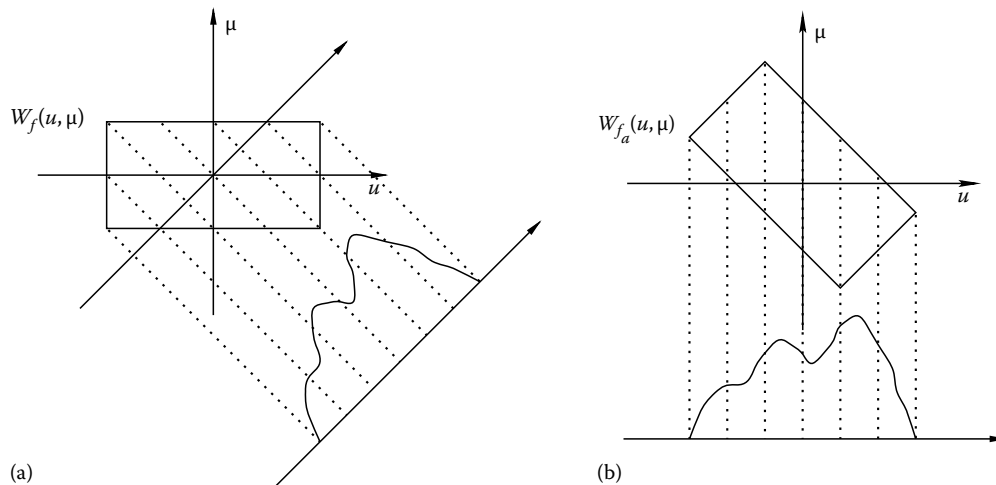


**FIGURE 14.3** (a) Projection of  $W_f(u, \mu)$  onto the  $u_a$  axis. (b) Projection of  $W_{f_a}(u, \mu)$  onto the  $u$  axis. (From Ozaktas, H. M. and Kutay, M. A., *Proceedings of the European Control Conference*. European Union Control Association and University of Porto, Porto, Portugal, 2001. With permission.)



is the prime example of a *correlative* time–frequency representation. The ambiguity function deserves this by virtue of the following properties [37,67]:

$$A_f(\bar{u}, 0) = \mathcal{S}_0[A_f(\bar{u}, \bar{\mu})] = \int_{-\infty}^{\infty} f(u' + \bar{u})f^*(u') du', \quad (14.28)$$

$$A_f(0, \bar{\mu}) = \mathcal{S}_{\pi/2}[A_f(\bar{u}, \bar{\mu})] = \int_{-\infty}^{\infty} F(\mu' + \bar{\mu})F^*(\mu') d\mu', \quad (14.29)$$

$$A_f(\bar{u}, \bar{\mu}) \leq A_f(0, 0) = \|f\|^2 = \text{En}[f] = \text{Signal energy}, \quad (14.30)$$

which say that the on-axis profiles of the ambiguity function are equal to the autocorrelation of the signal in the time and frequency domains, respectively. Here  $\mathcal{S}_\alpha$  denotes the slice operator that returns the slice  $A_f(\rho \cos \alpha, \rho \sin \alpha)$  of the two-dimensional function  $A_f(\bar{u}, \bar{\mu})$  (page 56 of [129]).

Now, it is possible to show that slices of the ambiguity function  $A_f(\bar{u}, \bar{\mu})$  satisfy

$$\mathcal{S}_\alpha[A_f(\bar{u}, \bar{\mu})](\rho) = A_f(\rho \cos \alpha, \rho \sin \alpha) = f_{2\alpha/\pi}(\rho) * f_{2\alpha/\pi}^*(-\rho), \quad (14.31)$$

where  $*$  denotes ordinary convolution. Just as oblique projections of the Wigner distribution correspond to the squared magnitudes of the fractional Fourier transforms of the function, the oblique slices of the ambiguity function correspond to the autocorrelations of the fractional Fourier transforms of the function.

Finally, we note that the ambiguity function is related to the Wigner distribution by what is essentially a two-dimensional Fourier transform:

$$A_f(\bar{u}, \bar{\mu}) = \int_{-\infty}^{\infty} \int_{-\infty}^{\infty} W_f(u, \mu) e^{-i2\pi(\bar{\mu}u - \bar{u}\mu)} du d\mu. \quad (14.32)$$

## 14.4 Fractional Fourier Transforms of Some Common Functions

Below we list the fractional Fourier transforms of some common functions. Transforms of most other functions must usually be computed numerically (Section 14.13).

**Unit function:** The fractional Fourier transform of  $f(u) = 1$  is

$$\mathcal{F}^a[1] = \sqrt{1 + i \tan \alpha} e^{-i\pi u^2 \tan \alpha}. \quad (14.33)$$

This equation is valid when  $a \neq 2j + 1$  where  $j$  is an arbitrary integer. The transform is  $\delta(u)$  when  $a = 2j + 1$ .

**Delta function:** The fractional Fourier transform of a delta function  $f(u) = \delta(u - u_0)$  is

$$\mathcal{F}^a[\delta(u - u_0)] = \sqrt{1 - i \cot \alpha} e^{i\pi(u^2 \cot \alpha - 2u u_0 \csc \alpha + u_0^2 \cot \alpha)}. \quad (14.34)$$

This expression is valid when  $a \neq 2j$ . The transform of  $\delta(u - u_0)$  is  $\delta(u - u_0)$  when  $a = 4j$  and  $\delta(u + u_0)$  when  $a = 4j + 2$ .

**Harmonic function:** The fractional Fourier transform of a harmonic function  $f(u) = \exp(i2\pi\mu_0 u)$  is

$$\mathcal{F}^a[e^{i2\pi\mu_0 u}] = \sqrt{1 + i \tan \alpha} e^{-i\pi(u^2 \tan \alpha - 2u\mu_0 \sec \alpha + \mu_0^2 \tan \alpha)}. \quad (14.35)$$

This equation is valid when  $a \neq 2j + 1$ . The transform of  $\exp(i2\pi\mu_0 u)$  is  $\delta(u - \mu_0)$  when  $a = 4j + 1$  and  $\delta(u + \mu_0)$  when  $a = 4j + 3$ .

**General chirp function:** The fractional Fourier transform of a general chirp function  $f(u) = \exp[i\pi(\chi u^2 + 2\xi u)]$  is

$$\begin{aligned} \mathcal{F}^a[e^{i\pi(\chi u^2 + 2\xi u)}] \\ = \sqrt{\frac{1 + i \tan \alpha}{1 + \chi \tan \alpha}} e^{i\pi[u^2(\chi - \tan \alpha) + 2u\xi \sec \alpha - \xi^2 \tan \alpha]/[1 + \chi \tan \alpha]}. \end{aligned} \quad (14.36)$$

This equation is valid when  $a - (2/\pi) \arctan \chi \neq 2j + 1$ . The transform of  $\exp(i\pi\chi u^2)$  is  $\sqrt{1/(1 - i\chi)} \delta(u)$  when  $[a - (2/\pi) \arctan \chi] = 2j + 1$  and  $\sqrt{1/(1 - i\chi)}$  when  $[a - (2/\pi) \arctan \chi] = 2j$ .

**Hermite–Gaussian functions:** The fractional Fourier transform of a Hermite–Gaussian function  $f(u) = \psi_n(u)$  is

$$\mathcal{F}^a[\psi_n(u)] = e^{-in\alpha} \psi_n(u). \quad (14.37)$$

**General Gaussian function:** The fractional Fourier transform of a general Gaussian function  $f(u) = \exp[-\pi(\chi u^2 + 2\xi u)]$  is

$$\begin{aligned} \mathcal{F}^a[e^{-\pi(\chi u^2 + 2\xi u)}] \\ = \sqrt{\frac{1 - i \cot \alpha}{\chi - i \cot \alpha}} e^{i\pi \cot \alpha [u^2(\chi^2 - 1) + 2u\xi \sec \alpha + \xi^2]/[\chi^2 + \cot \alpha]} \\ \times e^{-\pi \csc^2 \alpha (u^2 \chi + 2u\xi \cos \alpha - \chi \xi^2 \sin^2 \alpha)/(\chi^2 + \cot \alpha)}. \end{aligned} \quad (14.38)$$

Here  $\chi > 0$  is required for convergence.

## 14.5 Basic and Operational Properties of the Fractional Fourier Transform

Here we present a list of the more important basic and operational properties of the FRT. Readers can easily verify that the operational properties, such as those for scaling, coordinate multiplication, and differentiation, reduce to the corresponding property for the ordinary Fourier transform when  $a = 1$ .

**Linearity:** Let  $\mathcal{F}^a$  denote the  $a$ th order fractional Fourier transform operator. Then  $\mathcal{F}^a[\sum_k b_k f_k(u)] = \sum_k b_k [\mathcal{F}^a f_k(u)]$ .

**Integer orders:**  $\mathcal{F}^k = (\mathcal{F})^k$  where  $\mathcal{F}$  denotes the ordinary Fourier transform operator. This property states that when  $a$  is equal to an integer  $k$ , the  $a$ th order fractional Fourier transform is equivalent to the  $k$ th integer power of the ordinary Fourier transform, defined by repeated application. It also follows that  $\mathcal{F}^2 = \mathcal{P}$  (the parity operator),  $\mathcal{F}^3 = \mathcal{F}^{-1} = (\mathcal{F})^{-1}$  (the inverse transform operator),  $\mathcal{F}^4 = \mathcal{F}^0 = \mathcal{I}$  (the identity operator), and  $\mathcal{F}^j = \mathcal{F}^{j \bmod 4}$ .

**Inverse:**  $(\mathcal{F}^a)^{-1} = \mathcal{F}^{-a}$ . In terms of the kernel, this property is stated as  $K_a^{-1}(u, u') = K_{-a}(u, u')$ .

**Unitarity:**  $(\mathcal{F}^a)^{-1} = (\mathcal{F}^a)^H = \mathcal{F}^{-a}$  where  $()^H$  denotes the conjugate transpose of the operator. In terms of the kernel, this property can be stated as  $K_a^{-1}(u, u') = K_a^*(u', u)$ .

**Index additivity:**  $\mathcal{F}^{a_2} \mathcal{F}^{a_1} = \mathcal{F}^{a_2+a_1}$ . In terms of kernels this can be written as  $K_{a_2+a_1}(u, u') = \int K_{a_2}(u, u'') K_{a_1}(u'', u') du''$ .

**Commutativity:**  $\mathcal{F}^{a_2} \mathcal{F}^{a_1} = \mathcal{F}^{a_1} \mathcal{F}^{a_2}$ .

**Associativity:**  $\mathcal{F}^{a_3} (\mathcal{F}^{a_2} \mathcal{F}^{a_1}) = (\mathcal{F}^{a_3} \mathcal{F}^{a_2}) \mathcal{F}^{a_1}$ .

**Eigenfunctions:**  $\mathcal{F}^a[\psi_n(u)] = \exp(-ian\pi/2)\psi_n(u)$ . Here  $\psi_n(u)$  are the Hermite–Gaussian functions defined in Section 14.2.

**Parseval:**  $\int f^*(u)g(u)du = \int f_a^*(u)g_a(u)du$ . This property is equivalent to unitarity. Energy or norm conservation ( $\text{En}[f] = \text{En}[f_a]$  or  $\|f\| = \|f_a\|$ ) is a special case.

**Time reversal:** Let  $\mathcal{P}$  denote the parity operator:  $\mathcal{P}[f(u)] = f(-u)$ , then

$$\mathcal{F}^a \mathcal{P} = \mathcal{P} \mathcal{F}^a \quad (14.39)$$

$$\mathcal{F}^a [f(-u)] = f_a(-u) \quad (14.40)$$

**Transform of a scaled function:** Let  $\mathcal{M}(M)$  and  $\mathcal{Q}(q)$  denote the scaling  $\mathcal{M}(M)[f(u)] = |M|^{-1/2}f(u/M)$  and chirp multiplication  $\mathcal{Q}(q)[f(u)] = e^{-i\pi q u^2}f(u)$  operators, respectively. Here the notation  $\mathcal{M}(M)[f(u)]$  means that the operator  $\mathcal{M}(M)$  is applied to the function  $f(u)$ . Then

$$\begin{aligned} \mathcal{F}^a \mathcal{M}(M) &= \mathcal{Q}(-\cot \alpha (1 - (\cos^2 \alpha') / (\cos^2 \alpha))) \\ &\times \mathcal{M}(\sin \alpha / M \sin \alpha') \mathcal{F}^{a'}, \end{aligned} \quad (14.41)$$

$$\begin{aligned} \mathcal{F}^a [|M|^{-1/2}f(u/M)] &= \sqrt{\frac{1 - i \cot \alpha}{1 - iM^2 \cot \alpha}} e^{i\pi u^2 \cot \alpha (1 - (\cos^2 \alpha') / (\cos^2 \alpha))} \\ &\times f_{a'}\left(\frac{Mu \sin \alpha'}{\sin \alpha}\right). \end{aligned} \quad (14.42)$$

Here  $\alpha' = \arctan(M^{-2} \tan \alpha)$  and  $\alpha'$  is taken to be in the same quadrant as  $\alpha$ . This property is the generalization of the ordinary Fourier transform property stating that the Fourier transform of  $f(u/M)$  is  $|M|F(M\mu)$ . Notice that the fractional Fourier transform of  $f(u/M)$  cannot be expressed as a scaled version of  $f_a(u)$  for the same order  $a$ . Rather, the fractional Fourier transform of  $f(u/M)$  turns out to be a scaled and chirp modulated version of  $f_{a'}(u)$  where  $a' \neq a$  is a different order.

**Transform of a shifted function:** Let  $\mathcal{SH}(u_0)$  and  $\mathcal{PH}(\mu_0)$  denote the shift  $\mathcal{SH}(u_0)[f(u)] = f(u + u_0)$  and the phase shift  $\mathcal{PH}(\mu_0)[f(u)] = \exp(i2\pi\mu_0 u)f(u)$  operators, respectively. Then

$$\mathcal{F}^a \mathcal{SH}(u_0) = e^{i\pi u_0^2 \sin \alpha \cos \alpha} \mathcal{PH}(u_0 \sin \alpha) \mathcal{SH}(u_0 \cos \alpha) \mathcal{F}^a, \quad (14.43)$$

$$\mathcal{F}^a [f(u + u_0)] = e^{i\pi u_0^2 \sin \alpha \cos \alpha} e^{i2\pi u u_0 \sin \alpha} f_a(u + u_0 \cos \alpha). \quad (14.44)$$

We see that the  $\mathcal{SH}(u_0)$  operator, which simply results in a translation in the  $u$  domain, corresponds to a translation followed by a phase shift in the  $a$ th fractional domain. The amount of translation and phase shift is given by cosine and sine multipliers which can be interpreted in terms of “projections” between the axes.

**Transform of a phase-shifted function:**

$$\mathcal{F}^a \mathcal{PH}(\mu_0) = e^{-i\pi \mu_0^2 \sin \alpha \cos \alpha} \mathcal{PH}(\mu_0 \cos \alpha) \mathcal{SH}(-\mu_0 \sin \alpha) \mathcal{F}^a, \quad (14.45)$$

$$\begin{aligned} \mathcal{F}^a [\exp(i2\pi\mu_0 u)f(u)] &= e^{-i\pi \mu_0^2 \sin \alpha \cos \alpha} e^{i2\pi u \mu_0 \cos \alpha} \\ &f_a(u - \mu_0 \sin \alpha). \end{aligned} \quad (14.46)$$

Similar to the shift operator, the phase-shift operator, which simply results in a phase shift in the  $u$  domain, corresponds to a translation followed by a phase shift in the  $a$ th fractional domain. Again the amount of translation and phase shift are given by cosine and sine multipliers.

**Transform of a coordinate multiplied function:** Let  $\mathcal{U}$  and  $\mathcal{D}$  denote the coordinate multiplication  $\mathcal{U}[f(u)] = uf(u)$  and differentiation  $\mathcal{D}[f(u)] = (i2\pi)^{-1}df(u)/du$  operators, respectively. Then

$$\mathcal{F}^a \mathcal{U}^n = [\cos \alpha \mathcal{U} - \sin \alpha \mathcal{D}]^n \mathcal{F}^a, \quad (14.47)$$

$$\mathcal{F}^a [u^n f(u)] = [\cos \alpha u - \sin \alpha (i2\pi)^{-1}d/du]^n f_a(u). \quad (14.48)$$

When  $a = 1$ , the transform of a coordinate multiplied function  $uf(u)$  is the derivative of the transform of the original function  $f(u)$ , a well-known property of the Fourier transform. For arbitrary values of  $a$ , we see that the transform of  $uf(u)$  is a linear combination of the coordinate-multiplied transform of the original function and the derivative of the transform of the original function. The coefficients in the linear combination are  $\cos \alpha$  and  $-\sin \alpha$ . As  $a$  approaches 0, there is more  $uf(u)$  and less  $df(u)/du$  in the linear combination. As  $a$  approaches 1, there is more  $df(u)/du$  and less  $uf(u)$ .

**Transform of the derivative of a function:**

$$\mathcal{F}^a \mathcal{D}^n = [\sin \alpha \mathcal{U} + \cos \alpha \mathcal{D}]^n \mathcal{F}^a, \quad (14.49)$$

$$\mathcal{F}^a [[(i2\pi)^{-1}d/du]^n f(u)] = [\sin \alpha u + \cos \alpha (i2\pi)^{-1}d/du]^n f_a(u). \quad (14.50)$$

When  $a=1$  the transform of the derivative of a function  $df(u)/du$  is the coordinate-multiplied transform of the original function. For arbitrary values of  $a$ , we see that the transform is again a linear combination of the coordinate-multiplied transform of the original function and the derivative of the transform of the original function.

**Transform of a coordinate divided function:**

$$\mathcal{F}^a[f(u)/u] = -i \csc \alpha e^{i\pi u^2 \cot \alpha} \int_{-\infty}^{2\pi u} f_a(u') e^{-i\pi u'^2 \cot \alpha} du'. \quad (14.51)$$

**Transform of the integral of a function:**

$$\mathcal{F}^a \left[ \int_{u_0}^u f(u') du' \right] = \sec \alpha e^{-i\pi u^2 \tan \alpha} \int_{u_0}^u f_a(u') e^{i\pi u'^2 \tan \alpha} du'. \quad (14.52)$$

A few additional properties are

$$\mathcal{F}^a[f^*(u)] = f_{-a}^*(u), \quad (14.53)$$

$$\mathcal{F}^a[(f(u) + f(-u))/2] = (f_a(u) + f_a(-u))/2, \quad (14.54)$$

$$\mathcal{F}^a[(f(u) - f(-u))/2] = (f_a(u) - f_a(-u))/2. \quad (14.55)$$

It is also possible to write convolution and multiplication properties for the fractional Fourier transform, though these are not of great simplicity (page 157 of [129] and [9,174]).

A function and its  $a$ th order fractional Fourier transform satisfy an ‘‘uncertainty relation,’’ stating that the product of the spread of the two functions, as measured by their standard deviations, cannot be less than  $|\sin(a\pi/2)|/4\pi$  [116].

We may finally note that the transform is continuous in the order  $a$ . That is, small changes in the order  $a$  correspond to small changes in the transform  $f_a(u)$ . Nevertheless, care is always required in dealing with cases where  $a$  approaches an even integer, since in this case the kernel approaches a delta function.

## 14.6 Dual Operators and Their Fractional Generalizations

The dual of the operator  $\mathcal{A}$  will be denoted by  $\mathcal{A}^D$  and satisfies

$$\mathcal{A}^D = \mathcal{F}^{-1} \mathcal{A} \mathcal{F}. \quad (14.56)$$

$\mathcal{A}^D$  performs the same action on the frequency-domain representation  $F(\mu)$ , that  $\mathcal{A}$  performs on the time-domain representation  $f(u)$ . For instance, if  $\mathcal{A}$  represents the operation of multiplying with the coordinate variable  $u$ , then the dual  $\mathcal{A}^D$  represents the operation of multiplying  $F(\mu)$  with  $\mu$ , which in the time domain corresponds to the operator  $(i2\pi)^{-1}d/du$ .

The fractional operators we deal with in this section perform the same action in a fractional domain:

$$\mathcal{A}_a = \mathcal{F}^{-a} \mathcal{A} \mathcal{F}^a. \quad (14.57)$$

This equation generalizes Equation 14.56 and reduces to it when  $a=1$  with  $\mathcal{A}_1 = \mathcal{A}^D$ . If again  $\mathcal{A}$  corresponds to the multiplication of  $f(u)$  with  $u$ , then  $\mathcal{A}_a$  corresponds to the multiplication of  $f_a(u_a)$  with  $u_a$ , where  $u_a$  denotes the coordinate variable associated with the  $a$ th fractional Fourier domain. The effect of  $\mathcal{A}_a$  in the ordinary time domain can be expressed as  $\cos \alpha uf(u) + \sin \alpha (i2\pi)^{-1}df(u)/du$  (see ‘‘Transform of a coordinate multiplied function’’ in Section 14.5).

To distinguish the kind of fractional operators discussed in this section from the  $a$ th operator power of  $\mathcal{A}$  which is denoted by  $\mathcal{A}^a$ , we are denoting them by  $\mathcal{A}_a$ . The FRT is the  $a$ th operator power of the ordinary Fourier transform, but the fractional operators here are operators that perform the same action, such as coordinate multiplication, in different fractional Fourier domains. To further emphasize the difference, we note that for  $a=0$ ,  $\mathcal{A}_0 = \mathcal{A}$  while  $\mathcal{A}^0 = \mathcal{I}$ ; and for  $a=1$ ,  $\mathcal{A}_1 = \mathcal{A}^D$  while  $\mathcal{A}^1 = \mathcal{A}$ . In other words,  $\mathcal{A}_a$  interpolates between the operator  $\mathcal{A}$  and its dual  $\mathcal{A}^D$ , gradually evolving from one member of the dual pair to the other as the fractional order goes from zero to one. On the other hand,  $\mathcal{A}^a$  interpolates between the identity operator and the operator  $\mathcal{A}$ .

The first pair of dual operators we will consider are the coordinate multiplication  $\mathcal{U}$  and differentiation  $\mathcal{D}$  operators, whose effects in the time domain are to take a function  $f(u)$  to  $uf(u)$  and  $(i2\pi)^{-1}df(u)/du$ , respectively. The fractional forms of these operators  $\mathcal{U}_a$  and  $\mathcal{D}_a$  are defined so as to have the same functional effect in the  $a$ th domain; they take  $f_a(u_a)$  to  $u_a f_a(u_a)$  and  $(i2\pi)^{-1}df_a(u_a)du_a$ , respectively. In the time domain these operations correspond to taking  $f(u)$  to  $\cos \alpha uf(u) + \sin \alpha (i2\pi)^{-1}df(u)/du$  and  $-\sin \alpha uf(u) + \cos \alpha (i2\pi)^{-1}df(u)/du$ , respectively. (These and similar results are a consequence of the operational properties presented in Section 14.5.) These relationships can be captured elegantly in the following operator form:

$$\begin{aligned} \mathcal{U}_a &= \cos \alpha \mathcal{U} + \sin \alpha \mathcal{D}, \\ \mathcal{D}_a &= -\sin \alpha \mathcal{U} + \cos \alpha \mathcal{D}. \end{aligned} \quad (14.58)$$

The phase shift operator  $\mathcal{PH}(\eta)$  and the translation operator  $\mathcal{SH}(\xi)$  are also duals which are defined in terms of the  $\mathcal{U}$  and  $\mathcal{D}$  operators as  $\mathcal{PH}(\eta) = \exp(i2\pi\eta\mathcal{U})$  and  $\mathcal{SH}(\xi) = \exp(i2\pi\xi\mathcal{D})$ . (Such expressions are meant to be interpreted in terms of their series expansions.) These operators take  $f(u)$  to  $\exp(i2\pi\eta u)f(u)$  and  $f(u + \xi)$ , respectively. The fractional forms of these operators are defined as  $\mathcal{PH}_a(\eta) = \exp(i2\pi\eta\mathcal{U}_a)$  and  $\mathcal{SH}_a(\xi) = \exp(i2\pi\xi\mathcal{D}_a)$  and satisfy

$$\begin{aligned} \mathcal{PH}_a(\eta) &= \exp(i\pi\eta^2 \sin \alpha \cos \alpha) \mathcal{PH}(\eta \cos \alpha) \mathcal{SH}(\eta \sin \alpha), \\ \mathcal{SH}_a(\xi) &= \exp(-i\pi\xi^2 \sin \alpha \cos \alpha) \mathcal{PH}(-\xi \sin \alpha) \mathcal{SH}(\xi \cos \alpha). \end{aligned} \quad (14.59)$$

The scaling operator  $\mathcal{M}(M)$  can be defined as  $\mathcal{M}(M) = \exp[-i\pi(\ln M)(\mathcal{U}\mathcal{D} + \mathcal{D}\mathcal{U})]$  where  $M > 0$ . It takes  $f(u)$  to  $\sqrt{1/M}f(u/M)$ . This operator is its own dual in the sense that scaling in the time domain corresponds to descaling in the frequency domain: the Fourier transform of  $\sqrt{1/M}f(u/M)$  is  $\sqrt{M}F(M\mu)$ . The fractional form is defined as  $\mathcal{M}_a(M) = \exp[-i\pi(\ln M)(\mathcal{U}_a\mathcal{D}_a + \mathcal{D}_a\mathcal{U}_a)]$  and satisfies

$$\mathcal{M}_a(M) = \mathcal{F}^{-a}\mathcal{M}(M)\mathcal{F}^a. \quad (14.60)$$

The dual chirp multiplication  $\mathcal{Q}(q)$  and chirp convolution  $\mathcal{R}(r)$  operators are defined as  $\mathcal{Q}(q) = \exp(-i\pi q\mathcal{U}^2)$  and  $\mathcal{R}(r) = \exp(-i\pi r\mathcal{D}^2)$ . In the time domain they take  $f(u)$  to  $\exp(-i\pi qu^2)f(u)$  and  $\exp(-i\pi/4)\sqrt{1/r}\exp(i\pi u^2/r)*f(u)$ , respectively. Their fractional forms are defined as  $\mathcal{Q}_a(q) = \exp(-i\pi q\mathcal{U}_a^2)$  and  $\mathcal{R}_a(r) = \exp(-i\pi r\mathcal{D}_a^2)$  and satisfy

$$\begin{aligned} \mathcal{Q}_a(q) &= \mathcal{R}(-\tan \alpha) \mathcal{Q}(q \cos^2 \alpha) \mathcal{R}(\tan \alpha), \\ \mathcal{R}_a(r) &= \mathcal{Q}(-\tan \alpha) \mathcal{R}(r \cos^2 \alpha) \mathcal{Q}(\tan \alpha). \end{aligned} \quad (14.61)$$

We now turn our attention to the final pair of dual operators we will discuss. The discretization  $\mathcal{DI}(\Delta\mu)$  and periodization  $\mathcal{PE}(\Delta u)$  operators can be defined in terms of the phase shift and translation operators:  $\mathcal{DI}(\Delta\mu) = \sum_{k=-\infty}^{\infty} \mathcal{PH}(k\Delta\mu)$  and  $\mathcal{PE}(\Delta u) = \sum_{k=-\infty}^{\infty} \mathcal{SH}(k\Delta u)$ . The parameters  $\Delta u > 0$  and  $\Delta\mu > 0$  correspond to the period of replication in the time and frequency domains, respectively. Unlike the other operators defined above, these operators do not in general have inverses. Since sampling in the time domain corresponds to periodic replication in the frequency domain and vice versa, we also define  $\delta u = 1/\Delta\mu$  and  $\delta\mu = 1/\Delta u$ , denoting the sampling interval in the time and frequency domains, respectively. It is possible to show that the discretization and periodization operators take  $f(u)$  to  $\delta u \sum_{k=-\infty}^{\infty} \delta(u - k\delta u)f(k\delta u)$  and  $\sum_{k=-\infty}^{\infty} f(u - k\Delta u)$ , respectively. In the time domain, the discretization operator corresponds to multiplication with an impulse train, and the periodization operator corresponds to convolution with an impulse train (and vice versa in the frequency domain). Discretization in the time domain corresponds to periodization in the frequency domain and periodization in the time domain corresponds to discretization in the frequency domain. This is what is meant by the duality of these two operators. The fractional versions of these operators can be defined as  $\mathcal{DI}_a(\Delta\mu) = \sum_{k=-\infty}^{\infty} \mathcal{PH}_a(k\Delta\mu)$  and  $\mathcal{PE}_a(\Delta u) = \sum_{k=-\infty}^{\infty} \mathcal{SH}_a(k\Delta u)$  and satisfy

$$\begin{aligned} \mathcal{DI}_a(\Delta\mu) &= \mathcal{R}(-\tan \alpha) \mathcal{DI}(\Delta\mu \cos \alpha) \mathcal{R}(\tan \alpha), \\ \mathcal{PE}_a(\Delta u) &= \mathcal{Q}(-\tan \alpha) \mathcal{PE}(\Delta u \cos \alpha) \mathcal{Q}(\tan \alpha). \end{aligned} \quad (14.62)$$

Equations 14.58 through 14.62 all express the fractional operators in terms of their non-fractional counterparts. Equations 14.58 through 14.60 are directly related to the corresponding operational properties presented in Section 14.5, and may be considered

abstract ways of expressing them (transform of a coordinate multiplied or differentiated function, transform of a phase-shifted or shifted function, transform of a scaled function, respectively).

The fractional operators in Equation 14.62 interpolate between periodicity and discreteness with the smooth transition being governed by the parameter  $a$ . However, this is not the only significance of the fractional periodicity and discreteness operators. In practice, one cannot realize infinite periodic replication; any periodic replication must be limited to a finite number of periods. This corresponds to multiplying the infinite periodic replication operator with a window function, and will be referred to as partial periodization. Likewise, one cannot realize discretization with true impulses; any discretization will involve finite-width sampling pulses. This corresponds to convolving a true impulse sampling operator with a window function, and will be referred to as partial discretization. Thus, the partial periodization and discretization operations represent practical real-life replication and sampling operations. It has been shown that fractional periodization and discretization operators can be expressed in terms of partial periodization and discretization operators [128]. Therefore, the fractional periodization and discretization operators are also related to real-life sampling and periodic replication.

The subject matter of this section is further discussed in [128,156].

## 14.7 Time-Order and Space-Order Representations

Interpreting the fractional Fourier transforms  $f_a(u)$  of a function  $f(u)$  for different values of the order  $a$  as a two-dimensional function of  $u$  and  $a$  leads to the concept of time-order (or space-order) signal representations. Just like other time-frequency and time-scale (or space-frequency and space-scale) signal representations, they constitute an alternative way of displaying the content of a signal. These representations are redundant in that the information of a one-dimensional signal is displayed in two dimensions. There are two variations of the time-order representation, the rectangular time-order representation and the polar time-order representation.

For the rectangular time-order representation,  $f_a(u)$  is interpreted as a two-dimensional function, with  $u$  the horizontal coordinate and  $a$  the vertical coordinate. As such, the representations of the signal  $f(u)$  in all fractional domains are displayed simultaneously. Mathematically, the rectangular time-order representation  $T_f(u, a)$  of a signal  $f$  is defined as

$$T_f(u, a) = f_a(u). \quad (14.63)$$

Figure 14.4 illustrates the definition of the rectangular time-order representation. Such a display of the fractional Fourier transforms of the rectangle function is shown in Figure 14.1.

For the polar time-order representation,  $f_a(u) = f_{2\alpha/\pi}(\rho)$  is interpreted as a polar two-dimensional function where  $\rho$  is the

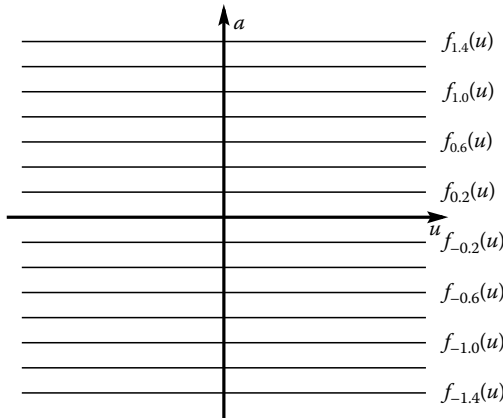


**FIGURE 14.4** The rectangular time-order representation. (From Ozaktas, H. M. and Kutay M. A., Technical Report BU-CE-0005, Bilkent University, Department of Computer Engineering, Ankara, January 2000; Ozaktas, H. M., Zalevsky, Z., and Kutay, M. A., *The Fractional Fourier Transform with Applications in Optics and Signal Processing*. John Wiley & Sons, New York, 2001. With permission.)

radial coordinate and  $\alpha$  is the angular coordinate. As such, all the fractional Fourier transforms of  $f(u)$  are displayed such that  $f_a(\rho)$  lies along the radial line making angle  $\alpha = a\pi/2$  with the horizontal axis. Mathematically, the polar time-order representation  $T_f(\rho, \alpha)$  of a signal  $f$  is defined as

$$T_f(\rho, \alpha) = f_{2\alpha/\pi}(\rho). \quad (14.64)$$

$T_f(\rho, \alpha)$  is periodic in  $\alpha$  with period  $2\pi$  as a result of the fact that  $f_a(\rho)$  is periodic in  $a$  with period 4.  $T_f(\rho, \alpha)$  can be consistently defined for negative values of  $\rho$  as well by using the property

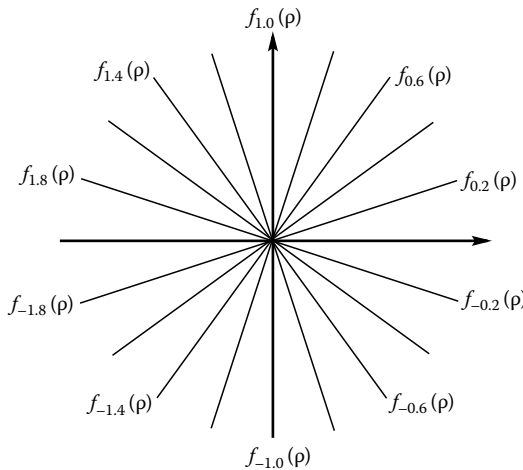


**FIGURE 14.5** The polar time-order representation. (From Ozaktas, H. M. and Kutay M. A., Technical Report BU-CE-0005, Bilkent University, Department of Computer Engineering, Ankara, January 2000; Ozaktas, H. M., Zalevsky, Z., and Kutay, M. A., *The Fractional Fourier Transform with Applications in Optics and Signal Processing*. John Wiley & Sons, New York, 2001. With permission.)

$f_{a\pm 2}(\rho) = f_a(-\rho)$ , from which it also follows that  $T_f(\rho, \alpha) = T_f(-\rho, \alpha \pm \pi)$ . Figure 14.5 illustrates the definition of the polar time-order representation.

As a consequence of its definition, there is a direct relation between the polar time-order representation and the concept of fractional Fourier domains. Each fractional Fourier transform  $f_a(\rho)$  of the signal  $f$  “lives” in the  $a$ th domain, defined by the radial line making angle  $\alpha = a\pi/2$  with the  $u$  axis. The polar time-order representation can be considered as a time–frequency space since the horizontal and vertical axes correspond to time and frequency. The oblique slices of the polar representation are simply equal to the fractional Fourier transforms. The slice at  $\alpha = 0$  is the time-domain representation  $f(\rho)$ , the slice at  $\alpha = \pi/2$  is the frequency-domain representation  $F(\rho)$ , and other slices correspond to fractional transforms of other orders.

We now discuss a number of properties of the polar time-order representation. The original function is obtained from the distribution as

$$f(u) = f_0(u) = T_f(u, 0). \quad (14.65)$$

The time-order representation of the  $a'$ th fractional Fourier transform of a function is simply a rotated version of the time-order representation of the original function

$$T_{f_{a'}}(\rho, \alpha) = T_f(\rho, \alpha + \alpha'), \quad (14.66)$$

where  $\alpha' = a'\pi/2$ . Since the time-order representation is linear, the representation of any linear combination of functions is the same as the linear combination of their representations.

We now discuss the relationship of time-order representations with the Wigner distribution and the ambiguity function. We had already encountered the Radon transform of the Wigner distribution:

$$\mathcal{R}_\alpha[W_f(u, \mu)](\rho) = |f_{2\alpha/\pi}(\rho)|^2 = |T_f(\rho, \alpha)|^2. \quad (14.67)$$

Thus, the Radon transform of the Wigner distribution, interpreted as a polar function, corresponds to the absolute square of the polar time-order representation. We also already encountered the following result, which is a consequence of the projection-slice theorem (page 56 of [129]):

$$\begin{aligned} \mathcal{S}_\alpha[A_f(\bar{u}, \bar{\mu})](\rho) &= A_f(\rho \cos \alpha, \rho \sin \alpha) \\ &= T_f(\rho, \alpha) * T_f^*(-\rho, \alpha) = f_{2\alpha/\pi}(\rho) * f_{2\alpha/\pi}^*(-\rho), \end{aligned} \quad (14.68)$$

where  $*$  denotes ordinary convolution. The Radon transforms and slices of the Wigner distribution and the ambiguity function are summarized in Table 14.1. For both the Wigner distribution and the ambiguity function, the Radon transform is of product form and the slice is of convolution form. The essential difference between the Wigner distribution and the ambiguity function lies in the scaling of  $\rho$  by 2 or 1/2 on the right-hand side.

**TABLE 14.1** Radon Transforms and Slices of the Wigner Distribution and the Ambiguity Function

---


$$\begin{aligned} \mathcal{RDN}_\alpha[W_f(u, \mu)](\rho) &= f_{2\alpha/\pi}(\rho) f_{2\alpha/\pi}^*(\rho) = T_f(\rho, \alpha) T_f^*(\rho, \alpha) \\ \mathcal{RDN}_\alpha[A_f(\bar{u}, \bar{\mu})](\rho) &= f_{2\alpha/\pi}(\rho/2) f_{2\alpha/\pi}^*(-\rho/2) = T_f(\rho/2, \alpha) T_f^*(-\rho/2, \alpha) \\ \mathcal{SLLC}_\alpha[W_f(u, \mu)](\rho) &= 2f_{2\alpha/\pi}(2\rho) * 2f_{2\alpha/\pi}^*(2\rho) = 2T_f(2\rho, \alpha) * 2T_f^*(2\rho, \alpha) \\ \mathcal{SLLC}_\alpha[A_f(\bar{u}, \bar{\mu})](\rho) &= f_{2\alpha/\pi}(\rho) * f_{2\alpha/\pi}^*(-\rho) = T_f(\rho, \alpha) * T_f^*(-\rho, \alpha) \end{aligned}$$


---

Sources: From Ozaktas, H. M. and Kutay, M. A., Technical Report BU-CE-0005, Bilkent University, Department of Computer Engineering, Ankara, January 2000; Ozaktas, H. M., et al., *The Fractional Fourier Transforms with Applications in Optics and Signal Processing*. John Wiley & Sons, New York, 2001. With permission.)

Note: The upper row can also be expressed as  $|f_{2\alpha/\pi}(\rho)|^2 = |T_f(\rho, \alpha)|^2$ .

Analogous expressions for the Radon transforms and slices of the polar time-order representation  $T_f(\rho, \alpha)$  and its two-dimensional Fourier transform  $\tilde{T}_f(\bar{\rho}, \bar{\alpha})$  are given in Table 14.2. The slice of  $T_f(\rho, \alpha)$  at a certain angle is simply equal to the fractional Fourier transform  $f_a(\rho)$  by definition (with  $\alpha = a\pi/2$ ). The Radon transform of  $\tilde{T}_f(\bar{\rho}, \bar{\alpha})$  at an angle  $\phi$  is given by  $f_{b+1}(\rho)$  or  $T_f(\rho, \phi + \pi/2)$ , a  $\pi/2$  rotated version of  $T_f(\rho, \alpha)$  (with  $\phi = b\pi/2$ ). We already know that the time-frequency representation whose projections are equal to  $|f_a(u)|^2$  is the Wigner distribution. We now see that the time-frequency representation whose projections are equal to  $f_a(u)$  is the two-dimensional Fourier transform of the polar time-order representation (within a rotation).

Thus in Tables 14.1 and 14.2 we present a total of eight expressions for the Radon transforms and slices of the Wigner distribution and its two-dimensional Fourier transform (the ambiguity function), and the Radon transforms and slices of the polar time-order representation and its two-dimensional Fourier transform.

The polar time-order representation is a linear time-frequency representation, unlike the Wigner distribution and ambiguity function which are quadratic. Its importance stems from the fact that the Radon transforms (integral projections) and slices of the Wigner distribution and the ambiguity function can be expressed in terms of products or convolutions of various scaled forms of the time-order representation and its two-dimensional

**TABLE 14.2** Radon Transforms and Slices of the Polar Time-Order Representation and Its Two-Dimensional Fourier Transform

---


$$\begin{aligned} \mathcal{RDN}_\phi[T_f(\rho, \alpha)](\varrho) &= \int_{-\pi/2}^{\pi/2} f_{2(\phi+\theta)/\pi}(\varrho \sec \theta) \varrho \sec^2 \theta d\theta \\ \mathcal{RDN}_\phi[\tilde{T}_f(\bar{\rho}, \bar{\alpha})](\varrho) &= f_{2\phi/\pi+1}(\varrho) \\ \mathcal{SLLC}_\phi[T_f(\rho, \alpha)](\varrho) &= f_{2\phi/\pi}(\varrho) \\ \mathcal{SLLC}_\phi[\tilde{T}_f(\bar{\rho}, \bar{\alpha})](\varrho) &= \frac{i}{2\pi} \int_{-\pi/2}^{\pi/2} f'_{2(\phi+\theta)/\pi+1}(\varrho \cos \theta) \sec \theta d\theta \end{aligned}$$


---

Sources: From Ozaktas, H. M. and Kutay, M. A., Technical Report BU-CE-0005, Bilkent University, Department of Computer Engineering, Ankara, January 2000; Ozaktas, H. M., et al., *The Fractional Fourier Transforms with Applications in Optics and Signal Processing*. John Wiley & Sons, New York, 2001. With permission.)

Fourier transform. These representations are discussed in greater detail in Chapter 5 of [129].

## 14.8 Linear Canonical Transforms

Linear canonical transforms (LCTs) are a three-parameter family of linear integral transforms. Many important operations and transforms including the FRT are special cases of linear canonical transforms. Readers wishing to learn more than we can cover here are referred to [129,164].

The linear canonical transform  $f_M(u)$  of  $f(u)$  with parameter  $\mathbf{M}$  is most conveniently defined as

$$f_M(u) = \int_{-\infty}^{\infty} C_M(u, u') f(u') du', \quad (14.69)$$

$$C_M(u, u') = \sqrt{\beta} e^{-i\pi/4} \exp[i\pi(\alpha u^2 - 2\beta uu' + \gamma u'^2)],$$

where  $\alpha$ ,  $\beta$ , and  $\gamma$  are real parameters. The label  $\mathbf{M}$  represents the three parameters  $\alpha$ ,  $\beta$ , and  $\gamma$  which completely specify the transform. Linear canonical transforms are unitary; that is, the inverse transform kernel is the Hermitian conjugate of the original transform kernel:  $C_M^{-1}(u, u') = C_M^*(u', u)$ .

The composition of any two linear canonical transforms is another linear canonical transform. In other words, the effect of consecutively applying two linear canonical transforms with different parameters is equivalent to applying another linear canonical transform whose parameters are related to those of the first two. (Actually this is strictly true only within a  $\pm$  sign factor [129,164].) Such compositions are not in general commutative, but they are associative.

Finding the parameters of the composite transform is made easier if we define a  $2 \times 2$  unit-determinant matrix to represent the parameters of the transform. We let the symbol  $\mathbf{M}$  (which until now denoted the three parameters  $\alpha$ ,  $\beta$ ,  $\gamma$ ) now be defined as a matrix of the form

$$\mathbf{M} = \begin{bmatrix} A & B \\ C & D \end{bmatrix} = \begin{bmatrix} \gamma/\beta & 1/\beta \\ -\beta + \alpha\gamma/\beta & \alpha/\beta \end{bmatrix} = \begin{bmatrix} \alpha/\beta & -1/\beta \\ \beta - \alpha\gamma/\beta & \gamma/\beta \end{bmatrix}^{-1}, \quad (14.70)$$

with determinant  $AD - BC = 1$ . The three original parameters can be expressed in terms of the matrix elements as  $\alpha = D/B$ ,  $\beta = 1/B$ , and  $\gamma = A/B$ , and the definition of linear canonical transforms can be rewritten as

$$f_M(u) = \int_{-\infty}^{\infty} C_M(u, u') f(u') du', \quad (14.71)$$

$$C_M(u, u') = \sqrt{1/B} e^{-i\pi/4} \exp\left[i\pi\left(\frac{D}{B}u^2 - 2\frac{1}{B}uu' + \frac{A}{B}u'^2\right)\right].$$

Now, it is easy to show the following results: The matrix  $\mathbf{M}_3$  corresponding to the composition of two systems is the matrix

product of the matrices  $M_2$  and  $M_1$  corresponding to the individual systems. That is,

$$M_3 = M_2 M_1, \tag{14.72}$$

where

- $M_1$  is the matrix of the transform that is applied first
- $M_2$  is the matrix of the transform that is applied next

Furthermore, the matrix corresponding to the inverse of a linear canonical transform is the inverse of the matrix corresponding to the original transform.

The set of linear canonical transforms satisfies all the axioms of a noncommutative group (closure, associativity, existence of identity, inverse of each element), just like the set of all unit-determinant  $2 \times 2$  matrices (again within a  $\pm$  sign). Certain subsets of the set of linear canonical transforms are groups in themselves and thus are subgroups. Some of them will be discussed below. For example, the fractional Fourier transform is a subgroup with one real parameter.

The effect of linear canonical transforms on the Wigner distribution of a function can be expressed quite elegantly in terms of the elements of the matrix  $M$ :

$$W_{f_M}(Au + B\mu, Cu + D\mu) = W_f(u, \mu), \tag{14.73}$$

$$W_{f_M}(u, \mu) = W_f(Du - B\mu, -Cu + A\mu). \tag{14.74}$$

A similar relationship holds for the ambiguity function as well. The above result means that the Wigner distribution of the transformed function is simply a linearly distorted form of the Wigner distribution of the original function, with the value of the Wigner distribution at each time/space–frequency point being mapped to another time/space–frequency point. Since the determinant of  $M$  is equal to unity, this pointwise geometrical distortion or deformation is area preserving; it distorts but does not concentrate or deconcentrate the Wigner distribution.

We now discuss several special cases of linear canonical transforms that correspond to specific forms of the matrix  $M$ . The last of these special cases will be the fractional Fourier transform which corresponds to the case where  $M$  is the rotation matrix.

The scaling operation takes  $f(u)$  to  $\sqrt{1/M}f(u/M)$ . The inverse of a scaling operation with parameter  $M > 0$  is a scaling operation with parameter  $1/M$ . The  $M$  matrix is of the form

$$\begin{bmatrix} M & 0 \\ 0 & 1/M \end{bmatrix} \tag{14.75}$$

and the Wigner distribution of the scaled function is  $W_f(u/M, M\mu)$  (Figure 14.6b shows how the Wigner distribution is scaled for  $M = 2$ ).

Let us now consider chirp multiplication which takes  $f(u)$  to  $e^{-i\pi q u^2} f(u)$ . The inverse of this operation with parameter  $q$  has the same form but with parameter  $-q$ . Its  $M$  matrix is

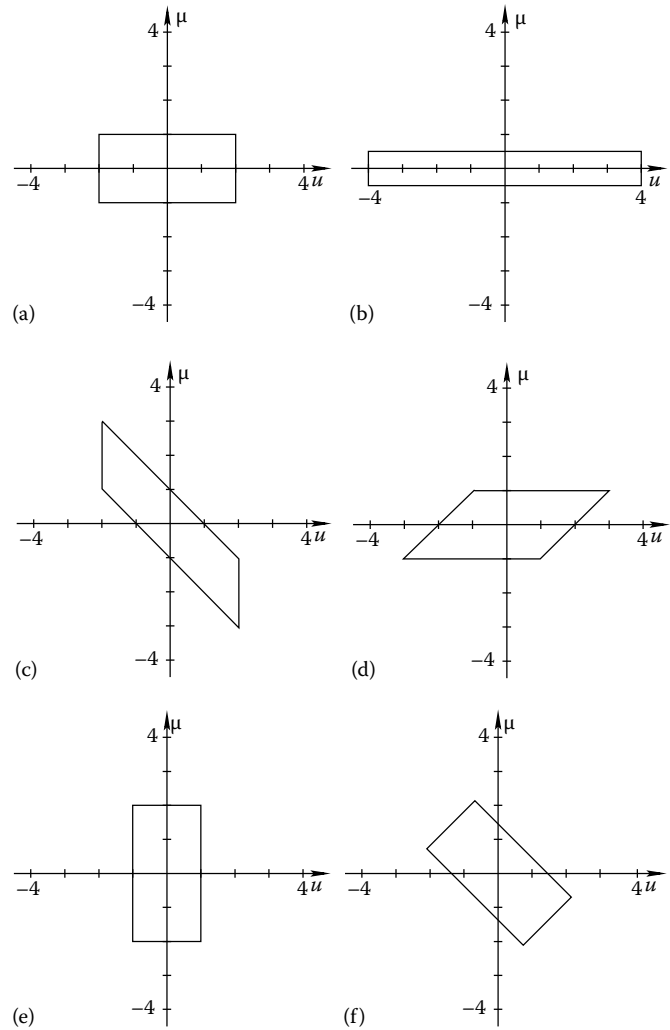


**FIGURE 14.6** (a) Rectangular region in the time/space–frequency plane, in which most of the signal energy is assumed to be concentrated. Effect of (b) scaling with  $M = 2$ , (c) chirp multiplication with  $q = 1$ , (d) chirp convolution with  $r = 1$ , (e) Fourier transformation, (f) fractional Fourier transformation with  $a = 0.5$ . (From Ozaktas, H. M., Zalevsky, Z., and Kutay, M. A., *The Fractional Fourier Transform with Applications in Optics and Signal Processing*. John Wiley & Sons, New York, 2001. With permission.)

$$\begin{bmatrix} 1 & 0 \\ -q & 1 \end{bmatrix} \tag{14.76}$$

and the Wigner distribution of the chirp multiplied function is  $W_f(u, \mu + qu)$  (Figure 14.6c shows this vertical shearing for  $q = 1$ ).

Now consider chirp convolution which takes  $f(u)$  to  $e^{-i\pi u^2/r} \sqrt{1/r} \exp(i\pi u^2/r) * f(u)$ . The inverse of this operation with parameter  $r$  has the same form but with parameter  $-r$ . Its  $M$  matrix is

$$\begin{bmatrix} 1 & r \\ 0 & 1 \end{bmatrix} \tag{14.77}$$

and the Wigner distribution of the chirp convolved function is  $W_f(u - r\mu, \mu)$  (Figure 14.6d shows this horizontal shearing for  $r = 1$ ).

The ordinary Fourier transform takes  $f(u)$  to  $\int_{-\infty}^{\infty} f(u')e^{-i2\pi uu'} du'$ . However, the Fourier transform that is a special case of linear canonical transforms has a slightly modified definition, taking  $f(u)$  to  $e^{-i\pi/4} \int f(u')e^{-i2\pi uu'} du'$ . The  $\mathbf{M}$  matrix is

$$\begin{bmatrix} 0 & 1 \\ -1 & 0 \end{bmatrix} \quad (14.78)$$

and the Wigner distribution of the Fourier transformed function is  $W_f(-\mu, u)$  (Figure 14.6e shows this  $\pi/2$  rotation).

Finally, we turn our attention to the fractional Fourier transform, which takes  $f(u)$  to  $f_a(u)$  as defined in Equation 14.1. The inverse of the  $a$ th order FRT is the  $-a$ th order FRT. The  $\mathbf{M}$  matrix is

$$\begin{bmatrix} \cos(a\pi/2) & \sin(a\pi/2) \\ -\sin(a\pi/2) & \cos(a\pi/2) \end{bmatrix} \quad (14.79)$$

and the Wigner distribution of the Fourier transformed function is

$$W_f[\cos(a\pi/2)u - \sin(a\pi/2)\mu, \sin(a\pi/2)u + \cos(a\pi/2)\mu]. \quad (14.80)$$

We have already encountered this expression before in Equation 14.25 (Figure 14.6f shows this rotation by angle  $\alpha = a\pi/2$  when  $a = 0.5$ ).

To summarize, we see that fractional Fourier transforms constitute a one-parameter subgroup of linear canonical transforms corresponding to the case where the  $\mathbf{M}$  matrix is the rotation matrix, and the fractional order parameter corresponds to the angle of rotation. Fractional Fourier transformation corresponds to rotation of the Wigner distribution in the time/space-frequency plane (phase space). The ordinary Fourier transform is a special case of the fractional Fourier transform, which in turn is a special case of linear canonical transforms.

The matrix formalism not only allows one to easily determine the parameters of the concatenation (composition) of several LCTs, it also allows a given LCT to be decomposed into more elementary operations such as scaling, chirp multiplication and convolution, and the fractional Fourier transform. This is often useful for both analytical and numerical purposes. Of the many such possible decompositions here we list only a few (see page 104 of [129]):

$$\begin{bmatrix} A & B \\ C & D \end{bmatrix} = \begin{bmatrix} 1 & (A-1)/C \\ 0 & 1 \end{bmatrix} \begin{bmatrix} 1 & 0 \\ C & 1 \end{bmatrix} \begin{bmatrix} 1 & (D-1)/C \\ 0 & 1 \end{bmatrix} \quad (14.81)$$

$$= \begin{bmatrix} 1 & 0 \\ (D-1)/B & 1 \end{bmatrix} \begin{bmatrix} 1 & B \\ 0 & 1 \end{bmatrix} \begin{bmatrix} 1 & 0 \\ (A-1)/B & 1 \end{bmatrix}. \quad (14.82)$$

Such decompositions usually show how an arbitrary LCT can be expressed in terms of its special cases. Specifically, the above two decompositions show how any unit-determinant matrix can be written as the product of lower and upper triangular matrices, which we have seen correspond to chirp multiplication and convolution operations.

Another important decomposition is the decomposition of an arbitrary LCT into a fractional Fourier transformation followed by scaling followed by chirp multiplication:

$$\begin{bmatrix} A & B \\ C & D \end{bmatrix} = \begin{bmatrix} 1 & 0 \\ -q & 1 \end{bmatrix} \begin{bmatrix} M & 0 \\ 0 & 1/M \end{bmatrix} \begin{bmatrix} \cos \alpha & \sin \alpha \\ -\sin \alpha & \cos \alpha \end{bmatrix}, \quad (14.83)$$

where

$$\alpha = \operatorname{arccot}(A/B), \quad (14.84)$$

$$M = \operatorname{sgn}(A)\sqrt{A^2 + B^2}, \quad (14.85)$$

$$q = \frac{A}{B(A^2 + B^2)} - \frac{D}{B}, \quad (14.86)$$

where  $\operatorname{sgn}(A)$  is the sign of  $A$ . The ranges of the square root and the arccotangent both lie in  $(-\pi/2, \pi/2]$ . Equation 14.83 can be interpreted geometrically as follows: any linear distortion in the time/space-frequency plane can be realized as a rotation followed by scaling followed by shearing. This decomposition is important because it forms the basis of a fast and accurate algorithm for digitally computing arbitrary linear canonical transforms [76,119]. These algorithms compute LCTs with a performance similar to that of the fast Fourier transform (FFT) algorithm in computing the Fourier transform, both in terms of speed and accuracy. Further discussion of decompositions of the type of Equation 14.83 may be found in [4]. Other works on the computation of LCTs include [64,65].

Many of the elementary and operational properties of LCTs are collected in Section 14.9, which can be recognized as generalizations of the corresponding properties of the fractional Fourier transform.

## 14.9 Basic and Operational Properties of Linear Canonical Transforms

Here we present a list of the more important basic and operational properties of the LCTs. Readers can easily verify that the operational properties reduce to the corresponding property for the fractional Fourier transform when  $\mathbf{M}$  is the rotation matrix.

**Linearity:** Let  $\mathcal{C}_{\mathbf{M}}$  denote the linear canonical transform operator with parameter matrix  $\mathbf{M}$ . Then  $\mathcal{C}_{\mathbf{M}}[\sum_k b_k f_k(u)] = \sum_k b_k [\mathcal{C}_{\mathbf{M}} f_k(u)]$ .

**Inverse:**  $(\mathcal{C}_{\mathbf{M}})^{-1} = \mathcal{C}_{\mathbf{M}^{-1}}$ .

**Unitarity:**  $(\mathcal{C}_{\mathbf{M}})^{-1} = (\mathcal{C}_{\mathbf{M}})^{\text{H}} = \mathcal{C}_{\mathbf{M}^{-1}}$  where  $()^{\text{H}}$  denotes the conjugate transpose of the operator.



**Associativity:**  $(C_{M_1}C_{M_2})C_{M_3} = C_{M_1}(C_{M_2}C_{M_3})$ .

**Eigenfunctions:** Eigenfunctions of linear canonical transforms are discussed in [133].

**Parseval:**  $\int f^*(u)g(u)du = \int f_M^*(u)g_M(u)du$ . This property is equivalent to unitarity. Energy or norm conservation ( $\text{En}[f] = \text{En}[f_M]$  or  $\|f\| = \|f_M\|$ ) is a special case.

**Time reversal:** Let  $\mathcal{P}$  denote the parity operator:  $\mathcal{P}[f(u)] = f(-u)$ , then

$$C_M\mathcal{P} = \mathcal{P}C_M, \quad (14.87)$$

$$C_M[f(-u)] = f_M(-u). \quad (14.88)$$

**Transform of a scaled function:**

$$C_M[|K|^{-1}f(u/K)] = C_{M'}[f(u)] = f_{M'}(u). \quad (14.89)$$

Here  $M'$  is the matrix that corresponds to the parameters  $\alpha' = \alpha$ ,  $\beta' = K\beta$ , and  $\gamma' = K^2\gamma$ .

**Transform of a shifted function:**

$$C_M[f(u - u_0)] = \exp[i\pi(2uu_0C - u_0^2AC)]f_M(u - Au_0). \quad (14.90)$$

Here  $u_0$  is real.

**Transform of a phase-shifted function:**

$$C_M[\exp(i2\pi\mu_0u)f(u)] = \exp[i\pi\mu_0D(2u - \mu_0B)]f_M(u - B\mu_0). \quad (14.91)$$

Here  $\mu_0$  is real.

**Transform of a coordinate multiplied function:**

$$C_M[u^n f(u)] = [Du - B(i2\pi)^{-1}d/du]^n f_M(u). \quad (14.92)$$

Here  $n$  is a positive integer.

**Transform of the derivative of a function:**

$$C_M[(i2\pi)^{-1}d/du]^n f(u) = [-Cu + A(i2\pi)^{-1}d/du]^n f_M(u). \quad (14.93)$$

Here  $n$  is a positive integer.

A few additional properties are

$$C_M[f^*(u)] = f_M^*(-(u)), \quad (14.94)$$

$$C_M[(f(u) + f(-u))/2] = (f_M(u) + f_M(-u))/2, \quad (14.95)$$

$$C_M[(f(u) - f(-u))/2] = (f_M(u) - f_M(-u))/2. \quad (14.96)$$

A function and its linear canonical transform satisfy an ‘‘uncertainty relation,’’ stating that the product of the spread of the two functions, as measured by their standard deviations, cannot be less than  $|B|/4\pi$  [129].

## 14.10 Filtering in Fractional Fourier Domains

Filtering, as conventionally understood, involves taking the Fourier transform of a signal, multiplying it with a Fourier-domain transfer function, and inverse transforming the result (Figure 14.7a). Here, we consider filtering in fractional Fourier domains, where we take the fractional Fourier transform, apply a filter function in the fractional Fourier domain, and inverse transform to the original domain (Figure 14.7b). Formally the filter output is written as

$$f_{\text{single}}(u) = [\mathcal{F}^{-a} \Lambda_h \mathcal{F}^a]f(u) = \mathcal{T}_{\text{single}}f(u), \quad (14.97)$$

where

$\mathcal{F}^a$  is the  $a$ th order fractional Fourier transform operator

$\Lambda_h$  denotes the operator corresponding to multiplication by the filter function  $h(u)$

$\mathcal{T}_{\text{single}}$  is the operator representing the overall filtering configuration

To understand the basic motivation for filtering in fractional Fourier domains, consider Figure 14.8, where the Wigner distributions of a desired signal and an undesired noise term are superimposed. We observe that the signal and noise overlap in both the 0th and 1st domains, but they do not overlap in the 0.5th domain (consider the projections onto the  $u_0 = u$ ,  $u_1 = \mu$ , and  $u_{0.5}$  axes). Although it is not possible to eliminate the noise in the time or frequency domains, we can eliminate it easily by using a simple amplitude mask in the 0.5th domain.

Fractional Fourier domain filtering can be applied to the problem of signal recovery or estimation from observations, where the signal to be recovered has been degraded by a known distortion or blur, and the observations are noisy. The problem is to reduce or eliminate these degradations and noise. The solution of such problems depends on the observation model and the prior knowledge available about the desired signal, degradation process, and noise. A commonly used observation model is

$$g(u) = \int h_d(u, u')f(u') du' + n(u), \quad (14.98)$$

where

$h_d(u, u')$  is the kernel of the linear system that distorts or blurs the desired signal  $f(u)$

$n(u)$  is an additive noise term

The problem is to find an estimation operator represented by the kernel  $h(u, u')$ , such that the estimated signal

$$f_{\text{est}}(u) = \int h(u, u')g(u') du' \quad (14.99)$$

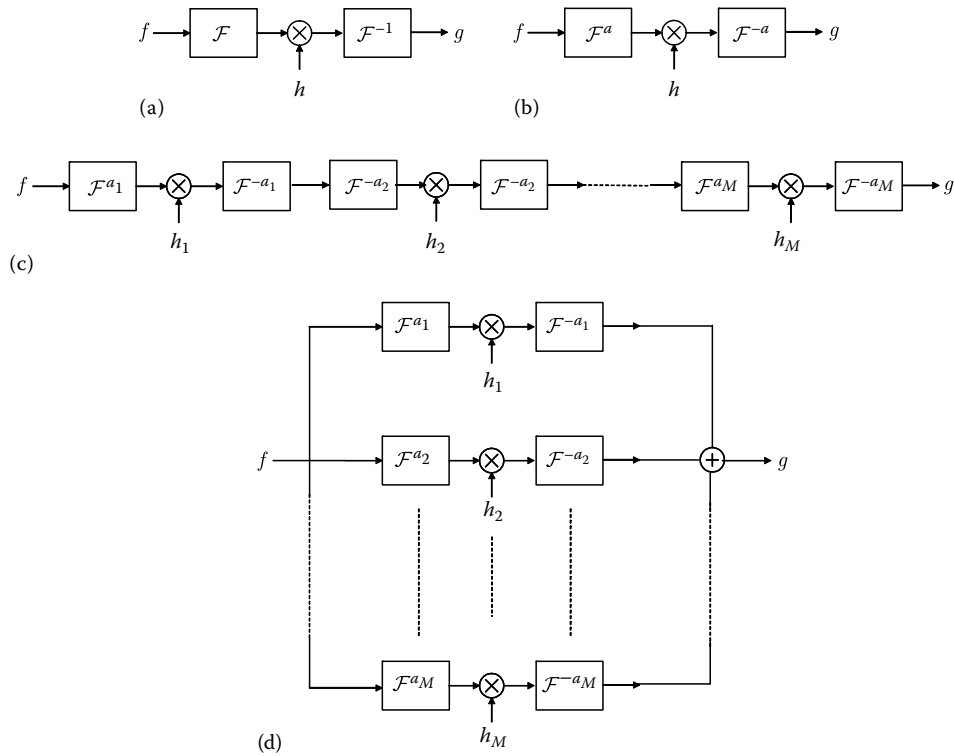


FIGURE 14.7 (a) Filtering in the frequency domain; (b) filtering in the  $a$ th order fractional Fourier domain; (c) multi-stage (series) filtering; (d) multi-channel (parallel) filtering.

optimizes some criteria. Despite its limitations, one of the most commonly used objectives is to minimize the mean square error  $\sigma_{\text{err}}^2$  defined as

$$\sigma_{\text{err}}^2 = \left\langle \int |f_{\text{est}}(u) - f(u)|^2 du \right\rangle, \quad (14.100)$$

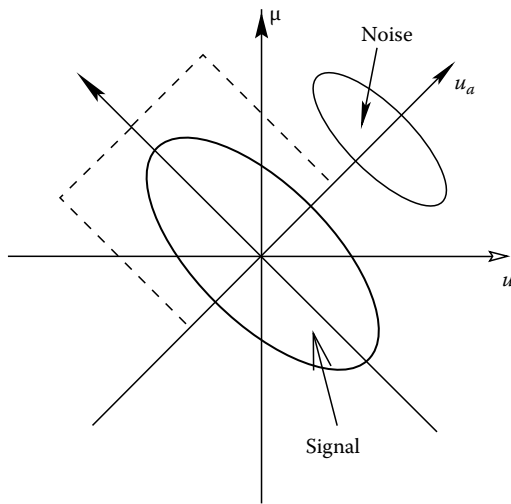


FIGURE 14.8 Filtering in a fractional Fourier domain as observed in the time- or space-frequency plane.  $a = 0.5$  as drawn. (From Ozaktas, H. M., et al., *J Opt Soc Am A-Opt Image Sci Vis*, 11:547-559, 1994. With permission.)

where the angle brackets denote an ensemble average. The estimation or recovery operator minimizing  $\sigma_{\text{err}}^2$  is known as the optimal Wiener filter. The kernel  $h(u, u')$  of this optimal filter satisfies the following relation [87]:

$$R_{fg}(u, u') = \int h(u, u'') R_{gg}(u'', u') du'' \quad \text{for all } u, u', \quad (14.101)$$

where

$$R_{fg}(u, u') \text{ is the statistical cross-correlation of } f(u) \text{ and } g(u)$$

$$R_{gg}(u, u') \text{ is the statistical autocorrelation of } g(u)$$

In the general case  $h_d(u, u')$  represents a time varying system, and there is no fast algorithm for obtaining  $f_{\text{est}}(u)$ .

We can formulate the problem of obtaining an estimate  $f_{\text{est}}(u) = f_{\text{single}}(u)$  of  $f(u)$  by using the  $a$ th order fractional Fourier domain filtering configuration (Equation 14.97). As we will see in Section 14.13, the fractional Fourier transform can be efficiently computed with an  $\sim N \log N$  algorithm similar to the fast Fourier transform algorithm used to compute the ordinary Fourier transform. Therefore, the fractional Fourier transform can be implemented nearly as efficiently as the ordinary Fourier transform, and the cost of fractional Fourier domain filtering is approximately the same as the cost of ordinary Fourier domain filtering. The optimal multiplicative filter function  $h(u)$  for a given order  $a$  that minimizes the mean square error defined in Equation 14.100

for the filtering configuration represented by Equation 14.97 is given by [85]:

$$h(u_a) = \frac{\iint K_a(u_a, u)K_{-a}(u_a, u')R_{fg}(u, u') du' du}{\iint K_a(u_a, u)K_{-a}(u_a, u')R_{gg}(u, u') du' du}, \quad (14.102)$$

where the statistical cross-correlation and autocorrelation functions  $R_{fg}(u, u')$  and  $R_{gg}(u, u')$  can be obtained from the functions  $R_{ff}(u, u')$  and  $R_{nn}(u, u')$ , which are assumed to be known. The corresponding mean square error can be calculated from Equation 14.100 for different values of  $a$ , and the value of  $a$  resulting in the smallest error can be determined.

Generalizations of the  $a$ th order fractional Fourier domain filtering configuration are the multistage (repeated or serial) and the multichannel (parallel) filtering configurations. These systems consist of  $M$  single-domain fractional Fourier filtering stages in series or in parallel (Figure 14.7).  $M = 1$  corresponds to single-domain filtering in both cases. In the multistage system shown in Figure 14.7c, the input is first transformed into the  $a_1$ th domain where it is multiplied by a filter  $h_1(u)$ . The result is then transformed back into the original domain and the same process is repeated  $M$  times consecutively. This amounts to sequentially visiting the domains  $a_1, a_2, a_3, \dots$ , and applying a filter in each. On the other hand, the multichannel system consists of  $M$  single-domain blocks in parallel (Figure 14.7d). For each channel  $k$ , the input is transformed to the  $a_k$ th domain, multiplied with a filter  $h_k(u)$ , and then transformed back. If these configurations are used to obtain an estimate  $f_{\text{ser}}(u)$  or  $f_{\text{par}}(u)$  of  $f(u)$  in terms of  $g(u)$ , we have

$$f_{\text{ser}}(u) = [\mathcal{F}^{-a_M} \Lambda_{h_M} \dots \mathcal{F}^{a_2 - a_1} \Lambda_{h_1} \mathcal{F}^{a_1}] g(u) = \mathcal{T}_{\text{ser}} g(u), \quad (14.103)$$

$$f_{\text{par}}(u) = \left[ \sum_{k=1}^M \mathcal{F}^{-a_k} \Lambda_{h_k} \mathcal{F}^{a_k} \right] g(u) = \mathcal{T}_{\text{par}} g(u), \quad (14.104)$$

where

- $\mathcal{F}^{a_k}$  represents the  $a_k$ th order fractional Fourier transform operator
- $\Lambda_{h_k}$  denotes the operator corresponding to multiplication by the filter function  $h_k(u)$
- $\mathcal{T}_{\text{ser}}, \mathcal{T}_{\text{par}}$  are the operators representing the overall filtering configurations

Both of these equations reduce to Equation 14.97 for  $M = 1$ .

Multistage and multichannel filtering systems as described above are a subclass of the class of general linear systems whose input-output relation is given in Equation 14.99. Such linear systems have in general  $N^2$  degrees of freedom, where  $N$  is the time-bandwidth product of the signals. Obtaining the output from the input normally takes  $\sim N^2$  time, unless the system kernel  $h(u, u')$  has some special structure which can be exploited. Shift-invariant (time- or space-invariant) systems are also a

subclass of general linear systems whose system kernels  $h(u, u')$  can always be expressed in the form  $h(u, u') = h(u - u')$ . They are a restricted subclass with only  $N$  degrees of freedom, but can be implemented in  $\sim N \log N$  time in the ordinary Fourier domain.

We may think of shift-invariant systems and general linear systems as representing two extremes in a cost-performance trade-off. Shift-invariant systems exhibit low cost and low performance, whereas general linear systems exhibit high cost and high performance. Sometimes use of shift-invariant systems may be inadequate, but at the same time use of general linear systems may be an overkill and prohibitively costly. Multistage and multichannel fractional Fourier domain filtering configurations interpolate between these two extremes, offering greater flexibility in trading off between cost and performance.

Both filtering configurations have at most  $MN + M$  degrees of freedom. Their digital implementation will take  $O(MN \log N)$  time since the fractional Fourier transform can be implemented in  $\sim N \log N$  time. These configurations interpolate between general linear systems and shift-invariant systems both in terms of cost and flexibility. If we choose  $M$  to be small, cost and flexibility are both low;  $M = 1$  corresponds to single-stage filtering. If we choose  $M$  to be larger, cost and flexibility are both higher; as  $M$  approaches  $N$ , the number of degrees of freedom approaches that of a general linear system.

Increasing  $M$  allows us to better approximate a given linear system. For a given value of  $M$ , we can approximate this system with a certain degree of accuracy (or error). For instance, a shift-invariant system can be realized with perfect accuracy with  $M = 1$ . In general, there will be a finite accuracy for each value of  $M$ . As  $M$  is increased, the accuracy will usually increase (but never decrease). In dealing with a specific application, we can seek the minimum value of  $M$  which results in the desired accuracy, or the highest accuracy that can be achieved for given  $M$ . Thus these systems give us considerable freedom in trading off efficiency and greater accuracy, enabling us to seek the best performance for a given cost, or the least cost for a given performance. In a given application, this flexibility may allow us to realize a system which is acceptable in terms of both cost and performance.

The cost-accuracy trade-off is illustrated in Figure 14.9, where we have plotted both the cost and the error as functions of the number of filters  $M$  for a hypothetical application. The two plots show how the cost increases and the error decreases as we increase  $M$ . Eliminating  $M$  from these two graphs leads us to a graph of error versus cost.

The multistage and multichannel configurations may be further extended to *generalized filtering configurations* or *generalized filter circuits* where we combine the serial and parallel filtering configurations in an arbitrary manner (Figure 14.10).

Having discussed quite generally the subject of filtering in fractional Fourier domains, we now discuss the closely related concepts of fractional convolution and fractional multiplication [108,117]. The convolution of two signals  $h$  and  $f$  in the

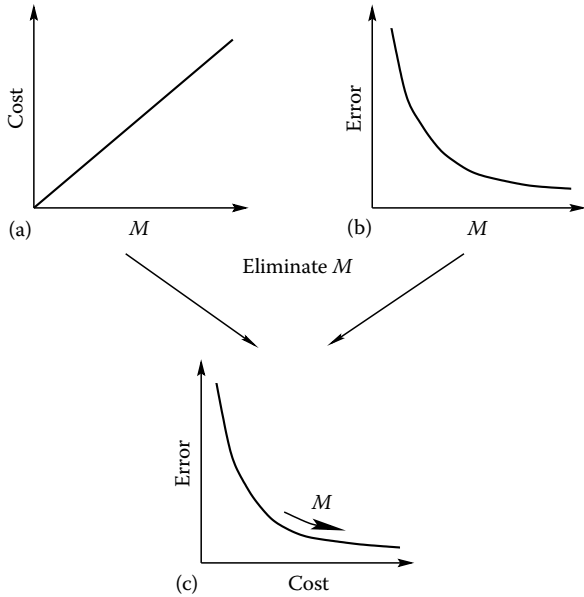


**FIGURE 14.9** (a) Cost versus  $M$ , (b) error versus  $M$ , (c) error versus cost. (From Kutay, M. A., PhD thesis, Bilkent University, Ankara, 1999; Ozaktas, H. M., et al., *The Fractional Fourier Transform with Applications in Optics and Signal Processing*. John Wiley & Sons, New York, 2001. With permission.)

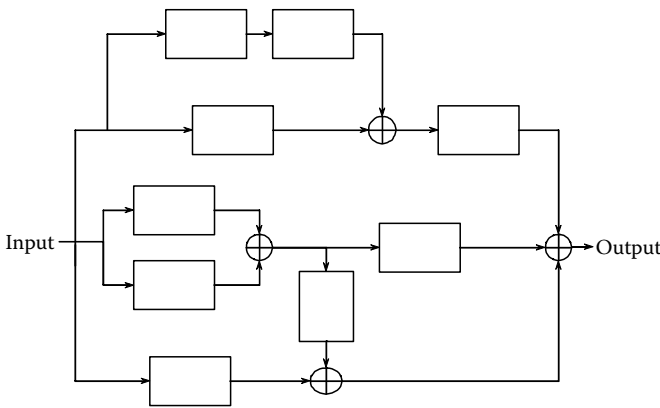


**FIGURE 14.10** Generalized filter circuits; each block is of the form  $F^{-ak} \Lambda_{h_k} F^{ak}$

$a$ th fractional Fourier domain is defined such that their  $a$ th order fractional Fourier domain representations  $h_a(u_a)$  and  $f_a(u_a)$  are convolved to give the corresponding representation of some new signal  $g$ :

$$g_a(u_a) = h_a(u_a) * f_a(u_a), \quad (14.105)$$

where  $*$  denotes ordinary convolution. Likewise, multiplication of two signals in the  $a$ th fractional Fourier domain is defined as

$$g_a(u_a) = h_a(u_a) f_a(u_a). \quad (14.106)$$

Of course, convolution (or multiplication) in the  $a=0$ th domain is ordinary convolution (or multiplication) and convolution (or multiplication) in the  $a=1$ st domain is ordinary multiplication (or convolution). More generally, convolution (or multiplication) in the  $a$ th domain is multiplication (or convolution) in the  $(a \pm 1)$ th domain (which is orthogonal to the  $a$ th domain), and convolution (or multiplication) in the  $a$ th domain is again convolution (or multiplication) in the  $(a \pm 2)$ th domain (the sign-flipped version of the  $a$ th domain). Convolution or multiplication in an arbitrary  $a$ th domain is an operation “interpolating” between the ordinary convolution and multiplication operations [129]. In light of these definitions, filtering in the  $a$ th fractional Fourier domain corresponds to the multiplication of two signals in the  $a$ th fractional Fourier domain or equivalently the convolution of two signals in the  $a \pm 1$ th fractional Fourier domain.

## 14.11 Fractional Fourier Domain Decompositions

The fractional Fourier domain decomposition (FFDD) [86] is closely related to multichannel filtering and is analogous to the singular-value decomposition in linear algebra [68,154].

The SVD of an arbitrary  $N_{\text{out}} \times N_{\text{in}}$  complex matrix  $\mathbf{H}$  is

$$\mathbf{H}_{N_{\text{out}} \times N_{\text{in}}} = \mathbf{U}_{N_{\text{out}} \times N_{\text{out}}} \mathbf{\Sigma}_{N_{\text{out}} \times N_{\text{in}}} \mathbf{V}_{N_{\text{in}} \times N_{\text{in}}}^{\text{H}}, \quad (14.107)$$

where  $\mathbf{U}$  and  $\mathbf{V}$  are unitary matrices whose columns are the eigenvectors of  $\mathbf{H}\mathbf{H}^{\text{H}}$  and  $\mathbf{H}^{\text{H}}\mathbf{H}$ , respectively. The superscript  $\text{H}$  denotes Hermitian transpose.  $\mathbf{\Sigma}$  is a diagonal matrix whose elements  $\lambda_k$  (the singular values) are the nonnegative square roots of the eigenvalues of  $\mathbf{H}\mathbf{H}^{\text{H}}$  and  $\mathbf{H}^{\text{H}}\mathbf{H}$ . The number of strictly positive singular values is equal to the rank  $R$  of  $\mathbf{H}$ . The SVD can also be written in the form of an outer product (or spectral) expansion

$$\mathbf{H} = \sum_{k=1}^R \lambda_k \mathbf{u}_k \mathbf{v}_k^{\text{H}}, \quad (14.108)$$

where  $\mathbf{u}_k$  and  $\mathbf{v}_k$  are the columns of  $\mathbf{U}$  and  $\mathbf{V}$ . It is common to assume that the  $\lambda_k$  are ordered in decreasing value.

Let  $\mathbf{F}_N^a$  denotes the  $N$ -point  $a$ th order discrete fractional Fourier transform matrix. The discrete fractional Fourier transform will be defined in Section 14.12. For the purpose of this section, it will suffice to think of this transform in analogy with the ordinary discrete Fourier transform. The discrete Fourier transform of a discrete signal represented by a vector of length  $N$  can be obtained by multiplying the vector by the  $N$ -point discrete Fourier transform matrix  $\mathbf{F}_N$ . Likewise, the  $a$ th order discrete fractional Fourier transform of a vector is obtained by multiplying it by  $\mathbf{F}_N^a$ . The discrete transforms can be used to approximately compute the continuous transforms.

The columns of the inverse discrete fractional Fourier transform matrix  $\mathbf{F}_N^{-a}$  constitute an orthonormal basis for the  $a$ th

domain, just as the columns of the identity matrix constitute a basis for the time domain and the columns of the ordinary inverse DFT matrix constitute a basis for the frequency domain. Now, let  $\mathbf{H}$  be a complex  $N_{\text{out}} \times N_{\text{in}}$  matrix and  $\{a_1, a_2, \dots, a_N\}$  a set of  $N = \max(N_{\text{out}}, N_{\text{in}})$  distinct real numbers such that  $-1 < a_1 < a_2 < \dots < a_N \leq 1$ . For instance,  $a_k$ s may be chosen uniformly spaced in this interval. We define the FFDD of  $\mathbf{H}$  as [86]

$$\mathbf{H}_{N_{\text{out}} \times N_{\text{in}}} = \sum_{k=1}^N \mathbf{F}_{N_{\text{out}}}^{-a_k} (\Lambda_{\mathbf{h}_k})_{N_{\text{out}} \times N_{\text{in}}} (\mathbf{F}_{N_{\text{in}}}^{-a_k})^H, \quad (14.109)$$

where the  $\Lambda_{\mathbf{h}_k}$  are  $N_{\text{out}} \times N_{\text{in}}$  diagonal matrices with  $N' = \min(N_{\text{out}}, N_{\text{in}})$  complex elements. Starting from the upper left corner, the  $l$ th diagonal element of  $\Lambda_{\mathbf{h}_k}$  is denoted as  $h_{kl}$ ,  $l = 1, 2, \dots, N'$  (the  $l$ th element of the column vector  $\mathbf{h}_k$ ). When  $\mathbf{H}$  is Hermitian (skew Hermitian),  $\mathbf{h}_k$  is real (imaginary). We also recall that  $(\mathbf{F}_{N_{\text{in}}}^{-a_k})^H = \mathbf{F}_{N_{\text{in}}}^{a_k}$ . The FFDD always exists and is unique [129].

If we compare one term in the summation on the right-hand side of Equation 14.109 with the right-hand side of Equation 14.107, we see that they are similar in that they both consist of three terms of corresponding dimensionality, the first and third being unitary matrices and the second being a diagonal matrix. Whereas the columns of  $\mathbf{U}$  and  $\mathbf{V}$  constitute orthonormal bases specific to  $\mathbf{H}$ , the columns of  $\mathbf{F}_{N_{\text{out}}}^{-a_k}$  and  $\mathbf{F}_{N_{\text{in}}}^{-a_k}$  constitute orthonormal bases for the  $a_k$ th fractional Fourier domain. Customization of FFDD is achieved through the coefficients  $h_{kl}$  and/or perhaps also the orders  $a_k$ .

When  $\mathbf{H}$  is a square matrix of dimension  $N$ , the FFDD becomes

$$\mathbf{H} = \sum_{k=1}^N \mathbf{F}^{-a_k} \Lambda_{\mathbf{h}_k} (\mathbf{F}^{-a_k})^H, \quad (14.110)$$

where all matrices are of dimension  $N$ . The continuous counterpart of the FFDD is similar to this equation, with the summation being replaced by an integral over  $a$  [167].

Equation 14.109 represents a decomposition of a matrix  $\mathbf{H}$  into  $N$  terms. Each term corresponds to filtering in the  $a_k$ th fractional Fourier domain (see Equation 14.97). All terms taken together, the FFDD can be interpreted as the decomposition of a matrix into fractional Fourier domain filters of different orders. An arbitrary matrix  $\mathbf{H}$  will in general not correspond to multiplicative filtering in the time or frequency domain or in any other single fractional Fourier domain. However,  $\mathbf{H}$  can always be expressed as a combination of filtering operations in different fractional domains.

*A sufficient number of different-ordered fractional Fourier domain filtering operations “span” the space of all linear operations.*

The fundamental importance of the FFDD is that it shows how an arbitrary linear system can be decomposed into this complete set of domains in the time-frequency plane.

Truncating some of the singular values in SVD of  $\mathbf{H}$  has many applications [68,154]. Similarly we can eliminate domains for which the coefficients  $h_{k1}, h_{k2}, \dots, h_{kN'}$  are small. This procedure, which we refer to as *pruning* the FFDD, is the counterpart of truncating the SVD. An alternative to this procedure will be referred to as *sparsening*, in which one simply employs a more coarsely spaced set of domains. In any event, the resulting smaller number of domains will be denoted by  $M < N$ . The upper limit of the summation in equation 109 is replaced by  $M$  and the equality is replaced by approximate equality. The equation  $\mathbf{H} = \tilde{\mathbf{P}}\mathbf{h}$  is likewise replaced by  $\mathbf{H} \approx \tilde{\mathbf{P}}\mathbf{h}$ . If we solve this in the least-squares sense, minimizing  $\|\mathbf{H} - \tilde{\mathbf{P}}\mathbf{h}\|$ , we can find the filter coefficients resulting in the best *M-domain approximation* to  $\mathbf{H}$ . (This procedure amounts to projecting  $\mathbf{H}$  onto the subspace spanned by the  $MN'$  basis matrices, which now do not span the whole space.) The correspondence between the pruned FFDD and multichannel filtering configurations is evident; it is possible to interpret multichannel filtering configurations as pruned FFDDs. These concepts have found application in to image compression [166].

## 14.12 Discrete Fractional Fourier Transforms

Ideally, a discrete version of a transform should exhibit a high level of analogy with its continuous counterpart. This analogy should include basic structural similarity and analogy of operational properties. Furthermore, it is desirable for the discrete transform to usefully approximate the samples of the continuous transform, so that it can provide a basis for digital computation of the continuous transform. The following can be posed as a minimal set of properties that we would like to see in a definition of the discrete fractional Fourier transform (DFRT):

1. Unitarity
2. Index additivity
3. Reduction to the ordinary discrete Fourier transform (DFT) when  $a = 1$
4. Approximation of the samples of the continuous FRT

Several definitions of the DFRT have been proposed in the literature. Some of these correspond to totally distinct continuous transforms. For example, one proposal was based on the power series expansion of the DFT matrix and employed the Cayley-Hamilton theorem [147]. If we let  $\mathbf{F}^a$  be the  $N \times N$  matrix representing the discrete fractional Fourier transform, this definition can be stated as follows:

$$\mathbf{F}^a = \sum_{n=0}^3 \exp\left(j\frac{3}{4}\pi(n-a)\right) \frac{\sin \pi(n-a)}{4 \sin \frac{1}{4}\pi(n-a)} \mathbf{F}^n, \quad (14.111)$$

where  $\mathbf{F}^n$  is the  $n$ th (integer) power of the DFT matrix. This definition satisfies all the desired properties listed above, except the critical fourth one: it can not be used to approximate the

samples of the continuous fractional Fourier transform which is the subject of this chapter. Rather, it corresponds to the continuous fractional Fourier transform based on principal powers of the eigenvalues discussed in Equation 14.9.

In the rest of this section, we focus on discrete fractional Fourier transforms that correspond to the continuous FRT defined in this chapter. The main task is to first find an eigenvector set of the DFT matrix which can serve as discrete versions of the Hermite–Gaussian functions. Such Hermite–Gaussian vectors have been defined in [26] based on [136]. It can be shown that [26] as  $h \rightarrow 0$  the difference equation

$$\frac{f(u+h) - 2f(u) + f(u-h)}{h^2} + \frac{2(\cos(2\pi hu) - 1)}{h^2} f(u) = \lambda f(u) \quad (14.112)$$

approximates the Hermite–Gaussian generating differential equation

$$\frac{d^2 f(t)}{dt^2} - 4\pi t^2 f(t) = \lambda f(t). \quad (14.113)$$

When  $h = \frac{1}{\sqrt{N}}$  the difference equation (Equation 14.112) has periodic coefficients. Therefore the solutions of the difference equation is also periodic and can be written as the eigenvectors of the following matrix, denoted by  $\mathbf{S}$ :

$$\mathbf{S} = \begin{bmatrix} 2 & 1 & 0 & \dots & 0 & 1 \\ 1 & 2 \cos(2\pi/N) & 1 & \dots & 0 & 0 \\ 0 & 1 & 2 \cos(2\pi 2/N) & \dots & 0 & 0 \\ \vdots & \vdots & \vdots & \ddots & \vdots & \vdots \\ 1 & 0 & 0 & \dots & 1 & 2 \cos(2\pi(N-1)/N) \end{bmatrix}. \quad (14.114)$$

In other words, the difference equation can be written as  $\mathbf{S}\mathbf{f} = \lambda\mathbf{f}$ . It can also be shown that  $\mathbf{S}$  commutes with DFT matrix. Since two commuting matrices share a common eigenvector set [154], the eigenvectors of  $\mathbf{S}$  are also eigenvectors of the DFT matrix. Thus the eigenvectors of  $\mathbf{S}$  constitute an orthogonal eigenvector set of the DFT matrix which are analogous to and which approximate the Hermite–Gaussian functions. Further details such as the distinctness of the eigenvectors and enumeration of the eigenvectors with respect to the continuous Hermite–Gaussian functions are discussed in [26].

Having obtained an appropriate set of eigenvectors, the discrete fractional Fourier transform matrix can now be defined as follows:

$$\mathbf{F}^a = \begin{cases} \sum_{k=0, k \neq N-1}^N \mathbf{u}_k e^{-j\frac{\pi}{2}ka} \mathbf{u}_k^T, & \text{when } N \text{ even} \\ \sum_{k=0, k \neq N}^N \mathbf{u}_k e^{-j\frac{\pi}{2}ka} \mathbf{u}_k^T, & \text{when } N \text{ odd} \end{cases} \quad (14.115)$$

where  $\mathbf{u}_k$  corresponds to the eigenvector of the  $\mathbf{S}$  matrix with  $k$  zero-crossings [26]. The necessity of separately writing the sum-

mation in equation 14.115 for even and odd dimensions  $N$  is a consequence of the eigenvalue multiplicity of the ordinary DFT matrix [26]. This definition of the fractional DFT satisfies all four of the desirable properties we had set out at the beginning. A complementary perspective to this line of development may be found in [13].

A MATLAB<sup>®</sup> routine “dFRT” for the calculation of the discrete fractional Fourier transform matrix defined above is available [25]. The following steps show how to use the routine to compute and plot the samples of the  $a$ th order FRT of a continuous function  $f(u)$ :

1.  $h = 1/\sqrt{N}$ ; tsamples =  $(-N/2 * h):h:(N/2 - 1) * h$ ;
2.  $f0 = f(\text{tsamples})$ ;
3.  $f0\text{shifted} = \text{fftshift}(f0)$ ;
4.  $Fa = \text{dFRT}(N,a,\text{order})$ ; {order can be any number in  $[2, N-1]$ }
5.  $fashifted = Fa * f0\text{shifted}$ ;
6.  $fa = \text{fftshift}(fashifted)$ ;
7.  $\text{plot}(\text{tsamples}, fa)$ ;

The “fftshift” operations are needed since the DFRT matrix follows the well-known circular indexing rule of the DFT matrix. Normally the approximation “order” is set to 2; higher values correspond to higher-order approximations to the continuous transform than have been discussed here. The approximation order should not be confused with the fractional Fourier transform order  $a$ . Figure 14.11 compares the  $N=64$  samples calculated with this routine with the continuous fractional Fourier transform of the example function  $f(u) = \sin(2\pi u)\text{rect}(u)$ . This function can be interpreted as the windowed version of a single period of the sine waveform between  $-0.5$  and  $0.5$ . As can be seen, the discrete transform fairly closely approximates the continuous one.

A number of other definitions of the discrete FRT which are still compatible with the continuous FRT discussed in this chapter have been proposed. In [138], the authors start with vectors formed by sampling the continuous Hermite–Gaussian functions. These are neither orthogonal nor eigenvectors of the DFT matrix. The authors orthogonalize these through a Gram–Schmidt process involving the  $\mathbf{S}$  matrix. These orthogonal vectors are then used to define the fractional DFRT. We find this method less desirable in that it is based on a numerical rather than an analytical approach. The approach of [101] is similar, but here the eigenvectors of the DFT matrix are constructed by sampling periodically replicated versions of the Hermite–Gaussian functions (which are not orthogonal either).

In [12] another finite dimensional approximation to the Fourier transform similar to the DFT is proposed. This transform has strong connections with the Fourier transform within a group theoretical framework [165]. Furthermore, analytical expressions for the transform can be written in terms of the so-called Kravchuk polynomials, which are known to approximate the Hermite polynomials. A major disadvantage of this approach

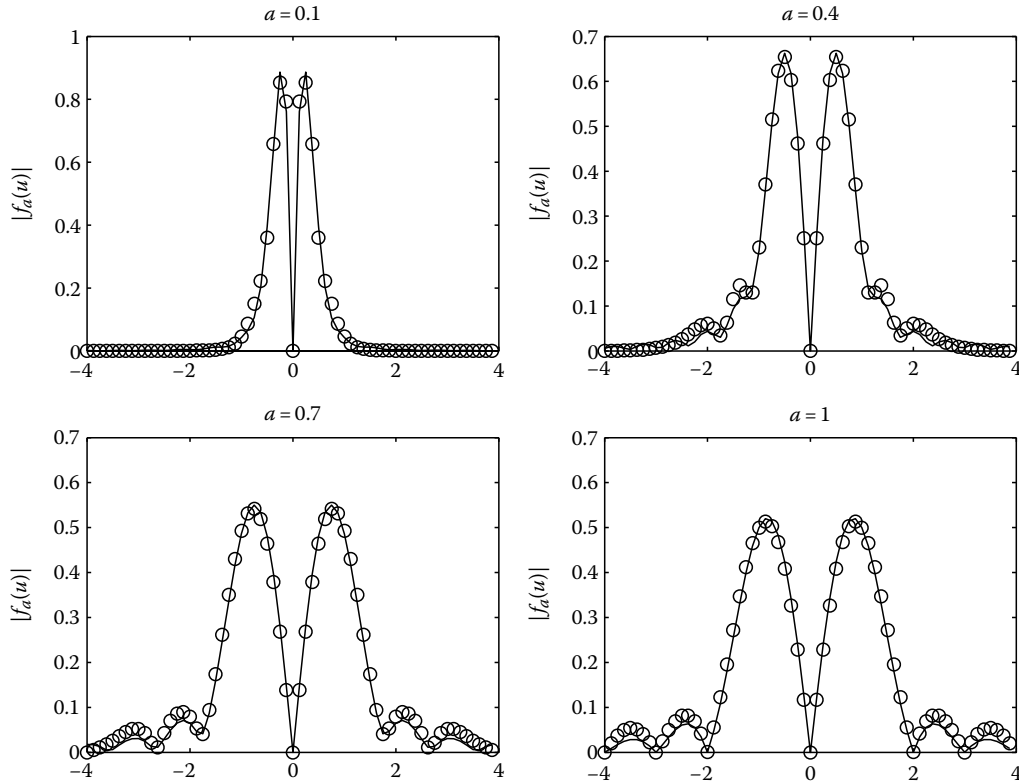


FIGURE 14.11 Approximation of the continuous fractional Fourier transform of  $f(u) = \sin(2\pi u)rect(u)$  with the discrete fractional Fourier transform.

is that the discrete FRT thus defined does not reduce to the ordinary DFT when  $a = 1$ .

In [26,61,135,148] yet other definitions are proposed based on the commuting matrices approach already discussed in relation to the  $S$  matrix. These matrices can be interpreted as higher-order approximation matrices which can be used to obtain increasingly accurate approximations to the continuous transform. A comparison of such matrices is given in [27].

### 14.13 Digital Computation of the Fractional Fourier Transform

The FRT of a continuous function whose time- or space-bandwidth product is  $N$  can be computed in the order of  $N \log N$  time [115], similar to the ordinary Fourier transform. Therefore, if in some application any improvements can be obtained by using the FRT instead of the ordinary Fourier transform, these improvements come at no additional cost.

The following formula allows one to compute the samples of the fractional Fourier transform  $f_a(u)$  of a function  $f(u)$ , in terms of the samples of  $f(u)$ , in  $\sim N \log N$  time where  $N = \Delta u^2$ , under the assumption that Wigner distribution of  $f(u)$  is approximately confined to a circle of diameter  $\Delta u$ :

$$f_a\left(\frac{k}{2\Delta u}\right) = \frac{A_\alpha}{2\Delta u} e^{j\pi(\cot\alpha - \csc\alpha)(k/2\Delta u)^2} \times \sum_{l=-N}^{N-1} e^{j\pi \csc\alpha((k-l)/2\Delta u)^2} e^{j\pi(\cot\alpha - \csc\alpha)(l/2\Delta u)^2} f\left(\frac{l}{2\Delta u}\right). \tag{14.116}$$

The summation is recognizable as a convolution, which can be computed in  $\sim N \log N$  time by using the fast Fourier transform (FFT). The result is then obtained by a final chirp multiplication. The overall procedure takes  $\sim N \log N$  time. A MATLAB code based on this formula may be found in [79]. A broader discussion of computational issues may be found in [115].

Note that this method is distinct from that discussed in Section 12. There, the discrete fractional Fourier transform was defined. The samples of the fractional Fourier transform of a function are then found by multiplying the discrete fractional Fourier transform matrix with the sample vector of the function to be transformed. Since a method for calculating this matrix product in  $\sim N \log N$  time is presently not available, the operation will take  $\sim N^2$  time. The approach in this section does not involve a definition of the discrete fractional Fourier transform, and can be viewed as a method to numerically compute the fractional Fourier transform integral.

## 14.14 Applications

The purpose of this section is to highlight some of the applications of the fractional Fourier transform which have received greater interest so far. The reader may consult [23,122,123,129] for further references.

The fractional Fourier transform is of potential usefulness in every area in which the ordinary Fourier transform is used. The typical pattern of discovery of a new application is to concentrate on an application where the ordinary Fourier transform is used and ask if any improvement or generalization might be possible by using the fractional Fourier transform instead. The additional order parameter often allows better performance or greater generality because it provides an additional degree of freedom over which to optimize.

Typically, improvements are observed or are greater when dealing with time/space-variant signals or systems. Furthermore, very large degrees of improvement often becomes possible when signals of a chirped nature or with nearly linearly increasing frequencies are in question, since chirp signals are the basis functions associated with the fractional Fourier transform (just as harmonic functions are the basis functions associated with the ordinary Fourier transform). Fractional Fourier transforms are also of special use when dealing with integral transforms whose kernels are of quadratic-exponential type, the diffraction integral being the most common example.

### 14.14.1 Applications in Signal and Image Processing

The FRT has found widespread application in signal and image processing, some of which are reviewed here (also see [157]).

One of the most striking applications is that of filtering in fractional Fourier domains, whose foundations have been discussed in Section 14.10 [117]. In traditional filtering, one takes the Fourier transform of a signal, multiplies it with a Fourier-domain transfer function, and inverse transforms the result. Here, one takes the fractional Fourier transform, applies a filter function in the fractional Fourier domain, and inverse transforms to the original domain. It has been shown that considerable improvement in performance is possible by exploiting the additional degree of freedom coming from the order parameter  $a$ . This improvement comes at no additional cost since computing the fractional Fourier transform is not more expensive than computing the ordinary Fourier transform (Section 14.13). The concept has been generalized to multistage and multichannel filtering systems which employ several fractional Fourier domain filters of different orders [81,82]. These schemes provide flexible and cost-efficient means of designing time/space-variant filtering systems to meet desired objectives. Fractional Fourier domain filtering has been useful in optical signal separation [43] and signal and image recovery and restoration in the presence of time/space-varying distortions such as space-varying blurs and nonstationary noise, with application to compensation of nonconstant velocity camera motion and atmospheric turbulence [48,50,83,85].

The FRT has also found many applications in pattern recognition and detection. Correlation is the underlying operation in matched filtering, which is used to detect signals. Fractional correlation has been defined in a number of different ways [71,92,103,180]. It has been shown how to control the degree of shift-invariance by adjusting the order  $a$ , which in turn allows one to design systems which detect objects within a certain region but reject them otherwise [92]. Joint-transform correlation is a well-known optical correlation technique, whose fractional version has received considerable attention [78,90]. The FRT has been studied as a preprocessing unit for neural network object recognition [14]. Some other applications in the pattern recognition area are face recognition [72] and realization and improvement of navigational tasks [149].

The windowed fractional Fourier transform has been studied in [29,46,104]. The possibility of changing the fractional order as the window is moved and/or choosing different orders in the two dimensions makes this a very flexible tool suited for various pattern recognition tasks, such as fingerprint recognition [171] or detection of targets in specific locations [59]. A review of applications of the FRT to pattern recognition as of 1998 is presented in [105].

The FRT has found a number of applications in radar signal processing. In [2], detection of linear frequency modulated signals is studied. In [69], radar return transients are analyzed in fractional domains. In [35,155], detection of moving targets for airborne radar systems is studied. In [11,10], synthetic aperture radar image reconstruction algorithms have been developed using the fractional Fourier transform.

The transform has found application to interpolation [53,150] and superresolution of multidimensional signals [32,62,151], phase retrieval from two or more intensity measurements [6,7,41,54,55], system and transform synthesis [50], processing of chirplets [22], signal and image compression [117,162,166], watermarking [40,112], speech processing [176], acoustic signal processing [60,173], ultrasound imaging [17], and antenna beamforming [168]. A large number of publications discuss the application of the FRT to encryption; for instance, see [33,63,66,111,161].

### 14.14.2 Applications in Communications

The FRT has found applications in spread spectrum communications systems [1], multicarrier communications systems [97], in the processing of time-varying channels [110], and beamforming for next generation wireless communication systems [75].

The concept of multiplexing in fractional Fourier domains, which generalizes time-domain and frequency-domain multiplexing, has been proposed in [117].

### 14.14.3 Applications in Optics and Wave Propagation

The fractional Fourier transform has received a great deal of interest in the area of optics and especially optical signal



processing (also known as Fourier optics or information optics) [5,18,91,118,127,129,139,159]. Optical signal processing is an analog signal processing method which relies on the representation of signals by light fields and their manipulation with optical elements such as lenses, prisms, transparencies, holograms, and so forth. Its key component is the optical Fourier transformer which can be realized using one or two lenses separated by certain distances from the input and output planes. It has been shown that the fractional Fourier transform can be optically implemented with equal ease as the ordinary Fourier transform [88,124,127,146], allowing a generalization of conventional approaches and results to their more flexible or general fractional counterparts.

The fractional Fourier transform has also been shown to be intimately related to wave and beam propagation and diffraction. The process of diffraction of light in free space (or any other disturbance satisfying a similar wave equation) has been shown to be nothing but a process of continual fractional Fourier transformation; the distribution of light becomes fractional Fourier transformed as it propagates, evolving through continuously increasing orders [118,126,127,139].

More generally, it is well known that a rather broad class of optical systems can be modeled as linear canonical transforms, which were discussed in Section 14.8 [15,129]. These include optical systems consisting of arbitrary concatenations of thin lenses and sections of free space, as well as sections of quadratic graded-index media. It has been shown that all such systems can be expressed in the form of a fractional Fourier transform operation followed by appropriate scaling and a residual chirp factor, which can be interpreted as a change in the radius of curvature of the output plane (Equation 14.83) [118,119]. Therefore, all such optical systems can be interpreted as fractional Fourier transformers [16,118,127], and the propagation of light through such systems can be viewed as a process of continual fractional Fourier transformation with the fractional transform order monotonically increasing as light propagates through the system. The case of free-space optical diffraction in the Fresnel approximation, discussed in the previous paragraph, is a special case of this more general result, and rests on expressing the Fresnel integral in terms of the FRT. Similar results hold for other wave and beam propagation modalities that satisfy a similar wave equation as the optical wave equation, or an equation similar to that of the quantum-mechanical harmonic oscillator, including electromagnetic and acoustic waves [47].

As noted above, the fractional Fourier transform plays a central role in the study of optical systems consisting of arbitrary sequences of lenses. Also of interest are systems in which thin optical filters (masks) are inserted at various points along the optical axis. Such systems can be modeled as multistage fractional Fourier domain filtering systems with multiplicative filters inserted between fractional Fourier transform stages, which were discussed in Section 14.10.

The fractional Fourier transform has also found application in the study of laser resonators and laser beams. The order of the fractional transform has been shown to be proportional to the

Gouy phase shift accumulated during Gaussian beam propagation [49,126] and also to be related to laser resonator stability [126,140,179]. Other laser applications have also been reported [94].

The FRT has also found use in increasing the resolution of low-resolution wave fields [32], optical phase retrieval from two or more intensity measurements [41,54,55], coherent and partially coherent wave field reconstruction using phase-space tomography [99,144,145], optical beam characterization and shaping [3,38,44,172,177], synthesis of mutual intensity functions [52], and the study of partially coherent light [20,24,51,153,160,163].

It has found further use in quantum optics [170], studies of the human eye [141,142], lens design problems [42], diffractive optics [58,158], optical profilometry [181], speckle photography [131] and metrology [73], holographic interferometry [152], holographic data storage [70], digital holography [34,36,178], holographic three-dimensional television [113,114], temporal pulse processing [21,45,89], solitons [39], and fiber Bragg gratings [98].

#### 14.14.4 Other Applications

The fractional Fourier transform has found several other applications not falling under the above categories. We discuss some of these here.

The FRT has been employed in quantum mechanics [56,57,93,96]. It has been shown that certain kinds of time-varying second-order differential equations (with nonconstant coefficients) can be solved by exploiting the additional degree of freedom associated with the fractional order parameter  $a$  [74,100,109]. Based on the relationship of the fractional Fourier transform to harmonic oscillation (Section 14.2), it may be expected to play an important role in the study of vibrating systems [84]. It has so far received only limited attention in the area of control theory and systems [28], but we believe it has considerable potential for use in this field. The FRT has been shown to be related to perspective projections [169]. The transform has been employed to realize free-space optical interconnection architectures [50].

## References

1. O. Akay and G. F. Boudreaux-Bartels. Broadband interference excision in spread spectrum communication systems via fractional Fourier transform. In *Proceedings of the 32nd Asilomar Conference on Signals, Systems, and Computers*, IEEE, Piscataway, NJ, 1998, pp. 832–837.
2. O. Akay and G. F. Boudreaux-Bartels. Fractional convolution and correlation via operator methods and an application to detection of linear FM signals. *IEEE Trans Signal Process*, 49:979–993, 2001.
3. T. Alieva and M. J. Bastiaans. Phase-space distributions in quasi-polar coordinates and the fractional Fourier transform. *J Opt Soc Am A-Opt Image Sci Vis*, 17:2324–2329, 2000.

4. T. Alieva and M. J. Bastiaans. Alternative representation of the linear canonical integral transform. *Opt Lett*, 30:3302–3304, 2005.
5. T. Alieva, M. J. Bastiaans, and M. L. Calvo. Fractional transforms in optical information processing. *EURASIP J Appl Signal Process*, 22:1498–1519, 2005.
6. T. Alieva, M. J. Bastiaans, and L. Stankovic. Signal reconstruction from two close fractional Fourier power spectra. *IEEE Trans Signal Process*, 51:112–123, 2003.
7. T. Alieva and M. L. Calvo. Image reconstruction from amplitude-only and phase-only data in the fractional Fourier domain. *Opt Spectrosc*, 95:110–113, 2003.
8. L. B. Almeida. The fractional Fourier transform and time-frequency representations. *IEEE Trans Signal Process*, 42:3084–3091, 1994.
9. L. B. Almeida. Product and convolution theorems for the fractional Fourier transform. *IEEE Signal Processing Lett*, 4:15–17, 1997.
10. A. S. Amein and J. J. Soraghan. Azimuth fractional transformation of the fractional chirp scaling algorithm (FrCSA). *IEEE Trans Geosci Remote Sensing*, 44:2871–2879, 2006.
11. A. S. Amein and J. J. Soraghan. Fractional chirp scaling algorithm: Mathematical model. *IEEE Trans Signal Process*, 55:4162–4172, 2007.
12. N. M. Atakishiyev and K. B. Wolf. Fractional Fourier-Kravchuk transform. *J Opt Soc Am A-Opt Image Sci Vis*, 14:1467–1477, 1997.
13. L. Barker, Ç. Candan, T. Hakioglu, M. A. Kutay, and H. M. Ozaktas. The discrete harmonic oscillator, Harper's equation, and the discrete fractional Fourier transform. *J Phys A-Math Gen*, 33:2209–2222, 2000.
14. B. Barshan and B. Ayrulu. Fractional Fourier transform pre-processing for neural networks and its application to object recognition. *Neural Netw*, 15:131–140, 2002.
15. M. J. Bastiaans. Wigner distribution function and its application to first-order optics. *J Opt Soc Am A-Opt Image Sci Vis*, 69:1710–1716, 1979.
16. M. J. Bastiaans and T. Alieva. First-order optical systems with unimodular eigenvalues. *J Opt Soc Am A-Opt Image Sci Vis*, 23:1875–1883, 2006.
17. M. J. Bennett, S. McLaughlin, T. Anderson, and N. McDicken. The use of the fractional Fourier transform with coded excitation in ultrasound imaging. *IEEE Trans Bio Eng*, 53:754–756, 2006.
18. L. M. Bernardo and O. D. D. Soares. Fractional Fourier transforms and imaging. *J Opt Soc Am A-Opt Image Sci Vis*, 11:2622–2626, 1994.
19. B. Borden. On the fractional wideband and narrowband ambiguity function in radar and sonar. *IEEE Signal Process Lett*, 13:545–548, 2006.
20. M. Brunel and S. Coetmellec. Fractional-order Fourier formulation of the propagation of partially coherent light pulses. *Opt Commun*, 230:1–5, 2004.
21. M. Brunel, S. Coetmellec, M. Lelek, and F. Louradour. Fractional-order Fourier analysis for ultrashort pulse characterization. *J Opt Soc Am A-Opt Image Sci Vis*, 24:1641–1646, 2007.
22. A. Bultan. A four-parameter atomic decomposition of chirplets. *IEEE Trans Signal Process*, 47:731–745, 1999.
23. A. Bultheel and H. Martínez-Sulbaran. Recent developments in the theory of the fractional Fourier and linear canonical transforms. *Bull Belg Math Soc*, 13:971–1005, 2006.
24. Y. J. Cai, D. Ge, and Q. Lin. Fractional Fourier transform for partially coherent and partially polarized Gaussian-Schell model beams. *J Opt A-Pure Appl Opt*, 5:453–459, 2003.
25. Ç. Candan. Matlab code for generating discrete fractional Fourier transform matrix, 1998. <http://www.ee.bilkent.edu.tr/haldun/wileybook.html>
26. Ç. Candan, M. A. Kutay, and H. M. Ozaktas. The discrete fractional Fourier transform. *IEEE Trans Signal Process*, 48:1329–1337, 2000.
27. C. Candan. On higher order approximations for Hermite-Gaussian functions and discrete fractional Fourier transforms. *IEEE Signal Process Lett*, 14:699–702, 2007.
28. U. O. Candoğan, H. Özbay, and Haldun M. Ozaktas. Controller implementation for a class of spatially-varying distributed parameter systems. In *Proceedings of the 17th IFAC World Congress*, IFAC, Laxenburg, Austria, 2008.
29. C. Capus and K. Brown. Short-time fractional Fourier methods for the time-frequency representation of chirp signals. *J Acoust Soc Am*, 113:3253–3263, 2003.
30. G. Cariolaro, T. Erseghe, and P. Kraniuskas. The fractional discrete cosine transform. *IEEE Trans Signal Process*, 50:902–911, 2002.
31. G. Cariolaro, T. Erseghe, P. Kraniuskas, and N. Laurenti. A unified framework for the fractional Fourier transform. *IEEE Trans Signal Process*, 46:3206–3219, 1998.
32. A. E. Çetin, H. Özaktaş, and H. M. Ozaktas. Resolution enhancement of low resolution wavefields with POCS algorithm. *Electron Lett*, 39:1808–1810, 2003.
33. L. F. Chen and D. M. Zhao. Optical color image encryption by wavelength multiplexing and lensless Fresnel transform holograms. *Opt Express*, 14:8552–8560, 2006.
34. L. F. Chen and D. M. Zhao. Color information processing (coding and synthesis) with fractional Fourier transforms and digital holography. *Opt Express*, 15:16080–16089, 2007.
35. S. Chiu. Application of fractional Fourier transform to moving target indication via along-track interferometry. *EURASIP J Appl Signal Process*, 20:3293–3303, 2005.
36. S. Coetmellec, D. Lebrun, and C. Ozkul. Application of the two-dimensional fractional-order Fourier transformation to particle field digital holography. *J Opt Soc Am A-Opt Image Sci Vis*, 19:1537–1546, 2002.
37. L. Cohen. *Time-Frequency Analysis*. Prentice Hall, Englewood Cliffs, NJ, 1995.
38. W. X. Cong, N. X. Chen, and B. Y. Gu. Beam shaping and its solution with the use of an optimization method. *Appl Opt*, 37:4500–4503, 1998.

39. S. De Nicola, R. Fedele, M. A. Manko, and V. I. Manko. Quantum tomography wave packets, and solitons. *J Russ Laser Res*, 25:1–29, 2004.
40. I. Djurovic, S. Stankovic, and I. Pitas. Digital watermarking in the fractional Fourier transformation domain. *J Netw Comput Appl*, 24:167–173, 2001.
41. B. Z. Dong, Y. Zhang, B. Y. Gu, and G. Z. Yang. Numerical investigation of phase retrieval in a fractional Fourier transform. *J Opt Soc Am A-Opt Image Sci Vis*, 14:2709–2714, 1997.
42. R. G. Dorsch and A. W. Lohmann. Fractional Fourier transform used for a lens design problem. *Appl Opt*, 34:4111–4112, 1995.
43. R. G. Dorsch, A. W. Lohmann, Y. Bitran, D. Mendlovic, and H. M. Ozaktas. Chirp filtering in the fractional Fourier domain. *Appl Opt*, 33:7599–7602, 1994.
44. D. Dragoman and M. Dragoman. Near and far field optical beam characterization using the fractional Fourier transform. *Opt Commun*, 141:5–9, 1997.
45. D. Dragoman, M. Dragoman, and K. H. Brenner. Variant fractional Fourier transformer for optical pulses. *Opt Lett*, 24:933–935, 1999.
46. L. Durak and O. Arikan. Short-time Fourier transform: Two fundamental properties and an optimal implementation. *IEEE Trans Signal Process*, 51:1231–1242, 2003.
47. N. Engheta. On fractional paradigm and intermediate zones in electromagnetism: I—Planar observation. *Microw Opt Technol Lett*, 22:236–241, 1999.
48. M. F. Erden, M. A. Kutay, and H. M. Ozaktas. Repeated filtering in consecutive fractional Fourier domains and its application to signal restoration. *IEEE Trans Signal Process*, 47:1458–1462, 1999.
49. M. F. Erden and H. M. Ozaktas. Accumulated Gouy phase shift in Gaussian beam propagation through first-order optical systems. *J Opt Soc Am A-Opt Image Sci Vis*, 14:2190–2194, 1997.
50. M. F. Erden and H. M. Ozaktas. Synthesis of general linear systems with repeated filtering in consecutive fractional Fourier domains. *J Opt Soc Am A-Opt Image Sci Vis*, 15:1647–1657, 1998.
51. M. F. Erden, H. M. Ozaktas, and D. Mendlovic. Propagation of mutual intensity expressed in terms of the fractional Fourier transform. *J Opt Soc Am A-Opt Image Sci Vis*, 13:1068–1071, 1996.
52. M. F. Erden, H. M. Ozaktas, and D. Mendlovic. Synthesis of mutual intensity distributions using the fractional Fourier transform. *Opt Commun*, 125:288–301, 1996.
53. T. Erseghe, P. Kraniuskas, and G. Cariolaro. Unified fractional Fourier transform and sampling theorem. *IEEE Trans Signal Process*, 47:3419–3423, 1999.
54. M. G. Ertosun, H. Atli, H. M. Ozaktas, and B. Barshan. Complex signal recovery from two fractional Fourier transform intensities: Order and noise dependence. *Opt Commun*, 244:61–70, 2005.
55. M. G. Ertosun, H. Atli, H.M. Ozaktas, and B. Barshan. Complex signal recovery from multiple fractional Fourier-transform intensities. *Appl Opt*, 44:4902–4908, 2005.
56. H. Y. Fan and Y. Fan. EPR entangled states and complex fractional Fourier transformation. *Eur Phys J D*, 21:233–238, 2002.
57. H. Y. Fan and Y. Fan. Fractional Fourier transformation for quantum mechanical wave functions studied by virtue of IWOP technique. *Commun Theor Phys*, 39:417–420, 2003.
58. D. Feng, Y. B. Yan, S. Lu, K. H. Tian, and G. F. Jin. Designing diffractive phase plates for beam smoothing in the fractional Fourier domain. *J Mod Opt*, 49:1125–1133, 2002.
59. J. García, D. Mendlovic, Z. Zalevsky, and A. Lohmann. Space-variant simultaneous detection of several objects by the use of multiple anamorphic fractional-Fourier-transform filters. *Appl Opt*, 35:3945–3952, 1996.
60. G. Gonon, O. Richoux, and C. Depollier. Acoustic wave propagation in a 1-D lattice: Analysis of nonlinear effects by the fractional Fourier transform method. *Signal Process*, 83:1269–2480, 2003.
61. F. A. Grunbaum. The eigenvectors of the discrete Fourier transform: A version of the Hermite functions. *J Math Anal Appl*, 88:355–363, 1982.
62. H. E. Guven, H. M. Ozaktas, A. E. Cetin, and B. Barshan. Signal recovery from partial fractional Fourier domain information and its applications. *IET Signal Process*, 2:15–25, 2008.
63. B. M. Hennelly and J. T. Sheridan. Image encryption and the fractional Fourier transform. *Optik*, 114:251–265, 2003.
64. B. M. Hennelly and J. T. Sheridan. Generalizing, optimizing, and inventing numerical algorithms for the fractional Fourier, Fresnel, and linear canonical transforms. *J Opt Soc Am A-Opt Image Sci Vis*, 22:917–927, 2005.
65. B. M. Hennelly and J. T. Sheridan. Fast numerical algorithm for the linear canonical transform. *J Opt Soc Am A-Opt Image Sci Vis*, 22:928–937, 2005.
66. B. M. Hennelly and J. T. Sheridan. Optical encryption and the space bandwidth product. *Opt Commun*, 247:291–305, 2005.
67. F. Hlawatsch and G. F. Boudreaux-Bartels. Linear and quadratic time-frequency signal representations. *IEEE Signal Processing Magazine*, pages 21–67, April 1992.
68. A. K. Jain. *Fundamentals of Digital Image Processing*. Prentice Hall, Englewood Cliffs, NJ, 1989.
69. S. Jang, W. S. Choi, T. K. Sarkar, M. Salazar-Palma, K. Kim, and CE. Baum. Exploiting early time response using the fractional Fourier transform for analyzing transient radar returns. *IEEE Trans Antennas Propag*, 52:3109–3121, 2004.
70. S. I. Jin, Y. S. Bae, and S. Y. Lee. Holographic data storage with fractional Fourier transform. *Opt Commun*, 198:57–63, 2001.
71. S. I. Jin, Y. S. Bae, and S. Y. Lee. Generalized Vander Lugt correlator as an optical pattern classifier and its optimal learning rate. *Opt Commun*, 206:19–25, 2002.

72. X. Y. Jing, H. S. Wong, and D. Zhang. Face recognition based on discriminant fractional Fourier feature extraction. *Pattern Recognit Lett*, 27:1465–1471, 2006.
73. D. P. Kelly, J. E. Ward, B. M. Hennelly, U. Gopinathan, F. T. O'Neill, and J. T. Sheridan. Paraxial speckle-based metrology systems with an aperture. *J Opt Soc Am A-Opt Image Sci Vis*, 23:2861–2870, 2006.
74. F. H. Kerr. Namias' fractional Fourier transforms on  $L^2$  and applications to differential equations. *J Math Anal Appl*, 136:404–418, 1988.
75. R. Khanna, K. Singh, and R. Saxena. Fractional Fourier transform based beamforming for next generation wireless communication systems. *IETE Tech Rev*, 21:357–366, 2004.
76. A. Koç, H. M. Ozaktas, C. Candan, and M. A. Kutay. Digital computation of linear canonical transforms. *IEEE Trans on Signal Process*, 56:2383–2394, 2008.
77. P. Kraniuskas, G. Cariolaro, and T. Erseghe. Method for defining a class of fractional operations. *IEEE Trans Signal Process*, 46:2804–2807, 1998.
78. C. J. Kuo and Y. Luo. Generalized joint fractional Fourier transform correlators: A compact approach. *Appl Opt*, 37:8270–8276, 1998.
79. M. A. Kutay. Matlab code for fast computation of the fractional Fourier transform, 1996. <http://www.ee.bilkent.edu.tr/haldun/wileybook.html>
80. M. A. Kutay. Generalized filtering configurations with applications in digital and optical signal and image processing. PhD thesis, Bilkent University, Ankara, 1999.
81. M. A. Kutay, M. F. Erden, H. M. Ozaktas, O. Arıkan, Ç. Candan, and Ö. Güleriyüz. Cost-efficient approximation of linear systems with repeated and multi-channel filtering configurations. In *Proceedings of the 1998 IEEE International Conference on Acoustics, Speech, Signal Processing*, IEEE, Piscataway, NJ, 1998, pp. 3433–3436.
82. M. A. Kutay, M. F. Erden, H. M. Ozaktas, O. Arıkan, Ö. Güleriyüz, and Ç. Candan. Space-bandwidth-efficient realizations of linear systems. *Opt Lett*, 23:1069–1071, 1998.
83. M. A. Kutay and H. M. Ozaktas. Optimal image restoration with the fractional Fourier transform. *J Opt Soc Am A-Opt Image Sci Vis*, 15:825–833, 1998.
84. M. A. Kutay and H. M. Ozaktas. The fractional Fourier transform and harmonic oscillation. *Nonlinear Dyn*, 29:157–172, 2002.
85. M. A. Kutay, H. M. Ozaktas, O. Arıkan, and L. Onural. Optimal filtering in fractional Fourier domains. *IEEE Trans Signal Process*, 45:1129–1143, 1997.
86. M. A. Kutay, H. Özaktas, H. M. Ozaktas, and O. Arıkan. The fractional Fourier domain decomposition. *Signal Process*, 77:105–109, 1999.
87. F. L. Lewis. *Optimal Estimation*. Wiley, New York, 1986.
88. A. W. Lohmann. Image rotation, Wigner rotation, and the fractional order Fourier transform. *J Opt Soc Am A-Opt Image Sci Vis*, 10:2181–2186, 1993.
89. A. W. Lohmann and D. Mendlovic. Fractional Fourier transform: Photonic implementation. *Appl Opt*, 33:7661–7664, 1994.
90. A. W. Lohmann and D. Mendlovic. Fractional joint transform correlator. *Appl Opt*, 36:7402–7407, 1997.
91. A. W. Lohmann, D. Mendlovic, and Z. Zalevsky. Fractional transformations in optics. In *Progress in Optics XXXVIII*, Elsevier, Amsterdam, the Netherlands, 1998. Chapter IV, pp. 263–342.
92. A. W. Lohmann, Z. Zalevsky, and D. Mendlovic. Synthesis of pattern recognition filters for fractional Fourier processing. *Opt Commun*, 128:199–204, 1996.
93. H. L. Lu, and H. Y. Fan. Two-variable Hermite function as quantum entanglement of harmonic oscillator's wave functions. *Commun Theor Phys*, 47:1024–1028, 2007.
94. A. A. Malyutin. Use of the fractional Fourier transform in  $\pi/2$  converters of laser modes. *Quantum Electron*, 34:165–171, 2004.
95. M. A. Manko. Fractional Fourier transform in information processing, tomography of optical signal, and green function of harmonic oscillator. *J Russ Laser Res*, 20:226–238, 1999.
96. M. A. Manko. Propagators, tomograms, wavelets and quasidistributions for multipartite quantum systems. *Open Syst Inf Dyn*, 14:179–188, 2007.
97. M. Martone. A multicarrier system based on the fractional Fourier transform for time-frequency-selective channels. *IEEE Trans Commun*, 49:1011–1020, 2001.
98. E. Mazzetto, C. G. Someda, J. A. Acebron, and R. Spigler. The fractional Fourier transform in the analysis and synthesis of fiber Bragg gratings. *Opt Quantum Electron*, 37:755–787, 2005.
99. D. F. McAlister, M. Beck, L. Clarke, A. Meyer, and M.G. Raymer. Optical phase-retrieval by phase-space tomography and fractional-order Fourier transforms. *Opt Lett*, 20:1181–1183, 1995.
100. A. C. McBride and F. H. Kerr. On Namias's fractional Fourier transforms. *IMA J Appl Math*, 39:159–175, 1987.
101. M. L. Mehta. Eigenvalues and eigenvectors of the finite Fourier transform. *J Math Phys*, 28:781–785, 1987.
102. D. Mendlovic and H. M. Ozaktas. Fractional Fourier transforms and their optical implementation: I. *J Opt Soc Am A-Opt Image Sci Vis*, 10:1875–1881, 1993.
103. D. Mendlovic, H. M. Ozaktas, and A.W. Lohmann. Fractional correlation. *Appl Opt*, 34:303–309, 1995.
104. D. Mendlovic, Z. Zalevsky, A. W. Lohmann, and R. G. Dorsch. Signal spatial-filtering using the localized fractional Fourier transform. *Opt Commun*, 126:14–18, 1996.
105. D. Mendlovic, Z. Zalevsky, and H. M. Ozaktas. Applications of the fractional Fourier transform to optical pattern recognition. In *Optical Pattern Recognition*, Cambridge University Press, Cambridge, U.K., 1998, Chapter 4, pp. 89–125.
106. D. A. Mustard. The fractional Fourier transform and a new uncertainty principle. School of Mathematics Preprint

- AM87/14, The University of New South Wales, Kensington, Australia, 1987.
107. D. Mustard. The fractional Fourier transform and the Wigner distribution. *J Aust Math Soc B*, 38:209–219, 1996.
  108. D. Mustard. Fractional convolution. *J Aust Math Soc B*, 40:257–265, 1998.
  109. V. Namias. The fractional order Fourier transform and its application to quantum mechanics. *J Inst Math Appl*, 25:241–265, 1980.
  110. R. Narasimhan. Adaptive channel partitioning and modulation for linear time-varying channels. *IEEE Trans Commun*, 51:1313–1324, 2003.
  111. N. K. Nishchal, J. Joseph, and K. Singh. Securing information using fractional Fourier transform in digital holography. *Opt Commun*, 235:253–259, 2004.
  112. X. M. Niu and S. H. Sun. Robust video watermarking based on discrete fractional Fourier transform. *Chin J Electron*, 10:428–434, 2001.
  113. L. Onural, A. Gotchev, H. M. Ozaktas, and E. Stoykova. A survey of signal processing problems and tools in holographic three-dimensional television. *IEEE Trans Circuits Syst Video Technol*, 17:1631–1646, 2007.
  114. L. Onural and H. M. Ozaktas. Signal processing issues in diffraction and holographic 3DTV. *Signal Process Image Commun*, 22:169–177, 2007.
  115. H. M. Ozaktas, O. Arikan, M. A. Kutay, and G. Bozdađı. Digital computation of the fractional Fourier transform. *IEEE Trans Signal Process*, 44:2141–2150, 1996.
  116. H. M. Ozaktas and O. Aytür. Fractional Fourier domains. *Signal Process*, 46:119–124, 1995.
  117. H. M. Ozaktas, B. Barshan, D. Mendlovic, and L. Onural. Convolution, filtering, and multiplexing in fractional Fourier domains and their relation to chirp and wavelet transforms. *J Opt Soc Am A-Opt Image Sci Vis*, 11:547–559, 1994.
  118. H. M. Ozaktas and M. F. Erden. Relationships among ray optical, Gaussian beam, and fractional Fourier transform descriptions of first-order optical systems. *Opt Commun*, 143:75–86, 1997.
  119. H. M. Ozaktas, A. Koç, I. Sari, and M. A. Kutay. Efficient computation of quadratic-phase integrals in optics. *Opt Lett*, 31:35–37, 2006.
  120. H. M. Ozaktas and M. A. Kutay. Time-order signal representations. Technical Report BU-CE-0005, Bilkent University, Department of Computer Engineering, Ankara, January 2000. Also in *Proceedings of the First IEEE Balkan Conference on Signal Processing, Communications, Circuits, Systems*, Bilkent University, Ankara, 2000. CD-ROM.
  121. H. M. Ozaktas and M. A. Kutay. The fractional Fourier transform. In *Proceedings of the European Control Conference*, European Union Control Association and University of Porto, Porto, Portugal, 2001.
  122. H. M. Ozaktas and M. A. Kutay. The fractional Fourier transform with applications in optics and signal processing—Supplementary bibliography, 2008. <http://www.ee.bilkent.edu.tr/haldun/wileybook.html>
  123. H. M. Ozaktas, M. A. Kutay, and D. Mendlovic. Introduction to the fractional Fourier transform and its applications. In *Advances in Imaging and Electron Physics 106*, Academic Press, San Diego, CA, 1999, pp. 239–291.
  124. H. M. Ozaktas and D. Mendlovic. Fourier transforms of fractional order and their optical interpretation. *Opt Commun*, 101:163–169, 1993.
  125. H. M. Ozaktas and D. Mendlovic. Fractional Fourier transforms and their optical implementation: II. *J Opt Soc Am A-Opt Image Sci Vis*, 10:2522–2531, 1993.
  126. H. M. Ozaktas and D. Mendlovic. Fractional Fourier transform as a tool for analyzing beam propagation and spherical mirror resonators. *Opt Lett*, 19:1678–1680, 1994.
  127. H. M. Ozaktas and D. Mendlovic. Fractional Fourier optics. *J Opt Soc Am A-Opt Image Sci Vis*, 12:743–751, 1995.
  128. H. M. Ozaktas and U. Sümbül. Interpolating between periodicity and discreteness through the fractional Fourier transform. *IEEE Trans Signal Process*, 54:4233–4243, 2006.
  129. H. M. Ozaktas, Z. Zalevsky, and M. A. Kutay. *The Fractional Fourier Transform with Applications in Optics and Signal Processing*. John Wiley & Sons, New York, 2001.
  130. L. Durak, A. K. Ozdemir, and O. Arikan. Efficient computation of joint fractional fourier domain signal representation. *J Opt Soc Am A-Opt Image Sci Vis*, 25:765–772, 2008.
  131. R. E. Patten, B. M. Hennelly, D. P. Kelly, F. T. O’Neill, Y. Liu, and J. T. Sheridan. Speckle photography: Mixed domain fractional Fourier motion detection. *Opt Lett*, 31:32–34, 2006.
  132. S. C. Pei and J. J. Ding. Relations between fractional operations and time-frequency distributions, and their applications. *IEEE Trans Signal Process*, 49:1638–1655, 2001.
  133. S. C. Pei and J. J. Ding. Eigenfunctions of linear canonical transform. *IEEE Trans Signal Process*, 50:11–26, 2002.
  134. S. C. Pei and J. J. Ding. Fractional cosine, sine, and Hartley transforms. *IEEE Trans Signal Process*, 50:1661–1680, 2002.
  135. S. C. Pei, W. L. Hsue, and J. J. Ding. Discrete fractional Fourier transform based on new nearly tridiagonal commuting matrices. *IEEE Trans Signal Process*, 54:3815–3828, 2006.
  136. S. C. Pei and M. H. Yeh. Improved discrete fractional Fourier transform. *Opt Lett*, 22:1047–1049, 1997.
  137. S. C. Pei and M. H. Yeh. Discrete fractional Hilbert transform. *Trans Circuits Syst II-Analog Digit Signal Process*, 47:1307–1311, 2000.
  138. S. C. Pei, M. H. Yeh, and C. C. Tseng. Discrete fractional Fourier transform based on orthogonal projections. *IEEE Trans Signal Process*, 47:1335–1348, 1999.
  139. P. Pellat-Finet. Fresnel diffraction and the fractional-order Fourier transform. *Opt Lett*, 19:1388–1390, 1994.
  140. P. Pellat-Finet and E. Fogret. Complex order, fractional Fourier transforms and their use in diffraction theory. Application to optical resonators. *Opt Commun*, 258:103–113, 2006.

141. J. Perez, D. Mas, C. Illueca, J. J. Miret, C. Vazquez, and C. Hernandez. Complete algorithm for the calculation light patterns inside the ocular media. *J Mod Opt*, 52:1161–1176, 2005.
142. A. M. Pons, A. Lorente, C. Illueca, D. Mas, and J. M. Artigas. Fresnel diffraction in a theoretical eye: a fractional Fourier transform approach. *J Mod Opt*, 46:1043–1050, 1999.
143. S. Qazi, A. Georgakis, L. K. Stergioulas, and M. Shikh-Bahaei. Interference suppression in the Wigner distribution using fractional Fourier transformation and signal synthesis. *IEEE Trans Signal Process*, 55:3150–3154, 2007.
144. M. G. Raymer, M. Beck, and D. F. McAlister. Complex wave-field reconstruction using phase-space tomography. *Phys Rev Lett*, 72:1137–1140, 1994.
145. M. G. Raymer, M. Beck, and D. McAlister. Spatial and temporal optical field reconstruction using phase-space tomography. In *Quantum Optics VI*, Springer, Berlin, Germany, 1994.
146. A. Sahin, H. M. Ozaktas, and D. Mendlovic. Optical implementations of two-dimensional fractional Fourier transforms and linear canonical transforms with arbitrary parameters. *Appl Opt*, 37:2130–2141, 1998.
147. B. Santhanam and J. H. McClellan. The discrete rotational Fourier transform. *IEEE Trans Signal Process*, 44:994–998, 1996.
148. B. Santhanam and T. S. Santhanam. Discrete Gauss Hermite functions and eigenvectors of the centered discrete Fourier transform. In *Proceedings of the International Conference on Acoust, Speech, Signal Processing*, IEEE, Piscataway, NJ, 2007, pp. 418–422.
149. D. Sazbon, Z. Zalevsky, E. Rivlin, and D. Mendlovic. Using Fourier/Mellin-based correlators and their fractional versions in navigational tasks. *Pattern Recog*, 35:2993–2999, 2002.
150. K. K. Sharma and S. D. Joshi. Signal reconstruction from the undersampled signal samples. *Opt Commun*, 268:245–252, 2006.
151. K. K. Sharma and S. D. Joshi. Papoulis-like generalized sampling expansions in fractional Fourier domains and their application to superresolution. *Opt Commun*, 278:52–59, 2007.
152. J. T. Sheridan, and R. Patten. Holographic interferometry and the fractional Fourier transformation. *Opt Lett*, 25:448–450, 2000.
153. R. Simon and N. Mukunda. Iwasawa decomposition in first-order optics: universal treatment of shape-invariant propagation for coherent and partially coherent beams. *J Opt Soc Am A-Opt Image Sci Vis*, 15:2146–2155, 1998.
154. G. Strang. *Linear Algebra and Its Applications*, 3rd edn. Harcourt Brace Jovanovich, New York, 1988.
155. H. Sun, G. S. Liu, H. Gu, and W. M. Su. Application of the fractional Fourier transform to moving target detection in airborne SAR. *IEEE Trans Aerosp Electron Syst*, 38:1416–1424, 2002.
156. U. Sümbül and H. M. Ozaktas. Fractional free space, fractional lenses, and fractional imaging systems. *J Opt Soc Am A-Opt Image Sci Vis*, 20:2033–2040, 2003.
157. R. Tao, B. Deng, and Y. Wang. Research progress of the fractional Fourier transform in signal processing. *Sci China Ser F-Inf Sci*, 49:1–25, 2006.
158. M. Testorf. Design of diffractive optical elements for the fractional Fourier transform domain: Phase-space approach. *Appl Opt*, 45:76–82, 2006.
159. A. Torre. The fractional Fourier transform and some of its applications to optics. *Progress Opt*, 66:531–596, 2002.
160. C. O. Torres and Y. Torres. The van Cittert-Zernike theorem: A fractional order Fourier transform point of view. *Opt Commun*, 232:11–14, 2004.
161. G. Unnikrishnan, and K. Singh. Double random fractional Fourier-domain encoding for optical security. *Opt Eng*, 39:2853–2859, 2000.
162. C. Vijaya, and J. S. Bhat. Signal compression using discrete fractional Fourier transform and set partitioning in hierarchical tree. *Signal Process*, 86:1976–1983, 2006.
163. F. Wang, and Y. J. Cai. Experimental observation of fractional Fourier transform for a partially coherent optical beam with Gaussian statistics. *J Opt Soc Am A-Opt Image Sci Vis*, 24:1937–1944, 2007.
164. K. B. Wolf. *Integral Transforms in Science and Engineering*. Plenum Press, New York, 1979.
165. K. B. Wolf and G. Krötzsch. Geometry and dynamics in the fractional discrete Fourier transform. *J Opt Soc Am A-Opt Image Sci Vis*, 24:651–658, 2007.
166. İ. Ş. Yetik, M. A. Kutay, and H. M. Ozaktas. Image representation and compression with the fractional Fourier transform. *Opt Commun*, 197:275–278, 2001.
167. İ. Ş. Yetik, M. A. Kutay, H. Özaktas, and H.M. Ozaktas. Continuous and discrete fractional Fourier domain decomposition. In *Proceedings of the IEEE International Conference on Acoustics, Speech, Signal Processing*, IEEE, Piscataway, NJ, 2000, pp. I:93–96.
168. İ. Ş. Yetik and A. Nehorai. Beamforming using the fractional Fourier transform. *IEEE Trans Signal Process*, 51:1663–1668, 2003.
169. İ. Ş. Yetik, H. M. Ozaktas, Billur Barshan, and L. Onural. Perspective projections in the space-frequency plane and fractional Fourier transforms. *J Opt Soc Am A-Opt Image Sci Vis*, 17:2382–2390, 2000.
170. Z. R. Yu. A new expression of the fractional Fourier transformation. *Commun Theor Phys*, 36:399–400, 2001.
171. Z. Zalevsky, D. Mendlovic, and J. H. Caulfield. Localized, partially space-invariant filtering. *Appl Opt*, 36:1086–1092, 1997.
172. Z. Zalevsky, D. Mendlovic, and R. G. Dorsch. Gerchberg-Saxton algorithm applied in the fractional Fourier or the Fresnel domain. *Opt Lett*, 21:842–844, 1996.
173. Z. Zalevsky, D. Mendlovic, M. A. Kutay, H. M. Ozaktas, and J. Solomon. Improved acoustic signals discrimination

- using fractional Fourier transform based phase-space representations. *Opt Commun*, 190:95–101, 2001.
174. A. I. Zayed. A convolution and product theorem for the fractional Fourier transform. *IEEE Signal Process. Lett*, 5:101–103, 1998.
175. A. I. Zayed. A class of fractional integral transforms: A generalization of the fractional Fourier transform. *IEEE Trans Signal Process*, 50:619–627, 2002.
176. F. Zhang, Y. Q. Chen, and G. Bi. Adaptive harmonic fractional Fourier transform. *IEEE Signal Process Lett*, 6:281–283, 1999.
177. Y. Zhang, B.-Z. Dong, B.-Y. Gu, and G.-Z. Yang. Beam shaping in the fractional Fourier transform domain. *J Opt Soc Am A-Opt Image Sci Vis*, 15:1114–1120, 1998.
178. Y. Zhang, G. Pedrini, W. Osten, and H. J. Tiziani. Applications of fractional transforms to object reconstruction from in-line holograms. *Opt Lett*, 29:1793–1795, 2004.
179. D. M. Zhao. Multi-element resonators and scaled fractional Fourier transforms. *Opt Commun*, 168:85–88, 1999.
180. B. H. Zhu and S. T. Liu. Multifractional correlation. *Opt Lett*, 26:578–580, 2001.
181. B. H. Zhu, S. T. Liu, and L. X. Chen. Fractional profilometry correlator for three dimensional object recognition. *Appl Opt*, 40:6474–6478, 2001.

# 15

## Lapped Transforms

15.1	Introduction.....	15-1
	Notation • Brief History • Block Transforms • Factorization of Discrete Transforms • Discrete MIMO Linear Systems • Block Transform as a MIMO System	
15.2	Lapped Transforms.....	15-4
	Orthogonal Lapped Transforms • Nonorthogonal Lapped Transforms	
15.3	LTs as MIMO Systems.....	15-8
15.4	Factorization of Lapped Transforms .....	15-9
15.5	Hierarchical Connection of LTs: Introduction.....	15-10
	Time-Frequency Diagram • Tree-Structured Hierarchical Lapped Transforms • Variable-Length LTs	
15.6	Practical Symmetric LTs.....	15-14
	The Lapped Orthogonal Transform: LOT • The Lapped Biorthogonal Transform: LBT • The Generalized LOT: GenLOT • The General Factorization: GLBT	
15.7	The Fast Lapped Transform: FLT .....	15-22
15.8	Modulated LTs.....	15-23
15.9	Finite-Length Signals.....	15-25
	Overall Transform • Recovering Distorted Samples • Symmetric Extensions	
15.10	Conclusions .....	15-28
	References .....	15-28

Ricardo L. de Queiroz  
*Xerox Corporation*

### 15.1 Introduction

In this chapter, an effort will be made to cover the basic aspects of lapped transforms. It is a subject that has been extensively studied, making available a large number of papers and books. This is mostly true because of the direct correspondence among lapped transforms, filter banks, wavelets, and time-frequency transformations. Some of those topics are well covered in other chapters in this handbook. In any case it will be certainly impractical to reference all the contributions in the field. Therefore, the presentation will be more focused rather than general. We refer the reader to chapters on wavelet and time-frequency transforms in this handbook, as well as Refs. [20,44,50,53] for a more detailed treatment of filter banks.

We expect the reader to have a background in digital signal processing. An introductory chapter in this handbook on signals and systems, the chapter on Z-transforms, and the chapter on the discrete cosine transform (DCT) are certainly useful.

#### 15.1.1 Notation

In terms of notation, our conventions are:  $\mathbf{I}_n$  is the  $n \times n$  identity matrix.  $\mathbf{O}_n$  is the  $n \times n$  null matrix, while  $\mathbf{O}_{n \times m}$  stands for the  $n \times m$  null matrix.  $\mathbf{J}_n$  is the  $n \times n$  counter-identity, or exchange, or reversing matrix, illustrated by the following example:

$$\mathbf{J}_3 = \begin{bmatrix} 0 & 0 & 1 \\ 0 & 1 & 0 \\ 1 & 0 & 1 \end{bmatrix}.$$

$\mathbf{J}$  reverses the order of elements of a vector.  $[\ ]^T$  means transposition.  $[\ ]^H$  means transposition combined with conjugation, where this combination is usually called the Hermitian of the vector or matrix. Unidimensional concatenation of matrices and vectors is indicated by a comma. In general, capital bold face letters are reserved for matrices, so that  $\mathbf{a}$  represents a (column) vector while  $\mathbf{A}$  represents a matrix.

#### 15.1.2 Brief History

In the early 1980s transform coding was maturing itself and the DCT<sup>38</sup> was the preferred transformation method. At that time, DCT-based image compression was state-of-the-art, but researchers were uncomfortable with the blocking artifacts which are common (and annoying) artifacts found at images which were compressed at low bit rates using block transforms. To resolve this problem, the idea of a lapped transform (LT, for short) was developed in the early 1980s at MIT. The idea was to extend the basis function beyond the block boundaries, creating an overlap, in order to eliminate the blocking effect. This idea was not new, but the new ingredient to overlapping blocks would



be the fact that the number of transform coefficients would be the same as if there was no overlap, and that the transform would maintain orthogonality. Cassereau<sup>3</sup> introduced the lapped orthogonal transform (LOT). However, it was Malvar<sup>12-14</sup> who gave the LOT an elegant design strategy and a fast algorithm, thus making the LOT practical and a serious contender to replace the DCT for image compression.

It was later pointed by Malvar<sup>16</sup> the equivalence between a LOT and a multirate filter bank which is now a very popular signal processing tool.<sup>50</sup> Based on cosine modulated filter banks,<sup>27</sup> modulated lapped transforms were designed.<sup>15,40</sup> Modulated transforms were generalized for an arbitrary overlap later, creating the class of extended lapped transforms (ELT).<sup>18-21</sup> Recently a new class of LTs with symmetric bases were developed yielding the class of generalized LOTs (GenLOTs).<sup>29,31,34</sup> The GenLOTs were made to have an arbitrary length (not a multiple of the block size),<sup>46</sup> extended to the nonorthogonal case<sup>49</sup> and even made to have filters of different lengths.<sup>48</sup> As we mentioned, filter banks and LTs are the same, although studied independently in the past. Because of this duality, it would be impractical to mention all related work in the field. Nevertheless, Vaidyanathan's book<sup>50</sup> is considered an excellent text on filter banks, while Malvar's book<sup>20</sup> is a good reference to bridge the gap between lapped transforms and filter banks. We, however, refer to LTs for uniform FIR filter banks with fast implementation algorithms based on special factorizations of the basis functions, with particular design attention for signal (mainly image) coding.<sup>10,14,15,20,30,36,46,55</sup>

### 15.1.3 Block Transforms

We assume a one-dimensional input sequence  $x(n)$  which is transformed into several coefficients  $y_i(n)$ , where  $y_i(n)$  would belong to the  $i$ th subband. In traditional block-transform processing, such as in image and audio coding, the signal is divided into blocks of  $M$  samples, and each block is processed independently,<sup>4,9,20,26,37-39</sup> Let the samples in the  $m$ th block be denoted as

$$\mathbf{x}_m^T = [x_0(m), x_1(m), \dots, x_{M-1}(m)], \quad (15.1)$$

for  $x_k(m) = x(mM + k)$  and let the corresponding transform vector be

$$\mathbf{y}_m^T = [y_0(m), y_1(m), \dots, y_{M-1}(m)]. \quad (15.2)$$

For a real unitary transform  $\mathbf{A}$ ,  $\mathbf{A}^T = \mathbf{A}^{-1}$ . The forward and inverse transforms for the  $m$ th block are

$$\mathbf{y}_m = \mathbf{A}\mathbf{x}_m, \quad (15.3)$$

and

$$\mathbf{x}_m = \mathbf{A}^T \mathbf{y}_m. \quad (15.4)$$

The rows of  $\mathbf{A}$ , denoted  $\mathbf{a}_n^T$  ( $0 \leq n \leq M-1$ ), are called the basis vectors because they form an orthogonal basis for the  $M$ -tuples over the real field.<sup>39</sup> The transform vector coefficients  $[y_0(m), y_1(m), \dots, y_{M-1}(m)]$  represent the corresponding weights of vector  $\mathbf{x}_m$  with respect to this basis.

If the input signal is represented by vector  $\mathbf{x}$  while the subbands are grouped into blocks in vector  $\mathbf{y}$ , we can represent the transform  $\mathbf{H}$  which operates over the entire signal as a block diagonal matrix:

$$\mathbf{H} = \text{diag}\{\dots, \mathbf{A}, \mathbf{A}, \mathbf{A}, \dots\}, \quad (15.5)$$

where, of course,  $\mathbf{H}$  is an orthogonal matrix if  $\mathbf{A}$  is also an orthogonal matrix. In summary, a signal is transformed by segmentation into blocks followed by transformation, which amounts to transforming the signal with a sparse matrix. Also, it is well known that the signal energy is preserved under an orthogonal transformation,<sup>9,38</sup> assuming stationary signals, i.e.,

$$M\sigma_x^2 = \sum_{i=0}^{M-1} \sigma_i^2, \quad (15.6)$$

where

$\sigma_i^2$  is the variance of  $y_i(m)$

$\sigma_x^2$  is the variance of the input samples

### 15.1.4 Factorization of Discrete Transforms

For our purposes, discrete transforms of interest are linear and governed by a square matrix with real entries. Square matrices can be factorized into a product of sparse matrices of the same size. Notably, orthogonal matrices can be factorized by a product of plane (Givens) rotations.<sup>8</sup> Let  $\mathbf{A}$  be an  $M \times M$  real orthogonal matrix and let  $\Theta(i, j, \theta_n)$  be a matrix with entries  $\Theta_{kl}$  which is like the identity matrix  $\mathbf{I}_M$  except for four entries:

$$\Theta_{ii} = \cos(\theta_n) \quad \Theta_{jj} = \cos(\theta_n) \quad \Theta_{ij} = \sin(\theta_n) \quad \Theta_{ji} = -\sin(\theta_n), \quad (15.7)$$

i.e.,  $\Theta(i, j, \theta_n)$  corresponds to a plane rotation along the  $i$ th and the  $j$ th axes by an angle  $\theta_n$ . Then,  $\mathbf{A}$  can be factorized as

$$\mathbf{A} = \mathbf{S} \prod_{i=0}^{M-2} \prod_{j=i+1}^{M-1} \Theta(i, j, \theta_n) \quad (15.8)$$

where  $n$  is increased by one for every matrix and  $\mathbf{S}$  is a diagonal matrix with entries  $\pm 1$  to correct for any sign error.<sup>8</sup> This correction is not necessary in most cases and is not required if we could apply variations of the rotation matrix defined in Equation 15.7 as

$$\Theta_{ii} = \cos(\theta_n) \quad \Theta_{jj} = -\cos(\theta_n) \quad \Theta_{ij} = \sin(\theta_n) \quad \Theta_{ji} = \sin(\theta_n). \quad (15.9)$$

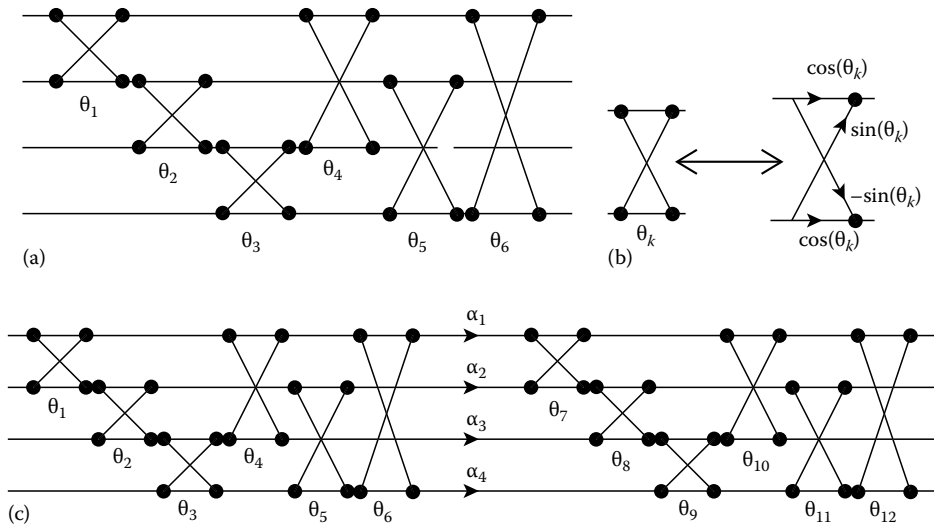


**FIGURE 15.1** Factorization of a  $4 \times 4$  matrix. (a) Orthogonal factorization into Givens rotations. (b) Detail of the rotation element. (c) Factorization of a nonorthogonal matrix through SVD with the respective factorization of SVD's orthogonal factors into rotations.

All combinations of pairs of axes shall be used for a complete factorization. Figure 15.1a shows an example of the factorization of a  $4 \times 4$  orthogonal matrix into plane rotations (the order differs from that in Equation 15.8, but the factorization is also complete). If the matrix is not orthogonal, we can always decompose the matrix using singular value decomposition (SVD).<sup>8</sup>  $\mathbf{A}$  is decomposed through SVD as

$$\mathbf{A} = \mathbf{U}\mathbf{\Lambda}\mathbf{V} \quad (15.10)$$

where

$\mathbf{U}$  and  $\mathbf{V}$  are orthogonal matrices

$\mathbf{\Lambda}$  is a diagonal matrix containing the singular values of  $\mathbf{A}$

While  $\mathbf{\Lambda}$  is already a sparse matrix, we can further decompose the orthogonal matrices using Equation 15.8, i.e.,

$$\mathbf{A} = \mathbf{S} \left( \prod_{i=0}^{M-2} \prod_{j=i+1}^{M-1} \Theta(i, j, \theta_n^U) \right) \mathbf{\Lambda} \left( \prod_{i=0}^{M-1} \prod_{j=i+1}^{M-1} \Theta(i, j, \theta_n^V) \right) \quad (15.11)$$

where  $\theta_n^U$  and  $\theta_n^V$  compose the set of angles for  $\mathbf{U}$  and  $\mathbf{V}$ , respectively. Figure 15.1c illustrates the factorization for a  $4 \times 4$  nonorthogonal matrix, where  $\alpha_i$  are the singular values.

The factorization is an invaluable tool for the design of block and lapped transforms as we will explain later. In the orthogonal case the angles are all the degrees of freedom. In an  $M \times M$  orthogonal matrix, there are  $M(M-1)/2$  angles, and by spanning all the angle spaces ( $0$  to  $2\pi$  for each one) one spans the space of all  $M \times M$  orthogonal matrices. The idea is to span the angles in order to design orthogonal matrices through unconstrained optimization. In the general case, there are  $M^2$  degrees of freedom either by utilizing the matrix entries directly or by using

the SVD decomposition. However, we are mainly concerned with invertible matrices. Using the SVD-based method, one can design invertible matrices by freely spanning the angles, with the only mild constraint to assure that all singular values are not zero. The author commonly uses unconstrained nonlinear optimization based on simplex search provided by MATLAB<sup>®</sup> to span all angles and possibly singular values as well.

### 15.1.5 Discrete MIMO Linear Systems

Let a multi-input multi-output (MIMO)<sup>50</sup> discrete linear FIR system have  $M$  input and  $M$  output sequences with respective  $Z$ -transforms  $X_i(z)$  and  $Y_i(z)$ , for  $0 \leq i \leq M-1$ . Then,  $X_i(z)$  and  $Y_i(z)$  are related by

$$\begin{bmatrix} Y_0(z) \\ Y_1(z) \\ \vdots \\ Y_{M-1}(z) \end{bmatrix} = \begin{bmatrix} E_{0,0}(z) & E_{0,1}(z) & \cdots & E_{0,M-1}(z) \\ E_{1,0}(z) & E_{1,1}(z) & \cdots & E_{1,M-1}(z) \\ \vdots & \vdots & \ddots & \vdots \\ E_{M-1,0}(z) & E_{M-1,1}(z) & \cdots & E_{M-1,M-1}(z) \end{bmatrix} \times \begin{bmatrix} X_0(z) \\ X_1(z) \\ \vdots \\ X_{M-1}(z) \end{bmatrix} \quad (15.12)$$

where  $E_{ij}(z)$  are entries of the given MIMO system  $\mathbf{E}(z)$ .  $\mathbf{E}(z)$  is called the transfer matrix of the system and we have chosen it to be square for simplicity. It is a regular matrix whose entries are polynomials. Of relevance to us is the case wherein the entries belong to the field of real-coefficient polynomials of  $z^{-1}$ , i.e., the entries represent real-coefficient FIR filters. The degree of  $\mathbf{E}(z)$  (or the McMillan degree,  $N_z$ ) is the minimum number of delays necessary to implement the system. The order of  $\mathbf{E}(z)$  is the

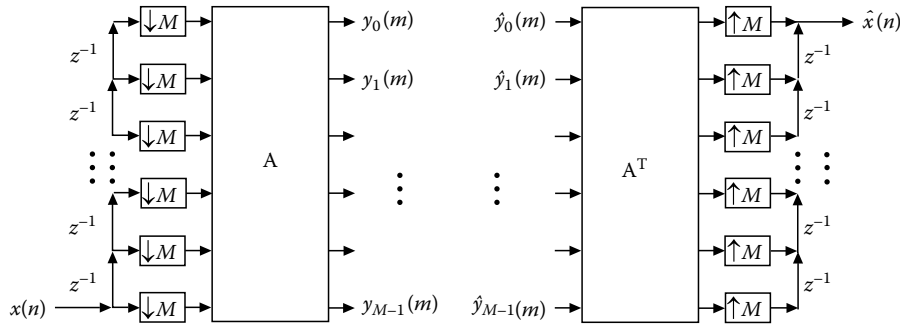


**FIGURE 15.2** The signal samples are parallelized into polyphase components through a sequence of delays and decimators ( $\downarrow M$  means subsampling by a factor of  $M$ ). Effectively the signal is “blocked” and each block is transformed by system  $\mathbf{A}$  into  $M$  subband samples (transformed samples). Inverse transform (for orthogonal transforms) is accomplished by system  $\mathbf{A}^T$  whose outputs are polyphase components of the reconstructed signal, which are then serialized by a sequence of up-samplers ( $\uparrow M$  means subsampling by a factor of  $M$ , padding the signal with  $M - 1$  zeros) and delays.

maximum degree among all  $E_{ij}(z)$ . In both cases, causal FIR filters are assumed.

A special subset of great interest comprises the transfer matrices which are normalized paraunitary. In the paraunitary case,  $\mathbf{E}(z)$  becomes a unitary matrix when evaluated on the unit circle:

$$\mathbf{E}^H(e^{j\omega})\mathbf{E}(e^{j\omega}) = \mathbf{E}(e^{j\omega})\mathbf{E}^H(e^{j\omega}) = \mathbf{I}_M. \quad (15.13)$$

Furthermore:

$$\mathbf{E}^{-1}(z) = \mathbf{E}^T(z^{-1}). \quad (15.14)$$

For causal inverses of paraunitary systems,

$$\mathbf{E}'(z) = z^{-n}\mathbf{E}^T(z^{-1}). \quad (15.15)$$

is often used, where  $n$  is the order of  $\mathbf{E}(z)$ , since  $\mathbf{E}'(z)\mathbf{E}(z) = z^{-n}\mathbf{I}_M$ .

For paraunitary systems, the determinant of  $\mathbf{E}(z)$  is of the form  $az^{-N_z}$ , for a real constant  $a$ ,<sup>50</sup> where we recall that  $N_z$  is the McMillan degree of the system. For FIR causal entries, they are also said to be lossless systems.<sup>50</sup> In fact, an orthogonal matrix is one where all  $E_{ij}(z)$  are constant for all  $z$ .

We also have interest in invertible, although nonparaunitary, transfer matrices. In this case, it is required that the matrix be invertible in the unit circle, i.e., for all  $z = e^{j\omega}$ ,  $\omega$  real. Nonparaunitary systems are also called biorthogonal or perfect reconstruction (PR).<sup>50</sup>

### 15.1.6 Block Transform as a MIMO System

The sequences  $x_i(m)$  in Equation 15.1 are called the polyphase components of the input signal  $x(n)$ . In the other hand, the sequences  $y_i(m)$  in Equation 15.2 are the subbands resulting from the transform process. In an alternative view of the transformation process, the signal samples are “blocked” or parallelized into polyphase components through a sequence of delays

and decimators as shown in Figure 15.2. Each block is transformed by system  $\mathbf{A}$  into  $M$  subband samples (transformed samples). Inverse transform (for orthogonal transforms) is accomplished by system  $\mathbf{A}^T$  whose output are polyphase components of the reconstructed signal, which are then serialized by a sequence of upsamplers and delays. In this system, blocks are processed independently. Therefore, the transform can be viewed as a MIMO system of order 0, i.e.,  $\mathbf{E}(z) = \mathbf{A}$ , and if  $\mathbf{A}$  is unitary, so is  $\mathbf{E}(z)$  which is obviously also paraunitary. The system matrix relating the polyphase components to the subbands is referred to as the polyphase transfer matrix (PTM).

## 15.2 Lapped Transforms

The motivation for a transform with overlap as we mentioned in the introduction was to try to improve the performance of block (nonoverlapped) transforms for image and signal compression. Compression commonly implies signal losses due to quantization.<sup>9</sup> As the bases of block transforms do not overlap, there may be discontinuities along the boundary regions of the blocks. Different approximations of those boundary regions in each side of the border may cause an artificial “edge” between blocks, the so-called *blocking* effect. In Figure 15.3 is shown an example signal which is to be projected into bases, by segmenting the signal into blocks and projecting each segment into the desired bases. Alternatively, one can view the process as projecting the whole signal into several translated bases (one translation per block). Figure 15.3a shows translated versions of the first basis of the DCT, in order to account for all the different blocks. In Figure 15.3b, shows the same diagram for the first basis of a typical short LT. Note that the bases overlap spatially. The idea is that overlap would help decrease, if not eliminate, the *blocking* effect.

Although Figure 15.3 shows just one basis for either DCT or LT, there are  $M$  of them. An example of the bases for  $M = 8$  is shown in Figure 15.4. It shows the bases for the DCT and for the LOT, which is a particular LT that will be discussed later.

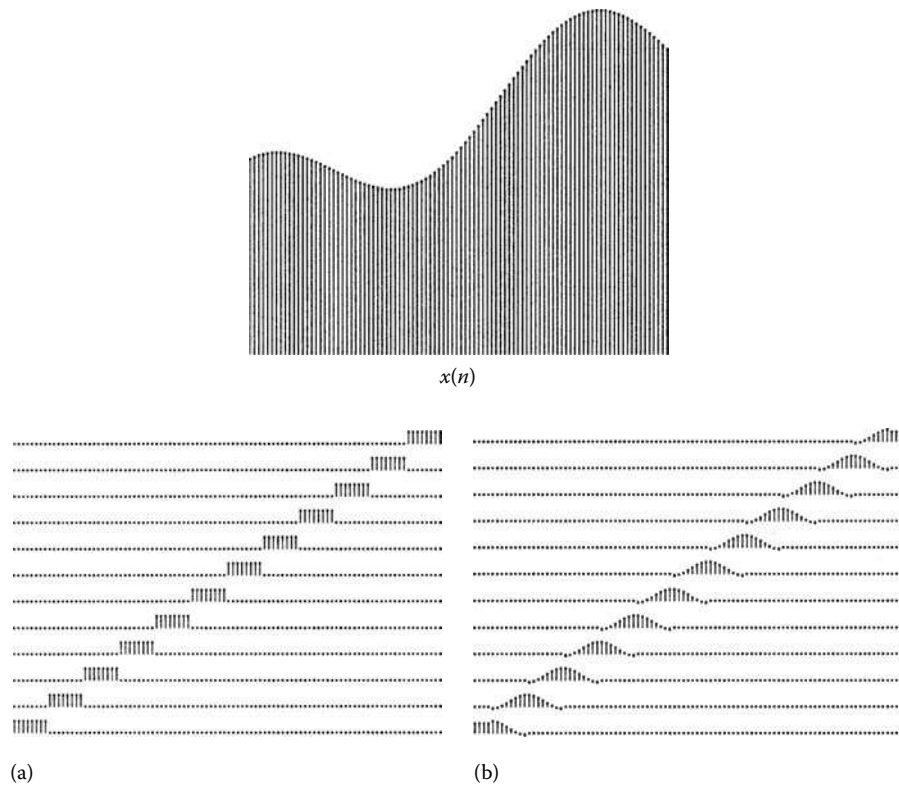


**FIGURE 15.3** The example discrete signal on top is to be projected into a number of bases. (a) spatially displaced versions of the first DCT basis, (b) spatially displaced versions of the first basis of a typical short LT.

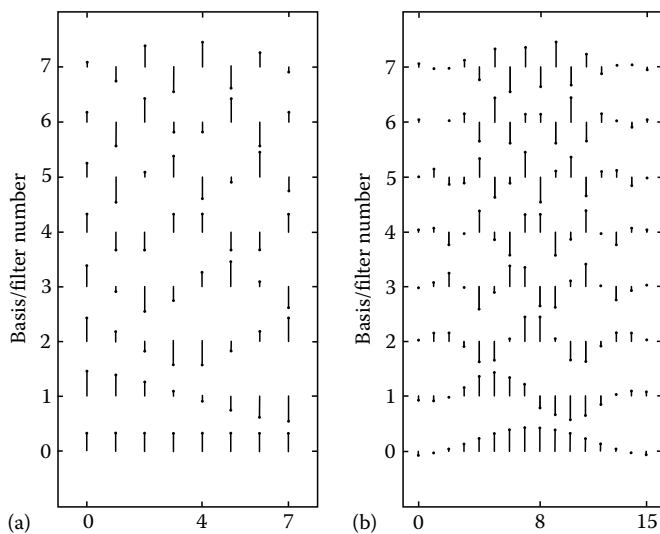


**FIGURE 15.4** Bases for the 8-point DCT ( $M=8$ ) (a) and for the LOT (b) with  $M=8$ . The LOT is a particular LT which will be explained later.

The reader may note that not only are the LOT bases longer, but they are also smoother than their DCT counterparts. Figure 15.5a shows an example of an image compressed using the standard JPEG baseline coder,<sup>26</sup> where the reader

can readily perceive the blocking artifacts at the boundaries of  $8 \times 8$  pixel blocks. By replacing the DCT with the LOT at the same compression ratio, we obtain the image shown in Figure 15.5b, where blocking is largely reduced. This brief introduction to the motivation behind the development of LTs helps to illustrate the overall problem, without detail on how to apply LTs. In this section we will develop the LT framework.

### 15.2.1 Orthogonal Lapped Transforms

For lapped transforms,<sup>20</sup> the basis vectors can have length  $L$ , such that  $L > M$ , extending across traditional block boundaries. Thus, the transform matrix is no longer square and most of the equations valid for block transforms do not apply to an LT. We will concentrate our efforts on *orthogonal* LTs<sup>20</sup> and consider  $L = NM$ , where  $N$  is the overlap factor. Note that  $N$ ,  $M$ , and hence  $L$  are all integers. As in the case of block transforms, we define the transform matrix as containing the orthonormal basis vectors as its rows. A LT matrix  $\mathbf{P}$  of dimensions  $M \times L$  can be divided into square  $M \times M$  submatrices  $\mathbf{P}_i$  ( $i = 0, 1, \dots, N-1$ ) as

$$\mathbf{P} = [\mathbf{P}_0, \mathbf{P}_1, \dots, \mathbf{P}_{N-1}]. \quad (15.16)$$

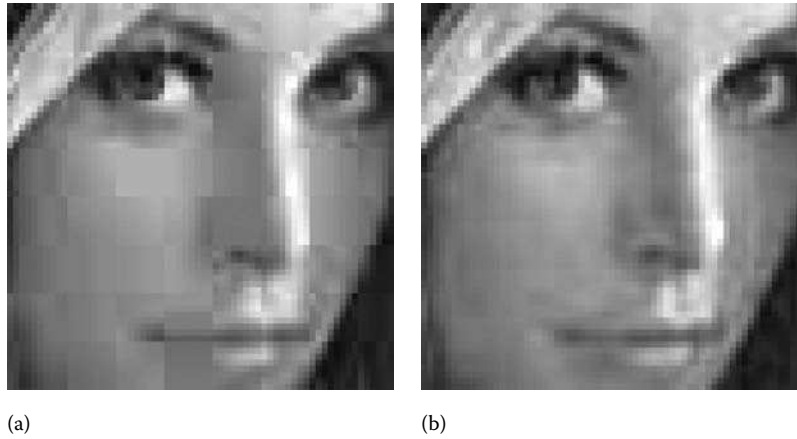


FIGURE 15.5 Zoom of image compressed using JPEG at 0.5 bit per pixel. (a) DCT, (b) LOT.

The orthogonality property does not hold because  $\mathbf{P}$  is no longer a square matrix and it is replaced by the PR property,<sup>20,23</sup> defined by

$$\sum_{i=0}^{N-1-l} \mathbf{P}_i \mathbf{P}_{i+l}^T = \sum_{i=0}^{N-1-l} \mathbf{P}_{i+l}^T \mathbf{P}_i = \delta(l) \mathbf{I}_M, \quad (15.17)$$

for  $l=0, 1, \dots, N-1$ , where  $\delta(l)$  is the Kronecker delta, i.e.,  $\delta(0)=1$  and  $\delta(l)=0$  for  $l \neq 0$ . As we will see later (Equation 15.17) states the PR conditions and orthogonality of the transform operating over the entire signal.

If we divide the signal into blocks, each of size  $M$ , we would have vectors  $\mathbf{x}_m$  and  $\mathbf{y}_m$  such as in Equations 15.1 and 15.2. These blocks are not used by LTs in a straightforward manner. The actual vector which is transformed by the matrix  $\mathbf{P}$  has to have  $L$  samples and, at block number  $m$ , it is composed of the samples of  $\mathbf{x}_m$  plus  $L-M$  samples. These samples are chosen by picking  $(L-M)/2$  samples at each side of the block  $\mathbf{x}_m$ , as shown in Figure 15.6, for  $N=2$ . However, the number of transform coefficients at each step is  $M$ , and, in this respect, there is no change in the way we represent the transform-domain blocks  $\mathbf{y}_m$ .

The input vector of length  $L$  is denoted as  $\mathbf{v}_m$ , which is centered around the block  $\mathbf{x}_m$ , and is defined as

$$\mathbf{v}_m^T \left[ x \left( mM - (N-1) \frac{M}{2} \right) \cdots x \left( mM + (N+1) \frac{M}{2} - 1 \right) \right]. \quad (15.18)$$

Then, we have

$$\mathbf{y}_m = \mathbf{P} \mathbf{v}_m. \quad (15.19)$$

The inverse transform is not direct as in the case of block transforms, i.e., with the knowledge of  $\mathbf{y}_m$  we do not know the samples in the support region of  $\mathbf{v}_m$ , or in the support region of  $\mathbf{x}_m$ . We can reconstruct a vector  $\hat{\mathbf{v}}_m$  from  $\mathbf{y}_m$ , as

$$\hat{\mathbf{v}}_m = \mathbf{P}^T \mathbf{y}_m, \quad (15.20)$$

where  $\hat{\mathbf{v}}_m \neq \mathbf{v}_m$ . To reconstruct the original sequence, it is necessary to accumulate the results of the vectors  $\hat{\mathbf{v}}_m$ , in a sense that a particular sample  $x(n)$  will be reconstructed from the sum of the contributions it receives from all  $\hat{\mathbf{v}}_m$ , such that  $x(n)$  was included in the region of support of the corresponding  $\mathbf{v}_m$ . This additional complication comes from the fact that  $\mathbf{P}$  is not a square matrix.<sup>20</sup> However, the whole analysis-synthesis system (applied to the entire input vector) is orthogonal, assuring the PR property using Equation 15.20.

We can also describe the process using a sliding rectangular window applied over the samples of  $x(n)$ . As an  $M$ -sample block  $\mathbf{y}_m$  is computed using  $\mathbf{v}_m$ ,  $\mathbf{y}_{m+1}$  is computed from  $\mathbf{v}_{m+1}$  which is obtained by shifting the window to the right by  $M$  samples, as shown in Figure 15.7.

As the reader may have noticed, the region of support of all vectors  $\mathbf{v}_m$  is greater than the region of support of the input vector. Hence, a special treatment has to be given to the

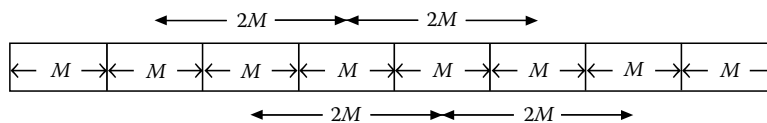


FIGURE 15.6 The signal samples are divided into blocks of  $M$  samples. The lapped transform uses neighboring block samples, as in this example for  $N=2$ , i.e.,  $L=2M$ , yielding an overlap of  $(L-M)/2=M/2$  samples on either side of a block.

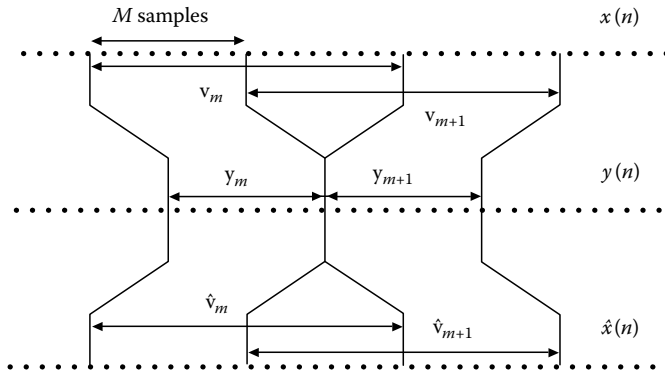


FIGURE 15.7 Illustration of a lapped transform with  $N=2$  applied to signal  $x(n)$ , yielding transform domain signal  $y(n)$ . The input  $L$ -tuple as vector  $\mathbf{v}_m$  is obtained by a sliding window advancing  $M$  samples, generating  $\mathbf{y}_m$ . This sliding is also valid for the synthesis side.

transform at the borders. We will discuss this fact later and assume infinite-length signals until then, or assume the length is very large and the borders of the signal are far enough from the region to which we are focusing our attention.

If we denote by  $\mathbf{x}$  the input vector and by  $\mathbf{y}$  the transform-domain vector, we can be consistent with our notation of transform matrices by defining a matrix  $\mathbf{H}$  such that  $\mathbf{y} = \mathbf{H}\mathbf{x}$  and  $\hat{\mathbf{x}} = \mathbf{H}^T\mathbf{y}$ . In this case, we have

$$\mathbf{H} = \begin{bmatrix} \ddots & & & & 0 \\ & \mathbf{P} & & & \\ & & \mathbf{P} & & \\ & & & \mathbf{P} & \\ 0 & & & & \ddots \end{bmatrix}. \quad (15.21)$$

Where the displacement of the matrices  $\mathbf{P}$  obeys the following:

$$\mathbf{H} = \begin{bmatrix} \ddots & \ddots & \ddots & \ddots & \ddots & 0 \\ & \mathbf{P}_0 & \mathbf{P}_1 & \ddots & \mathbf{P}_{N-1} & \\ & & \mathbf{P}_0 & \mathbf{P}_1 & \ddots & \mathbf{P}_{N-1} \\ 0 & & & \ddots & \ddots & \ddots \end{bmatrix}. \quad (15.22)$$

$\mathbf{H}$  has as many block-rows as transform operations over each vector  $\mathbf{v}_m$ .

Let the rows of  $\mathbf{P}$  be denoted by  $1 \times L$  vectors  $\mathbf{p}_i^T$  ( $0 \leq i \leq M-1$ ), so that  $\mathbf{P}^T = [\mathbf{p}_0, \dots, \mathbf{p}_{M-1}]$ . In an analogy to the block transform case, we have

$$y_i(m) = \mathbf{p}_i^T \mathbf{v}_m. \quad (15.23)$$

The vectors  $\mathbf{p}_i$  are the basis vectors of the lapped transform. They form an orthogonal basis for an  $M$ -dimensional subspace (there are only  $M$  vectors) of the  $L$ -tuples over the real field. As a remark, assuming infinite length signals, from the orthogonality

of the basis vectors and from the PR property in Equation 15.17, the energy is preserved, such that Equation 15.6 is valid.

In order to compute the variance of the subband signals of a block or lapped transform, assume that  $x(n)$  is a zero-mean stationary process with a given autocorrelation function. Let its  $L \times L$  autocorrelation matrix be  $\mathbf{R}_{xx}$ . Then, from Equation 15.23:

$$E[y_i(m)] = \mathbf{p}_i^T E[\mathbf{v}_m] = \mathbf{p}_i^T \mathbf{0}_{L \times 1} = 0, \quad (15.24)$$

so that:

$$\sigma_i^2 = E[y_i^2(m)] = \mathbf{p}_i^T E[\mathbf{v}_m \mathbf{v}_m^T] \mathbf{p}_i = \mathbf{p}_i^T \mathbf{R}_{xx} \mathbf{p}_i, \quad (15.25)$$

i.e., the output variance is easily computed from the input autocorrelation matrix for a given basis  $\mathbf{P}$ .

Assuming that the entire input and output signals are represented by the vectors  $\mathbf{x}$  and  $\mathbf{y}$ , respectively, and that the signals have infinite length, then, from Equation 15.21, we have

$$\mathbf{y} = \mathbf{H}\mathbf{x} \quad (15.26)$$

and, if  $\mathbf{H}$  is orthogonal,

$$\mathbf{x} = \mathbf{H}^T\mathbf{y}. \quad (15.27)$$

Note that  $\mathbf{H}$  is orthogonal if and only if Equation 15.17 is satisfied. Thus, the meaning for Equation 15.17 becomes clear, as it forces the transform operating over the entire input-output signals to be orthogonal. So, the LT is called orthogonal. For block transforms as there is no overlap, it is sufficient to state the orthogonality of  $\mathbf{A}$  because  $\mathbf{H}$  will be a block-diagonal matrix.

These formulations for LTs are general, and if the transform satisfies the PR property described in Equation 15.17, then the LTs are independent of the contents of the matrix  $\mathbf{P}$ . The definition of  $\mathbf{P}$  with a given  $N$  can accommodate any LT whose length of the basis vectors lies between  $M$  and  $NM$ . For the case of block transforms,  $N=1$ , i.e., no overlap. In fact, block transforms are a special case of lapped transforms and can be easily padded with zeroes. Similarly, basis functions can be increased by zero-padding as long as Equation 15.17 is respected.

*Causal notation*—If one is not concerned with particular localization of the transform with respect to the origin  $x(0)$  of the signal  $x(n)$ , it is possible to change the notation to apply a causal representation. In this case, we can represent  $\mathbf{v}_m$  as

$$\mathbf{v}_m^T = [\mathbf{x}_{m-N+1}^T, \dots, \mathbf{x}_{m-1}^T, \mathbf{x}_m^T], \quad (15.28)$$

which is identical to the previous representation, except for a shift in the origin to maintain causality. The block  $\mathbf{y}_m$  is found in a similar fashion as

$$\mathbf{y}_m = \mathbf{P}\mathbf{v}_m = \sum_{i=0}^{N-1} \mathbf{P}_{N-1-i} \mathbf{x}_{m-i}. \quad (15.29)$$

Similarly,  $\hat{\mathbf{v}}_m$  can be reconstructed as in Equation 15.20 where the support region for the vector is the same, except that the relation between it and the blocks  $\hat{\mathbf{x}}_m$  will be changed accordingly.

### 15.2.2 Nonorthogonal Lapped Transforms

So far, we have discussed orthogonal LTs. In those, a segment of the signal is projected onto the basis functions of  $\mathbf{P}$ , yielding the coefficients (subband samples). The signal is reconstructed by the overlapped projection of the same bases weighted by the subband samples. In the nonorthogonal case, we define another LT matrix  $\mathbf{Q}$  as

$$\mathbf{Q} = [\mathbf{Q}_0, \mathbf{Q}_1, \dots, \mathbf{Q}_{N-1}], \quad (15.30)$$

in the same way as we did for  $\mathbf{P}$  with the same size. The difference is that  $\mathbf{Q}$  instead of  $\mathbf{P}$  is used in the reconstruction process so that Equation 15.20 is replaced by

$$\hat{\mathbf{v}}_m = \mathbf{Q}^T \mathbf{y}_m. \quad (15.31)$$

We also define another transform matrix as

$$\mathbf{H}' = \begin{bmatrix} \ddots & \ddots & & \ddots & & & & 0 \\ & \mathbf{Q}_0 & \mathbf{Q}_1 & \cdots & \mathbf{Q}_{N-1} & & & \\ & & \mathbf{Q}_0 & \mathbf{Q}_1 & \cdots & \mathbf{Q}_{N-1} & & \\ 0 & & & \ddots & \ddots & & \ddots & \ddots \end{bmatrix}. \quad (15.32)$$

The forward and inverse transformation are now:

$$\mathbf{y} = \mathbf{H}_F \mathbf{x}, \quad \mathbf{x} = \mathbf{H}_I \mathbf{y}. \quad (15.33)$$

In the orthonormal case,  $\mathbf{H}_F = \mathbf{H}$  and  $\mathbf{H}_I = \mathbf{H}^T$ . In the general case, it is required that  $\mathbf{H}_I = \mathbf{H}_F^{-1}$ . With the choice of  $\mathbf{Q}$  as the inverse LT, then  $\mathbf{H}_I = \mathbf{H}'^T$ , while  $\mathbf{H}_F = \mathbf{H}$ . Therefore the perfect reconstruction condition is

$$\mathbf{H}'^T \mathbf{H} = \mathbf{I}_\infty. \quad (15.34)$$

The reader can check that the above equation can also be expressed in terms of the LTs  $\mathbf{P}$  and  $\mathbf{Q}$  as

$$\sum_{k=0}^{N-1-m} \mathbf{Q}_k^T \mathbf{P}_{k+m} = \sum_{k=0}^{N-1-m} \mathbf{Q}_{k+m}^T \mathbf{P}_k = \delta(m) \mathbf{I}_M, \quad (15.35)$$

which establish general necessary and sufficient conditions for the perfect reconstruction of the signal by using  $\mathbf{P}$  as a forward LT and  $\mathbf{Q}$  as an inverse LT. Unlike the orthogonal case in Equation 15.17, here both sets are necessary conditions, i.e., a total of  $2N - 1$  matrix equations.

### 15.3 LTs as MIMO Systems

As we discussed in Sections 15.1.3 and 15.1.6, the input signal can be decomposed into  $M$  polyphase signals  $x_i(m)$ , each sequence having one  $M$ th of the original rate. As there are  $M$  subbands  $y_i(m)$ , under some circumstances and since only linear operations are used to transform the signal, there is a MIMO system  $\mathbf{F}(z)$  that converts the  $M$  polyphase signals to the  $M$  subband signals. Those transfer matrices are also called PTM (Section 15.1.6). The same is true for the inverse transform (from subbands  $\hat{y}_i(m)$  to polyphase  $\hat{x}_i(m)$ ). Therefore, we can use the diagram shown in Figure 15.8 to represent the forward and inverse transforms. Note that Figure 15.8 is identical to Figure 15.2 except for the fact that the transforms have memory, i.e., depend not only on the present input vector, but also on past input vectors. One can view the system as a clocked one, in which at every clock, a block is input, transformed, and output. The parallelization and serialization of blocks is performed by the chain of delays, upsamplers and down-samplers as shown in Figure 15.8. If we express the forward and inverse PTM as matrix polynomials:

$$\mathbf{F}(z) = \sum_{i=0}^{N-1} \mathbf{F}_i z^{-i}, \quad (15.36)$$

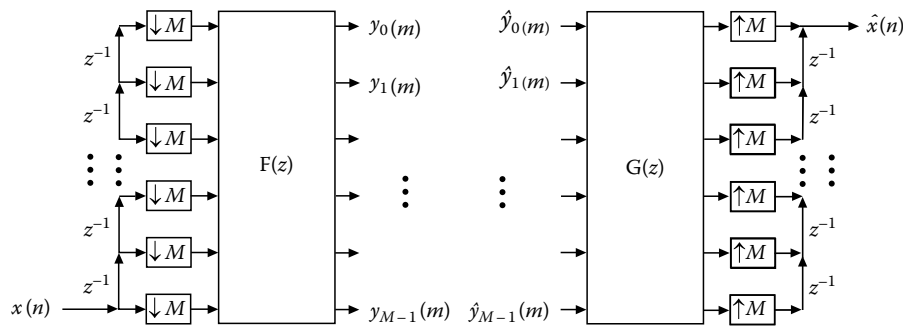


**FIGURE 15.8** The filter bank represented as a MIMO system is applied to the polyphase components of the signal. The matrices  $\mathbf{F}(z)$  and  $\mathbf{G}(z)$  are called polyphase transfer matrices. For a PR system both must be inverses of each other and for paraunitary filter banks they must be paraunitary matrices, i.e.,  $\mathbf{G}(z) = \mathbf{F}^{-1}(z) = \mathbf{F}^T(z^{-1})$ . For a PR paraunitary causal system of order  $N$ , we must choose  $\mathbf{G}(z) = z^{-(N-1)} \mathbf{F}^T(z^{-1})$ .

$$\mathbf{G}(z) = \sum_{i=0}^{N-1} \mathbf{G}_i z^{-i}, \quad (15.37)$$

then the forward and inverse transforms are given by

$$\mathbf{y}_m = \sum_{i=0}^{N-1} \mathbf{F}_i \mathbf{x}_{m-i}, \quad (15.38)$$

$$\hat{\mathbf{x}}_m = \sum_{i=0}^{N-1} \mathbf{G}_i \hat{\mathbf{y}}_{m-i}. \quad (15.39)$$

In the absence of any processing  $\hat{\mathbf{y}}_m = \mathbf{y}_m$  and  $\mathbf{F}(z)$  and  $\mathbf{G}(z)$  are connected together back-to-back, so that PR is possible if they are inverses of each other. Since the inverse of a causal FIR MIMO system may be noncausal, we can delay the entries of the inverse matrix to make it causal. Since the MIMO system's PTM is assumed to have order  $N$  (because  $N$  is the overlap factor of the equivalent LT), PR requires that:

$$\mathbf{G}(z)\mathbf{F}(z) = z^{-N+1}\mathbf{I}_M \rightarrow \mathbf{G}(z) = z^{-N+1}\mathbf{F}^{-1}(z). \quad (15.40)$$

In this case,  $\hat{\mathbf{x}} = \mathbf{x}_{m-N+1}$ , i.e., the signal is perfectly reconstructed after a system's delay. Because of the delay chains combined with the block delay (system's order), the reconstructed signal delay is  $\hat{x}(n) = x(n - NM + 1) = x(n - L - 1)$ .

By combining Equations 15.38 through 15.40 we can restate the PR conditions as

$$\sum_{i=0}^{N-1} \sum_{j=0}^{N-1} \mathbf{G}_i \mathbf{F}_j z^{-i-j} = z^{-N+1} \mathbf{I}_M, \quad (15.41)$$

which, by equating the powers of  $z$ , can be rewritten as

$$\sum_{k=0}^{N-1-m} \mathbf{G}_k \mathbf{F}_{k+m} = \sum_{k=0}^{N-1-m} \mathbf{G}_{k+m} \mathbf{F}_k = \delta(m) \mathbf{I}_M. \quad (15.42)$$

The reader should note the striking similarity of the above equation against Equation 15.35. In fact, the simple comparison of the transformation process in space domain notation (Equation 15.33) against the MIMO system notation in Equations 15.38 and 15.39 would reveal the following relations:

$$\mathbf{F}_k = \mathbf{P}_{N-1-k} \quad \mathbf{G}_k = \mathbf{Q}_k^T \quad (15.43)$$

for  $0 \leq k < N$ . In fact, the conditions imposed in Equations 15.34, 15.35, 15.40, and 15.42 are equivalent and each one of them implies the others. This is a powerful tool in the design of lapped transforms. As an LT, the matrix is nonsquare but the entries are real. As a MIMO system, the matrix is square, but the entries are polynomials. One form may complement the other, facilitating tasks such as factorization, design, and implementation.

As mentioned earlier, paraunitary (lossless) systems are a class of MIMO systems of interest. Let  $\mathbf{E}(z)$  be a paraunitary PTM so that  $\mathbf{E}^{-1}(z) = \mathbf{E}^T(z^{-1})$ , and let:

$$\mathbf{F}(z) = \mathbf{E}(z), \quad \mathbf{G}(z) = z^{-(N-1)} \mathbf{E}^T(z^{-1}). \quad (15.44)$$

As a result, the reader can verify that it implies that  $\mathbf{P}_i = \mathbf{Q}_i$  and that:

$$\sum_{i=0}^{N-1-l} \mathbf{P}_i \mathbf{P}_{i+l}^T = \sum_{i=0}^{N-1-l} \mathbf{P}_i^T \mathbf{P}_{i+l} = \delta(l) \mathbf{I}_M, \quad (15.45)$$

$$\mathbf{H}\mathbf{H}^T = \mathbf{H}^T \mathbf{H} = \mathbf{I}_\infty. \quad (15.46)$$

In other words, if the system's PTM is paraunitary, then the LT ( $\mathbf{H}$ ) is orthogonal and vice-versa.

## 15.4 Factorization of Lapped Transforms

There is an important results for paraunitary PTM which states that any paraunitary  $\mathbf{E}(z)$  can be decomposed into a series of orthogonal matrices and delay stages.<sup>6,51</sup> In this decomposition there are  $N_z$  delay stages and  $N_z + 1$  orthogonal matrices, where  $N_z$  is the McMillan degree of  $\mathbf{E}(z)$  (the degree of the determinant of  $\mathbf{E}(z)$ ). Then,

$$\mathbf{E}(z) = \mathbf{B}_0 \prod_{i=1}^{N_z} (\mathbf{Y}(z) \mathbf{B}_i) \quad (15.47)$$

where

$$\mathbf{Y}(z) = \text{diag}\{z^{-1}, 1, 1, \dots, 1\}$$

$\mathbf{B}_i$  are orthogonal matrices

It is well-known that an  $M \times M$  orthogonal matrix can be expressed as a product of  $M(M-1)/2$  plane rotations. However, in this case, only  $\mathbf{B}_0$  is a general orthogonal matrix, while the matrices  $\mathbf{B}_1$  through  $\mathbf{B}_{N_z}$  have only  $M-1$  degrees of freedom.<sup>52</sup>

This result states that it is possible to implement an orthogonal LT using a sequence of delays and orthogonal matrices. It also defines the total number of degrees of freedom in a lapped transform, i.e., if one changes arbitrarily any of the plane rotations composing the orthogonal transforms, one will span all possible orthogonal lapped transform, for given values of  $M$  and  $L$ . It is also possible to prove<sup>29</sup> that the (McMillan) degree of  $\mathbf{E}(z)$  is bounded by  $N_z \leq (L-M)/2$  with equality for a general structure to implement all LTs whose bases have length up to  $L = NM$ , i.e.,  $\mathbf{E}(z)$  of order  $N-1$ .

In fact Equation 15.47 may be able to implement all lapped transforms (orthogonal or not) whose degree is  $N_z$ . For that it is only required that all the multiplicative factors that compose the PTM are invertible. Let us consider a more particular factorization:



$$\mathbf{F}(z) = \prod_{i=0}^{(N-1)/(K-1)} \mathbf{B}_i(z) \quad (15.48)$$

where  $\mathbf{B}_i(z) = \sum_{k=0}^{K-1} \mathbf{B}_{ik} z^{-k}$  is a stage of order  $K-1$ . If  $\mathbf{F}(z)$  is paraunitary then all  $\mathbf{B}_i(z)$  must be paraunitary, so that perfect reconstruction is guaranteed if

$$\mathbf{G}(z) = z^{-N+1} \mathbf{F}^T(z^{-1}) = \prod_{i=(N-1)/(K-1)}^0 \left( \sum_{k=0}^{K-1} \mathbf{B}_{ik}^T z^{-(K-1-k)} \right). \quad (15.49)$$

In the case the PTM is not paraunitary, all factors have to be invertible in the unit circle for PR. More strongly put, there have to be factors  $\mathbf{C}_i(z)$  of order  $K$  such that:

$$\mathbf{C}_i(z) \mathbf{B}_i(z) = z^{-K+1} \mathbf{I}_M. \quad (15.50)$$

Being that the case, the inverse PTM is simply given by

$$\mathbf{G}(z) = \prod_{i=(N-1)/(K-1)}^0 \mathbf{C}_i(z) \quad (15.51)$$

With factorization, the design of  $\mathbf{F}(z)$  is broken down in the design of  $\mathbf{B}_i(z)$ . Lower order factors simplify the constraint analysis and facilitate the design of a useful transform, either paraunitary or allowing inverse. Even more desirable is to factorize the PTM as

$$\mathbf{F}(z) = \mathbf{B}_0 \prod_{i=0}^{N-1} \Lambda(z) \mathbf{B}_i \quad (15.52)$$

where  $\mathbf{B}_i$  are square matrices and  $\Lambda(z)$  is a paraunitary matrix containing only entries 1 and  $z^{-1}$ . In this case, if the PTM is paraunitary:

$$\mathbf{G}(z) = \left( \prod_{i=N-1}^0 \mathbf{B}_i^T \tilde{\Lambda}(z) \right) \mathbf{B}_0^T \quad (15.53)$$

where  $\tilde{\Lambda}(z) = z^{-1} \Lambda(1/z)$ . If the PTM is not paraunitary, then:

$$\mathbf{G}(z) = \left( \prod_{i=N-1}^0 \mathbf{B}_i^{-1} \tilde{\Lambda}(z) \right) \mathbf{B}_0^{-1}, \quad (15.54)$$

i.e., the design can be simplified by only applying invertible real matrices  $\mathbf{B}_i$ . This factorization approach is the basis for most useful LTs. It allows efficient implementation and design. We will discuss some useful LTs later on. For example, for  $M$  even, the symmetric delay factorization (SDF) is quite useful. In that,

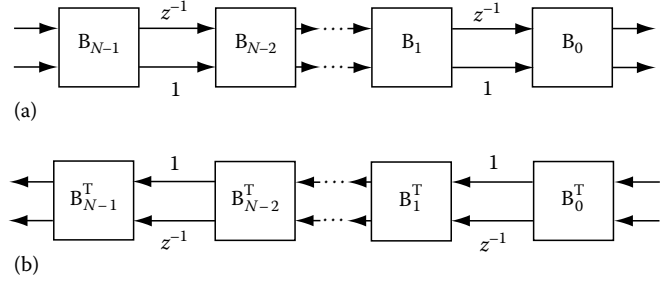


**FIGURE 15.9** Flow graph for implementing an LT where  $\mathbf{F}(z)$  can be factorized using symmetric delays and  $N$  stages. Signals  $x(n)$  and  $y(n)$  are segmented and processed using blocks of  $M$  samples, all branches carry  $M/2$  samples, and blocks  $\mathbf{B}_i$  are  $M \times M$  orthogonal or invertible matrices. (a) Forward transform section; (b) inverse transform section.

$$\Lambda(z) = \begin{bmatrix} z^{-1} \mathbf{I}_{M/2} & 0 \\ 0 & \mathbf{I}_{M/2} \end{bmatrix}, \quad \tilde{\Lambda}(z) = \begin{bmatrix} \mathbf{I}_{M/2} & 0 \\ 0 & z^{-1} \mathbf{I}_{M/2} \end{bmatrix}. \quad (15.55)$$

The flow graph for implementing an LT which can be parameterized using SDF is shown in Figure 15.9.

If we are given the SDF matrices instead of the basis coefficients, one can easily reconstruct the LT matrix. For this, start with the last stage and recur the structure in Equation 15.52 using Equation 15.55. Let  $\mathbf{P}^{(i)}$  be the partial reconstruction of  $\mathbf{P}$  after including up to the  $i$ th stage. Then,

$$\mathbf{P}^{(0)} = \mathbf{B}_{N-1} \quad (15.56)$$

$$\mathbf{P}^{(i)} = \mathbf{B}_{N-1-i} \begin{bmatrix} \mathbf{I}_{M/2} & \mathbf{0}_{M/2} & \mathbf{0}_{M/2} & \mathbf{0}_{M/2} \\ \mathbf{0}_{M/2} & \mathbf{0}_{M/2} & \mathbf{0}_{M/2} & \mathbf{I}_{M/2} \end{bmatrix} \begin{bmatrix} \mathbf{P}^{(i-1)} & \mathbf{0}_M \\ \mathbf{0}_M & \mathbf{P}^{(i-1)} \end{bmatrix} \quad (15.57)$$

$$\mathbf{P} = \mathbf{P}^{(N-1)} \quad (15.58)$$

Similarly, one can find  $\mathbf{Q}$  from the factors  $\mathbf{B}_i^{-1}$ .

## 15.5 Hierarchical Connection of LTs: Introduction

So far we have focused on the construction of a single LT resulting in  $M$  subband signals. What happens if we cascade LTs by connecting them hierarchically, in such a way that a subband signal is the actual input for another LT? Also, what are the consequences of submitting only part of the subband signals to further stages of LTs? We will try to introduce the answer to those questions.

The subject has been intensively studied and a large number of publications are available. Our intent, however, is just to provide a basic introduction, while leaving more detailed analysis to the references. The relation between filter banks and discrete wavelets<sup>42,50,52</sup> is well-known. Under conditions

that are easily satisfied,<sup>50</sup> an infinite cascade of filter banks will generate a set of continuous orthogonal wavelet bases. In general, if only the low-pass subband is connected to another filter bank, for a finite number of stages, we call the resulting filter bank a discrete wavelet transform (DWT).<sup>50,52</sup> A free cascading of filter banks, however, is better known as a discrete wavelet packet (DWP).<sup>5,28,42,54</sup> As LTs and filter banks are equivalent in most senses, the same relations apply to LTs and wavelets. The system resulting from the hierarchical association of several LTs will be called here a hierarchical lapped transform (HLT).<sup>17</sup>

### 15.5.1 Time–Frequency Diagram

The description of the cascaded connection of LTs is better carried with the aid of simplifying diagrams. The first is the time–frequency (TF) diagram. It is based on the TF plane, which is well known from the fields of spectral and time–frequency analysis.<sup>1,2,25</sup> The time–frequency representation of signals is a well-known method (for example, the time-dependent discrete Fourier transform (DFT) and the construction of spectrograms; see Refs. [1,2,25] for details on TF signal representation, and other chapters in this handbook for the DFT). The TF representation is obtained by expressing the signal  $x(n)$  with respect to bases that are functions of both frequency and time. For example, the size- $r$  DFT of a sequence extracted from  $x(n)$  (from  $x(n)$  to  $x(n+r-1)$ )<sup>25</sup> can be

$$\alpha(k, n) = \sum_{i=0}^{r-1} x(i+n) \exp\left(-\frac{j2\pi ki}{r}\right). \quad (15.59)$$

Using a sliding window  $w(m)$  of length  $r$  which is nonzero only in the interval  $n \leq m \leq n+r-1$ , (which in this case is rectangular), we can rewrite the last equation as

$$\alpha(k, n) = \sum_{i=-\infty}^{\infty} x(i)w(i) \exp\left(-\frac{jk(i-n)2\pi}{r}\right). \quad (15.60)$$

For more general bases we may write:

$$\alpha(k, n) = \sum_{i=-\infty}^{\infty} x(i)\phi(n-i, k) \quad (15.61)$$

where

$\phi(n, k)$  represents the bases for the space of the signal  
 $n$  represents the index where the basis is located in time  
 $k$  is the frequency index

As the signal is assumed to have an infinite number of samples, consider a segment of  $N_x$  samples extracted from signal  $x(n)$ , which can be extended in any fashion in order to account for the overlap of the window of  $r$  samples outside the signal domain. In such segment we can construct a spectrogram with a resolution of  $r$  samples in the frequency axis and  $N_x$  samples in the time axis. Assuming a maximum frequency resolution we can have a window with length up to  $r = N_x$ . In this case, the diagram for the spectrogram is given in Figure 15.10a. We call such diagrams TF diagrams, because they only indicate the number of samples used in the TF representation of the signal. Assuming an ideal partition of the TF plane (using filters with ideal frequency response and null transition regions), each TF coefficient would represent a distinct region in a TF diagram. Note that in such representation, the signal is represented by  $N_x^2$  TF coefficients. We are looking for maximally decimated TF representation which is defined as a representation of the signal where the TF plane diagram would be partitioned into  $N_x$  regions, i.e.,  $N_x$  TF coefficients will be generated. Also, we require that all  $N_x$  samples of  $x(n)$  can be reconstructed from the  $N_x$  TF coefficients. If we use less than  $N_x$  samples in the TF plane, we clearly cannot reconstruct all possible combinations of samples in  $x(n)$ , from the TF coefficients, solely using linear relations.

Under these assumptions, Figure 15.10b shows the TF diagram for the original signal (only resolution in the time axis) for  $N_x = 16$ . Also, for  $N_x = 16$ , Figure 15.10c shows a TF diagram with maximum frequency resolution, which could be achieved by transforming the original  $N_x$ -sample sequence with an  $N_x$ -sample DCT or DFT.

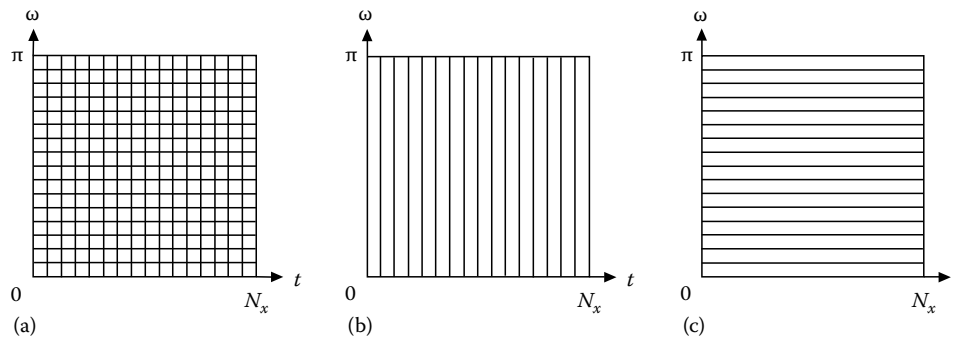


**FIGURE 15.10** Examples of rectangular partitions of the time–frequency plane for a signal which has  $N_x$  samples. (a) Spectrogram with a  $N_x$ -length window, resulting in  $N_x^2$  TF samples; (b) Input signal, no processing; (c) A transform such as the DCT or DFT is applied to all  $N_x$  samples.

### 15.5.2 Tree-Structured Hierarchical Lapped Transforms

The tree diagram is helpful to describe the hierarchical connection of filter banks. In this diagram we represent an  $M$ -band LT by nodes and branches of an  $M$ -ary tree. Figure 15.11a shows an  $M$ -band LT, where all the  $M$  subband signals have sampling rates  $M$  times smaller than that of  $x(n)$ . Figure 15.11b shows the equivalent notation for the LT in a tree diagram, i.e., a single-stage  $M$ -branch tree, which is called here a tree cell. Recalling Figure 15.10, the equivalent TF diagram for an  $M$ -band LT is shown in Figure 15.11c, for a 16-sample signal and for  $M=4$ . Note that the TF diagram of Figure 15.11c resembles that of Figure 15.10a. This is because for each 4 samples in  $x(n)$  there is a corresponding set of 4 transformed coefficients. So, the TF representation is maximally decimated. Compared to Figure 15.10b, Figure 15.11c implies an exchange of resolution from time to frequency domain achieved by the LT.

The exchange of resolution in the TF diagram is obtained by the LT. As we connect several LTs following the paths of a tree, each new set of branches (each new tree cell) connected to the tree will force the TF diagram to exchange from time to frequency resolution. We can achieve a more versatile TF

representation by connecting cells in unbalanced ways. For example, Figure 15.12, shows some examples of HLTs given by their tree diagrams and respective TF diagrams. Figure 15.12a shows the tree diagram for the 3-stages DWT. Note that only the lowpass subband is further processed. Also, as all stages are chosen to be 2-channel LTs, this HLT can be represented by a binary tree. In Figure 15.12b, a more generic hierarchical connection of 2-channel LTs is shown. First the signal is split into low- and high-pass. Each output branch is further connected to another 2-channel LT. In the third stage only the most low-pass subband signal is connected to another 2-channel LT. Figure 15.12c shows a 2-stage HLT obtaining the same TF diagram as Figure 15.12b. Note that the succession of 2-channel LTs was substituted by a single stage 4-channel LT, i.e., the signal is split into four subbands and, then, one subband is connected to another LT. Figure 15.12d shows the TF diagram corresponding to Figure 15.12a, while Figure 15.12e shows the TF diagram corresponding to Figure 15.12b and c. Note that, as the tree-paths are unbalanced, we have irregular partitions of the TF plane. For example, in the DWT, low-frequency TF coefficients have poor time localization and good frequency resolution, while high-frequency ones have poor frequency resolution and better time localization.

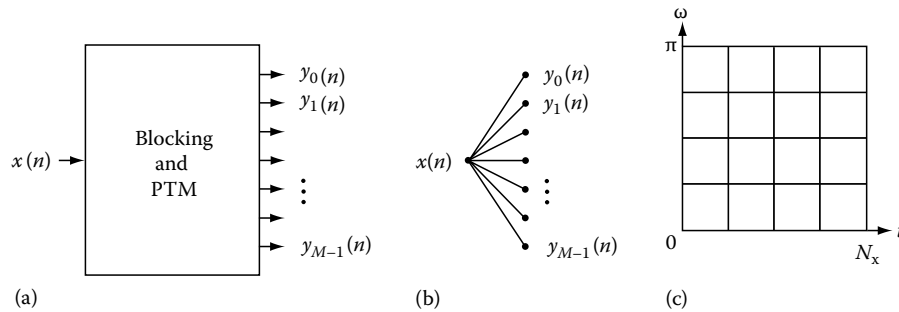


FIGURE 15.11 Representation of an  $M$ -channel LT as tree nodes and branches. (a) Forward section of an LT, including the blocking device. (b) Equivalent notation for (a) using an  $M$ -branch single-stage tree. (c) Equivalent TF diagram for (a) or (b) assuming  $M=4$  and  $N_x=16$ .

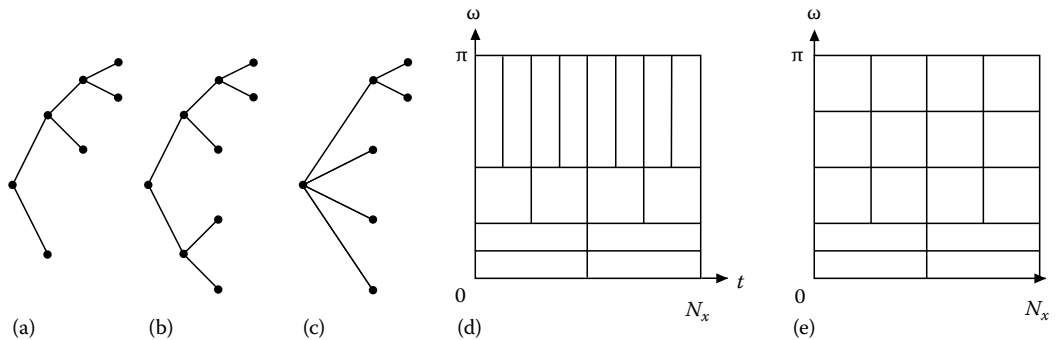
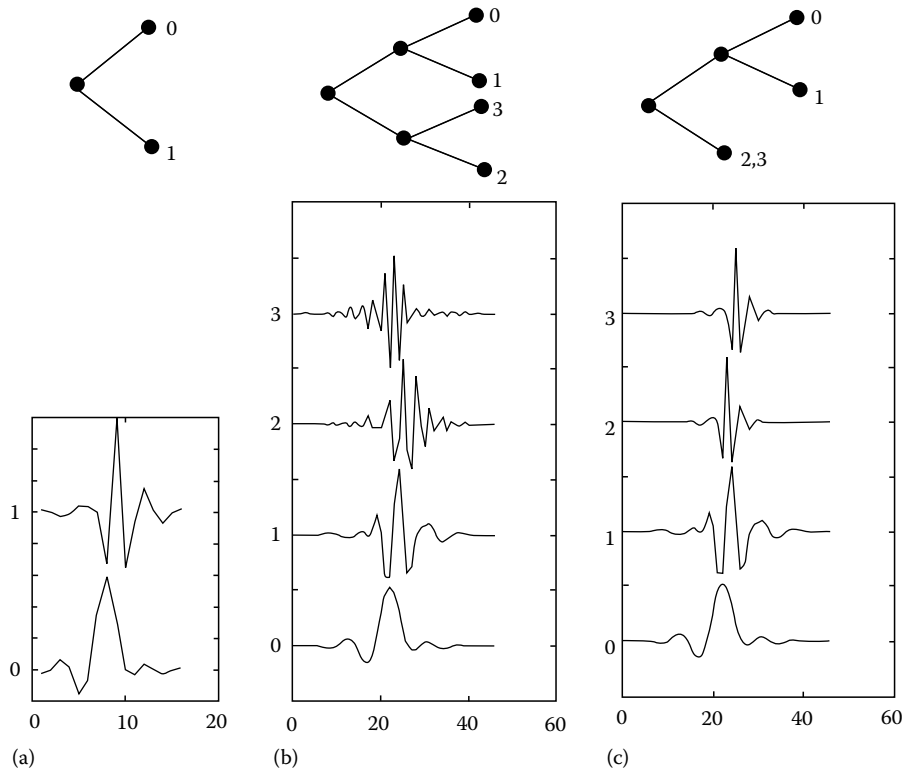


FIGURE 15.12 Tree and TF diagrams. (a) The 3-stage DWT binary-tree diagram, where only the low-pass subband is submitted to further LT states. (b) A more generic 3-stages tree diagram. (c) A 2-stages tree-diagram resulting in the same TF diagram as (b). (d) TF diagram for (a). (e) TF diagram for (b) or (c).



**FIGURE 15.13** Two HLTs and resulting bases. (a) The 2-channel 16-tap-bases LT, showing low-and high-frequency bases,  $f_0(n)$  and  $f_1(n)$ , respectively. (b) Resulting basis functions of a 2-stage HLT based on (a), given by  $f_0(n)$  through  $f_3(n)$ . Its respective tree diagram is also shown. (c) Resulting HLT, by pruning one high-frequency branch in (b). Note that the two high-frequency basis functions are identical to the high-frequency basis function of (a) and, instead of having two distinct bases for high frequencies occupying distinct spectral slots, the two bases are now shifted in time. Thus, better time localization is attainable, at the expense of frequency resolution.

To better understand how connecting an LT to the tree can achieve the exchange between time and frequency resolution, Figure 15.13 shows the basis functions resulting from two similar tree-structured HLTs. The difference between them is one tree cell which is applied or not to a terminal branch of the tree.

### 15.5.3 Variable-Length LTs

In the tree-structured method to cascade LTs, every time an LT is added to the structure, more subbands are created by further subdividing previous subbands, so that the overall TF diagram of the decomposition is altered. There is a useful alternative to the tree structure in which the number of subbands does not change. We refer to Figure 15.14, where the “blocking” part of the diagram corresponds to the chain of delays and decimators (as in Figure 15.8) that parallelizes the signal into polyphase components. System  $\mathbf{A}(z)$  of  $M$  bases of length  $N_A M$  is postprocessed by system  $\mathbf{B}(z)$  of  $K$  bases of length  $N_B K$ . Clearly, entries in  $\mathbf{A}(z)$  have order  $N_A - 1$  and entries in  $\mathbf{B}(z)$  have order  $N_B - 1$ . Without loss generality, we associate system  $\mathbf{B}(z)$  to the first  $K$  output subbands of  $\mathbf{A}(z)$ . The overall PTM is given by

$$F(x) = \begin{bmatrix} \mathbf{B}(z) & 0 \\ 0 & \mathbf{I}_{M-K} \end{bmatrix} \mathbf{A}(z), \quad (15.62)$$

where  $\mathbf{F}(z)$  has  $K$  bases of order  $N_A + N_B - 2$  and  $M - K$  bases of order  $N_A - 1$ . As the resulting LT has  $M$  channels the final orders dictate that the first  $K$  bases have length  $(N_A + N_B - 1) M$  while the others still have length  $N_A M$ . In other words the effect of cascading  $\mathbf{A}(z)$  and  $\mathbf{B}(z)$  was only to modify  $K$  bases, so that the length of the modified bases is equal or larger than the length of the initial bases. An example is shown in Figure 15.15. We start with the bases corresponding to  $\mathbf{A}(z)$  shown in Figure 15.15a. There are 8 bases of length 16 so that  $\mathbf{A}(z)$  has order 1.  $\mathbf{A}(z)$  is postprocessed by  $\mathbf{B}(z)$  which is a  $4 \times 4$  PTM of order 3 whose

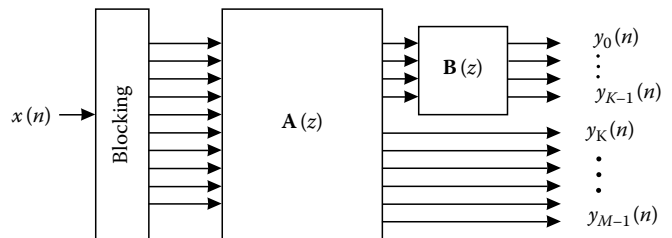


**FIGURE 15.14** Cascade of PTMs  $\mathbf{A}(z)$  of  $M$  channels and  $\mathbf{B}(z)$  of  $K$  channels. The total number of subbands does not change, however, of  $\mathbf{A}(z)$  bases are increased in length and order.

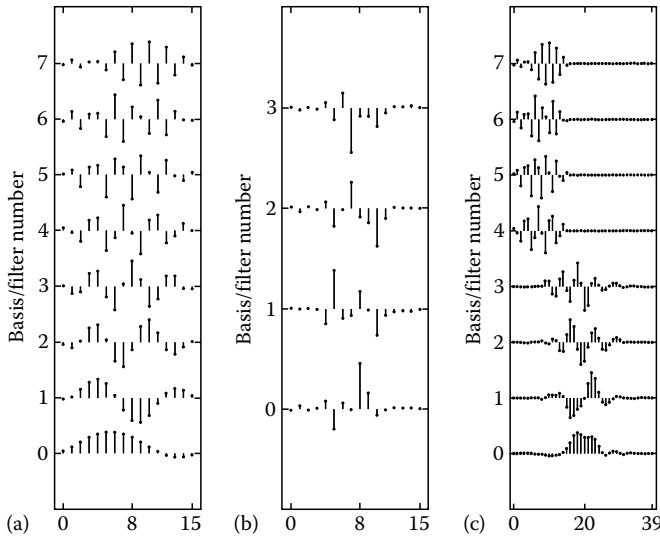


**FIGURE 15.15** Example of constructing variable-length bases through cascading LTs. (a) The basis corresponding to  $A(z)$ ; (b) an LT with 8 bases of length 16 (order 1). (c) The bases corresponding to  $F(z)$ : 4 of the 8 bases have order 1, i.e., length 16, while the remaining 4 have order 4, i.e., length 40.

corresponding bases are shown in Figure 15.15b. The resulting LT is shown in Figure 15.15c. There are 4 bases of length 16 and 4 of length 40. The shorter ones are identical to those in Figure 15.15b, while the longer ones have orders which are the sums of the others of  $A(z)$  and  $B(z)$ , i.e., order 4, and the shape of the longer bases in  $F(z)$  is very different from the corresponding ones in  $A(z)$ .

The effect of postprocessing few bases is a means to construct a new LT with larger bases from an initial one. In fact it can be shown that variable length LTs can be factorized using post-processing stage.<sup>47,48</sup> A general factorization of LTs is as shown in Figure 15.16. Assume a variable-length  $F(z)$  whose bases are arranged in decreasing length order. Such a PTM can be factorized as

$$F(z) = \prod_{i=0}^{M-2} \begin{bmatrix} \mathbf{B}_i(z) & 0 \\ 0 & \mathbf{I}_i \end{bmatrix} \quad (15.63)$$

where  $\mathbf{I}_0$  is understood to be nonexistent and  $\mathbf{B}_i(z)$  has size  $(M-i) \times (M-i)$ . The factors  $\mathbf{B}_i$  can have individual orders  $K_i$

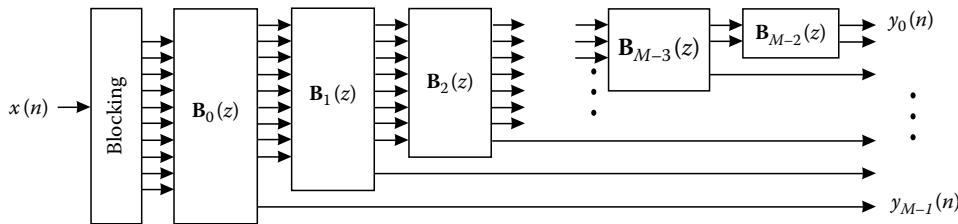


**FIGURE 15.16** General factorization of a variable-length LT.

and can be factorized differently into factors  $\mathbf{B}_{ik}(z)$  for  $0 \leq k < K_i$ . Hence,

$$F(z) = \prod_{i=0}^{M-2} \prod_{k=0}^{K_i-1} \begin{bmatrix} \mathbf{B}_{ik}(z) & 0 \\ 0 & \mathbf{I}_i \end{bmatrix}. \quad (15.64)$$

In a later section we will show a very useful LT which is based on the factorization principles of Equation 15.64.

## 15.6 Practical Symmetric LTs

We have discussed LTs in a general sense as a function of several parameters such as matrix entries, orthogonal or invertible factors, etc. The design of an LT suitable for a given application is the single most important step in the study of LTs. In order to do that, one may factorize the LT to facilitate optimization techniques.

An LT with symmetric bases is commonly used in image processing and compression applications. By symmetric bases we mean that:

$$p_{i,j} = (\pm 1)p_{i,L-1-j}. \quad (15.65)$$

The bases can be symmetric or antisymmetric. In terms of the PTM, this constraint is given by<sup>42,43</sup>

$$F(z) = z^{-(N-1)} \mathbf{S} F(z^{-1}) \mathbf{J}_M, \quad (15.66)$$

where  $\mathbf{S}$  is a diagonal matrix whose diagonal entries  $s_{ii}$  are  $\pm 1$ , depending whether the  $i$ th basis is symmetric (+1) or antisymmetric (-1). Note that we require that all bases share the same center of symmetry.

### 15.6.1 The Lapped Orthogonal Transform: LOT

LOT<sup>12-14</sup> was the first useful LT with a well defined factorization. Malvar developed the fast LOT based on the work by Cassereau<sup>3</sup> to provide not only a factorization, but a factorization based on the DCT. The DCT is attractive for many reasons, among them, fast implementation and near-optimal performance for block transform coding.<sup>38</sup> Also, since it is a popular transform, it has

a reduced cost and it easily available in either software or hardware. The DCT matrix  $\mathbf{D}$  is defined as having entries:

$$d_{ij} = \sqrt{\frac{2}{M}} k_i \cos\left(\frac{(2j+1)i\pi}{2M}\right) \quad (15.67)$$

where  $k_0 = 1$  and  $k_i = 1/\sqrt{2}$ , for  $1 \leq i \leq M-1$ .

The LOT as defined by Malvar is orthogonal. Then, according to our notation,  $\mathbf{P} = \mathbf{Q}$  and  $\mathbf{H}^{-1} = \mathbf{H}^T$ . It is also a symmetric LT with  $M$  even. The LT matrix is given by

$$\mathbf{P}_{\text{LOT}} = \begin{bmatrix} \mathbf{I}_M & 0 \\ 0 & \mathbf{V}_R \end{bmatrix} \begin{bmatrix} \mathbf{D}_e - \mathbf{D}_o & \mathbf{J}_{M/2}(\mathbf{D}_e - \mathbf{D}_o) \\ \mathbf{D}_e - \mathbf{D}_o & -\mathbf{J}_{M/2}(\mathbf{D}_e - \mathbf{D}_o) \end{bmatrix} \quad (15.68)$$

where

$\mathbf{D}_e$  is the  $M/2 \times M$  matrix with the even-symmetric basis functions of the DCT

$\mathbf{D}_o$  is the matrix of the same size with the odd-symmetric ones

In our notation,  $\mathbf{D}_e$  also corresponds to the even numbered rows of  $\mathbf{D}$  and  $\mathbf{D}_o$  corresponds to the odd numbered rows of  $\mathbf{D}$ .  $\mathbf{V}_R$  is an  $M/2 \times M/2$  orthogonal matrix, which according to Refs. [15,21] should be approximated by  $M/2 - 1$  plane rotations as

$$\mathbf{V}_R = \prod_{i=M/2-2}^0 \Theta(i, i+1, \theta_i) \quad (15.69)$$

where  $\Theta$  is defined in Section 15.1.4. Suggestions of rotation angles which were designed to yield a good transform for image compression are<sup>20</sup>

$$M = 4 \rightarrow \theta_0 = 0.1\pi \quad (15.70)$$

$$M = 8 \rightarrow \{\theta_0, \theta_1, \theta_2\} = \{0.13, 0.16, 0.13\} \times \pi \quad (15.71)$$

$$M = 16 \rightarrow \{\theta_0, \dots, \theta_7\} \\ = \{0.62, 0.53, 0.53, 0.50, 0.44, 0.35, 0.23, 0.11\} \times \pi. \quad (15.72)$$

For  $M \geq 16$  it is suggested to use:

$$\mathbf{V}_R = \mathbf{D}_{\text{IV}}^T \mathbf{D}^T \quad (15.73)$$

where  $\mathbf{D}_{\text{IV}}$  is the DCT type IV matrix<sup>38</sup> whose entries are

$$d_{ij}^{\text{IV}} = \sqrt{\frac{2}{M}} \cos\left(\frac{(2j+1)(2i+1)\pi}{4M}\right). \quad (15.74)$$

A block diagram for the implementation of the LOT is shown in Figure 15.17 for  $M=8$ .

### 15.6.2 The Lapped Biorthogonal Transform: LBT

The LOT is a large improvement over the DCT for image compression mainly because it reduces the so-called blocking

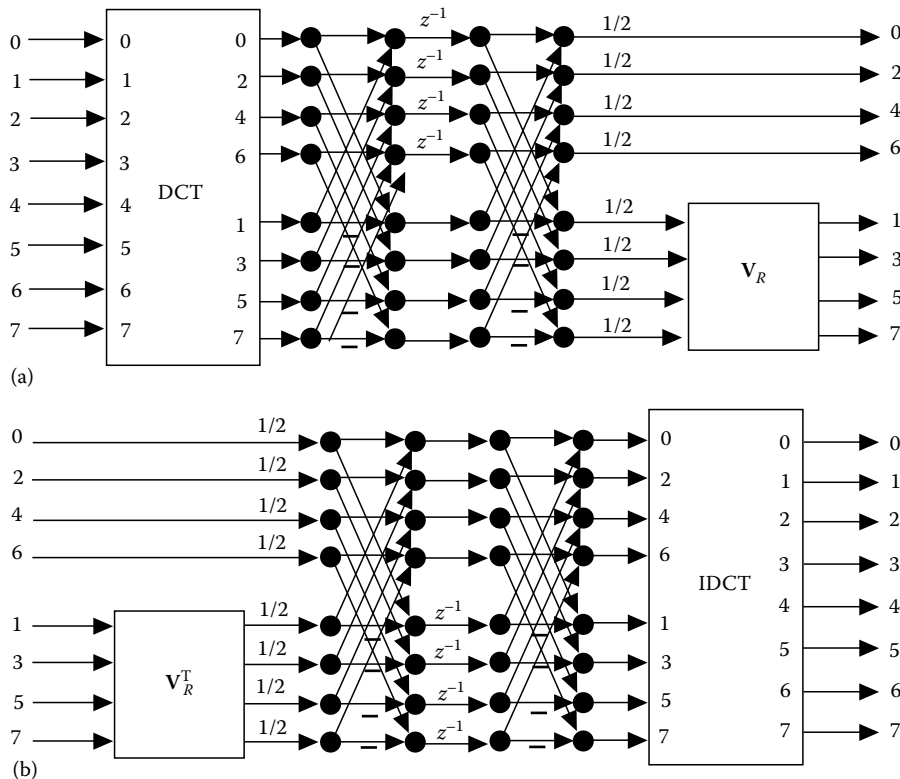
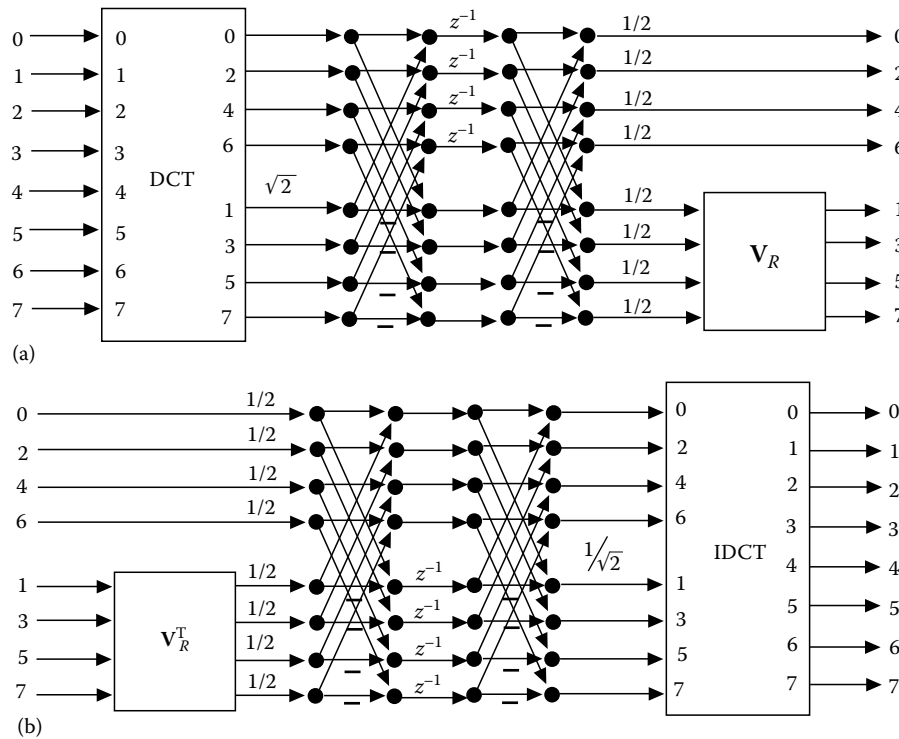


FIGURE 15.17 Implementation of the LOT for  $M=8$ . (a) Forward transform, (b) inverse transform.



**FIGURE 15.18** Implementation of the LBT for  $M=8$ . (a) forward transform, (b) inverse transform. Note that there is only one extra multiplication as compared to the LOT.

effects. Although there is a very large reduction, blocking is not eliminated. The reason for that lies in the format of the low frequency bases of LOT. In image compression, few bases are used to reconstruct the signal. From Figure 15.4, one can see that the “tails” of the lower frequency bases of the LOT do not exactly decay to zero. For that reason there is some blocking effect (Figure 15.4a) in images compressed using the LOT at lower bit rates.

To help resolve this problem, Malvar recently proposed to modify the LOT, creating the lapped biorthogonal transform (LBT).<sup>22</sup> (Biorthogonal is a jargon used in the filter banks community to designate transforms and filter banks which are not orthogonal.) In any case, the factorization of the LBT is almost identical to that of the LOT. However:

$$\mathbf{P}_{\text{LBT}} = \begin{bmatrix} \mathbf{I}_M & 0 \\ 0 & \mathbf{V}_R \end{bmatrix} \begin{bmatrix} \mathbf{D}_e - \mathbf{YD}_o & \mathbf{J}_{M/2}(\mathbf{D}_e - \mathbf{YD}_o) \\ \mathbf{D}_e - \mathbf{YD}_o & -\mathbf{J}_{M/2}(\mathbf{D}_e - \mathbf{YD}_o) \end{bmatrix} \quad (15.75)$$

where  $\mathbf{Y}$  is the  $M/2 \times M/2$  diagonal matrix given by  $\mathbf{Y} = \text{diag}\{\sqrt{2}, 1, \dots, 1\}$ . Note that it only implies that one of the DCT’s output in multiplied by a constant. The inverse is given by the LT  $\mathbf{Q}_{\text{LBT}}$  which is found in an identical manner as in Equation 15.75 except that the multiplier is inverted, i.e.,  $\mathbf{Y} = \text{diag}\{1/\sqrt{2}, 1, \dots, 1\}$ . The diagram for implementing an LBT for  $M=8$  is shown in Figure 15.18.

Because of the multiplicative factor, the LT is no longer orthogonal. However the factor is very easily inverted. The result

is a reduction of amplitude of lateral samples of the first bases of the LOT into the new bases of the forward LBT, as it can be seen in Figure 15.19. In Figure 15.19 the reader can note the reduction in the amplitude of the boundary samples of the LBT and an

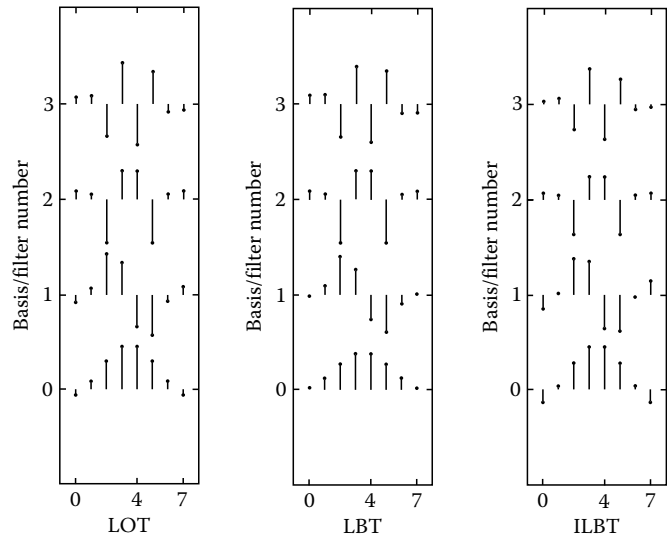


**FIGURE 15.19** Comparison of bases for the LOT ( $\mathbf{P}_{\text{LOT}}$ ), inverse LBT ( $\mathbf{Q}_{\text{LBT}}$ ) and forward LBT ( $\mathbf{P}_{\text{LBT}}$ ). The extreme samples of the lower frequency bases of the LOT are larger than those of the inverse LBT. This is an advantage for image compression.

enlargement of the same samples in the inverse LBT. This simple “trick” improved noticeably the performance of the LOT/LBT for image compression at negligible overhead. Design of the other parameters of the LOT are not changed. It is recommended to use the LBT instead of the LOT whenever a nonorthogonal LT can be used.

### 15.6.3 The Generalized LOT: GenLOT

The formulation for the LOT<sup>14</sup> which is shown in Equation 15.68, is not the most general there is for this kind of LT. In fact it can be generalized to become:

$$\mathbf{P} = \begin{bmatrix} \mathbf{U} & \mathbf{0} \\ \mathbf{0} & \mathbf{V} \end{bmatrix} \begin{bmatrix} \mathbf{D}_e - \mathbf{D}_o & \mathbf{J}_{M/2}(\mathbf{D}_e - \mathbf{D}_o) \\ \mathbf{D}_e - \mathbf{D}_o & -\mathbf{J}_{M/2}(\mathbf{D}_e - \mathbf{D}_o) \end{bmatrix}. \quad (15.76)$$

As long as  $\mathbf{U}$  and  $\mathbf{V}$  remain orthogonal matrices, the LT is orthogonal. In terms of the PTM,  $F(z)$  can be expressed similarly. Let:

$$\mathbf{W} = \frac{1}{\sqrt{2}} \begin{bmatrix} \mathbf{I}_{M/2} & \mathbf{I}_{M/2} \\ \mathbf{I}_{M/2} & -\mathbf{I}_{M/2} \end{bmatrix}, \quad (15.77)$$

$$\Phi_i = \begin{bmatrix} \mathbf{U}_i & \mathbf{0}_{M/2} \\ \mathbf{0}_{M/2} & \mathbf{V}_i \end{bmatrix}, \quad (15.78)$$

$$\Lambda(z) = \begin{bmatrix} \mathbf{I}_{M/2} & \mathbf{0}_{M/2} \\ \mathbf{0}_{M/2} & z^{-1}\mathbf{I}_{M/2} \end{bmatrix}, \quad (15.79)$$

and let  $\mathbf{D}$  bet the  $M \times M$  DCT matrix. The, for the general LOT,

$$\mathbf{F}(z) = \Phi_1 \mathbf{W} \Lambda(z) \mathbf{W} \mathbf{D}. \quad (15.80)$$

Where  $\mathbf{U}_1 = \mathbf{U}$  and  $\mathbf{V}_1 = -\mathbf{V}$ . Note that the regular LOT is the case where  $\mathbf{U}_1 = \mathbf{I}_{M/2}$  and  $\mathbf{V}_1 = -\mathbf{V}_R$ . The implementation diagram for  $M = 8$  is shown in Figure 15.20.

From this formulation along with other results it was realized<sup>34</sup> that all orthogonal symmetric LTs can be expressed as

$$\mathbf{F}(z) = \mathbf{K}_{N-1}(z) \mathbf{K}_{N-2}(z) \cdots \mathbf{K}_1(z) \mathbf{K}_0 \quad (15.81)$$

where

$$\mathbf{K}_i(z) = \Phi_i \mathbf{W} \Lambda(z) \mathbf{W}, \quad (15.82)$$

and where  $\mathbf{K}_0$  is any orthogonal symmetric matrix. The inverse is given by

$$\mathbf{G}(z) = \mathbf{K}_0^T \mathbf{K}'_1(z) \mathbf{K}'_2(z) \cdots \mathbf{K}'_{N-1}(z) \quad (15.83)$$

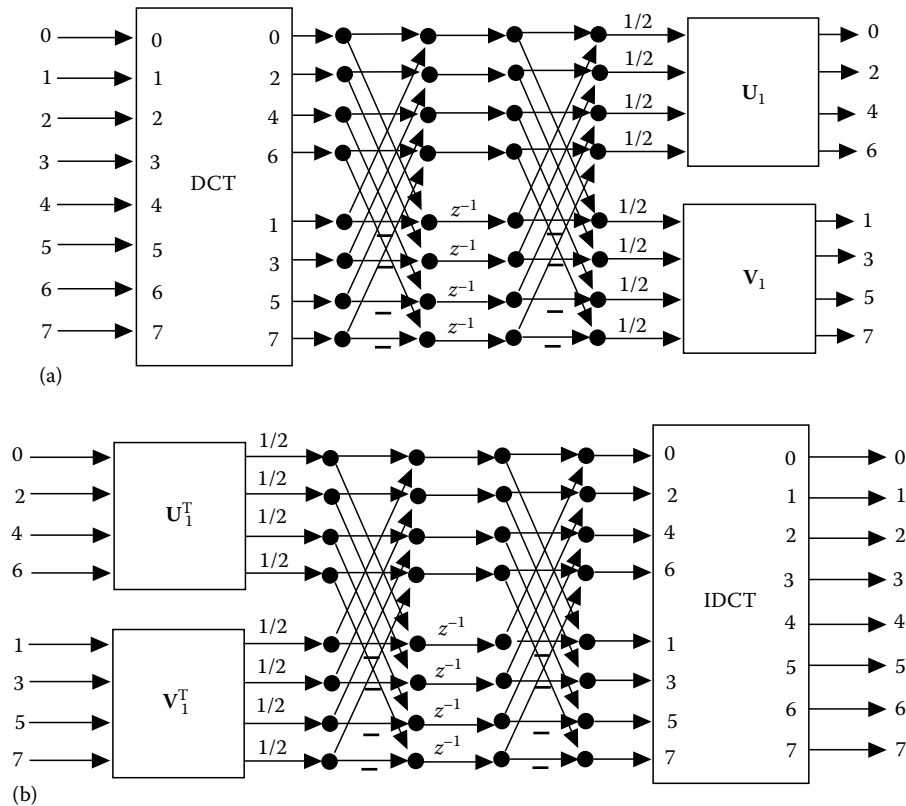


FIGURE 15.20 Implementation of a more general version of the LOT for  $M = 8$ . (a) Forward transform, (b) inverse transform.



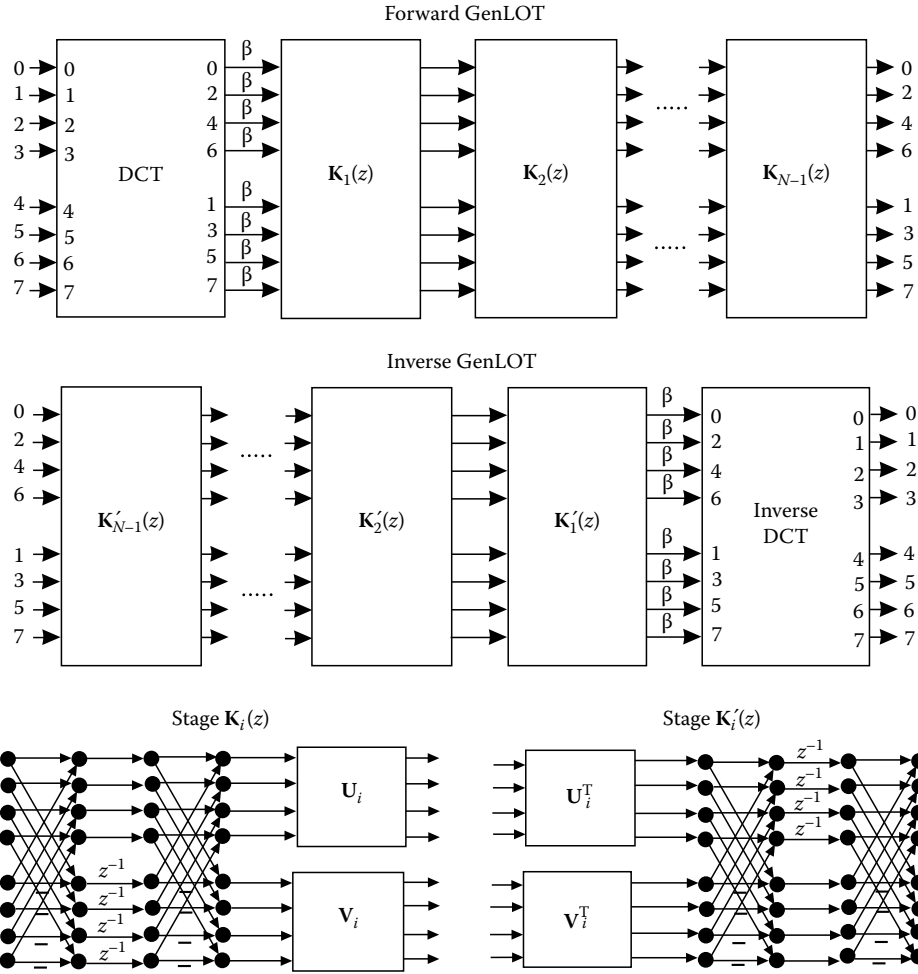


FIGURE 15.21 Implementation of a GenLOT for even  $M$ , ( $M=8$ ). Forward and inverse transforms are shown along with details of each stage.  $\beta = 2^{-(N-1)}$  accounts for all terms of the form  $1/\sqrt{2}$  which make the butterflies ( $W$ ) orthogonal.

where:

$$\mathbf{K}'_i(z) = z^{-1} \mathbf{W} \mathbf{\Lambda} (z^{-1}) \mathbf{W} \Phi_i^T. \quad (15.84)$$

From the perspective, the GenLOT is defined as the orthogonal LT as in Equation 15.81 in which  $\mathbf{K}_0 = \mathbf{D}$ , i.e.,

$$\mathbf{F}(z) = \mathbf{K}_{N-1}(z) \cdots \mathbf{K}_1(z) \mathbf{D}. \quad (15.85)$$

A diagram for implementing a GenLOT for even  $M$  is shown in Figure 15.21. In this diagram, the scaling parameters are  $\beta = 2^{-(N-1)}$  and account for the terms  $1/\sqrt{2}$  in the definition of  $\mathbf{W}$ .

The degrees of freedom of a GenLOT are the orthogonal matrices  $\mathbf{U}_i$  and  $\mathbf{V}_i$ . There are  $2(N-1)$  matrices to optimize, each of size  $M/2 \times M/2$ . From Section 15.1.4 we know that each one can be factorized into  $M(M-2)/8$  rotations. Thus, the total number of rotations is  $(L-M)(M-2)/4$ , which is less than the initial number of degrees of freedom in a symmetric  $M \times L$  matrix,  $LM/2$ . However, it is still a large number of parameters to design. In general, GenLOTs are designed through

nonlinear unconstrained optimization. Rotation angles are searched to minimize some cost function. GenLOT examples are given elsewhere<sup>34</sup> and we present two examples, for  $M=8$ , in Tables 15.1 and 15.2, which are also plotted in Figure 15.22.

In case  $M$  is odd, the GenLOT is defined as

$$\mathbf{F}(z) = \mathbf{K}_{(N-1)/2}(z) \cdots \mathbf{K}_1(z) \mathbf{D}. \quad (15.86)$$

where the stages  $\mathbf{K}_i$  have necessarily order 2 as

$$\mathbf{K}_i(z) = \Phi_{2i}^o \mathbf{W}^o \mathbf{\Lambda}^{o1}(z) \mathbf{W}^o \Phi_{2i-1}^o \mathbf{W}^o \mathbf{\Lambda}^{o2}(z) \mathbf{W}^o \quad (15.87)$$

and where:

$$\Phi_{2i}^o = \begin{bmatrix} \mathbf{U}_{2i} & 0 \\ 0 & \mathbf{V}_{2i} \end{bmatrix}, \quad (15.88)$$

$$\Phi_{2i-1}^o = \begin{bmatrix} \mathbf{U}_{2i-1} & 0 \\ 0 & 1 & \mathbf{V}_{2i-1} \end{bmatrix}, \quad (15.89)$$

TABLE 15.1 GenLot Example for  $N = 4$ 

$p_{0n}$	$p_{1n}$	$p_{2n}$	$p_{3n}$	$p_{4n}$	$p_{5n}$	$p_{6n}$	$p_{7n}$
0.004799	0.004829	0.002915	-0.002945	0.000813	-0.000109	0.000211	0.000483
0.009320	-0.000069	-0.005744	-0.010439	0.001454	0.003206	0.000390	-0.001691
0.006394	-0.005997	-0.011121	-0.010146	0.000951	0.004317	0.000232	-0.002826
-0.011794	-0.007422	-0.001800	0.009462	-0.001945	-0.001342	-0.000531	0.000028
-0.032408	-0.009604	0.008083	0.031409	-0.005262	-0.007504	-0.001326	0.003163
-0.035122	-0.016486	0.001423	0.030980	-0.005715	-0.006029	-0.001554	0.001661
-0.017066	-0.031155	-0.027246	0.003473	-0.003043	0.005418	-0.000789	-0.005605
0.000288	-0.035674	-0.043266	-0.018132	-0.000459	0.013004	-0.000165	-0.010084
-0.012735	-0.053050	0.007163	-0.083325	0.047646	0.011562	0.048534	0.043066
-0.018272	-0.090207	0.131531	0.046926	0.072761	-0.130875	-0.089467	-0.028641
0.021269	-0.054379	0.109817	0.224818	-0.224522	0.136666	0.022488	-0.025219
0.126784	0.112040	-0.123484	-0.032818	-0.035078	0.107446	0.147727	0.109817
0.261703	0.333730	-0.358887	-0.379088	0.384874	-0.378415	-0.339368	-0.216652
0.357269	0.450401	-0.292453	-0.126901	-0.129558	0.344379	0.439129	0.317070
0.383512	0.369819	0.097014	0.418643	-0.419231	0.045807	-0.371449	-0.392556
0.370002	0.140761	0.478277	0.318691	0.316307	-0.433937	0.146036	0.427668

Note: The even bases are symmetric while the odd ones are antisymmetric, so that only their first half is shown.

TABLE 15.2 GenLot Example for  $N = 6$ 

$p_{0n}$	$p_{1n}$	$p_{2n}$	$p_{3n}$	$p_{4n}$	$p_{5n}$	$p_{6n}$	$p_{7n}$
-0.000137	-0.000225	0.000234	0.000058	-0.000196	-0.000253	0.000078	0.000017
-0.000222	-0.000228	0.000388	0.000471	0.000364	0.000163	-0.000220	-0.000283
0.001021	0.000187	0.002439	0.001211	-0.000853	-0.002360	0.000157	-0.000823
0.000536	0.000689	0.000029	0.000535	0.000572	0.000056	0.000633	0.000502
-0.001855	0.000515	-0.006584	-0.002809	0.003177	0.006838	-0.000886	0.001658
0.001429	0.001778	-0.000243	0.000834	0.000977	-0.000056	0.001687	0.001429
0.001440	0.001148	0.000698	0.000383	0.000109	-0.000561	-0.000751	-0.001165
0.001056	0.001893	0.002206	0.005386	0.005220	0.001676	0.001673	0.000792
0.009734	0.002899	0.018592	0.004888	-0.006600	-0.018889	-0.000261	-0.006713
-0.005196	-0.013699	-0.008359	-0.021094	-0.020406	-0.009059	-0.012368	-0.005263
-0.000137	-0.001344	-0.027993	-0.028046	0.026048	0.024169	-0.001643	-0.000402
-0.007109	-0.002130	0.002484	0.013289	0.013063	0.002655	-0.002180	-0.006836
-0.011238	-0.002219	0.033554	0.062616	-0.058899	-0.031538	-0.001404	0.004060
-0.020287	-0.006775	0.003214	0.019082	0.018132	0.004219	-0.006828	-0.019040
-0.028214	-0.018286	-0.059401	-0.023539	0.024407	0.056646	0.009849	0.021475
-0.034379	-0.055004	-0.048827	-0.052703	-0.051123	-0.048429	-0.049853	-0.031732
-0.029911	-0.106776	0.070612	-0.088796	0.086462	-0.066383	0.097006	0.031014
-0.004282	-0.107167	0.197524	0.049701	0.051188	0.193302	-0.104953	-0.006324
0.058553	-0.026759	0.144748	0.241758	-0.239193	-0.143627	0.020370	-0.048085
0.133701	0.147804	-0.123524	0.026563	0.025910	-0.125263	0.147501	0.130959
0.231898	0.330343	-0.376982	-0.365965	0.366426	0.377886	-0.332858	-0.228016
0.318102	0.430439	-0.312564	-0.174852	-0.174803	-0.314092	0.431705	0.317994
0.381693	0.368335	0.061832	0.393949	-0.395534	-0.060887	-0.369244	-0.384842
0.417648	0.144412	0.409688	0.318912	0.319987	0.411214	0.145256	0.419936

Note: The even bases are symmetric while the odd ones are antisymmetric, so that only their first half is shown.

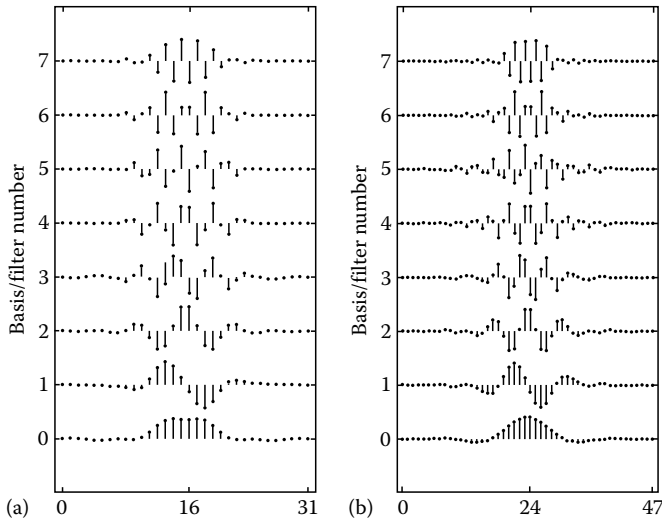


FIGURE 15.22 Example of optimized GenLOT bases for  $M = 8$  and for (a)  $N = 4$ , and (b)  $N = 6$ .

$$W^o = \begin{bmatrix} I_{(M-1)/2} & 0_{(M-1)/2 \times 1} & I_{(M-1)/2} \\ 0_{1 \times (M-1)/2} & 1 & 0_{1 \times (M-1)/2} \\ I_{(M-1)/2} & 0_{(M-1)/2 \times 1} & -I_{(M-1)/2} \end{bmatrix}, \quad (15.90)$$

$$\Lambda^{o1}(z) = \text{diag}\{ \underbrace{1, 1, \dots, 1}_{(M+1)/2 \times 1's}, \underbrace{z^{-1}, \dots, z^{-1}}_{(M-1)/2 \times z^{-1}} \}, \quad (15.91)$$

$$\Lambda^{o2}(z) = \text{diag}\{ \underbrace{1, 1, \dots, 1}_{(M-1)/2 \times 1's}, \underbrace{z^{-1}, \dots, z^{-1}}_{(M+1)/2 \times z^{-1}} \}, \quad (15.92)$$

Although it may seem that the formulation of the odd-channel case is more complex than the one for the even- $M$  case, the implementation is very similar in complexity as shown in Figure 15.23. The main difference is that two stages have to be connected together. The inverse transform is accomplished in the same way as for the even channel case:

$$G(z) = D^T K'_1(z) K'_2(z) \cdots K'_{N-1}(z) \quad (15.93)$$

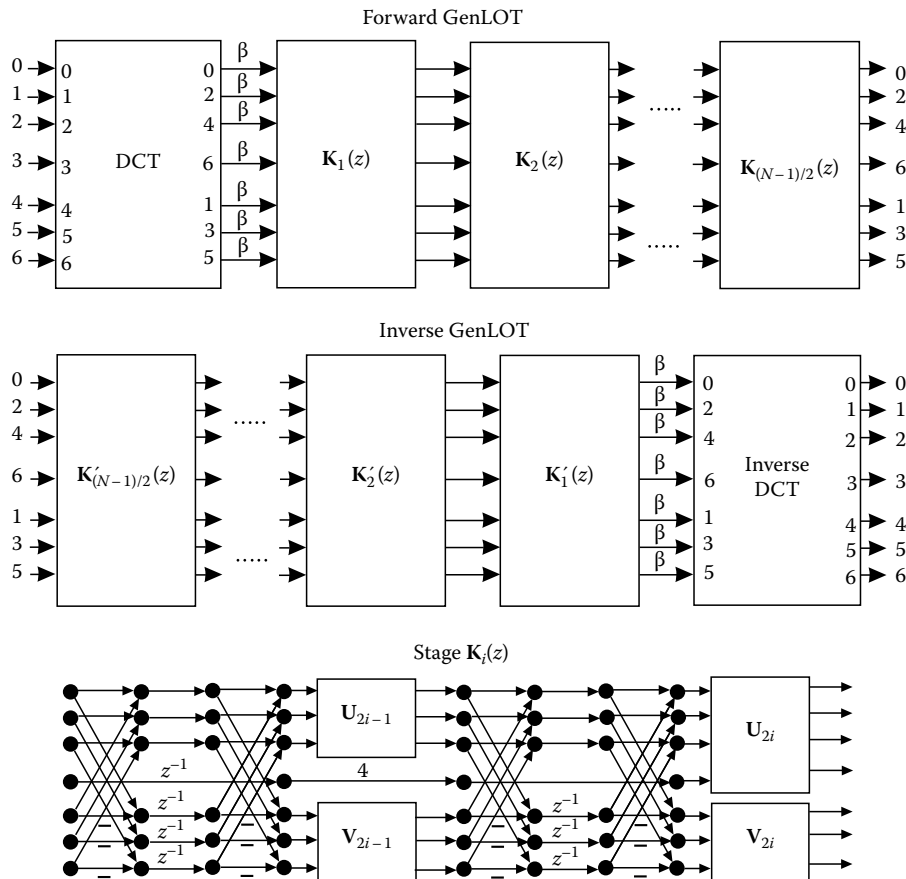


FIGURE 15.23 Implementation of a GenLOT for  $M$  odd. Forward and inverse transforms are shown along with details of each stage and  $\beta = 2^{-(N-1)}$ .

where the inverse factors are:

$$\mathbf{K}'_i(z) = z^{-2} \mathbf{K}_i^T(z^{-1}), \quad (15.94)$$

whose structure is evident from Figure 15.23.

### 15.6.4 The General Factorization: GLBT

The general factorization for all symmetric LTs<sup>49</sup> can be viewed either as an extension of GenLOTs or as a generalization of the LBT. It can be shown that for  $M$  even, all LTs obeying Equation 15.65 or Equation 15.66 can be factorized as in Equation 15.81, where the  $\mathbf{K}_i(z)$  factors are given in Equation 15.82 with the matrices  $\mathbf{U}_i$  and  $\mathbf{V}_i$  (which compose  $\Phi_i$ ) being only required to be general invertible matrices. From Section 15.1.4, each factor can be decomposed as

$$\mathbf{U}_i = \mathbf{U}_{iB} \mathbf{U}_{id} \mathbf{U}_{iA}, \quad \mathbf{V}_i = \mathbf{V}_{iB} \mathbf{V}_{id} \mathbf{V}_{iA}, \quad (15.95)$$

where  $\mathbf{U}_{iA}$ ,  $\mathbf{U}_{iB}$ ,  $\mathbf{V}_{iA}$ , and  $\mathbf{V}_{iB}$  are general  $M/2 \times M/2$  orthogonal matrices, while  $\mathbf{U}_{id}$  and  $\mathbf{V}_{id}$  are diagonal matrices with nonzero diagonal entries.

The first factor  $\mathbf{K}_0$  is given by

$$\mathbf{K}_0 = \Phi_0 \mathbf{W}, \quad (15.96)$$

where  $\Phi_i$  is given as in Equation 15.78, and factors  $\mathbf{U}_0$  and  $\mathbf{V}_0$  are only required to be invertible. The general factorization can be viewed as a generalized LBT (GLBT) and its implementation flow graph for  $M$  even is shown in Figure 15.24.

The inverse GLBT is similar to the GenLOT case, where:

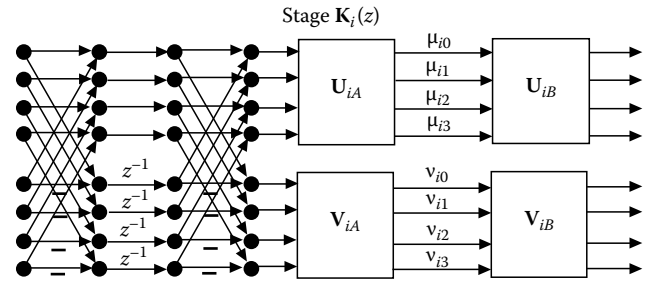
$$\mathbf{K}'_i(z) = z^{-1} \mathbf{W} \Lambda(z) \mathbf{W} \Phi_i^{-1}. \quad (15.97)$$

and

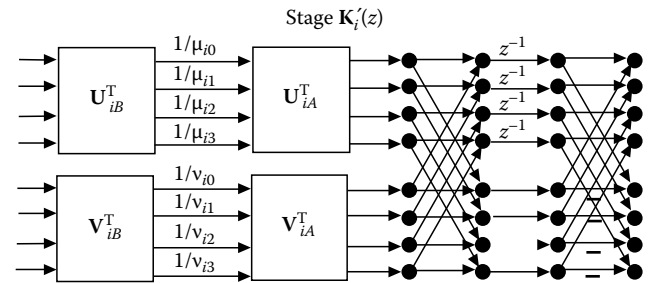
$$\Phi_i^{-1} = \begin{bmatrix} \mathbf{U}_i^{-1} & \mathbf{0}_{M/2} \\ \mathbf{0}_{M/2} & \mathbf{V}_i^{-1} \end{bmatrix} = \begin{bmatrix} \mathbf{U}_{iA}^T \mathbf{U}_{id}^{-1} \mathbf{U}_{iB}^T & \mathbf{0}_{M/2} \\ \mathbf{0}_{M/2} & \mathbf{V}_{iA}^T \mathbf{V}_{id}^{-1} \mathbf{V}_{iB}^T \end{bmatrix} \quad (15.98)$$

while

$$\mathbf{K}_0^{-1} = \mathbf{W} \Phi_0^{-1}. \quad (15.99)$$



(a)



(b)

**FIGURE 15.24** Implementation of the factors of the general factorization (GLBT) for  $M$  even. (a) factor of the forward transform:  $\mathbf{K}_i(z)$ . (b) factor of the inverse transform:  $\mathbf{K}'_i(z)$ .

The diagram for the implementation of the inverse stages of the GLBT is shown in Figure 15.24.

Examples of bases for the GLBT of particular interest to image compression are given in Tables 15.3 and 15.4.

For the odd case, the GLBT can be similarly defined. It follows the GenLOT factorization:

$$\mathbf{F}(z) = \mathbf{K}_{(N-1)/2}(z) \cdots \mathbf{K}_1(z) \mathbf{K}_0 \quad (15.100)$$

where the stages  $\mathbf{K}_i$  are as in Equation 15.87 with the following differences: (1) all factors  $\mathbf{U}_i$  and  $\mathbf{V}_i$  are only required to be invertible; (2) the center element of  $\Phi_{2i-1}$  is a nonzero constant  $u_0$  and not 1. Again  $\mathbf{K}_0$  is a symmetric invertible matrix. Forward and inverse stages for the odd-channel case are illustrated in Figure 15.25.

**TABLE 15.3** Forward GLBT Bases Example for  $M=8$  and  $N=2$

$p_{0n}$	$p_{1n}$	$p_{2n}$	$p_{3n}$	$p_{4n}$	$p_{5n}$	$p_{6n}$	$p_{7n}$
-0.21192	-0.18197	0.00011	-0.09426	0.03860	-0.03493	0.04997	0.01956
-0.13962	-0.19662	0.16037	0.05334	0.09233	0.12468	-0.09240	-0.03134
-0.03387	-0.09540	0.17973	0.25598	-0.24358	-0.12311	0.01067	-0.01991
0.09360	0.10868	-0.06347	-0.01332	-0.05613	-0.10218	0.16423	0.11627
0.23114	0.34101	-0.36293	-0.39498	0.42912	0.36084	-0.35631	-0.22434
0.35832	0.46362	-0.35056	-0.16415	-0.13163	-0.31280	0.47723	0.31907
0.46619	0.42906	0.00731	0.42662	-0.45465	-0.07434	-0.40585	-0.38322
0.53813	0.22604	0.42944	0.36070	0.32595	0.43222	0.15246	0.39834

Note: The even bases are symmetric while the odd ones are antisymmetric, so that only their first half is shown.

TABLE 15.4 Inverse GLBT Bases Example for  $M=8$  and  $N=2$

$p_{0n}$	$p_{1n}$	$p_{2n}$	$p_{3n}$	$p_{4n}$	$p_{5n}$	$p_{6n}$	$p_{7n}$
0.01786	-0.01441	0.06132	0.01952	0.05243	0.05341	0.04608	0.08332
0.05692	-0.01681	0.16037	0.12407	0.04888	0.16065	-0.09042	-0.02194
0.10665	0.06575	0.12462	0.24092	-0.21793	-0.13556	0.02108	-0.00021
0.16256	0.20555	-0.12304	-0.03560	-0.02181	-0.08432	0.13397	0.12747
0.22148	0.34661	-0.38107	-0.35547	0.36530	0.39610	-0.30170	-0.23278
0.27739	0.40526	-0.32843	-0.12298	-0.12623	-0.35462	0.41231	0.34133
0.32711	0.33120	0.03939	0.38507	-0.38248	-0.08361	-0.35155	-0.40906
0.36617	0.13190	0.44324	0.30000	0.28191	0.45455	0.13232	0.41414

Note: The even bases are symmetric while the odd ones are antisymmetric, so that only their first half is shown.

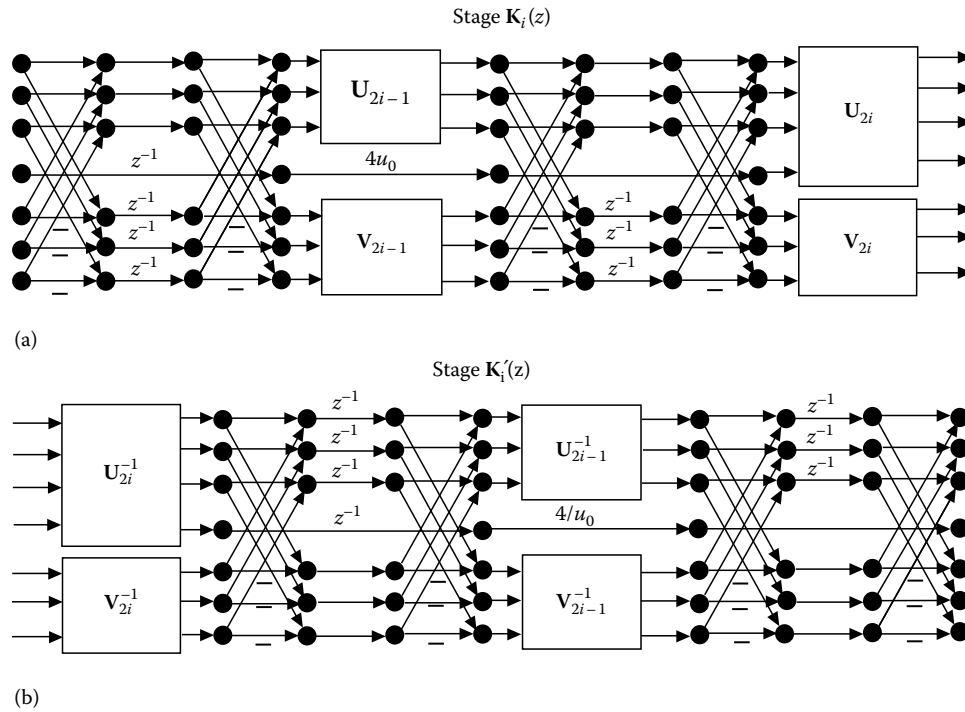


FIGURE 15.25 Implementation of the factors of the general factorization (GLBT) for  $M$  odd. (a) factor of the forward transform:  $K_i(z)$ . (b) factor of the inverse transform:  $K'_i(z)$ .

### 15.7 The Fast Lapped Transform: FLT

The motivation behind the fast lapped transform (FLT) is to design an LT with minimum possible complexity compared to a block transform and, yet, to provide some advantage over a block transform. For that we use the principles of Section 15.5.3 and define the FLT as the LT whose PTM is given by

$$F(z) = \begin{bmatrix} E(z) & 0 \\ 0 & I_{M-K} \end{bmatrix} D_M \quad (15.101)$$

where  $E(z)$  is a  $K \times K$  PTM and  $D_M$  is the  $M \times M$  DCT matrix. The PTM for the inverse LT is given by

$$G(z) = D_M^T \begin{bmatrix} E'(z) & 0 \\ 0 & I_{M-N} \end{bmatrix}, \quad (15.102)$$

where  $E'(z)$  is the inverse of  $E(z)$ .

The design of  $E(z)$  can be done in two basic ways. Firstly, one can use direct optimization. Secondly, one can design  $E(z)$  as

$$E(z) = \Psi(z) D_K^T \quad (15.103)$$

where  $\Psi(z)$  is a known LT and  $D_K$  is the  $K \times K$  DCT matrix, i.e., we perform an inverse DCT followed by a known LT. For example, if  $\Psi(z)$  is the LOT, GenLOT, or LBT, of  $K$  channels, the first stage ( $D_K$ ) cancels the inverse DCT. Examples of FLT are

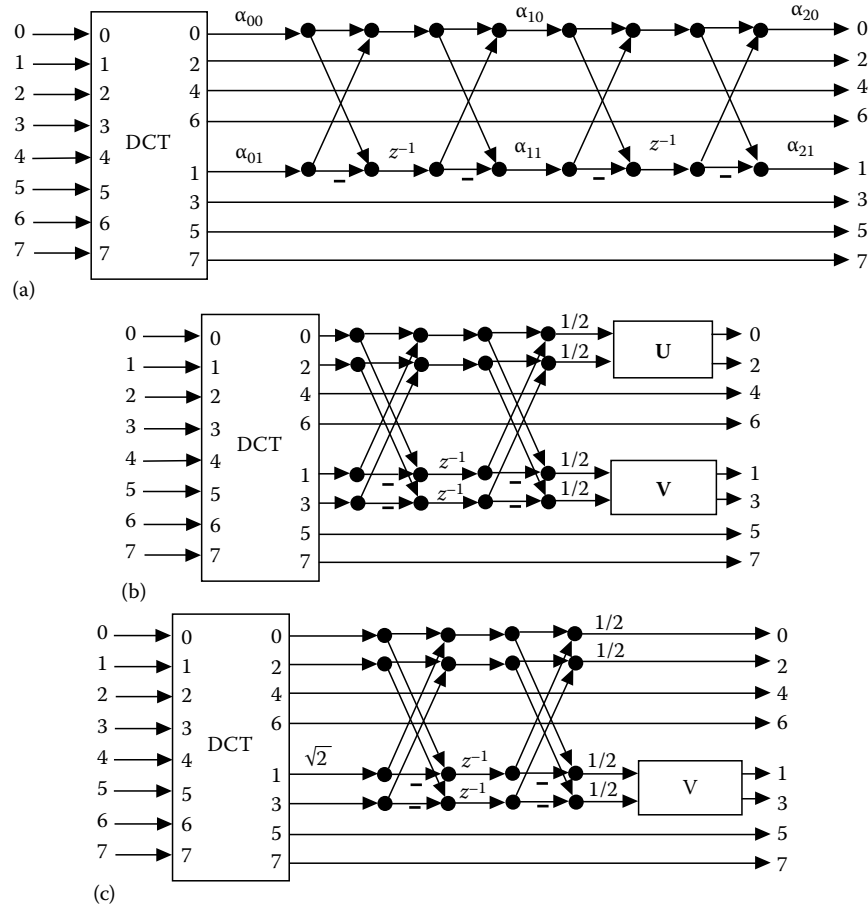


FIGURE 15.26 Implementation of examples of the FLT. On (a),  $K = 2$ ; (b), case  $K = 4$ ; (c), case  $K = 4$  where  $\Psi(z)$  is the LBT, thus having its DCT stage cancelled.

given in Figure 15.26. In that example, the first case where  $K = 2$ , direct optimization is recommended, for which the values  $\{\alpha_{00}, \alpha_{01}, \alpha_{10}, \alpha_{20}, \alpha_{21}\} = \{1.9965, 1.3193, 0.4388, 0.7136, 0.9385, 1.2878\}$  yield an excellent FLT for image compression. Figure 15.26b the case  $K = 4$  can be optimized by optimizing two invertible matrices. In the case where we use the method in Equation 15.103 and the LBT as the  $K$  channel postprocessing stage, we can see that the LBT's DCT stage is cancelled yielding a very simple flow-graph. The respective bases for forward and inverse transforms for the two FLTs ( $K = 2$  with the given parameters, and  $K = 4$  using the LBT) are shown in Figure 15.27. Both bases are excellent for image coding, virtually eliminating ringing, despite the minimal complexity added to the DCT (which by itself can be implemented in a very fast manner).<sup>38</sup>

### 15.8 Modulated LTs

Cosine modulated LTs<sup>50</sup> use a low-pass prototype to modulate a cosine sequence. By a proper choice of the phase of the cosine sequence, Malvar developed the modulated lapped transform (MLT),<sup>15</sup> which led to the so-called ELT.<sup>18-21</sup> The ELT allows several overlapping factors, generating a family of

orthogonal cosine modulated LTs. Both designations (MLT and ELT) are frequently applied to this class of filter banks. Other cosine-modulation approaches have also been developed and the most significant difference among them is the low-pass prototype choice and the phase of the cosine sequence.<sup>11,15,19,20,24,27,40,44,45,49</sup>

In the ELTs, the filters' length  $L$  is basically an even multiple of the block size  $M$ , as  $L = NM = 2KM$ . Thus,  $K$  is referred to as the overlap factor of the ELT. The MLT-ELT class is defined by

$$p_{k,n} = h(n) \cos \left[ \left( k + \frac{1}{2} \right) \left( \left( n - \frac{L-1}{2} \right) \frac{\pi}{M} + (N+1) \frac{\pi}{2} \right) \right] \tag{15.104}$$

for  $k = 0, 1, \dots, M-1$  and  $n = 0, 1, \dots, L-1$ .  $h(n)$  is a symmetric window modulating the cosine sequence and the impulse response of a low-pass prototype (with cutoff frequency at  $\pi/2M$ ) which is translated in frequency to  $M$  different frequency slots in order to construct the LT. A very useful ELT is the one with  $K = 2$ , which will be designated as ELT-2, while ELTs with other values of  $K$  will be referred as ELT- $K$ .

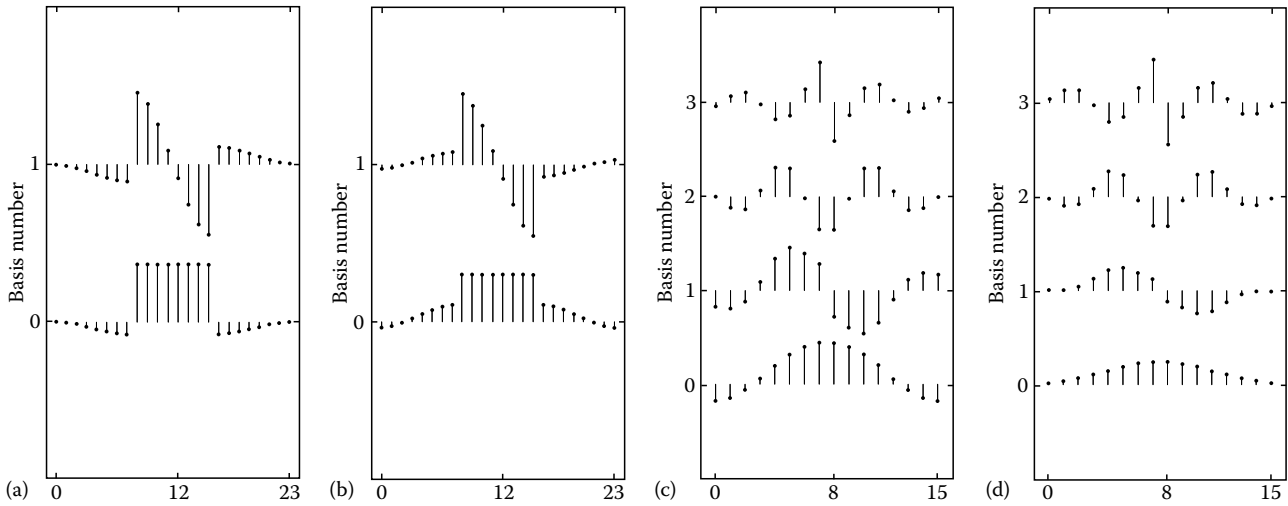


FIGURE 15.27 Bases of the FLT in the case  $M = 8$  for forward and inverse LTs. (a-d) Forward transform bases for the case  $K = 2$ , inverse transform bases for the case  $K = 2$ , forward transform bases for the case  $K = 4$ , inverse transform bases for the case  $K = 4$ . The remaining bases, not shown are the regular bases of the DCT and have length 8.

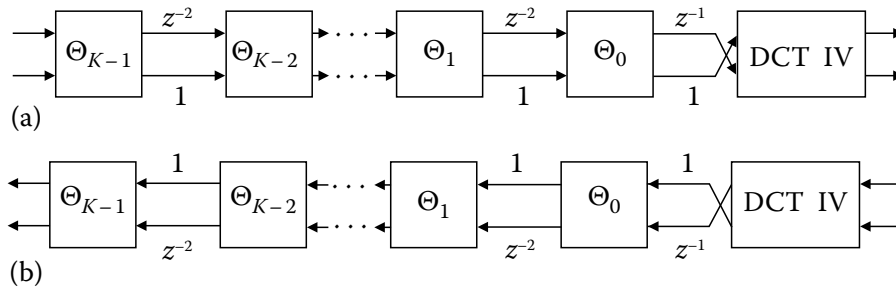


FIGURE 15.28 Flow graph for the direct (a) and inverse (b) ELT. Each branch carries  $M/2$  samples.

The ELTs have as their major plus a fast implementation algorithm. The algorithm is based on a factorization of the PTM into a series of plane rotation stages and delays and a DCT type IV<sup>38</sup> orthogonal transform in the last stage, which has fast implementation algorithms. The lattice-style algorithm is shown in Figure 15.28 for an ELT with generic overlap factor  $K$ . In Figure 15.28 each branch carries  $M/2$  samples and both analysis (forward transform) and synthesis (inverse transform) flow-graphs are shown. The plane rotation stages are of the form indicated in Figure 15.29 and contain  $M/2$  orthogonal butterflies to implement the  $M/2$  plane rotations. The stages  $\Theta_i$  contain the plane rotations and are defined by

$$\Theta_i = \begin{bmatrix} -C_i & S_i J_{M/2} \\ J_{M/2} S_i & J_{M/2} C_i J_{M/2} \end{bmatrix}, \quad (15.105)$$

$$C_i = \text{diag}\{\cos(\theta_{0,i}), \cos(\theta_{1,i}), \dots, \cos(\theta_{\frac{M}{2}-1,i})\}$$

$$S_i = \text{diag}\{\sin(\theta_{0,i}), \sin(\theta_{1,i}), \dots, \sin(\theta_{\frac{M}{2}-1,i})\}.$$

$\theta_{i,j}$  are rotation angles. These angles are the free parameters in the design of an ELT because they define the modulating window  $h(n)$ . Note that there are  $KM$  angles, while  $h(n)$  has

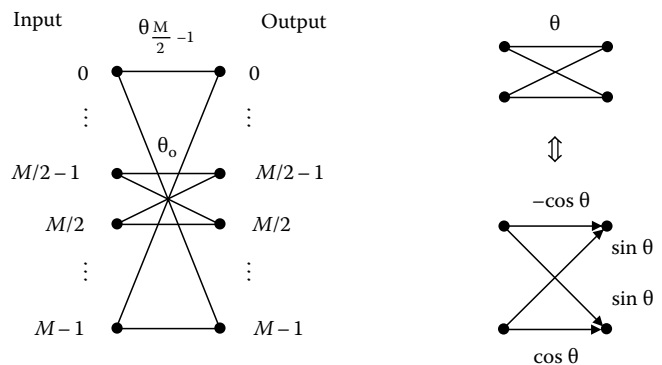


FIGURE 15.29 Implementation of plane rotations stage showing the displacement of the  $M/2$  butterflies.

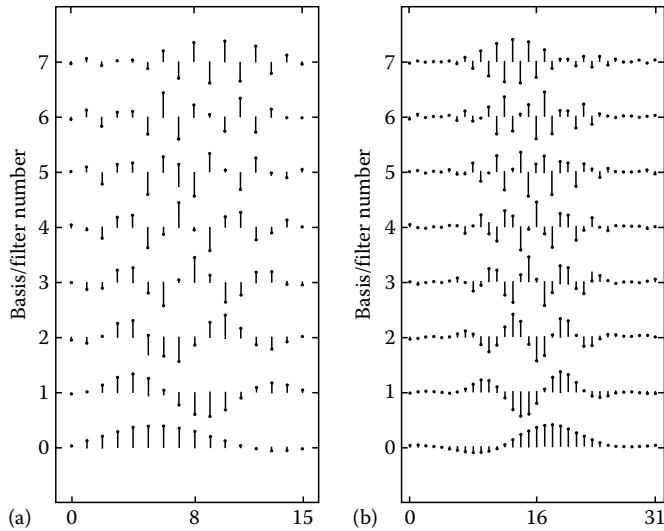


FIGURE 15.30 Example of ELT bases for the given angles design method for  $M=8$ . (a)  $K=1, N=2$ , (b)  $K=2, N=4$ .

$2KM$  samples, however,  $h(n)$  is symmetric and brings the total number of degrees of freedom to  $KM$ .

In general, there is no simple relation among the rotation angles and the window. Optimized angles for several values of  $M$  and  $K$  are presented in extensive tables in Ref. [21]. In the ELT-2 case, however, one can use a parameterized design.<sup>19-21</sup> In this design, we have

$$\theta_{k,0} = -\frac{\pi}{2} + \mu_{M/2+k} \quad (15.106)$$

$$\theta_{k,1} = -\frac{\pi}{2} + \mu_{M/2-1-k} \quad (15.107)$$

where

$$\mu_i = \left[ \left( \frac{1-\gamma}{2M} \right) (2k+1) + \gamma \right] \quad (15.108)$$

and  $\gamma$  is a control parameter, for  $0 \leq k \leq (M/2) - 1$ . In general, although suboptimal for individual applications,  $\gamma = 0.5$  provides a balanced trade-off of stopband attenuation and transition range for the equivalent filters (which are the bases of the LT viewed as a filter bank). The equivalent modulating window  $h(n)$  is related to the angles as

$$\begin{aligned} h(n) &= \cos(\theta_{n0}) \cos(\theta_{n1}) \\ h(M-1-n) &= \cos(\theta_{n0}) \sin(\theta_{n1}) \\ h(M+n) &= \sin(\theta_{n0}) \cos(\theta_{n1}) \\ h(2M-1-n) &= -\sin(\theta_{n0}) \sin(\theta_{n1}) \end{aligned} \quad (15.109)$$

for  $0 \leq n \leq (M/2) - 1$ . In the case  $K=1$ , some example angles are

$$\theta_{k,0} = \frac{\pi}{2} - \frac{\pi}{2M} \left( k + \frac{1}{2} \right) \quad (15.110)$$

for  $0 \leq k \leq (M/2) - 1$ . The corresponding modulating window  $h(n)$  is

$$\begin{aligned} h(n) &= h(2M-1-n) = -\cos(\theta_{n0}) \\ h(M+n) &= h(M-1-n) = -\sin(\theta_{n0}) \end{aligned} \quad (15.111)$$

for  $0 \leq n \leq (M/2) - 1$ . The bases for the ELT using the suggested angles are shown in Figure 15.30. In this figure, the 8-channel examples are for  $N=2$  ( $K=1$ ) and for  $N=4$  ( $K=2$ ).

## 15.9 Finite-Length Signals

Since the LT matrices are not square, in order to obtain  $n$  transformed subband samples one has to evaluate more than  $n$  samples of the input signal. For the same reason,  $n$  subband samples would generate more than  $n$  signals samples after inverse transformation. All the analysis so far has assumed infinite-length signals. Processing finite-length signals, however, is not trivial. Without proper consideration there will be a distortion in the reconstruction of the boundary samples of the signal. There are basically three methods to process finite-length signals with LTs:

- Signal extension and windowing of subband coefficients
- Same as above but using different extensions for different bases
- Using time-varying bases for the boundary regions

We will discuss the first method only. The second is just applicable to few transforms and filter banks and can be covered elsewhere. The subject of time-varying LTs is very rich and provides for solutions to several problems including the processing of boundary samples. We will not cover it in this chapter. The reader is referred to Refs. [7,28,29,32,41] and their references for further information on time-varying LTs.

### 15.9.1 Overall Transform

Here we assume the model of extension and windowing described in Figure 15.31.<sup>33</sup> The input vector  $x$  is assumed to have  $N_x = N_B M$  samples and is divided into three sections:  $x^T = [x_l^T, x_c^T, x_r^T]$ , where  $x_l$  and  $x_r$  contain the first and last  $\lambda$  samples of  $x$ , respectively. Following the signal extension model,  $x$  is extended into  $\tilde{x}$  as

$$\tilde{x}^T = [x_{e,l}^T, x_c^T, x_{e,r}^T] = [(\mathbf{R}_l x_l)^T, x_c^T, (\mathbf{R}_r x_r)^T]. \quad (15.112)$$

The extended sections are found by a linear transform of the boundary samples of  $x$  as shown in Figure 15.32, i.e.,

$$x_{e,l} = \mathbf{R}_l x_l, \quad x_{e,r} = \mathbf{R}_r x_r \quad (15.113)$$



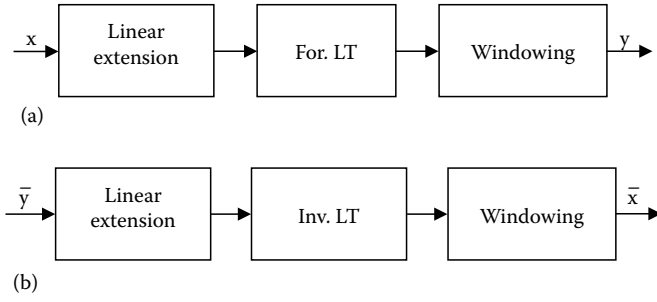


FIGURE 15.31 Extension and windowing in transformation of a finite-length signal using LTs. (a) Overall forward transform section. (b) Overall inverse transform section.

Note that there are  $N_B$  block rows and that  $\lambda = (N - 1)M/2$ . The difference between  $\tilde{\mathbf{P}}$  and  $\mathbf{H}$  defined in Equation 15.21 is that  $\mathbf{H}$  is assumed to be infinite and  $\tilde{\mathbf{P}}$  is assumed to have only  $N_B$  block rows. We can use the same notation for  $\tilde{\mathbf{Q}}$  with respect to  $Q_i$ , so that, again, the difference between  $\tilde{\mathbf{Q}}$  and  $\mathbf{H}'$  defined in Equation 15.32 is that  $\mathbf{H}'$  is assumed to be infinite and  $\tilde{\mathbf{Q}}$  is assumed to have only  $N_B$  block rows. The forward and inverse transform systems are given by

$$\tilde{\mathbf{y}} = \tilde{\mathbf{P}}\tilde{\mathbf{x}}, \quad \tilde{\mathbf{x}} = \tilde{\mathbf{Q}}^T\tilde{\mathbf{y}}. \quad (15.115)$$

In the absence of quantization or processing of the subband signals, then  $\tilde{\mathbf{y}} = \mathbf{y}$  and

$$\tilde{\mathbf{x}} = \tilde{\mathbf{Q}}^T\tilde{\mathbf{y}} = \tilde{\mathbf{Q}}^T\tilde{\mathbf{P}}\tilde{\mathbf{x}} = \tilde{\mathbf{T}}\tilde{\mathbf{x}} \quad (15.116)$$

where  $\tilde{\mathbf{x}}$  is the reconstructed vector in the absence of quantization and  $\tilde{\mathbf{T}} = \tilde{\mathbf{Q}}^T\tilde{\mathbf{P}}$  is the transform matrix between  $\tilde{\mathbf{x}}$  and  $\tilde{\mathbf{x}}$ . Note that  $\tilde{\mathbf{T}}$  has size  $(N_x + \lambda) \times (N_x + \lambda)$  because it maps two extended signals. From Equation 15.35 we can easily show that the transform matrix is

$$\tilde{\mathbf{T}} = \tilde{\mathbf{Q}}^T\tilde{\mathbf{P}} = \begin{bmatrix} \mathbf{T}_L & & 0 \\ & \mathbf{I}_{N_x-2\lambda} & \\ 0 & & \mathbf{T}_R \end{bmatrix} \quad (15.117)$$

where  $\mathbf{T}_L$  and  $\mathbf{T}_R$  are some  $2\lambda \times 2\lambda$  matrices. Thus, distortion is just incurred to the  $\lambda$  boundary samples in each side of  $\mathbf{x}$  ( $2\lambda$  samples in each side of  $\tilde{\mathbf{x}}$ ).

In another view of the process, regardless of the extension method, there is a transform  $\mathbf{T}$  such that

$$\mathbf{y} = \mathbf{T}\mathbf{x}, \quad \tilde{\mathbf{x}} = \mathbf{T}^{-1}\tilde{\mathbf{y}} \quad (15.118)$$

without resorting to signal extension. The key is to find  $\mathbf{T}$  and to invert it. If  $\mathbf{T}$  is made orthogonal one can easily invert it by applying transposition. This is the concept behind the use of time-varying LTs for correcting boundary distortions. For example, the LT can be changed near the borders to ensure  $\mathbf{T}$ 's orthogonality.<sup>32</sup> We will not use time-varying LTs here but rather use extended signals and transform matrices.

### 15.9.2 Recovering Distorted Samples

Let:

$$[\Phi_l | \Phi_r] = \begin{bmatrix} \mathbf{P}_0 & \mathbf{P}_1 & \cdots & \mathbf{P}_{N-2} & \mathbf{P}_{N-1} & & & 0 \\ & \mathbf{P}_0 & \mathbf{P}_1 & \cdots & \mathbf{P}_{N-2} & \mathbf{P}_{N-1} & & \\ & & \ddots & \ddots & \ddots & \ddots & \ddots & \\ 0 & & & \mathbf{P}_0 & \mathbf{P}_1 & \cdots & \mathbf{P}_{N-2} & \mathbf{P}_{N-1} \end{bmatrix}, \quad (15.119)$$

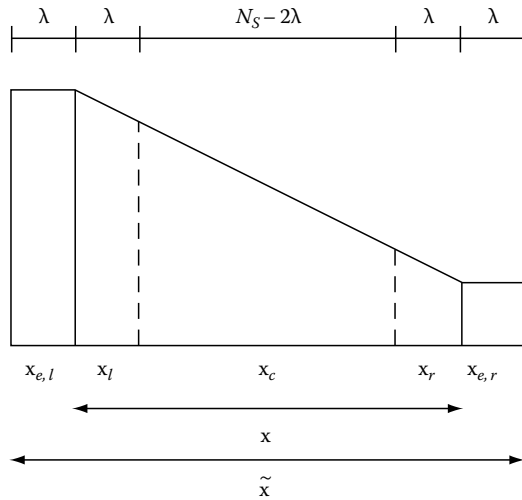


FIGURE 15.32 Illustration of signal extension of vector  $\mathbf{x}$  into vector  $\tilde{\mathbf{x}}$ . In each border,  $\lambda = (L - M)/2$  samples outside initial signal boundaries are found by linear relations applied to the  $\lambda$  boundary samples of  $\mathbf{x}$ , i.e.,  $x_{e,l} = \mathbf{R}_l x_l$  and  $x_{e,r} = \mathbf{R}_r x_r$ . As only  $\lambda$  samples are affected across the signal boundaries, it is not necessary to use an infinite-length extension. Also,  $x_l$  and  $x_r$  contain the samples possibly affected by the border distortions after the inverse transformation.

and  $\mathbf{R}_l$  and  $\mathbf{R}_r$  are arbitrary  $\lambda \times \lambda$  “extension” matrices. For example,  $\mathbf{R}_l = \mathbf{R}_r = \mathbf{J}_\lambda$  yields a symmetric extension.

The transformation from the  $N_x + 2\lambda$  samples in  $\tilde{\mathbf{x}}$  to vector  $\mathbf{y}$  with  $N_B M = N_x$  subband samples is achieved through the block-banded matrix  $\tilde{\mathbf{P}}$ , i.e.,

$$\tilde{\mathbf{P}} = \begin{pmatrix} \ddots & & & & & & & & & 0 \\ & \mathbf{P}_0 & \mathbf{P}_1 & \cdots & \mathbf{P}_{N-1} & & & & & \\ & & \mathbf{P}_0 & \mathbf{P}_1 & \cdots & \mathbf{P}_{N-1} & & & & \\ & & & \mathbf{P}_0 & \mathbf{P}_1 & \cdots & \mathbf{P}_{N-1} & & & \\ 0 & & & & & \ddots & & & & \\ & & & & & & & \ddots & & \end{pmatrix}. \quad (15.114)$$

$$[\Psi_l | \Psi_r] = \begin{bmatrix} \mathbf{Q}_0 & \mathbf{Q}_1 & \cdots & \mathbf{Q}_{N-2} & \mathbf{Q}_{N-1} & & & & 0 \\ & \mathbf{Q}_0 & \mathbf{Q}_1 & \cdots & \mathbf{Q}_{N-2} & \mathbf{Q}_{N-1} & & & \\ & & \ddots & \ddots & \ddots & \ddots & \ddots & & \\ 0 & & & \mathbf{Q}_0 & \mathbf{Q}_1 & \cdots & \mathbf{Q}_{N-2} & \mathbf{Q}_{N-1} & \end{bmatrix}. \quad (15.120)$$

Hence,

$$\mathbf{T}_l = \Psi_l^T \Phi_l, \quad \mathbf{T}_r = \Psi_r^T \Phi_r. \quad (15.121)$$

If we divide  $\bar{\bar{x}}$  in the same manner as  $\bar{x}$ ,

$$\bar{\bar{x}} = [\bar{x}_{e,l}^T, \bar{x}_l^T, \bar{x}_c^T, \bar{x}_r^T, \bar{x}_{e,r}^T], \quad (15.122)$$

then,

$$\begin{bmatrix} \bar{x}_{e,l} \\ \bar{x}_l \end{bmatrix} = \mathbf{T}_l \begin{bmatrix} x_{e,l} \\ x_l \end{bmatrix} = T_l \begin{bmatrix} \mathbf{R}_l x_l \\ x_l \end{bmatrix} = \mathbf{T}_l \begin{bmatrix} \mathbf{R}_l \\ \mathbf{I}_\lambda \end{bmatrix} x_l = \Gamma_l x_l \quad (15.123)$$

where

$$\Gamma_l = \mathbf{T}_l \begin{bmatrix} \mathbf{R}_l \\ \mathbf{I}_\lambda \end{bmatrix} \quad (15.124)$$

is a  $2\lambda \times \lambda$  matrix. If and only if  $\Gamma_l$  has rank  $\lambda$ , then  $x_l$  can be recovered through the pseudo-inverse of  $\Gamma_l$  as

$$x_l = \Gamma_l^+ \begin{bmatrix} \bar{x}_{e,l} \\ \bar{x}_l \end{bmatrix} = (\Gamma_l^T \Gamma_l)^{-1} \Gamma_l^T \begin{bmatrix} \bar{x}_{e,l} \\ \bar{x}_l \end{bmatrix}. \quad (15.125)$$

For the other ("right") border the identical result is trivially found to be

$$x_r = \Gamma_r^+ \begin{bmatrix} \bar{x}_r \\ \bar{x}_{e,r} \end{bmatrix} = (\Gamma_r^T \Gamma_r)^{-1} \Gamma_r^T \begin{bmatrix} \bar{x}_r \\ \bar{x}_{e,r} \end{bmatrix}, \quad (15.126)$$

where

$$\Gamma_r = \mathbf{T}_r \begin{bmatrix} \mathbf{I}_\lambda \\ \mathbf{R}_r \end{bmatrix} \quad (15.127)$$

is also assumed to have rank  $\lambda$ . It is necessary that  $\Phi_b$ ,  $\Phi_r$ ,  $\Psi_l$  and  $\Psi_r$  have rank  $\lambda$ , but not sufficient since rank can be reduced by the matrix products. It is also possible to express in more detail the conditions but without any useful analytical solution, so that numerical rank checking is the best choice.

Summarizing, the steps to achieve PR for given  $\mathbf{R}_l$  and  $\mathbf{R}_r$  are:

- Select P and Q and identify their submatrices  $\mathbf{P}_i$  and  $\mathbf{Q}_i$
- Find  $\Phi_b$ ,  $\Phi_r$ ,  $\Psi_b$ ,  $\Psi_r$  from Equations 15.119 and 15.120
- Find  $\mathbf{T}_l$  and  $\mathbf{T}_r$  from Equation 15.121
- Find  $\Gamma_l$  and  $\Gamma_r$  from Equations 15.124 and 15.127
- Test rank of  $\Gamma_l$  and  $\Gamma_r$
- If ranks are  $\lambda$ , obtain  $\Gamma_l^+$ ,  $\Gamma_r^+$  and reconstruct  $x_l$  and  $x_r$

This is an extension of Ref. [33] to nonorthogonal LTs, with the particular concern to test whether the pseudo inverses exist.

The model in Figure 15.31 and the proposed method are not applicable for some LTs. The notable classes of LTs include those LTs whose bases have different length and different symmetries. Examples are: (1) some two-channel nonorthogonal LTs with odd-length; (2) the FLT; (3) other composite systems, i.e., cascaded systems such as those used in Refs. [35,36]. For the first example, it is trivial to use symmetric extensions, but different symmetries for different bases.<sup>44</sup> The second example has the same reasoning, however an FLT can be efficiently implemented by applying the method just described to each of the stages of the transformation (i.e., first apply the DCT and then use the method above for the second part). The reason for problems is that different filters would require different extensions during the forward transformation process, therefore, the model in Figure 15.31 is not applicable.

The above method works very well for  $M$ -channel filter banks whose filters have same length. The phase of the filters and the extensions can be arbitrary, and the method has been shown to be consistent for all uniform-length filter banks of interest tested.

### 15.9.3 Symmetric Extensions

In case the LT is symmetric and obeys Equations 15.65 and 15.66, there is a much simpler method to implement the LT over a finite-length signal of  $N_B$  blocks of  $M$  samples.

In the forward transform section we perform symmetric extension as described, applied to the last  $\lambda = (L - M)/2$  samples on each border, resulting in a signal  $\bar{x}(n)$  with  $N_x + 2\lambda = N_x + L - M$  samples, as

$$x(\lambda - 1), \dots, x(0), x(0), \dots, x(N_x - 1), x(N_x - 1), \dots, x(N_x - \lambda). \quad (15.128)$$

The signal is processed by the PTM  $\mathbf{F}(z)$  as a clocked system, without concern for border locations. The internal states of the system  $\mathbf{F}(z)$  can be initialized in any way. So, the  $N_B + N - 1$  blocks of the extended signal are processed yielding an equal number of blocks of subband samples. Discard the first  $N - 1$  output blocks, obtaining  $N_B$  transform-domain blocks corresponding to  $N_B$  samples of each subband.

The general strategy to achieve perfect reconstruction without great increase in complexity or change in the implementation algorithm, is to extend the samples in the subbands, generating more blocks to be inverse transformed, in such a way that after inverse transformation, assuming no processing of the subband signals, the signal recovered is identical to the original at the borders. The extension of the  $k$ th subband signal depends on the symmetry of the  $k$ th basis. Let  $p_{kn} = v_k p_{k, L-1-n}$  for  $0 \leq k \leq M - 1$  and  $0 \leq n \leq L - 1$ , i.e.,  $v_k = 1$  if  $p_{kn}$  is symmetric and  $v_k = -1$  if  $p_{kn}$  is antisymmetric. Before inverse transformation, for each subband signal  $\bar{y}_k(m)$ , of  $N_B$  samples, fold the borders of  $\bar{y}_k(m)$ , (as in the analysis section) in order to find a signal  $\bar{\bar{y}}_k(m)$ , and invert the sign of the extended samples if  $p_{kn}$  is

antisymmetric. For  $s$  samples reflected around the borders, then the  $k$ th subband signal will have samples:

$$\begin{aligned} &v_k \hat{y}_k(s-1), \dots, v_k \hat{y}_k(0), \hat{y}_k(0), \dots, \hat{y}_k(N_B-1), \\ &v_k \hat{y}_k(N_B-1), \dots, v_k \hat{y}_k(N_B-s). \end{aligned}$$

The inverse transformation can be performed as

- *N odd*—Reflect  $s = (N-1)/2$  samples around each border, getting, thus,  $N_B + N - 1$  blocks with subband samples to be processed. To obtain the inverse transformed samples  $\hat{x}(n)$ , initialize the internal states in any way, run the system  $\mathbf{G}(z)$  over the  $N_B + N - 1$  blocks, and discard the first  $N - 1$  reconstructed blocks, retaining the  $N_x = N_B M$  remaining samples.
- *N even*—Reflect  $s = N/2$  samples around each border, getting, thus,  $N_B + N$  blocks to be processed. To obtain the inverse transformed samples  $\hat{x}(n)$ , initialize the internal states in any way and run the system  $\mathbf{G}(z)$  over the  $N_B + N$  blocks. Discard the first  $N - 1$  reconstructed blocks and the first  $M/2$  samples of the  $N$ th block. Include in the reconstructed signal the last  $M/2$  samples of the  $N$ th block and the subsequent  $(N_B - 1)M$  samples. In the last block, include the first  $M/2$  samples in the reconstructed signal and discard the rest.

The approach will assure the perfect reconstruction property and orthogonality of the overall transformation if the LT is orthogonal.<sup>32</sup> The price paid is to run the algorithm over extra  $N$  or  $N - 1$  blocks. As it is common to have  $N_B \gg N$ , the computational increase is only marginal.

## 15.10 Conclusions

We hope this material will serve as an introduction to lapped transforms and give some insight into their nature. This chapter should be viewed as a first step, whereas the references, and the references therein, should give a more detailed treatment of the subject.

It was shown how lapped transforms can replace block transforms allowing overlap of the basis functions. It was also shown that the analyses of MIMO systems, mainly their factorizations, are invaluable tools for the design of useful lapped transforms. That was the case in the design of transforms such as the LOT, LBT, GenLOT, GLBT, FLT, MLT, and ELT. Those practical LTs were presented by not only presenting the general factorization, but by also plotting bases and describing in detail how to construct at least a good design example, either by printing basis entries or by providing all parameters necessary to construct the bases. Even if the particular examples are not ideal for a particular application the reader might have in mind, they may provide an experimental example, from which one can build up on, by exploring the references and performing customized optimization.

It is worth pointing that we intentionally avoided viewing the transforms as filter banks, so that the bases were not discussed as

impulse responses of filters and their frequency response was not analyzed. Nevertheless the framework is the same and so is the analysis of MIMO systems. Therefore, this chapter should give insight in such a vast field which is based on the study of multi-rate systems.

Good luck in the field of lapped transforms!

## References

1. Boashash, B., Ed. 1992. *Time-Frequency Signal Analysis*, New York: John Wiley & Sons.
2. Bordreaux-Bartels, G. F. *Mixed Time-Frequency Signal Transformations*, Boca Raton, FL: CRC Press.
3. Cassereau, P. 1985. A new class of optimal unitary transforms for image processing, Master's thesis, Mass. Inst. Tech., Cambridge, MA.
4. Clarke, R. J. 1985. *Transform Coding of Images*, Orlando, FL: Academic Press.
5. Coifman, R., Meier, Y., Quaker, D., and Wickerhauser, V. 1991. Signal processing and compression using wavelet packets, Technical Report, Department of Mathematics, Yale University, New Haven, CT.
6. Doganata, Z., Vaidyanathan, P. P., and Nguyen, T. Q. 1988. General synthesis procedures for FIR lossless transfer matrices, for perfect reconstruction multirate filter banks applications, *IEEE Trans. Acoust. Speech Signal Process.*, 36 (10), 1561–1574.
7. Herley, C., Kovacevic, J., Ramchandran, K., and Vetterli, M. 1993. Tilings of the time-frequency plane: Construction of arbitrary orthogonal bases and fast tiling algorithms, *IEEE Trans. Signal Process.*, 41, 3341–3359.
8. Hohn, F. E. 1964. *Elementary Matrix Algebra*, 2nd edn., New York: Macmillan.
9. Jayant, N. S. and Noll, P. 1984. *Digital Coding of Waveforms*, Englewood Cliffs, NJ: Prentice-Hall.
10. Jozawa, H. and Watanabe, H. September 4–6, 1991. Intrafiled/Interfiled adaptive lapped transform for compatible HDTV coding, *Proceedings of the 4th International Workshop on HDTV and Beyond*, Torino, Italy.
11. Koilpillai, R. D. and Vaidyanathan, P. P. 1992. Cosine modulated FIR filter banks satisfying perfect reconstruction, *IEEE Trans. Signal Process.*, 40, 770–783.
12. Malvar, H. S. 1986. Optimal pre- and post-filtering in noisy sampled-data systems, PhD dissertation. Mass. Inst. Tech., Cambridge, MA.
13. Malvar, H. S. 1988. Reduction of blocking effects in imaging coding with a lapped orthogonal transform, *Proceedings of the International Conference on Acoustics Speech Signal Processing*, Glasgow, Scotland, pp. 781–784.
14. Malvar, H. S. and Staelin, D. H. 1989. The LOT: Transform coding without blocking effects, *IEEE Trans. Acoust. Speech Signal Process.*, ASSP-37, 553–559.
15. Malvar, H. S. 1990. Lapped transforms for efficient transform/subband coding, *IEEE Trans. Acoust. Speech Signal Process.*, ASSP-38, 969–978.

16. Malvar, H. S. 1988. The LOT: A link between block transform coding and multirate filter banks, *Proceedings of the International Symposium on Circuits and Systems*, Espoo, Finland, pp. 835–838.
17. Malvar, H. S. 1990. Efficient signal coding with hierarchical lapped transforms, *Proceedings of the International Conference on Acoustics, Speech, Signal Processing*, Albuquerque, NM, pp. 761–764.
18. Malvar, H. S. 1990. Modulated QMF filter banks with perfect reconstruction, *Electron. Lett.*, 26, 906–907.
19. Malvar, H. S. 1991. Extended lapped transform: Fast algorithms and applications, *Proceedings of the International Conference on Acoustics, Speech, Signal Processing*, Toronto, Canada, pp. 1797–1800.
20. Malvar, H. S. 1992. *Signal Processing with Lapped Transforms*. Norwood, MA: Artech House.
21. Malvar, H. S. 1992. Extended lapped transforms: Properties, applications and fast algorithms, *IEEE Trans. Signal Process.*, 40, 2703–2714.
22. Malvar, H. S. 1998. Biorthogonal and nonuniform lapped transforms for transform coding with reduced blocking and ringing artifacts, *IEEE Trans. Signal Process.*, 46, 1043–1053.
23. Nayebi, K., Barnwell, T. P., and Smith, M. J. 1992. The time domain filter bank analysis: A new design theory, *IEEE Trans. Signal Process.*, 40, 1412–1429.
24. Nguyen, T. Q. and Koilpillai, R. D. 1996. Theory and design of arbitrary-length cosine-modulated filter banks and wavelets satisfying perfect reconstruction, *IEEE Trans. Signal Process.*, 44, 473–483.
25. Oppenheim, A. V. and Schaffer, R. W. 1989. *Discrete-Time Signal Processing*, Englewoods Cliffs, NJ: Prentice-Hall.
26. Pennebaker, W. B. and Mitchell, J. L. 1993. *JPEG: Still Image Compression Standard*, New York: Van Nostrand Reinhold.
27. Princen, J. P. and Bradley, A. B. 1986. Analysis/synthesis filter bank design based on time domain aliasing cancellation, *IEEE Trans. Acoust. Speech Signal Process.*, ASSP-34, 1153–1161.
28. de Queiroz, R. L. and Rao, K. R. 1993. Time-varying lapped transforms and wavelet packets, *IEEE Trans. Signal Process.*, 41, 3293–3305.
29. de Queiroz, R. L. 1996. On lapped transforms, PhD dissertation, The University of Texas at Arlington, Arlington, TX.
30. de Queiroz, R. L. and Rao, K. R. 1995. The extended lapped transform for image coding, *IEEE Trans. Image Process.*, 4, 828–832.
31. de Queiroz, R. L., Nguyen, T. Q., and Rao, K. R. January 1994. The generalized lapped orthogonal transforms, *Electron. Lett.*, 30, 107–107.
32. de Queiroz, R. L. and Rao, K. R. 1995. On orthogonal transforms of images using paraunitary filter banks, *J. Vis. Commun. Image Rep.*, 6(2), 142–153.
33. de Queiroz, R. L. and Rao, K. R. 1995. On reconstruction methods for processing finite-length signals with paraunitary filter banks, *IEEE Trans. Signal Process.*, 43, 2407–2410.
34. de Queiroz, R. L., Nguyen, T. Q., and Rao, K. R. 1996. The GenLOT: Generalized linear-phase lapped orthogonal transform, *IEEE Trans. Signal Process.*, 44, 497–507.
35. de Queiroz, R.L. 1997. Uniform filter banks with non-uniform bands: Post-processing design, *Proc. of Intl. Cong. Acoust. Speech Signal Proc.*, Seattle, WA, Vol. III, 1341–1344.
36. de Queiroz, R. L. and Eschbach, R. 1997. Fast downscaled inverses for images compressed with M-channel lapped transforms, *IEEE Trans. Image Process.*, 6, 794–807.
37. Rabbani, M. and Jones, P. W. 1991. *Digital Image Compression Techniques*, Bellingham, WA: SPIE Optical Engineering Press.
38. Rao, K. R. and Yip, P. 1990. *Discrete Cosine Transform: Algorithms, Advantages, Applications*, San Diego, CA: Academic Press.
39. Rao, K. R. (ed.), 1985. *Discrete Transforms and Their Applications*, New York: Van Nostrand Reinhold.
40. Schiller, H. 1988. Overlapping block transform for image coding preserving equal number samples and coefficients, *Proc. SPIE, Vis. Commun. Image Process.*, 1001, 834–839.
41. Sodagar, I., Nayebi, K., and Barnwell, T. P. 1993. A class of time-varying wavelet transforms, *Proc. Intl. Conf. Acoust. Speech Signal Process.*, Minneapolis, MN, Vol. III, pp. 201–204.
42. Soman, A. K. and Vaidyanathan, P. P. 1992. Paraunitary filter banks and wavelet packets, *Proc. Intl. Conf. Acoust. Speech Signal Process.*, IV, 397–400.
43. Soman, A. K., Vaidyanathan, P. P., and Nguyen, T. Q. 1993. Linear-phase paraunitary filter banks: Theory, factorizations and applications, *IEEE Trans. Signal Process.*, 41, 3480–3496.
44. Strang, G. and Nguyen, T. 1996. *Wavelets and Filter Banks*, Wellesley, MA: Wellesley-Cambridge.
45. Temerinac, M. and Edler, B. 1992. A unified approach to lapped orthogonal transforms, *IEEE Trans. Image Process.*, 1, 111–116.
46. Tran, T. D., de Queiroz, R., and Nguyen, T. Q. 2000. Linear phase perfect reconstruction filter bank: Lattice structure, design, and application in image coding, *IEEE Trans. on Signal Processing.*, 48, 133–147. Available at [http://image.unb.br/queiroz/papers/fullpaper\\_glb.pdf](http://image.unb.br/queiroz/papers/fullpaper_glb.pdf)
47. Tran, T. D. 1998. Linear phase perfect reconstruction filter banks: Theory, structure, design, and application in image compression, PhD thesis, University of Wisconsin, Madison, WI.
48. Tran, T. D., de Queiroz, R. L., and Nguyen, T. Q. 1998. The variable-length generalized lapped biorthogonal transform, *Proc. Intl. Conf. Image Process.*, Chicago, IL, Vol. III, pp. 697–701.
49. Tran, T. D., de Queiroz, R., and Nguyen, T. Q. 1998. The generalized lapped biorthogonal transform, *Proc. Intl. Conf. Acoust. Speech Signal Proc.*, Seattle, WA, Vol. III, pp. 1441–1444.

50. Vaidyanathan, P. P. 1993. *Multirate Systems and Filter Banks*, Englewood Cliffs, NJ: Prentice-Hall.
51. Vaidyanathan, P. P. and Hoang, P. 1988. Lattice structures for optimal design and robust implementation of 2-channel PR-QMF banks, *IEEE Trans. Acoust. Speech Signal Process.*, ASSP-36, 81–94.
52. Vetterli, M. and Herley, C. 1992. Wavelets and filter banks: Theory and design, *IEEE Trans. Signal Process.*, 40, 2207–2232.
53. Vetterli, M. and Kovacevic, J. 1995. *Wavelets and Subband Coding*, Englewood Cliffs, NJ: Prentice-Hall.
54. Wickerhauser, M. V. 1992. Acoustical signal compression using wavelet packets, in *Wavelets: A Tutorial in Theory and Applications*, ed. C. K. Chui, San Diego, CA: Academic Press.
55. Young, R. W. and Kingsbury, N. G. 1993. Frequency domain estimation using a complex lapped transform, *IEEE Trans. Image Process.*, 2, 2–17.

# 16

## Zak Transform

---

16.1	Introduction.....	16-1
	Brief History of Zak Transform • Organization of the Chapter	
16.2	Preliminary Background.....	16-1
	Remarks about Notation • Linear Spaces of Functions	
16.3	Continuous Zak Transform.....	16-2
	Definitions • General Properties • Algebraic Properties • Topological Properties • Geometric Properties • Inverse Transform • Relationships to Other Transformations • Extensions of the Continuous Zak Transform	
16.4	Discrete Zak Transform.....	16-14
	Definitions • Properties • Inverse Transform • Extensions of the Discrete Zak Transform	
16.5	Finite Zak Transform.....	16-15
	Definition • Properties • Inverse Transform • Extensions of the Finite Zak Transform	
16.6	Applications.....	16-17
	Mathematics • Physics • Engineering • Suter–Stevens Fast Fourier Transform Algorithm	
16.7	Summary.....	16-19
	References.....	16-20

Mark E. Oxley  
*Air Force Institute of Technology*

Bruce W. Suter  
*Air Force Research Laboratory*

### 16.1 Introduction

---

The Zak transform inputs a signal and outputs a mixed time–frequency representation of the signal. The signal may be real-valued or complex-valued, defined on a continuum set (e.g., the real numbers) or a discrete set (e.g., the integers or a finite subset of integers). This chapter investigates the various properties and attributes of the Zak transform.

#### 16.1.1 Brief History of Zak Transform

The Zak transform was discovered by several people independently in different fields and, consequently, was called by different names. It was called the “Gel’fand mapping” in the Russian literature because I.M. Gel’fand introduced it in his work [15] on eigenfunction expansions associated with Schrödinger operators with periodic potentials. In 1967, the transform was rediscovered by a solid-state physicist, Zak [39–41] who called it the “k-q representation.” Zak introduced this representation to construct a quantum mechanical representation for the motion of a Bloch electron in the presence of a magnetic or electric field. In [29], W. Schempp mentions that some properties of another version of the Zak transform, called the “Weil–Brezin mapping” (see [10,38]), were known to the mathematician, Carl F. Gauss. Since Zak was, indeed, the first to systematically study this transform in a more general setting and recognize its usefulness,

the general consent among experts in the field is to call it the Zak transform.

#### 16.1.2 Organization of the Chapter

This chapter begins with some preliminary background material in Section 16.2 that will be used throughout the chapter. The continuous Zak transform is defined on continuum signals and investigated in Section 16.3. The discrete Zak transform is defined on discrete signals and investigated in Section 16.4. Whereas the finite signals are a special case of discrete signals, the finite Zak transform warrants its own study in Section 16.5. Applications follow in Section 16.6 with important references.

### 16.2 Preliminary Background

---

#### 16.2.1 Remarks about Notation

We will be consistent as possible with the notation and use the following fonts for certain objects.

**Special constants**— $e$ , Euler’s number;  $\pi$ ,  $\pi i$ ;  $i = \sqrt{-1}$ , the imaginary complex number.

**Set of scalars**—Roman, uppercase, blackboard bold, e.g.,  $\mathbb{R}$ , real numbers;  $\mathbb{C}$ , complex numbers.

**Vector**—Roman, lowercase, boldfaced, e.g.,  $\mathbf{t}$ ,  $\mathbf{m}$ .

**Matrix**—Roman, uppercase, Sans Serif, e.g.,  $M$ .

**Sets**—Roman, uppercase, italics, e.g.,  $C, S$ .

**Function**—Roman, lowercase, italics, e.g.,  $f, g$ ; except for the Dirac delta function,  $\delta$ .

**Variable**—Roman or Greek, lowercase, italics, e.g.,  $t, \omega$ .

**Linear space of functions**—Roman, uppercase, calligraphic, e.g.,  $\mathcal{L}$ .

**Transformation**—Roman, uppercase, boldfaced, e.g.,  $Z, F$ .

### 16.2.2 Linear Spaces of Functions

We will use various linear spaces of functions and use the following notation.

**Function:** The complex-valued function  $f$  defined on the nonempty set  $S$  will be denoted by  $f: S \rightarrow \mathbb{C}$ . Here the domain of definition of the function  $f$  is  $\mathcal{D}(f) = S$ . The image of  $f$  is the range set  $\mathcal{R}(f) \subseteq \mathbb{C}$ . The symbol  $f$  denotes the function (name). The symbols  $f(t)$  denote the unique output of function  $f$  given the input  $t$ . Hence,  $f(t)$  is “not” the function, but a complex number.

**Set of functions:** Define the set of complex-valued functions whose domain of definition is set  $S$ , by

$$\mathcal{F}(S, \mathbb{C}) = \{f: S \rightarrow \mathbb{C}: \mathcal{D}(f) = S\}.$$

**Linear spaces of functions:** We will use several linear spaces of functions.

$\mathcal{C}(\mathbb{R}, \mathbb{C})$ —Define the linear space of continuous functions that are defined over the set  $\mathbb{R}$ , by

$$\mathcal{C}(\mathbb{R}, \mathbb{C}) = \{f: \mathbb{R} \rightarrow \mathbb{C}: f \text{ is continuous at every } t \in \mathbb{R}\}.$$

For  $f, g \in \mathcal{C}(\mathbb{R}, \mathbb{C})$  we write  $f = g$  to mean point-wise equality, that is,  $f(t) = g(t)$  for every  $t \in \mathbb{R}$ .

$\mathcal{L}(\mathbb{R}, \mathbb{C})$ —Define the linear space of Lebesgue measurable functions that are defined over the set  $\mathbb{R}$ , by

$$\mathcal{L}(\mathbb{R}, \mathbb{C}) = \{f: \mathbb{R} \rightarrow \mathbb{C}: f \text{ is Lebesgue measurable}\}.$$

Recall that  $f$  may not be defined for every  $t \in \mathbb{R}$ , but this set will have Lebesgue measure zero. Function equality in this space is *almost everywhere*, that is,  $f = g$  if and only if the Lebesgue measure of the set where  $f$  and  $g$  differ, that is,  $\{t \in \mathbb{R}: f(t) \neq g(t)\}$  has Lebesgue measure zero, so

$$m(\{t \in \mathbb{R}: f(t) \neq g(t)\}) = 0.$$

Here,  $m$  denotes the Lebesgue measure. This set includes where  $f$  or  $g$  are not defined. We write  $f(t) = g(t)$  for almost every  $t \in \mathbb{R}$ , for brevity, just  $f(t) = g(t)$  a.e.  $t \in \mathbb{R}$ .

$\mathcal{L}^p(\mathbb{R}, \mathbb{C})$ —Define the linear space of Lebesgue measurable functions that are Lebesgue  $p$ -integrable over the set  $\mathbb{R}$ , by

$$\mathcal{L}^p(\mathbb{R}, \mathbb{C}) = \left\{ f \in \mathcal{L}(\mathbb{R}, \mathbb{C}): \int_{\mathbb{R}} |f(t)|^p dm < \infty \right\}$$

where  $dm$  represents integration with respect to the Lebesgue measure. The possible values of  $p \in [1, \infty)$ .

$\mathcal{L}_{loc}^p(\mathbb{R}, \mathbb{C})$ —Define the linear space of Lebesgue measurable functions that are locally Lebesgue  $p$ -integrable over the set  $\mathbb{R}$ , by

$$\mathcal{L}_{loc}^p(\mathbb{R}, \mathbb{C}) = \left\{ f \in \mathcal{L}(\mathbb{R}, \mathbb{C}): \int_K |f(t)|^p dm < \infty \text{ for every compact subset } K \subset \mathbb{R} \right\}.$$

The importance of this linear space of functions lies in the fact that the behavior at infinity is unimportant.

$\ell^p(S, \mathbb{F})$ —Given a field of scalars  $\mathbb{F}$  (e.g.,  $\mathbb{R}$  or  $\mathbb{C}$ ), and  $p \in [1, \infty)$ , define the linear space of  $\mathbb{F}$ -valued,  $p$ -summable sequences defined on the countable set  $S$  to be

$$\ell^p(S, \mathbb{F}) = \left\{ f \in \mathcal{F}(S, \mathbb{F}): \sum_{n \in S} |f(n)|^p < \infty \right\}.$$

The order of summation is arbitrary since the series is absolutely summable.

The relationships between these spaces are

$$\mathcal{C}(\mathbb{R}, \mathbb{C}) \subset \mathcal{L}^p(\mathbb{R}, \mathbb{C}) \subset \mathcal{L}_{loc}^p(\mathbb{R}, \mathbb{C}) \subset \mathcal{L}(\mathbb{R}, \mathbb{C}).$$

When we write an integration in the  $t$  variable, we will write

$$\int \text{expression}(t) dt \quad \text{instead of} \quad \int \text{expression}(t) dm.$$

## 16.3 Continuous Zak Transform

The continuous Zak transform is called “continuous” because of the domain of the function on which it acts. In this case, the domain of the functions is the entire set of real numbers  $\mathbb{R}$ , a *continuum* set.

### 16.3.1 Definitions

There are several slightly different definitions of the continuous Zak transform in the literature. We give four versions.

**Definition 16.1** (Version 1) The Zak transform  $\mathbf{Z}$  of  $f \in \mathcal{L}^1_{\text{loc}}(\mathbb{R}, \mathbb{C})$  is defined to be

$$[\mathbf{Z}f](t, \omega) = \sum_{k \in \mathbb{Z}} f(t+k) e^{-i2\pi k \omega} \quad (16.1)$$

for a.e.  $(t, \omega) \in \mathbb{R}^2$ .

For a fixed  $t \in \mathbb{R}$ , the Zak transform is computed by taking the discrete Fourier transform of the sequence of samples

$$(\dots, f(t-1), f(t+0), f(t+1), \dots).$$

Another version of the definition of the continuous Zak transform is the following.

**Definition 16.2** (Version 2) [24] Let  $T > 0$ . The Zak transform  $\mathbf{Z}_T$  of  $f \in \mathcal{L}^1_{\text{loc}}(\mathbb{R}, \mathbb{C})$  is defined to be

$$[\mathbf{Z}_T f](t, \omega) = \sqrt{T} \sum_{k \in \mathbb{Z}} f(t+kT) e^{-i2\pi k T \omega}$$

for a.e.  $(t, \omega) \in [0, T] \times [0, T^{-1}]$ .

When  $T = 1$  we will see that this definition reduces to Definition 16.1. Another version is the following.

**Definition 16.3** (Version 3) The Zak transform  $\mathbf{Z}$  of  $f \in \mathcal{L}^1_{\text{loc}}(\mathbb{R}, \mathbb{C})$  is defined to be

$$[\mathbf{Z}f](t, \nu) = \sum_{k \in \mathbb{Z}} f(t+k) e^{-ik\nu} \quad (16.2)$$

for a.e.  $(t, \nu) \in \mathbb{R}^2$ .

Choosing  $\nu = 2\pi\omega$  yields Definition 16.1.

**Definition 16.4** (Version 4) [24] Let  $a > 0$ . The Zak transform  $\mathbf{Z}_a$  of  $f \in \mathcal{L}^1_{\text{loc}}(\mathbb{R}, \mathbb{C})$  is defined to be

$$[\mathbf{Z}_a f](t, \omega) = \sqrt{a} \sum_{k \in \mathbb{Z}} f(at+ak) e^{-i2\pi k \omega}$$

for a.e.  $(t, \omega) \in \mathbb{R}^2$ .

Choosing  $a = 1$  yields Definition 16.1.

We will use Definition 16.1 throughout this chapter.

### 16.3.2 General Properties

The first question to answer is: When does the Zak transform “make sense?” That is, for what collection of functions does the Zak transform exist? The first three theorems give some answers to the convergence of the series.

### THEOREM 16.1

The Zak transform is defined for every  $f \in \mathcal{L}^1(\mathbb{R}, \mathbb{C})$ , and  $\mathbf{Z}f$  is defined for a.e.  $(t, \omega) \in \mathbb{R} \times \mathbb{R}$ , thus,  $\mathcal{D}(\mathbf{Z}) = \mathcal{L}^1(\mathbb{R}, \mathbb{C})$ . The corresponding range set of  $\mathbf{Z}$  is  $\mathcal{R}(\mathbf{Z}) \subseteq \mathcal{L}^1([0, 1]^2, \mathbb{C})$ .

*Proof* Let  $f \in \mathcal{L}^1(\mathbb{R}, \mathbb{C})$ , then for  $m, n \in \mathbb{N}$

$$\begin{aligned} & \int_0^1 \int_0^1 \left| \sum_{k=-n}^m f(t+k) e^{-i2\pi k \omega} \right| dt d\omega \\ & \leq \int_0^1 \int_0^1 \sum_{k=-n}^m |f(t+k)| |e^{-i2\pi k \omega}| dt d\omega \\ & = \int_0^1 \int_0^1 \sum_{k=-n}^m |f(t+k)| dt d\omega \\ & = \sum_{k=-n}^m \int_0^1 |f(t+k)| dt \\ & = \int_{-n}^{m+1} |f(t)| dt. \end{aligned}$$

Now, let  $m \rightarrow \infty$  and  $n \rightarrow \infty$  (any order) to get

$$\begin{aligned} & \lim_{m \rightarrow \infty} \lim_{n \rightarrow \infty} \int_0^1 \int_0^1 \left| \sum_{k=-n}^m f(t+k) e^{-i2\pi k \omega} \right| dt d\omega \\ & \leq \lim_{m \rightarrow \infty} \lim_{n \rightarrow \infty} \int_{-n}^{m+1} |f(t)| dt = \int_{-\infty}^{\infty} |f(t)| dt < \infty \quad (16.3) \end{aligned}$$

since  $f \in \mathcal{L}^1(\mathbb{R}, \mathbb{C})$ . Therefore, the series converges in the  $\mathcal{L}^1$  sense. By the Lebesgue dominated convergence theorem (LDCT) [25] we have

$$\begin{aligned} & \lim_{m \rightarrow \infty} \lim_{n \rightarrow \infty} \int_0^1 \int_0^1 \left| \sum_{k=-n}^m f(t+k) e^{-i2\pi k \omega} \right| dt d\omega \\ & = \int_0^1 \int_0^1 \lim_{m \rightarrow \infty} \lim_{n \rightarrow \infty} \left| \sum_{k=-n}^m f(t+k) e^{-i2\pi k \omega} \right| dt d\omega \\ & = \int_0^1 \int_0^1 \left| \sum_{k=-\infty}^{\infty} f(t+k) e^{-i2\pi k \omega} \right| dt d\omega \\ & = \int_0^1 \int_0^1 |[\mathbf{Z}f](t, \omega)| dt d\omega, \end{aligned}$$



so,

$$\int_0^1 \int_0^1 |[Zf](t, \omega)| dt d\omega = \int_{-\infty}^{\infty} |f(t)| dt < \infty.$$

Therefore,  $Zf \in \mathcal{L}^1([0, 1]^2, \mathbb{C})$  for every  $f \in \mathcal{L}^1(\mathbb{R}, \mathbb{C})$ , so  $\mathcal{D}(\mathbf{Z}) = \mathcal{L}^1(\mathbb{R}, \mathbb{C})$ . Also, this shows that,  $\mathcal{R}(\mathbf{Z}) \subseteq \mathcal{L}^1([0, 1]^2, \mathbb{C})$ .

This theorem shows the Zak transform  $\mathbf{Z}$  maps  $\mathcal{L}^1(\mathbb{R}, \mathbb{C})$  into  $\mathcal{L}^1([0, 1]^2, \mathbb{C})$ .

We are interested in signals with finite energy so we also consider the linear space  $\mathcal{L}^2(\mathbb{R}, \mathbb{C})$ .

---

### THEOREM 16.2

The Zak transform is defined for every  $f \in \mathcal{L}^2(\mathbb{R}, \mathbb{C})$ , and  $Zf$  is defined for a.e.  $(t, \omega) \in \mathbb{R} \times \mathbb{R}$ , thus,  $\mathcal{D}(\mathbf{Z}) = \mathcal{L}^2(\mathbb{R}, \mathbb{C})$ . The corresponding range set of  $\mathbf{Z}$  is  $\mathcal{R}(\mathbf{Z}) \subseteq \mathcal{L}^2([0, 1]^2, \mathbb{C})$ .

*Proof* Let  $f \in \mathcal{L}^2(\mathbb{R}, \mathbb{C})$  and  $m, n \in \mathbb{N}$ ,

$$\begin{aligned} & \int_0^1 \int_0^1 \left| \sum_{k=-n}^m f(t+k)e^{-i2\pi k\omega} \right|^2 dt d\omega \\ &= \int_0^1 \int_0^1 \left( \sum_{k=-n}^m f(t+k)e^{-i2\pi k\omega} \right) \overline{\left( \sum_{\ell=-n}^m f(t+\ell)e^{-i2\pi \ell\omega} \right)} dt d\omega \\ &= \int_0^1 \int_0^1 \left( \sum_{k=-n}^m f(t+k)e^{-i2\pi k\omega} \right) \left( \sum_{\ell=-n}^m \overline{f(t+\ell)} e^{i2\pi \ell\omega} \right) dt d\omega \\ &= \int_0^1 \int_0^1 \sum_{k=-n}^m \sum_{\ell=-n}^m f(t+k) \overline{f(t+\ell)} e^{-i2\pi k\omega} e^{i2\pi \ell\omega} dt d\omega \\ &= \int_0^1 \sum_{k=-n}^m \sum_{\ell=-n}^m f(t+k) \overline{f(t+\ell)} \left( \int_0^1 e^{-i2\pi(k-\ell)\omega} d\omega \right) dt \\ &= \int_0^1 \sum_{k=-n}^m \sum_{\ell=-n}^m f(t+k) \overline{f(t+\ell)} \delta(k-\ell) dt \\ &= \int_0^1 \sum_{k=-n}^m |f(t+k)|^2 dt \\ &= \sum_{k=-n}^m \int_0^1 |f(t+k)|^2 dt \\ &= \int_{-n}^{m+1} |f(t)|^2 dt. \end{aligned}$$

Now, let  $m \rightarrow \infty$  and  $n \rightarrow \infty$  (any order) to get

$$\begin{aligned} & \lim_{m \rightarrow \infty} \lim_{n \rightarrow \infty} \int_0^1 \int_0^1 \left| \sum_{k=-n}^m f(t+k)e^{-i2\pi k\omega} \right|^2 dt d\omega \\ &= \lim_{m \rightarrow \infty} \lim_{n \rightarrow \infty} \int_{-n}^{m+1} |f(t)|^2 dt = \int_{-\infty}^{\infty} |f(t)|^2 dt < \infty \end{aligned}$$

since  $f \in \mathcal{L}^2(\mathbb{R}, \mathbb{C})$ . Therefore, the series converges in the  $\mathcal{L}^2$  sense. By the LDCT [25] we have

$$\begin{aligned} & \lim_{m \rightarrow \infty} \lim_{n \rightarrow \infty} \int_0^1 \int_0^1 \left| \sum_{k=-n}^m f(t+k)e^{-i2\pi k\omega} \right|^2 dt d\omega \\ &= \int_0^1 \int_0^1 \lim_{m \rightarrow \infty} \lim_{n \rightarrow \infty} \left| \sum_{k=-n}^m f(t+k)e^{-i2\pi k\omega} \right|^2 dt d\omega \\ &= \int_0^1 \int_0^1 \left| \sum_{k=-\infty}^{\infty} f(t+k)e^{-i2\pi k\omega} \right|^2 dt d\omega \\ &= \int_0^1 \int_0^1 |[Zf](t, \omega)|^2 dt d\omega, \end{aligned}$$

so,

$$\int_0^1 \int_0^1 |[Zf](t, \omega)|^2 dt d\omega = \int_{-\infty}^{\infty} |f(t)|^2 dt < \infty.$$

Therefore,  $Zf \in \mathcal{L}^2([0, 1]^2, \mathbb{C})$  and so,  $\mathbf{Z}$  maps  $\mathcal{L}^2(\mathbb{R}, \mathbb{C})$  into  $\mathcal{L}^2([0, 1]^2, \mathbb{C})$ .

We are interested in continuous signals as well, so we consider the linear space  $\mathcal{C}(\mathbb{R}, \mathbb{C})$ .

---

### THEOREM 16.3

If  $f \in \mathcal{C}(\mathbb{R}, \mathbb{C})$  such that

$$|f(t)| \leq c(1 + |t|^{-1-\epsilon}) \quad \text{as } |t| \rightarrow \infty \quad (16.4)$$

for some constants  $c, \epsilon > 0$ , then  $Zf$  is defined and continuous at every  $(t, \omega) \in \mathbb{R} \times \mathbb{R}$ .

Condition (16.4) is called a *decay condition*. Two well-known properties unique to the Zak transform are the following theorems.

**THEOREM 16.4**

(Quasi-periodic) For  $f \in \mathcal{L}^1(\mathbb{R}, \mathbb{C})$  then

$$[\mathbf{Z}f](t+1, \omega) = e^{i2\pi\omega}[\mathbf{Z}f](t, \omega), \quad (16.5)$$

$$[\mathbf{Z}f](t, \omega+1) = [\mathbf{Z}f](t, \omega), \quad (16.6)$$

a.e.  $(t, \omega) \in \mathbb{R}^2$ .

*Proof* Property (16.5):

$$\begin{aligned} [\mathbf{Z}f](t+1, \omega) &= \sum_{k \in \mathbb{Z}} f(t+1+k) e^{-i2\pi k\omega} \\ &= \sum_{\ell \in \mathbb{Z}} f(t+\ell) e^{-i2\pi(\ell-1)\omega} \quad \text{where } \ell = 1+k \\ &= e^{i2\pi\omega} \sum_{\ell \in \mathbb{Z}} f(t+\ell) e^{-i2\pi\ell\omega} \\ &= e^{i2\pi\omega} [\mathbf{Z}f](t, \omega). \end{aligned}$$

Property (16.6):

$$\begin{aligned} [\mathbf{Z}f](t, \omega+1) &= \sum_{k \in \mathbb{Z}} f(t+k) e^{-i2\pi k(\omega+1)} \\ &= \sum_{k \in \mathbb{Z}} f(t+k) e^{-i2\pi k\omega} e^{-i2\pi k} \\ &= \sum_{k \in \mathbb{Z}} f(t+k) e^{-i2\pi k\omega} \quad \text{since } e^{-i2\pi k} = 1 \\ &= [\mathbf{Z}f](t, \omega). \end{aligned}$$

Property (16.6) implies  $\mathbf{Z}f$  is periodic in  $\omega$  with period 1. Therefore, we need only consider an interval of length 1, say,  $[0, 1]$ . Property (16.5) implies  $\mathbf{Z}f$  is almost periodic in  $t$  with period 1. The scale term  $e^{i2\pi\omega}$  keeps the periodic condition from holding true. This is the non-Abelian nature of the Zak transform [4]. But, the scale term  $e^{i2\pi\omega}$  has modulus one for all real values of  $\omega$ , consequently,  $\mathbf{Z}f$  is said to be *quasi-periodic* in  $t$ . Likewise, one need only consider an interval of length 1 for  $t$ . Define the unit square in  $\mathbb{R}^2$  in the first quadrant to be  $Q$ , that is,

$$\begin{aligned} Q &\equiv \{(t, \omega) \in \mathbb{R}^2 : 0 \leq t \leq 1, 0 \leq \omega \leq 1\} = [0, 1] \times [0, 1] \\ &= [0, 1]^2, \end{aligned}$$

then  $\mathbf{Z}f$  is completely determined on  $Q$ . The Zak transform is a mapping from  $\mathcal{L}^p(\mathbb{R}, \mathbb{C})$  into  $\mathcal{L}^p(Q, \mathbb{C})$  for  $p \in \{1, 2\}$ .

More general results are the following properties.

**THEOREM 16.5**

For every  $f \in \mathcal{L}^1(\mathbb{R}, \mathbb{C})$  and  $m, n \in \mathbb{Z}$ , then

$$[\mathbf{Z}f](t+m, \omega) = e^{-i2\pi m\omega} [\mathbf{Z}f](t, \omega),$$

$$[\mathbf{Z}f](t, \omega+n) = [\mathbf{Z}f](t, \omega),$$

a.e.  $(t, \omega) \in \mathbb{R}^2$ .

*Proof* These are simple extensions of Theorem 16.4 above.

Since  $\mathbf{Z}f$  is quasi-periodic then  $\mathbf{Z}f$  is not  $\mathcal{L}^1$  over  $\mathbb{R} \times \mathbb{R}$  (nor over  $\mathbb{R} \times [0, 1]$  nor  $[0, 1] \times \mathbb{R}$ ) but is locally integrable.

**THEOREM 16.6**

For every  $f \in \mathcal{L}^1(\mathbb{R}, \mathbb{C})$

1. (Conjugation)  $[\mathbf{Z}\bar{f}](t, \omega) = [\bar{\mathbf{Z}}f](t, -\omega)$ .
2. (Symmetry) if  $f$  is an odd function, then  $[\mathbf{Z}f](-t, -\omega) = -[\mathbf{Z}f](t, \omega)$ .
3. (Symmetry) if  $f$  is an even function, then  $[\mathbf{Z}f](-t, -\omega) = [\mathbf{Z}f](t, \omega)$ .

*Proof* The proofs are straightforward from using Definition 16.1.

Some numerical results from special evaluations are given.

**THEOREM 16.7**

For every  $f \in \mathcal{L}^1(\mathbb{R}, \mathbb{C})$

1.  $[\mathbf{Z}f](t, 0) = \sum_{k \in \mathbb{Z}} f(t+k)$
2.  $[\mathbf{Z}f](t, \frac{1}{2}) = \sum_{k \in \mathbb{Z}} (-1)^k f(t+k)$
3.  $[\mathbf{Z}f](0, 0) = \sum_{k \in \mathbb{Z}} f(k)$
4.  $[\mathbf{Z}f](0, \frac{1}{2}) = \sum_{k \in \mathbb{Z}} (-1)^k f(k)$
5.  $[\mathbf{Z}f](1, \frac{1}{2}) = -\sum_{k \in \mathbb{Z}} (-1)^k f(k)$

such that  $\mathbf{Z}f$  exists at these points in  $Q$ .

*Proof* For  $f \in \mathcal{L}^1(\mathbb{R}, \mathbb{C})$ :

1. Definition 16.1 and  $e^{-i2\pi k0} = 1$  for all  $k \in \mathbb{Z}$  implies this equation is true.
2. Definition 16.1 and  $e^{-i2\pi k(1/2)} = e^{-i\pi k} = (-1)^k$  for all  $k \in \mathbb{Z}$  implies this equation is true.
3. From Theorem 16.7, statement 1 with  $t = 0$ , this equation is true.
4. From Theorem 16.7, statement 2 with  $t = 0$ , this equation is true.
5. Definition 16.1 evaluated at  $(1, \frac{1}{2})$  yields

$$\begin{aligned} [\mathbf{Z}f]\left(1, \frac{1}{2}\right) &= \sum_{k \in \mathbb{Z}} f(1+k) e^{-i2\pi k(1/2)} \\ &= \sum_{\ell \in \mathbb{Z}} f(\ell) e^{-i\pi(\ell-1)} \quad \text{where } \ell = 1+k \\ &= \sum_{\ell \in \mathbb{Z}} (-1)^{\ell-1} f(\ell) \\ &= -\sum_{\ell \in \mathbb{Z}} (-1)^\ell f(\ell). \end{aligned}$$

**THEOREM 16.8**

(Zeroes) If  $f \in \mathcal{C}(\mathbb{R}, \mathbb{C})$  and satisfies the decay condition (16.4), then  $\mathbf{Z}f$  has at least one zero on the horizontal line segment connecting the points  $(0, \frac{1}{2})$  and  $(1, \frac{1}{2})$ .

*Proof* Statements 4 and 5 of Theorem 16.7 imply a sign change of the continuous function  $[\mathbf{Z}f](\cdot, \frac{1}{2})$ . The intermediate value theorem implies there exists at least one zero on the horizontal line segment connecting the points  $(0, \frac{1}{2})$  and  $(1, \frac{1}{2})$ .

**16.3.3 Algebraic Properties**

The Zak transform is a linear transformation from  $\mathcal{L}^p(\mathbb{R}, \mathbb{C})$  into  $\mathcal{L}^p(Q, \mathbb{C})$  for  $p \in \{1, 2\}$ .

**THEOREM 16.9**

The Zak transform  $\mathbf{Z}$  has the following properties:

1. (Total)  $\mathbf{Z}$  is defined on the set  $\mathcal{L}^2(\mathbb{R}, \mathbb{C})$ , that is,  $\mathcal{D}(\mathbf{Z}) = \mathcal{L}^2(\mathbb{R}, \mathbb{C})$  and  $\mathcal{R}(\mathbf{Z}) \subseteq \mathcal{L}^2(Q, \mathbb{C})$ .
2. (Linear)  $\mathbf{Z}$  is a linear transformation, that is, for any complex scalars  $\alpha, \beta \in \mathbb{C}$  and  $f, g \in \mathcal{L}^2(\mathbb{R}, \mathbb{C})$

$$\mathbf{Z}(\alpha f + \beta g) = \alpha \mathbf{Z}(f) + \beta \mathbf{Z}(g).$$

**Definition 16.5:** (Convolutions) Let  $f, g \in \mathcal{L}^1(\mathbb{R}, \mathbb{C})$  the convolution  $f * g \in \mathcal{L}^1(\mathbb{R}, \mathbb{C})$  is defined to be

$$[f * g](t) = \int_{-\infty}^{\infty} f(s)g(t-s)ds = \int_{-\infty}^{\infty} g(s)f(t-s)ds.$$

Let  $x, y \in \mathcal{L}^1(Q, \mathbb{C})$  the convolution  $x \overset{1}{*} y$  (with respect to the first variable) is defined to be

$$[x \overset{1}{*} y](t, \omega) = \int_0^1 x(s, \omega)y(t-s, \omega)ds = \int_0^1 y(s, \omega)x(t-s, \omega)ds.$$

The convolution  $x \overset{2}{*} y$  (with respect to the second variable) is defined to be

$$[x \overset{2}{*} y](t, \omega) = \int_0^1 x(t, \nu)y(t, \omega - \nu)d\nu = \int_0^1 y(t, \nu)x(t, \omega - \nu)d\nu.$$

For values of  $t, s \in [0, 1]$  such that  $t-s \notin [0, 1]$  we use the periodic extension of the function, or equivalently, use modulo 1 arithmetic. The same assumption is made for  $\nu, \omega \in [0, 1]$ .

**THEOREM 16.10**

Let  $f, g \in \mathcal{L}^1(\mathbb{R}, \mathbb{C})$  then

1.  $\mathbf{Z}f \overset{1}{*} \mathbf{Z}g = \mathbf{Z}(f * g)$ .
2.  $\mathbf{Z}f \overset{2}{*} \mathbf{Z}g = \mathbf{Z}(f \cdot g)$  where  $f \cdot g$  is the point-wise function multiplication of  $f$  with  $g$ .

*Proof* (1)

$$\begin{aligned} & [\mathbf{Z}f \overset{1}{*} \mathbf{Z}g](t, \omega) \\ &= \int_0^1 [\mathbf{Z}f](s, \omega)[\mathbf{Z}g](t-s, \omega)ds \\ &= \int_0^1 \left( \sum_{k \in \mathbb{Z}} f(s+k)e^{-i2\pi k\omega} \right) \left( \sum_{\ell \in \mathbb{Z}} g(t-s+\ell)e^{-i2\pi \ell\omega} \right) ds \\ &= \int_0^1 \sum_{k \in \mathbb{Z}} \sum_{\ell \in \mathbb{Z}} f(s+k)g(t-s+\ell)e^{-i2\pi(k+\ell)\omega} ds \\ &= \sum_{k \in \mathbb{Z}} \sum_{\ell \in \mathbb{Z}} \left( \int_0^1 f(s+k)g(t-s+\ell) ds \right) e^{-i2\pi(k+\ell)\omega} \\ & \text{by LDCT} \\ &= \sum_{\ell \in \mathbb{Z}} \sum_{k \in \mathbb{Z}} \left( \int_0^1 f(s+k)g(t+[k+\ell]-[s+k]) ds \right) e^{-i2\pi(k+\ell)\omega} \\ &= \sum_{m \in \mathbb{Z}} \sum_{k \in \mathbb{Z}} \left( \int_k^{k+1} f(\sigma)g(t+m-\sigma) d\sigma \right) e^{-i2\pi m\omega} \\ & \text{where } \sigma = s+k, m = k+\ell \\ &= \sum_{m \in \mathbb{Z}} \left( \int_{-\infty}^{\infty} f(\sigma)g(t+m-\sigma) d\sigma \right) e^{-i2\pi m\omega} \\ &= \sum_{m \in \mathbb{Z}} [f * g](t+m)e^{-i2\pi m\omega} \\ &= [\mathbf{Z}(f * g)](t, \omega). \end{aligned}$$

(2)

$$\begin{aligned}
& [\mathbf{Z}f \star \mathbf{Z}g](t, \omega) \\
&= \int_0^1 [\mathbf{Z}f](t, \nu)[\mathbf{Z}g](t, \omega - \nu) d\nu \\
&= \int_0^1 \left( \sum_{k \in \mathbb{Z}} f(t+k)e^{-i2\pi k\nu} \right) \left( \sum_{\ell \in \mathbb{Z}} g(t+\ell)e^{-i2\pi\ell(\omega-\nu)} \right) d\nu \\
&= \int_0^1 \sum_{k \in \mathbb{Z}} \sum_{\ell \in \mathbb{Z}} f(t+k)g(t+\ell)e^{-i2\pi k\nu} e^{-i2\pi\ell(\omega-\nu)} d\nu \\
&= \sum_{k \in \mathbb{Z}} \sum_{\ell \in \mathbb{Z}} f(t+k)g(t+\ell)e^{-i2\pi\ell\omega} \int_0^1 e^{-i2\pi(k-\ell)\nu} d\nu \quad \text{by LDCT} \\
&= \sum_{k \in \mathbb{Z}} \sum_{\ell \in \mathbb{Z}} f(t+k)g(t+\ell)e^{-i2\pi\ell\omega} \delta(k-\ell) \\
&= \sum_{k \in \mathbb{Z}} f(t+k)g(t+k)e^{-i2\pi k\omega} \\
&= \sum_{k \in \mathbb{Z}} [f \cdot g](t+k)e^{-i2\pi k\omega} \\
&= [\mathbf{Z}(f \cdot g)](t, \omega).
\end{aligned}$$

### 16.3.4 Topological Properties

Define the norm  $\|\cdot\|_{\text{in}}$  on the linear space  $\mathcal{L}^2(\mathbb{R}, \mathbb{C})$  to be, for each  $f \in \mathcal{L}^2(\mathbb{R}, \mathbb{C})$

$$\|f\|_{\text{in}} = \left( \int_{\mathbb{R}} |f(t)|^2 dt \right)^{1/2}$$

then  $(\mathcal{L}^2(\mathbb{R}, \mathbb{C}), \|\cdot\|_{\text{in}})$  is a complete normed linear space (i.e., a Banach space). Define the norm  $\|\cdot\|_{\text{out}}$  on the linear space  $\mathcal{L}^2(Q, \mathbb{C})$  to be, for each  $g \in \mathcal{L}^2(Q, \mathbb{C})$

$$\|g\|_{\text{out}} = \left( \int_Q |g(t, \omega)|^2 dt d\omega \right)^{1/2}$$

then  $(\mathcal{L}^2(Q, \mathbb{C}), \|\cdot\|_{\text{out}})$  is a Banach space.

---

#### THEOREM 16.11

The Zak transform is a continuous linear transformation from  $(\mathcal{L}^2(\mathbb{R}, \mathbb{C}), \|\cdot\|_{\text{in}})$  into  $(\mathcal{L}^2(Q, \mathbb{C}), \|\cdot\|_{\text{out}})$ . Also,

$$\|\mathbf{Z}f\|_{\text{out}} = \|f\|_{\text{in}}$$

for every  $f \in \mathcal{L}^2(\mathbb{R}, \mathbb{C})$ .

*Proof* For linear transformations, continuous and bounded are equivalent [25], therefore, we will show that  $\mathbf{Z}$  is bounded. Let  $f \in \mathcal{L}^2(\mathbb{R}, \mathbb{C})$  then

$$\begin{aligned}
\|\mathbf{Z}f\|_{\text{out}}^2 &= \int_Q |\mathbf{Z}f(t, \omega)|^2 dt d\omega \\
&= \int_Q \left| \sum_{k \in \mathbb{Z}} f(t+k)e^{-i2\pi k\omega} \right|^2 dt d\omega \\
&= \int_Q \sum_{k \in \mathbb{Z}} f(t+k)e^{-i2\pi k\omega} \overline{\sum_{\ell \in \mathbb{Z}} f(t+\ell)e^{-i2\pi\ell\omega}} dt d\omega \\
&= \int_0^1 \int_0^1 \sum_{k \in \mathbb{Z}} \sum_{\ell \in \mathbb{Z}} f(t+k)\overline{f(t+\ell)} e^{-i2\pi k\omega} e^{i2\pi\ell\omega} dt d\omega \\
&= \int_0^1 \sum_{k \in \mathbb{Z}} \sum_{\ell \in \mathbb{Z}} f(t+k)\overline{f(t+\ell)} \left( \int_0^1 e^{-i2\pi(k-\ell)\omega} d\omega \right) dt \\
&= \int_0^1 \sum_{k \in \mathbb{Z}} \sum_{\ell \in \mathbb{Z}} f(t+k)\overline{f(t+\ell)} \delta(k-\ell) dt \\
&= \int_0^1 \sum_{k \in \mathbb{Z}} |f(t+k)|^2 dt \\
&= \sum_{k \in \mathbb{Z}} \int_0^1 |f(t+k)|^2 dt \\
&= \int_{-\infty}^{\infty} |f(t)|^2 dt \\
&= \|f\|_{\text{in}}^2.
\end{aligned}$$

Hence,

$$\|\mathbf{Z}\| \equiv \sup \left\{ \frac{\|\mathbf{Z}f\|_{\text{out}}}{\|f\|_{\text{in}}} : 0 \neq f \in \mathcal{L}^2(\mathbb{R}, \mathbb{C}) \right\} = 1 < \infty.$$

Since  $\mathbf{Z}$  is a bounded linear transformation, then,  $\mathbf{Z}$  is a continuous linear transformation. Notice that  $\mathbf{Z}$  preserves the energy of the signal, since  $\|\mathbf{Z}f\|_{\text{out}} = \|f\|_{\text{in}}$  for every  $f \in \mathcal{L}^2(\mathbb{R}, \mathbb{C})$ .

### 16.3.5 Geometric Properties

Define the inner product  $\langle \cdot, \cdot \rangle_{\text{in}}$  on the linear space  $\mathcal{L}^2(\mathbb{R}, \mathbb{C})$  to be, for each  $f, g \in \mathcal{L}^2(\mathbb{R}, \mathbb{C})$

$$\langle f|g \rangle_{\text{in}} = \int_{-\infty}^{\infty} f(t)\overline{g(t)} dt,$$

then  $(\mathcal{L}^2(\mathbb{R}, \mathbb{C}), \langle \cdot | \cdot \rangle_{\text{in}})$  is a complete inner product space (i.e., a Hilbert space). Define the inner product  $\langle \cdot | \cdot \rangle_{\text{out}}$  on the linear space  $\mathcal{L}^2(Q, \mathbb{C})$  to be, for each  $x, y \in \mathcal{L}^2(Q, \mathbb{C})$

$$\langle x | y \rangle_{\text{out}} = \int_Q x(t, \omega) \overline{y(t, \omega)} dt d\omega,$$

then  $(\mathcal{L}^2(Q, \mathbb{C}), \langle \cdot | \cdot \rangle_{\text{out}})$  is a Hilbert space.

---

### THEOREM 16.12

(Unitary) The Zak transform is a unitary transformation, that is, for every  $f, g \in \mathcal{L}^2(\mathbb{R}, \mathbb{C})$

$$\langle \mathbf{Z}f | \mathbf{Z}g \rangle_{\text{out}} = \langle f | g \rangle_{\text{in}}.$$

*Proof*

$$\begin{aligned} \langle \mathbf{Z}f | \mathbf{Z}g \rangle_{\text{out}} &= \int_Q [\mathbf{Z}f](t, \omega) \overline{[\mathbf{Z}g](t, \omega)} dt d\omega \\ &= \int_Q \left( \sum_{k \in \mathbb{Z}} f(t+k) e^{-i2\pi k\omega} \right) \overline{\left( \sum_{\ell \in \mathbb{Z}} g(t+\ell) e^{-i2\pi \ell\omega} \right)} dt d\omega \\ &= \int_Q \left( \sum_{k \in \mathbb{Z}} f(t+k) e^{-i2\pi k\omega} \right) \left( \sum_{\ell \in \mathbb{Z}} \overline{g(t+\ell)} e^{i2\pi \ell\omega} \right) dt d\omega \\ &= \int_Q \sum_{k \in \mathbb{Z}} \sum_{\ell \in \mathbb{Z}} f(t+k) \overline{g(t+\ell)} e^{-i2\pi(k-\ell)\omega} dt d\omega \\ &= \int_0^1 \sum_{k \in \mathbb{Z}} \sum_{\ell \in \mathbb{Z}} f(t+k) \overline{g(t+\ell)} \left( \int_0^1 e^{-i2\pi(k-\ell)\omega} d\omega \right) dt \\ &= \int_0^1 \sum_{k \in \mathbb{Z}} \sum_{\ell \in \mathbb{Z}} f(t+k) \overline{g(t+\ell)} \delta(k-\ell) dt \\ &= \int_0^1 \sum_{k \in \mathbb{Z}} f(t+k) \overline{g(t+k)} dt \\ &= \sum_{k \in \mathbb{Z}} \int_0^1 f(t+k) \overline{g(t+k)} dt \\ &= \int_{-\infty}^{\infty} f(t) \overline{g(t)} dt \\ &= \langle f | g \rangle_{\text{in}}. \end{aligned}$$

This theorem implies that  $\mathbf{Z}$  preserves the “angle” between signals. The angle between  $f$  and  $g$  is defined to be

$$\text{Ang}(f, g) \equiv \text{Arc cos} \left( \frac{\langle f | g \rangle_{\text{in}}}{\|f\|_{\text{in}} \|g\|_{\text{in}}} \right).$$

This theorem says

$$\text{Ang}(\mathbf{Z}f, \mathbf{Z}g) = \text{Ang}(f, g)$$

for every pair  $(f, g) \in \mathcal{L}^2(\mathbb{R}, \mathbb{C}) \times \mathcal{L}^2(\mathbb{R}, \mathbb{C})$ .

---

### THEOREM 16.13

(Adjoint) The adjoint of  $\mathbf{Z}$  is  $\mathbf{Z}^{-1}$ , that is,  $\mathbf{Z}^* = \mathbf{Z}^{-1}$ .

*Proof* Since  $\mathbf{Z}$  is a unitary transformation then

$$\langle f | g \rangle_{\text{in}} = \langle \mathbf{Z}f | \mathbf{Z}g \rangle_{\text{out}} = \langle f | \mathbf{Z}^* \mathbf{Z}g \rangle_{\text{out}}$$

for all  $f \in \mathcal{L}^2(\mathbb{R}, \mathbb{C})$ . So

$$\langle f | g - \mathbf{Z}^* \mathbf{Z}g \rangle_{\text{in}} = 0$$

for all  $f \in \mathcal{L}^2(\mathbb{R}, \mathbb{C})$ , which implies  $\mathbf{Z}^* \mathbf{Z}g = g$  for all  $g \in \mathcal{L}^2(\mathbb{R}, \mathbb{C})$ . Hence,  $\mathbf{Z}^* \mathbf{Z} = \mathbf{I}$ , the identity operator, implying  $\mathbf{Z}^* = \mathbf{Z}^{-1}$ .

### 16.3.6 Inverse Transform

---

### THEOREM 16.14

The Zak transform  $\mathbf{Z}$  has the following properties:

1.  $\mathbf{Z}$  is a one-to-one transform.
2.  $\mathbf{Z}$  is onto  $\mathcal{L}^2(Q, \mathbb{C})$ , that is,  $\mathcal{R}(\mathbf{Z}) = \mathcal{L}^2(Q, \mathbb{C})$ .

*Proof* These follow from Theorem 16.13, since  $\mathbf{Z}^{-1}$  exists.

The next theorem gives ideas about the definition of the inverse Zak transform.

---

### THEOREM 16.15

(Marginals) For every  $f \in \mathcal{L}^2(\mathbb{R}, \mathbb{C})$  such that  $\mathbf{Z}f$  is continuous, then, in fact,  $f$  is continuous and  $\mathbf{F}f$  (the Fourier transform) is continuous. The marginals are

$$f(t) = \int_0^1 [\mathbf{Z}f](t, \omega) d\omega \quad \text{a.e. } t \in \mathbb{R},$$

$$[\mathbf{F}f](\omega) = \int_0^1 [\mathbf{Z}f](t, \omega) dt \quad \text{a.e. } \omega \in \mathbb{R}.$$

*Proof* For every  $f \in \mathcal{L}^2(\mathbb{R}, \mathbb{C})$  such that  $\mathbf{Z}f$  is continuous, then

$$\begin{aligned} \int_0^1 [\mathbf{Z}f](t, \omega) d\omega &= \int_0^1 \sum_{k \in \mathbb{Z}} f(t+k) e^{-i2\pi k\omega} d\omega \\ &= \sum_{k \in \mathbb{Z}} f(t+k) \int_0^1 e^{-i2\pi k\omega} d\omega \\ &= \sum_{k \in \mathbb{Z}} f(t+k) \delta(k) \\ &= f(t). \end{aligned}$$

The second result will be proved in Section 16.3.7.

This theorem demonstrates that the Zak transform is a linear time–frequency representation. The first result of this theorem motivates the definition of the inverse of the Zak transform. But, first we define marginal transformations.

---

**Definition 16.6:** (Marginal Transforms) For every  $g \in \mathcal{L}^2(Q, \mathbb{C})$  define the marginal transforms

$$\begin{aligned} [\mathbf{M}^{(1)}g](\omega) &= \int_0^1 g(t, \omega) dt, \\ [\mathbf{M}^{(2)}g](t) &= \int_0^1 g(t, \omega) d\omega, \end{aligned}$$

where the superscript denotes which variable is integrated.

These marginal transforms are continuous linear transformations from  $\mathcal{L}^2(Q, \mathbb{C})$  into  $\mathcal{L}^2([0, 1], \mathbb{C})$ .

---

**Definition 16.7:** (Inverse) The inverse Zak transform is defined, for every  $g \in \mathcal{L}^2(Q, \mathbb{C})$ , to be

$$[\mathbf{Z}^{-1}g](t) = \int_0^1 g(t, \omega) d\omega, \quad (16.7)$$

a.e.  $t \in [0, 1]$ .

Notice that  $\mathbf{Z}^{-1}$  is  $\mathbf{M}^{(2)}$ .

---

### THEOREM 16.16

The inverse Zak transform  $\mathbf{Z}^{-1}$  satisfies the following properties:

1.  $\mathbf{Z}^{-1}: \mathcal{L}^2(Q, \mathbb{C}) \rightarrow \mathcal{L}^2([0, 1], \mathbb{C})$ .
2.  $\mathbf{Z}^{-1}$  is linear transform.
3.  $\mathbf{Z}^{-1}$  is continuous transform.
4.  $\mathbf{Z}^{-1}$  is unitary transform.

*Proof* (1) Let  $g \in \mathcal{L}^2(Q, \mathbb{C})$  then

$$|[\mathbf{Z}^{-1}g](t)| = \left| \int_0^1 g(t, \omega) d\omega \right| \leq \left( \int_0^1 |g(t, \omega)|^2 d\omega \right)^{1/2},$$

so

$$\begin{aligned} \|\mathbf{Z}^{-1}g\|_{\text{in}}^2 &= \int_0^1 |[\mathbf{Z}^{-1}g](t)|^2 dt \leq \int_0^1 \int_0^1 |g(t, \omega)|^2 d\omega dt \\ &= \|g\|_{\text{out}}^2. \end{aligned}$$

- (2) Since  $\mathbf{Z}$  is linear, then  $\mathbf{Z}^{-1}$  is linear, (see [25]).
- (3) By (1)  $\mathbf{Z}^{-1}$  is bounded, therefore,  $\mathbf{Z}^{-1}$  is continuous.
- (4) Since  $\mathbf{Z}^{-1} = \mathbf{Z}^*$  then  $(\mathbf{Z}^{-1})^* = \mathbf{Z}^{**} = \mathbf{Z} = (\mathbf{Z}^{-1})^{-1}$ . So the adjoint of  $\mathbf{Z}^{-1}$  is  $(\mathbf{Z}^{-1})^{-1} = \mathbf{Z}$ , its own inverse. Thus,  $\mathbf{Z}^{-1}$  is a unitary transform.

## 16.3.7 Relationships to Other Transformations

### 16.3.7.1 Fourier

---

**Definition 16.8:** (1D Continuous Fourier Transform) The continuous Fourier transform of  $f \in \mathcal{L}^2(\mathbb{R}, \mathbb{C})$  is defined to be

$$[\mathbf{F}f](\omega) = \int_{-\infty}^{\infty} f(t) e^{-i2\pi t\omega} dt,$$

a.e.  $\omega \in \mathbb{R}$ , and  $\mathbf{F}: \mathcal{L}^2(\mathbb{R}, \mathbb{C}) \rightarrow \mathcal{L}^2(\mathbb{R}, \mathbb{C})$ . The inverse continuous Fourier transform of  $g \in \mathcal{L}^2(\mathbb{R}, \mathbb{C})$  is defined to be

$$[\mathbf{F}^{-1}g](t) = \int_{-\infty}^{\infty} g(\omega) e^{i2\pi t\omega} d\omega,$$

a.e.  $t \in \mathbb{R}$ .

---

**Definition 16.9:** (1D Discrete Fourier Transform) The discrete Fourier transform of  $f \in \ell^2(\mathbb{Z}, \mathbb{C})$  is defined to be

$$[\mathbf{F}_d f](\omega) = \sum_{k \in \mathbb{Z}} f(k) e^{-i2\pi k\omega},$$

a.e.  $\omega \in [0, 1]$ , and  $\mathbf{F}_d: \ell^2(\mathbb{Z}, \mathbb{C}) \rightarrow \mathcal{L}^2([0, 1], \mathbb{C})$ . The inverse discrete Fourier transform of  $g \in \mathcal{L}^2(\mathbb{R}, \mathbb{C})$  is defined to be

$$[\mathbf{F}_d^{-1}g](k) = \int_0^1 g(\omega)e^{i2\pi k\omega} d\omega$$

for  $k \in \mathbb{Z}$ .

---

**Definition 16.10:** (2D Fourier Transform) The continuous Fourier transform of  $x \in \mathcal{L}^2(Q, \mathbb{C})$  is defined to be

$$[\mathbf{F}_2x](s, \nu) = \int_0^1 \int_0^1 x(t, \omega)e^{-i2\pi(st+\nu\omega)} dt d\omega,$$

a.e.  $(s, \nu) \in Q$ , and  $\mathbf{F}_2 : \mathcal{L}^2(Q, \mathbb{C}) \rightarrow \mathcal{L}^2(Q, \mathbb{C})$ . The inverse continuous Fourier transform of  $y \in \mathcal{L}^2(Q, \mathbb{C})$  is defined to be

$$[\mathbf{F}_2^{-1}y](t, \omega) = \int_0^1 \int_0^1 y(s, \nu)e^{i2\pi(st+\nu\omega)} ds d\nu,$$

a.e.  $(t, \omega) \in Q$ .

---

### THEOREM 16.17

For every  $f \in \mathcal{L}^2(\mathbb{R}, \mathbb{C})$

$$[\mathbf{Z}f](0, \omega) = [\mathbf{F}_d f](\omega),$$

a.e.  $\omega \in [0, 1]$ .

*Proof* Let  $f \in \mathcal{L}^2(\mathbb{R}, \mathbb{C})$

$$[\mathbf{Z}f](0, \omega) = \sum_{k \in \mathbb{Z}} f(k)e^{-i2\pi k\omega} = [\mathbf{F}_d f](\omega),$$

a.e.  $\omega \in [0, 1]$ .

For  $f \in \mathcal{L}^2(\mathbb{R}, \mathbb{C})$  define the multiplication operator  $\mathbf{C}$  to be  $[\mathbf{C}f](t, \omega) = \chi_{[0,1]}(t) \cdot f(t)$  where  $\chi_{[0,1]}$  is the characteristic function on the interval  $[0, 1]$ .

---

### THEOREM 16.18

For  $f \in \mathcal{L}^2(\mathbb{R}, \mathbb{C})$

1.  $\int_0^1 [\mathbf{Z}f](t, \omega)e^{-i2\pi\omega t} dt = [\mathbf{FCZ}f](\omega) = [\mathbf{F}f](\omega)$ .
2.  $\mathbf{FCZF}^{-1}f = f$ .
3.  $[\mathbf{ZF}f](\omega, -t) = e^{-i2\pi t\omega} [\mathbf{Z}f](t, \omega)$ .
4.  $\mathbf{F}_2(\mathbf{Z}f \cdot \overline{\mathbf{Z}g})(m) = [\mathbf{F}(f \cdot g)](m)$  for  $m \in \mathbb{Z}$ , where  $[\mathbf{Z}g](t, \omega) \equiv [\mathbf{Z}g](t, -\omega)$ .

*Proof* Let  $f \in \mathcal{L}^2(\mathbb{R}, \mathbb{C})$  then

1. For  $\omega \in \mathbb{R}$

$$\begin{aligned} [\mathbf{FCZ}f](\omega) &= \int_{-\infty}^{\infty} (\chi_{[0,1]}(t)[\mathbf{Z}f](t, \omega))e^{-i2\pi\omega t} dt \\ &= \int_0^1 [\mathbf{Z}f](t, \omega)e^{-i2\pi\omega t} dt \\ &= \int_0^1 \sum_{k \in \mathbb{Z}} f(t+k)e^{-i2\pi k\omega} e^{-i2\pi\omega t} dt \\ &= \sum_{k \in \mathbb{Z}} \int_0^1 f(t+k)e^{-i2\pi\omega(t+k)} dt \\ &= \sum_{k \in \mathbb{Z}} \int_k^{k+1} f(\tau)e^{-i2\pi\omega\tau} d\tau \quad \text{where } \tau = t+k \in [k, k+1] \\ &= \int_{-\infty}^{\infty} f(\tau)e^{-i2\pi\omega\tau} d\tau \\ &= [\mathbf{F}f](\omega). \end{aligned}$$

2. Let  $f = \mathbf{F}^{-1}g$  then by (1)  $\mathbf{FCZ}f = \mathbf{F}f$  becomes

$$\mathbf{FCZF}^{-1}g = \mathbf{FF}^{-1}g = g.$$

Rename  $g$  to be  $f$ .

3. For  $(t, \omega) \in Q$  then

$$\begin{aligned} [\mathbf{ZF}f](\omega, -t) &= \sum_{k \in \mathbb{Z}} [\mathbf{F}f](\omega+k)e^{-i2\pi k(-t)} \\ &= \sum_{k \in \mathbb{Z}} \left( \int_{-\infty}^{\infty} f(s)e^{-i2\pi s(\omega+k)} ds \right) e^{-i2\pi k(-t)} \\ &= \int_{-\infty}^{\infty} f(s) \left[ \sum_{k \in \mathbb{Z}} e^{-i2\pi k(s-t)} \right] e^{-i2\pi s\omega} ds \\ &= \int_{-\infty}^{\infty} f(s) \left[ \sum_{k \in \mathbb{Z}} \delta(k - [s-t]) \right] e^{-i2\pi s\omega} ds \\ &= \sum_{k \in \mathbb{Z}} \int_{-\infty}^{\infty} f(s)\delta(k-s+t)e^{-i2\pi s\omega} ds \\ &= \sum_{k \in \mathbb{Z}} f(k+t)e^{-i2\pi(k+t)\omega} \\ &= e^{-i2\pi t\omega} \sum_{k \in \mathbb{Z}} f(k+t)e^{-i2\pi k\omega} \\ &= e^{-i2\pi t\omega} [\mathbf{Z}f](t, \omega). \end{aligned}$$

4. Let  $f, g \in \mathcal{L}^2(\mathbb{R}, \mathbb{C})$  then

$$\begin{aligned}
& [\mathbf{F}_2(\mathbf{Z}f \cdot \overline{\mathbf{Z}g})](m, \nu) \\
&= \int_0^1 \int_0^1 [\mathbf{Z}f](t, \omega) [\mathbf{Z}g](t, -\omega) e^{-i2\pi(mt+\nu\omega)} dt d\omega \\
&= \int_0^1 \int_0^1 \sum_{k \in \mathbb{Z}} f(t+k) e^{-i2\pi k\omega} \sum_{\ell \in \mathbb{Z}} g(t+\ell) e^{i2\pi\ell\omega} e^{-i2\pi(mt+\nu\omega)} dt d\omega \\
&= \int_0^1 \sum_{k \in \mathbb{Z}} \sum_{\ell \in \mathbb{Z}} f(t+k) g(t+\ell) \left( \int_0^1 e^{-i2\pi(k-\ell+\nu)\omega} d\omega \right) e^{-i2\pi mt} dt \\
&= \int_0^1 \sum_{k \in \mathbb{Z}} \sum_{\ell \in \mathbb{Z}} f(t+k) g(t+\ell) \delta(k-\ell) e^{-i2\pi mt} dt \\
&= \int_0^1 \sum_{k \in \mathbb{Z}} f(t+k) g(t+k) e^{-i2\pi mt} dt \\
&= \sum_{k \in \mathbb{Z}} \int_0^1 f(t+k) g(t+k) e^{-i2\pi mt} dt \\
&= \sum_{k \in \mathbb{Z}} \int_k^{k+1} f(\tau) g(\tau) e^{-i2\pi m(\tau-k)} d\tau \quad \text{where } \tau = t+k \\
&= \sum_{k \in \mathbb{Z}} \int_k^{k+1} f(\tau) g(\tau) e^{-i2\pi m\tau} d\tau e^{i2\pi mk} \\
&= \int_{-\infty}^{\infty} f(\tau) g(\tau) e^{-i2\pi m\tau} d\tau \quad \text{since } e^{i2\pi mk} = 1 \\
&= [\mathbf{F}(f \cdot g)](m).
\end{aligned}$$

### 16.3.7.2 Translations and Modulations

**Definition 16.11:** (Translation Operators) For every  $a, b \in \mathbb{R}$ , define the translation operators

- $\mathbf{T}_a$  acting on a function  $f \in \mathcal{L}^2(\mathbb{R}, \mathbb{C})$  to be

$$[\mathbf{T}_a f](t) = f(t+a)$$

a.e.  $t \in \mathbb{R}$ .

- $\mathbf{T}_a^{(1)}$  acting on the first variable of a function  $g \in \mathcal{L}^2(\mathbb{R}^2, \mathbb{C})$  to be

$$[\mathbf{T}_a^{(1)} g](t, \omega) = g(t+a, \omega)$$

a.e.  $(t, \omega) \in \mathbb{R}^2$ .

- $\mathbf{T}_a^{(2)}$  acting on the second variable of a function  $g \in \mathcal{L}^2(\mathbb{R}^2, \mathbb{C})$  to be

$$[\mathbf{T}_a^{(2)} g](t, \omega) = g(t, \omega+a)$$

a.e.  $(t, \omega) \in \mathbb{R}^2$ .

- $\mathbf{T}_{a,b}^{(1,2)}$  acting on both variables of a function  $g \in \mathcal{L}^2(\mathbb{R}^2, \mathbb{C})$  to be

$$[\mathbf{T}_{a,b}^{(1,2)} g](t, \omega) = g(t+a, \omega+b)$$

a.e.  $(t, \omega) \in \mathbb{R}^2$ .

---

### THEOREM 16.19

For every  $a \in \mathbb{R}$ , the translation operator  $\mathbf{T}_a$  satisfies the following properties:

1.  $\mathbf{T}_a$  is a linear operator on  $\mathcal{L}^2(\mathbb{R}, \mathbb{C})$ .
2.  $\mathbf{T}_0 = \mathbf{I}$ , the identity operator.
3.  $\mathbf{T}_a \mathbf{T}_b = \mathbf{T}_b \mathbf{T}_a = \mathbf{T}_{a+b}$ .
4.  $\mathbf{T}_a^{-1} = \mathbf{T}_{-a}$ .

The proofs are straightforward. There are similar statements for  $\mathbf{T}_a^{(1)}$ ,  $\mathbf{T}_b^{(2)}$ , and  $\mathbf{T}_{a,b}^{(1,2)}$ .

---

**Definition 16.12:** (Modulation Operators) For every  $a, b \in \mathbb{R}$  define the modulation operators

- $\mathbf{E}_a$  acting on a function  $f \in \mathcal{L}^2(\mathbb{R}, \mathbb{C})$  to be

$$[\mathbf{E}_a f](t) = e^{-i2\pi at} f(t)$$

a.e.  $t \in \mathbb{R}$ .

- $\mathbf{E}_a^{(1)}$  acting on the first variable of a function  $g \in \mathcal{L}^2(\mathbb{R}^2, \mathbb{C})$  to be

$$[\mathbf{E}_a^{(1)} g](t, \omega) = e^{-i2\pi at} g(t, \omega)$$

a.e.  $(t, \omega) \in \mathbb{R}^2$ .

- $\mathbf{E}_a^{(2)}$  acting on the second variable of a function  $g \in \mathcal{L}^2(\mathbb{R}^2, \mathbb{C})$  to be

$$[\mathbf{E}_a^{(2)} g](t, \omega) = e^{-i2\pi a\omega} g(t, \omega)$$

a.e.  $(t, \omega) \in \mathbb{R}^2$ .

- $\mathbf{E}_{a,b}^{(1,2)}$  acting on both variables of a function  $g \in \mathcal{L}^2(\mathbb{R}^2, \mathbb{C})$  to be

$$[\mathbf{E}_{a,b}^{(1,2)} g](t, \omega) = e^{-i2\pi(at+b\omega)} g(t, \omega)$$

a.e.  $(t, \omega) \in \mathbb{R}^2$ .



**THEOREM 16.20**

For every  $a, b \in \mathbb{R}$ , the modulation operator  $\mathbf{E}_a$  satisfies the following properties:

1.  $\mathbf{E}_a$  is a linear operator on  $\mathcal{L}^2(\mathbb{R}, \mathbb{C})$ .
2.  $\mathbf{E}_0 = \mathbf{I}$ , the identity operator.
3.  $\mathbf{E}_a \mathbf{E}_b = \mathbf{E}_b \mathbf{E}_a = \mathbf{E}_{a+b}$ .
4.  $\mathbf{E}_a^{-1} = \mathbf{E}_{-a}$ .

The following properties consider the relationships between translations, modulations, and the Zak transform. We list expressions where  $\mathbf{Z}$  is the last transform and  $\mathbf{Z}$  is the first transform in separate theorems.

**THEOREM 16.21**

( $\mathbf{Z}$  is last) Let  $f \in \mathcal{L}^2(\mathbb{R}, \mathbb{C})$ :

1.  $\mathbf{Z}f = \sum_{k \in \mathbb{Z}} \mathbf{E}_k^{(2)} \mathbf{T}_k f$ .
2.  $\mathbf{Z} \mathbf{T}_m f = \mathbf{E}_{-m}^{(2)} \mathbf{Z}f$  for  $m \in \mathbb{Z}$ .
3.  $\mathbf{Z} \mathbf{T}_a f = \mathbf{T}_a^{(1)} \mathbf{Z}f$  for  $a \in \mathbb{R} - \mathbb{Z}$ .
4.  $\mathbf{Z} \mathbf{E}_m f = \mathbf{E}_m^{(1)} \mathbf{Z}f$  for  $m \in \mathbb{Z}$ .
5.  $\mathbf{Z} \mathbf{E}_a f = \mathbf{E}_a^{(1)} \mathbf{T}_a^{(2)} \mathbf{Z}f$  for  $a \in \mathbb{R} - \mathbb{Z}$ .
6.  $\mathbf{Z} \mathbf{E}_m^{(2)} \mathbf{T}_m f = \mathbf{Z}f$  for  $m \in \mathbb{Z}$ .
7.  $\mathbf{Z} \mathbf{E}_m^{(2)} \mathbf{T}_n f = \mathbf{E}_{m-n}^{(2)} \mathbf{Z}f$  for  $m, n \in \mathbb{Z}$ .
8.  $\mathbf{Z} \mathbf{E}_a^{(2)} \mathbf{T}_a f = \mathbf{Z}f$  for  $a \in \mathbb{R} - \mathbb{Z}$ .
9.  $\mathbf{Z} \mathbf{T}_m \mathbf{E}_n f = \mathbf{E}_{n,m}^{(1,2)} \mathbf{Z}f$  for  $m, n \in \mathbb{Z}$ .

*Proof* For a.e.  $(t, \omega) \in \mathbb{Q}$

1.

$$\begin{aligned} [\mathbf{Z}f](t, \omega) &= \sum_{k \in \mathbb{Z}} f(t+k) e^{-i2\pi k \omega} \\ &= \sum_{k \in \mathbb{Z}} [\mathbf{T}_k f](t) e^{-i2\pi k \omega} \\ &= \sum_{k \in \mathbb{Z}} [\mathbf{E}_k^{(2)} \mathbf{T}_k f](t, \omega). \end{aligned}$$

2. For  $m \in \mathbb{Z}$

$$\begin{aligned} [\mathbf{Z} \mathbf{T}_m f](t, \omega) &= \sum_{k \in \mathbb{Z}} f(t+m+k) e^{-i2\pi k \omega} \\ &= \sum_{\ell \in \mathbb{Z}} f(t+\ell) e^{-i2\pi(\ell-m)\omega} \quad \text{where } \ell = m+k \\ &= e^{i2\pi m \omega} \sum_{\ell \in \mathbb{Z}} f(t+\ell) e^{-i2\pi \ell \omega} \\ &= e^{-i2\pi(-m)\omega} [\mathbf{Z}f](t, \omega) \\ &= [\mathbf{E}_{-m}^{(2)} \mathbf{Z}f](t, \omega). \end{aligned}$$

3. For  $a \in \mathbb{R} - \mathbb{Z}$

$$\begin{aligned} [\mathbf{Z} \mathbf{T}_a f](t, \omega) &= \sum_{k \in \mathbb{Z}} f(t+a+k) e^{-i2\pi k \omega} \\ &= [\mathbf{Z}f](t+a, \omega) \\ &= [\mathbf{T}_a^{(1)} \mathbf{Z}f](t, \omega). \end{aligned}$$

4. For  $m \in \mathbb{Z}$

$$\begin{aligned} [\mathbf{Z} \mathbf{E}_m f](t, \omega) &= \sum_{k \in \mathbb{Z}} e^{-i2\pi m(t+k)} f(t+k) e^{-i2\pi k \omega} \\ &= e^{-i2\pi m t} \sum_{k \in \mathbb{Z}} e^{-i2\pi m k} f(t+k) e^{-i2\pi k \omega} \\ &= e^{-i2\pi m t} \sum_{k \in \mathbb{Z}} f(t+k) e^{-i2\pi k \omega} \quad \text{since } e^{-i2\pi m k} = 1 \\ &= e^{-i2\pi m t} [\mathbf{Z}f](t, \omega) \\ &= [\mathbf{E}_m^{(1)} \mathbf{Z}f](t, \omega). \end{aligned}$$

5. For  $a \in \mathbb{R} - \mathbb{Z}$

$$\begin{aligned} [\mathbf{Z} \mathbf{E}_a f](t, \omega) &= \sum_{k \in \mathbb{Z}} e^{-i2\pi a(t+k)} f(t+k) e^{-i2\pi k \omega} \\ &= e^{-i2\pi a t} \sum_{k \in \mathbb{Z}} f(t+k) e^{-i2\pi k(\omega+a)} \\ &= e^{-i2\pi a t} [\mathbf{Z}f](t, \omega+a) \\ &= e^{-i2\pi a t} [\mathbf{T}_a^{(2)} \mathbf{Z}f](t, \omega) \\ &= [\mathbf{E}_a^{(1)} \mathbf{T}_a^{(2)} \mathbf{Z}f](t, \omega). \end{aligned}$$

6. For  $m \in \mathbb{Z}$

$$\begin{aligned} [\mathbf{Z} \mathbf{E}_m^{(2)} \mathbf{T}_m f](t, \omega) &= \sum_{k \in \mathbb{Z}} e^{-i2\pi m \omega} f(t+m+k) e^{-i2\pi k \omega} \\ &= \sum_{k \in \mathbb{Z}} f(t+m+k) e^{-i2\pi(m+k)\omega} \\ &= \sum_{\ell \in \mathbb{Z}} f(t+\ell) e^{-i2\pi \ell \omega} \quad \text{where } \ell = m+k \\ &= [\mathbf{Z}f](t, \omega). \end{aligned}$$

7. For  $m, n \in \mathbb{Z}$

$$\begin{aligned} [\mathbf{Z} \mathbf{E}_m^{(2)} \mathbf{T}_n f](t, \omega) &= \sum_{k \in \mathbb{Z}} e^{-i2\pi m \omega} f(t+n+k) e^{-i2\pi k \omega} \\ &= \sum_{k \in \mathbb{Z}} f(t+n+k) e^{-i2\pi(m+k)\omega} \\ &= \sum_{\ell \in \mathbb{Z}} f(t+\ell) e^{-i2\pi(m+\ell-n)\omega} \quad \text{where } \ell = n+k \\ &= e^{-i2\pi(m-n)\omega} \sum_{\ell \in \mathbb{Z}} f(t+\ell) e^{-i2\pi \ell \omega} \\ &= e^{-i2\pi(m-n)\omega} [\mathbf{Z}f](t, \omega) \\ &= [\mathbf{E}_{m-n}^{(2)} \mathbf{Z}f](t, \omega). \end{aligned}$$

8. For  $a, b \in \mathbb{R} - \mathbb{Z}$

$$\begin{aligned} [\mathbf{Z}\mathbf{E}_a^{(2)}\mathbf{T}_b f](t, \omega) &= \sum_{k \in \mathbb{Z}} e^{-i2\pi a \omega} f(t + b + k) e^{-i2\pi k \omega} \\ &= e^{-i2\pi a \omega} \sum_{k \in \mathbb{Z}} f(t + b + k) e^{-i2\pi k \omega} \\ &= e^{-i2\pi a \omega} [\mathbf{Z}f](t + b, \omega) \\ &= e^{-i2\pi a \omega} [\mathbf{T}_b^{(1)} \mathbf{Z}f](t, \omega) \\ &= [\mathbf{E}_a^{(2)} \mathbf{T}_b^{(1)} \mathbf{Z}f](t, \omega). \end{aligned}$$

9. For  $m, n \in \mathbb{Z}$

$$\begin{aligned} [\mathbf{Z}\mathbf{T}_m \mathbf{E}_n f](t, \omega) &= \sum_{k \in \mathbb{Z}} e^{-i2\pi n(t+m)} f(t + m + k) e^{-i2\pi k \omega} \\ &= e^{-i2\pi n t} \sum_{k \in \mathbb{Z}} e^{-i2\pi n m} f(t + m + k) e^{-i2\pi k \omega} \quad \text{since } e^{-i2\pi n m} = 1 \\ &= e^{-i2\pi n t} \sum_{k \in \mathbb{Z}} f(t + \ell) e^{-i2\pi(\ell-m)\omega} \quad \text{where } \ell = m + k \\ &= e^{-i2\pi n t} e^{i2\pi m \omega} \sum_{k \in \mathbb{Z}} f(t + \ell) e^{-i2\pi \ell \omega} \\ &= e^{-i2\pi n t} e^{i2\pi m \omega} \sum_{k \in \mathbb{Z}} f(t + \ell) e^{-i2\pi \ell \omega} \\ &= e^{-i2\pi n t} e^{i2\pi m \omega} [\mathbf{Z}f](t, \omega) \\ &= [\mathbf{E}_n^{(1)} \mathbf{E}_m^{(2)} \mathbf{Z}f](t, \omega) \\ &= [\mathbf{E}_{n,m}^{(1,2)} \mathbf{Z}f](t, \omega). \end{aligned}$$

---

### THEOREM 16.22

( $\mathbf{Z}$  is first) Let  $f \in \mathcal{L}^2(\mathbb{R}, \mathbb{C})$  and  $m \in \mathbb{Z}$ , then

$$\mathbf{T}_m^{(1)} \mathbf{Z}f = \mathbf{E}_m^{(2)} \mathbf{Z}f.$$

*Proof* For  $m \in \mathbb{Z}$

$$\begin{aligned} [\mathbf{T}_m^{(1)} \mathbf{Z}f](t, \omega) &= [\mathbf{Z}f](t + m, \omega) \\ &= \sum_{k \in \mathbb{Z}} f(t + m + k) e^{-i2\pi k \omega} \\ &= \sum_{\ell \in \mathbb{Z}} f(t + \ell) e^{-i2\pi(\ell-m)\omega} \quad \text{where } \ell = m + k \\ &= e^{i2\pi m \omega} \sum_{\ell \in \mathbb{Z}} f(t + \ell) e^{-i2\pi \ell \omega} \\ &= e^{i2\pi m \omega} [\mathbf{Z}f](t, \omega) \\ &= [\mathbf{E}_{-m}^{(2)} \mathbf{Z}f](t, \omega). \end{aligned}$$

## 16.3.8 Extensions of the Continuous Zak Transform

There have been several extensions to the Zak transform. We mention, without discussion, the multiplicative Zak transform and refer the reader to the article [17].

### 16.3.8.1 Multidimensional Continuous Zak Transform

---

**Definition 16.13:** The multidimensional continuous Zak transform of  $f \in \mathcal{L}^2(\mathbb{R}^d, \mathbb{C})$  is defined to be

$$[\mathbf{Z}f](\mathbf{t}, \boldsymbol{\omega}) = \sum_{\mathbf{k} \in \mathbb{Z}^d} f(\mathbf{t} + \mathbf{k}) e^{-i2\pi \mathbf{k} \cdot \boldsymbol{\omega}} \quad (16.8)$$

for a.e.  $(\mathbf{t}, \boldsymbol{\omega}) \in \mathbb{R}^d \times \mathbb{R}^d$ .

A quasi-periodic condition also holds true.

---

### THEOREM 16.23

Let  $f \in \mathcal{L}^2(\mathbb{R}^d, \mathbb{C})$

1. For  $\mathbf{m} \in \mathbb{Z}^d$  then  $[\mathbf{Z}f](\mathbf{t} + \mathbf{m}, \boldsymbol{\omega}) = e^{i2\pi \mathbf{m} \cdot \boldsymbol{\omega}} [\mathbf{Z}f](\mathbf{t}, \boldsymbol{\omega})$
2. For  $\mathbf{n} \in \mathbb{Z}^d$  then  $[\mathbf{Z}f](\mathbf{t}, \boldsymbol{\omega} + \mathbf{n}) = [\mathbf{Z}f](\mathbf{t}, \boldsymbol{\omega})$

for a.e.  $(\mathbf{t}, \boldsymbol{\omega}) \in \mathbb{R}^d \times \mathbb{R}^d T$ .

*Proof* 1. For  $\mathbf{m} \in \mathbb{Z}^d$

$$\begin{aligned} [\mathbf{Z}f](\mathbf{t} + \mathbf{m}, \boldsymbol{\omega}) &= \sum_{\mathbf{k} \in \mathbb{Z}^d} f(\mathbf{t} + \mathbf{m} + \mathbf{k}) e^{-i2\pi \mathbf{k} \cdot \boldsymbol{\omega}} \\ &= \sum_{\ell \in \mathbb{Z}^d} f(\mathbf{t} + \ell) e^{-i2\pi(\ell-m) \cdot \boldsymbol{\omega}} \quad \text{where } \ell = \mathbf{m} + \mathbf{k} \\ &= e^{i2\pi \mathbf{m} \cdot \boldsymbol{\omega}} \sum_{\ell \in \mathbb{Z}^d} f(\mathbf{t} + \ell) e^{-i2\pi \ell \cdot \boldsymbol{\omega}} \\ &= e^{i2\pi \mathbf{m} \cdot \boldsymbol{\omega}} [\mathbf{Z}f](\mathbf{t}, \boldsymbol{\omega}). \end{aligned}$$

2. For  $\mathbf{n} \in \mathbb{Z}^d$

$$\begin{aligned} [\mathbf{Z}f](\mathbf{t}, \boldsymbol{\omega} + \mathbf{n}) &= \sum_{\mathbf{k} \in \mathbb{Z}^d} f(\mathbf{t} + \mathbf{k}) e^{-i2\pi \mathbf{k} \cdot (\boldsymbol{\omega} + \mathbf{n})} \\ &= \sum_{\mathbf{k} \in \mathbb{Z}^d} f(\mathbf{t} + \mathbf{k}) e^{-i2\pi \mathbf{k} \cdot (\boldsymbol{\omega} + \mathbf{n})} e^{-i2\pi \mathbf{k} \cdot \mathbf{n}} \\ &= [\mathbf{Z}f](\mathbf{t}, \boldsymbol{\omega}) \end{aligned}$$

since the dot product  $\mathbf{k} \cdot \mathbf{n} \in \mathbb{Z}$ , then  $e^{-i2\pi \mathbf{k} \cdot \mathbf{n}} = 1$ .

**THEOREM 16.24**

The multidimensional continuous Zak transform  $\mathbf{Z}$ :

1. Is defined for all  $f \in \mathcal{L}^2(\mathbb{R}^d, \mathbb{C})$ , i.e.,  $\mathcal{D}(\mathbf{Z}) = \mathcal{L}^2(\mathbb{R}^d, \mathbb{C})$
2. Has range  $\mathcal{R}(\mathbf{Z}) \subseteq \mathcal{L}^2(Q^d, \mathbb{C})$  so  $\mathbf{Z} : \mathcal{L}^2(\mathbb{R}^d, \mathbb{C}) \rightarrow \mathcal{L}^2(Q^d, \mathbb{C})$
3. Is linear transform
4. Is continuous transform
5. Is unitary transform
6. Is invertible transform, defined by

$$[\mathbf{Z}^{-1}g](\mathbf{t}) = \int_{Q^d} g(\mathbf{t}, \boldsymbol{\omega}) d\boldsymbol{\omega}.$$

*Proof* All these results are simple extensions from the previous one-dimensional theorems.

**16.3.8.2 Multidimensional Weighted Continuous Zak Transform**

**Definition 16.14:** The multidimensional weighted continuous Zak transform of  $f \in \mathcal{L}^2(\mathbb{R}^d, \mathbb{C})$  is, for weight matrix  $\mathbf{M} \in \mathbb{R}^{d \times d}$ , defined to be

$$[\mathbf{Z}f](\mathbf{t}, \boldsymbol{\omega}) = \sum_{\mathbf{k} \in \mathbb{Z}^d} f(\mathbf{t} + \mathbf{M}\mathbf{k}) e^{-i2\pi\mathbf{k} \cdot \boldsymbol{\omega}} \quad (16.9)$$

a.e.  $(\mathbf{t}, \boldsymbol{\omega}) \in \mathbb{R}^d \times \mathbb{R}^d$ .

**16.3.8.3 Multidimensional Windowed, Weighted Continuous Zak Transform**

**Definition 16.15:** The multidimensional windowed, weighted continuous Zak transform of  $f \in \mathcal{L}^2(\mathbb{R}^d, \mathbb{C})$  is, for weight matrix  $\mathbf{M} \in \mathbb{R}^{d \times d}$  and window function  $w \in \mathcal{L}(\mathbb{R}^d, \mathbb{R}^+)$  with compact support, defined to be

$$[\mathbf{Z}f](\mathbf{t}, \boldsymbol{\omega}) = \sum_{\mathbf{k} \in \mathbb{Z}^d} f(\mathbf{t} + \mathbf{M}\mathbf{k}) w(\mathbf{k}) e^{-i2\pi\mathbf{k} \cdot \boldsymbol{\omega}} \quad (16.10)$$

a.e.  $(\mathbf{t}, \boldsymbol{\omega}) \in \mathbb{R}^d \times \mathbb{R}^d$ .

**16.4 Discrete Zak Transform**

The discrete Zak transform is analogous to the continuous Zak transform. The term “discrete” describes the input function. The input function will be a countable function, that is, a sequence. The output function will be discrete in  $t$  and continuum in  $\omega$ .

**16.4.1 Definitions**

**Definition 16.16:** The discrete Zak transform  $\mathbf{Z}$  of  $f \in \ell^2(\mathbb{Z}, \mathbb{C})$  is defined to be

$$[\mathbf{Z}f](m, \omega) = \sum_{k \in \mathbb{Z}} f(m+k) e^{-i2\pi k\omega}$$

for  $(m, \omega) \in \mathbb{Z} \times \mathbb{R}$ .

When  $f \in \mathcal{L}^2(\mathbb{R}, \mathbb{C})$  is defined at every integer, then the continuous Zak transform of  $f$  evaluated at the discrete times  $m \in \mathbb{Z}$  yields the same results as this discrete Zak transform.

**16.4.2 Properties**

The discrete Zak transform satisfies quasi-periodic conditions.

**THEOREM 16.25**

The discrete Zak transform  $\mathbf{Z} : \ell^2(\mathbb{Z}, \mathbb{C}) \rightarrow \ell^2(\mathbb{Z} \times \mathbb{R}, \mathbb{C})$  is

1. A total transform, that is,  $\mathcal{D}(\mathbf{Z}) = \ell^2(\mathbb{Z}, \mathbb{C})$ .
2. A linear transform, that is, for all  $\alpha, \beta \in \mathbb{C}$  and  $f, g \in \ell^2(\mathbb{Z}, \mathbb{C})$

$$\mathbf{Z}(\alpha f + \beta g) = \alpha \mathbf{Z}f + \beta \mathbf{Z}g$$

3. A continuous (equivalently, bounded) transform, and in particular,  $\|\mathbf{Z}f\|_{\text{out}} = \|f\|_{\text{in}}$  where

$$\|f\|_{\text{in}} = \left( \sum_{k \in \mathbb{Z}} |f(k)|^2 \right)^{1/2},$$

$$\|x\|_{\text{out}} = \left( \sum_{k \in \mathbb{Z}} \int_0^1 |x(k, \omega)|^2 d\omega \right)^{1/2}.$$

4. An unitary transform, that is,  $\langle \mathbf{Z}f | \mathbf{Z}g \rangle_{\text{out}} = \langle f | g \rangle_{\text{in}}$  for all  $f, g \in \ell^2(\mathbb{Z}, \mathbb{C})$  where

$$\langle f | g \rangle_{\text{in}} = \sum_{k \in \mathbb{Z}} f(k) \overline{g(k)},$$

$$\langle x | y \rangle_{\text{out}} = \sum_{k \in \mathbb{Z}} \int_0^1 x(k, \omega) \overline{y(k, \omega)} d\omega.$$

**16.4.3 Inverse Transform**

The unitary property of  $\mathbf{Z}$  implies that the inverse transform does exist. Observe the marginal property that motivates the inverse transform.

**THEOREM 16.26**

For every  $f \in \ell^2(\mathbb{Z}, \mathbb{C})$

$$f(m) = \int_0^1 [\mathbf{Z}f](m, \omega) d\omega$$

for  $m \in \mathbb{Z}$ .

*Proof* The proof is the same as for the inverse of the continuous Zak transform with  $t$  replaced with  $m$ .

**Definition 16.17:** The inverse discrete Zak transform of  $g \in \ell^2(\mathbb{Z} \times \mathbb{R}, \mathbb{C})$  is defined to be

$$[\mathbf{Z}^{-1}g](m) = \int_0^1 g(m, \omega) d\omega$$

for  $m \in \mathbb{Z}$ .

### 16.4.4 Extensions of the Discrete Zak Transform

Multidimensional discrete Zak transform takes as its input a complex-valued function  $f$  whose input is a multidimensional discrete set. That is,  $f \in \ell^2(\mathbb{Z}^d, \mathbb{C})$  where  $d \in \mathbb{N}$  is the dimension of the input set.

**Definition 16.18:** The multidimensional discrete Zak transform of  $f \in \ell^2(\mathbb{Z}^d, \mathbb{C})$  is defined to be

$$[\mathbf{Z}f](\mathbf{m}, \boldsymbol{\omega}) = \sum_{\mathbf{k} \in \mathbb{Z}^d} f(\mathbf{m} + \mathbf{k}) e^{-i2\pi \mathbf{k} \cdot \boldsymbol{\omega}}$$

for  $(\mathbf{m}, \boldsymbol{\omega}) \in \mathbb{Z}^d \times \mathbb{R}^d$ .

**Definition 16.19:** Let matrix  $\mathbf{M} \in \mathbb{Z}^{d \times d}$  generate a lattice of points in  $\mathbb{Z}^d$ , that is, for every  $\mathbf{k} \in \mathbb{Z}^d$  then  $\mathbf{M}\mathbf{k} \in \mathbb{Z}^d$ . The multidimensional weighted discrete Zak transform of  $f \in \ell^2(\mathbb{Z}^d, \mathbb{C})$  is defined to be

$$[\mathbf{Z}f](\mathbf{m}, \boldsymbol{\omega}) = \sum_{\mathbf{k} \in \mathbb{Z}^d} f(\mathbf{m} + \mathbf{M}\mathbf{k}) e^{-i2\pi \mathbf{k} \cdot \mathbf{M}^T \boldsymbol{\omega}}$$

for  $(\mathbf{m}, \boldsymbol{\omega}) \in \mathbb{Z}^d \times \mathbb{R}^d$ .

**Definition 16.20:** The multidimensional windowed, weighted discrete Zak transform of  $f \in \ell^2(\mathbb{Z}^d, \mathbb{C})$  is, for weight

matrix  $\mathbf{M} \in \mathbb{Z}^{d \times d}$  and window function  $w \in \ell^2(\mathbb{Z}^d, \mathbb{R}^+)$  with finite support, defined to be

$$[\mathbf{Z}_w f](\mathbf{m}, \boldsymbol{\omega}) = \sum_{\mathbf{k} \in \mathbb{Z}^d} f(\mathbf{t} + \mathbf{M}\mathbf{k}) w(\mathbf{k}) e^{-i2\pi \mathbf{k} \cdot \mathbf{M}^T \boldsymbol{\omega}} \quad (16.11)$$

for  $(\mathbf{m}, \boldsymbol{\omega}) \in \mathbb{Z}^d \times \mathbb{R}^d$ .

Consider the short-time discrete Fourier transform  $\mathbf{F}_w$  of  $f \in \ell^2(\mathbb{Z}, \mathbb{C})$  with window function  $w \in \ell^2(\mathbb{Z}, \mathbb{R}^+)$

$$[\mathbf{F}_w f](m, \omega) = \sum_{k \in \mathbb{Z}} f(k) w(k - m) e^{-i2\pi k \omega}.$$

Let  $\ell = k - m$  then  $k = \ell + m$  and

$$\begin{aligned} [\mathbf{F}_w f](m, \omega) &= \sum_{\ell \in \mathbb{Z}} f(\ell + m) w(\ell) e^{-i2\pi(\ell + m)\omega} \\ &= e^{-i2\pi m \omega} \sum_{\ell \in \mathbb{Z}} f(\ell + m) w(\ell) e^{-i2\pi \ell \omega} \\ &= e^{-i2\pi m \omega} [\mathbf{Z}_w f](m, \omega). \end{aligned}$$

**THEOREM 16.27**

For every  $f \in \ell^2(\mathbb{Z}, \mathbb{C})$

$$[\mathbf{F}_w f](m, \omega) = [\mathbf{E}_{-m}^{(1)} \mathbf{Z}_w f](m, \omega)$$

for  $(m, \omega) \in \mathbb{Z} \times \mathbb{R}$ .

The multidimensional versions of this theorem follow by simple extensions.

## 16.5 Finite Zak Transform

### 16.5.1 Definition

The finite Zak transform is a special case of the discrete Zak transform where the input sequence is always a finite length sequence. Assume the length is some  $L \in \mathbb{N}$ , then define the finite set  $S = \{0, 1, \dots, L-1\}$ . Let  $\mathcal{F}(S, \mathbb{C})$  be the set of functions  $f: S \rightarrow \mathbb{C}$ , then  $f$  is, in fact, a finite sequence. Actually,  $\mathcal{F}(S, \mathbb{C}) = \mathbb{C}^L$  the complex vector space, and  $f$  is, essentially, a complex vector of length  $L$ .

**Definition 16.21:** The finite Zak transform of  $f \in \mathcal{F}(S, \mathbb{C})$  is defined to be

$$[\mathbf{Z}f](m, n) = \sum_{k \in S} f(m + k) e^{-i2\pi nk/L} = \sum_{k=0}^{L-1} f(m + k) e^{-i2\pi nk/L}$$

for  $(m, n) \in S \times S$ . Here,  $\overset{L}{+}$  means modulo  $L$  addition in  $S$ . Equivalently, one can use the periodic extension of  $f$  for  $m + k \notin S$ .

### 16.5.2 Properties

The finite Zak transform satisfies a quasi-periodic condition, in fact, a periodic condition.

---

#### THEOREM 16.28

(Quasi-periodic) For every  $f \in \mathcal{F}(S, \mathbb{C})$

1.  $[\mathbf{Z}f](m + L, n) = [\mathbf{Z}f](m, n)$  for  $(m, n) \in S \times S$ .
2.  $[\mathbf{Z}f](m, n + L) = [\mathbf{Z}f](m, n)$  for  $(m, n) \in S \times S$ .

*Proof* For  $f \in \mathcal{F}(S, \mathbb{C})$

1. And  $(m, n) \in S \times S$

$$\begin{aligned} [\mathbf{Z}f](m + L, n) &= \sum_{k \in S} f\left(m + L + k\right) e^{-i2\pi nk/L} \\ &= \sum_{k \in S} f\left(m + k\right) e^{-i2\pi nk/L} \\ &= [\mathbf{Z}f](m, n). \end{aligned}$$

2. For  $(m, n) \in S \times S$

$$\begin{aligned} [\mathbf{Z}f](m, n + L) &= \sum_{k \in S} f(m + k) e^{-i2\pi \left(\frac{n+L}{L}\right) k/L} \\ &= \sum_{k \in S} f(m + k) e^{-i2\pi nk/L} \\ &= [\mathbf{Z}f](m, n). \end{aligned}$$

Notice that the addition of  $n + L$  in the exponent  $e^{-i2\pi(n+L)k/L}$  can be  $\frac{L}{+}$  or  $\frac{\mathbb{R}}{+}$  since they both give the same answer. That is,

$$e^{-i2\pi \left(\frac{\mathbb{R}}{n+L}\right) k/L} = e^{-i2\pi nk/L - i2\pi Lk/L} = e^{-i2\pi nk/L} e^{-i2\pi k} = e^{-i2\pi(n)k/L}.$$


---

#### THEOREM 16.29

The finite Zak transform  $\mathbf{Z}$  is

1. A total transform, that is,  $\mathcal{D}(\mathbf{Z}) = \mathcal{F}(S, \mathbb{C})$ .
2. A linear transform from  $\mathcal{F}(S, \mathbb{C})$  into  $\mathcal{F}(S^2, \mathbb{C})$ .
3. A continuous (equivalently, bounded) transform, and in particular,  $\|\mathbf{Z}f\|_{\text{out}} = \|f\|_{\text{in}}$  where

$$\begin{aligned} \|f\|_{\text{in}} &= \left( \sum_{k \in S} |f(k)|^2 \right)^{1/2} \\ \|x\|_{\text{out}} &= \left( \sum_{k \in S} \sum_{\ell \in S} |x(k, \ell)|^2 \right)^{1/2}. \end{aligned}$$

4. an unitary transform, that is,  $\langle \mathbf{Z}f | \mathbf{Z}g \rangle_{\text{out}} = \langle f | g \rangle_{\text{in}}$  for all  $f, g \in \ell^2(\mathbb{Z}, \mathbb{C})$  where

$$\begin{aligned} \langle f | g \rangle_{\text{in}} &= \sum_{k \in S} f(k) \overline{g(k)} \\ \langle x | y \rangle_{\text{out}} &= \sum_{k \in S} \sum_{\ell \in S} x(k, \omega) \overline{y(k, \omega)}. \end{aligned}$$

### 16.5.3 Inverse Transform

Since  $\mathbf{Z}$  is unitary then its inverse exists. We expect its inverse to be a marginal operation.

---

**Definition 16.22:** The inverse finite Zak transform is, for every  $x \in \mathcal{F}(S^2, \mathbb{C})$ , defined to be

$$[\mathbf{Z}^{-1}x](m) = \frac{1}{L} \sum_{n=0}^{L-1} x(m, n) \quad (16.12)$$

for  $m \in S$ .

Just to check that this is correct, we determine  $\mathbf{Z}^{-1}\mathbf{Z}f$  for any  $f \in \mathcal{F}(S, \mathbb{C})$

$$\begin{aligned} [\mathbf{Z}^{-1}\mathbf{Z}f](m) &= \frac{1}{L} \sum_{n=0}^{L-1} \left( \sum_{k=0}^{L-1} f(m + k) e^{-i2\pi nk/L} \right) \\ &= \frac{1}{L} \sum_{k=0}^{L-1} \sum_{n=0}^{L-1} f(m + k) e^{-i2\pi nk/L} \\ &= \frac{1}{L} \sum_{n=0}^{L-1} \sum_{\ell=0}^{L-1} f(\ell) e^{-i2\pi n(\ell-m)/L} \quad \text{where } \ell = m + k \\ &= \frac{1}{L} \sum_{\ell=0}^{L-1} f(\ell) \left( \sum_{n=0}^{L-1} e^{-i2\pi n(\ell-m)/L} \right). \end{aligned}$$

Observe that when  $\ell - m = 0$  then  $e^{-i2\pi n(\ell-m)/L} = 1$  so

$$\sum_{n=0}^{L-1} e^{-i2\pi n(\ell-m)/L} = L$$

but when  $\ell - m \neq 0$  then

$$\begin{aligned} \sum_{n=0}^{L-1} e^{-i2\pi n(\ell-m)/L} &= \frac{1 - e^{-i2\pi L(\ell-m)/L}}{1 - e^{-i2\pi(\ell-m)/L}} = \frac{1 - e^{-i2\pi(\ell-m)}}{1 - e^{-i2\pi(\ell-m)/L}} \\ &= \frac{1 - 1}{1 - e^{-i2\pi(\ell-m)/L}} = 0. \end{aligned}$$

Therefore,

$$\begin{aligned} \frac{1}{L} \sum_{\ell=0}^{L-1} f(\ell) \left( \sum_{n=0}^{L-1} e^{-i2\pi n(\ell-m)/L} \right) &= \frac{1}{L} \sum_{\ell=0}^{L-1} f(\ell) L \delta(\ell - m) \\ &= f(m) \end{aligned}$$

and so

$$\mathbf{Z}^{-1}\mathbf{Z}f = f.$$

Hence, Equation 16.12 is the definition for the inverse finite Zak transform.

## 16.5.4 Extensions of the Finite Zak Transform

**Definition 16.23:** [35] The weighted finite Zak transform, with scalar weights  $M, N \in \mathbb{N}$ , of  $f \in \mathcal{F}(S, \mathbb{C})$  is defined to be

$$[\mathbf{Z}f](m, n) = \sum_{k \in S} f(m + Mk) e^{-i2\pi n N k / L}$$

for  $(m, n) \in S \times S$ .

**Definition 16.24:** Let matrix  $M \in S^{d \times d}$  generate a lattice of points in  $S^d$ . The Multidimensional weighted finite Zak transform of  $f \in \ell^2(S^d, \mathbb{C})$  is defined to be

$$[\mathbf{Z}f](\mathbf{m}, \mathbf{n}) = \sum_{\mathbf{k} \in S^d} f(\mathbf{m} + M\mathbf{k}) e^{-i2\pi \mathbf{k}^t M \mathbf{n}}$$

for  $(\mathbf{m}, \mathbf{n}) \in S^d \times S^d$ .

## 16.6 Applications

This section discusses some application areas where the Zak transform is used. At the same time, we insert some important references.

### 16.6.1 Mathematics

#### 16.6.1.1 Jacobi Theta Functions

Jacobi's third theta function,  $\Theta_3$ , is defined to be [1],

$$\Theta_3(z, q) \equiv 1 + 2 \sum_{k=1}^{\infty} q^{k^2} \cos(2nz) = \sum_{k=-\infty}^{\infty} q^{k^2} e^{-i2kz}$$

for  $z \in \mathbb{C}$  and nome  $q$  (a special function). "Theta functions are important because every one of the Jacobi elliptic functions can be expressed as the ratio of two theta functions" [1].

If  $f(t) = \exp(-ct^2)$  for constant  $c > 0$  then  $\mathbf{Z}f$  is related to  $\Theta_3$  by

$$\begin{aligned} [\mathbf{Z}f](t, \omega) &= \sum_{k \in \mathbb{Z}} e^{-c(t+k)^2} e^{-i2\pi k \omega} \\ &= \sum_{k \in \mathbb{Z}} e^{-c(t^2 + 2kt + k^2)} e^{-i2\pi k \omega} \end{aligned}$$

$$\begin{aligned} &= e^{-ct^2} \sum_{k \in \mathbb{Z}} e^{-ck^2} e^{-i2k(\pi\omega - ict)} \\ &= e^{-ct^2} \Theta_3(\pi\omega - ict, e^{-c}). \end{aligned}$$

Articles of interest are [4,13], and the book by Igusa [22].

#### 16.6.1.2 Gabor Expansions

In 1946, Gabor [14] (born Gábor Dénes) suggested the expansion of a signal into a discrete set of shifted and modulated Gaussian signals, that is, an expansion of the form

$$\sum_{k \in \mathbb{Z}} c_k e^{-(t+k)^2} e^{-i2\pi kt}$$

for some set of scalars  $\{c_k\}$ . His idea has various mathematical implications as well as the signal analysis applications. "The Zak transform can be helpful in determining the window function that corresponds to a given elementary signal and how it can be used to Gabor's expansion coefficients" [7]. Papers of special interest are by Gel'fand [15], Weil [38], Auslander and Tolimieri [4], Brezin [10], Heil and Walnut [19], Hernandez and Weiss [20], Piao et al. [28], Grochenig [18], Benedetto and Walnut [8], Benedetto et al. [9].

### 16.6.2 Physics

The physics community has used the Zak transform to investigate solid-state physics. Zak introduced this representation to construct a quantum mechanical representation for the motion of a Bloch electron in the presence of a magnetic or electric field. Articles of interest are by Zak [39–41], and Janssen [23].

### 16.6.3 Engineering

#### 16.6.3.1 Time-Frequency Analysis

The time-frequency representation of a signal will reveal more information than a time representation or frequency representation. In the articles by Auslander et al. [2,3], they presented an algorithm to compute coefficients of the finite double sum expansion of time-varying nonstationary signals and to synthesize them from a finite number of expansion coefficients. The algorithms are based on the computation of the discrete Zak transform.

Brodzik and Tolimieri [11] proposed a new, time-frequency formulation of the Gerchberg-Papoulis algorithm for extrapolation of band-limited signals. The new formulation is obtained by translating the constituent operations of the Gerchberg-Papoulis procedure, the truncation and the Fourier transform, into the language of the finite Zak transform. They showed that the use of the Zak transform results in a significant reduction of the computational complexity of the Gerchberg-Papoulis procedure and in an increased flexibility of the algorithm.

Other articles of interest are by Janssen [23,27]. There are a few books of interest in the time-frequency community, in particular, Cohen [12], Suter [31], and Tolimieri and An [37].

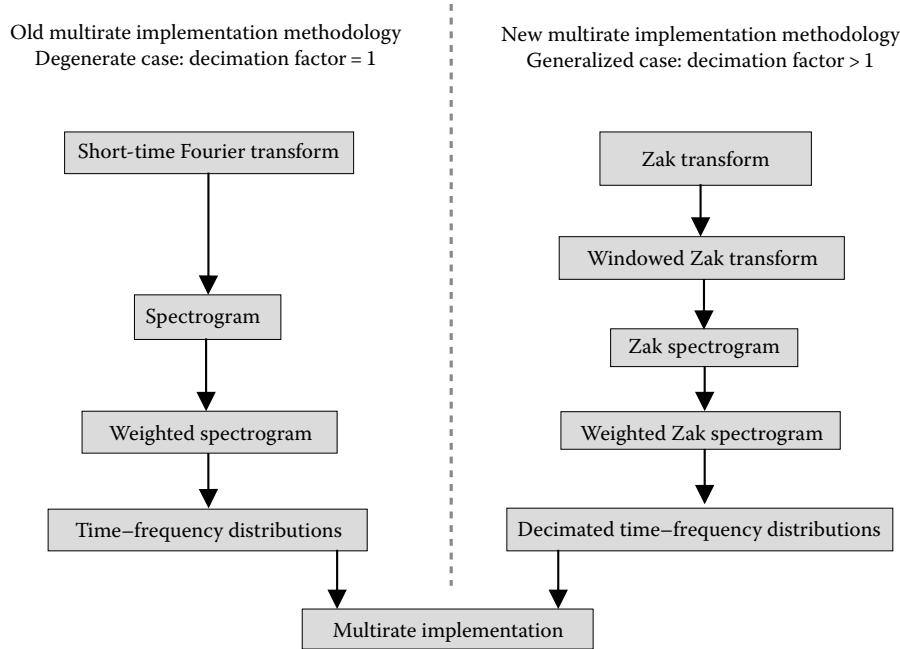


FIGURE 16.1 Interrelations of logical elements in O’Hair and Suter paper [26].

In [26], O’Hair and Suter define the Zak spectrogram and show the connection between the short-time Fourier transform (STFT) and the Zak transform. Figure 16.1 shows the relationship between old multirate implementation and new multirate implementation. The point of interest is how the Zak transform is key to the new implementation.

**16.6.3.2 Weighted Fast Fourier Transforms**

The main engine of almost every signal processing algorithm is the finite Fourier transform. The signal processing engineer has several goals when working with finite Fourier transforms: (1) make them fast, thus, the fast Fourier transform (FFT); and (2) make them big (i.e., large  $N$ ). The chip designer wishes to make the chip: (1) physically small; (2) small memory needs; and (3) a low power consumer. So, designing a chip that will compute the FFT has some conflicting goals.

In the mid-1960s, the problem of computing the FFT of a vector that was too large to fit into main memory was addressed by Gentleman and Sande [16]. In the late 1980s the approach was rediscovered by Bailey [5] for multiprocessor applications of the FFT algorithm running on hypercubes. The work done by Gentleman and Bailey, and even the work of Suter and Stevens [32] emphasized the connection to FFTs. As such, the Zak transform was not mentioned explicitly. In all of these papers, derivations were done in terms of FFTs, without realizing their intimate link to the Zak transform. In contrast, in the O’Hair and Suter paper [26], the Zak transform was explicitly mentioned. Also, the goal of the Suter–Stevens research (e.g., see [21]) was to “rediscover” the Zak transform approach as a mathematical abstraction to support the design of a low-power,

high-performance asynchronous FFT architecture. Their research produced a patent that we discuss next.

**16.6.3.2.1 Suter–Stevens Patent**

The patent by Suter and Stevens [33] uses the weighted finite Zak transform to perform the finite Fourier transform. We give the theory to demonstrate the application of the Zak transform.

Recall the finite Fourier transform of  $x \in \mathbb{R}^N$  to be

$$X(m) = [Fx](m) = \sum_{n=0}^{N-1} x(n)e^{-i2\pi mn/N} \quad \text{for } m = 0, 1, \dots, N - 1.$$

Assume  $N = N_1N_2$  for  $N_1, N_2 \in \mathbb{N}$ . Let

$$\begin{aligned} m &= m_1 + N_1m_2, \\ n &= N_2n_1 + n_2, \end{aligned}$$

where

$$\begin{aligned} m_1, n_1 &= 0, 1, \dots, N_1 - 1, \\ m_2, n_2 &= 0, 1, \dots, N_2 - 1. \end{aligned}$$

The polyphase components of  $x$  are  $x_{n_2}$  where, for each  $n_2 = 0, 1, \dots, N_2 - 1$ ,

$$x_{n_2}(n_1) = x(N_2n_1 + n_2) \quad \text{for } n_1 = 0, 1, \dots, N_1 - 1.$$

The finite Fourier transform of  $x_{n_2}$  yields for each  $m_1 = 0, 1, \dots, N_1 - 1$ ,

$$\begin{aligned}
X_{m_1}(m_2) &= \sum_{n_2=0}^{N_2-1} \sum_{n_1=0}^{N_1-1} x_{n_2}(n_1) e^{-i2\pi m_1 \frac{n_1}{N_1}} \\
&= \sum_{n_2=0}^{N_2-1} \sum_{n_1=0}^{N_1-1} x_{n_2}(n_1) \exp \left[ -i2\pi \left( \frac{m_1 + N_1 m_2}{N_1} \right) \left( \frac{N_2 n_1 + n_2}{N_2} \right) \right] \\
&= \sum_{n_2=0}^{N_2-1} \sum_{n_1=0}^{N_1-1} x_{n_2}(n_1) \exp \left[ -i2\pi \left( m_2 n_1 + \frac{m_1 n_1}{N_1} + \frac{m_2 n_2}{N_2} + \frac{m_1 n_2}{N_1 N_2} \right) \right] \\
&= \sum_{n_2=0}^{N_2-1} \sum_{n_1=0}^{N_1-1} x_{n_2}(n_1) e^{-i2\pi m_2 n_1} e^{-i2\pi \frac{m_1 n_1}{N_1}} e^{-i2\pi \frac{m_2 n_2}{N_2}} e^{-i2\pi \frac{m_1 n_2}{N_1 N_2}} \\
&= \sum_{n_2=0}^{N_2-1} \left[ e^{-i2\pi \frac{m_1 n_2}{N_1 N_2}} \left( \sum_{n_1=0}^{N_1-1} x_{n_2}(n_1) e^{-i2\pi \frac{m_1 n_1}{N_1}} \right) \right] e^{-i2\pi \frac{m_2 n_2}{N_2}} \\
&= \sum_{n_2=0}^{N_2-1} \left[ e^{-i2\pi \frac{m_1 n_2}{N_1 N_2}} \left( \sum_{n_1=0}^{N_1-1} x(n_1 N_2 + n_2) e^{-i2\pi \frac{m_1 n_1}{N_1}} \right) \right] e^{-i2\pi \frac{m_2 n_2}{N_2}} \\
&= X(m_2 N_1 + m_1).
\end{aligned}$$

Observe that

$$\sum_{n_1=0}^{N_1-1} x(n_1 N_2 + n_2) e^{-i2\pi \frac{m_1 n_1}{N_1}}$$

is the weighted finite Zak transform  $[\mathbf{Z}_{N_2} x](n_2, m_1)$  with weight  $N_2$ . This yields the algorithm generated in the patent.

### Suter–Stevens Fast Fourier Transform Algorithm [33]

Given:  $N = N_1 N_2$  for some  $N_1, N_2 \in \mathbb{N}$ . Given:  $f(n)$  for  $n = 0, 1, \dots, N - 1$

1. Compute the  $N_2$ -weighted finite Zak transform

$$[\mathbf{Z}_{N_2} f](n_2, m_1) = \sum_{n_1=0}^{N_1-1} f(n_2 + n_1 N_2) e^{-i2\pi m_1 \frac{n_1}{N_1}}$$

for  $n_2 = 0, 1, \dots, N_2 - 1$  and  $m_1 = 0, 1, \dots, N_1 - 1$ .

2. Scale the answer from 1.

$$g(m_1 + n_2 N_1) \equiv e^{-i2\pi \frac{n_2 m_1}{N}} [\mathbf{Z}_{N_2} f](n_2, m_1)$$

for  $n_2 = 0, 1, \dots, N_2 - 1$  and  $m_1 = 0, 1, \dots, N_1 - 1$ .

3. Compute the  $N_1$ -weighted finite Zak transform of  $g$

$$[\mathbf{Z}_{N_1} g](m_1, m_2) = \sum_{n_2=0}^{N_2-1} g(m_1 + n_2 N_1) e^{-i2\pi m_2 \frac{n_2}{N_2}}$$

for  $m_1 = 0, 1, \dots, N_1 - 1$  and  $m_2 = 0, 1, \dots, N_2 - 1$

The FFT of  $f$  is the vector  $F$

$$F(m) = F(m_1 + m_2 N_1) = [\mathbf{Z}_{N_1} g](m_1, m_2)$$

for  $m_1 = 0, 1, \dots, N_1 - 1$  and  $m_2 = 0, 1, \dots, N_2 - 1$ .

The novelty of this patent is the hardware realization. Other articles related to this patent are [6,30,34,36].

## 16.7 Summary

In this section we summarize the properties of the continuous Zak transform. The functions  $f, g$  are complex-valued unless stated otherwise. The pair  $(t, \omega) \in Q = [0, 1] \times [0, 1]$  unless stated otherwise.

1.  $[\mathbf{Z}\bar{f}](t, \omega) = [\bar{\mathbf{Z}}f](t, -\omega)$ .
2.  $[\mathbf{Z}f](t, \omega) = [\bar{\mathbf{Z}}f](t, -\omega)$  for  $f$  real-valued.
3.  $[\mathbf{Z}f](t, \omega) = [\mathbf{Z}f](-t, -\omega)$  for  $f$  even.
4.  $[\mathbf{Z}f](t, \omega) = -[\mathbf{Z}f](-t, -\omega)$  for  $f$  odd.
5.  $\mathbf{Z}(\alpha f + \beta g) = \alpha \mathbf{Z}f + \beta \mathbf{Z}g$ .
6.  $[\mathbf{Z}f](t + 1, \omega) = e^{i2\pi\omega} [\mathbf{Z}f](t, \omega)$ .
7.  $[\mathbf{Z}f](t, \omega) = [\bar{\mathbf{Z}}f](t, -\omega)$ .
8.  $[\mathbf{Z}f](t + m, \omega) = e^{-i2\pi m\omega} [\mathbf{Z}f](t, \omega)$  for  $m \in \mathbb{Z}$ .
9.  $[\mathbf{Z}f](t, \omega + n) = [\mathbf{Z}f](t, \omega)$  for  $n \in \mathbb{Z}$ .
10.  $\mathbf{Z}f \star \mathbf{Z}g = \mathbf{Z}(f \star g)$ .
11.  $\mathbf{Z}f \star^2 \mathbf{Z}g = \mathbf{Z}(f \cdot g)$ .
12.  $\|\mathbf{Z}f\|_{\text{out}} = \|f\|_{\text{in}}$ .
13.  $\langle \mathbf{Z}f | \mathbf{Z}g \rangle_{\text{out}} = \langle f | g \rangle_{\text{in}}$ .
14.  $[\mathbf{Z}^{-1}g](t) = \int_0^1 g(t, \omega) d\omega$ .
15.  $\int_0^1 [\mathbf{Z}f](t, \omega) e^{-i2\pi\omega t} dt = [\mathbf{F}f](\omega)$ .
16.  $[\mathbf{Z}\mathbf{E}f](\omega, -t) = e^{-i2\pi t\omega} [\mathbf{Z}f](t, \omega)$ .
17.  $\mathbf{F}_2(\mathbf{Z}f \cdot \bar{\mathbf{Z}}g)(m) = [\mathbf{F}(f \cdot g)](m)$  for  $m \in \mathbb{Z}$ , where  $[\bar{\mathbf{Z}}g](t, \omega) \equiv [\mathbf{Z}g](t, -\omega)$ .
18.  $\mathbf{Z}f = \sum_{k \in \mathbb{Z}} \mathbf{E}_k^{(2)} \mathbf{T}_k f$ .
19.  $\mathbf{Z}\mathbf{T}_m f = \mathbf{E}_m^{(2)} \mathbf{Z}f$  for  $m \in \mathbb{Z}$ .
20.  $\mathbf{Z}\mathbf{T}_a f = \mathbf{T}_a^{(1)} \mathbf{Z}f$  for  $a \in \mathbb{R} - \mathbb{Z}$ .
21.  $\mathbf{Z}\mathbf{E}_m f = \mathbf{E}_m^{(1)} \mathbf{Z}f$  for  $m \in \mathbb{Z}$ .
22.  $\mathbf{Z}\mathbf{E}_a f = \mathbf{E}_a^{(1)} \mathbf{T}_a^{(2)} \mathbf{Z}f$  for  $a \in \mathbb{R} - \mathbb{Z}$ .
23.  $\mathbf{Z}\mathbf{E}_m^{(2)} \mathbf{T}_m f = \mathbf{Z}f$  for  $m \in \mathbb{Z}$ .
24.  $\mathbf{Z}\mathbf{E}_m^{(2)} \mathbf{T}_n f = \mathbf{E}_{m-n}^{(2)} \mathbf{Z}f$  for  $m, n \in \mathbb{Z}$ .
25.  $\mathbf{Z}\mathbf{E}_a^{(2)} \mathbf{T}_a f = \mathbf{Z}f$  for  $a \in \mathbb{R} - \mathbb{Z}$ .
26.  $\mathbf{Z}\mathbf{T}_m \mathbf{E}_n f = \mathbf{E}_{n,m}^{(1,2)} \mathbf{Z}f$  for  $m, n \in \mathbb{Z}$ .



## References

1. Abramowitz, M. and Stegun, I, *Handbook of Mathematical Functions with Formulas, Graphs, and Mathematical Tables*. Washington, DC: U.S. Government Printing Office, 1964.
2. Auslander, L., Gertner, C., and Tolimieri, R., The discrete Zak transform application to time-frequency analysis and synthesis of nonstationary signals, *IEEE Trans. Signal Process.*, 39:825–835 (April 1991).
3. Auslander, L., Gertner, I., and Tolimieri, R., The finite Zak transform and the finite Fourier transform, *Institute for Mathematics and Its Applications*, 39:21–36 (1992).
4. Auslander, L. and Tolimieri, R., *Abelian Harmonic Analysis, Theta Functions and Function Algebra on Nilmanifolds*. New York: Springer-Verlag, 1975.
5. Bailey, D., FFTs in external or hierarchical memory, *J. Supercomput.*, 4:23–35 (1990).
6. Barnhart, D., Duggan, P., Suter, B., Brothers, C., and Stevens, K., Total ionizing dose characterization of a commercially fabricated asynchronous FFT for space applications, Government Microcircuit Application Conference (GOMAC – 200), Anaheim, CA, March 2000.
7. Bastiaans, M., Gabor's expansion and the Zak transform for continuous-time and discrete-time signals. *Signal and Image Representation in Combined Spaces 7. Wavelet Analysis and Its Applications*, R. R. Coifman Y. Y. Zeevi (eds.), Chapter 2, pp. 23–70. San Diego, CA: Academic Press, 1998.
8. Benedetto, J. and Walnut, D. Gabor Frames for  $L^2$  and related spaces, Chapter 3, pp. 97–162. *Wavelets: Mathematics and Applications*. Boca Raton, FL: CRC Press, 994.
9. Benedetto, J. J., Czaja, W., Gadzinski, P., and Powell, A. M. The Balian–Low theorem and regularity of Gabor systems, *J. Geom. Anal.*, 13(2):217–232 (2003).
10. Brezin, J. Function theory on metabelian solvmanifolds, *J. Funct. Anal.*, 10:33–51 (1972).
11. Brodzik, A. K. and Tolimieri, R. Gerchberg–Papoulis algorithm and the finite Zak transform. *Proceedings of SPIE, Wavelet Applications in Signal and Image Processing VIII*, vol. 4119, A. Aldroubi, et al. (eds.) pp. 1084–1093, San Diego, CA, December 2000.
12. Cohen, L. *Time Frequency Analysis: Theory and Applications*. Signal Processing Series. Englewood Cliffs, NJ: Prentice-Hall, 1995.
13. Foth, T. and Neretin, Y. A. Zak transform, Weil representation, and integral operators with theta-kernels, *International Mathematics Research Notices* (2004), pp. 2305–2327, Oxford, 2004.
14. Gabor, D. Theory of communication, *Proc. Inst. Electr. Eng.*, 93(III):429–457 (1946).
15. Gel'fand, I. Eigenfunction expansions for an equation with periodic coefficients, *Dokl. Akad. Nauk. SSR*, 76:1117–1120 (1950) (in Russian).
16. Gentleman, W. M. and Sande, G. Fast Fourier transforms for fun and profit. *1966 Fall Joint Computer Conf.* 29, pp. 563–578. Washington, DC: Spartan, 1966.
17. Gertner, I. and Tolimieri, R. Multiplicative Zak transform, *J. Vis. Commun. Image Represent.*, 6(1):89–95 (March 1996).
18. Gröchenig, K. *Foundations of Time–Frequency Analysis*. Borton, MA: Birkhäuser, 2001.
19. Heil, C. and Walnut, D. Continuous and discrete wavelet transforms, *SIAM Rev.*, 31(4):628–666 (December 1989).
20. Hernandez, E. and Weiss, G. *A First Course on Wavelets*. Boca Raton, FL: CRC Press, 1996.
21. Hunt, B. W., Stevens, K. S., Suter, B. W., and Gelosh., D. S. A single chip low power asynchronous implementation of an FFT algorithm for space applications. *Proceedings of the 4th International Symposium on Advanced Research in Asynchronous Circuits and Systems (ASYNC-98)*, pp. 216–223. San Diego, CA, 1998.
22. Igusa, J. *Theta Function*. Berlin, Germany/New York: Springer-Verlag, 1972.
23. Janssen, A. Bargmann transform, Zak transform, and coherent states, *J. Math. Phys.*, 23:720–731 (1982).
24. Janssen, A. The Zak transform: A signal transform for sampled time-continuous signals, *Philips J. Res.*, 43(1):23–69 (1988).
25. Naylor, A. W. and Sell, G. R. *Linear Operator Theory in Engineering and Science*, Vol. 40. Applied Mathematical Sciences. New York: Springer-Verlag, 1982.
26. O'Hair, J. R. and Suter, B. W. The Zak Transform and Decimated Time-Frequency Distributions, *IEEE Trans. Signal Process.*, 44(5):1099–1110 (May 1996).
27. Pei, S.-C. and Yeh, M.-H. Time and frequency split Zak transform for finite Gabor expansion, *Signal Process.*, 52(3):323–341 (1996).
28. Piao, Z., Zibulski, M., and Zeevi, Y. The multidimensional multi-window nonrectangular discrete Gabor schemes. *International Symposium on Time-Frequency and Time-Scale Analysis*, pp. 41–43. IEEE, Philadelphia, PA, October 1998.
29. Schempp, W. Radar ambiguity functions, the Heisenberg group and holomorphic theta series, *Proc. Am. Math. Soc.*, 92:103–110 (1984).
30. Stevens, K. S. and Suter, B. W. A mathematical approach to a low power FFT architecture. *International Symposium on Circuits and Systems (ISCAS-98)II*, pp. 21–24, Monterey, CA, June 1998.
31. Suter, B. W. *Multirate and Wavelet Signal Processing*, Vol. 8. *Wavelet Analysis and Its Applications*. San Diego, CA: Academic Press, 1998.
32. Suter, B. W. and Stevens, K. S. Low power, high performance FFT design. *IMACS World Congress on Scientific Computation, Modeling, and Applied Mathematics 1*, pp. 99–104, July 1997.
33. Suter, B. W. and Stevens, K. S., Low energy consumption, high performance fast Fourier transform. U.S. Patent 5,831,883, November 1998.
34. Suter, B. W. and Stevens, K. S. A low power, high performance approach for time-frequency time-scale computa-

- tions. *Proceedings of SPIE Conference on Advanced Signal Processing Algorithms, Architectures and Implementations VIII, vol. 3461*, pp. 86–90, San Diego, CA, July 1998.
35. Suter, B. W. and Stevens, K. A mathematical approach to a low power FFT architecture. *IEEE International Symposium on Circuits and Systems*, (ISCAS-98) pp. 21–24. IEEE, Monterey, CA, 1998.
  36. Suter, B. W., Stevens, K. S., Velazquez, S. R., and Nguyen, T. Multirate as a Hardware Paradigm. *International Conference on Acoustics, Speech, and Signal Processing (ICASSP-99) Vol IV*, pp. 1885–1888, Phoenix, AZ, March 1999.
  37. Tolimieri, R. and An, M. *Time-Frequency Representations*, 2nd edn. Boston, MA: Birkhauser, 1998.
  38. Weil, A. Sur certains groupes d'opérateurs unitaires, *Aeta Math.*, 111:143–211 (1964).
  39. Zak, J. Finite translation in solid state physics, *Phys. Rev. Lett.*, 19:1385–1397 (1967).
  40. Zak, J. Dynamics of electrons in solids in external fields, *Phys. Rev.*, 168:686–695 (1968).
  41. Zak, J. The kq-representation in the dynamics of electrons in solids, *Solid State Phys.*, 27:1–62 (1972).



# 17

## Discrete Time and Discrete Fourier Transforms

17.1	Introduction.....	17-1
17.2	Discrete-Time Fourier Transforms .....	17-1
	Definitions of Discrete-Time Fourier Transform (DTFT) • DTFT Properties • Finite Sequences • Frequency Response of LTI Discrete Systems • Approximation to Continuous-Time Fourier Transforms	
17.3	The Discrete Fourier Transform.....	17-5
	Definitions of the Discrete Fourier Transform • Properties of the DFT	
	References .....	17-12

Alexander D. Poularikas  
University of Alabama in Huntsville

### 17.1 Introduction

In this chapter we shall present both the discrete-time and discrete Fourier transforms (DFT). We shall also present their important properties and introduce examples to elucidate the mathematical relationships.

### 17.2 Discrete-Time Fourier Transforms

#### 17.2.1 Definitions of Discrete-Time Fourier Transform (DTFT)

The DTFT pair is

$$X(e^{j\omega}) \equiv \mathcal{F}_{\text{DT}}\{x(n)\} = \sum_{n=-\infty}^{\infty} x(n)e^{-j\omega n} \quad (17.1)$$

$$x(n) \equiv \mathcal{F}_{\text{DT}}^{-1}\{X(e^{j\omega})\} = \frac{1}{2\pi} \int_{-\pi}^{\pi} X(e^{j\omega})e^{j\omega n} d\omega \quad (17.2)$$

where  $X(e^{j\omega})$  is a periodic function with period  $2\pi$ . This implies that all the spectral information contained in the fundamental interval is necessary for the complete description of the signal.

If  $x(n)$  and  $X(e^{j\omega})$  are complex they have the form:

$$x(n) = x_r(n) + jx_i(n) \quad (17.3)$$

$$X(e^{j\omega}) = X_r(e^{j\omega}) + jX_i(e^{j\omega}) \quad (17.4)$$

Using the above equation, (Equations 17.1 and 17.2) become

$$X_r(e^{j\omega}) = \sum_{n=-\infty}^{\infty} (x_r(n) \cos \omega n + x_i(n) \sin \omega n) \quad (17.5)$$

$$X_i(e^{j\omega}) = \sum_{n=-\infty}^{\infty} (x_r(n) \sin \omega n - x_i(n) \cos \omega n) \quad (17.6)$$

$$x_r(e^{j\omega}) = \frac{1}{2\pi} \int_{-\pi}^{\pi} (X_r(e^{j\omega}) \cos \omega n - X_i(e^{j\omega}) \sin \omega n) d\omega \quad (17.7)$$

$$x_i(n) = \frac{1}{2\pi} \int_{-\pi}^{\pi} (X_r(e^{j\omega}) \sin \omega n + X_i(e^{j\omega}) \cos \omega n) d\omega \quad (17.8)$$

Based on the above equations, Table 17.1 can be easily completed.

#### Example:

Find the DTFT of the function:

$$x(n) = \begin{cases} e^{-an}n & 0 \leq n \leq N-1 \\ 0 & \text{otherwise} \end{cases} \quad (17.9)$$

#### Solution

Using Equation 17.1 we obtain

$$\begin{aligned} X(e^{j\omega}) &= \sum_{n=0}^{N-1} e^{-an} n e^{-j\omega n} \\ &= \frac{e^{-a} e^{-j\omega}}{(1 - e^{-a} e^{-j\omega})^2} [1 - N e^{-a(N-1)} e^{-j\omega(N-1)}] \\ &\quad + (N-1) e^{-aN} e^{-j\omega N} \end{aligned} \quad (17.10)$$

The signal  $x(n)$  and  $|X(e^{j\omega})|$  are shown in Figure 17.1 with  $a = 0.5$ .

**TABLE 17.1** Symmetry Properties of the Discrete-Time Fourier Transforms

Sequence	DTFT
<i>Complex signals</i>	
$x(n)$	$X(e^{j\omega})$
$x^*(n)$	$X^*(e^{-j\omega})$
$x^*(-n)$	$X^*(e^{j\omega})$
$x_r(n)$	$X_e(e^{j\omega}) = \frac{1}{2}[X(e^{j\omega}) + X^*(e^{-j\omega})]$
$jx_i(n)$	$X_o(e^{j\omega}) = \frac{1}{2}[X(e^{j\omega}) - X^*(e^{-j\omega})]$
$x_e(n) = \frac{1}{2}[x(n) + x^*(-n)]$	$X_r(e^{j\omega})$
$x_o(n) = \frac{1}{2}[x(n) - x^*(-n)]$	$jX_i(e^{j\omega})$
<i>Real signals</i>	
$x(n)$	$X(e^{j\omega}) = X^*(e^{-j\omega})$
$x(n)$	$X_r(e^{j\omega}) = X_r(e^{-j\omega})$
$x(n)$	$X_i(e^{j\omega}) = -X_i(e^{-j\omega})$
$x(n)$	$ X(e^{j\omega})  =  X(e^{-j\omega}) $
$x(n)$	$\text{angle } X(e^{j\omega}) = -\text{angle } X(e^{-j\omega})$
$x_e(n) = \frac{1}{2}[x(n) + x(-n)]$ (real and even)	$X_r(e^{j\omega})$ (real and even)
$x_o(n) = \frac{1}{2}[x(n) - x(-n)]$ (real and odd)	$jX_i(e^{j\omega})$ (imaginary and odd)

**17.2.2 DTFT Properties**

*Linearity:*

$$\begin{aligned} \mathcal{F}_{DT}\{x_1(n) + x_2(n)\} &= \mathcal{F}_{DT}\{x_1(n)\} + \mathcal{F}_{DT}\{x_2(n)\} \\ &= X_1(e^{j\omega}) + X_2(e^{j\omega}) \end{aligned} \quad (17.11)$$

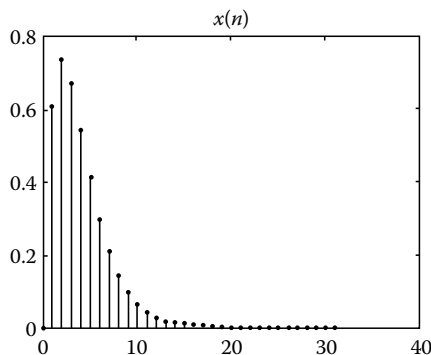
*Time shifting:*

If  $\mathcal{F}_{DT}\{x(n)\} = X(e^{j\omega})$ , then:

$$\mathcal{F}_{DT}\{x(n - n_0)\} = e^{-j\omega n_0} X(e^{j\omega}) \quad (17.12)$$

*Proof:*

$$\begin{aligned} \sum_{n=-\infty}^{\infty} x(n - n_0)e^{-j\omega n} &= \sum_{m=-\infty}^{\infty} x(m)e^{-j\omega(m+n_0)} \\ &= e^{-j\omega n_0} \sum_{m=-\infty}^{\infty} x(m)e^{-j\omega m} \end{aligned}$$



*Time reversal:* If  $\mathcal{F}_{DT}\{x(n)\} = X(e^{j\omega})$ , then:

$$\mathcal{F}_{DT}\{x(-n)\} = X(e^{-j\omega}) \quad (17.13)$$

*Convolution:* If  $\mathcal{F}_{DT}\{x(n)\} = X(e^{j\omega})$  and  $\mathcal{F}_{DT}\{y(n)\} = Y(e^{j\omega})$ , then:

$$G(e^{j\omega}) = \mathcal{F}_{DT}\{x(n) * y(n)\} = X(e^{j\omega})Y(e^{j\omega}) \quad (17.14)$$

*Proof:*

$$\begin{aligned} G(e^{j\omega}) &= \sum_{n=-\infty}^{\infty} \sum_{m=-\infty}^{\infty} x(m)y(n - m)e^{-j\omega n} \\ &= \sum_{n=-\infty}^{\infty} x(m) \sum_{m=-\infty}^{\infty} y(n - m)e^{-j\omega n} \\ &= \sum_{m=-\infty}^{\infty} x(m) \sum_{r=-\infty}^{\infty} y(r)e^{-j(m+r)\omega} \\ &= \sum_{m=-\infty}^{\infty} x(m)e^{-jm\omega} \sum_{r=-\infty}^{\infty} y(r)e^{-jr\omega} \end{aligned}$$

*Frequency shifting:* If  $\mathcal{F}_{DT}\{x(n)\} = X(e^{j\omega})$ , then:

$$\mathcal{F}_{DT}\{e^{j\omega_0 n} x(n)\} = X(e^{j(\omega - \omega_0)}), \quad (17.15)$$

*Time multiplication:* If  $\mathcal{F}_{DT}\{x(n)\} = X(e^{j\omega})$ , then:

$$\mathcal{F}_{DT}\{nx(n)\} = -z \frac{dX(z)}{dz} \Big|_{z=e^{j\omega}} \quad (17.16)$$

For proof, see Chapter 6.

*Modulation:* If  $\mathcal{F}_{DT}\{x(n)\} = X(e^{j\omega})$ , then:

$$\begin{aligned} \mathcal{F}_{DT}\{x(n) \cos \omega_0 n\} &= \frac{1}{2} \sum_{n=-\infty}^{\infty} x(n)e^{-j(\omega + \omega_0)n} \\ &\quad + \frac{1}{2} \sum_{n=-\infty}^{\infty} x(n)e^{-j(\omega - \omega_0)n} \\ &= \frac{1}{2} X(e^{j(\omega + \omega_0)}) + \frac{1}{2} X(e^{j(\omega - \omega_0)}) \end{aligned} \quad (17.17)$$

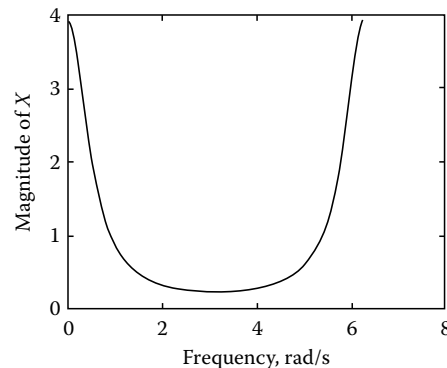


**FIGURE 17.1**

**Correlation:** If  $\mathcal{F}_{DT}\{x(n)\} = X(e^{j\omega})$  and  $\mathcal{F}_{DT}\{y(n)\} = Y(e^{j\omega})$ , then:

$$\begin{aligned} \mathcal{F}_{DT}\{x(n) \star y(n)\} &= \sum_{n=-\infty}^{\infty} \sum_{m=-\infty}^{\infty} x(m)y(m-n)e^{-j\omega n} \\ &= \sum_{m=-\infty}^{\infty} x(m) \sum_{n=-\infty}^{\infty} y(m-n)e^{-j\omega n} \\ &= \sum_{m=-\infty}^{\infty} x(m) \sum_{r=-\infty}^{\infty} y(r)e^{-j\omega(m-r)} \\ &= \sum_{m=-\infty}^{\infty} x(m)e^{-j\omega m} \sum_{r=-\infty}^{\infty} y(r)e^{-j(\omega-r)m} \\ &= X(e^{j\omega})Y(e^{-j\omega}) \end{aligned} \tag{17.18}$$

**Example:**

Find the autocorrelation of the signal  $x(n) = a^n u(n)$  for  $|a| < 1$ .

**Solution:**

Since  $\mathcal{F}_{DT}\{x(n)\} = \sum_{n=0}^{\infty} a^n e^{-j\omega n} = \sum_{n=0}^{\infty} (ae^{-j\omega})^n = \frac{1}{1-ae^{-j\omega}}$ , then from Equation 17.18

$$\mathcal{F}_{DT}\{x(n) \star y(n)\} = \frac{1}{1-ae^{-j\omega}} \frac{1}{1-ae^{-j\omega}} = \frac{1}{1-2a \cos \omega + a^2}$$

**Parseval's theorem:** If  $\mathcal{F}_{DT}\{x(n)\} = X(e^{j\omega})$  and  $\mathcal{F}_{DT}\{y(n)\} = Y(e^{j\omega})$ , then:

$$\sum_{n=-\infty}^{\infty} x(n)y^*(n) = \frac{1}{2\pi} \int_{-\pi}^{\pi} X(e^{j\omega})Y^*(e^{j\omega})d\omega \tag{17.19}$$

*Proof:*

$$\begin{aligned} &\frac{1}{2\pi} \int_{-\pi}^{\pi} \left[ \sum_{n=-\infty}^{\infty} x(n)e^{-jn\omega} \right] Y^*(e^{j\omega})d\omega \\ &= \sum_{n=-\infty}^{\infty} x(n) \frac{1}{2\pi} \int_{-\pi}^{\pi} Y^*(e^{j\omega})e^{-j\omega n} d\omega \end{aligned}$$

For the case  $x(n) = y(n)$ , then:

$$\sum_{n=-\infty}^{\infty} |x(n)|^2 = \frac{1}{2\pi} \int_{-\pi}^{\pi} |X(e^{j\omega})|^2 d\omega \tag{17.20}$$

**Multiplication of sequence:** If  $\mathcal{F}_{DT}\{x(n)\} = X(e^{j\omega})$  and  $\mathcal{F}_{DT}\{y(n)\} = Y(e^{j\omega})$ , then:

$$\begin{aligned} \mathcal{F}_{DT}\{x(n)y(n)\} &= \sum_{n=-\infty}^{\infty} x(n)y(n)e^{-j\omega n} \\ &= \sum_{n=-\infty}^{\infty} x(n) \left[ \frac{1}{2\pi} \int_{-\pi}^{\pi} Y(e^{j\lambda})e^{j\lambda n} d\lambda \right] e^{-j\omega n} \\ &= \frac{1}{2\pi} \int_{-\pi}^{\pi} Y(e^{j\lambda})d\lambda \sum_{n=-\infty}^{\infty} x(n)e^{-j(\omega-\lambda)n} \\ &= \frac{1}{2\pi} \int_{-\pi}^{\pi} Y(e^{j\lambda})X(e^{j(\omega-\lambda)})d\lambda \\ &= \frac{1}{2\pi} Y(e^{j\omega}) \star X(e^{j\omega}) \end{aligned} \tag{17.21}$$

**Differentiation in the frequency domain:** If  $\mathcal{F}_{DT}\{x(n)\} = X(e^{j\omega})$ , then:

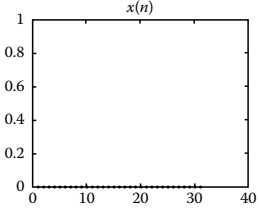
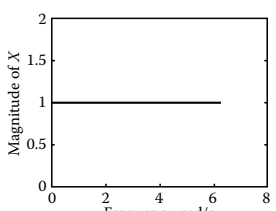
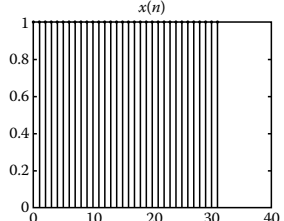
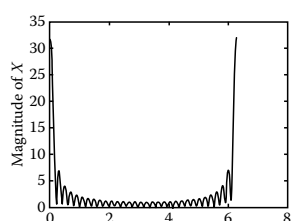
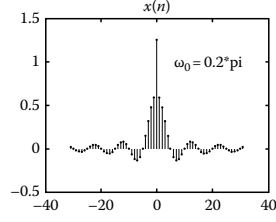
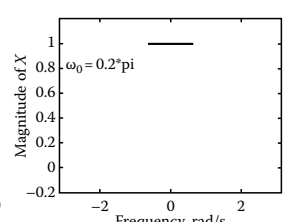
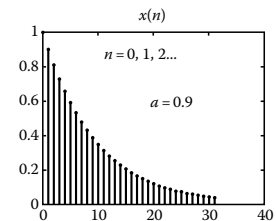
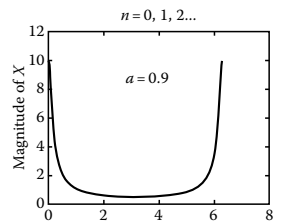
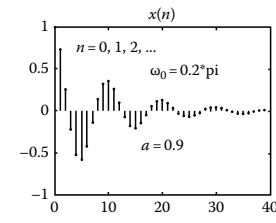
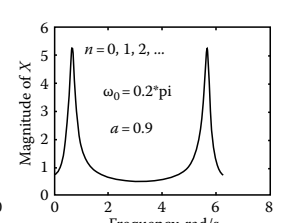
$$\begin{aligned} \frac{dX(e^{j\omega})}{d\omega} &= \frac{d}{d\omega} \left[ \sum_{n=-\infty}^{\infty} x(n)e^{-j\omega n} \right] \\ &= -j \sum_{n=-\infty}^{\infty} nx(n)e^{-j\omega n} = -j\mathcal{F}_{DT}\{nx(n)\} \end{aligned} \tag{17.22}$$

Table 17.2 presents the DTFT properties and Table 17.3 presents DTFT of some typical signals.

**TABLE 17.2** Properties of the Fourier Transform for Discrete-Time Signals

Property	Time Domain $x(n), y(n)$	Frequency Domain $X(e^{j\omega}), Y(e^{j\omega})$
Linearity	$ax(n) + by(n)$	$aX(e^{j\omega}) + bY(e^{j\omega})$
Time shifting	$x(n - n_0)$	$e^{-j\omega n_0} X(e^{j\omega})$
Time reversal	$x(-n)$	$X(e^{-j\omega})$
Convolution	$x(n) \star y(n)$	$X(e^{j\omega}) Y(e^{j\omega})$
Correlation	$x(n) \star y(n)$	$X(e^{j\omega}) Y(e^{-j\omega}) = X(e^{j\omega}) Y^*(e^{j\omega})$
Frequency shifting	$e^{j\omega_0 n} x(n)$	$X(e^{j(\omega-\omega_0)})$
Modulation	$x(n) \cos \omega_0 n$	$\frac{1}{2} X(e^{j(\omega+\omega_0)}) + \frac{1}{2} X(e^{j(\omega-\omega_0)})$
Multiplication	$x(n)y(n)$	$\frac{1}{2\pi} \int_{-\pi}^{\pi} X(e^{j\lambda})Y(e^{j(\omega-\lambda)})d\lambda$
Differentiation in the frequency domain	$nx(n)$	$j \frac{dX(e^{j\omega})}{d\omega}$
Conjugation	$x^*(n)$	$X^*(e^{-j\omega})$
Parseval's theorem	$\sum_{n=-\infty}^{\infty} x(n)y(n)$	$\frac{1}{2\pi} \int_{-\pi}^{\pi} X(e^{j\omega})Y^*(e^{j\omega})d\omega$

TABLE 17.3 DTFTs of Some Typical Discrete-Time Signals

Time Function $x(n)$	Magnitude of Spectrum $ X(e^{j\omega}) $
1. $x(n) = \delta(n)$	$X(e^{j\omega}) = 1$
	
2. $x(n) = u(n) - u(n - N - 1)$	$X(e^{j\omega}) = e^{-j\frac{\omega}{2}(N-1)} \frac{\sin \frac{\omega N}{2}}{\sin \frac{\omega}{2}}$
	
3. $x(n) = \frac{\sin \omega_0 n}{\pi n} \quad  \omega_0  < \pi$ $n = 0, \pm 1, \pm 2, \dots$	$X(e^{j\omega}) = \begin{cases} 1 &  \omega  < \omega_0 \\ 0 & \omega_0 \leq  \omega  \leq \pi \end{cases}$
	
4. $x(n) = a^n u(n)$	$X(e^{j\omega}) = \frac{1}{1 - ae^{-j\omega}}$
	
5. $x(n) = a^n \cos n\omega_0 u(n)$ $ \omega_0  < \pi$	$X(e^{j\omega}) = \frac{1}{2} \frac{1}{1 - ae^{-j(\omega - \omega_0)}} + \frac{1}{2} \frac{1}{1 - ae^{-j(\omega + \omega_0)}}$
	

### 17.2.3 Finite Sequences

Practical considerations usually dictate that we deal with truncated series. We must, therefore, consider the effect of the missing data, if, for example, the time series,  $x(n)$ , is defined in the whole interval  $0 \leq n < \infty$ .

The truncated Fourier transform is defined by

$$X_N(e^{j\omega}) = \sum_{n=0}^{N-1} x(n)e^{-j\omega n} \tag{17.23}$$

We introduce the Fourier transform of  $x(n)$  in this expression so that:

$$\begin{aligned} X_N(e^{j\omega}) &= \sum_{n=0}^{N-1} \left[ \frac{1}{2\pi} \int_{-\pi}^{\pi} X(e^{j\omega'}) e^{j\omega' n} d\omega' \right] e^{-j\omega n} \\ &= \frac{1}{2\pi} \int_{-\pi}^{\pi} X(e^{j\omega'}) \sum_{n=0}^{N-1} e^{-j(\omega - \omega') n} d\omega' \\ &= \frac{1}{2\pi} \int_{-\pi}^{\pi} X(e^{j\omega'}) W(e^{j(\omega - \omega')}) d\omega' = \frac{1}{2\pi} X(e^{j\omega}) * W(e^{j\omega}) \end{aligned} \tag{17.24}$$

where

$$W(e^{j\omega}) = \sum_{n=0}^{N-1} e^{-j\omega n} = e^{-j\omega(N-1)/2} \frac{\sin(\omega N/2)}{\sin(\omega/2)} \tag{17.25}$$

the transform function  $W(e^{j\omega})$  is the *rectangular window transform*. We observe that with a finite data sequence, a convolution operation appears. From Equation 17.24 we observe that to find  $X(e^{j\omega})$  we require  $W(e^{j\omega})$  to be a delta function in the interval  $-\pi \leq \omega \leq \pi$ . However, the amplitude of  $|W(e^{j\omega})| = \sin(\omega N/2)/\sin(\omega/2)$  has the properties of a delta function and approaches it as  $N \rightarrow \infty$ . Thus, the longer the time-data sequence that we observe, less distortion will occur in the spectrum of  $X(e^{j\omega})$ .

Because  $\mathcal{F}_{DT}^{-1}\{\pi\delta(\omega - \omega_0) + \pi\delta(\omega + \omega_0)\} = \cos \omega_0 n, \quad |\omega| < \pi$ , then its truncated Fourier transform is given by

$$\begin{aligned} X_N(e^{j\omega}) &\equiv \mathcal{F}_{DT}\{\cos \omega_0 n\} = e^{-j(\omega - \omega_0)(N-1)/2} \frac{\sin[(\omega - \omega_0)N/2]}{\sin[(\omega - \omega_0)/2]} \\ &\quad + e^{j(\omega - \omega_0)(N-1)/2} \frac{\sin[(\omega + \omega_0)N/2]}{\sin[(\omega + \omega_0)/2]} \end{aligned} \tag{17.26}$$

This indicates that instead of delta functions at  $\omega = \pm\omega_0$ , two sine functions appear. This phenomenon is known as the *smearing effect*.

### 17.2.4 Frequency Response of LTI Discrete Systems

The  $N$ th-order discrete system is characterized by the difference equation:

$$y(n) + a_1y(n - 1) + \dots + a_{N-1}y(n - N + 1) = b_0x(n) + b_1x(n - 1) + \dots + b_{N-1}x(n - N + 1) \quad (17.27)$$

Assuming that the transforms of  $y(n)$ ,  $x(n)$ , and the system impulse response  $h(n)$  exist, the above equation becomes:

$$H(e^{j\omega}) = \frac{Y(e^{j\omega})}{X(e^{j\omega})} = \frac{\sum_{i=0}^{N-1} b_i e^{-j\omega i}}{1 + \sum_{i=1}^{N-1} a_i e^{-j\omega i}} \quad (17.28)$$

where  $H(e^{j\omega})$  is its *transfer function*, a periodic function with period  $2\pi$ .

### 17.2.5 Approximation to Continuous-Time Fourier Transforms

The Fourier transform of a continuous time function is given by

$$X(\Omega) = \int_{-\infty}^{\infty} x(t)e^{-j\Omega t} dt \quad (17.29)$$

where  $\Omega$  is used to designate the frequency of a continuous-time function. We can approximate the above integral in the form:

$$X(\Omega) = \sum_{n=-\infty}^{\infty} \int_{nT}^{nT+T} x(t)e^{-j\Omega t} dt \cong \sum_{n=-\infty}^{\infty} Tx(nt)e^{-j\Omega Tn} \quad (17.30)$$

By comparing this equation with Equation 17.2, we observe the following correspondence:

$$x(n) = Tx(nT) \quad (17.31)$$

$$\omega = \Omega T \quad (17.32)$$

Therefore, the following steps can be taken to approximate the continuous-time Fourier transform:

1. Select the time interval  $T$  such that  $X(\Omega) \cong 0$  for all  $|\Omega| > \pi/T$
2. Sample  $x(t)$  at times,  $nT$ , to obtain  $x(nT)$
3. Compute the discrete time Fourier transform using the sequence  $\{Tx(nT)\}$
4. The resulting approximation is then:  $X(\Omega) \cong X(e^{j\omega})$  for  $-\pi/T < \Omega < \pi/T$

## 17.3 The Discrete Fourier Transform

### 17.3.1 Definitions of the Discrete Fourier Transform

The discrete Fourier transform pair is defined by

$$X(k) \equiv \mathcal{F}_D\{x(n)\} = \sum_{n=0}^{N-1} x(n)e^{-j2\pi kn/N}, \quad k = 0, 1, 2, \dots, N - 1 \quad (17.33)$$

$$x(n) \equiv \mathcal{F}_D^{-1}\{X(k)\} = \frac{1}{N} \sum_{k=0}^{N-1} X(k)e^{j2\pi kn/N}, \quad n = 0, 1, 2, \dots, N - 1 \quad (17.34)$$

where  $X(k) \equiv X(2\pi k/N)$ . If we substitute Equation 17.33 in Equation 17.34, we obtain

$$\begin{aligned} & \frac{1}{N} \sum_{k=0}^{N-1} \left[ \sum_{m=0}^{N-1} x(m)e^{-j2\pi km/N} \right] e^{j2\pi kn/N} \\ &= \frac{1}{N} \sum_{m=0}^{N-1} x(m) \sum_{k=0}^{N-1} e^{-j2\pi(m-n)k/N} \end{aligned}$$

But the last summation is equal to zero for  $m \neq n$  and equal to one for  $m = n$  and, thus, the last expression becomes  $x(n)N/N = x(n)$  which proves that Equations 17.33 and 17.34 are the DFT pair.

#### 17.3.1.1 DFT as a Linear Transformation

Equations 17.23 and 17.24 can be considered as linear transformations for the sequences  $x(n)$  and  $X(k)$ . Let  $x_N$  be an  $N$ -point vector of the signal sequence and  $X_N$  is an  $N$ -point sequence of the frequency samples. We can write Equation 17.33 in the form

$$\underline{X}_N = \underline{W}_N \underline{x}_N \quad (17.35)$$

where

$$\underline{X}_N = \begin{bmatrix} X(0) \\ X(1) \\ \vdots \\ X(N-1) \end{bmatrix}, \quad \underline{x}_N = \begin{bmatrix} x(0) \\ x(1) \\ \vdots \\ x(N-1) \end{bmatrix},$$

$$\underline{W}_N = \begin{bmatrix} 1 & 1 & 1 & \dots & 1 \\ 1 & e^{-j2\pi/N} & (e^{-j2\pi/N})^2 & \dots & (e^{-j2\pi/N})^{N-1} \\ \vdots & & & & \vdots \\ 1 & (e^{-j2\pi/N})^{N-1} & (e^{-j2\pi/N})^{2N-1} & \dots & (e^{-j2\pi/N})^{(N-1)(N-1)} \end{bmatrix} \quad (17.36)$$

If the inverse of  $\underline{W}_N$  exists, then Equation 17.35 gives

$$\underline{x}_N = \underline{W}_N^{-1} \underline{X}_N \quad (17.37)$$



which is the inverse discrete Fourier transform (IDFT). The matrix  $\underline{W}_N$  is symmetric and has the properties

$$\underline{W}_N^{-1} = \frac{1}{N} \underline{W}_N^*, \quad \underline{W}_N \underline{W}_N^* = N \underline{I}_N \quad (17.38)$$

where

$\underline{I}_N$  is an  $N \times N$  identity matrix

$\underline{W}_N$  is an orthogonal (unitary matrix)

### 17.3.2 Properties of the DFT

*Periodicity:* If  $x(n)$  and  $X(k)$  are DFT pair, then

$$x(n+N) = x(n) \quad \text{for all } n \quad (17.39)$$

$$X(k+N) = X(k) \quad \text{for all } k \quad (17.40)$$

which can easily be proved from Equations 17.33 and 17.34

*Linearity:* If  $\mathcal{F}_D\{x(n)\} = X(k)$  and  $\mathcal{F}_D\{y(n)\} = Y(k)$ , then

$$\mathcal{F}_D\{ax(n) + by(n)\} = aX(k) + bY(k) \quad (17.41)$$

This is easily proved using Equations 17.33 and 17.34 and applying the linearity property of the summation operator.

*Circular symmetries:* The DFT of finite duration sequence,  $x(n)$  for  $0 \leq n \leq N-1$ , is equivalent to  $N$ -point DFT of the periodic sequence

$$x_p(n) = \sum_{\ell=-\infty}^{\infty} x(n - \ell N) \quad (17.42)$$

The shifted form of this equation is

$$x_{sp} = x_p(n-k) = \sum_{\ell=-\infty}^{\infty} x(n-k-\ell N) \quad (17.43)$$

and from this we can define the new finite-duration sequence

$$x_s(n) = \begin{cases} x_{sp} & 0 \leq n \leq N-1 \\ 0 & \text{otherwise} \end{cases} \quad (17.44)$$

which is related to the original sequence  $x(n)$  by a circular shift. Hence, Equation 17.44 can be written in the form

$$x_s = x(n-k, \text{ modulo } N) \equiv x((n-k))_N \quad (17.45)$$

If an  $N$ -point sequence is folded; then modulo- $N$  operators are the argument  $x(-n)$  is defined by

$$x((-n)) = \begin{cases} x(0) & n = 0 \\ x(N-n) & 0 \leq n \leq N-1 \end{cases} \quad (17.46)$$

and is called a *circular folding*. The sequence  $x(n)$  is folded counterclockwise and the points  $n=0$  and  $n=N$  overlap. The DFT is given by

$$\mathcal{F}_D\{x((-n))_N\} = X((-k))_N \begin{cases} X(0) & k = 0 \\ X(N-k) & 1 \leq k \leq N-1 \end{cases} \quad (17.47)$$

For the circular shift of  $x_s(n)$  with  $k=2$  and  $N=4$ , we obtain  $x_s(n) = x((n-2))_4$  and, thus,

$$x_s(0) = x((-2))_4 = x(2) \quad x_s(1) = x((-1))_4 = x(3)$$

$$x_s(2) = x((0))_4 = x(0) \quad x_s(3) = x((1))_4 = x(1)$$

$$\text{Circularly even: } x(N-n) = x(n) \quad 1 \leq n \leq N-1 \quad (17.48)$$

$$\text{Circularly odd: } x(N-n) = -x(n) \quad 1 \leq n \leq N-1 \quad (17.49)$$

$$\text{Circularly even periodic: } x_p(n) = x_p(-n) = x_p(N-n) \quad (17.50)$$

$$\text{Circularly odd periodic: } x_p(n) = -x_p(-n) = -x_p(N-n) \quad (17.51)$$

$$\text{Conjugate even periodic: } x_p(n) = x_p^*(N-n) \quad (17.52)$$

$$\text{Conjugate odd periodic: } x_p(n) = -x_p^*(N-n) \quad (17.53)$$

The above suggests the following relationships:

$$x_p(n) = x_{pe}(n) + x_{po}(n) \quad (17.54)$$

$$x_{pe}(n) = \frac{1}{2} [x_p(n) + x_p^*(N-n)] \quad (17.55)$$

$$x_{po}(n) = \frac{1}{2} [x_p(n) - x_p^*(N-n)]$$

#### 17.3.2.1 Symmetry Properties of the DFT

Let an  $N$ -point sequence  $\{x(n)\}$  and its DFT are complex valued. Hence, we can express them in the form

$$x(n) = x_r(n) + jx_i(n) \quad 0 \leq n \leq N-1 \quad (17.56a)$$

$$X(k) = X_r(k) + jX_i(k) \quad 0 \leq k \leq N-1 \quad (17.56b)$$

Introducing these relationships into Equations 17.33 and 17.34, we obtain

$$X_r(k) = \sum_{n=0}^{N-1} \left[ x_r(n) \cos \frac{2\pi kn}{N} + x_i(n) \sin \frac{2\pi kn}{N} \right] \quad (17.57a)$$

$$X_i(k) = - \sum_{n=0}^{N-1} \left[ x_r(n) \sin \frac{2\pi kn}{N} - x_i(n) \cos \frac{2\pi kn}{N} \right] \quad (17.57b)$$

$$x_r(k) = \frac{1}{N} \sum_{n=0}^{N-1} \left[ X_r(k) \cos \frac{2\pi kn}{N} - X_i(k) \sin \frac{2\pi kn}{N} \right] \quad (17.58a)$$

$$x_i(k) = \frac{1}{N} \sum_{k=0}^{N-1} \left[ X_r(k) \sin \frac{2\pi kn}{N} + X_i(k) \cos \frac{2\pi kn}{N} \right] \quad (17.58b)$$

### 17.3.2.2 Real-Valued Sequences

If the sequence  $x(n)$  is real, it follows directly from the DFT pair that

$$X(N - k) = X^*(k) = X(-k) \quad (17.59)$$

As a result of the above equation, we obtain

$$|X(N - k)| = |X(k)|, \quad \text{angle}\{X(N - k)\} = -\text{angle}\{X(k)\} \quad (17.60)$$

Since  $x_i(n) = 0$ , the  $x(n)$  can be determined by Equation 17.58a.

### 17.3.2.3 Real and Even Sequences

If  $x(n)$  is real and even; that is

$$x(n) = x(N - n), \quad 0 \leq n \leq N - 1 \quad (17.61)$$

then Equation 17.57b yields  $X_i(k) = 0$  and, hence, the DFT becomes

$$X(k) = \sum_{n=0}^{N-1} x(n) \cos \frac{2\pi kn}{N}, \quad 0 \leq k \leq N - 1 \quad (17.62)$$

which is real and even. In addition,  $X_i(k) = 0$  and the IDFT reduces to

$$x(n) = \frac{1}{N} \sum_{k=0}^{N-1} X(k) \cos \frac{2\pi kn}{N}, \quad 0 \leq n \leq N - 1 \quad (17.63)$$

### 17.3.2.4 Real and Odd Sequences

If  $x(n)$  is real and odd ( $x_i(n) = 0$ ); that is

$$x(n) = -x(N - n) \quad (17.64)$$

then Equation 17.57a yields  $X_r(k) = 0$ , and hence, the DFT becomes (see also Equation 17.56b)

$$X(k) = -j \sum_{n=0}^{N-1} x(n) \sin \frac{2\pi kn}{N}, \quad 0 \leq k \leq N - 1 \quad (17.65)$$

which is purely imaginary and odd. Since  $X_r(k) = 0$ , the IDFT reduces to

$$x(n) = j \frac{1}{N} \sum_{k=0}^{N-1} X(k) \sin \frac{2\pi kn}{N}, \quad 0 \leq n \leq N - 1 \quad (17.66)$$

### 17.3.2.5 Imaginary Sequences

If  $x(n) = jx_i(n)$ , Equations 17.57a and 17.56b reduce to

$$X_r(k) = \sum_{n=0}^{N-1} x_i(n) \sin \frac{2\pi kn}{N} \quad (17.67a)$$

$$X_i(k) = \sum_{n=0}^{N-1} x_i(n) \cos \frac{2\pi kn}{N} \quad (17.67b)$$

$X_r(k)$  is odd and  $X_i(k)$  is even. If  $x_i(n)$  is odd,  $X_i(k) = 0$  and, hence,  $X(k)$  is purely real. If  $x_i(n)$  is even,  $X_r(k) = 0$  and, hence  $X(k)$  is purely imaginary.

The symmetry properties are given in Table 17.4.

### 17.3.2.6 Circular Convolution

Let  $x_1(n)$ ,  $x_2(n)$ , and  $x_3(n)$  are three sequences of length  $N$ . Then, if we take the inverse transform of the DFT product  $X_1(k)X_2(k)$ , we obtain:

$$x_3(n) = \frac{1}{N} \sum_{k=0}^{N-1} X_1(k)X_2(k)e^{j\frac{2\pi nk}{N}}, \quad 0 \leq n \leq N - 1 \quad (17.68)$$

Substituting the inverse transform of  $X_1(k)$  and  $X_2(k)$  in Equation 17.68, we obtain the relation

$$x_3(m) = \sum_{n=0}^{N-1} x_1(n)x_2((m - n)N), \quad 0 \leq m \leq N - 1 \quad (17.69)$$

**TABLE 17.4** Symmetries of DFT

$N$ -Point Sequence $x(n)$ $0 \leq n \leq N - 1$	DFT $X(k)$ $0 \leq k \leq N - 1$
<i>Complex signals</i>	
$x(n)$	$X(k)$
$x^*(n)$	$X^*(N - k)$
$x^*(N - n)$	$X^*(k)$
$x_r(n)$	$X_e(k) = \frac{1}{2}[X(k) + X^*(N - k)]$
$jx_i(n)$	$X_o(k) = \frac{1}{2}[X(k) - X^*(N - k)]$
$x_e(n) = \frac{1}{2}[x(n) + x^*(N - n)]$	$X_r(k)$
$x_o(n) = \frac{1}{2}[x(n) - x^*(N - n)]$	$jX_i(k)$
<i>Real signals</i>	
$x(n)$	$X(k) = X^*(N - k)$
$x(n)$	$X_r(k) = X_r(N - k)$
$x(n)$	$X_i(k) = -X_i(N - k)$
$x(n)$	$ X(k)  =  X(N - k) $
$x(n)$	$\text{angle}\{X(k)\} = \text{angle}\{X(N - k)\}$
$x_e(n) = \frac{1}{2}[x(n) + x(N - n)]$	$X_r(k)$
$x_o(n) = \frac{1}{2}[x(n) - x(N - n)]$	$jX_i(k)$

**Example:**

The circular convolution of  $x_1(n) = \{1, 2, 1, 4\}$ ,  $x_2(n) = \{1, 2, 3, 4\}$  is found as follows

$$\begin{aligned} x_3(m) &= \sum_{n=0}^{N-1} x_1(n)x_2((m-n))_N, \quad x_3(0) = \sum_{n=0}^{N-1} x_1(n)x_2((-n))_N \\ &= x_1(0)x_2(0) + x_1(1)x_2(4-1) + x_1(2)x_2(4-2) \\ &\quad + x_1(3)x_2(4-3) = 1 \cdot 1 + 2 \cdot 4 + 1 \cdot 3 + 4 \cdot 2 = 20, \text{ etc.} \end{aligned}$$

Therefore, we write

$$\mathcal{F}_D\{x_1(n) \otimes x_2(n)\} = X_1(k)X_2(k), \quad 0 \leq k \leq N-1 \quad (17.70)$$

**17.3.2.7 Time Reversal**

If  $\mathcal{F}_D\{x(n)\} = X(k)$ , then

$$\begin{aligned} \mathcal{F}_D\{x((-n))_N\} &= \mathcal{F}_D\{x(N-n)\} = X((-k))_N \\ &= X(N-k), \quad 0 \leq k \leq N-1 \end{aligned} \quad (17.71)$$

*Proof:*

$$\begin{aligned} \mathcal{F}_D\{x(N-n)\} &= \sum_{n=0}^{N-1} x(N-n)e^{-j2\pi kn/N} = \sum_{m=0}^{N-1} x(m)e^{-j2\pi k(N-m)/N} \\ &= \sum_{m=0}^{N-1} x(m)e^{j2\pi km/N} = \sum_{m=0}^{N-1} x(m)e^{-j2\pi m(N-k)/N} \\ &= X(N-k) \end{aligned}$$

**17.3.2.8 Circular Time Shift**

If  $\mathcal{F}_D\{x(n)\} = X(k)$ , then

$$\mathcal{F}_D\{x((n-\ell))_N\} = X(k)e^{-j2\pi k\ell/N} \quad (17.72)$$

*Proof:*

$$\begin{aligned} \mathcal{F}_D\{x((n-\ell))_N\} &= \sum_{n=0}^{\ell-1} x((n-\ell))_N e^{-j2\pi k\ell/N} \\ &\quad + \sum_{n=\ell}^{N-1} x(n-\ell)e^{-j2\pi kn/N} \\ &= \sum_{n=0}^{\ell-1} x(n-\ell+n)_N e^{-j2\pi k\ell/N} \\ &\quad + \sum_{n=\ell}^{N-1} x(n-\ell)e^{-j2\pi kn/N} \\ &= \sum_{m=N-\ell}^{N-1} x(m)e^{-j2\pi k(m+\ell)/N} \\ &\quad + \sum_{m=0}^{N-1-\ell} x(m)e^{-j2\pi k(m+\ell)/N} \\ &= \sum_{m=0}^{N-1} x(m)e^{-j2\pi k(m+\ell)/N} = X(k)e^{-j2\pi k\ell/N} \end{aligned}$$

**17.3.2.9 Circular Frequency Shift**

If  $\mathcal{F}_D\{x(n)\} = X(k)$ , then

$$\mathcal{F}_D\{x(n)e^{j2\pi \ell n/N}\} = X((k-\ell))_N \quad (17.73)$$

**17.3.2.10 Complex-Conjugate**

If  $\mathcal{F}_D\{x(n)\} = X(k)$ , then

$$\mathcal{F}_D\{x^*(n)\} = X^*((-k))_N = X^*(N-k) \quad (17.74)$$

and since

$$\frac{1}{N} \sum_{k=0}^{N-1} X^*(k)e^{j2\pi kn/N} = \left[ \frac{1}{N} \sum_{k=0}^{N-1} X(k)e^{j2\pi k(N-n)/N} \right]^*$$

implies that

$$x^*((-n))_N = x^*(N-n) = \mathcal{F}_D^{-1}\{X^*(k)\} \quad (17.75)$$

**17.3.2.11 Circular Correlation**

If  $\mathcal{F}_D\{x(n)\} = X(k)$  and  $\mathcal{F}_D\{h(n)\} = H(k)$ , then the DFT of a circular cross-correlation is

$$\mathcal{F}_D\left\{\sum_{n=0}^{N-1} x(n)h^*((n-\ell))_N\right\} = X(k)H^*(k) \quad (17.76)$$

*Proof:* The correlation of Equation 17.76 can be represented as a circular convolution. Hence,

$$\mathcal{F}_D\{x(m) \otimes h^*(-m)\} = X(k)H^*(k) \quad (17.77)$$

where Equation 17.70 was used. Furthermore, if  $x(n) = h(n)$ , an autocorrelation case, then

$$\mathcal{F}_D\{x(m) \otimes x^*(-m)\} = |X(k)|^2 \quad (17.78)$$

**17.3.2.12 Product**

If  $\mathcal{F}_D\{x(n)\} = X(k)$  and  $\mathcal{F}_D\{h(n)\} = H(k)$ , then

$$\mathcal{F}_D\{x(n)h(n)\} = \frac{1}{N} X(k) \otimes H(k) \quad (17.79)$$

By interchanging the roles of time and frequency in the expression for the circular convolution, Equation 17.79 results.

17.3.2.13 Parseval's Theorem

If  $\mathcal{F}_D\{x(n)\} = X(k)$  and  $\mathcal{F}_D\{h(n)\} = H(k)$ , then

$$\sum_{n=0}^{N-1} x(n)h^*(n) = \frac{1}{N} \sum_{k=0}^{N-1} X(k)H^*(k) \quad (17.80)$$

*Proof:*  $\sum_{n=0}^{N-1} x(n)h^*((n-\ell)_N) = \frac{1}{N} \sum_{k=0}^{N-1} X(k)H^*(k)e^{j2\pi k\ell/N}$   
 from Equation 17.76, taking its inverse transform.

Setting  $\ell = 0$ , we obtain Equation 17.80.

Table 17.5 presents the DFT properties.

Table 17.6 presents several DFT's of specific functions. The functions in this chapter were calculated using MATLAB<sup>®</sup> software.

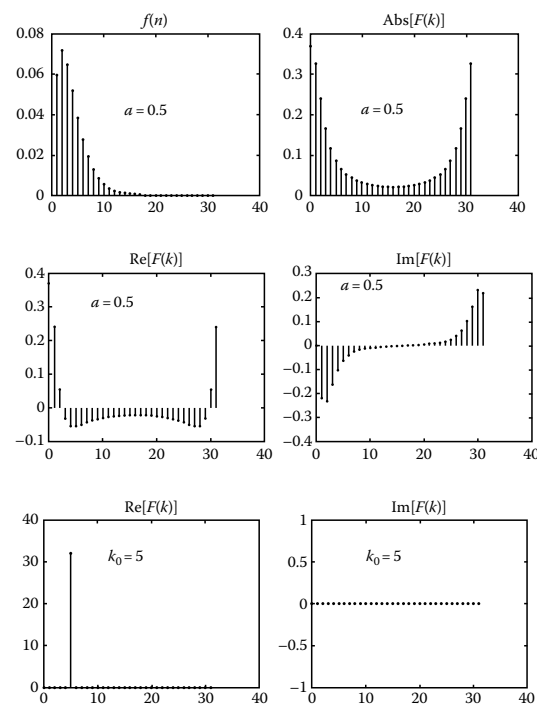
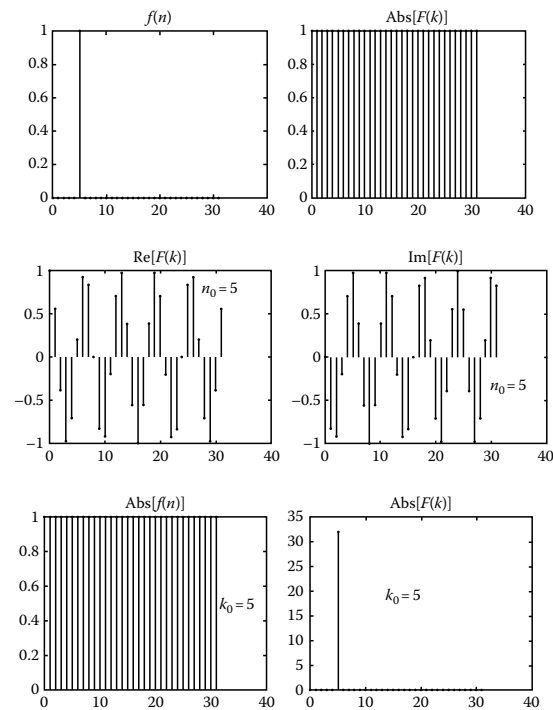
TABLE 17.5 Properties of DFT

Property	Time Functions $x(n), h(n)$	Frequency Domain Functions $X(k), H(k)$
Linearity	$ax(n) + bh(n)$	$aX(k) + bH(k)$
Periodicity	$x(n) = x(n+N)$	$X(k) = X(k+N)$
Time reversal	$x(N-n)$	$X(N-k)$
Circular time shift	$x((n-\ell)_N)$	$X(k)e^{-j2\pi k\ell/N}$
Circular frequency shift	$x(n)e^{j2\pi \ell n/N}$	$X((k-\ell)_N)$
Complex conjugate	$x^*(n)$	$X^*(N-k)$
Circular convolution	$x(n) \otimes h(n)$	$X(k)H(k)$
Circular correlation	$x(n) \otimes h^*(-n)$	$X(k)H^*(k)$
Multiplication	$x(n)h(n)$	$\frac{1}{N}X(k) \otimes H^*(k)$
Symmetry	$\frac{1}{N}X(n)$	$x(-k)$
Parseval's theorem	$\sum_{n=0}^{N-1} x(n)h^*(n) = \frac{1}{N} \sum_{k=0}^{N-1} X(k)H^*(k)$	

TABLE 17.6 Table of DFTs of Functions

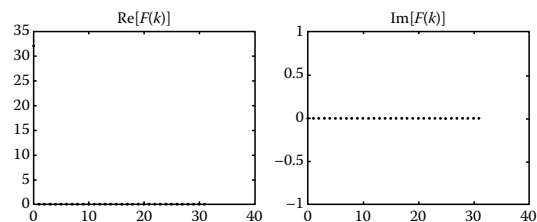
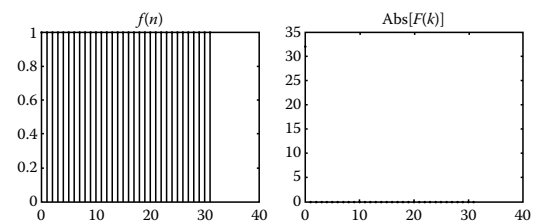
1.  $f(n) = \delta(n - n_0)$ ,  $0 \leq n_0 < N - 1$ ,  $n_0 = \text{integer}$   
 $0 \leq n < N - 1$

$$F(k) = e^{-j2\pi n_0 k/N}, \quad 0 \leq k \leq N - 1$$



2.  $f(n) = \exp(j2\pi k_0 n/N)$ ,  $0 < k_0 < N - 1$   
 $k_0 = \text{integer}$ ,  $0 \leq n \leq N - 1$

$$F(k) = \delta(k - k_0), \quad 0 \leq k \leq N - 1$$

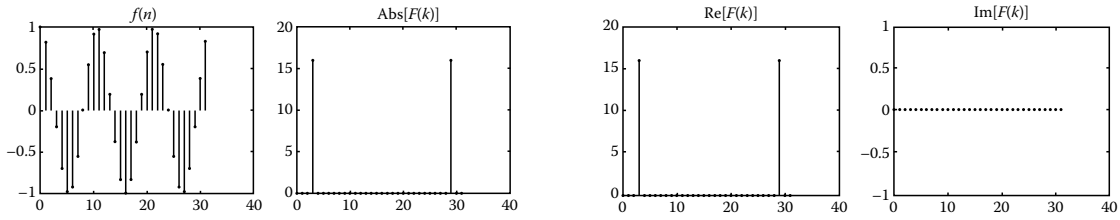


(continued)

TABLE 17.6 (continued) Table of DFTs of Functions

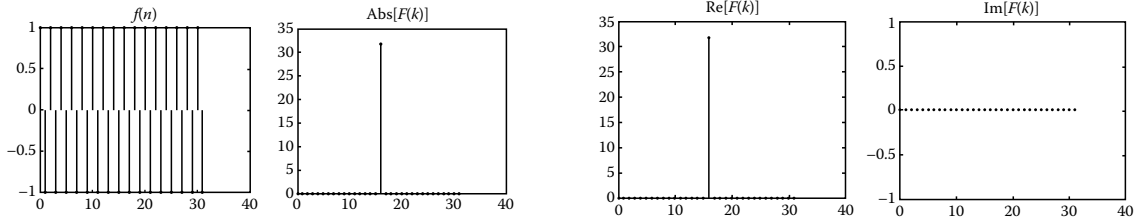
3.  $f(n) = u(n) - u(n - N), \quad 0 \leq n \leq N - 1$

$$F(k) = \begin{cases} 1 & k = 0 \\ 0 & \text{otherwise} \end{cases}$$



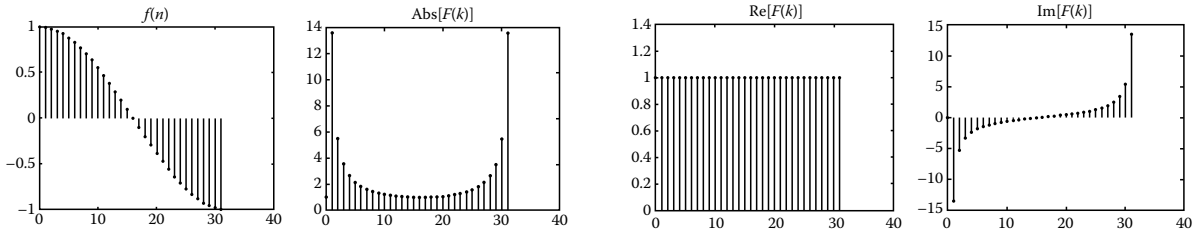
4.  $f(n) = \cos(2\pi k_0 n / N), \quad 0 < k_0 < N - 1$   
 $k_0 = \text{integer}, \quad 0 \leq n \leq N - 1$

$$F(k) \begin{cases} \frac{N}{2} \delta(k - k_0) & k = k_0 \\ \frac{N}{2} \delta[k - (N - k_0)] & k = N - k_0 \end{cases}$$



5.  $f(n) = \cos(\pi n), \quad 0 \leq n \leq N - 1$

$$F(k) = N\delta\left(k - \frac{N}{2}\right), \quad 0 \leq k \leq N - 1$$



6.  $f(n) = \cos\left(\frac{\pi n}{N}\right), \quad 0 \leq n \leq N - 1$

$$F(k) = \frac{1}{2} \frac{1 - \exp[-j(2\pi k - \pi)]}{1 - \exp\left[-j\left(\frac{2\pi k}{N} - \frac{\pi}{N}\right)\right]} + \frac{1}{2} \frac{1 - \exp[-j(2\pi k + \pi)]}{1 - \exp\left[-j\left(\frac{2\pi k}{N} + \frac{\pi}{N}\right)\right]}, \quad 0 \leq k \leq N - 1$$

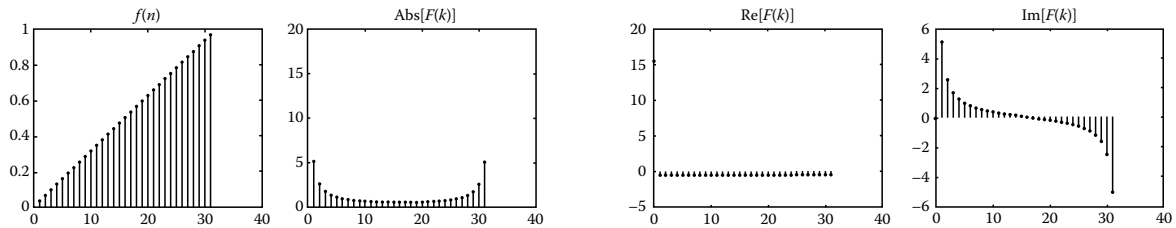
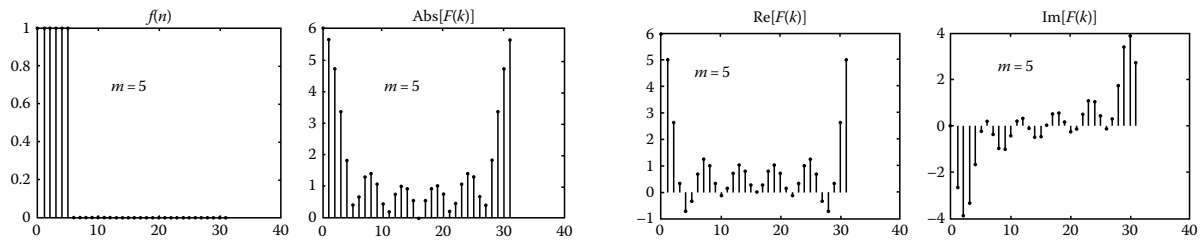


**TABLE 17.6 (continued)** Table of DFTs of Functions

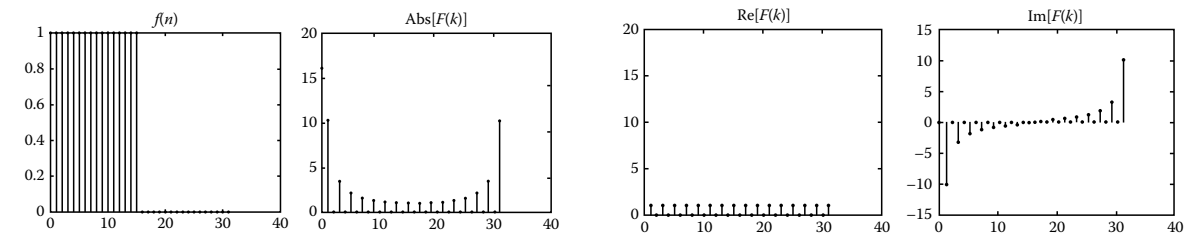
7.  $f(n) = n/N, \quad 0 \leq n \leq N - 1$

$$F(k) = \begin{cases} \frac{N}{2} & k = 0 \\ j \frac{\cos(k\pi) \sin(k\pi/N)}{2 \sin^2(k\pi/N)} & 0 < k \leq N - 1 \end{cases}$$



8.  $f(n) = \begin{cases} 1 & 0 \leq n \leq m \\ 0 & m < n \leq N - 1 \end{cases}$

$$F(k) = \exp\left(-j \frac{\pi k m}{N}\right) \frac{\sin\left(\frac{\pi k(m+1)}{N}\right)}{\sin\left(\frac{\pi k}{N}\right)}, \quad 0 \leq k \leq N - 1$$

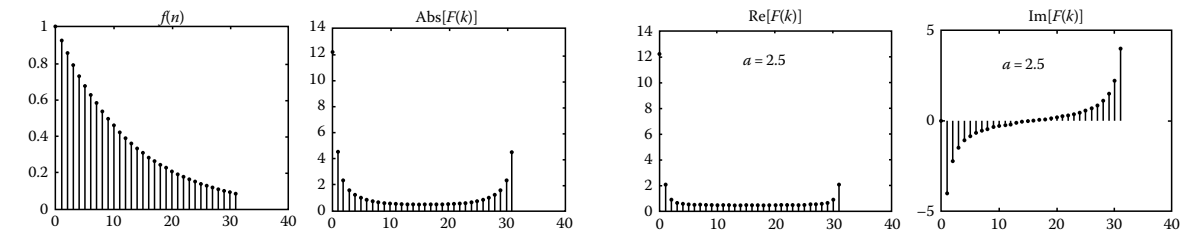


9.  $f(n) = \begin{cases} 1 & 0 \leq n \leq \frac{N}{2} - 1 \\ 0 & \frac{N}{2} < n \leq N - 1 \end{cases}$

$$F(k) = \exp\left[-j \frac{\pi k}{N} (N - 1)\right] \frac{\sin\left(\frac{\pi k}{2}\right)}{\sin\left(\frac{\pi k}{N}\right)}, \quad 0 \leq k \leq N - 1$$

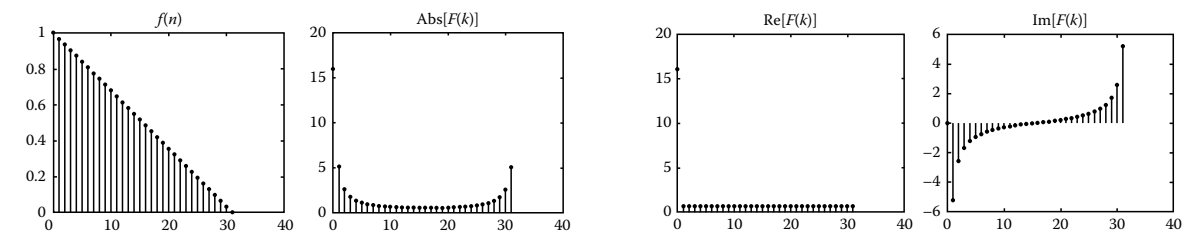
10.  $f(n) = \exp(-an/N), a = \text{positive constant}$   
 $0 \leq n \leq N - 1$

$$F(k) = \frac{1 - e^{-a} e^{-j2\pi k}}{1 - e^{-a/N} e^{-j2\pi k/N}}, \quad 0 \leq k \leq N - 1$$



11.  $f(n) = 1 - \frac{n}{N - 1}, \quad 0 \leq n \leq N - 1$

$$F(k) = \frac{1 - e^{-j2\pi k}}{1 - e^{-j2\pi k/N}} - \frac{1}{N - 1} \left[ e^{-j \frac{2\pi k}{N}} \left[ 1 - N e^{-j \frac{2\pi k(N-1)}{N}} + (N - 1) e^{-j2\pi k} \right] / \left( 1 - e^{-j \frac{2\pi k}{N}} \right)^2 \right], \quad 0 \leq k \leq N - 1$$



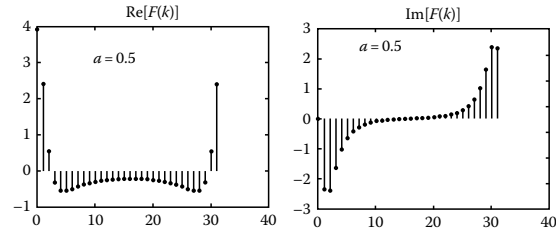
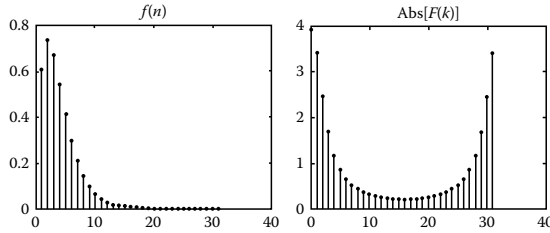
(continued)

TABLE 17.6 (continued) Table of DFTs of Functions

12.  $f(n) = ne^{-an}, \quad 0 \leq n \leq N - 1$   
 $a = \text{positive constant}$

$$F(k) = \frac{e^{-a} e^{-j\frac{2\pi k}{N}}}{\left(1 - e^{-a} e^{-j\frac{2\pi k}{N}}\right)^2} \times \left(1 - Ne^{-a(N-1)} e^{-j\frac{2\pi k(N-1)}{N}} + (N-1)e^{-aN} e^{-j\frac{2\pi k}{N}}\right),$$

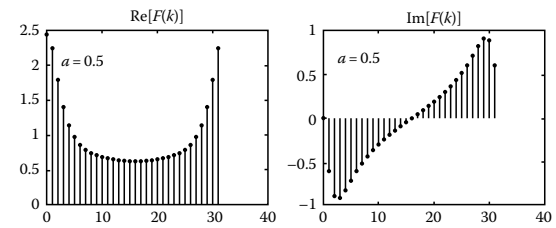
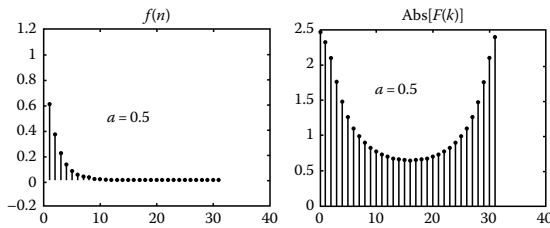
$0 \leq k \leq N - 1$



13.  $f(n) = e^{-an} \cos\left(\frac{\pi n}{N}\right), \quad 0 \leq n \leq N - 1$   
 $a = \text{positive constant}$

$$F(k) = \frac{1}{2} \frac{1 - e^{-aN} e^{-j\pi} e^{-j2\pi k}}{1 - e^{-a} e^{-j\frac{\pi}{N}} e^{-j\frac{2\pi k}{N}}} + \frac{1}{2} \frac{1 - e^{-aN} e^{j\pi} e^{-j2\pi k}}{1 - e^{-a} e^{j\frac{\pi}{N}} e^{-j\frac{2\pi k}{N}}}$$

$0 \leq k \leq N - 1$



14.  $f(n) = e^{an} \sin\left(\frac{\pi n}{N}\right), \quad 0 \leq n \leq N - 1$   
 $a = \text{positive constant}$

$$F(k) = \frac{1}{2j} \frac{1 - e^{-aN} e^{j\pi} e^{-j2\pi k}}{1 - e^{-a} e^{j\frac{\pi}{N}} e^{-j\frac{2\pi k}{N}}} - \frac{1}{2j} \frac{1 - e^{-aN} e^{-j\pi} e^{-j2\pi k}}{1 - e^{-a} e^{-j\frac{\pi}{N}} e^{-j\frac{2\pi k}{N}}}$$

$0 \leq k \leq N - 1$

## References

Oppenheim, A.V. and R.W. Schaffer. 1989. *Discrete-Time Signal Processing*, Prentice Hall, Englewood Cliffs, NJ.

Poularikas, A.D. 1998. *The Handbook of Formulas and Tables for Signal Processing*, CRC Press LLC, Boca Raton, FL.

Poularikas, A.D. and S. Seeley. 1995. *Signals and Systems*, 2nd edn., Krieger Publishing Co., Melbourne, FL.

Proakis, J.G. and D.G. Manolakis. 1996. *Digital Signal Processing*, Prentice Hall, Upper Saddle River, NJ.

# Discrete Chirp-Fourier Transform

---

18.1	Introduction.....	18-1
18.2	Discrete Chirp-Fourier Transform and Its Basic Properties for Single Component Chirp Signals.....	18-2
18.3	DCFT Properties for Multiple Component Chirp Signals .....	18-5
18.4	Connection to the Analog Chirp-Fourier Transform.....	18-6
18.5	Numerical Simulations.....	18-7
18.6	Conclusion .....	18-11
	References .....	18-14

Xiang-Gen Xia  
University of Delaware

Discrete Fourier transform (DFT) has found tremendous applications in almost all fields mainly because it can be used to match the multiple frequencies of a stationary signal with multiple harmonics. In many applications, wideband and nonstationary signals, however, often occur. One of the typical examples of such signals is chirp-type signals that are usually encountered in radar signal processing, such as synthetic aperture radar (SAR) and inverse SAR (ISAR) imaging. Due to the motion of a target, the radar return signals are usually chirps and their chirp rates include the information about the target, such as the location and the velocity.

In this chapter, we study discrete chirp-Fourier transform (DCFT), which is analogous to the DFT. Besides the multiple frequency matching similar to the DFT, the DCFT can be used to match the multiple chirp rates in a chirp-type signal with multiple chirp components. We show that, when the signal length  $N$  is prime, the magnitudes of all the sidelobes of the DCFT of a linear chirp signal are 1 while the magnitude of the mainlobe of the DCFT is  $\sqrt{N}$ . With this result, an upper bound for the number of the detectable chirp components using the DCFT is provided in terms of signal length, signal, and noise powers. We also show that the  $N$ -point DCFT performs optimally when  $N$  is a prime.

## 18.1 Introduction

Discrete Fourier transform (DFT) has been applied in almost all fields. The main reason is because the DFT matches the frequencies in a signal of multiple harmonics. In other words, if a signal has only several harmonics, the DFT of this signal has and only has peaks at the frequencies of the signal harmonics and the peak values correspond to the signal powers at the corresponding harmonic frequencies. Therefore, the DFT can be used to estimate the Fourier spectrum of a signal, which is known as

*spectrum estimation* that plays an important role in digital signal processing applications. However, in order to have the DFT work well, a signal has to be stationary. Although the stationarity assumption applies in many applications, nonstationary signals often occur in some real applications. Examples of nonstationary signals are chirp-type signals that are encountered in radar signal processing, such as in synthetic aperture radar (SAR) and inverse SAR (ISAR) imaging, see for example, Refs. [1,2]. In SAR imaging, when targets are moving, the radar return signals are chirps, in particular *linear chirps* when the velocities of the moving targets are constant. In ISAR imaging, when targets have maneuvering motions, the radar return signals are also chirps. It is well-known in the SAR and ISAR literature that the direct DFT applications to the radar return signals shall smear the SAR or ISAR images of the targets. Furthermore, the chirp rates in the radar return signals include the important information about the moving targets, such as the velocities and the location parameters of the moving targets in SAR imaging. Therefore, the estimation of the chirp rates are critically important in these applications.

For chirp-type signals, besides frequencies of multiple harmonics there are chirp rates of multiple chirps, and the DFT can be used only to match the multiple frequencies, but the multiple chirps in this case may even reduce the resolution of the frequency matching. The intent of this chapter is to generalize the DFT and its properties to discrete chirp-Fourier transform (DCFT) [3] and corresponding properties, which is used not only to match the multiple frequencies but also to match the multiple chirp rates, simultaneously.

It should be noticed that there have been many researches on chirp-type signals and their chirp rate estimations, such as high-order ambiguity functions [4–6], adaptive chirplet transforms [7], and other polynomial phase signal estimations [8–12]. Also, the

This work was supported in part by the Air Force Office of Scientific Research (AFOSR) under Grant No. FA9550-05-1-0161 and a DEPSCoR Grant W911NF-07-0422 through ARO.



chirp  $z$ -transform was proposed in Ref. [13] for the efficient DFT implementation but not for chirp rate estimation. However, the goal of this chapter is for chirp signal analysis and therefore different. We first generalize the DFT to the DCFT and then study the properties of the DCFT analogous to the DFT. In particular, we show that, when signal length  $N$  is a prime, the magnitudes of all the sidelobes (i.e., when the chirp rate is not matched) of the DCFT of a single linear chirp signal without noise are 1 while the magnitude of the mainlobe (i.e., when the chirp rate and the harmonic frequency are both matched) of the DCFT is  $\sqrt{N}$ . The mainlobe and sidelobe magnitude ratio in this case is  $\sqrt{N}$ , which is shown to be optimal for a given length  $N$ . In other words, the DCFT performs optimally in the matching of the constant frequency and the chirp rate, when the signal length  $N$  is a prime. When the chirp rate is precisely matched, the DCFT is reduced to the DFT. Notice that, for any signal length  $N$ , the magnitudes of all the sidelobes of the DFT of a single harmonic signal without noise are 0 while the magnitude of the mainlobe of the DFT is  $\sqrt{N}$ . The mainlobe and sidelobe magnitude ratio in this case is infinity, which tells us that  $N$  many different harmonics can be estimated using the DFT when there is no noise. In general, unlike the DFT for the harmonic estimation, less than  $\sqrt{N}$ , many different chirps can be estimated using the DCFT. This chapter is focused on linear chirps that are common in radar applications.

This chapter is organized as follows. In Section 18.2, we introduce the DCFT and study its basic properties for single component chirp signals. In Section 18.3, we study the properties of the DCFT for multiple component chirp signals. We present an upper bound for the number of the components such that they are detectable using the DCFT. In Section 18.4, we study its connection with the analog chirp-Fourier transform (ACFT). In Section 18.5, we present some numerical examples.

## 18.2 Discrete Chirp-Fourier Transform and Its Basic Properties for Single Component Chirp Signals

Before going to the DCFT, let us first briefly recall the DFT. For a signal  $x(n)$  with length  $N$ , its  $N$ -point DFT is defined as

$$X(k) = \frac{1}{\sqrt{N}} \sum_{n=0}^{N-1} x(n) W_N^{nk}, \quad 0 \leq k \leq N-1, \quad (18.1)$$

where  $W_N = \exp(-2\pi j/N)$ . The key properties of the DFT are based on the following elementary identity

$$\sum_{n=0}^{N-1} W_N^{nk} = N\delta(k), \quad 0 \leq k \leq N-1, \quad (18.2)$$

where  $\delta(k)$  takes 1 when  $k=0$ , and 0 otherwise. The identity 18.2 implies that, if  $x(n)$  is a single harmonic, i.e.,

$$x(n) = \exp\left(j2\pi \frac{k_0}{N} n\right),$$

for some integer  $k_0$  with  $0 \leq k_0 \leq N-1$ , then its DFT matches the frequency  $k_0$  perfectly, i.e.,

$$X(k) = \sqrt{N}\delta(k - k_0). \quad (18.3)$$

Based on this property, when  $x(n)$  has  $I$  harmonics with  $I \leq N$ , i.e.,

$$x(n) = \sum_{i=1}^I A_{k_i} \exp\left(j2\pi \frac{k_i}{N} n\right),$$

where  $k_{i_1} \neq k_{i_2}$  for  $i_1 \neq i_2$ , its DFT matches these frequencies perfectly, i.e.,

$$X(k) = \sqrt{N} \sum_{i=1}^I A_{k_i} \delta(k - k_i), \quad (18.4)$$

where the peaks in the DFT domain are shown at all  $k_i$  and the corresponding peak values are  $A_{k_i}$  for  $i=1, 2, \dots, I$ .

We now introduce the DCFT. Let  $x(n)$ ,  $0 \leq n \leq N-1$ , be a signal of length  $N$ . Its  $N$ -point DCFT is defined as

$$X_c(k, l) = \frac{1}{\sqrt{N}} \sum_{n=0}^{N-1} x(n) W_N^{ln^2 + kn}, \quad 0 \leq k, l \leq N-1, \quad (18.5)$$

where  $k$  represents the constant frequencies and  $l$  represents the chirp rates. From the above DCFT, one can see that, for each fixed  $l$ ,  $\{X_c(k, l)\}_{0 \leq k \leq N-1}$  is the DFT of the signal  $x(n)W_N^{ln^2}$ . When  $l=0$ , the DCFT is the same as the DFT. Therefore, the inverse DCFT (IDCFT) is

$$x(n) = W_N^{-ln^2} \frac{1}{\sqrt{N}} \sum_{k=0}^{N-1} X_c(k, l) W_N^{-kn}, \quad 0 \leq n \leq N-1, \quad (18.6)$$

where  $l$  is an arbitrarily fixed integer. The above connection between the DCFT and the DFT also suggests a fast algorithm to compute the DCFT, i.e., for each  $l$ , the Fast Fourier transform (FFT) may be used to compute  $X_c(k, l)$ ,  $0 \leq k \leq N-1$ . The computational complexity with this approach is, thus,  $O(N^2 \log(N))$ .

As a remark, the above chirp-Fourier transform is related to the fractional Fourier transform (FRFT), where the rotation angle is related to the variable  $l$  in the DCFT. For more about FRFT, see, for example, [14–18].

The above DCFT definition is not surprising to see by following the DFT definition. What is more interesting is its properties. Can it be used to match the chirp rates and the constant frequencies simultaneously? If so, how many of the chirp components can be matched simultaneously? Similar to the previous DFT study, let us first consider a single chirp signal

$$x(n) = W_N^{-(l_0 n^2 + k_0 n)}, \quad (18.7)$$

where  $k_0$  and  $l_0$  are two integers with  $0 \leq k_0, l_0 \leq N-1$ . When  $k$  and  $l$  in the DCFT (18.5) precisely match the above  $k_0$  and  $l_0$ , we have

$$X_c(k_0, l_0) = \sqrt{N},$$

which is called the mainlobe of the DCFT  $X_c(k, l)$ . The question of interest here is what happens when the chirp rate  $l$  and the constant frequency  $k$  do not match  $l_0$  and  $k_0$ , i.e., what the sidelobes of the DCFT are. Is there a similar property for the DCFT as Equation 18.3 for the DFT? To study these questions, we first have the following lemma.

---

### LEMMA 18.1

When  $N$  is a prime, we have the following identity: for  $0 \leq l, k \leq N-1$ ,

$$\left| \sum_{n=0}^{N-1} W_N^{ln^2+kn} \right| = \begin{cases} N, & l = 0 \text{ and } k = 0, \\ \sqrt{N}, & l \neq 0, \\ 0, & l = 0 \text{ but } k \neq 0. \end{cases} \quad (18.8)$$

*Proof* Let

$$P(k, l) \triangleq \sum_{n=0}^{N-1} W_N^{ln^2+kn}.$$

Then, for  $0 < l \leq N-1$ ,

$$\begin{aligned} |P(k, l)|^2 &= \sum_{n=0}^{N-1} W_N^{ln^2+kn} \sum_{m=0}^{N-1} W_N^{-lm^2-km} \\ &= \sum_{n=0}^{N-1} \sum_{m=0}^{N-1} W_N^{(n-m)(l(n+m)+k)} \\ &= \sum_{n=0}^{N-1} \sum_{e=0}^{N-1} W_N^{e(l(2n-e)+k)} \\ &= \sum_{e=0}^{N-1} \left( \sum_{n=0}^{N-1} W_N^{2eln} \right) W_N^{-e^2l+ek}, \end{aligned} \quad (18.9)$$

where  $e = n - m$  and the new range of  $e$  in the summation in Step 1 is from the periodicity of  $W_N^{ln}$  in terms of the integer variable  $n$  for any integer  $l$ . When  $N$  is a prime,  $2el$  for  $0 < l \leq N-1$  and  $0 \leq e \leq N-1$  is a multiple of  $N$  if and only if  $e$  is a multiple of  $N$ , i.e.,  $e = 0$ . Thus,

$$\sum_{n=0}^{N-1} W_N^{2eln} = 0 \quad \text{for } 0 < e, l \leq N-1.$$

Therefore,  $|P(k, l)|^2 = N$  when  $l \neq 0$ . When  $l = 0$ ,  $P(k, l)$  is reduced to Equation 18.2. This proves the lemma. q.e.d.

From the second half of the above proof, one can see why  $N$  needs to be prime in order for the second equality in Equation 18.8 to hold. From this lemma, we immediately have the following result.

---

### THEOREM 18.1 Let $x(n)$ be a single chirp

$$x(n) = W_N^{-(l_0 n^2 + k_0 n)}, \quad (18.10)$$

for some integers  $k_0$  and  $l_0$  with  $0 \leq k_0, l_0 \leq N-1$ . If the length  $N$  is a prime, then its DCFT magnitude has the following form

$$|X_c(k, l)| = \begin{cases} \sqrt{N}, & \text{when } l = l_0 \text{ and } k = k_0, \\ 1, & \text{when } l \neq l_0, \\ 0, & \text{when } l = l_0 \text{ but } k \neq k_0. \end{cases} \quad (18.11)$$

This result tells us that, for a single linear chirp, the peak or the mainlobe of its DCFT has value  $\sqrt{N}$  and appears at  $(k_0, l_0)$  in the DCFT domain, and the sidelobes are not above 1. In other words, the DCFT of a single linear chirp matches its chirp rate  $l_0$  and its constant frequency  $k_0$  simultaneously. Surprisingly, one can see that all the magnitudes of the sidelobes, unless the chirp rate is matched, are all the same, which are 1.

In chirp rate and the constant frequency estimation, the smaller the sidelobe magnitudes of the DCFT are, the better the performance of the estimation is. When  $N$  is a prime, from Equation 18.11 the maximal sidelobe magnitude of the DCFT is 1, i.e.,

$$\max_{(k, l) \neq (k_0, l_0)} |X_c(k, l)| = 1, \quad \text{when } N \text{ is a prime.} \quad (18.12)$$

One might want to ask what will happen when  $N$  is not a prime. The following result tells us that the maximal sidelobe magnitude is the minimal when  $N$  is a prime, i.e., the  $N$ -point DCFT performs the best when  $N$  is a prime in the estimation of chirp rates and constant frequencies. This shall be also seen from the numerical simulations in Section 18.5.

---

### THEOREM 18.2

Let  $x(n)$  be the same as in Theorem 18.1, i.e., have the form in Equation 18.10. If the length  $N$  is not a prime, then the maximal sidelobe magnitude of the DCFT satisfies

$$\max_{(k, l) \neq (k_0, l_0)} |X_c(k, l)| \geq \sqrt{2}. \quad (18.13)$$

*Proof* To prove Equation 18.13, it is enough to prove that, when  $N$  is not a prime, the following inequality holds

$$\max_{(k, l) \neq (0, 0)} |P(k, l)|^2 \geq 2N, \quad (18.14)$$

where  $P(k, l)$  is defined in the proof of Lemma 18.1. Assume  $N$  is not a prime and let  $N = N_1 N_2$  with  $N_1 \geq 2$  and  $N_2 \geq 2$ .

**Case (i):** Both  $N_1$  and  $N_2$  are odd. In this case, let  $l = N_1$  and  $k = 0$ . Then, by Equation 18.9,

$$\begin{aligned} |P(k, l)|^2 &= \sum_{e=0}^{N_1-1} \left( \sum_{n=0}^{N_2-1} W_{N_2}^{2en} \right) W_{N_2}^{-e^2} \\ &= N_1 \sum_{e=0}^{N_1-1} \left( \sum_{n=0}^{N_2-1} W_{N_2}^{2en} \right) W_{N_2}^{-e^2}. \end{aligned}$$

Since  $N_2$  is odd,  $2e$  is a multiple of  $N_2$  if and only if  $e$  is a multiple of  $N_2$ . Thus,

$$\sum_{n=0}^{N_2-1} W_{N_2}^{2en} = 0, \text{ if } e \text{ is not a multiple of } N_2.$$

Therefore, by setting  $e = e_1 N_2$  we have

$$\begin{aligned} |P(k, l)|^2 &= N_1 \sum_{e_1=0}^{N_1-1} \left( \sum_{n=0}^{N_2-1} W_{N_2}^{2e_1 N_2 n} \right) W_{N_2}^{-e_1^2 N_2^2} \\ &= N_1 \sum_{e_1=0}^{N_1-1} N_2 = N_1^2 N_2 \geq 2N \end{aligned}$$

**Case (ii):** One of  $N_1$  and  $N_2$  is even. Without loss of generality, we may assume  $N_2 = 2$ . Let  $k = l = N_1$ . In this case,  $W_N^{2eln} = 1$ . Thus, by Equation 18.9,

$$|P(k, l)|^2 = N \sum_{e=0}^{N-1} W_2^{-e(e-1)}.$$

Notice that  $e(e-1)$  is always even, which implies  $W_2^{-e(e-1)} = 1$ . Therefore,

$$|P(k, l)|^2 = N^2 \geq 2N.$$

By combining Case (i) and Case (ii), Equation 18.14 is proved. q.e.d.

By this result, in what follows we only consider prime  $N$ . The above results are based on the assumption that both  $l_0$  and  $k_0$  in Equation 18.10 are integers. In practice, these two parameters may not be precisely integers. Next, we want to briefly discuss the DCFT performance when they are not integers but close to integers. The reason why we only consider the case when  $l_0$  and  $k_0$  are close to integers is because of the following argument.

Let us consider an analog chirp signal

$$x_a(t) = \exp(j(\beta_0 t^2 + \alpha_0 t)), \quad (18.15)$$

and consider the sampling  $t = n/N^{1/3}$ . Then, the sampled chirp becomes

$$\begin{aligned} \tilde{x}(n) \triangleq x_a\left(\frac{n}{N^{1/3}}\right) &= \exp\left(j\left(\frac{\beta_0}{N^{2/3}} n^2 + \frac{\alpha_0}{N^{1/3}} n\right)\right) \\ &= W_N^{-(\tilde{l}_0 n^2 + \tilde{k}_0 n)}, \end{aligned} \quad (18.16)$$

where  $\tilde{l}_0 = \beta_0 N^{1/3}/(2\pi)$  and  $\tilde{k}_0 = \alpha_0 N^{2/3}/(2\pi)$ . Therefore, when  $N$  is large enough (i.e., the sampling rate is fast enough), there exist integers  $l_0$  and  $k_0$  such that

$$\tilde{l}_0 = \frac{\beta_0 N^{1/3}}{2\pi} \approx l_0 \quad \text{and} \quad \tilde{k}_0 = \frac{\alpha_0 N^{2/3}}{2\pi} \approx k_0. \quad (18.17)$$

This implies that the real chirp rate is  $\beta_0 \approx 2\pi l_0 N^{-1/3}$  and the real constant frequency is  $\alpha_0 \approx 2\pi k_0 N^{-2/3}$  when integers  $l_0$  and  $k_0$  are estimated. It also tells us that for a practical chirp signal  $x_a(t)$  in Equation 18.15, we only need to consider the discrete chirp signal  $\tilde{x}(n)$  in Equation 18.16 with parameters  $\tilde{l}_0$  and  $\tilde{k}_0$  close to integers.

We now consider a discrete chirp signal

$$\tilde{x}(n) = W_N^{-(\tilde{l}_0 n^2 + \tilde{k}_0 n)}, \quad (18.18)$$

where

$$|\tilde{l}_0 - l_0| < \epsilon \quad \text{and} \quad |\tilde{k}_0 - k_0| < \eta, \quad (18.19)$$

where  $l_0$  and  $k_0$  are two integers with  $0 \leq l_0, k_0 \leq N-1$ , and  $\epsilon$  and  $\eta$  are two positive numbers. By using the Taylor expansion of  $\exp(jy)$  in terms of  $jy$ , it is not hard to see that

$$|\exp(jy) - 1| \leq |y| \exp(|y|), \quad y \in \mathbf{R}. \quad (18.20)$$

Thus, for  $0 \leq n \leq N-1$ ,

$$\begin{aligned} |\tilde{x}(n) - x(n)| &\leq \frac{\epsilon n^2 + \eta n}{N} \exp(\epsilon n^2 + \eta n) \\ &< (\epsilon N + \eta) \exp(\epsilon N + \eta) \triangleq \xi, \end{aligned} \quad (18.21)$$

where  $x(n) = W_N^{-(l_0 n^2 + k_0 n)}$ , that is the same as in Equation 18.10. By using Theorem 18.1 and Equation 18.21, the following result is therefore proved.

---

### THEOREM 18.3

Let  $\tilde{x}(n)$  satisfy Equations 18.18 and 18.19 and  $\tilde{X}_c(k, l)$  be its DCFT. Then

$$|\tilde{X}_c(k, l)| \begin{cases} > \sqrt{N}(1 - \xi), & \text{if } l = l_0 \text{ and } k = k_0, \\ < 1 + \sqrt{N}\xi, & \text{if } l \neq l_0, \\ < \sqrt{N}\xi, & \text{if } l = l_0 \text{ and } k \neq k_0, \end{cases} \quad (18.22)$$

where  $\xi$  is defined in Equation 18.21.

From this theorem, one can see that as long as the chirp rate error level  $\epsilon$  and the constant frequency error level  $\eta$  are low enough (i.e.,  $\tilde{l}_0$  and  $\tilde{k}_0$  are close enough to integers  $l_0$  and  $k_0$ ,

i.e.,  $\epsilon, \eta \approx 0$ , which can be achieved when the sampling rate is fast enough), the DCFT of a linear chirp signal still has the peak property as in Theorem 18.1. We shall see some numerical examples in Section 18.5.

### 18.3 DCFT Properties for Multiple Component Chirp Signals

We next consider a multiple component chirp signal  $x(n)$  of the form

$$x(n) = \sum_{i=1}^I A_i W_N^{-(l_i n^2 + k_i n)} + z(n), \quad (18.23)$$

where  $z(n)$  is an additive i.i.d. noise with mean 0 and variance  $\sigma^2$ ,  $|A_i|^2 > 0$  is the signal power of the  $i$ th chirp component, and  $(k_{i_1}, l_{i_1}) \neq (k_{i_2}, l_{i_2})$  for  $i_1 \neq i_2$ . For  $i = 1, 2, \dots, I$ , let

$$x_i(n) = A_i W_N^{-(l_i n^2 + k_i n)}. \quad (18.24)$$

Then, the DCFT  $X_c(k, l)$  of  $x(n)$  is

$$X_c(k, l) = \sum_{i=1}^I X_c^{(i)}(k, l) + Z_c(k, l),$$

where  $X_c^{(i)}(k, l)$  is the DCFT of the  $i$ th chirp component  $x_i(n)$  and  $Z_c(k, l)$  is the DCFT of noise  $z(n)$ . From the study in Section 18.2, we know that each  $X_c^{(i)}(k, l)$  has a peak at  $(k_i, l_i)$  with peak value  $|A_i| \sqrt{N}$  and the maximal off-peak value is  $|A_i|$ . What we are interested here is whether there is a peak of  $X_c(k, l)$  at each  $(k_i, l_i)$ ,  $1 \leq i \leq I$ . If there is a peak at  $(k_i, l_i)$ , then a chirp component with constant frequency  $k_i$  and chirp rate  $l_i$  is detected. To study this question, let us calculate the mean magnitude of  $X_c(k, l)$ . We first calculate the mean  $|X_c(k, l)|$  at  $(k_i, l_i)$ . For  $i = 1, 2, \dots, I$ ,

$$\begin{aligned} E|X_c(k_i, l_i)| &\geq |X_c^{(i)}(k_i, l_i)| - \sum_{\tau \neq i} |X_c^{(\tau)}(k_i, l_i)| - E|Z_c(k_i, l_i)| \\ &\geq |A_i| \sqrt{N} - \sum_{\tau \neq i} |A_\tau| - (E|Z_c(k_i, l_i)|^2)^{1/2}, \end{aligned} \quad (18.25)$$

where the inequality in Step 1 is because  $E|Z_c(k_i, l_i)| \leq (E|Z_c(k_i, l_i)|^2)^{1/2}$  from the Schwarz inequality with respect to the expectation  $E$ . Thus, to estimate the lower bound of the mean magnitude  $|X_c(k_i, l_i)|$  we need to estimate the mean power of the DCFT of the noise  $z(n)$ . Since, for any fixed  $l$ ,  $Z_c(k, l)$  is the DFT of  $z(n)W_N^{ln^2}$ , the energy of  $Z_c(k, l)$  in terms of the frequency variable  $k$  is the same as the one of  $z(n)W_N^{ln^2}$ , i.e., the one of  $z(n)$ . This proves

$$E|Z_c(k, l)|^2 = \sigma^2. \quad (18.26)$$

Therefore, for  $i = 1, 2, \dots, I$ , by Equations 18.25 and 18.26 we have

$$E|X_c(k_i, l_i)| \geq \sqrt{N}|A_i| - \sum_{\tau \neq i} |A_\tau| - \sigma. \quad (18.27)$$

Furthermore, for  $(k, l) \neq (k_i, l_i)$  for  $i = 1, 2, \dots, I$ ,

$$\begin{aligned} E|X_c(k, l)| &\leq \sum_{i=1}^I |X_c^{(i)}(k, l)| + (E|Z_c(k, l)|^2)^{1/2} \\ &\leq \sum_{i=1}^I |A_i| + \sigma. \end{aligned} \quad (18.28)$$

By comparing Equations 18.27 and 18.28, there are peaks at  $(k_i, l_i)$  in the DCFT domain if

$$\sqrt{N}|A_i| - \sum_{\tau \neq i} |A_\tau| - \sigma > \sum_{i=1}^I |A_i| + \sigma.$$

Or,

$$|A_i| > \frac{2}{\sqrt{N} - 1} \left( \sum_{\tau \neq i} |A_\tau| + \sigma \right). \quad (18.29)$$

This concludes the following theorem.

#### THEOREM 18.4

Consider a multiple component chirp signal  $x(n)$  in Equation 18.23 with components at different constant frequency and chirp rate pairs  $(k_i, l_i)$  of power  $|A_i|^2$  for  $i = 1, 2, \dots, I$ . Its DCFT magnitudes at  $(k_i, l_i)$  are lower bounded by

$$E|X_c(k_i, l_i)| \geq \sqrt{N}|A_i| - \sum_{\tau \neq i} |A_\tau| - \sigma, \quad i = 1, 2, \dots, I, \quad (18.30)$$

and its DCFT magnitudes at other  $(k, l)$  are upper bounded by

$$E|X_c(k, l)| \leq \sum_{i=1}^I |A_i| + \sigma, \quad (k, l) \neq (k_i, l_i), \quad i = 1, 2, \dots, I. \quad (18.31)$$

For each  $i$  with  $1 \leq i \leq I$ , a peak in the DCFT domain appears at  $(k_i, l_i)$  if the inequality 18.29 holds.

From (18.29), one can see that, when the number  $I$  of multiple chirp components is fixed, all the peaks at  $(k_i, l_i)$  for  $i = 1, 2, \dots, I$  will appear in the DCFT domain as long as the signal length  $N$ , a prime, is sufficiently large. In other words, when the signal is sufficiently long, all the chirp components can be detected by using the DCFT.

We next consider the special case when all the signal powers  $|A_i|^2$  of the different chirp components are the same, i.e.,

$$|A_i| = A, \quad \text{for } i = 1, 2, \dots, I.$$

In this case, (18.29) becomes

$$1 > \frac{2}{\sqrt{N}-1} \left( I - 1 + \frac{\sigma}{A} \right) = \frac{2}{\sqrt{N}-1} \left( I - 1 + \frac{1}{\sqrt{\gamma}} \right),$$

where  $\gamma$  is the signal-to-noise (SNR) ratio

$$\gamma = \frac{A^2}{\sigma^2}. \quad (18.32)$$

In other words, given the SNR  $\gamma$ , all peaks at  $(k_i, l_i)$  for  $i = 1, 2, \dots, I$  appear in the DCFT domain if the number of chirp components satisfies

$$I < \frac{\sqrt{N} + 1}{2} - \frac{1}{\sqrt{\gamma}}. \quad (18.33)$$

This gives us the following corollary.

---

### COROLLARY 18.1

Let  $x(n)$  be of the form (18.23) with all equal powers  $|A_i|^2 = A^2$  and the SNR  $\gamma$  defined in Equation 18.32. Then, there are peaks at  $(k_i, l_i)$  for  $i = 1, 2, \dots, I$  if the number  $I$  of the chirp components satisfies the upper bound (18.33).

The above corollary basically says that, in the case when all signal powers of the multiple chirp components are the same, the chirp components can be detected using the DCFT if the number of them is less than  $\sqrt{N}/2$  when the signal length  $N$  is sufficiently large. From the simulation results in Section 18.5, one will see that the upper bound in Equation 18.33 is already optimal, i.e., tight.

Similar to the single chirp DCFT performance analysis in Theorem 18.3, when the chirp rate and the constant frequency parameters  $l_i$  and  $k_i$  are not integers, the above results for multiple chirp DCFT can be generalized. Some numerical examples will be presented in Section 18.5.

## 18.4 Connection to the Analog Chirp-Fourier Transform

In this section, we want to see the relationship of the DCFT and the ACFT. Let us first see the ACFT. For an analog signal  $x_a(t)$ , its ACFT is

$$X_{c,a}(\alpha, \beta) = \int_{-\infty}^{\infty} x_a(t) \exp(-j(\beta t^2 + \alpha t)) dt, \quad (18.34)$$

where  $\alpha$  and  $\beta$  are real. When  $x_a(t)$  is a linear chirp, i.e.,

$$x_a(t) = \exp(j(\beta_0 t^2 + \alpha_0 t)), \quad (18.35)$$

the ACFT is

$$\begin{aligned} X_{c,a}(\alpha, \beta) &= \int_{-\infty}^{\infty} \exp(j[(\beta_0 - \beta)t^2 + (\alpha_0 - \alpha)t]) dt \\ &= 2 \int_0^{\infty} \cos(\beta_0 - \beta)t^2 \cos(\alpha_0 - \alpha)t dt \\ &\quad + 2j \int_0^{\infty} \sin(\beta_0 - \beta)t^2 \cos(\alpha_0 - \alpha)t dt \\ &= \frac{1}{|\beta_0 - \beta|^{1/2}} (1 + \text{sign}(\beta_0 - \beta)) \\ &\quad \cdot \exp\left(-j \frac{(\alpha_0 - \alpha)^2}{4(\beta_0 - \beta)}\right), \end{aligned} \quad (18.36)$$

where Equation 18.36 is from [19]. Clearly, when the constant frequency  $\alpha_0$  and the chirp rate  $\beta_0$  are both matched, i.e., when  $\alpha = \alpha_0$  and  $\beta = \beta_0$ , the ACFT  $X_{c,a}(\alpha, \beta) = \infty$ , and otherwise  $X_{c,a}(\alpha, \beta)$  is a finite value, i.e.,  $X_{c,a}(\alpha, \beta) < \infty$  for  $\beta \neq \beta_0$  or  $\alpha \neq \alpha_0$ .

To consider the connection with the DCFT, let us consider the following samplings for the above analog parameters  $t$ ,  $\alpha$ , and  $\beta$ :

$$t := \frac{n}{N^{1/3}}, \quad \beta := \frac{2\pi n}{N^{1/3}}, \quad \alpha := \frac{2\pi n}{N^{2/3}}, \quad (18.37)$$

where  $N$  is a positive integer. The reason for this sampling method is for getting the DCFT form studied Sections 18.2 and 18.3 and the difference of the samplings between the chirp rate  $\beta$  and the constant frequency  $\alpha$  is due to the power difference between the chirp term  $t^2$  and the constant frequency term  $t$ . Truncate  $x_a(t)$  such that it is zero for  $t \notin [0, N^{2/3}]$ . Sample  $x_a(t)$  into  $x(n) = x_a(n/N^{1/3})$  for  $n = 0, 1, 2, \dots, N-1$ . In this case, the integral in Equation 18.34 can be discretized

$$\begin{aligned} X_{c,a}\left(\frac{2\pi k}{N^{2/3}}, \frac{2\pi l}{N^{1/3}}\right) &\approx \frac{1}{N^{1/3}} \sum_{n=0}^{N-1} x(n) W_N^{ln^2 + kn} \\ &= \frac{N^{1/2}}{N^{1/3}} X_c(k, l). \end{aligned}$$

In other words,

$$X_c(k, l) \approx N^{-1/6} X_{c,a}\left(\frac{2\pi k}{N^{2/3}}, \frac{2\pi l}{N^{1/3}}\right), \quad (18.38)$$

which gives a connection between the DCFT and the ACFT.

### 18.5 Numerical Simulations

In this section, we want to see some simple numerical simulations. Two signal lengths are considered:  $N = 67$  and  $N = 66$ . We first see some examples when  $N = 67$ . Two different SNRs  $\gamma$  in Equation 18.32 are considered, which are  $\gamma_1 = 1$  (0 dB) and  $\gamma_2 = 4$  (6 dB). For the first SNR  $\gamma_1$ , the upper bound in Equation 18.33 for the number  $I$  of the detectable chirp components is 3, i.e.,  $I \leq I_1 = 3$ . For the second SNR  $\gamma_2$ , the upper bound in

Equation 18.33 for the number  $I$  of the detectable chirp components is 4, i.e.,  $I \leq I_2 = 4$ . In the following, three different numbers  $I = 2, 3, 4$  of chirp components are simulated, where the constant frequencies  $k_i$  and the chirp rates  $l_i$  for  $i = 1, 2, \dots, I$  are arbitrarily chosen. The corresponding amplitudes  $A_i$  are set to be all 1.

Figures 18.1 and 18.2 show the DCFTs of signals with two chirp components at  $(k_i, l_i) = (42, 15), (45, 44)$ , and the SNRs  $\gamma = \gamma_1 = 0$  dB and  $\gamma = \gamma_2 = 6$  dB in Equation 18.32, respectively.

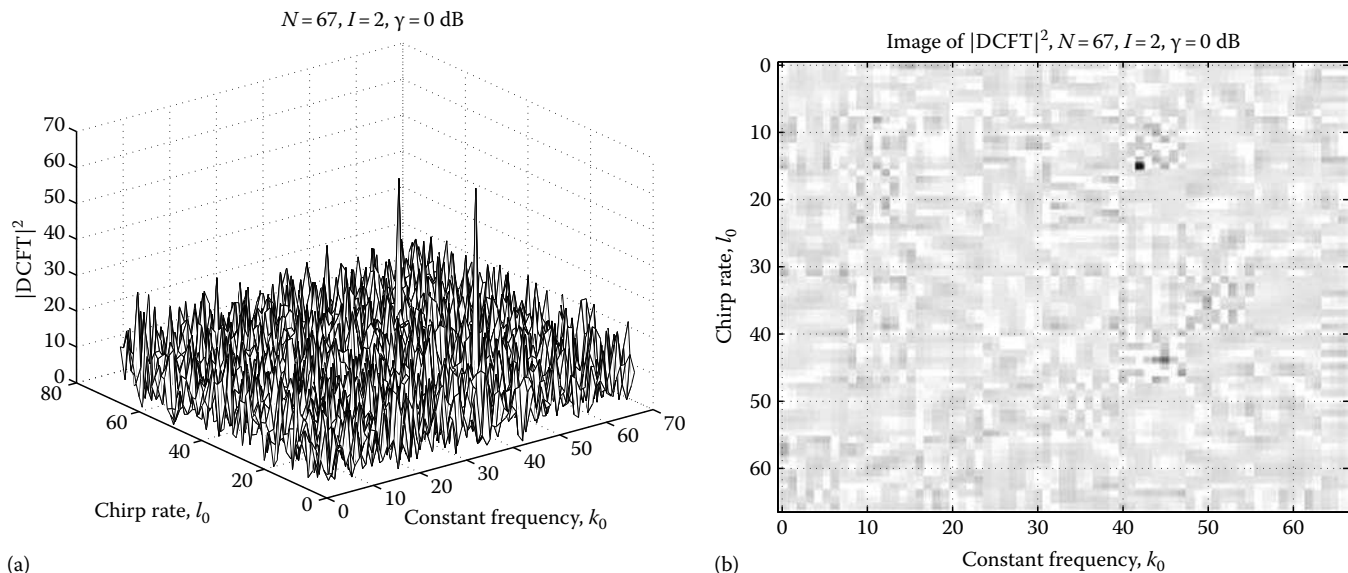


FIGURE 18.1 The DCFT of two chirp components with additive SNR  $\gamma = 0$  dB: (a) three-dimensional plot and (b) image.

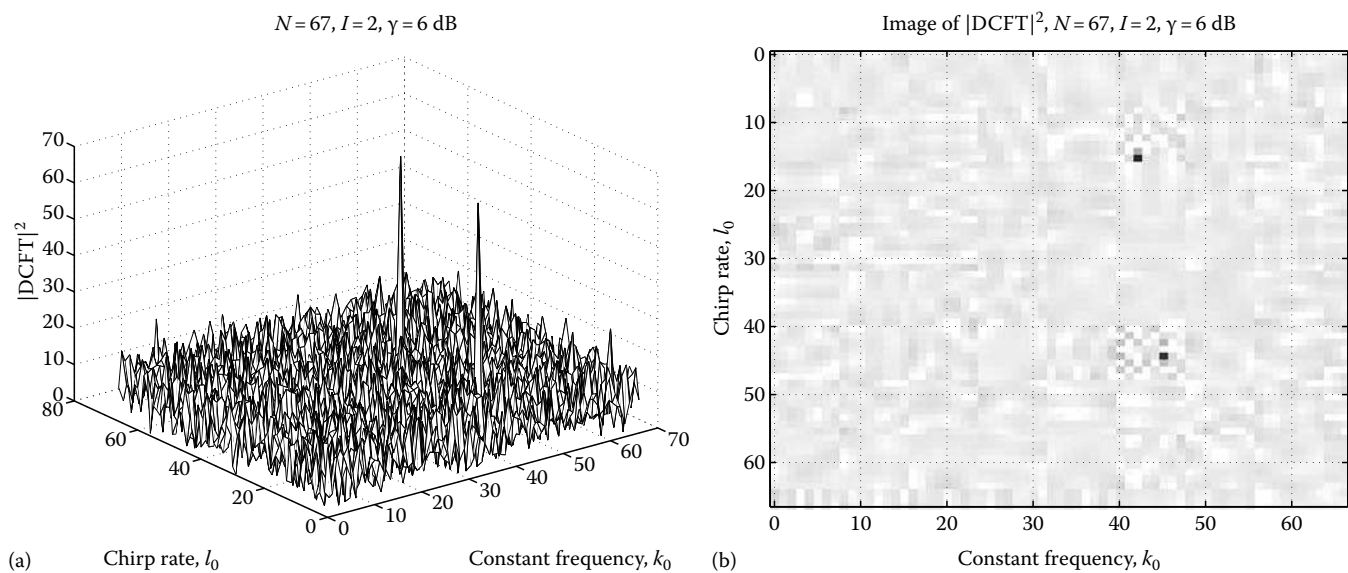


FIGURE 18.2 The DCFT of two chirp components with additive SNR  $\gamma = 6$  dB: (a) three-dimensional plot and (b) image.

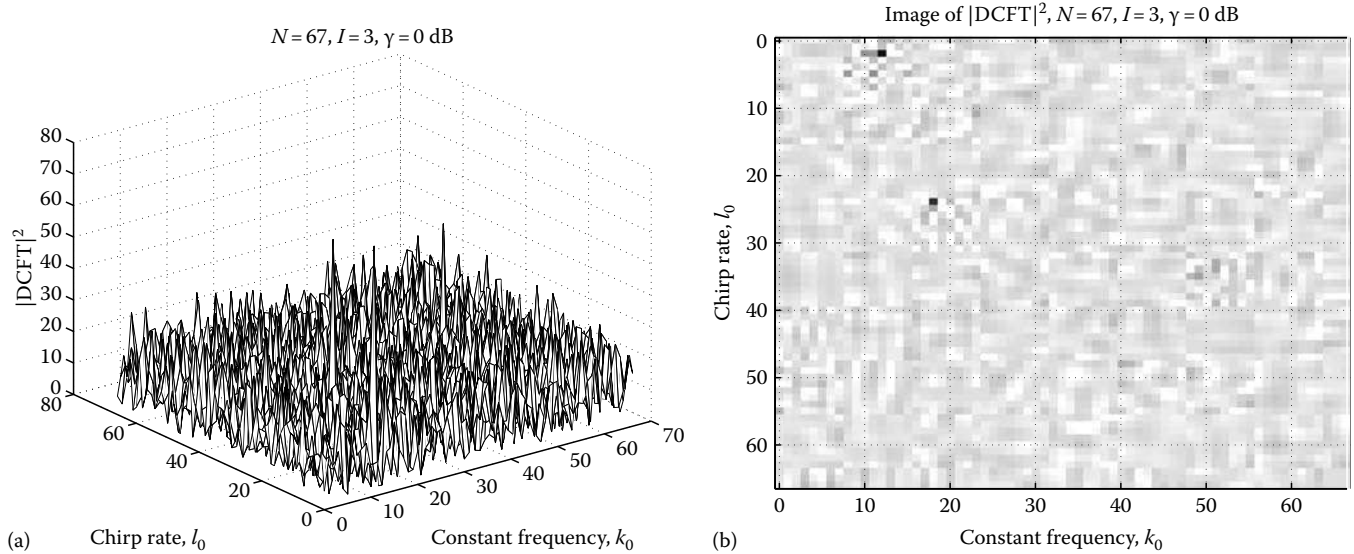


FIGURE 18.3 The DCFT of three chirp components with additive SNR  $\gamma = 0$  dB: (a) three-dimensional plot and (b) image.

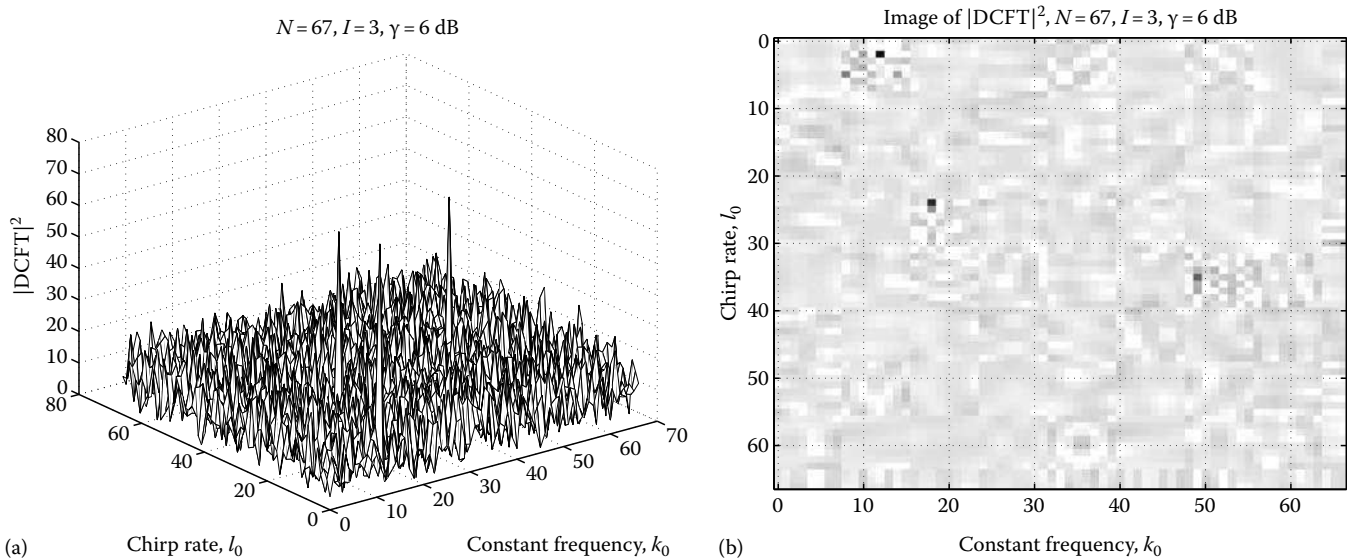


FIGURE 18.4 The DCFT of three chirp components with additive SNR  $\gamma = 6$  dB: (a) three-dimensional plot and (b) image.

Figures 18.3 and 18.4 show the DCFTs of signals with three chirp components at  $(k_i, l_i) = (12, 2), (49, 35), (18, 24)$ , and the SNRs  $\gamma = \gamma_1 = 0$  dB and  $\gamma = \gamma_2 = 6$  dB in Equation 18.32, respectively. Figures 18.5 and 18.6 show the DCFTs of signals with four chirp components at  $(k_i, l_i) = (44, 57), (38, 65), (53, 10), (55, 12)$ , and the SNRs  $\gamma = \gamma_1 = 0$  dB and  $\gamma = \gamma_2 = 6$  dB in Equation 18.32, respectively. One can see from Figure 18.5 that, although the

upper bound for  $I$  is 3 when the SNR  $\gamma = \gamma_1 = 0$  dB, the four peaks can be seen in the DCFT domain. This is, however, not always true from the following examples. Figures 18.7 and 18.8 show the DCFTs of another set of two signals with four chirp components at  $(k_i, l_i) = (64, 55), (21, 39), (8, 17), (53, 44)$ , and the SNRs  $\gamma = \gamma_1 = 0$  dB and  $\gamma = \gamma_2 = 6$  dB in Equation 18.32, respectively. One can see from Figures 18.7 that the four peaks

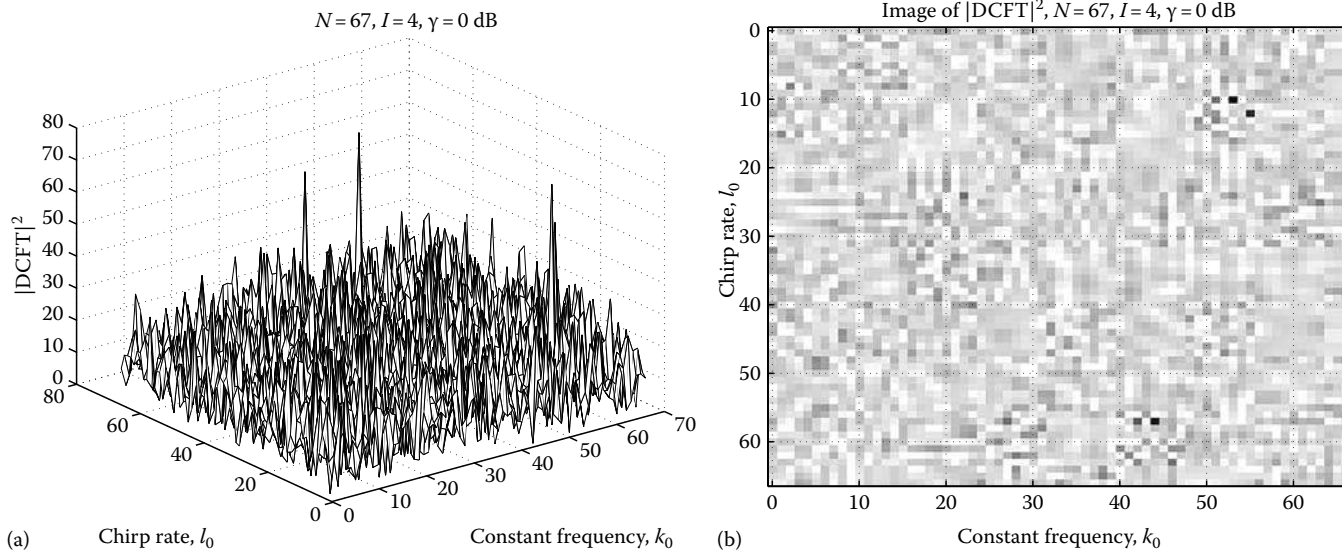


FIGURE 18.5 The DCFT of four chirp components with additive SNR  $\gamma = 0 \text{ dB}$ : (a) three-dimensional plot and (b) image.

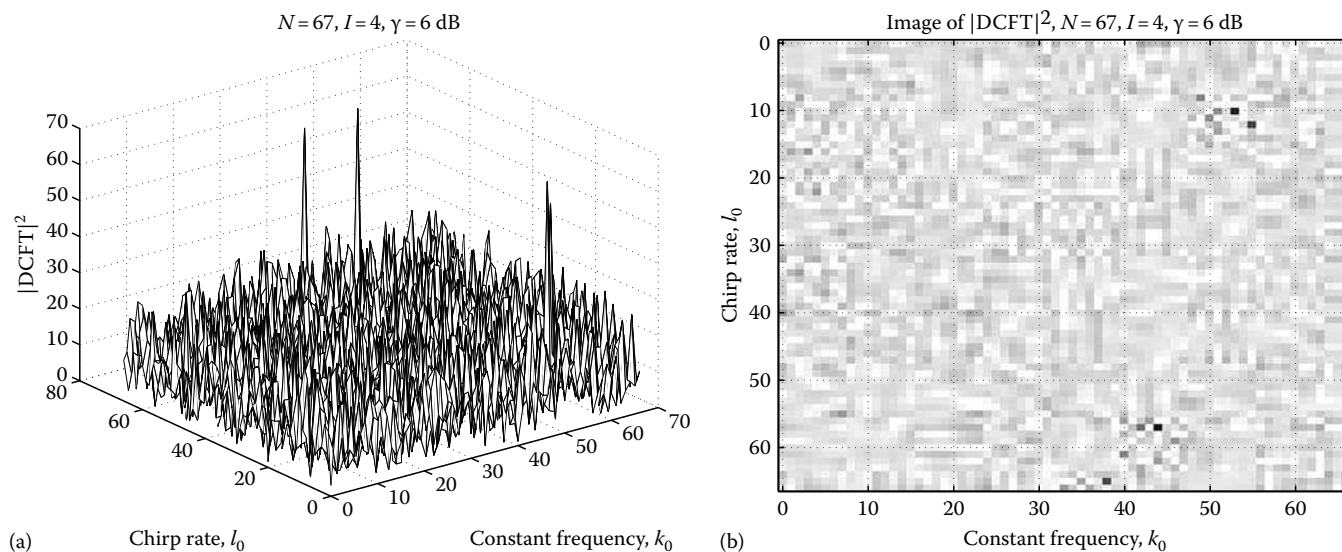


FIGURE 18.6 The DCFT of four chirp components with additive SNR  $\gamma = 6 \text{ dB}$ : (a) three-dimensional plot and (b) image.

( $I = 4$ ) are not clear, which is because the upper bound for  $I$  in Equation 18.33 is 3 when  $\gamma = \gamma_1 = 0 \text{ dB}$ . The four peaks in Figure 18.8 are, however, clear because the upper bound for  $I$  in Equation 18.33 is 4 when  $\gamma = \gamma_2 = 6 \text{ dB}$ .

When  $N = 66$ , we consider the two chirp components  $(k_i, l_i) = (42, 15), (45, 44)$  in Figure 18.2 with the SNR  $\gamma = \gamma_2 = 6 \text{ dB}$ . Its

DCFT is shown in Figure 18.9. Clearly, it fails to show the two peaks, which illustrates the difference of the DCFT with respect to having prime and nonprime length.

We next want to see some examples when the chirp rate and the constant frequency parameters  $l_i$  and  $k_i$  are not but close to integers, i.e.,  $\epsilon, \eta \approx 0$ . The parameter errors are randomly added



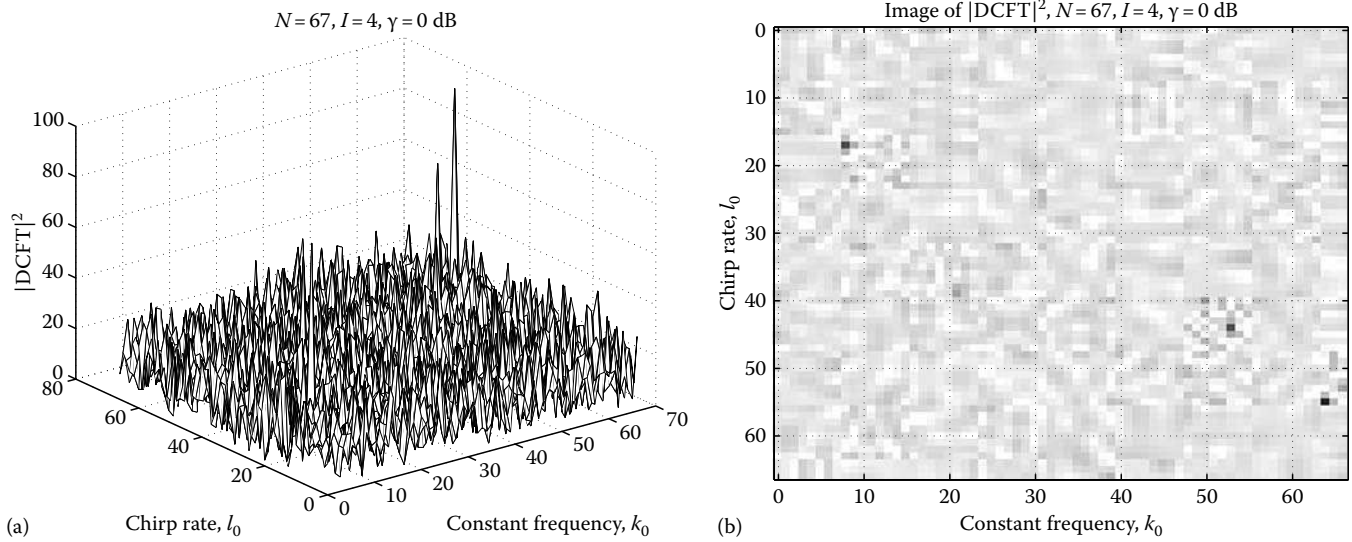


FIGURE 18.7 The DCFT of another set of four chirp components with additive SNR  $\gamma = 0$  dB: (a) three-dimensional plot and (b) image.

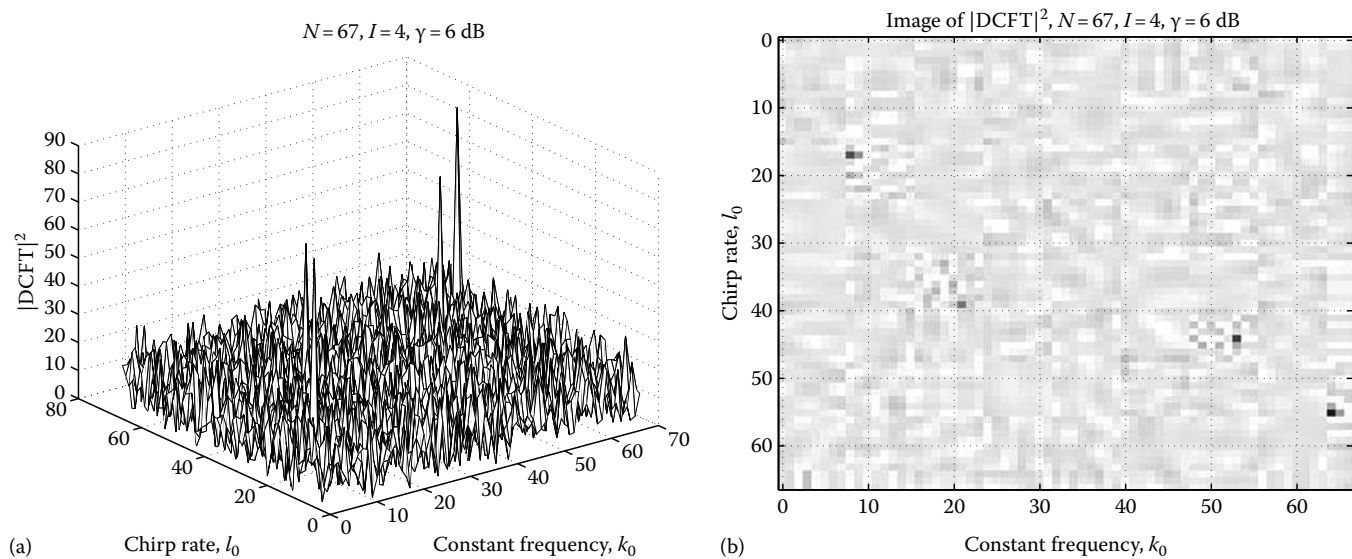


FIGURE 18.8 The DCFT of another set of four chirp components with additive SNR  $\gamma = 6$  dB: (a) three-dimensional plot and (b) image.

with Gaussian distributions. Figures 18.10 and 18.11 show the DCFTs of the two chirp components  $(k_i, l_i) = (41.9897, 15.0180)$ ,  $(45.0037, 43.9968)$  that are distorted from the chirp components in Figures 18.1 and 18.2. Figures 18.12 and 18.13 show the DCFTs of the three chirp components  $(k_i, l_i) = (12.0050, 1.9883)$ ,

$(48.9875, 35.0063)$ ,  $(17.9825, 24.0004)$  that are distorted from the chirp components in Figures 18.3 and 18.4. Figures 18.14 and 18.15 show the DCFTs of the four chirp components  $(k_i, l_i) = (43.9977, 56.9989)$ ,  $(38.0013, 64.9920)$ ,  $(52.9976, 9.9991)$ ,  $(54.9898, 12.0094)$  that are distorted from the chirp components

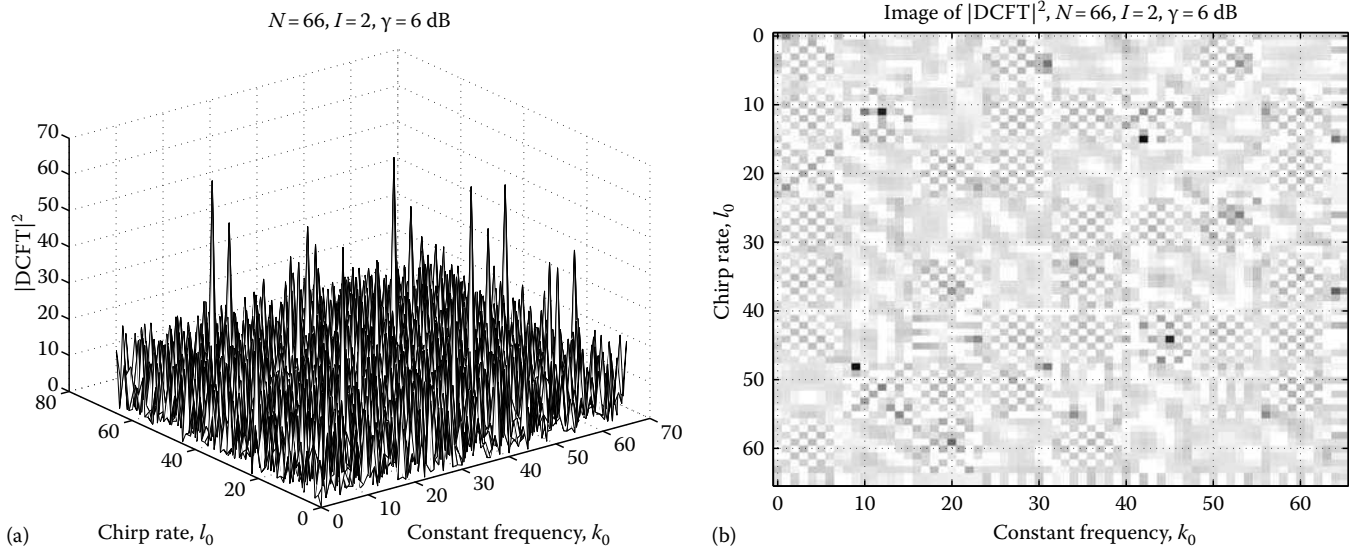


FIGURE 18.9 The DCFT of two chirp components with additive SNR  $\gamma = 6 \text{ dB}$ : and signal length  $N = 66$ : (a) three-dimensional plot and (b) image.

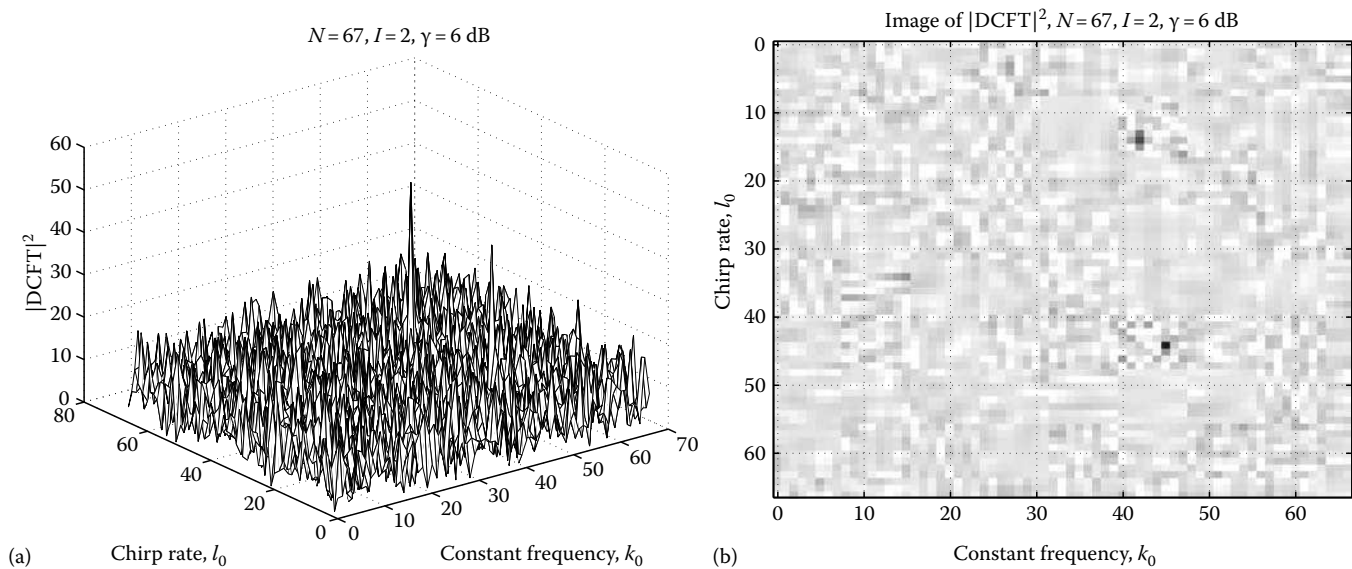
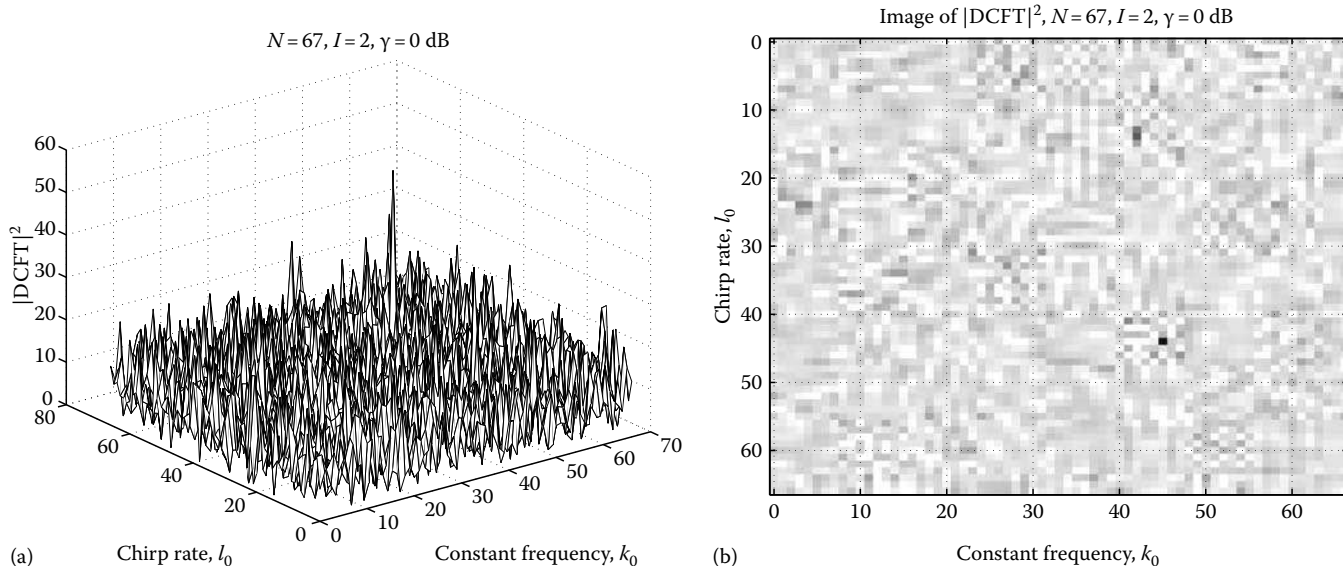


FIGURE 18.10 The DCFT of two chirp components  $(41.9897, 15.0180), (45.0037, 43.9968)$  with additive SNR  $\gamma = 6 \text{ dB}$ : (a) three-dimensional plot and (b) image.

in Figures 18.5 and 18.6. One can see that, unlike in Figures 18.5 and 18.6, in Figures 18.14 and 18.15 the four peaks are not all shown well, which is due to the additional distortions of the integer chirp rate and constant frequency parameters  $l_i$  and  $k_i$  as we studied in Theorem 18.3.

## 18.6 Conclusion

In this chapter, we studied the DCFT for discrete linear chirp signals. The approach is analogous to the one of the DFT. We showed that, when the signal length  $N$  is a prime, all the sidelobes



**FIGURE 18.11** The DCFT of two chirp components (41.9897, 15.0180), (45.0037, 43.9968) with additive SNR  $\gamma=0 \text{ dB}$ : (a) three-dimensional plot and (b) image.

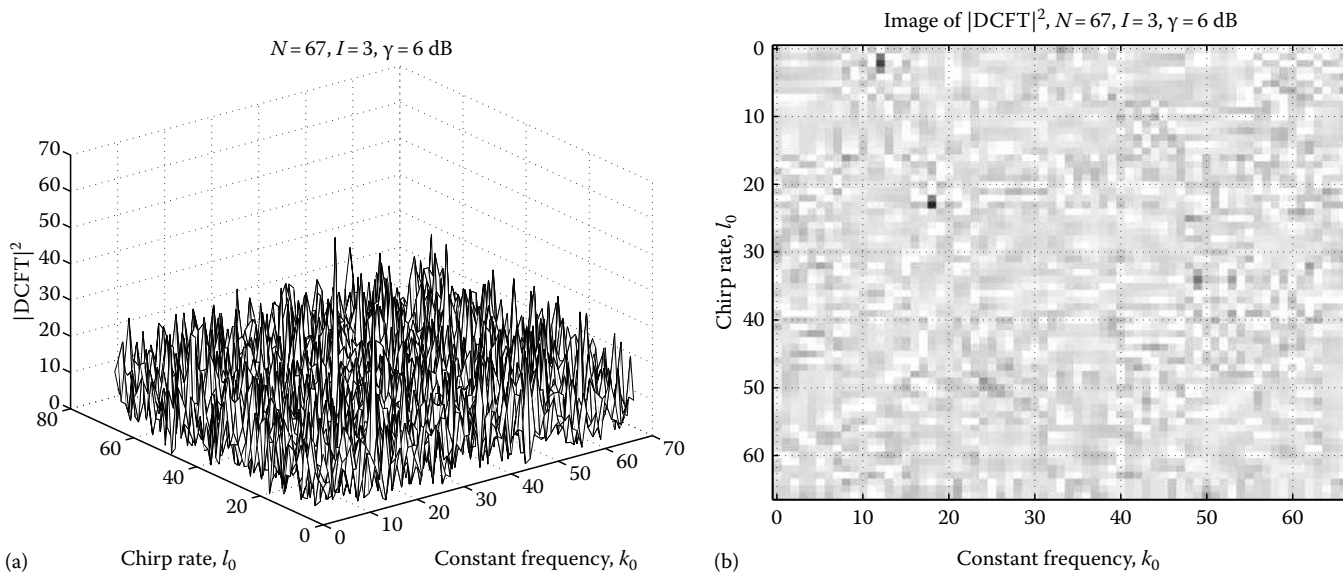


**FIGURE 18.12** The DCFT of three chirp components (12.0050, 1.9883), (48.9875, 35.0063), (17.9825, 24.0004) with additive SNR  $\gamma=6 \text{ dB}$ : (a) three-dimensional plot and (b) image.

(i.e., when the chirp rates or the constant frequencies are not matched) of the DCFT are not above 1 while the mainlobe (i.e., when the chirp rates and the constant frequencies are matched simultaneously) of the DCFT is  $\sqrt{N}$ . We showed that this is optimal, i.e., when  $N$  is not a prime, the maximal sidelobe magnitude of the DCFT is greater than 1 (in fact, we showed

that the maximal sidelobe magnitude of the DCFT is greater than  $\sqrt{2}$ ). We also presented an upper bound in terms of signal length  $N$  and SNR for the number of the detectable chirp components using the DCFT. Simulations were presented to illustrate the theory. A connection of the DCFT with the ACFT was also presented.

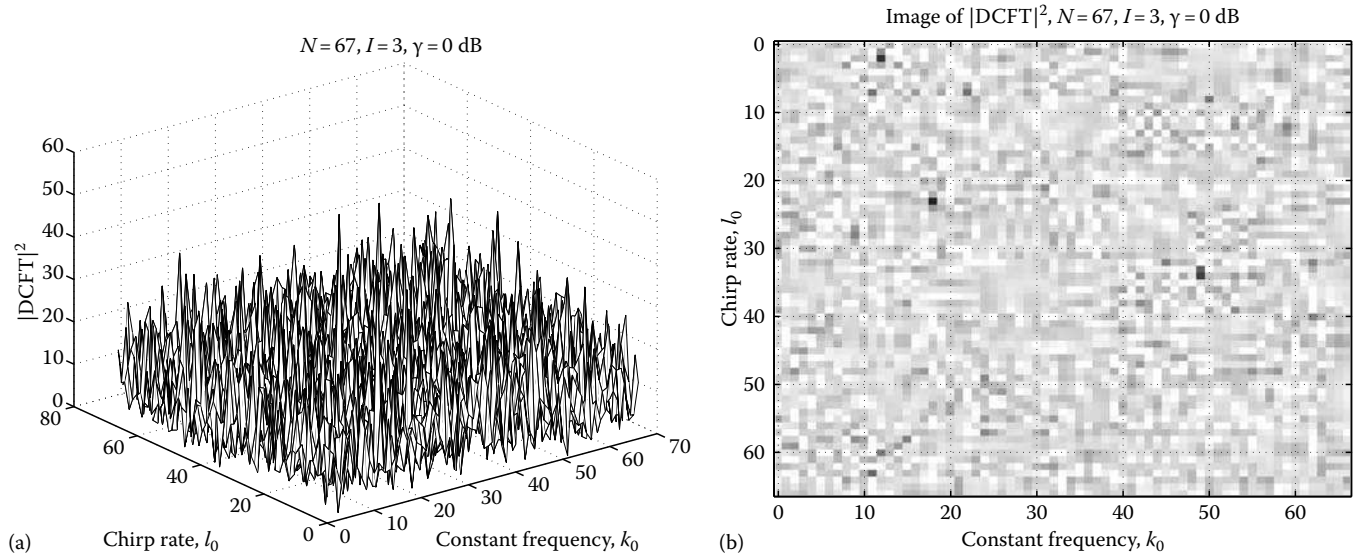


**FIGURE 18.13** The DCFT of three chirp components (12.0050, 1.9883), (48.9875, 35.0063), (17.9825, 24.0004) with additive SNR  $\gamma = 0$  dB: (a) three-dimensional plot and (b) image.

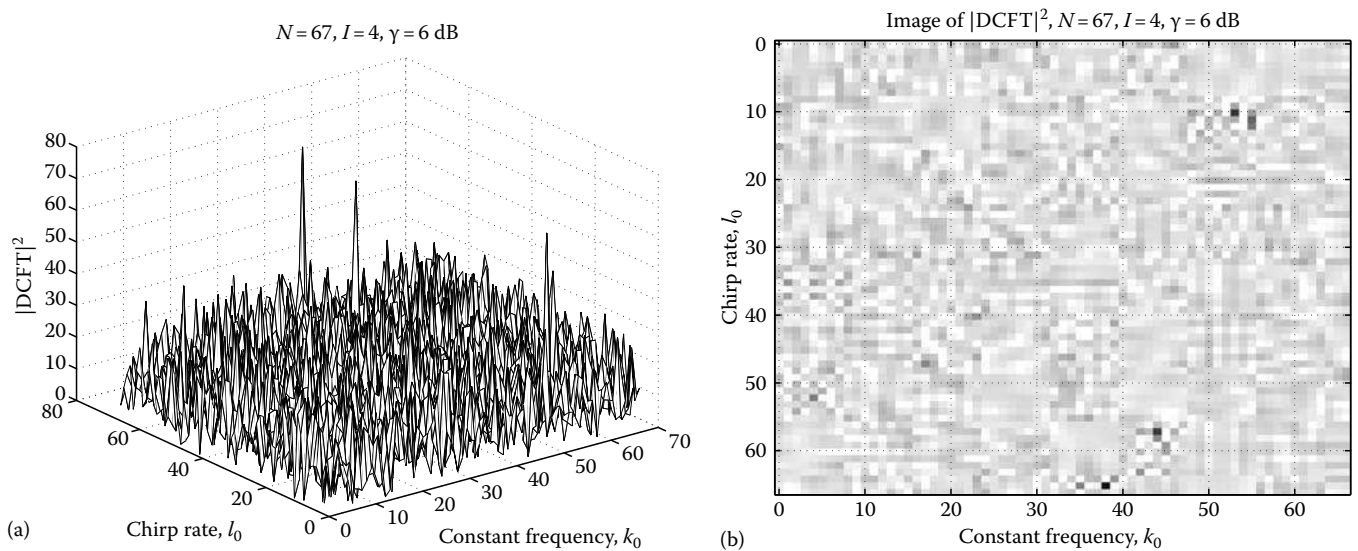


**FIGURE 18.14** The DCFT of four chirp components (43.9977, 56.9989), (38.0013, 64.9920), (52.9976, 9.9991), (54.9898, 12.0094) with additive SNR  $\gamma = 6$  dB: (a) three-dimensional plot and (b) image.

Although the DCFT was defined for linear chirps that are quite common in radar applications, it is not hard to generalize to higher order chirps. Notice that the DCFT for higher order chirps may not have the precise values but some roughly low values of the sidelobes obtained in Sections 18.2 through 18.5 for linear chirps. However, it might be possible but more tedious to calculate the

values of the sidelobes of the DCFT for higher order chirps when the higher order powers of  $P(k, l)$  in Equation 18.9 in the proof of Lemma 18.1 is used. Another comment we would like to make here is that, similar to the spectrum estimation, when the chirp rate and the constant frequency are not integers, other high resolution techniques may exist and are certainly interesting.

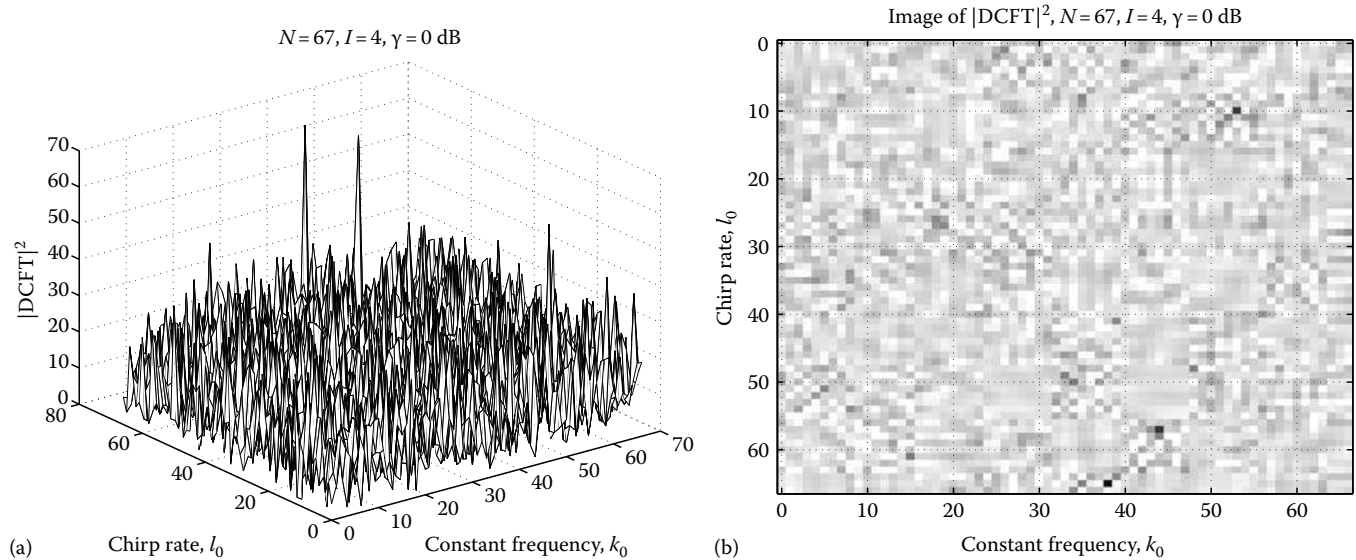


**FIGURE 18.15** The DCFT of four chirp components (43.9977, 56.9989), (38.0013, 64.9920), (52.9976, 9.9991), (54.9898, 12.0094) with additive SNR  $\gamma = 0$  dB: (a) three-dimensional plot and (b) image.

## References

1. D. R. Wehner, *High-Resolution Radar*, 2nd edn., Boston, MA-London, U.K., Artech House, 1995.
2. V. C. Chen and H. Lin, *Time-Frequency Transforms for Radar Imaging and Signal Analysis*, Artech House Publishing, Boston, MA, 2002.
3. X.-G. Xia, Discrete chirp-Fourier transform and its application to chirp rate estimation, *IEEE Trans. Signal Process.*, 48, 3122–3133, Nov. 2000.
4. S. Peleg and B. Porat, Estimation and classification of signals with polynomial phase, *IEEE Information Theory*, 37, pp.422–430, 1991.
5. B. Porat, *Digital Processing of Random Signals, Theory and Methods*, Prentice-Hall, Englewood Cliffs, NJ, 1994.
6. S. Peleg and B. Friedlander, The discrete polynomial-phase transform, *IEEE Trans. Signal Process.*, 43, 1901–1914, Aug. 1995.
7. S. Qian, D. Chen, and Q. Yin, Adaptive chirplet based signal approximation, Proceedings of ICASSP'98, Seattle, WA, May 12–15, 1998.
8. R. Kumaresan and S. Verma, On estimating the parameters of chirp signals using rank reduction techniques, *Proceedings of the 21st Asilomar Conference Signals, System, Computing*, Pacific Grove, CA, pp. 555–558, 1987.
9. P. M. Djuric and S. M. Kay, Parameter estimation of chirp signals, *IEEE Trans. Acoust. Speech Signal Process.*, 38, 2118–2126, Dec. 1990.
10. M. Z. Ikram, K. Abed-Meraim, and Y. Hua, Estimating the parameters of chirp signals: An iterative approach, *IEEE Trans. Signal Process.*, 46, 3436–3441, Dec. 1998.
11. T. J. Abatzoglou, Fast maximum likelihood joint estimation of frequency and frequency rate, *IEEE Trans. Aerosp. Electron. Syst.*, 22, 708–715, Nov. 1986.
12. S. Peleg and B. Porat, The Cramer–Rao lower bound for signals with constant amplitude and polynomial phase, *IEEE Trans. Signal Process.*, 39, 749–752, Mar. 1991.
13. L. R. Rabiner, R. W. Schafer, and C.M. Rader, The chirp z-transform algorithm and its applications, *Bell Syst. Tech. J.*, 48, 1249–1292, May–June 1969.
14. V. Namias, The fractional order Fourier transform and its application to quantum mechanics, *J. Inst. Math. Appl.*, 25, 241–265., 1980.
15. A. C. McBride and F. H. Kerr, On Namias' fractional Fourier transforms, *IMA J. Appl. Math.*, 39, 150–175, 1987.
16. L. B. Almeida, The fractional Fourier transform and time-frequency representations, *IEEE Trans. Signal Process.*, 42, 3084–3091, Nov. 1994.
17. A. W. Lohmann, Image rotation, Wigner rotation and the fractional Fourier transform, *J. Opt. Soc. Am. A*, 10, 2181–2186, 1993.
18. D. Mendlovic and H. M. Ozaktas, Fractional Fourier transformations and their optical implementation: I. *J. Opt. Soc. Am. A*, 10, 1875–1881, 1993.
19. I. N. Bronshtein and K. A. Semendyayev, *Handbook of Mathematics*, Van Nostrand Reinhold Company, New York, 1985.

# Multidimensional Discrete Unitary Transforms

---

19.1	Introduction.....	19-1
	Row-Column Algorithm • Vector Radix Algorithm • Method of the Polynomial Transforms	
19.2	Nontraditional Forms of Representation.....	19-5
19.3	Partitioning of Multidimensional Transforms .....	19-7
	Tensor Representation • Covering with Cyclic Groups	
19.4	Fourier Transform Tensor Representation .....	19-10
	2-D Directional Images	
19.5	Tensor Algorithm of the 2-D DFT .....	19-16
	$N$ Is a Prime • $N$ Is a Power of Two • Modified Tensor Algorithms • Recursive Tensor Algorithm • $n$ -Dimensional DFT	
19.6	Discrete Hartley Transforms .....	19-26
	3-D DHT Tensor Representation • $n$ -Dimensional DHT	
19.7	2-D Shifted DFT.....	19-32
	$2^r \times 2^r$ -Point SDFT • $L^r \times L^r$ -Point SDFT • $L_1 L_2 \times L_1 L_2$ -Point SDFT	
19.8	2-D DCT .....	19-35
	Modified Algorithms of the 2-D DCT	
19.9	3-D Paired Representation.....	19-41
	2D-to-3D Paired Transform • $N$ Is a Power of Two • $N$ Is a Power of Odd Prime • Set-Frequency Characteristics	
19.10	2-D DFT on the Hexagonal Lattice .....	19-55
	Paired Representation of the DHFT	
19.11	Paired Transform-Based Algorithms .....	19-62
	Calculation of the 2-D DHT • 2-D Discrete Cosine Transform • 2-D Discrete Hadamard Transform	
19.12	Conclusion .....	19-67
	References .....	19-67

Artyom M. Grigoryan  
The University of Texas

## 19.1 Introduction

---

The use of fast discrete unitary transforms has become a powerful technique in multidimensional signal processing, and in particular in image processing. Image processing in the frequency domain is used widely in image filtration, restoration, enhancement, compression, image reconstruction by projections, and other areas [1–4]. Among the unitary transforms, one should note the Fourier, Hartley, Hadamard, and cosine transforms. Theory of the Fourier transform is well developed, and effective methods (or, fast algorithms) of the discrete Fourier transforms (DFT's) are used for solving many problems in different areas of data processing such as signal and image processing, speech analysis, and communication, etc. We also observe the considerable interest to many applications of the discrete Hartley transform (DHT) together with the DFT, since the DHT relates closely to the DFT and has been created as an alternative form

of the complex DFT, to eliminate the necessity of using complex operations. Another transform is the discrete Hadamard transform (DHdT), which is real, binary, and computationally advantageous over the fast Fourier transform (FFT). The Hadamard functions can be used for a series expansion of the signal, being orthogonal and taking value  $\pm 1$  at each point. This transform has found useful applications in signal and image processing, communication systems, image coding, image enhancement, pattern recognition, and general two-dimensional filtering. The discrete cosine transform (DCT) is used in speech and image processing, especially in image compression and transform coding in telecommunication [5–9].

The application of the multidimensional transform involves the calculation of the transform, manipulation with transform coefficients, and then calculation of the inverse transform. For signals of large sizes, this process requires a great number of operations when performing multidimensional transforms. It is

desired to maximally reduce this number, and different methods of effective calculation of multidimensional unitary transforms have been developed. For instance, in most cases, the calculation of the 2-D transform is reduced by partitioning the entire image by one-dimensional (1-D) or two-dimensional (2-D) blocks and calculating the transforms of these blocks. We here stand on the traditional “row-column” algorithm, when 1-D transforms over all rows and then columns are calculated, as well as the “vector-radix” algorithm, when the image is divided consequently by four blocks of equal size. The method of the polynomial transformations developed by Nussbaumer is also considered. Then we describe, in detail, the partitionings of multidimensional transforms, which are based on the concepts of the tensor and paired representations of multidimensional signals, including 2-D and three-dimensional (3-D) images. In these new forms of representation, the multidimensional signals are described by sets of 1-D signals which carry the spectral information of multidimensional signals in different subsets of frequency-points. The processing of multidimensional signals thus is reduced to processing 1-D signals, which we call splitting-signals, since they represent the multidimensional signals and split the transforms of these signals. The splitting-signals are described for the 2-D and multidimensional Fourier, Hartley, Hadamard, and cosine transforms.

### 19.1.1 Row-Column Algorithm

Many of the multidimensional transformations are separable, meaning that these transforms over multidimensional signals can be performed by calculating 1-D transforms consequently along all dimensions of the signal. For instance, for a separable 2-D transformation  $T$ , the transform of a 2-D signal or image  $f = \{f_{n,m}\}$  of size  $(N \times N)$ ,  $N > 1$ , can be obtained by first calculating the 1-D transforms over all columns of the image and, then calculating the 1-D transforms by the rows of the obtained 2-D data, as shown in Figure 19.1.

In matrix form, the transform of  $f$  can be written as

$$[2-D T] [f] = [1-D T] [f] [1-D T]^t$$

where “ $t$ ” denotes the matrix operation of transposition, and square brackets  $[ \cdot ]$  are used to denote the matrices of the transformations  $T$  and image  $f$ .

As an example, we consider the 2-D DFT of the image  $f_{n,m}$ , which is defined by

$$F_{p,s} = (\mathcal{F}_{N,N} \circ f)_{p,s} = \sum_{n=0}^{N-1} \sum_{m=0}^{N-1} f_{n,m} W^{np+ms}, \quad p, s = 0: (N-1), \tag{19.1}$$

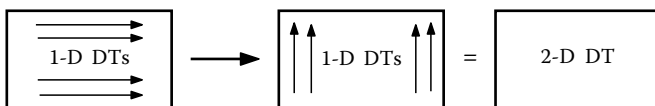


FIGURE 19.1 Block diagram of calculation of the 2-D discrete transform (DT) (separable).

where  $W = W_N = \exp(-2\pi j/N)$  is the kernel of the transformation, and  $j^2 = -1$ . The designation  $p = 0: (N-1)$  denotes  $p$  as an integer that runs from 0 to  $(N-1)$ . The kernel is separable,  $W^{np+ms} = W^{np} W^{ms}$ , and the transform can thus be written as

$$F_{p,s} = \sum_{n=0}^{N-1} \left[ F_n(s) = \sum_{m=0}^{N-1} f_{n,m} W^{ms} \right] W^{np}, \quad p, s = 0: (N-1), \tag{19.2}$$

where  $F_n(s)$  is the value of the 1-D DFT of row number  $n$  at point  $s$ . To calculate the 2-D DFT,  $2N$  1-D DFTs are used in the row-column algorithm. This algorithm is simple, but requires many operations of multiplication and addition. All twiddle coefficients,  $W^t$ ,  $t = 0: (N-1)$ , lie on  $N$  equidistant points of the unit circle, and many of them are irrational numbers.

We now consider the transformation whose kernel lies only on two points  $\pm 1$  on the unit circle. The 2-D separable DHdT of order  $N \times N$ , where  $N = 2^r$ ,  $r > 1$ , is defined as

$$A_{p,s} = (\mathcal{A}_{N,N} \circ f)_{p,s} = \sum_{n=0}^{N-1} \sum_{m=0}^{N-1} f_{n,m} a(p;n) a(s;m) = \sum_{n=0}^{N-1} \left[ \sum_{m=0}^{N-1} f_{n,m} a(s;m) \right] a(p;n). \tag{19.3}$$

The kernel of the transformation is defined by the binary function

$$a(p;n) = (-1)^{n_0 p_0 + n_1 p_1 + \dots + n_r p_r} \tag{19.4}$$

where  $(n_0, n_1, \dots, n_r)$  and  $(p_0, p_1, \dots, p_r)$  are the binary representations of numbers  $n$  and  $p$ , respectively.

As an example, Figure 19.2 shows an image  $(512 \times 512)$  in part (a), along with the 2-D discrete Fourier and Hadamard transforms of the image in (b) and (c), respectively. The realization of the Hadamard transformation requires only operations of addition (and subtraction). From the computational point of view, the 1-D Hadamard transform is faster than the complex Fourier transform. These two different transforms can share the same fast algorithm. For instance, the FFT by paired transforms can also be used for the fast Hadamard transform, when considering all twiddle coefficients  $W^t$  equal 1 [11].

### 19.1.2 Vector Radix Algorithm

The “row-column” method of calculation of a separable 2-D DT requires the transposition of the 2-D data table obtained after performing all 1-D transforms over the rows. For tables of large sizes, the transposition slows down the process of calculation of the transform, and therefore other methods of fast calculation of the transform have been developed to avoid the transposition. That can be done by partitioning the square period  $(N \times N)$  of the transform by other than row and column sets. We mention here the idea of generalization of the 2-D “butterfly” operation from the

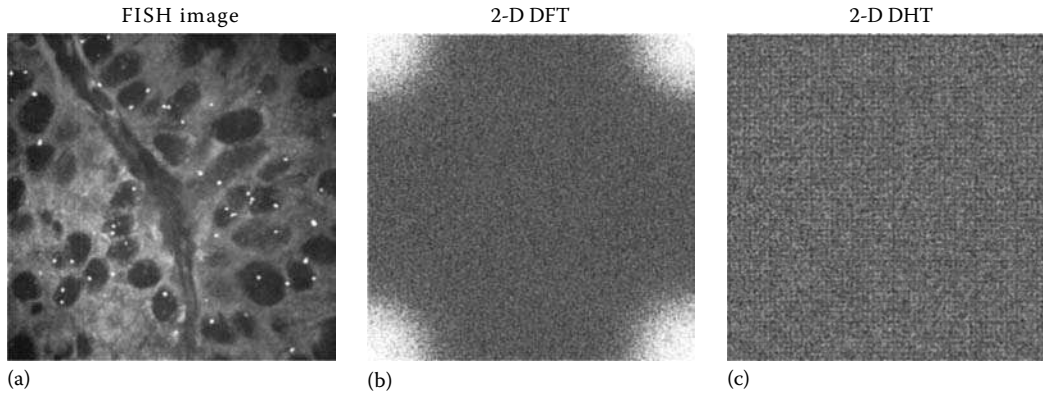


FIGURE 19.2 (a) Original image of size  $512 \times 512$ , (b) 2-D DFT (in absolute mode), and (c) 2-D DHdT.

1-D Cooley–Tukey algorithm [10] to the four-dimensional (4-D) operation, when dividing the transforms by four parts of size  $(N/2 \times N/2)$  each.

The vector-radix algorithm for the 2-D DFT uses the “butterfly”  $2 \times 2$  which is defined as the following Kronecker product of two 2-D butterflies:

$$\begin{bmatrix} 1 & W^{p_1} \\ 1 & -W^{p_1} \end{bmatrix} \otimes \begin{bmatrix} 1 & W^{s_1} \\ 1 & -W^{s_1} \end{bmatrix} = \begin{bmatrix} 1 & W^{p_1} & W^{s_1} & W^{p_1+s_1} \\ 1 & -W^{p_1} & W^{s_1} & -W^{p_1+s_1} \\ 1 & W^{p_1} & -W^{s_1} & -W^{p_1+s_1} \\ 1 & -W^{p_1} & -W^{s_1} & W^{p_1+s_1} \end{bmatrix} \quad (19.5)$$

where  $p_1, s_1 = 0: (N/2 - 1)$ . The block diagram of the vector-radix algorithm is given in Figure 19.3.

The image  $f_{n,m}$  is reorganized into four parts of size  $(N/2 \times N/2)$ , each of which contains only even–even, odd–even, even–odd, or odd–odd coordinates,

$$\{f_{n,m}\} \rightarrow \begin{cases} a_{n_1,m_1} = f_{2n_1,2m_1} \\ b_{n_1,m_1} = f_{2n_1+1,2m_1} \\ c_{n_1,m_1} = f_{2n_1,2m_1+1} \\ d_{n_1,m_1} = f_{2n_1+1,2m_1+1} \end{cases} \quad n_1, m_1 = 0: (N/2 - 1). \quad (19.6)$$

Then, the  $N/2 \times N/2$ -point DFT of each part is calculated,

$$A_{p_1,s_1} = (\mathcal{F}_{N/2,N/2} \circ a)_{p_1,s_1} = \sum_{n_1=0}^{N/2-1} \sum_{m_1=0}^{N/2-1} a_{n_1,m_1} W_{N/2}^{n_1 p_1 + m_1 s_1},$$

$$B_{p_1,s_1} = (\mathcal{F}_{N/2,N/2} \circ b)_{p_1,s_1},$$

$$C_{p_1,s_1} = (\mathcal{F}_{N/2,N/2} \circ c)_{p_1,s_1},$$

$$D_{p_1,s_1} = (\mathcal{F}_{N/2,N/2} \circ d)_{p_1,s_1}.$$

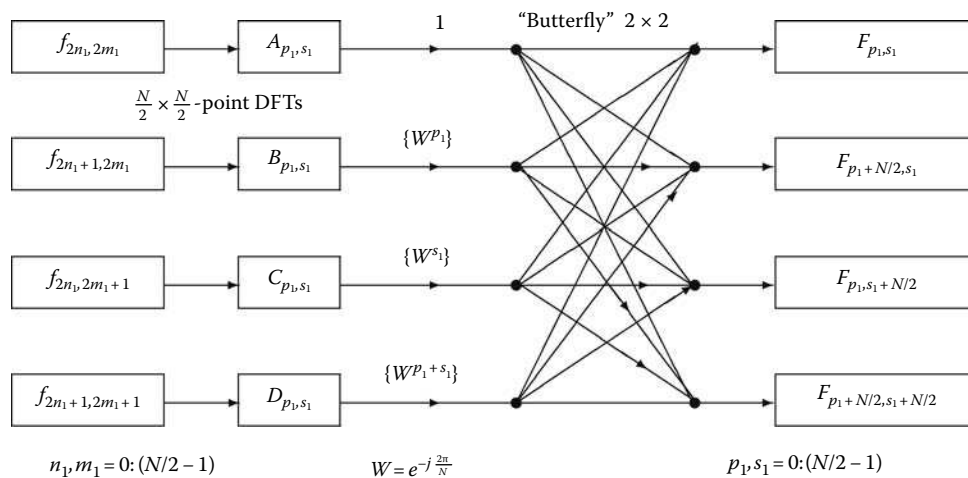


FIGURE 19.3 Diagram of 2-D  $N \times N$ -point DFT by using “butterfly”  $2 \times 2$ .



where  $p_1, s_1 = 0 : (N/2 - 1)$ . The 2-D DFT of the image  $f_{n,m}$  can be composed from these four 2-D DFTs by using the butterfly operation (Equation 19.5) as follows:

$$\begin{aligned} F_{p_1, s_1} &= A_{p_1, s_1} + W^{p_1} B_{p_1, s_1} + W^{s_1} C_{p_1, s_1} + W^{p_1+s_1} D_{p_1, s_1} \\ F_{p_1+N/2, s_1} &= A_{p_1, s_1} - W^{p_1} B_{p_1, s_1} + W^{s_1} C_{p_1, s_1} - W^{p_1+s_1} D_{p_1, s_1} \\ F_{p_1, s_1+N/2} &= A_{p_1, s_1} + W^{p_1} B_{p_1, s_1} - W^{s_1} C_{p_1, s_1} - W^{p_1+s_1} D_{p_1, s_1} \\ F_{p_1+N/2, s_1+N/2} &= A_{p_1, s_1} - W^{p_1} B_{p_1, s_1} - W^{s_1} C_{p_1, s_1} + W^{p_1+s_1} D_{p_1, s_1}. \end{aligned}$$

The same method of partitioning can be applied to each of the parts  $(N/2 \times N/2)$ , and then to each of the sixteen obtained  $(N/4 \times N/4)$  parts, and so on, until the parts be of size  $(2 \times 2)$ . The vector-radix algorithms reduce the number of arithmetic operations. For instance, the number of multiplications can be estimated by the recurrent formula

$$\begin{aligned} m_{N,N} &= 4m_{N/2, N/2} + 3(N/2)^2 \\ &= 4[4m_{N/4, N/4} + 3(N/4)^2] + 3(N/2)^2 \\ &= \frac{3}{4}N^2(\log_2 N - 2). \end{aligned} \quad (19.7)$$

The actual number of multiplications is smaller than  $m_{N,N}$ , since the number of trivial twiddle coefficients are not considered. For large  $N$ , the vector-radix algorithms reduces the number of multiplications by almost 25%, when compared with the row-column algorithm. Indeed, the number of multiplications in the row-column algorithm can be estimated by

$$m_{N,N} = 2Nm_N = 2N \left( \frac{N}{2}(\log_2 N - 3) + 2 \right) = N^2(\log_2 N - 3) + 4N. \quad (19.8)$$

We use the estimation  $m_N = N/2(\log_2 N - 3) + 2$ , ( $N > 8$ ), for the number of multiplications used in the  $N$ -point DFT by the fast paired transforms [11,12].

There are many modifications of the vector-radix technique to decompose the image into many smaller 2-D transforms. Another powerful method of calculation of the DFT is based on using polynomial transforms, which was developed by Nussbaumer [13,14].

### 19.1.3 Method of the Polynomial Transforms

The Nussbaumer algorithm uses the polynomial expansion of the field of rational and complex numbers, where the Fourier transformation exists. Such expansion represents the domain of polynomials, in which the operations of addition and multiplication of polynomials are considered modulo the given polynomial. We here briefly describe the cases of most interest, which correspond to the 2-D DFT of the equal orders  $N \times N$ , when  $N$  is a prime and a power of two.

Let us write the  $N \times N$ -point DFT of the sequence  $f_{n_1, n_2}$  in the separable form

$$F_{p_1, p_2} = \sum_{n_1=0}^{N-1} \left( \sum_{n_2=0}^{N-1} f_{n_1, n_2} W^{n_2 p_2} \right) W^{n_1 p_1}, \quad p_1, p_2 = 0 : (N-1). \quad (19.9)$$

The polynomial transforms represent themselves the polynomial expansion the 1-D DFTs when the complex exponents  $W^{p_2}$  are replaced by the variable  $z$  in the complex plane  $C^2$ . Thus, we consider the following transformation into polynomials:

$$\sum_{n_2=0}^{N-1} f_{n_1, n_2} W^{p_2 n_2} \rightarrow F_{n_1}(z) = \sum_{n_2=0}^{N-1} f_{n_1, n_2} z^{n_2}, \quad z \in C^2,$$

and, then, write the definition in (Equation 19.9) as

$$\begin{aligned} F_{p_1, p_2} &= \sum_{n_1=0}^{N-1} \left( \sum_{n_2=0}^{N-1} f_{n_1, n_2} z^{n_2} \right) \Big|_{z=W^{p_2}} W^{n_1 p_1} \\ &= \left( \sum_{n_1=0}^{N-1} F_{n_1}(z) W^{n_1 p_1} \right) \Big|_{z=W^{p_2}} \end{aligned} \quad (19.10)$$

or shortly

$$F_{p_1, p_2} = \sum_{n_1=0}^{N-1} F_{n_1}(z) W^{n_1 p_1} \bmod (z - W^{p_2}). \quad (19.11)$$

All twiddle coefficients  $W^{p_2}$ ,  $p_2 = 0 : (N-1)$ , are the  $N$ th roots of the unit, or the roots of the polynomial  $z^N - 1$ . We consider the sum of the above equation modulo  $z^N - 1$  and denote it by

$$G_{p_1}(z) = \sum_{n_1=0}^{N-1} F_{n_1}(z) W^{n_1 p_1} \bmod (z^N - 1). \quad (19.12)$$

Thus, the 2-D DFT can be written in the form of

$$F_{p_1, p_2} = G_{p_1}(z) \bmod (z - W^{p_2}), \quad p_2 = 0 : (N-1). \quad (19.13)$$

The polynomial  $z^N - 1$  can be represented as the product of the cyclotomic polynomials (i.e., indivisible polynomials with rational coefficients):

$$z^N - 1 = P_1(z)P_2(z) \cdots P_m(z), \quad m = m(N) \leq N,$$

and the residual of division of  $G_{p_1}(z)$  by the polynomial  $z^N - 1$  in Equation 19.13 can be reduced to residuals by such indivisible polynomials. For example, we consider the case when  $N$  is a prime number  $> 2$ . The following decomposition of the polynomial holds:

$$z^N - 1 = (z - 1)P_2(z) = (z - 1)(z^{N-1} + z^{N-2} + \cdots + 1). \quad (19.14)$$

Since  $N$  is prime, and  $p_2 \neq 0$ , the transformation  $p_1 \rightarrow (p_1 p_2) \bmod N$  maps the set of the integers  $p_1 = 0 : (N-1)$  into itself. The coefficients  $W^{p_2}$  are roots of the polynomial  $P_2(z)$ . Therefore, Equation 19.13 takes the form

$$\begin{aligned} F_{p_1 p_2, p_2} &= \sum_{n_1=0}^{N-1} F_{n_1}(z) W^{n_1 p_1 p_2} \bmod (z^N - 1) \\ &= \sum_{n_1=0}^{N-1} F_{n_1}(z) z^{n_1 p_1} \bmod P_2(z), \quad z = W^{p_2}, p_2 = 1 : (N-1), \end{aligned}$$

where  $p_1 = 0 : (N-1)$ . The compact form of this equation is

$$\begin{aligned} F_{p_1 p_2, p_2} &= \left( \sum_{n_1=0}^{N-1} F_{n_1}(z) z^{n_1 p_1} \bmod P_2(z) \right) \bmod (z - W^{p_2}), \\ p_1 &= 0 : (N-1), p_2 = 1 : (N-1). \end{aligned} \quad (19.15)$$

Thus, the 2-D DFT at the frequency-points  $\{(p_1 p_2, p_2); p_2 = 0 : (N-1)\}$  can be defined as

$$F_{p_1 p_2, p_2} = G_{p_1}(z) \bmod (z - W^{p_2}), \quad p_2 = 0 : (N-1), \quad (19.16)$$

where

$$G_{p_1}(z) = \sum_{n_1=0}^{N-1} F_{n_1}(z) z^{n_1 p_1} \bmod P_2(z), \quad p_1 = 0 : (N-1). \quad (19.17)$$

When  $p_2 = 0$ , the formula for the 2-D DFT takes the simple form of the 1-D DFT,

$$F_{p_1, 0} = \sum_{n_1=0}^{N-1} \sum_{n_2=0}^{N-1} f_{n_1, n_2} W^{n_1 p_1} = \sum_{n_1=0}^{N-1} F_{n_1}(1) W^{n_1 p_1}, \quad p_1 = 0 : (N-1). \quad (19.18)$$

The polynomial transform modulo  $P_2(z)$  in Equation 19.17 does not depend on  $p_2$  and is calculated without operations of multiplication. The multiplications are required to calculate the  $N$ -point DFT in Equation 19.18 and the  $N$ -point DFT in Equation 19.16, for each  $p_1 = 0 : (N-1)$ . Thus, the  $N \times N$ -point DFT is calculated by means of the polynomial transforms modulo  $P(z)$  and  $(N+1)$   $N$ -point DFTs.

In the case, when  $N$  equals a power of two, the following decomposition of the polynomial holds:

$$z^N - 1 = (z^{N/2} - 1)(z^{N/2} + 1),$$

and all exponents  $z = W^{p_2}$  with odd powers  $p_2$  are roots of the polynomial  $z^{N/2} - 1$ . Therefore it follows directly from Equation 19.10 through Equation 19.13, that all spectral components  $F_{p_1, p_2}$  at frequency-points  $(p_1, p_2)$ , both coordinates of which  $p_1$  and  $p_2$  are not even, can be calculated by means of the polynomial

transforms modulo  $z^{N/2} + 1$ ,  $3N/2$  reduced  $N$ -point DFTs and one  $N/2 \times N/2$ -point DFT for calculating all components of the spectrum at frequency-points  $(p_1, p_2)$  with even  $p_1$  and  $p_2$ . The  $N/2 \times N/2$ -point DFT can also be reduced by the polynomial transforms modulus  $z^{N/4} + 1$ , to  $3N/4$   $N/4$ -point reduced DFTs, and the  $N/4 \times N/4$ -point DFT. The sequential application of the polynomial transforms modulo  $z^{N/2^k} + 1$ , ( $k = 1 : (r-m)$ ), when  $m = 1 : (r-2)$ , yields the decomposition of the  $N \times N$ -point DFT by  $3N/2$   $N/2$ -point DFTs,  $3N/4$   $N/4$ -point DFTs, etc. In comparison with the row-column algorithm, the method of polynomial transforms uses approximately two times less operations of multiplication and a small number of additions.

We now present the tensor approach and its improvement for dividing the calculation of the 2-D DFT into the minimal number of short 1-D transforms. The approach is universal because it can be implemented to calculate other discrete unitary transforms, such as the Hadamard, cosine, and Hartley transforms [15,16], and transforms of high dimensions.

## 19.2 Nontraditional Forms of Representation

When processing a multidimensional signal  $f_{n_1, n_2, \dots, n_m}$ ,  $m \geq 2$ , in frequency domain by a specific unitary transformation, for instance the  $m$ -dimensional DFT, the signal can be represented in a form that splits the structure of both signal and transform in a way that yields an effective method of calculation of the transform with the following signal processing. Such forms are not necessarily of the matrix form, but other multidimensional figures. The work presented here does not rely on traditional methods of processing multidimensional transforms and signals, but more effective methods which are based on the discovery that can be briefly formulated as follows. Multidimensional spectra are split by appointed trajectories (such as orbits) and the movement of a spectral point along each such trajectory is of great interest in the process of formation of the spectra, as well as in processing the spectra. Trajectories do not intersect, and it is possible to extract the spectral information from such trajectories or change and put desired information into trajectories. Vast horizons lie before us in such an approach allowing new effective methods of processing multidimensional spectra to be discovered and applied in practice.

We present a theory of fast multidimension transforms based on the concept of partitioning that reveals the transforms. We stand in detail on the 2-D and 3-D cases; the application of the discussed methods to high-dimensional signals is straightforward. At the same time, we present our vision of developing and applying new methods of multidimensional signal processing, such as image processing. We propose to use new forms of image and transform representation, that simplify not only the calculation of 2-D (or 3-D) transforms, but also lead to effective solutions of different problems in image processing, such as image enhancement, computerized tomography, image filtration, and compression. We describe the theory of the so-called tensor and paired forms of representation. Their main task is to

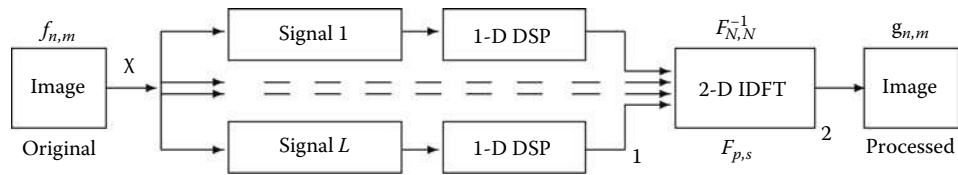


FIGURE 19.4 Block diagram of image processing by 1-D signals. DSP, digital signal processing.

represent uniquely the image in a form of a set of 1-D signals which can be processed separately and then transferred back to the image, as shown in the diagram of Figure 19.4 (with or without block 2). The calculation of the 2-D DFT is reduced to calculation of 1-D DFTs and processing of the 2-D image to processing all or a few 1-D signals. The mathematical structure of the 2-D DFT and other unitary transforms possess such representations.

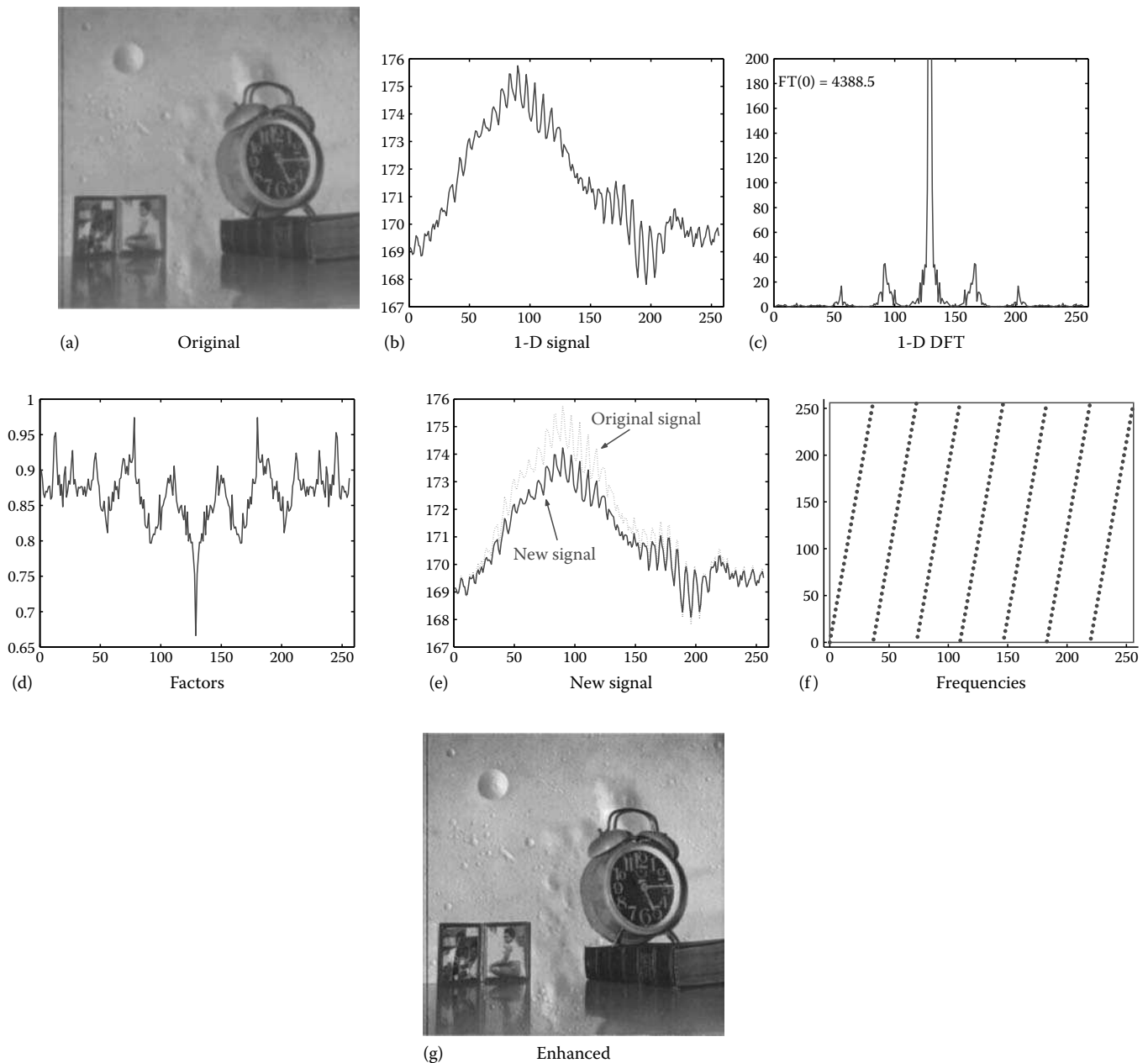


FIGURE 19.5 Fast transform-based method of image enhancement. (a) The original image, (b) the splitting-signal, (c) the amplitude spectrum of the signal, (d) factors, (e) the processed signal, (f) marked locations of 256 frequency-points, and (g) the image enhanced by one signal.

As an example, we consider the image enhancement by one such signal, instead of calculating the 2-D DFT of the image and manipulating its coefficients. Figure 19.5 shows the original image of size  $256 \times 256$  in part a, along with a 1-D signal derived from the image in (b), the 1-D DFT of the signal (in absolute scale and shifted to the center) in (c), the coefficients to be multiplied pointwise by the 1-D DFT in (d), a new 1-D signal in (e), 256 frequency-points at which the spectral information of the new signal will be recorded in the 2-D DFT of the processed image in (f), and the enhanced image in (g). The enhanced image can be obtained by the inverse 2-D DFT (2-D IDFT), as well as directly from the new signal (of e) by using the 1-D DFT [18]. Thus the problem of the 2-D image enhancement can be reduced to processing a 1-D signal (or a few such), by passing the calculation of the 2-D DFT of the original image as well as the inverse 2-D DFT (2-D IDFT) for the enhanced image. We now describe methods of deriving such 1-D signals, which lead to effective calculation of the 2-D DFT, as well as other unitary transforms.

### 19.3 Partitioning of Multidimensional Transforms

Let a sequence  $g = \{g_0, g_1, \dots, g_{N-1}\}$  of length  $N > 1$  be linearly and uniformly expressed by a sequence  $f = \{f_0, f_1, \dots, f_{N-1}\}$

$$g_p = \sum_{n=0}^{N-1} \varphi_p(n) f_n, \quad p = 0: (N-1). \quad (19.19)$$

The transformation of  $f$  into  $g$ , by using this formula is called a *linear transformation*, which we denote by  $\mathcal{A}$ . Coefficients  $a_{p,n} = \varphi_p(n)$  form a square  $(N \times N)$  matrix  $A = \|a_{p,n}\|$ , which is called the matrix of the transformation. The linear transformation can be written in matrix representation  $[g] = A[f]$ , where  $[g]$  and  $[f]$  denote the vector-columns of sequences  $g$  and  $f$ , respectively. Every linear 1-D transformation determines uniquely a 2-D matrix  $A$ , and vice versa, every matrix  $A$  determines the linear 1-D transformation. Similarly, each  $2n$ -dimensional ( $n > 1$ ) matrix determines a certain linear  $n$ -dimensional transformation  $\mathcal{A}$  of  $n$ -dimensional sequences,

$$\mathcal{A}: f = \{f_{n_1, n_2, \dots, n_n}\} \rightarrow g = \{g_{p_1, p_2, \dots, p_n}\} \quad (19.20)$$

where  $n_k, p_k = 0 : (N_k - 1)$  and  $N_k > 1, k = 1 : n$ . The numbers  $N_1, \dots, N_n$  are called *orders* of the transformation  $\mathcal{A}$ .  $g = \mathcal{A} \circ f$  is called the  $n$ -dimensional transform of  $f$ . For simplicity of future calculations, we will consider mainly the case of equal orders, when  $N_k = N, k = 1 : n$ .

The transform of  $f$  is described by the following relation:

$$g_{p_1, \dots, p_n} = \sum_{n_1=0}^{N_1-1} \dots \sum_{n_n=0}^{N_n-1} \varphi_{p_1, \dots, p_n}(n_1, \dots, n_n) f_{n_1, \dots, n_n} \quad (19.21)$$

where  $a_{p_1, \dots, p_n, n_1, \dots, n_n} = \varphi_{p_1, \dots, p_n}(n_1, \dots, n_n)$  are coefficients of the matrix of the transformation  $\mathcal{A}$ . Elements  $(p_1, \dots, p_n) \in X$  are referred to as *frequency-points*. We assume that sequences  $f$  and the transforms  $\mathcal{A} \circ f$  are defined on the same  $n$ -dimensional rectangular integer lattice of size  $N_1 \times \dots \times N_n$

$$X = X_{N_1, \dots, N_n} = \{(n_1, \dots, n_n); n_k = 0: (N_k - 1), k = 1: n\}. \quad (19.22)$$

This set  $X$  is called *the fundamental period* of the transformation  $\mathcal{A}$ .

#### Example 19.1 (3-D Fourier Transformation)

Let  $f$  be a 3-D  $N \times N \times N$ -point sequence  $f = \{f_{n_1, n_2, n_3}\}$ . The  $N \times N \times N$ -point Fourier transform of the sequence  $f$  is defined by

$$F_{p_1, p_2, p_3} = \sum_{n_1=0}^{N-1} \sum_{n_2=0}^{N-1} \sum_{n_3=0}^{N-1} W^{n_1 p_1 + n_2 p_2 + n_3 p_3} f_{n_1, n_2, n_3}, \quad p_1, p_2, p_3 = 0: (N-1) \quad (19.23)$$

where  $W = \exp(-2\pi j/N)$ . The arithmetic action  $f_{n_1, n_2, n_3} \rightarrow \{F_{p_1, p_2, p_3}\}$  is called a 3-D  $N \times N \times N$ -point *Fourier transformation*, which we shall denote by  $\mathcal{F}_{N,N,N}$ . The order of the transformation  $\mathcal{F}_{N,N,N}$  equals  $N \times N \times N$ , and its matrix is the six-dimensional matrix

$$[\mathcal{F}_{N,N,N}] = \| \| a_{p_1, p_2, p_3, n_1, n_2, n_3} = W^{n_1 p_1 + n_2 p_2 + n_3 p_3} \| \|, \quad n_k, p_k = 0: (N-1), k = 1: 3.$$

An  $n$ -dimensional DT  $\mathcal{A}$  is called *unitary*, if the matrix of the transformation is unitary, i.e.,  $AA^* = I$ , where  $I$  is the diagonal matrix, and  $A^*$  is the complex conjugate to  $A$ , which is defined by

$$A^* = \| \| \bar{a}_{n_1, \dots, n_n, p_1, \dots, p_n} \| \|$$

where the sign  $\bar{\phantom{x}}$  denotes the transition to the complex conjugate value, that is,  $\bar{z} = x - jy$ , if  $z = x + jy$ . A real unitary transformation is called *orthogonal*.

For a fixed  $(p_1, \dots, p_m)$ , the function  $\varphi_{p_1, \dots, p_m}(\cdot, \dots, \cdot)$  is said to be the  $(p_1, \dots, p_m)$ -th *basis function* of the transformation  $\mathcal{A}$ , and the collection of such functions  $\{\varphi = \{\varphi_{p_1, \dots, p_n}(\cdot, \dots, \cdot)\}\}$  is called a *basis or kernel* of  $\mathcal{A}$ . The unitary property of the transformation is also expressed by the following expression

$$\sum_{(n_1, \dots, n_n) \in X} \varphi_{p_1, \dots, p_n}(n_1, \dots, n_n) \bar{\varphi}_{s_1, \dots, s_n}(n_1, \dots, n_n) = \prod_{k=1}^n \delta(p_k, s_k) \quad (19.24)$$

$$(p_1, \dots, p_n), (s_1, \dots, s_n) \in X,$$

where  $\delta$  is the kronecker delta-function,  $\delta(n, k) = 1$ , if  $n = k$ , and  $\delta(n, k) = 0$ , otherwise. If the collection of functions  $\{\varphi\}$  satisfies this condition, then  $\{\varphi\}$  is said to be a *complete* and *orthonormal* set of functions (or *orthogonal*, if there is a factor different from 1 in the right side of Equation 19.24, before the multiplication sign) in the space of  $n$ -dimensional sequences defined on  $X$ . For the unitary transformation  $\mathcal{A}$ , the collection of functions is a complete and orthonormal set of basis functions.

### Example 19.2 (1-D Fourier Transformation)

Let  $f$  be a 1-D sequence  $f = \{f_0, f_1, \dots, f_{N-1}\}$ . The  $N$ -point Fourier transform of the sequence  $f$  is defined by

$$F_p = (\mathcal{F}_N \circ f)_p = \frac{1}{\sqrt{N}} \sum_{n=0}^{N-1} W^{np} f_n, \quad p = 0: (N-1). \quad (19.25)$$

The basis functions  $\varphi_p(n)$  are the pairs  $(1/\sqrt{N} \cos(\omega_p n), 1/\sqrt{N} \sin(\omega_p n))$  of discrete-time cosine and sine waves with frequencies  $\omega_p = (2\pi/N)p$ . The waves are orthonormal, since

$$\begin{aligned} \sum_{n=0}^{N-1} \varphi_p(n) \bar{\varphi}_s(n) &= \frac{1}{N} \sum_{n=0}^{N-1} W^{n(p-s)} \\ &= \frac{1}{N} \sum_{n=0}^{N-1} \left[ \cos \frac{2\pi(p-s)}{N} n - j \sin \frac{2\pi(p-s)}{N} n \right] \\ &= \begin{cases} 1, & p = s \\ 0, & p \neq s \end{cases} \end{aligned}$$

and the transformation is unitary. The matrices of the transformation and its conjugate are symmetric matrices

$$[\mathcal{F}_N] = \frac{1}{\sqrt{N}} \| e^{-\frac{j2\pi}{N} np} \|_{n,p=0:(N-1)}, \quad [\mathcal{F}_N^*] = \frac{1}{\sqrt{N}} \| e^{\frac{j2\pi}{N} np} \|_{n,p=0:(N-1)},$$

and  $[\mathcal{F}_N][\mathcal{F}_N^*] = I$ . The conjugate matrix is thus the matrix of the inverse 1-D DFT.

### 19.3.1 Tensor Representation

In this section, we describe a concept of covering that reveals the mathematical structure of many multidimensional transforms [19–23]. The covering is considered to be composed by cyclic groups of frequency-points of the period of transformations. This covering leads to the tensor, or vectorial representation of multidimensional signals.

In the general multidimensional case, the covering revealing the transform is described in the following way. Suppose  $\sigma = (T)$  is an irreducible covering of an  $n$ -dimensional lattice  $X$ ,  $n \geq 2$ . It means that the set-theoretic union of all subsets  $T$  coincides with  $X$  and any smaller family of subsets of  $T$  from  $\sigma$  does not cover  $X$ . We use *card* to denote the cardinality of a set. If a discrete  $n$ -dimensional unitary transformation with the fundamental period  $X$  can be split into a set of *card*  $\sigma$  one-dimensional

*card*  $T$ -point unitary transformations  $\mathcal{A}$ , then we say that the considered multidimensional transformation is revealed by the covering  $\sigma$ , or, the covering  $\sigma$  reveals the transformation. Let  $f$  be an  $N_1 \times \dots \times N_n$  sequence.

**Definition 19.1:** An  $N_1 \times \dots \times N_n$  transformation  $\mathcal{P}$  is said to be revealed by the covering  $\sigma$  of  $X$  if, for each set  $T \in \sigma$ , there exists a 1-D orthogonal transformation  $\mathcal{A} = \mathcal{A}(T)$  and a sequence  $f_T$  such that the restriction of the transform  $\mathcal{P} \circ f$  on the set of frequency-points  $T$  equals the transform  $\mathcal{A} \circ f_T$ , i.e.,

$$(\mathcal{P} \circ f)|_T = \mathcal{A} \circ f_T. \quad (19.26)$$

This condition is briefly written as  $\mathcal{P}|_{\sigma} \tilde{\sigma} \mathcal{A}$ .

The set of the 1-D transforms  $\{\mathcal{A}(T); T \in \sigma\}$  is called a  $\sigma$ -splitting of the  $n$ -dimensional transformation  $\mathcal{P}$  by the covering  $\sigma$  and denoted by  $\mathcal{R}(\mathcal{P}; \sigma)$ . The set of 1-D sequences  $\{f_T; T \in \sigma\}$  is the  $\sigma$ -representation of  $f$  with respect to the transformation  $\mathcal{P}$ .

In the above definition, each 1-D transformation  $\mathcal{A}$  is determined by the corresponding subset  $T$ , not  $f$ . It should also be noted, that the covering  $\sigma$  results in not only the splitting of the  $n$ -dimensional transformation  $\mathcal{P}$  by the 1-D transformations  $\mathcal{A}$  but also determines the corresponding representation of the  $n$ -dimensional sequence  $f$  as a set of 1-D sequences  $f_T$ . In other words, two representations are defined, one for the given sequence and another for its transform,

$$f \rightarrow \{f_T; T \in \sigma\}, \quad \text{and} \quad \mathcal{P} \circ f \rightarrow \{\mathcal{A} \circ f_T; T \in \sigma\}. \quad (19.27)$$

### 19.3.2 Covering with Cyclic Groups

We consider a class of  $n$ -dimensional discrete unitary transformations that are revealed by the irreducible covering  $\sigma$  composed only from additive cyclic groups

$$\sigma = \sigma_J = (T_{p_1, \dots, p_n})_{(p_1, \dots, p_n) \in J} \quad (19.28)$$

with generators  $(p_1, \dots, p_n)$  from a certain subset  $J \subset X = X_{N_1, \dots, N_n}$ . The cyclic group  $T$  with a generator  $(p_1, \dots, p_n)$  is defined as a set of frequency-points which are integer multiples to the generator,

$$T = T_{p_1, \dots, p_n} = \{(\overline{kp_1}, \dots, \overline{kp_n}); k = 0: (\text{card } T - 1)\} \quad (19.29)$$

We use the short notation  $\overline{kp_i} = (kp_i) \bmod N_i$  for  $i = 1 : n$ .

#### Example 19.3

Let  $X$  be the lattice  $5 \times 5$ , what corresponds to the  $N_1 = N_2 = 5$  case. The group  $T_{p_1, p_2}$  with a generatrix  $(p_1, p_2) \in X = X_{5,5}$  is

$$T_{p_1, p_2} = \{(0, 0), (p_1, p_2), (\overline{2p_1}, \overline{2p_2}), (\overline{3p_1}, \overline{3p_2}), (\overline{4p_1}, \overline{4p_2})\}.$$

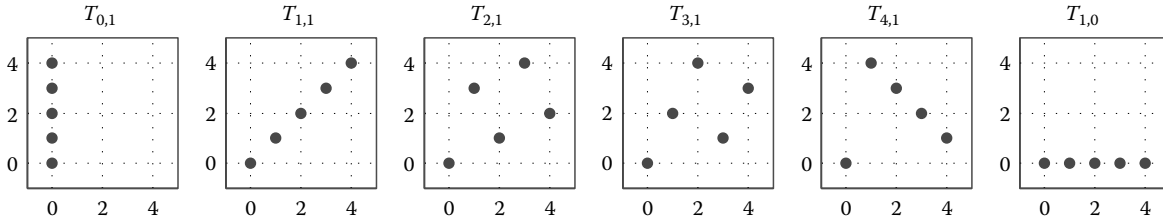


FIGURE 19.6 Arrangement of frequency-points of groups  $T_{p_1, p_2}$  covering the lattice  $5 \times 5$ .

There are six groups  $T$  which compose an irreducible covering  $\sigma = \sigma_J$  of  $X$ , namely

$$\begin{aligned}
 T_{0,1} &= \{(0, 0), (0, 1), (0, 2), (0, 3), (0, 4)\} \\
 T_{1,1} &= \{(0, 0), (1, 1), (2, 2), (3, 3), (4, 4)\} \\
 T_{2,1} &= \{(0, 0), (2, 1), (4, 2), (1, 3), (3, 4)\} \\
 T_{3,1} &= \{(0, 0), (3, 1), (1, 2), (4, 3), (2, 4)\} \\
 T_{4,1} &= \{(0, 0), (4, 1), (3, 2), (2, 3), (1, 4)\} \\
 T_{1,0} &= \{(0, 0), (1, 0), (2, 0), (3, 0), (4, 0)\}
 \end{aligned} \tag{19.30}$$

and the set of generators

$$J = J_{5,5} = \{(0, 1), (1, 1), (2, 1), (3, 1), (4, 1), (1, 0)\}. \tag{19.31}$$

Figure 19.6 shows the location of all frequency-points of these six groups. These groups intersect only at point  $(0, 0)$ . If the covering composed by these groups reveals a  $5 \times 5$ -point transformation, then that transformation can be split by six 5-point 1-D transformations. It will be shown, that such transformations are the Fourier, Hartley, and Hadamard transformations. To calculate, for instance the  $5 \times 5$ -point 2-D DFT, there are only six 1-D 5-points transforms required, instead of 10 transforms in the “row-column” method.

In the general  $N \times N$  case, the elements of the group  $T_{p_1, p_2}$  lie on parallel lines at angle  $\theta = \tan^{-1}(p_2/p_1)$  to the horizontal axis. The number  $l$  of such lines is determined as follows. If  $p_1 = 0$  or  $p_2 = 0$ , then  $l = 1$ . For other cases, let  $k_1$  and  $k_2$  be the least integers satisfying the relations  $\overline{k_1 p_1} = \overline{k_2 p_2} = N - 1$ . Then,  $l = k_1/k_2$  with  $k_1 \geq k_2$ , and  $l = k_2/k_1$  with  $k_1 < k_2$ . For instance, when  $N = 5$  and  $(p_1, p_2) = (2, 1)$ , we obtain  $\overline{2p_1} = \overline{4p_2} = 4$  and  $l = 4/2 = 2$ . The frequency-points of the group  $T_{2,1}$  lie on two parallel lines at angle  $\theta = \tan^{-1}(1/2) = 26.5651^\circ$  to the horizontal axis (see Figure 19.6). The points of this group can be also considered lying on three parallel lines at angle  $\theta_1 = \theta - 90^\circ = -63.4349^\circ$  to the horizontal axis. It should be noted, that if we splice the opposite sides of the lattice bounds, then the lattice will be represented as a net traced on the surface of a three-dimensional torus and the mentioned  $l$  lines will compose a closed spiral on the torus, which will pass through those points on the net, which correspond to the points  $(0, 0)$  and  $(p_1, p_2)$ . All elements of the cyclic group will be points of intersection of the spiral with the net. As an example, Figure 19.7 shows the points of the lattice  $X_{20,20}$  on the torus and two spirals with frequency-points of the groups  $T_{1,1}$  and  $T_{1,2}$  which intersect at the knot  $(0, 0)$ .

The irreducible covering  $\sigma$  of the domain  $X$  composed from groups (Equation 19.29) is unique. To illustrate this property, we consider the 2-D case with the square lattice  $X_{5,5}$ . The irreducible covering  $\sigma$  of  $X_{5,5}$  is the family of six groups given in Equation 19.30:

$$\sigma = (T_{0,1}, T_{1,1}, T_{2,1}, T_{3,1}, T_{4,1}, T_{1,0}).$$

The cyclic group  $T_{p_1, p_2}$  with any other generatrix  $(p_1, p_2) \neq (0, 0)$ , different from generatrices  $(0, 1), (1, 1), (2, 1), (3, 1), (4, 1)$ , and  $(1, 0)$ , coincides with one of the groups of the covering  $\sigma$ . For instance,

$$\begin{aligned}
 T_{1,2} &= \{(0, 0), (1, 2), (2, 4), (3, 1), (4, 3)\} = T_{3,1}, \\
 T_{3,2} &= \{(0, 0), (3, 2), (1, 4), (4, 1), (2, 3)\} = T_{4,1}, \\
 T_{2,2} &= \{(0, 0), (2, 2), (4, 4), (1, 1), (3, 3)\} = T_{1,1}.
 \end{aligned}$$

If an  $n$ -dimensional transformation  $\mathcal{P}$  is revealing by the covering  $\sigma$  composed by cyclic groups (Equation 19.29), then the  $\sigma_J$ -representation of a  $n$ -dimensional sequence  $f$  by  $\mathcal{P}$ , i.e., the totality of 1-D signals  $\{f_T; T \in \sigma\}$ , is called a *tensor*, or *vector* representation of  $f$  with respect to the transformation  $\mathcal{P}$  [12]. The 1-D signals  $f_T$  are called the *splitting-signals* of  $f$ .

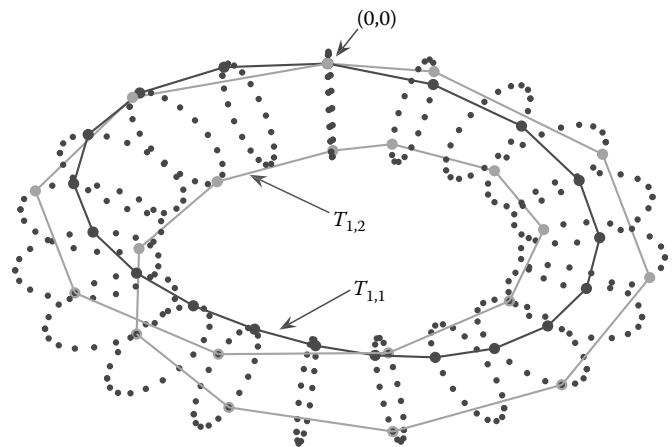


FIGURE 19.7 Torus of the lattice  $20 \times 20$  with two spirals corresponding to the groups  $T_{1,1}$  and  $T_{1,2}$ .

## 19.4 Fourier Transform Tensor Representation

In this section, we discuss in detail the construction and properties of the tensor representation of the multidimensional signals with respect to the DFT. We first consider the 2-D case as the simplest case among multidimensional ones.

Let  $f = \{f_{n_1, n_2}\}$  be a sequence of size  $N_1 \times N_2$ , and let  $N_0 = \text{g.c.d.}(N_1, N_2) > 1$ , i.e.,  $N_1 = N_0 N'_1$ ,  $N_2 = N_0 N'_2$ . Let  $\sigma = \sigma_{N_1, N_2}$  be the irreducible covering of the rectangular lattice  $X = X_{N_1, N_2}$  defined in Equation 19.28. We denote by  $\mathcal{F} = \mathcal{F}_{N_1, N_2}$  the  $N_1 \times N_2$ -point 2-D DFT. The 2-D DFT of the sequence  $f$ , accurate to the normalizing factor  $1/N_1 N_2$ , is defined by the following relation:

$$F_{p_1, p_2} = (\mathcal{F} \circ f)_{p_1, p_2} = \sum_{n_1=0}^{N_1-1} \sum_{n_2=0}^{N_2-1} f_{n_1, n_2} W_{N_1}^{n_1 p_1} W_{N_2}^{n_2 p_2}, \quad (p_1, p_2) \in X, \quad (19.32)$$

where  $W_{N_k} = \exp(-2\pi j/N_k)$ ,  $k = 1, 2$ .

For an arbitrary frequency-point  $(p_1, p_2)$ , we determine in the period  $X$  the sets of points

$$V_{p_1, p_2, t} = \{(n_1, n_2); N'_2 n_1 p_1 + N'_1 n_2 p_2 = t \bmod N\}, \quad t = 0: (N-1), \quad (19.33)$$

where  $N = N_1 N_2 / N_0$ . On these sets of points, we consider the sums of the sequence  $f$ , i.e., the following  $N$  quantities

$$f_{p_1, p_2, t} = \sum \{f_{n_1, n_2}; (n_2, n_2) \in V_{p_1, p_2, t}\}, \quad t = 0: (N-1). \quad (19.34)$$

For the spectral component  $F_{p_1, p_2}$ , the following calculations hold:

$$F_{p_1, p_2} = \sum_{n_1=0}^{N_1-1} \sum_{n_2=0}^{N_2-1} f_{n_1, n_2} W_N^{N'_2 n_1 p_1 + N'_1 n_2 p_2} = \sum_{t=0}^{N-1} f_{p_1, p_2, t} W^t, \quad (19.35)$$

where  $W = W_N = e^{-j2\pi/N}$ . The general formula is also valid,

$$F_{k p_1, k p_2} = \sum_{t=0}^{N-1} f_{p_1, p_2, t} W^{kt}, \quad k = 0: (N-1). \quad (19.36)$$

In other words,  $N$  components  $F_{k p_1, k p_2}$  of the 2-D DFT of  $f$  can be represented by the 1-D sequence of length  $N$ :

$$f_{T_{p_1, p_2}} = \{f_{p_1, p_2, 0}, f_{p_1, p_2, 1}, \dots, f_{p_1, p_2, N-1}\}. \quad (19.37)$$

The sequence  $f_{T_{p_1, p_2}}$  determines the spectral information of the image  $f$  at frequency-points of the set  $T_{p_1, p_2}$ . We call such a sequence *the splitting-signal*, or *the image-signal* if  $f$  is an image. The components of the splitting-signal are numbered by the set of three,  $(p_1, p_2, t)$ , where two components represent the

frequency  $(p_1, p_2)$  and  $t$  is referred to as the time. Thus the splitting-signal is a (2-D frequency)-(1-D time) representation of the 2-D sequence  $f$ , which determines completely the 2-D DFT of  $f$  at the frequency-points of the set  $T_{p_1, p_2}$ .

### Example 19.4

(5 × 5-point DFT) Let  $N = 5$  and  $f$  be the following image of size 5 × 5:

$$f = \begin{vmatrix} \underline{1} & 2 & 1 & 3 & 1 \\ 2 & 0 & 1 & 1 & 2 \\ 1 & 3 & 2 & 2 & 1 \\ 4 & 1 & 0 & 1 & 3 \\ 2 & 4 & 1 & 2 & 1 \end{vmatrix}.$$

The underlined unit shows the location of the zero point. We consider the frequency-point  $(p_1, p_2) = (2, 1)$ . All values of  $t$  in the equations  $n_1 p_1 + n_2 p_2 = t \bmod 5$  can be written in the form of the following matrix:

$$\|t = (n_1 \cdot 2 + n_2 \cdot 1) \bmod 5\|_{n_2, n_1=0:4} = \begin{vmatrix} \underline{0} & 1 & 2 & 3 & 4 \\ 2 & 3 & 4 & 0 & 1 \\ 4 & 0 & 1 & 2 & 3 \\ 1 & 2 & 3 & 4 & 0 \\ 3 & 4 & 0 & 1 & 2 \end{vmatrix}.$$

Therefore, the components of the splitting-signal  $f_{T_{2,1}}$  of  $f$  are defined as follows:

$$f_{T_{2,1}} = \begin{cases} f_{2,1,0} = f_{0,0} + f_{1,3} + f_{2,1} + f_{3,4} + f_{4,2} = 1 + 1 + 3 + 3 + 1 = 9 \\ f_{2,1,1} = f_{0,1} + f_{1,4} + f_{2,2} + f_{3,0} + f_{4,3} = 2 + 2 + 2 + 4 + 2 = 12 \\ f_{2,1,2} = f_{0,2} + f_{1,0} + f_{2,3} + f_{3,1} + f_{4,4} = 1 + 2 + 2 + 1 + 1 = 7 \\ f_{2,1,3} = f_{0,3} + f_{1,1} + f_{2,4} + f_{3,2} + f_{4,0} = 3 + 0 + 1 + 0 + 2 = 6 \\ f_{2,1,4} = f_{0,4} + f_{1,2} + f_{2,0} + f_{3,3} + f_{4,1} = 1 + 1 + 1 + 1 + 4 = 8 \end{cases} \quad (19.38)$$

and  $f_{T_{2,1}} = \{9, 12, 7, 6, 8\}$ . The power of this signal equals the power of the image  $f$ , i.e.,

$$\sum_{t=0}^4 f_{2,1,t} = 9 + 12 + 7 + 6 + 8 = 42 = \sum_{n_1=0}^4 \sum_{n_2=0}^4 f_{n_1, n_2}.$$

The 5-point DFT of the splitting-signal equals

$$\mathcal{F}_5 \circ f_{T_{2,1}} = \{42, 4.6631 - 4.3920j, -3.1631 - 1.4001j, -3.1631 + 1.4001j, 4.6631 + 4.3920j\}.$$

This transform coincides with the 2-D DFT of the image  $f$  at frequency-points of the group

$$T_{2,1} = \{(0, 0), (2, 1), (4, 2), (1, 3), (3, 4)\},$$

as shown in the following table:

$$\begin{bmatrix} 42 & 0 & 0 & 0 & 0 \\ 0 & 0 & 0 & -3.1631+1.4001j & 0 \\ 0 & 4.6631-4.3920j & 0 & 0 & 0 \\ 0 & 0 & 0 & 0 & 4.6631+4.3920j \\ 0 & 0 & -3.1631-1.4001j & 0 & 0 \end{bmatrix} \quad (19.39)$$

We can fill the rest values of the 2-D DFT of the image, by using other splitting-signals. For instance, for the signal corresponding to the generator  $(p_1, p_2) = (3, 1)$ , we have the following table of time-points:

$$\|t = (n_1 \cdot 3 + n_2 \cdot 1) \bmod 5\|_{n_2, n_1=0:4} = \begin{bmatrix} 0 & 1 & 2 & 3 & 4 \\ 3 & 4 & 0 & 1 & 2 \\ 1 & 2 & 3 & 4 & 0 \\ 4 & 0 & 1 & 2 & 3 \\ 2 & 3 & 4 & 0 & 1 \end{bmatrix}.$$

The components of the splitting-signal  $f_{T_{2,1}}$  are thus calculated as follows:

$$f_{T_{3,1}} = \begin{cases} f_{3,1,0} = f_{0,0} + f_{1,2} + f_{2,4} + f_{3,1} + f_{4,3} = 1 + 1 + 1 + 1 + 2 = 6 \\ f_{3,1,1} = f_{0,1} + f_{1,3} + f_{2,0} + f_{3,2} + f_{4,4} = 2 + 1 + 1 + 0 + 1 = 5 \\ f_{3,1,2} = f_{0,2} + f_{1,4} + f_{2,1} + f_{3,3} + f_{4,0} = 1 + 2 + 3 + 1 + 2 = 9 \\ f_{3,1,3} = f_{0,3} + f_{1,0} + f_{2,2} + f_{3,4} + f_{4,1} = 3 + 2 + 2 + 3 + 4 = 14 \\ f_{3,1,4} = f_{0,4} + f_{1,1} + f_{2,3} + f_{3,0} + f_{4,2} = 1 + 0 + 2 + 4 + 1 = 8 \end{cases} \quad (19.40)$$

and  $f_{T_{3,1}} = \{6, 5, 9, 14, 8\}$ . The 5-point DFT of this splitting-signal equals

$$\mathcal{F}_5 \circ f_{T_{3,1}} = \{42, -8.5902 + 5.7921j, 2.5902 - 2.9919j, 2.5902 + 2.9919j, -8.5902 - 5.7921j\}.$$

This transform defines the 2-D DFT of the image at frequency-points of the group

$$T_{3,1} = \{(0, 0), (3, 1), (1, 2), (4, 3), (2, 4)\}.$$

In this stage, we fill the 2-D DFT as shown in the following table:

$$\begin{bmatrix} 42 & 0 & 0 & 0 & 0 \\ 0 & 0 & 2.5902-2.9919j & -3.1631+1.4001j & 0 \\ 0 & 4.6631-4.3920j & 0 & 0 & -8.5902-5.7921j \\ 0 & -8.5902+5.7921j & 0 & 0 & 4.6631+4.3920j \\ 0 & 0 & -3.1631-1.4001j & 2.5902+2.9919j & 0 \end{bmatrix}.$$

In a similar way, the 1-D DFTs of the splitting-signals  $f_{T_{0,1}}$ ,  $f_{T_{1,1}}$ ,  $f_{T_{4,1}}$ , and  $f_{T_{1,0}}$ , fill the rest of the table of the 2-D DFT of the image  $f$ .

To illustrate the tensor representation in the general case, we consider the case when  $N = 256$  and the generator is  $(p_1, p_2) = (16, 1)$ . Figure 19.8 shows (a) the clock-and-moon image

$256 \times 256$  in part (a), along with the image-signal  $f_{T_{16,1}}$  of length 256 in (b), the 1-D DFT of the image-signal (in absolute scale) in (c), and 256 samples of this 1-D DFT at frequency-points of the subset  $T_{16,1}$  of  $X_{256,256}$  at which the 2-D DFT of the image is filled by the 1-D DFT in (d). The value of the 1-D DFT at point 0, which is the power 43,885 of the image, has been truncated in parts (c) and (d). Figure 19.9 shows another image-signal  $f_{T_{5,1}}$  in part (a), along with the 256-point DFT of this signal in (b), and the arrangement of values of the 1-D DFT in the 2-D DFT of the image in (c).

### 19.4.1 2-D Directional Images

The components  $f_{p_1, p_2, t}$ ,  $t = 0 : (N - 1)$ , of the splitting-signals of a 2-D sequence, or image  $f_{n_1, n_2}$ , are defined as sums of the image at points lying on the corresponding set  $V_{p_1, p_2, t}$  defined in Equation 19.33. To describe these sets, we first consider the case when  $N_1 = N_2 = N$ . Given a sample  $(p_1, p_2) \in X$  and a nonnegative integer  $t < N$ , the set

$$V_{p_1, p_2, t} = \{(n_1, n_2); n_1 p_1 + n_2 p_2 = t \bmod N, n_1, n_2 = 0 : (N - 1)\}$$

if it is not empty, is the set of points  $(n_1, n_2)$  along a family of parallel straight lines at the angle of  $\psi = -\arctan(p_2/p_1)$  to the horizontal axis. The equations for these lines are

$$\begin{cases} xp_1 + yp_2 = t \\ xp_1 + yp_2 = t + N \\ \dots & \dots \\ xp_1 + yp_2 = t + kN \end{cases} \quad (19.41)$$

where  $k \leq p_1 + p_2$ . We denote this family by  $\mathcal{L}_{p_1, p_2, t}$ . For different values of  $t_1 \neq t_2 < N$  the families of lines  $\mathcal{L}_{p_1, p_2, t_1}$  and  $\mathcal{L}_{p_1, p_2, t_2}$  do not intersect. All together, the sets  $V_{p_1, p_2, t}$ ,  $t = 0 : (N - 1)$ , compose a partition of the period  $X$ . It is interesting to note that the direction of parallel lines of  $\mathcal{L}_{p_1, p_2, t}$  is perpendicular to the direction of frequency-points of the cyclic group  $T_{p_1, p_2}$ .

#### Example 19.5

On the lattice  $X_{8,8}$ , we consider two sets of parallel lines  $\mathcal{L}_{2,1,1}$  and  $\mathcal{L}_{2,1,2}$ . Each family contains three parallel lines. For the family  $\mathcal{L}_{2,1,1}$ , the parallel lines are

$$y_1: 2x + y = 1, y_9: 2x + y = 9, y_{17}: 2x + y = 17.$$

One point  $(0, 1)$  of the set  $V_{2,1,1}$  lies on the first line of  $\mathcal{L}_{2,1,1}$ , four points  $(1, 7)$ ,  $(2, 5)$ ,  $(3, 3)$ ,  $(4, 1)$  on the second line and, three points  $(5, 7)$ ,  $(6, 5)$ ,  $(7, 3)$  on the third one. Therefore,  $f_{2,1,1} = (x_{0,1}) + (x_{1,7} + x_{2,5} + x_{3,3} + x_{4,1}) + (x_{5,7} + x_{6,5} + x_{7,3})$ . The parallel lines of the family  $\mathcal{L}_{2,1,2}$  are defined by

$$y_2: 2x + y = 2, y_{10}: 2x + y = 10, y_{18}: 2x + y = 18,$$



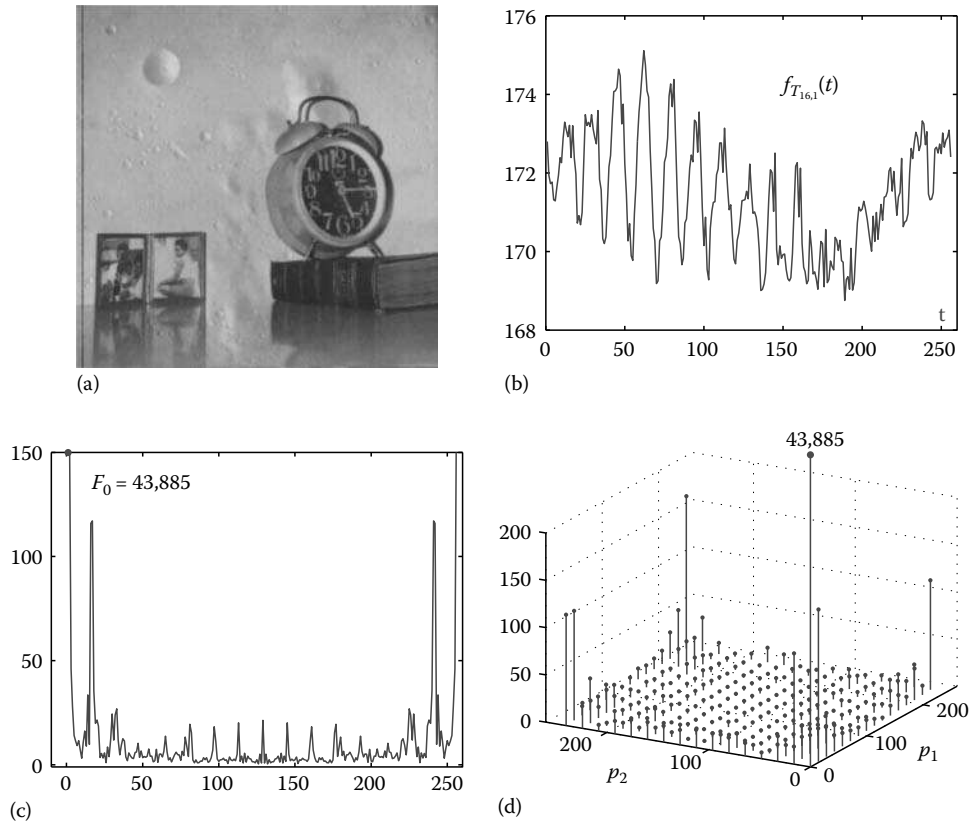


**FIGURE 19.8** (a) The image  $256 \times 256$ , (b) image-signal corresponding to the generator  $(p_1, p_2) = (16, 1)$ , (c) absolute spectrum of the image-signal (with the truncated zero component), and (d) the arrangement of values of the 1-D DFT in the 2-D DFT of the image (in the 3-D view).

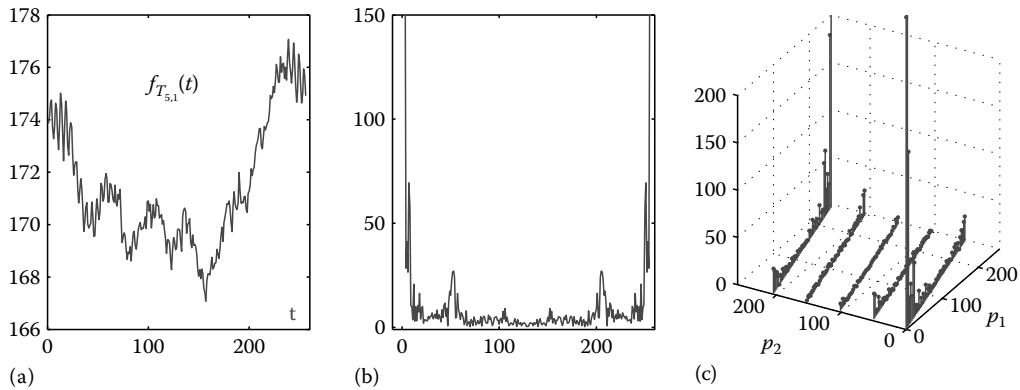


**FIGURE 19.9** (a) Image-signal corresponding to the generator  $(5, 1)$ , (b) absolute spectrum of the image-signal, and (c) the arrangement of values of the 1-D DFT in the 2-D DFT of the image.

and the component  $f_{2,1,2} = (x_{0,2} + x_{1,0}) + (x_{2,6} + x_{3,4} + x_{4,2} + x_{5,0}) + (x_{6,6} + x_{7,4})$ . The disposition of the points lying on the parallel lines of these sets is given in Figure 19.10. The location of the frequency-points of the group  $T_{2,1}$  is also shown in this figure. Two parallel lines pass through these frequency-points, which are defined in the frequency plane  $(w_1, w_2)$  as  $l_1 : 2w_2 - w_1 = 0$  and  $l_2 : 2w_2 - w_1 = 8$ . The parallel lines  $l_1$  and  $l_2$  are perpendicular to

the parallel lines  $y_n$  of  $\mathcal{L}_{2,1,1}$  and  $\mathcal{L}_{2,1,2}$ , as well as all other families  $\mathcal{L}_{2,1,t}$ ,  $t = 0, 3 : 7$ .

The disposition of the points of all disjoint eight sets  $V_{2,1,t}$  when  $t = 0 : 7$ , is given in Figure 19.11.

We can again identify the opposite sides of the boundaries of the square  $Y = [0, N] \times [0, N]$  and consider  $Y$  as a torus and the 2-D lattice  $X$  as a net traced on the torus in the 3-D space.

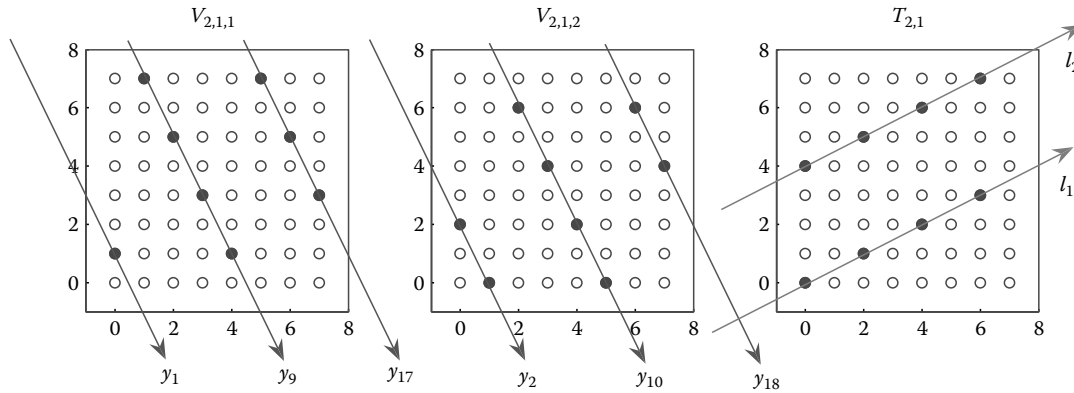


FIGURE 19.10 The locations of the points of sets  $V_{2,1,1}$  and  $V_{2,1,2}$  and frequency-points of the group  $T_{2,1}$ .

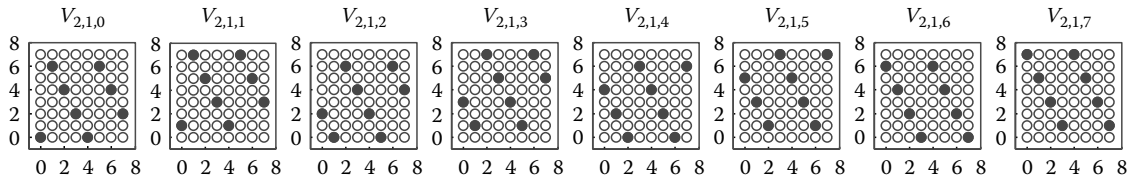


FIGURE 19.11 The disposition of eight sets of points of  $V_{2,1,t}$ , when  $t = 0 : 7$  (shown by filled circles).

Then, the straight lines of  $\mathcal{L}_{p_1, p_2, t}$  will compose a closed spiral  $S_t$  on the torus. The sums  $\{f_{p_1, p_2, t}\}$ , calculated on  $N$  parallel spirals  $S_t$ ,  $t = 0 : (N - 1)$ , represent the image  $f_{n_1, n_2}$  in the group of frequency-points  $T_{p_1, p_2}$ , which are also situated on a spiral that passes through the initial point  $(0, 0)$  of the net and make an angle  $\pi / 2$  with the spirals  $S_t$ .

The image-signals are the discrete integrals (or image projections) along the parallel lines of Equation 19.41. Therefore, any processing of the image-signal  $f_T$  yields the change in the Fourier spectrum at frequency-points of the corresponding cyclic group  $T$ . After performing the 2-D IDFT, the corresponding change can be observed in the image along the parallel lines of sets  $V_{p_1, p_2, t}$ ,  $t = 0 : (N - 1)$ . As an example, Figure 19.12 shows the tree image of size  $(256 \times 256)$  in part (a), along with the results of

amplifying only one image-signal  $f_{T_{2,1}}$  by the factor of 4 in (b), and signal  $f_{T_{5,1}}$  by the factor of 6 in (c). The directions of parallel lines of the corresponding families  $\mathcal{L}_{2,1,t}$ , and  $\mathcal{L}_{5,1,t}$ ,  $t = 0 : 255$ , on the image can easily be observed.

19.4.1.1 Superposition of Directions

The images of Figure 19.12 illustrates well that an image  $f = f_{n_1, n_2}$  can be composed by specific collection of directional images. To show that, we consider the tensor representation of  $f$ ,

$$\{f_{n_1, n_2}\} \rightarrow \{f_T; T = T_{p_1, p_2} \in \sigma_J\},$$

where  $\sigma$  is the irreducible covering of the period  $X$  whose size we assume equal,  $N \times N$ .

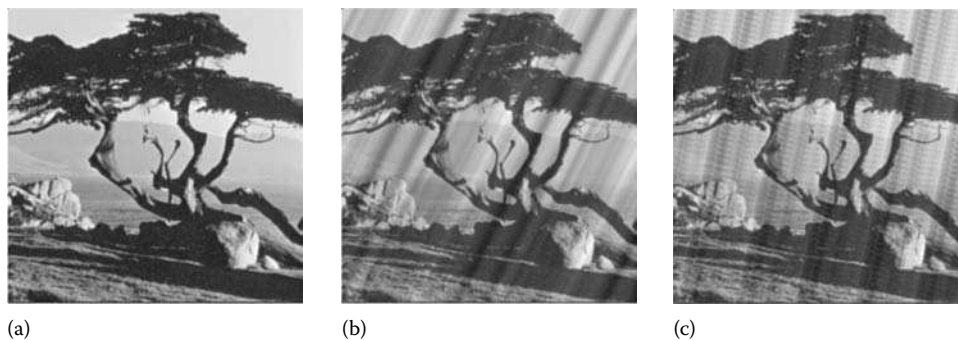


FIGURE 19.12 (a) Tree image before and after processing by the image-signals, (b)  $f_{T_{2,1}}$  and (c)  $f_{T_{5,1}}$ .

Given a generator  $(p, s) \in J$ , we define the complex data  $A = A(p, s)$  of size  $N \times N$  by

$$A_{p_1, p_2} = A(p, s)_{p_1, p_2} = \begin{cases} F_{\overline{kp, ks}}, & \text{if } (p_1, p_2) = (\overline{kp}, \overline{ks}), k = 0 : (N-1), \\ 0, & \text{otherwise,} \end{cases} \quad (19.42)$$

where  $p_1, p_2 = 0 : (N-1)$ . The data  $A$  represent an incomplete 2-D DFT of the image, that is zero at all frequency-points except the group  $T_{p,s}$ . Examples of such incomplete 2-D DFTs have been shown in Equation 19.39 for the  $N=5$  case, as well as in the 3-D view for the image  $256 \times 256$  in Figures 19.8d and 19.9c for groups  $T_{16,1}$  and  $T_{5,1}$ , respectively.

We define the “directional image”  $d_{n_1, n_2}$  as the 2-D IDFT of the data  $A$ ,

$$d_{n_1, n_2} = d_{n_1, n_2}^{(p,s)} = (\mathcal{F}_{N,N}^{-1} \circ A)_{n_1, n_2} = \frac{1}{N^2} \sum_{p_1=0}^{N-1} \sum_{p_2=0}^{N-1} A_{p_1, p_2} W^{n_1 p_1 + n_2 p_2} \quad (19.43)$$

$$n_1, n_2 = 0 : (N-1).$$

Since the splitting-signal  $f_{T_{p,s}}$  defines the 2-D DFT of the image at frequency-points of the group  $T = T_{p,s}$ ,

$$(\mathcal{F}_N \circ f_T)_k = F_{\overline{kp, ks}}, k = 0 : (N-1),$$

the following calculations hold:

$$\begin{aligned} d_{n_1, n_2} &= \frac{1}{N^2} \sum_{p_1=0}^{N-1} \sum_{p_2=0}^{N-1} A_{p_1, p_2} W^{n_1 p_1 + n_2 p_2} = \frac{1}{N^2} \sum_{k=0}^{N-1} F_{\overline{kp, ks}} W^{n_1(kp) + n_2(ks)} \\ &= \frac{1}{N} \frac{1}{N} \sum_{k=0}^{N-1} F_{\overline{kp, ks}} W^{k(n_1 p + n_2 s)} = \frac{1}{N} f_{p,s, (n_1 p + n_2 s) \bmod N} \end{aligned} \quad (19.44)$$

Thus,  $N$  values of the splitting-signal are placed in all  $N^2$  points of the square lattice  $X_{N,N}$ . Namely, each value  $f_{p,s,t}$  is placed at all points which are situated along the parallel lines of the corresponding family  $\mathcal{L}_{p,s,t}$ .

As an example, we consider an image of size  $257 \times 257$ , i.e., when  $N=257$ . The first 10 directional images  $d_{n_1, n_2}^{(p,s)}$ , for  $(p, s) = (0, 1), (1, 1), \dots$ , and  $(9, 1)$ , are shown in Figure 19.13, for the tree image (whose original size  $256 \times 256$  has been extended to the size  $257 \times 257$ ).

When  $N$  is a prime,  $N+1$  directional signal-images are required to compose the image  $f$ . Indeed, the covering  $\sigma = (T_{p,s}; (p, s) \in J)$  consists of  $(N+1)$  groups  $T_{p,s}$ . The set  $J$  of generators  $(p, s)$  can be taken as

$$J = \{(0, 1), (1, 1), (2, 1), (3, 1), \dots, (N-1, 1), (1, 0)\}.$$

The cyclic groups  $T$  of  $\sigma_J$  intersect only at the point  $(0, 0)$ . Therefore, for a given frequency-point  $(p_1, p_2)$ , the following holds

$$\sum_{T_{p,s} \in \sigma} A(p, s)_{p_1, p_2} = F_{p_1, p_2} + N s_0 \delta_{p_1, p_2},$$

where  $s_0 = F_{0,0}$  or the power of the image. Taking the 2-D IDFT of the sum of all incomplete 2-D DFTs, we obtain the following:

$$\begin{aligned} \sum_{(p,s) \in J} [\mathcal{F}_{N,N}^{-1} \circ A(p, s)_{p_1, p_2}] &= \mathcal{F}_{N,N}^{-1} \circ \left[ \sum_{(p,s) \in J} A(p, s)_{p_1, p_2} \right] \\ &= \mathcal{F}_{N,N}^{-1} \circ [F_{p_1, p_2}] + \frac{s_0}{N}. \end{aligned} \quad (19.45)$$

To simplify our calculations, we assume that the image is centered  $f_{n_1, n_2} \rightarrow f_{n_1, n_2} - s_0/N^2$ . Then, it directly follows from Equation 19.45 that

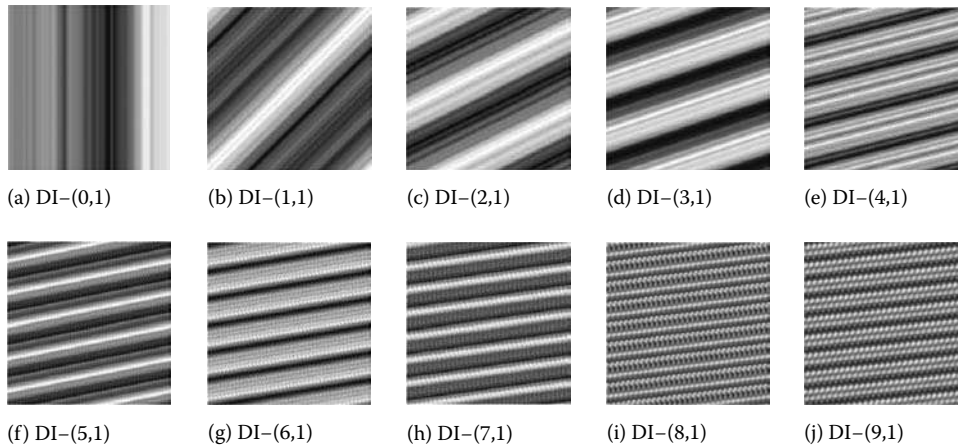


FIGURE 19.13 (a)–(j) The first 10 directional images of the tree image  $257 \times 257$ . (All images have been scaled.)

$$\sum_{(p,s) \in J} d_{n_1, n_2}^{(p,s)} = \sum_{(p,s) \in J} (\mathcal{F}_{N,N}^{-1} \circ A(p, s))_{n_1, n_2} = f_{n_1, n_2}. \quad (19.46)$$

The sum of the directional images equals to the image  $f_{n_1, n_2}$ . Each directional image can be determined by the corresponding splitting-signal as shown in Equation 19.44. Therefore, the whole image  $f_{n_1, n_2}$  can be reconstructed from  $(N + 1)$  splitting-signals as

$$f_{n_1, n_2} = \sum_{(p,s) \in J} d_{n_1, n_2}^{(p,s)} = \frac{1}{N} \sum_{(p,s) \in J} f_{p,s, (n_1 p + n_2 s) \bmod N}. \quad (19.47)$$

If the image is not centered, the reconstruction formula is

$$f_{n_1, n_2} = \sum_{(p,s) \in J} d_{n_1, n_2}^{(p,s)} - \frac{s_0}{N} = \frac{1}{N} \sum_{(p,s) \in J} f_{p,s, (n_1 p + n_2 s) \bmod N} - \frac{s_0}{N}. \quad (19.48)$$

Each directional  $d^{(p,s)}$  completes the original image with details, or parallel straight lines of different brightness in gray scale. The direction of these lines is defined by the generator  $(p, s)$ . Formula (19.48) describes the principle of the superposition of

directional images in image formation. Each directional image is determined by the corresponding splitting-signal which is calculated by the discrete linear integrals (sums) of the image  $f_{n_1, n_2}$  along the parallel lines of  $\mathcal{L}_{p,s,t}, t = 0 : (N - 1)$ . These integrals can be considered as the projection data along the angle defined by the generator  $(p, s)$ . Thus we obtain the simple formula of reconstruction of the image by its projection data, by using the splitting-signals of the tensor representation of the image with respect to the Fourier transform. The number of projections equals the number of generators, i.e.,  $(N + 1)$ , when  $N$  is prime. This is the required number of projections for the exact reconstruction of the image  $N \times N$ . As an example, Figure 19.14 shows the tree image after removing the projection data  $f_{p,s, (n_1 p + n_2 s) \bmod N}$  which corresponds to the generator  $(p, s) = (1, 0)$  in part (a),  $(p, s) = (1, 1)$  in (b), and  $(p, s) = (0, 1)$  in (c).

The angles of the required projections for reconstruction of an image of size  $257 \times 257$  by the splitting-signals (or direction images) compose the following set

$$\Phi_{257, 257} = \{ \text{arctg}(p); p = 0 : 257 \} \cup \{ \pi/2 \}.$$

Figure 19.15 illustrates all central angles of this set on the unit circle. One can see that the points on the circle are not uniformly

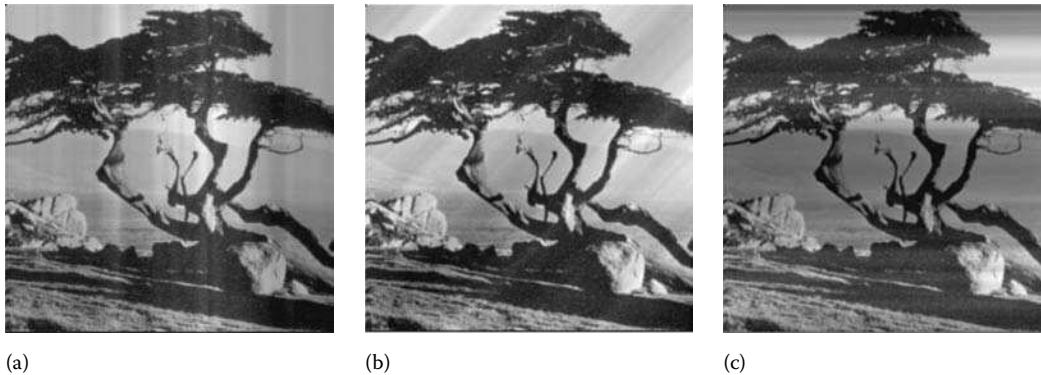


FIGURE 19.14 Images reconstructed by 256 projections by splitting-signals, when the projection data of one generator  $(p, s)$  have been removed, for  $(p, s)$  equals (a)  $(1, 0)$  (b)  $(1, 1)$ , and (c)  $(0, 1)$ .

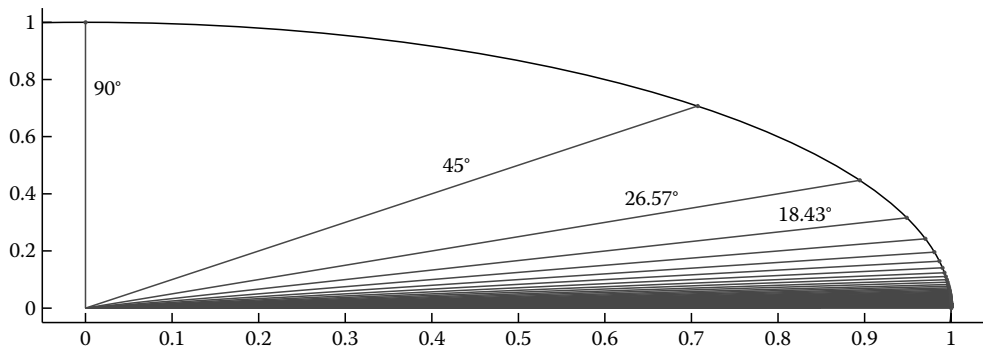


FIGURE 19.15 Central angles of 258 projections required for reconstructing an image  $257 \times 257$ .

distributed, and the increment of the angles is not a constant. The main part of the projections are taken along the small angles. For instance, there are no projections for angles in the intervals  $(45^\circ, 90^\circ)$  and  $(26.57^\circ, 45^\circ)$ , as well as  $(18.43^\circ, 26.57^\circ)$ .

## 19.5 Tensor Algorithm of the 2-D DFT

In this section, we consider the tensor algorithm for calculating the 2-D DFT of order  $N_1 \times N_2$ . Let  $\sigma = \sigma_J$  be an irreducible covering of the period  $X = X_{N_1, N_2}$  consisting of cyclic groups  $T$ . The algorithm of calculation of the 2-D DFT  $\mathcal{F}_{N_1, N_2} \circ f$  of a 2-D sequence  $f_{n_1, n_2}$  is performed by the following two steps.

*Step 1.* Calculate the 1-D splitting-signals  $f_T$  of the tensor-representation of the image, i.e., calculate the transform

$$\mathcal{X}_\sigma : f \rightarrow \{f_T; T \in \sigma\} \quad (19.49)$$

which we call *the tensor transform* of the image.

*Step 2.* Calculate the 1-D DFTs of the obtained splitting-signals,  $\mathcal{F}_N(T) \circ f_T$ ,  $T \in \sigma$ .

*Step 3.* Allocate the 1-D DFTs in the 2-D data by cyclic groups  $T \in \sigma$ ,

$$[\mathcal{F}_N \circ f_T] \rightarrow \{F_{p,s}; (p, s) \in T\}. \quad (19.50)$$

Each splitting-signal  $f_T$  defines the 2-D DFT at the frequency-points of the cyclic group  $T$ ,

$$F_{\overline{kp_1}, \overline{kp_2}} = (\mathcal{F}_N \circ f_T)_k, k = 0 : (N - 1),$$

where the number  $N = N_1 N_2 / g.c.d.(N_1, N_2)$ . The number of 1-D transforms required for calculating the 2-D DFT coincides with the cardinality, *card*  $\sigma$ , of the covering  $\sigma$ , or the cardinality of the set  $J$  of generators of these groups,

$$\sigma = \sigma_J = (T_{p_1, p_2})_{(p_1, p_2) \in J}. \quad (19.51)$$

We here separately consider the set of generators for the cases of most interest, when  $N_1 = N_2 = N$ , and  $N$  is a general prime, the product of two prime numbers, and then we describe the case when  $N_1$  and  $N_2$  are arbitrary unequal integers.

### 19.5.1 $N$ Is a Prime

Let  $N > 1$  be a general prime. The irreducible covering  $\sigma_J$  of the set  $X_{N, N}$  has the cardinality  $N + 1$ , i.e.,

$$\text{card} \sigma_J = N + 1. \quad (19.52)$$

In other words, the minimum number of cyclic groups  $T_{p,s}$  which together cover the period  $X$  equals  $(N + 1)$ . Indeed, the irreducible covering  $\sigma_J$  is determined by the following set of generatrices

$$J = J_{N, N} = \{(0, 1), (1, 1), (2, 1), \dots, (N - 1, 1), (1, 0)\}. \quad (19.53)$$

Other sets of  $(N + 1)$  generators can also be taken, for instance,  $J = \{(1, 0), (1, 1), (1, 2), \dots, (1, N - 1), (0, 1)\}$ . Therefore, to calculate the  $N \times N$ -point 2-D DFT, it is sufficient to fulfill  $(N + 1)$  1-D  $N$ -point DFTs.

### Example 19.6

We consider the  $3 \times 3$ -point DFT of the following 2-D sequence, or image:

$$f = \{f_{n_1, n_2}\} = \begin{bmatrix} 1 & 2 & 1 \\ 2 & 4 & 2 \\ 1 & 2 & 1 \end{bmatrix}.$$

The square lattice  $X_{3,3} = \{(n_1, n_2); n_1, n_2 = 0, 1, 2\}$  is covered by the totality of sets  $\sigma = (T_{0,1}, T_{1,1}, T_{2,1}, T_{1,0})$ . The tensor representation of  $f$  defines four splitting-signals,

$$\mathcal{X}_\sigma : \{f_{n_1, n_2}\} \rightarrow \{\{f_{0,1,t}\}, \{f_{1,1,t}\}, \{f_{2,1,t}\}, \{f_{1,0,t}\}\}, \quad t = 0, 1, 2. \quad (19.54)$$

*Step 1:* We denote by  $\mathbf{f}$  the vector-column composing from rows of the sequence  $f_{n_1, n_2}$ , i.e.,  $\mathbf{f} = (1, 2, 1, 2, 4, 2, 1, 2, 1)'$ . The first splitting-signal  $\{f_{0,1,t}\}$  is calculated by

$$\begin{bmatrix} f_{0,1,0} \\ f_{0,1,1} \\ f_{0,1,2} \end{bmatrix} = \begin{bmatrix} 1 & 0 & 0 & 1 & 0 & 0 & 1 & 0 & 0 \\ 0 & 1 & 0 & 0 & 1 & 0 & 0 & 1 & 0 \\ 0 & 0 & 1 & 0 & 0 & 1 & 0 & 0 & 1 \end{bmatrix} \mathbf{f} = [4, 8, 4], \quad (19.55)$$

and the next three splitting-signals are calculated as follows:

$$\begin{bmatrix} f_{1,1,0} \\ f_{1,1,1} \\ f_{1,1,2} \end{bmatrix} = \begin{bmatrix} 1 & 0 & 0 & 0 & 0 & 1 & 0 & 1 & 0 \\ 0 & 1 & 0 & 1 & 0 & 0 & 0 & 0 & 1 \\ 0 & 0 & 1 & 0 & 1 & 0 & 1 & 0 & 0 \end{bmatrix} \mathbf{f} = [5, 5, 6], \quad (19.56)$$

$$\begin{bmatrix} f_{2,1,0} \\ f_{2,1,1} \\ f_{2,1,2} \end{bmatrix} = \begin{bmatrix} 1 & 0 & 0 & 0 & 1 & 0 & 0 & 0 & 1 \\ 0 & 1 & 0 & 0 & 0 & 1 & 1 & 0 & 0 \\ 0 & 0 & 1 & 1 & 0 & 0 & 0 & 1 & 0 \end{bmatrix} \mathbf{f} = [6, 5, 5], \quad (19.57)$$

$$\begin{bmatrix} f_{1,0,0} \\ f_{1,0,1} \\ f_{1,0,2} \end{bmatrix} = \begin{bmatrix} 1 & 1 & 1 & 0 & 0 & 0 & 0 & 0 & 0 \\ 0 & 0 & 0 & 1 & 1 & 1 & 0 & 0 & 0 \\ 0 & 0 & 0 & 0 & 0 & 0 & 1 & 1 & 1 \end{bmatrix} \mathbf{f} = [4, 8, 4]. \quad (19.58)$$

*Step 2:* The three-point DFT of the first signal  $\{f_{0,1,0}, f_{0,1,1}, f_{0,1,2}\} = [4, 8, 4]$  is calculated by

$$\begin{bmatrix} A_0 \\ A_1 \\ A_2 \end{bmatrix} = \begin{bmatrix} 1 & 1 & 1 \\ 1 & W & W^2 \\ 1 & W^2 & W \end{bmatrix} \begin{bmatrix} 4 \\ 8 \\ 4 \end{bmatrix} = \begin{bmatrix} 16 \\ -2.0 - j3.4641 \\ -2.0 + j3.4641 \end{bmatrix},$$

where  $W = \exp(-j2\pi/3)$ . The power of each splitting-signal equals 16, and there is no need to calculate the three-point DFTs of other signals at zero. Therefore, we can perform three incomplete three-point DFTs of these splitting-signals:

$$\begin{bmatrix} B_1 \\ B_2 \end{bmatrix} = \begin{bmatrix} 1 & W & W^2 \\ 1 & W^2 & W \end{bmatrix} \begin{bmatrix} 5 \\ 5 \\ 6 \end{bmatrix} = \begin{bmatrix} -0.5 + j0.8660 \\ -0.5 - j0.8660 \end{bmatrix},$$

$$\begin{bmatrix} C_1 \\ C_2 \end{bmatrix} = \begin{bmatrix} 1 & W & W^2 \\ 1 & W^2 & W \end{bmatrix} \begin{bmatrix} 6 \\ 5 \\ 5 \end{bmatrix} = \begin{bmatrix} 1 \\ 1 \end{bmatrix},$$

$$\begin{bmatrix} D_1 \\ D_2 \end{bmatrix} = \begin{bmatrix} 1 & W & W^2 \\ 1 & W^2 & W \end{bmatrix} \begin{bmatrix} 4 \\ 8 \\ 4 \end{bmatrix} = \begin{bmatrix} -2.0 - j3.4641 \\ -2.0 + j3.4641 \end{bmatrix}.$$

The splitting-signals and the energy Fourier spectrums of these signals are shown in the first and second rows of Figure 19.16, respectively.

Step 3: The location of frequency-points of four cyclic groups  $T \in \sigma$  in the lattice  $3 \times 3$ , where the 1-D DFTs of the splitting-signals are placed, is shown in the last row of the figure. As a result, we obtain the following matrix expression for the  $3 \times 3$ -point DFT of the given sequence  $f$ :

$$\begin{bmatrix} F_{0,0} & F_{0,1} & F_{0,2} \\ F_{1,0} & F_{1,1} & F_{1,2} \\ F_{2,0} & F_{2,1} & F_{2,2} \end{bmatrix} = \begin{bmatrix} A_0 & A_1 & A_2 \\ D_1 & B_1 & C_2 \\ D_2 & C_1 & B_2 \end{bmatrix} = \begin{bmatrix} 16 & -2.0 - j3.4641 & -2 + j3.4641 \\ -2 - j3.4641 & -0.5 + j0.8660 & 1 \\ -2 + j3.4641 & 1 & -0.5 - j0.8660 \end{bmatrix}.$$

If we unite four binary matrices  $9 \times 3$  in Equations 19.55 through 19.58, we obtain the following matrix of the tensor transformation in Equation 19.54:

$$[\mathcal{X}_\sigma] = \begin{bmatrix} 1 & 0 & 0 & 1 & 0 & 0 & 1 & 0 & 0 \\ 0 & 1 & 0 & 0 & 1 & 0 & 0 & 1 & 0 \\ 0 & 0 & 1 & 0 & 0 & 1 & 0 & 0 & 1 \\ 1 & 0 & 0 & 0 & 0 & 1 & 0 & 1 & 0 \\ 0 & 1 & 0 & 1 & 0 & 0 & 0 & 0 & 1 \\ 0 & 0 & 1 & 0 & 1 & 0 & 1 & 0 & 0 \\ 1 & 0 & 0 & 0 & 1 & 0 & 0 & 0 & 1 \\ 0 & 1 & 0 & 0 & 0 & 1 & 1 & 0 & 0 \\ 0 & 0 & 1 & 1 & 0 & 0 & 0 & 1 & 0 \\ 1 & 1 & 1 & 0 & 0 & 0 & 0 & 0 & 0 \\ 0 & 0 & 0 & 1 & 1 & 1 & 0 & 0 & 0 \\ 0 & 0 & 0 & 0 & 0 & 0 & 1 & 1 & 1 \end{bmatrix}. \quad (19.59)$$

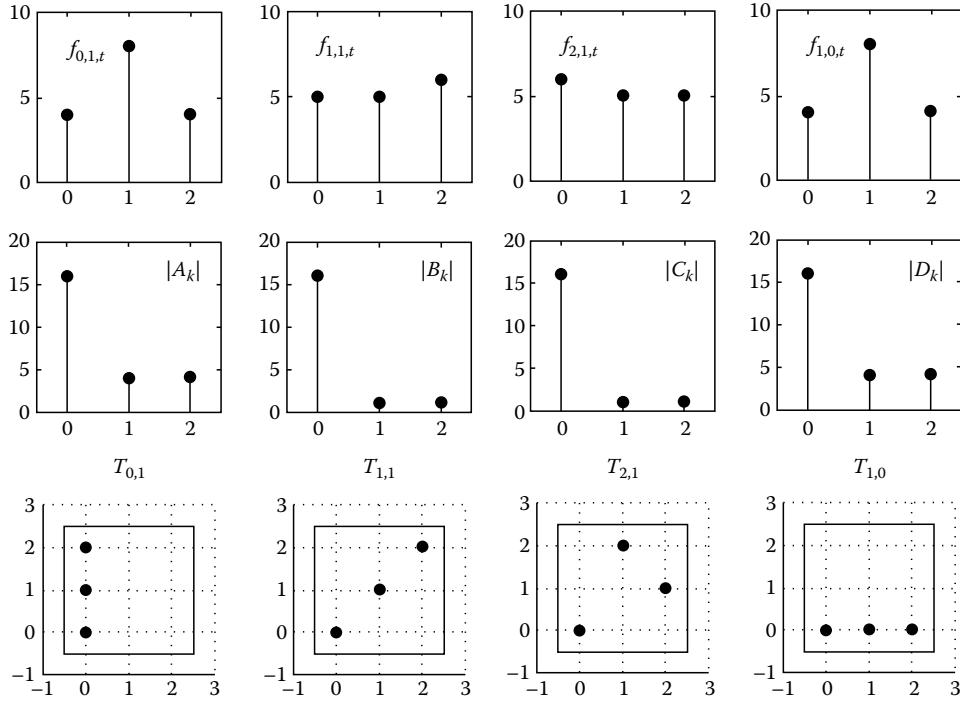


FIGURE 19.16 Four splitting-signals (the first row), the 3-point DFTs (in absolute scale) of the splitting-signals (the second row), and the location of the frequency-points of the cyclic groups  $T \in \sigma$  (the third row).

In matrix form, the described tensor algorithm of the  $3 \times 3$ -point DFT can be written as

$$\begin{bmatrix} F_{0,0} \\ F_{0,1} \\ F_{0,2} \\ F_{1,1} \\ F_{2,2} \\ F_{2,1} \\ F_{1,2} \\ F_{1,0} \\ F_{2,0} \end{bmatrix} = \begin{bmatrix} 1 & 1 & 1 & & & & & & \\ 1 & W & W^2 & & & & & & \\ 1 & W^2 & W & & & & & & \\ & & & 1 & W & W^2 & & & \\ & & & 1 & W^2 & W & & & \\ & & & & & & 1 & W & W^2 \\ & & & & & & 1 & W^2 & W \\ & & & & & & & & 1 & W & W^2 \\ & & & & & & & & 1 & W^2 & W \end{bmatrix} [\mathcal{X}_\sigma] \mathbf{f}.$$

The tensor algorithm of the  $3 \times 3$ -point DFT uses the following number of arithmetical operations: 4 real multiplications and 38 real additions, if the sequence  $f$  is real. Indeed, since  $W^2 = -1 - W$ , we have the following:

$$\begin{aligned} \begin{bmatrix} F_1 \\ F_2 \end{bmatrix} &= \begin{bmatrix} 1 & W & W^2 \\ 1 & W^2 & W \end{bmatrix} \begin{bmatrix} x \\ y \\ z \end{bmatrix} = \begin{bmatrix} x + W_y - (z + W_z) \\ x - (y + W_y) + W_z \end{bmatrix} \\ &= \begin{bmatrix} x - z + W(y - z) \\ x - y - W(y - z) \end{bmatrix}. \end{aligned} \tag{19.60}$$

The incomplete 3-point Fourier transform can thus be calculated by one complex multiplication. Moreover, since  $W^1 = (-\sqrt{3} - j)/2$  and the division by 2 is the elementary operation of shifting, the multiplication by  $W$  is equivalent to one real multiplication and shifting. The 3-point DFT of real data uses one operation of real multiplication, five additions, and one shifting. Three additions are required to calculate the incomplete 3-point DFT, since  $\bar{F}_2 = F_1$ . For the complex data, the 3-point DFT uses two multiplications, two shiftings, and 16 operations of real additions, and the incomplete DFT requires 12 additions. Further, the direct calculation of the matrix  $[\mathcal{X}]$  of order  $12 \times 8$  is fulfilled in the given example via 24 operations of real addition and subtraction. Therefore, the  $3 \times 3$ -point 2-D DFT requires  $(5 + 3 \times 3) + 24 = 38$  additions for the real sequence  $f$ . We note for comparison, the polynomial algorithm of the  $3 \times 3$ -point DFT also uses four 3-point DFTs, polynomial transforms, reductions, and Chinese remainder operations, which requires 25 additions (against 24 for the tensor transform). In the row-column algorithm, six 3-point DFTs are used, namely, three transforms with real inputs and three transforms with complex inputs. Therefore, the algorithm uses respectively  $3 + 2(3) = 9$  real multiplications and  $3 \times 5 + 3 \times 16 = 63$  additions, when data are real. Thus, in the tensor and polynomial algorithms, we get the advantage of the number of multiplications by 3 times, and 1.6 times for additions.

In the general case, for a prime number  $N > 3$ , in the traditional row-column algorithm,  $2N$  one-dimensional  $N$ -point DFTs are used. Therefore, the tensor algorithm decreases the number of multiplications by  $2N/(N + 1)$  times, i.e., almost by 2 times, for large  $N$ . The tensor transform  $\mathcal{X}_\sigma$  requires  $N^3 - N$  additions, and the polynomial transforms and reductions

and Chinese remainder operations require  $N^3 + N^2 - 5N + 4$  additions [14].

### 19.5.2 $N$ Is a Power of Two

When  $N = 2^r$ ,  $r > 1$ , the irreducible covering  $\sigma$  of the lattice  $X = X_{2^r, 2^r}$  can be taken as the following family of  $3N/2$  cyclic groups:

$$\sigma_J = \left( (T_{p_1, 1})_{p_1=0:(2^r-1)}, (T_{1, 2p_2})_{p_2=0:(2^{r-1}-1)} \right). \tag{19.61}$$

Thus, to calculate the  $2^r \times 2^r$ -point 2-D DFT,  $3 \cdot 2^{r-1}$  1-D DFTs are used in the tensor algorithm which is described by

$$\begin{aligned} F_{\bar{k}p, \bar{k}s} &= (\mathcal{F}^{2^r, 2^r} \circ f)_{\bar{k}p, \bar{k}s} = \sum_{n_1=0}^{2^r-1} \sum_{n_2=0}^{2^r-1} f_{n_1, n_2} W^{n_1 k p + n_2 k s} \\ &= (\mathcal{F}^{2^r} \circ f_T)_k = \sum_{t=0}^{2^r-1} f_{p, s, t} W^{kt}, \quad k = 0: (2^r - 1), \end{aligned} \tag{19.62}$$

where the generators  $(p, s)$  are taken from the set

$$\begin{aligned} J &= \{(0, 1), (1, 1), (2, 1), \dots, (2^r - 1, 1)\} \\ &\cup \{(1, 0), (1, 2), (1, 4), \dots, (1, 2^{r-2})\}. \end{aligned} \tag{19.63}$$

The components of splitting-signals  $f_T$  are calculated by the characteristic functions of sets  $V_{p, s, t}$

$$f_{p, s, t} = \mathcal{X}_{p, s, t} \circ f = \sum_{n_1=0}^{2^r-1} \sum_{n_2=0}^{2^r-1} \mathcal{X}_{p, s, t}(n_1, n_2) f_{n_1, n_2} = \sum_{(n_1, n_2) \in V_{p, s, t}} f_{n_1, n_2}. \tag{19.64}$$

These binary functions determine the tensor transform  $\mathcal{X}_\sigma$  and are defined as

$$\mathcal{X}_{p, s, t}(n_1, n_2) = \begin{cases} 1, & \text{if } n_1 p + n_2 s = t \pmod{2^r}, \\ 0, & \text{otherwise,} \end{cases} \quad (n_1, n_2) \in X. \tag{19.65}$$

All ones of the functions lie on parallel lines passing the knots of the corresponding sets  $V_{p, s, t}$ .

#### Example 19.7

Consider the following 2-D sequence  $f$  of size  $4 \times 4$ :

$$f = \begin{bmatrix} f_{0,0} & f_{0,1} & f_{0,2} & f_{0,3} \\ f_{1,0} & f_{1,1} & f_{1,2} & f_{1,3} \\ f_{2,0} & f_{2,1} & f_{2,2} & f_{2,3} \\ f_{3,0} & f_{3,1} & f_{3,2} & f_{3,3} \end{bmatrix} = \begin{bmatrix} 1 & 2 & 1 & 3 \\ 2 & 0 & 1 & 1 \\ 1 & 3 & 2 & 2 \\ 2 & 4 & 1 & 2 \end{bmatrix}.$$

The set of generators of the cyclic groups  $T_{p,s}$  of the covering  $\sigma_j$  equals

$$J = \{(0, 1), (1, 1), (2, 1), (3, 1)\} \cup \{(1, 0), (1, 2)\}. \quad (19.66)$$

We first describe the splitting-signal corresponding to the frequency-point  $(p, s) = (0, 1)$ . For that, we write all values  $t$  in equations  $np + ms = t \pmod 4$  in the form of the following matrix:

$$\|t = (n \cdot 0 + m \cdot 1) \pmod 4\|_{n,m=0:3} = \begin{bmatrix} \underline{0} & 1 & 2 & 3 \\ 0 & 1 & 2 & 3 \\ 0 & 1 & 2 & 3 \\ 0 & 1 & 2 & 3 \end{bmatrix}.$$

The components of this splitting-signal are calculated as follows:

$$\begin{aligned} f_{1,0,0} &= \mathcal{X}_{1,0,0} \circ f = \begin{bmatrix} \underline{1} & 0 & 0 & 0 \\ 1 & 0 & 0 & 0 \\ 1 & 0 & 0 & 0 \\ 1 & 0 & 0 & 0 \end{bmatrix} \circ \begin{bmatrix} \underline{1} & 2 & 1 & 3 \\ 2 & 0 & 1 & 1 \\ 1 & 3 & 2 & 2 \\ 2 & 4 & 1 & 2 \end{bmatrix} \\ &= 1 + 2 + 1 + 2 = 6 \end{aligned} \quad (19.67)$$

$$\begin{aligned} f_{1,0,1} &= \mathcal{X}_{1,0,1} \circ f = \begin{bmatrix} \underline{0} & 1 & 0 & 0 \\ 0 & 1 & 0 & 0 \\ 0 & 1 & 0 & 0 \\ 0 & 1 & 0 & 0 \end{bmatrix} \circ \begin{bmatrix} \underline{1} & 2 & 1 & 3 \\ 2 & 0 & 1 & 1 \\ 1 & 3 & 2 & 2 \\ 2 & 4 & 1 & 2 \end{bmatrix} \\ &= 2 + 0 + 3 + 4 = 9 \end{aligned} \quad (19.68)$$

$$\begin{aligned} f_{1,0,2} &= \mathcal{X}_{1,0,2} \circ f = \begin{bmatrix} \underline{0} & 0 & 1 & 0 \\ 0 & 0 & 1 & 0 \\ 0 & 0 & 1 & 0 \\ 0 & 0 & 1 & 0 \end{bmatrix} \circ \begin{bmatrix} \underline{1} & 2 & 1 & 3 \\ 2 & 0 & 1 & 1 \\ 1 & 3 & 2 & 2 \\ 2 & 4 & 1 & 2 \end{bmatrix} \\ &= 1 + 1 + 2 + 1 = 5 \end{aligned} \quad (19.69)$$

$$\begin{aligned} f_{1,0,3} &= \mathcal{X}_{1,0,3} \circ f = \begin{bmatrix} \underline{0} & 0 & 0 & 1 \\ 0 & 0 & 0 & 1 \\ 0 & 0 & 0 & 1 \\ 0 & 0 & 0 & 1 \end{bmatrix} \circ \begin{bmatrix} \underline{1} & 2 & 1 & 3 \\ 2 & 0 & 1 & 1 \\ 1 & 3 & 2 & 2 \\ 2 & 4 & 1 & 2 \end{bmatrix} \\ &= 3 + 1 + 2 + 2 = 8 \end{aligned} \quad (19.70)$$

The splitting-signal  $f_{T_{0,1}} = \{6, 9, 5, 8\}$ . The four-point DFT of this signal equals  $(F_0, F_1, F_2, F_3) = (28, 1-j, -6, 1+j)$ , which can be written in the table of the 2-D DFT of  $f$  at the frequency-points  $(0, 0)$ ,  $(0, 1)$ ,  $(0, 2)$ , and  $(0, 3)$  as follows:

$$\begin{bmatrix} F_0 & F_1 & F_2 & F_3 \\ 0 & 0 & 0 & 0 \\ 0 & 0 & 0 & 0 \\ 0 & 0 & 0 & 0 \end{bmatrix} = \begin{bmatrix} \underline{28} & 1-j & -6 & 1+j \\ 0 & 0 & 0 & 0 \\ 0 & 0 & 0 & 0 \\ 0 & 0 & 0 & 0 \end{bmatrix}.$$

We also consider the splitting-signal corresponding to the next generator  $(p, s) = (1, 1)$ . For this generator, equations  $np + ms = t \pmod 4$  result in the following matrix:

$$\|t = (n \cdot 1 + m \cdot 1) \pmod 4\|_{n,m=0:3} = \begin{bmatrix} \underline{0} & 1 & 2 & 3 \\ 1 & 2 & 3 & 0 \\ 2 & 3 & 0 & 1 \\ 3 & 0 & 1 & 2 \end{bmatrix}.$$

Therefore, the first component of this splitting-signal is calculated by

$$\begin{aligned} f_{1,1,0} &= \mathcal{X}_{1,1,0} \circ f = \begin{bmatrix} \underline{1} & 0 & 0 & 0 \\ 0 & 0 & 0 & 1 \\ 0 & 0 & 1 & 0 \\ 0 & 1 & 0 & 0 \end{bmatrix} \circ \begin{bmatrix} \underline{1} & 2 & 1 & 3 \\ 2 & 0 & 1 & 1 \\ 1 & 3 & 2 & 2 \\ 2 & 4 & 1 & 2 \end{bmatrix} \\ &= 1 + 1 + 2 + 4 = 8 \end{aligned} \quad (19.71)$$

and similarly we obtain the next three components

$$\begin{aligned} f_{1,1,1} &= \mathcal{X}_{1,1,1} \circ f = 2 + 2 + 2 + 1 = 7 \\ f_{1,1,2} &= \mathcal{X}_{1,1,2} \circ f = 1 + 0 + 1 + 2 = 4 \\ f_{1,1,3} &= \mathcal{X}_{1,1,3} \circ f = 3 + 1 + 3 + 2 = 9. \end{aligned} \quad (19.72)$$

Thus, the splitting-signal  $f_{T_{1,1}} = \{8, 7, 4, 9\}$ . The four-point DFT of this signal equals  $(A_0, A_1, A_2, A_3) = (28, 4+2j, -4, 4-2j)$ , which defines the 2-D DFT of  $f$  at the frequency-points  $(0, 0)$ ,  $(1, 1)$ ,  $(2, 2)$ , and  $(3, 3)$ . At this step, we can record the other three values of the 2-D DFT as follows:

$$\begin{bmatrix} F_0 & F_1 & F_2 & F_3 \\ 0 & A_1 & 0 & 0 \\ 0 & 0 & A_2 & 0 \\ 0 & 0 & 0 & A_3 \end{bmatrix} = \begin{bmatrix} \underline{28} & 1-j & -6 & 1+j \\ 0 & 4+2j & 0 & 0 \\ 0 & 0 & -4 & 0 \\ 0 & 0 & 0 & 4-2j \end{bmatrix}.$$

The first component  $A_0 = F_0 = 28$  and could be omitted from the calculations, to avoid the redundancy. The redundancy of calculation takes place for other splitting-signals not only at frequency-point  $(0, 0)$  but frequency-points with even coordinates, i.e., in the quarter of all frequency-points, as it can be seen from Figure 19.17.

For instance, the four-point DFT of the splitting-signal  $f_{T_{2,1}} = \{4, 8, 7, 9\}$  equals  $(B_0, B_1, B_2, B_3) = (28, -3+j, -6, -3-j)$ . These values define in the 2-D DFT at the frequency-points  $(0, 0)$ ,  $(2, 1)$ ,  $(0, 2)$ , and  $(2, 3)$ . At this step, we can record the other two values of the 2-D DFT as follows:

$$\begin{bmatrix} F_0 & F_1 & F_2 & F_3 \\ 0 & A_1 & 0 & 0 \\ 0 & B_1 & A_2 & B_3 \\ 0 & 0 & 0 & A_3 \end{bmatrix} = \begin{bmatrix} \underline{28} & 1-j & -6 & 1+j \\ 0 & 4+2j & 0 & 0 \\ 0 & -3+j & -4 & -3-j \\ 0 & 0 & 0 & 4-2j \end{bmatrix}.$$

It is clear, that the incomplete four-point DFT is required, to avoid calculations for components  $B_0$  and  $B_2$  that have already been calculated.



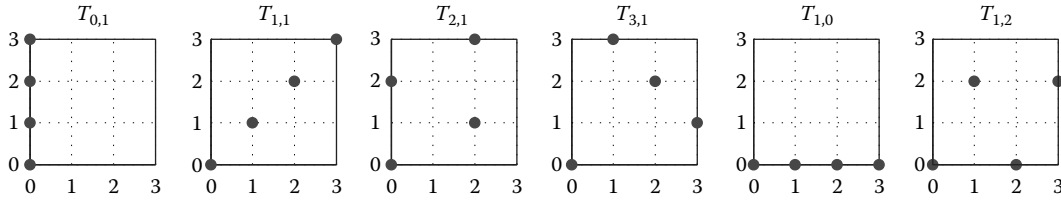


FIGURE 19.17 The disposition of frequency-points of six groups  $T$  of the covering  $\sigma_j$  of  $X_{4,4}$ .

We continue the calculation of the 2-D DFT. The 4 point DFT of the splitting-signal  $f_{T_{3,1}} = \{5, 7, 7, 9\}$  equals  $(C_0, C_1, C_2, C_3) = (28, -2 + 2j, -4, -2 - 2j)$ . It defines the 2-D DFT of  $f$  at the frequency-points  $(0, 0)$ ,  $(3, 1)$ ,  $(2, 2)$ , and  $(1, 3)$ . At this step, we can record two new values of the 2-D DFT as follows:

$$\begin{bmatrix} F_0 & F_1 & F_2 & F_3 \\ 0 & A_1 & 0 & C_3 \\ 0 & B_1 & A_2 & B_3 \\ 0 & C_1 & 0 & A_3 \end{bmatrix} = \begin{bmatrix} \underline{28} & 1-j & -6 & 1+j \\ 0 & 4+2j & 0 & -2-2j \\ 0 & -3+j & -4 & -3-j \\ 0 & -2+2j & 0 & 4-2j \end{bmatrix}.$$

For this signal, the incomplete four-point DFT is required to avoid calculations for components  $C_0$  and  $C_2$ , which have already been determined on the second step of our calculations (when  $(p, s)$  was  $(1, 1)$ ).

The remaining five values of the 2-D DFT will be calculated by the splitting-signals corresponding to the generators  $(1, 0)$  and  $(1, 2)$ . The splitting-signal  $f_{T_{1,0}} = \{7, 4, 8, 8\}$ . The 4-point DFT of this signal equals  $(D_0, D_1, D_2, D_3) = (28, -1 + 5j, 2, -1 - 5j)$  and defines the 2-D DFT of  $f$  at the frequency-points  $(0, 0)$ ,  $(1, 0)$ ,  $(2, 0)$ , and  $(3, 0)$ . At this step, we can record three new values of the 2-D DFT as follows:

$$\begin{bmatrix} F_0 & F_1 & F_2 & F_3 \\ D_1 & A_1 & 0 & C_3 \\ D_2 & B_1 & A_2 & B_3 \\ D_3 & C_1 & 0 & A_3 \end{bmatrix} = \begin{bmatrix} \underline{28} & 1-j & -6 & 1+j \\ -1+5j & 4+2j & 0 & -2-2j \\ 2 & -3+j & -4 & -3-j \\ -1-5j & -2+2j & 0 & 4-2j \end{bmatrix}.$$

The redundancy of calculation on this step is only at  $(0, 0)$ . At the last step, the four-point DFT of the splitting-signal  $f_{T_{1,2}} = \{7, 9, 8, 4\}$  is calculated. It equals  $(E_0, E_1, E_2, E_3) = (28, -1 - 5j, 2, -1 + 5j)$  and defines the 2-D DFT of  $f$  at the frequency-points  $(0, 0)$ ,  $(1, 2)$ ,  $(2, 0)$ , and  $(3, 2)$ . We fill the 2-D DFT by the values of  $E_1$  and  $E_2$ ,

$$\begin{bmatrix} F_0 & F_1 & F_2 & F_3 \\ D_1 & A_1 & E_1 & C_3 \\ D_2 & B_1 & A_2 & B_3 \\ D_3 & C_1 & E_3 & A_3 \end{bmatrix} = \begin{bmatrix} \underline{28} & 1-j & -6 & 1+j \\ -1+5j & 4+2j & -1-5j & -2-2j \\ 2 & -3+j & -4 & -3-j \\ -1-5j & -2+2j & -1+5j & 4-2j \end{bmatrix} = \begin{bmatrix} F_{0,0} & F_{0,1} & F_{0,2} & F_{0,3} \\ F_{1,0} & F_{1,1} & F_{1,2} & F_{1,3} \\ F_{2,0} & F_{2,1} & F_{2,2} & F_{2,3} \\ F_{3,0} & F_{3,1} & F_{3,2} & F_{3,3} \end{bmatrix}.$$

For this signal, it is sufficient to perform an incomplete 4-point DFT, to avoid the redundancy of calculations in two points.

Thus, the  $4 \times 4$ -point 2-D DFT is calculated in the tensor algorithm by six 4-point DFTs. Namely, one full 4-point DFT and five incomplete 4-point DFTs are required in this algorithm.

### 19.5.3 Modified Tensor Algorithms

When  $N$  is a power of two, many cyclic groups of the irreducible covering  $\sigma$  are intersected at frequency-points  $(p_1, p_2) \neq (0, 0)$ , which leads to a redundancy of the calculation. The demonstration of such a redundancy in the  $N = 4$  case has been shown in Example 19.7, when the repeated calculations have occurred at all frequency-points with even coordinates.

In general  $N = 2^r$  case, when  $r > 1$ , the following intersection holds

$$T_{p_1,1} \cap T_{p_1+2^{r-1},1} = T_{2p_1,2}, \quad T_{1,1p_2} \cap T_{1,2p_2+2^{r-1}} = T_{2,4p_2}, \quad (19.73)$$

when  $p_1 = 0 : (2^{r-1} - 1)$  and  $p_2 = 0 : (2^{r-2} - 1)$ . For large  $2^r$ , we can also consider other intersections:

$$T_{p_1,1} \cap T_{p_1+2^{r-k},1} = T_{2^k(p_1,1)}, \quad T_{1,2p_2} \cap T_{1,2p_2+2^{r-k}} = T_{2^k(1,2p_2)}, \quad (19.74)$$

when  $k = 2 : (r - 1)$  and  $p_1 = 0 : (2^{r-k} - 1)$  and  $p_2 = 0 : (2^{r-k-1} - 1)$ . Therefore, in the tensor algorithm, the calculation of many  $2^r$ -point DFTs of splitting-signals can be reduced to the calculation of incomplete DFTs, such as the  $2^{r-1}$ -point DFT, to remove all repeated calculations of spectral components. As a result, we can achieve the effective calculation of the  $2^r \times 2^r$ -point DFT with the number of multiplications estimated as

$$m_{2^r,2^r} \approx (2^r + 1)m_{2^r} = (2^r + 1)(2^{r-1}(r - 3) + 2), \quad (19.75)$$

where  $m_{2^r}$  denotes the number of multiplications required for the  $2^r$ -point DFT. We use the known estimate  $M_{2^r} = 2^{r-1}(r - 3) + 2$  for the Cooley-Tukey algorithm and the fast paired transforms [10,11].

In each group  $T_{p_1,1}$  or  $T_{1,2p_2}$  of the covering  $\sigma$ , we consider the set complement of the intersection  $T_{2^k(p_1,1)}$  or  $T_{2^k(1,2p_2)}$ , respectively. In other words, we define the following subsets

$$T_{p_1,1}^k = T_{p_1,1} \setminus T_{2^k(p_1,1)} \quad \text{and} \quad T_{1,2p_2}^k = T_{1,2p_2} \setminus T_{2^k(1,2p_2)} \quad (19.76)$$

with  $2^r - 2^{r-k}$  points each. When  $k = 1$ , and the totality of sets

$$\sigma_{(1)} = \left( \left( T_{p_1,1}, T_{p_1+2^{r-1},1}^1 \right)_{p_1=0:(2^{r-1}-1)}, \left( T_{1,2p_2}, T_{1,2p_2+2^{r-1}}^1 \right)_{p_2=0:(2^{r-2}-1)} \right)$$

is the covering of the period  $X_{2^r,2^r}$ . The calculation of the 2-D DFT at frequency-points of each set  $T^1$  can be reduced to the  $2^{r-1}$ -point DFT. For that, we can use, for instance, the FFT algorithm with decimation in frequency. Indeed, after the first iteration in this algorithm, the  $2^r$ -point DFT is reduced to two  $2^{r-1}$ -point DFTs. One of them defines the  $2^r$ -point DFT at all even frequencies and another at odd frequencies. Therefore, we can determine the components of the 2-D DFT at frequency-points of subsets  $T_{p_1,1}^1$  and  $T_{1,2p_2}^1$ , by fulfilling about half of the operations of multiplication that are used for calculating the 2-D DFT at frequency-points of the corresponding groups  $T_{p_1,1}$  and  $T_{1,2p_2}$ . Consequently, the number of multiplications in the tensor algorithm can be reduced to

$$m_{2^r,2^r} = 3 \cdot 2^{r-2}(m_{2^r} + m_{2^{r-1}} + 2^{r-1} - 2) \approx 9/8 \cdot 2^r m_{2^r}.$$

Continuing similar discussions, we can eliminate the intersections  $T_{2^k(p_1,1)}$  and  $T_{2^k(1,2p_2)}$ , at other groups of  $T$  of the covering  $\sigma_{(1)}$ , for  $k=2 : (r-1)$ . As a result, we achieve a good estimation of the number of multiplications,  $m_{2^r,2^r}^r \approx ((2^r + 1)/2^r) \cdot 2^r m_{2^r} = (2^r + 1)m_{2^r}$ . To demonstrate the described improvement of the tensor algorithm, we consider in detail the  $N = 8$  example.

### Example 19.8

Let  $f = \{f_{n_1,n_2}; n_1, n_2 = 0: 7\}$  be a two-dimensional sequence and let  $\mathcal{F}_{8,8}$  be the  $8 \times 8$ -point DFT. The tensor transform

$$f \rightarrow \{f_{T_{p_s}}; T_{p_s} \in \sigma_J\}$$

defines 12 splitting-signals with generators from the set

$$J = \{(p_1, 1); p_1 = 0: 7\} \cup \{(1, 2p_2); p_2 = 0: 3\}.$$

We consider all groups of the irreducible covering  $\sigma_J$ :

$$\begin{aligned} T_{0,1} &= \{(0, 0), (0, 1), (0, 2), (0, 3), (0, 4), (0, 5), (0, 6), (0, 7)\} \\ T_{1,1} &= \{(\underline{0}, 0), (1, 1), (2, 2), (3, 3), (4, 4), (5, 5), (6, 6), (7, 7)\} \\ T_{2,1} &= \{(\underline{0}, \underline{0}), (2, 1), (4, 1), (6, 3), (\underline{0}, \underline{4}), (2, 5), (4, 6), (6, 7)\} \\ T_{3,1} &= \{(\underline{0}, \underline{0}), (3, 1), (6, 2), (1, 3), (\underline{4}, \underline{4}), (7, 5), (2, 6), (5, 7)\} \\ T_{4,1} &= \{(\underline{0}, \underline{0}), (4, 1), (\underline{0}, \underline{2}), (4, 3), (\underline{0}, \underline{4}), (4, 5), (\underline{0}, \underline{6}), (4, 7)\} \\ T_{5,1} &= \{(\underline{0}, \underline{0}), (5, 1), (\underline{2}, \underline{2}), (7, 3), (\underline{4}, \underline{4}), (1, 5), (\underline{6}, \underline{6}), (3, 7)\} \\ T_{6,1} &= \{(\underline{0}, \underline{0}), (6, 1), (\underline{4}, \underline{2}), (2, 3), (\underline{0}, \underline{4}), (6, 5), (\underline{4}, \underline{6}), (2, 7)\} \\ T_{7,1} &= \{(\underline{0}, \underline{0}), (7, 1), (\underline{6}, \underline{2}), (5, 3), (\underline{4}, \underline{4}), (3, 5), (\underline{2}, \underline{6}), (1, 7)\} \\ T_{1,0} &= \{(\underline{0}, \underline{0}), (1, 0), (2, 0), (3, 0), (4, 0), (5, 0), (6, 0), (7, 0)\} \\ T_{1,2} &= \{(\underline{0}, \underline{0}), (1, 2), (2, 4), (3, 6), (\underline{4}, \underline{0}), (5, 2), (6, 4), (7, 6)\} \\ T_{1,4} &= \{(\underline{0}, \underline{0}), (1, 4), (\underline{2}, \underline{0}), (3, 4), (\underline{4}, \underline{0}), (5, 4), (\underline{6}, \underline{0}), (7, 4)\} \\ T_{1,6} &= \{(\underline{0}, \underline{0}), (1, 6), (\underline{2}, \underline{4}), (3, 2), (\underline{4}, \underline{0}), (5, 6), (\underline{6}, \underline{4}), (7, 2)\} \end{aligned} \quad (19.77)$$

(many frequency-points that lie in the intersections of the groups are underlined).

It directly follows from this covering, that to calculate the  $8 \times 8$ -point DFT, it is sufficient to fulfill the following full and incomplete DFTs.

*Step 1.* The 8-point DFT,  $\mathcal{F}_8$ , over the sequence  $f_{T_{0,1}}$ , to determine the 2-D DFT at frequency-points of the group  $T_{0,1}$ ,

$$F_{0,k} = (\mathcal{F}_8 \circ f_{T_{0,1}})_k, \quad k = 0: 7.$$

*Step 2.* Two incomplete DFTs over the splitting-signals  $f_{T_{1,1}}$  and  $f_{T_{1,0}}$ , to determine the 2-D DFT at frequency-points of the groups  $T_{1,1}$  and  $T_{1,0}$ , except zero point  $(0, 0)$ ,

$$F_{k,k} = (\mathcal{F}_8 \circ f_{T_{1,1}})_k, \quad F_{k,0} = (\mathcal{F}_8 \circ f_{T_{1,0}})_k, \quad k = 1: 7.$$

*Step 3.* Three incomplete DFTs over the splitting-signals  $f_{T_{2,1}}$ ,  $f_{T_{3,1}}$ , and  $f_{T_{1,2}}$ , to determine the 2-D DFT at frequency-points of the corresponding groups  $T_{2,1}$ ,  $T_{3,1}$ , and  $T_{1,2}$ , except the frequency-points with the coordinates which are integer multiple to four, i.e., the frequency-points  $(0, 0)$ ,  $(4, 0)$ ,  $(0, 4)$ , and  $(4, 4)$ ,

$$\begin{aligned} F_{2k,k}^- &= (\mathcal{F}_8 \circ f_{T_{2,1}})_k, \quad F_{3k,k}^- = (\mathcal{F}_8 \circ f_{T_{3,1}})_k, \\ F_{k,2k}^- &= (\mathcal{F}_8 \circ f_{T_{1,2}})_k, \quad k = 1, 2, 3, 5, 6, 7. \end{aligned}$$

*Step 4.* Six incomplete DFTs on the splitting-signals  $f_{T_{4,1}}$ ,  $f_{T_{5,1}}$ ,  $f_{T_{6,1}}$ ,  $f_{T_{7,1}}$ ,  $f_{T_{1,4}}$ , and  $f_{T_{1,6}}$ , to determine the 2-D DFT at frequency-points of corresponding groups  $T_{4,1}$ ,  $T_{5,1}$ ,  $T_{6,1}$ ,  $T_{7,1}$ ,  $T_{1,4}$ , and  $T_{1,6}$ , except the frequency-points with even coordinates,

$$\begin{aligned} F_{4k,k}^- &= (\mathcal{F}_8 \circ f_{T_{4,1}})_k, \quad F_{5k,k}^- = (\mathcal{F}_8 \circ f_{T_{5,1}})_k, \quad F_{6k,k}^- = (\mathcal{F}_8 \circ f_{T_{6,1}})_k, \\ F_{7k,k}^- &= (\mathcal{F}_8 \circ f_{T_{7,1}})_k, \quad F_{k,4k}^- = (\mathcal{F}_8 \circ f_{T_{1,4}})_k, \quad F_{k,6k}^- = (\mathcal{F}_8 \circ f_{T_{1,6}})_k, \quad k = 1, 3, 5, 7. \end{aligned}$$

All reiterations of calculation of the 2-D DFT in the tensor algorithm, the number of which equals 32, are eliminated in the improved algorithm.

For large values of  $r$ , the improvement of the tensor algorithm of the  $2^r \times 2^r$ -point DFT is estimated as 1.5 by the number of multiplications,

$$k(2^r) = \frac{3 \cdot 2^{r-1} m_{2^r}}{(2^r + 1) m_{2^r}} \approx \frac{3}{2}.$$

The known Cooley–Tukey algorithm with base  $(2 \times 2)$  uses  $4^{r-1}(3r - 4) + 1$  operations of multiplication, which exceeds 1.7 times the number of multiplications in the improved tensor algorithm (see Table 19.1). The efficiency of the tensor algorithm by operations of multiplication with respect to the Cooley–Tukey algorithm is also given in the table.

### 19.5.4 Recursive Tensor Algorithm

We now describe another, more elegant improved tensor algorithm for calculating the 2-D DFT, which we call *the recurrent tensor* algorithm, since it represents itself the recurrent

**TABLE 19.1** The Number of Operations of Multiplication Required for Calculating the  $2^r \times 2^r$ -Point DFT in the Tensor and Improved Tensor Algorithms, as well as by the Cooley–Tukey Algorithm with the Base  $(2 \times 2)$

$2^r$	$T = 3(2^{r-1})m_{2^r}$	$I = (2^r + 1)m_{2^r}$	$C = 4^{r-1} (3r - 4) + 1$	$C/T$	$C/I$
256	246,528	164,994	327,681	1.33	1.99
512	1,181,184	788,994	1,507,329	1.28	1.91
1024	5,508,096	3,675,650	6,815,745	1.24	1.85
2048	25,171,968	16,789,506	30,408,705	1.21	1.81
4096	113,258,496	75,524,098	134,217,729	1.19	1.78
8192	503,341,056	335,601,666	587,202,561	1.17	1.75

Note: It is assumed that  $m_{2^r} = 2^{r-1}(r - 3) + 2$ .

procedure of calculation of the 2-D DFT by means of the 2-D DFTs of small orders. The calculation of the  $2^r \times 2^r$ -point DFT is reduced to  $3 \cdot 2^{r-1}$  incomplete transformations  $\mathcal{F}_{2^r,2}$  and one  $2^{r-1} \times 2^{r-1}$ -point DFT.  $\mathcal{F}_{2^r,2}$  denotes the incomplete  $2^r$ -point DFT when all  $2^{r-1}$  components with even numbers are not calculated. The number of operations of multiplication in such a recurrent algorithm equals

$$m_{2^r,2^r} = 4^r/6(3r - 7) + 8/3. \tag{19.78}$$

In the tensor algorithm, the redundancy of the calculations ( $p_1, p_2$ ) occurs in all frequency-points with even coordinates. The set of these frequency-points can be written as  $2X_{2^{r-1},2^{r-1}}$ . We can define the following partition of the lattice  $X_{2^r,2^r}$ :

$$X_{2^r,2^r} = \bigcup_{(p,s) \in J} \left( T_{p,s} \setminus T_{2p,2s} \right) \cup 2X_{2^{r-1},2^{r-1}}.$$

The calculation of the 1-D DFTs of the splitting-signals  $f_{T_{p,s}}$  at only odd points can be reduced to the incomplete transforms  $\mathcal{F}_{2^r,2} \circ f_{T_{p,s}}$ . The calculation of the 2-D  $2^r \times 2^r$ -point DFT at all even frequency-points can be reduced to the  $2^{r-1} \times 2^{r-1}$ -point DFT. Indeed, the following holds:

$$\begin{aligned} F_{2p_1,2p_2} &= \sum_{n_1=1}^{2^r-1} \sum_{n_2=1}^{2^r-1} f_{n_1,n_2} W_{2^r}^{2n_1p_1+2n_2p_2} \\ &= \sum_{n_1=1}^{2^{r-1}-1} \sum_{n_2=1}^{2^{r-1}-1} g_{n_1,n_2} W_{2^{r-1}}^{n_1p_1+n_2p_2} = (\mathcal{F}_{2^{r-1},2^{r-1}} \circ g)_{p_1,p_2}, \end{aligned} \tag{19.79}$$

where the 2-D sequence  $g$  is defined as

$$g_{n_1,n_2} = f_{n_1,n_2} + f_{n_1+2^{r-1},n_2} + f_{n_1,n_2+2^{r-1}} + f_{n_1+2^{r-1},n_2+2^{r-1}},$$

for  $p_1, p_2 = 0 : (2^{r-1} - 1)$ . The number of operations of multiplication required to fulfill the incomplete transform  $\mathcal{F}_{2^r,2} \circ f_T$  equals

$$m_{2^r,2} = m_{2^r} - m_{2^{r-1}} = 2^{r-1} - 2 + m_{2^{r-1}} = 2^{r-2}(r - 2),$$

if we use the valuation  $m_{2^r} = 2^{r-1}(r - 3) + 2$ . The number of multiplications required in the recurrent algorithm of the  $2^r \times 2^r$ -point DFT can be estimated as follows:

$$\begin{aligned} m_{2^r,2^r} &= m_{2^{r-1},2^{r-1}} + 3 \cdot 2^{r-1} m_{2^r,2} = m_{2^{r-1},2^{r-1}} + 3 \cdot 2^{2r-3}(r - 2) \\ &= \frac{4^r}{6}(3r - 7) + 8/3, \end{aligned}$$

when we similarly continue the splitting of the  $2^{r-1} \times 2^{r-1}$ -point DFT, and then  $2^{r-2} \times 2^{r-2}$ -point DFT, and so on. Table 19.2 shows the number of multiplications in the recurrent algorithm in comparison with the tensor algorithm, for  $N = 2^r$ , when  $r = 8 : 15$ .

#### 19.5.4.1 $N$ Is a Power of an Odd Prime

We now consider a splitting of the  $N \times N$ -point DFT, when  $N = L^r$ ,  $L > 1$  is an arbitrary odd prime number, and  $r > 1$ . The irreducible covering  $\sigma_J = (T_{p,s})$  of the lattice  $X_{L^r,L^r}$  consists of

**TABLE 19.2** The Number of Operations of Multiplication Required for Calculation of the  $2^r \times 2^r$ -Point DFT by the Tensor Algorithm and Recurrent Tensor Algorithm

$r$	$2^r$	$T = 3(2^{r-1})m_{2^r}$	$R = 4^r/6(3r - 7) + 8/3$	$T / R$
8	256	246,528	185,688	1.33
9	512	1,181,184	873,816	1.35
10	1,024	5,508,096	4,019,544	1.37
11	2,048	25,171,968	18,175,320	1.38
12	4,096	113,258,496	81,089,880	1.40
13	8,192	503,341,056	357,913,944	1.41
14	16,384	2,214,641,664	1,565,873,496	1.41
15	32,768	9,663,774,720	6,800,364,888	1.42

$L^{r-1}(L+1)$  cyclic groups and can be defined by the following set of generators:

$$J = J_{L^r, L^r} = \bigcup_{p_1=0}^{L^r-1} (p_1, 1) \bigcup_{p_2=0}^{L^{r-1}-1} (1, L p_2). \quad (19.80)$$

Therefore, to calculate the  $L^r \times L^r$ -point DFT, it is sufficient to fulfill  $L^{r-1}(L+1)$   $L^r$ -point DFTs of the splitting-signals. The number of multiplications is estimated as

$$m_{L^r, L^r} = L^{r-1}(L+1)m_{L^r}.$$

The column-row algorithm uses  $2(L^r)$   $L^r$ -point DFTs and  $2(L^r)m_{L^r}$  multiplications. The tensor algorithm reduces the number of multiplications by  $2L/(L+1)$  times.

The tensor algorithm can be improved, when removing the redundancy of calculations in the intersections of the cyclic groups  $T_{p,s}$  of the covering. For instance, for the  $r=2$  case, the calculation of the  $L^2 \times L^2$ -point 2-D DFT can be reduced to one  $L^2$ -point DFT,  $L$  incomplete  $L^2$ -point DFTs (without calculation of the first component at zero point), and  $L^2 - 1$  incomplete  $L^2$ -point DFTs (without calculation of components at points which are integer multiple to  $L$ ).

The redundancy of the algorithm is in calculation of the spectral components at all frequency-points with coordinates which are integer multiple to  $L$ . The recurrent tensor algorithm can be constructed similar to the  $L=2$  case, when  $L^r \times L^r$ -point DFT is reduced to one  $L^{r-1} \times L^{r-1}$ -point 2-D DFT and  $L^{r-1}(L+1)$  incomplete transforms  $\mathcal{F}_{L^r, L} \circ f_T$ . The incomplete transforms are not calculated at points which are integer multiple to  $L$ . In such a recurrent algorithm, the number of operations of multiplication can be estimated by the following recursive formula:

$$m_{L^r, L^r} = m_{L^{r-1}, L^{r-1}} + (L+1)L^{r-1}(m_{L^r} - m_{L^{r-1}}). \quad (19.81)$$

The difference of number of multiplications in the tensor and recurrent tensor algorithms is estimated as:

$$\Delta m_{L^r, L^r} = (L+1)L^{r-1}m_{L^r} - m_{L^r, L^r} \geq (L^2 - 1)L^{r-2}m_{L^{r-1}}.$$

For example, for the  $25 \times 25$ -point DFT, the recurrent tensor algorithm saves more than 240 multiplications, and 768 multiplications for the  $49 \times 49$ -point DFT. We use the known valuations  $m_5 = 10$  and  $m_7 = 16$ , for the number of multiplications in the five-point and seven-point DFTs, respectively.

#### 19.5.4.2 Case $N = L_1 L_2$ ( $L_1 \neq L_2 > 1$ )

We consider the  $N = L_1 L_2$  case, where  $L_1$  and  $L_2$  are arbitrary coprime numbers  $> 1$ . The irreducible covering  $\sigma_J$  of the lattice  $X_{L_1 L_2, L_1 L_2}$  consists of  $(L_1 + 1)(L_2 + 1)$  cyclic groups  $T_{p,s}$ . Such a covering  $\sigma_J$  can be determined by the following set of generators:

$$J = \bigcup_{p_1=0}^{L_1 L_2 - 1} (p_1, 1) \cup \{(1, 0)\} \cup \left( \bigcup_{g.c.d.(p_2, L_1 L_2) > 1} (1, p_2) \right) \cup \{(L_1, L_2)\} \cup \{(L_2, L_1)\}. \quad (19.82)$$

To calculate the 2-D  $(L_1 L_2) \times (L_1 L_2)$ -point DFT, it is sufficient to perform  $(L_1 + 1)(L_2 + 1)$   $L_1 L_2$ -point 1-D DFTs of splitting-signals  $f_{T_{p,s}}$ . The number of multiplications required for this algorithm equals

$$m_{L_1 L_2, L_1 L_2} = (L_1 + 1)(L_2 + 1)m_{L_1 L_2}. \quad (19.83)$$

For instance, the calculation of the  $20 \times 20$ -point 2-D DFT is reduced to calculation of thirty 20-point DFTs, instead of forty 20-point DFTs in the column-row algorithm.

#### 19.5.4.3 Other Orders $N_1 \times N_2$

The tensor algorithm as well as the improved tensor algorithm can be constructed for other orders  $N_1 \times N_2$  of the 2-D DFT, when  $N_1 \neq N_2 > 1$ . The tensor algorithm is defined by the irreducible covering  $\sigma_J$  of the lattice  $X_{N_1, N_2}$  by the cyclic groups  $T_{p,s}$ . It is not difficult to compose such a covering for each  $N_1 \times N_2$  case under consideration. By analyzing the intersections of groups of the covering, where the calculations of the spectral components are repeated, we can obtain an effective improvement of the tensor algorithm.

#### Example 19.9

We consider  $3 \times 6$ -point DFT,  $\mathcal{F}_{3,6}$ , i.e., the case when  $N_1 = 3$  and  $N_2 = 6$ . Let  $f = f_{n_1, n_2}$  be a  $3 \times 6$ -point 2-D sequence. The irreducible covering  $\sigma_J$  of the lattice  $X_{3,6}$  can be defined by the following set of four generators:  $J = \{(0, 1), (1, 1), (2, 1), (1, 3)\}$ . All cyclic groups of this covering and their intersections are shown below:

$$\begin{aligned} T_{0,1} &= \{(0, 0), (0, 1), (0, 2), (0, 3), (0, 4), (0, 5)\} \\ T_{1,1} &= \{(0, 0), (1, 1), (2, 2), (0, 3), (1, 4), (2, 5)\} \\ T_{2,1} &= \{(0, 0), (2, 1), (1, 2), (0, 3), (2, 4), (1, 5)\} \\ T_{1,3} &= \left\{ \begin{array}{cc} (0, 0) & (0, 3) \\ (1, 0) & (1, 3) \\ (2, 0) & (2, 3) \end{array} \right\}. \end{aligned}$$

Figure 19.18 illustrates the locations of all frequency-points of these four groups. The groups are intersected only at two frequency-points  $(0, 0)$  and  $(0, 3)$ , i.e., when the coordinates of the points are integer multiple to 3. Therefore, the transformation  $\mathcal{F}_{3,6}$  can be split by one 6-point DFT and three incomplete 6-point DFTs,

$$\mathcal{F}_{3,6} \sim \{\mathcal{F}_6, \mathcal{F}_{6,3}, \mathcal{F}_{6,3}, \mathcal{F}_{6,3}\}.$$

These transforms can be performed in the following way:

*Step 1:* One 6-point DFT over the splitting-signal  $f_{T_{0,1}}$ , to determine the 2-D DFT at frequency-points of the group  $T_{0,1}$ ,

$$F_{0,k} = (\mathcal{F}_6 \circ f_{T_{0,1}})_k, \quad k = 0: 5.$$

*Step 2:* Three incomplete 6-point DFTs over the splitting-signals  $f_{T_{1,1}}$ ,  $f_{T_{2,1}}$ , and  $f_{T_{1,3}}$ , to determine the 2-D DFT at all

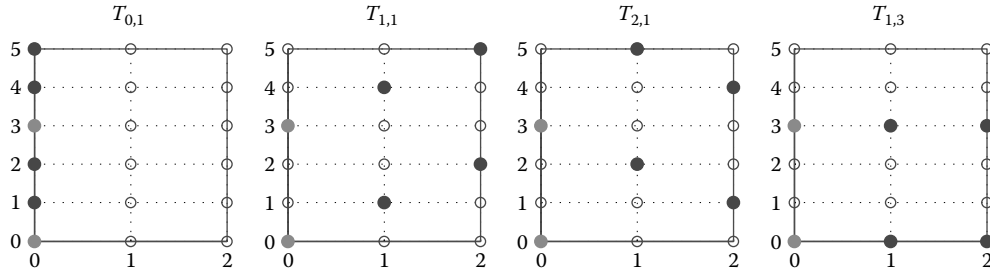


FIGURE 19.18 Arrangement of frequency-points of groups  $T_{p_1,p_2}$  covering the lattice  $X_{3,6}$ .

frequency-points of the corresponding groups  $T_{1,1}$ ,  $T_{2,1}$ , and  $T_{1,3}$ , except points  $(0, 0)$  and  $(0, 3)$ ,

$$F_{k \bmod 3,k} = (\mathcal{F}_{6;3} \circ f_{T_{1,1}})_k, \quad F_{2k \bmod 3,k} = (\mathcal{F}_{6;3} \circ f_{T_{2,1}})_k, \\ F_{k \bmod 3,3k \bmod 6} = (\mathcal{F}_{6;3} \circ f_{T_{1,3}})_k,$$

where  $k = 1, 2, 4, 5$ .

When the input is real, the 6-point DFT uses six operations of multiplication by factors  $W_6 = \exp(-j\pi/3) = (1 - j\sqrt{3})/2$ ,  $W_3 = \exp(-j2\pi/3) = -(1 + j\sqrt{3})/2$ , and  $W_3^2 = \exp(-j4\pi/3) = -(1 - j\sqrt{3})/2$ . We here consider the fast paired algorithm of the six-point DFT [16]. Each such multiplication requires one real multiplication by the factor of  $\sqrt{3}$  and two shifting operations. Six real operations of multiplication are required for the 6-point DFT. The incomplete Fourier transformation  $\mathcal{F}_{6,3}$  requires also six multiplications. Therefore, the  $3 \times 6$ -point DFT uses the real multiplications in number  $6 + 3(6) = 24$ . For comparison, in the column-row algorithm, three 6-point DFTs with real inputs and six 3-point DFTs with complex inputs are used, and the number of multiplications equals  $3(6) + 6(2) = 30$ .

$$T_{1,1} = \left\{ \begin{array}{l} (0, 0), (1, 1), (2, 2), (3, 3), (4, 4), (5, 5), (0, 6), (1, 7) \\ (2, 0), (3, 1), (4, 2), (5, 3), (0, 4), (1, 5), (2, 6), (3, 7) \\ (4, 0), (5, 1), (0, 2), (1, 3), (2, 4), (3, 5), (4, 6), (5, 7) \end{array} \right\} \\ T_{2,1} = \left\{ \begin{array}{l} \underline{(0, 0)}, (2, 1), \underline{(4, 2)}, (0, 3), \underline{(2, 4)}, (4, 5), \underline{(0, 6)}, (2, 7) \\ \underline{(4, 0)}, (0, 1), \underline{(2, 2)}, (4, 3), (0, 4), (2, 5), \underline{(4, 6)}, (0, 7) \\ \underline{(2, 0)}, (4, 1), \underline{(0, 2)}, (2, 3), \underline{(4, 4)}, (0, 5), \underline{(2, 6)}, (4, 7) \end{array} \right\} \\ T_{1,2} = \left\{ \begin{array}{l} (0, 0), (1, 2), (2, 4), (3, 6) \\ \underline{(4, 0)}, (5, 2), \underline{(0, 4)}, (1, 6) \\ (2, 0), (3, 2), (4, 4), (5, 6) \end{array} \right\} \\ T_{1,4} = \left\{ \begin{array}{l} \underline{(0, 0)}, (1, 4) \\ (2, 0), (3, 4) \\ \underline{(4, 0)}, (5, 4) \end{array} \right\} \\ T_{1,0} = \left\{ \begin{array}{l} \underline{(0, 0)} \\ (1, 0) \\ \underline{(2, 0)} \\ (3, 0) \\ \underline{(4, 0)} \\ (5, 0) \end{array} \right\}. \tag{19.84}$$

**Example 19.10**

We consider the  $6 \times 8$ -point Fourier transformation,  $\mathcal{F}_{6,8}$ . Let  $f = f_{n_1,n_2}$  be a  $6 \times 8$ -point 2-D sequence. The irreducible covering  $\sigma_j$  of the lattice  $X_{6,8}$  can be defined by the set of generators  $J = \{(1, 1), (2, 1), (1, 2), (1, 4), (1, 0)\}$ .

The intersections of the cyclic groups of this covering are shown below:

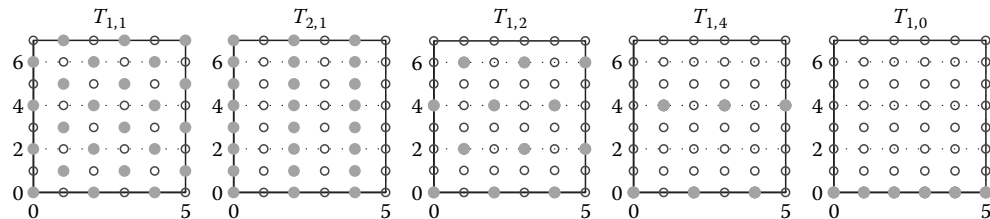


FIGURE 19.19 Arrangement of frequency-points of groups  $T_{p_s}$  covering the lattice  $X_{6,8}$ .

The location of frequency-points of the five cyclic groups  $T_{p_s}$  of the covering are shown in Figure 19.19

The groups are intersected only at 12 frequency-points with even coordinates. Therefore, the transformation  $\mathcal{F}_{6,8}$  can be split by one 24-point DFT, two incomplete 24- and 12-point DFTs, and two incomplete 6-point DFTs. Namely, the following splitting is valid:

$$\mathcal{F}_{6,8} \sim \{\mathcal{F}_{24}, \mathcal{F}_{24;2}, \mathcal{F}_{12;2}, \mathcal{F}_{6;2}, \mathcal{F}_{6;2}\}.$$

All these incomplete DFTs are not calculated for the components with even points, and, therefore, they can be reduced to calculation of the DFTs of twice smaller orders. Thus the  $6 \times 8$ -point DFT can be split by the 24-, 12-, 6-point DFTs, and two 3-point DFTs, and the redundancy of calculations in the tensor algorithm will be removed.

These transforms can be performed in the following way:

*Step 1:* One 24-point DFT over the splitting-signal  $f_{T_{1,1}}$ , to determine the 2-D DFT at frequency-points of the group  $T_{1,1}$ ,

$$F_{k \bmod 6, k \bmod 8} = (\mathcal{F}_{24} \circ f_{T_{1,1}})_k, \quad k = 0 : 23.$$

*Step 2:* One incomplete 24-point DFT over the splitting-signal  $f_{T_{2,1}}$ , to determine the 2-D DFT at 12 frequency-points of the group  $T_{2,1}$  with odd coordinates,

$$F_{2k \bmod 6, k \bmod 8} = (\mathcal{F}_{24} \circ f_{T_{2,1}})_k, \quad k = 1, 3, \dots, 21, 23.$$

*Step 3:* One incomplete 12-point DFT over the splitting-signal  $f_{T_{1,2}}$ , to determine the 2-D DFT at frequency-points of the group  $T_{2,1}$  with odd coordinates,

$$F_{k \bmod 6, 2k \bmod 8} = (\mathcal{F}_{12} \circ f_{T_{1,2}})_k, \quad k = 1, 3, \dots, 9, 11.$$

*Step 4:* Two incomplete 6-point DFTs over the splitting-signals  $f_{T_{1,4}}$  and  $f_{T_{1,0}}$ , to determine respectively the 2-D DFT at frequency-points of the groups  $T_{1,4}$  and  $T_{1,0}$  with odd coordinates,

$$F_{k \bmod 6, 4k \bmod 8} = (\mathcal{F}_{6;2} \circ f_{T_{1,4}})_k, F_{k,0} = (\mathcal{F}_{6;2} \circ f_{T_{1,0}})_k, \quad k = 1, 3, 5.$$

The location of all 48 frequency-points of the cyclic groups of the covering  $\sigma_j$ , at which the calculations of the Fourier transform components  $F_{p_1, p_2}$  are performed, are shown in Figure 19.20.

To estimate the number of real multiplications used in this algorithm, we use the valuations of the fast 1-D DFT by paired transforms [16]. The number of multiplications for the incomplete transforms  $\mathcal{F}_{6;2}$  and  $\mathcal{F}_{12;2}$  over real data equal 2 and 4, respectively. The 24-point DFT of real data is reduced to the 12-point DFT with additional 10 multiplications by twiddle factors, which results in the total  $16 + 20 = 36$  real multiplications, when

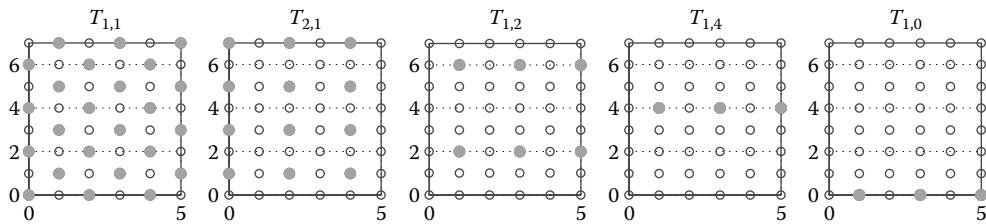


FIGURE 19.20 Arrangement of frequency-points of groups  $T_{p,s}$  which divide the lattice  $X_{6,8}$ , after removing their intersections.

considering  $m_{12} = 16$  for complex data. The incomplete 24-point DFT,  $\mathcal{F}_{24;2}$ , requires 18 real multiplications. Thus, the above described  $6 \times 8$ -point 2-D DFT uses  $36 + 18 + 4 + 2 + 2 = 62$  real multiplications for real data  $f_{n_1, n_2}$ . It should be noted for the comparison, that the column–row algorithm for this transform uses six 8-point DFTs of real inputs and eight 6-point DFTs of complex inputs with total  $6(2) + 8(12) = 108$  real multiplications.

### 19.5.5 $n$ -Dimensional DFT

The concepts of the tensor transform and representation can be extended for the  $n$ -dimensional DFT, when  $n > 2$ . Let  $f = \{f_{n_1, \dots, n_n}\}$  be an arbitrary  $n$ -dimensional sequence. We consider for simplicity of our calculations that the sizes of  $f$  are equal, i.e.,  $n_k = 0 : (N-1)$ ,  $k = 1 : n$ . The  $n$ -dimensional DFT of the sequence  $f$  at the frequency-point  $(p_1, \dots, p_n) \in X_{N, \dots, N}$ , accurate to the normalizing factor  $N^{n/2}$ , is defined as

$$F_{p_1, \dots, p_n} = \sum_{n_1=0}^{N-1} \dots \sum_{n_n=0}^{N-1} f_{n_1, \dots, n_n} W^{n_1 p_1 + \dots + n_n p_n} \quad (19.85)$$

where  $W = W_N = \exp(-2\pi j/N)$ . In the tensor representation, each spectral component  $F_{p_1, \dots, p_n}$  is represented by the corresponding vector of dimension  $N$ :

$$F_{p_1, \dots, p_n} \rightarrow (f_{p_1, \dots, p_n, 0}, f_{p_1, \dots, p_n, 1}, \dots, f_{p_1, \dots, p_n, N-1})' \quad (19.86)$$

whose superposition with the exponential wave of “the low frequency”  $\omega_0 = (2\pi/N)$  equals to the component,

$$F_{p_1, \dots, p_n} = \sum_{t=0}^{N-1} f_{p_1, \dots, p_n, t} W^t. \quad (19.87)$$

To open the complex number  $F_{p_1, \dots, p_n}$  as a vector, we perform a summation of the initial  $n$ -dimensional sequence at spacial points of the following  $N$  disjoint subsets of the lattice  $X$ :

$$V_{p_1, \dots, p_n, t} = \left\{ (n_1, \dots, n_n); \sum_{k=1}^n n_k p_k = t \bmod N \right\} \cap X \quad (19.88)$$

where  $t=0 : (N-1)$ . In other words, the components of the vector in Equation 19.86 are calculated by

$$f_{p_1, \dots, p_n, t} = \sum_{V_{p_1, \dots, p_n, t}} f_{n_1, \dots, n_n}, \quad t = 0 : (N-1). \quad (19.89)$$

The following assertion holds:

$$F_{\overline{kp_1}, \dots, \overline{kp_n}} = \sum_{t=0}^{N-1} f_{p_1, \dots, p_n, t} W^{kt}, \quad k = 0 : (N-1). \quad (19.90)$$

The frequency-points  $(\overline{kp_1}, \dots, \overline{kp_n}) = (kp_1 \bmod N, \dots, kp_n \bmod N)$  compose the cyclic group

$$T_{p_1, \dots, p_n} = \{(\overline{kp_1}, \dots, \overline{kp_n}); \quad k = 0 : (N-1)\}.$$

The 1-D signal

$$f_{T_{p_1, \dots, p_n}} = \{f_{p_1, \dots, p_n, t}, \quad t = 0 : (N-1)\} \quad (19.91)$$

is referred to as the splitting-signal, which carries the spectral information of the  $n$ -dimensional sequence  $f$  at frequency-points of  $T_{p_1, \dots, p_n}$ . To collect the whole spectral information of the sequence, we need to cover the lattice  $X$  by the cyclic groups. Let  $\sigma = (T_{p_1, \dots, p_n})$  be an irreducible covering of the lattice  $X$ . Then, the representation of the  $n$ -dimensional sequence as a set of splitting-signals

$$f_{n_1, \dots, n_n} \rightarrow \{f_{T_{p_1, \dots, p_n}}; \quad T_{p_1, \dots, p_n} \in \sigma\}$$

is called the *tensor transform* of  $f$ . Thus, in the tensor representation, the  $n$ -dimensional sequence is considered as the set of the splitting-signals. The number of splitting-signals increases with dimension  $n$ , but the lengths of all signals are the same and equal  $N$ .

## 19.6 Discrete Hartley Transforms

In this section, we consider the DHT [24,25], whose kernel is the sum of the cosine and sine waves of the exponential kernel of the Fourier transformation. The Hartley transform of real data is real, and it has many properties which are similar to the Fourier transform. From the standpoint of the arithmetical computation, both transforms have almost the same complexity in the multidimensional case, as well as in 1-D case. Both transformations lead to the same tensor representation of multi-dimensional signals and images, and the transforms thus are split by the same number of 1-D transforms. We first describe the 2-D case and then the 3-D case which at the same time will illustrate the tensor transformation for the 3-D Fourier transform.

We denote by  $\mathcal{H}_{N,N}$  the  $N \times N$ -point DHT, whose image  $\mathcal{H}_{N,N} \circ f$  upon an  $N \times N$  sequence  $f = \{f_{n_1, n_2}\}$  is defined as:

$$H_{p_1, p_2} = (\mathcal{H}_{N,N} \circ f)_{p_1, p_2} = \sum_{n_1=0}^{N-1} \sum_{n_2=0}^{N-1} f_{n_1, n_2} \text{Cas}(n_1 p_1 + n_2 p_2), \\ (p_1, p_2) \in X_{N,N}, \quad (19.92)$$

where the transform kernel is the real periodic function

$$\text{Cas}(x) = \text{Cas}_N(x) = \text{cas}\left(\frac{2\pi x}{N}\right) = \cos\left(\frac{2\pi x}{N}\right) + \sin\left(\frac{2\pi x}{N}\right). \quad (19.93)$$

The above defined 2-D DHT is a real-to-real and nonseparable transform. The inversion formula for the DHT coincides with the initial formula (accurate to the factor  $1/N^2$ ), i.e.,  $\mathcal{H}_{N,N}^{-1} = 1/N^2 \mathcal{H}_{N,N}$ .

The 1-D  $N$ -point DHT of a 1-D sequence  $f = \{f_n\}$  is defined by

$$H_p = (\mathcal{H}_N \circ f)_p = \sum_{n=0}^{N-1} f_n \text{Cas}(np), \quad p = 0 : (N-1). \quad (19.94)$$

For a given frequency-point  $(p_1, p_2)$  of the lattice  $X_{N,N}$ , the following property holds:

$$H_{\overline{kp_1}, \overline{kp_2}} = \sum_{t=0}^{N-1} f_{p_1, p_2, t} \text{Cas}(kt), \quad k = 0 : (N-1), \quad (19.95)$$

where  $f_{p_1, p_2, t}$  are components of the splitting-signals which are defined exactly as for the Fourier transform,

$$f_{p_1, p_2, t} = \sum_{V_{p_1, p_2, t}} f_{n_1, n_2}, \quad t = 0 : (N-1). \quad (19.96)$$

The uniqueness of the tensor representation for the Hartley and Fourier transforms follows from the identical form of the relation between the spatial points  $(n_1, n_2)$  and frequency-points  $(p_1, p_2)$  in the kernel of these transforms. This is the Diophantus form  $\mathcal{L}(n_1, n_2; p_1, p_2) = n_1 p_1 + n_2 p_2$ . Therefore, if  $\sigma_J$  is the irreducible covering of the lattice  $X_{N,N}$ , which is composed from the cyclic groups  $T_{p, s}$ , then the 2-D DHT is split by the  $\text{card}(J)$  1-D DHT. The splitting of the 2-D DFT and DHT are similar; both are defined by the same number of the 1-D transforms. We can thus apply all reasonings used for the Fourier transform to the Hartley transform in the 2-D case. The tensor algorithm of calculation of the  $N \times N$ -point 2-D DHT uses

$$m_{N,N} = (\text{card } J) m_N \quad (19.97)$$

operations of multiplication, where  $m_N$  denotes the number of multiplications for the 1-D  $N$ -point DHT. In many cases of  $N$ , we have  $\text{card } J < 2N$ , therefore the tensor algorithm uses less multiplications than the column-row method does for the separable 2-D DHT.

For instance, when  $N$  is an odd prime  $L > 2$ , then the calculation of the  $L \times L$ -point DHT is reduced to calculations of  $(L + 1)$  1-D  $L$ -point DHTs, and it is sufficient to fulfill

$$m_{L,L} = (L + 1)m_L \quad (19.98)$$

operations of multiplication. We can compare this estimation with the known estimation  $\mu_{L,L} = L^2 + 2L - 3$ , which has been obtained by Boussakta and Holt by using an index mapping scheme, when calculating the  $L \times L$ -point DHT [26]. Using the estimation  $m_L = (L - 1)$  introduced with the Fermat number transform [27], we gain the following number of multiplications:

$$\Delta(L) = \mu_{L,L} - m_{L,L} = (L^2 + 2L - 3) - (L + 1)(L - 1) = 2(L - 1). \quad (19.99)$$

### Example 19.11

Let  $N = 3$  and  $f$  be a 2-D sequence  $\{f_{n_1, n_2}; n_1, n_2 = 0, 1, 2\}$ . The tensor algorithm of the  $3 \times 3$ -point DHT of  $f$  uses 4 real multiplications and 45 real additions if  $f$  is real. Indeed, using the covering  $\sigma = (T_{0,1}, T_{1,1}, T_{2,1}, T_{1,0})$ , the  $3 \times 3$ -point DHT reduces to calculation of four splitting-signals  $f_{T_{0,1}}, f_{T_{1,1}}, f_{T_{2,1}}$ , and  $f_{T_{1,0}}$  as is described in Example 19.6. Then one three-point DHT of the first splitting-signal is calculated and three incomplete 3-point DHTs of other signals.

In matrix form, the tensor algorithm of the  $3 \times 3$ -point DHT can be written as follows:

$$\begin{bmatrix} H_{0,0} \\ H_{0,1} \\ H_{0,2} \\ H_{1,1} \\ H_{2,2} \\ H_{2,1} \\ H_{1,2} \\ H_{1,0} \\ H_{2,0} \end{bmatrix} = \begin{bmatrix} 1 & 1 & 1 \\ 1 & C_1 & C_2 \\ 1 & C_2 & C_1 \\ & & 1 & C_1 & C_2 \\ & & 1 & C_2 & C_1 \\ & & & 1 & C_1 & C_2 \\ & & & 1 & C_2 & C_1 \\ & & & & 1 & C_1 & C_2 \\ & & & & 1 & C_2 & C_1 \end{bmatrix} [\mathcal{X}_\sigma] \mathbf{f}$$

where the coefficients of the Hartley matrices equal  $C_1 = \text{Cas}_3(1)$  and  $C_2 = \text{Cas}_3(2)$ .

Each incomplete Hartley transform uses one real multiplication and five additions. Indeed, since  $\text{Cas}(1) = \cos(2\pi/3) + \sin(2\pi/3)$  and  $\text{Cas}(2) = \cos(2\pi/3) - \sin(2\pi/3)$ , we can write the transform as follows:

$$\begin{bmatrix} 1 & C_1 & C_2 \\ 1 & C_2 & C_1 \end{bmatrix} \begin{bmatrix} x \\ y \\ z \end{bmatrix} = \begin{bmatrix} x + (c_1 + s_1)y + (c_1 - s_1)z \\ x + (c_1 - s_1)y + (c_1 + s_1)z \end{bmatrix} \quad (19.100)$$

$$= \begin{bmatrix} x + c_1(y + z) + s_1(y - z) \\ x + c_1(y + z) - s_1(y - z) \end{bmatrix}$$

$$c_1 = -\sqrt{3}/2, \quad s_1 = -1/2.$$

The multiplication  $c_1(y + z)$  is the only nontrivial multiplication used in this transform. The 3-point DHT requires one more addition for calculating the first component at point 0, as  $x + (y + z)$ .

The direct calculation of the tensor transform  $[\mathcal{X}] \mathbf{f}$  requires 24 additions (subtractions). Therefore, to calculate the  $3 \times 3$ -point DHT by the tensor algorithm, it is sufficient to use  $6 + 3 \times 5 + 24 = 45$  real additions. In the column-row algorithm, the calculation of the  $3 \times 3$  separable DHT is fulfilled via six 3-point DHTs. Therefore, respectively  $6 \cdot 1 = 6$  and  $6 \cdot 6 = 36$  real operations of multiplication and addition are used in such an algorithm, i.e., three multiplications more, but nine additions less than in the tensor algorithm.

In the general  $N \times N$  case, the construction of the irreducible covering

$$\sigma_J = (T_{p,s})_{p,s \in J} \quad (19.101)$$

of the square lattice  $X_{N,N}$  can be implemented in the following way [16]. We first define the set  $B_N = \{n \in X_N; g.c.d.(n, N) > 1\}$  and function  $\beta(p)$  which equals the number of elements  $s \in B_N$  being coprime with  $p$  and such that  $ps < N$ . Then the set of generators can be defined as follows:

$$J = \bigcup_{p=0}^{N-1} (p, 1) \cup \left( \bigcup_{s \in B_N} (1, s) \right) \cup \left( \bigcup_{p, s \in B_N, g.c.d.(p,s)=1, p,s \leq N} (p, s) \right). \quad (19.102)$$

The number of generators in this set, or the number of 1-D DHTs required to calculate the 2-D  $N \times N$ -point DHT equals

$$\text{card} \sigma_J = 2N - \phi(N) + \sum_{p \in B_N} \beta(p) \quad (19.103)$$

where we denote by  $\phi(N)$  Euler's function, that is, the number of positive integers which are smaller than  $N$  and coprime with  $N$ . It is easy to verify, that  $\phi(N) \geq \sum \{\beta(p); p \in B_N\}$ , so that  $\text{card} \sigma \leq 2N$ . Herewith, the equality in this expression takes place when  $L_1 = 2$  and  $L_2 = 3$  (or when  $L_1 = 3$  and  $L_2 = 2$ ); since  $\text{card} \sigma = 2(3) + 2 + 3 + 1 = 2(6) = 12$ . In this case, the column-row and tensor algorithms use the same number, twelve, of the 6-point DHTs.

When  $r > 2$  and  $L$  is a prime, the calculation of the  $L' \times L'$ -point 2-D DHT is reduced to calculations of  $(L + 1)L'^{-1}$  1-D  $L'$ -point DHTs. The covering of the lattice  $X_{L',L'}$  is defined as

$$\sigma_J = ((T_{p,1})_{p=0:(L'-1)}, (T_{1,Ls})_{s=0:(L'-1-1)}). \quad (19.104)$$

For example, the covering of the lattice  $X_{9,9}$  equals

$$\sigma_J = ((T_{p,1}; p = 0:8), T_{1,0}, T_{1,3}, T_{1,6}). \quad (19.105)$$

Therefore, the  $9 \times 9$ -point 2-D DHT is calculated in the tensor algorithm by 12 1-D 9-point DHTs. In the column-row algorithm, this 2-D transform requires 18 9-point DHTs.



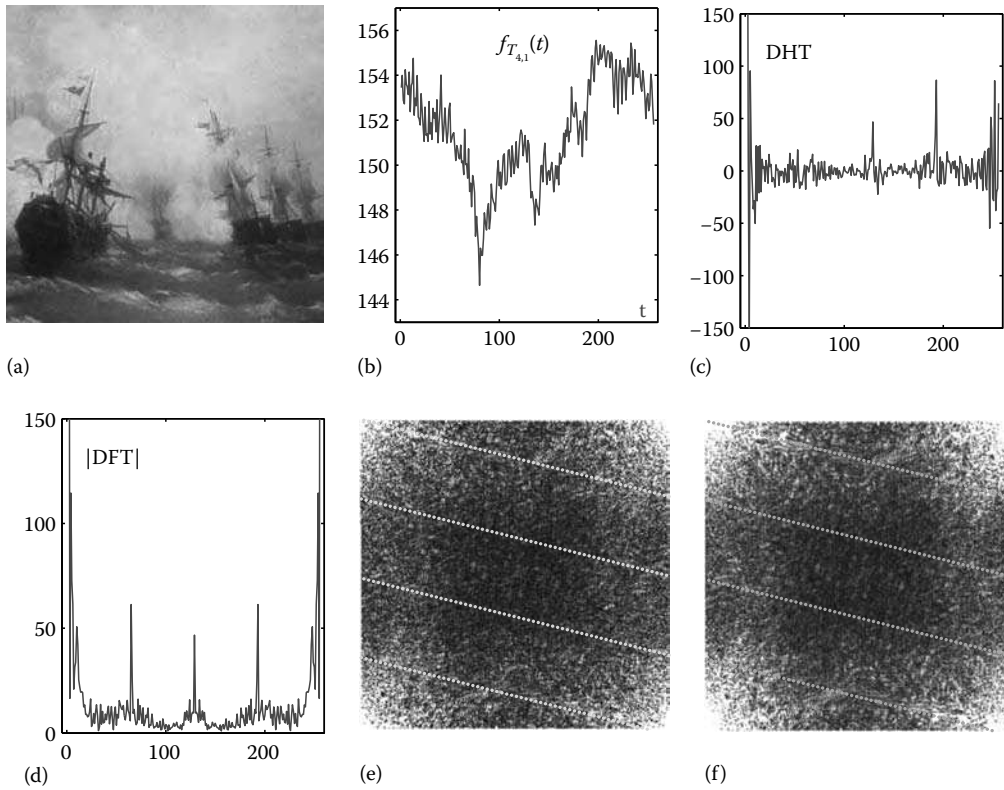


**FIGURE 19.21** (a) The image  $256 \times 256$ , (b) the image-signal  $f_{T_{4,1}}$ , (c) the 1-D DHT of the signal, (d) the 1-D DFT of the signal (in the absolute scale), (e) the 2-D DHT, and (f) the 2-D DFT of the image. (The frequency-points of the group  $T_{4,1}$  are marked on the 2-D transforms.)

In the  $L = 2$  case, the calculation of the  $2^r \times 2^r$ -point DHT of a 2-D sequence  $f_{n_1, n_2}$  is performed by  $3 \cdot 2^{r-1}$   $2^r$ -point DHTs of the splitting-signals  $f_{T_{p,s}}$  with generators  $(p, s) \in J$ . This is the main point in the tensor representation of the 2-D DHT, and 2-D DFT as well. The image in the tensor representation is not considered in the form of the 2-D square matrix in the spacial domain, but as another figure in the 3-D domain, namely the (2-D frequency)-(1-D time) domain,

$$f_{n_1, n_2} \rightarrow \{f_{p,s,t}; t = 0: (N - 1), (p, s) \in J\}.$$

As an example, Figure 19.21 shows the original image of size  $256 \times 256$  in part a, along with the image-signal  $f_{T_{4,1}}$  of length 256 in part (b), and the 256-point DHT of the signal in (c), and the magnitude of the Fourier transform of the signal in (d). For both transforms, this image-signal carries the spectral information of the image at frequency-points of the cyclic group  $T_{4,1}$ . The 2-D DHT and DFT of the image are shown in parts (e) and (f), respectively. The locations of all frequency-points  $(p_1, s_1)$  of this group in the frequency domain of both transforms are also shown. These points lie along four parallel lines at the angle  $\arctan(4) = 75.9638^\circ$  to the verticals (which are assigned for the first coordinates  $p_1$  of frequency-points).

The complete set of image-signals that represent a 2-D sequence (or image), as well its 2-D DHT and DFT can be shown in the 3-D space in different ways. As an example, Figure 19.22 shows a

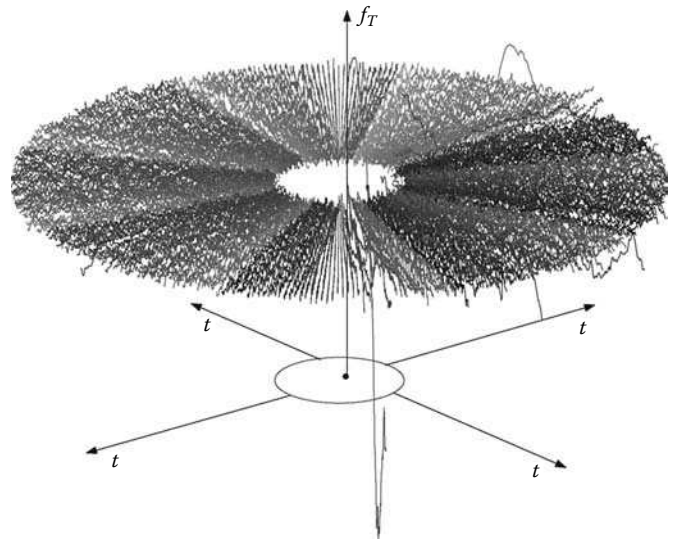


**FIGURE 19.22** The 3-D ring with 384 image-signals  $f_{T_{p,s}}$  of the image  $256 \times 256$ .

3-D figure for the set of 384 all image-signals  $f_{T_{p,s}}, (p, s) \in J$ , of the above considered image  $256 \times 256$ . Image-signals of length 256 are located along 384 directions in a ring with the inner circle of radius 32.

The presentation of the image  $f$  in the form of the ring is performed through the transform:

$$\mathcal{X}_\sigma: f \rightarrow \{f_{p,s,t}; (p,s) \in J, t = 0: (N-1)\}, \quad (19.106)$$

where the set  $J$  of the generatrices  $(p,s)$  of sets  $T \in \sigma$  is defined by Equation 19.102. We call the transformation  $\mathcal{X}_\sigma$  to be the tensor, or vector transformation, because it transfers the image  $f$  into the set of card  $\sigma$  vectors, or image-signals  $f_{T_{p,s}}, (p,s) \in J$ .

The number of required multiplication used in the  $2^r \times 2^r$ -point DHT can be estimated as follows:

$$m_{2^r, 2^r} = 3 \cdot 2^{r-1} m_{2^r} \leq 3[4^{r-1}(r-3) + 2^r]. \quad (19.107)$$

Here we use the well-known fact that, for computing the  $2^r$ -point DHT, it is enough to fulfill  $M_{2^r} = 2^{r-1}(r-3) + 2$  multiplications [28,29]. Comparing this estimation with the number of multiplications  $\mu_{2^r, 2^r} = 2 \cdot 4^r(r-2) + 2^{r+2}$  obtained in the Bracewell algorithm [30], we obtain that  $\mu_{2^r, 2^r}/M_{2^r, 2^r} \approx 4/3$ . In other words, the number of multiplications reduces 4/3 times. The number of multiplications can be reduced, by removing the redundancy of calculations at the intersections of the cyclic groups, as is done for the 2-D DFT, when we have constructed the improved and recurrent tensor algorithms.

### 19.6.1 3-D DHT Tensor Representation

In this section, we describe the tensor representation for dividing the calculation of the nonseparable 3-D DHT by the 1-D DHTs. For simplicity of future calculations, we discuss the case of the transform of the order  $N \times N \times N$ , when  $N = 2^r$ ,  $r > 1$ . However, the concept of tensor representation can be applied to the 3-D DHT transform of an arbitrary order. It will be shown, that the number of multiplications required for calculating the 3-D DHT can be reduced to  $7[8^{r-1}(r-3) + 4^{r-1}]$ . This number can be reduced about 1.6 times, when removing the redundancy of the tensor algorithm, which occurs because of intersections of many cyclic groups covering the 3-D lattice of the frequency-points. Such improvement or the recurrent tensor algorithm can be obtained similar to the algorithms described in Sections 19.5.3 and 19.5.4 for the 2-D DFT.

Let  $X$  be the cubic  $N \times N \times N$  lattice

$$X_{N,N,N} = \{(p_1, p_2, p_3); p_1, p_2, p_3 = 0: (N-1)\}. \quad (19.108)$$

We denote by  $\mathcal{H}_{N,N,N}$  the  $N \times N \times N$ -point DHT whose image  $\mathcal{H}_{N,N,N} \circ f$  on a 3-D sequence  $f = \{f_{n_1, n_2, n_3}\}$  is defined as follows:

$$\begin{aligned} H_{p_1, p_2, p_3} &= (\mathcal{H}_{N,N,N} \circ f)_{p_1, p_2, p_3} \\ &= \sum_{n_1=0}^{N-1} \sum_{n_2=0}^{N-1} \sum_{n_3=0}^{N-1} f_{n_1, n_2, n_3} \text{Cas}(n_1 p_1 + n_2 p_2 + n_3 p_3), \end{aligned} \quad (19.109)$$

where  $(p_1, p_2, p_3) \in X$ . The tensor representation of  $f$  is defined by the irreducible covering  $\sigma_J$  of the lattice  $X$ , which is composed by the following cyclic groups in  $X$ :

$$T = T_{p_1, p_2, p_3} = \{(\overline{k p_1}, \overline{k p_2}, \overline{k p_3}); k = 0: (N-1)\}, \quad (T_{0,0,0} = \{(0,0,0)\}). \quad (19.110)$$

For a given frequency-point  $(p_1, p_2, p_3) \neq (0, 0, 0)$ , the collection of subsets  $\{V_{p_1, p_2, p_3, t}; t = 0: (N-1)\}$  is a partition of  $X$ . Therefore, the following property holds for spectral components of the 3-D DHT:

$$H_{\overline{k p_1}, \overline{k p_2}, \overline{k p_3}} = \sum_{t=0}^{N-1} f_{p_1, p_2, p_3, t} \text{Cas}(kt), \quad k = 0: (N-1). \quad (19.111)$$

Thus the splitting-signal

$$f_{T_{p_1, p_2, p_3}} = \{f_{p_1, p_2, p_3, 0}, f_{p_1, p_2, p_3, 1}, \dots, f_{p_1, p_2, p_3, N-1}\} \quad (19.112)$$

carries the spectral information of the 3-D sequence  $f$  at frequency-points of  $T_{p_1, p_2, p_3}$ . The complete set of the splitting-signals  $f_T$ ,  $T \in \sigma$ , is the tensor representation of the sequence  $f$  with respect to the 3-D DHT. With respect to the 3-D Fourier transform, the sequence  $f$  has the same tensor representation, as is mentioned in 19.5.5. The components of splitting-signals are calculated by linear integrals

$$f_{p_1, p_2, p_3, t} = \sum_{V_{p_1, p_2, p_3, t}} f_{n_1, n_2, n_3}, \quad t = 0: (N-1), \quad (19.113)$$

along the parallel hyperplanes lying in the sets

$$V_{p_1, p_2, p_3, t} = \{(n_1, n_2, n_3); \overline{n_1 p_1 + n_2 p_2 + n_3 p_3} = t\}. \quad (19.114)$$

Indeed, each set  $V_{p_1, p_2, p_3, t}$ , if it is not empty, is the set of spatial points  $(n_1, n_2, n_3)$  along parallel hyperplanes:

$$\left. \begin{aligned} x p_1 + y p_2 + z p_3 &= t \\ x p_1 + y p_2 + z p_3 &= t + N \\ \dots &\dots \\ x p_1 + y p_2 + z p_3 &= t + (p_1 + p_2 + p_3 - 1)N \end{aligned} \right\} \quad (19.115)$$

in the cube  $[0, N] \times [0, N] \times [0, N]$ .

The number of 1-D DHTs splitting the 3-D DHT equals to the number of generators of the cyclic groups of the irreducible covering  $\sigma_J$  of the lattice  $X$ . The set of these generators can be constructed for any order of the transform, and we stand here on examples, when  $N = 4$  and 8.

**Example 19.12**

We consider the lattice  $4 \times 4 \times 4$  and the following 3-D image

$$f = \begin{array}{c|c|c|c} n_3 = 0 & n_3 = 1 & n_3 = 2 & n_3 = 3 \\ \hline \begin{array}{cccc} \underline{1} & 2 & 3 & 1 \\ 1 & 0 & 1 & 2 \\ 2 & 1 & 2 & 1 \\ 3 & 2 & 1 & 2 \end{array} & \begin{array}{cccc} 2 & 2 & 1 & 5 \\ 4 & 3 & 3 & 1 \\ 1 & 2 & 4 & 4 \\ 5 & 1 & 3 & 1 \end{array} & \begin{array}{cccc} 3 & 1 & 2 & 1 \\ 1 & 2 & 1 & 6 \\ 3 & 2 & 4 & 1 \\ 4 & 5 & 2 & 4 \end{array} & \begin{array}{cccc} 1 & 2 & 2 & 3 \\ 1 & 2 & 3 & 3 \\ 1 & 1 & 4 & 4 \\ 1 & 5 & 5 & 4 \end{array} \end{array}$$

which is presented separately by four 2-D matrices in planes  $n_3 = 0, 1, 2,$  and  $3$ . The value of  $f_{0,0,0} = 1$  is underlined.

Let the generator be  $(p_1, p_2, p_3) = (2, 1, 1)$ . All values of the time variable  $t$  in the Diophantus form  $n_1 p_1 + n_2 p_2 + n_3 p_3 = t \pmod{N}$  can be written in the form of the following four matrices  $4 \times 4$  that compose a 3-D matrix  $4 \times 4 \times 4$ :

$$\|t = (n_1 \cdot 2 + n_2 \cdot 1 + n_3 \cdot 1) \pmod{4}\|_{n_3, n_2, n_1=0:3} = \begin{array}{c|c|c|c} n_3 = 0 & n_3 = 1 & n_3 = 2 & n_3 = 3 \\ \hline \begin{array}{cccc} \underline{0} & 1 & 2 & 3 \\ 2 & 3 & 0 & 1 \\ 0 & 1 & 2 & 3 \\ 2 & 3 & 0 & 1 \end{array} & \begin{array}{cccc} 1 & 2 & 3 & 0 \\ 3 & 0 & 1 & 2 \\ 1 & 2 & 3 & 0 \\ 3 & 0 & 1 & 2 \end{array} & \begin{array}{cccc} 2 & 3 & 0 & 1 \\ 0 & 1 & 2 & 3 \\ 2 & 3 & 0 & 1 \\ 0 & 1 & 2 & 3 \end{array} & \begin{array}{cccc} 3 & 0 & 1 & 2 \\ 1 & 2 & 3 & 0 \\ 3 & 0 & 1 & 2 \\ 1 & 2 & 3 & 0 \end{array} \end{array}$$

Therefore, the image-signal  $f_{T_{2,1,1}}$  of  $f$  is defined as follows:

$$f_{2,1,1,0} = \sum \begin{cases} f_{0,0,0} + f_{1,2,0} + f_{2,0,0} + f_{3,2,0} = 1 + 1 + 2 + 1 = 5 \\ f_{0,3,1} + f_{1,1,1} + f_{2,3,1} + f_{3,1,1} = 5 + 3 + 4 + 1 = 13 \\ f_{0,2,2} + f_{1,0,2} + f_{2,2,2} + f_{3,0,2} = 2 + 1 + 4 + 4 = 11 \\ f_{0,1,3} + f_{1,3,3} + f_{2,1,3} + f_{3,3,3} = 2 + 3 + 1 + 4 = 10 \end{cases} = 39$$

$$f_{2,1,1,1} = \sum \begin{cases} f_{0,1,0} + f_{1,3,0} + f_{2,1,0} + f_{3,3,0} = 2 + 2 + 1 + 2 = 7 \\ f_{0,0,1} + f_{1,2,1} + f_{2,0,1} + f_{3,2,1} = 2 + 3 + 1 + 3 = 9 \\ f_{0,3,2} + f_{1,1,2} + f_{2,3,2} + f_{3,1,2} = 1 + 2 + 1 + 5 = 9 \\ f_{0,2,3} + f_{1,0,3} + f_{2,2,3} + f_{3,0,3} = 2 + 1 + 4 + 1 = 8 \end{cases} = 33$$

$$f_{2,1,1,2} = \sum \begin{cases} f_{0,2,0} + f_{1,0,0} + f_{2,2,0} + f_{3,0,0} = 3 + 1 + 2 + 3 = 9 \\ f_{0,1,1} + f_{1,3,1} + f_{2,1,1} + f_{3,3,1} = 2 + 1 + 2 + 1 = 6 \\ f_{0,0,2} + f_{1,2,2} + f_{2,0,2} + f_{3,2,2} = 3 + 1 + 3 + 2 = 9 \\ f_{0,3,3} + f_{1,1,3} + f_{2,3,3} + f_{3,1,3} = 3 + 2 + 4 + 5 = 14 \end{cases} = 38$$

$$f_{2,1,1,3} = \sum \begin{cases} f_{0,3,0} + f_{1,1,0} + f_{2,3,0} + f_{3,1,0} = 1 + 0 + 1 + 2 = 4 \\ f_{0,2,1} + f_{1,0,1} + f_{2,2,1} + f_{3,0,1} = 1 + 4 + 4 + 5 = 14 \\ f_{0,1,2} + f_{1,3,2} + f_{2,1,2} + f_{3,3,2} = 1 + 6 + 2 + 4 = 13 \\ f_{0,0,3} + f_{1,2,3} + f_{2,0,3} + f_{3,2,3} = 1 + 3 + 1 + 5 = 10 \end{cases} = 41$$

Thus  $f_{T_{2,1,1}} = \{39, 33, 38, 41\}$  and the 4-point DHT of this splitting-signal is calculated by

$$\begin{bmatrix} H_0 \\ H_1 \\ H_2 \\ H_3 \end{bmatrix} = \begin{bmatrix} 1 & 1 & 1 & 1 \\ 1 & 1 & -1 & -1 \\ 1 & -1 & 1 & -1 \\ 1 & -1 & -1 & 1 \end{bmatrix} \begin{bmatrix} 39 \\ 33 \\ 38 \\ 41 \end{bmatrix} = \begin{bmatrix} 151 \\ -7 \\ 3 \\ 9 \end{bmatrix}$$

This transform coincides with the 3-D DHT of  $f$  at the following frequency-points of the group  $T_{2,1,1} : (0, 0, 0), (2, 1, 1), (0, 2, 2),$  and  $(2, 3, 3)$ , as shown below

$$[\mathcal{H}_{4,4,4} \circ f] = \begin{array}{c|c|c|c} p_3 = 0 & p_3 = 1 & p_3 = 2 & p_3 = 3 \\ \hline \begin{array}{cccc} \underline{151} & \circ & \circ & \circ \\ \circ & \circ & \circ & \circ \\ \circ & \circ & \circ & \circ \\ \circ & \circ & \circ & \circ \end{array} & \begin{array}{cccc} \circ & \circ & \circ & \circ \\ \circ & \circ & \circ & \circ \\ \circ & -7 & \circ & \circ \\ \circ & \circ & \circ & \circ \end{array} & \begin{array}{cccc} \circ & \circ & 3 & \circ \\ \circ & \circ & \circ & \circ \\ \circ & \circ & \circ & \circ \\ \circ & \circ & \circ & \circ \end{array} & \begin{array}{cccc} \circ & \circ & \circ & \circ \\ \circ & \circ & \circ & \circ \\ \circ & \circ & \circ & 9 \\ \circ & \circ & \circ & \circ \end{array} \end{array}$$

We can construct similarly other splitting-signals and fill the 3-D DHT by the 1-D DHTs of these signals. For, instance, when the generator is  $(1, 1, 1)$ , we obtain the splitting-signal  $f_{T_{1,1,1}} = \{45, 30, 46, 30\}$  and its 4-point DHT equals

$$\begin{bmatrix} 151 \\ -1 \\ 31 \\ -1 \end{bmatrix} = \begin{bmatrix} 1 & 1 & 1 & 1 \\ 1 & 1 & -1 & -1 \\ 1 & -1 & 1 & -1 \\ 1 & -1 & -1 & 1 \end{bmatrix} \begin{bmatrix} 45 \\ 30 \\ 46 \\ 30 \end{bmatrix}$$

This transform coincides with the 3-D DHT at the frequency-points of the group  $T_{1,1,1}$ , i.e.,  $(0, 0, 0), (1, 1, 1), (2, 2, 2),$  and  $(3, 3, 3)$ . The first value, 151, has been already calculated in the previous step. We can fill other three values of the 3-D DHT as follows:

$$[\mathcal{H}_{4,4,4} \circ f] = \begin{array}{c|c|c|c} p_3 = 0 & p_3 = 1 & p_3 = 2 & p_3 = 3 \\ \hline \begin{array}{cccc} \underline{151} & \circ & \circ & \circ \\ \circ & \circ & \circ & \circ \\ \circ & \circ & \circ & \circ \\ \circ & \circ & \circ & \circ \end{array} & \begin{array}{cccc} \circ & \circ & \circ & \circ \\ \circ & -1 & \circ & \circ \\ \circ & -7 & \circ & \circ \\ \circ & \circ & \circ & \circ \end{array} & \begin{array}{cccc} \circ & \circ & 3 & \circ \\ \circ & \circ & \circ & \circ \\ \circ & \circ & 31 & \circ \\ \circ & \circ & \circ & \circ \end{array} & \begin{array}{cccc} \circ & \circ & \circ & \circ \\ \circ & \circ & \circ & \circ \\ \circ & \circ & \circ & 9 \\ \circ & \circ & \circ & -1 \end{array} \end{array}$$

We consider also the generator  $(1, 2, 0)$ , for which the splitting-signal and its Hartley transform are defined as follows:

$$f_{T_{1,2,0}} = \{31, 39, 38, 43\} \rightarrow \mathcal{H}_4 \circ f_{T_{1,2,0}} = \{151, -11, -13, -3\}.$$

As a result, we define other three components the 3-D DHT at the frequency-points of the group  $T_{1,2,0}$ , namely, at  $(1, 2, 0), (2, 0, 0),$  and  $(3, 2, 0)$ , as shown:

$$[\mathcal{H}_{4,4,4} \circ f] = \begin{array}{c|c|c|c} p_3 = 0 & p_3 = 1 & p_3 = 2 & p_3 = 3 \\ \hline \begin{array}{cccc} \underline{151} & \circ & \circ & \circ \\ \circ & \circ & -11 & \circ \\ -13 & \circ & \circ & \circ \\ \circ & \circ & -3 & \circ \end{array} & \begin{array}{cccc} \circ & \circ & \circ & \circ \\ \circ & -1 & \circ & \circ \\ \circ & -7 & \circ & \circ \\ \circ & \circ & \circ & \circ \end{array} & \begin{array}{cccc} \circ & \circ & 3 & \circ \\ \circ & \circ & \circ & \circ \\ \circ & \circ & 31 & \circ \\ \circ & \circ & \circ & \circ \end{array} & \begin{array}{cccc} \circ & \circ & \circ & \circ \\ \circ & \circ & \circ & \circ \\ \circ & \circ & \circ & 9 \\ \circ & \circ & \circ & -1 \end{array} \end{array}$$

To calculate all values of the 3-D DHT, we need cover the 3-D lattice  $4 \times 4 \times 4$  by cyclic groups  $T_{p_1, p_2, p_3}$ . No more than 28 generators are required for such a covering  $\sigma_j$ , and they can be taken from the following set:

$$J = \{(p, 1, z); p, z = 0: 3\} \cup \{(1, 2s, z); z = 0: 3, s = 0, 1\} \\ \cup \{(0, 2, 1), (2, 2, 1), (2, 0, 1), (0, 0, 1)\}.$$

Therefore, the  $4 \times 4 \times 4$ -point DHT can be calculated by 28 four-point DHTs.

**Example 19.13**

The number of 8-point DHTs required for calculation of the  $8 \times 8 \times 8$ -point DHT by using the tensor representation is equal to the minimum number of cyclic groups  $T_{p_1, p_2, p_3}$  covering the 3-D lattice  $8 \times 8 \times 8$ . The generators  $(p_1, p_2, p_3)$  of these groups can be defined from the following set of 112 triplets:

$$J = \{(p, 1, z); p, z = 0: 7\} \cup \{(1, 2s, z); z = 0: 7, s = 0: 3\} \cup \\ \cup \{(2p, 2, z); z = 1, 3, p = 0: 3\} \cup \{(2, 4s, z); z = 1, 3, s = 0, 1\} \cup \\ \cup \{(0, 4, 1), (4, 4, 1), (4, 0, 1), (0, 0, 1)\}.$$

Thus, from the perspective of the tensor representation, the  $8 \times 8 \times 8$ -DHT is calculated by 112 8-point DHTs.

It should be noted, that the 3-D DHT under the consideration is not separable, but it can be expressed through the separable 3-D DFT. Indeed, the kernel of the Harley transform is the sum of real and imaginary parts of the exponential kernel of the Fourier transform,

$$\text{cas}(t) = \cos(t) + \sin(t) = \text{Re}(e^{-jt}) - \text{Im}(e^{-jt}).$$

Therefore, the following relation holds:

$$H_{p_1, p_2, p_3} = \text{Re}(F_{p_1, p_2, p_3}) - \text{Im}(F_{p_1, p_2, p_3}). \quad (19.116)$$

The 3-D DFT of order  $8 \times 8 \times 8$  has the splitting similar to the Hartley transform, and it is calculated by 112 eight-point DFTs. For comparison, we consider the column-row approach for calculating the 3-D DFT, which is based on the expression

$$F_{p_1, p_2, p_3} = \sum_{n_3=0}^7 \left( \sum_{n_2=0}^7 \sum_{n_1=0}^7 f_{n_1, n_2, n_3} W^{n_1 p_1 + n_2 p_2} \right) W^{n_3 p_3},$$

where  $W = \exp(-2\pi j/8)$ . In this approach, eight  $8 \times 8$ -point DFTs are calculated first, and then 64 eight-point DFTs along the third dimension  $n_3$ . Totally,  $8(2 \cdot 8) + 64 = 3 \cdot 64 = 192$  eight-point DFTs are used, or 80 eight-point DFTs more than the tensor transform method uses. When using the row-column approach to the 3-D DFT of the order  $N \times N \times N$ , as in the above  $N = 8$  case, all  $N$ -point DFTs in calculations have complex input data, except the first  $N$  transforms in each  $(n_1, n_2)$ -plane, if the 3-D sequence  $f$  is real. However, all 1-D DFTs in the tensor algorithm are performed over the real splitting-signals, when  $f$  is real.

In the general case when  $N = 2^r$ ,  $r \geq 1$ , we can construct the irreducible covering  $\sigma_J$  of the 3-D lattice  $X_{2^r, 2^r, 2^r}$  by using the following set of  $7 \cdot 4^{r-1}$  generators:

$$J = \bigcup_{z=0}^{2^r-1} \{ \{(1, s, z); s = 0: 2^r - 1\} \cup \{(2p, 1, z); p = 0: 2^{r-1} - 1\} \} \\ \bigcup_{k=1}^{r-1} \bigcup_{z=1}^{2^{r-k}-1} \{ \{(2^k, 2^k s, 2^k z + 1); s = 0: 2^{r-k} - 1\}, \\ \{(2^{k+1} p, 2^k, 2^k z + 1); p = 0: 2^{r-k-1} - 1\} \} \cup \{(0, 0, 1)\}. \quad (19.117)$$

Therefore, the  $2^r \times 2^r \times 2^r$ -point DHT (or DFT) can be split by  $4^{r-1} \cdot 7$  1-D  $2^r$ -point DHTs (or DFTs). To estimate the total number of multiplications required to calculate the  $2^r \times 2^r \times 2^r$ -point DHT, we use the following estimate for the  $2^r$ -point DHT:

$$m_{2^r} = 2^{r-1}(r - 3) + 2 \quad (r \geq 3). \quad (19.118)$$

The 3-D DHT by the tensor transform uses operations of multiplication in the number

$$m_{2^r, 2^r, 2^r} = 7 \cdot 4^{r-1} m_{2^r} = 7[8^{r-1}(r - 3) + 2 \cdot 4^{r-1}]. \quad (19.119)$$

For the comparison, Table 19.3 shows the number of multiplications required by the column-row approach based on the radix-2 algorithm [31,32], the radix-2  $\times 2 \times 2$  algorithm [33], and the tensor algorithm, for calculating the  $2^r \times 2^r \times 2^r$ -point DHT when  $r = 7 : 12$ . In the radix-2  $\times 2 \times 2$  algorithm, the 3-D DHT is divided into eight  $2^{r-1} \times 2^{r-1} \times 2^{r-1}$ -point DHTs, and the process of division is similarly repeated  $(r - 2)$  times, until we receive the transforms of order  $2 \times 2 \times 2$ .

**19.6.2 n-Dimensional DHT**

The tensor transform of an  $n$ -dimensional sequence  $f$  defines the splitting-signals in the number which is determined by the covering  $\sigma_J$  of the lattice  $X$ . In the 2-D case, the square lattice  $X_{2^r, 2^r}$  is covered by  $3 \cdot 2^{r-1}$  cyclic groups  $T$ . In the 3-D case, the cubic lattice  $X_{2^r, 2^r, 2^r}$  is covered by  $7 \cdot 4^{r-1}$  groups  $T$ .

**TABLE 19.3** The Number of Multiplications per Sample, Which Are Required to Calculate the  $2^r \times 2^r \times 2^r$ -Point DHT by the Column-Row Radix-2 Algorithm (C-R), Radix-2  $\times 2 \times 2$  Algorithm, and the Tensor Algorithm (T)

$r$	C-R Radix-2	Radix-2 $\times 2 \times 2$	T
7	10.64	6.20	3.53
8	13.57	7.91	4.39
9	16.53	9.64	5.26
10	19.51	11.38	6.13
11	20.50	13.13	7.00
12	25.50	14.87	7.88

In the general  $n \geq 2$  case, the  $n$ -dimensional  $2^r \times 2^r \times \dots \times 2^r$ -point DHT is split by 1-D DHTs in the number equal to the cardinality of the covering  $\sigma_J$  which is calculated by

$$\text{card}\sigma_J = (2^n - 1)2^{(r-1)(n-1)}. \quad (19.120)$$

The number of multiplications required for computing the transform can be estimated thus by

$$m_{2^r, 2^r, \dots, 2^r} = (2^n - 1)2^{(r-1)(n-1)} [2^{r-1}(r-3) + 2]. \quad (19.121)$$

This number can be reduced, when removing repeated calculation of spectral components. For instance, in the 3-D case, we can remove the repeated calculations for all components at frequency-points  $2^k(p_1, p_2, p_3)$ , for  $k=1 : (r-1)$ . The number of these reiterations equals

$$\Delta = (7 \cdot 4^{r-1})2^r - 8^r = (3/4)8^r$$

which is a quite big value. To remove them, we consider the following partition of the set complement of all frequency-points with even coordinates

$$\sigma^1 = (T_{p_1, p_2, p_3} \setminus T_{2p_1, 2p_2, 2p_3}; (p_1, p_2, p_3) \in J).$$

Each cyclic group  $T$  in the covering  $\sigma$  is divided by two parts of frequency-points with all even and not all even coordinates. Each part consists of  $2^{r-1}$  points. Therefore, we can obtain the recurrent algorithm for computing  $\mathcal{H}_{2^r, 2^r, 2^r}$  via  $\mathcal{H}_{2^{r-1}, 2^{r-1}, 2^{r-1}}$  and  $7 \cdot 4^{r-1}$  incomplete 1-D  $2^r$ -point DHTs, which we denote by  $\mathcal{H}_{N;2}$  and for which only components with odd numbers are calculated. Each such incomplete transform can be reduced to  $2^{r-1}$ -point DHT. Herewith, for computing 3-D DHT, the number of real multiplications can be calculated by the following recurrent formula:

$$m'_{2^r, 2^r, 2^r} = m'_{2^{r-1}, 2^{r-1}, 2^{r-1}} + 7 \cdot 4^{r-1}(m_{2^r} - m_{2^{r-1}}) \leq 35 \cdot 8^{r-3}r, \quad (m_{8,8,8} = 214). \quad (19.122)$$

The reduction of multiplications in Equation 19.119 forms the 5/8 of all multiplications.

## 19.7 2-D Shifted DFT

In this section, tensor algorithms for calculating the two-dimensional DCT are described. We analyze the multiplicative complexity of the  $N \times N$ -point 2-D DCT, for cases of the most interest, when  $N = L^r$ , where  $L$  is a general prime number and  $r \geq 1$ , and  $N = L_1 L_2$ , where  $L_1$  and  $L_2$  are arbitrary coprime numbers. The tensor algorithm and its modification are described in detail for the  $8 \times 8$  and  $15 \times 15$  cases.

We first move on to the study of the tensor representation of the 2-D shifted discrete Fourier transform (SDFT) [34], which is applied to 2-D sequences defined on the 2-D lattice  $Y_{N,N}$  which

is the square lattice  $X_{N,N}$  shifted in the 2-D plane by the vector  $(1/2, 1/2)$ . The frequency-points of the transform are considered on the square lattice  $X$ . For simplicity of indexing, we denote points  $(n_1 + 1/2, n_2 + 1/2)$  of the lattice  $Y$  by  $(n_1, n_2)$ , as well as samples  $f_{n_1+1/2, n_2+1/2}$  of a sequence defined on  $Y$  by  $f_{n_1, n_2}$ .

The components of the 2-D SDFT,  $\mathcal{F}_{N,N}^s$ , of a 2-D sequence  $f = f_{n_1, n_2}$  are defined by

$$F_{p_1, p_2}^s = (\mathcal{F}_{N,N}^s \circ f)_{p_1, p_2} = \sum_{n_1=0}^{N-1} \sum_{n_2=0}^{N-1} f_{n_1, n_2} W^{(n_1 + \frac{1}{2})p_1 + (n_2 + \frac{1}{2})p_2}, \quad p_1, p_2 = 0: (N-1), \quad (19.123)$$

where  $W = \exp(-j2\pi/N)$ . The transform is periodic, but its fundamental period is the lattice  $X_{2N, 2N}$ , not  $X_{N,N}$ . The following properties are valid for this transform:

$$F_{N+p_1, p_2}^s = F_{p_1, N+p_2}^s = -F_{p_1, p_2}^s, F_{N+p_1, N+p_2}^s = F_{p_1, p_2}^s, \quad (19.124)$$

where  $p_1, p_2 = 0 : (N/2 - 1)$ . Therefore, it is enough to perform the calculations for the transform only at frequency-points of one-fourth of the lattice  $X_{2N, 2N}$ , i.e., in  $X_{N,N}$ . If  $f$  is real, then the following properties of complex conjugacy hold:

$$F_{N-p_1, p_2}^s = \overline{F_{p_1, N-p_2}^s}, F_{N-p_1, N-p_2}^s = \overline{F_{p_1, p_2}^s}, p_1, p_2 = 1: (N/2 - 1). \quad (19.125)$$

It follows directly from the definition, that the 2-D SDFT can be expressed through the 2-D DFT as

$$F_{p_1, p_2}^s = W^{\frac{j}{2}(p_1 + p_2)} F_{p_1, p_2}, p_1, p_2 = 0: (N-1). \quad (19.126)$$

Thus, in order to obtain the table of all values of the 2-D SDFT, the table of values of the 2-D DFT is multiplied point-wise by the table of  $(2N-1)$  twiddle coefficients  $W^{\frac{j}{2}t}$ ,  $t = 0: (2N-1)$ . For instance, for  $N=4$ , we have

$$\left[ W^{\frac{j}{2}(p_1 + p_2)} \right]_{p_1, p_2 = 0:3} = \begin{bmatrix} 1 & W^{\frac{1}{2}} & W^1 & W^{\frac{3}{2}} \\ W^{\frac{1}{2}} & W^1 & W^{\frac{3}{2}} & W^2 \\ W^1 & W^{\frac{3}{2}} & W^2 & W^{\frac{5}{2}} \\ W^{\frac{3}{2}} & W^2 & W^{\frac{5}{2}} & W^3 \end{bmatrix},$$

where  $W = W_4 = \exp(-2\pi j/4) = -j$ . The splitting-signals defined for the 2-D DFT can be applied to split the shifted 2-D DFT by cyclic groups  $T_{p,s}$  of the covering  $\sigma_J$  of the lattice  $X_{N,N}$ . The application can be described by the following three steps:

$$f_{n_1, n_2} \rightarrow f_{T_{p,s}} \rightarrow [F_k = (\mathcal{F} \circ f_{T_{p,s}})_k] \rightarrow [F_{kp, ks}^s = W^{\frac{j}{2}(p+s)k} F_k], \quad k = 0: (N-1), \quad (19.127)$$

which are performed for each generator  $(p, s)$  of the set  $J$ . Subscripts  $kp$  and  $ks$  are taken modulo  $2N$ . However, we can note that, if  $kp \bmod 2N = N + p_0$  and  $p_0 < N$ , then  $p_0 = kp \bmod N$  and the following is valid:  $F_{kp, ks}^s = F_{N+p_0, ks}^s = -F_{p_0, ks}^s$ , and if

$ks \bmod 2N = N + s_0$  and  $s_0 < N$ , then  $s_0 = ks \bmod N$  and  $F_{kp, ks}^s = F_{kp, N+s_0}^s = -F_{kp, s_0}^s$ . In addition,  $F_{kp, ks}^s = F_{N+p_0, N+s_0}^s = F_{p_1, s_0}^s$ . This is why, we can consider subscripts  $kp$  and  $ks$  by modulo  $N$ , and

$$F_{kp \bmod 2N, ks \bmod 2N}^s = \pm F_{kp \bmod N, ks \bmod N}^s, \quad k = 0: (N-1). \quad (19.128)$$

We also can define the concept of the tensor representation of  $f$  with respect to the 2-D SDFT, by using a method different from what is given in Equation 19.127. In the kernel of this transform, the relation between the spacial points and frequency-points is described by the nonlinear form

$$\mathcal{L}(n_1, n_2; p_1, p_2) = \left(n_1 + \frac{1}{2}\right)p_1 + \left(n_2 + \frac{1}{2}\right)p_2 = (n_1 p_1 + n_2 p_2) + \frac{1}{2}(p_1 + p_2),$$

and in arithmetic modulo  $N$  it takes integer values as well as mixed numbers with the fraction  $1/2$ . Therefore complex coefficients of the kernel lie on the  $N$  or  $2N$  equidistant points on the unit circle. The number of these points depends on the evenness of coordinates  $p_1$  and  $p_2$ .

For a given frequency-point  $(p_1, p_2)$ , we define the following sets of points

$$\tilde{V}_{p_1, p_2, t} = \{(n_1, n_2); \mathcal{L}(n_1, n_2; p_1, p_2) = t \bmod N\} \quad (19.129)$$

and components

$$\tilde{f}_{p_1, p_2, t} = \sum_{\tilde{V}_{p_1, p_2, t}} f_{n_1, n_2}, \quad t \in [0, N-1], \quad (19.130)$$

which allow for writing Equation 19.123 as

$$F_{kp_1, kp_2}^s = \sum_{t=1-\Delta t}^{N-\Delta t} \tilde{f}_{p_1, p_2, t} W^{kt}. \quad (19.131)$$

The number  $t$  in Equations 19.129 through 19.131 runs the interval  $[0, N-1]$  with the step  $\Delta t = 1$  or  $1/2$ , depending on the evenness of coordinates of the frequency-point  $(p_1, p_2)$ . For instance, if both the coordinates are simultaneously even or odd, then  $\Delta t = 1$  and the variable  $t$  takes only integer values in the interval  $[0, N-1]$ . If the evenness of the coordinates of the frequency-point  $(p_1, p_2)$  are different, then all numbers  $t$  in the above formulas have the fraction  $\Delta t = 1/2$ . We write the fact of equal evenness by  $e(p_1, p_2) = 0$ , and  $e(p_1, p_2) = 1$ , if the evenness of coordinates are different.

The following general formula is valid:

$$F_{kp_1, kp_2}^s = \sum_{t=1-\Delta t}^{N-\Delta t} \tilde{f}_{p_1, p_2, t} W^{kt}, \quad k = 0: (N-1). \quad (19.132)$$

This property is used in the tensor algorithm of the 2-D SDFT. Let  $\sigma_J$  be an irreducible covering of the lattice  $X_{N,N}$ , which is

composed by cyclic groups  $T_{p_1, p_2}$ . The spectral information of  $f$  at frequency-points of a group  $T_{p_1, p_2} \in \sigma_J$  is determined by the following splitting-signal:

$$\tilde{f}_{T_{p_1, p_2}} = \left(\tilde{f}_{p_1, p_2, 1-\Delta t}, \tilde{f}_{p_1, p_2, 2-\Delta t}, \dots, \tilde{f}_{p_1, p_2, N-\Delta t}\right). \quad (19.133)$$

Indeed, depending on the evenness of  $p_1$  and  $p_2$ , the expression in Equation 19.132 can be rewritten as follows:

$$F_{kp_1, kp_2}^s = \sum_{t=0}^{N-1} \tilde{f}_{p_1, p_2, t} W^{kt}, \quad \text{if } e(p_1, p_2) = 0, \quad (19.134)$$

$$F_{kp_1, kp_2}^s = W^{\frac{k}{2}} \sum_{t=0}^{N-1} \tilde{f}_{p_1, p_2, t+\frac{1}{2}} W^{kt}, \quad \text{if } e(p_1, p_2) = 1, \quad (19.135)$$

where  $k = 0 : (N-1)$ . The 2-D SDFT of  $f$  at the group  $T_{p_1, p_2}$  coincides with the 1-D DFT of the splitting-signal, if  $p_1$  and  $p_2$  have the same evenness, otherwise it coincides with the modified 1-D DFT. This property can be written shortly as

$$(\mathcal{F}_{N,N}^s[f])|_{T_{p_1, p_2}} = \begin{cases} \mathcal{F}_N[\tilde{f}_{T_{p_1, p_2}}], & e(p_1, p_2) = 0; \\ (\varepsilon_N \circ \mathcal{F}_N)[\tilde{f}_{T_{p_1, p_2}}], & e(p_1, p_2) = 1; \end{cases} \quad (19.136)$$

where  $\varepsilon_N$  is the  $N$ -point DT with the diagonal matrix

$$[\varepsilon_N] = \text{diag}\left(1, W^{\frac{1}{2}}, W^1, W^{\frac{3}{2}}, W^2, \dots, W^{\frac{N-1}{2}}, W^{\frac{N-1}{2}}\right). \quad (19.137)$$

Thus, we split the 2-D SDFT and this splitting set which we denote by  $\mathcal{R}(\mathcal{F}_{N,N}^s; \sigma_J)$  consists of the  $N$ -point transforms  $\mathcal{F}_N$  and  $\varepsilon_N \circ \mathcal{F}_N$ . We remind for comparison, that the splitting of the 2-D DFT by the covering  $\sigma_J$  consists only of the transforms  $\mathcal{F}_N$ . The representation of the 2-D sequence  $f$  as a set of splitting-signals  $\{\tilde{f}_T; T \in \sigma_J\}$  is called the tensor representation of  $f$  with respect to the 2-D SDFT, and the transformation  $f \rightarrow \{\tilde{f}_T; T \in \sigma_J\}$  is the tensor transformation.

### Example 19.14

We consider the  $N=8$  case. The irreducible covering  $\sigma_J$  of the lattice  $X_{8,8}$  consists of 12 cyclic groups whose generators  $(p, s)$  can be taken from the set  $J = \{(0, 1), (1, 1), (2, 1), \dots, (7, 1), (1, 0), (1, 2), (1, 4), (1, 6)\}$ . Four generators  $(p, s)$ , which are  $(1, 1), (3, 1), (5, 1)$ , and  $(7, 1)$ , have the same evenness, and the remaining eight generators have different evenness. Therefore, the  $8 \times 8$ -point SDFT is split into four 8-point DFTs,  $\mathcal{F}_8$ , and eight compositions of the 8-point Fourier transform and scalar transform  $\varepsilon_8$ , i.e.,

$$\mathcal{R}(\mathcal{F}_{8,8}^s; \sigma_J) = \left\{ \mathcal{F}_8, \mathcal{F}_8, \mathcal{F}_8, \mathcal{F}_8, \underbrace{\varepsilon_8 \circ \mathcal{F}_8, \dots, \varepsilon_8 \circ \mathcal{F}_8}_{8 \text{ times}} \right\}.$$

It is important to note, that the tensor representation of the shifted 2-D DFT can be derived directly from the tensor representation of the 2-D DFT. Indeed, the following relation is valid:

$$\tilde{V}_{p,s,t} = V_{p,s,(t-t_0) \bmod N}, \quad t_0 = (p+s)/2. \quad (19.138)$$

If  $e(p, s) = 0$ , the subscript  $t - t_0$  takes only integer values, and therefore  $\tilde{f}_{p,s,t} = f_{p,s,t-t_0 \bmod N}$ . If  $e(p, s) = 1$ , then the similar cyclic shift can be performed over the splitting-signal  $f_{T_{p,s}}$ , to obtain the signal  $\tilde{f}_{T_{p,s}}$ , namely, the cyclic shift by  $t_0 = \lfloor (p+s)/2 \rfloor$  elements to the right. We here denote by  $\lfloor x \rfloor$  the floor function, i.e., the greatest integer  $\leq x$ . For instance, in the considered  $8 \times 8$  case, the cyclic shifting for the generators (1, 1), (2, 1), and (3, 1) are performed by  $t_0 = 1, 1$ , and 2, respectively. Therefore, the following relations hold between the splitting-signals of these generators:

$$\begin{aligned} f_{T_{1,1}} &= (f_{1,1,0}, f_{1,1,1}, f_{1,1,2}, f_{1,1,3}, f_{1,1,4}, f_{1,1,5}, f_{1,1,6}, f_{1,1,7}) \\ \tilde{f}_{T_{1,1}} &= (f_{1,1,7}, f_{1,1,0}, f_{1,1,1}, f_{1,1,2}, f_{1,1,3}, f_{1,1,4}, f_{1,1,5}, f_{1,1,6}) \\ f_{T_{2,1}} &= (f_{2,1,0}, f_{2,1,1}, f_{2,1,2}, f_{2,1,3}, f_{2,1,4}, f_{2,1,5}, f_{2,1,6}, f_{2,1,7}) \\ \tilde{f}_{T_{2,1}} &= (f_{2,1,7}, f_{2,1,0}, f_{2,1,1}, f_{2,1,2}, f_{2,1,3}, f_{2,1,4}, f_{2,1,5}, f_{2,1,6}) \\ f_{T_{3,1}} &= (f_{3,1,0}, f_{3,1,1}, f_{3,1,2}, f_{3,1,3}, f_{3,1,4}, f_{3,1,5}, f_{3,1,6}, f_{3,1,7}) \\ \tilde{f}_{T_{3,1}} &= (f_{3,1,6}, f_{3,1,7}, f_{3,1,0}, f_{3,1,1}, f_{3,1,2}, f_{3,1,3}, f_{3,1,4}, f_{3,1,5}) \end{aligned}$$

Taking into consideration this property, we can write the expressions in Equations 19.134 and 19.135 respectively as follows:

$$F_{kp_1, kp_2}^s = \sum_{t=0}^{N-1} f_{p_1, p_2, t - \frac{t_1 + p_2}{2} \bmod N} W^{kt}, \quad (19.139)$$

$$F_{kp_1, kp_2}^s = W^{\frac{k}{2}} \sum_{t=0}^{N-1} f_{p_1, p_2, t - \lfloor \frac{p_1 + p_2}{2} \rfloor \bmod N} W^{kt}, \quad k = 0 : (N-1). \quad (19.140)$$

We now estimate the number of real multiplications used in the  $8 \times 8$ -point SDFT. When  $f$  is real, all splitting-signals are real, too. For each 8-point DFT,  $(F_0, F_1, \dots, F_7)$ , in Equation 19.140, it is enough to calculate only the first 5 components. For instance,  $F_5$  and  $F_3$  are complex conjugates, i.e.,  $F_5 = \overline{F_3}$  and  $W_8^{5/2} = W_{16}^5 = -\overline{W_{16}^3} = -\overline{W_8^{3/2}}$ . Therefore,  $W_8^{5/2} F_5 = -\overline{W_8^{3/2} F_3}$ . Two other equalities are  $W_8^{6/2} F_6 = -\overline{W_8^{2/2} F_2}$  and  $W_8^{7/2} F_7 = -\overline{W_8^{1/2} F_1}$ . The twiddle coefficients  $W_8^{k/2} = W_{16}^k$ , when  $k = 0 : 4$ , equal to 1,  $0.9239 - 0.3827j$ ,  $0.7071(1-j)$ ,  $0.3827 - 0.9239j$ , and  $-j$ , respectively. Multiplications of a complex number by  $0.7071(1-j)$  required two real multiplications. We consider that for each multiplications by  $W^{1/2}$  and  $W^{3/2}$  four real multiplications are used. Denoting by  $m_{8,8}^s$  and  $m_{8,8}$  respectively the numbers of multiplications required to calculate the  $8 \times 8$ -point SDFT and DFT by the corresponding splitting-signals  $\tilde{f}_T$  and  $f_T$ ,  $T \in \sigma_j$ , we obtain the following relation between these estimates:

$$\begin{aligned} m_{8,8}^s &= 4m_8 + [8(m_8 + (4 + 4 + 2))] = 12m_8 + 80 \\ &= m_{8,8} + 80 = 12 \cdot 2 + 80 = 104, \end{aligned} \quad (19.141)$$

since the 8-point DFT requires two multiplications and  $m_{8,8} = 12m_8 = 24$ .

### 19.7.1 $2^r \times 2^r$ -Point SDFT

In the general  $2^r \times 2^r$  case, when  $r > 2$ , the covering  $\sigma_j$  of the lattice  $X_{2^r, 2^r}$  consists of  $3 \cdot 2^r$  cyclic groups.  $2^{r-1}$  generators of these groups have the same evenness and  $2^r$  generators have a different evenness. The splitting of the  $2^r \times 2^r$ -point SDFT by the 1-D transforms can be written as

$$\mathcal{R}(\mathcal{F}_{2^r, 2^r}^s; \sigma) = \left\{ \underbrace{\mathcal{F}_{2^r}, \mathcal{F}_{2^r}, \dots, \mathcal{F}_{2^r}}_{2^{r-1} \text{ times}}, \underbrace{\varepsilon_{2^r} \circ \mathcal{F}_{2^r}, \dots, \varepsilon_{2^r} \circ \mathcal{F}_{2^r}}_{2^r \text{ times}} \right\}.$$

Therefore, the number of multiplications,  $m_{2^r, 2^r}^s$ , required to calculate the  $2^r \times 2^r$ -point SDFT can be estimated by

$$\begin{aligned} m_{2^r, 2^r}^s &= 2^{r-1} m_{2^r} + [2^r (m_{2^r} + (2^r - 2) \mu_1 - 2)] \\ &= m_{2^r, 2^r} + 2^r [(2^r - 2) \mu_1 - 2], \end{aligned} \quad (19.142)$$

where we denote by  $m_{2^r, 2^r}$  the number of multiplications used for calculating the  $2^r \times 2^r$ -point DFT.  $\mu_1$  is the number of real multiplications used for performing a complex multiplication, which is considered equal 4. The number of operations of complex multiplications is calculated as

$$m_{2^r, 2^r}^s = m_{2^r, 2^r} + 2^r (2^r - 2) = 4^r \left( \frac{r}{2} - \frac{1}{6} \right) - 2^{r+1} + \frac{8}{3}. \quad (19.143)$$

### 19.7.2 $L^r \times L^r$ -Point SDFT

We now consider the case when  $N = L^r$ , ( $r \geq 1$ ), and  $L$  is an odd prime number.

In the  $N = L$  case, the irreducible covering of  $X_{L,L}$  consists of  $(L+1)$  cyclic groups and can be taken as  $\sigma_j = (T_{0,1}, T_{1,1}, \dots, T_{L-1,1}, T_{1,0})$ . The number of the generators of the groups of  $\sigma$  that have the same evenness equals  $(L-1)/2$ , and the remaining  $(L+3)/2$  generators have a different evenness. Therefore, the splitting of the  $L \times L$ -point SDFT consists of  $(L-1)/2$   $L$ -point DFTs and  $(L+3)/2$  modified DFTs which are the compositions of the  $L$ -point DFT with the scalar transform  $\varepsilon_L$ , i.e.,

$$\mathcal{R}(\mathcal{F}_{L,L}^s; \sigma_j) = \left\{ \underbrace{\mathcal{F}_L, \mathcal{F}_L, \dots, \mathcal{F}_L}_{(L-1)/2 \text{ times}}, \underbrace{\varepsilon_L \circ \mathcal{F}_L, \dots, \varepsilon_L \circ \mathcal{F}_L}_{(L+3)/2 \text{ times}} \right\}.$$

For instance, when  $L = 5$ , two generators (1, 1) and (3, 1) have the same evenness, and the other four generators (0, 1), (2, 1), (4, 1)

and  $(1, 0)$  have a different evenness. Therefore, the tensor representation yields the following splitting of the  $5 \times 5$ -point SDFT:  $\mathcal{R}(\mathcal{F}_{5,5}^s; \sigma_J) = \{\mathcal{F}_5, \mathcal{F}_5, \varepsilon_5 \circ \mathcal{F}_5, \varepsilon_5 \circ \mathcal{F}_5, \varepsilon_5 \circ \mathcal{F}_5, \varepsilon_5 \circ \mathcal{F}_5\}$ . The number of multiplications required for calculating the  $L \times L$ -point SDFT can be written as follows:

$$m_{L,L}^s = \frac{L-1}{2}m_L + \frac{L+3}{2}(m_L + L - 1) = (L+1)m_L + \frac{(L+3)(L-1)}{2}, \quad (19.144)$$

or  $m_{L,L}^s = m_{L,L} + (L+3)(L-1)/2$ . For the above considered  $5 \times 5$  example, the  $5 \times 5$ -point SDFT uses 16 operations of multiplication more than the  $5 \times 5$ -point DFT, i.e.,  $m_{5,5}^s = m_{5,5} + 16$ .

In the  $N = L^r$  case, with  $r > 1$ , the irreducible covering of  $X_{L^r, L^r}$  can be taken as

$$\sigma_J = ((T_{p,1})_{p=0:(L^r-1)}, (T_{1, L_s})_{s=0:(L^r-1)}). \quad (19.145)$$

$(L^r + L^{r-1})/2 - 1$  generators of groups of this covering have the same evenness and  $(L^r + L^{r-1})/2 + 1$  generatrices have a different evenness. Therefore, the splitting of the shifted 2-D DFT consists of  $(L^{r-1} + L^r)/2 - 1$   $L^r$ -point DFTs and  $(L^{r-1} + L^r)/2 + 1$  modified  $L^r$ -point DFTs,

$$\mathcal{R}(\mathcal{F}_{L^r, L^r}^s; \sigma_J) = \left\{ \underbrace{\mathcal{F}_{L^r}, \mathcal{F}_{L^r}, \dots, \mathcal{F}_{L^r}}_{L^{r-1}(L+1)/2-1 \text{ times}}, \underbrace{\varepsilon_{L^r} \circ \mathcal{F}_{L^r}, \dots, \varepsilon_{L^r} \circ \mathcal{F}_{L^r}}_{L^{r-1}(L+1)/2+1 \text{ times}} \right\}.$$

For the number of multiplications required to calculate the  $L^r \times L^r$ -point SDFT, we have the following expression:

$$\begin{aligned} m_{L^r, L^r}^s &= \left( \frac{L^r + L^{r-1}}{2} - 1 \right) m_{L^r} + \left( \frac{L^r + L^{r-1}}{2} + 1 \right) (m_{L^r} + L^r - 1) \\ &= L^{r-1}(L+1)m_{L^r} + \frac{L^{2r-1}(L+1)}{2} - L^{r-1} \frac{(L+1)}{2} - 1 \end{aligned}$$

For example, the splitting set for the  $9 \times 9$ -point SDFT equals

$$\mathcal{R}(\mathcal{F}_{9,9}^s; \sigma_J) = \left\{ \underbrace{\mathcal{F}_9, \mathcal{F}_9, \dots, \mathcal{F}_9}_{5 \text{ times}}, \underbrace{\varepsilon_9 \circ \mathcal{F}_9, \dots, \varepsilon_9 \circ \mathcal{F}_9}_{7 \text{ times}} \right\}.$$

The number of operations of multiplication for this transform equals  $m_{9,9}^s = 12m_9 + 47$ . The 9-point DFT requires 11 real multiplications, when considering the paired fast transform, i.e.,  $m_9 = 11$ . Additional 47 complex multiplications are used for multiplications by twiddle factors  $W_9^{k/2}$ ,  $k = 1 : 8$ . Therefore, we can write  $m_{9,9}^s = 12 \cdot 11 + 47\mu_1 = 132 + 188 = 220$ .

### 19.7.3 $L_1 L_2 \times L_1 L_2$ -Point SDFT

We now consider the  $N = L_1 L_2$  case, with arbitrary coprime numbers  $L_1, L_2 > 1$ . The covering  $\sigma_J$  for the lattice  $X_{L_1 L_2, L_1 L_2}$  has

been described in Section 19.5.4.2 and it has  $(L_1 + 1)(L_2 + 1)$  generators. The simple analysis of the evenness of coordinates of these generators leads to the tensor algorithm of calculation of the  $(L_1 L_2) \times (L_1 L_2)$ -point SDFT.

For instance, if  $N = 3 \cdot 5 = 15$ , then we can consider the following covering of the lattice  $X_{15,15}$ :

$$\sigma_J = (T_{1,s})_{s=0:14} \cup (T_{0,1}, T_{3,1}, T_{5,1}, T_{6,1}, T_{9,1}, T_{10,1}, T_{12,1}, T_{3,5}, T_{5,3}).$$

24 generators are in this set, among which half of the generators have the same evenness and the other half different. Therefore, the splitting of  $15 \times 15$ -point SDFT equals

$$\mathcal{R}(\mathcal{F}_{15,15}^s; \sigma) = \left\{ \underbrace{\mathcal{F}_{15}, \mathcal{F}_{15}, \dots, \mathcal{F}_{15}}_{12 \text{ times}}, \underbrace{\varepsilon_{15} \circ \mathcal{F}_{15}, \dots, \varepsilon_{15} \circ \mathcal{F}_{15}}_{12 \text{ times}} \right\}. \quad (19.146)$$

The number of multiplications required to compute the  $15 \times 15$ -point SDFT can be calculated in the form  $m_{15,15}^s = 12m_{15} + 12(m_{15} + 14) = 24m_{15} + 168$ .

## 19.8 2-D DCT

In this section we consider the tensor representation of the 2-D DCT, by using the tensor algorithm of calculation of the 2-D SDFT.

Let  $N$  be an arbitrary even number and let  $f$  be a real even sequence  $f_{n_1, n_2}$  of the size  $N \times N$ , which is determined by the following relation:

$$\left. \begin{aligned} f_{N-n_1-1, N-n_2-1} &= f_{n_1, n_2} \\ f_{N-n_1, n_2} &= 0 \\ f_{n_1, N-n_2} &= 0 \end{aligned} \right\}, \quad n_1, n_2 = 0 : (N/2 - 1). \quad (19.147)$$

It is not difficult to see, that the shifted Fourier transform  $\mathcal{F}_{N,N}^s$  over the sequence  $f$  is real and can be expressed in the following form:

$$\begin{aligned} F_{p_1, p_2}^s &= 2 \sum_{n_1=0}^{N/2-1} \sum_{n_2=0}^{N/2-1} f_{n_1, n_2} \cos \left( \frac{2\pi}{N} \left[ \left( n_1 + \frac{1}{2} \right) p_1 + \left( n_2 + \frac{1}{2} \right) p_2 \right] \right), \\ p_1, p_2 &= 0 : (N-1). \end{aligned} \quad (19.148)$$

The following relations hold between components of this transform:

$$\begin{aligned} F_{N-p_1, N-p_2}^s &= F_{p_1, p_2}^s, \quad F_{0, N-p_2}^s = -F_{0, p_2}^s, \quad F_{N-p_1, 0}^s = -F_{p_1, 0}^s, \\ p_1, p_2 &= 1 : (N/2 - 1), \end{aligned} \quad (19.149)$$

and  $F_{N/2, 0}^s = F_{0, N/2}^s = 0$ . Therefore, the calculation in Equation 19.148 can be performed only for half of the frequency-points  $(p_1, p_2)$  of the lattice  $X_{N,N}$ . The factor of 2 can also be omitted from the definition.



**Example 19.15**

Let  $N=8$ , and let  $f$  be the following sequence  $f_{n_1, n_2}$  of size  $4 \times 4$ , which is extended to  $8 \times 8$  as follows:

$$f = \{f_{n_1, n_2}\} = \begin{bmatrix} 1 & 2 & 1 & 2 \\ 3 & 1 & 2 & 3 \\ 2 & 3 & 1 & 4 \\ 5 & 3 & 2 & 2 \end{bmatrix} \rightarrow \begin{bmatrix} 1 & 2 & 1 & 2 & & & & \\ 3 & 1 & 2 & 3 & & & & \\ & & & & 0 & & & \\ 2 & 3 & 1 & 4 & & & & \\ 5 & 3 & 2 & 2 & & & & \\ & & & & & 2 & 2 & 3 & 5 \\ & & & & & 4 & 1 & 3 & 2 \\ & & & & & 3 & 2 & 1 & 3 \\ & & 0 & & & & & & 2 & 1 & 2 & 1 \end{bmatrix}. \quad (19.150)$$

The sequence  $f$  is even. Below is the  $8 \times 8$ -point SDFT of this sequence, which is written in the form of the table:

74	2.2961	9.8995	-5.5433	0	5.5433	-9.8995	-2.2961
-11.8519	-35.3137	-2.9302	-20.3848	5.5433	-20.1421	1.2137	-22.7279
-1.4142	11.8519	2	4.4609	-1.4142	2.7444	8	0.3170
-2.7444	-16.3848	-8.1564	-12.6863	-2.2961	2.7279	-3.3785	-8.1421
0	4.9092	4.2426	6.6257	18	6.6257	4.2426	4.9092
2.7444	-8.1421	-3.3785	2.7279	-2.2961	-12.6863	-8.1564	-16.3848
1.4142	0.3170	8	2.7444	-1.4142	4.4609	2	11.8519
11.8519	-22.7279	1.2137	-20.1421	5.5433	-20.3848	-2.9302	-35.3137

The table is divided by nine parts, in correspondence with the properties of Equation 19.149.

Let us consider the values of the  $8 \times 8$ -point SDFT in the first subtable ( $4 \times 4$ ),

74	2.2961	9.8995	-5.5433
-11.8519	-35.3137	-2.9302	-20.3848
-1.4142	11.8519	2.0000	4.4609
-2.7444	-16.3848	-8.1564	-12.6863

(19.151)

which we call the  $4 \times 4$ -point DCT of  $f$ . These values are defined by the cosine kernel function, and all values of the transform, which are lying outside this subtable, are defined by transforms whose kernel is the sine function. Indeed, the following holds:

$$F_{N/2+p_1, p_2} = -2 \sum_{n_1=0}^{N/2-1} \sum_{n_2=0}^{N/2-1} (-1)^{n_1} f_{n_1, n_2} \times \sin\left(\frac{2\pi}{N} \left[ \left(n_1 + \frac{1}{2}\right)p_1 + \left(n_2 + \frac{1}{2}\right)p_2 \right]\right),$$

and

$$F_{p_1, N/2+p_2} = -2 \sum_{n_1=0}^{N/2-1} \sum_{n_2=0}^{N/2-1} (-1)^{n_2} f_{n_1, n_2} \times \sin\left(\frac{2\pi}{N} \left[ \left(n_1 + \frac{1}{2}\right)p_1 + \left(n_2 + \frac{1}{2}\right)p_2 \right]\right),$$

where  $p_1, p_2 = 0 : (N-1)$ .

In the general case, the 2-D SDFT is reduced to the transform with the cosine kernel function, which is why we call this transform the 2-D DCT. The  $N/2 \times N/2$ -point DCT of a sequence  $f = \{f_{n_1, n_2}; n_1, n_2 = 0 : (N/2 - 1)\}$  is defined by

$$C_{p_1, p_2} = (C_{N/2, N/2} \circ f)_{p_1, p_2} = \sum_{n_1=0}^{N/2-1} \sum_{n_2=0}^{N/2-1} f_{n_1, n_2} \cos\left(\frac{\pi}{N/2} \left[ \left(n_1 + \frac{1}{2}\right)p_1 + \left(n_2 + \frac{1}{2}\right)p_2 \right]\right), \quad p_1, p_2 = 0 : (N/2 - 1). \quad (19.152)$$

The 2-D DCT is nonseparable and periodical with the period  $(N, N)$ , not  $(N/2, N/2)$ . Since this transform is a special case of the shifted 2-D DFT, the tensor representation of the shifted 2-D DFT can be used for splitting the 2-D DCT by a minimum number of 1-D transforms.

Indeed, it directly follows from definitions (19.130) and (19.147), that the relation

$$\tilde{f}_{p_1, p_2, t} = \tilde{f}_{p_1, p_2, N-t} \quad (19.153)$$

is valid, when  $t = 1 : (N/2 - 1)$ . If  $e(p_1, p_2) = 0$ , then the splitting-signal corresponding to the generator  $(p_1, p_2)$  has the following form:

$$\tilde{f}_{T_{p_1, p_2}} = \left\{ \tilde{f}_{p_1, p_2, 0}, \tilde{f}_{p_1, p_2, 1}, \tilde{f}_{p_1, p_2, 2}, \dots, \tilde{f}_{p_1, p_2, N/2}, \dots, \tilde{f}_{p_1, p_2, 2}, \tilde{f}_{p_1, p_2, 1}, \tilde{f}_{p_1, p_2, 0} \right\}, \quad (19.154)$$

i.e., the signal is even.

Therefore, the following calculations can be performed for the transform in Equation 19.134:

$$\begin{aligned} \sum_{t=0}^{N-1} \tilde{f}_{p_1, p_2, t} W^{kt} &= \tilde{f}_{p_1, p_2, 0} + \sum_{t=1}^{N/2-1} \tilde{f}_{p_1, p_2, t} [W^{kt} + W^{k(N-t)}] + \tilde{f}_{p_1, p_2, N/2} W^{kN/2} \\ &= \tilde{f}_{p_1, p_2, 0} + 2 \sum_{t=1}^{N/2-1} \tilde{f}_{p_1, p_2, t} \cos\left(\frac{2\pi}{N} kt\right) + (-1)^k \tilde{f}_{p_1, p_2, N/2}. \end{aligned}$$

For simplicity of calculations, we denote  $\tilde{f}_{p_1, p_2, t} = \tilde{f}_{p_1, p_2, t}/2$ , when  $t = 0$  and  $N/2$ . Thus, we can write the following:

$$C_{k p_1, k p_2} = \sum_{t=0}^{N/2-1} \tilde{f}_{p_1, p_2, t} \cos\left(\frac{2\pi}{N} kt\right) + (-1)^k \tilde{f}_{p_1, p_2, N/2}, \quad \text{if } e(p_1, p_2) = 0. \quad (19.155)$$

The sum in this equation represents the  $N/2$ -point DCT of type I, which we denote by  $\mathcal{K}_{N/2}$ . The  $N/2 \times N/2$ -point DCT at frequency-points of the group  $T_{p_1, p_2}$  with generator having coordinates of the same evenness is defined by the  $N/2$ -point DCT of type I plus/minus the value of  $\tilde{f}_{p_1, p_2, N/2}$ . The equation can also be written as

$$C_{\overline{kp_1}, \overline{kp_2}} = \sum_{t=0}^{N/2} \tilde{f}_{p_1, p_2, t} \cos\left(\frac{2\pi}{N} kt\right), \text{ if } e(p_1, p_2) = 0.$$

We now consider the  $N/2 \times N/2$ -point DCT at frequency-points of the group  $T_{p_1, p_2}$ , when the coordinates of its generator have different evenness,  $e(p_1, p_2) = 1$ . In this case, the splitting-signal corresponding to the generator  $(p_1, p_2)$  has the following form:

$$\tilde{f}_{T_{p_1, p_2}} = \left\{ \tilde{f}_{p_1, p_2, \frac{1}{2}}, \tilde{f}_{p_1, p_2, \frac{3}{2}}, \dots, \tilde{f}_{p_1, p_2, N/2 - \frac{1}{2}}, \tilde{f}_{p_1, p_2, N/2 + \frac{1}{2}}, \dots, \tilde{f}_{p_1, p_2, \frac{3}{2}}, \tilde{f}_{p_1, p_2, \frac{1}{2}} \right\}. \quad (19.156)$$

The modified Fourier transform in Equation 19.135 can thus be written as follows:

$$\begin{aligned} F_{\overline{kp_1}, \overline{kp_2}}^s &= \sum_{t=0}^{N-1} \tilde{f}_{p_1, p_2, t + \frac{1}{2}} W^{k(t + \frac{1}{2})} = \sum_{t=0}^{N/2-1} \tilde{f}_{p_1, p_2, t + \frac{1}{2}} \left[ W^{k(t + \frac{1}{2})} + W^{k(N - t - \frac{1}{2})} \right] \\ &= 2 \sum_{t=0}^{N/2-1} \tilde{f}_{p_1, p_2, t + \frac{1}{2}} \cos\left(\frac{2\pi}{N} k \left(t + \frac{1}{2}\right)\right). \end{aligned}$$

Then, the 2-D DCT at frequency-points of this group can be written as

$$C_{\overline{kp_1}, \overline{kp_2}} = \sum_{t=0}^{N/2-1} \tilde{f}_{p_1, p_2, t + \frac{1}{2}} \cos\left(\frac{2\pi}{N} k \left(t + \frac{1}{2}\right)\right). \quad (19.157)$$

The sum in Equation 19.157 represents the  $N/2$ -point DCT of type II, which we denote by  $C_{N/2}$ . Thus, for the generator  $(p_1, p_2)$  with coordinates of the same evenness, the  $N$ -point DFT is reduced to the  $N/2$ -point DCT of type I. For the generator with coordinates of different evenness, the  $N$ -point modified transform  $\varepsilon_N \circ \mathcal{F}_N$  is reduced to the  $N/2$ -point DCT of type II. We note, that if  $g_n$  is a sequence of length  $N$ , then the following properties hold for these cosine transforms:

$$(\mathcal{K}_{N/2} \circ g_n)_{N-k} = (\mathcal{K}_{N/2} \circ g_n)_k \quad \text{and} \quad (C_{N/2} \circ g_n)_{N-k} = -(C_{N/2} \circ g_n)_k$$

when  $k = 1 : (N/2 - 1)$ . Therefore, we can consider  $\overline{kp_n} = kp_n \bmod (N/2)$ ,  $n = 1, 2$ , in both Equations 19.155 and 19.157, wherein  $k = 0 : (N/2 - 1)$ . As a result, the following property of the 2-D DCT is valid:

$$(C_{N/2, N/2} \circ f)|_{T_{p_1, p_2}} = \begin{cases} \mathcal{K}_{N/2} \circ \tilde{f}_{T_{p_1, p_2}} + P \cdot \tilde{f}_{p_1, p_2, N/2}, & e(p_1, p_2) = 0; \\ \mathcal{C}_{N/2} \circ \tilde{f}_{T_{p_1, p_2}}, & e(p_1, p_2) = 1, \end{cases} \quad (19.158)$$

where  $P = (1, -1, 1, -1, \dots, 1, -1)'$ .

Note that the sets  $\tilde{V}_{p_1, p_2, t}$  and components  $\tilde{f}_{p_1, p_2, t}$  of the splitting-signals, which are defined respectively in Equations 19.129 and 19.130, have been considered in the lattice  $X_{N, N}$ , and the 2-D DCT is considered for  $(n_1, n_2) \in X_{N/2, N/2}$ . Denoting by  $V_{p_1, p_2, t}^*$  the set intersection  $\tilde{V}_{p_1, p_2, t} \cap X_{N/2, N/2}$  and defining the components

$$f_{p_1, p_2, t} = \sum \left\{ f_{n_1, n_2}; (n_1, n_2) \in V_{p_1, p_2, t}^* \right\},$$

we obtain the following:

$$\begin{aligned} \tilde{f}_{p_1, p_2, t - \Delta} &= f_{p_1, p_2, t - \Delta} + f_{p_1, p_2, N - t + \Delta}, \quad t = 1, 2, \dots, N/2, \\ \tilde{f}_{p_1, p_2, 0} &= 2f_{p_1, p_2, 0}, \quad \tilde{f}_{p_1, p_2, N/2} = 2f_{p_1, p_2, N/2}. \end{aligned}$$

It follows from Equation 19.155 and 19.157, that for a given group  $T_{p_1, p_2} \in \sigma$ , the corresponding splitting-signal can be written as

$$\tilde{f}_{T_{p_1, p_2}} = \left\{ f_{p_1, p_2, 0}, f_{p_1, p_2, 1} + f_{p_1, p_2, N-1}, \dots, f_{p_1, p_2, N/2-1} + f_{p_1, p_2, N/2+1}, f_{p_1, p_2, N/2} \right\},$$

if  $p_1$  and  $p_2$  are the subscripts of the same evenness, or

$$\begin{aligned} \tilde{f}_{T_{p_1, p_2}} &= \left\{ f_{p_1, p_2, \frac{1}{2}} + f_{p_1, p_2, N - \frac{1}{2}}, f_{p_1, p_2, \frac{3}{2}} + f_{p_1, p_2, N - \frac{3}{2}}, \dots, \right. \\ &\quad \left. f_{p_1, p_2, N/2 - \frac{1}{2}} + f_{p_1, p_2, N/2 + \frac{1}{2}} \right\}, \end{aligned}$$

if  $p_1$  and  $p_2$  are the subscripts of different evenness.

### Example 19.16

When  $N = 8$ , the  $4 \times 4$ -point 2-D cosine transform of a sequence  $f_{n_1, n_2}$  is calculated by

$$\begin{aligned} C_{p_1, p_2} &= \sum_{n_1=0}^3 \sum_{n_2=0}^3 f_{n_1, n_2} \cos\left(\frac{\pi}{4} \left[ \left(n_1 + \frac{1}{2}\right)p_1 + \left(n_2 + \frac{1}{2}\right)p_2 \right]\right), \\ p_1, p_2 &= 0 : 3. \end{aligned} \quad (19.159)$$

We consider the 2-D sequence  $f$  defined in Equation 19.150 and two generators  $(p_1, p_2) = (1, 1)$  and  $(p_1, p_2) = (1, 2)$ , with the equal and different evenness. For the first generator, the values of the form  $\mathcal{L}(n_1, n_2, 1, 1)$  can be written as the following table:

$$|t = n_1 + n_2 + 1|_{n_1, n_2=0:7} = \begin{bmatrix} \underline{1} & 2 & 3 & 4 & & & & \\ 2 & 3 & 4 & 5 & & & & \\ & & & & & & 0 & \\ 3 & 4 & 5 & 6 & & & & \\ 4 & 5 & 6 & 7 & & & & \\ & & & & & & & 1 & 2 & 3 & 4 \\ & & & & & & & & 2 & 3 & 4 & 5 \\ & & & & & & 0 & & & 3 & 4 & 5 & 6 \\ & & & & & & & & & & 4 & 5 & 6 & 7 \end{bmatrix}.$$

The corresponding splitting-signal of the tensor representation  $f \rightarrow \{\tilde{f}_T; T \in \sigma\}$  is calculated as follows:

$$\tilde{f}_{T_{1,1}} = \left\{ \tilde{f}_{1,1,0}, \tilde{f}_{1,1,1}, \tilde{f}_{1,1,2}, \tilde{f}_{1,1,3}, \tilde{f}_{1,1,4} \right\} = \{0, 3, 11, 11, 12\},$$

where

$$\begin{aligned}\tilde{f}_{1,1,0} &= f_{1,1,0} = 0 \\ \tilde{f}_{1,1,1} &= f_{1,1,1} + f_{1,1,7} = f_{0,0} + f_{3,3} = 1 + 2 = 3, \\ \tilde{f}_{1,1,2} &= f_{1,1,2} + f_{1,1,6} = (f_{0,1} + f_{1,0}) + (f_{2,3} + f_{3,2}) \\ &= (2 + 3) + (4 + 2) = 11, \\ \tilde{f}_{1,1,3} &= f_{1,1,3} + f_{1,1,5} = (f_{0,2} + f_{1,1} + f_{2,0}) + (f_{1,3} + f_{2,2} + f_{3,1}) \\ &= (1 + 1 + 2) + (3 + 1 + 3) = 11, \\ \tilde{f}_{1,1,4} &= f_{1,1,4} = f_{0,3} + f_{1,2} + f_{2,1} + f_{3,0} = 2 + 2 + 3 + 5 = 12\end{aligned}$$

For the generator (1, 2), the values of the form  $\mathcal{L}(n_1, n_2, 1, 2)$  can be written as the following table:

$$\left| t = n_1 + 2n_2 + \frac{3}{2} \right|_{n_1, n_2=0:7} = \frac{1}{2} \begin{bmatrix} 3 & 7 & 11 & 15 & & & & \\ 5 & 9 & 13 & 1 & & & & \\ & & & & 0 & & & \\ 7 & 11 & 15 & 3 & & & & \\ 9 & 13 & 1 & 5 & & & & \\ & & & & & 11 & 15 & 3 & 7 \\ & & & & & & & & & 13 & 1 & 5 & 9 \\ & & & 0 & & & & & & & & & & 15 & 3 & 7 & 11 \\ & & & & & & & & & & & & & & & & & 1 & 5 & 9 & 13 \end{bmatrix}.$$

Therefore the components  $\tilde{f}_{1,2,t}$  of the splitting-signal are calculated by

$$\begin{aligned}\tilde{f}_{1,2,\frac{1}{2}} &= f_{1,2,\frac{1}{2}} + f_{1,2,\frac{15}{2}} = (f_{1,3} + f_{3,2}) + (f_{0,3} + f_{2,2}) = (3 + 2) + (2 + 1) = 8, \\ \tilde{f}_{1,2,\frac{3}{2}} &= f_{1,2,\frac{3}{2}} + f_{1,2,\frac{13}{2}} = (f_{0,0} + f_{2,3}) + (f_{1,2} + f_{3,1}) = (1 + 4) + (2 + 3) = 10, \\ \tilde{f}_{1,2,\frac{5}{2}} &= f_{1,2,\frac{5}{2}} + f_{1,2,\frac{11}{2}} = (f_{1,0} + f_{3,3}) + (f_{0,2} + f_{2,1}) = (3 + 2) + (1 + 3) = 9, \\ \tilde{f}_{1,2,\frac{7}{2}} &= f_{1,2,\frac{7}{2}} + f_{1,2,\frac{9}{2}} = (f_{0,1} + f_{2,0}) + (f_{1,1} + f_{3,0}) = (2 + 2) + (1 + 5) = 10,\end{aligned}$$

and

$$\tilde{f}_{T_{1,2}} = \left\{ \tilde{f}_{1,2,\frac{1}{2}}, \tilde{f}_{1,2,\frac{3}{2}}, \tilde{f}_{1,2,\frac{5}{2}}, \tilde{f}_{1,2,\frac{7}{2}} \right\} = \{8, 10, 9, 10\}.$$

The following formulas hold for the 2-D DCT at frequency-points of groups  $T_{1,1}$  and  $T_{1,2}$ :

$$\begin{aligned}C_{k,k} &= \sum_{t=0}^4 \tilde{f}_{1,1,t} \cos\left(\frac{\pi}{4} kt\right), \\ C_{k,2k} &= \sum_{t=0}^3 \tilde{f}_{1,2,t+\frac{1}{2}} \cos\left(\frac{\pi}{4} k\left(t + \frac{1}{2}\right)\right), \quad k = 0 : 3.\end{aligned}$$

Similarly, we can consider other four elements of the tensor representation, namely  $\tilde{f}_{T_{1,3}}$ ,  $\tilde{f}_{T_{1,0}}$ ,  $\tilde{f}_{T_{0,1}}$ , and  $\tilde{f}_{T_{2,1}}$ . In terms of the tensor representation, the  $4 \times 4$ -point DCT is split by two transforms  $\mathcal{K}_4$ , and four transforms  $\mathcal{C}_4$ , i.e.,  $\mathcal{R}(\mathcal{C}_{4,4}; \sigma) = \{\mathcal{K}_4, \mathcal{C}_4, \mathcal{C}_4, \mathcal{C}_4, \mathcal{C}_4, \mathcal{C}_4\}$ .

We now consider the general case:  $N = 2^r$ , when  $r \geq 2$ . The irreducible covering  $\sigma_J$  of the lattice  $X_{2^r, 2^r}$  consists of  $3N/2$

groups  $T_{p,s}$ . Among all  $3 \cdot 2^{r-1}$  generators ( $p, s$ ) of these groups,  $2^{r-1}$  generators have coordinates of the same evenness and the remaining  $2^r$  generators have coordinates of different evenness. The splitting of the  $2^r \times 2^r$ -point DCT consists thus of  $2^{r-1}$   $2^r$ -point cosine transforms  $\mathcal{K}_{2^r}$  and  $2^r$  cosine transforms  $\mathcal{C}_{2^r}$ , that is,

$$\mathcal{R}(\mathcal{C}_{2^r, 2^r}; \sigma_J) = \left\{ \underbrace{\mathcal{K}_{2^r}, \mathcal{K}_{2^r}, \dots, \mathcal{K}_{2^r}}_{2^{r-1} \text{ times}}, \underbrace{\mathcal{C}_{2^r}, \mathcal{C}_{2^r}, \dots, \mathcal{C}_{2^r}}_{2^r \text{ times}} \right\}. \quad (19.160)$$

The number of used multiplications,  $m_{2^r, 2^r}^c$ , for calculating the 2-D DCT can be estimated by two different ways. The calculation of the transform directly through the  $2^{r+1} \times 2^{r+1}$ -point SDFT yields the estimate

$$\begin{aligned}m_{2^r, 2^r; \text{SDFT}}^c &= \frac{1}{4} m_{2^{r+1}, 2^{r+1}}^s = \frac{1}{4} \left[ 4^{r+1} \left( \frac{r+1}{2} - \frac{1}{6} \right) - 2^{r+2} + \frac{8}{3} \right] \\ &= 4^r \left( \frac{r}{2} + \frac{1}{3} \right) - 2^r + \frac{2}{3}.\end{aligned} \quad (19.161)$$

In particular, for  $N=8$  and  $16$ , we obtain  $m_{8,8}^c = 110$  and  $m_{16,16}^c = 582$ . It is clear, that the estimate in Equation 19.161 can be improved, if we use the concept of the pruning algorithm [39], since the extended  $2^{r+1} \times 2^{r+1}$ -point input for the SDFT has  $2 \cdot 4^r$  zeros.

Another estimate can be obtained by using the calculation of the 2-D DCT in Equations 19.155 and 19.157 through the fast 1-D cosine transforms. Denoting by  $m(\mathcal{K}_{2^r})$  and  $m(\mathcal{C}_{2^r})$  respectively the number of multiplications required to calculate the cosine transforms  $\mathcal{K}_{2^r}$  and  $\mathcal{C}_{2^r}$ , we obtain from the splitting (19.160) the following estimate:

$$m_{2^r, 2^r}^c = 2^{r-1} m(\mathcal{K}_{2^r}) + 2^r m(\mathcal{C}_{2^r}). \quad (19.162)$$

The estimates for  $m(\mathcal{C}_{2^r})$  are well known, and we can use, for instance, the estimate [37,40]

$$m(\mathcal{C}_{2^r}) = 2^{r+1} - r - 2, \quad r > 2, \quad (m(\mathcal{C}_4) = 3). \quad (19.163)$$

For  $m(\mathcal{K}_{2^r})$ , we consider the following estimate obtained by the 1-D paired transforms [34]

$$m(\mathcal{K}_{2^r}) = 2^{r+1} - \frac{(r-2)(r+5)}{2} - 8, \quad (m(\mathcal{K}_4) = 4). \quad (19.164)$$

Substituting these estimates into Equation 19.162, we obtain the following multiplicative complexity of the 2-D DCT in the tensor representation:

$$m_{2^r, 2^r}^c = 3 \cdot 4^r - 2^{r-2}(r^2 + 7r + 14). \quad (19.165)$$

For  $N=8, 16$ , and  $32$ , we obtain respectively  $m_{8,8}^c = 104$ ,  $m_{16,16}^c = 536$ , and  $m_{32,32}^c = 2480$ .

### 19.8.1 Modified Algorithms of the 2-D DCT

The tensor representation of the 2-D sequence with respect to the 2-D DCT associates with the covering  $\sigma_j$  of the lattice  $X_{N,N}$ , which is not a partition. The deficiency of the tensor algorithm, which splits the 2-D DCT into 1-D cosine transforms, is its reiteration of the spectral component computations at the frequency-points  $(p_1, p_2)$  which lie in the intersections of the groups of the covering. For  $N=2^r$ , the number of these frequency-points equals  $4^r/2$ , which composes half of the total number of frequency-points. We can improve the tensor algorithm for the 2-D DCT, in order to avoid the reiteration of the computations. Such an improvement can be obtained similar to the way described above in the improved tensor algorithms for the 2-D DFT and 2-D DHT.

For that, we consider a new covering  $\sigma_j^1$  of the lattice, which contain  $3 \cdot 2^{r-2}$  groups  $T_{1,p_2}$  and  $T_{2p_1,1}$ ,  $p_2: 0: (2^{r-1}-1)$ ,  $p_1: 0: (2^{r-2}-1)$ , at which we can calculate the complete  $2^r$ -point DCTs. The rest of the covering consists of  $3 \cdot 2^{r-2}$  subgroups of  $T_{1,p_2+2^{r-1}}$  and  $T_{2p_1+2^{r-1},1}$ , where  $p_2: 0: (2^{r-1}-1)$ ,  $p_1: 0: (2^{r-2}-1)$ , at which each second element is omitted. The calculation of the 2-D DCT at frequency-points of these subgroups is reduced to incomplete 1-D DCTs (or  $2^{r-1}$ -point DCTs), when only components with odd numbers are calculated. We denote these incomplete DCTs of types I and II by  $\mathcal{K}_{2^r;2}$  and  $\mathcal{C}_{2^r;2}$  respectively. By using this covering  $\sigma_j^1$ , we obtain the following splitting of the 2-D DCT by  $3 \cdot 2^{r-2}$  complete and  $3 \cdot 2^{r-2}$  incomplete DCTs:

$$\mathcal{R}(\mathcal{C}_{2^r;2^r}; \sigma^1) = \left\{ \underbrace{\mathcal{K}_{2^r}, \dots, \mathcal{K}_{2^r}}_{2^{r-2} \text{ times}}, \underbrace{\mathcal{K}_{2^r;2}, \dots, \mathcal{K}_{2^r;2}}_{2^{r-2} \text{ times}}, \underbrace{\mathcal{C}_{2^r}, \dots, \mathcal{C}_{2^r}}_{2^{r-1} \text{ times}}, \right. \\ \left. \underbrace{\mathcal{C}_{2^r;2}, \dots, \mathcal{C}_{2^r;2}}_{2^{r-1} \text{ times}} \right\}. \quad (19.166)$$

The cyclic groups of the covering  $\sigma_j$  intersect at the original point,  $(0, 0)$ , as well as the following intersections take place

$$T_{1,p_2} \cap T_{1,p_2+2^{r-k}} = T_{2^k(1,p_2)}, \quad T_{p_1,1} \cap T_{p_1+2^{r-k},1} \\ = T_{2^k(p_1,1)}, \quad k = 1: (r-1), \quad (19.167)$$

for an arbitrary  $(p_1, p_2) \in X_{2^r, 2^r}$ . We denote by  $T^k$  the set-complements of these groups

$$T_{1,p_2}^k = T_{1,p_2} \setminus T_{2^k(1,p_2)}, \quad T_{p_1,1}^k = T_{p_1,1} \setminus T_{2^k(p_1,1)}, \quad (19.168)$$

which contain  $(2^r - 2^{r-k})$  frequency-points. The splitting described in Equation 19.166 corresponds to the  $k=1$  case, when the following covering of the lattice  $X_{2^r, 2^r}$  is composed:

$$\sigma_j^1 = \left( \left( T_{1,p_2}, T_{1,p_2+2^{r-1}} \right)_{p_2=0:(2^{r-1}-1)}, \left( T_{2p_1,1}, T_{2p_1+2^{r-1},1} \right)_{p_1=0:(2^{r-2}-1)} \right).$$

This covering is smaller than the initial covering  $\sigma$ , which means that each set of  $\sigma_j^1$  includes in a group of  $\sigma_j$ .

We can count the number of multiplications saved on this stage of calculations. Denoting by  $m(\mathcal{K}_{2^r;2})$  and  $m(\mathcal{C}_{2^r;2})$  respectively the numbers of multiplications required to compute the incomplete cosine transforms  $\mathcal{K}_{2^r;2}$  and  $\mathcal{C}_{2^r;2}$ , we can estimate the total number of multiplications used in the splitting Equation 19.166 as

$$m_{2^r, 2^r}^c = 2^{r-2} [m(\mathcal{K}_{2^r}) + m(\mathcal{K}_{2^r;2})] + 2^{r-1} [m(\mathcal{C}_{2^r}) + m(\mathcal{C}_{2^r;2})]. \quad (19.169)$$

We consider that  $m(\mathcal{K}_{2^r;2}) = m(\mathcal{K}_{2^r})$ . For the incomplete cosine transforms  $\mathcal{C}_{2^r;2}$ , we can use the recursive algorithm [35,36], which splits the transform  $\mathcal{C}_{2^r}$  into two transforms  $\mathcal{C}_{2^{r-1}}$ , by dividing the frequencies  $k=0 : (N-1)$  into two sets of the even and odd frequencies. Then, we can write that  $m(\mathcal{C}_{2^r;2}) = m(\mathcal{C}_{2^{r-1}}) + 2^{r-1}$ . Therefore the estimate in Equation 19.169 can be calculated by

$$m_{2^r, 2^r}^c = m_{2^r, 2^r | \text{step1}}^c = 2^{r-1} m(\mathcal{K}_{2^r}) + 2^{r-1} [m(\mathcal{C}_{2^r}) + m(\mathcal{C}_{2^{r-1}}) + 2^{r-1}]. \quad (19.170)$$

In particular, for the  $8 \times 8$ -point DCT we obtain  $m_{8,8 | \text{step1}}^c = 4 \cdot 4 + 4(11 + 3 + 4) = 88$ . In the general  $r > 3$  case, by substituting the considered estimates for  $m(\mathcal{K}_{2^r})$  and  $m(\mathcal{C}_{2^r})$  into Equation 19.170, we obtain

$$m_{2^r, 2^r | \text{step1}}^c = 11 \cdot 4^{r-1} - (r^2 + 7r + 12)2^{r-2}. \quad (19.171)$$

This number can be reduced if we consider other intersections  $T^k$ ,  $k=2 : (r-1)$ , of the groups of the covering, and, to show that, we describe the  $8 \times 8$  case in detail.

#### Example 19.17

For the  $N=8$  case, we consider all groups of the irreducible covering  $\sigma_j$  of the lattice  $X_{8,8}$ :

$$T_{1,0} = \{(0, 0), (1, 0), (2, 0), (3, 0), (4, 0), (5, 0), (6, 0), (7, 0)\}, \\ T_{1,1} = \{\underline{0}, 0, (1, 1), (2, 2), (3, 3), (4, 4), (5, 5), (6, 6), (7, 7)\}, \\ T_{1,2} = \{\underline{0}, \underline{0}, (1, 2), (2, 4), (3, 6), \underline{4}, 0, (5, 2), (6, 4), (7, 6)\}, \\ T_{1,3} = \{\underline{0}, \underline{0}, (1, 3), (2, 6), (3, 1), \underline{4}, \underline{4}, (5, 7), (6, 2), (7, 5)\}, \\ T_{1,4} = \{\underline{0}, \underline{0}, (1, 4), \underline{2}, 0, (3, 4), \underline{4}, 0, (5, 4), \underline{6}, 0, (7, 4)\}, \\ T_{1,5} = \{\underline{0}, \underline{0}, (1, 5), \underline{2}, 2, (3, 7), \underline{4}, 4, (5, 1), \underline{6}, 6, (7, 3)\}, \\ T_{1,6} = \{\underline{0}, \underline{0}, (1, 6), \underline{2}, 4, (3, 2), \underline{4}, 0, (5, 6), \underline{6}, 4, (7, 2)\}, \\ T_{1,7} = \{\underline{0}, \underline{0}, (1, 7), \underline{2}, 6, (3, 5), \underline{4}, 4, (5, 3), \underline{6}, 2, (7, 1)\}, \\ T_{0,1} = \{\underline{0}, \underline{0}, (0, 1), (0, 2), (0, 3), (0, 4), (0, 5), (0, 6), (0, 7)\}, \\ T_{2,1} = \{\underline{0}, \underline{0}, (2, 1), (4, 2), (6, 3), \underline{0}, 4, (2, 5), (4, 6), (6, 7)\}, \\ T_{4,1} = \{\underline{0}, \underline{0}, (4, 1), \underline{0}, 2, (3, 6), \underline{0}, 4, (4, 5), \underline{0}, 6, (4, 7)\}, \\ T_{6,1} = \{\underline{0}, \underline{0}, (6, 1), \underline{4}, 2, (2, 3), \underline{0}, 4, (6, 5), \underline{4}, 6, (2, 7)\}.$$

In accordance with this covering  $\sigma_j$ , the splitting of the 2-D DCT is

$$\mathcal{R}(\mathcal{C}_{8,8}; \sigma_j) = \{\mathcal{C}_8, \mathcal{K}_8, \mathcal{C}_8, \mathcal{K}_8, \mathcal{C}_8, \mathcal{K}_8, \mathcal{C}_8, \mathcal{K}_8, \mathcal{C}_8, \mathcal{C}_8, \mathcal{C}_8, \mathcal{C}_8\}.$$

Let  $f = \{f_{n_1, n_2}; n_1, n_2 = 0 : 7\}$  be a 2-D sequence and let  $\{\tilde{f}_T; T \in \sigma\}$  be the  $\sigma$ -representation, or tensor representation of the sequence  $f$  by the  $8 \times 8$ -point DCT. Then, to calculate the  $8 \times 8$ -point DCT, it is sufficient to fulfill:

*Step 1:* Four 8-point DCTs of type II,  $C_8$ , over the sequences  $\tilde{f}_{T_{1,0}}, \tilde{f}_{T_{1,2}}, \tilde{f}_{T_{0,1}}, \tilde{f}_{T_{2,1}}$ , as well as two 8-point DCTs of type I,  $K_8$ , over the sequences  $\tilde{f}_{T_{1,1}}$  and  $\tilde{f}_{T_{1,3}}$ , to determine the 2-D DCT at frequency-points of the corresponding six groups  $T_{1,0}, T_{1,2}, T_{0,1}, T_{2,1}, T_{1,1}$ , and  $T_{1,3}$ .

*Step 2:* Four incomplete 8-point DCTs of type II,  $C_{8;2}$ , over the sequences  $\tilde{f}_{T_{1,4}}, \tilde{f}_{T_{1,6}}, \tilde{f}_{T_{4,1}}, \tilde{f}_{T_{6,1}}$ , as well as two incomplete 8-point DCTs of type I,  $K_{8;2}$ , over the sequences  $\tilde{f}_{T_{1,5}}$  and  $\tilde{f}_{T_{1,7}}$ , to determine the 2-D DCT at frequency-points of the subgroups  $T_{1,4}^1, T_{1,6}^1, T_{4,1}^1, T_{6,1}^1, T_{1,5}^1$ , and  $T_{1,7}^1$ .

On Step 2, we save 4 multiplications every time we use the incomplete cosine transform  $C_{8;2}$  instead of  $C_8$ , thereby avoiding repeated calculations at the frequency-points with even coordinates. Therefore, we save 16 multiplications on this step of the algorithm, which results in the total number of used multiplications to be  $m_{8,8|step,1}^c = 104 - 16 = 88$ .

We can see that this process of the improvement can be continued. Indeed, to avoid the repeated calculations in the groups  $T_{1,2}, T_{1,3}$ , and  $T_{2,1}$  at frequency-points with both coordinates multiple to 4, we can perform two incomplete cosine transforms of type I,  $\tilde{C}_{8;4}$ , without outputs at points 0 and 4. The use of two transforms  $C_{8;4}$  saves in addition two multiplications by  $\sqrt{2}/2$ , and the total number of multiplications reduces to  $m_{8,8|step2}^c = 88 - 2 = 86$ .

At last, we have only intersections of the group  $T_{1,0}$  with  $T_{1,1}$  and  $T_{0,1}$  at (0, 0). Although, these reiterations of calculations do not reduce the multiplicative complexity of the algorithm, we can perform two incomplete cosine transforms  $K_{8;0}$  and  $C_{8;0}$  avoiding the repeated calculations at the origin point. As a result, we obtain a partition  $\sigma'$  of the lattice  $X_{8,8}$ . The sets of this partition and the 1-D DCTs used to calculate the 2-D DCT at frequency-points of these sets are given below in the form of the table:

$T_{1,0}$	$\{(0, 0), (1, 0), (2, 0), (3, 0), (4, 0), (5, 0), (6, 0), (7, 0)\}$	$C_8$
$T_{1,1}^3$	$\{(1, 1), (2, 2), (3, 3), (4, 4), (5, 5), (6, 6), (7, 7)\}$	$K_{8;0}$
$T_{1,2}^2$	$\{(1, 2), (2, 4), (3, 6), (5, 2), (6, 4), (7, 6)\}$	$C_{8;4}$
$T_{1,3}^2$	$\{(1, 3), (2, 6), (3, 1), (5, 7), (6, 2), (7, 5)\}$	$K_{8;4}$
$T_{1,4}^1$	$\{(1, 4), (3, 4), (5, 4), (7, 4)\}$	$C_{8;2}$
$T_{1,5}^1$	$\{(1, 5), (3, 7), (5, 1), (7, 3)\}$	$K_{8;2}$
$T_{1,6}^1$	$\{(1, 6), (3, 2), (5, 6), (7, 2)\}$	$C_{8;2}$
$T_{1,7}^1$	$\{(1, 7), (3, 5), (5, 3), (7, 1)\}$	$K_{8;2}$
$T_{0,1}^3$	$\{(0, 1), (0, 2), (0, 3), (0, 4), (0, 5), (0, 6), (0, 7)\}$	$C_{8;0}$
$T_{2,1}^2$	$\{(2, 1), (4, 2), (6, 3), (2, 5), (4, 6), (6, 7)\}$	$C_{8;4}$
$T_{4,1}^1$	$\{(4, 1), (3, 6), (4, 5), (4, 7)\}$	$C_{8;2}$
$T_{6,1}^1$	$\{(6, 1), (2, 3), (6, 5), (2, 7)\}$	$C_{8;2}$

Thus, all reiterations of computation of the 2-D DCT in the tensor algorithm has been eliminated by using the incomplete cosine transforms of types I and II.

In the general  $N \geq 8$  case, we can use the similar procedure in order to improve the tensor algorithm. So, for the next  $k = 2$  step, we can eliminate the intersections in other remained groups  $T$  of the covering  $\sigma^1$ , using equalities (19.167). Then, we obtain the following covering:

$$\sigma^2 = \left( \left( T_{1,p_2}, T_{1,p_2+2^{r-2}}^2 \right)_{p_2=0:(2^{r-2}-1)}, \left( T_{1,p_2+2^{r-1}}^1 \right)_{p_2=0:(2^{r-1}-1)}, \right. \\ \left. \left( T_{2p_1,1}, T_{2p_1+2^{r-2},1}^2 \right)_{p_1=0:(2^{r-3}-1)}, \left( T_{2p_1+2^{r-1},1}^1 \right)_{p_1=0:(2^{r-2}-1)} \right),$$

wherein the sets  $T^2$  contain  $3 \cdot 2^{r-2}$  frequency-points each. Continuing such an improvement, we can estimate the number,  $\Delta m'_{2^r}$ , of multiplications saved by this improvement as follows:

$$\Delta m'_{2^r} \geq 2^{r-1} m(C_{2^r;2}) + 2^{r-2} m(C_{2^r;4}) + \dots + 2m(C_{2^r;2^{r-1}}) \\ \geq 2^{r-1} \left[ m(C_{2^r}) - \frac{1}{2} m(C_{2^{r-1}}) - \frac{1}{4} m(C_{2^{r-2}}) - \dots - \frac{1}{2^{r-3}} m(C_8) \right] \\ - 2m(C_4) - \frac{1}{3}(4^r - 16) \\ \geq \frac{1}{3}(4^r - 4) - 2^r + 8,$$

where we consider that  $m(C_{2^k;2}) = m(C_{2^k}) - m(C_{2^{k-1}}) - 2^{k-1}$ , for  $k = 3 : r$ , and  $m(C_{2^r;2^{r-1}}) = 2$ . Therefore, at the last step of improvement, the total number of multiplications is reduced to

$$m_{2^r, 2^r|step(r-1)}^c = m_{2^r, 2^r}^c - \Delta m'_{2^r} \leq \frac{2}{3} 4^{r+1} - 2^{r-2}(r^2 + 7r + 10) - \frac{20}{3}. \tag{19.172}$$

So, using the tensor representation of the shifted Fourier transform, we obtain three estimates for the multiplicative complexity of the 2-D DCT, which are estimated respectively by formulae (19.161), (19.165), and (19.172). For some integers  $r$ , the values of these estimates and the known estimates, which have been received in the polynomial and recursive algorithms, are given in Table 19.4. We should note, that a few addition multiplications can be saved on the steps  $k = 2, 3, \dots, (r - 1)$  in the improved tensor algorithm, if we succeed in calculating the incomplete 1-D DCT of type I,  $K_{2^r;2^k}$ , by a method similar to the pruning algorithm [39,41].

**Example 19.18**

We here describe the improved tensor algorithm of the  $15 \times 15$ -point DCT. The splitting of the  $15 \times 15$ -point DFT is performed by twelve 15-point DFTs and twelve 15-point modified DFTs, as is shown in (19.146). Therefore, the  $15 \times 15$ -point DFT can be split by twelve 15-point DCTs of

**TABLE 19.4** The Number of Multiplications Required to Calculate the  $2^r \times 2^r$ -Point DCT by the SDFT, Tensor, Improved Tensor, Polynomial, and Recursive Algorithms

$2^r \times 2^r$	$m_{\text{SDFT}}^c$	$m_{\text{tensor}}^c$	$m_{\text{step1}}^c$	$m_{\text{step}(r-1)}^c$	$m_{\text{polyn}}^c$	$m_{\text{rec}}^c$
$8 \times 8$	110	104	88	86	96	112
$16 \times 16$	582	536	476	460	512	640
$32 \times 32$	2,870	2,480	2,236	2,164	2,560	3328
$64 \times 64$	13,590	10,816	9,820	9,508	12,288	—
$128 \times 128$	62,678	45,568	41,532	40,228	57,344	—
$256 \times 256$	283,734	188,032	171,772	166,436	262,144	—
$512 \times 512$	1,266,518	766,208	700,924	679,332	1,179,648	—
$1024 \times 1024$	5,591,382	3,098,624	2,836,988	2,750,116	5,242,880	—

type I, and twelve 15-point DCTs of type II. The number of multiplications required to calculate this 2-D DCT can be estimated as

$$m_{15,15}^c = 12[m(\mathcal{K}_{15}) + m(\mathcal{C}_{15})].$$

Taking the known estimate  $m(\mathcal{C}_{15}) = 18[38]$  and considering that  $m(\mathcal{K}_{15}) < m(\mathcal{C}_{15})$ , we obtain  $m_{15,15}^c < 24m(\mathcal{C}_{15}) = 432$ . However, this estimate can be essentially improved if we use the modified tensor algorithm. Indeed, by means of the calculations similar to the ones given in Example 19.17, we can obtain the following splitting  $\mathcal{R}(\mathcal{C}_{15,15}; \sigma')$  of the  $15 \times 15$ -point DCT:

$$\left\{ \begin{array}{l} \mathcal{C}_{15}, \mathcal{K}_{15,0}, \mathcal{C}_{15,0}, \mathcal{C}_{15,0}, \mathcal{K}_{15,5}, \mathcal{C}_{15,5}, \underbrace{\mathcal{K}_{15,3,5}, \dots, \mathcal{K}_{15,3,5}}_{10 \text{ times}}, \\ \underbrace{\mathcal{C}_{15,3,5}, \dots, \mathcal{C}_{15,3,5}}_{8 \text{ times}} \end{array} \right\} \quad (19.173)$$

where  $\mathcal{K}_{15,3,5}$  and  $\mathcal{C}_{15,3,5}$  denote respectively the incomplete 15-point DCTs of types I and II, wherein the outputs with numbers multiple to 3 and 5 are not calculated. Outputs are calculated only for eight points 1, 2, 4, 7, 8, 11, 13, and 14. In the incomplete cosine transforms  $\mathcal{K}_{15,5}$  and  $\mathcal{C}_{15,5}$ , the outputs with numbers 0, 5, and 10 are not calculated. It is not difficult to see, that the 15-point DCT can be split into three 5-point DCTs. For that we consider the sets  $T'_{p_0} = \{(p_0 + 6k) \bmod 15; k = 0 : 4\}$ , where  $p_0$  is a number of the integer interval  $[0, 14]$ . Then, three subsets  $T'_0$ ,  $T'_5$ , and  $T'_{10}$  form a partition  $\omega'$  of the set  $X_{15} = \{0, 1, \dots, 14\}$ :  $T'_0 = \{0, 6, 12, 3, 9\}$ ,  $T'_5 = \{5, 11, 2, 8, 14\}$ ,  $T'_{10} = \{10, 1, 7, 13, 4\}$ . This partition corresponds to the well-known Chinese remainder theorem mapping for  $N=15$ . The restriction of the 15-point DCT on each subset  $T' \in \omega'$  is the 5-point DCT. For instance, for  $p \in T'_0$ , we have the following:

$$\begin{aligned} C_p = C_{(0;k)} &= \sum_{n=0}^{14} f_n \cos\left(\frac{\pi}{15} n(0 + 6k)\right) = \sum_{n=0}^{14} f_n \cos\left(\frac{\pi}{5} 2nk\right) \\ &= \sum_{n=0}^4 (f_n + f_{n+5} + f_{n+10}) \cos\left(\frac{\pi}{5} n(2k)\right), \quad k = 0 : 4. \end{aligned}$$

To calculate the incomplete 15-point DCT of type II,  $\mathcal{C}_{15,3,5}$ , it is sufficient to calculate two incomplete 5-point DCTs,  $\mathcal{C}_{5,0}$ , which requires 12 multiplications. Therefore, using the splitting in Equation 19.173, we can estimate the multiplicative complexity of the  $15 \times 15$ -point DCT as

$$\begin{aligned} m_{15,15}^c &\leq m(\mathcal{C}_{15}) + 3m(\mathcal{C}_{15,0}) + 2m(\mathcal{C}_{15,5}) + 18m(\mathcal{C}_{15,3,5}) \\ &= 6 \cdot 18 + 18 \cdot 12 = 324. \end{aligned}$$

We note for comparison, that the same estimate have been obtained in [38].

## 19.9 3-D Paired Representation

In this section, we introduce a more advanced form of representation of multidimensional signals and images, than the tensor representation. Such a form associates with special partitions of the spatial lattice in the frequency-domain, that reveal the multidimensional DTs such as the Fourier, Hadamard, and cosine transforms. We stand in detail on the 2-D case, since the three- and more-dimensional cases are described similarly. In the tensor and the new forms of representation proposed here, multidimensional signals and images are represented by the sets of 1-D splitting-signals, and dimensions of the signals change only the cardinality of such sets.

The tensor representation of multidimensional signals is associated with an irreducible covering  $\sigma_J$  not being partitions of the lattice. This is why, there is a redundancy in calculations; the same spectral information contains in different groups of frequency-points and the splitting-signals together contains more points than the volume of the represented multidimensional signals. As an illustration, Figure 19.23 shows the image  $256 \times 256$  in part (a), along with the image of 384 1-D splitting-signals in (b), which are lying on rows of this image. These 1-D signals are also called image-signals; they describe uniquely the original image and at the same time they split the mathematical structure of the 2-D DFT (shown in (c)) into a set of separate 1-D transforms (shown all together as an image in (d)). The 2-D

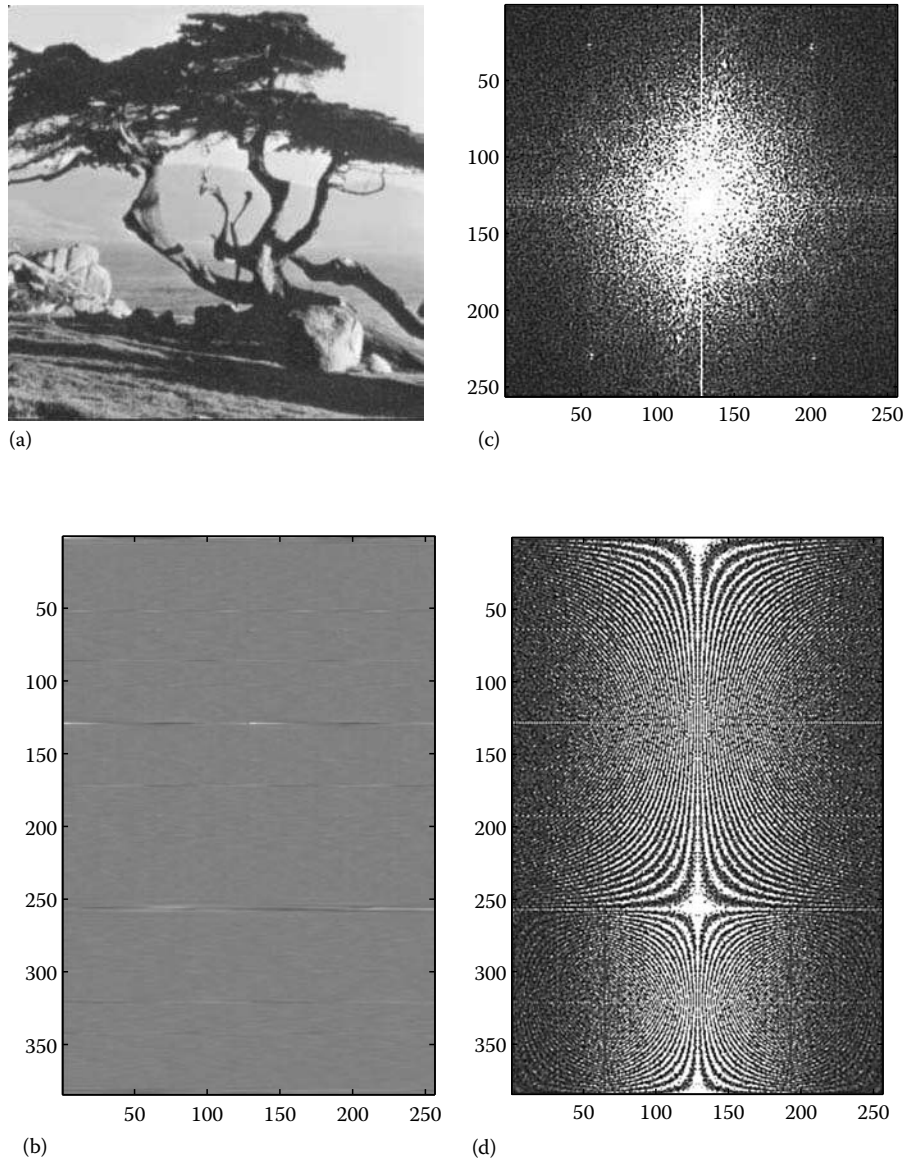


**FIGURE 19.23** Conventional and tensor representation of the image and its spectrum. (a) Tree image  $256 \times 256$ , (b) the image of all 384 splitting-signals. (c) the  $256 \times 256$ -point DFT of the image, and (d) the image of the 256-point DFTs of splitting-signals. (All DFTs are shifted to the centers.)

DFT is thus considered as a unique set of separate 1-D DFTs. The image in (b) is the tensor representation of the image, or the tensor transform of the image,

$$\mathcal{X} = \mathcal{X}_\sigma: f \rightarrow \{f_{T_{p,s}}; T_{p,s} \in \sigma_J\}. \quad (19.174)$$

One can note, that a few slitting-signals are well expressed, which can be seen also from the energy plot of all splitting-signals, which is given in Figure 19.24. For this image, the high

energy is concentrated in the splitting-signals of numbers 1, 129, 257, 172, 52, 258, and 2 that correspond to the generators  $(p, s) = (0, 1), (128, 1), (1, 0), (171, 1), (51, 1), (1, 2),$  and  $(1, 1)$ , respectively. The processing of only these signals may lead to good results, for instance in image enhancement [17,18]. One such example has been shown in Figure 19.5, where the image is enhanced by one splitting-signal of the generator  $(p, s) = (7, 1)$ . However, all together the splitting-signals contain  $384 \cdot 256$  points which is much greater than the original size  $256 \cdot 256$ .

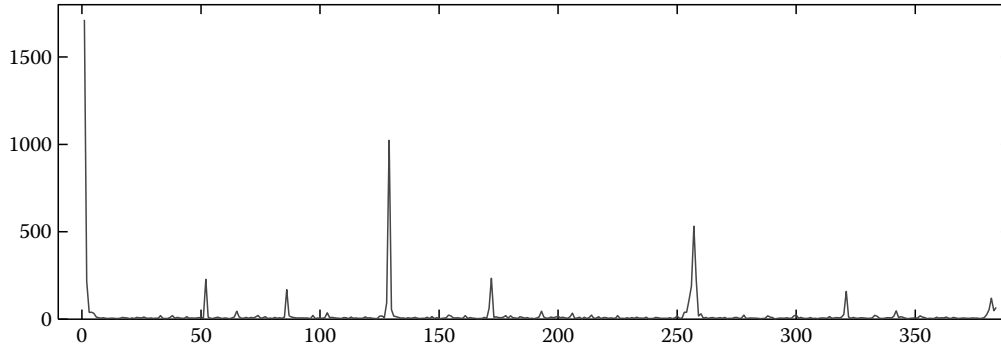


FIGURE 19.24 Energy of all 384 splitting-signals of the tree image.

In order to remove such a redundancy, we consider the concept of the paired representation of multidimensional signals and images. Unlike the tensor representation, the paired representation allows for distribution of the spectral information of multidimensional signals and images by disjoint sets of frequency-points. This property makes the paired representation the most attractive in multidimensional signal and image processing as well as in the construction of effective algorithms for calculating multidimensional transforms. As examples, we first consider the paired representation of images with respect to the discrete unitary Fourier, Hadamard, Hartley, and cosine transforms on the rectangular lattices. We also will describe the paired representation of images defined on the hexagonal lattices.

### 19.9.1 2D-to-3D Paired Transform

A complete system of functions can be derived from the 2-D DFT as a system that splits the transform [12,21]. In other words, there exists a system of functions that reveals completely the mathematical structure of the 2-D DFT when considering it as a minimal composition of short 1-D DFTs. Such a system is 3-D, i.e., the system of functions is numbered by three parameters, namely, two parameters for the spatial frequencies and one parameter for the time. The change in time determines a series of functions, and the total number of triples numbering the system of functions, since the system is complete, equals the size of the 2-D DFT, let us say  $N \times N$ . The complete systems of such functions, which are called the paired functions, exist also in the one- and multidimensional cases.

Let  $N$  be not a prime number. We consider an irreducible covering  $\sigma_J$  of the lattice  $X_{N,N}$  and for each generator  $(p, s) \in J$ , we determine the characteristic functions of the sets  $V_{p,s,t} = \{(n_1, n_2); n_1p + n_2s = t \pmod N\}$  as follows

$$\mathcal{X}_{p,s,t}(n_1, n_2) = \begin{cases} 1; & (n_1, n_2) \in V_{p,s,t}, \\ 0; & \text{otherwise,} \end{cases} \quad t = 0: (N-1). \quad (19.175)$$

These functions describe the tensor transformation of a 2-D sequence or image  $f$  with respect to the Fourier transformation.

Indeed, the components  $f_{p,s,t}$  of the splitting-signal  $f_{T_{p,s}}$  are defined as

$$f_{p,s,t} = \mathcal{X}_{p,s,t} \circ f = \sum_{n_1=0}^{N-1} \sum_{n_2=0}^{N-1} \mathcal{X}_{p,s,t}(n_1, n_2) f_{n_1, n_2}, \quad t = 0: (N-1). \quad (19.176)$$

Therefore, the tensor transformation  $\mathcal{X}_\sigma$  is described by the following system of binary functions

$$\mathcal{X}_\sigma = \{\mathcal{X}_{p,s,t}; T_{p,s} \in \sigma_J, t = 0: (N-1)\}. \quad (19.177)$$

The tensor transformation is not orthogonal, but, by means of this transformation, one can synthesize unitary transformations.

**Definition 19.2:** Let  $L$  be a nontrivial divisor of the number  $N$  and let  $W_L = \exp(-2\pi j/L)$ . For a given frequency-point  $(p, s) \in X_{N,N}$  and integer  $t \in \{0, 1, 2, \dots, N/L-1\}$ , the function

$$\mathcal{X}'_{p,s,t}(n_1, n_2) = \mathcal{X}'_{p,s,t;L}(n_1, n_2) = \sum_{k=0}^{L-1} W_L^k \mathcal{X}_{p,s,t+k\frac{N}{L}}(n_1, n_2) \quad (19.178)$$

is called an  $L$ -paired function.

The operation of the paired functions over a 2-D sequence  $f$  of size  $N \times N$  determines the components which can be calculated from components of the tensor representation by

$$f'_{p,s,t} = \mathcal{X}'_{p,s,t} \circ f = \sum_{k=0}^{L-1} f_{p,s,t+k\frac{N}{L}} W_L^k, \quad k = 0: (N/L-1). \quad (19.179)$$

The  $N/L$ -point signal

$$f'_{T_{p,s}} = (f'_{p,s,0}, f'_{p,s,1}, \dots, f'_{p,s,N/L-1}) \quad (19.180)$$



determines the 2-D DFT of  $f$  at frequency-points of the following subset of the cyclic group  $T_{p,s}$ :

$$T' = T'_{p,s,L} = \{(\overline{(kL+1)p}, \overline{(kL+1)s}); k = 0 : (N/L - 1)\}. \tag{19.181}$$

Indeed, the following formula holds:

$$F_{(kL+1)p, (kL+1)s} = F_{\overline{(kL+1)p}, \overline{(kL+1)s}} = \sum_{t=0}^{N/L-1} (f'_{p,s,t} W^t) W_{N/L}^{kt} \tag{19.182}$$

where  $k = 0 : (N/L - 1)$ . Thus, the  $N/L$ -point DFT of the modified signal

$$g_{T'_{p,s}} = f'_{T'_{p,s}} W = (f'_{p,s,0}, f'_{p,s,1} W, \dots, f'_{p,s,N/L-1} W^{N/L-1}) \tag{19.183}$$

defines the 2-D DFT at frequency-points of the subset  $T'_{p,s,L}$ . Here  $\mathbf{W}$  denotes the diagonal matrix with coefficients  $1, W, W^2, \dots, W^{N/L-1}$  on the diagonal. The signal  $f'_{T'_{p,s}}$  is called the *paired splitting-signal*, and the signal  $g_{T'_{p,s}}$  is the *modified paired splitting-signal*.

It is interesting to note, that the subsets  $T'_{p,s}$  compose a unique partition  $\sigma' = (T'_{p,s})$  of the lattice  $X_{N,N}$ . Indeed, each subset  $T'_{p,s}$  itself represents an orbit of the point  $(p, s)$  with respect to the movement group  $G = \{(kL+1) \bmod N; k = 0 : (N/L - 1)\}$ . All orbits are equal or disjoint between themselves, and together they compose the whole lattice. In the general case, such a partition is defined as

$$\sigma' = \sigma'_{J'} = \left( \left( (T'_{p,s,L})_{L \in D} \right)_{(p,s) \in J'} \right), \tag{19.184}$$

for a certain subset  $J'$  of generators  $(p, s)$  and a set of factors  $D$  of the number  $N$ . In many cases of  $N$ , the set  $D$  consists of only one factor.

### 19.9.2 $N$ Is a Power of Two

In this section, we consider the case of most interest, when  $N$  is a power of two. We describe the paired representation of 2-D

signals or images  $f$  of size  $N \times N$ , as well as the paired transform of  $f$  on the example when  $N = 8$ . The general case, when  $N = 2^r$ ,  $r > 1$ , is also considered.

#### Example 19.19

Let  $L = 2$  and let  $X$  be the lattice  $X_{8,8}$ . To compose a partition of the lattice, we first note, that each subset  $T'_{p,s}$  is the orbit of the point  $(p, s)$  with respect to the movement group  $G = \{1, 3, 5, 7\}$ . For instance, the subset  $T'_{1,1} = T'_{1,1,2} = \{(1, 1), (3, 3), (5, 5), (7, 7)\}$  is the orbit of the point  $(1, 1)$ . The point  $(1, 1)$  "is moving" starting (at time  $t = 0$ ) from itself and "returning" back in four units of time (at time  $t = 4$ ) as  $(1, 1) \rightarrow (3, 3) \rightarrow (5, 5) \rightarrow (7, 7) \rightarrow (1, 1)$ . In the orbit  $T'_{3,1}$ , the point "is moving" as follows:  $(3, 1) \rightarrow (1, 3) \rightarrow (7, 5) \rightarrow (5, 7) \rightarrow (3, 1)$ .

The set of all orbits dividing the lattice  $X_{8,8}$  in unique and can be described as follows:

$T'_{0,1}$	$T'_{1,1}$	$T'_{2,1}$	$T'_{3,1}$	$T'_{4,1}$	$T'_{5,1}$	$T'_{6,1}$	$T'_{7,1}$	$T'_{1,0}$	$T'_{1,2}$	$T'_{1,4}$	$T'_{1,6}$	4
$T'_{0,2}$	$T'_{2,2}$	$T'_{4,2}$	$T'_{6,2}$	$T'_{2,0}$	$T'_{2,4}$							2
$T'_{0,4}$	$T'_{4,4}$	$T'_{4,0}$										1
$T'_{0,0}$												1

(19.185)

22 orbits divide the lattice, and the orbits shown on the same row have equal cardinalities, which are shown in the right column of this table. For instance, the point  $(0, 1)$  runs around its orbit for time  $t = 4$ , and the orbit of the point  $(0, 2)$  is twice shorter,  $(0, 2) \rightarrow (0, 6) \rightarrow (0, 2)$ . The set of generators of these orbits are shown in Figure 19.25 in part a, by the filled circles. The locations of frequency-points of orbits  $T'_{p,s}$  for generators  $(p, s) = (1, 1), (3, 1),$  and  $(6, 1)$  are shown in parts (b) through (d), respectively.

Twenty-two splitting-signals defined for generators of the subsets, or orbits  $T'$  of the partition  $\sigma'$  determines the value of the 2-D DFT at frequency-points of these subsets. For instance, the signal  $f'_{T'_{1,1}}$  carries the spectral information of a 2-D signal  $f$  at frequency-points  $(1, 1), (3, 3), (5, 5),$  and  $(7, 7)$ . According to the table of (19.185), the 2-D  $8 \times 8$ -point DFT is split by twelve 4-point DFTs, six 2-point DFTs, and four 1-point DFTs (which are the identity transformations).

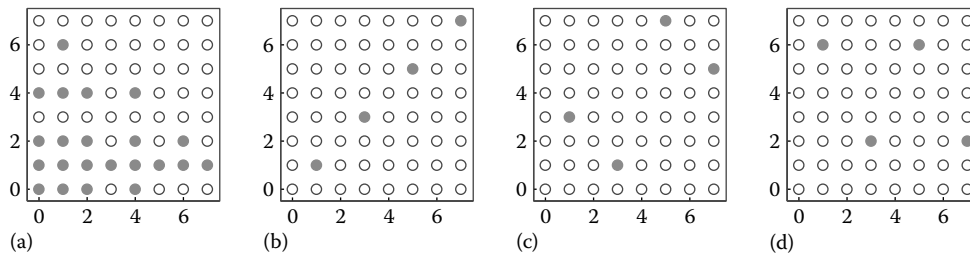


FIGURE 19.25 (a) Twenty-two generators on the lattice  $8 \times 8$ , and the orbits of points (b)  $(1, 1)$ , (c)  $(3, 1)$ , and (d)  $(6, 1)$ . (The generators and elements of the orbits are shown by the filled circles.)

This table shows also the way of composing the complete set of basis paired functions. Indeed, it follows from the definition (19.178), that 2-paired, or simply paired functions are calculated by

$$\begin{aligned} \mathcal{X}'_{p,s,t}(n_1, n_2) &= \mathcal{X}_{p,s,t}(n_1, n_2) - \mathcal{X}_{p,s,t+4}(n_1, n_2) \\ &= \begin{cases} 1; & \text{if } n_1p + n_2s = t \pmod 8, \\ -1; & \text{if } n_1p + n_2s = t + 4 \pmod 8. \\ 0; & \text{otherwise,} \end{cases} \end{aligned} \tag{19.186}$$

where  $t=0 : 3$ . For instance, the values of the function  $\mathcal{X}'_{3,1,2}(n_1, n_2)$  can be written in the form of the following mask:

$$[\mathcal{X}'_{3,1,2}] = \begin{bmatrix} 0 & 0 & 1 & 0 & 0 & 0 & -1 & 0 \\ 0 & 0 & 0 & -1 & 0 & 0 & 0 & 1 \\ -1 & 0 & 0 & 0 & 1 & 0 & 0 & 0 \\ 0 & 1 & 0 & 0 & 0 & -1 & 0 & 0 \\ 0 & 0 & -1 & 0 & 0 & 0 & 1 & 0 \\ 0 & 0 & 0 & 1 & 0 & 0 & 0 & -1 \\ 1 & 0 & 0 & 0 & -1 & 0 & 0 & 0 \\ 0 & -1 & 0 & 0 & 0 & 1 & 0 & 0 \end{bmatrix}.$$

The 64 triplets  $(p, s, t)$ , or numbers of the complete system of paired functions  $\mathcal{X}'_{p,s,t}$  are composed from the generators  $(p, s)$  and time variable  $t$ , which runs numbers 0, 1, 2, 3, for the orbits in the first row in the table of Equation 19.185. For short orbits in the second row,  $t$  takes only values of 0 and 2. Indeed, both coordinates of points on these orbits are even, therefore conditions  $(n_1p + n_2s = t \pmod 8)$  and  $(n_1p + n_2s = t + 4 \pmod 8)$  do not hold for odd  $t = 1$  and 3. In other words, for these triples  $(p, s, t)$ , we have  $\mathcal{X}'_{p,s,t} \equiv 0$ , and we do not consider such functions. There is no movement (or  $t=0$ ) in single-point orbits for  $(p, s) = (0, 4)$ ,  $(4, 4)$ ,  $(4, 0)$ , and  $(0, 0)$ . The set of 64 triplets for the complete system of paired functions are given in the following table:

$(p, s)$	$t$
$(0, 1), (1, 1), (2, 1), (3, 1), (4, 1), (5, 1), (6, 1), (7, 1), (1, 0), (1, 2), (1, 4), (1, 6), (0, 1, 2, 3)$	0, 1, 2, 3
$(0, 2), (2, 2), (4, 2), (6, 2), (2, 0), (2, 4)$	0, 2
$(0, 4), (4, 4), (4, 0)$	0
$(0, 0)$	0

(19.187)

Figure 19.26 shows all 64 basis paired functions  $\mathcal{X}'_{p,s,t}$ , which are placed in the order given in the above table, starting from the top on the left to the bottom to the right. For instance, the first

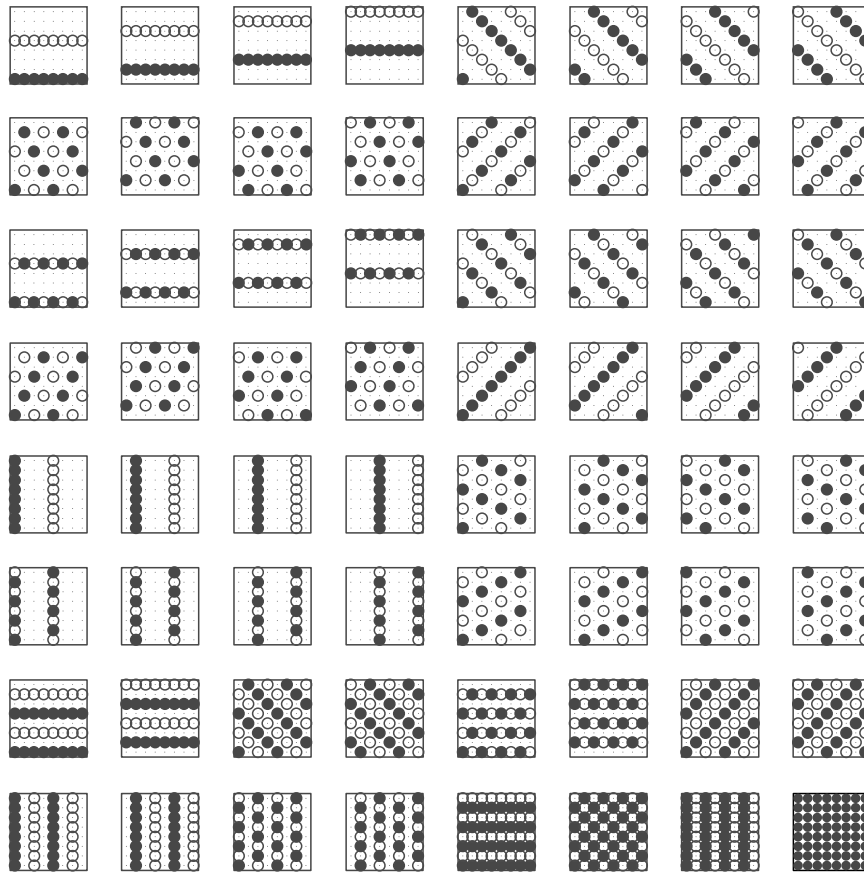


FIGURE 19.26 The complete system of 2-D basis functions of the  $8 \times 8$ -paired transform. (Values of 1 are shown by the filled circles, and  $-1$  by the open circles.)

four functions have numbers  $(0, 1, t)$ , where  $t=0: 3$ . The filled circle is used for value 1 and the open circle for  $-1$ . It is not difficult to see that all these functions are orthogonal. The complete set of paired functions define the paired representation of the 2-D sequence or image  $f$

$$f \rightarrow \{f_{T'_{p,s}}; T'_{p,s} \in \sigma'\}. \quad (19.188)$$

The components of these paired splitting-signals  $f_{T'_{p,s}}$  are calculated from the components of the splitting-signals  $f_{T_{p,s}}$  of the tensor representation of  $f$  by

$$f'_{p,s,t} = f_{p,s,t} - f_{p,s,t+4}, \quad t \in \{0, 1, 2, 3\}. \quad (19.189)$$

The transformation

$$\mathcal{X}': f \rightarrow \{f'_{p,s,t}; T'_{p,s} \in \sigma', t=0: (\text{card}(T'_{p,s}) - 1)\} \quad (19.190)$$

is called the paired transformation. Thus the paired transform is the representation of the image in the form of 1-D splitting-signals; components of all splitting-signals together compose the paired transform.

Let  $(p, s) = (3, 1)$  and let  $f$  be the following image of size  $8 \times 8$ :

$$f = \begin{bmatrix} \underline{1} & 2 & 1 & 3 & 1 & 2 & 1 & 3 \\ 2 & 0 & 1 & 2 & 2 & 4 & 2 & 1 \\ 1 & 3 & 2 & 2 & 1 & 1 & 1 & 2 \\ 4 & 1 & 0 & 1 & 3 & 1 & 3 & 1 \\ 2 & 4 & 1 & 2 & 1 & 3 & 2 & 2 \\ 2 & 4 & 1 & 2 & 1 & 2 & 2 & 1 \\ 2 & 4 & 1 & 2 & 1 & 5 & 2 & 1 \\ 2 & 4 & 1 & 2 & 1 & 1 & 3 & 2 \end{bmatrix}.$$

We will calculate the 2-D DFT of  $f$  at frequency-points of the orbit of the point  $(3, 1)$ . For that, first we write all values of  $t$  in the equations  $3n_1 + n_2 = t \pmod 8$  in the form of the following table:

$$\|t = (3n_1 + n_2) \pmod 8\|_{n_2, n_1=0:7} = \begin{bmatrix} \underline{0} & 1 & 2 & 3 & 4 & 5 & 6 & 7 \\ 3 & 4 & 5 & 6 & 7 & 0 & 1 & 2 \\ 6 & 7 & 0 & 1 & 2 & 3 & 4 & 5 \\ 1 & 2 & 3 & 4 & 5 & 6 & 7 & 0 \\ 4 & 5 & 6 & 7 & 0 & 1 & 2 & 3 \\ 7 & 0 & 1 & 2 & 3 & 4 & 5 & 6 \\ 2 & 3 & 4 & 5 & 6 & 7 & 0 & 1 \\ 5 & 6 & 7 & 0 & 1 & 2 & 3 & 4 \end{bmatrix}.$$

According to this table, the components of the splitting-signal  $f_{T'_{3,1}}$  are defined as follows:

$$f_{T'_{3,1}} = \begin{cases} f'_{3,1,0} = (f_{0,0} + f_{1,5} + f_{2,2} + f_{3,7} + f_{4,4} + f_{5,1} + f_{6,6} + f_{7,3}) - \\ (f_{0,4} + f_{1,1} + f_{2,6} + f_{3,3} + f_{4,0} + f_{5,5} + f_{6,2} + f_{7,7}) = \\ (1 + 4 + 2 + 1 + 1 + 4 + 2 + 2) - (1 + 0 + 1 + 1 + 2 + 2 + 1 + 2) = 7 \\ f'_{3,1,1} = (f_{0,1} + f_{1,6} + f_{2,3} + f_{3,0} + f_{4,5} + f_{5,2} + f_{6,7} + f_{7,4}) - \\ (f_{0,5} + f_{1,2} + f_{2,7} + f_{3,4} + f_{4,1} + f_{5,6} + f_{6,3} + f_{7,0}) = \\ (2 + 2 + 2 + 4 + 3 + 1 + 1 + 1) - (2 + 1 + 2 + 3 + 4 + 2 + 2 + 2) = -2 \\ f'_{3,1,2} = (f_{0,2} + f_{1,7} + f_{2,4} + f_{3,1} + f_{4,6} + f_{5,3} + f_{6,0} + f_{7,5}) - \\ (f_{0,6} + f_{1,3} + f_{2,0} + f_{3,5} + f_{4,2} + f_{5,7} + f_{6,4} + f_{7,1}) = \\ (1 + 1 + 1 + 1 + 2 + 2 + 2 + 1) - (1 + 2 + 1 + 1 + 1 + 1 + 1 + 4) = -1 \\ f'_{3,1,3} = (f_{0,3} + f_{1,0} + f_{2,5} + f_{3,2} + f_{4,7} + f_{5,4} + f_{6,1} + f_{7,6}) - \\ (f_{0,7} + f_{1,4} + f_{2,1} + f_{3,6} + f_{4,3} + f_{5,0} + f_{6,5} + f_{7,2}) = \\ (3 + 2 + 1 + 0 + 2 + 1 + 4 + 3) - (3 + 2 + 3 + 3 + 2 + 2 + 5 + 1) = -5 \end{cases}$$

This splitting-signal is modified as  $f_{T'_{3,1}} \mathbf{W}$ , where

$$\mathbf{W} = \text{diag}\{1, e^{-j\pi/4}, e^{-j2\pi/4}, e^{-j3\pi/4}\} \\ = \text{diag}\{1, a(1-j), -j, -a(1+j)\}$$

and  $a = \sqrt{2}/2 = 0.7071$ . The four-point DFT of the modified splitting-signal

$$g_{T'_{3,1}} = f_{T'_{3,1}} \mathbf{W} = \{7, -1.4142 + j1.4142, j, 3.5355 + j3.5355\}$$

is calculated as follows:

$$\begin{bmatrix} 1 & 1 & 1 & 1 \\ 1 & -j & -1 & j \\ 1 & -1 & 1 & -1 \\ 1 & j & -1 & -j \end{bmatrix} \begin{bmatrix} 1 & 0 & 0 & 0 \\ 0 & a(1-j) & 0 & 0 \\ 0 & 0 & -j & 0 \\ 0 & 0 & 0 & -a(1+j) \end{bmatrix} \begin{bmatrix} 7 \\ -2 \\ -1 \\ -5 \end{bmatrix} \\ = \begin{bmatrix} 9.1213 + j5.9497 \\ 4.8787 + j3.9497 \\ 4.8787 - j3.9497 \\ 9.1213 - j5.9497 \end{bmatrix}.$$

The obtained 4-point DFT coincides with the  $8 \times 8$ -point DFT of the image  $f$  at four frequency-points of the orbit  $T'_{3,1}$ , i.e.,

$$\begin{bmatrix} F_{3,1} \\ F_{1,3} \\ F_{7,5} \\ F_{5,7} \end{bmatrix} = \begin{bmatrix} 9.1213 + j5.9497 \\ 4.8787 + j3.9497 \\ 4.8787 - j3.9497 \\ 9.1213 - j5.9497 \end{bmatrix}.$$

We can also see from this example, that the pairs of complex conjugate components  $F_{3,1}$  and  $F_{5,7}$ , and  $F_{1,3}$  and  $F_{7,5}$  are obtained from the same splitting-signal. In general, if  $(p_1, p_2)$  lies on the orbit  $T'_{p,s}$ , then the point  $(N-p_1, N-p_2)$  lies also on this orbit.

In the  $N=2^r$  case, when  $r > 1$ , the partition  $\sigma' = (T')$  of the lattice  $X_{2^r, 2^r}$  is composed similarly to the case  $N=8$ . For integers  $n=0: (r-1)$ , we define the sets of generators

$$J_{2^n, 2^n} = \{(1, 0), (1, 1), \dots, (1, 2^n - 1), (0, 1), (2, 1), \\ (4, 1), \dots, (2^n - 2, 1)\}.$$

The totality of  $3 \cdot 2^r - 2$  subsets

$$\sigma' = \left( \left( \left( T'_{2^n p, 2^n s} \right)_{(p,s) \in J_{2^{r-n}, 2^{r-n}}} \right)_{n=0:(r-1)}, \{(0, 0)\} \right) \quad (19.191)$$

is the partition of the lattice  $X$ . The complete set of paired functions  $\mathcal{X}' = \{ \mathcal{X}'_{p,s,t}; (p, s, t) \in U \}$  can thus be defined by the following set of triplets:

$$U = \bigcup_{n=0}^{r-1} \{ 2^n(p, s, t); (p, s) \in J_{2^{r-n}, 2^{r-n}}, t = 0: (2^{r-n-1} - 1) \} \cup \{(0, 0, 0)\}. \quad (19.192)$$

The paired transform  $\mathcal{X}': f \rightarrow \{ f'_{p,s,t}; (p, s, t) \in U \}$  does not require multiplications, but only operations of addition and subtraction.

For  $L = 2$ , the equation in Equation 19.182 takes the following form:

$$F_{(2k+1)p, (2k+1)s} = \sum_{t=0}^{2^{r-1}-1} \left( f'_{p,s,t} W^{kt} \right) W_{2^{r-1}}^{kt}, \quad k = 0: (2^{r-1} - 1), \quad (19.193)$$

where the components

$$f'_{p,s,t} = f_{p,s,t} - f_{p,s,t+2^{r-1}}, \quad t = 0: (2^{r-1} - 1).$$

It directly follows from Equation 19.193 and the given set of triplets  $U$ , that the  $2^r \times 2^r$ -point DFT is split by the paired transform into a set of  $2^r 3 - 2$  short DFTs, namely  $3 \cdot 2^{r-1}$   $2^{r-1}$ -point DFTs,  $3 \cdot 2^{r-2}$   $2^{r-2}$ -point DFTs, ..., six 2-point DFTs, and four 1-point identity transforms, i.e.,

$$\mathcal{R}(\mathcal{F}_{2^r, 2^r}; \sigma') = \left\{ \underbrace{\mathcal{F}_{2^{r-1}, \dots, \mathcal{F}_{2^{r-1}}}}_{3 \cdot 2^{r-1} \text{ times}}, \underbrace{\mathcal{F}_{2^{r-2}, \dots, \mathcal{F}_{2^{r-2}}}}_{3 \cdot 2^{r-2} \text{ times}}, \right. \\ \left. \underbrace{\mathcal{F}_{2^{r-3}, \dots, \mathcal{F}_{2^{r-3}}}}_{3 \cdot 2^{r-3} \text{ times}}, \dots, \underbrace{\mathcal{F}_2, \dots, \mathcal{F}_2}_{6 \text{ times}}, \underbrace{\mathcal{F}_1, \dots, \mathcal{F}_1}_{4 \text{ times}} \right\}.$$

Indeed, at the frequency-points of the subset  $T'_{p,s}$  of the partition  $\sigma'$ , the 2-D DFT of  $f$  is completely determined by the  $2^{r-n-1}$ -point splitting-signal

$$f'_{T'_{p,s}} = \left\{ f'_{p,s,0}, f'_{p,s,2^n}, f'_{p,s,2 \cdot 2^n}, f'_{p,s,3 \cdot 2^n}, \dots, f'_{p,s,2^{r-1}-2^n} \right\},$$

where the integer  $n \geq 0$  is defined by the simple equation  $2^n = g.c.d(p, s)$ . Indeed, if  $t$  is not divisible by  $2^n$ , then the sets  $V_{p,s,t} = \emptyset$  and  $V_{p,s,t+2^{r-1}} = \emptyset$ , and therefore  $f'_{p,s,t} \equiv 0$ . Each  $2^{r-n-1}$ -point DFT in the right side of Equation 19.193 itself represents the

$2^{r-n-1}$ -point DFT. In other words, if  $(p, s) = 2^n(p_0, s_0)$  where  $(p_0, s_0) \in J_{2^{r-n}, 2^{r-n}}$ , then

$$F_{(2k+1)p, (2k+1)s} = \sum_{t=0}^{2^{r-n-1}-1} \left( f'_{p,s,2^n t} W_{2^{r-n}}^{t} \right) W_{2^{r-n-1}}^{kt}, \quad k = 0: (2^{r-n-1} - 1). \quad (19.194)$$

### Example 19.20

We consider the  $N = 8$  case, for which the partition  $\sigma'$  of the lattice  $X_{8,8}$  has been described in Example 19.19. Twelve subsets  $T'$  of this partition consist of four points each, six subsets of two points each, and the remaining four subsets are one-point sets. The splitting of the  $8 \times 8$ -point DFT thus equals

$$\mathcal{R}(\mathcal{F}_{8,8}; \sigma') = \left\{ \underbrace{\mathcal{F}_4, \dots, \mathcal{F}_4}_{12 \text{ times}}, \underbrace{\mathcal{F}_2, \dots, \mathcal{F}_2}_6 \text{ times}, \underbrace{\mathcal{F}_1, \dots, \mathcal{F}_1}_4 \text{ times} \right\}. \quad (19.195)$$

The first twelve 4-point DFTs are calculated over the modified splitting-signals

$$g_{T'_{p,s}} = \left\{ f'_{p,s,0}, f'_{p,s,1} W, f'_{p,s,2} W^2, f'_{p,s,3} W^3 \right\} \\ = \left\{ f'_{p,s,0}, a(1-j)f'_{p,s,1}, -j f'_{p,s,2}, -a(1+j)f'_{p,s,3} \right\} \quad (19.196)$$

where  $a = \sqrt{2}/2 = 0.7071$  and  $W = \exp(-j2\pi/8) = a(1-j)$ . The generators  $(p, s)$  of these signals lie on the first row in the table of Equation 19.187. The calculation in Equation 19.196 uses two operations of multiplication by the factor of  $a$ , for each splitting-signal. The next six 2-point DFTs are calculated over the short modified splitting-signals

$$g_{T'_{p,s}} = \left\{ f'_{p,s,0}, f'_{p,s,2} W^2 \right\} = \left\{ f'_{p,s,0}, -j f'_{p,s,2} \right\}$$

which do not use multiplications. The generators  $(p, s)$  of these signals lie on the second row in the above mentioned table. Thus, the total number of operations of multiplication for calculating the  $8 \times 8$ -point DFT through the splitting (19.195) equals  $m'_{8,8} = 12 \cdot 2 = 24$ .

### Example 19.21

The calculation of the  $16 \times 16$ -point DFT by the paired transform is performed by means of 216 operations of multiplication. Indeed, the splitting of the  $16 \times 16$ -point DFT by the partition  $\sigma' = (T')$  equals

$$\mathcal{R}(\mathcal{F}_{16,16}; \sigma') = \left\{ \underbrace{\mathcal{F}_8, \dots, \mathcal{F}_8}_{24 \text{ times}}, \underbrace{\mathcal{F}_4, \dots, \mathcal{F}_4}_{12 \text{ times}}, \right. \\ \left. \underbrace{\mathcal{F}_2, \dots, \mathcal{F}_2}_6 \text{ times}, \underbrace{\mathcal{F}_1, \dots, \mathcal{F}_1}_4 \text{ times} \right\}.$$

The cardinalities of the largest subsets  $T'_{p,s}$  of the partition  $\sigma'$  of the lattice  $X_{16,16}$  equal 8. The generators for these subsets are taken from the set  $J_{16,16}$ , and the corresponding modified splitting-signals have the following form:

$$g_{T'_{p,s}} = f_{T'_{p,s}} \mathbf{W} = \left\{ f'_{p,s,0}, f'_{p,s,1} W, f'_{p,s,2} W^2, f'_{p,s,3} W^3, \dots, f'_{p,s,7} W^7 \right\} \quad (19.197)$$

where  $W = \exp(-j2\pi/16) = 0.9239 - j0.3827$ . This product uses six nontrivial operations of multiplication by the twiddle factors  $W^t$ ,  $t = 1, 2, 3, 5, 6, 7$ . The 8-point DFT requires two operations of multiplication. Therefore the calculation of 24 eight-point DFTs in the splitting of the  $16 \times 16$ -point DFT requires  $24 \cdot 8$  operations of multiplication. The calculation of the 4-point DFTs over the modified splitting-signals of length four has been described in Example 19.20. Each such transform uses two operations of multiplication. The total number of operations of multiplication required to calculate the  $16 \times 16$ -point DFT by the paired transform is calculated by

$$\begin{aligned} m'_{16,16} &= 24(m_8 + 8 - 2) + 12(m_4 + 4 - 2) = 24(2 + 6) + 12(2) \\ &= 192 + 24 = 216. \end{aligned}$$

We note for comparison, that the tensor algorithm of the  $16 \times 16$ -point DFT uses  $24m_{16} = 24 \cdot 10 = 240$  operations of multiplication.

In the general  $N = 2^r$  case, the number of operations of multiplication required for calculating the  $2^r \times 2^r$ -point DFT by the paired transforms can be estimated as

$$m_{2^r, 2^r} = \sum_{n=1}^{r-2} 2^{r-n} 3(m_{2^{r-n}} + 2^{r-n} - 2) \leq 2 \cdot 4^{r-1} (r - 7/3) + 8/3, (r > 2). \quad (19.198)$$

When estimating this number, we use the fact that the  $2^n$ -point fast DFT requires  $m_{2^n} = 2^{n-1}(n - 3) + 2$  multiplications, when  $n \geq 3$  [11, 22].

As an illustration of the concept of the paired representation, Figure 19.27 shows the tree image of size  $256 \times 256$  in part (a), along with the splitting-signal  $f_{T'_{3,1}}$  of length 128 together with the modified signal  $f_{T'_{3,1}}$  in (b), the 128-point DFT of the modified signal in (c), and the samples of the 2-D DFT of the image at frequency-points of the subset  $T'_{3,1}$  on the lattice  $X_{256,256}$ , at which the 2-D DFT can be filled by the calculated 1-D DFT of the modified signal.

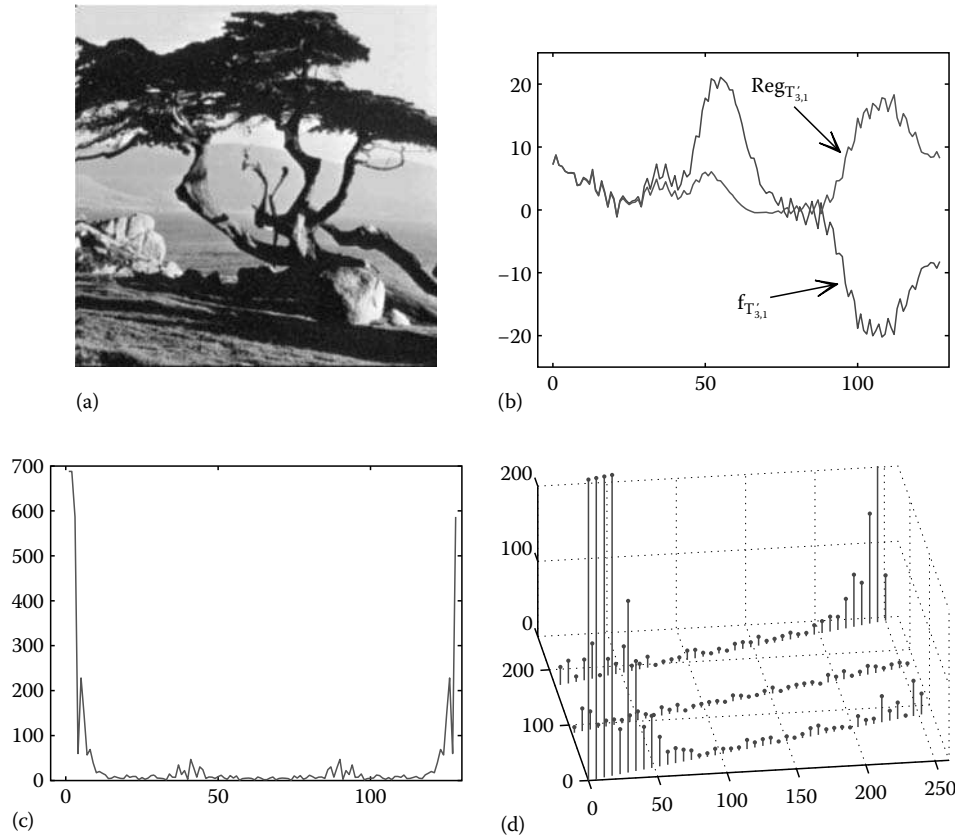


**FIGURE 19.27** (a) Tree image  $256 \times 256$ , (b) the paired splitting-signal  $f_{T'_{3,1}}$  and the real part of the modified signal, (c) the 1-D DFT of the modified signal, and (d) the arrangement of values of the 1-D DFT at frequency-points of the subset  $T'_{3,1}$ . (The 1-D DFT is shown in the absolute scale.)

The paired representation of 2-D signals or images in the form of separate 1-D splitting-signals of different lengths is the transformation of the 2-D data into 3-D space which is a space of 2-D frequency with 1-D time,

$$\mathcal{X}': f_{n_1, n_2} \rightarrow \left\{ f_{T'_{p,s}} = \{f'_{p,s,t}\} \right\}.$$

The paired transform is not separable, but the paired splitting-signals carry the spectral information of  $f_{n_1, n_2}$  at disjoint subsets of frequency-points, and the processing of 2-D signals and images thus can be reduced to processing their 1-D splitting-signals. To illustrate such splitting-signals for images of large sizes, Figure 19.28 shows the tree image  $f_{n_1, n_2}$  of size  $256 \times 256$  in part (a), along with the totality of all 766 splitting-signals of the image in (b). The first 384 splitting-signals of length 128 each are shown in the form of the “image”  $384 \times 128$ . The next 192 splitting-signals of length 64 each are shown in the form of the image  $192 \times 64$ , the splitting-signals of length 32 are shown in the form of the image  $96 \times 32$ , and so on. The whole picture represents the paired transform of the tree image. The set of the 1-D DFTs of all splitting-signals are shown in the form of a similar figure in (c). These 1-D DFTs represent the splitting of the 2-D DFT, by frequency-points which are distributed by disjoint subsets, or orbits in the lattice  $256 \times 256$ . The number of elements in both images (b) and (c) are equal to  $256^2$ . As compared with the tensor representation of the tree image and splitting of the 2-D DFT of the image, which are shown in Figure 19.23, the paired representation provides the representation of the image and the splitting of the 2-D DFT without redundancy.

### 19.9.3 $N$ Is a Power of Odd Prime

For the  $L^r \times L^r$  case, when  $L > 2$  is a prime number, the complete set of 2-D paired functions

$$\mathcal{X}' = \left\{ \mathcal{X}'_{p,s,t}; (p, s, t) \in U \right\} \quad (19.199)$$

is defined by the following set of triplets:

$$U = \bigcup_{n=0}^{r-1} \bigcup_{k=1}^{L-1} U_{k;n} \cup \{(0, 0, 0)\} \quad (19.200)$$

where the disjoint sets  $U_{k;n}$  are defined as

$$U_{k;n} = \{L^n(k, kp_2, t), L^n(kLp_1, k, t); p_2 = 0: (L^{r-n} - 1), p_1, t = 0: (L^{r-n-1} - 1)\}. \quad (19.201)$$

The number of all triplets  $(p, s, t)$  in Equation 19.200 is equal to  $L^{2r}$ . The set  $U$  is not unique; one can replace, for instance, each triplet  $(p, s, t)$  in  $U$  by  $(s, p, t)$ ; but that will change only the numbering of the paired basis functions, and the sign for some of them. Therefore, the new complete system of paired functions will be similar to  $\mathcal{X}'$ . The set  $J'$  of generators  $(p, s)$  in the triplets  $(p, s, t) \in U$  are taken from the partition of the lattice  $X_{L^r, L^r}$  by subsets  $T'_{p,s}$ , which are considered to be

$$\sigma_{J'} = \left( \left( \left( \left( T'_{p_1, p_2; L} \right)_{(p_1, p_2) \in kL^n J_{L^r-n, L^r-n}} \right)_{k=1:(L-1)} \right)_{n=0:(r-1)}, (0, 0) \right). \quad (19.202)$$

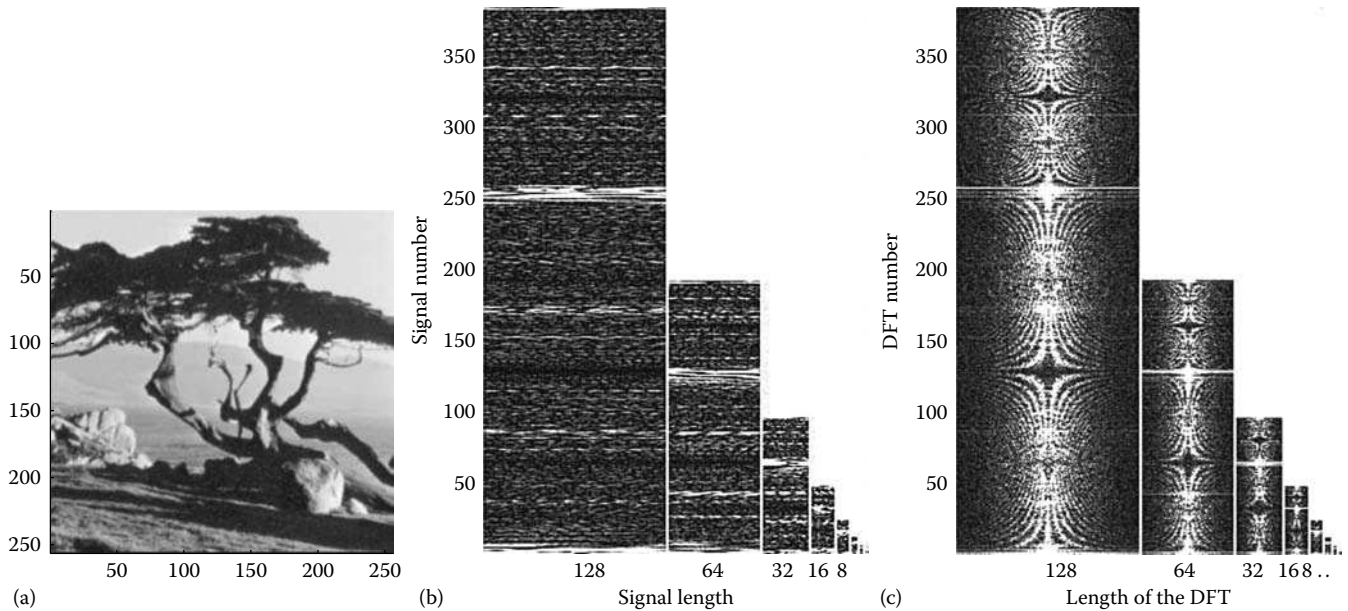


**FIGURE 19.28** (a) Tree image ( $\{f_{n,m}\}$ ), (b) the splitting-signals of lengths 128, 64, 32, 16, 8, 4, 2, 1 ( $\{f'_{p,s,t}\}$ ), and (c) 1-D DFTs of the modified splitting-signals (the transforms are shown in the absolute scale and shifted to the center) ( $\{F_{(2k+1)p, (2k+1)s}\}$ ).

In other words, this set equals

$$J' = J'_{L^r, L^r} = \bigcup_{n=0}^{r-1} \bigcup_{k=1}^{L-1} kL^n J_{L^{r-n}, L^{r-n}} \quad (19.203)$$

and has the cardinality  $(L+1)(L^r-1)+1$ . In the paired representation, the set of 1-D DFTs which split the 2-D DFT of order  $L^r \times L^r$  consists therefore of  $(L+1)(L^r-1)+1$  transforms,  $(L^2-1)L^{r-1}$  of which are  $L^{r-1}$ -point DFTs,  $(L^2-1)L^{r-2}$  are  $L^{r-2}$ -point DFTs, ..., and  $(L^2-1)L$  are  $L$ -point DFTs. The number of operations of multiplication which are used for calculating the  $L^r \times L^r$ -point DFT by such splitting is estimated as

$$m'_{L^r, L^r} \leq (L^2-1) \sum_{n=1}^{r-1} L^{r-n} m_{L^{r-n}} + [(L-1)L^{2r} - (L+1)L^r + 2]. \quad (19.204)$$

The number in the square brackets is referred to as the number of multiplications by all twiddle factors that are used for the calculation of the modified splitting-signals of Equation 19.183. It is supposed that each component  $f'_{p,s,t}$  of the paired transform is calculated directly by the formula (19.179) with  $(L-1)$  operations of complex multiplication by twiddle factors.

### Example 19.22 (9 × 9-Paired Transformation)

Let  $N=9$ , and let  $f$  be a sequence of size  $9 \times 9$ . The square lattice  $X_{9,9}$  can be divided by the following totality of subsets:

$$\sigma' = \left( \begin{array}{cccccccccc} T'_{1,0}, & T'_{1,1}, & T'_{1,2}, & T'_{1,3}, & T'_{1,4}, & T'_{1,5}, & T'_{1,6}, & T'_{1,7}, & T'_{1,8}, & T'_{0,1}, & T'_{3,1}, & T'_{6,1} \\ T'_{2,0}, & T'_{2,2}, & T'_{2,3}, & T'_{2,6}, & T'_{2,8}, & T'_{2,1}, & T'_{2,3}, & T'_{2,5}, & T'_{2,7}, & T'_{0,2}, & T'_{3,2}, & T'_{6,2} \\ T'_{3,0}, & T'_{3,3}, & T'_{3,3}, & T'_{0,3}, & T'_{6,0}, & T'_{6,6}, & T'_{6,3}, & T'_{0,6}, & T'_{0,0} \end{array} \right).$$

The first 24 subsets  $T'_{p,s}$  of this partition (which lie on the first two rows) consists of three elements each, and the remaining 9 subsets are 1-point each.

Using the tensor representation of  $f$  with respect to the 2-D DFT, it is not difficult to calculate all 33 splitting-signals of the 3-paired representation of  $f$ :

$$f_{n,m} \rightarrow \left\{ \begin{array}{l} f'_{T'_{1,0}}, f'_{T'_{1,1}}, f'_{T'_{1,2}}, f'_{T'_{1,3}}, f'_{T'_{1,4}}, f'_{T'_{1,5}}, f'_{T'_{1,6}}, f'_{T'_{1,7}}, f'_{T'_{1,8}}, f'_{T'_{0,1}}, f'_{T'_{3,1}}, f'_{T'_{6,1}}, \\ f'_{T'_{2,0}}, f'_{T'_{2,2}}, f'_{T'_{2,4}}, f'_{T'_{2,6}}, f'_{T'_{2,8}}, f'_{T'_{2,1}}, f'_{T'_{2,3}}, f'_{T'_{2,5}}, f'_{T'_{2,7}}, f'_{T'_{0,2}}, f'_{T'_{3,2}}, f'_{T'_{6,2}}, \\ f'_{T'_{3,0}}, f'_{T'_{3,3}}, f'_{T'_{3,6}}, f'_{T'_{0,3}}, f'_{T'_{6,0}}, f'_{T'_{6,6}}, f'_{T'_{6,3}}, f'_{T'_{0,6}}, f'_{T'_{0,0}} \end{array} \right.$$

The first 24 splitting-signals of the 3-paired representation of  $f$  are 3-point signals each, and they are modified as:

$$f'_{T'_{p,s}} \rightarrow g_{T'_{p,s}} = \left\{ f'_{p_1, p_2, 0}, f'_{p_1, p_2, 1} W, f'_{p_1, p_2, 2} W^2 \right\},$$

where  $W = \exp(-2\pi j/9)$ . The components of these signals are calculated by

$$\begin{aligned} f'_{p_1, p_2, 0} &= f_{p_1, p_2, 0} + f_{p_1, p_2, 3} W_3 + f_{p_1, p_2, 6} W_3^2, \\ f'_{p_1, p_2, 1} &= f_{p_1, p_2, 1} + f_{p_1, p_2, 4} W_3 + f_{p_1, p_2, 7} W_3^2, \\ f'_{p_1, p_2, 2} &= f_{p_1, p_2, 2} + f_{p_1, p_2, 5} W_3 + f_{p_1, p_2, 8} W_3^2, \end{aligned}$$

where  $W_3 = \exp(-2\pi j/3) = -0.5 - j0.8660$  and  $W_3^2 = \overline{W_3}$ . The calculation of the 2-D DFT of  $f$  at frequency-points of subsets  $T'_{p,s}$  can be calculated by the 3-point DFTs of the modified splitting-signals,

$$F_{(3k+1)p \bmod 9, (3k+1)s \bmod 9} = \sum_{t=0}^2 \left( f'_{p,s,t} W_9^t \right) W_3^{kt}, \quad k = 0, 1, 2.$$

Other splitting-signals with generators  $(p, s)$  whose both coordinates are multiple to 3, themselves represent one-point sequences,  $f'_{T'_{p,s}} = f'_{p,s,0}$ . We can also write, that  $f'_{T'_{p,s}} = \{f'_{p,s,0}, 0, 0\}$ . For example,  $f'_{T'_{3,0}} = \{f'_{3,0,0}, 0, 0\}$ , since  $f'_{3,0,1} = f'_{3,0,2} = 0$ . Therefore, the 2-D DFT of  $f$  at these generators equals to these 1-point signals, i.e.,  $F_{p,s} = f'_{p,s,0}$ . As a result, the 3-paired representation leads to the following splitting of the  $9 \times 9$  DFT:

$$\mathcal{R}(\mathcal{F}_{9,9}; \sigma') = \left\{ \underbrace{\mathcal{F}_3, \mathcal{F}_3, \dots, \mathcal{F}_3}_{24 \text{ times}}, \underbrace{1, 1, \dots, 1}_{9 \text{ times}} \right\}.$$

The number of operations of multiplication for calculating the 2-D DFT is estimated as

$$m'_{9,9} = 24(m_3 + 2 + 1) = 24m_3 + 72 = 96,$$

where we consider that the 3-point DFT uses one operation of multiplication, and each modified splitting-signal of length three requires three real multiplications by the factor of 0.8660, which can be counted as one complex multiplication. We note, that the tensor algorithm uses twelve 9-point DFTs and  $m_{9,9} = 12m_9 = 120$  operations of multiplication. We here consider that the 9-point DFT uses 10 operations of multiplication.

### 19.9.4 Set-Frequency Characteristics

Each subset  $T'_{p,s}$  of frequency-points generates the splitting-signal  $f'_{T'_{p,s}}$ , which carries the spectral information of the image  $f_{n,m}$  at these points. The splitting-signal is thus the set-frequency characteristics of the image. This signal defines the corresponding direction-image component of  $f_{n,m}$ . Indeed, let  $D_{p_1, s_1}$  be the following 2-D DFT composed only from the components of the 2-D DFT which lie on the given subset  $T'_{p,s}$ :

$$D_{p_1, s_1} = \begin{cases} F_{p_1, s_1}; & \text{if } (p_1, s_1) \in T'_{p,s}, \\ 0; & \text{otherwise} \end{cases} \quad (19.205)$$

We first consider the case when g.c.d.  $(p, s) = 1$ , i.e.,  $(p, s) \in J_{2^r, 2^r}$ . The inverse transform of the defined 2-D DFT can be calculated as follows:

$$\begin{aligned}
 d_{n,m} &= \frac{1}{N^2} \sum_{p_1=0}^{N-1} \sum_{s_1=0}^{N-1} D_{p_1, s_1} W^{-(np_1+ms_1)} = \frac{1}{N^2} \sum_{(p_1, s_1) \in T'_{p,s}} F_{p_1, s_1} W^{-(np_1+ms_1)} \\
 &= \frac{1}{N^2} \sum_{k=0}^{N/2-1} F_{(2k+1)p, (2k+1)s} W^{-(n(2k+1)p+m(2k+1)s)} \\
 &= \frac{1}{N^2} \sum_{k=0}^{N/2-1} F_{(2k+1)p, (2k+1)s} W^{-(2k+1)(np+ms)} \\
 &= \frac{1}{2N} \left( \frac{2}{N} \sum_{k=0}^{N/2-1} F_{(2k+1)p, (2k+1)s} W_{N/2}^{-kt} \right) W^{-t} \\
 &= \frac{1}{2N} \left( f'_{p,s,t} W^t \right) W^{-t} = \frac{1}{2N} f'_{p,s,t}
 \end{aligned}$$

where we denote  $t = (np + ms) \bmod N$  and consider  $f'_{p,s,t+N/2} = -f'_{p,s,t}$ ,  $t = 0: (N/2 - 1)$ . Thus the direction image is defined as

$$d_{n,m} = d_{n,m;p,s} = \frac{1}{2N} f'_{p,s,(np+ms) \bmod N}, \quad (n, m) \in X_{N,N}. \quad (19.206)$$

In other words, the direction image  $N \times N$  is filled by the  $N/2$  values of the splitting-signal  $f'_{p,s}$ , which are placed along the parallel lines  $np + ms = t \bmod N$ ,  $t = 0 : (N - 1)$ . The direction of these lines is defined by the coordinates of the frequency-point  $(p, s)$ . As an example, Figure 19.29 shows the splitting-signal  $f'_{T'_{1,1}}$  of the tree image in part a, along with the 128-point DFT (in absolute scale) of the modified splitting-signal in (b), the set of frequency-points  $T'_{1,1}$  on the square grid  $256 \times 256$  in (c), and the direction image  $d_{n,m}$  of the size  $256 \times 256$  in (d). The frequency-points of the set  $T'_{1,1}$  are located on the main diagonal of the grid; they occupy each second point on the diagonal.

In the case when g.c.d.  $(p, s) = 2^k$ ,  $k \geq 1$ , the 2-D IDFT of the transform  $D_{p_1, s_1}$  results in the following direction image (or the 2-D signal with positive and negative values)

$$d_{n,m} = d_{n,m;p,s} = \frac{1}{2^{k+1}N} f'_{p,s,(np+ms) \bmod N}, \quad (n, m) \in X_{N,N}. \quad (19.207)$$

All  $(3N - 2)$  subsets  $T'_{p,s}$ , with generators  $(p, s)$  from the set  $J'_{N,N}$  compose the partition of the grid  $X_{N,N}$ . Therefore, the sum of all directional images  $d_{n,m} = d_{n,m;p,s}$  results in the original image  $f_{n,m}$ . In other words, we obtain the following decomposition of the image by the direction images:

$$f_{n,m} = \sum_{(p,s) \in J'_{N,N}} d_{n,m;p,s} = \frac{1}{2N} \sum_{k=0}^r \frac{1}{2^k} \sum_{(p,s) \in 2^k J_{2^r-k, 2^r-k}} f'_{p,s,(np+ms) \bmod N} \quad (19.208)$$

where the  $k=r$  case corresponds to the set  $J_{0,0} = (0, 0)$  and normalize coefficient  $1/2^{k-1}$  instead of  $1/2^k$ . Equation 19.208 is the formula of reconstruction of the image by its paired transform, by using operations of addition and division by powers of two.

The processing of the splitting-signal  $f'_{p_0, s_0} \rightarrow \hat{f}'_{p_0, s_0}$  with number  $(p_0, s_0)$  leads to the change of the 2-D DFT of the image at frequency-points of the subset  $T'_{p_0, s_0}$ . The image is changed as

$$f_{n,m} \rightarrow f_{n,m} + \frac{1}{2^{k+1}N} \Delta f'_{p_0, s_0, (np_0+ms_0) \bmod N} \quad (19.209)$$

where  $\Delta f'_{p_0, s_0, t} = \hat{f}'_{p_0, s_0, t} - f'_{p_0, s_0, t}$ ,  $t = 0: (N - 1)$ . The processing of the image through its splitting-signals is the process along parallel lines in certain directions, which are referred to as projection data. Some splitting-signals, or direction images are highly expressed and other little, by their characteristics (see Figure 19.28). For instance, the splitting-signals have different energy,

$$E_{p,s} = \frac{1}{N} \sqrt{(f'_{p,s,0})^2 + (f'_{p,s,1})^2 + \dots + (f'_{p,s,N/2-1})^2}$$

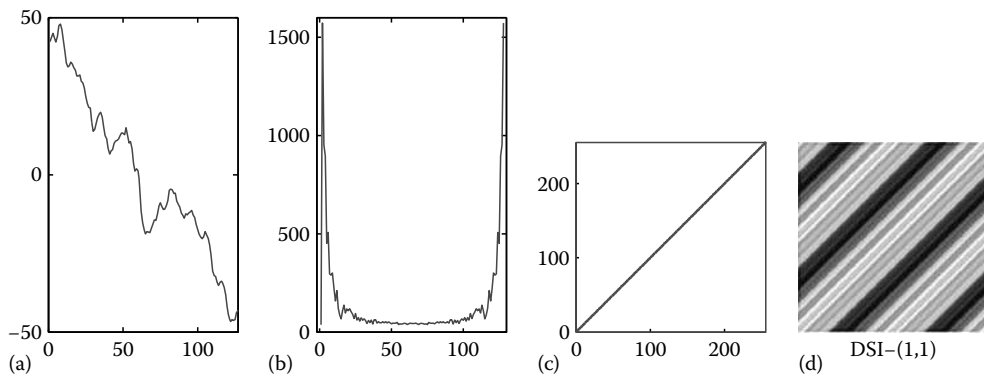


FIGURE 19.29 (a) The splitting-signal with number  $(p, s) = (1, 1)$ , (b) 128-point DFT of the modified splitting-signal, (c) subset of frequency-points  $T'_{1,1}$ , and (d) direction image  $256 \times 256$ .



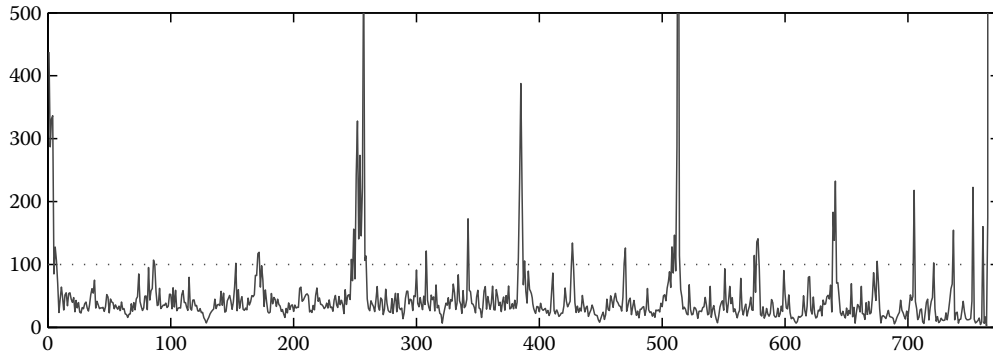


FIGURE 19.30 Energy of all splitting-signals of the tree image.

which can be used for selecting signals with high energies. The energy curve of all 766 splitting-signals of the tree image is given in Figure 19.30. The signals are numbered by the order of generators  $(p, s)$  in the set  $J$ , which is divided by the subsets  $J_{256,256}, 2J_{128,128}, \dots, 128J_{2,2}$ , plus  $(0, 0)$ . Taking the threshold for energy equal  $E_0 = 100$ , we obtain 50 splitting-signals with high energies  $E_{p,s} > E_0$ . All together, the images of these splitting-signals, or their direction images compose the image shown in Figure 19.31a, and the rest of the direction images compose the image in (b). The sum of these two images equals the original tree image. The image in (a) provides no details but a very smooth and “hot” picture of the image, and opposite, the image in (b) provides the details of the tree image but the lack of brightness.

**19.9.4.1 Series Images**

From each image specific periodic structures can be extracted, which all together compose the image. To illustrate this property, we call the sum of direction images corresponding to the subset of generators  $2^k J_{2^{r-k}, 2^{r-k}}$ ,

$$S_{n,m}^{(k)} = \sum_{(p,s) \in 2^k J_{2^{r-k}, 2^{r-k}}} d_{n,m;p,s} \left( S_{n,m}^{(r)} = d_{n,m;0,0} \equiv \frac{1}{N^2} F_{0,0} \right)$$

the  $k$ th series image, where  $k \in \{0, 1, \dots, r\}$ . Figure 19.32 shows the first five series images for the tree image in parts (a) through (e). One can see that each series image, starting from the second one, has a periodic structure with a resolution which increases exponentially with the number of the series. We call the number  $2^k$  the resolution of the  $k$ th series image. This is an interesting fact: each resolution is referred to as a periodic structure of one part of the image. The first series image is the component of the image with the lowest resolution, and the  $(r - 1)$ th series image is the component of the image with the highest resolution. The constant image  $S^{(r)}$  has 0 resolution. Sum of the series images equals the original image, as shown in (f) where the image is the sum of only the first five series images. The remaining three resolutions add more details in the image.

Periodic structure of the series images takes place for other images as well. As an example, Figure 19.33 shows the first series image of the girl image in part (a), along with the next six series images in (b)–(g), and the sum of these series images in (h). Series images have different ranges of intensities, which decrease when the resolution increases. For instance, the first four series images have values that vary in range 255, 101, 45, and 15, respectively. Therefore for better illustration, all series

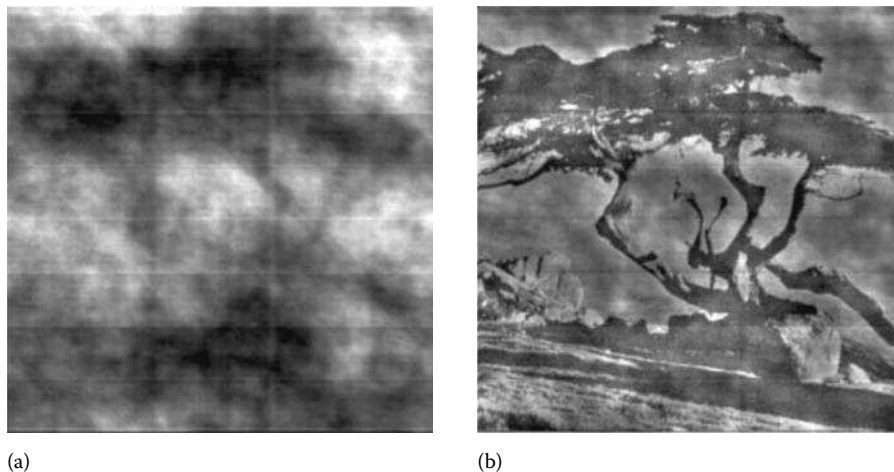


FIGURE 19.31 (a) The sum of 50 direction images defined by splitting-signals of high energy, and (b) the sum of the remaining direction images.

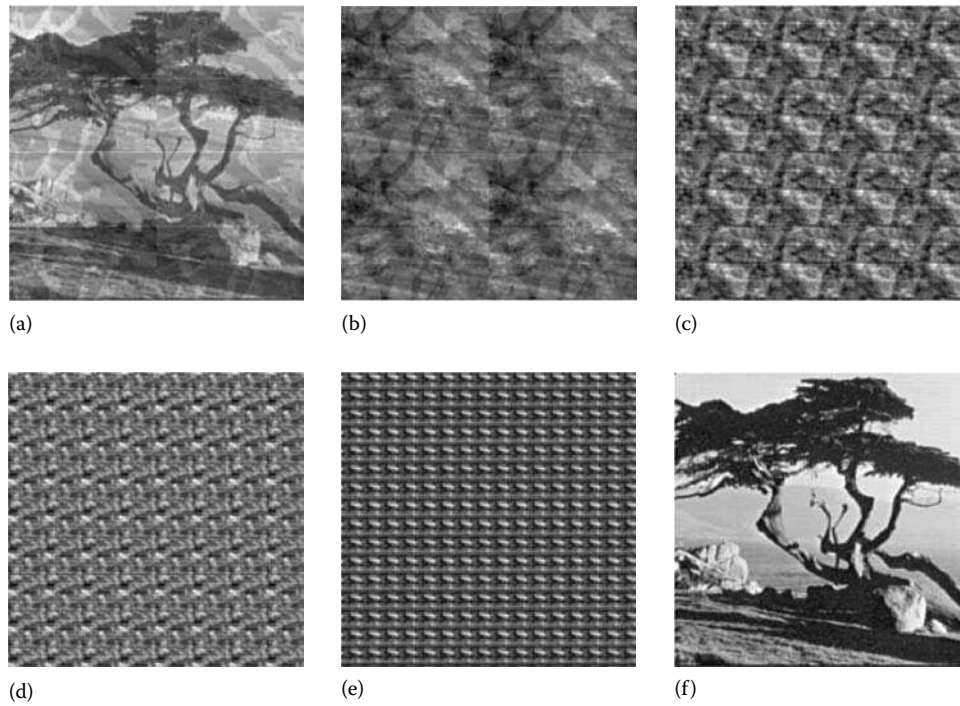


FIGURE 19.32 (a)–(e) The first five series images of the tree image, (f) and the sum of these series images.

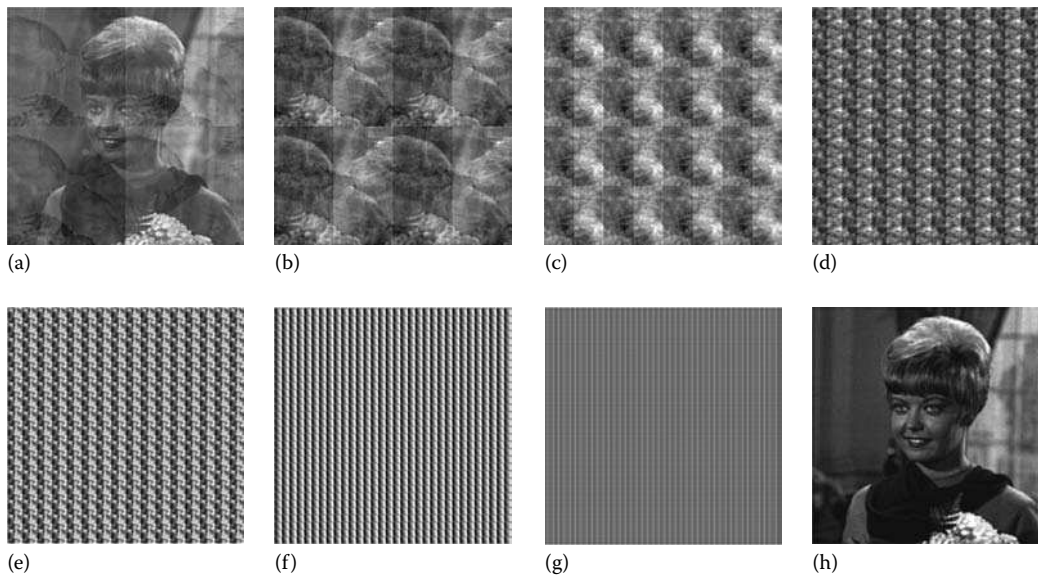


FIGURE 19.33 (a)–(g) The first seven series images of the girl image, and (h) the sum of these images.

images in this figure, as well as in Figure 19.32, have been scaled by using the MATLAB<sup>®</sup> command “imagesc(.)”.

**19.9.4.2 Resolution Map**

It is important to mention, that the first series image is also composed by periodic structures  $N/2 \times N/2$ . In this image, as well as the remaining series images, we can separate subsets of

direction images in the following way. The set of generators  $J_{2^k, 2^k}$  is divided by three parts as

$$\begin{aligned}
 J_{2^r, 2^r}^{(1)} &= \{(1, 2s); s = 0: (N/2 - 1)\}, \\
 J_{2^r, 2^r}^{(2)} &= \{(2p, 1); p = 0: (N/2 - 1)\}, \\
 J_{2^r, 2^r}^{(3)} &= \{(1, 2s + 1); s = 0: (N/2 - 1)\}.
 \end{aligned}$$

In the first two sets, the coordinates of the generators are replaced, i.e., these two sets are symmetric to each other. The directions of the direction images that correspond to the first set of generators are positive, and negative for the second set. The directions defined by the third set of generators are unique. We denote the division of the first series image  $S^{(0)}$  by these subsets as

$$P_{n,m}^{(0)} = \sum_{(p,s) \in J_{2^r, 2^r}^{(1)}} d_{n,m;p,s}, \quad N_{n,m}^{(0)} = \sum_{(p,s) \in J_{2^r, 2^r}^{(2)}} d_{n,m;p,s},$$

$$U_{n,m}^{(0)} = \sum_{(p,s) \in J_{2^r, 2^r}^{(3)}} d_{n,m;p,s},$$

so that  $S^{(0)} = P^{(0)} + N^{(0)} + U^{(0)}$ .

Figure 19.34 shows the image  $P^{(0)}$  for the girl image in part (a), along with the images  $N^{(0)}$  and  $U^{(0)}$  in (b) and (c), respectively. In these images, one can notice different parts of the girl image with their negative versions periodically shifted by 128 along the horizontal, vertical, and diagonal directions. Each image is divided by four parts  $N/2 \times N/2$  with similar structures, which can be used for composing the entire series image  $S^{(0)}$ . Indeed, it follows directly from the definition of the paired functions that the following equations are valid:

$$\begin{cases} f'_{1,2s,(n+N/2)+2ms \bmod N} = -f'_{1,2s,n+2ms \bmod N} \\ f'_{1,2s,n+2(m+N/2)s \bmod N} = f'_{1,2s,n+2ms \bmod N} \\ f'_{1,2s,(n+N/2)+2(m+N/2)s \bmod N} = -f'_{1,2s,n+2ms \bmod N} \\ f'_{1,2s+1,(n+N/2)+m(2s+1) \bmod N} = -f'_{1,2s+1,n+m(2s+1) \bmod N} \\ f'_{1,2s+1,n+(m+N/2)(2s+1) \bmod N} = -f'_{1,2s+1,n+m(2s+1) \bmod N} \\ f'_{1,2s+1,(n+N/2)+(m+N/2)(2s+1) \bmod N} = -f'_{1,2s+1,n+m(2s+1) \bmod N} \end{cases}$$

for  $s = 0 : (N/2 - 1)$ , and

$$\begin{cases} f'_{2p,1,2(n+N/2)p+m \bmod N} = f'_{2p,1,m+2np \bmod N} \\ f'_{2p,1,2np+(m+N/2) \bmod N} = -f'_{2p,1,m+2np \bmod N} \\ f'_{2p,1,2(n+N/2)p+(m+N/2) \bmod N} = -f'_{2p,1,m+2np \bmod N} \end{cases}$$

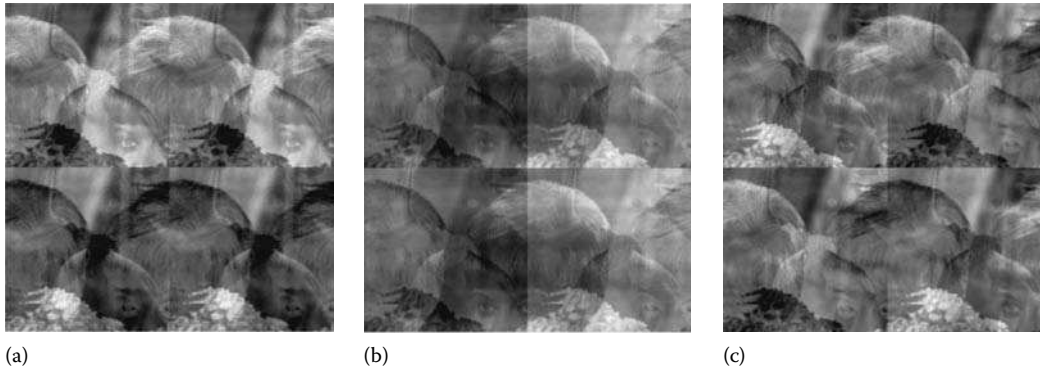


FIGURE 19.34 Three components of the first series images of the girl image.

for  $p = 0 : (N/2 - 1)$ . Therefore, the series image components  $P^{(0)}$ ,  $N^{(0)}$ , and  $U^{(0)}$  can be defined from their first quarters which we denote by  $P_1$ ,  $N_1$ , and  $U_1$ , respectively, as follows:

$$P^{(0)} = \begin{bmatrix} P_1 & P_1 \\ -P_1 & -P_1 \end{bmatrix}, \quad N^{(0)} = \begin{bmatrix} N_1 & -N_1 \\ N_1 & -N_1 \end{bmatrix},$$

$$U^{(0)} = \begin{bmatrix} U_1 & -U_1 \\ -U_1 & U_1 \end{bmatrix}.$$

Figure 19.35 shows the decomposition of the next series image  $S^{(1)}$  for the girl image. For this series image, as well as the remaining series images  $S^{(k)}$ ,  $k = 2 : (r - 1)$ , the similar decompositions take place. Each of such images can be defined by the three quarters  $P_{k+1}$ ,  $N_{k+1}$ , and  $U_{k+1}$  of their periods  $N/2^{k+1} \times N/2^{k+1}$  in the way similar to the first series image. As a result, the following resolution map (RM) associates with the image  $f$ :

$$\text{RM}[f] = \begin{array}{c|cc} & P_1 & U_1 \\ \hline & P_2 & U_2 \\ N_1 & N_2 & \begin{array}{c|c} P_3 & U_3 \\ \hline N_3 & \dots \end{array} \end{array} \quad (19.210)$$

This resolution map has the same size as the image and contains all periodic parts of the series images, i.e., all periods by means of which the original image can be reconstructed. Each periodic part is extracted from the direction image, whose directions are given by subsets of generators of  $J'_{N,N}$ . In other words, the RM represents itself the image packed by its periodic structures that correspond to specific set of projections. The resolution map can be used to change the resolution of the entire image, by processing direction images for desired directions.

Good results of image processing, including the enhancement, can be achieved when working with one or a few high energy splitting-signals, as well as the sets of splitting-signals which are combined by series and correspond to different resolutions written in the image RM. Figure 19.36 shows all 766 generators  $(p, s) \in J'_{256,256}$  in part (a), where the 12 generators for the 6th series image and six generators for the 7th series image are

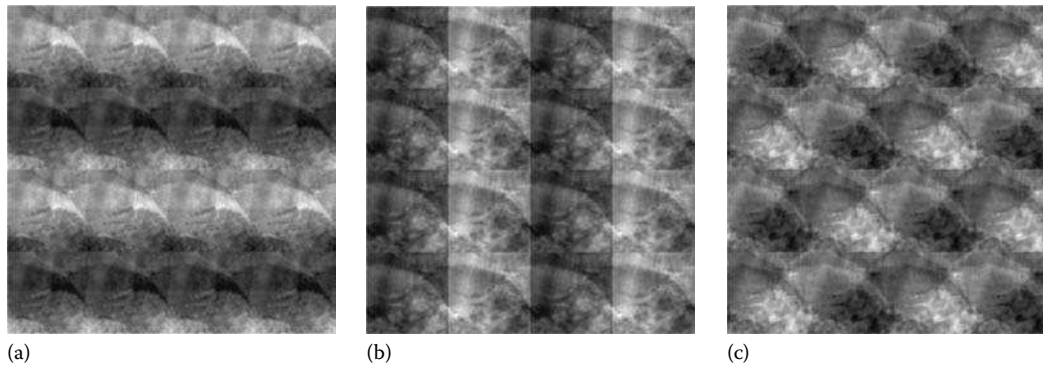


FIGURE 19.35 Three components of the 2nd series image of the girl image.

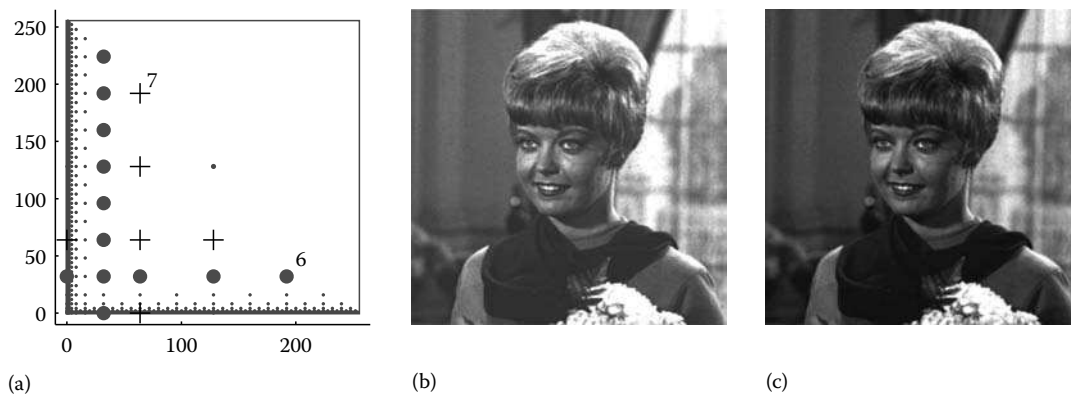


FIGURE 19.36 (a) 766 generators of the set  $J'_{256,256}$ , and the tree image with amplified (b) 7th series image, and (c) 6th and 7th series images.

marked by “•” and “+,” respectively. The girl image with amplified series image of number 7 by the factor of 2 is shown in (b), and the image with the amplified series images of numbers 6 and 7 respectively by the factors of 1.2 and 1.5 in (c). These two images are enhanced by resolutions 64 and 64 with 32, respectively.

Thus, the paired form of image representation leads to the splitting of the 2-D DFT of the image by the set of 1-D DFTs of splitting-signals which define the direction images as components of the image. This representation allows for extracting the periodic structures of the image, which are defined by direction images united in special groups of directions, which are referred to as series images. The image is packed and described by its resolution map, which can be used for image enhancement and compression. Each periodic structure in the resolution map can be also represented by its resolution map. In such a recursive way, the resolution map can be crushed into small pieces, from which the whole image can be reconstructed.

### 19.10 2-D DFT on the Hexagonal Lattice

In this section, we generalize concepts of the tensor and paired representations with respect to the 2-D DFTs whose fundamental periods are hexagonal lattices. Hexagonal lattices are important for many problems in image processing [42,43]. Sampling 2-D

isotropic functions on hexagonal lattices is significantly more efficient than sampling on rectangular lattices [44]. It also was shown that the vision system relates best to the regular hexagonal tessellation [45,46], which has a lower number of neighbors than the rectangular lattice.

Let us first consider the problem of splitting the 2-D DFT into a set of short 1-D transforms, when samples of both 2-D sequence  $f$  and transform  $F$  are arranged on the similar hexagonal lattices

$$F_{p_1+[p_2], p_2} = \sum_{n_1=0}^{N-1} \sum_{n_2=0}^{N-1} f_{n_1+[n_2], n_2} W^{(n_1+[n_2])(p_1+[p_2])+n_2 p_2} \quad (19.211)$$

where  $W = \exp(-2\pi j/N)$  and  $[n_2] = (1 - (-1)^{n_2})/4$ ,  $[p_2] = (1 - (-1)^{p_2})/4$ , for all  $n_2, p_2 = 0 : (N - 1)$ . Since  $[n] = 0$  when  $n$  is even, and  $[n] = 0.5$  when  $n$  is odd, each second row of knots of the hexagonal lattice is shifted by 0.5 with respect to the even rows. As an example, Figure 19.37 shows the rectangular lattice  $8 \times 8$  in part (a), along with the hexagonal lattice in (b).

It is clear that the traditional row-column method cannot be applied directly for fast computing the values  $F_{p_1+[p_2], p_2}$ . The complexity of the 2-D discrete hexagonal Fourier transform (DHFT) is due to the fact that the kernel of the transform has a

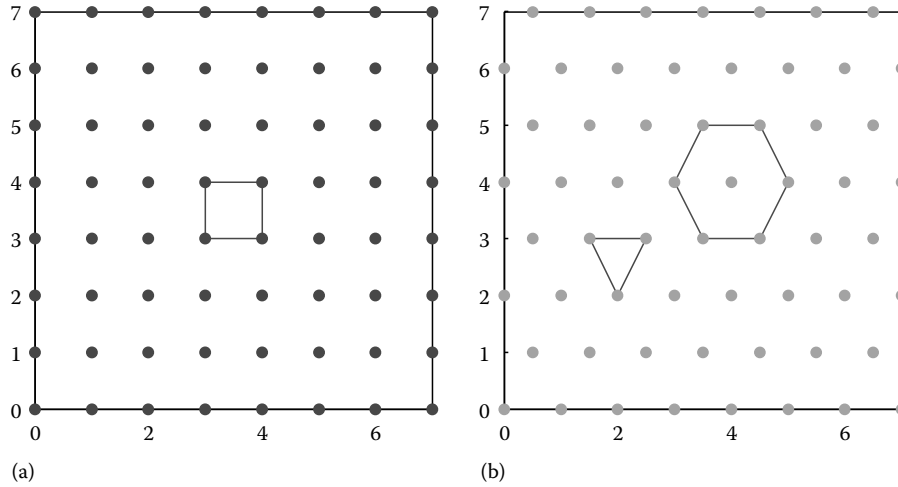


FIGURE 19.37 (a) Rectangular lattice and (b) hexagonal lattice.

more complex form than in the rectangular case, and in addition it is not separable.

For any integers  $p_1$  and  $p_2$ , the following relations hold between the spectral components of the transform:

$$\left. \begin{aligned} F_{(p_1+2N)+(p_2+N), p_2+N} &= F_{p_1+[p_2], p_2} \\ F_{(p_1+N)+(p_2+N), p_2+N} &\neq F_{p_1+[p_2], p_2} \end{aligned} \right\}. \quad (19.212)$$

The period of the transform is  $(2N, N)$ , not  $(N, N)$ . In other words, the hexagonal lattice  $X_{N,N}$  is not the fundamental period of this transform. Therefore, we consider the 2-D hexagonal lattice of size  $2N \times N$ ,

$$X_{2N,N} = \{(p_1 + [p_2], p_2); p_1 = 0 : (2N - 1), p_2 = 0 : (N - 1)\}, \quad (19.213)$$

and the 2-D sequence  $f = \{f_{n_1+[n_2], n_2}\}$  as a  $2N \times N$ -point sequence defined (or extended) on this lattice.

Hereinafter, we define the 2-D DFT,  $\mathcal{F}_{2N,N}$ , on the lattice  $X_{2N,N}$  by

$$F_{p_1+[p_2], p_2} = \sum_{n_1=0}^{2N-1} \sum_{n_2=0}^{N-1} f_{n_1+[n_2], n_2} W^{(n_1+[n_2])(p_1+[p_2])+n_2 p_2}, \quad (19.214)$$

$$(p_1 + [p_2], p_2) \in X_{2N,N},$$

and we call it the 2-D DHFT. We now describe a covering of the lattice  $X_{2N,N}$  that allows for splitting the structure of the 2-D DHFT. For that, we define the following subsets (or cyclic groups) of frequency-points on the lattice:

$$T_{p_1+[p_2], p_2} = \left\{ \left( \overline{k(p_1 + [p_2])}, \overline{k p_2} \right), k = 0 : (4N - 1) \right\} \quad (19.215)$$

where  $(\overline{k(p_1 + [p_2])}, \overline{k p_2}) = (k(p_1 + [p_2]) \bmod 2N, k p_2 \bmod N)$ .

### Example 19.23

Let  $X$  be the hexagonal lattice  $X_{8,4}$ . We consider two subsets  $T_{p_1+[p_2], p_2}$  for  $(p_1, p_2) = (1, 1)$  and  $(1, 2)$ ,

$$T_{1+[1], 1} = T_{1.5, 1} = \left\{ (0, 0), (1.5, 1), (3, 2), (4.5, 3), (6, 0), (7.5, 1), (1, 2), (2.5, 3) \right\}$$

$$\left\{ (4, 0), (5.5, 1), (7, 2), (0.5, 3), (2, 0), (3.5, 1), (5, 2), (6.5, 3) \right\}$$

$$T_{1+[2], 1} = T_{1, 1} = \{(0, 0), (1, 1), (2, 2), (3, 3), (4, 4), (5, 5), (6, 6), (7, 7)\}.$$

Since  $1 + [1] = 1.5$ ,  $1 + [2] = 1$ , and  $k = 0 : 15$ , the first subset consists of 16 frequency-points and the second subset has 8 frequency-points. The number of points of these sets is defined as the smallest integer  $k > 0$  for which  $k(p_1 + [p_2]) \bmod 8 = 0$ . These two subsets intersect only at  $(0, 0)$ .

As in the case of the 2-D DFT on the rectangular lattice, for a given  $(p_1 + [p_2], p_2) \in X_{2N,N}$ , we unite all spatial points  $(n_1 + [n_2], n_2)$  on the lattice, for which the form

$$\mathcal{L}(n_1 + [n_2], n_2; p_1 + [p_2], p_2) = (n_1 + [n_2])(p_1 + [p_2]) + n_2 p_2$$

takes the same values  $t$ , where  $t$  varies from 0 through  $N - \Delta$  with a step  $\Delta$  which depends on the values of  $p_1$  and  $p_2$ . In other words, we define the following disjoint subsets of points  $(n_1 + [n_2], n_2)$ :

$$V_{p_1+[p_2], p_2, t} = \{(n_1 + [n_2], n_2); \mathcal{L}(n_1 + [n_2], n_2; p_1 + [p_2], p_2) = t \bmod N\}. \quad (19.216)$$

The sums of the elements of the image  $f$  on these subsets of points are denoted by

$$f_{p_1+[p_2], p_2, t} = \sum_{V_{p_1+[p_2], p_2, t}} f_{n_1+[n_2], n_2}, \quad t = 0, \Delta, 2\Delta, \dots, N - \Delta. \quad (19.217)$$

We now compose the following 1-D signal, which we call the splitting-signal of the image,

$$f_T = \{f_{p_1+[p_2], p_2, 0}, f_{p_1+[p_2], p_2, \Delta}, f_{p_1+[p_2], p_2, 2\Delta}, \dots, f_{p_1+[p_2], p_2, N-\Delta}\}.$$

The step  $\Delta$  is calculated as follows:

$$\Delta = \begin{cases} 4^{-1}, & \text{if } p_2 \text{ is odd;} \\ 2^{-1}, & \text{if } p_1 \text{ is odd, } p_2 \text{ is even;} \\ 2^{n-1}, & \text{if } g.c.d(p_1, p_2) = 2^n, n \geq 1. \end{cases}$$

The splitting-signal  $f_T$  corresponding to the generator  $(p_1 + [p_2], p_2)$  has the following form:

$$f_T = \begin{cases} \{f_{p_1+\frac{1}{2}p_2, 0}, f_{p_1+\frac{1}{2}p_2, \frac{1}{2}\Delta}, f_{p_1+\frac{1}{2}p_2, \frac{3}{2}\Delta}, \dots, f_{p_1+\frac{1}{2}p_2, N-\frac{1}{2}\Delta}\}, & \text{if } p_2 \text{ is odd;} \\ \{f_{p_1, p_2, 0}, f_{p_1, p_2, \frac{1}{2}\Delta}, f_{p_1, p_2, \Delta}, \dots, f_{p_1, p_2, N-\frac{1}{2}\Delta}\}, & \text{if } p_1 \text{ is odd, } p_2 \text{ is even;} \\ \{f_{p_1, p_2, 0}, f_{p_1, p_2, 2^{n-1}\Delta}, f_{p_1, p_2, 2^n\Delta}, \dots, f_{p_1, p_2, N-2^{n-1}\Delta}\}, & \text{if } p_1 \text{ and } p_2 \text{ are even} \end{cases} \quad (19.218)$$

The following statement can be derived from the above definitions. Let  $(p_1 + [p_2], p_2)$  be a frequency-point of  $X_{2N, N}$ , then the 2-D DHFT at this frequency-point, as well as at other frequency-points of the subset  $T = T_{p_1+[p_2], p_2}$  can be calculated by the 1-D Fourier transform as

$$\overline{F_{k(p_1+[p_2]), kp_2}} = \sum_{t=0, \Delta}^{N-\Delta} f_{p_1+[p_2], p_2, t} W^{kt}, \quad k = 0 : (\text{card}(T) - 1). \quad (19.219)$$

The index  $t$  varies from 0 through  $N - \Delta$  with step  $\Delta$ . The cardinality of the set  $T$  equals  $N/\Delta$ . Therefore, the sum in this equation is referred to as the  $N/\Delta$ -point DFT. The 2-D DHFT on frequency-points of the subset  $T_{p_1+[p_2], p_2}$  represents itself thus as one of the following 1-D DFTs:

$$\mathcal{F}_{2N, N|_{T_{p_1+[p_2], p_2}}} \sim \begin{cases} \mathcal{F}_{4N}; & \text{if } p_2 \text{ is odd,} \\ \mathcal{F}_{2N}; & \text{if } p_1 \text{ is odd, } p_2 \text{ is even,} \\ \mathcal{F}_{N/2^{n-1}}; & \text{if } p_1 \text{ and } p_2 \text{ are even.} \end{cases} \quad (19.220)$$

As an example, Figure 19.38 illustrates the tree image  $512 \times 256$  written on the hexagonal lattice  $X_{512, 256}$ , along with the splitting-signal  $f_{T_{1+[1], 1}}$  of length 1024 in part (b), the 1024-point DFT of this signal in part (c), and 1024 samples of the 1-D DFT at frequency-points of the subset  $T_{1+[1], 1}$ , at which the 2-D DHFT of the image coincides with the 1-D DFT, in part (d). In this example,  $N = 256$ ,  $p_1 = 1$ ,  $p_2 = 1$ ,  $[p_2] = 0.5$ ,  $\text{card } T_{1+[1], 1} = 4 \cdot 256 = 1024$ . For this modeled image, all samples of the hexagonal lattice  $512 \times 256$  have been placed on the rectangular lattice  $1024 \times 256$  in a way shown in Figure 19.38a and b. Then the image has been extended at other points of the rectangular lattice, by calculating the means of the image at the nearest samples of the hexagonal lattice, as shown in Figure 19.39.

The interpolation of samples has been performed by the cross  $3 \times 3$ , such that  $a = (1 + 6 + 6 + 5)/4 = 4.5$ ,  $b = (1 + 6 + 3 + 5)/4 = 3.75$ , and  $c = (2 + 3 + 3 + 4)/4 = 3$ .

According to Equation 19.219, the calculation of the 2-D DHFT is reduced to the composition of an irreducible covering  $\sigma$  of the hexagonal lattice  $X_{2N, N}$ , which is composed of subsets (19.215), i.e.,

$$\sigma = \sigma_J = (T_{p_1+[p_2], p_2})_{(p_1+[p_2], p_2) \in J} \quad (19.221)$$

for a certain set of generators  $J \subseteq X_{2N, N}$ . The 1-D DFTs of the splitting-signals  $f_T$  are calculated for all subsets  $T = T_{p_1+[p_2], p_2} \in \sigma$ . These 1-D DFTs fill completely the 2-D DHFT.

### Example 19.24

In the  $N = 4$  case, the irreducible covering  $\sigma$  of the hexagonal lattice  $X_{8, 4}$  can be defined as follows:

$$\sigma_{8, 4} = (T_{0+[1], 1}, T_{1+[1], 1}, T_{1+[0], 0}, T_{0+[2], 2}, T_{2+[2], 2}, T_{4+[2], 2})$$

where the subsets  $T$  equal

$$T_{0+[1], 1} = T_{0.5, 1} = \left\{ \begin{array}{l} (0, 0), (0.5, 1), (1, 2), (1.5, 3) \\ (2, 0), (2.5, 1), (3, 2), (3.5, 3) \\ (4, 0), (4.5, 1), (5, 2), (5.5, 3) \\ (6, 0), (6.5, 1), (7, 2), (7.5, 3) \end{array} \right\}$$

$$T_{1+[1], 1} = T_{1.5, 1} = \left\{ \begin{array}{l} (0, 0), (1.5, 1), (3, 2), (4.5, 3) \\ (6, 0), (7.5, 1), (1, 2), (2.5, 3) \\ (4, 0), (5.5, 1), (7, 2), (0.5, 3) \\ (2, 0), (3.5, 1), (5, 2), (6.5, 3) \end{array} \right\}$$

$$T_{1+[0], 0} = T_{1, 0} = \left\{ \begin{array}{l} (0, 0), (1, 0), (2, 0), (3, 0) \\ (4, 0), (5, 0), (6, 0), (7, 0) \end{array} \right\}$$

$$T_{0+[2], 2} = T_{0, 2} = \{(0, 0), (0, 2)\}$$

$$T_{2+[2], 2} = T_{2, 2} = \{(0, 0), (2, 2), (4, 0), (6, 2)\}$$

$$T_{4+[2], 2} = T_{4, 2} = \{(0, 0), (4, 2)\}.$$

The  $8 \times 4$ -point DHFT at frequency-points of the subsets  $T_{0+[1], 1}$ ,  $T_{1+[1], 1}$ , and  $T_{1+[0], 0}$  is determined by the 16, 16, and 8-point DFTs, respectively. To calculate the DHFT at frequency-points of all subsets of the covering, it is enough to calculate the following:

1. One 16-point DFT of the splitting-signal  $f_{T_{0.5, 1}}$ , to define components of the DHFT at all 16 frequency-points of the set  $T_{0.5, 1}$ .
2. One incomplete 16-point DFT of the splitting-signal  $f_{T_{1.5, 1}}$ , when only spectral components with odd points are calculated. This transform can be reduced to the 8-point DFT (which requires six additional multiplications with the twiddle factors). The 2-D DHFT will be defined by the incomplete DFT at frequency-points  $(1.5, 1), (4.5, 3), (7.5, 1), (2.5, 1), (5.5, 1), (0.5, 1), (3.5, 1),$  and  $(6.5, 1)$ .

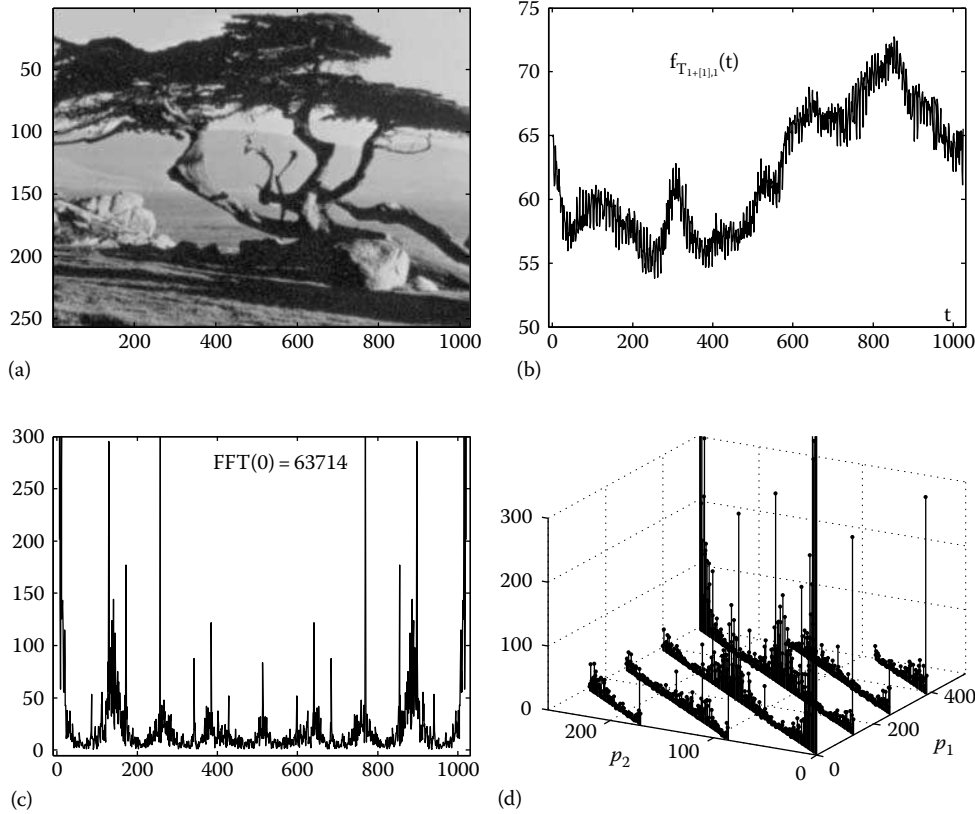


**FIGURE 19.38** (a) Tree image  $512 \times 256$  with the hexagonal lattice  $X_{512,256}$  written on the rectangular lattice  $1024 \times 256$ . (b) Splitting-signal  $f_{T_{1+[1],1}}(t)$  of length 1024. (c) Absolute value of the 1024-point DFT of the splitting-signal. (d) Samples of the subset  $T_{1+[1],1}$  of  $X_{512,256}$ , at which the 2-D DHFT of the image coincides with the 1024-point DFT.

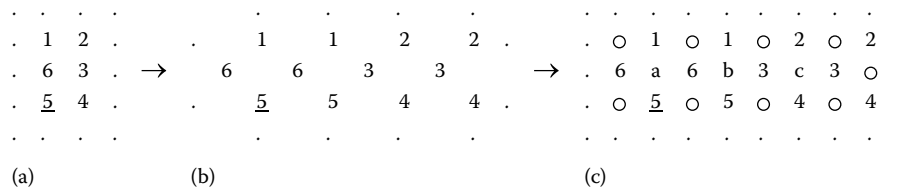


**FIGURE 19.39** Diagram for transferring (a) the tree image  $256 \times 256$  to (b) the hexagonal lattice  $512 \times 256$ , and, then, extending (c) the image to the rectangular lattice  $1024 \times 256$ .

3. One incomplete 8-point DFT of the splitting-signal  $f_{T_{1,0}}$ , which is calculated at odd frequencies 1, 3, 5, and 7. This transform can be reduced to the 4-point DFT, and for that two additional multiplications are required. The 2-D DHFT will be defined by the incomplete DFT at frequency-points (1, 0), (3, 0), (5, 0), and (7, 0).
4. Two trivial incomplete 2-point DFTs of the splitting-signals  $f_{T_{0,2}}$  and  $f_{T_{4,2}}$ , to calculate the DHFT at frequency-points (0, 2) and (4, 2), respectively.
5. One incomplete 4-point DFT of the splitting-signal  $f_{T_{2,2}}$ , to calculate the DHFT at frequency-points (2, 2) and (6, 2).

The calculation of the DHFT at frequency-points (0, 2), (2, 2), (4, 2), and (6, 2) can also be performed in a different way, if we note the following. In the case  $N \geq 4$ , we can write that

$$\begin{aligned}
 F_{2p_1+[2p_2], 2p_2} &= \sum_{n_1=0}^{2N-1} \sum_{n_2=0}^{N-1} f_{n_1+[n_2], n_2} W^{(n_1+[n_2])(2p_1+[2p_2])+n_2 2p_2} \\
 &= \sum_{n_1=0}^{N-1} \sum_{n_2=0}^{N/2-1} g_{1+[n_2], n_2}^n W_{N/2}^{(n_1+[n_2])p_1+n_2 p_2} = G_{p_1, p_2},
 \end{aligned}
 \tag{19.222}$$

where  $p_1 = 0 : (N-1)$  and  $p_2 = 1 : (N/2-1)$ . The sequence  $g$  is defined on the hexagonal lattice  $X_{N,N/2}$  as follows:

$$\begin{aligned} g_{n_1+[n_2], n_2} &= f_{n_1+[n_2], n_2} + f_{n_1+N/2+[n_2], n_2} + f_{n_1+[n_2+N/2], n_2+N/2} \\ &\quad + f_{n_1+N/2+[n_2+N/2], n_2+N/2} \\ &= f_{n_1+[n_2], n_2} + f_{n_1+N/2+[n_2], n_2} + f_{n_1+[n_2], n_2+N/2} \\ &\quad + f_{n_1+N/2+[n_2], n_2+N/2} \end{aligned}$$

for numbers  $n_1 = 0 : (N-1)$  and  $n_2 = 0 : (N/2-1)$ .

Therefore, for  $p_1 = 0 : (N-1)$  and  $p_2 = 1 : (N/2-1)$ , the set of values  $F_{2p_1, 2p_2}$  represents itself an incomplete  $N \times N/2$ -point DHFT whose spectral components at points  $(p_1, 0)$ ,  $p_1 = 0 : (N-1)$ , are not calculated. This transform is defined at frequency-points  $(p_1, p_2)$  that lie on the rectangular lattice  $X_{N, N/2}$ . We denote this transform by  $\mathcal{F}_{N, N/2}^o$  and the number of operations of multiplication required to calculate this transform by  $m_{N, N/2}^o$ .

In the  $N=4$  case, we obtain the splitting  $\{\mathcal{F}_{16}, \mathcal{F}_8^o, \mathcal{F}_4^o, \mathcal{F}_{4,2}^o\}$  of the  $8 \times 4$ -point DHFT. The number of the required multiplications can be estimated as  $m_{8,4} = m_{16} + (m_8 + 6) + (m_4 + 2) + (m_{4,2}^o = 0) = 10 + (2 + 6) + 2 = 20$ .

In the general  $N > 4$  case, we consider the following covering of the hexagonal lattice  $X_{2N,N}$ :

$$\sigma_{2N,N} = \left( (T_{p_1+[1],1})_{p_1=0:(N/2-1)}, (T_{1+[4p_2],4p_2})_{p_2=0:(N/4-1)}, 2X_{N,N/2}^o \right) \quad (19.223)$$

where  $2X_{N,N/2}^o$  is a subset of  $X_{2N,N}$  that contains all frequency-points with even coordinates, except the first column,

$$2X_{N,N/2}^o = \{(2p_1, 2p_2); p_1 = 0 : (N-1), p_2 = 1 : (N/2-1)\}.$$

The  $2N \times N$ -point DHFT can therefore be reduced to  $N/2$   $4N$ -point DFTs,  $N/4$   $2N$ -point DFTs, and one incomplete  $N \times N/2$ -point DHFT. The repeated calculations of the 2-D DHFT at intersections of subsets  $T \in \sigma_{2N,N}$  can be removed similar to the considered above  $N=4$  case.

The number of multiplications required to calculate the  $2N \times N$ -point DHFT is estimated as  $m_{2N,N} = N/2 m_{4N} + N/4 m_{2N} + m_{N,N/2}^o$ . Considering the estimate  $m_{N,N/2}^o = m_{N,N/2} - m_N$  for  $N = 2^r \geq 8$ , we obtain the following recursive formula:

$$\begin{aligned} m_{2N,N} &= m_{N, \frac{N}{2}} + \frac{N}{2} m_{4N} + \frac{N}{4} m_{2N} - m_N \\ &= m_{N, \frac{N}{2}} + \frac{N^2}{4} (5r - 6) - \frac{N}{2} (r - 6) - 2. \end{aligned} \quad (19.224)$$

### 19.10.1 Paired Representation of the DHFT

In this section, we describe a partition of the hexagonal lattice  $X_{2N,N}$ , which leads to the splitting of the 2-D DHFT by the 1-D

DFTs on disjoint subsets of the frequency-points. Such a partition allows also for representing the 2-D image defined on the hexagonal lattice by a set of splitting-signals, which are defined similarly to the paired-splitting signals for the 2-D DFT.

Let  $(p_1 + [p_2], p_2)$  be an arbitrary point of the lattice. Then, for integers  $m = 0 : (N/(2\Delta) - 1)$ , the following relation is valid:

$$F_{\overline{(2m+1)(p_1+[p_2])}, \overline{(2m+1)p_2}}} = \sum_{t=0, \Delta}^{N/2-\Delta} \left( f'_{p_1+[p_2], p_2, t} W^t \right) W_{N/2}^{mt}, \quad (19.225)$$

where

$$f'_{p_1+[p_2], p_2, t} = f_{p_1+[p_2], p_2, t} - f_{p_1+[p_2], p_2, t+N/2}, \quad (19.226)$$

and numbers  $t$  run from 0 to  $N/2 - \Delta$  with the step  $\Delta$  (which we write as  $t = 0 : \Delta : (N/2 - \Delta)$ ).

To construct the paired-representation of the hexagonal image  $f$  with respect to the DHFT, we define the following subsets of sets (19.215):

$$\begin{aligned} T'_{p_1+[p_2], p_2} &= \left\{ \overline{(2m+1)(p_1+[p_2])}, \overline{(2m+1)p_2} \right\}, \\ m = 0 : (N/(2\Delta) - 1). \end{aligned} \quad (19.227)$$

#### Example 19.25

We consider the hexagonal lattice  $X_{8,4}$ . For points  $(p_1, p_2) = (1, 1)$  and  $(1, 2)$ , we have the following:

$$\begin{aligned} T'_{1+[1],1} &= T'_{1.5,1} = \left\{ (1.5, 1), (4.5, 3), (7.5, 1), (2.5, 3) \right\} \\ &\quad \left\{ (5.5, 1), (0.5, 3), (3.5, 1), (6.5, 3) \right\} \\ T'_{1+[2],2} &= T'_{1,2} = \{(1, 2), (3, 2), (5, 2), (7, 2)\}. \end{aligned}$$

The subsets  $T'_{p_1+[p_2], p_2}$  with different generators are disjoint or coincide, and therefore, we can construct a unique partition of the hexagonal lattice  $X_{2N,N}$

$$\sigma' = \sigma'_{J'} = \left( T'_{p_1+[p_2], p_2} \right)_{(p_1+[p_2], p_2) \in J'} \quad (19.228)$$

for a certain set  $J'$  of generators. Depending on the evenness of generators, the 2-D DHFT at frequency-points of subsets  $T'_{p_1+[p_2], p_2}$  represents itself one of the following 1-D DFT:

$$\mathcal{F}_{2N, N'_{p_1+[p_2], p_2}} \sim \begin{cases} \mathcal{F}_{2N}; & \text{if } p_2 \text{ is odd,} \\ \mathcal{F}_N; & \text{if } p_1 \text{ is odd, } p_2 \text{ is even,} \\ \mathcal{F}_{N/2^n}; & \text{if } p_1 \text{ and } p_2 \text{ are even.} \end{cases} \quad (19.229)$$



The corresponding modified element of the  $\sigma'$ -representation, or the paired representation of  $f$  with respect to the 2-D DHFT has the following form:

$$g_{T'} = \begin{cases} \left\{ f'_{p_1+\frac{1}{2}, p_2, 0}, f'_{p_1+\frac{1}{2}, p_2, \frac{1}{4}} W_{4N}, \dots, f'_{p_1+\frac{1}{2}, p_2, \frac{N-1}{4}} W_{4N}^{2N-1} \right\}; \\ \quad \text{if } p_2 \text{ is odd,} \\ \left\{ f'_{p_1, p_2, 0}, f'_{p_1, p_2, \frac{1}{2}} W_{2N}, \dots, f'_{p_1, p_2, \frac{N-1}{2}} W_{2N}^{N-1} \right\}; \\ \quad \text{if } p_1 \text{ is odd, } p_2 \text{ is even,} \\ \left\{ f'_{p_1, p_2, 0}, f'_{p_1, p_2, 2^{n-1}} W_{N/2^{n-1}}, \dots, f'_{p_1, p_2, N/2-2^{n-1}} W_{N/2^{n-1}}^{N/2^{n-1}} \right\}; \\ \quad \text{if } p_1 \text{ and } p_2 \text{ are even} \end{cases} \quad (19.230)$$

For instance, when  $p_2$  is odd, we have the following  $2N$ -point DFT:

$$F_{(2m+1)(p_1+\frac{1}{2}), (2m+1)p_2} = \sum_{t=0}^{2N-1} \left( f'_{p_1+\frac{1}{2}, p_2, \frac{t}{4}} W_{4N}^t \right) W_{2N}^{mt}, \quad m=0: (2N-1).$$

The partition  $\sigma'$  of the hexagonal lattice can be constructed directly from the irreducible covering  $\sigma$  of the lattice. Indeed, each set  $T$  of the covering  $\sigma$  can be divided by disjoint or coincident subsets  $T'$ . The removal of those coincident subsets results in a partition of the lattice. To illustrate this property, we consider two examples.

### Example 19.26

Let  $N=4$  and let  $\sigma$  be the covering of the hexagonal lattice  $X_{8,4}$ , which has been composed in Example 19.24. The generators of sets  $T$  of this covering are taken from the set

$$J = J_{8,4} = \{(0 + [1], 1), (1 + [1], 1), (1 + [0], 0), (0 + [2], 2), (2 + [2], 2), (4 + [2], 2)\}.$$

We first consider the set  $T_{0+[1],1}$  that can be divided as follows:

$$\begin{aligned} T'_{0+[1],1} &= \left\{ (0.5, 1), (1.5, 3), (2.5, 1), (3.5, 3) \right. \\ &\quad \left. (4.5, 1), (5.5, 3), (6.5, 1), (7.5, 3) \right\} \\ T'_{1+[2],2} &= \{(1, 2), (3, 2), (5, 2), (7, 2)\} \\ T'_{2+[0],0} &= \{(2, 0), (6, 0)\} \\ T'_{4+[0],0} &= \{(4, 0)\} \\ T'_{0+[0],0} &= \{(0, 0)\}. \end{aligned}$$

The next set  $T_{1+[1],1}$  of the covering can be divided as

$$\begin{aligned} T'_{1+[1],1} &= \left\{ (1.5, 1), (4.5, 3), (7.5, 1), (2.5, 3) \right. \\ &\quad \left. (5.5, 1), (0.5, 3), (3.5, 1), (6.5, 3) \right\} \\ T'_{1+[2],2} &= \{(1, 2), (3, 2), (5, 2), (7, 2)\} \\ T'_{2+[0],0} &= \{(2, 0), (6, 0)\} \\ T'_{4+[0],0} &= \{(4, 0)\} \\ T'_{0+[0],0} &= \{(0, 0)\} \end{aligned}$$

and the set  $T_{1+[0],1}$  is divided as

$$\begin{aligned} T'_{1+[2],0} &= \{(1, 0), (3, 0), (5, 0), (7, 0)\} \\ T'_{2+[0],0} &= \{(2, 0), (6, 0)\} \\ T'_{4+[0],0} &= \{(4, 0)\} \\ T'_{0+[0],0} &= \{(0, 0)\} \end{aligned}$$

One can see that all subsets  $T'$  of the decomposition of these three sets  $T$  are disjoint or coincident. The first set  $T_{0+[1],1}$  together with two subsets  $T'_{1+[1],1}$  and  $T'_{1+[2],0}$  cover 28 frequency-points of the lattice. The rest are the frequency-points (2, 2), (6, 2), (2, 4), and (4, 2). Therefore, we can consider the following partition of the lattice  $X_{8,4}$ :

$$\sigma' = \begin{cases} T'_{0+[1],1} = \{(0.5, 1), (1.5, 3), (2.5, 1), (3.5, 3), \\ \quad (4.5, 1), (5.5, 3), (6.5, 1), (7.5, 3)\} \\ T'_{1+[2],2} = \{(1, 2), (3, 2), (5, 2), (7, 2)\} \\ T'_{2+[0],0} = \{(2, 0), (6, 0)\} \\ T'_{4+[0],0} = \{(4, 0)\} \\ T'_{0+[0],0} = \{(0, 0)\} \\ T'_{1+[1],1} = \{(1.5, 1), (4.5, 3), (7.5, 1), (2.5, 3), \\ \quad (5.5, 1), (0.5, 3), (3.5, 1), (6.5, 3)\} \\ T'_{1+[2],0} = \{(1, 0), (3, 0), (5, 0), (7, 0)\} \\ T'_{2+[2],2} = \{(2, 2), (6, 2)\} \\ T'_{2+[4],4} = \{(2, 4)\} \\ T'_{4+[2],2} = \{(4, 2)\}. \end{cases}$$

To calculate the  $8 \times 4$ -point DHFT, it is required to calculate two 8-point DFTs, two 4-point DFTs, two 2-point DFT, and four 1-point DFTs. Therefore, the following splitting of the  $8 \times 4$ -point DHFT holds:

$$\mathcal{R}(\mathcal{F}_{8,4}; \sigma') = \{\mathcal{F}_8, \mathcal{F}_8, \mathcal{F}_4, \mathcal{F}_4, \mathcal{F}_2, \mathcal{F}_2, 1, 1, 1, 1\}.$$

Since the paired transform is fulfilled without multiplications, the multiplicative complexity of the  $8 \times 4$ -point DHFT is estimated as

$$m'_{8,4} = 2(m_8 + 8 - 2) + 2(m_4 + 4 - 2) = 20.$$

It should be noted for comparison with the rectangular case, that in the tensor representation, the  $8 \times 4$ -point DFT is split by the covering  $\sigma_{8,4} = ((T_{1,p_2}; p_2 = 0 : 3), (T_{2p_1,1}; p_1 = 0 : 3))$  as

$$\mathcal{R}(\mathcal{F}_{8,4}; \sigma_{8,4}) = \{\mathcal{F}_8, \mathcal{F}_8, \mathcal{F}_8, \mathcal{F}_8, \mathcal{F}_4, \mathcal{F}_4, \mathcal{F}_4, \mathcal{F}_4\}$$

which requires  $4(m_8 + m_4) = 4m_8 = 8$  operations of multiplication.

**Example 19.27**

We now construct a partition  $\sigma'$  of the hexagonal lattice  $X_{16,8}$ . For that, we first consider the following covering of the lattice:

$$\sigma_{16,8} = \left( (T_{p_1+1,1})_{p_1=0:3}, T_{1+[0],0}, T_{1+[4],4}, T_{2+[2],2}, T_{6+[2],2}, (T_{4p_1+[2],2})_{p_1=0:3} \right). \quad (19.231)$$

The first four sets contain 32 elements each, the next two subsets contain 16 elements each,  $T_{2+[2],2}$  and  $T_{6+[2],2}$  contain 8 elements each, and the last four subsets  $T_{4p_1+[2],2}$  contain 4 elements each. The  $16 \times 8$ -point DHFT is thus split as

$$\mathcal{R}(\mathcal{F}_{16,4}; \sigma) = \{\mathcal{F}_{32}, \mathcal{F}_{32}, \mathcal{F}_{32}, \mathcal{F}_{32}, \mathcal{F}_{16}, \mathcal{F}_{16}, \mathcal{F}_8, \mathcal{F}_8, \mathcal{F}_4, \mathcal{F}_4, \mathcal{F}_4, \mathcal{F}_4\}.$$

To remove the redundancy of calculations that are due to the intersections between sets  $T$  of the covering  $\sigma_{16,8}$ , we consider the following decompositions of sets:

$$\begin{aligned} T_{0+[1],1} &= \underline{T'_{0.5,1}} + \underline{T'_{1,2}} + \underline{T'_{2,4}} + \underline{T'_{4,0}} + \underline{T'_{8,0}} + \underline{T'_{0,0}} \\ T_{1+[1],1} &= \underline{T'_{1.5,1}} + \underline{T'_{3,2}} + \underline{T'_{2,4}} + \underline{T'_{4,0}} + \underline{T'_{8,0}} + \underline{T'_{0,0}} \\ T_{2+[1],1} &= \underline{T'_{2.5,1}} + \underline{T'_{1,2}} + \underline{T'_{2,4}} + \underline{T'_{4,0}} + \underline{T'_{8,0}} + \underline{T'_{0,0}} \\ T_{3+[1],1} &= \underline{T'_{3.5,1}} + \underline{T'_{3,2}} + \underline{T'_{2,4}} + \underline{T'_{4,0}} + \underline{T'_{8,0}} + \underline{T'_{0,0}} \\ T_{1+[0],0} &= \underline{T'_{1,0}} + \underline{T'_{2,0}} + \underline{T'_{4,0}} + \underline{T'_{8,0}} + \underline{T'_{0,0}} \\ T_{1+[4],4} &= \underline{T'_{1,4}} + \underline{T'_{2,0}} + \underline{T'_{4,0}} + \underline{T'_{8,0}} + \underline{T'_{0,0}} \\ T_{2+[2],2} &= \underline{T'_{2,2}} + \underline{T'_{4,4}} + \underline{T'_{8,0}} + \underline{T'_{0,0}} \\ T_{6+[2],2} &= \underline{T'_{6,2}} + \underline{T'_{4,4}} + \underline{T'_{8,0}} + \underline{T'_{0,0}} \\ T_{0+[2],2} &= \underline{T'_{0,2}} + \underline{T'_{0,4}} + \underline{T'_{0,0}} \\ T_{4+[2],2} &= \underline{T'_{4,2}} + \underline{T'_{8,4}} + \underline{T'_{0,0}} \\ T_{8+[2],2} &= \underline{T'_{8,2}} + \underline{T'_{0,4}} + \underline{T'_{0,0}} \\ T_{12+[2],2} &= \underline{T'_{12,2}} + \underline{T'_{8,4}} + \underline{T'_{0,0}}. \end{aligned}$$

By removing all subsets that are not underlined above, we obtain the following partition of the hexagonal lattice  $X_{16,8}$ :

$$\sigma'_{16,8} = \{ \underline{T'_{0.5,1}}, \underline{T'_{1,2}}, \underline{T'_{2,4}}, \underline{T'_{1.5,1}}, \underline{T'_{3,2}}, \underline{T'_{2.5,1}}, \underline{T'_{3.5,1}}, \underline{T'_{1,0}}, \underline{T'_{2,0}}, \underline{T'_{4,0}}, \underline{T'_{8,0}}, \underline{T'_{0,0}}, \underline{T'_{1,4}}, \underline{T'_{2,2}}, \underline{T'_{4,4}}, \underline{T'_{6,2}}, \underline{T'_{0,2}}, \underline{T'_{0,4}}, \underline{T'_{4,2}}, \underline{T'_{8,4}}, \underline{T'_{8,2}}, \underline{T'_{12,2}} \}. \quad (19.232)$$

The cardinalities of these subsets equal 16, 8, 4, 16, 8, 16, 16, 8, 4, 2, 1, 1, 8, 4, 2, 4, 2, 1, 2, 1, 2, 2, respectively. The splitting of the

$16 \times 8$ -point DHFT by the partition  $\sigma'_{16,8}$  contains the following 1-D DFTs:

$$\mathcal{R}(\mathcal{F}_{16,4}; \sigma') = \left\{ \underbrace{\mathcal{F}_{16}, \dots, \mathcal{F}_{16}}_{4 \text{ times}}, \underbrace{\mathcal{F}_8, \dots, \mathcal{F}_8}_{4 \text{ times}}, \underbrace{\mathcal{F}_4, \dots, \mathcal{F}_4}_{4 \text{ times}}, \underbrace{\mathcal{F}_2, \dots, \mathcal{F}_2}_{6 \text{ times}}, 1, 1, 1, 1 \right\}.$$

Taking into account the multiplications by twiddle factors which are used to calculate the modified paired representation of  $f$  (see Equation 19.230), we can estimate the number of operations of multiplication required for the  $16 \times 8$ -point DHFT as

$$\begin{aligned} m'_{16,8} &= 4(m_{16} + 16 - 2) + 4(m_8 + 8 - 2) + 4(m_4 + 4 - 2) \\ &= 4(10 + 14) + 4(2 + 6) + 4(2) = 96 + 32 + 8 = 136. \end{aligned}$$

To construct the partition  $\sigma'$  of the hexagonal lattice in the general  $N \geq 8$  case, we can use the covering of the form (19.223) or take the following covering:

$$\sigma_{2N,N} = \left( (T_{p_1+1,1})_{p_1=0:(N/2-1)}, (T_{1+[4p_2],4p_2})_{p_2=0:(N/4-1)}, (T_{4p_1+[2],2})_{p_1=0:(N-1)} \right),$$

and, then, divide all its sets by the subsets  $T'$  as

$$T_{p_1+[p_2],p_2} = T'_{p_1+[p_2],p_2} \cup T'_{2p_1,2p_2} \cup T'_{4p_1,4p_2} \cup \dots \cup T'_{N,0} \cup T'_{0,0}.$$

After removing the equivalent subsets, we obtain a partition  $\sigma' = (T')$  of the hexagonal lattice  $X_{2N,N}$ . This partition yields a splitting of the  $2N \times N$ -point DHFT into a set of 1-D DFTs:

$$\mathcal{R}(\mathcal{F}_{2N,N}; \sigma') = \left\{ \underbrace{\mathcal{F}_{2N}, \dots, \mathcal{F}_{2N}}_{N/2 \text{ times}}, \underbrace{\mathcal{F}_N, \dots, \mathcal{F}_N}_{N/2 \text{ times}}, \dots, \underbrace{\mathcal{F}_4, \dots, \mathcal{F}_4}_{N/2 \text{ times}}, \underbrace{\mathcal{F}_2, \dots, \mathcal{F}_2}_{3N/4 \text{ times}}, \underbrace{1, \dots, 1}_{N/2 \text{ times}} \right\}. \quad (19.233)$$

The number of operations of multiplication required to calculate the  $2N \times N$ -point DHFT is estimated as follows:

$$\begin{aligned} m'_{2N,N} &= \frac{N}{2} \sum_{n=2}^{r+1} (m_{2^n} + 2^n - 2) \\ &= \frac{N}{2} \sum_{n=2}^{r+1} ([2^{n-1}(n-3) + 2] + 2^n - 2) \\ &= N^2(r-1) + N. \end{aligned} \quad (19.234)$$

The number of multiplications required to calculate the  $2N \times N$ -point DHFT at knots of the first part  $N \times N$  of the hexagonal lattice  $2N \times N$  is estimated as half of  $m'_{2N,N}$ , i.e., about  $N^2/2 (r-1) + N/2$ . Indeed, each subset  $T' \in \sigma'$  (except the one-point ones, such as  $T'_{N/2,0}$  and  $T'_{0,0}$ ) has the equal number of points in both the parts of the lattice.

For comparison, we consider the estimate  $m_{N_1}^* = N_1(8 \log_7 N_1 - 1)$  obtained in Ref. [47] for computing the 2-D DHFT by the radix-7 decimation-in-space algorithm developed for the  $N_1 = 7^\lambda$  case. Taking the number of hexagonal pixels equal  $N_2 = 8^\lambda$ , we can see that the proposed paired method uses  $m_{8^\lambda}^*|_{\text{sample}} = 0.75\lambda - 0.5$  operations of multiplication per sample. In the part of the lattice consisting of  $7^\lambda$  pixels which lie on the hierarchical structure of the hexagonal aggregates, the radix-7 decimation-in-space algorithm uses  $m_{7^\lambda}^*|_{\text{sample}} = 8\lambda - 1$  such operations of multiplication per sample, i.e., at least 10 times more operations than the proposed algorithm does.

### 19.10.1.1 2-D DHFT on Other Lattices

The concept of the 2-D DHFT can also be defined on hexagonal lattices which are constructed in ways different from the lattice considered in Equation 19.213. One can say, that the hexagonal lattice  $X_{2N,N}$  is constructed by the broken lines:

$$l_{n_1} = \left\{ n_1 + [n_2] = n + \frac{1 - (-1)^{n_2}}{4}; n_2 = 0 : (N-1) \right\}, \\ n_1 = 0 : (2N-1).$$

The 2-D DHFT can be defined on another hexagonal lattice  $X_{3N,N}$  by [42]

$$F_{p_1+[p_2], p_2} = \sum_{n_1=0}^{3N-1} \sum_{n_2=0}^{N-1} f_{n_1+[n_2], n_2} W^{(n_1+[n_2])(p_1+[p_2])+n_2 p_2} \\ = \sum_{n_1=0}^{3N-1} \sum_{n_2=0}^{N-1} f_{n_1+[n_2], n_2} W_{3N}^{[(2n_1-n_2)p_1+3n_2 p_2]}. \quad (19.235)$$

The period of this transformation equals  $(3N, N)$ . The first coordinates of spatial points  $(n_1 + [n_2], n_2)$  and frequency-points  $(p_1 + [p_2], p_2)$  on the hexagonal lattice  $X_{3N,N}$  are calculated by

$$n_1 + [n_2] = n_1 - \frac{n_1 + n_2}{3}, \quad p_1 + [p_2] = p_1 - \frac{p_1 + p_2}{3}.$$

In this case, we consider conditionally that  $[n_2] = -(n_1 + n_2)/3$  and  $[p_2] = -(p_1 + p_2)/3$ . The hexagonal lattice  $X_{3N,N}$  is constructed by the straight parallel lines

$$m_{n_1} = \left\{ n_1 - \frac{n_1 + n_2}{3}; n_2 = 0 : (N-1) \right\}, \quad n_1 = 0 : (3N-1).$$

The points of this lattice are arranged horizontally,  $3/2$  times more compactly than in the first lattice (see Figure 19.40). We obtain the  $3N \times N$ -point DHFT with the fundamental period  $X_{3N,N}$  being the hexagonal lattice of size  $3N \times N$ . The given

notation of this 2-D DHFT is identical to the notation considered in (214). The method of splitting the  $3N \times N$ -point DHFT into a set of 1-D DFTs is similar to the  $2N \times N$ -point DHFT case.

## 19.11 Paired Transform-Based Algorithms

In this section, we briefly describe the paired transform-based algorithms of calculation of the 2-D Hartley, cosine, and Hadamard transforms of order  $N \times N$ , when  $N = 2^r$ ,  $r > 1$ . The unitary paired transform as a core for each of these transforms is derived from the tensor transform in a way that all splitting-signals of the image are transformed into a set of short signals which carry the spectral information of the image at disjoint subsets of frequency-points. The redundancy of the tensor transform is thus removed completely.

### 19.11.1 Calculation of the 2-D DHT

The paired representation of an image  $f_{n_1, n_2}$  with respect to the Fourier transform can be used for splitting the 2-D DHT,  $\mathcal{H}_{N,N}$ , defined as

$$H_{p_1, p_2} = \sum_{n_1=0}^{N-1} \sum_{n_2=0}^{N-1} f_{n_1, n_2} \text{Cas}_N(n_1 p_1 + n_2 p_2), \quad p_1, p_2 = 0 : (N-1), \quad (19.236)$$

where  $\text{Cas}_N(x) = \text{cas}(2\pi x/N)$ . Both 2-D DHT and DFT result in the same tensor representation of the image,  $\{f_{n_1, n_2}\} \rightarrow \{f_{p_1, p_2, t}\}$ , as well as the paired representation

$$\mathcal{X}'_{N,N} : \{f_{n_1, n_2}\} \rightarrow \left\{ f'_{p_1, p_2, t} = f_{p_1, p_2, t} - f_{p_1, p_2, t+N/2} \right\}. \quad (19.237)$$

The set of triplets  $(p_1, p_2, t)$  is considered to be the set  $U$  defined in Equation 19.192. In other words,  $(p_1, p_2) = 2^n(p, s)$ , where  $(p, s) \in J_{2^{r-n}, 2^{r-n}}$  and  $t = 2^n t_1$ ,  $t_1 = 0 : (2^{r-n-1} - 1)$ . In terms of the paired representation, the 2-D DHT is considered as a transform composed by 1-D Hartley transforms of orders  $2^{r-n-1}$ ,  $n = 0 : (r-1)$ . Indeed, the following formula

$$H_{(2m+1)p_1, (2m+1)p_2} = \sum_{t=0}^{2^{r-n-1}-1} f'_{p_1, p_2, t} \text{Cas}_{2^{r-n-1}} \left( \left( m + \frac{1}{2} \right) t \right) \quad (19.238)$$

holds for integers  $m = 0 : (2^{r-n-1} - 1)$ . The  $N \times N$ -point DHT is thus determined at frequency-points of each orbit  $T'_{p_1, p_2}$  by the odd-frequency  $2^{r-n-1}$ -point DHT, which we denote by  $\mathcal{H}_{2^{r-n-1}|_{\text{of}}}$  and define over a sequence  $f_n$  by

$$(\mathcal{H}_{2^{r-n-1}|_{\text{of}}} \circ f)_m = \sum_{n=0}^{2^{r-n-1}-1} f_n \text{Cas}_{2^{r-n-1}} \left( \left( m + \frac{1}{2} \right) n \right), \quad (19.239) \\ m = 0 : (2^{r-n-1} - 1).$$

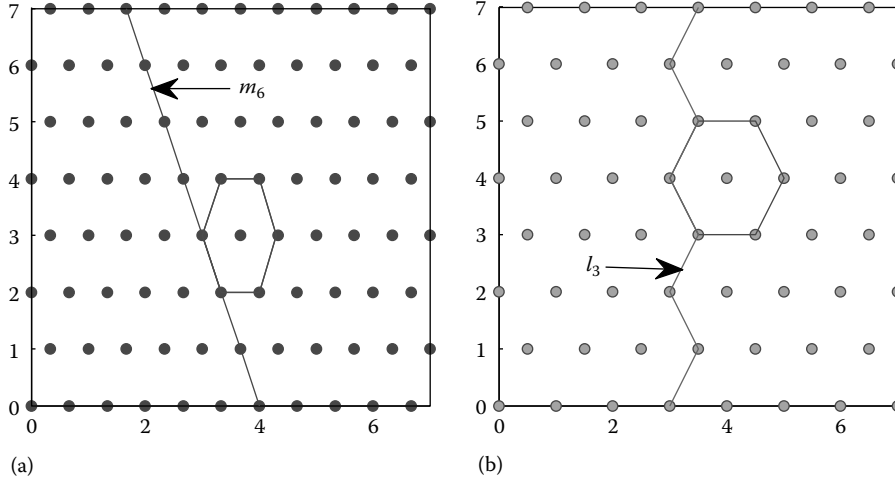


**FIGURE 19.40** (a) The hexagonal lattice defined by straight lines  $m_n$  (the line  $m_6$  is also shown), and (b) the hexagonal lattice defined by broken lines  $l_n$  (the line  $l_3$  is also shown).

To estimate the number  $m_{2^n|of}$  of multiplications required for computing  $\mathcal{H}_{2^n|of}$ , we can use the known recursive estimates  $m_{2^n|of} = 2^{n-1}n + m_{2^{n-1}|of}$ , for  $n \geq 2$  [48].

The sets  $J_{2^{r-n}, 2^{r-n}}$ ,  $n = 0 : (r-1)$ , consist of  $3 \cdot 2^{r-n-1}$  generators, respectively. Therefore, by means of the paired transform  $\mathcal{X}'_{2^r, 2^r}$ , the  $2^r \times 2^r$ -point DHT is split into  $2^3 - 2$  short odd-frequency DHTs, namely  $2^{r-1}$ -point DHTs in number  $3 \cdot 2^{r-1}$ ,  $2^{r-2}$ -point DHTs in number  $3 \cdot 2^{r-2}$ , ..., and six 2-point and four 1-point DHTs. This splitting is similar to the splitting of the 2-D DFT, and for calculating the  $2^r \times 2^r$ -point DHT, it is enough to fulfill

$$m'_{2^r, 2^r} \leq 2 \cdot 4^{r-1}(r - 7/3) + 8/3 - 12, \quad (r > 3), \quad (19.240)$$

operations of multiplication.

### Example 19.28

In the  $N = 8$  case, the lattice  $X_{8,8}$  is divided by 22 orbits  $T' \in \sigma'$ . Twelve of these orbits have 4 points each, six orbits have 2 points each, and the other four orbits are 1-point. Therefore, by using the paired transformation, we obtain the following splitting of the  $8 \times 8$ -point DHT by the off-frequency DHTs:

$$\mathcal{R}(\mathcal{H}_{8,8}; \sigma') = \left\{ \underbrace{\mathcal{H}_{4|of}, \dots, \mathcal{H}_{4|of}}_{12 \text{ times}}, \underbrace{\mathcal{H}_{2|of}, \dots, \mathcal{H}_{2|of}}_{6 \text{ times}}, 1, 1, 1, 1 \right\}.$$

The off-frequency 4-point DHT has the matrix

$$[\mathcal{H}_{4|of}] = \begin{bmatrix} 1 & 1 & 1 & 1 \\ 1.4142 & 0 & -1.4142 & 0 \\ 1 & -1 & 1 & -1 \\ 0 & 1.4142 & 0 & -1.4142 \end{bmatrix}$$

and requires only two multiplications. No multiplication is required for the off-frequency two-point DHT:  $(f_0, f_1) \rightarrow (f_0 + f_1, f_0 - f_1)$ . Therefore, the paired transform-based  $8 \times 8$ -point DHT uses  $m'_{8,8} = 12m_{4|of} = 24$  operations of multiplication.

### 19.11.2 2-D Discrete Cosine Transform

We now consider the paired transform-based algorithm for calculation of the 2-D DCT. We stand briefly on the main properties of the algorithm, which is a modification of the tensor algorithm described in detail in Section 19.8.

Let  $\mathcal{C}_{N,N}$  be the 2-D discrete nonseparable  $N \times N$ -point DCT calculated at frequency-points  $(p_1, p_2)$  of the lattice  $X_{N,N}$  by

$$C_{p_1, p_2} = \sum_{n_1=0}^{N-1} \sum_{n_2=0}^{N-1} f_{n_1, n_2} \text{Cos} \left( n_1 p_1 + n_2 p_2 + \frac{p_1 + p_2}{2} \right), \quad p_1, \quad p_2 = 0 : (N-1), \quad (19.241)$$

where  $\text{Cos}(x) = \cos(\pi x/N)$ .

The paired representation of the image  $f$  by the cosine transform is described as a complete set of paired splitting-signals, which are composed from the splitting-signals in the tensor representation, by substituting the first half of the signals from their second half. In other words, the paired splitting-signals corresponding to the generators  $(p_1, p_2)$  are defined as follows:

1. If  $e(p_1, p_2) = 0$ , then

$$\tilde{f}'_{T'_{p_1, p_2}} = \left\{ \tilde{f}'_{p_1, p_2, 0}, \tilde{f}'_{p_1, p_2, 1}, \tilde{f}'_{p_1, p_2, 2}, \dots, \tilde{f}'_{p_1, p_2, N/2-1} \right\}, \quad (19.242)$$

where

$$\tilde{f}'_{p_1, p_2, t} = \tilde{f}_{p_1, p_2, t} - \tilde{f}_{p_1, p_2, N-t}, \quad t = 0 : (N/2 - 1). \quad (19.243)$$

2. If  $e(p_1, p_2) = 1$ , then

$$\tilde{f}'_{T'_{p_1, p_2}} = \left\{ \tilde{f}'_{p_1, p_2, \frac{1}{2}}, \tilde{f}'_{p_1, p_2, \frac{3}{2}}, \dots, \tilde{f}'_{p_1, p_2, N/2 - \frac{1}{2}} \right\}, \quad (19.244)$$

where

$$\tilde{f}'_{p_1, p_2, t + \frac{1}{2}} = \tilde{f}_{p_1, p_2, t + \frac{1}{2}} - \tilde{f}_{p_1, p_2, N - t - \frac{1}{2}}, \quad t = 0 : (N/2 - 1). \quad (19.245)$$

Therefore, the slitting of the 2-D DCT is described by the following pair of equations:

$$C_{(2m+1)p_1, (2m+1)p_2} = \begin{cases} \sum_{t=0}^{N/2-1} \tilde{f}'_{p_1, p_2, t} \cos_{N/2} \left( \left( m + \frac{1}{2} \right) t \right), \\ \text{if } e(p_1, p_2) = 0, \\ \sum_{t=0}^{N/2-1} \tilde{f}'_{p_1, p_2, t + \frac{1}{2}} \cos_{N/2} \left( \left( m + \frac{1}{2} \right) \left( t + \frac{1}{2} \right) \right), \\ \text{if } e(p_1, p_2) = 1, \quad m = 0 : (N/2 - 1). \end{cases} \quad (19.246)$$

The right part of Equation 19.246 itself represents the  $N/2$ -point DCT of type-III,  $C_{N/2;3}$ , or the  $N/2$ -point DCT of type-IV,  $C_{N/2;4}$ , if  $p_1$  and  $p_2$  have the same or different evenness, respectively. We here remind that the partition  $\sigma' = (T')$  of the lattice  $X_{N,N}$  consists of  $(3N - 2)$  subsets  $T'_{p_1, p_2}$ , which are orbits of  $3N/2$  cyclic groups  $T_{p_1, p_2}$  composing the covering  $\sigma$  of the lattice. The generators  $(p_1, p_2)$  of  $N/2$  groups  $T_{p_1, p_2}$  of this covering have the same evenness and generators of the rest of  $N$  groups have different evenness. The  $N \times N$ -point DCT consists therefore of  $N/2$   $N/2$ -point DCTs  $C_{N/2;3}$ , and  $N$  DCTs  $C_{N/2;4}$ ,  $N/4N/4$ -point DCTs  $C_{N/4;3}$  and  $N/8$  DCTs  $C_{N/4;4}$ , etc. In other words, the splitting set of the  $N \times N$ -point DCT equals

$$\mathcal{R}(C_{N,N}; \sigma') = \left\{ \underbrace{C_{N/2;3}, C_{N/2;3}, \dots, C_{N/2;3}}_{N/2 \text{ times}}, \underbrace{C_{N/2;4}, C_{N/2;4}, \dots, C_{N/2;4}}_{N \text{ times}}, \right. \\ \underbrace{C_{N/4;3}, C_{N/4;3}, \dots, C_{N/4;3}}_{N/4 \text{ times}}, \underbrace{C_{N/4;4}, C_{N/4;4}, \dots, C_{N/4;4}}_{N/2 \text{ times}}, \\ \underbrace{C_{N/8;3}, C_{N/8;3}, \dots, C_{N/8;3}}_{N/8 \text{ times}}, \underbrace{C_{N/8;4}, C_{N/8;4}, \dots, C_{N/8;4}}_{N/4 \text{ times}}, \\ \dots \dots \dots \left. \underbrace{C_{2;3}, C_{2;3}, C_{2;4}, C_{2;4}, C_{2;4}, C_{2;4}}_{N/4 \text{ times}}, 1, 1, 1, 1 \right\}. \quad (19.247)$$

### Example 19.29

In the  $N=8$  case, we obtain the following splitting of the  $8 \times 8$ -point DCT by the paired transform:

$$\mathcal{R}(C_{8,8}; \sigma') = \left\{ \underbrace{C_{4;3}, \dots, C_{4;3}}_{4 \text{ times}}, \underbrace{C_{4;4}, C_{4;4}, \dots, C_{4;4}}_{8 \text{ times}}, \right. \\ \left. \underbrace{C_{2;3}, C_{2;3}}, \underbrace{C_{2;4}, C_{2;4}, C_{2;4}, C_{2;4}}, 1, 1, 1, 1 \right\}. \quad (19.248)$$

The similar, but more complicated splitting set holds for the  $2^r \times 2^r$ -point DCT, as well as for other orders  $N \times N$  of the transform, and we leave these cases to the reader as exercises.

### 19.11.3 2-D Discrete Hadamard Transform

The basis functions of the DHdT take value 1 or  $-1$  at each point. The DHdT has found useful applications in signal and image processing (image coding, enhancement, pattern recognition, and filtering). The two-dimensional DHdT of a 2-D sequence or image  $f = \{f_{n_1, n_2}\}$  of size  $N \times N$ , where  $N = 2^r$ ,  $r \geq 1$ , is defined by

$$A_{p_1, p_2} = (\mathcal{A}_{N,N} \circ f)_{p_1, p_2} = \sum_{n_2=0}^{N-1} \sum_{n_1=0}^{N-1} f_{n_1, n_2} a(p_1; n_1) a(p_2; n_2), \quad (19.249)$$

where  $p_1, p_2 = 0 : (N - 1)$ . The transform is separable; it can be calculated by the row-column method by using the 1-D DHdT,

$$A_p = (\mathcal{A}_N \circ f_n)_p = \sum_{n=0}^{N-1} f_n a(p; n), \quad p = 0 : (N - 1),$$

where  $a(p; n)$  is the kernel of the transform, which is defined in Equation 19.4. The matrix  $[\mathcal{A}_N]$  of the 1-D DHdT consists only of the elements  $\pm 1$  and can be constructed recursively:

$$[\mathcal{A}_N] = \begin{bmatrix} [\mathcal{A}_{N/2}] & -[\mathcal{A}_{N/2}] \\ [\mathcal{A}_{N/2}] & [\mathcal{A}_{N/2}] \end{bmatrix}, \quad (\mathcal{A}_1 = 1). \quad (19.250)$$

We here focus on the construction of the fast algorithm for calculating the 2-D DHdT, which is based on a concept of the paired transforms, which has been described above for the 2-D DFT. The paired transform reveals the 2-D DHdT and DFT, which means that the same splitting-signals

$$f_{T'_{p,s}} = \{f_{p,s,0}, f_{p,s,1}, \dots, f_{p,s,N/2-1}\}, \quad (p, s) \in I_{N,N},$$

can be used for calculating both transforms. Namely, the following property is valid for the 2-D DHdT. Let us consider the given

in Section 19.9 formula (19.193) of calculation of the 2-D DFT through the 1-D DFTs of the paired splitting-signals,

$$F_{(2m+1)p, (2m+1)s} = \sum_{t=0}^{N/2-1} \left( f'_{p,s,t} W^t \right) W_{N/2}^{mt}, \quad m = 0 : (N/2 - 1),$$

for the case when  $g.c.d(p, s) = 1$ . The  $N/2$ -point DFT of the modified splitting-signal defines the 2-D DFT at frequency-points of the subset  $T'_{p,s}$ . If we now omit all twiddle factors  $W^t$  (i.e., the splitting-signals are not modified) and consider, in the right side of this formula, the  $N/2$ -point DHdT instead of the  $N/2$ -point DFT, we obtain the 2-D DHdT at frequency-points of  $T'_{p,s}$ . In other words, the following is valid:

$$A_{(2m+1)p, (2m+1)s} = \sum_{t=0}^{N/2-1} f'_{p,s,t} a(m; t), \quad m = 0 : (N/2 - 1). \quad (19.251)$$

A similar result can easily be derived for the case when  $g.c.d(p, s) = 2^k$ , where  $k = 1 : (r - 1)$ , when the  $N/2$ -point DHdT in the right side of Equation 19.251 is reduced to the  $N/2^{k+1}$ -point DHdT. The illustration of this property can easily be seen in the 1-D case.

### 19.11.3.1 1-D DFT and DHdT

The 1-D  $N$ -point discrete paired transform (DPT)  $\mathcal{X}'_N$  is defined by the following complete system of the paired functions [12]:

$$\mathcal{X}'_{2^k, 2^k t}(n) = M \left( \cos \left( \frac{2\pi(n-t)}{2^{r-k}} \right) \right), \quad t = 0 : (2^{r-k-1} - 1),$$

$$k = 0 : (r - 1), \quad \mathcal{X}'_{0,0}(n) \equiv 1, \quad n = 0 : (N - 1), \quad (19.252)$$

where  $M$  is the real function which differs from zero only on the bounds of the interval  $[-1, 1]$  and takes values  $M(-1) = -1$ ,  $M(1) = 1$ . The double numbering of the paired functions refers to the frequency ( $p = 2^k$ ) and time ( $t$ ). The paired transform is a transform of the discrete-time signal  $f_n$  to the set of frequency-time signals,

$$f_n \rightarrow \left\{ \left\{ f'_{2^k, 0}, f'_{2^k, 2^k}, f'_{2^k, 2^{2k}}, \dots, f'_{2^k, N/2^{k+1}-1} \right\}, \quad k = 0 : (r - 1) \right\},$$

which splits the  $2^r$ -point DFT by the  $2^{r-k-1}$ -point DFTs,  $k = 0 : (r - 1)$ . The components of these splitting-signals are calculated by

$$f'_{2^k, 2^k t} = \mathcal{X}'_{2^k, 2^k t} \circ f_n = \sum_{n=0}^{2^r-1} \mathcal{X}'_{2^k, 2^k t}(n) f_n, \quad t = 0 : (2^{r-k-1} - 1).$$

### Example 19.30

The matrix of the 8-point DPT is defined as follows:

$$[\mathcal{X}'_8] = \begin{bmatrix} \mathcal{X}'_{1,0} \\ \mathcal{X}'_{1,1} \\ \mathcal{X}'_{1,2} \\ \mathcal{X}'_{1,3} \\ \mathcal{X}'_{2,0} \\ \mathcal{X}'_{2,2} \\ \mathcal{X}'_{4,0} \\ \mathcal{X}'_{0,0} \end{bmatrix} = \begin{bmatrix} 1 & 0 & 0 & 0 & -1 & 0 & 0 & 0 \\ 0 & 1 & 0 & 0 & 0 & -1 & 0 & 0 \\ 0 & 0 & 1 & 0 & 0 & 0 & -1 & 0 \\ 0 & 0 & 0 & 1 & 0 & 0 & 0 & -1 \\ 1 & 0 & -1 & 0 & 1 & 0 & -1 & 0 \\ 0 & 1 & 0 & -1 & 0 & 1 & 0 & -1 \\ 1 & -1 & 1 & -1 & 1 & -1 & 1 & -1 \\ 1 & 1 & 1 & 1 & 1 & 1 & 1 & 1 \end{bmatrix}.$$

The first four basis paired functions correspond to the frequency  $p = 1$ , the next two functions correspond to frequency  $p = 2$ , and the last two functions correspond to the frequencies  $p = 4$  and  $0$ , respectively. The process of composition of these functions from the corresponding cosine waves defined in the interval  $[0, 7]$  is illustrated in Figure 19.41.

Let  $f_n$  be the signal  $\{1, 2, 2, 4, 5, 3, 1, 3\}$ . The paired transform of this signal results in four splitting-signals as follows:

$$f_n \rightarrow \begin{cases} \{-4, -1, 1, 1\} \\ \{3, -2\} \\ \{-3\} \\ \{21\} \end{cases}$$

The splitting of the  $2^r$ -point DFT into  $(r + 1)$  short DFTs is described by

$$F_{(2m+1)2^k} = \sum_{t=0}^{2^{r-k-1}-1} \left( f'_{p,t} W_{2^{r-k}}^t \right) W_{2^{r-k-1}}^{mt}, \quad m = 0 : (2^{r-k-1} - 1). \quad (19.253)$$

The set of  $2^r$  frequency-points  $X_{2^r} = \{0, 1, 2, \dots, 2^r - 1\}$  is divided by  $(r + 1)$  subsets, or orbits  $T'_p = \{(2m + 1)p \bmod 2^r; m = 0 : (2^{r-1}/p - 1)\}$ , where  $p = 2^k$ ,  $k = 0 : (r - 1)$ , and  $T'_0 = \{0\}$ . These subsets compose a partition  $\sigma'$  of  $X_{2^r}$ , and the  $2^r$ -point DFT is split as follows:

$$\mathcal{R}(\mathcal{F}_{2^r}; \sigma') = \{\mathcal{F}_{2^{r-1}}, \mathcal{F}_{2^{r-2}}, \mathcal{F}_{2^{r-3}}, \dots, \mathcal{F}_2, 1, 1\}. \quad (19.254)$$

Using the similar splitting for each short transform  $\mathcal{F}_{2^{r-k-1}}$  of this splitting, we obtain the full decomposition of the  $2^r$ -point DFT, by the paired transforms.

The similar results are valid for the 1-D DHdT (up to a permutation),

$$A_{(2m+1)2^k} = \sum_{t=0}^{2^{r-k-1}-1} f'_{p,t} a(m, t), \quad m = 0 : (2^{r-k-1} - 1), \quad (19.255)$$

and the splitting of the  $2^r$ -point DHdT equals

$$\mathcal{R}(\mathcal{A}_{2^r}; \sigma') = \{\mathcal{A}_{2^{r-1}}, \mathcal{A}_{2^{r-2}}, \mathcal{A}_{2^{r-3}}, \dots, \mathcal{A}_2, 1, 1\}. \quad (19.256)$$

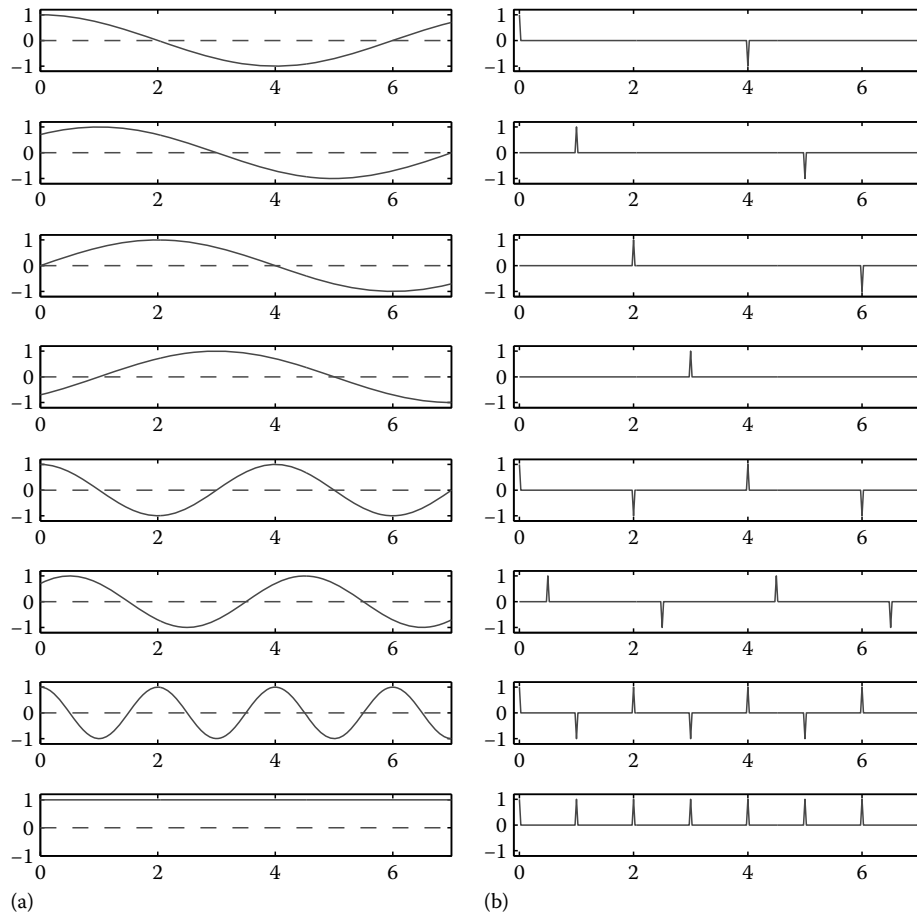


FIGURE 19.41 (a) Cosine waves and (b) discrete paired functions of the 8-point DPT.

**Example 19.31**

Let  $N=8$  and let  $f_n$  be the signal of Example 19.30. According to Equation 19.253, the calculation of the 8-point DFT of  $f_n$  can be written in the matrix form as

$$\begin{bmatrix} F_7 \\ F_3 \\ F_5 \\ F_1 \\ F_6 \\ F_2 \\ F_4 \\ F_0 \end{bmatrix} = \begin{bmatrix} [\mathcal{F}_2] & & & & & & & \\ & 1 & & & & & & \\ & & \text{diag} \left\{ \begin{matrix} 1 \\ -j \\ 1 \\ 1 \end{matrix} \right\} & & & & & \\ & & & [\mathcal{F}_2] & & & & \\ & & & & 1 & & & \\ & & & & & & & 1 \end{bmatrix} [\mathcal{X}'_4]$$

$$\text{diag} \left\{ \begin{matrix} 1 \\ W \\ -j \\ W^3 \\ 1 \\ -j \\ 1 \\ 1 \end{matrix} \right\} [\mathcal{X}'_8] = \begin{bmatrix} 1 \\ 2 \\ 2 \\ 4 \\ 5 \\ 3 \\ 1 \\ 3 \end{bmatrix} = \begin{bmatrix} -5.4142 + j \\ -2.5858 + j \\ -2.5858 - j \\ -5.4142 - j \\ 3 - 2j \\ 3 + 2j \\ -3 \\ 21 \end{bmatrix}$$

where the twiddle factors  $W = \exp(-2\pi j/8) = 0.7071(1 - j)$  and  $W^3 = -0.7071(1 + j)$ .

The construction of the matrix  $[\mathcal{A}_8]$  of the 8-point DHdT is illustrated in Table 19.5. The calculation of the Hadamard transform of the signal  $f_n$  is performed as

$$\begin{bmatrix} A_7 \\ A_{3 \rightarrow 6} \\ A_5 \\ A_{1 \rightarrow 4} \\ A_{6 \rightarrow 3} \\ A_2 \\ A_{4 \rightarrow 1} \\ A_0 \end{bmatrix} = \begin{bmatrix} [\mathcal{A}_2] & & & & & & & \\ & 1 & & & & & & \\ & & [\mathcal{X}'_4] & & & & & \\ & & & [\mathcal{A}_2] & & & & \\ & & & & 1 & & & \\ & & & & & & & 1 \end{bmatrix} [\mathcal{X}'_8] = \begin{bmatrix} 1 \\ 2 \\ 2 \\ 4 \\ 5 \\ 3 \\ 1 \\ 3 \end{bmatrix} = \begin{bmatrix} -3 \\ -7 \\ -3 \\ -3 \\ 5 \\ 1 \\ -3 \\ 21 \end{bmatrix}$$

where the permutation of the components  $A_p$  is performed as  $p = (p_0, p_1, p_2) \rightarrow (p_2, p_1, p_0)$ , and

$$[\mathcal{A}_2] = [\mathcal{F}_2] = \begin{bmatrix} 1 & -1 \\ 1 & 1 \end{bmatrix}$$

**TABLE 19.5** Construction of the Hadamard Matrix  $8 \times 8$

$n, p$	$n_0 n_1 n_2$	$p_0 p_1 p_2$	$[\mathcal{A}_8] = [(-1)^{n_0 p_0 + n_1 p_1 + n_2 p_2}]$
7	1 1 1	1 1 1	1, -1, -1, 1, -1, 1, 1, -1
6	0 1 1	0 1 1	1, 1, -1, -1, -1, -1, 1, 1
5	1 0 1	1 0 1	1, -1, 1, -1, -1, 1, -1, 1
4	0 0 1	0 0 1	1, 1, 1, 1, -1, -1, -1, -1
3	1 1 0	1 1 0	1, -1, -1, 1, 1, -1, -1, 1
2	0 1 0	0 1 0	1, 1, -1, -1, 1, 1, -1, -1
1	1 0 0	1 0 0	1, -1, 1, -1, 1, -1, 1, -1
0	0 0 0	0 0 0	1, 1, 1, 1, 1, 1, 1, 1

Thus, the following decomposition is valid:

$$\begin{aligned}
 [\mathcal{A}_8] &= \begin{bmatrix} [\mathcal{A}_4] & & & \\ & [\mathcal{A}_2] & & \\ & & 1 & \\ & & & 1 \end{bmatrix} [\mathcal{X}'_8] \\
 &= \begin{bmatrix} \begin{bmatrix} [\mathcal{A}_2] & & \\ & 1 & \\ & & 1 \end{bmatrix} [\mathcal{X}'_4] & & & \\ & & & [\mathcal{A}_2] & & \\ & & & & 1 & \\ & & & & & 1 \end{bmatrix} [\mathcal{X}'_8].
 \end{aligned}$$

In the general  $N = 2^r$  case, where  $r \geq 2$ , the following matrix decompositions hold for the 1-D DHdT and DFT:

$$\begin{aligned}
 [\mathcal{A}_{2^r}] &= \left[ \left( \bigoplus_{k=0}^{r-1} [\mathcal{A}_{2^{r-k-1}}] \right) \oplus 1 \right] [\mathcal{X}'_{2^r}], \\
 [\mathcal{F}_{2^r}] &= \left[ \left( \bigoplus_{k=0}^{r-1} [\mathcal{F}_{2^{r-k-1}}] \right) \oplus 1 \right] D_{2^r} [\mathcal{X}'_{2^r}], \quad (19.257)
 \end{aligned}$$

where  $\oplus$  denotes the operation of the Kronecker sum of matrices and the diagonal matrix

$$\begin{aligned}
 D_{2^r} = \text{diag} \{ &1, W, W^2, W^3, \dots, W^{2^r-1}, 1, W^2, W^4, \dots, \\
 &W^{2^r-2}, 1, W^4, W^8, \dots, W^{2^r-4}, 1, \dots, 1, 1 \}.
 \end{aligned}$$

Thus for the calculation of the  $2^r$ -point DHdT, we can use the paired algorithm of the DFT, from which all diagonal matrices with twiddle factors are removed, or considered to be the identity matrices. The paired transform splits the mathematical structures of both transforms. In the 2-D case, the paired algorithm of the 2-D DFT can also be used for the calculation of the 2-D DHdT, by removing all twiddle factors, or considering them equal 1.

### 19.12 Conclusion

The representation of the multidimensional signals and splitting of the unitary transforms of the signals by the tensor and paired transforms allows for developing effective methods of calculation

of the multidimensional transforms through the one-dimensional splitting-signals. The splitting-signals can be processed separately and in parallel; they carry the spectral information of the signals and define the images of the multidimensional signals along the different directions in the spatial domain. The paired transformations are unitary and transfer the  $n$ -dimensional signals from the spatial space to  $(n + 1)$ -dimensional space which is the  $n$ -dimensional space of frequency-points together with the 1-D time interval. The basis functions of the paired transforms are defined by linear integrals (sums) along specific parallel directions in the spatial domain. We can also call the paired transforms the directional unitary transforms which are derived from the kernels of the multidimensional transforms, such as the Fourier and cosine transforms. Therefore the paired transforms can be used not only in effective calculation of the multidimensional transforms, but in such practical applications as the image enhancement, or computer tomography, when the 2-D or 3-D image is reconstructed from the parallel projections directly from the paired transforms. The images can be defined on the multidimensional rectangular lattices, and other types of lattices, such as hexagonal lattices were described for the 2-D Fourier transforms. In this chapter, we have focused on the discrete Fourier, the Hartley, the Hadamard, and the cosine transforms, but other transforms can also be revealed by 1-D splitting-signals. The important orthogonal transformation, the Haar transformation has not been considered in this chapter. However, an attentive reader would have noticed that the Haar transformation in the 1-D case can easily be derived from the paired transformation of order  $N = 2^r$ ,  $r > 1$ . For that, a few permutations of columns and rows of the matrix of the paired transformation are required. In other words, the Haar transformation is a paired-like transformation which is present in the mathematical structure of the DFT [16]. In the two- and multidimensional cases, the paired transformations are not separable and exist not only for orders being powers of two, but for many other orders as well.

### References

1. N. Ahmed and K.R. Rao, *Orthogonal Transforms for Digital Image Processing*, Springer-Verlag, New York, 1975.
2. L.A. Zalmonzon, *Fourier, Walsh, and Haar Transforms and Their Application in Control, Communication and Other Fields*, Nauka, Moscow, 1989.
3. A.K. Jain, *Fundamentals of Digital Image Processing*, Prentice Hall, Inc. Englewood Cliffs, NJ, 1989.
4. O. Ersoy, *Fourier-Related Transform, Fast Algorithms and Applications*, Prentice Hall, Englewood Cliffs, NJ, 1997.
5. O.K. Ersoy and C.H. Chen, Transform-coding of images with reduced complexity, *CVGIP*, 42(1), 19–31, Apr. 1988.
6. K.R. Rao and P. Yip, *Discrete Cosine Transform—Algorithms, Advantages, Applications*, Academic Press, London, U.K., 1990.
7. W.B. Pennebaker and J.L. Mitchell, *JPEG Still Image Compression Standard*, Van Nostrand Reinhold, New York, 1993.



8. G. Mandyam, N. Ahmed, and N. Magotra, Lossless image compression using the discrete cosine transform, *JVCIR*, 8(1), 21–26, Mar. 1997.
9. M.S. Moellenhoff and M.W. Maier, DCT transform coding of stereo images for multimedia applications, *IndEle*, 45(1), 38–43, Feb. 1998.
10. J.W. Cooley and J.W. Tukey, An algorithm for the machine computation of complex Fourier series, *Math. Comput.*, 9(2), 297–301, 1965.
11. A.M. Grigoryan and S.S. Agaian, Split manageable efficient algorithm for Fourier and Hadamard transforms, *IEEE Trans. Signal Process.*, 48(1), 172–183, Jan. 2000.
12. A.M. Grigoryan, 2-D and 1-D multipaired transforms: Frequency-time type wavelets, *IEEE Trans. Signal Process.*, 49(2), 344–353, Feb. 2001.
13. H.J. Nussbaumer and P. Quandalle, Fast computation of discrete Fourier transforms using polynomial transforms, *IEEE Trans. Acoust. Speech Signal Process.*, 27, 169–181, 1979.
14. H.J. Nussbaumer, *Fast Fourier Transform and Convolution Algorithms*, 2nd edn., Springer-Verlag, Berlin, Heidelberg, 1982.
15. A.M. Grigoryan, New algorithms for calculating the discrete Fourier transforms, *Journal Vichislitelnoi Matematiki i Matematicheskoi Fiziki*, Academy Science USSR, Moscow, 26(9), 1407–1412, 1986.
16. A.M. Grigoryan and S.S. Agaian, *Multidimensional Discrete Unitary Transforms: Representation, Partitioning and Algorithms*, Marcel Dekker Inc., New York, 2003.
17. A.M. Grigoryan and S.S. Agaian, Transform-based image enhancement algorithms with performance measure, *Adv. Imaging Electron Phys.*, Acad. Press, 130, 165–242, May 2004.
18. F.T. Arslan and A.M. Grigoryan, Fast splitting alpha-rooting method of image enhancement: Tensor representation, *IEEE Trans. Image Process.*, 15(11), 3375–3384, Nov. 2006.
19. A.M. Grigoryan, Two-dimensional Fourier transform algorithm, *Izvestiya VUZ SSSR, Radioelectronica*, USSR, Kiev, 27(10), 52–57, 1984.
20. A.M. Grigoryan, An optimal algorithm for computing the two-dimensional discrete Fourier transform, *Izvestiya VUZ SSSR, Radioelectronica*, USSR, Kiev, 29(12), 20–25, 1986.
21. A.M. Grigoryan and M.M. Grigoryan, Tensor representation of the two-dimensional discrete Fourier transform and new orthogonal functions, *Avtometriya, AS USSR Siberian Section*, Novosibirsk, 1, 21–27, 1986.
22. A.M. Grigoryan, Algorithm for computing the discrete Fourier transform with arbitrary orders, *Journal Vichislitelnoi Matematiki i Matematicheskoi Fiziki*, AS USSR, 30(10), 1576–1581, 1991.
23. A.M. Grigoryan, Vectorial algorithms for computing the two-dimensional discrete Hartley transformation, *Doklady Nationalnoy Akademii Nauk Armenii*, AS RA, 1, 6–9, 1995.
24. R.N. Bracewell, Fast Hartley transformation, *Proc. IEEE*, 72(8), 19–27, 1984.
25. R.N. Bracewell, *Discrete Hartley transform*, Oxford University Press, New York, 1988.
26. S. Boussakta and A.G.J. Holt, Fast multidimensional discrete Hartley transform using Fermat number transform, *IEE Proc. G*, 135(6), 253–257, 1988.
27. S. Boussakta and A.G.J. Holt, Calculation of the discrete Hartley transform via the Fermat number transform using a VLSI chip, *IEE Proc. G*, 135(3), 101–103, 1988.
28. D. Yang, New fast algorithm to compute two-dimensional discrete Hartley transform, *Electron. Lett.*, 25(25), 1705–1706, 1989.
29. A.M. Grigoryan, A novel algorithm for computing the 1-D discrete Hartley transform, *IEEE Signal Process. Lett.*, 11(2), 156–159, Feb. 2004.
30. R.N. Bracewell, O. Buneman, H. Hao, and J. Villasenor, Fast two-dimensional Hartley transform, *Proc. IEEE*, 74, 1282–1283, 1986.
31. P. Duhamel and M. Vetterili, Improved Fourier and Hartley transform algorithms: Application to cyclic convolution of real data, *IEEE Trans. Acoust. Speech Signal Process.*, 35(5), 818–824, June 1987.
32. H.V. Sorensen, D.L. Jones, C.G. Burrus, and M.T. Heideman, On computing the discrete Hartley transform, *IEEE Trans. Acoust. Speech Signal Process.*, 33(5), 1231–1238, Oct. 1985.
33. S. Boussakta, O.H. Alshibami, and M.Y. Aziz, Radix- $2 \times 2 \times 2$  algorithm for the 3-D discrete Hartley transform, *IEEE Trans. Signal Process.*, 49(12), 3145–3156, Dec. 2001.
34. A.M. Grigoryan and S.S. Agaian, Shifted Fourier transform based tensor algorithms for 2-D DCT, *IEEE Trans. Signal Process.*, 49(9), 2113–2126, Sep. 2001.
35. Z. Cvetković and M.V. Popović, New fast recursive algorithms for the computation of the discrete cosine and sine transforms, *ICASSP '91*, Toronto, Ontario, Canada, p. 2201, 1991.
36. Z. Zhijin and Q. Huisheng, Recursive algorithms for discrete cosine transform, *ICASSP '96*, Atlanta, GA, pp. 115–118, 1996.
37. P. Duhamel and C. Guillemot, Polynomial transform computation of the two-dimensional DCT, *In Proc. ICASSP'90*, Albuquerque, NM, pp. 1515–1518, 1990.
38. Z. Wang, G. Jullien, and W. Miller, One- and two-dimensional algorithms for length 15 and 30 discrete cosine transform, *IEEE Trans. Circ. Syst. II Analog Dig. Signal Process.*, 43(2), 149–153, Feb. 1996.
39. H.V. Sorensen and C.S. Burrus, Efficient computation of the DFT with only a subset of input or output points, *IEEE Trans. Signal Process.*, 41(3), 1184–1200, Mar. 1993.
40. M.T. Heidemann, *Multiplicative Complexity, Convolution, and the DFT*, Springer-Verlag, New York, 1988.
41. Z. Wang, Pruning the fast discrete cosine transform, *IEEE Trans. Commun.*, 39(5), 640–643, May 1991.

42. D.E. Dudgeon and R.M. Mersereau, *Multidimensional Digital Signal Processing*, Prentice Hall, Englewood Cliffs, NJ, 1984.
43. R.C. Staunton, Hexagonal sampling in image processing, *Adv. Image Electron Phys.*, 107, 231–307, 1999.
44. D.P. Petersen and D. Middleton, Sampling and reconstruction of wave-number-limited functions in  $N$ -dimensional Euclidean spaces, *Inform. Control*, 5, 279–323, 1962.
45. D.H. Hubel, *Eye, Brain, and Vision*, Scientific American Books, New York, 1988.
46. A.B. Watson and A.J. Ahumada Jr., A hexagonal orthogonal-oriented pyramid as a model of image representation in visual cortex, *IEEE Trans. Biomed. Eng.*, 36(1), 97–106, Jan. 1989.
47. J.L. Zapata and G.X. Ritter, Fast Fourier transform for hexagonal aggregates, *J. Math. Imaging Vis.*, 12(3), 183–197, Jun. 2000.
48. G. Bi and Y. Chen, Fast generalized DFT and DHT algorithms, *Signal Process.*, 65, 383–390, 1998.



## Empirical Mode Decomposition and the Hilbert–Huang Transform

---

Albert Ayenu-Prah  
*University of Delaware*

Nii Attoh-Okine  
*University of Delaware*

Norden E. Huang  
*National Central University*

20.1	Introduction.....	20-1
20.2	Empirical Mode Decomposition and the Hilbert–Huang Transform .....	20-1
	Drawbacks • Hilbert Transform and Hilbert–Huang Transform •	
	Recent Developments • End Effects	
20.3	Bidimensional Empirical Mode Decomposition .....	20-6
	Extrema Detection and Scattered Data Interpolation • Boundary Effects	
20.4	Attempted Improvements on EMD.....	20-8
20.5	HHT for Global Health Monitoring of Civil Infrastructure .....	20-8
20.6	Applications and Potential Application of BEMD.....	20-9
20.7	Recommendations.....	20-9
	References.....	20-10

### 20.1 Introduction

This chapter discusses the empirical mode decomposition (EMD) and the bidimensional empirical mode decomposition (BEMD) as well as the Hilbert–Huang transform method (HHT). The HHT combines the EMD and the Hilbert spectral analysis; the Hilbert spectral analysis involves the Hilbert transform of the basis functions generated by the EMD. The HHT has been developed to handle nonstationary data, which are properties of almost all physical processes that are sampled for analysis. Traditionally, Fourier-based approaches have been the main analysis procedures for such physical processes, but stationarity must be assumed for Fourier-based methods. The HHT, by the nature of the method, presents a relative advantage over the Fourier analysis methods because it does not implicitly assume stationarity. The EMD has been extended to handle 2-D data, such as images, using the BEMD, which follows a similar procedure as the 1-D version.

### 20.2 Empirical Mode Decomposition and the Hilbert–Huang Transform

Huang et al. (1998) introduced the HHT as a signal-processing tool that adaptively decomposes nonstationary signals into basis functions called intrinsic mode functions (IMF). The Hilbert transform of each IMF is well behaved, and the instantaneous frequency and instantaneous amplitude can be determined from the subsequent analytic signal that is formed from the IMF and its Hilbert transform. The instantaneous frequency and instantaneous amplitude may be used to plot an energy–frequency–time spectrum of the original signal.

The HHT consists of two parts: the EMD and the Hilbert spectral analysis (HSA). The EMD generally separates nonstationary data into locally non-overlapping time scale components. The signal decomposition process will break down the signal into a set of complete and almost orthogonal components, which are the IMFs. An IMF is a function that satisfies the following two conditions:

- The number of extrema and the number of zero-crossings must either equal or differ by at most one in whole data sets;
- The mean value of the envelope defined by the local maxima and the envelope defined by the local minima is zero at every point.

To begin the EMD, a function or signal is decomposed as follows.

Identify all the local extrema; then connect all the local maxima by cubic spline as the upper envelope. Repeat the procedure for the local minima to produce the lower envelope. The upper and lower envelopes should include all the data. If the mean of the upper and lower envelopes is designated as  $m_1$  and the difference between the data and  $m_1$  is the first component  $h_1$ , then

$$x(t) - m_1 = h_1. \tag{20.1}$$

The mean  $m_1$  is given by

$$m_1 = \frac{L + U}{2}, \tag{20.2}$$

where

- $U$  is the local maxima
- $L$  is the local minima

Technically,  $h_1$  is supposed to be an IMF, except that some error might be introduced by the spline curve fitting process—in many cases there are overshoots and undershoots after the first round of processing; therefore, the sifting process has to be repeated many times. The sifting process serves two purposes (Huang et al., 1998): It eliminates riding waves (smaller waves that seem to “ride” bigger waves), and it makes the signal or profile more symmetric about the local zero-mean line.

In the second round of sifting,  $h_1$  is treated as the data or the first component. Then a new mean is computed as before. If the new mean is  $m_{11}$ , then

$$h_1 - m_{11} = h_{11}. \quad (20.3)$$

After repeating the sifting process up to  $k$  times,  $h_{1k}$  becomes an IMF; that is

$$h_{1(k-1)} - m_{1k} = h_{1k}. \quad (20.4)$$

Let  $h_{1k} = c_1$ , the first IMF from the data.  $c_1$  should contain the finest scale or the shortest period component of the data. The process to generate one IMF may be considered as the inner loop. Now  $c_1$  is separated from the original data begun with as

$$x(t) - c_1 = r_1, \quad (20.5)$$

where  $r_1$  is the residue, and it contains information on longer period components; it is now treated as the new data and subjected to the same sifting process. (This is now the beginning of the outer loop, which will go on to the next inner loop for the next IMF.) The procedure is repeated for all subsequent  $r_j$ 's resulting in

$$r_1 - c_2 = r_2; \dots r_{n-1} - c_n = r_n, \quad (20.6)$$

where  $c_2$  to  $c_n$  are the subsequent IMFs of the data. The inner and outer loops of the EMD can be pictured as in Figure 20.1.

There are stopping criteria for the sifting process for IMFs since allowing sifting to go beyond a certain point may smooth out important signal variations and features that arise from the natural dynamics of the system: The IMF components need to retain enough physical sense of both amplitude and frequency modulations. This can be achieved by limiting the value of the sum of the difference (SD) computed from two consecutive sifting results as

$$SD = \frac{\sum_{t=0}^T |h_{k-1}(t) - h_k(t)|^2}{\sum_{t=0}^T h_{k-1}^2(t)}. \quad (20.7)$$

A value of SD between 0.2 and 0.3 is usually preferable based on experimental analyses performed by Huang et al. (1998). To check that the number of zero-crossings is equal to, or differs by at most one from the number of extrema, an alternate stopping criterion is proposed by Huang et al. (2003). Sifting is

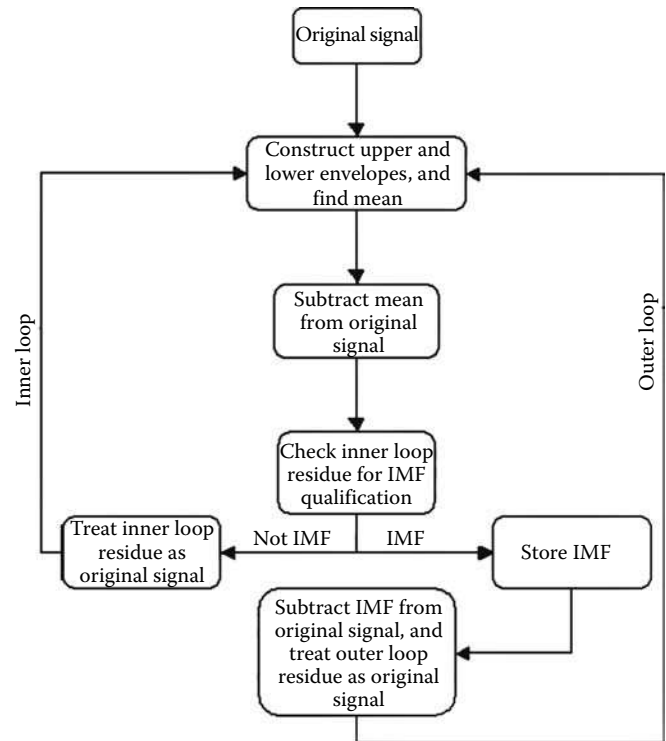


FIGURE 20.1 Pictorial depiction of EMD process.

stopped when the number of zero-crossings is equal to, or differs by at most one from the number of extrema for  $S$  successive sifting steps; the optimum value for  $S$  was found to be between 4 and 8. The optimum value for  $S$  came about while determining a confidence limit for the EMD. Traditionally, the Fourier spectral analysis has invoked the ergodic theory in computing the confidence limit, treating the temporal average as the ensemble average. The data span is cut into a certain number of sections, and the Fourier spectra found for each section; the confidence limit is then the statistical spread of the different spectra. However, for nonstationary processes, the ergodic assumption would not make much sense. Therefore, Huang et al. (2003) decomposed a data set with EMD using different stopping criteria—different  $S$  numbers, varying from 1 to 20. Since different stopping criteria can produce different numbers of IMFs, the intermittency criteria was invoked to force the same number of IMFs for each  $S$ -number used.

Intermittency, which is an attribute of turbulent dynamical systems, is defined as sudden erratic changes in wave heights. It is not uncommon for data from natural physical systems to show intermittency. According to Huang et al. (2003), intermittency can introduce mode mixing, that is, having different time or spatial scales mixed in one IMF. This has the effect of producing additional, albeit spurious, variations in the IMFs and, therefore, in the values of instantaneous frequency. To deal with intermittency, a number,  $n_1$ , is selected, which corresponds with the number of data points within a certain chosen data limit; only waves shorter than this limit are to be included in an IMF.

Therefore, the upper and lower envelopes and their mean would be available to extract IMFs only when the distance between extrema is less than  $n_1$ . The intermittency test can be difficult to invoke, for it is not trivial to choose  $n_1$ ; the test should be done only when serious mode mixing is detected after the data has first been processed by EMD. The intermittency test can then be applied, and waves of periods longer than a preset length scale can be ignored for successive IMFs; this has the effect of including waves of similar length in a single IMF. After getting IMFs using different  $S$ -numbers, the mean of specific IMFs are determined in order to get a range of standard deviations that will define the confidence limit.

The whole EMD process is stopped by any of the following predetermining criteria:

- Either when the residue  $r_n$  is a function having only one extremum, or
- When the residue  $r_n$  becomes a monotonic function from which no IMF can be extracted.

Summing Equations 20.5 and 20.6 yields the following equation:

$$x(t) = \sum_{j=1}^n c_j + r_n, \quad (20.8)$$

which indicates completeness, in that the sum of the IMFs and the residue recovers the original signal.  $c_j$  is the  $j$ th IMF, and  $n$  is the number of sifted IMFs;  $r_n$  can be interpreted as the general trend of the signal. A measure of orthogonality may be determined from two consecutive IMFs,  $C_f$  and  $C_g$ , as follows (Huang et al., 1998):

$$IO_{fg} = \sum_t \frac{C_f C_g}{C_f^2 + C_g^2} \quad (20.9)$$

where  $IO_{fg}$  is the index of orthogonality between  $C_f$  and  $C_g$ , which must be as close to zero as possible. Figure 20.2a through d depict a pictorial flow of the sifting process.

In the next step, the Hilbert transform is applied to each of the IMFs in order to compute instantaneous frequencies and instantaneous amplitudes so that the Hilbert amplitude spectra may be plotted. The Hilbert transform of a real-valued function  $x(t)$ , which belongs to  $L^p$ , is given by

$$H(x(t)) = y(t) = \frac{1}{\pi} P \int_{-\infty}^{\infty} \frac{x(\tau)}{t - \tau} d\tau, \quad (20.10)$$

where  $P$  is the Cauchy principal value.

The function,  $x(t)$ , and its Hilbert transform,  $y(t)$ , form an analytic signal,  $z(t)$ , given by

$$z(t) = x(t) + iy(t) = a(t)e^{i\theta(t)}, \quad (20.11)$$

where  $a(t)$  and  $\theta(t)$  represent the instantaneous amplitude and instantaneous phase respectively. Now,

$$a(t) = \sqrt{x^2 + y^2}, \quad (20.12)$$

$$\theta(t) = \tan^{-1} \frac{y}{x}. \quad (20.13)$$

By definition, the instantaneous frequency is given as

$$\omega(t) = \frac{d\theta(t)}{dt}. \quad (20.14)$$

From Equations 20.11 and 20.14, after Hilbert transformation, each IMF can be represented by

$$c_j = \text{Re} \left[ a_j(t) e^{i \int \omega_j(t) dt} \right], \quad (20.15)$$

and, therefore, the original data,  $x(t)$  can be recovered as

$$x(t) = \text{Re} \sum_{j=1}^n a_j(t) e^{i \int \omega_j(t) dt}. \quad (20.16)$$

Equation 20.15 gives both the amplitude and frequency of each component as a function of time, and Equation 20.16 gives a frequency–time distribution of the amplitude, which is called the Hilbert spectrum,  $H(\omega, t)$ . The corresponding Fourier representation would be as follows:

$$x(t) = \text{Re} \sum_{j=1}^{\infty} a_j e^{i\omega_j t}, \quad (20.17)$$

with both  $a_j$  and  $\omega_j$  constants.

The residual trend is not included in Equation 20.16 since, according to Huang et al. (1998), its energy could be overpowering;  $r_n$  should only be included if its inclusion can be well justified. Knowing the instantaneous frequencies and amplitudes of the IMFs, an energy–time–frequency spectrum, called the Hilbert spectrum, may be plotted for the signal,  $x(t)$ , in terms of the IMFs. Following from Equation 20.15, which presents the Hilbert spectrum, a marginal spectrum can be defined as

$$h(\omega) = \int_0^T H(\omega, t) dt, \quad (20.18)$$

where  $H(\omega, t)$  is used to represent the Hilbert spectrum. The marginal spectrum as given by Equation 20.18 gives an indication of the total energy contribution of each frequency value,  $\omega$ , over the data span; it is similar to the Fourier spectrum.

The preceding discussion of the HHT shows that no a priori basis sets are defined for the procedure, and the problem of the Heisenberg uncertainty principle is not encountered. Table 20.1 compares the Fourier transform, the Wavelet transform, and the HHT (Table 20.1)

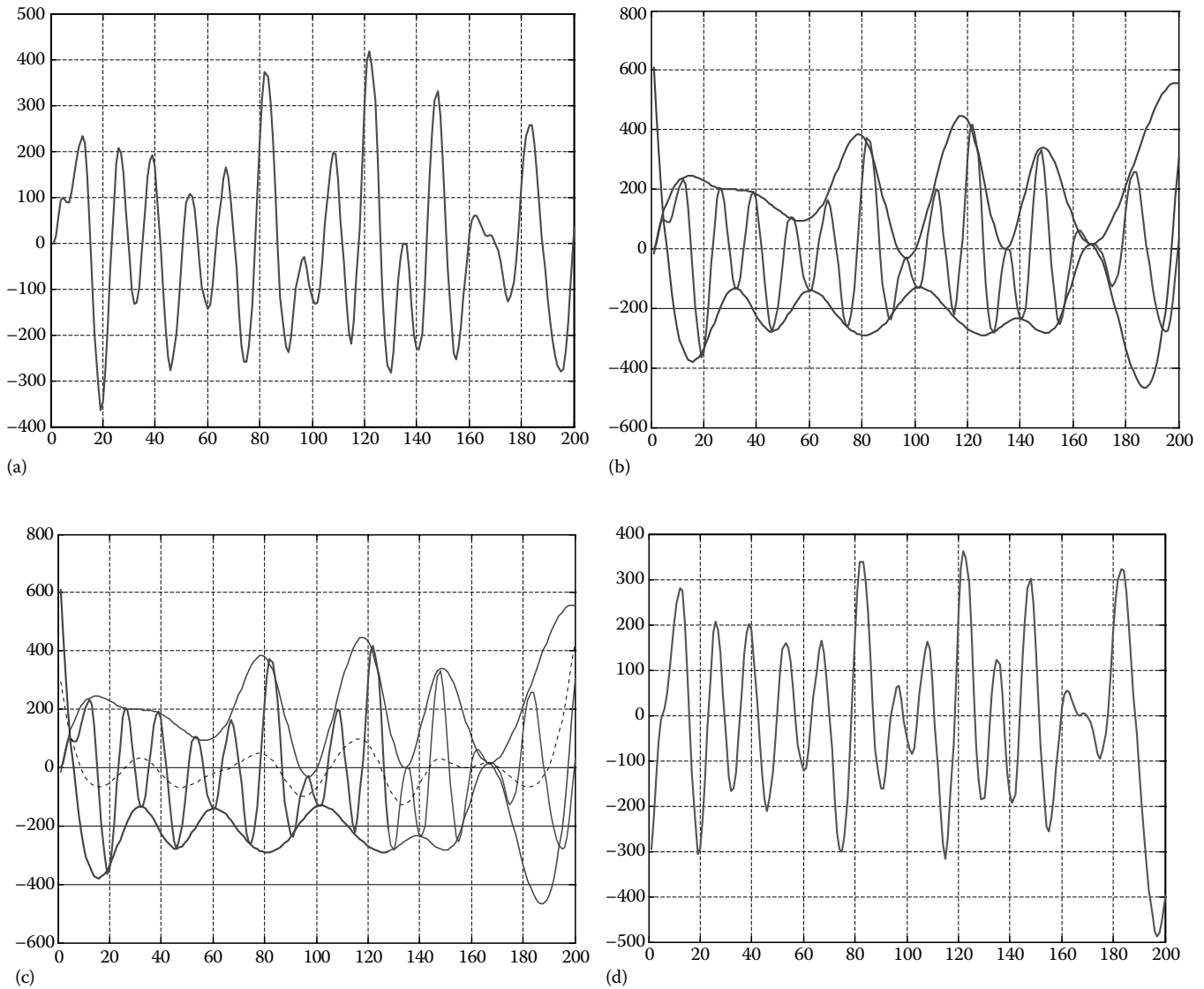


FIGURE 20.2 (a) Original signal. (b) Upper and Lower envelopes. (c) Mean envelope (dashed line). (d) IMF produced by subtracting mean envelope from original signal.

TABLE 20.1 Comparison between Fourier, Wavelet, and HHT

	Fourier	Wavelet	HHT
Basis	A priori	A priori	Adaptive
Frequency	Convolution: global, uncertainty	Convolution: regional, uncertainty	Differentiation: local, certainty
Presentation	Energy–frequency	Energy–time–frequency	Energy–time–frequency
Nonlinear	Not easily defined	Not easily defined	Not easily defined
Nonstationary	No	Yes	Yes
Feature extraction	No	Yes	Yes
Theoretical base	Theory complete	Theory complete	Empirical

Source: Modified from Huang, N.E. *The Hilbert–Huang Transform in Engineering*, Eds, Huang, N.E. and Attob-Okiné, N.O., CRC Press, Boca Raton, FL, 1, 2005.

### 20.2.1 Drawbacks

The HHT procedure is empirical and the most computationally intensive step is the EMD operation, which does not involve

convolution and other time-consuming operations (this makes HHT ideal for signals of large size). However, there are some drawbacks to the application of HHT. First, the EMD may generate undesired low- or high-amplitude IMFs at the

low-frequency region, and bring up some undesired frequency components; second, the first IMF may cover a wide frequency range at the high-frequency region and therefore cannot satisfy the monocomponent definition well—it has been observed to contain most of the noise in the original signal, though; and third, the EMD operation often cannot separate some low-energy components from the analysis signal, therefore, those components may not appear in the frequency–time plane.

### 20.2.2 Hilbert Transform and Hilbert–Huang Transform

The major difference between the conventional Hilbert transform and HHT is the definition of instantaneous frequency. The instantaneous frequency has more physical meaning through its definition within the IMF component; meanwhile, the classical Hilbert transform of the original data might possess unrealistic features (Huang et al., 1998). This implies that the IMF represents a generalized Fourier expansion basis. It has variable amplitude and instantaneous frequency, which enable the expansion to accommodate nonstationary data. Furthermore, since the instantaneous frequency is a derivative, it is very local and can, therefore, describe intra-wave variations within the signal. Physically, the definition of instantaneous frequency has a true meaning for “monocomponent” signals, which has one frequency, or at most a narrow range of frequencies, varying as a function of time (narrow band). Since most data do not show these necessary characteristics, sometimes the Hilbert transform makes little physical sense in practical applications. Explaining this sense of physical meaning, Huang (2005) directly Hilbert transformed the length-of-day (LOD) data shown in Figure 20.3 and plotted the analytic function in complex phase plane. Instead of simple circles, the data showed haphazardly intertwined curves that looped around showing no apparent order as depicted in

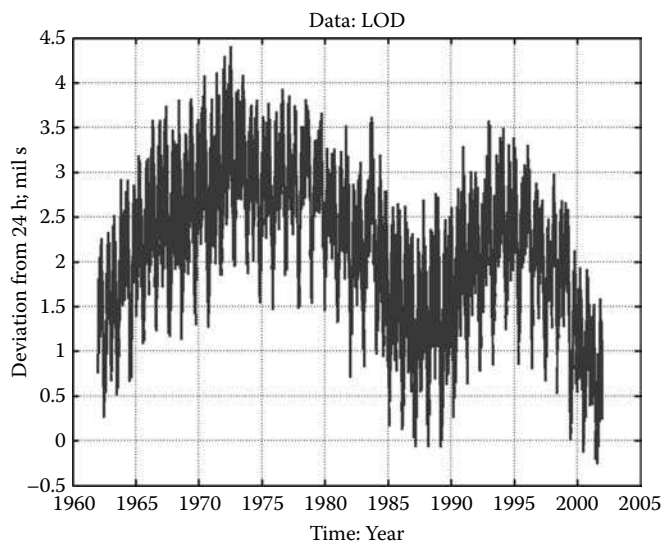


FIGURE 20.3 LOD data.

Figure 20.4. Additionally, plotting the phase function and the instantaneous frequency did not yield any meaningful result, with the phase function showing random but finite jumps (Figure 20.5) and the instantaneous frequency plot showing equally likely positive and negative frequencies (Figure 20.6). After performing EMD on the LOD data, the annual cycle is extracted and plotted; it showed apparent order with near-circles in the polar representation (also shown in Figure 20.4). This illustrates why some preprocessing of the data is needed before the Hilbert transform is performed on the data; this preprocessing step is the EMD, which decomposes the signal into IMFs that have better-behaved Hilbert transforms.

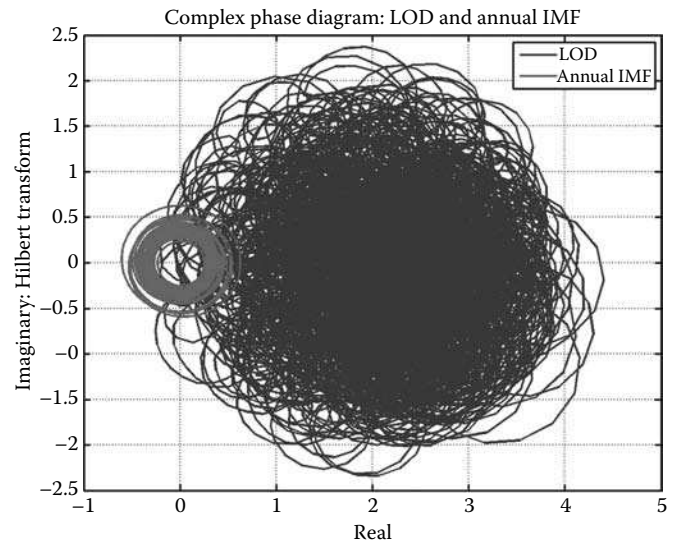


FIGURE 20.4 Analytic function in complex phase plane after Hilbert-transforming LOD data; after EMD, the plotted annual cycle is also shown.

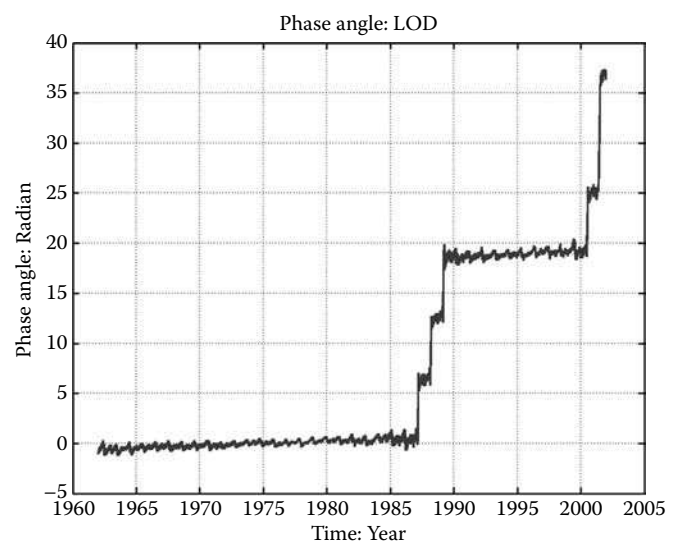


FIGURE 20.5 Phase function of analytic function from LOD data.



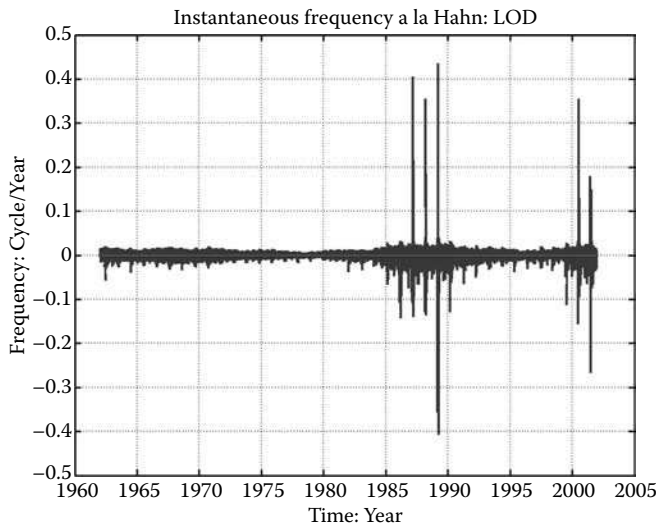


FIGURE 20.6 Instantaneous function from derivative of phase function without EMD.

### 20.2.3 Recent Developments

A number of recent developments have emerged regarding the HHT (Huang, 2005). A normalized HHT was developed because of two theorems concerning the Hilbert transform: the product theorem for Hilbert transforms (Bedrosian, 1963) and the quadrature approximation to the Hilbert transform of modulated signals (Nuttall, 1966).

According to the Bedrosian theorem, the Hilbert transform of the product of two signals,  $f(x)$  and  $g(x)$ , can be defined as

$$H[f(x)g(x)] = f(x)H[g(x)] \quad (20.19)$$

only if the Fourier spectra of the  $f(x)$  and  $g(x)$  are non-overlapping (disjoint) in frequency space and  $g(x)$  has a higher frequency content than  $f(x)$ , or both  $f(x)$  and  $g(x)$  are analytic. It would not be entirely possible to define the phase function as in Equation 20.13 and represent an IMF as in Equation 20.15 unless the following equation holds true:

$$H[a(t) \cos \theta(t)] = a(t)H[\cos \theta(t)]. \quad (20.20)$$

Equation 20.20 implies that  $a(t)$  has to have a very low frequency content compared to  $\cos \theta(t)$ . Therefore, a way to satisfy this condition would be to normalize the function with respect to  $a(t)$ , so that amplitude is always unity in the normalized function. Applying this normalization in the EMD, Huang (2005) proposed to find all the maxima of each IMF, connect the maxima by cubic spline to form an upper envelope,  $E(t)$ , and then divide the IMF by  $E(t)$ . In this way, the IMF is normalized with respect to amplitude.

The second condition to satisfy is given by the Nuttall theorem, which gives a measure of the discrepancy between the Hilbert transform and the quadrature of a carrier wave with amplitude or phase modulation or both. Let the signal be  $x(t)$  with a Hilbert transform,  $x_H(t)$ ; and let the quadrature of  $x(t)$  be

$x_q(t)$ . Nuttall (1966) presents the discrepancy in terms of the difference in energy of  $x_H(t)$  and the energy of  $x_q(t)$ ; if the difference in energy is  $E$ , then the ratio of  $E$  to the energy of the signal gives a relative measure of error in approximating  $x_H(t)$  by  $x_q(t)$ . This error measure is going to be constant over the whole data range, and according to Huang (2005), a constant error bound is not going to reveal the location of the error on the time axis of a nonstationary signal. Therefore, Huang (2005) proposed a variable error bound using the normalized IMF and also a new method to compute the instantaneous frequency through direct quadrature (Huang et al., in press). The squared amplitudes of the normalized IMF would equal one if the Hilbert transform were equal to the quadrature, and, therefore, the difference between the squared amplitude and unity should be zero; otherwise, the Hilbert transform cannot be exactly the quadrature. Therefore, the error is the difference between the squared normalized amplitude and unity, and is a function of time. According to Huang (2005), detailed comparisons gave satisfactory results. An error index calculated gave values that were 10% or less over the data span.

Though the intermittency test could alleviate the mode mixing to a certain degree, it is no longer totally adaptive. A better method is to use the ensemble empirical mode decomposition (EEMD) (Wu and Huang, 2009), in which noise is introduced to help scale separation and achieve a truly dyadic filter effect.

### 20.2.4 End Effects

The spline fitting for upper and lower envelopes can create problems at the ends of the data where large swings are prone to occur. These large swings can propagate into the data series and corrupt the whole signal leading to an ineffective EMD. In Huang et al. (1998), end effects are treated by adding characteristic waves at both ends of the signal that have the capacity to contain the wide swings that come from cubic spline fitting. Datig and Schlurmann (2004) implement a signal extension procedure that adds new maxima and minima to the front and rear of the signal, which new extrema are derived from the original time span of the signal. This has the effect of no information being canceled out and the original data series remaining unaffected. Rilling et al. (2003) mirrored the extrema close to the edges in order to contain wide swings. Chen et al. (2007) used axis-symmetry signal extension to handle end effects while Cheng et al. (2007) used support vector regression machines to process end effects. So far, the best approach is the one used by Wu and Huang (2009), where a combination of linear extension based on the two neighboring extrema was used in conjunction of the end point value.

## 20.3 Bidimensional Empirical Mode Decomposition

The potential of the 1-D EMD generated research interests in 2-D applications for image processing. Existing traditional methods are still Fourier-based and processing is global rather

than local so that essential information may be lost in the image during processing. To avoid loss of information a 2-D version of the EMD has been recently developed. Algorithms have been developed in the literature to do two-dimensional sifting for BEMD (Damerval et al., 2005; Linderhed, 2004; Nunes et al., 2003a,b), and they generally follow that for the one-dimensional case, only modified to handle two-dimensional signals.

Linderhed (2002) first introduced EMD in two dimensions, which is now popularly called the bidimensional empirical mode decomposition (BEMD); BEMD was used for image compression, using only the extrema of the IMFs in the coding scheme.

Nunes et al. (2003a,b) developed a BEMD method for texture image analysis; BEMD was used for texture feature extraction and image filtering. The sifting process used is as follows:

- Identify the extrema of the image,  $I$ , by morphological reconstruction based on geodesic operators
- Generate the 2-D envelope by connecting the maxima points with radial basis function (RBF)
- Determine the local mean,  $m_i$ , by averaging the two envelopes
- Do  $I - m_i = h_i$
- Repeat the process

For the envelope construction, the authors used RBF of the form

$$s(x) = p_m(x) + \sum_{i=1}^N \lambda_i \Phi(\|x - x_i\|), \quad (20.21)$$

where

$p_m$  is a low degree polynomial, of the  $m$ th degree polynomial in  $d$  variables

$\|\cdot\|$  denotes Euclidean norm

$\lambda_i$  are RBF coefficients

$\Phi$  is a real-valued function

$x_i$  are the RBF centers

The stopping criterion used is similar to that by Huang et al. (1998), using standard deviation as discussed in Section 20.2 above. Linderhed (2005) also developed a sifting process for 2-D time series. Although the stopping criterion for IMF extraction is relaxed, the stopping criterion for the whole EMD process is similar to that of Huang et al. (1998). The IMF stopping criterion is based on the condition that the extrema envelope is close enough to zero; therefore, there is no need to check for symmetry. The algorithm is similar to that of Nunes et al. (2003a,b). However, the author performs extrema detection by comparing a candidate data point with its eight nearest-connected neighbors, and suggests thin-plate splines, which are RBFs, for envelope construction.

Two general types of BEMD are presented in the literature. One uses tensor products to generate upper and lower envelopes for rows and columns of an image (Liu and Peng, 2005), and the other (the more popular) uses neighboring-window technique for extrema detection, and two-dimensional envelopes for interpolation; for instance, the use of RBFs and Delaunay triangulation.

The former method is faster but does not take into account the geometry of the image. In the literature, the preferred method seems to be the latter, which uses two-dimensional lower and upper envelopes to interpolate.

Just as in the 1-D EMD, intermittency can also pose problems in BEMD in terms of mode mixing. Nunes et al. (2005) introduced a modified algorithm for BEMD that included a treatment of intermittency. Similar to the 1-D, it also uses a period length criterion whereby a predetermined period length is set so that any period length above the predetermined length is ignored; subsequently waves of similar period lengths are included in corresponding IMFs.

### 20.3.1 Extrema Detection and Scattered Data Interpolation

Detection of extrema has been achieved with methods including morphological reconstruction based on geodesic operators (Nunes et al., 2003a,b), and neighboring windows (Damerval et al., 2005; Linderhed, 2005). An important step in BEMD after extrema detection is constructing the upper and lower envelopes when sifting for IMFs; envelope construction is done with scattered data interpolation. Scattered data interpolation (SDI) is the construction of a function that interpolates data values known at only some specific, scattered points; it is a single-valued function. In general, for  $n$ -dimensional space, a function is sought that maps  $R^n$  into  $R$ ; that is

$$f: R^n \rightarrow R. \quad (20.22)$$

Therefore, for BEMD, the SDI function maps  $R^2$  into  $R$ . SDI functions are effective interpolants because of their meshless capability. While other methods may need regular meshes to work, SDI interpolants do not need a regular mesh; they work on irregularly spaced data. There are two general approaches to SDI: global and local approaches. The global approach considers all other points for each interpolated point, while local approaches consider only points within a certain radius of support of each interpolated point. There are generally five SDI methods classified under global or local approaches as shown in Table 20.2.

The groupings in Table 20.2 are not rigid. Some global methods may be made local by slight modifications; CSRBFs are local variations of RBFs. Global approaches have higher computational costs for very large data points. Morse et al. (2001) identified some drawbacks when working with thin-plate RBFs, which are global methods.

**TABLE 20.2** Scattered Data Interpolation Methods

Global	Local
RBFs	Compactly supported RBFs (CSRBFs)
Inverse-distance weighted methods (Shepard's methods)	Triangulation-based methods Natural neighbor methods

Effective BEMD depends on proper scattered data interpolation of the extrema. The interpolant must have continuous second derivatives everywhere to ensure smoothness. Although overshoots should necessarily be avoided, few may sometimes persist that may generate spurious extrema, which can additionally exaggerate or shift existing extrema. However, their effect is indirect since the mean of the envelopes rather than the envelopes themselves are used in the sifting process; the essential modes are still well recovered. To overcome the problem of overshooting, a new method has been proposed recently by Xu et al. (2006). The authors use finite element basis functions to construct the local mean surface of the data instead of constructing it from the upper and lower envelopes. Damerval et al. (2005) used Delaunay triangulation on the extrema, and then performed piecewise cubic interpolation on triangles to build extrema envelopes. Linderhed (2005) investigated the issue of proper spline interpolation by using thin-plate smoothing splines and triangle-based cubic interpolation to generate upper and lower envelopes. For sparse data, thin-plate splines were smoother than triangle-based cubic interpolation. Results of comprehensive analyses performed by Bhuiyan et al. (2009) were not conclusive regarding the superiority of one SDI method over another when various methods were used in BEMD analyses of texture and real images. The appropriate SDI method would depend on the objective of the BEMD analysis.

### 20.3.2 Boundary Effects

Similar to end effects in 1-D EMD, boundary effect issues are important in BEMD. In constructing extrema envelopes, extra care is needed around image boundaries in order to prevent wide swings and other artifacts from corrupting the decomposition process. Basically, extension of the boundary has been the main objective of various authors while treating boundary effects in BEMD. Liu and Peng (2005) used texture synthesis to process image boundaries. A modified form of nonparametric-sampling-based texture synthesis is used to extend the image before BEMD is performed; finally, the corresponding parts of the 2-D IMFs are extracted from the extended versions. Linderhed (2004) added extra points at the borders to the set of extrema points; the extra points are placed at the corners of the image and also some equally spaced along the borders.

## 20.4 Attempted Improvements on EMD

Constructing extrema envelopes may usually result in overshoots and undershoots due to the nature of the cubic spline fitting process. In addition, adverse end effects may propagate inward into the signal during sifting, corrupting the whole resulting signal. In order to do a mathematical study of the EMD, Chen et al. (2006) introduced an innovative way of finding the mean of 1-D signals using B-splines, thereby avoiding the use of upper and lower envelopes and their attendant problems. Building on the idea by Chen et al. (2006), Xu et al. (2006) developed a new method of finding the mean of a 2-D signal by using finite

elements for 2-D EMD without constructing extrema envelopes. Frei and Osorio (2006) also introduced a new method of non-linear and nonstationary time series analysis that finds the mean of the signal without extrema envelopes and generates basis functions similar to the IMF, but without iteration.

## 20.5 HHT for Global Health Monitoring of Civil Infrastructure

HHT is being used in global health monitoring techniques whereby signals from infrastructure are analyzed to determine the presence of damage. Traditionally, Fourier analysis has been the signal analysis method of choice; however, Fourier methods cannot resolve signals locally, forcing the analysis to depend on averaging to determine a single parameter. Attempts at achieving temporal localization compromise frequency resolution and vice versa.

HHT is being used in determining mode shapes present in a complicated signal produced by a structure through sensors, and in feature identification. Signals produced by civil infrastructure systems are mostly from nonlinear systems and are nonstationary.

In the literature, HHT has been used in various infrastructure damage detection procedures. Xu and Chen (2004) use empirical mode decomposition (EMD) for damage detection. The study is motivated by the fact that current vibration-based structural damage detection methods are global rather than local so that the exact time instants of sudden damage events cannot be accurately known. These methods assume that measured modal parameters or properties derived from modal parameters are indicative of the physical characteristics and behavior of the structure, and therefore, changes in the modal parameters or their properties indicate changes in the physical behavior of the structure: the behavior of the structure is assumed to be linear. Experimental investigations are carried out on a three-story shear building model to identify structural damage caused by changes in structural stiffness using EMD. Changes in structural stiffness is induced by two pretensioned springs connecting the first floor to fixed steel frames away from the building; during vibration of the building the springs are released to simulate a sudden change in structural stiffness. This arrangement is based on the assumption that most damage occurs at the lower floors of a building under seismic excitation. The vibrations are measured with accelerometers installed on each floor in the building. Signals from the accelerometers are analyzed with EMD to detect exact damage instants; using intermittency check, the exact instant of damage appears as a spike in the first IMF of the accelerometers. Power spectral density analysis could not reveal the exact instant of damage since the Fourier transform is a global method. The spatial distribution of accelerometers is important in detecting structural damage; since the signal response of sudden damage is of high frequency and high decay rate, positioning accelerometers close to damage location enhances effective damage detection. However, it is not trivial to place accelerometers such that they will be close enough to detect locally occurring damage events.

Chen et al. (2007) used HHT in a vibration-based damage detection technique to detect damage in composite wingbox structures. A damage feature index vector, extracted based on HHT, is used for damage detection. Damage is simulated in a structural dynamic model developed with vibration analysis and finite element methods. The signal obtained from the vibration analysis is decomposed into IMFs; a comparison of instantaneous frequencies of undamaged and damaged wingbox signals reveals obvious changes. A nondimensional index matrix is composed from normalized instantaneous frequency values of undamaged and damaged wingbox IMFs; elements of the matrix are functions of the ratio of normalized instantaneous frequencies from undamaged and damaged IMFs. Traditionally, variation of structural vibration natural frequencies and mode shapes are used as parameters for damage detection. However, these parameters are unable to detect small damage events in the wingbox structures. In addition, the time-domain response signals of the damaged and undamaged states do not show any noticeable differences. But a comparison of IMFs of damaged and undamaged states does not show any observable differences, too. Therefore, IMFs are unable to detect damage directly. However, Hilbert transforming IMFs and comparing undamaged and damaged states reveal noticeable differences in instantaneous frequencies. Variations in instantaneous frequencies between undamaged and damaged states used in a damage feature index matrix can help in an online structural damage detection scheme.

Yang et al. (2004) detect damage time instants and locations by EMD and HHT using a model ASCE four-story benchmark building. Using EMD, an appropriate intermittency frequency is set such that sharp spikes reveal damage time instants and locations in the first IMF, and represent discontinuities in structural stiffness. The intermittency frequency is lower than the frequency of the discontinuity but higher than the highest frequency in the acceleration measurement of the structure. The effectiveness of damage detection is dependent on factors such as signal-to-noise ratio and damage severity. A second method based on EMD, random decrement technique (RDT), and Hilbert transform is used to detect damage time instants, natural frequencies, and damping ratios.

Zhang et al. (2003) use HHT to analyze dynamic and earthquake motion recordings. HHT is found to be suitable for analyzing nonstationary dynamic and earthquake motion recordings; it also found to be better than Fourier transform in this regard. However, although IMFs may contain some important inherent signal information, the physical meaning of IMFs is not clear.

## 20.6 Applications and Potential Application of BEMD

BEMD has been used for texture analysis (Nunes et al., 2005) and image compression (Linderherd, 2004). Recently, Sinclair and Pegram (2005) have used it for rainfall analysis and nowcasting. Computer scientists, mathematicians, and electrical engineers have usually used the method for image analyses.

The potential application for BEMD is in presmoothing of images before feature detection techniques are applied; this can pave the way for a hybrid method of edge detection that involves the BEMD and an edge detector that does not have a presmoothing step. Images usually tend to be noisy and so filtering out noise is essential to make the image ready for further analysis. The first few IMFs from BEMD usually contain most of the noise in the original image; therefore, removing them and reconstructing the image with the remaining IMFs tends to denoise the image. The number of IMFs needed to be removed depends on the level of noise in the image; very noisy images require more high frequency IMFs removed than do less noisy images. This method has been applied in a study of pavement cracks using two popular edge detection techniques: the Sobel and the Canny edge detectors (Ayenu-Prah and Attoh-Okine, 2008). The Canny edge detector has a prefiltering step in which images are denoised with a Gaussian filter before edge detection is accomplished. This detection method is computationally more expensive due to the convolution processes required in Gaussian smoothing. The Sobel edge detection method has no prefiltering step; however, it is more susceptible to noise. Therefore, the BEMD is used to first filter the images before the Sobel method is applied. An advantage BEMD has over Gaussian filtering is that it does not involve any convolution process, and it is a local method of denoising. This method has been applied to asphalt concrete and Portland cement concrete (PCC) pavement images to detect cracks. The asphalt images tend to be noisier than the PCC images, which is not unusual since PCC pavements tend to be generally smoother than asphalt surfaces. Therefore, for PCC images the first three IMFs are removed while only the first IMF is removed for asphalt images; this decision is arrived at after several trials. Results from the combination method of BEMD/Sobel are compared with that from the Canny edge detector; BEMD/Sobel method tends to be a very effective technique, easily comparable to the Canny method.

## 20.7 Recommendations

Fourier analysis has been around for almost two centuries and has subsequently become very dominant in signal processing; it has also been used to model many scientific phenomena such as heat transfer and wave propagation. For HHT to be considered a sound alternative, stakeholders have to know and appreciate the efficacy of the HHT in treating nonstationary signals. It is not the intention that HHT can or will replace Fourier transform; however, it is being presented as a powerful signal processing alternative that is relatively more efficient in dealing with nonstationary signals. Technology is getting to the point where accuracy is becoming ever more paramount as scientists and engineers continually operate in the nano realm; it is, therefore, reasonable to expect the possibility of the insufficiency of a stationary assumption at some point in the near future. HHT holds promise for the future of signal processing when stationary assumptions may likely not suffice. However, the staying power of Fourier analysis has been guaranteed by a sound mathematical

foundation, while HHT essentially remains an empirical method without the requisite mathematical support. For HHT to capture a wider support of stakeholders, mathematicians would be needed to develop a mathematical basis for the procedure without necessarily invoking assumptions that may compromise the a posteriori appeal of the method. Of concern also is the treatment of the end effects in 1-D EMD and the boundary effects in the BEMD; errors at the ends and boundaries during interpolation tend to propagate inward, corrupting the whole signal in the process. In addition, extrema points may shift or may be exaggerated or both; however, this phenomenon ultimately tends to average out by the end of the decomposition since essentially the procedure works with the mean of the envelopes rather than with the envelopes themselves. In any case, despite positive and encouraging but varying efforts at mitigating end and boundary effects such as adding characteristic waves at ends of signals and boundary extension in images, a move toward a universal method of processing the ends and boundaries during interpolation should be most sought after. While the original inventors of the HHT and a number of subsequent authors have endorsed the cubic spline for envelope construction, there remain questions about the most preferable scattered data interpolation method for BEMD envelope construction. Although the authors of this article have participated in a comprehensive study to determine an appropriately suitable method of scattered data interpolation, the results have not been sufficiently conclusive for endorsing one particular method over a number of candidate RBF methods; at best, it is observed that RBF methods generally seem to work best.

A persisting challenge has been the physical meaning of the IMFs before Hilbert-transforming them. Using structural models, researchers have attempted to analyze with EMD data acquired from the models after excitation. Modal parameters for the structure are known before the excitation force is applied, and, therefore, are compared with modal parameters after excitation in order to try and ultimately get the physical meaning of the IMFs. While the effort is highly commendable, and is in the right direction, usually the modal parameters for existing real-life structures are not known before, say, an earthquake strikes. Therefore, assuming the structure is instrumented to record data during vibration, analyzing the data with EMD would require interpreting each IMF without the benefit of knowledge of any before-excitation modal parameters; the task becomes more challenging in that regard. The ability to pick out relevant IMFs from any particular decomposition is a good first step toward interpreting them; however, more research needs to be performed in order to establish physical meaning for the IMFs.

## References

Ayenu-Prah, A. and Attoh-Okine, N. Evaluating pavement cracks with bidimensional empirical mode decomposition. *EURASIP Journal on Advances in Signal Processing*, 2008, Article ID 861701, 7pp, 2008.

- Bedrosian, E. A product theorem for Hilbert transforms. *Proceedings of the IEEE*, 51(5), 868–869, 1963.
- Bhuiyan, S., Attoh-Okine, N. O., Barner, K. E., and Ayenu-Prah, A. Bidimensional empirical mode decomposition using various interpolation techniques. *Advances in Adaptive Data Analysis*, 1(2), 309–338, 2009.
- Chen, Q., Huang, N., Riemenschneider, S., and Xu, Y. A B-spline approach for empirical mode decompositions. *Advances in Computational Mathematics*, 24, 171–195, 2006.
- Chen, H. G., Yan, Y. J., and Jiang, J. S. Vibration-based damage detection in composite wingbox structures by HHT. *Mechanical Systems and Signal Processing*, 21, 307–321, 2007.
- Damerval, C., Meignen, S., and Perrier, V. A fast algorithm for bidimensional EMD. *IEEE Signal Processing Letters*, 12(10), 701–704, October 2005.
- Datig, M. and Schlurmann, T. Performance and limitations of the Hilbert-Huang transformation (HHT) with an application to irregular water waves. *Ocean Engineering*, 31, 1783–1834, 2004.
- Frei, M. G. and Osorio, I. Intrinsic time-scale decomposition: Time-Frequency-Energy analysis and real-time filtering of non-stationary signals. *Proceedings of the Royal Society A, FirstCite Early Online Publishing*, London, U.K., 2006.
- Huang, N. E. Introduction to Hilbert-Huang transform and some recent developments. *The Hilbert-Huang Transform in Engineering*, Eds. Norden E. Huang and Nii O. Attoh-Okine, CRC Press, Boca Raton, FL, pp. 1–23, 2005.
- Huang, N. E., Shen, Z., Long, S. R., Wu, M. C., Shih, H. H., Zheng, Q., Yen, N.-C., Tung, C. C., and Liu, H. H. The empirical mode decomposition and the Hilbert spectrum for nonlinear and non-stationary time series analysis. *Proceedings of the Royal Society London A*, 454, 903–995, 1998.
- Huang, N. E., Wu, M. C., Long, S. R., Shen, S. S., Qu, W., Gloersen, P., and Fan, K. L. A confidence limit for the empirical mode decomposition and Hilbert spectral analysis. *Proceedings of the Royal Society London A*, 459, 2317–2345, 2003.
- Huang, N. E., Wu, Z., Long, S. R., Arnold, K. C., Chen, X., and Blank, K. On instantaneous frequency. *Advanced Adaptive data Analysis*, 2, in press.
- Linderherd, A. 2-D empirical mode decomposition—In the spirit of image compression. *Proceedings SPIE, Wavelet and Independent Component Analysis Applications IXI*, Orlando, FL, Vol. 4738, 2002.
- Linderherd, A. Image compression based on empirical mode decomposition. *Proceedings of the International Conference on Image and Graphics*, Hong Kong, China, pp. 430–433, 2004.
- Linderherd, A. Variable sampling of the empirical mode decomposition of two-dimensional signals. *International Journal of Wavelets, Multiresolution and Information Processing*, 3(3), 435–452, 2005.
- Liu, Z. and Peng, S. Boundary processing of bidimensional EMD using texture synthesis. *IEEE Signal Processing Letters*, 12(1), 33–36, 2005.

- Morse, B. S., Yoo, T. S., Rheingans, P., Chen, D. T., and Subramanian, K. R. Interpolating implicit surfaces from scattered surface data using compactly supported radial basis functions. SMI 2001, *International Conference on Shape Modelling and Applications*, Genova, Italy, May 2001.
- Nunes, J. C., Guyot, S., and Delechelle, E. Texture analysis based on local analysis of the bidimensional empirical mode decomposition. *Machine Vision and Applications*, 16, 177–188, 2005.
- Nuttall, A. H. On the quadrature approximation to the Hilbert transform of modulated signals. *Proceedings of the IEEE*, 54(10), 1458–1459, 1966.
- Rilling, G., Flandrin, P., and Goncalves, P. On empirical mode decomposition and its algorithms. *Proceedings IEEE EUR-ASIP Workshop on Nonlinear Signal Processing*, Grado, Italy, 2003.
- Sinclair, S. and Pogram, G. G. S. Empirical mode decomposition in 2-D space and time: A tool for space-time rainfall analysis and nowcasting. *Hydrology Earth System Science Discuss*, 2, 289–318, 2005.
- Wu, Z. and Huang, N. E. Ensemble mode decomposition: A noise-assisted data analysis method. *Advanced Adaptive data Analysis*, 1, 1–41, 2009.
- Xu, Y., Liu, B., Liu, J., and Riemenschneider, S. Two-dimensional empirical mode decomposition by finite elements. *Proceedings of the Royal Society A*, 462, 3081–3096, 2006.
- Xu, Y. L. and Chen, J. Structural damage detection using empirical mode decomposition: Experimental investigation. *Journal of Engineering Mechanics*, 130(11), 1279–1288, 2004.
- Yang, J. N., Lei, Y., Lin, S., and Huang, N. *Journal of Engineering Mechanics*, 130(1), 85–95, 2004.
- Zhang, R. R., Ma, S., Safak, E., and Hartgell, S. *Journal of Engineering Mechanics*, 129(8), 861–875, 2003.



# Appendix A: Functions of a Complex Variable\*

---

A.1	Basic Concepts .....	A-1
	Integration • Derivative of an Analytic Function $W(z)$ • Taylor's Theorem • Laurent's Theorem	
A.2	Sequences and Series .....	A-8
	Comparison Test • Limit Comparison Test • D'Alembert's Test • Root Test • Uniform Convergence (Weierstrass $M$ -Test) • Analyticity of a Sequence of Functions	
A.3	Power Series.....	A-9
A.4	Analytic Continuation.....	A-11
A.5	Singularities of Complex Functions .....	A-11
A.6	Theory of Residues .....	A-14
A.7	Aids to Integration.....	A-16
	Transformation of Contour	
A.8	The Bromwich Contour.....	A-19
	Finite Number of Poles • Branch Points and Branch Cuts	
A.9	Evaluation of Definite Integrals .....	A-25
	Evaluation of the Integrals of Certain Periodic Functions (0 to $2\pi$ ) • Evaluation of Integrals with Limits $-\infty$ and $+\infty$ • Certain Infinite Integrals Involving Sines and Cosines • Miscellaneous Definite Integrals	
A.10	Principal Value of an Integral.....	A-31
A.11	Integral of the Logarithmic Derivative.....	A-32

Alexander D. Poularikas  
University of Alabama in Huntsville

## A.1 Basic Concepts

---

A complex variable  $z$  defined by

$$z = x + jy \tag{A.1}$$

assumes certain values over a region  $R_z$  of the complex plane. If a complex quantity  $W(z)$  is so connected with  $z$  that each  $z$  in  $R_z$  corresponds with one value of  $W(z)$  in  $R_w$ , then we say that  $W(z)$  is a single-valued function of  $z$

$$W(z) = u(x, y) + jv(x, y) \tag{A.2}$$

which has a *domain*  $R_z$  and a *range*  $R_w$  (see Figure A.1). The function  $W(z)$  can be *single valued* or *multiple valued*. Examples of single-valued functions include

$$\begin{aligned} W &= a_0 + a_1z + a_2z^2 + \cdots + a_nz^n \quad n \text{ integer} \\ W &= e^z \end{aligned}$$

Examples of multiple-valued functions are

$$\begin{aligned} W &= z^n \quad n \text{ not an integer} \\ W &= \log z \\ W &= \sin^{-1} z \end{aligned}$$

---

**Definition A.1** A function  $W(z)$  is continuous at a point  $z = \lambda$  of  $R_z$  if, for each number  $\epsilon > 0$ , however small, there exists another number  $\delta > 0$  such that whenever

$$|z - \lambda| > \delta \quad \text{then} \quad |W(z) - W(\lambda)| < \epsilon \tag{A.3}$$

The geometric representation of this equation is shown in Figure A.1.

---

**Definition A.2** A function  $W(z)$  is analytic at a point  $z$  if, for each number  $\epsilon > 0$ , however small, there exist another number  $\delta > 0$  such that whenever

$$|z - \lambda| < \delta \quad \text{then} \quad \left| \frac{W(z) - W(\lambda)}{z - \lambda} - \frac{dW(\lambda)}{dz} \right| < \epsilon \tag{A.4}$$

---

\* All contour integrals are taken counterclockwise, unless specifically indicated.



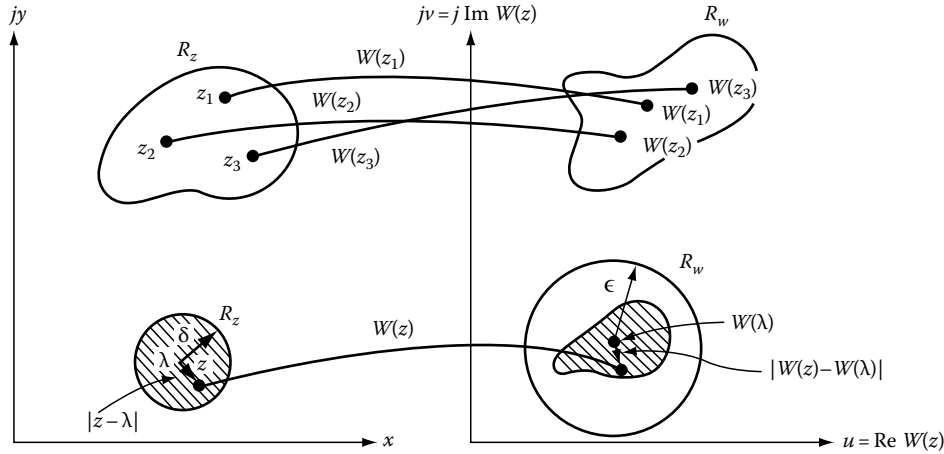


FIGURE A.1 Illustration of the range and domain of complex functions.

**Example A.1**

Show that the function  $W(z) = e^z$  satisfies Equation A.4.

**SOLUTION**

From Equation A.4, we obtain

$$\begin{aligned} \lim_{z \rightarrow \lambda} \frac{W(z) - W(\lambda)}{z - \lambda} &= \lim_{z \rightarrow \lambda} \frac{e^z - e^\lambda}{z - \lambda} \\ &= \lim_{z \rightarrow \lambda} e^z \left[ 1 - \frac{(z - \lambda)}{2!} + \frac{(z - \lambda)^2}{3!} - \dots \right] \\ &= e^\lambda = \left. \frac{de^z}{dz} \right|_{z=\lambda} \end{aligned}$$

which proves the assertion.

In this example, we did not mention the direction from which the  $z$  approaches  $\lambda$ . We might surmise from this that the derivative of our analytic function is independent of the path of  $z$  as it approaches the limiting point. However, this is not true in general. By setting  $\lambda = z$  and  $z = z + \Delta z$  in Equation A.4, we obtain an alternative form of that equation, namely,

$$\frac{dW}{dz} = \lim_{\Delta z \rightarrow 0} \left\{ \frac{W(z + \Delta z) - W(z)}{\Delta z} \right\} \quad (\text{A.5})$$

For a function to possess a unique derivative, it is required that

$$\frac{dW}{dz} = \lim_{\Delta z \rightarrow 0} \frac{\Delta W}{\Delta z} = \lim_{\substack{\Delta x \rightarrow 0 \\ \Delta y \rightarrow 0}} \frac{\Delta u + j\Delta v}{\Delta x + j\Delta y}$$

But because

$$\Delta u = \frac{\partial u}{\partial x} \Delta x + \frac{\partial u}{\partial y} \Delta y$$

$$\Delta v = \frac{\partial v}{\partial x} \Delta x + \frac{\partial v}{\partial y} \Delta y$$

the unique derivative becomes

$$\frac{dW}{dz} = \lim_{\substack{\Delta x \rightarrow 0 \\ \Delta y \rightarrow 0}} \frac{\left( \frac{\partial u}{\partial x} + j \frac{\partial v}{\partial x} \right) \Delta x + j \left( \frac{\partial v}{\partial y} - j \frac{\partial u}{\partial y} \right) \Delta y}{\Delta x + j\Delta y}$$

For this to be independent of how  $\Delta x$  and  $\Delta y$  approach zero (that is, for the derivative to be unique), it is necessary and sufficient that  $\Delta x + j \Delta y$  cancel in the numerator and denominator. This requires that

$$\frac{dW}{dz} = \frac{\partial u}{\partial x} + j \frac{\partial v}{\partial y} = \frac{\partial v}{\partial x} - j \frac{\partial u}{\partial y}$$

This condition can be met if

$$\frac{\partial u}{\partial x} = \frac{\partial v}{\partial y} \quad \frac{\partial v}{\partial x} = -\frac{\partial u}{\partial y} \quad (\text{A.6})$$

These are the *Cauchy-Riemann* conditions. If the function satisfies these equations, it possesses a unique derivative and it is analytic at that point. These conditions are necessary and sufficient.

**A.1.1 Integration**

Integration of a complex function is defined in a manner like that for a real function, except for the important difference that the path of integration as well as the end points must be specified. A number of important theorems relate to integration, as we will discuss later.

Recall that the real integral  $\int_a^b f(x) dx$  means that the  $x$ -axis is broken into tiny elements  $\Delta x$  from  $a$  to  $b$ , each element is multiplied by the mean value of  $f(x)$  in the element, and then the sum of all such products from  $a$  to  $b$  is taken as  $\Delta x \rightarrow 0$ . The same general procedure is used to define the integral in

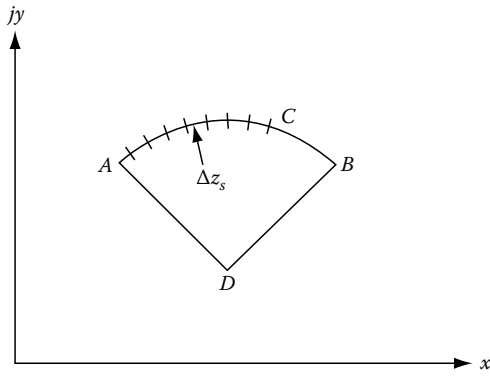


FIGURE A.2 The path of integration in the complex plane.

the complex plane. Instead of being restricted to the  $x$ -axis, the path of integration can be anywhere in the  $z$ -plane, for example, the arc  $ABC$  in Figure A.2. This arc is broken into  $n$  elements  $\Delta z_s$ , and the corresponding mean value of  $W(z)$  over each element is written  $W_s$ . Now from the sum  $\sum_{s=1}^n W_s \Delta z_s$ , over all values of  $s$  from  $a$  to  $b$ , and take the limit  $\Delta z_s \rightarrow 0, n \rightarrow \infty$ . This limit, if it exists, is the integral

$$I = \int_a^b W(z) dz \quad (\text{A.7})$$

The only innovation introduced here is that the path over which the integral is to be taken must be specified.

**Example A.2**

Evaluate the integral in Equation A.7 for the function  $W(z) = 1/z$  over the semicircles shown in Figure A.3.

**SOLUTION**

Refer first to Figure A.3a, and introduce the polar coordinates

$$z = re^{j\theta} \quad dz = jre^{j\theta} d\theta$$

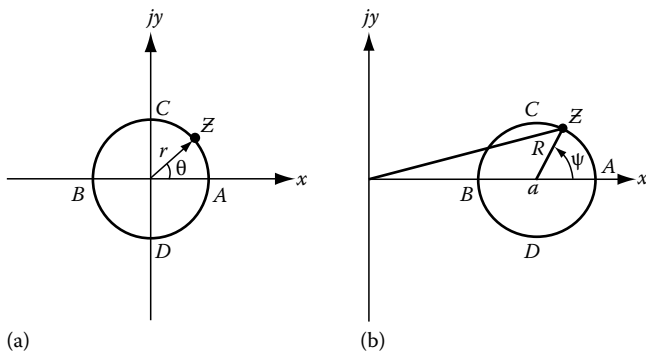


FIGURE A.3 Integral of the function  $W = 1/z$  over two paths.

Then

$$\int W(z) dz = \int \frac{dz}{z} = \int j d\theta$$

Over the path  $ACB$ ,  $\theta$  varies between 0 and  $\pi$ , and the integral equals  $j\pi$ . Over the path  $ADB$ ,  $\theta$  varies from 0 to  $-\pi$ , and the integral equals  $-j\pi$ . Thus, although the end points are the same, the integrals over the two paths are different. (The fact that one integral is numerically the negative of the other has no general significance.)

In evaluating the real integral by starting at  $A$  and integrating to  $B$  and then back to  $A$ , the result will be zero because the integral from  $A$  to  $B$  is the negative of the integral from  $B$  to  $A$ . The same result is not necessarily true for complex variables, unless the path from  $A$  to  $B$  coincides with the path from  $B$  to  $A$ . In the present complex integral, the integration from  $A$  to  $B$  via  $C$  and then back to  $A$  via  $D$  yields  $j\pi - (-j\pi) = j2\pi$  and no zero.

Now consider the integration over the semicircle displaced from the origin, as shown in Figure A.3b. Introduce the coordinates

$$z = a + Re^{j\psi} \quad dz = j Re^{j\psi} d\psi$$

Then

$$\int_{ACBDA} \frac{dz}{z} = \int_0^{2\pi} \frac{jRe^{j\psi}}{a + Re^{j\psi}} d\psi = \ln(a + Re^{j\psi}) \Big|_0^{2\pi} = \ln z \Big|_A^A = 0$$

The results of these calculations emphasize the fact that the two paths possess different features. The difference is that in Figure A.3a, the path encloses a singularity (the function becomes infinite) at the origin, whereas the path in Figure A.3b does not enclose the singularity and  $W = 1/z$  is analytic everywhere in the region and on the boundary.

It is easily shown that the integrals of the function

$$W(z) = \frac{1}{z^2}, W(z) = \frac{1}{z^3}, \dots, W(z) = \frac{1}{z^n}$$

around a contour encircling the origin of the coordinate axis are each equal to zero; that is,

$$\oint \frac{1}{z^2} dz = \oint \frac{1}{z^3} dz = \dots = \oint \frac{1}{z^n} dz = 0 \quad (\text{A.8})$$

where the contour is taken counterclockwise.

**Example A.3**

Find the value of the integral  $\int_0^{z_0} z dz$  from the point  $(0, 0)$  to  $(2, j4)$ .

**SOLUTION**

Because  $z$  is an analytic function along any path, then

$$\int_0^{z_0} z dz = \frac{z^2}{2} \Big|_0^{2+j4} = -6 + j8$$

Equivalently, we could write

$$\begin{aligned} \int_0^{z_0} z dz &= \int_0^2 x dz - \int_0^4 y dy + j \int_0^4 x dy = +\frac{x^2}{2} \Big|_0^2 - \frac{y^2}{2} \Big|_0^4 + jxy \Big|_0^4 \\ &= 2 - \frac{16}{2} + j2 \times 4 = -6 + j8 \end{aligned}$$

We now state a very important theorem, and this is often referred to as the *principal theorem of complex variable theory*. This is the *Cauchy first integral theorem*.

---

**THEOREM A.1**

Given a region of the complex plane within which  $W(z)$  is analytic and any closed curve that lies entirely within this region, then

$$\oint_C W(z) dz = 0 \tag{A.9}$$

where the contour  $C$  is taken counterclockwise.

The integration over a closed path is called a contour integral. Also, by convention the positive direction of integration is taken so that when traversing the contour, the enclosed region is always to the left. The proof of this theorem depends on the fact that everywhere within  $C$  the Cauchy–Riemann equations are satisfied,  $W(z)$  possesses a unique derivative at all points of the path.

---

**COROLLARY A.1**

If the contour  $C_2$  completely encloses  $C_1$ , and if  $W(z)$  is analytic in the region between  $C_1$  and  $C_2$  and also on  $C_1$  and  $C_2$ , then

$$\oint_{C_1} W(z) dz = \oint_{C_2} W(z) dz \tag{A.10}$$

*Proof* Refer to Figure A.4, which shows the two contours  $C_1$  and  $C_2$  and two connecting lines  $DE$  and  $GA$ . In the region closed by the contour  $ABDEFGA$ , the function  $W(z)$  is analytic everywhere, and  $\oint W dz = 0$  over the path. This means that

$$\int_{ABD} + \int_{DE} + \int_{EFG} + \int_{GA} = 0 \tag{A.11}$$

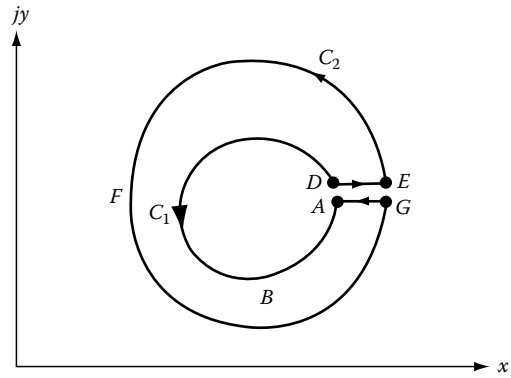


**FIGURE A.4** To prove the first corollary.

where  $W(z) dz$  is to be understood after each integral sign. Now allow  $A$  to approach  $D$ , and  $G$  to approach  $E$ , so that  $D E$  coincides with  $A G$ . Then

$$\int_{DE} = \int_{AG} = - \int_{GA}$$

Also

$$\int_{ABD} = - \int_{C_1} \quad \text{and} \quad \int_{EFG} = \int_{C_2} \tag{A.12}$$

where strict attention has been paid to the convention given in the determination of the positive direction of integration around a contour. Combine Equations A.11 and A.12 so that

$$- \int_{C_1} + \int_{C_2} = 0 \quad \text{or} \quad \int_{C_1} W(z) dz = \int_{C_2} W(z) dz$$

which was to be proved.

This is an important theorem because it allows the evaluation around one contour by replacing that contour with a simpler one, the only restriction being that in the region between the two contours the integral must be regular. It does not require that the function  $W(z)$  be analytic within  $C_1$ .

---

**COROLLARY A.2**

If  $W(z)$  has a finite number  $n$  of isolated singularities within a region  $G$  bounded by a curve  $C$ , then

$$\int_C W(z) dz = \sum_{s=1}^N \oint_{C_s} W(z) dz \tag{A.13}$$

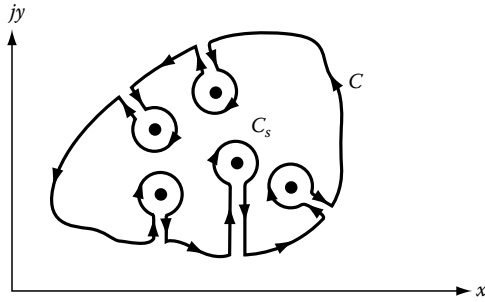


FIGURE A.5 A contour enclosing  $n$  isolated singularities.

where  $C_s$  is any contour surrounding the  $s$ th singularity. The contours are taken in the counterclockwise direction.

*Proof* Refer to Figure A.5. The proof for this case is evident from the manner in which the first corollary was proved.

**COROLLARY A.3**

The integral  $\int_A^B W(z) dz$  depends only upon the end points  $A$  and  $B$  (refer to Figure A.2) and does not depend on the path of integration, provided that this path lies entirely within the region in which  $W(z)$  is analytic.

*Proof* Consider  $ACBDA$  of Figure A.2 as a contour that encloses no singularity of  $W(z)$ . Then

$$\oint_C = 0 = \int_{ADB} + \int_{BCA} \quad \text{or} \quad \int_{ADB} = \int_{ACB} \quad (\text{A.14})$$

Hence, the integral is the same whether taken over path  $D$  or  $C$ , and thus is independent of the path and depends only on the end points  $A$  and  $B$ .

**THEOREM A.2 The Cauchy Second Integral Theorem**

If  $W(z)$  is the function  $W(z) = f(z)/(z - z_0)$  and the contour encloses the only singularity at  $z_0$ , then

$$\oint_C \frac{f(z)}{z - z_0} dz = j2\pi f(z_0) \quad (\text{A.15})$$

or

$$f(z_0) = \frac{1}{2\pi j} \oint_C \frac{f(z)}{z - z_0} dz \quad (\text{A.16})$$

(the contours are taken in the counterclockwise direction.)

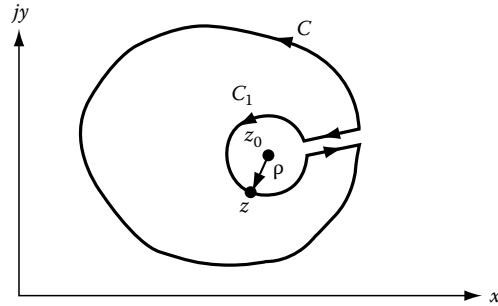


FIGURE A.6 To prove the Cauchy second integral theorem.

*Proof* Refer to Figure A.6. Begin with the second corollary and draw a circle  $C_1$  about the point  $z_0$ . Then

$$\int_C \frac{f(z)}{z - z_0} dz = \int_{C_1} \frac{f(z)}{z - z_0} dz \quad (\text{A.17})$$

Let  $z' = z - z_0 = \rho e^{j\theta}$ , which permits writing

$$\int_{C_1} \frac{f(z)}{z - z_0} dz = \int_0^{2\pi} \frac{f(z' + z_0)}{\rho e^{j\theta}} j\rho e^{j\theta} d\theta = j \int_0^{2\pi} f(z' + z_0) d\theta$$

In the limit as  $\rho \rightarrow 0, z' \rightarrow 0$ , and

$$j \int_0^{2\pi} f(z' + z_0) d\theta \Big|_{\lim \rho \rightarrow 0} = 2\pi j f(z_0)$$

Combine with Equation A.17 to find

$$\int_C \frac{f(z)}{z - z_0} dz = 2\pi j f(z_0)$$

which proves the theorem.

**A.1.2 Derivative of an Analytic Function  $W(z)$**

The derivative of an analytic function is also analytic, and consequently itself possesses a derivative. Let  $C$  be a contour within and upon which  $W(z)$  is analytic. Then if  $a$  is a point inside the contour (the prime indicates first-order derivative)

$$W'(a) = \lim_{|h| \rightarrow 0} \frac{W(a + h) - W(a)}{h} \quad (\text{A.18})$$

and can be shown that

$$W'(a) = \frac{1}{2\pi j} \oint_C \frac{W(z) dz}{(z - a)^2} \quad (\text{A.19})$$

where the contour  $C$  is taken in a counterclockwise direction. Proceeding, it can be shown that

$$W^{(n)}(a) = \frac{n!}{2\pi j} \oint_C \frac{W(z)dz}{(z-a)^{n+1}} \quad (A.20)$$

The exponent ( $n$ ) indicates  $n$ th derivative and the contour is taken counterclockwise.

### A.1.3 Taylor's Theorem

Let  $f(z)$  be analytic in the neighborhood of a point  $z = a$ . Let the contour  $C$  be a circle with center point  $a$  in the  $z$ -plane, and let the function  $f(z)$  not have any singularity within and on the contour. Let  $z = a + h$  be any point inside the contour; then by Equation A.15 we obtain

$$\begin{aligned} f(a+h) &= \frac{1}{2\pi j} \oint_C \frac{f(z)dz}{z-a-h} \\ &= \frac{1}{2\pi j} \oint_C f(z)dz \left\{ \frac{1}{z-a} + \frac{h}{(z-a)^2} + \dots \right. \\ &\quad \left. + \frac{h^n}{(z-a)^{n+1}} + \frac{h^{n+1}}{(z-a)^{n+1}(z-a-h)} \right\} \\ &= f(a) + hf^{(1)}(a) + \frac{h^2}{2!}f^{(2)}(a) + \dots \\ &\quad + \frac{h^n}{n!}f^{(n)}(a) + \frac{1}{2\pi j} \oint_C \frac{f(z)h^{n+1}dz}{(z-a)^{n+1}(z-a-h)} \end{aligned}$$

But where  $z$  is on  $C$  the modulus  $f(z)/(z-a-h)$  is continuous and therefore bounded. Its modulus will not exceed some finite number  $M$ . Hence, with  $|z-a|=R$  for points on the circle, we obtain

$$\left| \frac{1}{2\pi j} \oint_C \frac{f(z)h^{n+1}dz}{(z-a)^{n+1}(z-a-h)} \right| \leq \frac{M2\pi R}{2\pi} \left( \frac{|h|}{R} \right)^{n+1}$$

where  $|h|/R < 1$  and therefore tends to zero as  $n$  tends to infinity. Therefore, we have

$$f(a+h) = f(a) + hf^{(1)}(a) + \frac{h^2}{2!}f^{(2)}(a) + \dots + \frac{h^n}{n!}f^{(n)}(a) + \dots \quad (A.21)$$

or

$$f(z) = f(a) + (z-a)f^{(1)}(a) + \frac{(z-a)^2}{2!}f^{(2)}(a) + \dots + \frac{(z-a)^n}{n!}f^{(n)}(a) + \dots \quad (A.22)$$

where the numbers in the exponents indicate order of differentiation. The radius of convergence is such that it excludes from the interior of the circle that singularity of the function that is nearest to  $a$ .

### A.1.4 Laurent's Theorem

Let  $C_1$  and  $C_2$  be two concentric circles, as shown in Figure A.7, with their center at  $a$ . The function  $f(z)$  is analytic with the ring and  $(a+h)$  is any point in it. From the figure and Cauchy's theorem, we obtain

$$\frac{1}{2\pi j} \oint_{C_2} \frac{f(z)dz}{(z-a-h)} + \frac{1}{2\pi j} \oint_{C_1} \frac{f(z)dz}{(z-a-h)} + \frac{1}{2\pi j} \oint_{C_3} \frac{f(z)dz}{(z-a-h)} = 0$$

where the first contour is counterclockwise and the last two are clockwise. The above equation becomes

$$f(a+h) = \frac{1}{2\pi j} \oint_{C_2} \frac{f(z)dz}{(z-a-h)} - \frac{1}{2\pi j} \oint_{C_1} \frac{f(z)dz}{(z-a-h)} \quad (A.23)$$

where both the contours are taken counterclockwise. For the  $C_2$  contour  $|h| < |(z-a)|$  and for the  $C_1$   $|h| > |(z-a)|$ . Hence, we expand the above integral (contours in the counterclockwise direction) as follows:

$$\begin{aligned} f(a+h) &= \frac{1}{2\pi j} \oint_{C_2} f(z) \left\{ \frac{1}{z-a} + \frac{h}{(z-a)^2} + \dots \right. \\ &\quad \left. + \frac{h^n}{(z-a)^{n+1}} + \frac{h^{n+1}}{(z-a)^{n+1}(z-a-h)} \right\} dz \\ &\quad + \frac{1}{2\pi j} \oint_{C_1} f(z) \left\{ \frac{1}{h} + \frac{z-a}{h^2} + \dots + \frac{(z-a)^n}{h^{n+1}} \right. \\ &\quad \left. + \frac{(z-a)^{n+1}}{h^{n+1}(z-a-h)} \right\} dz \end{aligned}$$

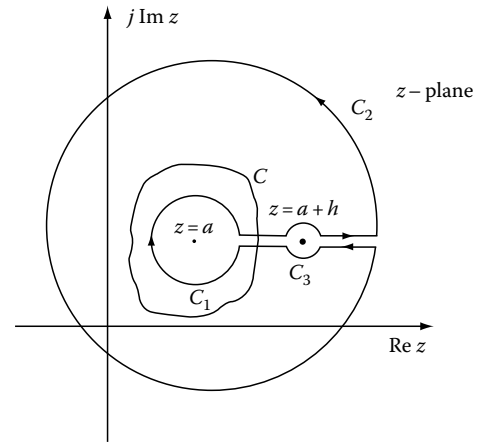


FIGURE A.7 Explaining Laurent's theorem.

From Taylor's theorem it was shown that the integrals of the last term in the two brackets tend to zero as  $n$  tends to infinity. Therefore, we have

$$f(a+h) = a_0 + a_1h + a_2h^2 + \dots + \frac{b_1}{h} + \frac{b_2}{h^2} + \dots \quad (\text{A.24})$$

where (contours in the counterclockwise direction)

$$a_n = \frac{1}{2\pi j} \oint_{C_2} \frac{f(z)dz}{(z-a)^{n+1}} \quad b_n = \frac{1}{2\pi j} \oint_{C_1} (z-a)^{n+1} f(z) dz$$

The above expansion can be put in more convenient form by substituting  $h = z - a$ , which gives

$$f(z) = c_0 + c_1(z-a) + c_2(z-a)^2 + \dots + \frac{d_1}{(z-a)} + \frac{d_2}{(z-a)^2} + \dots + \frac{d_n}{(z-a)^n} + \dots \quad (\text{A.25})$$

Because  $z = a + h$ , it means that  $z$  now is any point within the ring-shaped space between  $C_1$  and  $C_2$  where  $f(z)$  is analytic. Equation A.25 is the Laurent's expansion of  $f(z)$  at a point  $z + h$  within the ring. The coefficients  $c_n$  and  $d_n$  are obtained from Equation A.24 by replacing  $a_n, b_n, z$  by  $c_n, d_n, \zeta$ , respectively. Here  $\zeta$  is the variable on the contours and  $z$  is inside the ring. When  $f(z)$  has a simple pole at  $z = a$ , there is only one term, namely,  $d_1/(z-a)$ . If there exists an  $n$ th-order term, there are  $n$  terms of which the last is  $d_n/(z-a)^n$ ; some of the  $d_n$ 's may be zero.

If  $m$  is the highest index of the inverse power of  $f(z)$  in Equation A.25, it is said that  $f(z)$  has a pole of order  $m$  at  $z = a$ . Then

$$f(z) = \sum_{n=0}^{\infty} c_n(z-a)^n + \sum_{n=1}^m \frac{d_n}{(z-a)^n} \quad (\text{A.26})$$

The coefficient  $d_1$  is the *residue* at the pole.

If the series in inverse powers of  $(z-a)$  in Equation A.25 does not terminate, the function  $f(z)$  is said to have an *essential singularity* at  $z = a$ . Thus,

$$f(z) = \sum_{n=0}^{\infty} c_n(z-a)^n + \sum_{n=1}^{\infty} \frac{d_n}{(z-a)^n} \quad (\text{A.27})$$

The coefficient  $d_1$  is the *residue* of the singularity.

### Example A.4

Find the Laurent expansion of  $f(z) = 1/[(z-a)(z-b)^2]$  ( $n \geq 1, a \neq b \neq 0$ ) near each pole.

#### SOLUTION

First remove the origin to  $z = a$  by the transformation  $\zeta = (z-a)$ . Hence, we obtain

$$f(z) = \frac{1}{\zeta} \frac{1}{(\zeta+c)^2} = \frac{1}{c^n \zeta} \frac{1}{(1+\zeta/c)^2} \quad c = a-b$$

If  $|\zeta/c| < 1$ , then we have

$$f(z) = \frac{1}{c^n \zeta} \left[ 1 - \frac{n\zeta}{c} + \frac{n(n+1)}{2!} \frac{\zeta^2}{c^2} - \dots \right] = \left[ -\frac{n}{c^{n+1}} + \frac{n(n+1)\zeta}{2!c^{n+2}} - \dots \right] + \frac{1}{c^n \zeta}$$

which is the Laurent series expansion near the pole at  $z = a$ . The residue is  $1/c^n = 1/(a-b)^n$ .

For the second pole set  $\zeta = (z-b)$  and expand as above to find

$$f(z) = -\left( \frac{1}{c^{n+1}} + \frac{\zeta}{z^{n+2}} + \frac{\zeta^2}{c^{n+3}} + \dots \right) - \left( \frac{1}{c^n \zeta} + \frac{1}{c^{n-1} \zeta^2} + \dots + \frac{1}{c \zeta^n} \right)$$

The second part of the expansion is the principal expansion near  $z = b$  and the residue is  $-1/c^n = -1/(a-b)^n$ .

### Example A.5

Prove that

$$f(z) = \exp\left[\frac{x}{2}\left(z - \frac{1}{z}\right)\right] = J_0(x) + zJ_1(x) + z^2J_2(x) + \dots + z^nJ_n(x) + \dots - \frac{1}{z}J_1(x) + \frac{1}{z^2}J_2(x) - \dots + \frac{(-1)^n}{z^n}J_n(x) + \dots$$

where

$$J_n(x) = \frac{1}{2\pi} \int_0^{2\pi} \cos(n\theta - x \sin \theta) d\theta$$

#### SOLUTION

The function  $f(z)$  is analytic except the point  $z = a$ . Hence, by the Laurent's theorem, we obtain

$$f(z) = a_0 + a_1z + a_2z^2 + \dots + \frac{b_1}{z} + \frac{b_2}{z^2} + \dots$$

where (contours in the counterclockwise direction)

$$a_n = \frac{1}{2\pi j} \oint_{C_2} \exp\left[\frac{x}{2}\left(z - \frac{1}{z}\right)\right] \frac{dz}{z^{n+1}},$$

$$b_n = \frac{1}{2\pi j} \oint_{C_1} \exp\left[\frac{x}{2}\left(z - \frac{1}{z}\right)\right] z^{n-1} dz$$

where the contours are circles with center at the origin and are taken counterclockwise. Set  $C_2$  equal to a circle of unit radius and write  $z = \exp(j\theta)$ . Then we have

$$a_n = \frac{1}{2\pi j} \int_0^{2\pi} e^{jx \sin \theta} e^{-jn\theta} j d\theta = \frac{1}{2\pi} \int_0^{2\pi} \cos(n\theta - x \sin \theta) d\theta$$

because the last integral vanishes, as can be seen by writing  $2\pi - \varphi$  for  $\theta$ . Thus,  $a_n = J_n(x)$ , and  $b_n = (-1)^n a_n$  because the function is unaltered if  $-z^{-1}$  is substituted for  $z$ , so that  $b_n = (-1)^n J_n(x)$ .

## A.2 Sequences and Series

Consider a sequence of numbers, such as those that arise in connection with the Z-transform. Suppose that the sequence of complex numbers is given as  $z_0, z_1, z_2, \dots$ .

The sequence of complex numbers is said to *converge* to the limit  $L$ ; that is,

$$\lim_{n \rightarrow \infty} z_n = L$$

if for every positive  $\delta$  there exists an integer  $N$  such that

$$|z_n - L| < \delta \quad \text{for all } n > N$$

That is, a convergent sequence is one whose terms approach arbitrarily close to the limit  $L$  as  $n$  increases. If the series does not converge, it is said to *diverge*.

---

### THEOREM A.3

In order for a sequence  $\{z_n\}$  of complex numbers to be convergent, it is necessary and sufficient that for all  $\delta > 0$  there exists a number  $N(\delta)$  such that for all  $n > N$  and all  $p = 1, 2, 3, \dots$  the inequality  $|z_{n+p} - z_n| < \delta$  is fulfilled.

The sum of an infinite sequence of complex numbers  $z_0, z_1, \dots$  is given by

$$S = z_0 + z_1 + z_2 + \dots = \sum_{n=0}^{\infty} z_n \quad (\text{A.28})$$

Consider the partial sum sequence of  $n$  terms, which is designated  $S_n$ . The infinite series converges to the sum  $S$  if the partial sum sequence  $S_n$  converges to  $S$ . That is, the series converges if for

$$S_n = \sum_{n=0}^n z_n \quad \lim_{n \rightarrow \infty} S_n = S \quad (\text{A.29})$$

When the partial sum  $S_n$  diverges, the series is said to diverge.

### A.2.1 Comparison Test

Let the terms of the numerical series (Equation A.28) for all  $n \geq n_0 \geq 1$  satisfy the condition  $|z_n| \leq b_n$ . Then the convergence of the series of positive terms  $\sum_{n=1}^{\infty} b_n$  implies absolute convergence of the above series.

### A.2.2 Limit Comparison Test

If the numerical series  $\sum_{n=1}^{\infty} v_n$  converges absolutely and for the terms of the numerical series (Equation A.28) there takes place the relationship

$$\lim_{n \rightarrow \infty} \left| \frac{z_n}{v_n} \right| = q = \text{const} < \infty$$

then series (Equation A.28) converges absolutely.

### A.2.3 D'Alembert's Test

If for the terms of the numerical series (Equation A.29) the finite limit

$$\lim_{n \rightarrow \infty} \left| \frac{z_{n+1}}{z_n} \right| = l$$

then for  $0 \leq l < 1$  series (Equation A.28) converges absolutely, for  $l > 1$  series (Equation A.28) diverges, and for  $l = 1$  an additional test is required.

### A.2.4 Root Test

Consider the sequence

$$r_n = \sqrt[n]{|z_n|}$$

If this sequence converges to  $l$  as  $n$  approaches infinity, then the series (Equation A.28) converges absolutely if  $l < 1$  and diverges if  $l > 1$ .

### A.2.5 Uniform Convergence (Weierstrass M-Test)

If  $|u_n(z)| \leq M_n$ , where  $M_n$  is independent of  $z$  in a region  $U$  and  $\sum_{n=1}^{\infty} M_n$  converges, then  $\sum_{n=1}^{\infty} u_n(z)$  is uniformly convergent in  $U$ .

#### Example A.6

Show that  $\sum_{n=1}^{\infty} \frac{1}{n^2+z^2}$  is uniformly convergent in the interval  $1 < |z| < 2$ .

#### SOLUTION

$|n^2 + z^2| \geq |n^2| - |z^2| \geq n^2 - 4 \geq \frac{1}{2}n^2$  for  $n > 2$  (the convergence is not affected by dropping the first two terms of the

series). Therefore,  $\frac{1}{|n^2 + z^2|} \leq \frac{2}{n^2}$  and the series  $\sum_{n=3}^{\infty} \frac{2}{n^2}$  converges. From the  $M$  test with  $M_n = \frac{2}{n^2}$  implies that the series converges uniformly.

### A.2.6 Analyticity of a Sequence of Functions

If the functions of sequence  $\{f_k(z)\}$  are analytic in a region  $U$  and the sum

$$F(z) = \sum_{k=1}^{\infty} f_k(z)$$

is uniformly convergent, then  $F(z)$  is analytic in  $U$ .

*Proof* Because  $F(z)$  is uniformly convergent for any  $\varepsilon$ , we can find  $N$  such that  $|F(z) - S_k(z)| < \varepsilon$  for all  $n > N$ , where  $S_k$  = partial sum =  $\sum_{k=1}^{\infty} f_k(z)$ . Because  $F(z)$  is uniformly convergent, it implies that  $f_k(z)$  are continuous and, hence,  $F(z)$  is continuous. Integrating within the region  $U$ , we obtain (integration is performed counterclockwise)

$$\left| \oint_C F(z) dz - \sum_{k=1}^n \oint_C f_k(z) dz \right| < \varepsilon \oint_C dz = \varepsilon \ell(C)$$

where  $\ell(C)$  is the length of the contour. Since  $\varepsilon \rightarrow 0$  as  $n \rightarrow \infty$  implies that  $\oint_C F(z) dz = \sum_{k=1}^{\infty} \oint_C f_k(z) dz = 0$ , since  $f_k(z)$ 's are analytic. Hence,  $F(z)$  is also analytic.

## A.3 Power Series

A series of the form

$$\begin{aligned} W(z) &= a_0 + a_1(z - z_0) + a_2(z - z_0)^2 + \dots \\ &= \sum_{n=0}^{\infty} a_n(z - z_0)^n \end{aligned} \quad (\text{A.30})$$

where the coefficients  $a_n$  are given by

$$a_n = \frac{1}{n!} \left. \frac{d^n W(z)}{dz^n} \right|_{z=z_0} \quad (\text{A.31})$$

is a *Taylor* series that is expanded about the point  $z = z_0$ , where  $z_0$  is a complex constant. That is, the Taylor series expands an analytic function as an infinite sum of component functions. More precisely, the Taylor series expands a function  $W(z)$ , which is analytic in the neighborhood of the point  $z = z_0$ , into an infinite series whose coefficients are the successive derivatives of the function at the given point. However, we know that the definition of a derivative of any order does not require more than the knowledge of the function in an arbitrarily small neighborhood of the point  $z = z_0$ . This means, therefore, that the Taylor series indicates that the shape of the function at a finite distance  $z_0$  from  $z$  is determined by the behavior of the function in the infinitesimal vicinity of  $z = z_0$ . Thus, the Taylor's series implies

that any analytic function has a very strong interconnected structure, and that by studying the function in a small vicinity of the point  $z = z_0$ , we can precisely predict what happens at the point  $z = z_0 + \Delta z_0$ , which is a finite distance from the point of study.

If  $z_0 = 0$ , the expansion is said to be about the origin and is called a *Maclaurin* series.

A power series of negative powers of  $(z - z_0)$ ,

$$W(z) = a_0 + a_1(z - z_0)^{-1} + a_2(z - z_0)^{-2} + \dots \quad (\text{A.32})$$

is called a *negative power* series.

We first focus attention on the positive power series (Equation A.30). Clearly, this series converges to  $a_0$  when  $z = z_0$ . To ascertain whether it converges for other values of  $z$ , we write

---

### THEOREM A.4

A positive power series converges absolutely in a circle of radius  $R^+$  centered at  $z_0$  where  $|z - z_0| < R^+$ ; it diverges outside of this circle where  $|z - z_0| > R^+$ . The value of  $R^+$  may be zero, a positive number, or infinity. If  $R^+ = \text{infinity}$ , the series converges everywhere, and if it is equal to zero the series converges only at  $z = z_0$ . The radius  $R^+$  is found from the relation

$$R^+ = \lim_{n \rightarrow \infty} \left| \frac{a_n}{a_{n+1}} \right| \text{ if the limit exists} \quad (\text{A.33})$$

or by

$$R^+ = \lim_{n \rightarrow \infty} \frac{1}{\sqrt[n]{|a_n|}} \text{ if the limit exists} \quad (\text{A.34})$$

*Proof* For a fixed value  $z$ , apply the ratio test, where

$$z_n = a_n(z - z_0)^n$$

That is,

$$\left| \frac{z_{n+1}}{z_n} \right| = \left| \frac{a_{n+1}(z - z_0)^{n+1}}{a_n(z - z_0)^n} \right| = \left| \frac{a_{n+1}}{a_n} \right| |z - z_0|$$

For the power series to converge, the ratio test requires that

$$\lim_{n \rightarrow \infty} \left| \frac{a_{n+1}}{a_n} \right| |z - z_0| < 1 \quad \text{or} \quad |z - z_0| < \lim_{n \rightarrow \infty} \left| \frac{a_n}{a_{n+1}} \right| = R^+$$

That is, the power series converges absolutely for all  $z$  that satisfy this inequality. It diverges for all  $z$  for which  $|z - z_0| > R^+$ . The value of  $R^+$  specified by Equation 3.5 is reduced by applying the root test.



**Example A.7**

Determine the region of convergence for the power series

$$W(z) = \frac{1}{1+z} = 1 - z + z^2 - z^3 + \dots$$

**SOLUTION**

We have  $a_n = (-1)^n$ , from which

$$R^+ = \lim_{n \rightarrow \infty} \left| \frac{(-1)^n}{(-1)^{n+1}} \right| = |1|$$

The series converges for all  $z$  for which  $|z| < 1$ . Hence, this expansion converges for any value of  $z$  within a circle of unit radius about the origin. Note that there will be at least one singular point of  $W(z)$  on the circle of convergence. In the present case, the point  $z = -1$  is a singular point.

**Example A.8**

Determine the region of convergence for the power series

$$W(z) = e^z = 1 + z + \frac{z^2}{2!} + \frac{z^3}{3!} + \dots = \sum_{n=1}^{\infty} \frac{1}{n!} z^n$$

**SOLUTION**

We have  $a_n = 1/n!$  from which

$$R^+ = \lim_{n \rightarrow \infty} \left| \frac{(n+1)!}{n!} \right| = \lim_{n \rightarrow \infty} (n+1) = \infty$$

The circle of convergence is specified by  $R^+ = \text{infinity}$ ; hence,  $W(z) = e^z$  converges for all finite values of  $z$ .

If a function has a singularity at  $z = z_0$ , it cannot be expanded in a Taylor series about this point. However, if one deletes the neighborhood of  $z_0$ , it can be expressed in the form of a Laurent series. The Laurent series is written

$$W(z) = \dots + \frac{a_{-2}}{(z-z_0)^2} + \frac{a_{-1}}{(z-z_0)} + a_0 + a_1(z-z_0) + a_2(z-z_0)^2 + \dots$$

$$= \sum_{n=-\infty}^{\infty} a_n(z-z_0)^n \tag{A.37}$$

If a circle is drawn about the point  $z_0$  such that the nearest singularity of  $W(z)$  lies on the circle, then Equation A.37 defines an analytic function everywhere within this circle except at its center. The portion  $\sum_{n=0}^{\infty} a_n(z-z_0)^n$  is regular at  $z = z_0$ . The portion  $\sum_{n=-1}^{-\infty} a_n(z-z_0)^n$  is not regular and is called the principal part of  $W(z)$  at  $z = z_0$ .

The region of convergence for the positive series part of the Laurent series is of the form

$$|z - z_0| < R^+ \tag{A.38}$$

while that for the principal part is given by

$$|z - z_0| > R^- \tag{A.39}$$

The evaluation of  $R^+$  and  $R^-$  proceeds according to the methods already discussed. Hence, the region of convergence of the Laurent series is given by those points common to Equations A.38 and A.39 or for

$$R^- < |z - z_0| < R^+ \tag{A.40}$$

If  $R^- > R^+$ , the series converges nowhere. The annular region of convergence for a typical Laurent series is shown in Figure A.8.

**THEOREM A.5**

A negative power series (Equation A.32) converges absolutely outside a circle of radius  $R^-$  centered at  $z_0$ , where  $|z - z_0| > R^-$ ; it diverges inside of this circle where  $|z - z_0| < R^-$ . The radius of convergence is determined from

$$R^- = \lim_{n \rightarrow \infty} \left| \frac{a_{n+1}}{a_n} \right| \text{ if the limit exists} \tag{A.35}$$

or by

$$R^- = \lim_{n \rightarrow \infty} \sqrt[n]{|a_n|} \text{ if the limit exists} \tag{A.36}$$

*Proof* The proof of this theorem parallels that of Theorem A.4.

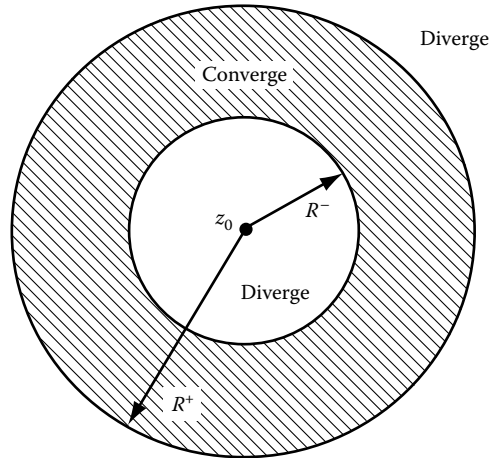


FIGURE A.8

**Example A.9**

Consider the Laurent series  $W(z) = \sum_n a_n z^n$  where

$$a_n \begin{cases} \left(\frac{1}{3}\right)^n & \text{for } n = 0, 1, 2, \dots \\ 2^n & \text{for } n = -1, -2, \dots \end{cases}$$

Determine the region of convergence.

**SOLUTION**

By Equations A.33 and A.38 we have  $R^+ = 3$ . By Equations A.35 and A.38 we have  $R^- = 2$ . Hence, the series converges for all  $z$  for which  $2 < |z| < 3$ .

No convenient expression for obtaining the coefficients of the Laurent series. However, because there is only one Laurent expansion for a given function, the resulting series, however derived, will be the appropriate one. For example,

$$e^{1/z} = 1 + \frac{1}{z} + \frac{1}{2!z^2} + \frac{1}{3!z^3} + \dots \quad (\text{A.41})$$

is obtained by replacing  $z$  by  $1/z$  in the Maclaurin expansion of  $\exp(z)$ . Note that in this case the coefficients of all positive powers of  $z$  in the Laurent expansion are zero. As a second illustration, consider the function  $W(z) = (\cos z)/z$ . This is found by dividing the Maclaurin series for  $\cos z$  by  $z$ , with the result

$$\frac{\cos z}{z} = \frac{1}{z} \left( 1 - \frac{z^2}{2!} + \frac{z^4}{4!} - \dots \right) = \frac{1}{z} - \frac{z}{2!} + \frac{z^3}{4!} - \dots \quad (\text{A.42})$$

In this case, the Laurent expansion includes only one term  $1/z$  in descending powers of  $z$ , but an infinite number of terms in ascending powers of  $z$ . That is,  $a_{-1} = 1$  and  $a_{-n} = 0$  if  $n \neq 1$ .

**A.4 Analytic Continuation**

The Taylor theorem shows that if a function  $f(z)$  is given by a power in  $z$ , it can also be represented as a power series in  $z - z_0 = f[(z - z_0) + z_0]$  where  $z_0$  is any point within the original circle of convergence, and this series will converge within any circle about  $z_0$  that does not pass beyond the original circle of convergence. Actually, it may converge within a circle that does not pass beyond the original circle of convergence. Consider, for example, the function

$$f(z) = 1 + z + z^2 + \dots = \frac{1}{1 - z} \quad \text{for } |z| < 1$$

Choose  $z_0 = j/2$ , and the Taylor expansion of

$$f(z) = \frac{1}{1 - [(z - \frac{1}{2}j) + \frac{1}{2}j]} = \frac{1}{(1 - \frac{1}{2}j) - z'} \quad z' = z - \frac{1}{2}j$$

in powers of  $z'$  is

$$f(z) = \frac{1}{1 - \frac{1}{2}j} + \frac{z'}{(1 - \frac{1}{2}j)^2} + \frac{z'^2}{(1 - \frac{1}{2}j)^3} + \dots$$

This series must converge and be equal to the original function if  $|z'| < 1/2$ , because  $j$  is the point of circle  $|z| = 1$  nearest to  $j/2$ , a requirement of Taylor's theorem. Actually this series converges if  $|z'| < |1 - \frac{1}{2}j| = \frac{1}{2}\sqrt{5}$ .

Suppose that the considered series represented no previously known function. In this case, the new Taylor series would define values of an analytic function over a range of  $z$  where no function is defined by the original series. Then we can extend the range of definition by taking a new Taylor series about a point in the new region. This process is called *analytic continuation*. In practice, when continuation is required, the direct use of the Taylor series is laborious and is seldom used. Of more convenience is the following theorem.

**THEOREM A.6**

If two functions  $f_1(z)$  and  $f_2(z)$  are analytic in a region  $D$  and equal in a region  $D'$  within  $D$ , they are equal everywhere in  $D$ .

**A.5 Singularities of Complex Functions**

A singularity has already been defined as a point at which a function ceases to be analytic. Thus, a discontinuation function has a singularity at the point of discontinuity, and multivalued functions have a singularity at a branch point. There are two important classes of singularities that a continuous, single-valued function may possess.

**Definition** A function has an *essential singularity* at  $z = z_0$  if its Laurent expansion about the point  $z_0$  contains an infinite number of terms in inverse powers of  $(z - z_0)$ .

**Definition** A function has a *nonessential singularity* or *pole of order  $m$*  if its Laurent expansion can be expressed in the form

$$W(z) = \sum_{n=-m}^{\infty} a_n (z - z_0)^n \quad (\text{A.43})$$

Note that the summation extends from  $-m$  to infinity and not from minus infinity to infinity; that is, the highest inverse power of  $(z - z_0)$  is  $m$ .

An alternative definition that is equivalent to this but somewhat simpler to apply is the following: if  $\lim_{z \rightarrow z_0} [(z - z_0)^m W(z)] = c$ ,

a nonzero constant (here  $m$  is a positive number), then  $W(z)$  is said to possess a pole of order  $m$  at  $z_0$ . The following examples illustrate these definitions:

1.  $\exp(1/z)$  (see Equation A.41) has an essential singularity at the origin.
2.  $\cos z/z$  (see Equation A.42) has a pole of order 1 at the origin.
3. Consider the function.

$$W(z) = \frac{e^z}{(z-4)^2(z^2+1)}$$

Note that functions of this general type exist frequently in the Laplace inversion integral. Because  $e^z$  is regular at all finite points of the  $z$ -plane, the singularities of  $W(z)$  must occur at the points for which the denominator vanishes; that is, for

$$(z-4)^2(z^2+1) = 0 \quad \text{or} \quad z = 4, +j, -j$$

By the second definition above, it is easily shown that  $W(z)$  has a second-order pole at  $z = 4$ , and first-order poles at the two points  $+j$  and  $-j$ . That is,

$$\lim_{z \rightarrow 4} (z-4)^2 \left[ \frac{e^z}{(z-4)^2(z^2+1)} \right] = \frac{e^4}{17} \neq 0$$

$$\lim_{z \rightarrow j} (z-j) \left[ \frac{e^z}{(z-4)^2(z^2+1)} \right] = \frac{e^j}{(j-4)^2 2j} \neq 0$$

4. An example of a function with an infinite number of singularities occurs in heat flow, wave motion, and similar problems. The function involved is

$$W(z) = 1/\sinh az$$

The singularities in this function occur when  $\sinh az = 0$  or  $az = js\pi$ , where  $s = 0, \pm 1, \pm 2, \dots$ . That each of these is a first-order pole follows from

$$\lim_{z \rightarrow j(s\pi/a)} \left( z - j \frac{s\pi}{a} \right) \frac{1}{\sinh az} = \frac{0}{0}$$

This can be evaluated in the usual manner by differentiating numerator and denominator (L'Hospital rule) to find

$$\lim_{z \rightarrow j(s\pi/a)} \frac{1}{a \cosh az} = \frac{1}{a \cosh js\pi} = \frac{1}{a \cos s\pi} \neq 0$$

---

**Definition (Isolated Singularities)** The point  $z = z_0$  is an *isolated singularity* of  $W(z)$  if we can always find  $\delta$  such that

the circle  $|z - z_0| = \delta$  does not contain another singularity. If no such  $\delta$  exists, the point  $z_0$  is known as a *nonisolated singularity*.

---

**Definition (Poles)** If  $\lim_{z \rightarrow z_0} (z - z_0)^n W(z) = \text{constant} \neq 0$ , where  $n$  is positive, then the point  $z = z_0$  is called a *pole of order  $n$* . If  $n = 1$ ,  $z_0$  is called a *simple pole*.

**Example A.10**

It is interesting to study the variation of  $f(z)$  close to the pole. For example, the function  $W(z) = 1/z = (1/r)e^{-j\theta}$  has a simple pole at zero. For any specific angle  $\theta_1$  the modulus  $|W(z)|$  increases to infinity as  $r \rightarrow 0$ , and this is true for all the angles from 0 to  $2\pi$ .

---

**Definition (Removable Singularities)** The point  $z = z_0$  is a *removable singularity* of  $W(z)$  if  $\lim_{z \rightarrow z_0} W(z)$  exists.

---

**Definition (Branch Points)** Multiple-valued functions contain singular points known as the *branch points*.

**Example A.11**

Investigate the function  $W(z) = z^{1/2}$ .

**SOLUTION**

In polar form we have  $W = \sqrt{z} = r^{1/2} (\cos \frac{1}{2}\theta + j \sin \frac{1}{2}\theta)$  (see Figure A.9) where  $z = x + jy$ ,  $r = \sqrt{x^2 + y^2}$ , and  $\theta = \tan^{-1}(y/x)$ . If we increase  $\theta$  by  $2\pi$ , we obtain  $W = \sqrt{z} = [\cos(\frac{1}{2}\theta + \pi) + j \sin(\frac{1}{2}\theta + \pi)] = -\sqrt{r} [\cos \frac{1}{2}\theta + j \sin \frac{1}{2}\theta]$  which is evident from Figure A.9b. This implies that  $W(z)$  has two values, one value for  $0 \leq \theta \leq \pi$  and the other from  $\pi \leq \theta \leq 2\pi$ . This indicates that  $W(z)$  is not analytic on the positive real axis when the angle ranges from  $0 \leq \theta \leq 2\pi$ . If we create a barrier (or cut) to exist along  $0x$  (see Figure A.9c) then  $\theta$  cannot take the values  $0, 2n\pi, n = 1, 2, \dots$ . Then for the angle  $0 < \theta < 2\pi$   $W$  is single valued and continuous and, therefore, analytic. This angle is known as the *principal branch* of the function.

The origin 0 is called the branch point. To make  $W = \sqrt{z}$  unique on each branch, the barrier must start from the branch point. The angular position of the barrier is arbitrary.

**Example A.12**

Investigate phase change in relation to branch points.

**SOLUTION**

If the contour is that shown in Figure A.10a for the function  $W(z) = z^{1/2}$ , then as  $z$  varies on the contour from  $A$  to  $B$  it

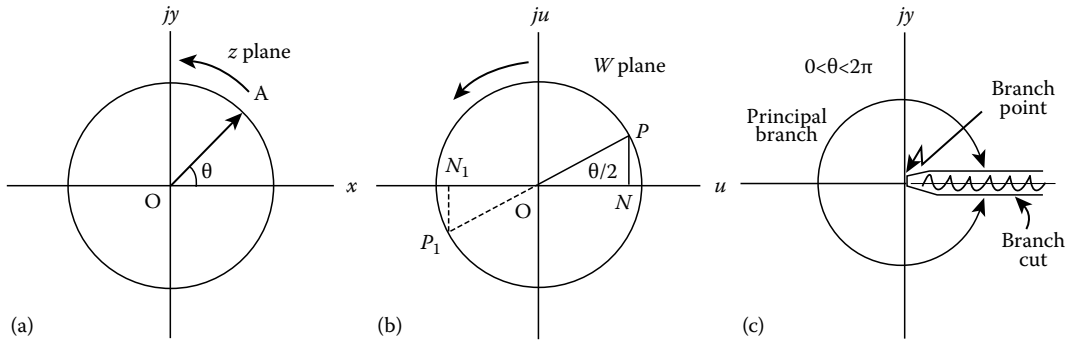


FIGURE A.9 Illustrating  $W(z) = z^{1/2}$ .

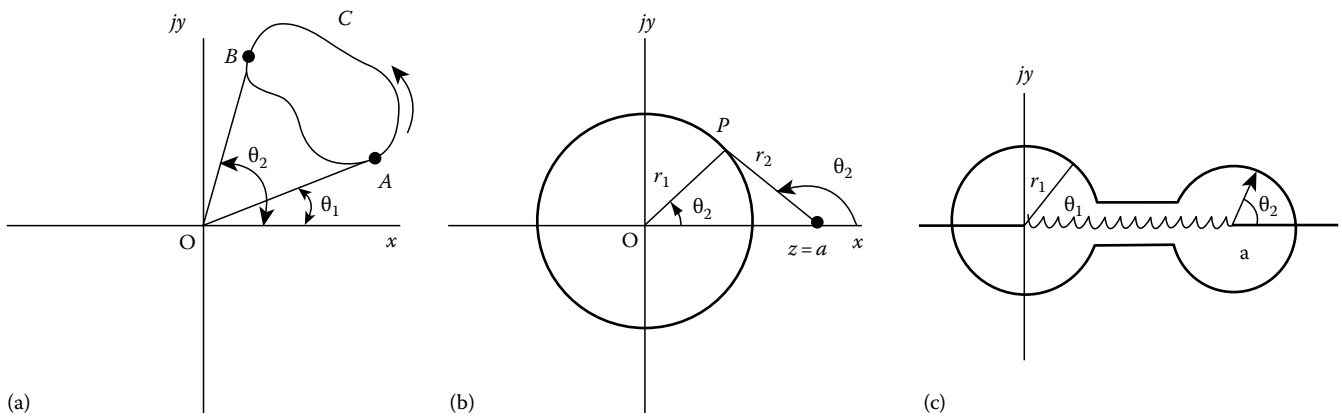


FIGURE A.10 Illustrating Example A.12.

sweeps the angle from  $\theta_1$  to  $\theta_2$ . Then if it varies from  $B$  to  $C$  continuous in the counterclockwise direction, the angle is swept from  $\theta_2$  to  $\theta_1$ . The angle swept out of  $OA$  is zero since it oscillated to  $B$  and back. Hence, the value of the function is that given by  $W = \sqrt{r}[\cos \frac{1}{2}\theta_1 + j \sin \frac{1}{2}\theta_1]$ .

Let's investigate the function  $W(z) = \sqrt{z(z-a)}$ , which has two branch points,  $z=0$  and  $z=a$ . From Figure A.10b we obtain

$$W = \sqrt{r_1 r_2} e^{j\frac{1}{2}(\theta_1 + \theta_2)}$$

$$= \sqrt{r_1 r_2} \left[ \cos \frac{1}{2}(\theta_1 + \theta_2) + j \sin \frac{1}{2}(\theta_1 + \theta_2) \right]$$

If we start from  $P$  moving counterclockwise,  $\theta_1$  varies by  $2\pi$  and  $\theta_2$  returns back to its original value. Hence,

$$W = \sqrt{r_1 r_2} \left[ \cos \frac{1}{2}(\theta_1 + 2\pi + \theta_2) + j \sin \frac{1}{2}(\theta_1 + 2\pi + \theta_2) \right]$$

$$= -\sqrt{r_1 r_2} \left[ \cos \frac{1}{2}(\theta_1 + \theta_2) + j \sin \frac{1}{2}(\theta_1 + \theta_2) \right]$$

which implies that the function enters a new branch. When  $P$  rotates twice,  $\theta_1$  becomes  $\theta_1 + 4\pi$  and the function has its original value.

From Figure A.10c, we observe that as we trace the contour  $\theta_1$  and  $\theta_2$  change by  $2\pi$  each. Therefore,

$$W = \sqrt{r_1 r_2} \left[ \cos \frac{1}{2}(\theta_1 + \theta_2 + 4\pi) + j \sin \frac{1}{2}(\theta_1 + \theta_2 + 4\pi) \right]$$

$$= \sqrt{r_1 r_2} \left[ \cos \frac{1}{2}(\theta_1 + \theta_2) + j \sin \frac{1}{2}(\theta_1 + \theta_2) \right]$$

and the function regains its original value. Hence, the branch cut can be from 0 to point  $a$  as indicated in the figure.

### Example A.13 (Essential Singularity)

Let us investigate the function  $W(z) = e^{1/z}$  as  $z \rightarrow 0$ . We write

$$W = e^{1/z} = e^{1/[re^{j\theta}]} = e^{\frac{1}{r}e^{-j\theta}} = e^{\frac{1}{r}\cos\theta} e^{-j\frac{\sin\theta}{r}} = e^{\frac{\cos\theta}{r}} \left[ \cos \frac{\sin\theta}{r} - j \sin \frac{\sin\theta}{r} \right]$$

$$= u + jv = r_1 e^{-j\theta_1} = r_1 \cos \theta_1 - jr_1 \sin \theta_1$$

where

$$r_1 = e^{\frac{1}{r}\cos\theta}, \theta_1 = \frac{\sin\theta}{r}, u = r_1 \cos \theta_1, v = -r_1 \sin \theta_1$$

We observe that for a specific value of  $0 < \theta < \pi/2$  as  $r \rightarrow 0$ ,  $r_1 = e^{\cos\theta/r}$  and  $\theta_1 = \sin \theta/r$  increase rapidly and, thus, the point  $W = r_1 \cos \theta_1 - j r_1 \sin \theta_1 = r_1[\cos \theta_1 - j \sin \theta_1]$  rotates with ever-increasing length and angular velocity (assuming  $r \rightarrow 0$  linearly with time). Although the function behaves peculiar near the singularity, it is analytic there and it is said that the singularity is isolated.

**Definition** (Singularity at  $\infty$ ) A singularity of  $W(z)$  at infinity is the same as that of  $W(1/\zeta)$  at  $\zeta = 0$ , where  $z = 1/\zeta$ .

**Example A.14**

The function  $W(z) = z^2$  has a double pole at  $\infty$  since  $W(1/\zeta) = 1/\zeta^2$  has a double pole at  $\zeta = 0$ .

In general: (1) if a function has a branch point at  $z = z_0$ , it has no other type of singularity there; (2) if a function has an essential singularity at  $z = z_0$ , it has no pole there.

**A.6 Theory of Residues**

It has already been shown that the contour integral of any function that encloses no singularities of the integrand will vanish. (In this section all the contour integrals are taken counterclockwise unless it is indicated otherwise.) Now our purpose is to examine the integral, the path of which encloses one singularity, say at  $z = z_0$ . The Laurent expansion of such a function is

$$W(z) = \sum_{n=-\infty}^{\infty} a_n(z - z_0)^n$$

and so

$$\oint_C W(z) dz = \sum_{n=-\infty}^{\infty} a_n \oint_{C_n} (z - z_0)^n dz$$

But by Equation A.11, each term in the sum vanishes except for  $n = -1$ , with

$$\oint_C (z - z_0)^{-1} dz = 2\pi j$$

In then follows that

$$\oint_C W(z) dz = \sum_{n=-\infty}^{\infty} \oint_{C_n} (z - z_0)^n dz = 2\pi j a_{-1} \quad (A.44)$$

Because the integral  $(1/2\pi j) \oint_C W(z) dz$  will appear frequently in subsequent applications, it is given a name; it is called the *residue of  $W(z)$  at  $z_0$*  and is abbreviated  $\text{Res}(W)$ .

From the second corollary Equation A.13, it follows that if  $W(z)$  has  $n$  isolated singularities within  $C$ , then

$$\frac{1}{2\pi j} \oint_C W(z) dz = \sum_{s=1}^n \frac{1}{2\pi j} \oint_{C_s} W(z) dz = \sum_{s=1}^n \text{Res}_s(W) \quad (A.45)$$

or, in other words, the value of the contour integral equals the sum of the residues within  $C$ . Observe that to evaluate integrals in the complex plane, it is only necessary to find the residues at the singularities of the integrand within the contour. One obvious way of doing this is (see Equation A.44) to find the coefficient  $a_{-1}$  in the Laurent expansion about each singularity. However, this is not always an easy task.

Several theorems exist that make evaluating residues relatively easy. We introduce these.

**THEOREM A.7**

If the  $\lim_{z \rightarrow z_0} [(z - z_0)W(z)]$  is finite, this limit is the residue of  $W(z)$  at  $z = z_0$ . If the limit is not finite, then  $W(z)$  has a pole of at least second order at  $z = z_0$  (it may possess an essential singularity here). If the limit is zero, then  $W(z)$  is regular at  $z = z_0$ .

*Proof* Suppose that the function is expanded into the Laurent series

$$W(z) = \frac{a_{-1}}{z - z_0} + a_0 + a_1(z - z_0) + a_2(z - z_0)^2 + \dots$$

Then the expression

$$\lim_{z \rightarrow z_0} [(z - z_0)W(z)] = \lim_{z \rightarrow z_0} [a_{-1} + a_0(z - z_0) + a_1(z - z_0)^2 + \dots] = a_{-1}$$

This proves the theorem.

This process was previously used to ascertain whether or not a function had a first-order pole at  $z = z_0$ . Thus, referring back to the examples in Section A.5, we have

$$\begin{aligned} \text{Res}\left(\frac{\cos z}{z}\right)_{z=0} &= 1 \\ \text{Res}\left[\frac{e^z}{(z-4)^2(z^2+1)}\right]_{z=j} &= \frac{e^j}{(j-4)^2 2j} \\ \text{Res}\left(\frac{1}{\sinh az}\right)_{z=j(s\pi/a)} &= \frac{1}{a \cos s\pi} \end{aligned}$$

Many of the singularities that arise in system function studies are first-order poles. The evaluation of the integral is relatively direct.

**Example A.15**

Evaluate the following integral

$$\frac{1}{2\pi j} \oint_C \frac{e^{zt}}{(z^2 + \omega^2)} dz$$

when the contour  $C$  encloses both first-order poles at  $z = \pm j\omega$ . Note that this is precisely the Laplace inversion integral of the function  $1/(z^2 + \omega^2)$ .

**SOLUTION**

This involves finding the following residues

$$\text{Res}\left(\frac{e^{zt}}{z^2 + \omega^2}\right)_{z=j\omega} = \frac{e^{j\omega t}}{2j\omega} \quad \text{Res}\left(\frac{e^{zt}}{z^2 + \omega^2}\right)_{z=-j\omega} = -\frac{e^{-j\omega t}}{2j\omega}$$

Hence,

$$\frac{1}{2\pi j} \oint_C \frac{e^{zt}}{z^2 + \omega^2} dz = \sum \text{Res} = \left(\frac{e^{j\omega t} - e^{-j\omega t}}{2j\omega}\right) = \frac{\sin \omega t}{\omega}$$

A slight modification of the method for finding residues of simple poles

$$\text{Res}W(z_0) = \lim_{z \rightarrow z_0} [(z - z_0)W(z)] \quad (\text{A.46})$$

makes the process even simpler. This is specified by the following theorem.

---

**THEOREM A.8**

Suppose that  $f(z)$  is analytic at  $z = z_0$  and suppose that  $g(z)$  is divisible by  $z - z_0$  but not by  $(z - z_0)^2$ . Then

$$\text{Res}\left[\frac{f(z)}{g(z)}\right]_{z=z_0} = \frac{f(z_0)}{g'(z_0)} \quad \text{where } g'(z) = \frac{dg(z)}{dz} \quad (\text{A.47})$$

*Proof* We write the relation  $(z - z_0) h(z) = g(z)$ , then  $g'(z) = (z - z_0) h'(z) + h(z)$  so that for  $z = z_0, g'(z_0) = h(z_0)$ . Then we have

$$\begin{aligned} \text{Res}\left[\frac{f(z)}{g(z)}\right]_{z=z_0} &= \lim_{z \rightarrow z_0} \left[ (z - z_0) \frac{f(z)}{g(z)} \right] = \lim_{z \rightarrow z_0} \left[ \frac{f(z)}{h(z)} \right] = \frac{f(z_0)}{h(z_0)} \\ &= \frac{f(z_0)}{g'(z_0)} \end{aligned}$$

which is the given result.

In reality, this theorem has already been used in the evaluation of  $\text{Res}(1/\sinh az)_{z=j(s\pi/a)}$ . Here  $f(z) = 1, g(z) = \sinh az$ , and  $g'(z) = a \cosh az$ .

As a second illustration, consider the previously used function

$$W(z) = \frac{e^z}{(z - 4)^2(z^2 + 1)}$$

Here, we take

$$f(z) = \frac{e^z}{(z - 4)^2}, \quad g(z) = z^2 + 1$$

thus,  $g'(z) = 2z$  and the previous result follows immediately with

$$\text{Res}\left[\frac{e^z}{(z - 4)^2(z^2 + 1)}\right] = \frac{e^j}{(j - 4)^2 2j}$$

Equation A.47 permits a simple proof of the Cauchy second integral theorem (A.15). This involves choosing  $g(z) = (z - z_0)$  in the integral

$$\frac{1}{2\pi j} \oint_C \frac{f(z)}{z - z_0} dz = \frac{f(z_0)}{1} = f(z_0) \quad (\text{A.48})$$

Suppose that Equation A.48 is differentiated  $n - 1$  times with respect to  $z_0$ . Then we write

$$\frac{d^{n-1}f(z_0)}{dz_0^{n-1}} = f^{(n-1)}(z_0) = \frac{(n - 1)!}{2\pi j} \oint_C \frac{f(z)}{(z - z_0)^n} dz \quad (\text{A.49})$$

This species an any-order derivative of a complex function expressed as a contour integral.

Our discussion so far has concentrated on finding the residue of a first-order pole. However, Equation A.49 permits finding the residue of a pole of any order. If, for example,  $W(z) = [f(z)/(z - z_0)^n]$ , then evidently  $W(z)$  has a pole of order  $n$  at  $z = z_0$  because  $f(z)$  is analytic at  $z = z_0$ . Then  $f(z) = (z - z_0)^n W(z)$ , and Equation A.49 becomes

$$\begin{aligned} \text{Res}(W(z))|_{z=z_0} &= \frac{1}{2\pi j} \oint_C W(z) dz \\ &= \frac{1}{(n - 1)!} \frac{d^{n-1}}{dz^{n-1}} [(z - z_0)^n W(z)]_{z=z_0} \quad (\text{A.50}) \end{aligned}$$

**Example A.16**

Evaluate the residue at the second-order pole at  $z = 4$  of the previously considered function

$$W(z) = \frac{e^z}{(z - 4)^2(z^2 + 1)}$$

**SOLUTION**

It follows from Equation A.50 that

$$\text{Res } W(z)|_{z=4} = \frac{1}{1!} \frac{d}{dz} \left[ \frac{e^z}{z^2 + 1} \right]_{z=4} = \frac{9e^4}{289}$$

**Example A.17**

Evaluate the residue at the third pole of the function

$$W(z) = \frac{e^{zt}}{(z+1)^3}$$

**SOLUTION**

A direct application of Equation A.50 yields

$$\text{Res } W(z)|_{z=-1} = \frac{1}{2!} \frac{d^2}{dz^2} (e^{zt}) \Big|_{z=-1} = \frac{1}{2} t^2 e^{-t}$$

There is no simple way of finding the residue at an essential singularity. The Laurent expansion must be found and the coefficient  $a_{-1}$  is thereby obtained. For example, from Equation A.41 it is seen that the residue of  $\exp(1/z)$  at the origin is unity. Fortunately, an essential singularity seldom arises in practical applications.

Sometimes the function takes the form

$$W(z) = \frac{f(z)}{zg(z)} \quad (\text{A.51})$$

where the numerator and denominator are prime to each other,  $g(z)$  has no zero at  $z=0$  and cannot be factored readily. The residue due to the pole at zero is given by

$$\text{Res } W(z) = \left. \frac{f(z)}{g(z)} \right|_{z=0} = \frac{f(0)}{g(0)} \quad (\text{A.52})$$

If  $z=a$  is the zero of  $g(z)$  then the residue at  $z=a$  is given by

$$\text{Res } W(z) = \frac{f(a)}{ag'(a)} \quad (\text{A.53})$$

If there are  $N$  poles of  $g(z)$  then the residues at all simple poles of  $W(z)$  are given by

$$\sum \text{Res} = \left. \frac{f(z)}{g(z)} \right|_{z=0} + \sum_{m=1}^N \left[ f(z) / \left( z \frac{dg(z)}{dz} \right) \right]_{z=a_m} \quad (\text{A.54})$$

If  $W(z)$  takes the form  $W(z) = f(z)/[h(z)g(z)]$  and the simple poles to the two functions are not common, then the residues at all simple poles are given by

$$\sum \text{Res} = \sum_{m=1}^N \frac{f(a_m)}{h(a_m)g'(a_m)} + \sum_{r=1}^R \frac{f(b_r)}{h'(b_r)g(b_r)} \quad (\text{A.55})$$

**Example A.18**

Find the sum of the residues  $e^{2z}/\sin mz$  at the first  $N+1$  poles on the negative axis.

**SOLUTION**

The simple poles occur at  $z = -n\pi/m$ ,  $n = 0, 1, 2, \dots$ . Thus

$$\sum \text{Res} = \sum_{n=0}^N \left[ \frac{e^{2z}}{m \cos mz} \right]_{z=-n\pi/m} = \frac{1}{m} \sum_{n=0}^N (-1)^n e^{-2n\pi/m}$$

**Example A.19**

Find the sum of the residues of  $e^{2z}/(z \cosh mz)$  at the origin and at the first  $N$  poles on each side of it.

**SOLUTION**

The zeros of  $\cosh mz$  are  $z = -j(n+1/2)\pi/m$ ,  $n$  integral. Because  $\cosh mz$  has no zero at  $z=0$ , then Equation A.55 gives

$$\sum \text{Res} = 1 + \sum_{n=-N}^{N-1} \left[ \frac{e^{2z}}{mz \sinh mz} \right]_{z=-(n+\frac{1}{2})\pi/m}$$

**Example A.20**

Find the residue of  $ze^z/\sin mz$  at the origin.

**SOLUTION**

Because near  $z=0$   $\sin mz \approx mz$  there is no pole at the origin and, hence, the integral  $(1/2\pi j) \int_C ze^z dz / \sin mz$  is equal to zero for a contour encircling the origin with radius less than  $\pi/m$ .

**A.7 Aids to Integration**

The following three theorems will substantially simplify the evaluation of certain integrals in the complex plane. Examples will be found in later applications.

**THEOREM A.9**

If  $AB$  is the arc of a circle of radius  $|z|=R$  for which  $\theta_1 \leq \theta \leq \theta_2$  and if  $\lim_{R \rightarrow \infty} (zW(z)) = k$ , a constant that may be zero, then

$$\lim_{R \rightarrow \infty} \int_{AB} W(z) dz = jk(\theta_2 - \theta_1) \quad (\text{A.56})$$

*Proof* Let  $zW(z) = k + \varepsilon$ , where  $\varepsilon \rightarrow 0$  as  $R$  approaches infinity. Then

$$\int_{AB} W(z)dz = \int_{AB} \frac{k + \varepsilon}{z} dz = (k + \varepsilon) \int_{\theta_1}^{\theta_2} j d\theta = (k + \varepsilon)j(\theta_2 - \theta_1)$$

In carrying out this integration, the procedure employed in Example A.2 is used. In the limit as  $R$  approaches infinity (Equation A.56) follows.

This theorem can be shown to be valid even if there are a finite number of points on the arc  $AB$  for which the  $\lim_{R \rightarrow \infty} (zW(z)) \neq k$ , provided only that the limit remains finite for finite  $R$  at these points. This theorem can also be proved true if we choose  $\lim_{R \rightarrow \infty} (z - a)W(z) = k$  when the integral is taken around the arc  $\theta_1 \leq \arg(z - a) \leq \theta_2$  of the circle  $|z - a| = r$ .

---

**THEOREM A.10**

If  $AB$  is the arc of a circle of radius  $|z - z_0| = r$  for which  $\varphi_1 \leq \varphi \leq \varphi_2$  (as shown in Figure A.11) and if  $\lim_{z \rightarrow z_0} [(z - z_0)W(z)] = k$ , a constant that may be zero, then

$$\lim_{r \rightarrow 0} \int_{AB} W(z)dz = jk(\varphi_2 - \varphi_1) \quad (\text{A.57})$$

where  $r$  and  $\varphi$  are introduced polar coordinates, with the point  $z = z_0$  as origin.

*Proof* The proof of this theorem follows along similar lines to that of Theorem A.9.

Note specifically that Theorem A.9 will allow the evaluation of integrals over infinitely large arcs, whereas Theorem A.10 will allow the evaluation over infinitely small arcs.

---

**THEOREM A.11**

If the maximum value of  $W(z)$  along a path  $C$  (not necessarily closed) is  $M$ , the maximum value of the integral of  $W(z)$  along  $C$

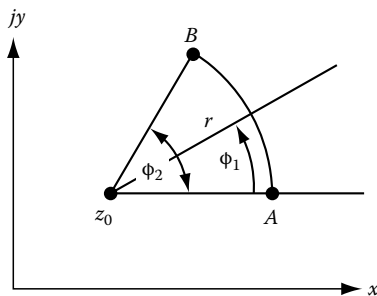


FIGURE A.11

is  $Ml$ , where  $l$  is the length of  $C$ . When expressed analytically, this specifies that

$$\left| \int_C W(z)dz \right| \leq Ml \quad (\text{A.58})$$

*Proof* The proof of this theorem is very simple if recourse is made to the definition of an integral. Thus, from Figure A.12

$$\left| \int_C W(z)dz \right| = \left| \lim_{n \rightarrow \infty} \sum_{s=1}^n W_s \Delta z_s \right| \leq M \lim_{n \rightarrow \infty} \sum_{s=1}^n |\Delta z_s| = Ml$$

---

**JORDAN'S LEMMA A.1**

If  $t < 0$  and

$$f(z) \rightarrow 0 \quad \text{as } z \rightarrow \infty \quad (\text{A.59})$$

then

$$\int_C e^{tz} f(z) dz \rightarrow 0 \quad \text{as } r \rightarrow \infty \quad (\text{A.60})$$

where  $C$  is the arc shown in Figure A.13a.

*Proof* We must assume that the angle of  $C$  does not exceed  $\pi$ ,  $0 \leq \arg z \leq \pi$ . This is not true if  $c < 0$ . However, the portion of  $C$  in the  $\text{Re } z < 0$  region will have length not exceeding  $\pi|c|$ . Hence, because of Equation A.59 the integration over this portion will tend to zero. From Equation A.59 it follows that, given  $\varepsilon > 0$ , we can find a constant  $r_0$  such that

$$|f(z)| < \varepsilon \quad \text{for } |z| > r_0$$

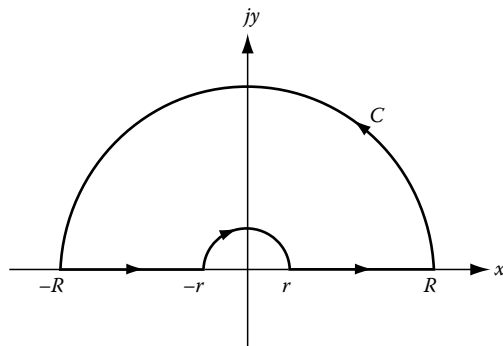


FIGURE A.12



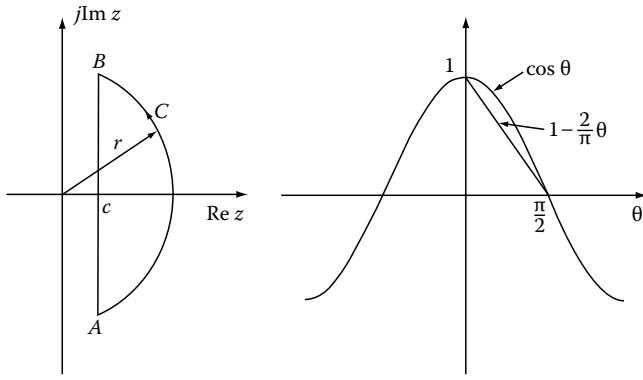


FIGURE A.13

Hence, with  $z = re^{j\theta}$ ,  $r > r_0$  we obtain ( $t < 0$ )

$$\begin{aligned} \left| \int_C e^{tz} f(z) dz \right| &= \left| \int_{-\pi/2}^{\pi/2} e^{tr(\cos \theta + j \sin \theta)} f(re^{j\theta}) j r e^{j\theta} d\theta \right| \\ &< \epsilon r \int_{-\pi/2}^{\pi/2} e^{tr \cos \theta} d\theta \leq \epsilon r 2 \int_0^{\pi/2} e^{tr(1-2\theta/\pi)} d\theta \\ &= \frac{\epsilon r \pi}{|t|r} (1 - e^{-t}) < \frac{\pi \epsilon}{|t|} \end{aligned}$$

Because  $\epsilon$  is arbitrarily small, the lemma is verified.

From the above lemma we conclude that if  $f(z)$  is analytic everywhere in the  $\text{Re } z \geq c$  region except at a number of poles, then

$$\int_{\text{Br}} e^{tz} f(z) dz = -2\pi j \sum_{k=1}^n \text{Res}_k \quad t < 0 \quad (\text{A.61})$$

where the Br stands for the Bromwich integration from  $c - j\infty$  to  $c + j\infty$ , which is the line  $AB$  in Figure A.13a.  $\text{Res}_k$  are the corresponding residues; the minus sign occurs because of the direction of integration along the Br line from  $B$  to  $A$ . The lemma can easily be extended for  $t > 0$  and  $C$  be an arc lying on the  $\text{Re } z < c$  plane. The residues are given by

$$\int_{\text{Br}} e^{tz} f(z) dz = 2\pi j \sum_{k=1}^n \text{Res}_k \quad t > 0 \quad (\text{A.62})$$

---

**THEOREM A.12 Mellin 1**

Let

- (a)  $\phi(z)$  be analytic in the strip  $\alpha < x < \beta$ , both alpha and beta being real
- (b)  $\int_{x-j\infty}^{x+j\infty} |\phi(z)| dz = \int_{-\infty}^{\infty} |\phi(x + jy)| dy$  converges

- (c)  $\phi(z) \rightarrow 0$  uniformly as  $|y| \rightarrow \infty$  in the strip  $\alpha < x < \beta$
- (d)  $\theta = \text{real and positive}$ : if

$$f(\theta) = \frac{1}{2\pi j} \int_{c-j\infty}^{c+j\infty} \theta^{-z} \phi(z) dz \quad (\text{A.63})$$

then

$$\phi(z) = \int_0^{\infty} \theta^{z-1} f(\theta) d\theta \quad (\text{A.64})$$

---

**THEOREM A.13 Mellin 2**

For  $\theta$  real and positive,  $\alpha < \text{Re } z < \beta$ , let  $f(\theta)$  be continuous or piecewise continuous, and integral (Equation A.64) be absolutely convergent. Then (Equation A.63) follows from (Equation A.64).

---

**THEOREM A.14 Mellin 3**

If in Equations A.63 and A.64 we write  $\theta = e^{-t}$ ,  $t$  being real, and in Equation A.64 put  $p$  for  $z$  and  $g(t)$  for  $f(e^{-t})$ , we get

$$g(t) = \frac{1}{2\pi j} \int_{c-j\infty}^{c+j\infty} e^{zt} \phi(z) dz \quad (\text{A.65})$$

$$\phi(p) = \int_{-\infty}^{\infty} e^{-pt} g(t) dt \quad (\text{A.66})$$

**A.7.1 Transformation of Contour**

To evaluate formally the integral

$$I = \int_0^a \cos xt \, dt \quad (\text{A.67})$$

we set  $v = xt$  that gives  $dx = dv/t$  and, thus,

$$I = \frac{1}{t} \int_0^{at} \cos v \, dv = \frac{\sin at}{t} \quad (\text{A.68})$$

Regarding this as a contour integral along the real axis for  $x = 0$  to  $a$ , the change to  $v = xt$  does not change the real axis. However, the contour is unaltered except in length.

Let  $t$  be real and positive. If we set  $z = \zeta t$  or  $\zeta = z/t$ , the contour in the  $\zeta$ -plane is identical in type with that in

the  $z$ -plane. If it were a circle of radius  $r$  in the  $z$ -plane, the contour in the  $\zeta$ -plane would be a circle of radius  $r/t$ . When  $t$  is complex  $z = r_1 e^{j\theta_1}$ ,  $t = r_2 e^{j\theta_2}$ , so  $\zeta = (r_1/r_2) e^{j(\theta_1-\theta_2)}$ ,  $r_1$ ,  $\theta_1$  being variables while  $r_2$  and  $\theta_2$  are fixed. If  $z = jy = |z| e^{j\pi/2} = |z| e^{j\pi/2}$  and if the phase of  $t$  was  $\theta_2 = \pi/4$  then the contour in the  $\zeta$ -plane would be a straight line at  $45^\circ$  with respect to the real axis. In effect, any figure in the  $z$ -plane transforms into a similar figure in the  $\zeta$ -plane, whose orientation and dimensions are governed by the factor  $1/t = e^{-j\theta_2}/r_2$ .

**Example A.21**

Make the transformation  $z = \zeta t$  to the integral  $I = \int_C e^{z/t} \frac{dz}{z}$ , where  $C$  is a circle of radius  $r_0$  around the origin.

**SOLUTION**

$dz/z = d\zeta/\zeta$  so  $I = \int_C e^{\zeta} \frac{d\zeta}{\zeta}$ , where  $C$  is a circle around the origin of radius  $r_0/r$  ( $r = |t|$ ).

**Example A.22**

Discuss the transformation  $z = (\zeta - a)$ ,  $a$  being complex and finite.

**SOLUTION**

This is equivalent to a shift of the origin to point  $z = -a$ . Neither the contour nor the position of the singularities are affected in relation to each other, so the transformation can be made without any alteration in technique.

**Example A.23**

Find the new contour due to transformation  $z = \zeta^2$  if the contour was the imaginary axis,  $z = jy$ .

**SOLUTION**

Choosing the positive square root we have  $\zeta = (jy)^{1/2}$  above and  $\zeta = (-jy)^{1/2}$  below the origin. Because

$$\sqrt{j} = (e^{j\pi/2})^{1/2} = e^{j\pi/4} \quad \text{and} \quad \sqrt{-j} = (e^{-j\pi/2})^{1/2} = e^{-j\pi/4}$$

the imaginary axis of the  $z$ -plane transforms to that in Figure A.14.

**Example A.24**

Evaluate the integral  $\int_C \frac{dz}{z}$ , where  $C$  is a circle of radius 4 units around the origin, under the transformation  $z = \zeta^2$ .

**SOLUTION**

The integral has a pole at  $z=0$  and its value is  $2\pi j$ . If we apply the transformation  $z = \zeta^2$  then  $dz = 2\zeta d\zeta$ . Also

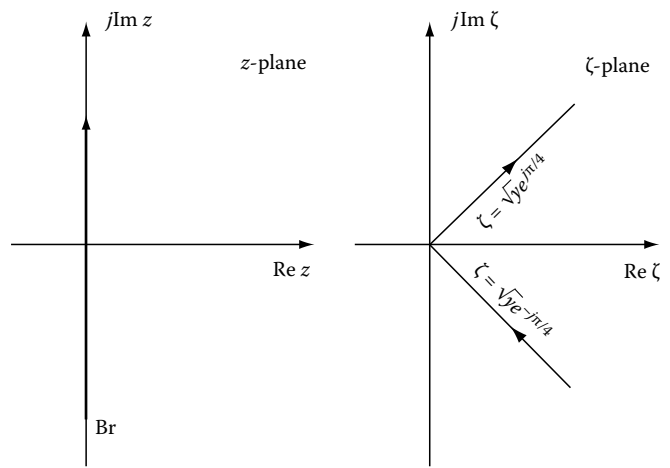


FIGURE A.14

$\zeta = \sqrt{z} = \sqrt{r} e^{j\theta/2}$  if we choose the positive root. From this relation we observe that as the  $z$  traces a circle around the origin, the  $\zeta$  traces a half-circle from 0 to  $\pi$ . Hence, the integral becomes

$$2 \int_C \frac{d\zeta}{\zeta} = 2 \int_0^\pi \frac{\rho j e^{j\theta}}{\rho e^{j\theta}} d\theta = 2\pi j$$

as was expected.

## A.8 The Bromwich Contour

The Bromwich contour takes the form

$$f(t) = \frac{1}{2\pi j} \int_{c-j\infty}^{c+j\infty} e^{zt} F(z) dz \tag{A.69}$$

where  $F(z)$  is a function of  $z$ , all of whose singularities lie on the left of the path, and  $t$  is the time, which is always real and positive,  $t > 0$ .

### A.8.1 Finite Number of Poles

Let us assume that  $F(z)$  has  $n$  poles at  $p_1, p_2, \dots, p_n$  and no other singularities; this case includes the important case of *rational transforms*. To utilize the Cauchy's integral theorem, we must express  $f(t)$  as an integral along a closed contour. Figure A.15 shows such a situation. We know from Jordan's lemma (see Section A.7) that if  $F(z) \rightarrow 0$  as  $|z| \rightarrow \infty$  on the contour  $C$  then for  $t > 0$

$$\lim_{R \rightarrow \infty} \int_C e^{tz} F(z) dz \rightarrow 0 \quad t > 0 \tag{A.70}$$

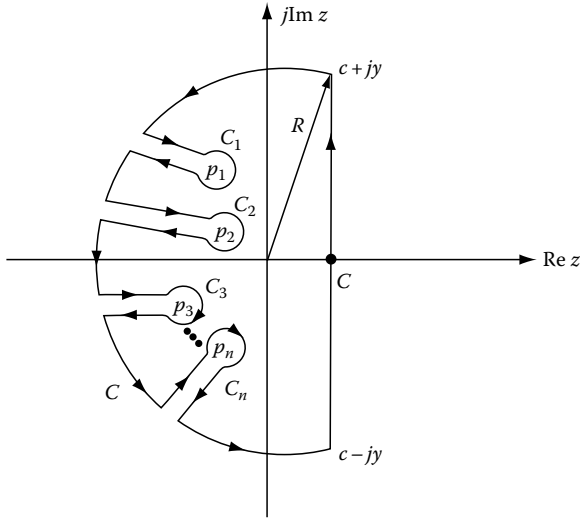


FIGURE A.15

and because

$$\int_{c-jy}^{c+jy} e^{tz} F(z) dz \rightarrow \int_{Br} e^{tz} F(z) dz \quad y \rightarrow \infty \quad (\text{A.71})$$

we conclude that  $f(t)$  can be written as a limit,

$$f(t) \xrightarrow{R \rightarrow \infty} \frac{1}{2\pi j} \int_C e^{zt} F(z) dz \quad (\text{A.72})$$

of an integral along the closed path as shown in Figure A.15. If we make  $R$  large enough to contain all the poles of  $F(z)$  then the integral along  $C$  is independent of  $R$ . Therefore, we write

$$f(t) = \frac{1}{2\pi j} \int_C e^{zt} F(z) dz \quad (\text{A.73})$$

Using Cauchy's theorem it follows that

$$\int_C e^{zt} F(z) dz = \sum_{k=1}^n \int_{C_k} e^{zt} F(z) dz \quad (\text{A.74})$$

where  $C_k$ 's are the contours around each pole.

1. For simple poles we obtain

$$f(t) = \sum_{k=1}^n F_k(z_k) e^{z_k t} \quad t > 0 \quad (\text{A.75})$$

$$F_k(z_k) = F(z)(z - z_k)|_{z=z_k}$$

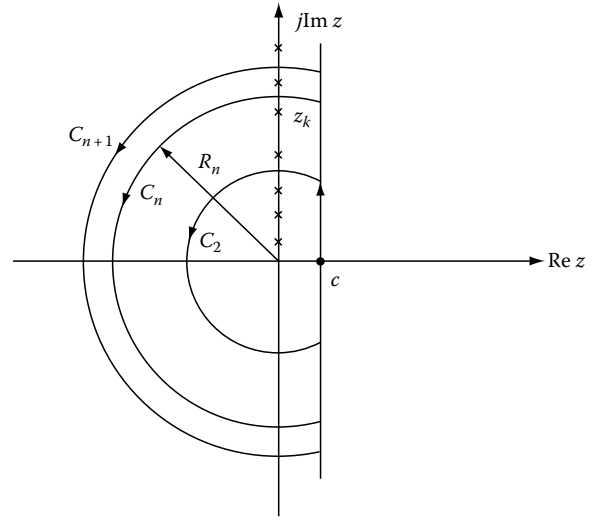


FIGURE A.16

2. For a multiple pole of  $m + 1$  multiplicity, we obtain

$$\begin{aligned} \int_{C_k} e^{zt} F(z) dz &= \int_{C_k} \frac{e^{zt} F_k(z)}{(z - z_k)^{m+1}} dz \\ &= \frac{2\pi j}{m!} \frac{d^m}{dz^m} [e^{zt} F_k(z)]|_{z=z_k} \end{aligned} \quad (\text{A.76})$$

3. Infinitely many poles (see Figure A.16).

If we can find circular arcs with radii tending to infinity such that

$$F(z) \rightarrow 0 \quad \text{as } z \rightarrow \infty \quad \text{on } C_n \quad (\text{A.77})$$

Applying Jordan's lemma to the integral along those arcs, we obtain

$$\int_{C_n} e^{zt} F(z) dz \xrightarrow{n \rightarrow \infty} 0 \quad t > 0 \quad (\text{A.78})$$

and with  $C_n'$  the closed curve, consisting of  $C_n$  and the vertical line  $\text{Re } z = c$ , we obtain

$$f(t) = \lim_{n \rightarrow \infty} \frac{1}{2\pi j} \int_{C_n'} e^{zt} F(z) dz \quad t > 0 \quad (\text{A.79})$$

Hence, for simple poles  $z_1, z_2, \dots, z_n$  of  $F(z)$ , we obtain

$$f(t) = \sum_{k=1}^{\infty} F_k(z_k) e^{z_k t} \quad (\text{A.80})$$

where  $F_k(z) = F(z)(z - z_k)$ .

**Example A.25**

Find  $f(t)$  from its transformed value  $F(z) = 1/(z \cosh az)$ ,  $a > 0$ .

**SOLUTION**

The poles of the above function are

$$z_0 = 0, \quad z_k = \pm j \frac{(2k-1)\pi}{2a} \quad k = 1, 2, 3, \dots$$

We select the arcs  $C_n$  such that their radii are  $R_n = jn\pi$ . It can be shown that  $1/\cosh az$  is bounded on  $C_n$  and, therefore,  $1/(z \cosh az) \rightarrow 0$  as  $z \rightarrow \infty$  on  $C_n$ . Hence,

$$zF(z)|_{z=0} = 1, \quad (z - z_k)F(z)|_{z=z_k} = \frac{(-1)^k 2}{(2k-1)\pi}$$

and from Equation A.80 we obtain

$$\begin{aligned} f(t) &= 1 + \frac{2}{\pi} \sum_{k=1}^{\infty} \frac{(-1)^k}{2k-1} e^{z_k t} + \frac{2}{\pi} \sum_{k=1}^{\infty} \frac{(-1)^k}{2k-1} e^{-z_k t} \\ &= 1 + \frac{4}{\pi} \sum_{k=1}^{\infty} \frac{(-1)^k}{2k-1} \cos \frac{(2k-1)\pi t}{2a} \end{aligned}$$

**A.8.2 Branch Points and Branch Cuts**

The singularities that have been considered are those points at which  $|W(z)|$  ceases to be finite. At a branch point the absolute value of  $W(z)$  may be finite but  $W(z)$  is not single-valued, and hence is not regular. One of the simplest functions with these properties is

$$W_1(z) = z^{1/2} = \sqrt{r}e^{j\theta/2} \tag{A.81}$$

which takes on two values for each value of  $z$ , one the negative of the other depending on the choice of  $\theta$ . This follows because we can write an equally valid form for  $z^{1/2}$  as

$$W_2(z) = \sqrt{r}e^{j(\theta+2\pi)/2} = -\sqrt{r}e^{j\theta/2} = -W_1(z) \tag{A.82}$$

Clearly,  $W_1(z)$  is not continuous at points on the positive real axis because

$$\lim_{\theta \rightarrow 2\pi} (\sqrt{r}e^{j\theta/2}) = -\sqrt{r} \text{ while } \lim_{\theta \rightarrow 0} (\sqrt{r}e^{j\theta/2}) = \sqrt{r}$$

Hence,  $W'(z)$  does not exist when  $z$  is real and positive. However, the branch  $W_1(z)$  is analytic in the region  $0 \leq \theta < 2\pi$ ,  $r \rightarrow 0$ . The part of the real axis where  $x \geq 0$  is called a *branch cut* for the branch  $W_1(z)$  and the branch is analytic except at points on the cut. Hence, the cut is a boundary introduced so that the corresponding branch is single valued and analytic throughout the open region bounded by the cut.

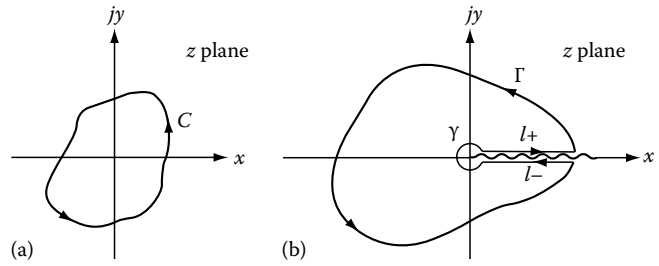


FIGURE A.17

Suppose that we consider the function  $W(z) = z^{1/2}$  and contour  $C$ , as shown in Figure A.17a, which encloses the origin. Clearly, after one complete circle in the positive direction enclosing the origin,  $\theta$  is increased by  $2\pi$ , given a value of  $W(z)$  that changes from  $W_1(z)$  to  $W_2(z)$ ; that is, the function has changed from one branch to the second. To avoid this and to make the function analytic, the contour  $C$  is replaced by a contour  $\Gamma$ , which consists of a small circle  $\gamma$  surrounding the branch point, a semi-infinite cut connecting the small circle and  $C$ , and  $C$  itself (as shown in Figure A.17b). Such a contour, which avoids crossing the branch cut, ensures that  $W(z)$  is single valued. Because  $W(z)$  is single valued and excludes the origin, we would write for this composite contour  $C$

$$\int_C W(z) dz = \int_{\Gamma} + \int_{l^-} + \int_{\gamma} + \int_{l^+} = 2\pi j \sum \text{Res} \tag{A.83}$$

The evaluation of the function along the various segments of  $C$  proceeds as before.

**Example A.26**

If  $0 < a < 1$ , show that

$$\int_0^{\infty} \frac{x^{a-1}}{1+x} dx = \frac{\pi}{\sin a\pi}$$

**SOLUTION**

Consider the integral

$$\oint_C \frac{z^{a-1}}{1+z} dz = \int_{\Gamma} + \int_{l^-} + \int_{\gamma} + \int_{l^+} = I_1 + I_2 + I_3 + I_4 = 2\pi j \sum \text{Res}$$

which we will evaluate using the contour shown in Figure A.18. Under the conditions

$$\begin{aligned} \left| \frac{z^a}{1+z} \right| &\rightarrow 0 \text{ as } |z| \rightarrow 0 \text{ if } a > 0 \\ \left| \frac{z^a}{z+1} \right| &\rightarrow 0 \text{ as } |z| \rightarrow \infty \text{ if } a < 1 \end{aligned}$$

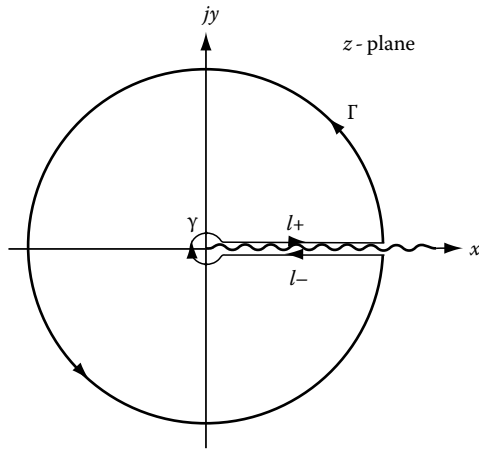


FIGURE A.18

the integral becomes by Equation A.56

$$\int_{\Gamma} \rightarrow 0 \quad \int_{l-} = -e^{2\pi ja} \int_0^{\infty}$$

by Equation A.57

$$\int_{\gamma} \rightarrow 0 \quad \int_{l+} = 1 \int_0^{\infty}$$

Thus

$$(1 - e^{2\pi ja}) \int_0^{\infty} \frac{x^{a-1}}{1+x} dx = 2\pi j \sum \text{Res}$$

Further, the residue at the pole  $z = -1$ , which is enclosed, is

$$\lim_{z \rightarrow -1} (1+z) \frac{z^{a-1}}{1+z} = e^{j\pi(a-1)} = -e^{j\pi a}$$

Therefore,

$$\int_0^{\infty} \frac{x^{a-1}}{x+1} dx = 2\pi j \frac{e^{j\pi a}}{e^{j\pi a} - 1} = \frac{\pi}{\sin \pi a}$$

If, for example, we have the integral  $(1/2\pi j) \int_{Br_1} \frac{e^{at} dz}{z^{v+1}}$  to evaluate with  $\text{Re } v > -1$  and  $t$  real and positive, we observe that the integral has a branch point at the origin if  $v$  is a nonintegral constant. Because the integral vanishes along the arcs as  $R \rightarrow \infty$ , the equivalent contour can assume the form depicted in Figure A.19a and marked  $Br_2$ . For the contour made up of  $Br_1, Br_2$ , the arc is closed and contains no singularities and, hence, the integral around the contour is zero. Because the arcs do not contribute any value, provided  $\text{Re } v > -1$ , the integral along  $Br_1$  is equal to that along  $Br_2$ , both being described positively. The angle  $\gamma$  between the barrier and the positive real axis may have any value between  $\pi/2$  and  $3\pi/2$ . When the only singularity is a branch point at the origin, the contour of Figure A.19b is an approximate one.

**Example A.27**

Evaluate the integral  $I = \frac{1}{2\pi j} \int_{Br_2} \frac{e^z dz}{\sqrt{z}}$ , where  $Br_2$  is the contour shown in Figure A.19b.

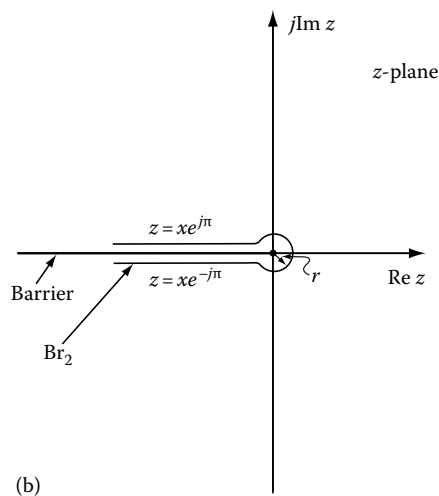
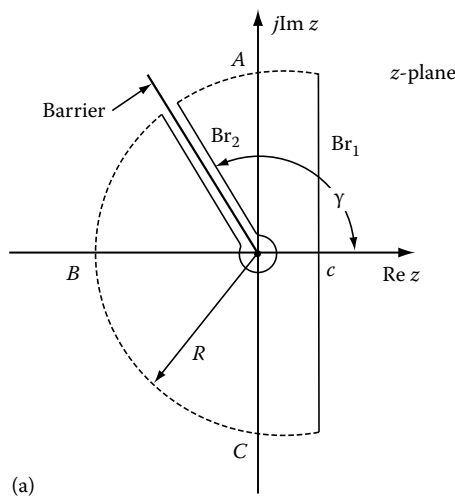


FIGURE A.19

**SOLUTION**

1. Write  $z = re^{j\theta}$  on the circle. Hence, we get

$$I_1 = \frac{1}{2\pi j} \int_{-\pi}^{\pi} \frac{e^{re^{j\theta}} d(re^{j\theta})}{\sqrt{re^{j\theta/2}}} = \frac{\sqrt{r}}{2\pi} \int_{-\pi}^{\pi} r^{(\cos\theta + j\sin\theta) + j\theta/2} d\theta$$

2. On the line below the barrier  $z = x \exp(-j\pi)$  where  $x = |x|$ . Hence, the integral becomes

$$I_2 = \frac{1}{2\pi j} \int_{\infty}^r \frac{e^{xe^{-j\pi}} d(xe^{-j\pi})}{\sqrt{x}e^{-j\pi/2}} = \frac{1}{2\pi} \int_r^{\infty} e^{-x} x^{-1/2} dx$$

3. On the line above the barrier  $z = x \exp(j\pi)$  and, hence,

$$I_3 = \frac{1}{2\pi j} \int_r^{\infty} \frac{e^{xe^{j\pi}} d(xe^{j\pi})}{\sqrt{x}e^{j\pi/2}} = \frac{1}{2\pi} \int_r^{\infty} e^{-x} x^{-1/2} dx$$

Hence, we have

$$I_2 + I_3 = \frac{1}{\pi} \int_r^{\infty} e^{-x} x^{-1/2} dx$$

As  $r \rightarrow 0$ ,  $I_1 \rightarrow 0$  and, hence,

$$I = I_1 + I_2 + I_3 = \frac{1}{\pi} \int_0^{\infty} e^{-x} x^{-1/2} dx = \frac{\Gamma(\frac{1}{2})}{\pi} \frac{\sqrt{\pi}}{\pi} = \frac{1}{\sqrt{\pi}}$$

**Example A.28**

Evaluate the integral  $f(t) = \frac{1}{2\pi j} \int_{Br} \frac{e^{zt} e^{-a\sqrt{z}}}{\sqrt{z}} dz, a > 0$  (see Figure A.20).

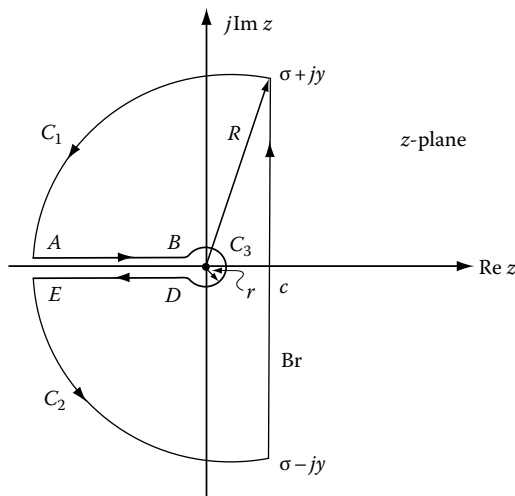


FIGURE A.20

**SOLUTION**

The origin is a point branch and we select the negative axis as the barrier. We select the positive of  $\sqrt{z}$  when  $z$  takes positive real values in order that the integral vanishes as  $z$  approaches infinity in the region  $\text{Re } z > \gamma$ , where  $\gamma$  indicates the region of convergence,  $\gamma \leq c$ . Hence, we obtain

$$z = re^{j\theta} - \pi < \theta \leq \pi \quad \sqrt{z} = \sqrt{r}e^{j\theta/2} \quad (\text{A.84})$$

The curve  $C = Br + C_1 + C_2 + C_3$  encloses a region with no singularities and, therefore, Cauchy's theorem applies (the integrand is analytic in the region). Hence,

$$\int_C e^{zt} \frac{e^{-a\sqrt{z}}}{\sqrt{z}} dz = 0 \quad (\text{A.85})$$

It is easy to see that the given function converges to zero as  $R$  approaches infinity and therefore the integration over  $C_1 + C_2$  does not contribute any value. For  $z$  on the circle, we obtain

$$\left| \frac{e^{-a\sqrt{z}}}{\sqrt{z}} \right| \rightarrow 0$$

Therefore, for fixed  $t > 0$ , we obtain

$$\left| \int_{C_3} e^{zt} \frac{e^{-a\sqrt{z}}}{\sqrt{z}} dz \right| \leq 2\pi r \frac{e^{rt}}{\sqrt{r}} = \lim_{r \rightarrow 0} 2\pi r \frac{e^{rt}}{\sqrt{r}} = 0$$

because

$$\left| \int_C f(z) dz \right| \leq ML$$

where  $L$  is the length of the contour and  $|f(z)| < M$  for  $z$  on  $C$ .

On  $AB, z = -x, \sqrt{z} = j\sqrt{x}$ , and on  $DE, z = -x, \sqrt{z} = -j\sqrt{x}$ . Therefore, we obtain

$$\int_{AB+DE} e^{zt} \frac{e^{-a\sqrt{z}}}{\sqrt{z}} dz \rightarrow_{R \rightarrow \infty} - \int_0^R e^{-xt} \frac{e^{ja\sqrt{x}}}{j\sqrt{x}} dx - \int_0^{\infty} e^{-xt} \times \frac{e^{-ja\sqrt{x}}}{-j\sqrt{x}} dx \quad (\text{A.86})$$

But from Equation A.69

$$\int_{Br} e^{zt} \frac{e^{-a\sqrt{z}}}{\sqrt{z}} dz = 2\pi j f(t) \quad (\text{A.87})$$

and, hence, Equations A.85 and A.87 reduce to

$$f(t) + \frac{1}{2\pi j} \int_0^{\infty} e^{-xt} \frac{e^{ja\sqrt{x}} + e^{-ja\sqrt{x}}}{j\sqrt{x}} dx = 0 \quad (\text{A.88})$$

If we set  $x = y^2$ , we have

$$\int_0^\infty e^{-xt} \frac{\cos a\sqrt{x}}{\sqrt{x}} dx = 2 \int_0^\infty e^{-y^2t} \cos ay dy \quad (A.89)$$

But (see Fourier transform of Gaussian function, Chapter 3)

$$2 \int_0^\infty e^{-y^2t} \cos ay dy = \sqrt{\frac{\pi}{t}} e^{-a^2/4t} \quad (A.90)$$

and, hence, Equation A.89 becomes

$$f(t) = \frac{1}{\sqrt{\pi t}} e^{-a^2/4t} \quad (A.91)$$

**Example A.29**

Evaluate the integral  $I = \frac{1}{2\pi j} \int_C \frac{e^{xz}}{\sqrt{z^2-1}}$  where  $C$  is the contour shown in Figure A.21.

**SOLUTION**

The Br contour is equivalent to the dumbbell-type contour shown in Figure A.21,  $B_1B_2A_2A_1B_1$ . Set the phase along the line  $A_2A_1$  equal to zero (it can also be set equal to  $\pi$ ). Then on  $A_2A_1$   $z = x$  from  $+1$  to  $-1$ . Hence, we have

$$I_1 = \frac{1}{2\pi j} \int_1^{-1} \frac{e^{xt}}{\sqrt{x^2-1}} dx = \frac{1}{2\pi} \int_{-1}^1 \frac{e^{xt}}{\sqrt{1-x^2}} dx \quad |x| < 1 \quad (A.92)$$

By passing around the  $z = -1$  point the phase changes by  $\pi$  and, hence, on  $B_1B_2$   $z = x \exp(2\pi j)$ . The change by  $2\pi$  is due

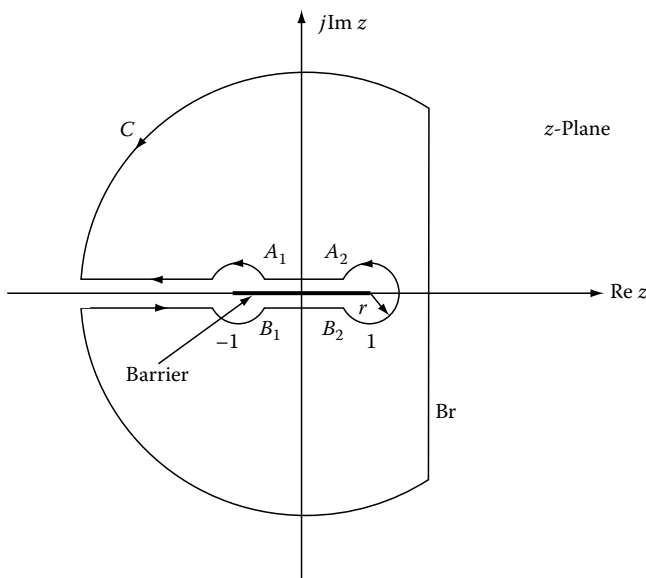


FIGURE A.21

to the complete transversal of the contour that contains two branch points. Hence, we obtain

$$I_2 = -\frac{1}{2\pi j} \int_{-1}^1 \frac{e^{xt}}{\sqrt{x^2-1}} dx = \frac{1}{2\pi} \int_{-1}^1 \frac{e^{xt}}{\sqrt{1-x^2}} dx \quad (A.93)$$

Changing the origin to  $-1$ , we set  $\zeta = z + 1$  or  $z = \zeta - 1$ , which gives

$$I_3 = \frac{e^{-t}}{2\pi j} \int \frac{e^{\zeta t}}{\sqrt{[(\zeta-2)\zeta]}} d\zeta \quad (A.94)$$

On the small circle with  $z = -1$  as center,  $\zeta = r \exp(j\theta)$  and we get

$$I_3 = \frac{e^{-t}}{2\pi} \int_{\pi}^{-\pi} \frac{e^{t(\cos\theta + j\sin\theta) + (j\theta/2)} \sqrt{r} d\theta}{\sqrt{r e^{j\theta} - 2}} \quad (A.95)$$

When  $\theta = 0$  the integrand has the value  $+\sqrt{r} e^t / \sqrt{r-2}$ ; and for  $\theta = 2\pi$  the value is  $-\sqrt{r} e^t / \sqrt{r-2}$ . Therefore, the integrand changes sign in rounding the branch point at  $z = -1$ . Similarly for the branch point at  $z = 1$ , where the change is from  $-$  to  $+$ . As  $r \rightarrow 0$ ,  $I_3 \rightarrow 0$ , and thus  $I_3$  vanishes. The same is true for the branch point at  $z = -1$ . Therefore, by setting  $x = \cos \theta$  we obtain

$$\begin{aligned} I &= I_1 + I_2 = \frac{1}{\pi} \int_{-1}^1 \frac{e^{xt}}{\sqrt{1-x^2}} dx = \frac{1}{\pi} \int_0^\pi e^{t \cos \theta} d\theta = \frac{1}{\pi} \int_0^\pi \sum_{k=0}^\infty \frac{(t \cos \theta)^k}{k!} d\theta \\ &= \frac{1}{\pi} \left[ \pi + \pi \frac{t^2}{2!} + \pi \frac{3! t^4}{4!} + \pi \frac{5! t^6}{6!} + \dots \right] \\ &= 1 + \frac{t^2}{2^2} + \frac{t^4}{2^2 4^2} + \frac{t^6}{2^2 4^2 6^2} + \dots = \sum_{k=0}^\infty \frac{(\frac{1}{2}t)^{2k}}{(k!)^2} = I_0(t) \end{aligned} \quad (A.96)$$

where  $I_0(t)$  is the modified Bessel function of the first kind and zero order.

**Example A.30**

Evaluate the integral  $I = \int_C \frac{e^{zt}}{\sqrt{z^2+1}}$  where  $C$  is the closed contour shown in Figure A.22.

**SOLUTION**

The Br contour is equal to the dumbbell-type contour as shown in Figure A.22,  $A B G D A = C_1$ . Hence, we have

$$f(t) = \frac{1}{2\pi j} \int_{C_1} \frac{e^{zt}}{\sqrt{z^2+1}} dz \quad (A.97)$$

But

$$\left| \frac{e^{zt}}{\sqrt{z^2+1}} \right| < \frac{e^t}{\sqrt{r}\sqrt{2-r}}$$

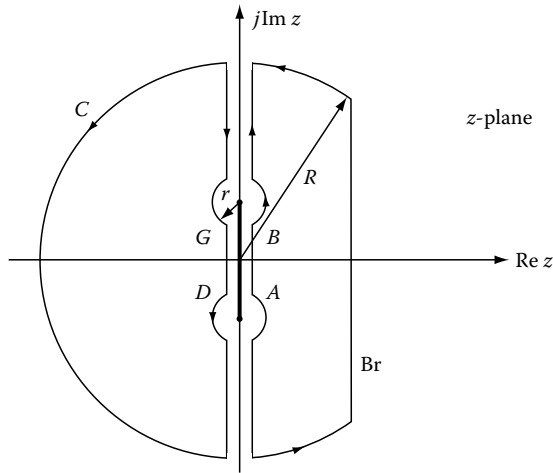


FIGURE A.22

on the circle on the  $+j$  branch point and, therefore, for  $t > 0$

$$\left| \int \frac{e^{zt}}{\sqrt{z^2 + 1}} dz \right| < \frac{2\pi\sqrt{r}e^{rt}}{\sqrt{2-r}} \rightarrow 0 \text{ as } r \rightarrow 0$$

We obtain similar results for the contour around the  $-j$  branch point. However,

$$\begin{aligned} \text{On } AB, z = j\omega, \sqrt{1+z^2} = \sqrt{1-\omega^2}; \text{ on } GD, z = j\omega, \sqrt{1+z^2} \\ = -\sqrt{1-\omega^2} \end{aligned}$$

and, therefore, for  $t > 0$  we obtain

$$\begin{aligned} f(t) &= \frac{j}{2\pi j} \int_{-1}^1 \frac{e^{j\omega t}}{\sqrt{1-\omega^2}} d\omega + \frac{j}{2\pi j} \int_1^{-1} \frac{e^{j\omega t}}{-\sqrt{1-\omega^2}} d\omega \\ &= \frac{1}{\pi} \int_{-1}^1 \frac{\cos \omega t}{\sqrt{1-\omega^2}} d\omega \end{aligned}$$

If we set  $\omega = \sin \theta$  (see also Chapter 1)

$$f(t) = \frac{1}{\pi} \int_{-\pi/2}^{\pi/2} \cos(t \sin \theta) d\theta = J_0(t)$$

where  $J_0(t)$  is the Bessel function of the first kind.

## A.9 Evaluation of Definite Integrals

The principles discussed above find considerable applicability in the evaluation of certain definite real integrals. This is a common application of the developed theory, as it is often extremely difficult to evaluate some of these real integrals by other methods. We employ such methods in the evaluation of Fourier integrals. In practice the given integral is replaced by

a complex function that yields the specified integrand in its appropriate limit. The integration is then carried out in the complex plane, with the real integral being extracted for the required result. The following several examples show this procedure.

### A.9.1 Evaluation of the Integrals of Certain Periodic Functions (0 to $2\pi$ )

An integral of the form

$$I = \int_0^{2\pi} F(\cos \theta, \sin \theta) d\theta \tag{A.98}$$

where the integral is a *rational function* of  $\cos \theta$  and  $\sin \theta$  finite on the range of integration, and can be integrated by setting  $z = \exp(j\theta)$ ,

$$\cos \theta = \frac{1}{2}(z + z^{-1}), \quad \sin \theta = \frac{1}{2j}(z - z^{-1}) \tag{A.99}$$

The integral (Equation A.98) takes the form

$$I = \int_C F(z) dz \tag{A.100}$$

where  $F(z)$  is a rational function of  $z$  finite on  $C$ , which is a circle of radius unity with center at the origin.

#### Example A.31

If  $0 < a < 1$ , find the value of the integral

$$I = \int_0^{2\pi} \frac{d\theta}{1 - 2a \cos \theta + a^2} \tag{A.101}$$

#### SOLUTION

Introducing Equation A.99 in A.101 we obtain

$$I = \int_C \frac{dz}{j(1 - az)(z - a)} \tag{A.102}$$

The only pole inside the unit circle is at  $a$ . Therefore, by residue theory we have

$$I = 2\pi j \lim_{z \rightarrow a} \frac{z - a}{j(1 - az)(z - a)} = \frac{2\pi}{1 - a^2}$$



### A.9.2 Evaluation of Integrals with Limits $-\infty$ and $+\infty$

We can evaluate the integral  $I = \int_{-\infty}^{\infty} F(x) dx$  provided that the function  $F(z)$  satisfies the following properties.

1. It is analytic when the imaginary part of  $z$  is positive or zero (except at a finite number of poles).
2. It has no poles on the real axis.
3. As  $|z| \rightarrow \infty$ ,  $zF(z) \rightarrow 0$  uniformly for all value of  $\arg z$  such that  $0 \leq \arg z \leq \pi$ , provided that when
4.  $x$  is real,  $xF(x) \rightarrow 0$  as  $x \rightarrow \pm\infty$ , in such a way that  $\int_0^{\infty} F(x) dx$  and  $\int_{-\infty}^0 F(x) dx$  both converge.

The integral is given by

$$I = \int_C F(z) dz = 2\pi j \sum \text{Res} \quad (\text{A.103})$$

where the contour is the real axis and a semicircle having its center in the origin and lying above the real axis.

#### Example A.32

Evaluate the integral  $I = \int_{-\infty}^{\infty} \frac{dx}{(x^2+1)^3}$ .

#### SOLUTION

The integral becomes

$$I = \int_C \frac{dz}{(z^2+1)^3} = \int_C \frac{dz}{(z+j)^3(z-j)^3}$$

which has one pole at  $j$  of order three (see Equation A.50). Hence, we obtain

$$I = \frac{1}{2!} \frac{d^2}{dz^2} \left[ \frac{1}{(z+j)^3} \right] \Big|_{z=j} = -j \frac{3}{16}$$

#### Example A.33

Evaluate the integral  $I = \int_0^{\infty} \frac{dx}{x^2+1}$ .

#### SOLUTION

The integral becomes

$$I = \int_C \frac{dz}{z^2+1}$$

where  $C$  is the contour of the real axis and the upper semicircle. From  $z^2+1=0$  we obtain  $z = \exp(j\pi/2)$  and  $z = \exp(-j\pi/2)$ . Only the pole  $z = \exp(j\pi/2)$  exists inside the contour. Hence, we obtain

$$2\pi j \lim_{z \rightarrow e^{j\pi/2}} \left( \frac{z - e^{j\pi/2}}{(z - e^{j\pi/2})(z - e^{-j\pi/2})} \right) = \pi$$

Therefore, we have

$$\int_{-\infty}^{\infty} \frac{dx}{x^2+1} = 2 \int_0^{\infty} \frac{dx}{x^2+1} = \pi \quad \text{or} \quad I = \frac{\pi}{2}$$

### A.9.3 Certain Infinite Integrals Involving Sines and Cosines

If  $F(z)$  satisfies conditions (1), (2), and (3) above, and if  $m > 0$ , then  $F(z)e^{jmx}$  also satisfies the same conditions. Hence,  $\int_0^{\infty} [F(x)e^{jmx} + F(-x)e^{-jmx}] dx$  is equal to  $2\pi j \sum \text{Res}$ , where  $\sum \text{Res}$  means the sum of the residues of  $F(z)e^{jmx}$  at its poles in the upper half-plane. Therefore,

1. If  $F(x)$  is an even function; that is,  $F(x) = F(-x)$ , then

$$\int_0^{\infty} F(x) \cos mx dx = j\pi \sum \text{Res} \quad (\text{A.104})$$

2. If  $F(x)$  is an odd function; that is,  $F(x) = -F(-x)$ , then

$$\int_0^{\infty} F(x) \sin mx dx = \pi \sum \text{Res} \quad (\text{A.105})$$

#### Example A.34

Evaluate the integral  $I = \int_0^{\infty} \frac{\cos x}{x^2+a^2} dx, a > 0$ .

#### SOLUTION

Consider the integral

$$I_1 = \int_C \frac{e^{jz}}{z^2+a^2} dz$$

where the contour is the real axis and the infinite semicircle on the upper side with respect to the real axis. The contour encircles the pole  $ja$ . Hence,

$$\int_C \frac{e^{jz}}{z^2+a^2} dz = 2\pi j \frac{e^{jja}}{2ja} = \frac{\pi}{a} e^{-a}$$

However,

$$\int_{-\infty}^{\infty} \frac{e^{jz}}{z^2+a^2} dz = \int_{-\infty}^{\infty} \frac{\cos x}{x^2+a^2} dx + j \int_{-\infty}^{\infty} \frac{\sin x}{x^2+a^2} dx = \int_{-\infty}^{\infty} \frac{\cos x}{(x^2+a^2)} dx$$

because the integrand of the third integral is odd and therefore is equal to zero. From the last two equations we find that

$$I = \int_{-\infty}^{\infty} \frac{\cos x}{x^2 + a^2} dx = \frac{\pi}{2a} e^{-a}$$

because the integrand is an even function.

**Example A.35**

Evaluate the integral  $I = \int_0^{\infty} \frac{x \sin ax}{x^2 + b^2} dx, k > 0$  and  $a > 0$ .

**SOLUTION**

Consider the integral

$$I_1 = \int_C \frac{ze^{jaz}}{z^2 + b^2} dz$$

where  $C$  is the same type of contour as in Example A.34. Because there is only one pole at  $z = jb$  in the upper half of the  $z$ -plane, then

$$I_1 = \int_{-\infty}^{\infty} \frac{ze^{jaz}}{z^2 + b^2} dz = 2\pi j \frac{jbe^{jab}}{2jb} = j\pi e^{-ab}$$

Because the integrand  $x \sin ax / (x^2 + b^2)$  is an even function, we obtain

$$I_1 = j \int_{-\infty}^{\infty} \frac{x \sin ax}{x^2 + b^2} dx = j\pi e^{-ab} \quad \text{or} \quad I = \frac{\pi}{2} e^{-ab}$$

**Example A.36**

Show that  $\int_{-\infty}^{\infty} \frac{x \sin \pi x}{x^2 + 2x + 5} dx = -\pi e^{-2\pi}$ .

**INTEGRALS OF THE FORM**  $\int_0^{\infty} x^{\alpha-1} f(x) dx, 0 < \alpha < 1$

It can be shown that the above integral has the value

$$I = \int_0^{\infty} x^{\alpha-1} f(x) dx = \frac{2\pi j}{1 - e^{j2\pi\alpha}} \sum_{k=1}^N \text{Res}[z^{\alpha-1} f(z)]_{z=z_k} \quad (\text{A.106})$$

where  $f(z)$  has  $N$  singularities and  $z^{\alpha-1} f(z)$  has a branch point at the origin.

**Example A.37**

Evaluate the integral  $I = \int_0^{\infty} \frac{x^{-1/2}}{x+1} dx$

**SOLUTION**

Because  $x^{-1/2} = x^{1/2-1}$ , it is simplified that  $\alpha = 1/2$ . From the integrand we observe that the origin is a branch point and the  $f(x) = 1/(x + 1)$  has a pole at  $-1$ . Hence, from Equation A.106 we obtain

$$I = \frac{2\pi j}{1 - e^{j2\pi/2}} \text{Res} \left[ \frac{z^{-1/2}}{z+1} \right]_{z=-1} = \frac{2\pi j}{j(1 - e^{j\pi})} = \pi$$

We can also proceed by considering the integral  $I = \int_C \frac{z^{-1/2}}{z+1} dz$ . Because  $z=0$  is a branch point, we choose the contour  $C$  as shown in Figure A.23. The integrand has a simple pole at  $z = -1$  inside the contour  $C$ . Hence, the residue at  $z = -1 = \exp(j\pi)$  and is

$$\text{Res}|_{z=-1} = \lim_{z \rightarrow -1} (z+1) \frac{z^{-1/2}}{z+1} = e^{-j\pi/2}$$

Therefore, we write

$$\oint_C \frac{z^{-1/2}}{z+1} dz = \int_{AB} + \int_{BDEFG} + \int_{GH} + \int_{HJA} = e^{-j\pi/2}$$

The above integrals take the following form:

$$\int_{\epsilon}^R \frac{x^{-1/2}}{x+1} dx + \int_0^{2\pi} \frac{(\text{Re}^{j\theta})^{-1/2} j \text{Re}^{j\theta} d\theta}{1 + \text{Re}^{j\theta}} + \int_R^{\epsilon} \frac{(xe^{j2\pi})^{-1/2}}{1 + xe^{j2\pi}} dx + \int_{2\pi}^0 \frac{(\epsilon e^{j\theta})^{-1/2} j \epsilon e^{j\theta} d\theta}{1 + \epsilon e^{j\theta}} = j2\pi e^{-j\pi/2}$$

where we have used  $z = x \exp(j2\pi)$  for the integral along  $GH$ , because the argument of  $z$  is increased by  $2\pi$  in going around the circle  $BDEFG$ .

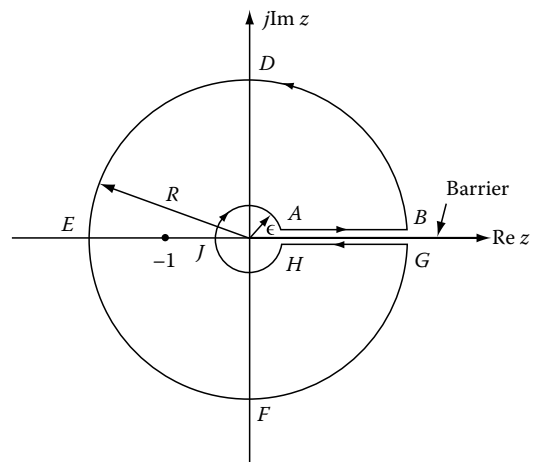


FIGURE A.23

Taking the limit as  $\epsilon \rightarrow 0$  and  $R \rightarrow \infty$  and noting that the second and fourth integrals approach zero, we find

$$\int_0^{\infty} \frac{x^{-1/2}}{x+1} dx + \int_{\infty}^0 \frac{e^{-j2\pi/2} x^{-1/2}}{x+1} dx = j2\pi e^{-j\pi/2}$$

or

$$(1 - e^{-j\pi}) \int_0^{\infty} \frac{x^{-1/2}}{x+1} dx = j2\pi e^{-j\pi/2} \quad \text{or}$$

$$\int_0^{\infty} \frac{x^{-1/2}}{x+1} dx = \frac{j2\pi(-j)}{2} = \pi$$

### A.9.4 Miscellaneous Definite Integrals

The following examples will elucidate some of the approaches that have been used to find the values of definite integrals.

#### Example A.38

Evaluate the integral  $I = \int_{-\infty}^{\infty} \frac{1}{x^2+a^2} dx, a > 0$ .

#### SOLUTION

We write (see Figure A.24)

$$\int_C \frac{dz}{z^2+a^2} = \int_{AB} + \int_{BDA} = 2\pi j \sum \text{Res}$$

As  $R \rightarrow \infty$

$$\int_{BDA} \frac{dz}{z^2+a^2} = \int_0^{\pi} \frac{Rje^{j\theta} d\theta}{R^2 e^{j2\theta} + a^2} \rightarrow 0_{R \rightarrow \infty}$$

and, therefore, we have

$$\int_{AB} \frac{dx}{x^2+a^2} = \int_{-\infty}^{\infty} \frac{dx}{x^2+a^2} = 2\pi j \left. \frac{z-ja}{z^2+a^2} \right|_{z=ja} = 2\pi j \frac{1}{2ja} = \frac{\pi}{a}$$

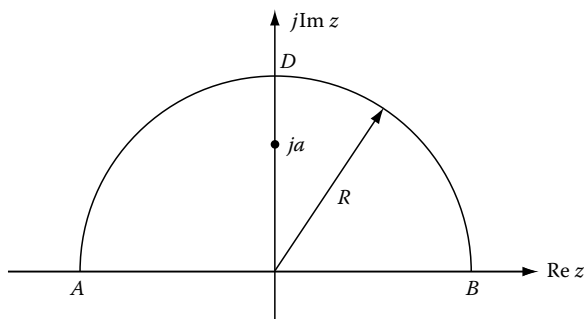


FIGURE A.24

#### Example A.39

Evaluate the integral  $I = \int_0^{\infty} \frac{\sin ax}{x} dx$ .

#### SOLUTION

Because  $\sin az/z$  is analytic near  $z=0$ , we indent the contour around the origin as shown in Figure A.25. With a positive we write

$$\begin{aligned} \int_0^{\infty} \frac{\sin ax}{x} dx &= \frac{1}{2} \int_{ABCD} \frac{\sin az}{z} dz = \frac{1}{4j} \int_{ABCD} \left[ \frac{e^{jaz}}{z} - \frac{e^{-jaz}}{z} \right] dz \\ &= \frac{1}{4j} \int_{ABCA} \frac{e^{jaz}}{z} dz - \frac{1}{4j} \int_{ABCFDA} \frac{e^{-jaz}}{z} dz = \frac{1}{4j} \left[ 2\pi j \frac{1}{1} - 0 \right] = \frac{\pi}{2} \end{aligned}$$

because the lower contour does not include any singularity. Because  $\sin ax$  is an odd function of  $a$  and  $\sin 0=0$ , we obtain

$$\int_0^{\infty} \frac{\sin x}{x} dx = \begin{cases} \frac{\pi}{2} & a > 0 \\ 0 & a = 0 \\ -\frac{\pi}{2} & a < 0 \end{cases}$$

#### Example A.40

Evaluate the integral  $I = \int_0^{\infty} \frac{dx}{1+x^3}$ .

#### SOLUTION

Because the integrand  $f(x)$  is odd, we introduce the  $\ln z$ . Taking a branch cut along the positive real axis, we obtain

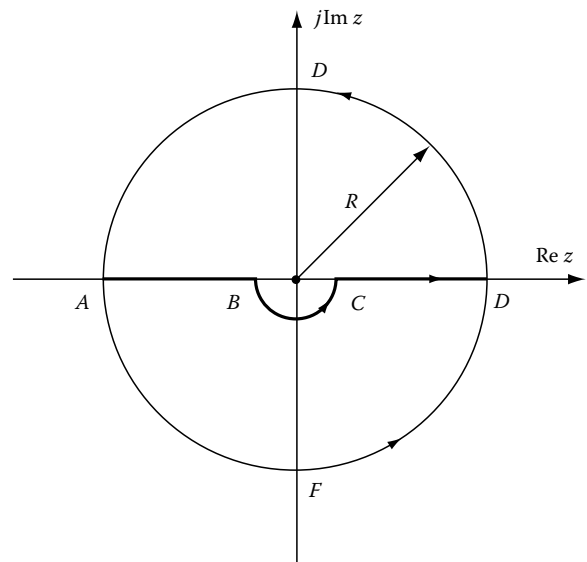


FIGURE A.25

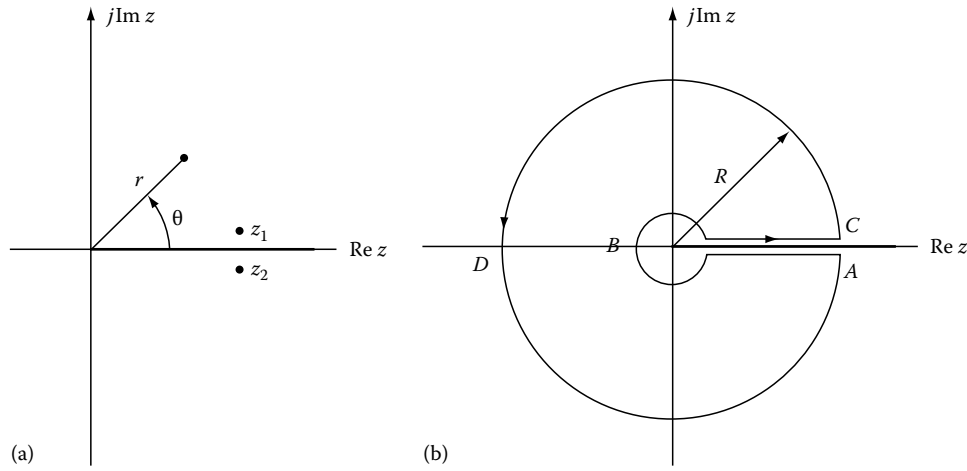


FIGURE A.26

$$\ln z = \ln r + j\theta \quad 0 \leq \theta < 2\pi$$

The discontinuity of  $\ln z$  across the cut is (see Figure A.26a)

$$\ln z_1 - \ln z_2 = -2\pi j$$

Therefore, if  $f(z)$  is analytic along the real axis and the contribution around an infinitesimal circle at the origin is vanishing, we obtain

$$\int_0^{\infty} f(x) dx = -\frac{1}{2\pi j} \int_{ABC} f(z) \ln(z) dz$$

If further  $f(z) \rightarrow 0$  as  $|z| \rightarrow \infty$ , the contour can be completed with  $CDA$  (see Figure A.26b). If  $f(z)$  has simple poles of order one at points  $z_k$  with residues  $\text{Res}(f, z_k)$ , we obtain

$$\int_0^{\infty} f(x) dx = -\sum_k \text{Res}(f, z_k) \ln z_k$$

Hence, because  $z^3 + 1 = 0$  has poles at  $z_1 = e^{j\pi/3}$ ,  $z_2 = e^{j2\pi/3}$ ,  $z_3 = e^{j5\pi/3}$ , then the integral is given by

$$I = \int_0^{\infty} \frac{dx}{x^3 + 1} = -\left[ \frac{j\pi/3}{3e^{2j\pi/3}} + \frac{j\pi}{3e^{j2\pi}} + \frac{j5\pi/3}{3e^{j10\pi/3}} \right] = \frac{2\pi\sqrt{3}}{9}$$

**Example A.41**

Show that  $\int_0^{\infty} \cos ax^2 dx = \int_0^{\infty} \sin ax^2 dx = \frac{1}{2} \sqrt{\frac{\pi}{2a}} a > 0$ .

**SOLUTION**

We first form the integral

$$F = \int_0^{\infty} \cos ax^2 dx + j \int_0^{\infty} \sin ax^2 dx = \int_0^{\infty} e^{jax^2} dx$$

Because  $\exp(jaz^2)$  is analytic in the entire  $z$ -plane, we can use Cauchy's theorem and write (see Figure A.27)

$$F = \int_{AB} e^{jaz^2} dz = \int_{AC} e^{jaz^2} dz + \int_{CB} e^{jaz^2} dz$$

Along the contour  $CB$ , we obtain

$$\begin{aligned} \left| -\int_0^{\pi/4} e^{jR^2 \cos 2\theta - R^2 \sin 2\theta} j R e^{j\theta} d\theta \right| &\leq \int_0^{\pi/4} e^{-R^2 \sin 2\theta} R d\theta = \frac{R}{2} \int_0^{\pi/2} e^{-R^2 \sin \phi} d\phi \\ &\leq \frac{R}{2} \int_0^{\pi/2} e^{-R^2 \phi/\pi} d\phi = \frac{\pi}{4R} (1 - e^{-R^2}) \end{aligned}$$

where the transformation  $2\theta = \phi$  and the inequality  $\sin \phi \geq \phi/\pi$  were used ( $0 \leq \phi \leq \pi/2$ ). Hence, as  $R$  approaches infinity the contribution from  $CB$  contour vanishes. Hence,

$$F = \int_{AB} e^{jaz^2} dz = e^{j\pi/4} \int_0^{\infty} e^{-ar^2} dr = \frac{1+j}{\sqrt{2}} \frac{1}{2} \sqrt{\frac{\pi}{a}}$$

from which we obtain the desired result.

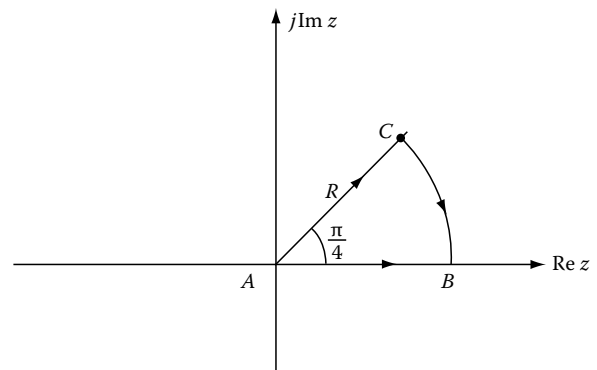


FIGURE A.27

**Example A.42**

Evaluate the integral  $I = \int_{-1}^1 \frac{dx}{\sqrt{1-x^2}(1+x^2)}$ .

**SOLUTION**

Consider the integral

$$\oint_C \frac{dz}{\sqrt{1-z^2}(1+z^2)}$$

whose contour  $C$  is that shown in Figure A.28. On the top side of the branch cut we obtain  $I$  and from the bottom we also get  $I$ . The contribution of the integral on the outer circle as  $R$  approaches infinity vanishes. Hence, due to two poles we obtain

$$2I = 2\pi j \left[ \frac{1}{2j\sqrt{2}} + \frac{1}{2j\sqrt{2}} \right] = \pi\sqrt{2} \quad \text{or} \quad I = \frac{\sqrt{2}}{2}\pi$$

**Example A.43**

Evaluate the integral  $I = \int_{-\infty}^{\infty} \frac{e^{ax}}{e^{bx}+1} dx, a, b > 0$ .

**SOLUTION**

From Figure A.29 we find

$$I = \int_C \frac{e^{az}}{e^{bz}+1} dz = \int_C \frac{e^{az/b}}{e^z+1} dz = 2\pi j \sum \text{Res}$$

There is an infinite number of poles: at  $z = j\pi/b$ , residue is  $-\exp(j\pi a/b)$ ; at  $z = 3j\pi/b$ , residue is  $-\exp(3j\pi a/b)$ , and so on. The sum of residue forms a geometric series and because we assume a small imaginary part of  $a$ ,  $|\exp(j2\pi a/b)| < 1$ .

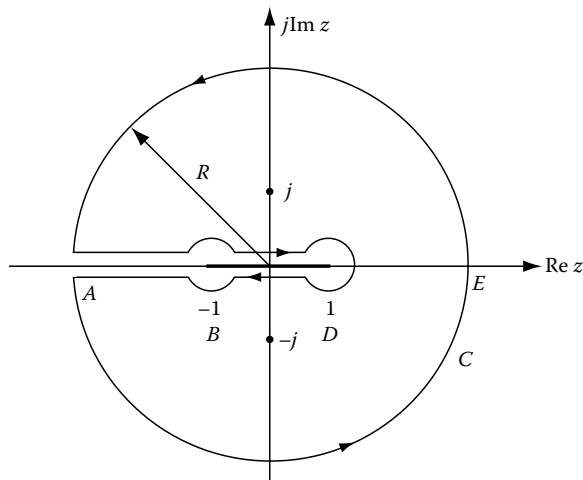


FIGURE A.28

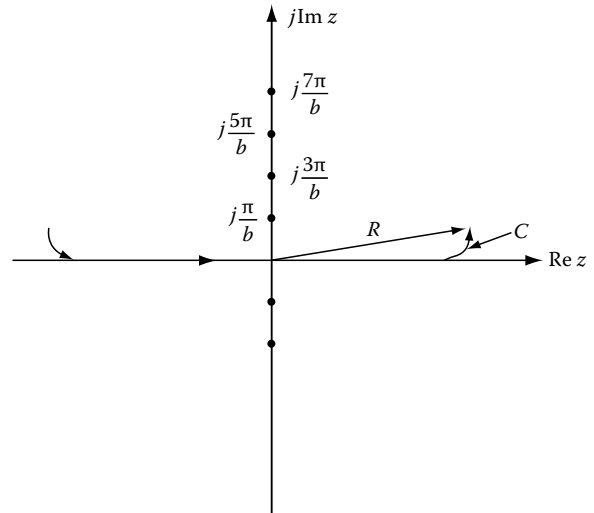


FIGURE A.29

Hence, by considering the common factor  $\exp(j\pi a/b)$ , we obtain

$$I = -\frac{2\pi j}{b} j \frac{e^{j\pi a/b}}{1 - e^{j2\pi a/b}} = \frac{1}{b} \frac{\pi}{\sin(\pi a/b)}$$

The integral is of the form  $\int e^{j\omega x} f(x) dx$  whose evaluation can be simplified by Jordan's lemma (see also Equation A.60)

$$\int_C e^{j\omega x} f(x) dx = 0$$

for the contour semicircle  $C$  at infinity for which  $\text{Im}(\omega x) > 0$ , provided  $|f(\text{Re}^{\theta})| < \epsilon(R) \rightarrow 0$  as  $R \rightarrow \infty$  (note that the bound on  $|f(x)|$  must be independent of  $\theta$ ).

**Example A.44**

A relaxed  $RL$  series circuit with an input voltage source  $v(t)$  is described by the equation  $L di/dt + Ri = v(t)$ . Find the current in the circuit using the inverse Fourier transform when the input voltage is a delta function.

**SOLUTION**

The Fourier transform of the differential equation with delta input voltage function is

$$Lj\omega I(\omega) + RI(\omega) = 1 \quad \text{or} \quad I(\omega) = \frac{1}{R + j\omega L}$$

and, hence,

$$i(t) = \frac{1}{2\pi} \int_{-\infty}^{\infty} \frac{e^{j\omega t}}{R + j\omega L} d\omega$$

If  $t < 0$ , the integral is exponentially small for  $\text{Im } \omega \rightarrow -\infty$ . If we complete the contour by a large semicircle in the lower  $\omega$ -plane, the integral vanishes by Jordan's lemma. Because the contour does not include any singularities,  $i(t) = 0$ ,  $t < 0$ . For  $t > 0$ , we complete the contour in the upper  $\omega$ -plane. Similarly no contribution exists from the semicircle. Because there is only one pole at  $\omega = jR/L$  inside the contour the value of the integral is

$$i(t) = 2\pi j \frac{1}{2\pi} \frac{1}{jL} e^{j(jR/L)t} = \frac{1}{L} e^{-\frac{R}{L}t}$$

which is known as the *impulse response of the system*.

### A.10 Principal Value of an Integral

Refer to the limiting process employed in Example A.39, which can be written in the form

$$\lim_{R \rightarrow \infty} \int_{-R}^R \frac{e^{jx}}{x} dx = j\pi$$

The limit is called the *Cauchy principal value* of the integral in the equation

$$\int_{-\infty}^{\infty} \frac{e^{jx}}{x} dx = j\pi$$

In general, if  $f(x)$  becomes infinite at a point  $x = c$  inside the range of integration, and if

$$\lim_{\varepsilon \rightarrow 0} \int_{-R}^R f(x) dx = \lim_{\varepsilon \rightarrow 0} \left[ \int_{-R}^{c-\varepsilon} f(x) dx + \int_{c+\varepsilon}^R f(x) dx \right]$$

and if the separate limits on the right also exist, then the integral is convergent and the integral is written as  $P \int$  where the  $P$  indicates the principal value. Whenever each of the integrals

$$\int_{-\infty}^0 f(x) dx \quad \int_0^{\infty} f(x) dx$$

has a value, here  $R \rightarrow \infty$ , the principal value is the same as the integral. For example, if  $f(x) = x$ , the principal value of the integral is zero, although the value of the integral itself does not exist.

As another example, consider the integral

$$\int_a^b \frac{dx}{x} = \log \frac{b}{a}$$

If  $a$  is negative and  $b$  is positive, the integral diverges at  $x = 0$ . However, we can still define

$$\begin{aligned} P \int_a^b \frac{dx}{x} &= \lim_{\varepsilon \rightarrow 0} \left[ \int_a^{-\varepsilon} \frac{dx}{x} + \int_{\varepsilon}^b \frac{dx}{x} \right] = \lim_{\varepsilon \rightarrow 0} \left( \log \frac{\varepsilon}{-a} + \log \frac{b}{\varepsilon} \right) \\ &= \log \frac{b}{|a|} \end{aligned}$$

This principal value integral is unambiguous. The condition that the same value of  $\varepsilon$  must be used in both sides is essential; otherwise, the limit could be almost anything by taking the first integral from  $a$  to  $-\varepsilon$  and the second from  $\kappa$  to  $b$  and making these two quantities tend to zero in a suitable ratio.

If the complex variables were used, we could complete the path by a semicircle from  $-\varepsilon$  to  $+\varepsilon$  about the origin, either above or below the real axis. If the upper semicircle were chosen, there would be a contribution  $-j\pi$ , whereas if the lower semicircle were chosen, the contribution to the integral would be  $+j\pi$ . Thus, according to the path permitted in the complex plane we should have

$$\int_a^b \frac{dz}{z} = \log \frac{b}{|a|} \pm j\pi$$

The principal value is the mean of these alternatives.

If a path in the complex plane passes through a simple pole at  $z = a$ , we can define a principal value of the integral along the path by using a hook of small radius  $\varepsilon$  about the point  $a$  and the making  $\varepsilon$  tend to zero, as already discussed. If we change the variable  $z$  to  $\zeta$  and  $dz/d\zeta$  is finite and not equal to zero at the pole, this procedure will define an integral in the  $\zeta$ -plane, but the values of the integrals will be the same. Suppose that the hook in the  $z$ -plane cuts the path at  $a - \varepsilon$  and  $a + \varepsilon'$ , where  $|\varepsilon| = |\varepsilon'|$ , and in the  $\zeta$ -plane the hook cuts the path at  $\alpha - \kappa$  and  $\alpha + \kappa'$ . Then, if  $\kappa$  and  $\kappa'$  tend to zero so that  $\varepsilon/\varepsilon' \rightarrow 1$ ,  $\kappa$  and  $\kappa'$  will tend to zero so that  $\kappa/\kappa' \rightarrow 1$ .

To illustrate this discussion, suppose we want to evaluate the integral

$$I = \int_0^{\pi} \frac{d\theta}{a - b \cos \theta}$$

where  $a$  and  $b$  are real and  $a > b > 0$ . A change of variable by writing  $z = \exp(j\theta)$  transforms this integral to (where a new constant  $\alpha$  is introduced)

$$I = \int_0^{\pi} \frac{2e^{j\theta} d\theta}{2ae^{j\theta} - b(e^{j2\theta} + 1)} = -\frac{1}{j} \int_C \frac{2dz}{bz^2 - 2az + b} = -\frac{1}{j} \int_C \frac{2dz}{b(z - \alpha)(z - \frac{1}{\alpha})}$$

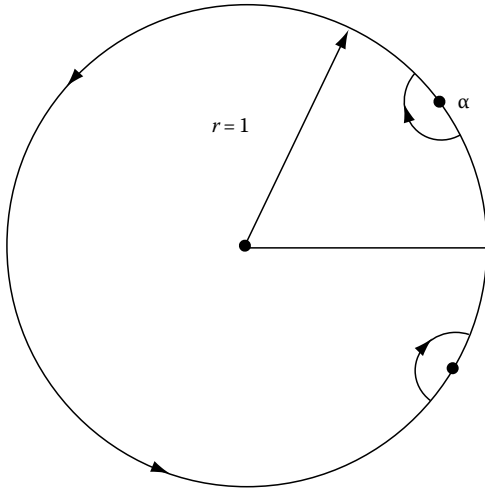


FIGURE A.30

where the path of integration is around the unit circle. Because the contour would pass through the poles, hooks are used to isolate the poles as shown in Figure A.30. Because no singularities are closed by the path, the integral is zero. The contributions of the hooks are  $-j\pi$  times the residues, where the residues are

$$-\frac{1}{j} \frac{\frac{2}{b}}{\alpha - \frac{1}{\alpha}} \quad -\frac{1}{j} \frac{\frac{2}{b}}{\frac{1}{\alpha} - \alpha}$$

These are equal and opposite and cancel each other. Therefore, the principal value of the integral around the unit circle is zero. This approach for finding principal values succeeds only at simple poles.

### A.11 Integral of the Logarithmic Derivative

Of importance in the study of mapping from  $z$ -plane to  $W(z)$ -plane is the integral of the logarithmic derivative. Consider, therefore, the function

$$F(z) = \log W(z) \tag{A.107}$$

Then

$$\frac{dF(z)}{dz} = \frac{1}{W(z)} \frac{dW(z)}{dz} = \frac{W'(z)}{W(z)}$$

The function to be examined is the following:

$$\int_C \frac{dF(z)}{dz} dz = \int_C \frac{W'(z)}{W(z)} dz \tag{A.108}$$

The integrand of this expression will be analytic within the contour  $C$  except for the points at which  $W(z)$  is either zero or infinity.

Suppose that  $W(z)$  has a pole of order  $n$  at  $z_0$ . This means that  $W(z)$  can be written

$$W(z) = (z - z_0)^n g(z) \tag{A.109}$$

with  $n$  positive for a zero and  $n$  negative for a pole. We differentiate this expression to get

$$W'(z) = n(z - z_0)^{n-1} g(z) + (z - z_0)^n g'(z)$$

and so

$$\frac{W'(z)}{W(z)} = \frac{n}{z - z_0} + \frac{g'(z)}{g(z)} \tag{A.110}$$

For  $n$  positive,  $W'(z)/W(z)$  will possess a pole of order one. Similarly, for  $n$  negative  $W'(z)/W(z)$  will possess a pole of order one, but with a negative sign. Thus, for the case of  $n$  positive or negative, the contour integral in the positive sense yields

$$\int_C \frac{W'(z)}{W(z)} dz = \pm \int_C \frac{n}{z - z_0} dz + \int_C \frac{g'(z)}{g(z)} dz \tag{A.111}$$

But because  $g(z)$  is analytic at the point  $z_0$ , then  $\int_C [g'(z)/g(z)] dz = 0$ , and by Equation A.44

$$\int_C \frac{W'(z)}{W(z)} dz = \pm 2\pi j n \tag{A.112}$$

Thus, the existence of a zero of  $W(z)$  introduces a contribution  $2\pi j n_z$  to the contour integral, where  $n_z$  is the multiplicity of the zero of  $W(z)$  at  $z_0$ . Clearly, if a number of zeros of  $W(z)$  exist, the total contribution to the contour integral is  $2\pi j N$ , where  $N$  is the weighted value of the zeros of  $W(z)$  (weight 1 to a first-order zero, weight 2 to a second-order zero, and so on).

For the case where  $n$  is negative, which specifies that  $W(z)$  has a pole of order  $n$  at  $z_0$ , then in Equation A.112  $n$  is negative and the contribution to the contour integral is now  $-2\pi j n_p$  for each pole of  $W(z)$ ; the total contribution is  $-2\pi j P$ , where  $P$  is the weighted number of poles. Clearly, because both zeros and poles of  $F(z)$  cause poles of  $W'(z)/W(z)$  with opposite signs, then the total value of the integral is

$$\int_C \frac{W'(z)}{W(z)} dz = \pm 2\pi j (N - P) \tag{A.113}$$

Note further that

$$\begin{aligned} \int_C W'(z) dz &= \int_C \frac{dW(z)}{dz} dz = \int d[\log W(z)] \\ &= \int d[\log|W(z)| + j \arg W(z)] \\ &= \log|W(z)|_0^{2\pi} + j[\arg W(2\pi) - \arg W(0)] \\ &= 0 + j[\arg W(2\pi) - \arg W(0)] \end{aligned}$$

so that

$$[\arg W(0) - \arg W(2\pi)] = 2\pi(N - P) \tag{A.114}$$

This relation can be given simple graphical interpretation. Suppose that the function  $W(z)$  is represented by its pole and zero configuration on the  $z$ -plane. As  $z$  traverses the prescribed contour on the  $z$ -plane,  $W(z)$  will move on the  $W(z)$ -plane according to its functional dependence on  $z$ . But the left-hand side of this equation denotes the total change in the phase angle of  $W(z)$  as  $z$  transverses around the complete contour. Therefore, the number of times that the moving point representing  $W(z)$  revolves around the origin in the  $W(z)$ -plane as  $z$  moves around the specified contour is given by  $N - P$ .

The foregoing is conveniently illustrated graphically. Figure A.31a shows the prescribed contour in the  $z$ -plane, and Figure A.31b shows a possible form for the variation of  $W(z)$ . For this particular case, the contour in the  $z$ -plane encloses one zero and no poles; hence,  $W(z)$  encloses the origin once in the clockwise direction in the  $W(z)$ -plane.

Note that corresponding to a point  $z_0$  within the contour in the  $z$ -plane, the point  $W(z_0)$  is mapped inside the  $W(z)$ -plane. In fact, every point on the inside of the contour in the  $z$ -plane maps onto the inside of the  $W(z)$ -contour in the  $W(z)$ -plane (for single-valued functions). Clearly, there is one point in the  $z$ -plane that maps into  $W(z)=0$ , the origin.

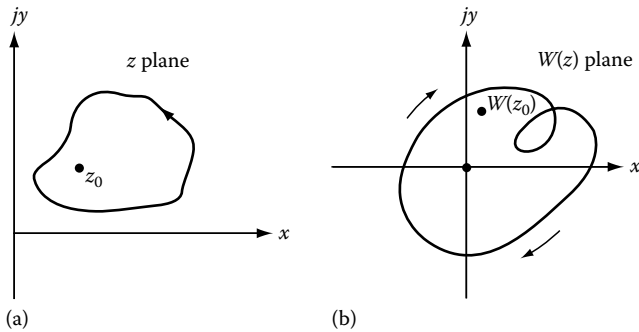


FIGURE A.31

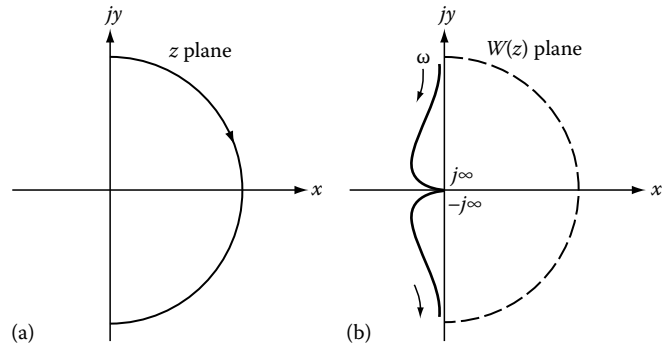


FIGURE A.32

On the other hand, if the contour includes a pole but no zeros, it can be shown by a similar argument that any point in the interior of the  $z$ -contour must correspond to a corresponding point outside of the  $W(z)$ -contour in the  $W(z)$ -plane. This is manifested by the fact that the  $W(z)$ -contour is traversed in a counterclockwise direction. With both zeros and poles present, the situation depends on the value of  $N$  and  $P$ .

Of special interest is the locus of the network function that contains no poles in the right-hand plane or on the  $j\omega$ -axis. In this case the frequency locus is completely traced as  $z$  varies along the  $\omega$ -axis from  $-j\infty$  to  $+j\infty$ . To show this, because  $W(z)$  is analytic along this path,  $W(z)$  can be written for the neighborhood of a point  $z_0$  in a Taylor series

$$W(z) = \alpha_0 + \alpha_1(z - z_0) + \alpha_2(z - z_0)^2 + \dots$$

For the neighborhood  $z \rightarrow \infty$ , we examine  $W(z')$ , where  $z' = 1/z$ . Because  $W(z)$  does not have a pole at infinity, then  $W(z')$  does not have a pole at zero. Therefore, we can expand  $W(z')$  in a Maclaurin series

$$W(z') = \alpha_0 + \alpha_1 z' + \alpha_2 (z')^2 + \dots$$

which means that

$$W(z) = \alpha_0 + \frac{\alpha_1}{z} + \frac{\alpha_2}{z^2} + \dots$$

But as  $z$  approaches infinity,  $W(\infty)$  approaches infinity. In a real network function when  $z^*$  is written for  $z$ , then  $W(z^*) = W^*(z)$ . This condition requires that  $\alpha_0 = \alpha_0 + j_0$  be a real number irrespective of how  $z$  approaches infinity; that is, as  $z$  approaches infinity,  $W(z)$  approaches a fixed point in the  $W(z)$ -plane. This shows that as  $z$  varies around the specific contour in the  $z$ -plane,  $W(z)$  varies from  $W(-j\infty)$  to  $W(+j\infty)$  as  $z$  varies along the imaginary axis. However,  $W(-j\infty) = W(+j\infty)$ , from the above, which thereby shows that the locus is completely determined. This is illustrated in Figure A.32.





# Appendix B: Series and Summations

---

B.1	Series .....	B-1
B.2	Binomial .....	B-1
B.3	Reversion of Series .....	B-1
B.4	Taylor .....	B-1
B.5	Maclaurin .....	B-2
B.6	Exponential .....	B-2
B.7	Logarithmic .....	B-2
B.8	Trigonometric .....	B-2
B.9	Hyperbolic and Inverse Hyperbolic .....	B-3

## B.1 Series

---

The expression in parentheses following certain of the series indicates the region of convergence. If not otherwise indicated, it is to be understood that the series converges for all finite values of  $x$ .

## B.2 Binomial

---

$$(x + y)^n = x^n + nx^{n-1}y + \frac{n(n-1)}{2!}x^{n-2}y^2 + \frac{n(n-1)(n-2)}{3!}x^{n-3}y^3 + \dots \quad (y^2 < x^2)$$

$$(1 \pm x)^n = 1 \pm nx + \frac{n(n-1)x^2}{2!} \pm \frac{n(n-1)(n-2)x^3}{3!} + \dots \quad (x^2 < 1)$$

$$(1 \pm x)^{-n} = 1 \mp nx + \frac{n(n+1)x^2}{2!} \mp \frac{n(n+1)(n+2)x^3}{3!} + \dots \quad (x^2 < 1)$$

$$(1 \pm x)^{-1} = 1 \mp x + x^2 \mp x^3 + x^4 \mp x^5 + \dots \quad (x^2 < 1)$$

$$(1 \pm x)^{-2} = 1 \mp 2x + 3x^2 \mp 4x^3 + 5x^4 \mp 6x^5 + \dots \quad (x^2 < 1)$$

## B.3 Reversion of Series

---

Let a series be represented by

$$y = a_1x + a_2x^2 + a_3x^3 + a_4x^4 + a_5x^5 + a_6x^6 + \dots \quad (a_1 \neq 0)$$

to find the coefficients of the series

$$x = A_1y + A_2y^2 + A_3y^3 + A_4y^4 + \dots$$

$$A_1 = \frac{1}{a_1} \quad A_2 = -\frac{a_2}{a_1^3} \quad A_3 = \frac{1}{a_1^5}(2a_2^2 - a_1a_3)$$

$$A_4 = \frac{1}{a_1^7}(5a_1a_2a_3 - a_1^2a_4 - 5a_2^3)$$

$$A_5 = \frac{1}{a_1^9}(6a_1^2a_2a_4 + 3a_1^2a_3^2 + 14a_2^4 - a_1^3a_5 - 21a_1a_2^2a_3)$$

$$A_6 = \frac{1}{a_1^{11}}(7a_1^3a_2a_5 + 7a_1^3a_3a_4 + 84a_1a_2^3a_3 - a_1^4a_6 - 28a_1^2a_2^2a_4 - 28a_1^2a_2a_3^2 - 42a_2^5)$$

$$A_7 = \frac{1}{a_1^{13}}(8a_1^4a_2a_6 + 8a_1^4a_3a_5 + 4a_1^4a_4^2 + 120a_1^2a_2^3a_4 + 180a_1^2a_2^2a_3^2 + 132a_2^6 - a_1^5a_7 - 36a_1^3a_2^2a_5 - 72a_1^3a_2a_3a_4 - 12a_1^3a_3^3 - 330a_1a_2^4a_3)$$

## B.4 Taylor

---

1.

$$f(x) = f(a) + (x-a)f'(a) + \frac{(x-a)^2}{2!}f''(a) + \frac{(x-a)^3}{3!}f'''(a) + \dots + \frac{(x-a)^n}{n!}f^{(n)}(a) + \dots \quad (\text{Taylor's series})$$

(Increment form)

2.

$$f(x+h) = f(x) + hf'(x) + \frac{h^2}{2!}f''(x) + \frac{h^3}{3!}f'''(x) + \dots$$

$$= f(h) + xf'(h) + \frac{x^2}{2!}f''(h) + \frac{x^3}{3!}f'''(h) + \dots$$

3. If  $f(x)$  is a function possessing derivatives of all orders throughout the interval  $a \leq x \leq b$ , then there is value  $X$ , with  $a < X < b$ , such that

$$f(b) = f(a) + (b-a)f'(a) + \frac{(b-a)^2}{2!}f''(a) + \dots$$

$$+ \frac{(b-a)^{n-1}}{(n-1)!}f^{(n-1)}(a) + \frac{(b-a)^n}{n!}f^{(n)}(X)$$

$$f(a+h) = f(a) + hf'(a) + \frac{h^2}{2!}f''(a) + \dots + \frac{h^{n-1}}{(n-1)!}f^{(n-1)}(a)$$

$$+ \frac{h^n}{n!}f^{(n)}(a+\theta h), \quad b = a+h, \quad 0 < \theta < 1.$$

or

$$f(x) = f(a) + (x-a)f'(a) + \frac{(x-a)^2}{2!}f''(a) + \dots + (x-a)^{n-1}$$

$$\times \frac{f^{(n-1)}(a)}{(n-1)!} + R_n,$$

where

$$R_n = \frac{f^{(n)}[a + \theta \cdot (x-a)]}{n!} (x-a)^n, \quad 0 < \theta < 1.$$

The above forms are known as Taylor's series with the remainder term.

#### 4. Taylor's series for a function of two variables

$$\text{If } \left( h \frac{\partial}{\partial x} + k \frac{\partial}{\partial y} \right) f(x, y) = h \frac{\partial f(x, y)}{\partial x} + k \frac{\partial f(x, y)}{\partial y};$$

$$\left( h \frac{\partial}{\partial x} + k \frac{\partial}{\partial y} \right)^2 f(x, y) = h^2 \frac{\partial^2 f(x, y)}{\partial x^2} + 2hk \frac{\partial^2 f(x, y)}{\partial x \partial y} + k^2 \frac{\partial^2 f(x, y)}{\partial y^2}$$

etc., and if  $h \left( \frac{\partial}{\partial x} + k \frac{\partial}{\partial y} \right)^n f(x, y) \Big|_{x=a, y=b}$  with the bar and subscripts means that after differentiation we are to replace  $x$  by  $a$  and  $y$  by  $b$ ,

$$f(a+h, b+k) = f(a, b) + \left( h \frac{\partial}{\partial x} + k \frac{\partial}{\partial y} \right) f(x, y) \Big|_{x=a, y=b}$$

$$+ \dots + \frac{1}{n!} \left( h \frac{\partial}{\partial x} + k \frac{\partial}{\partial y} \right)^n f(x, y) \Big|_{x=a, y=b} + \dots$$

## B.5 Maclaurin

$$f(x) = f(0) + xf'(0) + \frac{x^2}{2!}f''(0) + \frac{x^3}{3!}f'''(0) + \dots + x^{n-1} \frac{f^{(n-1)}(0)}{(n-1)!} + R_n,$$

where

$$R_n = \frac{x^n f^{(n)}(\theta x)}{n!}, \quad 0 < \theta < 1.$$

## B.6 Exponential

$$e = 1 + \frac{1}{1!} + \frac{1}{2!} + \frac{1}{3!} + \frac{1}{4!} + \dots$$

$$e^x = 1 + x + \frac{x^2}{2!} + \frac{x^3}{3!} + \frac{x^4}{4!} + \dots \quad (\text{all real values of } x)$$

$$a^x = 1 + x \log_e a + \frac{(x \log_e a)^2}{2!} + \frac{(x \log_e a)^3}{3!} + \dots$$

$$e^x = e^a \left[ 1 + (x-a) + \frac{(x-a)^2}{2!} + \frac{(x-a)^3}{3!} + \dots \right]$$

## B.7 Logarithmic

$$\log_e x = \frac{x-1}{x} + \frac{1}{2} \left( \frac{x-1}{x} \right)^2 + \frac{1}{3} \left( \frac{x-1}{x} \right)^3 + \dots \quad \left( x > \frac{1}{2} \right)$$

$$\log_e x = (x-1) - \frac{1}{2}(x-1)^2 + \frac{1}{3}(x-1)^3 - \dots \quad (2 \geq x > 0)$$

$$\log_e x = 2 \left[ \frac{x-1}{x+1} + \frac{1}{3} \left( \frac{x-1}{x+1} \right)^3 + \frac{1}{5} \left( \frac{x-1}{x+1} \right)^5 + \dots \right] \quad (x > 0)$$

$$\log_e (1+x) = x - \frac{1}{2}x^2 + \frac{1}{3}x^3 - \frac{1}{4}x^4 + \dots \quad (-1 < x < 1)$$

$$\log_e (n+1) - \log_e (n-1) = 2 \left[ \frac{1}{n} + \frac{1}{3n^3} + \frac{1}{5n^5} + \dots \right]$$

$$\log_e (a+x) = \log_e a + 2 \left[ \frac{x}{2a+x} + \frac{1}{3} \left( \frac{x}{2a+x} \right)^3 \right.$$

$$\left. + \frac{1}{5} \left( \frac{x}{2a+x} \right)^5 + \dots \right] \quad (a > 0, -a < x < +\infty)$$

$$\log_e \frac{1+x}{1-x} = 2 \left[ x + \frac{x^3}{3} + \frac{x^5}{5} + \dots + \frac{x^{2n-1}}{2n-1} + \dots \right], \quad -1 < x < 1$$

$$\log_e x = \log_e a + \frac{(x-a)}{a} - \frac{(x-a)^2}{2a^2} + \frac{(x-a)^3}{3a^3} - \dots, \quad 0 < x \leq 2a$$

## B.8 Trigonometric

$$\sin x = x - \frac{x^3}{3!} + \frac{x^5}{5!} - \frac{x^7}{7!} + \dots \quad (\text{all real values of } x)$$

$$\cos x = 1 - \frac{x^2}{2!} + \frac{x^4}{4!} - \frac{x^6}{6!} + \dots \quad (\text{all real values of } x)$$

$$\tan x = x + \frac{x^3}{3} + \frac{2x^5}{15} + \frac{17x^7}{315} + \frac{62x^9}{2835} + \cdots$$

$$+ \frac{2^{2n}(2^{2n}-1)B_n}{(2n)!}x^{2n-1} + \cdots,$$

$$\left[ x^2 < \frac{\pi^2}{4}, \text{ and } B_n \text{ represents the } n\text{th Bernoulli number.} \right]$$

$$\cot x = \frac{1}{x} - \frac{x}{3} + \frac{x^2}{45} - \frac{2x^5}{945} - \frac{x^7}{4725} - \cdots - \frac{2^{2n}B_n}{(2n)!}x^{2n-1} - \cdots,$$

$$[x^2 < \pi^2, \text{ and } B_n \text{ represents the } n\text{th Bernoulli number.}]$$

$$\sec x = 1 + \frac{x^2}{2} + \frac{5}{24}x^4 + \frac{61}{720}x^6 + \frac{277}{8064}x^8 + \cdots + \frac{E_n x^{2n}}{(2n)!} + \cdots,$$

$$\left[ x^2 < \frac{\pi^2}{4}, \text{ and } E_n \text{ represents the } n\text{th Euler number.} \right]$$

$$\csc x = \frac{1}{x} + \frac{x}{6} + \frac{7}{360}x^3 + \frac{31}{15,120}x^5 + \frac{127}{604,800}x^7 + \cdots$$

$$+ \frac{2(2^{2n-1}-1)B_n x^{2n-1}}{(2n)!} + \cdots,$$

$$[x^2 < \pi^2, \text{ and } B_n \text{ represents the } n\text{th Bernoulli number.}]$$

$$\sin x = x \left( 1 - \frac{x^2}{\pi^2} \right) \left( 1 - \frac{x^2}{2^2\pi^2} \right) \left( 1 - \frac{x^2}{3^2\pi^2} \right) \cdots \quad (x^2 < \infty)$$

$$\cos x = \left( 1 - \frac{4x^2}{\pi^2} \right) \left( 1 - \frac{4x^2}{3^2\pi^2} \right) \left( 1 - \frac{4x^2}{5^2\pi^2} \right) \cdots \quad (x^2 < \infty)$$

$$\sin^{-1} x = x + \frac{x^3}{2 \cdot 3} + \frac{1 \cdot 3}{2 \cdot 4 \cdot 5}x^5 + \frac{1 \cdot 3 \cdot 5}{2 \cdot 4 \cdot 6 \cdot 7}x^7$$

$$+ \cdots \quad \left( x^2 < 1, -\frac{\pi}{2} < \sin^{-1} x < \frac{\pi}{2} \right)$$

$$\cos^{-1} x = \frac{\pi}{2} - \left( x + \frac{x^3}{2 \cdot 3} + \frac{1 \cdot 3}{2 \cdot 4 \cdot 5}x^5 + \frac{1 \cdot 3 \cdot 5x^7}{2 \cdot 4 \cdot 6 \cdot 7} + \cdots \right)$$

$$(x^2 < 1, 0 < \cos^{-1} x < \pi)$$

$$\tan^{-1} x = x - \frac{x^3}{3} + \frac{x^5}{5} - \frac{x^7}{7} + \cdots \quad (x^2 < 1)$$

$$\tan^{-1} x = \frac{\pi}{2} - \frac{1}{x} + \frac{1}{3x^2} - \frac{1}{5x^4} + \frac{1}{7x^6} - \cdots \quad (x > 1)$$

$$\tan^{-1} x = -\frac{\pi}{2} - \frac{1}{x} + \frac{1}{3x^2} - \frac{1}{5x^4} + \frac{1}{7x^6} - \cdots \quad (x < -1)$$

$$\cot^{-1} x = \frac{\pi}{2} - x + \frac{x^3}{3} - \frac{x^5}{5} + \frac{x^7}{7} - \cdots \quad (x^2 < 1)$$

$$\log_e \sin x = \log_e x - \frac{x^2}{6} - \frac{x^4}{180} - \frac{x^6}{2835} - \cdots \quad (x^2 < \pi^2)$$

$$\log_e \cos x = -\frac{x^2}{2} - \frac{x^4}{12} - \frac{x^6}{45} - \frac{17x^8}{2520} - \cdots \quad \left( x^2 < \frac{\pi^2}{4} \right)$$

$$\log_e \tan x = \log_e x + \frac{x^2}{3} + \frac{7x^4}{90} + \frac{62x^6}{2835} + \cdots \quad \left( x^2 < \frac{\pi^2}{4} \right)$$

$$e^{\sin x} = 1 + x + \frac{x^2}{2!} - \frac{3x^4}{4!} - \frac{8x^5}{5!} - \frac{3x^6}{6!} + \frac{56x^7}{7!} + \cdots$$

$$e^{\cos x} = e \left( 1 - \frac{x^2}{2!} + \frac{4x^4}{4!} - \frac{31x^6}{6!} + \cdots \right)$$

$$e^{\tan x} = 1 + x + \frac{x^2}{2!} + \frac{3x^3}{3!} + \frac{9x^4}{4!} + \frac{37x^5}{5!} + \cdots \quad \left( x^2 < \frac{\pi^2}{4} \right)$$

$$\sin x = \sin a + (x-a) \cos a - \frac{(x-a)^2}{2!} \sin a - \frac{(x-a)^3}{3!}$$

$$\times \cos a + \frac{(x-a)^4}{4!} \sin a + \cdots$$

## B.9 Hyperbolic and Inverse Hyperbolic

Table of expansion of certain functions into power series

$$\sinh x = x + \frac{x^3}{3!} + \frac{x^5}{5!} + \frac{x^7}{7!} + \cdots + \frac{x^{2n+1}}{(2n+1)!} + \cdots \quad |x| < \infty$$

$$\cosh x = 1 + \frac{x^2}{2!} + \frac{x^4}{4!} + \frac{x^6}{6!} + \cdots + \frac{x^{2n}}{(2n)!} + \cdots \quad |x| < \infty$$

$$\tanh x = x - \frac{1}{3}x^3 + \frac{2}{15}x^5 - \frac{17}{315}x^7 + \frac{62}{2835}x^9 - \cdots$$

$$+ \frac{(-1)^{n+1}2^{2n}(2^{2n}-1)}{(2n)!}B_n x^{2n-1} \pm \cdots,$$

$$B_n \text{ denotes Bernoulli's numbers } |x| < \frac{\pi}{2}$$

$$\coth x = \frac{1}{x} + \frac{x}{3} - \frac{x^3}{45} + \frac{2x^5}{945} - \frac{x^7}{4725} + \cdots$$

$$+ \frac{(-1)^{n+1}2^{2n}}{(2n)!}B_n x^{2n-1} \pm \cdots,$$

$$B_n \text{ denotes Bernoulli's numbers } 0 < |x| < \pi$$

$$\operatorname{sech} x = 1 - \frac{1}{2!}x^2 + \frac{5}{4!}x^4 - \frac{61}{6!}x^6 + \frac{1385}{8!}x^8 - \cdots$$

$$+ \frac{(-1)^n}{(2n)!}E_n x^{2n} \pm \cdots, E_n \text{ denotes Euler's numbers}$$

$$|x| < \frac{\pi}{2}$$

$$\operatorname{cosech} x = \frac{1}{x} - \frac{x}{6} + \frac{7x^3}{360} - \frac{31x^5}{15,120} + \cdots + \frac{2(-1)^n(2^{2n-1}-1)}{(2n)!}$$

$$B_n x^{2n-1} + \cdots, B_n \text{ denotes Bernoulli's numbers}$$

$$0 < |x| < \pi$$

$$\begin{aligned} \arg \sinh x &= x - \frac{1}{2 \cdot 3} x^3 + \frac{1 \cdot 3}{2 \cdot 4 \cdot 5} x^5 - \frac{1 \cdot 3 \cdot 5}{2 \cdot 4 \cdot 6 \cdot 7} x^7 + \dots \\ &+ (-1)^n \cdot \frac{1 \cdot 3 \cdot 5 \cdot (2n-1)}{2 \cdot 4 \cdot 6 \dots 2n(2n+1)} x^{2n+1} \pm \dots \quad |x| < 1 \end{aligned}$$

$$\arg \cosh x = \pm \left[ \ln(2x) - \frac{1}{2 \cdot 2x^2} - \frac{1 \cdot 3}{2 \cdot 4 \cdot 4x^4} - \frac{1 \cdot 3 \cdot 5}{2 \cdot 4 \cdot 6 \cdot 6x^6} - \dots \right] \quad x > 1$$

$$\arg \tanh x = x + \frac{x^3}{3} + \frac{x^5}{5} + \frac{x^7}{7} + \dots + \frac{x^{2n+1}}{2n+1} + \dots \quad |x| < 1$$

$$\arg \coth x = \frac{1}{x} + \frac{1}{3x^3} + \frac{1}{5x^5} + \frac{1}{7x^7} + \dots + \frac{1}{(2n+1)x^{2n+1}} + \dots \quad |x| > 1$$

Arithmetic Progression of the first order (first differences constant), to  $n$  terms,

$$\begin{aligned} &a + (a + d) + (a + 2d) + (a + 3d) + \dots + \{a + (n - 1)d\} \\ &\equiv na + \frac{1}{2}n(n - 1)d \\ &\equiv \frac{n}{2}(1\text{st term} + n\text{th term}). \end{aligned}$$

Geometric Progression, to  $n$  terms,

$$\begin{aligned} a + ar + ar^2 + ar^3 + \dots + ar^{n-1} &\equiv a(1 - r^n)/(1 - r) \\ &\equiv a(r^n - 1)/(r - 1). \end{aligned}$$

If  $r^2 < 1$ , the limit of the sum of an infinite number of terms is  $a/(1 - r)$ .

The reciprocals of the terms of a series in arithmetic progression of the first order are in *Harmonic Progression*. Thus,

$$\frac{1}{a}, \frac{1}{a + d}, \frac{1}{a + 2d}, \dots, \frac{1}{a + (n - 1)d}$$

are in Harmonic Progression.

The *Arithmetic Mean* of  $n$  quantities is

$$\frac{1}{n}(a_1 + a_2 + a_3 + \dots + a_n).$$

The *Geometric Mean* of  $n$  quantities is

$$(a_1 a_2 a_3 \dots a_n)^{1/n}.$$

Let the *Harmonic Mean* of  $n$  quantities be  $H$ . Then

$$\frac{1}{H} = \frac{1}{n} \left( \frac{1}{a_1} + \frac{1}{a_2} + \frac{1}{a_3} + \dots + \frac{1}{a_n} \right).$$

The arithmetic mean of a number of positive quantities is  $\geq$  their geometric mean, which in turn is  $\geq$  their harmonic mean.

$$1 + 2 + 3 + \dots + n = \frac{n}{2}(n + 1) = \sum_{k=0}^n k$$

$$\begin{aligned} 1^2 + 2^2 + 3^2 + \dots + n^2 &= \frac{n}{6}(n + 1)(2n + 1) \\ &= \frac{n}{6}(2n^2 + 3n + 1) = \sum_{k=0}^n k^2 \end{aligned}$$

$$\begin{aligned} 1^3 + 2^3 + 3^3 + \dots + n^3 &= \frac{n^2}{4}(n + 1)^2 \\ &= \frac{n^2}{4}(n^2 + 2n + 1) = \sum_{k=0}^n k^3 \end{aligned}$$

$$1 + 3 + 5 + 7 + 9 + \dots + (2n - 1) = n^2 = \sum_{k=0}^{2n-1} (2k + 1)$$

$$1 + 8 + 16 + 24 + 32 + \dots + 8(n - 1) = (2n - 1)^2$$

$$1 + 3x + 5x^2 + 7x^3 + \dots = \frac{1 + x}{(1 - x)^2}$$

$$1 + ax + (a + b)x^2 + (a + 2b)x^3 + \dots = 1 + \frac{ax + (b - a)x^2}{(1 - x)^2}$$

$$1 + 2^2x + 3^2x^2 + 4^2x^3 + \dots = \frac{1 + x}{(1 - x)^3}$$

$$1 + 3^2x + 5^2x^2 + 7^2x^3 + \dots = \frac{1 + 6x + x^2}{(1 - x)^3}$$

$$\frac{a[1 - (n + 1)a^n + na^{n+1}]}{(1 - a)^2} = \sum_{k=0}^n ka^k$$

$$\frac{a[(1 + a) - (n + 1)^2a^n + (2n^2 + 2n - 1)a^{n+1} - n^2a^{n+2}]}{(1 - a)^3}$$

$$= \sum_{k=0}^n k^2 a^k$$

$$\frac{a}{(1 - a)^2} = \sum_{k=0}^{\infty} ka^k \quad |a| < 1$$

$$\frac{a^2 + a}{(1 - a)^3} = \sum_{k=0}^{\infty} k^2 a^k \quad |a| < 1$$

# Appendix C: Definite Integrals

---

$$\int_0^{\infty} x^{n-1} e^{-x} dx = \int_0^1 \left(\log \frac{1}{x}\right)^{n-1} dx = \frac{1}{n} \prod_{m=1}^{\infty} \frac{\left(1 + \frac{1}{m}\right)^n}{1 + \frac{n}{m}}$$

$$= \Gamma(n), \quad n \neq 0, -1, -2, -3, \dots$$

(Gamma Function)

$$\int_0^{\infty} t^n p^{-t} dt = \frac{n!}{(\log p)^{n+1}} \quad (n = 0, 1, 2, 3, \dots \text{ and } p > 0)$$

$$\int_0^{\infty} t^{n-1} e^{-(a+1)t} dt = \frac{\Gamma(n)}{(a+1)^n} \quad (n > 0, a > -1)$$

$$\int_0^1 x^m \left(\log \frac{1}{x}\right)^n dx = \frac{\Gamma(n+1)}{(m+1)^{n+1}} \quad (m > -1, n > -1)$$

$\Gamma(n)$  is finite if  $n > 0$ ,  $\Gamma(n+1) = n\Gamma(n)$

$$\Gamma(n) \cdot \Gamma(1-n) = \frac{\pi}{\sin n\pi}$$

$\Gamma(n) = (n-1)!$  if  $n = \text{integer} > 0$

$$\Gamma\left(\frac{1}{2}\right) = 2 \int_0^{\infty} e^{-t^2} dt = \sqrt{\pi} = 1.7724538509 \dots$$

$$\Gamma\left(n + \frac{1}{2}\right) = \frac{1 \cdot 3 \cdot 5 \cdot 7 \cdots (2n-1)}{2^n} \sqrt{\pi},$$

where  $n$  is an integer and  $> 0$

$$\int_0^1 x^{m-1} (1-x)^{n-1} dx = B(m, n) \quad (\text{Beta function})$$

$$B(m, n) = B(n, m) = \frac{\Gamma(m)\Gamma(n)}{\Gamma(m+n)}$$

where  $m$  and  $n$  are any positive real numbers

$$\int_0^1 x^{m-1} (1-x)^{n-1} dx = \int_0^{\infty} \frac{x^{m-1} dx}{(1+x)^{m+n}} = \frac{\Gamma(m)\Gamma(n)}{\Gamma(m+n)}$$

$$\int_a^b (x-a)^m (b-x)^n dx = (b-a)^{m+n+1} \frac{\Gamma(m+1) \cdot \Gamma(n+1)}{\Gamma(m+n+2)}$$

$(m > -1, n > -1, b > a)$

$$\int_0^{\infty} \frac{dx}{x^m} = \frac{1}{m-1} \quad (m > 1)$$

$$\int_0^{\infty} \frac{dx}{(1+x)x^p} = \pi \csc p\pi \quad (p < 1)$$

$$\int_0^{\infty} \frac{dx}{(1-x)x^p} = -\pi \cot p\pi \quad (p < 1)$$

$$\int_0^{\infty} \frac{x^{p-1} dx}{1+x} = \frac{\pi}{\sin p\pi}$$

$$= B(p, 1-p) = \Gamma(p)\Gamma(1-p) \quad (0 < p < 1)$$

$$\int_0^{\infty} \frac{x^{m-1} dx}{1+x^n} = \frac{\pi}{n \sin \frac{m\pi}{n}} \quad (0 < m < n)$$

$$\int_0^{\infty} \frac{x^a dx}{(m+x^b)^c} = m \frac{a+1}{b-c} \left[ \frac{\Gamma\left(\frac{a+1}{b}\right)\Gamma\left(c - \frac{a+1}{b}\right)}{\Gamma(c)} \right]$$

$(a > -1, b > 0, m > 0, c > \frac{a+1}{b})$

$$\int_0^{\infty} \frac{dx}{(1+x)\sqrt{x}} = \pi$$

$$\int_0^{\infty} \frac{a dx}{a^2 + x^2} = \frac{\pi}{2}, \quad \text{if } a > 0; \quad 0, \quad \text{if } a = 0; \quad -\frac{\pi}{2}, \quad \text{if } a < 0$$

$$\int_0^a x^m (a^2 - x^2)^{\frac{n}{2}} dx = \begin{cases} \frac{1}{2} a^{m+n+1} B\left(\frac{m+1}{2}, \frac{n+2}{2}\right) \\ \frac{1}{2} a^{m+n+1} \frac{\Gamma\left(\frac{m+1}{2}\right)\Gamma\left(\frac{n+2}{2}\right)}{\Gamma\left(\frac{m+n+3}{2}\right)} \end{cases}$$

$$\int_0^1 \frac{dx}{\sqrt{(1-x^n)}} = \frac{\sqrt{\pi}}{n} \frac{\Gamma(\frac{1}{n})}{\Gamma(\frac{1}{n} + \frac{1}{2})} \quad (n > 0)$$

$$\int_0^1 \frac{x^m dx}{\sqrt{(1-x^n)}} = \frac{\sqrt{\pi}}{n} \frac{\Gamma(\frac{m+1}{n})}{\Gamma(\frac{m+1}{n} + \frac{1}{2})} \quad (m+1, n > 0)$$

$$\int_0^1 x^m (1-x^2)^p dx = \frac{\Gamma(p+1)\Gamma(\frac{m+1}{2})}{2\Gamma(p + \frac{m+3}{2})} \quad (p+1, m+1 > 0)$$

$$\int_0^1 x^m (1-x^n)^p dx = \frac{\Gamma(p+1)\Gamma(\frac{m+1}{n})}{n\Gamma(p+1 + \frac{m+1}{n})} \quad (p+1, m+1, n > 0)$$

$$\int_0^1 \frac{x^m dx}{\sqrt{(1-x^2)}} = \frac{2 \cdot 4 \cdot 6 \cdots (m-1)}{3 \cdot 5 \cdot 7 \cdots m} \quad (m \text{ an odd integer } > 1)$$

$$= \frac{1 \cdot 3 \cdot 5 \cdots (m-1) \pi}{2 \cdot 4 \cdot 6 \cdots m} \quad (m \text{ an even, positive integer})$$

$$= \frac{\sqrt{\pi}}{2} \frac{\Gamma(\frac{m+1}{2})}{\Gamma(\frac{m}{2} + 1)} \quad (m \text{ any value } > -1)$$

$$\int_0^\infty \frac{x^{p-1} dx}{1+x} = \frac{\pi}{\sin(\pi - p\pi)} = \frac{\pi}{\sin p\pi} \quad (0 < p < 1)$$

$$\int_0^\infty \frac{dx}{(1+x)\sqrt{x}} = \pi$$

$$\int_0^\infty \frac{x^{p-1} dx}{a+x} = \frac{\pi a^{p-1}}{\sin p\pi} \quad (0 < p < 1)$$

$$\int_0^\infty \frac{dx}{1+x^p} = \frac{\pi}{p \sin \frac{\pi}{p}} \quad (p > 1)$$

$$\int_0^\infty \frac{x^p dx}{(1+ax)^2} = \frac{p\pi}{a^{p+1} \sin p\pi} \quad (0 < p < 1)$$

$$\int_0^\infty \frac{x^p dx}{1+x^2} = \frac{\pi}{2 \cos \frac{p\pi}{2}} \quad (-1 < p < 1)$$

$$\int_0^\infty \frac{x^{p-1} dx}{1+x^q} = \frac{\pi}{q \sin \frac{p\pi}{q}} \quad (0 < p < q)$$

$$\int_0^\infty \frac{x^{m-1} dx}{(1+x)^{m+n}} = \frac{\Gamma(m)\Gamma(n)}{\Gamma(m+n)} \quad (m, n > 0)$$

$$\int_0^\infty \frac{x^{m-1} dx}{(a+bx)^{m+n}} = \frac{\Gamma(m)\Gamma(n)}{a^n b^m \Gamma(m+n)} \quad (a, b, m, n > 0)$$

$$\int_0^\infty \frac{dx}{(a^2+x^2)^n} = \frac{1 \cdot 3 \cdot 5 \cdots (2n-3)}{2 \cdot 4 \cdot 6 \cdots (2n-2)} \times \frac{\pi}{2a^{2n-1}} \quad (a > 0; n = 2, 3, \dots)$$

$$\int_0^\infty \frac{dx}{(a^2+x^2)(b^2+x^2)} = \frac{\pi}{2ab(a+b)} \quad (a, b > 0)$$

$$\int_0^{\pi/2} (\cos^n x) dx = \begin{cases} \int_0^{\pi/2} (\cos^n x) dx \\ \frac{1 \cdot 3 \cdot 5 \cdot 7 \cdots (n-1) \pi}{2 \cdot 4 \cdot 6 \cdot 8 \cdots (n)} \frac{\pi}{2}, & (n \text{ an even integer, } n \neq 0) \\ \frac{2 \cdot 4 \cdot 6 \cdot 8 \cdots (n-1)}{1 \cdot 3 \cdot 5 \cdot 7 \cdots (n)}, & (n \text{ an odd integer, } n \neq 1) \\ \frac{\sqrt{\pi}}{2} \frac{\Gamma(\frac{n+1}{2})}{\Gamma(\frac{n}{2} + 1)}, & (n > -1) \end{cases}$$

$$\int_0^{\pi/2} (\sin^n x) dx = \begin{cases} \int_0^{\pi/2} (\sin^n x) dx \\ \frac{1 \cdot 3 \cdot 5 \cdot 7 \cdots (n-1) \pi}{2 \cdot 4 \cdot 6 \cdot 8 \cdots (n)} \frac{\pi}{2}, & (n \text{ an even integer, } n \neq 0) \\ \frac{2 \cdot 4 \cdot 6 \cdot 8 \cdots (n-1)}{1 \cdot 3 \cdot 5 \cdot 7 \cdots (n)}, & (n \text{ an odd integer, } n \neq 1) \\ \frac{\sqrt{\pi}}{2} \frac{\Gamma(\frac{n+1}{2})}{\Gamma(\frac{n}{2} + 1)}, & (n > -1) \end{cases}$$

$$\int_0^\infty \frac{\sin mx dx}{x} = \frac{\pi}{2}, \quad \text{if } m > 0; \quad \text{if } m = 0; \quad -\frac{\pi}{2}, \quad \text{if } m < 0$$

$$\int_0^\infty \frac{\cos x dx}{x} = \infty$$

$$\int_0^\infty \frac{\tan x dx}{x} = \frac{\pi}{2}$$

$$\int_0^\pi \sin ax \cdot \sin bx dx = \int_0^\pi \cos ax \cdot \cos bx dx = 0, \quad (a \neq b; a, b \text{ integers})$$

$$\int_0^{\pi/a} [\sin(ax)][\cos(ax)] dx = \int_0^\pi [\sin(ax)][\cos(ax)] dx = 0$$

$$\int_0^\pi [\sin(ax)][\cos(bx)] dx = \frac{2a}{a^2 - b^2}, \quad \text{if } a - b \text{ is odd,} \\ \text{or zero if } a - b \text{ is even}$$

$$\int_0^\infty \frac{\sin x \cos mx dx}{x} = 0, \text{ if } m < -1 \text{ or } m > 1, = \frac{\pi}{4}, \text{ if } m = \pm 1; \\ = \frac{\pi}{2}, \text{ if } m^2 < 1$$

$$\int_0^\infty \frac{\sin ax \sin bx dx}{x^2} = \frac{\pi a}{2} \quad (a \leq b)$$

$$\int_0^\pi \sin^2 mx dx = \int_0^\pi \cos^2 mx dx = \frac{\pi}{2}$$

$$\int_0^{\infty} \frac{\sin^2 x \, dx}{x^2} = \frac{\pi}{2}$$

$$\int \frac{\cos mx}{1+x^2} dx = \frac{\pi}{2} e^{-|m|}$$

$$\int_0^{\infty} \cos(x^2) dx = \int_0^{\infty} \sin(x^2) dx = \frac{1}{2} \sqrt{\frac{\pi}{2}}$$

$$\int_0^{\infty} \frac{\sin x \, dx}{\sqrt{x}} = \int_0^{\infty} \frac{\cos x \, dx}{\sqrt{x}} = \sqrt{\frac{\pi}{2}}$$

$$\int_0^{\pi/2} \frac{dx}{1+a \cos x} = \frac{\cos^{-1} a}{\sqrt{1-a^2}} \quad (a < 1)$$

$$\int_0^{\infty} \frac{dx}{a+b \cos x} = \frac{\pi}{\sqrt{a^2-b^2}} \quad (a > b \geq 0)$$

$$\int_0^{2\pi} \frac{dx}{1+a \cos x} = \frac{2\pi}{\sqrt{1-a^2}} \quad (a^2 < 1)$$

$$\int_0^{\infty} \frac{\cos ax - \cos bx}{x} dx = \log \frac{b}{a}$$

$$\int_0^{\pi/2} \frac{dx}{a^2 \sin^2 x + b^2 \cos^2 x} = \frac{\pi}{2ab}$$

$$\int_0^{\pi/2} \frac{dx}{(a^2 \sin^2 x + b^2 \cos^2 x)^2} = \frac{\pi(a^2+b^2)}{4a^3b^3} \quad (a, b > 0)$$

$$\int_0^{\pi/2} \sin^{n-1} x \cos^{m-1} x \, dx = \frac{1}{2} B\left(\frac{n}{2}, \frac{m}{2}\right) \quad (m \text{ and } n \text{ positive integers})$$

$$\int_0^{\pi/2} (\sin^{2n+1} \theta) d\theta = \frac{2 \cdot 4 \cdot 6 \cdots (2n)}{1 \cdot 3 \cdot 5 \cdots (2n+1)} \quad (n = 1, 2, 3 \dots)$$

$$\int_0^{\pi/2} (\sin^{2n} \theta) d\theta = \frac{1 \cdot 3 \cdot 5 \cdots (2n-1)}{2 \cdot 4 \cdots (2n)} \left(\frac{\pi}{2}\right) \quad (n = 1, 2, 3 \dots)$$

$$\int_0^{\pi/2} \sqrt{\cos \theta} \, d\theta = \frac{(2\pi)^{\frac{3}{2}}}{[\Gamma(\frac{1}{4})]^2}$$

$$\int_0^{\pi/2} (\tan^h \theta) d\theta = \frac{\pi}{2 \cos(\frac{h\pi}{2})} \quad (0 < h < 1)$$

$$\int_0^{\infty} \frac{\tan^{-1}(ax) - \tan^{-1}(bx)}{x} dx = \frac{\pi}{2} \log \frac{a}{b} \quad (a, b > 0)$$

The area enclosed by a curve defined through the equation  $x^{b/c} + y^{b/c} = a^{b/c}$  where  $a > 0$ ,  $c$  a positive odd integer, and  $b$  a positive even integer is given by

$$\frac{[\Gamma(\frac{c}{b})]^2}{\Gamma(\frac{2c}{b})} \left(\frac{2ca^2}{b}\right)$$

$I = \iiint_R x^{h-1} y^{m-1} z^{n-1} \, dv$ , where  $R$  denotes the region of space bounded by the coordinate planes and that portion of the surface  $(x/a)^p + (y/b)^q + (z/c)^k = 1$ , which lies in the first octant and where  $h, m, n, p, q, k, a, b, c$ , denote positive real numbers is given by

$$\int_0^a x^{h-1} dx \int_0^{b[1-(\frac{x}{a})^p]^{\frac{1}{q}}} y^m dy \int_0^{c[1-(\frac{x}{a})^p - (\frac{y}{b})^q]^{\frac{1}{k}}} z^{n-1} dz = \frac{a^h b^m c^n}{p q k} \frac{\Gamma(\frac{h}{p}) \Gamma(\frac{m}{q}) \Gamma(\frac{n}{k})}{\Gamma(\frac{h}{p} + \frac{m}{q} + \frac{n}{k} + 1)}$$

$$\int_0^{\pi/2} \frac{dx}{a^2 \sin^2 x + b^2 \cos^2 x} = \frac{\pi}{2ab} \quad (ab > 0)$$

$$\int_0^{\pi} \frac{dx}{a^2 \sin^2 x + b^2 \cos^2 x} = \frac{\pi}{ab} \quad (ab > 0)$$

$$\int_0^{\pi/2} \frac{\sin^2 x \, dx}{a^2 \sin^2 x + b^2 \cos^2 x} = \int_0^{\pi/2} \frac{dx}{a^2 + b^2 \cot^2 x} = \frac{\pi}{2a(a+b)} \quad (a, b > 0)$$

$$\int_0^{\pi/2} \frac{\cos^2 x \, dx}{a^2 \sin^2 x + b^2 \cos^2 x} = \int_0^{\pi/2} \frac{dx}{b^2 + a^2 \tan^2 x} = \frac{\pi}{2b(a+b)} \quad (a, b > 0)$$

$$\int_0^{\pi/2} \frac{dx}{(a^2 \sin^2 x + b^2 \cos^2 x)^2} = \frac{\pi}{4} \frac{(a^2+b^2)}{a^3b^3} \quad (ab > 0)$$



$$\int_0^{\pi/2} \frac{\sin^2 x \, dx}{(a^2 \sin^2 x + b^2 \cos^2 x)^2} = \frac{\pi}{4a^3 b} \quad (ab > 0)$$

$$\int_0^{\pi/2} \frac{\cos^2 x \, dx}{(a^2 \sin^2 x + b^2 \cos^2 x)^2} = \frac{\pi}{4ab^3} \quad (ab > 0)$$

$$\int_0^{\infty} \sin(a^2 x^2) \, dx = \int_0^{\infty} \cos(a^2 x^2) \, dx = \frac{\sqrt{\pi}}{2a\sqrt{2}} \quad (a > 0)$$

$$\int_0^{\infty} \sin \frac{\pi x^2}{2} \, dx = \int_0^{\infty} \cos \frac{\pi x^2}{2} \, dx = \frac{1}{2} \quad (\text{Fresnel's integrals})$$

$$\int_0^{\infty} \sin(x^p) \, dx = \Gamma\left(1 + \frac{1}{p}\right) \sin \frac{\pi}{2p} \quad (p > 1)$$

$$\int_0^{\infty} \cos(x^p) \, dx = \Gamma\left(1 + \frac{1}{p}\right) \cos \frac{\pi}{2p} \quad (p > 1)$$

$$\int_0^{\infty} \sin a^2 x^2 \cos mx \, dx = \frac{\sqrt{\pi}}{2a} \sin\left(\frac{\pi}{4} - \frac{m^2}{4a^2}\right) \quad (a > 0)$$

$$\int_0^{\infty} \cos a^2 x^2 \cos mx \, dx = \frac{\sqrt{\pi}}{2a} \cos\left(\frac{\pi}{4} - \frac{m^2}{4a^2}\right) \quad (a > 0)$$

$$\int_0^{\infty} \frac{\sin^{2p} mx}{x^2} \, dx = \frac{1 \cdot 3 \cdot 5 \cdots (2p-3)}{2 \cdot 4 \cdot 6 \cdots (2p-2)} \frac{|m|\pi}{2} \quad (p = 2, 3, 4, \dots)$$

$$\int_0^{\infty} \frac{\sin^3 mx}{x^3} \, dx = \frac{3}{8} m^2 \pi \quad (m > 0)$$

$$\int_0^{\infty} \frac{\sin mx \cos nx}{x} \, dx = \pi/2 \quad (m > n > 0)$$

$$\qquad \qquad \qquad = \pi/4 \quad (m = n > 0)$$

$$\qquad \qquad \qquad = 0 \quad (n > m > 0)$$

$$\int_0^{\infty} \frac{\sin mx \sin nx}{x} \, dx = \frac{1}{2} \log \frac{m+n}{m-n} \quad (m > n > 0)$$

$$\int_0^{\infty} \frac{\cos mx \cos nx}{x} \, dx = \infty$$

$$\int_0^{\infty} \frac{\sin^2 ax \sin mx}{x} \, dx = \frac{\pi}{4} \quad (2a > m > 0)$$

$$\qquad \qquad \qquad = \frac{\pi}{8} \quad (2a = m > 0)$$

$$\qquad \qquad \qquad = 0 \quad (m > 2a > 0)$$

$$\int_0^{\infty} \frac{\sin mx \sin nx}{x^2} \, dx = \frac{\pi m}{2} \quad (n \geq m > 0)$$

$$\qquad \qquad \qquad = \frac{\pi n}{2} \quad (m \geq n > 0)$$

$$\int_0^{\infty} \frac{\sin^2 ax \sin mx}{x^2} \, dx = \frac{m+2a}{4} \log|m+2a|$$

$$\qquad \qquad \qquad + \frac{m-2a}{4} \log|m-2a| - \frac{m}{2} \log m \quad (m > 0)$$

$$\int_0^{\infty} \frac{\cos mx}{a^2 + x^2} \, dx = \frac{\pi}{2a} e^{-ma} \quad (a > 0; m \geq 0)$$

$$\int_0^{\infty} \frac{\sin^2 mx}{a^2 + x^2} \, dx = \frac{\pi}{4a} (1 - e^{-2ma}) \quad (a > 0; m \geq 0)$$

$$\int_0^{\infty} \frac{\cos^2 mx}{a^2 + x^2} \, dx = \frac{\pi}{4a} (1 + e^{-2ma}) \quad (a > 0; m \geq 0)$$

$$\int_0^{\infty} \frac{x \sin mx}{a^2 + x^2} \, dx = \frac{\pi}{2} e^{-ma} \quad (a \geq 0; m > 0)$$

$$\int_0^{\infty} \frac{\sin mx}{x(a^2 + x^2)} \, dx = \frac{\pi}{2a^2} (1 - e^{-ma}) \quad (a > 0; m \geq 0)$$

$$\int_0^{\infty} \frac{\sin mx \sin nx}{a^2 + x^2} \, dx = \frac{\pi}{2a} e^{-ma} \sinh na \quad (a > 0; m \geq n \geq 0)$$

$$\qquad \qquad \qquad = \frac{\pi}{2a} e^{-na} \sinh ma \quad (a > 0; n \geq m \geq 0)$$

$$\int_0^{\infty} \frac{\cos mx \cos nx}{a^2 + x^2} \, dx = \frac{\pi}{2a} e^{-ma} \cosh na \quad (a > 0; m \geq n \geq 0)$$

$$\qquad \qquad \qquad = \frac{\pi}{2a} e^{-na} \cosh ma \quad (a > 0; n \geq m \geq 0)$$

$$\int_0^{\infty} \frac{x \sin mx \cos nx}{a^2 + x^2} \, dx = \frac{\pi}{2} e^{-ma} \cosh na \quad (a > 0; m > n > 0)$$

$$\qquad \qquad \qquad = -\frac{\pi}{2} e^{-na} \sinh ma \quad (a > 0; n > m > 0)$$

$$\int_0^{\infty} \frac{\cos mx}{(a^2 + x^2)^2} \, dx = \frac{\pi}{4a^3} (1 + ma) e^{-ma} \quad (a, m > 0)$$

$$\int_0^{\infty} \frac{x \sin mx}{(a^2 + x^2)^2} dx = \frac{\pi m}{4a} e^{-ma} \quad (a, m > 0) \quad \int_0^{\infty} x^2 e^{-x^2} dx = \frac{\sqrt{\pi}}{4}$$

$$\int_0^{\infty} \frac{x^2 \cos mx}{(a^2 + x^2)^2} dx = \frac{\pi}{4a} (1 - ma) e^{-ma} \quad (a, m > 0) \quad \int_0^{\infty} x^{2n} e^{-ax^2} dx = \frac{1 \cdot 3 \cdot 5 \cdots (2n-1)}{2^{n+1} a^n} \sqrt{\frac{\pi}{a}}$$

$$\int_0^{\infty} \frac{\sin^2 ax \cos mx}{x^2} dx = \frac{\pi}{2} \left( a - \frac{m}{2} \right) \quad \left( a > \frac{m}{2} > 0 \right) \quad \int_0^1 x^m e^{-ax} dx = \frac{m!}{a^{m+1}} \left[ 1 - e^{-a} \sum_{r=0}^m \frac{a^r}{r!} \right]$$

$$= 0 \quad \left( \frac{m}{2} \cong a \cong 0 \right) \quad \int_0^{\infty} e^{(-x^2 - \frac{a^2}{x^2})} dx = \frac{e^{-2a} \sqrt{\pi}}{2} \quad (a \geq 0)$$

$$\int_0^{\infty} \frac{1 - \cos mx}{x^2} dx = \frac{\pi |m|}{2} \quad \int_0^{\infty} e^{-nx} \sqrt{x} dx = \frac{1}{2n} \sqrt{\frac{\pi}{n}}$$

$$\int_0^{\infty} \frac{\sin^2 ax \sin mx}{x^3} dx = \frac{\pi am}{2} - \frac{\pi m^2}{8} \quad \left( a \cong \frac{m}{2} > 0 \right) \quad \int_0^{\infty} \frac{e^{-nx}}{\sqrt{x}} dx = \sqrt{\frac{\pi}{n}}$$

$$= \frac{\pi a^2}{2} \quad \left( \frac{m}{2} \cong a > 0 \right) \quad \int_0^{\infty} e^{-ax} \cos mx dx = \frac{a}{a^2 + m^2} \quad (a > 0)$$

$$\int_0^{\infty} \frac{\sin mx}{\sqrt{x}} dx = \int_0^{\infty} \frac{\cos mx}{\sqrt{x}} dx = \frac{\sqrt{\pi}}{\sqrt{2m}} \quad (m > 0) \quad \int_0^{\infty} e^{-ax} \sin mx dx = \frac{m}{a^2 + m^2} \quad (a > 0)$$

$$\int_0^{\infty} \frac{\sin mx}{x\sqrt{x}} dx = \sqrt{2\pi m} \quad (m > 0) \quad \int_0^{\infty} x e^{-ax} [\sin(bx)] dx = \frac{2ab}{(a^2 + b^2)^2} \quad (a > 0)$$

$$\int_0^{\infty} \frac{\sin mx}{x^p} dx = \frac{\pi m^{p-1}}{2 \sin(\frac{p\pi}{2}) \Gamma(p)} \quad (0 < p < 2; m > 0) \quad \int_0^{\infty} x e^{-ax} [\cos(bx)] dx = \frac{a^2 - b^2}{(a^2 + b^2)^2} \quad (a > 0)$$

$$\int_0^{\infty} e^{-ax} dx = \frac{1}{a} \quad (a > 0) \quad \int_0^{\infty} x^n e^{-ax} [\sin(bx)] dx = \frac{n! [(a - ib)^{n+1} - (a + ib)^{n+1}]}{2(a^2 + b^2)^{n+1}} \quad (i^2 = -1, a > 0)$$

$$\int_0^{\infty} \frac{e^{-ax} - e^{-bx}}{x} dx = \log \frac{b}{a} \quad (a, b > 0) \quad \int_0^{\infty} x^n e^{-ax} [\cos(bx)] dx = \frac{n! [(a - ib)^{n+1} + (a + ib)^{n+1}]}{2(a^2 + b^2)^{n+1}} \quad (i^2 = -1, a > 0)$$

$$\int_0^{\infty} x^n e^{-ax} dx = \frac{\Gamma(n+1)}{a^{n+1}} \quad (n > -1, a > 0) \quad \int_0^{\infty} \frac{e^{-ax} \sin x}{x} dx = \cot^{-1} a \quad (a > 0)$$

$$= \frac{n!}{a^{n+1}} \quad (n \text{ positive integer}, a > 0) \quad \int_0^{\infty} e^{-a^2 x^2} dx = \frac{1}{2a} \sqrt{\pi} = \frac{1}{2a} \Gamma\left(\frac{1}{2}\right) \quad (a > 0)$$

$$\int_0^{\infty} x e^{-x^2} dx = \frac{1}{2} \quad \int_0^{\infty} e^{-a^2 x^2} \cos bx dx = \frac{\sqrt{\pi}}{2a} e^{-\frac{b^2}{4a^2}} \quad (ab \neq 0)$$

$$\int_0^{\infty} e^{-t \cos \phi} t^{b-1} [\sin(t \sin \phi)] dt = [\Gamma(b)] \sin(b\phi) \quad (b > 0, -\frac{\pi}{2} < \phi < \frac{\pi}{2})$$

$$\int_0^{\infty} e^{-t \cos \phi} t^{b-1} [\cos(t \sin \phi)] dt = [\Gamma(b)] \cos(b\phi) \quad (b > 0, -\frac{\pi}{2} < \phi < \frac{\pi}{2})$$

$$\int_0^{\infty} \frac{e^{-ax^c} - e^{-bx^c}}{x} dx = \frac{1}{c} \log \frac{b}{a} \quad (a, b, c > 0)$$

$$\int_0^{\infty} \frac{1 - e^{-ax^2}}{x^2} dx = \sqrt{a\pi}$$

$$\int_0^{\infty} \exp\left[-a^2 x^2 - \frac{b^2}{x^2}\right] dx = \frac{\sqrt{\pi}}{2a} e^{-2ab}$$

$$\int_0^{\infty} \frac{dx}{e^{ax} - 1} = \infty \quad (a > 0)$$

$$\int_0^{\infty} \frac{x dx}{e^{ax} - 1} = \frac{\pi^2}{6a^2} \quad (a > 0)$$

$$\int_0^{\infty} \frac{e^{-ax} - e^{-bx}}{x} dx = \log \frac{b}{a} \quad (a, b > 0)$$

$$\int_0^{\infty} \frac{dx}{e^{ax} + 1} = \frac{\log 2}{a} \quad (a > 0)$$

$$\int_0^{\infty} \frac{x dx}{e^{ax} + 1} = \frac{\pi^2}{12a^2} \quad (a > 0)$$

$$\int_0^{\infty} \frac{e^{-ax}}{x} \sin mx dx = \tan^{-1} \frac{m}{a} \quad (a > 0)$$

$$\int_0^{\infty} \frac{e^{-ax}}{x} \cos mx dx = \infty$$

$$\int_0^{\infty} \frac{e^{-ax}}{x} (1 - \cos mx) dx = \frac{1}{2} \ln \left(1 + \frac{m^2}{a^2}\right) \quad (a > 0)$$

$$\int_0^{\infty} \frac{e^{-ax}}{x} (\cos mx - \cos nx) dx = \frac{1}{2} \ln \frac{a^2 + n^2}{a^2 + m^2} \quad (a > 0)$$

$$\int_0^{\infty} \frac{e^{-ax} - e^{-bx}}{x} \cos mx dx = \frac{1}{2} \ln \frac{b^2 + m^2}{a^2 + m^2} \quad (a, b > 0)$$

$$\int_0^{\infty} e^{-ax} \cos^2 mx dx = \frac{a^2 + 2m^2}{a(a^2 + 4m^2)} \quad (a > 0)$$

$$\int_0^{\infty} e^{-ax} \sin^2 mx dx = \frac{2m^2}{a(a^2 + 4m^2)} \quad (a > 0)$$

$$\int_0^{\infty} \frac{e^{-ax}}{x} \sin^2 mx dx = \frac{1}{4} \ln \left(1 + \frac{4m^2}{a^2}\right) \quad (a > 0)$$

$$\int_0^{\infty} \frac{e^{-ax}}{x^2} \sin^2 mx dx = m \tan^{-1} \frac{2m}{a} - \frac{a}{4} \ln \left(1 + \frac{4m^2}{a^2}\right) \quad (a > 0)$$

$$\int_0^{\infty} e^{-ax} \sin mx \sin nx dx = \frac{2amn}{\{a^2 + (m-n)^2\} \{a^2 + (m+n)^2\}} \quad (a > 0)$$

$$\int_0^{\infty} e^{-ax} \sin mx \cos nx dx = \frac{m(a^2 + m^2 - n^2)}{\{a^2 + (m-n)^2\} \{a^2 + (m+n)^2\}} \quad (a > 0)$$

$$\int_0^{\infty} e^{-ax} \cos mx \cos nx dx = \frac{a(a^2 + m^2 + n^2)}{\{a^2 + (m-n)^2\} \{a^2 + (m+n)^2\}} \quad (a > 0)$$

$$\int_0^{\infty} \frac{e^{-ax}}{x} \sin mx \sin nx dx = \frac{1}{4} \log \frac{a^2 + (m+n)^2}{a^2 + (m-n)^2} \quad (a > 0)$$

$$\int_0^{\infty} e^{-a^2 x^2} \cos mx dx = \frac{\sqrt{\pi}}{2a} e^{-m^2/(4a^2)} \quad (a > 0)$$

$$\int_0^{\infty} x e^{-a^2 x^2} \sin mx dx = \frac{m\sqrt{\pi}}{4a^3} e^{-m^2/(4a^2)} \quad (a > 0)$$

$$\int_0^{\infty} \frac{e^{-a^2 x^2}}{x} \sin mx dx = \frac{\pi}{2} \operatorname{erf} \left(\frac{m}{2a}\right) \quad (a > 0)$$

$$\int_0^{\infty} \frac{e^{-ax}}{\sqrt{x}} \cos mx dx = \frac{\{a + \sqrt{(a^2 + m^2)}\}^{1/2} \sqrt{\pi}}{(a^2 + m^2)^{1/2} \sqrt{2}} \quad (a > 0)$$

$$\int_0^{\infty} e^{-ax} \sin \sqrt{(mx)} dx = \frac{\sqrt{(\pi m)}}{2a\sqrt{a}} e^{-m/(4a)} \quad (a, m > 0)$$

$$\int_0^{\infty} \frac{e^{-ax}}{\sqrt{x}} \cos \sqrt{mx} dx = \frac{\sqrt{\pi}}{\sqrt{a}} e^{-m/(4a)}$$

$$\int_0^{\infty} e^{-ax} \sin(px+q) dx = \frac{a \sin q + p \cos q}{a^2 + p^2}$$

$$\int_0^{\infty} e^{-ax} \cos(px+q) dx = \frac{a \cos q - p \sin q}{a^2 + p^2}$$

$$\int_0^{\infty} t^{b-1} \cos t dt = [\Gamma(b)] \cos\left(\frac{b\pi}{2}\right)$$

$$\int_0^{\infty} t^{b-1} (\sin t) dt = [\Gamma(b)] \sin\left(\frac{b\pi}{2}\right)$$

$$\int_0^1 (\ln x)^n dx = (-1)^n \cdot n!$$

$$\int_0^1 \left(\ln \frac{1}{x}\right)^{\frac{1}{2}} dx = \frac{\sqrt{\pi}}{2}$$

$$\int_0^1 \left(\ln \frac{1}{x}\right)^{-\frac{1}{2}} dx = \sqrt{\pi}$$

$$\int_0^1 \left(\ln \frac{1}{x}\right)^n dx = n!$$

$$\int_0^1 x \ln(1-x) dx = -\frac{3}{4}$$

$$\int_0^1 x \ln(1+x) dx = \frac{1}{4}$$

$$\int_0^1 \frac{\ln x}{1+x} dx = -\frac{\pi^2}{12}$$

$$\int_0^1 \frac{\ln x}{1-x} dx = -\frac{\pi^2}{6}$$

$$\int_0^1 \frac{\ln x}{1-x^2} dx = -\frac{\pi^2}{8}$$

$$\int_0^1 \ln\left(\frac{1+x}{1-x}\right) \cdot \frac{dx}{x} = \frac{\pi^2}{4}$$

$$(a, m > 0) \int_0^1 \frac{\ln x dx}{\sqrt{1-x^2}} = -\frac{\pi}{2} \ln 2$$

$$(a > 0) \int_0^1 x^m \left[\ln\left(\frac{1}{x}\right)\right]^n dx = \frac{\Gamma(n+1)}{(m+1)^{n+1}}, \quad \text{if } m+1 > 0, n+1 > 0$$

$$(a > 0) \int_0^1 \frac{(x^p - x^q) dx}{\ln x} = \ln\left(\frac{p+1}{q+1}\right) \quad (p+1 > 0, q+1 > 0)$$

$$(0 < b < 1) \int_0^1 \frac{dx}{\sqrt{\ln\left(\frac{1}{x}\right)}} = \sqrt{\pi}$$

$$(0 < b < 1) \int_0^{\infty} \ln\left(\frac{e^x + 1}{e^x - 1}\right) dx = \frac{\pi^2}{4}$$

$$\int_0^{\pi/2} \ln \sin x dx = \int_0^{\pi/2} \ln \cos x dx = -\frac{\pi}{2} \ln 2$$

$$\int_0^{\pi/2} \ln \sec x dx = \int_0^{\pi/2} \ln \csc x dx = \frac{\pi}{2} \ln 2$$

$$\int_0^{\pi} x \ln \sin x dx = -\frac{\pi^2}{2} \ln 2$$

$$\int_0^{\pi/2} \sin x \ln \sin x dx = \ln 2 - 1$$

$$\int_0^{\pi/2} \ln \tan x dx = 0$$

$$\int_0^{\pi} \ln(a \pm b \cos x) dx = \pi \log\left(\frac{a + \sqrt{a^2 - b^2}}{2}\right) \quad (a \geq b)$$

$$\int_0^{\infty} \frac{dx}{\cosh ax} = \frac{\pi}{2a}$$

$$\int_0^{\infty} \frac{x dx}{\sinh ax} = \frac{\pi^2}{4a^2}$$

$$\int_0^{\infty} e^{-ax} \cosh bx dx = \frac{a}{a^2 - b^2} \quad (0 \leq |b| < a)$$

$$\int_0^{\infty} e^{-ax} \sinh bx \, dx = \frac{b}{a^2 - b^2} \quad (0 \leq |b| < a)$$

$$\int_{+\infty}^1 \frac{e^{-xu}}{u} \, du = \gamma + \ln x - x + \frac{x^2}{2 \cdot 2!} - \frac{x^3}{3 \cdot 3!} + \frac{x^4}{4 \cdot 4!} - \dots,$$

$$\text{where } \gamma = \lim_{z \rightarrow \infty} \left( 1 + \frac{1}{2} + \frac{1}{3} + \dots + \frac{1}{z} - \ln z \right) \\ = 0.5772157 \dots \quad (0 < x < \infty)$$

$$\int_0^{\pi/2} \frac{dx}{\sqrt{1 - k^2 \sin^2 x}} = \frac{\pi}{2} \left[ 1 + \left( \frac{1}{2} \right)^2 k^2 + \left( \frac{1 \cdot 3}{2 \cdot 4} \right)^2 k^4 \right. \\ \left. + \left( \frac{1 \cdot 3 \cdot 5}{2 \cdot 4 \cdot 6} \right)^2 k^6 + \dots \right], \quad \text{if } k^2 < 1$$

$$\int_0^{\pi/2} \sqrt{1 - k^2 \sin^2 x} \, dx = \frac{\pi}{2} \left[ 1 - \left( \frac{1}{2} \right)^2 k^2 - \left( \frac{1 \cdot 3}{2 \cdot 4} \right)^2 \frac{k^4}{3} \right. \\ \left. - \left( \frac{1 \cdot 3 \cdot 5}{2 \cdot 4 \cdot 6} \right)^2 \frac{k^6}{5} - \dots \right], \quad \text{if } k^2 < 1$$

$$\int_0^{\infty} e^{-x} \ln x \, dx = -\gamma = -0.5772157 \dots$$

$$\int_0^{\infty} \left( \frac{1}{1 - e^{-x}} - \frac{1}{x} \right) e^{-x} \, dx = \gamma = 0.5772157 \dots \text{ (Euler's constant)}$$

$$\int_0^{\infty} \frac{1}{x} \left( \frac{1}{1+x} - e^{-x} \right) \, dx = \gamma = 0.5772157 \dots$$

# Appendix D: Matrices and Determinants

---

D.1	General Definitions.....	D-1
D.2	Addition, Subtraction, and Multiplication .....	D-2
D.3	Recognition Rules and Special Forms .....	D-2
D.4	Determinants.....	D-3
D.5	Singularity and Rank.....	D-5
D.6	Inversion.....	D-5
D.7	Traces.....	D-7
D.8	Characteristics Roots and Vector .....	D-8
D.9	Conditional Inverses.....	D-9
D.10	Matrix Differentiation .....	D-11
D.11	Statistical Matrix Forms.....	D-13

## D.1 General Definitions

---

**1.1** A matrix is an array of numbers consisting of  $m$  rows and  $n$  columns. It is usually denoted by a boldface capital letter, e.g.,

$$\mathbf{A} \sum \mathbf{M}.$$

**1.2** The  $(i, j)$  element of a matrix is the element occurring in row  $i$  and column  $j$ . It is usually denoted by a lowercase letter with subscripts, e.g.,

$$a_{ij} \sigma_{ij} m_{ij}.$$

Exceptions to this convention will be stated where required.

**1.3** A matrix is called rectangular if  $m$  (number of rows)  $\neq n$  (number of columns).

**1.4** A matrix is called square if  $m = n$ .

**1.5a** In the transpose of a matrix  $\mathbf{A}$ , denoted by  $\mathbf{A}'$ , the element in the  $j$ th row and  $i$ th column of  $\mathbf{A}$  is equal to the element in the  $i$ th row and  $j$ th column of  $\mathbf{A}'$ . Formally,  $(\mathbf{A}')_{ij} = (\mathbf{A})_{ji}$  where the symbol  $(\mathbf{A}')_{ij}$  denotes the  $(i, j)$ th element of  $\mathbf{A}'$ .

**1.5b** The Hermitian conjugate of a matrix  $\mathbf{A}$ , denoted by  $\mathbf{A}^H$  or  $\mathbf{A}^\dagger$ , is obtained by transposing  $\mathbf{A}$  and replacing each element by its conjugate complex. Hence, if

$$a_{k1} = u_{k1} + i v_{k1},$$

then

$$(\mathbf{A}^H)_{kl} = u_{kl} - i v_{kl},$$

where typical elements have been denoted by  $(k, l)$  to avoid confusion with  $i = \sqrt{-1}$ .

**1.6a** A square matrix is called *symmetric* if  $\mathbf{A} = \mathbf{A}'$ .

**1.6b** A square matrix is called *Hermitian* if  $\mathbf{A} = \mathbf{A}^H$ .

**1.7** A matrix with  $m$  rows and one column is called a column vector and is usually denoted by boldface, lowercase letters, e.g.,

$$\boldsymbol{\beta} \times \mathbf{a}.$$

**1.8** A matrix with one row and  $n$  columns is called a row vector and is usually denoted by a primed, boldface, lowercase letter, e.g.,

$$\mathbf{a}' \mathbf{c}' \boldsymbol{\mu}'.$$

**1.9** A matrix with one row and one column is called a scalar and is usually denoted by a lowercase letter, occasionally italicized.

**1.10** The diagonal extending from upper left (NW) to lower right (SE) is called the principal diagonal of a square matrix.

**1.11a** A matrix with all elements above the principal diagonal equal to zero is called a lower triangular matrix.

### Example

$$\mathbf{T} = \begin{bmatrix} t_{11} & 0 & 0 \\ t_{21} & t_{22} & 0 \\ t_{31} & t_{32} & t_{33} \end{bmatrix} \text{ is lower triangular.}$$

**1.11b** The transpose of a lower triangular matrix is called an upper triangular matrix.

**1.12** A square matrix with all off-diagonal elements equal to zero is called a diagonal matrix, denoted by the letter  $\mathbf{D}$  with a subscript indicating the typical element in the principal diagonal.

**Example**

$$\mathbf{D}_a = \begin{bmatrix} a_1 & 0 & 0 \\ 0 & a_2 & 0 \\ 0 & 0 & a_3 \end{bmatrix} \text{ is diagonal.}$$

## D.2 Addition, Subtraction, and Multiplication

**2.1** Two matrices  $\mathbf{A}$  and  $\mathbf{B}$  can be added (subtracted) if the number of rows (columns) in  $\mathbf{A}$  equals the number of rows (columns) in  $\mathbf{B}$ .

$$\mathbf{A} \pm \mathbf{B} = \mathbf{C}$$

implies

$$a_{ij} \pm b_{ij} = c_{ij}, \quad i = 1, 2, \dots, m \\ j = 1, 2, \dots, n$$

**2.2** Multiplication of a matrix or vector by a scalar implies multiplication of each element by the scalar. If

$$\mathbf{B} = \gamma \mathbf{A},$$

then

$$b_{ij} = \gamma a_{ij}$$

for all elements.

**2.3a** Two matrices  $\mathbf{A}$  and  $\mathbf{B}$  can be multiplied if the number of columns in  $\mathbf{A}$  equals the number of rows in  $\mathbf{B}$ .

**2.3b** Let  $\mathbf{A}$  be of order  $(m \times n)$  (have  $m$  rows and  $n$  columns) and  $\mathbf{B}$  of order  $(n \times p)$ . Then the product of two matrices  $\mathbf{C} = \mathbf{AB}$  is a matrix of order  $(m \times p)$  with elements

$$c_{ij} = \sum_{k=1}^n a_{ik} b_{kj}.$$

The states that  $c_{ij}$  is the scalar product of the  $i$ th row vector of  $\mathbf{A}$  and the  $j$ th column vector of  $\mathbf{B}$ .

**Example**

$$\begin{bmatrix} 3 & 4 & 2 \\ 2 & 3 & -1 \end{bmatrix} \begin{bmatrix} 1 & -2 & -4 \\ 0 & -1 & 2 \\ 6 & -3 & 9 \end{bmatrix} = \begin{bmatrix} 15 & -16 & 14 \\ -4 & -4 & -11 \end{bmatrix}$$

e.g.,

$$c_{23} = [2 \quad 3 \quad -1] \begin{bmatrix} -4 \\ 2 \\ 9 \end{bmatrix} \\ = 2 \times (-4) + 3 \times 2 + (-1) \times 9 = -11$$

**2.3c** In general, matrix multiplication is not commutative:

$$\mathbf{AB} \neq \mathbf{BA}.$$

**2.3d** Matrix multiplication is associative:

$$\mathbf{A}(\mathbf{BC}) = (\mathbf{AB})\mathbf{C}.$$

**2.3e** The distributive law for multiplication and addition holds as in the case of scalars:

$$(\mathbf{A} + \mathbf{B})\mathbf{C} = \mathbf{AC} + \mathbf{BC}$$

$$\mathbf{C}(\mathbf{A} + \mathbf{B}) = \mathbf{CA} + \mathbf{CB}.$$

**2.4** In some applications, the term-by-term product of two matrices  $\mathbf{A}$  and  $\mathbf{B}$  of identical order is defined as

$$\mathbf{C} = \mathbf{A} * \mathbf{B}$$

where

$$c_{ij} = a_{ij} b_{ij}.$$

**2.5**  $(\mathbf{ABC})' = \mathbf{C}'\mathbf{B}'\mathbf{A}'$ .

**2.6**  $(\mathbf{ABC})^H = \mathbf{C}^H\mathbf{B}^H\mathbf{A}^H$ .

**2.7** If both  $\mathbf{A}$  and  $\mathbf{B}$  are symmetric, then  $(\mathbf{AB})' = \mathbf{BA}$ . Note that the product of two symmetric matrices is generally not symmetric.

## D.3 Recognition Rules and Special Forms

**3.1** A column (row) vector with all elements equal to zero is called a null vector and is usually denoted by the symbol  $\mathbf{0}$ .

**3.2** A null matrix has all elements equal to zero.

**3.3a** A diagonal matrix with all elements equal to one in the principal diagonal is called the identity matrix  $\mathbf{I}$ .

**3.3b**  $\gamma \mathbf{I}$ , i.e., a diagonal matrix with all diagonal elements equal to a constant  $\gamma$ , is called a scalar matrix.

**3.4** A matrix that has only one element equal to one and all others equal to zero is called an elementary matrix  $(\mathbf{EL})_{ij}$ .

**Example**

$$(\mathbf{EL})_{23} = \begin{bmatrix} 0 & 0 & 0 & 0 & 0 \\ 0 & 0 & 1 & 0 & 0 \\ 0 & 0 & 0 & 0 & 0 \\ 0 & 0 & 0 & 0 & 0 \\ 0 & 0 & 0 & 0 & 0 \end{bmatrix}$$

The order of the matrix is usually implicit.

- 3.5a The symbol  $\mathbf{j}$  is reserved for a column vector with all elements equal to 1.
- 3.5b The symbol  $\mathbf{j}'$  is reserved for a row vector with all elements equal to 1.
- 3.6 An expression ending with a column vector is a column vector.

**Example**

$$\mathbf{ABx} = \mathbf{y}$$

(It is assumed that rule 2.3a is satisfied, else matrix multiplication would not be defined.)

- 3.7 An expression beginning with a row vector is a row vector:

**Example**

$$\mathbf{y}'(\mathbf{A} + \mathbf{BC}) = \mathbf{d}'.$$

- 3.8 An expression beginning with a row vector and ending with a column vector is a scalar:

**Example**

$$\mathbf{a}'\mathbf{Bc} = \gamma.$$

- 3.9a If  $\mathbf{Q}$  is a square matrix, the scalar  $\mathbf{x}'\mathbf{Qx}$  is called a quadratic form. If  $\mathbf{Q}$  is nonsymmetric, one can always find a symmetric matrix  $\mathbf{Q}^*$  such that

$$\mathbf{x}'\mathbf{Qx} = \mathbf{x}'\mathbf{Q}^*\mathbf{x}$$

where

$$(\mathbf{Q}^*)_{ij} = \frac{1}{2}(q_{ij} + q_{ji}).$$

- 3.9b If  $\mathbf{Q}$  is a square matrix, the scalar  $\mathbf{x}^H\mathbf{Qx}$  is called a Hermitian form.
- 3.10 A scalar  $\mathbf{x}'\mathbf{Qy}$  is called a bilinear form.
- 3.11 The scalar  $\mathbf{x}'\mathbf{x} = \sum x_i^2$ , i.e., the sum of squares of all elements of  $\mathbf{x}$ .
- 3.12 The scalar  $\mathbf{x}'\mathbf{y} = \sum x_i y_i$ , i.e., the sum of products of elements in  $\mathbf{x}$  by those in  $\mathbf{y}$ .  $\mathbf{x}$  and  $\mathbf{y}$  have the same number of elements.
- 3.13 The scalar  $\mathbf{x}'\mathbf{D}_w\mathbf{x} = \sum w_i x_i^2$  is called a weighted sum of squares.
- 3.14 The scalar  $\mathbf{x}'\mathbf{D}_w\mathbf{y} = \sum w_i x_i y_i$  is called a weighted sum of products.
- 3.15a The vector  $\mathbf{Aj}$  is a column vector whose elements are the row sums of  $\mathbf{A}$ .

- 3.15b The vector  $\mathbf{j}'\mathbf{A}$  is a row vector whose elements are the column sums of  $\mathbf{A}$ .
- 3.15c The scalar  $\mathbf{j}'\mathbf{Aj}$  is the sum of all elements in  $\mathbf{A}$ . Schematically,

$$\begin{array}{c|c} \mathbf{A} & \mathbf{Aj} \\ \hline \mathbf{j}'\mathbf{A} & \mathbf{j}'\mathbf{Aj} \end{array}$$

- 3.16a If  $\mathbf{B} = \mathbf{D}_w\mathbf{A}$ , then  $b_{ij} = w_i a_{ij}$ .
- 3.16b If  $\mathbf{B} = \mathbf{AD}_w$ , then  $b_{ij} = a_{ij} w_j$ .
- 3.17 Interchanging summation and matrix notation:  
If

$$\mathbf{ABCD} = \mathbf{E},$$

then

$$e_{ij} = \sum_k \sum_l \sum_m a_{ik} b_{kl} c_{lm} d_{mj}.$$

The second subscript of an element must coincide with the first of the next one. Reordering and transposing may be required.

**Example**

If

$$\begin{aligned} e_{ij} &= \sum_k \sum_l \sum_m a_{kl} b_{ki} c_{jm} d_{ml} \\ &= \sum_k \sum_l \sum_m b_{ki} a_{kl} d_{ml} c_{jm}, \end{aligned}$$

then

$$\mathbf{E} = \mathbf{B}'\mathbf{A}\mathbf{D}'\mathbf{C}'.$$

- 3.18a  $\mathbf{A}'\mathbf{A}$  is a symmetric matrix whose  $(i, j)$  element is the scalar product of the  $i$ th column vector and the  $j$ th column vector of  $\mathbf{A}$ .
- 3.18b  $\mathbf{AA}'$  is the symmetric matrix whose  $(i, j)$  element is the scalar product of the  $i$ th row vector and the  $j$ th row vector of  $\mathbf{A}$ .

## D.4 Determinants

- 4.1a A determinant  $|\mathbf{A}|$  or  $\det(\mathbf{A})$  is a scalar function of a square matrix defined in such a way that

$$|\mathbf{A}| |\mathbf{B}| = |\mathbf{AB}|$$

and

$$\begin{vmatrix} a_{11} & a_{12} \\ a_{21} & a_{22} \end{vmatrix} = a_{11}a_{22} - a_{12}a_{21}.$$

- 4.1b  $|\mathbf{A}| = |\mathbf{A}'|$ .



4.2

$$\begin{vmatrix} a_{11} & a_{12} & a_{13} \\ a_{21} & a_{22} & a_{23} \\ a_{31} & a_{32} & a_{33} \end{vmatrix} = a_{11}a_{22}a_{33} + a_{12}a_{23}a_{31} + a_{13}a_{21}a_{32} \\ - a_{13}a_{22}a_{31} - a_{11}a_{23}a_{32} - a_{12}a_{21}a_{33}.$$

4.3

$$\begin{vmatrix} a_{11} & a_{12} & \cdots & a_{1n} \\ a_{21} & a_{22} & \cdots & a_{2n} \\ \vdots & \vdots & \ddots & \vdots \\ a_{n1} & a_{n2} & \cdots & a_{nn} \end{vmatrix} = \sum (-1)^\delta a_{1i_1} a_{2i_2} \cdots a_{ni_n}$$

where the sum is over all permutations

$$i_1 \neq i_2 \neq \cdots i_n$$

and  $\delta$  denotes the number of exchanges necessary to bring the sequence  $(i_1, i_2, \dots, i_n)$  back into the natural order  $(1, 2, \dots, n)$ .

- 4.4 If two rows (columns) in a matrix are exchanged, the determinant will change its sign.
- 4.5 A determinant does not change its value if a linear combination of other rows (columns) is added to any given row (column).

**Example**

$$\begin{vmatrix} a_{11} & a_{12} & a_{13} & a_{14} \\ b_{21} & b_{22} & b_{23} & b_{24} \\ a_{31} & a_{32} & a_{33} & a_{34} \\ a_{41} & a_{42} & a_{43} & a_{44} \end{vmatrix} = \begin{vmatrix} a_{11} & a_{12} & a_{13} & a_{14} \\ a_{21} & a_{22} & a_{23} & a_{24} \\ a_{31} & a_{32} & a_{33} & a_{34} \\ a_{41} & a_{42} & a_{43} & a_{44} \end{vmatrix}$$

where

$$b_{2i} = a_{2i} + \gamma_1 a_{1i} + \gamma_3 a_{3i} + \gamma_4 a_{4i}, \\ i = 1, 2, 3, 4,$$

$\gamma_1, \gamma_3, \gamma_4$  arbitrary.

- 4.6 If the  $i$ th row (column) equals (a constant times) the  $j$ th row (column) of a matrix, its determinant is equal to zero ( $i \neq j$ ).
- 4.7 If, in a matrix  $\mathbf{A}$ , each element of a row (column) is multiplied by a constant  $\gamma$ , the determinant is multiplied by  $\gamma$ .
- 4.8  $|\gamma \mathbf{A}| = \gamma^n |\mathbf{A}|$  assuming that  $\mathbf{A}$  is of order  $(n \times n)$ .
- 4.9 The cofactor of a square matrix  $\mathbf{A}$ ,  $\text{cof}_{ij}(\mathbf{A})$ , is the determinant of a matrix obtained by striking the  $i$ th row and  $j$ th column of  $\mathbf{A}$  and choosing positive (negative) sign if  $i + j$  is even (odd):

**Example**

$$\text{cof}_{23} \begin{vmatrix} 2 & 4 & 3 \\ 6 & 1 & 5 \\ -2 & 1 & 3 \end{vmatrix} = - \begin{vmatrix} 2 & 4 \\ -2 & 1 \end{vmatrix} \\ = -(2 + 8) = -10.$$

4.10 (Laplace development)

$$|\mathbf{A}| = a_{i1} \text{cof}_{i1}(\mathbf{A}) + a_{i2} \text{cof}_{i2}(\mathbf{A}) + \cdots + a_{in} \text{cof}_{in}(\mathbf{A}) \\ = a_{1j} \text{cof}_{1j}(\mathbf{A}) + a_{2j} \text{cof}_{2j}(\mathbf{A}) + \cdots + a_{nj} \text{cof}_{nj}(\mathbf{A})$$

for any row  $i$  or any column  $j$ .

4.11 Numerical evaluation of the determinant of a symmetric matrix.

Note: If  $\mathbf{A}$  is nonsymmetric, from  $\mathbf{A}'\mathbf{A}$  or  $\mathbf{A}\mathbf{A}'$  by rule 3.18, obtain its determinant, and take the square root. ("Forward Doolittle Scheme," "left side")

Let

$$p_{11} = a_{11}, \quad p_{12} = a_{12} = a_{21}, \dots, p_{1n} = a_{1n}$$

$$\begin{array}{cccccc} p_{11} & p_{12} & p_{13} & \cdots & p_{1n} & \\ \hline 1 & u_{12} & u_{13} & \cdots & u_{1n} & \\ & a_{22} & a_{23} & \cdots & a_{2n} & \\ & p_{22} & p_{23} & \cdots & p_{2n} & \\ & \hline & 1 & u_{23} & \cdots & u_{2n} & \\ & & a_{33} & \cdots & a_{3n} & \\ & & p_{33} & \cdots & p_{3n} & \\ & & \hline & & 1 & \cdots & u_{3n} & \\ & & & \cdots & \cdots & \cdots & \\ & & & & & & a_{nn} \\ & & & & & & p_{nn} \\ & & & & & & 1 \end{array}$$

$$u_{1i} = p_{1i}/p_{11} \quad i = 1, 2, \dots, n$$

$$p_{2i} = a_{2i} - u_{12}p_{1i} \quad i = 2, 3, \dots, n$$

$$u_{2i} = p_{2i}/p_{22}$$

$$p_{3i} = a_{3i} - u_{13}p_{1i} - u_{23}p_{2i} \quad i = 3, 4, \dots, n$$

$$u_{3i} = p_{3i}/p_{33}$$

$$p_{ki} = a_{ki} - u_{1k}p_{1i} - u_{2k}p_{2i} - \cdots - u_{k-1,k}p_{k-1,i} \quad i = k, k + 1, \dots, n \\ k = 2, 3, \dots, n$$

$$u_{ki} = p_{ki}/p_{kk}$$

If, at some stage,  $p_{kk} = 0$ , reordering of rows and columns may be required. If the matrix is positive-definite (see 8.16) (always true for  $\mathbf{A}\mathbf{A}'$  or  $\mathbf{A}'\mathbf{A}$ ; see rule 10.24), none of the  $p_{kk}$  will be zero. The  $p_{ii}$  are called pivots. Then

$$|\mathbf{A}| = \prod_{i=1}^n p_{ii}.$$

Further, if  $\mathbf{A}$  is partitioned

$$\mathbf{A} = \begin{bmatrix} \mathbf{A}_{11} & \mathbf{A}_{12} \\ \mathbf{A}'_{12} & \mathbf{A}_{22} \end{bmatrix}$$

where  $\mathbf{A}_{11}$  is of order  $(k \times k)$ , then

$$|\mathbf{A}_{11}| = \prod_{i=1}^n p_{ii}.$$

(Numerical examples: see 6.14.)

## D.5 Singularity and Rank

- 5.1 A matrix  $\mathbf{A}$  is called *singular* if there exists a vector  $\mathbf{x} \neq \mathbf{0}$  such that  $\mathbf{Ax} = \mathbf{0}$  or  $\mathbf{A}'\mathbf{x} = \mathbf{0}$ . Note  $\mathbf{x} \neq \mathbf{0}$  if a single element of  $\mathbf{x}$  is unequal to 0. If a matrix is not singular, it is called *nonsingular*.
- 5.2 If a matrix  $\mathbf{A}_1$  can be formed by selection of  $r$  rows and columns of  $\mathbf{A}$  such that  $\mathbf{A}_1\mathbf{x} \neq \mathbf{0}$  or  $\mathbf{A}'_1\mathbf{x} \neq \mathbf{0}$  for every  $\mathbf{x} \neq \mathbf{0}$ , and if addition of an  $(r + 1)$ st row and column would produce a singular matrix,  $r$  is called the *rank* of  $\mathbf{A}$ .

### Example

$$\mathbf{A} = \begin{bmatrix} 2 & 4 & 6 \\ 1 & 3 & 7 \\ 3 & 7 & 13 \\ 1 & 1 & -1 \end{bmatrix}$$

Note that

$$[1, \quad 1, \quad -1] \begin{bmatrix} 2 & 4 & 6 \\ 1 & 3 & 7 \\ 3 & 7 & 13 \end{bmatrix} = [0 \quad 0 \quad 0]$$

and

$$[1, \quad -1, \quad -1] \begin{bmatrix} 2 & 4 & 6 \\ 1 & 3 & 7 \\ 1 & 1 & -1 \end{bmatrix} = [0 \quad 0 \quad 0]$$

but

$$\begin{bmatrix} 2 & 4 \\ 1 & 3 \end{bmatrix} \begin{bmatrix} x_1 \\ x_2 \end{bmatrix} \neq \begin{bmatrix} 0 \\ 0 \end{bmatrix}$$

or

$$[x_1 \quad x_2] \begin{bmatrix} 2 & 4 \\ 1 & 3 \end{bmatrix} \neq [0, \quad 0]$$

for any arbitrary

$$[x_1, \quad x_2] \neq [0, \quad 0].$$

Hence, the matrix has rank 2.

- 5.3 If  $\mathbf{A}$  has rank  $r$  and if  $\mathbf{A}_1$  is a nonsingular submatrix consisting of  $r$  rows and columns of  $\mathbf{A}$ , then  $\mathbf{A}_1$  is called a *basis* of  $\mathbf{A}$ .
- 5.4a The determinant of a square singular matrix is 0.
- 5.4b The determinant of a nonsingular matrix is  $\neq 0$ .
- 5.5  $\text{rank}(\mathbf{AB}) \leq \min[\text{rank}(\mathbf{A}), \text{rank}(\mathbf{B})]$ .
- 5.6  $\text{rank}(\mathbf{AA}') = \text{rank}(\mathbf{A}'\mathbf{A}) = \text{rank}(\mathbf{A})$ .
- 5.7  $|\mathbf{A}'\mathbf{A}| = |\mathbf{AA}'| = |\mathbf{A}|^2$  if  $\mathbf{A}$  is square.
- 5.8  $|\mathbf{A}'\mathbf{A}| = |\mathbf{AA}'| \geq 0$  for every  $\mathbf{A}$  with real elements.

## D.6 Inversion

*Regular case, nonsingular matrices*

- 6.1 If  $\mathbf{A}$  is square and nonsingular ( $|\mathbf{A}| \neq 0$ ), there exists a unique matrix  $\mathbf{A}^{-1}$  such that  $\mathbf{AA}^{-1} = \mathbf{A}^{-1}\mathbf{A} = \mathbf{I}$ .
- 6.2  $(\mathbf{ABC})^{-1} = \mathbf{C}^{-1}\mathbf{B}^{-1}\mathbf{A}^{-1}$  (provided that all inverses exist).
- 6.3  $(\mathbf{A}^{-1})' = (\mathbf{A}')^{-1}$ .
- 6.4  $\mathbf{Ax} = \mathbf{b}$  is a system of linear equations. If  $\mathbf{A}$  is square and nonsingular, there exists a unique solution

$$\mathbf{x} = \mathbf{A}^{-1}\mathbf{b}.$$

- 6.5  $(\gamma\mathbf{A})^{-1} = (1/\gamma)\mathbf{A}^{-1}$ .
- 6.6  $|\mathbf{A}^{-1}| = 1/|\mathbf{A}|$ .
- 6.7  $\mathbf{D}_w^{-1} = \mathbf{D}_{1/w}$  where  $\mathbf{D}$  is a diagonal matrix.
- 6.8 If

$$\mathbf{A} = \mathbf{B} + \mathbf{uv}'$$

then

$$\mathbf{A}^{-1} = \mathbf{B}^{-1} - \lambda\mathbf{yz}'$$

where

$$\mathbf{y} = \mathbf{B}^{-1}\mathbf{u}, \quad \mathbf{z}' = \mathbf{v}'\mathbf{B}^{-1},$$

and

$$\lambda = 1/(1 + \mathbf{z}'\mathbf{u}).$$

### Example 6.8.1

$$\mathbf{A} = \begin{bmatrix} 4 & 2 & 4 & 5 \\ 3 & 9 & 12 & 15 \\ 2 & 4 & 11 & 10 \\ 1 & 2 & 4 & 10 \end{bmatrix}$$

This matrix can be written as

$$\begin{bmatrix} 3 & 0 & 0 & 0 \\ 0 & 3 & 0 & 0 \\ 0 & 0 & 3 & 0 \\ 0 & 0 & 0 & 5 \end{bmatrix} + \begin{bmatrix} 1 \\ 3 \\ 2 \\ 1 \end{bmatrix} [1 \quad 2 \quad 4 \quad 5] = \mathbf{B} + \mathbf{uv}'$$

$$\mathbf{B}^{-1} = \begin{bmatrix} 1/3 & 0 & 0 & 0 \\ 0 & 1/3 & 0 & 0 \\ 0 & 0 & 1/3 & 0 \\ 0 & 0 & 0 & 1/5 \end{bmatrix}$$

$$\mathbf{y} = \mathbf{B}^{-1}\mathbf{u} = \begin{bmatrix} 1/3 \\ 1 \\ 2/3 \\ 1/5 \end{bmatrix}$$

$$\mathbf{z}' = \mathbf{v}'\mathbf{B}^{-1} = [1/3 \quad 2/3 \quad 4/3 \quad 1]$$

$$\mathbf{z}'\mathbf{u} = 1/3 \times 1 + 2/3 \times 3 + 4/3 \times 2 + 1 \times 1 = 6$$

$$\lambda = 1/7$$

$$\mathbf{A}^{-1} = \begin{bmatrix} 1/3 & 0 & 0 & 0 \\ 0 & 1/3 & 0 & 0 \\ 0 & 0 & 1/3 & 0 \\ 0 & 0 & 0 & 1/5 \end{bmatrix} - (1/7) \begin{bmatrix} 1 \\ 1 \\ 2/3 \\ 1/5 \end{bmatrix} [1/3 \quad 2/3 \quad 4/3 \quad 1]$$

$$= (1/315) \begin{bmatrix} 100 & -10 & -20 & -15 \\ -15 & 75 & -60 & -45 \\ -10 & -20 & 65 & -30 \\ -3 & -6 & -12 & 54 \end{bmatrix}$$

(This rule is especially useful if all off-diagonal elements are equal; then  $\mathbf{u} = k\mathbf{j}$  and  $\mathbf{v}' = \mathbf{j}'$  and  $\mathbf{B}$  is diagonal.)

**6.9** Let  $\mathbf{B}$  (elements  $b_{ij}$ ) have a known inverse,  $\mathbf{B}^{-1}$  (elements  $b^{ij}$ ). Let  $\mathbf{A} = \mathbf{B}$  except for one element  $a_{rs} = b_{rs} + k$ . Then the elements of  $\mathbf{A}^{-1}$  are

$$a^{ij} = b^{ij} - \frac{kb^{ir}b^{sj}}{1 + kb^{sr}}$$

**6.10** (Partitioning)

Let

$$\mathbf{A} = \begin{matrix} & \begin{matrix} (p) & (q) \end{matrix} \\ \begin{matrix} (p) \\ (q) \end{matrix} & \begin{bmatrix} \mathbf{B} & \mathbf{C} \\ \mathbf{D} & \mathbf{E} \end{bmatrix} \end{matrix} \quad \begin{matrix} \text{(letters in parentheses} \\ \text{denote order of the submatrices).} \end{matrix}$$

Let  $\mathbf{B}^{-1}$  and  $\mathbf{E}^{-1}$  exist. Then

$$\mathbf{A}^{-1} = \begin{bmatrix} \mathbf{X} & \mathbf{Y} \\ \mathbf{Z} & \mathbf{U} \end{bmatrix}$$

where

$$\mathbf{X} = (\mathbf{B} - \mathbf{C}\mathbf{E}^{-1}\mathbf{D})^{-1}$$

$$\mathbf{U} = (\mathbf{E} - \mathbf{D}\mathbf{B}^{-1}\mathbf{C})^{-1}$$

$$\mathbf{Y} = -\mathbf{B}^{-1}\mathbf{C}\mathbf{U}$$

$$\mathbf{Z} = -\mathbf{E}^{-1}\mathbf{D}\mathbf{X}$$

**6.11** (Partitioning of determinants)

Let

$$|\mathbf{A}| = \begin{vmatrix} \mathbf{B} & \mathbf{C} \\ \mathbf{D} & \mathbf{E} \end{vmatrix} \quad \text{(structure as in Equation 6.10).}$$

Then

$$|\mathbf{A}| = |\mathbf{E}| |(\mathbf{B} - \mathbf{C}\mathbf{E}^{-1}\mathbf{D})| = |\mathbf{B}| |(\mathbf{E} - \mathbf{D}\mathbf{B}^{-1}\mathbf{C})|.$$

**6.12.** Let

$$\mathbf{A} = \mathbf{B} + \mathbf{UV}$$

where  $\mathbf{B}(n \times n)$  has an inverse

$\mathbf{U}$  is of order  $(n \times k)$ , with  $k$  usually very small

$\mathbf{V}$  is of order  $(k \times n)$

(the special case for  $k = 1$  is treated in 6.8).

Then

$$\mathbf{A}^{-1} = \mathbf{B}^{-1} - \mathbf{Y}\mathbf{\Lambda}\mathbf{Z}$$

where

$$\mathbf{Y} = \mathbf{B}^{-1}\mathbf{U}(n \times k)$$

$$\mathbf{Z} = \mathbf{V}\mathbf{B}^{-1}(k \times n)$$

and

$$\mathbf{\Lambda}(k \times k) = [\mathbf{I} + \mathbf{Z}\mathbf{U}]^{-1}$$

**6.13** Let  $a_{ij}$  denote the elements of  $\mathbf{A}$  and  $a^{ij}$  those of  $\mathbf{A}^{-1}$ . Then

$$a^{ij} = \text{cof}_{ji}(\mathbf{A})/|\mathbf{A}|$$

where cof is the determinant defined in 4.9.

**6.14** "Doolittle" Method of inverting symmetric matrices (see also 4.11). Let

$$p_{11} = a_{11}, p_{12} = a_{12} = a_{21}, \dots, p_{1n} = a_{1n} = a_{n1}.$$

Forward Solution

$p_{11}$	$p_{12}$	$p_{13}$	$\cdots$	$p_{1n}$	1					
1	$u_{12}$	$u_{13}$	$\cdots$	$u_{1n}$	$u_{1I}$	0	1	—		
	$a_{22}$	$a_{23}$	$\cdots$	$a_{2n}$	$p_{2I}$	$p_{2II}$	—			
	$p_{22}$	$p_{23}$	$\cdots$	$p_{2n}$	$u_{2I}$	$p_{2II}$				
	1	$u_{23}$	$\cdots$	$u_{2n}$		0	0	1		
		$a_{33}$	$\cdots$	$a_{3n}$		$p_{3I}$	$p_{3II}$	$p_{3III}$		
		$p_{33}$	$\cdots$	$p_{3n}$		$u_{3I}$	$u_{3II}$	$u_{3III}$		
		1	$\cdots$	$u_{3n}$		$u_{3I}$	$u_{3II}$	$u_{3III}$		
		$\cdots$	$\cdots$	$\cdots$		$\cdots$	$\cdots$	$\cdots$	—	
				$a_{nn}$		0	0	0	$\cdots$	1
				$p_{nn}$		$p_{nI}$	$p_{nII}$	$p_{nIII}$	$\cdots$	$p_{nN}$
				1		$u_{nI}$	$u_{nII}$	$u_{nIII}$	$\cdots$	$u_{nN}$

$$\begin{aligned}
 u_{1i} &= p_{1i}/p_{11} & i &= 1, 2, \dots, n, \text{ I} \\
 p_{2i} &= a_{2i} - u_{12}p_{1i} & i &= 2, 3, \dots, n, \text{ I, II} \\
 u_{2i} &= p_{2i}/p_{22} \\
 p_{3i} &= a_{3i} - u_{13}p_{1i} - u_{23}p_{2i} & i &= 3, 4, \dots, n, \text{ I, II, III} \\
 u_{3i} &= p_{3i}/p_{33} \\
 p_{ki} &= a_{ki} - u_{1k}p_{1i} - u_{2k}p_{2i} \\
 &\quad - \dots - u_{k-1,k}p_{k-1,i} & i &= k, k+1, \dots, n, \text{ I, II, } \dots, \text{ K} \\
 & & k &= 2, 3, \dots, n
 \end{aligned}$$

$$u_{ki} = p_{ki}/p_{kk}$$

**Backward Solution**

*j* refers to Arabic, *J* refers to Roman numerals

The elements of  $\mathbf{A}^{-1}$  are  $a^{ij}$

$$\begin{aligned}
 a^{nj} &= u_{nj} & j &= 1, 2, \dots, n; \\
 & & J &= \text{I, II, } \dots, \text{ N} \\
 a^{n-1j} &= u_{n-1,J} - u_{n-1,n}a^{nj} & j &= 1, 2, \dots, (n-1); \\
 & & J &= \text{I, II, } \dots, \text{ (N-1)} \\
 a^{n-2,j} &= u_{n-2,J} - u_{n-2,n}a^{nj} \\
 &\quad - u_{n-2,n-1}a^{n-1,j} & j &= 1, 2, \dots, (n-2); \\
 & & J &= \text{I, II, } \dots, \text{ (N-2)} \\
 a^{n-k,j} &= u_{n-k,J} - u_{n-k,n}a^{nj} \\
 &\quad - u_{n-k,n-1}a^{n-1,j} \\
 &\quad - \dots - u_{n-k,n-k+1}a^{n-k+1,j} & j &= 1, 2, \dots, (n-k); \\
 & & J &= \text{I, II, } \dots, \text{ (N-k)} \\
 & & k &= 1, 2, \dots, (n-1),
 \end{aligned}$$

and  $a^{ji} = a^{ij}$ .

**Numerical Example 6.14.1**

Invert the matrix

$$\begin{bmatrix} 25 & 30 & -10 \\ 30 & 40 & -6 \\ -10 & -6 & 17 \end{bmatrix}$$

$a_1$	25	30	-10	1	
$u_1$	1	1.2	-0.4	0.04	
$a_2$	40	-6	0	0	1
$p_2$	4	6	-1.2	0	1
$u_2$	1	1.5	-0.3	0.25	
$a_3$	17	0	0	0	1
$p_3$	4	2.2	-1.5	0	1
$u_3$	1	0.55	-0.375	0.25	

1.61	-1.125	0.55
-1.125	0.8125	-0.375
0.55	0.375	0.25

Enter row  $a_1$ .

Elements in  $u_1$  = elements in  $a_1$  divided by  $a_{11}$  (= 25).

Enter row  $a_2$ .

$$\begin{aligned}
 p_{22} &= 40 - 1.2 \times 30 = 4 \\
 p_{23} &= -6 - 1.2 \times (-10) = 6 \\
 p_{21} &= 0 - 1.2 \times 1 = -1.2 \\
 p_{311} &= 1
 \end{aligned}$$

Elements in  $u_2$  = elements in  $p_2$  divided by  $p_{22}$  (= 4).  
Enter row  $a_3$ .

$$\begin{aligned}
 p_{33} &= 17 - (-0.4) \times (-10) - 1.5 \times 6 = 4 \\
 p_{31} &= 0 - (-0.4) \times 1 - 1.5 \times (-1.2) = 2.2 \\
 p_{311} &= 0 - 1.5 \times 1 = -1.5 \\
 p_{3111} &= 1
 \end{aligned}$$

Elements in  $u_3$  = elements in  $p_3$  divided by  $p_{33}$  (= 4).

Copy the right-hand side of the last (third)  $u$ -row as the last column below the double line.

$$\begin{aligned}
 a^{21} &= -0.3 - 1.5 \times 0.55 = -1.125 \\
 a^{22} &= 0.25 - 1.5 \times (-0.375) = 0.8125 \\
 a^{23} &= 0 - 1.5 \times 0.25 = -0.375 \text{ (check against } a^{32}\text{)}.
 \end{aligned}$$

These are entered in the next to last (second) column below.

$$\begin{aligned}
 a^{11} &= 0.04 - (-0.4) \times 0.55 - 1.2 \times (-1.125) = 1.61 \\
 a^{12} &= 0 - (-0.4) \times (-0.375) - 1.2 \times 0.8125 = \\
 &\quad - 1.125 \text{ (check against } a^{21}\text{)} \\
 a^{13} &= 0 - (-0.4) \times (0.25) - 1.2 \times (-0.375) \\
 &\quad = .55 \text{ (check against } a^{31}\text{)}.
 \end{aligned}$$

**6.15** A matrix is called orthogonal is  $\mathbf{A}' = \mathbf{A}^{-1}$  (or  $\mathbf{A}\mathbf{A}' = \mathbf{I}$ ).

**D.7 Traces**

- 7.1** If  $\mathbf{A}$  is a square matrix, then the trace of  $\mathbf{A}$  is  $\text{tr } \mathbf{A} = \sum_i a_{ii}$  i.e., the sum of the diagonal elements.
- 7.2** If  $\mathbf{A}$  is of order  $(m \times k)$  and  $\mathbf{B}$  of order  $(k \times m)$  then  $\text{tr}(\mathbf{A}\mathbf{B}) = \text{tr}(\mathbf{B}\mathbf{A})$ .
- 7.3** If  $\mathbf{A}$  is of order  $(m \times k)$ ,  $\mathbf{B}$  of order  $(k \times r)$ , and  $\mathbf{C}$  of order  $(r \times m)$ , then

$$\text{tr}(\mathbf{A}\mathbf{B}\mathbf{C}) = \text{tr}(\mathbf{B}\mathbf{C}\mathbf{A}) = \text{tr}(\mathbf{C}\mathbf{A}\mathbf{B}).$$

**7.3a** If  $\mathbf{b}$  is a column vector and  $\mathbf{c}'$  a row vector, then

$$\text{tr}(\mathbf{A}\mathbf{b}\mathbf{c}') = \text{tr}(\mathbf{b}\mathbf{c}'\mathbf{A}) = \mathbf{c}'\mathbf{A}\mathbf{b}.$$

since the trace of a scalar is the scalar.

- 7.4**  $\text{tr}(\mathbf{A} + \gamma\mathbf{B}) = \text{tr } \mathbf{A} + \gamma \text{tr } \mathbf{B}$ , where  $\gamma$  is a scalar.
- 7.5**  $\text{tr}(\mathbf{E}\mathbf{L})_{ij}\mathbf{A} = \text{tr } \mathbf{A}(\mathbf{E}\mathbf{L})_{ij} = a_{ji}$ , where  $(\mathbf{E}\mathbf{L})_{ij}$  is an elementary matrix as defined in 3.4.

- 7.6  $\text{tr}(\mathbf{E}\mathbf{L})_{ij}\mathbf{A}(\mathbf{E}\mathbf{L})_{rs}\mathbf{B} = a_{jr}b_{si}$ .  
 (These rules are useful in matrix differentiation)
- 7.7 The trace of the second order of a square matrix  $\mathbf{A}$  is the sum of the determinants of all  $\binom{n}{2}$  matrices of order  $(2 \times 2)$  that can be formed by intersecting rows  $i$  and  $j$  with columns  $i$  and  $j$ .

$$\begin{aligned} \text{tr}_2 \mathbf{A} = & \begin{vmatrix} a_{11} & a_{12} \\ a_{21} & a_{22} \end{vmatrix} + \begin{vmatrix} a_{11} & a_{13} \\ a_{31} & a_{33} \end{vmatrix} \\ & + \dots + \begin{vmatrix} a_{11} & a_{1n} \\ a_{n1} & a_{nn} \end{vmatrix} + \begin{vmatrix} a_{22} & a_{23} \\ a_{32} & a_{33} \end{vmatrix} \\ & + \dots + \begin{vmatrix} a_{22} & a_{2n} \\ a_{n2} & a_{nn} \end{vmatrix} + \dots + \begin{vmatrix} a_{n-1,n-1} & a_{n-1,n} \\ a_{n,n-1} & a_{nn} \end{vmatrix}. \end{aligned}$$

- 7.8 The trace of the  $k$ th order of a square matrix is the sum of the determinants of all  $\binom{n}{k}$  matrices of order  $(k \times k)$  that can be formed by intersecting any  $k$  rows of  $\mathbf{A}$  with the same  $k$  columns.

$$\text{tr}_k \mathbf{A} = \sum \begin{vmatrix} a_{i_1 i_1} & a_{i_1 i_2} & \dots & a_{i_1 i_k} \\ a_{i_2 i_1} & a_{i_2 i_2} & \dots & a_{i_2 i_k} \\ \dots & \dots & \dots & \dots \\ a_{i_k i_1} & a_{i_k i_2} & \dots & a_{i_k i_k} \end{vmatrix}$$

where the sum extends over all combinations of  $n$  elements taken  $k$  at a time in order

$$i_1 < i_2 < \dots < i_k.$$

- 7.9 Rules 7.2 and 7.3 (cyclic exchange) are valid for trace of  $k$ th order.
- 7.10  $\text{tr}_n \mathbf{A} = |\mathbf{A}|$  if  $\mathbf{A}$  is of order  $(n \times n)$ .

## D.8 Characteristics Roots and Vector

- 8.1 If  $\mathbf{A}$  is a square matrix of order  $(n \times n)$ , then  $|\mathbf{A} - \lambda \mathbf{I}| = 0$  is called the characteristic equation of the matrix  $\mathbf{A}$ . It is a polynomial of the  $n$ th degree in  $\lambda$ .
- 8.2 The  $n$  roots of the characteristic equation (not necessarily distinct) are called the characteristic roots of  $\mathbf{A}$

$$\text{ch}(\mathbf{A}) = \lambda_1, \lambda_2, \dots, \lambda_n.$$

- 8.3 The characteristic equation of  $\mathbf{A}$  can be obtained by the relation

$$\begin{aligned} \lambda^n - (\text{tr} \mathbf{A})\lambda^{n-1} + (\text{tr}_2 \mathbf{A})\lambda^{n-2} - (\text{tr}_3 \mathbf{A})\lambda^{n-3} \dots \\ - (-1)^n (\text{tr}_{n-1} \mathbf{A})\lambda + (-1)^n |\mathbf{A}| = 0 \end{aligned}$$

where  $\text{tr}_k$  is defined in 7.8.

### Example 8.3.1

$$\mathbf{A} = \begin{bmatrix} 25 & 30 & -10 \\ 30 & 40 & -6 \\ -10 & -6 & 17 \end{bmatrix}$$

$$\text{tr} \mathbf{A} = 25 + 40 + 17 = 82$$

$$\begin{aligned} \text{tr}_2 \mathbf{A} = (25 \times 40 - 30 \times 30) + (25 \times 17 - 10 \times 10) \\ + (40 \times 17 - 6 \times 6) = 1069 \end{aligned}$$

$$\text{tr}_3 \mathbf{A} = |\mathbf{A}| = 25 \times 4 \times 4 = 400$$

(cf. 6.14 and procedure stated in 4.11)  
 Hence,

$$\lambda^3 - 82\lambda^2 + 1069\lambda - 400 = 0.$$

The solution (by Newton iteration) are

$$\lambda_1 = 65.86108$$

$$\lambda_2 = 15.75339$$

$$\lambda_3 = 0.38553.$$

These are the characteristic roots of  $\mathbf{A}$ .

- 8.4  $\text{ch}(\mathbf{A} + \gamma \mathbf{I}) = \gamma + \text{ch}(\mathbf{A})$ .
- 8.5  $\text{ch}(\mathbf{A}\mathbf{B}) = \text{ch}(\mathbf{B}\mathbf{A})$   
 except that  $\mathbf{A}\mathbf{B}$  or  $\mathbf{B}\mathbf{A}$  may have additional roots equal to zero.
- 8.6  $\text{ch}(\mathbf{A}^{-1}) = 1/\text{ch}(\mathbf{A})$ .
- 8.7 If  $\lambda_1, \lambda_2, \dots, \lambda_n$  are the roots of  $\mathbf{A}$ , then

$$\begin{aligned} \sum_i \lambda_i &= \text{tr} \mathbf{A} \\ \sum_{i < j} \lambda_i \lambda_j &= \text{tr}_2 \mathbf{A} \\ \sum_{i < j < k} \lambda_i \lambda_j \lambda_k &= \text{tr}_3 \mathbf{A} \\ \prod_i \lambda_i &= |\mathbf{A}|. \end{aligned}$$

- 8.8 If  $\mathbf{x}'$  denotes the radius vector (running coordinates  $[x, y, z]$ ) and if a matrix  $\mathbf{Q}$  is positive-definite, then

$$(\mathbf{x}' - \mathbf{x}'_0) \mathbf{Q}^{-1} (\mathbf{x} - \mathbf{x}_0) = 1$$

is the equation of an ellipsoid with center at  $[x_0, y_0, z_0] = \mathbf{x}'_0$  and semi-axes equal to the square roots of the characteristic roots of  $\mathbf{Q}$ .

- 8.9 The characteristic roots of a triangular (or diagonal) matrix are the diagonal elements of the matrix.
- 8.10 If  $\mathbf{A}$  is a real matrix with positive roots, then

$$\text{ch}_{\min}(\mathbf{A}\mathbf{A}') \leq [\text{ch}_{\min}(\mathbf{A})]^2 \leq [\text{ch}_{\max}(\mathbf{A})]^2 \leq \text{ch}_{\max}(\mathbf{A}\mathbf{A}')$$

where  $\text{ch}_{\min}$  denotes the smallest and  $\text{ch}_{\max}$  the largest root.

8.11 The ratio of two quadratic forms (**B** nonsingular)

$$u = \frac{\mathbf{x}'\mathbf{A}\mathbf{x}}{\mathbf{x}'\mathbf{B}\mathbf{x}}$$

attains stationary values at the roots of  $\mathbf{B}^{-1}\mathbf{A}$ . In particular,

$$u_{\max} = \text{ch}_{\max}(\mathbf{B}^{-1}\mathbf{A}) \text{ and } u_{\min} = \text{ch}_{\min}(\mathbf{B}^{-1}\mathbf{A}).$$

8.12 The equation system

$$\mathbf{A}\mathbf{x} = \lambda\mathbf{x}$$

permits nonzero solutions only if  $\lambda$  is one of the characteristic roots of **A**. Such a solution **x** is called a characteristic vector.

- 8.13 If **x** is a solution to 8.12, so is  $\gamma\mathbf{x}$  for an arbitrary scalar  $\gamma$ .
- 8.14 A solution **x** which has unit length ( $\mathbf{x}'\mathbf{x} = 1$ ) is called the eigenvector associated with the characteristic root  $\lambda$  of **A**. The vector is frequently denoted by **e**.
- 8.15 A real symmetric matrix has real roots.
- 8.16 A matrix **A** is called positive-definite (abbreviated p.d.) if the quadratic form  $\mathbf{x}'\mathbf{A}\mathbf{x} > 0$  for every  $\mathbf{x} \neq \mathbf{0}$ .
- 8.17 A matrix **A** is called positive-semidefinite (abbreviated p.s.d.) if the quadratic form  $\mathbf{x}'\mathbf{A}\mathbf{x} > 0$  and/or  $\mathbf{x}'\mathbf{A}\mathbf{x} = 0$  for some  $\mathbf{x} \neq \mathbf{0}$ .
- 8.18 A positive-definite real symmetric matrix has only positive characteristic roots.
- 8.19 If a real symmetric matrix is p.s.d., it has no negative roots. The number of nonzero roots equals the rank of the matrix.
- 8.20 If all roots of a real symmetric matrix are distinct, the associated eigenvectors are distinct.
- 8.21 The matrix of eigenvectors

$$\mathbf{E} = [\mathbf{e}_1, \mathbf{e}_2, \dots, \mathbf{e}_n]$$

of a real symmetric matrix is (or can be chosen to be) orthogonal.

- 8.22  $\mathbf{AE} = \mathbf{ED}_\lambda$ .
- 8.23 For a real symmetric matrix,  $\mathbf{A} = \mathbf{ED}_\lambda\mathbf{E}'$  (decomposition into matrices of unit rank)

$$\mathbf{E}'\mathbf{AE} = \mathbf{D}_\lambda$$

where  $\mathbf{D}_\lambda$  denotes the diagonal matrix of characteristic roots ordered in the same way as the eigenvector columns in **E**.

8.24 If  $f(\lambda)$  is a polynomial in  $\lambda$ , then

$$f(\mathbf{A}) = \mathbf{E}\mathbf{D}_{f(\lambda)}\mathbf{E}^{-1}$$

where

- $\lambda$  are the characteristic roots of **A**
- E** is the matrix of associated eigenvectors

If **A** is symmetric,  $\mathbf{E}^{-1} = \mathbf{E}'$ .

### Example 8.24.1

Consider the matrix in 8.3 (and 6.14).

$$\mathbf{A} = \begin{bmatrix} 25 & 30 & -10 \\ 30 & 40 & -6 \\ -10 & -6 & 17 \end{bmatrix}.$$

The characteristic roots were found in Example 8.3.1,

$$\lambda_1 = 65.86108 \quad \lambda_2 = 15.75339 \quad \lambda_3 = 0.38553.$$

To find some **x** such that  $\mathbf{Ax} = \lambda_1\mathbf{x}$ , we arbitrarily set the first element of **x** equal to 1. Using only the first two rows of **A**, we solve the equation system

$$\begin{aligned} 25 + 30x_2 - 10x_3 &= 65.86108 \\ 30 + 40x_2 - 6x_3 &= 65.86108x_2 \end{aligned}$$

which yields  $x_2 = 1.24294$  and  $x_3 = -0.35729$ . Substitution of these values into the third equation

$$-10 - 6x_2 + 17x_3 = 65.86108x_3$$

yields zero to five decimal places, indicating the accuracy of the first characteristic root. To reduce to unit length the characteristic vector

$$[1 \quad 1.24294 \quad -0.35729]$$

we divide each element by

$$\sqrt{1 + 1.24294^2 + 0.35729^2}$$

and thus obtain the first eigenvector

$$[0.61170 \quad 0.76030 \quad -0.21855].$$

This, written as a column vector, is  $\mathbf{e}_1$ . Repeating the same process for the second and third eigenvector we obtain

$$\mathbf{e}_2 = \begin{bmatrix} -0.08659 \\ 0.33896 \\ 0.93861 \end{bmatrix} \quad \mathbf{e}_3 = \begin{bmatrix} 0.78634 \\ -0.55412 \\ 0.27318 \end{bmatrix}$$

The three vectors can be placed into the eigenvector matrix **E**, which is easily seen to be orthogonal.

## D.9 Conditional Inverses

9.1 Any matrix **A** (singular or nonsingular, rectangular or square) has some conditional or generalized inverse  $\mathbf{A}^{(-1)}$  defined by the relation

$$\mathbf{AA}^{(-1)}\mathbf{A} = \mathbf{A}.$$

- 9.2 If (and only if)  $\mathbf{A}$  is square and nonsingular,  $\mathbf{A}^{(-1)}$  is unique and equals  $\mathbf{A}^{-1}$ . Otherwise there will be infinitely many matrices  $\mathbf{A}^{(-1)}$  which satisfy the defining relation 9.1.
- 9.3a If  $\mathbf{A}$  is rectangular ( $n \times m$ ) of rank  $m$ , with  $m < n$ , then  $\mathbf{A}^{(-1)}$  is of order ( $m \times n$ ) and  $\mathbf{A}^{(-1)}\mathbf{A} = \mathbf{I}(m \times m)$ . Then  $\mathbf{A}^{(-1)}$  is called an inverse from the right.  $\mathbf{AA}^{(-1)} \neq \mathbf{I}$  In this case.
- 9.3b If  $\mathbf{A}$  is rectangular ( $n \times m$ ) of rank  $n$  with  $m > n$ , then  $\mathbf{A}^{(-1)}$  is of order ( $m \times n$ ) and  $\mathbf{AA}^{(-1)} = \mathbf{I}(n \times n)$ . Then  $\mathbf{A}^{(-1)}$  is called an inverse to the right. In this case,

$$\mathbf{A}^{(-1)}\mathbf{A} \neq \mathbf{I}.$$

- 9.3c For a square, singular matrix,  $\mathbf{AA}^{(-1)} \neq \mathbf{I}$  and  $\mathbf{A}^{(-1)}\mathbf{A} \neq \mathbf{I}$ .

**Example 9.3.1**

$$\mathbf{A} = \begin{bmatrix} 3 \\ 2 \\ 1 \end{bmatrix}$$

The row vector  $[1/3 \ 0 \ 0]$  is an inverse from the left. The row vector

$$[x \ y \ (1 - 3x - 2y)]$$

is a conditional inverse of the above matrix  $\mathbf{A}$  for any values of  $x$  and  $y$ . It is called the generalized inverse of  $\mathbf{A}$ .

**Example 9.3.2**

$$\mathbf{A} = \begin{bmatrix} 1 & 2 & 3 \\ 2 & 5 & 6 \\ 3 & 7 & 9 \end{bmatrix}$$

A conditional inverse is

$$\mathbf{A}^{(-1)} = \begin{bmatrix} 5 & -2 & 0 \\ -2 & 1 & 0 \\ 0 & 0 & 0 \end{bmatrix}$$

Here it was obtained by inversion of the basis (the  $2 \times 2$  matrix in the upper left-hand corner) and replacement of the other elements in zeros.

- 9.4 A square matrix  $\mathbf{A}$  is called idempotent if  $\mathbf{AA} = \mathbf{A}^2 = \mathbf{A}$ .
- 9.5  $\mathbf{AA}^{(-1)}$  and  $\mathbf{A}^{(-1)}\mathbf{A}$  are idempotent.
- 9.6 All characteristic roots of idempotent matrices are either zero or one.
- 9.7 A system of linear equations ( $m$  equations in  $n$  unknowns)

$$\mathbf{Ax} = \mathbf{b}$$

is called consistent if there exists some solution  $\mathbf{x}$  that satisfies the equation system.

**Example 9.7.1**

The system

$$\begin{aligned} x + y &= 2 \\ 2x + 2y &= 4 \end{aligned}$$

is consistent.

**Example 9.7.2**

The system

$$\begin{aligned} x + y &= 2 \\ 2x + 2y &= 5 \end{aligned}$$

is inconsistent.

for no pair of values  $(x, y)$  will satisfy this system.

- 9.8 If, in a system of equations (rectangular or square)

$$\mathbf{Ax} = \mathbf{b}$$

$\mathbf{AA}^{(-1)}\mathbf{b} = \mathbf{b}$  for some conditional inverse  $\mathbf{A}^{(-1)}$ , then  $\mathbf{AA}^{(-1)}\mathbf{b} = \mathbf{b}$  for every conditional inverse of  $\mathbf{A}$ , and  $\mathbf{Ax} = \mathbf{b}$  is consistent. Conversely, if  $\mathbf{AA}^{(-1)}\mathbf{b} \neq \mathbf{b}$  for some conditional inverse  $\mathbf{A}^{(-1)}$ , then  $\mathbf{AA}^{(-1)}\mathbf{b} \neq \mathbf{b}$  for every conditional inverse of  $\mathbf{A}$ , and  $\mathbf{Ax} = \mathbf{b}$  is inconsistent.

- 9.9 If  $\mathbf{Ax} = \mathbf{b}$  is consistent, then  $\mathbf{x} = \mathbf{A}^{(-1)}\mathbf{b}$  is a solution (generally a different one for each  $\mathbf{A}^{(-1)}$ ).
- 9.10 Let  $\mathbf{y}(p \times 1)$  be a set of linear functions of the solutions  $\mathbf{x}(n \times 1)$  of a consistent system of equations  $\mathbf{Ax} = \mathbf{b}$ , given by the relation  $\mathbf{y} = \mathbf{Cx}$ . They  $\mathbf{y} = \mathbf{Cx}$  is called unique if the same values of  $\mathbf{y}$  will result regardless of which solution  $\mathbf{x}$  is used.

**Example 9.10.1**

$$\begin{aligned} 3x + 4y + 5z &= 22 \\ x + y + z &= 6 \end{aligned}$$

is a consistent system. One solution would be

$$x = 3 \quad y = 2 \quad z = 1.$$

Another solution is

$$x = 2 \quad y = 4 \quad z = 0.$$

The linear function

$$[7 \ 9 \ 11] \begin{bmatrix} x \\ y \\ z \end{bmatrix} = u$$

$(7x + 9y + 11z = u)$  will have the same value (50) regardless of which of the two (or any other) solutions is substituted. Thus,  $u$  is unique.

**9.11** Let  $\mathbf{Ax} = \mathbf{b}$  be a consistent system of equations. For  $\mathbf{Cx} = \mathbf{y}$  to be a unique linear combination of the solution  $\mathbf{x}$ , it is necessary and sufficient that  $\mathbf{CA}^{(-1)}\mathbf{A} = \mathbf{C}$ . If this relation holds for some  $\mathbf{A}^{(-1)}$ , it will hold for every conditional inverse of  $\mathbf{A}$ . If it is violated for some  $\mathbf{A}^{(-1)}$ , it will be violated for every  $\mathbf{A}^{(-1)}$ , and  $\mathbf{y}$  will be nonunique.

**9.12** Let  $\mathbf{A}$  be of rank  $r$  and select  $r$  rows and  $r$  columns that form a basis of  $\mathbf{A}$ . Then a conditional inverse of  $\mathbf{A}$  can be obtained as follows: Invert the  $(r \times r)$  matrix, place the inverse (without transposing) into the  $r$  rows corresponding to the column numbers and the  $r$  columns corresponding to the row numbers of the basis, and place zero into all remaining elements. Thus, if  $\mathbf{A}$  is of order  $(5 \times 4)$  and rank 3, and if rows 1, 2, 4 and columns 2, 3, 4 are selected as a basis,  $\mathbf{A}^{(-1)}$ , of order  $(4 \times 5)$ , will contain the inverse elements of the basis in rows 2, 3, 4 and columns 1, 2, 4, and zeros elsewhere. (See Example 9.3.2.)

**9.13** If  $\mathbf{A}$  is a square, singular matrix of order  $(n \times n)$  and rank  $r$ , let  $\mathbf{M}$  be a matrix of order  $[n \times (n - r)]$  and  $\mathbf{K}$  another matrix of order  $[(n - r) \times n]$  chosen in such a way that  $\mathbf{A} + \mathbf{MK}$  is nonsingular. Then  $(\mathbf{A} + \mathbf{MK})^{-1}$  is a conditional inverse of  $\mathbf{A}$ .

**Example 9.13.1**

$$\mathbf{A} = \begin{bmatrix} 3 & -1 & -1 & -1 \\ -1 & 3 & -1 & -1 \\ -1 & -1 & 3 & -1 \\ -1 & -1 & -1 & 3 \end{bmatrix}$$

is of order  $(4 \times 4)$  and rank 3. Take  $\mathbf{M} = \mathbf{j}$  (column vector of ones) and  $\mathbf{K} = \mathbf{j}'$  (row vector of ones). Then  $\mathbf{A} + \mathbf{MK} = \mathbf{A} + \mathbf{jj}' = 4\mathbf{I}$ . Hence  $(1/4)\mathbf{I}$  is a conditional inverse of  $\mathbf{A}$ .

**9.14** The “Doolittle” method (see 6.14) can be employed to obtain a conditional inverse of a symmetric matrix. If, at any stage, the leading element of the  $p$ -row is zero, that cycle is disregarded.

**Example 9.14.1**

Invert, conditionally, the matrix

$$\mathbf{A} = \begin{bmatrix} 4 & 2 & -2 & 4 \\ 2 & 17 & 11 & 6 \\ -2 & 11 & 10 & 1 \\ 4 & 6 & 1 & 30 \end{bmatrix}$$

4	2	-2	4	1	
1	.5	-.5	1	.25	
17	11	6	0	1	
16	12	4	-.5	1	
1	.75	.25	-.03125	.0625	
10	1	0	0	1	
0					
30	0	0	0	1	
25	-.875	-.25	0	1	
1	-.035	-.01	0	.04	

$$\begin{bmatrix} .29625 & -.0225 & 0 & -.035 \\ -.0225 & .065 & 0 & -.01 \\ 0 & 0 & 0 & 0 \\ -.035 & -.01 & 0 & .04 \end{bmatrix} = \mathbf{A}^{(-1)}$$

## D.10 Matrix Differentiation

**10.1a** If the elements of a matrix  $\mathbf{Y}(m \times n)$  are functions of a scalar,  $x$ , the expression

$$\partial \mathbf{Y} / \partial x$$

denotes a matrix of order  $(m \times n)$  with elements  $\partial y_{ij} / \partial x$ .

**10.1b** If the elements of a column (row) vector  $\mathbf{y}(y')$  are functions of a scalar,  $x$ , the expression

$$\partial \mathbf{Y} / \partial \mathbf{x} \quad (\partial \mathbf{y}' / \partial x)$$

denotes a column (row) vector with elements  $\partial y_i / \partial x$ .

**10.2a** If  $y$  is a scalar function of  $m \times n$  variables,  $x_{ij}$ , arranged into a matrix  $\mathbf{X}$ , the expression

$$\partial Y / \partial \mathbf{X}$$

denotes a matrix with elements  $\partial y / \partial x_{ij}$ .

(Note: Partial differentiation is performed with respect to the element in row  $i$  and column  $j$  of  $\mathbf{X}$ . If the same  $x$ -variable occurs in another place as, e.g., in a symmetric matrix, differentiation with respect to the distinct (repeated) variable is performed in two stages.)

**Example 10.2.1**

If  $y = \mathbf{j}'\mathbf{X}\mathbf{j}$  (sum of all elements of a square matrix),  $\partial y / \partial \mathbf{X}$  is a matrix of ones. If  $\mathbf{X}$  is symmetric, one can introduce a new notation  $x_{ij} = x_{ji} = z_{ji}$ . Then

$$\begin{aligned} \partial y / \partial z_{ij} &= (\partial y / \partial x_{ij})(\partial x_{ij} / \partial z_{ij}) + (\partial y / \partial x_{ji})(\partial x_{ji} / \partial z_{ij}) \\ &= 1 + 1 = 2 \quad (\text{if } i \neq j) \\ &= 1 \quad (\text{if } i = j) \end{aligned}$$

**10.2b** If  $y$  is a scalar function of  $n$  variables,  $x_i$ , arranged into a column (row) vector  $\mathbf{x}(x')$ , the expression

$$\partial y / \partial \mathbf{x} \quad (\partial y / \partial \mathbf{x}')$$

denotes a column (row) vector with elements  $\partial y / \partial x_i$ .

**10.3** If  $\mathbf{y}$  is a column vector with  $m$  elements, each a function of  $n$  variables,  $x_i$ , arranged into a row vector  $\mathbf{x}'$ , the expression  $\partial \mathbf{y} / \partial \mathbf{x}'$  denotes a matrix with  $m$  rows and  $n$  columns, with elements  $\partial y_i / \partial x_j$ .

**10.4**  $\partial \mathbf{Y} / \partial y_{ij} = (\mathbf{EL})_{ij}$  (see definition of  $(\mathbf{EL})$  in 3.4).



- 10.5  $\partial \mathbf{UV}/\partial x = (\partial \mathbf{U}/\partial x)\mathbf{V} + \mathbf{U}(\partial \mathbf{V}/\partial x)$ .
- 10.6  $\partial \mathbf{AY}/\partial x = \mathbf{A}(\partial \mathbf{Y}/\partial x)$  (if elements of  $\mathbf{A}$  are not functions of  $x$ ).
- 10.7  $\partial \mathbf{Y}'/\partial y_{ij} = (\mathbf{E}\mathbf{L})_{ji}$ .
- 10.8  $\partial \mathbf{A}'\mathbf{YA}/\partial x = \mathbf{A}'(\partial \mathbf{Y}/\partial x)\mathbf{A}$ .
- 10.9  $\partial \mathbf{Y}'\mathbf{AY}/\partial x = (\partial \mathbf{Y}'/\partial x)\mathbf{AY} + \mathbf{Y}'\mathbf{A}(\partial \mathbf{Y}/\partial x)$ .
- 10.10  $\partial \mathbf{a}'\mathbf{x}/\partial \mathbf{x} = \mathbf{a}$ .
- 10.11  $\partial \mathbf{x}'\mathbf{x}/\partial \mathbf{x} = 2\mathbf{x}$ .
- 10.12  $\partial \mathbf{x}'\mathbf{Ax}/\partial \mathbf{x} = \mathbf{Ax} + \mathbf{A}'\mathbf{x}$ .
- 10.13 (Chain Rule No. 1)  $\partial \mathbf{y}/\partial \mathbf{x}' = (\partial \mathbf{y}/\partial \mathbf{z}')(\partial \mathbf{z}'/\partial \mathbf{x}')$ .
- 10.14  $\partial \mathbf{Ax}/\partial \mathbf{x}' = \mathbf{A}$ .
- 10.15  $\partial \text{tr } \mathbf{X}/\partial \mathbf{X} = \mathbf{I}$ .
- 10.16  $\partial \text{tr } \mathbf{AX}/\partial \mathbf{X} = \partial \text{tr } \mathbf{XA}/\partial \mathbf{X} = \mathbf{A}'$ .
- 10.17  $\partial \text{tr } \mathbf{AXB}/\partial \mathbf{X} = \mathbf{A}'\mathbf{B}'$ .
- 10.18  $\partial \text{tr } \mathbf{X}'\mathbf{AX}/\partial \mathbf{X} = \mathbf{AX} + \mathbf{A}'\mathbf{X}$ .
- 10.19  $\partial \log |\mathbf{X}|/\partial \mathbf{X} = (\mathbf{X}')^{-1}$  (log to base  $e$ ).
- 10.20  $\partial \mathbf{Y}^{-1}/\partial x = -\mathbf{Y}^{-1}(\partial \mathbf{Y}/\partial x)\mathbf{Y}^{-1}$ .
- 10.21 (Chain Rule No. 2)

$$\partial y/\partial x = \text{tr}(\partial \mathbf{y}/\partial \mathbf{Z}) (\partial \mathbf{Z}'/\partial x)$$

where  $y$  and  $x$  are scalars. The scalar  $y$  is a function of  $m \times n$  variables  $z_{ij}$ , and each of the  $z_{ij}$  is a function of  $x$ .

### Example 10.21.1

Obtain  $\log |\mathbf{R} - \mathbf{FF}'|/\partial \mathbf{F}$ , where  $\mathbf{R}$  is symmetric. By Chain Rule No. 2:

$$\begin{aligned} \partial \log |\mathbf{R} - \mathbf{FF}'|/\partial f_{ij} &= \text{tr}[\partial \log |\mathbf{R} - \mathbf{FF}'|/\partial (\mathbf{R} - \mathbf{FF}')] [\partial (\mathbf{R} - \mathbf{FF}')/\partial f_{ij}] \\ &\quad (\text{since } \mathbf{R} \text{ and } \mathbf{FF}' \text{ are symmetric}) \\ &= \text{tr}(\mathbf{R} - \mathbf{FF}')^{-1} [\partial (\mathbf{R} - \mathbf{FF}')/\partial f_{ij}] \quad (\text{by 10.19}) \\ &= \text{tr}(\mathbf{R} - \mathbf{FF}')^{-1} [-(\partial \mathbf{F}/\partial f_{ij})\mathbf{F}' - \mathbf{F}(\partial \mathbf{F}'/\partial f_{ij})] \quad (\text{by 10.5}) \\ &= \text{tr}(\mathbf{R} - \mathbf{FF}')^{-1} [-(\mathbf{E}\mathbf{L})_{ij}\mathbf{F}' - \mathbf{F}(\mathbf{E}\mathbf{L})_{ji}] \quad (\text{by 10.4 and 10.7}) \\ &= -\text{tr}(\mathbf{R} - \mathbf{FF}')^{-1} (\mathbf{E}\mathbf{L})_{ij}\mathbf{F}' - \text{tr}(\mathbf{R} - \mathbf{FF}')^{-1} \mathbf{F}(\mathbf{E}\mathbf{L})_{ji} \\ &= -\text{tr}(\mathbf{E}\mathbf{L})_{ij}\mathbf{F}'(\mathbf{R} - \mathbf{FF}')^{-1} - \text{tr}(\mathbf{E}\mathbf{L})_{ji}\mathbf{F}(\mathbf{R} - \mathbf{FF}')^{-1} \mathbf{F} \quad (\text{by 7.3}) \\ &= -[\mathbf{F}'(\mathbf{R} - \mathbf{FF}')^{-1}]_{ji} - [(\mathbf{R} - \mathbf{FF}')^{-1}\mathbf{F}]_{ij}, \end{aligned}$$

where  $[\ ]_{ij}$  denotes the  $(i, j)$  element of the matrix in brackets (by 7.5),

$$\begin{aligned} &= -[(\mathbf{R} - \mathbf{FF}')^{-1}\mathbf{F}]_{ij} - [(\mathbf{R} - \mathbf{FF}')^{-1}\mathbf{F}]_{ij} \quad (\text{since } \mathbf{R} - \mathbf{FF}' \text{ is symmetric}) \\ &= -2[(\mathbf{R} - \mathbf{FF}')^{-1}\mathbf{F}]_{ij}. \end{aligned}$$

Hence, by definition 10.2a.

$$\partial \log |\mathbf{R} - \mathbf{FF}'|/\partial \mathbf{F} = -2(\mathbf{R} - \mathbf{FF}')^{-1}\mathbf{F}.$$

- 10.22  $|\partial \mathbf{y}/\partial \mathbf{x}'| = J(\mathbf{y}; \mathbf{x})$  is called the Jacobian or *functional determinant* used in variable transformation of multiple integrals. Formally, if  $\mathbf{y}$  is a column vector with  $m$  elements, each function of  $m$  variables  $x_i$  arranged into a row vector  $\mathbf{x}'$ ,

$$dx_1 dx_2 \dots dx_m = |\partial \mathbf{y}/\partial \mathbf{x}'|^{-1} dy_1 dy_2 \dots dy_m.$$

- 10.23 For a scalar  $y$  (a function of  $m$  variables  $x_i$ ) to attain a stationary value, it is necessary that

$$\partial y/\partial x = \mathbf{0}.$$

- 10.24 For a stationary value to be a minimum (maximum) it is necessary that

$$\partial(\partial y/\partial \mathbf{x})/\partial \mathbf{x}' \quad (-\partial(\partial y/\partial \mathbf{x})/\partial \mathbf{x}')$$

be a positive-definite matrix for the value of  $\mathbf{x}$  satisfying 10.23.

### Example 10.24.1

Find the values of  $\beta$  that minimize  $u = \mathbf{x}'\mathbf{x}$  (the sum of squares of  $x_i$ ) where  $\mathbf{x} = \mathbf{y} - \mathbf{A}\beta$  (with  $\mathbf{y}$  and  $\mathbf{A}$  known and fixed).

$$\begin{aligned} \partial u/\partial \beta' &= (\partial u/\partial \mathbf{x}')(\partial \mathbf{x}/\partial \beta') \quad (\text{by Chain Rule No.1}) \\ &= -2\mathbf{x}'\mathbf{A} \quad (\text{by 10.11 and 10.14}) \end{aligned}$$

Hence,

$$\begin{aligned} \partial u/\partial \beta &= -2\mathbf{A}'\mathbf{x} \\ &= -2\mathbf{A}'(\mathbf{y} - \mathbf{A}\beta) \end{aligned}$$

Hence, for a stationary value, by 10.23, it is necessary that

$$\mathbf{A}'\hat{\beta} = \mathbf{A}'\mathbf{y}$$

where  $\hat{\beta}$  denotes the values that make  $u$  stationary. Now,

$$\partial(\partial u/\partial \beta)/\partial \beta' = 2\partial(\mathbf{A}'\mathbf{A}\beta)/\partial \beta' = 2\mathbf{A}'\mathbf{A}.$$

If  $\mathbf{A}$  has real elements, and if  $\mathbf{A}'\mathbf{A}$  is nonsingular, then it is positive-definite (since, given an arbitrary real  $\mathbf{x} \neq \mathbf{0}$ ,  $\mathbf{x}'\mathbf{A}'\mathbf{A}\mathbf{x} = \mathbf{z}'\mathbf{z}$ , with  $\mathbf{z} = \mathbf{A}\mathbf{x}$ ; thus, this is a sum of squares). Hence,  $\hat{\beta}$  minimizes  $u$ .

### 10.25 (Generalized Newton Iteration)

Let  $\mathbf{x}_0'$  be an initial estimate ( $m$  elements) of the roots of the  $m$  equations

$$\mathbf{f}(\mathbf{x}') = \mathbf{0}$$

where the  $m$  elements of the column vector  $\mathbf{f}$  are each functions of  $x_1, x_2, \dots, x_m$ . Then an improved root is

$$\mathbf{x}_1 = \mathbf{x}_0 - \mathbf{Q}_0^{-1}\mathbf{f}(\mathbf{x}'_0),$$

where  $\mathbf{Q}_0$  is the matrix of derivatives  $\partial\mathbf{f}/\partial\mathbf{x}'$  evaluated at  $\mathbf{x} = \mathbf{x}_0$ . The usual procedure consists of evaluating  $\mathbf{f}(\mathbf{x}'_0)$ , then solving  $\mathbf{Q}_0\mathbf{u} = \mathbf{f}(\mathbf{x}'_0)$  for  $\mathbf{u}$ . Then  $\mathbf{x}_1 = \mathbf{x}_0 - \mathbf{u}$ .

### Example 10.23.1

Solve

$$f_1(x, y) = x^3 - x^2y + y^2 - 3.526 = 0$$

$$f_2(x, y) = x^3 + y^3 - 14.911 = 0$$

$$\mathbf{Q} = \begin{bmatrix} 3x^2 - 2xy & 2y - x^2 \\ 3x^2 & 3y^2 \end{bmatrix}$$

Take  $x_0 = 1, y_0 = 2$

$$f_1(x_0, y_0) = -0.526$$

$$f_2(x_0, y_0) = -5.911$$

$$\mathbf{Q}_0 = \begin{bmatrix} -1 & 3 \\ 3 & 12 \end{bmatrix}$$

$$-u + 3v = -0.526$$

$$3u + 12v = -5.911$$

$$\text{yields } u = -0.55, v = -0.36.$$

Then,

$$x_1 = x_0 - u = 1.55$$

$$y_1 = y_0 - v = 2.36$$

$$f_1(x_1, y_1) = 0.0976$$

$$f_2(x_1, y_1) = 1.9572$$

$$\mathbf{Q}_1 = \begin{bmatrix} -0.1085 & 2.3175 \\ 7.2075 & 16.7088 \end{bmatrix}$$

$$-0.1085u + 2.3175v = 0.0976$$

$$7.2075u + 16.7088v = 1.9572$$

$$\text{yields } u = 0.157, v = 0.049.$$

Then,

$$x_2 = x_1 - u = 1.393$$

$$y_2 = y_1 - v = 2.311$$

$$f_1(x_2, y_2) = 0.3337$$

$$f_2(x_2, y_2) = 0.13443$$

$$\mathbf{Q}_2 = \begin{bmatrix} -0.61710 & 2.68155 \\ 5.82135 & 16.02216 \end{bmatrix}$$

$$-0.61710u + 2.68155v = 0.03337$$

$$5.82135u + 16.02216v = 0.13443$$

$$\text{yields } u = -0.0068, v = 0.0109.$$

Then,

$$x_3 = x_2 - u = 1.3998$$

$$y_3 = y_2 - v = 2.3001$$

(The exact roots are  $x = 1.4$  and  $y = 2.3$ .)

## D.11 Statistical Matrix Forms

**11.1** Let  $E$  denote the expectation operator, and let  $\mathbf{y}$  be a set of  $p$  random variables. Then

$$E(\mathbf{y}) = \boldsymbol{\mu}$$

states that  $E(y_i) = \mu_i$  ( $i = 1, 2, \dots, p$ ).

**11.2** Let  $\text{var}$  denote variance. Then

$$\text{var}(\mathbf{y}) = \boldsymbol{\Sigma}$$

denotes a  $p \times p$  symmetric matrix whose elements are  $\text{cov}(y_i, y_j)$  and whose diagonal elements are  $\text{var}(y_i)$ , where  $\text{cov}$  denotes covariance.

**11.3**  $E(\mathbf{A}\mathbf{y} + \mathbf{b}) = \mathbf{A}E(\mathbf{y}) + \mathbf{b} = \mathbf{A}\boldsymbol{\mu} + \mathbf{b}$ .

**11.4**  $\text{var}(\mathbf{A}\mathbf{y} + \mathbf{b}) = \mathbf{A} \text{var}(\mathbf{y})\mathbf{A}' = \mathbf{A}\boldsymbol{\Sigma}\mathbf{A}'$ .

**11.5**  $\text{cov}(\mathbf{y}, \mathbf{z}')$  denotes a matrix with elements  $\text{cov}(y_i, z_j)$ .  $\text{cov}(\mathbf{z}, \mathbf{y}') = [\text{cov}(\mathbf{y}, \mathbf{z}')]'$ .

**11.6**  $\text{cov}(\mathbf{A}\mathbf{y} + \mathbf{b}, \mathbf{z}'\mathbf{C} + \mathbf{d}') = \mathbf{A} \text{cov}(\mathbf{y}, \mathbf{z}')\mathbf{C}$ .

**11.7**  $\text{var}(\mathbf{y}) = E(\mathbf{y}\mathbf{y}') - E(\mathbf{y})E(\mathbf{y}')$ .

**11.8**  $\text{cov}(\mathbf{y}, \mathbf{z}') = E(\mathbf{y}\mathbf{z}') - E(\mathbf{y})E(\mathbf{z}')$ .

**11.9** (Expected "sum of squares")

$$E(\mathbf{y}'\mathbf{Q}\mathbf{y}) = \text{tr}[\mathbf{Q} \text{var}(\mathbf{y})] + E(\mathbf{y}')\mathbf{Q}E(\mathbf{y}).$$

**11.10** If a matrix  $\mathbf{Q}$  is symmetric and positive-definite, one can find a lower triangular matrix  $\mathbf{T}$  (with positive diagonal terms, for uniqueness) such that  $\mathbf{T}\mathbf{T}' = \mathbf{Q}$ . The matrices  $\mathbf{T}$  and  $\mathbf{T}^{-1}$  can be obtained from the Doolittle pattern (6.14) (Gauss elimination or square-root method) as follows: In each cycle, divide the  $p$ -row (left- and right-hand side) by  $\sqrt{p_{ii}}$  (instead of  $p_{ii}$  for the  $u$ -row). Thus, obtain rows designated as  $t$ -rows. The left-hand side (Arabic subscripts) is  $\mathbf{T}'$ , and the right-hand side (Roman subscripts) is  $\mathbf{T}^{-1}$ .

**11.11** If a coordinate system  $\mathbf{x}$  is oblique, and if the cosines reference vectors (scalar products of basis vectors of unit length) are stated in a symmetric matrix  $\mathbf{Q}$ , then  $\mathbf{T}^{-1}\mathbf{x} = \mathbf{y}$  is an orthogonal system, where  $\mathbf{T}$  is obtained from  $\mathbf{Q}$  by 11.10.

**11.12** The likelihood function of a sample of size  $n$  from a multivariate normal distribution ( $p$  responses), with common variance-covariance matrix  $\boldsymbol{\Sigma}(p \times p)$ , and with means or main effects replaced by maximum-likelihood or least-squares estimates, can be written as

$$\log L = -\frac{np}{2} \log 2\pi - \frac{n}{2} \log |\boldsymbol{\Sigma}| - \frac{n}{2} \text{tr}\boldsymbol{\Sigma}^{-1}\mathbf{S}$$

where  $\Sigma$  ( $p \times p$ ) is the common variance-covariance matrix, and  $\mathbf{S}$  is its maximum-likelihood estimate (matrix of sums of squares and products due to error, divided by sample size  $n$ ) and  $\log$  is base  $e$ .

**11.13** If  $\Sigma$  has a structure under a model or null hypothesis, and if elements of  $\Sigma$  are to be estimated, by maximum-likelihood, two cases can be distinguished:

(11.14)  $\Sigma^{-1}$  has the same structure (intraclass correlation, mixed model, compound symmetry, factor analysis).

(11.15)  $\Sigma^{-1}$  has a different structure (autocorrelation, Simplex structure).

**11.14** If the structure of  $\Sigma$  and  $\Sigma^{-1}$  are identical, and if  $u$  and  $v$  are elements (or functions of elements) of  $\Sigma^{-1}$ , then estimates of  $\Sigma$  can be obtained from the relations (usually requiring Newton iteration; see 10.25):

$$\partial \log L / \partial u = \frac{n}{2} \text{tr} \mathbf{A}(\Sigma - \mathbf{S})$$

where  $\mathbf{A} = \partial \Sigma^{-1} / \partial u$  is frequently an elementary matrix (see 3.4, especially rules 7.5 and 7.6).

$$\partial^2 \log L / \partial u \partial v = \frac{n}{2} \text{tr} (\partial \mathbf{A} / \partial v)(\Sigma - \mathbf{S}) + \frac{n}{2} \text{tr} \mathbf{A} \Sigma^{-1} \mathbf{B} \Sigma^{-1}$$

where  $\mathbf{B} = \partial \Sigma^{-1} / \partial v$ . These rules are useful to obtain Newton iterations and asymptotic variance-covariance matrices of the estimates. The  $\log$  is base  $e$ .

**11.15** If the structures of  $\Sigma$  and  $\Sigma^{-1}$  are different, then an estimate of  $\Sigma$  can be obtained from the relations

$$\partial \log L / \partial x = -\frac{n}{2} \text{tr} \mathbf{A}(\Sigma^{-1} - \mathbf{Q}),$$

where

$$\mathbf{Q} = \Sigma^{-1} \mathbf{S} \Sigma^{-1}$$

and

$\mathbf{A} = \partial \Sigma / \partial x$  (see comments in 11.14).

$$\begin{aligned} \partial^2 \log L / \partial x \partial y &= -\frac{n}{2} \text{tr} (\partial \mathbf{A} / \partial y)(\Sigma^{-1} - \mathbf{Q}) \\ &+ \frac{n}{2} \text{tr} \mathbf{A} \Sigma^{-1} \mathbf{B}(\Sigma^{-1} - \mathbf{Q}) - \frac{n}{2} \text{tr} \mathbf{A} \mathbf{Q} \mathbf{B} \Sigma^{-1}, \end{aligned}$$

where

$$\mathbf{B} = \partial \Sigma / \partial y$$

$x$  and  $y$  are elements (or functions of elements) of  $\Sigma$ . The comments of 11.14 apply, but the iterative procedure is considerably more complex. The  $\log$  is base  $e$ .

# Appendix E: Vector Analysis

---

E.1	Definitions.....	E-1
E.2	Vector Algebra.....	E-1
E.3	Vectors in Space.....	E-1
E.4	The Scalar, Dot, or Inner Product of Two Vectors $\mathbf{V}_1$ and $\mathbf{V}_2$ .....	E-2
E.5	The Vector or Cross Product of Vectors $\mathbf{V}_1$ and $\mathbf{V}_2$ .....	E-2
E.6	Scalar Triple Product.....	E-3
E.7	Vector Triple Product.....	E-3
E.8	Geometry of the Plane, Straight Line, and Sphere.....	E-3
E.9	Differentiation of Vectors.....	E-5
E.10	Geometry of Curves in Space.....	E-6
E.11	Differential Operators—Rectangular Coordinates.....	E-7
E.12	Transformation of Integrals.....	E-8
E.13	Gauss' Theorem (Green's Theorem).....	E-9
E.14	Stokes' Theorem.....	E-9
E.15	Green's Theorem.....	E-9

## E.1 Definitions

---

Any quantity that is completely determined by its magnitude is called a *scalar*. Examples of such are mass, density, temperature, etc. Any quantity that is completely determined by its magnitude and direction is called a *vector*. Examples of such are velocity, acceleration, force, etc. A vector quantity is represented by a directed line segment, the length of which represents the magnitude of the vector. A vector quantity is usually represented by a boldface letter such as  $\mathbf{V}$ . Two vectors  $\mathbf{V}_1$  and  $\mathbf{V}_2$  are equal to one another if they have equal magnitudes and are acting in the same directions. A negative vector, written as  $-\mathbf{V}$ , is one that acts in the opposite direction to  $\mathbf{V}$ , but is of equal magnitude to it. If we represent the magnitude of  $\mathbf{V}$  by  $v$ , we write  $\mathbf{V} = v$ . A vector parallel to  $\mathbf{V}$ , but equal to the reciprocal of its magnitude, is written as  $\mathbf{V}^{-1}$  or  $1/\mathbf{V}$ .

The *unit vector*  $\mathbf{V}/v$  ( $v \neq 0$ ) is that vector which has the same direction as  $\mathbf{V}$ , but which has a magnitude of unity (sometimes represented as  $\mathbf{V}_0$  or  $\hat{\mathbf{v}}$ ).

## E.2 Vector Algebra

---

The vector sum of  $\mathbf{V}_1$  and  $\mathbf{V}_2$  is represented by  $\mathbf{V}_1 + \mathbf{V}_2$ . The vector sum of  $\mathbf{V}_1$  and  $-\mathbf{V}_2$ , or the difference of the vector  $\mathbf{V}_2$  from  $\mathbf{V}_1$ , is represented by  $\mathbf{V}_1 - \mathbf{V}_2$ .

If  $r$  is a scalar, then  $r\mathbf{V} = \mathbf{V}r$  and represents a vector  $r$  times the magnitude of  $\mathbf{V}$ , in the same direction as  $\mathbf{V}$  if  $r$  is positive, and in the opposite direction if  $r$  is negative. If  $r$  and  $s$  are scalars and  $\mathbf{V}_1, \mathbf{V}_2, \mathbf{V}_3$  vectors, then the following rules of scalars and vectors hold:

$$\begin{aligned} \mathbf{V}_1 + \mathbf{V}_2 &= \mathbf{V}_2 + \mathbf{V}_1 \\ (r + s)\mathbf{V}_1 &= r\mathbf{V}_1 + s\mathbf{V}_1; r(\mathbf{V}_1 + \mathbf{V}_2) = r\mathbf{V}_1 + r\mathbf{V}_2 \\ \mathbf{V}_1 + (\mathbf{V}_2 + \mathbf{V}_3) &= (\mathbf{V}_1 + \mathbf{V}_2) + \mathbf{V}_3 = \mathbf{V}_1 + \mathbf{V}_2 + \mathbf{V}_3. \end{aligned}$$

## E.3 Vectors in Space

---

A plane is described by two distinct vectors  $\mathbf{V}_1$  and  $\mathbf{V}_2$ . Should these vectors not intersect one another, then one is displaced parallel to itself until they do (Figure E.1). Any other vector  $\mathbf{V}$  lying in this plane is given by

$$\mathbf{V} = r\mathbf{V}_1 + s\mathbf{V}_2.$$

A *position vector* specifies the position in space of a point relative to a fixed origin. If, therefore,  $\mathbf{V}_1$  and  $\mathbf{V}_2$  are the position vectors of the points  $A$  and  $B$ , relative to the origin  $O$ , then any point  $P$  on the line  $AB$  has a position vector  $\mathbf{V}$  given by

$$\mathbf{V} = r\mathbf{V}_1 + (1 - r)\mathbf{V}_2.$$

The scalar “ $r$ ” can be taken as the parametric representation of  $P$  since  $r = 0$  implies  $P = B$  and  $r = 1$  implies  $P = A$  (Figure E.2). If  $P$  divides the line  $AB$  in the ratio  $r : s$ , then

$$\mathbf{V} = \left( \frac{r}{r + s} \right) \mathbf{V}_1 + \left( \frac{s}{r + s} \right) \mathbf{V}_2.$$

The vectors  $\mathbf{V}_1, \mathbf{V}_2, \mathbf{V}_3, \dots, \mathbf{V}_n$  are said to be *linearly dependent* if there exist scalars  $r_1, r_2, r_3, \dots, r_n$ , not all zero, such that

$$r_1\mathbf{V}_1 + r_2\mathbf{V}_2 + \dots + r_n\mathbf{V}_n = 0.$$

A vector  $\mathbf{V}$  is linearly dependent on the set of vectors  $\mathbf{V}_1, \mathbf{V}_2, \mathbf{V}_3, \dots, \mathbf{V}_n$  if

$$\mathbf{V} = r_1\mathbf{V}_1 + r_2\mathbf{V}_2 + r_3\mathbf{V}_3 + \dots + r_n\mathbf{V}_n.$$

Three vectors are linearly dependent if and only if they are coplanar.

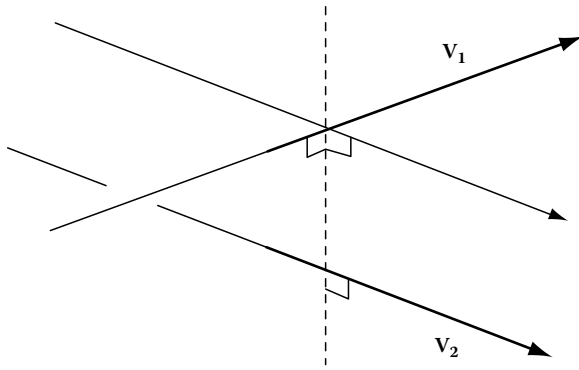


FIGURE E.1

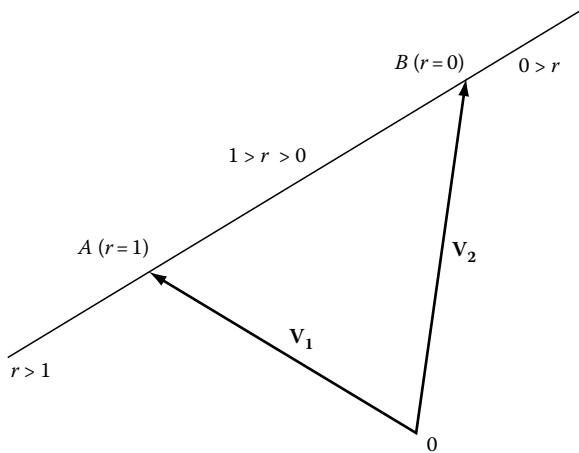


FIGURE E.2

All points in space can be uniquely determined by linear dependence on three *base vectors*, i.e., three vectors any one of which is linearly independent of the other two. The simplest set of base vectors are the unit vectors along the coordinate  $Ox$ ,  $Oy$ , and  $Oz$  axes. These are usually designated by  $\mathbf{i}$ ,  $\mathbf{j}$ , and  $\mathbf{k}$ , respectively.

If  $\mathbf{V}$  is a vector in space and  $a$ ,  $b$ , and  $c$  are the respective magnitudes of the projections of the vector along the axes, then

$$\mathbf{V} = a\mathbf{i} + b\mathbf{j} + c\mathbf{k}$$

and

$$v = \sqrt{a^2 + b^2 + c^2}$$

and the direction cosines of  $\mathbf{V}$  are

$$\cos \alpha = a/v, \quad \cos \beta = b/v, \quad \cos \gamma = c/v.$$

The law of addition yields

$$\mathbf{V}_1 + \mathbf{V}_2 = (a_1 + a_2)\mathbf{i} + (b_1 + b_2)\mathbf{j} + (c_1 + c_2)\mathbf{k}.$$

## E.4 The Scalar, Dot, or Inner Product of Two Vectors $\mathbf{V}_1$ and $\mathbf{V}_2$

This product is represented as  $\mathbf{V}_1 \cdot \mathbf{V}_2$  and is defined to be equal to  $v_1 v_2 \cos \theta$ , where  $\theta$  is the angle from  $\mathbf{V}_1$  to  $\mathbf{V}_2$ , i.e.,

$$\mathbf{V}_1 \cdot \mathbf{V}_2 = v_1 v_2 \cos \theta.$$

The following rules apply for this product:

$$\mathbf{V}_1 \cdot \mathbf{V}_2 = a_1 a_2 + b_1 b_2 + c_1 c_2 = \mathbf{V}_2 \cdot \mathbf{V}_1$$

It should be noted that scalar multiplication is commutative:

$$(\mathbf{V}_1 + \mathbf{V}_2) \cdot \mathbf{V}_3 = \mathbf{V}_1 \cdot \mathbf{V}_3 + \mathbf{V}_2 \cdot \mathbf{V}_3$$

$$\mathbf{V}_1 \cdot (\mathbf{V}_2 + \mathbf{V}_3) = \mathbf{V}_1 \cdot \mathbf{V}_2 + \mathbf{V}_1 \cdot \mathbf{V}_3.$$

If  $\mathbf{V}_1$  is perpendicular to  $\mathbf{V}_2$ , then  $\mathbf{V}_1 \cdot \mathbf{V}_2 = 0$ , and if  $\mathbf{V}_1$  is parallel to  $\mathbf{V}_2$ , then  $\mathbf{V}_1 \cdot \mathbf{V}_2 = v_1 v_2 = r w_1^2$ . In particular,

$$\mathbf{i} \cdot \mathbf{i} = \mathbf{j} \cdot \mathbf{j} = \mathbf{k} \cdot \mathbf{k} = 1,$$

and

$$\mathbf{i} \cdot \mathbf{j} = \mathbf{j} \cdot \mathbf{k} = \mathbf{k} \cdot \mathbf{i} = 0.$$

## E.5 The Vector or Cross Product of Vectors $\mathbf{V}_1$ and $\mathbf{V}_2$

This product is represented as  $\mathbf{V}_1 \times \mathbf{V}_2$  and is defined to be equal to  $v_1 v_2 (\sin \theta) \mathbf{1}$ , where  $\theta$  is the angle from  $\mathbf{V}_1$  to  $\mathbf{V}_2$  and  $\mathbf{1}$  is a unit vector perpendicular to the plane of  $\mathbf{V}_1$  and  $\mathbf{V}_2$  and so directed that a right-hand screw driven in the direction of  $\mathbf{1}$  would carry  $\mathbf{V}_1$  into  $\mathbf{V}_2$ , i.e.,

$$\mathbf{V}_1 \times \mathbf{V}_2 = v_1 v_2 (\sin \theta) \mathbf{1}$$

and

$$\tan \theta = \frac{|\mathbf{V}_1 \times \mathbf{V}_2|}{\mathbf{V}_1 \cdot \mathbf{V}_2}.$$

The following rules apply for vector products:

$$\mathbf{V}_1 \times \mathbf{V}_2 = -\mathbf{V}_2 \times \mathbf{V}_1$$

$$\mathbf{V}_1 \times (\mathbf{V}_2 + \mathbf{V}_3) = \mathbf{V}_1 \times \mathbf{V}_2 + \mathbf{V}_1 \times \mathbf{V}_3$$

$$(\mathbf{V}_1 + \mathbf{V}_2) \times \mathbf{V}_3 = \mathbf{V}_1 \times \mathbf{V}_3 + \mathbf{V}_2 \times \mathbf{V}_3$$

$$\mathbf{V}_1 \times (\mathbf{V}_2 \times \mathbf{V}_3) = \mathbf{V}_2(\mathbf{V}_3 \cdot \mathbf{V}_1) - \mathbf{V}_3(\mathbf{V}_1 \cdot \mathbf{V}_2)$$

$$\mathbf{i} \times \mathbf{i} = \mathbf{j} \times \mathbf{j} = \mathbf{k} \times \mathbf{k} = 0 \mathbf{1} \text{ (zero vector)}$$

$$= \mathbf{0}$$

$$\mathbf{i} \times \mathbf{j} = \mathbf{k}, \quad \mathbf{j} \times \mathbf{k} = \mathbf{i}, \quad \mathbf{k} \times \mathbf{i} = \mathbf{j}.$$

If  $\mathbf{V}_1 = a_1\mathbf{i} + b_1\mathbf{j} + c_1\mathbf{k}$ ,  $\mathbf{V}_2 = a_2\mathbf{i} + b_2\mathbf{j} + c_2\mathbf{k}$ ,  $\mathbf{V}_3 = a_3\mathbf{i} + b_3\mathbf{j} + c_3\mathbf{k}$ , then

$$\mathbf{V}_1 \times \mathbf{V}_2 = \begin{vmatrix} \mathbf{i} & \mathbf{j} & \mathbf{k} \\ a_1 & b_1 & c_1 \\ a_2 & b_2 & c_2 \end{vmatrix} = (b_1c_2 - b_2c_1)\mathbf{i} + (c_1a_2 - c_2a_1)\mathbf{j} + (a_1b_2 - a_2b_1)\mathbf{k}.$$

It should be noted that since  $\mathbf{V}_1 \times \mathbf{V}_2 = -\mathbf{V}_2 \times \mathbf{V}_1$ , the vector product is not commutative.

## E.6 Scalar Triple Product

There is only one possible interpretation of the expression  $\mathbf{V}_1 \cdot \mathbf{V}_2 \times \mathbf{V}_3$  and that is  $\mathbf{V}_1 \cdot (\mathbf{V}_2 \times \mathbf{V}_3)$ , which is obviously a scalar.

Further,  $\mathbf{V}_1 \cdot (\mathbf{V}_2 \times \mathbf{V}_3) = (\mathbf{V}_1 \times \mathbf{V}_2) \cdot \mathbf{V}_3 = \mathbf{V}_2 \cdot (\mathbf{V}_3 \times \mathbf{V}_1)$

$$= \begin{vmatrix} a_1 & b_1 & c_1 \\ a_2 & b_2 & c_2 \\ a_3 & b_3 & c_3 \end{vmatrix} = v_1v_2v_3 \cos \phi \sin \theta$$

where

$\theta$  is the angle between  $\mathbf{V}_2$  and  $\mathbf{V}_3$

$\phi$  is the angle between  $\mathbf{V}_1$  and the normal to the plane of  $\mathbf{V}_2$  and  $\mathbf{V}_3$

This product is called the *scalar triple product* and is written as  $[\mathbf{V}_1\mathbf{V}_2\mathbf{V}_3]$ .

The determinant indicates that it can be considered as the volume of the parallelepiped whose three determining edges are  $\mathbf{V}_1$ ,  $\mathbf{V}_2$ , and  $\mathbf{V}_3$ .

It also follows that cyclic permutation of the subscripts does not change the value of the scalar triple product so that

$$[\mathbf{V}_1\mathbf{V}_2\mathbf{V}_3] = [\mathbf{V}_2\mathbf{V}_3\mathbf{V}_1] = [\mathbf{V}_3\mathbf{V}_1\mathbf{V}_2]$$

but

$$[\mathbf{V}_1\mathbf{V}_2\mathbf{V}_3] = -[\mathbf{V}_2\mathbf{V}_1\mathbf{V}_3], \text{ etc.}$$

and

$$[\mathbf{V}_1\mathbf{V}_1\mathbf{V}_2] \equiv 0, \text{ etc.}$$

Given three noncoplanar reference vectors  $\mathbf{V}_1$ ,  $\mathbf{V}_2$ , and  $\mathbf{V}_3$  the *reciprocal system* is given by  $\mathbf{V}_1^*$ ,  $\mathbf{V}_2^*$ , and  $\mathbf{V}_3^*$ , where

$$1 = v_1v_1^* = v_2v_2^* = v_3v_3^* \\ 0 = v_1v_2^* = v_1v_3^* = v_2v_1^*, \text{ etc.}$$

$$\mathbf{V}_1^* = \frac{\mathbf{V}_2 \times \mathbf{V}_3}{[\mathbf{V}_1\mathbf{V}_2\mathbf{V}_3]}, \quad \mathbf{V}_2^* = \frac{\mathbf{V}_3 \times \mathbf{V}_1}{[\mathbf{V}_1\mathbf{V}_2\mathbf{V}_3]}, \quad \mathbf{V}_3^* = \frac{\mathbf{V}_1 \times \mathbf{V}_2}{[\mathbf{V}_1\mathbf{V}_2\mathbf{V}_3]}.$$

The system  $\mathbf{i}$ ,  $\mathbf{j}$ ,  $\mathbf{k}$  is its own reciprocal.

## E.7 Vector Triple Product

The product  $\mathbf{V}_1 \times (\mathbf{V}_2 \times \mathbf{V}_3)$  defines the *vector triple product*. Obviously, in this case, the brackets are vital to the definition:

$$\mathbf{V}_1 \times (\mathbf{V}_2 \times \mathbf{V}_3) = (\mathbf{V}_1 \cdot \mathbf{V}_3)\mathbf{V}_2 - (\mathbf{V}_1 \cdot \mathbf{V}_2)\mathbf{V}_3 \\ = \begin{vmatrix} \mathbf{i} & \mathbf{j} & \mathbf{k} \\ a_1 & b_1 & c_1 \\ b_2 & c_2 & c_3 \\ b_3 & c_3 & a_3 \end{vmatrix} - \begin{vmatrix} \mathbf{i} & \mathbf{j} & \mathbf{k} \\ a_1 & b_1 & c_1 \\ c_2 & a_2 & a_3 \\ a_2 & b_2 & b_3 \end{vmatrix},$$

i.e., it is a vector, perpendicular to  $\mathbf{V}_1$ , lying in the plane of  $\mathbf{V}_2$ ,  $\mathbf{V}_3$ . Similarly,

$$(\mathbf{V}_1 \times \mathbf{V}_2) \times \mathbf{V}_3 = \begin{vmatrix} \mathbf{i} & \mathbf{j} & \mathbf{k} \\ b_1 & c_1 & a_1 \\ b_2 & c_2 & a_2 \\ a_3 & b_3 & c_3 \end{vmatrix} - \begin{vmatrix} \mathbf{i} & \mathbf{j} & \mathbf{k} \\ c_1 & a_1 & a_2 \\ a_1 & b_1 & b_2 \\ a_2 & b_2 & c_2 \end{vmatrix}$$

$$\mathbf{V}_1 \times (\mathbf{V}_2 \times \mathbf{V}_3) + \mathbf{V}_2 \times (\mathbf{V}_3 \times \mathbf{V}_1) + \mathbf{V}_3 \times (\mathbf{V}_1 \times \mathbf{V}_2) \equiv 0.$$

If  $\mathbf{V}_1 \times (\mathbf{V}_2 \times \mathbf{V}_3) = (\mathbf{V}_1 \times \mathbf{V}_2) \times \mathbf{V}_3$ , then  $\mathbf{V}_1$ ,  $\mathbf{V}_2$ ,  $\mathbf{V}_3$  form an *orthogonal set*. Thus,  $\mathbf{i}$ ,  $\mathbf{j}$ ,  $\mathbf{k}$  form an orthogonal set.

## E.8 Geometry of the Plane, Straight Line, and Sphere

The position vectors of the fixed points  $A$ ,  $B$ ,  $C$ ,  $D$  relative to  $O$  are  $\mathbf{V}_1$ ,  $\mathbf{V}_2$ ,  $\mathbf{V}_3$ ,  $\mathbf{V}_4$ , and the position vector of the variable point  $P$  is  $\mathbf{V}$ .

The vector form of the equation of the straight line through  $A$  parallel to  $\mathbf{V}_2$  is

$$\mathbf{V} = \mathbf{V}_1 + r\mathbf{V}_2$$

$$\text{or } (\mathbf{V} - \mathbf{V}_1) = r\mathbf{V}_2$$

$$\text{or } (\mathbf{V} - \mathbf{V}_1) \times \mathbf{V}_2 = 0,$$

while that of the plane through  $A$  perpendicular to  $\mathbf{V}_2$  is

$$(\mathbf{V} - \mathbf{V}_1) \cdot \mathbf{V}_2 = 0.$$

The equation of the line  $AB$  is

$$\mathbf{V} = r\mathbf{V}_1 + (1 - r)\mathbf{V}_2$$

and those of the bisectors of the angles between  $\mathbf{V}_1$  and  $\mathbf{V}_2$  are

$$\mathbf{V} = r \left( \frac{\mathbf{V}_1}{v_1} \pm \frac{\mathbf{V}_2}{v_2} \right)$$

or

$$\mathbf{V} = r(\hat{\mathbf{v}}_1 + \hat{\mathbf{v}}_2).$$

The perpendicular from  $C$  to the line through  $A$  parallel to  $\mathbf{V}_2$  has as its equation

$$\mathbf{V} = \mathbf{V}_1 - \mathbf{V}_3 - \hat{\mathbf{v}}_2 \cdot (\mathbf{V}_1 - \mathbf{V}_3) \hat{\mathbf{v}}_2.$$

The condition for the intersection of the two lines,

$$\mathbf{V} = \mathbf{V}_1 + r\mathbf{V}_3$$

and

$$\mathbf{V} = \mathbf{V}_2 + s\mathbf{V}_4$$

is

$$[(\mathbf{V}_1 + \mathbf{V}_2)\mathbf{V}_3\mathbf{V}_4] = 0.$$

The common perpendicular to the above two lines is the line of intersection of the two planes

$$[(\mathbf{V} - \mathbf{V}_1)\mathbf{V}_3(\mathbf{V}_3 \times \mathbf{V}_4)] = 0$$

and

$$[(\mathbf{V} - \mathbf{V}_2)\mathbf{V}_4(\mathbf{V}_3 \times \mathbf{V}_4)] = 0$$

and the length of this perpendicular is

$$\frac{[(\mathbf{V} - \mathbf{V}_2)\mathbf{V}_3\mathbf{V}_4]}{|\mathbf{V}_3 \times \mathbf{V}_4|}.$$

The equation of the line perpendicular to the plane  $ABC$  is

$$\mathbf{V} = \mathbf{V}_1 \times \mathbf{V}_2 + \mathbf{V}_2 \times \mathbf{V}_3 + \mathbf{V}_3 \times \mathbf{V}_1,$$

and the distance of the plane from the origin is

$$\frac{[\mathbf{V}_1\mathbf{V}_2\mathbf{V}_3]}{|(\mathbf{V}_2 - \mathbf{V}_1) \times (\mathbf{V}_3 - \mathbf{V}_1)|}.$$

In general, the vector equation

$$\mathbf{V} \cdot \mathbf{V}_2 = r$$

defines the plane that is perpendicular to  $\mathbf{V}_2$ , and the perpendicular distance from  $A$  to this plane is

$$\frac{r - \mathbf{V}_1 \cdot \mathbf{V}_2}{v_2}.$$

The distance from  $A$ , measured along a line parallel to  $\mathbf{V}_3$ , is

$$\frac{r - \mathbf{V}_1 \cdot \mathbf{V}_2}{\mathbf{V}_2 \cdot \hat{\mathbf{v}}_3} \quad \text{or} \quad \frac{r - \mathbf{V}_1 \cdot \mathbf{V}_2}{v_2 \cos \theta}$$

where  $\theta$  is the angle between  $\mathbf{V}_2$  and  $\mathbf{V}_3$ .

(If this plane contains the point  $C$ , then  $r = \mathbf{V}_3 \cdot \mathbf{V}_2$ , and if it passes through the origin, then  $r = 0$ .) Given two planes

$$\mathbf{V} \cdot \mathbf{V}_1 = r$$

$$\mathbf{V} \cdot \mathbf{V}_2 = s,$$

any planes through the line of intersection of these two planes is given by

$$\mathbf{V} \cdot (\mathbf{V}_1 + \lambda\mathbf{V}_2) = r + \lambda s$$

where  $\lambda$  is a scalar parameter. In particular,  $\lambda = \pm v_1/v_2$  yields the equation of the two planes bisecting the angle between the given planes.

The plane through  $A$  parallel to the plane of  $\mathbf{V}_2, \mathbf{V}_3$  is

$$\mathbf{V} = \mathbf{V}_1 + r\mathbf{V}_2 + s\mathbf{V}_3$$

or

$$(\mathbf{V} - \mathbf{V}_1) \cdot \mathbf{V}_2 \times \mathbf{V}_3 = 0$$

or

$$[\mathbf{V}\mathbf{V}_2\mathbf{V}_3] - [\mathbf{V}_1\mathbf{V}_2\mathbf{V}_3] = 0$$

so that the expansion in rectangular Cartesian coordinates yields

$$\begin{vmatrix} (x - a_1) & (y - b_1) & (z - c_1) \\ a_2 & b_2 & c_2 \\ a_3 & b_3 & c_3 \end{vmatrix} = 0 \quad (\mathbf{V} \equiv x\mathbf{i} + y\mathbf{j} + z\mathbf{k}),$$

which is obviously the usual linear equation in  $x, y$ , and  $z$ .

The plane through  $AB$  parallel to  $\mathbf{V}_3$  is given by

$$[(\mathbf{V} - \mathbf{V}_1)(\mathbf{V}_1 - \mathbf{V}_2)\mathbf{V}_3] = 0$$

or

$$[\mathbf{V}\mathbf{V}_2\mathbf{V}_3] - [\mathbf{V}\mathbf{V}_1\mathbf{V}_3] - [\mathbf{V}_1\mathbf{V}_2\mathbf{V}_3] = 0.$$

The plane through the three points  $A, B$ , and  $C$  is

$$\mathbf{V} = \mathbf{V}_1 + s(\mathbf{V}_2 - \mathbf{V}_1) + t(\mathbf{V}_3 - \mathbf{V}_1)$$

or

$$\mathbf{V} = r\mathbf{V}_1 + s\mathbf{V}_2 + t\mathbf{V}_3 \quad (r + s + t \equiv 1)$$

or

$$[(\mathbf{V} - \mathbf{V}_1)(\mathbf{V}_1 - \mathbf{V}_2)(\mathbf{V}_2 - \mathbf{V}_3)] = 0$$

or

$$[\mathbf{V}\mathbf{V}_1\mathbf{V}_2] + [\mathbf{V}\mathbf{V}_2\mathbf{V}_3] + [\mathbf{V}\mathbf{V}_3\mathbf{V}_1] - [\mathbf{V}_1\mathbf{V}_2\mathbf{V}_3] = 0.$$

For four points  $A, B, C, D$  to be coplanar, then

$$r\mathbf{V}_1 + s\mathbf{V}_2 + t\mathbf{V}_3 + u\mathbf{V}_4 \equiv 0 \equiv r + s + t + u.$$

The following formulae relate to a sphere when the vectors are taken to lie in three-dimensional space and to a circle when the space is two-dimensional. For a circle in three dimensions, take the intersection of the sphere with a plane.

The equation of a sphere with center  $O$  and radius  $OA$  is

$$\mathbf{V} \cdot \mathbf{V} = v_1^2 \quad (\text{not } \mathbf{V} = \mathbf{V}_1)$$

or

$$(\mathbf{V} - \mathbf{V}_1) \cdot (\mathbf{V} + \mathbf{V}_1) = 0,$$

while that of a sphere with center  $B$  radius  $v_1$  is

$$(\mathbf{V} - \mathbf{V}_2) \cdot (\mathbf{V} - \mathbf{V}_2) = v_1^2$$

or

$$\mathbf{V} \cdot (\mathbf{V} - 2\mathbf{V}_2) = v_1^2 - v_2^2.$$

If the above sphere passes through the origin, then

$$\mathbf{V} \cdot (\mathbf{V} - 2\mathbf{V}_2) = 0.$$

Note that in two-dimensional polar coordinates this is simply

$$r = 2a \cdot \cos \theta$$

while in three-dimensional Cartesian coordinates, it is

$$x^2 + y^2 + z^2 - 2(a_2x + b_2y + c_2z) = 0.$$

The equation of a sphere having the points  $A$  and  $B$  as the extremities of a diameter is

$$(\mathbf{V} - \mathbf{V}_1) \cdot (\mathbf{V} - \mathbf{V}_2) = 0.$$

The square of the length of the tangent from  $C$  to the sphere with center  $B$  and radius  $v_1$  is given by

$$(\mathbf{V}_3 - \mathbf{V}_2) \cdot (\mathbf{V}_3 - \mathbf{V}_2) = v_1^2.$$

The condition that the plane  $\mathbf{V} \cdot \mathbf{V}_3 = s$  is tangential to the sphere  $(\mathbf{V} - \mathbf{V}_2) \cdot (\mathbf{V} - \mathbf{V}_2) = v_1^2$  is

$$(s - \mathbf{V}_3 \cdot \mathbf{V}_2) \cdot (s - \mathbf{V}_3 \cdot \mathbf{V}_2) = v_1^2 v_3^2.$$

The equation of the tangent plane at  $D$ , on the surface of sphere  $(\mathbf{V} - \mathbf{V}_2) \cdot (\mathbf{V} - \mathbf{V}_2) = v_1^2$ , is

$$(\mathbf{V} - \mathbf{V}_4) \cdot (\mathbf{V}_4 - \mathbf{V}_2) = 0$$

or

$$\mathbf{V} \cdot \mathbf{V}_4 - \mathbf{V}_2 \cdot (\mathbf{V} + \mathbf{V}_4) = v_1^2 - v_2^2.$$

The condition that the two circles  $(\mathbf{V} - \mathbf{V}_2) \cdot (\mathbf{V} - \mathbf{V}_2) = v_1^2$  and  $(\mathbf{V} - \mathbf{V}_4) \cdot (\mathbf{V} - \mathbf{V}_4) = v_3^2$  intersect orthogonally is clearly

$$(\mathbf{V}_2 - \mathbf{V}_4) \cdot (\mathbf{V}_2 - \mathbf{V}_4) = v_1^2 + v_3^2.$$

The polar plane of  $D$  with respect to the circle

$$\begin{aligned} (\mathbf{V} - \mathbf{V}_2) \cdot (\mathbf{V} - \mathbf{V}_2) &= v_1^2 \text{ is} \\ \mathbf{V} \cdot \mathbf{V}_4 - \mathbf{V}_2 \cdot (\mathbf{V} + \mathbf{V}_4) &= v_1^2 - v_2^2. \end{aligned}$$

Any sphere through the intersection of the two spheres  $(\mathbf{V} - \mathbf{V}_2) \cdot (\mathbf{V} - \mathbf{V}_2) = v_1^2$  and  $(\mathbf{V} - \mathbf{V}_4) \cdot (\mathbf{V} - \mathbf{V}_4) = v_3^2$  is given by

$$(\mathbf{V} - \mathbf{V}_2) \cdot (\mathbf{V} - \mathbf{V}_2) + \lambda(\mathbf{V} - \mathbf{V}_4) \cdot (\mathbf{V} - \mathbf{V}_4) = v_1^2 + \lambda v_3^2,$$

while the radical plane of two such spheres is

$$\mathbf{V} \cdot (\mathbf{V}_2 - \mathbf{V}_4) = -\frac{1}{2}(v_1^2 - v_2^2 - v_3^2 + v_4^2).$$

## E.9 Differentiation of Vectors

If  $\mathbf{V}_1 = a_1\mathbf{i} + b_1\mathbf{j} + c_1\mathbf{k}$  and  $\mathbf{V}_2 = a_2\mathbf{i} + b_2\mathbf{j} + c_2\mathbf{k}$  and if  $\mathbf{V}_1$  and  $\mathbf{V}_2$  are functions of the scalar  $t$ , then

$$\frac{d}{dt}(\mathbf{V}_1 + \mathbf{V}_2 + \dots) = \frac{d\mathbf{V}_1}{dt} + \frac{d\mathbf{V}_2}{dt} + \dots,$$

where

$$\begin{aligned} \frac{d\mathbf{V}_1}{dt} &= \frac{da_1}{dt}\mathbf{i} + \frac{db_1}{dt}\mathbf{j} + \frac{dc_1}{dt}\mathbf{k}, \text{ etc.} \\ \frac{d}{dt}(\mathbf{V}_1 \cdot \mathbf{V}_2) &= \frac{d\mathbf{V}_1}{dt} \cdot \mathbf{V}_2 + \mathbf{V}_1 \cdot \frac{d\mathbf{V}_2}{dt} \\ \frac{d}{dt}(\mathbf{V}_1 \times \mathbf{V}_2) &= \frac{d\mathbf{V}_1}{dt} \times \mathbf{V}_2 + \mathbf{V}_1 \times \frac{d\mathbf{V}_2}{dt} \\ \mathbf{V} \cdot \frac{d\mathbf{V}}{dt} &= v \frac{dv}{dt}. \end{aligned}$$

In particular, if  $\mathbf{V}$  is a vector of constant length then the right-hand side of the last equation is identically zero showing that  $\mathbf{V}$  is perpendicular to its derivative.



The derivatives of the triple products are

$$\frac{d}{dt}[\mathbf{V}_1\mathbf{V}_2\mathbf{V}_3] = \left[ \left( \frac{d\mathbf{V}_1}{dt} \right) \mathbf{V}_2\mathbf{V}_3 \right] + \left[ \mathbf{V}_1 \left( \frac{d\mathbf{V}_2}{dt} \right) \mathbf{V}_3 \right] + \left[ \mathbf{V}_1\mathbf{V}_2 \left( \frac{d\mathbf{V}_3}{dt} \right) \right]$$

and

$$\frac{d}{dt}\{\mathbf{V}_1 \times (\mathbf{V}_2 \times \mathbf{V}_3)\} = \left( \frac{d\mathbf{V}_1}{dt} \right) \times (\mathbf{V}_2 \times \mathbf{V}_3) + \mathbf{V}_1 \times \left( \left( \frac{d\mathbf{V}_2}{dt} \right) \times \mathbf{V}_3 \right) + \mathbf{V}_1 \times \left( \mathbf{V}_2 \times \left( \frac{d\mathbf{V}_3}{dt} \right) \right).$$

### E.10 Geometry of Curves in Space

- $s$  the length of arc, measured from some fixed point on the curve (Figure E.3).
- $\mathbf{V}_1$  the position vector of the point  $A$  on the curve.
- $\mathbf{V}_1 + \delta\mathbf{V}_1$  the position vector of the point  $P$  in the neighborhood of  $A$ .
- $\hat{\mathbf{t}}$  the unit tangent to the curve at the point  $A$ , measured in the direction of  $s$  increasing.

The normal plane is that plane which is perpendicular to the unit tangent. The principal normal is defined as the intersection of the normal plane with the plane defined by  $\mathbf{V}_1$  and  $\mathbf{V}_1 + \delta\mathbf{V}_1$  in the limit as  $\delta\mathbf{V}_1 \rightarrow 0$ .

- $\hat{\mathbf{n}}$  the unit normal (principal) at the point  $A$ . The plane defined by  $\hat{\mathbf{t}}$  and  $\hat{\mathbf{n}}$  is called the *osculating plane* (alternatively, plane of curvature or local plane).
- $\rho$  the radius of curvature of  $A$ .
- $\delta\theta$  the angle subtended at the origin by  $\delta\mathbf{V}_1$ .
- $\kappa = \frac{d\theta}{ds} = \frac{1}{\rho}$ .

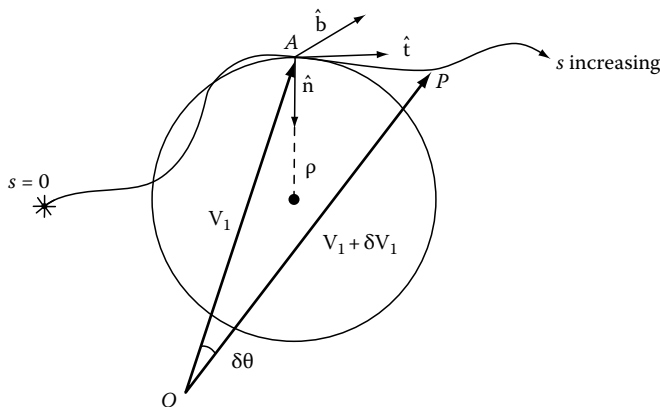


FIGURE E.3

- $\hat{\mathbf{b}}$  the unit binormal, i.e., the unit vector that is parallel to  $\hat{\mathbf{t}} \times \hat{\mathbf{n}}$  at the point  $A$ .
- $\lambda$  the torsion of the curve at  $A$ .

Frenet's formulae:

$$\begin{aligned} \frac{d\hat{\mathbf{t}}}{ds} &= \kappa\hat{\mathbf{n}} \\ \frac{d\hat{\mathbf{n}}}{ds} &= -\kappa\hat{\mathbf{t}} + \lambda\hat{\mathbf{b}} \\ \frac{d\hat{\mathbf{b}}}{ds} &= -\lambda\hat{\mathbf{n}} \end{aligned}$$

The following formulae are also applicable:

Unit tangent:

$$\hat{\mathbf{t}} = \frac{d\mathbf{V}_1}{ds}.$$

Equation of the tangent:

$$(\mathbf{V} - \mathbf{V}_1) \times \hat{\mathbf{t}} = 0$$

or

$$\mathbf{V} = \mathbf{V}_1 + q\hat{\mathbf{t}}.$$

Unit normal:

$$\hat{\mathbf{n}} = \frac{1}{\kappa ds^2} \frac{d^2\mathbf{V}_1}{ds^2}.$$

Equation of the normal plane:

$$(\mathbf{V} - \mathbf{V}_1) \cdot \hat{\mathbf{t}} = 0.$$

Equation of the normal:

$$(\mathbf{V} - \mathbf{V}_1) \times \hat{\mathbf{n}} = 0$$

or

$$\mathbf{V} = \mathbf{V}_1 + r\hat{\mathbf{n}}.$$

Unit binormal:

$$\hat{\mathbf{b}} = \hat{\mathbf{t}} \times \hat{\mathbf{n}}.$$

Equation of the binormal:

$$(\mathbf{V} - \mathbf{V}_1) \times \hat{\mathbf{b}} = 0$$

or

$$\mathbf{V} = \mathbf{V}_1 + u\hat{\mathbf{b}}$$

or

$$\mathbf{V} = \mathbf{V}_1 + w \frac{d\mathbf{V}_1}{ds} \times \frac{d^2\mathbf{V}_1}{ds^2}.$$

Equation of the osculating plane:

$$[(\mathbf{V} - \mathbf{V}_1)\hat{\mathbf{t}}\hat{\mathbf{n}}] = 0$$

or

$$\left[ (\mathbf{V} - \mathbf{V}_1) \left( \frac{d\mathbf{V}_1}{ds} \right) \left( \frac{d^2\mathbf{V}_1}{ds^2} \right) \right] = 0.$$

A *geodesic line* on a surface is a curve, the osculating plane of which is everywhere normal to the surface.

The differential equation of the geodesic is

$$[\hat{\mathbf{n}}d\mathbf{V}_1d^2\mathbf{V}_1] = 0.$$

## E.11 Differential Operators— Rectangular Coordinates

$$dS = \frac{\partial S}{\partial x} \cdot dx + \frac{\partial S}{\partial y} \cdot dy + \frac{\partial S}{\partial z} \cdot dz.$$

By definition,

$$\nabla \equiv \text{del} \equiv \mathbf{i} \frac{\partial}{\partial x} + \mathbf{j} \frac{\partial}{\partial y} + \mathbf{k} \frac{\partial}{\partial z}$$

$$\nabla^2 \equiv \text{Laplacian} \equiv \frac{\partial^2}{\partial x^2} + \frac{\partial^2}{\partial y^2} + \frac{\partial^2}{\partial z^2}.$$

If  $S$  is a scalar function, then

$$\nabla S \equiv \text{grad } S \equiv \frac{\partial S}{\partial x} \mathbf{i} + \frac{\partial S}{\partial y} \mathbf{j} + \frac{\partial S}{\partial z} \mathbf{k}.$$

Grad  $S$  defines both the direction and magnitude of the maximum rate of increase of  $S$  at any point. Hence the name *gradient* and also its vectorial nature.  $\nabla S$  is independent of the choice of rectangular coordinates.

$$\nabla S = \frac{\partial S}{\partial n} \hat{\mathbf{n}}$$

where  $\hat{\mathbf{n}}$  is the unit normal to the surface  $S = \text{constant}$ , in the direction of  $S$  increasing. The total derivative of  $S$  at a point having the position vector  $\mathbf{V}$  is given by (Figure E.4)

$$\begin{aligned} dS &= \frac{\partial S}{\partial n} \hat{\mathbf{n}} \cdot d\mathbf{V} \\ &= d\mathbf{V} \cdot \nabla S \end{aligned}$$

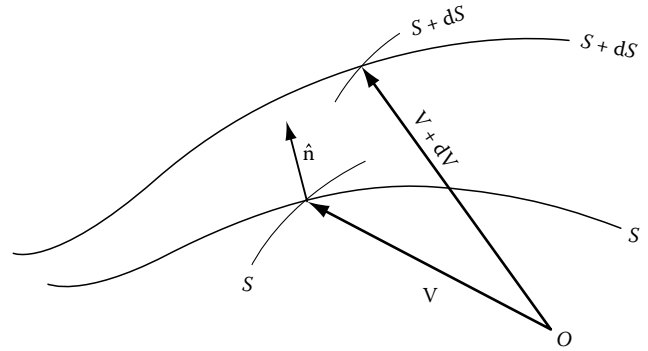


FIGURE E.4

and the directional derivative of  $S$  in the direction of  $\mathbf{U}$  is

$$\mathbf{U} \cdot \nabla S = \mathbf{U} \cdot (\nabla S) = (\mathbf{U} \cdot \nabla)S.$$

Similarly, the directional derivative of the vector  $\mathbf{V}$  in the direction of  $\mathbf{U}$  is

$$(\mathbf{U} \cdot \nabla)\mathbf{V}.$$

The *distributive* law holds for finding a gradient. Thus, if  $S$  and  $T$  are scalar functions,

$$\nabla(S + T) = \nabla S + \nabla T.$$

The *associative* law becomes the rule for differentiating a product:

$$\nabla(ST) = S\nabla T + T\nabla S.$$

If  $\mathbf{V}$  is a vector function with the magnitudes of the components parallel to the three coordinate axes,  $V_x, V_y, V_z$ , then

$$\nabla \cdot \mathbf{V} \equiv \text{div } \mathbf{V} \equiv \frac{\partial V_x}{\partial x} + \frac{\partial V_y}{\partial y} + \frac{\partial V_z}{\partial z}.$$

The divergence obeys the distributive law. Thus, if  $\mathbf{V}$  and  $\mathbf{U}$  are vectors functions, then

$$\nabla \cdot (\mathbf{V} + \mathbf{U}) = \nabla \cdot \mathbf{V} + \nabla \cdot \mathbf{U}$$

$$\nabla \cdot (S\mathbf{V}) = (\nabla S) \cdot \mathbf{V} + S(\nabla \cdot \mathbf{V})$$

$$\nabla \cdot (\mathbf{U} \times \mathbf{V}) = \mathbf{V} \cdot (\nabla \times \mathbf{U}) - \mathbf{U} \cdot (\nabla \times \mathbf{V}).$$

As with the gradient of a scalar, the divergence of a vector is invariant under a transformation from one set of rectangular coordinates to another:

$\nabla \times \mathbf{V} \equiv \text{curl } \mathbf{V}$  (sometimes  $\nabla \wedge \mathbf{V}$  or  $\text{rot } \mathbf{V}$ )

$$\begin{aligned} &\equiv \left( \frac{\partial V_z}{\partial y} - \frac{\partial V_y}{\partial z} \right) \mathbf{i} + \left( \frac{\partial V_x}{\partial z} - \frac{\partial V_z}{\partial x} \right) \mathbf{j} + \left( \frac{\partial V_y}{\partial x} - \frac{\partial V_x}{\partial y} \right) \mathbf{k} \\ &= \begin{vmatrix} \mathbf{i} & \mathbf{j} & \mathbf{k} \\ \frac{\partial}{\partial x} & \frac{\partial}{\partial y} & \frac{\partial}{\partial z} \\ V_x & V_y & V_z \end{vmatrix}. \end{aligned}$$

The *curl* (or *rotation*) of a vector is a vector that is invariant under a transformation from one set of rectangular coordinates to another

$$\begin{aligned}\nabla \times (\mathbf{U} + \mathbf{V}) &= \nabla \times \mathbf{U} + \nabla \times \mathbf{V} \\ \nabla \times (S\mathbf{V}) &= (\nabla S) \times \mathbf{V} + S(\nabla \times \mathbf{V}) \\ \nabla \times (\mathbf{U} \times \mathbf{V}) &= (\mathbf{V} \cdot \nabla)\mathbf{U} - (\mathbf{U} \cdot \nabla)\mathbf{V} + \mathbf{U}(\nabla \cdot \mathbf{V}) - \mathbf{V}(\nabla \cdot \mathbf{U}) \\ \text{grad}(\mathbf{U} \cdot \mathbf{V}) &= \nabla(\mathbf{U} \cdot \mathbf{V}) \\ &= (\mathbf{V} \cdot \nabla)\mathbf{U} + (\mathbf{U} \cdot \nabla)\mathbf{V} + \mathbf{V} \times (\nabla \times \mathbf{U}) \\ &\quad + \mathbf{U} \times (\nabla \times \mathbf{V}).\end{aligned}$$

If

$$\begin{aligned}\mathbf{V} &= V_x \mathbf{i} + V_y \mathbf{j} + V_z \mathbf{k} \\ \nabla \cdot \mathbf{V} &= \nabla V_x \cdot \mathbf{i} + \nabla V_y \cdot \mathbf{j} + \nabla V_z \cdot \mathbf{k}\end{aligned}$$

and

$$\nabla \times \mathbf{V} = \nabla V_x \times \mathbf{i} + \nabla V_y \times \mathbf{j} + \nabla V_z \times \mathbf{k}.$$

The operator  $\nabla$  can be used more than once. The number of possibilities where  $\nabla$  is used twice are

$$\begin{aligned}\nabla \cdot (\nabla \theta) &\equiv \text{div grad } \theta \\ \nabla \times (\nabla \theta) &\equiv \text{curl grad } \theta \\ \nabla(\nabla \cdot \mathbf{V}) &\equiv \text{grad div } \mathbf{V} \\ \nabla \cdot (\nabla \times \mathbf{V}) &\equiv \text{div curl } \mathbf{V} \\ \nabla \times (\nabla \times \mathbf{V}) &\equiv \text{curl curl } \mathbf{V}.\end{aligned}$$

The surface  $PRS \equiv u = \text{const.}$ , and the face of the curvilinear figure immediately opposite this is  $u + du = \text{const.}$  etc.

In terms of these surface constants

$$\begin{aligned}P &= P(u, v, w) \\ Q &= Q(u + du, v, w) \quad \text{and} \quad PQ = h_1 du \\ R &= R(u, v + dv, w) \quad PR = h_2 dv \\ S &= S(u, v, w + dw) \quad PS = h_3 dw\end{aligned}$$

where  $h_1, h_2,$  and  $h_3$  are functions of  $u, v,$  and  $w$ .

In rectangular Cartesians  $\mathbf{i}, \mathbf{j}, \mathbf{k}$ ,

$$\begin{aligned}h_1 &= 1, h_2 = 1, h_3 = 1. \\ \frac{\hat{\mathbf{a}}}{h_1} \frac{\partial}{\partial u} &= \mathbf{i} \frac{\partial}{\partial x}, \quad \frac{\hat{\mathbf{b}}}{h_2} \frac{\partial}{\partial v} = \mathbf{j} \frac{\partial}{\partial y}, \quad \frac{\hat{\mathbf{c}}}{h_3} \frac{\partial}{\partial w} = \mathbf{k} \frac{\partial}{\partial z}.\end{aligned}$$

In cylindrical coordinates  $\hat{\mathbf{r}}, \hat{\boldsymbol{\phi}}, \hat{\mathbf{k}}$ ,

$$\begin{aligned}h_1 &= 1, h_2 = r, h_3 = 1. \\ \frac{\hat{\mathbf{a}}}{h_1} \frac{\partial}{\partial u} &= \hat{\mathbf{r}} \frac{\partial}{\partial r}, \quad \frac{\hat{\mathbf{b}}}{h_2} \frac{\partial}{\partial v} = \frac{\hat{\boldsymbol{\phi}}}{r} \frac{\partial}{\partial \phi}, \quad \frac{\hat{\mathbf{c}}}{h_3} \frac{\partial}{\partial w} = \hat{\mathbf{k}} \frac{\partial}{\partial z}.\end{aligned}$$

In spherical coordinates  $\hat{\mathbf{r}}, \hat{\boldsymbol{\theta}}, \hat{\boldsymbol{\phi}}$

$$h_1 = 1, h_2 = r, h_3 = r \sin \theta$$

$$\frac{\hat{\mathbf{a}}}{h_1} \frac{\partial}{\partial u} = \hat{\mathbf{r}} \frac{\partial}{\partial r}, \quad \frac{\hat{\mathbf{b}}}{h_2} \frac{\partial}{\partial v} = \frac{\hat{\boldsymbol{\phi}}}{r} \frac{\partial}{\partial \theta}, \quad \frac{\hat{\mathbf{c}}}{h_3} \frac{\partial}{\partial w} = \frac{\hat{\boldsymbol{\phi}}}{r \sin \theta} \frac{\partial}{\partial \phi}.$$

The general expressions for grad, div, and curl, together with those for  $\nabla^2$  and the directional derivative, are in orthogonal curvilinear coordinates given by

$$\begin{aligned}\nabla S &= \frac{\hat{\mathbf{a}}}{h_1} \frac{\partial S}{\partial u} + \frac{\hat{\mathbf{b}}}{h_2} \frac{\partial S}{\partial v} + \frac{\hat{\mathbf{c}}}{h_3} \frac{\partial S}{\partial w} \\ (\mathbf{V} \cdot \nabla)S &= \frac{V_1}{h_1} \frac{\partial S}{\partial u} + \frac{V_2}{h_2} \frac{\partial S}{\partial v} + \frac{V_3}{h_3} \frac{\partial S}{\partial w} \\ \nabla \cdot \mathbf{V} &= \frac{1}{h_1 h_2 h_3} \left\{ \frac{\partial}{\partial u} (h_2 h_3 V_1) + \frac{\partial}{\partial v} (h_3 h_1 V_2) + \frac{\partial}{\partial w} (h_1 h_2 V_3) \right\} \\ \nabla \times \mathbf{V} &= \frac{\hat{\mathbf{a}}}{h_2 h_3} \left\{ \frac{\partial}{\partial v} (h_3 V_3) - \frac{\partial}{\partial w} (h_2 V_2) \right\} \\ &\quad + \frac{\hat{\mathbf{b}}}{h_3 h_1} \left\{ \frac{\partial}{\partial w} (h_1 V_1) - \frac{\partial}{\partial u} (h_3 V_3) \right\} \\ &\quad + \frac{\hat{\mathbf{c}}}{h_1 h_2} \left\{ \frac{\partial}{\partial u} (h_2 V_2) - \frac{\partial}{\partial v} (h_1 V_1) \right\} \\ \nabla^2 S &= \frac{1}{h_1 h_2 h_3} \left\{ \frac{\partial}{\partial u} \left( \frac{h_2 h_3}{h_1} \frac{\partial S}{\partial u} \right) + \frac{\partial}{\partial v} \left( \frac{h_3 h_1}{h_2} \frac{\partial S}{\partial v} \right) \right. \\ &\quad \left. + \frac{\partial}{\partial w} \left( \frac{h_1 h_2}{h_3} \frac{\partial S}{\partial w} \right) \right\}.\end{aligned}$$

## E.12 Transformation of Integrals

- $s$  the distance along some curve "C" in space and is measured from some fixed point
- $S$  a surface area
- $V$  a volume contained by a specified surface
- $\hat{\mathbf{t}}$  the unit tangent to C at the point P
- $\hat{\mathbf{n}}$  the unit outward pointing normal
- $F$  some vector function
- $ds$  is the vector element of curve ( $= \hat{\mathbf{t}} ds$ )
- $dS$  is the vector element of surface ( $= \hat{\mathbf{n}} dS$ ).

Then (Table E.1)

$$\int_{(c)} \mathbf{F} \cdot \hat{\mathbf{t}} ds = \int_{(c)} \mathbf{F} \cdot ds$$

and when

$$\mathbf{F} = \nabla \phi,$$

$$\int_{(c)} (\nabla \phi) \cdot \hat{\mathbf{t}} ds = \int_{(c)} d\phi.$$

TABLE E.1 Formulas of Vector Analysis

	Rectangular Coordinates	Cylindrical Coordinates	Spherical Coordinates
Conversion to rectangular coordinates		$x = r \cos \varphi \quad y = r \sin \varphi \quad z = z$	$x = r \cos \theta \sin \varphi \quad y = r \sin \theta \sin \varphi$ $z = r \cos \theta$
Gradient	$\nabla \phi = \frac{\partial \phi}{\partial x} \mathbf{i} + \frac{\partial \phi}{\partial y} \mathbf{j} + \frac{\partial \phi}{\partial z} \mathbf{k}$	$\nabla \phi = \frac{\partial \phi}{\partial r} \mathbf{r} + \frac{1}{r} \frac{\partial \phi}{\partial \varphi} \boldsymbol{\phi} + \frac{\partial \phi}{\partial z} \mathbf{k}$	$\nabla \phi = \frac{\partial \phi}{\partial r} \mathbf{r} + \frac{1}{r} \frac{\partial \phi}{\partial \theta} \boldsymbol{\theta} + \frac{1}{r \sin \theta} \frac{\partial \phi}{\partial \varphi} \boldsymbol{\phi}$
Divergence	$\nabla \cdot \mathbf{A} = \frac{\partial A_x}{\partial x} + \frac{\partial A_y}{\partial y} + \frac{\partial A_z}{\partial z}$	$\nabla \cdot \mathbf{A} = \frac{1}{r} \frac{\partial (r A_r)}{\partial r} + \frac{1}{r} \frac{\partial A_\varphi}{\partial \varphi} + \frac{\partial A_z}{\partial z}$	$\nabla \cdot \mathbf{A} = \frac{1}{r^2} \frac{\partial (r^2 A_r)}{\partial r} + \frac{1}{r \sin \theta} \frac{\partial (A_\theta \sin \theta)}{\partial \theta} + \frac{1}{r \sin \theta} \frac{\partial A_\varphi}{\partial \varphi}$
Curl	$\nabla \times \mathbf{A} = \begin{vmatrix} \mathbf{i} & \mathbf{j} & \mathbf{k} \\ \frac{\partial}{\partial x} & \frac{\partial}{\partial y} & \frac{\partial}{\partial z} \\ A_x & A_y & A_z \end{vmatrix}$	$\nabla \times \mathbf{A} = \begin{vmatrix} \frac{1}{r} \mathbf{r} & \boldsymbol{\phi} & \frac{1}{r} \mathbf{k} \\ \frac{\partial}{\partial r} & \frac{\partial}{\partial \varphi} & \frac{\partial}{\partial z} \\ A_r & r A_\varphi & A_z \end{vmatrix}$	$\nabla \times \mathbf{A} = \begin{vmatrix} \mathbf{r} & \boldsymbol{\theta} & \boldsymbol{\phi} \\ r^2 \sin \theta & r \sin \theta & r \\ \frac{\partial}{\partial r} & \frac{\partial}{\partial \theta} & \frac{\partial}{\partial \varphi} \\ A_r & r A_\theta & r A_\varphi \sin \theta \end{vmatrix}$
Laplacian	$\nabla^2 \phi = \frac{\partial^2 \phi}{\partial x^2} + \frac{\partial^2 \phi}{\partial y^2} + \frac{\partial^2 \phi}{\partial z^2}$	$\nabla^2 \phi = \frac{1}{r} \frac{\partial}{\partial r} \left( r \frac{\partial \phi}{\partial r} \right) + \frac{1}{r^2} \frac{\partial^2 \phi}{\partial \varphi^2} + \frac{\partial^2 \phi}{\partial z^2}$	$\nabla^2 \phi = \frac{1}{r^2} \frac{\partial}{\partial r} \left( r^2 \frac{\partial \phi}{\partial r} \right) + \frac{1}{r^2 \sin \theta} \frac{\partial}{\partial \theta} \left( \sin \theta \frac{\partial \phi}{\partial \theta} \right) + \frac{1}{r^2 \sin^2 \theta} \frac{\partial^2 \phi}{\partial \varphi^2}$

### E.13 Gauss' Theorem (Green's Theorem)

When  $S$  defines a closed region having a volume  $V$

$$\iiint_{(v)} (\nabla \cdot \mathbf{F}) dV = \iint_{(S)} (\mathbf{F} \cdot \hat{\mathbf{n}}) dS = \iint_{(S)} \mathbf{F} \cdot d\mathbf{s}$$

also

$$\iiint_{(v)} (\nabla \phi) dV = \iint_{(S)} \phi \hat{\mathbf{n}} dS$$

and

$$\iiint_{(v)} (\nabla \times \mathbf{F}) dV = \iint_{(S)} (\hat{\mathbf{n}} \times \mathbf{F}) dS.$$

### E.14 Stokes' Theorem

When  $C$  is closed and bounds the open surface  $S$ ,

$$\iint_{(S)} \hat{\mathbf{n}} \cdot (\nabla \times \mathbf{F}) dS = \int_{(C)} \mathbf{F} \cdot d\mathbf{s}$$

and

$$\iint_{(S)} (\hat{\mathbf{n}} \times \nabla \phi) dS = \int_{(C)} \phi d\mathbf{s}.$$

### E.15 Green's Theorem

$$\begin{aligned} \iint_{(S)} (\nabla \phi \times \nabla \theta) dS &= \iint_{(S)} \phi \hat{\mathbf{n}} \cdot (\nabla \theta) dS = \iiint_{(v)} \phi (\nabla^2 \theta) dV \\ &= \iint_{(a)} \theta \cdot \hat{\mathbf{n}} (\nabla \phi) dS = \iiint_{(v)} \theta (\nabla^2 \phi) dV. \end{aligned}$$



# Appendix F: Algebra Formulas and Coordinate Systems

---

F.1	Arithmetic Progression .....	F-1
F.2	Geometric Progression .....	F-1
F.3	Harmonic Progression .....	F-1
F.4	Factorials .....	F-1
F.5	Permutations .....	F-2
F.6	Combinations .....	F-2
F.7	Quadratic Equations .....	F-2
F.8	Cubic Equations .....	F-2
F.9	Trigonometric Solution of the Cubic Equation .....	F-2
F.10	Quartic Equation .....	F-3
F.11	Partial Fractions .....	F-3
F.12	Polar Coordinates in a Plane .....	F-5
F.13	Rectangular Coordinates in Space .....	F-6

## F.1 Arithmetic Progression \*

---

An arithmetic progression is a sequence of numbers such that each number differs from the previous number by a constant amount, called the *common difference*.

If  $a_1$  is the first term,  $a_n$  the  $n$ th term,  $d$  the common difference,  $n$  the number of terms, and  $s_n$  the sum of  $n$  terms.

$$a_n = a_1 + (n - 1)d, \quad s_n = \frac{n}{2}[a_1 + a_n],$$

$$s_n = \frac{n}{2}[2a_1 + (n - 1)d].$$

The arithmetic mean between  $a$  and  $b$  is given by  $\frac{a + b}{2}$ .

## F.2 Geometric Progression \*

---

A geometric progression is a sequence of numbers such that each number bears a constant ratio, called the *common ratio*, to the previous number.

If  $a_1$  is the first term,  $a_n$  the  $n$ th term,  $r$  the common ratio,  $n$  the number of terms, and  $s_n$  the sum of  $n$  terms.

$$a_n = a_1 r^{n-1}; \quad s_n = a_1 \frac{1 - r^n}{1 - r}$$

$$= a_1 \frac{r^n - 1}{r - 1} \quad (r \neq 1)$$

$$= \frac{a_1 - ra_n}{r - 1}$$

$$= \frac{1 - r}{ra_n - a_1}$$

---

\* It is customary to represent  $a_n$  by  $l$  in a finite progression and refer to it as the last term.

If  $|r| < 1$ , then the sum of an infinite geometrical progression converges to the limiting value

$$\frac{a_1}{1 - r}, \quad \left[ s_\infty = \lim_{n \rightarrow \infty} \frac{a_1(1 - r^n)}{1 - r} = \frac{a_1}{1 - r} \right]$$

The geometric mean between  $a$  and  $b$  is given by  $\sqrt{ab}$ .

## F.3 Harmonic Progression

---

A sequence of numbers whose reciprocals form an arithmetic progression is called an harmonic progression. Thus,

$$\frac{1}{a_1}, \frac{1}{a_1 + d}, \frac{1}{a_1 + 2d}, \dots, \frac{1}{a_1 + (n - 1)d}, \dots,$$

where

$$\frac{1}{a_n} = \frac{1}{a_1 + (n - 1)d}$$

forms a harmonic progression. The harmonic mean between  $a$  and  $b$  is given by  $\frac{2ab}{a + b}$ .

If  $A$ ,  $G$ ,  $H$ , respectively, represent the arithmetic mean, geometric mean, and harmonic mean between  $a$  and  $b$ , then  $G^2 = AH$ .

## F.4 Factorials

---

$$\angle n = n! = e^{-n} n^n \sqrt{2\pi n}, \text{ approximately.}$$

## F.5 Permutations

If  $M = {}_n P_r = P_{n:r}$  denotes the number of permutations of  $n$  distinct things taken  $r$  at a time,

$$M = n(n-1)(n-2)\dots(n-r+1) = \frac{n!}{(n-r)!}$$

## F.6 Combinations

If  $M = {}_n C_r = C_{n:r}$  denotes the number of combinations of  $n$  distinct things taken  $r$  at a time,

$$M = \frac{n(n-1)(n-2)\dots(n-r+1)}{r!} = \frac{n!}{r!(n-r)!}$$

By definition  $\binom{n}{0} = 1$ .

## F.7 Quadratic Equations

Any quadratic equation may be reduced to the form,

$$ax^2 + bx + c = 0.$$

Then

$$x = \frac{-b \pm \sqrt{b^2 - 4ac}}{2a}.$$

If  $a$ ,  $b$ , and  $c$  are real, then:

If  $b^2 - 4ac$  is positive, the roots are real and unequal.

If  $b^2 - 4ac$  is zero, the roots are real and equal.

If  $b^2 - 4ac$  is negative, the roots are imaginary and unequal.

## F.8 Cubic Equations

A cubic equation,  $y^3 + py^2 + qy + r = 0$  may be reduced to the form,

$$x^3 + ax + b = 0.$$

by substituting for  $y$  the value,  $x - \frac{p}{3}$ . Here

$$a = \frac{1}{3}(3q - p^2) \quad \text{and} \quad b = \frac{1}{27}(2p^3 - 9pq + 27r).$$

For solution, let

$$A = \sqrt[3]{-\frac{b}{2} + \sqrt{\frac{b^2}{4} + \frac{a^3}{27}}}, \quad B = \sqrt[3]{-\frac{b}{2} - \sqrt{\frac{b^2}{4} + \frac{a^3}{27}}}$$

then the values of  $x$  will be given by,

$$x = A + B, \quad -\frac{A+B}{2} + \frac{A-B}{2}\sqrt{-3}, \quad -\frac{A+B}{2} - \frac{A-B}{2}\sqrt{-3}.$$

If  $p$ ,  $q$ ,  $r$  are real, then:

If  $\frac{b^2}{4} + \frac{a^3}{27} > 0$ , there will be one real root and two conjugate imaginary roots.

If  $\frac{b^2}{4} + \frac{a^3}{27} = 0$ , there will be three real roots of which at least two are equal.

If  $\frac{b^2}{4} + \frac{a^3}{27} < 0$ , there will be three real and unequal roots.

## F.9 Trigonometric Solution of the Cubic Equation

The form  $x^3 + ax + b = 0$  with  $ab \neq 0$  can always be solved by transforming it to the trigonometric identity

$$4 \cos^3 \theta - 3 \cos \theta - \cos(3\theta) \equiv 0.$$

Let  $x = m \cos \theta$ , then

$$\begin{aligned} x^3 + ax + b &\equiv m^3 \cos^3 \theta + am \cos \theta + b \\ &\equiv 4 \cos^3 \theta - 3 \cos \theta - \cos(3\theta) \equiv 0. \end{aligned}$$

Hence,

$$\frac{4}{m^3} = -\frac{3}{am} = \frac{-\cos(3\theta)}{b},$$

from which follows that

$$m = 2\sqrt{-\frac{a}{3}}, \quad \cos(3\theta) = \frac{3b}{am}.$$

Any solution  $\theta_1$  which satisfies  $\cos(3\theta) = \frac{3b}{am}$ , will also have the solutions

$$\theta_1 + \frac{2\pi}{3} \quad \text{and} \quad \theta_1 + \frac{4\pi}{3}.$$

The roots of the cubic  $x^3 + ax + b = 0$  are

$$2\sqrt{-\frac{a}{3}} \cos \theta_1, \quad 2\sqrt{-\frac{a}{3}} \cos\left(\theta_1 + \frac{2\pi}{3}\right), \quad 2\sqrt{-\frac{a}{3}} \cos\left(\theta_1 + \frac{4\pi}{3}\right).$$

### Example Where Hyperbolic Functions Are Necessary for Solution with Latter Procedure

The roots of the equation  $x^3 - x + 2 = 0$  may be found as follows:

Here,

$$a = -1, \quad b = 2, \quad m = 2\sqrt{\frac{1}{3}} = 1.155$$

$$\cos(3\theta) = \frac{6}{-1.155} = -5.196$$

$$\cos(3\theta) = -\cos(3\theta - \pi) = -\cosh[i(3\theta - \pi)] = -5.196.$$

Using hyperbolic function tables for  $\cosh[i(3\theta + \pi)] = 5.196$ , it is found that

$$i(3\theta - \pi) = 2.332.$$

Thus,

$$\begin{aligned} 3\theta - \pi &= -i(2.332) \\ 3\theta &= \pi - i(2.332) \\ \theta_1 &= \frac{\pi}{3} - i(0.777) \\ \theta_1 + \frac{2\pi}{3} &= \pi - i(0.777) \\ \theta_1 + \frac{4\pi}{3} &= \frac{5\pi}{3} - i(0.777) \end{aligned}$$

$$\begin{aligned} \cos \theta_1 &= \cos \left[ \frac{\pi}{3} - i(0.777) \right] \\ &= \left( \cos \frac{\pi}{3} \right) [\cos i(0.777)] + \left( \sin \frac{\pi}{3} \right) [\sin i(0.777)] \\ &= \left( \cos \frac{\pi}{3} \right) (\cosh 0.777) + i \left( \sin \frac{\pi}{3} \right) (\sinh 0.777) \\ &= (0.5)(1.317) + i(0.866)(0.858) = 0.659 + i(0.743). \end{aligned}$$

Note that

$$\cos \mu = \cosh(i\mu) \quad \text{and} \quad \sin \mu = -i \sinh(i\mu).$$

Similarly,

$$\begin{aligned} \cos \left( \theta_1 + \frac{2\pi}{3} \right) &= \cos [\pi - i(0.777)] \\ &= (\cos \pi) (\cosh 0.777) + i (\sin \pi) (\sinh 0.777) \\ &= -1.317, \end{aligned}$$

and

$$\begin{aligned} \cos \left( \theta_1 + \frac{4\pi}{3} \right) &= \cos \left[ \frac{5\pi}{3} - i(0.777) \right] \\ &= \left( \cos \frac{5\pi}{3} \right) (\cosh 0.777) + i \left( \sin \frac{5\pi}{3} \right) (\sinh 0.777) \\ &= (0.5)(1.317) - i(0.866)(0.858) = 0.659 - i(0.743). \end{aligned}$$

The required roots are

$$\begin{aligned} 1.155[0.659 + i(0.743)] &= 0.760 + i(0.858) \\ (1.155)(-1.317) &= -1.520 \\ 1.155[0.659 - i(0.743)] &= 0.760 - i(0.858). \end{aligned}$$

## F.10 Quartic Equation

A quartic equation,

$$x^4 + ax^3 + bx^2 + cx + d = 0,$$

has the *resolvent cubic equation*

$$y^3 - by^2 + (ac - 4d)y - a^2d + 4bd - c^2 = 0.$$

Let  $y$  be any root of this equation and

$$R = \sqrt{\frac{a^2}{4} - b + y}.$$

If  $R \neq 0$ , then let

$$D = \sqrt{\frac{3a^2}{4} - R^2 - 2b + \frac{4ab - 8c - a^3}{4R}}$$

and

$$E = \sqrt{\frac{3a^2}{4} - R^2 - 2b - \frac{4ab - 8c - a^3}{4R}}.$$

If  $R = 0$ , then let

$$D = \sqrt{\frac{3a^2}{4} - 2b + 2\sqrt{y^2 - 4d}}$$

and

$$E = \sqrt{\frac{3a^2}{4} - 2b - 2\sqrt{y^2 - 4d}}.$$

Then the four roots of the original equation are given by

$$x = -\frac{a}{4} + \frac{R}{2} \pm \frac{D}{2}$$

and

$$x = -\frac{a}{4} - \frac{R}{2} \pm \frac{E}{2}.$$

## F.11 Partial Fractions

This section applies only to rational algebraic fractions with numerator of lower degree than the denominator. Improper fractions can be reduced to proper fractions by long division.

Every fraction may be expressed as the sum of component fractions whose denominators are factors of the denominator of the original fraction.

Let  $N(x)$  = numerator, a polynomial of the form

$$n_0 + n_1x + n_2x^2 + \cdots + n_ix^i$$



1. Nonrepeated Linear Factors

$$\frac{N(x)}{(x-a)G(x)} = \frac{A}{x-a} + \frac{F(x)}{G(x)}$$

$$A = \left[ \frac{N(x)}{G(x)} \right]_{x=a}$$

$F(x)$  is determined by methods discussed in the following sections.

Example

$$\frac{x^2 + 3}{x(x-2)(x^2 + 2x + 4)} = \frac{A}{x} + \frac{B}{x-2} + \frac{F(x)}{x^2 + 2x + 4}$$

$$A = \left[ \frac{x^2 + 3}{(x-2)(x^2 + 2x + 4)} \right]_{x=0} = -\frac{3}{8}$$

$$B = \left[ \frac{x^2 + 3}{x(x^2 + 2x + 4)} \right]_{x=2} = \frac{4 + 3}{2(4 + 4 + 4)} = \frac{7}{24}$$

2. Repeated Linear Factors

$$\frac{N(x)}{x^m G(x)} = \frac{A_0}{x^m} + \frac{A_1}{x^{m-1}} + \dots + \frac{A_{m-1}}{x} + \frac{F(x)}{G(x)}$$

$$F(x) = f_0 + f_1 + f_2x^2 + \dots, \quad G(x) = g_0 + g_1x + g_2x^2 + \dots$$

$$A_0 = \frac{n_0}{g_0}, \quad A_1 = \frac{n_1 - A_0g_1}{g_0}, \quad A_2 = \frac{n_2 - A_0g_2 - A_1g_1}{g_0}$$

General Term:\*

$$A_k = \frac{1}{g_0} \left[ n_k - \sum_{i=0}^{k-1} A_i g_{k-i} \right]$$

$$m = 1 \begin{cases} f_0 = n_1 - A_0g_1 \\ f_1 = n_2 - A_0g_2 \\ f_j = n_{j+1} - A_0g_{j+1} \end{cases}$$

$$m = 2 \begin{cases} f_0 = n_2 - A_0g_2 - A_1g_1 \\ f_1 = n_3 - A_0g_3 - A_1g_2 \\ f_j = n_{j+2} - [A_0g_{j+2} + A_1g_{j+1}] \end{cases}$$

$$m = 3 \begin{cases} f_0 = n_3 - A_0g_3 - A_1g_2 - A_2g_1 \\ f_1 = n_4 - A_0g_4 - A_1g_3 - A_2g_2 \\ f_j = n_{j+3} - [A_0g_{j+3} + A_1g_{j+2} + A_2g_{j+1}] \end{cases}$$

$$\text{any } m: f_j = n_{m+j} - \sum_{i=0}^{m-1} A_i g_{m+j-i}$$

\* Note: If  $G(x)$  contains linear factors,  $F(x)$  may be determined by Method 1.

Example

$$\frac{x^2 + 1}{x^3(x^2 - 3x + 6)} = \frac{A_0}{x^3} + \frac{A_1}{x^2} + \frac{A_2}{x} + \frac{f_1x + f_0}{x^2 - 3x + 6}$$

$$A_0 = \frac{1}{6},$$

$$A_1 = \frac{0 - \left(\frac{1}{6}\right)(-3)}{6} = \frac{1}{12},$$

$$A_2 = \frac{1 - \left(\frac{1}{6}\right)(1) - \left(\frac{1}{12}\right)(-3)}{6} = \frac{13}{72},$$

$$m = 3 \begin{cases} f_0 = 0 - \frac{1}{6}(0) + \frac{1}{12}(1) - \frac{13}{72}(-3) = \frac{11}{24} \\ f_1 = 0 - \frac{1}{6}(0) - \frac{1}{12}(0) - \frac{13}{72}(1) = -\frac{13}{72} \end{cases}$$

3. Repeated Linear Factors

$$\frac{N(x)}{(x-a)^m G(x)} = \frac{A_0}{(x-a)^m} + \frac{A_1}{(x-a)^{m-1}} + \dots + \frac{A_{m-1}}{(x-a)} + \frac{F(x)}{G(x)}$$

Change to form  $\frac{N'(y)}{y^m G'(y)}$  by substitution of  $x = y + a$ . Resolve into partial fractions in terms of  $y$  as described in Method 2. Then express in terms of  $x$  by substitution  $y = x - a$ .

Example

$$\frac{x-3}{(x-2)^2(x^2+x+1)}$$

Let  $x - 2 = y, x = y + 2$

$$\frac{(y+2)-3}{y^2[(y+2)^2+(y+2)+1]} = \frac{y-1}{y^2(y^2+5y+7)}$$

$$= \frac{A_0}{y^2} + \frac{A_1}{y} + \frac{f_1y+f_0}{y^2+5y+7}$$

$$A_0 = -\frac{1}{7}, \quad A_1 = \frac{1 - \left(-\frac{1}{7}\right)(5)}{7} = \frac{12}{49},$$

$$m = 2 \begin{cases} f_0 = 0 - \left(-\frac{1}{7}\right)(1) - \left(\frac{12}{49}\right)(5) = -\frac{53}{49} \\ f_1 = 0 - \left(-\frac{1}{7}\right)(0) - \left(\frac{12}{49}\right)(1) = -\frac{12}{49} \end{cases}$$

$$\therefore \frac{y-1}{y^2(y^2+5y+7)} = \frac{-\frac{1}{7}}{y^2} + \frac{12}{49y} + \frac{-\frac{12}{49}y - \frac{53}{49}}{y^2+5y+7}$$

Let  $y = x - 2$ , then

$$\frac{x-3}{(x-2)^2(x^2+x+1)} = \frac{-\frac{1}{7}}{(x-2)^2} + \frac{12}{35(x-2)} + \frac{-\frac{12}{49}(x-2) - \frac{53}{49}}{x^2+x+1}$$

$$= -\frac{1}{7(x-2)^2} + \frac{12}{35(x-2)} + \frac{-12x-29}{49(x^2+x+1)}$$

#### 4. Repeated Linear Factors

Alternative method of determining coefficients:

$$\frac{N(x)}{(x-a)^m G(x)} = \frac{A_0}{(x-a)^m} + \dots + \frac{A_k}{(x-a)^{m-k}} + \dots + \frac{A_{m-1}}{x-a} + \frac{F(x)}{G(x)}$$

$$A_k = \frac{1}{k!} \left\{ D_x^k \left[ \frac{N(x)}{G(x)} \right] \right\}_{x=a}$$

where  $D_x^k$  is the differentiating operator, and the derivative of zero order is defined as:

$$D_x^0 u = u.$$

#### 5. Factors of Higher Degree

Factors of higher degree have the corresponding numerators indicated.

$$\frac{N(x)}{(x^2 + h_1x + h_0)G(x)} = \frac{a_1x + a_0}{x^2 + h_1x + h_0} + \frac{F(x)}{G(x)}$$

$$\frac{N(x)}{(x^2 + h_1x + h_0)^2 G(x)} = \frac{a_1x + a_0}{(x^2 + h_1x + h_0)^2} + \frac{b_1x + b_0}{x^2 + h_1x + h_0} + \frac{F(x)}{G(x)}$$

$$\frac{N(x)}{(x^3 + h_2x^2 + h_1x + h_0)G(x)} = \frac{a_2x^2 + a_1x + a_0}{x^3 + h_2x^2 + h_1x + h_0} + \frac{F(x)}{G(x)}$$

⋮

Problems of this type are determined first by solving for the coefficients due to linear factors as shown above, and then determining the remaining coefficients by the general methods given below.

#### 6. General Methods for Evaluating Coefficients

1.

$$\frac{N(x)}{D(x)} = \frac{N(x)}{G(x)H(x)L(x)} = \frac{A(x)}{G(x)} + \frac{B(x)}{H(x)} + \frac{C(x)}{L(x)} + \dots$$

Multiply both sides of equation by  $D(x)$  to clear fractions. Then collect terms, equate like powers of  $x$ , and solve the resulting simultaneous equations for the unknown coefficients.

2. Clear fractions as above. Then let  $x$  assume certain convenient values ( $x = 1.0, -1, \dots$ ). Solve the resulting equations for the unknown coefficients.

3.

$$\frac{N(x)}{G(x)H(x)} = \frac{A(x)}{G(x)} + \frac{B(x)}{H(x)}$$

Then,

$$\frac{N(x)}{G(x)H(x)} - \frac{A(x)}{G(x)} = \frac{B(x)}{H(x)}$$

If  $A(x)$  can be determined, such as by Method 1, then  $B(x)$  can be found as above.

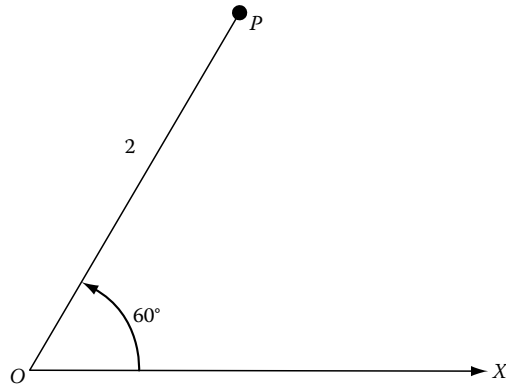
## F.12 Polar Coordinates in a Plane

### Polar Coordinates

In a plane, let  $O X$  (called the *initial line*) be a fixed ray radiating from point  $O$  (called the *pole* or *origin*). Then any point  $P$ , other than  $O$ , in the plane is located by angle  $\theta$  (called the *vectorial angle*) measured from  $O X$  to the line determined by  $O$  and  $P$  and the distance  $r$  (called the *radius vector*) from  $O$  to  $P$ , where  $\theta$  is taken as positive if measured counterclockwise and negative if measured clockwise, and  $r$  is taken as positive if measured along the terminal side of angle  $\theta$  and negative if measured along the terminal side of  $\theta$  produced through the pole. Such an ordered pair of numbers,  $(r, \theta)$ , is called *polar coordinates* of the point  $P$ . The polar coordinates of the pole  $O$  are taken as  $(0, \theta)$ , where  $\theta$  is arbitrary. It follows that, for a given initial line and pole, each point of the plane has infinitely many polar coordinates.

### Example

Some polar coordinates of  $P$  are  $(2, 60^\circ)$ ,  $(2, 420^\circ)$ ,  $(2, -300^\circ)$ ,  $(-2, 240^\circ)$ ,  $(-2, 120^\circ)$ .



### Points

Distance between  $P_1$  and  $P_2$ :

$$\sqrt{r_1^2 + r_2^2 - 2r_1r_2 \cos(\theta_1 - \theta_2)}$$

Points  $P_1, P_2, P_3$  are collinear if and only if

$$r_2r_3 \sin(\theta_3 - \theta_2) + r_3r_1 \sin(\theta_1 - \theta_3) + r_1r_2 \sin(\theta_2 - \theta_1) = 0.$$

### Polygonal Areas

Area of triangle  $P_1P_2P_3$ :

$$\frac{1}{2} [r_1r_2 \sin(\theta_2 - \theta_1) + r_2r_3 \sin(\theta_3 - \theta_2) + r_3r_1 \sin(\theta_1 - \theta_3)]$$

Area of polygon  $P_1P_2\dots P_n$ :

$$\frac{1}{2}[r_1r_2 \sin(\theta_2 - \theta_1) + r_2r_3 \sin(\theta_3 - \theta_2) + \dots + r_{n-1}r_n \sin(\theta_n - \theta_{n-1}) + r_nr_1 \sin(\theta_1 - \theta_n)]$$

The area is positive or negative according as  $P_1P_2\dots P_n$  is a counterclockwise or clockwise polygon.

**Straight Lines**

Let  $p$  = distance of line from  $O$ ,  $\omega$  = counterclockwise angle from  $OX$  to the perpendicular through  $O$  to the line:

Normal form:  $r \cos(\theta - \omega) = p$

Two-point form:  $r[r_1 \sin(\theta - \theta_1) + r_2 \sin(\theta - \theta_2)] = r_1r_2 \sin(\theta_2 - \theta_1)$

**Circles**

- Center at pole, radius  $a$ :  $r = a$
- Center at  $(a, 0)$  and passing through the pole:  $r = 2a \cos \theta$
- Center at  $(a, \frac{\pi}{2})$  and passing through the pole:  $r = 2a \sin \theta$
- Center  $(h, \alpha)$ , radius  $a$ :  $r^2 - 2hr \cos(\theta - \alpha) + h^2 - a^2 = 0$

**Conics**

Let  $2p$  = distance from directrix to focus,  $e$  = eccentricity.

- Focus at pole, directrix to left of pole:  $r = \frac{2ep}{1 - e \cos \theta}$
- Focus at pole, directrix to right of pole:  $r = \frac{2ep}{1 + e \cos \theta}$
- Focus at pole, directrix below pole:  $r = \frac{2ep}{1 - e \sin \theta}$
- Focus at pole, directrix above pole:  $r = \frac{2ep}{1 + e \sin \theta}$
- Parabola with vertex at pole, directrix to left of pole:

$$r = \frac{4p \cos \theta}{\sin^2 \theta}$$

Ellipse with center at pole, semiaxes  $a$  and  $b$  horizontal and vertical, respectively:

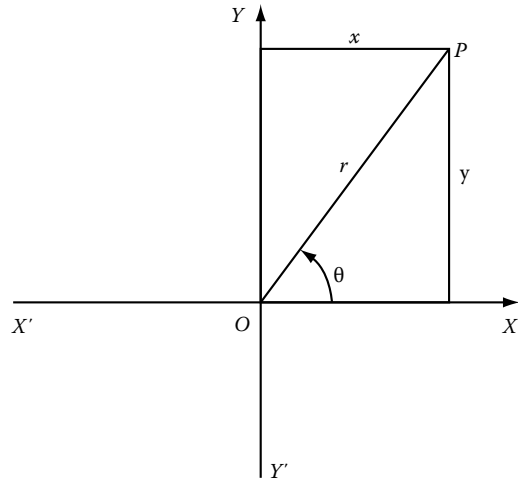
$$r^2 = \frac{a^2b^2}{a^2 \sin^2 \theta + b^2 \cos^2 \theta}$$

Hyperbola with center at pole, semiaxes  $a$  and  $b$  horizontal and vertical, respectively:

$$r^2 = \frac{a^2b^2}{a^2 \sin^2 \theta - b^2 \cos^2 \theta}$$

**Relations between Rectangular Polar Coordinates**

Let the positive  $x$ -axis coincide with the initial line and let  $r$  be nonnegative.

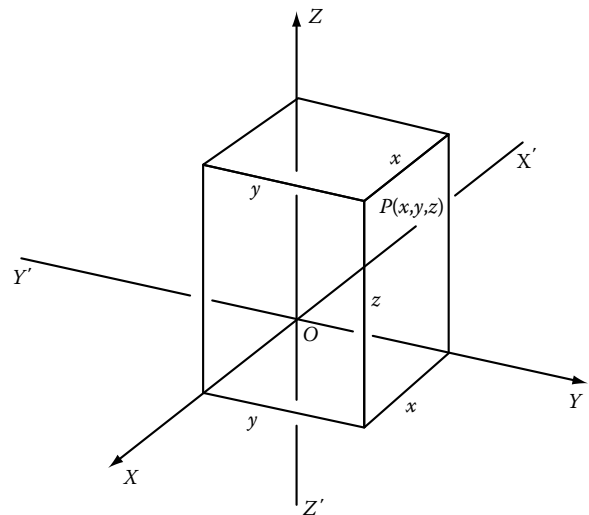


$$\begin{aligned} x &= r \cos \theta, & y &= r \sin \theta, \\ r &= \sqrt{x^2 + y^2}, & \theta &= \arctan \frac{y}{x}, \\ \sin \theta &= \frac{y}{\sqrt{x^2 + y^2}}, & \cos \theta &= \frac{x}{\sqrt{x^2 + y^2}} \end{aligned}$$

**F.13 Rectangular Coordinates in Space**

**Rectangular (Cartesian) Coordinates**

Let  $X'Y$ ,  $Y'Y$ ,  $Z'Z$  (called the  $y$ -axis, and the  $z$ -axis, respectively) be three mutually perpendicular lines in space intersecting in a point  $O$  (called the *origin*), forming in this way three mutually perpendicular planes  $XOY$ ,  $XOZ$ ,  $YOZ$  (called the  $xy$ -plane, the  $xz$ -plane, and the  $yz$ -plane, respectively). Then, any point  $P$  of space is located by its signed distances  $x$ ,  $y$ ,  $z$  from the  $yz$ -plane, the  $xz$ -plane, and the  $xy$ -plane, respectively, where  $x$  and  $y$  are the rectangular coordinates with respect to the axes  $X'X$  and  $Y'Y$  of the orthogonal projection  $P'$  of  $P$  on the  $xy$ -plane (here, taken horizontally) and  $z$  is taken as positive above and negative below the  $xy$ -plane. The ordered triple of numbers,  $(x, y, z)$ , are called *rectangular coordinates* of the point  $P$ .



**Points**

Let  $P_1(x_1, y_1, z_1)$  and  $P_2(x_2, y_2, z_2)$  be any two points.

Distance between  $P_1$  and  $P_2$ :  $\sqrt{(x_2-x_1)^2+(y_2-y_1)^2+(z_2-z_1)^2}$

Point dividing  $P_1P_2$  in ratio  $\frac{r}{s}$ :  $\left(\frac{rx_2+sx_1}{r+s}, \frac{ry_2+sy_1}{r+s}, \frac{rz_2+sz_1}{r+s}\right)$

Midpoint of  $P_1P_2$ :  $\left(\frac{x_1+x_2}{2}, \frac{y_1+y_2}{2}, \frac{z_1+z_2}{2}\right)$

Points  $P_1, P_2, P_3$  are collinear if and only if

$$x_2 - x_1 : y_2 - y_1 : z_2 - z_1 = x_3 - x_1 : y_3 - y_1 : z_3 - z_1.$$

Points  $P_1, P_2, P_3, P_4$  are coplanar if and only if

$$\begin{vmatrix} x_1 & y_1 & z_1 & 1 \\ x_2 & y_2 & z_2 & 1 \\ x_3 & y_3 & z_3 & 1 \\ x_4 & y_4 & z_4 & 1 \end{vmatrix} = 0.$$

Area of triangle  $P_1P_2P_3$ :

$$\frac{1}{2} \sqrt{\begin{vmatrix} y_1 & z_1 & 1 \\ y_2 & z_2 & 1 \\ y_3 & z_3 & 1 \end{vmatrix}^2 + \begin{vmatrix} z_1 & x_1 & 1 \\ z_2 & x_2 & 1 \\ z_3 & x_3 & 1 \end{vmatrix}^2 + \begin{vmatrix} x_1 & y_1 & 1 \\ x_2 & y_2 & 1 \\ x_3 & y_3 & 1 \end{vmatrix}^2}$$

Volume of tetrahedron  $P_1 P_2 P_3 P_4$ :

$$\frac{1}{6} \begin{vmatrix} x_1 & y_1 & z_1 & 1 \\ x_2 & y_2 & z_2 & 1 \\ x_3 & y_3 & z_3 & 1 \\ x_4 & y_4 & z_4 & 1 \end{vmatrix}$$

**Direction Numbers and Direction Cosines**

Let  $\alpha, \beta, \gamma$  (called *direction angles*) be the angles that  $P_1P_2$ , or any line parallel to  $P_1P_2$ , makes with the  $x$ -,  $y$ -, and  $z$ -axis, respectively. Let  $d$  = distance between  $P_1$  and  $P_2$ .

Direction cosines of  $P_1P_2$ :

$$\cos \alpha = \frac{x_2 - x_1}{d}, \quad \cos \beta = \frac{y_2 - y_1}{d}, \quad \cos \gamma = \frac{z_2 - z_1}{d}$$

$$\cos^2 \alpha + \cos^2 \beta + \cos^2 \gamma = 1$$

If  $a, b, c$  are direction numbers of  $P_1P_2$ , then:

$$a : b : c = x_2 - x_1 : y_2 - y_1 : z_2 - z_1$$

$$= \cos \alpha : \cos \beta : \cos \gamma$$

$$\cos \alpha = \frac{a}{\pm\sqrt{a^2 + b^2 + c^2}}, \quad \cos \beta = \frac{b}{\pm\sqrt{a^2 + b^2 + c^2}},$$

$$\cos \gamma = \frac{c}{\pm\sqrt{a^2 + b^2 + c^2}}$$

Angle between two lines with direction angles,  $\alpha_1, \beta_1, \gamma_1$ , and  $\alpha_2, \beta_2, \gamma_2$ :

$$\cos \theta = \cos \alpha_1 \cos \alpha_2 + \cos \beta_1 \cos \beta_2 + \cos \gamma_1 \cos \gamma_2$$

For parallel lines:  $\alpha_1 = \alpha_2, \beta_1 = \beta_2, \gamma_1 = \gamma_2$

For perpendicular lines:

$$\cos \alpha_1 \cos \alpha_2 + \cos \beta_1 \cos \beta_2 + \cos \gamma_1 \cos \gamma_2 = 0$$

Angle between two lines with directions  $(a_1, b_1, c_1)$  and  $(a_2, b_2, c_2)$ :

$$\cos \theta = \frac{a_1a_2 + b_1b_2 + c_1c_2}{\sqrt{a_1^2 + b_1^2 + c_1^2}\sqrt{a_2^2 + b_2^2 + c_2^2}}$$

$$\sin \theta = \frac{\sqrt{(b_1c_2 - c_1b_2)^2 + (c_1a_2 - a_1c_2)^2 + (a_1b_2 - b_1a_2)^2}}{\sqrt{a_1^2 + b_1^2 + c_1^2}\sqrt{a_2^2 + b_2^2 + c_2^2}}$$

For parallel lines:

$$a_1 : b_1 : c_1 = a_2 : b_2 : c_2$$

For perpendicular lines:

$$a_1a_2 + b_1b_2 + c_1c_2 = 0$$

The direction

$$(b_1c_2 - c_1b_2, c_1a_2 - a_1c_2, a_1b_2 - b_1a_2)$$

is perpendicular to both directions  $(a_1, b_1, c_1)$  and  $(a_2, b_2, c_2)$ .

The directions  $(a_1, b_1, c_1), (a_2, b_2, c_2), (a_3, b_3, c_3)$  are parallel to a common plane if and only if

$$\begin{vmatrix} a_1 & b_1 & c_1 \\ a_2 & b_2 & c_2 \\ a_3 & b_3 & c_3 \end{vmatrix} = 0.$$

**Straight Lines**

Point direction form:  $\frac{x - x_1}{a} = \frac{y - y_1}{b} = \frac{z - z_1}{c}$

Two-point form:  $\frac{x - x_1}{x_2 - x_1} = \frac{y - y_1}{y_2 - y_1} = \frac{z - z_1}{z_2 - z_1}$

Parametric form:  $x = x_1 + ta, y = y_1 + tb, z = z_1 + tc$

General form:  $\begin{cases} A_1x + B_1y + C_1z + D_1 = 0 \\ A_2x + B_2y + C_2z + D_2 = 0 \end{cases}$

Direction of line:  $(B_1C_2 - C_1B_2, C_1A_2 - A_1C_2, A_1B_2 - B_1A_2)$

Projection of segment  $P_1P_2$  on direction  $(a, b, c)$ :

$$\frac{(x_2 - x_1)a + (y_2 - y_1)b + (z_2 - z_1)c}{\sqrt{a^2 + b^2 + c^2}}$$

Distance from point  $P_0$  to line through  $P_1$  in direction  $(a, b, c)$ :

$$\sqrt{\frac{\begin{vmatrix} y_0 - y_1 & z_0 - z_1 \\ b & c \end{vmatrix}^2 + \begin{vmatrix} z_0 - z_1 & x_0 - x_1 \\ c & a \end{vmatrix}^2 + \begin{vmatrix} x_0 - x_1 & y_0 - y_1 \\ a & b \end{vmatrix}^2}{a^2 + b^2 + c^2}}$$

Distance between line through  $P_1$  in direction  $(a_1, b_1, c_1)$  and line through  $P_2$  in direction  $(a_2, b_2, c_2)$ :

$$\pm \frac{\begin{vmatrix} x_2 - x_1 & y_2 - y_1 & z_2 - z_1 \\ a_1 & b_1 & c_1 \\ a_2 & b_2 & c_2 \end{vmatrix}}{\sqrt{\begin{vmatrix} b_1 & c_1 \\ b_2 & c_2 \end{vmatrix}^2 + \begin{vmatrix} c_1 & a_1 \\ c_2 & a_2 \end{vmatrix}^2 + \begin{vmatrix} a_1 & b_1 \\ a_2 & b_2 \end{vmatrix}^2}}$$

The line through  $P_1$  in direction  $(a_1, b_1, c_1)$  and the line through  $P_2$  in direction  $(a_2, b_2, c_2)$  intersect if and only if

$$\begin{vmatrix} x_2 - x_1 & y_2 - y_1 & z_2 - z_1 \\ a_1 & b_1 & c_1 \\ a_2 & b_2 & c_2 \end{vmatrix} = 0.$$

**Planes**

- General form:  $Ax + By + Cz + D = 0$
- Direction to normal:  $(A, B, C)$
- Perpendicular to  $yz$ -plane:  $By + Cz + D = 0$
- Perpendicular to  $xz$ -plane:  $Ax + Cz + D = 0$
- Perpendicular to  $xy$ -plane:  $Ax + By + D = 0$
- Perpendicular to  $x$ -axis:  $Ax + D = 0$
- Perpendicular to  $y$ -axis:  $By + D = 0$
- Perpendicular to  $z$ -axis:  $Cz + D = 0$
- Intercept form:  $\frac{x}{a} + \frac{y}{b} + \frac{z}{c} = 1$

Plane through point  $P_1$  and perpendicular to direction  $(a, b, c)$ :

$$a(x - x_1) + b(y - y_1) + c(z - z_1) = 0$$

Plane through point  $P_1$  and parallel to directions  $(a_1, b_1, c_1)$  and  $(a_2, b_2, c_2)$ :

$$\begin{vmatrix} x - x_1 & y - y_1 & z - z_1 \\ a_1 & b_1 & c_1 \\ a_2 & b_2 & c_2 \end{vmatrix} = 0$$

Plane through points  $P_1$  and  $P_2$  parallel to direction  $(a, b, c)$ :

$$\begin{vmatrix} x - x_1 & y - y_1 & z - z_1 \\ x_2 - x_1 & y_2 - y_1 & z_2 - z_1 \\ a & b & c \end{vmatrix} = 0$$

Three-point form:

$$\begin{vmatrix} x & y & z & 1 \\ x_1 & y_1 & z_1 & 1 \\ x_2 & y_2 & z_2 & 1 \\ x_3 & y_3 & z_3 & 1 \end{vmatrix} = 0 \quad \text{or} \quad \begin{vmatrix} x - x_1 & y - y_1 & z - z_1 \\ x_2 - x_1 & y_2 - y_1 & z_2 - z_1 \\ x_3 - x_1 & y_3 - y_1 & z_3 - z_1 \end{vmatrix} = 0$$

Normal form ( $p$  = distance from origin to plane:  $\alpha, \beta, \gamma$  are direction angles of perpendicular to plane from origin):

$$x \cos \alpha + y \cos \beta + z \cos \gamma = p$$

To reduce  $Ax + By + Cz + D = 0$  to normal form, divide by  $\pm\sqrt{A^2 + B^2 + C^2}$ , where the sign of the radical is chosen opposite to the sign of  $D$  when  $D \neq 0$ , the same as the sign of  $C$  when  $D = 0$  and  $C \neq 0$ , the same as the sign of  $B$  when  $C = D = 0$ .

Distance from point  $P_1$  to plane  $Ax + By + Cz + D = 0$ :

$$\frac{Ax_1 + By_1 + Cz_1 + D}{\pm\sqrt{A^2 + B^2 + C^2}}$$

Angle  $\theta$  between planes  $A_1x + B_1y + C_1z + D_1 = 0$  and  $A_2x + B_2y + C_2z + D_2 = 0$ :

$$\cos \theta = \frac{A_1A_2 + B_1B_2 + C_1C_2}{\sqrt{A_1^2 + B_1^2 + C_1^2}\sqrt{A_2^2 + B_2^2 + C_2^2}}$$

Planes parallel:  $A_1 : B_1 : C_1 = A_2 : B_2 : C_2$

Planes perpendicular:  $A_1A_2 + B_1B_2 + C_1C_2 = 0$

**Spheres**

Center at origin, radius  $r$ :  $x^2 + y^2 + z^2 = r^2$

Center at  $(g, h, k)$ , radius  $r$ :  $(x - g)^2 + (y - h)^2 + (z - k)^2 = r^2$

General form:

$$\begin{cases} Ax^2 + Ay^2 + Az^2 + Dx + Ey + Fz + M = 0, & A \neq 0 \\ x^2 + y^2 + z^2 + 2dx + 2ey + 2fz + m = 0 \end{cases}$$

Center:  $(-d, -e, -f)$

Radius:  $r = \sqrt{d^2 + e^2 + f^2 - m}$

Sphere on  $P_1P_2$  as diameter:

$$(x - x_1)(x - x_2) + (y - y_1)(y - y_2) + (z - z_1)(z - z_2) = 0$$

Four-point form:

$$\begin{vmatrix} x^2 + y^2 + z^2 & x & y & z & 1 \\ x_1^2 + y_1^2 + z_1^2 & x_1 & y_1 & z_1 & 1 \\ x_2^2 + y_2^2 + z_2^2 & x_2 & y_2 & z_2 & 1 \\ x_3^2 + y_3^2 + z_3^2 & x_3 & y_3 & z_3 & 1 \\ x_4^2 + y_4^2 + z_4^2 & x_4 & y_4 & z_4 & 1 \end{vmatrix} = 0$$

**The 17 Quadric Surfaces in Standard Form**

1.	Real ellipsoid:	$x^2/a^2 + y^2/b^2 + z^2/c^2 = 1$
2.	Imaginary ellipsoid:	$x^2/a^2 + y^2/b^2 + z^2/c^2 = -1$
3.	Hyperboloid of one sheet:	$x^2/a^2 + y^2/b^2 - z^2/c^2 = 1$
4.	Hyperboloid of two sheets:	$x^2/a^2 + y^2/b^2 - z^2/c^2 = -1$
5.	Real quadratic cone:	$x^2/a^2 + y^2/b^2 - z^2/c^2 = 0$
6.	Imaginary quadric cone:	$x^2/a^2 + y^2/b^2 + z^2/c^2 = 0$
7.	Elliptic paraboloid:	$x^2/a^2 + y^2/b^2 + 2z = 0$
8.	Hyperbolic paraboloid:	$x^2/a^2 - y^2/b^2 + 2z = 0$
9.	Real elliptic cylinder:	$x^2/a^2 + y^2/b^2 = 1$
10.	Imaginary elliptic cylinder:	$x^2/a^2 + y^2/b^2 = -1$
11.	Hyperbolic cylinder:	$x^2/a^2 - y^2/b^2 = -1$
12.	Real intersecting planes:	$x^2/a^2 - y^2/b^2 = 0$
13.	Imaginary intersecting planes:	$x^2/a^2 + y^2/b^2 = 0$
14.	Parabolic cylinder:	$x^2 + 2rz = 0$
15.	Real parallel planes:	$x^2 = a^2$
16.	Imaginary parallel planes:	$x^2 = -a^2$
17.	Coincident planes:	$x^2 = 0$

8	2	4	+	No	Hyperbolic paraboloid
9	2	3		Yes	Real elliptic cylinder
10	2	3		Yes	Imaginary elliptic cylinder
11	2	3		No	Hyperbolic cylinder
12	2	2		No	Real intersecting planes
13	2	2		Yes	Imaginary intersecting planes
14	1	3			Parabolic cylinder
15	1	2			Real parallel planes
16	1	2			Imaginary parallel planes
17	1	1			Coincident planes

**General Equation of Second Degree**

The nature of the graph of the general quadratic equation in  $x, y, z$ ,

$$ax^2 + by^2 + cz^2 + 2fyz + 2gzx + 2hxy + 2px + 2qy + 2rz + d = 0,$$

is described in the following table in terms of  $\rho_3, \rho_4, \Delta, k_1, k_2, k_3$ , where

$$e = \begin{bmatrix} a & h & g \\ h & b & f \\ g & f & c \end{bmatrix}, \quad E = \begin{bmatrix} a & h & g & p \\ h & b & f & q \\ g & f & c & r \\ p & q & r & d \end{bmatrix},$$

$\rho_3 = \text{rank } e, \rho_4 = \text{rank } E,$   
 $\Delta = \text{determinant of } E,$

$$k_1, k_2, k_3 \text{ are the roots of } \begin{vmatrix} a-x & h & g \\ h & b-x & f \\ g & f & c-x \end{vmatrix} = 0.$$

Case	$\rho_3$	$\rho_4$	Sign of $\Delta$	Nonzero $k$ 's Same Sign?	Quadric Surface
1	3	4	-	Yes	Real ellipsoid
2	3	4	+	Yes	Imaginary ellipsoid
3	3	4	+	No	Hyperboloid of one sheet
4	3	4	-	No	Hyperboloid of two sheets
5	3	3		No	Real quadratic cone
6	3	3		Yes	Imaginary quadric cone
7	2	4	-	Yes	Elliptic paraboloid

**Cylindrical and Conical Surfaces**

Any equation in just two of the variables  $x, y, z$  represents a *cylindrical surface* whose elements are parallel to the axis of the missing variables.

Any equation homogeneous in the variables  $x, y, z$  represents a *conical surface* whose vertex is at the origin.

**Transformation of Coordinates**

To transform an equation of a surface from an old system of rectangular coordinates  $(x, y, z)$  to a new system of rectangular coordinates  $(x', y', z')$ , substitute for each old variable in the equation of the surface its expression in terms of the new variables.

Translation:

$$x = x' + h$$

The new axes are parallel to the old axes and the coordinates of

$$y = y' + k$$

the new origin in terms of the old system are  $(h, k, l)$ .

$$z = z' + l$$

Rotation about the origin:

$$x = \lambda_1 x' + \lambda_2 y' + \lambda_3 z'$$

The new origin is coincident with the old origin and

$$y = \mu_1 x' + \mu_2 y' + \mu_3 z'$$

the  $x'$ -axis,  $y'$ -axis,  $z'$ -axis have direction cosines

$$z = \nu_1 x' + \nu_2 y' + \nu_3 z' (\lambda_1, \mu_1, \nu_1), (\lambda_2, \mu_2, \nu_2), (\lambda_3, \mu_3, \nu_3)$$

respectively, with respect to the old system of axes.

$$x' = \lambda_1 x + \mu_1 y + \nu_1 z$$

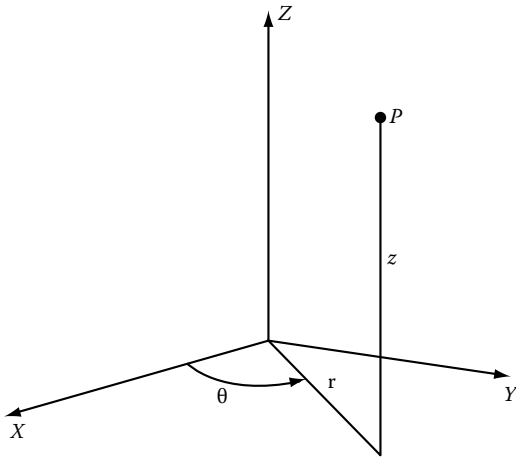
$$y' = \lambda_2 x + \mu_2 y + \nu_2 z$$

$$z' = \lambda_3 x + \mu_3 y + \nu_3 z$$

### Cylindrical Coordinates

If  $(r, \theta, z)$  are the cylindrical coordinates and  $(x, y, z)$  the rectangular coordinates of a point  $P$ , then

$$\begin{aligned} x &= r \cos \theta, & r &= \sqrt{x^2 + y^2}, \\ y &= r \sin \theta, & \theta &= \arctan \frac{y}{x}, \\ z &= z, & z &= z. \end{aligned}$$



### Spherical Coordinates

If  $(r, \theta, \phi)$  are the spherical coordinates and  $(x, y, z)$  the rectangular coordinates of a point  $P$ , then

$$x = r \sin \theta \cos \phi,$$

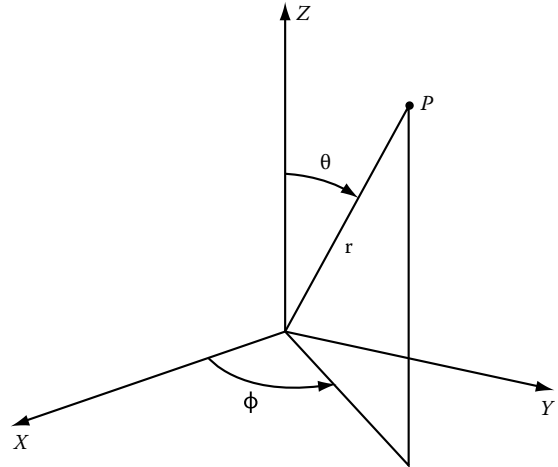
$$y = r \sin \theta \sin \phi,$$

$$z = r \cos \theta,$$

$$r = \sqrt{x^2 + y^2 + z^2},$$

$$\theta = \arccos \frac{z}{\sqrt{x^2 + y^2 + z^2}},$$

$$\phi = \arctan \frac{y}{x}.$$



## A

Abel transformation, 9-14

Algebra formulas and coordinate systems

- arithmetic progression, F-1
- combinations, F-2
- common difference, F-1
- common ratio, F-1
- cubic equations, F-2–F-3
- factorials, F-1
- geometric progression, F-1
- harmonic progression, F-1
- partial fractions
  - coefficients, F-5
  - expression, F-3
  - higher degree factors, F-5
  - nonrepeated linear factors, F-4
  - repeated linear factors, F-4–F-5
- permutations, F-2
- polar coordinates, F-5–F-6
- quadratic equation, F-2
- quartic equation, F-3
- rectangular (Cartesian) coordinates, F-6
  - cylindrical and conical surfaces, F-9
  - cylindrical coordinates, F-10
  - direction numbers and cosines, F-7
  - general quadratic equation, F-9
  - planes, F-8
  - points, F-7
  - quadric surfaces, F-9
  - spheres, F-8
  - spherical coordinates, F-10
  - straight lines, F-7–F-8
  - transformation, F-9–F-10

Algebraic reconstruction techniques (ART), 8-34

Altes Q distribution, 13-8–13-9

Analog all-pass filters, 7-62–7-63

Analog chirp Fourier transform, 18-6

Asymptotic sequence, 1-53

Attenuated Radon transform, 8-41

Autocorrelation sequence, 6-6

## B

Backprojection
 

- definition, 8-31
- filter, 8-32–8-33
- filtered projection
  - convolution methods, 8-31–8-32
  - feature space function, 8-31
  - frequency space implementation, 8-32
  - inverse Fourier transform, 8-31

Band-limited functions, 2-45
 

- sampling theorem, 2-43–2-44
- truncated sampling reconstruction, 2-44

Band-pass Hilbert transformers, 7-68–7-71

Bandwidth theorem
 

- absolutely integrable functions, 2-17–2-18
- finite energy functions, 2-18–2-19

Bedrosian's theorem, 7-69, 7-85

Bertrand  $P_k$  distributions, 13-10

Bessel functions
 

- Bessel's equations solution, 2-32–2-33
- Chebyshev polynomial, 7-30–7-31
- definition, 1-35
- finite Hankel transforms, 11-2, 11-5
- Fourier Bessel series, 1-39
- Fourier cosine transform (FCT), 3-9
- Fourier sine transform (FST), 3-16
- frequency domain differentiation, 7-30
- Hankel transform
  - elementary properties, 9-1–9-2
  - finite interval, 9-11–9-13
  - infinite interval, 9-13–9-15
- integral order Bessel functions, 2-34
- integral representation, 1-37
- inverse Fourier transformation, 7-31
- nonintegral order Bessel functions, 2-35
- power series representation, 7-28, 7-31–7-32
- properties, 1-41–1-43
- recurrence relation, 1-36
- second order Bessel differential equation, 7-28
- waveforms, 7-29–7-30
- zero-order Bessel function, 2-33–2-34

Bessel's equality, 2-15

Bessel's inequality
 

- Hartley series, 4-12
- signal orthogonality, 1-20

Beta function, 12-34

Bidimensional empirical mode decomposition (BEMD)
 

- applications, 20-9
- boundary effects, 20-8
- extrema detection, 20-7–20-8
- intermittency, 20-7
- scattered data interpolation (SDI), 20-7–20-8
- sifting process and stopping criterion, 20-7
- texture image analysis, 20-6–20-7
- types, 20-7

Bilateral Laplace transform, *see* Two-sided Laplace transform

Binomial distribution, 2-56–2-57

Biorthogonal filter bank, 10-32–10-33

Boundary value problems, 11-10–11-11

Bounded input bounded output (BIBO) stability, 1-17

Broad-band modulation index, 12-29

Bromwich contour
 

- branch points and cuts
  - analytic and single valued function, A-21
  - evaluation, A-22–A-25
  - singularity, A-22
- finite number of poles, A-19–A-21
- rational transforms, A-19

Butterworth IIR Hilbert transformers, 7-77

## C

Cauchy principal values, 2-7

Cauchy–Riemann equations, 7-4

Cauchy–Schwarz inequality, 1-20

Cauchy second integral theorem, 5-17

Cauchy's residue theorem, 6-24

Central-slice theorem, 8-2, 8-6–8-7



- Chebyshev polynomials
    - Bessel function, 7-30–7-31
    - circular harmonic decomposition, 8-35
    - Fourier cosine transform (FCT), 3-8
    - Fourier sine transform (FST), 3-15
    - functions and formulas, 8-43–8-44
    - integral order Bessel functions, 2-34
    - modified Clenshaw–Curtis quadrature method, 9-11–9-12
    - orthogonal functions, unit disk, 8-39
    - signal orthogonality, 1-34–1-35
  - Chirp signal analysis, 18-1–18-2; *see also*
    - Discrete chirp-Fourier transform (DCFT)
  - Choi–Williams exponential distribution (CWD), 13-29–13-30
  - Circular harmonic decomposition
    - Chebyshev polynomial, 8-35
    - extension, higher dimensions, 8-35
    - Fourier series, 8-34
    - three dimensions, 8-35–8-36
  - Classical time–frequency representations (TFRs)
    - Altes Q distribution, 13-8–13-9
    - Bertrand  $P_k$  distributions, 13-10
    - quadratic time–frequency representation
      - band-limited cosine, 13-13
      - interference geometry, 13-11–13-12
      - multicomponent signal, 13-11
      - nonlinear operation, 13-10
    - short-time Fourier transform (STFT), 13-4–13-5
    - TFR warping, 13-9–13-10
    - Wigner distribution and Woodward ambiguity function
      - Dirac function, 13-6
      - Fourier transform, 13-7–13-8
      - Gaussian signal, 13-6–13-7
      - quantum mechanics, 13-5
      - signal operations, 13-7
  - Complex variable functions
    - analytic continuation, A-11
    - Bromwich contour
      - branch points and cuts, A-21–A-25
      - finite number of poles, A-19–A-21
    - definite integral evaluation
      - infinite integrals, sines and cosines, A-26–A-28
      - miscellaneous integrals, A-28–A-31
      - periodic functions (0 to  $2\pi$ ), A-25
      - $-\infty$  to  $+\infty$ , A-26
    - derivative of analytic function, A-5–A-6
    - integration
      - Cauchy first integral theorem, A-4
      - Cauchy second integral theorem, A-5
      - contour integral, A-4
      - contour transformation, A-18–A-19
      - definition, A-2–A-3
      - evaluation theorem, A-16–A-18
      - logarithmic derivative, A-32–A-33
      - path, complex plane, A-3
  - Laurent’s theorem, A-6–A-7
  - power series
    - convergence, A-10–A-11
    - Maclaurin series, A-9
    - negative power series, A-10
    - positive power series, A-9
    - Taylor series, A-9
  - principal value integral, A-31–A-32
  - residue theory, A-14–A-16
  - sequences and series, A-8–A-9
  - single/multiple valued functions, A-1–A-2
  - singularities
    - at  $\infty$ , A-14
    - branch points, A-12–A-13
    - definition, A-11–A-12
    - essential and nonessential singularity, A-11, A-13–A-14
    - isolated and nonisolated singularity, A-12
    - phase change, A-12–A-13
    - poles, A-12
    - removable singularity, A-12
    - Taylor’s theorem, A-6
  - Computational algorithms
    - discrete sine and cosine transforms (DST and DCT) algorithms
      - decimation-in-frequency algorithms, 3-30–3-31
      - decimation-in-time algorithms, 3-28–3-30
    - Fourier cosine and sine transform (FCT and FST) algorithms, 3-28
  - Conditional inverses, D-9–D-11
  - Cosine-and-sine (cas) function, 4-2–4-3
  - Cramer–Rao bounds, velocity estimation
    - broad-band modulation index, 12-29
    - Doppler compression, 12-28
    - Fisher information matrix, 12-28–12-29
    - maximum-likelihood estimation, 12-28
    - Parseval’s formula, 12-28
    - variance, 12-30
    - zero mean white Gaussian noise, 12-29
  - Cross-power spectrum, 7-53
  - Cyclic convolution, 4-19–4-20
- D**
- Daubechies basis
    - maximum flatness filter, 10-45–10-46
    - time domain, 10-46–10-47
  - Definite integrals, C-1–C-8
    - impulse response, A-31
    - infinite integrals, A-26
    - miscellaneous integrals, A-28–A-31
    - periodic functions (0 to  $2\pi$ ), A-25
    - $-\infty$  to  $+\infty$ , A-26
  - Delta functions
    - periodic arrays, 2-26
    - regular arrays, 2-24–2-25
    - variables and derivatives, 2-27–2-28
  - Determinants, D-3–D-4
  - 2-D DFT tensor algorithm
    - algorithm steps, 19-16
    - modified tensor algorithms, 19-20–19-21
    - $n$ -dimensional DFT, 19-25–19-26
    - $N$ , power of two, 19-18
    - $N$ , prime, 19-16
    - recursive tensor algorithm
      - multiplication operation, 19-21–19-22
      - $N = L_1 L_2$ , 19-23
      - $N_1 \times N_2$ , 19-23–19-25
      - $N$ , power of odd prime, 19-22–19-23
    - tensor image transform, 19-16
  - Differentiating Hilbert transformers
    - cascade connection, 7-77
    - coefficients, 7-79
    - definition, 7-77
    - Fourier series, 7-78–7-79
    - impulse response, 7-78
    - transfer function, 7-77–7-78
  - Digital filters
    - finite impulse response (FIR) filters, 6-28–6-29
    - infinite impulse response (IIR) filters, 6-27–6-28
  - Digital Hilbert transformers
    - antisymmetric sequence, 7-71
    - frequency-independent group delay, 7-72
    - magnitude and phase function, 7-71–7-72
    - transfer function, 7-70–7-71
  - Digital phase splitters, 7-75
  - Dirac delta function, *see* Impulse delta function
  - Dirac function, 13-6
  - Direct matrix factorization
    - decimation-in-frequency algorithms, 3-30–3-31
    - decimation-in-time algorithms, 3-28–3-30
  - Discrete chirp-Fourier transform (DCFT)
    - analog chirp-Fourier transform, 18-6
    - chirp rate estimation, 18-1–18-2
    - frequency matching, 18-1
    - magnitude, 18-2
    - multiple component chirp signals, 18-5–18-6
    - numerical simulations
      - four chirp components, 18-9, 18-13–18-14
      - multiple chirp components, 18-10
      - three chirp components, 18-8, 18-12–18-13
      - two chirp components, 18-7, 18-11–18-12
    - single component chirp signal
      - DFT, 18-2–18-3
      - inverse DCFT (IDCFT), 18-2
      - linear chirp signal, 18-4–18-5
      - sidelobe magnitude *vs.* estimation performance, 18-3–18-4
  - 2-D Discrete cosine transform (DCT)
    - fast 1-D cosine transforms, 19-38
    - modified DCT, 19-39
    - $N/2$ -point DCT, 19-36–19-37
    - tensor representation, 19-35

- Discrete Fourier transforms (DFT),  
 2-41, 6-26–6-27  
 basic properties, 17-6  
 circular convolution and correlation,  
 17-7–17-8  
 circular time and frequency shift, 17-8  
 complex conjugate, 17-8  
 definition, 17-5  
 functions, 17-9–17-12  
 imaginary sequences, 17-7  
 linear transformation, 17-5–17-6  
 Parseval's theorem, 17-9  
 product, 17-8  
 properties, 17-9  
 real-valued sequences, 17-7  
 SAR and ISAR imaging, 18-1  
 spectrum estimation, 18-1  
 symmetry properties, 17-6–17-7  
 time reversal, 17-8
- Discrete Hartley transforms (DHT), 4-17  
 2-D DHT representation  
 3-D image-signals, 19-28–19-29  
 index mapping, 19-27  
 spectral information, frequency-points,  
 19-28  
 splitting-signals, 19-26  
 tensor algorithm, 19-26–19-27  
 3-D DHT tensor representation,  
 19-29–19-31  
 $n$ -dimensional DHT, 19-31–19-32
- 2-D Discrete hexagonal Fourier transform  
 (DHFT)  
 calculation, frequency-points,  
 19-57–19-59  
 complexity, 19-55–19-56  
 definition, 19-56–19-57  
 paired representation, 19-59–19-62  
 $8 \times 4$ -point DHFT, 19-59  
 rectangular and hexagonal lattice, 19-56  
 regular hexagonal tessellation, 19-55
- Discrete Hilbert transformation (DHT), 6-26  
 bilinear transformation, 7-59–7-60  
 circular convolution, 7-56  
 complex analytic discrete sequence, 7-58  
 discrete one-sided convolution, 7-55  
 exponential kernels, 7-54  
 impulse response, 7-55–7-56  
 inverse transformation, 7-54  
 linearity, 7-57–7-58  
 Parseval's theorem, 7-56–7-57  
 shifting property, 7-57  
 transfer function, 7-55–7-56
- Discrete, linear, and time-invariant (DLTI)  
 system, 7-43–7-44
- Discrete Mellin transform  
 dilatocycle function  $Z(\nu)$  with ratio  $Q$ , 12-25  
 $\nu$  and  $\beta$  sample connection,  
 12-26–12-27  
 number of samples, 12-27  
 periodize  $M_S(\beta)$ , period  $1/\ln q$ ,  
 12-25–12-26
- Discrete periodic Radon transform, 8-42–8-43
- Discrete-time Fourier transforms (DTFT)  
 approximated continuous-time Fourier  
 transforms, 17-5  
 definition, 17-1–17-2  
 discrete-time signals, 17-4  
 finite sequences, 17-4  
 LTI discrete system frequency response,  
 17-5  
 properties, 17-2–17-3  
 smearing effect, 17-4
- Discrete wavelet transform  
 timescale space lattices, 10-14–10-15  
 wavelet frame, 10-15–10-16
- Distortion power, 7-53
- Doppler compression, 12-28
- E**
- Electrical power, Hilbert transforms  
 complex power notion, 7-51  
 instantaneous power, 7-50  
 power notion generalization  
 Budeanu's vs. Fryze's definitions, 7-52  
 finite average power, 7-52–7-54  
 in-phase component, 7-51–7-52  
 nonsinusoidal periodic waveform, 7-51  
 quadrature component, 7-52  
 reactive power, 7-51–7-52  
 quadrature instantaneous power, 7-50  
 voltage and current harmonic waveforms,  
 7-50–7-51
- Empirical mode decomposition (EMD)  
 drawbacks, 20-4–20-5  
 end effects, 20-6  
 extrema envelope, 20-1  
 vs. Fourier and wavelet transform, 20-4  
 Hilbert transform, 20-5–20-6  
 intermittency, 20-2–20-3  
 pictorial depiction, 20-2  
 recent developments, 20-6  
 sifting process, 20-2–20-3  
 stopping criteria, 20-2, 20-3  
 without extrema envelopes, 20-8
- Euler–Cauchy differential equation, 12-13
- Euler's equation, 7-88
- Euler's transformation, 9-13
- F**
- Fast Hartley transform (FHT)  
 applications, 4-18  
 cyclic convolution, 4-19–4-20  
 DHT and IDHT, 4-17  
 FFT algorithm, 4-17  
 frequency domain, 4-19–4-20  
 nontrivial computation, 4-21  
 periodic load current, 4-20  
 program, 4-28–4-31  
 quasiperiodic transient inputs, 4-19  
 time-domain convolution, 4-18–4-19  
 transform domain, 4-19  
 zero padding, 4-20
- Fast lapped transform (FLT),  
 15-22–15-23, 15-24
- Filter bank  
 biorthogonal filter bank, 10-32–10-33  
 FIR filter bank, 10-27–10-28  
 orthonormal filter bank, 10-30–10-31  
 perfect reconstruction  
 aliasing cancellation, 10-29  
 down-sampling, 10-28  
 modulation matrix, 10-29–10-30  
 up-sampling, 10-29  
 time domain, orthonormal filters,  
 10-31–10-32
- Filtered backprojection algorithm, 8-31
- Final value theorem, 5-9
- Finite energy functions  
 bandwidth theorem, 2-18–2-19  
 square integrable function, 2-18
- Finite Hankel transforms, 9-9–9-10  
 definition, 11-1–11-2  
 long circular cylinder  
 temperature distribution, 11-3, 11-5  
 unsteady viscous flow, 11-3–11-4  
 vibrations, circular membrane, 11-4  
 operational properties, 11-2–11-3
- Finite impulse response (FIR) Hilbert  
 transformers  
 equiripple function, 7-74–7-75  
 impulse responses, 7-73  
 normalized dimensionless pass-band, 7-74  
 structure, 7-72  
 transfer function, 7-73–7-74  
 $Z$ -transform, 7-73
- Finite Sturm–Liouville transform, 11-11
- Fisher information matrix, 12-28–12-29
- Fourier–Bessel series, 9-9, 11-1
- Fourier cosine transform (FCT)  
 algebraic functions, 3-5–3-6, 3-32  
 Bessel functions, 3-9  
 complementary error function, 3-8  
 convolution property, 3-10  
 cosine integral function, 3-9  
 definitions, 3-1–3-2  
 differentiation-in- $t$ , 3-9–3-10  
 differentiation-in- $\omega$ , 3-10  
 exponential and logarithmic functions,  
 3-6–3-7, 3-32  
 exponential integral function, 3-9  
 orthogonal polynomials, 3-8  
 properties and operational rules, 3-2–3-5  
 real data sequence, 3-28  
 shift-in- $t$ , shift-in- $\omega$  and kernel product  
 property, 3-10  
 sine integral function, 3-8  
 trigonometric functions, 3-7, 3-32
- Fourier inverse transform, 2-2
- Fourier sine transform (FST)  
 algebraic functions, 3-13–3-14, 3-33  
 Bessel functions, 3-16  
 complementary error function, 3-15–3-16  
 cosine integral function, 3-16  
 definitions, 3-11

- exponential and logarithmic functions, 3-14, 3-33
  - exponential integral function, 3-16
  - orthogonal polynomials, 3-15
  - properties and operational rules, 3-11–3-13
  - real data sequence, 3-28
  - sine integral function, 3-16
  - trigonometric function, 3-14–3-15, 3-33
  - Fourier transforms
    - circularly symmetric functions and Hankel transform, 2-38–2-39
    - definitions
      - Cauchy principal values, 2-7
      - generalized transforms, 2-3–2-4
      - notation, and terminology, 2-2
      - residue theorem, 2-4
    - discrete Fourier transform, 2-41
    - functions, 2-65–2-66
      - absolutely integrable functions, 2-16–2-18
      - band-limited functions, 2-20
      - Bessel functions, 2-32–2-35
      - causal functions, 2-30
        - with finite duration, 2-20
      - finite energy functions, 2-18–2-19
      - on finite intervals, 2-32
      - finite power functions, 2-20–2-22
      - on half-line, 2-31–2-32
      - negative powers and step functions, 2-28
      - periodic arrays, delta functions, 2-26
      - periodic functions, 2-22–2-24
      - rational functions, 2-29
      - real/imaginary valued even/odd functions, 2-16
      - regular arrays, delta functions, 2-24–2-25
      - square integrable functions, 2-18
      - variables and derivatives, 2-27–2-28
    - fundamental Fourier identities, 2-65
    - general identities and relations
      - bandwidth theorem, 2-15
      - Bessel's equality, 2-15
      - conjugation, 2-8–2-9
      - correlation, 2-11
      - differentiation and multiplication, 2-11–2-12
      - integration, 2-13–2-14
      - invertibility, 2-8
      - linearity, 2-9
      - modulation, 2-10
      - moments, 2-13
      - near-equivalence, 2-8
      - Parseval's equality, 2-14–2-15
      - products and convolution, 2-10
      - scaling, 2-9
      - translation and multiplication, 2-9–2-10
    - graphical representations, 2-67–2-75
    - half-line sine and cosine transforms, 2-40
    - Hankel transform, 9-2–9-3
    - Hartley transform, 4-5
    - Laplace transform, 2-42–2-43
  - linear systems
    - casual systems, 2-52
    - complex exponentials and periodic functions, 2-51
    - correlation, 2-60
    - differential equations, 2-52
    - linear shift invariant systems, 2-49
    - modulation and demodulation, 2-54–2-55
    - random signals, 2-60–2-61
    - reality and stability, 2-50
    - RLC circuits, 2-54
  - Mellin transform, 12-3
  - multidimensional Fourier transforms, 2-35–2-36
  - one-dimensional spectral representations, 13-2–13-3
  - partial differential equations
    - half-infinite rod, 2-64
    - infinite rod, 2-63–2-64
    - one-dimensional heat equation, 2-62
  - Radon and Abel transforms, 8-7–8-8
  - random variables
    - correlation, 2-60
    - multiple random process and independence, 2-57
    - probability and statistics, 2-55–2-56
    - random signals and stationary random signals, 2-59
    - sums of random processes, 2-58–2-59
  - sampled signal reconstruction
    - band-limited functions, 2-43–2-45
    - finite duration functions, 2-47
    - fundamental sampling formulas and Poisson's formula, 2-47–2-48
  - separable functions, multidimensional transform, 2-36–2-37
  - signal analysis properties, 13-19–13-20
  - Wigner distribution, 13-7–13-8
  - Z-transform, 6-36
- Fourier transform tensor representation
- 2-D directional images
    - 2D IDTF, image-signal processing, 19-13–19-14
    - frequency point location, 19-11–19-12
    - image reconstruction, 19-15–19-16
    - point disposition, 19-12–19-13
    - superposition, 19-15
  - splitting-signal, 19-10–19-11
- Fractional Fourier transform (FRT)
- applications
    - communications, 14-21
    - optics and wave propagation, 14-21–14-22
    - quantum mechanics, 14-22
    - signal and image processing, 14-21
- nth order, 14-1
- definition
- differential equation, 14-3–14-4
  - eigenvalues and eigenfunctions, 14-2–14-3
  - harmonic oscillation, 14-3
- linear integral transforms, 14-2
    - square-integrable function, 14-3
  - digital computation, 14-19–14-20
  - discrete transform, 14-18–14-19
  - domains
    - frequency domain, 14-4
    - phase space, 14-4–14-5
    - space or time domain, 14-4
    - time-frequency domain, 14-4
    - Wigner distribution, 14-5–14-6
  - dual operators
    - chirp multiplication and chirp convolution operator, 14-9
    - differentiation and multiplication operator, 14-8
    - discretization and periodization operator, 14-9
    - phase shift operator and translation operator, 14-8
    - scaling operator, 14-9
  - filtering
    - convolution and multiplication operations, 14-17
    - cost-accuracy trade-off, 14-16
    - filter function, 14-14
    - generalized filtering configurations, 14-17
    - multistage and multichannel configuration, 14-15–14-16
    - optimal filter, 14-15
    - signal recovery, 14-15
  - fractional Fourier domain decomposition (FFDD), 14-17–14-18
  - functions, 14-6
  - linear canonical transforms (LCT)
    - basic properties, 14-13
    - composite transform, 14-11
    - decompositions, 14-13
    - noncommutative group sets, 14-11–14-12
    - operational properties, 14-14
    - Wigner distribution, 14-12–14-13
  - magnitude, 14-2
  - operational properties, 14-7–14-8
  - properties, 14-6–14-7
  - singular-value decomposition (SVD), 14-17–14-18
  - time-order and space-order representations
    - polar time-order representation, 14-9–14-10
    - rectangular time-order representation, 14-9
    - Wigner distribution and ambiguity function, 14-10–14-11
  - zeroth-order, 14-1
- Frequency matching, 18-1
- G**
- Gamma function, 12-4, 12-33–12-34
  - Gaussian distribution, 3-6
  - Gauss–Jacobi rules, 9-11, 9-14

- Gauss quadrature formulas, 9-11  
 Gauss' theorem, E-9  
 Gegenbauer polynomials, 1-34  
 Gegenbauer transform, 8-35  
   application, 11-16  
   definition, 11-14  
   operational properties, 11-14–11-15  
 Generalized lapped orthogonal transform (GenLOT), 15-19  
   definition, 15-17–15-18  
   degrees of freedom, 15-18  
   implementation, 15-18  
   inverse and forward transform, 15-20–15-21  
   nonlinear unconstrained optimization, 15-18, 15-20  
 Geometric Dirac comb, 12-21–12-22  
 Gram–Schmidt orthonormalization process, 1-21  
 Green's theorem, E-9
- H**
- Hankel transform, 8-29–8-30  
   applications  
     electrified disc, 9-6–9-7  
     electrostatic problem, 9-8–9-9  
     heat conduction, 9-8  
     Laplace equation, 9-8  
   Bessel functions  
     elementary properties, 9-1–9-2  
     finite interval, 9-11–9-13  
     infinite interval, 9-13–9-15  
   definition, 9-2  
   finite Hankel transform, 9-9–9-10  
   Fourier transform, 9-2–9-3  
   Fourier transforms, 2-38–2-39  
   numerical integration methods, 9-10–9-11  
   properties, 9-3–9-4  
   Radon and Abel transforms, 8-29–8-30  
   Weber's integral theorem, 9-10  
 Hartley oscillator, 4-1  
 Hartley transform  
   bus voltages, 4-24–4-25  
   cas function, 4-2–4-3  
   vs. classical complex-valued fast Fourier transform (FFT), 4-1  
   complex and real Mellin transforms, 4-7  
   definition, 4-1  
   Dirichlet conditions, 4-5  
   distribution network model, 4-21–4-22  
   electrostatic coupling, 4-22  
   elementary properties  
     autocorrelation, 4-9  
     convolution, 4-8–4-9  
     function shift/delay and reversal, 4-8  
     linearity, 4-7  
     modulation, 4-8  
      $n$ th derivative of a function, 4-9  
     power spectrum and phase, 4-8  
     product, 4-9  
     scaling/similarity, 4-8  
   energy signals, 4-26  
   engineering signals, 4-26–4-28  
   even and odd function, 4-4  
   expression, 4-2  
   fast Hartley transform (FHT)  
     applications, 4-18  
     cyclic convolution, 4-19–4-20  
     DHT and IDHT, 4-17  
     FFT algorithm, 4-17  
     frequency domain, 4-19–4-20  
     nontrivial computation, 4-21  
     periodic load current, 4-20  
     program, 4-28–4-31  
     quasiperiodic transient inputs, 4-19  
     time-domain convolution, 4-18–4-19  
     transform domain, 4-19  
     zero padding, 4-20  
   Fourier magnitude, 4-22–4-23  
   Fourier transforms, 4-5  
   greyqui hoy, 4-2  
   Hermitian symmetry, 4-5  
   Hilbert transforms, 4-6  
   impedance frequency components, 4-22  
   inverse Hartley transform, 4-2–4-3  
   Laplace transforms, 4-6  
   multiple dimensions, 4-10  
   nonsinusoidal waveform propagation, 4-21  
   power signals, 4-26  
   predictor–corrector method, 4-23  
   real Fourier transform (RFT), 4-6–4-7  
   scaling coefficient, 4-3  
   self-inverse property, 4-3  
   sine and cosine transforms, 4-5  
   systems analysis, Hartley series  
     Bessel's inequality, 4-12  
     electric power quality assessment, 4-15–4-17  
     finality of coefficients, 4-10, 4-12  
     impulse function, 4-10  
     linear system response problem, 4-14  
     orthogonal basis function, 4-13  
     orthonormal set, 4-12–4-13  
     Parseval's equality, 4-12  
     Riemann–Lebesgue lemma, 4-11–4-12  
     transfer function methodology, 4-15  
     truncation approximation, 4-11  
   transfer impedance, 4-23–4-24  
   transient/aperiodic excitations, 4-24–4-25  
   trigonometric properties and functions, 4-3  
 Heaviside expansion theorem, 5-12  
 Hermite polynomials, 8-17–8-18  
   definition, 1-28–1-29  
   Fourier cosine transform (FCT), 3-8  
   Fourier sine transform (FST), 3-15  
   functions and formulas, 8-44–8-45  
   integral representation and equation, 1-29  
   orthogonality relation, 1-29–1-30  
   properties, 1-31  
   recurrence relation, 1-29  
 Hermite transforms  
   basic operational properties, 11-23  
   even functions, 11-27  
   generalized convolution, 11-25  
   Laguerre transformation, 11-26  
   odd functions, 11-26  
   recurrence relations, 11-24–11-25  
   definition, 11-21–11-22  
 Hermitian symmetry, 4-5  
 Hierarchical lapped transform (HLT)  
   filter banks and discrete wavelets, 15-10–15-11  
   time–frequency diagram, 15-11  
   tree-structured transform  
     basis functions, 15-13  
     M-band LT, tree nodes and branches, 15-12  
     tree and TF diagram, 15-12  
   variable-length LT  
     cascading effect, 15-13–15-14  
     factorization, 15-14  
 High-pass filters, 10-22  
 Hilbert–Huang transform method (HHT)  
   bidimensional empirical mode decomposition (BEMD)  
     applications, 20-9  
     boundary effects, 20-8  
     extrema detection, 20-7–20-8  
     intermittency, 20-7  
     scattered data interpolation (SDI), 20-7–20-8  
     sifting process and stopping criterion, 20-7  
     texture image analysis, 20-6–20-7  
     types, 20-7  
   empirical mode decomposition (EMD)  
     drawbacks, 20-4–20-5  
     end effects, 20-6  
     extrema envelope, 20-1  
     vs. Fourier and wavelet transform, 20-4  
     Hilbert transform, 20-5–20-6  
     intermittency, 20-2–20-3  
     pictorial depiction, 20-2  
     recent developments, 20-6  
     sifting process, 20-2–20-3  
     stopping criteria, 20-2, 20-3  
     without extrema envelopes, 20-8  
   global health monitoring technique, 20-8–20-9  
   recommendations, 20-9–20-10  
 Hilbert space, 12-18  
 Hilbert transformers  
   analog all-pass filters, 7-62–7-63  
   band-pass Hilbert transformers, 7-68–7-71  
   delay, phase distortions, and equalization, 7-66–7-67  
   design methods, 7-72  
   differentiating Hilbert transformers, 7-77–7-79  
   digital Hilbert transformers, 7-70–7-72  
   digital phase splitters, 7-75  
   finite impulse response (FIR), 7-72–7-75

- infinite impulse response (IIR), 7-75–7-77
  - phase-splitter Hilbert transformers, 7-61–7-62
  - SSB filtering, 7-70
  - tapped delay-line filters, 7-67
  - Hilbert transforms
    - analytic functions
      - Cauchy–Riemann equations, 7-4
      - complex function, 7-3–7-4
      - Euler’s formula, 7-3, 7-5
    - analytic signal
      - instantaneous amplitude, complex phase, and complex frequency, 7-32–7-34
      - integration, 7-23, 7-25
      - multiplication, 7-28
      - wavelets, 7-99
    - autoconvolution and energy equality, 7-18–7-19
  - Bessel functions
    - Chebyshev polynomial, 7-30–7-31
    - Fourier series, 7-29
    - frequency domain differentiation, 7-30
    - integral form, 7-28
    - inverse Fourier transformation, 7-31
    - power series representation, 7-28, 7-31–7-32
    - second order Bessel differential equation, 7-28
    - waveforms, 7-29–7-30
  - Clifford analytic signal, 7-98–7-99
  - definitions, 7-2–7-3
  - differentiation, 7-20
  - discrete Hilbert transformation (DHT)
    - bilinear transformation, 7-59–7-60
    - circular convolution, 7-56
    - complex analytic discrete sequence, 7-58
    - discrete one-sided convolution, 7-55
    - exponential kernels, 7-54
    - impulse response, 7-55–7-56
    - inverse transformation, 7-54
    - linearity, 7-57–7-58
    - Parseval’s theorem, 7-56–7-57
    - shifting property, 7-57
    - transfer function, 7-55–7-56
  - distribution, 7-9–7-10
  - electrical power
    - complex power notion, 7-51
    - instantaneous power, 7-50
    - power notion generalization, 7-51–54
    - quadrature instantaneous power, 7-50
    - voltage and current harmonic waveforms, 7-50–7-51
  - Fourier transforms, 2-30
  - Hartley transform, 4-6
  - Hermite polynomials and functions
    - Fourier image, 7-23
    - Gaussian Fourier pair, 7-21
    - orthogonal function, 7-22–7-23
    - recursion formula, 7-22
    - waveforms, 7-22
    - weighting function, 7-23
  - Hilbert–Huang transform, 20-5–20-6
  - Hilbert pairs, 7-14–7-17
  - iteration, 7-14
  - linear systems, Kramers–Kronig relations
    - amplitude-phase relations, DLTI systems, 7-43–7-44
    - causality, 7-42
    - linear macroscopic continuous media, 7-44–7-45
    - linear, time-invariant (LTI) systems, 7-41–7-42
    - minimum phase property, 7-42–7-44
    - physical realizability, transfer functions, 7-42
    - signal delay, Hilbertian sense, 7-45
  - modulation theory
    - compatible single side-band modulation, 7-38–7-39, 7-41
    - generalized single side-band modulation, 7-37–7-38
    - harmonic carrier, modulation function, 7-35–7-37
  - monogenic 2-D signal
    - quaternionic Fourier transformation (QFT), 7-97
    - quaternion-valued function, 7-96
    - Riesz transform, 7-96–7-97
    - spherical coordinates representation, 7-97–7-98
  - multidimensional complex signals
    - conjugate 2-D complex signals, 7-90
    - definition, 7-89
    - 2-D modulation theory, 7-92–7-93
    - Euler’s equation, 7-88
    - labeling orthants, 7-94
    - local amplitudes, phases, and complex frequencies, 7-91
    - real and complex notation, 7-91–7-92
  - multidimensional Hilbert transformations
    - 2-D Hilbert transformation, 7-81, 7-84
    - evenness and oddness, 7-79–7-80
    - partial Hilbert transformation, 7-81
    - separable functions, 7-82
    - spectral description, 7-81–7-82
    - Stark’s extension, Bedrosian’s theorem, 7-85
  - one-sided spectrum
    - even and odd term, 7-5
    - Gaussian pulse and Fourier image, 7-8–7-9
    - Hartley transforms, 7-6–7-7
    - linear two-port network, 7-5
    - mean value, 7-8
    - periodic cosine signal, 7-7
    - two-sided symmetric unipolar square pulse, 7-7–7-8
  - periodic signals
    - cotangent Hilbert transformations, 7-12–7-13
    - generating function, 7-10
    - periodic function, Fourier series, 7-10–7-11
    - time domain, 7-11–7-12
    - properties, 7-17–7-18
  - quaternionic 2-D signals
    - Hermitian symmetry, 2-D Fourier spectrum, 7-95–7-96
    - quaternionic spectral analysis, 7-95
    - quaternion numbers and quaternion-valued functions, 7-94–7-95
  - sampling theory
    - band-pass signals, 7-48–7-49
    - delta sampling sequence, 7-46
    - interpolatory expansion, 7-48
    - low-pass band-limited spectrum, 7-47
    - low-pass sampled signal, 7-48–7-49
    - noncausal impulse response, 7-47
    - periodic sequence, 7-46
    - transfer function, 7-47–7-48
    - signal multiplication, nonoverlapping spectra, 7-27
    - Wigner distribution, 7-98, 13-5
- I**
- 
- Impulse delta function, 1-4
  - Infinite impulse response (IIR) Hilbert transformers, 7-75–7-77
  - Initial value theorem, 5-9
  - Integral order Bessel functions, 2-34
  - Integration
    - Cauchy first integral theorem, A-4
    - Cauchy second integral theorem, A-5
    - contour integral, A-4
    - contour transformation, A-18–A-19
    - definition, A-2–A-3
    - evaluation theorem, A-16–A-18
    - path, A-3
  - Interpolatory functions, 7-48
  - Inverse discrete Hartley transform (IDHT), 4-17
  - Inverse finite Hankel transform, 11-2
  - Inverse Fourier transform, 8-31
  - Inverse Hartley transform, 4-2–4-3
  - Inverse Hermite transform, 11-22
  - Inverse Jacobi transform, 11-12, 11-14
  - Inverse Laguerre transform, 11-16
  - Inverse Laplace transform
    - definition, 5-10
    - Heaviside expansion theorem, 5-12
    - partial fraction expansion, 5-10–5-11
    - proper fraction, 5-11
  - Inverse Legendre transform, 11-6
  - Inverse Z-transform
    - one-sided Z-transform
      - integration, 6-9
      - irrational function, 6-10
      - partial fraction expansion, 6-8
      - power series method, 6-7
      - simple and multiple poles, 6-9

two-sided Z-transform  
 integral inversion formula, 6-24  
 partial fraction expansion, 6-22  
 power series expansion, 6-21  
 Isotropic Hilbert transform, *see* Riesz transforms

**J**

Jacobi transforms  
 definition, 11-12  
 generalized heat conduction problem, 11-13-11-14  
 operational properties, 11-13

**K**

Karhunen–Loeve transform (KLT)  
 auto-covariance matrix  
 data vector, 3-19  
 signal vector, 3-20  
 diagonalization, 3-19-3-20  
 discrete cosine transform (DCT), 3-20  
 discrete sine transform (DST), 3-20-3-21  
 Markov-1 signal, 3-20  
 nonsingular symmetric Toeplitz matrix, 3-19  
 residual correlation, 3-21  
 signal decorrelation, 3-1  
 variance distribution, 3-20-3-21  
 Kelvin functions, 9-15

**L**

Laguerre polynomials  
 Fourier cosine transform (FCT), 3-8  
 Fourier sine transform (FST), 3-15  
 generating function, 1-30  
 Leibniz formula, 1-31  
 orthogonality, 1-32-1-33  
 properties, 1-33-1-34  
 Radon and Abel transforms, 8-18-8-19  
 recurrence relations, 1-31-1-32  
 Rodrigues formula, 1-31  
 Laguerre transforms  
 definition, 11-16  
 diffusion equation, 11-21  
 heat conduction problem, 11-20-11-21  
 operational properties, 11-18-11-20  
 Laplace equation, 9-8  
 Laplace transforms  
 Dirichlet conditions, 5-1  
 Fourier cosine transform (FCT)  
 exponential and logarithmic functions, 3-6  
 trigonometric functions, 3-7  
 Fourier sine transform (FST)  
 exponential and logarithmic functions, 3-14  
 trigonometric functions, 3-15  
 Hartley transform, 4-6  
 inverse Laplace transform  
 definition, 5-10

Heaviside expansion theorem, 5-12  
 partial fraction expansion, 5-10-5-11  
 proper fraction, 5-11  
 inversion integral  
 Cauchy second integral theorem, 5-17  
 region of convergence, 5-17  
 transformable function, 5-20  
 Laplace transform pairs, 5-29-5-42  
 Mellin transform, 12-3  
 ordinary linear equations, constant coefficients, 5-3  
 partial differential equations, 5-20  
 path of integration, 5-2  
 piecewise continuous function, 5-1  
 properties, 5-42-5-43  
 complex integration, 5-5  
 complex translation, 5-6-5-7  
 convolution, 5-7  
 differentiation, 5-3-5-4  
 final value theorem, 5-9  
 frequency convolution, s-plane, 5-8  
 initial value theorem, 5-9  
 integration, 5-4-5-5  
 linearity, 5-3  
 multiplication, 5-5  
 time delay, real translation, 5-6  
 two-sided Laplace transform, 5-27-5-28  
 Z-transform, 6-34-6-36  
 Lapped transforms (LT)  
 block transforms, 15-2, 15-4  
 vs. DCT, 15-4-15-5, 15-6  
 DCT-based image compression, 15-1  
 discrete MIMO linear systems, 15-3-15-4  
 discrete transform factorization, 15-2-15-3  
 extended lapped transforms (ELT), 15-2  
 factorization, 15-9-15-20  
 fast lapped transform (FLT), 15-22-15-23, 15-24  
 finite-length signals  
 distorted sample recovery, 15-26-15-27  
 overall transform, 15-25-15-26  
 symmetric extensions, 15-27-15-28  
 general factorization (GLBT), 15-21-15-22  
 generalized LOT (GenLOT), 15-19  
 definition, 15-17-15-18  
 degrees of freedom, 15-18  
 implementation, 15-18  
 inverse and forward transform, 15-20-15-21  
 nonlinear unconstrained optimization, 15-18, 15-20  
 hierarchical lapped transform (HLT)  
 filter banks and discrete wavelets, 15-10-15-11  
 time-frequency diagram, 15-11  
 tree-structured transform, 15-12-15-13  
 variable-length LT, 15-13-15-14  
 image and signal compression, 15-4-15-5, 15-6

lapped biorthogonal transform (LBT)  
 factorization, 15-16  
 frequency basis, 15-15-15-16  
 vs. LOT, 15-16-15-17  
 lapped orthogonal transform (LOT), 15-2, 15-14-15-15  
 modulated LT/extended lapped transform (ELT)  
 cosine sequence phase, 15-23  
 lattice-style algorithm, 15-24  
 plane rotation stages, 15-24-15-25  
 multi-input multi-output (MIMO) system, 15-8-15-9  
 nonorthogonal lapped transforms, 15-8  
 orthogonal lapped transforms  
 matrix, 15-5-15-6  
 notation, 15-7-15-8  
 PR property, 15-6  
 signal sampling, 15-6-15-7  
 subband signal variance, 15-7  
 vectors, 15-6-15-7  
 symmetric basis, 15-14  
 symmetric delay factorization (SDF), 15-20  
 Laurent's theorem, A-6-A-7  
 Legendre polynomials  
 associated Legendre polynomials, 1-24  
 complete orthonormal system, 1-22-1-23  
 definition, 1-21  
 Fourier cosine transform (FCT), 3-8  
 Fourier sine transform (FST), 3-15  
 properties, 1-26-1-27  
 Rodrigues and recursive formula, 1-22  
 Schlöfli's integral formula, 1-22  
 Legendre transforms  
 boundary value problems, 11-10-11-11  
 definition, 11-5-11-6  
 operational properties, 11-7-11-10  
 Linear canonical transforms (LCT)  
 basic properties, 14-13  
 composite transform, 14-11  
 decompositions, 14-13  
 noncommutative group sets, 14-11-14-12  
 operational properties, 14-14  
 Wigner distribution, 14-12-14-13  
 Linear discrete system analysis  
 causality, 6-26  
 discrete Fourier transform (DFT), 6-26-6-27  
 frequency characteristics, 6-26  
 Paley–Wiener theorem, 6-26  
 stability, 6-25-6-26  
 transfer function, 6-25  
 Linear discrete-time filters, 6-32-6-33  
 Linear-phase filters, 10-28  
 Linear systems  
 casual systems, 2-52  
 complex exponentials and periodic functions, 2-51  
 correlation, 2-60  
 differential equations, 2-52

- Kramers–Kronig relations  
   amplitude-phase relations, DLTI systems, 7-43–7-44  
   causality, 7-42  
   linear macroscopic continuous media, 7-44–7-45  
   linear, time-invariant (LTI) systems, 7-41–7-42  
   minimum phase property, 7-42–7-44  
   physical realizability, transfer functions, 7-42  
   signal delay, Hilbertian sense, 7-45  
   linear shift invariant systems, 2-49  
   modulation and demodulation, 2-54–2-55  
   random signals, 2-60–2-61  
   reality and stability, 2-50  
   RLC circuits, 2-54  
 Linz’s method, 9-14  
 Low-pass filters, 2-49–2-50, 10-22
- M**
- Matrices and determinants  
   addition, subtraction and multiplication, D-2  
   characteristics roots and vector, D-8–D-9  
   conditional inverses, D-9–D-11  
   definition, D-1–D-2  
   determinants, D-3–D-5  
   inversion, D-5–D-7  
   matrix differentiation, D-11–D-13  
   recognition rules and special forms, D-2–D-3  
   singularity and rank, D-5  
   statistical matrix forms, D-13–D-14  
   traces, D-7–D-8  
 Matrix differentiation, D-11–D-13  
 Matrix inversion, D-5–D-7  
 McCully’s theorem, 11-20  
 Mellin transforms, 4-7  
   beta function, 12-34  
   Cauchy’s theorem, 12-1, 12-3  
   definition, 12-2  
   discretization and fast computation  
     arithmetic sampling, Mellin space, 12-24  
     discrete Mellin transform, 12-25–12-27  
     geometric sampling, original space, 12-24–12-25  
     interpolation formula,  $v$ -space, 12-27  
   distribution transformation, 12-5–12-6, 12-21  
   gamma function, 12-33–12-34  
   hyperbolic class, 13-34  
   inversion formula, 12-3–12-5  
   Laplace and Fourier transformations, 12-3  
   multiplicative convolution, 12-8–12-9  
   practical inversion  
     inversion integral, 12-9  
     polar coordinates, 12-10–12-11  
     Slater’s theorem, 12-10  
   products and convolutions transformation, 12-22–12-23  
   properties, 12-7–12-8, 12-35–12-36  
   psi function, 12-34  
   Riemann’s zeta function, 12-34  
   signal analysis  
     affine time–frequency distributions, 12-32–12-33  
     Cramer–Rao bounds, velocity estimation, 12-28–12-30  
     dual Mellin variable interpretation, 12-30–12-31  
     numerical computation, 12-27  
     wavelet transform, 12-31–12-32  
   standard applications  
     asymptotic expansion, integrals, 12-15  
     convolution equations, 12-12–12-14  
     harmonic sums, asymptotic behavior, 12-16–12-17  
     integral computation, 12-12  
     potential problem, wedge, 12-14–12-15  
     summation of series, 12-11–12-12  
     transformation construction, 12-17–12-20  
     uncertainty relations, 12-20–12-21  
 Mexican-hat wavelet, 10-13  
 Minimum phase transfer function, 7-42  
 Minkowski inequality, 1-20  
 Mixed time–frequency signal transformations  
   affine class, 13-31  
     alternative formulation, 13-30, 13-32–13-33  
     expression, 13-30  
     kernels, 13-32  
   affine-Cohen subclass, 13-33  
   classical time–frequency representations (TFRs)  
     Altes Q distribution, 13-8–13-9  
     Bertrand  $P_k$  distributions, 13-10  
     quadratic time–frequency representations, 13-10–13-13  
     short-time Fourier transform (STFT), 13-4–13-5  
     TFR warping, 13-9–13-10  
     Wigner distribution and Woodward ambiguity function, 13-5–13-8  
 Cohen’s class, 13-27  
   alternative formulations, 13-23, 13-29  
   expression, 13-23  
   implementation consideration, 13-29  
   kernel constraints, 13-26, 13-29–13-30  
   shift covariant class, 13-28  
 covariance properties  
   convolution covariance, 13-16  
   frequency-shift covariance, 13-14  
   hyperbolic time-shift covariance, 13-15–13-16  
   modulation covariance, 13-16  
   scale covariance, 13-15  
   time-shift covariance, 13-15  
 hyperbolic class, 13-35  
   affine-hyperbolic subclass, 13-37  
   expression, 13-33  
   kernels, 13-36–13-37  
   Mellin transformation, 13-34  
   quadratic signal product, 13-33  
 inner products, 13-22–13-23  
 $k$ th power class, 13-38–13-39  
   central member, 13-38  
   expression, 13-37  
   inverse phase function, 13-38  
   kernels, 13-39–13-40  
   power AF, 13-38  
   signal product, 13-37  
   signal warping, 13-38  
 musical score, 13-1  
 one-dimensional spectral representations  
   Fourier transform, 13-2–13-3  
   instantaneous frequency and group delay, 13-3–13-4  
 signal analysis properties  
   finite frequency support, 13-19  
   finite time support, 13-18  
   Fourier transform, 13-19–13-20  
   group delay, 13-19  
   instantaneous frequency, 13-19  
 signal localization  
   chirp convolution, 13-21  
   chirp multiplication, 13-21–13-22  
   frequency localization, 13-20  
   hyperbolic chirp localization, 13-21  
   linear chirp localization, 13-20–13-21  
   time localization, 13-20  
 statistical energy density distribution properties  
   energy preservation, 13-17–13-18  
   frequency marginal preservation, 13-17  
   frequency moment preservation, 13-18  
   positivity, 13-17  
   real, 13-16–13-17  
   time marginal preservation, 13-17  
   time moment preservation, 13-18  
 Modified Clenshaw–Curtis (MCC) quadrature method, 9-11–9-13  
 Modified Schur–Cohn criterion, 6-25  
 Modulated lapped transform (MLT)/extended lapped transform (ELT)  
   cosine sequence phase, 15-23  
   lattice-style algorithm, 15-24  
   plane rotation stages, 15-24–15-25  
 Monogenic 2-D signal  
   isotropic Hilbert transform, 7-97  
   quaternionic Fourier transformation (QFT), 7-97  
   quaternion-valued function, 7-96  
   Riesz transform, 7-96–7-97  
   spherical coordinates representation, 7-97–7-98  
 Multidimensional complex signals  
   conjugate 2-D complex signals, 7-90  
   definition, 7-89  
   2-D modulation theory, 7-92–7-93  
   Euler’s equation, 7-88  
   labeling orthants, 7-94

- local amplitudes, phases, and complex frequencies, 7-91
  - real and complex notation, 7-91-7-92
  - Multidimensional discrete unitary transforms
    - butterfly operation, 19-2-19-4
    - calculation, 19-1-19-2
    - data processing, 19-1
    - 2-D DCT
      - fast 1-D cosine transforms, 19-38
      - modified DCT, 19-39-19-41
      - $N/2$ -point DCT, 19-36-19-37
      - tensor representation, 19-35
    - 2-D DFT, hexagonal lattice
      - calculation, frequency-points, 19-57-19-59
      - complexity, 19-55-19-56
      - definition, 19-56-19-57
      - paired representation, 19-59-19-62
      - $8 \times 4$ -point DHFT, 19-59
      - rectangular lattice, 19-56
      - regular hexagonal tessellation, 19-55
    - 2-D DFT tensor algorithm
      - modified tensor algorithms, 19-20-19-21
      - $n$ -dimensional DFT, 19-25-19-26
      - $N$ , power of two, 19-18-19-20
      - $N$ , prime, 19-16-19-18
      - recursive tensor algorithm, 19-21-19-25
    - discrete Hartley transforms
      - 2-D DHT representation, 19-26-19-29
      - 3-D DHT tensor representation, 19-29-19-31
      - $n$ -dimensional DHT, 19-31-19-32
    - 3-D paired representation
      - conventional and tensor representation, 19-41-19-42
      - 2D-to-3D paired transform, 19-43-19-44
      - $N$ , power of odd prime, 19-49-19-50
      - $N$ , power of two, 19-44-19-49
      - set-frequency characteristics, 19-50-19-55
      - signal processing, 19-42-19-43
      - splitting-signals, 19-42, 19-43
    - 2-D shifted DFT (SDFT)
      - components, 19-32
      - $L_1 L_2 \times L_1 L_2$ -point SDFT, 19-35
      - $L' \times L'$ -point SDFT, 19-34-19-35
      - $2^r \times 2^r$ -point SDFT, 19-34
      - tensor representation, 19-32-19-33
  - Fourier transform tensor representation
    - 2-D directional images, 19-11-19-16
    - splitting-signal, 19-10-19-11
  - nontraditional representation
    - image enhancement method, 19-6-19-7
    - image processing diagram, 19-5-19-6
    - spectral information processing, 19-5
  - Nussbaumer algorithm, 19-4
  - paired transform-based algorithms
    - 2-D DHT calculation, 19-62-19-63
    - 2-D discrete cosine transform, 19-63-19-64
    - 2-D discrete Hadamard transform, 19-64-19-67
  - partitioning
    - basis function, 19-7-19-8
    - covering, cyclic groups, 19-8-19-9
    - frequency-points, 19-8-19-9
    - fundamental period, 19-7
    - lattice torus, 19-9
    - linear transformation, 19-7
    - $\sigma$ -splitting, 19-8
    - tensor representation, 19-8
    - transformation orders, 19-7
  - polynomial transforms, 19-4-19-5
  - row-column algorithm, 19-2, 19-3
  - vector-radix algorithm, 19-2-19-4
  - Multidimensional Fourier transforms, 2-35-2-36
  - Multidimensional Hilbert transformations
    - 2-D Hilbert transformations, 7-81, 7-84
    - evenness and oddness, 7-79-7-80
    - partial Hilbert transformation, 7-81
    - separable functions, 7-82
    - spectral description, 7-81-7-82
    - Stark's extension, Bedrosian's theorem, 7-85
  - Multiresolution signal analysis
    - Gaussian pyramid, 10-16
    - Laplacian pyramid, 10-16-10-17
    - orthonormal wavelet transform, 10-18-10-19
    - power system signal, 10-50
    - scale and resolution, 10-18
    - subband coding, 10-17-10-18
  - Multiresolution wavelet analysis
    - band-pass filters, 10-9
    - constant fidelity analysis, 10-9-10-10
    - multiresolution filter bank, 10-9
    - scale and resolution, 10-10
    - time and frequency domain localization, 10-8
- N**
- 
- Neumann series, 9-12
  - Nonintegral order Bessel functions, 2-35
  - Nonsingular symmetric Toeplitz matrix, 3-19
  - Normal distribution, 2-56
  - Nyquist interval, 1-49
  - Nyquist rate, 7-47
- O**
- 
- Oliver's algorithm, 9-13
  - One-sided  $Z$ -transform
    - complex conjugate signal, 6-4-6-5
    - convolution, 6-3
    - correlation, 6-6
    - discrete functions, 6-1
    - final value, 6-4
  - initial value, 6-3-6-4
  - integration, 6-9
  - irrational function, 6-10
  - $(nT)^k$  multiplication, 6-4
  - linearity, 6-2
  - $n$  and  $nT$  multiplication, 6-3
  - parameters, 6-7
  - Parseval's theorem, 6-6
  - partial fraction expansion, 6-8
  - periodic sequence, 6-2
  - power series method, 6-7
  - product transform, 6-5
  - shifting property, 6-2
  - simple and multiple poles, 6-9
  - time scaling, 6-2
- Optimum linear filters, 6-33-6-34
  - Orthogonal Bessel functions, 8-39
  - Orthonormal filter bank, 10-30-10-31
  - Orthonormal wavelet transform
    - biorthogonal wavelet basis, 10-26-10-27
    - multiresolution signal analysis basis, 10-18-10-19
    - orthonormal basis, 10-19-10-20
    - orthonormal subspaces, 10-20-10-21
    - reconstruction, 10-25-10-26
    - wavelet series decomposition, 10-23-10-24
      - Haar wavelets, 10-24-10-25
      - low-pass and high-pass filters, 10-22
      - orthonormal projections, 10-21-10-22
      - recursive projections, 10-22-10-23
- P**
- 
- 3-D Paired representation
    - conventional and tensor representation, 19-41-19-42
    - 2D-to-3D paired transform, 19-43-19-44
    - $N$ , power of odd prime, 19-49-19-50
    - $N$ , power of two
      - basis paired functions, 19-45
      - concept, 19-48-19-49
      - generator and orbits of points, 19-44
      - set of triplets, 19-47
      - transformation, 19-46
    - set-frequency characteristics
      - direction-image component, 19-50
      - inverse 2-D DFT, 19-51
      - resolution map, 19-53-19-55
      - series images, 19-52-19-53
      - splitting-signal, 19-51-19-52
    - signal processing, 19-42-19-43
    - splitting-signals, 19-42, 19-43
  - Paired transform-based algorithms
    - 2-D DHT calculation, 19-62-19-63
    - 2-D discrete cosine transform, 19-63-19-64
    - 2-D discrete Hadamard transform (DHdT)
      - basis functions, 19-64
      - 1-D DHdT, 19-64, 19-65-19-66
      - properties, 19-64-19-65
  - Paley-Wiener theorem, 6-26
  - Parks-McClellan algorithm, 7-74



- Parseval's equality  
 Bessel's inequality, 4-12  
 Fourier transforms, 2-14-2-15
- Parseval's theorem  
 definition, 7-18  
 discrete Hilbert transformation (DHT), 7-56-7-57  
 one-sided  $Z$ -transform, 6-6  
 two-sided  $Z$ -transform, 6-20
- Partial differential equations, 5-20  
 half-infinite rod, boundary value problem, 2-64  
 infinite rod  
 heat sources and sinks, 2-63-2-64  
 initial value problem, 2-63  
 one-dimensional heat equation, 2-62
- Phase-splitter Hilbert transformers, 7-61-7-62
- Piecewise continuous function, 5-1
- Poincaré sense asymptotic sequence, 1-53
- Poisson integral formula, 11-11
- Power series  
 convergence, A-10-A-11  
 Maclaurin series, A-9  
 negative power series, A-10  
 positive power series, A-9  
 Taylor series, A-9
- Principal value integral, A-31-A-32
- Psi function, 12-34
- Q**
- Quadratic time-frequency representation  
 band-limited cosine, 13-13  
 interference geometry, 13-11-13-12  
 multicomponent signal, 13-11  
 nonlinear operation, 13-10
- Quadrature filter, *see* Hilbert transformers
- R**
- Radon and Abel transforms  
 Abel transform pairs, 8-24  
 circular harmonic decomposition  
 Chebyshev polynomial, 8-35  
 extension, higher dimensions, 8-35  
 Fourier series, 8-34  
 three dimensions, 8-35-8-36  
 component and matrix notations, 8-3  
 definitions  
 central-slice theorem, 8-6-8-7  
 feature, Radon, and Fourier space, 8-3  
 three and higher dimensions, 8-6  
 two dimensions, 8-3-8-5  
 derivatives, 8-15-8-16  
 discrete periodic Radon transform, 8-42-8-43  
 elliptic integral, 8-46  
 fractional integrals, 8-25  
 functions and formulas  
 Chebyshev polynomials, 8-43-8-44  
 Hermite polynomials, 8-44-8-45  
 selected integral formulas, 8-45  
 Zernike polynomials, 8-45  
 generalizations and wavelets, 8-41-8-42  
 Hankel transform, 8-29-8-30  
 integral equation, 8-2  
 inversion  
 backprojection, 8-31-8-33  
 direct Fourier method, 8-33-8-34  
 ill-posed problem, 8-30  
 indeterminacy theorem, 8-30  
 iterative and algebraic reconstruction techniques, 8-34  
 three dimensions, 8-20  
 two dimensions, 8-19-8-20  
 Laguerre polynomials, 8-18-8-19  
 linear transformations, 8-9-8-10  
 orthogonal functions, unit disk  
 Chebyshev polynomials, 8-39  
 Fourier space, 8-38  
 orthogonal Bessel functions, 8-39  
 Radon space, evaluation, 8-38  
 Zernike polynomials, 8-36-8-37  
 Parseval relation, 8-39  
 properties  
 convolution, 8-9  
 differentiation, 8-8-8-9  
 Fourier transform, 8-7-8-8  
 linearity, 8-8  
 similarity, symmetry and shifting, 8-8  
 reconstruction problem, 8-1-8-2  
 rotationally symmetric function, 8-28  
 sinc function, 8-46  
 singular integral equations, 8-21-8-22  
 spherical symmetry, 8-30  
 tauchrone problem generalization, 8-27
- Radon-Wigner transform, 8-42
- Random signal, 1-1
- Real Fourier transform (RFT), 4-6-4-7
- Reduced interference distributions (RID), 13-29
- Residue theory, A-14-A-16
- Riemann-Lebesgue lemma, 4-11-4-12
- Riemann's zeta function, 12-34
- Riess-Fischer theorem, 1-20
- Riesz transform, 7-96-7-97
- RLC circuits, 2-54
- S**
- Sampled signal reconstruction  
 band-limited functions, 2-45  
 sampling theorem, 2-43-2-44  
 truncated sampling reconstruction, 2-44  
 finite duration functions, 2-47  
 fundamental sampling formulas and Poisson's formula, 2-47-2-48
- Sampling theorem  
 aliasing, 1-49  
 delta sampling representation, 1-50-1-51  
 finite energy function, 1-49  
 frequency sampling, 1-51  
 Nyquist interval, 1-49
- Papoulis extensions, 1-52  
 rectangular pulse train, 1-51
- Schlafli's integral formula, 1-22
- Schwarz's inequality  
 finite power function, 2-21  
 stationary random signal and independence correlation, 2-60
- Series and summations  
 binomial, B-1  
 exponential, B-2  
 hyperbolic and inverse hyperbolic, B-3-B-4  
 logarithmic, B-2  
 Maclaurin, B-2  
 reversion, B-1  
 series, B-1  
 Taylor, B-1-B-2  
 trigonometric, B-2-B-3
- 2-D Shifted DFT (SDFT)  
 components, 19-32  
 $L_1L_2 \times L_1L_2$ -point SDFT, 19-35  
 $L^r \times L^r$ -point SDFT, 19-34-19-35  
 $2^r \times 2^r$ -point SDFT, 19-34  
 tensor representation, 19-32-19-33
- Short-time Fourier transform (STFT)  
 classical time-frequency representation, 13-4-13-5  
 definition, 10-3-10-4  
 discrete short-time Fourier transform, 10-5  
 Gabor function, 10-4  
 Gaussian window, 10-4-10-5  
 inverse short-time Fourier transform, 10-4  
 regular lattice, 10-5  
 time and frequency resolution, 10-4  
 uncertainty principle, 10-4
- Signals and systems  
 asymptotic series  
 asymptotic approximation, 1-53  
 asymptotic power series, 1-53-1-55  
 definition, 1-52-1-53  
 Poincaré sense asymptotic sequence, 1-53
- Bessel functions  
 definition, 1-35  
 Fourier Bessel series, 1-39  
 integral representation, 1-37  
 nonintegral order, 1-36  
 properties, 1-41-1-43  
 recurrence relation, 1-36
- beta function, 1-12-1-13
- Chebyshev polynomials, 1-34-1-35
- classification, 1-1
- complete orthonormal set, 1-21
- convolution  
 definition, 1-13-1-14  
 harmonic inputs, 1-18  
 impulse response, 1-15  
 nonanticipative convolution system, 1-15  
 properties, 1-16-1-18  
 stability, 1-17

- correlation, 1-19
  - delta function
    - definition, 1-4
    - properties, 1-6–1-7, 1-9
  - distance function, 1-20
  - distributions
    - definition, 1-5–1-6
    - generalized limit, 1-7–1-8
    - testing function, 1-4–1-5
  - energy and power signals, 1-4
  - functions (signals), variables, and point sets, 1-1–1-2
  - gamma function
    - definition, 1-10
    - integral expressions, 1-11
    - properties and specific evaluations, 1-11–1-12
  - Hermite polynomials
    - definition, 1-28–1-29
    - integral representation and equation, 1-29
    - orthogonality relation, 1-29–1-30
    - properties, 1-31
    - recurrence relation, 1-29
  - inner product, 1-19
  - Laguerre polynomials
    - generating function, 1-30
    - Leibniz formula, 1-31
    - orthogonality, 1-32–1-33
    - properties, 1-33–1-34
    - recurrence relations, 1-31–1-32
    - Rodrigues formula, 1-31
  - Legendre polynomials
    - associated Legendre polynomials, 1-24
    - complete orthonormal system, 1-22–1-23
    - definition, 1-21
    - properties, 1-26–1-27
    - Rodrigues and recursive formula, 1-22
    - Schläfli's integral formula, 1-22
  - limits and continuous functions, 1-2–1-3
  - normalization, 1-20
  - quadratically integrable functions, 1-19–1-20
  - series approximation, 1-21
  - signal sampling
    - aliasing, 1-49
    - delta sampling representation, 1-50–1-51
    - finite energy function, 1-49
    - Fourier transform, 1-48–1-49
    - frequency sampling, 1-51
    - Nyquist interval, 1-49
    - Papoulis extensions, 1-52
    - rectangular pulse train, 1-51
    - values and interval, 1-47–1-48
  - Zernike polynomials
    - definition, 1-40
    - piecewise continuous function, 1-45
    - Radial polynomials, 1-40, 1-45–1-46
    - Zernike moments, 1-45, 1-47–1-48
  - Sine and cosine transforms
    - cepstral analysis, speech processing, 3-23
    - computational algorithms
      - decimation-in-frequency algorithms, 3-30–3-31
      - decimation-in-time algorithms, 3-28–3-30
      - fast Fourier transform (FFT), 3-28
    - data compression, 3-23–3-24
    - differential equations
      - one-dimensional boundary value problem, 3-21–3-22
      - time-dependent one-dimensional boundary value problem, 3-22–3-23
      - two-dimensional boundary value problem, 3-22
    - discrete sine and cosine transforms (DST and DCT)
      - decimation-in-frequency algorithms, 3-30–3-31
      - decimation-in-time algorithms, 3-28–3-30
      - definitions, 3-17
      - Karhunen–Loeve transform (KLT), 3-19–3-21
      - properties and operational rules, 3-17–3-19
    - Fourier cosine transform (FCT)
      - algebraic functions, 3-5–3-6, 3-32
      - Bessel functions, 3-9
      - complementary error function, 3-8
      - convolution property, 3-10
      - cosine integral function, 3-9
      - definitions, 3-1–3-2
      - differentiation-in- $t$ , 3-9–3-10
      - differentiation-in- $\omega$ , 3-10
      - exponential and logarithmic functions, 3-6–3-7, 3-32
      - exponential integral function, 3-9
      - orthogonal polynomials, 3-8
      - properties and operational rules, 3-2–3-5
      - real data sequence, 3-28
      - shift-in- $t$ , shift-in- $\omega$  and kernel product property, 3-10
      - sine integral function, 3-8
      - trigonometric functions, 3-7, 3-32
    - Fourier sine transform (FST)
      - algebraic functions, 3-13–3-14, 3-33
      - Bessel functions, 3-16
      - complementary error function, 3-15–3-16
      - cosine integral function, 3-16
      - definitions, 3-11
      - exponential and logarithmic functions, 3-14, 3-33
      - exponential integral function, 3-16
      - orthogonal polynomials, 3-15
      - properties and operational rules, 3-11–3-13
      - real data sequence, 3-28
    - sine integral function, 3-16
    - trigonometric function, 3-14–3-15, 3-33
  - image compression
    - discrete local sine transform (DLS), 3-26
    - lapped orthogonal transform (LOT), 3-25
    - original vs. reconstructed image, 3-27
    - transform domain processing, 3-24
  - Single side-band (SSB) filtering, 7-70
  - Singularities
    - at  $\infty$ , A-15
    - branch points, A-12–A-13
    - definition, A-11–A-12
    - essential and nonessential singularity, A-11, A-13–A-14
    - isolated and nonisolated singularity, A-12
    - phase change, A-12–A-13
    - poles, A-12
    - removable singularity, A-12
  - Singular-value decomposition (SVD), 14-17–14-18
  - Slater's theorem, 12-10
  - Square matrix traces, D-7–D-8
  - Statistical matrix, D-13–D-14
  - Stokes' theorem, E-9
  - Struve functions, 9-15
  - Surface acoustic wave (SAW) filter, 7-70–7-71
  - Systems analysis, Hartley series
    - Bessel's inequality, 4-12
    - electric power quality assessment, 4-15–4-17
    - finality of coefficients, 4-10, 4-12
    - impulse function, 4-10
    - linear system response problem, 4-14
    - orthogonal basis function, 4-13
    - orthonormal set, 4-12–4-13
    - Parseval's equality, 4-12
    - Riemann–Lebesgue lemma, 4-11–4-12
    - transfer function methodology, 4-15
    - truncation approximation, 4-11
- ## T
- 
- Tapped delay-line filters, 7-67
  - Taylor's theorem, A-6
  - Tempered generalized functions, 2-4
  - Three-term recurrence formula, 1-36
  - Transversal filter structure, 6-29
  - Two-sided Laplace transform, 5-27–5-28
  - Two-sided Z-transform
    - complex conjugate signal, 6-21
    - convolution, 6-17
    - correlation, 6-18
    - discrete representation, 6-11
    - $e^{-anT}$  multiplication, 6-18
    - frequency translation, 6-18
    - integral inversion formula, 6-24
    - linearity, 6-16
    - $nT$ , multiplication, 6-17
    - Parseval's theorem, 6-20
    - partial fraction expansion, 6-22

power series expansion, 6-21  
 product, 6-18–6-20  
 region of convergence (ROC), 6-14–6-16  
 shifting and scaling, 6-16  
 time reversal, 6-16–6-17

## U

Unitarity property, *see* Parseval's formula

## V

### Vector analysis

cross product, E-2–E-3  
 definition, E-1  
 differential operators-rectangular  
   coordinates, E-7–E-8  
 differentiation, E-5–E-6  
 formulas, E-9  
 Gauss' theorem, E-9  
 geometry  
   curves in space, E-6–E-7  
   sphere, E-5  
   straight line and plane, E-3–E-4  
 Green's theorem, E-9  
 scalar, dot, and inner product, E-2  
 scalar triple product, E-3  
 Stokes' theorem, E-9  
 transformation of integrals, E-8–E-9  
 triple product, E-3  
 vector algebra, E-1

## W

### Wavelet theory

orthogonal filters, time domain,  
   10-37–10-38  
 orthonormality, 10-34–10-35  
 regularity  
   construction of scaling function,  
     10-40  
   convergence, wavelet reconstruction,  
     10-39–10-40  
   quadrature mirror filter, 10-40–10-41  
   smoothness measure, 10-39  
   time domain, 10-41–10-42  
 two scale relations, frequency domain  
   cross-filter orthogonality, 10-36  
   Fourier transforms, 10-35  
   Haar's basis, 10-37  
   paraunitary matrix, 10-36–10-37  
 wavelet and subband filters, 10-38–10-39

### Wavelet transform

ambiguity function, 10-6  
 B-spline basis, 10-42–10-43  
 constant-Q analysis, 10-1  
 continuous wavelet transform, 10-2–10-3  
 Daubechies basis  
   maximum flatness filter, 10-45–10-46  
   time domain, 10-46–10-47  
 discrete wavelet transform  
   timescale space lattices, 10-14–10-15  
   wavelet frame, 10-15–10-16

fast wavelet transform, 10-47–10-49  
 filter bank  
   biorthogonal filter bank, 10-32–10-33  
   FIR filter bank, 10-27–10-28  
   orthonormal filter bank, 10-30–10-31  
   perfect reconstruction, 10-28–10-30  
   time domain, orthonormal filters,  
     10-31–10-32  
 Gabor-wavelet, 10-13–10-14  
 Gaussian pyramid, 10-16  
 Gaussian wavelet, 10-13  
 Haar wavelet, 10-12–10-13  
 image compression, 10-53  
 image edge detection  
   edge detectors, 10-51–10-52  
   multiscale edges, 10-52–10-53  
   two-dimensional wavelet transform,  
     10-52  
 Laplacian pyramid, 10-16–10-17  
 Lemarie and Battle wavelet bases,  
   10-43–10-45  
 Mellin transform, 12-31–12-32  
 Mexican-hat wavelet, 10-13  
 orthonormal wavelet transform  
   biorthogonal wavelet basis, 10-26–10-27  
   multiresolution signal analysis basis,  
     10-18–10-19  
   orthonormal basis, 10-19–10-20  
   orthonormal subspaces, 10-20–10-21  
   reconstruction, 10-25–10-26  
   wavelet series decomposition,  
     10-21–10-25  
 power system signal, 10-50  
 properties  
   admissible condition, 10-6–10-7  
   linear transform property, 10-11–10-12  
   multiresolution wavelet analysis,  
     10-8–10-10  
   regularity, 10-7–10-8  
   scale and resolution, 10-18  
   scaling function basis, 10-1  
 short-time Fourier transform  
   definition, 10-3–10-4  
   discrete short-time Fourier transform,  
     10-5  
   Gabor function, 10-4  
   Gaussian window, 10-4–10-5  
   inverse short-time Fourier transform,  
     10-4  
   regular lattice, 10-5  
   time and frequency resolution, 10-4  
   uncertainty principle, 10-4  
 signal detection, 10-50–10-51  
 subband coding, 10-17–10-18  
 time-frequency space analysis, 10-3  
 Wigner distribution functions, 10-5–10-6  
 Weber's integral theorem, 9-10  
 Whittaker's interpolatory function, 7-48  
 Wiener-Khinchine theorem, 2-21  
 Wigner distribution  
   Fourier transforms, 13-7–13-8  
   fractional Fourier transform (FRT)

ambiguity function, 14-5–14-6  
 definition, 14-5  
 filtering, 14-15  
 properties, 14-5  
 Radon transforms and slices,  
   14-10–14-11

Hilbert transforms, 7-98, 13-5  
 linear canonical transforms (LCT),  
   14-12–14-13

Wavelet transform, 10-5–10-6

Woodward ambiguity function

Dirac function, 13-6  
 Fourier transform, 13-7–13-8  
 Gaussian signal, 13-6–13-7  
 quantum mechanics, 13-5  
 signal operations, 13-7

Wigner-Ville distribution, 13-5, 13-13

## Z

### Zak transform

#### applications

Gabor expansions, 16-17  
 Jacobi theta functions, 16-17  
 Suter-Stevens fast Fourier transform  
   algorithm, 16-19  
 time-frequency analysis, 16-17–16-18  
 weighted fast Fourier transforms,  
   16-18–16-19

#### continuous transform

algebraic property, 16-6–16-7  
 definition, 16-2–16-3  
 Fourier transform, 16-9–16-11  
 general property, 16-3–16-6  
 geometric property, 16-7–16-8  
 inverse transform, 16-8–16-9  
 multidimensional transform,  
   16-13–16-14  
 multidimensional weighted transform,  
   16-14  
 multidimensional windowed, weighted  
   transform, 16-14  
 topological property, 16-7  
 translation and modulation operator,  
   16-11–16-13

#### discrete transform

definition, 16-14  
 extensions, 16-15  
 inverse transform, 16-14–16-15  
 property, 16-14  
 finite transform  
   definition, 16-15  
   extensions, 16-17  
   inverse transform, 16-16–16-17  
   property, 16-16

#### history, 16-1

linear spaces, 16-2  
 notation, 16-1–16-2

### Zernike polynomials

definition, 1-40  
 functions and formulas, 8-45  
 orthogonal functions, unit disk, 8-36–8-37

- piecewise continuous function, 1-45
- Radial polynomials, 1-40, 1-45–1-46
- Zernike moments, 1-45, 1-47–1-48
- Zero-order Bessel function, 2-33–2-34
- Zero padding, 4-20
- Z-transform
  - difference equations, constant coefficients, 6-24
  - digital filters
    - finite impulse response (FIR) filters, 6-28–6-29
    - infinite impulse response (IIR) filters, 6-27–6-28
  - Fourier transform, 6-36
  - inverse transforms, partial fractions, 6-39
  - Laplace transform, 6-34–6-36
  - linear discrete system analysis
    - causality, 6-26
    - discrete Fourier transform (DFT), 6-26–6-27
    - frequency characteristics, 6-26
    - Paley–Wiener theorem, 6-26
    - stability, 6-25–6-26
    - transfer function, 6-25
  - linear, time-invariant, discrete-time, dynamical systems, 6-29
  - negative-time sequences, 6-38
  - one-sided Z-transform
    - complex conjugate signal, 6-4–6-5
    - convolution, 6-3
    - correlation, 6-6
    - discrete functions, 6-1
    - final value, 6-4
    - initial value, 6-3–6-4
    - integration, 6-9
    - irrational function, 6-10
    - $(nT)^k$  multiplication, 6-4
    - linearity, 6-2
    - $n$  and  $nT$  multiplication, 6-3
    - parameters, 6-7
    - Parseval’s theorem, 6-6
    - partial fraction expansion, 6-8
    - periodic sequence, 6-2
    - power series method, 6-7
    - product transform, 6-5
    - shifting property, 6-2
    - simple and multiple poles, 6-9
    - time scaling, 6-2
  - positive-time sequences, 6-36–6-38
  - random process
    - linear discrete-time filters, 6-32–6-33
    - optimum linear filtering, 6-33–6-34
    - power spectral densities, 6-32
  - two-sided Z-transform
    - complex conjugate signal, 6-21
    - convolution, 6-17
    - correlation, 6-18
    - discrete representation, 6-11
    - $e^{-anT}$  multiplication, 6-18
    - frequency translation, 6-18
    - integral inversion formula, 6-24
    - linearity, 6-16
    - $nT$ , multiplication, 6-17
    - Parseval’s theorem, 6-20
    - partial fraction expansion, 6-22
    - power series expansion, 6-21
    - product, 6-18–6-20
    - region of convergence (ROC), 6-14–6-16
    - shifting and scaling, 6-16
    - time reversal, 6-16–6-17
  - Z-transform pairs, 6-39–6-43



Math

THIRD EDITION

# TRANSFORMS AND APPLICATIONS HANDBOOK

*Editor-in-Chief*

ALEXANDER D. POULARIKAS

Updating the second edition, *Transforms and Applications Handbook, Third Edition* solidifies its place as the complete resource on those mathematical transforms most frequently used by engineers, scientists, and mathematicians. Highlighting the use of transforms and their properties, this latest edition of the bestseller begins with a solid introduction to signals and systems, including properties of the delta function and some classical orthogonal functions.

It then goes on to detail different transforms, including lapped, Mellin, wavelet, and Hartley varieties. Written by top experts, each chapter provides numerous examples and applications that clearly demonstrate the unique purpose and properties of each type. The material is presented in a way that makes it easy for readers from different backgrounds to familiarize themselves with the wide range of transform applications.

Revisiting transforms previously covered, this book adds information on other important ones, including:

- Finite Hankel, Legendre, Jacobi, Gegenbauer, Laguerre, and Hermite
- Fraction Fourier
- Zak
- Continuous and discrete chirp-Fourier
- Multidimensional discrete unitary
- Hilbert–Huang

Most comparable books cover only a few of the transforms addressed here, making this text by far the most useful for anyone involved in signal processing—including electrical and communication engineers, mathematicians, and any other scientist working in this field.

 **CRC Press**  
Taylor & Francis Group  
an informa business

6000 Broken Sound Parkway, NW  
Suite 300, Boca Raton, FL 33487  
270 Madison Avenue  
New York, NY 10016  
2 Park Square, Milton Park  
Abingdon, Oxon OX14 4RN, UK

66528  
ISBN: 978-1-4200-6652-4  
90000  
  
9 781420 066524

[www.crcpress.com](http://www.crcpress.com)